VISIT…

LANZAROTE
Caliente.com

Fundamentals of Materials Science and Engineering

An Interactive *e* • Text

FIFTH EDITION

Fundamentals of Materials Science and Engineering

An Interactive e . Text

William D. Callister, Jr.

Department of Metallurgical Engineering
The University of Utah

John Wiley & Sons, Inc.
New York Chichester Weinheim Brisbane Singapore Toronto

Front Cover: The object that appears on the front cover depicts a monomer unit for polycarbonate (or PC, the plastic that is used in many eyeglass lenses and safety helmets). Red, blue, and yellow spheres represent carbon, hydrogen, and oxygen atoms, respectively.

Back Cover: Depiction of a monomer unit for polyethylene terephthalate (or PET, the plastic used for beverage containers). Red, blue, and yellow spheres represent carbon, hydrogen, and oxygen atoms, respectively.

Editor *Wayne Anderson*
Marketing Manager *Katherine Hepburn*
Associate Production Director *Lucille Buonocore*
Senior Production Editor *Monique Calello*
Cover and Text Designer *Karin Gerdes Kincheloe*
Cover Illustration *Roy Wiemann*
Illustration Studio *Wellington Studio*

This book was set in 10/12 Times Roman by Bi-Comp, Inc., and printed and bound by Von Hoffmann Press. The cover was printed by Phoenix Color Corporation.

This book is printed on acid-free paper. ♾

The paper in this book was manufactured by a mill whose forest management programs include sustained yield harvesting of its timberlands. Sustained yield harvesting principles ensure that the number of trees cut each year does not exceed the amount of new growth.

Copyright © 2001, John Wiley & Sons, Inc. All rights reserved.

No part of this publication may be reproduced, stored in a retrieval system or transmitted in any form or by any means, electronic, mechanical, photocopying, recording, scanning or otherwise, except as permitted under Sections 107 or 108 of the 1976 United States Copyright Act, without either the prior written permission of the Publisher, or authorization through payment of the appropriate per-copy fee to the Copyright Clearance Center, 222 Rosewood Drive, Danvers, MA 01923, (508) 750-8400, fax (508) 750-4470. Requests to the Publisher for permission should be addressed to the Permissions Department, John Wiley & Sons, Inc., 605 Third Avenue, New York, NY 10158-0012, (212) 850-6011, fax (212) 850-6008, e-mail: PERMREQ@WILEY.COM.

To order books or for customer service call 1-800-CALL-WILEY (225-5945).

ISBN 0-471-39551-X

Printed in the United States of America

10 9 8 7 6 5 4 3 2 1

DEDICATED TO THE MEMORY OF
DAVID A. STEVENSON

MY ADVISOR, A COLLEAGUE,
AND FRIEND AT
STANFORD UNIVERSITY

Preface

Fundamentals of Materials Science and Engineering is an alternate version of my text, **Materials Science and Engineering: An Introduction, Fifth Edition.** The contents of both are the same, but the order of presentation differs and **Fundamentals** utilizes newer technologies to enhance teaching and learning.

With regard to the order of presentation, there are two common approaches to teaching materials science and engineering—one that I call the ''traditional'' approach, the other which most refer to as the ''integrated'' approach. With the traditional approach, structures/characteristics/properties of metals are presented first, followed by an analogous discussion of ceramic materials and polymers. **Introduction, Fifth Edition** is organized in this manner, which is preferred by many materials science and engineering instructors. With the integrated approach, one particular structure, characteristic, or property for all three material types is presented before moving on to the discussion of another structure/characteristic/property. This is the order of presentation in **Fundamentals.**

Probably the most common criticism of college textbooks is that they are too long. With most popular texts, the number of pages often increases with each new edition. This leads instructors and students to complain that it is impossible to cover all the topics in the text in a single term. After struggling with this concern (trying to decide what to delete without limiting the value of the text), we decided to divide the text into two components. The first is a set of ''core'' topics—sections of the text that are most commonly covered in an introductory materials course, and second, ''supplementary'' topics—sections of the text covered less frequently. Furthermore, we chose to provide only the core topics in print, but the entire text (both core and supplementary topics) is available on the CD-ROM that is included with the print component of **Fundamentals.** Decisions as to which topics to include in print and which to include only on the CD-ROM were based on the results of a recent survey of instructors and confirmed in developmental reviews. The result is a printed text of approximately 525 pages and an *Interactive eText* on the CD-ROM, which consists of, in addition to the complete text, a wealth of additional resources including interactive software modules, as discussed below.

The text on the CD-ROM with all its various links is navigated using Adobe Acrobat™. These links within the *Interactive eText* include the following: (1) from the Table of Contents to selected *eText* sections; (2) from the index to selected topics within the *eText;* (3) from reference to a figure, table, or equation in one section to the actual figure/table/equation in another section (all figures can be enlarged and printed); (4) from end-of-chapter Important Terms and Concepts to their definitions within the chapter; (5) from in-text boldfaced terms to their corresponding glossary definitions/explanations; (6) from in-text references to the corresponding appendices; (7) from some end-of-chapter problems to their answers; (8) from some answers to their solutions; (9) from software icons to the corresponding interactive modules; and (10) from the opening splash screen to the supporting web site.

The interactive software included on the CD-ROM and noted above is the same that accompanies **Introduction, Fifth Edition.** This software, *Interactive Materials Science and Engineering, Third Edition* consists of interactive simulations and animations that enhance the learning of key concepts in materials science and engineering, a materials selection database, and *E-Z Solve: The Engineer's Equation Solving and Analysis Tool.* Software components are executed when the user clicks on the icons in the margins of the *Interactive eText;* icons for these several components are as follows:

Crystallography and Unit Cells
Ceramic Structures
Polymer Structures
Dislocations
E-Z Solve
Tensile Tests
Diffusion and Design Problem
Solid Solution Strengthening
Phase Diagrams
Database

My primary objective in **Fundamentals** as in **Introduction, Fifth Edition** is to present the basic fundamentals of materials science and engineering on a level appropriate for university/college students who are well grounded in the fundamentals of calculus, chemistry, and physics. In order to achieve this goal, I have endeavored to use terminology that is familiar to the student who is encountering the discipline of materials science and engineering for the first time, and also to define and explain all unfamiliar terms.

The second objective is to present the subject matter in a logical order, from the simple to the more complex. Each chapter builds on the content of previous ones.

The third objective, or philosophy, that I strive to maintain throughout the text is that if a topic or concept is worth treating, then it is worth treating in sufficient detail and to the extent that students have the opportunity to fully understand it without having to consult other sources. In most cases, some practical relevance is provided. Discussions are intended to be clear and concise and to begin at appropriate levels of understanding.

The fourth objective is to include features in the book that will expedite the learning process. These learning aids include numerous illustrations and photographs to help visualize what is being presented, learning objectives, ''Why Study . . .'' items that provide relevance to topic discussions, end-of-chapter questions and problems, answers to selected problems, and some problem solutions to help in self-assessment, a glossary, list of symbols, and references to facilitate understanding the subject matter.

The fifth objective, specific to **Fundamentals,** is to enhance the teaching and learning process using the newer technologies that are available to most instructors and students of engineering today.

Most of the problems in **Fundamentals** require computations leading to numerical solutions; in some cases, the student is required to render a judgment on the basis of the solution. Furthermore, many of the concepts within the discipline of materials science and engineering are descriptive in nature. Thus, questions have also been included that require written, descriptive answers; having to provide a written answer helps the student to better comprehend the associated concept. The questions are of two types: with one type, the student needs only to restate in his/her own words an explanation provided in the text material; other questions require the student to reason through and/or synthesize before coming to a conclusion or solution.

The same engineering design instructional components found in **Introduction, Fifth Edition** are incorporated in **Fundamentals.** Many of these are in Chapter 20, ''Materials Selection and Design Considerations,'' that is on the CD-ROM. This chapter includes five different case studies (a cantilever beam, an automobile valve spring, the artificial hip, the thermal protection system for the Space Shuttle, and packaging for integrated circuits) relative to the materials employed and the rationale behind their use. In addition, a number of design-type (i.e., open-ended) questions/problems are found at the end of this chapter.

Other important materials selection/design features are Appendix B, ''Properties of Selected Engineering Materials,'' and Appendix C, ''Costs and Relative Costs for Selected Engineering Materials.'' The former contains values of eleven properties (e.g., density, strength, electrical resistivity, etc.) for a set of approximately one hundred materials. Appendix C contains prices for this same set of materials. The materials selection database on the CD-ROM is comprised of these data.

SUPPORTING WEB SITE

The web site that supports **Fundamentals** can be found at *www.wiley.com/college/callister.* It contains student and instructor's resources which consist of a more extensive set of learning objectives for all chapters, an index of learning styles (an electronic questionnaire that accesses preferences on ways to learn), a glossary (identical to the one in the text), and links to other web resources. Also included with the Instructor's Resources are suggested classroom demonstrations and lab experiments. Visit the web site often for new resources that we will make available to help teachers teach and students learn materials science and engineering.

INSTRUCTORS' RESOURCES

Resources are available on another CD-ROM specifically for instructors who have adopted **Fundamentals.** These include the following: 1) detailed solutions of all end-of-chapter questions and problems; 2) a list (with brief descriptions) of possible classroom demonstrations and laboratory experiments that portray phenomena and/or illustrate principles that are discussed in the book (also found on the web site); references are also provided that give more detailed accounts of these demonstrations; and 3) suggested course syllabi for several engineering disciplines.

Also available for instructors who have adopted **Fundamentals** as well as **Introduction, Fifth Edition** is an online assessment program entitled *eGrade.* It is a browser-based program that contains a large bank of materials science/engineering problems/questions and their solutions. Each instructor has the ability to construct homework assignments, quizzes, and tests that will be automatically scored, recorded in a gradebook, and calculated into the class statistics. These self-scoring problems/questions can also be made available to students for independent study or pre-class review. Students work online and receive immediate grading and feedback.

Tutorial and Mastery modes provide the student with hints integrated within each problem/question or a tailored study session that recognizes the student's demonstrated learning needs. For more information, visit *www.wiley.com/college/egrade.*

ACKNOWLEDGMENTS

Appreciation is expressed to those who have reviewed and/or made contributions to this alternate version of my text. I am especially indebted to the following individuals: Carl Wood of Utah State University, Rishikesh K. Bharadwaj of Systran Federal Corporation, Martin Searcy of the Agilent Technologies, John H. Weaver of The University of Minnesota, John B. Hudson of Rensselaer Polytechnic Institute, Alan Wolfenden of Texas A & M University, and T. W. Coyle of the University of Toronto.

I am also indebted to Wayne Anderson, Sponsoring Editor, to Monique Calello, Senior Production Editor, Justin Nisbet, Electronic Publishing Analyst at Wiley, and Lilian N. Brady, my proofreader, for their assistance and guidance in developing and producing this work. In addition, I thank Professor Saskia Duyvesteyn, Department of Metallurgical Engineering, University of Utah, for generating the *e-Grade* bank of questions/problems/solutions.

Since I undertook the task of writing my first text on this subject in the early 1980's, instructors and students, too numerous to mention, have shared their input and contributions on how to make this work more effective as a teaching and learning tool. To all those who have helped, I express my sincere thanks!

Last, but certainly not least, the continual encouragement and support of my family and friends is deeply and sincerely appreciated.

WILLIAM D. CALLISTER, JR.

Salt Lake City, Utah
August 2000

Contents

Chapters 1 through 13 discuss core topics (found in both print and on the CD-ROM) and supplementary topics (in the eText *only)*

LIST OF SYMBOLS xix

1. *Introduction 1*

Learning Objectives 2
1.1 Historical Perspective 2
1.2 Materials Science and Engineering 2
1.3 Why Study Materials Science and Engineering? 4
1.4 Classification of Materials 5
1.5 Advanced Materials 6
1.6 Modern Materials' Needs 6
References 7

2. *Atomic Structure and Interatomic Bonding 9*

Learning Objectives 10
2.1 Introduction 10

ATOMIC STRUCTURE 10

2.2 Fundamental Concepts 10
2.3 Electrons in Atoms 11
2.4 The Periodic Table 17

ATOMIC BONDING IN SOLIDS 18

2.5 Bonding Forces and Energies 18
2.6 Primary Interatomic Bonds 20
2.7 Secondary Bonding or Van der Waals Bonding 24
2.8 Molecules 26
Summary 27
Important Terms and Concepts 27
References 28
Questions and Problems 28

3. *Structures of Metals and Ceramics 30*

Learning Objectives 31
3.1 Introduction 31

CRYSTAL STRUCTURES 31

3.2 Fundamental Concepts 31
3.3 Unit Cells 32
3.4 Metallic Crystal Structures 33

3.5 Density Computations—Metals 37
3.6 Ceramic Crystal Structures 38
3.7 Density Computations—Ceramics 45
3.8 Silicate Ceramics 46
• **The Silicates (CD-ROM)** S-1
3.9 Carbon 47
• **Fullerenes (CD-ROM)** S-3
3.10 Polymorphism and Allotropy 49
3.11 Crystal Systems 49

CRYSTALLOGRAPHIC DIRECTIONS AND PLANES **51**

3.12 Crystallographic Directions 51
3.13 Crystallographic Planes 54
• **3.14 Linear and Planar Atomic Densities (CD-ROM)** S-4
3.15 Close-Packed Crystal Structures 58

CRYSTALLINE AND NONCRYSTALLINE MATERIALS **62**

3.16 Single Crystals 62
3.17 Polycrystalline Materials 62
3.18 Anisotropy 63
• **3.19 X-Ray Diffraction: Determination of Crystal Structures (CD-ROM)** S-6
3.20 Noncrystalline Solids 64
Summary 66
Important Terms and Concepts 67
References 67
Questions and Problems 68

4. Polymer Structures 76

Learning Objectives 77
4.1 Introduction 77
4.2 Hydrocarbon Molecules 77
4.3 Polymer Molecules 79
4.4 The Chemistry of Polymer Molecules 80
4.5 Molecular Weight 82
4.6 Molecular Shape 87
4.7 Molecular Structure 88
• **4.8 Molecular Configurations (CD-ROM)** S-11
4.9 Thermoplastic and Thermosetting Polymers 90
4.10 Copolymers 91
4.11 Polymer Crystallinity 92
4.12 Polymer Crystals 95
Summary 97
Important Terms and Concepts 98
References 98
Questions and Problems 99

5. Imperfections in Solids 102

Learning Objectives 103
5.1 Introduction 103

POINT DEFECTS **103**

5.2 Point Defects in Metals 103
5.3 Point Defects in Ceramics 105
5.4 Impurities in Solids 107
5.5 Point Defects in Polymers 110
5.6 Specification of Composition 110
• **Composition Conversions (CD-ROM)** S-14

MISCELLANEOUS IMPERFECTIONS **111**

5.7 Dislocations—Linear Defects 111
5.8 Interfacial Defects 115
5.9 Bulk or Volume Defects 118
5.10 Atomic Vibrations 118

MICROSCOPIC EXAMINATION **118**

5.11 General 118
• **5.12 Microscopic Techniques (CD-ROM)** S-17
5.13 Grain Size Determination 119
Summary 120
Important Terms and Concepts 121
References 121
Questions and Problems 122

6. Diffusion 126

Learning Objectives 127
6.1 Introduction 127
6.2 Diffusion Mechanisms 127
6.3 Steady-State Diffusion 130
6.4 Nonsteady-State Diffusion 132
6.5 Factors That Influence Diffusion 136
6.6 Other Diffusion Paths 141
6.7 Diffusion in Ionic and Polymeric Materials 141
Summary 142
Important Terms and Concepts 142
References 142
Questions and Problems 143

7. Mechanical Properties 147

Learning Objectives 148
7.1 Introduction 148
7.2 Concepts of Stress and Strain 149

ELASTIC DEFORMATION **153**

7.3 Stress–Strain Behavior 153
7.4 Anelasticity 157
7.5 Elastic Properties of Materials 157

MECHANICAL BEHAVIOR—METALS 160

7.6 Tensile Properties 160
7.7 True Stress and Strain 167
7.8 Elastic Recovery During Plastic Deformation 170
7.9 Compressive, Shear, and Torsional Deformation 170

MECHANICAL BEHAVIOR—CERAMICS 171

7.10 Flexural Strength 171
7.11 Elastic Behavior 173
• **7.12 Influence of Porosity on the Mechanical Properties of Ceramics (CD-ROM)** S-22

MECHANICAL BEHAVIOR—POLYMERS 173

7.13 Stress–Strain Behavior 173
7.14 Macroscopic Deformation 175
• **7.15 Viscoelasticity (CD-ROM)** S-22

HARDNESS AND OTHER MECHANICAL PROPERTY CONSIDERATIONS 176

7.16 Hardness 176
7.17 Hardness of Ceramic Materials 181
7.18 Tear Strength and Hardness of Polymers 181

PROPERTY VARIABILITY AND DESIGN/SAFETY FACTORS 183

7.19 Variability of Material Properties 183
• **Computation of Average and Standard Deviation Values (CD-ROM)** S-28
7.20 Design/Safety Factors 183
Summary 185
Important Terms and Concepts 186
References 186
Questions and Problems 187

8. Deformation and Strengthening Mechanisms 197

Learning Objectives 198
8.1 Introduction 198

DEFORMATION MECHANISMS FOR METALS 198

8.2 Historical 198
8.3 Basic Concepts of Dislocations 199
8.4 Characteristics of Dislocations 201
8.5 Slip Systems 203
• **8.6 Slip in Single Crystals (CD-ROM)** S-31
8.7 Plastic Deformation of Polycrystalline Metals 204
• **8.8 Deformation by Twinning (CD-ROM)** S-34

MECHANISMS OF STRENGTHENING IN METALS 206

8.9 Strengthening by Grain Size Reduction 206
8.10 Solid-Solution Strengthening 208
8.11 Strain Hardening 210

RECOVERY, RECRYSTALLIZATION, AND GRAIN GROWTH 213

8.12 Recovery 213
8.13 Recrystallization 213
8.14 Grain Growth 218

DEFORMATION MECHANISMS FOR CERAMIC MATERIALS 219

8.15 Crystalline Ceramics 220
8.16 Noncrystalline Ceramics 220

MECHANISMS OF DEFORMATION AND FOR STRENGTHENING OF POLYMERS 221

8.17 Deformation of Semicrystalline Polymers 221
• **8.18a Factors That Influence the Mechanical Properties of Semicrystalline Polymers [Detailed Version (CD-ROM)]** S-35
8.18b Factors That Influence the Mechanical Properties of Semicrystalline Polymers (Concise Version) 223
8.19 Deformation of Elastomers 224
Summary 227
Important Terms and Concepts 228
References 228
Questions and Problems 228

9. Failure 234

Learning Objectives 235
9.1 Introduction 235

FRACTURE 235

9.2 Fundamentals of Fracture 235
9.3 Ductile Fracture 236
• **Fractographic Studies (CD-ROM)** S-38
9.4 Brittle Fracture 238
• **9.5a Principles of Fracture Mechanics [Detailed Version (CD-ROM)]** S-38
9.5b Principles of Fracture Mechanics (Concise Version) 238
9.6 Brittle Fracture of Ceramics 248
• **Static Fatigue (CD-ROM)** S-53
9.7 Fracture of Polymers 249
9.8 Impact Fracture Testing 250

FATIGUE 255

9.9 Cyclic Stresses 255
9.10 The S-N Curve 257
9.11 Fatigue in Polymeric Materials 260
• **9.12a Crack Initiation and Propagation [Detailed Version (CD-ROM)]** S-54
9.12b Crack Initiation and Propagation (Concise Version) 260
• **9.13 Crack Propagation Rate (CD-ROM)** S-57
9.14 Factors That Affect Fatigue Life 263
• **9.15 Environmental Effects (CD-ROM)** S-62

CREEP 265

9.16 Generalized Creep Behavior 266
• **9.17a Stress and Temperature Effects [Detailed Version (CD-ROM)]** S-63
9.17b Stress and Temperature Effects (Concise Version) 267
• **9.18 Data Extrapolation Methods (CD-ROM)** S-65
9.19 Alloys for High-Temperature Use 268
9.20 Creep in Ceramic and Polymeric Materials 269
Summary 269
Important Terms and Concepts 272
References 272
Questions and Problems 273

10 Phase Diagrams 281

Learning Objectives 282
10.1 Introduction 282

DEFINITIONS AND BASIC CONCEPTS 282

10.2 Solubility Limit 283
10.3 Phases 283
10.4 Microstructure 284
10.5 Phase Equilibria 284

EQUILIBRIUM PHASE DIAGRAMS 285

10.6 Binary Isomorphous Systems 286
10.7 Interpretation of Phase Diagrams 288
• **10.8 Development of Microstructure in Isomorphous Alloys (CD-ROM)** S-67
10.9 Mechanical Properties of Isomorphous Alloys 292
10.10 Binary Eutectic Systems 292
• **10.11 Development of Microstructure in Eutectic Alloys (CD-ROM)** S-70
10.12 Equilibrium Diagrams Having Intermediate Phases or Compounds 297
10.13 Eutectoid and Peritectic Reactions 298
10.14 Congruent Phase Transformations 301
• **10.15 Ceramic Phase Diagrams (CD-ROM)** S-77
10.16 Ternary Phase Diagrams 301
• **10.17 The Gibbs Phase Rule (CD-ROM)** S-81

THE IRON–CARBON SYSTEM 302

10.18 The Iron–Iron Carbide (Fe–Fe_3C) Phase Diagram 302
10.19 Development of Microstructures in Iron–Carbon Alloys 305
• **10.20 The Influence of Other Alloying Elements (CD-ROM)** S-83
Summary 313
Important Terms and Concepts 314
References 314
Questions and Problems 315

11 Phase Transformations 323

Learning Objectives 324
11.1 Introduction 324

PHASE TRANSFORMATIONS IN METALS 324

11.2 Basic Concepts 325
11.3 The Kinetics of Solid-State Reactions 325
11.4 Multiphase Transformations 327

MICROSTRUCTURAL AND PROPERTY CHANGES IN IRON–CARBON ALLOYS 327

11.5 Isothermal Transformation Diagrams 328
• **11.6 Continuous Cooling Transformation Diagrams (CD-ROM)** S-85
11.7 Mechanical Behavior of Iron–Carbon Alloys 339
11.8 Tempered Martensite 344
11.9 Review of Phase Transformations for Iron–Carbon Alloys 346

PRECIPITATION HARDENING 347

11.10 Heat Treatments 347
11.11 Mechanism of Hardening 349
11.12 Miscellaneous Considerations 351

CRYSTALLIZATION, MELTING, AND GLASS TRANSITION PHENOMENA IN POLYMERS 352

11.13 Crystallization 353
11.14 Melting 354
11.15 The Glass Transition 354
11.16 Melting and Glass Transition Temperatures 354
• **11.17 Factors That Influence Melting and Glass Transition Temperatures (CD-ROM)** S-87

Summary 356
Important Terms and Concepts 357
References 357
Questions and Problems 358

12. Electrical Properties 365

Learning Objectives 366
12.1 Introduction 366

ELECTRICAL CONDUCTION **366**

12.2 Ohm's Law 366
12.3 Electrical Conductivity 367
12.4 Electronic and Ionic Conduction 368
12.5 Energy Band Structures in Solids 368
12.6 Conduction in Terms of Band and Atomic Bonding Models 371
12.7 Electron Mobility 372
12.8 Electrical Resistivity of Metals 373
12.9 Electrical Characteristics of Commercial Alloys 376

SEMICONDUCTIVITY **376**

12.10 Intrinsic Semiconduction 377
12.11 Extrinsic Semiconduction 379
12.12 The Temperature Variation of Conductivity and Carrier Concentration 383
• **12.13 The Hall Effect (CD-ROM)** S-91
• **12.14 Semiconductor Devices (CD-ROM)** S-93

ELECTRICAL CONDUCTION IN IONIC CERAMICS AND IN POLYMERS **389**

12.15 Conduction in Ionic Materials 389
12.16 Electrical Properties of Polymers 390

DIELECTRIC BEHAVIOR **391**

• **12.17 Capacitance (CD-ROM)** S-99
• **12.18 Field Vectors and Polarization (CD-ROM)** S-101
• **12.19 Types of Polarization (CD-ROM)** S-105
• **12.20 Frequency Dependence of the Dielectric Constant (CD-ROM)** S-106
• **12.21 Dielectric Strength (CD-ROM)** S-107
• **12.22 Dielectric Materials (CD-ROM)** S-107

OTHER ELECTRICAL CHARACTERISTICS OF MATERIALS **391**

• **12.23 Ferroelectricity (CD-ROM)** S-108
• **12.24 Piezoelectricity (CD-ROM)** S-109
Summary 391
Important Terms and Concepts 393
References 393
Questions and Problems 394

13. Types and Applications of Materials 401

Learning Objectives 402
13.1 Introduction 402

TYPES OF METAL ALLOYS **402**

13.2 Ferrous Alloys 402
13.3 Nonferrous Alloys 414

TYPES OF CERAMICS **422**

13.4 Glasses 423
13.5 Glass–Ceramics 423
13.6 Clay Products 424
13.7 Refractories 424
• **Fireclay, Silica, Basic, and Special Refractories (CD-ROM)** S-110
13.8 Abrasives 425
13.9 Cements 425
• **13.10 Advanced Ceramics (CD-ROM)** S-111
13.11 Diamond and Graphite 427

TYPES OF POLYMERS **428**

13.12 Plastics 428
13.13 Elastomers 431
13.14 Fibers 432
13.15 Miscellaneous Applications 433
• **13.16 Advanced Polymeric Materials (CD-ROM)** S-113
Summary 434
Important Terms and Concepts 435
References 435
Questions and Problems 436

Chapters 14 through 21 discuss just supplementary topics, and are found only on the CD-ROM (and not in print)

14. Synthesis, Fabrication, and Processing of Materials (CD-ROM) *S-118*

Learning Objectives S-119
14.1 Introduction S-119

FABRICATION OF METALS **S-119**

14.2 Forming Operations S-119
14.3 Casting S-121
14.4 Miscellaneous Techniques S-122

THERMAL PROCESSING OF METALS S-124

14.5 Annealing Processes S-124
14.6 Heat Treatment of Steels S-126

FABRICATION OF CERAMIC MATERIALS S-136

14.7 Fabrication and Processing of Glasses S-137
14.8 Fabrication of Clay Products S-142
14.9 Powder Pressing S-145
14.10 Tape Casting S-149

SYNTHESIS AND FABRICATION OF POLYMERS S-149

14.11 Polymerization S-150
14.12 Polymer Additives S-151
14.13 Forming Techniques for Plastics S-153
14.14 Fabrication of Elastomers S-155
14.15 Fabrication of Fibers and Films S-155
Summary S-156
Important Terms and Concepts S-157
References S-158
Questions and Problems S-158

15. *Composites* (CD-ROM) *S-162*

Learning Objectives S-163
15.1 Introduction S-163

PARTICLE-REINFORCED COMPOSITES S-165

15.2 Large-Particle Composites S-165
15.3 Dispersion-Strengthened Composites S-169

FIBER-REINFORCED COMPOSITES S-170

15.4 Influence of Fiber Length S-170
15.5 Influence of Fiber Orientation and Concentration S-171
15.6 The Fiber Phase S-180
15.7 The Matrix Phase S-180
15.8 Polymer–Matrix Composites S-182
15.9 Metal–Matrix Composites S-185
15.10 Ceramic–Matrix Composites S-186
15.11 Carbon–Carbon Composites S-188
15.12 Hybrid Composites S-189
15.13 Processing of Fiber-Reinforced Composites S-189

STRUCTURAL COMPOSITES S-195

15.14 Laminar Composites S-195
15.15 Sandwich Panels S-196
Summary S-196
Important Terms and Concepts S-198
References S-198
Questions and Problems S-199

16. *Corrosion and Degradation of Materials* (CD-ROM) *S-204*

Learning Objectives S-205
16.1 Introduction S-205

CORROSION OF METALS S-205

16.2 Electrochemical Considerations S-206
16.3 Corrosion Rates S-212
16.4 Prediction of Corrosion Rates S-214
16.5 Passivity S-221
16.6 Environmental Effects S-222
16.7 Forms of Corrosion S-223
16.8 Corrosion Environments S-231
16.9 Corrosion Prevention S-232
16.10 Oxidation S-234

CORROSION OF CERAMIC MATERIALS S-237

DEGRADATION OF POLYMERS S-237

16.11 Swelling and Dissolution S-238
16.12 Bond Rupture S-238
16.13 Weathering S-241
Summary S-241
Important Terms and Concepts S-242
References S-242
Questions and Problems S-243

17. *Thermal Properties* (CD-ROM) *S-247*

Learning Objectives S-248
17.1 Introduction S-248
17.2 Heat Capacity S-248
17.3 Thermal Expansion S-250
17.4 Thermal Conductivity S-253
17.5 Thermal Stresses S-256
Summary S-258
Important Terms and Concepts S-259
References S-259
Questions and Problems S-259

18. *Magnetic Properties* (CD-ROM) *S-263*

Learning Objectives S-264
18.1 Introduction S-264
18.2 Basic Concepts S-264
18.3 Diamagnetism and Paramagnetism S-268
18.4 Ferromagnetism S-270
18.5 Antiferromagnetism and Ferrimagnetism S-272
18.6 The Influence of Temperature on Magnetic Behavior S-276
18.7 Domains and Hysteresis S-276
18.8 Soft Magnetic Materials S-280
18.9 Hard Magnetic Materials S-282

18.10 Magnetic Storage S-284
18.11 Superconductivity S-287
Summary S-291
Important Terms and Concepts S-292
References S-292
Questions and Problems S-292

19. Optical Properties (CD-ROM) *S-297*

Learning Objectives S-298
19.1 Introduction S-298

BASIC CONCEPTS S-298

19.2 Electromagnetic Radiation S-298
19.3 Light Interactions with Solids S-300
19.4 Atomic and Electronic Interactions S-301

OPTICAL PROPERTIES OF METALS S-302
OPTICAL PROPERTIES OF NONMETALS S-303

19.5 Refraction S-303
19.6 Reflection S-304
19.7 Absorption S-305
19.8 Transmission S-308
19.9 Color S-309
19.10 Opacity and Translucency in Insulators S-310

APPLICATIONS OF OPTICAL PHENOMENA S-311

19.11 Luminescence S-311
19.12 Photoconductivity S-312
19.13 Lasers S-313
19.14 Optical Fibers in Communications S-315
Summary S-320
Important Terms and Concepts S-321
References S-321
Questions and Problems S-322

20. Materials Selection and Design Considerations (CD-ROM) *S-324*

Learning Objectives S-325
20.1 Introduction S-325

MATERIALS SELECTION FOR A TORSIONALLY STRESSED CYLINDRICAL SHAFT S-325

20.2 Strength S-326
20.3 Other Property Considerations and the Final Decision S-331

AUTOMOBILE VALVE SPRING S-332

20.4 Introduction S-332
20.5 Automobile Valve Spring S-334

ARTIFICIAL TOTAL HIP REPLACEMENT S-339

20.6 Anatomy of the Hip Joint S-339
20.7 Material Requirements S-341
20.8 Materials Employed S-343

THERMAL PROTECTION SYSTEM ON THE SPACE SHUTTLE ORBITER S-345

20.9 Introduction S-345
20.10 Thermal Protection System—Design Requirements S-345
20.11 Thermal Protection System—Components S-347

MATERIALS FOR INTEGRATED CIRCUIT PACKAGES S-351

20.12 Introduction S-351
20.13 Leadframe Design and Materials S-353
20.14 Die Bonding S-354
20.15 Wire Bonding S-356
20.16 Package Encapsulation S-358
20.17 Tape Automated Bonding S-360
Summary S-362
References S-363
Questions and Problems S-364

21. Economic, Environmental, and Societal Issues in Materials Science and Engineering (CD-ROM) *S-368*

Learning Objectives S-369
21.1 Introduction S-369

ECONOMIC CONSIDERATIONS S-369

21.2 Component Design S-370
21.3 Materials S-370
21.4 Manufacturing Techniques S-370

ENVIRONMENTAL AND SOCIETAL CONSIDERATIONS S-371

21.5 Recycling Issues in Materials Science and Engineering S-373
Summary S-376
References S-376

Appendix A The International System of Units (SI) 439

Appendix B Properties of Selected Engineering Materials 441

B.1 Density 441
B.2 Modulus of Elasticity 444
B.3 Poisson's Ratio 448
B.4 Strength and Ductility 449
B.5 Plane Strain Fracture Toughness 454
B.6 Linear Coefficient of Thermal Expansion 455
B.7 Thermal Conductivity 459

B.8 Specific Heat 462
B.9 Electrical Resistivity 464
B.10 Metal Alloy Compositions 467

Appendix C Costs and Relative Costs for Selected Engineering Materials 469

Appendix D Mer Structures for Common Polymers 475

Appendix E Glass Transition and Melting Temperatures for Common Polymeric Materials 479

Glossary 480

Answers to Selected Problems 495

Index 501

List of Symbols

The number of the section in which a symbol is introduced or explained is given in parentheses.

A = area
Å = angstrom unit
A_i = atomic weight of element i (2.2)
APF = atomic packing factor (3.4)
%RA = ductility, in percent reduction in area (7.6)
a = lattice parameter: unit cell x-axial length (3.4)
a = crack length of a surface crack (9.5a, 9.5b)
at% = atom percent (5.6)
B = magnetic flux density (induction) (18.2)
B_r = magnetic remanence (18.7)
BCC = body-centered cubic crystal structure (3.4)
b = lattice parameter: unit cell y-axial length (3.11)
$\mathbf{b}$ = Burgers vector (5.7)
C = capacitance (12.17)
C_i = concentration (composition) of component i in wt% (5.6)
C_i' = concentration (composition) of component i in at% (5.6)
C_v, C_p = heat capacity at constant volume, pressure (17.2)
CPR = corrosion penetration rate (16.3)
CVN = Charpy V-notch (9.8)
%CW = percent cold work (8.11)
c = lattice parameter: unit cell z-axial length (3.11)
c = velocity of electromagnetic radiation in a vacuum (19.2)
D = diffusion coefficient (6.3)
D = dielectric displacement (12.18)
d = diameter
d = average grain diameter (8.9)
d_{hkl} = interplanar spacing for planes of Miller indices h, k, and l (3.19)
E = energy (2.5)
E = modulus of elasticity or Young's modulus (7.3)
$\mathscr{E}$ = electric field intensity (12.3)
E_f = Fermi energy (12.5)
E_g = band gap energy (12.6)
$E_r(t)$ = relaxation modulus (7.15)
%EL = ductility, in percent elongation (7.6)
e = electric charge per electron (12.7)
e^- = electron (16.2)
erf = Gaussian error function (6.4)
exp = e, the base for natural logarithms
F = force, interatomic or mechanical (2.5, 7.2)
$\mathscr{F}$ = Faraday constant (16.2)
FCC = face-centered cubic crystal structure (3.4)
G = shear modulus (7.3)
H = magnetic field strength (18.2)
H_c = magnetic coercivity (18.7)
HB = Brinell hardness (7.16)
HCP = hexagonal close-packed crystal structure (3.4)
HK = Knoop hardness (7.16)
HRB, HRF = Rockwell hardness: B and F scales (7.16)

HR15N, HR45W = superficial Rockwell hardness: 15N and 45W scales (7.16)

HV = Vickers hardness (7.16)

h = Planck's constant (19.2)

(hkl) = Miller indices for a crystallographic plane (3.13)

I = electric current (12.2)

I = intensity of electromagnetic radiation (19.3)

i = current density (16.3)

i_C = corrosion current density (16.4)

J = diffusion flux (6.3)

J = electric current density (12.3)

K = stress intensity factor (9.5a)

K_c = fracture toughness (9.5a, 9.5b)

K_{Ic} = plane strain fracture toughness for mode I crack surface displacement (9.5a, 9.5b)

k = Boltzmann's constant (5.2)

k = thermal conductivity (17.4)

l = length

l_c = critical fiber length (15.4)

ln = natural logarithm

log = logarithm taken to base 10

M = magnetization (18.2)

$\overline{M}_n$ = polymer number-average molecular weight (4.5)

$\overline{M}_w$ = polymer weight-average molecular weight (4.5)

mol% = mole percent

N = number of fatigue cycles (9.10)

N_{A} = Avogadro's number (3.5)

N_f = fatigue life (9.10)

n = principal quantum number (2.3)

n = number of atoms per unit cell (3.5)

n = strain-hardening exponent (7.7)

n = number of electrons in an electrochemical reaction (16.2)

n = number of conducting electrons per cubic meter (12.7)

n = index of refraction (19.5)

n' = for ceramics, the number of formula units per unit cell (3.7)

n_n = number-average degree of polymerization (4.5)

n_w = weight-average degree of polymerization (4.5)

P = dielectric polarization (12.18)

P–B ratio = Pilling–Bedworth ratio (16.10)

p = number of holes per cubic meter (12.10)

Q = activation energy

Q = magnitude of charge stored (12.17)

R = atomic radius (3.4)

R = gas constant

r = interatomic distance (2.5)

r = reaction rate (11.3, 16.3)

r_{A}, r_{C} = anion and cation ionic radii (3.6)

S = fatigue stress amplitude (9.10)

SEM = scanning electron microscopy or microscope

T = temperature

T_c = Curie temperature (18.6)

T_C = superconducting critical temperature (18.11)

T_g = glass transition temperature (11.15)

T_m = melting temperature

TEM = transmission electron microscopy or microscope

TS = tensile strength (7.6)

t = time

t_r = rupture lifetime (9.16)

U_r = modulus of resilience (7.6)

$[uvw]$ = indices for a crystallographic direction (3.12)

V = electrical potential difference (voltage) (12.2)

V_C = unit cell volume (3.4)

V_C = corrosion potential (16.4)

V_{H} = Hall voltage (12.13)

V_i = volume fraction of phase i (10.7)

v = velocity

vol% = volume percent

W_i = mass fraction of phase i (10.7)

wt% = weight percent (5.6)

x = length
x = space coordinate
Y = dimensionless parameter or function in fracture toughness expression (9.5a, 9.5b)
y = space coordinate
z = space coordinate
α = lattice parameter: unit cell y-z interaxial angle (3.11)
α, β, γ = phase designations
α_l = linear coefficient of thermal expansion (17.3)
β = lattice parameter: unit cell x-z interaxial angle (3.11)
γ = lattice parameter: unit cell x-y interaxial angle (3.11)
γ = shear strain (7.2)
Δ = finite change in a parameter the symbol of which it precedes
ϵ = engineering strain (7.2)
ϵ = dielectric permittivity (12.17)
ϵ_r = dielectric constant or relative permittivity (12.17)
$\dot{\epsilon}_s$ = steady-state creep rate (9.16)
ϵ_T = true strain (7.7)
η = viscosity (8.16)
η = overvoltage (16.4)
θ = Bragg diffraction angle (3.19)
θ_{D} = Debye temperature (17.2)
λ = wavelength of electromagnetic radiation (3.19)
μ = magnetic permeability (18.2)
μ_{B} = Bohr magneton (18.2)
μ_r = relative magnetic permeability (18.2)
μ_e = electron mobility (12.7)
μ_h = hole mobility (12.10)
ν = Poisson's ratio (7.5)
ν = frequency of electromagnetic radiation (19.2)
ρ = density (3.5)
ρ = electrical resistivity (12.2)
ρ_t = radius of curvature at the tip of a crack (9.5a, 9.5b)
σ = engineering stress, tensile or compressive (7.2)
σ = electrical conductivity (12.3)
σ^* = longitudinal strength (composite) (15.5)
σ_c = critical stress for crack propagation (9.5a, 9.5b)
σ_{fs} = flexural strength (7.10)
σ_m = maximum stress (9.5a, 9.5b)
σ_m = mean stress (9.9)
σ'_m = stress in matrix at composite failure (15.5)
σ_T = true stress (7.7)
σ_w = safe or working stress (7.20)
σ_y = yield strength (7.6)
τ = shear stress (7.2)
τ_c = fiber–matrix bond strength/matrix shear yield strength (15.4)
τ_{crss} = critical resolved shear stress (8.6)
χ_m = magnetic susceptibility (18.2)

SUBSCRIPTS

c = composite
cd = discontinuous fibrous composite
cl = longitudinal direction (aligned fibrous composite)
ct = transverse direction (aligned fibrous composite)
f = final
f = at fracture
f = fiber
i = instantaneous
m = matrix
m, max = maximum
min = minimum
0 = original
0 = at equilibrium
0 = in a vacuum

Chapter 20 / Materials Selection and Design Considerations

Shown in this photograph is the landing of the *Atlantis* Space Shuttle Orbiter. This chapter discusses the materials that are used for its outer airframe's thermal protection system. [Photograph courtesy the National Aeronautics and Space Administration (NASA).]

Why Study *Materials Selection and Design Considerations?*

Perhaps one of the most important tasks that an engineer may be called upon to perform is that of materials selection with regard to component design. Inappropriate or improper decisions can be disastrous from both economic and safety perspectives. Therefore, it is essential that the engineering student become familiar with and versed in the procedures and protocols that are normally employed in this process. This chapter discusses materials selection issues in several contexts and from various perspectives.

Learning Objectives

After careful study of this chapter you should be able to do the following:

1. **Describe how the strength performance index for a solid cylindrical shaft is determined.**
2. **Describe the manner in which materials selection charts are employed in the materials selection process.**
3. **Briefly describe the steps that are used to ascertain whether or not a particular metal alloy is suitable for use in an automobile valve spring.**
4. **List and briefly explain six biocompatibility considerations relative to materials that are employed in artificial hip replacements.**
5. **Name the four components found in the artificial hip replacement, and, for each, list its specific material requirements.**
6. **(a) Name the three components of the thermal protection system for the Space Shuttle Orbiter. (b) Describe the composition, microstructure, and general properties of the ceramic tiles that are used on the Space Shuttle Orbiter.**
7. **Describe the components and their functions for an integrated circuit leadframe.**
8. **(a) Name and briefly describe the three processes that are carried out during integrated circuit packaging. (b) Note property requirements for each of these processes, and, in addition, cite at least two materials that are employed.**

20.1 INTRODUCTION

Virtually the entire book to this point has dealt with the properties of various materials, how the properties of a specific material are dependent on its structure, and, in many cases, how structure may be fashioned by the processing technique that is employed during production. Of late, there has been a trend to emphasize the element of *design* in engineering pedagogy. To a materials scientist or materials engineer, design can be taken in several contexts. First of all, it can mean designing new materials having unique property combinations. Alternatively, design can involve selecting a new material having a better combination of characteristics for a specific application; choice of material cannot be made without consideration of necessary manufacturing processes (e.g., forming, welding, etc.), which also rely on material properties. Or, finally, design might mean developing a process for producing a material having better properties.

One particularly effective technique for teaching design principles is the case study method. With this technique, the solutions to real-life engineering problems are carefully analyzed in detail so that the student may observe the procedures and rationale that are involved in the decision-making process. We have chosen to perform five case studies which draw upon principles that were introduced in previous chapters. These five studies involve materials that are used for the following: (1) a torsionally stressed cylindrical shaft; (2) an automobile valve spring; (3) the artificial total hip replacement; (4) the thermal protection system on the Space Shuttle Orbiter; and (5) integrated circuit packages.

MATERIALS SELECTION FOR A TORSIONALLY STRESSED CYLINDRICAL SHAFT

We begin by addressing the design process from the perspective of materials selection; that is, for some application, selecting a material having a desirable or optimum property or combination of properties. Elements of this materials selection process involve deciding on the constraints of the problem, and, from these, establishing criteria that can be used in materials selection to maximize performance.

The component or structural element we have chosen to discuss is a solid cylindrical shaft that is subjected to a torsional stress. Strength of the shaft will be considered in detail, and criteria will be developed for the maximization of strength with respect to both minimum material mass and minimum cost. Other parameters and properties that may be important in this selection process are also discussed briefly.

20.2 STRENGTH

For this portion of the problem, we will establish a criterion for selection of light and strong materials for this shaft. It will be assumed that the twisting moment and length of the shaft are specified, whereas the radius (or cross-sectional area) may be varied. We develop an expression for the mass of material required in terms of twisting moment, shaft length, and density and strength of the material. Using this expression, it will be possible to evaluate the performance—that is, maximize the strength of this torsionally stressed shaft with respect to mass and, in addition, relative to material cost.

Consider the cylindrical shaft of length L and radius r, as shown in Figure 20.1. The application of twisting moment (or torque), M_t produces an angle of twist ϕ. Shear stress τ at radius r is defined by the equation

$$\tau = \frac{M_t r}{J} \tag{20.1}$$

Here, J is the polar moment of inertia, which for a solid cylinder is

$$J = \frac{\pi r^4}{2} \tag{20.2}$$

Thus,

$$\tau = \frac{2M_t}{\pi r^3} \tag{20.3}$$

A safe design calls for the shaft to be able to sustain some twisting moment without fracture. In order to establish a materials selection criterion for a light and strong material, we replace the shear stress in Equation 20.3 with the shear strength of the material τ_f divided by a factor of safety N, as

$$\frac{\tau_f}{N} = \frac{2M_t}{\pi r^3} \tag{20.4}$$

It is now necessary to take into consideration material mass. The mass m of any given quantity of material is just the product of its density (ρ) and volume. Since the volume of a cylinder is just $\pi r^2 L$, then

$$m = \pi r^2 L\rho \tag{20.5}$$

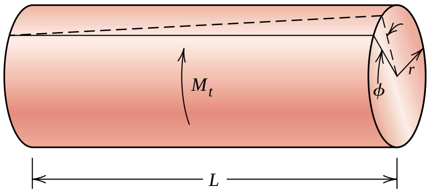

FIGURE 20.1 A solid cylindrical shaft that experiences an angle of twist ϕ in response to the application of a twisting moment M_t.

Or, the radius of the shaft in terms of its mass is just

$$r = \sqrt{\frac{m}{\pi L \rho}} \tag{20.6}$$

Substitution of this r expression into Equation 20.4 leads to

$$\frac{\tau_f}{N} = \frac{2M_t}{\pi\left(\sqrt{\dfrac{m}{\pi L \rho}}\right)^3}$$

$$= 2M_t\sqrt{\frac{\pi L^3 \rho^3}{m^3}} \tag{20.7}$$

Solving this expression for the mass m yields

$$m = (2NM_t)^{2/3}(\pi^{1/3}L)\left(\frac{\rho}{\tau_f^{2/3}}\right) \tag{20.8}$$

The parameters on the right-hand side of this equation are grouped into three sets of parentheses. Those contained within the first set (i.e., N and M_t) relate to the safe functioning of the shaft. Within the second parentheses is L, a geometric parameter. And, finally, the material properties of density and strength are contained within the last set.

The upshot of Equation 20.8 is that the best materials to be used for a light shaft which can safely sustain a specified twisting moment are those having low $\rho/\tau_f^{2/3}$ ratios. In terms of material suitability, it is sometimes preferable to work with what is termed a *performance index*, P, which is just the reciprocal of this ratio; that is

$$P = \frac{\tau_f^{2/3}}{\rho} \tag{20.9}$$

In this context we want to utilize a material having a large performance index.

At this point it becomes necessary to examine the performance indices of a variety of potential materials. This procedure is expedited by the utilization of what are termed *materials selection charts.*[1] These are plots of the values of one material property versus those of another property. Both axes are scaled logarithmically and usually span about five orders of magnitude, so as to include the properties of virtually all materials. For example, for our problem, the chart of interest is logarithm of strength versus logarithm of density, which is shown in Figure 20.2.[2] It may be noted on this plot that materials of a particular type (e.g., woods, engineering polymers, etc.) cluster together and are enclosed within an envelope delineated with a bold line. Subclasses within these clusters are enclosed using finer lines.

---

[1] A comprehensive collection of these charts may be found in M. F. Ashby, *Materials Selection in Mechanical Design,* Pergamon Press, Oxford, 1992.

[2] Strength for metals and polymers is taken as yield strength, for ceramics and glasses, compressive strength, for elastomers, tear strength, and for composites, tensile failure strength.

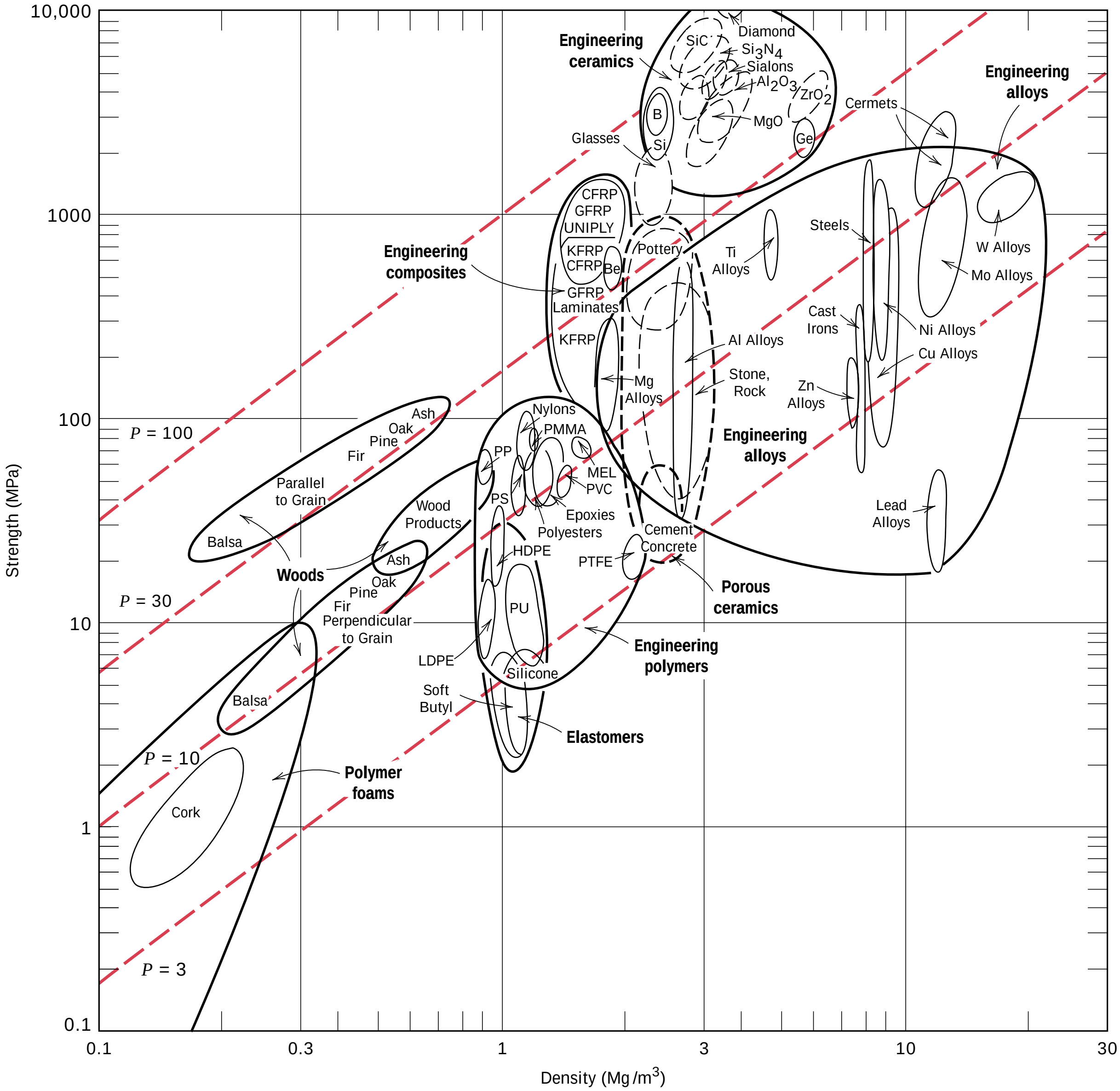

FIGURE 20.2 Strength versus density materials selection chart. Design guidelines for performance indices of 3, 10, 30, and 100 $(\text{MPa})^{2/3}\text{m}^3/\text{Mg}$ have been constructed, all having a slope of $\frac{3}{2}$. (Adapted from M. F. Ashby, *Materials Selection in Mechanical Design*. Copyright © 1992. Reprinted by permission of Butterworth-Heinemann Ltd.)

Now, taking the logarithm of both sides of Equation 20.9 and rearranging yields

$$\log \tau_f = \tfrac{3}{2} \log \rho + \tfrac{3}{2} \log P \tag{20.10}$$

This expression tells us that a plot of log τ_f versus log ρ will yield a family of straight and parallel lines all having a slope of $\frac{3}{2}$; each line in the family corresponds to a different performance index, P. These lines are termed *design guidelines*, and four have been included in Figure 20.2 for P values of 3, 10, 30, and 100 $(\text{MPa})^{2/3}\text{m}^3/\text{Mg}$. All materials that lie on one of these lines will perform equally well in terms of strength-per-mass basis; materials whose positions lie above a particular line will have higher performance indices, while those lying below will exhibit poorer performances. For example, a material on the $P = 30$ line will yield the same strength with one-third the mass as another material that lies along the $P = 10$ line.

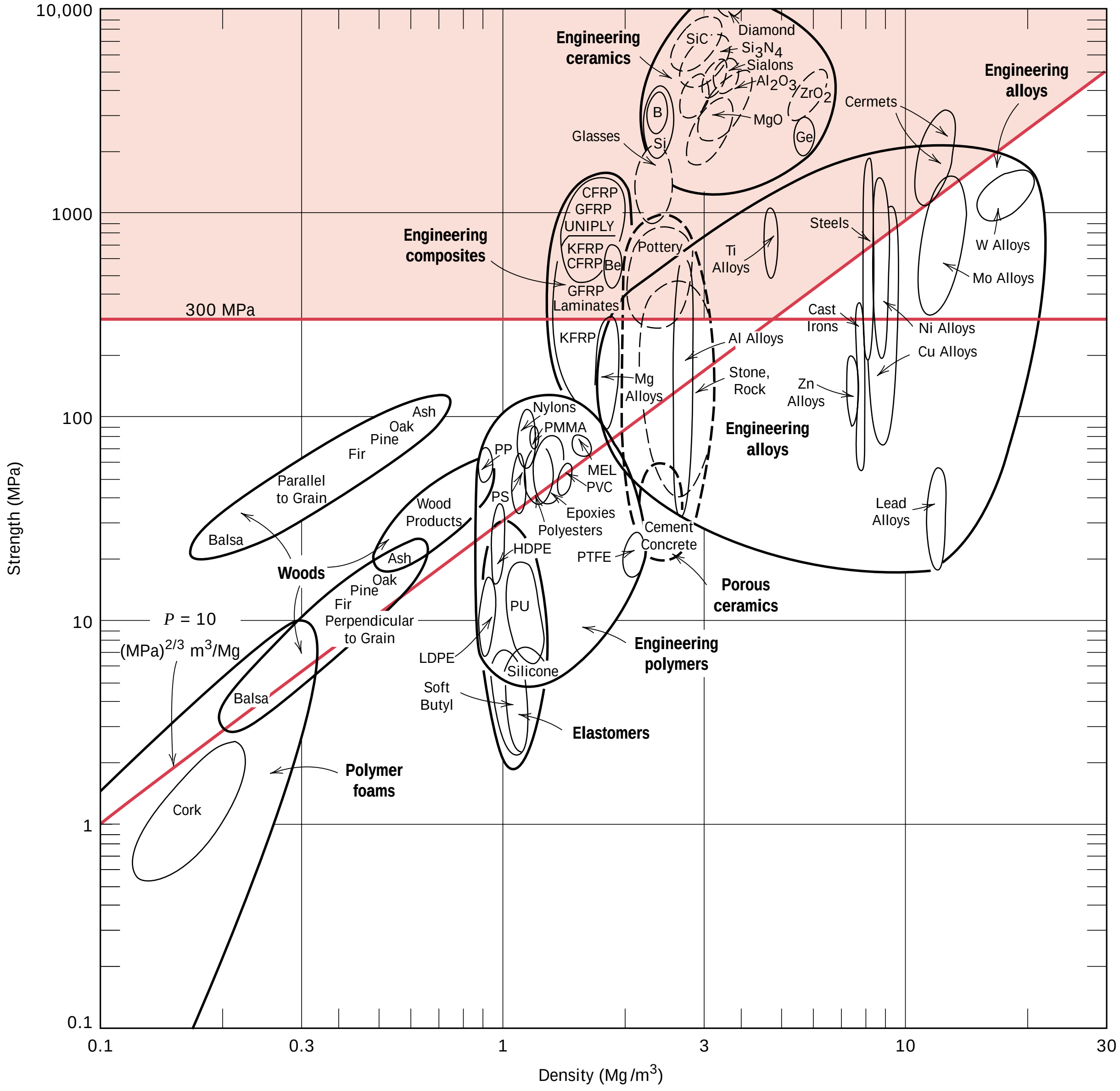

FIGURE 20.3 Strength versus density materials selection chart. Those materials lying within the shaded region are acceptable candidates for a solid cylindrical shaft which has a mass-strength performance index in excess of 10 $(\text{MPa})^{2/3}\text{m}^3/\text{Mg}$, and a strength of at least 300 MPa (43,500 psi). (Adapted from M. F. Ashby, *Materials Selection in Mechanical Design.* Copyright © 1992. Reprinted by permission of Butterworth-Heinemann Ltd.)

The selection process now involves choosing one of these lines, a ''selection line'' that includes some subset of these materials; for the sake of argument let us pick $P = 10\ (\text{MPa})^{2/3}\text{m}^3/\text{Mg}$, which is represented in Figure 20.3. Materials lying along this line or above it are in the ''search region'' of the diagram and are possible candidates for this rotating shaft. These include wood products, some plastics, a number of engineering alloys, the engineering composites, and glasses and engineering ceramics. On the basis of fracture toughness considerations, the engineering ceramics and glasses are ruled out as possibilities.

Let us now impose a further constraint on the problem, namely that the strength of the shaft must equal or exceed 300 MPa (43,500 psi). This may be represented on the materials selection chart by a horizontal line constructed at 300 MPa, Figure 20.3. Now the search region is further restricted to that area above both of these lines. Thus, all wood products, all engineering polymers, other engineering alloys (viz. Mg and some Al alloys), as well as some engineering composites are eliminated as candidates; steels, titanium alloys, high-strength aluminum alloys, and the engineering composites remain as possibilities.

At this point we are in a position to evaluate and compare the strength performance behavior of specific materials. Table 20.1 presents the density, strength, and strength performance index for three engineering alloys and two engineering composites, which were deemed acceptable candidates from the analysis using the materials selection chart. In this table, strength was taken as 0.6 times the tensile yield strength (for the alloys) and 0.6 times the tensile strength (for the composites); these approximations were necessary since we are concerned with strength in torsion and torsional strengths are not readily available. Furthermore, for the two engineering composites, it is assumed that the continuous and aligned glass and carbon fibers are wound in a helical fashion (Figure 15.14), and at a 45° angle referenced to the shaft axis. The five materials in Table 20.1 are ranked according to strength performance index, from highest to lowest: carbon fiber-reinforced and glass fiber-reinforced composites, followed by aluminum, titanium, and 4340 steel alloys.

Material cost is another important consideration in the selection process. In real-life engineering situations, economics of the application often is the overriding issue and normally will dictate the material of choice. One way to determine materi-

Table 20.1 Density (ρ), Strength (τ_f), the Performance Index (P) for Five Engineering Materials

Material	ρ (Mg/m^3)	τ_f (MPa)	$\tau_f^{2/3}/\rho = P$ $[(MPa)^{2/3}m^3/Mg]$
Carbon fiber-reinforced composite (0.65 fiber fraction)[a]	1.5	1140	72.8
Glass fiber-reinforced composite (0.65 fiber fraction)[a]	2.0	1060	52.0
Aluminum alloy (2024-T6)	2.8	300	16.0
Titanium alloy (Ti-6Al-4V)	4.4	525	14.8
4340 Steel (oil-quenched and tempered)	7.8	780	10.9

[a] The fibers in these composites are continuous, aligned, and wound in a helical fashion at a 45° angle relative to the shaft axis.

Table 20.2 Tabulation of the $\rho/\tau_f^{2/3}$ Ratio, Relative Cost ($\bar{c}$), and the Product of $\rho/\tau_f^{2/3}$ and $\bar{c}$ for Five Engineering Materials[a]

Material	$\rho/\tau_f^{2/3}$ [10^{-2} {Mg/(MPa)$^{2/3}$m^3}]	$\bar{c}$ (\$/\$)	$\bar{c}(\rho/\tau_f^{2/3})$ [10^{-2} (\$/\$){Mg/(MPa)$^{2/3}$m^3}]
4340 Steel (oil-quenched and tempered)	9.2	5	46
Glass fiber-reinforced composite (0.65 fiber fraction)[b]	1.9	40	76
Aluminum alloy (2024-T6)	6.2	15	93
Carbon fiber-reinforced composite (0.65 fiber fraction)[b]	1.4	80	112
Titanium alloy (Ti-6Al-4V)	6.8	110	748

[a] The relative cost is the ratio of the prices per unit mass of the material and low-carbon steel.

[b] The fibers in these composites are continuous, aligned, and wound in a helical fashion at a 45° angle relative to the shaft axis.

als cost is by taking the product of the price (on a per-unit mass basis) and the required mass of material.

Cost considerations for these five remaining candidate materials—steel, aluminum, and titanium alloys, and two engineering composites—are presented in Table 20.2. In the first column is tabulated $\rho/\tau_f^{2/3}$. The next column lists the approximate relative cost, denoted as $\bar{c}$; this parameter is simply the per-unit mass cost of material divided by the per-unit mass cost for low-carbon steel, one of the common engineering materials. The underlying rationale for using $\bar{c}$ is that while the price of a specific material will vary over time, the price ratio between that material and another will, most likely, change more slowly.

Finally, the right-hand column of Table 20.2 shows the product of $\rho/\tau_f^{2/3}$ and $\bar{c}$. This product provides a comparison of these several materials on the basis of the cost of materials for a cylindrical shaft that would not fracture in response to the twisting moment M_t. We use this product inasmuch as $\rho/\tau_f^{2/3}$ is proportional to the mass of material required (Equation 20.8) and $\bar{c}$ is the relative cost on a per-unit mass basis. Now the most economical is the 4340 steel, followed by the glass fiber-reinforced composite, 2024-T6 aluminum, the carbon fiber-reinforced composite, and the titanium alloy. Thus, when the issue of economics is considered, there is a significant alteration within the ranking scheme. For example, inasmuch as the carbon fiber-reinforced composite is relatively expensive, it is significantly less desirable; or, in other words, the higher cost of this material may not outweigh the enhanced strength it provides.

20.3 Other Property Considerations and the Final Decision

To this point in our materials selection process we have considered only the strength of materials. Other properties relative to the performance of the cylindrical shaft may be important—for example, stiffness, and, if the shaft rotates, fatigue behavior. Furthermore, fabrication costs should also be considered; in our analysis they have been neglected.

Relative to stiffness, a stiffness-to-mass performance analysis similar to that above could be conducted. For this case, the stiffness performance index P_s is

$$P_s = \frac{\sqrt{G}}{\rho} \tag{20.11}$$

where G is the shear modulus. The appropriate materials selection chart (log G versus log ρ) would be used in the preliminary selection process. Subsequently, performance index and per-unit-mass cost data would be collected on specific candidate materials; from these analyses the materials would be ranked on the basis of stiffness performance and cost.

In deciding on the best material, it may be worthwhile to make a table employing the results of the various criteria that were used. The tabulation would include, for all candidate materials, performance index, cost, etc. for each criterion, as well as comments relative to any other important considerations. This table puts in perspective the important issues and facilitates the final decision process.

AUTOMOBILE VALVE SPRING

20.4 INTRODUCTION

The basic function of a spring is to store mechanical energy as it is initially elastically deformed and then recoup this energy at a later time as the spring recoils. In this section helical springs that are used in mattresses and in retractable pens and as suspension springs in automobiles are discussed. A stress analysis will be conducted on this type of spring, and the results will then be applied to a valve spring that is utilized in automobile engines.

Consider the helical spring shown in Figure 20.4, which has been constructed of wire having a circular cross section of diameter d; the coil center-to-center diameter is denoted as D. The application of a compressive force F causes a twisting force, or moment, denoted T, as shown in the figure. A combination of shear stresses result, the sum of which, τ, is

$$\tau = \frac{8FD}{\pi d^3} K_w \tag{20.12}$$

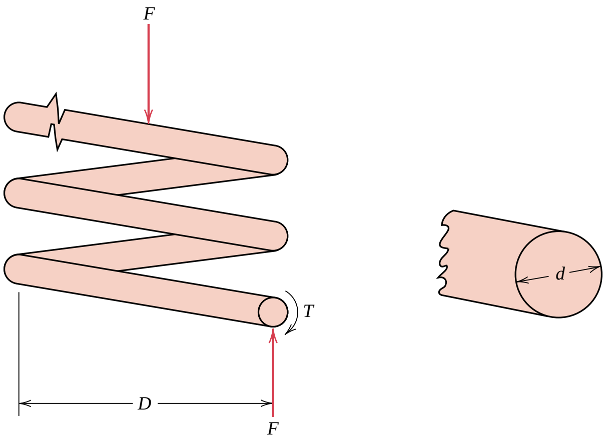

FIGURE 20.4 Schematic diagram of a helical spring showing the twisting moment T that results from the compressive force F. (Adapted from K. Edwards and P. McKee, *Fundamentals of Mechanical Component Design*. Copyright © 1991 by McGraw-Hill, Inc. Reproduced with permission of The McGraw-Hill Companies.)

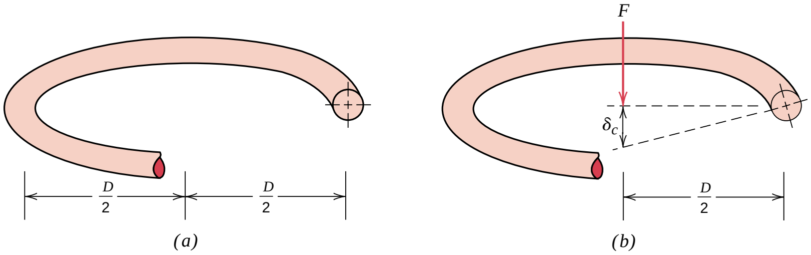

FIGURE 20.5 Schematic diagrams of one coil of a helical spring, (*a*) prior to being compressed, and (*b*) showing the deflection δ_c produced from the compressive force *F*. (Adapted from K. Edwards and P. McKee, *Fundamentals of Mechanical Component Design*. Copyright © 1991 by McGraw-Hill, Inc. Reproduced with permission of The McGraw-Hill Companies.)

where K_w is a force-independent constant that is a function of the D/d ratio:

$$K_w = 1.60\left(\frac{D}{d}\right)^{-0.140} \tag{20.13}$$

In response to the force *F*, the coiled spring will experience deflection, which will be assumed to be totally elastic. The amount of deflection per coil of spring, δ_c, as indicated in Figure 20.5, is given by the expression

$$\delta_c = \frac{8FD^3}{d^4G} \tag{20.14}$$

where *G* is the shear modulus of the material from which the spring is constructed. Furthermore, δ_c may be computed from the total spring deflection, δ_s, and the number of effective spring coils, N_c, as

$$\delta_c = \frac{\delta_s}{N_c} \tag{20.15}$$

Now, solving for *F* in Equation 20.14 gives

$$F = \frac{d^4\delta_c G}{8D^3} \tag{20.16}$$

and substituting for *F* in Equation 20.12 leads to

$$\tau = \frac{\delta_c Gd}{\pi D^2}K_w \tag{20.17}$$

Under normal circumstances, it is desired that a spring experience no permanent deformation upon loading; this means that the right-hand side of Equation 20.17 must be less than the shear yield strength τ_y of the spring material, or that

$$\tau_y > \frac{\delta_c Gd}{\pi D^2}K_w \tag{20.18}$$

20.5 AUTOMOBILE VALVE SPRING

We shall now apply the results of the preceding section to an automobile valve spring. A cut-away schematic diagram of an automobile engine showing these springs is presented in Figure 20.6. Functionally, springs of this type permit both intake and exhaust valves to alternately open and close as the engine is in operation. Rotation of the camshaft causes a valve to open and its spring to be compressed, so that the load on the spring is increased. The stored energy in the spring then forces the valve to close as the camshaft continues its rotation. This process occurs for each valve for each engine cycle, and over the lifetime of the engine it occurs many millions of times. Furthermore, during normal engine operation, the temperature of the springs is approximately 80°C (175°F).

A photograph of a typical valve spring is shown in Figure 20.7. The spring has a total length of 1.67 in. (42 mm), is constructed of wire having a diameter d of 0.170 in. (4.3 mm), has six coils (only four of which are active), and has a center-to-center diameter D of 1.062 in. (27 mm). Furthermore, when installed and when a valve is completely closed, its spring is compressed a total of 0.24 in. (6.1 mm), which, from Equation 20.15, gives an installed deflection per coil δ_{ic} of

$$\delta_{ic} = \frac{0.24 \text{ in.}}{4 \text{ coils}} = 0.060 \text{ in./coil } (1.5 \text{ mm/coil})$$

The cam lift is 0.30 in. (7.6 mm), which means that when the cam completely opens a valve, the spring experiences a maximum total deflection equal to the sum of the valve lift and the compressed deflection, namely, 0.30 in. + 0.24 in. = 0.54 in. (13.7

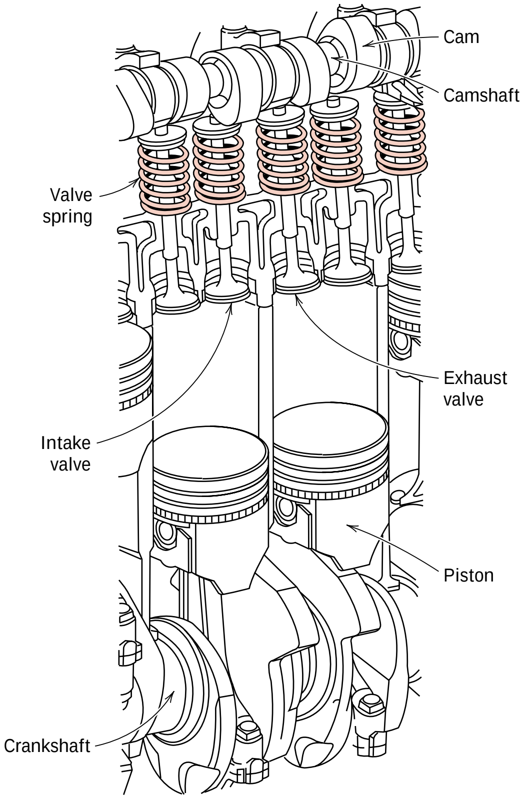

FIGURE 20.6 Cutaway drawing of a section of an automobile engine in which various components including valves and valve springs are shown.

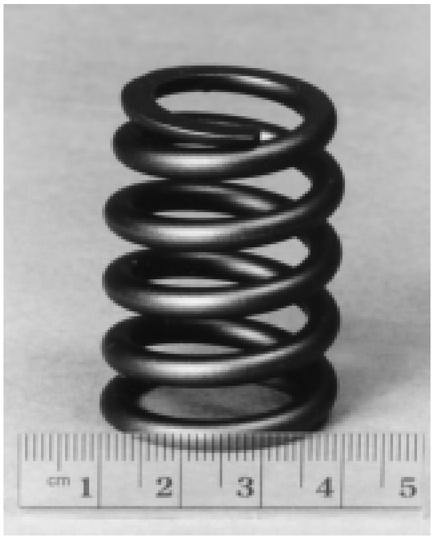

Figure 20.7 Photograph of a typical automobile valve spring.

mm). Hence, the maximum deflection per coil, δ_{mc}, is

$$\delta_{mc} = \frac{0.54 \text{ in.}}{4 \text{ coils}} = 0.135 \text{ in./coil } (3.4 \text{ mm/coil})$$

Thus, we have available all of the parameters in Equation 20.18 (taking $\delta_c = \delta_{mc}$), except for τ_y, the required shear yield strength of the spring material.

However, the material parameter of interest is really not τ_y inasmuch as the spring is continually stress cycled as the valve opens and closes during engine operation; this necessitates designing against the possibility of failure by fatigue rather than against the possibility of yielding. This fatigue complication is handled by choosing a metal alloy that has a fatigue limit (Figure 9.25*a*) that is greater than the cyclic stress amplitude to which the spring will be subjected. For this reason, steel alloys, which have fatigue limits, are normally employed for valve springs.

When using steel alloys in spring design, two assumptions may be made if the stress cycle is reversed (if $\tau_m = 0$, where τ_m is the mean stress, or, equivalently, if $\tau_{\max} = -\tau_{\min}$, in accordance with Equation 9.21 and as noted in Figure 20.8). The first of these assumptions is that the fatigue limit of the alloy (expressed as stress amplitude) is 45,000 psi (310 MPa), the threshold of which occurs at about 10^6 cycles. Secondly, for torsion and on the basis of experimental data, it has been

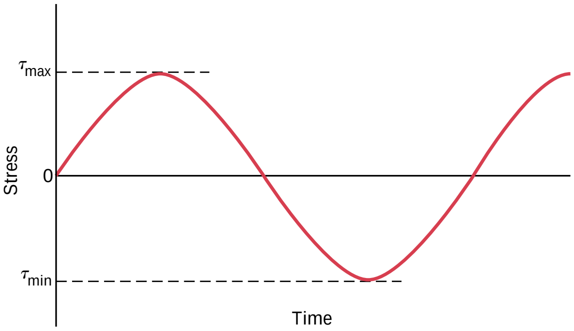

Figure 20.8 Stress versus time for a reversed cycle in shear.

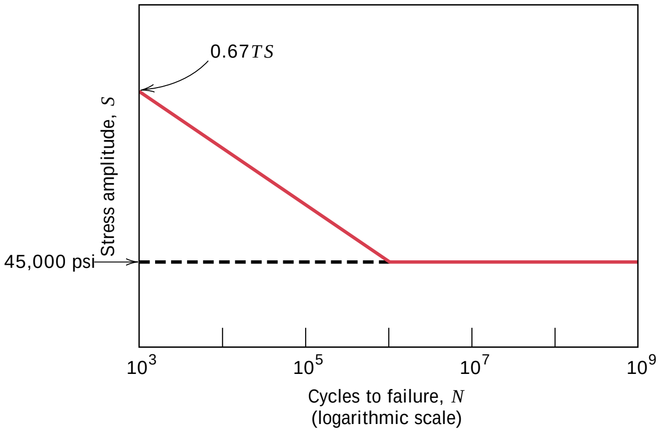

FIGURE 20.9 Shear stress amplitude versus logarithm of the number of cycles to fatigue failure for typical ferrous alloys.

found that the fatigue strength at 10^3 cycles is $0.67TS$, where TS is the tensile strength of the material (as measured from a pure tension test). The S–N fatigue diagram (i.e., stress amplitude versus logarithm of the number of cycles to failure) for these alloys is shown in Figure 20.9.

Now let us estimate the number of cycles to which a typical valve spring may be subjected in order to determine whether it is permissible to operate within the fatigue limit regime of Figure 20.9 (i.e., if the number of cycles exceeds 10^6). For the sake of argument, assume that the automobile in which the spring is mounted travels a minimum of 100,000 miles (161,000 km) at an average speed of 40 mph (64.4 km/h), with an average engine speed of 3000 rpm (rev/min). The total time it takes the automobile to travel this distance is 2500 h (100,000 mi/40 mph), or 150,000 min. At 3000 rpm, the total number of revolutions is (3000 rev/min)(150,000 min) $= 4.5 \times 10^8$ rev, and since there are 2 rev/cycle, the total number of cycles is 2.25×10^8. This result means that we may use the fatigue limit as the design stress inasmuch as the limit cycle threshold has been exceeded for the 100,000-mile distance of travel (i.e., since 2.25×10^8 cycles $> 10^6$ cycles).

Furthermore, this problem is complicated by the fact that the stress cycle is not completely reversed (i.e., $\tau_m \neq 0$) inasmuch as between minimum and maximum deflections the spring remains in compression; thus, the 45,000 psi (310 MPa) fatigue limit is not valid. What we would now like to do is first to make an appropriate extrapolation of the fatigue limit for this $\tau_m \neq 0$ case and then compute and compare with this limit the actual stress amplitude for the spring; if the stress amplitude is significantly below the extrapolated limit, then the spring design is satisfactory.

A reasonable extrapolation of the fatigue limit for this $\tau_m \neq 0$ situation may be made using the following expression (termed Goodman's law):

$$\tau_{al} = \tau_e \left(1 - \frac{\tau_m}{0.67TS}\right) \tag{20.19}$$

where τ_{al} is the fatigue limit for the mean stress τ_m; τ_e is the fatigue limit for $\tau_m = 0$ [i.e., 45,000 psi (310 MPa)]; and, again, TS is the tensile strength of the alloy. To determine the new fatigue limit τ_{al} from the above expression necessitates the computation of both the tensile strength of the alloy and the mean stress for the spring.

One common spring alloy is an ASTM 232 chrome–vanadium steel, having a composition of 0.48–0.53 wt% C, 0.80–1.10 wt% Cr, a minimum of 0.15 wt% V, and the balance being Fe. Spring wire is normally cold drawn (Section 14.2) to the desired diameter; consequently, tensile strength will increase with the amount of drawing (i.e., with decreasing diameter). For this alloy it has been experimentally verified that, for the diameter d in inches, the tensile strength is

$$TS\,(\text{psi}) = 169{,}000(d)^{-0.167} \tag{20.20}$$

Since $d = 0.170$ in. for this spring,

$$\begin{aligned} TS &= (169{,}000)(0.170\text{ in.})^{-0.167} \\ &= 227{,}200\text{ psi } (1570\text{ MPa}) \end{aligned}$$

Computation of the mean stress τ_m is made using Equation 9.21 modified to the shear stress situation as follows:

$$\tau_m = \frac{\tau_{\min} + \tau_{\max}}{2} \tag{20.21}$$

It now becomes necessary to determine the minimum and maximum shear stresses for the spring, using Equation 20.17. The value of $\tau_{\min}$ may be calculated from Equations 20.17 and 20.13 inasmuch as the minimum δ_c is known (i.e., $\delta_{ic} = 0.060$ in.). A shear modulus of 11.5×10^6 psi (79 GPa) will be assumed for the steel; this is the room-temperature value, which is also valid at the 80°C service temperature. Thus, $\tau_{\min}$ is just

$$\tau_{\min} = \frac{\delta_{ic} G d}{\pi D^2} K_w \tag{20.22a}$$

$$\begin{aligned} &= \frac{\delta_{ic} G d}{\pi D^2}\left[1.60\left(\frac{D}{d}\right)^{-0.140}\right] \\ &= \left[\frac{(0.060\text{ in.})(11.5 \times 10^6\text{ psi})(0.170\text{ in.})}{\pi(1.062\text{ in.})^2}\right]\left[1.60\left(\frac{1.062\text{ in.}}{0.170\text{ in.}}\right)^{-0.140}\right] \\ &= 41{,}000\text{ psi } (280\text{ MPa}) \end{aligned}$$

Now $\tau_{\max}$ may be determined taking $\delta_c = \delta_{mc} = 0.135$ in. as follows:

$$\tau_{\max} = \frac{\delta_{mc} G d}{\pi D^2}\left[1.60\left(\frac{D}{d}\right)^{-0.140}\right] \tag{20.22b}$$

$$\begin{aligned} &= \left[\frac{(0.135\text{ in.})(11.5 \times 10^6\text{ psi})(0.170\text{ in.})}{\pi(1.062\text{ in.})^2}\right]\left[1.60\left(\frac{1.062\text{ in.}}{0.170\text{ in.}}\right)^{-0.140}\right] \\ &= 92{,}200\text{ psi } (635\text{ MPa}) \end{aligned}$$

Now, from Equation 20.21,

$$\begin{aligned} \tau_m &= \frac{\tau_{\min} + \tau_{\max}}{2} \\ &= \frac{41{,}000\text{ psi} + 92{,}200\text{ psi}}{2} = 66{,}600\text{ psi } (460\text{ MPa}) \end{aligned}$$

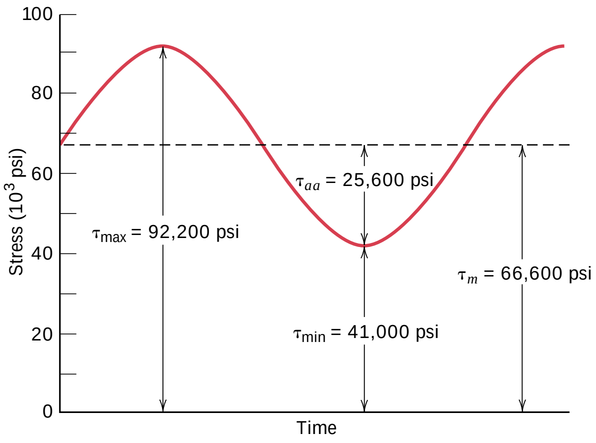

Figure 20.10 Shear stress versus time for an automobile valve spring.

The variation of shear stress with time for this valve spring is noted in Figure 20.10; the time axis is not scaled, inasmuch as the time scale will depend on engine speed.

Our next objective is to determine the fatigue limit amplitude (τ_{al}) for this τ_m = 66,600 psi (460 MPa) using Equation 20.19 and for τ_e and TS values of 45,000 psi (310 MPa) and 227,200 psi (1570 MPa), respectively. Thus,

$$\tau_{al} = \tau_e\left[1 - \frac{\tau_m}{0.67TS}\right]$$

$$= (45{,}000 \text{ psi})\left[1 - \frac{66{,}600 \text{ psi}}{(0.67)(227{,}200 \text{ psi})}\right]$$

$$= 25{,}300 \text{ psi } (175 \text{ MPa})$$

Now let us determine the actual stress amplitude τ_{aa} for the valve spring using Equation 9.23 modified to the shear stress condition:

$$\tau_{aa} = \frac{\tau_{\max} - \tau_{\min}}{2}$$
$$= \frac{92{,}200 \text{ psi} - 41{,}000 \text{ psi}}{2} = 25{,}600 \text{ psi } (177 \text{ MPa}) \qquad (20.23)$$

Thus, the actual stress amplitude is slightly greater than the fatigue limit, which means that this spring design is marginal.

The fatigue limit of this alloy may be increased to greater than 25,300 psi (175 MPa) by shot peening, a procedure described in Section 9.14. Shot peening involves the introduction of residual compressive surface stresses by plastically deforming outer surface regions; small and very hard particles are projected onto the surface at high velocities. This is an automated procedure commonly used to improve the fatigue resistance of valve springs; in fact, the spring shown in Figure 20.7 has been shot peened, which accounts for its rough surface texture. Shot peening has been observed to increase the fatigue limit of steel alloys in excess of 50% and, in addition, to reduce significantly the degree of scatter of fatigue data.

This spring design, including shot peening, may be satisfactory; however, its adequacy should be verified by experimental testing. The testing procedure is relatively complicated and, consequently, will not be discussed in detail. In essence, it involves performing a relatively large number of fatigue tests (on the order of 1000) on this shot-peened ASTM 232 steel, in shear, using a mean stress of 66,600 psi (460 MPa) and a stress amplitude of 25,600 psi (177 MPa), and for 10^6 cycles. On the basis of the number of failures, an estimate of the survival probability can be made. For the sake of argument, let us assume that this probability turns out to be 0.99999; this means that one spring in 100,000 produced will fail.

Suppose that you are employed by one of the large automobile companies that manufactures on the order of 1 million cars per year, and that the engine powering each automobile is a six-cylinder one. Since for each cylinder there are two valves, and thus two valve springs, a total of 12 million springs would be produced every year. For the above survival probability rate, the total number of spring failures would be approximately 120, which also corresponds to 120 engine failures. As a practical matter, one would have to weigh the cost of replacing these 120 engines against the cost of a spring redesign.

Redesign options would involve taking measures to reduce the shear stresses on the spring, by altering the parameters in Equations 20.13 and 20.17. This would include either (1) increasing the coil diameter D, which would also necessitate increasing the wire diameter d, or (2) increasing the number of coils N_c.

ARTIFICIAL TOTAL HIP REPLACEMENT

20.6 ANATOMY OF THE HIP JOINT

As a prelude to discussing the artificial hip, let us first briefly address some of the anatomical features of joints in general and the hip joint in particular. The joint is an important component of the skeletal system. It is located at bone junctions, where loads may be transmitted from bone to bone by muscular action; this is normally accompanied by some relative motion of the component bones. Bone tissue is a complex natural composite consisting of soft and strong protein collagen and brittle apatite, which has a density between 1.6 and 1.7 g/cm^3. Being an anisotropic material, the mechanical properties of bone differ in longitudinal (axial) and transverse (radial) directions (Table 20.3). The articulating (or connecting) surface of each joint is coated with cartilage, which consists of body fluids that lubricate

Table 20.3 Mechanical Characteristics of Human Long Bone Both Parallel and Perpendicular to the Bone Axis

Property	*Parallel to Bone Axis*	*Perpendicular to Bone Axis*
Elastic modulus, GPa (psi)	17.4 (2.48×10^6)	11.7 (1.67×10^6)
Ultimate strength, tension, MPa (ksi)	135 (19.3)	61.8 (8.96)
Ultimate strength, compression, MPa (ksi)	196 (28.0)	135 (19.3)
Elongation at fracture	3–4%	—

Source: From D. F. Gibbons, ‘‘Biomedical Materials,’’ pp. 253–254, in *Handbook of Engineering in Medicine and Biology,* D. G. Fleming, and B. N. Feinberg, CRC Press, Boca Raton, Florida, 1976. With permission.

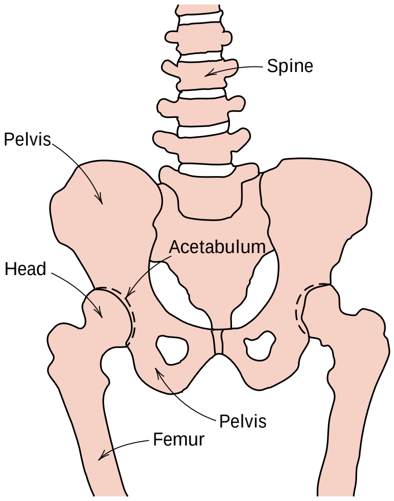

Figure 20.11 Schematic diagram of human hip joints and adjacent skeletal components.

and provide an interface having a very low coefficient of friction so as to facilitate the bone-sliding movement.

The human hip joint (Figure 20.11) occurs at the junction between the pelvis and the upper leg (thigh) bone, or femur. A relatively large range of rotary motion is permitted at the hip by a ball-and-socket type of joint; the top of the femur terminates in a ball-shaped head that fits into a cuplike cavity (the acetabulum) within the pelvis. An x-ray of a normal hip joint is shown in Figure 20.12*a*.

This joint is susceptible to fracture, which normally occurs at the narrow region just below the head. An x-ray of a fractured hip is shown in Figure 20.12*b*; the arrows show the two ends of the fracture line through the femoral neck. Furthermore, the hip may become diseased (osteoarthritis); in such a case small lumps of bone form on the rubbing surfaces of the joint, which causes pain as the head rotates in the

Figure 20.12 X-Rays of (*a*) a normal hip joint and (*b*) a fractured hip joint. The arrows in (*b*) show the two ends of the fracture line through the femoral neck.

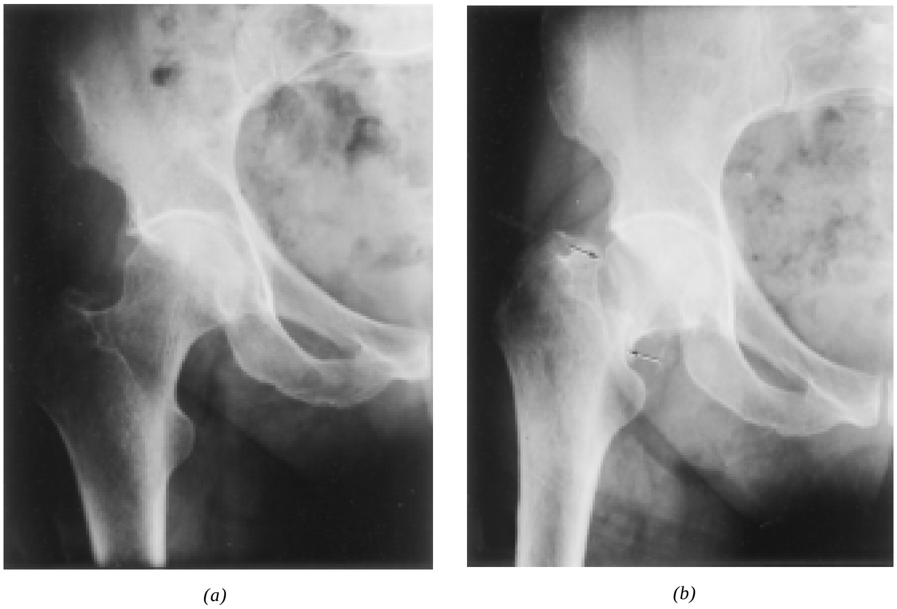
(*a*) (*b*)

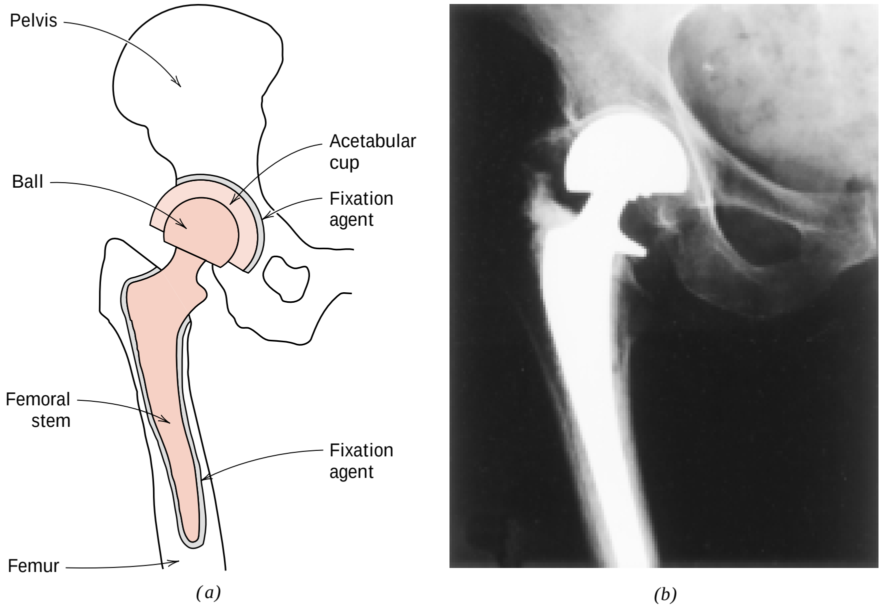

FIGURE 20.13 (*a*) Schematic diagram and (*b*) x-ray of an artificial total hip replacement.

acetabulum. Damaged and diseased hip joints have been replaced with artificial or prosthetic ones, with moderate success, beginning in the late 1950s. Total hip replacement surgery involves the removal of the head and the upper portion of the femur, and some of the bone marrow at the top of the remaining femur segment. Into this hole within the center of the femur is secured a metal anchorage stem onto which is attached, at its other end, the ball portion of the joint. In addition, the replacement cup socket must be attached to the pelvis. This is accomplished by removal of the old cup and its surrounding bone tissue. The new socket is affixed into this recess. A schematic diagram of the artificial hip joint is presented in Figure 20.13*a*; and Figure 20.13*b* shows an x-ray of a total hip replacement. In the remainder of this section we discuss material constraints and those materials that have been used with the greatest degree of success for the various artificial hip components.

20.7 MATERIAL REQUIREMENTS

In essence, there are four basic components to the artificial hip: (1) the femoral stem, (2) the ball that attaches to this stem, (3) the acetabular cup that is affixed to the pelvis, and (4) a fixation agent that secures the stem into the femur and the cup to the pelvis. The property constraints on the materials to be used for these elements are very stringent because of the chemical and mechanical complexity of the hip joint. Some of the requisite material characteristics will now be discussed.

Whenever any foreign material is introduced into the body environment, rejection reactions occur. The magnitude of rejection may range from mild irritation or inflammation to death. Any implant material must be *biocompatible,* that is, it must produce a minimum degree of rejection. Products resulting from reactions with body fluids must be tolerated by the surrounding body tissues such that normal tissue function is unimpaired. Biocompatibility is a function of the location of the implant, as well as of its chemistry and shape.

The body fluid consists of an aerated and warm solution containing approximately 1 wt% NaCl in addition to other salts and organic compounds in relatively minor concentrations. Thus, the body fluids are very corrosive, which, for metal alloys can lead not only to uniform corrosion, but also to crevice attack and pitting and, when stresses are present, to fretting, stress corrosion cracking, and corrosion fatigue. It has been estimated that the maximum tolerable corrosion rate for implant metal alloys is on the order of 0.01 mil per year (2.5×10^{-4} mm per year).

Another adverse consequence of corrosion is the generation of corrosion products that are either toxic or interfere with normal body functions. These substances are rapidly transported throughout the body; some may segregate in specific organs. Even though others may be excreted from the body, they may nevertheless still persist in relatively high concentrations by virtue of the ongoing corrosion process.

The bones and replacement components within the hip joint must support forces that originate from without the body, such as those due to gravity; in addition, they must transmit forces that result from muscular action such as walking. These forces are complex in nature and fluctuate with time in magnitude, in direction, and in rate of application. Thus, mechanical characteristics such as modulus of elasticity, yield strength, tensile strength, fatigue strength, fracture toughness, and ductility are all important considerations relative to the materials of choice for the prosthetic hip. For example, the material used for the femoral stem should have minimum yield and tensile strengths of approximately 500 MPa (72,500 psi) and 650 MPa (95,000 psi), respectively, and a minimum ductility of about 8%EL. In addition, the fatigue strength (for bending stresses that are fully reversed [Figure 9.23*a*]) should be at least 400 MPa (60,000 psi) at 10^7 cycles. For the average person, the load on the hip joint fluctuates on the order of 10^6 times per year. Furthermore, the modulus of elasticity of the prosthetic material should match that of bone; a significant difference can lead to deterioration of the bone tissue surrounding the implant.

Furthermore, since the ball-and-cup articulating surfaces rub against one another, wear of these surfaces is minimized by the employment of very hard materials. Excessive and uneven wear can lead to a change in shape of the articulating surfaces and cause the prosthesis to malfunction. In addition, particulate debris will be generated as the articulating surfaces wear against one another; accumulation of this debris in the surrounding tissues can also lead to inflammation.

Frictional forces at these rubbing counterfaces should also be minimized to prevent loosening of the femoral stem and acetabular cup assembly from their positions secured by the fixation agent. If these components do become loose over time, the hip will experience premature degradation that may require it to be replaced.

Three final important material factors are density, property reproducibility, and cost. It is highly desirable that lightweight components be used, that material properties from prosthesis to prosthesis remain consistent over time, and, of course, that the cost of the prosthesis components be reasonable.

Ideally, an artificial hip that has been surgically implanted should function satisfactorily for the lifetime of the recipient and not require replacement. For current designs, lifetimes range between only five and ten years; certainly longer ones are desirable.

Several final comments are in order relative to biocompatibility assessment. Biocompatibility of materials is usually determined empirically; that is, tests are conducted wherein materials are implanted in laboratory animals and the biocompatibility of each material is judged on the basis of rejection reactions, level of corrosion, generation of toxic substances, etc. This procedure is then repeated on humans for those materials that were found to be relatively biocompatible in animals. It is difficult to *a priori* predict the biocompatibility of a material. For example, mercury, when ingested into the body, is poisonous; however, dental amalgams, which have high mercury contents, have generally been found to be very biocompatible.

20.8 MATERIALS EMPLOYED

FEMORAL STEM AND BALL

Early prosthetic hip designs called for both the femoral stem and ball to be of the same material—a stainless steel. Subsequent improvements have been introduced, including the utilization of materials other than stainless steel and, in addition, constructing the stem and ball from different materials. Figure 20.14 is a photograph in which are shown two different hip replacement designs.

Currently, the femoral stem is constructed from a metal alloy of which there are three possible types: stainless steel, cobalt–nickel–chromium–molybdenum, and titanium. The most suitable stainless steel is 316L, which has a very low sulfur content ($<$0.002 wt%); its composition is given in Table 13.4. The principal disadvantages of this alloy are its susceptibility to crevice corrosion and pitting, and its relatively low fatigue strength. Fabrication technique may also have a significant influence on its characteristics. Cast 316L typically has poor mechanical properties and inadequate corrosion resistance. Consequently, prosthetic femoral stems are either forged or cold worked. Furthermore, heat treatment may also influence the characteristics of the material and must be taken into consideration. Normally, 316L is implanted in older and less active persons. The mechanical characteristics and corrosion rate range of this alloy (in the cold-worked state) are supplied in Table 20.4.

Various Co–Cr–Mo and Co–Ni–Cr–Mo alloys have been employed for artificial hip prostheses; one that has been found to be especially suitable, designated MP35N, has a composition of 35 wt% Co, 35 wt% Ni, 20 wt% Cr, and 10 wt% Mo. It is formed by hot forging and, as such, has tensile and yield strengths that are superior to 316L stainless steel (Table 20.4). Furthermore, its corrosion and fatigue characteristics are excellent.

Of those metal alloys that are implanted for prosthetic hip joints, probably the most biocompatible is the titanium alloy Ti–6Al–4V; its composition is 90 wt% Ti, 6 wt% Al, and 4 wt% V. The optimal properties for this material are produced by hot forging; any subsequent deformation and/or heat treatment should be avoided

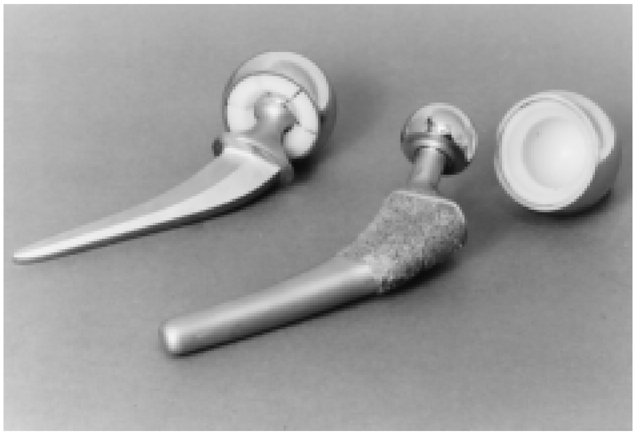

FIGURE 20.14 Photograph showing two artificial total hip replacement designs.

Table 20.4 **Mechanical and Corrosion Characteristics of Three Metal Alloys That Are Commonly Used for the Femoral Stem Component of the Prosthetic Hip**

Alloy	*Elastic Modulus [GPa (psi)]*	*0.2% Yield Strength [MPa (ksi)]*	*Tensile Strength [MPa (ksi)]*	*Elongation at Fracture (%)*	*Fatigue Strength or Limit, 10^7 Cycles [MPa (ksi)]*	*Corrosion Rate (mpy)*[a]
316L Stainless steel (cold worked)	196 (28.4×10^6)	700 (102)	875 (127)	12	383 (55.5)	0.001–0.002
MP35N (hot forged)	230 (33.4×10^6)	1000 (145)	1200 (174)	13	500 (72.5)	0.0012–0.002
Ti-6Al-4V (hot forged)	120 (17.4×10^6)	950 (138)	1075 (156)	13	580 (84.1)	0.007–0.04

[a] mpy means mils per year, or 0.001 in./yr

Sources: From Gladius Lewis, *Selection of Engineering Materials,* © 1990, p. 189. Adapted by permission of Prentice Hall, Englewood Cliffs, New Jersey. And D. F. Gibbons, ''Materials for Orthopedic Joint Prostheses,'' Ch. 4, p. 116, in *Biocompatibility of Orthopedic Implants,* Vol. I, D. F. Williams, CRC Press, Boca Raton, Florida, 1982. With permission.

to prevent the formation of microstructures that are deleterious to its bioperformance. The properties of this alloy are also listed in Table 20.4.

Recent improvements for this prosthetic device include using a ceramic material for the ball component rather than any of the aforementioned metal alloys. The ceramic of choice is a high-purity and polycrystalline aluminum oxide, which is harder and more wear resistant, and generates lower frictional stresses at the joint. However, the fracture toughness of alumina is relatively low and its fatigue characteristics are poor. Hence, the femoral stem, being subjected to significant stress levels, is still fabricated from one of the above alloys, and is then attached to the ceramic ball; this femoral stem–ball component thus becomes a two-piece unit.

The materials selected for use in an orthopedic implant come after years of research into the chemical and physical properties of a host of different candidate materials. Ideally, the material(s) of choice will not only be biocompatible, but have mechanical properties that match the biomaterial being replaced—viz., bone. However, no man-made material is both biocompatible and possesses the property combination of bone and the natural hip joint—i.e., low modulus of elasticity, relatively high strength and fracture toughness, low coefficient of friction, and excellent wear resistance. Consequently, material property compromises and trade-offs must be made. For example, recall that the modulus of elasticity of bone and femoral stem materials should be closely matched such that accelerated deterioration of the bone tissue adjacent to the implant is avoided. Unfortunately, man-made materials that are both biocompatible and relatively strong, also have high moduli of elasticity. Thus, for this application, it was decided to trade off a low modulus for biocompatibility and strength.

ACETABULAR CUP

Some acetabular cups are made from one of the biocompatible alloys or aluminum oxide. More commonly, however, ultrahigh molecular weight polyethylene (Section 13.16) is used. This material is virtually inert in the body environment and has excellent wear-resistance characteristics; furthermore, it has a very low coefficient of friction when in contact with the materials used for the ball component of the socket.

FIXATION

Successful performance of the artificial hip joint calls for the secure attachment of both the femoral stem to the femur and the acetabular cup to the pelvis. Insecure attachment of either component ultimately leads to a loosening of that component and the accelerated degradation of the joint. A fixation agent is sometimes used to bond these two prosthetic components to their surrounding bone structures. The most commonly used fixation agent is a polymethyl methacrylate (acrylic) bone cement that is polymerized *in situ* during surgery.

This acrylic bond cement has, in some cases, contributed to femoral stem loosening because it is brittle and does not bond well with the metallic implant and bone tissue. It has been found that a more secure implant–bone bond is formed when the stem is coated with a porous surface layer, consisting of a sintered metal powder. After implantation, bone tissue grows into the three-dimensional pore network, and thereby fixates the implant to the bone. Such a coating has been applied to the upper stem region of the right hip replacement shown in Figure 20.14.

THERMAL PROTECTION SYSTEM ON THE SPACE SHUTTLE ORBITER

20.9 INTRODUCTION

In 1969, the National Aeronautics and Space Administration (NASA) of the United States decided to direct its primary mission to the development of a *Space Transportation System* (*STS*), also commonly known as the *Space Shuttle Orbiter*. In essence, the Space Shuttle is a reusable cargo-carrying space vehicle that is launched aboard a rocket, and then orbits the earth. Upon mission completion, it reenters the atmosphere as a space craft, and, finally, once inside the lower atmosphere, lands in the manner of a normal aircraft. The maiden flight was made by the *Columbia* orbiter in April of 1981; since then, four other orbiters have been constructed—*Discovery*, *Atlantis*, *Endeavour*, and the ill-fated *Challenger*. A photograph of the *Atlantis* is shown in the chapter-opening photograph for this chapter.

The successful operation of the Space Shuttle is dependent on a fully reusable outer ‘‘skin,’’ termed a *Thermal Protection System* (*TPS*), that protects the inner airframe and its occupants from the searing heat generated during the reentry phase from space into the earth’s atmosphere. The development of this Thermal Protection System evolved over a twenty-year period, and is a classical and somewhat involved materials selection and design problem. In this section the primary components of the Shuttle’s TPS are discussed.

In reading this section, keep in mind that cost constraints relative to the design and fabrication of these materials were not as rigid as would be expected for normal commercial applications.

20.10 THERMAL PROTECTION SYSTEM—DESIGN REQUIREMENTS

Material requirements on the Thermal Protection System are, to say the least, awesome. For example, the TPS must do the following:

1. Maintain the temperature on the inner airframe below that to which it was designed [viz., 175°C (350°F)] for a maximum outer surface temperature of 1260°C (2300°F).

2. Remain usable for 100 missions, with a maximum turnaround time of 160 h.
3. Provide and maintain an aerodynamically smooth outer surface.
4. Be constructed of low-density materials.
5. Withstand temperature extremes between −110°C (−170°F) and 1260°C (2300°F).
6. Be resistant to severe thermal gradients and rapid temperature changes.
7. Be able to withstand stresses and vibrations that are experienced during launch, as well as thermally induced stresses imposed during temperature changes.
8. Experience a minimum absorption of moisture and other contaminants during storage between missions.
9. Be made to adhere to the airframe that is constructed of an aluminum alloy.

Thermal protection systems and materials developed previously by the aerospace industry proved unsuitable for the Space Shuttle because they were either too dense and/or nonreusable. Therefore, it became necessary to design a new set of complex materials. Furthermore, no single material is capable of meeting all of the criteria listed above. In addition, not all of these criteria are required over all surfaces of the spacecraft; for example, typical reentry maximum temperature profiles are shown in Figure 20.15.

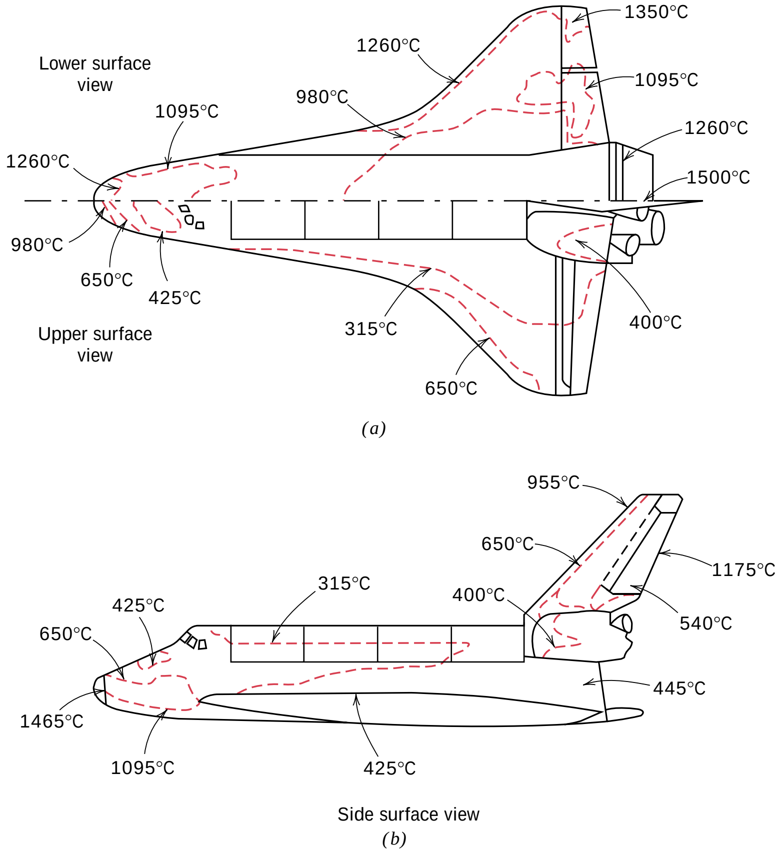
Lower surface view
1260°C
1350°C
980°C
1095°C
1095°C
1260°C
1260°C
1500°C
980°C
650°C
425°C
315°C
400°C
Upper surface view
650°C
(a)
955°C
650°C
1175°C
315°C
400°C
540°C
425°C
650°C
445°C
1465°C
1095°C
425°C
Side surface view
(b)

FIGURE 20.15 Approximate maximum outer surface temperature profiles for the Space Shuttle Orbiter during reentry: (*a*) upper and lower views; (*b*) side view. (From ''The Shuttle Orbiter Thermal Protection System,'' L. J. Korb, C. A. Morant, R. M. Calland, and C. S. Thatcher, *Ceramic Bulletin*, No. 11, Nov. 1981, p. 1188. Copyright 1981. Reprinted by permission of the American Ceramic Society.)

Table 20.5 Thermal Protection Systems Employed on the Space Shuttle Orbiter

Material Generic Name	*Minimum Operating Temperature, °C (°F)*	*Maximum Operating Temperature, °C (°F)*	*Material Composition*	*Orbiter Locations*
Felt reusable surface insulation (FRSI)	−130 (−200)	400 (750)	Nylon felt, silicone rubber coating	Wing upper surface, upper sides, cargo bay doors
Advanced flexible reusable surface insulation (AFRSI)	−130 (−200)	815 (1500)	Quartz batting sandwiched between quartz and glass fabrics	Upper surface regions
Low-temperature reusable surface insulation (LRSI)	−130 (−200)	650 (1200)	Silica tiles, borosilicate glass coating	Upper wing surfaces, tail surfaces, upper vehicle sides
High-temperature reusable insulation (HRSI)	−130 (−200)	1260 (2300)	Silica tiles, borosilicate glass coating with SiB_4 added	Lower surfaces and sides, tail leading and trailing edges
Reinforced carbon–carbon (RCC)	No lower limit identified	1650 (3000)	Pyrolized carbon–carbon, coated with SiC	Nose cap and wing leading edges

Source: Adapted from L. J. Korb, C. A. Morant, R. M. Calland and C. S. Thatcher, ''The Shuttle Orbiter Thermal Protection System,'' *Ceramic Bulletin*, No. 11, Nov. 1981, p. 1188. Copyright 1981. Reprinted by permission of the American Ceramic Society.

Therefore, the philosophy adopted was to design several different thermal protection materials systems, each with its particular set of properties, that satisfy the required criteria for a specific region of the spacecraft surface. Several different materials systems are employed on the Space Shuttles, the designs of which depend on the maximum outer surface temperature generated during vehicle reentry. These systems and their temperature ranges of operation, material compositions, and orbiter areas are listed in Table 20.5. Furthermore, the locations of these various systems are indicated in Figure 20.16.

20.11 Thermal Protection System—Components

FELT REUSABLE SURFACE INSULATION

Upper surface regions exposed up to temperatures of 400°C (750°F) are covered with what is termed *felt reusable surface insulation* (*FRSI*). This insulation consists of felt blankets of a nylon material the outer surface of which is coated with a silicone elastomer to achieve the necessary surface thermal properties. These blankets come in two thicknesses, 4 and 8 mm (0.16 and 0.32 in.), and are bonded to the aluminum airframe by a room-temperature vulcanizing (RTV) silicone adhesive.

Other upper surface regions that are exposed to higher temperatures, not to exceed 815°C (1500°F), are protected by blankets of an *advanced flexible reusable surface insulation (AFRSI)*. These blankets consist of a quartz fiber batting that is sandwiched between a high-temperature woven quartz fabric on the outer side and a lower-temperature glass fabric on the inner side. The outer surface of some regions is also protected with a ceramic coating. Furthermore, these three layers are stitched together using quartz and glass threads in a one-inch square pattern.

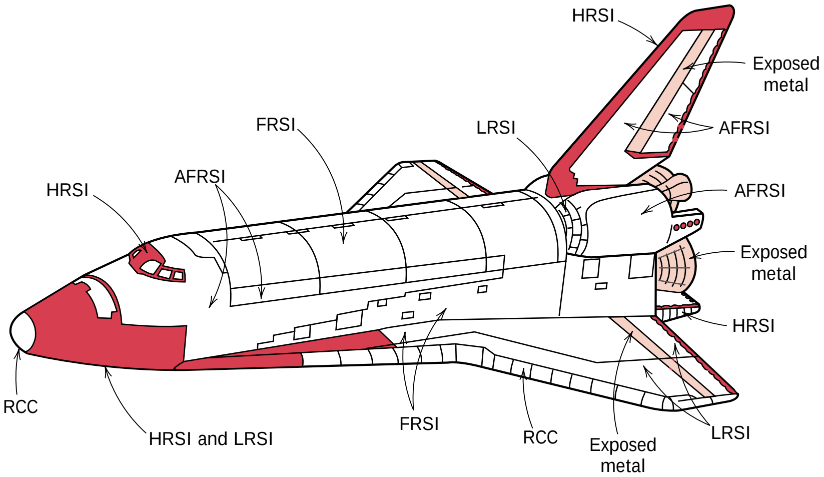

FIGURE 20.16 Locations of the various components of the thermal protection system on the Space Shuttle Orbiter: FRSI, felt reusable surface insulation; AFRSI, advanced flexible reusable surface insulation; LRSI, low-temperature reusable surface insulation; HRSI, high-temperature reusable surface insulation; RCC, reinforced carbon–carbon composite. (Adapted from L. J. Korb, C. A. Morant, R. M. Calland, and C. S. Thatcher, ''The Shuttle Orbiter Thermal Protection System,'' *Ceramic Bulletin*, No. 11, Nov. 1981, p. 1189. Copyright 1981. Reprinted by permission of the American Ceramic Society.)

AFRSI blanket thicknesses range between 10 mm (0.41 in.) and just under 50 mm (2 in.). Over most vehicle regions, these AFRSI blankets are bonded to the structure by a silicone RTV adhesive, as with the FRSI insulation.

CERAMIC TILE SYSTEMS

More rigid material restrictions are imposed on regions of the Space Shuttle that are exposed to temperatures in the range of 400 to 1260°C (750 to 2300°F). For these areas it was decided to use a relatively complex ceramic material in the form of tiles. Ceramics are intrinsically thermal insulators and, furthermore, will withstand these elevated temperatures. The tile design is utilized for the protection system to conform to the contours of the Shuttle's surface, and also to accommodate the thermal dimensional changes accompanying the extremes of temperature that are experienced during a typical mission.

Each Shuttle has on the average of 24,300 of these tiles, which comprise approximately 70% of the total orbiter exterior area. No two tiles have exactly the same configuration, but sizes range from between about 150 mm by 150 mm (6 in. by 6 in.) to about 200 mm by 200 mm (8 in. by 8 in.). Tile thicknesses vary between 5 mm (0.2 in.) and 90 mm (3.5 in.). Each tile is precisely machined to its individual shape using diamond tools on a computer-controlled mill. Figure 20.17 is a photograph that shows the tiles being installed.

Tiles having three densities are used, which are designated by LI-900, FRCI-12, and LI-2200; the respective densities of these materials are 0.14 g/cm^3 (9 lb$_m$/ft^3), 0.19 g/cm^3 (12 lb$_m$/ft^3), and 0.35 g/cm^3 (22 lb$_m$/ft^3). The LI-900 and LI-2200 materials are fabricated using very high-purity silica fibers, having diameters ranging between 1 and 4 μm and lengths on the order of 3 mm (0.13 in.). Fiber-to-fiber bonds are established by a sintering heat treatment at 1370°C (2500°F), which gives

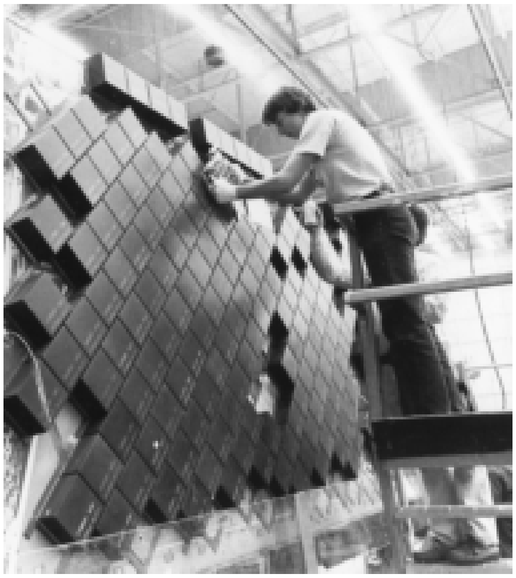

Figure 20.17 Photograph showing the installation of thermal protection ceramic tiles on the Space Shuttle Orbiter. [Photograph courtesy the National Aeronautics and Space Administration (NASA).]

rise to a very porous and lightweight material. The microstructure of a typical tile is shown in the scanning electron micrograph, Figure 20.18. On the other hand, FRCI tiles are composed of a 78% silica fiber-22% aluminum borosilicate fiber composite; the FRCI designation comes from *Fibrous Refractory Composite Insulation*.

The strengths of the LI-2200 and FRCI tiles are virtually equivalent, being greater than that of LI-900. LI-2200 and FRCI are used in those locations where a higher strength is required, such as around doors and access panels. Employment of FRCI instead of LI-2200 reduced orbiter weight by approximately 450 kg (1000 lb_m). Most tiles on the orbiters are the LI-900 type.

These low-density silica fiber materials are ideal for the Shuttle's Thermal Protection System. Being approximately 93 vol% void, they are excellent thermal insulators; this is confirmed by the chapter-opening photograph for Chapter 17, which shows a man holding a very hot cube of the tile material in his bare hands.

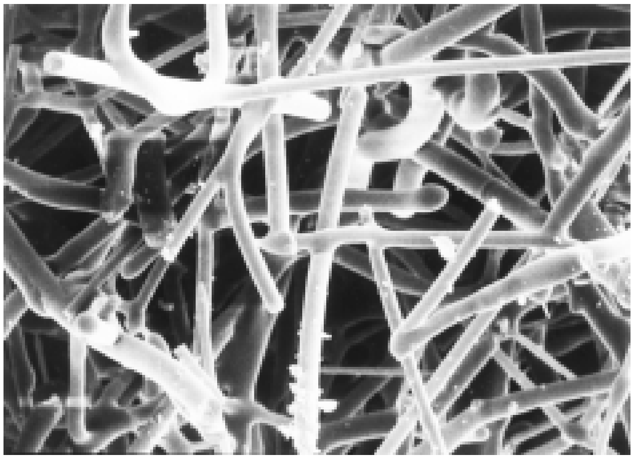

Figure 20.18 Scanning electron micrograph of a Space Shuttle Orbiter ceramic tile showing silica fibers that were bonded to one another during a sintering heat treatment. 750×. (Photograph provided courtesy of Lockheed Aerospace Ceramics Systems, Sunnyvale, California.)

Furthermore, silica has an extremely low coefficient of thermal expansion (Table 17.1) as well as a relatively small modulus of elasticity (Table 7.1); thus, it is very resistant to thermal shock associated with rapid temperature changes (Equation 17.8). Also, silica may be heated to relatively high temperatures without softening; short-term exposures to temperatures as high as 1480°C (2700°F) are possible.

The properties of the tiles are anisotropic; they are designed to be strongest in the plane of the tile and to be most thermally insulative in the direction perpendicular to this plane.

Tiles on surfaces exposed to maximum temperatures in the range of 400 to 650°C (750 to 1200°F) (i.e., upper vehicle sides, and upper wing and tail surfaces) are coated with a thin layer (0.30 mm [0.012 in.] thick) of a high-emittance borosilicate glass. This tile type is referred to as a *low-temperature reusable surface insulation* (*LRSI*); the tile surface is white, which reflects the sun's rays and keeps the Shuttle relatively cool while in orbit. Locations of the LRSI tiles are indicated in Figure 20.16.

Those tiles that are exposed to higher maximum temperatures between 650°C (1200°F) and 1260°C (2300°F) (i.e., the vehicle underbody, and tail leading and trailing edges) receive a black coating consisting of the same borosilicate glass and, in addition, silicon tetraboride (SiB_4); this coating material is sometimes termed a *reaction cured glass* (*RCG*). Being of high optical emittance, this coating is able to radiate approximately 90% of the reentry heat generated away from the Shuttle either into the earth's atmosphere or into deep space. This type of tile is termed a *high-temperature reusable surface insulation* (*HRSI*), and its locations on the Shuttle are also noted in Figure 20.16.

It is also necessary to isolate and cushion the brittle ceramic tiles from the mechanical and thermal strains sustained by the airframe and, in addition, to attach the tiles to the airframe. This is accomplished by an assembly consisting of a *strain isolator pad* (*SIP*), a *filler bar,* and a silicone RTV adhesive that bonds the tile to the SIP and the SIP and filler bar to the airframe structure. A schematic diagram of this assembly is shown in Figure 20.19. The strain isolator pad is composed of a nylon felt that will sustain repeated heatings to 290°C (550°F); this pad isolates the tiles from airframe deflections.

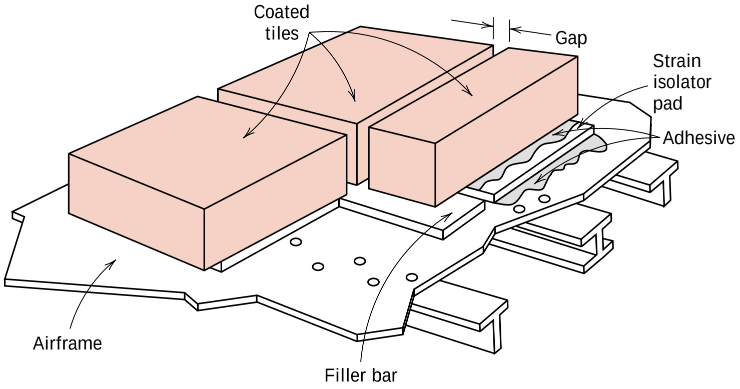

Figure 20.19 Schematic cross section of the tile component of the Space Shuttle Orbiter's thermal protection system. (From L. J. Korb, C. A. Morant, R. M. Calland, and C. S. Thatcher, "The Shuttle Orbiter Thermal Protection System," *Ceramic Bulletin*, No. 11, Nov. 1981, p. 1189. Copyright 1981. Reprinted by permission of the American Ceramic Society.)

Beneath the tile-to-tile junctions are located the filler bars. They are of the same nylon felt to which an RTV outer coating has been applied. The thickness of these bars is greater than the strain isolator pad, and, as such, they form a gasket seal to the undersurface of the tiles and protect the strain isolator pads from water or plasma penetration through the tile-to-tile junctions.

The adhesive that bonds this system together and to the airframe must survive repeated exposures to at least 290°C (550°F), must cure at room temperature, and must be capable of filling any irregularities in the airframe structure. The only material that fulfills all these requirements is a silicone RTV adhesive.

REINFORCED CARBON–CARBON

During reentry, some shuttle orbiter surface regions are exposed to temperatures in excess of those that the ceramic tiles are capable of sustaining (1260°C [2300°F]). Specifically, these areas are the nose cap and wing leading edges, Figure 20.15, where temperatures may reach as high as 1650°C (3000°F). The material that was designed for use in these locations is a *reinforced carbon–carbon* (*RCC*) composite. It is also a relatively complex material consisting of a carbon matrix that is reinforced with graphite fibers; the surface is coated with a thin layer of silicon carbide (SiC) as a protection against oxidation. This composite material is suitable for these high-temperature locations for the following reasons: strength and stiffness are retained up to the maximum service temperatures; it has a low coefficient of thermal expansion, and thus will not experience significant thermal stresses and deflections; it is highly resistant to thermal shock and fatigue; its density is very low; and fabrication into complex shapes is possible. Figure 20.16 shows those areas where this RCC composite material is employed.

Of course, materials other than those already cited are used on the Orbiter. For example, window ports are made of glass materials. Also, as may be noted from Figure 20.16, metal alloys are used for some exposed surfaces. These alloys will typically have high melting temperatures and, preferably, relatively low densities. Examples include beryllium, niobium, titanium, stainless steel (alloys 316), and several superalloys (Inconel alloys 718, 625, 750, and Haynes alloy 188).

MATERIALS FOR INTEGRATED CIRCUIT PACKAGES

20.12 INTRODUCTION

The microelectronic circuitry, including the integrated circuits that are used in our modern computers, calculators, and other electronic devices, was briefly discussed in Section 12.14. The heart of the integrated circuit (abbreviated *IC*) is the *chip*, a small rectangular substrate of high-purity and single-crystal silicon (or more recently gallium arsenide) onto which literally thousands of circuit elements are imprinted. Circuit elements (i.e., transistors, resistors, diodes, etc.) are created by selectively adding controlled concentrations of specific impurities to extremely minute and localized regions near the surface of the semiconducting material using involved photolithographic techniques. The chips are small in size, with the largest being on the order of 6 mm ($\frac{1}{4}$ in.) on each side and approximately 0.4 mm (0.015 in.) thick. Photographs of a typical chip are shown in Figure 12.25.

Furthermore, chips are very fragile inasmuch as silicon is a relatively brittle material and gallium arsenide is even more brittle. It is also necessary to fabricate conducting circuit paths over the surface of the chip so as to facilitate the passage of current from device to device; on silicon ICs the metal conductor used is aluminum or an aluminum–silicon alloy (99 wt% Al, 1 wt% Si) which is metallized onto the chip surface to form a very thin film. The chip design also calls for these circuit paths to terminate at contact pads on the chip periphery, at which points electrical connections may be made with the macroscopic world. It should be obvious that a functioning microelectronic chip is a very sophisticated electronic entity, that materials requirements are very stringent, and that elegant processing techniques are involved in its fabrication.

A large number of IC chips are fabricated onto a circular thin wafer of single-crystal Si, as shown in the photograph in Figure 20.20. Single crystals of Si having diameters as large as 200 mm (8 in.) are routinely grown. The small rectangular ICs arrayed in the manner shown in the photograph are collectively referred to as *dice*. Each IC or *die* (singular of dice) is first tested for functionality, after which it is removed from the wafer in a meticulous sawing or ''scribe and break'' operation. Next, the die is mounted in some type of *package*. The packaged IC may then be bonded to a printed circuit board. The purpose of this section is to discuss the material requirements and some of the materials that are used for the various IC package components.

Some of the functions that an integrated circuit package must perform include the following:

1. To permit electrical contact between the devices on the chip and the macroscopic world. The contact pads on the surface of the IC are so minuscule and numerous that accommodation of macroscopic wiring is simply not possible.
2. To dissipate excess heat. While in operation, the many electronic devices generate significant quantities of heat, which must be dissipated away from the chip.

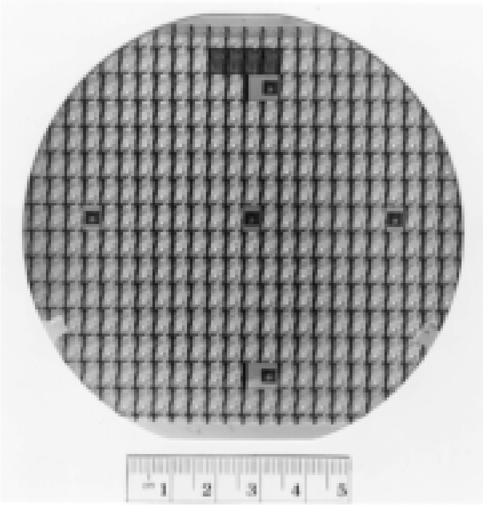

FIGURE 20.20 Photograph of a 100-mm-diameter (4-in.-diameter) silicon wafer. Each of the small rectangles shown is an individual IC chip or die.

3. To protect delicate electrical connections on the chip from chemical degradation and contamination.
4. To provide mechanical support so that the small and fragile chip may be handled.
5. To provide an adequate electrical interface such that the performance of the IC itself is not significantly degraded by the package design.

Thus, IC packaging also poses a host of material demands that are very challenging. In fact, it has been noted that the performance of some ICs is limited, not by the characteristics of the semiconducting materials nor by the metallization process, but rather by the quality of the package. There are a number of different package designs used by the various IC manufacturers. For one of the common designs, the *leadframe*, we have elected to discuss the various components and, for each component, the materials that are employed along with their property limitations. This package design is popular with digital IC manufacturers primarily because its production can be highly automated.

20.13 LEADFRAME DESIGN AND MATERIALS

The leadframe, as the name suggests, is a frame to which electrical leads may be made from the IC chip. A photograph of a leadframe-type package is shown in Figure 20.21. In essence, the leadframe consists of a central plate onto which the die is mounted, and an array of contact leads to which wire connections may be made from the contact pads on the chip. Some leadframe designs also call for a substrate onto which the die is mounted, which substrate is, in turn, bonded to the central plate. During the packaging process, and after the chip has been attached to the central plate (a procedure termed *die bonding*), the contact pads on the IC chip are cleaned, wires are attached to both the contact pads and the leadframe leads (called *wire bonding*), and, finally, this package is encapsulated in a protective

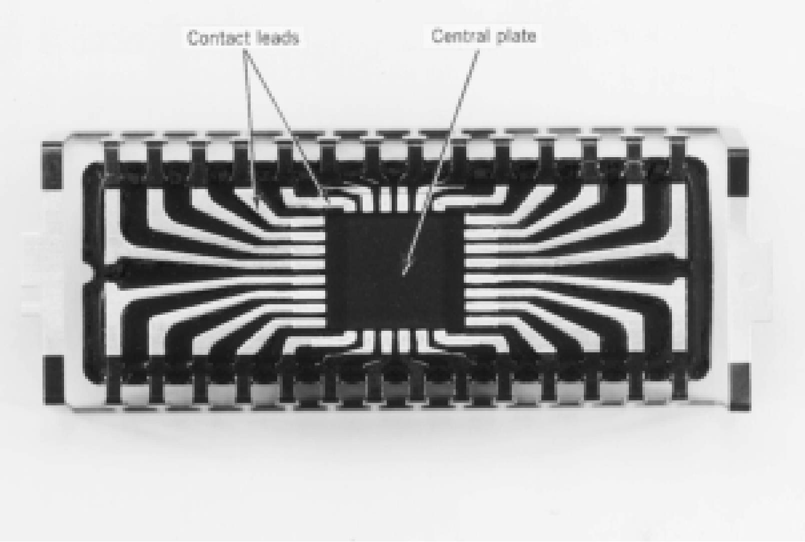

FIGURE 20.21 Photograph of a leadframe on which the central plate and contact leads are labeled. 2×. (Leadframe supplied by National Semiconductor Corporation. Photograph by Dennis Haynes.)

enclosure so as to seal out moisture, dust, and other contaminants. This procedure is called *hermetic sealing*.

There are some rather stringent requirements on the properties of the material to be used for the leadframe; these are as follows: (1) The leadframe material must have a high electrical conductivity, inasmuch as there will be current passage through its leads. (2) The leadframe, the die attach central plate, substrate (if present), and die-bonding adhesive must also be thermally conductive so as to facilitate the dissipation of heat generated by the IC. (3) A coefficient of thermal expansion comparable to that of Si is highly desirable; a thermal expansion mismatch could destroy the integrity of the bond between the IC and the central plate as a result of thermal cycling during normal operation. (4) The leadframe material and substrate must also adhere to the die-bonding adhesive, and the adhesive and substrate must also be electrically conductive. (5) A secure and electrically conductive joint between the leadframe and the connecting wires must be possible. (6) The leadframe must be resistant to oxidation and retain its mechanical strength during any thermal cycling that may accompany the die-bonding and encapsulation procedures. (7) The leadframe must also withstand corrosive environments at high temperatures and high humidities. (8) It must be possible to mass produce the leadframes economically. Normally, they are stamped from thin metal sheets.

A parenthetical comment is in order relative to the electrical characteristics of the substrate and die-bonding adhesive. In the preceding paragraph it was noted that the materials used for these two leadframe components must be electrically conductive. This is inconsistent with the ceramic materials used for packaging substrates which, as discussed in Section 13.10, must be electrical insulators. This discrepancy is resolved when it is realized that some package designs call for grounding of the IC chip through the substrate, whereas for other designs, grounding is through the contact wires.

Several alloys have been used for the leadframe with varying degrees of success. The most commonly used materials are copper-based alloys; the compositions, electrical and thermal conductivities, and coefficients of thermal expansion for two of the most popular ones (C19400 and C19500) are listed in Table 20.6. For the most part, they satisfy the criteria listed in the preceding paragraph. Also listed in the table are the compositions of two other alloys (Kovar and Alloy 42) that have been used extensively in leadframes. The desirability of these latter two alloys lies in their relatively low coefficients of thermal expansion, which are closely matched to that of Si [i.e., $2.5 \times 10^{-6}\ (^\circ\mathrm{C})^{-1}$]. However, from Table 20.6 it may also be noted that both electrical and thermal conductivities for Kovar and Alloy 42 are inferior to the conductivity values for the C19400 and C19500 alloys.

20.14 DIE BONDING

The die-bonding operation consists of attaching the IC chip to the central supporting leadframe plate. For the copper alloys noted in Table 20.6, attachment may be made using a gold–silicon eutectic solder; however, melting of the solder requires heating the assembly to 500°C (900°F).

Another adhesive possibility is an epoxy bonding agent, which is normally filled with metal particles (frequently Ag) so as to provide both a thermally and electrically conductive path between the chip and the leadframe. Curing of the epoxy is carried out at temperatures between 60°C (140°F) and 350°C (660°F) depending on the application. Since the amounts of thermal expansion are different for the Cu alloy leadframe plate and Si chip, the epoxy adhesive must be capable of absorbing any thermal strains produced during temperature changes such that the mechanical

Table 20.6 **Designations, Compositions, Electrical and Thermal Conductivities, and Coefficients of Thermal Expansion for Common IC Leadframe Alloys**

	Composition (*wt%*)					*Electrical Conductivity* [10^6 (Ω-m)$^{-1}$]	*Thermal Conductivity* (W/m-K)	*Coefficient of Thermal Expansion*[a] [10^{-6} (°C)$^{-1}$]
Alloy Designation	*Fe*	*Ni*	*Co*	*Cu*	*Other*			
C19400	2.35			Balance	0.03 P, 0.12 Zn, 0.03 Pb (max)	39.4	260	16.3
C19500	1.5		0.8	Balance	0.6 Sn, 0.03 P	29.1	200	16.9
Kovar (ASTM F15)	54	29	17			2.0	17	5.1
Alloy 42 (ASTM F30)	58	42				1.4	12	4.9

[a] Coefficient of thermal expansion values are averages measured between 20°C and 300°C.

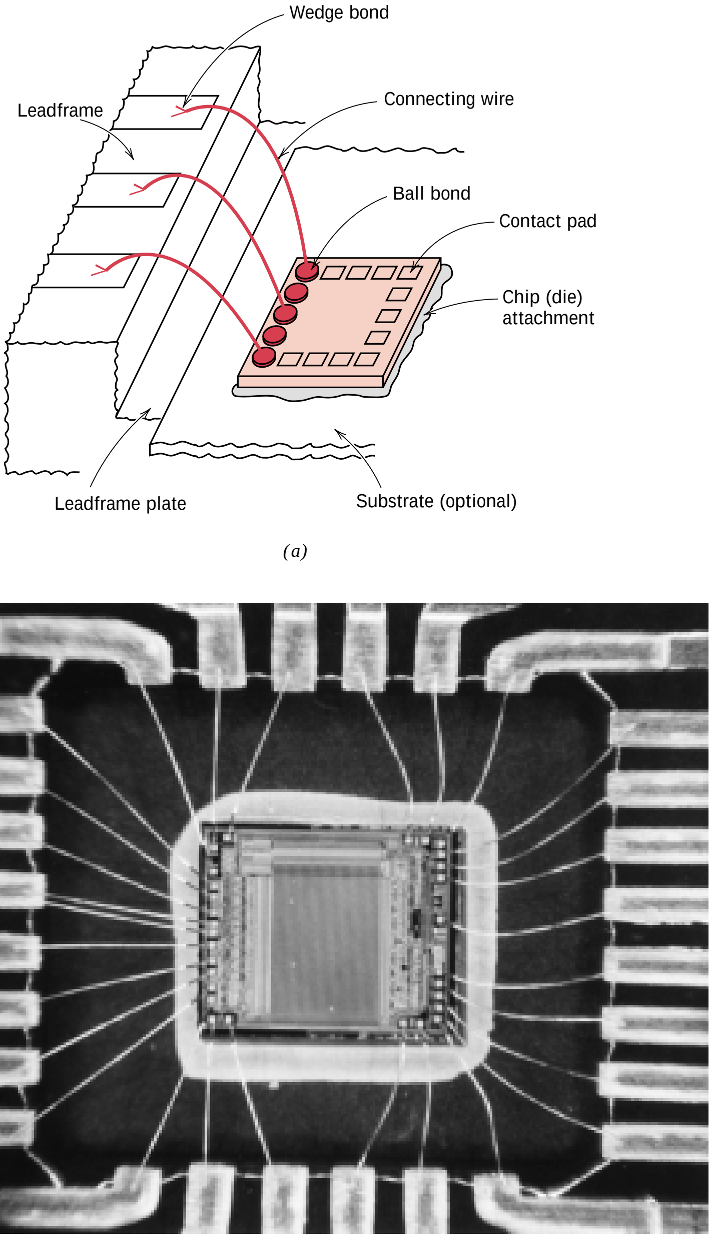
Wedge bond
Leadframe
Connecting wire
Ball bond
Contact pad
Chip (die) attachment
Leadframe plate
Substrate (optional)

(a)

(b)

FIGURE 20.22 (*a*) Schematic diagram showing the IC chip, its attachment to the substrate (or leadframe plate), and the connecting wires that run to the leadframe contact leads. (Adapted from *Electronic Materials Handbook*, Vol. 1, *Packaging*, C. A. Dostal, editor, ASM International, 1989, p. 225.) (*b*) Photograph showing a portion of a leadframe package. Included is the IC chip along with its connecting wires. One end of each wire is bonded to a chip pad; the other wire extremity is bonded to a leadframe contact lead. 7$\frac{1}{2}$×. (Photograph courtesy of National Semiconductor Corporation.)

integrity of the junction is maintained. Figure 20.22*a* shows a schematic diagram of a chip that is bonded to a substrate layer that is, in turn, bonded to the leadframe plate. Figure 20.22*b* is a photograph of a chip, its leadframe, and the connecting wires.

20.15 WIRE BONDING

The next step in the packaging process involves making electrical connections between the metallized chip pads and the leadframe; this is accomplished using connecting wires (Figures 20.22*a* and 20.22*b*). A wire-bonding procedure is normally carried out using a microjoining operation, since very fine wires are used to make the connections. Wire bonding is the slow step in the packaging process because several hundred wires may need to be installed; this procedure is usually automated.

Several important considerations must be taken into account relative to the choice of wire alloy. Of course, a high electrical conductivity is the prime prerequisite. In addition, consideration must be given to the ability of the alloy to bond, by welding or brazing, with both the Al alloy at the chip pad and the Cu alloy on the leadframe; the formation of a microjoint that is both mechanically and electrically stable is an absolute necessity.

The most commonly used wire material is gold—actually a gold alloy containing a small amount of beryllium–copper that is added to inhibit grain growth. Gold wires are round and have diameters that are typically 18 μm (0.0007 in.), 25 μm (0.001 in.), or 50 μm (0.002 in.). Less costly Cu and Al have also been employed for contact wires. Prior to making the microjoint, regions of the chip pad and leadframe surfaces at which the junctions are to be made may be coated with Au so as to improve bondability. During the actual microjoining process, one wire end is brought into the vicinity of one of the joint regions using a special tool. This wire end is then melted with a spark or flame heat source.

Two different types of microjoints are possible: ball and wedge. Figure 20.23 is a schematic diagram showing a connecting wire having a ball microjoint at its contact pad end and a wedge microjoint at the leadframe connection. Ball joints are possible for gold wires since the melted wire end forms into a small ball because of the high surface tension of gold. Bonding of this molten ball with the contact pad or leadframe is accomplished by making mechanical contact with the bonding surface while both wire and surface are subjected to ultrasonic vibrations. A scanning electron micrograph of a ball microjoint is shown in Figure 20.24*a*. This type of microjoint is especially desirable since, after the first of the two microjoints for each wire has been made (usually on the IC contact pad), the wire may then be bent in any direction in preparation for the microjoining of its other extremity.

The ends of copper and aluminum wires do not form balls upon melting. They are wedge microjoined by positioning the wire between a vibrating probe and the contact pad or leadframe surface; the vibrations loosen and remove surface contaminants, which results in intimate contact of the two surfaces. An electric current is then applied through the probe, which welds the wire to the surface. Unfortunately, the bending motion of wedge-bonded wires is restricted to a single direction. Gold wires may also be bonded using wedge microjoints. Figure 20.24*b* is a scanning electron micrograph of a wedge microjoint.

There are other considerations relative to wire bonding that deserve mentioning. Microjunction alloy combinations that form intermetallic phases should be avoided

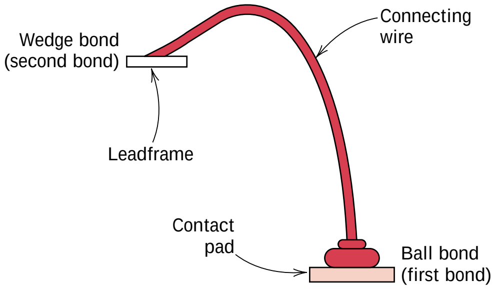

FIGURE 20.23 Schematic diagram showing a connecting wire that is ball bonded to the IC contact pad and wedge bonded to the leadframe. (Adapted from *Electronic Materials Handbook*, Vol. 1, *Packaging*, C. A. Dostal, editor, ASM International, 1989, p. 225.)

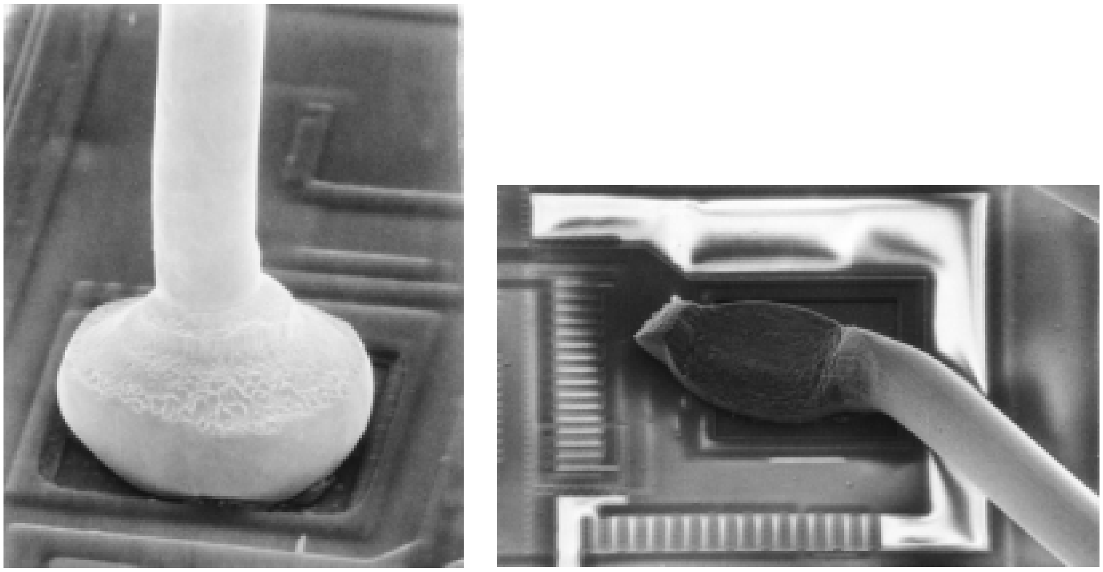
(*a*) (*b*)

Figure 20.24 Scanning electron micrographs of (*a*) a ball bond (475×), and (*b*) a wedge bond (275×). (Photographs courtesy of National Semiconductor Corporation.)

because these phases are normally brittle and yield microjoints lacking long-term mechanical stability. For example, Au and Al may react at elevated temperatures to form $AuAl_2$, termed the "purple plague"; this compound is not only very brittle (and purple), but also highly electrically resistive. Furthermore, mechanical integrity at each microjoint is important so as to (1) withstand vibrations that the package may experience, and (2) survive thermal stresses that are generated as the packaging materials change temperature.

20.16 PACKAGE ENCAPSULATION

The microelectronic package, as now constituted, must be provided some type of protection from corrosion, contamination, and damage during handling and while in service. The wire interconnection microjunctions are extremely fragile and may be easily damaged. Especially vulnerable to corrosion are the narrow Al circuit paths that have been metallized onto the surface of the IC chip; even the slightest corrosion of these elements will impair the operation of the chip. These Al-metallized layers experience corrosion when atmospheric moisture in which even minute concentrations of ionic contaminants are dissolved (especially chlorine and phosphorus) condenses on the chip surface. Furthermore, the corrosive reactions are accelerated as a consequence of electric currents that pass through these circuit paths. In addition, any sodium (as Na^+) that gets on the chip surface will eventually diffuse into the chip and destroy its operation.

The material used to encapsulate the package should:

1. Be electrically insulating;
2. Be easily molded to the desired shape around the chip die and its wire leads;

3. Be highly impervious to the penetration of moisture and contaminants;
4. Be able to form strong adhesive bonds with the chip surface, wires, and other leadframe components;
5. Exhibit mechanical and chemical stability for the expected lifetime of the package;
6. Not require exposure to excessively high temperatures during installation;
7. Have a coefficient of thermal expansion similar to those of other package components so as to avoid thermal stresses capable of fracturing the wire leads.

Figure 20.25 shows a schematic diagram of an encapsulated IC package.

Both ceramic and polymeric materials are used to encapsulate IC packages; of course each of these material types has its own set of assets and liabilities. Ceramics are extremely resistant to moisture penetration and are chemically stable and chemically inert. Glasses are the most commonly utilized ceramic materials. The principal disadvantage of glass is the requirement that it be heated to moderately high temperatures to lower its viscosity to the point where it will flow around and make intimate contact with all of the wires that are microjoined to the chip surface. Some common glass constituents should be avoided (notably Na_2O and K_2O) since volatile cation species (Na^+ and K^+) may be emitted from the molten glass. These species are notorious in accelerating corrosion reactions, and the ions will degrade the chip performance.

Polymeric materials are used in the largest volume for packaging encapsulation because they are not as costly as the ceramics, and they may be produced in a low-viscosity state at lower temperatures. Epoxies and polyurethanes are commonly used, with the former being the most common. However, these materials have a tendency to absorb water and do not form moisture-tight bonds with the lead wires. Some of these polymers require curing at a temperature on the order of 150°C, and during cooling to room temperature will shrink more than other package components to which they are attached. This difference in amounts of contraction can give rise to mechanical strains of sufficient magnitude to damage the connecting wires as well as other electronic components. The addition of appropriate fillers (such as fine silica or alumina particles) to the polymer can alleviate this problem but often has undesirable electrical consequences. A comparison of the important encapsulation characteristics of four different polymer types is given in Table 20.7.

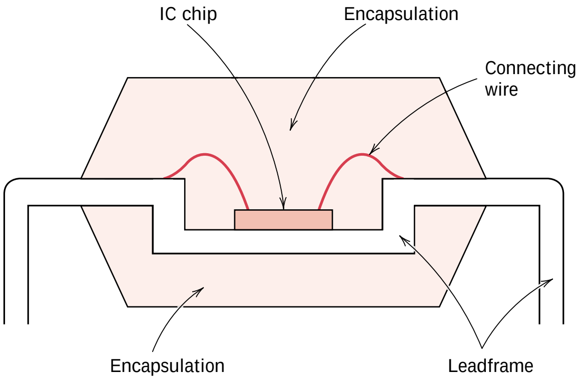

FIGURE 20.25 Schematic diagram showing an encapsulated IC leadframe package. (Adapted from *Electronic Materials Handbook*, Vol. 1, *Packaging*, C. A. Dostal, editor, ASM International, 1989, p. 241.)

Table 20.7 Property Comparisons of Four Classes of Polymers Used for IC Package Encapsulation

	Epoxy Resins	*Silicones*	*Polyurethanes*	*Polysulphides*
Dielectric strength	Good	Good	Good	Good
Elastic modulus	High	Low	Wide range	Low
Tensile strength	High	Low	Wide range	—
Precursor viscosity	Low	Low	Low	High
Adhesion to package	Excellent	Poor (to ceramics)	Good	Good
Moisture diffusion rate	High	High	Low	Very low

Source: From C. R. M. Grovenor, *Microelectronic Materials.* Copyright © 1989 by Institute of Physics Publishing, Bristol.

20.17 TAPE AUTOMATED BONDING

Another packaging design, *tape automated bonding* (or *TAB*), a variation of the leadframe discussed above, has found widespread use by virtue of its low cost. The tape-bonded package consists of a thin and flexible polyimide polymer backing film substrate; onto this substrate surface is patterned an array of copper ‘‘finger’’ high-conductivity conduction paths similar in configuration to the contact leads for the conventional leadframe. A schematic diagram of a tape-bonded film leadframe is shown in Figure 20.26.

Mechanical support for the assembly is provided by the polyimide film, onto which the die is bonded using an adhesive. Polyimide strip widths are typically 35 mm (1.38 in.), and sprocket holes are incorporated along opposing edges so as to facilitate movement and positioning of the TAB leadframes. Literally thousands of these individual units, attached end to end, are spooled onto reels in preparation for automated processing.

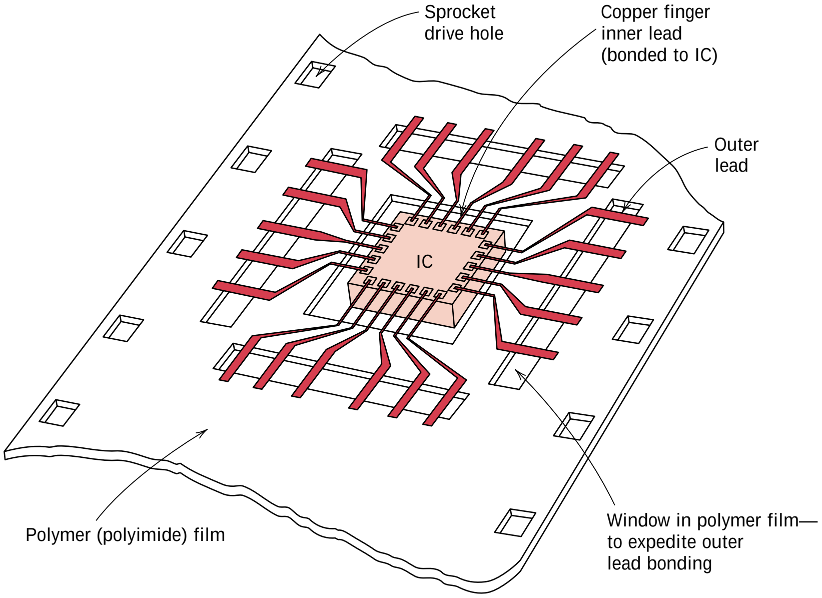
Sprocket drive hole
Copper finger inner lead (bonded to IC)
Outer lead
IC
Polymer (polyimide) film
Window in polymer film—to expedite outer lead bonding

FIGURE 20.26 Schematic diagram of a complete tape-bonded (TAB) leadframe. (From *Electronic Materials Handbook*, Vol. 1, *Packaging*, C. A. Dostal, editor, ASM International, 1989, p. 233.)

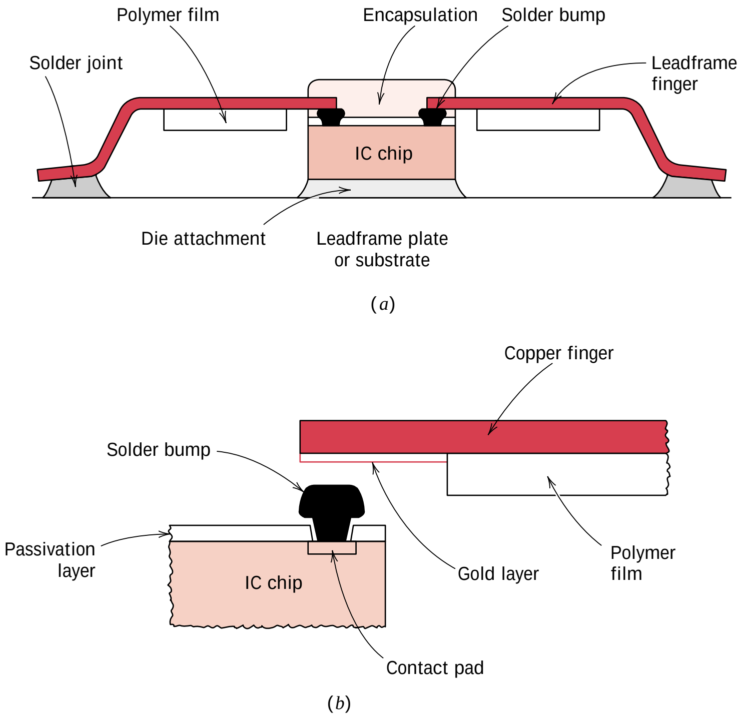

Figure 20.27 Schematic diagrams showing (*a*) the cross section of an encapsulated TAB leadframe package, and (*b*) how bonding between the IC chip and a copper finger is achieved with a solder bump. (Adapted from *Electronic Materials Handbook*, Vol. 1, *Packaging*, C. A. Dostal, editor, ASM International, 1989, pp. 233, 234.)

The copper fingers are extremely narrow and positioned close together. Separation distances of the inner contact leads are on the order of 50 μm, which is much smaller than is possible for the stamped leadframe. Furthermore, each die chip contact pad is microjoined directly to one of these copper fingers, which eliminates the need for any connecting wires. The copper fingers are very thin, so that, for this direct bonding to be achieved, the chip pad bonding sites must be raised above the metallized coating. This is accomplished using ‘‘solder bumps,’’ which are normally layers of gold (or gold-plated copper) approximately 25 μm thick. Schematic representations illustrating this attachment design are presented in Figure 20.27. The finger contacts are bonded to these raised bumps by soldering using a thermal-compression bonding tool. This tape-bonding design is fully automated in that all of the hundred or so microjoints can be made in a single step, a feature not possible with leadframes that require multiple wire-bonding operations.

The packaging operation for the TAB leadframe is completed, as with the stamped leadframe, by encapsulation of the assembly (i.e., tape leadframe and its attached chip) within a fluid polymeric material that subsequently cures so as to form a protective shield. Protruding from this package are the copper finger conducting paths to which external electrical connections are made. Furthermore, excess heat generated by the chip must be dissipated along these copper fingers inasmuch as the polymer tape backing does not provide an effective thermal conduction path because of its low thermal conductivity.

The ultimate design goal of the IC package is to allow for the proper electrical operation of the packaged device. As frequencies and computing speeds creep ever higher, the mechanical and electrical design considerations of the package design must become more and more integrated. The overall electrical performance of the package is as important to the end user as the overall reliability.

SUMMARY

In this chapter, we have illustrated the protocol of materials selection using five diverse examples. For the first case, a torsionally stressed cylindrical shaft, an expression for strength performance index was derived; then, using the appropriate materials selection chart, a preliminary candidate search was conducted. From the results of this search, several candidate engineering materials were ranked on both strength-per-unit mass and cost bases. Other factors that are relevant to the decision-making process were also discussed.

A stress analysis was next performed on a helical spring, which was then extended to an automobile valve spring. It was noted that the possibility of fatigue failure was crucial to the performance of this spring application. The shear stress amplitude was computed, the magnitude of which was almost identical to the calculated fatigue limit for a chrome–vanadium steel that is commonly used for valve springs. It was noted that the fatigue limit of valve springs is often enhanced by shot peening. Finally, a procedure was suggested for assessing the economic feasibility of this spring design incorporating the shot-peened chrome–vanadium steel.

For the third case study, the artificial total hip replacement was explored. The hip anatomy was first presented, which was followed by a discussion of the components and material requirements for the artificial replacement. Implant materials must be biocompatible with body tissues and fluids, must be corrosion resistant, and must also be mechanically compatible with interfacing replacement/body components. The femoral stem and ball are normally made of a cold-worked stainless steel, a hot-forged Co–Ni–Cr–Mo alloy, or a hot-forged titanium alloy. Some recent designs call for a polycrystalline aluminum oxide ball. Ultrahigh molecular weight polyethylene is commonly used for the acetabular cup, whereas acrylic bone cement is normally the fixation agent for attachment of the femoral stem (to the femur) and acetabular cup (to the pelvis).

The thermal protection system on the Space Shuttle was the fourth materials case study considered. Its design presented some very restrictive materials requirements; these were overcome by the incorporation of several different systems as well as by the development of new materials. A felt reusable surface insulation, consisting of silicone-coated nylon felt blankets, is used for those surface areas exposed to relatively low reentry temperatures. The ceramic tiles cover the major portion of the Space Shuttle's surface, areas that are exposed to higher temperatures. This porous insulation is composed of either silica fibers or a combination of silica and aluminum borosilicate fibers. Tiles having several different strengths, densities, and thermal properties are fabricated for utilization at the various locations. A thin glass surface coating is applied to each tile so as to improve either its reflectance or emissive characteristics. Those surface regions of the Shuttle that experience the highest reentry temperatures are constructed of a reinforced carbon–carbon composite that is coated with a thin layer of silicon carbide.

Materials utilized for the integrated circuit package incorporating the leadframe design were the topic of the final case study. An IC chip is bonded to the leadframe plate using either a eutectic solder or an epoxy resin. The leadframe material must be both electrically and thermally conductive, and, ideally, have a coefficient of thermal expansion that matches the IC chip material (i.e., silicon or gallium arsenide); copper alloys are commonly used leadframe materials. Very thin wires (preferably of gold, but often of copper or aluminum) are used to make electrical connections from the microscopic IC chip contact pads to the leadframe. Ultrasonic microjoining welding/brazing techniques are used where each connection joint may be in the form of either a ball or wedge. The final step is package encapsulation, wherein this leadframe–wire–chip assembly is encased in a protective enclosure. Ceramic glasses and polymeric resins are the most common encapsulation materials. Resins are less expensive than glasses and require lower encapsulation temperatures; however, glasses normally offer a higher level of protection.

REFERENCES

General

Ashby, M. F., *Materials Selection in Mechanical Design*, Pergamon Press, Oxford, 1992.

ASM Handbook, Vol. 20, *Materials Selection and Design,* ASM International, Materials Park, OH, 1997.

Budinski, K. G., *Engineering Materials: Properties and Selection,* 5th edition, Prentice Hall, Inc., Englewood Cliffs, NJ, 1995.

Creyke, W. E. C., I. E. J. Sainsbury, and R. Morrell, *Design with Nonductile Materials*, Applied Science Publishers, London, 1982.

Dieter, G. E., *Engineering Design, A Materials and Processing Approach*, 2nd edition, McGraw-Hill Book Company, New York, 1991.

Farag, M. M., *Materials Selection for Engineering Design,* Prentice Hall, Inc., Upper Saddle River, NJ, 1997.

Lewis, G., *Selection of Engineering Materials*, Prentice Hall, Inc., Englewood Cliffs, NJ, 1990.

Mangonon, P. L., *The Principles of Materials Selection for Engineering Design,* Prentice Hall, Saddle River, NJ, 1999.

Optimization of Strength

Ashby, M. F. and D. R. H. Jones, *Engineering Materials 1, An Introduction to Their Properties and Applications*, 2nd edition, Pergamon Press, Oxford, 1996.

Automotive Valve Springs

Edwards, K. S., Jr. and R. B. McKee, *Fundamentals of Mechanical Component Design*, Chapter 18, McGraw-Hill Book Company, New York, 1991.

Society of Automotive Engineers Handbook, 1991 edition, Section 6, Society of Automotive Engineers, Inc., 1991.

Artificial Hip Replacements

Williams, D. F. (Editor), *Biocompatibility of Orthopedic Implants*, Vol. I, CRC Press, Inc., Boca Raton, FL, 1982.

Pilliar, R. M., ''Manufacturing Processes of Metals: The Processing and Properties of Metal Implants,'' *Metal and Ceramic Biomaterials*, P. Ducheyne and G. Hastings (Editors), CRC Press, Inc., Boca Raton, FL, 1984.

Thermal Protection System on the Space Shuttle Orbiter

Korb, L. J., C. A. Morant, R. M. Calland, and C. S. Thatcher, ''The Shuttle Orbiter Thermal Protection System,'' *American Ceramic Society Bulletin*, Vol. 60, No. 11, 1981, pp. 1188–1193.

Cooper, P. A. and P. F. Holloway, ''The Shuttle Tile Story,'' *Astronautics and Aeronautics*, Vol. 19, No. 1, 1981, pp. 24–36.

Gordon, M. P., *The Space Shuttle Orbiter Thermal Protection System, Processing Assessment, Final Report*, http://ihm.arc.nasa.gov/repair/shuttle_report/index.html.

Integrated Circuit Packaging

Electronic Materials Handbook, Vol. I, *Packaging*, ASM International, Materials Park, OH, 1989.

Grovenor, C. R. M., *Microelectronic Materials*, Institute of Physics Publishing, Bristol, 1989.

QUESTIONS AND PROBLEMS

Design Problems

20.D1 **(a)** Using the procedure as outlined in Section 20.2 ascertain which of the metal alloys listed in Appendix B (and also the database on the CD-ROM), have torsional strength performance indices greater than 12.5 (in SI units), and, in addition, shear strengths greater than 300 MPa. **(b)** Also using the cost database (Appendix C), conduct a cost analysis in the same manner as Section 20.2. For those materials that satisfy the criteria noted in part a, and, on the basis of this cost analysis, which material would you select for a solid cylindrical shaft? Why?

20.D2 In a manner similar to the treatment of Section 20.2, perform a stiffness-to-mass performance analysis on a solid cylindrical shaft that is subjected to a torsional stress. Use the same engineering materials that are listed in Table 20.1. In addition, conduct a material cost analysis. Rank these materials both on the basis of mass of material required and material cost. For glass and carbon fiber-reinforced composites, assume that the shear moduli are 8.6 and 9.2 GPa, respectively.

20.D3 **(a)** A cylindrical cantilever beam is subjected to a force *F*, as indicated in the figure below. Derive strength and stiffness performance index expressions analogous to Equations 20.9 and 20.11 for this beam. The stress imposed on the unfixed end σ is

$$\sigma = \frac{FLr}{I} \tag{20.24}$$

L, r, and I are, respectively, the length, radius, and moment of inertia of the beam. Furthermore, the beam-end deflection δ is

$$\delta = \frac{FL^3}{3EI} \tag{20.25}$$

where E is the modulus of elasticity of the beam.

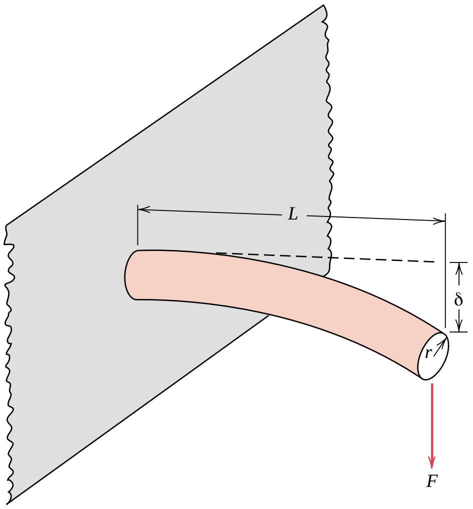

(b) From the properties database presented in Appendix B (or on the CD-ROM), select those metal alloys with stiffness performance indices greater than 3.0 (in SI units).

(c) Also using the cost database (Appendix C), conduct a cost analysis in the same manner as Section 20.2. Relative to this analysis and that in part b, which alloy would you select on a stiffness-per-mass basis?

(d) Now select those metal alloys having strength performance indices greater than 18.0 (in SI units), and rank them from highest to lowest *P*.

(e) And, using the cost database, rank the materials in part d from least to most costly. Relative to this analysis and that in part d, which alloy would you select on a strength-per-mass basis?

(f) Which material would you select if both stiffness and strength are to be considered relative to this application? Justify your choice.

20.D4 **(a)** A bar specimen having a square cross section of edge length *c* is subjected to a uniaxial tensile force *F*, as shown in the following figure. Derive strength and stiffness performance index expressions analogous to Equations 20.9 and 20.11 for this bar.

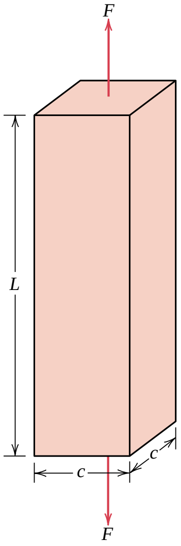

(b) From the properties database presented in Appendix B (or on the CD-ROM), select those metal alloys with stiffness performance indices greater than 26.3 (in SI units).

(c) Also using the cost database (Appendix C), conduct a cost analysis in the same manner as Section 20.2. Relative to this analysis and that in part b, which alloy would you select on a stiffness-per-mass basis?

(d) Now select those metal alloys having strength performance indices greater than 100 (in SI units), and rank them from highest to lowest P.

(e) And, using the cost database, rank the materials in part d from least to most costly. Relative to this analysis and that in part d, which alloy would you select on a strength-per-mass basis?

(f) Which material would you select if both stiffness and strength are to be considered relative to this application? Justify your choice.

20.D5 Consider the plate shown below that is supported at its ends and subjected to a force F that is uniformly distributed over the upper face as indicated. The deflection δ at the $L/2$ position is given by the expression

$$\delta = \frac{5FL^3}{32Ewt^3} \tag{20.26}$$

Furthermore, the tensile stress at the underside and also at the $L/2$ location is equal to

$$\sigma = \frac{3FL}{4wt^2} \tag{20.27}$$

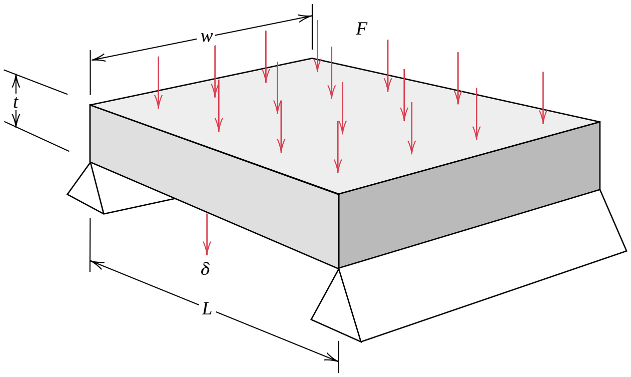

(a) Derive stiffness and strength performance index expressions analogous to Equations 20.9 and 20.11 for this plate. (*Hint:* solve for t in these two equations, and then substitute the resulting expressions into the mass equation, as expressed in terms of density and plate dimensions.)

(b) From the properties database in Appendix B (or on the CD-ROM), select those metal alloys with stiffness performance indices greater than 1.50 (in SI units)

(c) Also using the cost database (Appendix C), conduct a cost analysis in the same manner as Section 20.2. Relative to this analysis and that in part b, which alloy would you select on a stiffness-per-mass basis?

(d) Now select those metal alloys having strength performance indices greater than 6.0 (in SI units), and rank them from highest to lowest P.

(e) And, using the cost database, rank the materials in part d from least to most costly. Relative to this analysis and that in part d, which alloy would you select on a strength-per-mass basis?

(f) Which material would you select if both stiffness and strength are to be considered relative to this application? Justify your choice.

20.D6 A spring having a center-to-center diameter of 15 mm (0.6 in.) is to be constructed of cold-worked ($\frac{1}{4}$ hard) 304 stainless steel wire that is 2.0 mm (0.08 in.) in diameter; this spring design calls for ten coils.

(a) What is the maximum tensile load that may be applied such that the total spring deflection will be no more than 5 mm (0.2 in)?

(b) What is the maximum tensile load that may be applied without any permanent deformation of the spring wire? Assume that the shear yield strength is 0.6 σ_y, where σ_y is the yield strength in tension.

20.D7 You have been asked to select a material for a spring that is to be stressed in tension. It is to consist of 8 coils, and the coil-to-coil diameter called for is 12 mm; furthermore, the diameter of the spring wire must be 1.75 mm. Upon application of a tensile force of 30 N, the spring is to experience a deflection of no more than 10 mm, and not plastically deform.

(a) From those materials included in the database in Appendix B (or on the CD-ROM), make a list of those candidate materials that meet the above criteria. Assume that the shear yield strength is $0.6\sigma_y$, where σ_y is the yield strength in tension, and that the shear modulus is equal to $0.4E$, E being the modulus of elasticity.

(b) Now, from this list of candidate materials, select the one you would use for this spring application. In addition to the above criteria, the material must be relatively corrosion resistant, and, of course, capable of being fabricated into wire form. Justify your decision.

20.D8 A spring having 10 coils and a coil-to-coil diameter of 0.4 in. is to be made of cold-drawn steel wire. When a tensile load of 12.9 lb_f is applied the spring is to deflect no more than 0.80 in. The cold drawing operation will, of course, increase the shear yield strength of the wire, and it has been observed that τ_y (in ksi) depends on wire diameter d (in in.) according to

$$\tau_y = \frac{63}{d^{0.2}} \qquad (20.28)$$

If the shear modulus for this steel is 11.5 $\times$ 10^6 psi, calculate the minimum wire diameter required such that the spring will not plastically deform when subjected to the above load.

20.D9 A helical spring is to be constructed from a 4340 steel. The design calls for 12 coils, a coil-to-coil diameter of 12 mm, and a wire diameter of 2 mm. Furthermore, in response to a tensile force of 27 N, the total deflection is to be no more than 3.5 mm. Specify a heat treatment for this 4340 steel wire in order for the spring to meet the above criteria. Assume a shear modulus of 80 GPa for this steel alloy, and that $\tau_y = 0.6\sigma_y$.

20.D10 Using the *E-Z Solve* software included on the CD-ROM that accompanies this book, construct a routine for the automobile valve spring (Section 20.5) that allows the user to specify the number of effective coils (N), the spring coil-to-coil diameter (D), and the wire cross-section diameter (d), and calculates the fatigue limit (τ_{al}) as well as the actual stress amplitude (τ_{aa}). Incorporate into this routine values cited for installed and maximum deflections per coil (i.e., δ_{ic} = 0.24 in. and δ_{mc} = 0.54 in.), as well as for the shear modulus of steel (G = 11.5 $\times$ 10^6 psi).

20.D11 You have been asked to select a metal alloy to be used as leadframe plate in an integrated circuit package that is to house a silicon chip.

(a) Using the database in Appendix B (or on the CD-ROM) list those materials that are electrically conductive [$\sigma > 10 \times 10^6$ $(\Omega\text{-m})^{-1}$], have linear coefficients of thermal expansion of between 2×10^{-6} and 10×10^{-6} $(°\text{C})^{-1}$, and thermal conductivities of greater than 100 W/m-K. On the bases of properties and cost, would you consider any of these materials in preference to those listed in Table 20.6? Why or why not?

(b) Repeat this procedure for potential insulating leadframe plate materials that must have electrical conductivities less than 10^{-10} $(\Omega\text{-m})^{-1}$, as well as coefficients of thermal expansion between 2×10^{-6} and 10×10^{-6} $(^\circ\text{C})^{-1}$, and thermal conductivities of greater than 30 W/m-K. On the bases of properties and cost (Appendix C), would you consider any of the materials listed in Appendix B (or on the CD-ROM) in preference to aluminum oxide? Why or why not?

20.D12 After consultation of one of the following references, describe the shape memory effect, and then explain the mechanism (in terms of phase transformations, etc.) that is responsible for this phenomenon. Now suggest three practical applications in which an alloy displaying this shape memory effect may be utilized.

Schetky, L. M., ''Shape-Memory Alloys,'' *Scientific American*, Vol. 241, No. 5, November 1979, pp. 74–82.

''Shape-Memory Alloys—Metallurgical Solution Looking for a Problem,'' *Metallurgia*, Vol. 51, No. 1, January 1984, pp. 26–29.

20.D13 Write an essay on the replacement of metallic automobile components by polymers and composite materials. Address the following issues: (1) Which automotive components (e.g., crankshaft) now use polymers and/or composites? (2) Specifically what materials (e.g., high-density polyethylene) are now being used? (3) What are the reasons for these replacements?

20.D14 Perform a case study on material usage for the compact disc, after the manner of those studies described in this chapter. Begin with a brief description of the mechanism by which sounds are stored and then reproduced. Then, cite all of the requisite material properties for this application; finally, note which material is most commonly utilized, and the rationale for its use.

20.D15 One of the critical components of our modern video cassette recorders (VCRs) is the magnetic recording/playback head. Write an essay in which you address the following issues: (1) the mechanism by which the head records and plays back video/audio signals; (2) the requisite properties for the material from which the head is manufactured; then (3) present at least three likely candidate materials, and the property values for each that make it a viable candidate.

20.D16 Another group of new materials are the metallic glasses (or amorphous metals). Write an essay about these materials in which you address the following issues: (1) compositions of some of the common metallic glasses; (2) characteristics of these materials that make them technologically attractive; (3) characteristics that limit their utilization; (4) current and potential uses; and (5) at least one technique that is used to produce metallic glasses.

20.D17 The transdermal patch has recently become popular as a mechanism for delivering drugs into the human body.

(a) Cite at least one advantage of this drug-delivery system over oral administration using pills and caplets.

(b) Note the limitations on drugs that are administered by transdermal patches.

(c) Make a list of the characteristics required of materials (other than the delivery drug) that are incorporated in the transdermal patch.

20.D18 Glass, aluminum, and various plastic materials are utilized for beverage containers (chapter-opening photograph, Chapter 1). Make a list of the advantages and disadvantages of using each of these three material types; include such factors as cost, recyclability, and energy consumption for container production.

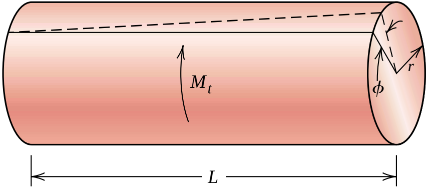

FIGURE 20.1 A solid cylindrical shaft that experiences an angle of twist ϕ in response to the application of a twisting moment M_t.

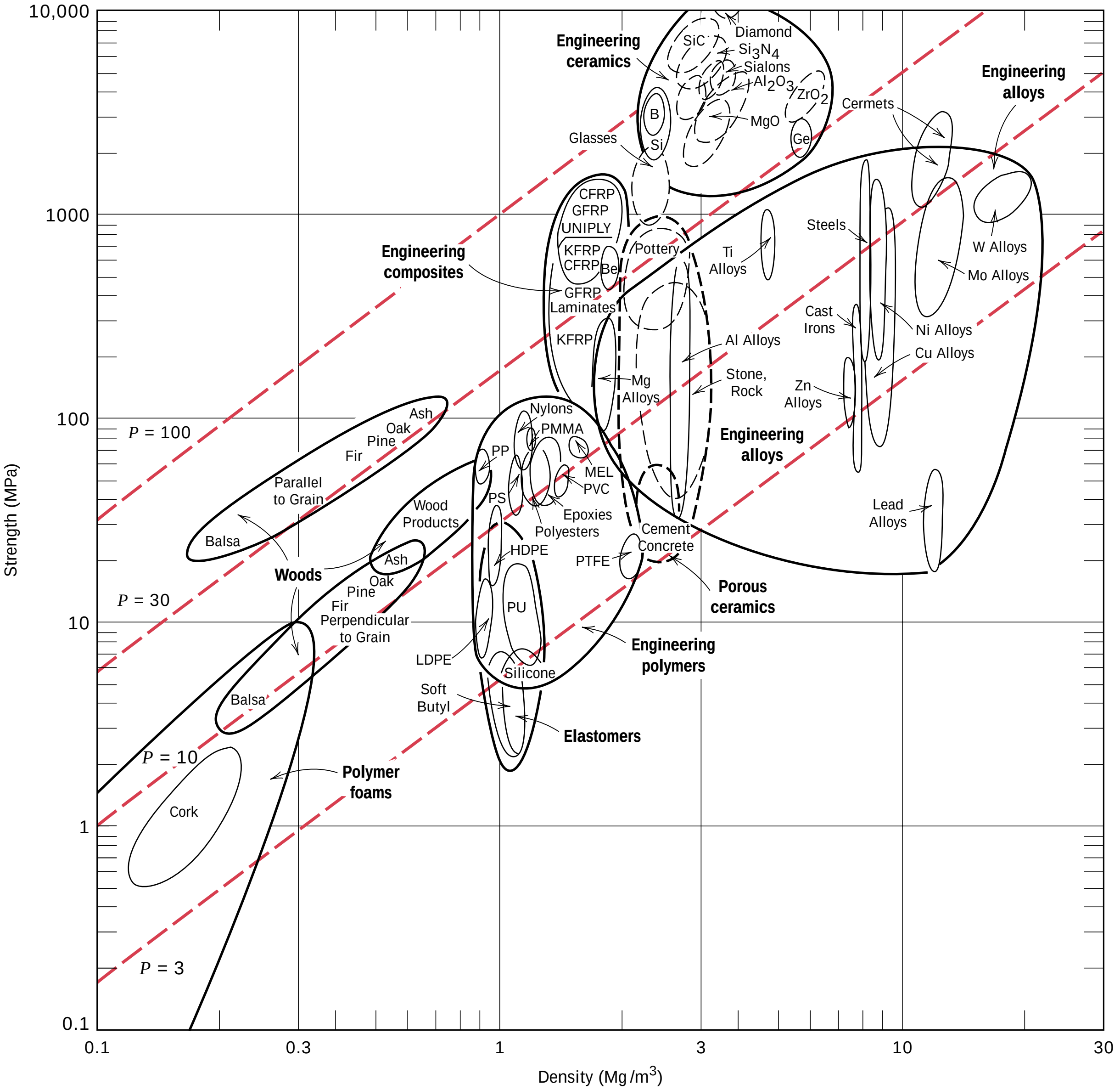

Figure 20.2 Strength versus density materials selection chart. Design guidelines for performance indices of 3, 10, 30, and 100 $(MPa)^{2/3}m^3/Mg$ have been constructed, all having a slope of $\frac{3}{2}$. (Adapted from M. F. Ashby, *Materials Selection in Mechanical Design*. Copyright © 1992. Reprinted by permission of Butterworth-Heinemann Ltd.)

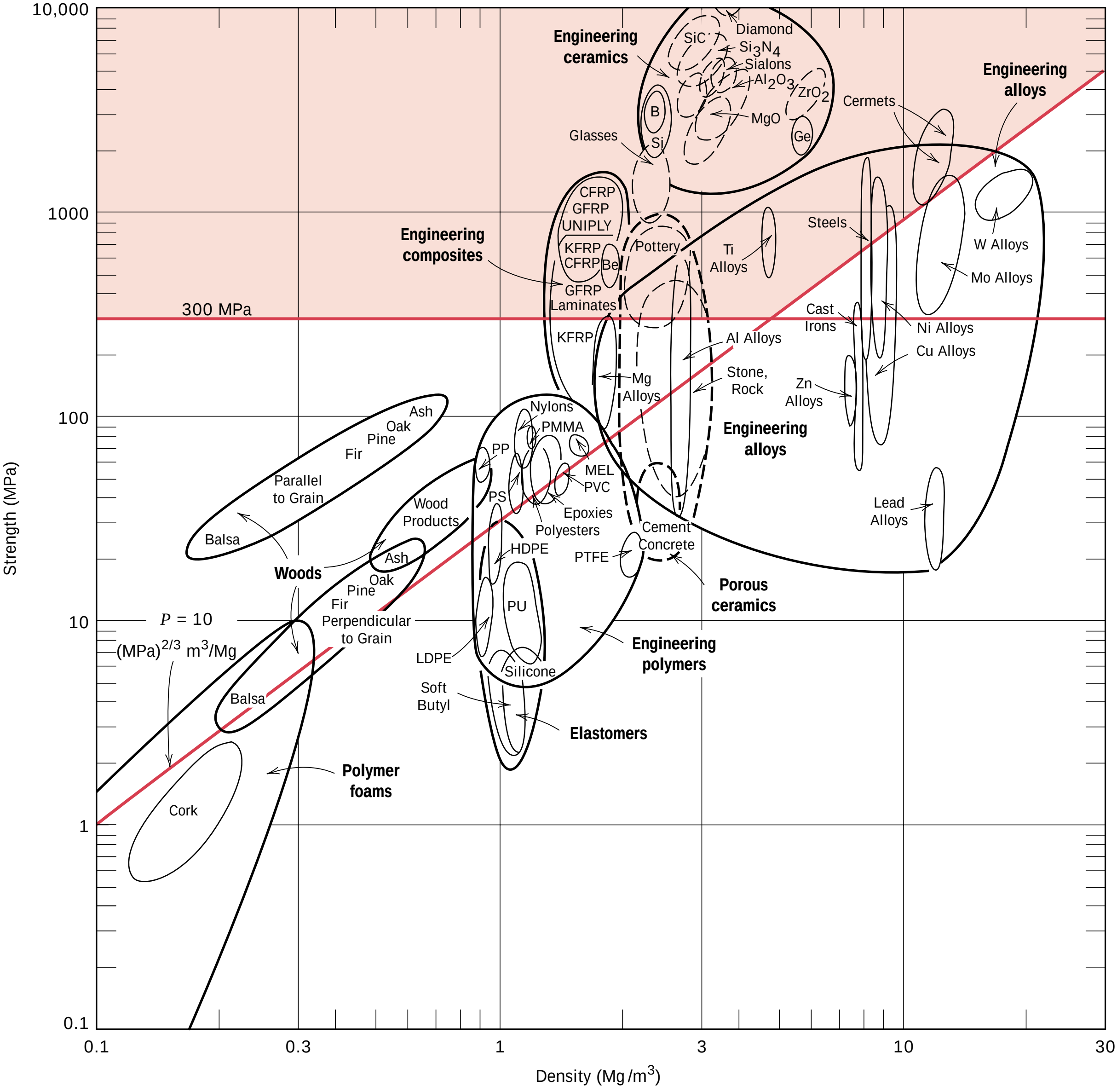

Figure 20.3 Strength versus density materials selection chart. Those materials lying within the shaded region are acceptable candidates for a solid cylindrical shaft which has a mass-strength performance index in excess of 10 (MPa)$^{2/3}$m^3/Mg, and a strength of at least 300 MPa (43,500 psi). (Adapted from M. F. Ashby, *Materials Selection in Mechanical Design*. Copyright © 1992. Reprinted by permission of Butterworth-Heinemann Ltd.)

Table 20.1 **Density (ρ), Strength (τ_f), the Performance Index (P) for Five Engineering Materials**

Material	ρ (Mg/m^3)	τ_f (MPa)	$\tau_f^{2/3}/\rho = P$ [$(MPa)^{2/3}m^3/Mg$]
Carbon fiber-reinforced composite (0.65 fiber fraction)[a]	1.5	1140	72.8
Glass fiber-reinforced composite (0.65 fiber fraction)[a]	2.0	1060	52.0
Aluminum alloy (2024-T6)	2.8	300	16.0
Titanium alloy (Ti-6Al-4V)	4.4	525	14.8
4340 Steel (oil-quenched and tempered)	7.8	780	10.9

[a] The fibers in these composites are continuous, aligned, and wound in a helical fashion at a 45° angle relative to the shaft axis.

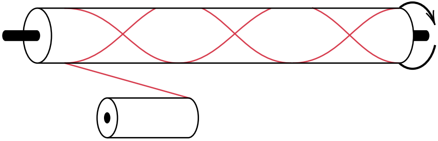

Helical winding

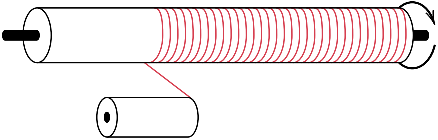

Circumferential winding

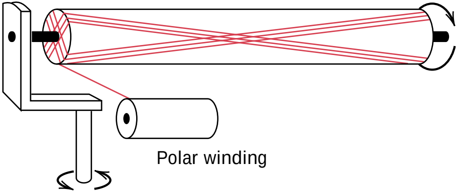

Polar winding

Figure 15.14 Schematic representations of helical, circumferential, and polar filament winding techniques. (From N. L. Hancox, Editor, *Fibre Composite Hybrid Materials*, The Macmillan Company, New York, 1981.)

Table 20.2 **Tabulation of the $\rho/\tau_f^{2/3}$ Ratio, Relative Cost ($\bar{c}$), and the Product of $\rho/\tau_f^{2/3}$ and $\bar{c}$ for Five Engineering Materials**[a]

Material	$\rho/\tau_f^{2/3}$ [10^{-2} {$Mg/(MPa)^{2/3}m^3$}]	$\bar{c}$ (\$/\$)	$\bar{c}(\rho/\tau_f^{2/3})$ [10^{-2} (\$/\$){$Mg/(MPa)^{2/3}m^3$}]
4340 Steel (oil-quenched and tempered)	9.2	5	46
Glass fiber-reinforced composite (0.65 fiber fraction)[b]	1.9	40	76
Aluminum alloy (2024-T6)	6.2	15	93
Carbon fiber-reinforced composite (0.65 fiber fraction)[b]	1.4	80	112
Titanium alloy (Ti-6Al-4V)	6.8	110	748

[a] The relative cost is the ratio of the prices per unit mass of the material and low-carbon steel.

[b] The fibers in these composites are continuous, aligned, and wound in a helical fashion at a 45° angle relative to the shaft axis.

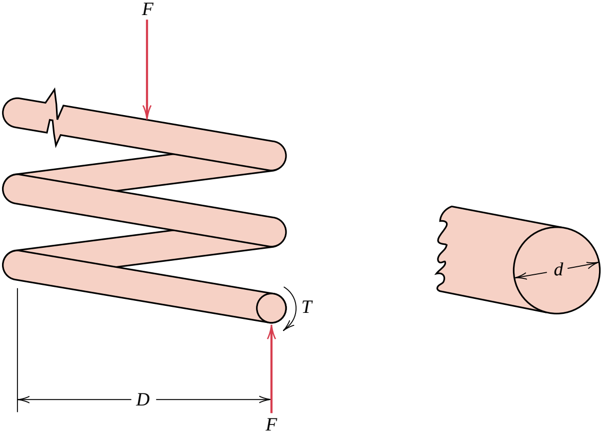

Figure 20.4 Schematic diagram of a helical spring showing the twisting moment T that results from the compressive force F. (Adapted from K. Edwards and P. McKee, *Fundamentals of Mechanical Component Design.* Copyright © 1991 by McGraw-Hill, Inc. Reproduced with permission of The McGraw-Hill Companies.)

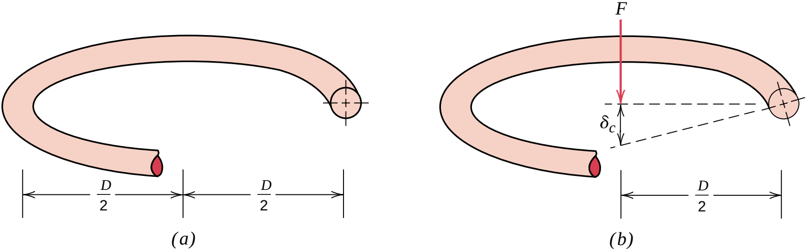

Figure 20.5 Schematic diagrams of one coil of a helical spring, (*a*) prior to being compressed, and (*b*) showing the deflection δ_c produced from the compressive force F. (Adapted from K. Edwards and P. McKee, *Fundamentals of Mechanical Component Design*. Copyright © 1991 by McGraw-Hill, Inc. Reproduced with permission of The McGraw-Hill Companies.)

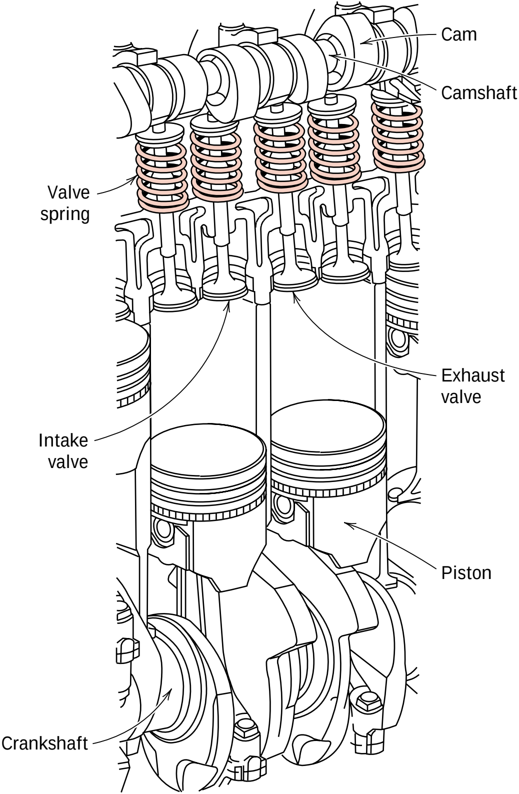
Cam
Camshaft
Valve spring
Exhaust valve
Intake valve
Piston
Crankshaft

FIGURE 20.6 Cutaway drawing of a section of an automobile engine in which various components including valves and valve springs are shown.

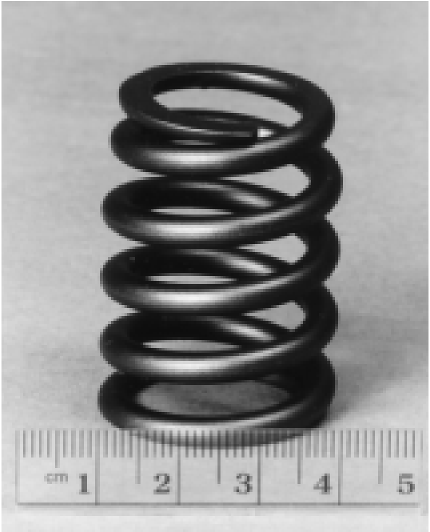

FIGURE 20.7 Photograph of a typical automobile valve spring.

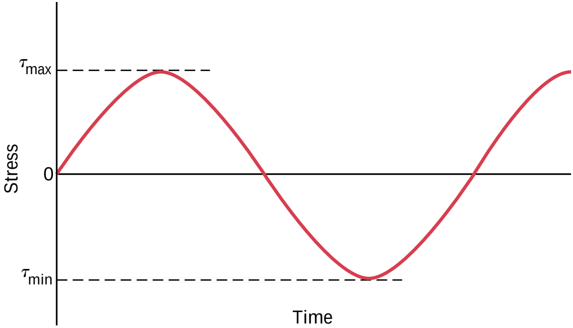

FIGURE 20.8 Stress versus time for a reversed cycle in shear.

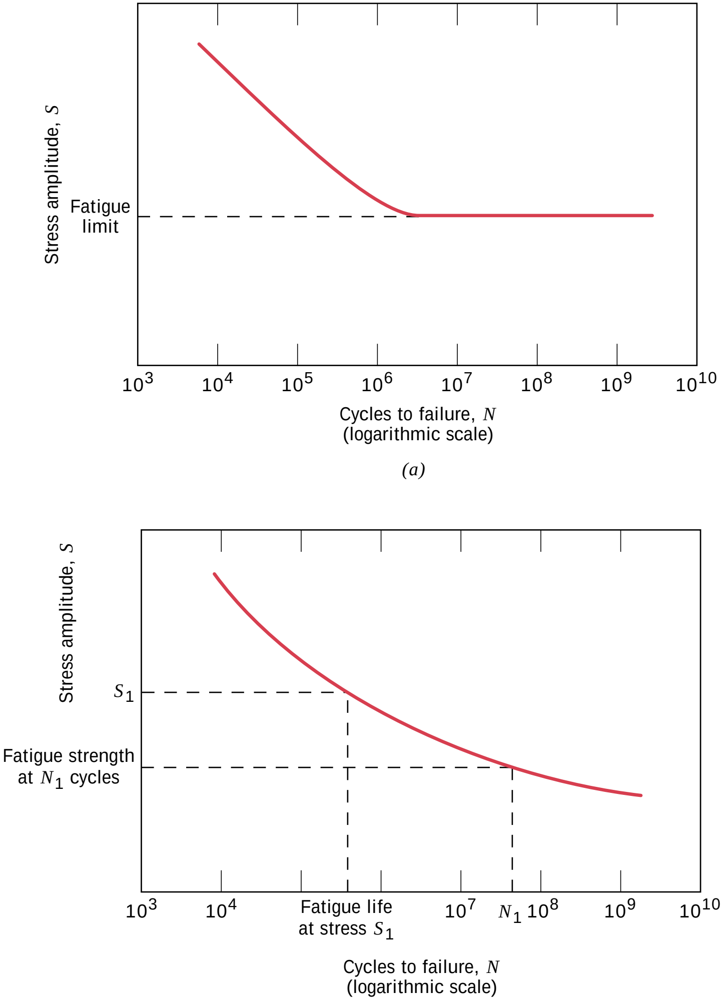

(a)

(b)

FIGURE 9.25 Stress amplitude (S) versus logarithm of the number of cycles to fatigue failure (N) for (*a*) a material that displays a fatigue limit, and (*b*) a material that does not display a fatigue limit.

Chapter 9 / Failure

An oil tanker that fractured in a brittle manner by crack propagation around its girth. (Photography by Neal Boenzi. Reprinted with permission from *The New York Times*.)

Why Study *Failure?*

The design of a component or structure often calls upon the engineer to minimize the possibility of failure. Thus, it is important to understand the mechanics of the various failure modes—i.e., fracture, fatigue, and creep—and, in addition, be familiar with appropriate design principles that may be employed to prevent in-service failures. {For example, we discuss in Section 20.5 material selection and processing issues relating to the fatigue of an automobile valve spring.}

Learning Objectives

After studying this chapter you should be able to do the following:

1. **Describe the mechanism of crack propagation for both ductile and brittle modes of fracture.**
2. **Explain why the strengths of brittle materials are much lower than predicted by theoretical calculations.**
3. **Define fracture toughness in terms of (a) a brief statement, and (b) an equation; define all parameters in this equation.**
4. {**Make distinctions between *stress intensity factor, fracture toughness,* and *plane strain fracture toughness.***}
5. **Briefly explain why there is normally significant scatter in the fracture strength for identical specimens of the same ceramic material.**
6. **Briefly describe the phenomenon of** *crazing.*
7. **Name and describe the two impact fracture testing techniques.**
8. **Define fatigue and specify the conditions under which it occurs.**
9. **From a fatigue plot for some material, determine (a) the fatigue lifetime (at a specified stress level), and (b) the fatigue strength (at a specified number of cycles).**
10. **Define creep and specify the conditions under which it occurs.**
11. **Given a creep plot for some material, determine (a) the steady-state creep rate, and (b) the rupture lifetime.**

9.1 INTRODUCTION

The failure of engineering materials is almost always an undesirable event for several reasons; these include human lives that are put in jeopardy, economic losses, and the interference with the availability of products and services. Even though the causes of failure and the behavior of materials may be known, prevention of failures is difficult to guarantee. The usual causes are improper materials selection and processing and inadequate design of the component or its misuse. It is the responsibility of the engineer to anticipate and plan for possible failure and, in the event that failure does occur, to assess its cause and then take appropriate preventive measures against future incidents.

Topics to be addressed in this chapter are the following: simple fracture (both ductile and brittle modes), fundamentals of fracture mechanics, impact fracture testing, the ductile-to-brittle transition, fatigue, and creep. These discussions include failure mechanisms, testing techniques, and methods by which failure may be prevented or controlled.

FRACTURE

9.2 FUNDAMENTALS OF FRACTURE

Simple fracture is the separation of a body into two or more pieces in response to an imposed stress that is static (i.e., constant or slowly changing with time) and at temperatures that are low relative to the melting temperature of the material. The applied stress may be tensile, compressive, shear, or torsional; the present discussion will be confined to fractures that result from uniaxial tensile loads. For engineering materials, two fracture modes are possible: **ductile** and **brittle.** Classification is based on the ability of a material to experience plastic deformation. Ductile materials typically exhibit substantial plastic deformation with high energy absorption before fracture. On the other hand, there is normally little or no plastic deformation with low energy absorption accompanying a brittle fracture. The tensile stress–strain behaviors of both fracture types may be reviewed in Figure 7.13.

''Ductile'' and ''brittle'' are relative terms; whether a particular fracture is one mode or the other depends on the situation. Ductility may be quantified in terms of percent elongation (Equation 7.11) and percent reduction in area (Equation 7.12). Furthermore, ductility is a function of temperature of the material, the strain rate, and the stress state. The disposition of normally ductile materials to fail in a brittle manner is discussed in Section 9.8.

Any fracture process involves two steps—crack formation and propagation—in response to an imposed stress. The mode of fracture is highly dependent on the mechanism of crack propagation. Ductile fracture is characterized by extensive plastic deformation in the vicinity of an advancing crack. Furthermore, the process proceeds relatively slowly as the crack length is extended. Such a crack is often said to be *stable*. That is, it resists any further extension unless there is an increase in the applied stress. In addition, there will ordinarily be evidence of appreciable gross deformation at the fracture surfaces (e.g., twisting and tearing). On the other hand, for brittle fracture, cracks may spread extremely rapidly, with very little accompanying plastic deformation. Such cracks may be said to be *unstable*, and crack propagation, once started, will continue spontaneously without an increase in magnitude of the applied stress.

Ductile fracture is almost always preferred for two reasons. First, brittle fracture occurs suddenly and catastrophically without any warning; this is a consequence of the spontaneous and rapid crack propagation. On the other hand, for ductile fracture, the presence of plastic deformation gives warning that fracture is imminent, allowing preventive measures to be taken. Second, more strain energy is required to induce ductile fracture inasmuch as ductile materials are generally tougher. Under the action of an applied tensile stress, most metal alloys are ductile, whereas ceramics are notably brittle, and polymers may exhibit both types of fracture.

9.3 DUCTILE FRACTURE

Ductile fracture surfaces will have their own distinctive features on both macroscopic and microscopic levels. Figure 9.1 shows schematic representations for two characteristic macroscopic fracture profiles. The configuration shown in Figure 9.1*a* is found for extremely soft metals, such as pure gold and lead at room temperature, and other metals, polymers, and inorganic glasses at elevated temperatures. These highly ductile materials neck down to a point fracture, showing virtually 100% reduction in area.

The most common type of tensile fracture profile for ductile metals is that represented in Figure 9.1*b*, which fracture is preceded by only a moderate amount

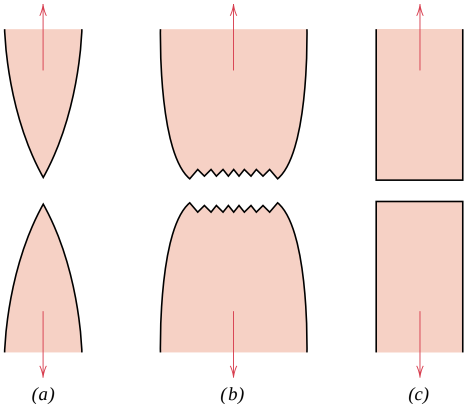

FIGURE 9.1 (*a*) Highly ductile fracture in which the specimen necks down to a point. (*b*) Moderately ductile fracture after some necking. (*c*) Brittle fracture without any plastic deformation.

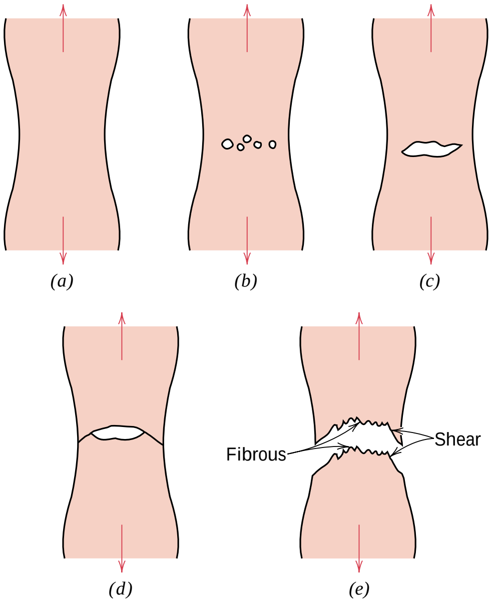

Figure 9.2 Stages in the cup-and-cone fracture. (*a*) Initial necking. (*b*) Small cavity formation. (*c*) Coalescence of cavities to form a crack. (*d*) Crack propagation. (*e*) Final shear fracture at a 45° angle relative to the tensile direction. (From K. M. Ralls, T. H. Courtney, and J. Wulff, *Introduction to Materials Science and Engineering*, p. 468. Copyright © 1976 by John Wiley & Sons, New York. Reprinted by permission of John Wiley & Sons, Inc.)

of necking. The fracture process normally occurs in several stages (Figure 9.2). First, after necking begins, small cavities, or microvoids, form in the interior of the cross section, as indicated in Figure 9.2*b*. Next, as deformation continues, these microvoids enlarge, come together, and coalesce to form an elliptical crack, which has its long axis perpendicular to the stress direction. The crack continues to grow in a direction parallel to its major axis by this microvoid coalescence process (Figure 9.2*c*). Finally, fracture ensues by the rapid propagation of a crack around the outer perimeter of the neck (Figure 9.2*d*), by shear deformation at an angle of about 45° with the tensile axis—this is the angle at which the shear stress is a maximum. Sometimes a fracture having this characteristic surface contour is termed a *cup-and-cone fracture* because one of the mating surfaces is in the form of a cup, the other like a cone. In this type of fractured specimen (Figure 9.3*a*), the central

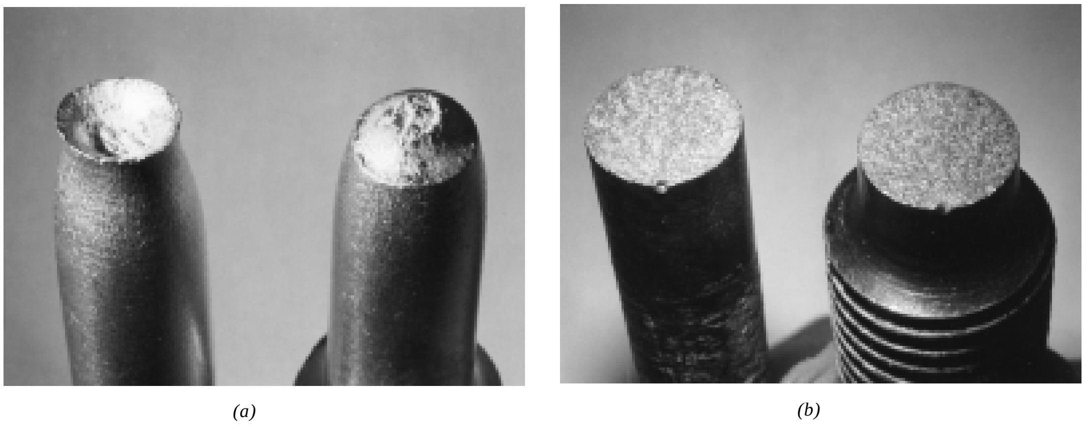
(*a*)
(*b*)

Figure 9.3 (*a*) Cup-and-cone fracture in aluminum. (*b*) Brittle fracture in a mild steel.

interior region of the surface has an irregular and fibrous appearance, which is indicative of plastic deformation.

FRACTOGRAPHIC STUDIES (CD-ROM)

9.4 BRITTLE FRACTURE

Brittle fracture takes place without any appreciable deformation, and by rapid crack propagation. The direction of crack motion is very nearly perpendicular to the direction of the applied tensile stress and yields a relatively flat fracture surface, as indicated in Figure 9.1*c*.

Fracture surfaces of materials that failed in a brittle manner will have their own distinctive patterns; any signs of gross plastic deformation will be absent. For example, in some steel pieces, a series of V-shaped ‘‘chevron’’ markings may form near the center of the fracture cross section that point back toward the crack initiation site (Figure 9.5*a*). Other brittle fracture surfaces contain lines or ridges that radiate from the origin of the crack in a fanlike pattern (Figure 9.5*b*). Often, both of these marking patterns will be sufficiently coarse to be discerned with the naked eye. For very hard and fine-grained metals, there will be no discernible fracture pattern. Brittle fracture in amorphous materials, such as ceramic glasses, yields a relatively shiny and smooth surface.

For most brittle crystalline materials, crack propagation corresponds to the successive and repeated breaking of atomic bonds along specific crystallographic planes; such a process is termed *cleavage.* This type of fracture is said to be **transgranular** (or *transcrystalline*), because the fracture cracks pass through the grains. Macroscopically, the fracture surface may have a grainy or faceted texture (Figure 9.3*b*), as a result of changes in orientation of the cleavage planes from grain to grain. This feature is more evident in the scanning electron micrograph shown in Figure 9.6*a*.

In some alloys, crack propagation is along grain boundaries; this fracture is termed **intergranular.** Figure 9.6*b* is a scanning electron micrograph showing a typical intergranular fracture, in which the three-dimensional nature of the grains may be seen. This type of fracture normally results subsequent to the occurrence of processes that weaken or embrittle grain boundary regions.

9.5a PRINCIPLES OF FRACTURE MECHANICS [DETAILED VERSION (CD-ROM)]

9.5b PRINCIPLES OF FRACTURE MECHANICS (CONCISE VERSION)

Brittle fracture of normally ductile materials, such as that shown in the chapter-opening photograph of this chapter, has demonstrated the need for a better understanding of the mechanisms of fracture. Extensive research endeavors over the past several decades have led to the evolution of the field of **fracture mechanics.** This subject allows quantification of the relationships between material properties, stress level, the presence of crack-producing flaws, and crack propagation mechanisms. Design engineers are now better equipped to anticipate, and thus prevent, structural failures. The present discussion centers on some of the fundamental principles of the mechanics of fracture.

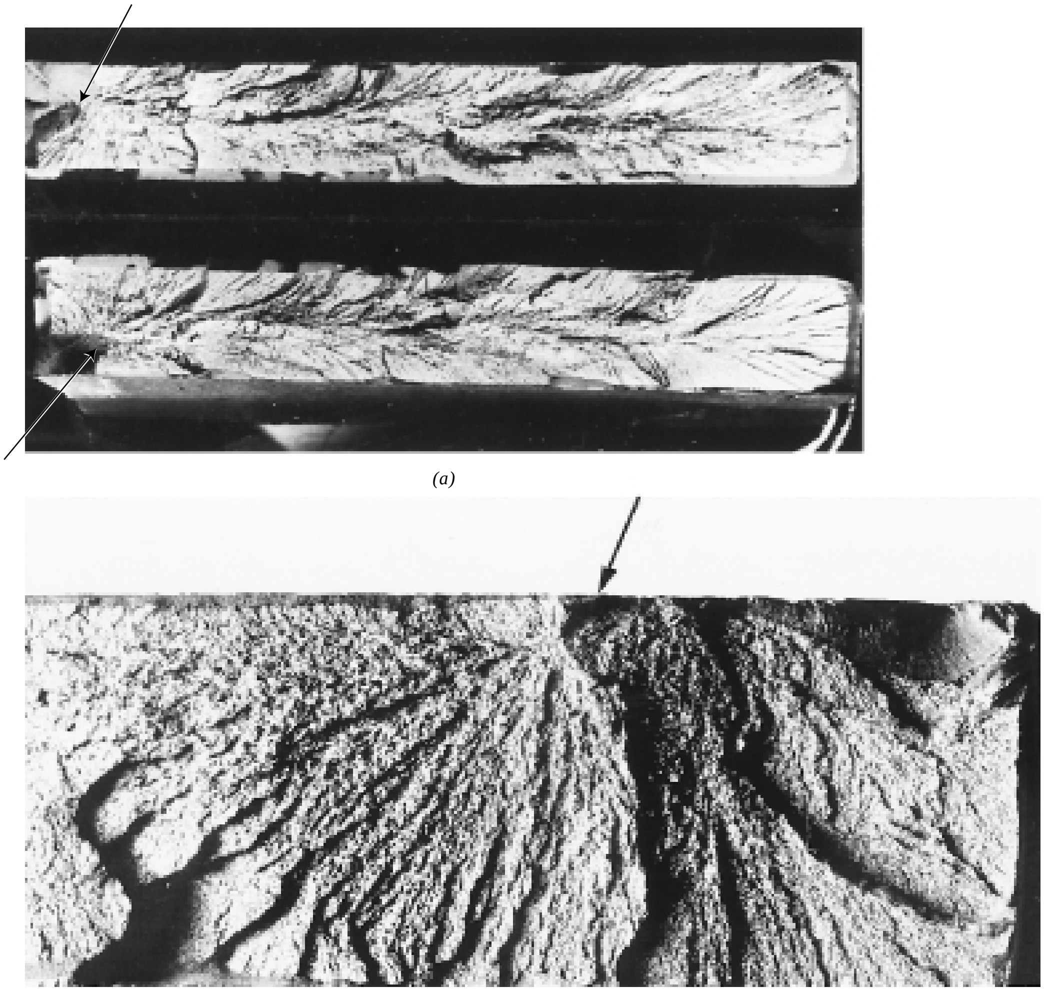

(a)

(b)

Figure 9.5 (*a*) Photograph showing V-shaped ''chevron'' markings characteristic of brittle fracture. Arrows indicate origin of crack. Approximately actual size. (From R. W. Hertzberg, *Deformation and Fracture Mechanics of Engineering Materials,* 3rd edition. Copyright © 1989 by John Wiley & Sons, New York. Reprinted by permission of John Wiley & Sons, Inc. Photograph courtesy of Roger Slutter, Lehigh University.) (*b*) Photograph of a brittle fracture surface showing radial fan-shaped ridges. Arrow indicates origin of crack. Approximately 2×. (Reproduced with permission from D. J. Wulpi, *Understanding How Components Fail,* American Society for Metals, Materials Park, OH, 1985.)

STRESS CONCENTRATION

The measured fracture strengths for most brittle materials are significantly lower than those predicted by theoretical calculations based on atomic bonding energies. This discrepancy is explained by the presence of very small, microscopic flaws or cracks that always exist under normal conditions at the surface and within the interior of a body of material. These flaws are a detriment to the fracture strength because an applied stress may be amplified or concentrated at the tip, the magnitude

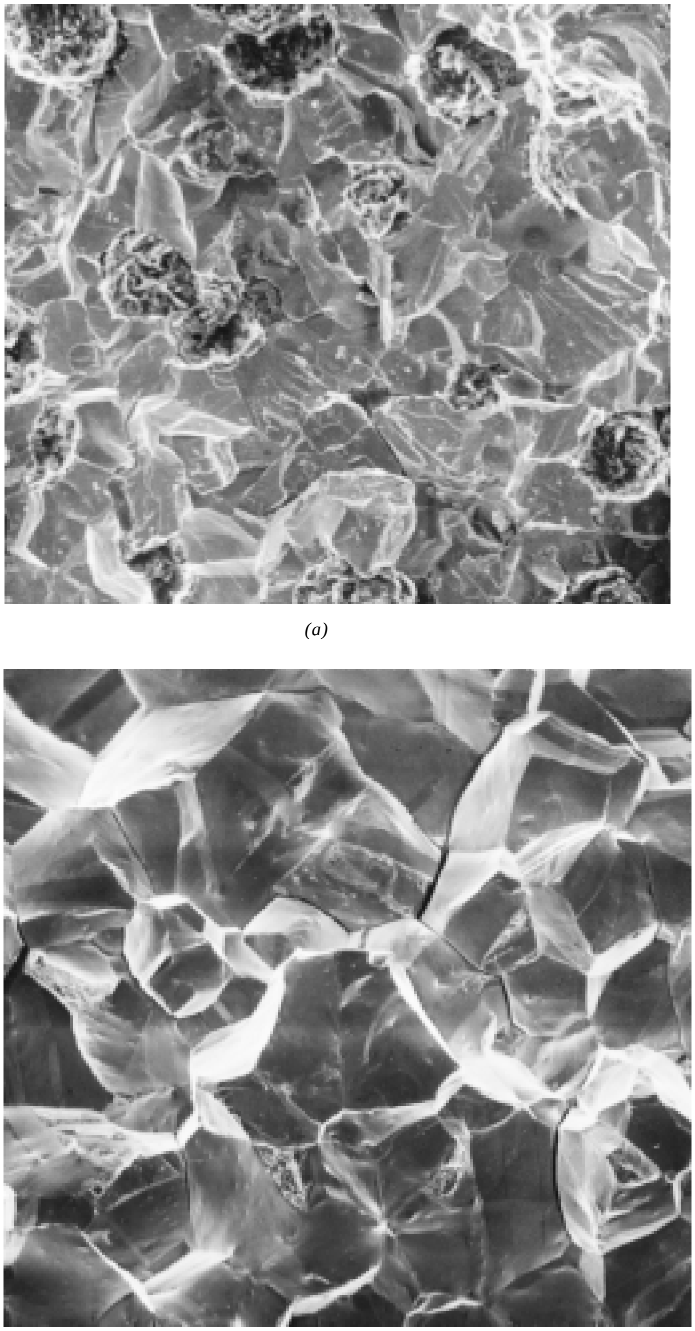

(a)

(b)

Figure 9.6 (*a*) Scanning electron fractograph of ductile cast iron showing a transgranular fracture surface. Magnification unknown. (From V. J. Colangelo and F. A. Heiser, *Analysis of Metallurgical Failures,* 2nd edition. Copyright © 1987 by John Wiley & Sons, New York. Reprinted by permission of John Wiley & Sons, Inc.) (*b*) Scanning electron fractograph showing an intergranular fracture surface. 50×. (Reproduced with permission from *ASM Handbook*, Vol. 12, *Fractography*, ASM International, Materials Park, OH, 1987.)

of this amplification depending on crack orientation and geometry. This phenomenon is demonstrated in Figure 9.7, a stress profile across a cross section containing an internal crack. As indicated by this profile, the magnitude of this localized stress diminishes with distance away from the crack tip. At positions far removed, the stress is just the nominal stress σ_0, or the load divided by the specimen cross-

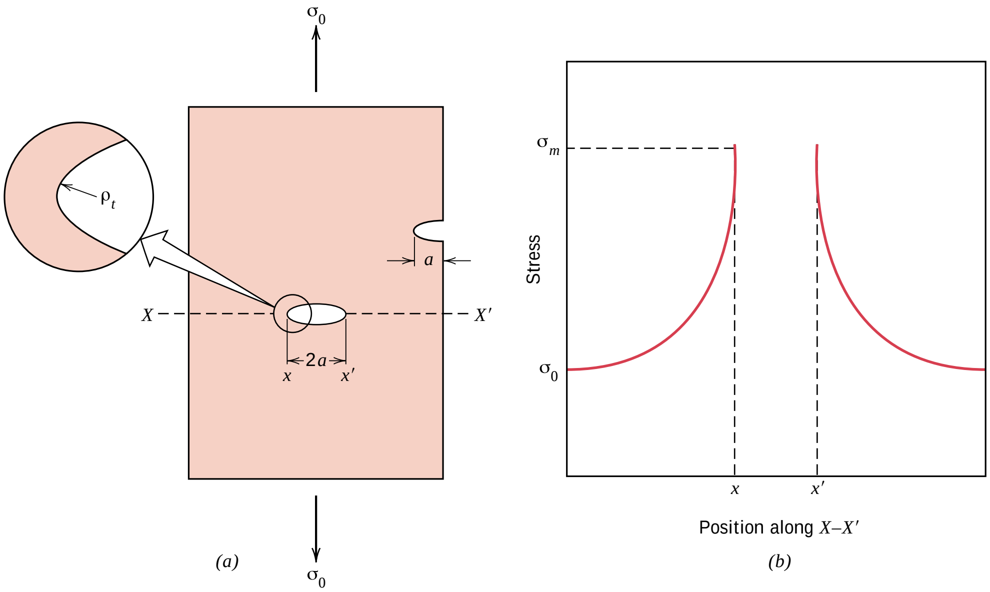

Figure 9.7 (*a*) The geometry of surface and internal cracks. (*b*) Schematic stress profile along the line $X–X'$ in (*a*), demonstrating stress amplification at crack tip positions.

sectional area (perpendicular to this load). Due to their ability to amplify an applied stress in their locale, these flaws are sometimes called **stress raisers.**

If it is assumed that a crack has an elliptical shape and is oriented perpendicular to the applied stress, the maximum stress at the crack tip, σ_m, may be approximated by

$$\sigma_m = 2\sigma_0\left(\frac{a}{\rho_t}\right)^{1/2} \tag{9.1b}$$

where σ_0 is the magnitude of the nominal applied tensile stress, ρ_t is the radius of curvature of the crack tip (Figure 9.7*a*), and a represents the length of a surface crack, or half of the length of an internal crack. For a relatively long microcrack that has a small tip radius of curvature, the factor $(a/\rho_t)^{1/2}$ may be very large. This will yield a value of σ_m that is many times the value of σ_0.

Sometimes the ratio σ_m/σ_0 is denoted as the *stress concentration factor* K_t:

$$K_t = \frac{\sigma_m}{\sigma_0} = 2\left(\frac{a}{\rho_t}\right)^{1/2} \tag{9.2}$$

which is simply a measure of the degree to which an external stress is amplified at the tip of a crack.

By way of comment, it should be said that stress amplification is not restricted to these microscopic defects; it may occur at macroscopic internal discontinuities (e.g., voids), at sharp corners, and at notches in large structures.

Furthermore, the effect of a stress raiser is more significant in brittle than in ductile materials. For a ductile material, plastic deformation ensues when the maximum stress exceeds the yield strength. This leads to a more uniform distribution of stress in the vicinity of the stress raiser and to the development of a maximum stress concentration factor less than the theoretical value. Such yielding and stress redistribution do not occur to any appreciable extent around flaws and discontinuities in brittle materials; therefore, essentially the theoretical stress concentration will result.

Using principles of fracture mechanics, it is possible to show that the critical stress σ_c required for crack propagation in a brittle material is described by the expression

$$\sigma_c = \left(\frac{2E\gamma_s}{\pi a}\right)^{1/2} \tag{9.3}$$

where

E = modulus of elasticity

γ_s = specific surface energy

a = one half the length of an internal crack

All brittle materials contain a population of small cracks and flaws that have a variety of sizes, geometries, and orientations. When the magnitude of a tensile stress at the tip of one of these flaws exceeds the value of this critical stress, a crack forms and then propagates, which results in fracture. Very small and virtually defect-free metallic and ceramic whiskers have been grown with fracture strengths that approach their theoretical values.

EXAMPLE PROBLEM 9.1

A relatively large plate of a glass is subjected to a tensile stress of 40 MPa. If the specific surface energy and modulus of elasticity for this glass are 0.3 J/m^2 and 69 GPa, respectively, determine the maximum length of a surface flaw that is possible without fracture.

SOLUTION

To solve this problem it is necessary to employ Equation 9.3. Rearrangement of this expression such that a is the dependent variable, and realizing that σ = 40 MPa, γ_s = 0.3 J/m^2, and E = 69 GPa leads to

$$\begin{aligned} a &= \frac{2E\gamma_s}{\pi\sigma^2} \\ &= \frac{(2)(69 \times 10^9\ \text{N/m}^2)(0.3\ \text{N/m})}{\pi(40 \times 10^6\ \text{N/m}^2)^2} \\ &= 8.2 \times 10^{-6}\ \text{m} = 0.0082\ \text{mm} = 8.2\ \mu\text{m} \end{aligned}$$

FRACTURE TOUGHNESS

Furthermore, using fracture mechanical principles, an expression has been developed that relates this critical stress for crack propagation (σ_c) to crack length (a) as

$$K_c = Y\sigma_c\sqrt{\pi a} \tag{9.9a}$$

In this expression K_c is the **fracture toughness,** a property that is a measure of a material's resistance to brittle fracture when a crack is present. Worth noting is that K_c has the unusual units of $\text{MPa}\sqrt{\text{m}}$ or $\text{psi}\sqrt{\text{in.}}$ (alternatively $\text{ksi}\sqrt{\text{in.}}$). Furthermore, Y is a dimensionless parameter or function that depends on both crack and specimen sizes and geometries, as well as the manner of load application.

Relative to this Y parameter, for planar specimens containing cracks that are much shorter than the specimen width, Y has a value of approximately unity. For example, for a plate of infinite width having a through-thickness crack (Figure 9.11*a*), $Y = 1.0$; whereas for a plate of semi-infinite width containing an edge crack of length a (Figure 9.11*b*), $Y \cong 1.1$. Mathematical expressions for Y have been determined for a variety of crack-specimen geometries; these expressions are often relatively complex.

For relatively thin specimens, the value of K_c will depend on specimen thickness. However, when specimen thickness is much greater than the crack dimensions, K_c becomes independent of thickness; under these conditions a condition of **plane strain** exists. By plane strain we mean that when a load operates on a crack in the manner represented in Figure 9.11*a*, there is no strain component perpendicular to the front and back faces. The K_c value for this thick-specimen situation is known as the **plane strain fracture toughness** K_{Ic}; furthermore, it is also defined by

$$K_{Ic} = Y\sigma\sqrt{\pi a} \tag{9.11}$$

K_{Ic} is the fracture toughness cited for most situations. The I (i.e., Roman numeral "one") subscript for K_{Ic} denotes that the plane strain fracture toughness is for mode I crack displacement, as illustrated in Figure 9.9*a*[5] (see page 244).

Brittle materials, for which appreciable plastic deformation is not possible in front of an advancing crack, have low K_{Ic} values and are vulnerable to catastrophic failure. On the other hand, K_{Ic} values are relatively large for ductile materials. Fracture mechanics is especially useful in predicting catastrophic failure in materials

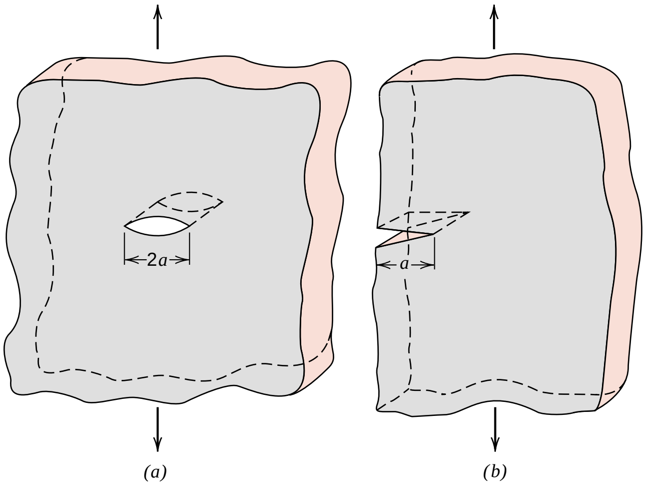

FIGURE 9.11 Schematic representations of (*a*) an interior crack in a plate of infinite width, and (*b*) an edge crack in a plate of semi-infinite width.

---

[5] Two other crack displacement modes denoted by II and III and as illustrated in Figures 9.9*b* and 9.9*c* are also possible; however, mode I is most commonly encountered.

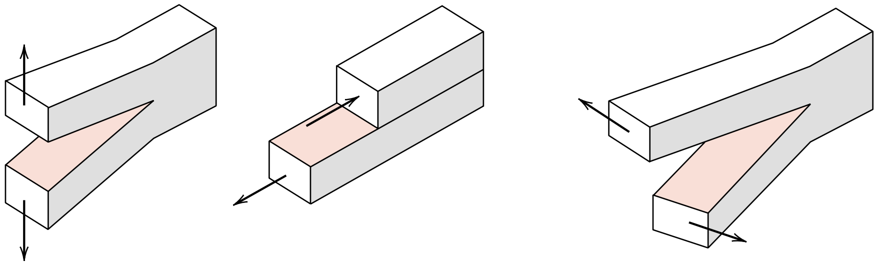
(a) (b) (c)

Figure 9.9 The three modes of crack surface displacement. (*a*) Mode I, opening or tensile mode; (*b*) mode II, sliding mode; and (*c*) mode III, tearing mode.

having intermediate ductilities. Plane strain fracture toughness values for a number of different materials are presented in Table 9.1; a more extensive list of K_{Ic} values is contained in Table B.5, Appendix B.

The plane strain fracture toughness K_{Ic} is a fundamental material property that depends on many factors, the most influential of which are temperature, strain rate, and microstructure. The magnitude of K_{Ic} diminishes with increasing strain rate and

Table 9.1 Room-Temperature Yield Strength and Plane Strain Fracture Toughness Data for Selected Engineering Materials

	Yield Strength		K_{Ic}	
Material	***MPa***	***ksi***	$MPa\sqrt{m}$	$ksi\sqrt{in.}$
	Metals			
Aluminum Alloy[a] (7075-T651)	495	72	24	22
Aluminum Alloy[a] (2024-T3)	345	50	44	40
Titanium Alloy[a] (Ti-6Al-4V)	910	132	55	50
Alloy Steel[a] (4340 tempered @ 260°C)	1640	238	50.0	45.8
Alloy Steel[a] (4340 tempered @ 425°C)	1420	206	87.4	80.0
	Ceramics			
Concrete	—	—	0.2–1.4	0.18–1.27
Soda-Lime Glass	—	—	0.7–0.8	0.64–0.73
Aluminum Oxide	—	—	2.7–5.0	2.5–4.6
	Polymers			
Polystyrene (PS)	—	—	0.7–1.1	0.64–1.0
Polymethyl Methacrylate (PMMA)	53.8–73.1	7.8–10.6	0.7–1.6	0.64–1.5
Polycarbonate (PC)	62.1	9.0	2.2	2.0

[a] **Source:** Reprinted with permission, *Advanced Materials and Processes,* ASM International, © 1990.

decreasing temperature. Furthermore, an enhancement in yield strength wrought by solid solution or dispersion additions or by strain hardening generally produces a corresponding decrease in K_{Ic}. Furthermore, K_{Ic} normally increases with reduction in grain size as composition and other microstructural variables are maintained constant. Yield strengths are included for some of the materials listed in Table 9.1. Furthermore, K_{Ic} normally increases with reduction in grain size as composition and other microstructural variables are maintained constant.

Several different testing techniques are used to measure K_{Ic}.[6] Virtually any specimen size and shape consistent with mode I crack displacement may be utilized, and accurate values will be realized provided that the Y scale parameter in Equation 9.11 has been properly determined.

DESIGN USING FRACTURE MECHANICS

According to Equations 9.9a and 9.11, three variables must be considered relative to the possibility for fracture of some structural component—viz. the fracture toughness (K_c) or plane strain fracture toughness (K_{Ic}), the imposed stress (σ), and the flaw size (a), assuming, of course, that Y has been determined. When designing a component, it is first important to decide which of these variables are constrained by the application and which are subject to design control. For example, material selection (and hence K_c or K_{Ic}) is often dictated by factors such as density (for lightweight applications) or the corrosion characteristics of the environment. Or, the allowable flaw size is either measured or specified by the limitations of available flaw detection techniques. It is important to realize, however, that once any combination of two of the above parameters is prescribed, the third becomes fixed (Equations 9.9a and 9.11). For example, assume that K_{Ic} and the magnitude of a are specified by application constraints; therefore, the design (or critical) stress σ_c must be

$$\sigma_c \leq \frac{K_{Ic}}{Y\sqrt{\pi a}} \tag{9.13}$$

On the other hand, if stress level and plane strain fracture toughness are fixed by the design situation, then the maximum allowable flaw size a_c is

$$a_c = \frac{1}{\pi}\left(\frac{K_{Ic}}{\sigma Y}\right)^2 \tag{9.14}$$

A number of nondestructive test (NDT) techniques have been developed that permit detection and measurement of both internal and surface flaws. Such NDT methods are used to avoid the occurrence of catastrophic failure by examining structural components for defects and flaws that have dimensions approaching the critical size.

DESIGN EXAMPLE 9.1

Consider the thin-walled spherical tank of radius r and thickness t (Figure 9.15) that may be used as a pressure vessel.

---

[6] See for example ASTM Standard E 399, ''Standard Test Method for Plane Strain Fracture Toughness of Metallic Materials.''

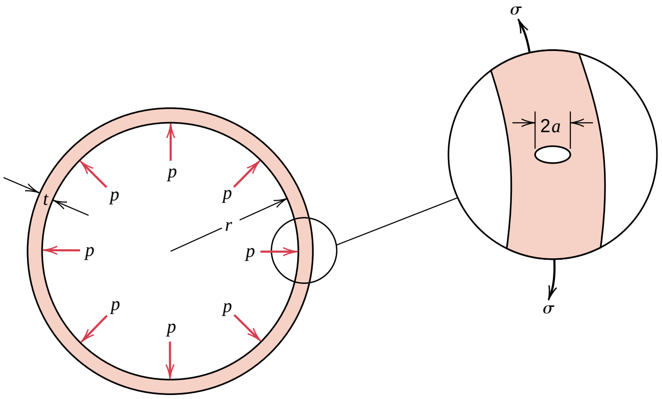

FIGURE 9.15 Schematic diagram showing the cross section of a spherical tank that is subjected to an internal pressure *p*, and that has a radial crack of length 2*a* in its wall.

(a) One design of such a tank calls for yielding of the wall material prior to failure as a result of the formation of a crack of critical size and its subsequent rapid propagation. Thus, plastic distortion of the wall may be observed and the pressure within the tank released before the occurrence of catastrophic failure. Consequently, materials having large critical crack lengths are desired. On the basis of this criterion, rank the metal alloys listed in Table B.5, Appendix B, as to critical crack size, from longest to shortest.

(b) An alternative design that is also often utilized with pressure vessels is termed *leak-before-break*. Using principles of fracture mechanics, allowance is made for the growth of a crack through the thickness of the vessel wall prior to the occurrence of rapid crack propagation (Figure 9.15). Thus, the crack will completely penetrate the wall without catastrophic failure, allowing for its detection by the leaking of pressurized fluid. With this criterion the critical crack length a_c (i.e., one-half of the total internal crack length) is taken to be equal to the pressure vessel thickness t. Allowance for $a_c = t$ instead of $a_c = t/2$ assures that fluid leakage will occur prior to the buildup of dangerously high pressures. Using this criterion, rank the metal alloys in Table B.5, Appendix B as to the maximum allowable pressure.

For this spherical pressure vessel, the circumferential wall stress σ is a function of the pressure p in the vessel and the radius r and wall thickness t according to

$$\sigma = \frac{pr}{2t} \tag{9.15}$$

For both parts (a) and (b) assume a condition of plane strain.

SOLUTION

(a) For the first design criterion, it is desired that the circumferential wall stress be less than the yield strength of the material. Substitution of σ_y for σ in Equation 9.11, and incorporation of a factor of safety N leads to

$$K_{Ic} = Y\left(\frac{\sigma_y}{N}\right)\sqrt{\pi a_c} \tag{9.16}$$

where a_c is the critical crack length. Solving for a_c yields the following expression:

$$a_c = \frac{N^2}{Y^2\pi}\left(\frac{K_{Ic}}{\sigma_y}\right)^2 \tag{9.17}$$

Table 9.2 **Ranking of Several Metal Alloys Relative to Critical Crack Length (Yielding Criterion) for a Thin-Walled Spherical Pressure Vessel**

Material	$\left(\frac{K_{Ic}}{\sigma_y}\right)^2$ ***(mm)***
Medium carbon (1040) steel	43.1
AZ31B magnesium	19.6
2024 aluminum (T3)	16.3
Ti-5Al-2.5Sn titanium	6.6
4140 steel (tempered @ 482°C)	5.3
4340 steel (tempered @ 425°C)	3.8
Ti-6Al-4V titanium	3.7
17-7PH steel	3.4
7075 aluminum (T651)	2.4
4140 steel (tempered @ 370°C)	1.6
4340 Steel (tempered @ 260°C)	0.93

Therefore, the critical crack length is proportional to the square of the K_{Ic}-σ_y ratio, which is the basis for the ranking of the metal alloys in Table B.5. The ranking is provided in Table 9.2, where it may be seen that the medium carbon (1040) steel with the largest ratio has the longest critical crack length, and, therefore, is the most desirable material on the basis of this criterion.

(b) As stated previously, the leak-before-break criterion is just met when one-half of the internal crack length is equal to the thickness of the pressure vessel—i.e., when $a = t$. Substitution of $a = t$ into Equation 9.11 gives

$$K_{Ic} = Y\sigma\sqrt{\pi t} \tag{9.18}$$

And, from Equation 9.15

$$t = \frac{pr}{2\sigma} \tag{9.19}$$

The stress is replaced by the yield strength, inasmuch as the tank should be designed to contain the pressure without yielding; furthermore, substitution of Equation 9.19 into Equation 9.18, after some rearrangement, yields the following expression:

$$p = \frac{2}{Y^2\pi r}\left(\frac{K_{Ic}^2}{\sigma_y}\right) \tag{9.20}$$

Hence, for some given spherical vessel of radius r, the maximum allowable pressure consistent with this leak-before-break criterion is proportional to K_{Ic}^2/σ_y. The same several materials are ranked according to this ratio in Table 9.3; as may be noted, the medium carbon steel will contain the greatest pressures.

Of the eleven metal alloys that are listed in Table B.5, the medium carbon steel ranks first according to both yielding and leak-before-break criteria. For these

Table 9.3 Ranking of Several Metal Alloys Relative to Maximum Allowable Pressure (Leak-Before-Break Criterion) for a Thin-Walled Spherical Pressure Vessel

Material	$\frac{K_{Ic}^2}{\sigma_y}$ *(MPa-m)*
Medium carbon (1040) steel	11.2
4140 steel (tempered @ 482°C)	6.1
Ti-5Al-2.5Sn titanium	5.8
2024 aluminum (T3)	5.6
4340 steel (tempered @ 425°C)	5.4
17-7PH steel	4.4
AZ31B magnesium	3.9
Ti-6Al-4V titanium	3.3
4140 steel (tempered @ 370°C)	2.4
4340 steel (tempered @ 260°C)	1.5
7075 aluminum (T651)	1.2

reasons, many pressure vessels are constructed of medium carbon steels, when temperature extremes and corrosion need not be considered.

9.6 Brittle Fracture of Ceramics

At room temperature, both crystalline and noncrystalline ceramics almost always fracture before any plastic deformation can occur in response to an applied tensile load. Furthermore, the mechanics of brittle fracture and principles of fracture mechanics developed earlier in this chapter also apply to the fracture of this group of materials.

It should be noted that stress raisers in brittle ceramics may be minute surface or interior cracks (microcracks), internal pores, and grain corners, which are virtually impossible to eliminate or control. For example, even moisture and contaminants in the atmosphere can introduce surface cracks in freshly drawn glass fibers; these cracks deleteriously affect the strength. In addition, plane strain fracture toughness values for ceramic materials are smaller than for metals; typically they are below $10\ \text{MPa}\sqrt{\text{m}}$ ($9\ \text{ksi}\sqrt{\text{in.}}$). Values of K_{Ic} for several ceramic materials are included in Table 9.1 and Table B.5, Appendix B.

There is usually considerable variation and scatter in the fracture strength for many specimens of a specific brittle ceramic material. A distribution of fracture strengths for portland cement is shown in Figure 9.16. This phenomenon may be explained by the dependence of fracture strength on the probability of the existence of a flaw that is capable of initiating a crack. This probability varies from specimen to specimen of the same material and depends on fabrication technique and any subsequent treatment. Specimen size or volume also influences fracture strength; the larger the specimen, the greater this flaw existence probability, and the lower the fracture strength.

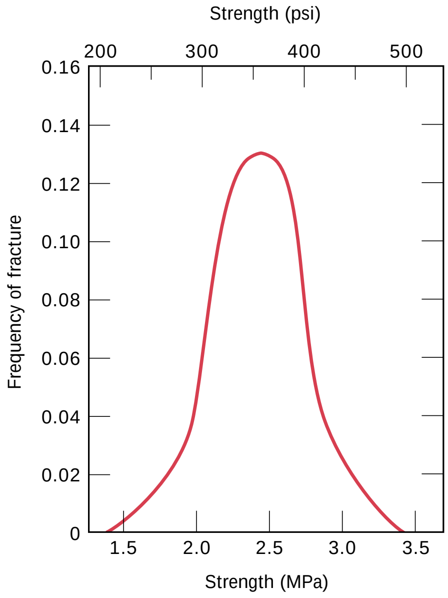

FIGURE 9.16 The frequency distribution of observed fracture strengths for a portland cement. (From W. Weibull, *Ing. Vetensk. Akad.*, Proc. 151, No. 153, 1939.)

For compressive stresses, there is no stress amplification associated with any existent flaws. For this reason, brittle ceramics display much higher strengths in compression than in tension (on the order of a factor of 10), and they are generally utilized when load conditions are compressive. Also, the fracture strength of a brittle ceramic may be enhanced dramatically by imposing residual compressive stresses at its surface. {One way this may be accomplished is by thermal tempering (see Section 14.7).}

Statistical theories have been developed that in conjunction with experimental data are used to determine the risk of fracture for a given material; a discussion of these is beyond the scope of the present treatment. However, due to the dispersion in the measured fracture strengths of brittle ceramic materials, average values and factors of safety as discussed in Sections 7.19 and 7.20 are not normally employed for design purposes.

STATIC FATIGUE (CD-ROM)

9.7 FRACTURE OF POLYMERS

The fracture strengths of polymeric materials are low relative to those of metals and ceramics. As a general rule, the mode of fracture in thermosetting polymers is brittle. In simple terms, associated with the fracture process is the formation of cracks at regions where there is a localized stress concentration (i.e., scratches, notches, and sharp flaws). Covalent bonds in the network or crosslinked structure are severed during fracture.

For thermoplastic polymers, both ductile and brittle modes are possible, and many of these materials are capable of experiencing a ductile-to-brittle transition. Factors that favor brittle fracture are a reduction in temperature, an increase in strain rate, the presence of a sharp notch, increased specimen thickness, and, in addition, a modification of the polymer structure (chemical, molecular, and/or

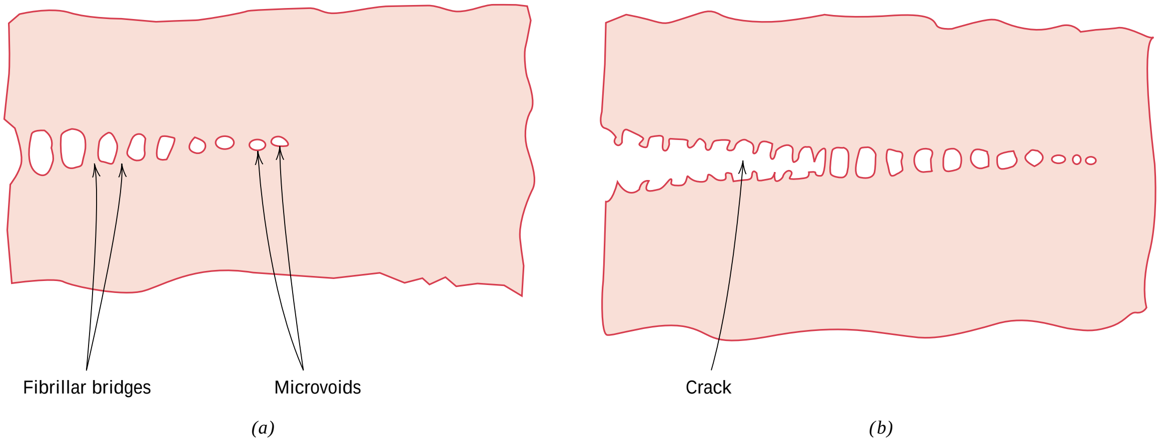

Figure 9.17 Schematic drawings of (*a*) a craze showing microvoids and fibrillar bridges, and (*b*) a craze followed by a crack. (From J. W. S. Hearle, *Polymers and Their Properties,* Vol. 1, *Fundamentals of Structure and Mechanics,* Ellis Horwood, Ltd., Chichester, West Sussex, England, 1982.)

microstructural). Glassy thermoplastics are brittle at relatively low temperatures; as the temperature is raised, they become ductile in the vicinity of their glass transition temperatures and experience plastic yielding prior to fracture. This behavior is demonstrated by the stress–strain characteristics of polymethyl methacrylate in Figure 7.24. At 4°C, PMMA is totally brittle, whereas at 60°C it becomes extremely ductile.

One phenomenon that frequently precedes fracture in some glassy thermoplastic polymers is *crazing.* Associated with crazes are regions of very localized yielding, which lead to the formation of small and interconnected microvoids (Figure 9.17*a*). Fibrillar bridges form between these microvoids wherein molecular chains become oriented. If the applied tensile load is sufficient, these bridges elongate and break, causing the microvoids to grow and coalesce; as the microvoids coalesce, cracks begin to form, as demonstrated in Figure 9.17*b*. A craze is different from a crack in that it can support a load across its face. Furthermore, this process of craze growth prior to cracking absorbs fracture energy and effectively increases the fracture toughness of the polymer. Crazes form at highly stressed regions associated with scratches, flaws, and molecular inhomogeneities; in addition, they propagate perpendicular to the applied tensile stress, and typically are 5 μm or less thick. Figure 9.18 is a photomicrograph in which a craze is shown.

Principles of fracture mechanics developed in Section 9.5 also apply to brittle and quasi-brittle polymers. The magnitude of K_{Ic} will depend on characteristics of the polymer (i.e., molecular weight, percent crystallinity, etc.) as well as temperature, strain rate, and the external environment. Representative values of K_{Ic} for several polymers are included in Table 9.1 and Table B.5, Appendix B.

9.8 IMPACT FRACTURE TESTING

Prior to the advent of fracture mechanics as a scientific discipline, impact testing techniques were established so as to ascertain the fracture characteristics of materials. It was realized that the results of laboratory tensile tests could not be extrapolated to predict fracture behavior; for example, under some circumstances normally

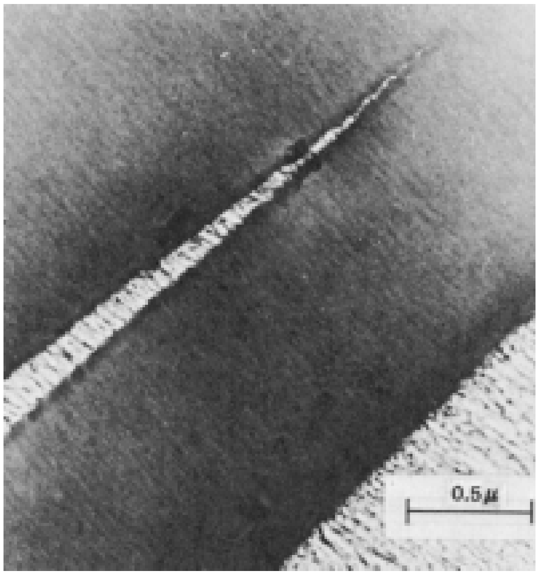

FIGURE 9.18 Photomicrograph of a craze in polyphenylene oxide. (From R. P. Kambour and R. E. Robertson, ''The Mechanical Properties of Plastics,'' in *Polymer Science, A Materials Science Handbook,* A. D. Jenkins, Editor. Reprinted with permission of Elsevier Science Publishers.)

ductile metals fracture abruptly and with very little plastic deformation. Impact test conditions were chosen to represent those most severe relative to the potential for fracture, namely, (1) deformation at a relatively low temperature, (2) a high strain rate (i.e., rate of deformation), and (3) a triaxial stress state (which may be introduced by the presence of a notch).

IMPACT TESTING TECHNIQUES

Two standardized tests,[7] the **Charpy** and **Izod,** were designed and are still used to measure the **impact energy,** sometimes also termed *notch toughness.* The Charpy V-notch (CVN) technique is most commonly used in the United States. For both Charpy and Izod, the specimen is in the shape of a bar of square cross section, into which a V-notch is machined (Figure 9.19*a*). The apparatus for making V-notch impact tests is illustrated schematically in Figure 9.19*b*. The load is applied as an impact blow from a weighted pendulum hammer that is released from a cocked position at a fixed height h. The specimen is positioned at the base as shown. Upon release, a knife edge mounted on the pendulum strikes and fractures the specimen at the notch, which acts as a point of stress concentration for this high velocity impact blow. The pendulum continues its swing, rising to a maximum height h', which is lower than h. The energy absorption, computed from the difference between h and h', is a measure of the impact energy. The primary difference between the Charpy and Izod techniques lies in the manner of specimen support, as illustrated in Figure 9.19*b*. Furthermore, these are termed impact tests in light of the manner of load application. Variables including specimen size and shape as well as notch configuration and depth influence the test results.

Both plane strain fracture toughness and these impact tests determine the fracture properties of materials. The former are quantitative in nature, in that a specific property of the material is determined (i.e., K_{Ic}). The results of the impact

---

[7] ASTM Standard E 23, ''Standard Test Methods for Notched Bar Impact Testing of Metallic Materials.''

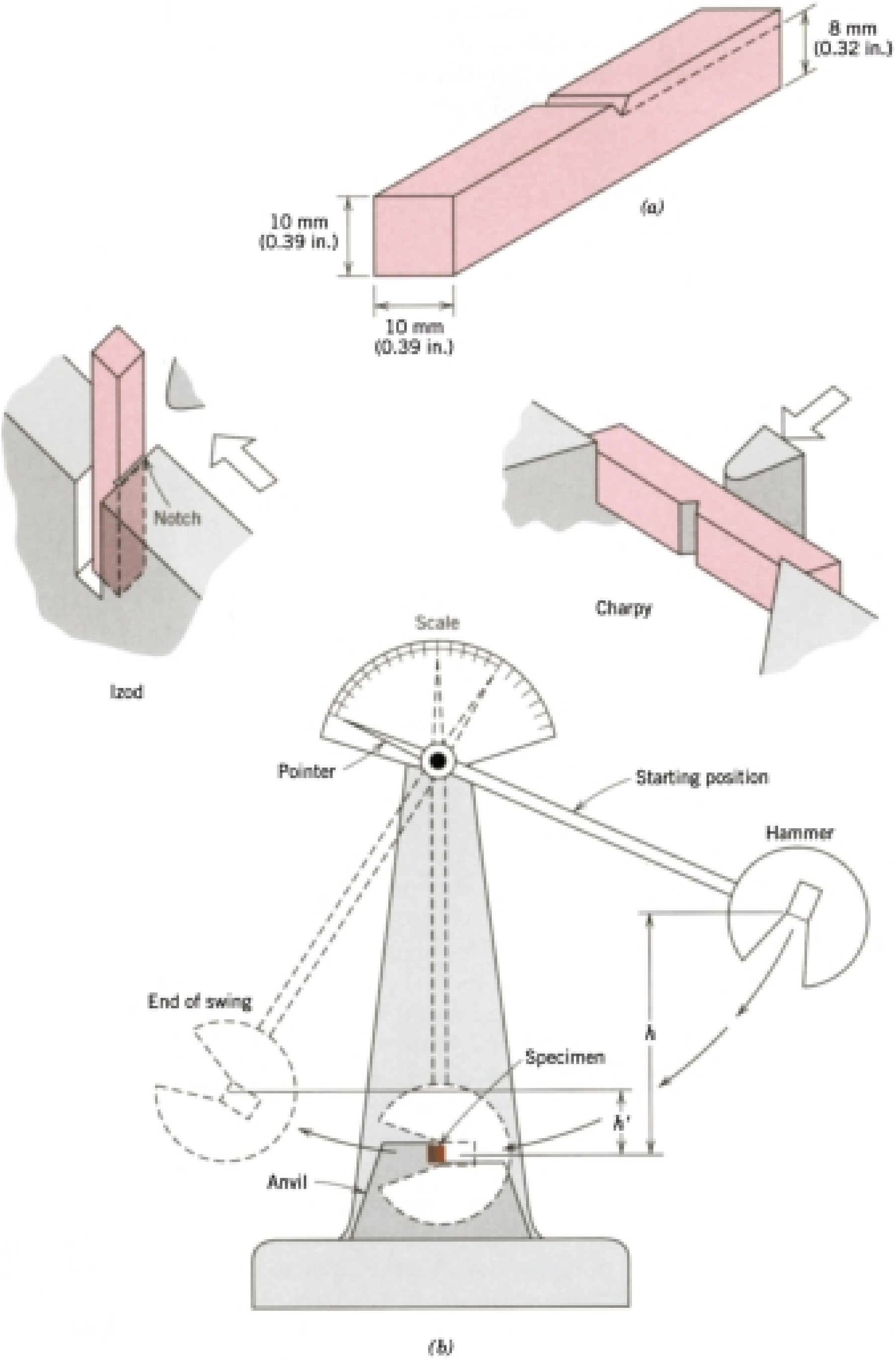
8 mm
(0.32 in.)
10 mm
(0.39 in.)
(a)
10 mm
(0.39 in.)
Notch
Izod
Charpy
Scale
Pointer
Starting position
Hammer
End of swing
Specimen
h
h'
Anvil
(b)

Figure 9.19 (*a*) Specimen used for Charpy and Izod impact tests. (*b*) A schematic drawing of an impact testing apparatus. The hammer is released from fixed height *h* and strikes the specimen; the energy expended in fracture is reflected in the difference between *h* and the swing height *h*′. Specimen placements for both Charpy and Izod tests are also shown. (Figure (*b*) adapted from H. W. Hayden, W. G. Moffatt, and J. Wulff, *The Structure and Properties of Materials*, Vol. III, *Mechanical Behavior*, p. 13. Copyright © 1965 by John Wiley & Sons, New York. Reprinted by permission of John Wiley & Sons, Inc.)

tests, on the other hand, are more qualitative and are of little use for design purposes. Impact energies are of interest mainly in a relative sense and for making comparisons—absolute values are of little significance. Attempts have been made to correlate plane strain fracture toughnesses and CVN energies, with only limited success. Plane strain fracture toughness tests are not as simple to perform as impact tests; furthermore, equipment and specimens are more expensive.

DUCTILE-TO-BRITTLE TRANSITION

One of the primary functions of Charpy and Izod tests is to determine whether or not a material experiences a **ductile-to-brittle transition** with decreasing temperature and, if so, the range of temperatures over which it occurs. The ductile-to-brittle transition is related to the temperature dependence of the measured impact energy absorption. This transition is represented for a steel by curve *A* in Figure 9.20. At higher temperatures the CVN energy is relatively large, in correlation with a ductile mode of fracture. As the temperature is lowered, the impact energy drops suddenly over a relatively narrow temperature range, below which the energy has a constant but small value; that is, the mode of fracture is brittle.

Alternatively, appearance of the failure surface is indicative of the nature of fracture, and may be used in transition temperature determinations. For ductile fracture this surface appears fibrous or dull (or of shear character); conversely, totally brittle surfaces have a granular (shiny) texture (or cleavage character). Over the ductile-to-brittle transition, features of both types will exist (Figure 9.21). Frequently, the percent shear fracture is plotted as a function of temperature—curve *B* in Figure 9.20.

For many alloys there is a range of temperatures over which the ductile-to-brittle transition occurs (Figure 9.20); this presents some difficulty in specifying a single ductile-to-brittle transition temperature. No explicit criterion has been established, and so this temperature is often defined as that temperature at which the CVN energy assumes some value (e.g., 20 J or 15 ft-lb$_f$), or corresponding to some given fracture appearance (e.g., 50% fibrous fracture). Matters are further complicated inasmuch as a different transition temperature may be realized for each of these criteria. Perhaps the most conservative transition temperature is that at which the fracture surface becomes 100% fibrous; on this basis, the transition temperature is approximately 110°C (230°F) for the steel alloy that is the subject of Figure 9.20.

FIGURE 9.20 Temperature dependence of the Charpy V-notch impact energy (curve *A*) and percent shear fracture (curve *B*) for an A283 steel. (Reprinted from *Welding Journal*. Used by permission of the American Welding Society.)

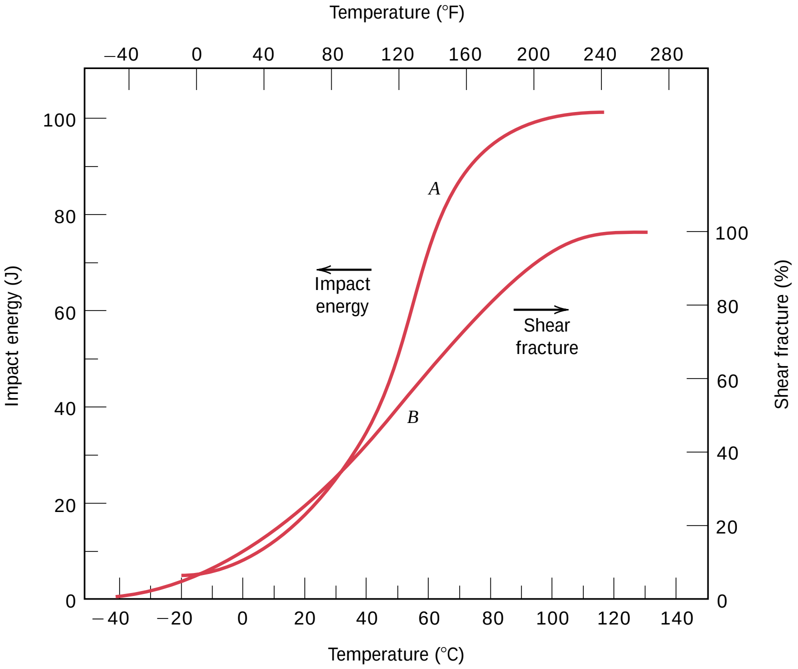

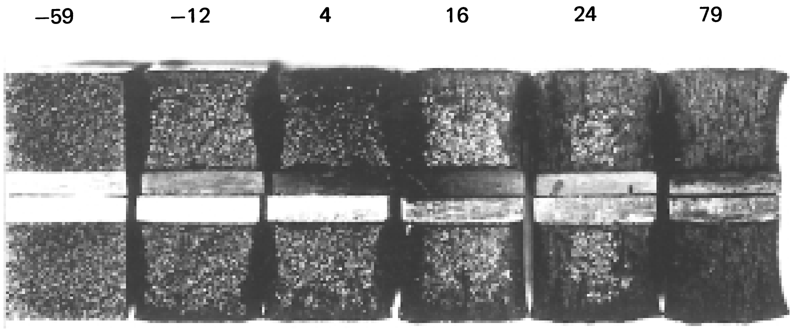

Figure 9.21 Photograph of fracture surfaces of A36 steel Charpy V-notch specimens tested at indicated temperatures (in °C). (From R. W. Hertzberg, *Deformation and Fracture Mechanics of Engineering Materials,* 3rd edition, Fig. 9.6, p. 329. Copyright © 1989 by John Wiley & Sons, Inc., New York. Reprinted by permission of John Wiley & Sons, Inc.)

Structures constructed from alloys that exhibit this ductile-to-brittle behavior should be used only at temperatures above the transition temperature, to avoid brittle and catastrophic failure. Classic examples of this type of failure occurred, with disastrous consequences, during World War II when a number of welded transport ships, away from combat, suddenly and precipitously split in half. The vessels were constructed of a steel alloy that possessed adequate ductility according to room-temperature tensile tests. The brittle fractures occurred at relatively low ambient temperatures, at about 4°C (40°F), in the vicinity of the transition temperature of the alloy. Each fracture crack originated at some point of stress concentration, probably a sharp corner or fabrication defect, and then propagated around the entire girth of the ship.

Not all metal alloys display a ductile-to-brittle transition. Those having FCC crystal structures (including aluminum- and copper-based alloys) remain ductile even at extremely low temperatures. However, BCC and HCP alloys experience this transition. For these materials the transition temperature is sensitive to both alloy composition and microstructure. For example, decreasing the average grain size of steels results in a lowering of the transition temperature. Hence, refining the grain size both strengthens (Section 8.9) and toughens steels. In contrast, increasing the carbon content, while increasing the strength of steels, also raises the CVN transition of steels, as indicated in Figure 9.22.

Izod or Charpy tests are also conducted to assess impact strength of polymeric materials. As with metals, polymers may exhibit ductile or brittle fracture under impact loading conditions, depending on the temperature, specimen size, strain rate, and mode of loading, as discussed in the preceding section. Both semicrystalline and amorphous polymers are brittle at low temperatures, and both have relatively low impact strengths. However, they experience a ductile-to-brittle transition over a relatively narrow temperature range, similar to that shown for a steel in Figure 9.20. Of course, impact strength undergoes a gradual decrease at still higher temperatures as the polymer begins to soften. Ordinarily, the two impact characteristics most sought after are a high impact strength at the ambient temperature and a ductile-to-brittle transition temperature that lies below room temperature.

Most ceramics also experience a ductile-to-brittle transition, which occurs only at elevated temperatures—ordinarily in excess of 1000°C (1850°F).

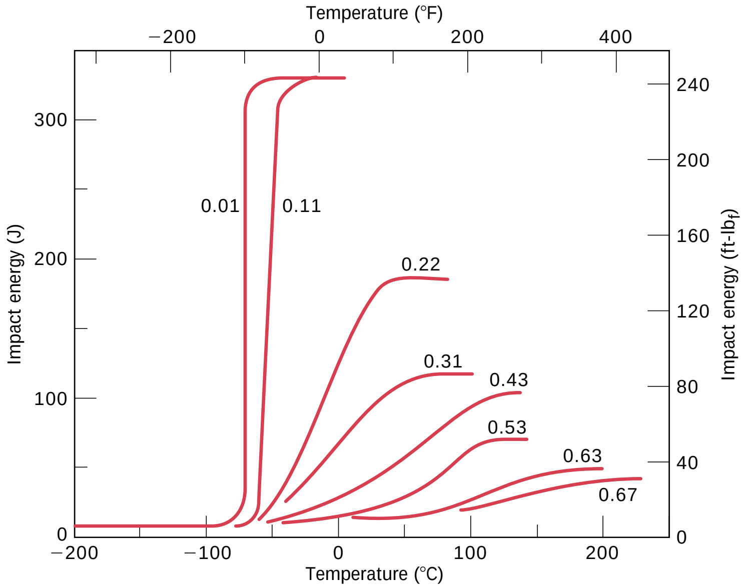

FIGURE 9.22 Influence of carbon content on the Charpy V-notch energy-versus-temperature behavior for steel. (Reprinted with permission from ASM International, Metals Park, OH 44073-9989, USA; J. A. Reinbolt and W. J. Harris, Jr., ''Effect of Alloying Elements on Notch Toughness of Pearlitic Steels,'' *Transactions of ASM*, Vol. 43, 1951.)

FATIGUE

Fatigue is a form of failure that occurs in structures subjected to dynamic and fluctuating stresses (e.g., bridges, aircraft, and machine components). Under these circumstances it is possible for failure to occur at a stress level considerably lower than the tensile or yield strength for a static load. The term ''fatigue'' is used because this type of failure normally occurs after a lengthy period of repeated stress or strain cycling. Fatigue is important inasmuch as it is the single largest cause of failure in metals, estimated to comprise approximately 90% of all metallic failures; polymers and ceramics (except for glasses) are also susceptible to this type of failure. Furthermore, it is catastrophic and insidious, occurring very suddenly and without warning.

Fatigue failure is brittlelike in nature even in normally ductile metals, in that there is very little, if any, gross plastic deformation associated with failure. The process occurs by the initiation and propagation of cracks, and ordinarily the fracture surface is perpendicular to the direction of an applied tensile stress.

9.9 CYCLIC STRESSES

The applied stress may be axial (tension-compression), flexural (bending), or torsional (twisting) in nature. In general, three different fluctuating stress–time modes are possible. One is represented schematically by a regular and sinusoidal time dependence in Figure 9.23*a*, wherein the amplitude is symmetrical about a mean zero stress level, for example, alternating from a maximum tensile stress ($\sigma_{\max}$) to a minimum compressive stress ($\sigma_{\min}$) of equal magnitude; this is referred to as a *reversed stress cycle.* Another type, termed *repeated stress cycle,* is illustrated in Figure 9.23*b*; the maxima and minima are asymmetrical relative to the zero stress level. Finally, the stress level may vary randomly in amplitude and frequency, as exemplified in Figure 9.23*c*.

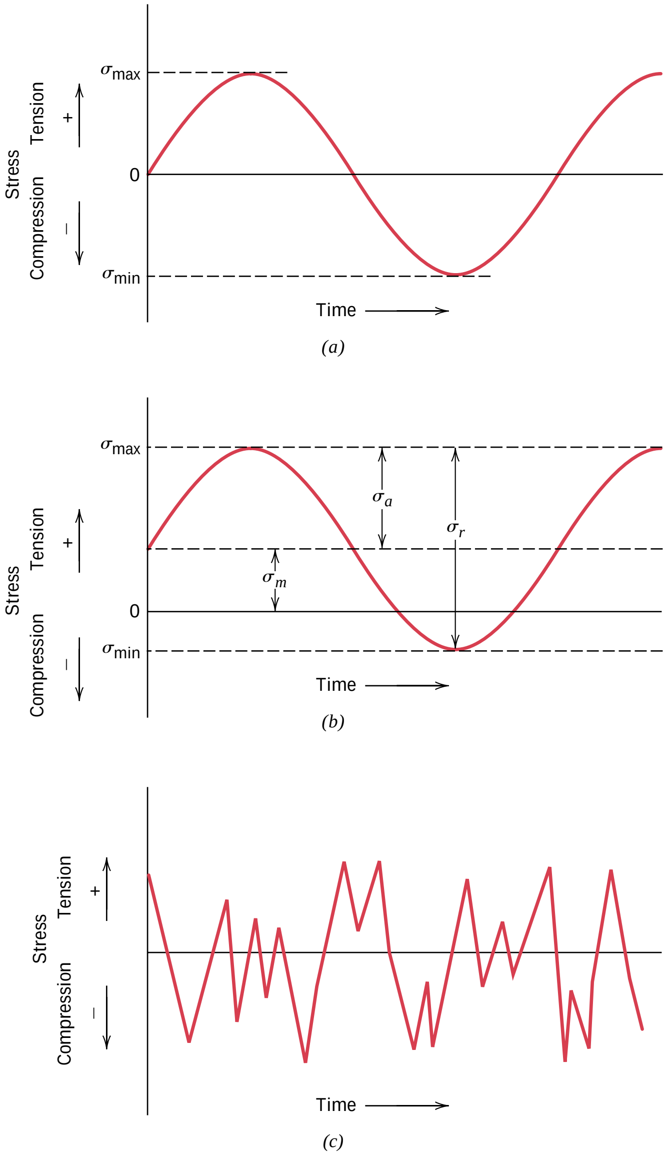

Figure 9.23 Variation of stress with time that accounts for fatigue failures. (*a*) Reversed stress cycle, in which the stress alternates from a maximum tensile stress (+) to a maximum compressive stress (−) of equal magnitude. (*b*) Repeated stress cycle, in which maximum and minimum stresses are asymmetrical relative to the zero stress level; mean stress σ_m, range of stress σ_r, and stress amplitude σ_a are indicated. (*c*) Random stress cycle.

Also indicated in Figure 9.23*b* are several parameters used to characterize the fluctuating stress cycle. The stress amplitude alternates about a *mean stress* σ_m, defined as the average of the maximum and minimum stresses in the cycle, or

$$\sigma_m = \frac{\sigma_{\max} + \sigma_{\min}}{2} \tag{9.21}$$

Furthermore, the *range of stress* σ_r is just the difference between $\sigma_{\max}$ and $\sigma_{\min}$, namely,

$$\sigma_r = \sigma_{\max} - \sigma_{\min} \tag{9.22}$$

Stress amplitude σ_a is just one half of this range of stress, or

$$\sigma_a = \frac{\sigma_r}{2} = \frac{\sigma_{\max} - \sigma_{\min}}{2} \tag{9.23}$$

Finally, the *stress ratio* R is just the ratio of minimum and maximum stress amplitudes:

$$R = \frac{\sigma_{\min}}{\sigma_{\max}} \tag{9.24}$$

By convention, tensile stresses are positive and compressive stresses are negative. For example, for the reversed stress cycle, the value of R is -1.

9.10 THE *S–N* CURVE

As with other mechanical characteristics, the fatigue properties of materials can be determined from laboratory simulation tests.[8] A test apparatus should be designed to duplicate as nearly as possible the service stress conditions (stress level, time frequency, stress pattern, etc.). A schematic diagram of a rotating-bending test apparatus, commonly used for fatigue testing, is shown in Figure 9.24; the compression and tensile stresses are imposed on the specimen as it is simultaneously bent and rotated. Tests are also frequently conducted using an alternating uniaxial tension-compression stress cycle.

A series of tests are commenced by subjecting a specimen to the stress cycling at a relatively large maximum stress amplitude ($\sigma_{\max}$), usually on the order of two thirds of the static tensile strength; the number of cycles to failure is counted. This procedure is repeated on other specimens at progressively decreasing maximum stress amplitudes. Data are plotted as stress S versus the logarithm of the number N of cycles to failure for each of the specimens. The values of S are normally taken as stress amplitudes (σ_a, Equation 9.23); on occasion, $\sigma_{\max}$ or $\sigma_{\min}$ values may be used.

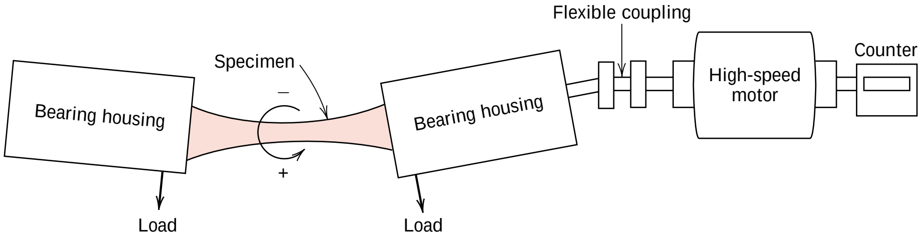

FIGURE 9.24 Schematic diagram of fatigue testing apparatus for making rotating-bending tests. (From *Materials Science in Engineering,* fourth edition, by Keyser, Carl A., © 1986. Reprinted by permission of Prentice-Hall, Inc., Upper Saddle River, NJ.)

---

[8] See ASTM Standard E 466, ''Standard Practice for Conducting Constant Amplitude Axial Fatigue Tests of Metallic Materials,'' and ASTM Standard E 468, ''Standard Practice for Presentation of Constant Amplitude Fatigue Test Results for Metallic Materials.''

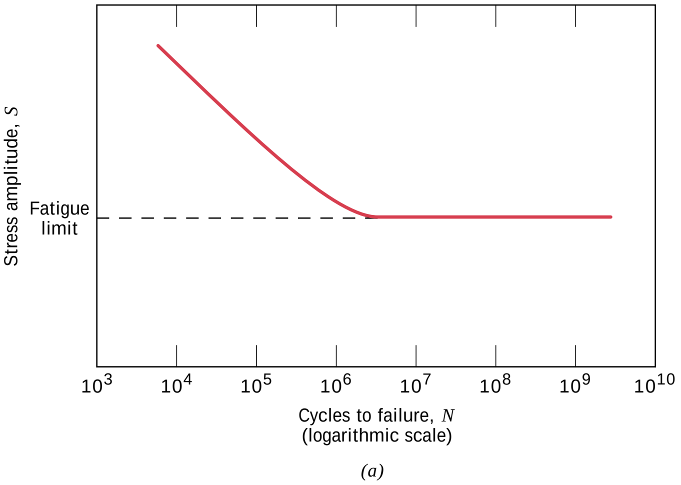

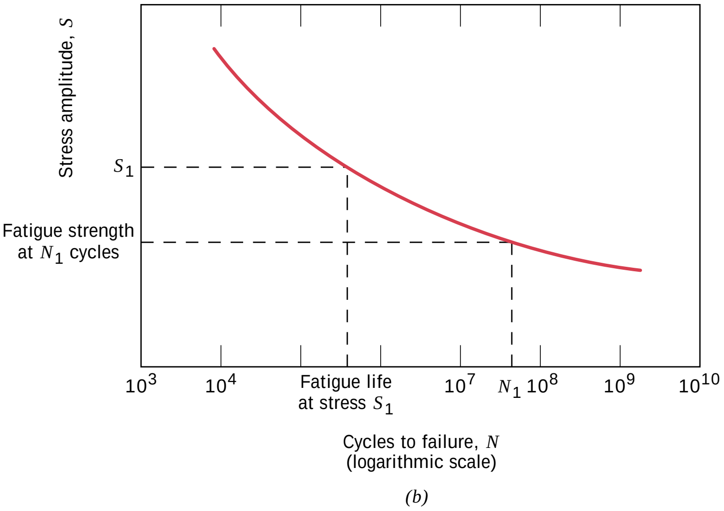

FIGURE 9.25 Stress amplitude (S) versus logarithm of the number of cycles to fatigue failure (N) for (*a*) a material that displays a fatigue limit, and (*b*) a material that does not display a fatigue limit.

Two distinct types of S–N behavior are observed, which are represented schematically in Figure 9.25. As these plots indicate, the higher the magnitude of the stress, the smaller the number of cycles the material is capable of sustaining before failure. For some ferrous (iron base) and titanium alloys, the S–N curve (Figure 9.25*a*) becomes horizontal at higher N values; or, there is a limiting stress level, called the **fatigue limit** (also sometimes the *endurance limit*), below which fatigue failure will not occur. This fatigue limit represents the largest value of fluctuating stress that will *not* cause failure for essentially an infinite number of cycles. For many steels, fatigue limits range between 35 and 60% of the tensile strength.

Most nonferrous alloys (e.g., aluminum, copper, magnesium) do not have a fatigue limit, in that the S–N curve continues its downward trend at increasingly greater N values (Figure 9.25*b*). Thus, fatigue will ultimately occur regardless of the magnitude of the stress. For these materials, the fatigue response is specified as **fatigue strength,** which is defined as the stress level at which failure will occur for some specified number of cycles (e.g., 10^7 cycles). The determination of fatigue strength is also demonstrated in Figure 9.25*b*.

Another important parameter that characterizes a material's fatigue behavior is **fatigue life** N_f. It is the number of cycles to cause failure at a specified stress level, as taken from the S–N plot (Figure 9.25*b*).

Unfortunately, there always exists considerable scatter in fatigue data, that is, a variation in the measured N value for a number of specimens tested at the same stress level. This may lead to significant design uncertainties when fatigue life and/or fatigue limit (or strength) are being considered. The scatter in results is a consequence of the fatigue sensitivity to a number of test and material parameters that are impossible to control precisely. These parameters include specimen fabrication and surface preparation, metallurgical variables, specimen alignment in the apparatus, mean stress, and test frequency.

Fatigue S–N curves similar to those shown in Figure 9.25 represent ''best fit'' curves which have been drawn through average-value data points. It is a little unsettling to realize that approximately one half of the specimens tested actually failed at stress levels lying nearly 25% below the curve (as determined on the basis of statistical treatments).

Several statistical techniques have been developed to specify fatigue life and fatigue limit in terms of probabilities. One convenient way of representing data treated in this manner is with a series of constant probability curves, several of which are plotted in Figure 9.26. The P value associated with each curve represents the probability of failure. For example, at a stress of 200 MPa (30,000 psi), we would expect 1% of the specimens to fail at about 10^6 cycles and 50% to fail at about 2×10^7 cycles, and so on. It should be remembered that S–N curves represented in the literature are normally average values, unless noted otherwise.

The fatigue behaviors represented in Figures 9.25*a* and 9.25*b* may be classified into two domains. One is associated with relatively high loads that produce not only elastic strain but also some plastic strain during each cycle. Consequently, fatigue lives are relatively short; this domain is termed *low-cycle fatigue* and occurs at less than about 10^4 to 10^5 cycles. For lower stress levels wherein deformations are totally elastic, longer lives result. This is called *high-cycle fatigue* inasmuch as relatively large numbers of cycles are required to produce

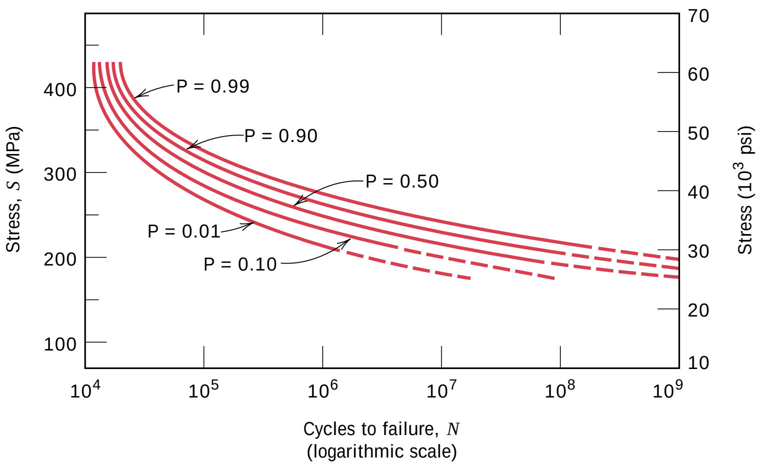

FIGURE 9.26 Fatigue S–N probability of failure curves for a 7075-T6 aluminum alloy; P denotes the probability of failure. (From G. M. Sinclair and T. J. Dolan, *Trans., ASME,* **75,** 1953, p. 867. Reprinted with permission of the American Society of Mechanical Engineers.)

fatigue failure. High-cycle fatigue is associated with fatigue lives greater than about 10^4 to 10^5 cycles.

9.11 FATIGUE IN POLYMERIC MATERIALS

Polymers may experience fatigue failure under conditions of cyclic loading. As with metals, fatigue occurs at stress levels that are low relative to the yield strength. Fatigue data are plotted in the same manner for both types of material, and the resulting curves have the same general shape. Fatigue curves for several common polymers are shown in Figure 9.27, as stress versus the number of cycles to failure (on a logarithmic scale). Some polymers have a fatigue limit. As would be expected, fatigue strengths and fatigue limits for polymeric materials are much lower than for metals.

The fatigue behavior of polymers is much more sensitive to loading frequency than for metals. Cycling polymers at high frequencies and/or relatively large stresses can cause localized heating; consequently, failure may be due to a softening of the material rather than as a result of typical fatigue processes.

9.12a CRACK INITIATION AND PROPAGATION [DETAILED VERSION (CD-ROM)]

9.12b CRACK INITIATION AND PROPAGATION (CONCISE VERSION)

The process of fatigue failure is characterized by three distinct steps: (1) crack initiation, wherein a small crack forms at some point of high stress concentration; (2) crack propagation, during which this crack advances incrementally with each stress cycle; and (3) final failure, which occurs very rapidly once the advancing

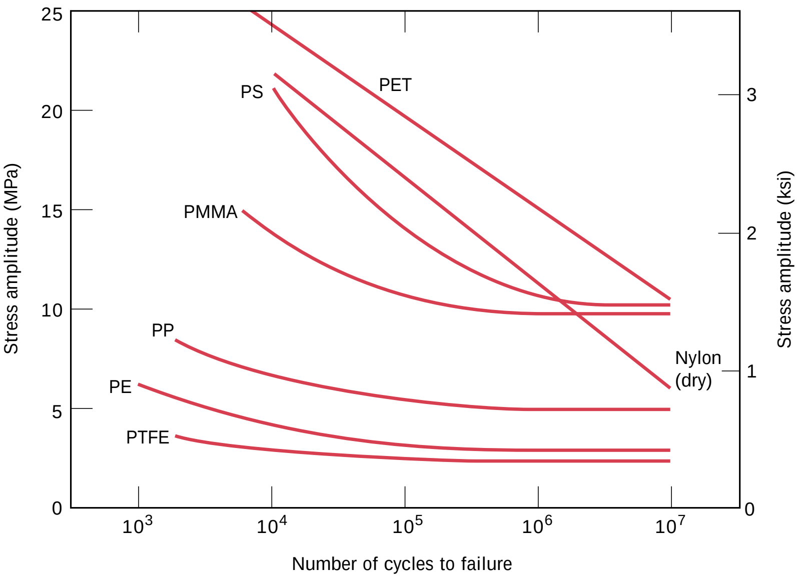

FIGURE 9.27 Fatigue curves (stress amplitude versus the number of cycles to failure) for polyethylene terephthalate (PET), nylon, polystyrene (PS), polymethyl methacrylate (PMMA), polypropylene (PP), polyethylene (PE), and polytetrafluoroethylene (PTFE). The testing frequency was 30 Hz. (From M. N. Riddell, ''A Guide to Better Testing of Plastics,'' *Plast. Eng.*, Vol. 30, No. 4, p. 78, 1974.)

crack has reached a critical size. Cracks associated with fatigue failure almost always initiate (or nucleate) on the surface of a component at some point of stress concentration. Crack nucleation sites include surface scratches, sharp fillets, keyways, threads, dents, and the like. In addition, cyclic loading can produce microscopic surface discontinuities resulting from dislocation slip steps which may also act as stress raisers, and therefore as crack initiation sites.

The region of a fracture surface that formed during the crack propagation step may be characterized by two types of markings termed *beachmarks* and *striations.* Both of these features indicate the position of the crack tip at some point in time and appear as concentric ridges that expand away from the crack initiation site(s), frequently in a circular or semicircular pattern. Beachmarks (sometimes also called ''clamshell marks'') are of macroscopic dimensions (Figure 9.30), and may be observed with the unaided eye. These markings are found for components that experienced interruptions during the crack propagation stage—for example, a machine that operated only during normal work-shift hours. Each beachmark band represents a period of time over which crack growth occurred.

On the other hand, fatigue striations are microscopic in size and subject to observation with the electron microscope (either TEM or SEM). Figure 9.31 is an electron fractograph which shows this feature. Each striation is thought to represent the advance distance of a crack front during a single load cycle. Striation width depends on, and increases with, increasing stress range.

At this point it should be emphasized that although both beachmarks and striations are fatigue fracture surface features having similar appearances, they are nevertheless different, both in origin and size. There may be literally thousands of striations within a single beachmark.

Often the cause of failure may be deduced after examination of the failure surfaces. The presence of beachmarks and/or striations on a fracture surface con-

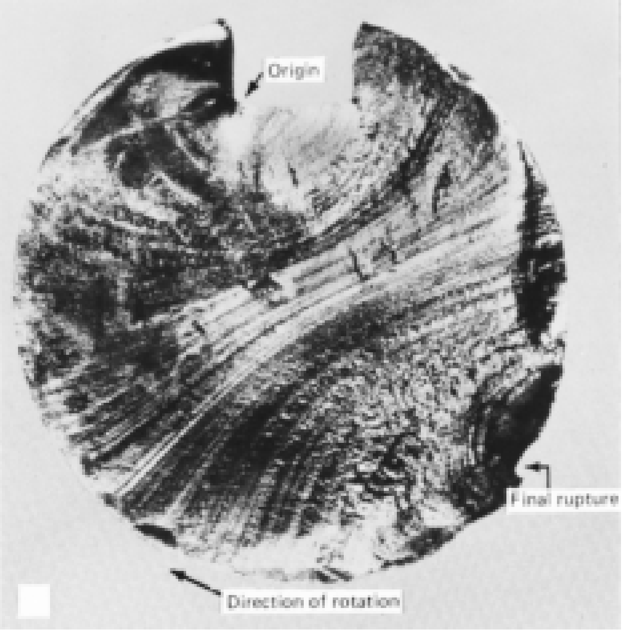

FIGURE 9.30 Fracture surface of a rotating steel shaft that experienced fatigue failure. Beachmark ridges are visible in the photograph. (Reproduced with permission from D. J. Wulpi, *Understanding How Components Fail,* American Society for Metals, Materials Park, OH, 1985.)

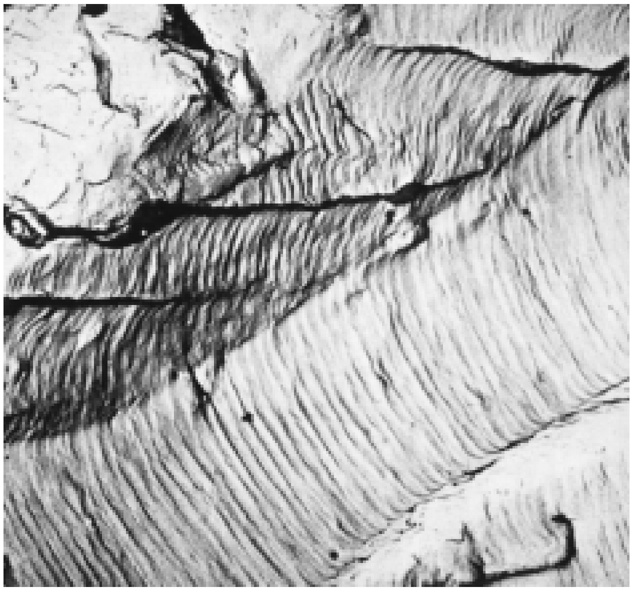

Figure 9.31 Transmission electron fractograph showing fatigue striations in aluminum. Magnification unknown. (From V. J. Colangelo and F. A. Heiser, *Analysis of Metallurgical Failures*, 2nd edition. Copyright © 1987 by John Wiley & Sons, New York. Reprinted by permission of John Wiley & Sons, Inc.)

firms that the cause of failure was fatigue. Nevertheless, the absence of either or both does not exclude fatigue as the cause of failure.

One final comment regarding fatigue failure surfaces: Beachmarks and striations will not appear on that region over which the rapid failure occurs. Rather, the rapid failure may be either ductile or brittle; evidence of plastic deformation will be present for ductile, and absent for brittle, failure. This region of failure may be noted in Figure 9.32.

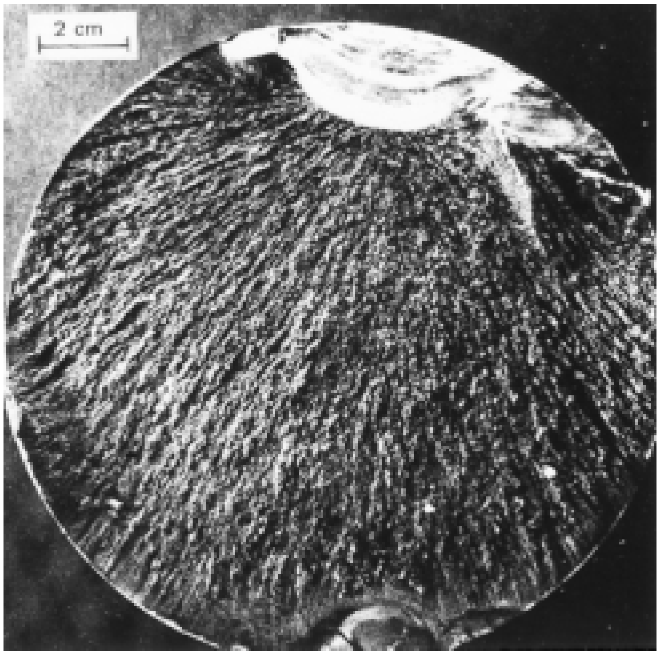

Figure 9.32 Fatigue failure surface. A crack formed at the top edge. The smooth region also near the top corresponds to the area over which the crack propagated slowly. Rapid failure occurred over the area having a dull and fibrous texture (the largest area). Approximately 0.5 ×. (Reproduced by permission from *Metals Handbook: Fractography and Atlas of Fractographs,* Vol. 9, 8th edition, H. E. Boyer, Editor, American Society for Metals, 1974.)

9.13 CRACK PROPAGATION RATE (CD-ROM)

9.14 FACTORS THAT AFFECT FATIGUE LIFE

As was mentioned in Section 9.10, the fatigue behavior of engineering materials is highly sensitive to a number of variables. Some of these factors include mean stress level, geometrical design, surface effects, and metallurgical variables, as well as the environment. This section is devoted to a discussion of these factors and, in addition, to measures that may be taken to improve the fatigue resistance of structural components.

MEAN STRESS

The dependence of fatigue life on stress amplitude is represented on the *S–N* plot. Such data are taken for a constant mean stress σ_m, often for the reversed cycle situation ($\sigma_m = 0$). Mean stress, however, will also affect fatigue life, which influence may be represented by a series of *S–N* curves, each measured at a different σ_m; this is depicted schematically in Figure 9.36. As may be noted, increasing the mean stress level leads to a decrease in fatigue life.

SURFACE EFFECTS

For many common loading situations, the maximum stress within a component or structure occurs at its surface. Consequently, most cracks leading to fatigue failure originate at surface positions, specifically at stress amplification sites. Therefore, it has been observed that fatigue life is especially sensitive to the condition and configuration of the component surface. Numerous factors influence fatigue resistance, the proper management of which will lead to an improvement in fatigue life. These include design criteria as well as various surface treatments.

Design Factors

The design of a component can have a significant influence on its fatigue characteristics. Any notch or geometrical discontinuity can act as a stress raiser and fatigue crack initiation site; these design features include grooves, holes, keyways, threads, and so on. The sharper the discontinuity (i.e., the smaller the radius of curvature),

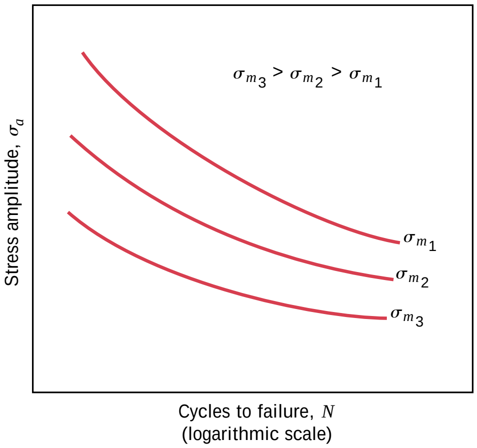

FIGURE 9.36 Demonstration of influence of mean stress σ_m on *S–N* fatigue behavior.

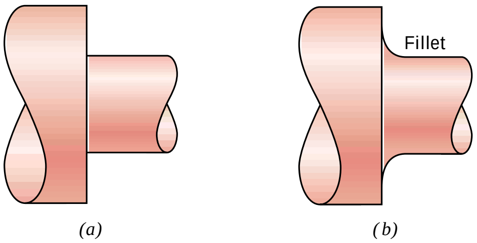

FIGURE 9.37 Demonstration of how design can reduce stress amplification. (*a*) Poor design: sharp corner. (*b*) Good design: fatigue lifetime improved by incorporating rounded fillet into a rotating shaft at the point where there is a change in diameter.

the more severe the stress concentration. The probability of fatigue failure may be reduced by avoiding (when possible) these structural irregularities, or by making design modifications whereby sudden contour changes leading to sharp corners are eliminated—for example, calling for rounded fillets with large radii of curvature at the point where there is a change in diameter for a rotating shaft (Figure 9.37).

Surface Treatments

During machining operations, small scratches and grooves are invariably introduced into the workpiece surface by cutting tool action. These surface markings can limit the fatigue life. It has been observed that improving the surface finish by polishing will enhance fatigue life significantly.

One of the most effective methods of increasing fatigue performance is by imposing residual compressive stresses within a thin outer surface layer. Thus, a surface tensile stress of external origin will be partially nullified and reduced in magnitude by the residual compressive stress. The net effect is that the likelihood of crack formation and therefore of fatigue failure is reduced.

Residual compressive stresses are commonly introduced into ductile metals mechanically by localized plastic deformation within the outer surface region. Commercially, this is often accomplished by a process termed *shot peening*. Small, hard particles (shot) having diameters within the range of 0.1 to 1.0 mm are projected at high velocities onto the surface to be treated. The resulting deformation induces compressive stresses to a depth of between one quarter and one half of the shot diameter. The influence of shot peening on the fatigue behavior of steel is demonstrated schematically in Figure 9.38.

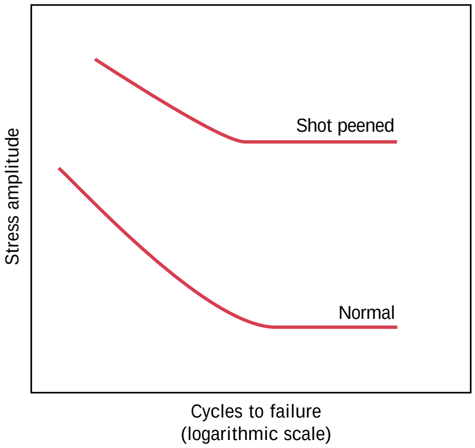

FIGURE 9.38 Schematic S–N fatigue curves for normal and shot-peened steel.

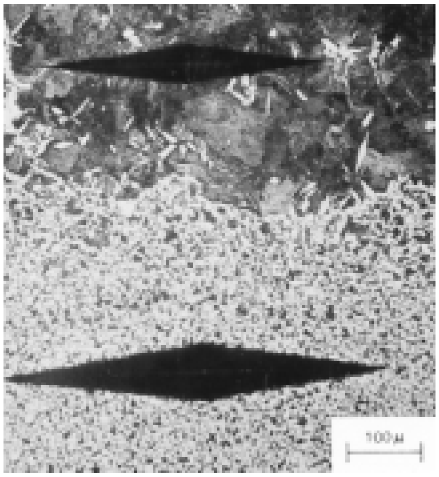

FIGURE 9.39 Photomicrograph showing both core (bottom) and carburized outer case (top) regions of a case-hardened steel. The case is harder as attested by the smaller microhardness indentation. 100×. (From R. W. Hertzberg, *Deformation and Fracture Mechanics of Engineering Materials*, 3rd edition. Copyright © 1989 by John Wiley & Sons, New York. Reprinted by permission of John Wiley & Sons, Inc.)

Case hardening is a technique whereby both surface hardness and fatigue life are enhanced for steel alloys. This is accomplished by a carburizing or nitriding process whereby a component is exposed to a carbonaceous or nitrogenous atmosphere at an elevated temperature. A carbon- or nitrogen-rich outer surface layer (or ''case'') is introduced by atomic diffusion from the gaseous phase. The case is normally on the order of 1 mm deep and is harder than the inner core of material. (The influence of carbon content on hardness for Fe–C alloys is demonstrated in Figure 11.21*a*.) The improvement of fatigue properties results from increased hardness within the case, as well as the desired residual compressive stresses the formation of which attends the carburizing or nitriding process. A carbon-rich outer case may be observed for the gear shown in the chapter-opening photograph for Chapter 6; it appears as a dark outer rim within the sectioned segment. The increase in case hardness is demonstrated in the photomicrograph appearing in Figure 9.39. The dark and elongated diamond shapes are Knoop microhardness indentations. The upper indentation, lying within the carburized layer, is smaller than the core indentation.

9.15 ENVIRONMENTAL EFFECTS (CD-ROM)

CREEP

Materials are often placed in service at elevated temperatures and exposed to static mechanical stresses (e.g., turbine rotors in jet engines and steam generators that experience centrifugal stresses, and high-pressure steam lines). Deformation under such circumstances is termed **creep.** Defined as the time-dependent and permanent deformation of materials when subjected to a constant load or stress, creep is normally an undesirable phenomenon and is often the limiting factor in the lifetime of a part. It is observed in all materials types; for metals it becomes important only for temperatures greater than about $0.4T_m$ (T_m = absolute melting temperature).

9.16 GENERALIZED CREEP BEHAVIOR

A typical creep test[10] consists of subjecting a specimen to a constant load or stress while maintaining the temperature constant; deformation or strain is measured and plotted as a function of elapsed time. Most tests are the constant load type, which yield information of an engineering nature; constant stress tests are employed to provide a better understanding of the mechanisms of creep.

Figure 9.40 is a schematic representation of the typical constant load creep behavior of metals. Upon application of the load there is an instantaneous deformation, as indicated in the figure, which is mostly elastic. The resulting creep curve consists of three regions, each of which has its own distinctive strain–time feature. *Primary* or *transient creep* occurs first, typified by a continuously decreasing creep rate; that is, the slope of the curve diminishes with time. This suggests that the material is experiencing an increase in creep resistance or strain hardening (Section 8.11)—deformation becomes more difficult as the material is strained. For *secondary creep*, sometimes termed *steady-state creep*, the rate is constant; that is, the plot becomes linear. This is often the stage of creep that is of the longest duration. The constancy of creep rate is explained on the basis of a balance between the competing processes of strain hardening and recovery, recovery (Section 8.12) being the process whereby a material becomes softer and retains its ability to experience deformation. Finally, for *tertiary creep*, there is an acceleration of the rate and ultimate failure. This failure is frequently termed *rupture* and results from microstructural and/or metallurgical changes; for example, grain boundary separation, and the formation of internal cracks, cavities, and voids. Also, for tensile loads, a neck may form at some point within the deformation region. These all lead to a decrease in the effective cross-sectional area and an increase in strain rate.

For metallic materials most creep tests are conducted in uniaxial tension using a specimen having the same geometry as for tensile tests (Figure 7.2). On the other hand, uniaxial compression tests are more appropriate for brittle materials; these provide a better measure of the intrinsic creep properties inasmuch as there is no stress amplification and crack propagation, as with tensile loads. Compressive test specimens are usually right cylinders or parallelepipeds having length-to-diameter

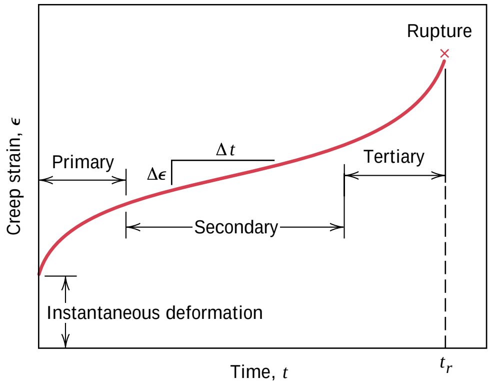

FIGURE 9.40 Typical creep curve of strain versus time at constant stress and constant elevated temperature. The minimum creep rate $\Delta\epsilon/\Delta t$ is the slope of the linear segment in the secondary region. Rupture lifetime t_r is the total time to rupture.

---

[10] ASTM Standard E 139, ''Standard Practice for Conducting Creep, Creep-Rupture, and Stress-Rupture Tests of Metallic Materials.''

ratios ranging from about 2 to 4. For most materials creep properties are virtually independent of loading direction.

Possibly the most important parameter from a creep test is the slope of the secondary portion of the creep curve ($\Delta\epsilon/\Delta t$ in Figure 9.40); this is often called the minimum or *steady-state creep rate* $\dot{\epsilon}_s$. It is the engineering design parameter that is considered for long-life applications, such as a nuclear power plant component that is scheduled to operate for several decades, and when failure or too much strain is not an option. On the other hand, for many relatively short-life creep situations (e.g., turbine blades in military aircraft and rocket motor nozzles), *time to rupture*, or the *rupture lifetime* t_r, is the dominant design consideration; it is also indicated in Figure 9.40. Of course, for its determination, creep tests must be conducted to the point of failure; these are termed *creep rupture* tests. Thus, a knowledge of these creep characteristics of a material allows the design engineer to ascertain its suitability for a specific application.

9.17a STRESS AND TEMPERATURE EFFECTS [DETAILED VERSION (CD-ROM)]

9.17b STRESS AND TEMPERATURE EFFECTS (CONCISE VERSION)

Both temperature and the level of the applied stress influence the creep characteristics (Figure 9.41). At a temperature substantially below $0.4T_m$, and after the initial deformation, the strain is virtually independent of time. With either increasing stress or temperature, the following will be noted: (1) the instantaneous strain at the time of stress application increases; (2) the steady-state creep rate is increased; and (3) the rupture lifetime is diminished.

The results of creep rupture tests are most commonly presented as the logarithm of stress versus the logarithm of rupture lifetime. Figure 9.42 is one such plot for a nickel alloy in which a linear relationship can be seen to exist at each temperature. For some alloys and over relatively large stress ranges, nonlinearity in these curves is observed.

Both temperature and stress effects on the steady-state creep rate are represented graphically as logarithm of stress versus logarithm of $\dot{\epsilon}_s$ for tests conducted

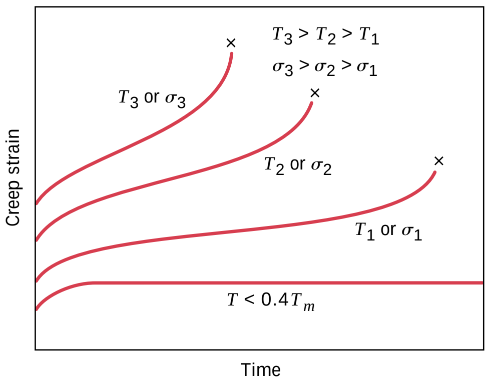

FIGURE 9.41 Influence of stress σ and temperature T on creep behavior.

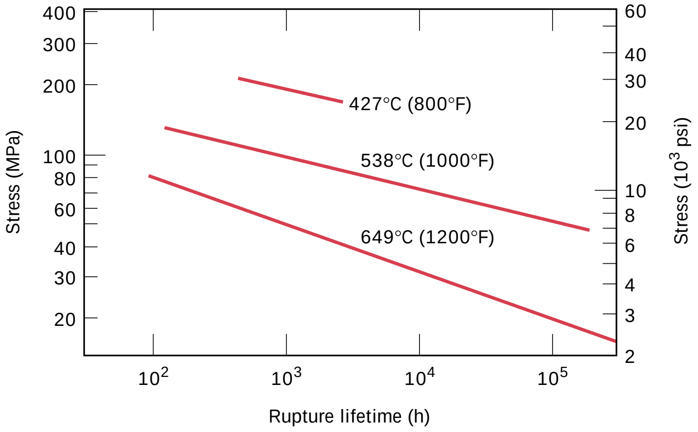

FIGURE 9.42 Stress (logarithmic scale) versus rupture lifetime (logarithmic scale) for a low carbon–nickel alloy at three temperatures. (From *Metals Handbook: Properties and Selection: Stainless Steels, Tool Materials and Special-Purpose Metals*, Vol. 3, 9th edition, D. Benjamin, Senior Editor, American Society for Metals, 1980, p. 130.)

at a variety of temperatures. Figure 9.43 shows data that were collected at three temperatures for the same nickel alloy. Clearly, a straight line segment is drawn at each temperature.

9.18 DATA EXTRAPOLATION METHODS (CD-ROM)

9.19 ALLOYS FOR HIGH-TEMPERATURE USE

There are several factors that affect the creep characteristics of metals. These include melting temperature, elastic modulus, and grain size. In general, the higher the melting temperature, the greater the elastic modulus, and the larger the grain

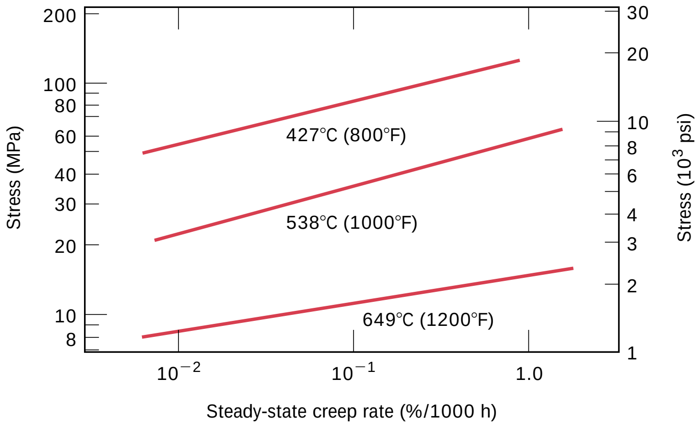

FIGURE 9.43 Stress (logarithmic scale) versus steady-state creep rate (logarithmic scale) for a low carbon–nickel alloy at three temperatures. (From *Metals Handbook: Properties and Selection: Stainless Steels, Tool Materials and Special-Purpose Metals*, Vol. 3, 9th edition, D. Benjamin, Senior Editor, American Society for Metals, 1980, p. 131.)

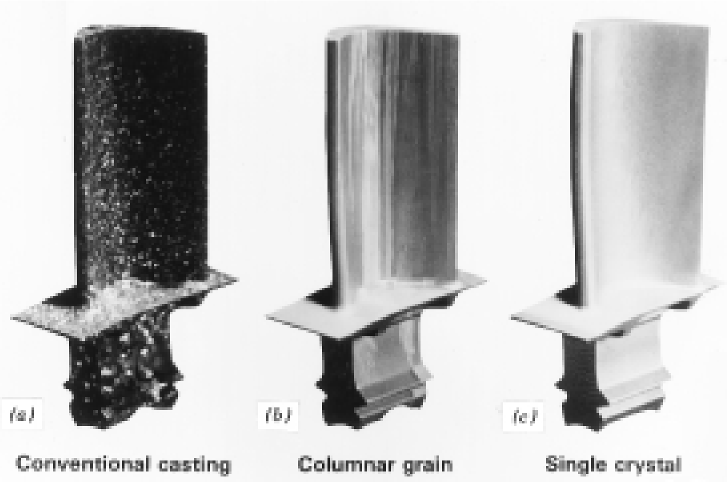

Figure 9.45 (*a*) Polycrystalline turbine blade that was produced by a conventional casting technique. High-temperature creep resistance is improved as a result of an oriented columnar grain structure (*b*) produced by a sophisticated directional solidification technique. Creep resistance is further enhanced when single-crystal blades (*c*) are used. (Courtesy of Pratt & Whitney.)

size, the better is a material's resistance to creep. Relative to grain size, smaller grains permit more grain-boundary sliding, which results in higher creep rates. This effect may be contrasted to the influence of grain size on the mechanical behavior at low temperatures [i.e., increase in both strength (Section 8.9) and toughness (Section 9.8)].

Stainless steels (Section 13.2), the refractory metals and the superalloys (Section 13.3) are especially resilient to creep and are commonly employed in high-temperature service applications. The creep resistance of the cobalt and nickel superalloys is enhanced by solid-solution alloying, and also by the addition of a dispersed phase which is virtually insoluble in the matrix. In addition, advanced processing techniques have been utilized; one such technique is directional solidification, which produces either highly elongated grains or single-crystal components (Figure 9.45). Another is the controlled unidirectional solidification of alloys having specially designed compositions wherein two-phase composites result.

9.20 CREEP IN CERAMIC AND POLYMERIC MATERIALS

Ceramic materials often experience creep deformation as a result of exposure to stresses (usually compressive) at elevated temperatures. In general, the time-deformation creep behavior of ceramics is similar to that of metals (Figure 9.40); however, creep occurs at higher temperatures in ceramics.

Viscoelastic creep is the term used to denote the creep phenomenon in polymeric materials. {It is one of the topics of discussion in Section 7.15.}

SUMMARY

Fracture, in response to tensile loading and at relatively low temperatures, may occur by ductile and brittle modes, both of which involve the formation and propagation of cracks. For ductile fracture, evidence will exist of gross plastic deformation at the fracture surface. In tension, highly ductile metals will neck down to essentially a point fracture; cup-and-cone mating fracture surfaces result for moderate ductility. {Microscopically, dimples (spherical and parabolic) are produced.} Cracks in ductile materials are said to be stable (i.e., resist extension without an increase in applied stress); and inasmuch as fracture is noncatastrophic, this fracture mode is almost always preferred.

For brittle fracture, cracks are unstable, and the fracture surface is relatively flat and perpendicular to the direction of the applied tensile load. Chevron and ridgelike patterns are possible, which indicate the direction of crack propagation. Transgranular (through-grain) and intergranular (between-grain) fractures are found in brittle polycrystalline materials.

The discipline of fracture mechanics allows for a better understanding of the fracture process and provides for structural design wherein the probability of failure is minimized. The significant discrepancy between actual and theoretical fracture strengths of brittle materials is explained by the existence of small flaws that are capable of amplifying an applied tensile stress in their vicinity, leading ultimately to crack formation. Stress amplification is greatest for long flaws that have small tip radii of curvature. Fracture ensues when the theoretical cohesive strength is exceeded at the tip of one of these flaws. Consideration of elastic strain and crack surface energies gives rise to an expression for a crack propagation critical stress in brittle materials; this parameter is a function of elastic modulus, specific surface energy, and crack length.

{The stress distributions in front of an advancing crack may be expressed in terms of position (as radial and angular coordinates) as well as stress intensity factor.} The critical value of the stress intensity factor (i.e., that at which fracture occurs) is termed the fracture toughness, which is related to stress level, crack length, and a geometrical factor. The fracture toughness of a material is indicative of its resistance to brittle fracture when a crack is present. It depends on specimen thickness, and, for relatively thick specimens (i.e., conditions of plane strain), is termed the plane strain fracture toughness. This parameter is the one normally cited for design purposes; its value is relatively large for ductile materials (and small for brittle ones), and is a function of microstructure, strain rate, and temperature. With regard to designing against the possibility of fracture, consideration must be given to material (its fracture toughness), the stress level, and the flaw size detection limit.

At room temperature, virtually all ceramics are brittle. Microcracks, the presence of which is very difficult to control, result in amplification of applied tensile stresses and account for relatively low fracture strengths (flexural strengths). This amplification does not occur with compressive loads, and, consequently, ceramics are stronger in compression.

Fracture strengths of polymeric materials are also low relative to metals. Both brittle and ductile fracture modes are possible, and some thermoplastic materials experience a ductile-to-brittle transition with a lowering of temperature, an increase in strain rate, and/or an alteration of specimen thickness or geometry. In some glassy thermoplastics, the crack formation process may be preceded by crazing; crazing can lead to an increase in ductility and toughness of the material.

Qualitatively, the fracture behavior of materials may be determined using Charpy and Izod impact testing techniques; impact energy (or notch toughness) is measured for specimens into which a V-shaped notch has been machined. On the basis of the temperature dependence of this impact energy (or appearance of the fracture surface), it is possible to ascertain whether or not a material experiences a ductile-to-brittle transition and the temperature range over which such a transition occurs. Metal alloys having BCC and HCP crystal structures experience this transition, and, for structural applications, should be used at temperatures in excess of this transition range.

Fatigue is a common type of catastrophic failure wherein the applied stress level fluctuates with time. Test data are plotted as stress versus the logarithm of the number of cycles to failure. For many materials, the number of cycles to failure increases continuously with diminishing stress. Fatigue strength represents the failure stress for a specified number of cycles. For some steels and titanium alloys, stress ceases to decrease with, and becomes independent of, the number of cycles; fatigue limit is the magnitude of this constant stress level, below which fatigue will not occur even for virtually an infinite number of cycles. Another fatigue property is fatigue life, which, for a specific stress, is the number of cycles to failure.

As a result of significant scatter in measured fatigue data, statistical analyses are performed that lead to specification of fatigue life and limit in terms of probabilities.

The processes of fatigue crack initiation and propagation were discussed. Cracks normally nucleate on the surface of a component at some point of stress concentration. Propagation proceeds in two stages, which are characterized by propagation direction and rate. {The mechanism for the more rapid stage II corresponds to a repetitive plastic blunting and sharpening process at the advancing crack tip.}

Two characteristic fatigue surface features are beachmarks and striations. Beachmarks form on components that experience applied stress interruptions; they normally may be observed with the naked eye. Fatigue striations are of microscopic dimensions, and each is thought to represent the crack tip advance distance over a single load cycle.

{An analytical expression was proposed for fatigue crack propagation rate in terms of the stress intensity range at the crack tip. Integration of the expression yields an equation whereby fatigue life may be estimated.}

Measures that may be taken to extend fatigue life include (1) reducing the mean stress level, (2) eliminating sharp surface discontinuities, (3) improving the surface finish by polishing, (4) imposing surface residual compressive stresses by shot peening, and (5) case hardening by using a carburizing or nitriding process.

{The fatigue behavior of materials may also be affected by the environment. Thermal stresses may be induced in components that are exposed to elevated temperature fluctuations and when thermal expansion and/or contraction is restrained; fatigue for these conditions is termed thermal fatigue. The presence of a chemically active environment may lead to a reduction in fatigue life for corrosion fatigue; small pit crack nucleation sites form on the component surface as a result of chemical reactions.}

The time-dependent plastic deformation of materials subjected to a constant load (or stress) and temperatures greater than about $0.4T_m$ is termed creep. A typical creep curve (strain versus time) will normally exhibit three distinct regions. For transient (or primary) creep, the rate (or slope) diminishes with time. The plot becomes linear (i.e., creep rate is constant) in the steady-state (or secondary) region. And finally, deformation accelerates for tertiary creep, just prior to failure (or rupture). Important design parameters available from such a plot include the steady-state creep rate (slope of the linear region) and rupture lifetime.

Both temperature and applied stress level influence creep behavior. Increasing either of these parameters produces the following effects: (1) an increase in the instantaneous initial deformation, (2) an increase in the steady-state creep rate, and (3) a diminishment of the rupture lifetime. {Analytical expressions were presented which relate $\dot{\epsilon}_s$ to both temperature and stress. Creep mechanisms may be discerned on the basis of steady-state rate stress exponent and creep activation energy values.}

{Extrapolation of creep test data to lower temperature–longer time regimes is possible using the Larson–Miller parameter.}

Metal alloys that are especially resistant to creep have high elastic moduli and melting temperatures; these include the superalloys, the stainless steels, and the refractory metals. Various processing techniques are employed to improve the creep properties of these materials.

The creep phenomenon is also observed in ceramic and polymeric materials.

IMPORTANT TERMS AND CONCEPTS

Brittle fracture
Case hardening
Charpy test
Corrosion fatigue
Creep
Ductile fracture
Ductile-to-brittle transition
Fatigue
Fatigue life
Fatigue limit
Fatigue strength
Fracture mechanics
Fracture toughness
Impact energy
Intergranular fracture
Izod test
Plane strain
Plane strain fracture toughness
Stress intensity factor
Stress raiser
Thermal fatigue
Transgranular fracture

REFERENCES

ASM Handbook, Vol. 11, *Failure Analysis and Prevention,* ASM International, Materials Park, OH, 1986.

ASM Handbook, Vol. 12, *Fractography,* ASM International, Materials Park, OH, 1987.

Boyer, H. E. (Editor), *Atlas of Creep and Stress–Rupture Curves,* ASM International, Materials Park, OH, 1988.

Boyer, H. E. (Editor), *Atlas of Fatigue Curves,* ASM International, Materials Park, OH, 1986.

Colangelo, V. J. and F. A. Heiser, *Analysis of Metallurgical Failures,* 2nd edition, John Wiley & Sons, New York, 1987.

Collins, J. A., *Failure of Materials in Mechanical Design,* 2nd edition, John Wiley & Sons, New York, 1993.

Courtney, T. H., *Mechanical Behavior of Materials,* McGraw-Hill Book Co., New York, 1990.

Davidge, R. W., *Mechanical Behaviour of Ceramics,* Cambridge University Press, Cambridge, 1979. Reprinted by TechBooks, Marietta, OH.

Dieter, G. E., *Mechanical Metallurgy,* 3rd edition, McGraw-Hill Book Co., New York, 1986.

Esaklul, K. A., *Handbook of Case Histories in Failure Analysis,* ASM International, Materials Park, OH, 1992 and 1993. In two volumes.

Fatigue Data Book: Light Structural Alloys, ASM International, Materials Park, OH, 1995.

Hertzberg, R. W., *Deformation and Fracture Mechanics of Engineering Materials,* 4th edition, John Wiley & Sons, New York, 1996.

Murakami, Y. (Editor), *Stress Intensity Factors Handbook,* Pergamon Press, Oxford, 1987. In two volumes.

Tetelman, A. S. and A. J. McEvily, *Fracture of Structural Materials,* John Wiley & Sons, New York, 1967. Reprinted by Books on Demand, Ann Arbor, MI.

Wachtman, J. B., *Mechanical Properties of Ceramics,* John Wiley & Sons, Inc., New York, 1996.

Ward, I. M. and D. W. Hadley, *An Introduction to the Mechanical Properties of Solid Polymers,* John Wiley & Sons, Chichester, UK, 1993.

Wulpi, D. J., *Understanding How Components Fail*, American Society for Metals, Materials Park, OH, 1985.

Young, R. J. and P. Lovell, *Introduction to Polymers*, 2nd edition, Chapman and Hall, London, 1991.

QUESTIONS AND PROBLEMS

Note: To solve those problems having an asterisk (*) by their numbers, consultation of supplementary topics [appearing only on the CD-ROM (and not in print)] will probably be necessary.

9.1 Cite at least two situations in which the possibility of failure is part of the design of a component or product.

9.2* Estimate the theoretical cohesive strengths of the ceramic materials listed in Table 7.1.

9.3 What is the magnitude of the maximum stress that exists at the tip of an internal crack having a radius of curvature of 2.5×10^{-4} mm (10^{-5} in.) and a crack length of 2.5×10^{-2} mm (10^{-3} in.) when a tensile stress of 170 MPa (25,000 psi) is applied?

9.4 Estimate the theoretical fracture strength of a brittle material if it is known that fracture occurs by the propagation of an elliptically shaped surface crack of length 0.25 mm (0.01 in.) and having a tip radius of curvature of 1.2×10^{-3} mm (4.7×10^{-5} in.) when a stress of 1200 MPa (174,000 psi) is applied.

9.5* A specimen of a ceramic material having a modulus of elasticity of 300 GPa (43.5×10^6 psi) is pulled in tension with a stress of 900 MPa (130,000 psi). Will the specimen fail if its ''most severe flaw'' is an internal crack that has a length of 0.30 mm (0.012 in.) and a tip radius of curvature of 5×10^{-4} mm (2×10^{-5} in.)? Why or why not?

9.6 Briefly explain **(a)** why there may be significant scatter in the fracture strength for some given ceramic material, and **(b)** why fracture strength increases with decreasing specimen size.

9.7 The tensile strength of brittle materials may be determined using a variation of Equation 9.1b. Compute the critical crack tip radius for an Al_2O_3 specimen that experiences tensile fracture at an applied stress of 275 MPa (40,000 psi). Assume a critical surface crack length of 2×10^{-3} mm and a theoretical fracture strength of $E/10$, where E is the modulus of elasticity.

9.8 If the specific surface energy for soda-lime glass is 0.30 J/m^2, using data contained in Table 7.1, compute the critical stress required for the propagation of a surface crack of length 0.05 mm.

9.9 A polystyrene component must not fail when a tensile stress of 1.25 MPa (180 psi) is applied. Determine the maximum allowable surface crack length if the surface energy of polystyrene is 0.50 J/m^2 (2.86×10^{-3} in.-lb_f/in.^{2}). Assume a modulus of elasticity of 3.0 GPa (0.435×10^6 psi).

9.10* The parameter K in Equations 9.7a, 9.7b, and 9.7c is a function of the applied nominal stress σ and crack length a as

$$K = \sigma\sqrt{\pi a}$$

Compute the magnitudes of the normal stresses σ_x and σ_y in front of a surface crack of length 2.5 mm (0.10 in.) (as depicted in Figure 9.10) in response to a nominal tensile stress of 75 MPa (10,875 psi) at the following positions:

(a) $r = 0.15$ mm (6.0×10^{-3} in.), $\theta = 30°$

(b) $r = 0.15$ mm (6.0×10^{-3} in.), $\theta = 60°$

(c) $r = 0.75$ mm (3.0×10^{-2} in.), $\theta = 30°$

(d) $r = 0.75$ mm (3.0×10^{-2} in.), $\theta = 60°$

9.11* The parameter K in Equations 9.7a, 9.7b, and 9.7c is defined in the previous problem.

(a) For a surface crack of length 3.0 mm (0.118 in.), determine the radial position at an angle θ of 45° at which the normal stress σ_x is 110 MPa (16,000 psi) when the magnitude of the nominal applied stress is 100 MPa (14,500 psi).

(b) Compute the normal stress σ_y at this same position.

9.12* A portion of a tensile specimen is shown as follows:

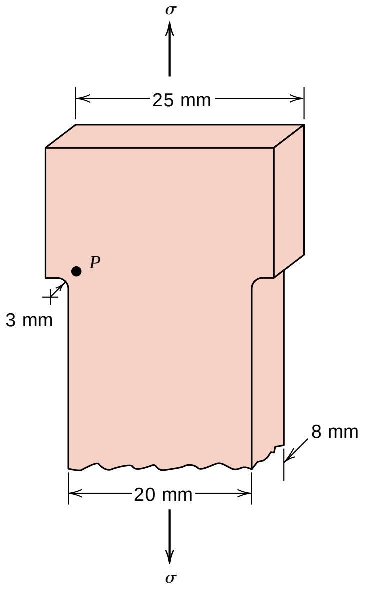

(a) Compute the magnitude of the stress at point *P* when the externally applied stress is 100 MPa (14,500 psi).

(b) How much will the radius of curvature at point *P* have to be increased to reduce this stress by 20%?

9.13* A cylindrical hole 25 mm (1.0 in.) in diameter passes entirely through the thickness of a steel plate 15 mm (0.6 in.) thick, 100 mm (4 in.) wide, and 400 mm (15.75 in.) long (see Figure 9.8*a*).

(a) Calculate the stress at the edge of this hole when a tensile stress of 50 MPa (7250 psi) is applied in a lengthwise direction.

(b) Calculate the stress at the hole edge when the same stress in part (a) is applied in a widthwise direction.

9.14* Cite the significant differences between the stress intensity factor, the plane stress fracture toughness, and the plane strain fracture toughness.

9.15* For each of the metal alloys listed in Table 9.1, compute the minimum component thickness for which the condition of plane strain is valid.

9.16 A specimen of a 4340 steel alloy having a plane strain fracture toughness of 45 MPa $\sqrt{\text{m}}$ (41 ksi $\sqrt{\text{in.}}$) is exposed to a stress of 1000 MPa (145,000 psi). Will this specimen experience fracture if it is known that the largest surface crack is 0.75 mm (0.03 in.) long? Why or why not? Assume that the parameter *Y* has a value of 1.0.

9.17 Some aircraft component is fabricated from an aluminum alloy that has a plane strain fracture toughness of 35 MPa $\sqrt{\text{m}}$ (31.9 ksi $\sqrt{\text{in.}}$). It has been determined that fracture results at a stress of 250 MPa (36,250 psi) when the maximum (or critical) internal crack length is 2.0 mm (0.08 in.). For this same component and alloy, will fracture occur at a stress level of 325 MPa (47,125 psi) when the maximum internal crack length is 1.0 mm (0.04 in.)? Why or why not?

9.18 Suppose that a wing component on an aircraft is fabricated from an aluminum alloy that has a plane strain fracture toughness of 40 MPa $\sqrt{\text{m}}$ (36.4 ksi $\sqrt{\text{in.}}$). It has been determined that fracture results at a stress of 365 MPa (53,000 psi) when the maximum internal crack length is 2.5 mm (0.10 in.). For this same component and alloy, compute the stress level at which fracture will occur for a critical internal crack length of 4.0 mm (0.16 in.).

9.19 A large plate is fabricated from a steel alloy that has a plane strain fracture toughness of 55 MPa $\sqrt{\text{m}}$ (50 ksi $\sqrt{\text{in.}}$). If, during service use, the plate is exposed to a tensile stress of 200 MPa (29,000 psi), determine the minimum length of a surface crack that will lead to fracture. Assume a value of 1.0 for *Y*.

9.20 Calculate the maximum internal crack length allowable for a 7075-T651 aluminum alloy (Table 9.1) component that is loaded to a stress one half of its yield strength. Assume that the value of *Y* is 1.35.

9.21 A structural component in the form of a wide plate is to be fabricated from a steel alloy that has a plane strain fracture toughness of 77 MPa $\sqrt{\text{m}}$ (70.1 ksi $\sqrt{\text{in.}}$) and a yield strength of 1400 MPa (205,000 psi). The flaw size resolution limit of the flaw detection apparatus is 4.0 mm (0.16 in.). If the design stress is one half of the yield strength and the value of Y is 1.0, determine whether or not a critical flaw for this plate is subject to detection.

9.22* A structural component in the shape of a flat plate 12.5 mm (0.5 in.) thick is to be fabricated from a metal alloy for which the yield strength and plane strain fracture toughness values are 350 MPa (50,750 psi) and 33 MPa$\sqrt{\text{m}}$ (30 ksi$\sqrt{\text{in.}}$), respectively; for this particular geometry, the value of Y is 1.75. Assuming a design stress of one half of the yield strength, is it possible to compute the critical length of a surface flaw? If so, determine its length; if this computation is not possible from the given data, then explain why.

9.23 After consultation of other references, write a brief report on one or two nondestructive test techniques that are used to detect and measure internal and/or surface flaws in metal alloys.

9.24 The fracture strength of glass may be increased by etching away a thin surface layer. It is believed that the etching may alter surface crack geometry (i.e., reduce crack length and increase the tip radius). Compute the ratio of the original and etched crack tip radii for an eightfold increase in fracture strength if two-thirds of the crack length is removed.

9.25 For thermoplastic polymers, cite five factors that favor brittle fracture.

9.26 Tabulated below are data that were gathered from a series of Charpy impact tests on a ductile cast iron:

Temperature (°C)	***Impact Energy (J)***
−25	124
−50	123
−75	115
−85	100
−100	73
−110	52
−125	26
−150	9
−175	6

(a) Plot the data as impact energy versus temperature.

(b) Determine a ductile-to-brittle transition temperature as that temperature corresponding to the average of the maximum and minimum impact energies.

(c) Determine a ductile-to-brittle transition temperature as that temperature at which the impact energy is 80 J.

9.27 Tabulated as follows are data that were gathered from a series of Charpy impact tests on a tempered 4140 steel alloy:

Temperature (°C)	***Impact Energy (J)***
100	89.3
75	88.6
50	87.6
25	85.4
0	82.9
−25	78.9
−50	73.1
−65	66.0
−75	59.3
−85	47.9
−100	34.3
−125	29.3
−150	27.1
−175	25.0

(a) Plot the data as impact energy versus temperature.

(b) Determine a ductile-to-brittle transition temperature as that temperature corresponding to the average of the maximum and minimum impact energies.

(c) Determine a ductile-to-brittle transition temperature as that temperature at which the impact energy is 70 J.

9.28 Briefly explain why BCC and HCP metal alloys may experience a ductile-to-brittle transition with decreasing temperature, whereas FCC alloys do not experience such a transition.

9.29 A fatigue test was conducted in which the mean stress was 50 MPa (7250 psi) and the stress amplitude was 225 MPa (32,625 psi).

(a) Compute the maximum and minimum stress levels.

(b) Compute the stress ratio.

(c) Compute the magnitude of the stress range.

9.30 A cylindrical 1045 steel bar (Figure 9.46) is subjected to repeated compression-tension stress cycling along its axis. If the load ampli-

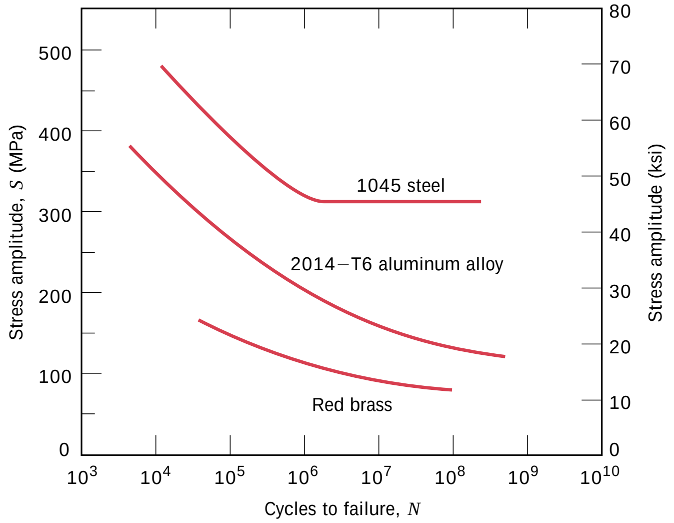

FIGURE 9.46 Stress magnitude S versus the logarithm of the number N of cycles to fatigue failure for red brass, an aluminum alloy, and a plain carbon steel. (Adapted from H. W. Hayden, W. G. Moffatt, and J. Wulff, *The Structure and Properties of Materials,* Vol. III, *Mechanical Behavior,* p. 15. Copyright © 1965 by John Wiley & Sons, New York. Reprinted by permission of John Wiley & Sons, Inc. Also adapted from *ASM Handbook*, Vol. 2, *Properties and Selection: Nonferrous Alloys and Special-Purpose Materials,* 1990. Reprinted by permission of ASM International.)

tude is 22,000 N (4950 lb_f), compute the minimum allowable bar diameter to ensure that fatigue failure will not occur. Assume a factor of safety of 2.0.

9.31 An 8.0 mm (0.31 in.) diameter cylindrical rod fabricated from a red brass alloy (Figure 9.46) is subjected to reversed tension-compression load cycling along its axis. If the maximum tensile and compressive loads are +7500 N (1700 lb_f) and −7500 N (−1700 lb_f), respectively, determine its fatigue life. Assume that the stress plotted in Figure 9.46 is stress amplitude.

9.32 A 12.5 mm (0.50 in.) diameter cylindrical rod fabricated from a 2014-T6 alloy (Figure 9.46) is subjected to a repeated tension-compression load cycling along its axis. Compute the maximum and minimum loads that will be applied to yield a fatigue life of 1.0×10^7 cycles. Assume that the stress plotted on the vertical axis is stress amplitude, and data were taken for a mean stress of 50 MPa (7250 psi).

9.33 The fatigue data for a brass alloy are given as follows:

Stress Amplitude (MPa)	***Cycles to Failure***
310	2×10^5
223	1×10^6
191	3×10^6
168	1×10^7
153	3×10^7
143	1×10^8
134	3×10^8
127	1×10^9

(a) Make an S–N plot (stress amplitude versus logarithm cycles to failure) using these data.

(b) Determine the fatigue strength at 5×10^5 cycles.

(c) Determine the fatigue life for 200 MPa.

9.34 Suppose that the fatigue data for the brass alloy in Problem 9.33 were taken from torsional tests, and that a shaft of this alloy is to be used for a coupling that is attached to an electric motor operating at 1500 rpm. Give the maximum torsional stress amplitude possible for each of the following lifetimes of the coupling: **(a)** 1 year, **(b)** 1 month, **(c)** 1 day, and **(d)** 2 hours.

9.35 The fatigue data for a ductile cast iron are given as follows:

Stress Amplitude [MPa (ksi)]	***Cycles to Failure***
248 (36.0)	1×10^5
236 (34.2)	3×10^5
224 (32.5)	1×10^6
213 (30.9)	3×10^6
201 (29.1)	1×10^7
193 (28.0)	3×10^7
193 (28.0)	1×10^8
193 (28.0)	3×10^8

(a) Make an S–N plot (stress amplitude versus logarithm cycles to failure) using the data.

(b) What is the fatigue limit for this alloy?

(c) Determine fatigue lifetimes at stress amplitudes of 230 MPa (33,500 psi) and 175 MPa (25,000 psi).

(d) Estimate fatigue strengths at 2×10^5 and 6×10^6 cycles.

9.36 Suppose that the fatigue data for the cast iron in Problem 9.35 were taken for bending-rotating tests, and that a rod of this alloy is to be used for an automobile axle that rotates at an average rotational velocity of 750 revolutions per minute. Give maximum lifetimes of continuous driving that are allowable for the following stress levels: **(a)** 250 MPa (36,250 psi), **(b)** 215 MPa (31,000 psi), **(c)** 200 MPa (29,000 psi), and **(d)** 150 MPa (21,750 psi).

9.37 Three identical fatigue specimens (denoted A, B, and C) are fabricated from a nonferrous alloy. Each is subjected to one of the maximum-minimum stress cycles listed below; the frequency is the same for all three tests.

Specimen	$\sigma_{\max}$ ***(MPa)***	$\sigma_{\min}$ ***(MPa)***
A	+450	−350
B	+400	−300
C	+340	−340

(a) Rank the fatigue lifetimes of these three specimens from the longest to the shortest.

(b) Now justify this ranking using a schematic S–N plot.

9.38 **(a)** Compare the fatigue limits for polystyrene (Figure 9.27) and the cast iron for which fatigue data are given in Problem 9.35.

(b) Compare the fatigue strengths at 10^6 cycles for polyethylene terephthalate (PET, Figure 9.27) and red brass (Figure 9.46).

9.39 Cite five factors that may lead to scatter in fatigue life data.

9.40 Make a schematic sketch of the fatigue behavior for some metal for which the stress ratio R has a value of $+1$.

9.41 Using Equations 9.23 and 9.24, demonstrate that increasing the value of the stress ratio R produces a decrease in stress amplitude σ_a.

9.42 Surfaces for some steel specimens that have failed by fatigue have a bright crystalline or grainy appearance. Laymen may explain the failure by saying that the metal crystallized while in service. Offer a criticism for this explanation.

9.43 Briefly explain the difference between fatigue striations and beachmarks both in terms of **(a)** size and **(b)** origin.

9.44 List four measures that may be taken to increase the resistance to fatigue of a metal alloy.

9.45 Give the approximate temperature at which creep deformation becomes an important consideration for each of the following metals: nickel, copper, iron, tungsten, lead, and aluminum.

9.46 Superimpose on the same strain-versus-time plot schematic creep curves for both constant tensile stress and constant load, and explain the differences in behavior.

9.47 The following creep data were taken on an aluminum alloy at 400°C (750°F) and a constant stress of 25 MPa (3660 psi). Plot the data as strain versus time, then determine the steady-state or minimum creep rate. *Note:* The initial and instantaneous strain is not included.

Time (min)	Strain	Time (min)	Strain
0	0.000	16	0.135
2	0.025	18	0.153
4	0.043	20	0.172
6	0.065	22	0.193
8	0.078	24	0.218
10	0.092	26	0.255
12	0.109	28	0.307
14	0.120	30	0.368

9.48 A specimen 750 mm (30 in.) long of a low carbon–nickel alloy (Figure 9.43) is to be exposed to a tensile stress of 40 MPa (5800 psi) at 538°C (1000°F). Determine its elongation after 5000 h. Assume that the total of both instantaneous and primary creep elongations is 1.5 mm (0.06 in.).

9.49 For a cylindrical low carbon–nickel alloy specimen (Figure 9.43) originally 10 mm (0.40 in.) in diameter and 500 mm (20 in.) long, what tensile load is necessary to produce a total elongation of 3.2 mm (0.13 in.) after 10,000 h at 427°C (800°F)? Assume that the sum of instantaneous and primary creep elongations is 0.8 mm (0.03 in.).

9.50 If a component fabricated from a low carbon–nickel alloy (Figure 9.42) is to be exposed to a tensile stress of 60 MPa (8700 psi) at 538°C (1000°F), estimate its rupture lifetime.

9.51 A cylindrical component constructed from a low carbon–nickel alloy (Figure 9.42) has a diameter of 12 mm (0.50 in.). Determine the maximum load that may be applied for it to survive 500 h at 649°C (1200°F).

9.52* From Equation 9.33, if the logarithm of $\dot{\epsilon}_s$ is plotted versus the logarithm of σ, then a straight line should result, the slope of which is the stress exponent n. Using Figure 9.43, determine the value of n for the low carbon–nickel alloy at each of the three temperatures.

9.53* **(a)** Estimate the activation energy for creep (i.e., Q_c in Equation 9.34) for the low carbon–nickel alloy having the steady-state creep behavior shown in Figure 9.43. Use data taken at a stress level of 55 MPa (8000 psi) and temperatures of 427°C and 538°C. Assume that the stress exponent n is independent of temperature. **(b)** Estimate $\dot{\epsilon}_s$ at 649°C (922 K).

9.54* Steady-state creep rate data are given below for nickel at 1000°C (1273 K):

$\dot{\epsilon}_s$ (s^{-1})	σ[MPa (psi)]
10^{-4}	15 (2175)
10^{-6}	4.5 (650)

If it is known that the activation energy for creep is 272,000 J/mol, compute the steady-state creep rate at a temperature of 850°C (1123 K) and a stress level of 25 MPa (3625 psi).

9.55* Steady-state creep data taken for a stainless steel at a stress level of 70 MPa (10,000 psi) are given as follows:

$\dot{\epsilon}_s$ (s^{-1})	T(K)
1×10^{-5}	977
2.5×10^{-3}	1089

If it is known that the value of the stress exponent n for this alloy is 7.0, compute the steady-state creep rate at 1250 K and a stress level of 50 MPa (7250 psi).

9.56 Cite three metallurgical/processing techniques that are employed to enhance the creep resistance of metal alloys.

Design Problems

9.D1* Consider a flat plate of width 90 mm (3.5 in.) that contains a centrally positioned, through-thickness crack (Figure 9.12) of length (i.e., $2a$) 20 mm (0.8 in.). Determine the minimum plane strain fracture toughness necessary to ensure that fracture will not occur for a design stress of 375 MPa (54,400 psi). The $\pi a/W$ ratio is in radians.

9.D2* A flat plate of some metal alloy contains a centrally positioned, through-thickness crack (Figure 9.12). Determine the critical crack length if the plane strain fracture toughness of the alloy is 38 MPa $\sqrt{\text{m}}$ (34.6 ksi $\sqrt{\text{in.}}$), the plate width is 50 mm (2 in.), and the design stress is 300 MPa (43,500 psi). The $\pi a/W$ ratio is in radians.

9.D3* Consider a steel plate having a through-thickness edge crack similar to that shown in Figure 9.13*a*. If it is known that the minimum crack length subject to detection is 2 mm (0.08 in.), determine the minimum allowable plate width assuming a plane strain fracture toughness of 80 MPa$\sqrt{\text{m}}$ (72.8 ksi$\sqrt{\text{in.}}$), a yield strength of 825 MPa (125,000 psi), and that the plate is to be loaded to one half of its yield strength.

9.D4* Consider a steel plate having a through-thickness edge crack similar to that shown in Figure 9.13*a*; the plate width (W) is 75 mm (3 in.), and its thickness (B) is 12.0 mm (0.50 in.). Furthermore, plane strain fracture toughness and yield strength values for this material are 80 MPa $\sqrt{\text{m}}$ (72.8 ksi$\sqrt{\text{in.}}$) and 1200 MPa (175,000 psi), respectively. If the plate is to be loaded to a stress of 300 MPa (43,500 psi), would you expect failure to occur if the crack length a is 15 mm (0.60 in.)? Why or why not?

9.D5* A small and thin flat plate of a brittle material having a through-thickness surface crack is to be loaded in the manner of Figure 9.13*c*; the K_{Ic} value for this material is 0.45 MPa$\sqrt{\text{m}}$ (0.41 ksi$\sqrt{\text{in.}}$). For a crack length of 0.25 mm (0.01 in.), determine the maximum load that may be applied without failure for B = 4 mm (0.16 in.), S = 8 mm (0.31 in.), and W = 1 mm (0.04 in.). Assume that the crack is located at the $S/2$ position.

9.D6 **(a)** For the thin-walled spherical tank discussed in Design Example 9.1, on the basis of critical crack size criterion [as addressed in part (a)], rank the following polymers from longest to shortest critical crack length: nylon 6,6 (50% relative humidity), polycarbonate, polyethylene terephthalate, and polymethyl methacrylate. Comment on the magnitude range of the computed values used in the ranking relative to those tabulated for metal alloys as provided in Table 9.2. For these computations, use data contained in Tables B.4 and B.5 in Appendix B.

(b) Now rank these same four polymers relative to maximum allowable pressure according to the leak-before-break criterion, as described in the (b) portion of Design Example 9.1. As above, comment on these values in relation to those for the metal alloys that are tabulated in Table 9.3.

9.D7* Consider a flat plate of some metal alloy that is to be exposed to repeated tensile-compressive cycling in which the mean stress is 25 MPa. If the initial and critical surface crack lengths are 0.15 and 4.5 mm, respectively, and the values of m and A are 3.5 and 2×10^{-14}, respectively (for $\Delta\sigma$ in MPa and a in m), estimate the maximum tensile stress to yield a fatigue life of 2.5×10^{7} cycles. Assume the parameter Y has a value of 1.4, which is independent of crack length.

9.D8* Consider a large, flat plate of a titanium alloy which is to be exposed to reversed tensile-compressive cycles of stress amplitude 100 MPa. If initially the length of the largest surface crack in this specimen is 0.30 mm and the plane strain fracture toughness is 55 MPa$\sqrt{\text{m}}$, whereas the values of m and A are 3.0 and 2×10^{-11}, respectively (for $\Delta\sigma$ in MPa and a in m), estimate the fatigue life of this plate. Assume that the parameter Y has a value of 1.45 which is independent of crack length.

9.D9* Consider a metal component that is exposed to cyclic tensile-compressive stresses. If the fatigue lifetime must be a minimum of 1×10^{7} cycles and it is known that the maximum initial surface crack length is 0.01 in. and the maximum tensile stress is 15,000 psi, compute the critical surface crack length. Assume that Y is independent of crack length and has a value of 1.75, and that m and A have values of 2.5 and 1.5×10^{-18}, respectively, for $\Delta\sigma$ and a in units of psi and in., respectively.

9.D10* Consider a thin metal plate 20 mm wide which contains a centrally positioned, through-thickness crack in the manner shown in Figure 9.12. This plate is to be exposed to reversed tensile-compressive cycles of stress amplitude 125 MPa. If the initial and critical crack lengths are 0.20 and 8.0 mm, respectively, and the values of m and A are 4 and 5×10^{-12}, respectively (for $\Delta\sigma$ in MPa and a in m), estimate the fatigue life of this plate.

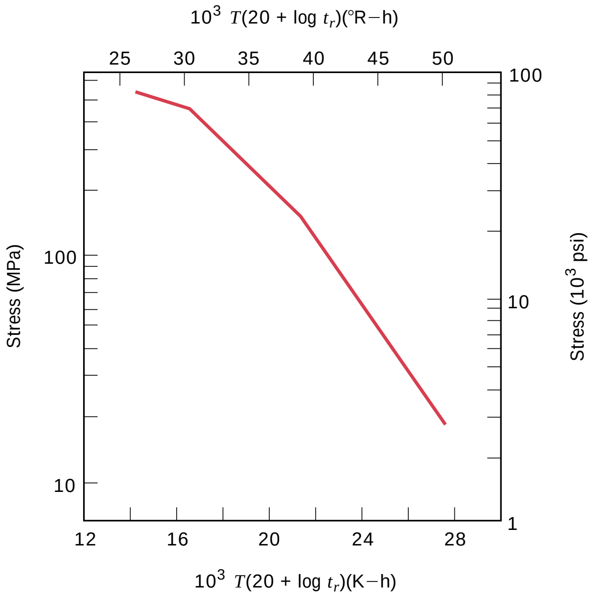

Figure 9.47 Logarithm stress versus the Larson–Miller parameter for an 18-8 Mo stainless steel. (From F. R. Larson and J. Miller, *Trans. ASME*, **74,** 765, 1952. Reprinted by permission of ASME.)

9.D11* For an edge crack in a plate of finite width (Figure 9.13*a*), Y is a function of the crack length–specimen width ratio as

$$Y = \frac{1.1\left(1 - \dfrac{0.2a}{W}\right)}{\left(1 - \dfrac{a}{W}\right)^{3/2}} \qquad (9.36)$$

Now consider a 60 mm wide plate that is exposed to cyclic tensile-compressive stresses (reversed stress cycle) for which $\sigma_{\text{min}} = -135$ MPa. Estimate the fatigue life of this plate if the initial and critical crack lengths are 5 mm and 12 mm, respectively. Assume values of 3.5 and 1.5×10^{-12} for the m and A parameters, respectively, for σ in units of megapascals and a in meters.

9.D12* The spherical tank shown in Figure 9.15 is alternately pressurized and depressurized between atmospheric pressure and a positive pressure p; thus, fatigue failure is a possibility. Utilizing Equation 9.31, derive an expression for the fatigue life N_f in terms of p, the tank radius r and thickness t, and other parameters subject to the following assumptions: Y is independent of crack length, $m \neq 2$, and the original and critical crack lengths are variable parameters.

9.D13* An S-590 iron component (Figure 9.44) must have a creep rupture lifetime of at least 100 days at 500°C (773 K). Compute the maximum allowable stress level.

9.D14* Consider an S-590 iron component (Figure 9.44) that is subjected to a stress of 200 MPa (29,000 psi). At what temperature will the rupture lifetime be 500 h?

9.D15* For an 18-8 Mo stainless steel (Figure 9.47), predict the time to rupture for a component that is subjected to a stress of 80 MPa (11,600 psi) at 700°C (973 K).

9.D16* Consider an 18-8 Mo stainless steel component (Figure 9.47) that is exposed to a temperature of 500°C (773 K). What is the maximum allowable stress level for a rupture lifetime of 5 years? 20 years?

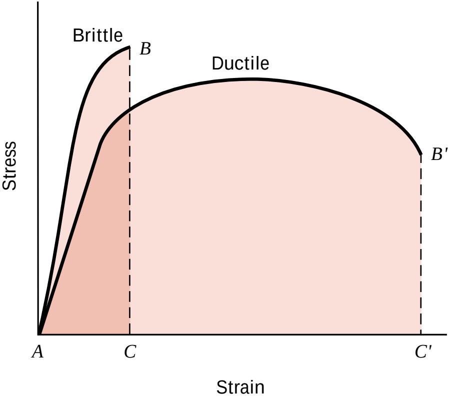

Figure 7.13 Schematic representations of tensile stress–strain behavior for brittle and ductile materials loaded to fracture.

Glossary

A

Abrasive. A hard and wear-resistant material (commonly a ceramic) that is used to wear, grind, or cut away other material.

Absorption. The optical phenomenon whereby the energy of a photon of light is assimilated within a substance, normally by electronic polarization or by an electron excitation event.

Acceptor level. For a semiconductor or insulator, an energy level lying within yet near the bottom of the energy band gap, which may accept electrons from the valence band, leaving behind holes. The level is normally introduced by an impurity atom.

Activation energy (Q). The energy required to initiate a reaction, such as diffusion.

Activation polarization. The condition wherein the rate of an electrochemical reaction is controlled by the one slowest step in a sequence of steps that occur in series.

Addition (or chain reaction) polymerization. The process by which bifunctional monomer units are attached one at a time, in chainlike fashion, to form a linear polymer macromolecule.

Adhesive. A substance that bonds together the surfaces of two other materials (termed adherends).

Age hardening. See **Precipitation hardening.**

Allotropy. The possibility of existence of two or more different crystal structures for a substance (generally an elemental solid).

Alloy. A metallic substance that is composed of two or more elements.

Alloy steel. A ferrous (or iron-based) alloy that contains appreciable concentrations of alloying elements (other than C and residual amounts of Mn, Si, S, and P). These alloying elements are usually added to improve mechanical and corrosion resistance properties.

Alternating copolymer. A copolymer in which two different mer units alternate positions along the molecular chain.

Amorphous. Having a noncrystalline structure.

Anelastic deformation. Time-dependent elastic (nonpermanent) deformation.

Anion. A negatively charged, nonmetallic ion.

Anisotropic. Exhibiting different values of a property in different crystallographic directions.

Annealing. A generic term used to denote a heat treatment wherein the microstructure and, consequently, the properties of a material are altered. ''Annealing'' frequently refers to a heat treatment whereby a previously cold-worked metal is softened by allowing it to recrystallize.

Annealing point (glass). That temperature at which residual stresses in a glass are eliminated within about 15 min; this corresponds to a glass viscosity of about 10^{12} Pa-s (10^{13} P).

Anode. The electrode in an electrochemical cell or galvanic couple that experiences oxidation, or gives up electrons.

Antiferromagnetism. A phenomenon observed in some materials (e.g., MnO); complete magnetic moment cancellation occurs as a result of antiparallel coupling of adjacent atoms or ions. The macroscopic solid possesses no net magnetic moment.

Artificial aging. For precipitation hardening, aging above room temperature.

Atactic. A type of polymer chain configuration wherein side groups are randomly positioned on one side of the chain or the other.

Athermal transformation. A reaction that is not thermally activated, and usually diffusionless, as with the martensitic transformation. Normally, the transformation takes place with great speed (i.e., is independent of time), and the extent of reaction depends on temperature.

Atomic mass unit (amu). A measure of atomic mass; one twelfth of the mass of an atom of C^{12}.

Atomic number (Z). For a chemical element, the number of protons within the atomic nucleus.

Atomic packing factor (APF). The fraction of the volume of a unit cell that is occupied by ''hard sphere'' atoms or ions.

Atomic vibration. The vibration of an atom about its normal position in a substance.

Atomic weight (A). The weighted average of the atomic masses of an atom's naturally occurring isotopes. It may be expressed in terms of atomic mass units (on an atomic basis), or the mass per mole of atoms.

Atom percent (at%). Concentration specification on the basis of the number of moles (or atoms) of a particular element relative to the total number of moles (or atoms) of all elements within an alloy.

Austenite. Face-centered cubic iron; also iron and steel alloys that have the FCC crystal structure.

Austenitizing. Forming austenite by heating a ferrous alloy above its upper critical temperature—to within the austenite phase region from the phase diagram.

B

Bainite. An austenitic transformation product found in some steels and cast irons. It forms at temperatures between those at which pearlite and martensite transformations occur. The microstructure consists of α-ferrite and a fine dispersion of cementite.

Band gap energy (E_g). For semiconductors and insulators, the energies that lie between the valence and conduction bands; for intrinsic materials, electrons are forbidden to have energies within this range.

Bifunctional. Designating monomer units that have two active bonding positions.

Block copolymer. A linear copolymer in which identical mer units are clustered in blocks along the molecular chain.

Body-centered cubic (BCC). A common crystal structure found in some elemental metals. Within the cubic unit cell, atoms are located at corner and cell center positions.

Bohr atomic model. An early atomic model, in which electrons are assumed to revolve around the nucleus in discrete orbitals.

Bohr magneton (μ_B). The most fundamental magnetic moment, of magnitude 9.27×10^{-24} A-m^2.

Boltzmann's constant (k). A thermal energy constant having the value of 1.38×10^{-23} J/atom-K (8.62×10^{-5} eV/atom-K). See also **Gas constant.**

Bonding energy. The energy required to separate two atoms that are chemically bonded to each other. It may be expressed on a per-atom basis, or per mole of atoms.

Bragg's law. A relationship {(Equation 3.10)} which stipulates the condition for diffraction by a set of crystallographic planes.

Branched polymer. A polymer having a molecular structure of secondary chains that extend from the primary main chains.

Brass. A copper-rich copper–zinc alloy.

Brazing. A metal joining technique that uses a molten filler metal alloy having a melting temperature greater than about 425°C (800°F).

Brittle fracture. Fracture that occurs by rapid crack propagation and without appreciable macroscopic deformation.

Bronze. A copper-rich copper–tin alloy; aluminum, silicon, and nickel bronzes are also possible.

Burgers vector (b). A vector that denotes the magnitude and direction of lattice distortion associated with a dislocation.

C

Calcination. A high-temperature reaction whereby one solid material dissociates to form a gas and another solid. It is one step in the production of cement.

Capacitance (C). The charge-storing ability of a capacitor, defined as the magnitude of charge stored on either plate divided by the applied voltage.

Carbon-carbon composite. A composite that is composed of continuous fibers of carbon that are imbedded in a carbon matrix. The matrix was originally a polymer resin that was subsequently pyrolyzed to form carbon.

Carburizing. The process by which the surface carbon concentration of a ferrous alloy is increased by diffusion from the surrounding environment.

Case hardening. Hardening of the outer surface (or ''case'') of a steel component by a carburizing or nitriding process; used to improve wear and fatigue resistance.

Cast iron. Generically, a ferrous alloy, the carbon content of which is greater than the maximum solubility in austenite at the eutectic temperature. Most commercial cast irons contain between 3.0 and 4.5 wt% C, and between 1 and 3 wt% Si.

Cathode. The electrode in an electrochemical cell or galvanic couple at which a reduction reaction occurs; thus the electrode that receives electrons from an external circuit.

Cathodic protection. A means of corrosion prevention whereby electrons are supplied to the structure to be protected from an external source such as another more reactive metal or a dc power supply.

Cation. A positively charged metallic ion.

Cement. A substance (often a ceramic) that by chemical reaction binds particulate aggregates into a cohesive structure. With hydraulic cements the chemical reaction is one of hydration, involving water.

Cementite. Iron carbide (Fe_3C).

Ceramic. A compound of metallic and nonmetallic elements, for which the interatomic bonding is predominantly ionic.

Ceramic-matrix composite (CMC). A composite for which both matrix and dispersed phases are ceramic materials. The dispersed phase is normally added to improve fracture toughness.

Cermet. A composite material consisting of a combination of ceramic and metallic materials. The most common cermets are the cemented carbides, composed of an extremely hard ceramic (e.g., WC, TiC), bonded together by a ductile metal such as cobalt or nickel.

Chain-folded model. For crystalline polymers, a model that describes the structure of platelet crystallites. Molecular alignment is accomplished by chain folding that occurs at the crystallite faces.

Charpy test. One of two tests (see also **Izod test**) that may be used to measure the impact energy or notch toughness of a standard notched specimen. An impact blow is imparted to the specimen by means of a weighted pendulum.

Cis. For polymers, a prefix denoting a type of molecular structure. For some unsaturated carbon chain atoms within a mer unit, a side atom or group may be situated on one side of the chain or directly opposite at a 180° rotation position. In a cis structure, two such side groups within the same mer reside on the same side (e.g., *cis*-isoprene).

Coarse pearlite. Pearlite for which the alternating ferrite and cementite layers are relatively thick.

Coercivity (or coercive field, H_c). The applied magnetic field necessary to reduce to zero the magnetic flux density of a magnetized ferromagnetic or ferrimagnetic material.

Cold working. The plastic deformation of a metal at a temperature below that at which it recrystallizes.

Color. Visual perception that is stimulated by the combination of wavelengths of light that are transmitted to the eye.

Colorant. An additive that imparts a specific color to a polymer.

Component. A chemical constituent (element or compound) of an alloy, which may be used to specify its composition.

Composition (C_i). The relative content of a particular element or constituent (i) within an alloy, usually expressed in weight percent or atom percent.

Concentration. See **Composition.**

Concentration gradient (dC/dx). The slope of the concentration profile at a specific position.

Concentration polarization. The condition wherein the rate of an electrochemical reaction is limited by the rate of diffusion in the solution.

Concentration profile. The curve that results when the concentration of a chemical species is plotted versus position in a material.

Concrete. A composite material consisting of aggregate particles bound together in a solid body by a cement.

Condensation (or step reaction) polymerization. The formation of polymer macromolecules by an intermolecular reaction involving at least two monomer species, usually with the production of a by-product of low molecular weight, such as water.

Conduction band. For electrical insulators and semiconductors, the lowest lying electron energy band that is empty of electrons at 0 K. Conduction electrons are those that have been excited to states within this band.

Conductivity, electrical (σ). The proportionality constant between current density and applied electric field; also a measure of the ease with which a material is capable of conducting an electric current.

Congruent transformation. A transformation of one phase to another of the same composition.

Continuous cooling transformation (CCT) diagram. A plot of temperature versus the logarithm of time for a steel alloy of definite composition. Used to indicate when transformations occur as the initially austenitized material is continuously cooled at a specified rate; in addition, the final microstructure and mechanical characteristics may be predicted.

Coordination number. The number of atomic or ionic nearest neighbors.

Copolymer. A polymer that consists of two or more dissimilar mer units in combination along its molecular chains.

Corrosion. Deteriorative loss of a metal as a result of dissolution environmental reactions.

Corrosion fatigue. A type of failure that results from the simultaneous action of a cyclic stress and chemical attack.

Corrosion penetration rate (CPR). Thickness loss of material per unit of time as a result of corrosion; usually expressed in terms of mils per year or millimeters per year.

Coulombic force. A force between charged particles such as ions; the force is attractive when the particles are of opposite charge.

Covalent bond. A primary interatomic bond that is formed by the sharing of electrons between neighboring atoms.

Creep. The time-dependent permanent deformation that occurs under stress; for most materials it is important only at elevated temperatures.

Crevice corrosion. A form of corrosion that occurs within narrow crevices and under deposits of dirt or corrosion products (i.e., in regions of localized depletion of oxygen in the solution).

Critical resolved shear stress (τ_{crss}). That shear stress, resolved within a slip plane and direction, which is required to initiate slip.

Crosslinked polymer. A polymer in which adjacent linear molecular chains are joined at various positions by covalent bonds.

Crystalline. The state of a solid material characterized by a periodic and repeating three-dimensional array of atoms, ions, or molecules.

Crystallinity. For polymers, the state wherein a periodic and repeating atomic arrangement is achieved by molecular chain alignment.

Crystallite. A region within a crystalline polymer in which all the molecular chains are ordered and aligned.

Crystal structure. For crystalline materials, the manner in which atoms or ions are arrayed in space. It is defined in terms of the unit cell geometry and the atom positions within the unit cell.

Crystal system. A scheme by which crystal structures are classified according to unit cell geometry. This geometry is specified in terms of the relationships between edge lengths and interaxial angles. There are seven different crystal systems.

Curie temperature (T_c). That temperature above which a ferromagnetic or ferrimagnetic material becomes paramagnetic.

D

Defect structure. Relating to the kinds and concentrations of vacancies and interstitials in a ceramic compound.

Degradation. A term used to denote the deteriorative processes that occur with polymeric materials. These processes include swelling, dissolution, and chain scission.

Degree of polymerization. The average number of mer units per polymer chain molecule.

Design stress (σ_d). Product of the calculated stress level (on the basis of estimated maximum load) and a design factor (which has a value greater than unity). Used to protect against unanticipated failure.

Devitrification. The process in which a glass (noncrystalline or vitreous solid) transforms to a crystalline solid.

Diamagnetism. A weak form of induced or nonpermanent magnetism for which the magnetic susceptibility is negative.

Dielectric. Any material that is electrically insulating.

Dielectric constant (ϵ_r). The ratio of the permittivity of a medium to that of a vacuum. Often called the relative dielectric constant or relative permittivity.

Dielectric displacement (D). The magnitude of charge per unit area of capacitor plate.

Dielectric (breakdown) strength. The magnitude of an electric field necessary to cause significant current passage through a dielectric material.

Diffraction (x-ray). Constructive interference of x-ray beams that are scattered by atoms of a crystal.

Diffusion. Mass transport by atomic motion.

Diffusion coefficient (D). The constant of proportionality between the diffusion flux and the concentration gradient in Fick's first law. Its magnitude is indicative of the rate of atomic diffusion.

Diffusion flux (J). The quantity of mass diffusing through and perpendicular to a unit cross-sectional area of material per unit time.

Diode. An electronic device that rectifies an electrical current—i.e., allows current flow in one direction only.

Dipole (electric). A pair of equal yet opposite electrical charges that are separated by a small distance.

Dislocation. A linear crystalline defect around which there is atomic misalignment. Plastic deformation corresponds to the motion of dislocations in response to an applied shear stress. Edge, screw, and mixed dislocations are possible.

Dislocation density. The total dislocation length per unit volume of material; alternately, the number of dislocations that intersect a unit area of a random surface section.

Dislocation line. The line that extends along the end of the extra half-plane of atoms for an edge dislocation, and along the center of the spiral of a screw dislocation.

Dispersed phase. For composites and some two-phase alloys, the discontinuous phase that is surrounded by the matrix phase.

Dispersion strengthening. A means of strengthening materials wherein very small particles (usually less than 0.1 μm) of a hard yet inert phase are uniformly dispersed within a load-bearing matrix phase.

Domain. A volume region of a ferromagnetic or ferrimagnetic material in which all atomic or ionic magnetic moments are aligned in the same direction.

Donor level. For a semiconductor or insulator, an energy level lying within yet near the top of the energy band gap, and from which electrons may be excited into the conduction band. It is normally introduced by an impurity atom.

Doping. The intentional alloying of semiconducting materials with controlled concentrations of donor or acceptor impurities.

Drawing (metals). A forming technique used to fabricate metal wire and tubing. Deformation is accomplished by pulling the material through a die by means of a tensile force applied on the exit side.

Drawing (polymers). A deformation technique wherein polymer fibers are strengthened by elongation.

Driving force. The impetus behind a reaction, such as diffusion, grain growth, or a phase transformation. Usually attendant to the reaction is a reduction in some type of energy (e.g., free energy).

Ductile fracture. A mode of fracture that is attended by extensive gross plastic deformation.

Ductile iron. A cast iron that is alloyed with silicon and a small concentration of magnesium and/or cerium and in which the free graphite exists in nodular form. Sometimes called nodular iron.

Ductile-to-brittle transition. The transition from ductile to brittle behavior with a decrease in temperature exhibited by BCC alloys; the temperature range over which the transition occurs is determined by Charpy and Izod impact tests.

Ductility. A measure of a material's ability to undergo appreciable plastic deformation before fracture; it may be expressed as percent elongation (%EL) or percent reduction in area (%RA) from a tensile test.

E

Edge dislocation. A linear crystalline defect associated with the lattice distortion produced in the vicinity of the end of an extra half-plane of atoms within a crystal. The Burgers vector is perpendicular to the dislocation line.

Elastic deformation. Deformation that is nonpermanent, that is, totally recovered upon release of an applied stress.

Elastic recovery. Nonpermanent deformation that is recovered or regained upon the release of a mechanical stress.

Elastomer. A polymeric material that may experience large and reversible elastic deformations.

Electrical conductivity. See **Conductivity, electrical.**

Electric dipole. See **Dipole (electric).**

Electric field ($\mathscr{E}$). The gradient of voltage.

Electroluminescence. The emission of visible light by a p–n junction across which a forward-biased voltage is applied.

Electrolyte. A solution through which an electric current may be carried by the motion of ions.

Electromotive force (emf) series. A ranking of metallic elements according to their standard electrochemical cell potentials.

Electron configuration. For an atom, the manner in which possible electron states are filled with electrons.

Electronegative. For an atom, having a tendency to accept valence electrons. Also, a term used to describe nonmetallic elements.

Electron energy band. A series of electron energy states that are very closely spaced with respect to energy.

Electroneutrality. The state of having exactly the same numbers of positive and negative electrical charges (ionic and electronic), that is, of being electrically neutral.

Electron state (level). One of a set of discrete, quantized energies that are allowed for electrons. In the atomic case each state is specified by four quantum numbers.

Electron volt (eV). A convenient unit of energy for atomic and subatomic systems. It is equivalent to the energy acquired by an electron when it falls through an electric potential of 1 volt.

Electropositive. For an atom, having a tendency to release valence electrons. Also, a term used to describe metallic elements.

Endurance limit. See **Fatigue limit.**

Energy band gap. See **Band gap energy.**

Engineering strain. See **Strain, engineering.**

Engineering stress. See **Stress, engineering.**

Equilibrium (phase). The state of a system where the phase characteristics remain constant over indefinite time periods. At equilibrium the free energy is a minimum.

Erosion–corrosion. A form of corrosion that arises from the combined action of chemical attack and mechanical wear.

Eutectic phase. One of the two phases found in the eutectic structure.

Eutectic reaction. A reaction wherein, upon cooling, a liquid phase transforms isothermally and reversibly into two intimately mixed solid phases.

Eutectic structure. A two-phase microstructure resulting from the solidification of a liquid having the eutectic composition; the phases exist as lamellae that alternate with one another.

Eutectoid reaction. A reaction wherein, upon cooling, one solid phase transforms isothermally and reversibly into two new solid phases that are intimately mixed.

Excited state. An electron energy state, not normally occupied, to which an electron may be promoted (from a lower energy state) by the absorption of some type of energy (e.g., heat, radiative).

Extrinsic semiconductor. A semiconducting material for which the electrical behavior is determined by impurities.

Extrusion. A forming technique whereby a material is forced, by compression, through a die orifice.

F

Face-centered cubic (FCC). A crystal structure found in some of the common elemental metals. Within the cubic unit cell, atoms are located at all corner and face-centered positions.

Fatigue. Failure, at relatively low stress levels, of structures that are subjected to fluctuating and cyclic stresses.

Fatigue life (N_f). The total number of stress cycles that will cause a fatigue failure at some specified stress amplitude.

Fatigue limit. For fatigue, the maximum stress amplitude level below which a material can endure an essentially infinite number of stress cycles and not fail.

Fatigue strength. The maximum stress level that a material can sustain, without failing, for some specified number of cycles.

Fermi energy (E_f). For a metal, the energy corresponding to the highest filled electron state at 0 K.

Ferrimagnetism. Permanent and large magnetizations found in some ceramic materials. It results from antiparallel spin coupling and incomplete magnetic moment cancellation.

Ferrite (ceramic). Ceramic oxide materials composed of both divalent and trivalent cations (e.g., Fe^{2+} and Fe^{3+}), some of which are ferrimagnetic.

Ferrite (iron). Body-centered cubic iron; also iron and steel alloys that have the BCC crystal structure.

Ferroelectric. A dielectric material that may exhibit polarization in the absence of an electric field.

Ferromagnetism. Permanent and large magnetizations found in some metals (e.g., Fe, Ni, and Co), which result from the parallel alignment of neighboring magnetic moments.

Ferrous alloy. A metal alloy for which iron is the prime constituent.

Fiber. Any polymer, metal, or ceramic that has been drawn into a long and thin filament.

Fiber-reinforced composite. A composite in which the dispersed phase is in the form of a fiber (i.e., a filament that has a large length-to-diameter ratio).

Fiber reinforcement. Strengthening or reinforcement of a relatively weak material by embedding a strong fiber phase within the weak matrix material.

Fick's first law. The diffusion flux is proportional to the concentration gradient. This relationship is employed for steady-state diffusion situations.

Fick's second law. The time rate of change of concentration is proportional to the second derivative of concentration. This relationship is employed in nonsteady-state diffusion situations.

Filler. An inert foreign substance added to a polymer to improve or modify its properties.

Fine pearlite. Pearlite for which the alternating ferrite and cementite layers are relatively thin.

Firing. A high temperature heat treatment that increases the density and strength of a ceramic piece.

Flame retardant. A polymer additive that increases flammability resistance.

Flexural strength (σ_{fs}). Stress at fracture from a bend (or flexure) test.

Fluorescence. Luminescence that occurs for times much less than a second after an electron excitation event.

Foam. A polymer that has been made porous (or spongelike) by the incorporation of gas bubbles.

Forging. Mechanical forming of a metal by heating and hammering.

Forward bias. The conducting bias for a p–n junction rectifier such that electron flow is to the n side of the junction.

Fracture mechanics. A technique of fracture analysis used to determine the stress level at which preexisting cracks of known size will propagate, leading to fracture.

Fracture toughness (K_c). Critical value of the stress intensity factor for which crack extension occurs.

Free electron. An electron that has been excited into an energy state above the Fermi energy (or into the conduction band for semiconductors and insulators) and may participate in the electrical conduction process.

Free energy. A thermodynamic quantity that is a function of both the internal energy and entropy (or randomness) of a system. At equilibrium, the free energy is at a minimum.

Frenkel defect. In an ionic solid, a cation–vacancy and cation–interstitial pair.

Full annealing. For ferrous alloys, austenitizing, followed by cooling slowly to room temperature.

G

Galvanic corrosion. The preferential corrosion of the more chemically active of two metals that are electrically coupled and exposed to an electrolyte.

Galvanic series. A ranking of metals and alloys as to their relative electrochemical reactivity in seawater.

Gas constant (R). Boltzmann's constant per mole of atoms. R = 8.31 J/mol-K (1.987 cal/mol-K).

Gibbs phase rule. For a system at equilibrium, an equation {(Equation 10.16)} that expresses the relationship between the number of phases present and the number of externally controllable variables.

Glass–ceramic. A fine-grained crystalline ceramic material that was formed as a glass and subsequently devitrified (or crystallized).

Glass transition temperature (T_g). That temperature at which, upon cooling, a noncrystalline ceramic or polymer transforms from a supercooled liquid to a rigid glass.

Graft copolymer. A copolymer wherein homopolymer side branches of one mer type are grafted to homopolymer main chains of a different mer.

Grain. An individual crystal in a polycrystalline metal or ceramic.

Grain boundary. The interface separating two adjoining grains having different crystallographic orientations.

Grain growth. The increase in average grain size of a polycrystalline material; for most materials, an elevated-temperature heat treatment is necessary.

Grain size. The average grain diameter as determined from a random cross section.

Gray cast iron. A cast iron alloyed with silicon in which the graphite exists in the form of flakes. A fractured surface appears gray.

Green ceramic body. A ceramic piece, formed as a particulate aggregate, that has been dried but not fired.

Ground state. A normally filled electron energy state from which electron excitation may occur.

H

Hall effect. The phenomenon whereby a force is brought to bear on a moving electron or hole by a magnetic field that is applied perpendicular to the direction of motion. The force direction is perpendicular to both the magnetic field and the particle motion directions.

Hardenability. A measure of the depth to which a specific ferrous alloy may be hardened by the formation of martensite upon quenching from a temperature above the upper critical temperature.

Hard magnetic material. A ferrimagnetic or ferromagnetic material that has large coercive field and remanence values, normally used in permanent magnet applications.

Hardness. The measure of a material's resistance to deformation by surface indentation or by abrasion.

Heat capacity (C_p, C_v). The quantity of heat required to produce a unit temperature rise per mole of material.

Hexagonal close-packed (HCP). A crystal structure found for some metals. The HCP unit cell is of hexagonal geometry and is generated by the stacking of close-packed planes of atoms.

High polymer. A solid polymeric material having a molecular weight greater than about 10,000 g/mol.

High-strength, low-alloy (HSLA) steels. Relatively strong, low-carbon steels, with less than about 10 wt% total of alloying elements.

Hole (electron). For semiconductors and insulators, a vacant electron state in the valence band that behaves as a positive charge carrier in an electric field.

Homopolymer. A polymer having a chain structure in which all mer units are of the same type.

Hot working. Any metal forming operation that is performed above a metal's recrystallization temperature.

Hybrid composite. A composite that is fiber reinforced by two or more types of fibers (e.g., glass and carbon).

Hydrogen bond. A strong secondary interatomic bond that exists between a bound hydrogen atom (its unscreened proton) and the electrons of adjacent atoms.

Hydrogen embrittlement. The loss or reduction of ductility of a metal alloy (often steel) as a result of the diffusion of atomic hydrogen into the material.

Hydroplastic forming. The molding or shaping of clay-based ceramics that have been made plastic and pliable by adding water.

Hypereutectoid alloy. For an alloy system displaying a eutectoid, an alloy for which the concentration of solute is greater than the eutectoid composition.

Hypoeutectoid alloy. For an alloy system displaying a eutectoid, an alloy for which the concentration of solute is less than the eutectoid composition.

Hysteresis (magnetic). The irreversible magnetic flux density-versus-magnetic field strength (B-versus-H) behavior found for ferromagnetic and ferrimagnetic materials; a closed B–H loop is formed upon field reversal.

I

Impact energy (notch toughness). A measure of the energy absorbed during the fracture of a specimen of standard dimensions and geometry when subjected to very rapid (impact) loading. Charpy and Izod impact tests are used to measure this parameter, which is important in assessing the ductile-to-brittle transition behavior of a material.

Imperfection. A deviation from perfection; normally applied to crystalline materials wherein there is a deviation from atomic/molecular order and/or continuity.

Index of refraction (n). The ratio of the velocity of light in a vacuum to the velocity in some medium.

Inhibitor. A chemical substance that, when added in relatively low concentrations, retards a chemical reaction.

Insulator (electrical). A nonmetallic material that has a filled valence band at 0 K and a relatively wide energy band gap. Consequently, the room-temperature electrical conductivity is very low, less than about 10^{-10} $(\Omega\text{-m})^{-1}$.

Integrated circuit. Thousands of electronic circuit elements (transistors, diodes, resistors, capacitors, etc.) incorporated on a very small silicon chip.

Interdiffusion. Diffusion of atoms of one metal into another metal.

Intergranular corrosion. Preferential corrosion along grain boundary regions of polycrystalline materials.

Intergranular fracture. Fracture of polycrystalline materials by crack propagation along grain boundaries.

Intermediate solid solution. A solid solution or phase having a composition range that does not extend to either of the pure components of the system.

Intermetallic compound. A compound of two metals that has a distinct chemical formula. On a phase diagram it appears as an intermediate phase that exists over a very narrow range of compositions.

Interstitial diffusion. A diffusion mechanism whereby atomic motion is from interstitial site to interstitial site.

Interstitial solid solution. A solid solution wherein relatively small solute atoms occupy interstitial positions between the solvent or host atoms.

Intrinsic semiconductor. A semiconductor material for which the electrical behavior is characteristic of the pure material; that is, electrical conductivity depends only on temperature and the band gap energy.

Invariant point. A point on a binary phase diagram at which three phases are in equilibrium.

Ionic bond. A coulombic interatomic bond that exists between two adjacent and oppositely charged ions.

Isomerism. The phenomenon whereby two or more polymer molecules or mer units have the same composition but different structural arrangements and properties.

Isomorphous. Having the same structure. In the phase diagram sense, isomorphicity means having the same crystal structure or complete solid solubility for all compositions (see Figure 10.2*a*).

Isotactic. A type of polymer chain configuration wherein all side groups are positioned on the same side of the chain molecule.

Isothermal. At a constant temperature.

Isothermal transformation (*T*–*T*–*T*) diagram. A plot of temperature versus the logarithm of time for a steel alloy of definite composition. Used to determine when transformations begin and end for an isothermal (constant-temperature) heat treatment of a previously austenitized alloy.

Isotopes. Atoms of the same element that have different atomic masses.

Isotropic. Having identical values of a property in all crystallographic directions.

Izod test. One of two tests (see also **Charpy test**) that may be used to measure the impact energy of a standard notched specimen. An impact blow is imparted to the specimen by a weighted pendulum.

J

Jominy end-quench test. A standardized laboratory test that is used to assess the hardenability of ferrous alloys.

Junction transistor. A semiconducting device composed of appropriately biased *n–p–n* or *p–n–p* junctions, used to amplify an electrical signal.

K

Kinetics. The study of reaction rates and the factors that affect them.

L

Laminar composite. A series of two-dimensional sheets, each having a preferred high-strength direction, fastened one on top of the other at different orientations; strength in the plane of the laminate is highly isotropic.

Large-particle composite. A type of particle-reinforced composite wherein particle-matrix interactions cannot be treated on an atomic level; the particles reinforce the matrix phase.

Laser. Acronym for light amplification by stimulated emission of radiation—a source of light that is coherent.

Lattice. The regular geometrical arrangement of points in crystal space.

Lattice parameters. The combination of unit cell edge lengths and interaxial angles that defines the unit cell geometry.

Lattice strains. Slight displacements of atoms relative to their normal lattice positions, normally imposed by crystalline defects such as dislocations, and interstitial and impurity atoms.

Lever rule. Mathematical expression, such as Equation 10.1b or Equation 10.2b, whereby the relative phase amounts in a two-phase alloy at equilibrium may be computed.

Linear coefficient of thermal expansion. See **Thermal expansion coefficient, linear.**

Linear polymer. A polymer in which each molecule consists of bifunctional mer units joined end to end in a single chain.

Liquid crystal polymer (*LCP*). A group of polymeric materials having extended and rod-shaped molecules, which, structurally, do not fall within traditional liquid, amorphous, crystalline, or semicrystalline classifications. They are used in digital displays and a variety of applications in electronics and medical equipment industries.

Liquidus line. On a binary phase diagram, that line or boundary separating liquid and liquid + solid phase regions. For an alloy, the liquidus temperature is that temperature at which a solid phase first forms under conditions of equilibrium cooling.

Longitudinal direction. The lengthwise dimension. For a rod or fiber, in the direction of the long axis.

Lower critical temperature. For a steel alloy, the temperature below which, under equilibrium conditions, all austenite has transformed to ferrite and cementite phases.

Luminescence. The emission of visible light as a result of electron decay from an excited state.

M

Macromolecule. A huge molecule made up of thousands of atoms.

Magnetic field strength (*H*). The intensity of an externally applied magnetic field.

Magnetic flux density (*B*). The magnetic field produced in a substance by an external magnetic field.

Magnetic induction (*B*). See **Magnetic flux density.**

Magnetic susceptibility (χ_m). The proportionality constant between the magnetization *M* and the magnetic field strength *H*.

Magnetization (*M*). The total magnetic moment per unit volume of material. Also, a measure of the contribution to the magnetic flux by some material within an *H* field.

Malleable cast iron. White cast iron that has been heat treated to convert the cementite into graphite clusters; a relatively ductile cast iron.

Martensite. A metastable iron phase supersaturated in carbon that is the product of a diffusionless (athermal) transformation from austenite.

Matrix phase. The phase in a composite or two-phase alloy microstructure that is continuous or completely surrounds the other (or dispersed) phase.

Matthiessen's rule. The total electrical resistivity of a metal is equal to the sum of temperature-, impurity-, and cold work-dependent contributions.

Melting point (glass). The temperature at which the viscosity of a glass material is 10 Pa-s (100 P).

Mer. The group of atoms that constitutes a polymer chain repeat unit.

Metal. The electropositive elements and alloys based on these elements. The electron band structure of metals is characterized by a partially filled electron band.

Metallic bond. A primary interatomic bond involving the nondirectional sharing of nonlocalized valence electrons (''sea of electrons'') that are mutually shared by all the atoms in the metallic solid.

Metal-matrix composite (*MMC*). A composite material which has a metal or metal alloy as the matrix phase. The dispersed phase may be particulates, fibers, or whiskers that normally are stiffer, stronger, and/or harder than the matrix.

Metastable. Nonequilibrium state that may persist for a very long time.

Microconstituent. An element of the microstructure that has an identifiable and characteristic structure. It may consist of more than one phase such as with pearlite.

Microscopy. The investigation of microstructural elements using some type of microscope.

Microstructure. The structural features of an alloy (e.g., grain and phase structure) that are subject to observation under a microscope.

Miller indices. A set of three integers (four for hexagonal) that designate crystallographic planes, as determined from reciprocals of fractional axial intercepts.

Mixed dislocation. A dislocation that has both edge and screw components.

Mobility (electron, μ_e, and hole, μ_h). The proportionality constant between the carrier drift velocity and applied electric field; also, a measure of the ease of charge carrier motion.

Modulus of elasticity (E). The ratio of stress to strain when deformation is totally elastic; also a measure of the stiffness of a material.

Molarity (M). Concentration in a liquid solution, in terms of the number of moles of a solute dissolved in 10^6 mm^3 (10^3 cm^3) of solution.

Molding (plastics). Shaping a plastic material by forcing it, under pressure and at an elevated temperature, into a mold cavity.

Mole. The quantity of a substance corresponding to 6.023×10^{23} atoms or molecules.

Molecular chemistry (polymer). With regard only to composition, not the structure of a mer.

Molecular structure (polymer). With regard to atomic arrangements within and interconnections between polymer molecules.

Molecular weight. The sum of the atomic weights of all the atoms in a molecule.

Molecule. A group of atoms that are bound together by primary interatomic bonds.

Monomer. A molecule consisting of a single mer.

MOSFET. Metal-oxide-silicon field effect transistor, an integrated circuit element.

N

***n*-Type semiconductor.** A semiconductor for which the predominant charge carriers responsible for electrical conduction are electrons. Normally, donor impurity atoms give rise to the excess electrons.

Natural aging. For precipitation hardening, aging at room temperature.

Network polymer. A polymer composed of trifunctional mer units that form three-dimensional molecules.

Nodular iron. See **Ductile iron.**

Noncrystalline. The solid state wherein there is no long-range atomic order. Sometimes the terms *amorphous*, *glassy*, and *vitreous* are used synonymously.

Nonferrous alloy. A metal alloy for which iron is *not* the prime constituent.

Nonsteady-state diffusion. The diffusion condition for which there is some net accumulation or depletion of diffusing species. The diffusion flux is dependent on time.

Normalizing. For ferrous alloys, austenitizing above the upper critical temperature, then cooling in air. The objective of this heat treatment is to enhance toughness by refining the grain size.

Nucleation. The initial stage in a phase transformation. It is evidenced by the formation of small particles (nuclei) of the new phase, which are capable of growing.

O

Octahedral position. The void space among close-packed, hard sphere atoms or ions for which there are six nearest neighbors. An octahedron (double pyramid) is circumscribed by lines constructed from centers of adjacent spheres.

Ohm's law. The applied voltage is equal to the product of the current and resistance; equivalently, the current density is equal to the product of the conductivity and electric field intensity.

Opaque. Being impervious to the transmission of light as a result of absorption, reflection, and/or scattering of incident light.

Overaging. During precipitation hardening, aging beyond the point at which strength and hardness are at their maxima.

Oxidation. The removal of one or more electrons from an atom, ion, or molecule.

P

Paramagnetism. A relatively weak form of magnetism that results from the independent alignment of atomic dipoles (magnetic) with an applied magnetic field.

Particle-reinforced composite. A composite for which the dispersed phase is equiaxed.

Passivity. The loss of chemical reactivity, under particular environmental conditions, by some active metals and alloys.

Pauli exclusion principle. The postulate that for an individual atom, at most two electrons, which necessarily have opposite spins, can occupy the same state.

Pearlite. A two-phase microstructure found in some steels and cast irons; it results from the transformation of austenite of eutectoid composition and consists of alternating layers (or lamellae) of α-ferrite and cementite.

Periodic table. The arrangement of the chemical elements with increasing atomic number according to the periodic variation in electron structure. Nonmetallic elements are positioned at the far right-hand side of the table.

Peritectic reaction. A reaction wherein, upon cooling, a solid and a liquid phase transform isothermally and reversibly to a solid phase having a different composition.

Permeability (magnetic, μ). The proportionality constant between B and H fields. The value of the permeability of a vacuum (μ_0) is 1.257×10^{-6} H/m.

Permittivity (ϵ). The proportionality constant between the dielectric displacement D and the electric field $\mathscr{E}$. The value of the permittivity ϵ_0 for a vacuum is 8.85×10^{-12} F/m.

Phase. A homogeneous portion of a system that has uniform physical and chemical characteristics.

Phase diagram. A graphical representation of the relationships between environmental constraints (e.g., temperature and sometimes pressure), composition, and regions of phase stability, ordinarily under conditions of equilibrium.

Phase equilibrium. See **Equilibrium (phase).**

Phase transformation. A change in the number and/or character of the phases that constitute the microstructure of an alloy.

Phonon. A single quantum of vibrational or elastic energy.

Phosphorescence. Luminescence that occurs at times greater than on the order of a second after an electron excitation event.

Photoconductivity. Electrical conductivity that results from photon-induced electron excitations in which light is absorbed.

Photomicrograph. The photograph made with a microscope, which records a microstructural image.

Photon. A quantum unit of electromagnetic energy.

Piezoelectric. A dielectric material in which polarization is induced by the application of external forces.

Pilling–Bedworth ratio (P–B ratio). The ratio of metal oxide volume to metal volume; used to predict whether or not a scale that forms will protect a metal from further oxidation.

Pitting. A form of very localized corrosion wherein small pits or holes form, usually in a vertical direction.

Plain carbon steel. A ferrous alloy in which carbon is the prime alloying element.

Planck's constant (h). A universal constant that has a value of 6.63×10^{-34} J-s. The energy of a photon of electromagnetic radiation is the product of h and the radiation frequency.

Plane strain. The condition, important in fracture mechanical analyses, wherein, for tensile loading, there is zero strain in a direction perpendicular to both the stress axis and the direction of crack propagation; this condition is found in thick plates, and the zero-strain direction is perpendicular to the plate surface.

Plane strain fracture toughness (K_{Ic}). The critical value of the stress intensity factor (i.e., at which crack propagation occurs) for the condition of plane strain.

Plastic. A solid material the primary ingredient of which is an organic polymer of high molecular weight; it may also contain additives such as fillers, plasticizers, flame retardants, and the like.

Plastic deformation. Deformation that is permanent or nonrecoverable after release of the applied load. It is accompanied by permanent atomic displacements.

Plasticizer. A low molecular weight polymer additive that enhances flexibility and workability and reduces stiffness and brittleness.

Point defect. A crystalline defect associated with one or, at most, several atomic sites.

Poisson's ratio (ν). For elastic deformation, the negative ratio of lateral and axial strains that result from an applied axial stress.

Polar molecule. A molecule in which there exists a permanent electric dipole moment by virtue of the asymmetrical distribution of positively and negatively charged regions.

Polarization (P). The total electric dipole moment per unit volume of dielectric material. Also, a measure of the contribution to the total dielectric displacement by a dielectric material.

Polarization (corrosion). The displacement of an electrode potential from its equilibrium value as a result of current flow.

Polarization (electronic). For an atom, the displacement of the center of the negatively charged electron cloud relative to the positive nucleus, which is induced by an electric field.

Polarization (ionic). Polarization as a result of the displacement of anions and cations in opposite directions.

Polarization (orientation). Polarization resulting from the alignment (by rotation) of permanent electric dipole moments with an applied electric field.

Polycrystalline. Referring to crystalline materials that are composed of more than one crystal or grain.

Polymer. A solid, nonmetallic (normally organic) compound of high molecular weight the structure of which is composed of small repeat (or mer) units.

Polymer-matrix composite (*PMC*). A composite material for which the matrix is a polymer resin, and having fibers (normally glass, carbon, or aramid) as the dispersed phase.

Polymorphism. The ability of a solid material to exist in more than one form or crystal structure.

Powder metallurgy (P/M). The fabrication of metal pieces having intricate and precise shapes by the compaction of metal powders, followed by a densification heat treatment.

Precipitation hardening. Hardening and strengthening of a metal alloy by extremely small and uniformly dispersed particles that precipitate from a supersaturated solid solution; sometimes also called *age hardening*.

Precipitation heat treatment. A heat treatment used to precipitate a new phase from a supersaturated solid solution. For precipitation hardening, it is termed *artificial aging*.

Prepreg. Continuous fiber reinforcement preimpregnated with a polymer resin that is then partially cured.

Prestressed concrete. Concrete into which compressive stresses have been introduced using steel wires or rods.

Primary bonds. Interatomic bonds that are relatively strong and for which bonding energies are relatively large. Primary bonding types are ionic, covalent, and metallic.

Primary phase. A phase that exists in addition to the eutectic structure.

Principle of combined action. The supposition, often valid, that new properties, better properties, better property combinations, and/or a higher level of properties can be fashioned by the judicious combination of two or more distinct materials.

Process annealing. Annealing of previously cold-worked products (commonly steel alloys in sheet or wire form) below the lower critical (eutectoid) temperature.

Proeutectoid cementite. Primary cementite that exists in addition to pearlite for hypereutectoid steels.

Proeutectoid ferrite. Primary ferrite that exists in addition to pearlite for hypoeutectoid steels.

Property. A material trait expressed in terms of the measured response to a specific imposed stimulus.

Proportional limit. The point on a stress–strain curve at which the straight line proportionality between stress and strain ceases.

***p*-Type semiconductor.** A semiconductor for which the predominant charge carriers responsible for electrical conduction are holes. Normally, acceptor impurity atoms give rise to the excess holes.

Q

Quantum mechanics. A branch of physics that deals with atomic and subatomic systems; it allows only discrete values of energy that are separated from one another. By contrast, for classical mechanics, continuous energy values are permissible.

Quantum numbers. A set of four numbers, the values of which are used to label possible electron states. Three of the quantum numbers are integers, which also specify the size, shape, and spatial orientation of an electron's probability density; the fourth number designates spin orientation.

R

Random copolymer. A polymer in which two different mer units are randomly distributed along the molecular chain.

Recovery. The relief of some of the internal strain energy of a previously cold-worked metal, usually by heat treatment.

Recrystallization. The formation of a new set of strain-free grains within a previously cold-worked material; normally an annealing heat treatment is necessary.

Recrystallization temperature. For a particular alloy, the minimum temperature at which complete recrystallization will occur within approximately one hour.

Rectifying junction. A semiconductor p–n junction that is conductive for a current flow in one direction and highly resistive for the opposite direction.

Reduction. The addition of one or more electrons to an atom, ion, or molecule.

Reflection. Deflection of a light beam at the interface between two media.

Refraction. Bending of a light beam upon passing from one medium into another; the velocity of light differs in the two media.

Refractory. A metal or ceramic that may be exposed to extremely high temperatures without deteriorating rapidly or without melting.

Reinforced concrete. Concrete that is reinforced (or strengthened in tension) by the incorporation of steel rods, wires, or mesh.

Relative magnetic permeability (μ_r). The ratio of the magnetic permeability of some medium to that of a vacuum.

Relaxation frequency. The reciprocal of the minimum reorientation time for an electric dipole within an alternating electric field.

Relaxation modulus [$E_r(t)$]. For viscoelastic polymers, the time-dependent modulus of elasticity. It is determined from stress relaxation measurements as the ratio of stress (taken at some time after the load application—normally 10 s) to strain.

Remanence (remanent induction, B_r). For a ferromagnetic or ferrimagnetic material, the magnitude of residual flux density that remains when a magnetic field is removed.

Residual stress. A stress that persists in a material that is free of external forces or temperature gradients.

Resilience. The capacity of a material to absorb energy when it is elastically deformed.

Resistivity (ρ). The reciprocal of electrical conductivity, and a measure of a material's resistance to the passage of electric current.

Resolved shear stress. An applied tensile or compressive stress resolved into a shear component along a specific plane and direction within that plane.

Reverse bias. The insulating bias for a p–n junction rectifier; electrons flow into the p side of the junction.

Rolling. A metal-forming operation that reduces the thickness of sheet stock; also elongated shapes may be fashioned using grooved circular rolls.

Rule of mixtures. The properties of a multiphase alloy or composite material are a weighted average (usually on the basis of volume) of the properties of the individual constituents.

Rupture. Failure that is accompanied by significant plastic deformation; often associated with creep failure.

S

Sacrificial anode. An active metal or alloy that preferentially corrodes and protects another metal or alloy to which it is electrically coupled.

Safe stress (σ_w). A stress used for design purposes; for ductile metals, it is the yield strength divided by a factor of safety.

Sandwich panel. A type of structural composite consisting of two stiff and strong outer faces that are separated by a lightweight core material.

Saturated. A term describing a carbon atom that participates in only single covalent bonds with four other atoms.

Saturation magnetization, flux density (M_s, B_s). The maximum magnetization (or flux density) for a ferromagnetic or ferrimagnetic material.

Scanning electron microscope (SEM). A microscope that produces an image by using an electron beam that scans the surface of a specimen; an image is produced by reflected electron beams. Examination of surface and/or microstructural features at high magnifications is possible.

Scanning probe microscope (SPM). A microscope that does not produce an image using light radiation. Rather, a very small and sharp probe raster scans across the specimen surface; out-of-surface plane deflections in response to electronic or other interactions with the probe are monitored, from which a topographical map of the specimen surface (on a nanometer scale) is produced.

Schottky defect. In an ionic solid, a defect consisting of a cation–vacancy and anion–vacancy pair.

Scission. A polymer degradation process whereby molecular chain bonds are ruptured by chemical reactions or by exposure to radiation or heat.

Screw dislocation. A linear crystalline defect associated with the lattice distortion created when normally parallel planes are joined together to form a helical ramp. The Burgers vector is parallel to the dislocation line.

Secondary bonds. Interatomic and intermolecular bonds that are relatively weak and for which bonding energies are relatively small. Normally atomic or molecular dipoles are involved. Secondary bonding types are van der Waals and hydrogen.

Selective leaching. A form of corrosion wherein one element or constituent of an alloy is preferentially dissolved.

Self-diffusion. Atomic migration in pure metals.

Self-interstitial. A host atom or ion that is positioned on an interstitial lattice site.

Semiconductor. A nonmetallic material that has a filled valence band at 0 K and a relatively narrow energy band gap. The room temperature electrical conductivity ranges between about 10^{-6} and 10^4 $(\Omega\text{-m})^{-1}$.

Shear. A force applied so as to cause or tend to cause two adjacent parts of the same body to slide relative to each other, in a direction parallel to their plane of contact.

Shear strain (γ). The tangent of the shear angle that results from an applied shear load.

Shear stress (τ). The instantaneous applied shear load divided by the original cross-sectional area across which it is applied.

Single crystal. A crystalline solid for which the periodic and repeated atomic pattern extends throughout its entirety without interruption.

Sintering. Particle coalescence of a powdered aggregate by diffusion that is accomplished by firing at an elevated temperature.

Slip. Plastic deformation as the result of dislocation motion; also, the shear displacement of two adjacent planes of atoms.

Slip casting. A forming technique used for some ceramic materials. A slip, or suspension of solid particles in water, is poured into a porous mold. A solid layer forms on the inside wall as water is absorbed by the mold, leaving a shell (or ultimately a solid piece) having the shape of the mold.

Slip system. The combination of a crystallographic plane and, within that plane, a crystallographic direction along which slip (i.e., dislocation motion) occurs.

Softening point (glass). The maximum temperature at which a glass piece may be handled without permanent deformation; this corresponds to a viscosity of approximately 4×10^6 Pa-s (4×10^7 P).

Soft magnetic material. A ferromagnetic or ferrimagnetic material having a small B versus H hysteresis loop, which may be magnetized and demagnetized with relative ease.

Soldering. A technique for joining metals using a filler metal alloy that has a melting temperature less than about 425°C (800°F). Lead–tin alloys are common solders.

Solid solution. A homogeneous crystalline phase that contains two or more chemical species. Both substitutional and interstitial solid solutions are possible.

Solid-solution strengthening. Hardening and strengthening of metals that result from alloying in which a solid solution is formed. The presence of impurity atoms restricts dislocation mobility.

Solidus line. On a phase diagram, the locus of points at which solidification is complete upon equilibrium cooling, or at which melting begins upon equilibrium heating.

Solubility limit. The maximum concentration of solute that may be added without forming a new phase.

Solute. One component or element of a solution present in a minor concentration. It is dissolved in the solvent.

Solution heat treatment. The process used to form a solid solution by dissolving precipitate particles. Often, the solid solution is supersaturated and metastable at ambient conditions as a result of rapid cooling from an elevated temperature.

Solvent. The component of a solution present in the greatest amount. It is the component that dissolves a solute.

Solvus line. The locus of points on a phase diagram representing the limit of solid solubility as a function of temperature.

Specific heat (c_p, c_v). The heat capacity per unit mass of material.

Specific modulus (specific stiffness). The ratio of elastic modulus to specific gravity for a material.

Specific strength. The ratio of tensile strength to specific gravity for a material.

Spheroidite. Microstructure found in steel alloys consisting of spherelike cementite particles within an α-ferrite matrix. It is produced by an appropriate elevated-temperature heat treatment of pearlite, bainite, or martensite, and is relatively soft.

Spheroidizing. For steels, a heat treatment carried out at a temperature just below the eutectoid in which the spheroidite microstructure is produced.

Spherulite. An aggregate of ribbonlike polymer crystallites radiating from a common center, which crystallites are separated by amorphous regions.

Spinning. The process by which fibers are formed. A multitude of fibers are spun as molten material is forced through many small orifices.

Stabilizer. A polymer additive that counteracts deteriorative processes.

Stainless steel. A steel alloy that is highly resistant to corrosion in a variety of environments. The predominant alloying element is chromium, which must be present in a concentration of at least 11 wt%; other alloy additions, to include nickel and molybdenum, are also possible.

Standard half-cell. An electrochemical cell consisting of a pure metal immersed in a 1*M* aqueous solution of its ions, which is electrically coupled to the standard hydrogen electrode.

Steady-state diffusion. The diffusion condition for which there is no net accumulation or depletion of diffusing species. The diffusion flux is independent of time.

Stereoisomerism. Polymer isomerism in which side groups within mer units are bonded along the molecular chain in the same order, but in different spatial arrangements.

Stoichiometry. For ionic compounds, the state of having exactly the ratio of cations to anions specified by the chemical formula.

Strain, engineering (ϵ). The change in gauge length of a specimen (in the direction of an applied stress) divided by its original gauge length.

Strain hardening. The increase in hardness and strength of a ductile metal as it is plastically deformed below its recrystallization temperature.

Strain point (glass). The maximum temperature at which glass fractures without plastic deformation; this corresponds to a viscosity of about 3×10^{13} Pa-s (3×10^{14} P).

Strain, true. See **True strain.**

Stress concentration. The concentration or amplification of an applied stress at the tip of a notch or small crack.

Stress corrosion (cracking). A form of failure that results from the combined action of a tensile stress and a corrosion environment; it occurs at lower stress levels than are required when the corrosion environment is absent.

Stress, engineering (σ). The instantaneous load applied to a specimen divided by its cross-sectional area before any deformation.

Stress intensity factor (K). A factor used in fracture mechanics to specify the stress intensity at the tip of a crack.

Stress raiser. A small flaw (internal or surface) or a structural discontinuity at which an applied tensile stress will be amplified and from which cracks may propagate.

Stress relief. A heat treatment for the removal of residual stresses.

Stress, true. See **True stress.**

Structural clay products. Ceramic products made principally of clay and used in applications where structural integrity is important (e.g., bricks, tiles, pipes).

Structural composite. A composite the properties of which depend on the geometrical design of the structural elements. Laminar composites and sandwich panels are two subclasses.

Structure. The arrangement of the internal components of matter: electron structure (on a subatomic level), crystal structure (on an atomic level), and microstructure (on a microscopic level).

Substitutional solid solution. A solid solution wherein the solute atoms replace or substitute for the host atoms.

Superconductivity. A phenomenon observed in some materials: the disappearance of the electrical resistivity at temperatures approaching 0 K.

Supercooling. Cooling to below a phase transition temperature without the occurrence of the transformation.

Superheating. Heating to above a phase transition temperature without the occurrence of the transformation.

Syndiotactic. A type of polymer chain configuration in which side groups regularly alternate positions on opposite sides of the chain.

System. Two meanings are possible: (1) a specific body of material that is being considered, and (2) a series of possible alloys consisting of the same components.

T

Temper designation. A letter–digit code used to designate the mechanical and/or thermal treatment to which a metal alloy has been subjected.

Tempered martensite. The microstructural product resulting from a tempering heat treatment of a martensitic steel. The microstructure consists of extremely small and uniformly dispersed cementite particles embedded within a continuous α-ferrite matrix. Toughness and ductility are enhanced significantly by tempering.

Tempering (glass). See **Thermal tempering.**

Tensile strength (*TS*). The maximum engineering stress, in tension, that may be sustained without fracture. Often termed *ultimate* (*tensile*) *strength*.

Terminal solid solution. A solid solution that exists over a composition range extending to either composition extremity of a binary phase diagram.

Tetrahedral position. The void space among close-packed, hard sphere atoms or ions for which there are four nearest neighbors.

Thermal conductivity (*k*). For steady-state heat flow, the proportionality constant between the heat flux and the temperature gradient. Also, a parameter characterizing the ability of a material to conduct heat.

Thermal expansion coefficient, linear (α_l). The fractional change in length divided by the change in temperature.

Thermal fatigue. A type of fatigue failure wherein the cyclic stresses are introduced by fluctuating thermal stresses.

Thermal shock. The fracture of a brittle material as a result of stresses that are introduced by a rapid temperature change.

Thermal stress. A residual stress introduced within a body resulting from a change in temperature.

Thermal tempering. Increasing the strength of a glass piece by the introduction of residual compressive stresses within the outer surface using an appropriate heat treatment.

Thermally activated transformation. A reaction that depends on atomic thermal fluctuations; the atoms having energies greater than an activation energy will spontaneously react or transform. The rate of this type of transformation depends on temperature according to Equation 11.3.

Thermoplastic (polymer). A polymeric material that softens when heated and hardens upon cooling. While in the softened state, articles may be formed by molding or extrusion.

Thermoplastic elastomer (*TPE*). A copolymeric material that exhibits elastomeric behavior yet is thermoplastic in nature. At the ambient temperature, domains of one mer type form at molecular chain ends that act as physical crosslinks.

Thermosetting (polymer). A polymeric material that, once having cured (or hardened) by a chemical reaction, will not soften or melt when subsequently heated.

Tie line. A horizontal line constructed across a two-phase region of a binary phase diagram; its intersections with the phase boundaries on either end represent the equilibrium compositions of the respective phases at the temperature in question.

Time–temperature–transformation (*T–T–T*) diagram. See **Isothermal transformation diagram.**

Toughness. A measure of the amount of energy absorbed by a material as it fractures. Toughness is indicated by the total area under the material's tensile stress–strain curve.

Trans. For polymers, a prefix denoting a type of molecular structure. To some unsaturated carbon chain atoms within a mer unit, a single side atom or group may be situated on one side of the chain, or directly opposite at a 180° rotation position. In a trans structure, two such side groups within the same mer reside on opposite chain sides (e.g., *trans*-isoprene).

Transformation rate. The reciprocal of the time necessary for a reaction to proceed halfway to its completion.

Transgranular fracture. Fracture of polycrystalline materials by crack propagation through the grains.

Translucent. Having the property of transmitting light only diffusely; objects viewed through a translucent medium are not clearly distinguishable.

Transmission electron microscope (TEM). A microscope that produces an image by using electron beams that are transmitted (pass through) the specimen. Examination of internal features at high magnifications is possible.

Transparent. Having the property of transmitting light with relatively little absorption, reflection, and scattering, such that objects viewed through a transparent medium can be distinguished readily.

Transverse direction. A direction that crosses (usually perpendicularly) the longitudinal or lengthwise direction.

Trifunctional mer. Designating mer units that have three active bonding positions.

True strain (ϵ_T). The natural logarithm of the ratio of instantaneous gauge length to original gauge length of a specimen being deformed by a uniaxial force.

True stress (σ_T). The instantaneous applied load divided by the instantaneous cross-sectional area of a specimen.

U

Ultimate (tensile) strength. See **Tensile strength.**

Ultrahigh molecular weight polyethylene (*UHMWPE*). A polyethylene polymer that has an extremely high molecular weight (approximately 4×10^6 g/mol). Distinctive characteristics of this material include high impact and abrasion resistance, and a low coefficient of friction.

Unit cell. The basic structural unit of a crystal structure. It is generally defined in terms of atom (or ion) positions within a parallelepiped volume.

Unsaturated. A term describing carbon atoms that participate in double or triple covalent bonds and, therefore, do not bond to a maximum of four other atoms.

Upper critical temperature. For a steel alloy, the minimum temperature above which, under equilibrium conditions, only austenite is present.

V

Vacancy. A normally occupied lattice site from which an atom or ion is missing.

Vacancy diffusion. The diffusion mechanism wherein net atomic migration is from lattice site to an adjacent vacancy.

Valence band. For solid materials, the electron energy band that contains the valence electrons.

Valence electrons. The electrons in the outermost occupied electron shell, which participate in interatomic bonding.

van der Waals bond. A secondary interatomic bond between adjacent molecular dipoles, which may be permanent or induced.

Viscoelasticity. A type of deformation exhibiting the mechanical characteristics of viscous flow and elastic deformation.

Viscosity (η). The ratio of the magnitude of an applied shear stress to the velocity gradient that it produces; that is, a measure of a noncrystalline material's resistance to permanent deformation.

Vitrification. During firing of a ceramic body, the formation of a liquid phase that upon cooling becomes a glass-bonding matrix.

Vulcanization. Nonreversible chemical reaction involving sulfur or other suitable agent wherein crosslinks are formed between molecular chains in rubber materials. The rubber's modulus of elasticity and strength are enhanced.

W

Wave-mechanical model. Atomic model in which electrons are treated as being wavelike.

Weight percent (wt%). Concentration specification on the basis of weight (or mass) of a particular element relative to the total alloy weight (or mass).

Weld decay. Intergranular corrosion that occurs in some welded stainless steels at regions adjacent to the weld.

Welding. A technique for joining metals in which actual melting of the pieces to be joined occurs in the vicinity of the bond. A filler metal may be used to facilitate the process.

Whisker. A very thin, single crystal of high perfection that has an extremely large length-to-diameter ratio. Whiskers are used as the reinforcing phase in some composites.

White cast iron. A low-silicon and very brittle cast iron, in which the carbon is in combined form as cementite; a fractured surface appears white.

Whiteware. A clay-based ceramic product that becomes white after high-temperature firing; whitewares include porcelain, china, and plumbing sanitary ware.

Working point (glass). The temperature at which a glass is easily deformed, which corresponds to a viscosity of 10^3 Pa-s (10^4 P).

Wrought alloy. A metal alloy that is relatively ductile and amenable to hot working or cold working during fabrication.

Y

Yielding. The onset of plastic deformation.

Yield strength (σ_y). The stress required to produce a very slight yet specified amount of plastic strain; a strain offset of 0.002 is commonly used.

Young's modulus. See **Modulus of elasticity.**

Figure 10.2 (*a*) The copper–nickel phase diagram. (Adapted from *Phase Diagrams of Binary Nickel Alloys*, P. Nash, Editor, 1991. Reprinted by permission of ASM International, Materials Park, OH.) (*b*) A portion of the copper–nickel phase diagram for which compositions and phase amounts are determined at point *B*.

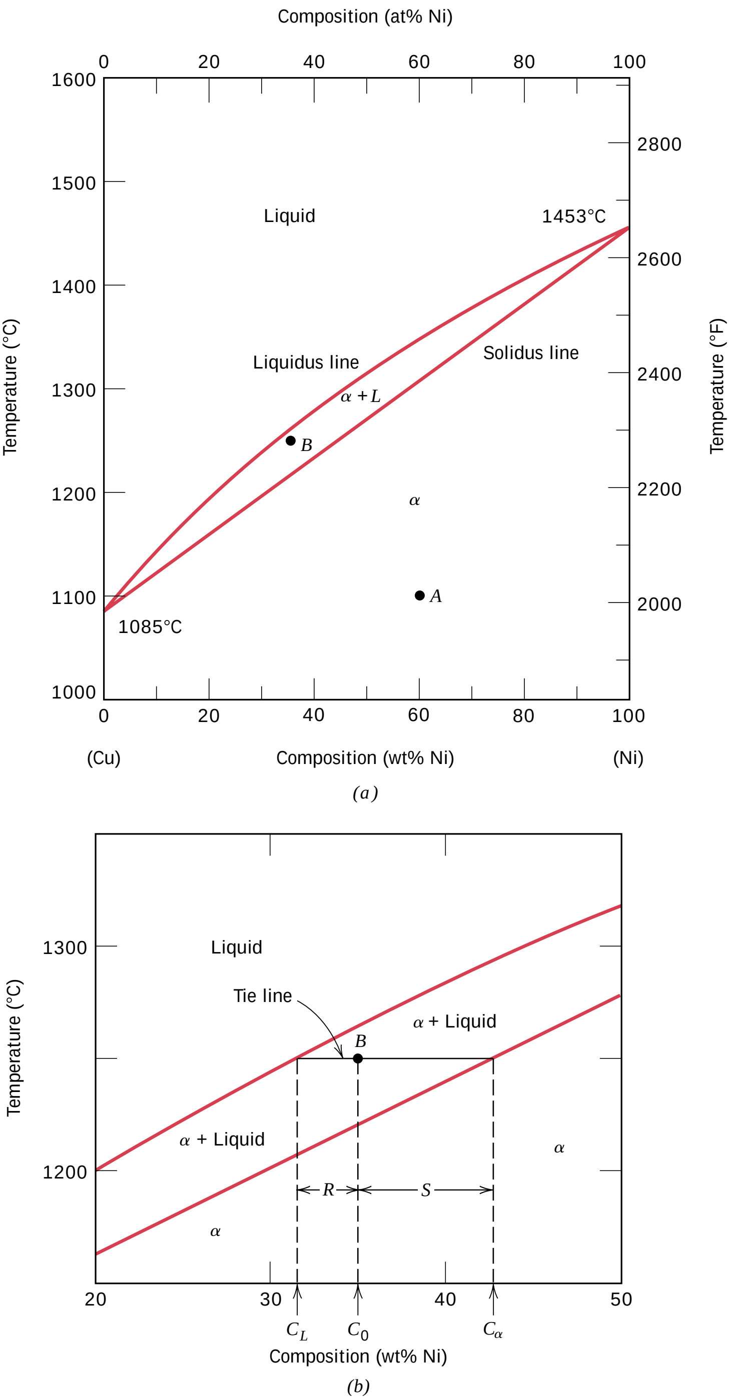

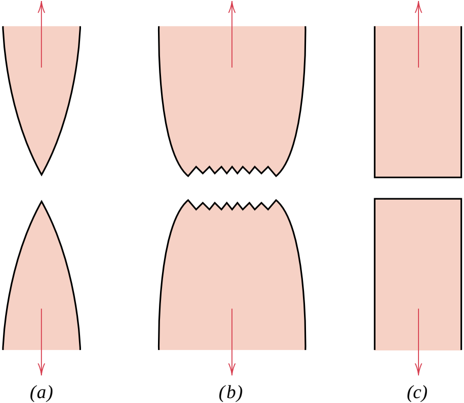

FIGURE 9.1 (*a*) Highly ductile fracture in which the specimen necks down to a point. (*b*) Moderately ductile fracture after some necking. (*c*) Brittle fracture without any plastic deformation.

Chapter 7 / Mechanical Properties

A modern Rockwell hardness tester. (Photograph courtesy of Wilson Instruments Division, Instron Corporation, originator of the Rockwell® Hardness Tester.)

Why Study *Mechanical Properties?*

It is incumbent on engineers to understand how the various mechanical properties are measured and what these properties represent; they may be called upon to design structures/components using predetermined materials such that unacceptable levels of deformation and/or failure will not occur. We demonstrate this procedure with respect to the design of a tensile-testing apparatus in Design Example 7.1.

Learning Objectives

After studying this chapter you should be able to do the following:

1. **Define engineering stress and engineering strain.**
2. **State Hooke's law, and note the conditions under which it is valid.**
3. **Define Poisson's ratio.**
4. **Given an engineering stress–strain diagram, determine (a) the modulus of elasticity, (b) the yield strength (0.002 strain offset), and (c) the tensile strength, and (d) estimate the percent elongation.**
5. **For the tensile deformation of a ductile cylindrical specimen, describe changes in specimen profile to the point of fracture.**
6. **Compute ductility in terms of both percent elongation and percent reduction of area for a material that is loaded in tension to fracture.**
7. **Compute the flexural strengths of ceramic rod specimens that have bent to fracture in three-point loading.**
8. **Make schematic plots of the three characteristic stress–strain behaviors observed for polymeric materials.**
9. **Name the two most common hardness-testing techniques; note two differences between them.**
10. **(a) Name and briefly describe the two different microhardness testing techniques, and (b) cite situations for which these techniques are generally used.**
11. **Compute the working stress for a ductile material.**

7.1 INTRODUCTION

Many materials, when in service, are subjected to forces or loads; examples include the aluminum alloy from which an airplane wing is constructed and the steel in an automobile axle. In such situations it is necessary to know the characteristics of the material and to design the member from which it is made such that any resulting deformation will not be excessive and fracture will not occur. The mechanical behavior of a material reflects the relationship between its response or deformation to an applied load or force. Important mechanical properties are strength, hardness, ductility, and stiffness.

The mechanical properties of materials are ascertained by performing carefully designed laboratory experiments that replicate as nearly as possible the service conditions. Factors to be considered include the nature of the applied load and its duration, as well as the environmental conditions. It is possible for the load to be tensile, compressive, or shear, and its magnitude may be constant with time, or it may fluctuate continuously. Application time may be only a fraction of a second, or it may extend over a period of many years. Service temperature may be an important factor.

Mechanical properties are of concern to a variety of parties (e.g., producers and consumers of materials, research organizations, government agencies) that have differing interests. Consequently, it is imperative that there be some consistency in the manner in which tests are conducted, and in the interpretation of their results. This consistency is accomplished by using standardized testing techniques. Establishment and publication of these standards are often coordinated by professional societies. In the United States the most active organization is the American Society for Testing and Materials (ASTM). Its *Annual Book of ASTM Standards* comprises numerous volumes, which are issued and updated yearly; a large number of these standards relate to mechanical testing techniques. Several of these are referenced by footnote in this and subsequent chapters.

The role of structural engineers is to determine stresses and stress distributions within members that are subjected to well-defined loads. This may be accomplished by experimental testing techniques and/or by theoretical and mathematical stress analyses. These topics are treated in traditional stress analysis and strength of materials texts.

Materials and metallurgical engineers, on the other hand, are concerned with producing and fabricating materials to meet service requirements as predicted by these stress analyses. This necessarily involves an understanding of the relationships between the microstructure (i.e., internal features) of materials and their mechanical properties.

Materials are frequently chosen for structural applications because they have desirable combinations of mechanical characteristics. This chapter discusses the stress–strain behaviors of metals, ceramics, and polymers and the related mechanical properties; it also examines their other important mechanical characteristics. Discussions of the microscopic aspects of deformation mechanisms and methods to strengthen and regulate the mechanical behaviors are deferred to Chapter 8.

7.2 Concepts of Stress and Strain

If a load is static or changes relatively slowly with time and is applied uniformly over a cross section or surface of a member, the mechanical behavior may be ascertained by a simple stress–strain test; these are most commonly conducted for metals at room temperature. There are three principal ways in which a load may be applied: namely, tension, compression, and shear (Figures 7.1*a, b, c*). In engineering practice many loads are torsional rather than pure shear; this type of loading is illustrated in Figure 7.1*d*.

TENSION TESTS[1]

One of the most common mechanical stress–strain tests is performed in *tension.* As will be seen, the tension test can be used to ascertain several mechanical properties of materials that are important in design. A specimen is deformed, usually to fracture, with a gradually increasing tensile load that is applied uniaxially along the long axis of a specimen. A standard tensile specimen is shown in Figure 7.2. Normally, the cross section is circular, but rectangular specimens are also used. During testing, deformation is confined to the narrow center region, which has a uniform cross section along its length. The standard diameter is approximately 12.8 mm (0.5 in.), whereas the reduced section length should be at least four times this diameter; 60 mm ($2\frac{1}{4}$ in.) is common. Gauge length is used in ductility computations, as discussed in Section 7.6; the standard value is 50 mm (2.0 in.). The specimen is mounted by its ends into the holding grips of the testing apparatus (Figure 7.3). The tensile testing machine is designed to elongate the specimen at a constant rate, and to continuously and simultaneously measure the instantaneous applied load (with a load cell) and the resulting elongations (using an extensometer). A stress–strain test typically takes several minutes to perform and is destructive; that is, the test specimen is permanently deformed and usually fractured.

The output of such a tensile test is recorded on a strip chart (or by a computer) as load or force versus elongation. These load–deformation characteristics are dependent on the specimen size. For example, it will require twice the load to produce the same elongation if the cross-sectional area of the specimen is doubled. To minimize these geometrical factors, load and elongation are normalized to the respective parameters of **engineering stress** and **engineering strain.** Engineering

---

[1] ASTM Standards E 8 and E 8M, ‘‘Standard Test Methods for Tension Testing of Metallic Materials.’’

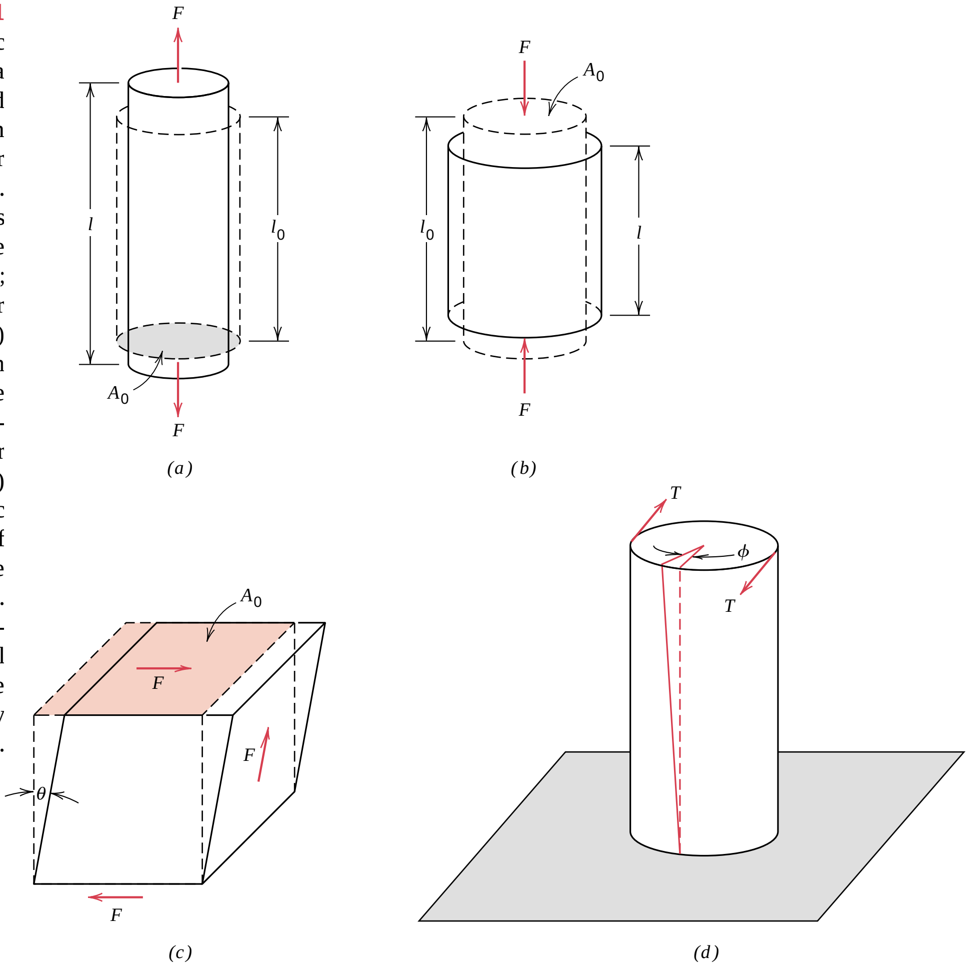
F
A0
l
l0
F
(a)
F
A0
l0
l
F
(b)
A0
F
F
θ
F
(c)
T
ϕ
T
(d)

FIGURE 7.1 (*a*) Schematic illustration of how a tensile load produces an elongation and positive linear strain. Dashed lines represent the shape before deformation; solid lines, after deformation. (*b*) Schematic illustration of how a compressive load produces contraction and a negative linear strain. (*c*) Schematic representation of shear strain γ, where $\gamma = \tan \theta$. (*d*) Schematic representation of torsional deformation (i.e., angle of twist ϕ) produced by an applied torque T.

stress σ is defined by the relationship

$$\sigma = \frac{F}{A_0} \tag{7.1}$$

in which F is the instantaneous load applied perpendicular to the specimen cross section, in units of newtons (N) or pounds force ($\mathrm{lb_f}$), and A_0 is the original cross-sectional area before any load is applied (m^2 or $\mathrm{in.}^2$). The units of engineering

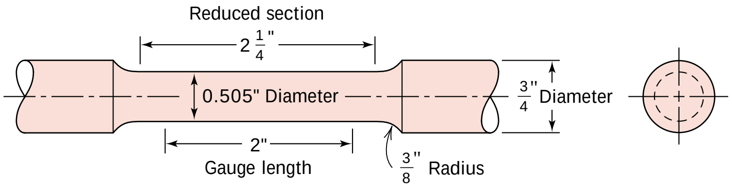
Reduced section
2 1/4"
0.505" Diameter
3/4" Diameter
2"
Gauge length
3/8" Radius

FIGURE 7.2 A standard tensile specimen with circular cross section.

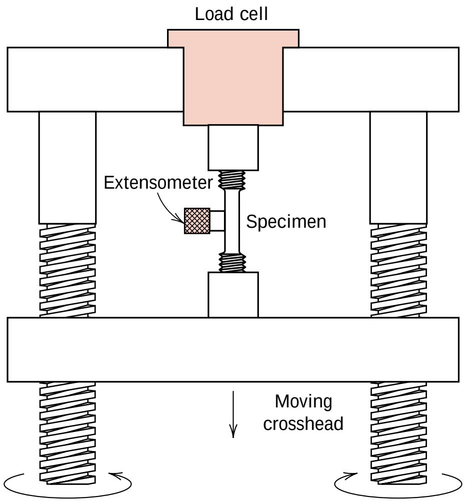

FIGURE 7.3 Schematic representation of the apparatus used to conduct tensile stress–strain tests. The specimen is elongated by the moving crosshead; load cell and extensometer measure, respectively, the magnitude of the applied load and the elongation. (Adapted from H. W. Hayden, W. G. Moffatt, and J. Wulff, *The Structure and Properties of Materials,* Vol. III, *Mechanical Behavior,* p. 2. Copyright © 1965 by John Wiley & Sons, New York. Reprinted by permission of John Wiley & Sons, Inc.)

stress (referred to subsequently as just stress) are megapascals, MPa (SI) (where 1 MPa $= 10^6$ N/m^2), and pounds force per square inch, psi (Customary U.S.).[2]

Engineering strain ϵ is defined according to

$$\epsilon = \frac{l_i - l_0}{l_0} = \frac{\Delta l}{l_0} \tag{7.2}$$

in which l_0 is the original length before any load is applied, and l_i is the instantaneous length. Sometimes the quantity $l_i - l_0$ is denoted as Δl, and is the deformation elongation or change in length at some instant, as referenced to the original length. Engineering strain (subsequently called just strain) is unitless, but meters per meter or inches per inch are often used; the value of strain is obviously independent of the unit system. Sometimes strain is also expressed as a percentage, in which the strain value is multiplied by 100.

COMPRESSION TESTS[3]

Compression stress–strain tests may be conducted if in-service forces are of this type. A compression test is conducted in a manner similar to the tensile test, except that the force is compressive and the specimen contracts along the direction of the stress. Equations 7.1 and 7.2 are utilized to compute compressive stress and strain, respectively. By convention, a compressive force is taken to be negative, which yields a negative stress. Furthermore, since l_0 is greater than l_i, compressive strains computed from Equation 7.2 are necessarily also negative. Tensile tests are more common because they are easier to perform; also, for most materials used in structural applications, very little additional information is obtained from compressive tests. Compressive tests are used when a material's behavior under large and permanent (i.e., plastic) strains is desired, as in manufacturing applications, or when the material is brittle in tension.

---

[2] Conversion from one system of stress units to the other is accomplished by the relationship 145 psi = 1 MPa.

[3] ASTM Standard E 9, ''Standard Test Methods of Compression Testing of Metallic Materials at Room Temperature.''

SHEAR AND TORSIONAL TESTS[4]

For tests performed using a pure shear force as shown in Figure 7.1*c*, the shear stress τ is computed according to

$$\tau = \frac{F}{A_0} \tag{7.3}$$

where F is the load or force imposed parallel to the upper and lower faces, each of which has an area of A_0. The shear strain γ is defined as the tangent of the strain angle θ, as indicated in the figure. The units for shear stress and strain are the same as for their tensile counterparts.

Torsion is a variation of pure shear, wherein a structural member is twisted in the manner of Figure 7.1*d*; torsional forces produce a rotational motion about the longitudinal axis of one end of the member relative to the other end. Examples of torsion are found for machine axles and drive shafts, and also for twist drills. Torsional tests are normally performed on cylindrical solid shafts or tubes. A shear stress τ is a function of the applied torque T, whereas shear strain γ is related to the angle of twist, ϕ in Figure 7.1*d*.

GEOMETRIC CONSIDERATIONS OF THE STRESS STATE

Stresses that are computed from the tensile, compressive, shear, and torsional force states represented in Figure 7.1 act either parallel or perpendicular to planar faces of the bodies represented in these illustrations. It should be noted that the stress state is a function of the orientations of the planes upon which the stresses are taken to act. For example, consider the cylindrical tensile specimen of Figure 7.4

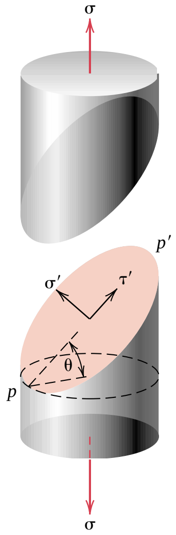

FIGURE 7.4 Schematic representation showing normal (σ') and shear (τ') stresses that act on a plane oriented at an angle θ relative to the plane taken perpendicular to the direction along which a pure tensile stress (σ) is applied.

---

[4] ASTM Standard E 143, ‘‘Standard Test for Shear Modulus.’’

that is subjected to a tensile stress σ applied parallel to its axis. Furthermore, consider also the plane p-p' that is oriented at some arbitrary angle θ relative to the plane of the specimen end-face. Upon this plane p-p', the applied stress is no longer a pure tensile one. Rather, a more complex stress state is present that consists of a tensile (or normal) stress σ' that acts normal to the p-p' plane, and, in addition, a shear stress τ' that acts parallel to this plane; both of these stresses are represented in the figure. Using mechanics of materials principles,[5] it is possible to develop equations for σ' and τ' in terms of σ and θ, as follows:

$$\sigma' = \sigma \cos^2 \theta = \sigma \left(\frac{1 + \cos 2\theta}{2} \right) \tag{7.4a}$$

$$\tau' = \sigma \sin \theta \cos \theta = \sigma \left(\frac{\sin 2\theta}{2} \right) \tag{7.4b}$$

These same mechanics principles allow the transformation of stress components from one coordinate system to another coordinate system that has a different orientation. Such treatments are beyond the scope of the present discussion.

ELASTIC DEFORMATION

7.3 STRESS–STRAIN BEHAVIOR

The degree to which a structure deforms or strains depends on the magnitude of an imposed stress. For most metals that are stressed in tension and at relatively low levels, stress and strain are proportional to each other through the relationship

$$\sigma = E\epsilon \tag{7.5}$$

This is known as Hooke's law, and the constant of proportionality E (GPa or psi)[6] is the **modulus of elasticity,** or *Young's modulus.* For most typical metals the magnitude of this modulus ranges between 45 GPa (6.5×10^6 psi), for magnesium, and 407 GPa (59×10^6 psi), for tungsten. The moduli of elasticity are slightly higher for ceramic materials, which range between about 70 and 500 GPa (10×10^6 and 70×10^6 psi). Polymers have modulus values that are smaller than both metals and ceramics, and which lie in the range 0.007 and 4 GPa (10^3 and 0.6×10^6 psi). Room temperature modulus of elasticity values for a number of metals, ceramics, and polymers are presented in Table 7.1. A more comprehensive modulus list is provided in Table B.2, Appendix B.

Deformation in which stress and strain are proportional is called **elastic deformation;** a plot of stress (ordinate) versus strain (abscissa) results in a linear relationship, as shown in Figure 7.5. The slope of this linear segment corresponds to the modulus of elasticity E. This modulus may be thought of as stiffness, or a material's resistance to elastic deformation. The greater the modulus, the stiffer the material, or the smaller the elastic strain that results from the application of a given stress. The modulus is an important design parameter used for computing elastic deflections.

Elastic deformation is nonpermanent, which means that when the applied load is released, the piece returns to its original shape. As shown in the stress–strain

---

[5] See, for example, W. F. Riley, L. D. Sturges, and D. H. Morris, *Mechanics of Materials,* 5th edition, John Wiley & Sons, New York, 1999.

[6] The SI unit for the modulus of elasticity is gigapascal, GPa, where 1 GPa $= 10^9$ N/m^2 $= 10^3$ MPa.

Table 7.1 **Room-Temperature Elastic and Shear Moduli, and Poisson's Ratio for Various Materials**

	Modulus of Elasticity		*Shear Modulus*		*Poisson's Ratio*
Material	*GPa*	*10^6 psi*	*GPa*	*10^6 psi*	
Metal Alloys					
Tungsten	407	59	160	23.2	0.28
Steel	207	30	83	12.0	0.30
Nickel	207	30	76	11.0	0.31
Titanium	107	15.5	45	6.5	0.34
Copper	110	16	46	6.7	0.34
Brass	97	14	37	5.4	0.34
Aluminum	69	10	25	3.6	0.33
Magnesium	45	6.5	17	2.5	0.35
Ceramic Materials					
Aluminum oxide (Al_2O_3)	393	57	—	—	0.22
Silicon carbide (SiC)	345	50	—	—	0.17
Silicon nitride (Si_3N_4)	304	44	—	—	0.30
Spinel ($MgAl_2O_4$)	260	38	—	—	—
Magnesium oxide (MgO)	225	33	—	—	0.18
Zirconia[a]	205	30	—	—	0.31
Mullite ($3Al_2O_3$-$2SiO_2$)	145	21	—	—	0.24
Glass–ceramic (Pyroceram)	120	17	—	—	0.25
Fused silica (SiO_2)	73	11	—	—	0.17
Soda–lime glass	69	10	—	—	0.23
Polymers[b]					
Phenol-formaldehyde	2.76–4.83	0.40–0.70	—	—	—
Polyvinyl chloride (PVC)	2.41–4.14	0.35–0.60	—	—	0.38
Polyester (PET)	2.76–4.14	0.40–0.60	—	—	—
Polystyrene (PS)	2.28–3.28	0.33–0.48	—	—	0.33
Polymethyl methacrylate (PMMA)	2.24–3.24	0.33–0.47	—	—	—
Polycarbonate (PC)	2.38	0.35	—	—	0.36
Nylon 6,6	1.58–3.80	0.23–0.55	—	—	0.39
Polypropylene (PP)	1.14–1.55	0.17–0.23	—	—	—
Polyethylene—high density (HDPE)	1.08	0.16	—	—	—
Polytetrafluoroethylene (PTFE)	0.40–0.55	0.058–0.080	—	—	0.46
Polyethylene—low density (LDPE)	0.17–0.28	0.025–0.041	—	—	—

[a] Partially stabilized with 3 mol% Y_2O_3.

[b] **Source:** *Modern Plastics Encyclopedia '96.* Copyright 1995, The McGraw-Hill Companies. Reprinted with permission.

plot (Figure 7.5), application of the load corresponds to moving from the origin up and along the straight line. Upon release of the load, the line is traversed in the opposite direction, back to the origin.

There are some materials (e.g., gray cast iron, concrete, and many polymers) for which this initial elastic portion of the stress–strain curve is not linear (Figure

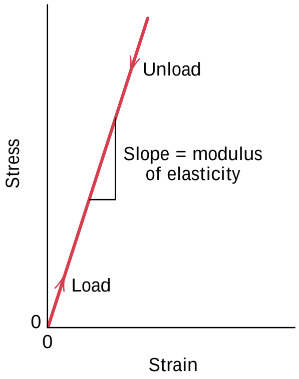

FIGURE 7.5 Schematic stress–strain diagram showing linear elastic deformation for loading and unloading cycles.

7.6); hence, it is not possible to determine a modulus of elasticity as described above. For this nonlinear behavior, either *tangent* or *secant modulus* is normally used. Tangent modulus is taken as the slope of the stress–strain curve at some specified level of stress, while secant modulus represents the slope of a secant drawn from the origin to some given point of the σ–ϵ curve. The determination of these moduli is illustrated in Figure 7.6.

On an atomic scale, macroscopic elastic strain is manifested as small changes in the interatomic spacing and the stretching of interatomic bonds. As a consequence, the magnitude of the modulus of elasticity is a measure of the resistance to separation of adjacent atoms/ions/molecules, that is, the interatomic bonding forces. Furthermore, this modulus is proportional to the slope of the interatomic force–separation curve (Figure 2.8*a*) at the equilibrium spacing:

$$E \propto \left(\frac{dF}{dr}\right)_{r_0} \tag{7.6}$$

Figure 7.7 shows the force–separation curves for materials having both strong and weak interatomic bonds; the slope at r_0 is indicated for each.

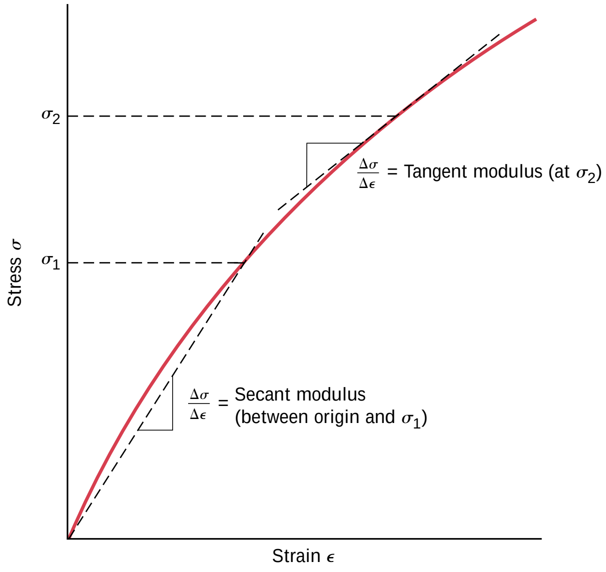

FIGURE 7.6 Schematic stress–strain diagram showing nonlinear elastic behavior, and how secant and tangent moduli are determined.

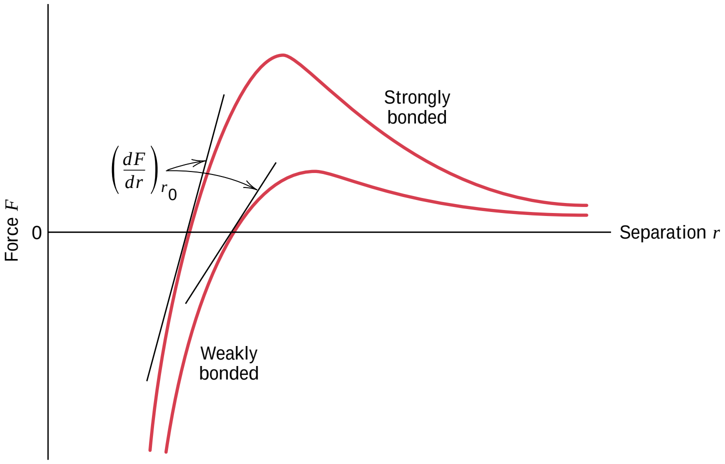

Figure 7.7 Force versus interatomic separation for weakly and strongly bonded atoms. The magnitude of the modulus of elasticity is proportional to the slope of each curve at the equilibrium interatomic separation r_0.

Differences in modulus values between metals, ceramics, and polymers are a direct consequence of the different types of atomic bonding that exist for the three materials types. Furthermore, with increasing temperature, the modulus of elasticity diminishes for all but some of the rubber materials; this effect is shown for several metals in Figure 7.8.

As would be expected, the imposition of compressive, shear, or torsional stresses also evokes elastic behavior. The stress–strain characteristics at low stress levels are virtually the same for both tensile and compressive situations, to include the magnitude of the modulus of elasticity. Shear stress and strain are proportional to each other through the expression

$$\tau = G\gamma \tag{7.7}$$

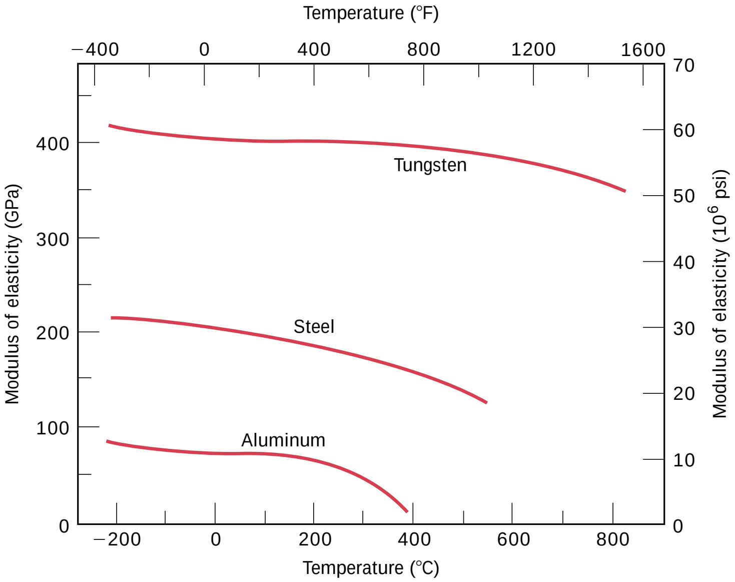

Figure 7.8 Plot of modulus of elasticity versus temperature for tungsten, steel, and aluminum. (Adapted from K. M. Ralls, T. H. Courtney, and J. Wulff, *Introduction to Materials Science and Engineering*. Copyright © 1976 by John Wiley & Sons, New York. Reprinted by permission of John Wiley & Sons, Inc.)

where G is the *shear modulus*, the slope of the linear elastic region of the shear stress–strain curve. Table 7.1 also gives the shear moduli for a number of the common metals.

7.4 ANELASTICITY

Up to this point, it has been assumed that elastic deformation is time independent, that is, that an applied stress produces an instantaneous elastic strain that remains constant over the period of time the stress is maintained. It has also been assumed that upon release of the load the strain is totally recovered, that is, that the strain immediately returns to zero. In most engineering materials, however, there will also exist a time-dependent elastic strain component. That is, elastic deformation will continue after the stress application, and upon load release some finite time is required for complete recovery. This time-dependent elastic behavior is known as **anelasticity,** and it is due to time-dependent microscopic and atomistic processes that are attendant to the deformation. For metals the anelastic component is normally small and is often neglected. However, for some polymeric materials its magnitude is significant; in this case it is termed *viscoelastic behavior,* {which is the discussion topic of Section 7.15.}

EXAMPLE PROBLEM 7.1

A piece of copper originally 305 mm (12 in.) long is pulled in tension with a stress of 276 MPa (40,000 psi). If the deformation is entirely elastic, what will be the resultant elongation?

SOLUTION

Since the deformation is elastic, strain is dependent on stress according to Equation 7.5. Furthermore, the elongation Δl is related to the original length l_0 through Equation 7.2. Combining these two expressions and solving for Δl yields

$$\sigma = \epsilon E = \left(\frac{\Delta l}{l_0}\right) E$$

$$\Delta l = \frac{\sigma l_0}{E}$$

The values of σ and l_0 are given as 276 MPa and 305 mm, respectively, and the magnitude of E for copper from Table 7.1 is 110 GPa (16×10^6 psi). Elongation is obtained by substitution into the expression above as

$$\Delta l = \frac{(276\text{ MPa})(305\text{ mm})}{110 \times 10^3\text{ MPa}} = 0.77\text{ mm }(0.03\text{ in.})$$

7.5 ELASTIC PROPERTIES OF MATERIALS

When a tensile stress is imposed on virtually all materials, an elastic elongation and accompanying strain ϵ_z result in the direction of the applied stress (arbitrarily taken to be the z direction), as indicated in Figure 7.9. As a result of this elongation,

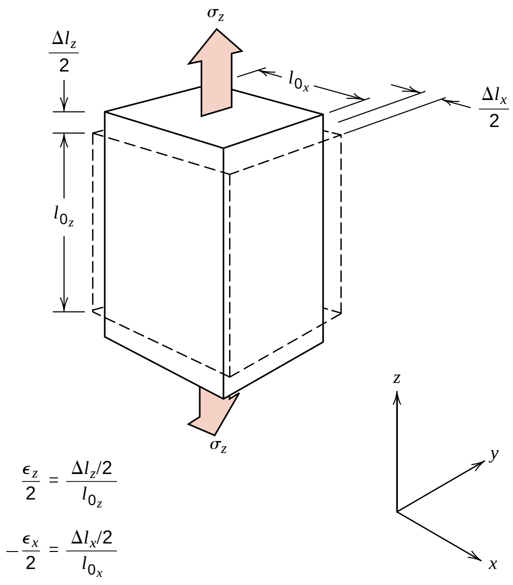
σ_z
$\frac{\Delta l_z}{2}$
l_{0_x}
$\frac{\Delta l_x}{2}$
l_{0_z}
σ_z
z
y
x
$\frac{\epsilon_z}{2} = \frac{\Delta l_z/2}{l_{0_z}}$
$-\frac{\epsilon_x}{2} = \frac{\Delta l_x/2}{l_{0_x}}$

FIGURE 7.9 Axial (z) elongation (positive strain) and lateral (x and y) contractions (negative strains) in response to an imposed tensile stress. Solid lines represent dimensions after stress application; dashed lines, before.

there will be constrictions in the lateral (x and y) directions perpendicular to the applied stress; from these contractions, the compressive strains ϵ_x and ϵ_y may be determined. If the applied stress is uniaxial (only in the z direction), and the material is isotropic, then $\epsilon_x = \epsilon_y$. A parameter termed **Poisson's ratio** ν is defined as the ratio of the lateral and axial strains, or

$$\nu = -\frac{\epsilon_x}{\epsilon_z} = -\frac{\epsilon_y}{\epsilon_z} \tag{7.8}$$

The negative sign is included in the expression so that ν will always be positive, since ϵ_x and ϵ_z will always be of opposite sign. Theoretically, Poisson's ratio for isotropic materials should be $\frac{1}{4}$; furthermore, the maximum value for ν (or that value for which there is no net volume change) is 0.50. For many metals and other alloys, values of Poisson's ratio range between 0.25 and 0.35. Table 7.1 shows ν values for several common materials; a more comprehensive list is given in Table B.3, Appendix B.

For isotropic materials, shear and elastic moduli are related to each other and to Poisson's ratio according to

$$E = 2G(1 + \nu) \tag{7.9}$$

In most metals G is about $0.4E$; thus, if the value of one modulus is known, the other may be approximated.

Many materials are elastically anisotropic; that is, the elastic behavior (e.g., the magnitude of E) varies with crystallographic direction (see Table 3.7). For these materials the elastic properties are completely characterized only by the specification of several elastic constants, their number depending on characteristics of the crystal structure. Even for isotropic materials, for complete characterization of the elastic properties, at least two constants must be given. Since the grain orientation is random in most polycrystalline materials, these may be considered to be isotropic;

inorganic ceramic glasses are also isotropic. The remaining discussion of mechanical behavior assumes isotropy and polycrystallinity (for metals and crystalline ceramics) because such is the character of most engineering materials.

EXAMPLE PROBLEM 7.2

A tensile stress is to be applied along the long axis of a cylindrical brass rod that has a diameter of 10 mm (0.4 in.). Determine the magnitude of the load required to produce a 2.5×10^{-3} mm (10^{-4} in.) change in diameter if the deformation is entirely elastic.

SOLUTION

This deformation situation is represented in the accompanying drawing.

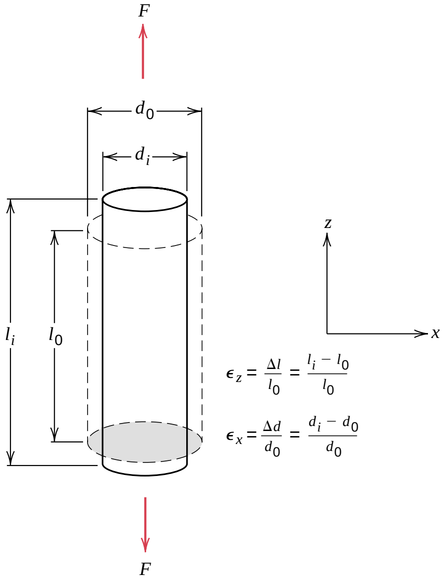
F
d_0
d_i
z
x
l_i
l_0
$\epsilon_z = \frac{\Delta l}{l_0} = \frac{l_i - l_0}{l_0}$
$\epsilon_x = \frac{\Delta d}{d_0} = \frac{d_i - d_0}{d_0}$
F

When the force F is applied, the specimen will elongate in the z direction and at the same time experience a reduction in diameter, Δd, of 2.5×10^{-3} mm in the x direction. For the strain in the x direction,

$$\epsilon_x = \frac{\Delta d}{d_0} = \frac{-2.5 \times 10^{-3}\text{ mm}}{10\text{ mm}} = -2.5 \times 10^{-4}$$

which is negative, since the diameter is reduced.

It next becomes necessary to calculate the strain in the z direction using Equation 7.8. The value for Poisson's ratio for brass is 0.34 (Table 7.1), and thus

$$\epsilon_z = -\frac{\epsilon_x}{\nu} = -\frac{(-2.5 \times 10^{-4})}{0.34} = 7.35 \times 10^{-4}$$

The applied stress may now be computed using Equation 7.5 and the modulus of elasticity, given in Table 7.1 as 97 GPa (14×10^6 psi), as

$$\sigma = \epsilon_z E = (7.35 \times 10^{-4})(97 \times 10^3\text{ MPa}) = 71.3\text{ MPa}$$

Finally, from Equation 7.1, the applied force may be determined as

$$F = \sigma A_0 = \sigma \left(\frac{d_0}{2}\right)^2 \pi$$

$$= (71.3 \times 10^6 \text{ N/m}^2) \left(\frac{10 \times 10^{-3} \text{ m}}{2}\right)^2 \pi = 5600 \text{ N } (1293 \text{ lb}_\text{f})$$

MECHANICAL BEHAVIOR—METALS

For most metallic materials, elastic deformation persists only to strains of about 0.005. As the material is deformed beyond this point, the stress is no longer proportional to strain (Hooke's law, Equation 7.5, ceases to be valid), and permanent, nonrecoverable, or **plastic deformation** occurs. Figure 7.10*a* plots schematically the tensile stress–strain behavior into the plastic region for a typical metal. The transition from elastic to plastic is a gradual one for most metals; some curvature results at the onset of plastic deformation, which increases more rapidly with rising stress.

From an atomic perspective, plastic deformation corresponds to the breaking of bonds with original atom neighbors and then reforming bonds with new neighbors as large numbers of atoms or molecules move relative to one another; upon removal of the stress they do not return to their original positions. This permanent deformation for metals is accomplished by means of a process called slip, which involves the motion of dislocations as discussed in Section 8.3.

7.6 TENSILE PROPERTIES

YIELDING AND YIELD STRENGTH

Most structures are designed to ensure that only elastic deformation will result when a stress is applied. It is therefore desirable to know the stress level at which

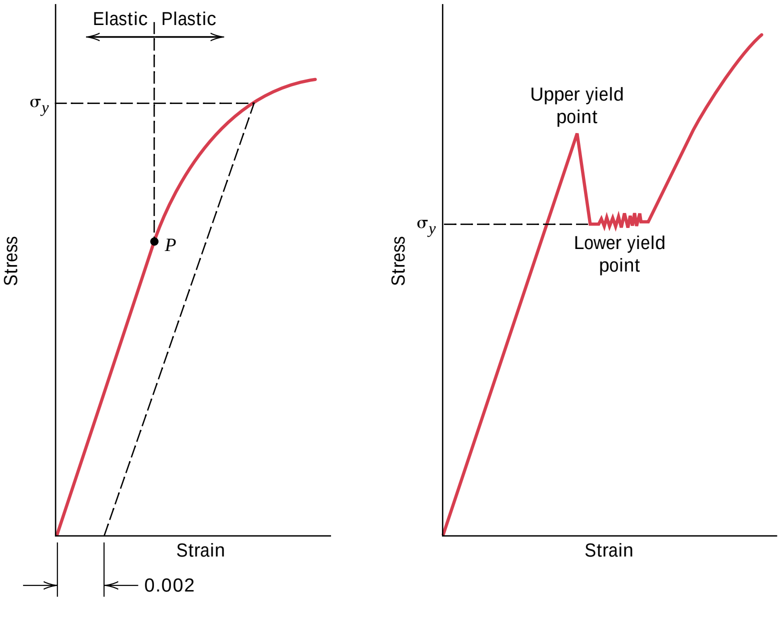

(*a*) (*b*)

FIGURE 7.10 (*a*) Typical stress–strain behavior for a metal showing elastic and plastic deformations, the proportional limit *P*, and the yield strength σ_y, as determined using the 0.002 strain offset method. (*b*) Representative stress–strain behavior found for some steels demonstrating the yield point phenomenon.

plastic deformation begins, or where the phenomenon of **yielding** occurs. For metals that experience this gradual elastic–plastic transition, the point of yielding may be determined as the initial departure from linearity of the stress–strain curve; this is sometimes called the **proportional limit,** as indicated by point P in Figure 7.10*a*. In such cases the position of this point may not be determined precisely. As a consequence, a convention has been established wherein a straight line is constructed parallel to the elastic portion of the stress–strain curve at some specified strain offset, usually 0.002. The stress corresponding to the intersection of this line and the stress–strain curve as it bends over in the plastic region is defined as the **yield strength** σ_y.[7] This is demonstrated in Figure 7.10*a*. Of course, the units of yield strength are MPa or psi.[8]

For those materials having a nonlinear elastic region (Figure 7.6), use of the strain offset method is not possible, and the usual practice is to define the yield strength as the stress required to produce some amount of strain (e.g., $\epsilon = 0.005$).

Some steels and other materials exhibit the tensile stress–strain behavior as shown in Figure 7.10*b*. The elastic–plastic transition is very well defined and occurs abruptly in what is termed a *yield point phenomenon.* At the upper yield point, plastic deformation is initiated with an actual decrease in stress. Continued deformation fluctuates slightly about some constant stress value, termed the lower yield point; stress subsequently rises with increasing strain. For metals that display this effect, the yield strength is taken as the average stress that is associated with the lower yield point, since it is well defined and relatively insensitive to the testing procedure.[9] Thus, it is not necessary to employ the strain offset method for these materials.

The magnitude of the yield strength for a metal is a measure of its resistance to plastic deformation. Yield strengths may range from 35 MPa (5000 psi) for a low-strength aluminum to over 1400 MPa (200,000 psi) for high-strength steels.

TENSILE STRENGTH

After yielding, the stress necessary to continue plastic deformation in metals increases to a maximum, point M in Figure 7.11, and then decreases to the eventual fracture, point F. The **tensile strength** TS (MPa or psi) is the stress at the maximum on the engineering stress–strain curve (Figure 7.11). This corresponds to the maximum stress that can be sustained by a structure in tension; if this stress is applied and maintained, fracture will result. All deformation up to this point is uniform throughout the narrow region of the tensile specimen. However, at this maximum stress, a small constriction or neck begins to form at some point, and all subsequent deformation is confined at this neck, as indicated by the schematic specimen insets in Figure 7.11. This phenomenon is termed ''necking,'' and fracture ultimately occurs at the neck. The fracture strength corresponds to the stress at fracture.

Tensile strengths may vary anywhere from 50 MPa (7000 psi) for an aluminum to as high as 3000 MPa (450,000 psi) for the high-strength steels. Ordinarily, when the strength of a metal is cited for design purposes, the yield strength is used. This is because by the time a stress corresponding to the tensile strength has been

---

[7] ''Strength'' is used in lieu of ''stress'' because strength is a property of the metal, whereas stress is related to the magnitude of the applied load.

[8] For Customary U.S. units, the unit of kilopounds per square inch (ksi) is sometimes used for the sake of convenience, where

$$1 \text{ ksi} = 1000 \text{ psi}$$

[9] It should be pointed out that to observe the yield point phenomenon, a ''stiff'' tensile-testing apparatus must be used; by stiff is meant that there is very little elastic deformation of the machine during loading.

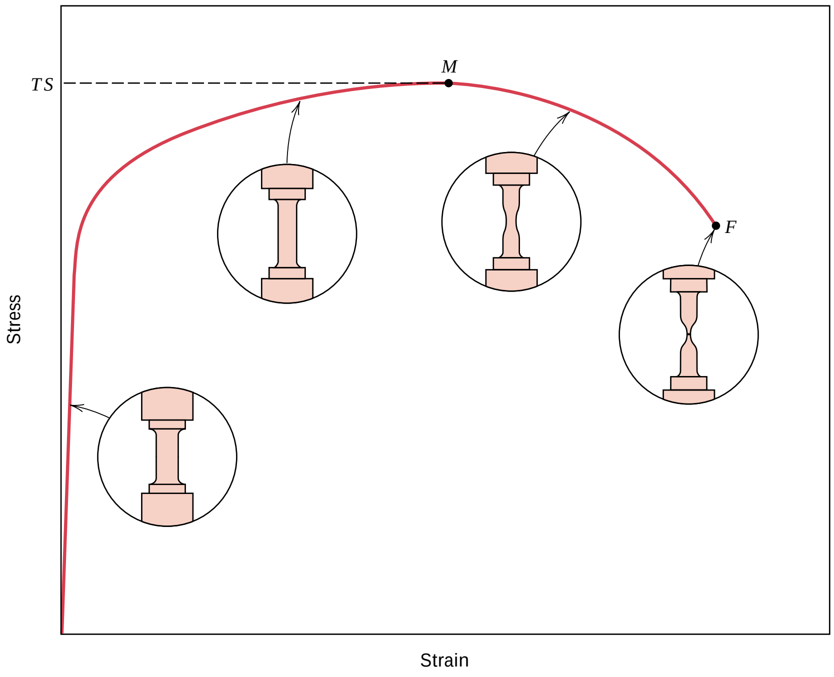

Figure 7.11 Typical engineering stress–strain behavior to fracture, point *F*. The tensile strength *TS* is indicated at point *M*. The circular insets represent the geometry of the deformed specimen at various points along the curve.

applied, often a structure has experienced so much plastic deformation that it is useless. Furthermore, fracture strengths are not normally specified for engineering design purposes.

EXAMPLE PROBLEM 7.3

From the tensile stress–strain behavior for the brass specimen shown in Figure 7.12, determine the following:

(a) The modulus of elasticity.

(b) The yield strength at a strain offset of 0.002.

(c) The maximum load that can be sustained by a cylindrical specimen having an original diameter of 12.8 mm (0.505 in.).

(d) The change in length of a specimen originally 250 mm (10 in.) long that is subjected to a tensile stress of 345 MPa (50,000 psi).

SOLUTION

(a) The modulus of elasticity is the slope of the elastic or initial linear portion of the stress–strain curve. The strain axis has been expanded in the inset, Figure 7.12, to facilitate this computation. The slope of this linear region is the rise over the run, or the change in stress divided by the corresponding change in strain; in mathematical terms,

$$E = \text{slope} = \frac{\Delta\sigma}{\Delta\epsilon} = \frac{\sigma_2 - \sigma_1}{\epsilon_2 - \epsilon_1} \tag{7.10}$$

Inasmuch as the line segment passes through the origin, it is convenient to take both σ_1 and ϵ_1 as zero. If σ_2 is arbitrarily taken as 150 MPa, then ϵ_2 will have

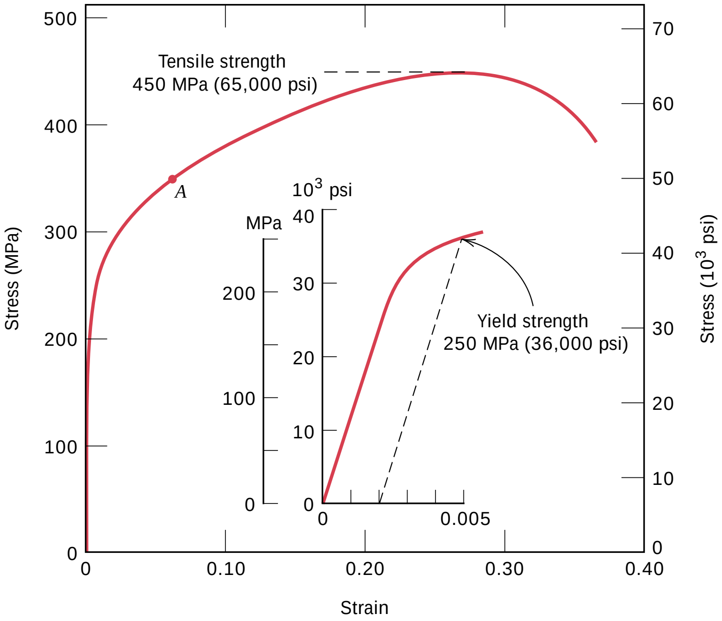

FIGURE 7.12 The stress–strain behavior for the brass specimen discussed in Example Problem 7.3.

a value of 0.0016. Therefore,

$$E = \frac{(150 - 0)\ \text{MPa}}{0.0016 - 0} = 93.8\ \text{GPa}\ (13.6 \times 10^6\ \text{psi})$$

which is very close to the value of 97 GPa (14×10^6 psi) given for brass in Table 7.1.

(b) The 0.002 strain offset line is constructed as shown in the inset; its intersection with the stress–strain curve is at approximately 250 MPa (36,000 psi), which is the yield strength of the brass.

(c) The maximum load that can be sustained by the specimen is calculated by using Equation 7.1, in which σ is taken to be the tensile strength, from Figure 7.12, 450 MPa (65,000 psi). Solving for F, the maximum load, yields

$$F = \sigma A_0 = \sigma \left(\frac{d_0}{2}\right)^2 \pi$$

$$= (450 \times 10^6\ \text{N/m}^2) \left(\frac{12.8 \times 10^{-3}\ \text{m}}{2}\right)^2 \pi = 57{,}900\ \text{N}\ (13{,}000\ \text{lb}_\text{f})$$

(d) To compute the change in length, Δl, in Equation 7.2, it is first necessary to determine the strain that is produced by a stress of 345 MPa. This is accomplished by locating the stress point on the stress–strain curve, point A, and reading the corresponding strain from the strain axis, which is approximately 0.06. Inasmuch as $l_0 = 250$ mm, we have

$$\Delta l = \epsilon l_0 = (0.06)(250\ \text{mm}) = 15\ \text{mm}\ (0.6\ \text{in.})$$

DUCTILITY

Ductility is another important mechanical property. It is a measure of the degree of plastic deformation that has been sustained at fracture. A material that experiences very little or no plastic deformation upon fracture is termed *brittle.* The tensile stress–strain behaviors for both ductile and brittle materials are schematically illustrated in Figure 7.13.

Ductility may be expressed quantitatively as either *percent elongation* or *percent reduction in area.* The percent elongation %EL is the percentage of plastic strain at fracture, or

$$\%\mathrm{EL} = \left(\frac{l_f - l_0}{l_0}\right) \times 100 \tag{7.11}$$

where l_f is the fracture length[10] and l_0 is the original gauge length as above. Inasmuch as a significant proportion of the plastic deformation at fracture is confined to the neck region, the magnitude of %EL will depend on specimen gauge length. The shorter l_0, the greater is the fraction of total elongation from the neck and, consequently, the higher the value of %EL. Therefore, l_0 should be specified when percent elongation values are cited; it is commonly 50 mm (2 in.).

Percent reduction in area %RA is defined as

$$\%\mathrm{RA} = \left(\frac{A_0 - A_f}{A_0}\right) \times 100 \tag{7.12}$$

where A_0 is the original cross-sectional area and A_f is the cross-sectional area at the point of fracture.[10] Percent reduction in area values are independent of both l_0 and A_0. Furthermore, for a given material the magnitudes of %EL and %RA will, in general, be different. Most metals possess at least a moderate degree of ductility at room temperature; however, some become brittle as the temperature is lowered (Section 9.8).

A knowledge of the ductility of materials is important for at least two reasons. First, it indicates to a designer the degree to which a structure will deform plastically

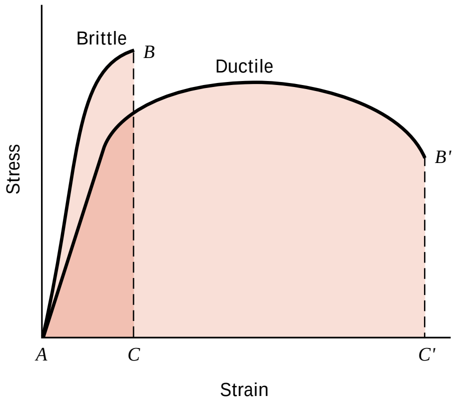

FIGURE 7.13 Schematic representations of tensile stress–strain behavior for brittle and ductile materials loaded to fracture.

---

[10] Both l_f and A_f are measured subsequent to fracture, and after the two broken ends have been repositioned back together.

before fracture. Second, it specifies the degree of allowable deformation during fabrication operations. We sometimes refer to relatively ductile materials as being ''forgiving,'' in the sense that they may experience local deformation without fracture should there be an error in the magnitude of the design stress calculation.

Brittle materials are *approximately* considered to be those having a fracture strain of less than about 5%.

Thus, several important mechanical properties of metals may be determined from tensile stress–strain tests. Table 7.2 presents some typical room-temperature

Table 7.2 Room-Temperature Mechanical Properties (in Tension) for Various Materials

	Yield Strength		*Tensile Strength*		
Material	***MPa***	***ksi***	***MPa***	***ksi***	***Ductility, %EL [in 50 mm (2 in.)]***[a]
			Metal Alloys[b]		
Molybdenum	565	82	655	95	35
Titanium	450	65	520	75	25
Steel (1020)	180	26	380	55	25
Nickel	138	20	480	70	40
Iron	130	19	262	38	45
Brass (70 Cu–30 Zn)	75	11	300	44	68
Copper	69	10	200	29	45
Aluminum	35	5	90	13	40
			Ceramic Materials[c]		
Zirconia (ZrO_2)[d]	—	—	800–1500	115–215	—
Silicon nitride (Si_3N_4)	—	—	250–1000	35–145	—
Aluminum oxide (Al_2O_3)	—	—	275–700	40–100	—
Silicon carbide (SiC)	—	—	100–820	15–120	—
Glass–ceramic (Pyroceram)	—	—	247	36	—
Mullite ($3Al_2O_3$-$2SiO_2$)	—	—	185	27	—
Spinel ($MgAl_2O_4$)	—	—	110–245	16–36	—
Fused silica (SiO_2)	—	—	110	16	—
Magnesium oxide (MgO)[e]	—	—	105	15	—
Soda–lime glass	—	—	69	10	—
			Polymers		
Nylon 6,6	44.8–82.8	6.5–12	75.9–94.5	11.0–13.7	15–300
Polycarbonate (PC)	62.1	9.0	62.8–72.4	9.1–10.5	110–150
Polyester (PET)	59.3	8.6	48.3–72.4	7.0–10.5	30–300
Polymethyl methacrylate (PMMA)	53.8–73.1	7.8–10.6	48.3–72.4	7.0–10.5	2.0–5.5
Polyvinyl chloride (PVC)	40.7–44.8	5.9–6.5	40.7–51.7	5.9–7.5	40–80
Phenol-formaldehyde	—	—	34.5–62.1	5.0–9.0	1.5–2.0
Polystyrene (PS)	—	—	35.9–51.7	5.2–7.5	1.2–2.5
Polypropylene (PP)	31.0–37.2	4.5–5.4	31.0–41.4	4.5–6.0	100–600
Polyethylene—high density (HDPE)	26.2–33.1	3.8–4.8	22.1–31.0	3.2–4.5	10–1200
Polytetrafluoroethylene (PTFE)	—	—	20.7–34.5	3.0–5.0	200–400
Polyethylene—low density (LDPE)	9.0–14.5	1.3–2.1	8.3–31.4	1.2–4.55	100–650

[a] For polymers, percent elongation at break.

[b] Property values are for metal alloys in an annealed state.

[c] The tensile strength of ceramic materials is taken as flexural strength (Section 7.10).

[d] Partially stabilized with 3 mol% Y_2O_3.

[e] Sintered and containing approximately 5% porosity.

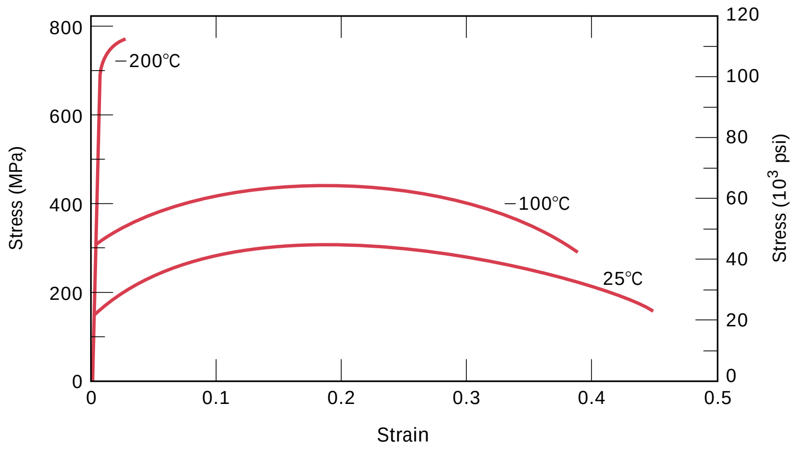

Figure 7.14 Engineering stress–strain behavior for iron at three temperatures.

values of yield strength, tensile strength, and ductility for several common metals (and also for a number of polymers and ceramics). These properties are sensitive to any prior deformation, the presence of impurities, and/or any heat treatment to which the metal has been subjected. The modulus of elasticity is one mechanical parameter that is insensitive to these treatments. As with modulus of elasticity, the magnitudes of both yield and tensile strengths decline with increasing temperature; just the reverse holds for ductility—it usually increases with temperature. Figure 7.14 shows how the stress–strain behavior of iron varies with temperature.

RESILIENCE

Resilience is the capacity of a material to absorb energy when it is deformed elastically and then, upon unloading, to have this energy recovered. The associated property is the *modulus of resilience*, U_r, which is the strain energy per unit volume required to stress a material from an unloaded state up to the point of yielding.

Computationally, the modulus of resilience for a specimen subjected to a uniaxial tension test is just the area under the engineering stress–strain curve taken to yielding (Figure 7.15), or

$$U_r = \int_0^{\epsilon_y} \sigma \, d\epsilon \tag{7.13a}$$

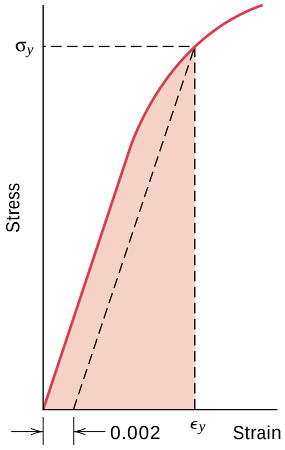

Figure 7.15 Schematic representation showing how modulus of resilience (corresponding to the shaded area) is determined from the tensile stress–strain behavior of a material.

Assuming a linear elastic region,

$$U_r = \tfrac{1}{2}\sigma_y \epsilon_y \tag{7.13b}$$

in which ϵ_y is the strain at yielding.

The units of resilience are the product of the units from each of the two axes of the stress–strain plot. For SI units, this is joules per cubic meter (J/m^3, equivalent to Pa), whereas with Customary U.S. units it is inch-pounds force per cubic inch (in.-lb$_f$/in.^{3}, equivalent to psi). Both joules and inch-pounds force are units of energy, and thus this area under the stress–strain curve represents energy absorption per unit volume (in cubic meters or cubic inches) of material.

Incorporation of Equation 7.5 into Equation 7.13b yields

$$U_r = \tfrac{1}{2}\sigma_y \epsilon_y = \tfrac{1}{2}\sigma_y \left(\frac{\sigma_y}{E}\right) = \frac{\sigma_y^2}{2E} \tag{7.14}$$

Thus, resilient materials are those having high yield strengths and low moduli of elasticity; such alloys would be used in spring applications.

TOUGHNESS

Toughness is a mechanical term that is used in several contexts; loosely speaking, it is a measure of the ability of a material to absorb energy up to fracture. Specimen geometry as well as the manner of load application are important in toughness determinations. For dynamic (high strain rate) loading conditions and when a notch (or point of stress concentration) is present, *notch toughness* is assessed by using an impact test, as discussed in Section 9.8. Furthermore, fracture toughness is a property indicative of a material's resistance to fracture when a crack is present (Section 9.5).

For the static (low strain rate) situation, toughness may be ascertained from the results of a tensile stress–strain test. It is the area under the σ–ϵ curve up to the point of fracture. The units for toughness are the same as for resilience (i.e., energy per unit volume of material). For a material to be tough, it must display both strength and ductility; and often, ductile materials are tougher than brittle ones. This is demonstrated in Figure 7.13, in which the stress–strain curves are plotted for both material types. Hence, even though the brittle material has higher yield and tensile strengths, it has a lower toughness than the ductile one, by virtue of lack of ductility; this is deduced by comparing the areas ABC and $AB'C'$ in Figure 7.13.

7.7 TRUE STRESS AND STRAIN

From Figure 7.11, the decline in the stress necessary to continue deformation past the maximum, point M, seems to indicate that the metal is becoming weaker. This is not at all the case; as a matter of fact, it is increasing in strength. However, the cross-sectional area is decreasing rapidly within the neck region, where deformation is occurring. This results in a reduction in the load-bearing capacity of the specimen. The stress, as computed from Equation 7.1, is on the basis of the original cross-sectional area before any deformation, and does not take into account this diminution in area at the neck.

Sometimes it is more meaningful to use a true stress–true strain scheme. **True stress** σ_T is defined as the load F divided by the instantaneous cross-sectional area

A_i over which deformation is occurring (i.e., the neck, past the tensile point), or

$$\sigma_T = \frac{F}{A_i} \tag{7.15}$$

Furthermore, it is occasionally more convenient to represent strain as **true strain** ϵ_T, defined by

$$\epsilon_T = \ln \frac{l_i}{l_0} \tag{7.16}$$

If no volume change occurs during deformation, that is, if

$$A_i l_i = A_0 l_0 \tag{7.17}$$

true and engineering stress and strain are related according to

$$\sigma_T = \sigma(1 + \epsilon) \tag{7.18a}$$

$$\epsilon_T = \ln(1 + \epsilon) \tag{7.18b}$$

Equations 7.18a and 7.18b are valid only to the onset of necking; beyond this point true stress and strain should be computed from actual load, cross-sectional area, and gauge length measurements.

A schematic comparison of engineering and true stress–strain behavior is made in Figure 7.16. It is worth noting that the true stress necessary to sustain increasing strain continues to rise past the tensile point M'.

Coincident with the formation of a neck is the introduction of a complex stress state within the neck region (i.e., the existence of other stress components in addition to the axial stress). As a consequence, the correct stress (*axial*) within the neck is slightly lower than the stress computed from the applied load and neck cross-sectional area. This leads to the ''corrected'' curve in Figure 7.16.

For some metals and alloys the region of the true stress-strain curve from the onset of plastic deformation to the point at which necking begins may be approximated by

$$\sigma_T = K\epsilon_T^n \tag{7.19}$$

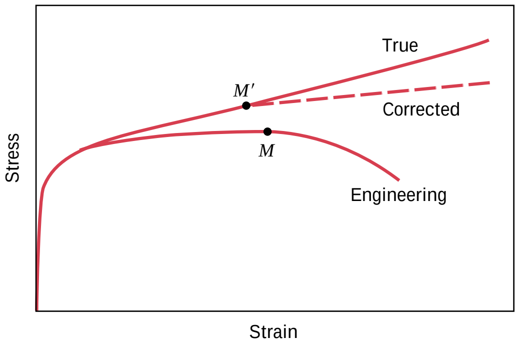

FIGURE 7.16 A comparison of typical tensile engineering stress–strain and true stress–strain behaviors. Necking begins at point M on the engineering curve, which corresponds to M' on the true curve. The ''corrected'' true stress–strain curve takes into account the complex stress state within the neck region.

Table 7.3 **Tabulation of *n* and *K* Values (Equation 7.19) for Several Alloys**

		K	
Material	***n***	***MPa***	***psi***
Low-carbon steel (annealed)	0.26	530	77,000
Alloy steel (Type 4340, annealed)	0.15	640	93,000
Stainless steel (Type 304, annealed)	0.45	1275	185,000
Aluminum (annealed)	0.20	180	26,000
Aluminum alloy (Type 2024, heat treated)	0.16	690	100,000
Copper (annealed)	0.54	315	46,000
Brass (70Cu–30Zn, annealed)	0.49	895	130,000

Source: From *Manufacturing Processes for Engineering Materials* by Seope Kalpakjian, © 1997. Reprinted by permission of Prentice-Hall, Inc., Upper Saddle River, NJ.

In this expression, K and n are constants, which values will vary from alloy to alloy, and will also depend on the condition of the material (i.e., whether it has been plastically deformed, heat treated, etc.). The parameter n is often termed the *strain-hardening exponent* and has a value less than unity. Values of n and K for several alloys are contained in Table 7.3.

EXAMPLE PROBLEM 7.4

A cylindrical specimen of steel having an original diameter of 12.8 mm (0.505 in.) is tensile tested to fracture and found to have an engineering fracture strength σ_f of 460 MPa (67,000 psi). If its cross-sectional diameter at fracture is 10.7 mm (0.422 in.), determine:

(a) The ductility in terms of percent reduction in area.

(b) The true stress at fracture.

SOLUTION

(a) Ductility is computed using Equation 7.12, as

$$\%\mathrm{RA} = \frac{\left(\dfrac{12.8\text{ mm}}{2}\right)^2 \pi - \left(\dfrac{10.7\text{ mm}}{2}\right)^2 \pi}{\left(\dfrac{12.8\text{ mm}}{2}\right)^2 \pi} \times 100$$

$$= \frac{128.7\text{ mm}^2 - 89.9\text{ mm}^2}{128.7\text{ mm}^2} \times 100 = 30\%$$

(b) True stress is defined by Equation 7.15, where in this case the area is taken as the fracture area A_f. However, the load at fracture must first be computed from the fracture strength as

$$F = \sigma_f A_0 = (460 \times 10^6 \text{ N/m}^2)(128.7 \text{ mm}^2)\left(\frac{1 \text{ m}^2}{10^6 \text{ mm}^2}\right) = 59{,}200 \text{ N}$$

Thus, the true stress is calculated as

$$\sigma_T = \frac{F}{A_f} = \frac{59{,}200 \text{ N}}{(89.9 \text{ mm}^2)\left(\frac{1 \text{ m}^2}{10^6 \text{ mm}^2}\right)}$$

$$= 6.6 \times 10^8 \text{ N/m}^2 = 660 \text{ MPa (95,700 psi)}$$

EXAMPLE PROBLEM 7.5

Compute the strain-hardening exponent n in Equation 7.19 for an alloy in which a true stress of 415 MPa (60,000 psi) produces a true strain of 0.10; assume a value of 1035 MPa (150,000 psi) for K.

SOLUTION

This requires some algebraic manipulation of Equation 7.19 so that n becomes the dependent parameter. This is accomplished by taking logarithms and rearranging. Solving for n yields

$$n = \frac{\log \sigma_T - \log K}{\log \epsilon_T}$$

$$= \frac{\log(415 \text{ MPa}) - \log(1035 \text{ MPa})}{\log(0.1)} = 0.40$$

7.8 ELASTIC RECOVERY DURING PLASTIC DEFORMATION

Upon release of the load during the course of a stress–strain test, some fraction of the total deformation is recovered as elastic strain. This behavior is demonstrated in Figure 7.17, a schematic engineering stress–strain plot. During the unloading cycle, the curve traces a near straight-line path from the point of unloading (point D), and its slope is virtually identical to the modulus of elasticity, or parallel to the initial elastic portion of the curve. The magnitude of this elastic strain, which is regained during unloading, corresponds to the strain recovery, as shown in Figure 7.17. If the load is reapplied, the curve will traverse essentially the same linear portion in the direction opposite to unloading; yielding will again occur at the unloading stress level where the unloading began. There will also be an elastic strain recovery associated with fracture.

7.9 COMPRESSIVE, SHEAR, AND TORSIONAL DEFORMATION

Of course, metals may experience plastic deformation under the influence of applied compressive, shear, and torsional loads. The resulting stress–strain behavior into

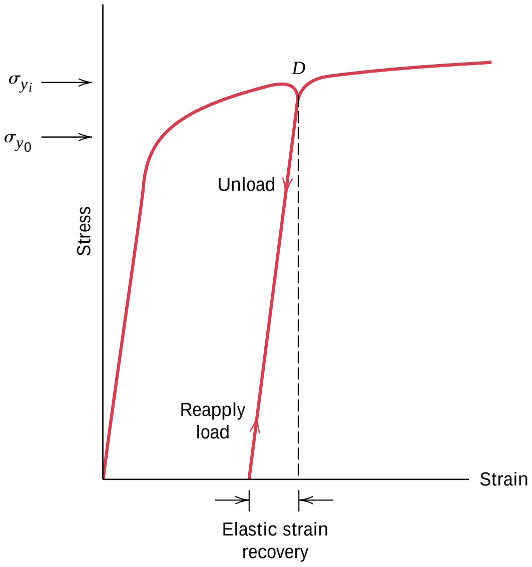

Figure 7.17 Schematic tensile stress–strain diagram showing the phenomena of elastic strain recovery and strain hardening. The initial yield strength is designated as σ_{y_0}; σ_{y_i} is the yield strength after releasing the load at point *D*, and then upon reloading.

the plastic region will be similar to the tensile counterpart (Figure 7.10*a*: yielding and the associated curvature). However, for compression, there will be no maximum, since necking does not occur; furthermore, the mode of fracture will be different from that for tension.

MECHANICAL BEHAVIOR—CERAMICS

Ceramic materials are somewhat limited in applicability by their mechanical properties, which in many respects are inferior to those of metals. The principal drawback is a disposition to catastrophic fracture in a brittle manner with very little energy absorption. In this section we explore the salient mechanical characteristics of these materials and how these properties are measured.

7.10 Flexural Strength

The stress–strain behavior of brittle ceramics is not usually ascertained by a tensile test as outlined in Section 7.2, for three reasons. First, it is difficult to prepare and test specimens having the required geometry. Second, it is difficult to grip brittle materials without fracturing them; and third, ceramics fail after only about 0.1% strain, which necessitates that tensile specimens be perfectly aligned in order to avoid the presence of bending stresses, which are not easily calculated. Therefore, a more suitable transverse bending test is most frequently employed, in which a rod specimen having either a circular or rectangular cross section is bent until fracture using a three- or four-point loading technique;[11] the three-point loading scheme is illustrated in Figure 7.18. At the point of loading, the top surface of the specimen is placed in a state of compression, whereas the bottom surface is in tension. Stress is computed from the specimen thickness, the bending moment, and

---

[11] ASTM Standard C 1161, ‘‘Standard Test Method for Flexural Strength of Advanced Ceramics at Ambient Temperature.’’

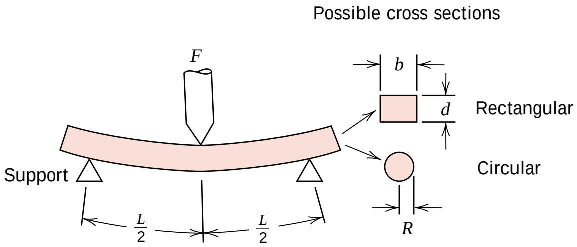

σ = stress = $\frac{Mc}{I}$

where M = maximum bending moment
c = distance from center of specimen to outer fibers
I = moment of inertia of cross section
F = applied load

	M	c	I	σ
Rectangular	$\frac{FL}{4}$	$\frac{d}{2}$	$\frac{bd^3}{12}$	$\frac{3FL}{2bd^2}$
Circular	$\frac{FL}{4}$	R	$\frac{\pi R^4}{4}$	$\frac{FL}{\pi R^3}$

Figure 7.18 A three-point loading scheme for measuring the stress–strain behavior and flexural strength of brittle ceramics, including expressions for computing stress for rectangular and circular cross sections.

the moment of inertia of the cross section; these parameters are noted in Figure 7.18 for rectangular and circular cross sections. The maximum tensile stress (as determined using these stress expressions) exists at the bottom specimen surface directly below the point of load application. Since the tensile strengths of ceramics are about one-tenth of their compressive strengths, and since fracture occurs on the tensile specimen face, the flexure test is a reasonable substitute for the tensile test.

The stress at fracture using this flexure test is known as the **flexural strength,** *modulus of rupture, fracture strength*, or the *bend strength*, an important mechanical parameter for brittle ceramics. For a rectangular cross section, the flexural strength σ_{fs} is equal to

$$\sigma_{fs} = \frac{3F_f L}{2bd^2} \tag{7.20a}$$

where F_f is the load at fracture, L is the distance between support points, and the other parameters are as indicated in Figure 7.18. When the cross section is circular, then

$$\sigma_{fs} = \frac{F_f L}{\pi R^3} \tag{7.20b}$$

R being the specimen radius.

Characteristic flexural strength values for several ceramic materials are given in Table 7.2. Since, during bending, a specimen is subjected to both compressive and tensile stresses, the magnitude of its flexural strength is greater than the tensile fracture strength. Furthermore, σ_{fs} will depend on specimen size; as explained in Section 9.6, with increasing specimen volume (under stress) there is an increase in the probability of the existence of a crack-producing flaw and, consequently, a decrease in flexural strength.

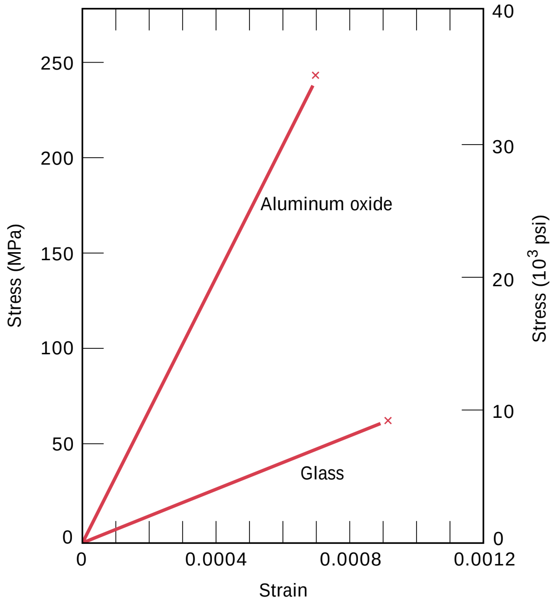

Figure 7.19 Typical stress–strain behavior to fracture for aluminum oxide and glass.

7.11 Elastic Behavior

The elastic stress–strain behavior for ceramic materials using these flexure tests is similar to the tensile test results for metals: a linear relationship exists between stress and strain. Figure 7.19 compares the stress–strain behavior to fracture for aluminum oxide (alumina) and glass. Again, the slope in the elastic region is the modulus of elasticity; also, the moduli of elasticity for ceramic materials are slightly higher than for metals (Table 7.2 and Table B.2, Appendix B). From Figure 7.19 it may be noted that neither of the materials experiences plastic deformation prior to fracture.

7.12 Influence of Porosity on the Mechanical Properties of Ceramics (CD-ROM)

MECHANICAL BEHAVIOR—POLYMERS

7.13 Stress–Strain Behavior

The mechanical properties of polymers are specified with many of the same parameters that are used for metals, that is, modulus of elasticity, and yield and tensile strengths. For many polymeric materials, the simple stress–strain test is employed for the characterization of some of these mechanical parameters.[12] The mechanical characteristics of polymers, for the most part, are highly sensitive to the rate of deformation (strain rate), the temperature, and the chemical nature of the environment (the presence of water, oxygen, organic solvents, etc.). Some modifications of the testing techniques and specimen configurations used for metals are necessary with polymers, especially for the highly elastic materials, such as rubbers.

---

[12] ASTM Standard D 638, ''Standard Test Method for Tensile Properties of Plastics.''

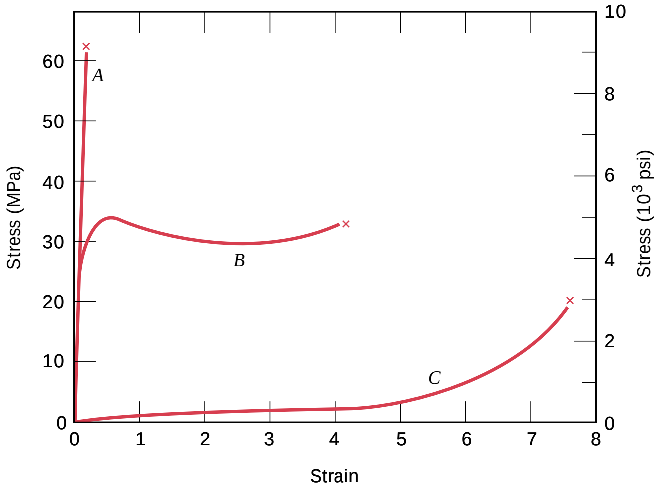

Figure 7.22 The stress–strain behavior for brittle (curve *A*), plastic (curve *B*), and highly elastic (elastomeric) (curve *C*) polymers.

Three typically different types of stress–strain behavior are found for polymeric materials, as represented in Figure 7.22. Curve *A* illustrates the stress–strain character for a brittle polymer, inasmuch as it fractures while deforming elastically. The behavior for the plastic material, curve *B*, is similar to that found for many metallic materials; the initial deformation is elastic, which is followed by yielding and a region of plastic deformation. Finally, the deformation displayed by curve *C* is totally elastic; this rubberlike elasticity (large recoverable strains produced at low stress levels) is displayed by a class of polymers termed the **elastomers.**

Modulus of elasticity (termed *tensile modulus* or sometimes just *modulus* for polymers) and ductility in percent elongation are determined for polymers in the same manner as for metals (Section 7.6). For plastic polymers (curve *B*, Figure 7.22), the yield point is taken as a maximum on the curve, which occurs just beyond the termination of the linear-elastic region (Figure 7.23); the stress at this maximum is the yield strength (σ_y). Furthermore, tensile strength (*TS*) corresponds to the stress at which fracture occurs (Figure 7.23); *TS* may be greater than or less than σ_y. Strength, for these plastic polymers, is normally taken as tensile strength. Table 7.2 and Tables B.2, B.3, and B.4 in Appendix B give these mechanical properties for a number of polymeric materials.

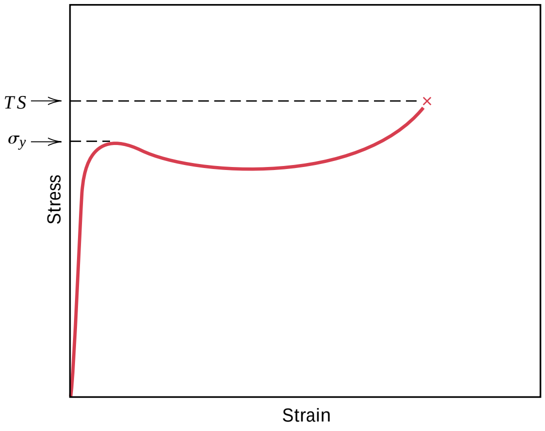

Figure 7.23 Schematic stress–strain curve for a plastic polymer showing how yield and tensile strengths are determined.

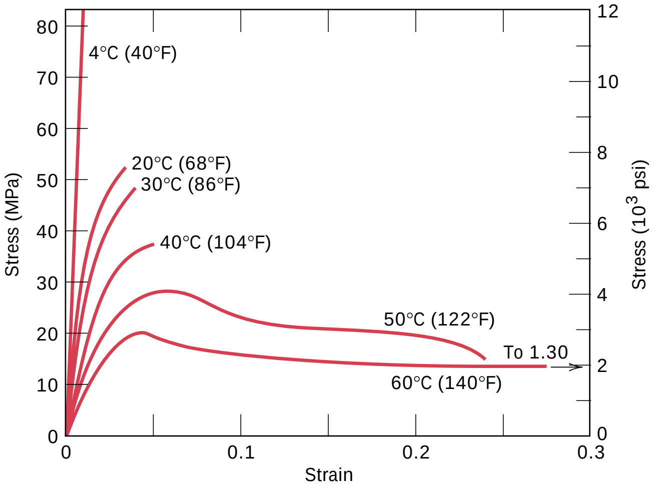

Figure 7.24 The influence of temperature on the stress–strain characteristics of polymethyl methacrylate. (From T. S. Carswell and H. K. Nason, ''Effect of Environmental Conditions on the Mechanical Properties of Organic Plastics,'' *Symposium on Plastics,* American Society for Testing and Materials, Philadelphia, 1944. Copyright, ASTM. Reprinted with permission.)

Polymers are, in many respects, mechanically dissimilar to metals (and ceramic materials). For example, the modulus for highly elastic polymeric materials may be as low as 7 MPa (10^3 psi), but may run as high as 4 GPa (0.6×10^6 psi) for some of the very stiff polymers; modulus values for metals are much larger (Table 7.1). Maximum tensile strengths for polymers are on the order of 100 MPa (15,000 psi)—for some metal alloys 4100 MPa (600,000 psi). And, whereas metals rarely elongate plastically to more than 100%, some highly elastic polymers may experience elongations to as much as 1000%.

In addition, the mechanical characteristics of polymers are much more sensitive to temperature changes within the vicinity of room temperature. Consider the stress–strain behavior for polymethyl methacrylate (Plexiglas) at several temperatures between 4 and 60°C (40 and 140°F) (Figure 7.24). Several features of this figure are worth noting, as follows: increasing the temperature produces (1) a decrease in elastic modulus, (2) a reduction in tensile strength, and (3) an enhancement of ductility—at 4°C (40°F) the material is totally brittle, whereas considerable plastic deformation is realized at both 50 and 60°C (122 and 140°F).

The influence of strain rate on the mechanical behavior may also be important. In general, decreasing the rate of deformation has the same influence on the stress–strain characteristics as increasing the temperature; that is, the material becomes softer and more ductile.

7.14 Macroscopic Deformation

Some aspects of the macroscopic deformation of semicrystalline polymers deserve our attention. The tensile stress–strain curve for a semicrystalline material, which was initially unoriented, is shown in Figure 7.25; also included in the figure are

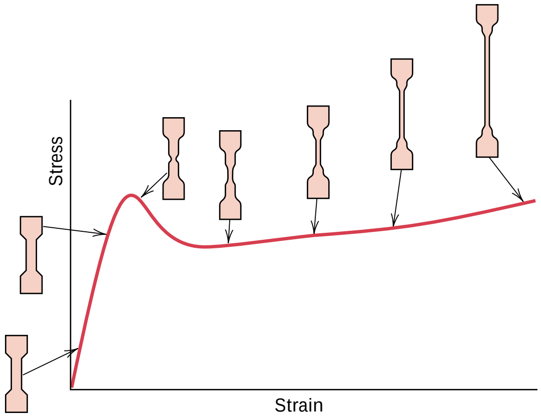

FIGURE 7.25 Schematic tensile stress–strain curve for a semicrystalline polymer. Specimen contours at several stages of deformation are included. (From Jerold M. Schultz, *Polymer Materials Science*, copyright © 1974, p. 488. Reprinted by permission of Prentice-Hall, Inc., Englewood Cliffs, NJ.)

schematic representations of specimen profile at various stages of deformation. Both upper and lower yield points are evident on the curve, which are followed by a near horizontal region. At the upper yield point, a small neck forms within the gauge section of the specimen. Within this neck, the chains become oriented (i.e., chain axes become aligned parallel to the elongation direction, a condition that is represented schematically in Figure 8.27*e*), which leads to localized strengthening. Consequently, there is a resistance to continued deformation at this point, and specimen elongation proceeds by the propagation of this neck region along the gauge length; the chain orientation phenomenon (Figure 8.27*e*) accompanies this neck extension. This tensile behavior may be contrasted to that found for ductile metals (Section 7.6), wherein once a neck has formed, all subsequent deformation is confined to within the neck region.

7.15 VISCOELASTICITY (CD-ROM)

HARDNESS AND OTHER MECHANICAL PROPERTY CONSIDERATIONS

7.16 HARDNESS

Another mechanical property that may be important to consider is **hardness,** which is a measure of a material's resistance to localized plastic deformation (e.g., a small dent or a scratch). Early hardness tests were based on natural minerals with a scale constructed solely on the ability of one material to scratch another that was softer. A qualitative and somewhat arbitrary hardness indexing scheme was devised, termed the Mohs scale, which ranged from 1 on the soft end for talc to 10 for diamond. Quantitative hardness techniques have been developed over the years in which a small indenter is forced into the surface of a material to be tested, under controlled conditions of load and rate of application. The depth or size of the resulting indentation is measured, which in turn is related to a hardness number; the softer the material, the larger and deeper the indentation, and the lower the hardness index number. Measured hardnesses are only relative (rather than absolute), and care should be exercised when comparing values determined by different techniques.

Hardness tests are performed more frequently than any other mechanical test for several reasons:

1. They are simple and inexpensive—ordinarily no special specimen need be prepared, and the testing apparatus is relatively inexpensive.
2. The test is nondestructive—the specimen is neither fractured nor excessively deformed; a small indentation is the only deformation.
3. Other mechanical properties often may be estimated from hardness data, such as tensile strength (see Figure 7.31).

ROCKWELL HARDNESS TESTS[13]

The Rockwell tests constitute the most common method used to measure hardness because they are so simple to perform and require no special skills. Several different scales may be utilized from possible combinations of various indenters and different loads, which permit the testing of virtually all metal alloys (as well as some polymers). Indenters include spherical and hardened steel balls having diameters of $\frac{1}{16}$, $\frac{1}{8}$, $\frac{1}{4}$, and $\frac{1}{2}$ in. (1.588, 3.175, 6.350, and 12.70 mm), and a conical diamond (Brale) indenter, which is used for the hardest materials.

With this system, a hardness number is determined by the difference in depth of penetration resulting from the application of an initial minor load followed by a larger major load; utilization of a minor load enhances test accuracy. On the basis of the magnitude of both major and minor loads, there are two types of tests: Rockwell and superficial Rockwell. For Rockwell, the minor load is 10 kg, whereas major loads are 60, 100, and 150 kg. Each scale is represented by a letter of the alphabet; several are listed with the corresponding indenter and load in Tables 7.4 and 7.5a. For superficial tests, 3 kg is the minor load; 15, 30, and 45 kg are the possible major load values. These scales are identified by a 15, 30, or 45 (according to load), followed by N, T, W, X, or Y, depending on indenter. Superficial tests are frequently performed on thin specimens. Table 7.5b presents several superficial scales.

When specifying Rockwell and superficial hardnesses, both hardness number and scale symbol must be indicated. The scale is designated by the symbol HR followed by the appropriate scale identification.[14] For example, 80 HRB represents a Rockwell hardness of 80 on the B scale, and 60 HR30W indicates a superficial hardness of 60 on the 30W scale.

For each scale, hardnesses may range up to 130; however, as hardness values rise above 100 or drop below 20 on any scale, they become inaccurate; and because the scales have some overlap, in such a situation it is best to utilize the next harder or softer scale.

Inaccuracies also result if the test specimen is too thin, if an indentation is made too near a specimen edge, or if two indentations are made too close to one another. Specimen thickness should be at least ten times the indentation depth, whereas allowance should be made for at least three indentation diameters between the center of one indentation and the specimen edge, or to the center of a second indentation. Furthermore, testing of specimens stacked one on top of another is not recommended. Also, accuracy is dependent on the indentation being made into a smooth flat surface.

---

[13] ASTM Standard E 18, ‘‘Standard Test Methods for Rockwell Hardness and Rockwell Superficial Hardness of Metallic Materials.’’

[14] Rockwell scales are also frequently designated by an R with the appropriate scale letter as a subscript, for example, R_C denotes the Rockwell C scale.

Table 7.4 Hardness Testing Techniques

		Shape of Indentation			
Test	***Indenter***	***Side View***	***Top View***	***Load***	***Formula for Hardness Number***[a]
Brinell	10-mm sphere of steel or tungsten carbide	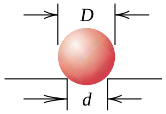	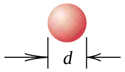	P	$\mathrm{HB} = \dfrac{2P}{\pi D[D - \sqrt{D^2 - d^2}]}$
Vickers microhardness	Diamond pyramid	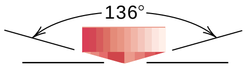	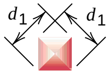	P	$\mathrm{HV} = 1.854P/d_1^2$
Knoop microhardness	Diamond pyramid	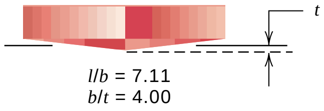	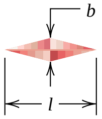	P	$\mathrm{HK} = 14.2P/l^2$
Rockwell and Superficial Rockwell	Diamond cone $\frac{1}{16}$, $\frac{1}{8}$, $\frac{1}{4}$, $\frac{1}{2}$ in. diameter steel spheres	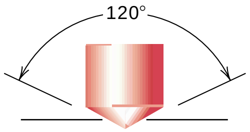 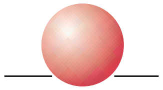	 	60 kg 100 kg 150 kg 15 kg 30 kg 45 kg	Rockwell Superficial Rockwell

[a] For the hardness formulas given, P (the applied load) is in kg, while D, d, d_1, and l are all in mm.

Source: Adapted from H. W. Hayden, W. G. Moffatt, and J. Wulff, *The Structure and Properties of Materials*, Vol. III, *Mechanical Behavior.* Copyright © 1965 by John Wiley & Sons, New York. Reprinted by permission of John Wiley & Sons, Inc.

Table 7.5a **Rockwell Hardness Scales**

Scale Symbol	*Indenter*	*Major Load (kg)*
A	Diamond	60
B	$\frac{1}{16}$ in. ball	100
C	Diamond	150
D	Diamond	100
E	$\frac{1}{8}$ in. ball	100
F	$\frac{1}{16}$ in. ball	60
G	$\frac{1}{16}$ in. ball	150
H	$\frac{1}{8}$ in. ball	60
K	$\frac{1}{8}$ in. ball	150

Table 7.5b **Superficial Rockwell Hardness Scales**

Scale Symbol	*Indenter*	*Major Load (kg)*
15N	Diamond	15
30N	Diamond	30
45N	Diamond	45
15T	$\frac{1}{16}$ in. ball	15
30T	$\frac{1}{16}$ in. ball	30
45T	$\frac{1}{16}$ in. ball	45
15W	$\frac{1}{8}$ in. ball	15
30W	$\frac{1}{8}$ in. ball	30
45W	$\frac{1}{8}$ in. ball	45

The modern apparatus for making Rockwell hardness measurements (see the chapter-opening photograph for this chapter) is automated and very simple to use; hardness is read directly, and each measurement requires only a few seconds.

The modern testing apparatus also permits a variation in the time of load application. This variable must also be considered in interpreting hardness data.

BRINELL HARDNESS TESTS[15]

In Brinell tests, as in Rockwell measurements, a hard, spherical indenter is forced into the surface of the metal to be tested. The diameter of the hardened steel (or tungsten carbide) indenter is 10.00 mm (0.394 in.). Standard loads range between 500 and 3000 kg in 500-kg increments; during a test, the load is maintained constant for a specified time (between 10 and 30 s). Harder materials require greater applied loads. The Brinell hardness number, HB, is a function of both the magnitude of the load and the diameter of the resulting indentation (see Table 7.4).[16] This diameter is measured with a special low-power microscope, utilizing a scale that is etched on the eyepiece. The measured diameter is then converted to the appropriate HB number using a chart; only one scale is employed with this technique.

Maximum specimen thickness as well as indentation position (relative to specimen edges) and minimum indentation spacing requirements are the same as for Rockwell tests. In addition, a well-defined indentation is required; this necessitates a smooth flat surface in which the indentation is made.

---

[15] ASTM Standard E 10, ‘‘Standard Test Method for Brinell Hardness of Metallic Materials.’’

[16] The Brinell hardness number is also represented by BHN.

KNOOP AND VICKERS MICROHARDNESS TESTS[17]

Two other hardness testing techniques are Knoop (pronounced *nūp*) and Vickers (sometimes also called diamond pyramid). For each test a very small diamond indenter having pyramidal geometry is forced into the surface of the specimen. Applied loads are much smaller than for Rockwell and Brinell, ranging between 1 and 1000 g. The resulting impression is observed under a microscope and measured; this measurement is then converted into a hardness number (Table 7.4). Careful specimen surface preparation (grinding and polishing) may be necessary to ensure a well-defined indentation that may be accurately measured. The Knoop and Vickers hardness numbers are designated by HK and HV, respectively,[18] and hardness scales for both techniques are approximately equivalent. Knoop and Vickers are referred to as microhardness testing methods on the basis of load and indenter size. Both are well suited for measuring the hardness of small, selected specimen regions; furthermore, Knoop is used for testing brittle materials such as ceramics.

There are other hardness-testing techniques that are frequently employed, but which will not be discussed here; these include ultrasonic microhardness, dynamic (Scleroscope), durometer (for plastic and elastomeric materials), and scratch hardness tests. These are described in references provided at the end of the chapter.

HARDNESS CONVERSION

The facility to convert the hardness measured on one scale to that of another is most desirable. However, since hardness is not a well-defined material property, and because of the experimental dissimilarities among the various techniques, a comprehensive conversion scheme has not been devised. Hardness conversion data have been determined experimentally and found to be dependent on material type and characteristics. The most reliable conversion data exist for steels, some of which are presented in Figure 7.30 for Knoop, Brinell, and two Rockwell scales; the Mohs scale is also included. Detailed conversion tables for various other metals and alloys are contained in ASTM Standard E 140, ‘‘Standard Hardness Conversion Tables for Metals.’’ In light of the preceding discussion, care should be exercised in extrapolation of conversion data from one alloy system to another.

CORRELATION BETWEEN HARDNESS AND TENSILE STRENGTH

Both tensile strength and hardness are indicators of a metal’s resistance to plastic deformation. Consequently, they are roughly proportional, as shown in Figure 7.31, on page 182, for tensile strength as a function of the HB for cast iron, steel, and brass. The same proportionality relationship does not hold for all metals, as Figure 7.31 indicates. As a rule of thumb for most steels, the HB and the tensile strength are related according to

$$TS(\text{MPa}) = 3.45 \times \text{HB} \tag{7.25a}$$

$$TS(\text{psi}) = 500 \times \text{HB} \tag{7.25b}$$

---

[17] ASTM Standard E 92, ‘‘Standard Test Method for Vickers Hardness of Metallic Materials,’’ and ASTM Standard E 384, ‘‘Standard Test for Microhardness of Materials.’’

[18] Sometimes KHN and VHN are used to denote Knoop and Vickers hardness numbers, respectively.

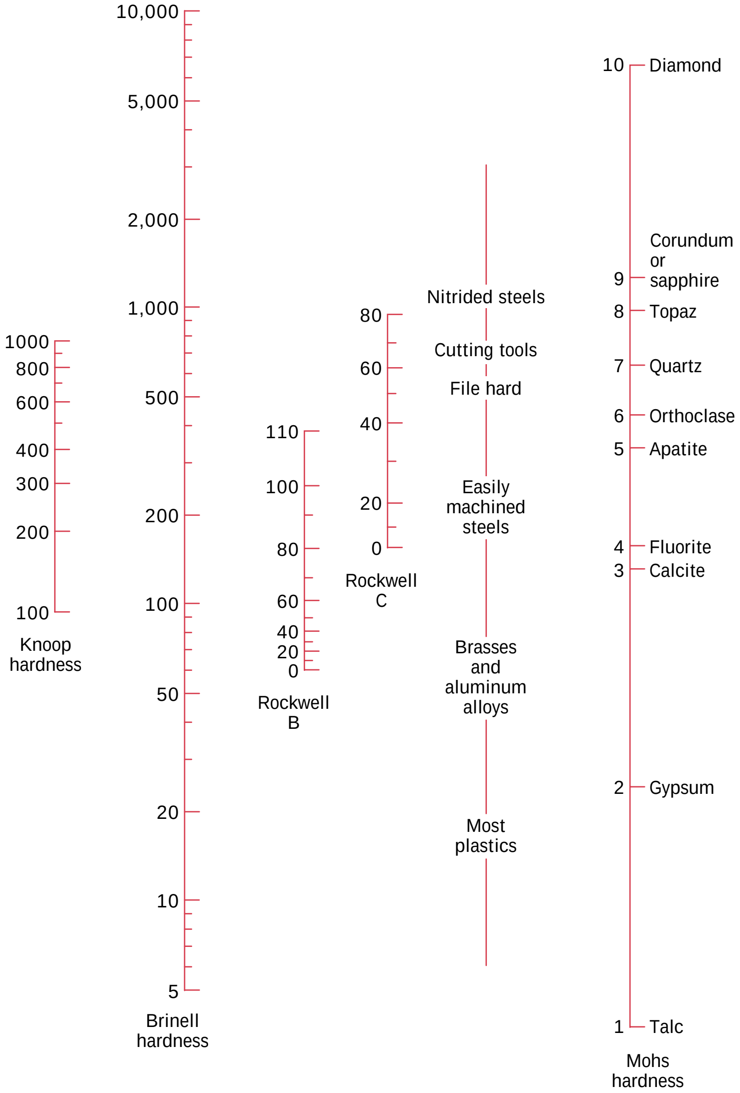

FIGURE 7.30 Comparison of several hardness scales. (Adapted from G. F. Kinney, *Engineering Properties and Applications of Plastics*, p. 202. Copyright © 1957 by John Wiley & Sons, New York. Reprinted by permission of John Wiley & Sons, Inc.)

7.17 HARDNESS OF CERAMIC MATERIALS

One beneficial mechanical property of ceramics is their hardness, which is often utilized when an abrasive or grinding action is required; in fact, the hardest known materials are ceramics. A listing of a number of different ceramic materials according to Knoop hardness is contained in Table 7.6. Only ceramics having Knoop hardnesses of about 1000 or greater are utilized for their abrasive characteristics (Section 13.8).

7.18 TEAR STRENGTH AND HARDNESS OF POLYMERS

Mechanical properties that are sometimes influential in the suitability of a polymer for some particular application include tear resistance and hardness. The ability to resist tearing is an important property of some plastics, especially those used for thin films in packaging. *Tear strength*, the mechanical parameter that is measured,

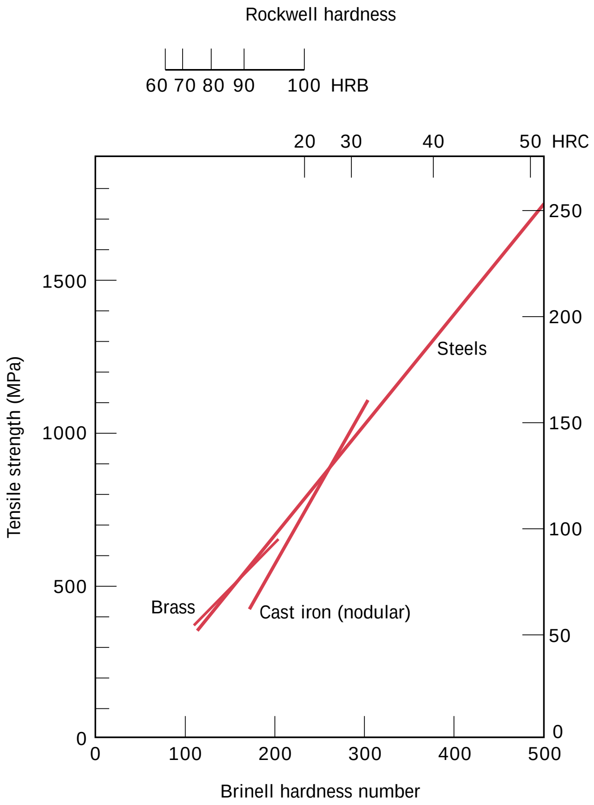

FIGURE 7.31 Relationships between hardness and tensile strength for steel, brass, and cast iron. (Data taken from *Metals Handbook: Properties and Selection: Irons and Steels,* Vol. 1, 9th edition, B. Bardes, Editor, American Society for Metals, 1978, pp. 36 and 461; and *Metals Handbook: Properties and Selection: Nonferrous Alloys and Pure Metals,* Vol. 2, 9th edition, H. Baker, Managing Editor, American Society for Metals, 1979, p. 327.)

is the energy required to tear apart a cut specimen that has a standard geometry. The magnitude of tensile and tear strengths are related.

Polymers are softer than metals and ceramics, and most hardness tests are conducted by penetration techniques similar to those described for metals in the previous section. Rockwell tests are frequently used for polymers.[19] Other indentation techniques employed are the Durometer and Barcol.[20]

Table 7.6 Approximate Knoop Hardness (100 g load) for Seven Ceramic Materials

Material	*Approximate Knoop Hardness*
Diamond (carbon)	7000
Boron carbide (B_4C)	2800
Silicon carbide (SiC)	2500
Tungsten carbide (WC)	2100
Aluminum oxide (Al_2O_3)	2100
Quartz (SiO_2)	800
Glass	550

---

[19] ASTM Standard D 785, ''Rockwell Hardness of Plastics and Electrical Insulating Materials.''

[20] ASTM Standard D 2240, ''Standard Test Method for Rubber Property—Durometer Hardness;'' and ASTM Standard D 2583, ''Standard Test Method for Indentation of Rigid Plastics by Means of a Barcol Impressor.''

PROPERTY VARIABILITY AND DESIGN/SAFETY FACTORS

7.19 VARIABILITY OF MATERIAL PROPERTIES

At this point it is worthwhile to discuss an issue that sometimes proves troublesome to many engineering students, namely, that measured material properties are not exact quantities. That is, even if we have a most precise measuring apparatus and a highly controlled test procedure, there will always be some scatter or variability in the data that are collected from specimens of the same material. For example, consider a number of identical tensile samples that are prepared from a single bar of some metal alloy, which samples are subsequently stress–strain tested in the same apparatus. We would most likely observe that each resulting stress–strain plot is slightly different from the others. This would lead to a variety of modulus of elasticity, yield strength, and tensile strength values. A number of factors lead to uncertainties in measured data. These include the test method, variations in specimen fabrication procedures, operator bias, and apparatus calibration. Furthermore, inhomogeneities may exist within the same lot of material, and/or slight compositional and other differences from lot to lot. Of course, appropriate measures should be taken to minimize the possibility of measurement error, and also to mitigate those factors that lead to data variability.

It should also be mentioned that scatter exists for other measured material properties such as density, electrical conductivity, and coefficient of thermal expansion.

It is important for the design engineer to realize that scatter and variability of materials properties are inevitable and must be dealt with appropriately. On occasion, data must be subjected to statistical treatments and probabilities determined. For example, instead of asking the question, ''What is the fracture strength of this alloy?'' the engineer should become accustomed to asking the question, ''What is the probability of failure of this alloy under these given circumstances?''

It is often desirable to specify a typical value and degree of dispersion (or scatter) for some measured property; such is commonly accomplished by taking the average and the standard deviation, respectively.

COMPUTATION OF AVERAGE AND STANDARD DEVIATION VALUES (CD-ROM)

7.20 DESIGN/SAFETY FACTORS

There will always be uncertainties in characterizing the magnitude of applied loads and their associated stress levels for in-service applications; ordinarily load calculations are only approximate. Furthermore, as noted in the previous section, virtually all engineering materials exhibit a variability in their measured mechanical properties. Consequently, design allowances must be made to protect against unanticipated failure. One way this may be accomplished is by establishing, for the particular application, a **design stress,** denoted as σ_d. For static situations and when ductile materials are used, σ_d is taken as the calculated stress level σ_c (on the basis of the estimated maximum load) multiplied by a *design factor, N'*, that is

$$\sigma_d = N'\sigma_c \tag{7.28}$$

where N' is greater than unity. Thus, the material to be used for the particular application is chosen so as to have a yield strength at least as high as this value of σ_d.

Alternatively, a **safe stress** or *working stress*, σ_w, is used instead of design stress. This safe stress is based on the yield strength of the material and is defined as the yield strength divided by a *factor of safety*, N, or

$$\sigma_w = \frac{\sigma_y}{N} \tag{7.29}$$

Utilization of design stress (Equation 7.28) is usually preferred since it is based on the anticipated maximum applied stress instead of the yield strength of the material; normally there is a greater uncertainty in estimating this stress level than in the specification of the yield strength. However, in the discussion of this text, we are concerned with factors that influence yield strengths, and not in the determination of applied stresses; therefore, the succeeding discussion will deal with working stresses and factors of safety.

The choice of an appropriate value of N is necessary. If N is too large, then component overdesign will result, that is, either too much material or a material having a higher-than-necessary strength will be used. Values normally range between 1.2 and 4.0. Selection of N will depend on a number of factors, including economics, previous experience, the accuracy with which mechanical forces and material properties may be determined, and, most important, the consequences of failure in terms of loss of life and/or property damage.

Design Example 7.1

A tensile-testing apparatus is to be constructed that must withstand a maximum load of 220,000 N (50,000 lb_f). The design calls for two cylindrical support posts, each of which is to support half of the maximum load. Furthermore, plain-carbon (1045) steel ground and polished shafting rounds are to be used; the minimum yield and tensile strengths of this alloy are 310 MPa (45,000 psi) and 565 MPa (82,000 psi), respectively. Specify a suitable diameter for these support posts.

Solution

The first step in this design process is to decide on a factor safety, N, which then allows determination of a working stress according to Equation 7.29. In addition, to ensure that the apparatus will be safe to operate, we also want to minimize any elastic deflection of the rods during testing; therefore, a relatively conservative factor of safety is to be used, say $N = 5$. Thus, the working stress σ_w is just

$$\begin{aligned}\sigma_w &= \frac{\sigma_y}{N} \\ &= \frac{310\ \text{MPa}}{5} = 62\ \text{MPa (9000 psi)}\end{aligned}$$

From the definition of stress, Equation 7.1,

$$A_0 = \left(\frac{d}{2}\right)^2 \pi = \frac{F}{\sigma_w}$$

where d is the rod diameter and F is the applied force; furthermore, each of the two rods must support half of the total force or 110,000 N (25,000 psi). Solving for *d* leads to

$$
\begin{aligned}
d &= 2\sqrt{\frac{F}{\pi\sigma_w}} \\
&= 2\sqrt{\frac{110{,}000\ \text{N}}{\pi\,(62 \times 10^6\ \text{N/m}^2)}} \\
&= 4.75 \times 10^{-2}\ \text{m} = 47.5\ \text{mm}\ (1.87\ \text{in.})
\end{aligned}
$$

Therefore, the diameter of each of the two rods should be 47.5 mm or 1.87 in.

SUMMARY

A number of the important mechanical properties of materials have been discussed in this chapter. Concepts of stress and strain were first introduced. Stress is a measure of an applied mechanical load or force, normalized to take into account cross-sectional area. Two different stress parameters were defined—engineering stress and true stress. Strain represents the amount of deformation induced by a stress; both engineering and true strains are used.

Some of the mechanical characteristics of materials can be ascertained by simple stress–strain tests. There are four test types: tension, compression, torsion, and shear. Tensile are the most common. A material that is stressed first undergoes elastic, or nonpermanent, deformation, wherein stress and strain are proportional. The constant of proportionality is the modulus of elasticity for tension and compression, and is the shear modulus when the stress is shear. Poisson's ratio represents the negative ratio of transverse and longitudinal strains.

For metals, the phenomenon of yielding occurs at the onset of plastic or permanent deformation; yield strength is determined by a strain offset method from the stress–strain behavior, which is indicative of the stress at which plastic deformation begins. Tensile strength corresponds to the maximum tensile stress that may be sustained by a specimen, whereas percents elongation and reduction in area are measures of ductility—the amount of plastic deformation that has occurred at fracture. Resilience is the capacity of a material to absorb energy during elastic deformation; modulus of resilience is the area beneath the engineering stress–strain curve up to the yield point. Also, static toughness represents the energy absorbed during the fracture of a material, and is taken as the area under the entire engineering stress–strain curve. Ductile materials are normally tougher than brittle ones.

For the brittle ceramic materials, flexural strengths are determined by performing transverse bending tests to fracture. {Many ceramic bodies contain residual porosity, which is deleterious to both their moduli of elasticity and flexural strengths.}

On the basis of stress–strain behavior, polymers fall within three general classifications: brittle, plastic, and highly elastic. These materials are neither as strong nor as stiff as metals, and their mechanical properties are sensitive to changes in temperature and strain rate.

{Viscoelastic mechanical behavior, being intermediate between totally elastic and totally viscous, is displayed by a number of polymeric materials. It is characterized by the relaxation modulus, a time-dependent modulus of elasticity. The magnitude of the relaxation modulus is very sensitive to temperature; critical to the in-service temperature range for elastomers is this temperature dependence.}

Hardness is a measure of the resistance to localized plastic deformation. In several popular hardness-testing techniques (Rockwell, Brinell, Knoop, and Vickers) a small indenter is forced into the surface of the material, and an index number is determined on the basis of the size or depth of the resulting indentation. For many metals, hardness and tensile strength are approximately proportional to each other. In addition to their inherent brittleness, ceramic materials are distinctively hard. And polymers are relatively soft in comparison to the other material types.

Measured mechanical properties (as well as other material properties) are not exact and precise quantities, in that there will always be some scatter for the measured data. Typical material property values are commonly specified in terms of averages, whereas magnitudes of scatter may be expressed as standard deviations.

As a result of uncertainties in both measured mechanical properties and inservice applied stresses, safe or working stresses are normally utilized for design purposes. For ductile materials, safe stress is the ratio of the yield strength and a factor of safety.

IMPORTANT TERMS AND CONCEPTS

Anelasticity
Design stress
Ductility
Elastic deformation
Elastic recovery
Elastomer
Engineering strain
Engineering stress
Flexural strength
Hardness
Modulus of elasticity
Plastic deformation
Poisson's ratio
Proportional limit
{Relaxation modulus}
Resilience
Safe stress
Shear
Tensile strength
Toughness
True strain
True stress
{Viscoelasticity}
Yielding
Yield strength

REFERENCES

ASM Handbook, Vol. 8, *Mechanical Testing*, ASM International, Materials Park, OH, 1985.

Billmeyer, F. W., Jr., *Textbook of Polymer Science*, 3rd edition, Wiley-Interscience, New York, 1984. Chapter 11.

Boyer, H. E. (Editor), *Atlas of Stress–Strain Curves*, ASM International, Materials Park, OH, 1986.

Boyer, H. E. (Editor), *Hardness Testing*, ASM International, Materials Park, OH, 1987.

Davidge, R. W., *Mechanical Behaviour of Ceramics*, Cambridge University Press, Cambridge, 1979. Reprinted by TechBooks, Marietta, OH.

Dieter, G. E., *Mechanical Metallurgy*, 3rd edition, McGraw-Hill Book Co., New York, 1986.

Dowling, N. E., *Mechanical Behavior of Materials*, Prentice Hall, Inc., Englewood Cliffs, NJ, 1993.

Engineered Materials Handbook, Vol. 2, *Engineering Plastics*, ASM International, Materials Park, OH, 1988.

Engineered Materials Handbook, Vol. 4, *Ceramics and Glasses*, ASM International, Materials Park, OH, 1991.

Han, P. (Editor), *Tensile Testing*, ASM International, Materials Park, OH, 1992.

Harper, C. A. (Editor), *Handbook of Plastics, Elastomers and Composites*, 3rd edition, McGraw-Hill Book Company, New York, 1996.

Kingery, W. D., H. K. Bowen, and D. R. Uhlmann, *Introduction to Ceramics*, 2nd edition, John Wiley & Sons, New York, 1976. Chapters 14 and 15.

McClintock, F. A. and A. S. Argon, *Mechanical Behavior of Materials*, Addison-Wesley Publishing Co., Reading, MA, 1966. Reprinted by TechBooks, Marietta, OH.

Meyers, M. A. and K. K. Chawla, *Mechanical Metallurgy, Principles and Applications,* Prentice Hall, Inc., Englewood Cliffs, NJ, 1984.

Modern Plastics Encyclopedia, McGraw-Hill Book Company, New York. Revised and published annually.

Nielsen, L. E., *Mechanical Properties of Polymers and Composites*, 2nd edition, Marcel Dekker, New York, 1994.

Richerson, D. W., *Modern Ceramic Engineering,* 2nd edition, Marcel Dekker, New York, 1992.

Rosen, S. L., *Fundamental Principles of Polymeric Materials*, 2nd edition, John Wiley & Sons, New York, 1993.

Tobolsky, A. V., *Properties and Structures of Polymers,* John Wiley & Sons, New York, 1960. Advanced treatment.

Wachtman, J. B., *Mechanical Properties of Ceramics*, John Wiley & Sons, Inc., New York, 1996.

Ward, I. M. and D. W. Hadley, *An Introduction to the Mechanical Properties of Solid Polymers,* John Wiley & Sons, Chichester, UK, 1993.

Young, R. J. and P. Lovell, *Introduction to Polymers,* 2nd edition, Chapman and Hall, London, 1991.

QUESTIONS AND PROBLEMS

Note: To solve those problems having an asterisk (*) by their numbers, consultation of supplementary topics [appearing only on the CD-ROM (and not in print)] will probably be necessary.

7.1 Using mechanics of materials principles (i.e., equations of mechanical equilibrium applied to a free-body diagram), derive Equations 7.4a and 7.4b.

7.2 **(a)** Equations 7.4a and 7.4b are expressions for normal (σ') and shear (τ') stresses, respectively, as a function of the applied tensile stress (σ) and the inclination angle of the plane on which these stresses are taken (θ of Figure 7.4). Make a plot on which is presented the orientation parameters of these expressions (i.e., $\cos^2\theta$ and $\sin\theta\cos\theta$) versus θ.

(b) From this plot, at what angle of inclination is the normal stress a maximum?

(c) Also, at what inclination angle is the shear stress a maximum?

7.3 A specimen of aluminum having a rectangular cross section 10 mm × 12.7 mm (0.4 in. × 0.5 in.) is pulled in tension with 35,500 N (8000 lb_f) force, producing only elastic deformation. Calculate the resulting strain.

7.4 A cylindrical specimen of a titanium alloy having an elastic modulus of 107 GPa (15.5×10^6 psi) and an original diameter of 3.8 mm (0.15 in.) will experience only elastic deformation when a tensile load of 2000 N (450 lb_f) is applied. Compute the maximum length of the specimen before deformation if the maximum allowable elongation is 0.42 mm (0.0165 in.).

7.5 A steel bar 100 mm (4.0 in.) long and having a square cross section 20 mm (0.8 in.) on an edge is pulled in tension with a load of 89,000 N (20,000 lb_f), and experiences an elongation of 0.10 mm (4.0×10^{-3} in.). Assuming that the deformation is entirely elastic, calculate the elastic modulus of the steel.

7.6 Consider a cylindrical titanium wire 3.0 mm (0.12 in.) in diameter and 2.5×10^4 mm (1000 in.) long. Calculate its elongation when a load of 500 N (112 lb_f) is applied. Assume that the deformation is totally elastic.

7.7 For a bronze alloy, the stress at which plastic deformation begins is 275 MPa (40,000 psi), and the modulus of elasticity is 115 GPa (16.7×10^6 psi).

(a) What is the maximum load that may be applied to a specimen with a cross-sectional area of 325 mm^2 (0.5 in.^2) without plastic deformation?

(b) If the original specimen length is 115 mm (4.5 in.), what is the maximum length to which it may be stretched without causing plastic deformation?

7.8 A cylindrical rod of copper ($E = 110$ GPa,

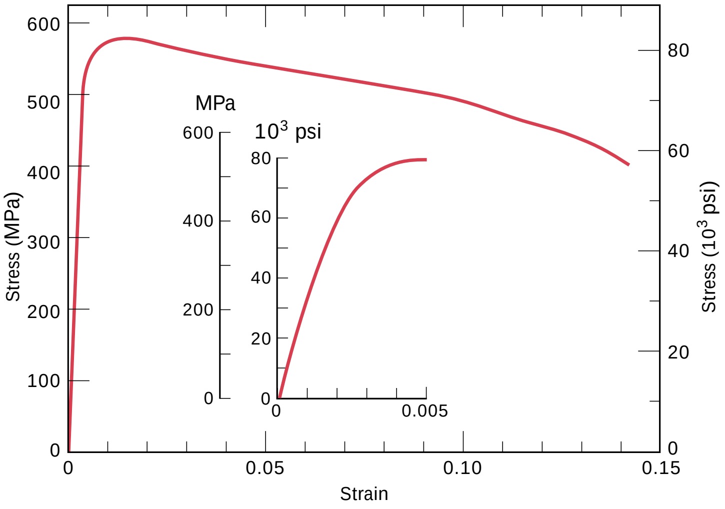

Figure 7.33 Tensile stress–strain behavior for a plain carbon steel.

16 × 10^6 psi) having a yield strength of 240 MPa (35,000 psi) is to be subjected to a load of 6660 N (1500 lb_f). If the length of the rod is 380 mm (15.0 in.), what must be the diameter to allow an elongation of 0.50 mm (0.020 in.)?

7.9 Consider a cylindrical specimen of a steel alloy (Figure 7.33) 10 mm (0.39 in.) in diameter and 75 mm (3.0 in.) long that is pulled in tension. Determine its elongation when a load of 23,500 N (5300 lb_f) is applied.

7.10 Figure 7.34 shows, for a gray cast iron, the tensile engineering stress–strain curve in the elastic region. Determine (**a**) the secant modulus taken to 35 MPa (5000 psi), and (**b**) the tangent modulus taken from the origin.

7.11 As was noted in Section 3.18, for single crystals of some substances, the physical properties are anisotropic, that is, they are dependent on crystallographic direction. One such property is the modulus of elasticity. For cubic single crystals, the modulus of elasticity in a general $[uvw]$ direction, E_{uvw}, is described by the relationship

$$\frac{1}{E_{uvw}} = \frac{1}{E_{\langle 100\rangle}} - 3\left(\frac{1}{E_{\langle 100\rangle}} - \frac{1}{E_{\langle 111\rangle}}\right)$$
$$(\alpha^2\beta^2 + \beta^2\gamma^2 + \gamma^2\alpha^2)$$

where $E_{\langle 100\rangle}$ and $E_{\langle 111\rangle}$ are the moduli of elasticity in [100] and [111] directions, respectively; α, β, and γ are the cosines of the

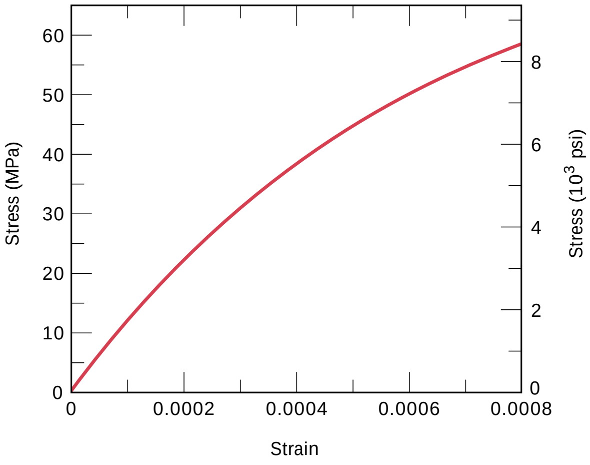

Figure 7.34 Tensile stress–strain behavior for a gray cast iron.

angles between [*uvw*] and the respective [100], [010], and [001] directions. Verify that the $E_{\langle 110\rangle}$ values for aluminum, copper, and iron in Table 3.7 are correct.

7.12 In Section 2.6 it was noted that the net bonding energy E_N between two isolated positive and negative ions is a function of interionic distance r as follows:

$$E_N = -\frac{A}{r} + \frac{B}{r^n} \tag{7.30}$$

where A, B, and n are constants for the particular ion pair. Equation 7.30 is also valid for the bonding energy between adjacent ions in solid materials. The modulus of elasticity E is proportional to the slope of the interionic force-separation curve at the equilibrium interionic separation; that is,

$$E \propto \left(\frac{dF}{dr}\right)_{r_0}$$

Derive an expression for the dependence of the modulus of elasticity on these A, B, and n parameters (for the two-ion system) using the following procedure:

1. Establish a relationship for the force F as a function of r, realizing that

$$F = \frac{dE_N}{dr}$$

2. Now take the derivative dF/dr.

3. Develop an expression for r_0, the equilibrium separation. Since r_0 corresponds to the value of r at the minimum of the E_N-versus-r-curve (Figure 2.8*b*), take the derivative dE_N/dr, set it equal to zero, and solve for r, which corresponds to r_0.

4. Finally, substitute this expression for r_0 into the relationship obtained by taking dF/dr.

7.13 Using the solution to Problem 7.12, rank the magnitudes of the moduli of elasticity for the following hypothetical X, Y, and Z materials from the greatest to the least. The appropriate A, B, and n parameters (Equation 7.30) for these three materials are tabulated below; they yield E_N in units of electron volts and r in nanometers:

Material	*A*	*B*	*n*
X	2.5	2×10^{-5}	8
Y	2.3	8×10^{-6}	10.5
Z	3.0	1.5×10^{-5}	9

7.14 A cylindrical specimen of aluminum having a diameter of 19 mm (0.75 in.) and length of 200 mm (8.0 in.) is deformed elastically in tension with a force of 48,800 N (11,000 lb_f). Using the data contained in Table 7.1, determine the following:

(a) The amount by which this specimen will elongate in the direction of the applied stress.

(b) The change in diameter of the specimen. Will the diameter increase or decrease?

7.15 A cylindrical bar of steel 10 mm (0.4 in.) in diameter is to be deformed elastically by application of a force along the bar axis. Using the data in Table 7.1, determine the force that will produce an elastic reduction of 3×10^{-3} mm (1.2×10^{-4} in.) in the diameter.

7.16 A cylindrical specimen of some alloy 8 mm (0.31 in.) in diameter is stressed elastically in tension. A force of 15,700 N (3530 lb_f) produces a reduction in specimen diameter of 5×10^{-3} mm (2×10^{-4} in.). Compute Poisson's ratio for this material if its modulus of elasticity is 140 GPa (20.3×10^6 psi).

7.17 A cylindrical specimen of a hypothetical metal alloy is stressed in compression. If its original and final diameters are 20.000 and 20.025 mm, respectively, and its final length is 74.96 mm, compute its original length if the deformation is totally elastic. The elastic and shear moduli for this alloy are 105 GPa and 39.7 GPa, respectively.

7.18 Consider a cylindrical specimen of some hypothetical metal alloy that has a diameter of 8.0 mm (0.31 in.). A tensile force of 1000 N (225 lb_f) produces an elastic reduction in diameter of 2.8×10^{-4} mm (1.10×10^{-5} in.). Compute the modulus of elasticity for this alloy, given that Poisson's ratio is 0.30.

7.19 A brass alloy is known to have a yield strength of 275 MPa (40,000 psi), a tensile strength of 380 MPa (55,000 psi), and an elastic modulus of 103 GPa (15.0×10^6 psi). A cylindrical specimen of this alloy 12.7 mm (0.50 in.) in diameter and 250 mm (10.0 in.) long is stressed in tension and found to elongate 7.6 mm (0.30 in.). On the basis of the information given, is it possible to compute the magnitude of the load that is necessary to produce this change in length? If so, calculate the load. If not, explain why.

7.20 A cylindrical metal specimen 15.0 mm (0.59 in.) in diameter and 150 mm (5.9 in.) long is to be subjected to a tensile stress of 50 MPa (7250 psi); at this stress level the resulting deformation will be totally elastic.

(a) If the elongation must be less than 0.072 mm (2.83×10^{-3} in.), which of the metals in Table 7.1 are suitable candidates? Why?

(b) If, in addition, the maximum permissible diameter decrease is 2.3×10^{-3} mm (9.1×10^{-5} in.), which of the metals in Table 7.1 may be used? Why?

7.21 Consider the brass alloy with stress–strain behavior shown in Figure 7.12. A cylindrical specimen of this material 6 mm (0.24 in.) in diameter and 50 mm (2 in.) long is pulled in tension with a force of 5000 N (1125 lb_f). If it is known that this alloy has a Poisson's ratio of 0.30, compute: **(a)** the specimen elongation, and **(b)** the reduction in specimen diameter.

7.22 Cite the primary differences between elastic, anelastic, and plastic deformation behaviors.

7.23 A cylindrical rod 100 mm long and having a diameter of 10.0 mm is to be deformed using a tensile load of 27,500 N. It must not experience either plastic deformation or a diameter reduction of more than 7.5×10^{-3} mm. Of the materials listed as follows, which are possible candidates? Justify your choice(s).

Material	*Modulus of Elasticity (GPa)*	*Yield Strength (MPa)*	*Poisson's Ratio*
Aluminum alloy	70	200	0.33
Brass alloy	101	300	0.35
Steel alloy	207	400	0.27
Titanium alloy	107	650	0.36

7.24 A cylindrical rod 380 mm (15.0 in.) long, having a diameter of 10.0 mm (0.40 in.), is to be subjected to a tensile load. If the rod is to experience neither plastic deformation nor an elongation of more than 0.9 mm (0.035 in.) when the applied load is 24,500 N (5500 lb_f), which of the four metals or alloys listed below are possible candidates? Justify your choice(s).

Material	*Modulus of Elasticity (GPa)*	*Yield Strength (MPa)*	*Tensile Strength (MPa)*
Aluminum alloy	70	255	420
Brass alloy	100	345	420
Copper	110	250	290
Steel alloy	207	450	550

7.25 Figure 7.33 shows the tensile engineering stress–strain behavior for a steel alloy.

(a) What is the modulus of elasticity?

(b) What is the proportional limit?

(c) What is the yield strength at a strain offset of 0.002?

(d) What is the tensile strength?

7.26 A cylindrical specimen of a brass alloy having a length of 60 mm (2.36 in.) must elongate only 10.8 mm (0.425 in.) when a tensile load of 50,000 N (11,240 lb_f) is applied. Under these circumstances, what must be the radius of the specimen? Consider this brass alloy to have the stress–strain behavior shown in Figure 7.12.

7.27 A load of 44,500 N (10,000 lb_f) is applied to a cylindrical specimen of steel (displaying the stress–strain behavior shown in Figure 7.33) that has a cross-sectional diameter of 10 mm (0.40 in.).

(a) Will the specimen experience elastic or plastic deformation? Why?

(b) If the original specimen length is 500 mm (20 in.), how much will it increase in length when this load is applied?

7.28 A bar of a steel alloy that exhibits the stress–strain behavior shown in Figure 7.33 is subjected to a tensile load; the specimen is 300 mm (12 in.) long, and of square cross section 4.5 mm (0.175 in.) on a side.

(a) Compute the magnitude of the load necessary to produce an elongation of 0.46 mm (0.018 in.).

(b) What will be the deformation after the load is released?

7.29 A cylindrical specimen of aluminum having a diameter of 0.505 in. (12.8 mm) and a gauge length of 2.000 in. (50.800 mm) is pulled in tension. Use the load–elongation characteristics tabulated below to complete problems a through f.

Load		***Length***	
lb$_f$	***N***	***in.***	***mm***
0	0	2.000	50.800
1,650	7,330	2.002	50.851
3,400	15,100	2.004	50.902
5,200	23,100	2.006	50.952
6,850	30,400	2.008	51.003
7,750	34,400	2.010	51.054
8,650	38,400	2.020	51.308
9,300	41,300	2.040	51.816
10,100	44,800	2.080	52.832
10,400	46,200	2.120	53.848
10,650	47,300	2.160	54.864
10,700	47,500	2.200	55.880
10,400	46,100	2.240	56.896
10,100	44,800	2.270	57.658
9,600	42,600	2.300	58.420
8,200	36,400	2.330	59.182
Fracture			

(a) Plot the data as engineering stress versus engineering strain.

(b) Compute the modulus of elasticity.

(c) Determine the yield strength at a strain offset of 0.002.

(d) Determine the tensile strength of this alloy.

(e) What is the approximate ductility, in percent elongation?

(f) Compute the modulus of resilience.

7.30 A specimen of ductile cast iron having a rectangular cross section of dimensions 4.8 mm × 15.9 mm ($\frac{3}{16}$ in. × $\frac{5}{8}$ in.) is deformed in tension. Using the load-elongation data tabulated below, complete problems a through f.

Load		***Length***	
N	***lb$_f$***	***mm***	***in.***
0	0	75.000	2.953
4,740	1065	75.025	2.954
9,140	2055	75.050	2.955
12,920	2900	75.075	2.956
16,540	3720	75.113	2.957
18,300	4110	75.150	2.959
20,170	4530	75.225	2.962
22,900	5145	75.375	2.968
25,070	5635	75.525	2.973
26,800	6025	75.750	2.982
28,640	6440	76.500	3.012
30,240	6800	78.000	3.071
31,100	7000	79.500	3.130
31,280	7030	81.000	3.189
30,820	6930	82.500	3.248
29,180	6560	84.000	3.307
27,190	6110	85.500	3.366
24,140	5430	87.000	3.425
18,970	4265	88.725	3.493
Fracture			

(a) Plot the data as engineering stress versus engineering strain.

(b) Compute the modulus of elasticity.

(c) Determine the yield strength at a strain offset of 0.002.

(d) Determine the tensile strength of this alloy.

(e) Compute the modulus of resilience.

(f) What is the ductility, in percent elongation?

7.31 A cylindrical metal specimen having an original diameter of 12.8 mm (0.505 in.) and gauge length of 50.80 mm (2.000 in.) is pulled in tension until fracture occurs. The diameter at the point of fracture is 6.60 mm (0.260 in.), and the fractured gauge length is 72.14 mm (2.840 in.). Calculate the ductility in terms of percent reduction in area and percent elongation.

7.32 Calculate the moduli of resilience for the materials having the stress–strain behaviors shown in Figures 7.12 and 7.33.

7.33 Determine the modulus of resilience for each of the following alloys:

	Yield Strength	
Material	***MPa***	***psi***
Steel alloy	550	80,000
Brass alloy	350	50,750
Aluminum alloy	250	36,250
Titanium alloy	800	116,000

Use modulus of elasticity values in Table 7.1.

7.34 A brass alloy to be used for a spring application must have a modulus of resilience of at least 0.75 MPa (110 psi). What must be its minimum yield strength?

7.35 **(a)** Make a schematic plot showing the tensile true stress–strain behavior for a typical metal alloy.

(b) Superimpose on this plot a schematic curve for the compressive true stress–strain behavior for the same alloy. Explain any difference between this curve and the one in part a.

(c) Now superimpose a schematic curve for the compressive engineering stress–strain behavior for this same alloy, and explain any difference between this curve and the one in part b.

7.36 Show that Equations 7.18a and 7.18b are valid when there is no volume change during deformation.

7.37 Demonstrate that Equation 7.16, the expression defining true strain, may also be represented by

$$\epsilon_T = \ln\left(\frac{A_0}{A_i}\right)$$

when specimen volume remains constant during deformation. Which of these two expressions is more valid during necking? Why?

7.38 Using the data in Problem 7.29 and Equations 7.15, 7.16, and 7.18a, generate a true stress–true strain plot for aluminum. Equation 7.18a becomes invalid past the point at which necking begins; therefore, measured diameters are given below for the last four data points, which should be used in true stress computations.

Load		***Length***		***Diameter***	
lb_f	***N***	***in.***	***mm***	***in.***	***mm***
10,400	46,100	2.240	56.896	0.461	11.71
10,100	44,800	2.270	57.658	0.431	10.95
9,600	42,600	2.300	58.420	0.418	10.62
8,200	36,400	2.330	59.182	0.370	9.40

7.39 A tensile test is performed on a metal specimen, and it is found that a true plastic strain of 0.20 is produced when a true stress of 575 MPa (83,500 psi) is applied; for the same metal, the value of K in Equation 7.19 is 860 MPa (125,000 psi). Calculate the true strain that results from the application of a true stress of 600 MPa (87,000 psi).

7.40 For some metal alloy, a true stress of 415 MPa (60,175 psi) produces a plastic true strain of 0.475. How much will a specimen of this material elongate when a true stress of 325 MPa (46,125 psi) is applied if the original length is 300 mm (11.8 in.)? Assume a value of 0.25 for the strain-hardening exponent n.

7.41 The following true stresses produce the corresponding true plastic strains for a brass alloy:

True Stress (psi)	***True Strain***
50,000	0.10
60,000	0.20

What true stress is necessary to produce a true plastic strain of 0.25?

7.42 For a brass alloy, the following engineering stresses produce the corresponding plastic engineering strains, prior to necking:

Engineering Stress (MPa)	***Engineering Strain***
235	0.194
250	0.296

On the basis of this information, compute the *engineering* stress necessary to produce an *engineering* strain of 0.25.

7.43 Find the toughness (or energy to cause fracture) for a metal that experiences both elastic and plastic deformation. Assume Equation 7.5 for elastic deformation, that the modulus of elasticity is 172 GPa (25×10^6 psi), and that elastic deformation terminates at a strain of 0.01. For plastic deformation, assume that the relationship between stress and strain is described by Equation 7.19, in which the values for K and n are 6900 MPa (1×10^6 psi) and 0.30, respectively. Furthermore, plastic deformation occurs between strain values of 0.01 and 0.75, at which point fracture occurs.

7.44 For a tensile test, it can be demonstrated that necking begins when

$$\frac{d\sigma_T}{d\epsilon_T} = \sigma_T \tag{7.31}$$

Using Equation 7.19, determine the value of the true strain at this onset of necking.

7.45 Taking the logarithm of both sides of Equation 7.19 yields

$$\log \sigma_T = \log K + n \log \epsilon_T \tag{7.32}$$

Thus, a plot of $\log \sigma_T$ versus $\log \epsilon_T$ in the plastic region to the point of necking should yield a straight line having a slope of n and an intercept (at $\log \sigma_T = 0$) of $\log K$.

Using the appropriate data tabulated in Problem 7.29, make a plot of $\log \sigma_T$ versus $\log \epsilon_T$ and determine the values of n and K. It will be necessary to convert engineering stresses and strains to true stresses and strains using Equations 7.18a and 7.18b.

7.46 A cylindrical specimen of a brass alloy 7.5 mm (0.30 in.) in diameter and 90.0 mm (3.54 in.) long is pulled in tension with a force of 6000 N (1350 lb_f); the force is subsequently released.

(a) Compute the final length of the specimen at this time. The tensile stress–strain behavior for this alloy is shown in Figure 7.12.

(b) Compute the final specimen length when the load is increased to 16,500 N (3700 lb_f) and then released.

7.47 A steel specimen having a rectangular cross section of dimensions 19 mm × 3.2 mm ($\frac{3}{4}$ in. × $\frac{1}{8}$ in.) has the stress–strain behavior shown in Figure 7.33. If this specimen is subjected to a tensile force of 33,400 N (7,500 lb_f), then

(a) Determine the elastic and plastic strain values.

(b) If its original length is 460 mm (18 in.), what will be its final length after the load in part a is applied and then released?

7.48 A three-point bending test is performed on a glass specimen having a rectangular cross section of height d 5 mm (0.2 in.) and width b 10 mm (0.4 in.); the distance between support points is 45 mm (1.75 in.).

(a) Compute the flexural strength if the load at fracture is 290 N (65 lb_f).

(b) The point of maximum deflection Δy occurs at the center of the specimen and is described by

$$\Delta y = \frac{FL^3}{48EI}$$

where E is the modulus of elasticity and I the cross-sectional moment of inertia. Compute Δy at a load of 266 N (60 lb_f).

7.49 A circular specimen of MgO is loaded using a three-point bending mode. Compute the minimum possible radius of the specimen without fracture, given that the applied load is 425 N (95.5 lb_f), the flexural strength is 105 MPa (15,000 psi), and the separation between load points is 50 mm (2.0 in.).

7.50 A three-point bending test was performed on an aluminum oxide specimen having a circular cross section of radius 3.5 mm (0.14 in.); the specimen fractured at a load of 950 N (215 lb_f) when the distance between the support points was 50 mm (2.0 in.). Another test is to be performed on a specimen of this same material, but one that has a square cross section of 12 mm (0.47 in.) length on each edge. At what load would you expect this specimen to fracture if the support point separation is 40 mm (1.6 in.)?

7.51 **(a)** A three-point transverse bending test is conducted on a cylindrical specimen of aluminum oxide having a reported flexural strength of 390 MPa (56,600 psi). If the specimen radius is 2.5 mm (0.10 in.) and the support point separation distance is 30 mm (1.2 in.), predict whether or not you would expect the specimen to fracture when a load of 620 N (140 $\mathrm{lb_f}$) is applied. Justify your prediction.

(b) Would you be 100% certain of the prediction in part a? Why or why not?

7.52* The modulus of elasticity for beryllium oxide (BeO) having 5 vol% porosity is 310 GPa (45×10^6 psi).

(a) Compute the modulus of elasticity for the nonporous material.

(b) Compute the modulus of elasticity for 10 vol% porosity.

7.53* The modulus of elasticity for boron carbide (B_4C) having 5 vol% porosity is 290 GPa (42×10^6 psi).

(a) Compute the modulus of elasticity for the nonporous material.

(b) At what volume percent porosity will the modulus of elasticity be 235 GPa (34×10^6 psi)?

7.54* Using the data in Table 7.2, do the following:

(a) Determine the flexural strength for nonporous MgO assuming a value of 3.75 for *n* in Equation 7.22.

(b) Compute the volume fraction porosity at which the flexural strength for MgO is 62 MPa (9000 psi).

7.55* The flexural strength and associated volume fraction porosity for two specimens of the same ceramic material are as follows:

σ_{fs} *(MPa)*	*P*
100	0.05
50	0.20

(a) Compute the flexural strength for a completely nonporous specimen of this material.

(b) Compute the flexural strength for a 0.1 volume fraction porosity.

7.56 From the stress–strain data for polymethyl methacrylate shown in Figure 7.24, determine the modulus of elasticity and tensile strength at room temperature [20°C (68°F)], and compare these values with those given in Tables 7.1 and 7.2.

7.57 When citing the ductility as percent elongation for semicrystalline polymers, it is not necessary to specify the specimen gauge length, as is the case with metals. Why is this so?

7.58* In your own words, briefly describe the phenomenon of viscoelasticity.

7.59* For some viscoelastic polymers that are subjected to stress relaxation tests, the stress decays with time according to

$$\sigma(t) = \sigma(0) \exp\left(-\frac{t}{\tau}\right) \tag{7.33}$$

where $\sigma(t)$ and $\sigma(0)$ represent the time-dependent and initial (i.e., time = 0) stresses, respectively, and t and τ denote elapsed time and the relaxation time; τ is a time-independent constant characteristic of the material. A specimen of some viscoelastic polymer the stress relaxation of which obeys Equation 7.33 was suddenly pulled in tension to a measured strain of 0.6; the stress necessary to maintain this constant strain was measured as a function of time. Determine $E_r(10)$ for this material if the initial stress level was 2.76 MPa (400 psi), which dropped to 1.72 MPa (250 psi) after 60 s.

7.60* In Figure 7.35, the logarithm of $E_r(t)$ versus the logarithm of time is plotted for polyisobutylene at a variety of temperatures. Make a plot of log $E_r(10)$ versus temperature and then estimate the T_g.

7.61* On the basis of the curves in Figure 7.26, sketch schematic strain-time plots for the following polystyrene materials at the specified temperatures:

(a) Amorphous at 120°C.

(b) Crosslinked at 150°C.

(c) Crystalline at 230°C.

(d) Crosslinked at 50°C.

7.62* **(a)** Contrast the manner in which stress relaxation and viscoelastic creep tests are conducted.

(b) For each of these tests, cite the experimental parameter of interest and how it is determined.

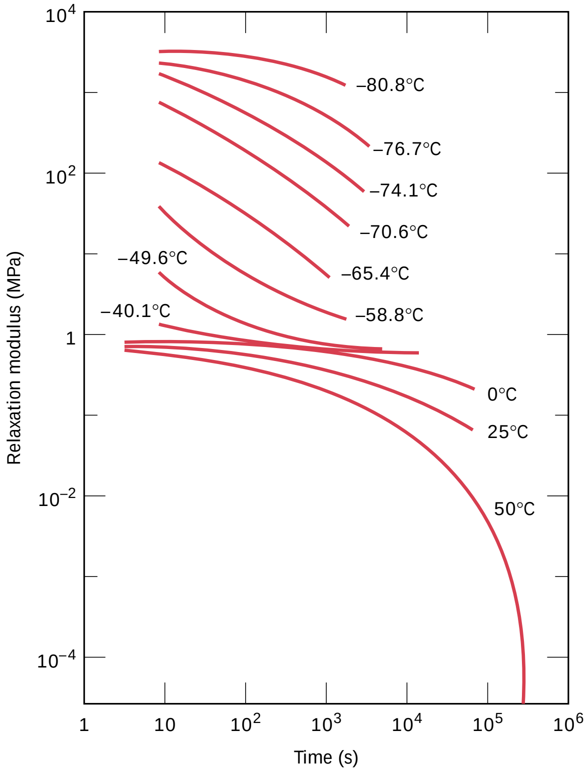

FIGURE 7.35 Logarithm of relaxation modulus versus logarithm of time for polyisobutylene between −80 and 50°C. (Adapted from E. Catsiff and A. V. Tobolsky, ''Stress-Relaxation of Polyisobutylene in the Transition Region [1,2],'' *J. Colloid Sci.*, **10,** 377 [1955]. Reprinted by permission of Academic Press, Inc.)

7.63* Make two schematic plots of the logarithm of relaxation modulus versus temperature for an amorphous polymer (curve *C* in Figure 7.29).

(a) On one of these plots demonstrate how the behavior changes with increasing molecular weight.

(b) On the other plot, indicate the change in behavior with increasing crosslinking.

7.64 **(a)** A 10-mm-diameter Brinell hardness indenter produced an indentation 1.62 mm in diameter in a steel alloy when a load of 500 kg was used. Compute the HB of this material.

(b) What will be the diameter of an indentation to yield a hardness of 450 HB when a 500 kg load is used?

7.65 Estimate the Brinell and Rockwell hardnesses for the following:

(a) The naval brass for which the stress–strain behavior is shown in Figure 7.12.

(b) The steel for which the stress–strain behavior is shown in Figure 7.33.

7.66 Using the data represented in Figure 7.31, specify equations relating tensile strength and Brinell hardness for brass and nodular cast iron, similar to Equations 7.25a and 7.25b for steels.

7.67 Cite five factors that lead to scatter in measured material properties.

7.68* Below are tabulated a number of Rockwell B hardness values that were measured on a single steel specimen. Compute average and standard deviation hardness values.

83.3	80.7	86.4
88.3	84.7	85.2
82.8	87.8	86.9
86.2	83.5	84.4
87.2	85.5	86.3

7.69 Upon what three criteria are factors of safety based?

7.70 Determine working stresses for the two alloys the stress–strain behaviors of which are shown in Figures 7.12 and 7.33.

Design Problems

7.D1 A large tower is to be supported by a series of steel wires. It is estimated that the load on each wire will be 11,100 N (2500 $\mathrm{lb_f}$). Determine the minimum required wire diameter assuming a factor of safety of 2 and a yield strength of 1030 MPa (150,000 psi).

7.D2 **(a)** Gaseous hydrogen at a constant pressure of 1.013 MPa (10 atm) is to flow within the inside of a thin-walled cylindrical tube of nickel that has a radius of 0.1 m. The temperature of the tube is to be 300°C and the pressure of hydrogen outside of the tube will be maintained at 0.01013 MPa (0.1 atm). Calculate the minimum wall thickness if the diffusion flux is to be no greater than 1×10^{-7} mol/m^2-s. The concentration of hydrogen in the nickel, C_H (in moles hydrogen per m^3 of Ni) is a function of hydrogen pressure, p_{H_2} (in MPa) and absolute temperature (T) according to

$$C_H = 30.8\sqrt{p_{H_2}}\exp\left(-\frac{12.3\text{ kJ/mol}}{RT}\right) \tag{7.34}$$

Furthermore, the diffusion coefficient for the diffusion of H in Ni depends on temperature as

$$D_H(\mathrm{m^2/s}) = 4.76 \times 10^{-7}\exp\left(-\frac{39.56\text{ kJ/mol}}{RT}\right) \tag{7.35}$$

(b) For thin-walled cylindrical tubes that are pressurized, the circumferential stress is a function of the pressure difference across the wall (Δp), cylinder radius (r), and tube thickness (Δx) as

$$\sigma = \frac{r\,\Delta p}{4\,\Delta x} \tag{7.36}$$

Compute the circumferential stress to which the walls of this pressurized cylinder are exposed.

(c) The room-temperature yield strength of Ni is 100 MPa (15,000 psi) and, furthermore, σ_y diminishes about 5 MPa for every 50°C rise in temperature. Would you expect the wall thickness computed in part (b) to be suitable for this Ni cylinder at 300°C? Why or why not?

(d) If this thickness is found to be suitable, compute the minimum thickness that could be used without any deformation of the tube walls. How much would the diffusion flux increase with this reduction in thickness? On the other hand, if the thickness determined in part (c) is found to be unsuitable, then specify a minimum thickness that you would use. In this case, how much of a diminishment in diffusion flux would result?

7.D3 Consider the steady-state diffusion of hydrogen through the walls of a cylindrical nickel tube as described in Problem 7.D2. One design calls for a diffusion flux of 5×10^{-8} mol/m^2-s, a tube radius of 0.125 m, and inside and outside pressures of 2.026 MPa (20 atm) and 0.0203 MPa (0.2 atm), respectively; the maximum allowable temperature is 450°C. Specify a suitable temperature and wall thickness to give this diffusion flux and yet ensure that the tube walls will not experience any permanent deformation.

7.D4 It is necessary to select a ceramic material to be stressed using a three-point loading scheme (Figure 7.18). The specimen must have a circular cross section and a radius of 2.5 mm (0.10 in.), and must not experience fracture or a deflection of more than 6.2×10^{-2} mm (2.4×10^{-3} in.) at its center when a load of 275 N (62 $\mathrm{lb_f}$) is applied. If the distance between support points is 45 mm (1.77 in.), which of the ceramic materials in Tables 7.1 and 7.2 are candidates? The magnitude of the centerpoint deflection may be computed using the equation supplied in Problem 7.48.

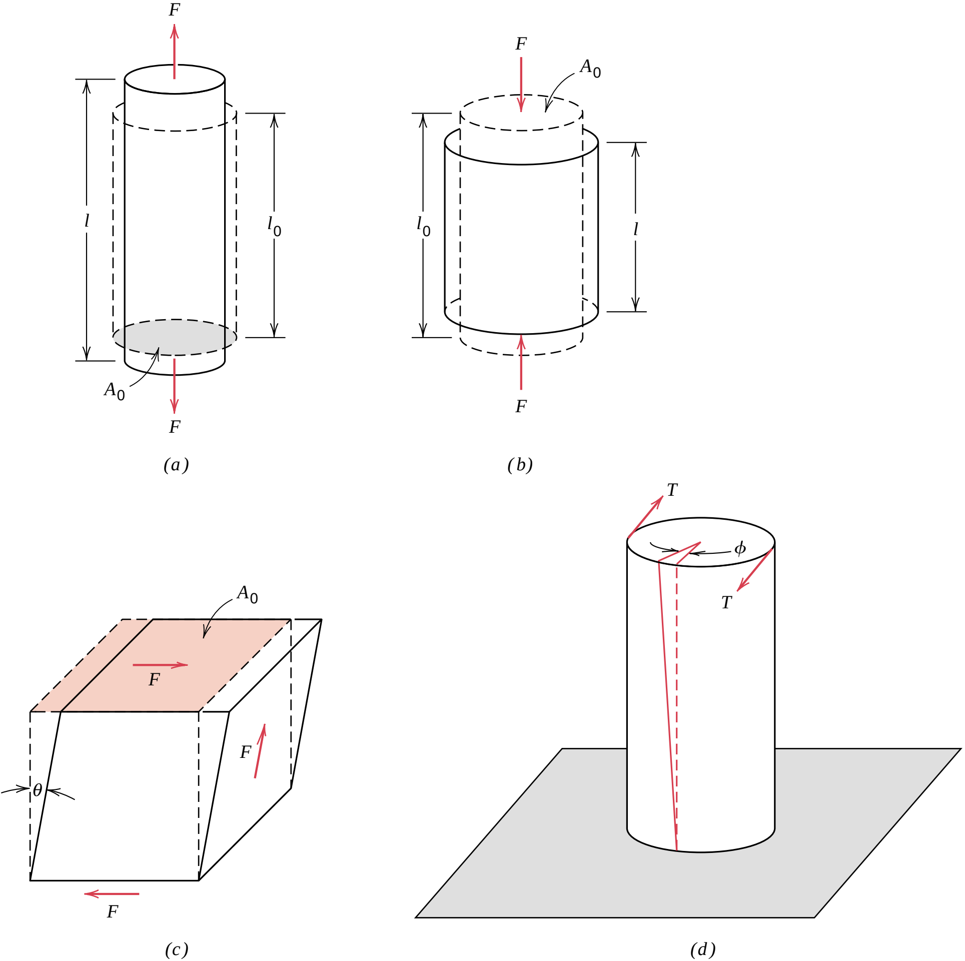

FIGURE 7.1 (*a*) Schematic illustration of how a tensile load produces an elongation and positive linear strain. Dashed lines represent the shape before deformation; solid lines, after deformation. (*b*) Schematic illustration of how a compressive load produces contraction and a negative linear strain. (*c*) Schematic representation of shear strain γ, where $\gamma = \tan\,\theta$. (*d*) Schematic representation of torsional deformation (i.e., angle of twist ϕ) produced by an applied torque *T*.

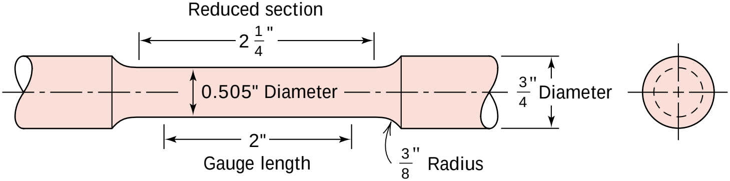
Reduced section
2 1/4"
0.505" Diameter
3/4" Diameter
2"
Gauge length
3/8" Radius

FIGURE 7.2 A standard tensile specimen with circular cross section.

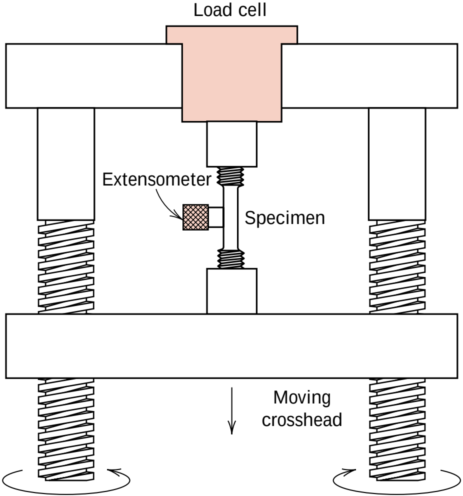
Load cell
Extensometer
Specimen
Moving
crosshead

Figure 7.3 Schematic representation of the apparatus used to conduct tensile stress–strain tests. The specimen is elongated by the moving crosshead; load cell and extensometer measure, respectively, the magnitude of the applied load and the elongation. (Adapted from H. W. Hayden, W. G. Moffatt, and J. Wulff, *The Structure and Properties of Materials,* Vol. III, *Mechanical Behavior,* p. 2. Copyright © 1965 by John Wiley & Sons, New York. Reprinted by permission of John Wiley & Sons, Inc.)

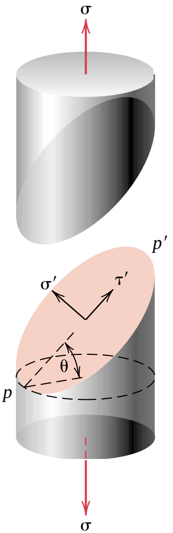

Figure 7.4 Schematic representation showing normal (σ') and shear (τ') stresses that act on a plane oriented at an angle θ relative to the plane taken perpendicular to the direction along which a pure tensile stress (σ) is applied.

Table 7.1 Room-Temperature Elastic and Shear Moduli, and Poisson's Ratio for Various Materials

	Modulus of Elasticity		*Shear Modulus*		
Material	*GPa*	*10^6 psi*	*GPa*	*10^6 psi*	*Poisson's Ratio*
	Metal Alloys				
Tungsten	407	59	160	23.2	0.28
Steel	207	30	83	12.0	0.30
Nickel	207	30	76	11.0	0.31
Titanium	107	15.5	45	6.5	0.34
Copper	110	16	46	6.7	0.34
Brass	97	14	37	5.4	0.34
Aluminum	69	10	25	3.6	0.33
Magnesium	45	6.5	17	2.5	0.35
	Ceramic Materials				
Aluminum oxide (Al_2O_3)	393	57	—	—	0.22
Silicon carbide (SiC)	345	50	—	—	0.17
Silicon nitride (Si_3N_4)	304	44	—	—	0.30
Spinel ($MgAl_2O_4$)	260	38	—	—	—
Magnesium oxide (MgO)	225	33	—	—	0.18
Zirconia[a]	205	30	—	—	0.31
Mullite ($3Al_2O_3$-$2SiO_2$)	145	21	—	—	0.24
Glass–ceramic (Pyroceram)	120	17	—	—	0.25
Fused silica (SiO_2)	73	11	—	—	0.17
Soda–lime glass	69	10	—	—	0.23
	Polymers[b]				
Phenol-formaldehyde	2.76–4.83	0.40–0.70	—	—	—
Polyvinyl chloride (PVC)	2.41–4.14	0.35–0.60	—	—	0.38
Polyester (PET)	2.76–4.14	0.40–0.60	—	—	—
Polystyrene (PS)	2.28–3.28	0.33–0.48	—	—	0.33
Polymethyl methacrylate (PMMA)	2.24–3.24	0.33–0.47	—	—	—
Polycarbonate (PC)	2.38	0.35	—	—	0.36
Nylon 6,6	1.58–3.80	0.23–0.55	—	—	0.39
Polypropylene (PP)	1.14–1.55	0.17–0.23	—	—	—
Polyethylene—high density (HDPE)	1.08	0.16	—	—	—
Polytetrafluoroethylene (PTFE)	0.40–0.55	0.058–0.080	—	—	0.46
Polyethylene—low density (LDPE)	0.17–0.28	0.025–0.041	—	—	—

[a] Partially stabilized with 3 mol% Y_2O_3.

[b] **Source:** *Modern Plastics Encyclopedia '96*. Copyright 1995, The McGraw-Hill Companies. Reprinted with permission.

Table B.2 Room-Temperature Modulus of Elasticity Values for Various Engineering Materials

Material	*Modulus of Elasticity* *GPa*	*Modulus of Elasticity* *10^6 psi*
METALS AND METAL ALLOYS		
Plain Carbon and Low Alloy Steels		
Steel alloy A36	207	30
Steel alloy 1020	207	30
Steel alloy 1040	207	30
Steel alloy 4140	207	30
Steel alloy 4340	207	30

Table B.2 (*Continued*)

	Modulus of Elasticity	
Material	***GPa***	***10^6 psi***
Stainless Steels		
Stainless alloy 304	193	28
Stainless alloy 316	193	28
Stainless alloy 405	200	29
Stainless alloy 440A	200	29
Stainless alloy 17-7PH	204	29.5
Cast Irons		
Gray irons		
• Grade G1800	66–97[a]	9.6–14[a]
• Grade G3000	90–113[a]	13.0–16.4[a]
• Grade G4000	110–138[a]	16–20[a]
Ductile irons		
• Grade 60-40-18	169	24.5
• Grade 80-55-06	168	24.4
• Grade 120-90-02	164	23.8
Aluminum Alloys		
Alloy 1100	69	10
Alloy 2024	72.4	10.5
Alloy 6061	69	10
Alloy 7075	71	10.3
Alloy 356.0	72.4	10.5
Copper Alloys		
C11000 (electrolytic tough pitch)	115	16.7
C17200 (beryllium–copper)	128	18.6
C26000 (cartridge brass)	110	16
C36000 (free-cutting brass)	97	14
C71500 (copper–nickel, 30%)	150	21.8
C93200 (bearing bronze)	100	14.5
Magnesium Alloys		
Alloy AZ31B	45	6.5
Alloy AZ91D	45	6.5
Titanium Alloys		
Commercially pure (ASTM grade 1)	103	14.9
Alloy Ti-5Al-2.5Sn	110	16
Alloy Ti-6Al-4V	114	16.5
Precious Metals		
Gold (commercially pure)	77	11.2
Platinum (commercially pure)	171	24.8
Silver (commercially pure)	74	10.7
Refractory Metals		
Molybdenum (commercially pure)	320	46.4
Tantalum (commercially pure)	185	27
Tungsten (commercially pure)	400	58
Miscellaneous Nonferrous Alloys		
Nickel 200	204	29.6
Inconel 625	207	30
Monel 400	180	26
Haynes alloy 25	236	34.2

Table B.2 (*Continued*)

Material	Modulus of Elasticity	
	GPa	10^6 psi
Invar	141	20.5
Super invar	144	21
Kovar	207	30
Chemical lead	13.5	2
Tin (commercially pure)	44.3	6.4
Lead–Tin solder (60Sn-40Pb)	30	4.4
Zinc (commercially pure)	104.5	15.2
Zirconium, reactor grade 702	99.3	14.4
GRAPHITE, CERAMICS, AND SEMICONDUCTING MATERIALS		
Aluminum oxide		
• 99.9% pure	380	55
• 96%	303	44
• 90%	275	40
Concrete	25.4–36.6[a]	3.7–5.3[a]
Diamond		
• Natural	700–1200	102–174
• Synthetic	800–925	116–134
Gallium arsenide, single crystal		
• In the ⟨100⟩ direction	85	12.3
• In the ⟨110⟩ direction	122	17.7
• In the ⟨111⟩ direction	142	20.6
Glass, borosilicate (Pyrex)	70	10.1
Glass, soda–lime	69	10
Glass ceramic (Pyroceram)	120	17.4
Graphite		
• Extruded	11	1.6
• Isostatically molded	11.7	1.7
Silica, fused	73	10.6
Silicon, single crystal		
• In the ⟨100⟩ direction	129	18.7
• In the ⟨110⟩ direction	168	24.4
• In the ⟨111⟩ direction	187	27.1
Silicon carbide		
• Hot pressed	207–483	30–70
• Sintered	207–483	30–70
Silicon nitride		
• Hot pressed	304	44.1
• Reaction bonded	304	44.1
• Sintered	304	44.1
Zirconia, 3 mol% Y_2O_3	205	30
POLYMERS		
Elastomers		
• Butadiene-acrylonitrile (nitrile)	0.0034[b]	0.00049[b]
• Styrene-butadiene (SBR)	0.002–0.010[b]	0.0003–0.0015[b]
Epoxy	2.41	0.35
Nylon 6,6	1.59–3.79	0.230–0.550
Phenolic	2.76–4.83	0.40–0.70
Polybutylene terephthalate (PBT)	1.93–3.00	0.280–0.435
Polycarbonate (PC)	2.38	0.345
Polyester (thermoset)	2.06–4.41	0.30–0.64

Table B.2 (*Continued*)

Material	*Modulus of Elasticity*	
	GPa	***10^6 psi***
Polyetheretherketone (PEEK)	1.10	0.16
Polyethylene		
• Low density (LDPE)	0.172–0.282	0.025–0.041
• High density (HDPE)	1.08	0.157
• Ultrahigh molecular weight (UHMWPE)	0.69	0.100
Polyethylene terephthalate (PET)	2.76–4.14	0.40–0.60
Polymethyl methacrylate (PMMA)	2.24–3.24	0.325–0.470
Polypropylene (PP)	1.14–1.55	0.165–0.225
Polystyrene (PS)	2.28–3.28	0.330–0.475
Polytetrafluoroethylene (PTFE)	0.40–0.55	0.058–0.080
Polyvinyl chloride (PVC)	2.41–4.14	0.35–0.60
FIBER MATERIALS		
Aramid (Kevlar 49)	131	19
Carbon (PAN precursor)		
• Standard modulus	230	33.4
• Intermediate modulus	285	41.3
• High modulus	400	58
E Glass	72.5	10.5
COMPOSITE MATERIALS		
Aramid fibers-epoxy matrix ($V_f = 0.60$)		
Longitudinal	76	11
Transverse	5.5	0.8
High modulus carbon fibers-epoxy matrix ($V_f = 0.60$)		
Longitudinal	220	32
Transverse	6.9	1.0
E glass fibers-epoxy matrix ($V_f = 0.60$)		
Longitudinal	45	6.5
Transverse	12	1.8
Wood		
• Douglas fir (12% moisture)		
Parallel to grain	10.8–13.6[c]	1.57–1.97[c]
Perpendicular to grain	0.54–0.68[c]	0.078–0.10[c]
• Red oak (12% moisture)		
Parallel to grain	11.0–14.1[c]	1.60–2.04[c]
Perpendicular to grain	0.55–0.71[c]	0.08–0.10[c]

[a] Secant modulus taken at 25% of ultimate strength.

[b] Modulus taken at 100% elongation.

[c] Measured in bending.

Sources: *ASM Handbooks, Volumes 1 and 2, Engineered Materials Handbooks, Volumes 1 and 4, Metals Handbook: Properties and Selection: Nonferrous Alloys and Pure Metals,* Vol. 2, 9th edition, and *Advanced Materials & Processes,* Vol. 146, No. 4, ASM International, Materials Park, OH; *Modern Plastics Encyclopedia '96,* The McGraw-Hill Companies, New York, NY; R. F. Floral and S. T. Peters, ''Composite Structures and Technologies,'' tutorial notes, 1989; and manufacturers' technical data sheets.

Appendix B / Properties of Selected Engineering Materials

B.1: Density 441
B.2: Modulus of Elasticity 444
B.3: Poisson's Ratio 448
B.4: Strength and Ductility 449
B.5: Plane Strain Fracture Toughness 454
B.6: Linear Coefficient of Thermal Expansion 455
B.7: Thermal Conductivity 459
B.8: Specific Heat 462
B.9: Electrical Resistivity 464
B.10: Metal Alloy Compositions 467

This appendix represents a compilation of important properties for approximately one hundred common engineering materials. Each table contains data values of one particular property for this chosen set of materials; also included is a tabulation of the compositions of the various metal alloys that are considered (Table B.10). Data are tabulated by material type (viz., metals and metal alloys; graphite, ceramics, and semiconducting materials; polymers; fiber materials; and composites); within each classification, the materials are listed alphabetically.

A couple of comments are appropriate relative to the content of these tables. First, data entries are expressed either as ranges of values or as single values that are typically measured. Also, on occasion, ''(min)'' is associated with an entry; this means that the value cited is a minimum one.

Table B.1 **Room-Temperature Density Values for Various Engineering Materials**

Material	*Density* g/cm^3	*Density* $lb_m/in.^3$
METALS AND METAL ALLOYS		
Plain Carbon and Low Alloy Steels		
Steel alloy A36	7.85	0.283
Steel alloy 1020	7.85	0.283
Steel alloy 1040	7.85	0.283
Steel alloy 4140	7.85	0.283
Steel alloy 4340	7.85	0.283
Stainless Steels		
Stainless alloy 304	8.00	0.289
Stainless alloy 316	8.00	0.289

Table B.1 (*Continued*)

Material	*Density* g/cm^3	*Density* $lb_m/in.^3$
Stainless alloy 405	7.80	0.282
Stainless alloy 440A	7.80	0.282
Stainless alloy 17-7PH	7.65	0.276
Cast Irons		
Gray irons		
• Grade G1800	7.30	0.264
• Grade G3000	7.30	0.264
• Grade G4000	7.30	0.264
Ductile irons		
• Grade 60-40-18	7.10	0.256
• Grade 80-55-06	7.10	0.256
• Grade 120-90-02	7.10	0.256
Aluminum Alloys		
Alloy 1100	2.71	0.0978
Alloy 2024	2.77	0.100
Alloy 6061	2.70	0.0975
Alloy 7075	2.80	0.101
Alloy 356.0	2.69	0.0971
Copper Alloys		
C11000 (electrolytic tough pitch)	8.89	0.321
C17200 (beryllium–copper)	8.25	0.298
C26000 (cartridge brass)	8.53	0.308
C36000 (free-cutting brass)	8.50	0.307
C71500 (copper–nickel, 30%)	8.94	0.323
C93200 (bearing bronze)	8.93	0.322
Magnesium Alloys		
Alloy AZ31B	1.77	0.0639
Alloy AZ91D	1.81	0.0653
Titanium Alloys		
Commercially pure (ASTM grade 1)	4.51	0.163
Alloy Ti-5Al-2.5Sn	4.48	0.162
Alloy Ti-6Al-4V	4.43	0.160
Precious Metals		
Gold (commercially pure)	19.32	0.697
Platinum (commercially pure)	21.45	0.774
Silver (commercially pure)	10.49	0.379
Refractory Metals		
Molybdenum (commercially pure)	10.22	0.369
Tantalum (commercially pure)	16.6	0.599
Tungsten (commercially pure)	19.3	0.697
Miscellaneous Nonferrous Alloys		
Nickel 200	8.89	0.321
Inconel 625	8.44	0.305
Monel 400	8.80	0.318
Haynes alloy 25	9.13	0.330
Invar	8.05	0.291

Table B.1 (*Continued*)

Material	*Density* g/cm^3	*Density* $lb_m/in.^3$
Super invar	8.10	0.292
Kovar	8.36	0.302
Chemical lead	11.34	0.409
Antimonial lead (6%)	10.88	0.393
Tin (commercially pure)	7.17	0.259
Lead–Tin solder (60Sn-40Pb)	8.52	0.308
Zinc (commercially pure)	7.14	0.258
Zirconium, reactor grade 702	6.51	0.235
GRAPHITE, CERAMICS, AND SEMICONDUCTING MATERIALS		
Aluminum oxide		
• 99.9% pure	3.98	0.144
• 96%	3.72	0.134
• 90%	3.60	0.130
Concrete	2.4	0.087
Diamond		
• Natural	3.51	0.127
• Synthetic	3.20–3.52	0.116–0.127
Gallium arsenide	5.32	0.192
Glass, borosilicate (Pyrex)	2.23	0.0805
Glass, soda–lime	2.5	0.0903
Glass ceramic (Pyroceram)	2.60	0.0939
Graphite		
• Extruded	1.71	0.0616
• Isostatically molded	1.78	0.0643
Silica, fused	2.2	0.079
Silicon	2.33	0.0841
Silicon carbide		
• Hot pressed	3.3	0.119
• Sintered	3.2	0.116
Silicon nitride		
• Hot pressed	3.3	0.119
• Reaction bonded	2.7	0.0975
• Sintered	3.3	0.119
Zirconia, 3 mol% Y_2O_3, sintered	6.0	0.217
POLYMERS		
Elastomers		
• Butadiene-acrylonitrile (nitrile)	0.98	0.0354
• Styrene-butadiene (SBR)	0.94	0.0339
• Silicone	1.1–1.6	0.040–0.058
Epoxy	1.11–1.40	0.0401–0.0505
Nylon 6,6	1.14	0.0412
Phenolic	1.28	0.0462
Polybutylene terephthalate (PBT)	1.34	0.0484
Polycarbonate (PC)	1.20	0.0433
Polyester (thermoset)	1.04–1.46	0.038–0.053
Polyetheretherketone (PEEK)	1.31	0.0473
Polyethylene		
• Low density (LDPE)	0.925	0.0334
• High density (HDPE)	0.959	0.0346

Table B.1 (*Continued*)

Material	*Density* g/cm^3	*Density* lb$_m$/in.^{3}
• Ultrahigh molecular weight (UHMWPE)	0.94	0.0339
Polyethylene terephthalate (PET)	1.35	0.0487
Polymethyl methacrylate (PMMA)	1.19	0.0430
Polypropylene (PP)	0.905	0.0327
Polystyrene (PS)	1.05	0.0379
Polytetrafluoroethylene (PTFE)	2.17	0.0783
Polyvinyl chloride (PVC)	1.30–1.58	0.047–0.057
FIBER MATERIALS		
Aramid (Kevlar 49)	1.44	0.0520
Carbon (PAN precursor)		
• Standard modulus	1.78	0.0643
• Intermediate modulus	1.78	0.0643
• High modulus	1.81	0.0653
E Glass	2.58	0.0931
COMPOSITE MATERIALS		
Aramid fibers-epoxy matrix ($V_f = 0.60$)	1.4	0.050
High modulus carbon fibers-epoxy matrix ($V_f = 0.60$)	1.7	0.061
E glass fibers-epoxy matrix ($V_f = 0.60$)	2.1	0.075
Wood		
• Douglas fir (12% moisture)	0.46–0.50	0.017–0.018
• Red oak (12% moisture)	0.61–0.67	0.022–0.024

Sources: *ASM Handbooks, Volumes 1 and 2, Engineered Materials Handbook, Volume 4, Metals Handbook: Properties and Selection: Nonferrous Alloys and Pure Metals,* Vol. 2, 9th edition, and *Advanced Materials & Processes,* Vol. 146, No. 4, ASM International Materials Park, OH; *Modern Plastics Encyclopedia '96,* The McGraw-Hill Companies, New York, NY; R. F. Floral and S. T. Peters, ''Composite Structures and Technologies,'' tutorial notes, 1989; and manufacturers' technical data sheets.

Table B.2 Room-Temperature Modulus of Elasticity Values for Various Engineering Materials

Material	*Modulus of Elasticity* GPa	*Modulus of Elasticity* 10^6 psi
METALS AND METAL ALLOYS		
Plain Carbon and Low Alloy Steels		
Steel alloy A36	207	30
Steel alloy 1020	207	30
Steel alloy 1040	207	30
Steel alloy 4140	207	30
Steel alloy 4340	207	30

Table B.2 (*Continued*)

Material	*Modulus of Elasticity*	
	GPa	*10^6 psi*
Stainless Steels		
Stainless alloy 304	193	28
Stainless alloy 316	193	28
Stainless alloy 405	200	29
Stainless alloy 440A	200	29
Stainless alloy 17-7PH	204	29.5
Cast Irons		
Gray irons		
• Grade G1800	66–97^a	9.6–14^a
• Grade G3000	90–113^a	13.0–16.4^a
• Grade G4000	110–138^a	16–20^a
Ductile irons		
• Grade 60-40-18	169	24.5
• Grade 80-55-06	168	24.4
• Grade 120-90-02	164	23.8
Aluminum Alloys		
Alloy 1100	69	10
Alloy 2024	72.4	10.5
Alloy 6061	69	10
Alloy 7075	71	10.3
Alloy 356.0	72.4	10.5
Copper Alloys		
C11000 (electrolytic tough pitch)	115	16.7
C17200 (beryllium–copper)	128	18.6
C26000 (cartridge brass)	110	16
C36000 (free-cutting brass)	97	14
C71500 (copper–nickel, 30%)	150	21.8
C93200 (bearing bronze)	100	14.5
Magnesium Alloys		
Alloy AZ31B	45	6.5
Alloy AZ91D	45	6.5
Titanium Alloys		
Commercially pure (ASTM grade 1)	103	14.9
Alloy Ti-5Al-2.5Sn	110	16
Alloy Ti-6Al-4V	114	16.5
Precious Metals		
Gold (commercially pure)	77	11.2
Platinum (commercially pure)	171	24.8
Silver (commercially pure)	74	10.7
Refractory Metals		
Molybdenum (commercially pure)	320	46.4
Tantalum (commercially pure)	185	27
Tungsten (commercially pure)	400	58
Miscellaneous Nonferrous Alloys		
Nickel 200	204	29.6
Inconel 625	207	30
Monel 400	180	26
Haynes alloy 25	236	34.2

Table B.2 (*Continued*)

Material	*Modulus of Elasticity*	
	GPa	*10^6 psi*
Invar	141	20.5
Super invar	144	21
Kovar	207	30
Chemical lead	13.5	2
Tin (commercially pure)	44.3	6.4
Lead–Tin solder (60Sn-40Pb)	30	4.4
Zinc (commercially pure)	104.5	15.2
Zirconium, reactor grade 702	99.3	14.4
GRAPHITE, CERAMICS, AND SEMICONDUCTING MATERIALS		
Aluminum oxide		
• 99.9% pure	380	55
• 96%	303	44
• 90%	275	40
Concrete	25.4–36.6[a]	3.7–5.3[a]
Diamond		
• Natural	700–1200	102–174
• Synthetic	800–925	116–134
Gallium arsenide, single crystal		
• In the ⟨100⟩ direction	85	12.3
• In the ⟨110⟩ direction	122	17.7
• In the ⟨111⟩ direction	142	20.6
Glass, borosilicate (Pyrex)	70	10.1
Glass, soda–lime	69	10
Glass ceramic (Pyroceram)	120	17.4
Graphite		
• Extruded	11	1.6
• Isostatically molded	11.7	1.7
Silica, fused	73	10.6
Silicon, single crystal		
• In the ⟨100⟩ direction	129	18.7
• In the ⟨110⟩ direction	168	24.4
• In the ⟨111⟩ direction	187	27.1
Silicon carbide		
• Hot pressed	207–483	30–70
• Sintered	207–483	30–70
Silicon nitride		
• Hot pressed	304	44.1
• Reaction bonded	304	44.1
• Sintered	304	44.1
Zirconia, 3 mol% Y_2O_3	205	30
POLYMERS		
Elastomers		
• Butadiene-acrylonitrile (nitrile)	0.0034[b]	0.00049[b]
• Styrene-butadiene (SBR)	0.002–0.010[b]	0.0003–0.0015[b]
Epoxy	2.41	0.35
Nylon 6,6	1.59–3.79	0.230–0.550
Phenolic	2.76–4.83	0.40–0.70
Polybutylene terephthalate (PBT)	1.93–3.00	0.280–0.435
Polycarbonate (PC)	2.38	0.345
Polyester (thermoset)	2.06–4.41	0.30–0.64

Table B.2 (*Continued*)

Material	*Modulus of Elasticity* GPa	*Modulus of Elasticity* 10^6 psi
Polyetheretherketone (PEEK)	1.10	0.16
Polyethylene		
• Low density (LDPE)	0.172–0.282	0.025–0.041
• High density (HDPE)	1.08	0.157
• Ultrahigh molecular weight (UHMWPE)	0.69	0.100
Polyethylene terephthalate (PET)	2.76–4.14	0.40–0.60
Polymethyl methacrylate (PMMA)	2.24–3.24	0.325–0.470
Polypropylene (PP)	1.14–1.55	0.165–0.225
Polystyrene (PS)	2.28–3.28	0.330–0.475
Polytetrafluoroethylene (PTFE)	0.40–0.55	0.058–0.080
Polyvinyl chloride (PVC)	2.41–4.14	0.35–0.60
FIBER MATERIALS		
Aramid (Kevlar 49)	131	19
Carbon (PAN precursor)		
• Standard modulus	230	33.4
• Intermediate modulus	285	41.3
• High modulus	400	58
E Glass	72.5	10.5
COMPOSITE MATERIALS		
Aramid fibers-epoxy matrix ($V_f = 0.60$)		
Longitudinal	76	11
Transverse	5.5	0.8
High modulus carbon fibers-epoxy matrix ($V_f = 0.60$)		
Longitudinal	220	32
Transverse	6.9	1.0
E glass fibers-epoxy matrix ($V_f = 0.60$)		
Longitudinal	45	6.5
Transverse	12	1.8
Wood		
• Douglas fir (12% moisture)		
Parallel to grain	10.8–13.6[c]	1.57–1.97[c]
Perpendicular to grain	0.54–0.68[c]	0.078–0.10[c]
• Red oak (12% moisture)		
Parallel to grain	11.0–14.1[c]	1.60–2.04[c]
Perpendicular to grain	0.55–0.71[c]	0.08–0.10[c]

[a] Secant modulus taken at 25% of ultimate strength.

[b] Modulus taken at 100% elongation.

[c] Measured in bending.

Sources: *ASM Handbooks, Volumes 1 and 2, Engineered Materials Handbooks, Volumes 1 and 4, Metals Handbook: Properties and Selection: Nonferrous Alloys and Pure Metals,* Vol. 2, 9th edition, and *Advanced Materials & Processes,* Vol. 146, No. 4, ASM International, Materials Park, OH; *Modern Plastics Encyclopedia '96,* The McGraw-Hill Companies, New York, NY; R. F. Floral and S. T. Peters, ''Composite Structures and Technologies,'' tutorial notes, 1989; and manufacturers' technical data sheets.

Table B.3 Room-Temperature Poisson's Ratio Values for Various Engineering Materials

Material	*Poisson's Ratio*
METALS AND METAL ALLOYS	
Plain Carbon and Low Alloy Steels	
Steel alloy A36	0.30
Steel alloy 1020	0.30
Steel alloy 1040	0.30
Steel alloy 4140	0.30
Steel alloy 4340	0.30
Stainless Steels	
Stainless alloy 304	0.30
Stainless alloy 316	0.30
Stainless alloy 405	0.30
Stainless alloy 440A	0.30
Stainless alloy 17-7PH	0.30
Cast Irons	
Gray irons	
• Grade G1800	0.26
• Grade G3000	0.26
• Grade G4000	0.26
Ductile irons	
• Grade 60-40-18	0.29
• Grade 80-55-06	0.31
• Grade 120-90-02	0.28
Aluminum Alloys	
Alloy 1100	0.33
Alloy 2024	0.33
Alloy 6061	0.33
Alloy 7075	0.33
Alloy 356.0	0.33
Copper Alloys	
C11000 (electrolytic tough pitch)	0.33
C17200 (beryllium–copper)	0.30
C26000 (cartridge brass)	0.35
C36000 (free-cutting brass)	0.34
C71500 (copper–nickel, 30%)	0.34
C93200 (bearing bronze)	0.34
Magnesium Alloys	
Alloy AZ31B	0.35
Alloy AZ91D	0.35
Titanium Alloys	
Commercially pure (ASTM grade 1)	0.34
Alloy Ti-5Al-2.5Sn	0.34
Alloy Ti-6Al-4V	0.34
Precious Metals	
Gold (commercially pure)	0.42
Platinum (commercially pure)	0.39
Silver (commercially pure)	0.37

Material	*Poisson's Ratio*
Refractory Metals	
Molybdenum (commercially pure)	0.32
Tantalum (commercially pure)	0.35
Tungsten (commercially pure)	0.28
Miscellaneous Nonferrous Alloys	
Nickel 200	0.31
Inconel 625	0.31
Monel 400	0.32
Chemical lead	0.44
Tin (commercially pure)	0.33
Zinc (commercially pure)	0.25
Zirconium, reactor grade 702	0.35
GRAPHITE, CERAMICS, AND SEMICONDUCTING MATERIALS	
Aluminum oxide	
• 99.9% pure	0.22
• 96%	0.21
• 90%	0.22
Concrete	0.20
Diamond	
• Natural	0.10–0.30
• Synthetic	0.20
Gallium arsenide	
• ⟨100⟩ orientation	0.30
Glass, borosilicate (Pyrex)	0.20
Glass, soda–lime	0.23
Glass ceramic (Pyroceram)	0.25
Silica, fused	0.17
Silicon	
• ⟨100⟩ orientation	0.28
• ⟨111⟩ orientation	0.36
Silicon carbide	
• Hot pressed	0.17
• Sintered	0.16
Silicon nitride	
• Hot pressed	0.30
• Reaction bonded	0.22
• Sintered	0.28
Zirconia, 3 mol% Y_2O_3	0.31
POLYMERS	
Nylon 6,6	0.39
Polycarbonate (PC)	0.36
Polystyrene (PS)	0.33
Polytetrafluoroethylene (PTFE)	0.46
Polyvinyl chloride (PVC)	0.38
FIBER MATERIALS	
E Glass	0.22

Table B.3 (*Continued*)

Material	*Poisson's Ratio*	*Material*	*Poisson's Ratio*
COMPOSITE MATERIALS		E glass fibers-epoxy matrix ($V_f = 0.6$)	0.19
Aramid fibers-epoxy matrix ($V_f = 0.6$)	0.34		
High modulus carbon fibers-epoxy matrix ($V_f = 0.6$)	0.25		

Sources: *ASM Handbooks, Volumes 1 and 2,* and *Engineered Materials Handbooks, Volumes 1 and 4,* ASM International, Materials Park, OH; R. F. Floral and S. T. Peters, ‘‘Composite Structures and Technologies,’’ tutorial notes, 1989; and manufacturers' technical data sheets.

Table B.4 **Typical Room-Temperature Yield Strength, Tensile Strength, and Ductility (Percent Elongation) Values for Various Engineering Materials**

Material/Condition	*Yield Strength* (*MPa* [*ksi*])	*Tensile Strength* (*MPa* [*ksi*])	*Percent Elongation*
METALS AND METAL ALLOYS			
Plain Carbon and Low Alloy Steels			
Steel alloy A36			
• Hot rolled	220–250 (32–36)	400–500 (58–72.5)	23
Steel alloy 1020			
• Hot rolled	210 (30) (min)	380 (55) (min)	25 (min)
• Cold drawn	350 (51) (min)	420 (61) (min)	15 (min)
• Annealed (@ 870°C)	295 (42.8)	395 (57.3)	36.5
• Normalized (@ 925°C)	345 (50.3)	440 (64)	38.5
Steel alloy 1040			
• Hot rolled	290 (42) (min)	520 (76) (min)	18 (min)
• Cold drawn	490 (71) (min)	590 (85) (min)	12 (min)
• Annealed (@ 785°C)	355 (51.3)	520 (75.3)	30.2
• Normalized (@ 900°C)	375 (54.3)	590 (85)	28.0
Steel alloy 4140			
• Annealed (@ 815°C)	417 (60.5)	655 (95)	25.7
• Normalized (@ 870°C)	655 (95)	1020 (148)	17.7
• Oil-quenched and tempered (@ 315°C)	1570 (228)	1720 (250)	11.5
Steel alloy 4340			
• Annealed (@ 810°C)	472 (68.5)	745 (108)	22
• Normalized (@ 870°C)	862 (125)	1280 (185.5)	12.2
• Oil-quenched and tempered (@ 315°C)	1620 (235)	1760 (255)	12
Stainless Steels			
Stainless alloy 304			
• Hot finished and annealed	205 (30) (min)	515 (75) (min)	40 (min)
• Cold worked ($\frac{1}{4}$ hard)	515 (75) (min)	860 (125) (min)	10 (min)
Stainless alloy 316			
• Hot finished and annealed	205 (30) (min)	515 (75) (min)	40 (min)
• Cold drawn and annealed	310 (45) (min)	620 (90) (min)	30 (min)
Stainless alloy 405			
• Annealed	170 (25)	415 (60)	20

Table B.4 *(Continued)*

Material/Condition	*Yield Strength (MPa [ksi])*	*Tensile Strength (MPa [ksi])*	*Percent Elongation*
Stainless alloy 440A			
• Annealed	415 (60)	725 (105)	20
• Tempered @ 315°C	1650 (240)	1790 (260)	5
Stainless alloy 17-7PH			
• Cold rolled	1210 (175) (min)	1380 (200) (min)	1 (min)
• Precipitation hardened @ 510°C	1310 (190) (min)	1450 (210) (min)	3.5 (min)
Cast Irons			
Gray irons			
• Grade G1800 (as cast)	—	124 (18) (min)	—
• Grade G3000 (as cast)	—	207 (30) (min)	—
• Grade G4000 (as cast)	—	276 (40) (min)	—
Ductile irons			
• Grade 60-40-18 (annealed)	276 (40) (min)	414 (60) (min)	18 (min)
• Grade 80-55-06 (as cast)	379 (55) (min)	552 (80) (min)	6 (min)
• Grade 120-90-02 (oil quenched and tempered)	621 (90) (min)	827 (120) (min)	2 (min)
Aluminum Alloys			
Alloy 1100			
• Annealed (O temper)	34 (5)	90 (13)	40
• Strain hardened (H14 temper)	117 (17)	124 (18)	15
Alloy 2024			
• Annealed (O temper)	75 (11)	185 (27)	20
• Heat treated and aged (T3 temper)	345 (50)	485 (70)	18
• Heat treated and aged (T351 temper)	325 (47)	470 (68)	20
Alloy 6061			
• Annealed (O temper)	55 (8)	124 (18)	30
• Heat treated and aged (T6 and T651 tempers)	276 (40)	310 (45)	17
Alloy 7075			
• Annealed (O temper)	103 (15)	228 (33)	17
• Heat treated and aged (T6 temper)	505 (73)	572 (83)	11
Alloy 356.0			
• As cast	124 (18)	164 (24)	6
• Heat treated and aged (T6 temper)	164 (24)	228 (33)	3.5
Copper Alloys			
C11000 (electrolytic tough pitch)			
• Hot rolled	69 (10)	220 (32)	50
• Cold worked (H04 temper)	310 (45)	345 (50)	12
C17200 (beryllium–copper)			
• Solution heat treated	195–380 (28–55)	415–540 (60–78)	35–60
• Solution heat treated, aged @ 330°C	965–1205 (140–175)	1140–1310 (165–190)	4–10
C26000 (cartridge brass)			
• Annealed	75–150 (11–22)	300–365 (43.5–53.0)	54–68
• Cold worked (H04 temper)	435 (63)	525 (76)	8
C36000 (free-cutting brass)			
• Annealed	125 (18)	340 (49)	53
• Cold worked (H02 temper)	310 (45)	400 (58)	25
C71500 (copper–nickel, 30%)			
• Hot rolled	140 (20)	380 (55)	45
• Cold worked (H80 temper)	545 (79)	580 (84)	3

Table B.4 (*Continued*)

Material/Condition	*Yield Strength* (*MPa* [*ksi*])	*Tensile Strength* (*MPa* [*ksi*])	*Percent Elongation*
C93200 (bearing bronze)			
• Sand cast	125 (18)	240 (35)	20
Magnesium Alloys			
Alloy AZ31B			
• Rolled	220 (32)	290 (42)	15
• Extruded	200 (29)	262 (38)	15
Alloy AZ91D			
• As cast	97–150 (14–22)	165–230 (24–33)	3
Titanium Alloys			
Commercially pure (ASTM grade 1)			
• Annealed	170 (25) (min)	240 (35) (min)	30
Alloy Ti-5Al-2.5Sn			
• Annealed	760 (110) (min)	790 (115) (min)	16
Alloy Ti-6Al-4V			
• Annealed	830 (120) (min)	900 (130) (min)	14
• Solution heat treated and aged	1103 (160)	1172 (170)	10
Precious Metals			
Gold (commercially pure)			
• Annealed	nil	130 (19)	45
• Cold worked (60% reduction)	205 (30)	220 (32)	4
Platinum (commercially pure)			
• Annealed	<13.8 (2)	125–165 (18–24)	30–40
• Cold worked (50%)	—	205–240 (30–35)	1–3
Silver (commercially pure)			
• Annealed	—	170 (24.6)	44
• Cold worked (50%)	—	296 (43)	3.5
Refractory Metals			
Molybdenum (commercially pure)	500 (72.5)	630 (91)	25
Tantalum (commercially pure)	165 (24)	205 (30)	40
Tungsten (commercially pure)	760 (110)	960 (139)	2
Miscellaneous Nonferrous Alloys			
Nickel 200 (annealed)	148 (21.5)	462 (67)	47
Inconel 625 (annealed)	517 (75)	930 (135)	42.5
Monel 400 (annealed)	240 (35)	550 (80)	40
Haynes alloy 25	445 (65)	970 (141)	62
Invar (annealed)	276 (40)	517 (75)	30
Super invar (annealed)	276 (40)	483 (70)	30
Kovar (annealed)	276 (40)	517 (75)	30
Chemical lead	6–8 (0.9–1.2)	16–19 (2.3–2.7)	30–60
Antimonial lead (6%) (chill cast)	—	47.2 (6.8)	24
Tin (commercially pure)	11 (1.6)	—	57
Lead–Tin solder (60Sn-40Pb)	—	52.5 (7.6)	30–60
Zinc (commercially pure)			
• Hot rolled (anisotropic)	—	134–159 (19.4–23.0)	50–65
• Cold rolled (anisotropic)	—	145–186 (21–27)	40–50
Zirconium, reactor grade 702			
• Cold worked and annealed	207 (30) (min)	379 (55) (min)	16 (min)

Table B.4 (*Continued*)

Material/Condition	*Yield Strength (MPa [ksi])*	*Tensile Strength (MPa [ksi])*	*Percent Elongation*
GRAPHITE, CERAMICS, AND SEMICONDUCTING MATERIALS[a]			
Aluminum oxide			
• 99.9% pure	—	282–551 (41–80)	—
• 96%	—	358 (52)	—
• 90%	—	337 (49)	—
Concrete[b]	—	37.3–41.3 (5.4–6.0)	—
Diamond			
• Natural	—	1050 (152)	—
• Synthetic	—	800–1400 (116–203)	—
Gallium arsenide			
• {100} orientation, polished surface	—	66 (9.6)[c]	—
• {100} orientation, as-cut surface	—	57 (8.3)[c]	—
Glass, borosilicate (Pyrex)	—	69 (10)	—
Glass, soda–lime	—	69 (10)	—
Glass ceramic (Pyroceram)	—	123–370 (18–54)	—
Graphite			
• Extruded (with the grain direction)	—	13.8–34.5 (2.0–5.0)	—
• Isostatically molded	—	31–69 (4.5–10)	—
Silica, fused	—	104 (15)	—
Silicon			
• {100} orientation, as-cut surface	—	130 (18.9)	—
• {100} orientation, laser scribed	—	81.8 (11.9)	—
Silicon carbide			
• Hot pressed	—	230–825 (33–120)	—
• Sintered	—	96–520 (14–75)	—
Silicon nitride			
• Hot pressed	—	700–1000 (100–150)	—
• Reaction bonded	—	250–345 (36–50)	—
• Sintered	—	414–650 (60–94)	—
Zirconia, 3 mol% Y_2O_3 (sintered)	—	800–1500 (116–218)	—
POLYMERS			
Elastomers			
• Butadiene-acrylonitrile (nitrile)	—	6.9–24.1 (1.0–3.5)	400–600
• Styrene-butadiene (SBR)	—	12.4–20.7 (1.8–3.0)	450–500
• Silicone	—	10.3 (1.5)	100–800
Epoxy	—	27.6–90.0 (4.0–13)	3–6
Nylon 6,6			
• Dry, as molded	55.1–82.8 (8–12)	94.5 (13.7)	15–80
• 50% relative humidity	44.8–58.6 (6.5–8.5)	75.9 (11)	150–300
Phenolic	—	34.5–62.1 (5.0–9.0)	1.5–2.0
Polybutylene terephthalate (PBT)	56.6–60.0 (8.2–8.7)	56.6–60.0 (8.2–8.7)	50–300
Polycarbonate (PC)	62.1 (9)	62.8–72.4 (9.1–10.5)	110–150
Polyester (thermoset)	—	41.4–89.7 (6.0–13.0)	<2.6
Polyetheretherketone (PEEK)	91 (13.2)	70.3–103 (10.2–15.0)	30–150
Polyethylene			
• Low density (LDPE)	9.0–14.5 (1.3–2.1)	8.3–31.4 (1.2–4.55)	100–650
• High density (HDPE)	26.2–33.1 (3.8–4.8)	22.1–31.0 (3.2–4.5)	10–1200
• Ultrahigh molecular weight (UHMWPE)	21.4–27.6 (3.1–4.0)	38.6–48.3 (5.6–7.0)	350–525
Polyethylene terephthalate (PET)	59.3 (8.6)	48.3–72.4 (7.0–10.5)	30–300

Table B.4 (*Continued*)

Material/Condition	***Yield Strength (MPa [ksi])***	***Tensile Strength (MPa [ksi])***	***Percent Elongation***
Polymethyl methacrylate (PMMA)	53.8–73.1 (7.8–10.6)	48.3–72.4 (7.0–10.5)	2.0–5.5
Polypropylene (PP)	31.0–37.2 (4.5–5.4)	31.0–41.4 (4.5–6.0)	100–600
Polystyrene (PS)	—	35.9–51.7 (5.2–7.5)	1.2–2.5
Polytetrafluoroethylene (PTFE)	—	20.7–34.5 (3.0–5.0)	200–400
Polyvinyl chloride (PVC)	40.7–44.8 (5.9–6.5)	40.7–51.7 (5.9–7.5)	40–80
FIBER MATERIALS			
Aramid (Kevlar 49)	—	3600–4100 (525–600)	2.8
Carbon (PAN precursor)			
• Standard modulus (longitudinal)	—	3800–4200 (550–610)	2
• Intermediate modulus (longitudinal)	—	4650–6350 (675–920)	1.8
• High modulus (longitudinal)	—	2500–4500 (360–650)	0.6
E Glass	—	3450 (500)	4.3
COMPOSITE MATERIALS			
Aramid fibers-epoxy matrix (aligned, $V_f = 0.6$)			
• Longitudinal direction	—	1380 (200)	1.8
• Transverse direction	—	30 (4.3)	0.5
High modulus carbon fibers-epoxy matrix (aligned, $V_f = 0.6$)			
• Longitudinal direction	—	760 (110)	0.3
• Transverse direction	—	28 (4)	0.4
E glass fibers-epoxy matrix (aligned, $V_f = 0.6$)			
• Longitudinal direction	—	1020 (150)	2.3
• Transverse direction	—	40 (5.8)	0.4
Wood			
• Douglas fir (12% moisture)			
Parallel to grain	—	108 (15.6)	—
Perpendicular to grain	—	2.4 (0.35)	—
• Red oak (12% moisture)			
Parallel to grain	—	112 (16.3)	—
Perpendicular to grain	—	7.2 (1.05)	—

[a] The strength of graphite, ceramics, and semiconducting materials is taken as flexural strength.

[b] The strength of concrete is measured in compression.

[c] Flexural strength value at 50% fracture probability.

Sources: *ASM Handbooks, Volumes 1 and 2, Engineered Materials Handbooks, Volumes 1 and 4, Metals Handbook: Properties and Selection: Nonferrous Alloys and Pure Metals*, Vol. 2, 9th edition, *Advanced Materials & Processes*, Vol. 146, No. 4, and *Materials & Processing Databook (1985)*, ASM International, Materials Park, OH; *Modern Plastics Encyclopedia '96*, The McGraw-Hill Companies, New York, NY; R. F. Floral and S. T. Peters, ''Composite Structures and Technologies,'' tutorial notes, 1989; and manufacturers' technical data sheets.

Table B.5 Room-Temperature Plane Strain Fracture Toughness and Strength Values for Various Engineering Materials

Material	*Fracture Toughness* $MPa\sqrt{m}$	*Fracture Toughness* $ksi\sqrt{in.}$	*Strength*[a] (*MPa*)
METALS AND METAL ALLOYS			
Plain Carbon and Low Alloy Steels			
Steel alloy 1040	54.0	49.0	260
Steel alloy 4140			
• Tempered @ 370°C	55–65	50–59	1375–1585
• Tempered @ 482°C	75–93	68.3–84.6	1100–1200
Steel alloy 4340			
• Tempered @ 260°C	50.0	45.8	1640
• Tempered @ 425°C	87.4	80.0	1420
Stainless Steels			
Stainless alloy 17-7PH			
• Precipitation hardened @ 510°C	76	69	1310
Aluminum Alloys			
Alloy 2024-T3	44	40	345
Alloy 7075-T651	24	22	495
Magnesium Alloys			
Alloy AZ31B			
• Extruded	28.0	25.5	200
Titanium Alloys			
Alloy Ti-5Al-2.5Sn			
• Air cooled	71.4	65.0	876
Alloy Ti-6Al-4V			
• Equiaxed grains	44–66	40–60	910
GRAPHITE, CERAMICS, AND SEMICONDUCTING MATERIALS			
Aluminum oxide			
• 99.9% pure	4.2–5.9	3.8–5.4	282–551
• 96%	3.85–3.95	3.5–3.6	358
Concrete	0.2–1.4	0.18–1.27	—
Diamond			
• Natural	3.4	3.1	1050
• Synthetic	6.0–10.7	5.5–9.7	800–1400
Gallium arsenide			
• In the {100} orientation	0.43	0.39	66
• In the {110} orientation	0.31	0.28	—
• In the {111} orientation	0.45	0.41	—
Glass, borosilicate (Pyrex)	0.77	0.70	69
Glass, soda-lime	0.75	0.68	69
Glass ceramic (Pyroceram)	1.6–2.1	1.5–1.9	123–370
Silica, fused	0.79	0.72	104
Silicon			
• In the {100} orientation	0.95	0.86	—
• In the {110} orientation	0.90	0.82	—
• In the {111} orientation	0.82	0.75	—
Silicon carbide			
• Hot pressed	4.8–6.1	4.4–5.6	230–825
• Sintered	4.8	4.4	96–520

Table B.5 (*Continued*)

Material	*Fracture Toughness* $MPa\sqrt{m}$	*Fracture Toughness* $ksi\sqrt{in.}$	*Strength*[a] (*MPa*)
Silicon nitride			
• Hot pressed	4.1–6.0	3.7–5.5	700–1000
• Reaction bonded	3.6	3.3	250–345
• Sintered	5.3	4.8	414–650
Zirconia, 3 mol% Y_2O_3	7.0–12.0	6.4–10.9	800–1500
POLYMERS			
Epoxy	0.6	0.55	—
Nylon 6,6	2.5–3.0	2.3–2.7	44.8–58.6
Polycarbonate (PC)	2.2	2.0	62.1
Polyester (thermoset)	0.6	0.55	—
Polyethylene terephthalate (PET)	5.0	4.6	59.3
Polymethyl methacrylate (PMMA)	0.7–1.6	0.6–1.5	53.8–73.1
Polypropylene (PP)	3.0–4.5	2.7–4.1	31.0–37.2
Polystyrene (PS)	0.7–1.1	0.6–1.0	—
Polyvinyl chloride (PVC)	2.0–4.0	1.8–3.6	40.7–44.8

[a] For metal alloys and polymers, strength is taken as yield strength; for ceramic materials, flexural strength is used.

Sources: *ASM Handbooks, Volumes 1 and 19, Engineered Materials Handbooks, Volumes 2* and *4*, and *Advanced Materials & Processes*, Vol. 137, No. 6, ASM International, Materials Park, OH.

Table B.6 Room-Temperature Linear Coefficient of Thermal Expansion Values for Various Engineering Materials

Material	*Coefficient of Thermal Expansion* $10^{-6}\ (°C)^{-1}$	*Coefficient of Thermal Expansion* $10^{-6}\ (°F)^{-1}$
METALS AND METAL ALLOYS		
Plain Carbon and Low Alloy Steels		
Steel alloy A36	11.7	6.5
Steel alloy 1020	11.7	6.5
Steel alloy 1040	11.3	6.3
Steel alloy 4140	12.3	6.8
Steel alloy 4340	12.3	6.8
Stainless Steels		
Stainless alloy 304	17.2	9.6
Stainless alloy 316	15.9	8.8
Stainless alloy 405	10.8	6.0
Stainless alloy 440A	10.2	5.7
Stainless alloy 17-7PH	11.0	6.1
Cast Irons		
Gray irons		
• Grade G1800	11.4	6.3
• Grade G3000	11.4	6.3
• Grade G4000	11.4	6.3

Table B.6 (*Continued*)

Material	*Coefficient of Thermal Expansion* $10^{-6}\ (^\circ C)^{-1}$	*Coefficient of Thermal Expansion* $10^{-6}\ (^\circ F)^{-1}$
Ductile irons		
• Grade 60-40-18	11.2	6.2
• Grade 80-55-06	10.6	5.9
Aluminum Alloys		
Alloy 1100	23.6	13.1
Alloy 2024	22.9	12.7
Alloy 6061	23.6	13.1
Alloy 7075	23.4	13.0
Alloy 356.0	21.5	11.9
Copper Alloys		
C11000 (electrolytic tough pitch)	17.0	9.4
C17200 (beryllium–copper)	16.7	9.3
C26000 (cartridge brass)	19.9	11.1
C36000 (free-cutting brass)	20.5	11.4
C71500 (copper–nickel, 30%)	16.2	9.0
C93200 (bearing bronze)	18.0	10.0
Magnesium Alloys		
Alloy AZ31B	26.0	14.4
Alloy AZ91D	26.0	14.4
Titanium Alloys		
Commercially pure (ASTM grade 1)	8.6	4.8
Alloy Ti-5Al-2.5Sn	9.4	5.2
Alloy Ti-6Al-4V	8.6	4.8
Precious Metals		
Gold (commerically pure)	14.2	7.9
Platinum (commercially pure)	9.1	5.1
Silver (commercially pure)	19.7	10.9
Refractory Metals		
Molybdenum (commercially pure)	4.9	2.7
Tantalum (commercially pure)	6.5	3.6
Tungsten (commercially pure)	4.5	2.5
Miscellaneous Nonferrous Alloys		
Nickel 200	13.3	7.4
Inconel 625	12.8	7.1
Monel 400	13.9	7.7
Haynes alloy 25	12.3	6.8
Invar	1.6	0.9
Super invar	0.72	0.40
Kovar	5.1	2.8
Chemical lead	29.3	16.3
Antimonial lead (6%)	27.2	15.1
Tin (commercially pure)	23.8	13.2
Lead–Tin solder (60Sn-40Pb)	24.0	13.3
Zinc (commercially pure)	23.0–32.5	12.7–18.1
Zirconium, reactor grade 702	5.9	3.3

Table B.6 (*Continued*)

Material	*Coefficient of Thermal Expansion* 10^{-6} (°C)$^{-1}$	*Coefficient of Thermal Expansion* 10^{-6} (°F)$^{-1}$
GRAPHITE, CERAMICS, AND SEMICONDUCTING MATERIALS		
Aluminum oxide		
• 99.9% pure	7.4	4.1
• 96%	7.4	4.1
• 90%	7.0	3.9
Concrete	10.0–13.6	5.6–7.6
Diamond (natural)	0.11–1.23	0.06–0.68
Gallium arsenide	5.9	3.3
Glass, borosilicate (Pyrex)	3.3	1.8
Glass, soda–lime	9.0	5.0
Glass ceramic (Pyroceram)	6.5	3.6
Graphite		
• Extruded	2.0–2.7	1.1–1.5
• Isostatically molded	2.2–6.0	1.2–3.3
Silica, fused	0.4	0.22
Silicon	2.5	1.4
Silicon carbide		
• Hot pressed	4.6	2.6
• Sintered	4.1	2.3
Silicon nitride		
• Hot pressed	2.7	1.5
• Reaction bonded	3.1	1.7
• Sintered	3.1	1.7
Zirconia, 3 mol% Y_2O_3	9.6	5.3
POLYMERS		
Elastomers		
• Butadiene-acrylonitrile (nitrile)	235	130
• Styrene-butadiene (SBR)	220	125
• Silicone	270	150
Epoxy	81–117	45–65
Nylon 6,6	144	80
Phenolic	122	68
Polybutylene terephthalate (PBT)	108–171	60–95
Polycarbonate (PC)	122	68
Polyester (thermoset)	100–180	55–100
Polyetheretherketone (PEEK)	72–85	40–47
Polyethylene		
• Low density (LDPE)	180–400	100–220
• High density (HDPE)	106–198	59–110
• Ultrahigh molecular weight (UHMWPE)	234–360	130–200
Polyethylene terephthalate (PET)	117	65
Polymethyl methacrylate (PMMA)	90–162	50–90
Polypropylene (PP)	146–180	81–100
Polystyrene (PS)	90–150	50–83
Polytetrafluoroethylene (PTFE)	126–216	70–120
Polyvinyl chloride (PVC)	90–180	50–100

Table B.6 (*Continued*)

	Coefficient of Thermal Expansion	
Material	***10^{-6} (°C)$^{-1}$***	***10^{-6} (°F)$^{-1}$***
FIBER MATERIALS		
Aramid (Kevlar 49)		
• Longitudinal direction	−2.0	−1.1
• Transverse direction	60	33
Carbon (PAN precursor)		
• Standard modulus		
Longitudinal direction	−0.6	−0.3
Transverse direction	10.0	5.6
• Intermediate modulus		
Longitudinal direction	−0.6	−0.3
• High modulus		
Longitudinal direction	−0.5	−0.28
Transverse direction	7.0	3.9
E Glass	5.0	2.8
COMPOSITE MATERIALS		
Aramid fibers-epoxy matrix ($V_f = 0.6$)		
• Longitudinal direction	−4.0	−2.2
• Transverse direction	70	40
High modulus carbon fibers-epoxy matrix ($V_f = 0.6$)		
• Longitudinal direction	−0.5	−0.3
• Transverse direction	32	18
E glass fibers-epoxy matrix ($V_f = 0.6$)		
• Longitudinal direction	6.6	3.7
• Transverse direction	30	16.7
Wood		
• Douglas fir (12% moisture)		
Parallel to grain	3.8–5.1	2.2–2.8
Perpendicular to grain	25.4–33.8	14.1–18.8
• Red oak (12% moisture)		
Parallel to grain	4.6–5.9	2.6–3.3
Perpendicular to grain	30.6–39.1	17.0–21.7

Sources: *ASM Handbooks, Volumes 1* and *2, Engineered Materials Handbooks, Volumes 1* and *4, Metals Handbook: Properties and Selection: Nonferrous Alloys and Pure Metals*, Vol. 2, 9th edition, and *Advanced Materials & Processes,* Vol. 146, No. 4, ASM International, Materials Park, OH; *Modern Plastics Encyclopedia '96,* The McGraw-Hill Companies, New York, NY; R. F. Floral and S. T. Peters, ''Composite Structures and Technologies,'' tutorial notes, 1989; and manufacturers' technical data sheets.

Table B.7 Room-Temperature Thermal Conductivity Values for Various Engineering Materials

	Thermal Conductivity	
Material	*W/m-K*	*Btu/ft-h-°F*
METALS AND METAL ALLOYS		
Plain Carbon and Low Alloy Steels		
Steel alloy A36	51.9	30
Steel alloy 1020	51.9	30
Steel alloy 1040	51.9	30
Stainless Steels		
Stainless alloy 304 (annealed)	16.2	9.4
Stainless alloy 316 (annealed)	16.2	9.4
Stainless alloy 405 (annealed)	27.0	15.6
Stainless alloy 440A (annealed)	24.2	14.0
Stainless alloy 17-7PH (annealed)	16.4	9.5
Cast Irons		
Gray irons		
• Grade G1800	46.0	26.6
• Grade G3000	46.0	26.6
• Grade G4000	46.0	26.6
Ductile irons		
• Grade 60-40-18	36.0	20.8
• Grade 80-55-06	36.0	20.8
• Grade 120-90-02	36.0	20.8
Aluminum Alloys		
Alloy 1100 (annealed)	222	128
Alloy 2024 (annealed)	190	110
Alloy 6061 (annealed)	180	104
Alloy 7075-T6	130	75
Alloy 356.0-T6	151	87
Copper Alloys		
C11000 (electrolytic tough pitch)	388	224
C17200 (beryllium–copper)	105–130	60–75
C26000 (cartridge brass)	120	70
C36000 (free-cutting brass)	115	67
C71500 (copper–nickel, 30%)	29	16.8
C93200 (bearing bronze)	59	34
Magnesium Alloys		
Alloy AZ31B	96[a]	55[a]
Alloy AZ91D	72[a]	43[a]
Titanium Alloys		
Commercially pure (ASTM grade 1)	16	9.2
Alloy Ti-5Al-2.5Sn	7.6	4.4
Alloy Ti-6Al-4V	6.7	3.9
Precious Metals		
Gold (commercially pure)	315	182
Platinum (commercially pure)	71[b]	41[b]
Silver (commercially pure)	428	247

Table B.7 (*Continued*)

Material	*Thermal Conductivity* W/m-K	*Thermal Conductivity* Btu/ft-h-°F
Refractory Metals		
Molybdenum (commercially pure)	142	82
Tantalum (commercially pure)	54.4	31.4
Tungsten (commercially pure)	155	89.4
Miscellaneous Nonferrous Alloys		
Nickel 200	70	40.5
Inconel 625	9.8	5.7
Monel 400	21.8	12.6
Haynes alloy 25	9.8	5.7
Invar	10	5.8
Super invar	10	5.8
Kovar	17	9.8
Chemical lead	35	20.2
Antimonial lead (6%)	29	16.8
Tin (commercially pure)	60.7	35.1
Lead–Tin solder (60Sn-40Pb)	50	28.9
Zinc (commercially pure)	108	62
Zirconium, reactor grade 702	22	12.7
GRAPHITE, CERAMICS, AND SEMICONDUCTING MATERIALS		
Aluminum oxide		
• 99.9% pure	39	22.5
• 96%	35	20
• 90%	16	9.2
Concrete	1.25–1.75	0.72–1.0
Diamond		
• Natural	1450–4650	840–2700
• Synthetic	3150	1820
Gallium arsenide	45.5	26.3
Glass, borosilicate (Pyrex)	1.4	0.81
Glass, soda–lime	1.7	1.0
Glass ceramic (Pyroceram)	3.3	1.9
Graphite		
• Extruded	130–190	75–110
• Isostatically molded	104–130	60–75
Silica, fused	1.4	0.81
Silicon	141	82
Silicon carbide		
• Hot pressed	80	46.2
• Sintered	71	41
Silicon nitride		
• Hot pressed	29	17
• Reaction bonded	10	6
• Sintered	33	19.1
Zirconia, 3 mol% Y_2O_3	2.0–3.3	1.2–1.9
POLYMERS		
Elastomers		
• Butadiene-acrylonitrile (nitrile)	0.25	0.14
• Styrene-butadiene (SBR)	0.25	0.14
• Silicone	0.23	0.13

Table B.7 (*Continued*)

Material	*Thermal Conductivity* W/m-K	*Thermal Conductivity* Btu/ft-h-°F
Epoxy	0.19	0.11
Nylon 6,6	0.24	0.14
Phenolic	0.15	0.087
Polybutylene terephthalate (PBT)	0.18–0.29	0.10–0.17
Polycarbonate (PC)	0.20	0.12
Polyester (thermoset)	0.17	0.10
Polyethylene		
• Low density (LDPE)	0.33	0.19
• High density (HDPE)	0.48	0.28
• Ultrahigh molecular weight (UHMWPE)	0.33	0.19
Polyethylene terephthalate (PET)	0.15	0.087
Polymethyl methacrylate (PMMA)	0.17–0.25	0.10–0.15
Polypropylene (PP)	0.12	0.069
Polystyrene (PS)	0.13	0.075
Polytetrafluoroethylene (PTFE)	0.25	0.14
Polyvinyl chloride (PVC)	0.15–0.21	0.08–0.12
FIBER MATERIALS		
Carbon (PAN precursor), longitudinal		
• Standard modulus	11	6.4
• Intermediate modulus	15	8.7
• High modulus	70	40
E Glass	1.3	0.75
COMPOSITE MATERIALS		
Wood		
• Douglas fir (12% moisture)		
Perpendicular to grain	0.14	0.08
• Red oak (12% moisture)		
Perpendicular to grain	0.18	0.11

[a] At 100°C.

[b] At 0°C.

Sources: *ASM Handbooks, Volumes 1 and 2, Engineered Materials Handbooks, Volumes 1 and 4, Metals Handbook: Properties and Selection: Nonferrous Alloys and Pure Metals,* Vol. 2, 9th edition, and *Advanced Materials & Processes,* Vol. 146, No. 4, ASM International, Materials Park, OH; *Modern Plastics Encyclopedia '96* and *Modern Plastics Encyclopedia 1977–1978,* The McGraw-Hill Companies, New York, NY; and manufacturers' technical data sheets.

Table B.8 **Room-Temperature Specific Heat Values for Various Engineering Materials**

	Specific Heat	
Material	*J/kg-K*	*10^{-2}Btu/lb_m–°F*
METALS AND METAL ALLOYS		
Plain Carbon and Low Alloy Steels		
Steel alloy A36	486[a]	11.6[a]
Steel alloy 1020	486[a]	11.6[a]
Steel alloy 1040	486[a]	11.6[a]
Stainless Steels		
Stainless alloy 304	500	12.0
Stainless alloy 316	500	12.0
Stainless alloy 405	460	11.0
Stainless alloy 440A	460	11.0
Stainless alloy 17-7PH	460	11.0
Cast Irons		
Gray irons		
• Grade G1800	544	13
• Grade G3000	544	13
• Grade G4000	544	13
Ductile irons		
• Grade 60-40-18	544	13
• Grade 80-55-06	544	13
• Grade 120-90-02	544	13
Aluminum Alloys		
Alloy 1100	904	21.6
Alloy 2024	875	20.9
Alloy 6061	896	21.4
Alloy 7075	960[b]	23.0[b]
Alloy 356.0	963[b]	23.0[b]
Copper Alloys		
C11000 (electrolytic tough pitch)	385	9.2
C17200 (beryllium–copper)	420	10.0
C26000 (cartridge brass)	375	9.0
C36000 (free-cutting brass)	380	9.1
C71500 (copper–nickel, 30%)	380	9.1
C93200 (bearing bronze)	376	9.0
Magnesium Alloys		
Alloy AZ31B	1024	24.5
Alloy AZ91D	1050	25.1
Titanium Alloys		
Commercially pure (ASTM grade 1)	528[c]	12.6[c]
Alloy Ti-5Al-2.5Sn	470[c]	11.2[c]
Alloy Ti-6Al-4V	610[c]	14.6[c]
Precious Metals		
Gold (commercially pure)	130	3.1
Platinum (commercially pure)	132[d]	3.2[d]
Silver (commercially pure)	235	5.6

Table B.8 (*Continued*)

Material	*Specific Heat*	
	J/kg-K	*10^{-2}Btu/lb_m–°F*
Refractory Metals		
Molybdenum (commercially pure)	276	6.6
Tantalum (commercially pure)	139	3.3
Tungsten (commercially pure)	138	3.3
Miscellaneous Nonferrous Alloys		
Nickel 200	456	10.9
Inconel 625	410	9.8
Monel 400	427	10.2
Haynes alloy 25	377	9.0
Invar	500	12.0
Super invar	500	12.0
Kovar	460	11.0
Chemical lead	129	3.1
Antimonial lead (6%)	135	3.2
Tin (commercially pure)	222	5.3
Lead–Tin solder (60Sn-40Pb)	150	3.6
Zinc (commercially pure)	395	9.4
Zirconium, reactor grade 702	285	6.8
GRAPHITE, CERAMICS, AND SEMICONDUCTING MATERIALS		
Aluminum oxide		
• 99.9% pure	775	18.5
• 96%	775	18.5
• 90%	775	18.5
Concrete	850–1150	20.3–27.5
Diamond (natural)	520	12.4
Gallium arsenide	350	8.4
Glass, borosilicate (Pyrex)	850	20.3
Glass, soda–lime	840	20.0
Glass ceramic (Pyroceram)	975	23.3
Graphite		
• Extruded	830	19.8
• Isostatically molded	830	19.8
Silica, fused	740	17.7
Silicon	700	16.7
Silicon carbide		
• Hot pressed	670	16.0
• Sintered	590	14.1
Silicon nitride		
• Hot pressed	750	17.9
• Reaction bonded	870	20.7
• Sintered	1100	26.3
Zirconia, 3 mol% Y_2O_3	481	11.5
POLYMERS		
Epoxy	1050	25
Nylon 6,6	1670	40
Phenolic	1590–1760	38–42
Polybutylene terephthalate (PBT)	1170–2300	28–55
Polycarbonate (PC)	840	20

Table B.8 (*Continued*)

Material	*Specific Heat* J/kg-K	*Specific Heat* 10^{-2}Btu/lb$_m$–°F
Polyester (thermoset)	710–920	17–22
Polyethylene		
• Low density (LDPE)	2300	55
• High density (HDPE)	1850	44.2
Polyethylene terephthalate (PET)	1170	28
Polymethyl methacrylate (PMMA)	1460	35
Polypropylene (PP)	1925	46
Polystyrene (PS)	1170	28
Polytetrafluoroethylene (PTFE)	1050	25
Polyvinyl chloride (PVC)	1050–1460	25–35
FIBER MATERIALS		
Aramid (Kevlar 49)	1300	31
E Glass	810	19.3
COMPOSITE MATERIALS		
Wood		
• Douglas fir (12% moisture)	2900	69.3
• Red oak (12% moisture)	2900	69.3

[a] At temperatures between 50°C and 100°C.
[b] At 100°C.
[c] At 50°C.
[d] At 0°C.

Sources: *ASM Handbooks, Volumes 1 and 2, Engineered Materials Handbooks, Volumes 1, 2, and 4, Metals Handbook: Properties and Selection: Nonferrous Alloys and Pure Metals*, Vol. 2, 9th edition, and *Advanced Materials & Processes*, Vol. 146, No. 4, ASM International, Materials Park, OH; *Modern Plastics Encyclopedia 1977–1978*, The McGraw-Hill Companies, New York, NY; and manufacturers' technical data sheets.

Table B.9 **Room-Temperature Electrical Resistivity Values for Various Engineering Materials**

Material	*Electrical Resistivity, Ω-m*
METALS AND METAL ALLOYS	
Plain Carbon and Low Alloy Steels	
Steel alloy A36[a]	1.60×10^{-7}
Steel alloy 1020 (annealed)[a]	1.60×10^{-7}
Steel alloy 1040 (annealed)[a]	1.60×10^{-7}
Steel alloy 4140 (quenched and tempered)	2.20×10^{-7}
Steel alloy 4340 (quenched and tempered)	2.48×10^{-7}
Stainless Steels	
Stainless alloy 304 (annealed)	7.2×10^{-7}
Stainless alloy 316 (annealed)	7.4×10^{-7}
Stainless alloy 405 (annealed)	6.0×10^{-7}
Stainless alloy 440A (annealed)	6.0×10^{-7}
Stainless alloy 17-7PH (annealed)	8.3×10^{-7}

Table B.9 (*Continued*)

Material	*Electrical Resistivity, Ω-m*
Cast Irons	
Gray irons	
• Grade G1800	15.0×10^{-7}
• Grade G3000	9.5×10^{-7}
• Grade G4000	8.5×10^{-7}
Ductile irons	
• Grade 60-40-18	5.5×10^{-7}
• Grade 80-55-06	6.2×10^{-7}
• Grade 120-90-02	6.2×10^{-7}
Aluminum Alloys	
Alloy 1100 (annealed)	2.9×10^{-8}
Alloy 2024 (annealed)	3.4×10^{-8}
Alloy 6061 (annealed)	3.7×10^{-8}
Alloy 7075 (T6 treatment)	5.22×10^{-8}
Alloy 356.0 (T6 treatment)	4.42×10^{-8}
Copper Alloys	
C11000 (electrolytic tough pitch, annealed)	1.72×10^{-8}
C172000 (beryllium–copper)	5.7×10^{-8}–1.15×10^{-7}
C26000 (cartridge brass)	6.2×10^{-8}
C36000 (free-cutting brass)	6.6×10^{-8}
C71500 (copper–nickel, 30%)	37.5×10^{-8}
C93200 (bearing bronze)	14.4×10^{-8}
Magnesium Alloys	
Alloy AZ31B	9.2×10^{-8}
Alloy AZ91D	17.0×10^{-8}
Titanium Alloys	
Commercially pure (ASTM grade 1)	4.2×10^{-7}–5.2×10^{-7}
Alloy Ti-5Al-2.5Sn	15.7×10^{-7}
Alloy Ti-6Al-4V	17.1×10^{-7}
Precious Metals	
Gold (commercially pure)	2.35×10^{-8}
Platinum (commercially pure)	10.60×10^{-8}
Silver (commercially pure)	1.47×10^{-8}
Refractory Metals	
Molybdenum (commercially pure)	5.2×10^{-8}
Tantalum (commercially pure)	13.5×10^{-8}
Tungsten (commercially pure)	5.3×10^{-8}
Miscellaneous Nonferrous Alloys	
Nickel 200	0.95×10^{-7}
Inconel 625	12.90×10^{-7}
Monel 400	5.47×10^{-7}
Haynes alloy 25	8.9×10^{-7}
Invar	8.2×10^{-7}
Super invar	8.0×10^{-7}
Kovar	4.9×10^{-7}
Chemical lead	2.06×10^{-7}
Antimonial lead (6%)	2.53×10^{-7}
Tin (commercially pure)	1.11×10^{-7}
Lead–Tin solder (60Sn-40Pb)	1.50×10^{-7}

Table B.9 (*Continued*)

Material	*Electrical Resistivity, Ω-m*
Zinc (commercially pure)	62.0×10^{-7}
Zirconium, reactor grade 702	3.97×10^{-7}
GRAPHITE, CERAMICS, AND SEMICONDUCTING MATERIALS	
Aluminum oxide	
• 99.9% pure	$>10^{13}$
• 96%	$>10^{12}$
• 90%	$>10^{12}$
Concrete (dry)	10^{9}
Diamond	
• Natural	$10–10^{14}$
• Synthetic	1.5×10^{-2}
Gallium arsenide (intrinsic)	10^{6}
Glass, borosilicate (Pyrex)	$\sim 10^{13}$
Glass, soda–lime	$10^{10}–10^{11}$
Glass ceramic (Pyroceram)	2×10^{14}
Graphite	
• Extruded (with grain direction)	$7 \times 10^{-6}–20 \times 10^{-6}$
• Isostatically molded	$10 \times 10^{-6}–18 \times 10^{-6}$
Silica, fused	$>10^{18}$
Silicon (intrinsic)	2500
Silicon carbide	
• Hot pressed	$1.0–10^{9}$
• Sintered	$1.0–10^{9}$
Silicon nitride	
• Hot isostatic pressed	$>10^{12}$
• Reaction bonded	$>10^{12}$
• Sintered	$>10^{12}$
Zirconia, 3 mol% Y_2O_3	10^{10}
POLYMERS	
Elastomers	
• Butadiene-acrylonitrile (nitrile)	3.5×10^{8}
• Styrene-butadiene (SBR)	6×10^{11}
• Silicone	10^{13}
Epoxy	$10^{10}–10^{13}$
Nylon 6,6	$10^{12}–10^{13}$
Phenolic	$10^{9}–10^{10}$
Polybutylene terephthalate (PBT)	4×10^{14}
Polycarbonate (PC)	2×10^{14}
Polyester (thermoset)	10^{13}
Polyetheretherketone (PEEK)	6×10^{14}
Polyethylene	
• Low density (LDPE)	$10^{15}–5 \times 10^{16}$
• High density (HDPE)	$10^{15}–5 \times 10^{16}$
• Ultrahigh molecular weight (UHMWPE)	$>5 \times 10^{14}$
Polyethylene terephthalate (PET)	10^{12}
Polymethyl methacrylate (PMMA)	$>10^{12}$
Polypropylene (PP)	$>10^{14}$
Polystyrene (PS)	$>10^{14}$
Polytetrafluoroethylene (PTFE)	10^{17}
Polyvinyl chloride (PVC)	$>10^{14}$

Table B.9 (*Continued*)

Material	*Electrical Resistivity, Ω-m*
FIBER MATERIALS	
Carbon (PAN precursor)	
• Standard modulus	17×10^{-6}
• Intermediate modulus	15×10^{-6}
• High modulus	9.5×10^{-6}
E Glass	4×10^{14}
COMPOSITE MATERIALS	
Wood	
• Douglas fir (oven dry)	
Parallel to grain	10^{14}–10^{16}
Perpendicular to grain	10^{14}–10^{16}
• Red oak (oven dry)	
Parallel to grain	10^{14}–10^{16}
Perpendicular to grain	10^{14}–10^{16}

[a] At 0°C.

Sources: *ASM Handbooks, Volumes 1 and 2, Engineered Materials Handbooks, Volumes 1, 2, and 4, Metals Handbook: Properties and Selection: Nonferrous Alloys and Pure Metals,* Vol. 2, 9th edition, and *Advanced Materials & Processes,* Vol. 146, No. 4, ASM International, Materials Park, OH; *Modern Plastics Encyclopedia 1977–1978,* The McGraw-Hill Companies, New York, NY; and manufacturers' technical data sheets.

Table B.10 **Compositions of Metal Alloys for Which Data Are Included in Tables B.1 through B.9**

Alloy (*UNS Designation*)	*Composition* (*wt%*)
PLAIN-CARBON AND LOW-ALLOY STEELS	
A 36 (ASTM A 36)	98.0 Fe (min), 0.29 C, 1.0 Mn, 0.28 Si
1020 (G10200)	99.1 Fe (min), 0.20 C, 0.45 Mn
1040 (G10400)	98.6 Fe (min), 0.40 C, 0.75 Mn
4140 (G41400)	96.8 Fe (min), 0.40 C, 0.90 Cr, 0.20 Mo, 0.9 Mn
4340 (G43400)	95.2 Fe (min), 0.40 C, 1.8 Ni, 0.80 Cr, 0.25 Mo, 0.7 Mn
STAINLESS STEELS	
304 (S30400)	66.4 Fe (min), 0.08 C, 19.0 Cr, 9.25 Ni, 2.0 Mn
316 (S31600)	61.9 Fe (min), 0.08 C, 17.0 Cr, 12.0 Ni, 2.5 Mo, 2.0 Mn
405 (S40500)	83.1 Fe (min), 0.08 C, 13.0 Cr, 0.20 Al, 1.0 Mn
440A (S44002)	78.4 Fe (min), 0.70 C, 17.0 Cr, 0.75 Mo. 1.0 Mn
17-7PH (S17700)	70.6 Fe (min), 0.09 C, 17.0 Cr, 7.1 Ni, 1.1 Al, 1.0 Mn
CAST IRONS	
Grade G1800 (F10004)	Fe (bal), 3.4–3.7 C, 2.8–2.3 Si, 0.65 Mn, 0.15 P, 0.15 S
Grade G3000 (F10006)	Fe (bal), 3.1–3.4 C, 2.3–1.9 Si, 0.75 Mn, 0.10 P, 0.15 S
Grade G4000 (F10008)	Fe (bal), 3.0–3.3 C, 2.1–1.8 Si, 0.85 Mn, 0.07 P, 0.15 S
Grade 60-40-18 (F32800)	Fe (bal), 3.4–4.0 C, 2.0–2.8 Si, 0–1.0 Ni, 0.05 Mg
Grade 80-55-06 (F33800)	Fe (bal), 3.3–3.8 C, 2.0–3.0 Si, 0–1.0 Ni, 0.05 Mg
Grade 120-90-02 (F36200)	Fe (bal), 3.4–3.8 C, 2.0–2.8 Si, 0–2.5 Ni, 0–1.0 Mo, 0.05 Mg

Table B.10 (*Continued*)

Alloy (***UNS Designation***)	***Composition*** (***wt%***)
	ALUMINUM ALLOYS
1100 (A91100)	99.00 Al (min), 0.20 Cu (max)
2024 (A92024)	90.75 Al (min), 4.4 Cu, 0.6 Mn, 1.5 Mg
6061 (A96061)	95.85 Al (min), 1.0 Mg, 0.6 Si, 0.30 Cu, 0.20 Cr
7075 (A97075)	87.2 Al (min), 5.6 Zn, 2.5 Mg, 1.6 Cu, 0.23 Cr
356.0 (A03560)	90.1 Al (min), 7.0 Si, 0.3 Mg
	COPPER ALLOYS
(C11000)	99.90 Cu (min), 0.04 O (max)
(C17200)	96.7 Cu (min), 1.9 Be, 0.20 Co
(C26000)	Zn (bal), 70 Cu, 0.07 Pb, 0.05 Fe (max)
(C36000)	60.0 Cu (min), 35.5 Zn, 3.0 Pb
(C71500)	63.75 Cu (min), 30.0 Ni
(C93200)	81.0 Cu (min), 7.0 Sn, 7.0 Pb, 3.0 Zn
	MAGNESIUM ALLOYS
AZ31B (M11311)	94.4 Mg (min), 3.0 Al, 0.20 Mn (min), 1.0 Zn, 0.1 Si (max)
AZ91D (M11916)	89.0 Mg (min), 9.0 Al, 0.13 Mn (min), 0.7 Zn, 0.1 Si (max)
	TITANIUM ALLOYS
Commercial, grade 1 (R50250)	99.5 Ti (min)
Ti-5Al-2.5Sn (R54520)	90.2 Ti (min), 5.0 Al, 2.5 Sn
Ti-6Al-4V (R56400)	87.7 Ti (min), 6.0 Al, 4.0 V
	MISCELLANEOUS ALLOYS
Nickel 200	99.0 Ni (min)
Inconel 625	58.0 Ni (min), 21.5 Cr, 9.0 Mo, 5.0 Fe, 3.65 Nb + Ta, 1.0 Co
Monel 400	63.0 Ni (min), 31.0 Cu, 2.5 Fe, 0.2 Mn, 0.3 C, 0.5 Si
Haynes alloy 25	49.4 Co (min), 20 Cr, 15 W, 10 Ni, 3 Fe (max), 0.10 C, 1.5 Mn
Invar (K93601)	64 Fe, 36 Ni
Super invar	63 Fe, 32 Ni, 5 Co
Kovar	54 Fe, 29 Ni, 17 Co
Chemical lead (L51120)	99.90 Pb (min)
Antimonial lead, 6% (L53105)	94 Pb, 6 Sb
Tin (commercially pure) (ASTM B339A)	98.85 Pb (min)
Lead–Tin solder (60Sn-40Pb) (ASTM B32 grade 60)	60 Sn, 40 Pb
Zinc (commercially pure) (Z21210)	99.9 Zn (min), 0.10 Pb (max)
Zirconium, reactor grade 702 (R60702)	99.2 Zr + Hf (min), 4.5 Hf (max), 0.2 Fe + Cr

Sources: *ASM Handbooks, Volumes 1 and 2,* ASM International, Materials Park, OH.

Table B.1 Room-Temperature Density Values for Various Engineering Materials

Material	*Density*	
	g/cm³	*lbm/in.³*
METALS AND METAL ALLOYS		
Plain Carbon and Low Alloy Steels		
Steel alloy A36	7.85	0.283
Steel alloy 1020	7.85	0.283
Steel alloy 1040	7.85	0.283
Steel alloy 4140	7.85	0.283
Steel alloy 4340	7.85	0.283
Stainless Steels		
Stainless alloy 304	8.00	0.289
Stainless alloy 316	8.00	0.289

Table B.1 (*Continued*)

	Density	
Material	***g/cm^3***	***lb$_\mathrm{m}$/in.^{3}***
Stainless alloy 405	7.80	0.282
Stainless alloy 440A	7.80	0.282
Stainless alloy 17-7PH	7.65	0.276
Cast Irons		
Gray irons		
• Grade G1800	7.30	0.264
• Grade G3000	7.30	0.264
• Grade G4000	7.30	0.264
Ductile irons		
• Grade 60-40-18	7.10	0.256
• Grade 80-55-06	7.10	0.256
• Grade 120-90-02	7.10	0.256
Aluminum Alloys		
Alloy 1100	2.71	0.0978
Alloy 2024	2.77	0.100
Alloy 6061	2.70	0.0975
Alloy 7075	2.80	0.101
Alloy 356.0	2.69	0.0971
Copper Alloys		
C11000 (electrolytic tough pitch)	8.89	0.321
C17200 (beryllium–copper)	8.25	0.298
C26000 (cartridge brass)	8.53	0.308
C36000 (free-cutting brass)	8.50	0.307
C71500 (copper–nickel, 30%)	8.94	0.323
C93200 (bearing bronze)	8.93	0.322
Magnesium Alloys		
Alloy AZ31B	1.77	0.0639
Alloy AZ91D	1.81	0.0653
Titanium Alloys		
Commercially pure (ASTM grade 1)	4.51	0.163
Alloy Ti-5Al-2.5Sn	4.48	0.162
Alloy Ti-6Al-4V	4.43	0.160
Precious Metals		
Gold (commercially pure)	19.32	0.697
Platinum (commercially pure)	21.45	0.774
Silver (commercially pure)	10.49	0.379
Refractory Metals		
Molybdenum (commercially pure)	10.22	0.369
Tantalum (commercially pure)	16.6	0.599
Tungsten (commercially pure)	19.3	0.697
Miscellaneous Nonferrous Alloys		
Nickel 200	8.89	0.321
Inconel 625	8.44	0.305
Monel 400	8.80	0.318
Haynes alloy 25	9.13	0.330
Invar	8.05	0.291

Table B.1 (*Continued*)

Material	*Density*	
	g/cm^3	*lb*$_m$*/in.*^{3}
Super invar	8.10	0.292
Kovar	8.36	0.302
Chemical lead	11.34	0.409
Antimonial lead (6%)	10.88	0.393
Tin (commercially pure)	7.17	0.259
Lead–Tin solder (60Sn-40Pb)	8.52	0.308
Zinc (commercially pure)	7.14	0.258
Zirconium, reactor grade 702	6.51	0.235
GRAPHITE, CERAMICS, AND SEMICONDUCTING MATERIALS		
Aluminum oxide		
• 99.9% pure	3.98	0.144
• 96%	3.72	0.134
• 90%	3.60	0.130
Concrete	2.4	0.087
Diamond		
• Natural	3.51	0.127
• Synthetic	3.20–3.52	0.116–0.127
Gallium arsenide	5.32	0.192
Glass, borosilicate (Pyrex)	2.23	0.0805
Glass, soda–lime	2.5	0.0903
Glass ceramic (Pyroceram)	2.60	0.0939
Graphite		
• Extruded	1.71	0.0616
• Isostatically molded	1.78	0.0643
Silica, fused	2.2	0.079
Silicon	2.33	0.0841
Silicon carbide		
• Hot pressed	3.3	0.119
• Sintered	3.2	0.116
Silicon nitride		
• Hot pressed	3.3	0.119
• Reaction bonded	2.7	0.0975
• Sintered	3.3	0.119
Zirconia, 3 mol% Y_2O_3, sintered	6.0	0.217
POLYMERS		
Elastomers		
• Butadiene-acrylonitrile (nitrile)	0.98	0.0354
• Styrene-butadiene (SBR)	0.94	0.0339
• Silicone	1.1–1.6	0.040–0.058
Epoxy	1.11–1.40	0.0401–0.0505
Nylon 6,6	1.14	0.0412
Phenolic	1.28	0.0462
Polybutylene terephthalate (PBT)	1.34	0.0484
Polycarbonate (PC)	1.20	0.0433
Polyester (thermoset)	1.04–1.46	0.038–0.053
Polyetheretherketone (PEEK)	1.31	0.0473
Polyethylene		
• Low density (LDPE)	0.925	0.0334
• High density (HDPE)	0.959	0.0346

Table B.1 (*Continued*)

Material	**Density**	
	g/cm³	***lbₘ/in.³***
• Ultrahigh molecular weight (UHMWPE)	0.94	0.0339
Polyethylene terephthalate (PET)	1.35	0.0487
Polymethyl methacrylate (PMMA)	1.19	0.0430
Polypropylene (PP)	0.905	0.0327
Polystyrene (PS)	1.05	0.0379
Polytetrafluoroethylene (PTFE)	2.17	0.0783
Polyvinyl chloride (PVC)	1.30–1.58	0.047–0.057
FIBER MATERIALS		
Aramid (Kevlar 49)	1.44	0.0520
Carbon (PAN precursor)		
• Standard modulus	1.78	0.0643
• Intermediate modulus	1.78	0.0643
• High modulus	1.81	0.0653
E Glass	2.58	0.0931
COMPOSITE MATERIALS		
Aramid fibers-epoxy matrix ($V_f = 0.60$)	1.4	0.050
High modulus carbon fibers-epoxy matrix ($V_f = 0.60$)	1.7	0.061
E glass fibers-epoxy matrix ($V_f = 0.60$)	2.1	0.075
Wood		
• Douglas fir (12% moisture)	0.46–0.50	0.017–0.018
• Red oak (12% moisture)	0.61–0.67	0.022–0.024

Sources: *ASM Handbooks, Volumes 1 and 2, Engineered Materials Handbook, Volume 4, Metals Handbook: Properties and Selection: Nonferrous Alloys and Pure Metals,* Vol. 2, 9th edition, and *Advanced Materials & Processes,* Vol. 146, No. 4, ASM International Materials Park, OH; *Modern Plastics Encyclopedia ’96,* The McGraw-Hill Companies, New York, NY; R. F. Floral and S. T. Peters, ‘‘Composite Structures and Technologies,’’ tutorial notes, 1989; and manufacturers’ technical data sheets.

Table B.10 Compositions of Metal Alloys for Which Data Are Included in Tables B.1 through B.9

Alloy (*UNS Designation*)	*Composition* (*wt%*)
PLAIN-CARBON AND LOW-ALLOY STEELS	
A 36 (ASTM A 36)	98.0 Fe (min), 0.29 C, 1.0 Mn, 0.28 Si
1020 (G10200)	99.1 Fe (min), 0.20 C, 0.45 Mn
1040 (G10400)	98.6 Fe (min), 0.40 C, 0.75 Mn
4140 (G41400)	96.8 Fe (min), 0.40 C, 0.90 Cr, 0.20 Mo, 0.9 Mn
4340 (G43400)	95.2 Fe (min), 0.40 C, 1.8 Ni, 0.80 Cr, 0.25 Mo, 0.7 Mn
STAINLESS STEELS	
304 (S30400)	66.4 Fe (min), 0.08 C, 19.0 Cr, 9.25 Ni, 2.0 Mn
316 (S31600)	61.9 Fe (min), 0.08 C, 17.0 Cr, 12.0 Ni, 2.5 Mo, 2.0 Mn
405 (S40500)	83.1 Fe (min), 0.08 C, 13.0 Cr, 0.20 Al, 1.0 Mn
440A (S44002)	78.4 Fe (min), 0.70 C, 17.0 Cr, 0.75 Mo. 1.0 Mn
17-7PH (S17700)	70.6 Fe (min), 0.09 C, 17.0 Cr, 7.1 Ni, 1.1 Al, 1.0 Mn
CAST IRONS	
Grade G1800 (F10004)	Fe (bal), 3.4–3.7 C, 2.8–2.3 Si, 0.65 Mn, 0.15 P, 0.15 S
Grade G3000 (F10006)	Fe (bal), 3.1–3.4 C, 2.3–1.9 Si, 0.75 Mn, 0.10 P, 0.15 S
Grade G4000 (F10008)	Fe (bal), 3.0–3.3 C, 2.1–1.8 Si, 0.85 Mn, 0.07 P, 0.15 S
Grade 60-40-18 (F32800)	Fe (bal), 3.4–4.0 C, 2.0–2.8 Si, 0–1.0 Ni, 0.05 Mg
Grade 80-55-06 (F33800)	Fe (bal), 3.3–3.8 C, 2.0–3.0 Si, 0–1.0 Ni, 0.05 Mg
Grade 120-90-02 (F36200)	Fe (bal), 3.4–3.8 C, 2.0–2.8 Si, 0–2.5 Ni, 0–1.0 Mo, 0.05 Mg

Table B.10 *(Continued)*

Alloy (***UNS Designation***)	***Composition*** (***wt%***)
ALUMINUM ALLOYS	
1100 (A91100)	99.00 Al (min), 0.20 Cu (max)
2024 (A92024)	90.75 Al (min), 4.4 Cu, 0.6 Mn, 1.5 Mg
6061 (A96061)	95.85 Al (min), 1.0 Mg, 0.6 Si, 0.30 Cu, 0.20 Cr
7075 (A97075)	87.2 Al (min), 5.6 Zn, 2.5 Mg, 1.6 Cu, 0.23 Cr
356.0 (A03560)	90.1 Al (min), 7.0 Si, 0.3 Mg
COPPER ALLOYS	
(C11000)	99.90 Cu (min), 0.04 O (max)
(C17200)	96.7 Cu (min), 1.9 Be, 0.20 Co
(C26000)	Zn (bal), 70 Cu, 0.07 Pb, 0.05 Fe (max)
(C36000)	60.0 Cu (min), 35.5 Zn, 3.0 Pb
(C71500)	63.75 Cu (min), 30.0 Ni
(C93200)	81.0 Cu (min), 7.0 Sn, 7.0 Pb, 3.0 Zn
MAGNESIUM ALLOYS	
AZ31B (M11311)	94.4 Mg (min), 3.0 Al, 0.20 Mn (min), 1.0 Zn, 0.1 Si (max)
AZ91D (M11916)	89.0 Mg (min), 9.0 Al, 0.13 Mn (min), 0.7 Zn, 0.1 Si (max)
TITANIUM ALLOYS	
Commercial, grade 1 (R50250)	99.5 Ti (min)
Ti-5Al-2.5Sn (R54520)	90.2 Ti (min), 5.0 Al, 2.5 Sn
Ti-6Al-4V (R56400)	87.7 Ti (min), 6.0 Al, 4.0 V
MISCELLANEOUS ALLOYS	
Nickel 200	99.0 Ni (min)
Inconel 625	58.0 Ni (min), 21.5 Cr, 9.0 Mo, 5.0 Fe, 3.65 Nb + Ta, 1.0 Co
Monel 400	63.0 Ni (min), 31.0 Cu, 2.5 Fe, 0.2 Mn, 0.3 C, 0.5 Si
Haynes alloy 25	49.4 Co (min), 20 Cr, 15 W, 10 Ni, 3 Fe (max), 0.10 C, 1.5 Mn
Invar (K93601)	64 Fe, 36 Ni
Super invar	63 Fe, 32 Ni, 5 Co
Kovar	54 Fe, 29 Ni, 17 Co
Chemical lead (L51120)	99.90 Pb (min)
Antimonial lead, 6% (L53105)	94 Pb, 6 Sb
Tin (commercially pure) (ASTM B339A)	98.85 Pb (min)
Lead–Tin solder (60Sn-40Pb) (ASTM B32 grade 60)	60 Sn, 40 Pb
Zinc (commercially pure) (Z21210)	99.9 Zn (min), 0.10 Pb (max)
Zirconium, reactor grade 702 (R60702)	99.2 Zr + Hf (min), 4.5 Hf (max), 0.2 Fe + Cr

Sources: *ASM Handbooks, Volumes 1 and 2,* ASM International, Materials Park, OH.

Table B.3 **Room-Temperature Poisson's Ratio Values for Various Engineering Materials**

Material	*Poisson's Ratio*
METALS AND METAL ALLOYS	
Plain Carbon and Low Alloy Steels	
Steel alloy A36	0.30
Steel alloy 1020	0.30
Steel alloy 1040	0.30
Steel alloy 4140	0.30
Steel alloy 4340	0.30
Stainless Steels	
Stainless alloy 304	0.30
Stainless alloy 316	0.30
Stainless alloy 405	0.30
Stainless alloy 440A	0.30
Stainless alloy 17-7PH	0.30
Cast Irons	
Gray irons	
• Grade G1800	0.26
• Grade G3000	0.26
• Grade G4000	0.26
Ductile irons	
• Grade 60-40-18	0.29
• Grade 80-55-06	0.31
• Grade 120-90-02	0.28
Aluminum Alloys	
Alloy 1100	0.33
Alloy 2024	0.33
Alloy 6061	0.33
Alloy 7075	0.33
Alloy 356.0	0.33
Copper Alloys	
C11000 (electrolytic tough pitch)	0.33
C17200 (beryllium–copper)	0.30
C26000 (cartridge brass)	0.35
C36000 (free-cutting brass)	0.34
C71500 (copper–nickel, 30%)	0.34
C93200 (bearing bronze)	0.34
Magnesium Alloys	
Alloy AZ31B	0.35
Alloy AZ91D	0.35
Titanium Alloys	
Commercially pure (ASTM grade 1)	0.34
Alloy Ti-5Al-2.5Sn	0.34
Alloy Ti-6Al-4V	0.34
Precious Metals	
Gold (commercially pure)	0.42
Platinum (commercially pure)	0.39
Silver (commercially pure)	0.37

Material	*Poisson's Ratio*
Refractory Metals	
Molybdenum (commercially pure)	0.32
Tantalum (commercially pure)	0.35
Tungsten (commercially pure)	0.28
Miscellaneous Nonferrous Alloys	
Nickel 200	0.31
Inconel 625	0.31
Monel 400	0.32
Chemical lead	0.44
Tin (commercially pure)	0.33
Zinc (commercially pure)	0.25
Zirconium, reactor grade 702	0.35
GRAPHITE, CERAMICS, AND SEMICONDUCTING MATERIALS	
Aluminum oxide	
• 99.9% pure	0.22
• 96%	0.21
• 90%	0.22
Concrete	0.20
Diamond	
• Natural	0.10–0.30
• Synthetic	0.20
Gallium arsenide	
• ⟨100⟩ orientation	0.30
Glass, borosilicate (Pyrex)	0.20
Glass, soda–lime	0.23
Glass ceramic (Pyroceram)	0.25
Silica, fused	0.17
Silicon	
• ⟨100⟩ orientation	0.28
• ⟨111⟩ orientation	0.36
Silicon carbide	
• Hot pressed	0.17
• Sintered	0.16
Silicon nitride	
• Hot pressed	0.30
• Reaction bonded	0.22
• Sintered	0.28
Zirconia, 3 mol% Y_2O_3	0.31
POLYMERS	
Nylon 6,6	0.39
Polycarbonate (PC)	0.36
Polystyrene (PS)	0.33
Polytetrafluoroethylene (PTFE)	0.46
Polyvinyl chloride (PVC)	0.38
FIBER MATERIALS	
E Glass	0.22

Table B.3 *(Continued)*

Material	*Poisson's Ratio*
COMPOSITE MATERIALS	
Aramid fibers-epoxy matrix ($V_f = 0.6$)	0.34
High modulus carbon fibers-epoxy matrix ($V_f = 0.6$)	0.25
E glass fibers-epoxy matrix ($V_f = 0.6$)	0.19

Sources: *ASM Handbooks, Volumes 1 and 2,* and *Engineered Materials Handbooks, Volumes 1 and 4,* ASM International, Materials Park, OH; R. F. Floral and S. T. Peters, ''Composite Structures and Technologies,'' tutorial notes, 1989; and manufacturers' technical data sheets.

Table B.4 Typical Room-Temperature Yield Strength, Tensile Strength, and Ductility (Percent Elongation) Values for Various Engineering Materials

Material/Condition	*Yield Strength* (*MPa* [*ksi*])	*Tensile Strength* (*MPa* [*ksi*])	*Percent Elongation*
METALS AND METAL ALLOYS			
Plain Carbon and Low Alloy Steels			
Steel alloy A36			
• Hot rolled	220–250 (32–36)	400–500 (58–72.5)	23
Steel alloy 1020			
• Hot rolled	210 (30) (min)	380 (55) (min)	25 (min)
• Cold drawn	350 (51) (min)	420 (61) (min)	15 (min)
• Annealed (@ 870°C)	295 (42.8)	395 (57.3)	36.5
• Normalized (@ 925°C)	345 (50.3)	440 (64)	38.5
Steel alloy 1040			
• Hot rolled	290 (42) (min)	520 (76) (min)	18 (min)
• Cold drawn	490 (71) (min)	590 (85) (min)	12 (min)
• Annealed (@ 785°C)	355 (51.3)	520 (75.3)	30.2
• Normalized (@ 900°C)	375 (54.3)	590 (85)	28.0
Steel alloy 4140			
• Annealed (@ 815°C)	417 (60.5)	655 (95)	25.7
• Normalized (@ 870°C)	655 (95)	1020 (148)	17.7
• Oil-quenched and tempered (@ 315°C)	1570 (228)	1720 (250)	11.5
Steel alloy 4340			
• Annealed (@ 810°C)	472 (68.5)	745 (108)	22
• Normalized (@ 870°C)	862 (125)	1280 (185.5)	12.2
• Oil-quenched and tempered (@ 315°C)	1620 (235)	1760 (255)	12
Stainless Steels			
Stainless alloy 304			
• Hot finished and annealed	205 (30) (min)	515 (75) (min)	40 (min)
• Cold worked ($\frac{1}{4}$ hard)	515 (75) (min)	860 (125) (min)	10 (min)
Stainless alloy 316			
• Hot finished and annealed	205 (30) (min)	515 (75) (min)	40 (min)
• Cold drawn and annealed	310 (45) (min)	620 (90) (min)	30 (min)
Stainless alloy 405			
• Annealed	170 (25)	415 (60)	20

Table B.4 (*Continued*)

Material/Condition	***Yield Strength*** (***MPa*** [***ksi***])	***Tensile Strength*** (***MPa*** [***ksi***])	***Percent Elongation***
Stainless alloy 440A			
• Annealed	415 (60)	725 (105)	20
• Tempered @ 315°C	1650 (240)	1790 (260)	5
Stainless alloy 17-7PH			
• Cold rolled	1210 (175) (min)	1380 (200) (min)	1 (min)
• Precipitation hardened @ 510°C	1310 (190) (min)	1450 (210) (min)	3.5 (min)
Cast Irons			
Gray irons			
• Grade G1800 (as cast)	—	124 (18) (min)	—
• Grade G3000 (as cast)	—	207 (30) (min)	—
• Grade G4000 (as cast)	—	276 (40) (min)	—
Ductile irons			
• Grade 60-40-18 (annealed)	276 (40) (min)	414 (60) (min)	18 (min)
• Grade 80-55-06 (as cast)	379 (55) (min)	552 (80) (min)	6 (min)
• Grade 120-90-02 (oil quenched and tempered)	621 (90) (min)	827 (120) (min)	2 (min)
Aluminum Alloys			
Alloy 1100			
• Annealed (O temper)	34 (5)	90 (13)	40
• Strain hardened (H14 temper)	117 (17)	124 (18)	15
Alloy 2024			
• Annealed (O temper)	75 (11)	185 (27)	20
• Heat treated and aged (T3 temper)	345 (50)	485 (70)	18
• Heat treated and aged (T351 temper)	325 (47)	470 (68)	20
Alloy 6061			
• Annealed (O temper)	55 (8)	124 (18)	30
• Heat treated and aged (T6 and T651 tempers)	276 (40)	310 (45)	17
Alloy 7075			
• Annealed (O temper)	103 (15)	228 (33)	17
• Heat treated and aged (T6 temper)	505 (73)	572 (83)	11
Alloy 356.0			
• As cast	124 (18)	164 (24)	6
• Heat treated and aged (T6 temper)	164 (24)	228 (33)	3.5
Copper Alloys			
C11000 (electrolytic tough pitch)			
• Hot rolled	69 (10)	220 (32)	50
• Cold worked (H04 temper)	310 (45)	345 (50)	12
C17200 (beryllium–copper)			
• Solution heat treated	195–380 (28–55)	415–540 (60–78)	35–60
• Solution heat treated, aged @ 330°C	965–1205 (140–175)	1140–1310 (165–190)	4–10
C26000 (cartridge brass)			
• Annealed	75–150 (11–22)	300–365 (43.5–53.0)	54–68
• Cold worked (H04 temper)	435 (63)	525 (76)	8
C36000 (free-cutting brass)			
• Annealed	125 (18)	340 (49)	53
• Cold worked (H02 temper)	310 (45)	400 (58)	25
C71500 (copper–nickel, 30%)			
• Hot rolled	140 (20)	380 (55)	45
• Cold worked (H80 temper)	545 (79)	580 (84)	3

Table B.4 (*Continued*)

Material/Condition	*Yield Strength (MPa [ksi])*	*Tensile Strength (MPa [ksi])*	*Percent Elongation*
C93200 (bearing bronze)			
• Sand cast	125 (18)	240 (35)	20
Magnesium Alloys			
Alloy AZ31B			
• Rolled	220 (32)	290 (42)	15
• Extruded	200 (29)	262 (38)	15
Alloy AZ91D			
• As cast	97–150 (14–22)	165–230 (24–33)	3
Titanium Alloys			
Commercially pure (ASTM grade 1)			
• Annealed	170 (25) (min)	240 (35) (min)	30
Alloy Ti-5Al-2.5Sn			
• Annealed	760 (110) (min)	790 (115) (min)	16
Alloy Ti-6Al-4V			
• Annealed	830 (120) (min)	900 (130) (min)	14
• Solution heat treated and aged	1103 (160)	1172 (170)	10
Precious Metals			
Gold (commercially pure)			
• Annealed	nil	130 (19)	45
• Cold worked (60% reduction)	205 (30)	220 (32)	4
Platinum (commercially pure)			
• Annealed	<13.8 (2)	125–165 (18–24)	30–40
• Cold worked (50%)	—	205–240 (30–35)	1–3
Silver (commercially pure)			
• Annealed	—	170 (24.6)	44
• Cold worked (50%)	—	296 (43)	3.5
Refractory Metals			
Molybdenum (commercially pure)	500 (72.5)	630 (91)	25
Tantalum (commercially pure)	165 (24)	205 (30)	40
Tungsten (commercially pure)	760 (110)	960 (139)	2
Miscellaneous Nonferrous Alloys			
Nickel 200 (annealed)	148 (21.5)	462 (67)	47
Inconel 625 (annealed)	517 (75)	930 (135)	42.5
Monel 400 (annealed)	240 (35)	550 (80)	40
Haynes alloy 25	445 (65)	970 (141)	62
Invar (annealed)	276 (40)	517 (75)	30
Super invar (annealed)	276 (40)	483 (70)	30
Kovar (annealed)	276 (40)	517 (75)	30
Chemical lead	6–8 (0.9–1.2)	16–19 (2.3–2.7)	30–60
Antimonial lead (6%) (chill cast)	—	47.2 (6.8)	24
Tin (commercially pure)	11 (1.6)	—	57
Lead–Tin solder (60Sn-40Pb)	—	52.5 (7.6)	30–60
Zinc (commercially pure)			
• Hot rolled (anisotropic)	—	134–159 (19.4–23.0)	50–65
• Cold rolled (anisotropic)	—	145–186 (21–27)	40–50
Zirconium, reactor grade 702			
• Cold worked and annealed	207 (30) (min)	379 (55) (min)	16 (min)

Table B.4 *(Continued)*

Material/Condition	*Yield Strength (MPa [ksi])*	*Tensile Strength (MPa [ksi])*	*Percent Elongation*
GRAPHITE, CERAMICS, AND SEMICONDUCTING MATERIALS[a]			
Aluminum oxide			
• 99.9% pure	—	282–551 (41–80)	—
• 96%	—	358 (52)	—
• 90%	—	337 (49)	—
Concrete[b]	—	37.3–41.3 (5.4–6.0)	—
Diamond			
• Natural	—	1050 (152)	—
• Synthetic	—	800–1400 (116–203)	—
Gallium arsenide			
• {100} orientation, polished surface	—	66 (9.6)[c]	—
• {100} orientation, as-cut surface	—	57 (8.3)[c]	—
Glass, borosilicate (Pyrex)	—	69 (10)	—
Glass, soda–lime	—	69 (10)	—
Glass ceramic (Pyroceram)	—	123–370 (18–54)	—
Graphite			
• Extruded (with the grain direction)	—	13.8–34.5 (2.0–5.0)	—
• Isostatically molded	—	31–69 (4.5–10)	—
Silica, fused	—	104 (15)	—
Silicon			
• {100} orientation, as-cut surface	—	130 (18.9)	—
• {100} orientation, laser scribed	—	81.8 (11.9)	—
Silicon carbide			
• Hot pressed	—	230–825 (33–120)	—
• Sintered	—	96–520 (14–75)	—
Silicon nitride			
• Hot pressed	—	700–1000 (100–150)	—
• Reaction bonded	—	250–345 (36–50)	—
• Sintered	—	414–650 (60–94)	—
Zirconia, 3 mol% Y_2O_3 (sintered)	—	800–1500 (116–218)	—
POLYMERS			
Elastomers			
• Butadiene-acrylonitrile (nitrile)	—	6.9–24.1 (1.0–3.5)	400–600
• Styrene-butadiene (SBR)	—	12.4–20.7 (1.8–3.0)	450–500
• Silicone	—	10.3 (1.5)	100–800
Epoxy	—	27.6–90.0 (4.0–13)	3–6
Nylon 6,6			
• Dry, as molded	55.1–82.8 (8–12)	94.5 (13.7)	15–80
• 50% relative humidity	44.8–58.6 (6.5–8.5)	75.9 (11)	150–300
Phenolic	—	34.5–62.1 (5.0–9.0)	1.5–2.0
Polybutylene terephthalate (PBT)	56.6–60.0 (8.2–8.7)	56.6–60.0 (8.2–8.7)	50–300
Polycarbonate (PC)	62.1 (9)	62.8–72.4 (9.1–10.5)	110–150
Polyester (thermoset)	—	41.4–89.7 (6.0–13.0)	<2.6
Polyetheretherketone (PEEK)	91 (13.2)	70.3–103 (10.2–15.0)	30–150
Polyethylene			
• Low density (LDPE)	9.0–14.5 (1.3–2.1)	8.3–31.4 (1.2–4.55)	100–650
• High density (HDPE)	26.2–33.1 (3.8–4.8)	22.1–31.0 (3.2–4.5)	10–1200
• Ultrahigh molecular weight (UHMWPE)	21.4–27.6 (3.1–4.0)	38.6–48.3 (5.6–7.0)	350–525
Polyethylene terephthalate (PET)	59.3 (8.6)	48.3–72.4 (7.0–10.5)	30–300

Table B.4 *(Continued)*

Material/Condition	***Yield Strength* (*MPa* [*ksi*])**	***Tensile Strength* (*MPa* [*ksi*])**	***Percent Elongation***
Polymethyl methacrylate (PMMA)	53.8–73.1 (7.8–10.6)	48.3–72.4 (7.0–10.5)	2.0–5.5
Polypropylene (PP)	31.0–37.2 (4.5–5.4)	31.0–41.4 (4.5–6.0)	100–600
Polystyrene (PS)	—	35.9–51.7 (5.2–7.5)	1.2–2.5
Polytetrafluoroethylene (PTFE)	—	20.7–34.5 (3.0–5.0)	200–400
Polyvinyl chloride (PVC)	40.7–44.8 (5.9–6.5)	40.7–51.7 (5.9–7.5)	40–80
FIBER MATERIALS			
Aramid (Kevlar 49)	—	3600–4100 (525–600)	2.8
Carbon (PAN precursor)			
• Standard modulus (longitudinal)	—	3800–4200 (550–610)	2
• Intermediate modulus (longitudinal)	—	4650–6350 (675–920)	1.8
• High modulus (longitudinal)	—	2500–4500 (360–650)	0.6
E Glass	—	3450 (500)	4.3
COMPOSITE MATERIALS			
Aramid fibers-epoxy matrix (aligned, $V_f = 0.6$)			
• Longitudinal direction	—	1380 (200)	1.8
• Transverse direction	—	30 (4.3)	0.5
High modulus carbon fibers-epoxy matrix (aligned, $V_f = 0.6$)			
• Longitudinal direction	—	760 (110)	0.3
• Transverse direction	—	28 (4)	0.4
E glass fibers-epoxy matrix (aligned, $V_f = 0.6$)			
• Longitudinal direction	—	1020 (150)	2.3
• Transverse direction	—	40 (5.8)	0.4
Wood			
• Douglas fir (12% moisture)			
Parallel to grain	—	108 (15.6)	—
Perpendicular to grain	—	2.4 (0.35)	—
• Red oak (12% moisture)			
Parallel to grain	—	112 (16.3)	—
Perpendicular to grain	—	7.2 (1.05)	—

[a] The strength of graphite, ceramics, and semiconducting materials is taken as flexural strength.

[b] The strength of concrete is measured in compression.

[c] Flexural strength value at 50% fracture probability.

Sources: *ASM Handbooks, Volumes 1 and 2, Engineered Materials Handbooks, Volumes 1 and 4, Metals Handbook: Properties and Selection: Nonferrous Alloys and Pure Metals,* Vol. 2, 9th edition, *Advanced Materials & Processes,* Vol. 146, No. 4, and *Materials & Processing Databook (1985),* ASM International, Materials Park, OH; *Modern Plastics Encyclopedia '96,* The McGraw-Hill Companies, New York, NY; R. F. Floral and S. T. Peters, ‘‘Composite Structures and Technologies,’’ tutorial notes, 1989; and manufacturers' technical data sheets.

Table B.5 Room-Temperature Plane Strain Fracture Toughness and Strength Values for Various Engineering Materials

Material	*Fracture Toughness*		*Strength*[a]
	MPa$\sqrt{m}$	*ksi*$\sqrt{in.}$	(*MPa*)
METALS AND METAL ALLOYS			
Plain Carbon and Low Alloy Steels			
Steel alloy 1040	54.0	49.0	260
Steel alloy 4140			
• Tempered @ 370°C	55–65	50–59	1375–1585
• Tempered @ 482°C	75–93	68.3–84.6	1100–1200
Steel alloy 4340			
• Tempered @ 260°C	50.0	45.8	1640
• Tempered @ 425°C	87.4	80.0	1420
Stainless Steels			
Stainless alloy 17-7PH			
• Precipitation hardened @ 510°C	76	69	1310
Aluminum Alloys			
Alloy 2024-T3	44	40	345
Alloy 7075-T651	24	22	495
Magnesium Alloys			
Alloy AZ31B			
• Extruded	28.0	25.5	200
Titanium Alloys			
Alloy Ti-5Al-2.5Sn			
• Air cooled	71.4	65.0	876
Alloy Ti-6Al-4V			
• Equiaxed grains	44–66	40–60	910
GRAPHITE, CERAMICS, AND SEMICONDUCTING MATERIALS			
Aluminum oxide			
• 99.9% pure	4.2–5.9	3.8–5.4	282–551
• 96%	3.85–3.95	3.5–3.6	358
Concrete	0.2–1.4	0.18–1.27	—
Diamond			
• Natural	3.4	3.1	1050
• Synthetic	6.0–10.7	5.5–9.7	800–1400
Gallium arsenide			
• In the {100} orientation	0.43	0.39	66
• In the {110} orientation	0.31	0.28	—
• In the {111} orientation	0.45	0.41	—
Glass, borosilicate (Pyrex)	0.77	0.70	69
Glass, soda-lime	0.75	0.68	69
Glass ceramic (Pyroceram)	1.6–2.1	1.5–1.9	123–370
Silica, fused	0.79	0.72	104
Silicon			
• In the {100} orientation	0.95	0.86	—
• In the {110} orientation	0.90	0.82	—
• In the {111} orientation	0.82	0.75	—
Silicon carbide			
• Hot pressed	4.8–6.1	4.4–5.6	230–825
• Sintered	4.8	4.4	96–520

Table B.5 (*Continued*)

Material	***Fracture Toughness***		***Strength***[a]
	MPa $\sqrt{m}$	***ksi $\sqrt{in.}$***	**(*MPa*)**
Silicon nitride			
• Hot pressed	4.1–6.0	3.7–5.5	700–1000
• Reaction bonded	3.6	3.3	250–345
• Sintered	5.3	4.8	414–650
Zirconia, 3 mol% Y_2O_3	7.0–12.0	6.4–10.9	800–1500
POLYMERS			
Epoxy	0.6	0.55	—
Nylon 6,6	2.5–3.0	2.3–2.7	44.8–58.6
Polycarbonate (PC)	2.2	2.0	62.1
Polyester (thermoset)	0.6	0.55	—
Polyethylene terephthalate (PET)	5.0	4.6	59.3
Polymethyl methacrylate (PMMA)	0.7–1.6	0.6–1.5	53.8–73.1
Polypropylene (PP)	3.0–4.5	2.7–4.1	31.0–37.2
Polystyrene (PS)	0.7–1.1	0.6–1.0	—
Polyvinyl chloride (PVC)	2.0–4.0	1.8–3.6	40.7–44.8

[a] For metal alloys and polymers, strength is taken as yield strength; for ceramic materials, flexural strength is used.

Sources: *ASM Handbooks, Volumes 1 and 19, Engineered Materials Handbooks, Volumes 2* and *4*, and *Advanced Materials & Processes*, Vol. 137, No. 6, ASM International, Materials Park, OH.

Table B.6 Room-Temperature Linear Coefficient of Thermal Expansion Values for Various Engineering Materials

Material	*Coefficient of Thermal Expansion* $10^{-6}\ (°C)^{-1}$	$10^{-6}\ (°F)^{-1}$
METALS AND METAL ALLOYS		
Plain Carbon and Low Alloy Steels		
Steel alloy A36	11.7	6.5
Steel alloy 1020	11.7	6.5
Steel alloy 1040	11.3	6.3
Steel alloy 4140	12.3	6.8
Steel alloy 4340	12.3	6.8
Stainless Steels		
Stainless alloy 304	17.2	9.6
Stainless alloy 316	15.9	8.8
Stainless alloy 405	10.8	6.0
Stainless alloy 440A	10.2	5.7
Stainless alloy 17-7PH	11.0	6.1
Cast Irons		
Gray irons		
• Grade G1800	11.4	6.3
• Grade G3000	11.4	6.3
• Grade G4000	11.4	6.3

Table B.6 *(Continued)*

	Coefficient of Thermal Expansion	
Material	***10^{-6} (°C)$^{-1}$***	***10^{-6} (°F)$^{-1}$***
Ductile irons		
• Grade 60-40-18	11.2	6.2
• Grade 80-55-06	10.6	5.9
Aluminum Alloys		
Alloy 1100	23.6	13.1
Alloy 2024	22.9	12.7
Alloy 6061	23.6	13.1
Alloy 7075	23.4	13.0
Alloy 356.0	21.5	11.9
Copper Alloys		
C11000 (electrolytic tough pitch)	17.0	9.4
C17200 (beryllium–copper)	16.7	9.3
C26000 (cartridge brass)	19.9	11.1
C36000 (free-cutting brass)	20.5	11.4
C71500 (copper–nickel, 30%)	16.2	9.0
C93200 (bearing bronze)	18.0	10.0
Magnesium Alloys		
Alloy AZ31B	26.0	14.4
Alloy AZ91D	26.0	14.4
Titanium Alloys		
Commercially pure (ASTM grade 1)	8.6	4.8
Alloy Ti-5Al-2.5Sn	9.4	5.2
Alloy Ti-6Al-4V	8.6	4.8
Precious Metals		
Gold (commerically pure)	14.2	7.9
Platinum (commercially pure)	9.1	5.1
Silver (commercially pure)	19.7	10.9
Refractory Metals		
Molybdenum (commercially pure)	4.9	2.7
Tantalum (commercially pure)	6.5	3.6
Tungsten (commercially pure)	4.5	2.5
Miscellaneous Nonferrous Alloys		
Nickel 200	13.3	7.4
Inconel 625	12.8	7.1
Monel 400	13.9	7.7
Haynes alloy 25	12.3	6.8
Invar	1.6	0.9
Super invar	0.72	0.40
Kovar	5.1	2.8
Chemical lead	29.3	16.3
Antimonial lead (6%)	27.2	15.1
Tin (commercially pure)	23.8	13.2
Lead–Tin solder (60Sn-40Pb)	24.0	13.3
Zinc (commercially pure)	23.0–32.5	12.7–18.1
Zirconium, reactor grade 702	5.9	3.3

Table B.6 *(Continued)*

	Coefficient of Thermal Expansion	
Material	***10^{-6} (°C)$^{-1}$***	***10^{-6} (°F)$^{-1}$***
GRAPHITE, CERAMICS, AND SEMICONDUCTING MATERIALS		
Aluminum oxide		
• 99.9% pure	7.4	4.1
• 96%	7.4	4.1
• 90%	7.0	3.9
Concrete	10.0–13.6	5.6–7.6
Diamond (natural)	0.11–1.23	0.06–0.68
Gallium arsenide	5.9	3.3
Glass, borosilicate (Pyrex)	3.3	1.8
Glass, soda–lime	9.0	5.0
Glass ceramic (Pyroceram)	6.5	3.6
Graphite		
• Extruded	2.0–2.7	1.1–1.5
• Isostatically molded	2.2–6.0	1.2–3.3
Silica, fused	0.4	0.22
Silicon	2.5	1.4
Silicon carbide		
• Hot pressed	4.6	2.6
• Sintered	4.1	2.3
Silicon nitride		
• Hot pressed	2.7	1.5
• Reaction bonded	3.1	1.7
• Sintered	3.1	1.7
Zirconia, 3 mol% Y_2O_3	9.6	5.3
POLYMERS		
Elastomers		
• Butadiene-acrylonitrile (nitrile)	235	130
• Styrene-butadiene (SBR)	220	125
• Silicone	270	150
Epoxy	81–117	45–65
Nylon 6,6	144	80
Phenolic	122	68
Polybutylene terephthalate (PBT)	108–171	60–95
Polycarbonate (PC)	122	68
Polyester (thermoset)	100–180	55–100
Polyetheretherketone (PEEK)	72–85	40–47
Polyethylene		
• Low density (LDPE)	180–400	100–220
• High density (HDPE)	106–198	59–110
• Ultrahigh molecular weight (UHMWPE)	234–360	130–200
Polyethylene terephthalate (PET)	117	65
Polymethyl methacrylate (PMMA)	90–162	50–90
Polypropylene (PP)	146–180	81–100
Polystyrene (PS)	90–150	50–83
Polytetrafluoroethylene (PTFE)	126–216	70–120
Polyvinyl chloride (PVC)	90–180	50–100

Table B.6 (*Continued*)

	Coefficient of Thermal Expansion	
Material	***10^{-6} (°C)$^{-1}$***	***10^{-6} (°F)$^{-1}$***
FIBER MATERIALS		
Aramid (Kevlar 49)		
• Longitudinal direction	−2.0	−1.1
• Transverse direction	60	33
Carbon (PAN precursor)		
• Standard modulus		
Longitudinal direction	−0.6	−0.3
Transverse direction	10.0	5.6
• Intermediate modulus		
Longitudinal direction	−0.6	−0.3
• High modulus		
Longitudinal direction	−0.5	−0.28
Transverse direction	7.0	3.9
E Glass	5.0	2.8
COMPOSITE MATERIALS		
Aramid fibers-epoxy matrix ($V_f = 0.6$)		
• Longitudinal direction	−4.0	−2.2
• Transverse direction	70	40
High modulus carbon fibers-epoxy matrix ($V_f = 0.6$)		
• Longitudinal direction	−0.5	−0.3
• Transverse direction	32	18
E glass fibers-epoxy matrix ($V_f = 0.6$)		
• Longitudinal direction	6.6	3.7
• Transverse direction	30	16.7
Wood		
• Douglas fir (12% moisture)		
Parallel to grain	3.8–5.1	2.2–2.8
Perpendicular to grain	25.4–33.8	14.1–18.8
• Red oak (12% moisture)		
Parallel to grain	4.6–5.9	2.6–3.3
Perpendicular to grain	30.6–39.1	17.0–21.7

Sources: *ASM Handbooks, Volumes 1* and *2, Engineered Materials Handbooks, Volumes 1* and *4, Metals Handbook: Properties and Selection: Nonferrous Alloys and Pure Metals*, Vol. 2, 9th edition, and *Advanced Materials & Processes*, Vol. 146, No. 4, ASM International, Materials Park, OH; *Modern Plastics Encyclopedia '96*, The McGraw-Hill Companies, New York, NY; R. F. Floral and S. T. Peters, "Composite Structures and Technologies," tutorial notes, 1989; and manufacturers' technical data sheets.

Table B.7 Room-Temperature Thermal Conductivity Values for Various Engineering Materials

Material	Thermal Conductivity W/m-K	Thermal Conductivity Btu/ft-h-°F
METALS AND METAL ALLOYS		
Plain Carbon and Low Alloy Steels		
Steel alloy A36	51.9	30
Steel alloy 1020	51.9	30
Steel alloy 1040	51.9	30
Stainless Steels		
Stainless alloy 304 (annealed)	16.2	9.4
Stainless alloy 316 (annealed)	16.2	9.4
Stainless alloy 405 (annealed)	27.0	15.6
Stainless alloy 440A (annealed)	24.2	14.0
Stainless alloy 17-7PH (annealed)	16.4	9.5
Cast Irons		
Gray irons		
• Grade G1800	46.0	26.6
• Grade G3000	46.0	26.6
• Grade G4000	46.0	26.6
Ductile irons		
• Grade 60-40-18	36.0	20.8
• Grade 80-55-06	36.0	20.8
• Grade 120-90-02	36.0	20.8
Aluminum Alloys		
Alloy 1100 (annealed)	222	128
Alloy 2024 (annealed)	190	110
Alloy 6061 (annealed)	180	104
Alloy 7075-T6	130	75
Alloy 356.0-T6	151	87
Copper Alloys		
C11000 (electrolytic tough pitch)	388	224
C17200 (beryllium–copper)	105–130	60–75
C26000 (cartridge brass)	120	70
C36000 (free-cutting brass)	115	67
C71500 (copper–nickel, 30%)	29	16.8
C93200 (bearing bronze)	59	34
Magnesium Alloys		
Alloy AZ31B	96[a]	55[a]
Alloy AZ91D	72[a]	43[a]
Titanium Alloys		
Commercially pure (ASTM grade 1)	16	9.2
Alloy Ti-5Al-2.5Sn	7.6	4.4
Alloy Ti-6Al-4V	6.7	3.9
Precious Metals		
Gold (commercially pure)	315	182
Platinum (commercially pure)	71[b]	41[b]
Silver (commercially pure)	428	247

Material	***Thermal Conductivity*** W/m-K	***Thermal Conductivity*** Btu/ft-h-°F
Refractory Metals		
Molybdenum (commercially pure)	142	82
Tantalum (commercially pure)	54.4	31.4
Tungsten (commercially pure)	155	89.4
Miscellaneous Nonferrous Alloys		
Nickel 200	70	40.5
Inconel 625	9.8	5.7
Monel 400	21.8	12.6
Haynes alloy 25	9.8	5.7
Invar	10	5.8
Super invar	10	5.8
Kovar	17	9.8
Chemical lead	35	20.2
Antimonial lead (6%)	29	16.8
Tin (commercially pure)	60.7	35.1
Lead–Tin solder (60Sn-40Pb)	50	28.9
Zinc (commercially pure)	108	62
Zirconium, reactor grade 702	22	12.7
GRAPHITE, CERAMICS, AND SEMICONDUCTING MATERIALS		
Aluminum oxide		
• 99.9% pure	39	22.5
• 96%	35	20
• 90%	16	9.2
Concrete	1.25–1.75	0.72–1.0
Diamond		
• Natural	1450–4650	840–2700
• Synthetic	3150	1820
Gallium arsenide	45.5	26.3
Glass, borosilicate (Pyrex)	1.4	0.81
Glass, soda–lime	1.7	1.0
Glass ceramic (Pyroceram)	3.3	1.9
Graphite		
• Extruded	130–190	75–110
• Isostatically molded	104–130	60–75
Silica, fused	1.4	0.81
Silicon	141	82
Silicon carbide		
• Hot pressed	80	46.2
• Sintered	71	41
Silicon nitride		
• Hot pressed	29	17
• Reaction bonded	10	6
• Sintered	33	19.1
Zirconia, 3 mol% Y_2O_3	2.0–3.3	1.2–1.9
POLYMERS		
Elastomers		
• Butadiene-acrylonitrile (nitrile)	0.25	0.14
• Styrene-butadiene (SBR)	0.25	0.14
• Silicone	0.23	0.13

Table B.7 *(Continued)*

Material	Thermal Conductivity W/m-K	Thermal Conductivity Btu/ft-h-°F
Epoxy	0.19	0.11
Nylon 6,6	0.24	0.14
Phenolic	0.15	0.087
Polybutylene terephthalate (PBT)	0.18–0.29	0.10–0.17
Polycarbonate (PC)	0.20	0.12
Polyester (thermoset)	0.17	0.10
Polyethylene		
• Low density (LDPE)	0.33	0.19
• High density (HDPE)	0.48	0.28
• Ultrahigh molecular weight (UHMWPE)	0.33	0.19
Polyethylene terephthalate (PET)	0.15	0.087
Polymethyl methacrylate (PMMA)	0.17–0.25	0.10–0.15
Polypropylene (PP)	0.12	0.069
Polystyrene (PS)	0.13	0.075
Polytetrafluoroethylene (PTFE)	0.25	0.14
Polyvinyl chloride (PVC)	0.15–0.21	0.08–0.12
FIBER MATERIALS		
Carbon (PAN precursor), longitudinal		
• Standard modulus	11	6.4
• Intermediate modulus	15	8.7
• High modulus	70	40
E Glass	1.3	0.75
COMPOSITE MATERIALS		
Wood		
• Douglas fir (12% moisture) Perpendicular to grain	0.14	0.08
• Red oak (12% moisture) Perpendicular to grain	0.18	0.11

[a] At 100°C.

[b] At 0°C.

Sources: *ASM Handbooks, Volumes 1 and 2, Engineered Materials Handbooks, Volumes 1 and 4, Metals Handbook: Properties and Selection: Nonferrous Alloys and Pure Metals,* Vol. 2, 9th edition, and *Advanced Materials & Processes*, Vol. 146, No. 4, ASM International, Materials Park, OH; *Modern Plastics Encyclopedia '96* and *Modern Plastics Encyclopedia 1977–1978*, The McGraw-Hill Companies, New York, NY; and manufacturers' technical data sheets.

Table B.8 Room-Temperature Specific Heat Values for Various Engineering Materials

Material	Specific Heat	
	$J/kg\text{-}K$	$10^{-2} Btu/lb_m\text{-}°F$
METALS AND METAL ALLOYS		
Plain Carbon and Low Alloy Steels		
Steel alloy A36	486[a]	11.6[a]
Steel alloy 1020	486[a]	11.6[a]
Steel alloy 1040	486[a]	11.6[a]
Stainless Steels		
Stainless alloy 304	500	12.0
Stainless alloy 316	500	12.0
Stainless alloy 405	460	11.0
Stainless alloy 440A	460	11.0
Stainless alloy 17-7PH	460	11.0
Cast Irons		
Gray irons		
• Grade G1800	544	13
• Grade G3000	544	13
• Grade G4000	544	13
Ductile irons		
• Grade 60-40-18	544	13
• Grade 80-55-06	544	13
• Grade 120-90-02	544	13
Aluminum Alloys		
Alloy 1100	904	21.6
Alloy 2024	875	20.9
Alloy 6061	896	21.4
Alloy 7075	960[b]	23.0[b]
Alloy 356.0	963[b]	23.0[b]
Copper Alloys		
C11000 (electrolytic tough pitch)	385	9.2
C17200 (beryllium–copper)	420	10.0
C26000 (cartridge brass)	375	9.0
C36000 (free-cutting brass)	380	9.1
C71500 (copper–nickel, 30%)	380	9.1
C93200 (bearing bronze)	376	9.0
Magnesium Alloys		
Alloy AZ31B	1024	24.5
Alloy AZ91D	1050	25.1
Titanium Alloys		
Commercially pure (ASTM grade 1)	528[c]	12.6[c]
Alloy Ti-5Al-2.5Sn	470[c]	11.2[c]
Alloy Ti-6Al-4V	610[c]	14.6[c]
Precious Metals		
Gold (commercially pure)	130	3.1
Platinum (commercially pure)	132[d]	3.2[d]
Silver (commercially pure)	235	5.6

Table B.8 (*Continued*)

Material	*Specific Heat* *J/kg-K*	 10^{-2}*Btu/lb*$_m$*–°F*
Refractory Metals		
Molybdenum (commercially pure)	276	6.6
Tantalum (commercially pure)	139	3.3
Tungsten (commercially pure)	138	3.3
Miscellaneous Nonferrous Alloys		
Nickel 200	456	10.9
Inconel 625	410	9.8
Monel 400	427	10.2
Haynes alloy 25	377	9.0
Invar	500	12.0
Super invar	500	12.0
Kovar	460	11.0
Chemical lead	129	3.1
Antimonial lead (6%)	135	3.2
Tin (commercially pure)	222	5.3
Lead–Tin solder (60Sn-40Pb)	150	3.6
Zinc (commercially pure)	395	9.4
Zirconium, reactor grade 702	285	6.8
GRAPHITE, CERAMICS, AND SEMICONDUCTING MATERIALS		
Aluminum oxide		
• 99.9% pure	775	18.5
• 96%	775	18.5
• 90%	775	18.5
Concrete	850–1150	20.3–27.5
Diamond (natural)	520	12.4
Gallium arsenide	350	8.4
Glass, borosilicate (Pyrex)	850	20.3
Glass, soda–lime	840	20.0
Glass ceramic (Pyroceram)	975	23.3
Graphite		
• Extruded	830	19.8
• Isostatically molded	830	19.8
Silica, fused	740	17.7
Silicon	700	16.7
Silicon carbide		
• Hot pressed	670	16.0
• Sintered	590	14.1
Silicon nitride		
• Hot pressed	750	17.9
• Reaction bonded	870	20.7
• Sintered	1100	26.3
Zirconia, 3 mol% Y_2O_3	481	11.5
POLYMERS		
Epoxy	1050	25
Nylon 6,6	1670	40
Phenolic	1590–1760	38–42
Polybutylene terephthalate (PBT)	1170–2300	28–55
Polycarbonate (PC)	840	20

Table B.8 (*Continued*)

Material	**Specific Heat** **J/kg-K**	 **10^{-2}Btu/lb$_m$–°F**
Polyester (thermoset)	710–920	17–22
Polyethylene		
• Low density (LDPE)	2300	55
• High density (HDPE)	1850	44.2
Polyethylene terephthalate (PET)	1170	28
Polymethyl methacrylate (PMMA)	1460	35
Polypropylene (PP)	1925	46
Polystyrene (PS)	1170	28
Polytetrafluoroethylene (PTFE)	1050	25
Polyvinyl chloride (PVC)	1050–1460	25–35
FIBER MATERIALS		
Aramid (Kevlar 49)	1300	31
E Glass	810	19.3
COMPOSITE MATERIALS		
Wood		
• Douglas fir (12% moisture)	2900	69.3
• Red oak (12% moisture)	2900	69.3

[a] At temperatures between 50°C and 100°C.

[b] At 100°C.

[c] At 50°C.

[d] At 0°C.

Sources: *ASM Handbooks, Volumes 1 and 2, Engineered Materials Handbooks, Volumes 1, 2, and 4, Metals Handbook: Properties and Selection: Nonferrous Alloys and Pure Metals*, Vol. 2, 9th edition, and *Advanced Materials & Processes*, Vol. 146, No. 4, ASM International, Materials Park, OH; *Modern Plastics Encyclopedia 1977–1978*, The McGraw-Hill Companies, New York, NY; and manufacturers' technical data sheets.

Table B.9 Room-Temperature Electrical Resistivity Values for Various Engineering Materials

Material	*Electrical Resistivity, Ω-m*
METALS AND METAL ALLOYS	
Plain Carbon and Low Alloy Steels	
Steel alloy A36[a]	1.60×10^{-7}
Steel alloy 1020 (annealed)[a]	1.60×10^{-7}
Steel alloy 1040 (annealed)[a]	1.60×10^{-7}
Steel alloy 4140 (quenched and tempered)	2.20×10^{-7}
Steel alloy 4340 (quenched and tempered)	2.48×10^{-7}
Stainless Steels	
Stainless alloy 304 (annealed)	7.2×10^{-7}
Stainless alloy 316 (annealed)	7.4×10^{-7}
Stainless alloy 405 (annealed)	6.0×10^{-7}
Stainless alloy 440A (annealed)	6.0×10^{-7}
Stainless alloy 17-7PH (annealed)	8.3×10^{-7}

Table B.9 (*Continued*)

Material	*Electrical Resistivity, Ω-m*
Cast Irons	
Gray irons	
• Grade G1800	15.0×10^{-7}
• Grade G3000	9.5×10^{-7}
• Grade G4000	8.5×10^{-7}
Ductile irons	
• Grade 60-40-18	5.5×10^{-7}
• Grade 80-55-06	6.2×10^{-7}
• Grade 120-90-02	6.2×10^{-7}
Aluminum Alloys	
Alloy 1100 (annealed)	2.9×10^{-8}
Alloy 2024 (annealed)	3.4×10^{-8}
Alloy 6061 (annealed)	3.7×10^{-8}
Alloy 7075 (T6 treatment)	5.22×10^{-8}
Alloy 356.0 (T6 treatment)	4.42×10^{-8}
Copper Alloys	
C11000 (electrolytic tough pitch, annealed)	1.72×10^{-8}
C172000 (beryllium–copper)	5.7×10^{-8}–1.15×10^{-7}
C26000 (cartridge brass)	6.2×10^{-8}
C36000 (free-cutting brass)	6.6×10^{-8}
C71500 (copper–nickel, 30%)	37.5×10^{-8}
C93200 (bearing bronze)	14.4×10^{-8}
Magnesium Alloys	
Alloy AZ31B	9.2×10^{-8}
Alloy AZ91D	17.0×10^{-8}
Titanium Alloys	
Commercially pure (ASTM grade 1)	4.2×10^{-7}–5.2×10^{-7}
Alloy Ti-5Al-2.5Sn	15.7×10^{-7}
Alloy Ti-6Al-4V	17.1×10^{-7}
Precious Metals	
Gold (commercially pure)	2.35×10^{-8}
Platinum (commercially pure)	10.60×10^{-8}
Silver (commercially pure)	1.47×10^{-8}
Refractory Metals	
Molybdenum (commercially pure)	5.2×10^{-8}
Tantalum (commercially pure)	13.5×10^{-8}
Tungsten (commercially pure)	5.3×10^{-8}
Miscellaneous Nonferrous Alloys	
Nickel 200	0.95×10^{-7}
Inconel 625	12.90×10^{-7}
Monel 400	5.47×10^{-7}
Haynes alloy 25	8.9×10^{-7}
Invar	8.2×10^{-7}
Super invar	8.0×10^{-7}
Kovar	4.9×10^{-7}
Chemical lead	2.06×10^{-7}
Antimonial lead (6%)	2.53×10^{-7}
Tin (commercially pure)	1.11×10^{-7}
Lead–Tin solder (60Sn-40Pb)	1.50×10^{-7}

Table B.9 *(Continued)*

Material	*Electrical Resistivity, Ω-m*
Zinc (commercially pure)	62.0×10^{-7}
Zirconium, reactor grade 702	3.97×10^{-7}
GRAPHITE, CERAMICS, AND SEMICONDUCTING MATERIALS	
Aluminum oxide	
• 99.9% pure	$>10^{13}$
• 96%	$>10^{12}$
• 90%	$>10^{12}$
Concrete (dry)	10^{9}
Diamond	
• Natural	$10–10^{14}$
• Synthetic	1.5×10^{-2}
Gallium arsenide (intrinsic)	10^{6}
Glass, borosilicate (Pyrex)	$\sim 10^{13}$
Glass, soda–lime	$10^{10}–10^{11}$
Glass ceramic (Pyroceram)	2×10^{14}
Graphite	
• Extruded (with grain direction)	$7 \times 10^{-6}–20 \times 10^{-6}$
• Isostatically molded	$10 \times 10^{-6}–18 \times 10^{-6}$
Silica, fused	$>10^{18}$
Silicon (intrinsic)	2500
Silicon carbide	
• Hot pressed	$1.0–10^{9}$
• Sintered	$1.0–10^{9}$
Silicon nitride	
• Hot isostatic pressed	$>10^{12}$
• Reaction bonded	$>10^{12}$
• Sintered	$>10^{12}$
Zirconia, 3 mol% Y_2O_3	10^{10}
POLYMERS	
Elastomers	
• Butadiene-acrylonitrile (nitrile)	3.5×10^{8}
• Styrene-butadiene (SBR)	6×10^{11}
• Silicone	10^{13}
Epoxy	$10^{10}–10^{13}$
Nylon 6,6	$10^{12}–10^{13}$
Phenolic	$10^{9}–10^{10}$
Polybutylene terephthalate (PBT)	4×10^{14}
Polycarbonate (PC)	2×10^{14}
Polyester (thermoset)	10^{13}
Polyetheretherketone (PEEK)	6×10^{14}
Polyethylene	
• Low density (LDPE)	$10^{15}–5 \times 10^{16}$
• High density (HDPE)	$10^{15}–5 \times 10^{16}$
• Ultrahigh molecular weight (UHMWPE)	$>5 \times 10^{14}$
Polyethylene terephthalate (PET)	10^{12}
Polymethyl methacrylate (PMMA)	$>10^{12}$
Polypropylene (PP)	$>10^{14}$
Polystyrene (PS)	$>10^{14}$
Polytetrafluoroethylene (PTFE)	10^{17}
Polyvinyl chloride (PVC)	$>10^{14}$

Table B.9 *(Continued)*

Material	*Electrical Resistivity, Ω-m*
FIBER MATERIALS	
Carbon (PAN precursor)	
• Standard modulus	17×10^{-6}
• Intermediate modulus	15×10^{-6}
• High modulus	9.5×10^{-6}
E Glass	4×10^{14}
COMPOSITE MATERIALS	
Wood	
• Douglas fir (oven dry)	
Parallel to grain	10^{14}–10^{16}
Perpendicular to grain	10^{14}–10^{16}
• Red oak (oven dry)	
Parallel to grain	10^{14}–10^{16}
Perpendicular to grain	10^{14}–10^{16}

[a] At 0°C.

Sources: *ASM Handbooks, Volumes 1 and 2, Engineered Materials Handbooks, Volumes 1, 2, and 4, Metals Handbook: Properties and Selection: Nonferrous Alloys and Pure Metals,* Vol. 2, 9th edition, and *Advanced Materials & Processes,* Vol. 146, No. 4, ASM International, Materials Park, OH; *Modern Plastics Encyclopedia 1977–1978,* The McGraw-Hill Companies, New York, NY; and manufacturers' technical data sheets.

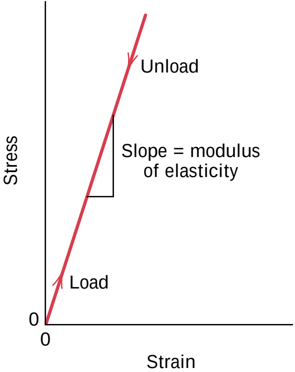

Figure 7.5 Schematic stress–strain diagram showing linear elastic deformation for loading and unloading cycles.

```
[Loader]
Program=mse5e
CommandLine=TensileMetal
```

```
[Loader]
Program=matdb
```

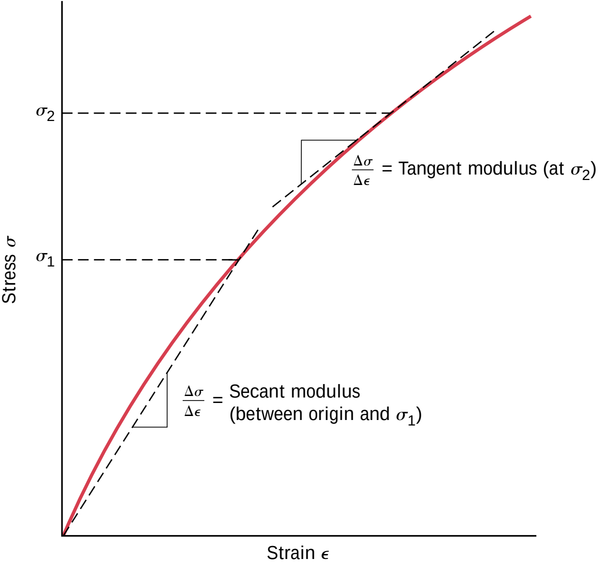

σ_2
σ_1
Stress σ
Strain ϵ
$\frac{\Delta\sigma}{\Delta\epsilon}$ = Tangent modulus (at σ_2)
$\frac{\Delta\sigma}{\Delta\epsilon}$ = Secant modulus (between origin and σ_1)

FIGURE 7.6 Schematic stress–strain diagram showing nonlinear elastic behavior, and how secant and tangent moduli are determined.

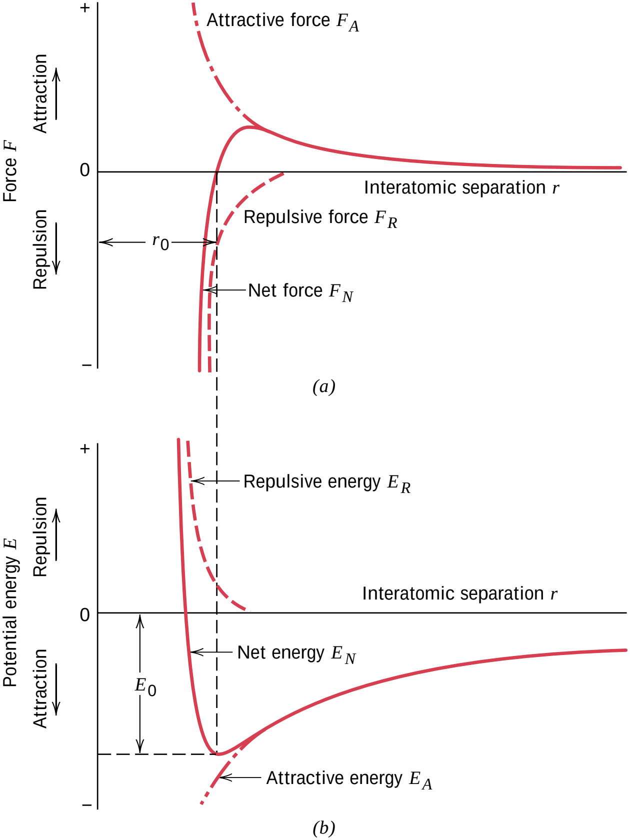

Figure 2.8 (*a*) The dependence of repulsive, attractive, and net forces on interatomic separation for two isolated atoms. (*b*) The dependence of repulsive, attractive, and net potential energies on interatomic separation for two isolated atoms.

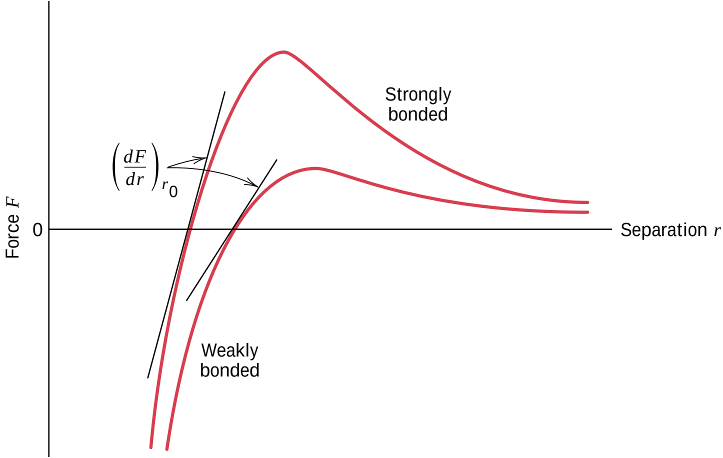

Figure 7.7 Force versus interatomic separation for weakly and strongly bonded atoms. The magnitude of the modulus of elasticity is proportional to the slope of each curve at the equilibrium interatomic separation r_0.

FIGURE 7.8 Plot of modulus of elasticity versus temperature for tungsten, steel, and aluminum. (Adapted from K. M. Ralls, T. H. Courtney, and J. Wulff, *Introduction to Materials Science and Engineering*. Copyright © 1976 by John Wiley & Sons, New York. Reprinted by permission of John Wiley & Sons, Inc.)

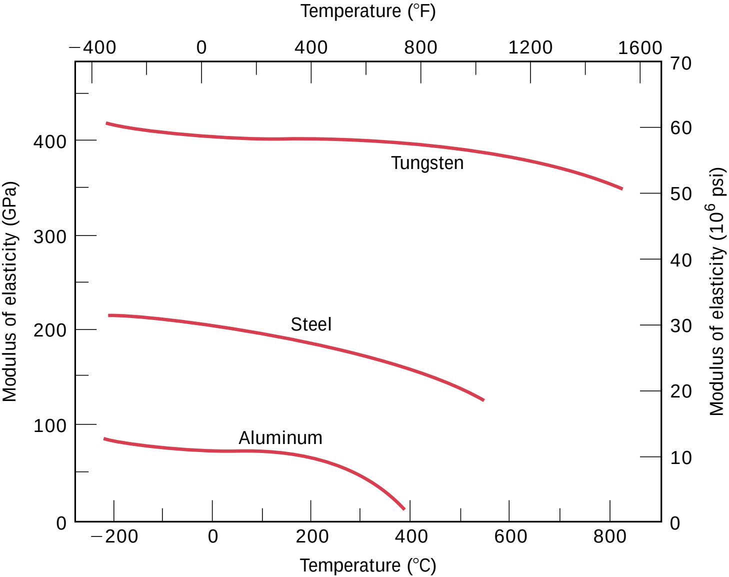

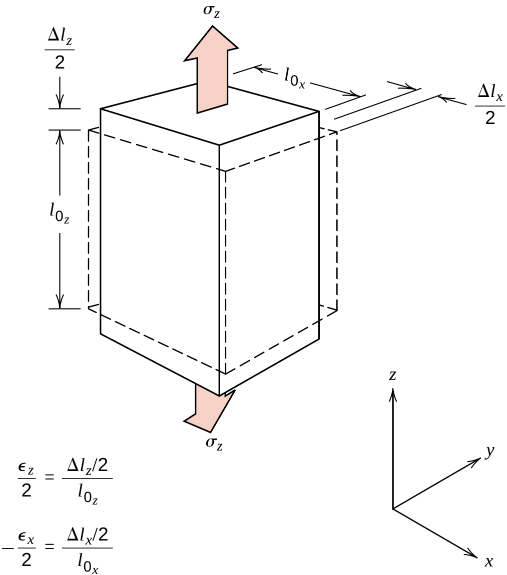
σ_z
$\frac{\Delta l_z}{2}$
l_{0_x}
$\frac{\Delta l_x}{2}$
l_{0_z}
σ_z
z
y
x
$\frac{\epsilon_z}{2} = \frac{\Delta l_z/2}{l_{0_z}}$
$-\frac{\epsilon_x}{2} = \frac{\Delta l_x/2}{l_{0_x}}$

FIGURE 7.9 Axial (z) elongation (positive strain) and lateral (x and y) contractions (negative strains) in response to an imposed tensile stress. Solid lines represent dimensions after stress application; dashed lines, before.

Table 3.7 Modulus of Elasticity Values for Several Metals at Various Crystallographic Orientations

	Modulus of Elasticity (GPa)		
Metal	**[*100*]**	**[*110*]**	**[*111*]**
Aluminum	63.7	72.6	76.1
Copper	66.7	130.3	191.1
Iron	125.0	210.5	272.7
Tungsten	384.6	384.6	384.6

Source: R. W. Hertzberg, *Deformation and Fracture Mechanics of Engineering Materials,* 3rd edition. Copyright © 1989 by John Wiley & Sons, New York. Reprinted by permission of John Wiley & Sons, Inc.

Chapter 3 / Structures of Metals and Ceramics

3.8 SILICATE CERAMICS

THE SILICATES

For the various silicate minerals, one, two, or three of the corner oxygen atoms of the SiO_4^{4-} tetrahedra are shared by other tetrahedra to form some rather complex structures. Some of these, represented in Figure 3.12, have formulas SiO_4^{4-}, $Si_2O_7^{6-}$, $Si_3O_9^{6-}$, and so on; single-chain structures are also possible, as in Figure 3.12*e*. Positively charged cations such as Ca^{2+}, Mg^{2+}, and Al^{3+} serve two roles. First, they compensate the negative charges from the SiO_4^{4-} units so that charge neutrality is achieved; and second, these cations ionically bond the SiO_4^{4-} tetrahedra together.

Simple Silicates

Of these silicates, the most structurally simple ones involve isolated tetrahedra (Figure 3.12*a*). For example, forsterite (Mg_2SiO_4) has the equivalent of two Mg^{2+} ions associated with each tetrahedron in such a way that every Mg^{2+} ion has six oxygen nearest neighbors.

The $Si_2O_7^{6-}$ ion is formed when two tetrahedra share a common oxygen atom (Figure 3.12*b*). Akermanite ($Ca_2MgSi_2O_7$) is a mineral having the equivalent of two Ca^{2+} ions and one Mg^{2+} ion bonded to each $Si_2O_7^{6-}$ unit.

Layered Silicates

A two-dimensional sheet or layered structure can also be produced by the sharing of three oxygen ions in each of the tetrahedra (Figure 3.13); for this structure the repeating unit formula may be represented by $(Si_2O_5)^{2-}$. The net negative charge is associated with the unbonded oxygen atoms projecting out of the plane of the page. Electroneutrality is ordinarily established by a second planar sheet structure having an excess of cations, which bond to these unbonded oxygen atoms from the Si_2O_5 sheet. Such materials are called the sheet or layered silicates, and their basic structure is characteristic of the clays and other minerals.

One of the most common clay minerals, kaolinite, has a relatively simple two-layer silicate sheet structure. Kaolinite clay has the formula $Al_2(Si_2O_5)(OH)_4$ in which the silica tetrahedral layer, represented by $(Si_2O_5)^{2-}$, is made electrically neutral by an adjacent $Al_2(OH)_4^{2+}$ layer. A single sheet of this structure is shown in Figure 3.14, which is exploded in the vertical direction to provide a better perspective of the ion positions; the two distinct layers are indicated in the figure. The midplane of anions consists of O^{2-} ions from the $(Si_2O_5)^{2-}$ layer, as well as OH^- ions that are a part of the $Al_2(OH)_4^{2+}$ layer. Whereas the bonding within this two-layered sheet is strong and intermediate ionic-covalent, adjacent sheets are only loosely bound to one another by weak van der Waals forces.

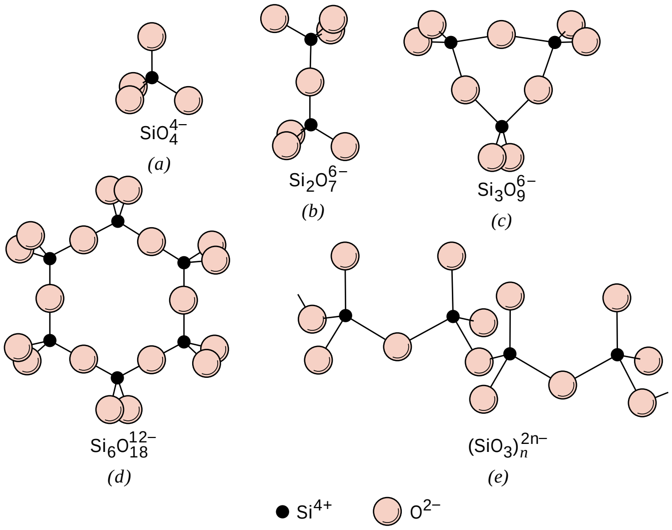

FIGURE 3.12 Five silicate ion structures formed from SiO_4^{4-} tetrahedra.

A crystal of kaolinite is made of a series of these double layers or sheets stacked parallel to each other, which form small flat plates typically less than 1 μm in diameter and nearly hexagonal. Figure 3.15 is an electron micrograph of kaolinite crystals at a high magnification, showing the hexagonal crystal plates some of which are piled one on top of the other.

These silicate sheet structures are not confined to the clays; other minerals also in this group are talc [$Mg_3(Si_2O_5)_2(OH)_2$] and the micas [e.g., muscovite, $KAl_3Si_3O_{10}(OH)_2$], which are important ceramic raw materials. As might be deduced from the chemical formulas, the structures for some silicates are among the most complex of all the inorganic materials.

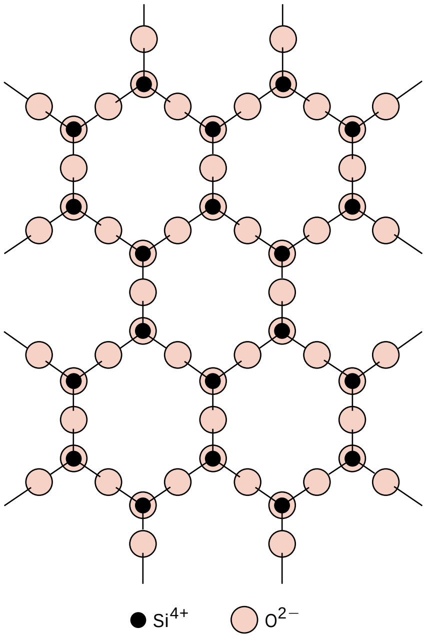

FIGURE 3.13 Schematic representation of the two-dimensional silicate sheet structure having a repeat unit formula of $(Si_2O_5)^{2-}$.

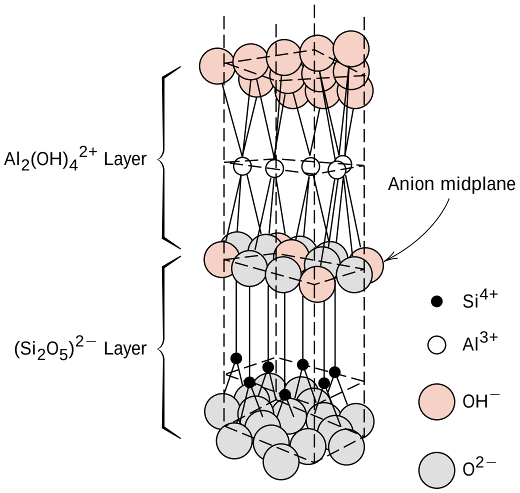

FIGURE 3.14 The structure of kaolinite clay. (Adapted from W. E. Hauth, ''Crystal Chemistry of Ceramics,'' *American Ceramic Society Bulletin,* Vol. 30, No. 4, 1951, p. 140.)

3.9 CARBON

FULLERENES

Another polymorphic form of carbon was discovered in 1985. It exists in discrete molecular form, and consists of a hollow spherical cluster of sixty carbon atoms; a single molecule is denoted by C_{60}. Each molecule is composed of groups of carbon atoms that are bonded to one another to form both hexagon (six-carbon atom) and pentagon (five-carbon atom) geometrical configurations. One such molecule, shown in Figure 3.18, is found to consist of 20 hexagons and 12 pentagons, which are arrayed such that no two pentagons share a common side; the molecular surface thus exhibits the symmetry of a soccer ball. The material composed of C_{60} molecules is known as *buckminsterfullerene,* named in honor of R. Buckminster Fuller, who

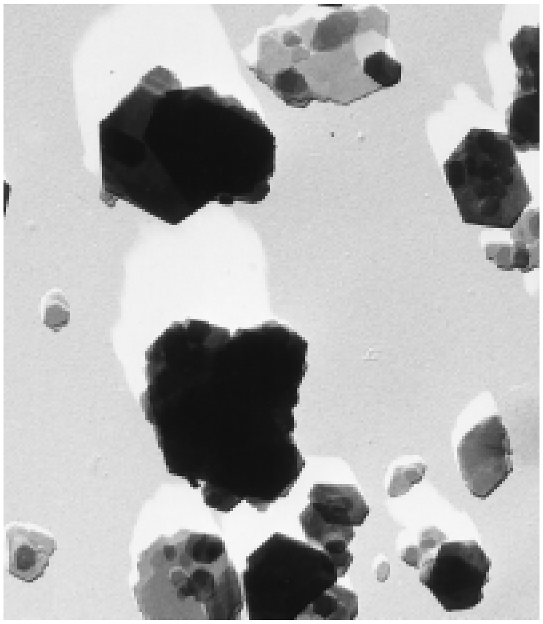

FIGURE 3.15 Electron micrograph of kaolinite crystals. They are in the form of hexagonal plates, some of which are stacked on top of one another. 15,000×. (Photograph courtesy of Georgia Kaolin Co., Inc.)

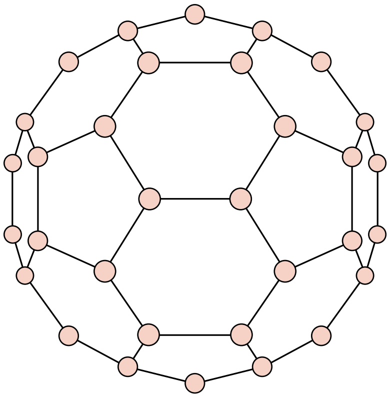

FIGURE 3.18 The structure of a C_{60} molecule.

invented the geodesic dome; each C_{60} is simply a molecular replica of such a dome, which is often referred to as ''buckyball'' for short. The term *fullerene* is used to denote the class of materials that are composed of this type of molecule.

Diamond and graphite are what may be termed *network solids,* in that all of the carbon atoms form primary bonds with adjacent atoms throughout the entirety of the solid. By way of contrast, the carbon atoms in buckminsterfullerene bond together so as to form these spherical molecules. In the solid state, the C_{60} units form a crystalline structure and pack together in a face-centered cubic array.

As a pure crystalline solid, this material is electrically insulating. However, with proper impurity additions, it can be made highly conductive and semiconductive. As a final note, molecular shapes other than the ball clusters recently have been discovered; these include nanoscale tubular and polyhedral structures. It is anticipated that, with further developments, the fullerenes will become technologically important materials.

3.14 LINEAR AND PLANAR ATOMIC DENSITIES

The two previous sections discussed the equivalency of nonparallel crystallographic directions and planes. Directional equivalency is related to the *atomic linear density* in the sense that equivalent directions have identical linear densities. The direction vector is positioned so as to pass through atom centers, and the fraction of line length intersected by these atoms is equal to the linear density.

Correspondingly, crystallographic planes that are equivalent have the same *atomic planar density*. The plane of interest is positioned so as to pass through atom centers. And planar density is simply the fraction of total crystallographic plane area that is occupied by atoms (represented as circles). It should be noted that the concepts of linear and planar densities are one- and two-dimensional analogs of the atomic packing factor; their determinations are illustrated in the following two example problems.

EXAMPLE PROBLEM 3.11

Calculate the linear density of the [100] direction for BCC.

SOLUTION

A BCC unit cell (reduced sphere) and the [100] direction therein are shown in Figure 3.26*a*; represented in Figure 3.26*b* is the linear packing in this direction.

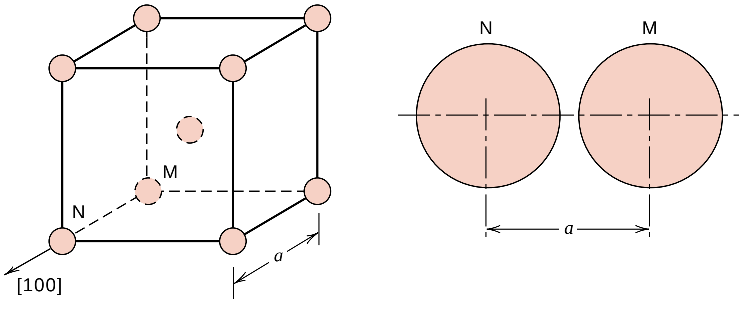

(a) (b)

FIGURE 3.26 (*a*) Reduced-sphere BCC unit cell with the [100] direction indicated. (*b*) Atomic spacing in the [100] direction for the BCC crystal structure—between atoms M and N in (*a*).

As a basis for our computation let us use the line length within the unit cell, L_l, which in this case is the lattice parameter a—the distance between the centers of atoms M and N. In terms of the atomic radius R,

$$L_l = a = \frac{4R}{\sqrt{3}} \qquad \text{(see Equation 3.3)}$$

Now, the total line length intersecting circles (atoms M and N), L_c, is equal to $2R$. And the linear density LD is just the following ratio:

$$\text{LD} = \frac{L_c}{L_l} = \frac{2R}{4R/\sqrt{3}} = 0.866$$

EXAMPLE PROBLEM 3.12

Calculate the planar density of the (110) plane for FCC.

SOLUTION

The atomic packing of this plane is represented in Figure 3.24*b*. Consider that portion of the plane that intersects a unit cell (Figure 3.24*b*), and then compute both this planar area and total circle area in terms of the atomic radius R. Planar density, then, is just the ratio of these two areas.

The unit cell plane area, A_p, is simply that of the rectangle circumscribed by the centers of the atoms A, C, D, and F (Figure 3.24*b*). The rectangle length ($\overline{\text{AC}}$) and width ($\overline{\text{AD}}$) are, respectively,

$$\begin{aligned} \overline{\text{AC}} &= 4R \\ \overline{\text{AD}} &= 2R\sqrt{2} \qquad \text{(see Equation 3.1)} \end{aligned}$$

Therefore,

$$\begin{aligned} A_p &= (\overline{\text{AC}})(\overline{\text{AD}}) \\ &= (4R)(2R\sqrt{2}) = 8R^2\sqrt{2} \end{aligned}$$

Now, for the total circle area, one fourth of each of atoms A, C, D, and F and one half of atoms B and E reside within this rectangle, which gives a total of 2 equivalent circles. Thus the total circle area A_c is just

$$A_c = (2)\pi R^2$$

Finally, the planar density PD is just

$$\text{PD} = \frac{A_c}{A_p} = \frac{2\pi R^2}{8R^2\sqrt{2}} = 0.555$$

Linear and planar densities are important considerations relative to the process of slip—that is, the mechanism by which metals plastically deform (Section 8.5). Slip occurs on the most densely packed crystallographic planes and, in those planes, along directions having the greatest atomic packing.

3.19 X-RAY DIFFRACTION: DETERMINATION OF CRYSTAL STRUCTURES

Historically much of our understanding regarding the atomic and molecular arrangements in solids has resulted from x-ray diffraction investigations; furthermore, x-rays are still very important in developing new materials. A brief overview of the diffraction phenomenon and how, using x-rays, atomic interplanar distances and crystal structures are deduced will now be given.

THE DIFFRACTION PHENOMENON

Diffraction occurs when a wave encounters a series of regularly spaced obstacles that (1) are capable of scattering the wave, and (2) have spacings that are comparable in magnitude to the wavelength. Furthermore, diffraction is a consequence of specific phase relationships that are established between two or more waves that have been scattered by the obstacles.

Consider waves 1 and 2 in Figure 3.34*a*, which have the same wavelength (λ) and are in phase at point O–O'. Now let us suppose that both waves are scattered in such a way that they traverse different paths. The phase relationship between the scattered waves, which will depend upon the difference in path length, is important. One possibility results when this path length difference is an integral number of wavelengths. As noted in Figure 3.34*a*, these scattered waves (now labeled $1'$ and $2'$) are still in phase. They are said to mutually reinforce (or constructively interfere with) one another; and, when amplitudes are added, the wave shown on the right side of the figure results. This is a manifestation of **diffraction,** and we refer to a diffracted beam as one composed of a large number of scattered waves that mutually reinforce one another.

Other phase relationships are possible between scattered waves that will not lead to this mutual reinforcement. The other extreme is that demonstrated in Figure 3.34*b*, wherein the path length difference after scattering is some integral number of *half* wavelengths. The scattered waves are out of phase—that is, corresponding amplitudes cancel or annul one another, or destructively interfere (i.e., the resultant wave has zero amplitude), as indicated on the extreme right side of the figure. Of course, phase relationships intermediate between these two extremes exist, resulting in only partial reinforcement.

X-RAY DIFFRACTION AND BRAGG'S LAW

X-rays are a form of electromagnetic radiation that have high energies and short wavelengths—wavelengths on the order of the atomic spacings for solids. When a

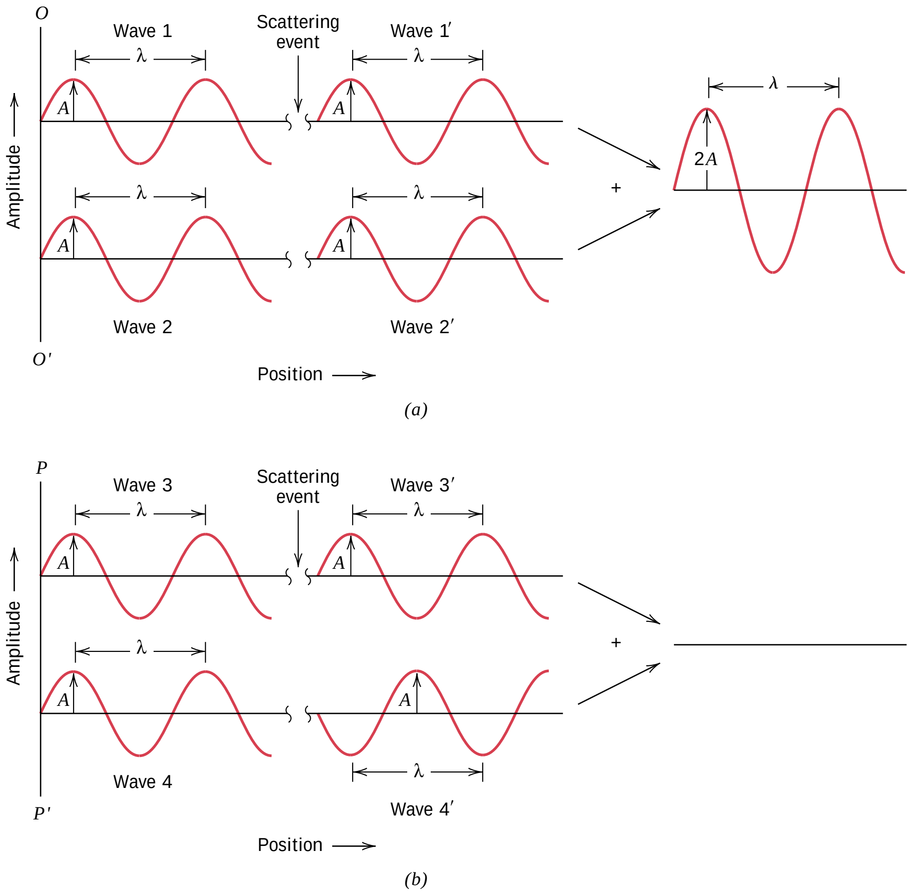

FIGURE 3.34 (*a*) Demonstration of how two waves (labeled 1 and 2) that have the same wavelength λ and remain in phase after a scattering event (waves 1′ and 2′) constructively interfere with one another. The amplitudes of the scattered waves add together in the resultant wave. (*b*) Demonstration of how two waves (labeled 3 and 4) that have the same wavelength and become out of phase after a scattering event (waves 3′ and 4′) destructively interfere with one another. The amplitudes of the two scattered waves cancel one another.

beam of x-rays impinges on a solid material, a portion of this beam will be scattered in all directions by the electrons associated with each atom or ion that lies within the beam's path. Let us now examine the necessary conditions for diffraction of x-rays by a periodic arrangement of atoms.

Consider the two parallel planes of atoms A–A′ and B–B′ in Figure 3.35, which have the same *h*, *k*, and *l* Miller indices and are separated by the interplanar spacing d_{hkl}. Now assume that a parallel, monochromatic, and coherent (in-phase) beam of x-rays of wavelength λ is incident on these two planes at an angle θ. Two rays in this beam, labeled 1 and 2, are scattered by atoms *P* and *Q*. Constructive interference of the scattered rays 1′ and 2′ occurs also at an angle θ to the planes, if the path length difference between 1–*P*–1′ and 2–*Q*–2′ (i.e., $\overline{SQ} + \overline{QT}$) is equal to a whole number, *n*, of wavelengths. That is, the condition for diffraction is

$$n\lambda = \overline{SQ} + \overline{QT} \tag{3.9}$$

or

$$n\lambda = d_{hkl}\sin\theta + d_{hkl}\sin\theta = 2d_{hkl}\sin\theta \tag{3.10}$$

Equation 3.10 is known as **Bragg's law;** also, *n* is the order of reflection, which may be any integer (1, 2, 3, . . .) consistent with sin θ not exceeding unity. Thus, we have a simple expression relating the x-ray wavelength and interatomic spacing to the angle of the diffracted beam. If Bragg's law is not satisfied, then the interfer-

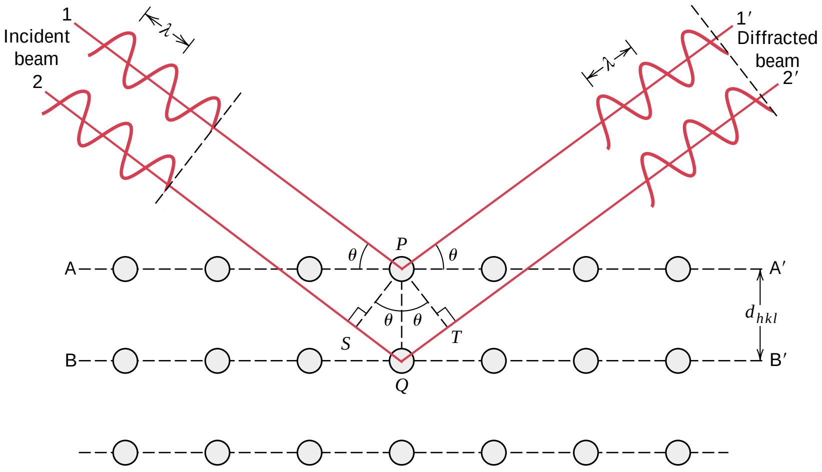

FIGURE 3.35 Diffraction of x-rays by planes of atoms (A–A′ and B–B′).

ence will be nonconstructive in nature so as to yield a very low-intensity diffracted beam.

The magnitude of the distance between two adjacent and parallel planes of atoms (i.e., the interplanar spacing d_{hkl}) is a function of the Miller indices (h, k, and l) as well as the lattice parameter(s). For example, for crystal structures having cubic symmetry,

$$d_{hkl} = \frac{a}{\sqrt{h^2 + k^2 + l^2}} \tag{3.11}$$

in which a is the lattice parameter (unit cell edge length). Relationships similar to Equation 3.11, but more complex, exist for the other six crystal systems noted in Table 3.6.

Bragg's law, Equation 3.10, is a necessary but not sufficient condition for diffraction by real crystals. It specifies when diffraction will occur for unit cells having atoms positioned only at cell corners. However, atoms situated at other sites (e.g., face and interior unit cell positions as with FCC and BCC) act as extra scattering centers, which can produce out-of-phase scattering at certain Bragg angles. The net result is the absence of some diffracted beams that, according to Equation 3.10, should be present. For example, for the BCC crystal structure, $h + k + l$ must be even if diffraction is to occur, whereas for FCC, h, k, and l must all be either odd or even.

DIFFRACTION TECHNIQUES

One common diffraction technique employs a powdered or polycrystalline specimen consisting of many fine and randomly oriented particles that are exposed to monochromatic x-radiation. Each powder particle (or grain) is a crystal, and having a large number of them with random orientations ensures that some particles are properly oriented such that every possible set of crystallographic planes will be available for diffraction.

The *diffractometer* is an apparatus used to determine the angles at which diffraction occurs for powdered specimens; its features are represented schematically in Figure 3.36. A specimen S in the form of a flat plate is supported so that rotations about the axis labeled O are possible; this axis is perpendicular to the plane of the

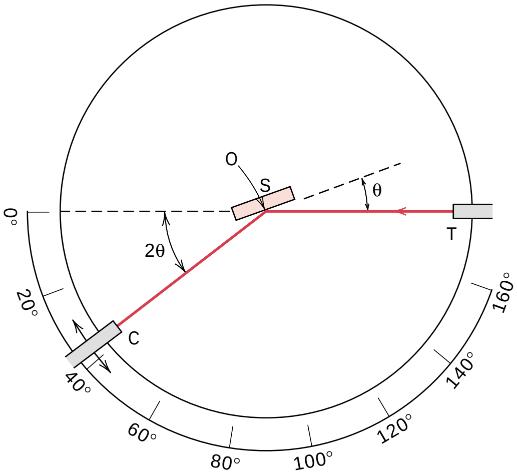

Figure 3.36 Schematic diagram of an x-ray diffractometer; T = x-ray source, S = specimen, C = detector, and O = the axis around which the specimen and detector rotate.

page. The monochromatic x-ray beam is generated at point T, and the intensities of diffracted beams are detected with a counter labeled C in the figure. The specimen, x-ray source, and counter are all coplanar.

The counter is mounted on a movable carriage that may also be rotated about the O axis; its angular position in terms of 2θ is marked on a graduated scale.[3] Carriage and specimen are mechanically coupled such that a rotation of the specimen through θ is accompanied by a 2θ rotation of the counter; this assures that the incident and reflection angles are maintained equal to one another (Figure 3.36). Collimators are incorporated within the beam path to produce a well-defined and focused beam. Utilization of a filter provides a near-monochromatic beam.

As the counter moves at constant angular velocity, a recorder automatically plots the diffracted beam intensity (monitored by the counter) as a function of 2θ; 2θ is termed the *diffraction angle,* which is measured experimentally. Figure 3.37 shows a diffraction pattern for a polycrystalline specimen of iron. The high-intensity peaks result when the Bragg diffraction condition is satisfied by some set of crystallographic planes. These peaks are plane-indexed in the figure.

Other powder techniques have been devised wherein diffracted beam intensity and position are recorded on a photographic film instead of being measured by a counter.

One of the primary uses of x-ray diffractometry is for the determination of crystal structure. The unit cell size and geometry may be resolved from the angular positions of the diffraction peaks, whereas arrangement of atoms within the unit cell is associated with the relative intensities of these peaks.

X-rays, as well as electron and neutron beams, are also used in other types of material investigations. For example, crystallographic orientations of single crystals are possible using x-ray diffraction (or Laue) photographs. The chapter-opening photograph for this chapter was generated using an incident electron beam that was directed on a gallium arsenide crystal; each spot (with the exception of the brightest one near the center) resulted from an electron beam that was diffracted

---

[3] It should be pointed out that the symbol θ has been used in two different contexts for this discussion. Here, θ represents the angular locations of both x-ray source and counter relative to the specimen surface. Previously (e.g., Equation 3.10), it denoted the angle at which the Bragg criterion for diffraction is satisfied.

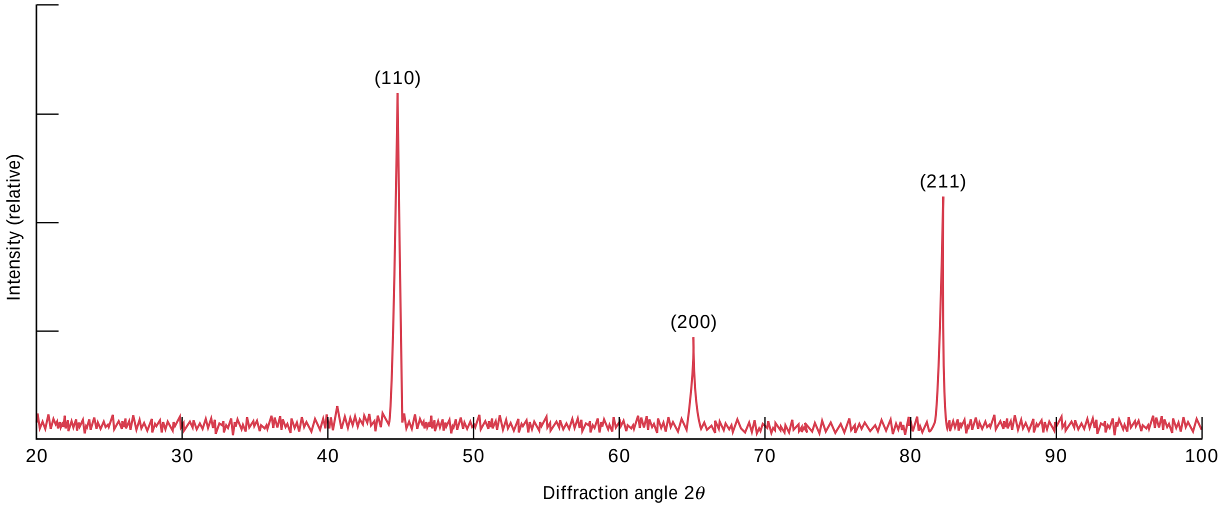

FIGURE 3.37 Diffraction pattern for polycrystalline α-iron.

by a specific set of crystallographic planes. Other uses of x-rays include qualitative and quantitative chemical identifications, and the determination of residual stresses and crystal size.

EXAMPLE PROBLEM 3.13

For BCC iron, compute (a) the interplanar spacing, and (b) the diffraction angle for the (220) set of planes. The lattice parameter for Fe is 0.2866 nm (2.866 Å). Also, assume that monochromatic radiation having a wavelength of 0.1790 nm (1.790 Å) is used, and the order of reflection is 1.

SOLUTION

(a) The value of the interplanar spacing d_{hkl} is determined using Equation 3.11, with $a = 0.2866$ nm, and $h = 2$, $k = 2$, and $l = 0$, since we are considering the (220) planes. Therefore,

$$d_{hkl} = \frac{a}{\sqrt{h^2 + k^2 + l^2}}$$

$$= \frac{0.2866 \text{ nm}}{\sqrt{(2)^2 + (2)^2 + (0)^2}} = 0.1013 \text{ nm } (1.013 \text{ Å})$$

(b) The value of θ may now be computed using Equation 3.10, with $n = 1$, since this is a first-order reflection:

$$\sin\theta = \frac{n\lambda}{2d_{hkl}} = \frac{(1)(0.1790 \text{ nm})}{(2)(0.1013 \text{ nm})} = 0.884$$

$$\theta = \sin^{-1}(0.884) = 62.13°$$

The diffraction angle is 2θ, or

$$2\theta = (2)(62.13°) = 124.26°$$

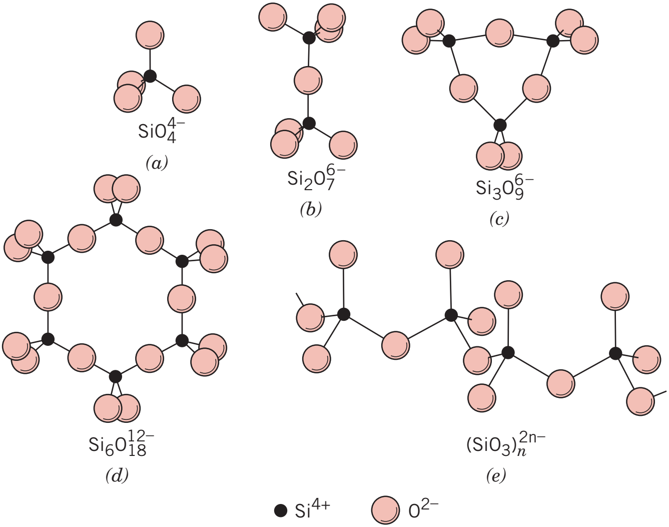
SiO_4^{4-}
(a)
$Si_2O_7^{6-}$
(b)
$Si_3O_9^{6-}$
(c)
$Si_6O_{18}^{12-}$
(d)
$(SiO_3)_n^{2n-}$
(e)
Si^{4+}
O^{2-}

FIGURE 3.12 Five silicate ion structures formed from SiO_4^{4-} tetrahedra.

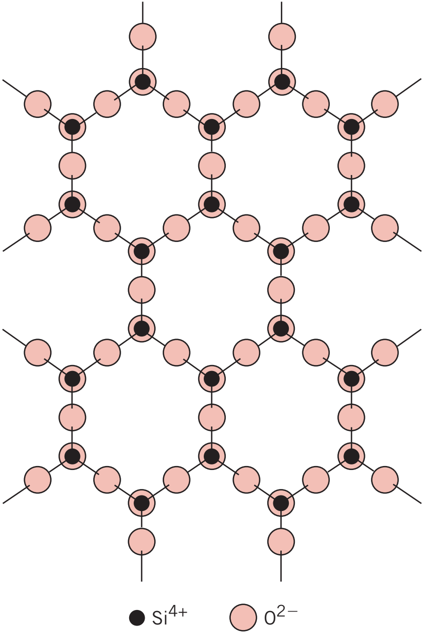

Figure 3.13 Schematic representation of the two-dimensional silicate sheet structure having a repeat unit formula of $(Si_2O_5)^{2-}$.

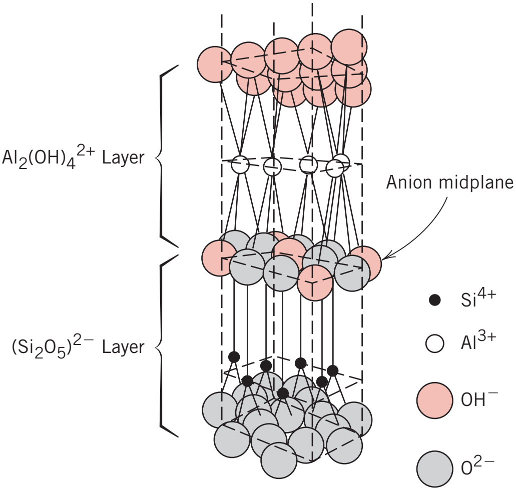
$Al_2(OH)_4^{2+}$ Layer
Anion midplane
$(Si_2O_5)^{2-}$ Layer
Si^{4+}
Al^{3+}
OH^-
O^{2-}

Figure 3.14 The structure of kaolinite clay. (Adapted from W. E. Hauth, “Crystal Chemistry of Ceramics,” *American Ceramic Society Bulletin,* Vol. 30, No. 4, 1951, p. 140.)

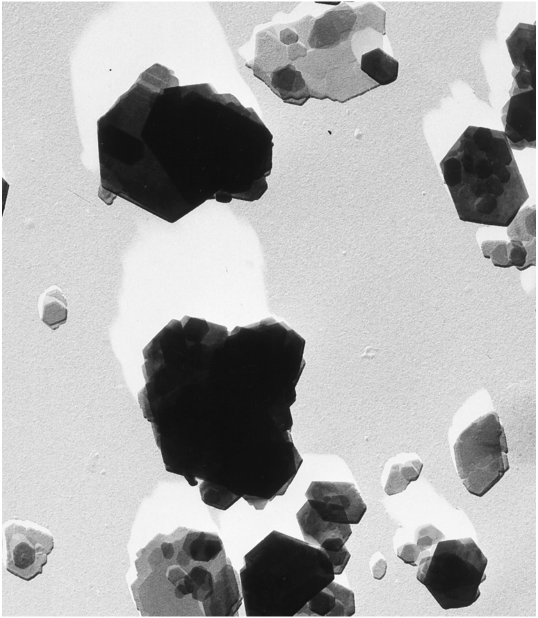

FIGURE 3.15 Electron micrograph of kaolinite crystals. They are in the form of hexagonal plates, some of which are stacked on top of one another. 21,000×. (Photograph courtesy of Georgia Kaolin Co., Inc.)

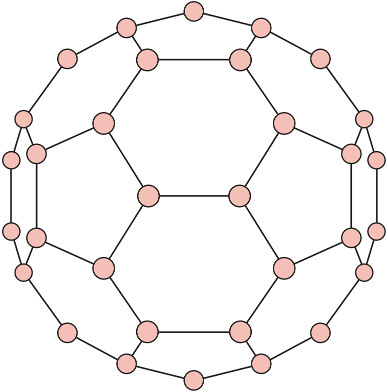

FIGURE 3.18 The structure of a C_{60} molecule.

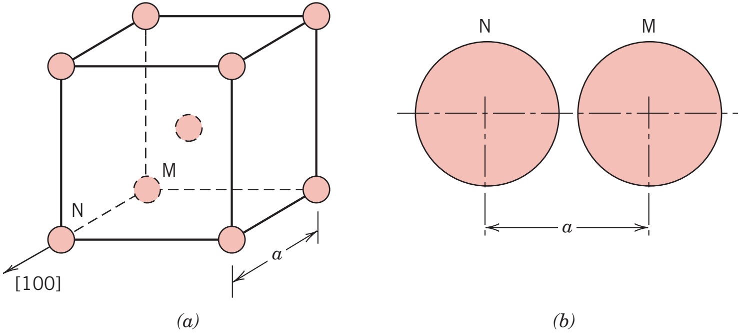

Figure 3.26 (*a*) Reduced-sphere BCC unit cell with the [100] direction indicated. (*b*) Atomic spacing in the [100] direction for the BCC crystal structure—between atoms M and N in (*a*).

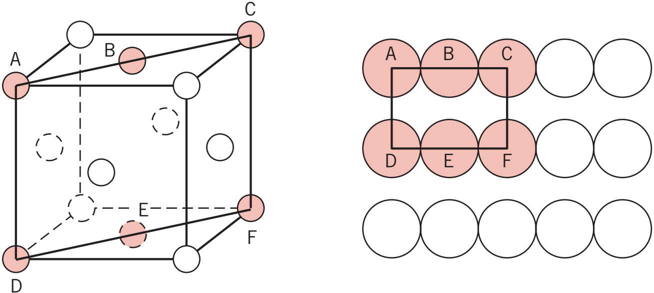

(*a*) (*b*)

Figure 3.24 (*a*) Reduced-sphere FCC unit cell with (110) plane. (*b*) Atomic packing of an FCC (110) plane. Corresponding atom positions from (*a*) are indicated.

Chapter 3 / Structures of Metals and Ceramics

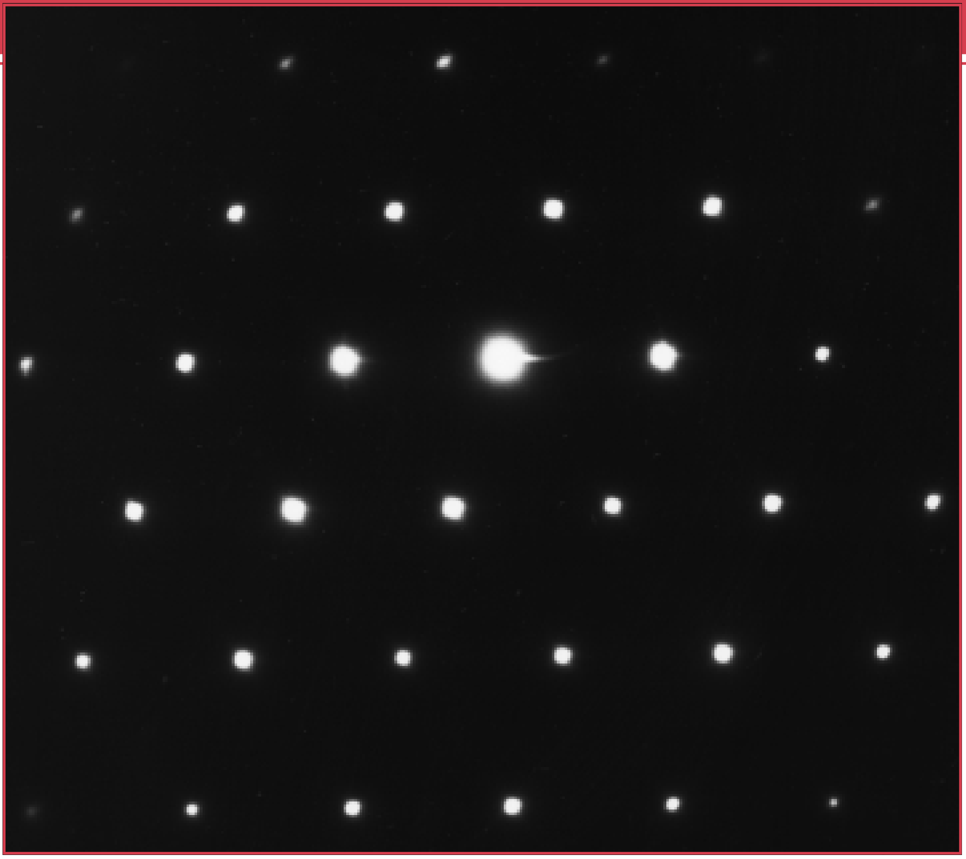

High velocity electron beams that are produced when electrons are accelerated across large voltages become wavelike in character. Their wavelengths are shorter than interatomic spacings, and thus these beams may be diffracted by atomic planes in crystalline materials, in the same manner as x-rays experience diffraction.

This photograph shows a diffraction pattern produced for a single crystal of gallium arsenide using a transmission electron microscope. The brightest spot near the center is produced by the incident electron beam, which is parallel to a ⟨110⟩ crystallographic direction. Each of the other white spots results from an electron beam that is diffracted by a specific set of crystallographic planes. (Photograph courtesy of Dr. Raghaw S. Rai, Motorola, Inc., Austin, Texas.)

Why Study *Structures of Metals and Ceramics*?

The properties of some materials are directly related to their crystal structures. For example, pure and undeformed magnesium and beryllium, having one crystal structure, are much more brittle (i.e., fracture at lower degrees of deformation) than are pure and undeformed metals such as gold and silver that have yet another crystal structure (see Section 8.5). {Also, the permanent magnetic and ferroelectric behaviors of some ceramic materials are explained by their crystal structures (Sections 18.4 and 12.23).}

Furthermore, significant property differences exist between crystalline and noncrystalline materials having the same composition. For example, noncrystalline ceramics and polymers normally are optically transparent; the same materials in crystalline (or semicrystalline) form tend to be opaque or, at best, translucent.

Learning Objectives

After studying this chapter you should be able to do the following:

1. **Describe the difference in atomic/molecular structure between crystalline and noncrystalline materials.**
2. **Draw unit cells for face-centered cubic, body-centered cubic, and hexagonal close-packed crystal structures.**
3. **Derive the relationships between unit cell edge length and atomic radius for face-centered cubic and body-centered cubic crystal structures.**
4. **Compute the densities for metals having face-centered cubic and body-centered cubic crystal structures given their unit cell dimensions.**
5. **Sketch/describe unit cells for sodium chloride, cesium chloride, zinc blende, diamond cubic, fluorite, and perovskite crystal structures. Do likewise for the atomic structures of graphite and a silica glass.**
6. **Given the chemical formula for a ceramic compound, the ionic radii of its component ions, determine the crystal structure.**
7. **Given three direction index integers, sketch the direction corresponding to these indices within a unit cell.**
8. **Specify the Miller indices for a plane that has been drawn within a unit cell.**
9. **Describe how face-centered cubic and hexagonal close-packed crystal structures may be generated by the stacking of close-packed planes of atoms. Do the same for the sodium chloride crystal structure in terms of close-packed planes of anions.**
10. **Distinguish between single crystals and polycrystalline materials.**
11. **Define *isotropy* and *anisotropy* with respect to material properties.**

3.1 INTRODUCTION

Chapter 2 was concerned primarily with the various types of atomic bonding, which are determined by the electron structure of the individual atoms. The present discussion is devoted to the next level of the structure of materials, specifically, to some of the arrangements that may be assumed by atoms in the solid state. Within this framework, concepts of crystallinity and noncrystallinity are introduced. For crystalline solids the notion of crystal structure is presented, specified in terms of a unit cell. Crystal structures found in both metals and ceramics are then detailed, along with the scheme by which crystallographic directions and planes are expressed. Single crystals, polycrystalline, and noncrystalline materials are considered.

CRYSTAL STRUCTURES

3.2 FUNDAMENTAL CONCEPTS

Solid materials may be classified according to the regularity with which atoms or ions are arranged with respect to one another. A **crystalline** material is one in which the atoms are situated in a repeating or periodic array over large atomic distances; that is, long-range order exists, such that upon solidification, the atoms will position themselves in a repetitive three-dimensional pattern, in which each atom is bonded to its nearest-neighbor atoms. All metals, many ceramic materials, and certain polymers form crystalline structures under normal solidification conditions. For those that do not crystallize, this long-range atomic order is absent; these *noncrystalline* or *amorphous* materials are discussed briefly at the end of this chapter.

Some of the properties of crystalline solids depend on the **crystal structure** of the material, the manner in which atoms, ions, or molecules are spatially arranged. There is an extremely large number of different crystal structures all having long-range atomic order; these vary from relatively simple structures for metals, to exceedingly complex ones, as displayed by some of the ceramic and polymeric

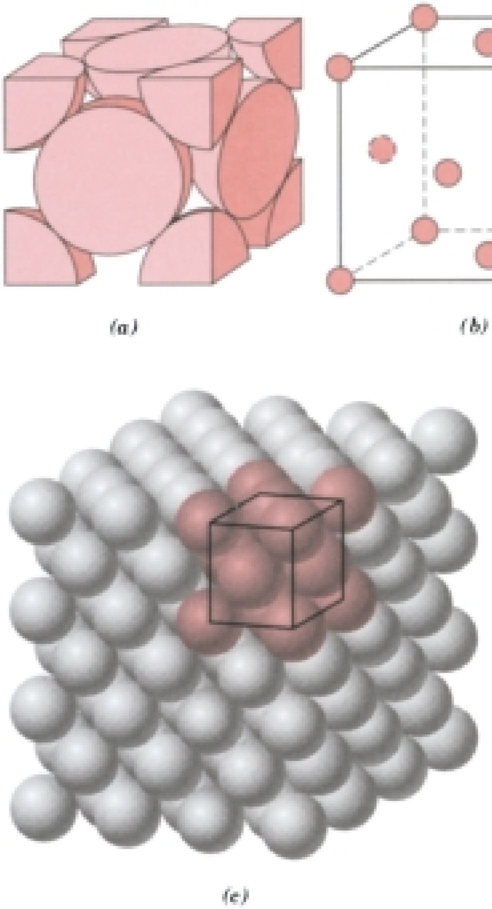

Figure 3.1 For the face-centered cubic crystal structure: (*a*) a hard sphere unit cell representation, (*b*) a reduced-sphere unit cell, and (*c*) an aggregate of many atoms. (Figure *c* adapted from W. G. Moffatt, G. W. Pearsall, and J. Wulff, *The Structure and Properties of Materials,* Vol. I, *Structure,* p. 51. Copyright © 1964 by John Wiley & Sons, New York. Reprinted by permission of John Wiley & Sons, Inc.)

materials. The present discussion deals with several common metallic and ceramic crystal structures. The next chapter is devoted to structures for polymers.

When describing crystalline structures, atoms (or ions) are thought of as being solid spheres having well-defined diameters. This is termed the *atomic hard sphere model* in which spheres representing nearest-neighbor atoms touch one another. An example of the hard sphere model for the atomic arrangement found in some of the common elemental metals is displayed in Figure 3.1*c*. In this particular case all the atoms are identical. Sometimes the term **lattice** is used in the context of crystal structures; in this sense ''lattice'' means a three-dimensional array of points coinciding with atom positions (or sphere centers).

3.3 UNIT CELLS

The atomic order in crystalline solids indicates that small groups of atoms form a repetitive pattern. Thus, in describing crystal structures, it is often convenient to subdivide the structure into small repeat entities called **unit cells.** Unit cells for most crystal structures are parallelepipeds or prisms having three sets of parallel faces; one is drawn within the aggregate of spheres (Figure 3.1*c*), which in this case happens to be a cube. A unit cell is chosen to represent the symmetry of the crystal structure, wherein all the atom positions in the crystal may be generated by translations of the unit cell integral distances along each of its edges. Thus, the unit cell is the basic structural unit or building block of the crystal structure and defines the crystal structure by virtue of its geometry and the atom positions within. Convenience usually dictates that parallelepiped corners coincide with centers of the hard sphere atoms. Furthermore, more than a single unit cell may be chosen for a particular crystal structure; however, we generally use the unit cell having the highest level of geometrical symmetry.

3.4 METALLIC CRYSTAL STRUCTURES

The atomic bonding in this group of materials is metallic, and thus nondirectional in nature. Consequently, there are no restrictions as to the number and position of nearest-neighbor atoms; this leads to relatively large numbers of nearest neighbors and dense atomic packings for most metallic crystal structures. Also, for metals, using the hard sphere model for the crystal structure, each sphere represents an ion core. Table 3.1 presents the atomic radii for a number of metals. Three relatively simple crystal structures are found for most of the common metals: face-centered cubic, body-centered cubic, and hexagonal close-packed.

THE FACE-CENTERED CUBIC CRYSTAL STRUCTURE

The crystal structure found for many metals has a unit cell of cubic geometry, with atoms located at each of the corners and the centers of all the cube faces. It is aptly called the **face-centered cubic (FCC)** crystal structure. Some of the familiar metals having this crystal structure are copper, aluminum, silver, and gold (see also Table 3.1). Figure 3.1*a* shows a hard sphere model for the FCC unit cell, whereas in Figure 3.1*b* the atom centers are represented by small circles to provide a better perspective of atom positions. The aggregate of atoms in Figure 3.1*c* represents a section of crystal consisting of many FCC unit cells. These spheres or ion cores touch one another across a face diagonal; the cube edge length a and the atomic radius R are related through

$$a = 2R\sqrt{2} \tag{3.1}$$

This result is obtained as an example problem.

For the FCC crystal structure, each corner atom is shared among eight unit cells, whereas a face-centered atom belongs to only two. Therefore, one eighth of

Table 3.1 Atomic Radii and Crystal Structures for 16 Metals

Metal	*Crystal Structure*[a]	*Atomic Radius*[b] *(nm)*	*Metal*	*Crystal Structure*	*Atomic Radius (nm)*
Aluminum	FCC	0.1431	Molybdenum	BCC	0.1363
Cadmium	HCP	0.1490	Nickel	FCC	0.1246
Chromium	BCC	0.1249	Platinum	FCC	0.1387
Cobalt	HCP	0.1253	Silver	FCC	0.1445
Copper	FCC	0.1278	Tantalum	BCC	0.1430
Gold	FCC	0.1442	Titanium (α)	HCP	0.1445
Iron (α)	BCC	0.1241	Tungsten	BCC	0.1371
Lead	FCC	0.1750	Zinc	HCP	0.1332

[a] FCC = face-centered cubic; HCP = hexagonal close-packed; BCC = body-centered cubic.

[b] A nanometer (nm) equals 10^{-9} m; to convert from nanometers to angstrom units (Å), multiply the nanometer value by 10.

each of the eight corner atoms and one half of each of the six face atoms, or a total of four whole atoms, may be assigned to a given unit cell. This is depicted in Figure 3.1*a*, where only sphere portions are represented within the confines of the cube. The cell comprises the volume of the cube, which is generated from the centers of the corner atoms as shown in the figure.

Corner and face positions are really equivalent; that is, translation of the cube corner from an original corner atom to the center of a face atom will not alter the cell structure.

Two other important characteristics of a crystal structure are the **coordination number** and the **atomic packing factor (APF).** For metals, each atom has the same number of nearest-neighbor or touching atoms, which is the coordination number. For face-centered cubics, the coordination number is 12. This may be confirmed by examination of Figure 3.1*a*; the front face atom has four corner nearest-neighbor atoms surrounding it, four face atoms that are in contact from behind, and four other equivalent face atoms residing in the next unit cell to the front, which is not shown.

The APF is the fraction of solid sphere volume in a unit cell, assuming the atomic hard sphere model, or

$$\text{APF} = \frac{\text{volume of atoms in a unit cell}}{\text{total unit cell volume}} \tag{3.2}$$

For the FCC structure, the atomic packing factor is 0.74, which is the maximum packing possible for spheres all having the same diameter. Computation of this APF is also included as an example problem. Metals typically have relatively large atomic packing factors to maximize the shielding provided by the free electron cloud.

THE BODY-CENTERED CUBIC CRYSTAL STRUCTURE

Another common metallic crystal structure also has a cubic unit cell with atoms located at all eight corners and a single atom at the cube center. This is called a **body-centered cubic (BCC)** crystal structure. A collection of spheres depicting this crystal structure is shown in Figure 3.2*c*, whereas Figures 3.2*a* and 3.2*b* are diagrams

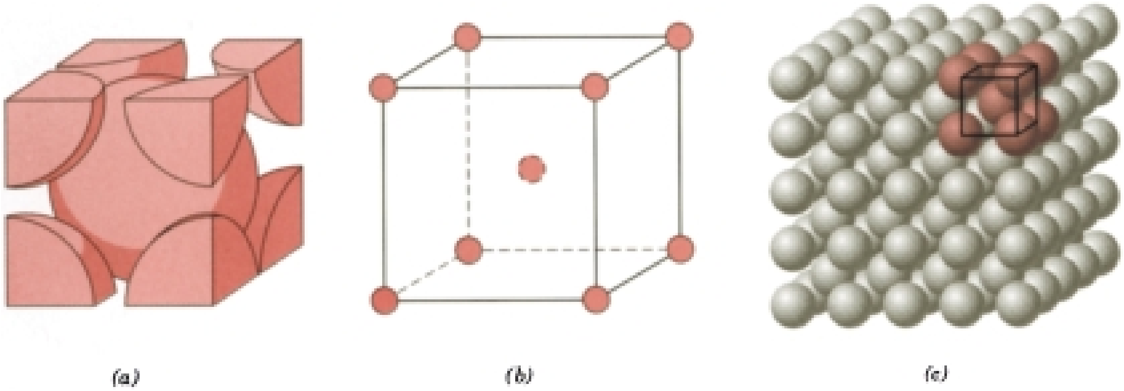

FIGURE 3.2 For the body-centered cubic crystal structure, (*a*) a hard sphere unit cell representation, (*b*) a reduced-sphere unit cell, and (*c*) an aggregate of many atoms. (Figure (*c*) from W. G. Moffatt, G. W. Pearsall, and J. Wulff, *The Structure and Properties of Materials*, Vol. I, *Structure*, p. 51. Copyright © 1964 by John Wiley & Sons, New York. Reprinted by permission of John Wiley & Sons, Inc.)

of BCC unit cells with the atoms represented by hard sphere and reduced-sphere models, respectively. Center and corner atoms touch one another along cube diagonals, and unit cell length *a* and atomic radius *R* are related through

$$a = \frac{4R}{\sqrt{3}} \tag{3.3}$$

Chromium, iron, tungsten, as well as several other metals listed in Table 3.1 exhibit a BCC structure.

Two atoms are associated with each BCC unit cell: the equivalent of one atom from the eight corners, each of which is shared among eight unit cells, and the single center atom, which is wholly contained within its cell. In addition, corner and center atom positions are equivalent. The coordination number for the BCC crystal structure is 8; each center atom has as nearest neighbors its eight corner atoms. Since the coordination number is less for BCC than FCC, so also is the atomic packing factor for BCC lower—0.68 versus 0.74.

THE HEXAGONAL CLOSE-PACKED CRYSTAL STRUCTURE

Not all metals have unit cells with cubic symmetry; the final common metallic crystal structure to be discussed has a unit cell that is hexagonal. Figure 3.3*a* shows a reduced-sphere unit cell for this structure, which is termed **hexagonal close-packed (HCP);** an assemblage of several HCP unit cells is presented in Figure 3.3*b*. The top and bottom faces of the unit cell consist of six atoms that form regular hexagons and surround a single atom in the center. Another plane that provides three additional atoms to the unit cell is situated between the top and bottom planes. The atoms in this midplane have as nearest neighbors atoms in both of the adjacent two planes. The equivalent of six atoms is contained in each unit cell; one-sixth of each of the 12 top and bottom face corner atoms, one-half of each of the 2 center face atoms, and all the 3 midplane interior atoms. If *a* and *c* represent, respectively,

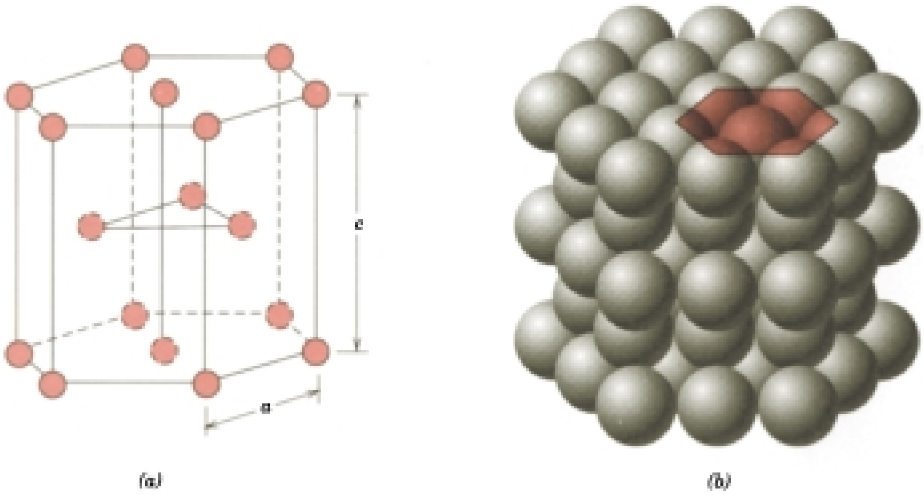

FIGURE 3.3 For the hexagonal close-packed crystal structure, (*a*) a reduced-sphere unit cell (*a* and *c* represent the short and long edge lengths, respectively), and (*b*) an aggregate of many atoms. (Figure (*b*) from W. G. Moffatt, G. W. Pearsall, and J. Wulff, *The Structure and Properties of Materials,* Vol. I, *Structure,* p. 51. Copyright © 1964 by John Wiley & Sons, New York. Reprinted by permission of John Wiley & Sons, Inc.)

the short and long unit cell dimensions of Figure 3.3*a*, the c/a ratio should be 1.633; however, for some HCP metals this ratio deviates from the ideal value.

The coordination number and the atomic packing factor for the HCP crystal structure are the same as for FCC: 12 and 0.74, respectively. The HCP metals include cadmium, magnesium, titanium, and zinc; some of these are listed in Table 3.1.

EXAMPLE PROBLEM 3.1

Calculate the volume of an FCC unit cell in terms of the atomic radius R.

SOLUTION

In the FCC unit cell illustrated,

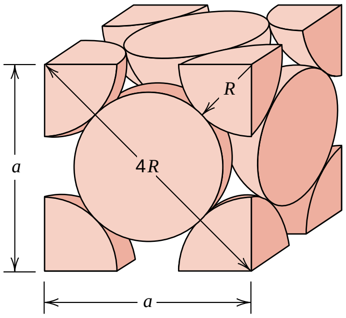

the atoms touch one another across a face-diagonal the length of which is $4R$. Since the unit cell is a cube, its volume is a^3, where a is the cell edge length. From the right triangle on the face,

$$a^2 + a^2 = (4R)^2$$

or, solving for a,

$$a = 2R\sqrt{2} \tag{3.1}$$

The FCC unit cell volume V_C may be computed from

$$V_C = a^3 = (2R\sqrt{2})^3 = 16R^3\sqrt{2} \tag{3.4}$$

EXAMPLE PROBLEM 3.2

Show that the atomic packing factor for the FCC crystal structure is 0.74.

SOLUTION

The APF is defined as the fraction of solid sphere volume in a unit cell, or

$$\text{APF} = \frac{\text{total sphere volume}}{\text{total unit cell volume}} = \frac{V_S}{V_C}$$

Both the total sphere and unit cell volumes may be calculated in terms of the atomic radius R. The volume for a sphere is $\frac{4}{3}\pi R^3$, and since there are four atoms per FCC unit cell, the total FCC sphere volume is

$$V_S = (4)\frac{4}{3}\pi R^3 = \frac{16}{3}\pi R^3$$

From Example Problem 3.1, the total unit cell volume is

$$V_C = 16R^3\sqrt{2}$$

Therefore, the atomic packing factor is

$$\text{APF} = \frac{V_S}{V_C} = \frac{(\frac{16}{3})\pi R^3}{16R^3\sqrt{2}} = 0.74$$

3.5 DENSITY COMPUTATIONS—METALS

A knowledge of the crystal structure of a metallic solid permits computation of its theoretical density ρ through the relationship

$$\rho = \frac{nA}{V_C N_A} \tag{3.5}$$

where

n = number of atoms associated with each unit cell
A = atomic weight
V_C = volume of the unit cell
N_A = Avogadro's number (6.023×10^{23} atoms/mol)

EXAMPLE PROBLEM 3.3

Copper has an atomic radius of 0.128 nm (1.28 Å), an FCC crystal structure, and an atomic weight of 63.5 g/mol. Compute its theoretical density and compare the answer with its measured density.

SOLUTION

Equation 3.5 is employed in the solution of this problem. Since the crystal structure is FCC, n, the number of atoms per unit cell, is 4. Furthermore, the atomic weight A_Cu is given as 63.5 g/mol. The unit cell volume V_C for FCC was determined in Example Problem 3.1 as $16R^3\sqrt{2}$, where R, the atomic radius, is 0.128 nm.

Substitution for the various parameters into Equation 3.5 yields

$$\rho = \frac{nA_\text{Cu}}{V_C N_\text{A}} = \frac{nA_\text{Cu}}{(16R^3\sqrt{2})N_\text{A}}$$

$$= \frac{(4 \text{ atoms/unit cell})(63.5 \text{ g/mol})}{[16\sqrt{2}(1.28 \times 10^{-8} \text{ cm})^3/\text{unit cell}](6.023 \times 10^{23} \text{ atoms/mol})}$$

$$= 8.89 \text{ g/cm}^3$$

The literature value for the density of copper is 8.94 g/cm^3, which is in very close agreement with the foregoing result.

3.6 CERAMIC CRYSTAL STRUCTURES

Because ceramics are composed of at least two elements, and often more, their crystal structures are generally more complex than those for metals. The atomic bonding in these materials ranges from purely ionic to totally covalent; many ceramics exhibit a combination of these two bonding types, the degree of ionic character being dependent on the electronegativities of the atoms. Table 3.2 presents the percent ionic character for several common ceramic materials; these values were determined using Equation 2.10 and the electronegativities in Figure 2.7.

For those ceramic materials for which the atomic bonding is predominantly ionic, the crystal structures may be thought of as being composed of electrically charged ions instead of atoms. The metallic ions, or **cations,** are positively charged, because they have given up their valence electrons to the nonmetallic ions, or **anions,** which are negatively charged. Two characteristics of the component ions in crystalline ceramic materials influence the crystal structure: the magnitude of the electrical charge on each of the component ions, and the relative sizes of the cations and anions. With regard to the first characteristic, the crystal must be electrically neutral; that is, all the cation positive charges must be balanced by an equal number of anion negative charges. The chemical formula of a compound indicates the ratio of cations to anions, or the composition that achieves this charge balance. For example, in calcium fluoride, each calcium ion has a +2 charge (Ca^{2+}), and associated with each fluorine ion is a single negative charge (F^-). Thus, there must be twice as many F^- as Ca^{2+} ions, which is reflected in the chemical formula CaF_2.

The second criterion involves the sizes or ionic radii of the cations and anions, r_C and r_A, respectively. Because the metallic elements give up electrons when ionized, cations are ordinarily smaller than anions, and, consequently, the ratio r_C/r_A is less than unity. Each cation prefers to have as many nearest-neighbor anions as possible. The anions also desire a maximum number of cation nearest neighbors.

Stable ceramic crystal structures form when those anions surrounding a cation are all in contact with that cation, as illustrated in Figure 3.4. The coordination number (i.e., number of anion nearest neighbors for a cation) is related to the cation–anion radius ratio. For a specific coordination number, there is a critical or minimum r_C/r_A ratio for which this cation–anion contact is established (Figure 3.4), which ratio may be determined from pure geometrical considerations (see Example Problem 3.4).

Table 3.2 **For Several Ceramic Materials, Percent Ionic Character of the Interatomic Bonds**

Material	*Percent Ionic Character*
CaF_2	89
MgO	73
NaCl	67
Al_2O_3	63
SiO_2	51
Si_3N_4	30
ZnS	18
SiC	12

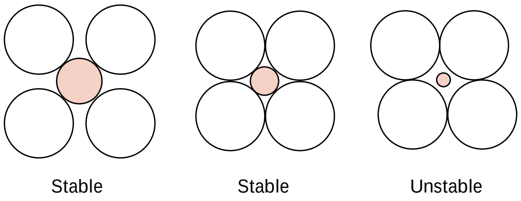

Figure 3.4 Stable and unstable anion–cation coordination configurations. Open circles represent anions; colored circles denote cations.

The coordination numbers and nearest-neighbor geometries for various r_C/r_A ratios are presented in Table 3.3. For r_C/r_A ratios less than 0.155, the very small cation is bonded to two anions in a linear manner. If r_C/r_A has a value between 0.155 and 0.225, the coordination number for the cation is 3. This means each cation is surrounded by three anions in the form of a planar equilateral triangle, with the cation located in the center. The coordination number is 4 for r_C/r_A between 0.225 and 0.414; the cation is located at the center of a tetrahedron, with anions at each of the four corners. For r_C/r_A between 0.414 and 0.732, the cation may be thought of as being situated at the center of an octahedron surrounded by six anions, one at each corner, as also shown in the table. The coordination number is 8 for r_C/r_A between 0.732 and 1.0, with anions at all corners of a cube and a cation positioned at the center. For a radius ratio greater than unity, the coordination number is 12. The most common coordination numbers for ceramic materials are 4, 6, and 8. Table 3.4 gives the ionic radii for several anions and cations that are common in ceramic materials.

Example Problem 3.4

Show that the minimum cation-to-anion radius ratio for the coordination number 3 is 0.155.

Solution

For this coordination, the small cation is surrounded by three anions to form an equilateral triangle as shown below—triangle ABC; the centers of all four ions are coplanar.

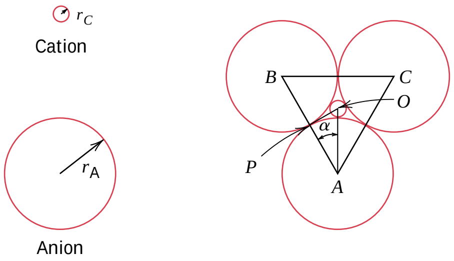

This boils down to a relatively simple plane trigonometry problem. Consideration of the right triangle APO makes it clear that the side lengths are related to the anion and cation radii r_A and r_C as

$$\overline{AP} = r_A$$

Table 3.3 Coordination Numbers and Geometries for Various Cation-Anion Radius Ratios (r_C/r_A)

Coordination Number	*Cation–Anion Radius Ratio*	*Coordination Geometry*
2	<0.155	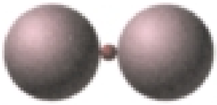
3	0.155–0.225	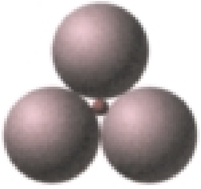
4	0.225–0.414	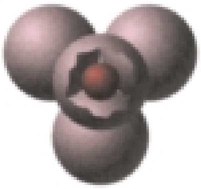
6	0.414–0.732	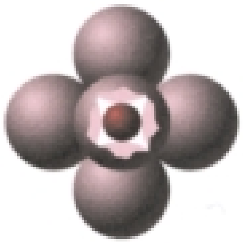
8	0.732–1.0	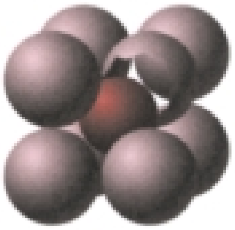

Source: W. D. Kingery, H. K. Bowen, and D. R. Uhlmann, *Introduction to Ceramics,* 2nd edition. Copyright © 1976 by John Wiley & Sons, New York. Reprinted by permission of John Wiley & Sons, Inc.

and

$$\overline{AO} = r_A + r_C$$

Furthermore, the side length ratio $\overline{AP}/\overline{AO}$ is a function of the angle α as

$$\frac{\overline{AP}}{\overline{AO}} = \cos\alpha$$

Table 3.4 Ionic Radii for Several Cations and Anions (for a Coordination Number of 6)

Cation	*Ionic Radius (nm)*	*Anion*	*Ionic Radius (nm)*
Al^{3+}	0.053	Br^-	0.196
Ba^{2+}	0.136	Cl^-	0.181
Ca^{2+}	0.100	F^-	0.133
Cs^+	0.170	I^-	0.220
Fe^{2+}	0.077	O^{2-}	0.140
Fe^{3+}	0.069	S^{2-}	0.184
K^+	0.138		
Mg^{2+}	0.072		
Mn^{2+}	0.067		
Na^+	0.102		
Ni^{2+}	0.069		
Si^{4+}	0.040		
Ti^{4+}	0.061		

The magnitude of α is 30°, since line $\overline{AO}$ bisects the 60° angle BAC. Thus,

$$\frac{\overline{AP}}{\overline{AO}} = \frac{r_A}{r_A + r_C} = \cos 30° = \frac{\sqrt{3}}{2}$$

Or, solving for the cation–anion radius ratio,

$$\frac{r_C}{r_A} = \frac{1 - \sqrt{3}/2}{\sqrt{3}/2} = 0.155$$

AX-TYPE CRYSTAL STRUCTURES

Some of the common ceramic materials are those in which there are equal numbers of cations and anions. These are often referred to as AX compounds, where A denotes the cation and X the anion. There are several different crystal structures for AX compounds; each is normally named after a common material that assumes the particular structure.

Rock Salt Structure

Perhaps the most common AX crystal structure is the *sodium chloride* (NaCl), or *rock salt,* type. The coordination number for both cations and anions is 6, and therefore the cation–anion radius ratio is between approximately 0.414 and 0.732. A unit cell for this crystal structure (Figure 3.5) is generated from an FCC arrangement of anions with one cation situated at the cube center and one at the center of each of the 12 cube edges. An equivalent crystal structure results from a face-centered arrangement of cations. Thus, the rock salt crystal structure may be thought of as two interpenetrating FCC lattices, one composed of the cations, the other of anions. Some of the common ceramic materials that form with this crystal structure are NaCl, MgO, MnS, LiF, and FeO.

Cesium Chloride Structure

Figure 3.6 shows a unit cell for the *cesium chloride* (CsCl) crystal structure; the coordination number is 8 for both ion types. The anions are located at each of the corners of a cube, whereas the cube center is a single cation. Interchange of anions

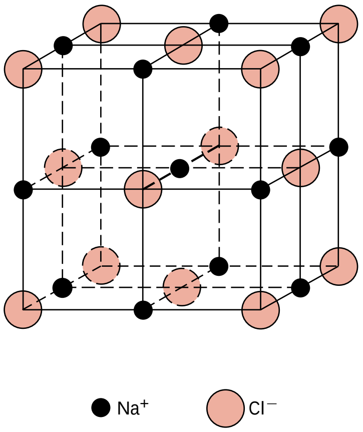

FIGURE 3.5 A unit cell for the rock salt, or sodium chloride (NaCl), crystal structure.

with cations, and vice versa, produces the same crystal structure. This is *not* a BCC crystal structure because ions of two different kinds are involved.

Zinc Blende Structure

A third AX structure is one in which the coordination number is 4; that is, all ions are tetrahedrally coordinated. This is called the *zinc blende,* or *sphalerite,* structure, after the mineralogical term for zinc sulfide (ZnS). A unit cell is presented in Figure 3.7; all corner and face positions of the cubic cell are occupied by S atoms, while the Zn atoms fill interior tetrahedral positions. An equivalent structure results if Zn and S atom positions are reversed. Thus, each Zn atom is bonded to four S atoms, and vice versa. Most often the atomic bonding is highly covalent in compounds exhibiting this crystal structure (Table 3.2), which include ZnS, ZnTe, and SiC.

A_mX_p-TYPE CRYSTAL STRUCTURES

If the charges on the cations and anions are not the same, a compound can exist with the chemical formula A_mX_p, where m and/or $p \neq 1$. An example would be AX_2, for which a common crystal structure is found in *fluorite* (CaF_2). The ionic radii ratio r_C/r_A for CaF_2 is about 0.8 which, according to Table 3.3, gives a coordination number of 8. Calcium ions are positioned at the centers of cubes, with fluorine

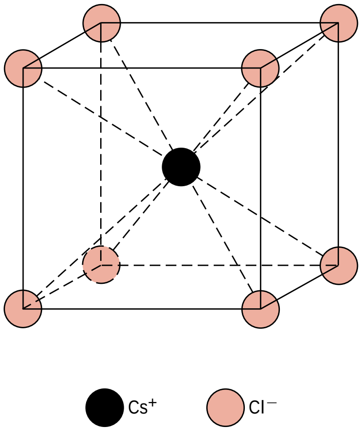

FIGURE 3.6 A unit cell for the cesium chloride (CsCl) crystal structure.

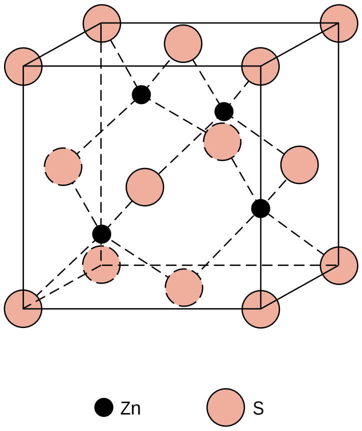

Figure 3.7 A unit cell for the zinc blende (ZnS) crystal structure.

ions at the corners. The chemical formula shows that there are only half as many Ca^{2+} ions as F^- ions, and therefore the crystal structure would be similar to CsCl (Figure 3.6), except that only half the center cube positions are occupied by Ca^{2+} ions. One unit cell consists of eight cubes, as indicated in Figure 3.8. Other compounds that have this crystal structure include UO_2, PuO_2, and ThO_2.

$A_mB_nX_p$-TYPE CRYSTAL STRUCTURES

It is also possible for ceramic compounds to have more than one type of cation; for two types of cations (represented by A and B), their chemical formula may be designated as $A_mB_nX_p$. Barium titanate ($BaTiO_3$), having both Ba^{2+} and Ti^{4+} cations, falls into this classification. This material has a *perovskite crystal structure* and rather interesting electromechanical properties to be discussed later. At temperatures above 120°C (248°F), the crystal structure is cubic. A unit cell of this structure is shown in Figure 3.9; Ba^{2+} ions are situated at all eight corners of the cube and a single Ti^{4+} is at the cube center, with O^{2-} ions located at the center of each of the six faces.

Table 3.5 summarizes the rock salt, cesium chloride, zinc blende, fluorite, and perovskite crystal structures in terms of cation–anion ratios and coordination numbers, and gives examples for each. Of course, many other ceramic crystal structures are possible.

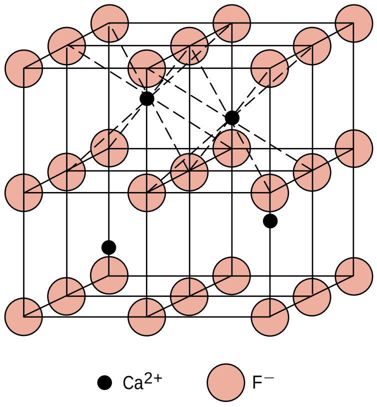

Figure 3.8 A unit cell for the fluorite (CaF_2) crystal structure.

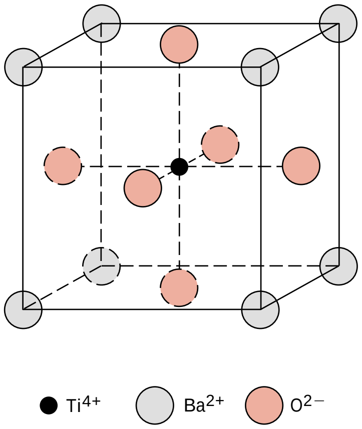

FIGURE 3.9 A unit cell for the perovskite crystal structure.

EXAMPLE PROBLEM 3.5

On the basis of ionic radii, what crystal structure would you predict for FeO?

SOLUTION

First, note that FeO is an AX-type compound. Next, determine the cation–anion radius ratio, which from Table 3.4 is

$$\frac{r_{\mathrm{Fe}^{2+}}}{r_{\mathrm{O}^{2-}}} = \frac{0.077\ \mathrm{nm}}{0.140\ \mathrm{nm}} = 0.550$$

This value lies between 0.414 and 0.732, and, therefore, from Table 3.3 the coordination number for the Fe^{2+} ion is 6; this is also the coordination number of O^{2-}, since there are equal numbers of cations and anions. The predicted crystal structure will be rock salt, which is the AX crystal structure having a coordination number of 6, as given in Table 3.5.

Table 3.5 Summary of Some Common Ceramic Crystal Structures

Structure Name	*Structure Type*	*Anion Packing*	*Coordination Numbers*		*Examples*
			Cation	*Anion*	
Rock salt (sodium chloride)	AX	FCC	6	6	NaCl, MgO, FeO
Cesium chloride	AX	Simple cubic	8	8	CsCl
Zinc blende (sphalerite)	AX	FCC	4	4	ZnS, SiC
Fluorite	AX_2	Simple cubic	8	4	CaF_2, UO_2, ThO_2
Perovskite	ABX_3	FCC	12(A) 6(B)	6	$BaTiO_3$, $SrZrO_3$, $SrSnO_3$
Spinel	AB_2X_4	FCC	4(A) 6(B)	4	$MgAl_2O_4$, $FeAl_2O_4$

Source: W. D. Kingery, H. K. Bowen, and D. R. Uhlmann, *Introduction to Ceramics*, 2nd edition. Copyright © 1976 by John Wiley & Sons, New York. Reprinted by permission of John Wiley & Sons, Inc.

3.7 DENSITY COMPUTATIONS—CERAMICS

It is possible to compute the theoretical density of a crystalline ceramic material from unit cell data in a manner similar to that described in Section 3.5 for metals. In this case the density ρ may be determined using a modified form of Equation 3.5, as follows:

$$\rho = \frac{n'(\Sigma A_C + \Sigma A_A)}{V_C N_A} \tag{3.6}$$

where

n' = the number of formula units[1] within the unit cell

ΣA_C = the sum of the atomic weights of all cations in the formula unit

ΣA_A = the sum of the atomic weights of all anions in the formula unit

V_C = the unit cell volume

N_A = Avogadro's number, 6.023×10^{23} formula units/mol

EXAMPLE PROBLEM 3.6

On the basis of crystal structure, compute the theoretical density for sodium chloride. How does this compare with its measured density?

SOLUTION

The density may be determined using Equation 3.6, where n', the number of NaCl units per unit cell, is 4 because both sodium and chloride ions form FCC lattices. Furthermore,

$$\Sigma A_C = A_{Na} = 22.99 \text{ g/mol}$$
$$\Sigma A_A = A_{Cl} = 35.45 \text{ g/mol}$$

Since the unit cell is cubic, $V_C = a^3$, a being the unit cell edge length. For the face of the cubic unit cell shown below,

$$a = 2r_{Na^+} + 2r_{Cl^-}$$

r_{Na^+} and r_{Cl^-} being the sodium and chlorine ionic radii, given in Table 3.4 as 0.102 and 0.181 nm, respectively.

Thus,

$$V_C = a^3 = (2r_{Na^+} + 2r_{Cl^-})^3$$

---

[1] By "formula unit" we mean all the ions that are included in the chemical formula unit. For example, for $BaTiO_3$, a formula unit consists of one barium ion, a titanium ion, and three oxygen ions.

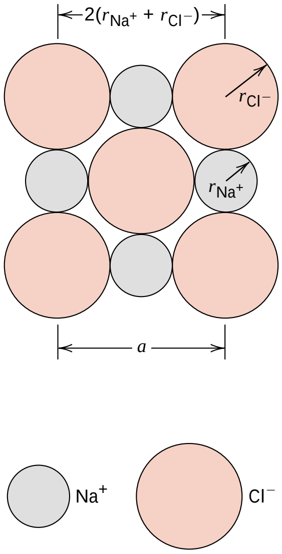

And finally,

$$\rho = \frac{n'(A_{\mathrm{Na}} + A_{\mathrm{Cl}})}{(2r_{\mathrm{Na}^+} + 2r_{\mathrm{Cl}^-})^3 N_{\mathrm{A}}}$$

$$= \frac{4(22.99 + 35.45)}{[2(0.102 \times 10^{-7}) + 2(0.181 \times 10^{-7})]^3(6.023 \times 10^{23})}$$

$$= 2.14 \text{ g/cm}^3$$

This compares very favorably with the experimental value of 2.16 g/cm^3.

3.8 SILICATE CERAMICS

Silicates are materials composed primarily of silicon and oxygen, the two most abundant elements in the earth's crust; consequently, the bulk of soils, rocks, clays, and sand come under the silicate classification. Rather than characterizing the crystal structures of these materials in terms of unit cells, it is more convenient to use various arrangements of an SiO_4^{4-} tetrahedron (Figure 3.10). Each atom of silicon is bonded to four oxygen atoms, which are situated at the corners of the tetrahedron; the silicon atom is positioned at the center. Since this is the basic unit of the silicates, it is often treated as a negatively charged entity.

Often the silicates are not considered to be ionic because there is a significant covalent character to the interatomic Si–O bonds (Table 3.2), which bonds are directional and relatively strong. Regardless of the character of the Si–O bond, there is a -4 charge associated with every SiO_4^{4-} tetrahedron, since each of the four oxygen atoms requires an extra electron to achieve a stable electronic structure. Various silicate structures arise from the different ways in which the SiO_4^{4-} units can be combined into one-, two-, and three-dimensional arrangements.

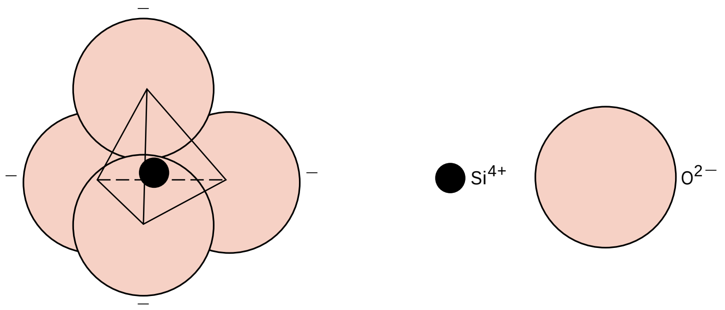

Figure 3.10 A silicon–oxygen (SiO_4^{4-}) tetrahedron.

SILICA

Chemically, the most simple silicate material is silicon dioxide, or silica (SiO_2). Structurally, it is a three-dimensional network that is generated when every corner oxygen atom in each tetrahedron is shared by adjacent tetrahedra. Thus, the material is electrically neutral and all atoms have stable electronic structures. Under these circumstances the ratio of Si to O atoms is 1 : 2, as indicated by the chemical formula.

If these tetrahedra are arrayed in a regular and ordered manner, a crystalline structure is formed. There are three primary polymorphic crystalline forms of silica: quartz, cristobalite (Figure 3.11), and tridymite. Their structures are relatively complicated, and comparatively open; that is, the atoms are not closely packed together. As a consequence, these crystalline silicas have relatively low densities; for example, at room temperature quartz has a density of only 2.65 g/cm^3. The strength of the Si–O interatomic bonds is reflected in a relatively high melting temperature, 1710°C (3110°F).

Silica can also be made to exist as a noncrystalline solid or glass; its structure is discussed in Section 3.20.

THE SILICATES (CD-ROM)

3.9 Carbon

Carbon is an element that exists in various polymorphic forms, as well as in the amorphous state. This group of materials does not really fall within any one of the traditional metal, ceramic, polymer classification schemes. However, it has been decided to discuss these materials in this chapter since graphite, one of the polymorphic forms, is sometimes classified as a ceramic. This treatment focuses on the

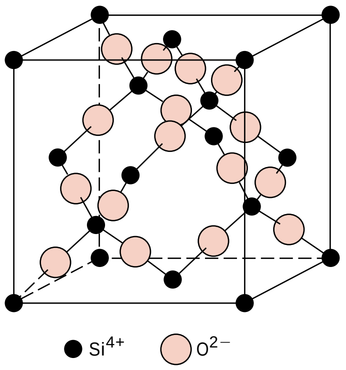

Figure 3.11 The arrangement of silicon and oxygen atoms in a unit cell of cristobalite, a polymorph of SiO_2.

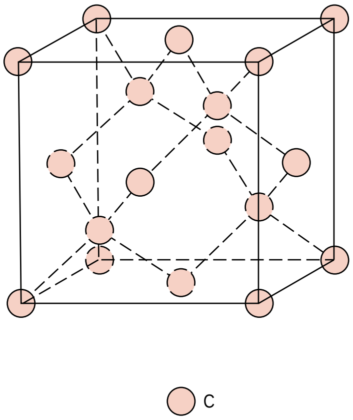

Figure 3.16 A unit cell for the diamond cubic crystal structure.

structures of graphite and diamond {and the new fullerenes.} The characteristics and current and potential uses of these materials are discussed in Section 13.11.

DIAMOND

Diamond is a metastable carbon polymorph at room temperature and atmospheric pressure. Its crystal structure is a variant of the zinc blende, in which carbon atoms occupy all positions (both Zn and S), as indicated in the unit cell shown in Figure 3.16. Thus, each carbon bonds to four other carbons, and these bonds are totally covalent. This is appropriately called the *diamond cubic* crystal structure, which is also found for other Group IVA elements in the periodic table [e.g., germanium, silicon, and gray tin, below 13°C (55°F)].

GRAPHITE

Graphite has a crystal structure (Figure 3.17) distinctly different from that of diamond and is also more stable than diamond at ambient temperature and pressure. The graphite structure is composed of layers of hexagonally arranged carbon atoms; within the layers, each carbon atom is bonded to three coplanar neighbor atoms by strong covalent bonds. The fourth bonding electron participates in a weak van der Waals type of bond between the layers.

FULLERENES (CD-ROM)

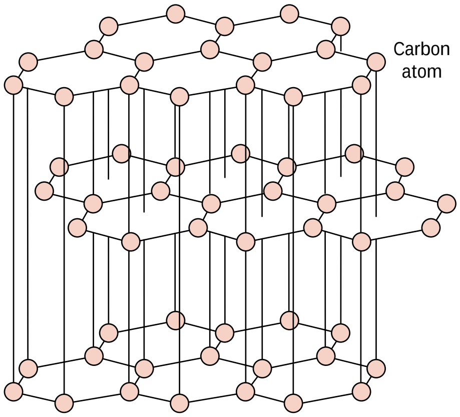

Figure 3.17 The structure of graphite.

3.10 POLYMORPHISM AND ALLOTROPY

Some metals, as well as nonmetals, may have more than one crystal structure, a phenomenon known as **polymorphism.** When found in elemental solids, the condition is often termed **allotropy.** The prevailing crystal structure depends on both the temperature and the external pressure. One familiar example is found in carbon as discussed in the previous section: graphite is the stable polymorph at ambient conditions, whereas diamond is formed at extremely high pressures. Also, pure iron has a BCC crystal structure at room temperature, which changes to FCC iron at 912°C (1674°F). Most often a modification of the density and other physical properties accompanies a polymorphic transformation.

3.11 CRYSTAL SYSTEMS

Since there are many different possible crystal structures, it is sometimes convenient to divide them into groups according to unit cell configurations and/or atomic arrangements. One such scheme is based on the unit cell geometry, that is, the shape of the appropriate unit cell parallelepiped without regard to the atomic positions in the cell. Within this framework, an x, y, z coordinate system is established with its origin at one of the unit cell corners; each of the x, y, and z axes coincides with one of the three parallelepiped edges that extend from this corner, as illustrated in Figure 3.19. The unit cell geometry is completely defined in terms of six parameters: the three edge lengths a, b, and c, and the three interaxial angles α, β, and γ. These are indicated in Figure 3.19, and are sometimes termed the **lattice parameters** of a crystal structure.

On this basis there are found crystals having seven different possible combinations of a, b, and c, and α, β, and γ, each of which represents a distinct **crystal system.** These seven crystal systems are cubic, tetragonal, hexagonal, orthorhombic, rhombohedral, monoclinic, and triclinic. The lattice parameter relationships and unit cell sketches for each are represented in Table 3.6. The cubic system, for which $a = b = c$ and $\alpha = \beta = \gamma = 90°$, has the greatest degree of symmetry. Least symmetry is displayed by the triclinic system, since $a \neq b \neq c$ and $\alpha \neq \beta \neq \gamma$.

From the discussion of metallic crystal structures, it should be apparent that both FCC and BCC structures belong to the cubic crystal system, whereas HCP falls within hexagonal. The conventional hexagonal unit cell really consists of three parallelepipeds situated as shown in Table 3.6.

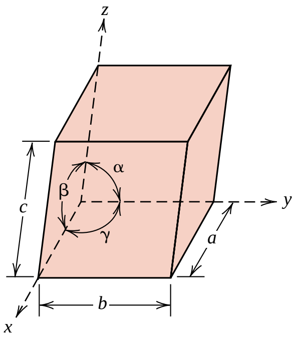

FIGURE 3.19 A unit cell with x, y, and z coordinate axes, showing axial lengths (a, b, and c) and interaxial angles (α, β, and γ).

Table 3.6 **Lattice Parameter Relationships and Figures Showing Unit Cell Geometries for the Seven Crystal Systems**

Crystal System	*Axial Relationships*	*Interaxial Angles*	*Unit Cell Geometry*
Cubic	$a = b = c$	$\alpha = \beta = \gamma = 90°$	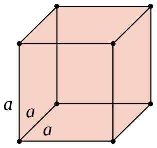
Hexagonal	$a = b \neq c$	$\alpha = \beta = 90°, \gamma = 120°$	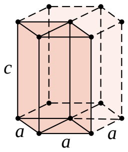
Tetragonal	$a = b \neq c$	$\alpha = \beta = \gamma = 90°$	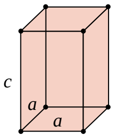
Rhombohedral	$a = b = c$	$\alpha = \beta = \gamma \neq 90°$	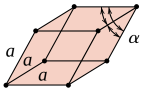
Orthorhombic	$a \neq b \neq c$	$\alpha = \beta = \gamma = 90°$	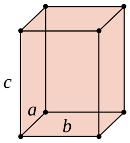
Monoclinic	$a \neq b \neq c$	$\alpha = \gamma = 90° \neq \beta$	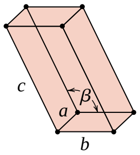
Triclinic	$a \neq b \neq c$	$\alpha \neq \beta \neq \gamma \neq 90°$	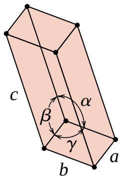

CRYSTALLOGRAPHIC DIRECTIONS AND PLANES

When dealing with crystalline materials, it often becomes necessary to specify some particular crystallographic plane of atoms or a crystallographic direction. Labeling conventions have been established in which three integers or indices are used to designate directions and planes. The basis for determining index values is the unit cell, with a coordinate system consisting of three (x, y, and z) axes situated at one of the corners and coinciding with the unit cell edges, as shown in Figure 3.19. For some crystal systems—namely, hexagonal, rhombohedral, monoclinic, and triclinic—the three axes are *not* mutually perpendicular, as in the familiar Cartesian coordinate scheme.

3.12 CRYSTALLOGRAPHIC DIRECTIONS

A crystallographic direction is defined as a line between two points, or a vector. The following steps are utilized in the determination of the three directional indices:

1. A vector of convenient length is positioned such that it passes through the origin of the coordinate system. Any vector may be translated throughout the crystal lattice without alteration, if parallelism is maintained.
2. The length of the vector projection on each of the three axes is determined; *these are measured in terms of the unit cell dimensions a, b, and c.*
3. These three numbers are multiplied or divided by a common factor to reduce them to the smallest integer values.
4. The three indices, not separated by commas, are enclosed in square brackets, thus: $[uvw]$. The u, v, and w integers correspond to the reduced projections along the x, y, and z axes, respectively.

For each of the three axes, there will exist both positive and negative coordinates. Thus negative indices are also possible, which are represented by a bar over the appropriate index. For example, the $[1\bar{1}1]$ direction would have a component in the $-y$ direction. Also, changing the signs of all indices produces an antiparallel

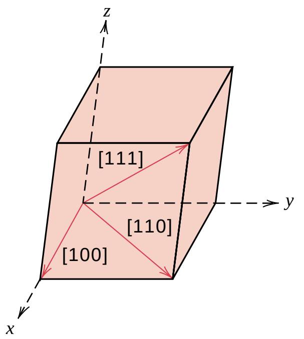

FIGURE 3.20 The [100], [110], and [111] directions within a unit cell.

direction; that is, $[\bar{1}1\bar{1}]$ is directly opposite to $[1\bar{1}1]$. If more than one direction or plane is to be specified for a particular crystal structure, it is imperative for the maintaining of consistency that a positive–negative convention, once established, not be changed.

The [100], [110], and [111] directions are common ones; they are drawn in the unit cell shown in Figure 3.20.

Example Problem 3.7

Determine the indices for the direction shown in the accompanying figure.

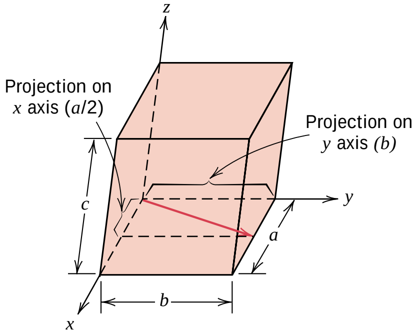

Solution

The vector, as drawn, passes through the origin of the coordinate system, and therefore no translation is necessary. Projections of this vector onto the x, y, and z axes are, respectively, $a/2$, b, and $0c$, which become $\frac{1}{2}$, 1, and 0 in terms of the unit cell parameters (i.e., when the a, b, and c are dropped). Reduction of these numbers to the lowest set of integers is accompanied by multiplication of each by the factor 2. This yields the integers 1, 2, and 0, which are then enclosed in brackets as [120].

This procedure may be summarized as follows:

	x	y	z
Projections	$a/2$	b	$0c$
Projections (in terms of a, b, and c)	$\frac{1}{2}$	1	0
Reduction	1	2	0
Enclosure		[120]	

Example Problem 3.8

Draw a $[1\bar{1}0]$ direction within a cubic unit cell.

Solution

First construct an appropriate unit cell and coordinate axes system. In the accompanying figure the unit cell is cubic, and the origin of the coordinate system, point O, is located at one of the cube corners.

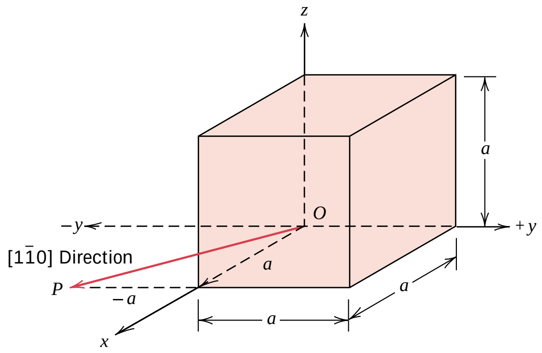

This problem is solved by reversing the procedure of the preceding example. For this [1$\bar{1}$0] direction, the projections along the x, y, z axes are a, $-a$, and $0a$, respectively. This direction is defined by a vector passing from the origin to point P, which is located by first moving along the x axis a units, and from this position, parallel to the y axis $-a$ units, as indicated in the figure. There is no z component to the vector, since the z projection is zero.

For some crystal structures, several nonparallel directions with different indices are actually equivalent; this means that the spacing of atoms along each direction is the same. For example, in cubic crystals, all the directions represented by the following indices are equivalent: [100], [$\bar{1}$00], [010], [0$\bar{1}$0], [001], and [00$\bar{1}$]. As a convenience, equivalent directions are grouped together into a *family*, which are enclosed in angle brackets, thus: ⟨100⟩. Furthermore, directions in cubic crystals having the same indices without regard to order or sign, for example, [123] and [$\bar{2}$1$\bar{3}$], are equivalent. This is, in general, not true for other crystal systems. For example, for crystals of tetragonal symmetry, [100] and [010] directions are equivalent, whereas [100] and [001] are not.

HEXAGONAL CRYSTALS

A problem arises for crystals having hexagonal symmetry in that some crystallographic equivalent directions will not have the same set of indices. This is circumvented by utilizing a four-axis, or *Miller–Bravais*, coordinate system as shown in Figure 3.21. The three a_1, a_2, and a_3 axes are all contained within a single plane

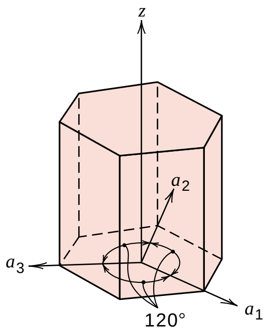

FIGURE 3.21 Coordinate axis system for a hexagonal unit cell (Miller–Bravais scheme).

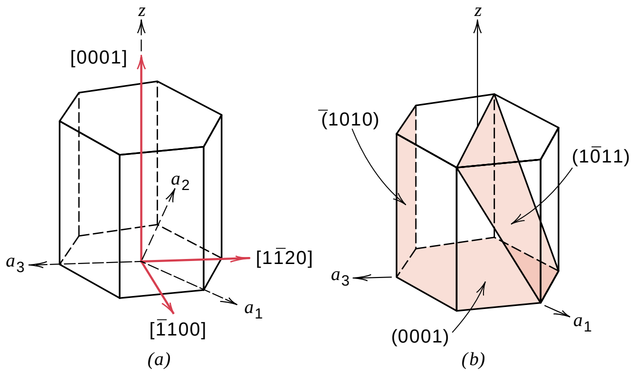

Figure 3.22 For the hexagonal crystal system, (*a*) $[0001]$, $[1\bar{1}00]$, and $[11\bar{2}0]$ directions, and (*b*) the (0001), $(10\bar{1}1)$, and $(\bar{1}010)$ planes.

(called the basal plane), and at 120° angles to one another. The z axis is perpendicular to this basal plane. Directional indices, which are obtained as described above, will be denoted by four indices, as $[uvtw]$; by convention, the first three indices pertain to projections along the respective a_1, a_2, and a_3 axes in the basal plane.

Conversion from the three-index system to the four-index system,

$$[u'v'w'] \longrightarrow [uvtw]$$

is accomplished by the following formulas:

$$u = \frac{n}{3}(2u' - v') \tag{3.7a}$$

$$v = \frac{n}{3}(2v' - u') \tag{3.7b}$$

$$t = -(u + v) \tag{3.7c}$$

$$w = nw' \tag{3.7d}$$

where primed indices are associated with the three-index scheme and unprimed, with the new Miller–Bravais four-index system; n is a factor that may be required to reduce u, v, t, and w to the smallest integers. For example, using this conversion, the $[010]$ direction becomes $[\bar{1}2\bar{1}0]$. Several different directions are indicated in the hexagonal unit cell (Figure 3.22*a*).

3.13 CRYSTALLOGRAPHIC PLANES

The orientations of planes for a crystal structure are represented in a similar manner. Again, the unit cell is the basis, with the three-axis coordinate system as represented in Figure 3.19. In all but the hexagonal crystal system, crystallographic planes are specified by three **Miller indices** as (hkl). Any two planes parallel to each other are equivalent and have identical indices. The procedure employed in determination of the h, k, and l index numbers is as follows:

1. If the plane passes through the selected origin, either another parallel plane must be constructed within the unit cell by an appropriate translation, or a new origin must be established at the corner of another unit cell.
2. At this point the crystallographic plane either intersects or parallels each of the three axes; the length of the planar intercept for each axis is determined in terms of the lattice parameters a, b, and c.

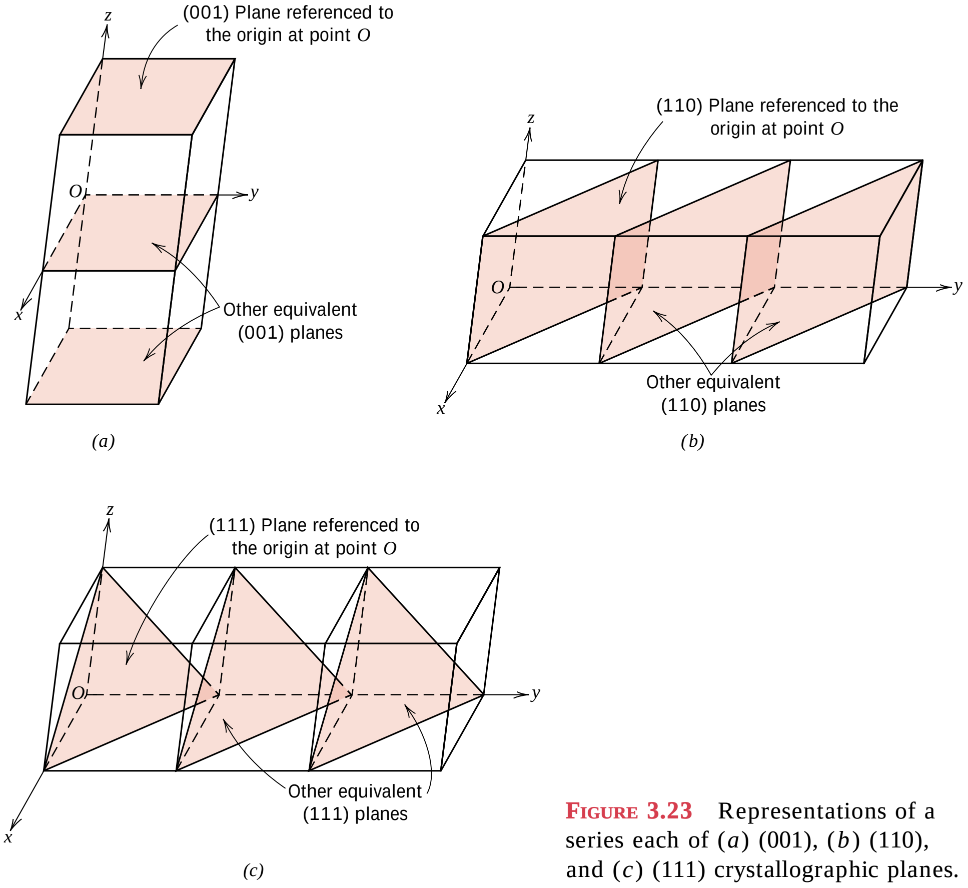
(001) Plane referenced to the origin at point O
z
y
x
O
Other equivalent (001) planes
(110) Plane referenced to the origin at point O
Other equivalent (110) planes
(111) Plane referenced to the origin at point O
Other equivalent (111) planes

(a) (b) (c)

FIGURE 3.23 Representations of a series each of (*a*) (001), (*b*) (110), and (*c*) (111) crystallographic planes.

3. The reciprocals of these numbers are taken. A plane that parallels an axis may be considered to have an infinite intercept, and, therefore, a zero index.
4. If necessary, these three numbers are changed to the set of smallest integers by multiplication or division by a common factor.[2]
5. Finally, the integer indices, not separated by commas, are enclosed within parentheses, thus: (hkl).

An intercept on the negative side of the origin is indicated by a bar or minus sign positioned over the appropriate index. Furthermore, reversing the directions of all indices specifies another plane parallel to, on the opposite side of and equidistant from, the origin. Several low-index planes are represented in Figure 3.23.

One interesting and unique characteristic of cubic crystals is that planes and directions having the same indices are perpendicular to one another; however, for other crystal systems there are no simple geometrical relationships between planes and directions having the same indices.

---

[2] On occasion, index reduction is not carried out {(e.g., for x-ray diffraction studies that are described in Section 3.19);} for example, (002) is not reduced to (001). In addition, for ceramic materials, the ionic arrangement for a reduced-index plane may be different from that for a nonreduced one.

Example Problem 3.9

Determine the Miller indices for the plane shown in the accompanying sketch (*a*).

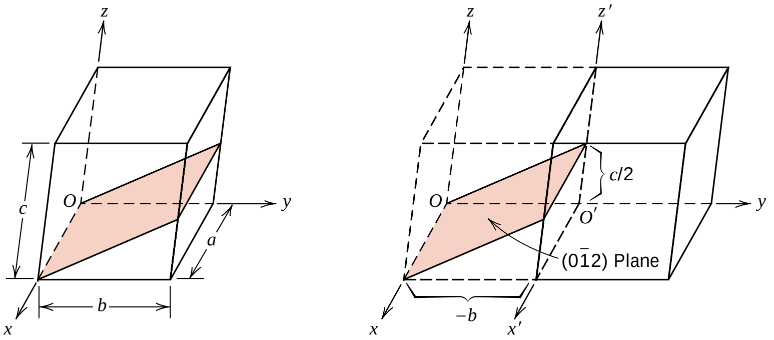

(*a*) (*b*)

Solution

Since the plane passes through the selected origin O, a new origin must be chosen at the corner of an adjacent unit cell, taken as O' and shown in sketch (*b*). This plane is parallel to the x axis, and the intercept may be taken as ∞a. The y and z axes intersections, referenced to the new origin O', are $-b$ and $c/2$, respectively. Thus, in terms of the lattice parameters a, b, and c, these intersections are ∞, -1, and $\frac{1}{2}$. The reciprocals of these numbers are 0, -1, and 2; and since all are integers, no further reduction is necessary. Finally, enclosure in parentheses yields $(0\bar{1}2)$.

These steps are briefly summarized below:

	x	y	z
Intercepts	∞a	$-b$	$c/2$
Intercepts (in terms of lattice parameters)	∞	-1	$\frac{1}{2}$
Reciprocals	0	-1	2
Reductions (unnecessary)			
Enclosure		$(0\bar{1}2)$	

Example Problem 3.10

Construct a $(0\bar{1}1)$ plane within a cubic unit cell.

Solution

To solve this problem, carry out the procedure used in the preceding example in reverse order. To begin, the indices are removed from the parentheses, and reciprocals are taken, which yields ∞, -1, and 1. This means that the particular plane parallels the x axis while intersecting the y and z axes at $-b$ and c, respectively, as indicated in the accompanying sketch (*a*). This plane has been drawn in sketch (*b*). A plane is indicated by lines representing its intersections with the planes that constitute the faces of the unit cell or their extensions. For example, in this figure, line *ef* is the intersection between the $(0\bar{1}1)$ plane and

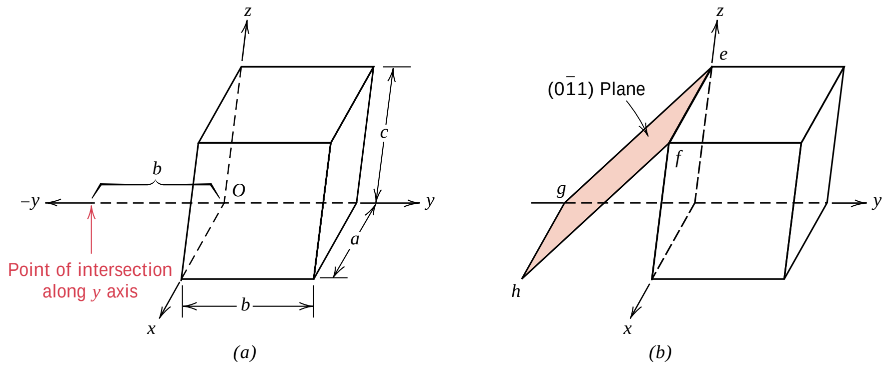

the top face of the unit cell; also, line *gh* represents the intersection between this same $(0\bar{1}1)$ plane and the plane of the bottom unit cell face extended. Similarly, lines *eg* and *fh* are the intersections between $(0\bar{1}1)$ and back and front cell faces, respectively.

ATOMIC ARRANGEMENTS

The atomic arrangement for a crystallographic plane, which is often of interest, depends on the crystal structure. The (110) atomic planes for FCC and BCC crystal structures are represented in Figures 3.24 and 3.25; reduced-sphere unit cells are also included. Note that the atomic packing is different for each case. The circles represent atoms lying in the crystallographic planes as would be obtained from a slice taken through the centers of the full-sized hard spheres.

A ''family'' of planes contains all those planes that are crystallographically equivalent—that is, having the same atomic packing; and a family is designated by indices that are enclosed in braces—e.g., {100}. For example, in cubic crystals the (111), $(\bar{1}\bar{1}\bar{1})$, $(\bar{1}11)$, $(1\bar{1}\bar{1})$, $(11\bar{1})$, $(\bar{1}\bar{1}1)$, $(\bar{1}1\bar{1})$, and $(1\bar{1}1)$ planes all belong to the {111} family. On the other hand, for tetragonal crystal structures, the {100} family would contain only the (100), $(\bar{1}00)$, (010), and $(0\bar{1}0)$ since the (001) and $(00\bar{1})$ planes are not crystallographically equivalent. Also, in the cubic system only, planes having the same indices, irrespective of order and sign, are equivalent. For example, both $(1\bar{2}3)$ and $(3\bar{1}2)$ belong to the {123} family.

HEXAGONAL CRYSTALS

For crystals having hexagonal symmetry, it is desirable that equivalent planes have the same indices; as with directions, this is accomplished by the Miller–Bravais

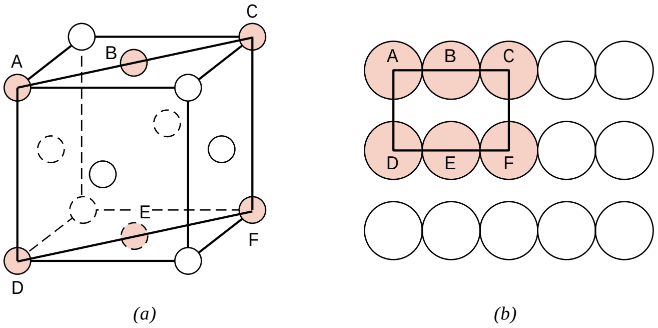

FIGURE 3.24 (*a*) Reduced-sphere FCC unit cell with (110) plane. (*b*) Atomic packing of an FCC (110) plane. Corresponding atom positions from (*a*) are indicated.

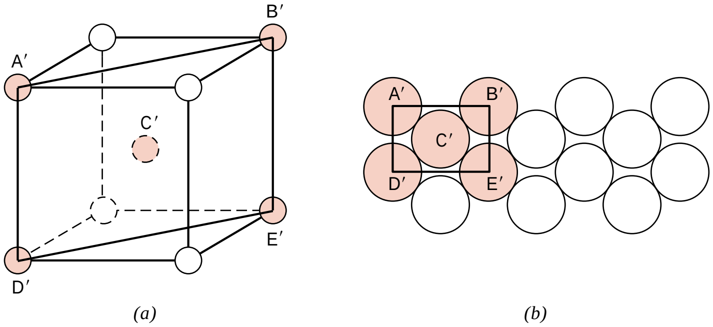

FIGURE 3.25 (*a*) Reduced-sphere BCC unit cell with (110) plane. (*b*) Atomic packing of a BCC (110) plane. Corresponding atom positions from (*a*) are indicated.

system shown in Figure 3.21. This convention leads to the four-index (*hkil*) scheme, which is favored in most instances, since it more clearly identifies the orientation of a plane in a hexagonal crystal. There is some redundancy in that *i* is determined by the sum of *h* and *k* through

$$i = -(h + k) \tag{3.8}$$

Otherwise the three *h*, *k*, and *l* indices are identical for both indexing systems. Figure 3.22*b* presents several of the common planes that are found for crystals having hexagonal symmetry.

3.14 LINEAR AND PLANAR ATOMIC DENSITIES (CD-ROM)

3.15 CLOSE-PACKED CRYSTAL STRUCTURES

METALS

It may be remembered from the discussion on metallic crystal structures (Section 3.4) that both face-centered cubic and hexagonal close-packed crystal structures have atomic packing factors of 0.74, which is the most efficient packing of equal-sized spheres or atoms. In addition to unit cell representations, these two crystal structures may be described in terms of close-packed planes of atoms (i.e., planes having a maximum atom or sphere-packing density); a portion of one such plane is illustrated in Figure 3.27*a*. Both crystal structures may be generated by the stacking of these close-packed planes on top of one another; the difference between the two structures lies in the stacking sequence.

Let the centers of all the atoms in one close-packed plane be labeled *A*. Associated with this plane are two sets of equivalent triangular depressions formed by three adjacent atoms, into which the next close-packed plane of atoms may rest. Those having the triangle vertex pointing up are arbitrarily designated as *B* positions, while the remaining depressions are those with the down vertices, which are marked *C* in Figure 3.27*a*.

A second close-packed plane may be positioned with the centers of its atoms over either *B* or *C* sites; at this point both are equivalent. Suppose that the *B* positions are arbitrarily chosen; the stacking sequence is termed *AB*, which is illustrated in Figure 3.27*b*. The real distinction between FCC and HCP lies in where

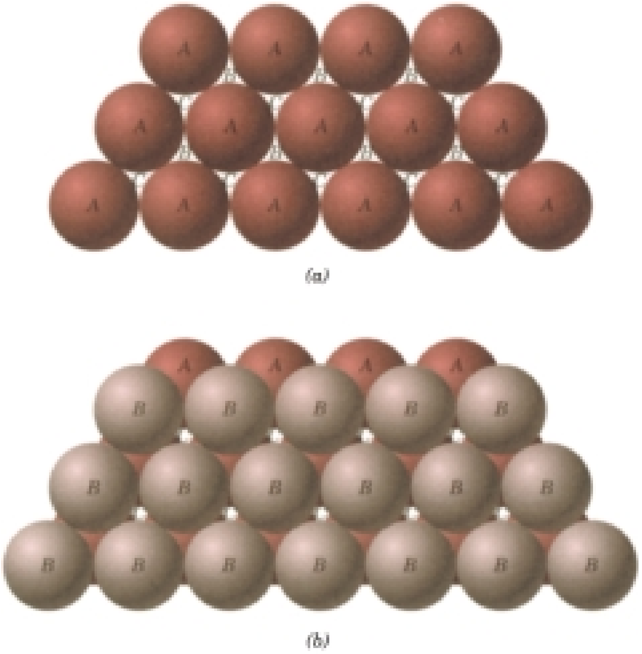

FIGURE 3.27 (*a*) A portion of a close-packed plane of atoms; *A*, *B*, and *C* positions are indicated. (*b*) The *AB* stacking sequence for close-packed atomic planes. (Adapted from W. G. Moffatt, G. W. Pearsall, and J. Wulff, *The Structure and Properties of Materials,* Vol. I, *Structure,* p. 50. Copyright © 1964 by John Wiley & Sons, New York. Reprinted by permission of John Wiley & Sons, Inc.)

the third close-packed layer is positioned. For HCP, the centers of this layer are aligned directly above the original *A* positions. This stacking sequence, *ABABAB* . . . , is repeated over and over. Of course, the *ACACAC* . . . arrangement would be equivalent. These close-packed planes for HCP are (0001)-type planes, and the correspondence between this and the unit cell representation is shown in Figure 3.28.

For the face-centered crystal structure, the centers of the third plane are situated over the *C* sites of the first plane (Figure 3.29*a*). This yields an *ABCABCABC* . . . stacking sequence; that is, the atomic alignment repeats every third plane. It is more difficult to correlate the stacking of close-packed planes to the FCC unit cell. However, this relationship is demonstrated in Figure 3.29*b*; these planes are of the (111) type. The significance of these FCC and HCP close-packed planes will become apparent in Chapter 8.

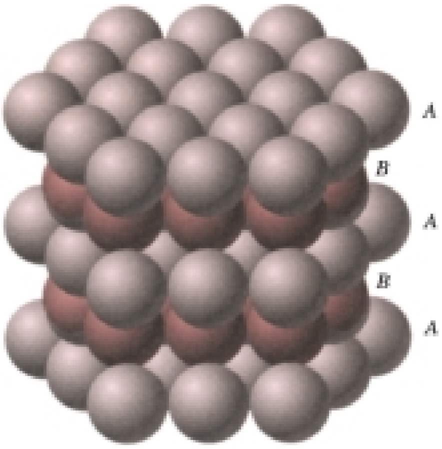

FIGURE 3.28 Close-packed plane stacking sequence for hexagonal close-packed. (Adapted from W. G. Moffatt, G. W. Pearsall, and J. Wulff, *The Structure and Properties of Materials,* Vol. I, *Structure,* p. 51. Copyright © 1964 by John Wiley & Sons, New York. Reprinted by permission of John Wiley & Sons, Inc.)

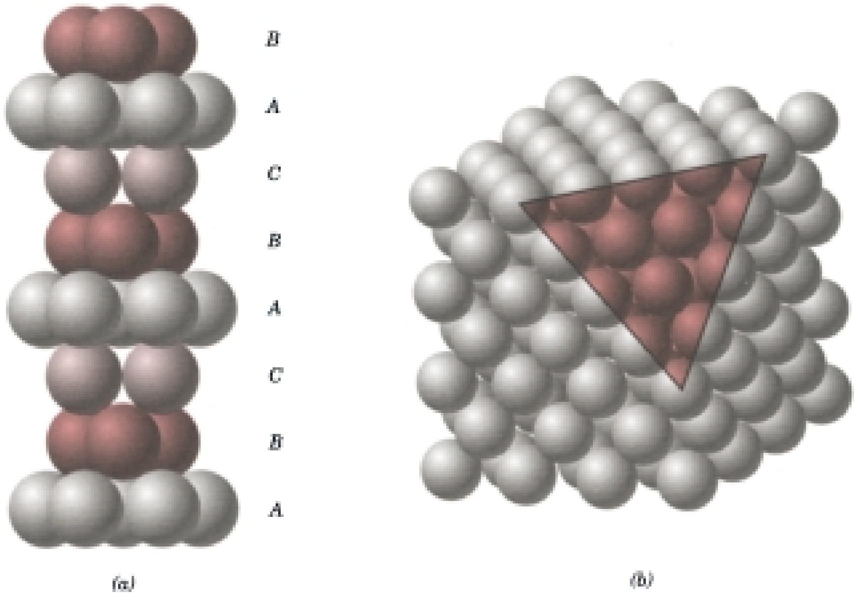

Figure 3.29 (*a*) Close-packed stacking sequence for face-centered cubic. (*b*) A corner has been removed to show the relation between the stacking of close-packed planes of atoms and the FCC crystal structure; the heavy triangle outlines a (111) plane. (Figure (*b*) from W. G. Moffatt, G. W. Pearsall, and J. Wulff, *The Structure and Properties of Materials,* Vol. I, *Structure,* p. 51. Copyright © 1964 by John Wiley & Sons, New York. Reprinted by permission of John Wiley & Sons, Inc.)

CERAMICS

A number of ceramic crystal structures may also be considered in terms of close-packed planes of ions (as opposed to *atoms* for metals), as well as unit cells. Ordinarily, the close-packed planes are composed of the large anions. As these planes are stacked atop each other, small interstitial sites are created between them in which the cations may reside.

These interstitial positions exist in two different types, as illustrated in Figure 3.30. Four atoms (three in one plane, and a single one in the adjacent plane) surround one type, labeled *T* in the figure; this is termed a **tetrahedral position,** since straight lines drawn from the centers of the surrounding spheres form a four-sided tetrahedron. The other site type, denoted as *O* in Figure 3.30, involves six ion spheres, three in each of the two planes. Because an octahedron is produced by joining these six sphere centers, this site is called an **octahedral position.** Thus, the coordination numbers for cations filling tetrahedral and octahedral positions are 4 and 6, respectively. Furthermore, for each of these anion spheres, one octahedral and two tetrahedral positions will exist.

Ceramic crystal structures of this type depend on two factors: (1) the stacking of the close-packed anion layers (both FCC and HCP arrangements are possible, which correspond to *ABCABC* . . . and *ABABAB* . . . sequences, respectively), and (2) the manner in which the interstitial sites are filled with cations. For example, consider the rock salt crystal structure discussed above. The unit cell has cubic symmetry, and each cation (Na^+ ion) has six Cl^- ion nearest neighbors, as may be verified from Figure 3.5. That is, the Na^+ ion at the center has as nearest neighbors

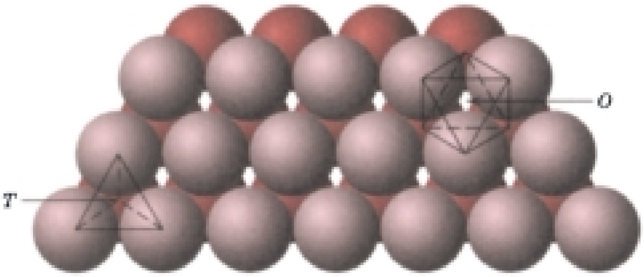

Figure 3.30 The stacking of one plane of close-packed spheres (anions) on top of another; tetrahedral and octahedral positions between the planes are designated by *T* and *O*, respectively. (From W. G. Moffatt, G. W. Pearsall, and J. Wulff, *The Structure and Properties of Materials*, Vol. 1, *Structure*. Copyright © 1964 by John Wiley & Sons, New York. Reprinted by permission of John Wiley & Sons, Inc.)

the six Cl^- ions that reside at the centers of each of the cube faces. The crystal structure, having cubic symmetry, may be considered in terms of an FCC array of close-packed planes of anions, and all planes are of the {111} type. The cations reside in octahedral positions because they have as nearest neighbors six anions. Furthermore, all octahedral positions are filled, since there is a single octahedral site per anion, and the ratio of anions to cations is 1:1. For this crystal structure, the relationship between the unit cell and close-packed anion plane stacking schemes is illustrated in Figure 3.31.

Other, but not all, ceramic crystal structures may be treated in a similar manner; included are the zinc blende and perovskite structures. The *spinel structure* is one of the $A_mB_nX_p$ types, which is found for magnesium aluminate or spinel ($MgAl_2O_4$). With this structure, the O^{2-} ions form an FCC lattice, whereas Mg^{2+} ions fill tetrahedral sites and Al^{3+} reside in octahedral positions. Magnetic ceramics, or ferrites, have a crystal structure that is a slight variant of this spinel structure; and the magnetic characteristics are affected by the occupancy of tetrahedral and octahedral positions {(see Section 18.5).}

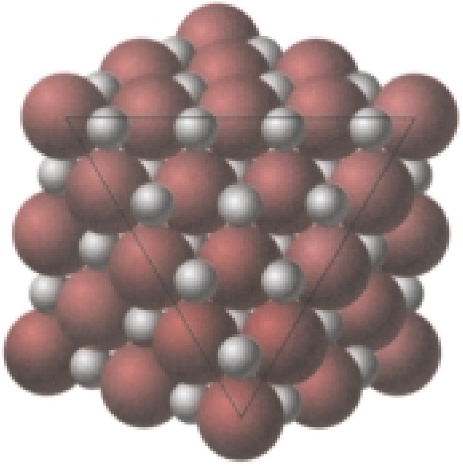

Figure 3.31 A section of the rock salt crystal structure from which a corner has been removed. The exposed plane of anions (light spheres inside the triangle) is a {111}-type plane; the cations (dark spheres) occupy the interstitial octahedral positions.

CRYSTALLINE AND NONCRYSTALLINE MATERIALS

3.16 Single Crystals

For a crystalline solid, when the periodic and repeated arrangement of atoms is perfect or extends throughout the entirety of the specimen without interruption, the result is a **single crystal.** All unit cells interlock in the same way and have the same orientation. Single crystals exist in nature, but they may also be produced artificially. They are ordinarily difficult to grow, because the environment must be carefully controlled.

If the extremities of a single crystal are permitted to grow without any external constraint, the crystal will assume a regular geometric shape having flat faces, as with some of the gem stones; the shape is indicative of the crystal structure. A photograph of several single crystals is shown in Figure 3.32. Within the past few years, single crystals have become extremely important in many of our modern technologies, in particular electronic microcircuits, which employ single crystals of silicon and other semiconductors.

3.17 Polycrystalline Materials

Most crystalline solids are composed of a collection of many small crystals or **grains;** such materials are termed **polycrystalline.** Various stages in the solidification of a polycrystalline specimen are represented schematically in Figure 3.33. Initially, small crystals or nuclei form at various positions. These have random crystallographic orientations, as indicated by the square grids. The small grains grow by the successive addition from the surrounding liquid of atoms to the structure of each. The extremities of adjacent grains impinge on one another as the solidification process approaches completion. As indicated in Figure 3.33, the crystallographic orientation varies from grain to grain. Also, there exists some atomic mismatch within the region where two grains meet; this area, called a **grain boundary,** is discussed in more detail in Section 5.8.

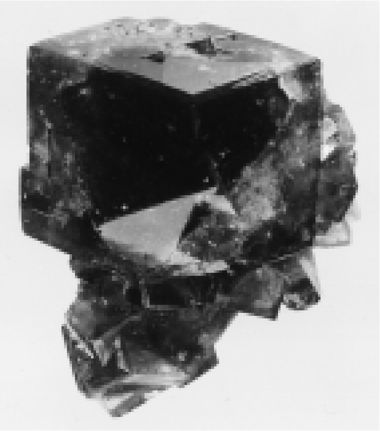

Figure 3.32 Photograph showing several single crystals of fluorite, CaF_2. (Smithsonian Institution photograph number 38181P.)

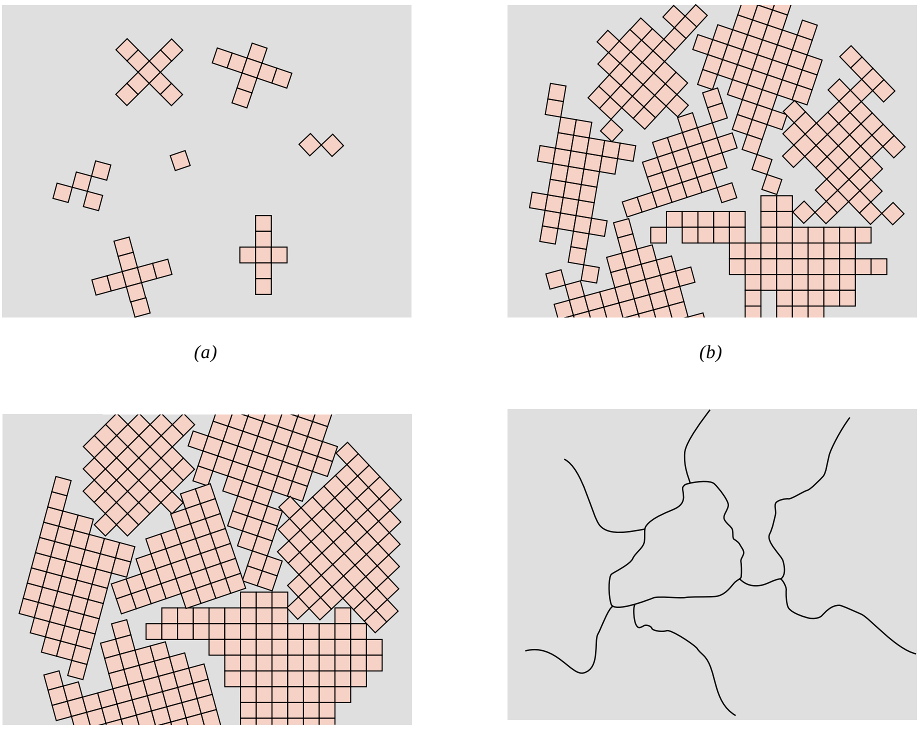

(a)

(b)

(c)

(d)

FIGURE 3.33 Schematic diagrams of the various stages in the solidification of a polycrystalline material; the square grids depict unit cells. (*a*) Small crystallite nuclei. (*b*) Growth of the crystallites; the obstruction of some grains that are adjacent to one another is also shown. (*c*) Upon completion of solidification, grains having irregular shapes have formed. (*d*) The grain structure as it would appear under the microscope; dark lines are the grain boundaries. (Adapted from W. Rosenhain, *An Introduction to the Study of Physical Metallurgy*, 2nd edition, Constable & Company Ltd., London, 1915.)

3.18 ANISOTROPY

The physical properties of single crystals of some substances depend on the crystallographic direction in which measurements are taken. For example, the elastic modulus, the electrical conductivity, and the index of refraction may have different values in the [100] and [111] directions. This directionality of properties is termed **anisotropy,** and it is associated with the variance of atomic or ionic spacing with crystallographic direction. Substances in which measured properties are independent of the direction of measurement are **isotropic.** The extent and magnitude of anisotropic effects in crystalline materials are functions of the symmetry of the crystal structure; the degree of anisotropy increases with decreasing structural symmetry—triclinic structures normally are highly anisotropic. The modulus of elasticity values at [100], [110], and [111] orientations for several materials are presented in Table 3.7.

For many polycrystalline materials, the crystallographic orientations of the individual grains are totally random. Under these circumstances, even though each

Table 3.7 **Modulus of Elasticity Values for Several Metals at Various Crystallographic Orientations**

	Modulus of Elasticity (GPa)		
Metal	**[*100*]**	**[*110*]**	**[*111*]**
Aluminum	63.7	72.6	76.1
Copper	66.7	130.3	191.1
Iron	125.0	210.5	272.7
Tungsten	384.6	384.6	384.6

Source: R. W. Hertzberg, *Deformation and Fracture Mechanics of Engineering Materials,* 3rd edition. Copyright © 1989 by John Wiley & Sons, New York. Reprinted by permission of John Wiley & Sons, Inc.

grain may be anisotropic, a specimen composed of the grain aggregate behaves isotropically. Also, the magnitude of a measured property represents some average of the directional values. Sometimes the grains in polycrystalline materials have a preferential crystallographic orientation, in which case the material is said to have a ''texture.''

3.19 X-RAY DIFFRACTION: DETERMINATION OF CRYSTAL STRUCTURES (CD-ROM)

3.20 NONCRYSTALLINE SOLIDS

It has been mentioned that **noncrystalline** solids lack a systematic and regular arrangement of atoms over relatively large atomic distances. Sometimes such materials are also called **amorphous** (meaning literally without form), or supercooled liquids, inasmuch as their atomic structure resembles that of a liquid.

An amorphous condition may be illustrated by comparison of the crystalline and noncrystalline structures of the ceramic compound silicon dioxide (SiO_2), which may exist in both states. Figures 3.38*a* and 3.38*b* present two-dimensional schematic diagrams for both structures of SiO_2, in which the SiO_4^{4-} tetrahedron is the basic unit (Figure 3.10). Even though each silicon ion bonds to four oxygen ions for both states, beyond this, the structure is much more disordered and irregular for the noncrystalline structure.

Whether a crystalline or amorphous solid forms depends on the ease with which a random atomic structure in the liquid can transform to an ordered state during solidification. Amorphous materials, therefore, are characterized by atomic or molecular structures that are relatively complex and become ordered only with some difficulty. Furthermore, rapidly cooling through the freezing temperature favors the formation of a noncrystalline solid, since little time is allowed for the ordering process.

Metals normally form crystalline solids; but some ceramic materials are crystalline, whereas others (i.e., the silica glasses) are amorphous. Polymers may be completely noncrystalline and semicrystalline consisting of varying degrees of crystallin-

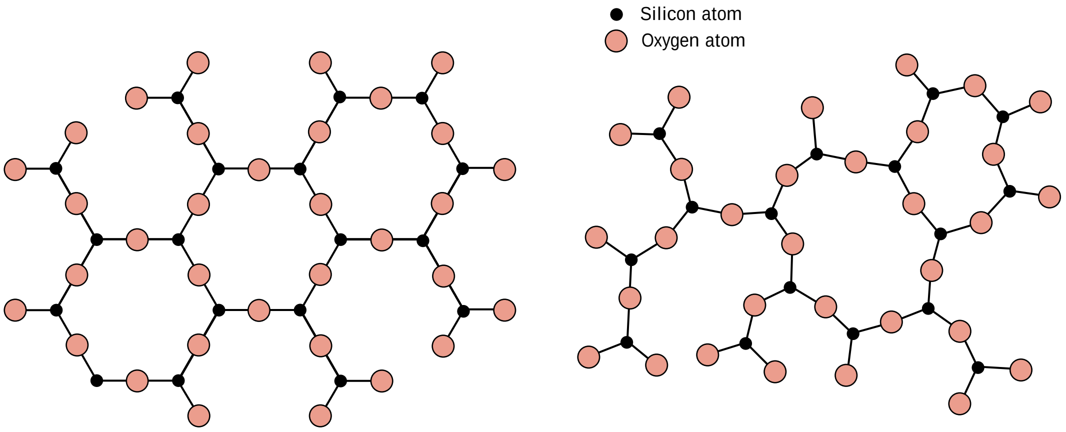

(*a*) (*b*)

Figure 3.38 Two-dimensional schemes of the structure of (*a*) crystalline silicon dioxide and (*b*) noncrystalline silicon dioxide.

ity. More about the structure and properties of these amorphous materials is discussed below and in subsequent chapters.

SILICA GLASSES

Silicon dioxide (or silica, SiO_2) in the noncrystalline state is called *fused silica,* or *vitreous silica;* again, a schematic representation of its structure is shown in Figure 3.38*b*. Other oxides (e.g., B_2O_3 and GeO_2) may also form glassy structures (and polyhedral oxide structures {similar to those shown in Figure 3.12}); these materials, as well as SiO_2, are *network formers.*

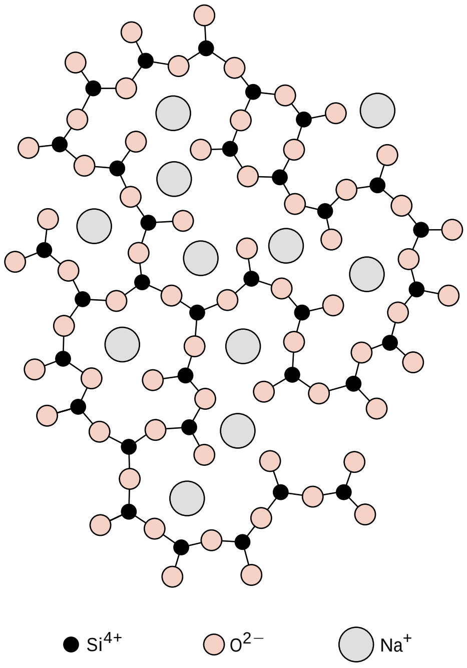

Figure 3.39 Schematic representation of ion positions in a sodium–silicate glass.

The common inorganic glasses that are used for containers, windows, and so on are silica glasses to which have been added other oxides such as CaO and Na_2O. These oxides do not form polyhedral networks. Rather, their cations are incorporated within and modify the SiO_4^{4-} network; for this reason, these oxide additives are termed *network modifiers.* For example, Figure 3.39 is a schematic representation of the structure of a sodium–silicate glass. Still other oxides, such as TiO_2 and Al_2O_3, while not network formers, substitute for silicon and become part of and stabilize the network; these are called *intermediates.* From a practical perspective, the addition of these modifiers and intermediates lowers the melting point and viscosity of a glass, and makes it easier to form at lower temperatures {(Section 14.7).}

SUMMARY

Atoms in crystalline solids are positioned in an orderly and repeated pattern that is in contrast to the random and disordered atomic distribution found in noncrystalline or amorphous materials. Atoms may be represented as solid spheres, and, for crystalline solids, crystal structure is just the spatial arrangement of these spheres. The various crystal structures are specified in terms of parallelepiped unit cells, which are characterized by geometry and atom positions within.

Most common metals exist in at least one of three relatively simple crystal structures: face-centered cubic (FCC), body-centered cubic (BCC), and hexagonal close-packed (HCP). Two features of a crystal structure are coordination number (or number of nearest-neighbor atoms) and atomic packing factor (the fraction of solid sphere volume in the unit cell). Coordination number and atomic packing factor are the same for both FCC and HCP crystal structures.

For ceramics both crystalline and noncrystalline states are possible. The crystal structures of those materials for which the atomic bonding is predominantly ionic are determined by the charge magnitude and the radius of each kind of ion. Some of the simpler crystal structures are described in terms of unit cells; several of these were discussed (rock salt, cesium chloride, zinc blende, diamond cubic, graphite, fluorite, perovskite, and spinel structures).

Theoretical densities of metallic and crystalline ceramic materials may be computed from unit cell and atomic weight data.

Generation of face-centered cubic and hexagonal close-packed crystal structures is possible by the stacking of close-packed planes of atoms. For some ceramic crystal structures, cations fit into interstitial positions that exist between two adjacent close-packed planes of anions.

For the silicates, structure is more conveniently represented by means of interconnecting SiO_4^{4-} tetrahedra. Relatively complex structures may result when other cations (e.g., Ca^{2+}, Mg^{2+}, Al^{3+}) and anions (e.g., OH^-) are added. The structures of silica (SiO_2), silica glass, {and several of the simple and layered silicates} were presented.

Structures for the various forms of carbon—diamond, graphite, {and the fullerenes}—were also discussed.

Crystallographic planes and directions are specified in terms of an indexing scheme. The basis for the determination of each index is a coordinate axis system defined by the unit cell for the particular crystal structure. Directional indices are computed in terms of vector projections on each of the coordinate axes, whereas planar indices are determined from the reciprocals of axial intercepts. For hexagonal unit cells, a four-index scheme for both directions and planes is found to be more convenient.

{Crystallographic directional and planar equivalencies are related to atomic linear and planar densities, respectively.} The atomic packing (i.e., planar density) of spheres in a crystallographic plane depends on the indices of the plane as well as the crystal structure. For a given crystal structure, planes having identical atomic packing yet different Miller indices belong to the same family.

Single crystals are materials in which the atomic order extends uninterrupted over the entirety of the specimen; under some circumstances, they may have flat faces and regular geometric shapes. The vast majority of crystalline solids, however, are polycrystalline, being composed of many small crystals or grains having different crystallographic orientations.

Other concepts introduced in this chapter were: crystal system (a classification scheme for crystal structures on the basis of unit cell geometry); polymorphism (or allotropy) (when a specific material can have more than one crystal structure); and anisotropy (the directionality dependence of properties).

{X-ray diffractometry is used for crystal structure and interplanar spacing determinations. A beam of x-rays directed on a crystalline material may experience diffraction (constructive interference) as a result of its interaction with a series of parallel atomic planes according to Bragg's law. Interplanar spacing is a function of the Miller indices and lattice parameter(s) as well as the crystal structure.}

IMPORTANT TERMS AND CONCEPTS

Allotropy
Amorphous
Anion
Anisotropy
Atomic packing factor (APF)
Body-centered cubic (BCC)
Bragg's law
Cation
Coordination number
Crystal structure
Crystal system
Crystalline
Diffraction
Face-centered cubic (FCC)
Grain
Grain boundary
Hexagonal close-packed (HCP)
Isotropic
Lattice
Lattice parameters
Miller indices
Noncrystalline
Octahedral position
Polycrystalline
Polymorphism
Single crystal
Tetrahedral position
Unit cell

REFERENCES

Azaroff, L. F., *Elements of X-Ray Crystallography*, McGraw-Hill Book Company, New York, 1968. Reprinted by TechBooks, Marietta, OH, 1990.

Barrett, C. S. and T. B. Massalski, *Structure of Metals*, 3rd edition, Pergamon Press, Oxford, 1980.

Barsoum, M. W., *Fundamentals of Ceramics*, The McGraw-Hill Companies, Inc., New York, 1997.

Budworth, D. W., *An Introduction to Ceramic Science*, Pergamon Press, Oxford, 1970.

Buerger, M. J., *Elementary Crystallography*, John Wiley & Sons, New York, 1956.

Charles, R. J., ''The Nature of Glasses,'' *Scientific American*, Vol. 217, No. 3, September 1967, pp. 126–136.

Chiang, Y. M., D. P. Birnie, III, and W. D. Kingery, *Physical Ceramics: Principles for Ceramic Science and Engineering*, John Wiley & Sons, Inc., New York, 1997.

Cullity, B. D., *Elements of X-Ray Diffraction*, 3rd edition, Addison-Wesley Publishing Co., Reading, MA, 1998.

Curl, R. F. and R. E. Smalley, ''Fullerenes,'' *Scientific American*, Vol. 265, No. 4, October 1991, pp. 54–63.

Gilman, J. J., ''The Nature of Ceramics,'' *Scientific American*, Vol. 217, No. 3, September 1967, pp. 112–124.

Hauth, W. E., ''Crystal Chemistry in Ceramics,'' *American Ceramic Society Bulletin*, Vol. 30, 1951: No. 1, pp. 5–7; No. 2, pp. 47–49; No. 3, pp. 76–77; No. 4, pp. 137–142; No. 5, pp. 165–167; No. 6, pp. 203–205. A good overview of silicate structures.

Kingery, W. D., H. K. Bowen, and D. R. Uhlmann, *Introduction to Ceramics*, 2nd edition, John Wiley & Sons, New York, 1976. Chapters 1–4.

Richerson, D. W., *Modern Ceramic Engineering*, 2nd edition, Marcel Dekker, New York, 1992.

Schwartz, L. H. and J. B. Cohen, *Diffraction from Materials*, 2nd edition, Springer-Verlag, New York, 1987.

Van Vlack, L. H., *Physical Ceramics for Engineers*, Addison-Wesley Publishing Company, Reading, MA, 1964. Chapters 1–4 and 6–8.

Wyckoff, R. W. G., *Crystal Structures*, 2nd edition, Interscience Publishers, 1963. Reprinted by Krieger Publishing Company, Melbourne, FL, 1986.

QUESTIONS AND PROBLEMS

Note: To solve those problems having an asterisk (*) by their numbers, consultation of supplementary topics [appearing only on the CD-ROM (and not in print)] will probably be necessary.

3.1 What is the difference between atomic structure and crystal structure?

3.2 What is the difference between a crystal structure and a crystal system?

3.3 If the atomic radius of aluminum is 0.143 nm, calculate the volume of its unit cell in cubic meters.

3.4 Show for the body-centered cubic crystal structure that the unit cell edge length a and the atomic radius R are related through $a = 4R/\sqrt{3}$.

3.5 For the HCP crystal structure, show that the ideal c/a ratio is 1.633.

3.6 Show that the atomic packing factor for BCC is 0.68.

3.7 Show that the atomic packing factor for HCP is 0.74.

3.8 Iron has a BCC crystal structure, an atomic radius of 0.124 nm, and an atomic weight of 55.85 g/mol. Compute and compare its density with the experimental value found inside the front cover.

3.9 Calculate the radius of an iridium atom given that Ir has an FCC crystal structure, a density of 22.4 g/cm^3, and an atomic weight of 192.2 g/mol.

3.10 Calculate the radius of a vanadium atom, given that V has a BCC crystal structure, a density of 5.96 g/cm^3, and an atomic weight of 50.9 g/mol.

3.11 Some hypothetical metal has the simple cubic crystal structure shown in Figure 3.40. If its atomic weight is 70.4 g/mol and the atomic radius is 0.126 nm, compute its density.

3.12 Zirconium has an HCP crystal structure and a density of 6.51 g/cm^3.

(a) What is the volume of its unit cell in cubic meters?

(b) If the c/a ratio is 1.593, compute the values of c and a.

3.13 Using atomic weight, crystal structure, and atomic radius data tabulated inside the front cover, compute the theoretical densities of lead, chromium, copper, and cobalt, and then

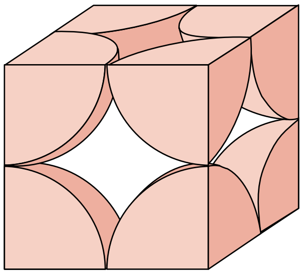

FIGURE 3.40 Hard-sphere unit cell representation of the simple cubic crystal structure.

compare these values with the measured densities listed in this same table. The c/a ratio for cobalt is 1.623.

3.14 Rhodium has an atomic radius of 0.1345 nm (1.345 Å) and a density of 12.41 g/cm^3. Determine whether it has an FCC or BCC crystal structure.

3.15 Below are listed the atomic weight, density, and atomic radius for three hypothetical alloys. For each determine whether its crystal structure is FCC, BCC, or simple cubic and then justify your determination. A simple cubic unit cell is shown in Figure 3.40.

Alloy	***Atomic Weight (g/mol)***	***Density*** (g/cm^3)	***Atomic Radius (nm)***
A	77.4	8.22	0.125
B	107.6	13.42	0.133
C	127.3	9.23	0.142

3.16 The unit cell for tin has tetragonal symmetry, with a and b lattice parameters of 0.583 and 0.318 nm, respectively. If its density, atomic weight, and atomic radius are 7.30 g/cm^3, 118.69 g/mol, and 0.151 nm, respectively, compute the atomic packing factor.

3.17 Iodine has an orthorhombic unit cell for which the a, b, and c lattice parameters are 0.479, 0.725, and 0.978 nm, respectively.

(a) If the atomic packing factor and atomic radius are 0.547 and 0.177 nm, respectively, determine the number of atoms in each unit cell.

(b) The atomic weight of iodine is 126.91 g/mol; compute its density.

3.18 Titanium has an HCP unit cell for which the ratio of the lattice parameters c/a is 1.58. If the radius of the Ti atom is 0.1445 nm, **(a)** determine the unit cell volume, and **(b)** calculate the density of Ti and compare it with the literature value.

3.19 Zinc has an HCP crystal structure, a c/a ratio of 1.856, and a density of 7.13 g/cm^3. Calculate the atomic radius for Zn.

3.20 Rhenium has an HCP crystal structure, an atomic radius of 0.137 nm, and a c/a ratio of 1.615. Compute the volume of the unit cell for Re.

3.21 This is a unit cell for a hypothetical metal:

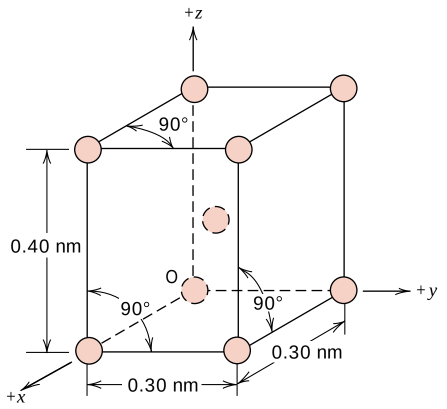

(a) To which crystal system does this unit cell belong?

(b) What would this crystal structure be called?

(c) Calculate the density of the material, given that its atomic weight is 141 g/mol.

3.22 Using the Molecule Definition File (MDF) on the CD-ROM that accompanies this book, generate a three-dimensional unit cell for the intermetallic compound $AuCu_3$ given the following: 1) the unit cell is cubic with an edge length of 0.374 nm, 2) gold atoms are situated at all cube corners, and 3) copper atoms are positioned at the centers of all unit cell faces.

3.23 Using the Molecule Definition File (MDF) on the CD-ROM that accompanies this book, generate a three-dimensional unit cell for the intermetallic compound AuCu given the following: 1) the unit cell is tetragonal with $a = 0.289$ nm and $c = 0.367$ nm (see Table 3.6), 2) gold atoms are situated at all unit cell corners, and 3) a copper atom is positioned at the center of the unit cell.

3.24 Sketch a unit cell for the body-centered orthorhombic crystal structure.

3.25 For a ceramic compound, what are the two characteristics of the component ions that determine the crystal structure?

3.26 Show that the minimum cation-to-anion radius ratio for a coordination number of 4 is 0.225.

3.27 Show that the minimum cation-to-anion radius ratio for a coordination number of 6 is 0.414. *Hint:* Use the NaCl crystal structure (Figure 3.5), and assume that anions and cations are just touching along cube edges and across face diagonals.

3.28 Demonstrate that the minimum cation-to-anion radius ratio for a coordination number of 8 is 0.732.

3.29 On the basis of ionic charge and ionic radii, predict the crystal structures for the following materials: **(a)** CsI, **(b)** NiO, **(c)** KI, and **(d)** NiS. Justify your selections.

3.30 Which of the cations in Table 3.4 would you predict to form iodides having the cesium chloride crystal structure? Justify your choices.

3.31 Compute the atomic packing factor for the cesium chloride crystal structure in which $r_C/r_A = 0.732$.

3.32 Table 3.4 gives the ionic radii for K^+ and O^{2-} as 0.138 and 0.140 nm, respectively. What would be the coordination number for each O^{2-} ion? Briefly describe the resulting crystal structure for K_2O. Explain why this is called the antifluorite structure.

3.33 Using the Molecule Definition File (MDF) on the CD-ROM that accompanies this book, generate a three-dimensional unit cell for lead oxide, PbO, given the following: (1) the unit cell is tetragonal with $a = 0.397$ nm and $c = 0.502$ nm, (2) oxygen ions are situated at all cube corners, and, in addition, at the centers of the two square faces, (3) one oxygen ion is positioned on each of two of the other opposing faces (rectangular) at the $0.5a$-$0.237c$ coordinate, and (4) for the other two rectangular and opposing faces, oxygen ions are located at the $0.5a$-$0.763c$ coordinate.

3.34 Calculate the density of FeO, given that it has the rock salt crystal structure.

3.35 Magnesium oxide has the rock salt crystal structure and a density of 3.58 g/cm^3.

(a) Determine the unit cell edge length.

(b) How does this result compare with the edge length as determined from the radii in Table 3.4, assuming that the Mg^{2+} and O^{2-} ions just touch each other along the edges?

3.36 Compute the theoretical density of diamond given that the C—C distance and bond angle are 0.154 nm and 109.5°, respectively. How does this value compare with the measured density?

3.37 Compute the theoretical density of ZnS given that the Zn—S distance and bond angle are 0.234 nm and 109.5°, respectively. How does this value compare with the measured density?

3.38 Cadmium sulfide (CdS) has a cubic unit cell, and from x-ray diffraction data it is known that the cell edge length is 0.582 nm. If the measured density is 4.82 g/cm^3, how many Cd^{2+} and S^{2-} ions are there per unit cell?

3.39 **(a)** Using the ionic radii in Table 3.4, compute the density of CsCl. *Hint:* Use a modification of the result of Problem 3.4.

(b) The measured density is 3.99 g/cm^3. How do you explain the slight discrepancy between your calculated value and the measured one?

3.40 From the data in Table 3.4, compute the density of CaF_2, which has the fluorite structure.

3.41 A hypothetical AX type of ceramic material is known to have a density of 2.65 g/cm^3 and a unit cell of cubic symmetry with a cell edge length of 0.43 nm. The atomic weights of the A and X elements are 86.6 and 40.3 g/mol, respectively. On the basis of this information, which of the following crystal structures is (are) possible for this material: rock salt, cesium chloride, or zinc blende? Justify your choice(s).

3.42 The unit cell for $MgFe_2O_4$ (MgO-Fe_2O_3) has cubic symmetry with a unit cell edge length of 0.836 nm. If the density of this material is 4.52 g/cm^3, compute its atomic packing factor. For this computation, you will need to use ionic radii listed in Table 3.4.

3.43 The unit cell for Al_2O_3 has hexagonal symmetry with lattice parameters $a = 0.4759$ nm and $c = 1.2989$ nm. If the density of this material is 3.99 g/cm^3, calculate its atomic packing factor. For this computation use ionic radii listed in Table 3.4.

3.44 Compute the atomic packing factor for the diamond cubic crystal structure (Figure 3.16).

Assume that bonding atoms touch one another, that the angle between adjacent bonds is 109.5°, and that each atom internal to the unit cell is positioned $a/4$ of the distance away from the two nearest cell faces (a is the unit cell edge length).

3.45 Compute the atomic packing factor for cesium chloride using the ionic radii in Table 3.4 and assuming that the ions touch along the cube diagonals.

3.46 In terms of bonding, explain why silicate materials have relatively low densities.

3.47 Determine the angle between covalent bonds in an SiO_4^{4-} tetrahedron.

3.48 Draw an orthorhombic unit cell, and within that cell a $[12\bar{1}]$ direction and a (210) plane.

3.49 Sketch a monoclinic unit cell, and within that cell a $[0\bar{1}1]$ direction and a (002) plane.

3.50 Here are unit cells for two hypothetical metals:

(a) What are the indices for the directions indicated by the two vectors in sketch (*a*)?

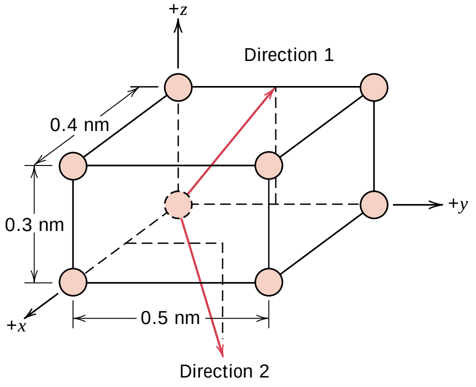

(a)

(b) What are the indices for the two planes drawn in sketch (*b*)?

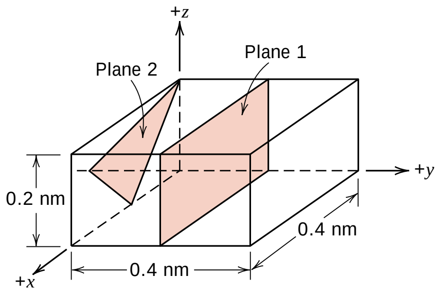

(b)

3.51 Within a cubic unit cell, sketch the following directions:

(a) $[\bar{1}10]$; **(e)** $[\bar{1}\bar{1}1]$;
(b) $[\bar{1}\bar{2}1]$; **(f)** $[\bar{1}22]$;
(c) $[0\bar{1}2]$; **(g)** $[1\bar{2}\bar{3}]$;
(d) $[1\bar{3}3]$; **(h)** $[\bar{1}03]$.

3.52 Determine the indices for the directions shown in the following cubic unit cell:

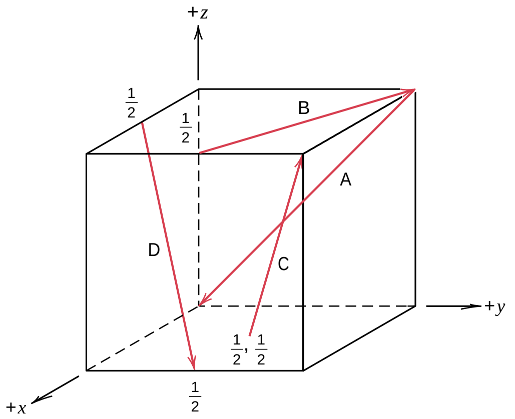

3.53 Determine the indices for the directions shown in the following cubic unit cell:

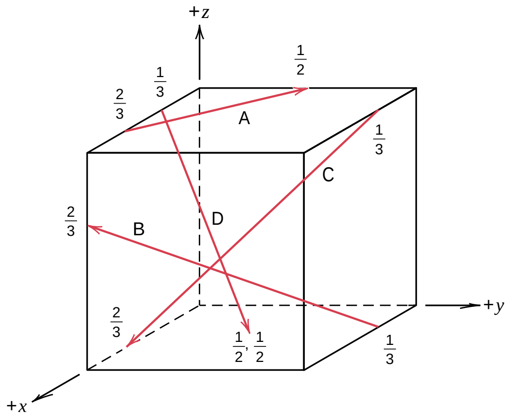

3.54 For tetragonal crystals, cite the indices of directions that are equivalent to each of the following directions:

(a) [101];
(b) [110];
(c) [010].

3.55 **(a)** Convert the [100] and [111] directions into the four-index Miller–Bravais scheme for hexagonal unit cells.

(b) Make the same conversion for the (010) and (101) planes.

3.56 Determine the Miller indices for the planes shown in the following unit cell:

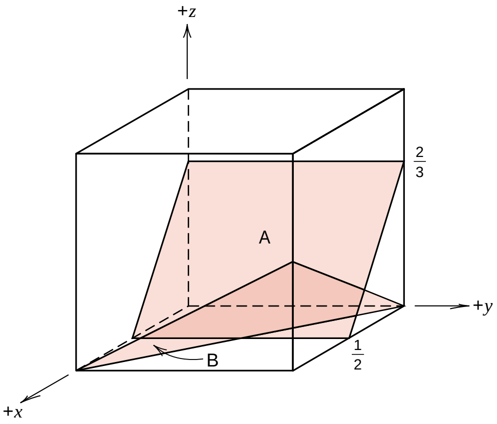
+z
$\frac{2}{3}$
A
+y
B
$\frac{1}{2}$
+x

3.57 Determine the Miller indices for the planes shown in the following unit cell:

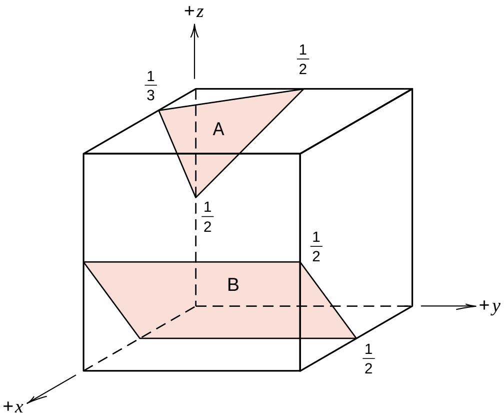
+z
$\frac{1}{3}$
$\frac{1}{2}$
A
$\frac{1}{2}$
$\frac{1}{2}$
B
+y
$\frac{1}{2}$
+x

3.58 Determine the Miller indices for the planes shown in the following unit cell:

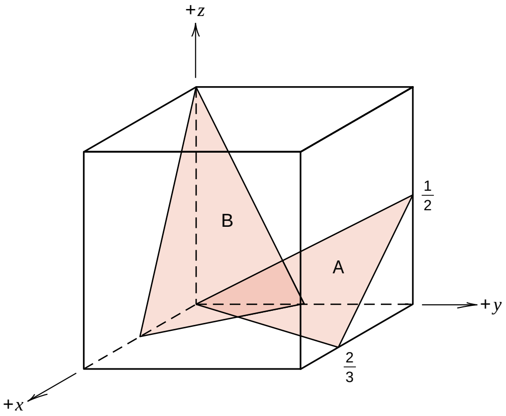
+z
$\frac{1}{2}$
B
A
+y
$\frac{2}{3}$
+x

3.59 Sketch the $(1\bar{1}01)$ and $(11\bar{2}0)$ planes in a hexagonal unit cell.

3.60 Determine the indices for the planes shown in the hexagonal unit cells shown below.

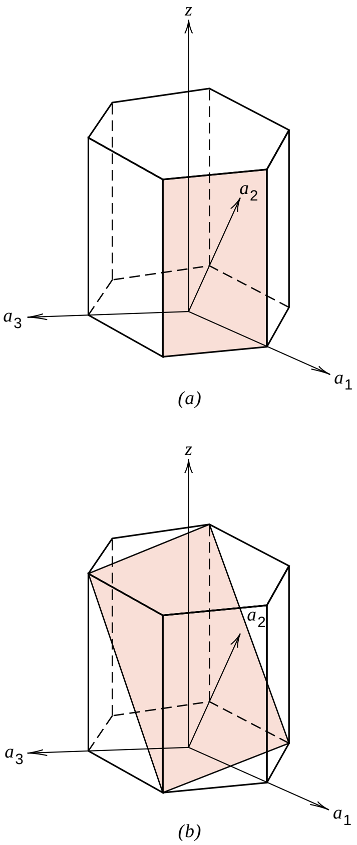
z
a_2
a_3
a_1
z
a_2
a_3
a_1

(a)

(b)

3.61 Sketch within a cubic unit cell the following planes:

(a) $(0\bar{1}\bar{1})$; **(e)** $(\bar{1}1\bar{1})$;
(b) $(11\bar{2})$; **(f)** $(1\bar{2}\bar{2})$;
(c) $(10\bar{2})$; **(g)** $(\bar{1}2\bar{3})$;
(d) $(1\bar{3}1)$; **(h)** $(0\bar{1}\bar{3})$.

3.62 Sketch the atomic packing of **(a)** the (100) plane for the FCC crystal structure, and **(b)** the (111) plane for the BCC crystal structure (similar to Figures 3.24*b* and 3.25*b*).

3.63 For each of the following crystal structures, represent the indicated plane in the manner of Figures 3.24 and 3.25, showing both anions and cations: **(a)** (100) plane for the rock salt crystal structure, **(b)** (110) plane for the cesium chloride crystal structure, **(c)** (111) plane for the zinc blende crystal structure, and **(d)** (110) plane for the perovskite crystal structure.

3.64 Consider the reduced-sphere unit cell shown in Problem 3.21, having an origin of the coordinate system positioned at the atom labeled with an O. For the following sets of planes, determine which are equivalent:

(a) (100), $(0\bar{1}0)$, and (001).

(b) (110), (101), (011), and $(\bar{1}10)$.

(c) (111), $(1\bar{1}1)$, $(11\bar{1})$, and $(\bar{1}1\bar{1})$.

3.65 Cite the indices of the direction that results from the intersection of each of the following pair of planes within a cubic crystal: **(a)** (110) and (111) planes; **(b)** (110) and $(1\bar{1}0)$ planes; and **(c)** $(10\bar{1})$ and (001) planes.

3.66 The zinc blende crystal structure is one that may be generated from close-packed planes of anions.

(a) Will the stacking sequence for this structure be FCC or HCP? Why?

(b) Will cations fill tetrahedral or octahedral positions? Why?

(c) What fraction of the positions will be occupied?

3.67 The corundum crystal structure, found for Al_2O_3, consists of an HCP arrangement of O^{2-} ions; the Al^{3+} ions occupy octahedral positions.

(a) What fraction of the available octahedral positions are filled with Al^{3+} ions?

(b) Sketch two close-packed O^{2-} planes stacked in an *AB* sequence, and note octahedral positions that will be filled with the Al^{3+} ions.

3.68 Iron sulfide (FeS) may form a crystal structure that consists of an HCP arrangement of S^{2-} ions.

(a) Which type of interstitial site will the Fe^{2+} ions occupy?

(b) What fraction of these available interstitial sites will be occupied by Fe^{2+} ions?

3.69 Magnesium silicate, Mg_2SiO_4, forms in the olivine crystal structure which consists of an HCP arrangement of O^{2-} ions.

(a) Which type of interstitial site will the Mg^{2+} ions occupy? Why?

(b) Which type of interstitial site will the Si^{4+} ions occupy? Why?

(c) What fraction of the total tetrahedral sites will be occupied?

(d) What fraction of the total octahedral sites will be occupied?

3.70* Compute and compare the linear densities of the [100], [110], and [111] directions for FCC.

3.71* Compute and compare the linear densities of the [110] and [111] directions for BCC.

3.72* Calculate and compare the planar densities of the (100) and (111) planes for FCC.

3.73* Calculate and compare the planar densities of the (100) and (110) planes for BCC.

3.74* Calculate the planar density of the (0001) plane for HCP.

3.75 Here are shown the atomic packing schemes for several different crystallographic directions for some hypothetical metal. For each direction the circles represent only those atoms contained within a unit cell, which circles are reduced from their actual size.

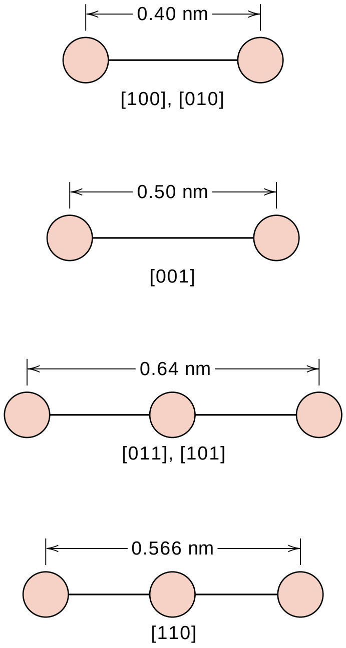

(a) To what crystal system does the unit cell belong?

(b) What would this crystal structure be called?

3.76 Below are shown three different crystallographic planes for a unit cell of some hypothetical metal; the circles represent atoms:

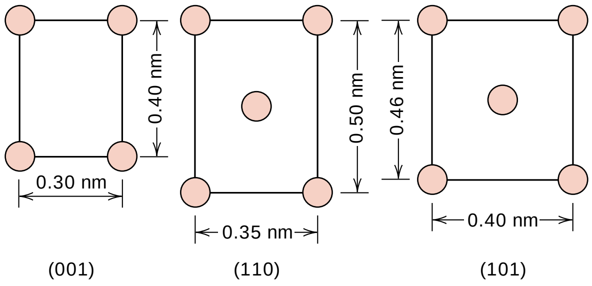

(a) To what crystal system does the unit cell belong?

(b) What would this crystal structure be called?

(c) If the density of this metal is 8.95 g/cm^3, determine its atomic weight.

3.77 Explain why the properties of polycrystalline materials are most often isotropic.

3.78* Using the data for molybdenum in Table 3.1, compute the interplanar spacing for the (111) set of planes.

3.79* Determine the expected diffraction angle for the first-order reflection from the (113) set of planes for FCC platinum when monochromatic radiation of wavelength 0.1542 nm is used.

3.80* Using the data for aluminum in Table 3.1, compute the interplanar spacings for the (110) and (221) sets of planes.

3.81* The metal iridium has an FCC crystal structure. If the angle of diffraction for the (220) set of planes occurs at 69.22° (first-order reflection) when monochromatic x-radiation having a wavelength of 0.1542 nm is used, compute **(a)** the interplanar spacing for this set of planes, and **(b)** the atomic radius for an iridium atom.

3.82* The metal rubidium has a BCC crystal structure. If the angle of diffraction for the (321) set of planes occurs at 27.00° (first-order reflection) when monochromatic x-radiation having a wavelength of 0.0711 nm is used, compute **(a)** the interplanar spacing for this set of planes, and **(b)** the atomic radius for the rubidium atom.

3.83* For which set of crystallographic planes will a first-order diffraction peak occur at a diffraction angle of 46.21° for BCC iron when monochromatic radiation having a wavelength of 0.0711 nm is used?

3.84* Figure 3.37 shows an x-ray diffraction pattern for α-iron taken using a diffractometer and monochromatic x-radiation having a wavelength of 0.1542 nm; each diffraction peak on the pattern has been indexed. Compute the interplanar spacing for each set of planes indexed; also determine the lattice parameter of Fe for each of the peaks.

3.85* The diffraction peaks shown in Figure 3.37 are indexed according to the reflection rules for BCC (i.e., the sum $h + k + l$ must be even). Cite the h, k, and l indices for the first four diffraction peaks for FCC crystals consistent with h, k, and l all being either odd or even.

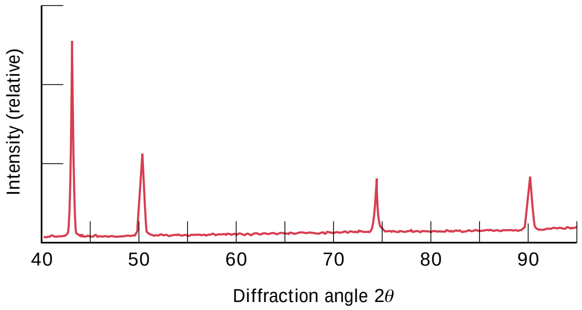

FIGURE 3.41 Diffraction pattern for polycrystalline copper.

3.86* Figure 3.41 shows the first four peaks of the x-ray diffraction pattern for copper, which has an FCC crystal structure; monochromatic x-radiation having a wavelength of 0.1542 nm was used.

(a) Index (i.e., give h, k, and l indices for) each of these peaks.

(b) Determine the interplanar spacing for each of the peaks.

(c) For each peak, determine the atomic radius for Cu and compare these with the value presented in Table 3.1.

3.87 Would you expect a material in which the atomic bonding is predominantly ionic in nature to be more or less likely to form a noncrystalline solid upon solidification than a covalent material? Why? (See Section 2.6.)

Design Problem

3.D1* Gallium arsenide (GaAs) and gallium phosphide (GaP) both have the zinc blende crystal structure and are soluble in one another at all concentrations. Determine the concentration in weight percent of GaP that must be added to GaAs to yield a unit cell edge length of 0.5570 nm. The densities of GaAs and GaP are 5.307 and 4.130 g/cm^3, respectively.

Chapter 18 / Magnetic Properties

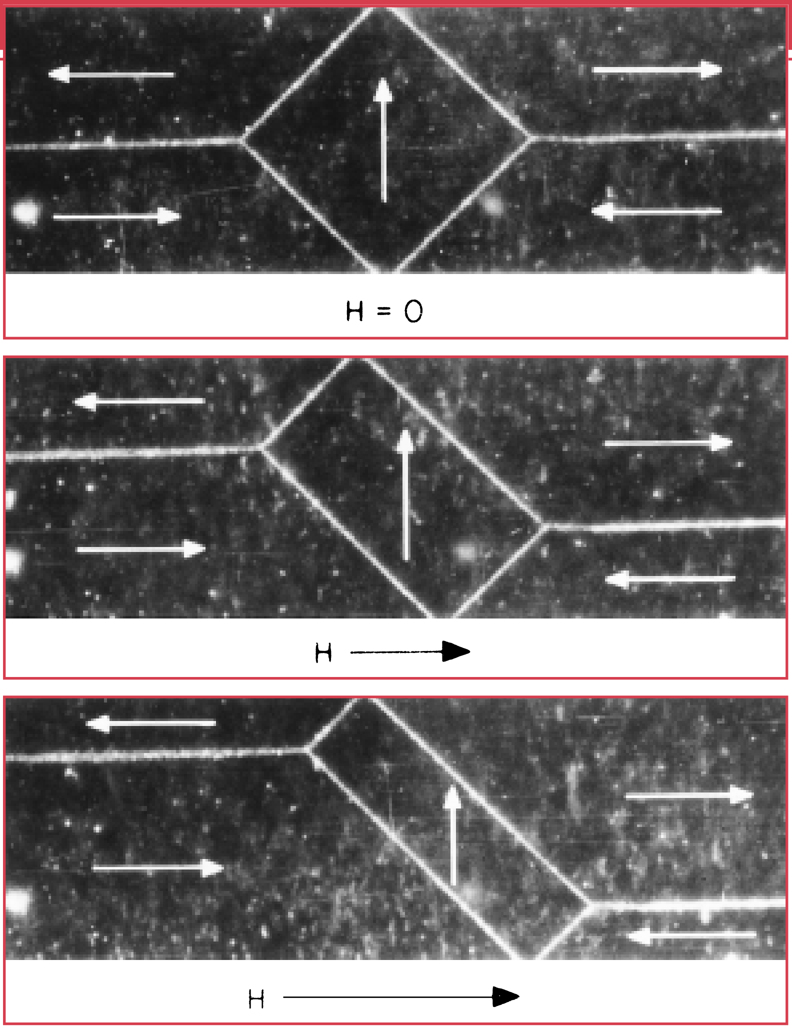

Photomicrographs of an iron single crystal, showing magnetic domains and their change in shape as a magnetic field (*H*) is applied. The magnetization direction of each domain is indicated by an arrow. Those domains that are favorably oriented with the applied field grow at the expense of the unfavorably oriented domains. (Photomicrographs courtesy of General Electric Research Laboratory.)

Why Study the *Magnetic Properties* of Materials?

An understanding of the mechanism that explains the permanent magnetic behavior of some materials may allow us to alter and in some cases tailor the magnetic properties. For example, in Design Example 18.1 we note how the behavior of a ceramic magnetic material may be enhanced by changing its composition.

Learning Objectives

After careful study of this chapter you should be able to do the following:

1. **Determine the magnetization of some material given its magnetic susceptibility and the applied magnetic field strength.**
2. **From an electronic perspective note and briefly explain the two sources of magnetic moments in materials.**
3. **Briefly explain the nature and source of (a) diamagnetism, (b) paramagnetism, and (c) ferromagnetism.**
4. **In terms of crystal structure, explain the source of ferrimagnetism for cubic ferrites.**
5. **(a) Describe magnetic hysteresis; (b) explain why ferromagnetic and ferrimagnetic materials experience magnetic hysteresis; and (c) explain why these materials may become permanent magnets.**
6. **Note the distinctive magnetic characteristics for both soft and hard magnetic materials.**
7. **Describe the phenomenon of *superconductivity*.**

18.1 INTRODUCTION

Magnetism, the phenomenon by which materials assert an attractive or repulsive force or influence on other materials, has been known for thousands of years. However, the underlying principles and mechanisms that explain the magnetic phenomenon are complex and subtle, and their understanding has eluded scientists until relatively recent times. Many of our modern technological devices rely on magnetism and magnetic materials; these include electrical power generators and transformers, electric motors, radio, television, telephones, computers, and components of sound and video reproduction systems.

Iron, some steels, and the naturally occurring mineral lodestone are well-known examples of materials that exhibit magnetic properties. Not so familiar, however, is the fact that all substances are influenced to one degree or another by the presence of a magnetic field. This chapter provides a brief description of the origin of magnetic fields and discusses the various magnetic field vectors and magnetic parameters; the phenomena of diamagnetism, paramagnetism, ferromagnetism, and ferrimagnetism; some of the different magnetic materials; and the phenomenon of superconductivity.

18.2 BASIC CONCEPTS

MAGNETIC DIPOLES

Magnetic forces are generated by moving electrically charged particles; these magnetic forces are in addition to any electrostatic forces that may prevail. Many times it is convenient to think of magnetic forces in terms of fields. Imaginary lines of force may be drawn to indicate the direction of the force at positions in the vicinity of the field source. The magnetic field distributions as indicated by lines of force are shown for a current loop and also a bar magnet in Figure 18.1.

Magnetic dipoles are found to exist in magnetic materials, which, in some respects, are analogous to electric dipoles (Section 12.18). Magnetic dipoles may be thought of as small bar magnets composed of north and south poles instead of positive and negative electric charges. In the present discussion, magnetic dipole moments are represented by arrows, as shown in Figure 18.2. Magnetic dipoles are influenced by magnetic fields in a manner similar to the way in which electric dipoles are affected by electric fields (Figure 12.28). Within a magnetic field, the force of the field itself exerts a torque that tends to orient the dipoles with the field. A familiar example is the way in which a magnetic compass needle lines up with the earth's magnetic field.

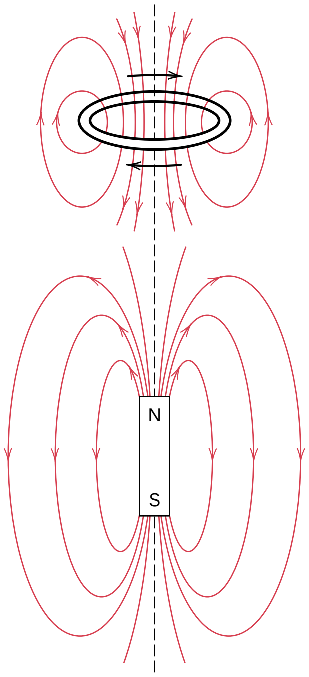

Figure 18.1 Magnetic field lines of force around a current loop and a bar magnet.

MAGNETIC FIELD VECTORS

Before discussing the origin of magnetic moments in solid materials, we describe magnetic behavior in terms of several field vectors. The externally applied magnetic field, sometimes called the **magnetic field strength,** is designated by H. If the magnetic field is generated by means of a cylindrical coil (or solenoid) consisting of N closely spaced turns, having a length l, and carrying a current of magnitude I, then

$$H = \frac{NI}{l} \tag{18.1}$$

A schematic diagram of such an arrangement is shown in Figure 18.3*a*. The magnetic field that is generated by the current loop and the bar magnet in Figure 18.1 is an H field. The units of H are ampere-turns per meter, or just amperes per meter.

The **magnetic induction,** or **magnetic flux density,** denoted by B, represents the magnitude of the internal field strength within a substance that is subjected to an H field. The units for B are teslas [or webers per square meter (Wb/m^2)]. Both B and H are field vectors, being characterized not only by magnitude, but also by direction in space.

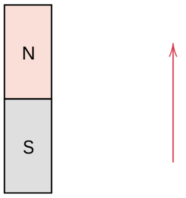

Figure 18.2 The magnetic moment as designated by an arrow.

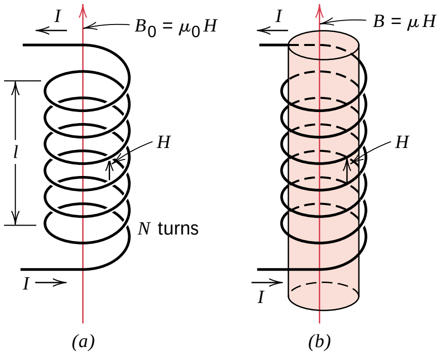

FIGURE 18.3 (*a*) The magnetic field H as generated by a cylindrical coil is dependent on the current I, the number of turns N, and the coil length l, according to Equation 18.1. The magnetic flux density B_0 in the presence of a vacuum is equal to $\mu_0 H$, where μ_0 is the permeability of a vacuum, $4\pi \times 10^{-7}$ H/m. (*b*) The magnetic flux density B within a solid material is equal to μH, where μ is the permeability of the solid material. (Adapted from A. G. Guy, *Essentials of Materials Science,* McGraw-Hill Book Company, New York, 1976.)

The magnetic field strength and flux density are related according to

$$B = \mu H \tag{18.2}$$

The parameter μ is called the **permeability,** which is a property of the specific medium through which the H field passes and in which B is measured, as illustrated in Figure 18.3*b*. The permeability has dimensions of webers per ampere-meter (Wb/A-m) or henries per meter (H/m).

In a vacuum,

$$B_0 = \mu_0 H \tag{18.3}$$

where μ_0 is the *permeability of a vacuum,* a universal constant, which has a value of $4\pi \times 10^{-7}$ (1.257×10^{-6}) H/m. The parameter B_0 represents the flux density within a vacuum as demonstrated in Figure 18.3*a*.

Several parameters may be used to describe the magnetic properties of solids. One of these is the ratio of the permeability in a material to the permeability in a vacuum, or

$$\mu_r = \frac{\mu}{\mu_0} \tag{18.4}$$

where μ_r is called the *relative permeability,* which is unitless. The permeability or relative permeability of a material is a measure of the degree to which the material can be magnetized, or the ease with which a B field can be induced in the presence of an external H field.

Another field quantity, M, called the **magnetization** of the solid, is defined by the expression

$$B = \mu_0 H + \mu_0 M \tag{18.5}$$

Table 18.1 **Magnetic Units and Conversion Factors for the SI and cgs–emu Systems**

		SI Units		*cgs–emu*	
Quantity	***Symbol***	***Derived***	***Primary***	***Unit***	***Conversion***
Magnetic induction (flux density)	B	tesla (Wb/m^2)[a]	kg/s-C	gauss	1 Wb/m^2 = 10^4 gauss
Magnetic field strength	H	amp-turn/m	C/m-s	oersted	1 amp-turn/m = $4\pi \times 10^{-3}$ oersted
Magnetization	M (SI) I (cgs–emu)	amp-turn/m	C/m-s	maxwell/cm^2	1 amp-turn/m = 10^{-3} maxwell/cm^2
Permeability of a vacuum	μ_0	henry/m[b]	kg-m/C^2	Unitless (emu)	$4\pi \times 10^{-7}$ henry/m = 1 emu
Relative permeability	μ_r (SI) μ' (cgs–emu)	Unitless	Unitless	Unitless	$\mu_r = \mu'$
Susceptibility	χ_m (SI) χ'_m (cgs–emu)	Unitless	Unitless	Unitless	$\chi_m = 4\pi\chi'_m$

[a] Units of the weber (Wb) are volt-seconds.

[b] Units of the henry are webers per ampere.

In the presence of an H field, the magnetic moments within a material tend to become aligned with the field and to reinforce it by virtue of their magnetic fields; the term $\mu_0 M$ in Equation 18.5 is a measure of this contribution.

The magnitude of M is proportional to the applied field as follows:

$$M = \chi_m H \tag{18.6}$$

and χ_m is called the **magnetic susceptibility,** which is unitless.[1] The magnetic susceptibility and the relative permeability are related as follows:

$$\chi_m = \mu_r - 1 \tag{18.7}$$

There is a dielectric analogue for each of the foregoing magnetic field parameters. The B and H fields are, respectively, analogous to the dielectric displacement D and the electric field $\mathscr{E}$, whereas the permeability μ parallels the permittivity ϵ (cf. Equations 18.2 and 12.33). Furthermore, the magnetization M and polarization P are correlates (Equations 18.5 and 12.34).

Magnetic units may be a source of confusion because there are really two systems in common use. The ones used thus far are SI [rationalized *MKS* (meter-kilogram-second)]; the others come from the *cgs–emu* (centimeter-gram-second-electromagnetic unit) system. The units for both systems as well as the appropriate conversion factors are contained in Table 18.1.

ORIGINS OF MAGNETIC MOMENTS

The macroscopic magnetic properties of materials are a consequence of *magnetic moments* associated with individual electrons. Some of these concepts are relatively complex and involve some quantum-mechanical principles beyond the scope of this

---

[1] This χ_m is taken to be the volume susceptibility in SI units, which, when multiplied by H, yields the magnetization per unit volume (cubic meter) of material. Other susceptibilities are also possible; see Problem 18.4.

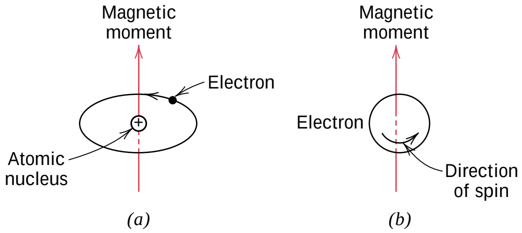

Figure 18.4 Demonstration of the magnetic moment associated with (*a*) an orbiting electron and (*b*) a spinning electron.

discussion; consequently, simplifications have been made and some of the details omitted. Each electron in an atom has magnetic moments that originate from two sources. One is related to its orbital motion around the nucleus; being a moving charge, an electron may be considered to be a small current loop, generating a very small magnetic field, and having a magnetic moment along its axis of rotation, as schematically illustrated in Figure 18.4*a*.

Each electron may also be thought of as spinning around an axis; the other magnetic moment originates from this electron spin, which is directed along the spin axis as shown in Figure 18.4*b*. Spin magnetic moments may be only in an ''up'' direction or in an antiparallel ''down'' direction. Thus each electron in an atom may be thought of as being a small magnet having permanent orbital and spin magnetic moments.

The most fundamental magnetic moment is the **Bohr magneton** μ_B, which is of magnitude 9.27×10^{-24} A-m^2. For each electron in an atom the spin magnetic moment is $\pm\mu_B$ (plus for spin up, minus for spin down). Furthermore, the orbital magnetic moment contribution is equal to $m_l\mu_B$, m_l being the magnetic quantum number of the electron, as mentioned in Section 2.3.

In each individual atom, orbital moments of some electron pairs cancel each other; this also holds for the spin moments. For example, the spin moment of an electron with spin up will cancel that of one with spin down. The net magnetic moment, then, for an atom is just the sum of the magnetic moments of each of the constituent electrons, including both orbital and spin contributions, and taking into account moment cancellation. For an atom having completely filled electron shells or subshells, when all electrons are considered, there is total cancellation of both orbital and spin moments. Thus materials composed of atoms having completely filled electron shells are not capable of being permanently magnetized. This category includes the inert gases (He, Ne, Ar, etc.) as well as some ionic materials. The types of magnetism include diamagnetism, paramagnetism, and ferromagnetism; in addition, antiferromagnetism and ferrimagnetism are considered to be subclasses of ferromagnetism. All materials exhibit at least one of these types, and the behavior depends on the response of electron and atomic magnetic dipoles to the application of an externally applied magnetic field.

18.3 Diamagnetism and Paramagnetism

Diamagnetism is a very weak form of magnetism that is nonpermanent and persists only while an external field is being applied. It is induced by a change in the orbital motion of electrons due to an applied magnetic field. The magnitude of the induced magnetic moment is extremely small, and in a direction opposite to that of the applied field. Thus, the relative permeability μ_r is less than unity (however, only very slightly), and the magnetic susceptibility is negative; that is, the magnitude of

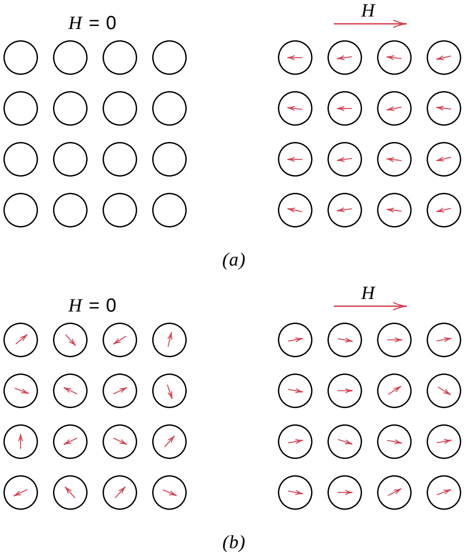

FIGURE 18.5 (*a*) The atomic dipole configuration for a diamagnetic material with and without a magnetic field. In the absence of an external field, no dipoles exist; in the presence of a field, dipoles are induced that are aligned opposite to the field direction. (*b*) Atomic dipole configuration with and without an external magnetic field for a paramagnetic material.

the B field within a diamagnetic solid is less than that in a vacuum. The volume susceptibility χ_m for diamagnetic solid materials is on the order of -10^{-5}. When placed between the poles of a strong electromagnet, diamagnetic materials are attracted toward regions where the field is weak.

Figure 18.5*a* illustrates schematically the atomic magnetic dipole configurations for a diamagnetic material with and without an external field; here, the arrows represent atomic dipole moments, whereas for the preceding discussion, arrows denoted only electron moments. The dependence of B on the external field H for a material that exhibits diamagnetic behavior is presented in Figure 18.6. Table 18.2 gives the susceptibilities of several diamagnetic materials. Diamagnetism is found in all materials; but because it is so weak, it can be observed only when

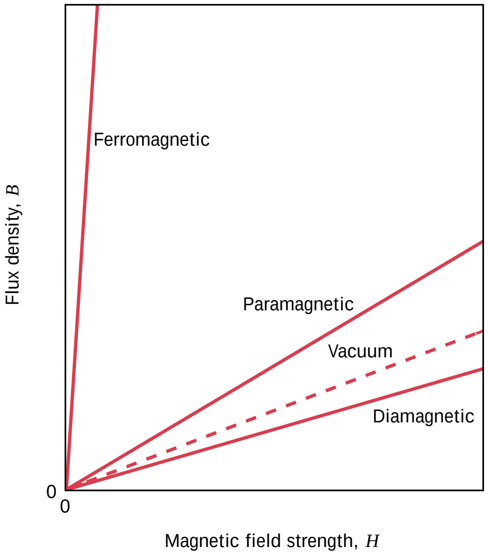

FIGURE 18.6 Schematic representation of the flux density B versus the magnetic field strength H for diamagnetic, paramagnetic, and ferromagnetic materials.

Table 18.2 Room-Temperature Magnetic Susceptibilities for Diamagnetic and Paramagnetic Materials

Diamagnetics		*Paramagnetics*	
Material	*Susceptibility χ_m (volume) (SI units)*	*Material*	*Susceptibility χ_m (volume) (SI units)*
Aluminum oxide	-1.81×10^{-5}	Aluminum	2.07×10^{-5}
Copper	-0.96×10^{-5}	Chromium	3.13×10^{-4}
Gold	-3.44×10^{-5}	Chromium chloride	1.51×10^{-3}
Mercury	-2.85×10^{-5}	Manganese sulfate	3.70×10^{-3}
Silicon	-0.41×10^{-5}	Molybdenum	1.19×10^{-4}
Silver	-2.38×10^{-5}	Sodium	8.48×10^{-6}
Sodium chloride	-1.41×10^{-5}	Titanium	1.81×10^{-4}
Zinc	-1.56×10^{-5}	Zirconium	1.09×10^{-4}

other types of magnetism are totally absent. This form of magnetism is of no practical importance.

For some solid materials, each atom possesses a permanent dipole moment by virtue of incomplete cancellation of electron spin and/or orbital magnetic moments. In the absence of an external magnetic field, the orientations of these atomic magnetic moments are random, such that a piece of material possesses no net macroscopic magnetization. These atomic dipoles are free to rotate, and **paramagnetism** results when they preferentially align, by rotation, with an external field as shown in Figure 18.5*b*. These magnetic dipoles are acted on individually with no mutual interaction between adjacent dipoles. Inasmuch as the dipoles align with the external field, they enhance it, giving rise to a relative permeability μ_r that is greater than unity, and to a relatively small but positive magnetic susceptibility. Susceptibilities for paramagnetic materials range from about 10^{-5} to 10^{-2} (Table 18.2). A schematic B-versus-H curve for a paramagnetic material is also shown in Figure 18.6.

Both diamagnetic and paramagnetic materials are considered to be nonmagnetic because they exhibit magnetization only when in the presence of an external field. Also, for both, the flux density B within them is almost the same as it would be in a vacuum.

18.4 FERROMAGNETISM

Certain metallic materials possess a permanent magnetic moment in the absence of an external field, and manifest very large and permanent magnetizations. These are the characteristics of **ferromagnetism,** and they are displayed by the transition metals iron (as BCC α ferrite), cobalt, nickel, and some of the rare earth metals such as gadolinium (Gd). Magnetic susceptibilities as high as 10^6 are possible for ferromagnetic materials. Consequently, $H \ll M$, and from Equation 18.5 we write

$$B \cong \mu_0 M \tag{18.8}$$

Permanent magnetic moments in ferromagnetic materials result from atomic magnetic moments due to electron spin—uncancelled electron spins as a consequence of the electron structure. There is also an orbital magnetic moment contribu-

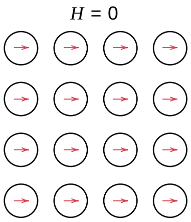

FIGURE 18.7 Schematic illustration of the mutual alignment of atomic dipoles for a ferromagnetic material, which will exist even in the absence of an external magnetic field.

tion that is small in comparison to the spin moment. Furthermore, in a ferromagnetic material, coupling interactions cause net spin magnetic moments of adjacent atoms to align with one another, even in the absence of an external field. This is schematically illustrated in Figure 18.7. The origin of these coupling forces is not completely understood, but it is thought to arise from the electronic structure of the metal. This mutual spin alignment exists over relatively large volume regions of the crystal called **domains** (see Section 18.7).

The maximum possible magnetization, or **saturation magnetization** M_s, of a ferromagnetic material represents the magnetization that results when all the magnetic dipoles in a solid piece are mutually aligned with the external field; there is also a corresponding saturation flux density B_s. The saturation magnetization is equal to the product of the net magnetic moment for each atom and the number of atoms present. For each of iron, cobalt, and nickel, the net magnetic moments per atom are 2.22, 1.72, and 0.60 Bohr magnetons, respectively.

EXAMPLE PROBLEM 18.1

Calculate **(a)** the saturation magnetization and **(b)** the saturation flux density for nickel, which has a density of 8.90 g/cm^3.

SOLUTION

(a) The saturation magnetization is just the product of the number of Bohr magnetons per atom (0.60 as given above), the magnitude of the Bohr magneton μ_B, and the number N of atoms per cubic meter, or

$$M_s = 0.60\mu_B N$$

Now, the number of atoms per cubic meter is related to the density ρ, the atomic weight A_{Ni}, and Avogadro's number N_A, as follows:

$$N = \frac{\rho N_A}{A_{Ni}}$$

$$= \frac{(8.90 \times 10^6 \text{ g/m}^3)(6.023 \times 10^{23} \text{ atoms/mol})}{58.71 \text{ g/mol}}$$

$$= 9.13 \times 10^{28} \text{ atoms/m}^3$$

Finally,

$$M_s = \left(\frac{0.60\ \text{Bohr magneton}}{\text{atom}}\right)\left(\frac{9.27 \times 10^{-24}\ \text{A-m}^2}{\text{Bohr magneton}}\right)\left(\frac{9.13 \times 10^{28}\ \text{atoms}}{\text{m}^3}\right)$$

$$= 5.1 \times 10^5\ \text{A/m}$$

(b) From Equation 18.8, the saturation flux density is just

$$B_s = \mu_0 M_s$$

$$= \left(\frac{4\pi \times 10^{-7}\ \text{H}}{\text{m}}\right)\left(\frac{5.1 \times 10^5\ \text{A}}{\text{m}}\right)$$

$$= 0.64\ \text{tesla}$$

18.5 ANTIFERROMAGNETISM AND FERRIMAGNETISM

ANTIFERROMAGNETISM

This phenomenon of magnetic moment coupling between adjacent atoms or ions occurs in materials other than those that are ferromagnetic. In one such group, this coupling results in an antiparallel alignment; the alignment of the spin moments of neighboring atoms or ions in exactly opposite directions is termed **antiferromagnetism.** Manganese oxide (MnO) is one material that displays this behavior. Manganese oxide is a ceramic material that is ionic in character, having both Mn^{2+} and O^{2-} ions. No net magnetic moment is associated with the O^{2-} ions, since there is a total cancellation of both spin and orbital moments. However, the Mn^{2+} ions possess a net magnetic moment that is predominantly of spin origin. These Mn^{2+} ions are arrayed in the crystal structure such that the moments of adjacent ions are antiparallel. This arrangement is represented schematically in Figure 18.8. Obviously, the opposing magnetic moments cancel one another, and, as a consequence, the solid as a whole possesses no net magnetic moment.

FERRIMAGNETISM

Some ceramics also exhibit a permanent magnetization, termed **ferrimagnetism.** The macroscopic magnetic characteristics of ferromagnets and ferrimagnets are similar; the distinction lies in the source of the net magnetic moments. The principles

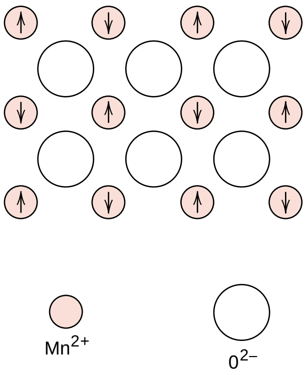

FIGURE 18.8 Schematic representation of antiparallel alignment of spin magnetic moments for antiferromagnetic manganese oxide.

of ferrimagnetism are illustrated with the cubic ferrites.[2] These ionic materials may be represented by the chemical formula MFe_2O_4, in which M represents any one of several metallic elements. The prototype ferrite is Fe_3O_4, the mineral magnetite, sometimes called lodestone.

The formula for Fe_3O_4 may be written as $Fe^{2+}O^{2-}\text{–}(Fe^{3+})_2(O^{2-})_3$ in which the Fe ions exist in both +2 and +3 valence states in the ratio of 1:2. A net spin magnetic moment exists for each Fe^{2+} and Fe^{3+} ion, which corresponds to 4 and 5 Bohr magnetons, respectively, for the two ion types. Furthermore, the O^{2-} ions are magnetically neutral. There are antiparallel spin-coupling interactions between the Fe ions, similar in character to antiferromagnetism. However, the net ferrimagnetic moment arises from the incomplete cancellation of spin moments.

Cubic ferrites have the inverse spinel crystal structure, which is cubic in symmetry, and similar to the spinel structure (Section 3.15). It might be thought of as having been generated by the stacking of close-packed planes of O^{2-} ions. Again, there are two types of positions that may be occupied by the iron cations, as illustrated in Figure 3.30. For one, the coordination number is 4 (tetrahedral coordination); that is, each Fe ion is surrounded by four oxygen nearest neighbors. For the other, the coordination number is 6 (octahedral coordination). With this inverse spinel structure, half the trivalent (Fe^{3+}) ions are situated in octahedral positions, the other half, in tetrahedral positions. The divalent Fe^{2+} ions are all located in octahedral positions. The critical factor is the arrangement of the spin moments of the Fe ions, as represented in Figure 18.9 and Table 18.3. The spin moments of all the Fe^{3+} ions in the octahedral positions are aligned parallel to one another; however, they are directed oppositely to the Fe^{3+} ions disposed in the tetrahedral positions, which are also aligned. This results from the antiparallel coupling of adjacent iron ions. Thus, the spin moments of all Fe^{3+} ions cancel one another and make no net contribution to the magnetization of the solid. All the Fe^{2+} ions have their moments aligned in the same direction, which total moment is responsible for the net magnetization (see Table 18.3). Thus, the saturation magnetization of a ferrimagnetic solid may be computed from the product of the net spin magnetic moment for each Fe^{2+} ion and the number of Fe^{2+} ions; this would correspond to the mutual alignment of all the Fe^{2+} ion magnetic moments in the Fe_3O_4 specimen.

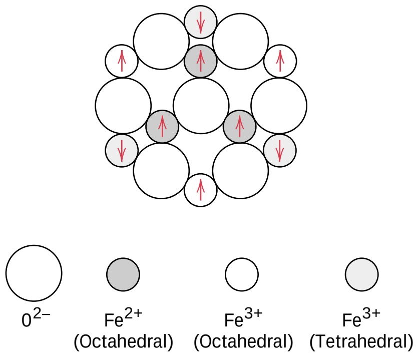

FIGURE 18.9 Schematic diagram showing the spin magnetic moment configuration for Fe^{2+} and Fe^{3+} ions in Fe_3O_4. (From Richard A. Flinn and Paul K. Trojan, *Engineering Materials and Their Applications,* 4th edition. Copyright © 1990 by John Wiley & Sons, Inc. Adapted by permission of John Wiley & Sons, Inc.)

---

[2] Ferrite in the magnetic sense should not be confused with the ferrite α-iron discussed in Section 10.18; in the remainder of this chapter, the term **ferrite** implies the magnetic ceramic.

Table 18.3 **The Distribution of Spin Magnetic Moments for Fe^{2+} and Fe^{3+} Ions in a Unit Cell of Fe_3O_4**[a]

Cation	*Octahedral Lattice Site*	*Tetrahedral Lattice Site*	*Net Magnetic Moment*
Fe^{3+}	↑ ↑ ↑ ↑ ↑ ↑ ↑ ↑	↓ ↓ ↓ ↓ ↓ ↓ ↓ ↓	Complete cancellation
Fe^{2+}	↑ ↑ ↑ ↑ ↑ ↑ ↑ ↑	—	↑ ↑ ↑ ↑ ↑ ↑ ↑ ↑

[a] Each arrow represents the magnetic moment orientation for one of the cations.

Cubic ferrites having other compositions may be produced by adding metallic ions that substitute for some of the iron in the crystal structure. Again, from the ferrite chemical formula, $M^{2+}O^{2-}$–$(Fe^{3+})_2(O^{2-})_3$, in addition to Fe^{2+}, M^{2+} may represent divalent ions such as Ni^{2+}, Mn^{2+}, Co^{2+}, and Cu^{2+}, each of which possesses a net spin magnetic moment different from 4; several are listed in Table 18.4. Thus, by adjustment of composition, ferrite compounds having a range of magnetic properties may be produced. For example, nickel ferrite has the formula $NiFe_2O_4$. Other compounds may also be produced containing mixtures of two divalent metal ions such as $(Mn,Mg)Fe_2O_4$, in which the $Mn^{2+}:Mg^{2+}$ ratio may be varied; these are called mixed ferrites.

Ceramic materials other than the cubic ferrites are also ferrimagnetic; these include the hexagonal ferrites and garnets. Hexagonal ferrites have a crystal structure similar to the inverse spinel, with hexagonal symmetry rather than cubic. The chemical formula for these materials may be represented by $AB_{12}O_{19}$, in which A is a divalent metal such as barium, lead, or strontium, and B is a trivalent metal such as aluminum, gallium, chromium, or iron. The two most common examples of the hexagonal ferrites are $PbFe_{12}O_{19}$ and $BaFe_{12}O_{19}$.

The garnets have a very complicated crystal structure, which may be represented by the general formula $M_3Fe_5O_{12}$; here, M represents a rare earth ion such as

Table 18.4 **Net Magnetic Moments for Six Cations**

Cation	*Net Spin Magnetic Moment (Bohr magnetons)*
Fe^{3+}	5
Fe^{2+}	4
Mn^{2+}	5
Co^{2+}	3
Ni^{2+}	2
Cu^{2+}	1

samarium, europium, gadolinium, or yttrium. Yttrium iron garnet ($Y_3Fe_5O_{12}$), sometimes denoted YIG, is the most common material of this type.

The saturation magnetizations for ferrimagnetic materials are not as high as for ferromagnets. On the other hand, ferrites, being ceramic materials, are good electrical insulators. For some magnetic applications, such as high-frequency transformers, a low electrical conductivity is most desirable.

Example Problem 18.2

Calculate the saturation magnetization for Fe_3O_4 given that each cubic unit cell contains 8 Fe^{2+} and 16 Fe^{3+} ions, and that the unit cell edge length is 0.839 nm.

Solution

This problem is solved in a manner similar to Example Problem 18.1, except that the computational basis is per unit cell as opposed to per atom or ion.

The saturation magnetization will be equal to the product of the number N' of Bohr magnetons per cubic meter of Fe_3O_4, and the magnetic moment per Bohr magneton μ_B,

$$M_s = N'\mu_B \tag{18.9}$$

Now, N' is just the number of Bohr magnetons per unit cell n_B divided by the unit cell volume V_C, or

$$N' = \frac{n_B}{V_C} \tag{18.10}$$

Again, the net magnetization results from the Fe^{2+} ions only. Since there are 8 Fe^{2+} ions per unit cell and 4 Bohr magnetons per Fe^{2+} ion, n_B is 32. Furthermore, the unit cell is a cube, and $V_C = a^3$, a being the unit cell edge length. Therefore,

$$M_s = \frac{n_B \mu_B}{a^3} \tag{18.11}$$

$$= \frac{(32 \text{ Bohr magnetons/unit cell})(9.27 \times 10^{-24} \text{ A-m}^2\text{/Bohr magneton})}{(0.839 \times 10^{-9} \text{ m})^3\text{/unit cell}}$$

$$= 5.0 \times 10^5 \text{ A/m}$$

Design Example 18.1

Design a cubic mixed-ferrite magnetic material that has a saturation magnetization of 5.25×10^5 A/m.

Solution

According to Example Problem 18.2 the saturation magnetization for Fe_3O_4 is 5.0×10^5 A/m. In order to increase the magnitude of M_s it is necessary to replace some fraction of the Fe^{2+} with a divalent metal ion that has a greater magnetic moment—for example Mn^{2+}; from Table 18.4, it may be noted that there are 5 Bohr magnetons/Mn^{2+} ion as compared to 4 Bohr magnetons/Fe^{2+}. Let us first employ Equation 18.11 to compute the number of Bohr magnetons per unit cell (n_B), assuming that the Mn^{2+} addition does not change the unit cell edge length (0.839 nm). Thus,

$$n_B = \frac{M_s a^3}{\mu_B}$$

$$= \frac{(5.25 \times 10^5 \text{ A/m})(0.839 \times 10^{-9} \text{ m})^3/\text{unit cell}}{9.27 \times 10^{-24} \text{ A-m}^2/\text{Bohr magneton}}$$

$$= 33.45 \text{ Bohr magnetons/unit cell}$$

If we let x represent the fraction of Mn^{2+} that have substituted for Fe^{2+}, then the remaining unsubstituted Fe^{2+} fraction is equal to $(1 - x)$. Furthermore, inasmuch as there are 8 divalent ions per unit cell, we may write the following expression:

$$8[5x + 4(1 - x)] = 33.45$$

which leads to $x = 0.181$. Thus, if 18.1 at% of the Fe^{2+} in Fe_3O_4 are replaced with Mn^{2+}, the saturation magnetization will be increased to 5.25×10^5 A/m.

18.6 THE INFLUENCE OF TEMPERATURE ON MAGNETIC BEHAVIOR

Temperature can also influence the magnetic characteristics of materials. It may be recalled that raising the temperature of a solid results in an increase in the magnitude of the thermal vibrations of atoms. The atomic magnetic moments are free to rotate; hence, with rising temperature, the increased thermal motion of the atoms tends to randomize the directions of any moments that may be aligned.

For ferromagnetic, antiferromagnetic, and ferrimagnetic materials, the atomic thermal motions counteract the coupling forces between the adjacent atomic dipole moments, causing some dipole misalignment, regardless of whether an external field is present. This results in a decrease in the saturation magnetization for both ferro- and ferrimagnets. The saturation magnetization is a maximum at 0 K, at which temperature the thermal vibrations are a minimum. With increasing temperature, the saturation magnetization diminishes gradually and then abruptly drops to zero at what is called the **Curie temperature** T_c. The magnetization-temperature behavior for iron and Fe_3O_4 is represented in Figure 18.10. At T_c the mutual spin coupling forces are completely destroyed, such that for temperatures above T_c both ferromagnetic and ferrimagnetic materials are paramagnetic. The magnitude of the Curie temperature varies from material to material; for example, for iron, cobalt, nickel, and Fe_3O_4, the respective values are 768, 1120, 335, and 585°C.

Antiferromagnetism is also affected by temperature; this behavior vanishes at what is called the *Néel temperature.* At temperatures above this point, antiferromagnetic materials also become paramagnetic.

18.7 DOMAINS AND HYSTERESIS

Any ferromagnetic or ferrimagnetic material that is at a temperature below T_c is composed of small-volume regions in which there is a mutual alignment in the same

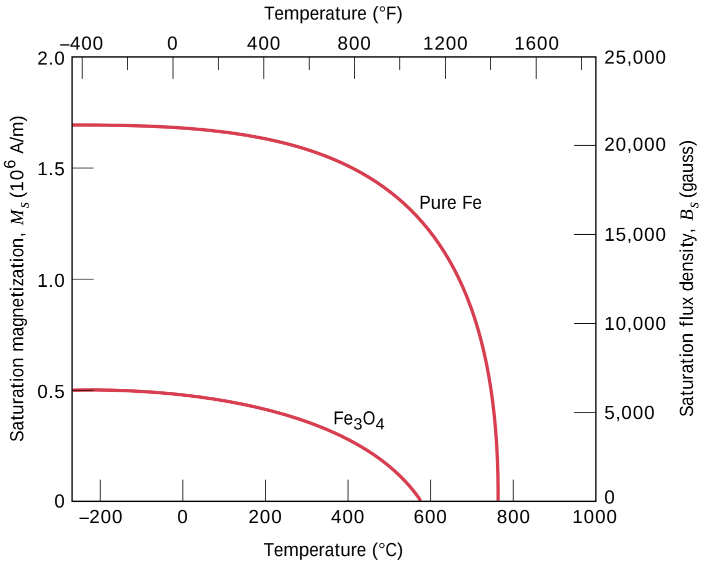

FIGURE 18.10 Plot of saturation magnetization as a function of temperature for iron and Fe_3O_4. [Adapted from J. Smit and H. P. J. Wijn, *Ferrites.* Copyright © 1959 by N. V. Philips Gloeilampenfabrieken, Eindhoven (Holland). Reprinted by permission.]

direction of all magnetic dipole moments, as illustrated in Figure 18.11. Such a region is called a domain, and each one is magnetized to its saturation magnetization. Adjacent domains are separated by domain boundaries or walls, across which the direction of magnetization gradually changes (Figure 18.12). Normally, domains are microscopic in size, and for a polycrystalline specimen, each grain may consist of more than a single domain. Thus, in a macroscopic piece of material, there will be a large number of domains, and all may have different magnetization orientations. The magnitude of the *M* field for the entire solid is the vector sum of the magnetizations of all the domains, each domain contribution being weighted by its volume fraction. For an unmagnetized specimen, the appropriately weighted vector sum of the magnetizations of all the domains is zero.

Flux density *B* and field intensity *H* are not proportional for ferromagnets and ferrimagnets. If the material is initially unmagnetized, then *B* varies as a function of *H* as shown in Figure 18.13. The curve begins at the origin, and as *H* is increased,

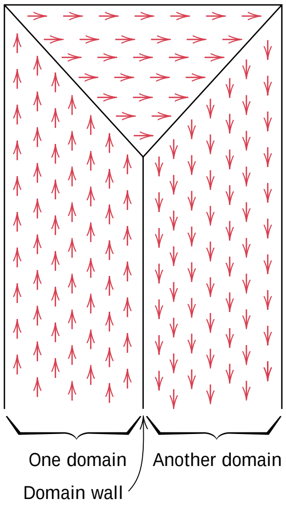

FIGURE 18.11 Schematic depiction of domains in a ferromagnetic or ferrimagnetic material; arrows represent atomic magnetic dipoles. Within each domain, all dipoles are aligned, whereas the direction of alignment varies from one domain to another.

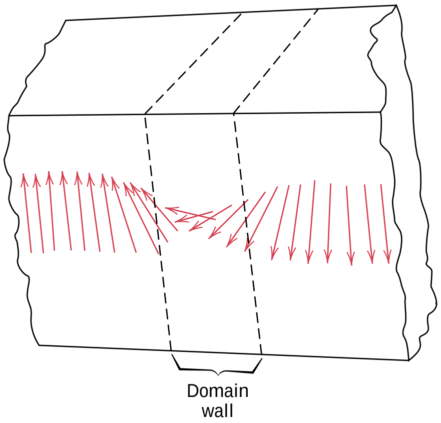

Figure 18.12 The gradual change in magnetic dipole orientation across a domain wall. (From W. D. Kingery, H. K. Bowen, and D. R. Uhlmann, *Introduction to Ceramics*, 2nd edition. Copyright © 1976 by John Wiley & Sons, New York. Reprinted by permission of John Wiley & Sons, Inc.)

the B field begins to increase slowly, then more rapidly, finally leveling off and becoming independent of H. This maximum value of B is the saturation flux density B_s, and the corresponding magnetization is the saturation magnetization M_s, mentioned previously. Since the permeability μ from Equation 18.2 is the slope of the B-versus-H curve, it may be noted from Figure 18.13 that the permeability changes with and is dependent on H. On occasion, the slope of the B-versus-H curve at $H = 0$ is specified as a material property, which is termed the *initial permeability* μ_i, as indicated in Figure 18.13.

As an H field is applied, the domains change shape and size by the movement of domain boundaries. Schematic domain structures are represented at several points along the B-versus-H curve in Figure 18.13. Initially, the moments of the constituent domains are randomly oriented such that there is no net B (or M) field. As the external field is applied, the domains that are oriented in directions favorable to (or nearly aligned with) the applied field grow at the expense of those that are unfavorably oriented. This process continues with increasing field strength until the macroscopic specimen becomes a single domain, which is nearly aligned with the field. Saturation is achieved when this domain, by means of rotation, becomes

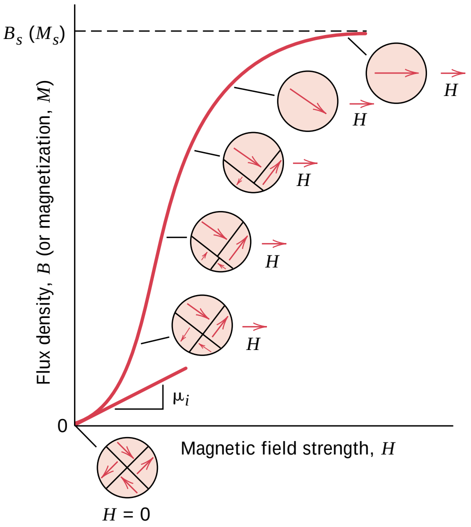

Figure 18.13 The B-versus-H behavior for a ferromagnetic or ferrimagnetic material that was initially unmagnetized. Domain configurations during several stages of magnetization are represented. Saturation flux density B_s, magnetization M_s, and initial permeability μ_i are also indicated. (Adapted from O. H. Wyatt and D. Dew-Hughes, *Metals, Ceramics and Polymers*, Cambridge University Press, 1974.)

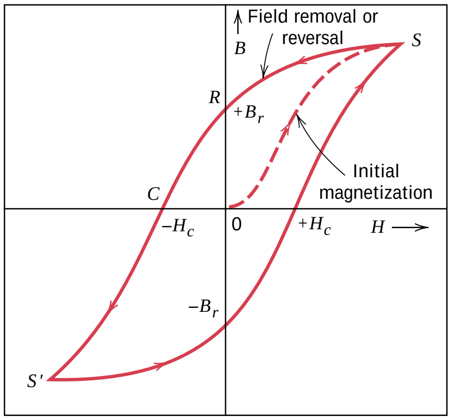

FIGURE 18.14 Magnetic flux density versus the magnetic field strength for a ferromagnetic material that is subjected to forward and reverse saturations (points S and S'). The hysteresis loop is represented by the solid curve; the dashed curve indicates the initial magnetization. The remanence B_r and the coercive force H_c are also shown.

oriented with the H field. Alteration of the domain structure with magnetic field for an iron single crystal is shown in the chapter-opening photograph for this chapter.

From saturation, point S in Figure 18.14, as the H field is reduced by reversal of field direction, the curve does not retrace its original path. A **hysteresis** effect is produced in which the B field lags behind the applied H field, or decreases at a lower rate. At zero H field (point R on the curve), there exists a residual B field that is called the **remanence,** or remanent flux density, B_r; the material remains magnetized in the absence of an external H field.

Hysteresis behavior and permanent magnetization may be explained by the motion of domain walls. Upon reversal of the field direction from saturation (point S in Figure 18.14), the process by which the domain structure changes is reversed. First, there is a rotation of the single domain with the reversed field. Next, domains having magnetic moments aligned with the new field form and grow at the expense of the former domains. Critical to this explanation is the resistance to movement of domain walls that occurs in response to the increase of the magnetic field in the opposite direction; this accounts for the lag of B with H, or the hysteresis. When the applied field reaches zero, there is still some net volume fraction of domains oriented in the former direction, which explains the existence of the remanence B_r.

To reduce the B field within the specimen to zero (point C on Figure 18.14), an H field of magnitude $-H_c$ must be applied in a direction opposite to that of the original field; H_c is called the **coercivity,** or sometimes the coercive force. Upon continuation of the applied field in this reverse direction, as indicated in the figure, saturation is ultimately achieved in the opposite sense, corresponding to point S'. A second reversal of the field to the point of the initial saturation (point S) completes the symmetrical hysteresis loop and also yields both a negative remanence ($-B_r$) and a positive coercivity ($+H_c$).

The B-versus-H curve in Figure 18.14 represents a hysteresis loop taken to saturation. Of course, it is not necessary to increase the H field to saturation before reversing the field direction; in Figure 18.15, loop NP is a hysteresis curve corresponding to less than saturation. Furthermore, it is possible to reverse the direction of the field at any point along the curve and generate other hysteresis loops. One such loop is indicated on the saturation curve in Figure 18.15: for loop LM, the H field is reversed to zero. One method of demagnetizing a ferromagnet or ferrimagnet is to repeatedly cycle it in an H field that alternates direction and decreases in magnitude.

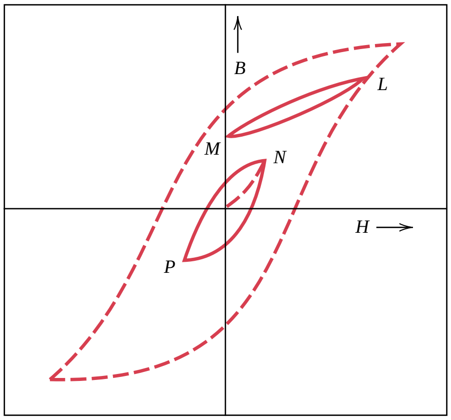

FIGURE 18.15 A hysteresis curve at less than saturation (curve NP) within the saturation loop for a ferromagnetic material. The B–H behavior for field reversal at other than saturation is indicated by curve LM.

18.8 SOFT MAGNETIC MATERIALS

The size and shape of the hysteresis curve for ferromagnetic and ferrimagnetic materials is of considerable practical importance. The area within a loop represents a magnetic energy loss per unit volume of material per magnetization–demagnetization cycle; this energy loss is manifested as heat that is generated within the magnetic specimen and is capable of raising its temperature.

Both ferromagnetic and ferrimagnetic materials are classified as either *soft* or *hard* on the basis of their hysteresis characteristics. **Soft magnetic materials** are used in devices that are subjected to alternating magnetic fields and in which energy losses must be low; one familiar example consists of transformer cores. For this reason the relative area within the hysteresis loop must be small; it is characteristically thin and narrow, as represented in Figure 18.16. Consequently, a soft magnetic material must have a high initial permeability and a low coercivity. A material

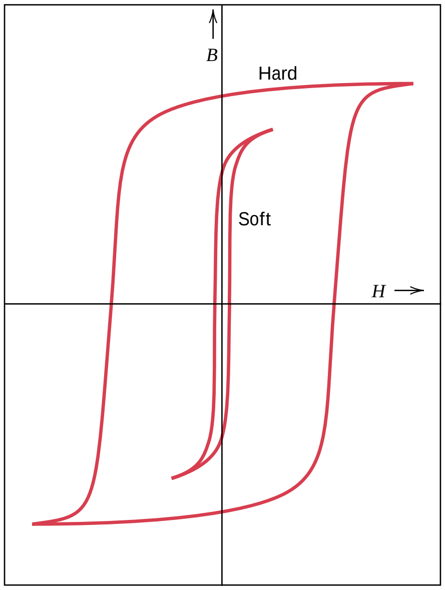

FIGURE 18.16 Schematic magnetization curves for soft and hard magnetic materials. (From K. M. Ralls, T. H. Courtney, and J. Wulff, *Introduction to Materials Science and Engineering*. Copyright © 1976 by John Wiley & Sons, New York. Reprinted by permission of John Wiley & Sons, Inc.)

possessing these properties may reach its saturation magnetization with a relatively low applied field (i.e., is easily magnetized and demagnetized) and still has low hysteresis energy losses.

The saturation field or magnetization is determined only by the composition of the material. For example, in cubic ferrites, substitution of a divalent metal ion such as Ni^{2+} for Fe^{2+} in $FeO–Fe_2O_3$ will change the saturation magnetization. However, susceptibility and coercivity (H_c), which also influence the shape of the hysteresis curve, are sensitive to structural variables rather than to composition. For example, a low value of coercivity corresponds to the easy movement of domain walls as the magnetic field changes magnitude and/or direction. Structural defects such as particles of a nonmagnetic phase or voids in the magnetic material tend to restrict the motion of domain walls, and thus increase the coercivity. Consequently, a soft magnetic material must be free of such structural defects.

Another property consideration for soft magnetic materials is electrical resistivity. In addition to the hysteresis energy losses described above, energy losses may result from electrical currents that are induced in a magnetic material by a magnetic field that varies in magnitude and direction with time; these are called *eddy currents*. It is most desirable to minimize these energy losses in soft magnetic materials by increasing the electrical resistivity. This is accomplished in ferromagnetic materials by forming solid solution alloys; iron–silicon and iron–nickel alloys are examples. The ceramic ferrites are commonly used for applications requiring soft magnetic materials because they are intrinsically electrical insulators. Their applicability is somewhat limited, however, inasmuch as they have relatively small susceptibilities. The properties of a half-dozen soft magnetic materials are shown in Table 18.5.

The hysteresis characteristics of soft magnetic materials may be enhanced for some applications by an appropriate heat treatment in the presence of a magnetic field. Using such a technique, a square hysteresis loop may be produced, which is desirable in some magnetic amplifier and pulse transformer applications. In addition, soft magnetic materials are used in generators, motors, dynamos, and switching circuits.

Table 18.5 **Typical Properties for Several Soft Magnetic Materials**

Material	*Composition (wt%)*	*Initial Relative Permeability* μ_i	*Saturation Flux Density* B_s *[tesla (gauss)]*	*Hysteresis Loss/Cycle* [J/m^3 (erg/cm^3)]	*Resistivity* ρ (Ω-m)
Commercial iron ingot	99.95Fe	150	2.14 (21,400)	270 (2700)	1.0×10^{-7}
Silicon–iron (oriented)	97Fe, 3Si	1400	2.01 (20,100)	40 (400)	4.7×10^{-7}
45 Permalloy	55Fe, 45Ni	2500	1.60 (16,000)	120 (1200)	4.5×10^{-7}
Supermalloy	79Ni, 15Fe, 5Mo, 0.5Mn	75,000	0.80 (8000)	—	6.0×10^{-7}
Ferroxcube A	$48MnFe_2O_4$, $52ZnFe_2O_4$	1400	0.33 (3300)	~40 (~400)	2000
Ferroxcube B	$36NiFe_2O_4$, $64ZnFe_2O_4$	650	0.36 (3600)	~35 (~350)	10^7

Source: Adapted from *Metals Handbook: Properties and Selection: Stainless Steels, Tool Materials and Special-Purpose Metals,* Vol. 3, 9th edition, D. Benjamin, Senior Editor, American Society for Metals, 1980.

18.9 HARD MAGNETIC MATERIALS

Hard magnetic materials are utilized in permanent magnets, which must have a high resistance to demagnetization. In terms of hysteresis behavior, a **hard magnetic material** has a high remanence, coercivity, and saturation flux density, as well as a low initial permeability, and high hysteresis energy losses. The hysteresis characteristics for hard and soft magnetic materials are compared in Figure 18.16. The two most important characteristics relative to applications for these materials are the coercivity and what is termed the ‘‘energy product,’’ designated as $(BH)_{\max}$. This $(BH)_{\max}$ corresponds to the area of the largest B-H rectangle that can be constructed within the second quadrant of the hysteresis curve, Figure 18.17; its units are kJ/m^3 (MGOe).[3] The value of the energy product is representative of the energy required to demagnetize a permanent magnet; that is, the larger $(BH)_{\max}$ the harder is the material in terms of its magnetic characteristics.

Again, hysteresis behavior is related to the ease with which the magnetic domain boundaries move; by impeding domain wall motion, the coercivity and susceptibility are enhanced, such that a large external field is required for demagnetization. Furthermore, these characteristics are interrelated to the microstructure of the material.

CONVENTIONAL HARD MAGNETIC MATERIALS

Hard magnetic materials fall within two main categories—conventional and high energy. The conventional materials have $(BH)_{\max}$ values that range between about 2

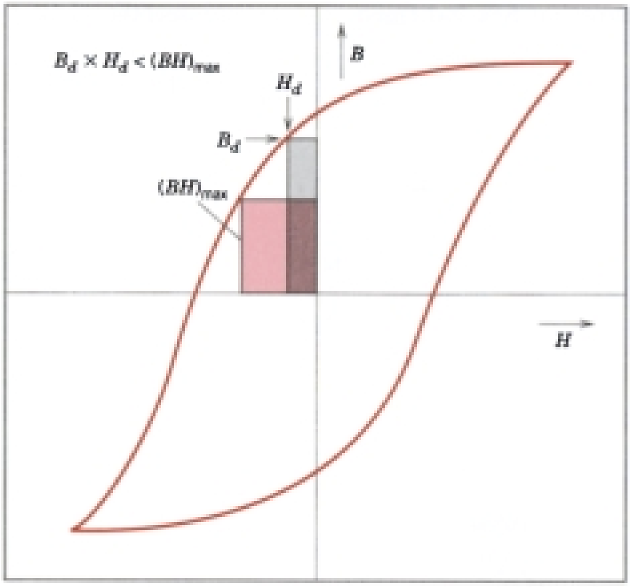

FIGURE 18.17 Schematic magnetization curve that displays hysteresis. Within the second quadrant are drawn two B-H energy product rectangles; the area of that rectangle labeled $(BH)_{\max}$ is the largest possible, which is greater than the area defined by B_d-H_d.

---

[3] MGOe is defined as

$$1 \text{ MGOe} = 10^6 \text{ gauss-oersted}$$

Furthermore, conversion from cgs-emu to SI units is accomplished by the relationship

$$1 \text{ MGOe} = 7.96 \text{ kJ/m}^3$$

and 80 kJ/m^3 (0.25 and 10 MGOe). These include ferromagnetic materials—magnet steels, cunife (Cu-Ni-Fe) alloys, alnico (Al-Ni-Co) alloys—as well as the hexagonal ferrites (BaO-$6Fe_2O_3$). Table 18.6 presents some of the critical properties of several of these hard magnetic materials.

The hard magnet steels are normally alloyed with tungsten and/or chromium. Under the proper heat-treating conditions these two elements readily combine with carbon in the steel to form tungsten and chromium carbide precipitate particles, which are especially effective in obstructing domain wall motion. For the other metal alloys, an appropriate heat-treatment forms extremely small single-domain and strongly magnetic iron-cobalt particles within a nonmagnetic matrix phase.

HIGH-ENERGY HARD MAGNETIC MATERIALS

Permanent magnetic materials having energy products in excess of about 80 kJ/m^3 (10 MGOe) are considered to be of the high-energy type. These are recently developed intermetallic compounds that have a variety of compositions; the two that have found commercial exploitation are $SmCo_5$ and $Nd_2Fe_{14}B$. Their magnetic properties are also listed in Table 18.6.

Samarium-Cobalt Magnets

$SmCo_5$ is a member of a group of alloys that are combinations of cobalt or iron and a light rare earth element; a number of these alloys exhibit high-energy, hard magnetic behavior, but $SmCo_5$ is the only one of commercial significance. The energy products of these $SmCo_5$ materials [between 120 and 240 kJ/m^3 (15 and 30 MGOe)] are considerably higher than the conventional hard magnetic materials (Table 18.6); in addition, they have relatively large coercivities. Powder metallurgical

Table 18.6 **Typical Properties for Several Hard Magnetic Materials**

Material	*Composition (wt%)*	*Remanence B_r [tesla (gauss)]*	*Coercivity H_c [amp-turn/m (Oe)]*	*$(BH)_{max}$ [kJ/m^3 (MGOe)]*	*Curie Temperature T_c [°C (°F)]*	*Resistivity ρ (Ω-m)*
Tungsten steel	92.8 Fe, 6 W, 0.5 Cr, 0.7 C	0.95 (9500)	5900 (74)	2.6 (0.33)	760 (1400)	3.0×10^{-7}
Cunife	20 Fe, 20 Ni, 60 Cu	0.54 (5400)	44,000 (550)	12 (1.5)	410 (770)	1.8×10^{-7}
Sintered alnico 8	34 Fe, 7 Al, 15 Ni, 35 Co, 4 Cu, 5 Ti	0.76 (7600)	125,000 (1550)	36 (4.5)	860 (1580)	—
Sintered ferrite 3	BaO-$6Fe_2O_3$	0.32 (3200)	240,000 (3000)	20 (2.5)	450 (840)	$\sim 10^4$
Cobalt rare earth 1	$SmCo_5$	0.92 (9200)	720,000 (9,000)	170 (21)	725 (1340)	5.0×10^{-7}
Sintered neodymium-iron-boron	$Nd_2Fe_{14}B$	1.16 (11,600)	848,000 (10,600)	255 (32)	310 (590)	1.6×10^{-6}

Source: Adapted from *ASM Handbook*, Vol. 2, *Properties and Selection: Nonferrous Alloys and Special-Purpose Materials*. Copyright © 1990 by ASM International. Reprinted by permission of ASM International, Materials Park, OH.

techniques are used to fabricate $SmCo_5$ magnets. The appropriately alloyed material is first ground into a fine powder; the powder particles are aligned using an external magnetic field, and then pressed into the desired shape. The piece is then sintered at an elevated temperature, followed by another heat treatment that improves the magnetic properties.

Neodymium-Iron-Boron Magnets

Samarium is a rare and relatively expensive material; furthermore, the price of cobalt is variable and its sources are unreliable. Consequently, the $Nd_2Fe_{14}B$ alloys have become the materials of choice for a large number and wide diversity of applications requiring hard magnetic materials. Coercivities and energy products of these materials rival those of the samarium-cobalt alloys (Table 18.6).

The magnetization–demagnetization behavior of these materials is a function of domain wall mobility, which, in turn, is controlled by the final microstructure—that is, the size, shape, and orientation of the crystallites or grains, as well as the nature and distribution of any second-phase particles that are present. Of course, microstructure will depend on how the material is processed. Two different processing techniques are available for the fabrication of $Nd_2Fe_{14}B$ magnets: powder metallurgy (sintering) and rapid solidification (melt spinning). The powder metallurgical approach is similar to that used for the $SmCo_5$ materials. For rapid solidification, the alloy, in molten form, is quenched very rapidly such that either an amorphous or very fine grained and thin solid ribbon is produced. This ribbon material is then pulverized, compacted into the desired shape, and subsequently heat treated. Rapid solidification is the more involved of the two fabrication processes; nevertheless, it is continuous, whereas powder metallurgy is a batch process, which has its inherent disadvantages.

These high-energy hard magnetic materials are employed in a host of different devices in a variety of technological fields. One common application is in motors. Permanent magnets are far superior to electromagnets in that their magnetic fields are continuously maintained and without the necessity of having to expend electrical power; furthermore, no heat is generated during operation. Motors using permanent magnets are much smaller than their electromagnet counterparts and are utilized extensively in fractional horse-power units. Familiar motor applications include the following: in cordless drills and screw drivers; in automobiles (starting, window winder, wiper, washer, and fan motors); in audio and video recorders; and clocks. Other common devices that employ these magnetic materials are speakers in audio systems, lightweight earphones, hearing aids, and computer peripherals.

18.10 MAGNETIC STORAGE

Within the past few years, magnetic materials have become increasingly important in the area of information storage; in fact, magnetic recording has become virtually the universal technology for the storage of electronic information. This is evidenced by the preponderance of audio tapes, VCRs, computer hard disks, floppy disks, credit cards, etc. Whereas with computers, semiconductor elements serve as primary memory, magnetic disks are used for secondary memory because they are capable of storing larger quantities of information and at a lower cost. Furthermore, the recording and television industries rely heavily on magnetic tapes for the storage and reproduction of audio and video sequences.

In essence, computer bytes, sound, or visual images in the form of electrical signals are recorded on very small segments of the magnetic storage medium—a tape or disk. Transference to and retrieval from the tape or disk is accomplished by means of an inductive read–write head, which consists basically of a wire coil wound around a magnetic material core into which a gap is cut. Data are introduced (or ''written'') by the electrical signal within the coil, which generates a magnetic field across the gap. This field in turn magnetizes a very small area of the disk or tape within the proximity of the head. Upon removal of the field, the magnetization remains; that is, the signal has been stored. The essential features of this recording process are shown in Figure 18.18.

Furthermore, the same head may be utilized to retrieve (or ''read'') the stored information. A voltage is induced when there is a change in the magnetic field as the tape or disk passes by the head coil gap; this may be amplified and then converted back into its original form or character. This process is also represented in Figure 18.18.

Recently hybrid heads that consist of an inductive-write and a magnetoresistive read head in a single unit have been introduced. In the magnetoresistive head, the electrical resistance of the magnetoresistive thin film element is changed as a result of magnetic field changes when the tape or disk passes by the read head. Higher sensitivies and higher data transfer rates make magnetoresistive heads very attractive.

There are two principal types of magnetic media—*particulate* and *thin film*. Particulate media consist of very small needlelike or acicular particles, normally of γ-Fe_2O_3 ferrite or CrO_2; these are applied and bonded to a polymeric film (for magnetic tapes) or to a metal or polymer disk. During manufacture, these particles are aligned with their long axes in a direction that parallels the direction of motion past the head (see Figures 18.18 and 18.19). Each particle is a single domain that may be magnetized only with its magnetic moment lying along this axis. Two magnetic states are possible, corresponding to the saturation magnetization in one axial direction, and its opposite. These two states make possible the storage of information in digital form, as 1's and 0's. In one system, a 1 is represented by a

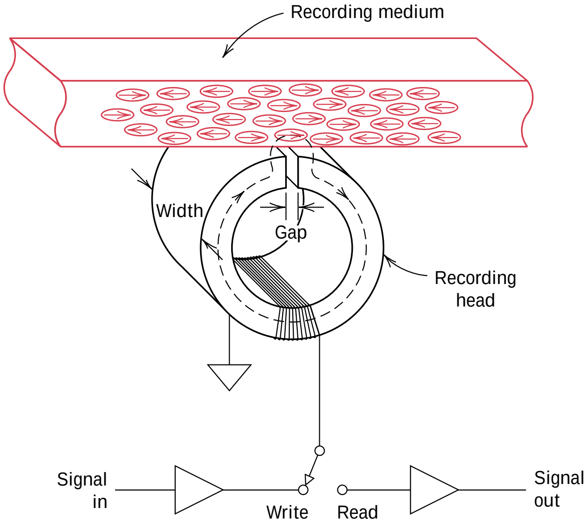

FIGURE 18.18 Schematic representation showing how information is stored and retrieved using a magnetic storage medium. (From J. U. Lemke, *MRS Bulletin*, Vol. XV, No. 3, p. 31, 1990. Reprinted with permission.)

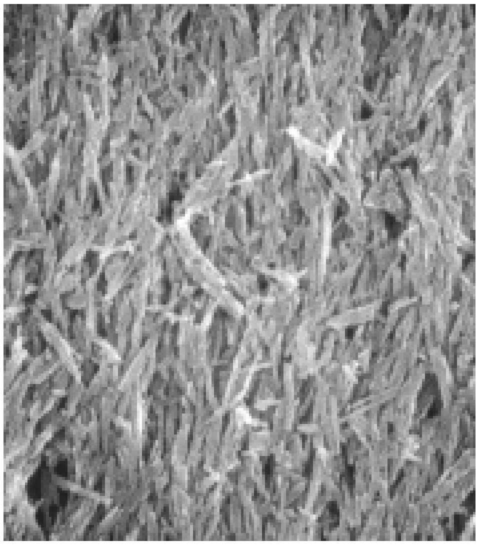

Figure 18.19 A scanning electron micrograph showing the microstructure of a magnetic storage disk. Needle-shaped particles of γ-Fe_2O_3 are oriented and embedded within an epoxy phenolic resin. 8000×. (Photograph courtesy of P. Rayner and N. L. Head, IBM Corporation.)

reversal in the magnetic field direction from one small area of the storage medium to another as the numerous acicular particles of each such region pass by the head. A lack of reversal between adjacent regions is indicated by a 0.

The thin-film storage technology is relatively new and provides higher storage capacities at lower costs. It is employed mainly on rigid disk drives and consists of a multilayered structure. A magnetic thin-film layer is the actual storage component (see Figure 18.20). This film is normally either a CoPtCr or CoCrTa alloy, with a thickness of between 10 and 50 nm (100 and 500 Å). A substrate layer below and upon which the thin film resides is pure chromium or a chromium alloy. The thin film itself is polycrystalline, having an average grain size that is typically between 10 and 30 nm (100 and 300 Å). Each grain within the thin film is a single magnetic domain, and it is highly desirable that grain shape and size be relatively uniform. For magnetic storage disks that employ these thin films, the crystallographic direction of easy magnetization for each grain is aligned in the direction of disk motion (or the direction opposite) (see Figure 18.20). The mechanism of magnetic storage within each of these single-domain grains is the same as for the needle-shaped particles, as described above—i.e., the two magnetic states correspond to domain magnetization in one direction or its antiparallel equivalent.

The storage density of thin films is greater than for particulate media because the packing efficiency of thin-film domains is greater than for the acicular particles; particles will always be separated with void space in between. At the time of this writing, areal storage densities for particulate media are on the order of 1×10^8 bit/in.^{2} (1.5×10^5 bit/mm^2); for thin films, storage densities are approximately an order of magnitude greater [i.e., $\sim 2 \times 10^9$ bit/in.^{2} (3×10^6 bit/mm^2)].

Regarding specific magnetic properties, the hysteresis loops for these magnetic storage media should be relatively large and square. These characteristics ensure that storage will be permanent, and, in addition, magnetization reversal will result over a narrow range of applied field strengths. For particulate recording media, saturation flux density normally ranges from 0.4 to 0.6 tesla (4000 and 6000 gauss); for thin films, B_s will lie between 0.6 and 1.2 tesla (6000 and 12,000 gauss). Coercivity values are typically in the range of 1.5×10^5 to 2.5×10^5 A/m (2000 to 3000 Oe).

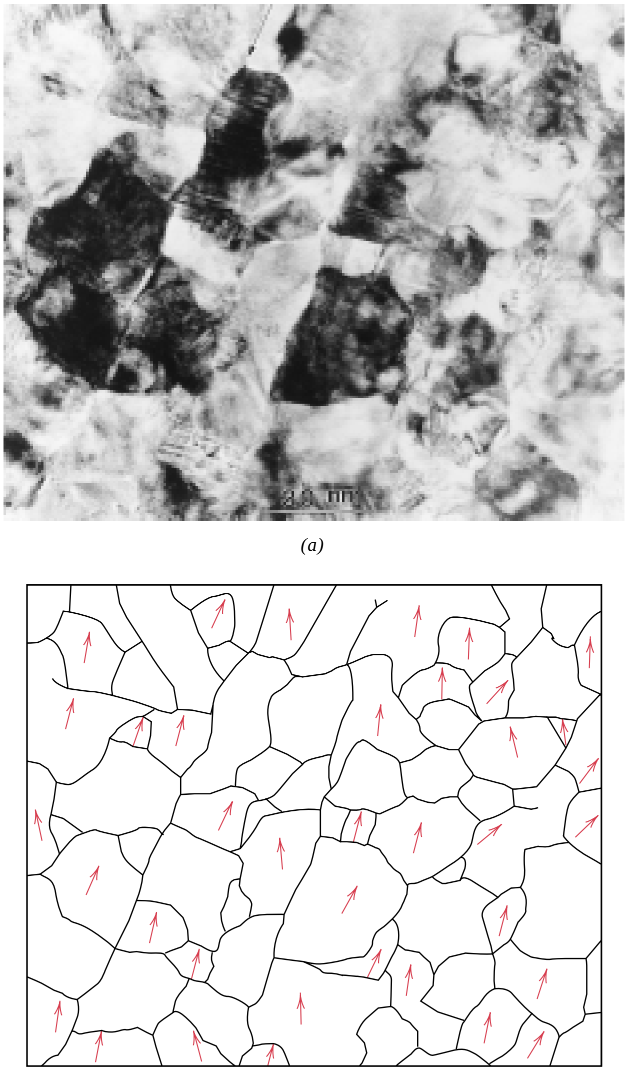
(a)

(b)

Figure 18.20 (*a*) A high-resolution transmission electron micrograph showing the microstructure of a cobalt–chromium–platinum thin film that is used as a high-density magnetic storage medium. The arrow at the top indicates the motion direction of the medium. 500,000×. (*b*) A representation of the grain structure for the electron micrograph in (*a*); the arrows in some of the grains indicate the texture, or the direction of easy magnetization. (From M. R. Kim, S. Guruswamy, and K. E. Johnson, *J. Appl. Phys.*, Vol. 74, No. 7, p. 4646, 1993. Reprinted with permission.)

18.11 SUPERCONDUCTIVITY

Superconductivity is basically an electrical phenomenon; however, its discussion has been deferred to this point because there are magnetic implications relative to the superconducting state, and, in addition, superconducting materials are used primarily in magnets capable of generating high fields.

As most high-purity metals are cooled down to temperatures nearing 0 K, the electrical resistivity decreases gradually, approaching some small yet finite value that is characteristic of the particular metal. There are a few materials, however, for which the resistivity, at a very low temperature, abruptly plunges from a finite value to one that is virtually zero and remains there upon further cooling. Materials that display this latter behavior are called *superconductors*, and the temperature

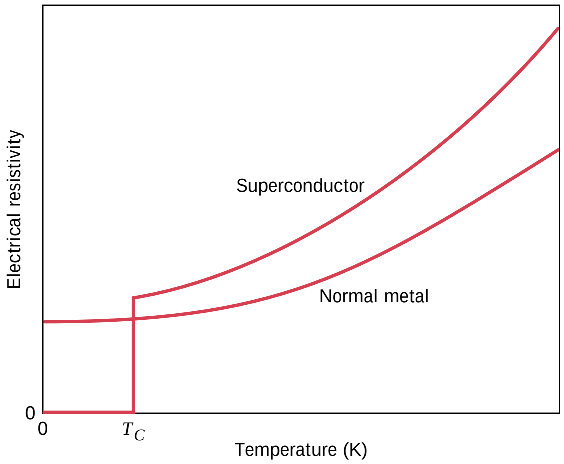

Figure 18.21 Temperature dependence of the electrical resistivity for normally conducting and superconducting materials in the vicinity of 0 K.

at which they attain **superconductivity** is called the critical temperature T_C.[4] The resistivity–temperature behaviors for superconductive and nonsuperconductive materials are contrasted in Figure 18.21. The critical temperature varies from superconductor to superconductor but lies between less than 1 K and approximately 20 K for metals and metal alloys. Recently, it has been demonstrated that some complex oxide ceramics have critical temperatures in excess of 100 K.

At temperatures below T_C, the superconducting state will cease upon application of a sufficiently large magnetic field, termed the critical field H_C, which depends on temperature and decreases with increasing temperature. The same may be said for current density; that is, a critical applied current density J_C exists below which a material is superconductive. Figure 18.22 shows schematically the boundary in temperature-magnetic field-current density space separating normal and supercon-

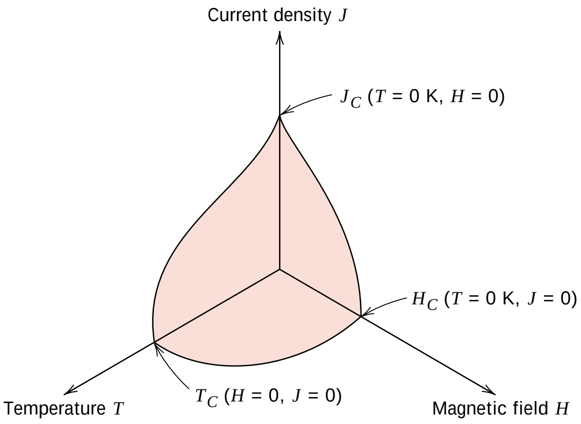

Figure 18.22 Critical temperature, current density, and magnetic field boundary separating superconducting and normal conducting states (schematic).

---

[4] The symbol T_c is used to represent both the Curie temperature (Section 18.6) and the superconducting critical temperature in the scientific literature. They are totally different entities and should not be confused. In this discussion they are denoted by T_c and T_C, respectively.

ducting states. The position of this boundary will, of course, depend on the material. For temperature, magnetic field, and current density values lying between the origin and this boundary, the material will be superconductive; outside the boundary, conduction is normal.

The superconductivity phenomenon has been satisfactorily explained by means of a rather involved theory. In essence, the superconductive state results from attractive interactions between pairs of conducting electrons; the motions of these paired electrons become coordinated such that scattering by thermal vibrations and impurity atoms is highly inefficient. Thus, the resistivity, being proportional to the incidence of electron scattering, is zero.

On the basis of magnetic response, superconducting materials may be divided into two classifications designated as type I and type II. Type I materials, while in the superconducting state, are completely diamagnetic; that is, all of an applied magnetic field will be excluded from the body of material, a phenomenon known as the *Meissner effect*, which is illustrated in Figure 18.23. As H is increased, the material remains diamagnetic until the critical magnetic field H_C is reached. At this point, conduction becomes normal, and complete magnetic flux penetration takes place. Several metallic elements including aluminum, lead, tin, and mercury belong to the type I group.

Type II superconductors are completely diamagnetic at low applied fields, and field exclusion is total. However, the transition from the superconducting state to the normal state is gradual and occurs between lower critical and upper critical fields, designated H_{C1} and H_{C2}, respectively. The magnetic flux lines begin to penetrate into the body of material at H_{C1}, and with increasing applied magnetic field, this penetration continues; at H_{C2}, field penetration is complete. For fields between H_{C1} and H_{C2}, the material exists in what is termed a mixed state—both normal and superconducting regions are present.

Type II superconductors are preferred over type I for most practical applications by virtue of their higher critical temperatures and critical magnetic fields. At present, the three most commonly utilized superconductors are niobium-zirconium (Nb–Zr) and niobium-titanium (Nb–Ti) alloys and the niobium-tin intermetallic compound Nb_3Sn. Table 18.7 lists several type I and II superconductors, their critical temperatures, and their critical magnetic flux densities.

Recently, a family of ceramic materials that are normally electrically insulative have been found to be superconductors with inordinately high critical temperatures. Initial research has centered on yttrium barium copper oxide, $YBa_2Cu_3O_7$, which has a critical temperature of about 92 K. This material has a complex perovskite-type crystal structure (Section 3.6). New superconducting ceramic materials reported

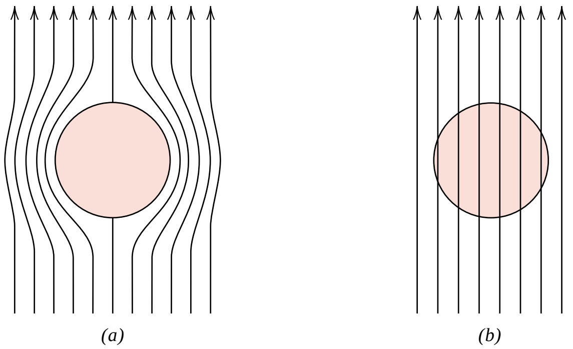

FIGURE 18.23 Representation of the Meissner effect. (*a*) While in the superconducting state, a body of material (circle) excludes a magnetic field (arrows) from its interior. (*b*) The magnetic field penetrates the same body of material once it becomes normally conductive.

Table 18.7 Critical Temperatures and Magnetic Fluxes for Selected Superconducting Materials

Material	*Critical Temperature T_C (K)*	*Critical Magnetic Flux Density B_C (tesla)*[a]
	Elements[b]	
Tungsten	0.02	0.0001
Titanium	0.40	0.0056
Aluminum	1.18	0.0105
Tin	3.72	0.0305
Mercury (α)	4.15	0.0411
Lead	7.19	0.0803
	Compounds and Alloys[b]	
Nb-Ti alloy	10.2	12
Nb-Zr alloy	10.8	11
$PbMo_6S_8$	14.0	45
V_3Ga	16.5	22
Nb_3Sn	18.3	22
Nb_3Al	18.9	32
Nb_3Ge	23.0	30
	Ceramic Compounds	
$YBa_2Cu_3O_7$	92	—
$Bi_2Sr_2Ca_2Cu_3O_{10}$	110	—
$Tl_2Ba_2Ca_2Cu_3O_{10}$	125	—
$HgBa_2Ca_2Cu_2O_8$	153	—

[a] The critical magnetic flux density ($\mu_0 H_C$) for the elements was measured at 0 K. For alloys and compounds, the flux is taken as $\mu_0 H_{C2}$ (in teslas), measured at 0 K.

[b] **Source:** Adapted with permission from *Materials at Low Temperatures*, R. P. Reed and A. F. Clark, Editors, American Society for Metals, Metals Park, OH, 1983.

to have even higher critical temperatures have been and are currently being developed. Several of these materials and their critical temperatures are listed in Table 18.7. The technological potential of these materials is extremely promising inasmuch as their critical temperatures are above 77 K, which permits the use of liquid nitrogen, a very inexpensive coolant in comparison to liquid hydrogen and liquid helium. These new ceramic superconductors are not without drawbacks, chief of which is their brittle nature. This characteristic limits the ability of these materials to be fabricated into useful forms such as wires.

The phenomenon of superconductivity has many important practical implications. Superconducting magnets capable of generating high fields with low power consumption are currently being employed in scientific test and research equipment. In addition, they are also used for magnetic resonance imaging (MRI) in the medical field as a diagnostic tool. Abnormalities in body tissues and organs can be detected on the basis of the production of cross-sectional images. Chemical analysis of body tissues is also possible using magnetic resonance spectroscopy (MRS). Numerous other potential applications of superconducting materials also exist. Some of the areas being explored include (1) electrical power transmission through superconducting materials—power losses would be extremely low, and the equipment would operate at low voltage levels; (2) magnets for high-energy particle accelerators; (3) higher-speed switching and signal transmission for computers; and (4) high-speed magnetically levitated trains, wherein the levitation results from magnetic field repulsion. The chief deterrent to the widespread application of these superconducting materials is, of course, the difficulty in attaining and maintaining extremely low temperatures. Hopefully, this problem will be overcome with the development of the new generation of superconductors with reasonably high critical temperatures.

SUMMARY

The macroscopic magnetic properties of a material are a consequence of interactions between an external magnetic field and the magnetic dipole moments of the constituent atoms. Associated with each individual electron are both orbital and spin magnetic moments. The net magnetic moment for an atom is just the sum of the contributions of each of its electrons, wherein there will be spin and orbital moment cancellation of electron pairs.

Diamagnetism results from changes in electron orbital motion that are induced by an external field. The effect is extremely small and in opposition to the applied field. All materials are diamagnetic. Paramagnetic materials are those having permanent atomic dipoles, which are acted on individually and are aligned in the direction of an external field. Since the magnetizations are relatively small and persist only while an applied field is present, diamagnetic and paramagnetic materials are considered to be nonmagnetic.

Large and permanent magnetizations may be established within the ferromagnetic metals (Fe, Co, Ni). Atomic magnetic dipole moments are of spin origin, which are coupled and mutually aligned with moments of adjacent atoms.

Antiparallel coupling of adjacent cation spin moments is found for some ionic materials. Those in which there is total cancellation of spin moments are termed antiferromagnetic. With ferrimagnetism, permanent magnetization is possible because spin moment cancellation is incomplete. For cubic ferrites, the net magnetization results from the divalent ions (e.g., Fe^{2+}) that reside on octahedral lattice sites, the spin moments of which are all mutually aligned.

With rising temperature, increased thermal vibrations tend to counteract the dipole coupling forces in ferromagnetic and ferrimagnetic materials. Consequently, the saturation magnetization gradually diminishes with temperature, up to the Curie temperature, at which point it drops to near zero; above T_c, these materials are paramagnetic.

Below its Curie temperature, a ferromagnetic or ferrimagnetic material is composed of domains—small-volume regions wherein all net dipole moments are mutually aligned and the magnetization is saturated. The total magnetization of the solid is just the appropriately weighted vector sum of the magnetizations of all these domains. As an external magnetic field is applied, domains having magnetization vectors oriented in the direction of the field grow at the expense of domains that have unfavorable magnetization orientations. At total saturation, the entire solid is a single domain and the magnetization is aligned with the field direction. The change in domain structure with increase or reversal of a magnetic field is accomplished by the motion of domain walls. Both hysteresis (the lag of the B field behind the applied H field) as well as permanent magnetization (or remanence) result from the resistance to movement of these domain walls.

For soft magnetic materials, domain wall movement is easy during magnetization and demagnetization. Consequently, they have small hysteresis loops and low energy losses. Domain wall motion is much more difficult for the hard magnetic materials, which results in larger hysteresis loops; because greater fields are required to demagnetize these materials, the magnetization is more permanent.

Information storage is accomplished using magnetic materials in both needle-shaped particulate and thin-film forms.

Superconductivity has been observed in a number of materials, in which, upon cooling and in the vicinity of absolute zero temperature, the electrical resistivity vanishes. The superconducting state ceases to exist if temperature, magnetic field, or current density exceeds the critical value. For type I superconductors, magnetic field exclusion is complete below a critical field, and field penetration is complete once H_C is exceeded. This penetration is gradual with increasing magnetic field for type II materials. New complex oxide ceramics are being developed with relatively high critical temperatures, which allow inexpensive liquid nitrogen to be used as a coolant.

IMPORTANT TERMS AND CONCEPTS

Antiferromagnetism
Bohr magneton
Coercivity
Curie temperature
Diamagnetism
Domain
Ferrimagnetism
Ferrite (ceramic)
Ferromagnetism
Hard magnetic material
Hysteresis
Magnetic field strength
Magnetic flux density
Magnetic induction
Magnetic susceptibility
Magnetization
Paramagnetism
Permeability
Remanence
Saturation magnetization
Soft magnetic material
Superconductivity

REFERENCES

Azaroff, L. V. and J. J. Brophy, *Electronic Processes in Materials*, McGraw-Hill Book Company, New York, 1963, Chapter 13. Reprinted by TechBooks, Marietta, OH.

Brockman, F. G., ''Magnetic Ceramics—A Review and Status Report,'' *American Ceramic Society Bulletin*, Vol. 47, No. 2, February 1968, pp. 186–194.

Cullity, B. D., *Introduction to Magnetic Materials*, Addison-Wesley Publishing Co., Reading, MA, 1972.

Keffer, F., ''The Magnetic Properties of Materials,'' *Scientific American*, Vol. 217, No. 3, September 1967, pp. 222–234.

Rose, R. M., L. A. Shepard, and J. Wulff, *The Structure and Properties of Materials*, Vol. IV, *Electronic Properties*, John Wiley & Sons, New York, 1966, Chapters 9–11.

Teeble, R. S. and D. J. Craik, *Magnetic Materials*, Wiley-Interscience, New York, 1969. Reprinted by Books on Demand, Ann Arbor, MI.

Wert, C. A. and R. M. Thomson, *Physics of Solids*, 2nd edition, McGraw-Hill Book Company, New York, 1970, Chapters 20–22.

QUESTIONS AND PROBLEMS

18.1 A coil of wire 0.20 m long and having 200 turns carries a current of 10 A.

(a) What is the magnitude of the magnetic field strength H?

(b) Compute the flux density B if the coil is in a vacuum.

(c) Compute the flux density inside a bar of titanium that is positioned within the coil. The susceptibility for titanium is found in Table 18.2.

(d) Compute the magnitude of the magnetization M.

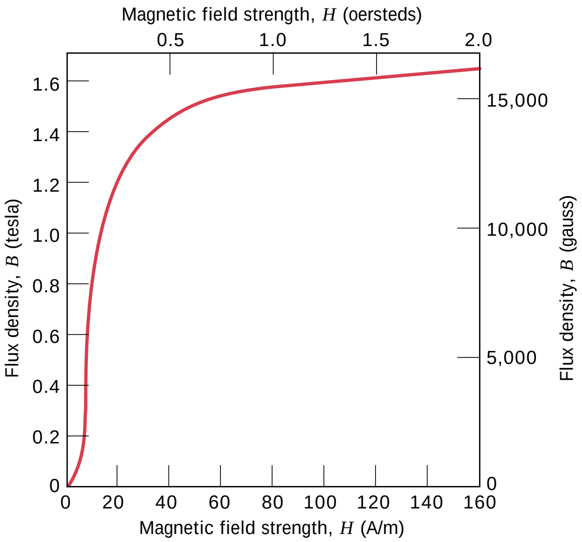

FIGURE 18.24 Initial magnetization B-versus-H curve for an iron-silicon alloy.

18.2 A coil of wire 0.1 m long and having 15 turns carries a current of 1.0 A.

(a) Compute the flux density if the coil is within a vacuum.

(b) A bar of an iron-silicon alloy, the B–H behavior for which is shown in Figure 18.24, is positioned within the coil. What is the flux density within this bar?

(c) Suppose that a bar of molybdenum is now situated within the coil. What current must be used to produce the same B field in the Mo as was produced in the iron–silicon alloy (part b) using 1.0 A?

18.3 Demonstrate that the relative permeability and the magnetic susceptibility are related according to Equation 18.7.

18.4 It is possible to express the magnetic susceptibility χ_m in several different units. For the discussion of this chapter, χ_m was used to designate the volume susceptibility in SI units, that is, the quantity that gives the magnetization per unit volume (m^3) of material when multiplied by H. The mass susceptibility $\chi_m(\text{kg})$ yields the magnetic moment (or magnetization) per kilogram of material when multiplied by H; and, similarly, the atomic susceptibility $\chi_m(\text{a})$ gives the magnetization per kilogram-mole. The latter two quantities are related to χ_m through the relationships

$$\chi_m = \chi_m(\text{kg}) \times \text{mass density (in kg/m}^3)$$

$$\chi_m(\text{a}) = \chi_m(\text{kg}) \times \text{atomic weight (in kg)}$$

When using the cgs-emu system, comparable parameters exist, which may be designated by χ'_m, $\chi'_m(\text{g})$, and $\chi'_m(\text{a})$; the χ_m and χ'_m are related in accordance with Table 18.1. From Table 18.2, χ_m for silver is -2.38×10^{-5}; convert this value into the other five susceptibilities.

18.5 **(a)** Explain the two sources of magnetic moments for electrons.

(b) Do all electrons have a net magnetic moment? Why or why not?

(c) Do all atoms have a net magnetic moment? Why or why not?

18.6 The magnetic flux density within a bar of some material is 0.435 tesla at an H field of 3.44×10^5 A/m. Compute the following for this material: **(a)** the magnetic permeability, and **(b)** the magnetic susceptibility. **(c)** What type(s) of magnetism would you suggest as being displayed by this material? Why?

18.7 The magnetization within a bar of some metal alloy is 3.2×10^5 A/m at an H field of 50 A/m. Compute the following: **(a)** the magnetic susceptibility, **(b)** the permeability, and **(c)** the magnetic flux density within this material. **(d)** What type(s) of magnetism would you suggest as being displayed by this material? Why?

18.8 Compute **(a)** the saturation magnetization and **(b)** the saturation flux density for cobalt, which has a net magnetic moment per atom of 1.72 Bohr magnetons and a density of 8.90 g/cm^3.

18.9 Confirm that there are 2.2 Bohr magnetons associated with each iron atom, given that the saturation magnetization is 1.70×10^6 A/m, that iron has a BCC crystal structure, and that the unit cell edge length is 0.2866 nm.

18.10 Assume there exists some hypothetical metal that exhibits ferromagnetic behavior and that has (1) a simple cubic crystal structure (Figure 3.40), (2) an atomic radius of 0.153 nm, and (3) a saturation flux density of 0.76 tesla. Determine the number of Bohr magnetons per atom for this material.

18.11 There is associated with each atom in paramagnetic and ferromagnetic materials a net magnetic moment. Explain why ferromagnetic materials can be permanently magnetized whereas paramagnetic ones cannot.

18.12 Cite the major similarities and differences between ferromagnetic and ferrimagnetic materials.

18.13 What is the difference between the spinel and inverse spinel crystal structures?

18.14 Consult another reference in which Hund's rule is outlined, and on its basis explain the net magnetic moments for each of the cations listed in Table 18.4.

18.15 Estimate **(a)** the saturation magnetization, and **(b)** the saturation flux density of nickel ferrite [$(NiFe_2O_4)_8$], which has a unit cell edge length of 0.8337 nm.

18.16 The chemical formula for manganese ferrite may be written as $(MnFe_2O_4)_8$ because there are eight formula units per unit cell. If this material has a saturation magnetization of 5.6×10^5 A/m and a density of 5.00 g/cm^3, estimate the number of Bohr magnetons associated with each Mn^{2+} ion.

18.17 The formula for yttrium iron garnet ($Y_3Fe_5O_{12}$) may be written in the form $Y_3^cFe_2^aFe_3^dO_{12}$, where the superscripts *a*, *c*, and *d* represent different sites on which the Y^{3+} and Fe^{3+} ions are located. The spin magnetic moments for the Y^{3+} and Fe^{3+} ions positioned in the *a* and *c* sites are oriented parallel to one another and antiparallel to the Fe^{3+} ions in *d* sites. Compute the number of Bohr magnetons associated with each Y^{3+} ion, given the following information: (1) each unit cell consists of eight formula ($Y_3Fe_5O_{12}$) units; (2) the unit cell is cubic with an edge length of 1.2376 nm; (3) the saturation magnetization for this material is 1.0×10^4 A/m; and (4) assume that there are 5 Bohr magnetons associated with each Fe^{3+} ion.

18.18 Explain why repeatedly dropping a permanent magnet on the floor will cause it to become demagnetized.

18.19 Briefly explain why the magnitude of the saturation magnetization decreases with increasing temperature for ferromagnetic materials, and why ferromagnetic behavior ceases above the Curie temperature.

18.20 Briefly describe the phenomenon of magnetic hysteresis, and why it occurs for ferromagnetic and ferrimagnetic materials.

18.21 Schematically sketch on a single plot the *B*-versus-*H* behavior for a ferromagnetic material **(a)** at 0 K, **(b)** at a temperature just below its Curie temperature, and **(c)** at a temperature just above its Curie temperature. Briefly explain why these curves have different shapes.

18.22 Schematically sketch the hysteresis behavior for a ferromagnet which is gradually demagnetized by cycling in an *H* field that alternates direction and decreases in magnitude.

18.23 Cite the differences between hard and soft magnetic materials in terms of both hysteresis behavior and typical applications.

18.24 Assume that the commercial iron (99.95 wt% Fe) in Table 18.5 just reaches the point of saturation when inserted within the coil in Problem 18.1. Compute the saturation magnetization.

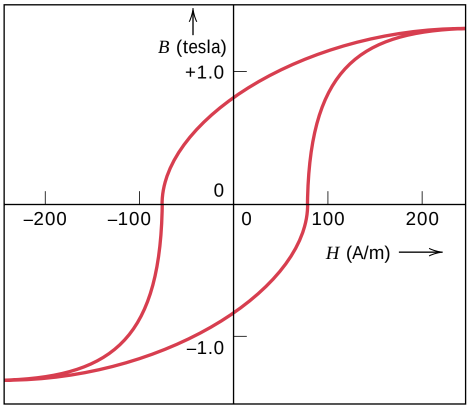

Figure 18.25 Complete magnetic hysteresis loop for a steel alloy.

18.25 Figure 18.25 shows the *B*-versus-*H* curve for a steel alloy.

(a) What is the saturation flux density?

(b) What is the saturation magnetization?

(c) What is the remanence?

(d) What is the coercivity?

(e) On the basis of the data in Tables 18.5 and 18.6, would you classify this material as a soft or hard magnetic material? Why?

18.26 A ferromagnetic material has a remanence of 1.25 teslas and a coercivity of 50,000 A/m. Saturation is achieved at a magnetic field intensity of 100,000 A/m, at which the flux density is 1.50 teslas. Using these data, sketch the entire hysteresis curve in the range $H = -100{,}000$ to $+100{,}000$ A/m. Be sure to scale and label both coordinate axes.

18.27 The following data are for a transformer steel:

***H* (A/m)**	***B* (teslas)**	***H* (A/m)**	***B* (teslas)**
0	0	200	1.04
10	0.03	400	1.28
20	0.07	600	1.36
50	0.23	800	1.39
100	0.70	1000	1.41
150	0.92		

(a) Construct a graph of *B* versus *H*.

(b) What are the values of the initial permeability and initial relative permeability?

(c) What is the value of the maximum permeability?

(d) At about what *H* field does this maximum permeability occur?

(e) To what magnetic susceptibility does this maximum permeability correspond?

18.28 An iron bar magnet having a coercivity of 4000 A/m is to be demagnetized. If the bar is inserted within a cylindrical wire coil 0.15 m long and having 100 turns, what electric current is required to generate the necessary magnetic field?

18.29 A bar of an iron-silicon alloy having the *B*–*H* behavior shown in Figure 18.24 is inserted within a coil of wire 0.20 m long and having 60 turns, through which passes a current of 0.1 A.

(a) What is the *B* field within this bar?

(b) At this magnetic field,
  (i) What is the permeability?
  (ii) What is the relative permeability?
  (iii) What is the susceptibility?
  (iv) What is the magnetization?

18.30 It is possible, by various means (e.g., alteration of microstructure and impurity additions), to control the ease with which domain walls move as the magnetic field is changed for ferromagnetic and ferrimagnetic materials. Sketch a schematic *B*-versus-*H* hysteresis loop for a ferromagnetic material, and superimpose on this plot the loop alterations that would occur if domain boundary movement were hindered.

18.31 Briefly explain the manner in which information is stored magnetically.

18.32 For a superconducting material at a temperature T below the critical temperature T_C, the critical field $H_C(T)$, depends on temperature according to the relationship

$$H_C(T) = H_C(0)\left(1 - \frac{T^2}{T_C^2}\right) \qquad (18.12)$$

where $H_C(0)$ is the critical field at 0 K.

(a) Using the data in Table 18.7, calculate the critical magnetic fields for tin at 1.5 and 2.5 K.

(b) To what temperature must lead be cooled in a magnetic field of 20,000 A/m for it to be superconductive?

18.33 Using Equation 18.12, determine which of the superconducting elements in Table 18.7 are superconducting at 3 K and in a magnetic field of 15,000 A/m.

18.34 Cite the differences between type I and type II superconductors.

18.35 Briefly describe the Meissner effect.

18.36 Cite the primary limitation of the new superconducting materials that have relatively high critical temperatures.

Design Problems

18.D1 A cobalt-nickel alloy is desired that has a saturation magnetization of 1.3×10^6 A/m. Specify its composition in weight percent nickel. Cobalt has an HCP crystal structure with a c/a ratio of 1.623, whereas the maximum solubility of Ni in Co at room temperature is approximately 35 wt%. Assume that the unit cell volume for this alloy is the same as for pure Co.

18.D2 Design a cubic mixed-ferrite magnetic material that has a saturation magnetization of 4.6×10^5 A/m.

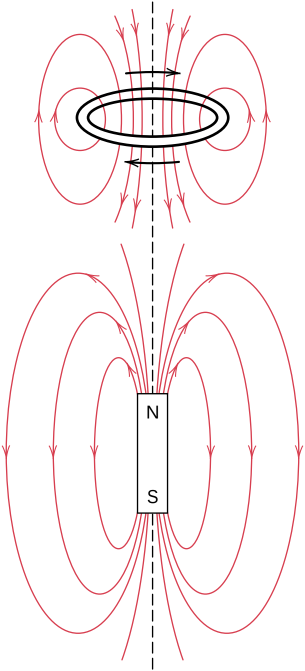

FIGURE 18.1 Magnetic field lines of force around a current loop and a bar magnet.

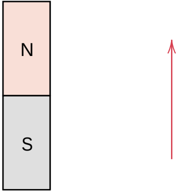

Figure 18.2 The magnetic moment as designated by an arrow.

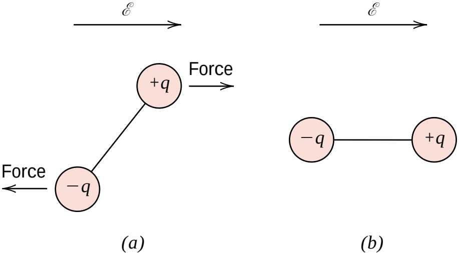

$\mathscr{E}$
Force
$+q$
Force
$-q$
(a)
$\mathscr{E}$
$-q$
$+q$
(b)

FIGURE 12.28 (*a*) Imposed forces (torque) acting on a dipole by an electric field. (*b*) Final dipole alignment with the field.

Chapter 12 / Electrical Properties

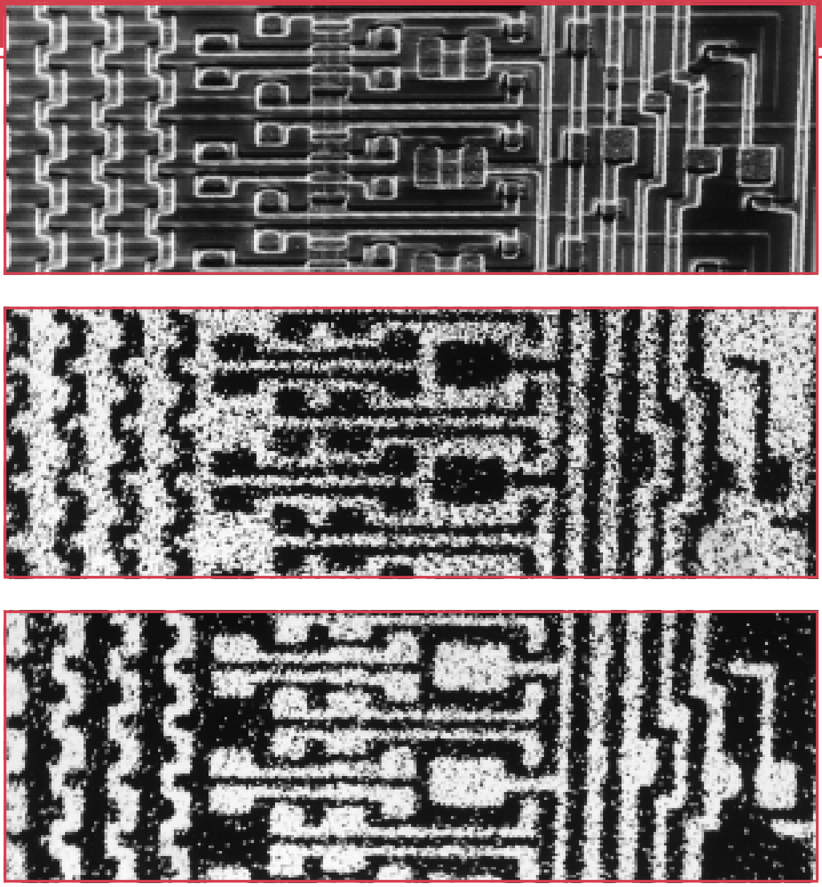

It was noted in {Section 5.12} that an image is generated on a scanning electron micrograph as a beam of electrons scans the surface of the specimen being examined. The electrons in this beam cause some of the specimen surface atoms to emit x-rays; the energy of an x-ray photon depends on the particular atom from which it radiates. It is possible to selectively filter out all but the x-rays emitted from one kind of atom. When projected on a cathode ray tube, small white dots are produced indicating the locations of the particular atom type; thus, a "dot map" of the image is generated.

Top: Scanning electron micrograph of an integrated circuit.

Center: A silicon dot map for the integrated circuit above, showing regions where silicon atoms are concentrated. Doped silicon is the semiconducting material from which integrated circuit elements are made.

Bottom: An aluminum dot map. Metallic aluminum is an electrical conductor and, as such, wires the circuit elements together. Approximately 200×.

Why Study the *Electrical Properties* of Materials?

Consideration of the electrical properties of materials is often important when materials selection and processing decisions are being made during the design of a component or structure. {For example, we discuss in Sections 20.12 through 20.17 materials that are used in the several components of one type of integrated circuit package.} The electrical behaviors of the various materials are diverse. Some need to be highly electrically conductive (e.g., connecting wires), whereas electrical insulativity is required of others (e.g., the protective package encapsulation).

Learning Objectives

After careful study of this chapter you should be able to do the following:

1. **Describe the four possible electron band structures for solid materials.**
2. **Briefly describe electron excitation events that produce free electrons/holes in (a) metals, (b) semiconductors (intrinsic and extrinsic), and (c) insulators.**
3. **Calculate the electrical conductivities of metals, semiconductors (intrinsic and extrinsic), and insulators given their charge carrier density(s) and mobility(s).**
4. **Distinguish between *intrinsic* and *extrinsic* semiconducting materials.**
5. **Note the manner in which electrical conductivity changes with increasing temperature for (a) metals, (b) semiconductors, and (c) insulating materials.**

{**6. For a *p–n* junction, explain the rectification process in terms of electron and hole motions.**}

{**7. Calculate the capacitance of a parallel-plate capacitor.**}

{**8. Define dielectric constant in terms of permittivities.**}

{**9. Briefly explain how the charge storing capacity of a capacitor may be increased by the insertion and polarization of a dielectric material between its plates.**}

{**10. Name and describe the three types of polarization.**}

12.1 INTRODUCTION

The prime objective of this chapter is to explore the electrical properties of materials, that is, their responses to an applied electric field. We begin with the phenomenon of electrical conduction: the parameters by which it is expressed, the mechanism of conduction by electrons, and how the electron energy band structure of a material influences its ability to conduct. These principles are extended to metals, semiconductors, and insulators. Particular attention is given to the characteristics of semiconductors, and then to semiconducting devices. Also treated are the dielectric characteristics of insulating materials. The final sections are devoted to the peculiar phenomena of ferroelectricity and piezoelectricity.

ELECTRICAL CONDUCTION

12.2 OHM'S LAW

One of the most important electrical characteristics of a solid material is the ease with which it transmits an electric current. **Ohm's law** relates the current I—or time rate of charge passage—to the applied voltage V as follows:

$$V = IR \tag{12.1}$$

where R is the resistance of the material through which the current is passing. The units for V, I, and R are, respectively, volts (J/C), amperes (C/s), and ohms (V/A). The value of R is influenced by specimen configuration, and for many materials is independent of current. The **resistivity** ρ is independent of specimen geometry but related to R through the expression

$$\rho = \frac{RA}{l} \tag{12.2}$$

where l is the distance between the two points at which the voltage is measured, and A is the cross-sectional area perpendicular to the direction of the current. The units for ρ are ohm-meters (Ω-m). From the expression for Ohm's law and

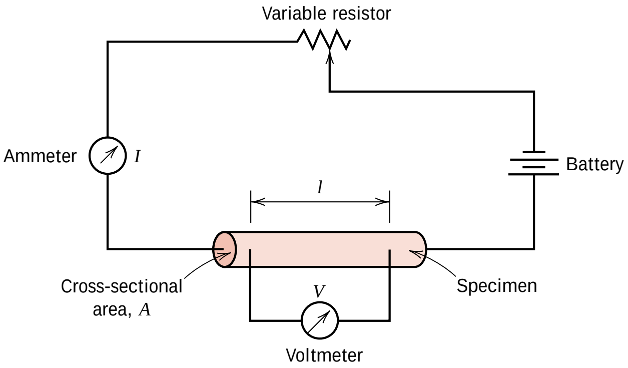

FIGURE 12.1 Schematic representation of the apparatus used to measure electrical resistivity.

Equation 12.2,

$$\rho = \frac{VA}{Il} \tag{12.3}$$

Figure 12.1 is a schematic diagram of an experimental arrangement for measuring electrical resistivity.

12.3 ELECTRICAL CONDUCTIVITY

Sometimes, **electrical conductivity** σ is used to specify the electrical character of a material. It is simply the reciprocal of the resistivity, or

$$\sigma = \frac{1}{\rho} \tag{12.4}$$

and is indicative of the ease with which a material is capable of conducting an electric current. The units for σ are reciprocal ohm-meters [$(\Omega\text{-m})^{-1}$, or mho/m]. The following discussions on electrical properties use both resistivity and conductivity.

In addition to Equation 12.1, Ohm's law may be expressed as

$$J = \sigma \mathscr{E} \tag{12.5}$$

in which J is the current density, the current per unit of specimen area I/A, and $\mathscr{E}$ is the electric field intensity, or the voltage difference between two points divided by the distance separating them, that is,

$$\mathscr{E} = \frac{V}{l} \tag{12.6}$$

The demonstration of the equivalence of the two Ohm's law expressions (Equations 12.1 and 12.5) is left as a homework exercise.

Solid materials exhibit an amazing range of electrical conductivities, extending over 27 orders of magnitude; probably no other physical property experiences this breadth of variation. In fact, one way of classifying solid materials is according to the ease with which they conduct an electric current; within this classification scheme there are three groupings: *conductors*, *semiconductors*, and *insulators*. **Metals** are good conductors, typically having conductivities on the order of 10^7 $(\Omega\text{-m})^{-1}$. At the other extreme are materials with very low conductivities, ranging between 10^{-10} and 10^{-20} $(\Omega\text{-m})^{-1}$; these are electrical **insulators.** Materials with intermediate conductivities, generally from 10^{-6} to 10^4 $(\Omega\text{-m})^{-1}$, are termed **semiconductors.**

12.4 ELECTRONIC AND IONIC CONDUCTION

An electric current results from the motion of electrically charged particles in response to forces that act on them from an externally applied electric field. Positively charged particles are accelerated in the field direction, negatively charged particles in the direction opposite. Within most solid materials a current arises from the flow of electrons, which is termed *electronic conduction.* In addition, for ionic materials a net motion of charged ions is possible that produces a current; such is termed **ionic conduction.** The present discussion deals with electronic conduction; ionic conduction is treated briefly in Section 12.15.

12.5 ENERGY BAND STRUCTURES IN SOLIDS

In all conductors, semiconductors, and many insulating materials, only electronic conduction exists, and the magnitude of the electrical conductivity is strongly dependent on the number of electrons available to participate in the conduction process. However, not all electrons in every atom will accelerate in the presence of an electric field. The number of electrons available for electrical conduction in a particular material is related to the arrangement of electron states or levels with respect to energy, and then the manner in which these states are occupied by electrons. A thorough exploration of these topics is complicated and involves principles of quantum mechanics that are beyond the scope of this book; the ensuing development omits some concepts and simplifies others.

Concepts relating to electron energy states, their occupancy, and the resulting electron configuration for isolated atoms were discussed in Section 2.3. By way of review, for each individual atom there exist discrete energy levels that may be occupied by electrons, arranged into shells and subshells. Shells are designated by integers (1, 2, 3, etc.), and subshells by letters (s, p, d, and f). For each of s, p, d, and f subshells, there exist, respectively, one, three, five, and seven states. The electrons in most atoms fill just the states having the lowest energies, two electrons of opposite spin per state, in accordance with the Pauli exclusion principle. The electron configuration of an isolated atom represents the arrangement of the electrons within the allowed states.

Let us now make an extrapolation of some of these concepts to solid materials. A solid may be thought of as consisting of a large number, say, N, of atoms initially separated from one another, which are subsequently brought together and bonded to form the ordered atomic arrangement found in the crystalline material. At relatively large separation distances, each atom is independent of all the others and will have the atomic energy levels and electron configuration as if isolated. However, as the atoms come within close proximity of one another, electrons are acted upon, or perturbed, by the electrons and nuclei of adjacent atoms. This influence is such that each distinct atomic state may split into a series of closely spaced electron states in the solid, to form what is termed an **electron energy band.** The extent of splitting depends on interatomic separation (Figure 12.2) and begins with the outermost electron shells, since they are the first to be perturbed as the atoms coalesce. Within each band, the energy states are discrete, yet the difference between

FIGURE 12.2 Schematic plot of electron energy versus interatomic separation for an aggregate of 12 atoms ($N = 12$). Upon close approach, each of the 1*s* and 2*s* atomic states splits to form an electron energy band consisting of 12 states.

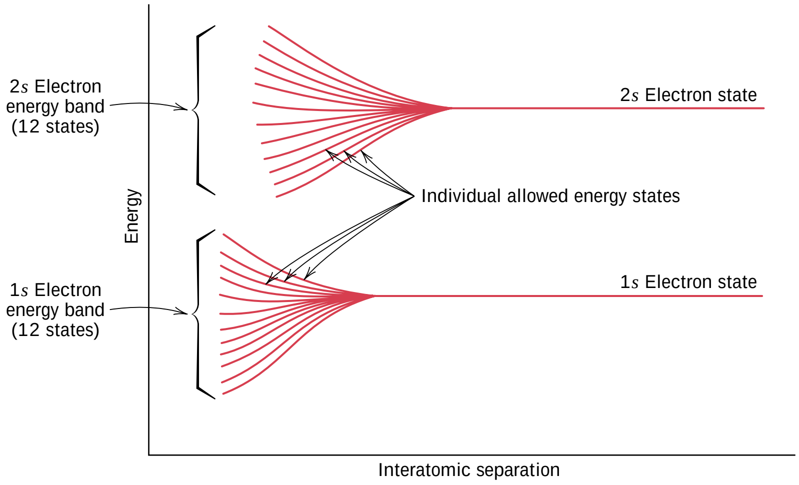
2*s* Electron energy band (12 states)
2*s* Electron state
Individual allowed energy states
Energy
1*s* Electron energy band (12 states)
1*s* Electron state
Interatomic separation

adjacent states is exceedingly small. At the equilibrium spacing, band formation may not occur for the electron subshells nearest the nucleus, as illustrated in Figure 12.3*b*. Furthermore, gaps may exist between adjacent bands, as also indicated in the figure; normally, energies lying within these band gaps are not available for electron occupancy. The conventional way of representing electron band structures in solids is shown in Figure 12.3*a*.

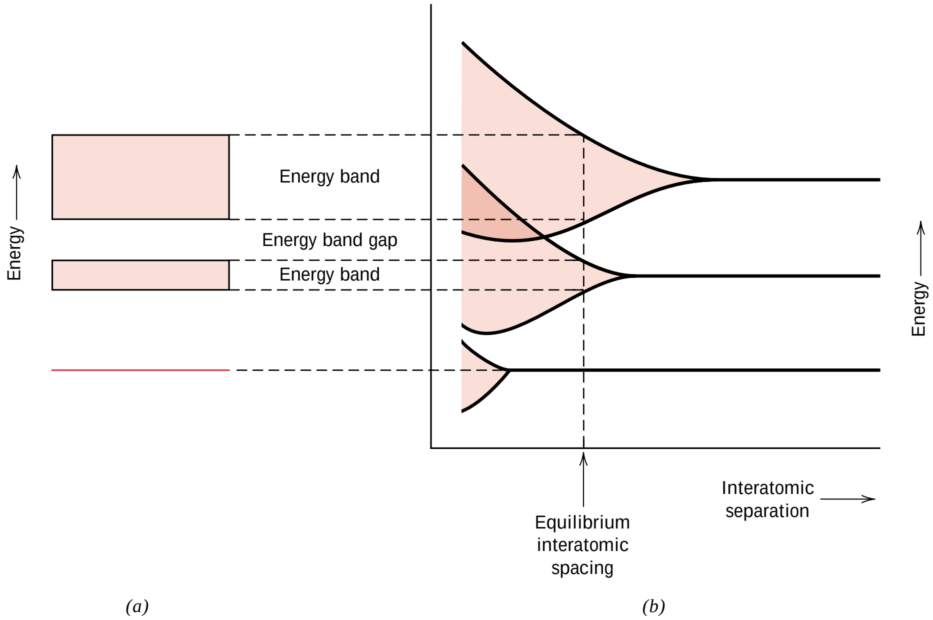
Energy
Energy band
Energy band gap
Energy band
Energy
Equilibrium interatomic spacing
Interatomic separation
(*a*)
(*b*)

FIGURE 12.3 (*a*) The conventional representation of the electron energy band structure for a solid material at the equilibrium interatomic separation. (*b*) Electron energy versus interatomic separation for an aggregate of atoms, illustrating how the energy band structure at the equilibrium separation in (*a*) is generated. (From Z. D. Jastrzebski, *The Nature and Properties of Engineering Materials*, 3rd edition. Copyright © 1987 by John Wiley & Sons, Inc. Reprinted by permission of John Wiley & Sons, Inc.)

The number of states within each band will equal the total of all states contributed by the N atoms. For example, an s band will consist of N states, and a p band of $3N$ states. With regard to occupancy, each energy state may accommodate two electrons, which must have oppositely directed spins. Furthermore, bands will contain the electrons that resided in the corresponding levels of the isolated atoms; for example, a 4s energy band in the solid will contain those isolated atom's 4s electrons. Of course, there will be empty bands and, possibly, bands that are only partially filled.

The electrical properties of a solid material are a consequence of its electron band structure, that is, the arrangement of the outermost electron bands and the way in which they are filled with electrons.

Four different types of band structures are possible at 0 K. In the first (Figure 12.4*a*), one outermost band is only partially filled with electrons. The energy corresponding to the highest filled state at 0 K is called the **Fermi energy** E_f, as indicated. This energy band structure is typified by some metals, in particular those that have a single s valence electron (e.g., copper). Each copper atom has one 4s electron; however, for a solid comprised of N atoms, the 4s band is capable of accommodating $2N$ electrons. Thus only half the available electron positions within this 4s band are filled.

For the second band structure, also found in metals (Figure 12.4*b*), there is an overlap of an empty band and a filled band. Magnesium has this band structure. Each isolated Mg atom has two 3s electrons. However, when a solid is formed, the 3s and 3p bands overlap. In this instance and at 0 K, the Fermi energy is taken as that energy below which, for N atoms, N states are filled, two electrons per state.

The final two band structures are similar; one band (the **valence band**) that is completely filled with electrons is separated from an empty **conduction band;** and an **energy band gap** lies between them. For very pure materials, electrons may not have energies within this gap. The difference between the two band structures lies in the magnitude of the energy gap; for materials that are insulators, the band gap is relatively wide (Figure 12.4*c*), whereas for semiconductors it is narrow (Figure

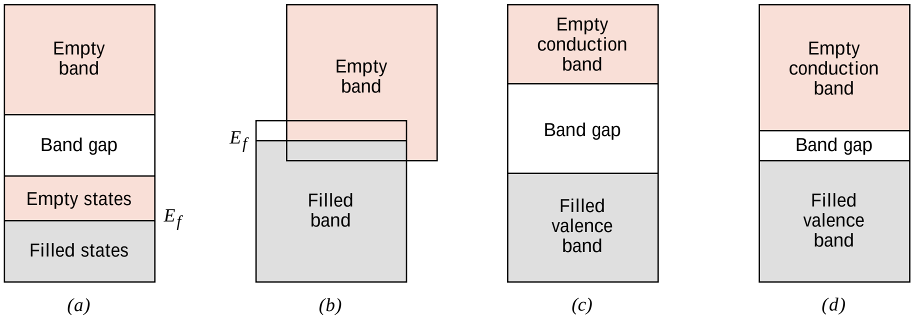

FIGURE 12.4 The various possible electron band structures in solids at 0 K. (*a*) The electron band structure found in metals such as copper, in which there are available electron states above and adjacent to filled states, in the same band. (*b*) The electron band structure of metals such as magnesium, wherein there is an overlap of filled and empty outer bands. (*c*) The electron band structure characteristic of insulators; the filled valence band is separated from the empty conduction band by a relatively large band gap (>2 eV). (*d*) The electron band structure found in the semiconductors, which is the same as for insulators except that the band gap is relatively narrow (<2 eV).

12.4*d*). The Fermi energy for these two band structures lies within the band gap—near its center.

12.6 CONDUCTION IN TERMS OF BAND AND ATOMIC BONDING MODELS

At this point in the discussion, it is vital that another concept be understood, namely, that only electrons with energies greater than the Fermi energy may be acted on and accelerated in the presence of an electric field. These are the electrons that participate in the conduction process, which are termed **free electrons.** Another charged electronic entity called a **hole** is found in semiconductors and insulators. Holes have energies less than E_f and also participate in electronic conduction. As the ensuing discussion reveals, the electrical conductivity is a direct function of the numbers of free electrons and holes. In addition, the distinction between conductors and nonconductors (insulators and semiconductors) lies in the numbers of these free electron and hole charge carriers.

METALS

For an electron to become free, it must be excited or promoted into one of the empty and available energy states above E_f. For metals having either of the band structures shown in Figures 12.4*a* and 12.4*b*, there are vacant energy states adjacent to the highest filled state at E_f. Thus, very little energy is required to promote electrons into the low-lying empty states, as shown in Figure 12.5. Generally, the energy provided by an electric field is sufficient to excite large numbers of electrons into these conducting states.

For the metallic bonding model discussed in Section 2.6, it was assumed that all the valence electrons have freedom of motion and form an ''electron gas,'' which is uniformly distributed throughout the lattice of ion cores. Even though these electrons are not locally bound to any particular atom, they, nevertheless, must experience some excitation to become conducting electrons that are truly free. Thus, although only a fraction are excited, this still gives rise to a relatively large number of free electrons and, consequently, a high conductivity.

INSULATORS AND SEMICONDUCTORS

For insulators and semiconductors, empty states adjacent to the top of the filled valence band are not available. To become free, therefore, electrons must be pro-

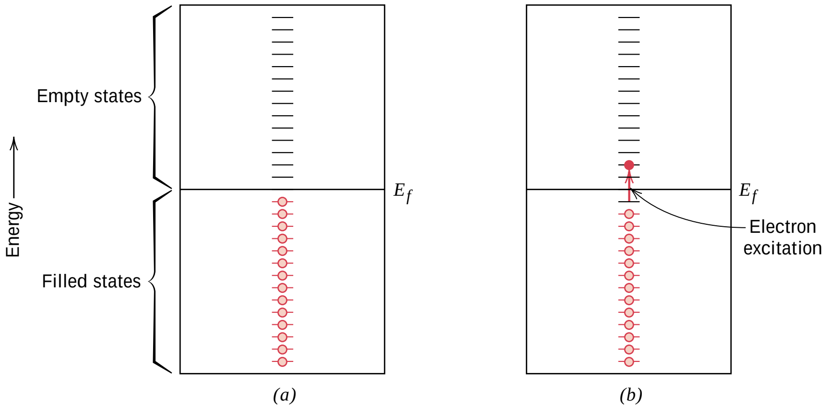

FIGURE 12.5 For a metal, occupancy of electron states (*a*) before and (*b*) after an electron excitation.

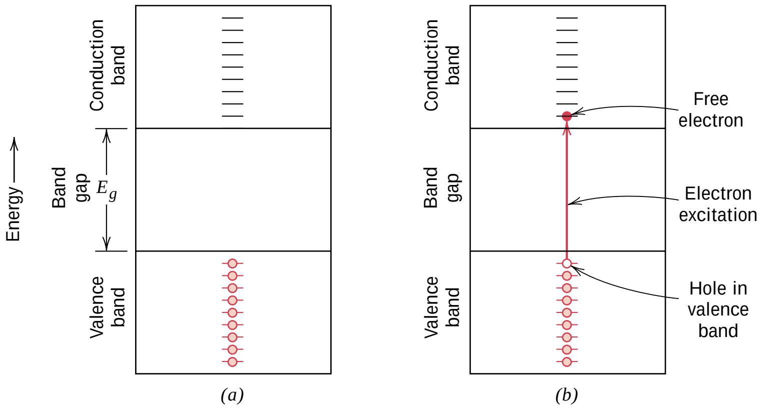

Figure 12.6 For an insulator or semiconductor, occupancy of electron states (*a*) before and (*b*) after an electron excitation from the valence band into the conduction band, in which both a free electron and a hole are generated.

moted across the energy band gap and into empty states at the bottom of the conduction band. This is possible only by supplying to an electron the difference in energy between these two states, which is approximately equal to the band gap energy E_g. This excitation process is demonstrated in Figure 12.6. For many materials this band gap is several electron volts wide. Most often the excitation energy is from a nonelectrical source such as heat or light, usually the former.

The number of electrons excited thermally (by heat energy) into the conduction band depends on the energy band gap width as well as temperature. At a given temperature, the larger the E_g, the lower the probability that a valence electron will be promoted into an energy state within the conduction band; this results in fewer conduction electrons. In other words, the larger the band gap, the lower the electrical conductivity at a given temperature. Thus, the distinction between semiconductors and insulators lies in the width of the band gap; for semiconductors it is narrow, whereas for insulating materials it is relatively wide.

Increasing the temperature of either a semiconductor or an insulator results in an increase in the thermal energy that is available for electron excitation. Thus, more electrons are promoted into the conduction band, which gives rise to an enhanced conductivity.

The conductivity of insulators and semiconductors may also be viewed from the perspective of atomic bonding models discussed in Section 2.6. For electrically insulating materials, interatomic bonding is ionic or strongly covalent. Thus, the valence electrons are tightly bound to or shared with the individual atoms. In other words, these electrons are highly localized and are not in any sense free to wander throughout the crystal. The bonding in semiconductors is covalent (or predominantly covalent) and relatively weak, which means that the valence electrons are not as strongly bound to the atoms. Consequently, these electrons are more easily removed by thermal excitation than they are for insulators.

12.7 ELECTRON MOBILITY

When an electric field is applied, a force is brought to bear on the free electrons; as a consequence, they all experience an acceleration in a direction opposite to that of the field, by virtue of their negative charge. According to quantum mechanics, there is no interaction between an accelerating electron and atoms in a perfect crystal lattice. Under such circumstances all the free electrons should accelerate as long as the electric field is applied, which would give rise to a continuously increasing

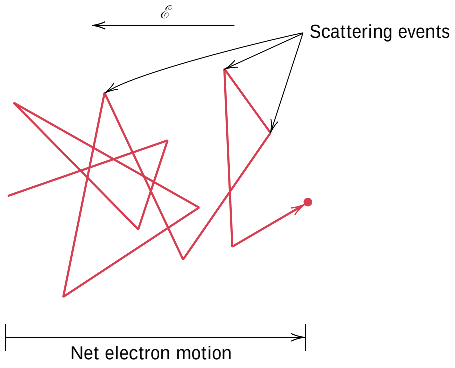

Figure 12.7 Schematic diagram showing the path of an electron that is deflected by scattering events.

electric current with time. However, we know that a current reaches a constant value the instant that a field is applied, indicating that there exist what might be termed ''frictional forces,'' which counter this acceleration from the external field. These frictional forces result from the scattering of electrons by imperfections in the crystal lattice, including impurity atoms, vacancies, interstitial atoms, dislocations, and even the thermal vibrations of the atoms themselves. Each scattering event causes an electron to lose kinetic energy and to change its direction of motion, as represented schematically in Figure 12.7. There is, however, some net electron motion in the direction opposite to the field, and this flow of charge is the electric current.

The scattering phenomenon is manifested as a resistance to the passage of an electric current. Several parameters are used to describe the extent of this scattering, these include the *drift velocity* and the **mobility** of an electron. The drift velocity v_d represents the average electron velocity in the direction of the force imposed by the applied field. It is directly proportional to the electric field as follows:

$$v_d = \mu_e \mathscr{E} \tag{12.7}$$

The constant of proportionality μ_e is called the electron mobility, which is an indication of the frequency of scattering events; its units are square meters per volt-second (m^2/V-s).

The conductivity σ of most materials may be expressed as

$$\sigma = n|e|\mu_e \tag{12.8}$$

where n is the number of free or conducting electrons per unit volume (e.g., per cubic meter), and $|e|$ is the absolute magnitude of the electrical charge on an electron (1.6×10^{-19} C). Thus, the electrical conductivity is proportional to both the number of free electrons and the electron mobility.

12.8 ELECTRICAL RESISTIVITY OF METALS

As mentioned previously, most metals are extremely good conductors of electricity; room-temperature conductivities for several of the more common metals are contained in Table 12.1. (Table B.9 in Appendix B lists the electrical resistivities of a large number of metals and alloys.) Again, metals have high conductivities because

Table 12.1 Room-Temperature Electrical Conductivities for Nine Common Metals and Alloys

Metal	*Electrical Conductivity* $[(\Omega\text{-}m)^{-1}]$
Silver	6.8×10^7
Copper	6.0×10^7
Gold	4.3×10^7
Aluminum	3.8×10^7
Iron	1.0×10^7
Brass (70 Cu–30 Zn)	1.6×10^7
Platinum	0.94×10^7
Plain carbon steel	0.6×10^7
Stainless steel	0.2×10^7

of the large numbers of free electrons that have been excited into empty states above the Fermi energy. Thus n has a large value in the conductivity expression, Equation 12.8.

At this point it is convenient to discuss conduction in metals in terms of the resistivity, the reciprocal of conductivity; the reason for this switch should become apparent in the ensuing discussion.

Since crystalline defects serve as scattering centers for conduction electrons in metals, increasing their number raises the resistivity (or lowers the conductivity). The concentration of these imperfections depends on temperature, composition, and the degree of cold work of a metal specimen. In fact, it has been observed experimentally that the total resistivity of a metal is the sum of the contributions from thermal vibrations, impurities, and plastic deformation; that is, the scattering mechanisms act independently of one another. This may be represented in mathematical form as follows:

$$\rho_{\text{total}} = \rho_t + \rho_i + \rho_d \tag{12.9}$$

in which ρ_t, ρ_i, and ρ_d represent the individual thermal, impurity, and deformation resistivity contributions, respectively. Equation 12.9 is sometimes known as **Matthiessen's rule.** The influence of each ρ variable on the total resistivity is demonstrated in Figure 12.8, as a plot of resistivity versus temperature for copper and several copper–nickel alloys in annealed and deformed states. The additive nature of the individual resistivity contributions is demonstrated at −100°C.

INFLUENCE OF TEMPERATURE

For the pure metal and all the copper–nickel alloys shown in Figure 12.8, the resistivity rises linearly with temperature above about −200°C. Thus,

$$\rho_t = \rho_0 + aT \tag{12.10}$$

where ρ_0 and a are constants for each particular metal. This dependence of the thermal resistivity component on temperature is due to the increase with temperature in thermal vibrations and other lattice irregularities (e.g., vacancies), which serve as electron-scattering centers.

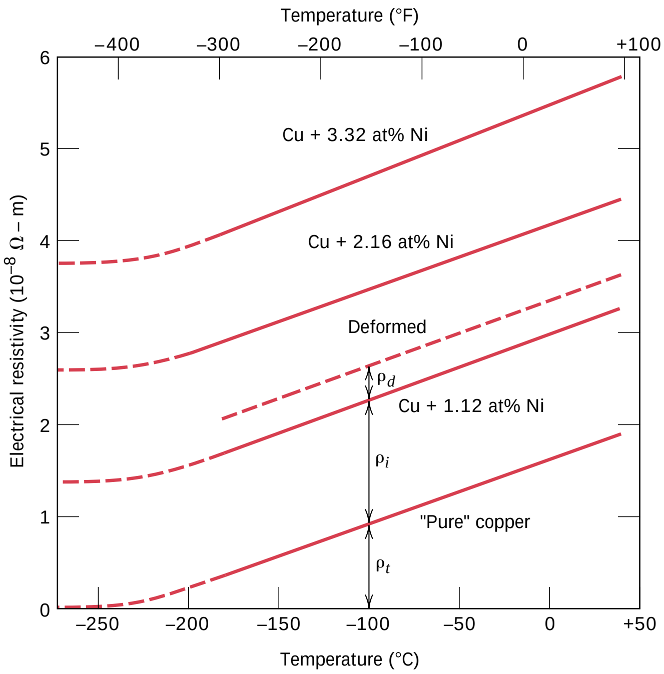

FIGURE 12.8 The electrical resistivity versus temperature for copper and three copper–nickel alloys, one of which has been deformed. Thermal, impurity, and deformation contributions to the resistivity are indicated at −100°C. [Adapted from J. O. Linde, *Ann. Physik*, **5,** 219 (1932); and C. A. Wert and R. M. Thomson, *Physics of Solids*, 2nd edition, McGraw-Hill Book Company, New York, 1970.]

INFLUENCE OF IMPURITIES

For additions of a single impurity that forms a solid solution, the impurity resistivity ρ_i is related to the impurity concentration c_i in terms of the atom fraction (at%/100) as follows:

$$\rho_i = Ac_i(1 - c_i) \tag{12.11}$$

where A is a composition-independent constant that is a function of both the impurity and host metals. The influence of nickel impurity additions on the room-temperature resistivity of copper is demonstrated in Figure 12.9, up to 50 wt% Ni; over this composition range nickel is completely soluble in copper (Figure 10.2). Again, nickel atoms in copper act as scattering centers, and increasing the concentration of nickel in copper results in an enhancement of resistivity.

For a two-phase alloy consisting of α and β phases, a rule-of-mixtures expression may be utilized to approximate the resistivity as follows:

$$\rho_i = \rho_\alpha V_\alpha + \rho_\beta V_\beta \tag{12.12}$$

where the V's and ρ's represent volume fractions and individual resistivities for the respective phases.

INFLUENCE OF PLASTIC DEFORMATION

Plastic deformation also raises the electrical resistivity as a result of increased numbers of electron-scattering dislocations. The effect of deformation on resistivity is also represented in Figure 12.8.

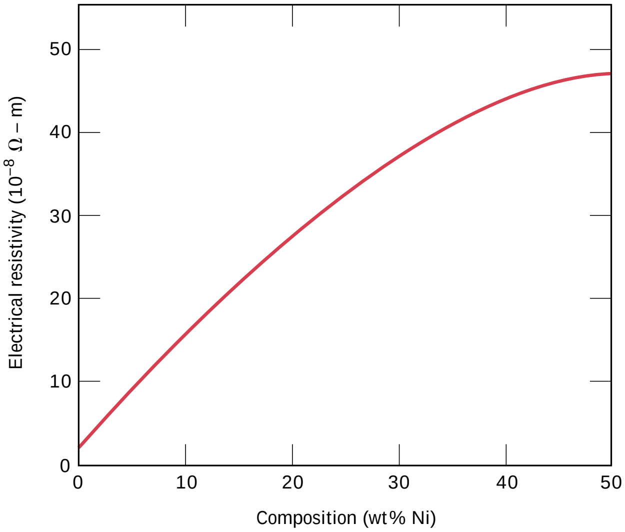

FIGURE 12.9 Room-temperature electrical resistivity versus composition for copper–nickel alloys.

12.9 ELECTRICAL CHARACTERISTICS OF COMMERCIAL ALLOYS

Electrical and other properties of copper render it the most widely used metallic conductor. Oxygen-free high-conductivity (OFHC) copper, having extremely low oxygen and other impurity contents, is produced for many electrical applications. Aluminum, having a conductivity only about one half that of copper, is also frequently used as an electrical conductor. Silver has a higher conductivity than either copper or aluminum; however, its use is restricted on the basis of cost.

On occasion, it is necessary to improve the mechanical strength of a metal alloy without impairing significantly its electrical conductivity. Both solid solution alloying and cold working (Section 8.11) improve strength at the expense of conductivity, and thus, a tradeoff must be made for these two properties. Most often, strength is enhanced by introducing a second phase that does not have so adverse an effect on conductivity. For example, copper–beryllium alloys are precipitation hardened (Section 11.11); but even so, the conductivity is reduced by about a factor of 5 over high-purity copper.

For some applications, such as furnace heating elements, a high electrical resistivity is desirable. The energy loss by electrons that are scattered is dissipated as heat energy. Such materials must have not only a high resistivity, but also a resistance to oxidation at elevated temperatures and, of course, a high melting temperature. Nichrome, a nickel–chromium alloy, is commonly employed in heating elements.

SEMICONDUCTIVITY

The electrical conductivity of the semiconducting materials is not as high as that of the metals; nevertheless, they have some unique electrical characteristics that render them especially useful. The electrical properties of these materials are extremely sensitive to the presence of even minute concentrations of impurities. **Intrinsic semiconductors** are those in which the electrical behavior is based on the electronic structure inherent to the pure material. When the electrical characteristics are dictated by impurity atoms, the semiconductor is said to be **extrinsic.**

12.10 INTRINSIC SEMICONDUCTION

Intrinsic semiconductors are characterized by the electron band structure shown in Figure 12.4*d*: at 0 K, a completely filled valence band, separated from an empty conduction band by a relatively narrow forbidden band gap, generally less than 2 eV. The two elemental semiconductors are silicon (Si) and germanium (Ge), having band gap energies of approximately 1.1 and 0.7 eV, respectively. Both are found in Group IVA of the periodic table (Figure 2.6) and are covalently bonded.[1] In addition, a host of compound semiconducting materials also display intrinsic behavior. One such group is formed between elements of Groups IIIA and VA, for example, gallium arsenide (GaAs) and indium antimonide (InSb); these are frequently called III–V compounds. The compounds composed of elements of Groups IIB and VIA also display semiconducting behavior; these include cadmium sulfide (CdS) and zinc telluride (ZnTe). As the two elements forming these compounds become more widely separated with respect to their relative positions in the periodic table (i.e., the electronegativities become more dissimilar, Figure 2.7), the atomic bonding becomes more ionic and the magnitude of the band gap energy increases—the materials tend to become more insulative. Table 12.2 gives the band gaps for some compound semiconductors.

CONCEPT OF A HOLE

In intrinsic semiconductors, for every electron excited into the conduction band there is left behind a missing electron in one of the covalent bonds, or in the band scheme, a vacant electron state in the valence band, as shown in Figure 12.6*b*. Under the influence of an electric field, the position of this missing electron within

Table 12.2 Band Gap Energies, Electron and Hole Mobilities, and Intrinsic Electrical Conductivities at Room Temperature for Semiconducting Materials

Material	*Band Gap (eV)*	*Electrical Conductivity* $[(\Omega\text{-}m)^{-1}]$	*Electron Mobility* $(m^2/V\text{-}s)$	*Hole Mobility* $(m^2/V\text{-}s)$
		Elemental		
Si	1.11	4×10^{-4}	0.14	0.05
Ge	0.67	2.2	0.38	0.18
		III–V Compounds		
GaP	2.25	—	0.05	0.002
GaAs	1.42	10^{-6}	0.85	0.45
InSb	0.17	2×10^{4}	7.7	0.07
		II–VI Compounds		
CdS	2.40	—	0.03	—
ZnTe	2.26	—	0.03	0.01

---

[1] The valence bands in silicon and germanium correspond to sp^3 hybrid energy levels for the isolated atom; these hybridized valence bands are completely filled at 0 K.

the crystalline lattice may be thought of as moving by the motion of other valence electrons that repeatedly fill in the incomplete bond (Figure 12.10). This process is expedited by treating a missing electron from the valence band as a positively charged particle called a *hole.* A hole is considered to have a charge that is of the same magnitude as that for an electron, but of opposite sign ($+1.6 \times 10^{-19}$ C).

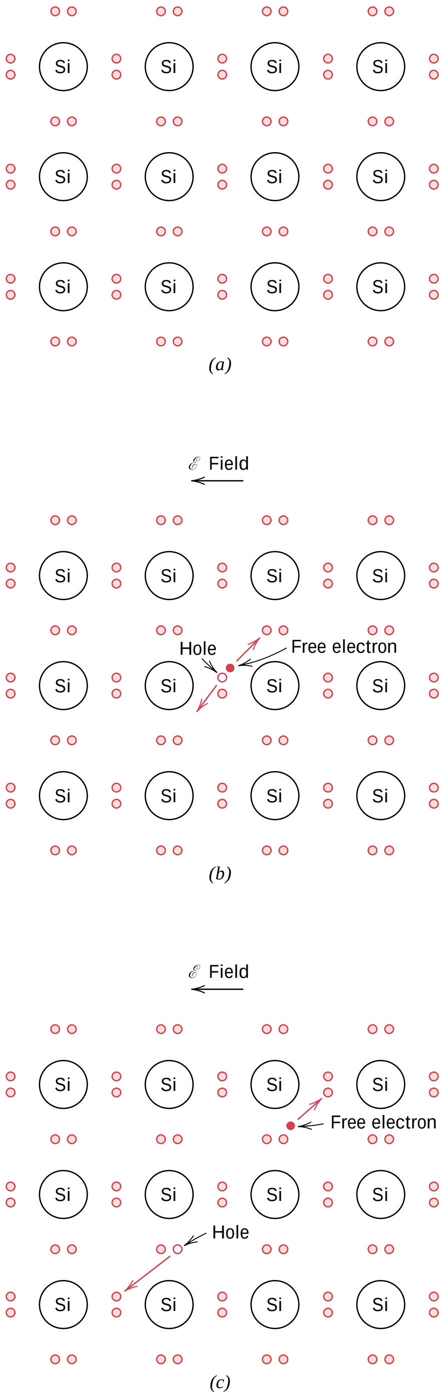

Figure 12.10 Electron bonding model of electrical conduction in intrinsic silicon: (*a*) before excitation; (*b*) and (*c*) after excitation (the subsequent free-electron and hole motions in response to an external electric field).

Thus, in the presence of an electric field, excited electrons and holes move in opposite directions. Furthermore, in semiconductors both electrons and holes are scattered by lattice imperfections.

INTRINSIC CONDUCTIVITY

Since there are two types of charge carrier (free electrons and holes) in an intrinsic semiconductor, the expression for electrical conduction, Equation 12.8, must be modified to include a term to account for the contribution of the hole current. Therefore, we write

$$\sigma = n|e|\mu_e + p|e|\mu_h \tag{12.13}$$

where p is the number of holes per cubic meter and μ_h is the hole mobility. The magnitude of μ_h is always less than μ_e for semiconductors. For intrinsic semiconductors, every electron promoted across the band gap leaves behind a hole in the valence band, thus,

$$n = p \tag{12.14}$$

and

$$\sigma = n|e|(\mu_e + \mu_h) = p|e|(\mu_e + \mu_h) \tag{12.15}$$

The room-temperature intrinsic conductivities and electron and hole mobilities for several semiconducting materials are also presented in Table 12.2.

EXAMPLE PROBLEM 12.1

For intrinsic silicon, the room-temperature electrical conductivity is 4×10^{-4} $(\Omega\text{-m})^{-1}$; the electron and hole mobilities are, respectively, 0.14 and 0.048 $\text{m}^2/\text{V-s}$. Compute the electron and hole concentrations at room temperature.

SOLUTION

Since the material is intrinsic, electron and hole concentrations will be the same, and therefore, from Equation 12.15,

$$\begin{aligned} n = p &= \frac{\sigma}{|e|(\mu_e + \mu_h)} \\ &= \frac{4 \times 10^{-4}\ (\Omega\text{-m})^{-1}}{(1.6 \times 10^{-19}\ \text{C})(0.14 + 0.048\ \text{m}^2/\text{V-s})} \\ &= 1.33 \times 10^{16}\ \text{m}^{-3} \end{aligned}$$

12.11 EXTRINSIC SEMICONDUCTION

Virtually all commercial semiconductors are extrinsic; that is, the electrical behavior is determined by impurities, which, when present in even minute concentrations, introduce excess electrons or holes. For example, an impurity concentration of one atom in 10^{12} is sufficient to render silicon extrinsic at room temperature.

n-TYPE EXTRINSIC SEMICONDUCTION

To illustrate how extrinsic semiconduction is accomplished, consider again the elemental semiconductor silicon. An Si atom has four electrons, each of which is covalently bonded with one of four adjacent Si atoms. Now, suppose that an impurity atom with a valence of 5 is added as a substitutional impurity; possibilities would include atoms from the Group VA column of the periodic table (e.g., P, As, and Sb). Only four of five valence electrons of these impurity atoms can participate in the bonding because there are only four possible bonds with neighboring atoms.

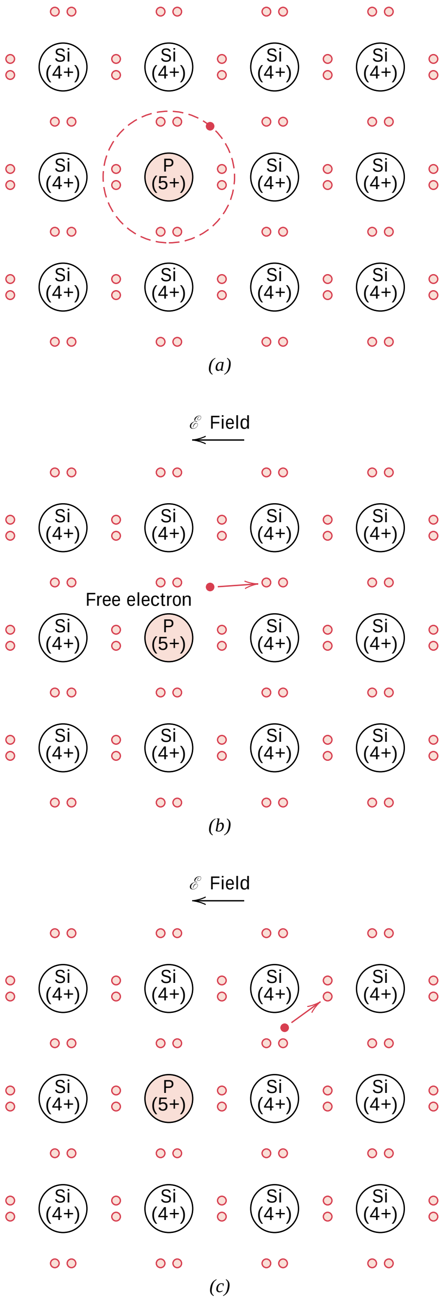

Figure 12.11 Extrinsic *n*-type semiconduction model (electron bonding). (*a*) An impurity atom such as phosphorus, having five valence electrons, may substitute for a silicon atom. This results in an extra bonding electron, which is bound to the impurity atom and orbits it. (*b*) Excitation to form a free electron. (*c*) The motion of this free electron in response to an electric field.

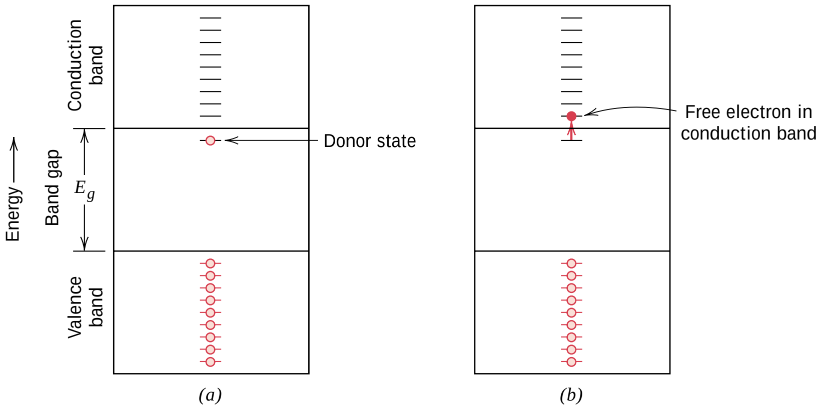

FIGURE 12.12 (*a*) Electron energy band scheme for a donor impurity level located within the band gap and just below the bottom of the conduction band. (*b*) Excitation from a donor state in which a free electron is generated in the conduction band.

The extra nonbonding electron is loosely bound to the region around the impurity atom by a weak electrostatic attraction, as illustrated in Figure 12.11*a*. The binding energy of this electron is relatively small (on the order of 0.01 eV); thus, it is easily removed from the impurity atom, in which case it becomes a free or conducting electron (Figures 12.11*b* and 12.11*c*).

The energy state of such an electron may be viewed from the perspective of the electron band model scheme. For each of the loosely bound electrons, there exists a single energy level, or energy state, which is located within the forbidden band gap just below the bottom of the conduction band (Figure 12.12*a*). The electron binding energy corresponds to the energy required to excite the electron from one of these impurity states to a state within the conduction band. Each excitation event (Figure 12.12*b*), supplies or donates a single electron to the conduction band; an impurity of this type is aptly termed a *donor*. Since each donor electron is excited from an impurity level, no corresponding hole is created within the valence band.

At room temperature, the thermal energy available is sufficient to excite large numbers of electrons from **donor states;** in addition, some intrinsic valence–conduction band transitions occur, as in Figure 12.6*b*, but to a negligible degree. Thus, the number of electrons in the conduction band far exceeds the number of holes in the valence band (or $n \gg p$), and the first term on the right-hand side of Equation 12.13 overwhelms the second; that is,

$$\sigma \cong n|e|\mu_e \tag{12.16}$$

A material of this type is said to be an *n-type* extrinsic semiconductor. The electrons are *majority carriers* by virtue of their density or concentration; holes, on the other hand, are the *minority charge carriers.* For *n*-type semiconductors, the Fermi level is shifted upward in the band gap, to within the vicinity of the donor state; its exact position is a function of both temperature and donor concentration.

p-TYPE EXTRINSIC SEMICONDUCTION

An opposite effect is produced by the addition to silicon or germanium of trivalent substitutional impurities such as aluminum, boron, and gallium from Group IIIA of the periodic table. One of the covalent bonds around each of these atoms is deficient in an electron; such a deficiency may be viewed as a hole that is weakly bound to the impurity atom. This hole may be liberated from the impurity atom by the transfer of an electron from an adjacent bond as illustrated in Figure 12.13.

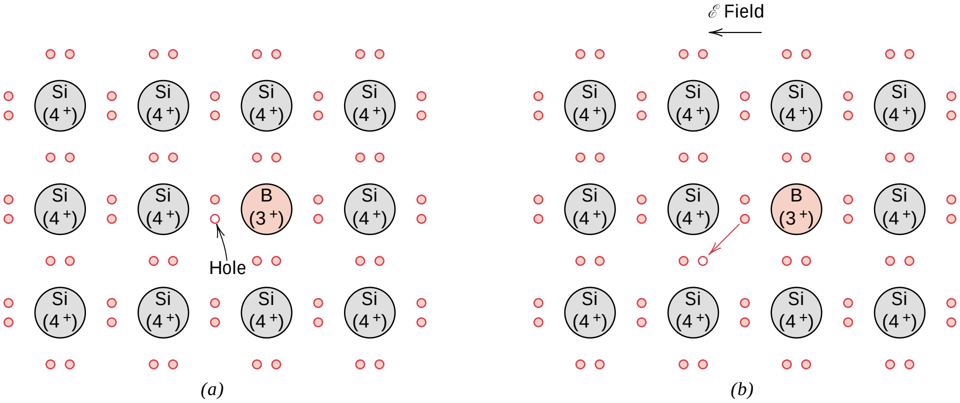

Figure 12.13 Extrinsic *p*-type semiconduction model (electron bonding). (*a*) An impurity atom such as boron, having three valence electrons, may substitute for a silicon atom. This results in a deficiency of one valence electron, or a hole associated with the impurity atom. (*b*) The motion of this hole in response to an electric field.

In essence, the electron and the hole exchange positions. A moving hole is considered to be in an excited state and participates in the conduction process, in a manner analogous to an excited donor electron, as described above.

Extrinsic excitations, in which holes are generated, may also be represented using the band model. Each impurity atom of this type introduces an energy level within the band gap, above yet very close to the top of the valence band (Figure 12.14*a*). A hole is imagined to be created in the valence band by the thermal excitation of an electron from the valence band into this impurity electron state, as demonstrated in Figure 12.14*b*. With such a transition, only one carrier is produced—a hole in the valence band; a free electron is *not* created in either the impurity level or the conduction band. An impurity of this type is called an *acceptor*, because it is capable of accepting an electron from the valence band, leaving behind a hole. It follows that the energy level within the band gap introduced by this type of impurity is called an **acceptor state.**

For this type of extrinsic conduction, holes are present in much higher concentrations than electrons (i.e., $p \gg n$), and under these circumstances a material is

Figure 12.14 (*a*) Energy band scheme for an acceptor impurity level located within the band gap and just above the top of the valence band. (*b*) Excitation of an electron into the acceptor level, leaving behind a hole in the valence band.

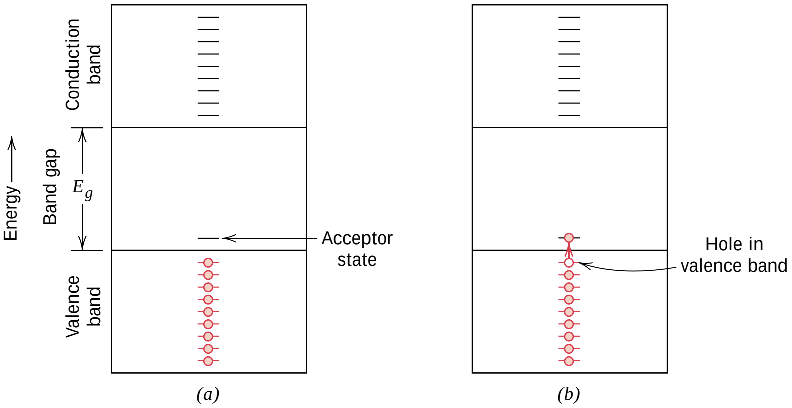

termed *p-type* because positively charged particles are primarily responsible for electrical conduction. Of course, holes are the majority carriers, and electrons are present in minority concentrations. This gives rise to a predominance of the second term on the right-hand side of Equation 12.13, or

$$\sigma \cong p|e|\mu_h \tag{12.17}$$

For *p*-type semiconductors, the Fermi level is positioned within the band gap and near to the acceptor level.

Extrinsic semiconductors (both *n*- and *p*-type) are produced from materials that are initially of extremely high purity, commonly having total impurity contents on the order of 10^{-7} at%. Controlled concentrations of specific donors or acceptors are then intentionally added, using various techniques. Such an alloying process in semiconducting materials is termed **doping.**

In extrinsic semiconductors, large numbers of charge carriers (either electrons or holes, depending on the impurity type) are created at room temperature, by the available thermal energy. As a consequence, relatively high room-temperature electrical conductivities are obtained in extrinsic semiconductors. Most of these materials are designed for use in electronic devices to be operated at ambient conditions.

EXAMPLE PROBLEM 12.2

Phosphorus is added to high-purity silicon to give a concentration of 10^{23} m^{-3} of charge carriers at room temperature.

(a) Is this material *n*-type or *p*-type?

(b) Calculate the room-temperature conductivity of this material, assuming that electron and hole mobilities are the same as for the intrinsic material.

SOLUTION

(a) Phosphorus is a Group VA element (Figure 2.6) and, therefore, will act as a donor in silicon. Thus, the 10^{23} m^{-3} charge carriers will be virtually all electrons. This electron concentration is greater than that for the intrinsic case (1.33×10^{16} m^{-3}, Example Problem 12.1); hence, this material is extrinsically *n*-type.

(b) In this case the conductivity may be determined using Equation 12.16, as follows:

$$\begin{aligned}\sigma = n|e|\mu_e &= (10^{23}\ \text{m}^{-3})(1.6 \times 10^{-19}\ \text{C})(0.14\ \text{m}^2/\text{V-s})\\ &= 2240\ (\Omega\text{-m})^{-1}\end{aligned}$$

12.12 THE TEMPERATURE VARIATION OF CONDUCTIVITY AND CARRIER CONCENTRATION

Figure 12.15 plots the logarithm of the electrical conductivity as a function of the logarithm of absolute temperature for intrinsic silicon, and also for silicon that has been doped with 0.0013 and 0.0052 at% boron; again, boron acts as an acceptor in silicon. Worth noting from this figure is that the electrical conductivity in the intrinsic

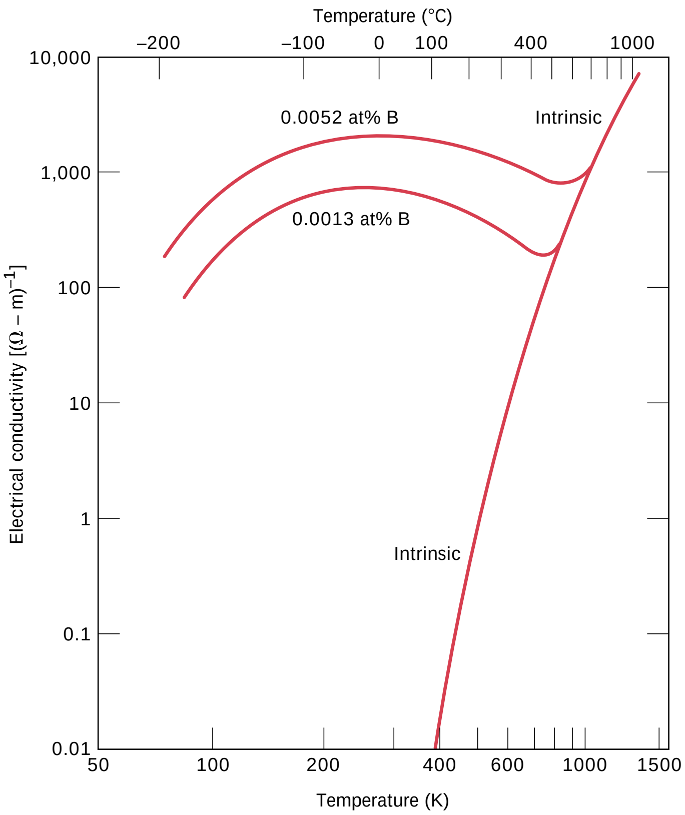

FIGURE 12.15 The temperature dependence of the electrical conductivity (log–log scales) for intrinsic silicon and boron-doped silicon at two doping levels. [Adapted from G. L. Pearson and J. Bardeen, *Phys. Rev.*, **75,** 865 (1949).]

specimen increases dramatically with rising temperature. The numbers of both electrons and holes increase with temperature because more thermal energy is available to excite electrons from the valence to the conduction band. Thus, both the values of n and p in the intrinsic conductivity expression, Equation 12.15, are enhanced. The magnitudes of electron and hole mobilities decrease slightly with temperature as a result of more effective electron and hole scattering by the thermal vibrations. However, these reductions in μ_e and μ_h by no means offset the increase in n and p, and the net effect of a rise in temperature is to produce a conductivity increase.

Mathematically, the dependence of intrinsic conductivity σ on the absolute temperature T is approximately

$$\ln \sigma \cong C - \frac{E_g}{2kT} \tag{12.18}$$

where C represents a temperature-independent constant and E_g and k are the band gap energy and Boltzmann's constant, respectively. Since the increase of n and p with rising temperature is so much greater than the decrease in μ_e and μ_h, the dependence of carrier concentration on temperature for intrinsic behavior is virtually the same as for the conductivity, or

$$\ln n = \ln p \cong C' - \frac{E_g}{2kT} \tag{12.19}$$

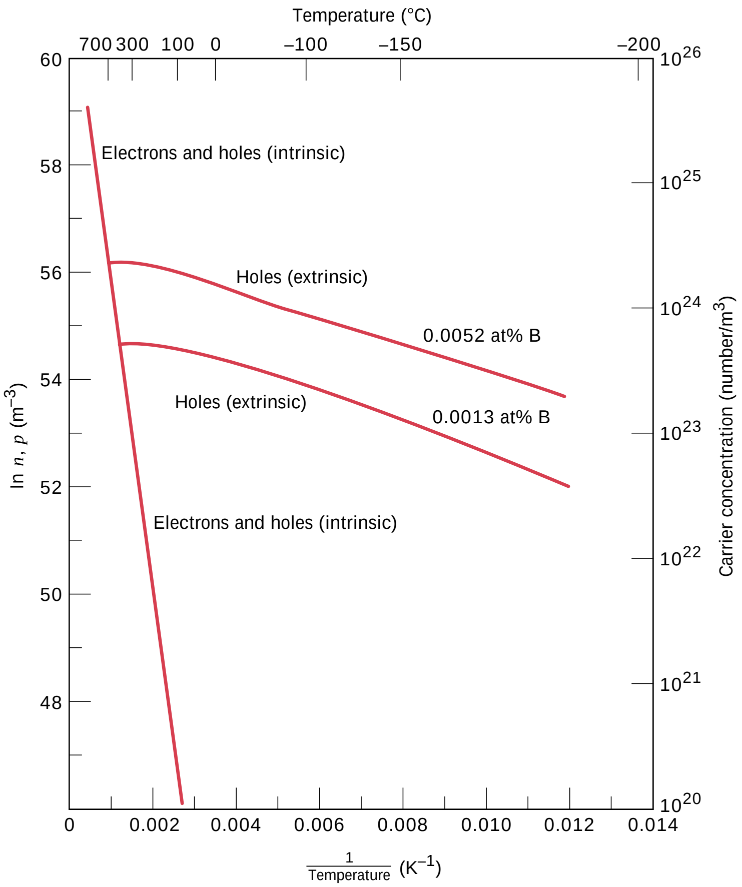

Figure 12.16 The logarithm of carrier (electron and hole) concentration as a function of the reciprocal of the absolute temperature for intrinsic silicon and two boron-doped silicon materials. (Adapted from G. L. Pearson and J. Bardeen, *Phys. Rev.*, **75,** 865, 1949.)

The parameter C' is a constant that is independent of temperature, yet is different from C in Equation 12.18.

In light of Equation 12.19, another method of representing the temperature dependence of the electrical behavior of semiconductors is as the natural logarithm of electron and hole concentrations versus the reciprocal of the absolute temperature. Figure 12.16 is such a plot using data taken from Figure 12.15; and, as may be noted (Figure 12.16), a straight line segment results for the intrinsic material; such a plot expedites the determination of the band gap energy. According to Equation 12.19, the slope of this line segment is equal to $-E_g/2k$, or E_g may be determined as follows:

$$E_g = -2k\left(\frac{\Delta \ln p}{\Delta(1/T)}\right)$$

$$= -2k\left(\frac{\Delta \ln n}{\Delta(1/T)}\right) \tag{12.20}$$

This is indicated in the schematic plot of Figure 12.17.

Another important feature of the behavior shown in Figures 12.15 and 12.16 is that at temperatures below about 800 K (527°C), the boron-doped materials are extrinsically p-type; that is, virtually all the carrier holes result from extrinsic

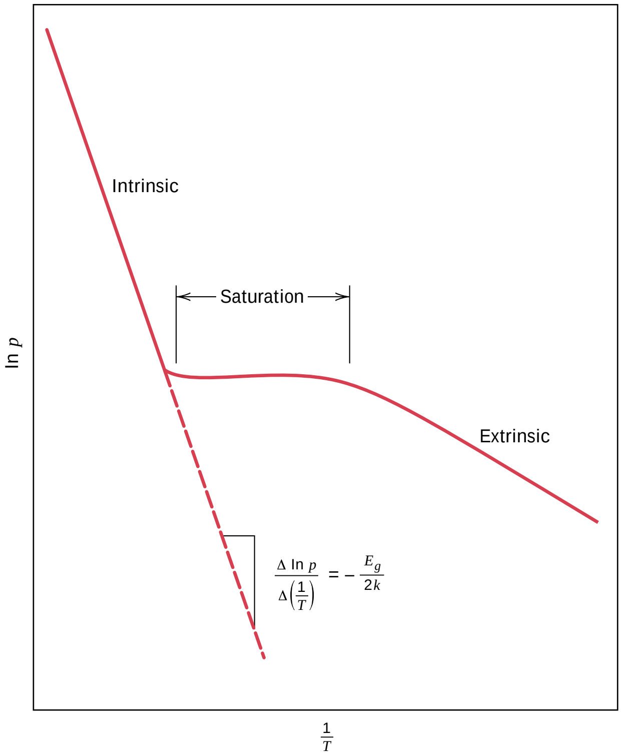

FIGURE 12.17 Schematic plot of the natural logarithm of hole concentration as a function of the reciprocal of absolute temperature for a *p*-type semiconductor that exhibits extrinsic, saturation, and intrinsic behavior.

excitations—electron transitions from the valence band into the boron acceptor level, which leave behind valence band holes (Figure 12.14). The available thermal energies at these temperatures are sufficient to promote significant numbers of these excitations, yet insufficient to stimulate many electrons from the valence band across the band gap. Thus, the extrinsic conductivity far exceeds that of the intrinsic material. For example, at 400 K (127°C) the conductivities for intrinsic silicon and extrinsic 0.0013 at% boron-doped material are approximately 10^{-2} and 600 $(\Omega\text{-m})^{-1}$, respectively (Figure 12.15). This comparison indicates the sensitivity of conductivity to even extremely small concentrations of some impurity elements.

Furthermore, the extrinsic conductivity is also sensitive to temperature, as indicated in Figure 12.15, for both boron-doped materials. Beginning at about 75 K (−200°C), the conductivity first increases with temperature, reaches a maximum, and then decreases slightly prior to becoming intrinsic. Or, in terms of carrier (i.e., hole) concentration, Figure 12.16, ln p first increases linearly with decreasing $1/T$ (or increasing temperature). Large numbers of extrinsic excitations are possible even at these relatively low temperatures inasmuch as the acceptor level lies just above the top of the valence band. With further temperature increase ($1/T$ decrease), the hole concentration eventually becomes independent of temperature, Figure 12.16. At this point virtually all of the boron atoms have accepted electrons from the valence band, or are said to be *saturated;* this is appropriately termed the *saturation region* (Figure 12.17). (Donor impurities become *exhausted* instead of saturated.) The number of holes in this region is approximately equal to the number of dopant impurity (i.e., boron) atoms.

The decrease of conductivity with increasing temperature within the saturation region for the two extrinsic curves in Figure 12.15 may be explained by the reduction in hole mobility with rising temperature. From the extrinsic conductivity expression, Equation 12.17, both e and p are independent of temperature in this region, and the only temperature dependence comes from the mobility.

Also worth noting from Figures 12.15 and 12.16 is that at about 800 K (527°C), the conductivity of both boron-doped materials becomes intrinsic. At the outset of intrinsic behavior, the number of intrinsic valence band-to-conduction band transitions becomes greater than the number of holes that are extrinsically generated.

A couple of final comments relate to the influence of boron acceptor content on the electrical behavior of silicon. First, the extrinsic and saturation conductivities and hole concentrations are greater for the material with the higher boron content (Figures 12.15 and 12.16), a result not unexpected, since more B atoms are present from which holes may be produced. Also, the intrinsic outset temperature becomes elevated as the dopant content increases.

Example Problem 12.3

If the room-temperature [25°C (298 K)] electrical conductivity of intrinsic germanium is 2.2 $(\Omega\text{-m})^{-1}$, estimate its conductivity at 150°C (423 K).

Solution

This problem is solved by employment of Equation 12.18. First, we determine the value of the constant C using the room-temperature data, after which the value at 150°C may be computed. From Table 12.2, the value of E_g for germanium is 0.67 eV, and, therefore,

$$C = \ln \sigma + \frac{E_g}{2kT}$$

$$= \ln(2.2) + \frac{0.67 \text{ eV}}{(2)(8.62 \times 10^{-5} \text{ eV/K})(298 \text{ K})} = 13.83$$

Now, at 150°C (423 K),

$$\ln \sigma = C - \frac{E_g}{2kT}$$

$$= 13.83 - \frac{0.67 \text{ eV}}{(2)(8.62 \times 10^{-5} \text{ eV/K})(423 \text{ K})} = 4.64$$

or

$$\sigma = 103.8 \ (\Omega\text{-m})^{-1}$$

Design Example 12.1

The room-temperature electrical conductivity of intrinsic silicon is 4×10^{-4} $(\Omega\text{-m})^{-1}$ (Table 12.2). An extrinsic n-type silicon material is desired having a room-temperature conductivity of 150 $(\Omega\text{-m})^{-1}$. Specify a donor impurity type that may be used as well as its concentration in atom percent to yield these electrical characteristics. Assume that the electron and hole mobilities are the same as for the intrinsic material, and that at room temperature the donor impurities are exhausted.

SOLUTION

First of all, those elements which, when added to silicon render it *n*-type, lie one group to the right of silicon in the periodic table; these include the group VA elements (Figure 2.6)—i.e., nitrogen, phosphorus, arsenic, and antimony.

Since this material is extrinsic and *n*-type, $n \gg p$, the electrical conductivity is a function of the free electron concentration according to Equation 12.16. Furthermore, the design stipulates that the donor impurity atoms are exhausted; therefore, the number of free electrons is about equal to the number of donor impurities, N_d. That is

$$n \sim N_d$$

We now solve Equation 12.16 for n using the stipulated conductivity [150 $(\Omega\text{-m})^{-1}$] and the electron mobility value provided in Table 12.2 (0.14 $\text{m}^2/\text{V-s}$). Thus

$$\begin{aligned} n = N_d &= \frac{\sigma}{|e|\mu_e} \\ &= \frac{150\ (\Omega\text{-m})^{-1}}{(1.6 \times 10^{-19}\ \text{C})(0.14\ \text{m}^2/\text{V-s})} \\ &= 6.7 \times 10^{21}\ \text{m}^{-3} \end{aligned}$$

It next becomes necessary to calculate the concentration of donor impurities in atom percent. This computation first requires the determination of the number of silicon atoms per cubic meter, N_{Si}, using Equation 5.2, which is as follows:

$$\begin{aligned} N_{\text{Si}} &= \frac{N_{\text{A}}\rho_{\text{Si}}}{A_{\text{Si}}} \\ &= \frac{(6.023 \times 10^{23}\ \text{atoms/mol})(2.33\ \text{g/cm}^3)(10^6\ \text{cm}^3/\text{m}^3)}{28.09\ \text{g/mol}} \\ &= 5 \times 10^{28}\ \text{m}^{-3} \end{aligned}$$

The concentration of donor impurities in atom percent (C'_d) is just the ratio of N_d and $N_d + N_{\text{Si}}$ multiplied by 100 as

$$\begin{aligned} C'_d &= \frac{N_d}{N_d + N_{\text{Si}}} \times 100 \\ &= \frac{6.7 \times 10^{21}\ \text{m}^{-3}}{(6.7 \times 10^{21}\ \text{m}^{-3}) + (5 \times 10^{28}\ \text{m}^{-3})} \times 100 = 1.34 \times 10^{-5} \end{aligned}$$

Thus, a silicon material having a room-temperature *n*-type electrical conductivity of 150 $(\Omega\text{-m})^{-1}$ must contain 1.34×10^{-5} at% nitrogen, phosphorus, arsenic, or antimony.

12.13 THE HALL EFFECT (CD-ROM)

12.14 SEMICONDUCTOR DEVICES (CD-ROM)

ELECTRICAL CONDUCTION IN IONIC CERAMICS AND IN POLYMERS

Most polymers and ionic ceramics are insulating materials at room temperature and, therefore, have electron energy band structures similar to that represented in Figure 12.4*c*; a filled valence band is separated from an empty conduction band by a relatively large band gap, usually greater than 2 eV. Thus, at normal temperatures only very few electrons may be excited across the band gap by the available thermal energy, which accounts for the very small values of conductivity; Table 12.3 gives the room-temperature electrical conductivity of several of these materials. (The electrical resistivities of a large number of ceramic and polymeric materials are provided in Table B.9, Appendix B.) Of course, many materials are utilized on the basis of their ability to insulate, and thus a high electrical resistivity is desirable. With rising temperature insulating materials experience an increase in electrical conductivity, which may ultimately be greater than that for semiconductors.

12.15 CONDUCTION IN IONIC MATERIALS

Both cations and anions in ionic materials possess an electric charge and, as a consequence, are capable of migration or diffusion when an electric field is present. Thus an electric current will result from the net movement of these charged ions, which will be present in addition to that due to any electron motion. Of course, anion and cation migrations will be in opposite directions. The total conductivity of an ionic material σ_{total} is thus equal to the sum of both electronic and ionic contributions, as follows:

$$\sigma_{\text{total}} = \sigma_{\text{electronic}} + \sigma_{\text{ionic}} \tag{12.25}$$

Table 12.3 **Typical Room-Temperature Electrical Conductivities for 13 Nonmetallic Materials**

Material	***Electrical Conductivity* [(Ω-*m*)$^{-1}$]**
Graphite	3×10^4–2×10^5
Ceramics	
Concrete (dry)	10^{-9}
Soda–lime glass	10^{-10}–10^{-11}
Porcelain	10^{-10}–10^{-12}
Borosilicate glass	$\sim 10^{-13}$
Aluminum oxide	$<10^{-13}$
Fused silica	$<10^{-18}$
Polymers	
Phenol-formaldehyde	10^{-9}–10^{-10}
Polymethyl methacrylate	$<10^{-12}$
Nylon 6,6	10^{-12}–10^{-13}
Polystyrene	$<10^{-14}$
Polyethylene	10^{-15}–10^{-17}
Polytetrafluoroethylene	$<10^{-17}$

Either contribution may predominate depending on the material, its purity, and, of course, temperature.

A mobility μ_i may be associated with each of the ionic species as follows:

$$\mu_i = \frac{n_i e D_i}{kT} \tag{12.26}$$

where n_i and D_i represent, respectively, the valence and diffusion coefficient of a particular ion; e, k, and T denote the same parameters as explained earlier in the chapter. Thus, the ionic contribution to the total conductivity increases with increasing temperature, as does the electronic component. However, in spite of the two conductivity contributions, most ionic materials remain insulative, even at elevated temperatures.

12.16 Electrical Properties of Polymers

Most polymeric materials are poor conductors of electricity (Table 12.3) because of the unavailability of large numbers of free electrons to participate in the conduction process. The mechanism of electrical conduction in these materials is not well understood, but it is felt that conduction in polymers of high purity is electronic.

CONDUCTING POLYMERS

Within the past several years, polymeric materials have been synthesized that have electrical conductivities on par with metallic conductors; they are appropriately termed *conducting polymers.* Conductivities as high as 1.5×10^7 $(\Omega\text{-m})^{-1}$ have been achieved in these materials; on a volume basis, this value corresponds to one fourth of the conductivity of copper, or twice its conductivity on the basis of weight.

This phenomenon is observed in a dozen or so polymers, including polyacetylene, polyparaphenylene, polypyrrole, and polyaniline that have been doped with appropriate impurities. As is the case with semiconductors, these polymers may be made either *n*-type (i.e., free-electron dominant) or *p*-type (i.e., hole dominant) depending on the dopant. However, unlike semiconductors, the dopant atoms or molecules do not substitute for or replace any of the polymer atoms.

High-purity polymers have electron band structures characteristic of electrical insulators (Figure 12.4*c*). The mechanism by which large numbers of free electrons and holes are generated in these conducting polymers is complex and not well understood. In very simple terms, it appears that the dopant atoms lead to the formation of new energy bands that overlap the valence and conduction bands of the intrinsic polymer, giving rise to a partially filled band, and the production at room temperature of a high concentration of free electrons or holes. Orienting the polymer chains, either mechanically (Section 8.17) or magnetically, during synthesis results in a highly anisotropic material having a maximum conductivity along the direction of orientation.

These conducting polymers have the potential to be used in a host of applications inasmuch as they have low densities, are highly flexible, and are easy to produce. Rechargeable batteries are currently being manufactured that employ polymer electrodes; in many respects these are superior to their metallic counterpart batteries. Other possible applications include wiring in aircraft and aerospace components, antistatic coatings for clothing, electromagnetic screening materials, and electronic devices (e.g., transistors and diodes).

DIELECTRIC BEHAVIOR

12.17 CAPACITANCE (CD-ROM)

12.18 FIELD VECTORS AND POLARIZATION (CD-ROM)

12.19 TYPES OF POLARIZATION (CD-ROM)

12.20 FREQUENCY DEPENDENCE OF THE DIELECTRIC CONSTANT (CD-ROM)

12.21 DIELECTRIC STRENGTH (CD-ROM)

12.22 DIELECTRIC MATERIALS (CD-ROM)

OTHER ELECTRICAL CHARACTERISTICS OF MATERIALS

12.23 FERROELECTRICITY (CD-ROM)

12.24 PIEZOELECTRICITY (CD-ROM)

SUMMARY

The ease with which a material is capable of transmitting an electric current is expressed in terms of electrical conductivity or its reciprocal, resistivity. On the basis of its conductivity, a solid material may be classified as a metal, a semiconductor, or an insulator.

For most materials, an electric current results from the motion of free electrons, which are accelerated in response to an applied electric field. The number of these free electrons depends on the electron energy band structure of the material. An electron band is just a series of electron states that are closely spaced with respect to energy, and one such band may exist for each electron subshell found in the isolated atom. By ‘‘electron energy band structure’’ is meant the manner in which the outermost bands are arranged relative to one another and then filled with electrons. A distinctive band structure type exists for metals, for semiconductors, and for insulators. An electron becomes free by being excited from a filled state in one band, to an available empty state above the Fermi energy. Relatively small energies are required for electron excitations in metals, giving rise to large numbers of free electrons. Larger energies are required for electron excitations in semiconductors and insulators, which accounts for their lower free electron concentrations and smaller conductivity values.

Free electrons being acted on by an electric field are scattered by imperfections in the crystal lattice. The magnitude of electron mobility is indicative of the frequency of these scattering events. In many materials, the electrical conductivity is proportional to the product of the electron concentration and the mobility.

For metallic materials, electrical resistivity increases with temperature, impurity content, and plastic deformation. The contribution of each to the total resistivity is additive.

Semiconductors may be either elements (Si and Ge) or covalently bonded compounds. With these materials, in addition to free electrons, holes (missing electrons in the valence band) may also participate in the conduction process. On the basis of electrical behavior, semiconductors are classified as either intrinsic or extrinsic. For intrinsic behavior, the electrical properties are inherent to the pure material, and electron and hole concentrations are equal; electrical behavior is dictated by impurities for extrinsic semiconductors. Extrinsic semiconductors may be either *n*- or *p*-type depending on whether electrons or holes, respectively, are the predominant charge carriers. Donor impurities introduce excess electrons; acceptor impurities, excess holes.

The electrical conductivity of semiconducting materials is particularly sensitive to impurity type and content, as well as to temperature. The addition of even minute concentrations of some impurities enhances the conductivity drastically. Furthermore, with rising temperature, intrinsic conductivity experiences an exponential increase. Extrinsic conductivity may also increase with temperature.

{A number of semiconducting devices employ the unique electrical characteristics of these materials to perform specific electronic functions. Included are the *p–n* rectifying junction, and junction and MOSFET transistors. Transistors are used for amplification of electrical signals, as well as for switching devices in computer circuitries.}

{Dielectric materials are electrically insulative, yet susceptible to polarization in the presence of an electric field. This polarization phenomenon accounts for the ability of the dielectrics to increase the charge storing capability of capacitors, the efficiency of which is expressed in terms of a dielectric constant. Polarization results from the inducement by, or orientation with the electric field of atomic or molecular dipoles; a dipole is said to exist when there is a net spatial separation of positively and negatively charged entities. Possible polarization types include electronic, ionic, and orientation; not all types need be present in a particular dielectric. For alternating electric fields, whether a specific polarization type contributes to the total polarization and dielectric constant depends on frequency; each polarization mechanism ceases to function when the applied field frequency exceeds its relaxation frequency.}

{This chapter concluded with brief discussions of two other electrical phenomena. Ferroelectric materials are those that may exhibit polarization spontaneously, that is, in the absence of any external electric field. Finally, piezoelectricity is the phenomenon whereby polarization is induced in a material by the imposition of external forces.}

IMPORTANT TERMS AND CONCEPTS

Acceptor state
Capacitance
Conduction band
Conductivity, electrical
Dielectric
Dielectric constant
Dielectric displacement
Dielectric strength
Diode
Dipole, electric
Donor state
Doping
Electrical resistance
Electron energy band
Energy band gap
Extrinsic semiconductor
Fermi energy
Ferroelectric
Forward bias
Free electron
Hall effect
Hole
Insulator
Integrated circuit
Intrinsic semiconductor
Ionic conduction
Junction transistor
Matthiessen's rule
Metal
Mobility
MOSFET
Ohm's law
Permittivity
Piezoelectric
Polarization
Polarization, electronic
Polarization, ionic
Polarization, orientation
Rectifying junction
Relaxation frequency
Resistivity, electrical
Reverse bias
Semiconductor
Valence band

REFERENCES

Azaroff, L. V. and J. J. Brophy, *Electronic Processes in Materials,* McGraw-Hill Book Company, New York, 1963. Reprinted by TechBooks, Marietta, OH, 1990. Chapters 6–12.

Bube, R. H., *Electrons in Solids,* 3rd edition, Academic Press, San Diego, 1992.

Bylander, E. G., *Materials for Semiconductor Functions,* Hayden Book Company, New York, 1971. Good fundamental treatment of the physics of semiconductors and various semiconducting devices.

Chaudhari, P., ''Electronic and Magnetic Materials,'' *Scientific American,* Vol. 255, No. 4, October 1986, pp. 136–144.

Ehrenreich, H., ''The Electrical Properties of Materials,'' *Scientific American,* Vol. 217, No. 3, September 1967, pp. 194–204.

Hummel, R. E., *Electronic Properties of Materials,* 2nd edition, Springer-Verlag New York, Inc., New York, 1994.

Kingery, W. D., H. K. Bowen, and D. R. Uhlmann, *Introduction to Ceramics,* 2nd edition, John Wiley & Sons, New York, 1976. Chapters 17 and 18.

Kittel, C., *Introduction to Solid State Physics,* 7th edition, John Wiley & Sons, Inc., New York, 1995. An advanced treatment.

Kwok, H. L., *Electronic Materials,* Brooks/Cole Publishing Company, Pacific Grove, CA, 1997.

Livingston, J., *Electronic Properties,* John Wiley & Sons, New York, 1999.

Meindl, J. D., ''Microelectronic Circuit Elements,'' *Scientific American,* Vol. 237, No. 3, September 1977, pp. 70–81.

Navon, D. H., *Semiconductor Microdevices and Materials,* Oxford University, Oxford, 1995.

Noyce, R. N., ''Microelectronics,'' *Scientific American*, Vol. 237, No. 3, September 1977, pp. 62–69.

Oldham, W. G., ''The Fabrication of Microelectronic Circuits,'' *Scientific American*, Vol. 237, No. 3, September 1977, pp. 110–128.

Rose, R. M., L. A. Shepard, and J. Wulff, *The Structure and Properties of Materials,* Vol. IV, *Electronic Properties,* John Wiley & Sons, New York, 1966. Chapters 1, 2, 4–8, and 12.

Warnes, L. A. A., *Electronic Materials,* Chapman and Hall, New York, 1990.

Wert, C. A. and R. M. Thomson, *Physics of Solids,* 2nd edition, McGraw-Hill Book Company, New York, 1970. Chapters 9 and 11–19.

QUESTIONS AND PROBLEMS

Note: To solve those problems having an asterisk (*) by their numbers, consultation of supplementary topics [appearing only on the CD-ROM (and not in print)] will probably be necessary.

12.1 **(a)** Compute the electrical conductivity of a 5.1-mm (0.2-in.) diameter cylindrical silicon specimen 51 mm (2 in.) long in which a current of 0.1 A passes in an axial direction. A voltage of 12.5 V is measured across two probes that are separated by 38 mm (1.5 in.). **(b)** Compute the resistance over the entire 51 mm (2 in.) of the specimen.

12.2 A copper wire 100 m long must experience a voltage drop of less than 1.5 V when a current of 2.5 A passes through it. Using the data in Table 12.1, compute the minimum diameter of the wire.

12.3 An aluminum wire 4 mm in diameter is to offer a resistance of no more than 2.5 Ω. Using the data in Table 12.1, compute the maximum wire length.

12.4 Demonstrate that the two Ohm's law expressions, Equations 12.1 and 12.5, are equivalent.

12.5 **(a)** Using the data in Table 12.1, compute the resistance of a copper wire 3 mm (0.12 in.) in diameter and 2 m (78.7 in.) long. **(b)** What would be the current flow if the potential drop across the ends of the wire is 0.05 V? **(c)** What is the current density? **(d)** What is the magnitude of the electric field across the ends of the wire?

12.6 What is the distinction between electronic and ionic conduction?

12.7 How does the electron structure of an isolated atom differ from that of a solid material?

12.8 In terms of electron energy band structure, discuss reasons for the difference in electrical conductivity between metals, semiconductors, and insulators.

12.9 If a metallic material is cooled through its melting temperature at an extremely rapid rate, it will form a noncrystalline solid (i.e., a metallic glass). Will the electrical conductivity of the noncrystalline metal be greater or less than its crystalline counterpart? Why?

12.10 Briefly tell what is meant by the drift velocity and mobility of a free electron.

12.11 **(a)** Calculate the drift velocity of electrons in germanium at room temperature and when the magnitude of the electric field is 1000 V/m. **(b)** Under these circumstances, how long does it take an electron to traverse a 25 mm (1 in.) length of crystal?

12.12 An *n*-type semiconductor is known to have an electron concentration of 3×10^{18} m^{-3}. If the electron drift velocity is 100 m/s in an electric field of 500 V/m, calculate the conductivity of this material.

12.13 At room temperature the electrical conductivity and the electron mobility for copper are 6.0×10^7 $(\Omega\text{-m})^{-1}$ and 0.0030 m^2/V-s, respectively. **(a)** Compute the number of free electrons per cubic meter for copper at room temperature. **(b)** What is the number of free electrons per copper atom? Assume a density of 8.9 g/cm^3.

12.14 **(a)** Calculate the number of free electrons per cubic meter for gold assuming that there

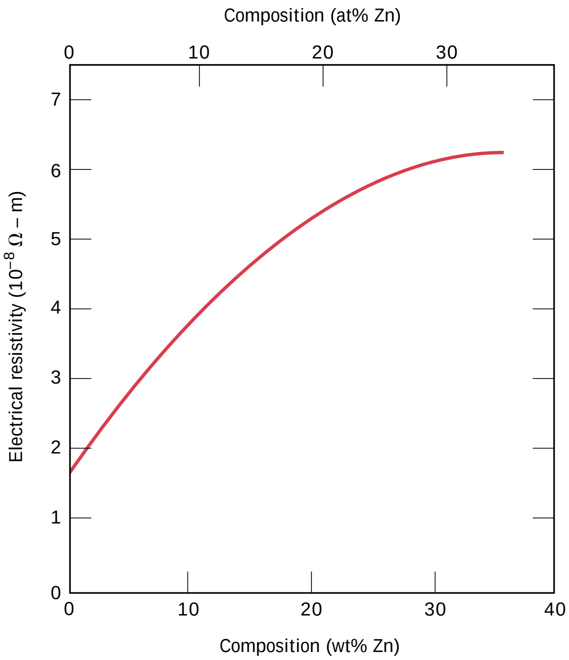

FIGURE 12.35 Room-temperature electrical resistivity versus composition for copper–zinc alloys. (Adapted from *Metals Handbook: Properties and Selection: Nonferrous Alloys and Pure Metals*, Vol. 2, 9th edition, H. Baker, Managing Editor, American Society for Metals, 1979, p. 315.)

are 1.5 free electrons per gold atom. The electrical conductivity and density for Au are 4.3×10^7 $(\Omega\text{-m})^{-1}$ and 19.32 g/cm^3, respectively. **(b)** Now compute the electron mobility for Au.

12.15 From Figure 12.35, estimate the value of A in Equation 12.11 for zinc as an impurity in copper–zinc alloys.

12.16 **(a)** Using the data in Figure 12.8, determine the values of ρ_0 and a from Equation 12.10 for pure copper. Take the temperature T to be in degrees Celsius. **(b)** Determine the value of A in Equation 12.11 for nickel as an impurity in copper, using the data in Figure 12.8. **(c)** Using the results of parts a and b, estimate the electrical resistivity of copper containing 1.75 at% Ni at 100°C.

12.17 Determine the electrical conductivity of a Cu-Ni alloy that has a yield strength of 125 MPa (18,000 psi). You will find Figure 8.16*b* helpful.

12.18 Tin bronze has a composition of 92 wt% Cu and 8 wt% Sn, and consists of two phases at room temperature: an α phase, which is copper containing a very small amount of tin in solid solution, and an ϵ phase, which consists of approximately 37 wt% Sn. Compute the room temperature conductivity of this alloy given the following data:

Phase	***Electrical Resistivity (Ω-m)***	***Density (g/cm³)***
α	1.88×10^{-8}	8.94
ϵ	5.32×10^{-7}	8.25

12.19 The room-temperature electrical resistivities of pure lead and pure tin are 2.06×10^{-7} and 1.11×10^{-7} Ω-m, respectively.

(a) Make a schematic graph of the room-temperature electrical resistivity versus composition for all compositions between pure lead and pure tin.

(b) On this same graph schematically plot electrical resistivity versus composition at 150°C.

(c) Explain the shapes of these two curves, as well as any differences between them.

12.20 A cylindrical metal wire 2 mm (0.08 in.) in diameter is required to carry a current of 10 A with a minimum of 0.03 V drop per foot (300 mm) of wire. Which of the metals and alloys listed in Table 12.1 are possible candidates?

12.21 **(a)** Compute the number of free electrons and holes that exist in intrinsic germanium at room temperature, using the data in Table 12.2. **(b)** Now calculate the number of free electrons per atom for germanium and silicon (Example Problem 12.1). **(c)** Explain the difference. You will need the densities for Ge and Si, which are 5.32 and 2.33 g/cm^3, respectively.

12.22 For intrinsic semiconductors, both electron and hole concentrations depend on temperature as follows:

$$n, p \propto \exp\left(-\frac{E_g}{2kT}\right) \qquad (12.38)$$

or, taking natural logarithms,

$$\ln n, \ln p \propto -\frac{E_g}{2kT}$$

Thus, a plot of the intrinsic ln n (or ln p) versus $1/T$ (K)$^{-1}$ should be linear and yield a slope of $-E_g/2k$. Using this information and Figure 12.16, determine the band gap energy for silicon. Compare this value with the one given in Table 12.2.

12.23 Define the following terms as they pertain to semiconducting materials: intrinsic, extrinsic, compound, elemental. Now provide an example of each.

12.24 Is it possible for compound semiconductors to exhibit intrinsic behavior? Explain your answer.

12.25 For each of the following pairs of semiconductors, decide which will have the smaller band gap energy E_g and then cite the reason for your choice: **(a)** ZnS and CdSe, **(b)** Si and C (diamond), **(c)** Al_2O_3 and ZnTe, **(d)** InSb and ZnSe, and **(e)** GaAs and AlP.

12.26 **(a)** In your own words, explain how donor impurities in semiconductors give rise to free electrons in numbers in excess of those generated by valence band–conduction band excitations. **(b)** Also explain how acceptor impurities give rise to holes in numbers in excess of those generated by valence band–conduction band excitations.

12.27 **(a)** Explain why no hole is generated by the electron excitation involving a donor impurity atom. **(b)** Explain why no free electron is generated by the electron excitation involving an acceptor impurity atom.

12.28 Will each of the following elements act as a donor or an acceptor when added to the indicated semiconducting material? Assume that the impurity elements are substitutional.

Impurity	*Semiconductor*
N	Si
B	Ge
Zn	GaAs
S	InSb
In	CdS
As	ZnTe

12.29 **(a)** At approximately what position is the Fermi energy for an intrinsic semiconductor? **(b)** At approximately what position is the Fermi energy for an *n*-type semiconductor? **(c)** Make a schematic plot of Fermi energy versus temperature for an *n*-type semiconductor up to a temperature at which it becomes intrinsic. Also note on this plot energy positions corresponding to the top of the valence band and the bottom of the conduction band.

12.30 **(a)** The room-temperature electrical conductivity of a silicon specimen is 10^3 (Ω-m)$^{-1}$. The hole concentration is known to be 1.0×10^{23} m^{-3}. Using the electron and hole mobilities for silicon in Table 12.2, compute the electron concentration. **(b)** On the basis of the result in part a, is the specimen intrinsic, *n*-type extrinsic, or *p*-type extrinsic? Why?

12.31 Using the data in Table 12.2, compute the electron and hole concentrations for intrinsic InSb at room temperature.

12.32 Germanium to which 5×10^{22} m^{-3} Sb atoms have been added is an extrinsic semiconductor at room temperature, and virtually all the Sb atoms may be thought of as being ionized (i.e., one charge carrier exists for each Sb atom). **(a)** Is this material *n*-type or *p*-type? **(b)** Calculate the electrical conductivity of this material, assuming electron and hole mobilities of 0.1 and 0.05 $m^2/V\text{-}s$, respectively.

12.33 The following electrical characteristics have been determined for both intrinsic and *p*-type extrinsic indium phosphide (InP) at room temperature:

	$\sigma(\Omega\text{-}m)^{-1}$	$n\ (m^{-3})$	$p\ (m^{-3})$
Intrinsic	2.5×10^{-6}	3.0×10^{13}	3.0×10^{13}
Extrinsic (*n*-type)	3.6×10^{-5}	4.5×10^{14}	2.0×10^{12}

Calculate electron and hole mobilities.

12.34 Compare the temperature dependence of the conductivity for metals and intrinsic semiconductors. Briefly explain the difference in behavior.

12.35 Using the data in Table 12.2, estimate the electrical conductivity of intrinsic GaAs at 150°C (423 K).

12.36 Briefly explain the presence of the factor 2 in the denominator of the second term on the right-hand side of Equation 12.19.

12.37 Using the data in Table 12.2, estimate the temperature at which the electrical conductivity of intrinsic GaAs is $4 \times 10^{-4}\ (\Omega\text{-m})^{-1}$.

12.38 The intrinsic electrical conductivities of a semiconductor at 20 and 100°C (293 and 373 K) are 1.0 and 500 $(\Omega\text{-m})^{-1}$, respectively. Determine the approximate band gap energy for this material.

12.39 Below, the intrinsic electrical conductivity of a semiconductor at two temperatures is tabulated:

T (*K*)	$\sigma\ (\Omega\text{-}m)^{-1}$
450	0.12
550	2.25

(a) Determine the band gap energy (in eV) for this material.

(b) Estimate the electrical conductivity at 300 K (27°C).

12.40 At room temperature, the temperature dependence of electron and hole mobilities for intrinsic germanium is found to be proportional to $T^{-3/2}$ for *T* in Kelvins; thus, a more accurate form of Equation 12.18 is as follows:

$$\sigma = C'' T^{-3/2} \exp\left(-\frac{E_g}{2kT}\right) \tag{12.39a}$$

or, in logarithmic form

$$\ln \sigma = \ln C'' - \frac{3}{2} \ln T - \frac{E_g}{2kT} \tag{12.39b}$$

where C'' is a temperature-independent constant.

(a) Calculate the intrinsic electrical conductivity for intrinsic germanium at 150°C, and compare this value with that obtained in Example Problem 12.3, which uses Equation 12.18.

(b) Now compute the number of free electrons and holes for intrinsic germanium at 150°C assuming this $T^{-3/2}$ dependence of electron and hole mobilities.

12.41 Estimate the temperature at which GaAs has an electrical conductivity of 3.7×10^{-3} $(\Omega\text{-m})^{-1}$ assuming the temperature dependence for σ of Equation 12.39a. The data shown in Table 12.2 might prove helpful.

12.42 The slope of the extrinsic portions of the curves in Figure 12.16 is related to the position of the acceptor level in the band gap (Figure 12.14). Write an expression for the dependence of *p* on the position of this level.

12.43 We noted in Section 5.3 (Figure 5.4) that in FeO (wüstite), the iron ions can exist in both Fe^{2+} and Fe^{3+} states. The number of each of these ion types depends on temperature and the ambient oxygen pressure. Furthermore, it was also noted that in order to retain electroneutrality, one Fe^{2+} vacancy will be created for every two Fe^{3+} ions that are formed; consequently, in order to reflect the existence of these vacancies the formula for wüstite is often represented as $Fe_{(1-x)}O$ where *x* is some small fraction less than unity.

In this nonstoichiometric $Fe_{(1-x)}O$ material, conduction is electronic, and, in fact, it behaves as a *p*-type semiconductor. That is, the Fe^{3+} ions act as electron acceptors, and it is relatively easy to excite an electron from the valence band into an Fe^{3+} acceptor state, with the formation of a hole. Determine the electrical conductivity of a specimen of wüstite that has a hole mobility of 1.0×10^{-5} m^2/V-s and for which the value of x is 0.060. Assume that the acceptor states are saturated (i.e., one hole exists for every Fe^{3+} ion). Wüstite has the sodium chloride crystal structure with a unit cell edge length of 0.437 nm.

12.44* Some hypothetical metal is known to have an electrical resistivity of 4×10^{-8} (Ω-m). Through a specimen of this metal that is 25 mm thick is passed a current of 30 A; when a magnetic field of 0.75 tesla is simultaneously imposed in a direction perpendicular to that of the current, a Hall voltage of -1.26×10^{-7} V is measured. Compute **(a)** the electron mobility for this metal, and **(b)** the number of free electrons per cubic meter.

12.45* Some metal alloy is known to have electrical conductivity and electron mobility values of 1.5×10^7 (Ω-m)$^{-1}$ and 0.0020 m^2/V-s, respectively. Through a specimen of this alloy that is 35 mm thick is passed a current of 45 A. What magnetic field would need to be imposed to yield a Hall voltage of -1.0×10^{-7} V?

12.46* Briefly describe electron and hole motions in a *p–n* junction for forward and reverse biases; then explain how these lead to rectification.

12.47* How is the energy in the reaction described by Equation 12.24 dissipated?

12.48* What are the two functions that a transistor may perform in an electronic circuit?

12.49* Would you expect increasing temperature to influence the operation of *p–n* junction rectifiers and transistors? Explain.

12.50* Cite the differences in operation and application for junction transistors and MOSFETs.

12.51 At temperatures between 775°C (1048 K) and 1100°C (1373 K), the activation energy and preexponential for the diffusion coefficient of Fe^{2+} in FeO are 102,000 J/mol and 7.3×10^{-8} m^2/s, respectively. Compute the mobility for an Fe^{2+} ion at 1000°C (1273 K).

12.52* A parallel-plate capacitor using a dielectric material having an ϵ_r of 2.5 has a plate spacing of 1 mm (0.04 in.). If another material having a dielectric constant of 4.0 is used and the capacitance is to be unchanged, what must be the new spacing between the plates?

12.53* A parallel-plate capacitor with dimensions of 100 mm by 25 mm and a plate separation of 3 mm must have a minimum capacitance of 38 pF (3.8×10^{-11} F) when an ac potential of 500 V is applied at a frequency of 1 MHz. Which of those materials listed in Table 12.4 are possible candidates? Why?

12.54* Consider a parallel-plate capacitor having an area of 2500 mm^2 and a plate separation of 2 mm, and with a material of dielectric constant 4.0 positioned between the plates. **(a)** What is the capacitance of this capacitor? **(b)** Compute the electric field that must be applied for a charge of 8.0×10^{-9} C to be stored on each plate.

12.55* In your own words, explain the mechanism by which charge storing capacity is increased by the insertion of a dielectric material within the plates of a capacitor.

12.56* For NaCl, the ionic radii for Na^+ and Cl^- ions are 0.102 and 0.181 nm, respectively. If an externally applied electric field produces a 5% expansion of the lattice, compute the dipole moment for each Na^+–Cl^- pair. Assume that this material is completely unpolarized in the absence of an electric field.

12.57* The polarization P of a dielectric material positioned within a parallel-plate capacitor is to be 1.0×10^{-6} C/m^2.

(a) What must be the dielectric constant if an electric field of 5×10^4 V/m is applied?

(b) What will be the dielectric displacement D?

12.58* A charge of 3.5×10^{-11} C is to be stored on each plate of a parallel-plate capacitor having an area of 160 mm^2 (0.25 in.^{2}) and a plate separation of 3.5 mm (0.14 in.).

(a) What voltage is required if a material having a dielectric constant of 5.0 is positioned within the plates?

(b) What voltage would be required if a vacuum is used?

(c) What are the capacitances for parts a and b?

(d) Compute the dielectric displacement for part a.

(e) Compute the polarization for part a.

12.59* **(a)** For each of the three types of polarization, briefly describe the mechanism by which dipoles are induced and/or oriented by the action of an applied electric field. **(b)** For solid lead titanate ($PbTiO_3$), gaseous neon, diamond, solid KCl, and liquid NH_3 what kind(s) of polarization is (are) possible? Why?

12.60* The dielectric constant for a soda–lime glass measured at very high frequencies (on the order of 10^{15} Hz) is approximately 2.3. What fraction of the dielectric constant at relatively low frequencies (1 MHz) is attributed to ionic polarization? Neglect any orientation polarization contributions.

12.61* **(a)** Compute the magnitude of the dipole moment associated with each unit cell of $BaTiO_3$, as illustrated in Figure 12.33.

(b) Compute the maximum polarization that is possible for this material.

12.62* Briefly explain why the ferroelectric behavior of $BaTiO_3$ ceases above its ferroelectric Curie temperature.

12.63* Would you expect the physical dimensions of a piezoelectric material such as $BaTiO_3$ to change when it is subjected to an electric field? Why or why not?

Design Problems

12.D1 A 95 wt% Pt-5 wt% Ni alloy is known to have an electrical resistivity of 2.35×10^{-7} Ω-m at room temperature (25°C). Calculate the composition of a platinum-nickel alloy that gives a room-temperature resistivity of 1.75×10^{-7} Ω-m. The room-temperature resistivity of pure platinum may be determined from the data in Table 12.1; assume that platinum and nickel form a solid solution.

12.D2 Using information contained in Figures 12.8 and 12.35, determine the electrical conductivity of an 80 wt% Cu-20 wt% Zn alloy at −150°C (−240°F).

12.D3 Is it possible to alloy copper with nickel to achieve a minimum tensile strength of 375 MPa (54,400 psi) and yet maintain an electrical conductivity of 2.5×10^6 $(\Omega\text{-m})^{-1}$? If not, why? If so, what concentration of nickel is required? You may want to consult Figure 8.16*a*.

12.D4 Specify an acceptor impurity type and concentration (in weight percent) that will produce a *p*-type silicon material having a room temperature electrical conductivity of 50 $(\Omega\text{-m})^{-1}$. Use intrinsic electron and hole mobilities, and assume that the acceptor impurities are saturated.

12.D5 One integrated circuit design calls for diffusing boron into very high purity silicon at an elevated temperature. It is necessary that at a distance 0.2 μm from the surface of the silicon wafer, the room-temperature electrical conductivity be 1.2×10^4 $(\Omega\text{-m})^{-1}$. The concentration of B at the surface of the Si is maintained at a constant level of 1.0×10^{25} m^{-3}; furthermore, it is assumed that the concentration of B in the original Si material is negligible, and that at room temperature the boron atoms are saturated. Specify the temperature at which this diffusion heat treatment is to take place if the treatment time is to be one hour. The diffusion coefficient for the diffusion of B in Si is a function of temperature as

$$D(\text{m}^2/\text{s}) = 2.4 \times 10^{-4} \exp\left(-\frac{347\ \text{kJ/mol}}{RT}\right)$$

12.D6 Problem 12.43 noted that FeO (wüstite) may behave as a semiconductor by virtue of the transformation of Fe^{2+} to Fe^{3+} and the creation of Fe^{2+} vacancies; the maintenance of electroneutrality requires that for every two Fe^{3+} ions, one vacancy is formed. The existence of these vacancies is reflected in the chemical formula of this nonstoichiometric wüstite as $Fe_{(1-x)}O$, where x is a small number having a value less than unity. The degree of nonstoichiometry (i.e., the value of x) may be varied by changing temperature and oxygen partial pressure. Compute the value of x that is required to produce an $Fe_{(1-x)}O$ material having a p-type electrical conductivity of 2000 $(\Omega\text{-m})^{-1}$; assume that the hole mobility is 1.0×10^{-5} $m^2/V\text{-s}$, and that the acceptor states are saturated.

12.D7 The base semiconducting material used in virtually all of our modern integrated circuits is silicon. However, silicon has some limitations and restrictions. Write an essay comparing the properties and applications (and/or potential applications) of silicon and gallium arsenide.

Chapter 5 / Imperfections in Solids

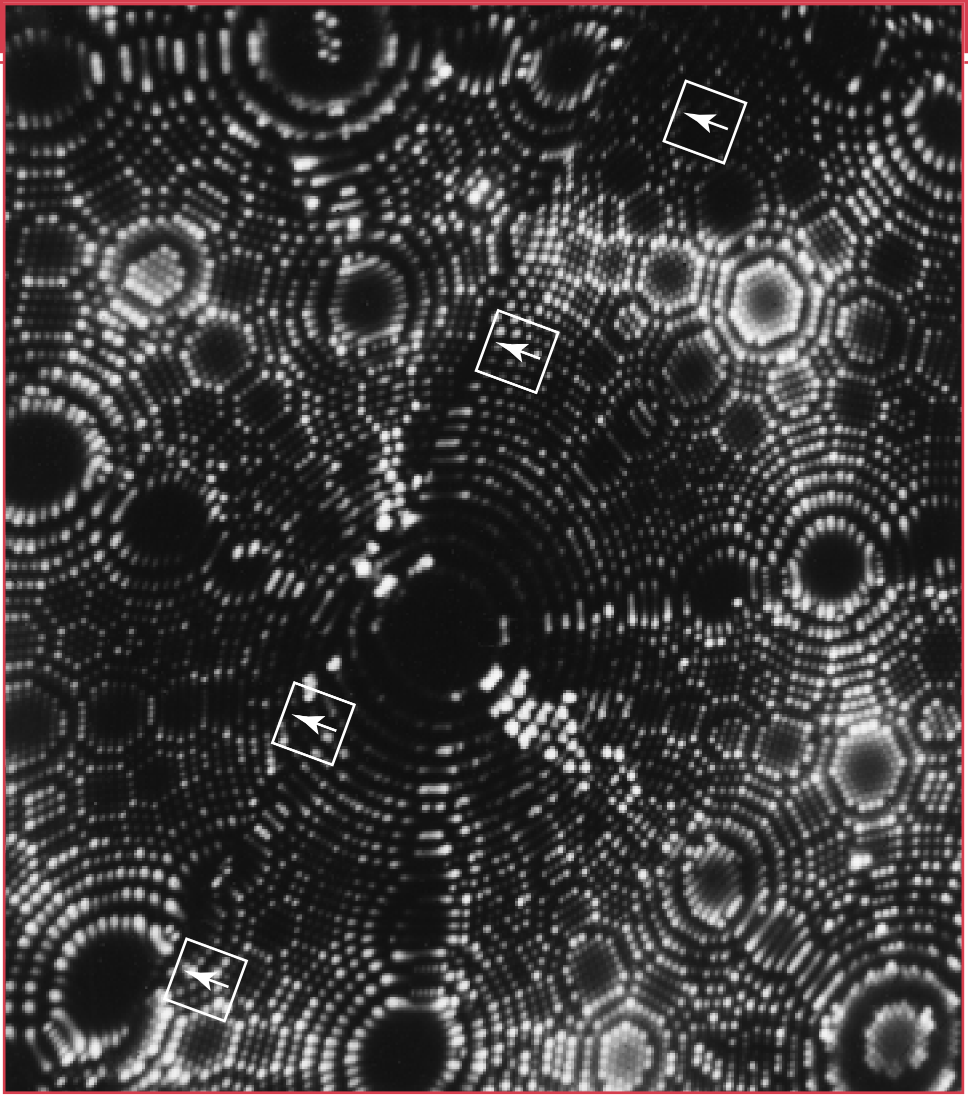

A field ion micrograph taken at the tip of a pointed tungsten specimen. Field ion microscopy is a sophisticated and fascinating technique that permits observation of individual atoms in a solid, which are represented by white spots. The symmetry and regularity of the atom arrangements are evident from the positions of the spots in this micrograph. A disruption of this symmetry occurs along a grain boundary, which is traced by the arrows. Approximately 3,460,000×. (Photomicrograph courtesy of J. J. Hren and R. W. Newman.)

Why Study *Imperfections in Solids?*

The properties of some materials are profoundly influenced by the presence of imperfections. Consequently, it is important to have a knowledge about the types of imperfections that exist, and the roles they play in affecting the behavior of materials. For example, the mechanical properties of pure metals experience significant alterations when alloyed (i.e., when impurity atoms are added)—e.g., sterling silver (92.5% silver-7.5% copper) is much harder and stronger than pure silver (Section 8.10).

Also, integrated circuit microelectronic devices found in our computers, calculators, and home appliances function because of highly controlled concentrations of specific impurities that are incorporated into small, localized regions of semiconducting materials (Sections 12.11 {and 12.14}).

Learning Objectives

After studying this chapter you should be able to do the following:

1. **Describe both vacancy and self-interstitial crystalline defects.**
2. **Calculate the equilibrium number of vacancies in a material at some specified temperature, given the relevant constants.**
3. **Name the two types of solid solutions, and provide a brief written definition and/or schematic sketch of each.**
4. **Name and describe eight different ionic point defects that are found in ceramic compounds.**
5. **Given the masses and atomic weights of two or more elements in a metal alloy, calculate the weight percent and atomic percent for each element.**
6. **For each of edge, screw, and mixed dislocations:**
   - **(a) describe and make a drawing of the dislocation;**
   - **(b) note the location of the dislocation line; and**
   - **(c) indicate the direction along which the dislocation line extends.**
7. **Describe the atomic structure within the vicinity of (a) a grain boundary, and (b) a twin boundary.**

5.1 INTRODUCTION

For a crystalline solid we have tacitly assumed that perfect order exists throughout the material on an atomic scale. However, such an idealized solid does not exist; all contain large numbers of various defects or imperfections. As a matter of fact, many of the properties of materials are profoundly sensitive to deviations from crystalline perfection; the influence is not always adverse, and often specific characteristics are deliberately fashioned by the introduction of controlled amounts or numbers of particular defects, as detailed in succeeding chapters.

By ‘‘crystalline defect’’ is meant a lattice irregularity having one or more of its dimensions on the order of an atomic diameter. Classification of crystalline imperfections is frequently made according to geometry or dimensionality of the defect. Several different imperfections are discussed in this chapter, including point defects (those associated with one or two atomic positions), linear (or one-dimensional) defects, as well as interfacial defects, or boundaries, which are two-dimensional. Impurities in solids are also discussed, since impurity atoms may exist as point defects. {Finally, techniques for the microscopic examination of defects and the structure of materials are briefly described.}

POINT DEFECTS

5.2 POINT DEFECTS IN METALS

The simplest of the point defects is a **vacancy,** or vacant lattice site, one normally occupied from which an atom is missing (Figure 5.1). All crystalline solids contain vacancies and, in fact, it is not possible to create such a material that is free of these defects. The necessity of the existence of vacancies is explained using principles of thermodynamics; in essence, the presence of vacancies increases the entropy (i.e., the randomness) of the crystal.

The equilibrium number of vacancies N_v for a given quantity of material depends on and increases with temperature according to

$$N_v = N \exp\left(-\frac{Q_v}{kT}\right) \tag{5.1}$$

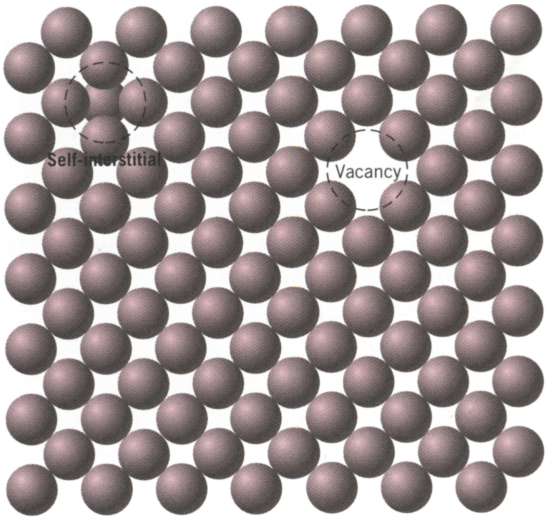

Figure 5.1 Two-dimensional representations of a vacancy and a self-interstitial. (Adapted from W. G. Moffatt, G. W. Pearsall, and J. Wulff, *The Structure and Properties of Materials,* Vol. I, *Structure,* p. 77. Copyright © 1964 by John Wiley & Sons, New York. Reprinted by permission of John Wiley & Sons, Inc.)

In this expression, N is the total number of atomic sites, Q_v is the energy required for the formation of a vacancy, T is the absolute temperature[1] in kelvins, and k is the gas or **Boltzmann's constant.** The value of k is 1.38×10^{-23} J/atom-K, or 8.62×10^{-5} eV/atom-K, depending on the units of Q_v.[2] Thus, the number of vacancies increases exponentially with temperature; that is, as T in Equation 5.1 increases, so does also the expression $\exp -(Q_v/kT)$. For most metals, the fraction of vacancies N_v/N just below the melting temperature is on the order of 10^{-4}; that is, one lattice site out of 10,000 will be empty. As ensuing discussions indicate, a number of other material parameters have an exponential dependence on temperature similar to that of Equation 5.1.

A **self-interstitial** is an atom from the crystal that is crowded into an interstitial site, a small void space that under ordinary circumstances is not occupied. This kind of defect is also represented in Figure 5.1. In metals, a self-interstitial introduces relatively large distortions in the surrounding lattice because the atom is substantially larger than the interstitial position in which it is situated. Consequently, the formation of this defect is not highly probable, and it exists in very small concentrations, which are significantly lower than for vacancies.

EXAMPLE PROBLEM 5.1

Calculate the equilibrium number of vacancies per cubic meter for copper at 1000°C. The energy for vacancy formation is 0.9 eV/atom; the atomic weight and density (at 1000°C) for copper are 63.5 g/mol and 8.40 g/cm^3, respectively.

SOLUTION

This problem may be solved by using Equation 5.1; it is first necessary, however, to determine the value of N, the number of atomic sites per cubic meter for copper, from its atomic weight A_{Cu}, its density ρ, and Avogadro's number N_{A}, according to

---

[1] Absolute temperature in kelvins (K) is equal to °C + 273.

[2] Boltzmann's constant per mole of atoms becomes the gas constant R; in such a case R = 8.31 J/mol-K, or 1.987 cal/mol-K.

$$N = \frac{N_{\text{A}}\rho}{A_{\text{Cu}}} \tag{5.2}$$

$$= \frac{(6.023 \times 10^{23}\ \text{atoms/mol})(8.40\ \text{g/cm}^3)(10^6\ \text{cm}^3/\text{m}^3)}{63.5\ \text{g/mol}}$$

$$= 8.0 \times 10^{28}\ \text{atoms/m}^3$$

Thus, the number of vacancies at 1000°C (1273 K) is equal to

$$N_v = N \exp\left(-\frac{Q_v}{kT}\right)$$

$$= (8.0 \times 10^{28}\ \text{atoms/m}^3) \exp\left[-\frac{(0.9\ \text{eV})}{(8.62 \times 10^{-5}\ \text{eV/K})(1273\ \text{K})}\right]$$

$$= 2.2 \times 10^{25}\ \text{vacancies/m}^3$$

5.3 POINT DEFECTS IN CERAMICS

Point defects also may exist in ceramic compounds. As with metals, both vacancies and interstitials are possible; however, since ceramic materials contain ions of at least two kinds, defects for each ion type may occur. For example, in NaCl, Na interstitials and vacancies and Cl interstitials and vacancies may exist. It is highly improbable that there would be appreciable concentrations of anion (Cl^-) interstitials. The anion is relatively large, and to fit into a small interstitial position, substantial strains on the surrounding ions must be introduced. Anion and cation vacancies and a cation interstitial are represented in Figure 5.2.

The expression **defect structure** is often used to designate the types and concentrations of atomic defects in ceramics. Because the atoms exist as charged ions, when defect structures are considered, conditions of electroneutrality must be maintained.

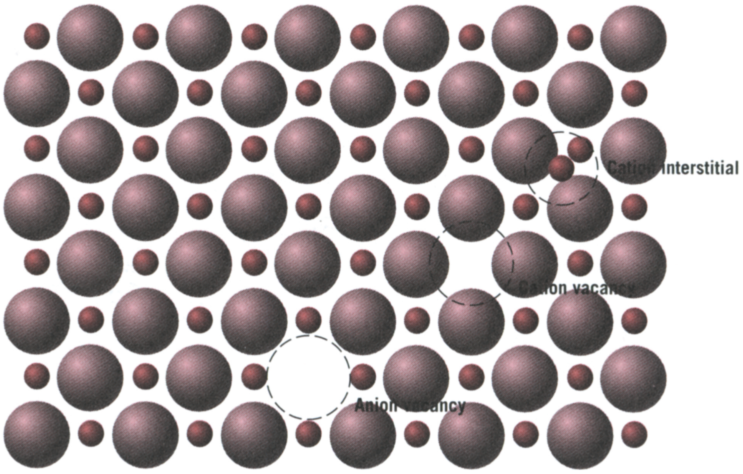

FIGURE 5.2 Schematic representations of cation and anion vacancies and a cation interstitial. (From W. G. Moffatt, G. W. Pearsall, and J. Wulff, *The Structure and Properties of Materials*, Vol. 1, *Structure*, p. 78. Copyright © 1964 by John Wiley & Sons, New York. Reprinted by permission of John Wiley & Sons, Inc.)

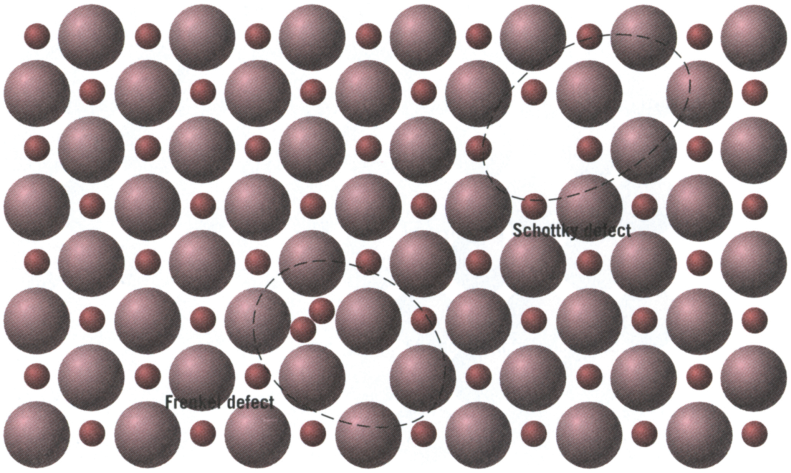

FIGURE 5.3 Schematic diagram showing Frenkel and Schottky defects in ionic solids. (From W. G. Moffatt, G. W. Pearsall, and J. Wulff, *The Structure and Properties of Materials*, Vol. 1, *Structure*, p. 78. Copyright © 1964 by John Wiley & Sons, New York. Reprinted by permission of John Wiley & Sons, Inc.)

Electroneutrality is the state that exists when there are equal numbers of positive and negative charges from the ions. As a consequence, defects in ceramics do not occur alone. One such type of defect involves a cation–vacancy and a cation–interstitial pair. This is called a **Frenkel defect** (Figure 5.3). It might be thought of as being formed by a cation leaving its normal position and moving into an interstitial site. There is no change in charge because the cation maintains the same positive charge as an interstitial.

Another type of defect found in AX materials is a cation vacancy–anion vacancy pair known as a **Schottky defect,** also schematically diagrammed in Figure 5.3. This defect might be thought of as being created by removing one cation and one anion from the interior of the crystal and then placing them both at an external surface. Since both cations and anions have the same charge, and since for every anion vacancy there exists a cation vacancy, the charge neutrality of the crystal is maintained.

The ratio of cations to anions is not altered by the formation of either a Frenkel or a Schottky defect. If no other defects are present, the material is said to be stoichiometric. **Stoichiometry** may be defined as a state for ionic compounds wherein there is the exact ratio of cations to anions as predicted by the chemical formula. For example, NaCl is stoichiometric if the ratio of Na^+ ions to Cl^- ions is exactly 1:1. A ceramic compound is *nonstoichiometric* if there is any deviation from this exact ratio.

Nonstoichiometry may occur for some ceramic materials in which two valence (or ionic) states exist for one of the ion types. Iron oxide (wüstite, FeO) is one such material, for the iron can be present in both Fe^{2+} and Fe^{3+} states; the number of each of these ion types depends on temperature and the ambient oxygen pressure. The formation of an Fe^{3+} ion disrupts the electroneutrality of the crystal by introducing an excess $+1$ charge, which must be offset by some type of defect. This may be accomplished by the formation of one Fe^{2+} vacancy (or the removal of two positive charges) for every two Fe^{3+} ions that are formed (Figure 5.4). The crystal is no longer stoichiometric because there is one more O ion than Fe ion; however, the crystal remains electrically neutral. This phenomenon is fairly common in iron oxide, and, in fact, its chemical formula is often written as $Fe_{1-x}O$ (where x is some

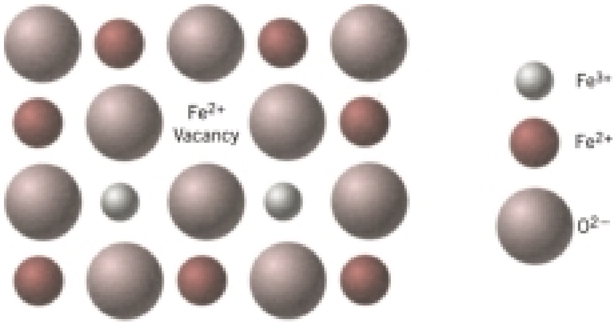

Figure 5.4 Schematic representation of an Fe^{2+} vacancy in FeO that results from the formation of two Fe^{3+} ions.

small and variable fraction substantially less than unity) to indicate a condition of nonstoichiometry with a deficiency of Fe.

5.4 IMPURITIES IN SOLIDS

IMPURITIES IN METALS

A pure metal consisting of only one type of atom just isn't possible; impurity or foreign atoms will always be present, and some will exist as crystalline point defects. In fact, even with relatively sophisticated techniques, it is difficult to refine metals to a purity in excess of 99.9999%. At this level, on the order of 10^{22} to 10^{23} impurity atoms will be present in one cubic meter of material. Most familiar metals are not highly pure; rather, they are **alloys,** in which impurity atoms have been added intentionally to impart specific characteristics to the material. Ordinarily alloying is used in metals to improve mechanical strength and corrosion resistance. For example, sterling silver is a 92.5% silver–7.5% copper alloy. In normal ambient environments, pure silver is highly corrosion resistant, but also very soft. Alloying with copper enhances the mechanical strength significantly, without depreciating the corrosion resistance appreciably.

The addition of impurity atoms to a metal will result in the formation of a **solid solution** and/or a new *second phase,* depending on the kinds of impurity, their concentrations, and the temperature of the alloy. The present discussion is concerned with the notion of a solid solution; treatment of the formation of a new phase is deferred to Chapter 10.

Several terms relating to impurities and solid solutions deserve mention. With regard to alloys, **solute** and **solvent** are terms that are commonly employed. ''Solvent'' represents the element or compound that is present in the greatest amount; on occasion, solvent atoms are also called *host atoms.* ''Solute'' is used to denote an element or compound present in a minor concentration.

SOLID SOLUTIONS

A solid solution forms when, as the solute atoms are added to the host material, the crystal structure is maintained, and no new structures are formed. Perhaps it is useful to draw an analogy with a liquid solution. If two liquids, soluble in each other (such as water and alcohol) are combined, a liquid solution is produced as the molecules intermix, and its composition is homogeneous throughout. A solid solution is also compositionally homogeneous; the impurity atoms are randomly and uniformly dispersed within the solid.

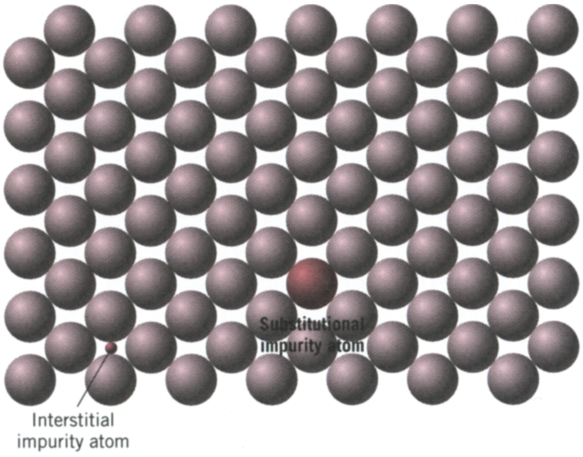

FIGURE 5.5 Two-dimensional schematic representations of substitutional and interstitial impurity atoms. (Adapted from W. G. Moffatt, G. W. Pearsall, and J. Wulff, *The Structure and Properties of Materials,* Vol. I, *Structure,* p. 77. Copyright © 1964 by John Wiley & Sons, New York. Reprinted by permission of John Wiley & Sons, Inc.)

Impurity point defects are found in solid solutions, of which there are two types: **substitutional** and **interstitial.** For substitutional, solute or impurity atoms replace or substitute for the host atoms (Figure 5.5). There are several features of the solute and solvent atoms that determine the degree to which the former dissolves in the latter; these are as follows:

1. *Atomic size factor.* Appreciable quantities of a solute may be accommodated in this type of solid solution only when the difference in atomic radii between the two atom types is less than about ±15%. Otherwise the solute atoms will create substantial lattice distortions and a new phase will form.
2. *Crystal structure.* For appreciable solid solubility the crystal structures for metals of both atom types must be the same.
3. *Electronegativity.* The more electropositive one element and the more electronegative the other, the greater is the likelihood that they will form an intermetallic compound instead of a substitutional solid solution.
4. *Valences.* Other factors being equal, a metal will have more of a tendency to dissolve another metal of higher valency than one of a lower valency.

An example of a substitutional solid solution is found for copper and nickel. These two elements are completely soluble in one another at all proportions. With regard to the aforementioned rules that govern degree of solubility, the atomic radii for copper and nickel are 0.128 and 0.125 nm, respectively, both have the FCC crystal structure, and their electronegativities are 1.9 and 1.8 (Figure 2.7); finally, the most common valences are +1 for copper (although it sometimes can be +2) and +2 for nickel.

For interstitial solid solutions, impurity atoms fill the voids or interstices among the host atoms (see Figure 5.5). For metallic materials that have relatively high atomic packing factors, these interstitial positions are relatively small. Consequently, the atomic diameter of an interstitial impurity must be substantially smaller than that of the host atoms. Normally, the maximum allowable concentration of interstitial impurity atoms is low (less than 10%). Even very small impurity atoms are ordinarily larger than the interstitial sites, and as a consequence they introduce some lattice strains on the adjacent host atoms. Problem 5.9 calls for determination of the radii of impurity atoms (in terms of R, the host atom radius) that will just fit into interstitial positions without introducing any lattice strains for both FCC and BCC crystal structures.

Carbon forms an interstitial solid solution when added to iron; the maximum concentration of carbon is about 2%. The atomic radius of the carbon atom is much less than that for iron: 0.071 nm versus 0.124 nm.

IMPURITIES IN CERAMICS

Impurity atoms can form solid solutions in ceramic materials much as they do in metals. Solid solutions of both substitutional and interstitial types are possible. For an interstitial, the ionic radius of the impurity must be relatively small in comparison to the anion. Since there are both anions and cations, a substitutional impurity will substitute for the host ion to which it is most similar in an electrical sense: if the impurity atom normally forms a cation in a ceramic material, it most probably will substitute for a host cation. For example, in sodium chloride, impurity Ca^{2+} and O^{2-} ions would most likely substitute for Na^+ and Cl^- ions, respectively. Schematic representations for cation and anion substitutional as well as interstitial impurities are shown in Figure 5.6. To achieve any appreciable solid solubility of substituting impurity atoms, the ionic size and charge must be very nearly the same as those of one of the host ions. For an impurity ion having a charge different from the host ion for which it substitutes, the crystal must compensate for this difference in charge so that electroneutrality is maintained with the solid. One way this is accomplished is by the formation of lattice defects—vacancies or interstitials of both ion types, as discussed above.

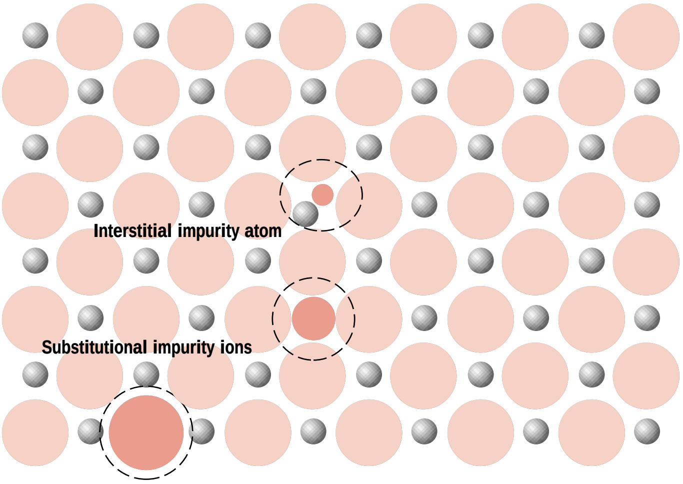

FIGURE 5.6 Schematic representations of interstitial, anion-substitutional, and cation-substitutional impurity atoms in an ionic compound. (Adapted from W. G. Moffatt, G. W. Pearsall, and J. Wulff, *The Structure and Properties of Materials,* Vol. 1, *Structure,* p. 78. Copyright © 1964 by John Wiley & Sons, New York. Reprinted by permission of John Wiley & Sons, Inc.)

EXAMPLE PROBLEM 5.2

If electroneutrality is to be preserved, what point defects are possible in NaCl when a Ca^{2+} substitutes for an Na^+ ion? How many of these defects exist for every Ca^{2+} ion?

SOLUTION

Replacement of an Na^+ by a Ca^{2+} ion introduces one extra positive charge. Electroneutrality is maintained when either a single positive charge is eliminated or another single negative charge is added. Removal of a positive charge is accomplished by the formation of one Na^+ vacancy. Alternatively, a Cl^- interstitial will supply an additional negative charge, negating the effect of each Ca^{2+} ion. However, as mentioned above, the formation of this defect is highly unlikely.

5.5 POINT DEFECTS IN POLYMERS

It should be noted that the defect concept is different in polymers (than in metals and ceramics) as a consequence of the chainlike macromolecules and the nature of the crystalline state for polymers. Point defects similar to those found in metals have been observed in crystalline regions of polymeric materials; these include vacancies and interstitial atoms and ions. Chain ends are considered to be defects inasmuch as they are chemically dissimilar to normal chain units; vacancies are also associated with the chain ends. Impurity atoms/ions or groups of atoms/ions may be incorporated in the molecular structure as interstitials; they may also be associated with main chains or as short side branches.

5.6 SPECIFICATION OF COMPOSITION

It is often necessary to express the **composition** (or *concentration*)[3] of an alloy in terms of its constituent elements. The two most common ways to specify composition are weight (or mass) percent and atom percent. The basis for **weight percent** (wt%) is the weight of a particular element relative to the total alloy weight. For an alloy that contains two hypothetical atoms denoted by 1 and 2, the concentration of 1 in wt%, C_1, is defined as

$$C_1 = \frac{m_1}{m_1 + m_2} \times 100 \tag{5.3}$$

where m_1 and m_2 represent the weight (or mass) of elements 1 and 2, respectively. The concentration of 2 would be computed in an analogous manner.

The basis for **atom percent** (at%) calculations is the number of moles of an element in relation to the total moles of the elements in the alloy. The number of moles in some specified mass of a hypothetical element 1, n_{m1}, may be computed as follows:

---

[3] The terms *composition* and *concentration* will be assumed to have the same meaning in this book (i.e., the relative content of a specific element or constituent in an alloy) and will be used interchangeably.

$$n_{m1} = \frac{m_1'}{A_1} \tag{5.4}$$

Here, m_1' and A_1 denote the mass (in grams) and atomic weight, respectively, for element 1.

Concentration in terms of atom percent of element 1 in an alloy containing 1 and 2 atoms, C_1', is defined by[4]

$$C_1' = \frac{n_{m1}}{n_{m1} + n_{m2}} \times 100 \tag{5.5}$$

In like manner, the atom percent of 2 may be determined.

Atom percent computations also can be carried out on the basis of the number of atoms instead of moles, since one mole of all substances contains the same number of atoms.

COMPOSITION CONVERSIONS (CD-ROM)

MISCELLANEOUS IMPERFECTIONS

5.7 Dislocations—Linear Defects

A *dislocation* is a linear or one-dimensional defect around which some of the atoms are misaligned. One type of dislocation is represented in Figure 5.7: an extra portion

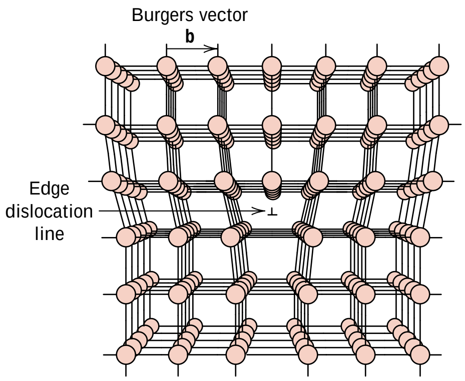

Figure 5.7 The atom positions around an edge dislocation; extra half-plane of atoms shown in perspective. (Adapted from A. G. Guy, *Essentials of Materials Science,* McGraw-Hill Book Company, New York, 1976, p. 153.)

---

[4] In order to avoid confusion in notations and symbols that are being used in this section, it should be pointed out that the prime (as in C_1' and m_1') is used to designate both composition, in atom percent, as well as mass of material in units of grams.

of a plane of atoms, or half-plane, the edge of which terminates within the crystal. This is termed an **edge dislocation;** it is a linear defect that centers around the line that is defined along the end of the extra half-plane of atoms. This is sometimes termed the **dislocation line,** which, for the edge dislocation in Figure 5.7, is perpendicular to the plane of the page. Within the region around the dislocation line there is some localized lattice distortion. The atoms above the dislocation line in Figure 5.7 are squeezed together, and those below are pulled apart; this is reflected in the slight curvature for the vertical planes of atoms as they bend around this extra half-plane. The magnitude of this distortion decreases with distance away from the dislocation line; at positions far removed, the crystal lattice is virtually perfect. Sometimes the edge dislocation in Figure 5.7 is represented by the symbol $\perp$, which also indicates the position of the dislocation line. An edge dislocation may also be formed by an extra half-plane of atoms that is included in the bottom portion of the crystal; its designation is a $\top$.

Another type of dislocation, called a **screw dislocation,** exists, which may be thought of as being formed by a shear stress that is applied to produce the distortion shown in Figure 5.8*a*: the upper front region of the crystal is shifted one atomic distance to the right relative to the bottom portion. The atomic distortion associated with a screw dislocation is also linear and along a dislocation line, line AB in Figure 5.8*b*. The screw dislocation derives its name from the spiral or helical path or ramp that is traced around the dislocation line by the atomic planes of atoms. Sometimes the symbol ↻ is used to designate a screw dislocation.

Most dislocations found in crystalline materials are probably neither pure edge nor pure screw, but exhibit components of both types; these are termed **mixed dislocations.** All three dislocation types are represented schematically in Figure 5.9; the lattice distortion that is produced away from the two faces is mixed, having varying degrees of screw and edge character.

The magnitude and direction of the lattice distortion associated with a dislocation is expressed in terms of a **Burgers vector,** denoted by a $\mathbf{b}$. Burgers vectors are indicated in Figures 5.7 and 5.8 for edge and screw dislocations, respectively. Furthermore, the nature of a dislocation (i.e., edge, screw, or mixed) is defined by the relative orientations of dislocation line and Burgers vector. For an edge, they are perpendicular (Figure 5.7), whereas for a screw, they are parallel (Figure 5.8); they are neither perpendicular nor parallel for a mixed dislocation. Also, even though a dislocation changes direction and nature within a crystal (e.g., from edge to mixed to screw), the Burgers vector will be the same at all points along its line. For example, all positions of the curved dislocation in Figure 5.9 will have the Burgers vector shown. For metallic materials, the Burgers vector for a dislocation will point in a close-packed crystallographic direction and will be of magnitude equal to the interatomic spacing.

Dislocations can be observed in crystalline materials using electron-microscopic techniques. In Figure 5.10, a high-magnification transmission electron micrograph, the dark lines are the dislocations.

Virtually all crystalline materials contain some dislocations that were introduced during solidification, during plastic deformation, and as a consequence of thermal stresses that result from rapid cooling. Dislocations are involved in the plastic deformation of these materials, as discussed in Chapter 8. Dislocations have been observed in polymeric materials; however, some controversy exists as to the nature of dislocation structures in polymers and the mechanism(s) by which polymers plastically deform.

Figure 5.8 (*a*) A screw dislocation within a crystal. (*b*) The screw dislocation in (*a*) as viewed from above. The dislocation line extends along line *AB*. Atom positions above the slip plane are designated by open circles, those below by solid circles. (Figure (*b*) from W. T. Read, Jr., *Dislocations in Crystals*, McGraw-Hill Book Company, New York, 1953.)

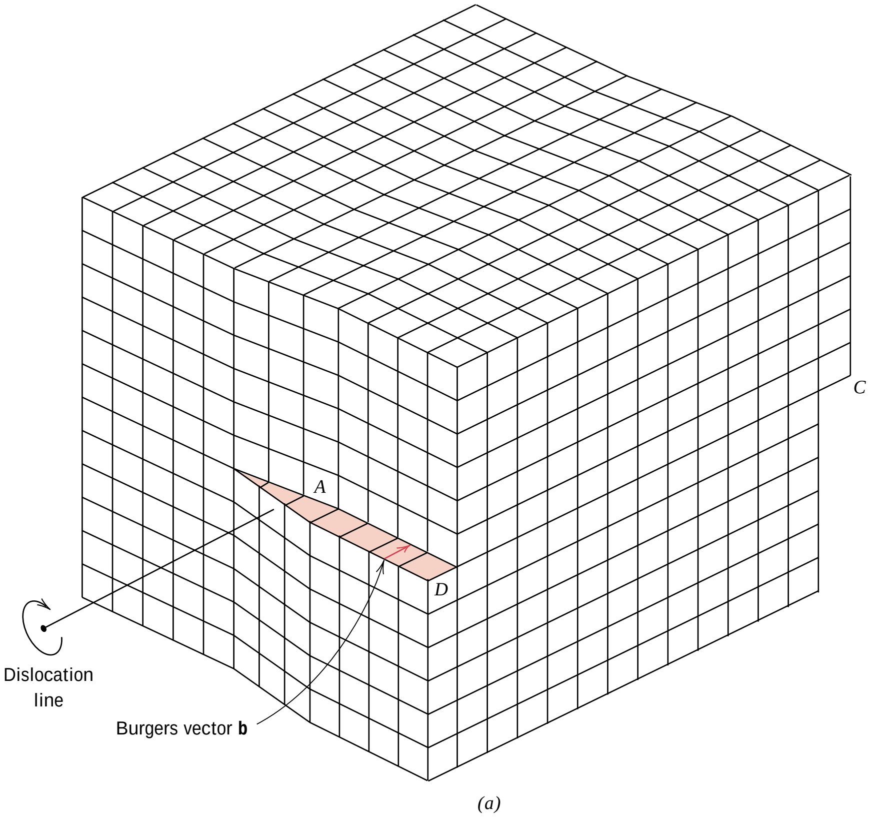
A
C
D
Dislocation line
Burgers vector **b**
(a)

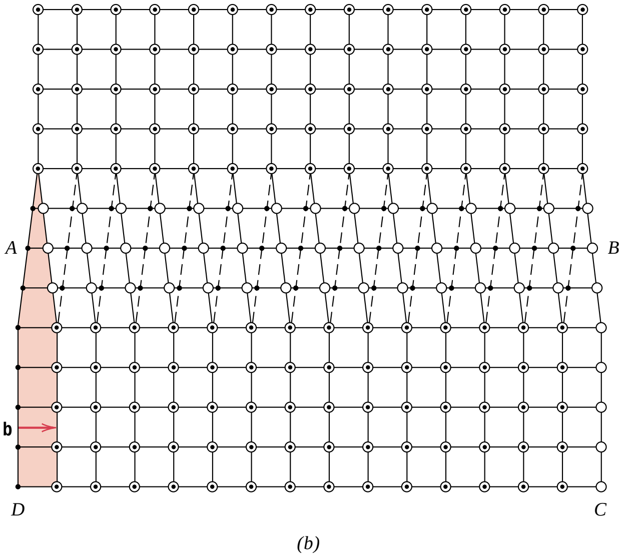

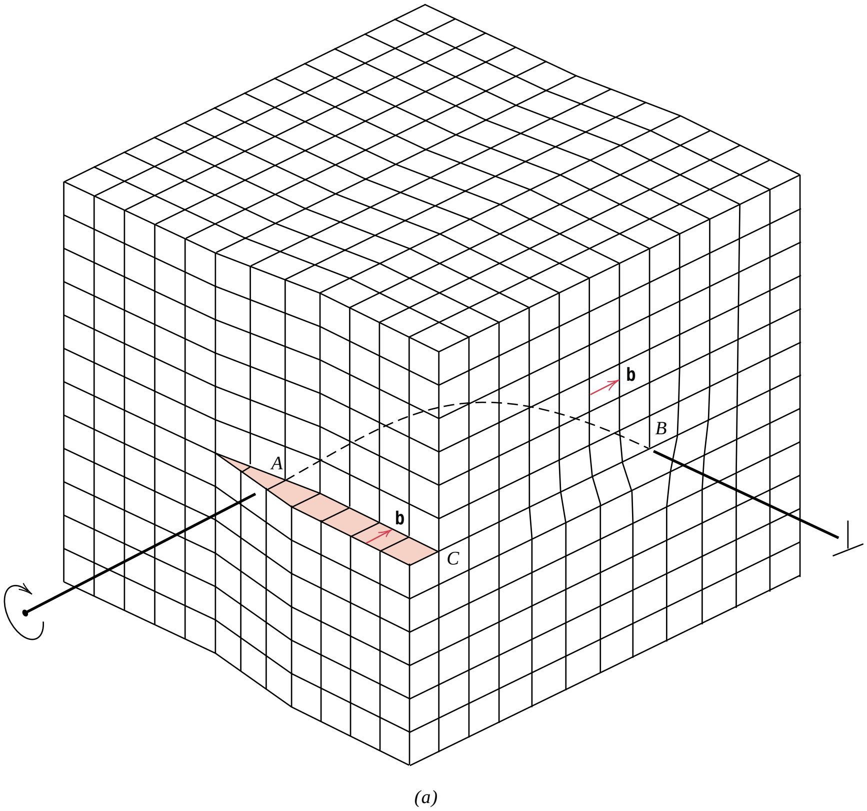

(a)

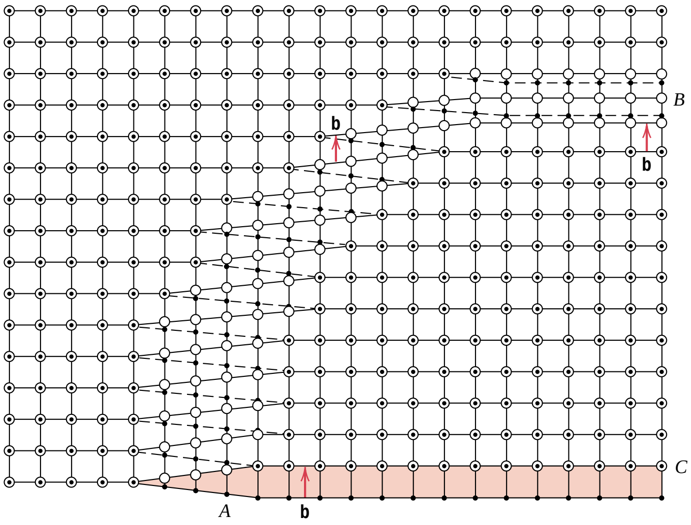

(b)

FIGURE 5.9 (*a*) Schematic representation of a dislocation that has edge, screw, and mixed character. (*b*) Top view, where open circles denote atom positions above the slip plane. Solid circles, atom positions below. At point *A*, the dislocation is pure screw, while at point *B*, it is pure edge. For regions in between where there is curvature in the dislocation line, the character is mixed edge and screw. (Figure (*b*) from W. T. Read, Jr., *Dislocations in Crystals*, McGraw-Hill Book Company, New York, 1953.)

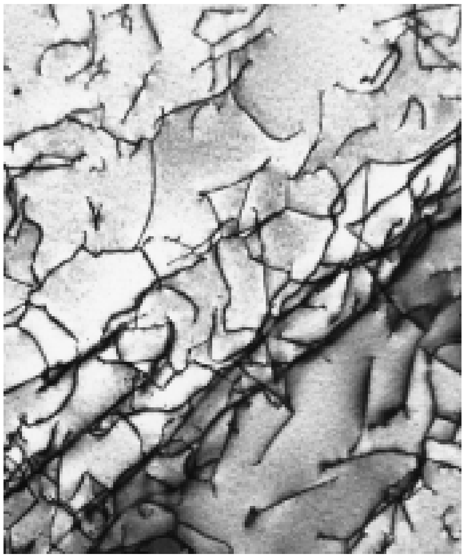

Figure 5.10 A transmission electron micrograph of a titanium alloy in which the dark lines are dislocations. 51,450×. (Courtesy of M. R. Plichta, Michigan Technological University.)

5.8 Interfacial Defects

Interfacial defects are boundaries that have two dimensions and normally separate regions of the materials that have different crystal structures and/or crystallographic orientations. These imperfections include external surfaces, grain boundaries, twin boundaries, stacking faults, and phase boundaries.

EXTERNAL SURFACES

One of the most obvious boundaries is the external surface, along which the crystal structure terminates. Surface atoms are not bonded to the maximum number of nearest neighbors, and are therefore in a higher energy state than the atoms at interior positions. The bonds of these surface atoms that are not satisfied give rise to a surface energy, expressed in units of energy per unit area (J/m^2 or erg/cm^2). To reduce this energy, materials tend to minimize, if at all possible, the total surface area. For example, liquids assume a shape having a minimum area—the droplets become spherical. Of course, this is not possible with solids, which are mechanically rigid.

GRAIN BOUNDARIES

Another interfacial defect, the grain boundary, was introduced in Section 3.17 as the boundary separating two small grains or crystals having different crystallographic orientations in polycrystalline materials. A grain boundary is represented schematically from an atomic perspective in Figure 5.11. Within the boundary region, which is probably just several atom distances wide, there is some atomic mismatch in a transition from the crystalline orientation of one grain to that of an adjacent one.

Various degrees of crystallographic misalignment between adjacent grains are possible (Figure 5.11). When this orientation mismatch is slight, on the order of a few degrees, then the term *small-* (or *low-*) *angle grain boundary* is used. These boundaries can be described in terms of dislocation arrays. One simple small-angle grain boundary is formed when edge dislocations are aligned in the manner of Figure 5.12. This type is called a *tilt boundary;* the angle of misorientation, θ, is

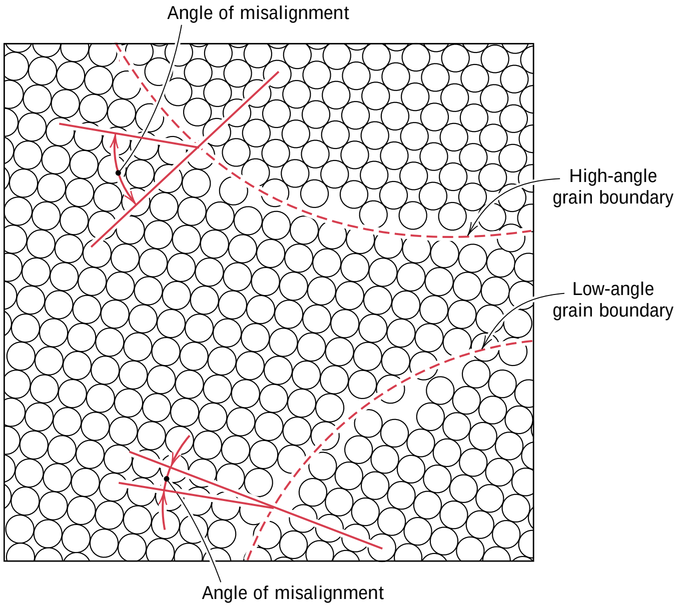
Angle of misalignment
High-angle grain boundary
Low-angle grain boundary
Angle of misalignment

Figure 5.11 Schematic diagram showing low- and high-angle grain boundaries and the adjacent atom positions.

also indicated in the figure. When the angle of misorientation is parallel to the boundary, a *twist boundary* results, which can be described by an array of screw dislocations.

The atoms are bonded less regularly along a grain boundary (e.g., bond angles are longer), and consequently, there is an interfacial or grain boundary energy

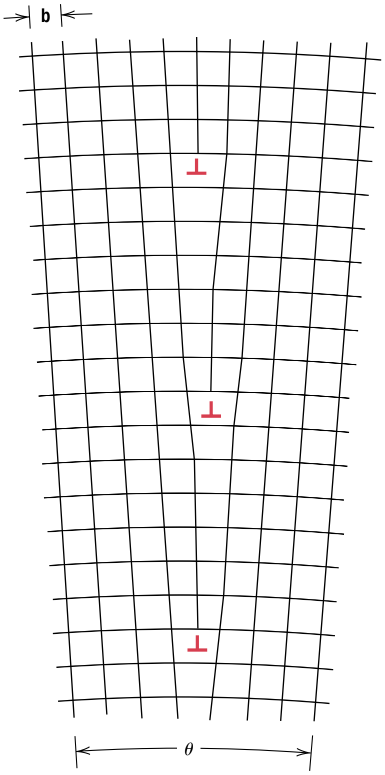

Figure 5.12 Demonstration of how a tilt boundary having an angle of misorientation θ results from an alignment of edge dislocations.

similar to the surface energy described above. The magnitude of this energy is a function of the degree of misorientation, being larger for high-angle boundaries. Grain boundaries are more chemically reactive than the grains themselves as a consequence of this boundary energy. Furthermore, impurity atoms often preferentially segregate along these boundaries because of their higher energy state. The total interfacial energy is lower in large or coarse-grained materials than in fine-grained ones, since there is less total boundary area in the former. Grains grow at elevated temperatures to reduce the total boundary energy, a phenomenon explained in Section 8.14.

In spite of this disordered arrangement of atoms and lack of regular bonding along grain boundaries, a polycrystalline material is still very strong; cohesive forces within and across the boundary are present. Furthermore, the density of a polycrystalline specimen is virtually identical to that of a single crystal of the same material.

TWIN BOUNDARIES

A *twin boundary* is a special type of grain boundary across which there is a specific mirror lattice symmetry; that is, atoms on one side of the boundary are located in mirror image positions of the atoms on the other side (Figure 5.13). The region of material between these boundaries is appropriately termed a *twin*. Twins result from atomic displacements that are produced from applied mechanical shear forces (mechanical twins), and also during annealing heat treatments following deformation (annealing twins). Twinning occurs on a definite crystallographic plane and in a specific direction, both of which depend on the crystal structure. Annealing twins are typically found in metals that have the FCC crystal structure, while mechanical twins are observed in BCC and HCP metals. {The role of mechanical twins in the deformation process is discussed in Section 8.8. Annealing twins may be observed in the photomicrograph of the polycrystalline brass specimen shown in Figure 5.15*c*. The twins correspond to those regions having relatively straight and parallel sides and a different visual contrast than the untwinned regions of the grains within which they reside. An explanation for the variety of textural contrasts in this photomicrograph is provided in Section 5.12.}

MISCELLANEOUS INTERFACIAL DEFECTS

Other possible interfacial defects include stacking faults, phase boundaries, and ferromagnetic domain walls. Stacking faults are found in FCC metals when there is an interruption in the *ABCABCABC* . . . stacking sequence of close-packed planes (Section 3.15). Phase boundaries exist in multiphase materials (Section 10.3)

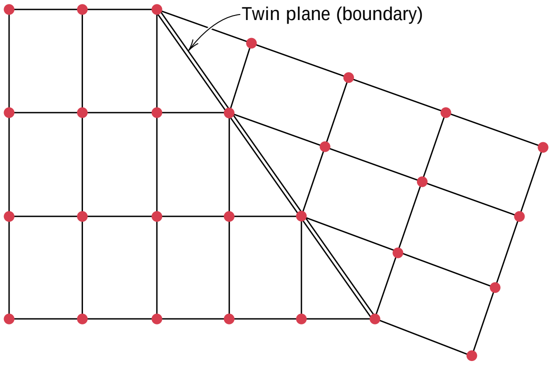

FIGURE 5.13 Schematic diagram showing a twin plane or boundary and the adjacent atom positions (dark circles).

across which there is a sudden change in physical and/or chemical characteristics. {For ferromagnetic and ferrimagnetic materials, the boundary that separates regions having different directions of magnetization is termed a domain wall, which is discussed in Section 18.7.}

With regard to polymeric materials, the surfaces of chain-folded layers (Figure 4.14) are considered to be interfacial defects, as are boundaries between two adjacent crystalline regions.

Associated with each of the defects discussed in this section is an interfacial energy, the magnitude of which depends on boundary type, and which will vary from material to material. Normally, the interfacial energy will be greatest for external surfaces and least for domain walls.

5.9 Bulk or Volume Defects

Other defects exist in all solid materials that are much larger than those heretofore discussed. These include pores, cracks, foreign inclusions, and other phases. They are normally introduced during processing and fabrication steps. Some of these defects and their effects on the properties of materials are discussed in subsequent chapters.

5.10 Atomic Vibrations

Every atom in a solid material is vibrating very rapidly about its lattice position within the crystal. In a sense, these vibrations may be thought of as imperfections or defects. At any instant of time not all atoms vibrate at the same frequency and amplitude, nor with the same energy. At a given temperature there will exist a distribution of energies for the constituent atoms about an average energy. Over time the vibrational energy of any specific atom will also vary in a random manner. With rising temperature, this average energy increases, and, in fact, the temperature of a solid is really just a measure of the average vibrational activity of atoms and molecules. At room temperature, a typical vibrational frequency is on the order of 10^{13} vibrations per second, whereas the amplitude is a few thousandths of a nanometer.

Many properties and processes in solids are manifestations of this vibrational atomic motion. For example, melting occurs when the vibrations are vigorous enough to rupture large numbers of atomic bonds. {A more detailed discussion of atomic vibrations and their influence on the properties of materials is presented in Chapter 17.}

MICROSCOPIC EXAMINATION

5.11 General

On occasion it is necessary or desirable to examine the structural elements and defects that influence the properties of materials. Some structural elements are of *macroscopic* dimensions, that is, are large enough to be observed with the unaided eye. For example, the shape and average size or diameter of the grains for a polycrystalline specimen are important structural characteristics. Macroscopic grains are often evident on aluminum streetlight posts and also on garbage cans. Relatively large grains having different textures are clearly visible on the surface of the sectioned lead ingot shown in Figure 5.14. However, in most materials the constituent

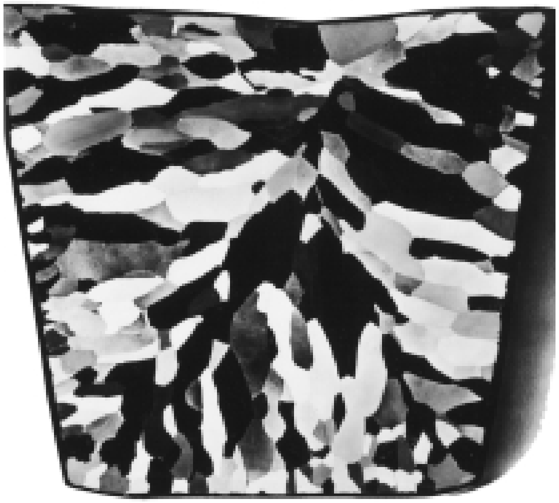

FIGURE 5.14 High-purity polycrystalline lead ingot in which the individual grains may be discerned. 0.7×. (Reproduced with permission from *Metals Handbook,* Vol. 9, 9th edition, *Metallography and Microstructures,* American Society for Metals, Metals Park, OH, 1985.)

grains are of *microscopic* dimensions, having diameters that may be on the order of microns,[5] and their details must be investigated using some type of microscope. Grain size and shape are only two features of what is termed the **microstructure;** these and other microstructural characteristics are discussed in subsequent chapters.

Optical, electron, and scanning probe microscopes are commonly used in **microscopy.** These instruments aid in investigations of the microstructural features of all material types. Some of these techniques employ photographic equipment in conjunction with the microscope; the photograph on which the image is recorded is called a **photomicrograph.** In addition, some microstructural images are computer generated and/or enhanced.

Microscopic examination is an extremely useful tool in the study and characterization of materials. Several important applications of microstructural examinations are as follows: to ensure that the associations between the properties and structure (and defects) are properly understood; to predict the properties of materials once these relationships have been established; to design alloys with new property combinations; to determine whether or not a material has been correctly heat treated; and to ascertain the mode of mechanical fracture. {Several techniques that are commonly used in such investigations are discussed next.}

5.12 MICROSCOPIC TECHNIQUES (CD-ROM)

5.13 GRAIN SIZE DETERMINATION

The **grain size** is often determined when the properties of a polycrystalline material are under consideration. In this regard, there exist a number of techniques by which size is specified in terms of average grain volume, diameter, or area. Grain size may be estimated by using an intercept method, described as follows. Straight lines all the same length are drawn through several photomicrographs that show the

---

[5] A micron (μm), sometimes called a micrometer, is 10^{-6} m.

grain structure. The grains intersected by each line segment are counted; the line length is then divided by an average of the number of grains intersected, taken over all the line segments. The average grain diameter is found by dividing this result by the linear magnification of the photomicrographs.

Probably the most common method utilized, however, is that devised by the American Society for Testing and Materials (ASTM).[6] The ASTM has prepared several standard comparison charts, all having different average grain sizes. To each is assigned a number ranging from 1 to 10, which is termed the *grain size number;* the larger this number, the smaller the grains. A specimen must be properly prepared to reveal the grain structure, which is photographed at a magnification of 100×. Grain size is expressed as the grain size number of the chart that most nearly matches the grains in the micrograph. Thus, a relatively simple and convenient visual determination of grain size number is possible. Grain size number is used extensively in the specification of steels.

The rationale behind the assignment of the grain size number to these various charts is as follows. Let n represent the grain size number, and N the average number of grains per square inch at a magnification of 100×. These two parameters are related to each other through the expression

$$N = 2^{n-1} \tag{5.16}$$

SUMMARY

All solid materials contain large numbers of imperfections or deviations from crystalline perfection. The several types of imperfection are categorized on the basis of their geometry and size. Point defects are those associated with one or two atomic positions; in metals these include vacancies (or vacant lattice sites), self-interstitials (host atoms that occupy interstitial sites), and impurity atoms.

With regard to atomic point defects in ceramics, interstitials and vacancies for each anion and cation type are possible. These imperfections often occur in pairs as Frenkel and Schottky defects to ensure that crystal electroneutrality is maintained.

A solid solution may form when impurity atoms are added to a solid, in which case the original crystal structure is retained and no new phases are formed. For substitutional solid solutions, impurity atoms substitute for host atoms, and appreciable solubility is possible only when atomic diameters and electronegativities for both atom types are similar, when both elements have the same crystal structure, and when the impurity atoms have a valence that is the same as or less than the host material. Interstitial solid solutions form for relatively small impurity atoms that occupy interstitial sites among the host atoms.

For ceramic materials, the addition of impurity atoms may result in the formation of substitutional or interstitial solid solutions. Any charge imbalance created by the impurity ions may be compensated by the generation of host ion vacancies or interstitials.

Composition of an alloy may be specified in weight percent or atom percent. The basis for weight percent computations is the weight (or mass) of each alloy constituent relative to the total alloy weight. Atom percents are calculated in terms of the number of moles for each constituent relative to the total moles of all the elements in the alloy. {Equations were provided for the conversion of one composition scheme to another.}

---

[6] ASTM Standard E 112, ''Standard Methods for Estimating the Average Grain Size for Metals.''

Dislocations are one-dimensional crystalline defects of which there are two pure types: edge and screw. An edge may be thought of in terms of the lattice distortion along the end of an extra half-plane of atoms; a screw, as a helical planar ramp. For mixed dislocations, components of both pure edge and screw are found. The magnitude and direction of lattice distortion associated with a dislocation is specified by its Burgers vector. The relative orientations of Burgers vector and dislocation line are (1) perpendicular for edge, (2) parallel for screw, and (3) neither perpendicular nor parallel for mixed.

Other imperfections include interfacial defects [external surfaces, grain boundaries (both small- and high-angle), twin boundaries, etc.], volume defects (cracks, pores, etc.), and atomic vibrations. Each type of imperfection has some influence on the properties of a material.

Many of the important defects and structural elements of materials are of microscopic dimensions, and observation is possible only with the aid of a microscope. {Both optical and electron microscopes are employed, usually in conjunction with photographic equipment. Transmissive and reflective modes are possible for each microscope type; preference is dictated by the nature of the specimen as well as the structural element or defect to be examined.}

{More recent scanning probe microscopic techniques have been developed that generate topographical maps representing the surface features and characteristics of the specimen. Examinations on the atomic and molecular levels are possible using these techniques.}

Grain size of polycrystalline materials is frequently determined using photomicrographic techniques. Two methods are commonly employed: intercept and standard comparison charts.

IMPORTANT TERMS AND CONCEPTS

Alloy
Atom percent
Atomic vibration
Boltzmann's constant
Burgers vector
Composition
Defect structure
Dislocation line
Edge dislocation
Electroneutrality
Frenkel defect
Grain size
Imperfection
Interstitial solid solution
Microscopy
Microstructure
Mixed dislocation
Photomicrograph
Point defect
Scanning electron microscope (SEM)
Scanning probe microscope (SPM)
Schottky defect
Screw dislocation
Self-interstitial
Solid solution
Solute
Solvent
Stoichiometry
Substitutional solid solution
Transmission electron microscope (TEM)
Vacancy
Weight percent

REFERENCES

ASM Handbook, Vol. 9, *Metallography and Microstructures*, ASM International, Materials Park, OH, 1985.

Barsoum, M. W., *Fundamentals of Ceramics*, The McGraw-Hill Companies, Inc., New York, 1997.

Chiang, Y. M., D. P. Birnie, III, and W. D. Kingery, *Physical Ceramics: Principles for Ceramic Science and Engineering*, John Wiley & Sons, Inc., New York, 1997.

Kingery, W. D., H. K. Bowen, and D. R. Uhlmann, *Introduction to Ceramics*, 2nd edition, John Wiley & Sons, New York, 1976. Chapters 4 and 5.

Moffatt, W. G., G. W. Pearsall, and J. Wulff, *The Structure and Properties of Materials*, Vol. 1, *Structure*, John Wiley & Sons, New York, 1964.

Phillips, V. A., *Modern Metallographic Techniques and Their Applications*, Wiley-Interscience, New York, 1971.

Van Bueren, H. G., *Imperfections in Crystals*, North-Holland Publishing Co., Amsterdam (Wiley-Interscience, New York), 1960.

Vander Voort, G. F., *Metallography, Principles and Practice*, McGraw-Hill Book Co., New York, 1984.

QUESTIONS AND PROBLEMS

Note: To solve those problems having an asterisk (*) by their numbers, consultation of supplementary topics [appearing only on the CD-ROM (and not in print)] will probably be necessary.

5.1 Calculate the fraction of atom sites that are vacant for lead at its melting temperature of 327°C (600°F). Assume an energy for vacancy formation of 0.55 eV/atom.

5.2 Calculate the number of vacancies per cubic meter in iron at 850°C. The energy for vacancy formation is 1.08 eV/atom. Furthermore, the density and atomic weight for Fe are 7.65 g/cm^3 and 55.85 g/mol, respectively.

5.3 Calculate the energy for vacancy formation in silver, given that the equilibrium number of vacancies at 800°C (1073 K) is 3.6×10^{23} m^{-3}. The atomic weight and density (at 800°C) for silver are, respectively, 107.9 g/mol and 9.5 g/cm^3.

5.4 Calculate the number of atoms per cubic meter in aluminum.

5.5 Would you expect Frenkel defects for anions to exist in ionic ceramics in relatively large concentrations? Why or why not?

5.6 In your own words, briefly define the term ''stoichiometric.''

5.7 If cupric oxide (CuO) is exposed to reducing atmospheres at elevated temperatures, some of the Cu^{2+} ions will become Cu^+.

(a) Under these conditions, name one crystalline defect that you would expect to form in order to maintain charge neutrality.

(b) How many Cu^+ ions are required for the creation of each defect?

(c) How would you express the chemical formula for this nonstoichiometric material?

5.8 Below, atomic radius, crystal structure, electronegativity, and the most common valence are tabulated, for several elements; for those that are nonmetals, only atomic radii are indicated.

Element	*Atomic Radius (nm)*	*Crystal Structure*	*Electronegativity*	*Valence*
Cu	0.1278	FCC	1.9	+2
C	0.071			
H	0.046			
O	0.060			
Ag	0.1445	FCC	1.9	+1
Al	0.1431	FCC	1.5	+3
Co	0.1253	HCP	1.8	+2
Cr	0.1249	BCC	1.6	+3
Fe	0.1241	BCC	1.8	+2
Ni	0.1246	FCC	1.8	+2
Pd	0.1376	FCC	2.2	+2
Pt	0.1387	FCC	2.2	+2
Zn	0.1332	HCP	1.6	+2

Which of these elements would you expect to form the following with copper:

(a) A substitutional solid solution having complete solubility?

(b) A substitutional solid solution of incomplete solubility?

(c) An interstitial solid solution?

5.9 For both FCC and BCC crystal structures, there are two different types of interstitial sites. In each case, one site is larger than the other, which site is normally occupied by impurity atoms. For FCC, this larger one is located at the center of each edge of the unit cell; it is termed an octahedral interstitial site. On the other hand, with BCC the larger site type is found at 0, $\frac{1}{2}$, $\frac{1}{4}$ positions—that is, lying on {100} faces, and situated midway between two unit cell edges on this face and one-quarter of the distance between the other two unit cell edges; it is termed a tetrahedral interstitial site. For both FCC and BCC crystal structures, compute the radius r of an impurity atom that will just fit into one of these sites in terms of the atomic radius R of the host atom.

5.10 **(a)** Suppose that Li_2O is added as an impurity to CaO. If the Li^+ substitutes for Ca^{2+}, what kind of vacancies would you expect to form? How many of these vacancies are created for every Li^+ added?

(b) Suppose that $CaCl_2$ is added as an impurity to CaO. If the Cl^- substitutes for O^{2-}, what kind of vacancies would you expect to form? How many of the vacancies are created for every Cl^- added?

5.11 What point defects are possible for MgO as an impurity in Al_2O_3? How many Mg^{2+} ions must be added to form each of these defects?

5.12 What is the composition, in atom percent, of an alloy that consists of 30 wt% Zn and 70 wt% Cu?

5.13 What is the composition, in weight percent, of an alloy that consists of 6 at% Pb and 94 at% Sn?

5.14 Calculate the composition, in weight percent, of an alloy that contains 218.0 kg titanium, 14.6 kg of aluminum, and 9.7 kg of vanadium.

5.15 What is the composition, in atom percent, of an alloy that contains 98 g tin and 65 g of lead?

5.16 What is the composition, in atom percent, of an alloy that contains 99.7 lb_m copper, 102 lb_m zinc, and 2.1 lb_m lead?

5.17* Derive the following equations:
(a) Equation 5.7a.
(b) Equation 5.9a.
(c) Equation 5.10a.
(d) Equation 5.11b.

5.18* What is the composition, in atom percent, of an alloy that consists of 97 wt% Fe and 3 wt% Si?

5.19* Convert the atom percent composition in Problem 5.16 to weight percent.

5.20* The concentration of carbon in an iron-carbon alloy is 0.15 wt%. What is the concentration in kilograms of carbon per cubic meter of alloy?

5.21* Determine the approximate density of a high-leaded brass that has a composition of 64.5 wt% Cu, 33.5 wt% Zn, and 2 wt% Pb.

5.22* For a solid solution consisting of two elements (designated as 1 and 2), sometimes it is desirable to determine the number of atoms per cubic centimeter of one element in a solid solution, N_1, given the concentration of that element specified in weight percent, C_1. This computation is possible using the following expression:

$$N_1 = \frac{N_A C_1}{\dfrac{C_1 A_1}{\rho_1} + \dfrac{A_1}{\rho_2}(100 - C_1)} \qquad (5.17)$$

where

N_A = Avogadro's number
ρ_1 and ρ_2 = densities of the two elements
A_1 = the atomic weight of element 1

Derive Equation 5.17 using Equation 5.2 and expressions contained in Section 5.3.

5.23 Gold forms a substitutional solid solution with silver. Compute the number of gold atoms per cubic centimeter for a silver-gold alloy that contains 10 wt% Au and 90 wt% Ag. The densities of pure gold and silver are 19.32 and 10.49 g/cm^3, respectively.

5.24 Germanium forms a substitutional solid solution with silicon. Compute the number of germanium atoms per cubic centimeter for a germanium-silicon alloy that contains 15 wt% Ge and 85 wt% Si. The densities of pure germanium and silicon are 5.32 and 2.33 g/cm^3, respectively.

5.25* Sometimes it is desirable to be able to determine the weight percent of one element, C_1, that will produce a specified concentration in terms of the number of atoms per cubic centimeter, N_1, for an alloy composed of two types of atoms. This computation is possible using the following expression:

$$C_1 = \frac{100}{1 + \dfrac{N_A \rho_2}{N_1 A_1} - \dfrac{\rho_2}{\rho_1}} \tag{5.18}$$

where

N_A = Avogadro's number

ρ_1 and ρ_2 = densities of the two elements

A_1 and A_2 = the atomic weights of the two elements

Derive Equation 5.18 using Equation 5.2 and expressions contained in Section 5.3.

5.26 Molybdenum forms a substitutional solid solution with tungsten. Compute the weight percent of molybdenum that must be added to tungsten to yield an alloy that contains 1.0×10^{22} Mo atoms per cubic centimeter. The densities of pure Mo and W are 10.22 and 19.30 g/cm^3, respectively.

5.27 Niobium forms a substitutional solid solution with vanadium. Compute the weight percent of niobium that must be added to vanadium to yield an alloy that contains 1.55×10^{22} Nb atoms per cubic centimeter. The densities of pure Nb and V are 8.57 and 6.10 g/cm^3, respectively.

5.28 Copper and platinum both have the FCC crystal structure and Cu forms a substitutional solid solution for concentrations up to approximately 6 wt% Cu at room temperature. Compute the unit cell edge length for a 95 wt% Pt-5 wt% Cu alloy.

5.29 Cite the relative Burgers vector–dislocation line orientations for edge, screw, and mixed dislocations.

5.30 For both FCC and BCC crystal structures, the Burgers vector **b** may be expressed as

$$\mathbf{b} = \frac{a}{2}[hkl]$$

where a is the unit cell edge length and $[hkl]$ is the crystallographic direction having the greatest linear atomic density.

(a) What are the Burgers vector representations for FCC, BCC, and simple cubic crystal structures? See Problems 3.70 and 3.71 at the end of Chapter 3.

(b) If the magnitude of the Burgers vector $|\mathbf{b}|$ is

$$|\mathbf{b}| = \frac{a}{2}(h^2 + k^2 + l^2)^{1/2}$$

determine the values of $|\mathbf{b}|$ for aluminum and tungsten. You may want to consult Table 3.1.

5.31 **(a)** The surface energy of a single crystal depends on the crystallographic orientation with respect to the surface. Explain why this is so.

(b) For an FCC crystal, such as aluminum, would you expect the surface energy for a (100) plane to be greater or less than that for a (111) plane? Why?

5.32 **(a)** For a given material, would you expect the surface energy to be greater than, the same as, or less than the grain boundary energy? Why?

(b) The grain boundary energy of a low-angle grain boundary is less than for a high-angle one. Why is this so?

5.33 **(a)** Briefly describe a twin and a twin boundary.

(b) Cite the difference between mechanical and annealing twins.

5.34 For each of the following stacking sequences found in FCC metals, cite the type of planar defect that exists:

(a) . . . *A B C A B C B A C B A* . . .

(b) . . . *A B C A B C B C A B C* . . .

Now, copy the stacking sequences and indicate the position(s) of planar defect(s) with a vertical dashed line.

5.35* Using the intercept method, determine the average grain size, in millimeters, of the specimen whose microstructure is shown in Figure 5.16*b*; assume that the magnification is 100×, and use at least seven straight-line segments.

5.36 Employing the intercept technique, determine the average grain size for the steel specimen whose microstructure is shown in Figure 10.27*a*; use at least seven straight-line segments.

5.37* **(a)** For an ASTM grain size of 4, approximately how many grains would there be per square inch in a micrograph taken at a magnification of 100×?

(b) Estimate the grain size number for the photomicrograph in Figure 5.16*b*, assuming a magnification of 100×.

5.38 A photomicrograph was taken of some metal at a magnification of 100× and it was determined that the average number of grains per square inch is 10. Compute the ASTM grain size number for this alloy.

Design Problems

5.D1* Aluminum-lithium alloys have been developed by the aircraft industry in order to reduce the weight and improve the performance of its aircraft. A commercial aircraft skin material having a density of 2.55 g/cm^3 is desired. Compute the concentration of Li (in wt%) that is required.

5.D2* Iron and vanadium both have the BCC crystal structure and V forms a substitutional solid solution in Fe for concentrations up to approximately 20 wt% V at room temperature. Determine the concentration in weight percent of V that must be added to iron to yield a unit cell edge length of 0.289 nm.

Chapter 8 / Deformation and Strengthening Mechanisms

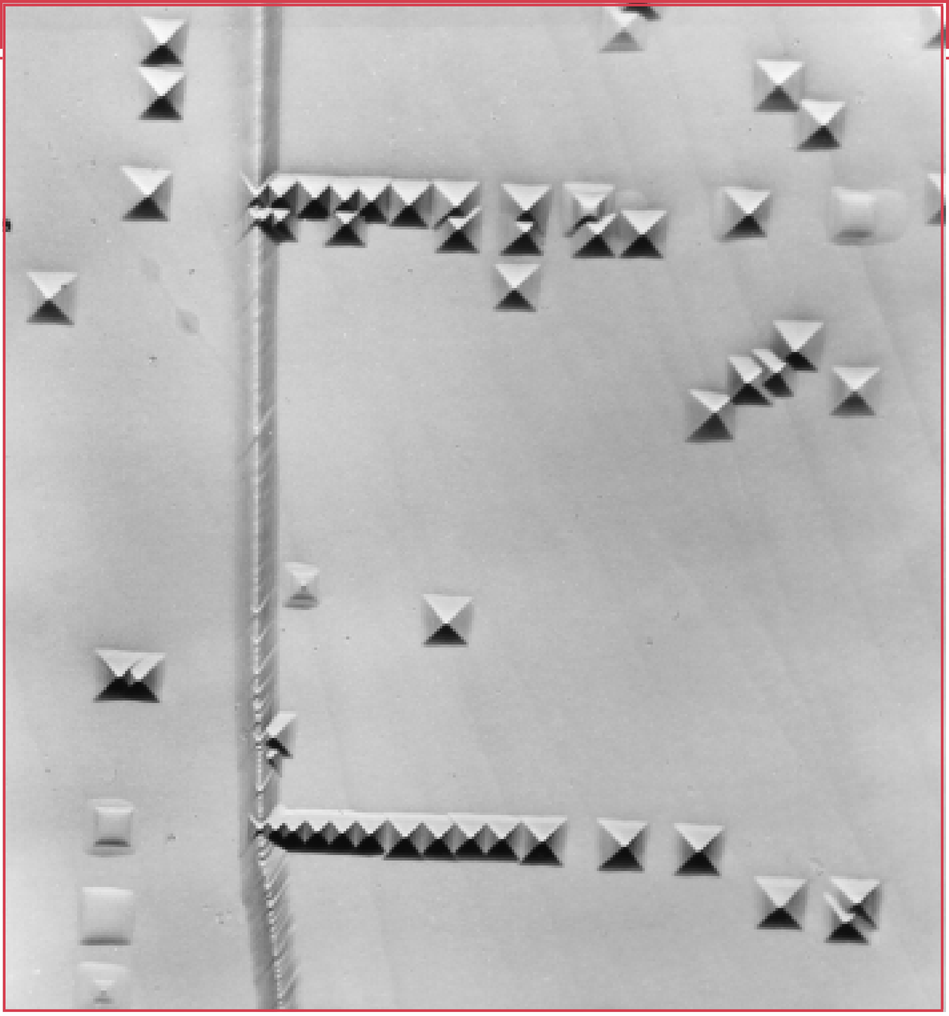

In this photomicrograph of a lithium fluoride (LiF) single crystal, the small pyramidal pits represent those positions at which dislocations intersect the surface. The surface was polished and then chemically treated; these "etch pits" result from localized chemical attack around the dislocations and indicate the distribution of the dislocations. 750×. (Photomicrograph courtesy of W. G. Johnston, General Electric Co.)

Why Study *Deformation and Strengthening Mechanisms?*

With a knowledge of the nature of dislocations and the role they play in the plastic deformation process, we are able to understand the underlying mechanisms of the techniques that are used to strengthen and harden metals and their alloys; thus, it becomes possible to design and tailor the mechanical properties of materials—for example, the strength or toughness of a metal-matrix composite.

Also, understanding the mechanisms by which polymers elastically and plastically deform allows one to alter and control their moduli of elasticity and strengths (Sections 8.17 and 8.18).

Learning Objectives

After studying this chapter you should be able to do the following:

1. **Describe edge and screw dislocation motion from an atomic perspective.**
2. **Describe how plastic deformation occurs by the motion of edge and screw dislocations in response to applied shear stresses.**
3. **Define slip system and cite one example.**
4. **Describe how the grain structure of a polycrystalline metal is altered when it is plastically deformed.**
5. **Explain how grain boundaries impede dislocation motion and why a metal having small grains is stronger than one having large grains.**
6. **Describe and explain solid-solution strengthening for substitutional impurity atoms in terms of lattice strain interactions with dislocations.**
7. **Describe and explain the phenomenon of strain hardening (or cold working) in terms of dislocations and strain field interactions.**
8. **Describe recrystallization in terms of both the alteration of microstructure and mechanical characteristics of the material.**
9. **Describe the phenomenon of grain growth from both macroscopic and atomic perspectives.**
10. **On the basis of slip considerations, explain why crystalline ceramic materials are normally brittle.**
11. **Describe/sketch the various stages in the plastic deformation of a semicrystalline (spherulitic) polymer.**
12. **Discuss the influence of the following factors on polymer tensile modulus and/or strength: (a) molecular weight, (b) degree of crystallinity, (c) predeformation, and (d) heat treating of undeformed materials.**
13. **Describe the molecular mechanism by which elastomeric polymers deform elastically.**

8.1 INTRODUCTION

In this chapter we explore various deformation mechanisms that have been proposed to explain the deformation behaviors of metals, ceramics, and polymeric materials. Techniques that may be used to strengthen the various material types are described and explained in terms of these deformation mechanisms.

DEFORMATION MECHANISMS FOR METALS

Chapter 7 explained that metallic materials may experience two kinds of deformation: elastic and plastic. Plastic deformation is permanent, and strength and hardness are measures of a material's resistance to this deformation. On a microscopic scale, plastic deformation corresponds to the net movement of large numbers of atoms in response to an applied stress. During this process, interatomic bonds must be ruptured and then reformed. Furthermore, plastic deformation most often involves the motion of dislocations, linear crystalline defects that were introduced in Section 5.7. This section discusses the characteristics of dislocations and their involvement in plastic deformation. Sections 8.9, 8.10, and 8.11 present several techniques for strengthening single-phase metals, the mechanisms of which are described in terms of dislocations.

8.2 HISTORICAL

Early materials studies led to the computation of the theoretical strengths of perfect crystals, which were many times greater than those actually measured. During the 1930s it was theorized that this discrepancy in mechanical strengths could be explained by a type of linear crystalline defect that has since come to be known as a dislocation. It was not until the 1950s, however, that the existence of such dislocation defects was established by direct observation with the electron microscope. Since then, a theory of dislocations has evolved that explains many of the physical and mechanical phenomena in metals [as well as crystalline ceramics (Section 8.15)].

8.3 BASIC CONCEPTS OF DISLOCATIONS

Edge and screw are the two fundamental dislocation types. In an edge dislocation, localized lattice distortion exists along the end of an extra half-plane of atoms, which also defines the dislocation line (Figure 5.7). A screw dislocation may be thought of as resulting from shear distortion; its dislocation line passes through the center of a spiral, atomic plane ramp (Figure 5.8). Many dislocations in crystalline materials have both edge and screw components; these are mixed dislocations (Figure 5.9).

Plastic deformation corresponds to the motion of large numbers of dislocations. An edge dislocation moves in response to a shear stress applied in a direction perpendicular to its line; the mechanics of dislocation motion are represented in Figure 8.1. Let the initial extra half-plane of atoms be plane *A*. When the shear stress is applied as indicated (Figure 8.1*a*), plane *A* is forced to the right; this in turn pushes the top halves of planes *B*, *C*, *D*, and so on, in the same direction. If the applied shear stress is of sufficient magnitude, the interatomic bonds of plane *B* are severed along the shear plane, and the upper half of plane *B* becomes the extra half-plane as plane *A* links up with the bottom half of plane *B* (Figure 8.1*b*). This process is subsequently repeated for the other planes, such that the extra half-plane, by discrete steps, moves from left to right by successive and repeated breaking of bonds and shifting by interatomic distances of upper half-planes. Before and after the movement of a dislocation through some particular region of the crystal, the atomic arrangement is ordered and perfect; it is only during the passage of the extra half-plane that the lattice structure is disrupted. Ultimately this extra half-plane may emerge

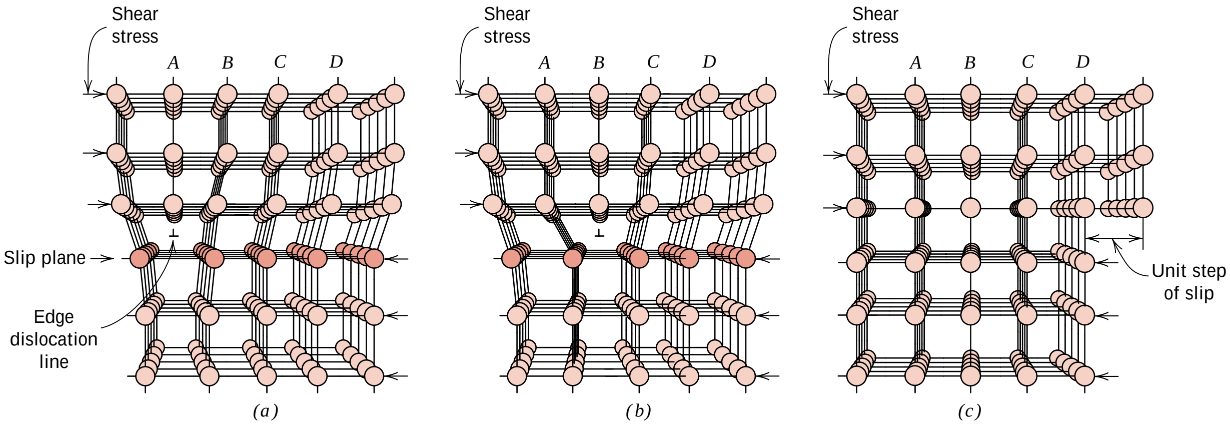

FIGURE 8.1 Atomic rearrangements that accompany the motion of an edge dislocation as it moves in response to an applied shear stress. (*a*) The extra half-plane of atoms is labeled *A*. (*b*) The dislocation moves one atomic distance to the right as *A* links up to the lower portion of plane *B*; in the process, the upper portion of *B* becomes the extra half-plane. (*c*) A step forms on the surface of the crystal as the extra half-plane exits. (Adapted from A. G. Guy, *Essentials of Materials Science*, McGraw-Hill Book Company, New York, 1976, p. 153.)

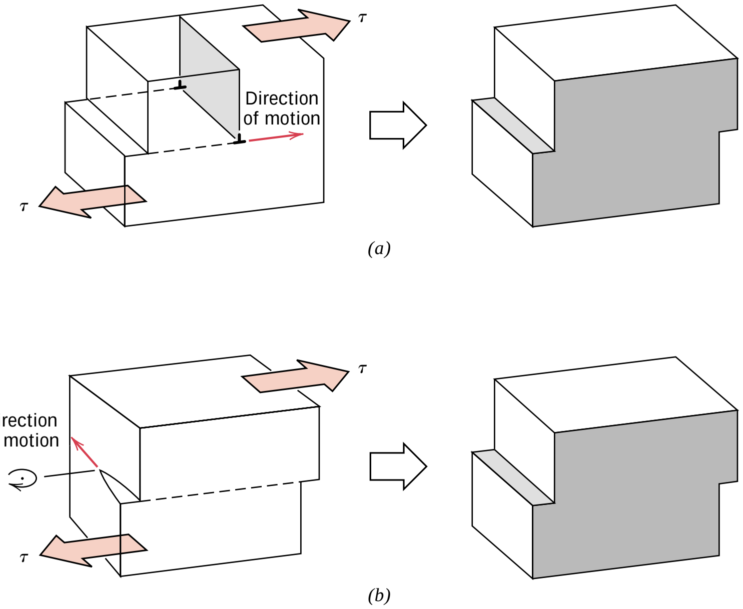

Figure 8.2 The formation of a step on the surface of a crystal by the motion of (*a*) an edge dislocation and (*b*) a screw dislocation. Note that for an edge, the dislocation line moves in the direction of the applied shear stress τ; for a screw, the dislocation line motion is perpendicular to the stress direction. (Adapted from H. W. Hayden, W. G. Moffatt, and J. Wulff, *The Structure and Properties of Materials,* Vol. III, *Mechanical Behavior,* p. 70. Copyright © 1965 by John Wiley & Sons, New York. Reprinted by permission of John Wiley & Sons, Inc.)

from the right surface of the crystal, forming an edge that is one atomic distance wide; this is shown in Figure 8.1*c*.

The process by which plastic deformation is produced by dislocation motion is termed **slip;** the crystallographic plane along which the dislocation line traverses is the *slip plane,* as indicated in Figure 8.1. Macroscopic plastic deformation simply corresponds to permanent deformation that results from the movement of dislocations, or slip, in response to an applied shear stress, as represented in Figure 8.2*a*.

Dislocation motion is analogous to the mode of locomotion employed by a caterpillar (Figure 8.3). The caterpillar forms a hump near its posterior end by pulling in its last pair of legs a unit leg distance. The hump is propelled forward by repeated lifting and shifting of leg pairs. When the hump reaches the anterior

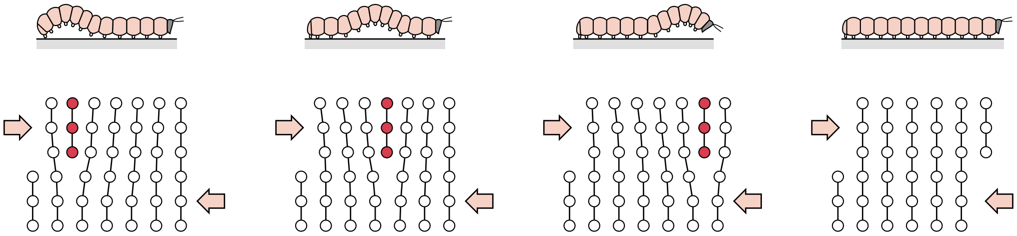

Figure 8.3 Representation of the analogy between caterpillar and dislocation motion.

end, the entire caterpillar has moved forward by the leg separation distance. The caterpillar hump and its motion correspond to the extra half-plane of atoms in the dislocation model of plastic deformation.

The motion of a screw dislocation in response to the applied shear stress is shown in Figure 8.2*b*; the direction of movement is perpendicular to the stress direction. For an edge, motion is parallel to the shear stress. However, the net plastic deformation for the motion of both dislocation types is the same (see Figure 8.2). The direction of motion of the mixed dislocation line is neither perpendicular nor parallel to the applied stress, but lies somewhere in between.

All metals and alloys contain some dislocations that were introduced during solidification, during plastic deformation, and as a consequence of thermal stresses that result from rapid cooling. The number of dislocations, or **dislocation density** in a material, is expressed as the total dislocation length per unit volume, or, equivalently, the number of dislocations that intersect a unit area of a random section. The units of dislocation density are millimeters of dislocation per cubic millimeter or just per square millimeter. Dislocation densities as low as 10^3 mm^{-2} are typically found in carefully solidified metal crystals. For heavily deformed metals, the density may run as high as 10^9 to 10^{10} mm^{-2}. Heat treating a deformed metal specimen can diminish the density to on the order of 10^5 to 10^6 mm^{-2}. By way of contrast, a typical dislocation density for ceramic materials is between 10^2 and 10^4 mm^{-2}; also, for silicon single crystals used in integrated circuits the value normally lies between 0.1 and 1 mm^{-2}.

8.4 Characteristics of Dislocations

Several characteristics of dislocations are important with regard to the mechanical properties of metals. These include strain fields that exist around dislocations, which are influential in determining the mobility of the dislocations, as well as their ability to multiply.

When metals are plastically deformed, some fraction of the deformation energy (approximately 5%) is retained internally; the remainder is dissipated as heat. The major portion of this stored energy is as strain energy associated with dislocations. Consider the edge dislocation represented in Figure 8.4. As already mentioned, some atomic lattice distortion exists around the dislocation line because of the presence of the extra half-plane of atoms. As a consequence, there are regions in which compressive, tensile, and shear **lattice strains** are imposed on the neighboring atoms. For example, atoms immediately above and adjacent to the dislocation line

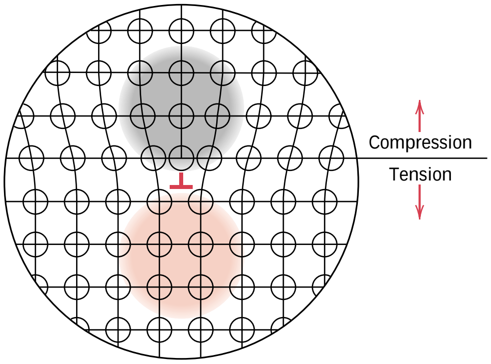

Figure 8.4 Regions of compression (dark) and tension (colored) located around an edge dislocation. (Adapted from W. G. Moffatt, G. W. Pearsall, and J. Wulff, *The Structure and Properties of Materials,* Vol. I, *Structure,* p. 85. Copyright © 1964 by John Wiley & Sons, New York. Reprinted by permission of John Wiley & Sons, Inc.)

are squeezed together. As a result, these atoms may be thought of as experiencing a compressive strain relative to atoms positioned in the perfect crystal and far removed from the dislocation; this is illustrated in Figure 8.4. Directly below the half-plane, the effect is just the opposite; lattice atoms sustain an imposed tensile strain, which is as shown. Shear strains also exist in the vicinity of the edge dislocation. For a screw dislocation, lattice strains are pure shear only. These lattice distortions may be considered to be strain fields that radiate from the dislocation line. The strains extend into the surrounding atoms, and their magnitudes decrease with radial distance from the dislocation.

The strain fields surrounding dislocations in close proximity to one another may interact such that forces are imposed on each dislocation by the combined interactions of all its neighboring dislocations. For example, consider two edge dislocations that have the same sign and the identical slip plane, as represented in Figure 8.5*a*. The compressive and tensile strain fields for both lie on the same side of the slip plane; the strain field interaction is such that there exists between these two isolated dislocations a mutual repulsive force that tends to move them apart. On the other hand, two dislocations of opposite sign and having the same slip plane will be attracted to one another, as indicated in Figure 8.5*b*, and dislocation annihilation will occur when they meet. That is, the two extra half-planes of atoms will align and become a complete plane. Dislocation interactions are possible between edge, screw, and/or mixed dislocations, and for a variety of orientations. These strain fields and associated forces are important in the strengthening mechanisms for metals.

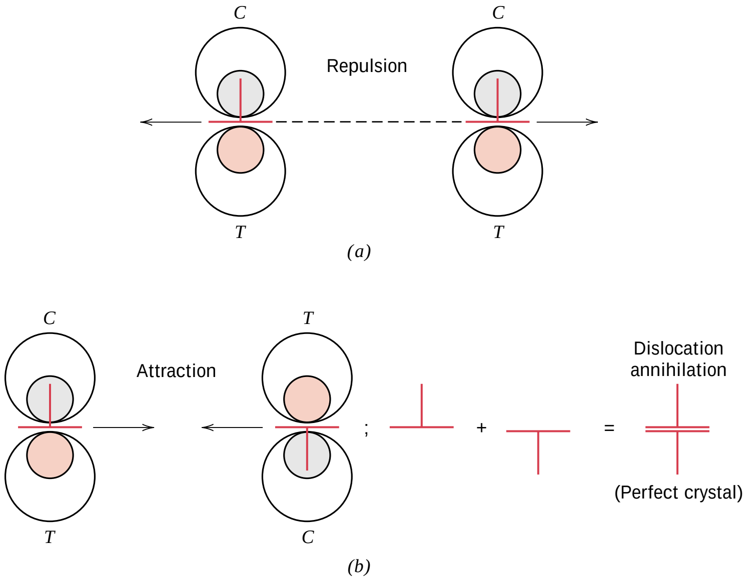

FIGURE 8.5 (*a*) Two edge dislocations of the same sign and lying on the same slip plane exert a repulsive force on each other; *C* and *T* denote compression and tensile regions, respectively. (*b*) Edge dislocations of opposite sign and lying on the same slip plane exert an attractive force on each other. Upon meeting, they annihilate each other and leave a region of perfect crystal. (Adapted from H. W. Hayden, W. G. Moffatt, and J. Wulff, *The Structure and Properties of Materials*, Vol. III, *Mechanical Behavior*, p. 75. Copyright © 1965 by John Wiley & Sons, New York. Reprinted by permission of John Wiley & Sons.)

During plastic deformation, the number of dislocations increases dramatically. We know that the dislocation density in a metal that has been highly deformed may be as high as 10^{10} mm^{-2}. One important source of these new dislocations is existing dislocations, which multiply; furthermore, grain boundaries, as well as internal defects and surface irregularities such as scratches and nicks, which act as stress concentrations, may serve as dislocation formation sites during deformation.

8.5 SLIP SYSTEMS

Dislocations do not move with the same degree of ease on all crystallographic planes of atoms and in all crystallographic directions. Ordinarily there is a preferred plane, and in that plane there are specific directions along which dislocation motion occurs. This plane is called the *slip plane;* it follows that the direction of movement is called the *slip direction.* This combination of the slip plane and the slip direction is termed the **slip system.** The slip system depends on the crystal structure of the metal and is such that the atomic distortion that accompanies the motion of a dislocation is a minimum. For a particular crystal structure, the slip plane is that plane having the most dense atomic packing, that is, has the greatest planar density. The slip direction corresponds to the direction, in this plane, that is most closely packed with atoms, that is, has the highest linear density. {Planar and linear atomic densities were discussed in Section 3.14.}

Consider, for example, the FCC crystal structure, a unit cell of which is shown in Figure 8.6*a*. There is a set of planes, the {111} family, all of which are closely packed. A (111)-type plane is indicated in the unit cell; in Figure 8.6*b*, this plane is positioned within the plane of the page, in which atoms are now represented as touching nearest neighbors.

Slip occurs along ⟨110⟩-type directions within the {111} planes, as indicated by arrows in Figure 8.6. Hence, {111}⟨110⟩ represents the slip plane and direction combination, or the slip system for FCC. Figure 8.6*b* demonstrates that a given slip plane may contain more than a single slip direction. Thus, several slip systems may exist for a particular crystal structure; the number of independent slip systems represents the different possible combinations of slip planes and directions. For example, for face-centered cubic, there are 12 slip systems: four unique {111} planes and, within each plane, three independent ⟨110⟩ directions.

The possible slip systems for BCC and HCP crystal structures are listed in Table 8.1. For each of these structures, slip is possible on more than one family of planes (e.g., {110}, {211}, and {321} for BCC). For metals having these two crystal structures, some slip systems are often operable only at elevated temperatures.

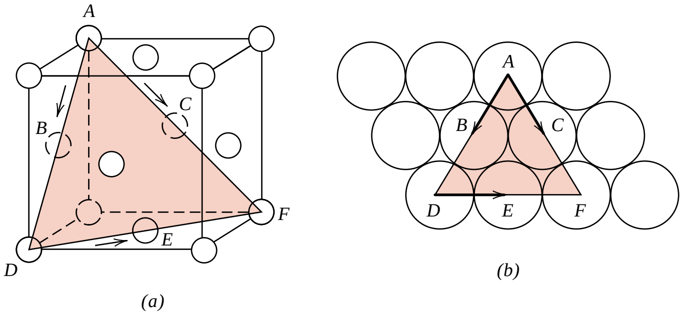

(a) *(b)*

FIGURE 8.6 (*a*) A {111}⟨110⟩ slip system shown within an FCC unit cell. (*b*) The (111) plane from (*a*) and three ⟨110⟩ slip directions (as indicated by arrows) within that plane comprise possible slip systems.

Table 8.1 **Slip Systems for Face-Centered Cubic, Body-Centered Cubic, and Hexagonal Close-Packed Metals**

Metals	*Slip Plane*	*Slip Direction*	*Number of Slip Systems*
	Face-Centered Cubic		
Cu, Al, Ni, Ag, Au	$\{111\}$	$\langle 1\bar{1}0 \rangle$	12
	Body-Centered Cubic		
α-Fe, W, Mo	$\{110\}$	$\langle \bar{1}11 \rangle$	12
α-Fe, W	$\{211\}$	$\langle \bar{1}11 \rangle$	12
α-Fe, K	$\{321\}$	$\langle \bar{1}11 \rangle$	24
	Hexagonal Close-Packed		
Cd, Zn, Mg, Ti, Be	$\{0001\}$	$\langle 11\bar{2}0 \rangle$	3
Ti, Mg, Zr	$\{10\bar{1}0\}$	$\langle 11\bar{2}0 \rangle$	3
Ti, Mg	$\{10\bar{1}1\}$	$\langle 11\bar{2}0 \rangle$	6

Metals with FCC or BCC crystal structures have a relatively large number of slip systems (at least 12). These metals are quite ductile because extensive plastic deformation is normally possible along the various systems. Conversely, HCP metals, having few active slip systems, are normally quite brittle.

8.6 Slip in Single Crystals (CD-ROM)

8.7 Plastic Deformation of Polycrystalline Metals

For polycrystalline metals, because of the random crystallographic orientations of the numerous grains, the direction of slip varies from one grain to another. For each, dislocation motion occurs along the slip system that has the most favorable orientation (i.e., the highest shear stress). This is exemplified by a photomicrograph of a polycrystalline copper specimen that has been plastically deformed (Figure 8.10); before deformation the surface was polished. Slip lines[1] are visible, and it appears that two slip systems operated for most of the grains, as evidenced by two sets of parallel yet intersecting sets of lines. Furthermore, variation in grain orientation is indicated by the difference in alignment of the slip lines for the several grains.

Gross plastic deformation of a polycrystalline specimen corresponds to the comparable distortion of the individual grains by means of slip. During deformation, mechanical integrity and coherency are maintained along the grain boundaries; that is, the grain boundaries usually do not come apart or open up. As a consequence, each individual grain is constrained, to some degree, in the shape it may assume by its neighboring grains. The manner in which grains distort as a result of gross plastic deformation is indicated in Figure 8.11. Before deformation the grains are equiaxed, or have approximately the same dimension in all directions. For this

---

[1] Surface steps or ledges produced by dislocations (Figure 8.1*c*) that have exited from a grain and that appear as lines when viewed with a microscope are called *slip lines.*

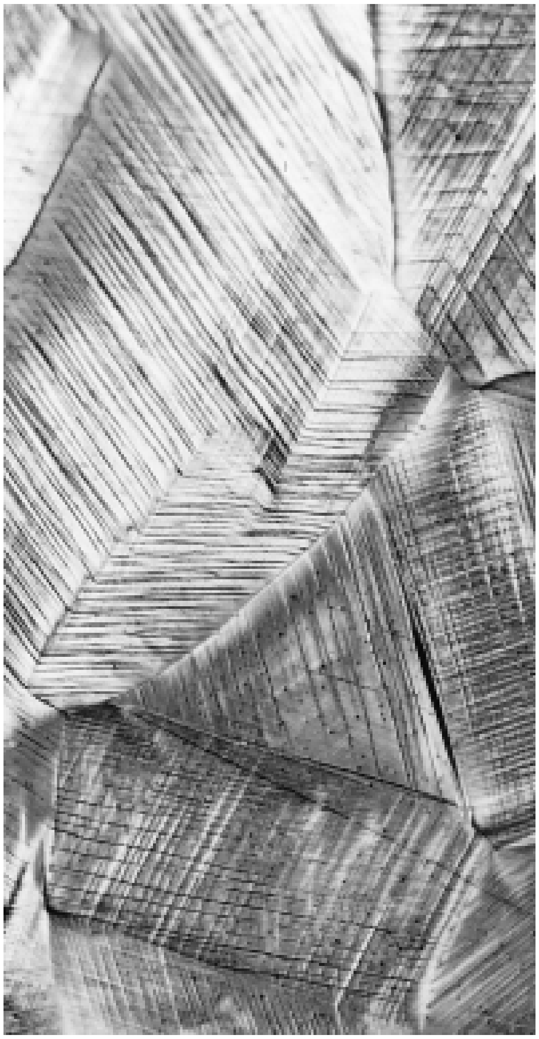

FIGURE 8.10 Slip lines on the surface of a polycrystalline specimen of copper that was polished and subsequently deformed. 173×. (Photomicrograph courtesy of C. Brady, National Bureau of Standards.)

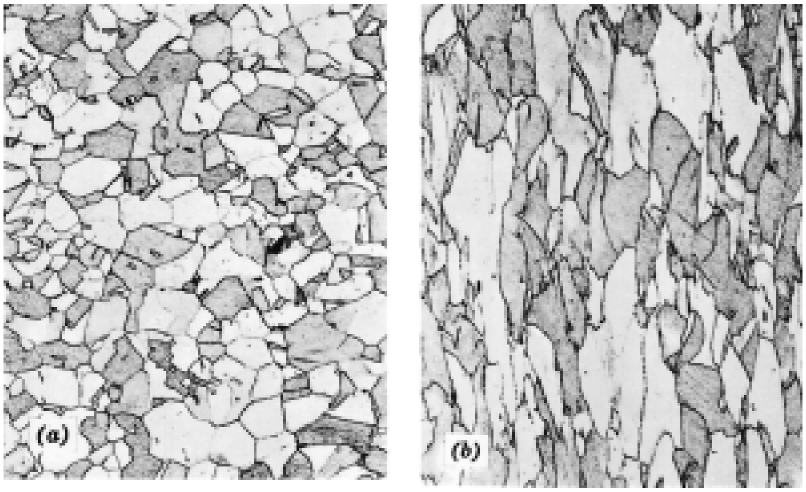

FIGURE 8.11 Alteration of the grain structure of a polycrystalline metal as a result of plastic deformation. (*a*) Before deformation the grains are equiaxed. (*b*) The deformation has produced elongated grains. 170×. (From W. G. Moffatt, G. W. Pearsall, and J. Wulff, *The Structure and Properties of Materials,* Vol. I, *Structure,* p. 140. Copyright © 1964 by John Wiley & Sons, New York. Reprinted by permission of John Wiley & Sons, Inc.)

particular deformation, the grains become elongated along the direction in which the specimen was extended.

Polycrystalline metals are stronger than their single-crystal equivalents, which means that greater stresses are required to initiate slip and the attendant yielding. This is, to a large degree, also a result of geometrical constraints that are imposed on the grains during deformation. Even though a single grain may be favorably oriented with the applied stress for slip, it cannot deform until the adjacent and less favorably oriented grains are capable of slip also; this requires a higher applied stress level.

8.8 DEFORMATION BY TWINNING (CD-ROM)

MECHANISMS OF STRENGTHENING IN METALS

Metallurgical and materials engineers are often called on to design alloys having high strengths yet some ductility and toughness; ordinarily, ductility is sacrificed when an alloy is strengthened. Several hardening techniques are at the disposal of an engineer, and frequently alloy selection depends on the capacity of a material to be tailored with the mechanical characteristics required for a particular application.

Important to the understanding of strengthening mechanisms is the relation between dislocation motion and mechanical behavior of metals. Because macroscopic plastic deformation corresponds to the motion of large numbers of dislocations, *the ability of a metal to plastically deform depends on the ability of dislocations to move.* Since hardness and strength (both yield and tensile) are related to the ease with which plastic deformation can be made to occur, by reducing the mobility of dislocations, the mechanical strength may be enhanced; that is, greater mechanical forces will be required to initiate plastic deformation. In contrast, the more unconstrained the dislocation motion, the greater the facility with which a metal may deform, and the softer and weaker it becomes. Virtually all strengthening techniques rely on this simple principle: *restricting or hindering dislocation motion renders a material harder and stronger.*

The present discussion is confined to strengthening mechanisms for single-phase metals, by grain size reduction, solid-solution alloying, and strain hardening. Deformation and strengthening of multiphase alloys are more complicated, involving concepts yet to be discussed.

8.9 STRENGTHENING BY GRAIN SIZE REDUCTION

The size of the grains, or average grain diameter, in a polycrystalline metal influences the mechanical properties. Adjacent grains normally have different crystallographic orientations and, of course, a common grain boundary, as indicated in Figure 8.14. During plastic deformation, slip or dislocation motion must take place across this common boundary, say, from grain A to grain B in Figure 8.14. The grain boundary acts as a barrier to dislocation motion for two reasons:

1. Since the two grains are of different orientations, a dislocation passing into grain B will have to change its direction of motion; this becomes more difficult as the crystallographic misorientation increases.

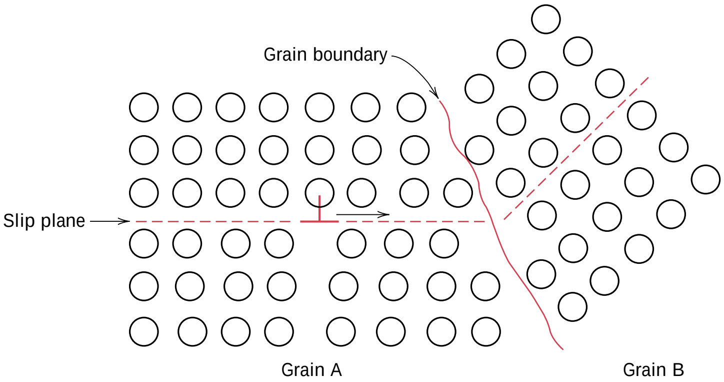

FIGURE 8.14 The motion of a dislocation as it encounters a grain boundary, illustrating how the boundary acts as a barrier to continued slip. Slip planes are discontinuous and change directions across the boundary. (From *A Textbook of Materials Technology* by Van Vlack, © 1973. Reprinted by permission of Prentice-Hall, Inc., Upper Saddle River, NJ.)

2. The atomic disorder within a grain boundary region will result in a discontinuity of slip planes from one grain into the other.

It should be mentioned that, for high-angle grain boundaries, it may not be the case that dislocations traverse grain boundaries during deformation; rather, a stress concentration ahead of a slip plane in one grain may activate sources of new dislocations in an adjacent grain.

A fine-grained material (one that has small grains) is harder and stronger than one that is coarse grained, since the former has a greater total grain boundary area to impede dislocation motion. For many materials, the yield strength σ_y varies with grain size according to

$$\sigma_y = \sigma_0 + k_y d^{-1/2} \tag{8.5}$$

In this expression, termed the *Hall-Petch equation*, d is the average grain diameter, and σ_0 and k_y are constants for a particular material. It should be noted that Equation 8.5 is not valid for both very large (i.e., coarse) grain and extremely fine grain polycrystalline materials. Figure 8.15 demonstrates the yield strength dependence on grain size for a brass alloy. Grain size may be regulated by the rate of solidification from the liquid phase, and also by plastic deformation followed by an appropriate heat treatment, as discussed in Section 8.14.

It should also be mentioned that grain size reduction improves not only strength, but also the toughness of many alloys.

Small-angle grain boundaries (Section 5.8) are not effective in interfering with the slip process because of the slight crystallographic misalignment across the boundary. On the other hand, twin boundaries (Section 5.8) will effectively block slip and increase the strength of the material. Boundaries between two different phases are also impediments to movements of dislocations; this is important in the strengthening of more complex alloys. The sizes and shapes of the constituent phases significantly affect the mechanical properties of multiphase alloys; these are the topics of discussion in Sections 11.7, 11.8, {and 15.1.}

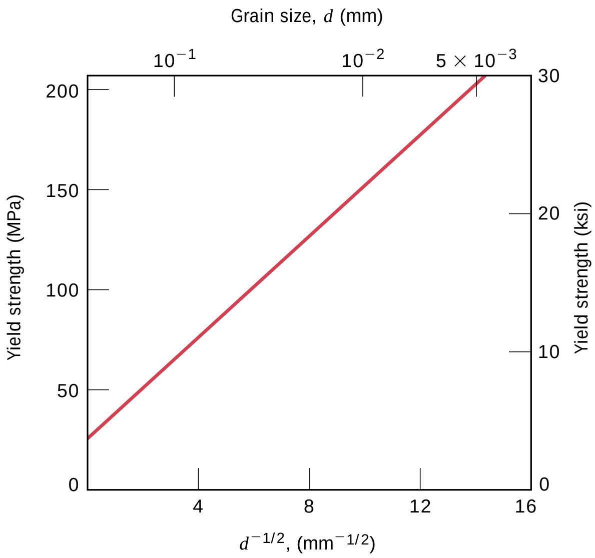

Figure 8.15 The influence of grain size on the yield strength of a 70 Cu–30 Zn brass alloy. Note that the grain diameter increases from right to left and is not linear. (Adapted from H. Suzuki, "The Relation Between the Structure and Mechanical Properties of Metals," Vol. II, *National Physical Laboratory, Symposium No. 15,* 1963, p. 524.)

8.10 SOLID-SOLUTION STRENGTHENING

Another technique to strengthen and harden metals is alloying with impurity atoms that go into either substitutional or interstitial solid solution. Accordingly, this is called **solid-solution strengthening.** High-purity metals are almost always softer and weaker than alloys composed of the same base metal. Increasing the concentration of the impurity results in an attendant increase in tensile and yield strengths, as indicated in Figures 8.16*a* and 8.16*b* for nickel in copper; the dependence of ductility on nickel concentration is presented in Figure 8.16*c*.

Alloys are stronger than pure metals because impurity atoms that go into solid solution ordinarily impose lattice strains on the surrounding host atoms. Lattice strain field interactions between dislocations and these impurity atoms result, and, consequently, dislocation movement is restricted. For example, an impurity atom that is smaller than a host atom for which it substitutes exerts tensile strains on the surrounding crystal lattice, as illustrated in Figure 8.17*a*. Conversely, a larger substitutional atom imposes compressive strains in its vicinity (Figure 8.18*a*). These solute atoms tend to diffuse to and segregate around dislocations in a way so as to reduce the overall strain energy, that is, to cancel some of the strain in the lattice surrounding a dislocation. To accomplish this, a smaller impurity atom is located where its tensile strain will partially nullify some of the dislocation's compressive strain. For the edge dislocation in Figure 8.17*b*, this would be adjacent to the dislocation line and above the slip plane. A larger impurity atom would be situated as in Figure 8.18*b*.

The resistance to slip is greater when impurity atoms are present because the overall lattice strain must increase if a dislocation is torn away from them. Furthermore, the same lattice strain interactions (Figures 8.17*b* and 8.18*b*) will exist between impurity atoms and dislocations that are in motion during plastic deformation. Thus, a greater applied stress is necessary to first initiate and then continue plastic deformation for solid-solution alloys, as opposed to pure metals; this is evidenced by the enhancement of strength and hardness.

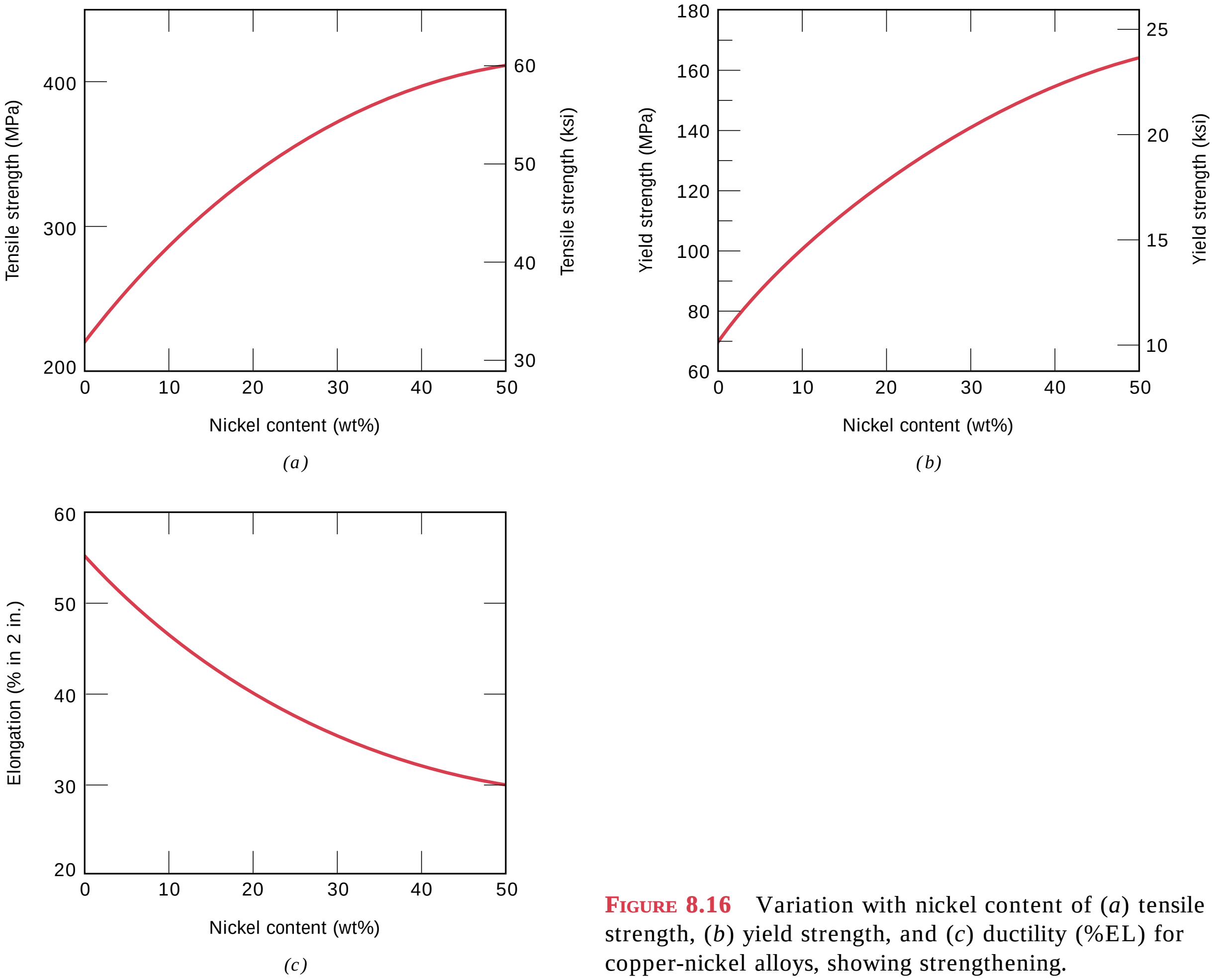

FIGURE 8.16 Variation with nickel content of (*a*) tensile strength, (*b*) yield strength, and (*c*) ductility (%EL) for copper-nickel alloys, showing strengthening.

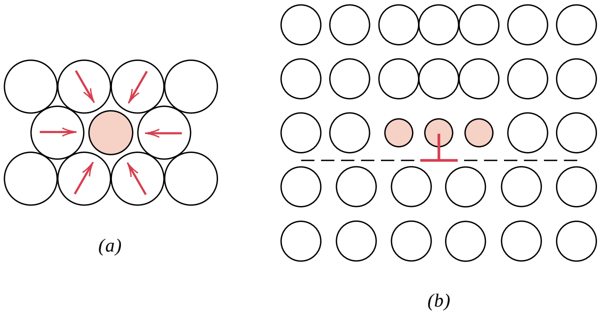

FIGURE 8.17 (*a*) Representation of tensile lattice strains imposed on host atoms by a smaller substitutional impurity atom. (*b*) Possible locations of smaller impurity atoms relative to an edge dislocation such that there is partial cancellation of impurity–dislocation lattice strains.

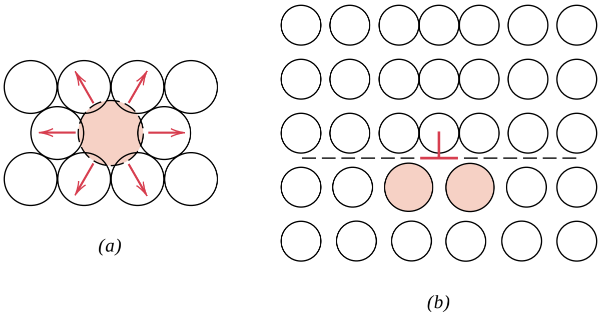

FIGURE 8.18 (*a*) Representation of compressive strains imposed on host atoms by a larger substitutional impurity atom. (*b*) Possible locations of larger impurity atoms relative to an edge dislocation such that there is partial cancellation of impurity–dislocation lattice strains.

8.11 STRAIN HARDENING

Strain hardening is the phenomenon whereby a ductile metal becomes harder and stronger as it is plastically deformed. Sometimes it is also called *work hardening*, or, because the temperature at which deformation takes place is ''cold'' relative to the absolute melting temperature of the metal, **cold working.** Most metals strain harden at room temperature.

It is sometimes convenient to express the degree of plastic deformation as *percent cold work* rather than as strain. Percent cold work (%CW) is defined as

$$\%\mathrm{CW} = \left(\frac{A_0 - A_d}{A_0}\right) \times 100 \tag{8.6}$$

where A_0 is the original area of the cross section that experiences deformation, and A_d is the area after deformation.

Figures 8.19*a* and 8.19*b* demonstrate how steel, brass, and copper increase in yield and tensile strength with increasing cold work. The price for this enhancement of hardness and strength is in the ductility of the metal. This is shown in Figure 8.19*c*, in which the ductility, in percent elongation, experiences a reduction with increasing percent cold work for the same three alloys. The influence of cold work on the stress–strain behavior of a steel is vividly portrayed in Figure 8.20.

Strain hardening is demonstrated in a stress–strain diagram presented earlier (Figure 7.17). Initially, the metal with yield strength σ_{y_0} is plastically deformed to point D. The stress is released, then reapplied with a resultant new yield strength, σ_{y_i}. The metal has thus become stronger during the process because σ_{y_i} is greater than σ_{y_0}.

The strain hardening phenomenon is explained on the basis of dislocation–dislocation strain field interactions similar to those discussed in Section 8.4. The dislocation density in a metal increases with deformation or cold work, due to dislocation multiplication or the formation of new dislocations, as noted previously. Consequently, the average distance of separation between dislocations decreases—the dislocations are positioned closer together. On the average, dislocation–dislocation strain interactions are repulsive. The net result is that the motion of a dislocation is hindered by the presence of other dislocations. As the dislocation density increases, this resistance to dislocation motion by other dislocations becomes more pronounced. Thus, the imposed stress necessary to deform a metal increases with increasing cold work.

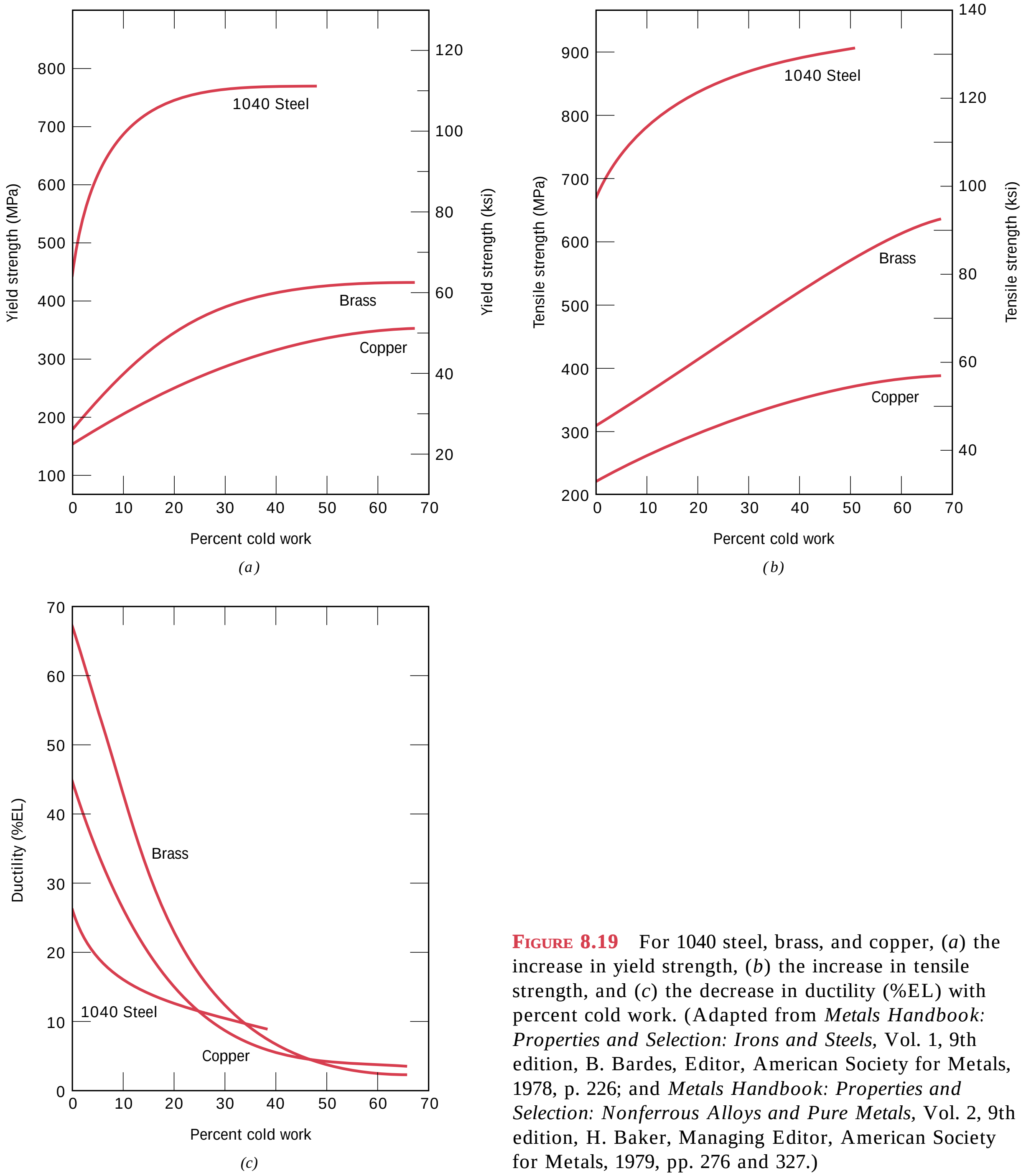

Figure 8.19 For 1040 steel, brass, and copper, (*a*) the increase in yield strength, (*b*) the increase in tensile strength, and (*c*) the decrease in ductility (%EL) with percent cold work. (Adapted from *Metals Handbook: Properties and Selection: Irons and Steels*, Vol. 1, 9th edition, B. Bardes, Editor, American Society for Metals, 1978, p. 226; and *Metals Handbook: Properties and Selection: Nonferrous Alloys and Pure Metals*, Vol. 2, 9th edition, H. Baker, Managing Editor, American Society for Metals, 1979, pp. 276 and 327.)

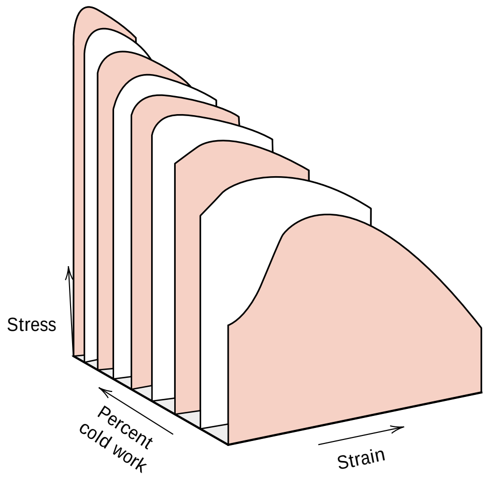

FIGURE 8.20 The influence of cold work on the stress–strain behavior for a low-carbon steel. (From *Metals Handbook: Properties and Selection: Irons and Steels,* Vol. 1, 9th edition, B. Bardes, Editor, American Society for Metals, 1978, p. 221.)

Strain hardening is often utilized commercially to enhance the mechanical properties of metals during fabrication procedures. The effects of strain hardening may be removed by an annealing heat treatment, {as discussed in Section 14.5.}

In passing, for the mathematical expression relating true stress and strain, Equation 7.19, the parameter n is called the *strain hardening exponent,* which is a measure of the ability of a metal to strain harden; the larger its magnitude, the greater the strain hardening for a given amount of plastic strain.

EXAMPLE PROBLEM 8.2

Compute the tensile strength and ductility (%EL) of a cylindrical copper rod if it is cold worked such that the diameter is reduced from 15.2 mm to 12.2 mm (0.60 in. to 0.48 in.).

SOLUTION

It is first necessary to determine the percent cold work resulting from the deformation. This is possible using Equation 8.6:

$$\%\text{CW} = \frac{\left(\dfrac{15.2\text{ mm}}{2}\right)^2 \pi - \left(\dfrac{12.2\text{ mm}}{2}\right)^2 \pi}{\left(\dfrac{15.2\text{ mm}}{2}\right)^2 \pi} \times 100 = 35.6\%$$

The tensile strength is read directly from the curve for copper (Figure 8.19*b*) as 340 MPa (50,000 psi). From Figure 8.19*c*, the ductility at 35.6%CW is about 7%EL.

In summary, we have just discussed the three mechanisms that may be used to strengthen and harden single-phase metal alloys—strengthening by grain size reduction, solid solution strengthening, and strain hardening. Of course they may be used in conjunction with one another; for example, a solid-solution strengthened alloy may also be strain hardened.

RECOVERY, RECRYSTALLIZATION, AND GRAIN GROWTH

As outlined in the preceding paragraphs of this chapter, plastically deforming a polycrystalline metal specimen at temperatures that are low relative to its absolute melting temperature produces microstructural and property changes that include (1) a change in grain shape (Section 8.7), (2) strain hardening (Section 8.11), and (3) an increase in dislocation density (Section 8.4). Some fraction of the energy expended in deformation is stored in the metal as strain energy, which is associated with tensile, compressive, and shear zones around the newly created dislocations (Section 8.4). Furthermore, other properties such as electrical conductivity (Section 12.8) and corrosion resistance may be modified as a consequence of plastic deformation.

These properties and structures may revert back to the precold-worked states by appropriate heat treatment (sometimes termed an annealing treatment). Such restoration results from two different processes that occur at elevated temperatures: **recovery** and **recrystallization,** which may be followed by **grain growth.**

8.12 RECOVERY

During recovery, some of the stored internal strain energy is relieved by virtue of dislocation motion (in the absence of an externally applied stress), as a result of enhanced atomic diffusion at the elevated temperature. There is some reduction in the number of dislocations, and dislocation configurations (similar to that shown in Figure 5.12) are produced having low strain energies. In addition, physical properties such as electrical and thermal conductivities and the like are recovered to their precold-worked states.

8.13 RECRYSTALLIZATION

Even after recovery is complete, the grains are still in a relatively high strain energy state. Recrystallization is the formation of a new set of strain-free and equiaxed grains (i.e., having approximately equal dimensions in all directions) that have low dislocation densities and are characteristic of the precold-worked condition. The driving force to produce this new grain structure is the difference in internal energy between the strained and unstrained material. The new grains form as very small nuclei and grow until they completely replace the parent material, processes that involve short-range diffusion. Several stages in the recrystallization process are represented in Figures 8.21*a* to 8.21*d*; in these photomicrographs, the small speckled grains are those that have recrystallized. Thus, recrystallization of cold-worked metals may be used to refine the grain structure.

Also, during recrystallization, the mechanical properties that were changed as a result of cold working are restored to their precold-worked values; that is, the metal becomes softer, weaker, yet more ductile. Some heat treatments are designed to allow recrystallization to occur with these modifications in the mechanical characteristics {(Section 14.5).}

Recrystallization is a process the extent of which depends on both time and temperature. The degree (or fraction) of recrystallization increases with time, as may be noted in the photomicrographs shown in Figures 8.21*a–d*. The explicit time dependence of recrystallization is addressed in more detail in Section 11.3.

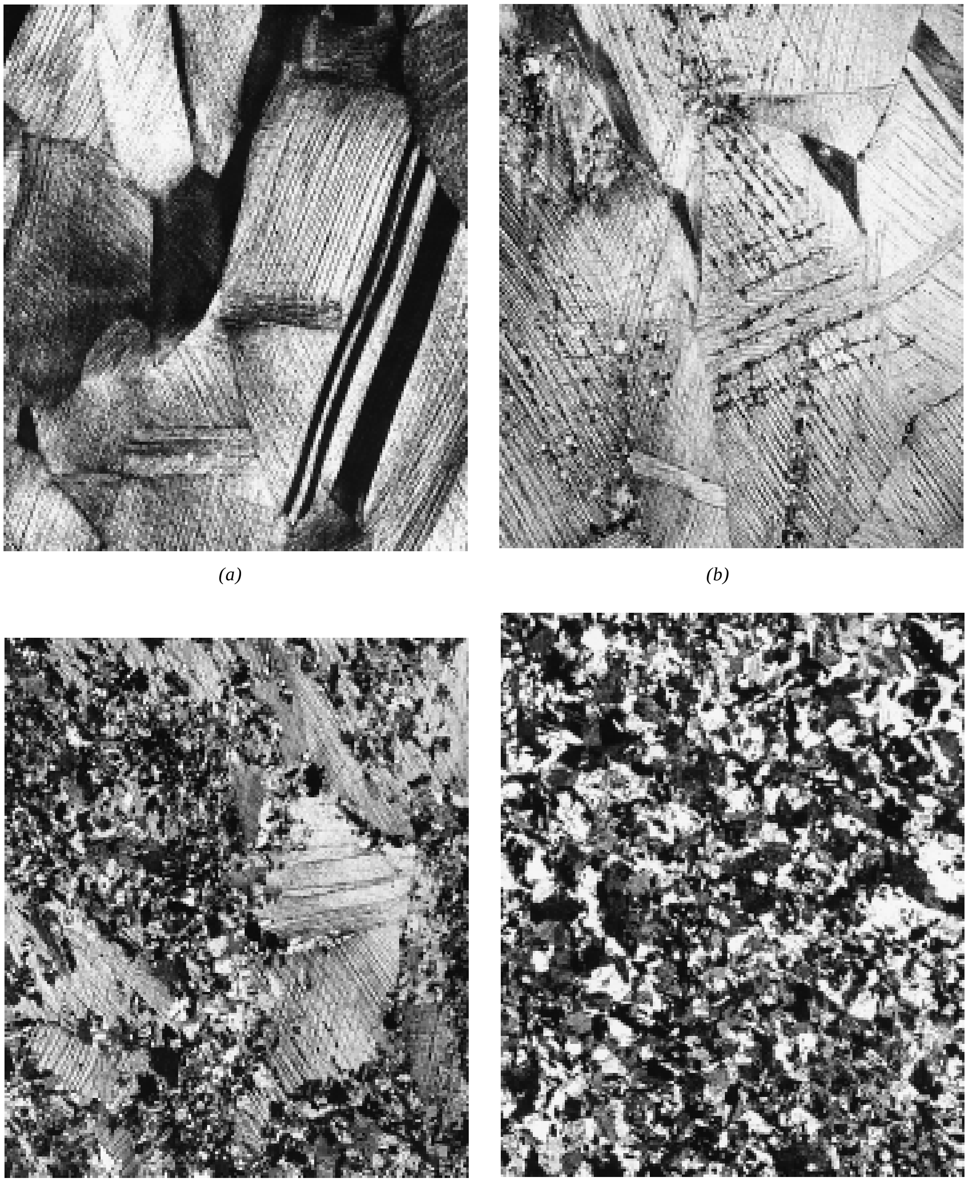

(a) (b)

(c) (d)

Figure 8.21 Photomicrographs showing several stages of the recrystallization and grain growth of brass. (*a*) Cold-worked (33%CW) grain structure. (*b*) Initial stage of recrystallization after heating 3 s at 580°C (1075°F); the very small grains are those that have recrystallized. (*c*) Partial replacement of cold-worked grains by recrystallized ones (4 s at 580°C). (*d*) Complete recrystallization (8 s at 580°C). (*e*) Grain growth after 15 min at 580°C. (*f*) Grain growth after 10 min at 700°C (1290°F). All photomicrographs 75×. (Photomicrographs courtesy of J. E. Burke, General Electric Company.)

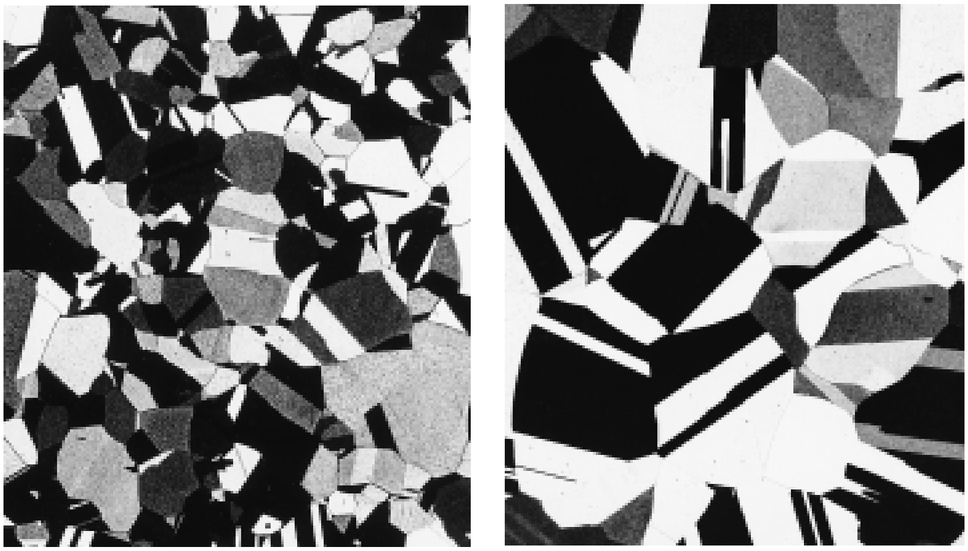

(e) (f)

Figure 8.21 (*continued*)

The influence of temperature is demonstrated in Figure 8.22, which plots tensile strength and ductility (at room temperature) of a brass alloy as a function of the temperature and for a constant heat treatment time of 1 h. The grain structures found at the various stages of the process are also presented schematically.

The recrystallization behavior of a particular metal alloy is sometimes specified in terms of a **recrystallization temperature,** the temperature at which recrystallization just reaches completion in 1 h. Thus, the recrystallization temperature for the brass alloy of Figure 8.22 is about 450°C (850°F). Typically, it is between one third and one half of the absolute melting temperature of a metal or alloy and depends on several factors, including the amount of prior cold work and the purity of the alloy. Increasing the percentage of cold work enhances the rate of recrystallization, with the result that the recrystallization temperature is lowered, and approaches a constant or limiting value at high deformations; this effect is shown in Figure 8.23. Furthermore, it is this limiting or minimum recrystallization temperature that is normally specified in the literature. There exists some critical degree of cold work below which recrystallization cannot be made to occur, as shown in the figure; normally, this is between 2 and 20% cold work.

Recrystallization proceeds more rapidly in pure metals than in alloys. Thus, alloying raises the recrystallization temperature, sometimes quite substantially. For pure metals, the recrystallization temperature is normally $0.3T_m$, where T_m is the absolute melting temperature; for some commercial alloys it may run as high as $0.7T_m$. Recrystallization and melting temperatures for a number of metals and alloys are listed in Table 8.2.

Plastic deformation operations are often carried out at temperatures above the recrystallization temperature in a process termed *hot working,* {described in Section 14.2.} The material remains relatively soft and ductile during deformation because it does not strain harden, and thus large deformations are possible.

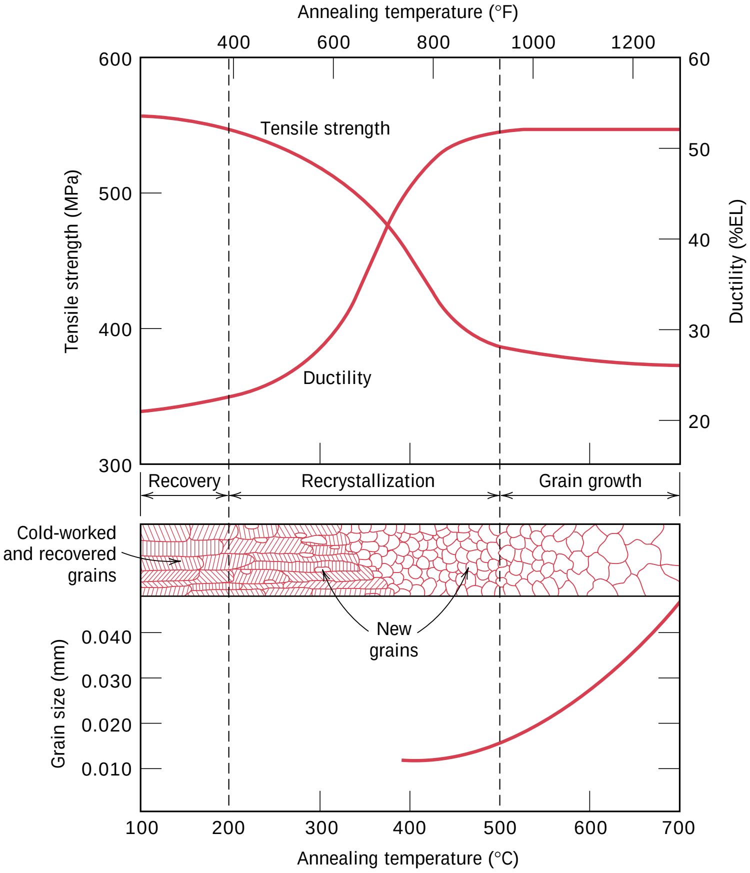

FIGURE 8.22 The influence of annealing temperature on the tensile strength and ductility of a brass alloy. Grain size as a function of annealing temperature is indicated. Grain structures during recovery, recrystallization, and grain growth stages are shown schematically. (Adapted from G. Sachs and K. R. Van Horn, *Practical Metallurgy, Applied Metallurgy and the Industrial Processing of Ferrous and Nonferrous Metals and Alloys*, American Society for Metals, 1940, p. 139.)

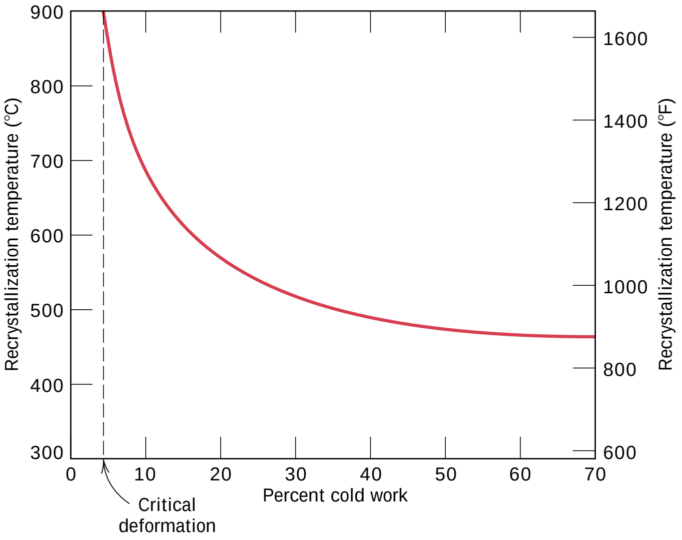

FIGURE 8.23 The variation of recrystallization temperature with percent cold work for iron. For deformations less than the critical (about 5%CW), recrystallization will not occur.

Table 8.2 Recrystallization and Melting Temperatures for Various Metals and Alloys

Metal	*Recrystallization Temperature* °C	*Recrystallization Temperature* °F	*Melting Temperature* °C	*Melting Temperature* °F
Lead	−4	25	327	620
Tin	−4	25	232	450
Zinc	10	50	420	788
Aluminum (99.999 wt%)	80	176	660	1220
Copper (99.999 wt%)	120	250	1085	1985
Brass (60 Cu–40 Zn)	475	887	900	1652
Nickel (99.99 wt%)	370	700	1455	2651
Iron	450	840	1538	2800
Tungsten	1200	2200	3410	6170

DESIGN EXAMPLE 8.1

A cylindrical rod of noncold-worked brass having an initial diameter of 6.4 mm (0.25 in.) is to be cold worked by drawing such that the cross-sectional area is reduced. It is required to have a cold-worked yield strength of at least 345 MPa (50,000 psi) and a ductility in excess of 20%EL; in addition, a final diameter of 5.1 mm (0.20 in.) is necessary. Describe the manner in which this procedure may be carried out.

SOLUTION

Let us first consider the consequences (in terms of yield strength and ductility) of cold working in which the brass specimen diameter is reduced from 6.4 mm (designated by d_0) to 5.1 mm (d_i). The %CW may be computed from Equation 8.6 as

$$\%\text{CW} = \frac{\left(\frac{d_0}{2}\right)^2 \pi - \left(\frac{d_i}{2}\right)^2 \pi}{\left(\frac{d_0}{2}\right)^2 \pi} \times 100$$

$$= \frac{\left(\frac{6.4\text{ mm}}{2}\right)^2 \pi - \left(\frac{5.1\text{ mm}}{2}\right)^2 \pi}{\left(\frac{6.4\text{ mm}}{2}\right)^2 \pi} \times 100 = 36.5\%\text{CW}$$

From Figures 8.19*a* and 8.19*c*, a yield strength of 410 MPa (60,000 psi) and a ductility of 8%EL are attained from this deformation. According to the stipulated criteria, the yield strength is satisfactory; however, the ductility is too low.

Another processing alternative is a partial diameter reduction, followed by a recrystallization heat treatment in which the effects of the cold work are nullified. The required yield strength, ductility, and diameter are achieved through a second drawing step.

Again, reference to Figure 8.19*a* indicates that 20%CW is required to give a yield strength of 345 MPa. On the other hand, from Figure 8.19*c*, ductilities greater than 20%EL are possible only for deformations of 23%CW or less. Thus during the final drawing operation, deformation must be between 20%CW and 23%CW. Let's take the average of these extremes, 21.5%CW, and then calculate the final diameter for the first drawing d_0', which becomes the original diameter for the second drawing. Again, using Equation 8.6,

$$21.5\%\text{CW} = \frac{\left(\dfrac{d_0'}{2}\right)^2 \pi - \left(\dfrac{5.1\text{ mm}}{2}\right)^2 \pi}{\left(\dfrac{d_0'}{2}\right)^2 \pi} \times 100$$

Now, solving from d_0' from the expression above gives

$$d_0' = 5.8 \text{ mm } (0.226 \text{ in.})$$

8.14 GRAIN GROWTH

After recrystallization is complete, the strain-free grains will continue to grow if the metal specimen is left at the elevated temperature (Figures 8.21*d*–*f*); this phenomenon is called **grain growth.** Grain growth does not need to be preceded by recovery and recrystallization; it may occur in all polycrystalline materials, metals and ceramics alike.

An energy is associated with grain boundaries, as explained in Section 5.8. As grains increase in size, the total boundary area decreases, yielding an attendant reduction in the total energy; this is the driving force for grain growth.

Grain growth occurs by the migration of grain boundaries. Obviously, not all grains can enlarge, but large ones grow at the expense of small ones that shrink. Thus, the average grain size increases with time, and at any particular instant there will exist a range of grain sizes. Boundary motion is just the short-range diffusion of atoms from one side of the boundary to the other. The directions of boundary movement and atomic motion are opposite to each other, as shown in Figure 8.24.

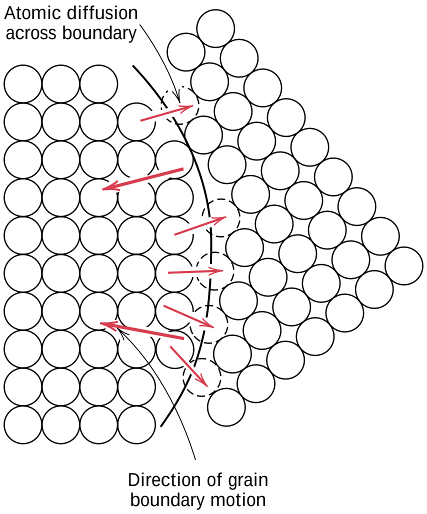
Atomic diffusion across boundary
Direction of grain boundary motion

FIGURE 8.24 Schematic representation of grain growth via atomic diffusion. (From *Elements of Materials Science and Engineering* by Van Vlack, © 1989. Reprinted by permission of Prentice-Hall, Inc., Upper Saddle River, NJ.)

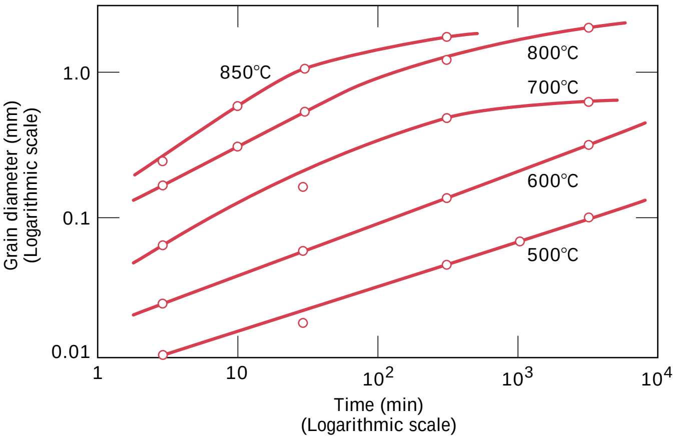

FIGURE 8.25 The logarithm of grain diameter versus the logarithm of time for grain growth in brass at several temperatures. (From J. E. Burke, ''Some Factors Affecting the Rate of Grain Growth in Metals.'' Reprinted with permission from *Metallurgical Transactions*, Vol. 180, 1949, a publication of The Metallurgical Society of AIME, Warrendale, Pennsylvania.)

For many polycrystalline materials, the grain diameter d varies with time t according to the relationship

$$d^n - d_0^n = Kt \tag{8.7}$$

where d_0 is the initial grain diameter at $t = 0$, and K and n are time-independent constants; the value of n is generally equal to or greater than 2.

The dependence of grain size on time and temperature is demonstrated in Figure 8.25, a plot of the logarithm of grain size as a function of the logarithm of time for a brass alloy at several temperatures. At lower temperatures the curves are linear. Furthermore, grain growth proceeds more rapidly as temperature increases; that is, the curves are displaced upward to larger grain sizes. This is explained by the enhancement of diffusion rate with rising temperature.

The mechanical properties at room temperature of a fine-grained metal are usually superior (i.e., higher strength and toughness) to those of coarse-grained ones. If the grain structure of a single-phase alloy is coarser than that desired, refinement may be accomplished by plastically deforming the material, then subjecting it to a recrystallization heat treatment, as described above.

DEFORMATION MECHANISMS FOR CERAMIC MATERIALS

Although at room temperature most ceramic materials suffer fracture before the onset of plastic deformation, a brief exploration into the possible mechanisms is worthwhile. Plastic deformation is different for crystalline and noncrystalline ceramics; however, each is discussed.

8.15 CRYSTALLINE CERAMICS

For crystalline ceramics, plastic deformation occurs, as with metals, by the motion of dislocations. One reason for the hardness and brittleness of these materials is the difficulty of slip (or dislocation motion). For crystalline ceramic materials for which the bonding is predominantly ionic, there are very few slip systems (crystallographic planes and directions within those planes) along which dislocations may move. This is a consequence of the electrically charged nature of the ions. For slip in some directions, ions of like charge are brought into close proximity to one another; because of electrostatic repulsion, this mode of slip is very restricted. This is not a problem in metals, since all atoms are electrically neutral.

On the other hand, for ceramics in which the bonding is highly covalent, slip is also difficult and they are brittle for the following reasons: (1) the covalent bonds are relatively strong; (2) there are also limited numbers of slip systems; and (3) dislocation structures are complex.

8.16 NONCRYSTALLINE CERAMICS

Plastic deformation does not occur by dislocation motion for noncrystalline ceramics because there is no regular atomic structure. Rather, these materials deform by *viscous flow*, the same manner in which liquids deform; the rate of deformation is proportional to the applied stress. In response to an applied shear stress, atoms or ions slide past one another by the breaking and reforming of interatomic bonds. However, there is no prescribed manner or direction in which this occurs, as with dislocations. Viscous flow on a macroscopic scale is demonstrated in Figure 8.26.

The characteristic property for viscous flow, **viscosity,** is a measure of a noncrystalline material's resistance to deformation. For viscous flow in a liquid that originates from shear stresses imposed by two flat and parallel plates, the viscosity η is the ratio of the applied shear stress τ and the change in velocity dv with distance dy in a direction perpendicular to and away from the plates, or

$$\eta = \frac{\tau}{dv/dy} = \frac{F/A}{dv/dy} \tag{8.8}$$

This scheme is represented in Figure 8.26.

The units for viscosity are poises (P) and pascal-seconds (Pa-s); 1 P = 1 dyne-s/cm^2, and 1 Pa-s = 1 N-s/m^2. Conversion from one system of units to the other is

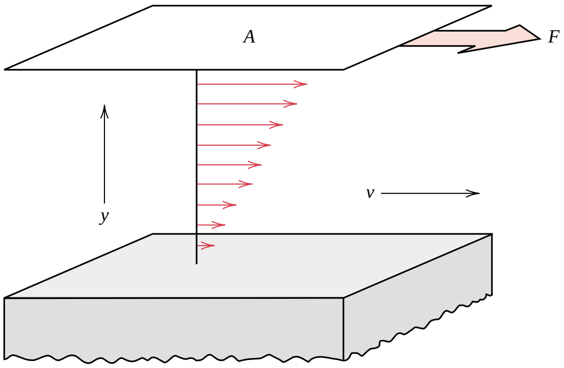

FIGURE 8.26 Representation of the viscous flow of a liquid or fluid glass in response to an applied shear force.

according to

$$10\ \text{P} = 1\ \text{Pa-s}$$

Liquids have relatively low viscosities; for example, the viscosity of water at room temperature is about 10^{-3} Pa-s. On the other hand, glasses have extremely large viscosities at ambient temperatures, which is accounted for by strong interatomic bonding. As the temperature is raised, the magnitude of the bonding is diminished, the sliding motion or flow of the atoms or ions is facilitated, and subsequently there is an attendant decrease in viscosity. {A discussion of the temperature dependence of viscosity for glasses is deferred to Section 14.7.}

MECHANISMS OF DEFORMATION AND FOR STRENGTHENING OF POLYMERS

An understanding of deformation mechanisms of polymers is important in order for us to be able to manage the mechanical characteristics of these materials. In this regard, deformation models for two different types of polymers—semicrystalline and elastomeric—deserve our attention. The stiffness and strength of semicrystalline materials are often important considerations; elastic and plastic deformation mechanisms are treated in the succeeding section, whereas methods used to stiffen and strengthen these materials are discussed in Section 8.18. On the other hand, elastomers are utilized on the basis of their unusual elastic properties; the deformation mechanism of elastomers is also treated.

8.17 Deformation of Semicrystalline Polymers

Many semicrystalline polymers in bulk form will have the spherulitic structure described in Section 4.12. By way of review, let us repeat here that each spherulite consists of numerous chain-folded ribbons, or lamellae, that radiate outward from the center. Separating these lamellae are areas of amorphous material (Figure 4.14); adjacent lamellae are connected by tie chains that pass through these amorphous regions.

MECHANISM OF ELASTIC DEFORMATION

The mechanism of elastic deformation in semicrystalline polymers in response to tensile stresses is the elongation of the chain molecules from their stable conformations, in the direction of the applied stress, by the bending and stretching of the strong chain covalent bonds. In addition, there may be some slight displacement of adjacent molecules, which is resisted by relatively weak secondary or van der Waals bonds. Furthermore, inasmuch as semicrystalline polymers are composed of both crystalline and amorphous regions, they may, in a sense, be considered composite materials. As such, the elastic modulus may be taken as some combination of the moduli of crystalline and amorphous phases.

MECHANISM OF PLASTIC DEFORMATION

The mechanism of plastic deformation is best described by the interactions between lamellar and intervening amorphous regions in response to an applied tensile load. This process occurs in several stages, which are schematically diagrammed in Figure 8.27. Two adjacent chain-folded lamellae and the interlamel-

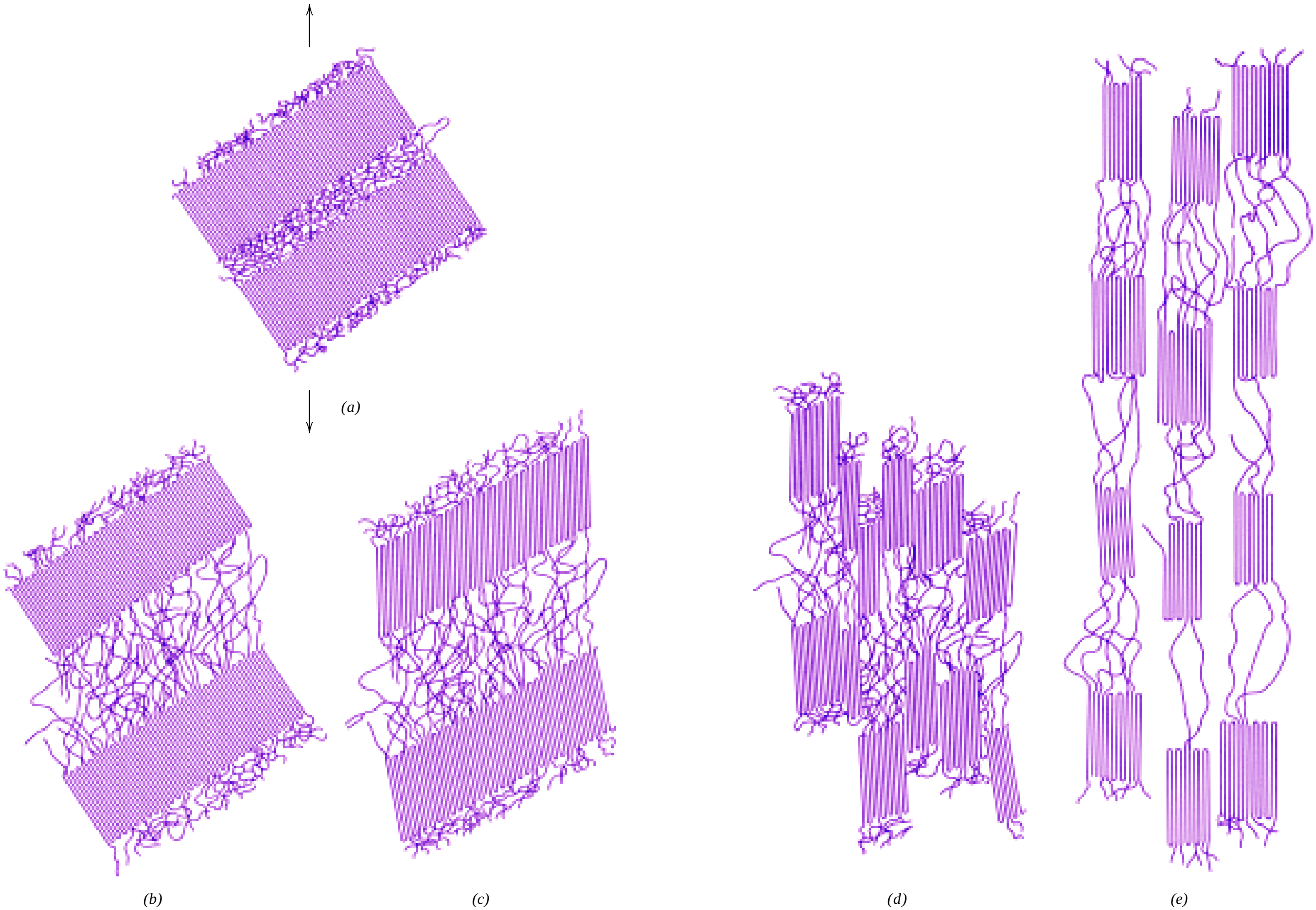

Figure 8.27 Stages in the deformation of a semicrystalline polymer. (*a*) Two adjacent chain-folded lamellae and interlamellar amorphous material before deformation. (*b*) Elongation of amorphous tie chains during the first stage of deformation. (*c*) Tilting of lamellar chain folds during the second stage. (*d*) Separation of crystalline block segments during the third stage. (*e*) Orientation of block segments and tie chains with the tensile axis in the final deformation stage. (From Jerold M. Schultz, *Polymer Materials Science*, copyright © 1974, pp. 500–501. Reprinted by permoission of Prentice-Hall, Inc., Englewood Cliffs, NJ.)

lar amorphous material, prior to deformation, are shown in Figure 8.27*a*. During the initial stage of deformation (Figure 8.27*b*) the chains in the amorphous regions slip past each other and align in the loading direction. This causes the lamellar ribbons simply to slide past one another as the tie chains within the amorphous regions become extended. Continued deformation in the second stage occurs by the tilting of the lamellae so that the chain folds become aligned with the tensile axis (Figure 8.27*c*). Next, crystalline block segments separate from the lamellae, which segments remain attached to one another by tie chains (Figure 8.27*d*). In the final stage (Figure 8.27*e*), the blocks and tie chains become oriented in the direction of the tensile axis. Thus appreciable tensile deformation of semicrystalline polymers produces a highly oriented structure. During deformation the spherulites experience shape changes for moderate levels of elongation. However, for large deformations, the spherulitic structure is virtually destroyed. Also, it is interesting to note that, to a large degree, the processes represented in Figure 8.27 are reversible. That is, if deformation is terminated at some arbitrary stage, and the specimen is heated to an elevated temperature near its melting point (i.e., annealed), the material will revert back to having the spherulitic structure that was characteristic of its undeformed state. Furthermore, the specimen will tend to shrink back to the shape it had prior to deformation; the extent of this shape and structural recovery will depend on the annealing temperature and also the degree of elongation.

8.18a FACTORS THAT INFLUENCE THE MECHANICAL PROPERTIES OF SEMICRYSTALLINE POLYMERS [DETAILED VERSION (CD-ROM)]

8.18b FACTORS THAT INFLUENCE THE MECHANICAL PROPERTIES OF SEMICRYSTALLINE POLYMERS (CONCISE VERSION)

A number of factors influence the mechanical characteristics of polymeric materials. For example, we have already discussed the effect of temperature and strain rate on stress–strain behavior (Section 7.13, Figure 7.24). Again, increasing the temperature or diminishing the strain rate leads to a decrease in the tensile modulus, a reduction in tensile strength, and an enhancement of ductility.

In addition, several structural/processing factors have decided influences on the mechanical behavior (i.e., strength and modulus) of polymeric materials. An increase in strength results whenever any restraint is imposed on the process illustrated in Figure 8.27; for example, a significant degree of intermolecular bonding or extensive chain entanglements inhibit relative chain motions. It should be noted that even though secondary intermolecular (e.g., van der Waals) bonds are much weaker than the primary covalent ones, significant intermolecular forces result from the formation of large numbers of van der Waals interchain bonds. Furthermore, the modulus rises as both the secondary bond strength and chain alignment increase. The mechanical behavior of polymers is affected by several structural/processing

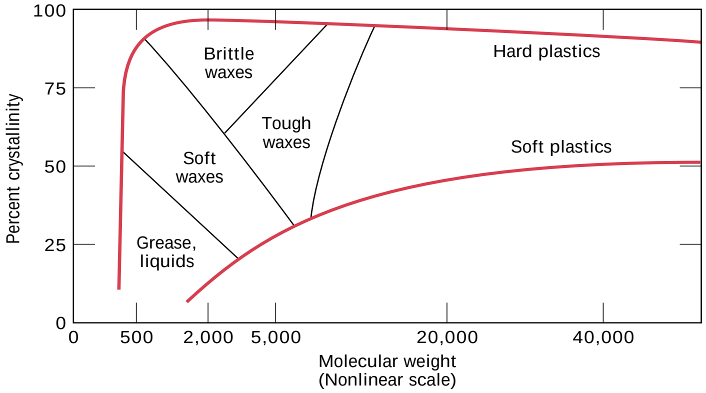

Figure 8.28 The influence of degree of crystallinity and molecular weight on the physical characteristics of polyethylene. (From R. B. Richards, ''Polyethylene—Structure, Crystallinity and Properties,'' *J. Appl. Chem.*, **1,** 370, 1951.)

factors that include molecular weight, degree of crystallinity, and predeformation (drawing).

The magnitude of the tensile modulus does not seem to be influenced by molecular weight alterations. On the other hand, for many polymers, it has been observed that tensile strength increases with increasing molecular weight.

For a specific polymer, the degree of crystallinity can have a rather significant influence on the mechanical properties, since it affects the extent of intermolecular secondary bonding. It has been observed that, for semicrystalline polymers, tensile modulus increases significantly with degree of crystallinity; in most cases, strength is also enhanced, and the material becomes more brittle. The influences of chain chemistry and structure (branching, stereoisomerism, etc.) on degree of crystallinity were discussed in Chapter 4.

The effects of both percent crystallinity and molecular weight on the physical state of polyethylene are represented in Figure 8.28.

On a commercial basis, one important technique that is used to improve mechanical strength and tensile modulus is permanently deforming the polymer in tension. This procedure, sometimes called *drawing,* produces the neck extension illustrated schematically in Figure 7.25. It is an important stiffening and strengthening technique that is employed in the production of fibers and films {(Section 14.15).} During drawing, the molecular chains slip past one another and become highly oriented; for semicrystalline materials the chains assume conformations similar to those represented schematically in Figure 8.27*e*. It should also be noted that the mechanical properties of drawn polymers are normally anisotropic.

8.19 DEFORMATION OF ELASTOMERS

One of the fascinating properties of the elastomeric materials is their rubberlike elasticity. That is, they have the ability to be deformed to quite large deformations, and then elastically spring back to their original form. This behavior was probably first observed in natural rubber; however, the past few years have brought about the synthesis of a large number of elastomers with a wide variety of properties. Typical stress–strain characteristics of elastomeric materials are displayed in Figure 7.22, curve *C*. Their moduli of elasticity are quite small and, furthermore, vary with strain since the stress–strain curve is nonlinear.

In an unstressed state, an elastomer will be amorphous and composed of molecular chains that are highly twisted, kinked, and coiled. Elastic deformation, upon application of a tensile load, is simply the partial uncoiling, untwisting, and straightening, and the resultant elongation of the chains in the stress direction, a phenomenon represented in Figure 8.29. Upon release of the stress, the chains spring back to their prestressed conformations, and the macroscopic piece returns to its original shape.

The driving force for elastic deformation is a thermodynamic parameter called *entropy*, which is a measure of the degree of disorder within a system; entropy increases with increasing disorder. As an elastomer is stretched and the chains straighten and become more aligned, the system becomes more ordered. From this state, the entropy increases if the chains return to their original kinked and coiled contours. Two intriguing phenomena result from this entropic effect. First, when stretched, an elastomer experiences a rise in temperature; second, the modulus of elasticity increases with increasing temperature, which is opposite to the behavior found in other materials (see Figure 7.8).

Several criteria must be met in order for a polymer to be elastomeric: (1) It must not easily crystallize; elastomeric materials are amorphous, having molecular chains that are naturally coiled and kinked in the unstressed state. (2) Chain bond rotations must be relatively free in order for the coiled chains to readily respond to an applied force. (3) For elastomers to experience relatively large elastic deformations, the onset of plastic deformation must be delayed. Restricting the motions of chains past one another by crosslinking accomplishes this objective. The crosslinks act as anchor points between the chains and prevent chain slippage from occurring; the role of crosslinks in the deformation process is illustrated in Figure 8.29. Crosslinking in many elastomers is carried out in a process called vulcanization, as discussed below. (4) Finally, the elastomer must be above its glass transition temperature (Section 11.16). The lowest temperature at which rubberlike behavior persists for many of the common elastomers is between −50 and −90°C (−60 and −130°F). Below its glass transition temperature, an elastomer becomes brittle such that its stress–strain behavior resembles curve *A* in Figure 7.22.

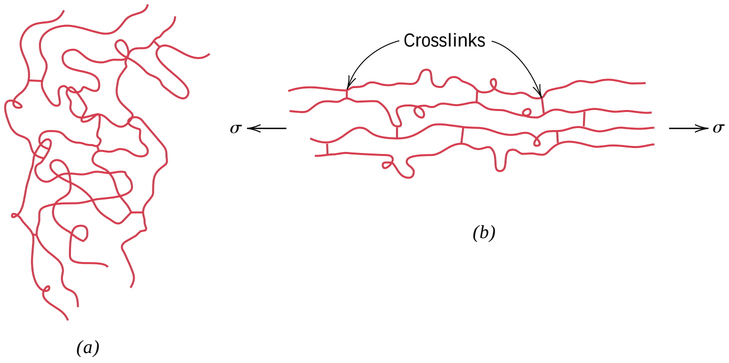

Figure 8.29 Schematic representation of crosslinked polymer chain molecules (*a*) in an unstressed state and (*b*) during elastic deformation in response to an applied tensile stress. (Adapted from Z. D. Jastrzebski, *The Nature and Properties of Engineering Materials*, 3rd edition. Copyright © 1987 by John Wiley & Sons, New York. Reprinted by permission of John Wiley & Sons, Inc.)

VULCANIZATION

The crosslinking process in elastomers is called **vulcanization,** which is achieved by a nonreversible chemical reaction, ordinarily carried out at an elevated temperature. In most vulcanizing reactions, sulfur compounds are added to the heated elastomer; chains of sulfur atoms bond with adjacent polymer backbone chains and crosslink them, which is accomplished according to the following reaction:

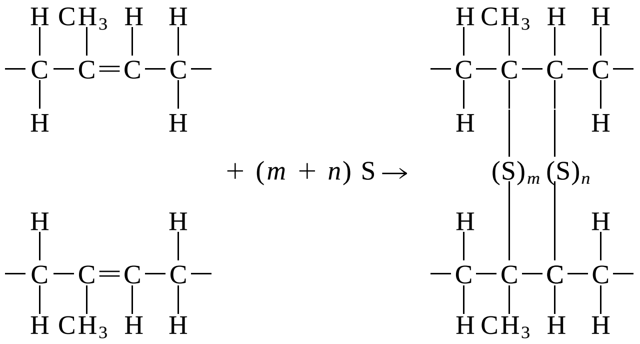

$$\begin{array}{ccc}
-\underset{\mathrm{H}}{\overset{\mathrm{H}}{\mathrm{C}}}-\overset{\mathrm{CH_3}}{\mathrm{C}}=\overset{\mathrm{H}}{\mathrm{C}}-\underset{\mathrm{H}}{\overset{\mathrm{H}}{\mathrm{C}}}- & & -\underset{\mathrm{H}}{\overset{\mathrm{H}}{\mathrm{C}}}-\overset{\mathrm{CH_3}}{\mathrm{C}}-\overset{\mathrm{H}}{\mathrm{C}}-\underset{\mathrm{H}}{\overset{\mathrm{H}}{\mathrm{C}}}- \\
 & +\ (m+n)\ \mathrm{S} \rightarrow & \qquad (\mathrm{S})_m\ (\mathrm{S})_n \\
-\underset{\mathrm{H}}{\overset{\mathrm{H}}{\mathrm{C}}}-\underset{\mathrm{CH_3}}{\mathrm{C}}=\underset{\mathrm{H}}{\mathrm{C}}-\underset{\mathrm{H}}{\overset{\mathrm{H}}{\mathrm{C}}}- & & -\underset{\mathrm{H}}{\overset{\mathrm{H}}{\mathrm{C}}}-\underset{\mathrm{CH_3}}{\mathrm{C}}-\underset{\mathrm{H}}{\mathrm{C}}-\underset{\mathrm{H}}{\overset{\mathrm{H}}{\mathrm{C}}}-
\end{array} \qquad (8.10)$$

in which the two crosslinks shown consist of m and n sulfur atoms. Crosslink main chain sites are carbon atoms that were doubly bonded before vulcanization, but, after vulcanization, have become singly bonded.

Unvulcanized rubber is soft and tacky, and has poor resistance to abrasion. Modulus of elasticity, tensile strength, and resistance to degradation by oxidation are all enhanced by vulcanization. The magnitude of the modulus of elasticity is directly proportional to the density of the crosslinks. Stress–strain curves for vulcanized and unvulcanized natural rubber are presented in Figure 8.30. To produce a rubber that is capable of large extensions without rupture of the primary chain bonds, there must be relatively few crosslinks, and these must be widely separated. Useful rubbers result when about 1 to 5 parts (by weight) of sulfur is added to 100 parts of rubber. Increasing the sulfur content further hardens the rubber and also reduces its extensibility. Also, since they are crosslinked, elastomeric materials are thermosetting in nature.

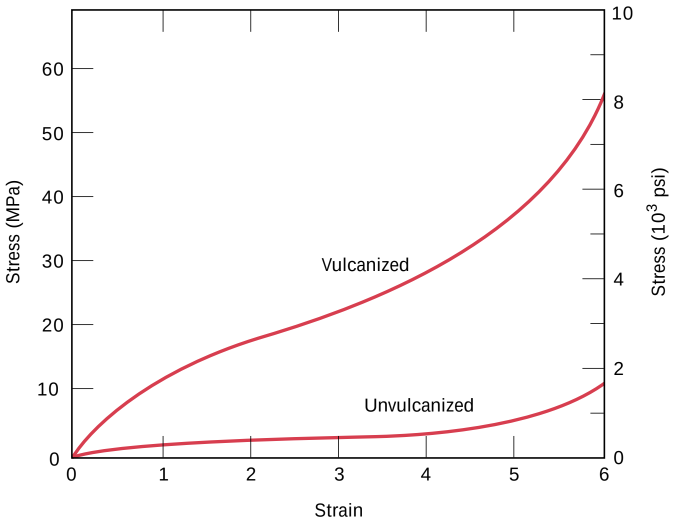

FIGURE 8.30 Stress–strain curves to 600% elongation for unvulcanized and vulcanized natural rubber.

SUMMARY

On a microscopic level, plastic deformation of metals corresponds to the motion of dislocations in response to an externally applied shear stress, a process termed ''slip.'' Slip occurs on specific crystallographic planes and within these planes only in certain directions. A slip system represents a slip plane–slip direction combination, and operable slip systems depend on the crystal structure of the material.

{The critical resolved shear stress is the minimum shear stress required to initiate dislocation motion; the yield strength of a metal single crystal depends on both the magnitude of the critical resolved shear stress and the orientation of slip components relative to the direction of the applied stress.}

For polycrystalline metals, slip occurs within each grain along the slip systems that are most favorably oriented with the applied stress; furthermore, during deformation, grains change shape in such a manner that coherency at the grain boundaries is maintained.

{Under some circumstances limited plastic deformation may occur in BCC and HCP metals by mechanical twinning. Normally, twinning is important to the degree that accompanying crystallographic reorientations make the slip process more favorable.}

Since the ease with which a metal is capable of plastic deformation is a function of dislocation mobility, restricting dislocation motion increases hardness and strength. On the basis of this principle, three different strengthening mechanisms were discussed. Grain boundaries serve as barriers to dislocation motion; thus refining the grain size of a polycrystalline metal renders it harder and stronger. Solid solution strengthening results from lattice strain interactions between impurity atoms and dislocations. And, finally, as a metal is plastically deformed, the dislocation density increases, as does also the extent of repulsive dislocation–dislocation strain field interactions; strain hardening is just the enhancement of strength with increased plastic deformation.

The microstructural and mechanical characteristics of a plastically deformed metal specimen may be restored to their predeformed states by an appropriate heat treatment, during which recovery, recrystallization, and grain growth processes are allowed to occur. During recovery there is a reduction in dislocation density and alterations in dislocation configurations. Recrystallization is the formation of a new set of grains that are strain free; in addition, the material becomes softer and more ductile. Grain growth is the increase in average grain size of polycrystalline materials, which proceeds by grain boundary motion.

Any plastic deformation of crystalline ceramics is a result of dislocation motion; the brittleness of these materials is, in part, explained by the limited number of operable slip systems. The mode of plastic deformation for noncrystalline materials is by viscous flow; a material's resistance to deformation is expressed as viscosity. At room temperature, the viscosity of many noncrystalline ceramics is extremely high.

During the elastic deformation of a semicrystalline polymer that is stressed in tension, the constituent molecules elongate in the stress direction by the bending and stretching of covalent chain bonds. Slight molecular displacements are resisted by weak secondary bonds.

The mechanism of plastic deformation for semicrystalline polymers having the spherulitic structure was presented. Tensile deformation is thought to occur in several stages as both amorphous tie chains and chain-folded block segments (which separate from the ribbonlike lamellae) become oriented with the tensile axis. Also, during deformation the shapes of spherulites are altered (for moderate deformations); relatively large degrees of deformation lead to a complete destruction of the spherulites. Furthermore, the predeformed spherulitic structure and macroscopic shape may be virtually restored by annealing at an elevated temperature below the polymer's melting temperature.

The mechanical behavior of a polymer will be influenced by both inservice and structural/processing factors. With regard to the former, increasing the temperature and/or diminishing the strain rate leads to reductions in tensile modulus and tensile strength, and an enhancement of ductility. In addition, other factors that affect the mechanical properties include molecular weight, degree of crystallinity, predeformation drawing, and heat treating. The influence of each of these factors was discussed.

Large elastic extensions are possible for the elastomeric materials that are amorphous and lightly crosslinked. Deformation corresponds to the unkinking and uncoiling of chains in response to an applied tensile stress. Crosslinking is often achieved during a vulcanization process.

IMPORTANT TERMS AND CONCEPTS

Cold working
Critical resolved shear stress
Dislocation density
Grain growth
Lattice strain
Recovery
Recrystallization
Recrystallization temperature
Resolved shear stress
Slip
Slip system
Solid-solution strengthening
Strain hardening
Viscosity
Vulcanization

REFERENCES

Hirth, J. P. and J. Lothe, *Theory of Dislocations,* 2nd edition, Wiley-Interscience, New York, 1982. Reprinted by Krieger Publishing Company, Melbourne, FL, 1992.

Hull, D., *Introduction to Dislocations,* 3rd edition, Pergamon Press, Inc., Elmsford, NY, 1984.

Kingery, W. D., H. K. Bowen, and D. R. Uhlmann, *Introduction to Ceramics,* 2nd edition, John Wiley & Sons, New York, 1976. Chapter 14.

Read, W. T., Jr., *Dislocations in Crystals,* McGraw-Hill Book Company, New York, 1953.

Richerson, D. W., *Modern Ceramic Engineering,* 2nd edition, Marcel Dekker, New York, 1992. Chapter 5.

Schultz, J., *Polymer Materials Science,* Prentice-Hall, Englewood Cliffs, NJ, 1974.

Weertman, J. and J. R. Weertman, *Elementary Dislocation Theory,* The Macmillan Co., New York, 1964. Reprinted by Oxford University Press, Oxford, 1992.

QUESTIONS AND PROBLEMS

Note: To solve those problems having an asterisk (*) by their numbers, consultation of supplementary topics [appearing only on the CD-ROM (and not in print)] will probably be necessary.

8.1 To provide some perspective on the dimensions of atomic defects, consider a metal specimen that has a dislocation density of 10^4 mm^{-2}. Suppose that all the dislocations in 1000 mm^3 (1 cm^3) were somehow removed and linked end to end. How far (in miles) would this chain extend? Now suppose that the density is increased to 10^{10} mm^{-2} by cold working. What would be the chain length of dislocations in 1000 mm^3 of material?

8.2 Consider two edge dislocations of opposite sign and having slip planes that are separated by several atomic distances as indicated in the diagram. Briefly describe the defect that results when these two dislocations become aligned with each other.

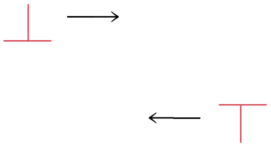

8.3 Is it possible for two screw dislocations of opposite sign to annihilate each other? Explain your answer.

8.4 For each of edge, screw, and mixed dislocations, cite the relationship between the direction of the applied shear stress and the direction of dislocation line motion.

8.5 **(a)** Define a slip system.

(b) Do all metals have the same slip system? Why or why not?

8.6* **(a)** Compare planar densities (Section 3.14) for the (100), (110), and (111) planes for FCC.

(b) Compare planar densities for the (100), (110), and (111) planes for BCC.

8.7 One slip system for the BCC crystal structure is $\{110\}\langle 111\rangle$. In a manner similar to Figure 8.6*b* sketch a {110}-type plane for the BCC structure, representing atom positions with circles. Now, using arrows, indicate two different $\langle 111\rangle$ slip directions within this plane.

8.8 One slip system for the HCP crystal structure is $\{0001\}\langle 11\bar{2}0\rangle$. In a manner similar to Figure 8.6*b*, sketch a {0001}-type plane for the HCP structure, and using arrows, indicate three different $\langle 11\bar{2}0\rangle$ slip directions within this plane. You might find Figure 3.22 helpful.

8.9* Explain the difference between resolved shear stress and critical resolved shear stress.

8.10* Sometimes $\cos\phi \cos\lambda$ in Equation 8.1 is termed the *Schmid factor*. Determine the magnitude of the Schmid factor for an FCC single crystal oriented with its [100] direction parallel to the loading axis.

8.11* Consider a metal single crystal oriented such that the normal to the slip plane and the slip direction are at angles of 43.1° and 47.9°, respectively, with the tensile axis. If the critical resolved shear stress is 20.7 MPa (3000 psi), will an applied stress of 45 MPa (6500 psi) cause the single crystal to yield? If not, what stress will be necessary?

8.12* A single crystal of aluminum is oriented for a tensile test such that its slip plane normal makes an angle of 28.1° with the tensile axis. Three possible slip directions make angles of 62.4°, 72.0°, and 81.1° with the same tensile axis.

(a) Which of these three slip directions is most favored?

(b) If plastic deformation begins at a tensile stress of 1.95 MPa (280 psi), determine the critical resolved shear stress for aluminum.

8.13* Consider a single crystal of silver oriented such that a tensile stress is applied along a [001] direction. If slip occurs on a (111) plane and in a $[\bar{1}01]$ direction, and is initiated at an applied tensile stress of 1.1 MPa (160 psi), compute the critical resolved shear stress.

8.14* The critical resolved shear stress for iron is 27 MPa (4000 psi). Determine the maximum possible yield strength for a single crystal of Fe pulled in tension.

8.15* List four major differences between deformation by twinning and deformation by slip relative to mechanism, conditions of occurrence, and final result.

8.16 Briefly explain why small-angle grain boundaries are not as effective in interfering with the slip process as are high-angle grain boundaries.

8.17 Briefly explain why HCP metals are typically more brittle than FCC and BCC metals.

8.18 Describe in your own words the three strengthening mechanisms discussed in this chapter (i.e., grain size reduction, solid solution strengthening, and strain hardening). Be sure to explain how dislocations are involved in each of the strengthening techniques.

8.19 **(a)** From the plot of yield strength versus (grain diameter)$^{-1/2}$ for a 70 Cu–30 Zn cartridge brass, Figure 8.15, determine values for the constants σ_0 and k_y in Equation 8.5.

(b) Now predict the yield strength of this alloy when the average grain diameter is 1.0×10^{-3} mm.

8.20 The lower yield point for an iron that has an average grain diameter of 5×10^{-2} mm is 135 MPa (19,500 psi). At a grain diameter of 8×10^{-3} mm, the yield point increases to 260 MPa (37,500 psi). At what grain diameter will the lower yield point be 205 MPa (30,000 psi)?

8.21 If it is assumed that the plot in Figure 8.15 is for noncold-worked brass, determine the grain size of the alloy in Figure 8.19; assume its composition is the same as the alloy in Figure 8.15.

8.22 In the manner of Figures 8.17*b* and 8.18*b* indicate the location in the vicinity of an edge dislocation at which an interstitial impurity atom would be expected to be situated. Now briefly explain in terms of lattice strains why it would be situated at this position.

8.23 When making hardness measurements, what will be the effect of making an indentation very close to a preexisting indentation? Why?

8.24 **(a)** Show, for a tensile test, that

$$\%\text{CW} = \left(\frac{\epsilon}{\epsilon + 1}\right) \times 100$$

if there is no change in specimen volume during the deformation process (i.e., $A_0 l_0 = A_d l_d$).

(b) Using the result of part a, compute the percent cold work experienced by naval brass (the stress–strain behavior of which is shown in Figure 7.12) when a stress of 400 MPa (58,000 psi) is applied.

8.25 Two previously undeformed cylindrical specimens of an alloy are to be strain hardened by reducing their cross-sectional areas (while maintaining their circular cross sections). For one specimen, the initial and deformed radii are 16 mm and 11 mm, respectively. The second specimen, with an initial radius of 12 mm, must have the same deformed hardness as the first specimen; compute the second specimen's radius after deformation.

8.26 Two previously undeformed specimens of the same metal are to be plastically deformed by reducing their cross-sectional areas. One has a circular cross section, and the other is rectangular; during deformation the circular cross section is to remain circular, and the rectangular is to remain as such. Their original and deformed dimensions are as follows:

	Circular (diameter, mm)	***Rectangular (mm)***
Original dimensions	15.2	125 × 175
Deformed dimensions	11.4	75 × 200

Which of these specimens will be the hardest after plastic deformation, and why?

8.27 A cylindrical specimen of cold-worked copper has a ductility (%EL) of 25%. If its cold-worked radius is 10 mm (0.40 in.), what was its radius before deformation?

8.28 **(a)** What is the approximate ductility (%EL) of a brass that has a yield strength of 275 MPa (40,000 psi)?

(b) What is the approximate Brinell hardness of a 1040 steel having a yield strength of 690 MPa (100,000 psi)?

8.29 Experimentally, it has been observed for single crystals of a number of metals that the critical resolved shear stress τ_{crss} is a function of the dislocation density ρ_D as

$$\tau_{\text{crss}} = \tau_0 + A\sqrt{\rho_D}$$

where τ_0 and A are constants. For copper, the critical resolved shear stress is 2.10 MPa (305 psi) at a dislocation density of 10^5 mm^{-2}. If it is known that the value of A for copper is 6.35×10^{-3} MPa-mm (0.92 psi-mm), compute the τ_{crss} at a dislocation density of 10^7 mm^{-2}.

8.30 Briefly cite the differences between recovery and recrystallization processes.

8.31 Estimate the fraction of recrystallization from the photomicrograph in Figure 8.21*c*.

8.32 Explain the differences in grain structure for a metal that has been cold worked and one that has been cold worked and then recrystallized.

8.33 Briefly explain why some metals (e.g., lead and tin) do not strain harden when deformed at room temperature.

8.34 **(a)** What is the driving force for recrystallization?

(b) For grain growth?

8.35 **(a)** From Figure 8.25, compute the length of time required for the average grain diameter to increase from 0.01 to 0.1 mm at 500°C for this brass material.

(b) Repeat the calculation at 600°C.

8.36 The average grain diameter for a brass material was measured as a function of time at 650°C, which is tabulated below at two different times:

Time (min)	*Grain Diameter (mm)*
30	3.9×10^{-2}
90	6.6×10^{-2}

(a) What was the original grain diameter?

(b) What grain diameter would you predict after 150 min at 650°C?

8.37 An undeformed specimen of some alloy has an average grain diameter of 0.040 mm. You are asked to reduce its average grain diameter to 0.010 mm. Is this possible? If so, explain the procedures you would use and name the processes involved. If it is not possible, explain why.

8.38 Grain growth is strongly dependent on temperature (i.e., rate of grain growth increases with increasing temperature), yet temperature is not explicitly given as a part of Equation 8.7.

(a) Into which of the parameters in this expression would you expect temperature to be included?

(b) On the basis of your intuition, cite an explicit expression for this temperature dependence.

8.39 An uncold-worked brass specimen of average grain size 0.008 mm has a yield strength of 160 MPa (23,500 psi). Estimate the yield strength of this alloy after it has been heated to 600°C for 1000 s, if it is known that the value of k_y is 12.0 MPa-mm$^{1/2}$ (1740 psi-mm$^{1/2}$).

8.40 Cite one reason why ceramic materials are, in general, harder yet more brittle than metals.

8.41 In your own words, describe the mechanisms by which semicrystalline polymers **(a)** elastically deform and **(b)** plastically deform, and **(c)** by which elastomers elastically deform.

8.42 Briefly explain how each of the following influences the tensile modulus of a semicrystalline polymer and why:

(a) molecular weight;

(b) degree of crystallinity;

(c) deformation by drawing;

(d) annealing of an undeformed material;

(e) annealing of a drawn material.

8.43* Briefly explain how each of the following influences the tensile or yield strength of a semicrystalline polymer and why:

(a) molecular weight;

(b) degree of crystallinity;

(c) deformation by drawing;

(d) annealing of an undeformed material.

8.44 Normal butane and isobutane have boiling temperatures of −0.5 and −12.3°C (31.1 and 9.9°F), respectively. Briefly explain this behavior on the basis of their molecular structures, as presented in Section 4.2.

8.45* The tensile strength and number-average molecular weight for two polymethyl methacrylate materials are as follows:

Tensile Strength (MPa)	*Number Average Molecular Weight (g/mol)*
107	40,000
170	60,000

Estimate the tensile strength at a number-average molecular weight of 30,000 g/mol.

8.46* The tensile strength and number-average molecular weight for two polyethylene materials are as follows:

Tensile Strength (MPa)	*Number Average Molecular Weight (g/mol)*
85	12,700
150	28,500

Estimate the number-average molecular weight that is required to give a tensile strength of 195 MPa.

8.47* For each of the following pairs of polymers, do the following: (1) state whether or not it is possible to decide if one polymer has a higher tensile modulus than the other; (2) if this is possible, note which has the higher tensile modulus and then cite the reason(s) for your choice; and (3) if it is not possible to decide, then state why.

(a) Syndiotactic polystyrene having a number-average molecular weight of 400,000 g/mol; isotactic polystyrene having a number-average molecular weight of 650,000 g/mol.

(b) Branched and atactic polyvinyl chloride with a weight-average molecular weight of 100,000 g/mol; linear and isotactic polyvinyl chloride having a weight-average molecular weight of 75,000 g/mol.

(c) Random styrene-butadiene copolymer with 5% of possible sites crosslinked; block styrene-butadiene copolymer with 10% of possible sites crosslinked.

(d) Branched polyethylene with a number-average molecular weight of 100,000 g/mol; atactic polypropylene with a number-average molecular weight of 150,000 g/mol.

8.48* For each of the following pairs of polymers, do the following: (1) state whether or not it is possible to decide if one polymer has a higher tensile strength than the other; (2) if this is possible, note which has the higher tensile strengh and then cite the reason(s) for your choice; and (3) if it is not possible to decide, then state why.

(a) Syndiotactic polystyrene having a number-average molecular weight of 600,000 g/mol; isotactic polystyrene having a number-average molecular weight of 500,000 g/mol.

(b) Linear and isotactic polyvinyl chloride with a weight-average molecular weight of 100,000 g/mol; branched and atactic polyvinyl chloride having a weight-average molecular weight of 75,000 g/mol.

(c) Graft acrylonitrile-butadiene copolymer with 10% of possible sites crosslinked; alternating acrylonitrile-butadiene copolymer with 5% of possible sites crosslinked.

(d) Network polyester; lightly branched polytetrafluoroethylene.

8.49 Would you expect the tensile strength of polychlorotrifluoroethylene to be greater than, the same as, or less than that of a polytetrafluoroethylene specimen having the same molecular weight and degree of crystallinity? Why?

8.50* For each of the following pairs of polymers, plot and label schematic stress–strain curves on the same graph (i.e., make separate plots for parts a, b, c, and d).

(a) Isotactic and linear polypropylene having a weight-average molecular weight of 120,000 g/mol; atactic and linear polypropylene having a weight-average molecular weight of 100,000 g/mol.

(b) Branched polyvinyl chloride having a number-average degree of polymerization of 2000; heavily crosslinked polyvinyl chloride having a number-average degree of polymerization of 2000.

(c) Poly(styrene-butadiene) random copolymer having a number-average molecular weight of 100,000 g/mol and 10% of the available sites crosslinked and tested at 20°C; poly(styrene-butadiene) random copolymer having a number-average molecular weight of 120,000 g/mol and 15% of the available sites crosslinked and tested at −85°C. *Hint:* poly(styrene-butadiene) copolymers may exhibit elastomeric behavior.

(d) Polyisoprene, molecular weight of 100,000 g/mol having 10% of available sites crosslinked; polyisoprene, molecular weight of 100,000 g/mol having 20% of available sites crosslinked. *Hint:* polyisoprene is a natural rubber that may display elastomeric behavior.

8.51 List the two molecular characteristics that are essential for elastomers.

8.52 Which of the following would you expect to be elastomers and which thermosetting polymers at room temperature? Justify each choice.

(a) Epoxy having a network structure.

(b) Lightly crosslinked poly(styrene-butadiene) random copolymer that has a glass-transition temperature of −50°C.

(c) Lightly branched and semicrystalline polytetrafluoroethylene that has a glass-transition temperature of −100°C.

(d) Heavily crosslinked poly(ethylene-propylene) random copolymer that has a glass-transition temperature of 0°C.

(e) Thermoplastic elastomer that has a glass-transition temperature of 75°C.

8.53 In terms of molecular structure, explain why phenol-formaldehyde (Bakelite) will not be an elastomer.

8.54 Ten kilograms of polybutadiene is vulcanized with 4.8 kg sulfur. What fraction of the possible crosslink sites is bonded to sulfur crosslinks, assuming that, on the average, 4.5 sulfur atoms participate in each crosslink?

8.55 Compute the weight percent sulfur that must be added to completely crosslink an alternating chloroprene-acrylonitrile copolymer, assuming that five sulfur atoms participate in each crosslink.

8.56 The vulcanization of polyisoprene is accomplished with sulfur atoms according to Equation 8.10. If 57 wt% sulfur is combined with polyisoprene, how many crosslinks will be associated with each isoprene mer if it is assumed that, on the average, six sulfur atoms participate in each crosslink?

8.57 For the vulcanization of polyisoprene, compute the weight percent of sulfur that must be added to ensure that 8% of possible sites will be crosslinked; assume that, on the average, three sulfur atoms are associated with each crosslink.

8.58 Demonstrate, in a manner similar to Equation 8.10, how vulcanization may occur in a chloroprene rubber.

Design Problems

8.D1 Determine whether or not it is possible to cold work steel so as to give a minimum Brinell hardness of 225 and at the same time have a ductility of at least 12%EL. Justify your decision.

8.D2 Determine whether or not it is possible to cold work brass so as to give a minimum Brinell hardness of 120 and at the same time have a ductility of at least 20%EL. Justify your decision.

8.D3 A cylindrical specimen of cold-worked steel has a Brinell hardness of 250.

(a) Estimate its ductility in percent elongation.

(b) If the specimen remained cylindrical during deformation and its uncold-worked radius was 5 mm (0.20 in.), determine its radius after deformation.

8.D4 It is necessary to select a metal alloy for an application that requires a yield strength of at least 345 MPa (50,000 psi) while maintaining a minimum ductility (%EL) of 20%. If the metal may be cold worked, decide which of the following are candidates: copper, brass, and a 1040 steel. Why?

8.D5 A cylindrical rod of 1040 steel originally 15.2 mm (0.60 in.) in diameter is to be cold worked by drawing; the circular cross section will be maintained during deformation. A cold-worked tensile strength in excess of 840 MPa (122,000 psi) and a ductility of at least 12%EL are desired. Furthermore, the final diameter must be 10 mm (0.40 in.). Explain how this may be accomplished.

8.D6 A cylindrical rod of copper originally 16.0 mm (0.625 in.) in diameter is to be cold worked by drawing; the circular cross section will be maintained during deformation. A cold-worked yield strength in excess of 250 MPa (36,250 psi) and a ductility of at least 12%EL are desired. Furthermore, the final diameter must be 11.3 mm (0.445 in.). Explain how this may be accomplished.

8.D7 A cylindrical 1040 steel rod having a minimum tensile strength of 865 MPa (125,000 psi), a ductility of at least 10%EL, and a final diameter of 6.0 mm (0.25 in.) is desired. Some 7.94 mm (0.313 in.) diameter 1040 steel stock, which has been cold worked 20%, is available. Describe the procedure you would follow to obtain this material. Assume that 1040 steel experiences cracking at 40%CW.

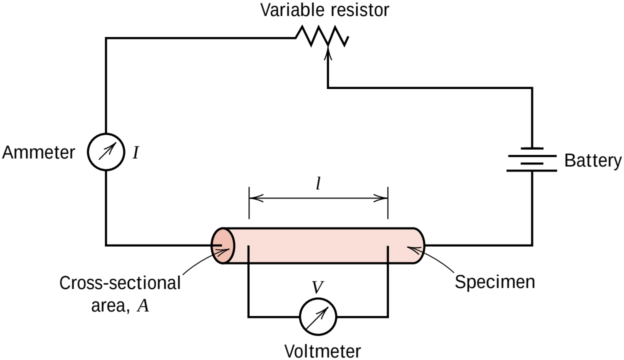
Variable resistor
Ammeter
I
Battery
l
V
Cross-sectional area, A
Specimen
Voltmeter

Figure 12.1 Schematic representation of the apparatus used to measure electrical resistivity.

FIGURE 12.2 Schematic plot of electron energy versus interatomic separation for an aggregate of 12 atoms ($N = 12$). Upon close approach, each of the 1*s* and 2*s* atomic states splits to form an electron energy band consisting of 12 states.

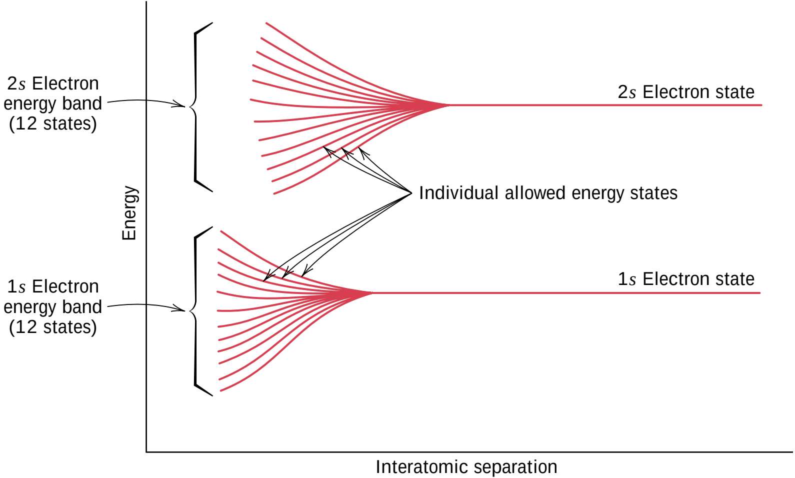
2*s* Electron energy band (12 states)
2*s* Electron state
Individual allowed energy states
Energy
1*s* Electron energy band (12 states)
1*s* Electron state
Interatomic separation

Chapter 2 / Atomic Structure and Interatomic Bonding

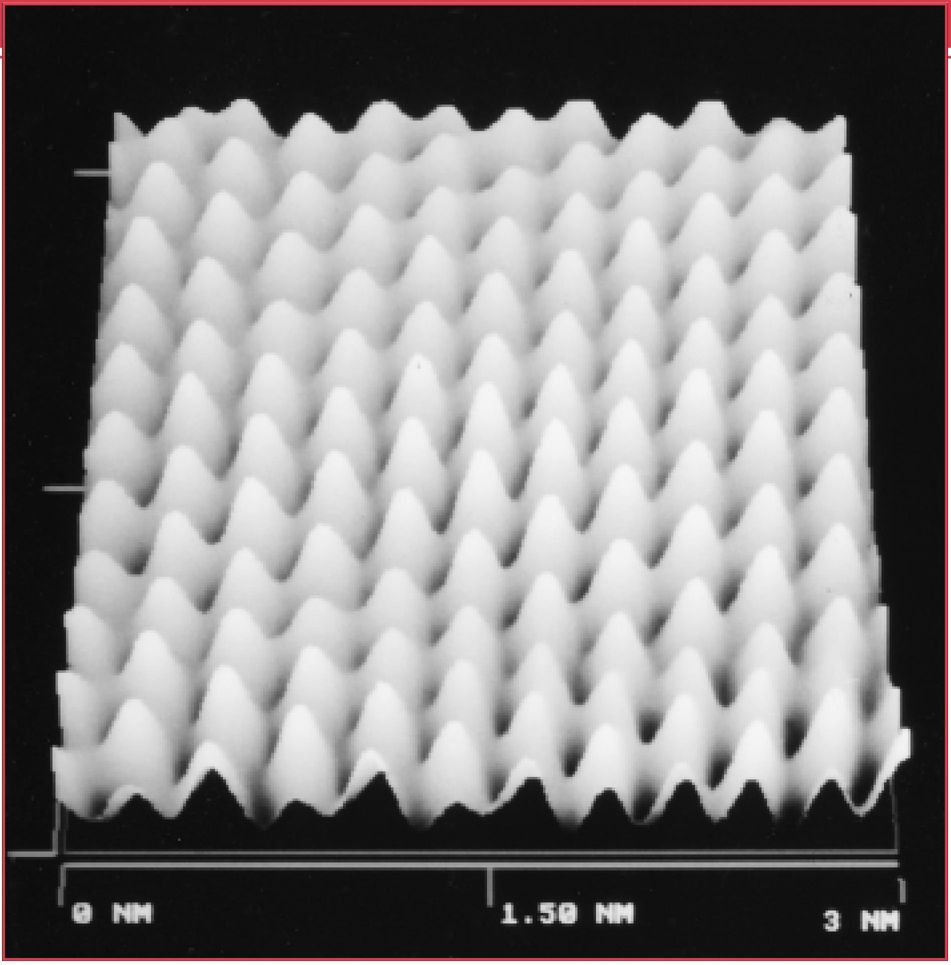

This micrograph, which represents the surface of a gold specimen, was taken with a sophisticated atomic force microscope (AFM). Individual atoms for this (111) crystallographic surface plane are resolved. Also note the dimensional scale (in the nanometer range) below the micrograph. (Image courtesy of Dr. Michael Green, TopoMetrix Corporation.)

Why Study *Atomic Structure and Interatomic Bonding?*

An important reason to have an understanding of interatomic bonding in solids is that, in some instances, the type of bond allows us to explain a material's properties. For example, consider carbon, which may exist as both graphite and diamond. Whereas graphite is relatively soft and has a "greasy" feel to it, diamond is the hardest known material. This dramatic disparity in properties is directly attributable to a type of interatomic bonding found in graphite that does not exist in diamond (see Section 3.9).

Learning Objectives

After careful study of this chapter you should be able to do the following:

1. **Name the two atomic models cited, and note the differences between them.**
2. **Describe the important quantum-mechanical principle that relates to electron energies.**
3. **(a) Schematically plot attractive, repulsive, and net energies versus interatomic separation for two atoms or ions.**
   (b) Note on this plot the equilibrium separation and the bonding energy.
4. **(a) Briefly describe ionic, covalent, metallic, hydrogen, and van der Waals bonds.**
   (b) Note what materials exhibit each of these bonding types.

2.1 INTRODUCTION

Some of the important properties of solid materials depend on geometrical atomic arrangements, and also the interactions that exist among constituent atoms or molecules. This chapter, by way of preparation for subsequent discussions, considers several fundamental and important concepts, namely: atomic structure, electron configurations in atoms and the periodic table, and the various types of primary and secondary interatomic bonds that hold together the atoms comprising a solid. These topics are reviewed briefly, under the assumption that some of the material is familiar to the reader.

ATOMIC STRUCTURE

2.2 FUNDAMENTAL CONCEPTS

Each atom consists of a very small nucleus composed of protons and neutrons, which is encircled by moving electrons. Both electrons and protons are electrically charged, the charge magnitude being 1.60×10^{-19} C, which is negative in sign for electrons and positive for protons; neutrons are electrically neutral. Masses for these subatomic particles are infinitesimally small; protons and neutrons have approximately the same mass, 1.67×10^{-27} kg, which is significantly larger than that of an electron, 9.11×10^{-31} kg.

Each chemical element is characterized by the number of protons in the nucleus, or the **atomic number** (Z).[1] For an electrically neutral or complete atom, the atomic number also equals the number of electrons. This atomic number ranges in integral units from 1 for hydrogen to 92 for uranium, the highest of the naturally occurring elements.

The *atomic mass* (A) of a specific atom may be expressed as the sum of the masses of protons and neutrons within the nucleus. Although the number of protons is the same for all atoms of a given element, the number of neutrons (N) may be variable. Thus atoms of some elements have two or more different atomic masses, which are called **isotopes.** The **atomic weight** of an element corresponds to the weighted average of the atomic masses of the atom's naturally occurring isotopes.[2] The **atomic mass unit (amu)** may be used for computations of atomic weight. A scale has been established whereby 1 amu is defined as $\frac{1}{12}$ of the atomic mass of the most common isotope of carbon, carbon 12 (^{12}C) ($A = 12.00000$). Within this scheme, the masses of protons and neutrons are slightly greater than unity, and

---

[1] Terms appearing in boldface type are defined in the Glossary, which follows Appendix E.

[2] The term "atomic mass" is really more accurate than "atomic weight" inasmuch as, in this context, we are dealing with masses and not weights. However, atomic weight is, by convention, the preferred terminology, and will be used throughout this book. The reader should note that it is *not* necessary to divide molecular weight by the gravitational constant.

$$A \cong Z + N \tag{2.1}$$

The atomic weight of an element or the molecular weight of a compound may be specified on the basis of amu per atom (molecule) or mass per mole of material. In one **mole** of a substance there are 6.023×10^{23} (Avogadro's number) atoms or molecules. These two atomic weight schemes are related through the following equation:

$$1 \text{ amu/atom (or molecule)} = 1 \text{ g/mol}$$

For example, the atomic weight of iron is 55.85 amu/atom, or 55.85 g/mol. Sometimes use of amu per atom or molecule is convenient; on other occasions g (or kg)/mol is preferred; the latter is used in this book.

2.3 ELECTRONS IN ATOMS

ATOMIC MODELS

During the latter part of the nineteenth century it was realized that many phenomena involving electrons in solids could not be explained in terms of classical mechanics. What followed was the establishment of a set of principles and laws that govern systems of atomic and subatomic entities that came to be known as **quantum mechanics.** An understanding of the behavior of electrons in atoms and crystalline solids necessarily involves the discussion of quantum-mechanical concepts. However, a detailed exploration of these principles is beyond the scope of this book, and only a very superficial and simplified treatment is given.

One early outgrowth of quantum mechanics was the simplified **Bohr atomic model,** in which electrons are assumed to revolve around the atomic nucleus in discrete orbitals, and the position of any particular electron is more or less well defined in terms of its orbital. This model of the atom is represented in Figure 2.1.

Another important quantum-mechanical principle stipulates that the energies of electrons are quantized; that is, electrons are permitted to have only specific values of energy. An electron may change energy, but in doing so it must make a quantum jump either to an allowed higher energy (with absorption of energy) or to a lower energy (with emission of energy). Often, it is convenient to think of these allowed electron energies as being associated with *energy levels* or *states.*

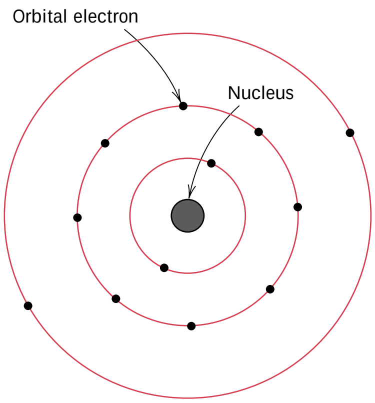

FIGURE 2.1 Schematic representation of the Bohr atom.

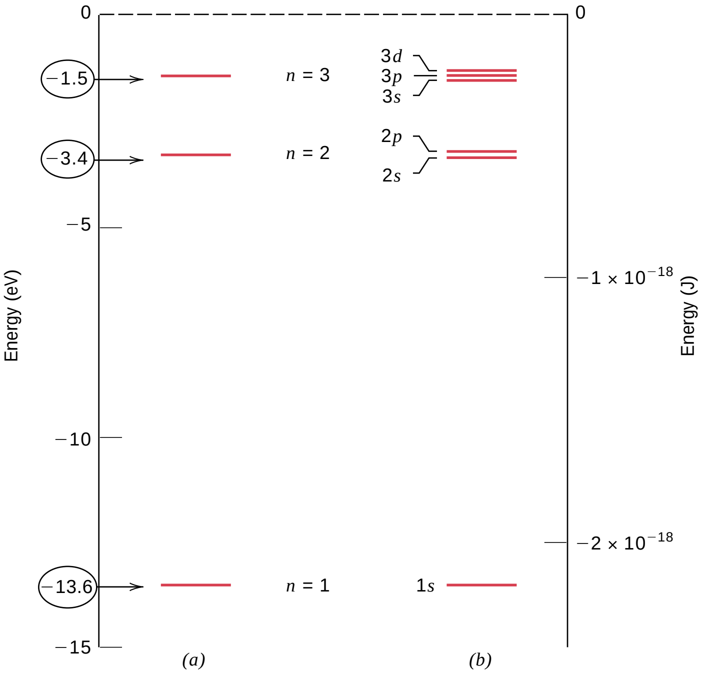

Figure 2.2 (*a*) The first three electron energy states for the Bohr hydrogen atom. (*b*) Electron energy states for the first three shells of the wave-mechanical hydrogen atom. (Adapted from W. G. Moffatt, G. W. Pearsall, and J. Wulff, *The Structure and Properties of Materials,* Vol. I, *Structure,* p. 10. Copyright © 1964 by John Wiley & Sons, New York. Reprinted by permission of John Wiley & Sons, Inc.)

These states do not vary continuously with energy; that is, adjacent states are separated by finite energies. For example, allowed states for the Bohr hydrogen atom are represented in Figure 2.2*a*. These energies are taken to be negative, whereas the zero reference is the unbound or free electron. Of course, the single electron associated with the hydrogen atom will fill only one of these states.

Thus, the Bohr model represents an early attempt to describe electrons in atoms, in terms of both position (electron orbitals) and energy (quantized energy levels).

This Bohr model was eventually found to have some significant limitations because of its inability to explain several phenomena involving electrons. A resolution was reached with a **wave-mechanical model,** in which the electron is considered to exhibit both wavelike and particle-like characteristics. With this model, an electron is no longer treated as a particle moving in a discrete orbital; but rather, position is considered to be the probability of an electron's being at various locations around the nucleus. In other words, position is described by a probability distribution or electron cloud. Figure 2.3 compares Bohr and wave-mechanical models for the hydrogen atom. Both these models are used throughout the course of this book; the choice depends on which model allows the more simple explanation.

QUANTUM NUMBERS

Using wave mechanics, every electron in an atom is characterized by four parameters called **quantum numbers.** The size, shape, and spatial orientation of an electron's probability density are specified by three of these quantum numbers. Furthermore, Bohr energy levels separate into electron subshells, and quantum numbers dictate the number of states within each subshell. Shells are specified by a *principal quantum number n*, which may take on integral values beginning with unity; sometimes these shells are designated by the letters *K*, *L*, *M*, *N*, *O*, and so on, which correspond, respectively, to $n = 1, 2, 3, 4, 5, \ldots$, as indicated in Table 2.1. It should also be

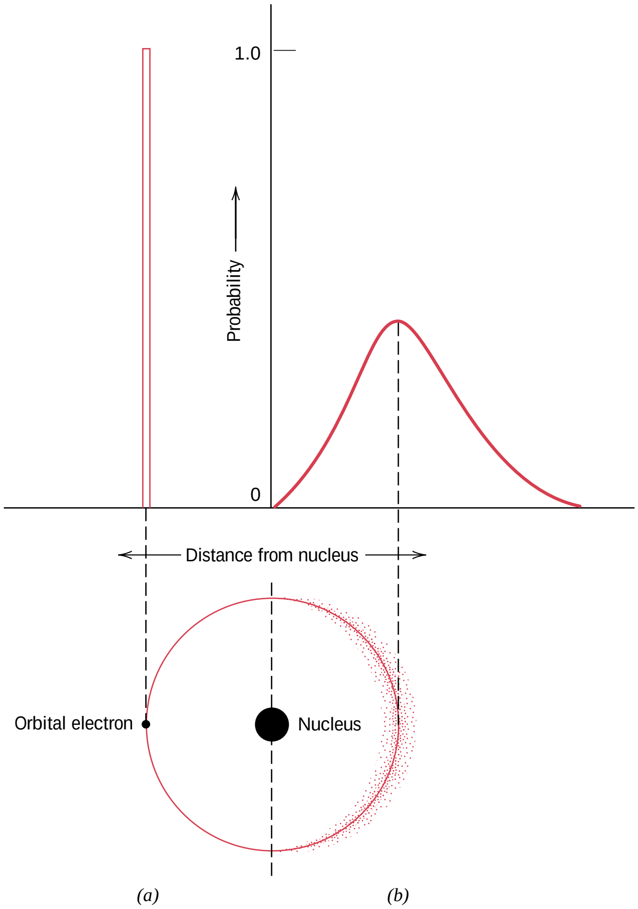
1.0
Probability
0
Distance from nucleus
Orbital electron
Nucleus
(a)
(b)

FIGURE 2.3 Comparison of the (*a*) Bohr and (*b*) wave-mechanical atom models in terms of electron distribution. (Adapted from Z. D. Jastrzebski, *The Nature and Properties of Engineering Materials,* 3rd edition, p. 4. Copyright © 1987 by John Wiley & Sons, New York. Reprinted by permission of John Wiley & Sons, Inc.)

Table 2.1 The Number of Available Electron States in Some of the Electron Shells and Subshells

Principal Quantum Number n	*Shell Designation*	*Subshells*	*Number of States*	*Number of Electrons*	
				Per Subshell	*Per Shell*
1	*K*	*s*	1	2	2
2	*L*	*s* *p*	1 3	2 6	8
3	*M*	*s* *p* *d*	1 3 5	2 6 10	18
4	*N*	*s* *p* *d* *f*	1 3 5 7	2 6 10 14	32

noted that this quantum number, and it only, is also associated with the Bohr model. This quantum number is related to the distance of an electron from the nucleus, or its position.

The second quantum number, *l*, signifies the subshell, which is denoted by a lowercase letter—an *s, p, d*, or *f*; it is related to the shape of the electron subshell. In addition, the number of these subshells is restricted by the magnitude of *n*. Allowable subshells for the several *n* values are also presented in Table 2.1. The number of energy states for each subshell is determined by the third quantum number, m_l. For an *s* subshell, there is a single energy state, whereas for *p, d*, and *f* subshells, three, five, and seven states exist, respectively (Table 2.1). In the absence of an external magnetic field, the states within each subshell are identical. However, when a magnetic field is applied these subshell states split, each state assuming a slightly different energy.

Associated with each electron is a *spin moment*, which must be oriented either up or down. Related to this spin moment is the fourth quantum number, m_s, for which two values are possible ($+\frac{1}{2}$ and $-\frac{1}{2}$), one for each of the spin orientations.

Thus, the Bohr model was further refined by wave mechanics, in which the introduction of three new quantum numbers gives rise to electron subshells within each shell. A comparison of these two models on this basis is illustrated, for the hydrogen atom, in Figures 2.2*a* and 2.2*b*.

A complete energy level diagram for the various shells and subshells using the wave-mechanical model is shown in Figure 2.4. Several features of the diagram are worth noting. First, the smaller the principal quantum number, the lower the energy level; for example, the energy of a 1*s* state is less than that of a 2*s* state, which in turn is lower than the 3*s*. Second, within each shell, the energy of a subshell level increases with the value of the *l* quantum number. For example, the energy of a 3*d* state is greater than a 3*p*, which is larger than 3*s*. Finally, there may be overlap in energy of a state in one shell with states in an adjacent shell, which is especially true of *d* and *f* states; for example, the energy of a 3*d* state is greater than that for a 4*s*.

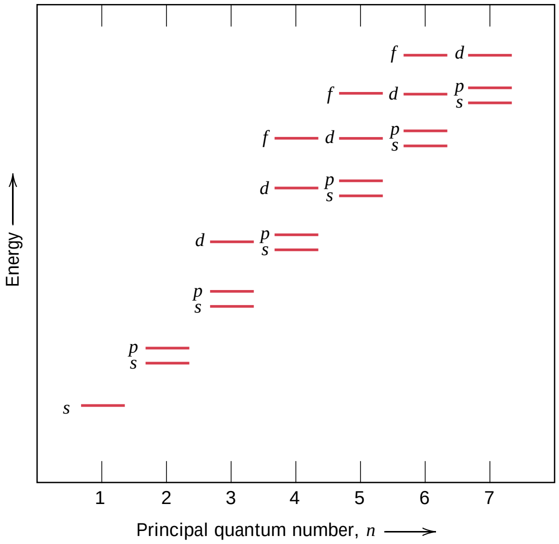

Figure 2.4 Schematic representation of the relative energies of the electrons for the various shells and subshells. (From K. M. Ralls, T. H. Courtney, and J. Wulff, *Introduction to Materials Science and Engineering*, p. 22. Copyright © 1976 by John Wiley & Sons, New York. Reprinted by permission of John Wiley & Sons, Inc.)

ELECTRON CONFIGURATIONS

The preceding discussion has dealt primarily with **electron states**—values of energy that are permitted for electrons. To determine the manner in which these states are filled with electrons, we use the **Pauli exclusion principle,** another quantum-mechanical concept. This principle stipulates that each electron state can hold no more than two electrons, which must have opposite spins. Thus, *s*, *p*, *d*, and *f* subshells may each accommodate, respectively, a total of 2, 6, 10, and 14 electrons; Table 2.1 summarizes the maximum number of electrons that may occupy each of the first four shells.

Of course, not all possible states in an atom are filled with electrons. For most atoms, the electrons fill up the lowest possible energy states in the electron shells and subshells, two electrons (having opposite spins) per state. The energy structure for a sodium atom is represented schematically in Figure 2.5. When all the electrons occupy the lowest possible energies in accord with the foregoing restrictions, an atom is said to be in its **ground state.** However, electron transitions to higher energy states are possible, as discussed in Chapters 12 {and 19.} The **electron configuration** or structure of an atom represents the manner in which these states are occupied. In the conventional notation the number of electrons in each subshell is indicated by a superscript after the shell–subshell designation. For example, the electron configurations for hydrogen, helium, and sodium are, respectively, $1s^1$, $1s^2$, and $1s^2 2s^2 2p^6 3s^1$. Electron configurations for some of the more common elements are listed in Table 2.2.

At this point, comments regarding these electron configurations are necessary. First, the **valence electrons** are those that occupy the outermost filled shell. These electrons are extremely important; as will be seen, they participate in the bonding between atoms to form atomic and molecular aggregates. Furthermore, many of the physical and chemical properties of solids are based on these valence electrons.

In addition, some atoms have what are termed ''stable electron configurations''; that is, the states within the outermost or valence electron shell are completely filled. Normally this corresponds to the occupation of just the *s* and *p* states for the outermost shell by a total of eight electrons, as in neon, argon, and krypton; one exception is helium, which contains only two 1*s* electrons. These elements (Ne, Ar, Kr, and He) are the inert, or noble, gases, which are virtually unreactive chemically. Some atoms of the elements that have unfilled valence shells assume

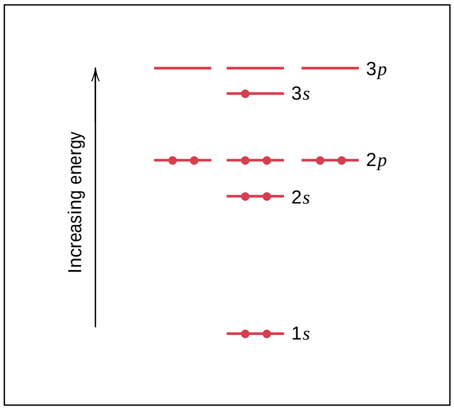

FIGURE 2.5 Schematic representation of the filled energy states for a sodium atom.

Table 2.2 A Listing of the Expected Electron Configurations for Some of the Common Elements[a]

Element	*Symbol*	*Atomic Number*	*Electron Configuration*
Hydrogen	H	1	$1s^1$
Helium	He	2	$1s^2$
Lithium	Li	3	$1s^2 2s^1$
Beryllium	Be	4	$1s^2 2s^2$
Boron	B	5	$1s^2 2s^2 2p^1$
Carbon	C	6	$1s^2 2s^2 2p^2$
Nitrogen	N	7	$1s^2 2s^2 2p^3$
Oxygen	O	8	$1s^2 2s^2 2p^4$
Fluorine	F	9	$1s^2 2s^2 2p^5$
Neon	Ne	10	$1s^2 2s^2 2p^6$
Sodium	Na	11	$1s^2 2s^2 2p^6 3s^1$
Magnesium	Mg	12	$1s^2 2s^2 2p^6 3s^2$
Aluminum	Al	13	$1s^2 2s^2 2p^6 3s^2 3p^1$
Silicon	Si	14	$1s^2 2s^2 2p^6 3s^2 3p^2$
Phosphorus	P	15	$1s^2 2s^2 2p^6 3s^2 3p^3$
Sulfur	S	16	$1s^2 2s^2 2p^6 3s^2 3p^4$
Chlorine	Cl	17	$1s^2 2s^2 2p^6 3s^2 3p^5$
Argon	Ar	18	$1s^2 2s^2 2p^6 3s^2 3p^6$
Potassium	K	19	$1s^2 2s^2 2p^6 3s^2 3p^6 4s^1$
Calcium	Ca	20	$1s^2 2s^2 2p^6 3s^2 3p^6 4s^2$
Scandium	Sc	21	$1s^2 2s^2 2p^6 3s^2 3p^6 3d^1 4s^2$
Titanium	Ti	22	$1s^2 2s^2 2p^6 3s^2 3p^6 3d^2 4s^2$
Vanadium	V	23	$1s^2 2s^2 2p^6 3s^2 3p^6 3d^3 4s^2$
Chromium	Cr	24	$1s^2 2s^2 2p^6 3s^2 3p^6 3d^5 4s^1$
Manganese	Mn	25	$1s^2 2s^2 2p^6 3s^2 3p^6 3d^5 4s^2$
Iron	Fe	26	$1s^2 2s^2 2p^6 3s^2 3p^6 3d^6 4s^2$
Cobalt	Co	27	$1s^2 2s^2 2p^6 3s^2 3p^6 3d^7 4s^2$
Nickel	Ni	28	$1s^2 2s^2 2p^6 3s^2 3p^6 3d^8 4s^2$
Copper	Cu	29	$1s^2 2s^2 2p^6 3s^2 3p^6 3d^{10} 4s^1$
Zinc	Zn	30	$1s^2 2s^2 2p^6 3s^2 3p^6 3d^{10} 4s^2$
Gallium	Ga	31	$1s^2 2s^2 2p^6 3s^2 3p^6 3d^{10} 4s^2 4p^1$
Germanium	Ge	32	$1s^2 2s^2 2p^6 3s^2 3p^6 3d^{10} 4s^2 4p^2$
Arsenic	As	33	$1s^2 2s^2 2p^6 3s^2 3p^6 3d^{10} 4s^2 4p^3$
Selenium	Se	34	$1s^2 2s^2 2p^6 3s^2 3p^6 3d^{10} 4s^2 4p^4$
Bromine	Br	35	$1s^2 2s^2 2p^6 3s^2 3p^6 3d^{10} 4s^2 4p^5$
Krypton	Kr	36	$1s^2 2s^2 2p^6 3s^2 3p^6 3d^{10} 4s^2 4p^6$

[a] When some elements covalently bond, they form *sp* hybrid bonds. This is especially true for C, Si, and Ge.

stable electron configurations by gaining or losing electrons to form charged ions, or by sharing electrons with other atoms. This is the basis for some chemical reactions, and also for atomic bonding in solids, as explained in Section 2.6.

Under special circumstances, the *s* and *p* orbitals combine to form hybrid sp^n orbitals, where *n* indicates the number of *p* orbitals involved, which may have a value of 1, 2, or 3. The 3A, 4A, and 5A group elements of the periodic table (Figure 2.6) are those which most often form these hybrids. The driving force for the formation of hybrid orbitals is a lower energy state for the valence electrons. For carbon the sp^3 hybrid is of primary importance in organic and polymer chemistries.

The shape of the sp^3 hybrid is what determines the 109° (or tetrahedral) angle found in polymer chains (Chapter 4).

2.4 THE PERIODIC TABLE

All the elements have been classified according to electron configuration in the **periodic table** (Figure 2.6). Here, the elements are situated, with increasing atomic number, in seven horizontal rows called periods. The arrangement is such that all elements that are arrayed in a given column or group have similar valence electron structures, as well as chemical and physical properties. These properties change gradually and systematically, moving horizontally across each period.

The elements positioned in Group 0, the rightmost group, are the inert gases, which have filled electron shells and stable electron configurations. Group VIIA and VIA elements are one and two electrons deficient, respectively, from having stable structures. The Group VIIA elements (F, Cl, Br, I, and At) are sometimes termed the halogens. The alkali and the alkaline earth metals (Li, Na, K, Be, Mg, Ca, etc.) are labeled as Groups IA and IIA, having, respectively, one and two electrons in excess of stable structures. The elements in the three long periods, Groups IIIB through IIB, are termed the transition metals, which have partially filled *d* electron states and in some cases one or two electrons in the next higher energy shell. Groups IIIA, IVA, and VA (B, Si, Ge, As, etc.) display characteristics that are intermediate between the metals and nonmetals by virtue of their valence electron structures.

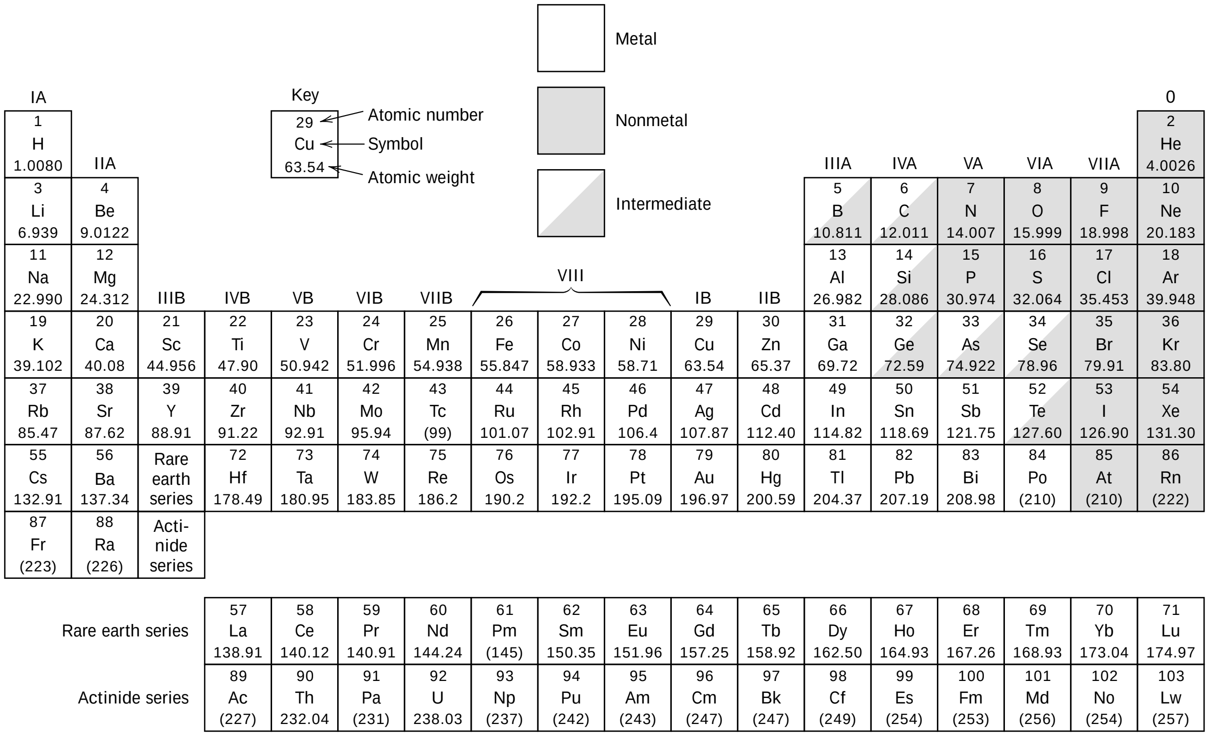

Key
29 ← Atomic number
Cu ← Symbol
63.54 ← Atomic weight

☐ Metal
▨ Nonmetal
◩ Intermediate

IA	IIA	IIIB	IVB	VB	VIB	VIIB	VIII	VIII	VIII	IB	IIB	IIIA	IVA	VA	VIA	VIIA	0
1 H 1.0080																	2 He 4.0026
3 Li 6.939	4 Be 9.0122											5 B 10.811	6 C 12.011	7 N 14.007	8 O 15.999	9 F 18.998	10 Ne 20.183
11 Na 22.990	12 Mg 24.312											13 Al 26.982	14 Si 28.086	15 P 30.974	16 S 32.064	17 Cl 35.453	18 Ar 39.948
19 K 39.102	20 Ca 40.08	21 Sc 44.956	22 Ti 47.90	23 V 50.942	24 Cr 51.996	25 Mn 54.938	26 Fe 55.847	27 Co 58.933	28 Ni 58.71	29 Cu 63.54	30 Zn 65.37	31 Ga 69.72	32 Ge 72.59	33 As 74.922	34 Se 78.96	35 Br 79.91	36 Kr 83.80
37 Rb 85.47	38 Sr 87.62	39 Y 88.91	40 Zr 91.22	41 Nb 92.91	42 Mo 95.94	43 Tc (99)	44 Ru 101.07	45 Rh 102.91	46 Pd 106.4	47 Ag 107.87	48 Cd 112.40	49 In 114.82	50 Sn 118.69	51 Sb 121.75	52 Te 127.60	53 I 126.90	54 Xe 131.30
55 Cs 132.91	56 Ba 137.34	Rare earth series	72 Hf 178.49	73 Ta 180.95	74 W 183.85	75 Re 186.2	76 Os 190.2	77 Ir 192.2	78 Pt 195.09	79 Au 196.97	80 Hg 200.59	81 Tl 204.37	82 Pb 207.19	83 Bi 208.98	84 Po (210)	85 At (210)	86 Rn (222)
87 Fr (223)	88 Ra (226)	Acti-nide series															

Rare earth series	57 La 138.91	58 Ce 140.12	59 Pr 140.91	60 Nd 144.24	61 Pm (145)	62 Sm 150.35	63 Eu 151.96	64 Gd 157.25	65 Tb 158.92	66 Dy 162.50	67 Ho 164.93	68 Er 167.26	69 Tm 168.93	70 Yb 173.04	71 Lu 174.97
Actinide series	89 Ac (227)	90 Th 232.04	91 Pa (231)	92 U 238.03	93 Np (237)	94 Pu (242)	95 Am (243)	96 Cm (247)	97 Bk (247)	98 Cf (249)	99 Es (254)	100 Fm (253)	101 Md (256)	102 No (254)	103 Lw (257)

FIGURE 2.6 The periodic table of the elements. The numbers in parentheses are the atomic weights of the most stable or common isotopes.

IA	IIA	IIIB	IVB	VB	VIB	VIIB	VIII			IB	IIB	IIIA	IVA	VA	VIA	VIIA	0
1 H 2.1																	2 He –
3 Li 1.0	4 Be 1.5											5 B 2.0	6 C 2.5	7 N 3.0	8 O 3.5	9 F 4.0	10 Ne –
11 Na 0.9	12 Mg 1.2											13 Al 1.5	14 Si 1.8	15 P 2.1	16 S 2.5	17 Cl 3.0	18 Ar –
19 K 0.8	20 Ca 1.0	21 Sc 1.3	22 Ti 1.5	23 V 1.6	24 Cr 1.6	25 Mn 1.5	26 Fe 1.8	27 Co 1.8	28 Ni 1.8	29 Cu 1.9	30 Zn 1.6	31 Ga 1.6	32 Ge 1.8	33 As 2.0	34 Se 2.4	35 Br 2.8	36 Kr –
37 Rb 0.8	38 Sr 1.0	39 Y 1.2	40 Zr 1.4	41 Nb 1.6	42 Mo 1.8	43 Tc 1.9	44 Ru 2.2	45 Rh 2.2	46 Pd 2.2	47 Ag 1.9	48 Cd 1.7	49 In 1.7	50 Sn 1.8	51 Sb 1.9	52 Te 2.1	53 I 2.5	54 Xe –
55 Cs 0.7	56 Ba 0.9	57–71 La–Lu 1.1–1.2	72 Hf 1.3	73 Ta 1.5	74 W 1.7	75 Re 1.9	76 Os 2.2	77 Ir 2.2	78 Pt 2.2	79 Au 2.4	80 Hg 1.9	81 Tl 1.8	82 Pb 1.8	83 Bi 1.9	84 Po 2.0	85 At 2.2	86 Rn –
87 Fr 0.7	88 Ra 0.9	89–102 Ac–No 1.1–1.7															

FIGURE 2.7 The electronegativity values for the elements. (Adapted from Linus Pauling, *The Nature of the Chemical Bond*, 3rd edition. Copyright 1939 and 1940, 3rd edition copyright © 1960, by Cornell University. Used by permission of the publisher, Cornell University Press.)

As may be noted from the periodic table, most of the elements really come under the metal classification. These are sometimes termed **electropositive** elements, indicating that they are capable of giving up their few valence electrons to become positively charged ions. Furthermore, the elements situated on the right-hand side of the table are **electronegative;** that is, they readily accept electrons to form negatively charged ions, or sometimes they share electrons with other atoms. Figure 2.7 displays electronegativity values that have been assigned to the various elements arranged in the periodic table. As a general rule, electronegativity increases in moving from left to right and from bottom to top. Atoms are more likely to accept electrons if their outer shells are almost full, and if they are less ''shielded'' from (i.e., closer to) the nucleus.

ATOMIC BONDING IN SOLIDS

2.5 BONDING FORCES AND ENERGIES

An understanding of many of the physical properties of materials is predicated on a knowledge of the interatomic forces that bind the atoms together. Perhaps the principles of atomic bonding are best illustrated by considering the interaction between two isolated atoms as they are brought into close proximity from an infinite separation. At large distances, the interactions are negligible; but as the atoms approach, each exerts forces on the other. These forces are of two types, attractive and repulsive, and the magnitude of each is a function of the separation or interatomic distance. The origin of an attractive force F_A depends on the particular type of bonding that exists between the two atoms. Its magnitude varies with the distance, as represented schematically in Figure 2.8*a*. Ultimately, the outer electron shells of the two atoms begin to overlap, and a strong repulsive force F_R comes into play. The net force F_N between the two atoms is just the sum of both attractive and repulsive components; that is,

$$F_N = F_A + F_R \tag{2.2}$$

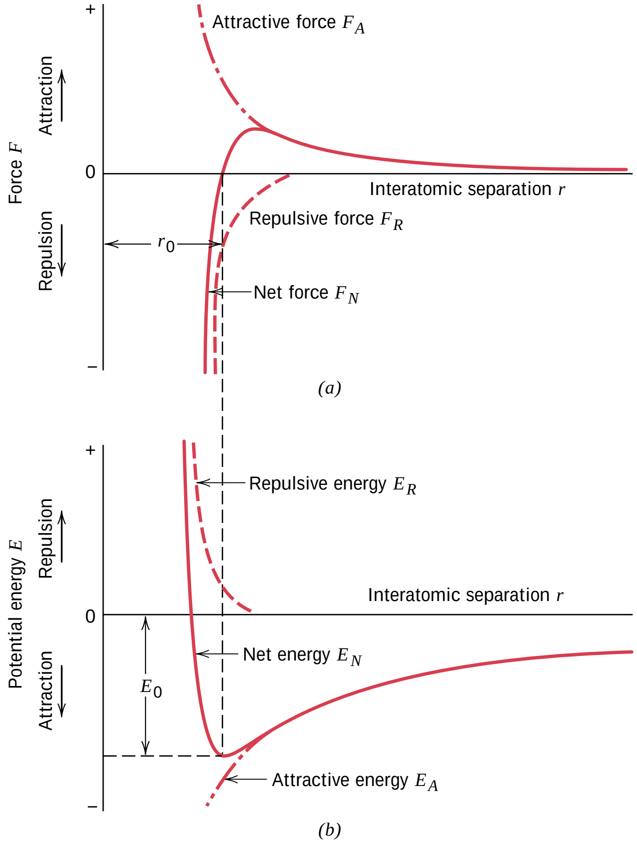

(*a*) (*b*)

FIGURE 2.8 (*a*) The dependence of repulsive, attractive, and net forces on interatomic separation for two isolated atoms. (*b*) The dependence of repulsive, attractive, and net potential energies on interatomic separation for two isolated atoms.

which is also a function of the interatomic separation, as also plotted in Figure 2.8*a*. When F_A and F_R balance, or become equal, there is no net force; that is,

$$F_A + F_R = 0 \tag{2.3}$$

Then a state of equilibrium exists. The centers of the two atoms will remain separated by the equilibrium spacing r_0, as indicated in Figure 2.8*a*. For many atoms, r_0 is approximately 0.3 nm (3 Å). Once in this position, the two atoms will counteract any attempt to separate them by an attractive force, or to push them together by a repulsive action.

Sometimes it is more convenient to work with the potential energies between two atoms instead of forces. Mathematically, energy (E) and force (F) are related as

$$E = \int F\,dr \tag{2.4}$$

Or, for atomic systems,

$$E_N = \int_\infty^r F_N\,dr \tag{2.5}$$

$$= \int_\infty^r F_A\,dr + \int_\infty^r F_R\,dr \tag{2.6}$$

$$= E_A + E_R \tag{2.7}$$

in which E_N, E_A, and E_R are respectively the net, attractive, and repulsive energies for two isolated and adjacent atoms.

Figure 2.8*b* plots attractive, repulsive, and net potential energies as a function of interatomic separation for two atoms. The net curve, which is again the sum of the other two, has a potential energy trough or well around its minimum. Here, the same equilibrium spacing, r_0, corresponds to the separation distance at the minimum of the potential energy curve. The **bonding energy** for these two atoms, E_0, corresponds to the energy at this minimum point (also shown in Figure 2.8*b*); it represents the energy that would be required to separate these two atoms to an infinite separation.

Although the preceding treatment has dealt with an ideal situation involving only two atoms, a similar yet more complex condition exists for solid materials because force and energy interactions among many atoms must be considered. Nevertheless, a bonding energy, analogous to E_0 above, may be associated with each atom. The magnitude of this bonding energy and the shape of the energy-versus-interatomic separation curve vary from material to material, and they both depend on the type of atomic bonding. Furthermore, a number of material properties depend on E_0, the curve shape, and bonding type. For example, materials having large bonding energies typically also have high melting temperatures; at room temperature, solid substances are formed for large bonding energies, whereas for small energies the gaseous state is favored; liquids prevail when the energies are of intermediate magnitude. In addition, as discussed in Section 7.3, the mechanical stiffness (or modulus of elasticity) of a material is dependent on the shape of its force-versus-interatomic separation curve (Figure 7.7). The slope for a relatively stiff material at the $r = r_0$ position on the curve will be quite steep; slopes are shallower for more flexible materials. Furthermore, how much a material expands upon heating or contracts upon cooling (that is, its linear coefficient of thermal expansion) is related to the shape of its E_0-versus-r_0 curve {(see Section 17.3).} A deep and narrow ''trough,'' which typically occurs for materials having large bonding energies, normally correlates with a low coefficient of thermal expansion and relatively small dimensional alterations for changes in temperature.

Three different types of primary or chemical bond are found in solids—ionic, covalent, and metallic. For each type, the bonding necessarily involves the valence electrons; furthermore, the nature of the bond depends on the electron structures of the constituent atoms. In general, each of these three types of bonding arises from the tendency of the atoms to assume stable electron structures, like those of the inert gases, by completely filling the outermost electron shell.

Secondary or physical forces and energies are also found in many solid materials; they are weaker than the primary ones, but nonetheless influence the physical properties of some materials. The sections that follow explain the several kinds of primary and secondary interatomic bonds.

2.6 PRIMARY INTERATOMIC BONDS

IONIC BONDING

Perhaps **ionic bonding** is the easiest to describe and visualize. It is always found in compounds that are composed of both metallic and nonmetallic elements, elements that are situated at the horizontal extremities of the periodic table. Atoms of a metallic element easily give up their valence electrons to the nonmetallic atoms. In the process all the atoms acquire stable or inert gas configurations and, in addition, an electrical charge; that is, they become ions. Sodium chloride (NaCl) is the classical ionic material. A sodium atom can assume the electron structure of neon (and a net single positive charge) by a transfer of its one valence 3*s* electron

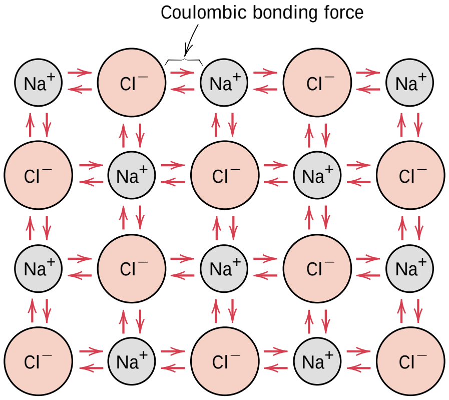

Figure 2.9 Schematic representation of ionic bonding in sodium chloride (NaCl).

to a chlorine atom. After such a transfer, the chlorine ion has a net negative charge and an electron configuration identical to that of argon. In sodium chloride, all the sodium and chlorine exist as ions. This type of bonding is illustrated schematically in Figure 2.9.

The attractive bonding forces are **coulombic**; that is, positive and negative ions, by virtue of their net electrical charge, attract one another. For two isolated ions, the attractive energy E_A is a function of the interatomic distance according to[3]

$$E_A = -\frac{A}{r} \tag{2.8}$$

An analogous equation for the repulsive energy is

$$E_R = \frac{B}{r^n} \tag{2.9}$$

In these expressions, A, B, and n are constants whose values depend on the particular ionic system. The value of n is approximately 8.

Ionic bonding is termed nondirectional, that is, the magnitude of the bond is equal in all directions around an ion. It follows that for ionic materials to be stable, all positive ions must have as nearest neighbors negatively charged ions in a three-dimensional scheme, and vice versa. The predominant bonding in ceramic materials is ionic. Some of the ion arrangements for these materials are discussed in Chapter 3.

Bonding energies, which generally range between 600 and 1500 kJ/mol (3 and 8 eV/atom), are relatively large, as reflected in high melting temperatures.[4] Table

---

[3] The constant A in Equation 2.8 is equal to

$$\frac{1}{4\pi\epsilon_0}(Z_1e)(Z_2e)$$

where ϵ_0 is the permittivity of a vacuum (8.85×10^{-12} F/m), Z_1 and Z_2 are the valences of the two ion types, and e is the electronic charge (1.602×10^{-19} C).

[4] Sometimes bonding energies are expressed per atom or per ion. Under these circumstances the electron volt (eV) is a conveniently small unit of energy. It is, by definition, the energy imparted to an electron as it falls through an electric potential of one volt. The joule equivalent of the electron volt is as follows: 1.602×10^{-19} J = 1 eV.

Table 2.3 **Bonding Energies and Melting Temperatures for Various Substances**

		Bonding Energy		
Bonding Type	***Substance***	***kJ/mol (kcal/mol)***	***eV/Atom, Ion, Molecule***	***Melting Temperature (°C)***
Ionic	NaCl	640 (153)	3.3	801
	MgO	1000 (239)	5.2	2800
Covalent	Si	450 (108)	4.7	1410
	C (diamond)	713 (170)	7.4	>3550
Metallic	Hg	68 (16)	0.7	−39
	Al	324 (77)	3.4	660
	Fe	406 (97)	4.2	1538
	W	849 (203)	8.8	3410
van der Waals	Ar	7.7 (1.8)	0.08	−189
	Cl_2	31 (7.4)	0.32	−101
Hydrogen	NH_3	35 (8.4)	0.36	−78
	H_2O	51 (12.2)	0.52	0

2.3 contains bonding energies and melting temperatures for several ionic materials. Ionic materials are characteristically hard and brittle and, furthermore, electrically and thermally insulative. As discussed in subsequent chapters, these properties are a direct consequence of electron configurations and/or the nature of the ionic bond.

COVALENT BONDING

In **covalent bonding** stable electron configurations are assumed by the sharing of electrons between adjacent atoms. Two atoms that are covalently bonded will each contribute at least one electron to the bond, and the shared electrons may be considered to belong to both atoms. Covalent bonding is schematically illustrated in Figure 2.10 for a molecule of methane (CH_4). The carbon atom has four valence electrons, whereas each of the four hydrogen atoms has a single valence electron. Each hydrogen atom can acquire a helium electron configuration (two 1*s* valence electrons) when the carbon atom shares with it one electron. The carbon now has four additional shared electrons, one from each hydrogen, for a total of eight valence

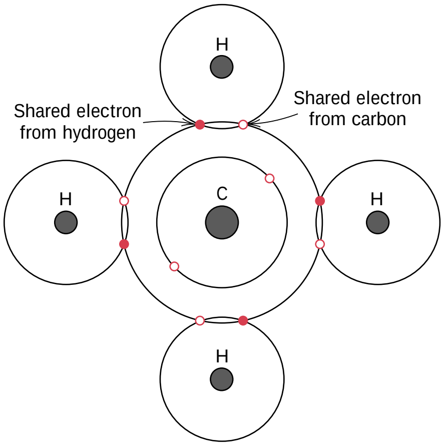

Figure 2.10 Schematic representation of covalent bonding in a molecule of methane (CH_4).

electrons, and the electron structure of neon. The covalent bond is directional; that is, it is between specific atoms and may exist only in the direction between one atom and another that participates in the electron sharing.

Many nonmetallic elemental molecules (H_2, Cl_2, F_2, etc.) as well as molecules containing dissimilar atoms, such as CH_4, H_2O, HNO_3, and HF, are covalently bonded. Furthermore, this type of bonding is found in elemental solids such as diamond (carbon), silicon, and germanium and other solid compounds composed of elements that are located on the right-hand side of the periodic table, such as gallium arsenide (GaAs), indium antimonide (InSb), and silicon carbide (SiC).

The number of covalent bonds that is possible for a particular atom is determined by the number of valence electrons. For N' valence electrons, an atom can covalently bond with at most $8 - N'$ other atoms. For example, $N' = 7$ for chlorine, and $8 - N' = 1$, which means that one Cl atom can bond to only one other atom, as in Cl_2. Similarly, for carbon, $N' = 4$, and each carbon atom has $8 - 4$, or four, electrons to share. Diamond is simply the three-dimensional interconnecting structure wherein each carbon atom covalently bonds with four other carbon atoms. This arrangement is represented in Figure 3.16.

Covalent bonds may be very strong, as in diamond, which is very hard and has a very high melting temperature, $>3550°C$ (6400°F), or they may be very weak, as with bismuth, which melts at about 270°C (518°F). Bonding energies and melting temperatures for a few covalently bonded materials are presented in Table 2.3. Polymeric materials typify this bond, the basic molecular structure being a long chain of carbon atoms that are covalently bonded together with two of their available four bonds per atom. The remaining two bonds normally are shared with other atoms, which also covalently bond. Polymeric molecular structures are discussed in detail in Chapter 4.

It is possible to have interatomic bonds that are partially ionic and partially covalent, and, in fact, very few compounds exhibit pure ionic or covalent bonding. For a compound, the degree of either bond type depends on the relative positions of the constituent atoms in the periodic table (Figure 2.6) or the difference in their electronegativities (Figure 2.7). The wider the separation (both horizontally—relative to Group IVA—and vertically) from the lower left to the upper-right-hand corner (i.e., the greater the difference in electronegativity), the more ionic the bond. Conversely, the closer the atoms are together (i.e., the smaller the difference in electronegativity), the greater the degree of covalency. The percent ionic character of a bond between elements A and B (A being the most electronegative) may be approximated by the expression

$$\%\ \text{ionic character} = \{1 - \exp[-(0.25)(X_A - X_B)^2]\} \times 100 \qquad (2.10)$$

where X_A and X_B are the electronegativities for the respective elements.

METALLIC BONDING

Metallic bonding, the final primary bonding type, is found in metals and their alloys. A relatively simple model has been proposed that very nearly approximates the bonding scheme. Metallic materials have one, two, or at most, three valence electrons. With this model, these valence electrons are not bound to any particular atom in the solid and are more or less free to drift throughout the entire metal. They may be thought of as belonging to the metal as a whole, or forming a ‘‘sea of electrons’’ or an ‘‘electron cloud.’’ The remaining nonvalence electrons and atomic nuclei form what are called *ion cores,* which possess a net positive charge equal in magnitude to the total valence electron charge per atom. Figure 2.11 is a

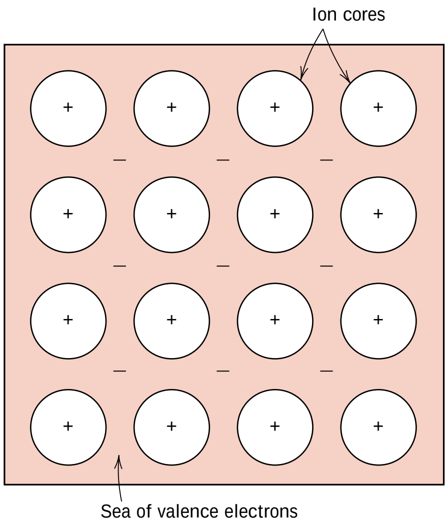

FIGURE 2.11 Schematic illustration of metallic bonding.

schematic illustration of metallic bonding. The free electrons shield the positively charged ion cores from mutually repulsive electrostatic forces, which they would otherwise exert upon one another; consequently the metallic bond is nondirectional in character. In addition, these free electrons act as a ''glue'' to hold the ion cores together. Bonding energies and melting temperatures for several metals are listed in Table 2.3. Bonding may be weak or strong; energies range from 68 kJ/mol (0.7 eV/atom) for mercury to 850 kJ/mol (8.8 eV/atom) for tungsten. Their respective melting temperatures are −39 and 3410°C (−38 and 6170°F).

Metallic bonding is found for Group IA and IIA elements in the periodic table, and, in fact, for all elemental metals.

Some general behaviors of the various material types (i.e., metals, ceramics, polymers) may be explained by bonding type. For example, metals are good conductors of both electricity and heat, as a consequence of their free electrons (see Sections 12.5, 12.6, {and 17.4}). By way of contrast, ionically and covalently bonded materials are typically electrical and thermal insulators, due to the absence of large numbers of free electrons.

Furthermore, in Section 8.5 we note that at room temperature, most metals and their alloys fail in a ductile manner; that is, fracture occurs after the materials have experienced significant degrees of permanent deformation. This behavior is explained in terms of deformation mechanism (Section 8.3), which is implicitly related to the characteristics of the metallic bond. Conversely, at room temperature ionically bonded materials are intrinsically brittle as a consequence of the electrically charged nature of their component ions (see Section 8.15).

2.7 SECONDARY BONDING OR VAN DER WAALS BONDING

Secondary, van der Waals, or physical bonds are weak in comparison to the primary or chemical ones; bonding energies are typically on the order of only 10 kJ/mol (0.1 eV/atom). Secondary bonding exists between virtually all atoms or molecules, but its presence may be obscured if any of the three primary bonding types is present. Secondary bonding is evidenced for the inert gases, which have stable

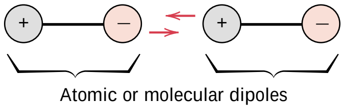

FIGURE 2.12 Schematic illustration of van der Waals bonding between two dipoles.

electron structures, and, in addition, between molecules in molecular structures that are covalently bonded.

Secondary bonding forces arise from atomic or molecular **dipoles.** In essence, an electric dipole exists whenever there is some separation of positive and negative portions of an atom or molecule. The bonding results from the coulombic attraction between the positive end of one dipole and the negative region of an adjacent one, as indicated in Figure 2.12. Dipole interactions occur between induced dipoles, between induced dipoles and polar molecules (which have permanent dipoles), and between polar molecules. **Hydrogen bonding,** a special type of secondary bonding, is found to exist between some molecules that have hydrogen as one of the constituents. These bonding mechanisms are now discussed briefly.

FLUCTUATING INDUCED DIPOLE BONDS

A dipole may be created or induced in an atom or molecule that is normally electrically symmetric; that is, the overall spatial distribution of the electrons is symmetric with respect to the positively charged nucleus, as shown in Figure 2.13*a*. All atoms are experiencing constant vibrational motion that can cause instantaneous and short-lived distortions of this electrical symmetry for some of the atoms or molecules, and the creation of small electric dipoles, as represented in Figure 2.13*b*. One of these dipoles can in turn produce a displacement of the electron distribution of an adjacent molecule or atom, which induces the second one also to become a dipole that is then weakly attracted or bonded to the first; this is one type of van der Waals bonding. These attractive forces may exist between large numbers of atoms or molecules, which forces are temporary and fluctuate with time.

The liquefaction and, in some cases, the solidification of the inert gases and other electrically neutral and symmetric molecules such as H_2 and Cl_2 are realized because of this type of bonding. Melting and boiling temperatures are extremely low in materials for which induced dipole bonding predominates; of all possible intermolecular bonds, these are the weakest. Bonding energies and melting temperatures for argon and chlorine are also tabulated in Table 2.3.

POLAR MOLECULE-INDUCED DIPOLE BONDS

Permanent dipole moments exist in some molecules by virtue of an asymmetrical arrangement of positively and negatively charged regions; such molecules are termed **polar molecules.** Figure 2.14 is a schematic representation of a hydrogen

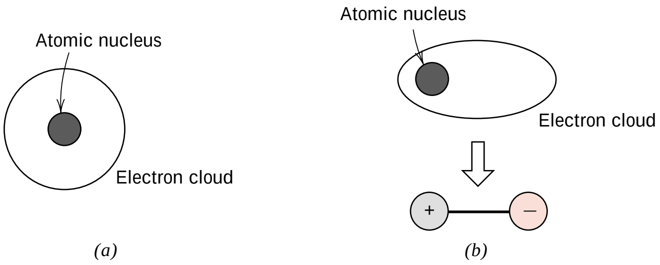

FIGURE 2.13 Schematic representations of (*a*) an electrically symmetric atom and (*b*) an induced atomic dipole.

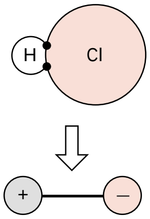

FIGURE 2.14 Schematic representation of a polar hydrogen chloride (HCl) molecule.

chloride molecule; a permanent dipole moment arises from net positive and negative charges that are respectively associated with the hydrogen and chlorine ends of the HCl molecule.

Polar molecules can also induce dipoles in adjacent nonpolar molecules, and a bond will form as a result of attractive forces between the two molecules. Furthermore, the magnitude of this bond will be greater than for fluctuating induced dipoles.

PERMANENT DIPOLE BONDS

Van der Waals forces will also exist between adjacent polar molecules. The associated bonding energies are significantly greater than for bonds involving induced dipoles.

The strongest secondary bonding type, the hydrogen bond, is a special case of polar molecule bonding. It occurs between molecules in which hydrogen is covalently bonded to fluorine (as in HF), oxygen (as in H_2O), and nitrogen (as in NH_3). For each H—F, H—O, or H—N bond, the single hydrogen electron is shared with the other atom. Thus, the hydrogen end of the bond is essentially a positively charged bare proton that is unscreened by any electrons. This highly positively charged end of the molecule is capable of a strong attractive force with the negative end of an adjacent molecule, as demonstrated in Figure 2.15 for HF. In essence, this single proton forms a bridge between two negatively charged atoms. The magnitude of the hydrogen bond is generally greater than that of the other types of secondary bonds, and may be as high as 51 kJ/mol (0.52 eV/molecule), as shown in Table 2.3. Melting and boiling temperatures for hydrogen fluoride and water are abnormally high in light of their low molecular weights, as a consequence of hydrogen bonding.

2.8 MOLECULES

At the conclusion of this chapter, let us take a moment to discuss the concept of a **molecule** in terms of solid materials. A molecule may be defined as a group of atoms that are bonded together by strong primary bonds. Within this context, the entirety of ionic and metallically bonded solid specimens may be considered as a single molecule. However, this is not the case for many substances in which covalent bonding predominates; these include elemental diatomic molecules (F_2, O_2, H_2, etc.) as well as a host of compounds (H_2O, CO_2, HNO_3, C_6H_6, CH_4, etc.). In the

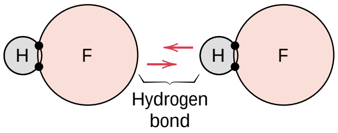

FIGURE 2.15 Schematic representation of hydrogen bonding in hydrogen fluoride (HF).

condensed liquid and solid states, bonds between molecules are weak secondary ones. Consequently, molecular materials have relatively low melting and boiling temperatures. Most of those that have small molecules composed of a few atoms are gases at ordinary, or ambient, temperatures and pressures. On the other hand, many of the modern polymers, being molecular materials composed of extremely large molecules, exist as solids; some of their properties are strongly dependent on the presence of van der Waals and hydrogen secondary bonds.

SUMMARY

This chapter began with a survey of the fundamentals of atomic structure, presenting the Bohr and wave-mechanical models of electrons in atoms. Whereas the Bohr model assumes electrons to be particles orbiting the nucleus in discrete paths, in wave mechanics we consider them to be wavelike and treat electron position in terms of a probability distribution.

Electron energy states are specified in terms of quantum numbers that give rise to electron shells and subshells. The electron configuration of an atom corresponds to the manner in which these shells and subshells are filled with electrons in compliance with the Pauli exclusion principle. The periodic table of the elements is generated by arrangement of the various elements according to valence electron configuration.

Atomic bonding in solids may be considered in terms of attractive and repulsive forces and energies. The three types of primary bond in solids are ionic, covalent, and metallic. For ionic bonds, electrically charged ions are formed by the transference of valence electrons from one atom type to another; forces are coulombic. There is a sharing of valence electrons between adjacent atoms when bonding is covalent. With metallic bonding, the valence electrons form a ''sea of electrons'' that is uniformly dispersed around the metal ion cores and acts as a form of glue for them.

Both van der Waals and hydrogen bonds are termed secondary, being weak in comparison to the primary ones. They result from attractive forces between electric dipoles, of which there are two types—induced and permanent. For the hydrogen bond, highly polar molecules form when hydrogen covalently bonds to a nonmetallic element such as fluorine.

IMPORTANT TERMS AND CONCEPTS

Atomic mass unit (amu)
Atomic number
Atomic weight
Bohr atomic model
Bonding energy
Coulombic force
Covalent bond
Dipole (electric)
Electron configuration
Electron state
Electronegative
Electropositive
Ground state
Hydrogen bond
Ionic bond
Isotope
Metallic bond
Mole
Molecule
Pauli exclusion principle
Periodic table
Polar molecule
Primary bonding
Quantum mechanics
Quantum number
Secondary bonding
Valence electron
van der Waals bond
Wave-mechanical model

Note: In each chapter, most of the terms listed in the ''Important Terms and Concepts'' section are defined in the Glossary, which follows Appendix E. The others are important enough to warrant treatment in a full section of the text and can be referenced from the table of contents or the index.

REFERENCES

Most of the material in this chapter is covered in college-level chemistry textbooks. Below, two are listed as references.

Kotz, J. C. and P. Treichel, Jr., *Chemistry and Chemical Reactivity,* 4th edition, Saunders College Publishing, Fort Worth, TX, 1999.

Masterton, W. L. and C. N. Hurley, *Chemistry, Principles and Reactions,* 3rd edition, Saunders College Publishing, Philadelphia, 1996.

QUESTIONS AND PROBLEMS

2.1 **(a)** What is an isotope?

(b) Why are the atomic weights of the elements not integers? Cite two reasons.

2.2 Cite the difference between atomic mass and atomic weight.

2.3 **(a)** How many grams are there in 1 amu of a material?

(b) Mole, in the context of this book, is taken in units of gram-mole. On this basis, how many atoms are there in a pound-mole of a substance?

2.4 **(a)** Cite two important quantum-mechanical concepts associated with the Bohr model of the atom.

(b) Cite two important additional refinements that resulted from the wave-mechanical atomic model.

2.5 Relative to electrons and electron states, what does each of the four quantum numbers specify?

2.6 Allowed values for the quantum numbers of electrons are as follows:

$$n = 1, 2, 3, \ldots$$

$$l = 0, 1, 2, 3, \ldots, n - 1$$

$$m_l = 0, \pm 1, \pm 2, \pm 3, \ldots, \pm l$$

$$m_s = \pm \tfrac{1}{2}$$

The relationships between n and the shell designations are noted in Table 2.1. Relative to the subshells,

$l = 0$ corresponds to an *s* subshell

$l = 1$ corresponds to a *p* subshell

$l = 2$ corresponds to a *d* subshell

$l = 3$ corresponds to an *f* subshell

For the *K* shell, the four quantum numbers for each of the two electrons in the 1*s* state, in the order of nlm_lm_s, are $100(\frac{1}{2})$ and $100(-\frac{1}{2})$. Write the four quantum numbers for all of the electrons in the *L* and *M* shells, and note which correspond to the *s*, *p*, and *d* subshells.

2.7 Give the electron configurations for the following ions: Fe^{2+}, Fe^{3+}, Cu^{+}, Ba^{2+}, Br^{-}, and S^{2-}.

2.8 Cesium bromide (CsBr) exhibits predominantly ionic bonding. The Cs^{+} and Br^{-} ions have electron structures that are identical to which two inert gases?

2.9 With regard to electron configuration, what do all the elements in Group VIIA of the periodic table have in common?

2.10 Without consulting Figure 2.6 or Table 2.2, determine whether each of the electron configurations given below is an inert gas, a halogen, an alkali metal, an alkaline earth metal, or a transition metal. Justify your choices.

(a) $1s^2 2s^2 2p^6 3s^2 3p^6 3d^7 4s^2$.

(b) $1s^2 2s^2 2p^6 3s^2 3p^6$.

(c) $1s^2 2s^2 2p^5$.

(d) $1s^2 2s^2 2p^6 3s^2$.

(e) $1s^2 2s^2 2p^6 3s^2 3p^6 3d^2 4s^2$.

(f) $1s^2 2s^2 2p^6 3s^2 3p^6 4s^1$.

2.11 **(a)** What electron subshell is being filled for the rare earth series of elements on the periodic table?

(b) What electron subshell is being filled for the actinide series?

2.12 Calculate the force of attraction between a K^{+} and an O^{2-} ion the centers of which are separated by a distance of 1.5 nm.

2.13 The net potential energy between two adjacent ions, E_N, may be represented by the sum of Equations 2.8 and 2.9, that is,

$$E_N = -\frac{A}{r} + \frac{B}{r^n} \qquad (2.11)$$

Calculate the bonding energy E_0 in terms of the parameters A, B, and n using the following procedure:

1. Differentiate E_N with respect to r, and then set the resulting expression equal to zero, since the curve of E_N versus r is a minimum at E_0.

2. Solve for r in terms of A, B, and n, which yields r_0, the equilibrium interionic spacing.

3. Determine the expression for E_0 by substitution of r_0 into Equation 2.11.

2.14 For a K^+–Cl^- ion pair, attractive and repulsive energies E_A and E_R, respectively, depend on the distance between the ions r, according to

$$E_A = -\frac{1.436}{r}$$

$$E_R = \frac{5.86 \times 10^{-6}}{r^9}$$

For these expressions, energies are expressed in electron volts per K^+–Cl^- pair, and r is the distance in nanometers. The net energy E_N is just the sum of the two expressions above.

(a) Superimpose on a single plot E_N, E_R, and E_A versus r up to 1.0 nm.

(b) On the basis of this plot, determine (i) the equilibrium spacing r_0 between the K^+ and Cl^- ions, and (ii) the magnitude of the bonding energy E_0 between the two ions.

(c) Mathematically determine the r_0 and E_0 values using the solutions to Problem 2.13 and compare these with the graphical results from part b.

2.15 Consider some hypothetical $X^+ - Y^-$ ion pair for which the equilibrium interionic spacing and bonding energy values are 0.35 nm and -6.13 eV, respectively. If it is known that n in Equation 2.11 has a value of 10, using the results of Problem 2.13, determine explicit expressions for attractive and repulsive energies, E_A and E_R of Equations 2.8 and 2.9.

2.16 The net potential energy E_N between two adjacent ions is sometimes represented by the expression

$$E_N = -\frac{C}{r} + D \exp\left(-\frac{r}{\rho}\right) \qquad (2.12)$$

in which r is the interionic separation and C, D, and ρ are constants whose values depend on the specific material.

(a) Derive an expression for the bonding energy E_0 in terms of the equilibrium interionic separation r_0 and the constants D and ρ using the following procedure:

1. Differentiate E_N with respect to r and set the resulting expression equal to zero.
2. Solve for C in terms of D, ρ, and r_0.
3. Determine the expression for E_0 by substitution for C in Equation 2.12.

(b) Derive another expression for E_0 in terms of r_0, C, and ρ using a procedure analogous to the one outlined in part a.

2.17 **(a)** Briefly cite the main differences between ionic, covalent, and metallic bonding.

(b) State the Pauli exclusion principle.

2.18 Offer an explanation as to why covalently bonded materials are generally less dense than ionically or metallically bonded ones.

2.19 Compute the percents ionic character of the interatomic bonds for the following compounds: TiO_2, ZnTe, CsCl, InSb, and $MgCl_2$.

2.20 Make a plot of bonding energy versus melting temperature for the metals listed in Table 2.3. Using this plot, approximate the bonding energy for copper, which has a melting temperature of 1084°C.

2.21 Using Table 2.2, determine the number of covalent bonds that are possible for atoms of the following elements: germanium, phosphorus, selenium, and chlorine.

2.22 What type(s) of bonding would be expected for each of the following materials: brass (a copper-zinc alloy), rubber, barium sulfide (BaS), solid xenon, bronze, nylon, and aluminum phosphide (AlP)?

2.23 Explain why hydrogen fluoride (HF) has a higher boiling temperature than hydrogen chloride (HCl) (19.4 vs. −85°C), even though HF has a lower molecular weight.

2.24 On the basis of the hydrogen bond, explain the anomalous behavior of water when it freezes. That is, why is there volume expansion upon solidification?

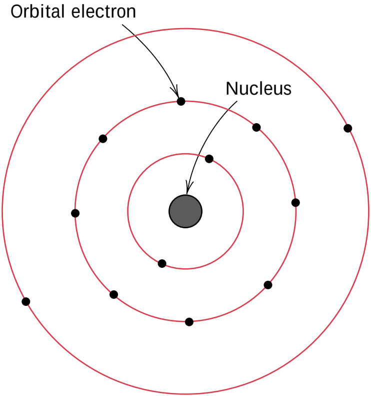
Orbital electron
Nucleus

Figure 2.1 Schematic representation of the Bohr atom.

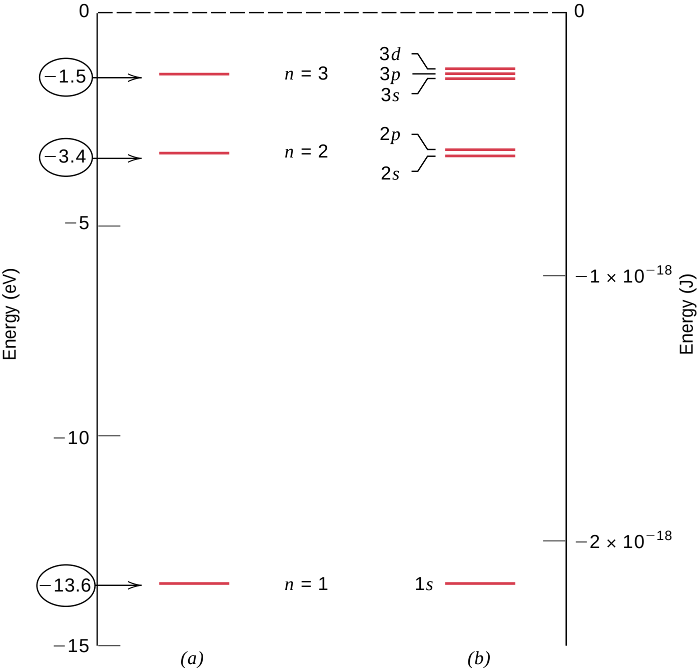
0
−1.5
−3.4
−5
−10
−13.6
−15
Energy (eV)
n = 3
n = 2
n = 1
3d
3p
3s
2p
2s
1s
0
−1 × 10^−18
−2 × 10^−18
Energy (J)
(a)
(b)

FIGURE 2.2 (*a*) The first three electron energy states for the Bohr hydrogen atom. (*b*) Electron energy states for the first three shells of the wave-mechanical hydrogen atom. (Adapted from W. G. Moffatt, G. W. Pearsall, and J. Wulff, *The Structure and Properties of Materials*, Vol. I, *Structure*, p. 10. Copyright © 1964 by John Wiley & Sons, New York. Reprinted by permission of John Wiley & Sons, Inc.)

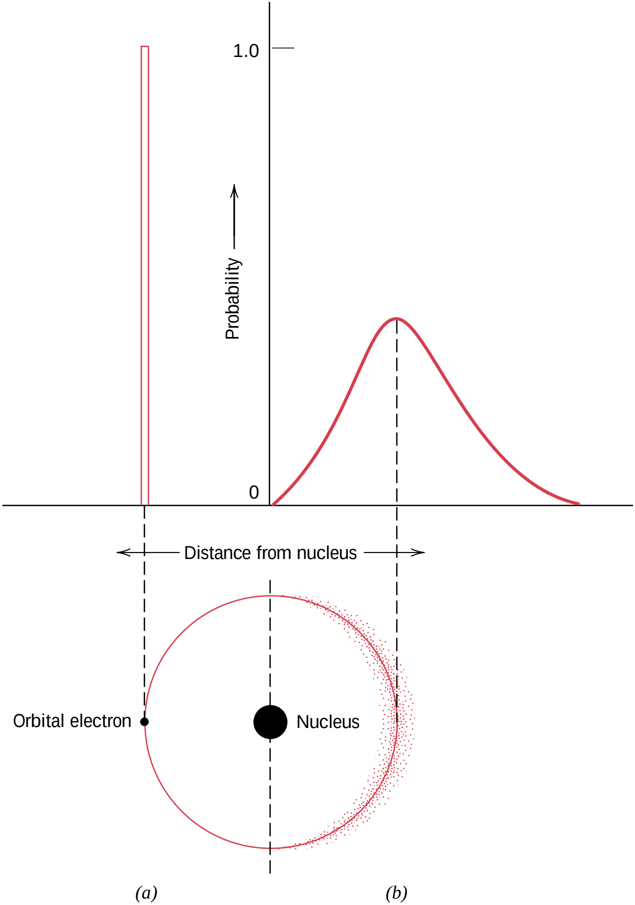
1.0
Probability
0
Distance from nucleus
Orbital electron
Nucleus
(a)
(b)

FIGURE 2.3 Comparison of the (*a*) Bohr and (*b*) wave-mechanical atom models in terms of electron distribution. (Adapted from Z. D. Jastrzebski, *The Nature and Properties of Engineering Materials*, 3rd edition, p. 4. Copyright © 1987 by John Wiley & Sons, New York. Reprinted by permission of John Wiley & Sons, Inc.)

Table 2.1 **The Number of Available Electron States in Some of the Electron Shells and Subshells**

Principal Quantum Number n	*Shell Designation*	*Subshells*	*Number of States*	*Number of Electrons*	
				Per Subshell	*Per Shell*
1	*K*	*s*	1	2	2
2	*L*	*s*	1	2	8
		p	3	6	
3	*M*	*s*	1	2	18
		p	3	6	
		d	5	10	
4	*N*	*s*	1	2	32
		p	3	6	
		d	5	10	
		f	7	14	

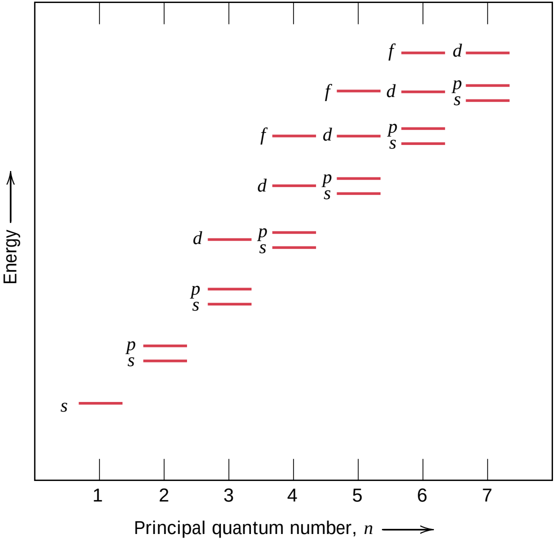

Energy
s
p
s
p
s
d
p
s
d
p
s
d
f
p
s
d
f
p
s
d
f
1
2
3
4
5
6
7
Principal quantum number, n

FIGURE 2.4 Schematic representation of the relative energies of the electrons for the various shells and subshells. (From K. M. Ralls, T. H. Courtney, and J. Wulff, *Introduction to Materials Science and Engineering*, p. 22. Copyright © 1976 by John Wiley & Sons, New York. Reprinted by permission of John Wiley & Sons, Inc.)

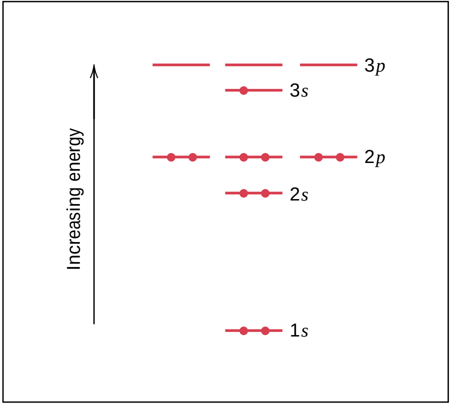
3p
3s
2p
2s
1s
Increasing energy

FIGURE 2.5 Schematic representation of the filled energy states for a sodium atom.

Table 2.2 A Listing of the Expected Electron Configurations for Some of the Common Elements[a]

Element	*Symbol*	*Atomic Number*	*Electron Configuration*
Hydrogen	H	1	$1s^1$
Helium	He	2	$1s^2$
Lithium	Li	3	$1s^22s^1$
Beryllium	Be	4	$1s^22s^2$
Boron	B	5	$1s^22s^22p^1$
Carbon	C	6	$1s^22s^22p^2$
Nitrogen	N	7	$1s^22s^22p^3$
Oxygen	O	8	$1s^22s^22p^4$
Fluorine	F	9	$1s^22s^22p^5$
Neon	Ne	10	$1s^22s^22p^6$
Sodium	Na	11	$1s^22s^22p^63s^1$
Magnesium	Mg	12	$1s^22s^22p^63s^2$
Aluminum	Al	13	$1s^22s^22p^63s^23p^1$
Silicon	Si	14	$1s^22s^22p^63s^23p^2$
Phosphorus	P	15	$1s^22s^22p^63s^23p^3$
Sulfur	S	16	$1s^22s^22p^63s^23p^4$
Chlorine	Cl	17	$1s^22s^22p^63s^23p^5$
Argon	Ar	18	$1s^22s^22p^63s^23p^6$
Potassium	K	19	$1s^22s^22p^63s^23p^64s^1$
Calcium	Ca	20	$1s^22s^22p^63s^23p^64s^2$
Scandium	Sc	21	$1s^22s^22p^63s^23p^63d^14s^2$
Titanium	Ti	22	$1s^22s^22p^63s^23p^63d^24s^2$
Vanadium	V	23	$1s^22s^22p^63s^23p^63d^34s^2$
Chromium	Cr	24	$1s^22s^22p^63s^23p^63d^54s^1$
Manganese	Mn	25	$1s^22s^22p^63s^23p^63d^54s^2$
Iron	Fe	26	$1s^22s^22p^63s^23p^63d^64s^2$
Cobalt	Co	27	$1s^22s^22p^63s^23p^63d^74s^2$
Nickel	Ni	28	$1s^22s^22p^63s^23p^63d^84s^2$
Copper	Cu	29	$1s^22s^22p^63s^23p^63d^{10}4s^1$
Zinc	Zn	30	$1s^22s^22p^63s^23p^63d^{10}4s^2$
Gallium	Ga	31	$1s^22s^22p^63s^23p^63d^{10}4s^24p^1$
Germanium	Ge	32	$1s^22s^22p^63s^23p^63d^{10}4s^24p^2$
Arsenic	As	33	$1s^22s^22p^63s^23p^63d^{10}4s^24p^3$
Selenium	Se	34	$1s^22s^22p^63s^23p^63d^{10}4s^24p^4$
Bromine	Br	35	$1s^22s^22p^63s^23p^63d^{10}4s^24p^5$
Krypton	Kr	36	$1s^22s^22p^63s^23p^63d^{10}4s^24p^6$

---

[a] When some elements covalently bond, they form *sp* hybrid bonds. This is especially true for C, Si, and Ge.

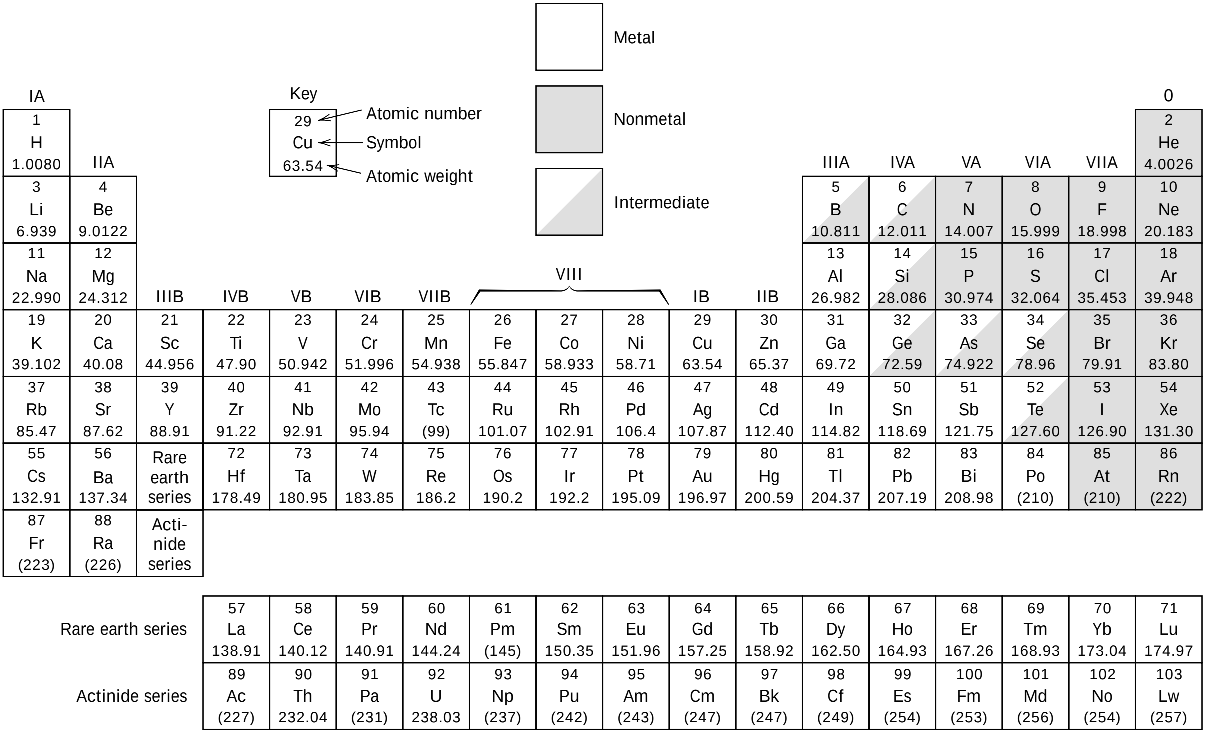

Key

29 ← Atomic number
Cu ← Symbol
63.54 ← Atomic weight

☐ Metal

▨ Nonmetal

◪ Intermediate

IA	IIA	IIIB	IVB	VB	VIB	VIIB	VIII	VIII	VIII	IB	IIB	IIIA	IVA	VA	VIA	VIIA	0
1 H 1.0080																	2 He 4.0026
3 Li 6.939	4 Be 9.0122											5 B 10.811	6 C 12.011	7 N 14.007	8 O 15.999	9 F 18.998	10 Ne 20.183
11 Na 22.990	12 Mg 24.312											13 Al 26.982	14 Si 28.086	15 P 30.974	16 S 32.064	17 Cl 35.453	18 Ar 39.948
19 K 39.102	20 Ca 40.08	21 Sc 44.956	22 Ti 47.90	23 V 50.942	24 Cr 51.996	25 Mn 54.938	26 Fe 55.847	27 Co 58.933	28 Ni 58.71	29 Cu 63.54	30 Zn 65.37	31 Ga 69.72	32 Ge 72.59	33 As 74.922	34 Se 78.96	35 Br 79.91	36 Kr 83.80
37 Rb 85.47	38 Sr 87.62	39 Y 88.91	40 Zr 91.22	41 Nb 92.91	42 Mo 95.94	43 Tc (99)	44 Ru 101.07	45 Rh 102.91	46 Pd 106.4	47 Ag 107.87	48 Cd 112.40	49 In 114.82	50 Sn 118.69	51 Sb 121.75	52 Te 127.60	53 I 126.90	54 Xe 131.30
55 Cs 132.91	56 Ba 137.34	Rare earth series	72 Hf 178.49	73 Ta 180.95	74 W 183.85	75 Re 186.2	76 Os 190.2	77 Ir 192.2	78 Pt 195.09	79 Au 196.97	80 Hg 200.59	81 Tl 204.37	82 Pb 207.19	83 Bi 208.98	84 Po (210)	85 At (210)	86 Rn (222)
87 Fr (223)	88 Ra (226)	Acti- nide series															

Rare earth series	57 La 138.91	58 Ce 140.12	59 Pr 140.91	60 Nd 144.24	61 Pm (145)	62 Sm 150.35	63 Eu 151.96	64 Gd 157.25	65 Tb 158.92	66 Dy 162.50	67 Ho 164.93	68 Er 167.26	69 Tm 168.93	70 Yb 173.04	71 Lu 174.97
Actinide series	89 Ac (227)	90 Th 232.04	91 Pa (231)	92 U 238.03	93 Np (237)	94 Pu (242)	95 Am (243)	96 Cm (247)	97 Bk (247)	98 Cf (249)	99 Es (254)	100 Fm (253)	101 Md (256)	102 No (254)	103 Lw (257)

FIGURE 2.6 The periodic table of the elements. The numbers in parentheses are the atomic weights of the most stable or common isotopes.

IA	IIA	IIIB	IVB	VB	VIB	VIIB	VIII			IB	IIB	IIIA	IVA	VA	VIA	VIIA	0
1 H 2.1																	2 He –
3 Li 1.0	4 Be 1.5											5 B 2.0	6 C 2.5	7 N 3.0	8 O 3.5	9 F 4.0	10 Ne –
11 Na 0.9	12 Mg 1.2											13 Al 1.5	14 Si 1.8	15 P 2.1	16 S 2.5	17 Cl 3.0	18 Ar –
19 K 0.8	20 Ca 1.0	21 Sc 1.3	22 Ti 1.5	23 V 1.6	24 Cr 1.6	25 Mn 1.5	26 Fe 1.8	27 Co 1.8	28 Ni 1.8	29 Cu 1.9	30 Zn 1.6	31 Ga 1.6	32 Ge 1.8	33 As 2.0	34 Se 2.4	35 Br 2.8	36 Kr –
37 Rb 0.8	38 Sr 1.0	39 Y 1.2	40 Zr 1.4	41 Nb 1.6	42 Mo 1.8	43 Tc 1.9	44 Ru 2.2	45 Rh 2.2	46 Pd 2.2	47 Ag 1.9	48 Cd 1.7	49 In 1.7	50 Sn 1.8	51 Sb 1.9	52 Te 2.1	53 I 2.5	54 Xe –
55 Cs 0.7	56 Ba 0.9	57–71 La–Lu 1.1–1.2	72 Hf 1.3	73 Ta 1.5	74 W 1.7	75 Re 1.9	76 Os 2.2	77 Ir 2.2	78 Pt 2.2	79 Au 2.4	80 Hg 1.9	81 Tl 1.8	82 Pb 1.8	83 Bi 1.9	84 Po 2.0	85 At 2.2	86 Rn –
87 Fr 0.7	88 Ra 0.9	89–102 Ac–No 1.1–1.7															

FIGURE 2.7 The electronegativity values for the elements. (Adapted from Linus Pauling, *The Nature of the Chemical Bond*, 3rd edition. Copyright 1939 and 1940, 3rd edition copyright © 1960, by Cornell University. Used by permission of the publisher, Cornell University Press.)

Chapter 17 / Thermal Properties

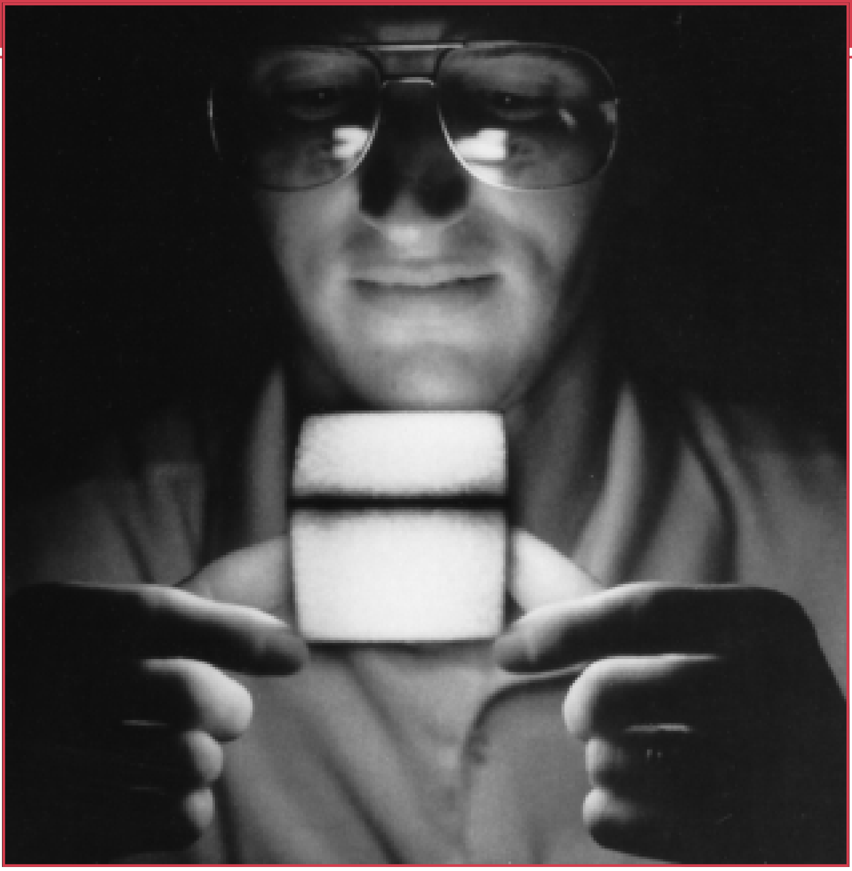

This photograph shows a white-hot cube of a silica fiber insulation material, which, only seconds after having been removed from a hot furnace, can be held by its edges with the bare hands. Initially, the heat transfer from the surface is relatively rapid; however, the thermal conductivity of this material is so small that heat conduction from the interior [maximum temperature approximately 1250°C (2300°F)] is extremely slow.

This material was developed especially for the tiles that cover the Space Shuttle Orbiters and protect and insulate them during their fiery reentry into the atmosphere. Other attractive features of this *high-temperature reusable surface insulation* (*HRSI*) include low density and a low coefficient of thermal expansion. (Photograph courtesy of Lockheed Missiles & Space Company, Inc.)

Why Study the *Thermal Properties* of Materials?

Materials selection decisions for components that are exposed to elevated/subambient temperatures, temperature changes, and/or thermal gradients require the design engineer to have an understanding of the thermal responses of materials, as well as access to the thermal properties of a wide variety of materials. For example, in the discussion on materials that are used for the leadframe component of an integrated circuit package (Section 20.13), we note restrictions that are imposed on the thermal characteristics of the adhesive material that attaches the integrated circuit chip to the leadframe plate. This adhesive must be thermally conductive so as to facilitate the dissipation of heat generated by the chip. In addition, its thermal expansion/contraction on heating/cooling must match that of the chip such that the integrity of the adhesive-chip bond is maintained during thermal cycling.

Learning Objectives

After careful study of this chapter you should be able to do the following:

1. **Define *heat capacity* and *specific heat*.**
2. **Note the primary mechanism by which thermal energy is assimilated in solid materials.**
3. **Determine the linear coefficient of thermal expansion given the length alteration that accompanies a specified temperature change.**
4. **Briefly explain the phenomenon of thermal expansion from an atomic perspective using a potential energy-versus-interatomic separation plot.**
5. **Define *thermal conductivity*.**
6. **Note the two principal mechanisms of heat condition in solids, and compare the relative magnitudes of these contributions for each of metals, ceramics, and polymeric materials.**

17.1 INTRODUCTION

By ''thermal property'' is meant the response of a material to the application of heat. As a solid absorbs energy in the form of heat, its temperature rises and its dimensions increase. The energy may be transported to cooler regions of the specimen if temperature gradients exist, and ultimately, the specimen may melt. Heat capacity, thermal expansion, and thermal conductivity are properties that are often critical in the practical utilization of solids.

17.2 HEAT CAPACITY

A solid material, when heated, experiences an increase in temperature signifying that some energy has been absorbed. **Heat capacity** is a property that is indicative of a material's ability to absorb heat from the external surroundings; it represents the amount of energy required to produce a unit temperature rise. In mathematical terms, the heat capacity C is expressed as follows:

$$C = \frac{dQ}{dT} \tag{17.1}$$

where dQ is the energy required to produce a dT temperature change. Ordinarily, heat capacity is specified per mole of material (e.g., J/mol-K, or cal/mol-K). **Specific heat** (often denoted by a lowercase c) is sometimes used; this represents the heat capacity per unit mass and has various units (J/kg-K, cal/g-K, Btu/lb$_m$-°F).

There are really two ways in which this property may be measured, according to the environmental conditions accompanying the transfer of heat. One is the heat capacity while maintaining the specimen volume constant, C_v; the other is for constant external pressure, which is denoted C_p. The magnitude of C_p is always greater than C_v; however, this difference is very slight for most solid materials at room temperature and below.

VIBRATIONAL HEAT CAPACITY

In most solids the principal mode of thermal energy assimilation is by the increase in vibrational energy of the atoms. Again, atoms in solid materials are constantly vibrating at very high frequencies and with relatively small amplitudes. Rather than being independent of one another, the vibrations of adjacent atoms are coupled by virtue of the atomic bonding. These vibrations are coordinated in such a way that traveling lattice waves are produced, a phenomenon represented in Figure 17.1. These may be thought of as elastic waves or simply sound waves, having short wavelengths and very high frequencies, which propagate through the crystal at the

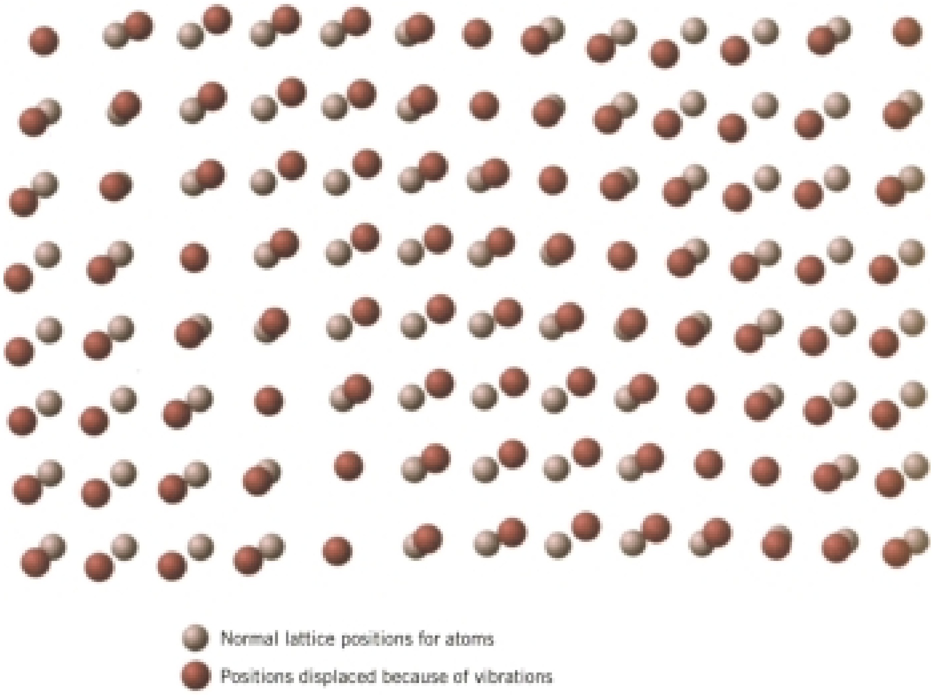
Normal lattice positions for atoms
Positions displaced because of vibrations

FIGURE 17.1 Schematic representation of the generation of lattice waves in a crystal by means of atomic vibrations. (Adapted from ‘‘The Thermal Properties of Materials’’ by J. Ziman. Copyright © 1967 by Scientific American, Inc. All rights reserved.)

velocity of sound. The vibrational thermal energy for a material consists of a series of these elastic waves, which have a range of distributions and frequencies. Only certain energy values are allowed (the energy is said to be quantized), and a single quantum of vibrational energy is called a **phonon.** (A phonon is analogous to the quantum of electromagnetic radiation, the **photon.**) On occasion, the vibrational waves themselves are termed phonons.

The thermal scattering of free electrons during electronic conduction (Section 12.7) is by these vibrational waves, and these elastic waves also participate in the transport of energy during thermal conduction (see Section 17.4).

TEMPERATURE DEPENDENCE OF THE HEAT CAPACITY

The variation with temperature of the vibrational contribution to the heat capacity at constant volume for many relatively simple crystalline solids is shown in Figure 17.2. The C_v is zero at 0 K, but it rises rapidly with temperature; this corresponds to an increased ability of the lattice waves to enhance their average energy with ascending temperature. At low temperatures the relationship between C_v and the absolute temperature T is

$$C_v = AT^3 \tag{17.2}$$

where A is a temperature-independent constant. Above what is called the *Debye temperature* θ_D, C_v levels off and becomes essentially independent of temperature at a value of approximately $3R$, R being the gas constant. Thus even though the

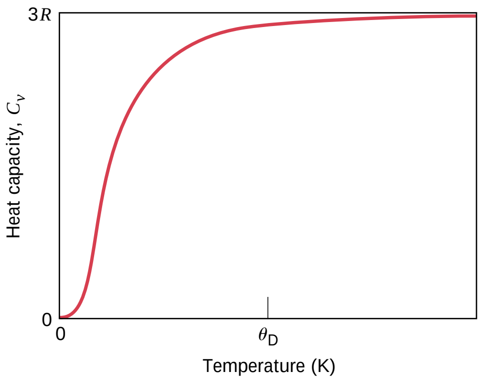

FIGURE 17.2 The temperature dependence of the heat capacity at constant volume; θ_D is the Debye temperature.

total energy of the material is increasing with temperature, the quantity of energy required to produce a one-degree temperature change is constant. The value of θ_D is below room temperature for many solid materials, and 25 J/mol-K (6 cal/mol-K) is a reasonable room-temperature approximation for C_v. Table 17.1 presents experimental specific heats for a number of materials; c_p values for still more materials are tabulated in Table B.8 of Appendix B.

OTHER HEAT CAPACITY CONTRIBUTIONS

Other energy-absorptive mechanisms also exist that can add to the total heat capacity of a solid. In most instances, however, these are minor relative to the magnitude of the vibrational contribution. There is an electronic contribution in that electrons absorb energy by increasing their kinetic energy. However, this is possible only for free electrons—those that have been excited from filled states to empty states above the Fermi energy (Section 12.6). In metals, only electrons at states near the Fermi energy are capable of such transitions, and these represent only a very small fraction of the total number. An even smaller proportion of electrons experiences excitations in insulating and semiconducting materials. Hence, this electronic contribution is ordinarily insignificant, except at temperatures near 0 K.

Furthermore, in some materials other energy-absorptive processes occur at specific temperatures, for example, the randomization of electron spins in a ferromagnetic material as it is heated through its Curie temperature. A large spike is produced on the heat capacity-versus-temperature curve at the temperature of this transformation.

17.3 THERMAL EXPANSION

Most solid materials expand upon heating and contract when cooled. The change in length with temperature for a solid material may be expressed as follows:

$$\frac{l_f - l_0}{l_0} = \alpha_l (T_f - T_0) \tag{17.3a}$$

or

$$\frac{\Delta l}{l_0} = \alpha_l \Delta T \tag{17.3b}$$

where l_0 and l_f represent, respectively, initial and final lengths with the temperature change from T_0 to T_f. The parameter α_l is called the **linear coefficient of thermal**

Table 17.1 Tabulation of the Thermal Properties for a Variety of Materials

Material	c_p *(J/kg-K)*[a]	α_l $[(°C)^{-1} \times 10^{-6}]$[b]	*k* *(W/m-K)*[c]	*L* $[\Omega\text{-}W/(K)^2 \times 10^{-8}]$
Metals				
Aluminum	900	23.6	247	2.20
Copper	386	17.0	398	2.25
Gold	128	14.2	315	2.50
Iron	448	11.8	80	2.71
Nickel	443	13.3	90	2.08
Silver	235	19.7	428	2.13
Tungsten	138	4.5	178	3.20
1025 Steel	486	12.0	51.9	—
316 Stainless steel	502	16.0	15.9	—
Brass (70Cu-30Zn)	375	20.0	120	—
Kovar (54Fe-29Ni-17Co)	460	5.1	17	2.80
Invar (64Fe-36Ni)	500	1.6	10	2.75
Super Invar (63Fe-32Ni-5Co)	500	0.72	10	2.68
Ceramics				
Alumina (Al_2O_3)	775	7.6	39	—
Magnesia (MgO)	940	13.5[d]	37.7	—
Spinel ($MgAl_2O_4$)	790	7.6[d]	15.0[e]	—
Fused silica (SiO_2)	740	0.4	1.4	—
Soda–lime glass	840	9.0	1.7	—
Borosilicate (Pyrex) glass	850	3.3	1.4	—
Polymers				
Polyethylene (high density)	1850	106–198	0.46–0.50	—
Polypropylene	1925	145–180	0.12	—
Polystyrene	1170	90–150	0.13	—
Polytetrafluoroethylene (Teflon)	1050	126–216	0.25	—
Phenol-formaldehyde, phenolic (Bakelite)	1590–1760	122	0.15	—
Nylon 6,6	1670	144	0.24	—
Polyisoprene	—	220	0.14	—

[a] To convert to cal/g-K, multiply by 2.39×10^{-4}; to convert to Btu/lb_m-°F, multiply by 2.39×10^{-4}.

[b] To convert to $(°F)^{-1}$, multiply by 0.56.

[c] To convert to cal/s-cm-K, multiply by 2.39×10^{-3}; to convert to Btu/ft-h-°F, multiply by 0.578.

[d] Value measured at 100°C.

[e] Mean value taken over the temperature range 0–1000°C.

expansion; it is a material property that is indicative of the extent to which a material expands upon heating, and has units of reciprocal temperature $[(°C)^{-1}$ or $(°F)^{-1}]$. Of course, heating or cooling affects all the dimensions of a body, with a resultant change in volume. Volume changes with temperature may be computed from

$$\frac{\Delta V}{V_0} = \alpha_v \Delta T \tag{17.4}$$

where ΔV and V_0 are the volume change and the original volume, respectively, and α_v symbolizes the volume coefficient of thermal expansion. In many materials, the value of α_v is anisotropic; that is, it depends on the crystallographic direction along which it is measured. For materials in which the thermal expansion is isotropic, α_v is approximately $3\alpha_l$.

From an atomic perspective, thermal expansion is reflected by an increase in the average distance between the atoms. This phenomenon can best be understood by consultation of the potential energy versus interatomic spacing curve for a solid material introduced previously (Figure 2.8*b*), and reproduced in Figure 17.3*a*. The curve is in the form of a potential energy trough, and the equilibrium interatomic spacing at 0 K, r_0, corresponds to the trough minimum. Heating to successively higher temperatures (T_1, T_2, T_3, etc.) raises the vibrational energy from E_1 to E_2 to E_3, and so on. The average vibrational amplitude of an atom corresponds to the trough width at each temperature, and the average interatomic distance is represented by the mean position, which increases with temperature from r_0 to r_1 to r_2, and so on.

Thermal expansion is really due to the asymmetric curvature of this potential energy trough, rather than the increased atomic vibrational amplitudes with rising temperature. If the potential energy curve were symmetric (Figure 17.3*b*), there would be no net change in interatomic separation and, consequently, no thermal expansion.

For each class of materials (metals, ceramics, and polymers), the greater the atomic bonding energy, the deeper and more narrow this potential energy trough. As a result, the increase in interatomic separation with a given rise in temperature will be lower, yielding a smaller value of α_l. Table 17.1 lists the linear coefficients of thermal expansion for several materials. With regard to temperature dependence, the magnitude of the coefficient of expansion increases with rising temperature. The values in Table 17.1 are taken at room temperature unless indicated otherwise. A more comprehensive list of coefficients of thermal expansion is provided in Table B.6 of Appendix B.

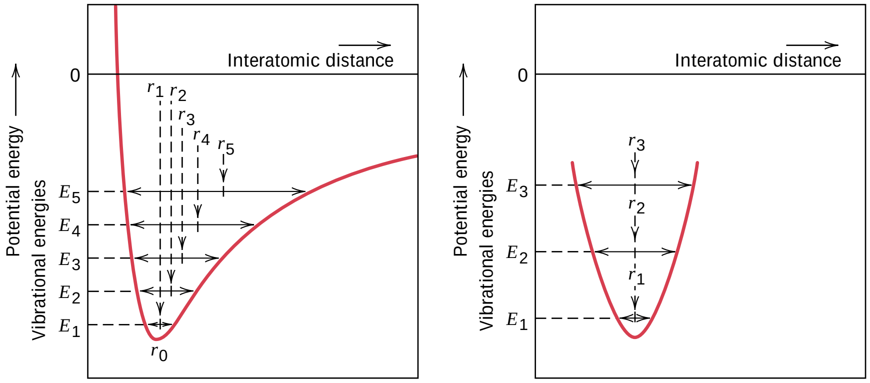

(*a*) (*b*)

FIGURE 17.3 (*a*) Plot of potential energy versus interatomic distance, demonstrating the increase in interatomic separation with rising temperature. With heating, the interatomic separation increases from r_0 to r_1 to r_2, and so on. (*b*) For a symmetric potential energy-versus-interatomic distance curve, there is no increase in interatomic separation with rising temperature (i.e., $r_1 = r_2 = r_3$). (Adapted from R. M. Rose, L. A. Shepard, and J. Wulff, *The Structure and Properties of Materials,* Vol. 4, *Electronic Properties.* Copyright © 1966 by John Wiley & Sons, New York. Reprinted by permission of John Wiley & Sons, Inc.)

METALS

As noted in Table 17.1, linear coefficients of thermal expansion for some of the common metals range between about 5×10^{-6} and 25×10^{-6} $(^\circ\text{C})^{-1}$. For some applications, a high degree of dimensional stability with temperature fluctuations is essential. This has resulted in the development of a family of iron-nickel and iron-nickel-cobalt alloys that have α_l values on the order of 1×10^{-6} $(^\circ\text{C})^{-1}$. One such alloy, tradename of Kovar (Table 17.1), has been designed to have expansion characteristics close to those of borosilicate (or Pyrex) glass; when joined to Pyrex and subjected to temperature variations, thermal stresses and possible fracture at the junction are avoided. Kovar and two other low-expansion alloys (Invar and Super-Invar) which have small α_l values are also included in Table 17.1.

CERAMICS

Relatively strong interatomic bonding forces are found in many ceramic materials as reflected in comparatively low coefficients of thermal expansion; values typically range between about 0.5×10^{-6} and 15×10^{-6} $(^\circ\text{C})^{-1}$. For noncrystalline ceramics and also those having cubic crystal structures, α_l is isotropic. Otherwise, it is anisotropic; and, in fact, some ceramic materials, upon heating, contract in some crystallographic directions while expanding in others. For inorganic glasses, the coefficient of expansion is dependent on composition. Fused silica (high-purity SiO_2 glass) has a small expansion coefficient, 0.4×10^{-6} $(^\circ\text{C})^{-1}$. This is explained by a low atomic packing density such that interatomic expansion produces relatively small macroscopic dimensional changes.

Ceramic materials that are to be subjected to temperature changes must have coefficients of thermal expansion that are relatively low, and in addition, isotropic. Otherwise, these brittle materials may experience fracture as a consequence of nonuniform dimensional changes in what is termed **thermal shock,** as discussed later in the chapter.

POLYMERS

Some polymeric materials experience very large thermal expansions upon heating as indicated by coefficients that range from approximately 50×10^{-6} to 400×10^{-6} $(^\circ\text{C})^{-1}$. The highest α_l values are found in linear and branched polymers because the secondary intermolecular bonds are weak, and there is a minimum of crosslinking. With increased crosslinking, the magnitude of the expansion coefficient diminishes; the lowest coefficients are found in the thermosetting network polymers such as phenol-formaldehyde, in which the bonding is almost entirely covalent.

17.4 THERMAL CONDUCTIVITY

Thermal conduction is the phenomenon by which heat is transported from high- to low-temperature regions of a substance. The property that characterizes the ability of a material to transfer heat is the **thermal conductivity.** It is best defined in terms of the expression

$$q = -k\frac{dT}{dx} \tag{17.5}$$

where q denotes the *heat flux*, or heat flow, per unit time per unit area (area being taken as that perpendicular to the flow direction), k is the thermal conductivity, and dT/dx is the *temperature gradient* through the conducting medium.

The units of q and k are W/m^2 (Btu/ft^2-h) and W/m-K (Btu/ft-h-°F), respectively. Equation 17.5 is valid only for steady-state heat flow, that is, for situations in which the heat flux does not change with time. Also, the minus sign in the expression indicates that the direction of heat flow is from hot to cold, or down the temperature gradient.

Equation 17.5 is similar in form to Fick's first law (Equation 6.3) for atomic diffusion. For these expressions, k is analogous to the diffusion coefficient D, and the temperature gradient parallels the concentration gradient, dC/dx.

MECHANISMS OF HEAT CONDUCTION

Heat is transported in solid materials by both lattice vibration waves (phonons) and free electrons. A thermal conductivity is associated with each of these mechanisms, and the total conductivity is the sum of the two contributions, or

$$k = k_l + k_e \tag{17.6}$$

where k_l and k_e represent the lattice vibration and electron thermal conductivities, respectively; usually one or the other predominates. The thermal energy associated with phonons or lattice waves is transported in the direction of their motion. The k_l contribution results from a net movement of phonons from high- to low-temperature regions of a body across which a temperature gradient exists.

Free or conducting electrons participate in electronic thermal conduction.To the free electrons in a hot region of the specimen is imparted a gain in kinetic energy. They then migrate to colder areas, where some of this kinetic energy is transferred to the atoms themselves (as vibrational energy) as a consequence of collisions with phonons or other imperfections in the crystal. The relative contribution of k_e to the total thermal conductivity increases with increasing free electron concentrations, since more electrons are available to participate in this heat transference process.

METALS

In high-purity metals, the electron mechanism of heat transport is much more efficient than the phonon contribution because electrons are not as easily scattered as phonons and have higher velocities. Furthermore, metals are extremely good conductors of heat because relatively large numbers of free electrons exist that participate in thermal conduction. The thermal conductivities of several of the common metals are given in Table 17.1; values generally range between about 20 and 400 W/m-K.

Since free electrons are responsible for both electrical and thermal conduction in pure metals, theoretical treatments suggest that the two conductivities should be related according to the *Wiedemann–Franz law:*

$$L = \frac{k}{\sigma T} \tag{17.7}$$

where σ is the electrical conductivity, T is the absolute temperature, and L is a constant. The theoretical value of L, 2.44×10^{-8} Ω-W/(K)^2, should be independent of temperature and the same for all metals if the heat energy is transported entirely by free electrons. Included in Table 17.1 are the experimental L values for these several metals; note that the agreement between these and the theoretical value is quite reasonable (well within a factor of 2).

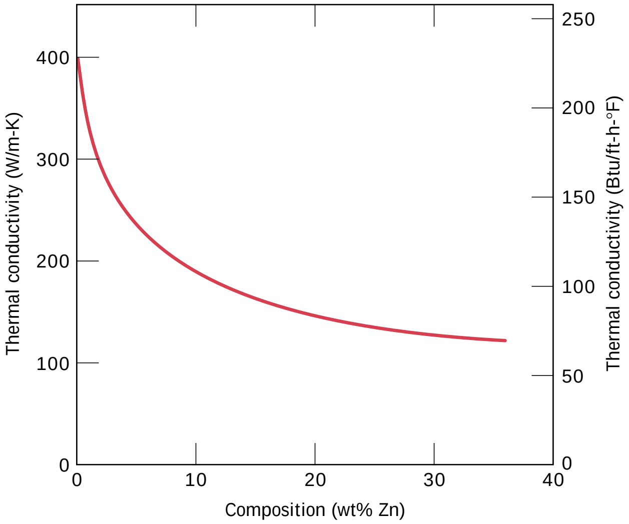

Figure 17.4 Thermal conductivity versus composition for copper–zinc alloys. (Adapted from *Metals Handbook: Properties and Selection: Nonferrous Alloys and Pure Metals,* Vol. 2, 9th edition, H. Baker, Managing Editor, American Society for Metals, 1979, p. 315.)

Alloying metals with impurities results in a reduction in the thermal conductivity, for the same reason that the electrical conductivity is diminished (Section 12.8); namely, the impurity atoms, especially if in solid solution, act as scattering centers, lowering the efficiency of electron motion. A plot of thermal conductivity versus composition for copper–zinc alloys (Figure 17.4) displays this effect. Also, stainless steels, which are highly alloyed, become relatively resistive to heat transport.

CERAMICS

Nonmetallic materials are thermal insulators inasmuch as they lack large numbers of free electrons. Thus the phonons are primarily responsible for thermal conduction: k_e is much smaller than k_l. Again, the phonons are not as effective as free electrons in the transport of heat energy as a result of the very efficient phonon scattering by lattice imperfections.

Thermal conductivity values for a number of ceramic materials are contained in Table 17.1; room-temperature thermal conductivities range between approximately 2 and 50 W/m-K. Glass and other amorphous ceramics have lower conductivities than crystalline ceramics, since the phonon scattering is much more effective when the atomic structure is highly disordered and irregular.

The scattering of lattice vibrations becomes more pronounced with rising temperature; hence, the thermal conductivity of most ceramic materials normally diminishes with increasing temperature, at least at relatively low temperatures (Figure 17.5). As Figure 17.5 indicates, the conductivity begins to increase at higher temperatures, which is due to radiant heat transfer: significant quantities of infrared radiant heat may be transported through a transparent ceramic material. The efficiency of this process increases with temperature.

Porosity in ceramic materials may have a dramatic influence on thermal conductivity; increasing the pore volume will, under most circumstances, result in a reduction of the thermal conductivity. In fact, many ceramics that are used for thermal insulation are porous. Heat transfer across pores is ordinarily slow and inefficient. Internal pores normally contain still air, which has an extremely low thermal conductivity—approximately 0.02 W/m-K. Furthermore, gaseous convection within the pores is also comparatively ineffective.

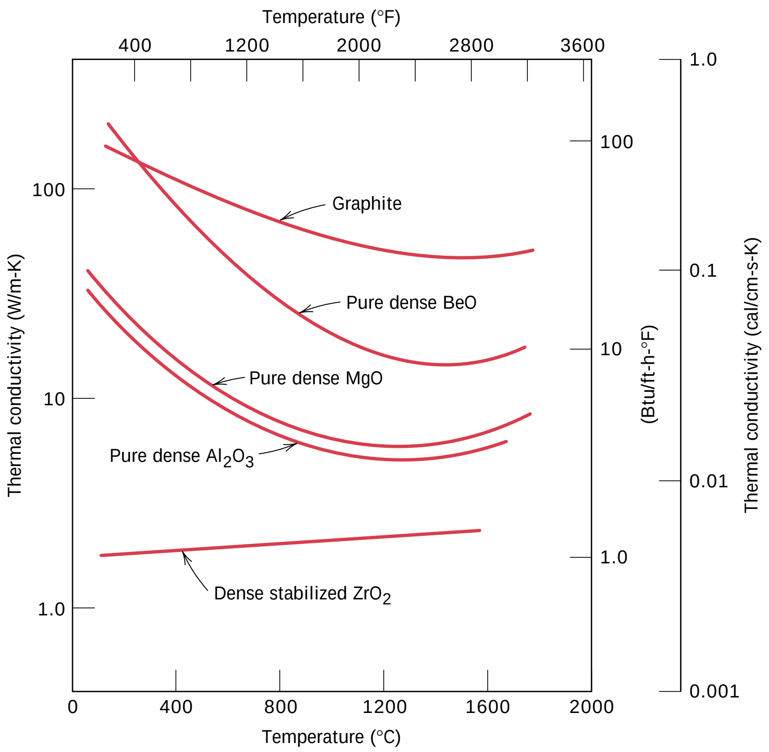

FIGURE 17.5 Dependence of thermal conductivity on temperature for several ceramic materials. (Adapted from W. D. Kingery, H. K. Bowen, and D. R. Uhlmann, *Introduction to Ceramics*, 2nd edition. Copyright © 1976 by John Wiley & Sons, New York. Reprinted by permission of John Wiley & Sons, Inc.)

POLYMERS

As noted in Table 17.1, thermal conductivities for most polymers are on the order of 0.3 W/m-K. For these materials, energy transfer is accomplished by the vibration and rotation of the chain molecules. The magnitude of the thermal conductivity depends on the degree of crystallinity; a polymer with a highly crystalline and ordered structure will have a greater conductivity than the equivalent amorphous material. This is due to the more effective coordinated vibration of the molecular chains for the crystalline state.

Polymers are often utilized as thermal insulators because of their low thermal conductivities. As with ceramics, their insulative properties may be further enhanced by the introduction of small pores, which are ordinarily introduced by foaming during polymerization (Section 13.15). Foamed polystyrene (Styrofoam) is commonly used for drinking cups and insulating chests.

17.5 THERMAL STRESSES

Thermal stresses are stresses induced in a body as a result of changes in temperature. An understanding of the origins and nature of thermal stresses is important because these stresses can lead to fracture or undesirable plastic deformation.

STRESSES RESULTING FROM RESTRAINED THERMAL EXPANSION AND CONTRACTION

Let us first consider a homogeneous and isotropic solid rod that is heated or cooled uniformly; that is, no temperature gradients are imposed. For free expansion or contraction, the rod will be stress free. If, however, axial motion of the rod is restrained by rigid end supports, thermal stresses will be introduced. The magnitude of the stress σ resulting from a temperature change from T_0 to T_f is

$$\sigma = E\alpha_l(T_0 - T_f) = E\alpha_l\Delta T \tag{17.8}$$

where E is the modulus of elasticity and α_l is the linear coefficient of thermal expansion. Upon heating ($T_f > T_0$), the stress is compressive ($\sigma < 0$), since rod expansion has been constrained. Of course, if the rod specimen is cooled ($T_f < T_0$), a tensile stress will be imposed ($\sigma > 0$). Also, the stress in Equation 17.8 is the same as that which would be required to elastically compress (or elongate) the rod specimen back to its original length after it had been allowed to freely expand (or contract) with the $T_0 - T_f$ temperature change.

EXAMPLE PROBLEM 17.1

A brass rod is to be used in an application requiring its ends to be held rigid. If the rod is stress free at room temperature [20°C (68°F)], what is the maximum temperature to which the rod may be heated without exceeding a compressive stress of 172 MPa (25,000 psi)? Assume a modulus of elasticity of 100 GPa (14.6×10^6 psi) for brass.

SOLUTION

Use Equation 17.8 to solve this problem, where the stress of 172 MPa is taken to be negative. Also, the initial temperature T_0 is 20°C, and the magnitude of the linear coefficient of thermal expansion from Table 17.1 is $20.0 \times 10^{-6}\ (°\text{C})^{-1}$. Thus, solving for the final temperature T_f yields

$$\begin{aligned} T_f &= T_0 - \frac{\sigma}{E\alpha_l} \\ &= 20° - \frac{-172\ \text{MPa}}{(100 \times 10^3\ \text{MPa})[20 \times 10^{-6}\ (°\text{C})^{-1}]} \\ &= 20°\text{C} + 86°\text{C} = 106°\text{C}\ (223°\text{F}) \end{aligned}$$

STRESSES RESULTING FROM TEMPERATURE GRADIENTS

When a solid body is heated or cooled, the internal temperature distribution will depend on its size and shape, the thermal conductivity of the material, and the rate of temperature change. Thermal stresses may be established as a result of temperature gradients across a body, which are frequently caused by rapid heating or cooling, in that the outside changes temperature more rapidly than the interior; differential dimensional changes serve to restrain the free expansion or contraction of adjacent volume elements within the piece. For example, upon heating, the exterior of a specimen is hotter and, therefore, will have expanded more than the interior regions. Hence, compressive surface stresses are induced and are balanced by tensile interior stresses. The interior–exterior stress conditions are reversed for rapid cooling such that the surface is put into a state of tension.

THERMAL SHOCK OF BRITTLE MATERIALS

For ductile metals and polymers, alleviation of thermally induced stresses may be accomplished by plastic deformation. However, the nonductility of most ceramics enhances the possibility of brittle fracture from these stresses. Rapid cooling of a brittle body is more likely to inflict such thermal shock than heating, since the induced surface stresses are tensile. Crack formation and propagation from surface flaws are more probable when an imposed stress is tensile (Section 9.6).

The capacity of a material to withstand this kind of failure is termed its *thermal shock resistance.* For a ceramic body that is rapidly cooled, the resistance to thermal shock depends not only on the magnitude of the temperature change, but also on the mechanical and thermal properties of the material. The thermal shock resistance is best for ceramics that have high fracture strengths σ_f and high thermal conductivities, as well as low moduli of elasticity and low coefficients of thermal expansion. The resistance of many materials to this type of failure may be approximated by a thermal shock resistance parameter TSR:

$$TSR \cong \frac{\sigma_f k}{E\alpha_l} \tag{17.9}$$

Thermal shock may be prevented by altering the external conditions to the degree that cooling or heating rates are reduced and temperature gradients across a body are minimized. Modification of the thermal and/or mechanical characteristics in Equation 17.9 may also enhance the thermal shock resistance of a material. Of these parameters, the coefficient of thermal expansion is probably most easily changed and controlled. For example, common soda–lime glasses, which have an α_l of approximately 9×10^{-6} $(°\text{C})^{-1}$, are particularly susceptible to thermal shock, as anyone who has baked can probably attest. Reducing the CaO and Na_2O contents while at the same time adding B_2O_3 in sufficient quantities to form borosilicate (or Pyrex) glass will reduce the coefficient of expansion to about 3×10^{-6} $(°\text{C})^{-1}$; this material is entirely suitable for kitchen oven heating and cooling cycles. The introduction of some relatively large pores or a ductile second phase may also improve the thermal shock characteristics of a material; both serve to impede the propagation of thermally induced cracks.

It is often necessary to remove thermal stresses in ceramic materials as a means of improving their mechanical strengths and optical characteristics. This may be accomplished by an annealing heat treatment, as discussed for glasses in Section 14.7.

SUMMARY

This chapter discussed heat absorption, thermal expansion, and thermal conduction—three important thermal phenomena. Heat capacity represents the quantity of heat required to produce a unit rise in temperature for one mole of a substance; on a per-unit mass basis, it is termed specific heat. Most of the energy assimilated by many solid materials is associated with increasing the vibrational energy of the atoms; contributions to the total heat capacity by other energy-absorptive mechanisms (i.e., increased free-electron kinetic energies) are normally insignificant.

For many crystalline solids and at temperatures within the vicinity of 0 K, the heat capacity measured at constant volume varies as the cube of the absolute temperature; in excess of the Debye temperature, C_v becomes temperature independent, assuming a value of approximately $3R$.

Solid materials expand when heated and contract when cooled. The fractional change in length is proportional to the temperature change, the constant of proportionality being the coefficient of thermal expansion. Thermal expansion is reflected by an increase in the average interatomic separation, which is a consequence of the asymmetric nature of the potential energy versus interatomic spacing curve trough. The larger the interatomic bonding energy, the lower the coefficient of thermal expansion.

The transport of thermal energy from high- to low-temperature regions of a material is termed thermal conduction. For steady-state heat transport, the flux is proportional to the temperature gradient along the direction of flow; the proportionality constant is the thermal conductivity.

For solid materials, heat is transported by free electrons and by vibrational lattice waves, or phonons. The high thermal conductivities for relatively pure metals are due to the large numbers of free electrons, and also the efficiency with which these electrons transport thermal energy. By way of contrast, ceramics and polymers are poor thermal conductors because free-electron concentrations are low and phonon conduction predominates.

Thermal stresses, which are introduced in a body as a consequence of temperature changes, may lead to fracture or undesirable plastic deformation. The two prime sources of thermal stresses are restrained thermal expansion (or contraction), and temperature gradients established during heating or cooling.

Thermal shock is the fracture of a body resulting from thermal stresses induced by rapid temperature changes. Because ceramic materials are brittle, they are especially susceptible to this type of failure. The thermal shock resistance of many materials is proportional to the fracture strength and thermal conductivity, and inversely proportional to both the modulus of elasticity and the coefficient of thermal expansion.

IMPORTANT TERMS AND CONCEPTS

Heat capacity
Linear coefficient of thermal expansion
Phonon
Specific heat
Thermal conductivity
Thermal shock
Thermal stress

REFERENCES

Kingery, W. D., H. K. Bowen, and D. R. Uhlmann, *Introduction to Ceramics*, 2nd edition, John Wiley & Sons, New York, 1976. Chapters 12 and 16.

Rose, R. M., L. A. Shepard, and J. Wulff, *The Structure and Properties of Materials*, Vol. IV, *Electronic Properties*, John Wiley & Sons, New York, 1966. Chapters 3 and 8.

Ziman, J., ''The Thermal Properties of Materials,'' *Scientific American*, Vol. 217, No. 3, September 1967, pp. 180–188.

QUESTIONS AND PROBLEMS

17.1 Estimate the energy required to raise the temperature of 2 kg (4.42 lb_m) of the following materials from 20 to 100°C (68 to 212°F): aluminum, steel, soda–lime glass, and high-density polyethylene.

17.2 To what temperature would 25 lb_m of a 1025 steel specimen at 25°C (77°F) be raised if 125 Btu of heat is supplied?

17.3 **(a)** Determine the room temperature heat capacities at constant pressure for the following materials: aluminum, silver, tungsten, and 70Cu-30Zn brass. **(b)** How do these values compare with one another? How do you explain this?

17.4 For aluminum, the heat capacity at constant volume C_v at 30 K is 0.81 J/mol-K, and the

Debye temperature is 375 K. Estimate the specific heat **(a)** at 50 K and **(b)** at 425 K.

17.5 The constant A in Equation 17.2 is $12\pi^4 R/5\theta_D^3$, where R is the gas constant and θ_D is the Debye temperature (K). Estimate θ_D for copper, given that the specific heat is 0.78 J/kg-K at 10 K.

17.6 **(a)** Briefly explain why C_v rises with increasing temperature at temperatures near 0 K. **(b)** Briefly explain why C_v becomes virtually independent of temperature at temperatures far removed from 0 K.

17.7 A bimetallic strip is constructed from strips of two different metals that are bonded along their lengths. Explain how such a device may be used in a thermostat to regulate temperature.

17.8 **(a)** Explain why a brass lid ring on a glass canning jar will loosen when heated. **(b)** Suppose the ring is made of tungsten instead of brass. What will be the effect of heating the lid and jar? Why?

17.9 An aluminum wire 10 m (32.8 ft) long is cooled from 38 to −1°C (100 to 30°F). How much change in length will it experience?

17.10 A 0.1 m (3.9 in.) rod of a metal elongates 0.2 mm (0.0079 in.) on heating from 20 to 100°C (68 to 212°F). Determine the value of the linear coefficient of thermal expansion for this material.

17.11 Briefly explain thermal expansion using the potential energy-versus-interatomic spacing curve.

17.12 When a metal is heated its density decreases. There are two sources that give rise to this diminishment of ρ: (1) the thermal expansion of the solid, and (2) the formation of vacancies (Section 5.2). Consider a specimen of copper at room temperature (20°C) that has a density of 8.940 g/cm^3. **(a)** Determine its density upon heating to 1000°C when only thermal expansion is considered. And **(b)** repeat the calculation when the introduction of vacancies is taken into account. Assume that the energy of vacancy formation is 0.90 eV/atom, and that the volume coefficient of thermal expansion, α_v, is equal to $3\alpha_l$.

17.13 The difference between the specific heats at constant pressure and volume is described by the expression

$$c_p - c_v = \frac{\alpha_v^2 v_0 T}{\beta} \tag{17.10}$$

where α_v is the volume coefficient of thermal expansion, v_0 is the specific volume (i.e., volume per unit mass, or the reciprocal of density), β is the compressibility, and T is the absolute temperature. Compute the values of c_v at room temperature (293 K) for copper and nickel using the data in Table 17.1, assume that $\alpha_v = 3\alpha_l$ and given that the values of β for Cu and Ni are 8.35×10^{-12} and 5.51×10^{-12} (Pa)$^{-1}$, respectively.

17.14 To what temperature must a cylindrical rod of tungsten 10.000 mm in diameter and a plate of 316 stainless steel having a circular hole 9.988 mm in diameter have to be heated for the rod to just fit into the hole? Assume that the initial temperature is 25°C.

17.15 Explain why, on a cold day, the metal door handle of an automobile feels colder to the touch than a plastic steering wheel, even though both are at the same temperature.

17.16 **(a)** Calculate the heat flux through a sheet of steel 10 mm (0.39 in.) thick if the temperatures at the two faces are 300 and 100°C (572 and 212°F); assume steady-state heat flow. **(b)** What is the heat loss per hour if the area of the sheet is 0.25 m^2 (2.7 ft^2)? **(c)** What will be the heat loss per hour if soda–lime glass instead of steel is used? **(d)** Calculate the heat loss per hour if steel is used and the thickness is increased to 20 mm (0.79 in.).

17.17 **(a)** Would you expect Equation 17.7 to be valid for ceramic and polymeric materials? Why or why not? **(b)** Estimate the value for the Wiedemann–Franz constant L [in Ω-W/(K)^2] at room temperature (293 K) for the following nonmetals: silicon (intrinsic), glass-ceramic (Pyroceram), fused silica, polycarbonate, and polytetrafluoroethylene. Consult Tables B.7 and B.9, Appendix B.

17.18 **(a)** The thermal conductivity of a single-crystal specimen is slightly greater than a polycrystalline one of the same material. Why is this so? **(b)** The thermal conductivity of a plain carbon steel is greater than for a stainless steel. Why is this so?

17.19 Briefly explain why the thermal conductivities are higher for crystalline than noncrystalline ceramics.

17.20 Briefly explain why metals are typically better thermal conductors than ceramic materials.

17.21 **(a)** Briefly explain why porosity decreases the thermal conductivity of ceramic and polymeric materials, rendering them more thermally insulative. **(b)** Briefly explain how the degree of crystallinity affects the thermal conductivity of polymeric materials and why.

17.22 For some ceramic materials, why does the thermal conductivity first decrease and then increase with rising temperature?

17.23 For each of the following pairs of materials, decide which has the larger thermal conductivity. Justify your choices.

(a) Pure silver; sterling silver (92.5 wt% Ag–7.5 wt% Cu).

(b) Fused silica; polycrystalline silica.

(c) Linear polyethylene (M_n = 450,000 g/mol); lightly branched polyethylene (M_n = 650,000 g/mol).

(d) Atactic polypropylene ($M_w = 10^6$ g/mol); isotactic polypropylene ($M_w = 5 \times 10^5$ g/mol).

17.24 We might think of a porous material as being a composite wherein one of the phases is a pore phase. Estimate upper and lower limits for the room-temperature thermal conductivity of a magnesium oxide material having a volume fraction of 0.30 of pores that are filled with still air.

17.25 Nonsteady-state heat flow may be described by the following partial differential equation:

$$\frac{\partial T}{\partial t} = D_T \frac{\partial^2 T}{\partial x^2}$$

where D_T is the thermal diffusivity; this expression is the thermal equivalent of Fick's second law of diffusion (Equation 6.4b). The thermal diffusivity is defined according to

$$D_T = \frac{k}{\rho c_p}$$

In this expression, k, ρ, and c_p represent the thermal conductivity, the mass density, and the specific heat at constant pressure, respectively.

(a) What are the SI units for D_T?

(b) Determine values of D_T for aluminum, steel, aluminum oxide, soda–lime glass, polystyrene, and nylon 6,6 using the data in Table 17.1. Density values are included in Table B.1, Appendix B.

17.26 Beginning with Equation 17.3, show that Equation 17.8 is valid.

17.27 **(a)** Briefly explain why thermal stresses may be introduced into a structure by rapid heating or cooling. **(b)** For cooling, what is the nature of the surface stresses? **(c)** For heating, what is the nature of the surface stresses? **(d)** For a ceramic material, is thermal shock more likely to occur on rapid heating or cooling? Why?

17.28 **(a)** If a rod of 1025 steel 0.5 m (19.7 in.) long is heated from 20 to 80°C (68 to 176°F) while its ends are maintained rigid, determine the type and magnitude of stress that develops. Assume that at 20°C the rod is stress free. **(b)** What will be the stress magnitude if a rod 1 m (39.4 in.) long is used? **(c)** If the rod in part a is cooled from 20° to −10°C (68 to 14°F), what type and magnitude of stress will result?

17.29 A copper wire is stretched with a stress of 70 MPa (10,000 psi) at 20°C (68°F). If the length is held constant, to what temperature must the wire be heated to reduce the stress to 35 MPa (5000 psi)?

17.30 If a cylindrical rod of nickel 100.00 mm long and 8.000 mm in diameter is heated from 20°C to 200°C while its ends are maintained rigid, determine its change in diameter. You may want to consult Table 7.1.

17.31 The two ends of a cylindrical rod of 1025 steel 75.00 mm long and 10.000 mm in diameter are maintained rigid. If the rod is initially at 25°C, to what temperature must it be cooled to have a 0.008-mm reduction in diameter?

17.32 What measures may be taken to reduce the likelihood of thermal shock of a ceramic piece?

Design Problems

17.D1 Railroad tracks made of 1025 steel are to be laid during the time of year when the temperature averages 10°C (50°F). If a joint space of 4.6 mm (0.180 in.) is allowed between the standard 11.9-m (39-ft) long rails, what is the hottest possible temperature that can be tolerated without the introduction of thermal stresses?

17.D2 The ends of a cylindrical rod 6.4 mm (0.25 in.) in diameter and 250 mm (10 in.) long are mounted between rigid supports. The rod is stress free at room temperature [20°C (68°F)]; and upon cooling to −40°C (−40°F), a maximum thermally induced tensile stress of 125 MPa (18,125 psi) is possible. Of which of the following metals or alloys may the rod be fabricated: aluminum, copper, brass, 1025 steel, and tungsten? Why?

17.D3 **(a)** What are the units for the thermal shock resistance parameter (TSR)? **(b)** Rank the following ceramic materials according to their thermal shock resistance: glass-ceramic (Pyroceram), partially stabilized zirconia, and borosilicate (Pyrex) glass. Appropriate data may be found in Tables B.2, B.4, B.6, and B.7, Appendix B.

17.D4 Equation 17.9, for the thermal shock resistance of a material, is valid for relatively low rates of heat transfer. When the rate is high, then, upon cooling of a body, the maximum temperature change allowable without thermal shock, ΔT_f, is approximately

$$\Delta T_f \cong \frac{\sigma_f}{E\alpha_l}$$

where σ_f is the fracture strength. Using the data in Tables B.2, B.4, and B.6 (Appendix B), determine ΔT_f for a glass-ceramic (Pyroceram), partially stabilized zirconia, and fused silica.

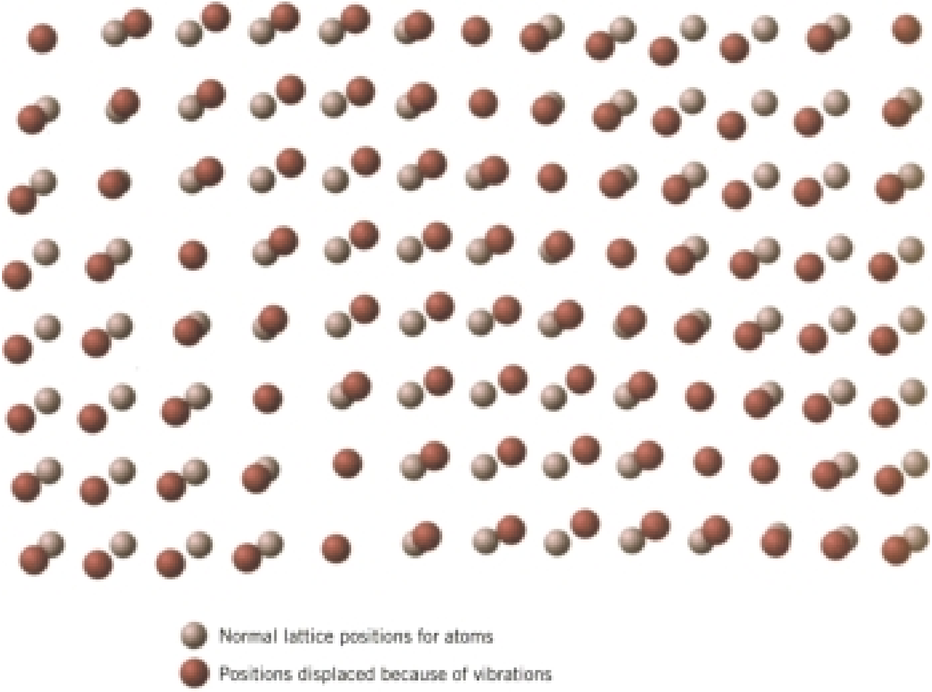
Normal lattice positions for atoms
Positions displaced because of vibrations

FIGURE 17.1 Schematic representation of the generation of lattice waves in a crystal by means of atomic vibrations. (Adapted from ‘‘The Thermal Properties of Materials’’ by J. Ziman. Copyright © 1967 by Scientific American, Inc. All rights reserved.)

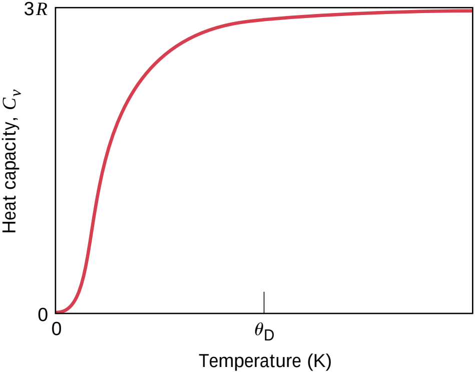

Figure 17.2 The temperature dependence of the heat capacity at constant volume; θ_D is the Debye temperature.

Table 17.1 Tabulation of the Thermal Properties for a Variety of Materials

Material	c_p *(J/kg-K)*[a]	α_l $[(°C)^{-1} \times 10^{-6}]$[b]	*k* *(W/m-K)*[c]	*L* $[\Omega\text{-}W/(K)^2 \times 10^{-8}]$
		Metals		
Aluminum	900	23.6	247	2.20
Copper	386	17.0	398	2.25
Gold	128	14.2	315	2.50
Iron	448	11.8	80	2.71
Nickel	443	13.3	90	2.08
Silver	235	19.7	428	2.13
Tungsten	138	4.5	178	3.20
1025 Steel	486	12.0	51.9	—
316 Stainless steel	502	16.0	15.9	—
Brass (70Cu-30Zn)	375	20.0	120	—
Kovar (54Fe-29Ni-17Co)	460	5.1	17	2.80
Invar (64Fe-36Ni)	500	1.6	10	2.75
Super Invar (63Fe-32Ni-5Co)	500	0.72	10	2.68
		Ceramics		
Alumina (Al_2O_3)	775	7.6	39	—
Magnesia (MgO)	940	13.5[d]	37.7	—
Spinel ($MgAl_2O_4$)	790	7.6[d]	15.0[e]	—
Fused silica (SiO_2)	740	0.4	1.4	—
Soda–lime glass	840	9.0	1.7	—
Borosilicate (Pyrex) glass	850	3.3	1.4	—
		Polymers		
Polyethylene (high density)	1850	106–198	0.46–0.50	—
Polypropylene	1925	145–180	0.12	—
Polystyrene	1170	90–150	0.13	—
Polytetrafluoroethylene (Teflon)	1050	126–216	0.25	—
Phenol-formaldehyde, phenolic (Bakelite)	1590–1760	122	0.15	—
Nylon 6,6	1670	144	0.24	—
Polyisoprene	—	220	0.14	—

[a] To convert to cal/g-K, multiply by 2.39×10^{-4}; to convert to Btu/lb_m-°F, multiply by 2.39×10^{-4}.

[b] To convert to $(°F)^{-1}$, multiply by 0.56.

[c] To convert to cal/s-cm-K, multiply by 2.39×10^{-3}; to convert to Btu/ft-h-°F, multiply by 0.578.

[d] Value measured at 100°C.

[e] Mean value taken over the temperature range 0–1000°C.

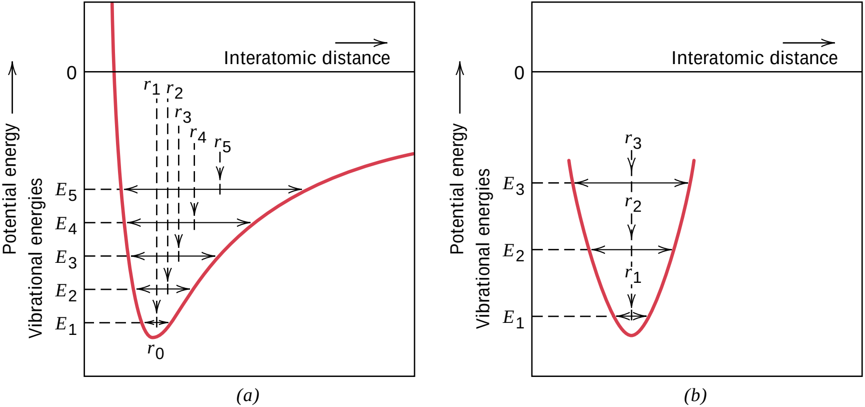

FIGURE 17.3 (*a*) Plot of potential energy versus interatomic distance, demonstrating the increase in interatomic separation with rising temperature. With heating, the interatomic separation increases from r_0 to r_1 to r_2, and so on. (*b*) For a symmetric potential energy-versus-interatomic distance curve, there is no increase in interatomic separation with rising temperature (i.e., $r_1 = r_2 = r_3$). (Adapted from R. M. Rose, L. A. Shepard, and J. Wulff, *The Structure and Properties of Materials*, Vol. 4, *Electronic Properties*. Copyright © 1966 by John Wiley & Sons, New York. Reprinted by permission of John Wiley & Sons, Inc.)

Chapter 6 / Diffusion

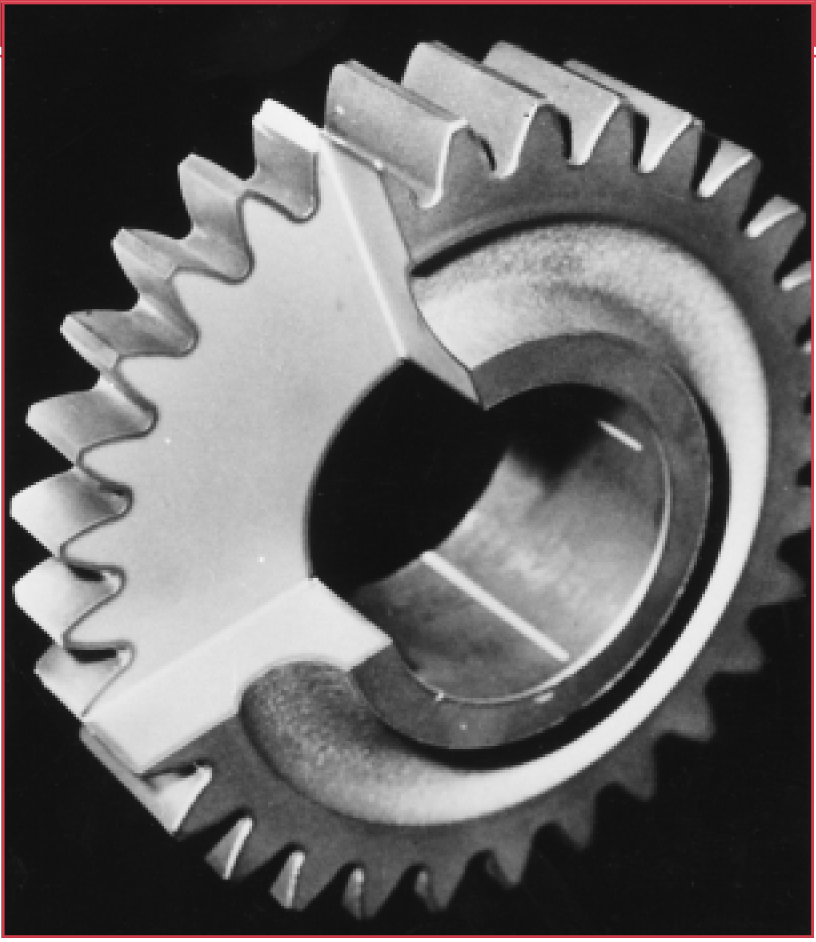

Photograph of a steel gear that has been "case hardened." The outer surface layer was selectively hardened by a high-temperature heat treatment during which carbon from the surrounding atmosphere diffused into the surface. The "case" appears as the dark outer rim of that segment of the gear that has been sectioned. Actual size. (Photograph courtesy of Surface Division Midland-Ross.)

Why Study *Diffusion*?

Materials of all types are often heat treated to improve their properties. The phenomena that occur during a heat treatment almost always involve atomic diffusion. Often an enhancement of diffusion rate is desired; on occasion measures are taken to reduce it. Heat-treating temperatures and times, and/or cooling rates are often predictable using the mathematics of diffusion and appropriate diffusion constants. The steel gear shown on this page has been case hardened (Section 9.14); that is, its hardness and resistance to failure by fatigue have been enhanced by diffusing excess carbon or nitrogen into the outer surface layer.

Learning Objectives

After studying this chapter you should be able to do the following:

1. **Name and describe the two atomic mechanisms of diffusion.**
2. **Distinguish between steady-state and nonsteady-state diffusion.**
3. **(a) Write Fick's first and second laws in equation form, and define all parameters.**
   (b) Note the kind of diffusion for which each of these equations is normally applied.
4. **Write the solution to Fick's second law for diffusion into a semi-infinite solid when the concentration of diffusing species at the surface is held constant. Define all parameters in this equation.**
5. **Calculate the diffusion coefficient for some material at a specified temperature, given the appropriate diffusion constants.**
6. **Note one difference in diffusion mechanisms for metals and ionic solids.**

6.1 INTRODUCTION

Many reactions and processes that are important in the treatment of materials rely on the transfer of mass either within a specific solid (ordinarily on a microscopic level) or from a liquid, a gas, or another solid phase. This is necessarily accomplished by **diffusion,** the phenomenon of material transport by atomic motion. This chapter discusses the atomic mechanisms by which diffusion occurs, the mathematics of diffusion, and the influence of temperature and diffusing species on the rate of diffusion.

The phenomenon of diffusion may be demonstrated with the use of a *diffusion couple,* which is formed by joining bars of two different metals together so that there is intimate contact between the two faces; this is illustrated for copper and nickel in Figure 6.1, which includes schematic representations of atom positions and composition across the interface. This couple is heated for an extended period at an elevated temperature (but below the melting temperature of both metals), and cooled to room temperature. Chemical analysis will reveal a condition similar to that represented in Figure 6.2, namely, pure copper and nickel at the two extremities of the couple, separated by an alloyed region. Concentrations of both metals vary with position as shown in Figure 6.2*c*. This result indicates that copper atoms have migrated or diffused into the nickel, and that nickel has diffused into copper. This process, whereby atoms of one metal diffuse into another, is termed **interdiffusion,** or **impurity diffusion.**

Interdiffusion may be discerned from a macroscopic perspective by changes in concentration which occur over time, as in the example for the Cu–Ni diffusion couple. There is a net drift or transport of atoms from high to low concentration regions. Diffusion also occurs for pure metals, but all atoms exchanging positions are of the same type; this is termed **self-diffusion.** Of course, self-diffusion is not normally subject to observation by noting compositional changes.

6.2 DIFFUSION MECHANISMS

From an atomic perspective, diffusion is just the stepwise migration of atoms from lattice site to lattice site. In fact, the atoms in solid materials are in constant motion, rapidly changing positions. For an atom to make such a move, two conditions must be met: (1) there must be an empty adjacent site, and (2) the atom must have sufficient energy to break bonds with its neighbor atoms and then cause some lattice distortion during the displacement. This energy is vibrational in nature (Section 5.10). At a specific temperature some small fraction of the total number of atoms

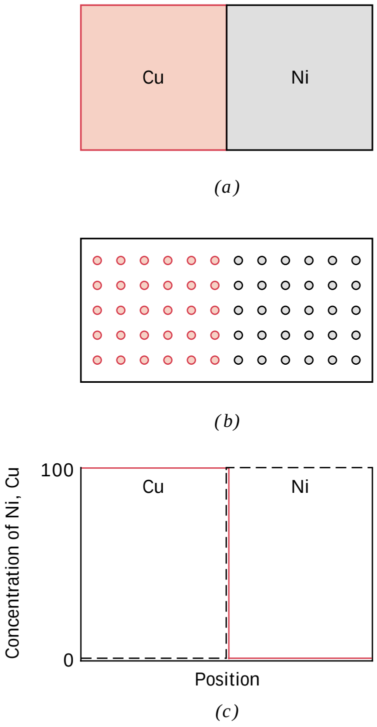
Cu
Ni
(a)
(b)
100
0
Concentration of Ni, Cu
Cu
Ni
Position
(c)

Figure 6.1 (*a*) A copper–nickel diffusion couple before a high-temperature heat treatment. (*b*) Schematic representations of Cu (colored circles) and Ni (gray circles) atom locations within the diffusion couple. (*c*) Concentrations of copper and nickel as a function of position across the couple.

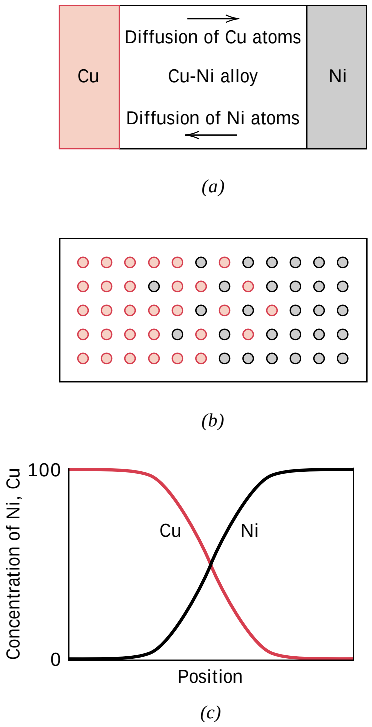
Cu
Diffusion of Cu atoms
Cu-Ni alloy
Diffusion of Ni atoms
Ni
(a)
(b)
100
0
Concentration of Ni, Cu
Cu
Ni
Position
(c)

Figure 6.2 (*a*) A copper–nickel diffusion couple after a high-temperature heat treatment, showing the alloyed diffusion zone. (*b*) Schematic representations of Cu (colored circles) and Ni (gray circles) atom locations within the couple. (*c*) Concentrations of copper and nickel as a function of position across the couple.

is capable of diffusive motion, by virtue of the magnitudes of their vibrational energies. This fraction increases with rising temperature.

Several different models for this atomic motion have been proposed; of these possibilities, two dominate for metallic diffusion.

VACANCY DIFFUSION

One mechanism involves the interchange of an atom from a normal lattice position to an adjacent vacant lattice site or vacancy, as represented schematically in Figure 6.3*a*. This mechanism is aptly termed **vacancy diffusion.** Of course, this process necessitates the presence of vacancies, and the extent to which vacancy diffusion can occur is a function of the number of these defects that are present; significant concentrations of vacancies may exist in metals at elevated temperatures (Section 5.2). Since diffusing atoms and vacancies exchange positions, the diffusion of atoms in one direction corresponds to the motion of vacancies in the opposite direction. Both self-diffusion and interdiffusion occur by this mechanism; for the latter, the impurity atoms must substitute for host atoms.

INTERSTITIAL DIFFUSION

The second type of diffusion involves atoms that migrate from an interstitial position to a neighboring one that is empty. This mechanism is found for interdiffusion of impurities such as hydrogen, carbon, nitrogen, and oxygen, which have atoms that are small enough to fit into the interstitial positions. Host or substitutional impurity atoms rarely form interstitials and do not normally diffuse via this mechanism. This phenomenon is appropriately termed **interstitial diffusion** (Figure 6.3*b*).

In most metal alloys, interstitial diffusion occurs much more rapidly than diffusion by the vacancy mode, since the interstitial atoms are smaller, and thus more

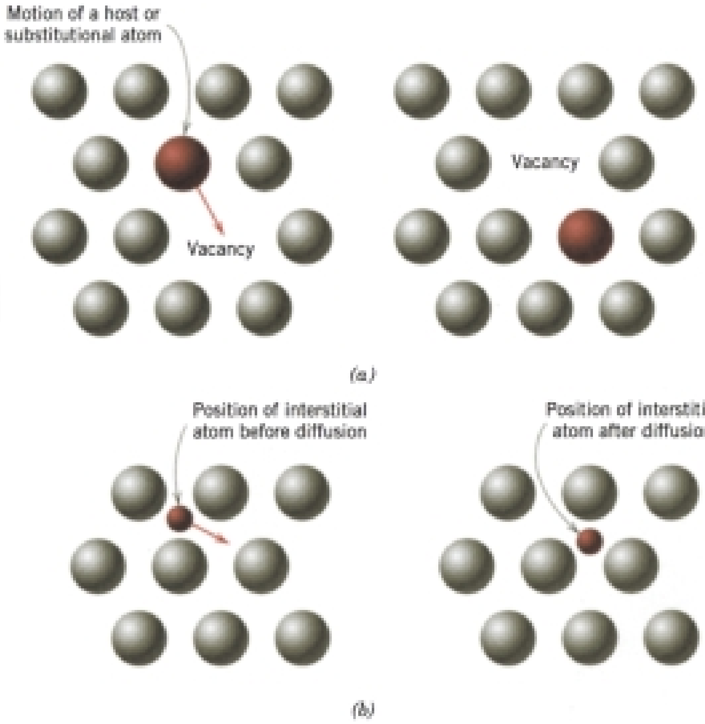
Motion of a host or substitutional atom
Vacancy
Vacancy
(a)
Position of interstitial atom before diffusion
Position of interstitial atom after diffusion
(b)

FIGURE 6.3 Schematic representations of (*a*) vacancy diffusion and (*b*) interstitial diffusion.

mobile. Furthermore, there are more empty interstitial positions than vacancies; hence, the probability of interstitial atomic movement is greater than for vacancy diffusion.

6.3 STEADY-STATE DIFFUSION

Diffusion is a time-dependent process—that is, in a macroscopic sense, the quantity of an element that is transported within another is a function of time. Often it is necessary to know how fast diffusion occurs, or the rate of mass transfer. This rate is frequently expressed as a **diffusion flux** (J), defined as the mass (or, equivalently, the number of atoms) M diffusing through and perpendicular to a unit cross-sectional area of solid per unit of time. In mathematical form, this may be represented as

$$J = \frac{M}{At} \tag{6.1a}$$

where A denotes the area across which diffusion is occurring and t is the elapsed diffusion time. In differential form, this expression becomes

$$J = \frac{1}{A}\frac{dM}{dt} \tag{6.1b}$$

The units for J are kilograms or atoms per meter squared per second (kg/m^2-s or atoms/m^2-s).

If the diffusion flux does not change with time, a steady-state condition exists. One common example of **steady-state diffusion** is the diffusion of atoms of a gas through a plate of metal for which the concentrations (or pressures) of the diffusing species on both surfaces of the plate are held constant. This is represented schematically in Figure 6.4*a*.

When concentration C is plotted versus position (or distance) within the solid x, the resulting curve is termed the **concentration profile;** the slope at a particular

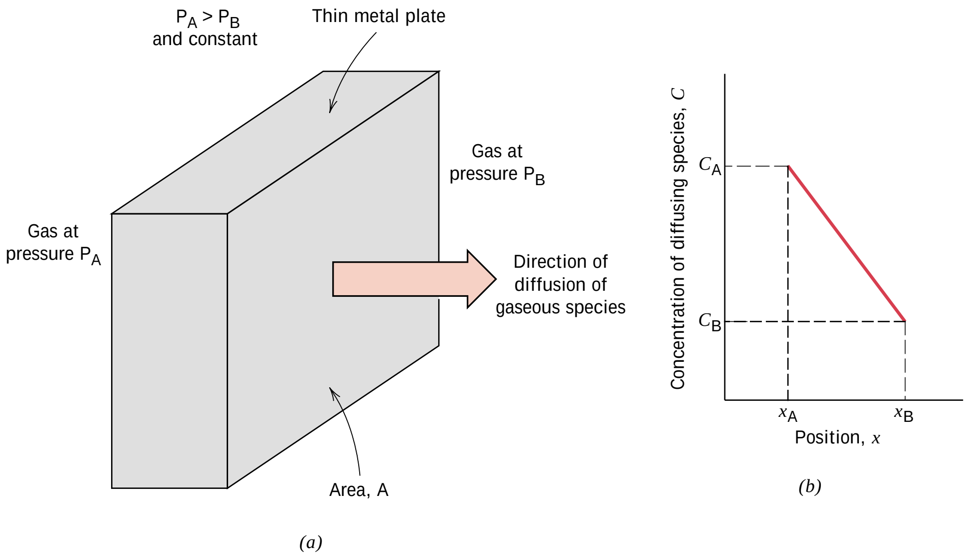
$P_A > P_B$
and constant
Thin metal plate
Gas at
pressure P_B
Gas at
pressure P_A
Direction of
diffusion of
gaseous species
Area, A
(a)
Concentration of diffusing species, C
C_A
C_B
x_A
x_B
Position, x
(b)

FIGURE 6.4 (*a*) Steady-state diffusion across a thin plate. (*b*) A linear concentration profile for the diffusion situation in (*a*).

point on this curve is the **concentration gradient:**

$$\text{concentration gradient} = \frac{dC}{dx} \tag{6.2a}$$

In the present treatment, the concentration profile is assumed to be linear, as depicted in Figure 6.4*b*, and

$$\text{concentration gradient} = \frac{\Delta C}{\Delta x} = \frac{C_A - C_B}{x_A - x_B} \tag{6.2b}$$

For diffusion problems, it is sometimes convenient to express concentration in terms of mass of diffusing species per unit volume of solid (kg/m^3 or g/cm^3).[1]

The mathematics of steady-state diffusion in a single (x) direction is relatively simple, in that the flux is proportional to the concentration gradient through the expression

$$J = -D\frac{dC}{dx} \tag{6.3}$$

The constant of proportionality D is called the **diffusion coefficient,** which is expressed in square meters per second. The negative sign in this expression indicates that the direction of diffusion is down the concentration gradient, from a high to a low concentration. Equation 6.3 is sometimes called **Fick's first law.**

Sometimes the term **driving force** is used in the context of what compels a reaction to occur. For diffusion reactions, several such forces are possible; but when diffusion is according to Equation 6.3, the concentration gradient is the driving force.

One practical example of steady-state diffusion is found in the purification of hydrogen gas. One side of a thin sheet of palladium metal is exposed to the impure gas composed of hydrogen and other gaseous species such as nitrogen, oxygen, and water vapor. The hydrogen selectively diffuses through the sheet to the opposite side, which is maintained at a constant and lower hydrogen pressure.

EXAMPLE PROBLEM 6.1

A plate of iron is exposed to a carburizing (carbon-rich) atmosphere on one side and a decarburizing (carbon-deficient) atmosphere on the other side at 700°C (1300°F). If a condition of steady state is achieved, calculate the diffusion flux of carbon through the plate if the concentrations of carbon at positions of 5 and 10 mm (5×10^{-3} and 10^{-2} m) beneath the carburizing surface are 1.2 and 0.8 kg/m^3, respectively. Assume a diffusion coefficient of 3×10^{-11} m^2/s at this temperature.

SOLUTION

Fick's first law, Equation 6.3, is utilized to determine the diffusion flux. Substitution of the values above into this expression yields

$$J = -D\frac{C_A - C_B}{x_A - x_B} = -(3 \times 10^{-11}\ \text{m}^2/\text{s})\frac{(1.2 - 0.8)\ \text{kg/m}^3}{(5 \times 10^{-3} - 10^{-2})\ \text{m}}$$

$$= 2.4 \times 10^{-9}\ \text{kg/m}^2\text{-s}$$

---

[1] Conversion of concentration from weight percent to mass per unit volume (in kg/m^3) is possible using {Equation 5.9.}

6.4 NONSTEADY-STATE DIFFUSION

Most practical diffusion situations are nonsteady-state ones. That is, the diffusion flux and the concentration gradient at some particular point in a solid vary with time, with a net accumulation or depletion of the diffusing species resulting. This is illustrated in Figure 6.5, which shows concentration profiles at three different diffusion times. Under conditions of nonsteady state, use of Equation 6.3 is no longer convenient; instead, the partial differential equation

$$\frac{\partial C}{\partial t} = \frac{\partial}{\partial x}\left(D\frac{\partial C}{\partial x}\right) \tag{6.4a}$$

known as **Fick's second law,** is used. If the diffusion coefficient is independent of composition (which should be verified for each particular diffusion situation), Equation 6.4a simplifies to

$$\frac{\partial C}{\partial t} = D\frac{\partial^2 C}{\partial x^2} \tag{6.4b}$$

Solutions to this expression (concentration in terms of both position and time) are possible when physically meaningful boundary conditions are specified. Comprehensive collections of these are given by Crank, and Carslaw and Jaeger (see References).

One practically important solution is for a semi-infinite solid[2] in which the surface concentration is held constant. Frequently, the source of the diffusing species is a gas phase, the partial pressure of which is maintained at a constant value. Furthermore, the following assumptions are made:

1. Before diffusion, any of the diffusing solute atoms in the solid are uniformly distributed with concentration of C_0.
2. The value of x at the surface is zero and increases with distance into the solid.

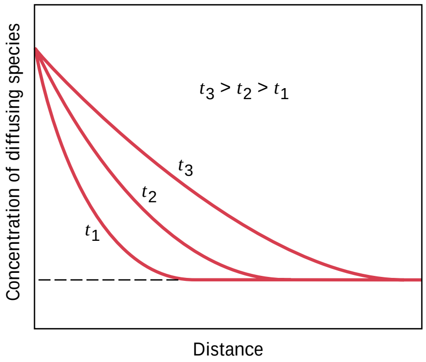

FIGURE 6.5 Concentration profiles for nonsteady-state diffusion taken at three different times, t_1, t_2, and t_3.

---

[2] A bar of solid is considered to be semi-infinite if none of the diffusing atoms reaches the bar end during the time over which diffusion takes place. A bar of length l is considered to be semi-infinite when $l > 10\sqrt{Dt}$.

3. The time is taken to be zero the instant before the diffusion process begins.

These boundary conditions are simply stated as

For $t = 0$, $C = C_0$ at $0 \leq x \leq \infty$

For $t > 0$, $C = C_s$ (the constant surface concentration) at $x = 0$

$C = C_0$ at $x = \infty$

Application of these boundary conditions to Equation 6.4b yields the solution

$$\frac{C_x - C_0}{C_s - C_0} = 1 - \operatorname{erf}\left(\frac{x}{2\sqrt{Dt}}\right) \tag{6.5}$$

where C_x represents the concentration at depth x after time t. The expression $\operatorname{erf}(x/2\sqrt{Dt})$ is the Gaussian error function,[3] values of which are given in mathematical tables for various $x/2\sqrt{Dt}$ values; a partial listing is given in Table 6.1. The concentration parameters that appear in Equation 6.5 are noted in Figure 6.6, a concentration profile taken at a specific time. Equation 6.5 thus demonstrates the relationship between concentration, position, and time, namely, that C_x, being a function of the dimensionless parameter $x/\sqrt{Dt}$, may be determined at any time and position if the parameters C_0, C_s, and D are known.

Suppose that it is desired to achieve some specific concentration of solute, C_1, in an alloy; the left-hand side of Equation 6.5 now becomes

$$\frac{C_1 - C_0}{C_s - C_0} = \text{constant}$$

Table 6.1 Tabulation of Error Function Values

z	*erf(z)*	*z*	*erf(z)*	*z*	*erf(z)*
0	0	0.55	0.5633	1.3	0.9340
0.025	0.0282	0.60	0.6039	1.4	0.9523
0.05	0.0564	0.65	0.6420	1.5	0.9661
0.10	0.1125	0.70	0.6778	1.6	0.9763
0.15	0.1680	0.75	0.7112	1.7	0.9838
0.20	0.2227	0.80	0.7421	1.8	0.9891
0.25	0.2763	0.85	0.7707	1.9	0.9928
0.30	0.3286	0.90	0.7970	2.0	0.9953
0.35	0.3794	0.95	0.8209	2.2	0.9981
0.40	0.4284	1.0	0.8427	2.4	0.9993
0.45	0.4755	1.1	0.8802	2.6	0.9998
0.50	0.5205	1.2	0.9103	2.8	0.9999

---

[3] This Gaussian error function is defined by

$$\operatorname{erf}(z) = \frac{2}{\sqrt{\pi}} \int_0^z e^{-y^2}\, dy$$

where $x/2\sqrt{Dt}$ has been replaced by the variable z.

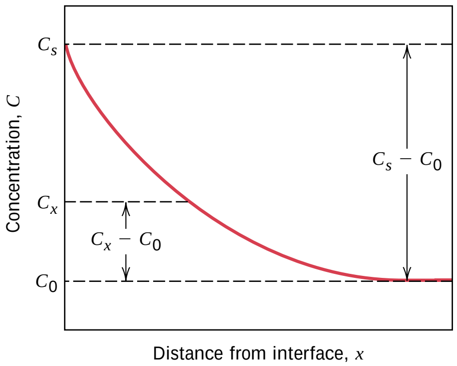

Figure 6.6 Concentration profile for nonsteady-state diffusion; concentration parameters relate to Equation 6.5.

This being the case, the right-hand side of this same expression is also a constant, and subsequently

$$\frac{x}{2\sqrt{Dt}} = \text{constant} \tag{6.6a}$$

or

$$\frac{x^2}{Dt} = \text{constant} \tag{6.6b}$$

Some diffusion computations are thus facilitated on the basis of this relationship, as demonstrated in Example Problem 6.3.

EXAMPLE PROBLEM 6.2

For some applications, it is necessary to harden the surface of a steel (or iron-carbon alloy) above that of its interior. One way this may be accomplished is by increasing the surface concentration of carbon in a process termed **carburizing;** the steel piece is exposed, at an elevated temperature, to an atmosphere rich in a hydrocarbon gas, such as methane (CH_4).

Consider one such alloy that initially has a uniform carbon concentration of 0.25 wt% and is to be treated at 950°C (1750°F). If the concentration of carbon at the surface is suddenly brought to and maintained at 1.20 wt%, how long will it take to achieve a carbon content of 0.80 wt% at a position 0.5 mm below the surface? The diffusion coefficient for carbon in iron at this temperature is 1.6×10^{-11} m^2/s; assume that the steel piece is semi-infinite.

SOLUTION

Since this is a nonsteady-state diffusion problem in which the surface composition is held constant, Equation 6.5 is used. Values for all the parameters in this expression except time t are specified in the problem as follows:

$$C_0 = 0.25 \text{ wt\% C}$$

$$C_s = 1.20 \text{ wt\% C}$$

$$C_x = 0.80 \text{ wt\% C}$$

$$x = 0.50 \text{ mm} = 5 \times 10^{-4} \text{ m}$$

$$D = 1.6 \times 10^{-11} \text{ m}^2\text{/s}$$

Thus,

$$\frac{C_x - C_0}{C_s - C_0} = \frac{0.80 - 0.25}{1.20 - 0.25} = 1 - \text{erf}\left[\frac{(5 \times 10^{-4}\ \text{m})}{2\sqrt{(1.6 \times 10^{-11}\ \text{m}^2/\text{s})(t)}}\right]$$

$$0.4210 = \text{erf}\left(\frac{62.5\ \text{s}^{1/2}}{\sqrt{t}}\right)$$

We must now determine from Table 6.1 the value of z for which the error function is 0.4210. An interpolation is necessary, as

z	erf(z)
0.35	0.3794
z	0.4210
0.40	0.4284

$$\frac{z - 0.35}{0.40 - 0.35} = \frac{0.4210 - 0.3794}{0.4284 - 0.3794}$$

or

$$z = 0.392$$

Therefore,

$$\frac{62.5\ \text{s}^{1/2}}{\sqrt{t}} = 0.392$$

and solving for t,

$$t = \left(\frac{62.5\ \text{s}^{1/2}}{0.392}\right)^2 = 25{,}400\ \text{s} = 7.1\ \text{h}$$

EXAMPLE PROBLEM 6.3

The diffusion coefficients for copper in aluminum at 500 and 600°C are 4.8×10^{-14} and $5.3 \times 10^{-13}\ \text{m}^2/\text{s}$, respectively. Determine the approximate time at 500°C that will produce the same diffusion result (in terms of concentration of Cu at some specific point in Al) as a 10-h heat treatment at 600°C.

SOLUTION

This is a diffusion problem in which Equation 6.6b may be employed. The composition in both diffusion situations will be equal at the same position (i.e., x is also a constant), thus

$$Dt = \text{constant} \tag{6.7}$$

at both temperatures. That is,

$$D_{500}t_{500} = D_{600}t_{600}$$

or

$$t_{500} = \frac{D_{600}t_{600}}{D_{500}} = \frac{(5.3 \times 10^{-13}\ \text{m}^2/\text{s})(10\ \text{h})}{4.8 \times 10^{-14}\ \text{m}^2/\text{s}} = 110.4\ \text{h}$$

6.5 FACTORS THAT INFLUENCE DIFFUSION

DIFFUSING SPECIES

The magnitude of the diffusion coefficient D is indicative of the rate at which atoms diffuse. Coefficients, both self- and interdiffusion, for several metallic systems are listed in Table 6.2. The diffusing species as well as the host material influence the diffusion coefficient. For example, there is a significant difference in magnitude between self- and carbon interdiffusion in α iron at 500°C, the D value being greater for the carbon interdiffusion (3.0×10^{-21} vs. 2.4×10^{-12} m^2/s). This comparison also provides a contrast between rates of diffusion via vacancy and interstitial modes as discussed above. Self-diffusion occurs by a vacancy mechanism, whereas carbon diffusion in iron is interstitial.

TEMPERATURE

Temperature has a most profound influence on the coefficients and diffusion rates. For example, for the self-diffusion of Fe in α-Fe, the diffusion coefficient increases approximately six orders of magnitude (from 3.0×10^{-21} to 1.8×10^{-15} m^2/s) in rising temperature from 500 to 900°C (Table 6.2). The temperature dependence of diffusion coefficients is related to temperature according to

$$D = D_0 \exp\left(-\frac{Q_d}{RT}\right) \tag{6.8}$$

where

D_0 = a temperature-independent preexponential (m^2/s)

Q_d = the **activation energy** for diffusion (J/mol, cal/mol, or eV/atom)

Table 6.2 A Tabulation of Diffusion Data

Diffusing Species	*Host Metal*	D_0*(m²/s)*	*Activation Energy* Q_d		*Calculated Values*	
			kJ/mol	*eV/atom*	T*(°C)*	D*(m²/s)*
Fe	α-Fe	2.8×10^{-4}	251	2.60	500	3.0×10^{-21}
	(BCC)				900	1.8×10^{-15}
Fe	γ-Fe	5.0×10^{-5}	284	2.94	900	1.1×10^{-17}
	(FCC)				1100	7.8×10^{-16}
C	α-Fe	6.2×10^{-7}	80	0.83	500	2.4×10^{-12}
					900	1.7×10^{-10}
C	γ-Fe	2.3×10^{-5}	148	1.53	900	5.9×10^{-12}
					1100	5.3×10^{-11}
Cu	Cu	7.8×10^{-5}	211	2.19	500	4.2×10^{-19}
Zn	Cu	2.4×10^{-5}	189	1.96	500	4.0×10^{-18}
Al	Al	2.3×10^{-4}	144	1.49	500	4.2×10^{-14}
Cu	Al	6.5×10^{-5}	136	1.41	500	4.1×10^{-14}
Mg	Al	1.2×10^{-4}	131	1.35	500	1.9×10^{-13}
Cu	Ni	2.7×10^{-5}	256	2.65	500	1.3×10^{-22}

Source: E. A. Brandes and G. B. Brook (Editors), *Smithells Metals Reference Book*, 7th edition, Butterworth-Heinemann, Oxford, 1992.

R = the gas constant, 8.31 J/mol-K, 1.987 cal/mol-K, or 8.62×10^{-5} eV/atom-K

T = absolute temperature (K)

The activation energy may be thought of as that energy required to produce the diffusive motion of one mole of atoms. A large activation energy results in a relatively small diffusion coefficient. Table 6.2 also contains a listing of D_0 and Q_d values for several diffusion systems.

Taking natural logarithms of Equation 6.8 yields

$$\ln D = \ln D_0 - \frac{Q_d}{R}\left(\frac{1}{T}\right) \tag{6.9a}$$

Or in terms of logarithms to the base 10

$$\log D = \log D_0 - \frac{Q_d}{2.3R}\left(\frac{1}{T}\right) \tag{6.9b}$$

Since D_0, Q_d, and R are all constants, Equation 6.9b takes on the form of an equation of a straight line:

$$y = b + mx$$

where y and x are analogous, respectively, to the variables $\log D$ and $1/T$. Thus, if $\log D$ is plotted versus the reciprocal of the absolute temperature, a straight line should result, having slope and intercept of $-Q_d/2.3R$ and $\log D_0$, respectively. This is, in fact, the manner in which the values of Q_d and D_0 are determined experimentally. From such a plot for several alloy systems (Figure 6.7), it may be noted that linear relationships exist for all cases shown.

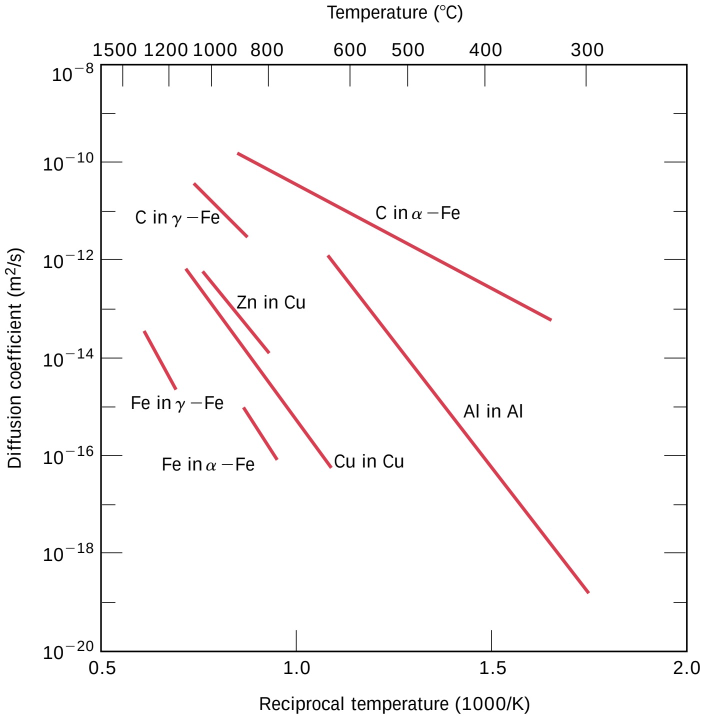

FIGURE 6.7 Plot of the logarithm of the diffusion coefficient versus the reciprocal of absolute temperature for several metals. [Data taken from E. A. Brandes and G. B. Brook (Editors), *Smithells Metals Reference Book*, 7th edition, Butterworth-Heinemann, Oxford, 1992.]

EXAMPLE PROBLEM 6.4

Using the data in Table 6.2, compute the diffusion coefficient for magnesium in aluminum at 550°C.

SOLUTION

This diffusion coefficient may be determined by applying Equation 6.8; the values of D_0 and Q_d from Table 6.2 are 1.2×10^{-4} m^2/s and 131 kJ/mol, respectively. Thus,

$$D = (1.2 \times 10^{-4}\ \text{m}^2/\text{s}) \exp\left[-\frac{(131{,}000\ \text{J/mol})}{(8.31\ \text{J/mol-K})(550 + 273\ \text{K})}\right]$$

$$= 5.8 \times 10^{-13}\ \text{m}^2/\text{s}$$

EXAMPLE PROBLEM 6.5

In Figure 6.8 is shown a plot of the logarithm (to the base 10) of the diffusion coefficient versus reciprocal of absolute temperature, for the diffusion of copper in gold. Determine values for the activation energy and the preexponential.

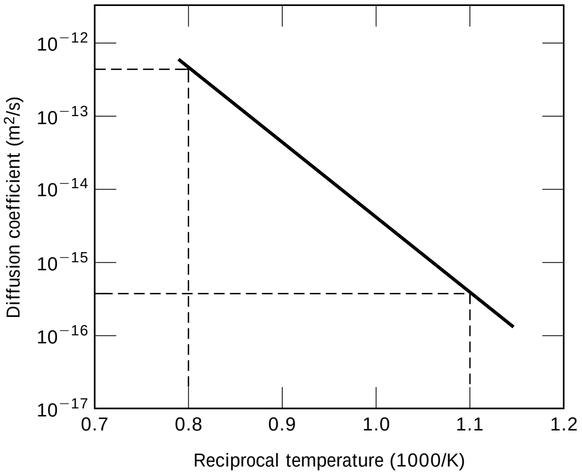

FIGURE 6.8 Plot of the logarithm of the diffusion coefficient versus the reciprocal of absolute temperature for the diffusion of copper in gold.

SOLUTION

From Equation 6.9b the slope of the line segment in Figure 6.8 is equal to $-Q_d/2.3R$, and the intercept at $1/T = 0$ gives the value of $\log D_0$. Thus, the activation energy may be determined as

$$Q_d = -2.3R\ (\text{slope}) = -2.3R\left[\frac{\Delta\,(\log D)}{\Delta\left(\dfrac{1}{T}\right)}\right]$$

$$= -2.3R\left[\frac{\log D_1 - \log D_2}{\dfrac{1}{T_1} - \dfrac{1}{T_2}}\right]$$

where D_1 and D_2 are the diffusion coefficient values at $1/T_1$ and $1/T_2$, respectively. Let us arbitrarily take $1/T_1 = 0.8 \times 10^{-3}$ (K)$^{-1}$ and $1/T_2 = 1.1 \times 10^{-3}$ (K)$^{-1}$. We may now read the corresponding log D_1 and log D_2 values from the line segment in Figure 6.8.

[Before this is done, however, a parenthetic note of caution is offered. The vertical axis in Figure 6.8 is scaled logarithmically (to the base 10); however, the actual diffusion coefficient values are noted on this axis. For example, for $D = 10^{-14}$ m^2/s, the logarithm of D is -14.0 *not* 10^{-14}. Furthermore, this logarithmic scaling affects the readings between decade values; for example, at a location midway between 10^{-14} and 10^{-15}, the value is not 5×10^{-15}, but rather, $10^{-14.5} = 3.2 \times 10^{-15}$].

Thus, from Figure 6.8, at $1/T_1 = 0.8 \times 10^{-3}$ (K)$^{-1}$, log $D_1 = -12.40$, while for $1/T_2 = 1.1 \times 10^{-3}$ (K)$^{-1}$, log $D_2 = -15.45$, and the activation energy, as determined from the slope of the line segment in Figure 6.8, is

$$Q_d = -2.3R \left[\frac{\log D_1 - \log D_2}{\dfrac{1}{T_1} - \dfrac{1}{T_2}} \right]$$

$$= -2.3\,(8.31 \text{ J/mol-K}) \left[\frac{-12.40 - (-15.45)}{0.8 \times 10^{-3}\,(\text{K})^{-1} - 1.1 \times 10^{-3}\,(\text{K})^{-1}} \right]$$

$$= 194{,}000 \text{ J/mol} = 194 \text{ kJ/mol}$$

Now, rather than trying to make a graphical extrapolation to determine D_0, a more accurate value is obtained analytically using Equation 6.9b, and a specific value of D (or log D) and its corresponding T (or $1/T$) from Figure 6.8. Since we know that log $D = -15.45$ at $1/T = 1.1 \times 10^{-3}$ (K)$^{-1}$, then

$$\log D_0 = \log D + \frac{Q_d}{2.3R}\left(\frac{1}{T}\right)$$

$$= -15.45 + \frac{(194{,}000 \text{ J/mol})(1.1 \times 10^{-3}\,[\text{K}]^{-1})}{(2.3)(8.31 \text{ J/mol-K})}$$

$$= -4.28$$

Thus, $D_0 = 10^{-4.28}$ m^2/s $= 5.2 \times 10^{-5}$ m^2/s.

DESIGN EXAMPLE 6.1

The wear resistance of a steel gear is to be improved by hardening its surface. This is to be accomplished by increasing the carbon content within an outer surface layer as a result of carbon diffusion into the steel; the carbon is to be supplied from an external carbon-rich gaseous atmosphere at an elevated and constant temperature. The initial carbon content of the steel is 0.20 wt%, whereas the surface concentration is to be maintained at 1.00 wt%. In order for this treatment to be effective, a carbon content of 0.60 wt% must be established at a position 0.75 mm below the surface. Specify an appropriate heat treatment in terms of temperature and time for temperatures between 900°C and 1050°C. Use data in Table 6.2 for the diffusion of carbon in γ-iron.

SOLUTION

Since this is a nonsteady-state diffusion situation, let us first of all employ Equation 6.5, utilizing the following values for the concentration parameters:

$$C_0 = 0.20 \text{ wt\% C}$$

$$C_s = 1.00 \text{ wt\% C}$$

$$C_x = 0.60 \text{ wt\% C}$$

Therefore

$$\frac{C_x - C_0}{C_s - C_0} = \frac{0.60 - 0.20}{1.00 - 0.20} = 1 - \operatorname{erf}\left(\frac{x}{2\sqrt{Dt}}\right)$$

And thus

$$0.5 = \operatorname{erf}\left(\frac{x}{2\sqrt{Dt}}\right)$$

Using an interpolation technique as demonstrated in Example Problem 6.2 and the data presented in Table 6.1

$$\frac{x}{2\sqrt{Dt}} = 0.4747 \qquad (6.10)$$

The problem stipulates that $x = 0.75 \text{ mm} = 7.5 \times 10^{-4}$ m. Therefore

$$\frac{7.5 \times 10^{-4} \text{ m}}{2\sqrt{Dt}} = 0.4747$$

This leads to

$$Dt = 6.24 \times 10^{-7} \text{ m}^2$$

Furthermore, the diffusion coefficient depends on temperature according to Equation 6.8; and, from Table 6.2 for the diffusion of carbon in γ-iron, $D_0 = 2.3 \times 10^{-5}$ m^2/s and $Q_d = 148{,}000$ J/mol. Hence

$$Dt = D_0 \exp\left(-\frac{Q_d}{RT}\right)(t) = 6.24 \times 10^{-7} \text{ m}^2$$

$$(2.3 \times 10^{-5} \text{ m}^2\text{/s}) \exp\left[-\frac{148{,}000 \text{ J/mol}}{(8.31 \text{ J/mol-K})(T)}\right](t) = 6.24 \times 10^{-7} \text{ m}^2$$

And solving for the time t

$$t \text{ (in s)} = \frac{0.0271}{\exp\left(-\dfrac{17{,}810}{T}\right)}$$

Thus, the required diffusion time may be computed for some specified temperature (in K). Below are tabulated t values for four different temperatures that lie within the range stipulated in the problem.

Temperature (°C)	***Time***	
	s	***h***
900	106,400	29.6
950	57,200	15.9
1000	32,300	9.0
1050	19,000	5.3

6.6 OTHER DIFFUSION PATHS

Atomic migration may also occur along dislocations, grain boundaries, and external surfaces. These are sometimes called ''*short-circuit*'' *diffusion paths* inasmuch as rates are much faster than for bulk diffusion. However, in most situations short-circuit contributions to the overall diffusion flux are insignificant because the cross-sectional areas of these paths are extremely small.

6.7 DIFFUSION IN IONIC AND POLYMERIC MATERIALS

We now extrapolate some of the diffusion principles discussed above to ionic and polymeric materials.

IONIC MATERIALS

For ionic compounds, the situation is more complicated than for metals inasmuch as it is necessary to consider the diffusive motion of two types of ions that have opposite charges. Diffusion in these materials occurs by a vacancy mechanism (Figure 6.3*a*). And, as we noted in Section 5.3, in order to maintain charge neutrality in an ionic material, the following may be said about vacancies: (1) ion vacancies occur in pairs [as with Schottky defects (Figure 5.3)], (2) they form in nonstoichiometric compounds (Figure 5.4), and (3) they are created by substitutional impurity ions having different charge states than the host ions (Example Problem 5.2). In any event, associated with the diffusive motion of a single ion is a transference of electrical charge. And in order to maintain localized charge neutrality in the vicinity of this moving ion, it is necessary that another species having an equal and opposite charge accompany the ion's diffusive motion. Possible charged species include another vacancy, an impurity atom, or an electronic carrier [i.e., a free electron or hole (Section 12.6)]. It follows that the rate of diffusion of these electrically charged couples is limited by the diffusion rate of the slowest moving species.

When an external electric field is applied across an ionic solid, the electrically charged ions migrate (i.e., diffuse) in response to forces that are brought to bear on them. And, as we discuss in Section 12.15, this ionic motion gives rise to an electric current. Furthermore, the electrical conductivity is a function of the diffusion coefficient (Equation 12.26). Consequently, much of the diffusion data for ionic solids comes from electrical conductivity measurements.

POLYMERIC MATERIALS

For polymeric materials, we are more interested in the diffusive motion of small foreign molecules (e.g., O_2, H_2O, CO_2, CH_4) between the molecular chains than in the diffusive motion of atoms within the chain structures. A polymer's permeability and absorption characteristics relate to the degree to which foreign substances diffuse into the material. Penetration of these foreign substances can lead to swelling and/or chemical reactions with the polymer molecules, and often to a depreciation of the material's mechanical and physical properties {(Section 16.11).}

Rates of diffusion are greater through amorphous regions than through crystalline regions; the structure of amorphous material is more ''open.'' This diffusion mechanism may be considered to be analogous to interstitial diffusion in metals—that is, in polymers, diffusive movement from one open amorphous region to an adjacent open one.

Foreign molecule size also affects the diffusion rate: smaller molecules diffuse faster than larger ones. Furthermore, diffusion is more rapid for foreign molecules that are chemically inert than for those that react with the polymer.

For some applications low diffusion rates through polymeric materials are desirable, as with food and beverage packaging and with automobile tires and inner tubes. Polymer membranes are often used as filters to selectively separate one chemical species from another (or others) (e.g., the desalinization of water). In such instances it is normally the case that the diffusion rate of the substance to be filtered is significantly greater than that for the other substance(s).

SUMMARY

Solid-state diffusion is a means of mass transport within solid materials by stepwise atomic motion. The term ''self-diffusion'' refers to the migration of host atoms; for impurity atoms, the term ''interdiffusion'' is used. Two mechanisms are possible: vacancy and interstitial. For a given host metal, interstitial atomic species generally diffuse more rapidly.

For steady-state diffusion, the concentration profile of the diffusing species is time independent, and the flux or rate is proportional to the negative of the concentration gradient according to Fick's first law. The mathematics for nonsteady state are described by Fick's second law, a partial differential equation. The solution for a constant surface composition boundary condition involves the Gaussian error function.

The magnitude of the diffusion coefficient is indicative of the rate of atomic motion, being strongly dependent on and increasing exponentially with increasing temperature.

Diffusion in ionic materials occurs by a vacancy mechanism; localized charge neutrality is maintained by the coupled diffusive motion of a charged vacancy and some other charged entity. In polymers, small molecules of foreign substances diffuse between molecular chains by an interstitial-type mechanism from one amorphous region to an adjacent one.

IMPORTANT TERMS AND CONCEPTS

Activation energy
Carburizing
Concentration gradient
Concentration profile
Diffusion
Diffusion coefficient
Diffusion flux
Driving force
Fick's first and second laws
Interdiffusion (impurity diffusion)
Interstitial diffusion
Nonsteady-state diffusion
Self-diffusion
Steady-state diffusion
Vacancy diffusion

REFERENCES

Borg, R. J. and G. J. Dienes (Editors), *An Introduction to Solid State Diffusion*, Academic Press, San Diego, 1988.

Brandes, E. A. and G. B. Brook (Editors), *Smithells Metals Reference Book*, 7th edition, Butterworth-Heinemann Ltd., Oxford, 1992.

Carslaw, H. S. and J. C. Jaeger, *Conduction of Heat in Solids*, 2nd edition, Clarendon Press, Oxford, 1986.

Crank, J., *The Mathematics of Diffusion*, 2nd edition, Clarendon Press, Oxford, 1980.

Girifalco, L. A., *Atomic Migration in Crystals*, Blaisdell Publishing Company, New York, 1964.

Shewmon, P. G., *Diffusion in Solids*, McGraw-Hill Book Company, New York, 1963. Reprinted by The Minerals, Metals and Materials Society, Warrendale, PA, 1989.

QUESTIONS AND PROBLEMS

Note: To solve those problems having an asterisk (*) by their numbers, consultation of supplementary topics [appearing only on the CD-ROM (and not in print)] will probably be necessary.

6.1 Briefly explain the difference between self-diffusion and interdiffusion.

6.2 Self-diffusion involves the motion of atoms that are all of the same type; therefore it is not subject to observation by compositional changes, as with interdiffusion. Suggest one way in which self-diffusion may be monitored.

6.3 **(a)** Compare interstitial and vacancy atomic mechanisms for diffusion.

(b) Cite two reasons why interstitial diffusion is normally more rapid than vacancy diffusion.

6.4 Briefly explain the concept of steady state as it applies to diffusion.

6.5 **(a)** Briefly explain the concept of a driving force.

(b) What is the driving force for steady-state diffusion?

6.6 The purification of hydrogen gas by diffusion through a palladium sheet was discussed in Section 6.3. Compute the number of kilograms of hydrogen that pass per hour through a 5-mm thick sheet of palladium having an area of 0.20 m^2 at 500°C. Assume a diffusion coefficient of 1.0×10^{-8} m^2/s, that the concentrations at the high- and low-pressure sides of the plate are 2.4 and 0.6 kg of hydrogen per cubic meter of palladium, and that steady-state conditions have been attained.

6.7 A sheet of steel 1.5 mm thick has nitrogen atmospheres on both sides at 1200°C and is permitted to achieve a steady-state diffusion condition. The diffusion coefficient for nitrogen in steel at this temperature is 6×10^{-11} m^2/s, and the diffusion flux is found to be 1.2×10^{-7} kg/m^2-s. Also, it is known that the concentration of nitrogen in the steel at the high-pressure surface is 4 kg/m^3. How far into the sheet from this high-pressure side will the concentration be 2.0 kg/m^3? Assume a linear concentration profile.

6.8* A sheet of BCC iron 1 mm thick was exposed to a carburizing gas atmosphere on one side and a decarburizing atmosphere on the other side at 725°C. After having reached steady state, the iron was quickly cooled to room temperature. The carbon concentrations at the two surfaces of the sheet were determined to be 0.012 and 0.0075 wt%. Compute the diffusion coefficient if the diffusion flux is 1.4×10^{-8} kg/m^2-s. *Hint:* Use Equation 5.9 to convert the concentrations from weight percent to kilograms of carbon per cubic meter of iron.

6.9 When α-iron is subjected to an atmosphere of hydrogen gas, the concentration of hydrogen in the iron, C_H (in weight percent), is a function of hydrogen pressure, p_{H_2} (in MPa), and absolute temperature (T) according to

$$C_H = 1.34 \times 10^{-2} \sqrt{p_{H_2}} \exp\left(-\frac{27.2 \text{ kJ/mol}}{RT}\right) \tag{6.11}$$

Furthermore, the values of D_0 and Q_d for this diffusion system are 1.4×10^{-7} m^2/s and 13,400 J/mol, respectively. Consider a thin iron membrane 1 mm thick that is at 250°C. Compute the diffusion flux through this membrane if the hydrogen pressure on one side of the membrane is 0.15 MPa (1.48 atm), and on the other side 7.5 MPa (74 atm).

6.10 Show that

$$C_x = \frac{B}{\sqrt{Dt}} \exp\left(-\frac{x^2}{4Dt}\right)$$

is also a solution to Equation 6.4b. The parameter B is a constant, being independent of both x and t.

6.11 Determine the carburizing time necessary to achieve a carbon concentration of 0.45 wt% at a position 2 mm into an iron–carbon alloy that initially contains 0.20 wt% C. The surface concentration is to be maintained at 1.30 wt% C, and the treatment is to be conducted at 1000°C. Use the diffusion data for γ-Fe in Table 6.2.

6.12 An FCC iron–carbon alloy initially containing 0.35 wt% C is exposed to an oxygen-rich and virtually carbon-free atmosphere at 1400 K (1127°C). Under these circumstances the carbon diffuses from the alloy and reacts at the surface with the oxygen in the atmosphere; that is, the carbon concentration at the surface position is maintained essentially at 0 wt% C. (This process of carbon depletion is termed *decarburization*.) At what position will the carbon concentration be 0.15 wt% after a 10-h treatment? The value of D at 1400 K is 6.9×10^{-11} m^2/s.

6.13 Nitrogen from a gaseous phase is to be diffused into pure iron at 700°C. If the surface concentration is maintained at 0.1 wt% N, what will be the concentration 1 mm from the surface after 10 h? The diffusion coefficient for nitrogen in iron at 700°C is 2.5×10^{-11} m^2/s.

6.14 **(a)** Consider a diffusion couple composed of two semi-infinite solids of the same metal. Each side of the diffusion couple has a different concentration of the same elemental impurity; furthermore, each impurity level is constant throughout its side of the diffusion couple. Solve Fick's second law for this diffusion situation assuming that the diffusion coefficient for the impurity is independent of concentration, and for the following boundary conditions:

$$C = C_1 \text{ for } x < 0, \text{ and } t = 0$$

$$C = C_2 \text{ for } x > 0, \text{ and } t = 0$$

Here we take the $x = 0$ position to be at the initial diffusion couple boundary.

(b) Using the result of part a, consider a diffusion couple composed of two silver-gold alloys; these alloys have compositions of 98 wt% Ag-2 wt% Au and 95 wt% Ag-5 wt% Au. Determine the time this diffusion couple must be heated at 750°C (1023 K) in order for the composition to be 2.5 wt% Au at the 50 μm position into the 2 wt% Au side of the diffusion couple. Preexponential and activation energy values for Au diffusion in Ag are 8.5×10^{-5} m^2/s and 202,100 J/mol, respectively.

6.15 For a steel alloy it has been determined that a carburizing heat treatment of 10 h duration will raise the carbon concentration to 0.45 wt% at a point 2.5 mm from the surface. Estimate the time necessary to achieve the same concentration at a 5.0-mm position for an identical steel and at the same carburizing temperature.

6.16 Cite the values of the diffusion coefficients for the interdiffusion of carbon in both α-iron (BCC) and γ-iron (FCC) at 900°C. Which is larger? Explain why this is the case.

6.17 Using the data in Table 6.2, compute the value of D for the diffusion of zinc in copper at 650°C.

6.18 At what temperature will the diffusion coefficient for the diffusion of copper in nickel have a value of 6.5×10^{-17} m^2/s? Use the diffusion data in Table 6.2.

6.19 The preexponential and activation energy for the diffusion of iron in cobalt are 1.1×10^{-5} m^2/s and 253,300 J/mol, respectively. At what temperature will the diffusion coefficient have a value of 2.1×10^{-14} m^2/s?

6.20 The activation energy for the diffusion of carbon in chromium is 111,000 J/mol. Calculate the diffusion coefficient at 1100 K (827°C), given that D at 1400 K (1127°C) is 6.25×10^{-11} m^2/s.

6.21 The diffusion coefficients for iron in nickel are given at two temperatures:

T(K)	D(m^2/s)
1273	9.4×10^{-16}
1473	2.4×10^{-14}

(a) Determine the values of D_0 and the activation energy Q_d.
(b) What is the magnitude of D at 1100°C (1373 K)?

6.22 The diffusion coefficients for silver in copper are given at two temperatures:

T(°C)	D(m^2/s)
650	5.5×10^{-16}
900	1.3×10^{-13}

(a) Determine the values of D_0 and Q_d.
(b) What is the magnitude of D at 875°C?

6.23 Below is shown a plot of the logarithm (to the base 10) of the diffusion coefficient versus reciprocal of the absolute temperature, for the diffusion of iron in chromium. Deter-

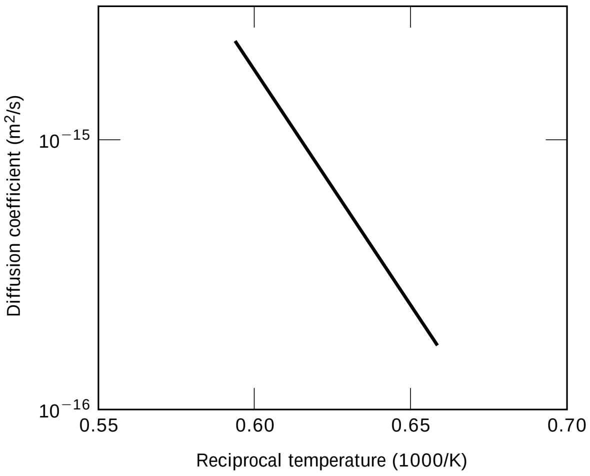

mine values for the activation energy and preexponential.

6.24 Carbon is allowed to diffuse through a steel plate 15 mm thick. The concentrations of carbon at the two faces are 0.65 and 0.30 kg C/m^3 Fe, which are maintained constant. If the preexponential and activation energy are 6.2×10^{-7} m^2/s and 80,000 J/mol, respectively, compute the temperature at which the diffusion flux is 1.43×10^{-9} kg/m^2-s.

6.25 The steady-state diffusion flux through a metal plate is 5.4×10^{-10} kg/m^2-s at a temperature of 727°C (1000 K) and when the concentration gradient is -350 kg/m^4. Calculate the diffusion flux at 1027°C (1300 K) for the same concentration gradient and assuming an activation energy for diffusion of 125,000 J/mol.

6.26 At approximately what temperature would a specimen of γ-iron have to be carburized for 2 h to produce the same diffusion result as at 900°C for 15 h?

6.27 **(a)** Calculate the diffusion coefficient for copper in aluminum at 500°C.
(b) What time will be required at 600°C to produce the same diffusion result (in terms of concentration at a specific point) as for 10 h at 500°C?

6.28 A copper-nickel diffusion couple similar to that shown in Figure 6.1*a* is fashioned. After a 700-h heat treatment at 1100°C (1373 K) the concentration of Cu is 2.5 wt% at the 3.0-mm position within the nickel. At what temperature must the diffusion couple need to be heated to produce this same concentration (i.e., 2.5 wt% Cu) at a 2.0-mm position after 700 h? The preexponential and activation energy for the diffusion of Cu in Ni are given in Table 6.2.

6.29 A diffusion couple similar to that shown in Figure 6.1*a* is prepared using two hypothetical metals A and B. After a 30-h heat treatment at 1000 K (and subsequently cooling to room temperature) the concentration of A in B is 3.2 wt% at the 15.5-mm position within metal B. If another heat treatment is conducted on an identical diffusion couple, only at 800 K for 30 h, at what position will the composition be 3.2 wt% A? Assume that the preexponential and activation energy for the diffusion coefficient are 1.8×10^{-5} m^2/s and 152,000 J/mol, respectively.

6.30 The outer surface of a steel gear is to be hardened by increasing its carbon content. The carbon is to be supplied from an external carbon-rich atmosphere, which is maintained at an elevated temperature. A diffusion heat treatment at 850°C (1123 K) for 10 min increases the carbon concentration to 0.90 wt% at a position 1.0 mm below the surface. Estimate the diffusion time required at 650°C (923 K) to achieve this same concentration also at a 1.0-mm position. Assume that the surface carbon content is the same for both heat treatments, which is maintained constant. Use the diffusion data in Table 6.2 for C diffusion in α-Fe.

6.31 An FCC iron-carbon alloy initially containing 0.20 wt% C is carburized at an elevated temperature and in an atmosphere wherein the surface carbon concentration is maintained at 1.0 wt%. If after 49.5 h the concentration of carbon is 0.35 wt% at a position 4.0 mm below the surface, determine the temperature at which the treatment was carried out.

Design Problems

6.D1 It is desired to enrich the partial pressure of hydrogen in a hydrogen-nitrogen gas mixture for which the partial pressures of both gases are 0.1013 MPa (1 atm). It has been proposed to accomplish this by passing both gases through a thin sheet of some metal at an elevated temperature; inasmuch as hydrogen diffuses through the plate at a higher rate than does nitrogen, the partial pressure of hydrogen will be higher on the exit side of the sheet. The design calls for partial pressures of 0.051 MPa (0.5 atm) and 0.01013 MPa (0.1 atm), respectively, for hydrogen and nitrogen. The concentrations of hydrogen and nitrogen (C_H and C_N, in mol/m^3) in this metal are functions of gas partial pressures (p_{H_2} and p_{N_2}, in MPa) and absolute temperature and are given by the following expressions:

$$C_\text{H} = 584\sqrt{p_{\text{H}_2}}\exp\left(-\frac{27.8\text{ kJ/mol}}{RT}\right) \tag{6.12a}$$

$$C_\text{N} = 2.75 \times 10^3\sqrt{p_{\text{N}_2}}\exp\left(-\frac{37.6\text{ kJ/mol}}{RT}\right) \tag{6.12b}$$

Furthermore, the diffusion coefficients for the diffusion of these gases in this metal are functions of the absolute temperature as follows:

$$D_\text{H}\ (\text{m}^2/\text{s}) = 1.4 \times 10^{-7}\exp\left(-\frac{13.4\text{ kJ/mol}}{RT}\right) \tag{6.13a}$$

$$D_\text{N}\ (\text{m}^2/\text{s}) = 3.0 \times 10^{-7}\exp\left(-\frac{76.15\text{ kJ/mol}}{RT}\right) \tag{6.13b}$$

Is it possible to purify hydrogen gas in this manner? If so, specify a temperature at which the process may be carried out, and also the thickness of metal sheet that would be required. If this procedure is not possible, then state the reason(s) why.

6.D2 A gas mixture is found to contain two diatomic A and B species for which the partial pressures of both are 0.1013 MPa (1 atm). This mixture is to be enriched in the partial pressure of the A species by passing both gases through a thin sheet of some metal at an elevated temperature. The resulting enriched mixture is to have a partial pressure of 0.051 MPa (0.5 atm) for gas A, and 0.0203 MPa (0.2 atm) for gas B. The concentrations of A and B (C_A and C_B, in mol/m^3) are functions of gas partial pressures (p_{A_2} and p_{B_2}, in MPa) and absolute temperature according to the following expressions:

$$C_\text{A} = 500\sqrt{p_{\text{A}_2}}\exp\left(-\frac{20.0\text{ kJ/mol}}{RT}\right) \tag{6.14a}$$

$$C_\text{B} = 2.0 \times 10^3\sqrt{p_{\text{B}_2}}\exp\left(-\frac{27.0\text{ kJ/mol}}{RT}\right) \tag{6.14b}$$

Furthermore, the diffusion coefficients for the diffusion of these gases in the metal are functions of the absolute temperature as follows:

$$D_\text{A}\ (\text{m}^2/\text{s}) = 5.0 \times 10^{-7}\exp\left(-\frac{13.0\text{ kJ/mol}}{RT}\right) \tag{6.15a}$$

$$D_\text{B}\ (\text{m}^2/\text{s}) = 3.0 \times 10^{-6}\exp\left(-\frac{21.0\text{ kJ/mol}}{RT}\right) \tag{6.15b}$$

Is it possible to purify the A gas in this manner? If so, specify a temperature at which the process may be carried out, and also the thickness of metal sheet that would be required. If this procedure is not possible, then state the reason(s) why.

6.D3 The wear resistance of a steel shaft is to be improved by hardening its surface. This is to be accomplished by increasing the nitrogen content within an outer surface layer as a result of nitrogen diffusion into the steel. The nitrogen is to be supplied from an external nitrogen-rich gas at an elevated and constant temperature. The initial nitrogen content of the steel is 0.002 wt%, whereas the surface concentration is to be maintained at 0.50 wt%. In order for this treatment to be effective, a nitrogen content of 0.10 wt% must be established at a position 0.40 mm below the surface. Specify appropriate heat treatments in terms of temperature and time for temperatures between 475°C and 625°C. The preexponential and activation energy for the diffusion of nitrogen in iron are 3×10^{-7} m^2/s and 76,150 J/mol, respectively, over this temperature range.

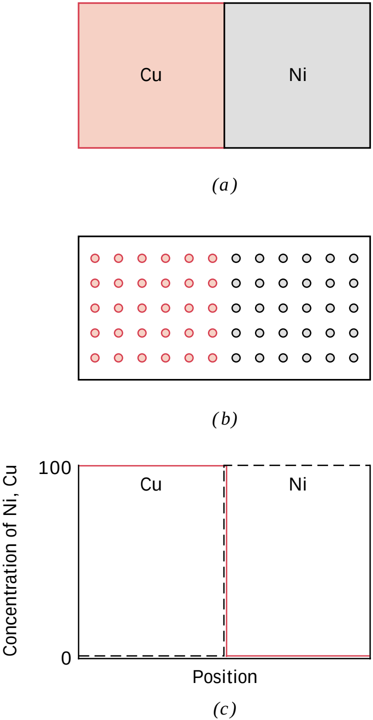
Cu
Ni
(a)
(b)
100
0
Concentration of Ni, Cu
Cu
Ni
Position
(c)

FIGURE 6.1 (*a*) A copper–nickel diffusion couple before a high-temperature heat treatment. (*b*) Schematic representations of Cu (colored circles) and Ni (gray circles) atom locations within the diffusion couple. (*c*) Concentrations of copper and nickel as a function of position across the couple.

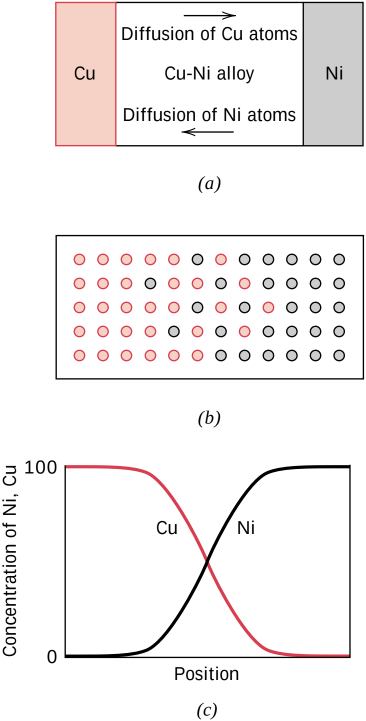

Diffusion of Cu atoms
Cu
Cu-Ni alloy
Ni
Diffusion of Ni atoms
(a)
(b)
100
0
Concentration of Ni, Cu
Cu
Ni
Position
(c)

Figure 6.2 (*a*) A copper–nickel diffusion couple after a high-temperature heat treatment, showing the alloyed diffusion zone. (*b*) Schematic representations of Cu (colored circles) and Ni (gray circles) atom locations within the couple. (*c*) Concentrations of copper and nickel as a function of position across the couple.

Figure 6.3 Schematic representations of (*a*) vacancy diffusion and (*b*) interstitial diffusion.

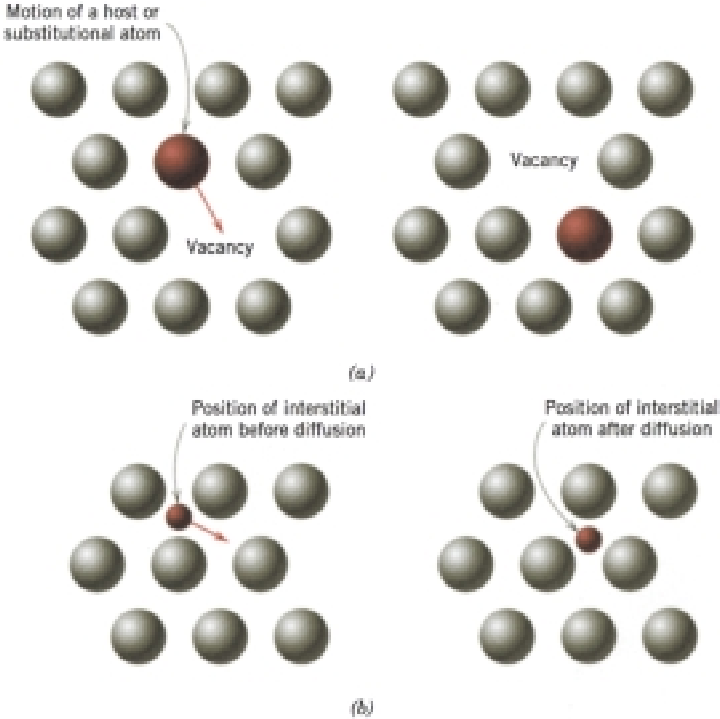
Motion of a host or substitutional atom
Vacancy
Vacancy
(a)
Position of interstitial atom before diffusion
Position of interstitial atom after diffusion
(b)

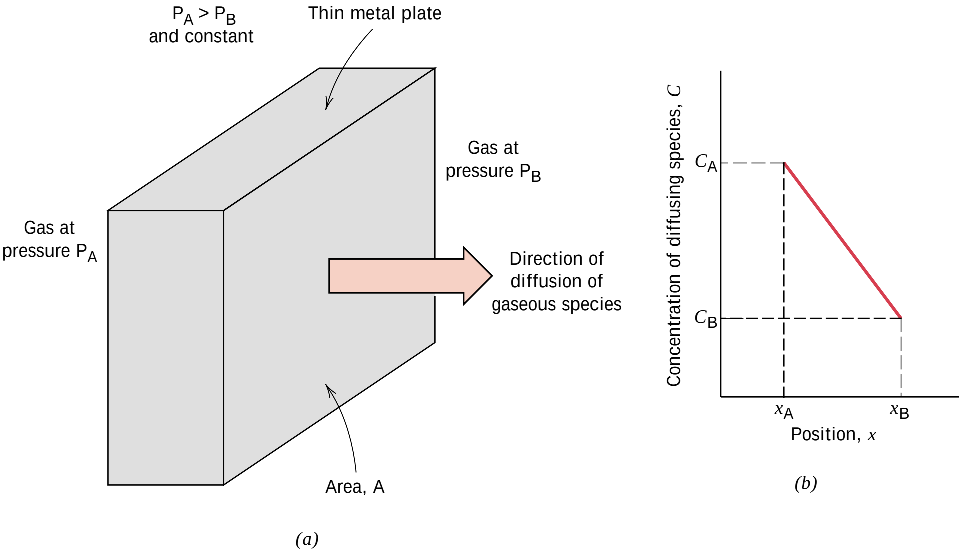

Figure 6.4 (*a*) Steady-state diffusion across a thin plate. (*b*) A linear concentration profile for the diffusion situation in (*a*).

$P_A > P_B$
and constant
Thin metal plate
Gas at
pressure P_B
Gas at
pressure P_A
Direction of
diffusion of
gaseous species
Area, A
(a)
Concentration of diffusing species, C
C_A
C_B
x_A
x_B
Position, x
(b)

Chapter 5 / Imperfections in Solids

5.6 Specification of Composition

COMPOSITION CONVERSIONS

Sometimes it is necessary to convert from one composition scheme to another—e.g., from weight percent to atom percent. We will now present equations for making these conversions in terms of the two hypothetical elements 1 and 2. Using the convention of the previous section (i.e., weight percents denoted by C_1 and C_2, atom percents by C'_1 and C'_2, and atomic weights as A_1 and A_2), these conversion expressions are as follows:

$$C'_1 = \frac{C_1A_2}{C_1A_2 + C_2A_1} \times 100 \tag{5.6a}$$

$$C'_2 = \frac{C_2A_1}{C_1A_2 + C_2A_1} \times 100 \tag{5.6b}$$

$$C_1 = \frac{C'_1A_1}{C'_1A_1 + C'_2A_2} \times 100 \tag{5.7a}$$

$$C_2 = \frac{C'_2A_2}{C'_1A_1 + C'_2A_2} \times 100 \tag{5.7b}$$

Since we are considering only two elements, computations involving the preceding equations are simplified when it is realized that

$$C_1 + C_2 = 100 \tag{5.8a}$$

$$C'_1 + C'_2 = 100 \tag{5.8b}$$

In addition, it sometimes becomes necessary to convert concentration from weight percent to mass of one component per unit volume of material (i.e., from units of wt% to kg/m^3); this latter composition scheme is often used in diffusion computations (Section 6.3). Concentrations in terms of this basis will be denoted using a double prime (i.e., C''_1 and C''_2), and the relevant equations are as follows:

$$C''_1 = \left(\frac{C_1}{\dfrac{C_1}{\rho_1} + \dfrac{C_2}{\rho_2}} \right) \times 10^3 \tag{5.9a}$$

$$C''_2 = \left(\frac{C_2}{\dfrac{C_1}{\rho_1} + \dfrac{C_2}{\rho_2}} \right) \times 10^3 \tag{5.9b}$$

For density ρ in units of g/cm^3, these expressions yield C''_1 and C''_2 in kg/m^3.

Furthermore, on occasion we desire to determine the density and atomic weight of a binary alloy given the composition in terms of either weight percent or atom percent. If we represent alloy density and atomic weight by ρ_{ave} and A_{ave}, respectively, then

$$\rho_{\text{ave}} = \frac{100}{\dfrac{C_1}{\rho_1} + \dfrac{C_2}{\rho_2}} \tag{5.10a}$$

$$\rho_{\text{ave}} = \frac{C'_1 A_1 + C'_2 A_2}{\dfrac{C'_1 A_1}{\rho_1} + \dfrac{C'_2 A_2}{\rho_2}} \tag{5.10b}$$

$$A_{\text{ave}} = \frac{100}{\dfrac{C_1}{A_1} + \dfrac{C_2}{A_2}} \tag{5.11a}$$

$$A_{\text{ave}} = \frac{C'_1 A_1 + C'_2 A_2}{100} \tag{5.11b}$$

It should be noted that Equations 5.9 and 5.11 are not always exact. In their derivations, it is assumed that total alloy volume is exactly equal to the sum of the volumes of the individual elements. This normally is not the case for most alloys; however, it is a reasonably valid assumption and does not lead to significant errors for dilute solutions and over composition ranges where solid solutions exist.

EXAMPLE PROBLEM 5.3

Derive Equation 5.6a.

SOLUTION

To simplify this derivation, it will be assumed that masses are expressed in units of grams, and denoted with a prime (e.g., m'_1). Furthermore, the total alloy mass (in grams) M' is

$$M' = m'_1 + m'_2 \tag{5.12}$$

Using the definition of C'_1 (Equation 5.5) and incorporating the expression for n_{m1}, Equation 5.4, and the analogous expression for n_{m2} yields

$$\begin{aligned} C'_1 &= \frac{n_{m1}}{n_{m1} + n_{m2}} \times 100 \\ &= \frac{\dfrac{m'_1}{A_1}}{\dfrac{m'_1}{A_1} + \dfrac{m'_2}{A_2}} \times 100 \end{aligned} \tag{5.13}$$

Rearrangement of the mass-in-grams equivalent of Equation 5.3 leads to

$$m'_1 = \frac{C_1 M'}{100} \tag{5.14}$$

Substitution of this expression and its m'_2 equivalent into Equation 5.13 gives

$$C'_1 = \frac{\dfrac{C_1 M'}{100 A_1}}{\dfrac{C_1 M'}{100 A_1} + \dfrac{C_2 M'}{100 A_2}} \times 100 \tag{5.15}$$

And upon simplification we have

$$C'_1 = \frac{C_1 A_2}{C_1 A_2 + C_2 A_1} \times 100$$

which is identical to Equation 5.6a.

EXAMPLE PROBLEM 5.4

Determine the composition, in atom percent, of an alloy that consists of 97 wt% aluminum and 3 wt% copper.

SOLUTION

If we denote the respective weight percent compositions as $C_{\text{Al}} = 97$ and $C_{\text{Cu}} = 3$, substitution into Equations 5.6a and 5.6b yields

$$\begin{aligned} C'_{\text{Al}} &= \frac{C_{\text{Al}} A_{\text{Cu}}}{C_{\text{Al}} A_{\text{Cu}} + C_{\text{Cu}} A_{\text{Al}}} \times 100 \\ &= \frac{(97)(63.55 \text{ g/mol})}{(97)(63.55 \text{ g/mol}) + (3)(26.98 \text{ g/mol})} \times 100 \\ &= 98.7 \text{ at\%} \end{aligned}$$

and

$$C'_{\mathrm{Cu}} = \frac{C_{\mathrm{Cu}}A_{\mathrm{Al}}}{C_{\mathrm{Cu}}A_{\mathrm{Al}} + C_{\mathrm{Al}}A_{\mathrm{Cu}}} \times 100$$

$$= \frac{(3)(26.98\ \mathrm{g/mol})}{(3)(26.98\ \mathrm{g/mol}) + (97)(63.55\ \mathrm{g/mol})} \times 100$$

$$= 1.30\ \mathrm{at\%}$$

5.12 MICROSCOPIC TECHNIQUES

OPTICAL MICROSCOPY

With optical microscopy, the light microscope is used to study the microstructure; optical and illumination systems are its basic elements. For materials that are opaque to visible light (all metals and many ceramics and polymers), only the surface is subject to observation, and the light microscope must be used in a reflecting mode. Contrasts in the image produced result from differences in reflectivity of the various regions of the microstructure. Investigations of this type are often termed *metallographic*, since metals were first examined using this technique.

Normally, careful and meticulous surface preparations are necessary to reveal the important details of the microstructure. The specimen surface must first be ground and polished to a smooth and mirrorlike finish. This is accomplished by using successively finer abrasive papers and powders. The microstructure is revealed by a surface treatment using an appropriate chemical reagent in a procedure termed *etching*. The chemical reactivity of the grains of some single-phase materials depends on crystallographic orientation. Consequently, in a polycrystalline specimen, etching characteristics vary from grain to grain. Figure 5.15*b* shows how normally incident light is reflected by three etched surface grains, each having a different orientation. Figure 5.15*a* depicts the surface structure as it might appear when viewed with the microscope; the luster or texture of each grain depends on its reflectance properties. A photomicrograph of a polycrystalline specimen exhibiting these characteristics is shown in Figure 5.15*c*.

Also, small grooves form along grain boundaries as a consequence of etching. Since atoms along grain boundary regions are more chemically active, they dissolve at a greater rate than those within the grains. These grooves become discernible when viewed under a microscope because they reflect light at an angle different from that of the grains themselves; this effect is displayed in Figure 5.16*a*. Figure 5.16*b* is a photomicrograph of a polycrystalline specimen in which the grain boundary grooves are clearly visible as dark lines.

When the microstructure of a two-phase alloy is to be examined, an etchant is often chosen that produces a different texture for each phase so that the different phases may be distinguished from each other.

ELECTRON MICROSCOPY

The upper limit to the magnification possible with an optical microscope is approximately 2000 diameters. Consequently, some structural elements are too fine or small to permit observation using optical microscopy. Under such circumstances the electron microscope, which is capable of much higher magnifications, may be employed.

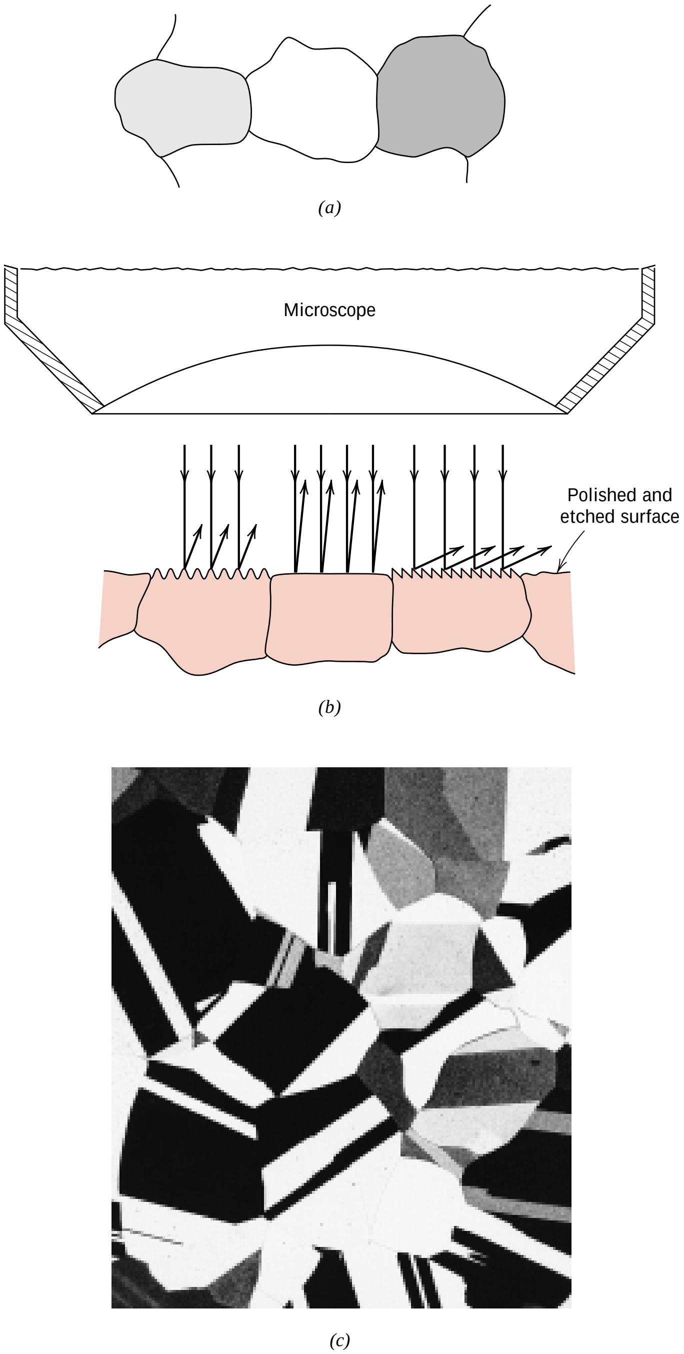

Figure 5.15 (*a*) Polished and etched grains as they might appear when viewed with an optical microscope. (*b*) Section taken through these grains showing how the etching characteristics and resulting surface texture vary from grain to grain because of differences in crystallographic orientation. (*c*) Photomicrograph of a polycrystalline brass specimen. 60×. (Photomicrograph courtesy of J. E. Burke, General Electric Co.)

An image of the structure under investigation is formed using beams of electrons instead of light radiation. According to quantum mechanics, a high-velocity electron will become wavelike, having a wavelength that is inversely proportional to its velocity. When accelerated across large voltages, electrons can be made to have wavelengths on the order of 0.003 nm (3 pm). High magnifications and resolving powers of these microscopes are consequences of the short wavelengths of electron

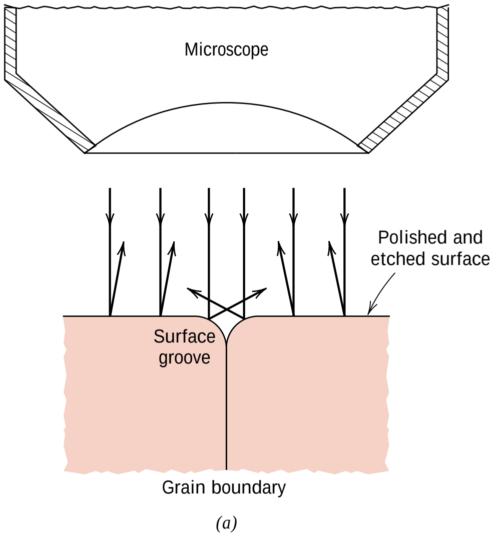

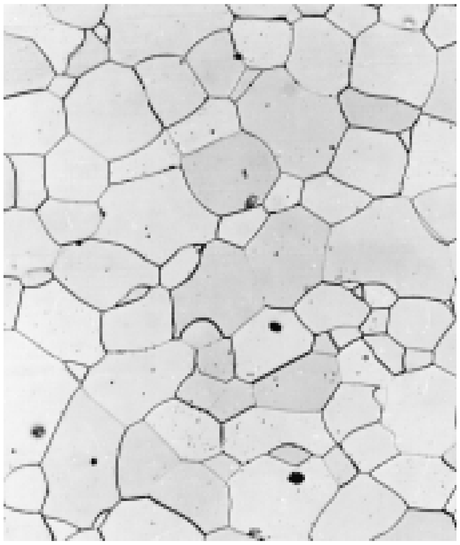
(b)

Figure 5.16 (*a*) Section of a grain boundary and its surface groove produced by etching; the light reflection characteristics in the vicinity of the groove are also shown. (*b*) Photomicrograph of the surface of a polished and etched polycrystalline specimen of an iron-chromium alloy in which the grain boundaries appear dark. 100×. (Photomicrograph courtesy of L. C. Smith and C. Brady, the National Bureau of Standards, Washington, DC.)

beams. The electron beam is focused and the image formed with magnetic lenses; otherwise the geometry of the microscope components is essentially the same as with optical systems. Both transmission and reflection beam modes of operation are possible for electron microscopes.

Transmission Electron Microscopy

The image seen with a **transmission electron microscope (TEM)** is formed by an electron beam that passes through the specimen. Details of internal microstructural features are accessible to observation; contrasts in the image are produced by differences in beam scattering or diffraction produced between various elements of the microstructure or defect. Since solid materials are highly absorptive to electron beams, a specimen to be examined must be prepared in the form of a very thin foil; this ensures transmission through the specimen of an appreciable fraction of the incident beam. The transmitted beam is projected onto a fluorescent screen or a photographic film so that the image may be viewed. Magnifications approaching 1,000,000× are possible with transmission electron microscopy, which is frequently utilized in the study of dislocations.

Scanning Electron Microscopy

A more recent and extremely useful investigative tool is the **scanning electron microscope (SEM).** The surface of a specimen to be examined is scanned with an electron beam, and the reflected (or back-scattered) beam of electrons is collected, then displayed at the same scanning rate on a cathode ray tube (similar to a TV screen). The image on the screen, which may be photographed, represents the surface features of the specimen. The surface may or may not be polished and etched, but it must be electrically conductive; a very thin metallic surface coating must be applied to nonconductive materials. Magnifications ranging from 10 to in excess of 50,000 diameters are possible, as are also very great depths-of-field. Accessory equipment permits qualitative and semiquantitative analysis of the elemental composition of very localized surface areas.

SCANNING PROBE MICROSCOPY

In the past decade and a half, the field of microscopy has experienced a revolution with the development of a new family of scanning probe microscopes. This **scanning probe microscope (SPM),** of which there are several varieties, differs from the optical and electron microscopes in that neither light nor electrons is used to form an image. Rather, the microscope generates a topographical map, on an atomic scale, that is a representation of surface features and characteristics of the specimen being examined. Some of the features that differentiate the SPM from other microscopic techniques are as follows:

- Examination on the nanometer scale is possible inasmuch as magnifications as high as $10^9\times$ are possible; much better resolutions are attainable than with other microscopic techniques.
- Three-dimensional magnified images are generated that provide topographical information about features of interest.
- Some SPMs may be operated in a variety of environments (e.g., vacuum, air, liquid); thus, a particular specimen may be examined in its most suitable environment.

Scanning probe microscopes employ a tiny probe with a very sharp tip that is brought into very close proximity (i.e., to within on the order of a nanometer) of the specimen surface. This probe is then raster-scanned across the plane of the surface. During scanning, the probe experiences deflections perpendicular to this plane, in response to electronic or other interactions between the probe and specimen surface. The in-surface-plane and out-of-plane motions of the probe are controlled by piezoelectric (Section 12.24) ceramic components that have nanometer resolutions. Furthermore, these probe movements are monitored electronically, and transferred to and stored in a computer, which then generates the three-dimensional surface image.

Specific scanning probe microscopic techniques differ from one another with regard to the type of interaction that is monitored. The chapter-opening photograph for Chapter 2 is an atomic force micrograph that shows, on an atomic scale, the surface of a gold specimen.

These new SPMs, which allow examination of the surface of materials at the atomic and molecular level, have provided a wealth of information about a host of materials, from integrated circuit chips to biological molecules. Indeed, the advent of the SPMs has helped to usher in the era of nanomaterials—materials whose properties are designed by engineering atomic and molecular structures.

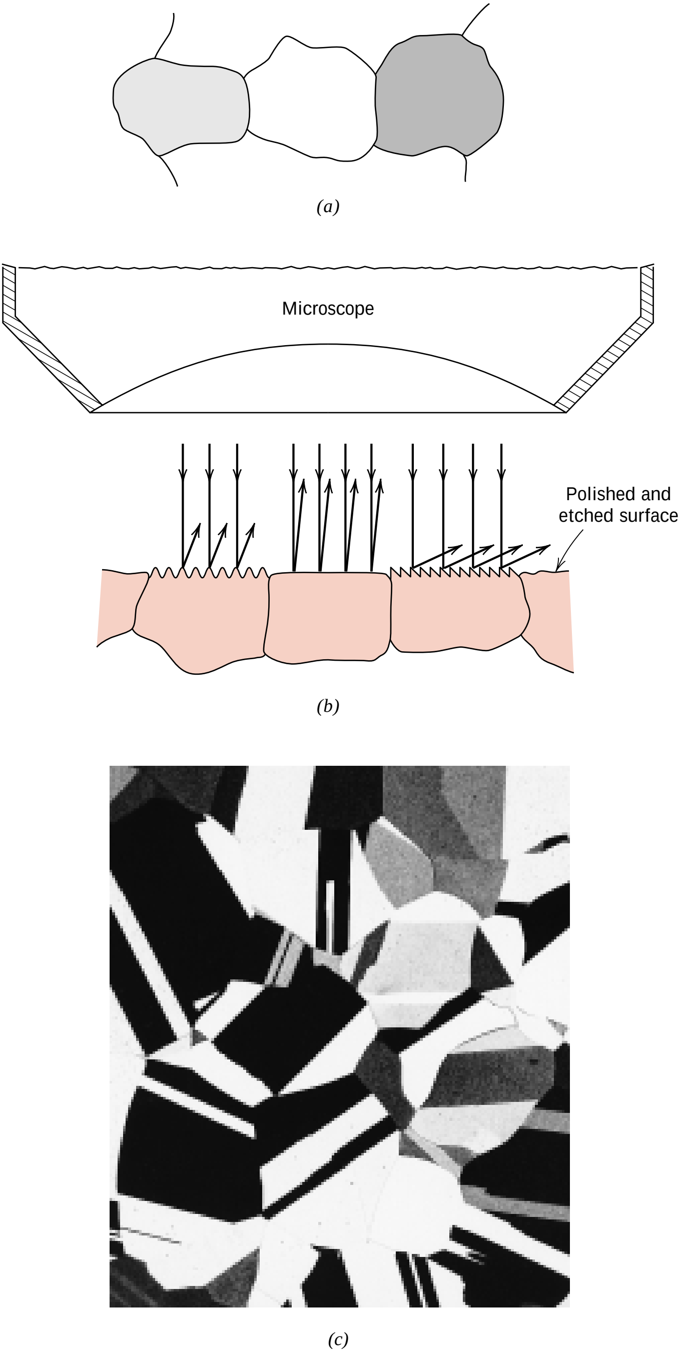

Figure 5.15 (*a*) Polished and etched grains as they might appear when viewed with an optical microscope. (*b*) Section taken through these grains showing how the etching characteristics and resulting surface texture vary from grain to grain because of differences in crystallographic orientation. (*c*) Photomicrograph of a polycrystalline brass specimen. 60×. (Photomicrograph courtesy of J. E. Burke, General Electric Co.)

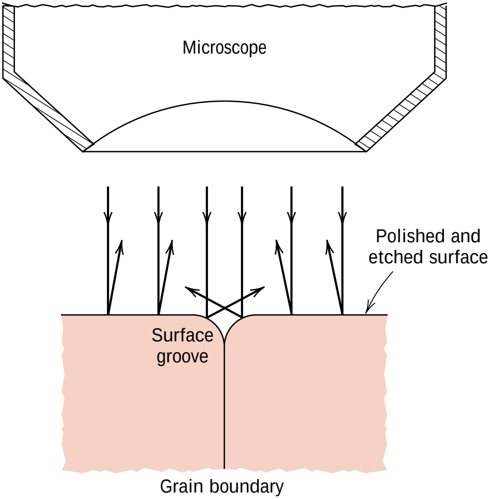
Microscope
Polished and etched surface
Surface groove
Grain boundary

(a)

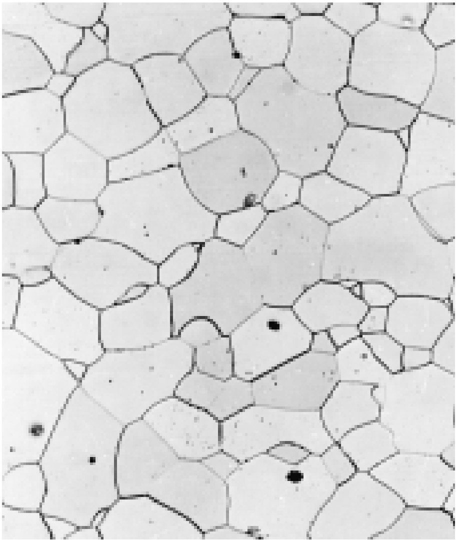

(b)

FIGURE 5.16 (*a*) Section of a grain boundary and its surface groove produced by etching; the light reflection characteristics in the vicinity of the groove are also shown. (*b*) Photomicrograph of the surface of a polished and etched polycrystalline specimen of an iron-chromium alloy in which the grain boundaries appear dark. 100×. (Photomicrograph courtesy of L. C. Smith and C. Brady, the National Bureau of Standards, Washington, DC.)

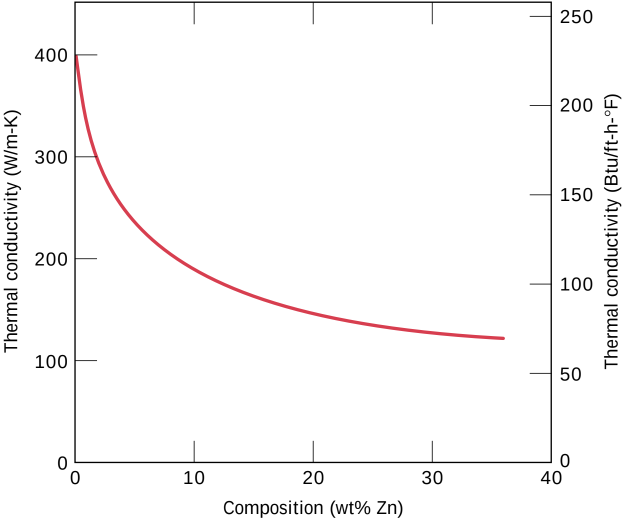

FIGURE 17.4 Thermal conductivity versus composition for copper–zinc alloys. (Adapted from *Metals Handbook: Properties and Selection: Nonferrous Alloys and Pure Metals*, Vol. 2, 9th edition, H. Baker, Managing Editor, American Society for Metals, 1979, p. 315.)

FIGURE 17.5 Dependence of thermal conductivity on temperature for several ceramic materials. (Adapted from W. D. Kingery, H. K. Bowen, and D. R. Uhlmann, *Introduction to Ceramics*, 2nd edition. Copyright © 1976 by John Wiley & Sons, New York. Reprinted by permission of John Wiley & Sons, Inc.)

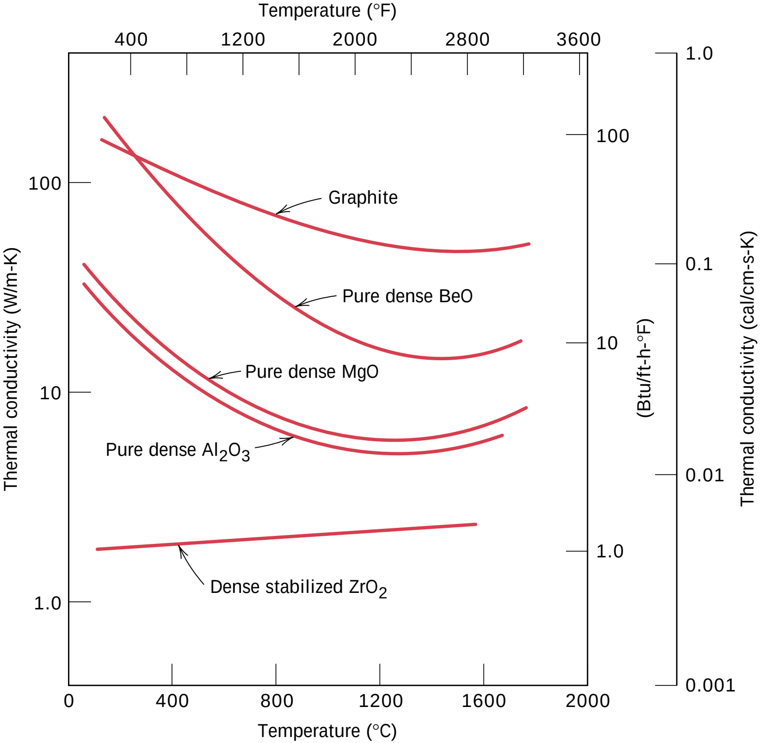

Chapter 13 / Types and Applications of Materials

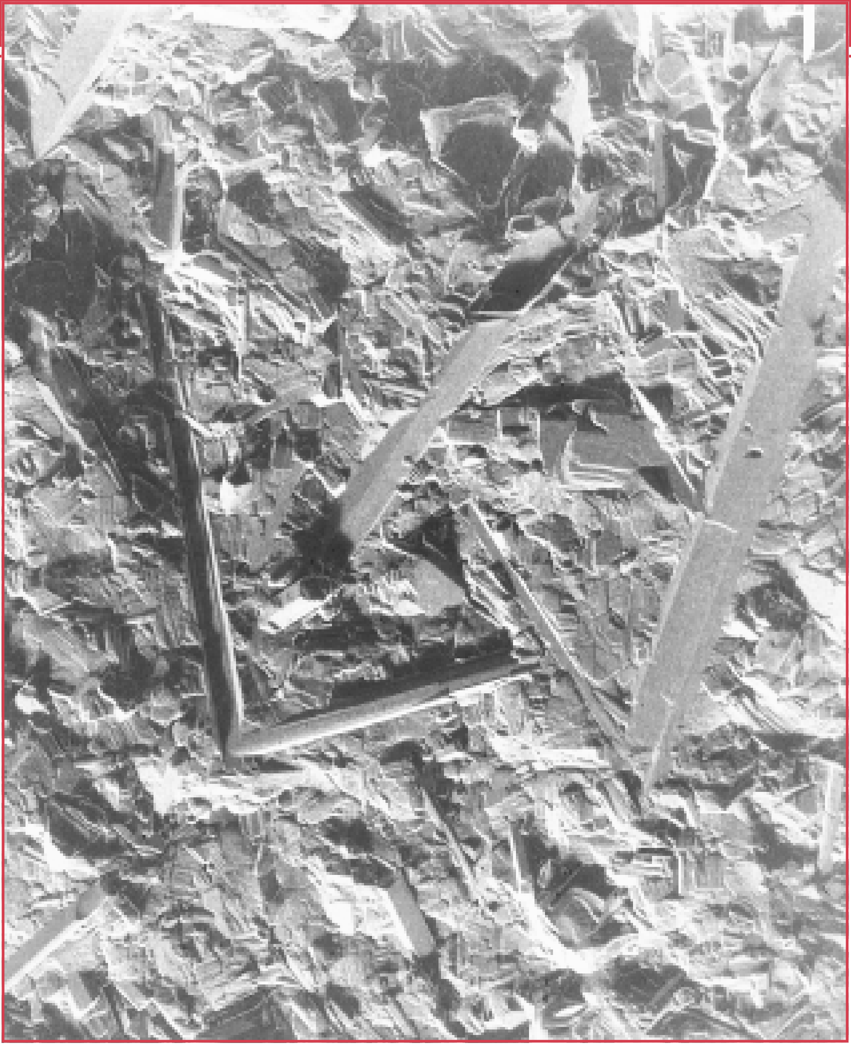

Scanning electron micrograph showing the microstructure of a glass–ceramic material. The long acicular blades yield a material with unusual strength and toughness. 65,000×. (Photograph courtesy of L. R. Pinckney and G. J. Fine of Corning Incorporated.)

Why Study *Types and Applications of Materials?*

Engineers are often involved in materials selection decisions, which necessitates that they have some familiarity with the general characteristics of a wide variety of materials. In addition, access to data bases containing property values for a large number of materials may be required. {For example, in Section 20.2 we discuss a materials selection process that is applied to a cylindrical shaft that is stressed in torsion.}

Learning Objectives

After careful study of this chapter you should be able to do the following:

1. **Name four different types of steels and, for each, cite compositional differences, distinctive properties, and typical uses.**
2. **Name the four cast iron types and, for each, describe its microstructure and note its general mechanical characteristics.**
3. **Name seven different types of nonferrous alloys and, for each, cite its distinctive physical and mechanical characteristics; in addition, list at least three typical applications.**
4. **Describe the process that is used to produce glass–ceramics.**
5. **Name the two types of clay products and give two examples of each.**
6. **Cite three important requirements that normally must be met by refractory ceramics and abrasive ceramics.**
7. **Describe the mechanism by which cement hardens when water is added.**
8. **Cite the seven different polymer application types and, for each, note its general characteristics.**

13.1 INTRODUCTION

Many times a materials problem is really one of selecting that material which has the right combination of characteristics for a specific application. Therefore, the persons who are involved in the decision making should have some knowledge of the available options. This extremely abbreviated presentation provides an overview of some of the types of metal alloys, ceramics, and polymeric materials, their general properties, and their limitations.

TYPES OF METAL ALLOYS

Metal alloys, by virtue of composition, are often grouped into two classes—ferrous and nonferrous. Ferrous alloys, those in which iron is the principal constituent, include steels and cast irons. These alloys and their characteristics are the first topics of discussion of this section. The nonferrous ones—all the alloys that are not iron based—are treated next.

13.2 FERROUS ALLOYS

Ferrous alloys—those of which iron is the prime constituent—are produced in larger quantities than any other metal type. They are especially important as engineering construction materials. Their widespread use is accounted for by three factors: (1) iron-containing compounds exist in abundant quantities within the earth's crust; (2) metallic iron and steel alloys may be produced using relatively economical extraction, refining, alloying, and fabrication techniques; and (3) ferrous alloys are extremely versatile, in that they may be tailored to have a wide range of mechanical and physical properties. The principal disadvantage of many ferrous alloys is their susceptibility to corrosion. These sections discuss compositions, microstructures, and properties of a number of different classes of steels and cast irons. A taxonomic classification scheme for the various ferrous alloys is presented in Figure 13.1.

STEELS

Steels are iron–carbon alloys that may contain appreciable concentrations of other alloying elements; there are thousands of alloys that have different compositions and/or heat treatments. The mechanical properties are sensitive to the content of

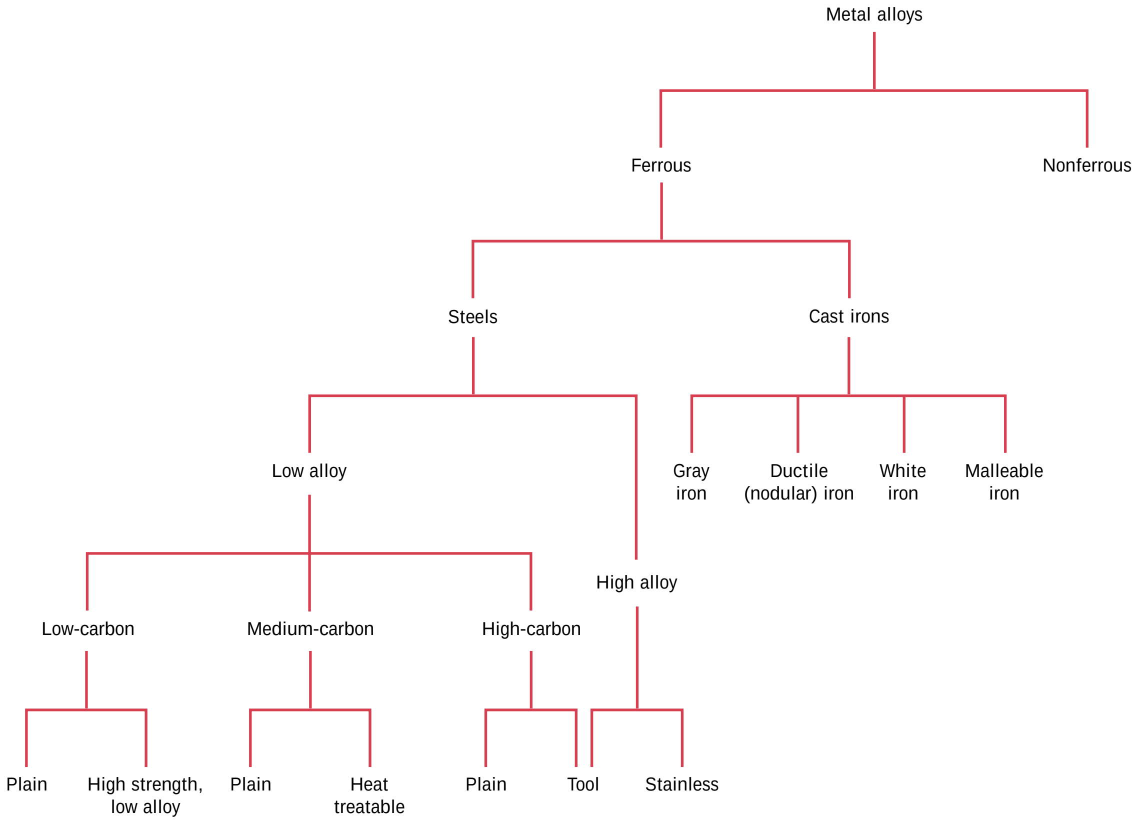
Metal alloys
Ferrous
Nonferrous
Steels
Cast irons
Low alloy
High alloy
Gray iron
Ductile (nodular) iron
White iron
Malleable iron
Low-carbon
Medium-carbon
High-carbon
Plain
High strength, low alloy
Plain
Heat treatable
Plain
Tool
Stainless

Figure 13.1 Classification scheme for the various ferrous alloys.

carbon, which is normally less than 1.0 wt%. Some of the more common steels are classified according to carbon concentration, namely, into low-, medium-, and high-carbon types. Subclasses also exist within each group according to the concentration of other alloying elements. **Plain carbon steels** contain only residual concentrations of impurities other than carbon and a little manganese. For **alloy steels,** more alloying elements are intentionally added in specific concentrations.

Low-Carbon Steels

Of all the different steels, those produced in the greatest quantities fall within the low-carbon classification. These generally contain less than about 0.25 wt% C and are unresponsive to heat treatments intended to form martensite; strengthening is accomplished by cold work. Microstructures consist of ferrite and pearlite constituents. As a consequence, these alloys are relatively soft and weak, but have outstanding ductility and toughness; in addition, they are machinable, weldable, and, of all steels, are the least expensive to produce. Typical applications include automobile body components, structural shapes (I-beams, channel and angle iron), and sheets that are used in pipelines, buildings, bridges, and tin cans. Tables 13.1a and 13.1b, respectively, present the compositions and mechanical properties of several plain low-carbon steels. They typically have a yield strength of 275 MPa (40,000 psi), tensile strengths between 415 and 550 MPa (60,000 and 80,000 psi), and a ductility of 25%EL.

Table 13.1a **Compositions of Five Plain Low-Carbon Steels and Three High-Strength, Low-Alloy Steels**

Designation[a]		*Composition (wt%)*[b]		
AISI/SAE or ASTM Number	***UNS Number***	***C***	***Mn***	***Other***
		Plain Low-Carbon Steels		
1010	G10100	0.10	0.45	
1020	G10200	0.20	0.45	
A36	K02600	0.29	1.00	0.20 Cu (min)
A516 Grade 70	K02700	0.31	1.00	0.25 Si
		High-Strength, Low-Alloy Steels		
A440	K12810	0.28	1.35	0.30 Si (max), 0.20 Cu (min)
A633 Grade E	K12002	0.22	1.35	0.30 Si, 0.08 V, 0.02 N, 0.03 Nb
A656 Grade 1	K11804	0.18	1.60	0.60 Si, 0.1 V, 0.20 Al, 0.015 N

[a] The codes used by the American Iron and Steel Institute (AISI), the Society of Automotive Engineers (SAE), and the American Society for Testing and Materials (ASTM), and in the Uniform Numbering System (UNS) are explained in the text.

[b] Also a maximum of 0.04 wt% P, 0.05 wt% S, and 0.30 wt% Si (unless indicated otherwise).

Source: Adapted from *Metals Handbook: Properties and Selection: Irons and Steels*, Vol. 1, 9th edition, B. Bardes (Editor), American Society for Metals, 1978, pp. 185, 407.

Table 13.1b **Mechanical Characteristics of Hot-Rolled Material and Typical Applications for Various Plain Low-Carbon and High-Strength, Low-Alloy Steels**

AISI/SAE or ASTM Number	***Tensile Strength [MPa (ksi)]***	***Yield Strength [MPa (ksi)]***	***Ductility [%EL in 50 mm (2 in.)]***	***Typical Applications***
		Plain Low-Carbon Steels		
1010	325 (47)	180 (26)	28	Automobile panels, nails, and wire
1020	380 (55)	205 (30)	25	Pipe; structural and sheet steel
A36	400 (58)	220 (32)	23	Structural (bridges and buildings)
A516 Grade 70	485 (70)	260 (38)	21	Low-temperature pressure vessels
		High-Strength, Low-Alloy Steels		
A440	435 (63)	290 (42)	21	Structures that are bolted or riveted
A633 Grade E	520 (75)	380 (55)	23	Structures used at low ambient temperatures
A656 Grade 1	655 (95)	552 (80)	15	Truck frames and railway cars

Another group of low-carbon alloys are the **high-strength, low-alloy (HSLA) steels.** They contain other alloying elements such as copper, vanadium, nickel, and molybdenum in combined concentrations as high as 10 wt%, and possess higher strengths than the plain low-carbon steels. Most may be strengthened by heat treatment, giving tensile strengths in excess of 480 MPa (70,000 psi); in addition, they are ductile, formable, and machinable. Several are listed in Table 13.1. In normal atmospheres, the HSLA steels are more resistant to corrosion than the plain carbon steels, which they have replaced in many applications where structural strength is critical (e.g., bridges, towers, support columns in high-rise buildings, and pressure vessels).

Medium-Carbon Steels

The medium-carbon steels have carbon concentrations between about 0.25 and 0.60 wt%. These alloys may be heat treated by austenitizing, quenching, and then tempering to improve their mechanical properties. They are most often utilized in the tempered condition, having microstructures of tempered martensite. The plain medium-carbon steels have low hardenabilities {(Section 14.6)} and can be successfully heat treated only in very thin sections and with very rapid quenching rates. Additions of chromium, nickel, and molybdenum improve the capacity of these alloys to be heat treated, giving rise to a variety of strength–ductility combinations. These heat-treated alloys are stronger than the low-carbon steels, but at a sacrifice of ductility and toughness. Applications include railway wheels and tracks, gears, crankshafts, and other machine parts and high-strength structural components calling for a combination of high strength, wear resistance, and toughness.

The compositions of several of these alloyed medium-carbon steels are presented in Table 13.2a. Some comment is in order regarding the designation schemes that are also included. The Society of Automotive Engineers (SAE), the American Iron and Steel Institute (AISI), and the American Society for Testing and Materials (ASTM) are responsible for the classification and specification of steels as well as other alloys. The AISI/SAE designation for these steels is a four-digit number: the first two digits indicate the alloy content; the last two, the carbon concentration. For plain carbon steels, the first two digits are 1 and 0; alloy steels are designated by other initial two-digit combinations (e.g., 13, 41, 43). The third and fourth digits represent the weight percent carbon multiplied by 100. For example, a 1060 steel is a plain carbon steel containing 0.60 wt% C.

A unified numbering system (UNS) is used for uniformly indexing both ferrous and nonferrous alloys. Each UNS number consists of a single-letter prefix followed by a five-digit number. The letter is indicative of the family of metals to which an alloy belongs. The UNS designation for these alloys begins with a G, followed by the AISI/SAE number; the fifth digit is a zero. Table 13.2b contains the mechanical characteristics and typical applications of several of these steels, which have been quenched and tempered.

High-Carbon Steels

The high-carbon steels, normally having carbon contents between 0.60 and 1.4 wt%, are the hardest, strongest, and yet least ductile of the carbon steels. They are almost always used in a hardened and tempered condition and, as such, are especially wear resistant and capable of holding a sharp cutting edge. The tool and die steels are high-carbon alloys, usually containing chromium, vanadium, tungsten, and molybdenum. These alloying elements combine with carbon to form very hard and wear-resistant

Table 13.2a AISI/SAE and UNS Designation Systems and Composition Ranges for Plain Carbon Steel and Various Low-Alloy Steels

AISI/SAE Designation[a]	UNS Designation	Composition Ranges (wt% of Alloying Elements in Addition to C)[b]			
		Ni	Cr	Mo	Other
10xx, Plain carbon	G10xx0				
11xx, Free machining	G11xx0				0.08–0.33S
12xx, Free machining	G12xx0				0.10–0.35S, 0.04–0.12P
13xx	G13xx0				1.60–1.90Mn
40xx	G40xx0			0.20–0.30	
41xx	G41xx0		0.80–1.10	0.15–0.25	
43xx	G43xx0	1.65–2.00	0.40–0.90	0.20–0.30	
46xx	G46xx0	0.70–2.00		0.15–0.30	
48xx	G48xx0	3.25–3.75		0.20–0.30	
51xx	G51xx0		0.70–1.10		
61xx	G61xx0		0.50–1.10		0.10–0.15V
86xx	G86xx0	0.40–0.70	0.40–0.60	0.15–0.25	
92xx	G92xx0				1.80–2.20Si

[a] The carbon concentration, in weight percent times 100, is inserted in the place of ''xx'' for each specific steel.

[b] Except for 13xx alloys, manganese concentration is less than 1.00 wt%.
Except for 12xx alloys, phosphorus concentration is less than 0.35 wt%.
Except for 11xx and 12xx alloys, sulfur concentration is less than 0.04 wt%.
Except for 92xx alloys, silicon concentration varies between 0.15 and 0.35 wt%.

Table 13.2b Typical Applications and Mechanical Property Ranges for Oil-Quenched and Tempered Plain Carbon and Alloy Steels

AISI Number	UNS Number	Tensile Strength [MPa (ksi)]	Yield Strength [MPa (ksi)]	Ductility [%EL in 50 mm (2 in.)]	Typical Applications
			Plain Low-Carbon Steels		
1040	G10400	605–780 (88–113)	430–585 (62–85)	33–19	Crankshafts, bolts
1080[a]	G10800	800–1310 (116–190)	480–980 (70–142)	24–13	Chisels, hammers
1095[a]	G10950	760–1280 (110–186)	510–830 (74–120)	26–10	Knives, hacksaw blades
			Alloy Steels		
4063	G40630	786–2380 (114–345)	710–1770 (103–257)	24–4	Springs, hand tools
4340	G43400	980–1960 (142–284)	895–1570 (130–228)	21–11	Bushings, aircraft tubing
6150	G61500	815–2170 (118–315)	745–1860 (108–270)	22–7	Shafts, pistons, gears

[a] Classified as high-carbon steels.

Table 13.3 Designations, Compositions, and Applications for Six Tool Steels

AISI Number	*UNS Number*	*Composition (wt%)*[a]						*Typical Applications*
		C	*Cr*	*Ni*	*Mo*	*W*	*V*	
M1	T11301	0.85	3.75	0.30 max	8.70	1.75	1.20	Drills, saws; lathe and planer tools
A2	T30102	1.00	5.15	0.30 max	1.15	—	0.35	Punches, embossing dies
D2	T30402	1.50	12	0.30 max	0.95	—	1.10 max	Cutlery, drawing dies
O1	T31501	0.95	0.50	0.30 max	—	0.50	0.30 max	Shear blades, cutting tools
S1	T41901	0.50	1.40	0.30 max	0.50 max	2.25	0.25	Pipe cutters, concrete drills
W1	T72301	1.10	0.15 max	0.20 max	0.10 max	0.15 max	0.10 max	Blacksmith tools, wood-working tools

[a] The balance of the composition is iron. Manganese concentrations range between 0.10 and 1.4 wt%, depending on alloy; silicon concentrations between 0.20 and 1.2 wt% depending on alloy.

Source: Adapted from *ASM Handbook*, Vol. 1, *Properties and Selection: Irons, Steels, and High-Performance Alloys*, 1990. Reprinted by permission of ASM International, Materials Park, OH.

carbide compounds (e.g., $Cr_{23}C_6$, V_4C_3, and WC). Some tool steel compositions and their applications are listed in Table 13.3. These steels are utilized as cutting tools and dies for forming and shaping materials, as well as in knives, razors, hacksaw blades, springs, and high-strength wire.

Stainless Steels

The **stainless steels** are highly resistant to corrosion (rusting) in a variety of environments, especially the ambient atmosphere. Their predominant alloying element is chromium; a concentration of at least 11 wt% Cr is required. Corrosion resistance may also be enhanced by nickel and molybdenum additions.

Stainless steels are divided into three classes on the basis of the predominant phase constituent of the microstructure—martensitic, ferritic, or austenitic. Table 13.4 lists several stainless steels, by class, along with composition, typical mechanical properties, and applications. A wide range of mechanical properties combined with excellent resistance to corrosion make stainless steels very versatile in their applicability.

Martensitic stainless steels are capable of being heat treated in such a way that martensite is the prime microconstituent. Additions of alloying elements in significant concentrations produce dramatic alterations in the iron–iron carbide phase diagram (Figure 10.26). For austenitic stainless steels, the austenite (or γ) phase field is extended to room temperature. Ferritic stainless steels are composed of the α ferrite (BCC) phase. Austenitic and ferritic stainless steels are hardened and strengthened by cold work because they are not heat treatable. The austenitic stainless steels are the most corrosion resistant because of the high chromium contents and also the nickel additions; and they are produced in the largest quantities. Both martensitic and ferritic stainless steels are magnetic; the austenitic stainlesses are not.

Table 13.4 **Designations, Compositions, Mechanical Properties, and Typical Applications for Austenitic, Ferritic, Martensitic, and Precipitation-Hardenable Stainless Steels**

				Mechanical Properties			
AISI Number	*UNS Number*	*Composition (wt%)*[a]	*Condition*[b]	*Tensile Strength [MPa (ksi)]*	*Yield Strength [MPa (ksi)]*	*Ductility [%EL in 50 mm (2 in.)]*	*Typical Applications*
			Ferritic				
409	S40900	0.08 C, 11.0 Cr, 1.0 Mn, 0.50 Ni, 0.75 Ti	Annealed	380 (55)	205 (30)	20	Automotive exhaust components, tanks for agricultural sprays
446	S44600	0.20 C, 25 Cr, 1.5 Mn	Annealed	515 (75)	275 (40)	20	Valves (high temperature), glass molds, combustion chambers
			Austenitic				
304	S30400	0.08 C, 19 Cr, 9 Ni, 2.0 Mn	Annealed	515 (75)	205 (30)	40	Chemical and food processing equipment, cryogenic vessels
316L	S31603	0.03 C, 17 Cr, 12 Ni, 2.5 Mo, 2.0 Mn	Annealed	485 (70)	170 (25)	40	Welding construction
			Martensitic				
410	S41000	0.15 C, 12.5 Cr, 1.0 Mn	Annealed Q & T	485 (70) 825 (120)	275 (40) 620 (90)	20 12	Rifle barrels, cutlery, jet engine parts
440A	S44002	0.70 C, 17 Cr, 0.75 Mo, 1.0 Mn	Annealed Q & T	725 (105) 1790 (260)	415 (60) 1650 (240)	20 5	Cutlery, bearings, surgical tools
			Precipitation Hardenable				
17-7PH	S17700	0.09 C, 17 Cr, 7 Ni, 1.0 Al, 1.0 Mn	Precipitation hardened	1450 (210)	1310 (190)	1–6	Springs, knives, pressure vessels

[a] The balance of the composition is iron.

[b] Q & T denotes quenched and tempered.

Source: Adapted from *ASM Handbook,* Vol. 1, *Properties and Selection: Irons, Steels, and High-Performance Alloys,* 1990. Reprinted by permission of ASM International, Materials Park, OH.

Some stainless steels are frequently used at elevated temperatures and in severe environments because they resist oxidation and maintain their mechanical integrity under such conditions; the upper temperature limit in oxidizing atmospheres is about 1000°C (1800°F). Equipment employing these steels includes gas turbines, high-temperature steam boilers, heat-treating furnaces, aircraft, missiles, and nuclear power generating units. Also included in Table 13.4 is one ultrahigh-strength stainless steel (17-7PH), which is unusually strong and corrosion resistant. Strengthening is accomplished by precipitation-hardening heat treatments (Section 11.10).

CAST IRONS

Generically, **cast irons** are a class of ferrous alloys with carbon contents above 2.14 wt%; in practice, however, most cast irons contain between 3.0 and 4.5 wt% C and, in addition, other alloying elements. A reexamination of the iron–iron carbide phase diagram (Figure 10.26) reveals that alloys within this composition range become completely liquid at temperatures between approximately 1150 and 1300°C (2100 and 2350°F), which is considerably lower than for steels. Thus, they are easily melted and amenable to casting. Furthermore, some cast irons are very brittle, and casting is the most convenient fabrication technique.

Cementite (Fe_3C) is a metastable compound, and under some circumstances it can be made to dissociate or decompose to form α ferrite and graphite, according to the reaction

$$Fe_3C \rightarrow 3Fe\ (\alpha) + C\ (\text{graphite}) \tag{13.1}$$

Thus, the true equilibrium diagram for iron and carbon is not that presented in Figure 10.26, but rather as shown in Figure 13.2. The two diagrams are virtually identical on the iron-rich side (e.g., eutectic and eutectoid temperatures for the Fe–Fe_3C system are 1147 and 727°C, respectively, as compared to 1153 and 740°C for Fe–C); however, Figure 13.2 extends to 100 wt% carbon such that graphite is the carbon-rich phase, instead of cementite at 6.7 wt% C (Figure 10.26).

This tendency to form graphite is regulated by the composition and rate of cooling. Graphite formation is promoted by the presence of silicon in concentrations greater than about 1 wt%. Also, slower cooling rates during solidification favor graphitization (the formation of graphite). For most cast irons, the carbon exists

FIGURE 13.2 The true equilibrium iron–carbon phase diagram with graphite instead of cementite as a stable phase. (Adapted from *Binary Alloy Phase Diagrams*, T. B. Massalski, Editor-in-Chief, 1990. Reprinted by permission of ASM International, Materials Park, OH.)

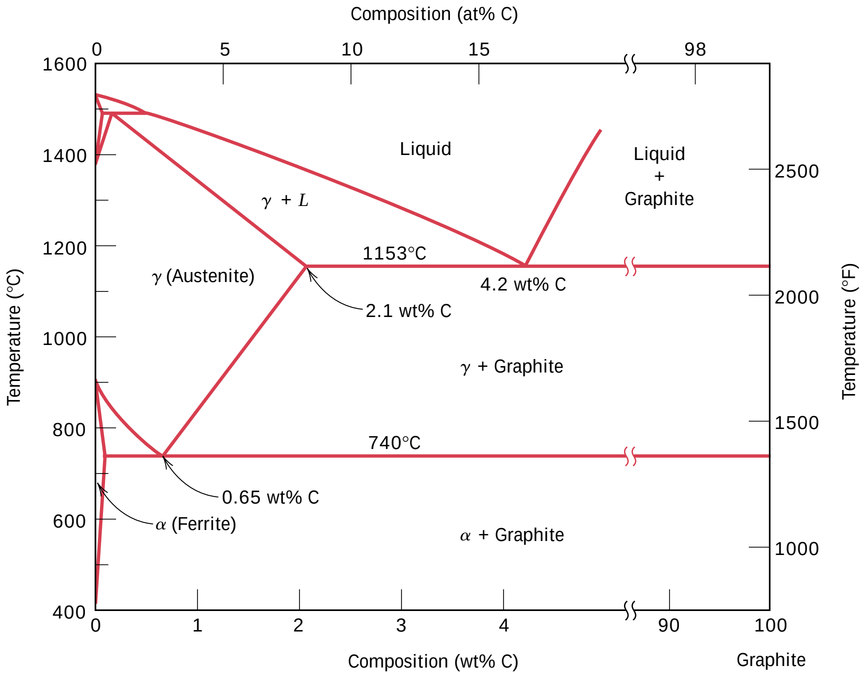

as graphite, and both microstructure and mechanical behavior depend on composition and heat treatment. The most common cast iron types are gray, nodular, white, and malleable.

Gray Iron

The carbon and silicon contents of **gray cast irons** vary between 2.5 and 4.0 wt% and 1.0 and 3.0 wt%, respectively. For most of these cast irons, the graphite exists in the form of flakes (similar to corn flakes), which are normally surrounded by an α ferrite or pearlite matrix; the microstructure of a typical gray iron is shown in Figure 13.3*a*. Because of these graphite flakes, a fractured surface takes on a gray appearance, hence its name.

Mechanically, gray iron is comparatively weak and brittle in tension as a consequence of its microstructure; the tips of the graphite flakes are sharp and pointed, and may serve as points of stress concentration when an external tensile stress is applied. Strength and ductility are much higher under compressive loads. Typical mechanical properties and compositions of several of the common gray cast irons are listed in Table 13.5. Gray irons do have some desirable characteristics and, in fact, are utilized extensively. They are very effective in damping vibrational energy; this is represented in Figure 13.4, which compares the relative damping capacities of steel and gray iron. Base structures for machines and heavy equipment that are exposed to vibrations are frequently constructed of this material. In addition, gray irons exhibit a high resistance to wear. Furthermore, in the molten state they have a high fluidity at casting temperature, which permits casting pieces having intricate shapes; also, casting shrinkage is low. Finally, and perhaps most important, gray cast irons are among the least expensive of all metallic materials.

Gray irons having microstructures different from that shown in Figure 13.3*a* may be generated by adjustment of composition and/or by using an appropriate treatment. For example, lowering the silicon content or increasing the cooling rate may prevent the complete dissociation of cementite to form graphite (Equation 13.1). Under these circumstances the microstructure consists of graphite flakes embedded in a pearlite matrix. Figure 13.5 compares schematically the several cast iron microstructures obtained by varying the composition and heat treatment.

Ductile (or Nodular) Iron

Adding a small amount of magnesium and/or cerium to the gray iron before casting produces a distinctly different microstructure and set of mechanical properties. Graphite still forms, but as nodules or spherelike particles instead of flakes. The resulting alloy is called **nodular** or **ductile iron,** and a typical microstructure is shown in Figure 13.3*b*. The matrix phase surrounding these particles is either pearlite or ferrite, depending on heat treatment (Figure 13.5); it is normally pearlite for an as-cast piece. However, a heat treatment for several hours at about 700°C (1300°F) will yield a ferrite matrix as in this photomicrograph. Castings are stronger and much more ductile than gray iron, as a comparison of their mechanical properties in Table 13.5 shows. In fact, ductile iron has mechanical characteristics approaching those of steel. For example, ferritic ductile irons have tensile strengths ranging between 380 and 480 MPa (55,000 and 70,000 psi), and ductilities (as percent elongation) from 10 to 20%. Typical applications for this material include valves, pump bodies, crankshafts, gears, and other automotive and machine components.

White Iron and Malleable Iron

For low-silicon cast irons (containing less than 1.0 wt% Si) and rapid cooling rates, most of the carbon exists as cementite instead of graphite, as indicated in Figure

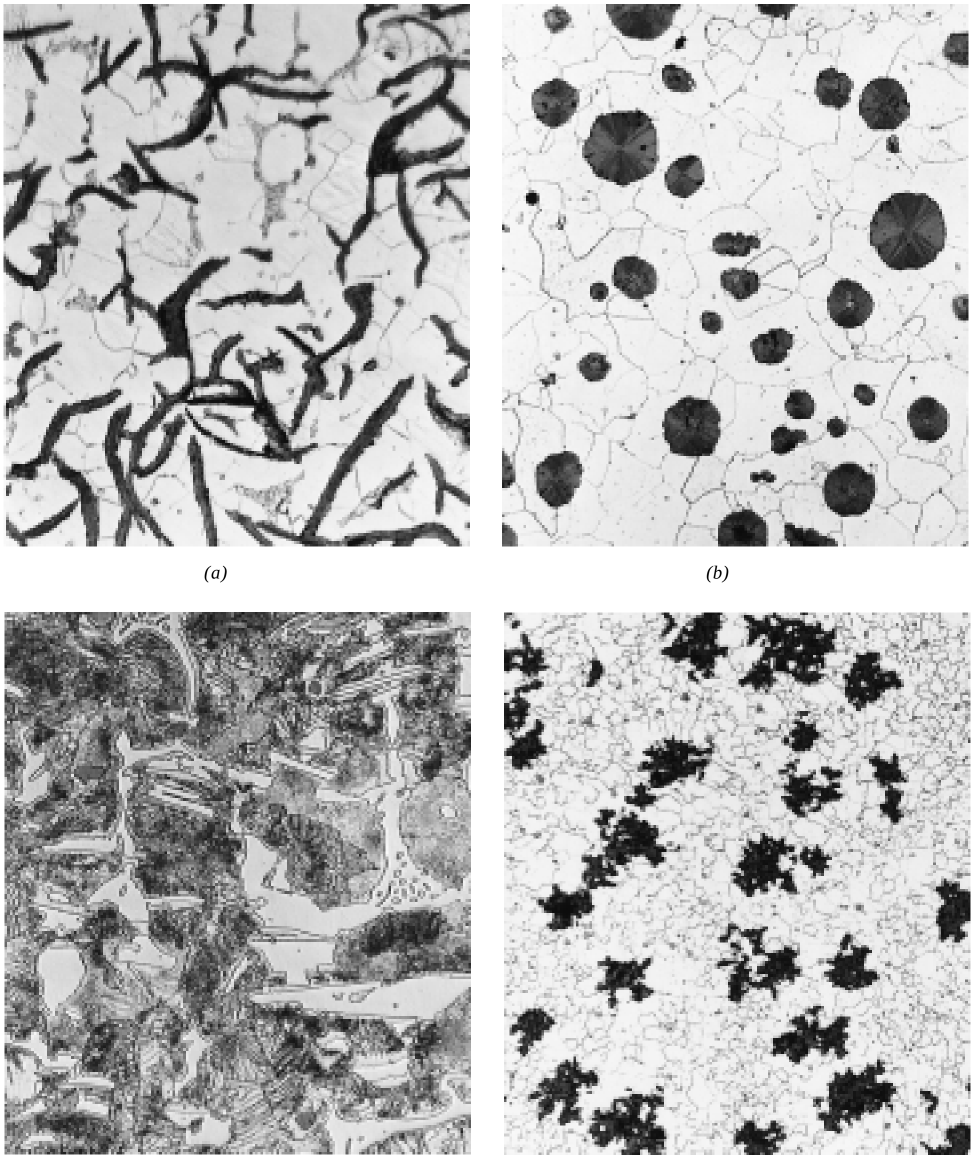

(a) (b)

(c) (d)

FIGURE 13.3 Optical photomicrographs of various cast irons. (*a*) Gray iron: the dark graphite flakes are embedded in an α-ferrite matrix. 500×. (Courtesy of C. H. Brady, National Bureau of Standards, Washington, DC.) (*b*) Nodular (ductile) iron: the dark graphite nodules are surrounded by an α-ferrite matrix. 200×. (Courtesy of C. H. Brady and L. C. Smith, National Bureau of Standards, Washington, DC.) (*c*) White iron: the light cementite regions are surrounded by pearlite, which has the ferrite–cementite layered structure. 400×. (Courtesy of Amcast Industrial Corporation.) (*d*) Malleable iron: dark graphite rosettes (temper carbon) in an α-ferrite matrix. 150×. (Reprinted with permission of the Iron Castings Society, Des Plaines, IL.)

Table 13.5 **Designations, Minimum Mechanical Properties, Approximate Compositions, and Typical Applications for Various Gray, Nodular, and Malleable Cast Irons**

				Mechanical Properties			
Grade	*UNS Number*	*Composition (wt%)*[a]	*Matrix Structure*	*Tensile Strength [MPa (ksi)]*	*Yield Strength [MPa (ksi)]*	*Ductility [%EL in 50 mm (2 in.)]*	*Typical Applications*
				Gray Iron			
SAE G1800	F10004	3.40–3.7 C, 2.55 Si, 0.7 Mn	Ferrite + Pearlite	124 (18)	—	—	Miscellaneous soft iron castings in which strength is not a primary consideration
SAE G2500	F10005	3.2–3.5 C, 2.20 Si, 0.8 Mn	Ferrite + Pearlite	173 (25)	—	—	Small cylinder blocks, cylinder heads, pistons, clutch plates, transmission cases
SAE G4000	F10008	3.0–3.3 C, 2.0 Si, 0.8 Mn	Pearlite	276 (40)	—	—	Diesel engine castings, liners, cylinders, and pistons
				Ductile (Nodular) Iron			
ASTM A536							
60-40-18	F32800	3.5–3.8 C, 2.0–2.8 Si, 0.05 Mg, <0.20 Ni, <0.10 Mo	Ferrite	414 (60)	276 (40)	18	Pressure-containing parts such as valve and pump bodies
100-70-03	F34800		Pearlite	689 (100)	483 (70)	3	High-strength gears and machine components
120-90-02	F36200		Tempered martensite	827 (120)	621 (90)	2	Pinions, gears, rollers, slides
				Malleable Iron			
32510	F22200	2.3–2.7 C, 1.0–1.75 Si, <0.55 Mn	Ferrite	345 (50)	224 (32)	10	General engineering service at normal and elevated temperatures
45006	—	2.4–2.7 C, 1.25–1.55 Si, <0.55 Mn	Ferrite + Pearlite	448 (65)	310 (45)	6	

[a] The balance of the composition is iron.

Source: Adapted from *ASM Handbook*, Vol. 1, *Properties and Selection: Irons, Steels, and High-Performance Alloys*, 1990. Reprinted by permission of ASM International, Materials Park, OH.

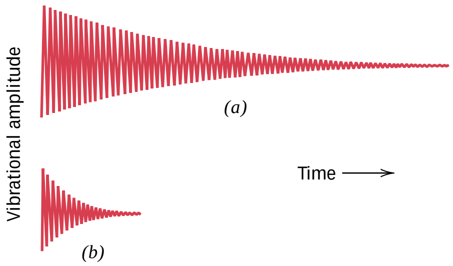

Figure 13.4 Comparison of the relative vibrational damping capacities of (*a*) steel and (*b*) gray cast iron. (From *Metals Engineering Quarterly*, February 1961. Copyright 1961 American Society for Metals.)

13.5. A fracture surface of this alloy has a white appearance, and thus it is termed **white cast iron.** An optical photomicrograph showing the microstructure of white iron is presented in Figure 13.3*c*. Thick sections may have only a surface layer of white iron that was ''chilled'' during the casting process; gray iron forms at interior regions, which cool more slowly. As a consequence of large amounts of the cementite

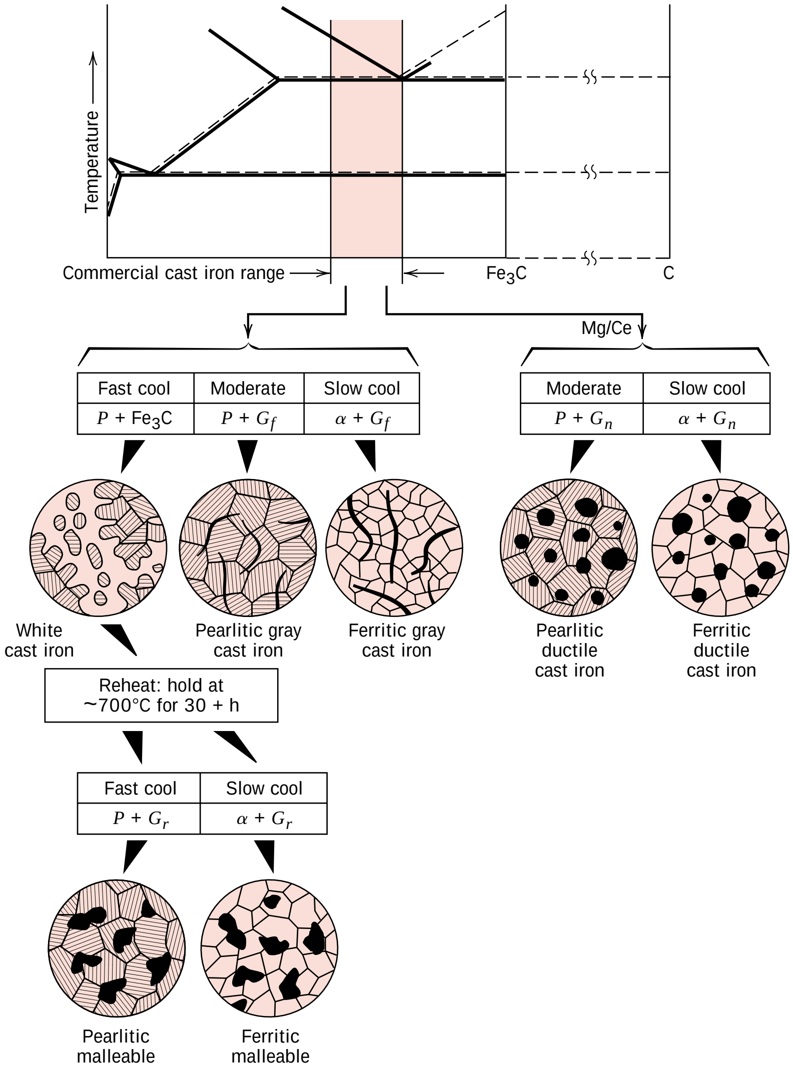
Temperature
Commercial cast iron range
Fe_3C
C
Mg/Ce
Fast cool
Moderate
Slow cool
$P + Fe_3C$
$P + G_f$
$\alpha + G_f$
Moderate
Slow cool
$P + G_n$
$\alpha + G_n$
White cast iron
Pearlitic gray cast iron
Ferritic gray cast iron
Pearlitic ductile cast iron
Ferritic ductile cast iron
Reheat: hold at ~700°C for 30 + h
Fast cool
Slow cool
$P + G_r$
$\alpha + G_r$
Pearlitic malleable
Ferritic malleable

Figure 13.5 From the iron–carbon phase diagram, composition ranges for commercial cast irons. Also shown are microstructures that result from a variety of heat treatments. G_f, flake graphite; G_r, graphite rosettes; G_n, graphite nodules; P, pearlite; α, ferrite. (Adapted from W. G. Moffatt, G. W. Pearsall, and J. Wulff, *The Structure and Properties of Materials*, Vol. 1, *Structure*, p. 195. Copyright © 1964 by John Wiley & Sons, New York. Reprinted by permission of John Wiley & Sons, Inc.)

phase, white iron is extremely hard but also very brittle, to the point of being virtually unmachinable. Its use is limited to applications that necessitate a very hard and wear-resistant surface, and without a high degree of ductility—for example, as rollers in rolling mills. Generally, white iron is used as an intermediary in the production of yet another cast iron, **malleable iron.**

Heating white iron at temperatures between 800 and 900°C (1470 and 1650°F) for a prolonged time period and in a neutral atmosphere (to prevent oxidation) causes a decomposition of the cementite, forming graphite, which exists in the form of clusters or rosettes surrounded by a ferrite or pearlite matrix, depending on cooling rate, as indicated in Figure 13.5. A photomicrograph of a ferritic malleable iron is presented in Figure 13.3*d*. The microstructure is similar to that for nodular iron (Figure 13.3*b*), which accounts for relatively high strength and appreciable ductility or malleability. Some typical mechanical characteristics are also listed in Table 13.5. Representative applications include connecting rods, transmission gears, and differential cases for the automotive industry, and also flanges, pipe fittings, and valve parts for railroad, marine, and other heavy-duty services.

13.3 NONFERROUS ALLOYS

Steel and other ferrous alloys are consumed in exceedingly large quantities because they have such a wide range of mechanical properties, may be fabricated with relative ease, and are economical to produce. However, they have some distinct limitations, chiefly: (1) a relatively high density, (2) a comparatively low electrical conductivity, and (3) an inherent susceptibility to corrosion in some common environments. Thus, for many applications it is advantageous or even necessary to utilize other alloys having more suitable property combinations. Alloy systems are classified either according to the base metal or according to some specific characteristic that a group of alloys share. This section discusses the following metal and alloy systems: copper, aluminum, magnesium, and titanium alloys, the refractory metals, the superalloys, the noble metals, and miscellaneous alloys, including those that have nickel, lead, tin, zirconium, and zinc as base metals.

On occasion, a distinction is made between cast and wrought alloys. Alloys that are so brittle that forming or shaping by appreciable deformation is not possible ordinarily are cast; these are classified as *cast alloys.* On the other hand, those that are amenable to mechanical deformation are termed **wrought alloys.**

In addition, the heat treatability of an alloy system is mentioned frequently. ''Heat treatable'' designates an alloy whose mechanical strength is improved by precipitation hardening or a martensitic transformation (normally the former), both of which involve specific heat-treating procedures.

COPPER AND ITS ALLOYS

Copper and copper-based alloys, possessing a desirable combination of physical properties, have been utilized in quite a variety of applications since antiquity. Unalloyed copper is so soft and ductile that it is difficult to machine; also, it has an almost unlimited capacity to be cold worked. Furthermore, it is highly resistant to corrosion in diverse environments including the ambient atmosphere, seawater, and some industrial chemicals. The mechanical and corrosion-resistance properties of copper may be improved by alloying. Most copper alloys cannot be hardened or strengthened by heat-treating procedures; consequently, cold working and/or solid-solution alloying must be utilized to improve these mechanical properties.

The most common copper alloys are the **brasses** for which zinc, as a substitutional impurity, is the predominant alloying element. As may be observed for the copper–zinc phase diagram (Figure 10.17), the α phase is stable for concentrations up to approximately 35 wt% Zn. This phase has an FCC crystal structure, and α brasses are relatively soft, ductile, and easily cold worked. Brass alloys having a higher zinc content contain both α and β' phases at room temperature. The β' phase has an ordered BCC crystal structure and is harder and stronger than the α phase; consequently, $\alpha + \beta'$ alloys are generally hot worked.

Some of the common brasses are yellow, naval, and cartridge brass, muntz metal, and gilding metal. The compositions, properties, and typical uses of several of these alloys are listed in Table 13.6. Some of the common uses for brass alloys include costume jewelry, cartridge casings, automotive radiators, musical instruments, electronic packaging, and coins.

Table 13.6 Compositions, Mechanical Properties, and Typical Applications for Eight Copper Alloys

Alloy Name	*UNS Number*	*Composition (wt%)*[a]	*Condition*	*Mechanical Properties*			*Typical Applications*
				Tensile Strength [MPa (ksi)]	*Yield Strength [MPa (ksi)]*	*Ductility [%EL in 50 mm (2 in.)]*	
				Wrought Alloys			
Electrolytic tough pitch	C11000	0.04 O	Annealed	220 (32)	69 (10)	45	Electrical wire, rivets, screening, gaskets, pans, nails, roofing
Beryllium copper	C17200	1.9 Be, 0.20 Co	Precipitation hardened	1140–1310 (165–190)	690–860 (100–125)	4–10	Springs, bellows, firing pins, bushings, valves, diaphragms
Cartridge brass	C26000	30 Zn	Annealed Cold-worked (H04 hard)	300 (44) 525 (76)	75 (11) 435 (63)	68 8	Automotive radiator cores, ammunition components, lamp fixtures, flashlight shells, kickplates
Phosphor bronze, 5% A	C51000	5 Sn, 0.2 P	Annealed Cold-worked (H04 hard)	325 (47) 560 (81)	130 (19) 515 (75)	64 10	Bellows, clutch disks, diaphragms, fuse clips, springs, welding rods
Copper-nickel, 30%	C71500	30 Ni	Annealed Cold-worked (H02 hard)	380 (55) 515 (75)	125 (18) 485 (70)	36 15	Condenser and heat-exchanger components, saltwater piping
				Cast Alloys			
Leaded yellow brass	C85400	29 Zn, 3 Pb, 1 Sn	As cast	234 (34)	83 (12)	35	Furniture hardware, radiator fittings, light fixtures, battery clamps
Tin bronze	C90500	10 Sn, 2 Zn	As cast	310 (45)	152 (22)	25	Bearings, bushings, piston rings, steam fittings, gears
Aluminum bronze	C95400	4 Fe, 11 Al	As cast	586 (85)	241 (35)	18	Bearings, gears, worms, bushings, valve seats and guards, pickling hooks

[a] The balance of the composition is copper.

Source: Adapted from *ASM Handbook*, Vol. 2, *Properties and Selection: Nonferrous Alloys and Special-Purpose Materials*, 1990. Reprinted by permission of ASM International, Materials Park, OH.

The **bronzes** are alloys of copper and several other elements, including tin, aluminum, silicon, and nickel. These alloys are somewhat stronger than the brasses, yet they still have a high degree of corrosion resistance. Table 13.6 contains several of the bronze alloys, their compositions, properties, and applications. Generally they are utilized when, in addition to corrosion resistance, good tensile properties are required.

The most common precipitation hardenable copper alloys are the beryllium coppers. They possess a remarkable combination of properties: tensile strengths as high as 1400 MPa (200,000 psi), excellent electrical and corrosion properties, and wear resistance when properly lubricated; they may be cast, hot worked, or cold worked. High strengths are attained by precipitation-hardening heat treatments. These alloys are costly because of the beryllium additions, which range between 1.0 and 2.5 wt%. Applications include jet aircraft landing gear bearings and bushings, springs, and surgical and dental instruments. One of these alloys (C17200) is included in Table 13.6.

ALUMINUM AND ITS ALLOYS

Aluminum and its alloys are characterized by a relatively low density (2.7 g/cm^3 as compared to 7.9 g/cm^3 for steel), high electrical and thermal conductivities, and a resistance to corrosion in some common environments, including the ambient atmosphere. Many of these alloys are easily formed by virtue of high ductility; this is evidenced by the thin aluminum foil sheet into which the relatively pure material may be rolled. Since aluminum has an FCC crystal structure, its ductility is retained even at very low temperatures. The chief limitation of aluminum is its low melting temperature [660°C (1220°F)], which restricts the maximum temperature at which it can be used.

The mechanical strength of aluminum may be enhanced by cold work and by alloying; however, both processes tend to diminish resistance to corrosion. Principal alloying elements include copper, magnesium, silicon, manganese, and zinc. Non-heat-treatable alloys consist of a single phase, for which an increase in strength is achieved by solid solution strengthening. Others are rendered heat treatable (capable of being precipitation hardened) as a result of alloying. In several of these alloys precipitation hardening is due to the precipitation of two elements other than aluminum, to form an intermetallic compound such as $MgZn_2$.

Generally, aluminum alloys are classified as either cast or wrought. Composition for both types is designated by a four-digit number that indicates the principal impurities, and in some cases, the purity level. For cast alloys, a decimal point is located between the last two digits. After these digits is a hyphen and the basic **temper designation**—a letter and possibly a one- to three-digit number, which indicates the mechanical and/or heat treatment to which the alloy has been subjected. For example, F, H, and O represent, respectively, the as-fabricated, strain-hardened, and annealed states; T3 means that the alloy was solution heat treated, cold worked, and then naturally aged (age hardened). A solution heat treatment followed by artificial aging is indicated by T6. The compositions, properties, and applications of several wrought and cast alloys are contained in Table 13.7. Some of the more common applications of aluminum alloys include aircraft structural parts, beverage cans, bus bodies, and automotive parts (engine blocks, pistons, and manifolds).

Recent attention has been given to alloys of aluminum and other low-density metals (e.g., Mg and Ti) as engineering materials for transportation, to effect reductions in fuel consumption. An important characteristic of these materials is **specific**

Table 13.7 Compositions, Mechanical Properties, and Typical Applications for Several Common Aluminum Alloys

Aluminum Association Number	*UNS Number*	*Composition (wt%)*[a]	*Condition (Temper Designation)*	*Mechanical Properties* *Tensile Strength [MPa (ksi)]*	*Mechanical Properties* *Yield Strength [MPa (ksi)]*	*Mechanical Properties* *Ductility [%EL in 50 mm (2 in.)]*	*Typical Applications/ Characteristics*
			Wrought, Nonheat-Treatable Alloys				
1100	A91100	0.12 Cu	Annealed (O)	90 (13)	35 (5)	35–45	Food/chemical handling & storage equipment, heat exchangers, light reflectors
3003	A93003	0.12 Cu, 1.2 Mn, 0.1 Zn	Annealed (O)	110 (16)	40 (6)	30–40	Cooking utensils, pressure vessels and piping
5052	A95052	2.5 Mg, 0.25 Cr	Strain hardened (H32)	230 (33)	195 (28)	12–18	Aircraft fuel & oil lines, fuel tanks, appliances, rivets, and wire
			Wrought, Heat-Treatable Alloys				
2024	A92024	4.4 Cu, 1.5 Mg, 0.6 Mn	Heat treated (T4)	470 (68)	325 (47)	20	Aircraft structures, rivets, truck wheels, screw machine products
6061	A96061	1.0 Mg, 0.6 Si, 0.30 Cu, 0.20 Cr	Heat treated (T4)	240 (35)	145 (21)	22–25	Trucks, canoes, railroad cars, furniture, pipelines
7075	A97075	5.6 Zn, 2.5 Mg, 1.6 Cu, 0.23 Cr	Heat treated (T6)	570 (83)	505 (73)	11	Aircraft structural parts and other highly stressed applications
			Cast, Heat-Treatable Alloys				
295.0	A02950	4.5 Cu, 1.1 Si	Heat treated (T4)	221 (32)	110 (16)	8.5	Flywheel and rear-axle housings, bus and aircraft wheels, crankcases
356.0	A03560	7.0 Si, 0.3 Mg	Heat treated (T6)	228 (33)	164 (24)	3.5	Aircraft pump parts, automotive transmission cases, water-cooled cylinder blocks
			Aluminum–Lithium Alloys				
2090	—	2.7 Cu, 0.25 Mg, 2.25 Li, 0.12 Zr	Heat treated, cold worked (T83)	455 (66)	455 (66)	5	Aircraft structures and cryogenic tankage structures
8090	—	1.3 Cu, 0.95 Mg, 2.0 Li, 0.1 Zr	Heat treated, cold worked (T651)	465 (67)	360 (52)	—	Aircraft structures that must be highly damage tolerant

[a] The balance of the composition is aluminum.

Source: Adapted from *ASM Handbook*, Vol. 2, *Properties and Selection: Nonferrous Alloys and Special-Purpose Materials*, 1990. Reprinted by permission of ASM International, Materials Park, OH.

strength, which is quantified by the tensile strength–specific gravity ratio. Even though an alloy of one of these metals may have a tensile strength that is inferior to a more dense material (such as steel), on a weight basis it will be able to sustain a larger load.

A generation of new aluminum-lithium alloys have been developed recently for use by the aircraft and aerospace industries. These materials have relatively low densities (between about 2.5 and 2.6 g/cm^3), high specific moduli (elastic modulus-specific gravity ratios), and excellent fatigue and low-temperature toughness properties. Furthermore, some of them may be precipitation hardened. However, these materials are more costly to manufacture than the conventional aluminum alloys because special processing techniques are required as a result of lithium's chemical reactivity.

MAGNESIUM AND ITS ALLOYS

Perhaps the most outstanding characteristic of magnesium is its density, 1.7 g/cm^3, which is the lowest of all the structural metals; therefore, its alloys are used where light weight is an important consideration (e.g., in aircraft components). Magnesium has an HCP crystal structure, is relatively soft, and has a low elastic modulus: 45 GPa (6.5×10^6 psi). At room temperature magnesium and its alloys are difficult to deform; in fact, only small degrees of cold work may be imposed without annealing. Consequently, most fabrication is by casting or hot working at temperatures between 200 and 350°C (400 and 650°F). Magnesium, like aluminum, has a moderately low melting temperature [651°C (1204°F)]. Chemically, magnesium alloys are relatively unstable and especially susceptible to corrosion in marine environments. On the other hand, corrosion or oxidation resistance is reasonably good in the normal atmosphere; it is believed that this behavior is due to impurities rather than being an inherent characteristic of Mg alloys. Fine magnesium powder ignites easily when heated in air; consequently, care should be exercised when handling it in this state.

These alloys are also classified as either cast or wrought, and some of them are heat treatable. Aluminum, zinc, manganese, and some of the rare earths are the major alloying elements. A composition–temper designation scheme similar to that for aluminum alloys is also used. Table 13.8 lists several common magnesium alloys, their compositions, properties, and applications. These alloys are used in aircraft and missile applications, as well as in luggage. Furthermore, in the last several years the demand for magnesium alloys has increased dramatically in a host of different industries. For many applications, magnesium alloys have replaced engineering plastics that have comparable densities inasmuch as the magnesium materials are stiffer, more recyclable, and less costly to produce. For example, magnesium is now employed in a variety of hand-held devices (e.g., chain saws, power tools, hedge clippers), in automobiles (e.g., steering wheels and columns, seat frames, transmission cases), and in audio-video-computer-communications equipment (e.g., laptop computers, camcorders, TV sets, cellular telephones).

TITANIUM AND ITS ALLOYS

Titanium and its alloys are relatively new engineering materials that possess an extraordinary combination of properties. The pure metal has a relatively low density (4.5 g/cm^3), a high melting point [1668°C (3035°F)], and an elastic modulus of 107 GPa (15.5×10^6 psi). Titanium alloys are extremely strong; room temperature tensile strengths as high as 1400 MPa (200,000 psi) are attainable, yielding remarkable specific strengths. Furthermore, the alloys are highly ductile and easily forged and machined.

Table 13.8 **Compositions, Mechanical Properties, and Typical Applications for Six Common Magnesium Alloys**

ASTM Number	UNS Number	Composition (wt%)[a]	Condition	Mechanical Properties: Tensile Strength [MPa (ksi)]	Yield Strength [MPa (ksi)]	Ductility [%EL in 50 mm (2 in.)]	Typical Applications
Wrought Alloys							
AZ31B	M11311	3.0 Al, 1.0 Zn, 0.2 Mn	As extruded	262 (38)	200 (29)	15	Structures and tubing, cathodic protection
HK31A	M13310	3.0 Th, 0.6 Zr	Strain hardened, partially annealed	255 (37)	200 (29)	9	High strength to 315°C (600°F)
ZK60A	M16600	5.5 Zn, 0.45 Zr	Artificially aged	350 (51)	285 (41)	11	Forgings of maximum strength for aircraft
Cast Alloys							
AZ91D	M11916	9.0 Al, 0.15 Mn, 0.7 Zn	As cast	230 (33)	150 (22)	3	Die-cast parts for automobiles, luggage, and electronic devices
AM60A	M10600	6.0 Al, 0.13 Mn	As cast	220 (32)	130 (19)	6	Automotive wheels
AS41A	M10410	4.3 Al, 1.0 Si, 0.35 Mn	As cast	210 (31)	140 (20)	6	Die castings requiring good creep resistance

[a] The balance of the composition is magnesium.

Source: Adapted from *ASM Handbook*, Vol. 2, *Properties and Selection: Nonferrous Alloys and Special-Purpose Materials*, 1990. Reprinted by permission of ASM International, Materials Park, OH.

The major limitation of titanium is its chemical reactivity with other materials at elevated temperatures. This property has necessitated the development of nonconventional refining, melting, and casting techniques; consequently, titanium alloys are quite expensive. In spite of this high temperature reactivity, the corrosion resistance of titanium alloys at normal temperatures is unusually high; they are virtually immune to air, marine, and a variety of industrial environments. Table 13.9 presents several titanium alloys along with their typical properties and applications. They are commonly utilized in airplane structures, space vehicles, surgical implants, and in the petroleum and chemical industries.

THE REFRACTORY METALS

Metals that have extremely high melting temperatures are classified as the refractory metals. Included in this group are niobium (Nb), molybdenum (Mo), tungsten (W), and tantalum (Ta). Melting temperatures range between 2468°C (4474°F) for niobium and 3410°C (6170°F), the highest melting temperature of any metal, for tungsten. Interatomic bonding in these metals is extremely strong, which accounts for the melting temperatures, and, in addition, large elastic moduli and high strengths and hardnesses, at ambient as well as elevated temperatures. The applications of these metals are varied. For example, tantalum and molybdenum are alloyed with stainless steel to improve its corrosion resistance. Molybdenum alloys are utilized for extrusion dies and structural parts in space vehicles; incandescent light filaments,

Table 13.9 Compositions, Mechanical Properties, and Typical Applications for Several Common Titanium Alloys

				Average Mechanical Properties			
Alloy Type	***Common Name (UNS Number)***	***Composition (wt%)***	***Condition***	***Tensile Strength [MPa (ksi)]***	***Yield Strength [MPa (ksi)]***	***Ductility [%EL in 50 mm (2 in.)]***	***Typical Applications***
Commercially pure	Unalloyed (R50500)	99.1 Ti	Annealed	484 (70)	414 (60)	25	Jet engine shrouds, cases and airframe skins, corrosion-resistant equipment for marine and chemical processing industries
α	Ti-5Al-2.5Sn (R54520)	5 Al, 2.5 Sn, balance Ti	Annealed	826 (120)	784 (114)	16	Gas turbine engine casings and rings; chemical processing equipment requiring strength to temperatures of 480°C (900°F)
Near α	Ti-8Al-1Mo-1V (R54810)	8 Al, 1 Mo, 1 V, balance Ti	Annealed (duplex)	950 (138)	890 (129)	15	Forgings for jet engine components (compressor disks, plates, and hubs)
α-β	Ti-6Al-4V (R56400)	6 Al, 4 V, balance Ti	Annealed	947 (137)	877 (127)	14	High-strength prosthetic implants, chemical-processing equipment, airframe structural components
α-β	Ti-6Al-6V-2Sn (R56620)	6 Al, 2 Sn, 6 V, 0.75 Cu, balance Ti	Annealed	1050 (153)	985 (143)	14	Rocket engine case airframe applications and high-strength airframe structures
β	Ti-10V-2Fe-3Al	10 V, 2 Fe, 3 Al, balance Ti	Solution + aging	1223 (178)	1150 (167)	10	Best combination of high strength and toughness of any commercial titanium alloy; used for applications requiring uniformity of tensile properties at surface and center locations; high-strength airframe components

Source: Adapted from *ASM Handbook*, Vol. 2, *Properties and Selection: Nonferrous Alloys and Special-Purpose Materials*, 1990. Reprinted by permission of ASM International, Materials Park, OH.

x-ray tubes, and welding electrodes employ tungsten alloys. Tantalum is immune to chemical attack by virtually all environments at temperatures below 150°C, and is frequently used in applications requiring such a corrosion-resistant material.

THE SUPERALLOYS

The superalloys have superlative combinations of properties. Most are used in aircraft turbine components, which must withstand exposure to severely oxidizing environments and high temperatures for reasonable time periods. Mechanical integrity under these conditions is critical; in this regard, density is an important consideration because centrifugal stresses are diminished in rotating members when the density is reduced. These materials are classified according to the predominant metal in the alloy, which may be cobalt, nickel, or iron. Other alloying elements include the refractory metals (Nb, Mo, W, Ta), chromium, and titanium. In addition to turbine applications, these alloys are utilized in nuclear reactors and petrochemical equipment.

THE NOBLE METALS

The noble or precious metals are a group of eight elements that have some physical characteristics in common. They are expensive (precious) and are superior or notable (noble) in properties—i.e., characteristically soft, ductile, and oxidation resistant. The noble metals are silver, gold, platinum, palladium, rhodium, ruthenium, iridium, and osmium; the first three are most common and are used extensively in jewelry. Silver and gold may be strengthened by solid-solution alloying with copper; sterling silver is a silver–copper alloy containing approximately 7.5 wt% Cu. Alloys of both silver and gold are employed as dental restoration materials; also, some integrated circuit electrical contacts are of gold. Platinum is used for chemical laboratory equipment, as a catalyst (especially in the manufacture of gasoline), and in thermocouples to measure elevated temperatures.

MISCELLANEOUS NONFERROUS ALLOYS

The discussion above covers the vast majority of nonferrous alloys; however, a number of others are found in a variety of engineering applications, and a brief exposure of these is worthwhile.

Nickel and its alloys are highly resistant to corrosion in many environments, especially those that are basic (alkaline). Nickel is often coated or plated on some metals that are susceptible to corrosion as a protective measure. Monel, a nickel-based alloy containing approximately 65 wt% Ni and 28 wt% Cu (the balance iron), has very high strength and is extremely corrosion resistant; it is used in pumps, valves, and other components that are in contact with some acid and petroleum solutions. As already mentioned, nickel is one of the principal alloying elements in stainless steels, and one of the major constituents in the superalloys.

Lead, tin, and their alloys find some use as engineering materials. Both are mechanically soft and weak, have low melting temperatures, are quite resistant to many corrosion environments, and have recrystallization temperatures below room temperature. Many common solders are lead–tin alloys, which have low melting temperatures. Applications for lead and its alloys include x-ray shields and storage batteries. The primary use of tin is as a very thin coating on the inside of plain carbon steel cans (tin cans) that are used for food containers; this coating inhibits chemical reactions between the steel and the food products.

Unalloyed zinc also is a relatively soft metal having a low melting temperature and a subambient recrystallization temperature. Chemically, it is reactive in a number of common environments and, therefore, susceptible to corrosion. Galvanized steel is just plain carbon steel that has been coated with a thin zinc layer; the zinc preferentially corrodes and protects the steel {(Section 16.9).} Typical applications of galvanized steel are familiar (sheet metal, fences, screen, screws, etc.). Common applications of zinc alloys include padlocks, automotive parts (door handles and grilles), and office equipment.

Although zirconium is relatively abundant in the earth's crust, it was not until quite recent times that commercial refining techniques were developed. Zirconium and its alloys are ductile and have other mechanical characteristics that are comparable to those of titanium alloys and the austenitic stainless steels. However, the primary asset of these alloys is their resistance to corrosion in a host of corrosive media, including superheated water. Furthermore, zirconium is transparent to thermal neutrons, so that its alloys have been used as cladding for uranium fuel in water-cooled nuclear reactors. In terms of cost, these alloys are also often the materials of choice for heat exchangers, reactor vessels, and piping systems for the chemical-processing and nuclear industries. They are also used in incendiary ordnance and in sealing devices for vacuum tubes.

In Appendix B is tabulated a wide variety of properties (e.g., density, elastic modulus, yield and tensile strengths, electrical conductivity, coefficient of thermal expansion, etc.) for a large number of metals and alloys.

TYPES OF CERAMICS

The preceding discussions of the properties of materials have demonstrated that there is a significant disparity between the physical characteristics of metals and ceramics. Consequently, these materials are utilized in totally different kinds of applications and, in this regard, tend to complement each other, and also the polymers. Most ceramic materials fall into an application–classification scheme that includes the following groups: glasses, structural clay products, whitewares, refractories, abrasives, cements, {and the newly developed advanced ceramics.} Figure 13.6 presents a taxonomy of these several types; some discussion is devoted to each. We have also chosen to discuss the characteristics and applications of diamond and graphite in this section.

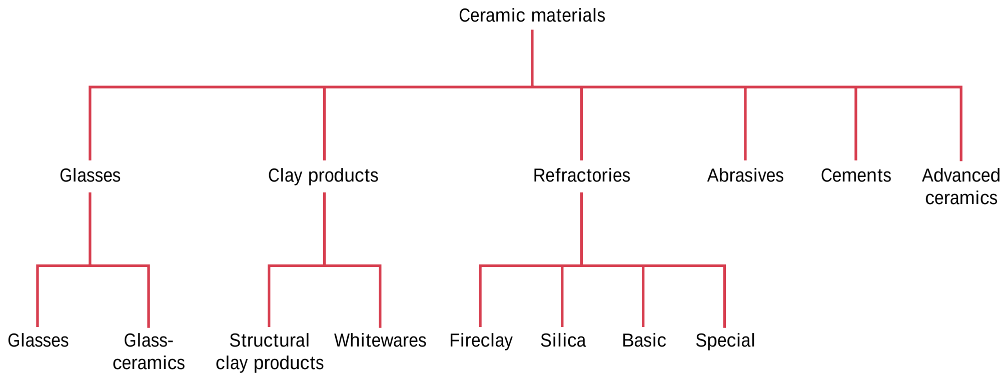

FIGURE 13.6 Classification of ceramic materials on the basis of application.

Table 13.10 Compositions and Characteristics of Some of the Common Commercial Glasses

	Composition (wt%)						
Glass Type	***SiO_2***	***Na_2O***	***CaO***	***Al_2O_3***	***B_2O_3***	***Other***	***Characteristics and Applications***
Fused silica	>99.5						High melting temperature, very low coefficient of expansion (shock resistant)
96% Silica (Vycor)	96				4		Thermally shock and chemically resistant—laboratory ware
Borosilicate (Pyrex)	81	3.5		2.5	13		Thermally shock and chemically resistant—ovenware
Container (soda–lime)	74	16	5	1		4MgO	Low melting temperature, easily worked, also durable
Fiberglass	55		16	15	10	4MgO	Easily drawn into fibers—glass–resin composites
Optical flint	54	1				37PbO, $8K_2O$	High density and high index of refraction—optical lenses
Glass–ceramic (Pyroceram)	43.5	14		30	5.5	$6.5TiO_2$, $0.5As_2O_3$	Easily fabricated; strong; resists thermal shock—ovenware

13.4 GLASSES

The glasses are a familiar group of ceramics; containers, windows, lenses, and fiberglass represent typical applications. As already mentioned, they are noncrystalline silicates containing other oxides, notably CaO, Na_2O, K_2O, and Al_2O_3, which influence the glass properties. A typical soda–lime glass consists of approximately 70 wt% SiO_2, the balance being mainly Na_2O (soda) and CaO (lime). The compositions of several common glass materials are contained in Table 13.10. Possibly the two prime assets of these materials are their optical transparency and the relative ease with which they may be fabricated.

13.5 GLASS–CERAMICS

Most inorganic glasses can be made to transform from a noncrystalline state to one that is crystalline by the proper high-temperature heat treatment. This process is called **devitrification,** and the product is a fine-grained polycrystalline material which is often called a **glass–ceramic.** A nucleating agent (frequently titanium dioxide) must be added to induce the crystallization or devitrification process. Desirable characteristics of glass–ceramics include a low coefficient of thermal expansion, such that the glass–ceramic ware will not experience thermal shock; in addition, relatively high mechanical strengths and thermal conductivities are achieved. Some glass–ceramics may be made optically transparent; others are opaque. Possibly the most attractive attribute of this class of materials is the ease with which they may be fabricated; conventional glass-forming techniques may be used conveniently in the mass production of nearly pore-free ware.

Glass–ceramics are manufactured commercially under the trade names of Pyroceram, Corningware, Cercor, and Vision. The most common uses for these materials are as ovenware and tableware, primarily because of their strength, excellent resistance to thermal shock, and their high thermal conductivity. They also serve as electrical insulators and as substrates for printed circuit boards, and are utilized for architectural cladding, and for heat exchangers and regenerators. A typical glass–ceramic is also included in Table 13.10, and the microstructure of a commercial material is shown in the chapter-opening photograph for this chapter.

13.6 CLAY PRODUCTS

One of the most widely used ceramic raw materials is clay. This inexpensive ingredient, found naturally in great abundance, often is used as mined without any upgrading of quality. Another reason for its popularity lies in the ease with which clay products may be formed; when mixed in the proper proportions, clay and water form a plastic mass that is very amenable to shaping. The formed piece is dried to remove some of the moisture, after which it is fired at an elevated temperature to improve its mechanical strength.

Most of the clay-based products fall within two broad classifications: the **structural clay products** and the **whitewares.** Structural clay products include building bricks, tiles, and sewer pipes—applications in which structural integrity is important. The whiteware ceramics become white after the high-temperature **firing.** Included in this group are porcelain, pottery, tableware, china, and plumbing fixtures (sanitary ware). In addition to clay, many of these products also contain other ingredients, each of which has some role to play in the processing and characteristics of the finished piece {(Section 14.8).}

13.7 REFRACTORIES

Another important class of ceramics that are utilized in large tonnages is the **refractory ceramics.** The salient properties of these materials include the capacity to withstand high temperatures without melting or decomposing, and the capacity to remain unreactive and inert when exposed to severe environments. In addition, the ability to provide thermal insulation is often an important consideration. Refractory materials are marketed in a variety of forms, but bricks are the most common. Typical applications include furnace linings for metal refining, glass manufacturing, metallurgical heat treatment, and power generation.

Of course, the performance of a refractory ceramic, to a large degree, depends on its composition. On this basis, there are several classifications, namely, fireclay, silica, basic, and special refractories. Compositions for a number of commercial refractories are listed in Table 13.11. For many commercial materials, the raw ingredients consist of both large (or grog) particles and fine particles, which may

Table 13.11 Compositions of Five Common Ceramic Refractory Materials

	Composition *(wt%)*							
Refractory Type	Al_2O_3	SiO_2	MgO	Cr_2O_3	Fe_2O_3	CaO	TiO_2	***Apparent Porosity*** *(%)*
Fireclay	25–45	70–50	0–1		0–1	0–1	1–2	10–25
High-alumina fireclay	90–50	10–45	0–1		0–1	0–1	1–4	18–25
Silica	0.2	96.3	0.6			2.2		25
Periclase	1.0	3.0	90.0	0.3	3.0	2.5		22
Periclase–chrome ore	9.0	5.0	73.0	8.2	2.0	2.2		21

Source: From W. D. Kingery, H. K. Bowen, and D. R. Uhlmann, *Introduction to Ceramics*, 2nd edition. Copyright © 1976 by John Wiley & Sons, New York. Reprinted by permission of John Wiley & Sons, Inc.

have different compositions. Upon firing, the fine particles normally are involved in the formation of a bonding phase, which is responsible for the increased strength of the brick; this phase may be predominantly either glassy or crystalline. The service temperature is normally below that at which the refractory piece was fired.

Porosity is one microstructural variable that must be controlled to produce a suitable refractory brick. Strength, load-bearing capacity, and resistance to attack by corrosive materials all increase with porosity reduction. At the same time, thermal insulation characteristics and resistance to thermal shock are diminished. Of course, the optimum porosity depends on the conditions of service.

FIRECLAY REFRACTORIES (CD-ROM)

SILICA REFRACTORIES (CD-ROM)

BASIC REFRACTORIES (CD-ROM)

SPECIAL REFRACTORIES (CD-ROM)

13.8 ABRASIVES

Abrasive ceramics are used to wear, grind, or cut away other material, which necessarily is softer. Therefore, the prime requisite for this group of materials is hardness or wear resistance; in addition, a high degree of toughness is essential to ensure that the abrasive particles do not easily fracture. Furthermore, high temperatures may be produced from abrasive frictional forces, so some refractoriness is also desirable.

Diamonds, both natural and synthetic, are utilized as abrasives; however, they are relatively expensive. The more common ceramic abrasives include silicon carbide, tungsten carbide (WC), aluminum oxide (or corundum), and silica sand.

Abrasives are used in several forms—bonded to grinding wheels, as coated abrasives, and as loose grains. In the first case, the abrasive particles are bonded to a wheel by means of a glassy ceramic or an organic resin. The surface structure should contain some porosity; a continual flow of air currents or liquid coolants within the pores that surround the refractory grains will prevent excessive heating. Figure 13.7 shows the microstructure of a bonded abrasive, revealing abrasive grains, the bonding phase, and pores.

Coated abrasives are those in which an abrasive powder is coated on some type of paper or cloth material; sandpaper is probably the most familiar example. Wood, metals, ceramics, and plastics are all frequently ground and polished using this form of abrasive.

Grinding, lapping, and polishing wheels often employ loose abrasive grains that are delivered in some type of oil- or water-based vehicle. Diamonds, corundum, silicon carbide, and rouge (an iron oxide) are used in loose form over a variety of grain size ranges.

13.9 CEMENTS

Several familiar ceramic materials are classified as inorganic **cements:** cement, plaster of paris, and lime, which, as a group, are produced in extremely large quantities. The characteristic feature of these materials is that when mixed with water, they form a paste that subsequently sets and hardens. This trait is especially useful in

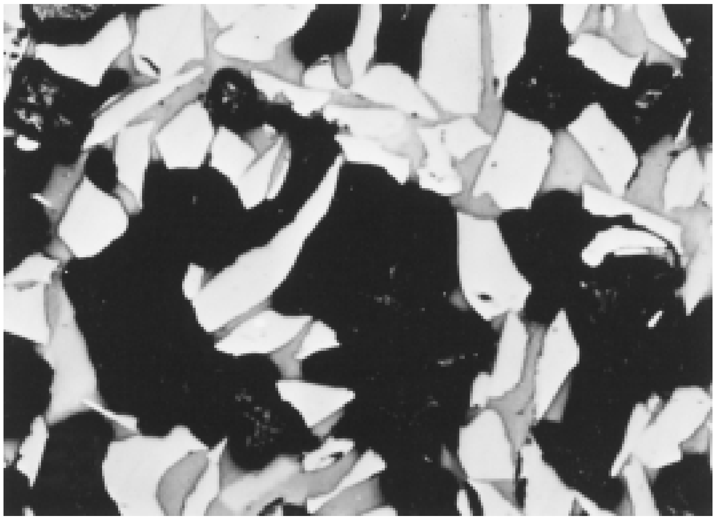

Figure 13.7 Photomicrograph of an aluminum oxide bonded ceramic abrasive. The light regions are the Al_2O_3 abrasive grains; the gray and dark areas are the bonding phase and porosity, respectively. 100×. (From W. D. Kingery, H. K. Bowen, and D. R. Uhlmann, *Introduction to Ceramics,* 2nd edition, p. 568. Copyright © 1976 by John Wiley & Sons. Reprinted by permission of John Wiley & Sons, Inc.)

that solid and rigid structures having just about any shape may be expeditiously formed. Also, some of these materials act as a bonding phase that chemically binds particulate aggregates into a single cohesive structure. Under these circumstances, the role of the cement is similar to that of the glassy bonding phase that forms when clay products and some refractory bricks are fired. One important difference, however, is that the cementitious bond develops at room temperature.

Of this group of materials, portland cement is consumed in the largest tonnages. It is produced by grinding and intimately mixing clay and lime-bearing minerals in the proper proportions, and then heating the mixture to about 1400°C (2550°F) in a rotary kiln; this process, sometimes called **calcination,** produces physical and chemical changes in the raw materials. The resulting ''clinker'' product is then ground into a very fine powder to which is added a small amount of gypsum ($CaSO_4$–$2H_2O$) to retard the setting process. This product is portland cement. The properties of portland cement, including setting time and final strength, to a large degree depend on its composition.

Several different constituents are found in portland cement, the principal ones being tricalcium silicate ($3CaO$–SiO_2) and dicalcium silicate ($2CaO$–SiO_2). The setting and hardening of this material result from relatively complicated hydration reactions that occur between the various cement constituents and the water that is added. For example, one hydration reaction involving dicalcium silicate is as follows:

$$2CaO\text{–}SiO_2 + xH_2O = 2CaO\text{–}SiO_2\text{–}xH_2O \tag{13.2}$$

where x is variable and depends on how much water is available. These hydrated products are in the form of complex gels or crystalline substances that form the cementitious bond. Hydration reactions begin just as soon as water is added to the cement. These are first manifested as setting (i.e., the stiffening of the once-plastic paste), which takes place soon after mixing, usually within several hours. Hardening of the mass follows as a result of further hydration, a relatively slow process that may continue for as long as several years. It should be emphasized that the process by which cement hardens is not one of drying, but rather, of hydration in which water actually participates in a chemical bonding reaction.

Portland cement is termed a hydraulic cement because its hardness develops by chemical reactions with water. It is used primarily in mortar and concrete to bind, into a cohesive mass, aggregates of inert particles (sand and/or gravel); these are considered to be composite materials {(see Section 15.2).} Other cement materials, such as lime, are nonhydraulic; that is, compounds other than water (e.g., CO_2) are involved in the hardening reaction.

13.10 ADVANCED CERAMICS (CD-ROM)

13.11 DIAMOND AND GRAPHITE

DIAMOND

The physical properties of diamond make it an extremely attractive material. It is extremely hard (the hardest known material) and has a very low electrical conductivity; these characteristics are due to its crystal structure and the strong interatomic covalent bonds. Furthermore, it has an unusually high thermal conductivity for a nonmetallic material, is optically transparent in the visible and infrared regions of the electromagnetic spectrum, and has a high index of refraction. Relatively large diamond single crystals are used as gem stones. Industrially, diamonds are utilized to grind or cut other softer materials (Section 13.8). Techniques to produce synthetic diamonds have been developed, beginning in the mid-1950s, that have been refined to the degree that today a large proportion of the industrial-quality materials are man-made, in addition to some of those of gem quality.

Over the last several years, diamond in the form of thin films has been produced. Film growth techniques involve vapor-phase chemical reactions followed by the film deposition. Maximum film thicknesses are on the order of a millimeter. Furthermore, none of the films yet produced has the long-range crystalline regularity of natural diamond. The diamond is polycrystalline and may consist of very small and/or relatively large grains; in addition, amorphous carbon and graphite may be present. A scanning electron micrograph of the surface of a diamond thin film is shown in Figure 13.8. The mechanical, electrical, and optical properties of diamond films approach those of the bulk diamond material. These desirable properties have been and will continue to be exploited so as to create new and better products. For example, the surfaces of drills, dies, bearings, knives, and other tools have been coated with diamond films to increase surface hardness; some lenses and radomes have been made stronger while remaining transparent by the application of diamond coatings; coatings have also been applied to loudspeaker tweeters and to high-precision micrometers. Potential applications for these films include application to the surface of machine components such as gears and bearings, to optical recording heads and disks, and as substrates for semiconductor devices.

GRAPHITE

The structure of graphite is represented in Figure 3.17; in addition, the discussion of graphite in Section 3.9 noted that the electron bonding between the layers of hexagonally arranged carbon atoms is of the van der Waals type. As a consequence

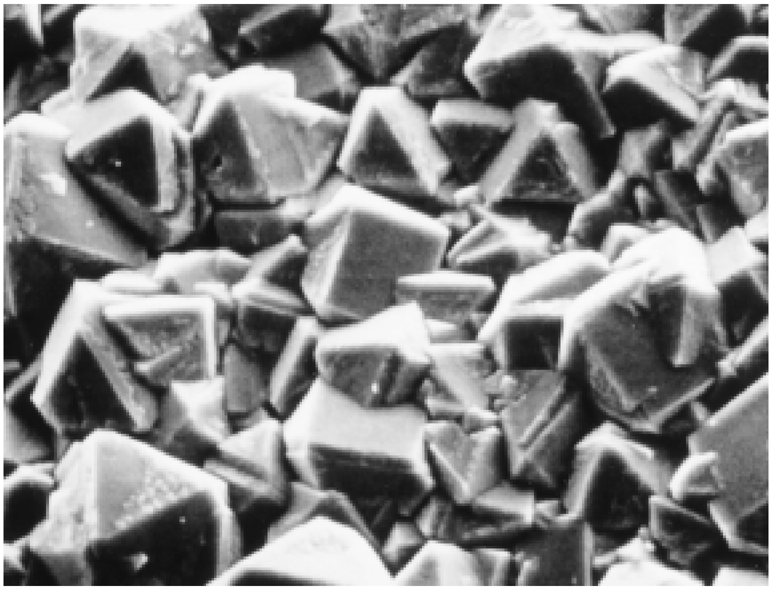

Figure 13.8 Scanning electron micrograph of a diamond thin film in which is shown numerous multifaceted microcrystals. 1000×. (Photograph courtesy of the Norton Company.)

of these weak interplanar bonds, interplanar cleavage is facile, which gives rise to the excellent lubricative properties of graphite. Also, the electrical conductivity is relatively high in crystallographic directions parallel to the hexagonal sheets.

Other desirable properties of graphite include the following: high strength and good chemical stability at elevated temperatures and in nonoxidizing atmospheres, high thermal conductivity, low coefficient of thermal expansion and high resistance to thermal shock, high adsorption of gases, and good machinability. Graphite is commonly used as heating elements for electric furnaces, as electrodes for arc welding, in metallurgical crucibles, in casting molds for metal alloys and ceramics, for high-temperature refractories and insulations, in rocket nozzles, in chemical reactor vessels, for electrical contacts, brushes and resistors, as electrodes in batteries, and in air purification devices.

TYPES OF POLYMERS

There are many different polymeric materials that are familiar to us and find a wide variety of applications. These include plastics, elastomers (or rubbers), fibers, coatings, adhesives, foams, and films. Depending on its properties, a particular polymer may be used in two or more of these application categories. For example, a plastic, if crosslinked and utilized above its glass transition temperature, may make a satisfactory elastomer. Or, a fiber material may be used as a plastic if it is not drawn into filaments. This portion of the chapter includes a brief discussion of each of these types of polymer.

13.12 PLASTICS

Possibly the largest number of different polymeric materials come under the plastic classification. Polyethylene, polypropylene, polyvinyl chloride, polystyrene, and the fluorocarbons, epoxies, phenolics, and polyesters may all be classified as **plastics.**

They have a wide variety of combinations of properties. Some plastics are very rigid and brittle; others are flexible, exhibiting both elastic and plastic deformations when stressed, and sometimes experiencing considerable deformation before fracture.

Polymers falling within this classification may have any degree of crystallinity, and all molecular structures and configurations (linear, branched, isotactic, etc.) are possible. Plastic materials may be either thermoplastic or thermosetting; in fact, this is the manner in which they are usually subclassified. The trade names, characteristics, and typical applications for a number of plastics are given in Table 13.12.

Table 13.12 **Trade Names, Characteristics, and Typical Applications for a Number of Plastic Materials**

Material Type	*Trade Names*	*Major Application Characteristics*	*Typical Applications*
		Thermoplastics	
Acrylonitrile-butadiene-styrene (ABS)	Abson Cycolac Kralastic Lustran Novodur Tybrene	Outstanding strength and toughness, resistant to heat distortion; good electrical properties; flammable and soluble in some organic solvents	Refrigerator linings, lawn and garden equipment, toys, highway safety devices
Acrylics (polymethyl methacrylate)	Acrylite Diakon Lucite Plexiglas	Outstanding light transmission and resistance to weathering; only fair mechanical properties	Lenses, transparent aircraft enclosures, drafting equipment, outdoor signs
Fluorocarbons (PTFE or TFE)	Teflon Fluon Halar Halon Hostaflon TF	Chemically inert in almost all environments, excellent electrical properties; low coefficient of friction; may be used to 260°C (500°F); relatively weak and poor cold-flow properties	Anticorrosive seals, chemical pipes and valves, bearings, antiadhesive coatings, high-temperature electronic parts
Polyamides (nylons)	Nylon Durethan Herox Nomex Ultramid Zytel	Good mechanical strength, abrasion resistance, and toughness; low coefficient of friction; absorbs water and some other liquids	Bearings, gears, cams, bushings, handles, and jacketing for wires and cables
Polycarbonates	Baylon Iupilon Lexan Makrolon Merlon Nuclon	Dimensionally stable; low water absorption; transparent; very good impact resistance and ductility; chemical resistance not outstanding	Safety helmets, lenses, light globes, base for photographic film
Polyethylene	Alathon Alkathene Ethron Fortiflex Hi-fax Petrothene Rigidex Zendel	Chemically resistant, and electrically insulating; tough and relatively low coefficient of friction; low strength and poor resistance to weathering	Flexible bottles, toys, tumblers, battery parts, ice trays, film wrapping materials

Table 13.12 (*Continued*)

Material Type	*Trade Names*	*Major Application Characteristics*	*Typical Applications*
Polypropylene	Bexphane Herculon Meraklon Moplen Poly-pro Pro-fax Propathene	Resistant to heat distortion; excellent electrical properties and fatigue strength; chemically inert; relatively inexpensive; poor resistance to UV light	Sterilizable bottles, packaging film, TV cabinets, luggage
Polystyrene	Carinex Celatron Hostyren Lustrex Styron Vestyron	Excellent electrical properties and optical clarity; good thermal and dimensional stability; relatively inexpensive	Wall tile, battery cases, toys, indoor lighting panels, appliance housings
Vinyls	Darvic Exon Geon Pee Vee Cee Pliovic Saran Tygon	Good low-cost, general-purpose materials; ordinarily rigid, but may be made flexible with plasticizers; often copolymerized; susceptible to heat distortion	Floor coverings, pipe, electrical wire insulation, garden hose, phonograph records
Polyester (PET or PETE)	Celanar Crastin Dacron Hylar Melinex Mylar Terylem	One of the toughest of plastic films; excellent fatigue and tear strength, and resistance to humidity, acids, greases, oils, and solvents	Magnetic recording tapes, clothing, automotive tire cords, beverage containers
		Thermosetting Polymers	
Epoxies	Araldite Epikote Epon Epi-rez Lekutherm Nepoxide	Excellent combination of mechanical properties and corrosion resistance; dimensionally stable; good adhesion; relatively inexpensive; good electrical properties	Electrical moldings, sinks, adhesives, protective coatings, used with fiberglass laminates
Phenolics	Bakelite Amberol Arofene Durite Resinox	Excellent thermal stability to over 150°C (300°F); may be compounded with a large number of resins, fillers, etc.; inexpensive	Motor housings, telephones, auto distributors, electrical fixtures
Polyesters	Aropol Baygal Derakane Laguval Laminac Selectron	Excellent electrical properties and low cost; can be formulated for room- or high-temperature use; often fiber reinforced	Helmets, fiberglass boats, auto body components, chairs, fans

Source: Adapted from C. A. Harper, Editor, *Handbook of Plastics and Elastomers.* Copyright © 1975 by McGraw-Hill Book Company. Reproduced with permission.

Several plastics exhibit especially outstanding properties. For applications in which optical transparency is critical, polystyrene and polymethyl methacrylate are especially well suited; however, it is imperative that the material be highly amorphous or, if semicrystalline, have very small crystallites. The fluorocarbons have a low coefficient of friction and are extremely resistant to attack by a host of chemicals, even at relatively high temperatures. They are utilized as coatings on nonstick cookware, in bearings and bushings, and for high-temperature electronic components.

13.13 ELASTOMERS

The characteristics of and deformation mechanism for elastomers were treated previously (Section 8.19). The present discussion, therefore, focuses on the types of elastomeric materials.

Table 13.13 lists properties and applications of common elastomers; these properties are typical and, of course, depend on the degree of vulcanization and on whether any reinforcement is used. Natural rubber is still utilized to a large degree because it has an outstanding combination of desirable properties. However, the

Table 13.13 Tabulation of Important Characteristics and Typical Applications for Five Commercial Elastomers

Chemical Type	*Trade (Common) Name*	*Elongation (%)*	*Useful Temperature Range [°C (°F)]*	*Major Application Characteristics*	*Typical Applications*
Natural polyisoprene	Natural Rubber (NR)	500–760	−60 to 120 (−75 to 250)	Excellent physical properties; good resistance to cutting, gouging, and abrasion; low heat, ozone, and oil resistance; good electrical properties	Pneumatic tires and tubes; heels and soles; gaskets
Styrene–butadiene copolymer	GRS, Buna S (SBR)	450–500	−60 to 120 (−75 to 250)	Good physical properties; excellent abrasion resistance; not oil, ozone, or weather resistant; electrical properties good, but not outstanding	Same as natural rubber
Acrylonitrile–butadiene copolymer	Buna A, Nitrile (NBR)	400–600	−50 to 150 (−60 to 300)	Excellent resistance to vegetable, animal, and petroleum oils; poor low-temperature properties; electrical properties not outstanding	Gasoline, chemical, and oil hose; seals and O-rings; heels and soles
Chloroprene	Neoprene (CR)	100–800	−50 to 105 (−60 to 225)	Excellent ozone, heat, and weathering resistance; good oil resistance; excellent flame resistance; not as good in electrical applications as natural rubber	Wire and cable; chem. tank linings; belts, hoses, seals, and gaskets
Polysiloxane	Silicone (VMQ)	100–800	−115 to 315 (−175 to 600)	Excellent resistance to high and low temperatures; low strength; excellent electrical properties	High- and low-temperature insulation; seals, diaphragms; tubing for food and medical uses

Sources: Adapted from: C. A. Harper, Editor, *Handbook of Plastics and Elastomers.* Copyright © 1975 by McGraw-Hill Book Company, reproduced with permission; and Materials Engineering's *Materials Selector,* copyright Penton/IPC.

most important synthetic elastomer is SBR, which is used predominantly in automobile tires, reinforced with carbon black. NBR, which is highly resistant to degradation and swelling, is another common synthetic elastomer.

For many applications (e.g., automobile tires), the mechanical properties of even vulcanized rubbers are not satisfactory in terms of tensile strength, abrasion and tear resistance, and stiffness. These characteristics may be further improved by additives such as carbon black {(Section 15.2).}

Finally, some mention should be made of the silicone rubbers. For these materials, the backbone carbon chain is replaced by a chain that alternates silicon and oxygen atoms:

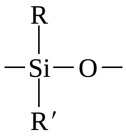

$$-\overset{\displaystyle R}{\underset{\displaystyle R'}{\overset{|}{\underset{|}{Si}}}}-O-$$

where R and R′ represent side-bonded atoms such as hydrogen or groups of atoms such as CH_3. For example, polydimethylsiloxane has the mer structure

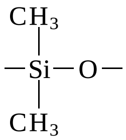

$$-\overset{\displaystyle CH_3}{\underset{\displaystyle CH_3}{\overset{|}{\underset{|}{Si}}}}-O-$$

Of course, as elastomers, these materials are crosslinked.

The silicone elastomers possess a high degree of flexibility at low temperatures [to −90°C (−130°F)] and yet are stable to temperatures as high as 250°C (480°F). In addition, they are resistant to weathering and lubricating oils. A further attractive characteristic is that some silicone rubbers vulcanize at room temperature (RTV rubbers).

13.14 Fibers

The **fiber** polymers are capable of being drawn into long filaments having at least a 100 : 1 length-to-diameter ratio. Most commercial fiber polymers are utilized in the textile industry, being woven or knit into cloth or fabric. In addition, the aramid fibers are employed in composite materials, {Section 15.8.} To be useful as a textile material, a fiber polymer must have a host of rather restrictive physical and chemical properties. While in use, fibers may be subjected to a variety of mechanical deformations—stretching, twisting, shearing, and abrasion. Consequently, they must have a high tensile strength (over a relatively wide temperature range) and a high modulus of elasticity, as well as abrasion resistance. These properties are governed by the chemistry of the polymer chains and also by the fiber drawing process.

The molecular weight of fiber materials should be relatively high. Also, since the tensile strength increases with degree of crystallinity, the structure and configuration of the chains should allow the production of a highly crystalline polymer; that translates into a requirement for linear and unbranched chains that are symmetrical and have regularly repeating mer units.

Convenience in washing and maintaining clothing depends primarily on the thermal properties of the fiber polymer, that is, its melting and glass transition temperatures. Furthermore, fiber polymers must exhibit chemical stability to a rather extensive variety of environments, including acids, bases, bleaches, dry cleaning solvents, and sunlight. In addition, they must be relatively nonflammable and amenable to drying.

13.15 MISCELLANEOUS APPLICATIONS

COATINGS

Coatings are frequently applied to the surface of materials to serve one or more of the following functions: (1) to protect the item from the environment that may produce corrosive or deteriorative reactions; (2) to improve the item's appearance; and (3) to provide electrical insulation. Many of the ingredients in coating materials are polymers, the majority of which are organic in origin. These organic coatings fall into several different classifications, as follows: paint, varnish, enamel, lacquer, and shellac.

ADHESIVES

An **adhesive** is a substance used to join together the surfaces of two solid materials (termed ''adherends'') to produce a joint with a high shear strength. The bonding forces between the adhesive and adherend surfaces are thought to be electrostatic, similar to the secondary bonding forces between the molecular chains in thermoplastic polymers. Even though the inherent strength of the adhesive may be much less than that of the adherend materials, nevertheless, a strong joint may be produced if the adhesive layer is thin and continuous. If a good joint is formed, the adherend material may fracture or rupture before the adhesive.

Polymeric materials that fall within the classifications of thermoplastics, thermosetting resins, elastomeric compounds, and natural adhesives (animal glue, casein, starch, and rosin) may serve adhesive functions. Polymer adhesives may be used to join a large variety of material combinations: metal–metal, metal–plastic, metal–ceramic, and so on. The primary drawback is the service temperature limitation. Organic polymers maintain their mechanical integrity only at relatively low temperatures, and strength decreases rapidly with increasing temperature.

FILMS

Within relatively recent times, polymeric materials have found widespread use in the form of thin *films.* Films having thicknesses between 0.025 and 0.125 mm (0.001 and 0.005 in.) are fabricated and used extensively as bags for packaging food products and other merchandise, as textile products, and a host of other uses. Important characteristics of the materials produced and used as films include low density, a high degree of flexibility, high tensile and tear strengths, resistance to attack by moisture and other chemicals, and low permeability to some gases, especially water vapor. Some of the polymers that meet these criteria and are manufactured in film form are polyethylene, polypropylene, cellophane, and cellulose acetate.

FOAMS

Foams are plastic materials that contain a relatively high volume percent of small pores. Both thermoplastic and thermosetting materials are used as foams; these include polyurethane, rubber, polystyrene, and polyvinyl chloride. Foams are commonly used as cushions in automobiles and furniture as well as in packaging and thermal insulation. The foaming process is carried out by incorporating into the batch of material a blowing agent that upon heating, decomposes with the liberation of a gas. Gas bubbles are generated throughout the now-fluid mass, which remain as pores upon cooling and give rise to a spongelike structure. The same effect is produced by bubbling an inert gas through a material while it is in a molten state.

13.16 ADVANCED POLYMERIC MATERIALS (CD-ROM)

SUMMARY

With regard to composition, metals and alloys are classified as either ferrous or nonferrous. Ferrous alloys (steels and cast irons) are those in which iron is the prime constituent. Most steels contain less than 1.0 wt% C, and, in addition, other alloying elements, which render them susceptible to heat treatment (and an enhancement of mechanical properties) and/or more corrosion resistant. Plain low-carbon steels and high-strength low-alloy, medium-carbon, tool, and stainless steels are the most common types.

Cast irons contain a higher carbon content, normally between 3.0 and 4.5 wt% C, and other alloying elements, notably silicon. For these materials, most of the carbon exists in graphite form rather than combined with iron as cementite. Gray, ductile (or nodular), and malleable irons are the three most widely used cast irons; the latter two are reasonably ductile.

All other alloys fall within the nonferrous category, which is further subdivided according to base metal or some distinctive characteristic that is shared by a group of alloys. The compositions, typical properties, and applications of copper, aluminum, magnesium, titanium, nickel, lead, tin, zirconium, and zinc alloys, as well as the refractory metals, the superalloys, and the noble metals were discussed.

Also discussed in this chapter were various types of ceramic materials. The familiar glass materials are noncrystalline silicates that contain other oxides; the most desirable trait of these materials is their optical transparency. Glass–ceramics are initially fabricated as a glass, then crystallized or devitrified.

Clay is the principal component of the whitewares and structural clay products. Other ingredients may be added, such as feldspar and quartz, which influence the changes that occur during firing.

The materials that are employed at elevated temperatures and often in reactive environments are the refractory ceramics; on occasion, their ability to thermally insulate is also utilized. On the basis of composition and application, the four main subdivisions are fireclay, silica, basic, and special.

The abrasive ceramics, being hard and tough, are utilized to cut, grind, and polish other softer materials. Diamond, silicon carbide, tungsten carbide, corundum, and silica sand are the most common examples. The abrasives may be employed in the form of loose grains, bonded to an abrasive wheel, or coated on paper or a fabric.

When mixed with water, inorganic cements form a paste that is capable of assuming just about any desired shape. Subsequent setting or hardening is a result of chemical reactions involving the cement particles and occurs at the ambient temperature. For hydraulic cements, of which portland cement is the most common, the chemical reaction is one of hydration.

{Many of our modern technologies utilize and will continue to utilize advanced ceramics because of their unique mechanical, chemical, electrical, magnetic, and optical properties and property combinations. Advanced materials characterization, processing, and reliability techniques need to be developed to make these materials cost effective.}

The properties and some applications for diamond and graphite were presented. Diamond is a gemstone and, because of its hardness, is used to cut and grind softer materials. Furthermore, it is now being produced and utilized in thin films. The layered structure of graphite gives rise to its excellent lubricative properties and a relatively high electrical conductivity. Graphite is also known for its high strength and chemical stability at elevated temperatures and in nonoxidizing atmospheres.

The various types and applications of polymeric materials were also discussed. Plastic materials are perhaps the most widely used group of polymers, which include the following: polyethylene, polypropylene, polyvinyl chloride, polystyrene, and the fluorocarbons, epoxies, phenolics, and polyesters.

Another polymer classification includes the elastomeric materials that may experience very large elastic deformations. Most of these materials are copolymers, whereas the silicone elastomers are really inorganic materials.

Many polymeric materials may be spun into fibers, which are used primarily in textiles. Mechanical, thermal, and chemical characteristics of these materials are especially critical.

Other miscellaneous applications that employ polymers include coatings, adhesives, films, and foams.

{This chapter concluded with discussions of three advanced polymeric materials—ultrahigh molecular weight polyethylene, liquid crystal polymers, and thermoplastic elastomers. These materials have unusual properties and are used in a host of high-technology applications.}

IMPORTANT TERMS AND CONCEPTS

Abrasive (ceramic)
Adhesive
Alloy steel
Brass
Bronze
Calcination
Cast iron
Cement
Devitrification
Ductile (nodular) iron
Ferrous alloy
Fiber
Foam
Glass–ceramic
Gray cast iron
High-strength, low-alloy (HSLA) steel
Liquid crystal polymer
Malleable iron
Nonferrous alloy
Plain carbon steel
Plastic
Refractory (ceramic)
Specific strength
Stainless steel
Structural clay product
Temper designation
Thermoplastic elastomer
Ultrahigh molecular weight polyethylene
White cast iron
Whiteware
Wrought alloy

REFERENCES

ASM Handbook, Vol. 1, *Properties and Selection: Irons, Steels, and High-Performance Alloys*, ASM International, Materials Park, OH, 1990.

ASM Handbook, Vol. 2, *Properties and Selection: Nonferrous Alloys and Special-Purpose Materials*, ASM International, Materials Park, OH, 1991.

Billmeyer, F. W., Jr., *Textbook of Polymer Science*, 3rd edition, Wiley-Interscience, New York, 1984.

Bowen, H. K., "Advanced Ceramics." *Scientific American*, Vol. 255, No. 4, October 1986, pp. 168–176.

Brick, R. M., A. W. Pense, and R. B. Gordon, *Structure and Properties of Engineering Materials*, 4th edition, McGraw-Hill Book Company, New York, 1977.

Coes, L., Jr., *Abrasives*, Springer-Verlag, New York, 1971.

Engineered Materials Handbook, Vol. 2, *Engineering Plastics*, ASM International, Metals Park, OH, 1988.

Engineered Materials Handbook, Vol. 4, *Ceramics and Glasses*, ASM International, Materials Park, OH, 1991.

Frick, J. (Editor), *Woldman's Engineering Alloys*, 8th edition, ASM International, Materials Park, OH, 1994.

Harper, C. A. (Editor), *Handbook of Plastics, Elastomers and Composites*, 3rd edition, McGraw-Hill Book Company, New York, 1996.

Lea, F. M., *The Chemistry of Cement and Concrete*, Chemical Publishing Company, New York, 1971.

Metals and Alloys in the Unified Numbering System, 7th edition, Society of Automotive Engineers, and American Society for Testing and Materials, Warrendale, PA, 1996.

Walton, C. F. and T. F. Opar (Editors), *Iron Castings Handbook*, Iron Castings Society, Des Plaines, IL, 1981.

Worldwide Guide to Equivalent Irons and Steels, 3rd edition, ASM International, Materials Park, OH, 1993.

Worldwide Guide to Equivalent Nonferrous Metals and Alloys, 3rd edition, ASM International, Materials Park, OH, 1996.

QUESTIONS AND PROBLEMS

Note: To solve those problems having an asterisk (*) by their numbers, consultation of supplementary topics [appearing only on the CD-ROM (and not in print)] will probably be necessary.

13.1 **(a)** List the four classifications of steels. **(b)** For each, briefly describe the properties and typical applications.

13.2 **(a)** Cite three reasons why ferrous alloys are used so extensively. **(b)** Cite three characteristics of ferrous alloys that limit their utilization.

13.3 Briefly explain why ferritic and austenitic stainless steels are not heat treatable.

13.4 What is the function of alloying elements in tool steels?

13.5 Compute the volume percent of graphite V_{Gr} in a 3.5 wt% C cast iron, assuming that all the carbon exists as the graphite phase. Assume densities of 7.9 and 2.3 g/cm^3 for ferrite and graphite, respectively.

13.6 On the basis of microstructure, briefly explain why gray iron is brittle and weak in tension.

13.7 Compare gray and malleable cast irons with respect to **(a)** composition and heat treatment, **(b)** microstructure, and **(c)** mechanical characteristics.

13.8 It is possible to produce cast irons that consist of a martensite matrix in which graphite is embedded in either flake, nodule, or rosette form. Briefly describe the treatment necessary to produce each of these three microstructures.

13.9 Compare white and nodular cast irons with respect to **(a)** composition and heat treatment, **(b)** microstructure, and **(c)** mechanical characteristics.

13.10 Is it possible to produce malleable cast iron in pieces having large cross-sectional dimensions? Why or why not?

13.11 What is the principal difference between wrought and cast alloys?

13.12 What is the main difference between a brass and a bronze?

13.13 Why must rivets of a 2017 aluminum alloy be refrigerated before they are used?

13.14 Explain why, under some circumstances, it is not advisable to weld a structure that is fabricated with a 3003 aluminum alloy.

13.15 What is the chief difference between heat-treatable and nonheat-treatable alloys?

13.16 Give the distinctive features, limitations, and applications of the following alloy groups: titanium alloys, refractory metals, superalloys, and noble metals.

13.17 Cite the two desirable characteristics of glasses.

13.18 **(a)** What is devitrification?

(b) Cite two properties that may be improved by devitrification and two that may be impaired.

13.19* Briefly explain why glass–ceramics are generally not transparent. You may want to consult Chapter 19.

13.20 For refractory ceramic materials, cite three characteristics that improve with and two characteristics that are adversely affected by increasing porosity.

13.21* Find the maximum temperature to which the following two magnesia–alumina refractory materials may be heated before a liquid phase will appear.

(a) A spinel-bonded alumina material of composition 95 wt% Al_2O_3-5 wt% MgO.

(b) A magnesia–alumina spinel of composition 65 wt% Al_2O_3-35 wt% MgO. Consult Figure 10.22.

13.22* Upon consideration of the SiO_2–Al_2O_3 phase diagram, Figure 10.24, for each pair of the following list of compositions, which would you judge to be the more desirable refractory? Justify your choices.

(a) 20 wt% Al_2O_3-80 wt% SiO_2 and 25 wt% Al_2O_3-75 wt% SiO_2.

(b) 70 wt% Al_2O_3-30 wt% SiO_2 and 80 wt% Al_2O_3-20 wt% SiO_2.

13.23* Compute the mass fractions of liquid in the following refractory materials at 1600°C (2910°F):

(a) 6 wt% Al_2O_3-94 wt% SiO_2.

(b) 10 wt% Al_2O_3-90 wt% SiO_2.

(c) 30 wt% Al_2O_3-70 wt% SiO_2.

(d) 80 wt% Al_2O_3-20 wt% SiO_2.

13.24* **(a)** For the SiO_2–Al_2O_3 system, what is the maximum temperature that is possible without the formation of a liquid phase? At what composition or over what range of compositions will this maximum temperature be achieved?

(b) For the MgO–Al_2O_3 system, what is the maximum temperature that is possible without the formation of a liquid phase? At what composition or over what range of compositions will this maximum temperature be achieved?

13.25 Compare the manner in which the aggregate particles become bonded together in clay-based mixtures during firing and in cements during setting.

13.26 Explain why it is important to grind cement into a fine powder.

13.27 During the winter months, the temperature in some parts of Alaska may go as low as −55°C (−65°F). Of the elastomers natural isoprene, styrene-butadiene, acrylonitrile-butadiene, chloroprene, and polysiloxane, which would be suitable for automobile tires under these conditions? Why?

13.28 Briefly explain the difference in molecular chemistry between silicone polymers and other polymeric materials.

13.29 Silicone polymers may be prepared to exist as liquids at room temperature. Cite differences in molecular structure between them and the silicone elastomers.

13.30 List two important characteristics for polymers that are to be used in fiber applications.

13.31 Cite five important characteristics for polymers that are to be used in thin-film applications.

Design Problems

13.D1 Of the following alloys, pick the one(s) that may be strengthened by heat treatment, cold work, or both: R50500 titanium, AZ31B magnesium, 6061 aluminum, C51000 phosphor bronze, lead, 6150 steel, 304 stainless steel, and C17200 beryllium copper.

13.D2 A structural member 100 mm (4 in.) long must be able to support a load of 50,000 N (11,250 lb_f) without experiencing any plastic deformation. Given the following data for brass, steel, aluminum, and titanium, rank them from least to greatest weight in accordance with these criteria.

Alloy	*Yield Strength MPa (ksi)*	*Density (g/cm^3)*
Brass	415 (60)	8.5
Steel	860 (125)	7.9
Aluminum	310 (45)	2.7
Titanium	550 (80)	4.5

13.D3 Discuss whether it would be advisable to hot work or cold work the following metals and alloys on the basis of melting temperature, oxidation resistance, yield strength, and degree of brittleness: tin, tungsten, aluminum alloys, magnesium alloys, and a 4140 steel.

13.D4 Below is a list of metals and alloys:

Plain carbon steel
Brass
Gray cast iron
Platinum
Stainless steel
Titanium alloy
Magnesium
Zinc
Tool steel
Aluminum
Tungsten

Select from this list the one metal or alloy that is best suited for each of the following applications, and cite at least one reason for your choice:

(a) The base for a milling machine.

(b) The walls of a steam boiler.

(c) High-speed aircraft.

(d) Drill bit.

(e) Cryogenic (i.e., very low temperature) container.

(f) As a pyrotechnic (i.e., in flares and fireworks).

(g) High-temperature furnace elements to be used in oxidizing atmospheres.

13.D5 **(a)** List at least three important characteristics required of metal alloys that are used for coins. **(b)** Write an essay in which you cite which metal alloys are employed in the coinage of your country, and then provide the rationale for their use.

13.D6 Some of our modern kitchen cookware is made of ceramic materials.

(a) List at least three important characteristics required of a material to be used for this application.

(b) Make a comparison of three ceramic materials as to their relative properties, and, in addition, to cost.

(c) On the basis of this comparison, select that material most suitable for the cookware.

13.D7 **(a)** List several advantages and disadvantages of using transparent polymeric materials for eyeglass lenses.

(b) Cite four properties (in addition to being transparent) that are important for this application.

(c) Note three polymers that may be candidates for eyeglass lenses, and then tabulate values of the properties noted in part b for these three materials.

13.D8 Write an essay on polymeric materials that are used in the packaging of food products and drinks. Include a list of the general requisite characteristics of materials that are used for these applications. Now cite a specific material that is utilized for each of three different container types and the rationale for each choice.

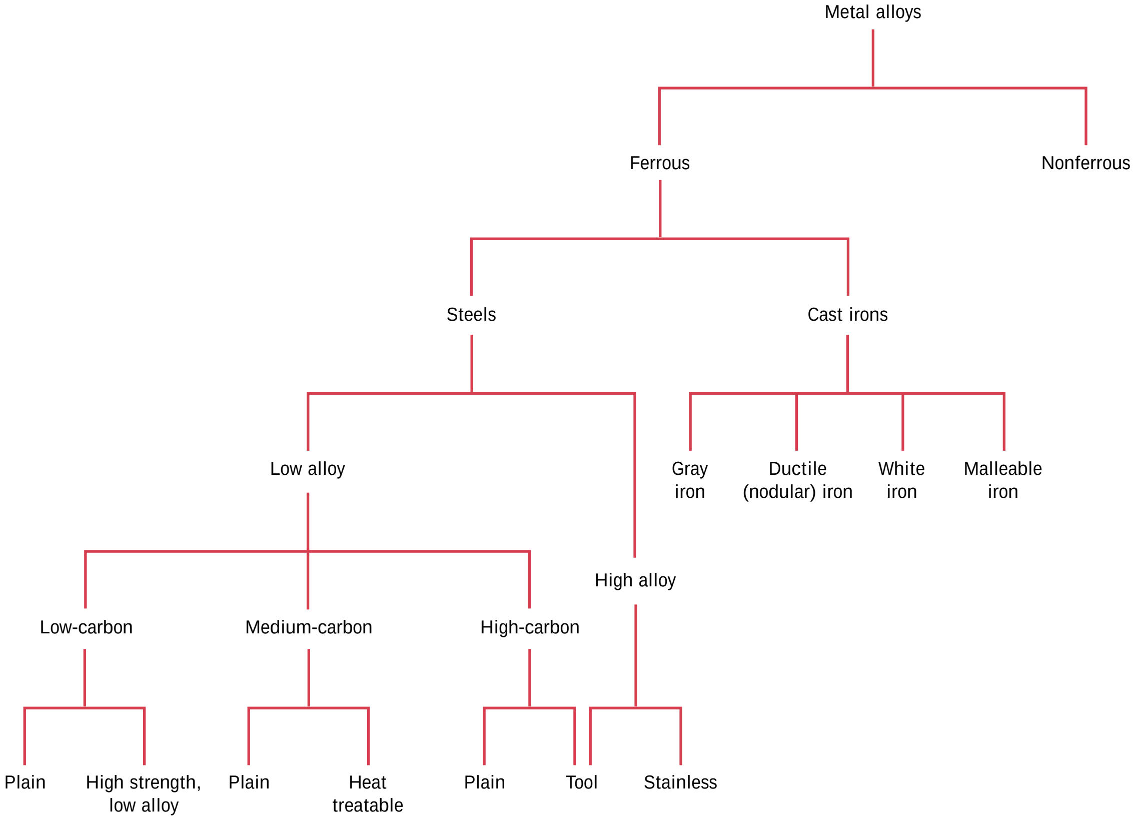
Metal alloys
Ferrous
Nonferrous
Steels
Cast irons
Low alloy
High alloy
Gray iron
Ductile (nodular) iron
White iron
Malleable iron
Low-carbon
Medium-carbon
High-carbon
Plain
High strength, low alloy
Plain
Heat treatable
Plain
Tool
Stainless

Figure 13.1 Classification scheme for the various ferrous alloys.

Table 13.1a Compositions of Five Plain Low-Carbon Steels and Three High-Strength, Low-Alloy Steels

Designation[a]		*Composition (wt%)*[b]		
AISI/SAE or ASTM Number	***UNS Number***	***C***	***Mn***	***Other***
		Plain Low-Carbon Steels		
1010	G10100	0.10	0.45	
1020	G10200	0.20	0.45	
A36	K02600	0.29	1.00	0.20 Cu (min)
A516 Grade 70	K02700	0.31	1.00	0.25 Si
		High-Strength, Low-Alloy Steels		
A440	K12810	0.28	1.35	0.30 Si (max), 0.20 Cu (min)
A633 Grade E	K12002	0.22	1.35	0.30 Si, 0.08 V, 0.02 N, 0.03 Nb
A656 Grade 1	K11804	0.18	1.60	0.60 Si, 0.1 V, 0.20 Al, 0.015 N

[a] The codes used by the American Iron and Steel Institute (AISI), the Society of Automotive Engineers (SAE), and the American Society for Testing and Materials (ASTM), and in the Uniform Numbering System (UNS) are explained in the text.

[b] Also a maximum of 0.04 wt% P, 0.05 wt% S, and 0.30 wt% Si (unless indicated otherwise).

Source: Adapted from *Metals Handbook: Properties and Selection: Irons and Steels*, Vol. 1, 9th edition, B. Bardes (Editor), American Society for Metals, 1978, pp. 185, 407.

Table 13.1b **Mechanical Characteristics of Hot-Rolled Material and Typical Applications for Various Plain Low-Carbon and High-Strength, Low-Alloy Steels**

AISI/SAE or ASTM Number	*Tensile Strength [MPa (ksi)]*	*Yield Strength [MPa (ksi)]*	*Ductility [%EL in 50 mm (2 in.)]*	*Typical Applications*
		Plain Low-Carbon Steels		
1010	325 (47)	180 (26)	28	Automobile panels, nails, and wire
1020	380 (55)	205 (30)	25	Pipe; structural and sheet steel
A36	400 (58)	220 (32)	23	Structural (bridges and buildings)
A516 Grade 70	485 (70)	260 (38)	21	Low-temperature pressure vessels
		High-Strength, Low-Alloy Steels		
A440	435 (63)	290 (42)	21	Structures that are bolted or riveted
A633 Grade E	520 (75)	380 (55)	23	Structures used at low ambient temperatures
A656 Grade 1	655 (95)	552 (80)	15	Truck frames and railway cars

Table 13.2a AISI/SAE and UNS Designation Systems and Composition Ranges for Plain Carbon Steel and Various Low-Alloy Steels

AISI/SAE Designation[a]	UNS Designation	Composition Ranges (wt% of Alloying Elements in Addition to C)[b]			
		Ni	*Cr*	*Mo*	*Other*
10xx, Plain carbon	G10xx0				
11xx, Free machining	G11xx0				0.08–0.33S
12xx, Free machining	G12xx0				0.10–0.35S, 0.04–0.12P
13xx	G13xx0				1.60–1.90Mn
40xx	G40xx0			0.20–0.30	
41xx	G41xx0		0.80–1.10	0.15–0.25	
43xx	G43xx0	1.65–2.00	0.40–0.90	0.20–0.30	
46xx	G46xx0	0.70–2.00		0.15–0.30	
48xx	G48xx0	3.25–3.75		0.20–0.30	
51xx	G51xx0		0.70–1.10		
61xx	G61xx0		0.50–1.10		0.10–0.15V
86xx	G86xx0	0.40–0.70	0.40–0.60	0.15–0.25	
92xx	G92xx0				1.80–2.20Si

[a] The carbon concentration, in weight percent times 100, is inserted in the place of ‘‘xx’’ for each specific steel.

[b] Except for 13xx alloys, manganese concentration is less than 1.00 wt%.
Except for 12xx alloys, phosphorus concentration is less than 0.35 wt%.
Except for 11xx and 12xx alloys, sulfur concentration is less than 0.04 wt%.
Except for 92xx alloys, silicon concentration varies between 0.15 and 0.35 wt%.

Table 13.2b Typical Applications and Mechanical Property Ranges for Oil-Quenched and Tempered Plain Carbon and Alloy Steels

AISI Number	*UNS Number*	*Tensile Strength [MPa (ksi)]*	*Yield Strength [MPa (ksi)]*	*Ductility [%EL in 50 mm (2 in.)]*	*Typical Applications*
			Plain Low-Carbon Steels		
1040	G10400	605–780 (88–113)	430–585 (62–85)	33–19	Crankshafts, bolts
1080[a]	G10800	800–1310 (116–190)	480–980 (70–142)	24–13	Chisels, hammers
1095[a]	G10950	760–1280 (110–186)	510–830 (74–120)	26–10	Knives, hacksaw blades
			Alloy Steels		
4063	G40630	786–2380 (114–345)	710–1770 (103–257)	24–4	Springs, hand tools
4340	G43400	980–1960 (142–284)	895–1570 (130–228)	21–11	Bushings, aircraft tubing
6150	G61500	815–2170 (118–315)	745–1860 (108–270)	22–7	Shafts, pistons, gears

---

[a] Classified as high-carbon steels.

Chapter 14 / Synthesis, Fabrication, and Processing of Materials

This photograph shows the aluminum beverage can in various stages of production. The can is formed from a single sheet of an aluminum alloy. Production operations include drawing, dome forming, trimming, cleaning, decorating, and neck and flange forming. (PEPSI is a registered trademark of PepsiCo, Inc. Used by permission.)

Why Study *Synthesis, Fabrication, and Processing of Materials?*

On occasion, fabrication and processing procedures adversely affect some of the properties of materials. For example, in Section 11.8 we note that some steels may become embrittled during tempering heat treatments. Also, some stainless steels are made susceptible to intergranular corrosion (Section 16.7) when they are heated for long time periods within a specific temperature range. And, as discussed in Section 14.4, regions adjacent to weld junctions may experience diminishments in strength and toughness as a result of undesirable microstructural alterations. It is important that engineers become familiar with possible consequences attendant to processing and fabricating procedures in order to prevent unanticipated material failures.

Learning Objectives

After careful study of this chapter you should be able to do the following:

1. **Name and describe four forming operations that are used to shape metal alloys.**
2. **Name and describe four casting techniques.**
3. **State the purposes of and describe procedures for the following heat treatments: process annealing, stress relief annealing, normalizing, full annealing, and spheroidizing.**
4. **Define *hardenability*.**
5. **Generate a hardness profile for a cylindrical steel specimen that has been austenitized and then quenched, given the hardenability curve for the specific alloy, as well as quenching rate-versus-bar diameter information.**
6. **Name and briefly describe four forming methods that are used to fabricate glass pieces.**
7. **Briefly describe and explain the procedure by which glass pieces are thermally tempered.**
8. **Briefly describe processes that occur during the drying and firing of clay-based ceramic ware.**
9. **Briefly describe/diagram the sintering process of powder particle aggregates.**
10. **Briefly describe addition and condensation polymerization mechanisms.**
11. **Name the five types of polymer additives and, for each, indicate how it modifies the properties.**
12. **Name and briefly describe five fabrication techniques used for plastic polymers.**

14.1 INTRODUCTION

Fabrication techniques are those methods by which materials are formed or manufactured into components that may be incorporated in useful products. Sometimes it also may be necessary to subject the component to some type of processing treatment in order to achieve the required properties. And, on occasion, the suitability of a material for an application is dictated by economic considerations with respect to fabrication and processing operations. In this chapter we discuss various techniques that are used to fabricate and process metals, ceramics, and polymers (and also for polymers, how they are synthesized).

FABRICATION OF METALS

Metal fabrication techniques are normally preceded by refining, alloying, and often heat-treating processes that produce alloys with the desired characteristics. The classifications of fabrication techniques include various metal-forming methods, casting, powder metallurgy, welding, and machining; often two or more of them must be used before a piece is finished. The methods chosen depend on several factors; the most important are the properties of the metal, the size and shape of the finished piece, and, of course, cost. The metal fabrication techniques we discuss are classified according to the scheme illustrated in Figure 14.1.

14.2 FORMING OPERATIONS

Forming operations are those in which the shape of a metal piece is changed by plastic deformation; for example, forging, rolling, extrusion, and drawing are common forming techniques. Of course, the deformation must be induced by an external force or stress, the magnitude of which must exceed the yield strength of the material. Most metallic materials are especially amenable to these procedures, being at least moderately ductile and capable of some permanent deformation without cracking or fracturing.

When deformation is achieved at a temperature above that at which recrystallization occurs, the process is termed **hot working** (Section 8.13); otherwise, it is

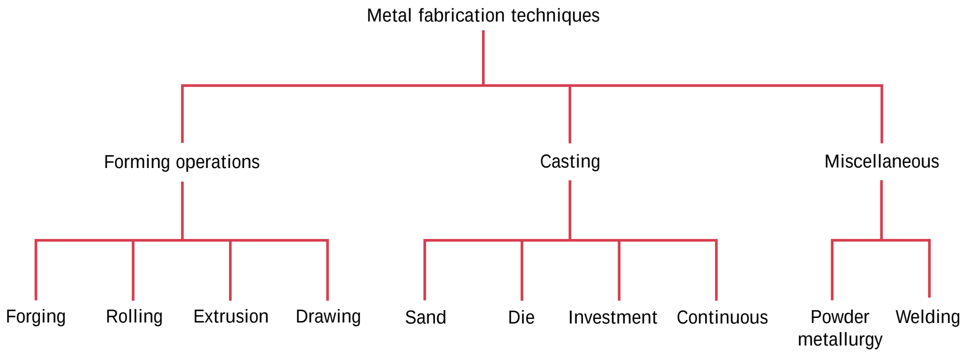

FIGURE 14.1 Classification scheme of metal fabrication techniques discussed in this chapter.

cold working. With most of the forming techniques, both hot- and cold-working procedures are possible. For hot-working operations, large deformations are possible, which may be successively repeated because the metal remains soft and ductile. Also, deformation energy requirements are less than for cold working. However, most metals experience some surface oxidation, which results in material loss and a poor final surface finish. **Cold working** produces an increase in strength with the attendant decrease in ductility, since the metal strain hardens; advantages over hot working include a higher quality surface finish, better mechanical properties and a greater variety of them, and closer dimensional control of the finished piece. On occasion, the total deformation is accomplished in a series of steps in which the piece is successively cold worked a small amount and then process annealed (Section 14.5); however, this is an expensive and inconvenient procedure.

These forming techniques are illustrated schematically in Figure 14.2.

FORGING

Forging is mechanically working or deforming a single piece of a normally hot metal; this may be accomplished by the application of successive blows or by continuous squeezing. Forgings are classified as either closed or open die. For closed die, a force is brought to bear on two or more die halves having the finished shape such that the metal is deformed in the cavity between them (Figure 14.2*a*). For open die, two dies having simple geometric shapes (e.g., parallel flat, semicircular) are employed, normally on large workpieces. Forged articles have outstanding grain structures and the best combination of mechanical properties. Wrenches, and automotive crankshafts and piston connecting rods are typical articles formed using this technique.

ROLLING

Rolling, the most widely used deformation process, consists of passing a piece of metal between two rolls; a reduction in thickness results from compressive stresses exerted by the rolls. Cold rolling may be used in the production of sheet, strip, and foil with high quality surface finish. Circular shapes as well as I-beams and railroad rails are fabricated using grooved rolls.

EXTRUSION

For **extrusion,** a bar of metal is forced through a die orifice by a compressive force that is applied to a ram; the extruded piece that emerges has the desired shape and a reduced cross-sectional area. Extrusion products include rods and tubing that

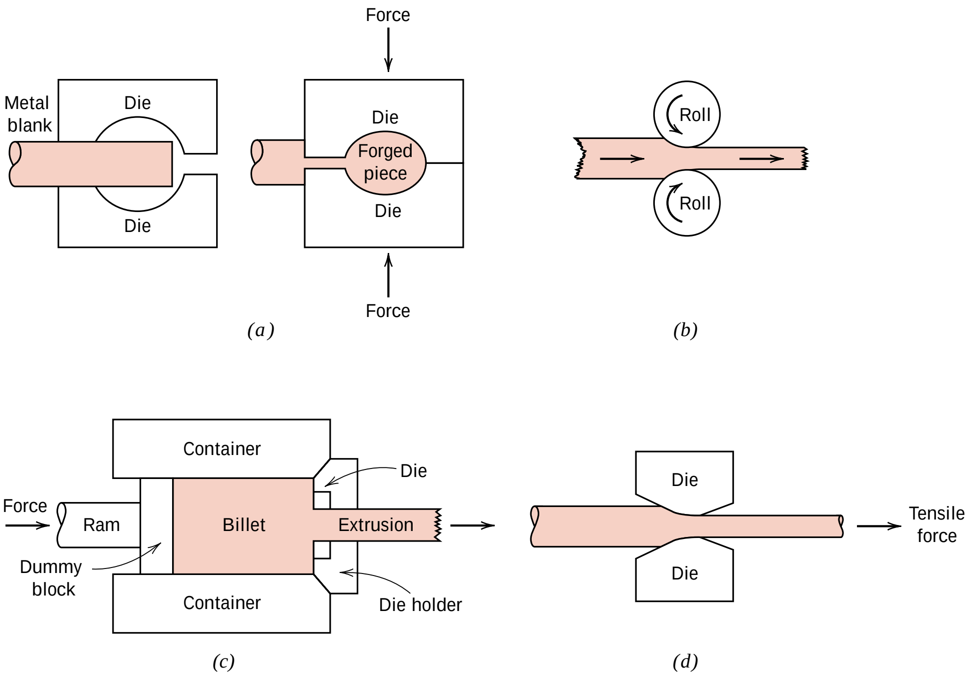

FIGURE 14.2 Metal deformation during (*a*) forging, (*b*) rolling, (*c*) extrusion, and (*d*) drawing.

have rather complicated cross-sectional geometries; seamless tubing may also be extruded.

DRAWING

Drawing is the pulling of a metal piece through a die having a tapered bore by means of a tensile force that is applied on the exit side. A reduction in cross section results, with a corresponding increase in length. The total drawing operation may consist of a number of dies in a series sequence. Rod, wire, and tubing products are commonly fabricated in this way.

14.3 CASTING

Casting is a fabrication process whereby a totally molten metal is poured into a mold cavity having the desired shape; upon solidification, the metal assumes the shape of the mold but experiences some shrinkage. Casting techniques are employed when (1) the finished shape is so large or complicated that any other method would be impractical, (2) a particular alloy is so low in ductility that forming by either hot or cold working would be difficult, and (3) in comparison to other fabrication processes, casting is the most economical. Furthermore, the final step in the refining of even ductile metals may involve a casting process. A number of different casting techniques are commonly employed, including sand, die, investment, and continuous casting. Only a cursory treatment of each of these is offered.

SAND CASTING

With sand casting, probably the most common method, ordinary sand is used as the mold material. A two-piece mold is formed by packing sand around a pattern that has the shape of the intended casting. Furthermore, a *gating system* is usually incorporated into the mold to expedite the flow of molten metal into the cavity and to minimize internal casting defects. Sand-cast parts include automotive cylinder blocks, fire hydrants, and large pipe fittings.

DIE CASTING

In die casting, the liquid metal is forced into a mold under pressure and at a relatively high velocity, and allowed to solidify with the pressure maintained. A two-piece permanent steel mold or die is employed; when clamped together, the two pieces form the desired shape. When complete solidification has been achieved, the die pieces are opened and the cast piece is ejected. Rapid casting rates are possible, making this an inexpensive method; furthermore, a single set of dies may be used for thousands of castings. However, this technique lends itself only to relatively small pieces and to alloys of zinc, aluminum, and magnesium, which have low melting temperatures.

INVESTMENT CASTING

For investment (sometimes called lost-wax) casting, the pattern is made from a wax or plastic that has a low melting temperature. Around the pattern is poured a fluid slurry, which sets up to form a solid mold or investment; plaster of paris is usually used. The mold is then heated, such that the pattern melts and is burned out, leaving behind a mold cavity having the desired shape. This technique is employed when high dimensional accuracy, reproduction of fine detail, and an excellent finish are required—for example, in jewelry and dental crowns and inlays. Also, blades for gas turbines and jet engine impellers are investment cast.

CONTINUOUS CASTING

At the conclusion of extraction processes, many molten metals are solidified by casting into large ingot molds. The ingots are normally subjected to a primary hot rolling operation, the product of which is a flat sheet or slab; these are more convenient shapes as starting points for subsequent secondary metal-forming operations (i.e., forging, extrusion, drawing). These casting and rolling steps may be combined by a *continuous casting* (sometimes also termed ‘‘strand casting’’) process. Using this technique, the refined and molten metal is cast directly into a continuous strand which may have either a rectangular or circular cross section; solidification occurs in a water-cooled die having the desired cross-sectional geometry. The chemical composition and mechanical properties are more uniform throughout the cross sections for continuous castings than for ingot-cast products. Furthermore, continuous casting is highly automated and more efficient.

14.4 MISCELLANEOUS TECHNIQUES

POWDER METALLURGY

Yet another fabrication technique involves the compaction of powdered metal, followed by a heat treatment to produce a more dense piece. The process is appropriately called **powder metallurgy,** frequently designated as P/M. Powder metallurgy makes it possible to produce a virtually nonporous piece having properties almost equivalent to the fully dense parent material. Diffusional processes during the heat treatment are central to the development of these properties. This method is especially suitable for metals having low ductilities, since only small plastic deformation of the powder particles need occur. Metals having high melting temperatures are difficult to melt and cast, and fabrication is expedited using P/M. Furthermore, parts that require very close dimensional tolerances (e.g., bushings and gears) may be economically produced using this technique.

WELDING

In a sense, welding may be considered to be a fabrication technique. In **welding,** two or more metal parts are joined to form a single piece when one-part fabrication is expensive or inconvenient. Both similar and dissimilar metals may be welded. The joining bond is metallurgical (involving some diffusion) rather than just mechanical, as with riveting and bolting. A variety of welding methods exist, including arc and gas welding, as well as brazing and soldering.

During arc and gas welding, the workpieces to be joined and the filler material (i.e., welding rod) are heated to a sufficiently high temperature to cause both to melt; upon solidification, the filler material forms a fusion joint between the workpieces. Thus, there is a region adjacent to the weld that may have experienced microstructural and property alterations; this region is termed the *heat-affected zone* (sometimes abbreviated *HAZ*). Possible alterations include the following:

1. If the workpiece material was previously cold worked, this heat-affected zone may have experienced recrystallization and grain growth, and thus a diminishment of strength, hardness, and toughness. The HAZ for this situation is represented schematically in Figure 14.3.
2. Upon cooling, residual stresses may form in this region that weaken the joint.
3. For steels, the material in this zone may have been heated to temperatures sufficiently high so as to form austenite. Upon cooling to room temperature, the microstructural products that form depend on cooling rate and alloy composition. For plain carbon steels that have low hardenabilities, normally pearlite and a proeutectoid phase will be present. However, for alloy steels, one microstructural product may be martensite, which is ordinarily undesirable because it is so brittle.
4. Some stainless steels may be ''sensitized'' during welding, which renders them susceptible to intergranular corrosion, as explained in Section 16.7.

A relatively modern joining technique is that of laser beam welding, wherein a highly focused and intense laser beam is used as the heat source. The laser beam melts the parent metal, and, upon solidification, a fusion joint is produced; often

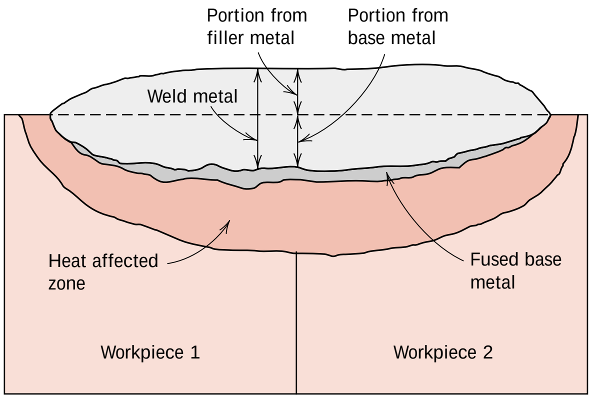

FIGURE 14.3 Schematic cross-sectional representation showing the zones in the vicinity of a typical fusion weld. (From *Iron Castings Handbook,* C. F. Walton and T. J. Opar, Editors, 1981.)

a filler material need not be used. Some of the advantages of this technique are as follows: (1) it is a noncontact process, which eliminates mechanical distortion of the workpieces; (2) it can be rapid and highly automated; (3) energy input to the workpiece is low, and therefore, the heat-affected zone size is minimal; (4) welds may be small in size and very precise; (5) a large variety of metals and alloys may be joined using this technique; and (6) porosity-free welds with strengths equal to or in excess of the base metal are possible. Laser beam welding is used extensively in the automotive and electronic industries where high quality and rapid welding rates are required.

THERMAL PROCESSING OF METALS

Earlier chapters have discussed a number of phenomena that occur in metals and alloys at elevated temperatures, for example, recrystallization and the decomposition of austenite. These are effective in altering the mechanical characteristics when appropriate heat treatments or thermal processes are employed. In fact, the use of heat treatments on commercial alloys is an exceedingly common practice. Therefore, we consider the details of some of these processes, including annealing procedures and the heat treating of steels.

14.5 Annealing Processes

The term **annealing** refers to a heat treatment in which a material is exposed to an elevated temperature for an extended time period and then slowly cooled. Ordinarily, annealing is carried out to (1) relieve stresses; (2) increase softness, ductility, and toughness; and/or (3) produce a specific microstructure. A variety of annealing heat treatments are possible; they are characterized by the changes that are induced, which many times are microstructural and are responsible for the alteration of the mechanical properties.

Any annealing process consists of three stages: (1) heating to the desired temperature, (2) holding or ‘‘soaking’’ at that temperature, and (3) cooling, usually to room temperature. Time is an important parameter in these procedures. During heating and cooling, there exist temperature gradients between the outside and interior portions of the piece; their magnitudes depend on the size and geometry of the piece. If the rate of temperature change is too great, temperature gradients and internal stresses may be induced that may lead to warping or even cracking. Also, the actual annealing time must be long enough to allow for any necessary transformation reactions. Annealing temperature is also an important consideration; annealing may be accelerated by increasing the temperature, since diffusional processes are normally involved.

PROCESS ANNEALING

Process annealing is a heat treatment that is used to negate the effects of cold work, that is, to soften and increase the ductility of a previously strain-hardened metal. It is commonly utilized during fabrication procedures that require extensive plastic deformation, to allow a continuation of deformation without fracture or excessive energy consumption. Recovery and recrystallization processes are allowed to occur. Ordinarily a fine-grained microstructure is desired, and therefore, the heat treatment is terminated before appreciable grain growth has occurred. Surface oxidation or scaling may be prevented or minimized by annealing at a relatively low temperature (but above the recrystallization temperature) or in a nonoxidizing atmosphere.

STRESS RELIEF

Internal residual stresses may develop in metal pieces in response to the following: (1) plastic deformation processes such as machining and grinding; (2) nonuniform cooling of a piece that was processed or fabricated at an elevated temperature, such as a weld or a casting; and (3) a phase transformation that is induced upon cooling wherein parent and product phases have different densities. Distortion and warpage may result if these residual stresses are not removed. They may be eliminated by a **stress relief** annealing heat treatment in which the piece is heated to the recommended temperature, held there long enough to attain a uniform temperature, and finally cooled to room temperature in air. The annealing temperature is ordinarily a relatively low one such that effects resulting from cold working and other heat treatments are not affected.

ANNEALING OF FERROUS ALLOYS

Several different annealing procedures are employed to enhance the properties of steel alloys. However, before they are discussed, some comment relative to the labeling of phase boundaries is necessary. Figure 14.4 shows the portion of the iron–iron carbide phase diagram in the vicinity of the eutectoid. The horizontal line at the eutectoid temperature, conventionally labeled A_1, is termed the **lower critical temperature,** below which, under equilibrium conditions, all austenite will have transformed into ferrite and cementite phases. The phase boundaries denoted as A_3 and A_{cm} represent the **upper critical temperature** lines, for hypoeutectoid and hypereutectoid steels, respectively. For temperatures and compositions above these boundaries, only the austenite phase will prevail. As explained in Section 10.20, other alloying elements will shift the eutectoid and the positions of these phase boundary lines.

Normalizing

Steels that have been plastically deformed by, for example, a rolling operation, consist of grains of pearlite (and most likely a proeutectoid phase), which are

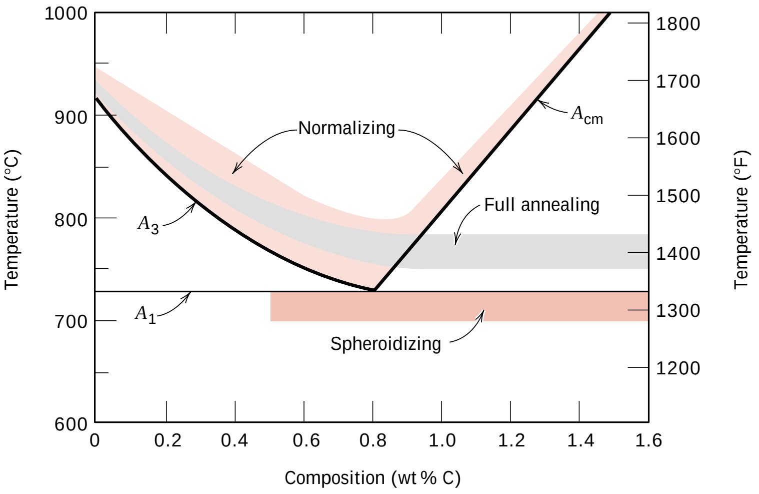

FIGURE 14.4 The iron–iron carbide phase diagram in the vicinity of the eutectoid, indicating heat treating temperature ranges for plain carbon steels. (Adapted from *Metals Handbook*, T. Lyman, Editor, American Society for Metals, 1948, p. 661.)

irregularly shaped and relatively large, but vary substantially in size. An annealing heat treatment called **normalizing** is used to refine the grains (i.e., to decrease the average grain size) and produce a more uniform and desirable size distribution; fine-grained pearlitic steels are tougher than coarse-grained ones. Normalizing is accomplished by heating at approximately 55 to 85°C (100 to 150°F) above the upper critical temperature, which is, of course, dependent on composition, as indicated in Figure 14.4. After sufficient time has been allowed for the alloy to completely transform to austenite—a procedure termed **austenitizing—**the treatment is terminated by cooling in air. A normalizing cooling curve is superimposed on the continuous cooling transformation diagram (Figure 11.18).

Full Anneal

A heat treatment known as **full annealing** is often utilized in low- and medium-carbon steels that will be machined or will experience extensive plastic deformation during a forming operation. The alloy is austenitized by heating to 15 to 40°C (30 to 70°F) above the A_3 or A_1 lines as indicated in Figure 14.4 until equilibrium is achieved. The alloy is then furnace cooled; that is, the heat-treating furnace is turned off and both furnace and steel cool to room temperature at the same rate, which takes several hours. The microstructural product of this anneal is coarse pearlite (in addition to any proeutectoid phase) that is relatively soft and ductile. The full-anneal cooling procedure (also shown in Figure 11.18) is time consuming; however, a microstructure having small grains and a uniform grain structure results.

Spheroidizing

Medium- and high-carbon steels having a microstructure containing even coarse pearlite may still be too hard to conveniently machine or plastically deform. These steels, and in fact any steel, may be heat treated or annealed to develop the spheroidite structure as described in Section 11.5. Spheroidized steels have a maximum softness and ductility and are easily machined or deformed. The **spheroidizing** heat treatment consists of heating the alloy at a temperature just below the eutectoid [line A_1 in Figure 14.4, or at about 700°C (1300°F)] in the $\alpha + Fe_3C$ region of the phase diagram. If the precursor microstructure contains pearlite, spheroidizing times will ordinarily range between 15 and 25 h. During this annealing there is a coalescence of the Fe_3C to form the spheroid particles (see Figure 11.11).

Still other annealing treatments are possible. For example, glasses are annealed, as outlined in Section 14.7, to remove residual internal stresses that render the material excessively weak. In addition, microstructural alterations and the attendant modification of mechanical properties of cast irons, as discussed in Section 13.2, result from what are in a sense annealing treatments.

14.6 HEAT TREATMENT OF STEELS

Conventional heat treatment procedures for producing martensitic steels ordinarily involve continuous and rapid cooling of an austenitized specimen in some type of quenching medium, such as water, oil, or air. The optimum properties of a steel that has been quenched and then tempered can be realized only if, during the quenching heat treatment, the specimen has been converted to a high content of martensite; the formation of any pearlite and/or bainite will result in other than the best combination of mechanical characteristics. During the quenching treatment, it is impossible to cool the specimen at a uniform rate throughout—the surface will always cool more rapidly than interior regions. Therefore, the austenite will transform over a range of temperatures, yielding a possible variation of microstructure and properties with position within a specimen.

The successful heat treating of steels to produce a predominantly martensitic microstructure throughout the cross section depends mainly on three factors: (1) the composition of the alloy, (2) the type and character of the quenching medium, and (3) the size and shape of the specimen. The influence of each of these factors is now addressed.

HARDENABILITY

The influence of alloy composition on the ability of a steel alloy to transform to martensite for a particular quenching treatment is related to a parameter called **hardenability.** For every different steel alloy there is a specific relationship between the mechanical properties and the cooling rate. ''Hardenability'' is a term that is used to describe the ability of an alloy to be hardened by the formation of martensite as a result of a given heat treatment. Hardenability is not ''hardness,'' which is the resistance to indentation; rather, hardenability is a qualitative measure of the rate at which hardness drops off with distance into the interior of a specimen as a result of diminished martensite content. A steel alloy that has a high hardenability is one that hardens, or forms martensite, not only at the surface but to a large degree throughout the entire interior.

The Jominy End-Quench Test

One standard procedure that is widely utilized to determine hardenability is the **Jominy end-quench test.**[1] With this procedure, except for alloy composition, all factors that may influence the depth to which a piece hardens (i.e., specimen size and shape, and quenching treatment) are maintained constant. A cylindrical specimen 25.4 mm (1.0 in.) in diameter and 100 mm (4 in.) long is austenitized at a prescribed temperature for a prescribed time. After removal from the furnace, it is quickly mounted in a fixture as diagrammed in Figure 14.5*a*. The lower end is quenched by a jet of water of specified flow rate and temperature. Thus, the cooling rate is a maximum at the quenched end and diminishes with position from this point along the length of the specimen. After the piece has cooled to room temperature, shallow flats 0.4 mm (0.015 in.) deep are ground along the specimen length and Rockwell hardness measurements are made for the first 50 mm (2 in.) along each flat (Figure 14.5*b*); for the first 12.8 mm ($\frac{1}{2}$ in.), hardness readings are taken at 1.6 mm ($\frac{1}{16}$ in.) intervals, and for the remaining 38.4 mm ($1\frac{1}{2}$ in.), every 3.2 mm ($\frac{1}{8}$ in.). A hardenability curve is produced when hardness is plotted as a function of position from the quenched end.

Hardenability Curves

A typical hardenability curve is represented in Figure 14.6. The quenched end is cooled most rapidly and exhibits the maximum hardness; 100% martensite is the product at this position for most steels. Cooling rate decreases with distance from the quenched end, and the hardness also decreases, as indicated in the figure. With diminishing cooling rate more time is allowed for carbon diffusion and the formation of a greater proportion of the softer pearlite, which may be mixed with martensite and bainite. Thus, a steel that is highly hardenable will retain large hardness values

---

[1] ASTM Standard A 255, ''Standard Test Method for End-Quench Test for Hardenability of Steel.''

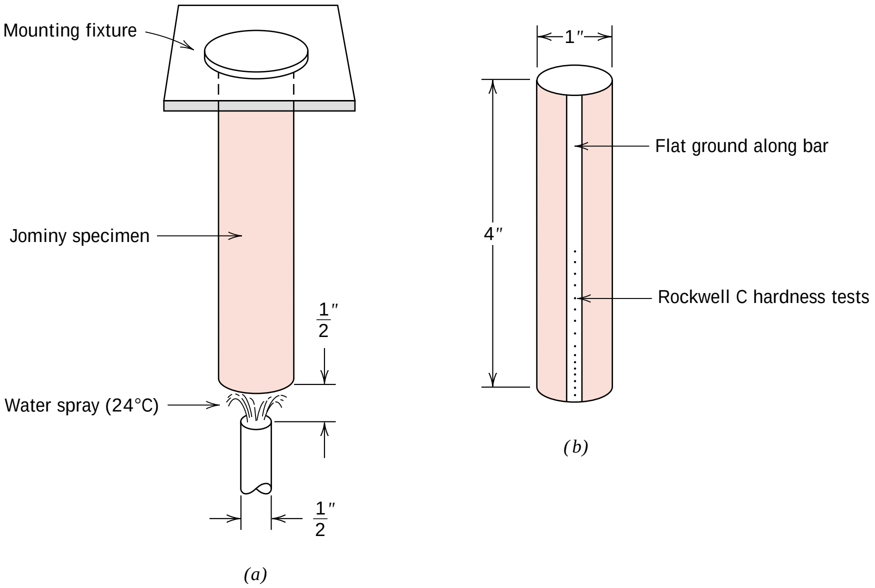

FIGURE 14.5 Schematic diagram of Jominy end-quench specimen (*a*) mounted during quenching and (*b*) after hardness testing from the quenched end along a ground flat. (Adapted from A. G. Guy, *Essentials of Materials Science.* Copyright 1978 by McGraw-Hill Book Company, New York.)

for relatively long distances; a low hardenable one will not. Also, each steel alloy has its own unique hardenability curve.

Sometimes, it is convenient to relate hardness to a cooling rate rather than to the location from the quenched end of a standard Jominy specimen. Cooling rate [taken at 700°C (1300°F)] is ordinarily shown on the upper horizontal axis of a hardenability diagram; this scale is included with the hardenability plots presented here. This correlation between position and cooling rate is the same for plain carbon and many alloy steels because the rate of heat transfer is nearly independent of composition. On occasion, cooling rate or position from the quenched end is specified in terms of Jominy distance, one Jominy distance unit being 1.6 mm ($\frac{1}{16}$ in.).

A correlation may be drawn between position along the Jominy specimen and continuous cooling transformations. For example, Figure 14.7 is a continuous transformation diagram for a eutectoid iron–carbon alloy onto which is superimposed the cooling curves at four different Jominy positions, and corresponding microstructures that result for each. The hardenability curve for this alloy is also included.

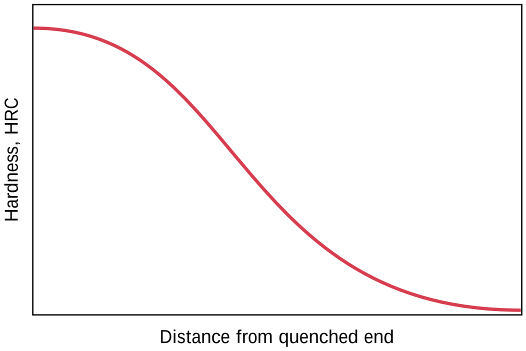

FIGURE 14.6 Typical hardenability plot of Rockwell C hardness as a function of distance from the quenched end.

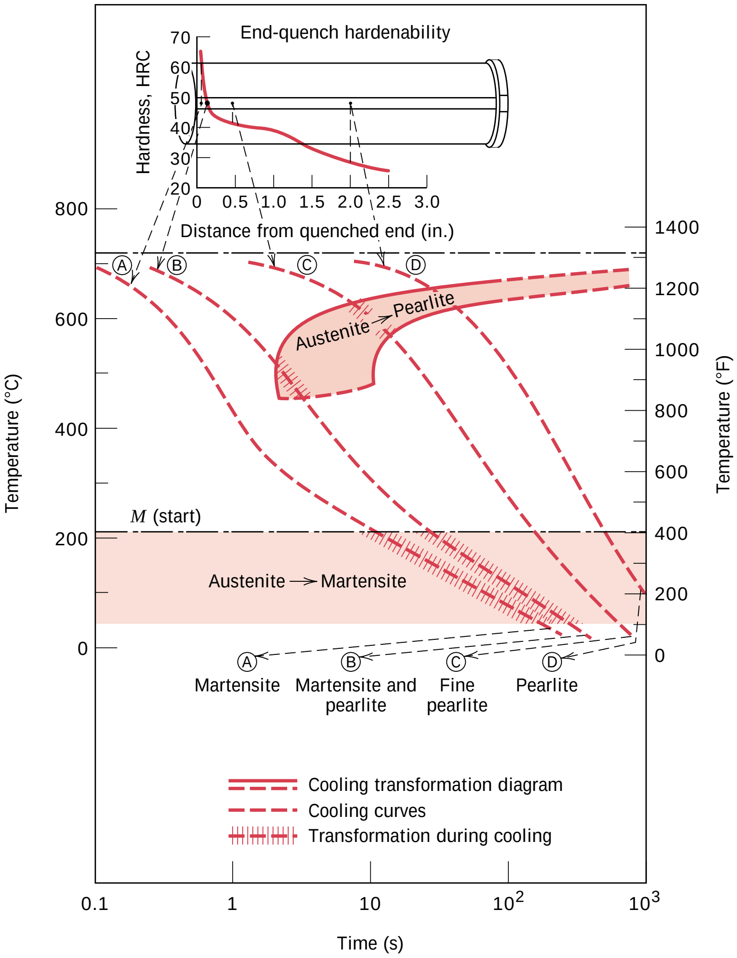

Figure 14.7 Correlation of hardenability and continuous cooling information for an iron–carbon alloy of eutectoid composition. (Adapted from H. Boyer, Editor, *Atlas of Isothermal Transformation and Cooling Transformation Diagrams,* American Society for Metals, 1977, p. 376.)

The hardenability curves for five different steel alloys all having 0.40 wt% C, yet differing amounts of other alloying elements, are shown in Figure 14.8. One specimen is a plain carbon steel (1040); the other four (4140, 4340, 5140, and 8640) are alloy steels. The compositions of the four alloy steels are included with the figure. The significance of the alloy designation numbers (e.g., 1040) is explained in Chapter 13. Several details are worth noting from this figure. First, all five alloys have identical hardnesses at the quenched end (57 HRC); this hardness is a function of carbon content only, which is the same for all these alloys.

Probably the most significant feature of these curves is shape, which relates to hardenability. The hardenability of the plain carbon 1040 steel is low because the hardness drops off precipitously (to about 30 HRC) after a relatively short Jominy distance (6.4 mm, $\frac{1}{4}$ in.). By way of contrast, the decreases in hardness for the other four alloy steels are distinctly more gradual. For example, at a Jominy distance of 50 mm (2 in.), the hardnesses of the 4340 and 8640 alloys are approximately 50 and 32 HRC, respectively; thus, of these two alloys, the 4340 is more hardenable. A water-quenched specimen of the 1040 plain carbon steel would harden only to a shallow depth below the surface, whereas for the other four alloy steels the high quenched hardness would persist to a much greater depth.

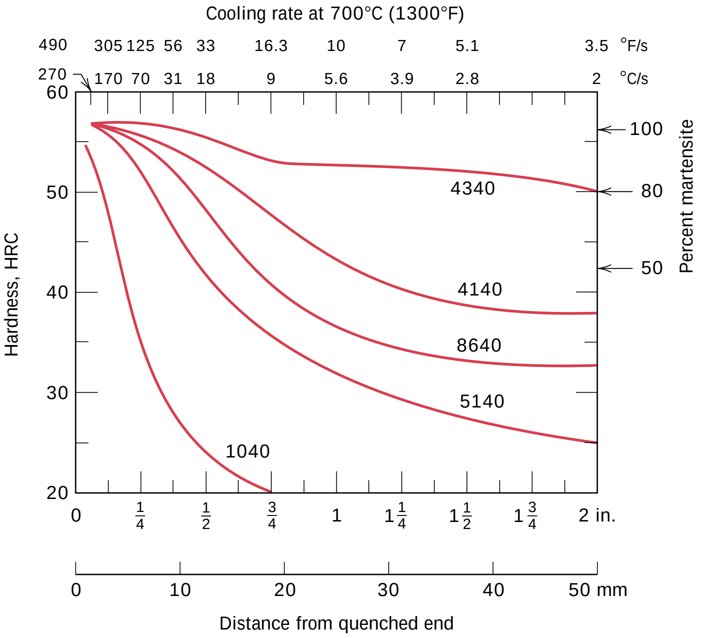

Figure 14.8 Hardenability curves for five different steel alloys, each containing 0.4 wt% C. Approximate alloy compositions (wt%) are as follows: 4340–1.85 Ni, 0.80 Cr, and 0.25 Mo; 4140–1.0 Cr and 0.20 Mo; 8640–0.55 Ni, 0.50 Cr, and 0.20 Mo; 5140–0.85 Cr; 1040 is an unalloyed steel. (Adapted from figure furnished courtesy Republic Steel Corporation.)

The hardness profiles in Figure 14.8 are indicative of the influence of cooling rate on the microstructure. At the quenched end, where the quenching rate is approximately 600°C/s (1100°F/s), 100% martensite is present for all five alloys. For cooling rates less than about 70°C/s (125°F/s) or Jominy distances greater than about 6.4 mm ($\frac{1}{4}$ in.), the microstructure of the 1040 steel is predominantly pearlitic, with some proeutectoid ferrite. However, the microstructures of the four alloy steels consist primarily of a mixture of martensite and bainite; bainite content increases with decreasing cooling rate.

This disparity in hardenability behavior for the five alloys in Figure 14.8 is explained by the presence of nickel, chromium, and molybdenum in the alloy steels. These alloying elements delay the austenite-to-pearlite and/or bainite reactions, as explained in Sections 11.5 and 11.6; this permits more martensite to form for a particular cooling rate, yielding a greater hardness. The right-hand axis of Figure 14.8 shows the approximate percent of martensite that is present at various hardnesses for these alloys.

The hardenability curves also depend on carbon content. This effect is demonstrated in Figure 14.9 for a series of alloy steels in which only the concentration of carbon is varied. The hardness at any Jominy position increases with the concentration of carbon.

Also, during the industrial production of steel, there is always a slight, unavoidable variation in composition and average grain size from one batch to another. This results in some scatter in measured hardenability data, which frequently are plotted as a band representing the maximum and minimum values that would be expected for the particular alloy. Such a hardenability band is plotted in Figure 14.10 for an 8640 steel. An H following the designation specification for an alloy (e.g., 8640H) indicates that the composition and characteristics of the alloy are such that its hardenability curve will lie within a specified band.

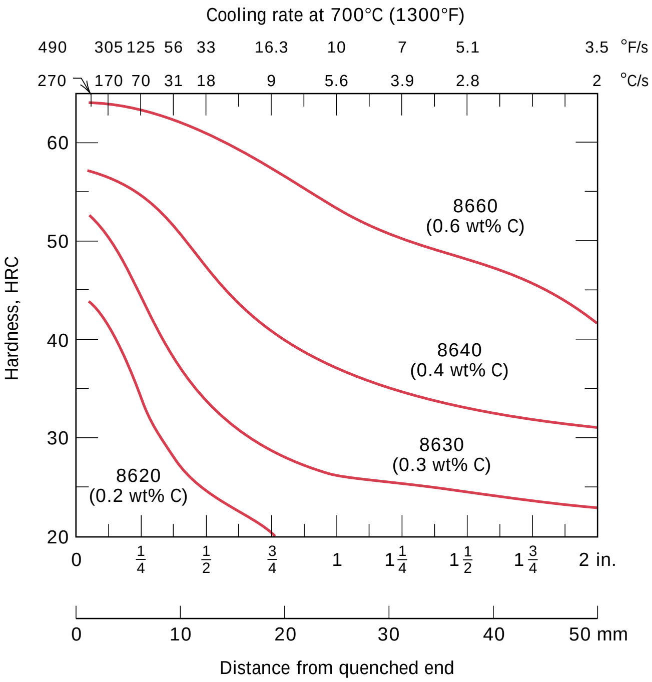

FIGURE 14.9 Hardenability curves for four 8600 series alloys of indicated carbon content. (Adapted from figure furnished courtesy Republic Steel Corporation.)

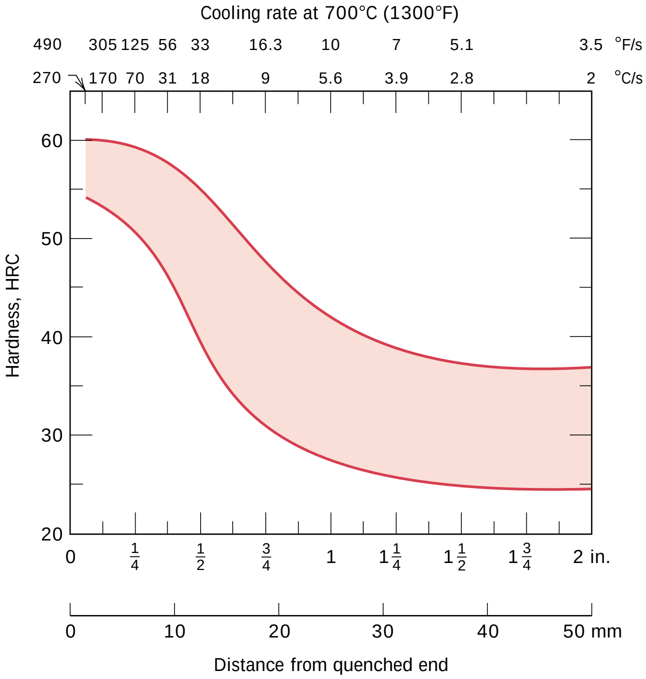

FIGURE 14.10 The hardenability band for an 8640 steel indicating maximum and minimum limits. (Adapted from figure furnished courtesy Republic Steel Corporation.)

INFLUENCE OF QUENCHING MEDIUM, SPECIMEN SIZE, AND GEOMETRY

The preceding treatment of hardenability discussed the influence of both alloy composition and cooling or quenching rate on the hardness. The cooling rate of a specimen depends on the rate of heat energy extraction, which is a function of the characteristics of the quenching medium in contact with the specimen surface, as well as the specimen size and geometry.

''Severity of quench'' is a term often used to indicate the rate of cooling; the more rapid the quench, the more severe the quench. Of the three most common quenching media—water, oil, and air—water produces the most severe quench, followed by oil, which is more effective than air. The degree of agitation of each medium also influences the rate of heat removal. Increasing the velocity of the quenching medium across the specimen surface enhances the quenching effectiveness. Oil quenches are suitable for the heat treating of many alloy steels. In fact, for higher-carbon steels, a water quench is too severe because cracking and warping may be produced. Air cooling of austenitized plain carbon steels ordinarily produces an almost totally pearlitic structure.

During the quenching of a steel specimen, heat energy must be transported to the surface before it can be dissipated into the quenching medium. As a consequence, the cooling rate within and throughout the interior of a steel structure varies with position and depends on the geometry and size. Figures 14.11*a* and 14.11*b* show the quenching rate [at 700°C (1300°F)] as a function of diameter for cylindrical bars at four radial positions (surface, three-quarters radius, midradius, and center). Quenching is in mildly agitated water (Figure 14.11*a*) and oil (Figure 14.11*b*); cooling rate is also expressed as equivalent Jominy distance, since these data are often used in conjunction with hardenability curves. Diagrams similar to those in Figure 14.11 have also been generated for geometries other than cylindrical (e.g., flat plates).

One utility of such diagrams is in the prediction of the hardness traverse along the cross section of a specimen. For example, Figure 14.12*a* compares the radial hardness distributions for cylindrical plain carbon (1040) and alloy (4140) steel specimens; both have a diameter of 50 mm (2 in.) and are water quenched. The difference in hardenability is evident from these two profiles. Specimen diameter also influences the hardness distribution, as demonstrated in Figure 14.12*b*, which plots the hardness profiles for water-quenched 4140 cylinders 50 and 100 mm (2 and 4 in.) in diameter. Example Problem 14.1 illustrates how these hardness profiles are determined.

As far as specimen shape is concerned, since the heat energy is dissipated to the quenching medium at the specimen surface, the rate of cooling for a particular quenching treatment depends on the ratio of surface area to the mass of the specimen. The larger this ratio, the more rapid will be the cooling rate and, consequently, the deeper the hardening effect. Irregular shapes with edges and corners have larger surface-to-mass ratios than regular and rounded shapes (e.g., spheres and cylinders) and are thus more amenable to hardening by quenching.

There are a multitude of steels that are responsive to a martensitic heat treatment, and one of the most important criteria in the selection process is hardenability. Hardenability curves, when utilized in conjunction with plots such as those in Figure 14.11 for various quenching media, may be used to ascertain the suitability of a specific steel alloy for a particular application. Or, conversely, the appropriateness of a quenching procedure for an alloy may be determined. For parts that are to be involved in relatively high stress applications, a minimum of 80% martensite must

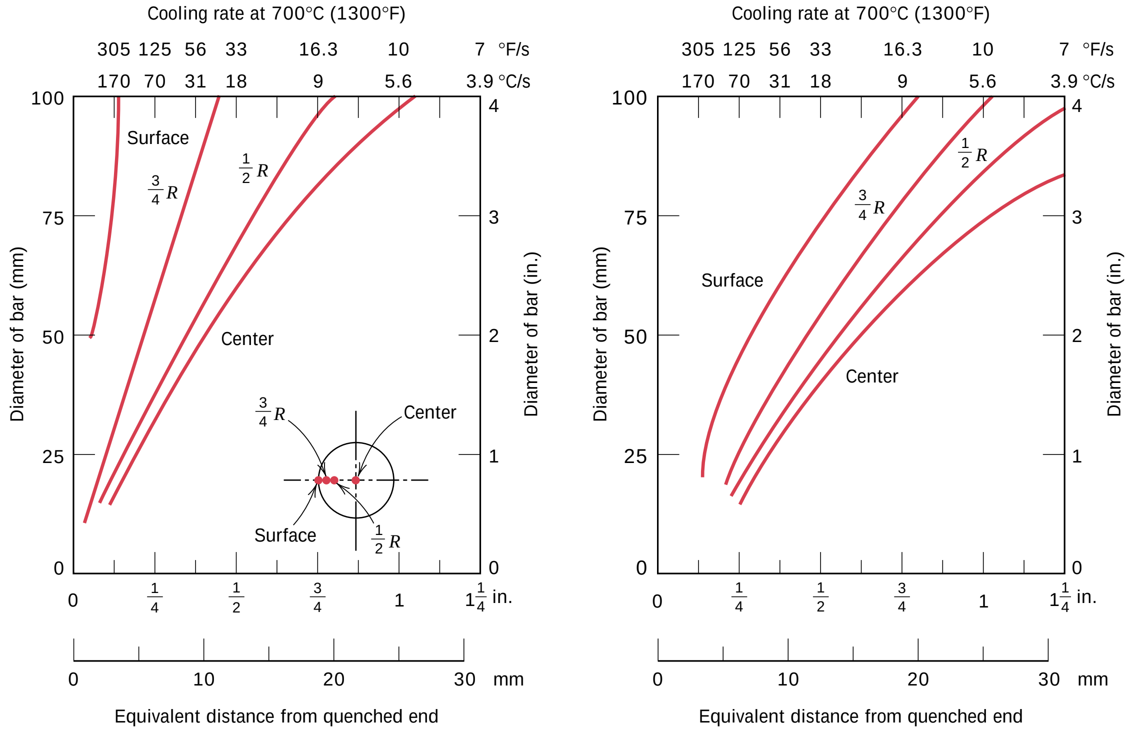

(a) *(b)*

Figure 14.11 Cooling rate as a function of diameter at surface, three-quarters radius ($\frac{3}{4}R$), midradius ($\frac{1}{2}R$), and center positions for cylindrical bars quenched in mildly agitated (*a*) water and (*b*) oil. Equivalent Jominy positions are included along the bottom axis. (Adapted from *Metals Handbook: Properties and Selection: Irons and Steels,* Vol. 1, 9th edition, B. Bardes, Editor, American Society for Metals, 1978, p. 492.)

Figure 14.12 Radial hardness profiles for (*a*) 50 mm (2 in.) diameter cylindrical 1040 and 4140 steel specimens quenched in mildly agitated water, and (*b*) 50 and 100 mm (2 and 4 in.) diameter cylindrical specimens of 4140 steel quenched in mildly agitated water.

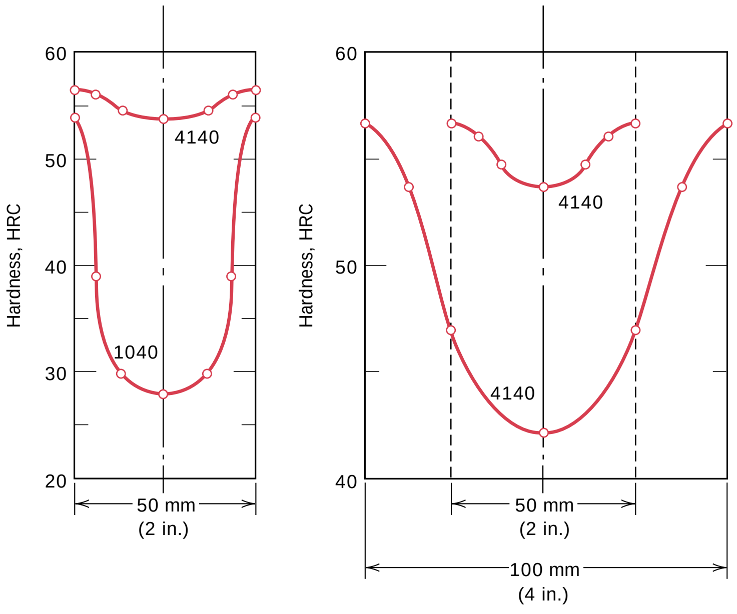

(a) *(b)*

be produced throughout the interior as a consequence of the quenching procedure. Only a 50% minimum is required for moderately stressed parts.

EXAMPLE PROBLEM 14.1

Determine the radial hardness profile for a 50 mm (2 in.) diameter cylindrical specimen of 1040 steel that has been quenched in moderately agitated water.

SOLUTION

First, evaluate the cooling rate (in terms of the Jominy end-quench distance) at center, surface, mid-, and three-quarter radial positions of the cylindrical specimen. This is accomplished using the cooling rate-versus-bar diameter plot for the appropriate quenching medium, in this case, Figure 14.11*a*. Then, convert the cooling rate at each of these radial positions into a hardness value from a hardenability plot for the particular alloy. Finally, determine the hardness profile by plotting the hardness as a function of radial position.

This procedure is demonstrated in Figure 14.13, for the center position.

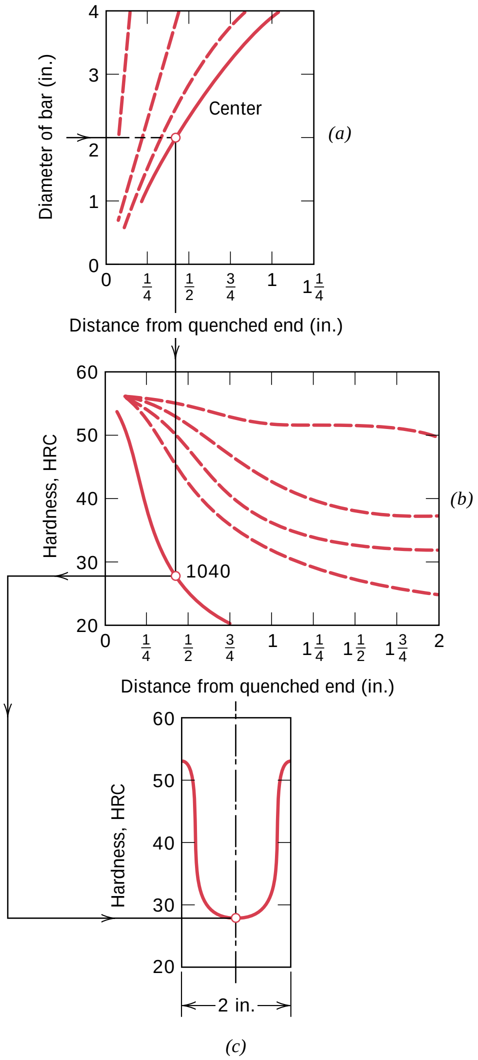

FIGURE 14.13 Use of hardenability data in the generation of hardness profiles. (*a*) The cooling rate at the center of a water-quenched 50 mm (2 in.) diameter specimen is determined. (*b*) The cooling rate is converted into an HRC hardness for a 1040 steel. (*c*) The Rockwell hardness is plotted on the radial hardness profile.

Note that for a water-quenched cylinder of 50 mm (2 in.) diameter, the cooling rate at the center is equivalent to that approximately 9.5 mm ($\frac{3}{8}$ in.) from the Jominy specimen quenched end (Figure 14.13*a*). This corresponds to a hardness of about 28 HRC, as noted from the hardenability plot for the 1040 steel alloy (Figure 14.13*b*). Finally, this data point is plotted on the hardness profile in Figure 14.13*c*.

Surface, midradius, and three-quarter radius hardnesses would be determined in a similar manner. The complete profile has been included, and the data that were used are tabulated below.

Radial Position	***Equivalent Distance from Quenched End [mm (in.)]***	***Hardness HRC***
Center	9.5 ($\frac{3}{8}$)	28
Midradius	8 ($\frac{5}{16}$)	30
Three-quarters radius	4.8 ($\frac{3}{16}$)	39
Surface	1.6 ($\frac{1}{16}$)	54

DESIGN EXAMPLE 14.1

It is necessary to select a steel alloy for a gearbox output shaft. The design calls for a 1-in. diameter cylindrical shaft having a surface hardness of at least 38 HRC and a minimum ductility of 12%EL. Specify an alloy and treatment that meet these criteria.

SOLUTION

First of all, cost is also most likely an important design consideration. This would probably eliminate relatively expensive steels, such as stainless and those that are precipitation hardenable. Therefore, let us begin by examining plain-carbon and low-alloy steels, and what treatments are available to alter their mechanical characteristics.

It is unlikely that merely cold-working one of these steels would produce the desired combination of hardness and ductility. For example, from Figure 7.31, a hardness of 38 HRC corresponds to a tensile strength of 1200 MPa (175,000 psi). The tensile strength as a function of percent cold work for a 1040 steel is represented in Figure 8.19*b*. Here it may be noted that at 50%CW, a tensile strength of only about 900 MPa (130,000 psi) is achieved; furthermore, the corresponding ductility is approximately 10%EL (Figure 8.19*c*). Hence, both of these properties fall short of those specified in the design; furthermore, cold working other plain-carbon or low-alloy steels would probably not achieve the required minimum values.

Another possibility is to perform a series of heat treatments in which the steel is austenitized, quenched (to form martensite), and finally tempered. Let us now examine the mechanical properties of various plain-carbon and low-alloy steels that have been heat treated in this manner. To begin, the surface hardness of the quenched material (which ultimately affects the tempered hardness) will depend on both alloy content and shaft diameter, as discussed in the previous two sections. For example, the degree to which surface hardness decreases with diameter is represented in Table 14.1 for a 1060 steel that was oil quenched. Furthermore, the tempered surface hardness will also depend on tempering temperature and time.

Table 14.1 **Surface Hardnesses for Oil-Quenched Cylinders of 1060 Steel Having Various Diameters**

Diameter (in.)	*Surface Hardness (HRC)*
0.5	59
1	34
2	30.5
4	29

As-quenched and tempered hardness and ductility data were collected for one plain-carbon (AISI/SAE 1040) and several common and readily available low-alloy steels, data for which are presented in Table 14.2. The quenching medium (either oil or water) is indicated, and tempering temperatures were 540°C (1000°F), 595°C (1100°F), and 650°C (1200°F). As may be noted, the only alloy-heat treatment combinations that meet the stipulated criteria are 4150/oil-540°C temper, 4340/oil-540°C temper, and 6150/oil-540°C temper; data for these alloys/heat treatments are boldfaced in the table. The costs of these three materials are probably comparable; however, a cost analysis should be conducted. Furthermore, the 6150 alloy has the highest ductility (by a narrow margin), which would give it a slight edge in the selection process.

FABRICATION OF CERAMIC MATERIALS

One chief concern in the application of ceramic materials is the method of fabrication. Many of the metal-forming operations discussed above rely on casting and/or techniques that involve some form of plastic deformation. Since ceramic materials have relatively high melting temperatures, casting them is normally impractical. Furthermore, in most instances the brittleness of these materials precludes deformation. Some ceramic pieces are formed from powders (or particulate collections) that must ultimately be dried and fired. Glass shapes are formed at elevated tempera-

Table 14.2 **Rockwell C Hardness (Surface) and Percent Elongation Values for 1-in. Diameter Cylinders of Six Steel Alloys, in the As-Quenched Condition and for Various Tempering Heat Treatments**

	As-Quenched	*Tempered at 540°C (1000°F)*		*Tempered at 595°C (1100°F)*		*Tempered at 650°C (1200°F)*	
Alloy Designation/ Quenching Medium	*Hardness (HRC)*	*Hardness (HRC)*	*Ductility (%EL)*	*Hardness (HRC)*	*Ductility (%EL)*	*Hardness (HRC)*	*Ductility (%EL)*
1040/oil	23	(12.5)[a]	26.5	(10)[a]	28.2	(5.5)[a]	30.0
1040/water	50	(17.5)[a]	23.2	(15)[a]	26.0	(12.5)[a]	27.7
4130/water	51	31	18.5	26.5	21.2	—	—
4140/oil	55	33	15.5	30	19.5	27.5	21.0
4150/oil	62	**38**	**14.0**	35.5	15.7	30	18.7
4340/oil	57	**38**	**14.2**	35.5	16.5	29	20.0
6150/oil	60	**38**	**14.5**	33	16.0	31	18.7

[a] These hardness values are only approximate because they are less than 20 HRC.

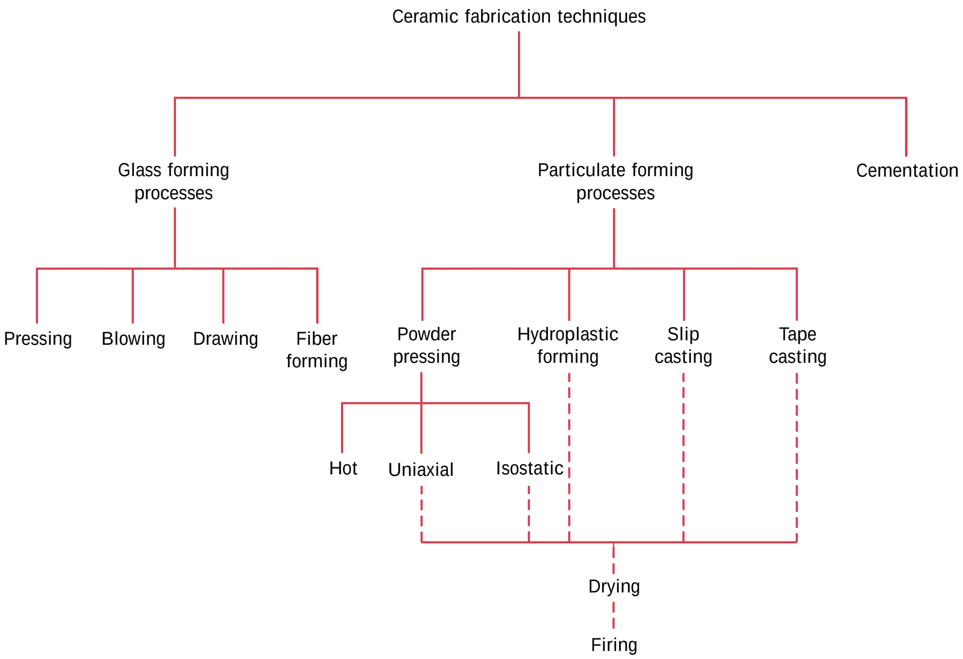
Ceramic fabrication techniques
Glass forming processes
Particulate forming processes
Cementation
Pressing
Blowing
Drawing
Fiber forming
Powder pressing
Hydroplastic forming
Slip casting
Tape casting
Hot
Uniaxial
Isostatic
Drying
Firing

Figure 14.14 A classification scheme for the ceramic-forming techniques discussed in this chapter.

tures from a fluid mass that becomes very viscous upon cooling. Cements are shaped by placing into forms a fluid paste that hardens and assumes a permanent set by virtue of chemical reactions. A taxonomical scheme for the several types of ceramic-forming techniques is presented in Figure 14.14.

14.7 FABRICATION AND PROCESSING OF GLASSES

GLASS PROPERTIES

Before we discuss specific glass-forming techniques, some of the temperature-sensitive properties of glass materials must be presented. Glassy, or noncrystalline, materials do not solidify in the same sense as do those that are crystalline. Upon cooling, a glass becomes more and more viscous in a continuous manner with decreasing temperature; there is no definite temperature at which the liquid transforms to a solid as with crystalline materials. In fact, one of the distinctions between crystalline and noncrystalline materials lies in the dependence of specific volume (or volume per unit mass—the reciprocal of density) on temperature, as illustrated in Figure 14.15; this same behavior is exhibited by highly crystalline and amorphous polymers (Figure 11.36). For crystalline materials, there is a discontinuous decrease in volume at the melting temperature T_m. However, for glassy materials, volume decreases continuously with temperature reduction; a slight decrease in slope of the curve occurs at what is called the **glass transition temperature,** or *fictive* temperature, T_g. Below this temperature, the material is considered to be a glass; above, it is first a supercooled liquid, and finally a liquid.

Also important in glass-forming operations are the viscosity–temperature characteristics of the glass. Figure 14.16 plots the logarithm of viscosity versus the temperature for fused silica, high silica, borosilicate, and soda–lime glasses. On the

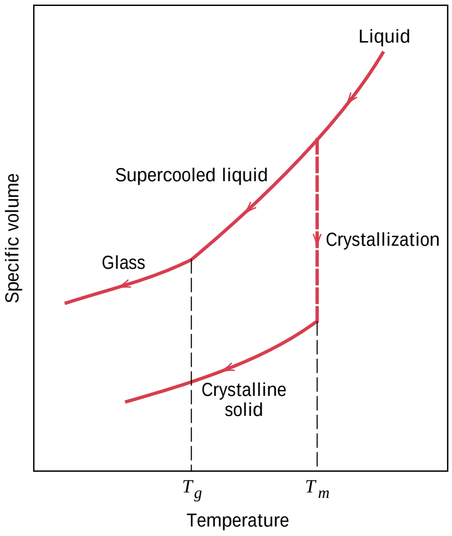

FIGURE 14.15 Contrast of specific volume-versus-temperature behavior of crystalline and noncrystalline materials. Crystalline materials solidify at the melting temperature T_m. Characteristic of the noncrystalline state is the glass transition temperature T_g.

viscosity scale several specific points that are important in the fabrication and processing of glasses are labeled:

1. The **melting point** corresponds to the temperature at which the viscosity is 10 Pa-s (100 P); the glass is fluid enough to be considered a liquid.
2. The **working point** represents the temperature at which the viscosity is 10^3 Pa-s (10^4 P); the glass is easily deformed at this viscosity.

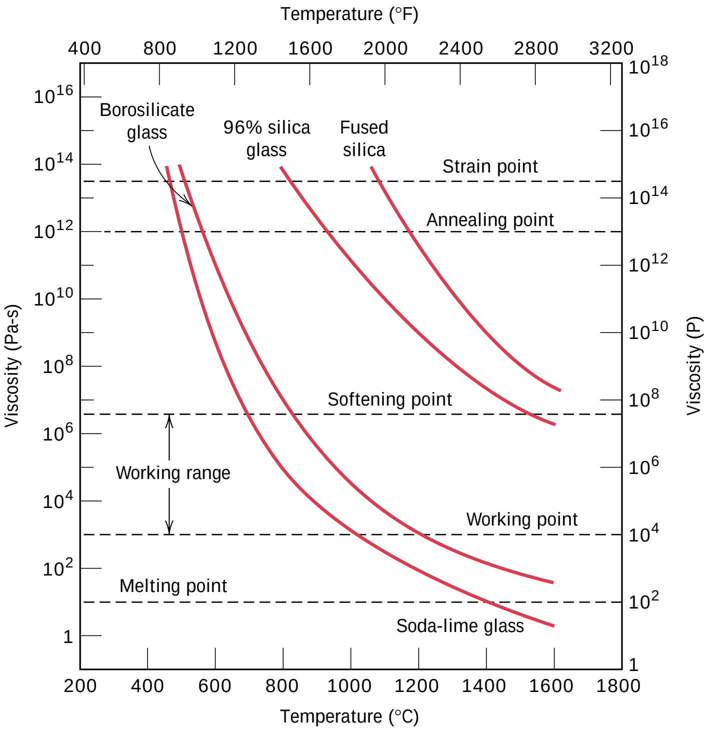

FIGURE 14.16 Logarithm of viscosity versus temperature for fused silica and several silica glasses. (From E. B. Shand, *Engineering Glass, Modern Materials,* Vol. 6, Academic Press, New York, 1968, p. 262.)

3. The **softening point,** the temperature at which the viscosity is 4 × 10^6 Pa-s (4 × 10^7 P), is the maximum temperature at which a glass piece may be handled without causing significant dimensional alterations.
4. The **annealing point** is the temperature at which the viscosity is 10^{12} Pa-s (10^{13} P); at this temperature, atomic diffusion is sufficiently rapid that any residual stresses may be removed within about 15 min.
5. The **strain point** corresponds to the temperature at which the viscosity becomes 3 × 10^{13} Pa-s (3 × 10^{14} P); for temperatures below the strain point, fracture will occur before the onset of plastic deformation. The glass transition temperature will be above the strain point.

Most glass-forming operations are carried out within the working range—between the working and softening temperatures.

Of course, the temperature at which each of these points occurs depends on glass composition. For example, the softening points for soda–lime and 96% silica glasses from Figure 14.16 are about 700 and 1550°C (1300 and 2825°F), respectively. That is, forming operations may be carried out at significantly lower temperatures for the soda–lime glass. The formability of a glass is tailored to a large degree by its composition.

GLASS FORMING

Glass is produced by heating the raw materials to an elevated temperature above which melting occurs. Most commercial glasses are of the silica–soda–lime variety; the silica is usually supplied as common quartz sand, whereas Na_2O and CaO are added as soda ash (Na_2CO_3) and limestone ($CaCO_3$). For most applications, especially when optical transparency is important, it is essential that the glass product be homogeneous and pore free. Homogeneity is achieved by complete melting and mixing of the raw ingredients. Porosity results from small gas bubbles that are produced; these must be absorbed into the melt or otherwise eliminated, which requires proper adjustment of the viscosity of the molten material.

Four different forming methods are used to fabricate glass products: pressing, blowing, drawing, and fiber forming. Pressing is used in the fabrication of relatively thick-walled pieces such as plates and dishes. The glass piece is formed by pressure application in a graphite-coated cast iron mold having the desired shape; the mold is ordinarily heated to ensure an even surface.

Although some glass blowing is done by hand, especially for art objects, the process has been completely automated for the production of glass jars, bottles, and light bulbs. The several steps involved in one such technique are illustrated in Figure 14.17. From a raw gob of glass, a *parison*, or temporary shape, is formed by mechanical pressing in a mold. This piece is inserted into a finishing or blow mold and forced to conform to the mold contours by the pressure created from a blast of air.

Drawing is used to form long glass pieces such as sheet, rod, tubing, and fibers, which have a constant cross section. One process by which sheet glass is formed is illustrated in Figure 14.18; it may also be fabricated by hot rolling. Flatness and the surface finish may be improved significantly by floating the sheet on a bath of molten tin at an elevated temperature; the piece is slowly cooled and subsequently heat treated by annealing.

Continuous glass fibers are formed in a rather sophisticated drawing operation. The molten glass is contained in a platinum heating chamber. Fibers are formed

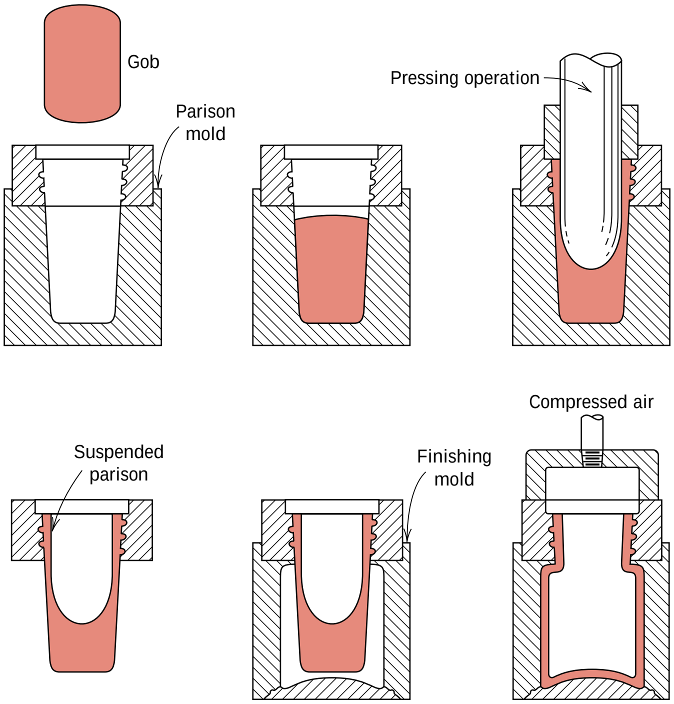
Gob
Parison mold
Pressing operation
Suspended parison
Finishing mold
Compressed air

Figure 14.17 The press-and-blow technique for producing a glass bottle. (Adapted from C. J. Phillips, *Glass: The Miracle Maker*. Reproduced by permission of Pitman Publishing Ltd., London.)

by drawing the molten glass through many small orifices at the chamber base. The glass viscosity, which is critical, is controlled by chamber and orifice temperatures.

HEAT TREATING GLASSES

Annealing

When a ceramic material is cooled from an elevated temperature, internal stresses, called thermal stresses, may be introduced as a result of the difference in cooling rate and thermal contraction between the surface and interior regions. These thermal stresses are important in brittle ceramics, especially glasses, since they may weaken the material or, in extreme cases, lead to fracture, which is termed **thermal**

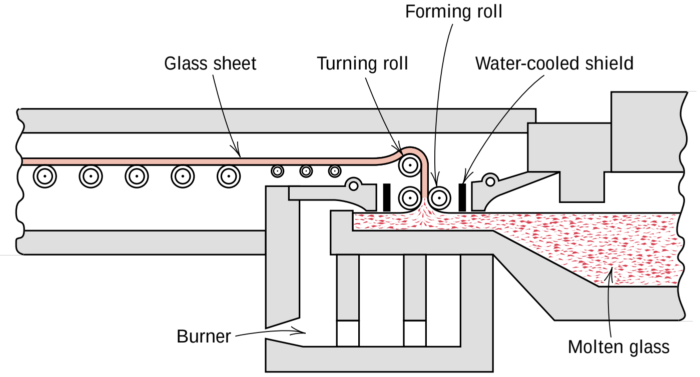
Forming roll
Glass sheet
Turning roll
Water-cooled shield
Burner
Molten glass

Figure 14.18 A process for the continuous drawing of sheet glass. (From W. D. Kingery, *Introduction to Ceramics*. Copyright © 1960 by John Wiley & Sons, New York. Reprinted by permission of John Wiley & Sons, Inc.)

shock (see Section 17.5). Normally, attempts are made to avoid thermal stresses, which may be accomplished by cooling the piece at a sufficiently slow rate. Once such stresses have been introduced, however, elimination, or at least a reduction in their magnitude, is possible by an annealing heat treatment in which the glassware is heated to the annealing point, then slowly cooled to room temperature.

Glass Tempering

The strength of a glass piece may be enhanced by intentionally inducing compressive residual surface stresses. This can be accomplished by a heat treatment procedure called **thermal tempering.** With this technique, the glassware is heated to a temperature above the glass transition region yet below the softening point. It is then cooled to room temperature in a jet of air or, in some cases, an oil bath. The residual stresses arise from differences in cooling rates for surface and interior regions. Initially, the surface cools more rapidly and, once having dropped to a temperature below the strain point, becomes rigid. At this time, the interior, having cooled less rapidly, is at a higher temperature (above the strain point) and, therefore, is still plastic. With continued cooling, the interior attempts to contract to a greater degree than the now rigid exterior will allow. Thus, the inside tends to draw in the outside, or to impose inward radial stresses. As a consequence, after the glass piece has cooled to room temperature, it sustains compressive stresses on the surface, with tensile stresses at interior regions. The room-temperature stress distribution over a cross section of a glass plate is represented schematically in Figure 14.19.

The failure of ceramic materials almost always results from a crack that is initiated at the surface by an applied tensile stress. To cause fracture of a tempered glass piece, the magnitude of an externally applied tensile stress must be great enough to first overcome the residual compressive surface stress and, in addition, to stress the surface in tension sufficiently to initiate a crack, which may then propagate. For an untempered glass, a crack will be introduced at a lower external stress level, and, consequently, the fracture strength will be smaller.

Tempered glass is used for applications in which high strength is important; these include large doors, automobile windshields, and eyeglass lenses.

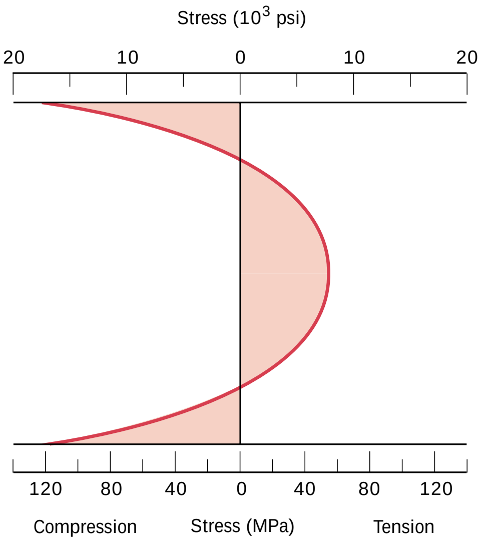

Figure 14.19 Room-temperature residual stress distribution over the cross section of a tempered glass plate. (From W. D. Kingery, H. K. Bowen, and D. R. Uhlmann, *Introduction to Ceramics,* 2nd edition. Copyright © 1976 by John Wiley & Sons, New York. Reprinted by permission of John Wiley & Sons, Inc.)

14.8 FABRICATION OF CLAY PRODUCTS

As Section 13.6 noted, this class of materials includes the structural clay products and the whitewares. In addition to clay, many of these products also contain other ingredients. After having been formed, pieces most often must be subjected to drying and firing operations; each of the ingredients influences the changes that take place during these processes and the characteristics of the finished piece.

THE CHARACTERISTICS OF CLAY

The clay minerals play two very important roles in ceramic bodies. First, when water is added, they become very plastic, a condition termed hydroplasticity. This property is very important in forming operations, as discussed below. In addition, clay fuses or melts over a range of temperatures; thus, a dense and strong ceramic piece may be produced during firing without complete melting such that the desired shape is maintained. This fusion temperature range, of course, depends on the composition of the clay.

Clays are aluminosilicates, being composed of alumina (Al_2O_3) and silica (SiO_2), that contain chemically bound water. They have a broad range of physical characteristics, chemical compositions, and structures; common impurities include compounds (usually oxides) of barium, calcium, sodium, potassium, and iron, and also some organic matter. Crystal structures for the clay minerals are relatively complicated; however, one prevailing characteristic is a layered structure. The most common clay minerals that are of interest have what is called the kaolinite structure. Kaolinite clay [$Al_2(Si_2O_5)(OH)_4$] has the crystal structure shown in Figure 3.14. When water is added, the water molecules fit in between these layered sheets and form a thin film around the clay particles. The particles are thus free to move over one another, which accounts for the resulting plasticity of the water–clay mixture.

COMPOSITIONS OF CLAY PRODUCTS

In addition to clay, many of these products (in particular the whitewares) also contain some nonplastic ingredients; the nonclay minerals include flint, or finely ground quartz, and a flux such as feldspar. The quartz is used primarily as a filler material, being inexpensive, relatively hard, and chemically unreactive. It experiences little change during high-temperature heat treatment because it has a high melting temperature; when melted, however, quartz has the ability to form a glass.

When mixed with clay, a flux forms a glass that has a relatively low melting point. The feldspars are some of the more common fluxing agents; they are a group of aluminosilicate materials that contain K^+, Na^+, and Ca^{2+} ions.

As would be expected, the changes that take place during drying and firing processes, and also the characteristics of the finished piece, are influenced by the proportions of these three constituents: clay, quartz, and flux. A typical porcelain might contain approximately 50% clay, 25% quartz, and 25% feldspar.

FABRICATION TECHNIQUES

The as-mined raw materials usually have to go through a milling or grinding operation in which particle size is reduced; this is followed by screening or sizing to yield a powdered product having a desired range of particle sizes. For multicomponent systems, powders must be thoroughly mixed with water and perhaps other ingredients to give flow characteristics that are compatible with the particular forming technique. The formed piece must have sufficient mechanical strength to remain intact during transporting, drying, and firing operations. Two common shaping techniques are utilized for forming clay-based compositions: **hydroplastic forming** and **slip casting.**

Hydroplastic Forming

As mentioned above, clay minerals, when mixed with water, become highly plastic and pliable and may be molded without cracking; however, they have extremely low yield strengths. The consistency (water–clay ratio) of the hydroplastic mass must give a yield strength sufficient to permit a formed ware to maintain its shape during handling and drying.

The most common hydroplastic forming technique is extrusion, in which a stiff plastic ceramic mass is forced through a die orifice having the desired cross-sectional geometry; it is similar to the extrusion of metals (Figure 14.2*c*). Brick, pipe, ceramic blocks, and tiles are all commonly fabricated using hydroplastic forming. Usually the plastic ceramic is forced through the die by means of a motor-driven auger, and often air is removed in a vacuum chamber to enhance the density. Hollow internal columns in the extruded piece (e.g., building brick) are formed by inserts situated within the die.

Slip Casting

Another forming process used for clay-based compositions is slip casting. A slip is a suspension of clay and/or other nonplastic materials in water. When poured into a porous mold (commonly made of plaster of paris), water from the slip is absorbed into the mold, leaving behind a solid layer on the mold wall the thickness of which depends on the time. This process may be continued until the entire mold cavity becomes solid (solid casting), as demonstrated in Figure 14.20*a*. Or it may be

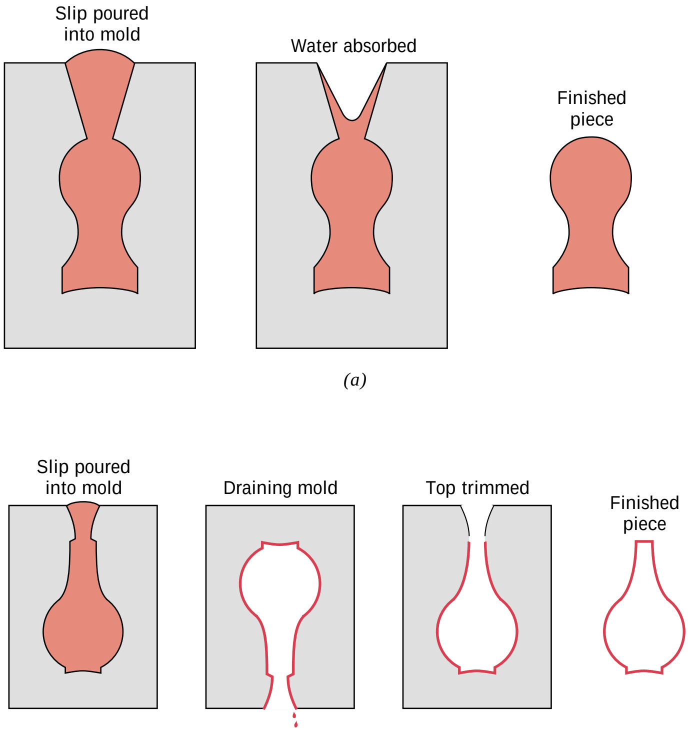

(*a*)

(*b*)

Figure 14.20 The steps in (*a*) solid and (*b*) drain slip casting using a plaster of paris mold. (From W. D. Kingery, *Introduction to Ceramics.* Copyright © 1960 by John Wiley & Sons, New York. Reprinted by permission of John Wiley & Sons, Inc.)

terminated when the solid shell wall reaches the desired thickness, by inverting the mold and pouring out the excess slip; this is termed drain casting (Figure 14.20*b*). As the cast piece dries and shrinks, it will pull away (or release) from the mold wall; at this time the mold may be disassembled and the cast piece removed.

The nature of the slip is extremely important; it must have a high specific gravity and yet be very fluid and pourable. These characteristics depend on the solid-to-water ratio and other agents that are added. A satisfactory casting rate is an essential requirement. In addition, the cast piece must be free of bubbles, and it must have a low drying shrinkage and a relatively high strength.

The properties of the mold itself influence the quality of the casting. Normally, plaster of paris, which is economical, relatively easy to fabricate into intricate shapes, and reusable, is used as the mold material. Most molds are multipiece items that must be assembled before casting. Also, the mold porosity may be varied to control the casting rate. The rather complex ceramic shapes that may be produced by means of slip casting include sanitary lavatory ware, art objects, and specialized scientific laboratory ware such as ceramic tubes.

DRYING AND FIRING

A ceramic piece that has been formed hydroplastically or by slip casting retains significant porosity and insufficient strength for most practical applications. In addition, it may still contain some liquid (e.g., water), which was added to assist in the forming operation. This liquid is removed in a drying process; density and strength are enhanced as a result of a high-temperature heat treatment or firing procedure. A body that has been formed and dried but not fired is termed **green.** Drying and firing techniques are critical inasmuch as defects that ordinarily render the ware useless (e.g., warpage, distortion, and cracks) may be introduced during the operation. These defects normally result from stresses that are set up from nonuniform shrinkage.

Drying

As a clay-based ceramic body dries, it also experiences some shrinkage. In the early stages of drying the clay particles are virtually surrounded by and separated from one another by a thin film of water. As drying progresses and water is removed, the interparticle separation decreases, which is manifested as shrinkage (Figure 14.21). During drying it is critical to control the rate of water removal. Drying at interior regions of a body is accomplished by the diffusion of water molecules to

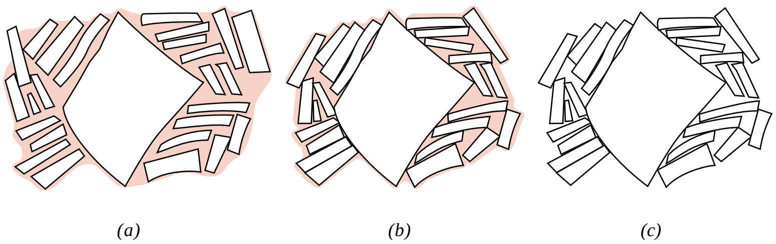
(*a*) (*b*) (*c*)

FIGURE 14.21 Several stages in the removal of water from between clay particles during the drying process. (*a*) Wet body. (*b*) Partially dry body. (*c*) Completely dry body. (From W. D. Kingery, *Introduction to Ceramics.* Copyright © 1960 by John Wiley & Sons, New York. Reprinted by permission of John Wiley & Sons, Inc.)

the surface where evaporation occurs. If the rate of evaporation is greater than the rate of diffusion, the surface will dry (and as a consequence shrink) more rapidly than the interior, with a high probability of the formation of the aforementioned defects. The rate of surface evaporation should be diminished to, at most, the rate of water diffusion; evaporation rate may be controlled by temperature, humidity, and the rate of airflow.

Other factors also influence shrinkage. One of these is body thickness; nonuniform shrinkage and defect formation are more pronounced in thick pieces than in thin ones. Water content of the formed body is also critical: the greater the water content, the more extensive the shrinkage. Consequently, the water content is ordinarily kept as low as possible. Clay particle size also has an influence; shrinkage is enhanced as the particle size is decreased. To minimize shrinkage, the size of the particles may be increased, or nonplastic materials having relatively large particles may be added to the clay.

Microwave energy may also be used to dry ceramic wares. One advantage of this technique is that the high temperatures used in conventional methods are avoided; drying temperatures may be kept to below 50°C (120°F). This is important because the drying of some temperature-sensitive materials should be kept as low as possible.

Firing

After drying, a body is usually fired at a temperature between 900 and 1400°C (1650 and 2550°F); the firing temperature depends on the composition and desired properties of the finished piece. During the firing operation, the density is further increased (with an attendant decrease in porosity) and the mechanical strength is enhanced.

When clay-based materials are heated to elevated temperatures, some rather complex and involved reactions occur. One of these is **vitrification,** the gradual formation of a liquid glass that flows into and fills some of the pore volume. The degree of vitrification depends on firing temperature and time, as well as the composition of the body. The temperature at which the liquid phase forms is lowered by the addition of fluxing agents such as feldspar. This fused phase flows around the remaining unmelted particles and fills in the pores as a result of surface tension forces (or capillary action); shrinkage also accompanies this process. Upon cooling, this fused phase forms a glassy matrix that results in a dense, strong body. Thus, the final microstructure consists of the vitrified phase, any unreacted quartz particles, and some porosity. Figure 14.22 is a scanning electron micrograph of a fired porcelain in which may be seen these microstructural elements.

The degree of vitrification, of course, controls the room-temperature properties of the ceramic ware; strength, durability, and density are all enhanced as it increases. The firing temperature determines the extent to which vitrification occurs; that is, vitrification increases as the firing temperature is raised. Building bricks are ordinarily fired around 900°C (1650°F) and are relatively porous. On the other hand, firing of highly vitrified porcelain, which borders on being optically translucent, takes place at much higher temperatures. Complete vitrification is avoided during firing, since a body becomes too soft and will collapse.

14.9 POWDER PRESSING

Several ceramic-forming techniques have already been discussed relative to the fabrication of glass and clay products. Another important and commonly used

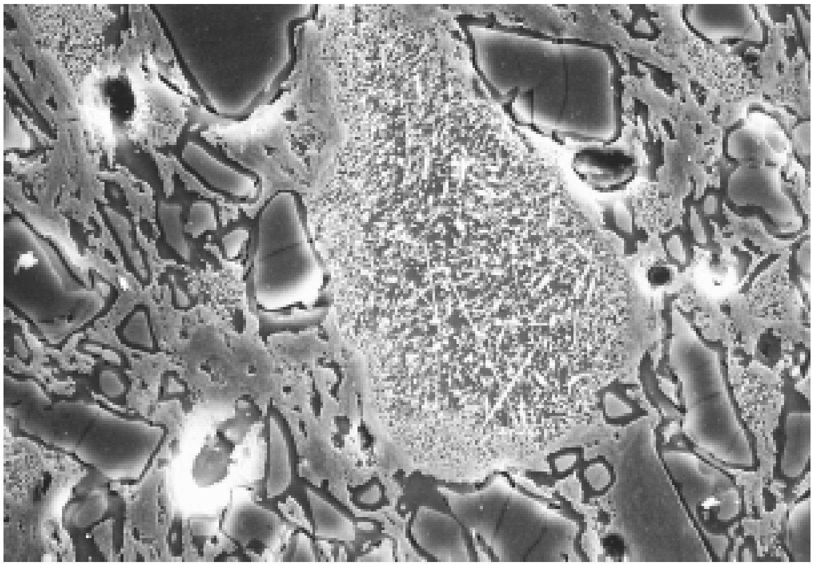

FIGURE 14.22 Scanning electron micrograph of a fired porcelain specimen (etched 15 s, 5°C, 10% HF) in which may be seen the following features: quartz grains (large dark particles) which are surrounded by dark glassy solution rims; partially dissolved feldspar regions (small unfeatured areas); mullite needles; and pores (dark holes with white border regions). Also, cracks within the quartz particles may be noted, which were formed during cooling, as a result of the difference in shrinkage between the glassy matrix and the quartz. 1500×. (Courtesy of H. G. Brinkies, Swinburne University of Technology, Hawthorn Campus, Hawthorn, Victoria, Australia.)

method that warrants a brief treatment is powder pressing. Powder pressing, the ceramic analogue to powder metallurgy, is used to fabricate both clay and nonclay compositions, including electronic and magnetic ceramics as well as some refractory brick products. In essence, a powdered mass, usually containing a small amount of water or other binder, is compacted into the desired shape, by pressure. The degree of compaction is maximized and fraction of void space is minimized by using coarse and fine particles mixed in appropriate proportions. There is no plastic deformation of the particles during compaction, as there may be with metal powders. One function of the binder is to lubricate the powder particles as they move past one another in the compaction process.

There are three basic powder pressing procedures: uniaxial, isostatic (or hydrostatic), and hot pressing. For uniaxial pressing, the powder is compacted in a metal die by pressure that is applied in a single direction. The formed piece takes on the configuration of die and platens through which the pressure is applied. This method is confined to shapes that are relatively simple; however, production rates are high and the process is inexpensive. The steps involved in one technique are illustrated in Figure 14.23.

For isostatic pressing, the powdered material is contained in a rubber envelope and the pressure is applied by a fluid, isostatically (i.e., it has the same magnitude in all directions). More complicated shapes are possible than with uniaxial pressing; however, the isostatic technique is more time consuming and expensive.

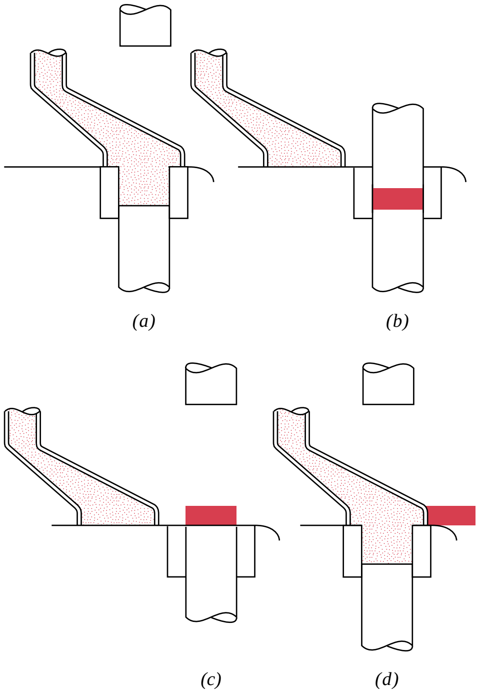

FIGURE 14.23 Schematic representation of the steps in uniaxial powder pressing. (*a*) The die cavity is filled with powder. (*b*) The powder is compacted by means of pressure applied to the top die. (*c*) The compacted piece is ejected by rising action of the bottom punch. (*d*) The fill shoe pushes away the compacted piece, and the fill step is repeated. (From W. D. Kingery, Editor, *Ceramic Fabrication Processes*, MIT Press. Copyright © 1958 by the Massachusetts Institute of Technology.)

For both uniaxial and isostatic procedures, a firing operation is required after the pressing operation. During firing the formed piece shrinks, and experiences a reduction of porosity and an improvement in mechanical integrity. These changes occur by the coalescence of the powder particles into a more dense mass in a process termed **sintering.** The mechanism of sintering is schematically illustrated in Figure 14.24. After pressing, many of the powder particles touch one another (Figure 14.24*a*). During the initial sintering stage, necks form along the contact regions between adjacent particles; in addition, a grain boundary forms within each neck, and every interstice between particles becomes a pore (Figure 14.24*b*). As sintering progresses, the pores become smaller and more spherical in shape (Figure 14.24*c*). A scanning electron micrograph of a sintered alumina material is shown in Figure 14.25. The driving force for sintering is the reduction in total particle surface area; surface energies are larger in magnitude than grain boundary energies. Sintering is carried out below the melting temperature so that a liquid phase is normally not present. Mass transport necessary to effect the changes shown in Figure 14.24 is accomplished by atomic diffusion from the bulk particles to the neck regions.

With hot pressing, the powder pressing and heat treatment are performed simultaneously—the powder aggregate is compacted at an elevated temperature. The procedure is used for materials that do not form a liquid phase except at very high and impractical temperatures; in addition, it is utilized when high densities without appreciable grain growth are desired. This is an expensive fabrication technique that has some limitations. It is costly in terms of time, since both mold and die must be heated and cooled during each cycle. In addition, the mold is usually expensive to fabricate and ordinarily has a short lifetime.

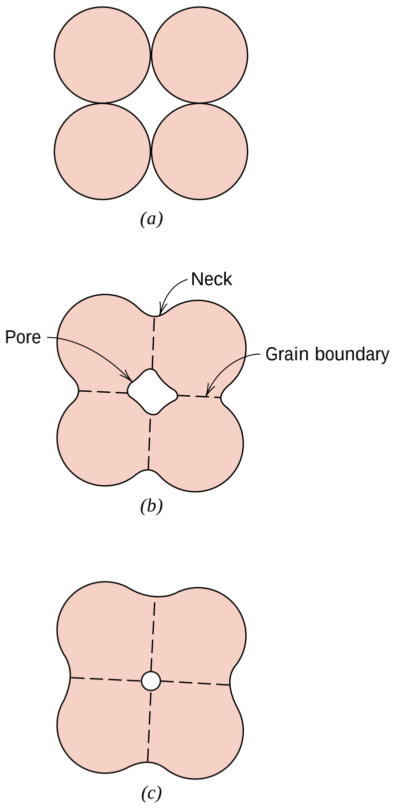

FIGURE 14.24 For a powder compact, microstructural changes that occur during firing. (*a*) Powder particles after pressing. (*b*) Particle coalescence and pore formation as sintering begins. (*c*) As sintering proceeds, the pores change size and shape.

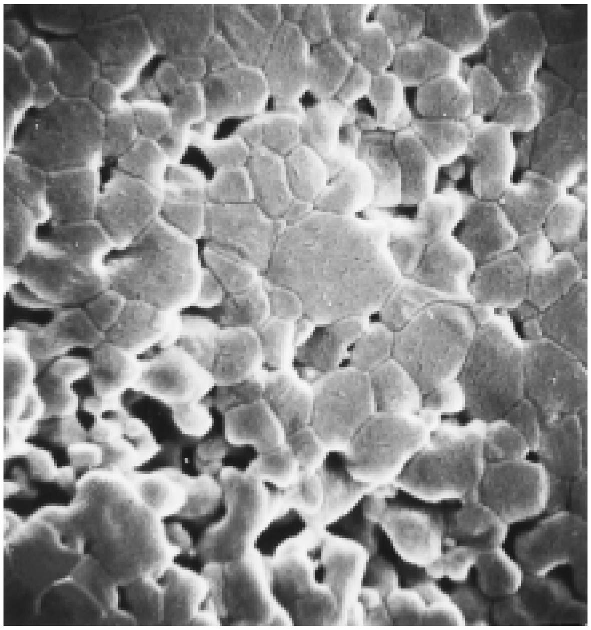

FIGURE 14.25 Scanning electron micrograph of an aluminum oxide powder compact that was sintered at 1700°C for 6 min. 5000×. (From W. D. Kingery, H. K. Bowen, and D. R. Uhlmann, *Introduction to Ceramics*, 2nd edition, p. 483. Copyright © 1976 by John Wiley & Sons, New York. Reprinted by permission of John Wiley & Sons, Inc.)

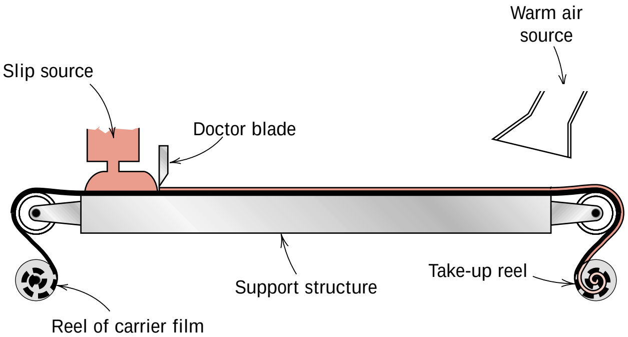

Figure 14.26 Schematic diagram showing the tape casting process using a doctor blade. (From D. W. Richerson, *Modern Ceramic Engineering,* 2nd edition, Marcel Dekker, Inc., NY, 1992. Reprinted from *Modern Ceramic Engineering,* 2nd edition, p. 472 by courtesy of Marcel Dekker, Inc.)

14.10 Tape Casting

A relatively new and important ceramic fabrication technique, tape casting, will now be briefly discussed. As the name implies, thin sheets of a flexible tape are produced by means of a casting process. These sheets are prepared from slips, in many respects similar to those that are employed for slip casting (Section 14.8). This type of slip consists of a suspension of ceramic particles in an organic liquid that also contains binders and plasticizers that are incorporated to impart strength and flexibility to the cast tape. De-airing in a vacuum may also be necessary to remove any entrapped air or solvent vapor bubbles, which may act as crack-initiation sites in the finished piece. The actual tape is formed by pouring the slip onto a flat surface (of stainless steel, glass, a polymeric film, or paper); a doctor blade spreads the slip into a thin tape of uniform thickness, as shown schematically in Figure 14.26. In the drying process, volatile slip components are removed by evaporation; this green product is a flexible tape that may be cut or into which holes may be punched prior to a firing operation. Tape thicknesses normally range between 0.1 and 2 mm (0.004 to 0.08 in.). Tape casting is widely used in the production of ceramic substrates that are used for integrated circuits and for multilayered capacitors.

Cementation is also considered to be a ceramic fabrication process (Figure 14.14). The cement material, when mixed with water, forms a paste that, after being fashioned into a desired shape, subsequently hardens as a result of complex chemical reactions. Cements and the cementation process were discussed briefly in Section 13.9.

SYNTHESIS AND FABRICATION OF POLYMERS

The large macromolecules of the commercially useful polymers must be synthesized from substances having smaller molecules in a process termed polymerization. Furthermore, the properties of a polymer may be modified and enhanced by the inclusion of additive materials. Finally, a finished piece having a desired shape must be fashioned during a forming operation. This section treats polymerization processes and the various forms of additives, as well as specific forming procedures.

14.11 POLYMERIZATION

The synthesis of the large molecular weight polymers is termed *polymerization;* it is simply the process by which monomer units are joined over and over, to generate each of the constituent giant molecules. Most generally, the raw materials for synthetic polymers are derived from coal and petroleum products, which are composed of molecules having low molecular weights. The reactions by which polymerization occurs are grouped into two general classifications—addition and condensation—according to the reaction mechanism, as discussed below.

ADDITION POLYMERIZATION

Addition polymerization (sometimes called *chain reaction polymerization*) is a process by which bifunctional monomer units are attached one at a time in chainlike fashion to form a linear macromolecule; the composition of the resultant product molecule is an exact multiple for that of the original reactant monomer.

Three distinct stages—initiation, propagation, and termination—are involved in addition polymerization. During the initiation step, an active center capable of propagation is formed by a reaction between an initiator (or catalyst) species and the monomer unit. This process has already been demonstrated for polyethylene (Equation 4.1), which is repeated as follows:

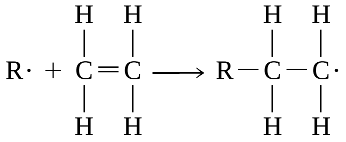

$$\mathrm{R\cdot} + \underset{\mathrm{H}}{\overset{\mathrm{H}}{\mathrm{C}}}{=}\underset{\mathrm{H}}{\overset{\mathrm{H}}{\mathrm{C}}} \longrightarrow \mathrm{R}-\underset{\mathrm{H}}{\overset{\mathrm{H}}{\mathrm{C}}}-\underset{\mathrm{H}}{\overset{\mathrm{H}}{\mathrm{C}}}\cdot \qquad (14.1)$$

Again, R· represents the active initiator, and · is an unpaired electron.

Propagation involves the linear growth of the molecule as monomer units become attached to one another in succession to produce the chain molecule, which is represented, again for polyethylene, as follows:

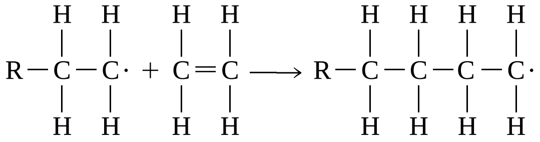

$$\mathrm{R}-\underset{\mathrm{H}}{\overset{\mathrm{H}}{\mathrm{C}}}-\underset{\mathrm{H}}{\overset{\mathrm{H}}{\mathrm{C}}}\cdot + \underset{\mathrm{H}}{\overset{\mathrm{H}}{\mathrm{C}}}{=}\underset{\mathrm{H}}{\overset{\mathrm{H}}{\mathrm{C}}} \longrightarrow \mathrm{R}-\underset{\mathrm{H}}{\overset{\mathrm{H}}{\mathrm{C}}}-\underset{\mathrm{H}}{\overset{\mathrm{H}}{\mathrm{C}}}-\underset{\mathrm{H}}{\overset{\mathrm{H}}{\mathrm{C}}}-\underset{\mathrm{H}}{\overset{\mathrm{H}}{\mathrm{C}}}\cdot \qquad (14.2)$$

Chain growth is relatively rapid; the period required to grow a molecule consisting of, say, 1000 mer units is on the order of 10^{-2} to 10^{-3} s.

Propagation may end or terminate in different ways. First, the active ends of two propagating chains may react or link together to form a nonreactive molecule, as follows:

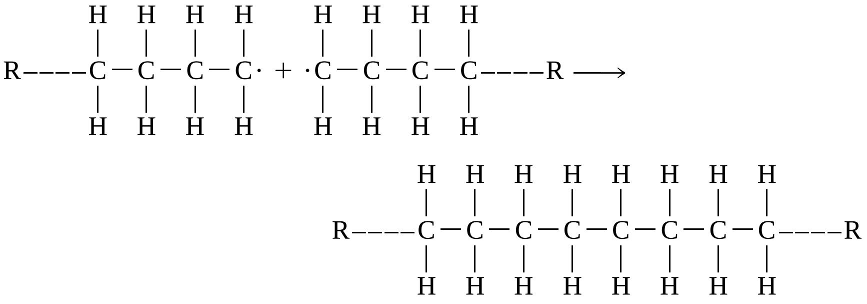

$$\mathrm{R}{----}\underset{\mathrm{H}}{\overset{\mathrm{H}}{\mathrm{C}}}-\underset{\mathrm{H}}{\overset{\mathrm{H}}{\mathrm{C}}}-\underset{\mathrm{H}}{\overset{\mathrm{H}}{\mathrm{C}}}-\underset{\mathrm{H}}{\overset{\mathrm{H}}{\mathrm{C}}}\cdot + \cdot\underset{\mathrm{H}}{\overset{\mathrm{H}}{\mathrm{C}}}-\underset{\mathrm{H}}{\overset{\mathrm{H}}{\mathrm{C}}}-\underset{\mathrm{H}}{\overset{\mathrm{H}}{\mathrm{C}}}-\underset{\mathrm{H}}{\overset{\mathrm{H}}{\mathrm{C}}}{----}\mathrm{R} \longrightarrow$$

$$\mathrm{R}{----}\underset{\mathrm{H}}{\overset{\mathrm{H}}{\mathrm{C}}}-\underset{\mathrm{H}}{\overset{\mathrm{H}}{\mathrm{C}}}-\underset{\mathrm{H}}{\overset{\mathrm{H}}{\mathrm{C}}}-\underset{\mathrm{H}}{\overset{\mathrm{H}}{\mathrm{C}}}-\underset{\mathrm{H}}{\overset{\mathrm{H}}{\mathrm{C}}}-\underset{\mathrm{H}}{\overset{\mathrm{H}}{\mathrm{C}}}-\underset{\mathrm{H}}{\overset{\mathrm{H}}{\mathrm{C}}}-\underset{\mathrm{H}}{\overset{\mathrm{H}}{\mathrm{C}}}{----}\mathrm{R} \qquad (14.3)$$

thus terminating the growth of each chain. Or, an active chain end may react with an initiator or other chemical species having a single active bond, as follows:

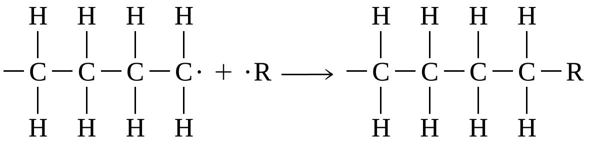

$$-\underset{\mathrm{H}}{\overset{\mathrm{H}}{\mathrm{C}}}-\underset{\mathrm{H}}{\overset{\mathrm{H}}{\mathrm{C}}}-\underset{\mathrm{H}}{\overset{\mathrm{H}}{\mathrm{C}}}-\underset{\mathrm{H}}{\overset{\mathrm{H}}{\mathrm{C}}}\cdot + \cdot\mathrm{R} \longrightarrow -\underset{\mathrm{H}}{\overset{\mathrm{H}}{\mathrm{C}}}-\underset{\mathrm{H}}{\overset{\mathrm{H}}{\mathrm{C}}}-\underset{\mathrm{H}}{\overset{\mathrm{H}}{\mathrm{C}}}-\underset{\mathrm{H}}{\overset{\mathrm{H}}{\mathrm{C}}}-\mathrm{R}$$

(14.4)

with the resultant cessation of chain growth.

Molecular weight is governed by the relative rates of initiation, propagation, and termination. Ordinarily, they are controlled to ensure the production of a polymer having the desired degree of polymerization.

Addition polymerization is used in the synthesis of polyethylene, polypropylene, polyvinyl chloride, and polystyrene, as well as many of the copolymers.

CONDENSATION POLYMERIZATION

Condensation (or *step reaction*) **polymerization** is the formation of polymers by stepwise intermolecular chemical reactions that normally involve more than one monomer species; there is usually a small molecular weight by-product such as water, which is eliminated. No reactant species has the chemical formula of the mer repeat unit, and the intermolecular reaction occurs every time a mer repeat unit is formed. For example, consider the formation of a polyester from the reaction between ethylene glycol and adipic acid; the intermolecular reaction is as follows:

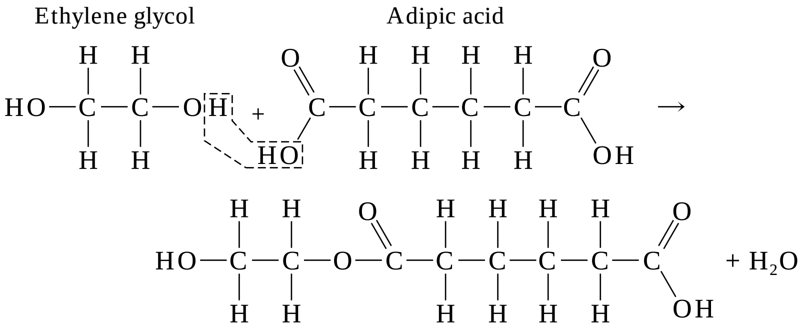

(14.5)

This stepwise process is successively repeated, producing, in this case, a linear molecule. The chemistry of the specific reaction is not important, but rather, the condensation polymerization mechanism. Furthermore, reaction times for condensation are generally longer than for addition polymerization.

Condensation reactions often produce trifunctional monomers capable of forming crosslinked and network polymers. The thermosetting polyesters and phenol-formaldehyde, the nylons, and the polycarbonates are produced by condensation polymerization. Some polymers, such as nylon, may be polymerized by either technique.

14.12 POLYMER ADDITIVES

Most of the properties of polymers discussed in previous chapters are intrinsic ones—that is, characteristic of or fundamental to the specific polymer. Some of these properties are related to and controlled by the molecular structure. Many times, however, it is necessary to modify the mechanical, chemical, and physical properties to a much greater degree than is possible by the simple alteration of this fundamental molecular structure. Foreign substances called *additives* are intentionally introduced to enhance or modify many of these properties, and thus render a polymer more serviceable. Typical additives include filler materials, plasticizers, stabilizers, colorants, and flame retardants.

FILLERS

Filler materials are most often added to polymers to improve tensile and compressive strengths, abrasion resistance, toughness, dimensional and thermal stability, and other properties. Materials used as particulate fillers include wood flour (finely powdered sawdust), silica flour and sand, glass, clay, talc, limestone, and even some synthetic polymers. Particle sizes range all the way from 10 nm to macroscopic dimensions. Because these inexpensive materials replace some volume of the more expensive polymer, the cost of the final product is reduced.

PLASTICIZERS

The flexibility, ductility, and toughness of polymers may be improved with the aid of additives called **plasticizers.** Their presence also produces reductions in hardness and stiffness. Plasticizers are generally liquids having low vapor pressures and low molecular weights. The small plasticizer molecules occupy positions between the large polymer chains, effectively increasing the interchain distance with a reduction in the secondary intermolecular bonding. Plasticizers are commonly used in polymers that are intrinsically brittle at room temperature, such as polyvinyl chloride and some of the acetate copolymers. In effect, the plasticizer lowers the glass transition temperature, so that at ambient conditions the polymers may be used in applications requiring some degree of pliability and ductility. These applications include thin sheets or films, tubing, raincoats, and curtains.

STABILIZERS

Some polymeric materials, under normal environmental conditions, are subject to rapid deterioration, generally in terms of mechanical integrity. Most often, this deterioration is a result of exposure to light, in particular ultraviolet radiation, and also oxidation (Section 16.12). Ultraviolet radiation interacts with, and causes a severance of some of the covalent bonds along the molecular chain, which may also result in some crosslinking. Oxidation deterioration is a consequence of the chemical interaction between oxygen atoms and the polymer molecules. Additives that counteract these deteriorative processes are called **stabilizers.**

COLORANTS

Colorants impart a specific color to a polymer; they may be added in the form of dyes or pigments. The molecules in a dye actually dissolve and become part of the molecular structure of the polymer. Pigments are filler materials that do not dissolve, but remain as a separate phase; normally they have a small particle size, are transparent, and have a refractive index near to that of the parent polymer. Others may impart opacity as well as color to the polymer.

FLAME RETARDANTS

The flammability of polymeric materials is a major concern, especially in the manufacture of textiles and children's toys. Most polymers are flammable in their pure form; exceptions include those containing significant contents of chlorine and/or fluorine, such as polyvinyl chloride and polytetrafluoroethylene. The flammability resistance of the remaining combustible polymers may be enhanced by additives called **flame retardants.** These retardants may function by interfering with the combustion process through the gas phase, or by initiating a chemical reaction that causes a cooling of the combustion region and a cessation of burning.

14.13 FORMING TECHNIQUES FOR PLASTICS

Quite a variety of different techniques are employed in the forming of polymeric materials. The method used for a specific polymer depends on several factors: (1) whether the material is thermoplastic or thermosetting; (2) if thermoplastic, the temperature at which it softens; (3) the atmospheric stability of the material being formed; and (4) the geometry and size of the finished product. There are numerous similarities between some of these techniques and those utilized for fabricating metals and ceramics.

Fabrication of polymeric materials normally occurs at elevated temperatures and often by the application of pressure. Thermoplastics are formed above their glass transition temperatures, if amorphous, or above their melting temperatures, if semicrystalline; an applied pressure must be maintained as the piece is cooled so that the formed article will retain its shape. One significant economic benefit of using thermoplastics is that they may be recycled; scrap thermoplastic pieces may be remelted and reformed into new shapes.

Fabrication of thermosetting polymers is ordinarily accomplished in two stages. First comes the preparation of a linear polymer (sometimes called a prepolymer) as a liquid, having a low molecular weight. This material is converted into the final hard and stiff product during the second stage, which is normally carried out in a mold having the desired shape. This second stage, termed ‘‘curing,’’ may occur during heating and/or by the addition of catalysts, and often under pressure. During curing, chemical and structural changes occur on a molecular level: a crosslinked or a network structure forms. After curing, thermoset polymers may be removed from a mold while still hot, since they are now dimensionally stable. Thermosets are difficult to recycle, do not melt, are usable at higher temperatures than thermoplastics, and are more chemically inert.

Molding is the most common method for forming plastic polymers. The several molding techniques used include compression, transfer, blow, injection, and extrusion molding. For each, a finely pelletized or granulized plastic is forced, at an elevated temperature and by pressure, to flow into, fill, and assume the shape of a mold cavity.

COMPRESSION AND TRANSFER MOLDING

For compression molding, the appropriate amounts of thoroughly mixed polymer and necessary additives are placed between male and female mold members, as illustrated in Figure 14.27. Both mold pieces are heated; however, only one is movable. The mold is closed, and heat and pressure are applied, causing the plastic material to become viscous and conform to the mold shape. Before molding, raw materials may be mixed and cold pressed into a disc, which is called a preform. Preheating of the preform reduces molding time and pressure, extends the die lifetime, and produces a more uniform finished piece. This molding technique lends itself to the fabrication of both thermoplastic and thermosetting polymers; however, its use with thermoplastics is more time consuming and expensive.

In transfer molding, a variation of compression molding, the solid ingredients are first melted in a heated transfer chamber. As the molten material is injected

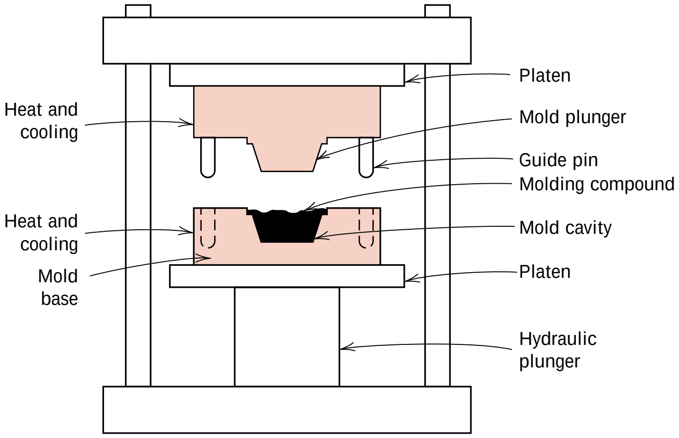
Heat and cooling
Heat and cooling
Mold base
Platen
Mold plunger
Guide pin
Molding compound
Mold cavity
Platen
Hydraulic plunger

Figure 14.27 Schematic diagram of a compression molding apparatus. (From F. W. Billmeyer, Jr., *Textbook of Polymer Science*, 3rd edition. Copyright © 1984 by John Wiley & Sons, New York. Reprinted by permission of John Wiley & Sons, Inc.)

into the mold chamber, the pressure is distributed more uniformly over all surfaces. This process is used with thermosetting polymers and for pieces having complex geometries.

INJECTION MOLDING

Injection molding, the polymer analogue of die casting for metals, is the most widely used technique for fabricating thermoplastic materials. A schematic cross section of the apparatus used is illustrated in Figure 14.28. The correct amount of pelletized material is fed from a loading hopper into a cylinder by the motion of a plunger or ram. This charge is pushed forward into a heating chamber, at which point the thermoplastic material melts to form a viscous liquid. Next, the molten plastic is impelled, again by ram motion, through a nozzle into the enclosed mold cavity; pressure is maintained until the molding has solidified. Finally, the mold is opened, the piece is ejected, the mold is closed, and the entire cycle is repeated. Probably the most outstanding feature of this technique is the speed with which pieces may be produced. For thermoplastics, solidification of the injected charge is almost immediate; consequently, cycle times for this process are short (commonly within the range of 10 to 30 s). Thermosetting polymers may also be injection molded; curing takes place while the material is under pressure in a heated mold, which

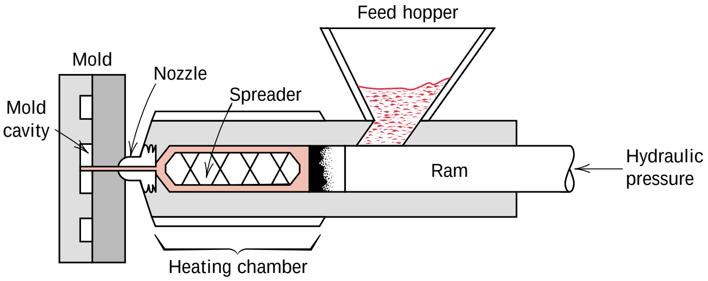
Feed hopper
Mold
Nozzle
Spreader
Mold cavity
Ram
Hydraulic pressure
Heating chamber

Figure 14.28 Schematic diagram of an injection molding apparatus. (Adapted from F. W. Billmeyer, Jr., *Textbook of Polymer Science*, 2nd edition. Copyright © 1971 by John Wiley & Sons, New York. Reprinted by permission of John Wiley & Sons, Inc.)

results in longer cycle times than for thermoplastics. This process is sometimes termed reaction injection molding (RIM).

EXTRUSION

The extrusion process is simply injection molding of a viscous thermoplastic through an open-ended die, similar to the extrusion of metals (Figure 14.2*c*). A mechanical screw or auger propels through a chamber the pelletized material, which is successively compacted, melted, and formed into a continuous charge of viscous fluid. Extrusion takes place as this molten mass is forced through a die orifice. Solidification of the extruded length is expedited by blowers or a water spray just before passing onto a moving conveyor. The technique is especially adapted to producing continuous lengths having constant cross-sectional geometries, for example, rods, tubes, hose channels, sheets, and filaments.

BLOW MOLDING

The blow molding process for the fabrication of plastic containers is similar to that used for blowing glass bottles, as represented in Figure 14.17. First, a parison, or length of polymer tubing is extruded. While still in a semimolten state, the parison is placed in a two-piece mold having the desired container configuration. The hollow piece is formed by blowing air or steam under pressure into the parison, forcing the tube walls to conform to the contours of the mold. Of course the temperature and viscosity of the parison must be carefully regulated.

CASTING

Like metals, polymeric materials may be cast, as when a molten plastic material is poured into a mold and allowed to solidify. Both thermoplastic and thermosetting plastics may be cast. For thermoplastics, solidification occurs upon cooling from the molten state; however, for thermosets, hardening is a consequence of the actual polymerization or curing process, which is usually carried out at an elevated temperature.

14.14 FABRICATION OF ELASTOMERS

Techniques used in the actual fabrication of rubber parts are essentially the same as those discussed for plastics as described above, that is, compression molding, extrusion, and so on. Furthermore, most rubber materials are vulcanized (Section 8.19) and some are reinforced with carbon black (Section 15.2).

14.15 FABRICATION OF FIBERS AND FILMS

FIBERS

The process by which fibers are formed from bulk polymer material is termed **spinning.** Most often, fibers are spun from the molten state in a process called melt spinning. The material to be spun is first heated until it forms a relatively viscous liquid. Next, it is pumped down through a plate called a spinnerette, which contains numerous small, round holes. As the molten material passes through each of these orifices, a single fiber is formed, which solidifies almost immediately upon passing into the air.

The crystallinity of a spun fiber will depend on its rate of cooling during spinning. The strength of fibers is improved by a postforming process called **drawing,** as discussed in Section 8.18. Again, drawing is simply the mechanical elongation of a fiber in the direction of its axis. During this process the molecular chains become oriented in the direction of drawing (Figure 8.27*e*), such that the tensile strength, modulus of elasticity, and toughness are improved. Although the mechanical strength of a drawn fiber is improved in this axial direction, strength is reduced in a transverse or radial direction. However, since fibers are normally stressed only along the axis, this strength differential is not critical. The cross section of drawn fibers is nearly circular, and the properties are uniform throughout the cross section.

FILMS

Many films are simply extruded through a thin die slit; this may be followed by a rolling operation that serves to reduce thickness and improve strength. Alternatively, film may be blown: continuous tubing is extruded through an annular die; then, by maintaining a carefully controlled positive gas pressure inside the tube, wall thickness may be continuously reduced to produce a thin cylindrical film, which may be cut and laid flat. Some of the newer films are produced by coextrusion; that is, multilayers of more than one polymer type are extruded simultaneously.

SUMMARY

This chapter began with a discussion of various fabrication techniques that may be applied to metallic materials. Forming operations are those in which a metal piece is shaped by plastic deformation. When deformation is carried out above the recrystallization temperature, it is termed hot working; otherwise, it is cold working. Forging, rolling, extrusion, and drawing are four of the more common forming techniques. Depending on the properties and shape of the finished piece, casting may be the most desirable and economical fabrication process; sand, die, investment, and continuous casting methods were also treated. Additional fabrication procedures, including powder metallurgy and welding, may be utilized alone or in combination with other methods.

Heat treatments that are used to fashion the mechanical properties of metal alloys were discussed. The exposure to an elevated temperature for an extended time period followed by cooling to room temperature at a relatively slow rate is termed annealing; several specific annealing treatments were discussed briefly. During process annealing, a cold-worked piece is rendered softer yet more ductile as a consequence of recrystallization. Internal residual stresses that have been introduced are eliminated during a stress relief anneal. For ferrous alloys, normalizing is used to refine and improve the grain structure. Fabrication characteristics may also be enhanced by full anneal and spheroidizing treatments that produce microstructures consisting of coarse pearlite and spheroidite, respectively.

For high-strength steels, the best combination of mechanical characteristics may be realized if a predominantly martensitic microstructure is developed over the entire cross section; this is converted to tempered martensite during a tempering heat treatment. Hardenability is a parameter used to ascertain the influence of composition on the susceptibility to the formation of a predominantly martensitic structure for some specific heat treatment. Determination of hardenability is accomplished by the standard Jominy end-quench test, from which hardenability curves are generated.

Other factors also influence the extent to which martensite will form. Of the common quenching media, water is the most efficient, followed by oil and air, in that order. The relationships between cooling rate and specimen size and geometry for a specific quenching medium frequently are expressed on empirical charts; two were introduced for cylindrical specimens. These may be used in conjunction with hardenability data to generate cross-sectional hardness profiles.

The next major section of this chapter discussed the principal techniques used for the fabrication of ceramic materials. Since glasses are formed at elevated temperatures, the temperature–viscosity behavior is an important consideration. Melting, working, softening, annealing, and strain points represent temperatures that correspond to specific viscosity values. Knowledge of these points is important in the fabrication and processing of a glass of given composition. Four of the more common glass-forming techniques—pressing, blowing, drawing, and fiber forming—were discussed briefly. After fabrication, glasses may be annealed and/or tempered to improve mechanical characteristics.

For clay products, two fabrication techniques that are frequently utilized are hydroplastic forming and slip casting. After forming, a body must be first dried and then fired at an elevated temperature to reduce porosity and enhance strength. Shrinkage that is excessive or too rapid may result in cracking and/or warping, and a worthless ware. Densification during firing is accomplished by vitrification, the formation of a glassy bonding phase.

Some ceramic pieces are formed by powder compaction; uniaxial and isostatic techniques are possible. Densification of pressed pieces takes place by a sintering mechanism during a high-temperature firing procedure. Hot pressing is also possible in which pressing and sintering operations are carried out simultaneously.

Thin ceramic substrate layers are often fabricated by tape casting.

The final sections of this chapter treated synthesis and fabrication techniques for polymeric materials. Synthesis of large molecular weight polymers is attained by polymerization, of which there are two types: addition and condensation. The various properties of polymers may be further modified by using additives; these include fillers, plasticizers, stabilizers, colorants, and flame retardants.

Fabrication of plastic polymers is usually accomplished by plastic deformation at an elevated temperature, using at least one of several different molding techniques—compression, transfer, injection, and blow. Casting is also possible.

Some fibers are spun from a viscous melt, after which they are plastically elongated during a drawing operation, which improves the mechanical strength. Films are formed by extrusion and blowing, which may be followed by rolling.

IMPORTANT TERMS AND CONCEPTS

Addition polymerization
Annealing
Annealing point (glass)
Austenitizing
Cold working
Colorant
Condensation polymerization
Drawing
Extrusion
Filler
Firing
Flame retardant
Forging
Full annealing
Glass transition temperature
Green ceramic body
Hardenability
Hot working
Hydroplastic forming
Jominy end-quench test
Lower critical temperature
Melting point (glass)
Molding
Normalizing
Plasticizer
Powder metallurgy (P/M)
Process annealing
Rolling
Sintering
Slip casting
Softening point (glass)
Spheroidizing
Spinning
Stabilizer
Strain point (glass)
Stress relief
Thermal shock
Thermal tempering
Upper critical temperature
Vitrification
Welding
Working point (glass)

REFERENCES

ASM Handbook, Vol. 6, *Welding, Brazing and Soldering,* ASM International, Materials Park, OH, 1993.

ASM Handbook, Vol. 14, *Forming and Forging,* ASM International, Materials Park, OH, 1988.

ASM Handbook, Vol. 15, *Casting,* ASM International, Materials Park, OH, 1988.

Billmeyer, F. W., Jr., *Textbook of Polymer Science,* 3rd edition, Wiley-Interscience, New York, 1984.

Dieter, G. E., *Mechanical Metallurgy,* 3rd edition, McGraw-Hill Book Company, New York, 1986. Chapters 15–21 provide an excellent discussion of various metal-forming techniques.

Kalpakjian, W., *Manufacturing Processes for Engineering Materials,* 2nd edition, Addison-Wesley Publishing Co., Reading, MA, 1991.

McCrum, N. G., C. P. Buckley, and C. B. Bucknall, *Principles of Polymer Engineering,* 2nd edition, Oxford University Press, Oxford, 1997.

Muccio, E. A., *Plastic Part Technology,* ASM International, Materials Park, OH, 1991.

Muccio, E. A., *Plastics Processing Technology,* ASM International, Materials Park, OH, 1994.

Norton, F. H., *Elements of Ceramics,* 2nd edition, Addison-Wesley Publishing Company, Reading, MA, 1974.

Reed, J. S., *Introduction to the Principles of Ceramic Processing,* 3rd edition, John Wiley & Sons, New York, 1995.

Richerson, D. W., *Modern Ceramic Engineering,* 2nd edition, Marcel Dekker, New York, 1992.

Tooley, F. V. (Editor), *Handbook of Glass Manufacture,* Ashlee Publishing Company, Inc., New York, 1985. In two volumes.

Welding Handbook, 7th edition, American Welding Society, Miami, FL, 1976. In five volumes.

QUESTIONS AND PROBLEMS

14.1 Cite advantages and disadvantages of hot working and cold working.

14.2 **(a)** Cite advantages of forming metals by extrusion as opposed to rolling. **(b)** Cite some disadvantages.

14.3 List four situations in which casting is the preferred fabrication technique.

14.4 Compare sand, die, investment, and continuous casting techniques.

14.5 **(a)** Cite some advantages of powder metallurgy over casting. **(b)** Cite some disadvantages.

14.6 What are the principal differences between welding, brazing, and soldering? You may need to consult another reference.

14.7 If it is assumed that, for steel alloys, the average cooling rate of the heat-affected zone in the vicinity of a weld is 10°C/s, compare the microstructures and associated properties that will result for 1080 (eutectoid) and 4340 alloys in their HAZs.

14.8 Describe one problem that might exist with a steel weld that was cooled very rapidly.

14.9 In your own words describe the following heat treatment procedures for steels and, for each, the intended final microstructure: full annealing, normalizing, quenching, and tempering.

14.10 Cite three sources of internal residual stresses in metal components. What are two possible adverse consequences of these stresses?

14.11 Give the temperature range over which it is possible to austenitize each of the following iron–carbon alloys during a normalizing heat treatment: **(a)** 0.20 wt% C, **(b)** 0.76 wt% C, and **(c)** 0.95 wt% C.

14.12 Give the temperature range over which it is desirable to austenitize each of the following iron–carbon alloys during a full anneal heat treatment: **(a)** 0.25 wt% C, **(b)** 0.45 wt% C, **(c)** 0.85 wt% C, and **(d)** 1.10 wt% C.

14.13 What is the purpose of a spheroidizing heat treatment? On what classes of alloys is it normally used?

14.14 Briefly explain the difference between hardness and hardenability.

14.15 What influence does the presence of alloying elements (other than carbon) have on the shape of a hardenability curve? Briefly explain this effect.

14.16 How would you expect a decrease in the austenite grain size to affect the hardenability of a steel alloy? Why?

14.17 **(a)** Name the three factors that influence the degree to which martensite is formed throughout the cross section of a steel specimen.

(b) For each, tell how the extent of martensite formation may be increased.

14.18 Name two thermal properties of a liquid medium that will influence its quenching effectiveness.

14.19 Construct radial hardness profiles for the following:

(a) A 50-mm (2-in.) diameter cylindrical specimen of an 8640 steel alloy that has been quenched in moderately agitated oil.

(b) A 75-mm (3-in.) diameter cylindrical specimen of a 5140 steel alloy that has been quenched in moderately agitated oil.

(c) A 65-mm ($2\frac{1}{2}$-in.) diameter cylindrical specimen of an 8620 steel alloy that has been quenched in moderately agitated water.

(d) A 70-mm ($2\frac{3}{4}$-in.) diameter cylindrical specimen of a 1040 steel alloy that has been quenched in moderately agitated water.

14.20 Compare the effectiveness of quenching in moderately agitated water and oil by graphing, on a single plot, radial hardness profiles for 65-mm ($2\frac{1}{2}$-in.) diameter cylindrical specimens of an 8630 steel that have been quenched in both media.

14.21 Soda and lime are added to a glass batch in the form of soda ash (Na_2CO_3) and limestone ($CaCO_3$). During heating, these two ingredients decompose to give off carbon dioxide (CO_2), the resulting products being soda and lime. Compute the weight of soda ash and limestone that must be added to 100 lb_m of quartz (SiO_2) to yield a glass of composition 75 wt% SiO_2, 15 wt% Na_2O, and 10 wt% CaO.

14.22 What is the distinction between glass transition temperature and melting temperature?

14.23 On the basis of mechanical characteristics associated with the behaviors shown in Figure 14.15, explain why glass may be drawn into fibers whereas crystalline aluminum oxide may not.

14.24 Compare the temperatures at which soda–lime, borosilicate, 96% silica, and fused silica may be annealed.

14.25 Compare the softening points for 96% silica, borosilicate, and soda–lime glasses.

14.26 The viscosity η of a glass varies with temperature according to the relationship

$$\eta = A \exp\left(\frac{Q_\text{vis}}{RT}\right)$$

where Q_vis is the energy of activation for viscous flow, A is a temperature-independent constant, and R and T are, respectively, the gas constant and the absolute temperature. A plot of ln η versus $1/T$ should be nearly linear, and with a slope of Q_vis/R. Using the data in Figure 14.16, **(a)** make such a plot for the borosilicate glass, and **(b)** determine the activation energy between temperatures of 500 and 900°C.

14.27 For many viscous materials, the viscosity η may be defined in terms of the expression

$$\eta = \frac{\sigma}{d\epsilon/dt}$$

where σ and $d\epsilon/dt$ are, respectively, the tensile stress and the strain rate. A cylindrical specimen of a soda–lime glass of diameter 5 mm (0.2 in.) and length 100 mm (4 in.) is subjected to a tensile force of 1 N (0.224 lb_f) along its axis. If its deformation is to be less than 1 mm (0.04 in.) over a week's time, using Figure 14.16, determine the maximum temperature to which the specimen may be heated.

14.28 **(a)** Explain why residual thermal stresses are introduced into a glass piece when it is cooled.

(b) Are thermal stresses introduced upon heating? Why or why not?

(c) How does the thickness of a glass ware affect the magnitude of the thermal stresses? Why?

14.29 Borosilicate glasses and fused silica are resistant to thermal shock. Why is this so?

14.30 In your own words, briefly describe what happens as a glass piece is thermally tempered.

14.31 Glass pieces may also be strengthened by chemical tempering. With this procedure, the glass surface is put in a state of compression by exchanging some of the cations near the surface with other cations having a larger diameter. Suggest one type of cation which, by replacing Na^+, will induce chemical tempering in a soda–lime glass.

14.32 Cite the two desirable characteristics of clay minerals relative to fabrication processes.

14.33 From a molecular perspective, briefly explain the mechanism by which clay minerals become hydroplastic when water is added.

14.34 Thick ceramic wares are more likely to crack upon drying than thin wares. Why is this so?

14.35 Explain why a clay, once having been fired at an elevated temperature, loses its hydroplasticity.

14.36 **(a)** What are the three main components of a whiteware ceramic such as porcelain?

(b) What role does each component play in the forming and firing procedures?

14.37 **(a)** Why is it so important to control the rate of drying of a ceramic body that has been hydroplastically formed or slip cast?

(b) Cite three factors that influence the rate of drying, and explain how each affects the rate.

14.38 Cite one reason why drying shrinkage is greater for slip cast or hydroplastic products that have smaller clay particles.

14.39 **(a)** Name three factors that influence the degree to which vitrification occurs in clay-based ceramic wares.

(b) Explain how density, firing distortion, strength, corrosion resistance, and thermal conductivity are affected by the extent of vitrification.

14.40 Some ceramic materials are fabricated by hot isostatic pressing. Cite some of the limitations and difficulties associated with this technique.

14.41 Cite the primary differences between addition and condensation polymerization techniques.

14.42 Cite whether the molecular weight of a polymer that is synthesized by addition polymerization is relatively high, medium, or relatively low for the following situations:

(a) Rapid initiation, slow propagation, and rapid termination.

(b) Slow initiation, rapid propagation, and slow termination.

(c) Rapid initiation, rapid propagation, and slow termination.

(d) Slow initiation, slow propagation, and rapid termination.

14.43 **(a)** How much adipic acid must be added to 50 kg of ethylene glycol to produce a linear chain structure of polyester according to Equation 14.5?

(b) What is the mass of the resulting polymer?

14.44 Nylon 6,6 may be formed by means of a condensation polymerization reaction in which hexamethylene diamine $[NH_2{-}(CH_2)_6{-}NH_2]$ and adipic acid react with one another with the formation of water as a by-product. Write out this reaction in the manner of Equation 14.5.

14.45 It is desired to produce nylon 6,6 by condensation polymerization using hexamethylene diamine and adipic acid as described in Problem 14.44. What masses of these two components are necessary to yield 37.5 kg of completely linear nylon 6,6?

14.46 **(a)** Why must the vapor pressure of a plasticizer be relatively low?

(b) How will the crystallinity of a polymer be affected by the addition of a plasticizer? Why?

(c) Is it possible for a crosslinked polymer to be plasticized? Why or why not?

(d) How does the addition of a plasticizer influence the tensile strength of a polymer? Why?

14.47 What is the distinction between dye and pigment colorants?

14.48 Cite four factors that determine what fabrication technique is used to form polymeric materials.

14.49 Contrast compression, injection, and transfer molding techniques that are used to form plastic materials.

14.50 It is desired that some rubber component in its final form be vulcanized. Should vulcanization be carried out prior or subsequent to the forming operation? Why?

14.51 Why must fiber materials that are melt spun and then drawn be thermoplastic? Cite two reasons.

14.52 Which of the following polyethylene thin films would have the better mechanical characteristics: (1) formed by blowing, or (2) formed by extrusion and then rolled? Why?

Design Problems

14.D1 A cylindrical piece of steel 25 mm (1.0 in.) in diameter is to be quenched in moderately agitated oil. Surface and center hardnesses must be at least 55 and 50 HRC, respectively. Which of the following alloys will satisfy these requirements: 1040, 5140, 4340, 4140, and 8640? Justify your choices.

14.D2 A cylindrical piece of steel 75 mm (3 in.) in diameter is to be austenitized and quenched such that a minimum hardness of 40 HRC is to be produced throughout the entire piece. Of the alloys 8660, 8640, 8630, and 8620, which will qualify if the quenching medium is **(a)** moderately agitated water and **(b)** moderately agitated oil? Justify your choice(s).

14.D3 A cylindrical piece of steel 38 mm ($1\frac{1}{2}$ in.) in diameter is to be austenitized and quenched such that a microstructure consisting of at least 80% martensite will be produced throughout the entire piece. Of the alloys 4340, 4140, 8640, 5140, and 1040, which will qualify if the quenching medium is **(a)** moderately agitated oil and **(b)** moderately agitated water? Justify your choice(s).

14.D4 A cylindrical piece of steel 90 mm ($3\frac{1}{2}$ in.) in diameter is to be quenched in moderately agitated water. Surface and center hardnesses must be at least 55 and 40 HRC, respectively. Which of the following alloys will satisfy these requirements: 1040, 5140, 4340, 4140, 8620, 8630, 8640, and 8660? Justify your choices.

14.D5 A cylindrical piece of 4140 steel is to be austenitized and quenched in moderately agitated oil. If the microstructure is to consist of at least 50% martensite throughout the entire piece, what is the maximum allowable diameter? Justify your answer.

14.D6 A cylindrical shaft 45 mm (1.75 in.) in diameter of a 1040 steel must be heat treated so as to produce a uniform tensile strength of at least 620 MPa (90,000 psi) over the entirety of its cross section. Describe a heat treatment that may be used.

14.D7 A cylindrical piece of 8640 steel is to be austenitized and quenched in moderately agitated oil. If the hardness at the surface of the piece must be at least 49 HRC, what is the maximum allowable diameter? Justify your answer.

Chapter 11 / Phase Transformations

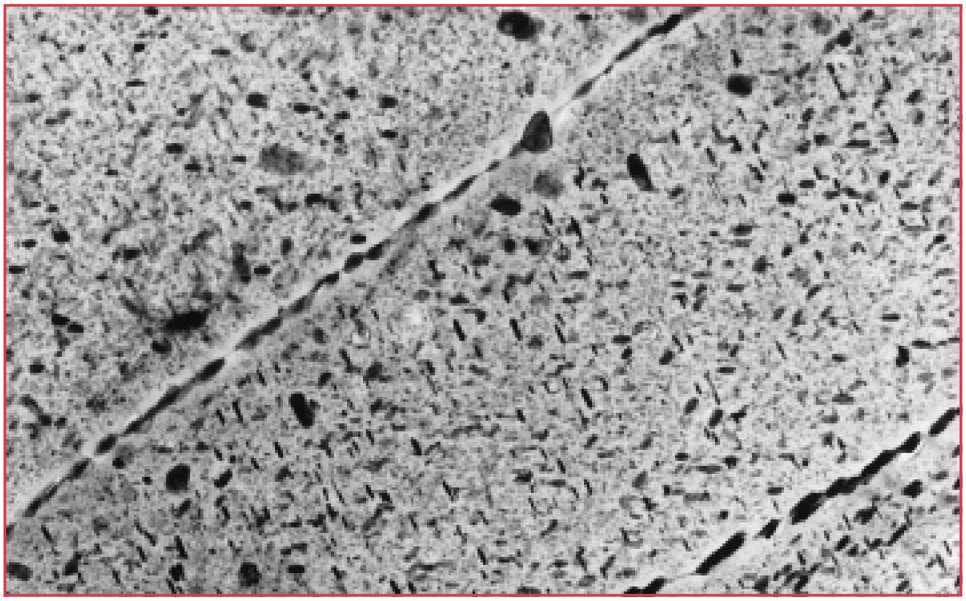

Top: A Boeing 767 airplane in flight. (Photograph courtesy of the Boeing Commercial Airplane Company.) Bottom: A transmission electron micrograph showing the microstructure of the aluminum alloy that is used for the upper wing skins, parts of the internal wing structures, and selected areas of the fuselage of the Boeing 767 above. This is a 7150–T651 alloy (6.2Zn, 2.3Cu, 2.3Mg, 0.12Zr, the balance Al) that has been precipitation hardened. The light matrix phase in the micrograph is an aluminum solid solution. The majority of the small plate-shaped dark precipitate particles are a transition η' phase, the remainder being the equilibrium η ($MgZn_2$) phase. Note that grain boundaries are "decorated" by some of these particles. 80,475×. (Electron micrograph courtesy of G. H. Narayanan and A. G. Miller, Boeing Commercial Airplane Company.)

Why Study *Phase Transformations?*

The development of a set of desirable mechanical characteristics for a material often results from a phase transformation, which is wrought by a heat treatment. The time and temperature dependencies of some phase transformations are conveniently represented on modified phase diagrams. It is important to know how to use these diagrams in order to design a heat treatment for some alloy that will yield the desired room-temperature mechanical properties. For example, the tensile strength of an iron–carbon alloy of eutectoid composition (0.76 wt% C) can be varied between approximately 700 MPa (100,000 psi) and 2000 MPa (300,000 psi) depending on the heat treatment employed.

Learning Objectives

After careful study of this chapter you should be able to do the following:

1. **Make a schematic fraction transformation-versus-logarithm of time plot for a typical solid–solid transformation; cite the equation that describes this behavior.**
2. **Briefly describe the microstructure for each of the following microconstituents that are found in steel alloys: fine pearlite, coarse pearlite, spheroidite, bainite, martensite, and tempered martensite.**
3. **Cite the general mechanical characteristics for each of the following microconstituents: fine pearlite, coarse pearlite, spheroidite, bainite, martensite, and tempered martensite. Now, in terms of microstructure (or crystal structure), briefly explain these behaviors.**
4. **Given the isothermal transformation (or continuous cooling transformation) diagram for some iron–carbon alloy, design a heat treatment that will produce a specified microstructure.**
5. **Using a phase diagram, describe and explain the two heat treatments that are used to precipitation-harden a metal alloy.**
6. **Make a schematic plot of room-temperature strength (or hardness) versus the logarithm of time for a precipitation heat treatment at constant temperature. Explain the shape of this curve in terms of the mechanism of precipitation hardening.**
7. **Schematically plot specific volume versus temperature for crystalline, semicrystalline, and amorphous polymers, noting glass transition and melting temperatures.**

{**8. List four characteristics or structural components of a polymer that affect both its melting and glass transition temperatures.**}

11.1 INTRODUCTION

Mechanical and other properties of many materials depend on their microstructures, which are often produced as a result of phase transformations. In the first portion of this chapter we discuss the basic principles of phase transformations. Next, we address the role these transformations play in the development of microstructure for iron–carbon, as well as other alloys, and how the mechanical properties are affected by these microstructural changes. Finally, we treat crystallization, melting, and glass transition transformations in polymers.

PHASE TRANSFORMATIONS IN METALS

One reason for the versatility of metallic materials lies in the wide range of mechanical properties they possess, which are accessible to management by various means. Three strengthening mechanisms were discussed in Chapter 8, namely, grain size refinement, solid-solution strengthening, and strain hardening. Additional techniques are available wherein the mechanical properties are reliant on the characteristics of the microstructure.

The development of microstructure in both single- and two-phase alloys ordinarily involves some type of phase transformation—an alteration in the number and/or character of the phases. The first portion of this chapter is devoted to a brief discussion of some of the basic principles relating to transformations involving solid phases. Inasmuch as most phase transformations do not occur instantaneously, consideration is given to the dependence of reaction progress on time, or the **transformation rate.** This is followed by a discussion of the development of two-phase microstructures for iron–carbon alloys. Modified phase diagrams are introduced which permit determination of the microstructure that results from a specific heat treatment. Finally, other microconstituents in addition to pearlite are presented, and, for each, the mechanical properties are discussed.

11.2 BASIC CONCEPTS

A variety of **phase transformations** are important in the processing of materials, and usually they involve some alteration of the microstructure. For purposes of this discussion, these transformations are divided into three classifications. In one group are simple diffusion-dependent transformations in which there is no change in either the number or composition of the phases present. These include solidification of a pure metal, allotropic transformations, and, recrystallization and grain growth (see Sections 8.13 and 8.14).

In another type of diffusion-dependent transformation, there is some alteration in phase compositions and often in the number of phases present; the final microstructure ordinarily consists of two phases. The eutectoid reaction, described by Equation 10.19, is of this type; it receives further attention in Section 11.5.

The third kind of transformation is diffusionless, wherein a metastable phase is produced. As discussed in Section 11.5, a martensitic transformation, which may be induced in some steel alloys, falls into this category.

11.3 THE KINETICS OF SOLID-STATE REACTIONS

Most solid-state transformations do not occur instantaneously because obstacles impede the course of the reaction and make it dependent on time. For example, since most transformations involve the formation of at least one new phase that has a composition and/or crystal structure different from that of the parent one, some atomic rearrangements via diffusion are required. Diffusion is a time-dependent phenomenon, as discussed in Section 6.4. A second impediment to the formation of a new phase is the increase in energy associated with the phase boundaries that are created between parent and product phases.

From a microstructural standpoint, the first process to accompany a phase transformation is **nucleation**—the formation of very small (often submicroscopic) particles, or nuclei, of the new phase, which are capable of growing. Favorable positions for the formation of these nuclei are imperfection sites, especially grain boundaries. The second stage is *growth*, in which the nuclei increase in size; during this process, of course, some volume of the parent phase disappears. The transformation reaches completion if growth of these new phase particles is allowed to proceed until the equilibrium fraction is attained.

As would be expected, the time dependence of the transformation rate (which is often termed the **kinetics** of a transformation) is an important consideration in the heat treatment of materials. With many kinetic investigations, the fraction of reaction that has occurred is measured as a function of time, while the temperature is maintained constant. Transformation progress is usually ascertained by either microscopic examination or measurement of some physical property (such as electrical conductivity) the magnitude of which is distinctive of the new phase. Data are plotted as the fraction of transformed material versus the logarithm of time; an S-shaped curve similar to that in Figure 11.1 represents the typical kinetic behavior for most solid-state reactions. Nucleation and growth stages are indicated in the figure.

For solid-state transformations displaying the kinetic behavior in Figure 11.1, the fraction of transformation y is a function of time t as follows:

$$y = 1 - \exp(-kt^n) \tag{11.1}$$

where k and n are time-independent constants for the particular reaction. The above expression is often referred to as the *Avrami equation*.

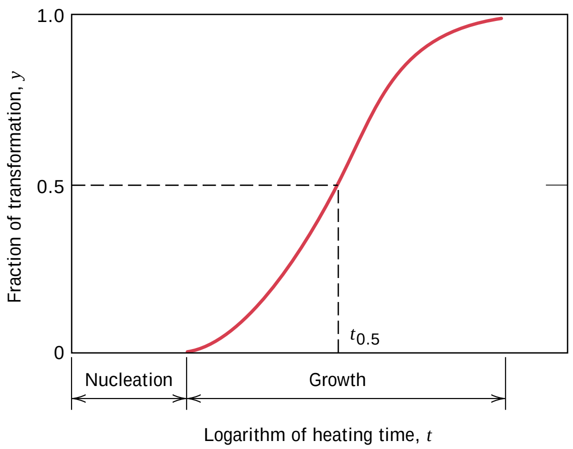

FIGURE 11.1 Plot of fraction reacted versus the logarithm of time typical of many solid-state transformations in which temperature is held constant.

By convention, the rate of a transformation r is taken as the reciprocal of time required for the transformation to proceed halfway to completion, $t_{0.5}$, or

$$r = \frac{1}{t_{0.5}} \tag{11.2}$$

This $t_{0.5}$ is also noted in Figure 11.1.

Temperature is one variable in a heat treatment process that is subject to control, and it may have a profound influence on the kinetics and thus on the rate of a transformation. This is demonstrated in Figure 11.2, where y-versus-log t S-shaped curves at several temperatures for the recrystallization of copper are shown.

For most reactions and over specific temperature ranges, rate increases with temperature according to

$$r = Ae^{-Q/RT} \tag{11.3}$$

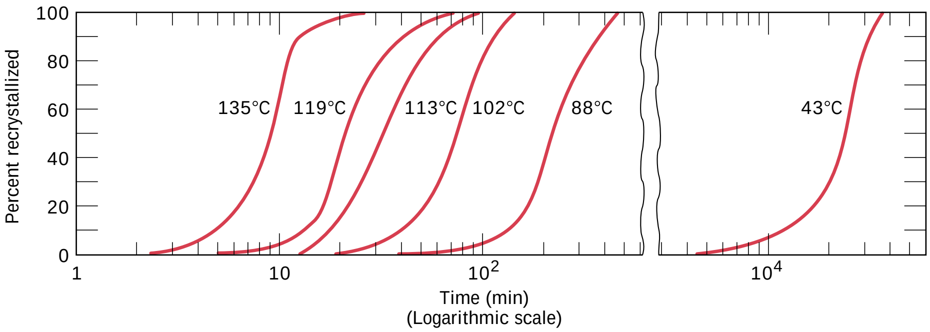

FIGURE 11.2 Percent recrystallization as a function of time and at constant temperature for pure copper. (Reprinted with permission from *Metallurgical Transactions,* Vol. 188, 1950, a publication of The Metallurgical Society of AIME, Warrendale, Pennsylvania. Adapted from B. F. Decker and D. Harker, "Recrystallization in Rolled Copper," *Trans. AIME,* **188,** 1950, p. 888.)

where

R = the gas constant

T = absolute temperature

A = a temperature-independent constant

Q = an activation energy for the particular reaction

It may be recalled that the diffusion coefficient has the same temperature dependence (Equation 6.8). Processes the rates of which exhibit this relationship with temperature are sometimes termed **thermally activated.**

11.4 MULTIPHASE TRANSFORMATIONS

Phase transformations may be wrought in metal alloy systems by varying temperature, composition, and the external pressure; however, temperature changes by means of heat treatments are most conveniently utilized to induce phase transformations. This corresponds to crossing a phase boundary on the composition–temperature phase diagram as an alloy of given composition is heated or cooled.

During a phase transformation, an alloy proceeds toward an equilibrium state that is characterized by the phase diagram in terms of the product phases, their compositions, and relative amounts. Most phase transformations require some finite time to go to completion, and the speed or rate is often important in the relationship between the heat treatment and the development of microstructure. One limitation of phase diagrams is their inability to indicate the time period required for the attainment of equilibrium.

The rate of approach to equilibrium for solid systems is so slow that true equilibrium structures are rarely achieved. Equilibrium conditions are maintained only if heating or cooling is carried out at extremely slow and unpractical rates. For other than equilibrium cooling, transformations are shifted to lower temperatures than indicated by the phase diagram; for heating, the shift is to higher temperatures. These phenomena are termed **supercooling** and **superheating,** respectively. The degree of each depends on the rate of temperature change; the more rapid the cooling or heating, the greater the supercooling or superheating. For example, for normal cooling rates the iron–carbon eutectoid reaction is typically displaced 10 to 20°C (18 to 36°F) below the equilibrium transformation temperature.

For many technologically important alloys, the preferred state or microstructure is a metastable one, intermediate between the initial and equilibrium states; on occasion, a structure far removed from the equilibrium one is desired. It thus becomes imperative to investigate the influence of time on phase transformations. This kinetic information is, in many instances, of greater value than a knowledge of the final equilibrium state.

MICROSTRUCTURAL AND PROPERTY CHANGES IN IRON–CARBON ALLOYS

Some of the basic kinetic principles of solid-state transformations are now extended and applied specifically to iron–carbon alloys in terms of the relationships between heat treatment, the development of microstructure, and mechanical properties.

This system has been chosen because it is familiar and because a wide variety of microstructures and mechanical properties are possible for iron–carbon (or steel) alloys.

11.5 ISOTHERMAL TRANSFORMATION DIAGRAMS

PEARLITE

Consider again the iron–iron carbide eutectoid reaction

$$\gamma(0.76\text{ wt\% C}) \underset{\text{heating}}{\overset{\text{cooling}}{\rightleftharpoons}} \alpha(0.022\text{ wt\% C}) + \text{Fe}_3\text{C}(6.70\text{ wt\% C}) \qquad (10.19)$$

which is fundamental to the development of microstructure in steel alloys. Upon cooling, austenite, having an intermediate carbon concentration, transforms to a ferrite phase, having a much lower carbon content, and also cementite, with a much higher carbon concentration. Pearlite is one microstructural product of this transformation (Figure 10.29), and the mechanism of pearlite formation was discussed previously (Section 10.19) and demonstrated in Figure 10.30.

Temperature plays an important role in the rate of the austenite-to-pearlite transformation. The temperature dependence for an iron–carbon alloy of eutectoid composition is indicated in Figure 11.3, which plots S-shaped curves of the percentage transformation versus the logarithm of time at three different temperatures. For each curve, data were collected after rapidly cooling a specimen composed of 100% austenite to the temperature indicated; that temperature was maintained constant throughout the course of the reaction.

A more convenient way of representing both the time and temperature dependence of this transformation is in the bottom portion of Figure 11.4. Here, the vertical and horizontal axes are, respectively, temperature and the logarithm of time. Two solid curves are plotted; one represents the time required at each temperature for the initiation or start of the transformation; the other is for the transformation conclusion. The dashed curve corresponds to 50% of transformation completion. These curves were generated from a series of plots of the percentage transformation versus the logarithm of time taken over a range of temperatures. The S-shaped curve [for 675°C (1247°F)], in the upper portion of Figure 11.4, illustrates how the data transfer is made.

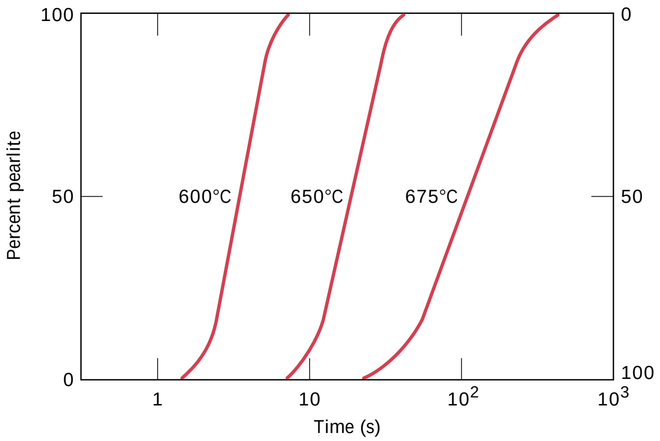

FIGURE 11.3 For an iron–carbon alloy of eutectoid composition (0.76 wt% C), isothermal fraction reacted versus the logarithm of time for the austenite-to-pearlite transformation.

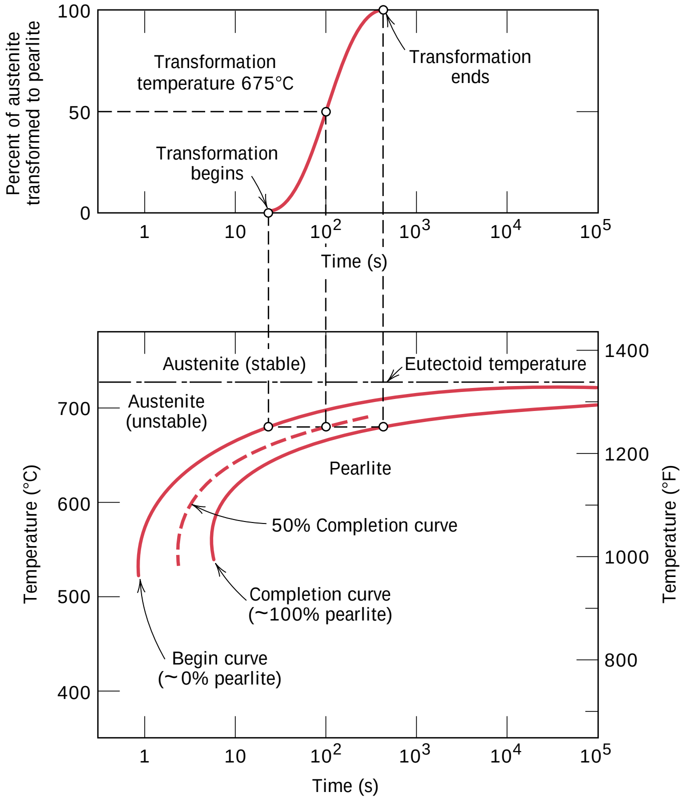

Figure 11.4 Demonstration of how an isothermal transformation diagram (bottom) is generated from percent transformation-versus-logarithm of time measurements (top). (Adapted from H. Boyer, Editor, *Atlas of Isothermal Transformation and Cooling Transformation Diagrams,* American Society for Metals, 1977, p. 369.)

In interpreting this diagram, note first that the eutectoid temperature [727°C (1341°F)] is indicated by a horizontal line; at temperatures above the eutectoid and for all times, only austenite will exist, as indicated in the figure. The austenite-to-pearlite transformation will occur only if an alloy is supercooled to below the eutectoid; as indicated by the curves, the time necessary for the transformation to begin and then end depends on temperature. The start and finish curves are nearly parallel, and they approach the eutectoid line asymptotically. To the left of the transformation start curve, only austenite (which is unstable) will be present, whereas to the right of the finish curve, only pearlite will exist. In between, the austenite is in the process of transforming to pearlite, and thus both microconstituents will be present.

According to Equation 11.2, the transformation rate at some particular temperature is inversely proportional to the time required for the reaction to proceed to 50% completion (to the dashed curve in Figure 11.4). That is, the shorter this time, the higher the rate. Thus, from Figure 11.4, at temperatures just below the eutectoid (corresponding to just a slight degree of undercooling) very long times (on the order of 10^5 s) are required for the 50% transformation, and therefore the reaction rate is very slow. The transformation rate increases with decreasing temperature such that at 540°C (1000°F) only about 3 s is required for the reaction to go to 50% completion.

This rate–temperature behavior is in apparent contradiction of Equation 11.3, which stipulates that rate *increases* with increasing temperature. The reason for this disparity is that over this range of temperatures (i.e., 540 to 727°C), the transformation rate is controlled by the rate of pearlite nucleation, and nucleation rate decreases with rising temperature (i.e., less supercooling). This behavior may be explained by Equation 11.3, wherein the activation energy Q for nucleation is a function of, and increases with, increasing temperature. We shall find that at lower temperatures, the austenite decomposition transformation is diffusion-controlled and that the rate behavior is as predicted by Equation 11.3, with a temperature-independent activation energy for diffusion.

Several constraints are imposed on using diagrams like Figure 11.4. First, this particular plot is valid only for an iron–carbon alloy of eutectoid composition; for other compositions, the curves will have different configurations. In addition, these plots are accurate only for transformations in which the temperature of the alloy is held constant throughout the duration of the reaction. Conditions of constant temperature are termed *isothermal;* thus, plots such as Figure 11.4 are referred to as **isothermal transformation diagrams,** or sometimes as *time–temperature–transformation* (or T–T–T) plots.

An actual isothermal heat treatment curve ($ABCD$) is superimposed on the isothermal transformation diagram for a eutectoid iron–carbon alloy in Figure 11.5. Very rapid cooling of austenite to a temperature is indicated by the near-vertical line AB, and the isothermal treatment at this temperature is represented by the horizontal segment BCD. Of course, time increases from left to right along this line. The transformation of austenite to pearlite begins at the intersection, point C (after approximately 3.5 s), and has reached completion by about 15 s, corresponding

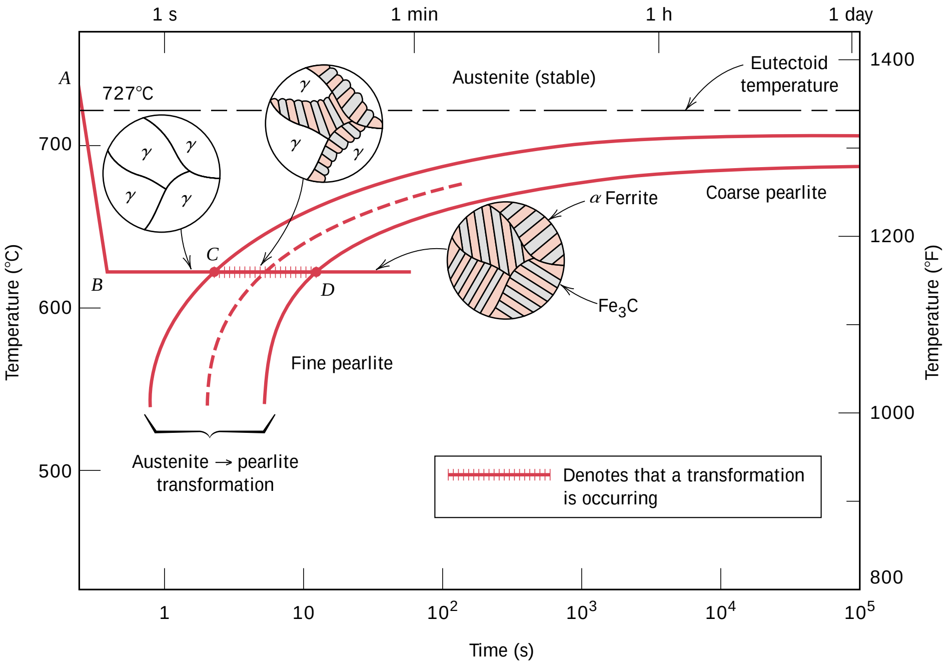

FIGURE 11.5 Isothermal transformation diagram for a eutectoid iron–carbon alloy, with superimposed isothermal heat treatment curve ($ABCD$). Microstructures before, during, and after the austenite-to-pearlite transformation are shown. (Adapted from H. Boyer, Editor, *Atlas of Isothermal Transformation and Cooling Transformation Diagrams,* American Society for Metals, 1977, p. 28.)

to point *D*. Figure 11.5 also shows schematic microstructures at various times during the progression of the reaction.

The thickness ratio of the ferrite and cementite layers in pearlite is approximately 8 to 1. However, the absolute layer thickness depends on the temperature at which the isothermal transformation is allowed to occur. At temperatures just below the eutectoid, relatively thick layers of both the α-ferrite and Fe_3C phases are produced; this microstructure is called **coarse pearlite,** and the region at which it forms is indicated to the right of the completion curve on Figure 11.5. At these temperatures, diffusion rates are relatively high, such that during the transformation illustrated in Figure 10.30 carbon atoms can diffuse relatively long distances, which results in the formation of thick lamellae. With decreasing temperature, the carbon diffusion rate decreases, and the layers become progressively thinner. The thin-layered structure produced in the vicinity of 540°C is termed **fine pearlite;** this is also indicated in Figure 11.5. To be discussed in Section 11.7 is the dependence of mechanical properties on lamellar thickness. Photomicrographs of coarse and fine pearlite for a eutectoid composition are shown in Figure 11.6.

For iron–carbon alloys of other compositions, a proeutectoid phase (either ferrite or cementite) will coexist with pearlite, as discussed in Section 10.19. Thus additional curves corresponding to a proeutectoid transformation also must be included on the isothermal transformation diagram. A portion of one such diagram for a 1.13 wt% C alloy is shown in Figure 11.7.

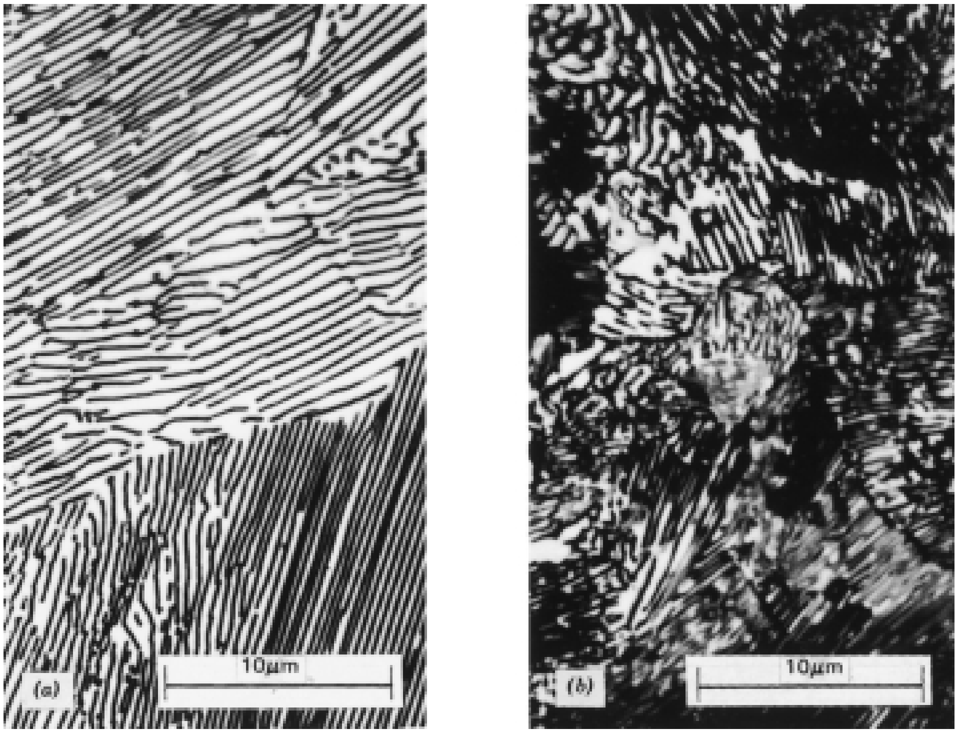

FIGURE 11.6 Photomicrographs of (*a*) coarse pearlite and (*b*) fine pearlite. 3000×. (From K. M. Ralls, et al., *An Introduction to Materials Science and Engineering,* p. 361. Copyright © 1976 by John Wiley & Sons, New York. Reprinted by permission of John Wiley & Sons, Inc.)

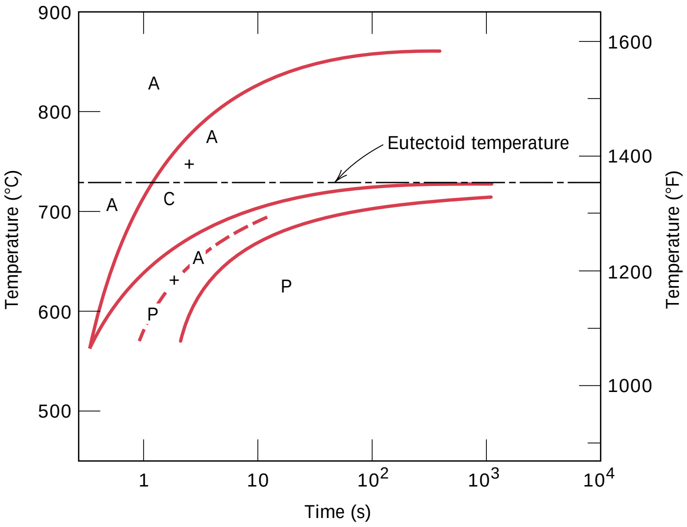

FIGURE 11.7 Isothermal transformation diagram for a 1.13 wt% C iron–carbon alloy: A, austenite; C, proeutectoid cementite; P, pearlite. (Adapted from H. Boyer, Editor, *Atlas of Isothermal Transformation and Cooling Transformation Diagrams*, American Society for Metals, 1977, p. 33.)

BAINITE

In addition to pearlite, other microconstituents that are products of the austenitic transformation exist; one of these is called **bainite.** The microstructure of bainite consists of ferrite and cementite phases, and thus diffusional processes are involved in its formation. Bainite forms as needles or plates, depending on the temperature of the transformation; the microstructural details of bainite are so fine that their resolution is possible only using electron microscopy. Figure 11.8 is an electron micrograph that shows a grain of bainite (positioned diagonally from lower left to upper right); it is composed of needles of ferrite that are separated by elongated particles of the Fe_3C phase; the various phases in this micrograph have been labeled. In addition, the phase that surrounds the needle is martensite, the topic to which a subsequent section is addressed. Furthermore, no proeutectoid phase forms with bainite.

The time–temperature dependence of the bainite transformation may also be represented on the isothermal transformation diagram. It occurs at temperatures below those at which pearlite forms; begin-, end-, and half-reaction curves are just extensions of those for the pearlitic transformation, as shown in Figure 11.9, the isothermal transformation diagram for an iron–carbon alloy of eutectoid composition that has been extended to lower temperatures. All three curves are C-shaped and have a ''nose'' at point N, where the rate of transformation is a maximum. As may be noted, whereas pearlite forms above the nose—that is, over the temperature range of about 540 to 727°C (1000 to 1341°F)—for isothermal treatments at temperatures between about 215 and 540°C (420 and 1000°F), bainite is the transformation product.

It should also be noted that pearlitic and bainitic transformations are really competitive with each other, and once some portion of an alloy has transformed to either pearlite or bainite, transformation to the other microconstituent is not possible without reheating to form austenite.

In passing, it should be mentioned that the kinetics of the bainite transformation (below the nose in Figure 11.9) obey Equation 11.3; that is, rate ($1/t_{0.5}$, Equation 11.2) increases exponentially with rising temperature. Furthermore, the kinetics of

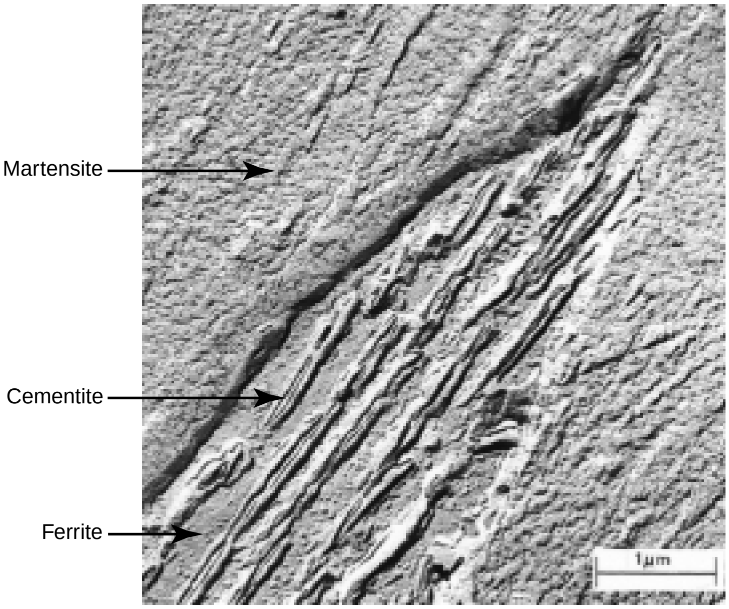

Figure 11.8 Replica transmission electron micrograph showing the structure of bainite. A grain of bainite passes from lower left to upper right-hand corners, which consists of elongated and needle-shaped particles of Fe_3C within a ferrite matrix. The phase surrounding the bainite is martensite. (Reproduced with permission from *Metals Handbook,* Vol. 8, 8th edition, *Metallography, Structures and Phase Diagrams,* American Society for Metals, Materials Park, OH, 1973.)

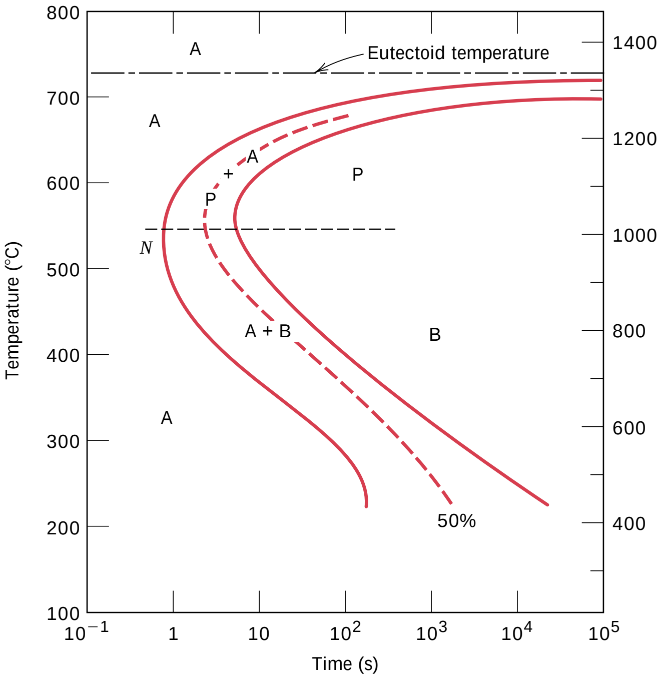

Figure 11.9 Isothermal transformation diagram for an iron–carbon alloy of eutectoid composition, including austenite-to-pearlite (A–P) and austenite-to-bainite (A–B) transformations. (Adapted from H. Boyer, Editor, *Atlas of Isothermal Transformation and Cooling Transformation Diagrams,* American Society for Metals, 1977, p. 28.)

many solid-state transformations are represented by this characteristic C-shaped curve (Figure 11.9).

SPHEROIDITE

If a steel alloy having either pearlitic or bainitic microstructures is heated to, and left at, a temperature below the eutectoid for a sufficiently long period of time—for example, at about 700°C (1300°F) for between 18 and 24 h—yet another microstructure will form. It is called **spheroidite** (Figure 11.10). Instead of the alternating ferrite and cementite lamellae (pearlite), or the microstructures observed for bainite, the Fe_3C phase appears as spherelike particles embedded in a continuous α phase matrix. This transformation has occurred by additional carbon diffusion with no change in the compositions or relative amounts of ferrite and cementite phases. The photomicrograph in Figure 11.11 shows a pearlitic steel that has partially transformed to spheroidite. The driving force for this transformation is the reduction in α–Fe_3C phase boundary area. The kinetics of spheroidite formation are not included on isothermal transformation diagrams.

MARTENSITE

Yet another microconstituent or phase called **martensite** is formed when austenitized iron–carbon alloys are rapidly cooled (or quenched) to a relatively low temperature (in the vicinity of the ambient). Martensite is a nonequilibrium single-phase structure that results from a diffusionless transformation of austenite. It may be thought of as a transformation product that is competitive with pearlite and bainite. The martensitic transformation occurs when the quenching rate is rapid enough to prevent carbon diffusion. Any diffusion whatsoever will result in the formation of ferrite and cementite phases.

The martensitic transformation is not well understood. However, large numbers of atoms experience cooperative movements, in that there is only a slight displacement of each atom relative to its neighbors. This occurs in such a way that the FCC austenite experiences a polymorphic transformation to a body-centered tetragonal (BCT) martensite. A unit cell of this crystal structure (Figure

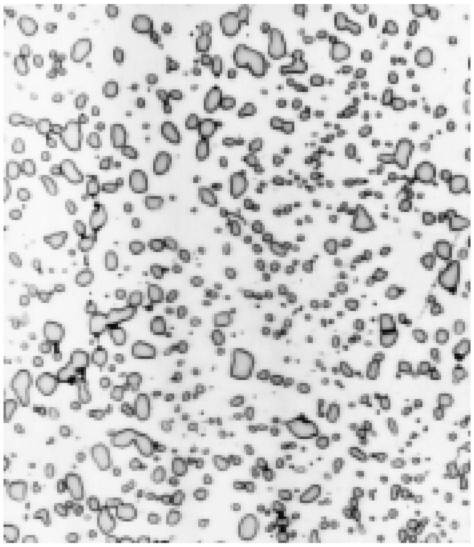

FIGURE 11.10 Photomicrograph of a steel having a spheroidite microstructure. The small particles are cementite; the continuous phase is α ferrite. 1000×. (Copyright 1971 by United States Steel Corporation.)

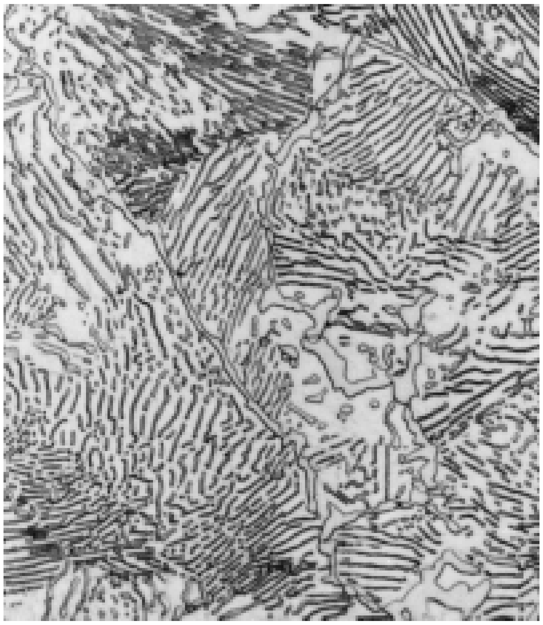

Figure 11.11 A photomicrograph of a pearlitic steel that has partially transformed to spheroidite. 1400×. (Courtesy of United States Steel Corporation.)

11.12) is simply a body-centered cube that has been elongated along one of its dimensions; this structure is distinctly different from that for BCC ferrite. All the carbon atoms remain as interstitial impurities in martensite; as such, they constitute a supersaturated solid solution that is capable of rapidly transforming to other structures if heated to temperatures at which diffusion rates become appreciable. Many steels, however, retain their martensitic structure almost indefinitely at room temperature.

The martensitic transformation is not, however, unique to iron–carbon alloys. It is found in other systems and is characterized, in part, by the diffusionless transformation.

Since the martensitic transformation does not involve diffusion, it occurs almost instantaneously; the martensite grains nucleate and grow at a very rapid rate—the velocity of sound within the austenite matrix. Thus the martensitic transformation rate, for all practical purposes, is time independent.

Martensite grains take on a platelike or needlelike appearance, as indicated in Figure 11.13. The white phase in the micrograph is austenite (retained austenite)

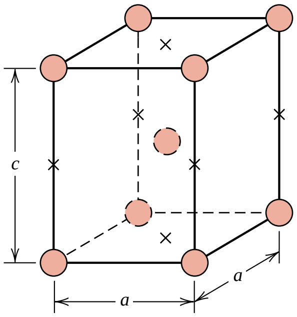

Figure 11.12 The body-centered tetragonal unit cell for martensitic steel showing iron atoms (circles) and sites that may be occupied by carbon atoms (crosses). For this tetragonal unit cell, $c > a$.

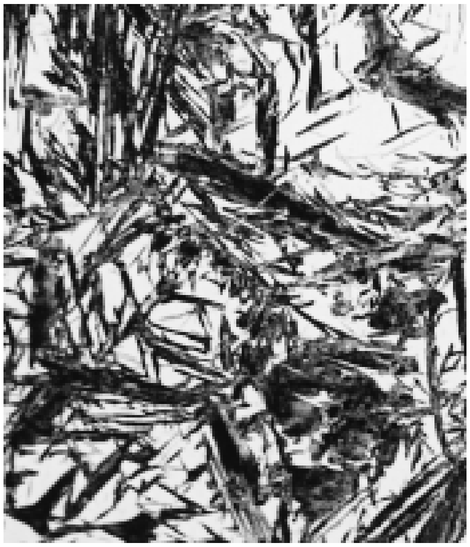

Figure 11.13 Photomicrograph showing the martensitic microstructure. The needle-shaped grains are the martensite phase, and the white regions are austenite that failed to transform during the rapid quench. 1220×. (Photomicrograph courtesy of United States Steel Corporation.)

that did not transform during the rapid quench. As has already been mentioned, martensite as well as other microconstituents (e.g., pearlite) can coexist.

Being a nonequilibrium phase, martensite does not appear on the iron–iron carbide phase diagram (Figure 10.26). The austenite-to-martensite transformation is, however, represented on the isothermal transformation diagram. Since the mar-

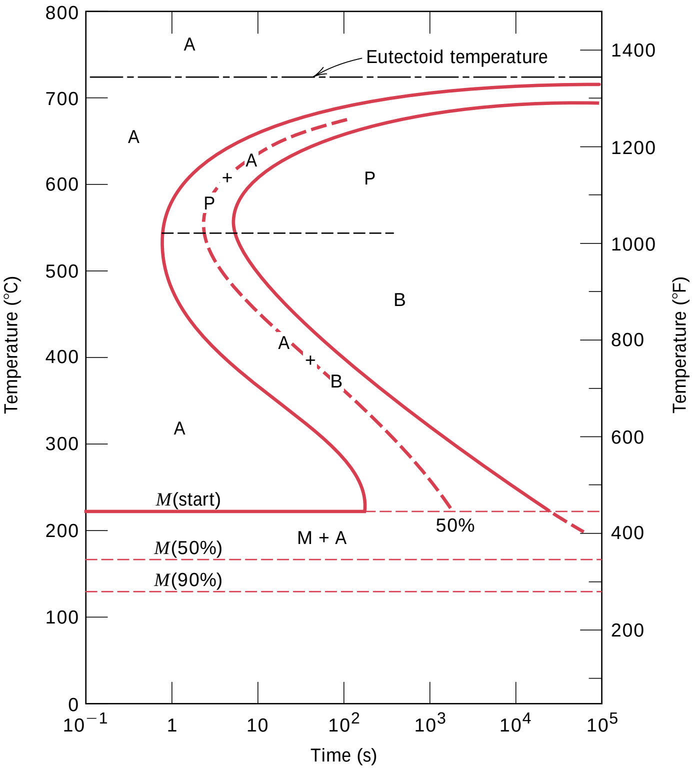

Figure 11.14 The complete isothermal transformation diagram for an iron–carbon alloy of eutectoid composition: A, austenite; B, bainite; M, martensite; P, pearlite.

tensitic transformation is diffusionless and instantaneous, it is not depicted in this diagram like the pearlitic and bainitic reactions. The beginning of this transformation is represented by a horizontal line designated *M*(start) (Figure 11.14). Two other horizontal and dashed lines, labeled *M*(50%) and *M*(90%), indicate percentages of the austenite-to-martensite transformation. The temperatures at which these lines are located vary with alloy composition but, nevertheless, must be relatively low because carbon diffusion must be virtually nonexistent. The horizontal and linear character of these lines indicates that the martensitic transformation is independent of time; it is a function only of the temperature to which the alloy is quenched or rapidly cooled. A transformation of this type is termed an **athermal transformation.**

Consider an alloy of eutectoid composition that is very rapidly cooled from a temperature above 727°C (1341°F) to, say, 165°C (330°F). From the isothermal transformation diagram (Figure 11.14) it may be noted that 50% of the austenite will immediately transform to martensite; and as long as this temperature is maintained, there will be no further transformation.

The presence of alloying elements other than carbon (e.g., Cr, Ni, Mo, and W) may cause significant changes in the positions and shapes of the curves in the isothermal transformation diagrams. These include (1) shifting to longer times the nose of the austenite-to-pearlite transformation (and also a proeutectoid phase nose, if such exists), and (2) the formation of a separate bainite nose. These alterations may be observed by comparing Figures 11.14 and 11.15, which are isothermal transformation diagrams for carbon and alloy steels, respectively.

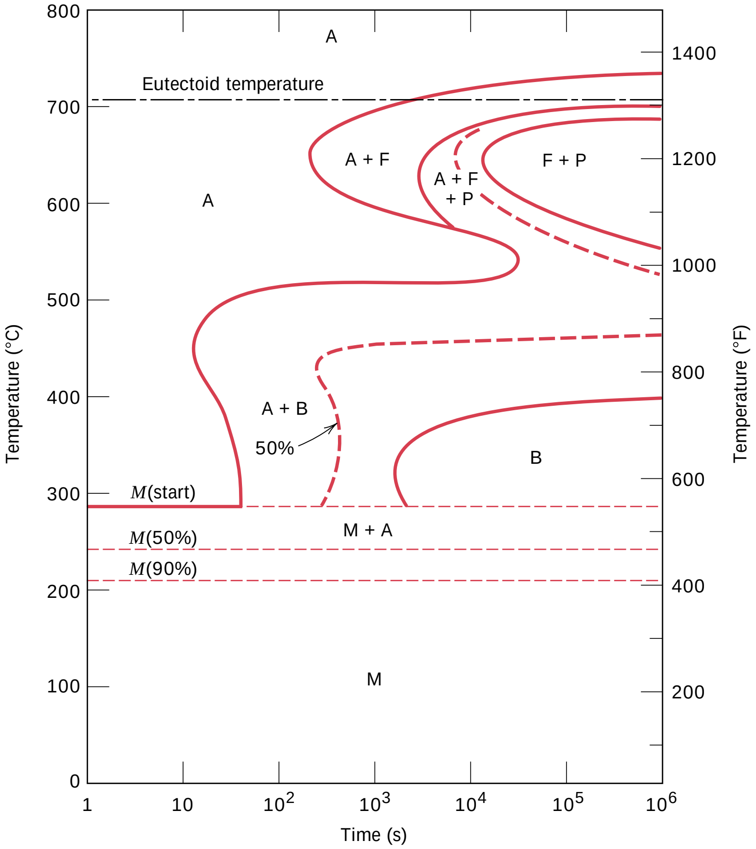

FIGURE 11.15 Isothermal transformation diagram for an alloy steel (type 4340): A, austenite; B, bainite; P, pearlite; M, martensite; F, proeutectoid ferrite. (Adapted from H. Boyer, Editor, *Atlas of Isothermal Transformation and Cooling Transformation Diagrams*, American Society for Metals, 1977, p. 181.)

Steels in which carbon is the prime alloying element are termed **plain carbon steels,** whereas **alloy steels** contain appreciable concentrations of other elements, including those cited in the preceding paragraph. Chapter 13 tells more about the classification and properties of ferrous alloys.

EXAMPLE PROBLEM 11.1

Using the isothermal transformation diagram for an iron–carbon alloy of eutectoid composition (Figure 11.14), specify the nature of the final microstructure (in terms of microconstituents present and approximate percentages) of a small specimen that has been subjected to the following time–temperature treatments. In each case assume that the specimen begins at 760°C (1400°F) and that it has been held at this temperature long enough to have achieved a complete and homogeneous austenitic structure.

(a) Rapidly cool to 350°C (660°F), hold for 10^4 s, and quench to room temperature.

(b) Rapidly cool to 250°C (480°F), hold for 100 s, and quench to room temperature.

(c) Rapidly cool to 650°C (1200°F), hold for 20 s, rapidly cool to 400°C (750°F), hold for 10^3 s, and quench to room temperature.

SOLUTION

The time–temperature paths for all three treatments are shown in Figure 11.16. In each case the initial cooling is rapid enough to prevent any transformation from occurring.

(a) At 350°C austenite isothermally transforms to bainite; this reaction begins after about 10 s and reaches completion at about 500 s elapsed time. Therefore, by 10^4 s, as stipulated in this problem, 100% of the specimen is bainite, and no further transformation is possible, even though the final quenching line passes through the martensite region of the diagram.

(b) In this case it takes about 150 s at 250°C for the bainite transformation to begin, so that at 100 s the specimen is still 100% austenite. As the specimen is cooled through the martensite region, beginning at about 215°C, progressively more of the austenite instantaneously transforms to martensite. This transformation is complete by the time room temperature is reached, such that the final microstructure is 100% martensite.

(c) For the isothermal line at 650°C, pearlite begins to form after about 7 s; by the time 20 s has elapsed, only approximately 50% of the specimen has transformed to pearlite. The rapid cool to 400°C is indicated by the vertical line; during this cooling, very little, if any, remaining austenite will transform to either pearlite or bainite, even though the cooling line passes through pearlite and bainite regions of the diagram. At 400°C, we begin timing at essentially zero time (as indicated in Figure 11.16); thus, by the time 10^3 s has elapsed, all of the remaining 50% austenite will have completely transformed to bainite. Upon quenching to room temperature, any further transformation is not possible inasmuch as no austenite remains; and so the final microstructure at room temperature consists of 50% pearlite and 50% bainite.

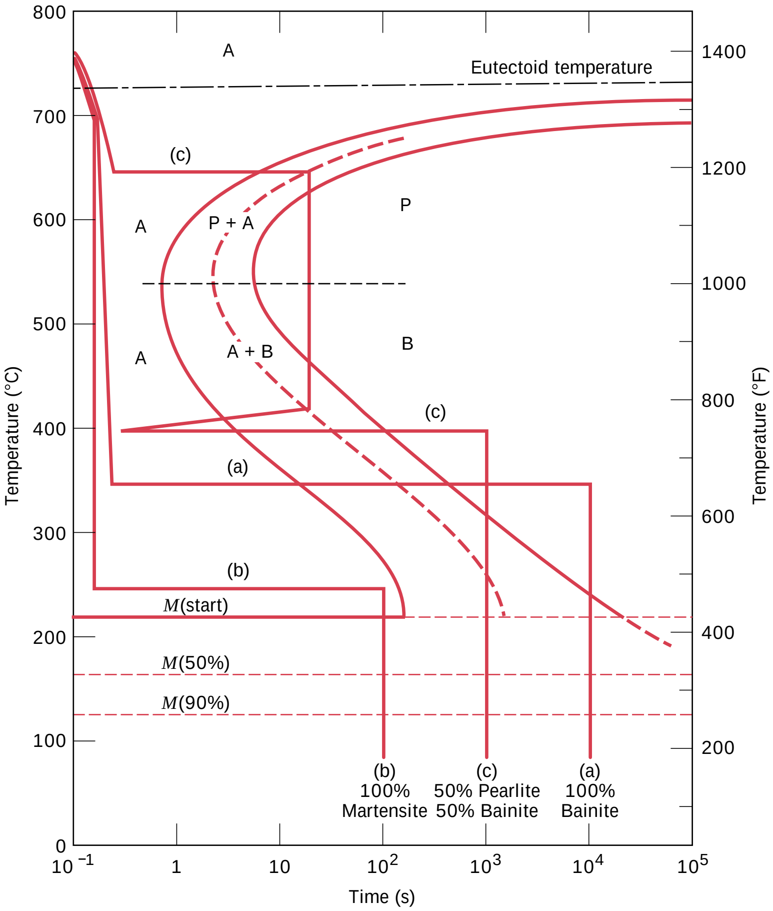

Figure 11.16 Isothermal transformation diagram for an iron–carbon alloy of eutectoid composition and the isothermal heat treatments (a), (b), and (c) in Example Problem 11.1.

11.6 CONTINUOUS COOLING TRANSFORMATION DIAGRAMS (CD-ROM)

11.7 MECHANICAL BEHAVIOR OF IRON–CARBON ALLOYS

We shall now discuss the mechanical behavior of iron–carbon alloys having the microstructures discussed heretofore, namely, fine and coarse pearlite, spheroidite, bainite, and martensite. For all but martensite, two phases are present (i.e., ferrite and cementite); and so an opportunity is provided to explore several mechanical property–microstructure relationships that exist for these alloys.

PEARLITE

Cementite is much harder but more brittle than ferrite. Thus, increasing the fraction of Fe_3C in a steel alloy while holding other microstructural elements constant will result in a harder and stronger material. This is demonstrated in Figure 11.21*a*, in which the tensile and yield strengths as well as the Brinell hardness number are plotted as a function of the weight percent carbon (or equivalently as the percent of Fe_3C) for steels that are composed of fine pearlite. All three parameters increase with increasing carbon concentration. Inasmuch as cementite is more brittle, increasing its content will result in a decrease in both ductility and toughness (or impact energy). These effects are shown in Figure 11.21*b* for the same fine pearlitic steels.

The layer thickness of each of the ferrite and cementite phases in the microstructure also influences the mechanical behavior of the material. Fine pearlite is harder and stronger than coarse pearlite, as demonstrated in Figure 11.22*a*, which plots hardness versus the carbon concentration.

The reasons for this behavior relate to phenomena that occur at the α–Fe_3C phase boundaries. First, there is a large degree of adherence between the two phases across a boundary. Therefore, the strong and rigid cementite phase severely restricts deformation of the softer ferrite phase in the regions adjacent to the boundary; thus the cementite may be said to reinforce the ferrite. The degree of this reinforcement is substantially higher in fine pearlite because of the greater phase boundary area per unit volume of material. In addition, phase boundaries serve as barriers to dislocation motion in much the same way as grain boundaries (Section 8.9). For fine pearlite there are more boundaries through which a dislocation must pass during plastic deformation. Thus, the greater reinforcement and restriction of dislocation motion in fine pearlite account for its greater hardness and strength.

Coarse pearlite is more ductile than fine pearlite, as illustrated in Figure 11.22*b*, which plots percent reduction in area versus carbon concentration for both microstructure types. This behavior results from the greater restriction to plastic deformation of the fine pearlite.

SPHEROIDITE

Other elements of the microstructure relate to the shape and distribution of the phases. In this respect, the cementite phase has distinctly different shapes and arrangements in the pearlite and spheroidite microstructures (Figures 11.6 and 11.10). Alloys containing pearlitic microstructures have greater strength and hardness than do those with spheroidite. This is demonstrated in Figure 11.22*a*, which compares the hardness as a function of the weight percent carbon for spheroidite with both the other pearlite structure types. This behavior is again explained in terms of reinforcement at, and impedance to, dislocation motion across the ferrite–cementite boundaries as discussed above. There is less boundary area per unit volume in spheroidite, and consequently plastic deformation is not nearly as constrained, which gives rise to a relatively soft and weak material. In fact, of all steel alloys, those that are softest and weakest have a spheroidite microstructure.

As would be expected, spheroidized steels are extremely ductile, much more than either fine or coarse pearlite (Figure 11.22*b*). In addition, they are notably tough because any crack can encounter only a very small fraction of the brittle cementite particles as it propagates through the ductile ferrite matrix.

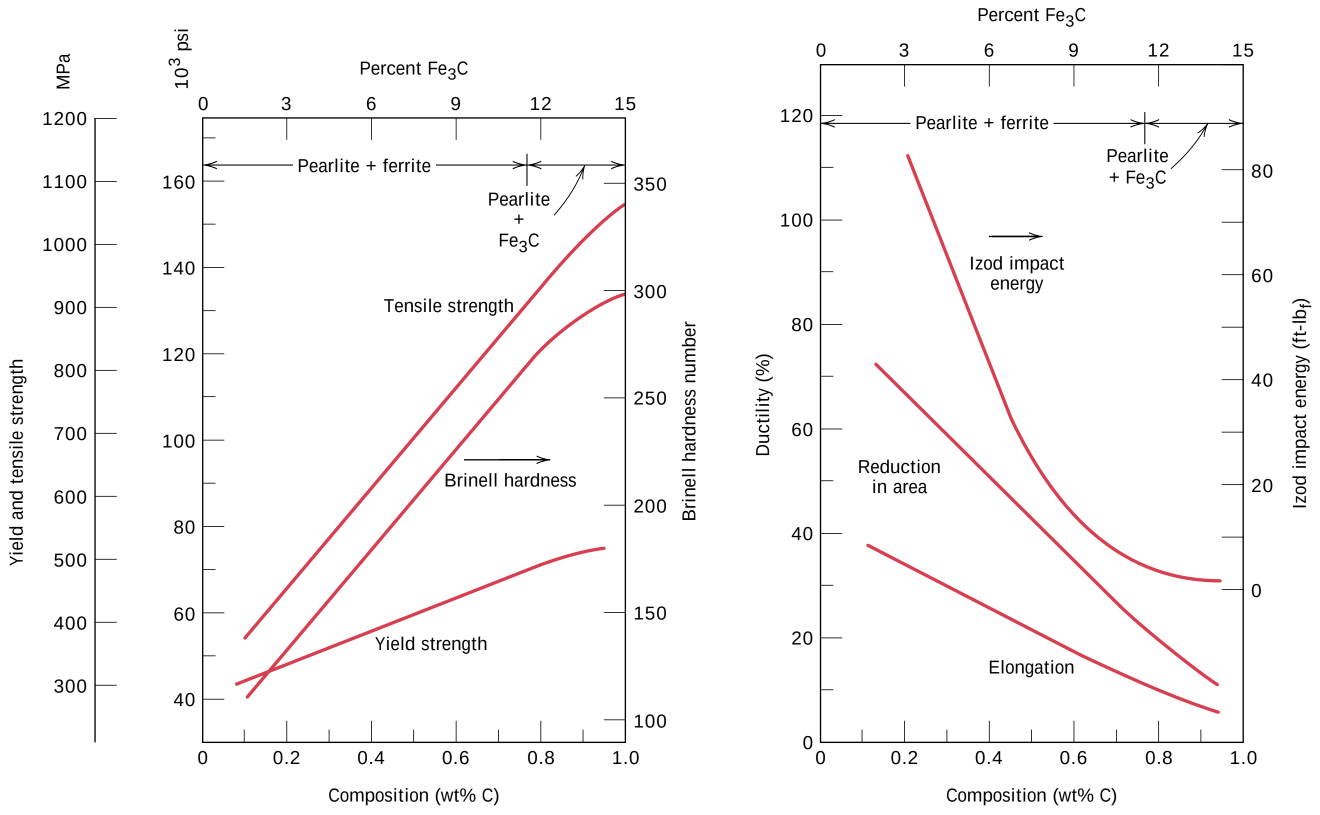

(a) (b)

Figure 11.21 (*a*) Yield strength, tensile strength, and Brinell hardness versus carbon concentration for plain carbon steels having microstructures consisting of fine pearlite. (*b*) Ductility (%EL and %RA) and Izod impact energy versus carbon concentration for plain carbon steels having microstructures consisting of fine pearlite. (Data taken from *Metals Handbook: Heat Treating*, Vol. 4, 9th edition, V. Masseria, Managing Editor, American Society for Metals, 1981, p. 9.)

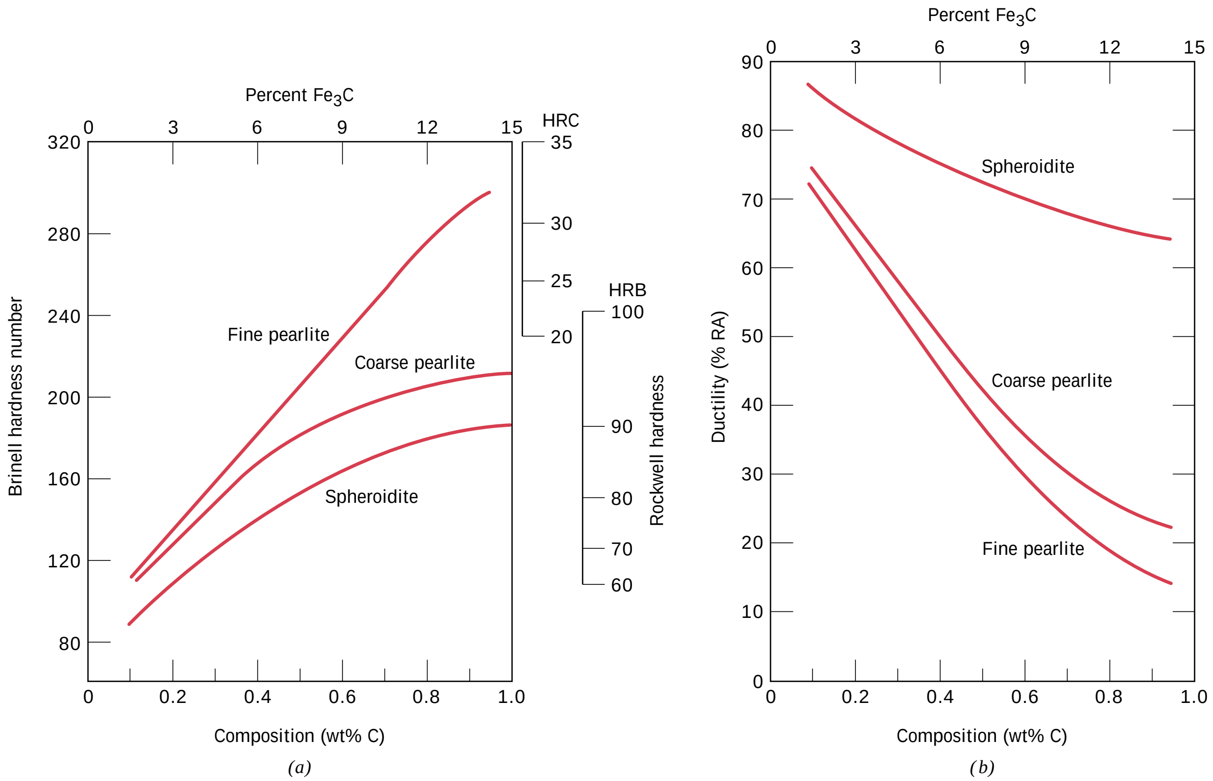

FIGURE 11.22 (*a*) Brinell and Rockwell hardness as a function of carbon concentration for plain carbon steels having fine and coarse pearlite as well as spheroidite microstructures. (*b*) Ductility (%RA) as a function of carbon concentration for plain carbon steels having fine and coarse pearlite as well as spheroidite microstructures. (Data taken from *Metals Handbook: Heat Treating,* Vol. 4, 9th edition, V. Masseria, Managing Editor, American Society for Metals, 1981, pp. 9 and 17.)

BAINITE

Because bainitic steels have a finer structure (i.e., smaller α-ferrite and Fe_3C particles), they are generally stronger and harder than pearlitic ones; yet they exhibit a desirable combination of strength and ductility. Figure 11.23 shows the influence of transformation temperature on the tensile strength and hardness for an iron–carbon alloy of eutectoid composition; temperature ranges over which pearlite and bainite form (consistent with the isothermal transformation diagram for this alloy, Figure 11.9) are noted at the top of Figure 11.23.

MARTENSITE

Of the various microstructures that may be produced for a given steel alloy, martensite is the hardest and strongest and, in addition, the most brittle; it has, in fact, negligible ductility. Its hardness is dependent on the carbon content, up to about 0.6 wt% as demonstrated in Figure 11.24, which plots the hardness of martensite and fine pearlite as a function of weight percent carbon. In contrast to pearlitic steels, strength and hardness of martensite are not thought to be related to microstructure.

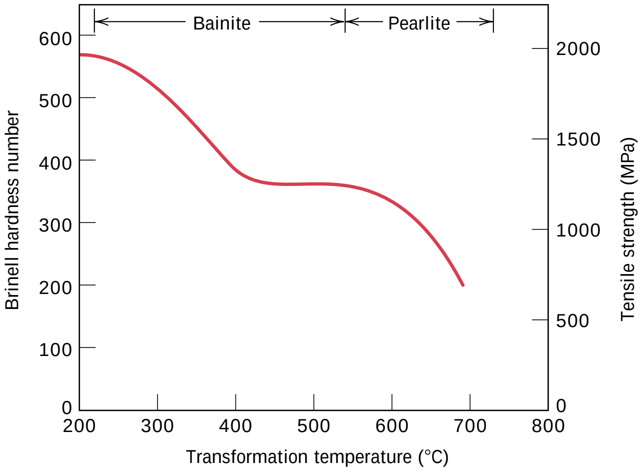

FIGURE 11.23 Brinell hardness and tensile strength as a function of isothermal transformation temperature for an iron–carbon alloy of eutectoid composition, taken over the temperature range at which bainitic and pearlitic microstructures form. (Adapted from E. S. Davenport, ''Isothermal Transformation in Steels,'' *Trans. ASM,* **27,** 1939, p. 847. Reprinted by permission of ASM International.)

Rather, these properties are attributed to the effectiveness of the interstitial carbon atoms in hindering dislocation motion (as a solid-solution effect, Section 8.10), and to the relatively few slip systems (along which dislocations move) for the BCT structure.

Austenite is slightly denser than martensite, and therefore, during the phase transformation upon quenching, there is a net volume increase. Consequently, relatively large pieces that are rapidly quenched may crack as a result of internal stresses; this becomes a problem especially when the carbon content is greater than about 0.5 wt%.

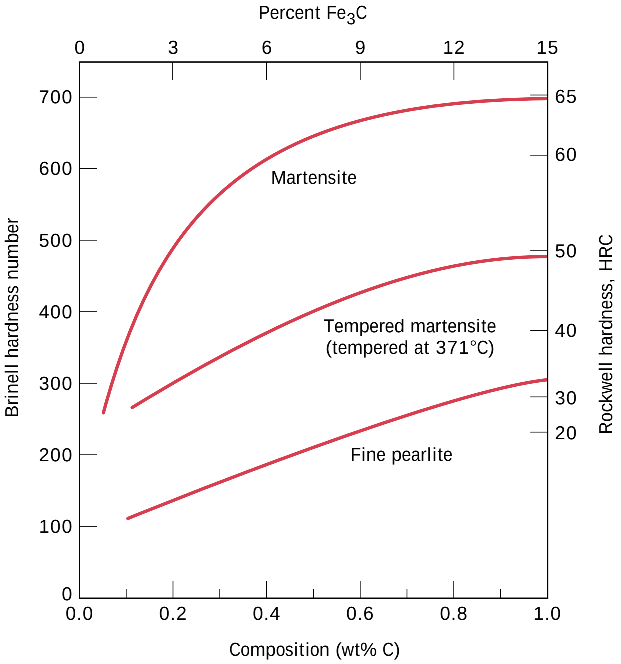

FIGURE 11.24 Hardness as a function of carbon concentration for plain carbon martensitic, tempered martensitic [tempered at 371°C (700°F)], and pearlitic steels. (Adapted from Edgar C. Bain, *Functions of the Alloying Elements in Steel,* American Society for Metals, 1939, p. 36; and R. A. Grange, C. R. Hribal, and L. F. Porter: *Metall. Trans. A,* Vol. 8A, p. 1776.)

11.8 TEMPERED MARTENSITE

In the as-quenched state, martensite, in addition to being very hard, is so brittle that it cannot be used for most applications; also, any internal stresses that may have been introduced during quenching have a weakening effect. The ductility and toughness of martensite may be enhanced and these internal stresses relieved by a heat treatment known as *tempering.*

Tempering is accomplished by heating a martensitic steel to a temperature below the eutectoid for a specified time period. Normally, tempering is carried out at temperatures between 250 and 650°C (480 and 1200°F); internal stresses, however, may be relieved at temperatures as low as 200°C (390°F). This tempering heat treatment allows, by diffusional processes, the formation of **tempered martensite,** according to the reaction

$$\text{martensite (BCT, single phase)} \rightarrow \text{tempered martensite } (\alpha + \text{Fe}_3\text{C phases}) \tag{11.4}$$

where the single-phase BCT martensite, which is supersaturated with carbon, transforms to the tempered martensite, composed of the stable ferrite and cementite phases, as indicated on the iron–iron carbide phase diagram.

The microstructure of tempered martensite consists of extremely small and uniformly dispersed cementite particles embedded within a continuous ferrite matrix. This is similar to the microstructure of spheroidite except that the cementite particles are much, much smaller. An electron micrograph showing the microstructure of tempered martensite at a very high magnification is presented in Figure 11.25.

Tempered martensite may be nearly as hard and strong as martensite, but with substantially enhanced ductility and toughness. For example, on the hardness-versus-weight percent carbon plot of Figure 11.24 is included a curve for tempered martensite. The hardness and strength may be explained by the large ferrite–cementite phase boundary area per unit volume that exists for the very fine and numerous cementite particles. Again, the hard cementite phase reinforces the ferrite matrix along the boundaries, and these boundaries also act as barriers to dislocation motion during plastic deformation. The continuous ferrite phase is also very ductile and relatively tough, which accounts for the improvement of these two properties for tempered martensite.

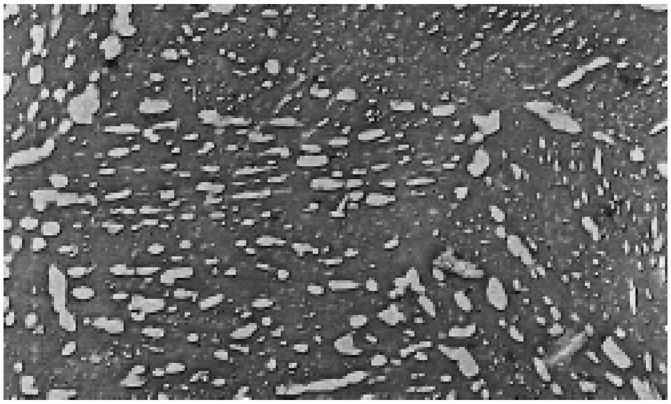

FIGURE 11.25 Electron micrograph of tempered martensite. Tempering was carried out at 594°C (1100°F). The small particles are the cementite phase; the matrix phase is α ferrite. 9300×. (Copyright 1971 by United States Steel Corporation.)

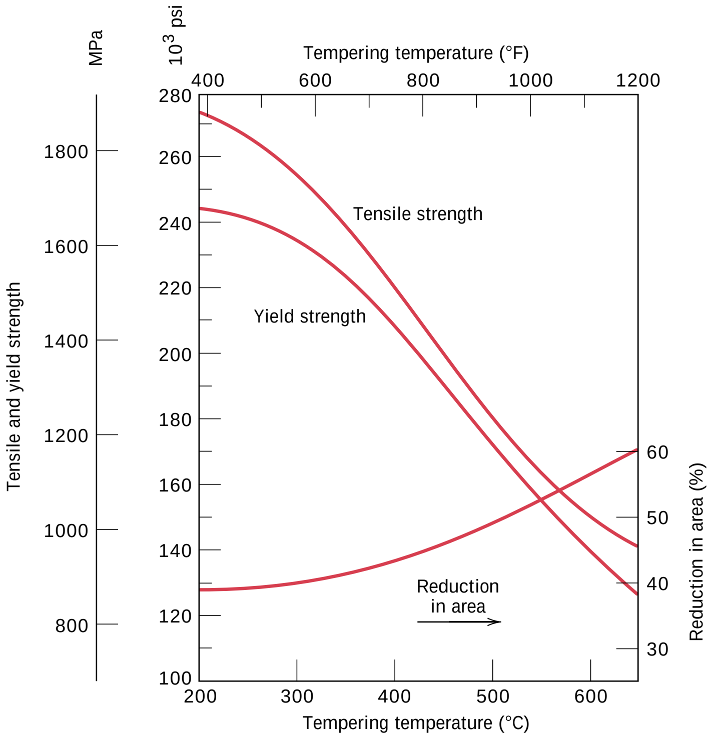

Figure 11.26 Tensile and yield strengths and ductility (%RA) versus tempering temperature for an oil-quenched alloy steel (type 4340). (Adapted from figure furnished courtesy Republic Steel Corporation.)

The size of the cementite particles influences the mechanical behavior of tempered martensite; increasing the particle size decreases the ferrite–cementite phase boundary area and, consequently, results in a softer and weaker material yet one that is tougher and more ductile. Furthermore, the tempering heat treatment determines the size of the cementite particles. Heat treatment variables are temperature and time, and most treatments are constant-temperature processes. Since carbon diffusion is involved in the martensite-tempered martensite transformation, increasing the temperature will accelerate diffusion, the rate of cementite particle growth, and, subsequently, the rate of softening. The dependence of tensile and yield strength and ductility on tempering temperature for an alloy steel is shown in Figure 11.26. Before tempering, the material was quenched in oil to produce the martensitic structure; the tempering time at each temperature was 1 h. This type of tempering data is ordinarily provided by the steel manufacturer.

The time dependence of hardness at several different temperatures is presented in Figure 11.27 for a water-quenched steel of eutectoid composition; the time scale is logarithmic. With increasing time the hardness decreases, which corresponds to the growth and coalescence of the cementite particles. At temperatures approaching the eutectoid [700°C (1300°F)] and after several hours, the microstructure will have become spheroiditic (Figure 11.10), with large cementite spheroids embedded within the continuous ferrite phase. Correspondingly, overtempered martensite is relatively soft and ductile.

TEMPER EMBRITTLEMENT

The tempering of some steels may result in a reduction of toughness as measured by impact tests (Section 9.8); this is termed *temper embrittlement.* The phenomenon

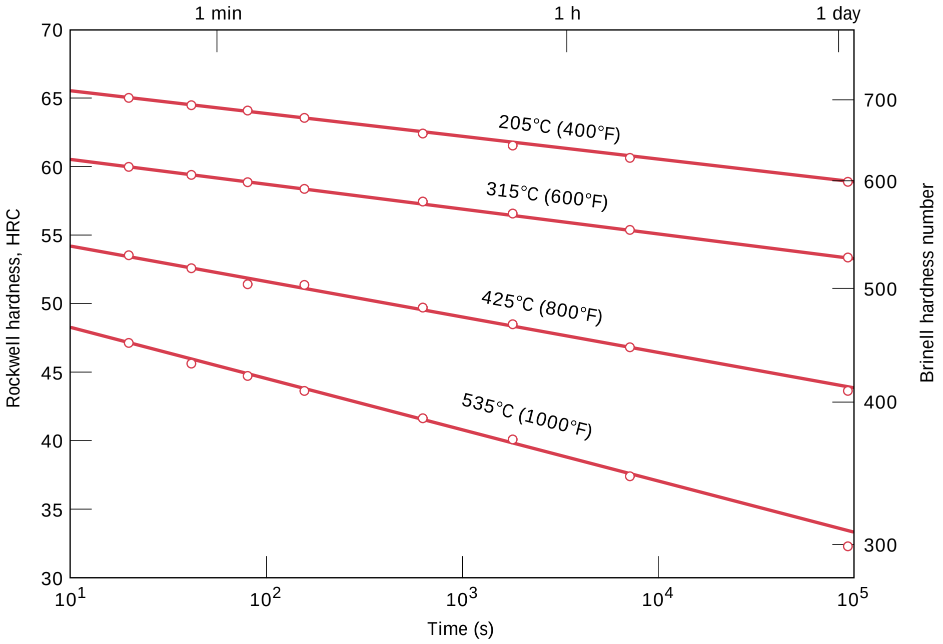

Figure 11.27 Hardness versus tempering time for a water-quenched eutectoid plain carbon (1080) steel. (Adapted from Edgar C. Bain, *Functions of the Alloying Elements in Steel*, American Society for Metals, 1939, p. 233.)

occurs when the steel is tempered at a temperature above about 575°C (1070°F) followed by slow cooling to room temperature, or when tempering is carried out at between approximately 375 and 575°C (700 and 1070°F). Steel alloys that are susceptible to temper embrittlement have been found to contain appreciable concentrations of the alloying elements manganese, nickel, or chromium and, in addition, one or more of antimony, phosphorus, arsenic, and tin as impurities in relatively low concentrations. The presence of these alloying elements and impurities shifts the ductile-to-brittle transition to significantly higher temperatures; the ambient temperature thus lies below this transition in the brittle regime. It has been observed that crack propagation of these embrittled materials is intergranular; that is, the fracture path is along the grain boundaries of the precursor austenite phase. Furthermore, alloy and impurity elements have been found to preferentially segregate in these regions.

Temper embrittlement may be avoided by (1) compositional control; and/or (2) tempering above 575°C or below 375°C, followed by quenching to room temperature. Furthermore, the toughness of steels that have been embrittled may be improved significantly by heating to about 600°C (1100°F) and then rapidly cooling to below 300°C (570°F).

11.9 Review of Phase Transformations for Iron–Carbon Alloys

In this chapter several different microstructures that may be produced in iron–carbon alloys depending on heat treatment have been discussed. Figure 11.28 sum-

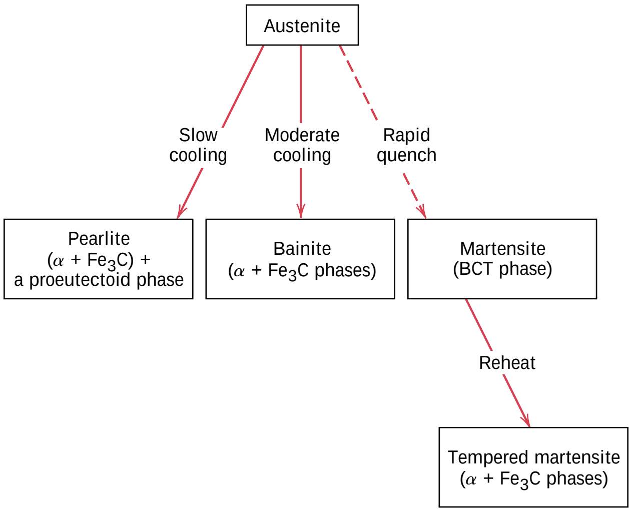
Austenite
Slow cooling
Moderate cooling
Rapid quench
Pearlite (α + Fe_3C) + a proeutectoid phase
Bainite (α + Fe_3C phases)
Martensite (BCT phase)
Reheat
Tempered martensite (α + Fe_3C phases)

Figure 11.28 Possible transformations involving the decomposition of austenite. Solid arrows, transformations involving diffusion; dashed arrow, diffusionless transformation.

marizes the transformation paths that produce these various microstructures. Here, it is assumed that pearlite, bainite, and martensite result from continuous cooling treatments; furthermore, the formation of bainite is only possible for alloy steels (not plain carbon ones) as outlined above.

PRECIPITATION HARDENING

The strength and hardness of some metal alloys may be enhanced by the formation of extremely small uniformly dispersed particles of a second phase within the original phase matrix; this must be accomplished by phase transformations that are induced by appropriate heat treatments. The process is called **precipitation hardening** because the small particles of the new phase are termed ''precipitates.'' ''Age hardening'' is also used to designate this procedure because the strength develops with time, or as the alloy ages. Examples of alloys that are hardened by precipitation treatments include aluminum–copper, copper–beryllium, copper–tin, and magnesium–aluminum; some ferrous alloys are also precipitation hardenable.

Precipitation hardening and the treating of steel to form tempered martensite are totally different phenomena, even though the heat treatment procedures are similar; therefore, the processes should not be confused. The principal difference lies in the mechanisms by which hardening and strengthening are achieved. These should become apparent as precipitation hardening is explained.

11.10 Heat Treatments

Inasmuch as precipitation hardening results from the development of particles of a new phase, an explanation of the heat treatment procedure is facilitated by use of a phase diagram. Even though, in practice, many precipitation-hardenable alloys contain two or more alloying elements, the discussion is simplified by reference to a binary system. The phase diagram must be of the form shown for the hypothetical A–B system in Figure 11.29.

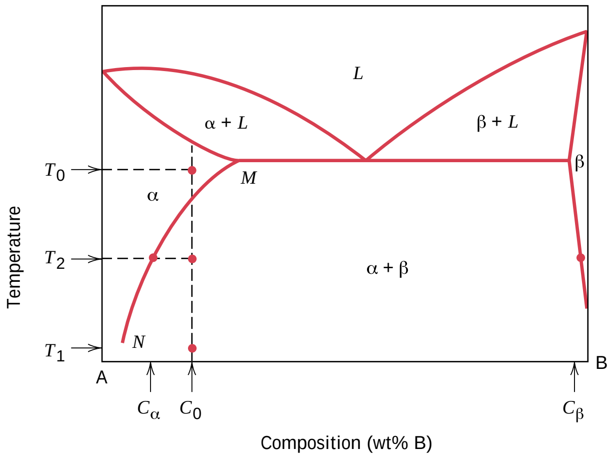

FIGURE 11.29 Hypothetical phase diagram for a precipitation hardenable alloy of composition C_0.

Two requisite features must be displayed by the phase diagrams of alloy systems for precipitation hardening: an appreciable maximum solubility of one component in the other, on the order of several percent; and a solubility limit that rapidly decreases in concentration of the major component with temperature reduction. Both these conditions are satisfied by this hypothetical phase diagram (Figure 11.29). The maximum solubility corresponds to the composition at point *M*. In addition, the solubility limit boundary between the α and $\alpha + \beta$ phase fields diminishes from this maximum concentration to a very low B content in A at point *N*. Furthermore, the composition of a precipitation-hardenable alloy must be less than the maximum solubility. These conditions are necessary but *not* sufficient for precipitation hardening to occur in an alloy system. An additional requirement is discussed below.

SOLUTION HEAT TREATING

Precipitation hardening is accomplished by two different heat treatments. The first is a **solution heat treatment** in which all solute atoms are dissolved to form a single-phase solid solution. Consider an alloy of composition C_0 in Figure 11.29. The treatment consists of heating the alloy to a temperature within the α phase field—say, T_0—and waiting until all the β phase that may have been present is completely dissolved. At this point, the alloy consists only of an α phase of composition C_0. This procedure is followed by rapid cooling or quenching to temperature T_1, which for many alloys is room temperature, to the extent that any diffusion and the accompanying formation of any of the β phase is prevented. Thus, a nonequilibrium situation exists in which only the α phase solid solution supersaturated with B atoms is present at T_1; in this state the alloy is relatively soft and weak. Furthermore, for most alloys diffusion rates at T_1 are extremely slow, such that the single α phase is retained at this temperature for relatively long periods.

PRECIPITATION HEAT TREATING

For the second or **precipitation heat treatment,** the supersaturated α solid solution is ordinarily heated to an intermediate temperature T_2 (Figure 11.29) within the $\alpha + \beta$ two-phase region, at which temperature diffusion rates become appreciable. The β precipitate phase begins to form as finely dispersed particles of composition C_β, which process is sometimes termed ''aging.'' After the appropriate aging time

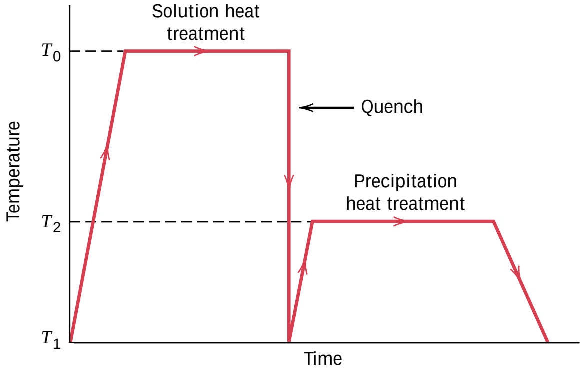

Figure 11.30 Schematic temperature-versus-time plot showing both solution and precipitation heat treatments for precipitation hardening.

at T_2, the alloy is cooled to room temperature; normally, this cooling rate is not an important consideration. Both solution and precipitation heat treatments are represented on the temperature-versus-time plot, Figure 11.30. The character of these β particles, and subsequently the strength and hardness of the alloy, depend on both the precipitation temperature T_2 and the aging time at this temperature. For some alloys, aging occurs spontaneously at room temperature over extended time periods.

The dependence of the growth of the precipitate β particles on time and temperature under isothermal heat treatment conditions may be represented by C-shaped curves similar to those in Figure 11.9 for the eutectoid transformation in steels. However, it is more useful and convenient to present the data as tensile strength, yield strength, or hardness at room temperature as a function of the logarithm of aging time, at constant temperature T_2. The behavior for a typical precipitation-hardenable alloy is represented schematically in Figure 11.31. With increasing time, the strength or hardness increases, reaches a maximum, and finally diminishes. This reduction in strength and hardness that occurs after long time periods is known as **overaging.** The influence of temperature is incorporated by the superposition, on a single plot, of curves at a variety of temperatures.

11.11 MECHANISM OF HARDENING

Precipitation hardening is commonly employed with high-strength aluminum alloys. Although a large number of these alloys have different proportions and combina-

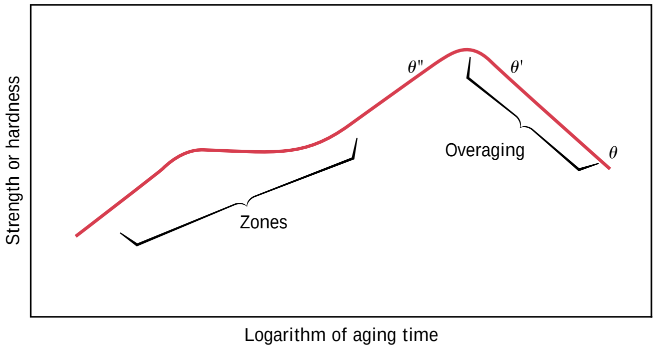

Figure 11.31 Schematic diagram showing strength and hardness as a function of the logarithm of aging time at constant temperature during the precipitation heat treatment.

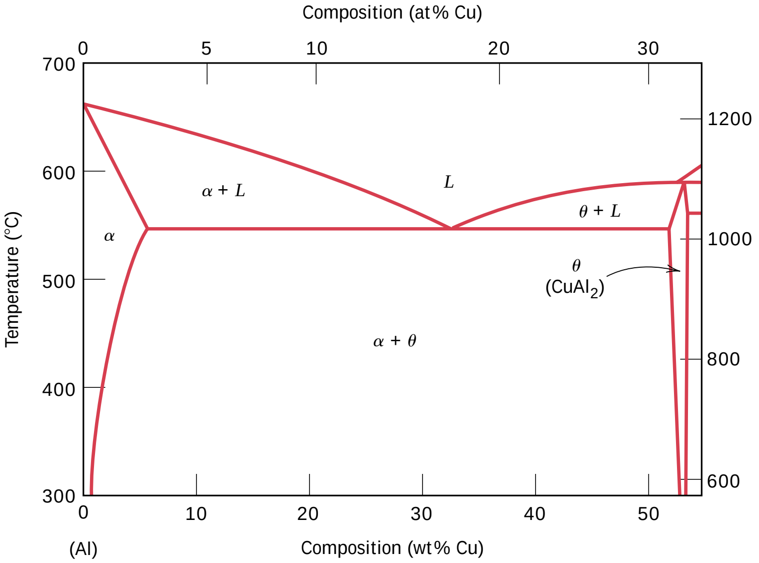

FIGURE 11.32 The aluminum-rich side of the aluminum–copper phase diagram. (Adapted from J. L. Murray, *International Metals Review*, **30,** 5, 1985. Reprinted by permission of ASM International.)

tions of alloying elements, the mechanism of hardening has perhaps been studied most extensively for the aluminum–copper alloys. Figure 11.32 presents the aluminum-rich portion of the aluminum–copper phase diagram. The α phase is a substitutional solid solution of copper in aluminum, whereas the intermetallic compound $CuAl_2$ is designated the θ phase. For an aluminum–copper alloy of, say, composition 96 wt% Al–4 wt% Cu, in the development of this equilibrium θ phase during the precipitation heat treatment, several transition phases are first formed in a specific sequence. The mechanical properties are influenced by the character of the particles of these transition phases. During the initial hardening stage (at short times, Figure 11.31), copper atoms cluster together in very small and thin discs that are only one or two atoms thick and approximately 25 atoms in diameter; these form at countless positions within the α phase. The clusters, sometimes called zones, are so small that they are really not regarded as distinct precipitate particles. However, with time and the subsequent diffusion of copper atoms, zones become particles as they increase in size. These precipitate particles then pass through two transition phases (denoted as θ'' and θ'), before the formation of the equilibrium θ phase (Figure 11.33*c*). Transition phase particles for a precipitation-hardened 7150 aluminum alloy are shown in the electron micrograph of the chapter-opening photograph for this chapter.

The strengthening and hardening effects shown in Figure 11.31 result from the innumerable particles of these transition and metastable phases. As noted in the figure, maximum strength coincides with the formation of the θ'' phase, which may be preserved upon cooling the alloy to room temperature. Overaging results from continued particle growth and the development of θ' and θ phases.

The strengthening process is accelerated as the temperature is increased. This is demonstrated in Figure 11.34*a*, a plot of tensile strength versus the logarithm of time for a 2014 aluminum alloy at several different precipitation temperatures. Ideally, temperature and time for the precipitation heat treatment should be designed to produce a hardness or strength in the vicinity of the maximum. Associated with an increase in strength is a reduction in ductility. This is demonstrated in Figure 11.34*b* for the same 2014 aluminum alloy at the several temperatures.

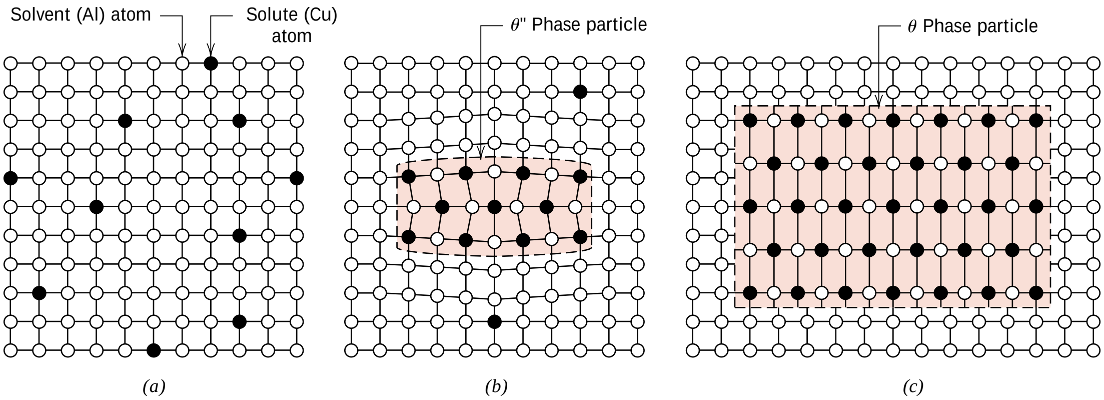

Figure 11.33 Schematic depiction of several stages in the formation of the equilibrium precipitate (θ) phase. (*a*) A supersaturated α solid solution. (*b*) A transition, θ'', precipitate phase. (*c*) The equilibrium θ phase, within the α matrix phase. Actual phase particle sizes are much larger than shown here.

Not all alloys that satisfy the aforementioned conditions relative to composition and phase diagram configuration are amenable to precipitation hardening. In addition, lattice strains must be established at the precipitate–matrix interface. For aluminum–copper alloys, there is a distortion of the crystal lattice structure around and within the vicinity of particles of these transition phases (Figure 11.33*b*). During plastic deformation, dislocation motions are effectively impeded as a result of these distortions, and, consequently, the alloy becomes harder and stronger. As the θ phase forms, the resultant overaging (softening and weakening) is explained by a reduction in the resistance to slip that is offered by these precipitate particles.

Alloys that experience appreciable precipitation hardening at room temperature and after relatively short time periods must be quenched to and stored under refrigerated conditions. Several aluminum alloys that are used for rivets exhibit this behavior. They are driven while still soft, then allowed to age harden at the normal ambient temperature. This is termed **natural aging**; **artificial aging** is carried out at elevated temperatures.

11.12 MISCELLANEOUS CONSIDERATIONS

The combined effects of strain hardening and precipitation hardening may be employed in high-strength alloys. The order of these hardening procedures is important in the production of alloys having the optimum combination of mechanical properties. Normally, the alloy is solution heat treated and then quenched. This is followed by cold working and finally by the precipitation hardening heat treatment. In the final treatment, little strength loss is sustained as a result of recrystallization. If the alloy is precipitation hardened before cold working, more energy must be expended in its deformation; in addition, cracking may also result because of the reduction in ductility that accompanies the precipitation hardening.

Most precipitation-hardened alloys are limited in their maximum service temperatures. Exposure to temperatures at which aging occurs may lead to a loss of strength due to overaging.

Figure 11.34 The precipitation hardening characteristics of a 2014 aluminum alloy (0.9 wt% Si, 4.4 wt% Cu, 0.8 wt% Mn, 0.5 wt% Mg) at four different aging temperatures: (*a*) tensile strength, and (*b*) ductility (%EL). (Adapted from *Metals Handbook: Properties and Selection: Nonferrous Alloys and Pure Metals*, Vol. 2, 9th edition, H. Baker, Managing Editor, American Society for Metals, 1979, p. 41.)

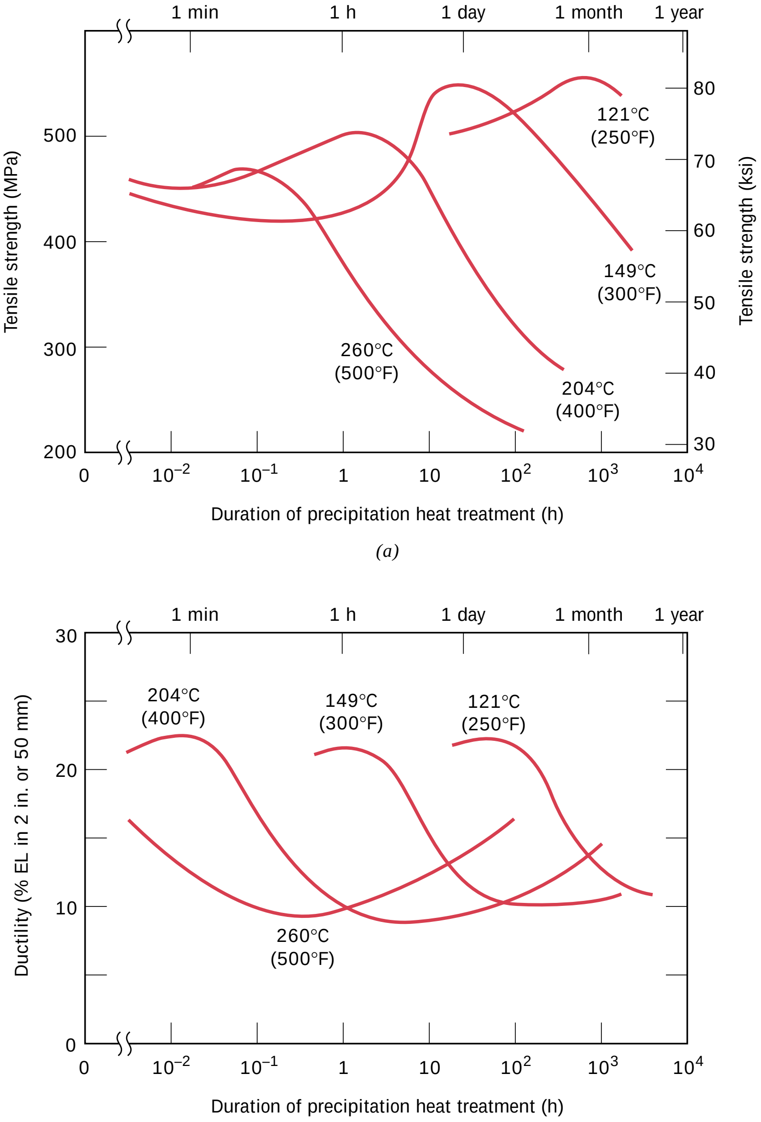

(*a*)

(*b*)

CRYSTALLIZATION, MELTING, AND GLASS TRANSITION PHENOMENA IN POLYMERS

Phase transformation phenomena are important with respect to the design and processing of polymeric materials. In the succeeding sections we discuss three of these phenomena—viz., crystallization, melting, and the glass transition.

Crystallization is the process by which, upon cooling, an ordered (i.e., crystalline) solid phase is produced from a liquid melt having a highly random molecular structure. The melting transformation is the reverse process that occurs when a polymer is heated. The glass-transition phenomenon occurs with amorphous or noncrystallizable polymers which, when cooled from a liquid melt, become rigid solids yet retain the disordered molecular structure that is characteristic of the liquid state. Of course, alterations of physical and mechanical properties attend crystallization, melting, and the glass transition. Furthermore, for semicrystalline polymers, crystalline regions will experience melting (and crystallization), while noncrystalline areas pass through the glass transition.

11.13 CRYSTALLIZATION

An understanding of the mechanism and kinetics of polymer crystallization is important inasmuch as the degree of crystallinity influences the mechanical and thermal properties of these materials. The crystallization of a molten polymer occurs by nucleation and growth processes, topics discussed in the context of phase transformations for metals in Section 11.3. For polymers, upon cooling through the melting temperature, nuclei form wherein small regions of the tangled and random molecules become ordered and aligned in the manner of chain-folded layers, Figure 4.13. At temperatures in excess of the melting temperature, these nuclei are unstable due to the thermal atomic vibrations that tend to disrupt the ordered molecular arrangements. Subsequent to nucleation and during the crystallization growth stage, nuclei grow by the continued ordering and alignment of additional molecular chain segments; that is, the chain-folded layers increase in lateral dimensions, or, for spherulitic structures (Figure 4.14) there is an increase in spherulite radius.

The time dependence of crystallization is the same as for many solid-state transformations—Figure 11.1; that is, a sigmoidal-shaped curve results when fraction transformation (i.e., fraction crystallized) is plotted versus the logarithm of time (at constant temperature). Such a plot is presented in Figure 11.35 for the crystallization of polypropylene at three temperatures. Mathematically, fraction crystallized y is a function of time t according to the Avrami equation, Equation 11.1, as

$$y = 1 - \exp(-kt^n) \tag{11.1}$$

where k and n are time-independent constants, which values depend on the crystallizing system. Normally, the extent of crystallization is measured by specimen volume changes since there will be a difference in volume for liquid and crystallized phases. Rate of crystallization may be specified in the same manner as for the

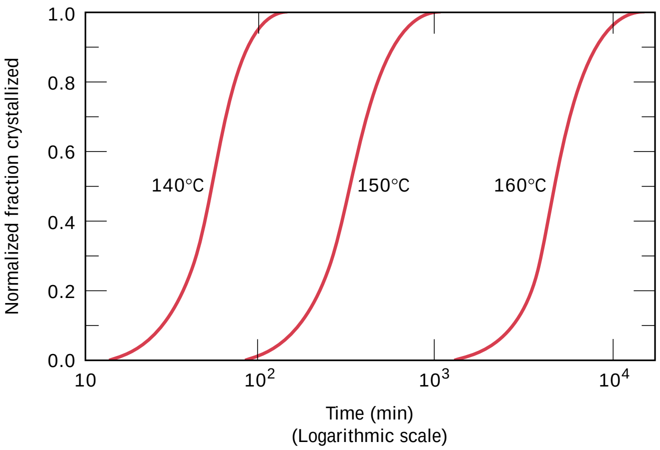

FIGURE 11.35 Plot of normalized fraction crystallized versus the logarithm of time for polypropylene at constant temperatures of 140°C, 150°C, and 160°C. (Adapted from P. Parrini and G. Corrieri, *Makromol. Chem.*, **62,** 83, 1963. Reprinted by permission of Hüthig & Wepf Publishers, Zug, Switzerland.)

transformations discussed in Section 11.3, and according to Equation 11.2; that is, rate is equal to the reciprocal of time required for crystallization to proceed to 50% completion. This rate is dependent on crystallization temperature (Figure 11.35) and also on the molecular weight of the polymer; rate decreases with increasing molecular weight.

For polypropylene, the attainment of 100% crystallinity is not possible. Therefore, in Figure 11.35, the vertical axis is scaled as ''normalized fraction crystallized.'' A value of 1.0 for this parameter corresponds to the highest level of crystallization that is achieved during the tests, which, in reality, is less than complete crystallization.

11.14 Melting

The melting of a polymer crystal corresponds to the transformation of a solid material, having an ordered structure of aligned molecular chains, to a viscous liquid in which the structure is highly random; this phenomenon occurs, upon heating, at the **melting temperature,** T_m. There are several features distinctive to the melting of polymers that are not normally observed with metals and ceramics; these are consequences of the polymer molecular structures and lamellar crystalline morphology. First of all, melting of polymers takes place over a range of temperatures; this phenomenon is discussed in more detail below. In addition, the melting behavior depends on the history of the specimen, in particular the temperature at which it crystallized. The thickness of chain-folded lamellae will depend on crystallization temperature; the thicker the lamellae, the higher the melting temperature. And finally, the apparent melting behavior is a function of the rate of heating; increasing this rate results in an elevation of the melting temperature.

{As Section 8.18 notes, polymeric materials are responsive to heat treatments that produce structural and property alterations. An increase in lamellar thickness may be induced by annealing just below the melting temperature. Annealing also raises the melting temperature of the polymer.}

11.15 The Glass Transition

The glass transition occurs in amorphous (or glassy) and semicrystalline polymers, and is due to a reduction in motion of large segments of molecular chains with decreasing temperature. Upon cooling, the glass transition corresponds to the gradual transformation from a liquid to a rubbery material, and finally, to a rigid solid. The temperature at which the polymer experiences the transition from rubbery to rigid states is termed the **glass transition temperature,** T_g. Of course, this sequence of events occurs in the reverse order when a rigid glass at a temperature below T_g is heated. In addition, abrupt changes in other physical properties accompany this glass transition: e.g., stiffness {(Figure 7.28),} heat capacity, and coefficient of thermal expansion.

11.16 Melting and Glass Transition Temperatures

Melting and glass transition temperatures are important parameters relative to in-service applications of polymers. They define, respectively, the upper and lower temperature limits for numerous applications, especially for semicrystalline poly-

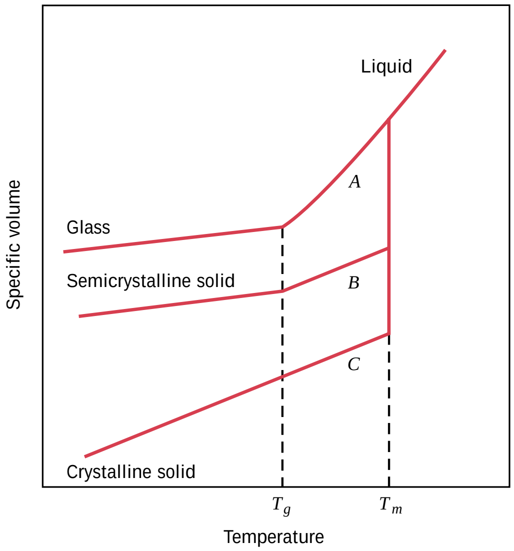

FIGURE 11.36 Specific volume versus temperature, upon cooling from the liquid melt, for totally amorphous (curve *A*), semicrystalline (curve *B*), and crystalline (curve *C*) polymers.

mers. The glass transition temperature may also define the upper use temperature for glassy amorphous materials. Furthermore, T_m and T_g also influence the fabrication and processing procedures for polymers and polymer-matrix composites. {These issues are discussed in other chapters.}

The temperatures at which melting and/or the glass transition occur for a polymer are determined in the same manner as for ceramic materials—from a plot of specific volume (the reciprocal of density) versus temperature. Figure 11.36 is such a plot, wherein curves *A* and *C*, for amorphous and crystalline polymers, respectively.[1] For the crystalline material, there is a discontinuous change in specific volume at the melting temperature T_m. The curve for the totally amorphous material is continuous but it experiences a slight decrease in slope at the glass transition temperature, T_g. The behavior is intermediate between these extremes for a semicrystalline polymer (curve *B*), in that both melting and glass transition phenomena are observed; T_m and T_g are properties of the respective crystalline and amorphous phases in this semicrystalline material. As discussed above, the behaviors represented in Figure 11.36 will depend on the rate of cooling or heating. Representative melting and glass transition temperatures of a number of polymers are contained in Table 11.1 and Appendix E.

11.17 FACTORS THAT INFLUENCE MELTING AND GLASS TRANSITION TEMPERATURES (CD-ROM)

---

[1] It should be noted that no engineering polymer is 100% crystalline; curve *C* is included in Figure 11.36 to illustrate the extreme behavior that would be displayed by a totally crystalline material.

Table 11.1 **Melting and Glass Transition Temperatures for Some of the More Common Polymeric Materials**

Material	*Glass Transition Temperature* [°C (°F)]	*Melting Temperature* [°C (°F)]
Polyethylene (low density)	−110 (−165)	115 (240)
Polytetrafluoroethylene	−97 (−140)	327 (620)
Polyethylene (high density)	−90 (−130)	137 (279)
Polypropylene	−18 (0)	175 (347)
Nylon 6,6	57 (135)	265 (510)
Polyester (PET)	69 (155)	265 (510)
Polyvinyl chloride	87 (190)	212 (415)
Polystyrene	100 (212)	240 (465)
Polycarbonate	150 (300)	265 (510)

SUMMARY

The first set of discussion topics for this chapter has included phase transformations in metals—modifications in the phase structure or microstructure—and how they affect mechanical properties. Some transformations involve diffusional phenomena, which means that their progress is time dependent. For these, some of the basic kinetic concepts were explored, including the relation between degree of reaction completion and time, the notion of transformation rate, and how rate depends on temperature.

As a practical matter, phase diagrams are severely restricted relative to transformations in multiphase alloys, because they provide no information as to phase transformation rates. The element of time is incorporated into both isothermal transformation and continuous cooling transformation diagrams; transformation progress as a function of temperature and elapsed time is expressed for a specific alloy at constant temperature {and for continuous cooling} treatments, respectively. Diagrams of both types were presented for iron–carbon steel alloys, and their utility with regard to the prediction of microstructural products was discussed.

Several microconstituents are possible for steels, the formation of which depends on composition and heat treatment. These microconstituents include fine and coarse pearlite, and bainite, which are composed of ferrite and cementite phases and result from the decomposition of austenite via diffusional processes. A spheroidite microstructure (also consisting of ferrite and cementite phases) may be produced when a steel specimen composed of any of the preceding microstructures is heat treated at a temperature just below the eutectoid. The mechanical characteristics of pearlitic, bainitic, and spheroiditic steels were compared and also explained in terms of their microconstituents.

Martensite, yet another transformation product in steels, results when austenite is cooled very rapidly. It is a metastable and single-phase structure that may be produced in steels by a diffusionless and almost instantaneous transformation of austenite. Transformation progress is dependent on temperature rather than time, and may be represented on both isothermal {and continuous cooling} transformation diagrams. Furthermore, alloying element additions retard the formation rate of pearlite and bainite, thus rendering the martensitic transformation more competitive. Mechanically, martensite is extremely hard; applicability, however, is limited by its brittleness. A tempering heat treatment increases the ductility at some sacrifice of strength and hardness. During tempering, martensite transforms to tempered martensite, which consists of the equilibrium ferrite and cementite phases. Embrittlement of some steel alloys results when specific alloying and impurity elements are present, and upon tempering within a definite temperature range.

Some alloys are amenable to precipitation hardening, that is, to strengthening by the formation of very small particles of a second, or precipitate, phase. Control of particle size, and subsequently the strength, is accomplished by two heat treatments. For the second or precipitation treatment at constant temperature, strength increases with time to a maximum and decreases during overaging. This process is accelerated with rising temperature. The strengthening phenomenon is explained in terms of an increased resistance to dislocation motion by lattice strains, which are established in the vicinity of these microscopically small precipitate particles.

Relative to polymeric materials, the molecular mechanics of crystallization, melting, and the glass transition were discussed. The manner in which melting and glass transition temperatures are determined was outlined; these parameters are important relative to the temperature range over which a particular polymer may be utilized and processed. {The magnitudes of T_m and T_g increase with increasing chain stiffness; stiffness is enhanced by the presence of chain double bonds and side groups that are either bulky or polar. Molecular weight and degree of branching also affect T_m and T_g.}

IMPORTANT TERMS AND CONCEPTS

Alloy steel
Artificial aging
Athermal transformation
Bainite
Coarse pearlite
Continuous cooling transformation diagram
Fine pearlite
Glass transition temperature
Isothermal transformation diagram
Kinetics
Martensite
Melting temperature
Natural aging
Nucleation
Overaging
Phase transformation
Plain carbon steel
Precipitation hardening
Precipitation heat treatment
Solution heat treatment
Spheroidite
Supercooling
Superheating
Tempered martensite
Thermally activated transformation
Transformation rate

REFERENCES

Atkins, M., *Atlas of Continuous Cooling Transformation Diagrams for Engineering Steels*, British Steel Corporation, Sheffield, England, 1980.

Atlas of Isothermal Transformation and Cooling Transformation Diagrams, American Society for Metals, Metals Park, OH, 1977.

Billmeyer, F. W., Jr., *Textbook of Polymer Science*, 3rd edition, Wiley-Interscience, New York, 1984. Chapter 10.

Brooks, C. R., *Principles of the Heat Treatment of Plain Carbon and Low Alloy Steels*, ASM International, Materials Park, OH, 1996.

Brophy, J. H., R. M. Rose, and J. Wulff, *The Structure and Properties of Materials*, Vol. II, *Thermodynamics of Structure*, John Wiley & Sons, New York, 1964. Reprinted by Books on Demand, Ann Arbor, MI.

Porter, D. A. and K. E. Easterling, *Phase Transformations in Metals and Alloys*, Van Nostrand Reinhold (International) Co. Ltd., Workingham, Berkshire, England, 1981. Reprinted by Chapman and Hall, New York, 1992.

Shewmon, P. G., *Transformations in Metals,* McGraw-Hill Book Company, New York, 1969. Reprinted by Williams Book Company, Tulsa, OK.

Vander Voort, G. (Editor), *Atlas of Time–Temperature Diagrams for Irons and Steels,* ASM International, Materials Park, OH, 1991.

Vander Voort, G. (Editor), *Atlas of Time–Temperature Diagrams for Nonferrous Alloys,* ASM International, Materials Park, OH, 1991.

Young, R. J. and P. Lovell, *Introduction to Polymers,* 2nd edition, Chapman and Hall, London, 1991.

QUESTIONS AND PROBLEMS

Note: To solve those problems having an asterisk (*) by their numbers, consultation of supplementary topics [appearing only on the CD-ROM (and not in print)] will probably be necessary.

11.1 Name the two stages involved in the formation of particles of a new phase. Briefly describe each.

11.2 For some transformation having kinetics that obey the Avrami equation (Equation 11.1), the parameter n is known to have a value of 1.7. If, after 100 s, the reaction is 50% complete, how long (total time) will it take the transformation to go to 99% completion?

11.3 Compute the rate of some reaction that obeys Avrami kinetics, assuming that the constants n and k have values of 3.0 and 7×10^{-3}, respectively, for time expressed in seconds.

11.4 It is known that the kinetics of recrystallization for some alloy obey the Avrami equation and that the value of n in the exponential is 2.5. If, at some temperature, the fraction recrystallized is 0.40 after 200 min, determine the rate of recrystallization at this temperature.

11.5 The kinetics of the austenite-to-pearlite transformation obey the Avrami relationship. Using the fraction transformed–time data given below, determine the total time required for 95% of the austenite to transform to pearlite:

Fraction Transformed	*Time (s)*
0.2	12.6
0.8	28.2

11.6 Below, the fraction recrystallized–time data for the recrystallization at 600°C of a previously deformed steel are tabulated. Assuming that the kinetics of this process obey the Avrami relationship, determine the fraction recrystallized after a total time of 22.8 min.

Fraction Recrystallized	*Time (min)*
0.20	13.1
0.70	29.1

11.7 **(a)** From the curves shown in Figure 11.2 and using Equation 11.2, determine the rate of recrystallization for pure copper at the several temperatures.

(b) Make a plot of ln(rate) versus the reciprocal of temperature (in K^{-1}), and determine the activation energy for this recrystallization process. (See Section 6.5.)

(c) By extrapolation, estimate the length of time required for 50% recrystallization at room temperature, 20°C (293 K).

11.8 In terms of heat treatment and the development of microstructure, what are two major limitations of the iron–iron carbide phase diagram?

11.9 **(a)** Briefly describe the phenomena of superheating and supercooling.

(b) Why do they occur?

11.10 Suppose that a steel of eutectoid composition is cooled to 550°C (1020°F) from 760°C

(1400°F) in less than 0.5 s and held at this temperature.

(a) How long will it take for the austenite-to-pearlite reaction to go to 50% completion? To 100% completion?

(b) Estimate the hardness of the alloy that has completely transformed to pearlite.

11.11 Briefly explain why the reaction rate for the austenite-to-pearlite transformation, as determined from Figure 11.5 and utilizing Equation 11.2, decreases with increasing temperature, in apparent contradiction with Equation 11.3.

11.12 Briefly cite the differences between pearlite, bainite, and spheroidite relative to microstructure and mechanical properties.

11.13 What is the driving force for the formation of spheroidite?

11.14 Using the isothermal transformation diagram for an iron–carbon alloy of eutectoid composition (Figure 11.14), specify the nature of the final microstructure (in terms of microconstituents present and approximate percentages of each) of a small specimen that has been subjected to the following time–temperature treatments. In each case assume that the specimen begins at 760°C (1400°F) and that it has been held at this temperature long enough to have achieved a complete and homogeneous austenitic structure.

(a) Cool rapidly to 700°C (1290°F), hold for 10^4 s, then quench to room temperature.

(b) Reheat the specimen in part a to 700°C (1290°F) for 20 h.

(c) Rapidly cool to 600°C (1110°F), hold for 4 s, rapidly cool to 450°C (840°F), hold for 10 s, then quench to room temperature.

(d) Cool rapidly to 400°C (750°F), hold for 2 s, then quench to room temperature.

(e) Cool rapidly to 400°C (750°F), hold for 20 s, then quench to room temperature.

(f) Cool rapidly to 400°C (750°F), hold for 200 s, then quench to room temperature.

(g) Rapidly cool to 575°C (1065°F), hold for 20 s, rapidly cool to 350°C (660°F), hold for 100 s, then quench to room temperature.

(h) Rapidly cool to 250°C (480°F), hold for 100 s, then quench to room temperature in water. Reheat to 315°C (600°F) for 1 h and slowly cool to room temperature.

11.15 Make a copy of the isothermal transformation diagram for an iron–carbon alloy of eutectoid composition (Figure 11.14) and then sketch and label on this diagram time–temperature paths to produce the following microstructures:

(a) 100% coarse pearlite.

(b) 100% tempered martensite.

(c) 50% coarse pearlite, 25% bainite, and 25% martensite.

11.16 Using the isothermal transformation diagram for a 0.45 wt% C steel alloy (Figure 11.38), determine the final microstructure (in terms of just the microconstituents present) of a small specimen that has been subjected to the following time–temperature treatments. In each case assume that the specimen begins at 845°C (1550°F), and that it has been held at this temperature long enough to have achieved a complete and homogeneous austenitic structure.

(a) Rapidly cool to 250°C (480°F), hold for 10^3 s, then quench to room temperature.

(b) Rapidly cool to 700°C (1290°F), hold for 30 s, then quench to room temperature.

(c) Rapidly cool to 400°C (750°F), hold for 500 s, then quench to room temperature.

(d) Rapidly cool to 700°C (1290°F), hold at this temperature for 10^5 s, then quench to room temperature.

(e) Rapidly cool to 650°C (1200°F), hold at this temperature for 3 s, rapidly cool to 400°C (750°F), hold for 10 s, then quench to room temperature.

(f) Rapidly cool to 450°C (840°F), hold for 10 s, then quench to room temperature.

(g) Rapidly cool to 625°C (1155°F), hold for 1 s, then quench to room temperature.

(h) Rapidly cool to 625°C (1155°F), hold at this temperature for 10 s, rapidly cool to 400°C (750°F), hold at this temperature for 5 s, then quench to room temperature.

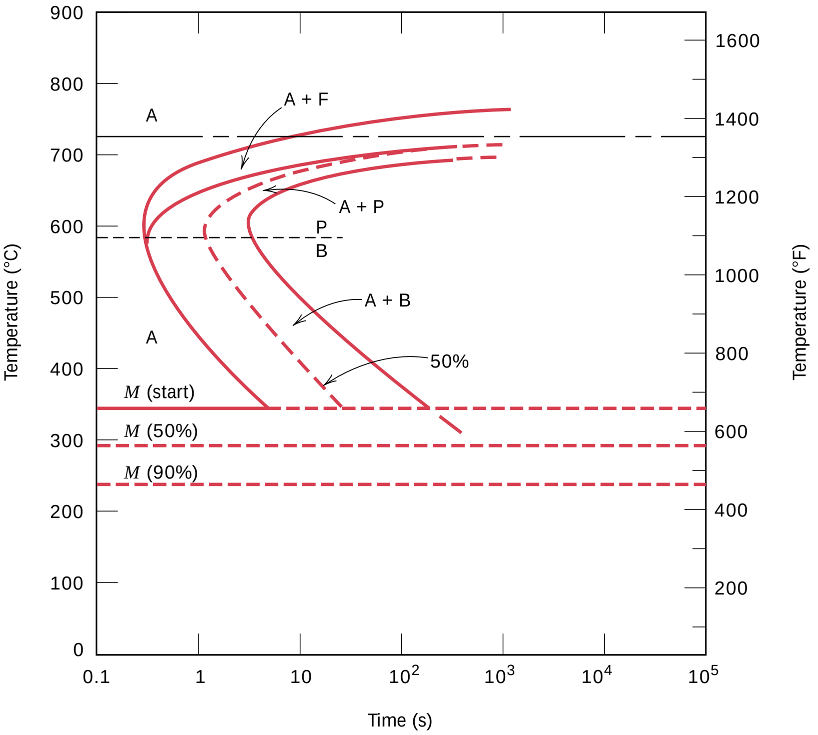

Figure 11.38 Isothermal transformation diagram for a 0.45 wt% C iron–carbon alloy: A, austenite; B, bainite; F, proeutectoid ferrite; M, martensite; P, pearlite. (Adapted from *Atlas of Time-Temperature Diagrams for Irons and Steels,* G. F. Vander Voort, Editor, 1991. Reprinted by permission of ASM International, Materials Park, OH.)

11.17 For parts a, c, d, f, and h of Problem 11.16, determine the approximate percentages of the microconstituents that form.

11.18 Make a copy of the isothermal transformation diagram for a 0.45 wt% C iron–carbon alloy (Figure 11.38), and then sketch and label on this diagram the time–temperature paths to produce the following microstructures:

(a) 42% proeutectoid ferrite and 58% coarse pearlite.

(b) 50% fine pearlite and 50% bainite.

(c) 100% martensite.

(d) 50% martensite and 50% austenite.

11.19* Name the microstructural products of eutectoid iron–carbon alloy (0.76 wt% C) specimens that are first completely transformed to austenite, then cooled to room temperature at the following rates: **(a)** 200°C/s, **(b)** 100°C/s, and **(c)** 20°C/s.

11.20* Figure 11.39 shows the continuous cooling transformation diagram for a 1.13 wt% C iron–carbon alloy. Make a copy of this figure and then sketch and label continuous cooling curves to yield the following microstructures:

(a) Fine pearlite and proeutectoid cementite.

(b) Martensite.

(c) Martensite and proeutectoid cementite.

(d) Coarse pearlite and proeutectoid cementite.

(e) Martensite, fine pearlite, and proeutectoid cementite.

11.21 Cite two major differences between martensitic and pearlitic transformations.

11.22* Cite two important differences between continuous cooling transformation diagrams for plain carbon and alloy steels.

11.23* Briefly explain why there is no bainite transformation region on the continuous cooling transformation diagram for an iron–carbon alloy of eutectoid composition.

11.24* Name the microstructural products of 4340 alloy steel specimens that are first completely transformed to austenite, then

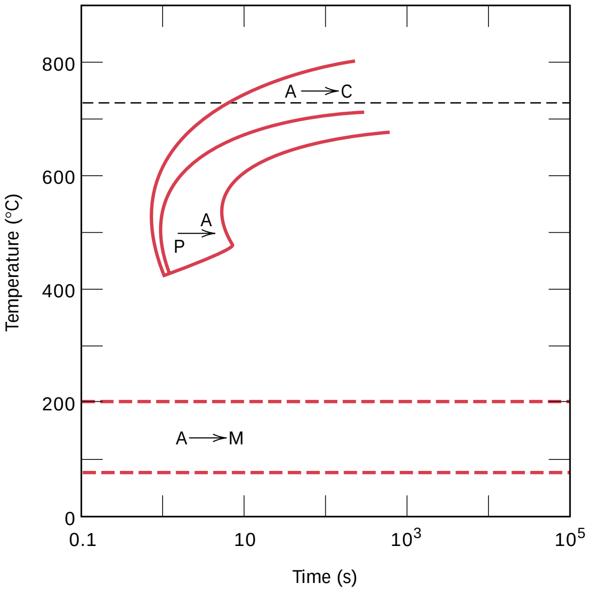

FIGURE 11.39 Continuous cooling transformation diagram for a 1.13 wt% C iron–carbon alloy.

cooled to room temperature at the following rates: **(a)** 10°C/s, **(b)** 1°C/s, **(c)** 0.1°C/s, and **(d)** 0.01°C/s.

11.25* Briefly describe the simplest continuous cooling heat treatment procedure that would be used in converting a 4340 steel from one microstructure to another.

(a) (Martensite + bainite) to (ferrite + pearlite).

(b) (Martensite + bainite) to spheroidite.

(c) (Martensite + bainite) to (martensite + bainite + ferrite).

11.26* On the basis of diffusion considerations, explain why fine pearlite forms for the moderate cooling of austenite through the eutectoid temperature, whereas coarse pearlite is the product for relatively slow cooling rates.

11.27 **(a)** Which is the more stable, the pearlitic or the spheroiditic microstructure?

(b) Why?

11.28 Briefly explain why fine pearlite is harder and stronger than coarse pearlite, which in turn is harder and stronger than spheroidite.

11.29 Cite two reasons why martensite is so hard and brittle.

11.30 Rank the following iron–carbon alloys and associated microstructures from the highest to the lowest tensile strength: **(a)** 0.25 wt%C with spheroidite, **(b)** 0.25 wt%C with coarse pearlite, **(c)** 0.6 wt%C with fine pearlite, and **(d)** 0.6 wt%C with coarse pearlite. Justify this ranking.

11.31 Briefly explain why the hardness of tempered martensite diminishes with tempering time (at constant temperature) and with increasing temperature (at constant tempering time).

11.32* Briefly describe the simplest heat treatment procedure that would be used in converting a 0.76 wt% C steel from one microstructure to the other, as follows:

(a) Spheroidite to tempered martensite.

(b) Tempered martensite to pearlite.

(c) Bainite to martensite.

(d) Martensite to pearlite.

(e) Pearlite to tempered martensite.

(f) Tempered martensite to pearlite.

(g) Bainite to tempered martensite.

(h) Tempered martensite to spheroidite.

11.33 **(a)** Briefly describe the microstructural difference between spheroidite and tempered martensite.

(b) Explain why tempered martensite is much harder and stronger.

11.34 Estimate the Rockwell hardnesses for specimens of an iron–carbon alloy of eutectoid composition that have been subjected to the heat treatments described in parts b, d, f, g, and h of Problem 11.14.

11.35 Estimate the Brinell hardnesses for specimens of a 0.45 wt% C iron–carbon alloy that have been subjected to the heat treatments described in parts a, d, and h of Problem 11.16.

11.36* Determine the approximate tensile strengths for specimens of a eutectoid iron–carbon alloy that have experienced the heat treatments described in parts a and c of Problem 11.19.

11.37 For a eutectoid steel, describe isothermal heat treatments that would be required to yield specimens having the following Rockwell hardnesses: **(a)** 93 HRB, **(b)** 40 HRC, and **(c)** 27 HRC.

11.38 The room-temperature tensile strengths of pure copper and pure silver are 209 MPa and 125 MPa, respectively.

(a) Make a schematic graph of the room-temperature tensile strength versus composition for all compositions between pure copper and pure silver.

(b) On this same graph schematically plot tensile strength versus composition at 600°C.

(c) Explain the shapes of these two curves, as well as any differences between them.

11.39 Compare precipitation hardening (Sections 11.10 and 11.11) and the hardening of steel by quenching and tempering (Sections 11.5, 11.6, and 11.8) with regard to

(a) The total heat treatment procedure.

(b) The microstructures that develop.

(c) How the mechanical properties change during the several heat treatment stages.

11.40 What is the principal difference between natural and artificial aging processes?

11.41* For each of the following pairs of polymers, plot and label schematic specific volume-versus-temperature curves on the same graph (i.e., make separate plots for parts a, b, and c):

(a) Spherulitic polypropylene, of 25% crystallinity, and having a weight-average molecular weight of 75,000 g/mol; spherulitic polystyrene, of 25% crystallinity, and having a weight-average molecular weight of 100,000 g/mol.

(b) Graft poly(styrene-butadiene) copolymer with 10% of available sites crosslinked; random poly(styrene-butadiene) copolymer with 15% of available sites crosslinked.

(c) Polyethylene having a density of 0.985 g/cm^3 and a number-average degree of polymerization of 2500; polyethylene having a density of 0.915 g/cm^3 and a degree of polymerization of 2000.

11.42* For each of the following pairs of polymers, do the following: (1) state whether or not it is possible to determine whether one polymer has a higher melting temperature than the other; (2) if it is possible, note which has the higher melting temperature and then cite reason(s) for your choice; and (3) if it is not possible to decide, then state why.

(a) Isotactic polystyrene that has a density of 1.12 g/cm^3 and a weight-average molecular weight of 150,000 g/mol; syndiotactic polystyrene that has a density of 1.10 g/cm^3 and a weight-average molecular weight of 125,000 g/mol.

(b) Linear polyethylene that has a number-average degree of polymerization of 5,000; linear and isotactic polypropylene that has a number-average degree of polymerization of 6,500.

(c) Branched and isotactic polystyrene that has a weight-average degree of polymerization of 4,000; linear and isotactic polypropylene that has a weight-average degree of polymerization of 7,500.

11.43* Make a schematic plot showing how the modulus of elasticity of an amorphous polymer depends on the glass transition temperature. Assume that molecular weight is held constant.

11.44 Name the following polymer(s) that would be suitable for the fabrication of cups to contain hot coffee: polyethylene, polypropylene, polyvinyl chloride, PET polyester, and polycarbonate. Why?

11.45 Of those polymers listed in Table 11.1, which polymer(s) would be best suited for use as ice cube trays? Why?

Design Problems

11.D1 Is it possible to produce an iron–carbon alloy of eutectoid composition that has a minimum hardness of 90 HRB and a minimum ductility of 35%RA? If so, describe the continuous cooling heat treatment to which the alloy would be subjected to achieve these properties. If it is not possible, explain why.

11.D2 Is it possible to produce an iron–carbon alloy that has a minimum tensile strength of 690 MPa (100,000 psi) and a minimum ductility of 40%RA? If so, what will be its composition and microstructure (coarse and fine pearlites and spheroidite are alternatives)? If this is not possible, explain why.

11.D3 It is desired to produce an iron–carbon alloy that has a minimum hardness of 175 HB and a minimum ductility of 52%RA. Is such an alloy possible? If so, what will be its composition and microstructure (coarse and fine pearlites and spheroidite are alternatives)? If this is not possible, explain why.

11.D4 **(a)** For a 1080 steel that has been water quenched, estimate the tempering time at 425°C (800°F) to achieve a hardness of 50 HRC.

(b) What will be the tempering time at 315°C (600°F) necessary to attain the same hardness?

11.D5 An alloy steel (4340) is to be used in an application requiring a minimum tensile strength of 1380 MPa (200,000 psi) and a minimum ductility of 43%RA. Oil quenching followed by tempering is to be used. Briefly describe the tempering heat treatment.

11.D6 Is it possible to produce an oil-quenched and tempered 4340 steel that has a minimum yield strength of 1400 MPa (203,000 psi) and a ductility of at least 42%RA? If this is possible, describe the tempering heat treatment. If it is not possible, explain why.

11.D7 Copper-rich copper–beryllium alloys are precipitation hardenable. After consulting

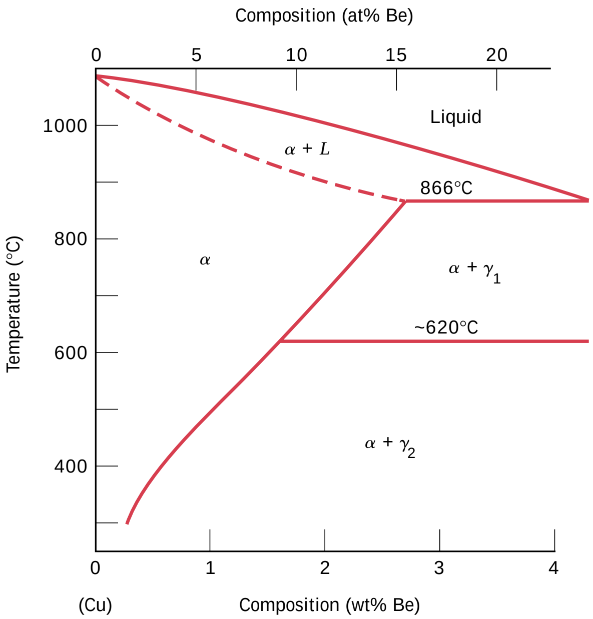

FIGURE 11.40 The copper-rich side of the copper–beryllium phase diagram. (Adapted from *Binary Alloy Phase Diagrams*, 2nd edition, Vol. 2, T. B. Massalski, Editor-in-Chief, 1990. Reprinted by permission of ASM International, Materials Park, OH.)

the portion of the phase diagram (Figure 11.40), do the following:

(a) Specify the range of compositions over which these alloys may be precipitation hardened.

(b) Briefly describe the heat-treatment procedures (in terms of temperatures) that would be used to precipitation harden an alloy having a composition of your choosing, yet lying within the range given for part a.

11.D8 A solution heat-treated 2014 aluminum alloy is to be precipitation hardened to have a minimum tensile strength of 450 MPa (65,250 psi) and a ductility of at least 15%EL. Specify a practical precipitation heat treatment in terms of temperature and time that would give these mechanical characteristics. Justify your answer.

11.D9 Is it possible to produce a precipitation-hardened 2014 aluminum alloy having a minimum tensile strength of 425 MPa (61,625 psi) and a ductility of at least 12%EL? If so, specify the precipitation heat treatment. If it is not possible, explain why.

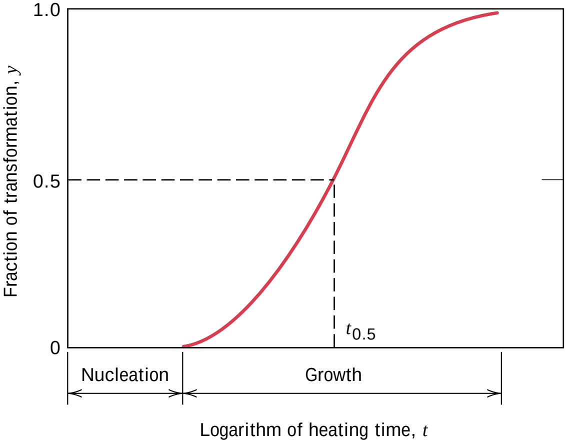

Figure 11.1 Plot of fraction reacted versus the logarithm of time typical of many solid-state transformations in which temperature is held constant.

Chapter 10 / Phase Diagrams

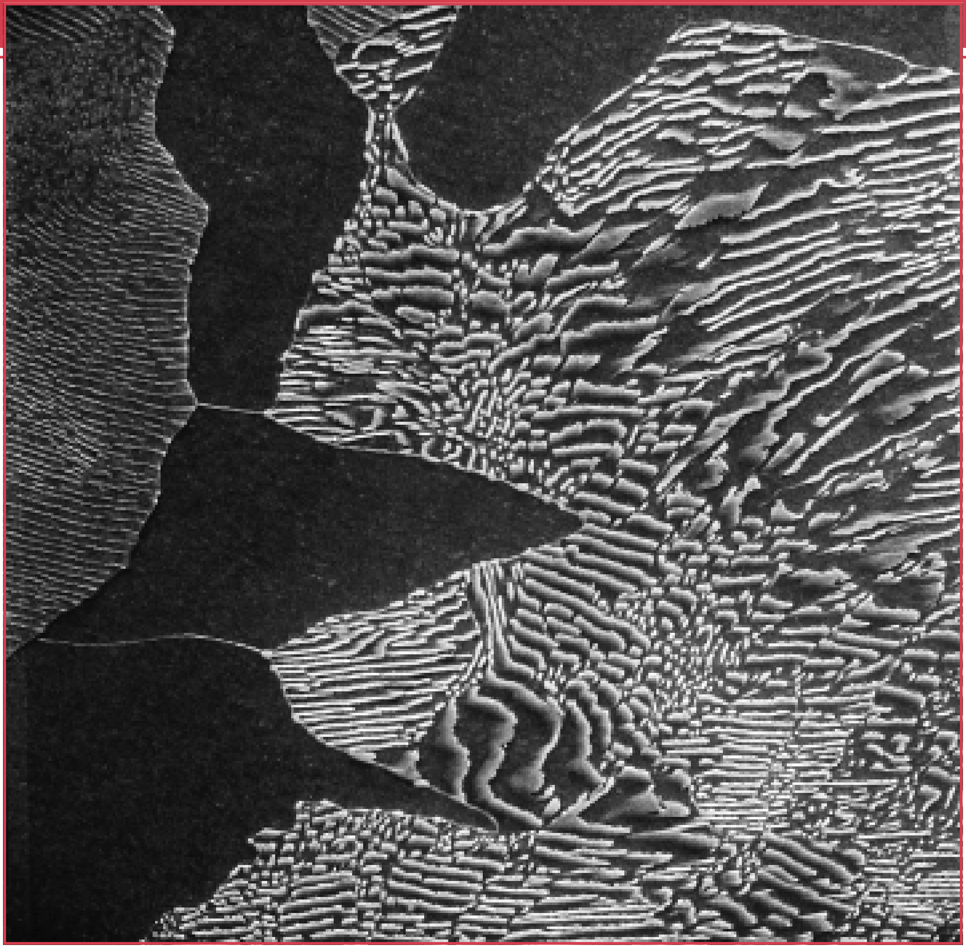

A scanning electron micrograph which shows the microstructure of a plain carbon steel that contains 0.44 wt% C. The large dark areas are proeutectoid ferrite. Regions having the alternating light and dark lamellar structure are pearlite; the dark and light layers in the pearlite correspond, respectively, to ferrite and cementite phases. During etching of the surface prior to examination, the ferrite phase was preferentially dissolved; thus, the pearlite appears in topographical relief with cementite layers being elevated above the ferrite layers. 3000×. (Micrograph courtesy of Republic Steel Corporation.)

Why Study *Phase Diagrams?*

One reason why a knowledge and understanding of phase diagrams is important to the engineer relates to the design and control of heat treating procedures; some properties of materials are functions of their microstructures, and, consequently, of their thermal histories. Even though most phase diagrams represent stable (or equilibrium) states and microstructures, they are, nevertheless useful in understanding the development and preservation of nonequilibrium structures and their attendant properties; it is often the case that these properties are more desirable than those associated with the equilibrium state. This is aptly illustrated by the phenomenon of precipitation hardening (Sections 11.10 and 11.11).

Learning Objectives

After studying this chapter you should be able to do the following:

1. **(a) Schematically sketch simple isomorphous and eutectic phase diagrams.**
   (b) On these diagrams label the various phase regions.
   (c) Label liquidus, solidus, and solvus lines.
2. **Given a binary phase diagram, the composition of an alloy, its temperature, and assuming that the alloy is at equilibrium, determine:**
   (a) what phase(s) is (are) present;
   (b) the composition(s) of the phase(s); and
   (c) the mass fraction(s) of the phase(s).
3. **For some given binary phase diagram, do the following:**
   (a) locate the temperatures and compositions of all eutectic, eutectoid, peritectic, and congruent phase transformations; and
   (b) write reactions for all these transformations for either heating or cooling.
4. **Given the composition of an iron–carbon alloy containing between 0.022 wt% C and 2.14 wt% C, be able to**
   (a) specify whether the alloy is hypoeutectoid or hypereutectoid;
   (b) name the proeutectoid phase;
   (c) compute the mass fractions of proeutectoid phase and pearlite; and
   (d) make a schematic diagram of the microstructure at a temperature just below the eutectoid.

10.1 INTRODUCTION

The understanding of phase diagrams for alloy systems is extremely important because there is a strong correlation between microstructure and mechanical properties, and the development of microstructure of an alloy is related to the characteristics of its phase diagram. In addition, phase diagrams provide valuable information about melting, casting, crystallization, and other phenomena.

This chapter presents and discusses the following topics: (1) terminology associated with phase diagrams and phase transformations; (2) the interpretation of phase diagrams; (3) some of the common and relatively simple binary phase diagrams, including that for the iron–carbon system; and (4) the development of equilibrium microstructures, upon cooling, for several situations.

DEFINITIONS AND BASIC CONCEPTS

It is necessary to establish a foundation of definitions and basic concepts relating to alloys, phases, and equilibrium before delving into the interpretation and utilization of phase diagrams. The term **component** is frequently used in this discussion; components are pure metals and/or compounds of which an alloy is composed. For example, in a copper–zinc brass, the components are Cu and Zn. *Solute* and *solvent*, which are also common terms, were defined in Section 5.4. Another term used in this context is **system,** which has two meanings. First, ''system'' may refer to a specific body of material under consideration (e.g., a ladle of molten steel). Or, it may relate to the series of possible alloys consisting of the same components, but without regard to alloy composition (e.g., the iron–carbon system).

The concept of a solid solution was introduced in Section 5.4. By way of review, a solid solution consists of atoms of at least two different types; the solute atoms occupy either substitutional or interstitial positions in the solvent lattice, and the crystal structure of the solvent is maintained.

10.2 SOLUBILITY LIMIT

For many alloy systems and at some specific temperature, there is a maximum concentration of solute atoms that may dissolve in the solvent to form a solid solution; this is called a **solubility limit.** The addition of solute in excess of this solubility limit results in the formation of another solid solution or compound that has a distinctly different composition. To illustrate this concept, consider the sugar–water ($C_{12}H_{22}O_{11}$–H_2O) system. Initially, as sugar is added to water, a sugar–water solution or syrup forms. As more sugar is introduced, the solution becomes more concentrated, until the solubility limit is reached, or the solution becomes saturated with sugar. At this time the solution is not capable of dissolving any more sugar, and further additions simply settle to the bottom of the container. Thus, the system now consists of two separate substances: a sugar–water syrup liquid solution and solid crystals of undissolved sugar.

This solubility limit of sugar in water depends on the temperature of the water and may be represented in graphical form on a plot of temperature along the ordinate and composition (in weight percent sugar) along the abscissa, as shown in Figure 10.1. Along the composition axis, increasing sugar concentration is from left to right, and percentage of water is read from right to left. Since only two components are involved (sugar and water), the sum of the concentrations at any composition will equal 100 wt%. The solubility limit is represented as the nearly vertical line in the figure. For compositions and temperatures to the left of the solubility line, only the syrup liquid solution exists; to the right of the line, syrup and solid sugar coexist. The solubility limit at some temperature is the composition that corresponds to the intersection of the given temperature coordinate and the solubility limit line. For example, at 20°C the maximum solubility of sugar in water is 65 wt%. As Figure 10.1 indicates, the solubility limit increases slightly with rising temperature.

10.3 PHASES

Also critical to the understanding of phase diagrams is the concept of a **phase.** A phase may be defined as a homogeneous portion of a system that has uniform physical and chemical characteristics. Every pure material is considered to be a

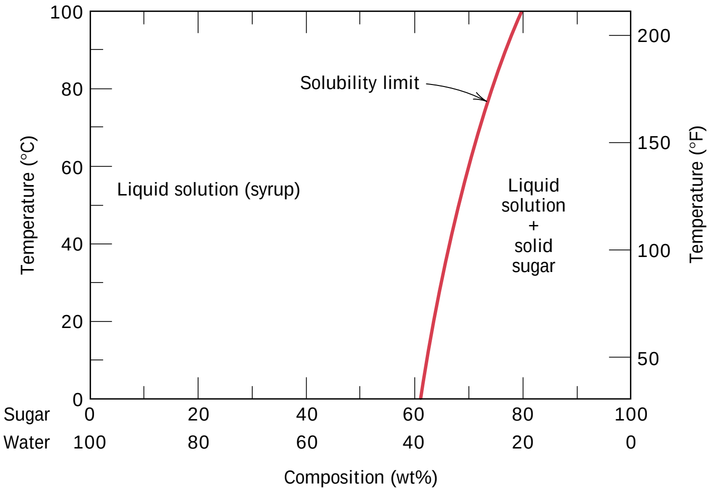

FIGURE 10.1 The solubility of sugar ($C_{12}H_{22}O_{11}$) in a sugar–water syrup.

phase; so also is every solid, liquid, and gaseous solution. For example, the sugar–water syrup solution just discussed is one phase, and solid sugar is another. Each has different physical properties (one is a liquid, the other is a solid); furthermore, each is different chemically (i.e., has a different chemical composition); one is virtually pure sugar, the other is a solution of H_2O and $C_{12}H_{22}O_{11}$. If more than one phase is present in a given system, each will have its own distinct properties, and a boundary separating the phases will exist across which there will be a discontinuous and abrupt change in physical and/or chemical characteristics. When two phases are present in a system, it is not necessary that there be a difference in both physical and chemical properties; a disparity in one or the other set of properties is sufficient. When water and ice are present in a container, two separate phases exist; they are physically dissimilar (one is a solid, the other is a liquid) but identical in chemical makeup. Also, when a substance can exist in two or more polymorphic forms (e.g., having both FCC and BCC structures), each of these structures is a separate phase because their respective physical characteristics differ.

Sometimes, a single-phase system is termed ''homogeneous.'' Systems composed of two or more phases are termed ''mixtures'' or ''heterogeneous systems.'' Most metallic alloys, and, for that matter, ceramic, polymeric, and composite systems are heterogeneous. Ordinarily, the phases interact in such a way that the property combination of the multiphase system is different from, and more attractive than, either of the individual phases.

10.4 MICROSTRUCTURE

Many times, the physical properties and, in particular, the mechanical behavior of a material depend on the microstructure. Microstructure is subject to direct microscopic observation, using optical or electron microscopes; {this topic was touched on in Section 5.12.} In metal alloys, microstructure is characterized by the number of phases present, their proportions, and the manner in which they are distributed or arranged. The microstructure of an alloy depends on such variables as the alloying elements present, their concentrations, and the heat treatment of the alloy (i.e., the temperature, the heating time at temperature, and the rate of cooling to room temperature).

{The procedure of specimen preparation for microscopic examination was briefly outlined in Section 5.12. After appropriate polishing and etching, the different phases may be distinguished by their appearance.} For example, for a two-phase alloy, one phase may appear light, and the other phase dark, as in the chapter-opening photograph for this chapter. When only a single phase or solid solution is present, the texture will be uniform, except for grain boundaries that may be revealed {(Figure 5.16*b*).}

10.5 PHASE EQUILIBRIA

Equilibrium is another essential concept. It is best described in terms of a thermodynamic quantity called the **free energy.** In brief, free energy is a function of the internal energy of a system, and also the randomness or disorder of the atoms or molecules (or entropy). A system is at equilibrium if its free energy is at a minimum under some specified combination of temperature, pressure, and composition. In a macroscopic sense, this means that the characteristics of the system do not change with time but persist indefinitely; that is, the system is stable. A change in temperature, pressure, and/or composition for a system in equilibrium will result in an increase in the free energy and in a possible spontaneous change to another state whereby the free energy is lowered.

The term **phase equilibrium,** often used in the context of this discussion, refers to equilibrium as it applies to systems in which more than one phase may exist. Phase equilibrium is reflected by a constancy with time in the phase characteristics of a system. Perhaps an example best illustrates this concept. Suppose that a sugar–water syrup is contained in a closed vessel and the solution is in contact with solid sugar at 20°C. If the system is at equilibrium, the composition of the syrup is 65 wt% $C_{12}H_{22}O_{11}$–35 wt% H_2O (Figure 10.1), and the amounts and compositions of the syrup and solid sugar will remain constant with time. If the temperature of the system is suddenly raised—say, to 100°C—this equilibrium or balance is temporarily upset in that the solubility limit has been increased to 80 wt% $C_{12}H_{22}O_{11}$ (Figure 10.1). Thus, some of the solid sugar will go into solution in the syrup. This will continue until the new equilibrium syrup concentration is established at the higher temperature.

This sugar–syrup example has illustrated the principle of phase equilibrium using a liquid–solid system. In many metallurgical and materials systems of interest, phase equilibrium involves just solid phases. In this regard the state of the system is reflected in the characteristics of the microstructure, which necessarily include not only the phases present and their compositions but, in addition, the relative phase amounts and their spatial arrangement or distribution.

Free energy considerations and diagrams similar to Figure 10.1 provide information about the equilibrium characteristics of a particular system, which is important; but they do not indicate the time period necessary for the attainment of a new equilibrium state. It is often the case, especially in solid systems, that a state of equilibrium is never completely achieved because the rate of approach to equilibrium is extremely slow; such a system is said to be in a nonequilibrium or **metastable** state. A metastable state or microstructure may persist indefinitely, experiencing only extremely slight and almost imperceptible changes as time progresses. Often, metastable structures are of more practical significance than equilibrium ones. For example, some steel and aluminum alloys rely for their strength on the development of metastable microstructures during carefully designed heat treatments (Sections 11.5 and 11.10).

Thus not only is an understanding of equilibrium states and structures important, but the speed or rate at which they are established and, in addition, the factors that affect the rate must be considered. This chapter is devoted almost exclusively to equilibrium structures; the treatment of reaction rates and nonequilibrium structures is deferred to Chapter 11.

EQUILIBRIUM PHASE DIAGRAMS

Much of the information about the control of microstructure or phase structure of a particular alloy system is conveniently and concisely displayed in what is called a **phase diagram,** also often termed an *equilibrium* or *constitutional diagram*. Many microstructures develop from phase transformations, the changes that occur between phases when the temperature is altered (ordinarily upon cooling). This may involve the transition from one phase to another, or the appearance or disappearance of a phase. Phase diagrams are helpful in predicting phase transformations and the resulting microstructures, which may have equilibrium or nonequilibrium character.

Equilibrium phase diagrams represent the relationships between temperature and the compositions and the quantities of phases at equilibrium. There are several different varieties; but in the present discussion, temperature and composition are the variable parameters, for binary alloys. A binary alloy is one that contains two components. If more than two components are present, phase diagrams become extremely complicated and difficult to represent. The principles of microstructural control with the aid of phase diagrams can be illustrated with binary alloys even though, in reality, most alloys contain more than two components. External pressure is also a parameter that influences the phase structure. However, in practicality, pressure remains virtually constant in most applications; thus, the phase diagrams presented here are for a constant pressure of one atmosphere (1 atm).

10.6 BINARY ISOMORPHOUS SYSTEMS

Possibly the easiest type of binary phase diagram to understand and interpret is that which is characterized by the copper–nickel system (Figure 10.2*a*). Temperature is plotted along the ordinate, and the abscissa represents the composition of the alloy, in weight percent (bottom) and atom percent (top) of nickel. The composition ranges from 0 wt% Ni (100 wt% Cu) on the left horizontal extremity to 100 wt% Ni (0 wt% Cu) on the right. Three different phase regions, or fields, appear on the diagram, an alpha (α) field, a liquid (L) field, and a two-phase $\alpha + L$ field. Each region is defined by the phase or phases that exist over the range of temperatures and compositions delimited by the phase boundary lines.

The liquid L is a homogeneous liquid solution composed of both copper and nickel. The α phase is a substitutional solid solution consisting of both Cu and Ni atoms, and having an FCC crystal structure. At temperatures below about 1080°C, copper and nickel are mutually soluble in each other in the solid state for all compositions. This complete solubility is explained by the fact that both Cu and Ni have the same crystal structure (FCC), nearly identical atomic radii and electronegativities, and similar valences, as discussed in Section 5.4. The copper–nickel system is termed **isomorphous** because of this complete liquid and solid solubility of the two components.

A couple of comments are in order regarding nomenclature. First, for metallic alloys, solid solutions are commonly designated by lowercase Greek letters (α, β, γ, etc.). Furthermore, with regard to phase boundaries, the line separating the L and $\alpha + L$ phase fields is termed the *liquidus line,* as indicated in Figure 10.2*a*; the liquid phase is present at all temperatures and compositions above this line. The *solidus line* is located between the α and $\alpha + L$ regions, below which only the solid α phase exists.

For Figure 10.2*a*, the solidus and liquidus lines intersect at the two composition extremities; these correspond to the melting temperatures of the pure components. For example, the melting temperatures of pure copper and nickel are 1085°C and 1453°C, respectively. Heating pure copper corresponds to moving vertically up the left-hand temperature axis. Copper remains solid until its melting temperature is reached. The solid-to-liquid transformation takes place at the melting temperature, and no further heating is possible until this transformation has been completed.

For any composition other than pure components, this melting phenomenon will occur over the range of temperatures between the solidus and liquidus lines;

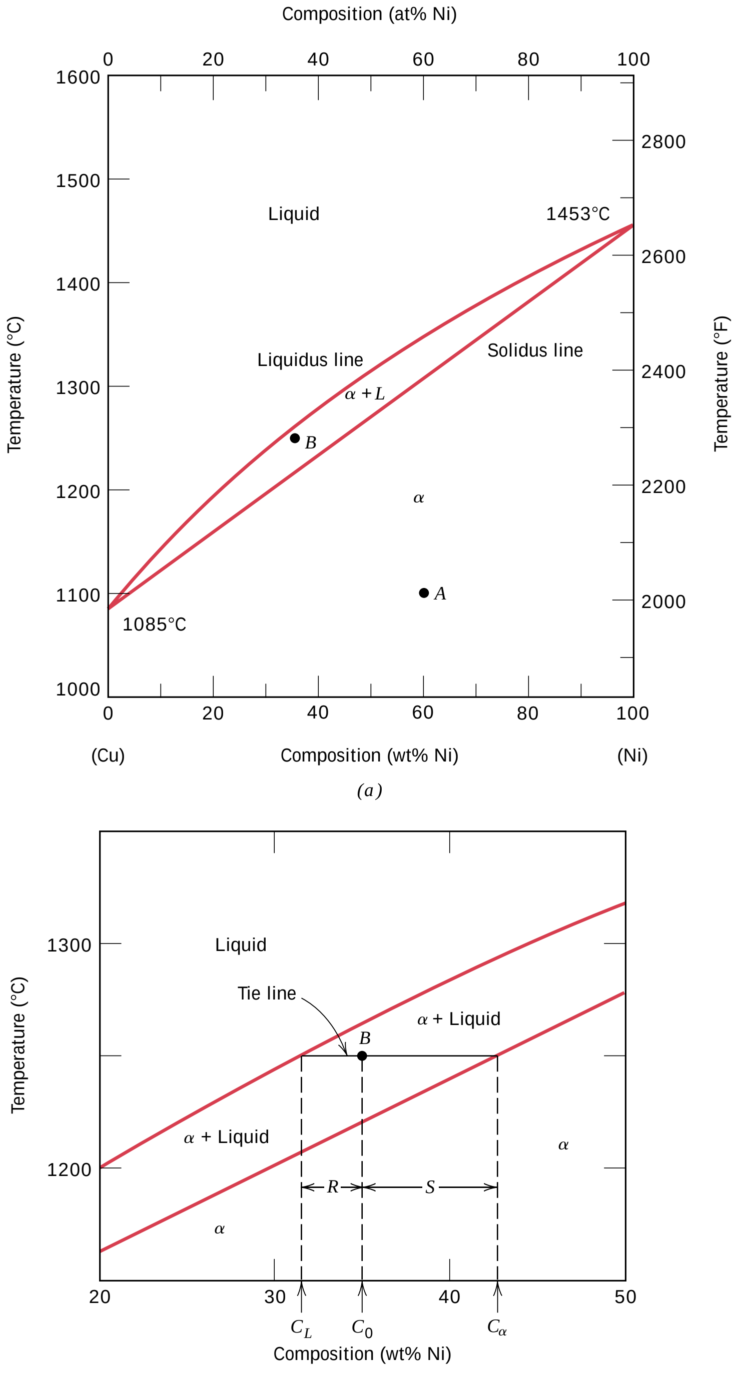

(a)

(b)

FIGURE 10.2 (*a*) The copper–nickel phase diagram. (Adapted from *Phase Diagrams of Binary Nickel Alloys,* P. Nash, Editor, 1991. Reprinted by permission of ASM International, Materials Park, OH.) (*b*) A portion of the copper–nickel phase diagram for which compositions and phase amounts are determined at point *B*.

both solid α and liquid phases will be in equilibrium within this temperature range. For example, upon heating an alloy of composition 50 wt% Ni–50 wt% Cu (Figure 10.2*a*), melting begins at approximately 1280°C (2340°F); the amount of liquid phase continuously increases with temperature until about 1320°C (2410°F), at which the alloy is completely liquid.

10.7 INTERPRETATION OF PHASE DIAGRAMS

For a binary system of known composition and temperature that is at equilibrium, at least three kinds of information are available: (1) the phases that are present, (2) the compositions of these phases, and (3) the percentages or fractions of the phases. The procedures for making these determinations will be demonstrated using the copper–nickel system.

PHASES PRESENT

The establishment of what phases are present is relatively simple. One just locates the temperature–composition point on the diagram and notes the phase(s) with which the corresponding phase field is labeled. For example, an alloy of composition 60 wt% Ni–40 wt% Cu at 1100°C would be located at point *A* in Figure 10.2*a*; since this is within the α region, only the single α phase will be present. On the other hand, a 35 wt% Ni–65 wt% Cu alloy at 1250°C (point *B*) will consist of both α and liquid phases at equilibrium.

DETERMINATION OF PHASE COMPOSITIONS

The first step in the determination of phase compositions (in terms of the concentrations of the components) is to locate the temperature–composition point on the phase diagram. Different methods are used for single- and two-phase regions. If only one phase is present, the procedure is trivial: the composition of this phase is simply the same as the overall composition of the alloy. For example, consider the 60 wt% Ni–40 wt% Cu alloy at 1100°C (point *A*, Figure 10.2*a*). At this composition and temperature, only the α phase is present, having a composition of 60 wt% Ni–40 wt% Cu.

For an alloy having composition and temperature located in a two-phase region, the situation is more complicated. In all two-phase regions (and in two-phase regions only), one may imagine a series of horizontal lines, one at every temperature; each of these is known as a **tie line,** or sometimes as an isotherm. These tie lines extend across the two-phase region and terminate at the phase boundary lines on either side. To compute the equilibrium concentrations of the two phases, the following procedure is used:

1. A tie line is constructed across the two-phase region at the temperature of the alloy.
2. The intersections of the tie line and the phase boundaries on either side are noted.
3. Perpendiculars are dropped from these intersections to the horizontal composition axis, from which the composition of each of the respective phases is read.

For example, consider again the 35 wt% Ni–65 wt% Cu alloy at 1250°C, located at point *B* in Figure 10.2*b* and lying within the $\alpha + L$ region. Thus, the problem is to determine the composition (in wt% Ni and Cu) for both the α and liquid phases. The tie line has been constructed across the $\alpha + L$ phase region, as shown in Figure 10.2*b*. The perpendicular from the intersection of the tie line with the liquidus boundary meets the composition axis at 31.5 wt% Ni–68.5 wt% Cu, which is the composition of the liquid phase, C_L. Likewise, for the solidus–tie line intersection, we find a composition for the α solid-solution phase, C_α, of 42.5 wt% Ni–57.5 wt% Cu.

DETERMINATION OF PHASE AMOUNTS

The relative amounts (as fraction or as percentage) of the phases present at equilibrium may also be computed with the aid of phase diagrams. Again, the single- and two-phase situations must be treated separately. The solution is obvious in the single-phase region: Since only one phase is present, the alloy is composed entirely of that phase; that is, the phase fraction is 1.0 or, alternatively, the percentage is 100%. From the previous example for the 60 wt% Ni–40 wt% Cu alloy at 1100°C (point A in Figure 10.2*a*), only the α phase is present; hence, the alloy is completely or 100% α.

If the composition and temperature position is located within a two-phase region, things are more complex. The tie line must be utilized in conjunction with a procedure that is often called the **lever rule** (or the *inverse lever rule*), which is applied as follows:

1. The tie line is constructed across the two-phase region at the temperature of the alloy.
2. The overall alloy composition is located on the tie line.
3. The fraction of one phase is computed by taking the length of tie line from the overall alloy composition to the phase boundary for the *other* phase, and dividing by the total tie line length.
4. The fraction of the other phase is determined in the same manner.
5. If phase percentages are desired, each phase fraction is multiplied by 100. When the composition axis is scaled in weight percent, the phase fractions computed using the lever rule are mass fractions—the mass (or weight) of a specific phase divided by the total alloy mass (or weight). The mass of each phase is computed from the product of each phase fraction and the total alloy mass.

In the employment of the lever rule, tie line segment lengths may be determined either by direct measurement from the phase diagram using a linear scale, preferably graduated in millimeters, or by subtracting compositions as taken from the composition axis.

Consider again the example shown in Figure 10.2*b*, in which at 1250°C both α and liquid phases are present for a 35 wt% Ni–65 wt% Cu alloy. The problem is to compute the fraction of each of the α and liquid phases. The tie line has been constructed that was used for the determination of α and L phase compositions. Let the overall alloy composition be located along the tie line and denoted as C_0, and mass fractions be represented by W_L and W_α for the respective phases. From the lever rule, W_L may be computed according to

$$W_L = \frac{S}{R + S} \tag{10.1a}$$

or, by subtracting compositions,

$$W_L = \frac{C_\alpha - C_0}{C_\alpha - C_L} \tag{10.1b}$$

Composition need be specified in terms of only one of the constituents for a binary alloy; for the computation above, weight percent nickel will be used (i.e., $C_0 = 35$

wt% Ni, $C_\alpha = 42.5$ wt% Ni, and $C_L = 31.5$ wt% Ni), and

$$W_L = \frac{42.5 - 35}{42.5 - 31.5} = 0.68$$

Similarly, for the α phase,

$$W_\alpha = \frac{R}{R + S} \tag{10.2a}$$

$$= \frac{C_0 - C_L}{C_\alpha - C_L} \tag{10.2b}$$

$$= \frac{35 - 31.5}{42.5 - 31.5} = 0.32$$

Of course, identical answers are obtained if compositions are expressed in weight percent copper instead of nickel.

Thus, the lever rule may be employed to determine the relative amounts or fractions of phases in any two-phase region for a binary alloy if the temperature and composition are known and if equilibrium has been established. Its derivation is presented as an example problem.

It is easy to confuse the foregoing procedures for the determination of phase compositions and fractional phase amounts; thus, a brief summary is warranted. *Compositions* of phases are expressed in terms of weight percents of the components (e.g., wt% Cu, wt% Ni). For any alloy consisting of a single phase, the composition of that phase is the same as the total alloy composition. If two phases are present, the tie line must be employed, the extremities of which determine the compositions of the respective phases. With regard to *fractional phase amounts* (e.g., mass fraction of the α or liquid phase), when a single phase exists, the alloy is completely that phase. For a two-phase alloy, on the other hand, the lever rule is utilized, in which a ratio of tie line segment lengths is taken.

EXAMPLE PROBLEM 10.1

Derive the lever rule.

SOLUTION

Consider the phase diagram for copper and nickel (Figure 10.2*b*) and alloy of composition C_0 at 1250°C, and let C_α, C_L, W_α, and W_L represent the same parameters as above. This derivation is accomplished through two conservation-of-mass expressions. With the first, since only two phases are present, the sum of their mass fractions must be equal to unity, that is,

$$W_\alpha + W_L = 1 \tag{10.3}$$

For the second, the mass of one of the components (either Cu or Ni) that is present in both of the phases must be equal to the mass of that component in the total alloy, or

$$W_\alpha C_\alpha + W_L C_L = C_0 \tag{10.4}$$

Simultaneous solution of these two equations leads to the lever rule expressions for this particular situation, Equations 10.1b and 10.2b:

$$W_L = \frac{C_\alpha - C_0}{C_\alpha - C_L} \tag{10.1b}$$

$$W_\alpha = \frac{C_0 - C_L}{C_\alpha - C_L} \tag{10.2b}$$

For multiphase alloys, it is often more convenient to specify relative phase amount in terms of volume fraction rather than mass fraction. Phase volume fractions are preferred because they (rather than mass fractions) may be determined from examination of the microstructure; furthermore, the properties of a multiphase alloy may be estimated on the basis of volume fractions.

For an alloy consisting of α and β phases, the volume fraction of the α phase, V_α, is defined as

$$V_\alpha = \frac{v_\alpha}{v_\alpha + v_\beta} \tag{10.5}$$

where v_α and v_β denote the volumes of the respective phases in the alloy. Of course, an analogous expression exists for V_β; and, for an alloy consisting of just two phases, it is the case that $V_\alpha + V_\beta = 1$.

On occasion conversion from mass fraction to volume fraction (or vice versa) is desired. Equations that facilitate these conversions are as follows:

$$V_\alpha = \frac{\dfrac{W_\alpha}{\rho_\alpha}}{\dfrac{W_\alpha}{\rho_\alpha} + \dfrac{W_\beta}{\rho_\beta}} \tag{10.6a}$$

$$V_\beta = \frac{\dfrac{W_\beta}{\rho_\beta}}{\dfrac{W_\alpha}{\rho_\alpha} + \dfrac{W_\beta}{\rho_\beta}} \tag{10.6b}$$

and

$$W_\alpha = \frac{V_\alpha \rho_\alpha}{V_\alpha \rho_\alpha + V_\beta \rho_\beta} \tag{10.7a}$$

$$W_\beta = \frac{V_\beta \rho_\beta}{V_\alpha \rho_\alpha + V_\beta \rho_\beta} \tag{10.7b}$$

In these expressions, ρ_α and ρ_β are the densities of the respective phases; {these may be determined approximately using Equations 5.10a and 5.10b.}

When the densities of the phases in a two-phase alloy differ significantly, there will be quite a disparity between mass and volume fractions; conversely, if the phase densities are the same, mass and volume fractions are identical.

10.8 DEVELOPMENT OF MICROSTRUCTURE IN ISOMORPHOUS ALLOYS

EQUILIBRIUM COOLING (CD-ROM)

NONEQUILIBRIUM COOLING (CD-ROM)

10.9 MECHANICAL PROPERTIES OF ISOMORPHOUS ALLOYS

We shall now briefly explore how the mechanical properties of solid isomorphous alloys are affected by composition as other structural variables (e.g., grain size) are held constant. For all temperatures and compositions below the melting temperature of the lowest-melting component, only a single solid phase will exist. Therefore, each component will experience solid-solution strengthening (Section 8.10), or an increase in strength and hardness by additions of the other component. This effect is demonstrated in Figure 10.5*a* as tensile strength versus composition for the copper–nickel system at room temperature; at some intermediate composition, the curve necessarily passes through a maximum. Plotted in Figure 10.5*b* is the ductility (%EL)–composition behavior, which is just the opposite of tensile strength; that is, ductility decreases with additions of the second component, and the curve exhibits a minimum.

10.10 BINARY EUTECTIC SYSTEMS

Another type of common and relatively simple phase diagram found for binary alloys is shown in Figure 10.6 for the copper–silver system; this is known as a binary eutectic phase diagram. A number of features of this phase diagram are important and worth noting. First of all, three single-phase regions are found on the diagram: α, β, and liquid. The α phase is a solid solution rich in copper; it has silver as the solute component and an FCC crystal structure. The β phase solid solution also

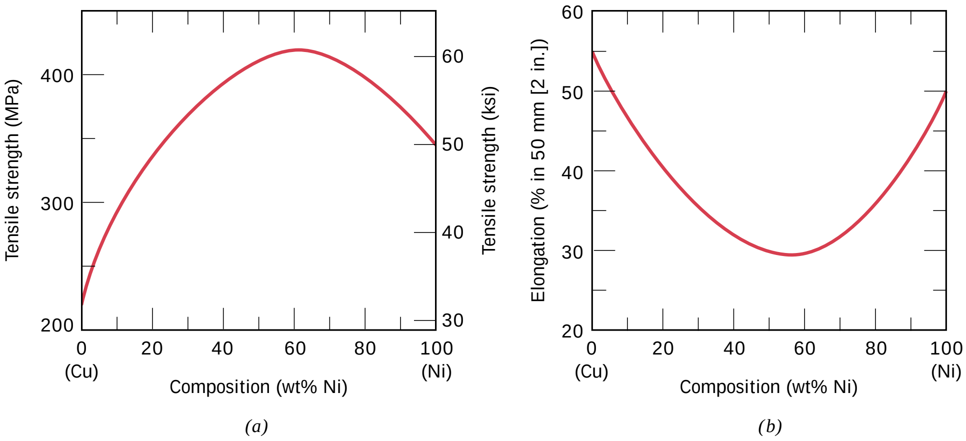

FIGURE 10.5 For the copper–nickel system, (*a*) tensile strength versus composition, and (*b*) ductility (%EL) versus composition at room temperature. A solid solution exists over all compositions for this system.

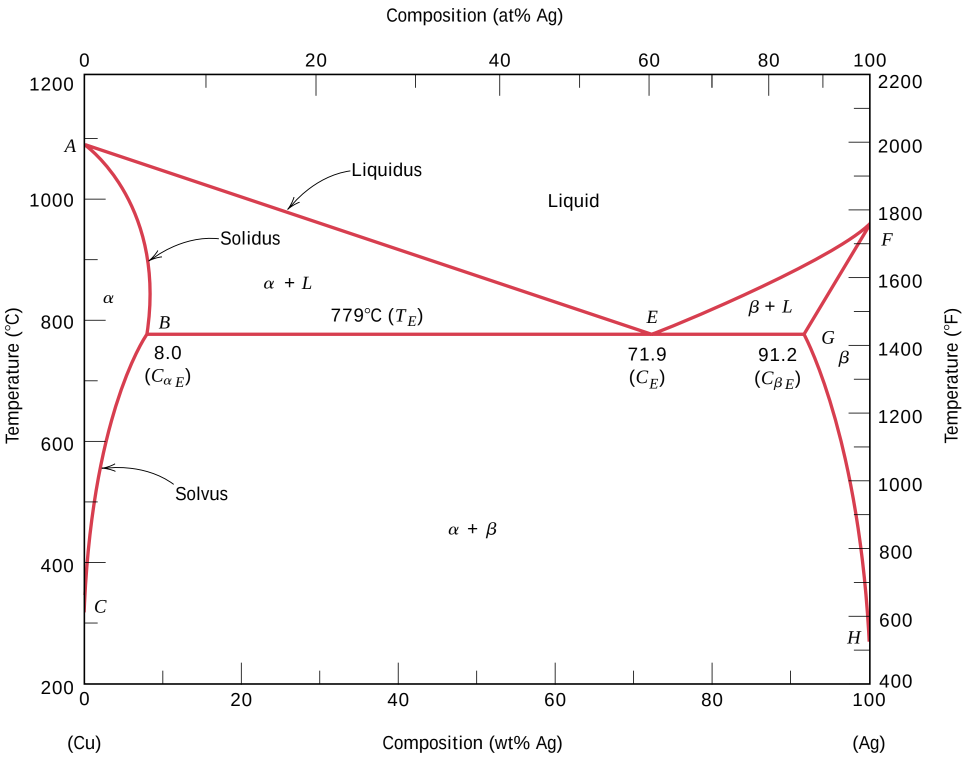

Figure 10.6 The copper–silver phase diagram. (Adapted from *Binary Alloy Phase Diagrams,* 2nd edition, Vol. 1, T. B. Massalski, Editor-in-Chief, 1990. Reprinted by permission of ASM International, Materials Park, OH.)

has an FCC structure, but copper is the solute. The α and β phases are considered to include pure copper and pure silver, respectively.

Thus, the solubility in each of these solid phases is limited, in that at any temperature below line BEG only a limited concentration of silver will dissolve in copper (for the α phase), and similarly for copper in silver (for the β phase). The solubility limit for the α phase corresponds to the boundary line, labeled CBA, between the $\alpha/(\alpha + \beta)$ and $\alpha/(\alpha + L)$ phase regions; it increases with temperature to a maximum [8.0 wt% Ag at 779°C (1434°F)] at point B, and decreases back to zero at the melting temperature of pure copper, point A [1085°C (1985°F)]. At temperatures below 779°C (1434°F), the solid solubility limit line separating the α and $\alpha + \beta$ phase regions is termed a **solvus line;** the boundary AB between the α and $\alpha + L$ fields is the **solidus line,** as indicated in Figure 10.6. For the β phase, both solvus and solidus lines also exist, HG and GF, respectively, as shown. The maximum solubility of copper in the β phase, point G (8.8 wt% Cu), also occurs at 779°C (1434°F). This horizontal line BEG, which is parallel to the composition axis and extends between these maximum solubility positions, may also be considered to be a solidus line; it represents the lowest temperature at which a liquid phase may exist for any copper–silver alloy that is at equilibrium.

There are also three two-phase regions found for the copper–silver system (Figure 10.6): $\alpha + L$, $\beta + L$, and $\alpha + \beta$. The α and β phase solid solutions coexist for all compositions and temperatures within the $\alpha + \beta$ phase field; the α + liquid and β + liquid phases also coexist in their respective phase regions. Furthermore, compositions and relative amounts for the phases may be determined using tie lines and the lever rule as outlined previously.

As silver is added to copper, the temperature at which the alloys become totally liquid decreases along the liquidus line, line AE; thus, the melting temperature of copper is lowered by silver additions. The same may be said for silver: the introduction of copper reduces the temperature of complete melting along the other liquidus line, FE. These liquidus lines meet at the point E on the phase diagram, through which also passes the horizontal isotherm line BEG. Point E is called an **invariant point,** which is designated by the composition C_E and temperature T_E; for the copper–silver system, the values of C_E and T_E are 71.9 wt% Ag and 779°C (1434°F), respectively.

An important reaction occurs for an alloy of composition C_E as it changes temperature in passing through T_E; this reaction may be written as follows:

$$L(C_E) \underset{\text{heating}}{\overset{\text{cooling}}{\rightleftharpoons}} \alpha(C_{\alpha E}) + \beta(C_{\beta E}) \tag{10.8}$$

Or, upon cooling, a liquid phase is transformed into the two solid α and β phases at the temperature T_E; the opposite reaction occurs upon heating. This is called a **eutectic reaction** (eutectic means easily melted), and C_E and T_E represent the eutectic composition and temperature, respectively; $C_{\alpha E}$ and $C_{\beta E}$ are the respective compositions of the α and β phases at T_E. Thus, for the copper–silver system, the eutectic reaction, Equation 10.8, may be written as follows:

$$L(71.9\text{ wt\% Ag}) \underset{\text{heating}}{\overset{\text{cooling}}{\rightleftharpoons}} \alpha(8.0\text{ wt\% Ag}) + \beta(91.2\text{ wt\% Ag})$$

Often, the horizontal solidus line at T_E is called the *eutectic isotherm.*

The eutectic reaction, upon cooling, is similar to solidification for pure components in that the reaction proceeds to completion at a constant temperature, or isothermally, at T_E. However, the solid product of eutectic solidification is always two solid phases, whereas for a pure component only a single phase forms. Because of this eutectic reaction, phase diagrams similar to that in Figure 10.6 are termed eutectic phase diagrams; components exhibiting this behavior comprise a eutectic system.

In the construction of binary phase diagrams, it is important to understand that one or at most two phases may be in equilibrium within a phase field. This holds true for the phase diagrams in Figures 10.2*a* and 10.6. For a eutectic system, three phases (α, β, and L) may be in equilibrium, but only at points along the eutectic isotherm. Another general rule is that single-phase regions are always separated from each other by a two-phase region that consists of the two single phases that it separates. For example, the $\alpha + \beta$ field is situated between the α and β single-phase regions in Figure 10.6.

Another common eutectic system is that for lead and tin; the phase diagram (Figure 10.7) has a general shape similar to that for copper–silver. For the lead–tin system the solid solution phases are also designated by α and β; in this case, α represents a solid solution of tin in lead, and for β, tin is the solvent and lead is the solute. The eutectic invariant point is located at 61.9 wt% Sn and 183°C (361°F). Of course, maximum solid solubility compositions as well as component melting temperatures will be different for the copper–silver and lead–tin systems, as may be observed by comparing their phase diagrams.

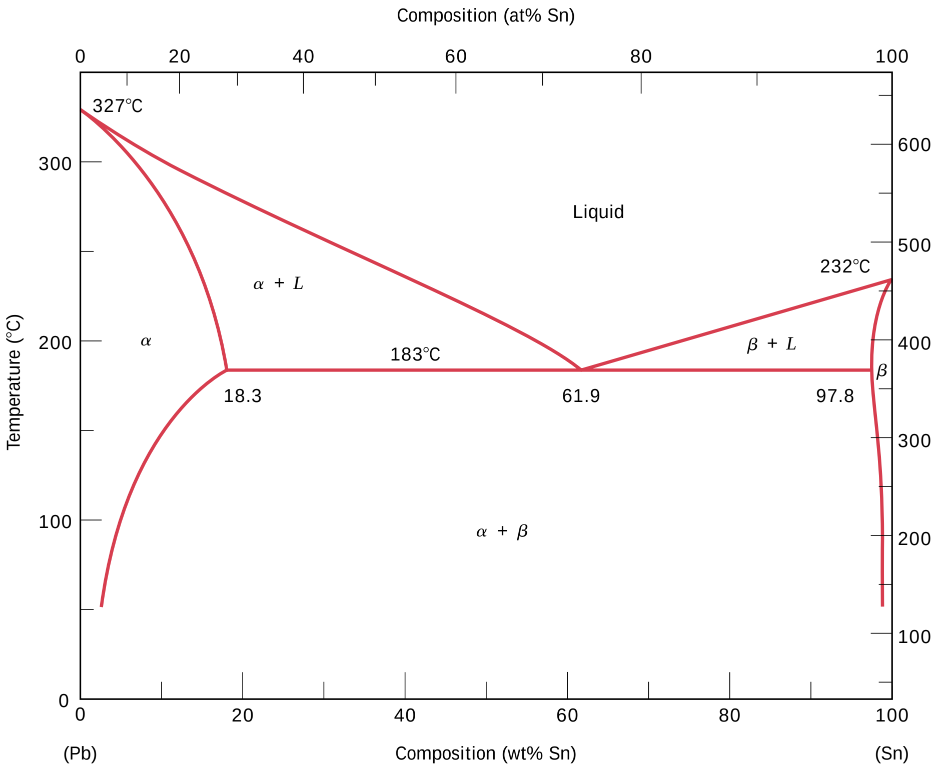

Figure 10.7 The lead–tin phase diagram. (Adapted from *Binary Alloy Phase Diagrams,* 2nd edition, Vol. 3, T. B. Massalski, Editor-in-Chief, 1990. Reprinted by permission of ASM International, Materials Park, OH.)

On occasion, low-melting-temperature alloys are prepared having near-eutectic compositions. A familiar example is the 60–40 solder, containing 60 wt% Sn and 40 wt% Pb. Figure 10.7 indicates that an alloy of this composition is completely molten at about 185°C (365°F), which makes this material especially attractive as a low-temperature solder, since it is easily melted.

EXAMPLE PROBLEM 10.2

For a 40 wt% Sn–60 wt% Pb alloy at 150°C (300°F), (a) What phase(s) is (are) present? (b) What is (are) the composition(s) of the phase(s)?

SOLUTION

(a) Locate this temperature–composition point on the phase diagram (point *B* in Figure 10.8). Inasmuch as it is within the $\alpha + \beta$ region, both α and β phases will coexist.

(b) Since two phases are present, it becomes necessary to construct a tie line across the $\alpha + \beta$ phase field at 150°C, as indicated in Figure 10.8. The composition of the α phase corresponds to the tie line intersection with the $\alpha/(\alpha + \beta)$ solvus phase boundary—about 10 wt% Sn–90 wt% Pb, denoted as C_α. Similarly for the β phase, which will have a composition approximately 98 wt% Sn–2 wt% Pb (C_β).

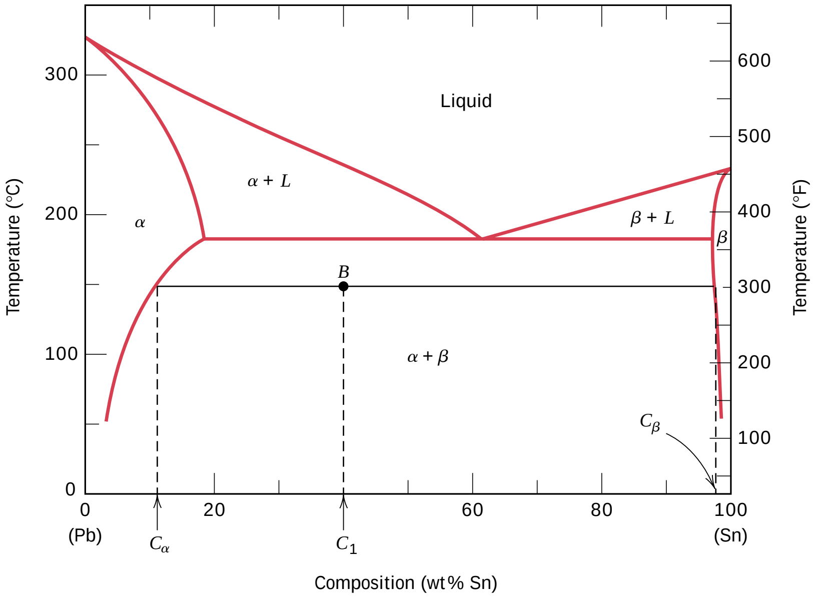

FIGURE 10.8 The lead–tin phase diagram. For a 40 wt% Sn–60 wt% Pb alloy at 150°C (point *B*), phase compositions and relative amounts are computed in Example Problems 10.2 and 10.3.

EXAMPLE PROBLEM 10.3

For the lead–tin alloy in Example Problem 10.2, calculate the relative amount of each phase present in terms of (a) mass fraction and (b) volume fraction. At 150°C take the densities of Pb and Sn to be 11.23 and 7.24 g/cm^3, respectively.

SOLUTION

(a) Since the alloy consists of two phases, it is necessary to employ the lever rule. If C_1 denotes the overall alloy composition, mass fractions may be computed by subtracting compositions, in terms of weight percent tin, as follows:

$$W_\alpha = \frac{C_\beta - C_1}{C_\beta - C_\alpha} = \frac{98 - 40}{98 - 10} = 0.66$$

$$W_\beta = \frac{C_1 - C_\alpha}{C_\beta - C_\alpha} = \frac{40 - 10}{98 - 10} = 0.34$$

(b) To compute volume fractions it is first necessary to determine the density of each phase {using Equation 5.10a.} Thus

$$\rho_\alpha = \frac{100}{\dfrac{C_{\text{Sn}(\alpha)}}{\rho_{\text{Sn}}} + \dfrac{C_{\text{Pb}(\alpha)}}{\rho_{\text{Pb}}}}$$

where $C_{\text{Sn}(\alpha)}$ and $C_{\text{Pb}(\alpha)}$ denote the concentrations in weight percent of tin and lead, respectively, in the α phase. From Example Problem 10.2, these values are 10 wt% and 90 wt%. Incorporation of these values along with the densities of the two components lead to

$$\rho_\alpha = \frac{100}{\dfrac{10}{7.24\ \text{g/cm}^3} + \dfrac{90}{11.23\ \text{g/cm}^3}} = 10.64\ \text{g/cm}^3$$

Similarly for the β phase

$$\rho_\beta = \frac{100}{\dfrac{C_{\text{Sn}(\beta)}}{\rho_{\text{Sn}}} + \dfrac{C_{\text{Pb}(\beta)}}{\rho_{\text{Pb}}}}$$

$$= \frac{100}{\dfrac{98}{7.24\ \text{g/cm}^3} + \dfrac{2}{11.23\ \text{g/cm}^3}} = 7.29\ \text{g/cm}^3$$

Now it becomes necessary to employ Equations 10.6a and 10.6b to determine V_α and V_β as

$$V_\alpha = \frac{\dfrac{W_\alpha}{\rho_\alpha}}{\dfrac{W_\alpha}{\rho_\alpha} + \dfrac{W_\beta}{\rho_\beta}}$$

$$= \frac{\dfrac{0.66}{10.64\ \text{g/cm}^3}}{\dfrac{0.66}{10.64\ \text{g/cm}^3} + \dfrac{0.34}{7.29\ \text{g/cm}^3}} = 0.57$$

$$V_\beta = \frac{\dfrac{W_\beta}{\rho_\beta}}{\dfrac{W_\alpha}{\rho_\alpha} + \dfrac{W_\beta}{\rho_\beta}}$$

$$= \frac{\dfrac{0.34}{7.29\ \text{g/cm}^3}}{\dfrac{0.66}{10.64\ \text{g/cm}^3} + \dfrac{0.34}{7.29\ \text{g/cm}^3}} = 0.43$$

10.11 DEVELOPMENT OF MICROSTRUCTURE IN EUTECTIC ALLOYS (CD-ROM)

10.12 EQUILIBRIUM DIAGRAMS HAVING INTERMEDIATE PHASES OR COMPOUNDS

The isomorphous and eutectic phase diagrams discussed thus far are relatively simple, but those for many binary alloy systems are much more complex. The eutectic copper–silver and lead–tin phase diagrams (Figures 10.6 and 10.7) have only two solid phases, α and β; these are sometimes termed **terminal solid solutions,** because they exist over composition ranges near the concentration extremities of the phase diagram. For other alloy systems, **intermediate solid solutions** (or *intermediate phases*) may be found at other than the two composition extremes. Such is the case for the copper–zinc system. Its phase diagram (Figure 10.17) may at first appear formidable because there are some invariant points and reactions similar to the eutectic that have not yet been discussed. In addition, there are six different solid solutions—two terminal (α and η) and four intermediate (β, γ, δ, and ϵ). (The β' phase is termed an ordered solid solution, one in which the copper and zinc atoms are situated in a specific and ordered arrangement within each unit cell.) Some phase boundary lines near the bottom of Figure 10.17 are dashed to indicate that their positions have not been exactly determined. The reason for this is that at low temperatures, diffusion rates are very slow and inordinately long times are required for the attainment of equilibrium. Again, only single- and two-phase regions are found on the diagram, and the same rules outlined in Section 10.7 are utilized for computing phase compositions and relative amounts. The commercial brasses are copper-rich copper–zinc alloys; for example, cartridge brass has a composition of 70 wt% Cu–30 wt% Zn and a microstructure consisting of a single α phase.

For some systems, discrete intermediate compounds rather than solid solutions may be found on the phase diagram, and these compounds have distinct chemical formulas; for metal–metal systems, they are called **intermetallic compounds.** For example, consider the magnesium–lead system (Figure 10.18). The compound Mg_2Pb has a composition of 19 wt% Mg–81 wt% Pb (33 at% Pb), and is represented as a vertical line on the diagram, rather than as a phase region of finite width; hence, Mg_2Pb can exist by itself only at this precise composition.

Several other characteristics are worth noting for this magnesium–lead system. First, the compound Mg_2Pb melts at approximately 550°C (1020°F), as indicated by point *M* in Figure 10.18. Also, the solubility of lead in magnesium is rather extensive, as indicated by the relatively large composition span for the α phase field. On the other hand, the solubility of magnesium in lead is extremely limited. This is evident from the very narrow β terminal solid-solution region on the right or lead-rich side of the diagram. Finally, this phase diagram may be thought of as two simple eutectic diagrams joined back to back, one for the Mg–Mg_2Pb system, the other for Mg_2Pb–Pb; as such, the compound Mg_2Pb is really considered to be a component. This separation of complex phase diagrams into smaller-component units may simplify them and, furthermore, expedite their interpretation.

10.13 EUTECTOID AND PERITECTIC REACTIONS

In addition to the eutectic, other invariant points involving three different phases are found for some alloy systems. One of these occurs for the copper–zinc system (Figure 10.17) at 560°C (1040°F) and 74 wt% Zn–26 wt% Cu. A portion of the phase diagram in this vicinity appears enlarged in Figure 10.19. Upon cooling, a solid δ phase transforms into two other solid phases (γ and ϵ) according to the reaction

$$\delta \underset{\text{heating}}{\overset{\text{cooling}}{\rightleftharpoons}} \gamma + \epsilon \tag{10.14}$$

The reverse reaction occurs upon heating. It is called a **eutectoid** (or eutecticlike) **reaction,** and the invariant point (point *E*, Figure 10.19) and the horizontal tie line

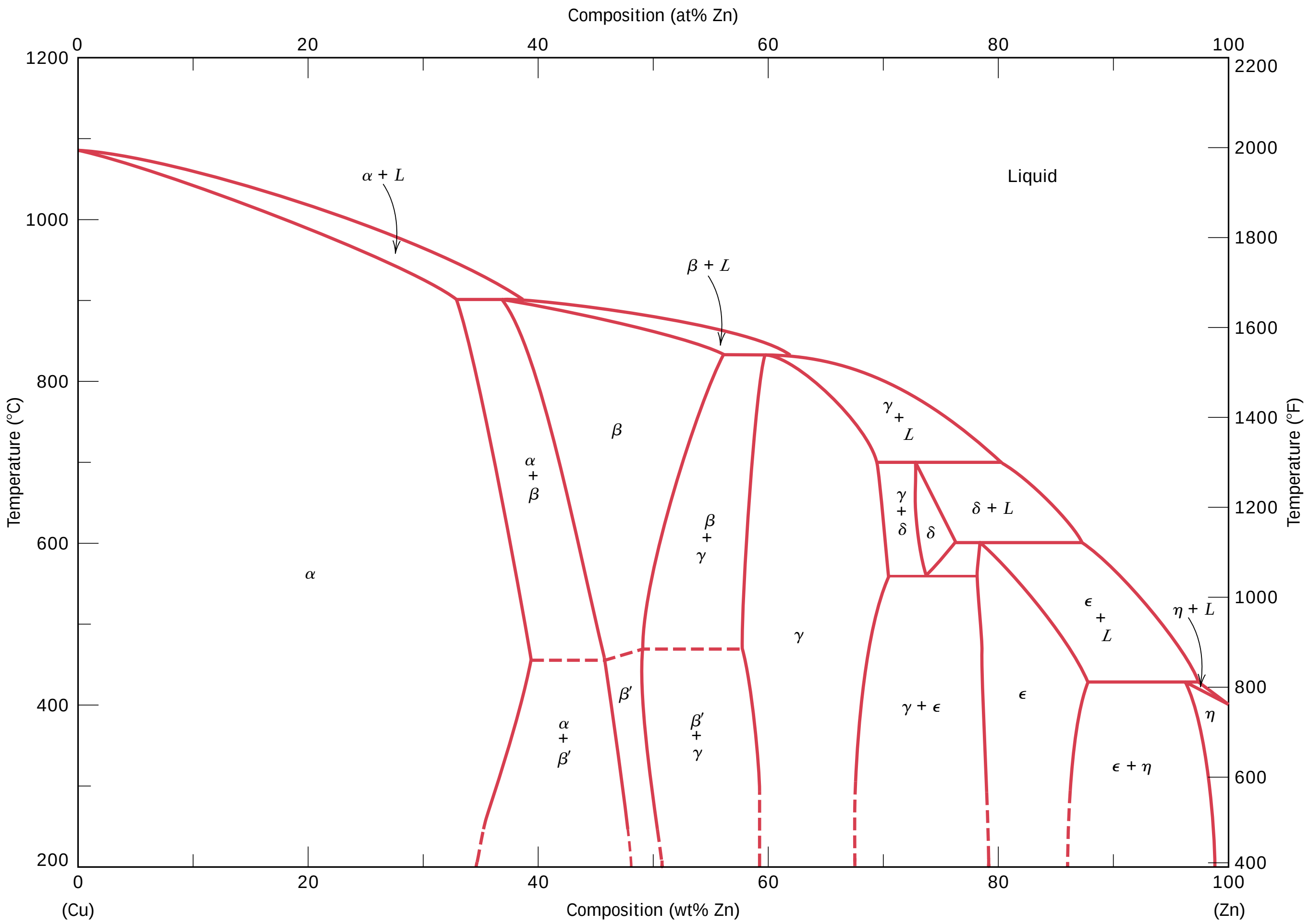

FIGURE 10.17 The copper–zinc phase diagram. (Adapted from *Binary Alloy Phase Diagrams*, 2nd edition, Vol. 2, T. B. Massalski, Editor-in-Chief, 1990. Reprinted by permission of ASM International, Materials Park, OH.)

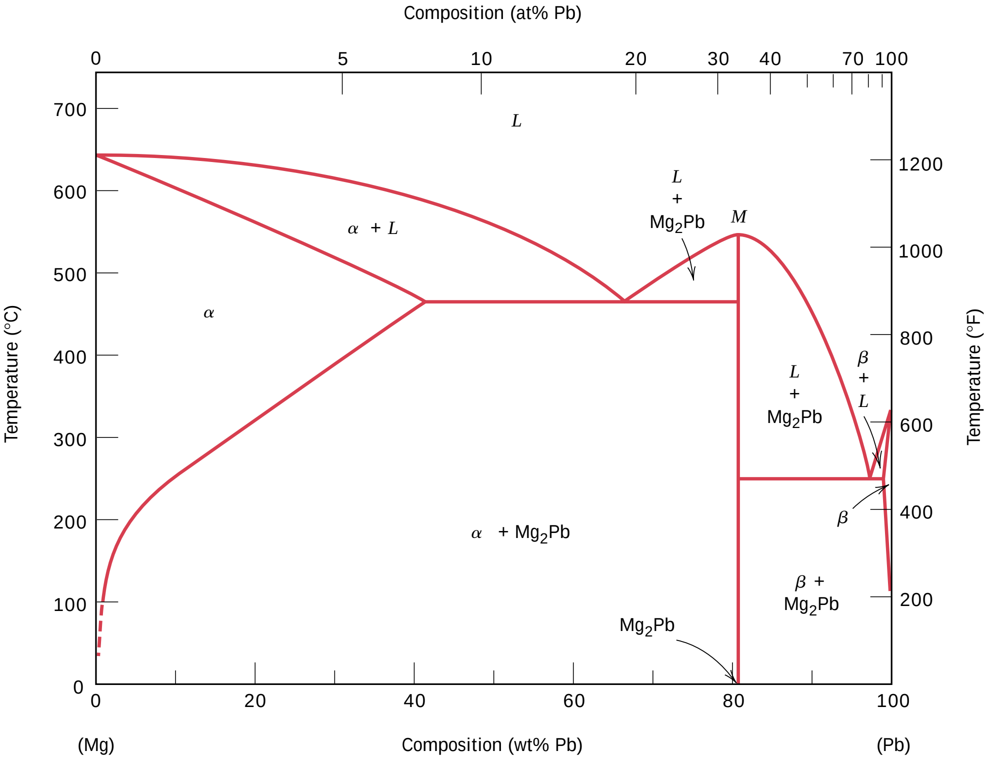

Figure 10.18 The magnesium–lead phase diagram. (Adapted from *Phase Diagrams of Binary Magnesium Alloys*, A. A. Nayeb-Hashemi and J. B. Clark, Editors, 1988. Reprinted by permission of ASM International, Materials Park, OH.)

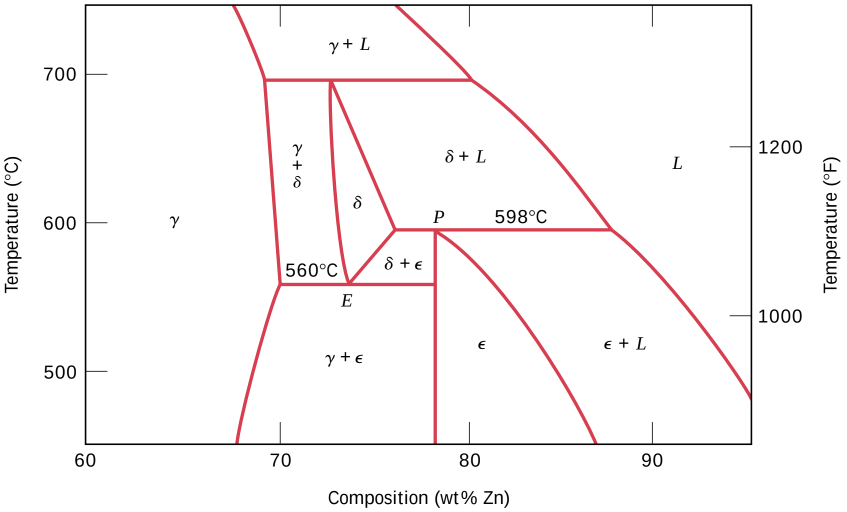

Figure 10.19 A region of the copper–zinc phase diagram that has been enlarged to show eutectoid and peritectic invariant points, labeled *E* (560°C, 74 wt% Zn) and *P* (598°C, 78.6 wt% Zn), respectively. (Adapted from *Binary Alloy Phase Diagrams*, 2nd edition, Vol. 2, T. B. Massalski, Editor-in-Chief, 1990. Reprinted by permission of ASM International, Materials Park, OH.)

at 560°C are termed the *eutectoid* and *eutectoid isotherm*, respectively. The feature distinguishing ''eutectoid'' from ''eutectic'' is that one solid phase instead of a liquid transforms into two other solid phases at a single temperature. A eutectoid reaction is found in the iron–carbon system (Section 10.18) that is very important in the heat treating of steels.

The **peritectic reaction** is yet another invariant reaction involving three phases at equilibrium. With this reaction, upon heating, one solid phase transforms into a liquid phase and another solid phase. A peritectic exists for the copper–zinc system (Figure 10.19, point *P*) at 598°C (1108°F) and 78.6 wt% Zn–21.4 wt% Cu; this reaction is as follows:

$$\delta + L \underset{\text{heating}}{\overset{\text{cooling}}{\rightleftharpoons}} \epsilon \qquad (10.15)$$

The low-temperature solid phase may be an intermediate solid solution (e.g., ϵ in the above reaction), or it may be a terminal solid solution. One of the latter peritectics exists at about 97 wt% Zn and 435°C (815°F) (see Figure 10.17), wherein the η phase, when heated, transforms to ϵ and liquid phases. Three other peritectics are found for the Cu–Zn system, the reactions of which involve β, δ, and γ intermediate solid solutions as the low-temperature phases that transform upon heating.

10.14 CONGRUENT PHASE TRANSFORMATIONS

Phase transformations may be classified according to whether or not there is any change in composition for the phases involved. Those for which there are no compositional alterations are said to be **congruent transformations.** Conversely, for *incongruent transformations,* at least one of the phases will experience a change in composition. Examples of congruent transformations include allotropic transformations (Section 3.10) and melting of pure materials. Eutectic and eutectoid reactions, as well as the melting of an alloy that belongs to an isomorphous system, all represent incongruent transformations.

Intermediate phases are sometimes classified on the basis of whether they melt congruently or incongruently. The intermetallic compound Mg_2Pb melts congruently at the point designated *M* on the magnesium–lead phase diagram, Figure 10.18. Also, for the nickel–titanium system, Figure 10.20, there is a congruent melting point for the γ solid solution that corresponds to the point of tangency for the pairs of liquidus and solidus lines, at 1310°C and 44.9 wt% Ti. Furthermore, the peritectic reaction is an example of incongruent melting for an intermediate phase.

10.15 CERAMIC PHASE DIAGRAMS (CD-ROM)

10.16 TERNARY PHASE DIAGRAMS

Phase diagrams have also been determined for metallic (as well as ceramic) systems containing more than two components; however, their representation and interpretation may be exceedingly complex. For example, a ternary, or three-component, composition–temperature phase diagram in its entirety is depicted by a three-dimensional model. Portrayal of features of the diagram or model in two dimensions is possible but somewhat difficult.

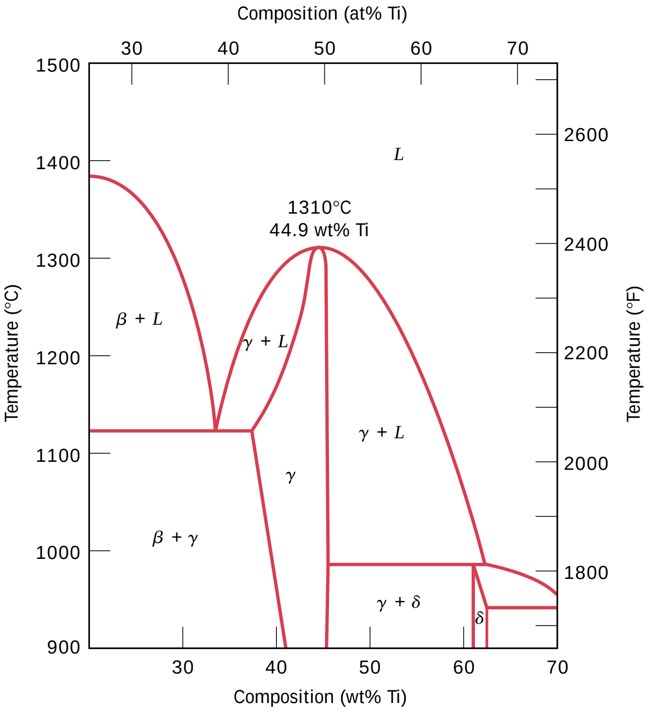

FIGURE 10.20 A portion of the nickel–titanium phase diagram on which is shown a congruent melting point for the γ phase solid solution at 1310°C and 44.9 wt% Ti. (Adapted from *Phase Diagrams of Binary Nickel Alloys,* P. Nash, Editor, 1991. Reprinted by permission of ASM International, Materials Park, OH.)

10.17 THE GIBBS PHASE RULE (CD-ROM)

THE IRON–CARBON SYSTEM

Of all binary alloy systems, the one that is possibly the most important is that for iron and carbon. Both steels and cast irons, primary structural materials in every technologically advanced culture, are essentially iron–carbon alloys. This section is devoted to a study of the phase diagram for this system and the development of several of the possible microstructures. The relationships between heat treatment, microstructure, and mechanical properties are explored in Chapter 11.

10.18 THE IRON–IRON CARBIDE (Fe–Fe_3C) PHASE DIAGRAM

A portion of the iron–carbon phase diagram is presented in Figure 10.26. Pure iron, upon heating, experiences two changes in crystal structure before it melts. At room temperature the stable form, called **ferrite,** or α iron, has a BCC crystal structure. Ferrite experiences a polymorphic transformation to FCC **austenite,** or γ iron, at 912°C (1674°F). This austenite persists to 1394°C (2541°F), at which temperature the FCC austenite reverts back to a BCC phase known as δ ferrite, which finally melts at 1538°C (2800°F). All these changes are apparent along the left vertical axis of the phase diagram.

The composition axis in Figure 10.26 extends only to 6.70 wt% C; at this concentration the intermediate compound iron carbide, or **cementite** (Fe_3C), is

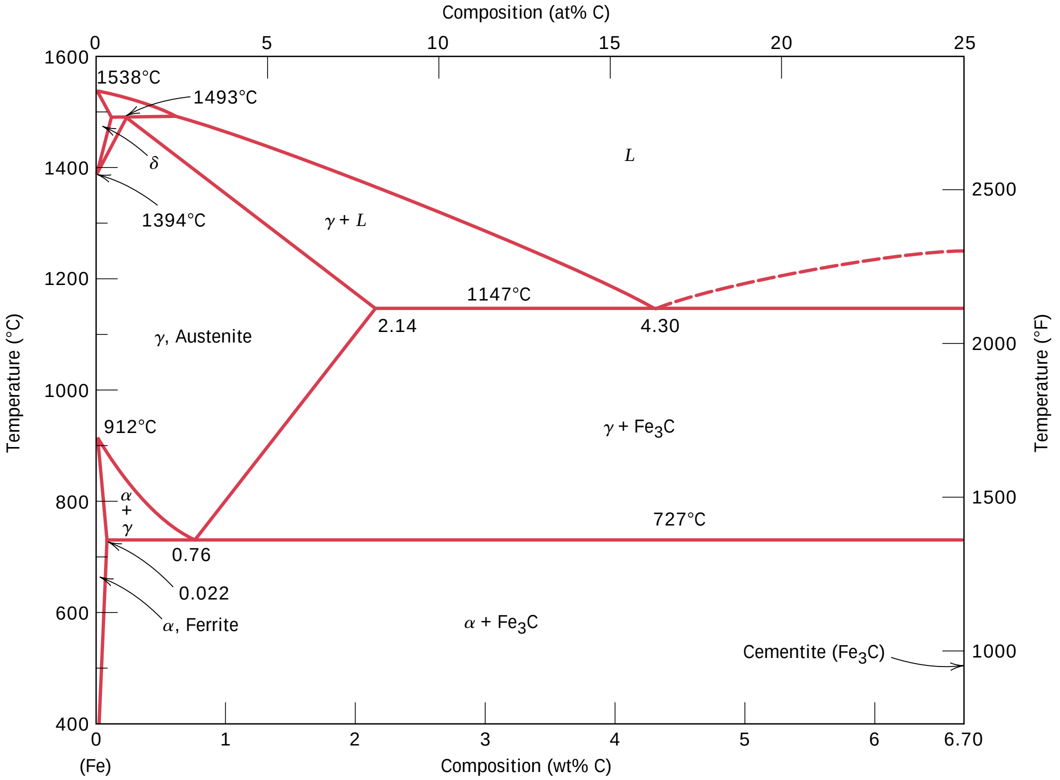

FIGURE 10.26 The iron–iron carbide phase diagram. (Adapted from *Binary Alloy Phase Diagrams,* 2nd edition, Vol. 1, T. B. Massalski, Editor-in-Chief, 1990. Reprinted by permission of ASM International, Materials Park, OH.)

formed, which is represented by a vertical line on the phase diagram. Thus, the iron–carbon system may be divided into two parts: an iron-rich portion, as in Figure 10.26; and the other (not shown) for compositions between 6.70 and 100 wt% C (pure graphite). In practice, all steels and cast irons have carbon contents less than 6.70 wt% C; therefore, we consider only the iron–iron carbide system. Figure 10.26 would be more appropriately labeled the Fe–Fe$_3$C phase diagram, since Fe$_3$C is now considered to be a component. Convention and convenience dictate that composition still be expressed in ''wt% C'' rather than ''wt% Fe$_3$C''; 6.70 wt% C corresponds to 100 wt% Fe$_3$C.

Carbon is an interstitial impurity in iron and forms a solid solution with each of α and δ ferrites, and also with austenite, as indicated by the α, δ, and γ single-phase fields in Figure 10.26. In the BCC α ferrite, only small concentrations of carbon are soluble; the maximum solubility is 0.022 wt% at 727°C (1341°F). The limited solubility is explained by the shape and size of the BCC interstitial positions, which make it difficult to accommodate the carbon atoms. Even though present in relatively low concentrations, carbon significantly influences the mechanical properties of ferrite. This particular iron–carbon phase is relatively soft, may be made magnetic at temperatures below 768°C (1414°F), and has a density of 7.88 g/cm^3. Figure 10.27*a* is a photomicrograph of α ferrite.

The austenite, or γ phase of iron, when alloyed with just carbon, is not stable below 727°C (1341°F), as indicated in Figure 10.26. The maximum solubility of

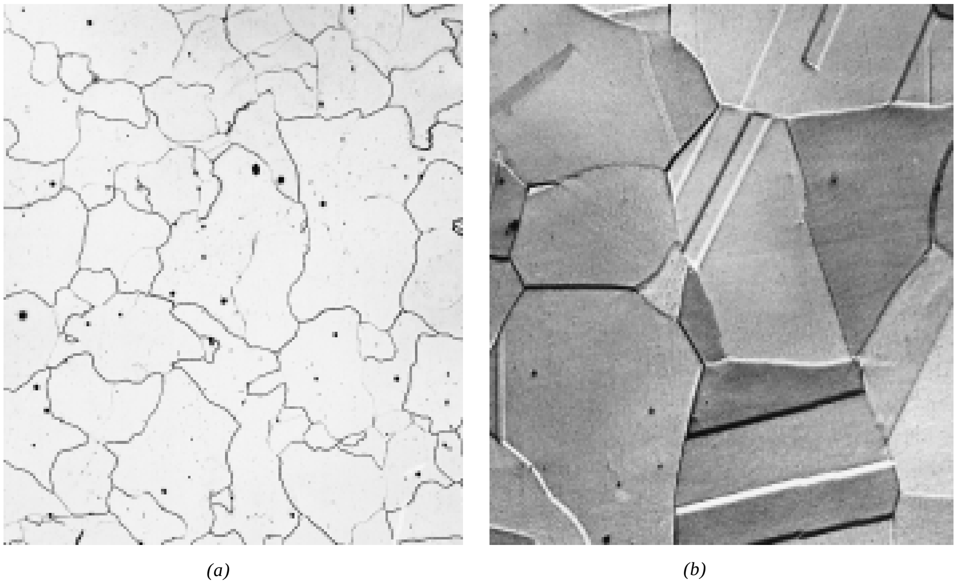

Figure 10.27 Photomicrographs of (*a*) α ferrite (90×) and (*b*) austenite (325×). (Copyright 1971 by United States Steel Corporation.)

carbon in austenite, 2.14 wt%, occurs at 1147°C (2097°F). This solubility is approximately 100 times greater than the maximum for BCC ferrite, since the FCC interstitial positions are larger (see the results of Problem 5.9), and, therefore, the strains imposed on the surrounding iron atoms are much lower. As the discussions that follow demonstrate, phase transformations involving austenite are very important in the heat treating of steels. In passing, it should be mentioned that austenite is nonmagnetic. Figure 10.27*b* shows a photomicrograph of this austenite phase.

The δ ferrite is virtually the same as α ferrite, except for the range of temperatures over which each exists. Since the δ ferrite is stable only at relatively high temperatures, it is of no technological importance and is not discussed further.

Cementite (Fe_3C) forms when the solubility limit of carbon in α ferrite is exceeded below 727°C (1341°F) (for compositions within the $\alpha + Fe_3C$ phase region). As indicated in Figure 10.26, Fe_3C will also coexist with the γ phase between 727 and 1147°C (1341 and 2097°F). Mechanically, cementite is very hard and brittle; the strength of some steels is greatly enhanced by its presence.

Strictly speaking, cementite is only metastable; that is, it will remain as a compound indefinitely at room temperature. But if heated to between 650 and 700°C (1200 and 1300°F) for several years, it will gradually change or transform into α iron and carbon, in the form of graphite, which will remain upon subsequent cooling to room temperature. Thus, the phase diagram in Figure 10.26 is not a true equilibrium one because cementite is not an equilibrium compound. However, inasmuch as the decomposition rate of cementite is extremely sluggish, virtually all the carbon in steel will be as Fe_3C instead of graphite, and the iron–iron carbide phase diagram is, for all practical purposes, valid. As will be seen in Section 13.2, addition of silicon to cast irons greatly accelerates this cementite decomposition reaction to form graphite.

The two-phase regions are labeled in Figure 10.26. It may be noted that one eutectic exists for the iron–iron carbide system, at 4.30 wt% C and 1147°C (2097°F);

for this eutectic reaction,

$$L \underset{\text{heating}}{\overset{\text{cooling}}{\rightleftharpoons}} \gamma + \mathrm{Fe_3C} \tag{10.18}$$

the liquid solidifies to form austenite and cementite phases. Of course, subsequent cooling to room temperature will promote additional phase changes.

It may be noted that a eutectoid invariant point exists at a composition of 0.76 wt% C and a temperature of 727°C (1341°F). This eutectoid reaction may be represented by

$$\gamma(0.76\text{ wt\% C}) \underset{\text{heating}}{\overset{\text{cooling}}{\rightleftharpoons}} \alpha(0.022\text{ wt\% C}) + \mathrm{Fe_3C}\ (6.7\text{ wt\% C}) \tag{10.19}$$

or, upon cooling, the solid γ phase is transformed into α iron and cementite. (Eutectoid phase transformations were addressed in Section 10.13.) The eutectoid phase changes described by Equation 10.19 are very important, being fundamental to the heat treatment of steels, as explained in subsequent discussions.

Ferrous alloys are those in which iron is the prime component, but carbon as well as other alloying elements may be present. In the classification scheme of ferrous alloys based on carbon content, there are three types: iron, steel, and cast iron. Commercially pure iron contains less than 0.008 wt% C and, from the phase diagram, is composed almost exclusively of the ferrite phase at room temperature. The iron–carbon alloys that contain between 0.008 and 2.14 wt% C are classified as steels. In most steels the microstructure consists of both α and $\mathrm{Fe_3C}$ phases. Upon cooling to room temperature, an alloy within this composition range must pass through at least a portion of the γ phase field; distinctive microstructures are subsequently produced, as discussed below. Although a steel alloy may contain as much as 2.14 wt% C, in practice, carbon concentrations rarely exceed 1.0 wt%. The properties and various classifications of steels are treated in Section 13.2. Cast irons are classified as ferrous alloys that contain between 2.14 and 6.70 wt% C. However, commercial cast irons normally contain less than 4.5 wt% C. These alloys are also discussed in Section 13.2.

10.19 DEVELOPMENT OF MICROSTRUCTURES IN IRON–CARBON ALLOYS

Several of the various microstructures that may be produced in steel alloys and their relationships to the iron–iron carbon phase diagram are now discussed, and it is shown that the microstructure that develops depends on both the carbon content and heat treatment. The discussion is confined to very slow cooling of steel alloys, in which equilibrium is continuously maintained. A more detailed exploration of the influence of heat treatment on microstructure, and ultimately on the mechanical properties of steels, is contained in Chapter 11.

Phase changes that occur upon passing from the γ region into the $\alpha + \mathrm{Fe_3C}$ phase field (Figure 10.26) are relatively complex {and similar to those described for the eutectic systems in Section 10.11.} Consider, for example, an alloy of eutectoid composition (0.76 wt% C) as it is cooled from a temperature within the γ phase region, say, 800°C, that is, beginning at point *a* in Figure 10.28 and moving down the vertical line xx'. Initially, the alloy is composed entirely of the austenite phase

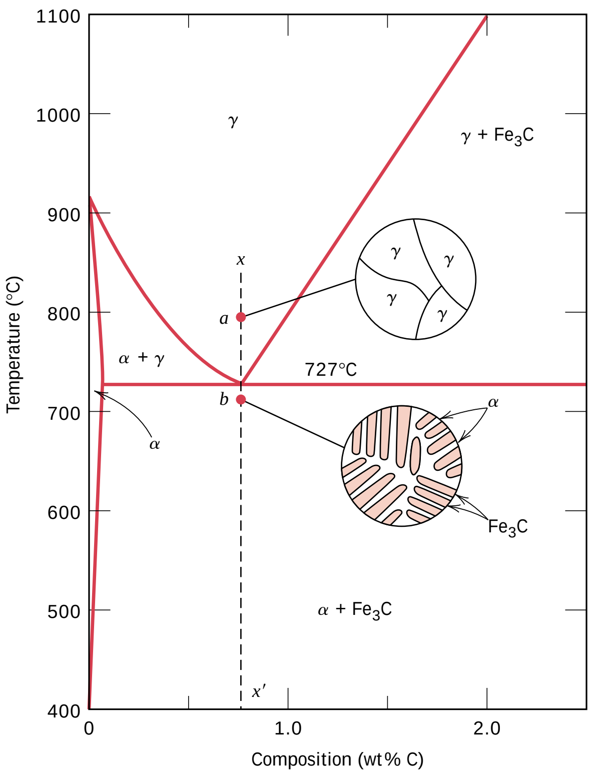

FIGURE 10.28 Schematic representations of the microstructures for an iron–carbon alloy of eutectoid composition (0.76 wt% C) above and below the eutectoid temperature.

having a composition of 0.76 wt% C and corresponding microstructure, also indicated in Figure 10.28. As the alloy is cooled, there will occur no changes until the eutectoid temperature (727°C) is reached. Upon crossing this temperature to point *b*, the austenite transforms according to Equation 10.19.

The microstructure for this eutectoid steel that is slowly cooled through the eutectoid temperature consists of alternating layers or lamellae of the two phases (α and Fe_3C) that form simultaneously during the transformation. In this case, the relative layer thickness is approximately 8 to 1. This microstructure, represented schematically in Figure 10.28, point *b*, is called **pearlite** because it has the appearance of mother of pearl when viewed under the microscope at low magnifications. Figure 10.29 is a photomicrograph of a eutectoid steel showing the pearlite. The pearlite exists as grains, often termed ''colonies''; within each colony the layers are oriented in essentially the same direction, which varies from one colony to another. The thick light layers are the ferrite phase, and the cementite phase appears as thin lamellae most of which appear dark. Many cementite layers are so thin that adjacent phase boundaries are indistinguishable, which layers appear dark at this magnification. Mechanically, pearlite has properties intermediate between the soft, ductile ferrite and the hard, brittle cementite.

The alternating α and Fe_3C layers in pearlite form {as such for the same reason that the eutectic structure (Figures 10.11 and 10.12) forms}—because the composition of the parent phase [in this case austenite (0.76 wt% C)] is different from either of the product phases [ferrite (0.022 wt% C) and cementite (6.7 wt% C)], and the phase transformation requires that there be a redistribution of the carbon by diffusion. Figure 10.30 illustrates schematically microstructural changes that accompany this eutectoid reaction; here the directions of carbon diffusion are

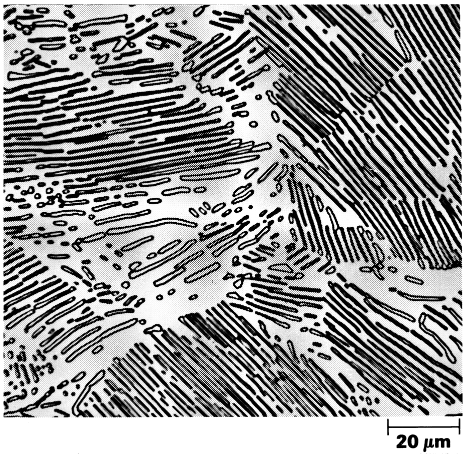

FIGURE 10.29 Photomicrograph of a eutectoid steel showing the pearlite microstructure consisting of alternating layers of α ferrite (the light phase) and Fe_3C (thin layers most of which appear dark). 500×. (Reproduced with permission from *Metals Handbook,* Vol. 9, 9th edition, *Metallography and Microstructures,* American Society for Metals, Materials Park, OH, 1985.)

indicated by arrows. Carbon atoms diffuse away from the 0.022 wt% ferrite regions and to the 6.7 wt% cementite layers, as the pearlite extends from the grain boundary into the unreacted austenite grain. The layered pearlite forms because carbon atoms need diffuse only minimal distances with the formation of this structure.

Furthermore, subsequent cooling of the pearlite from point b in Figure 10.28 will produce relatively insignificant microstructural changes.

HYPOEUTECTOID ALLOYS

Microstructures for iron–iron carbide alloys having other than the eutectoid composition are now explored; {these are analogous to the fourth case described in Section 10.11 and illustrated in Figure 10.14 for the eutectic system.} Consider a composition C_0 to the left of the eutectoid, between 0.022 and 0.76 wt% C; this is termed a **hypoeutectoid** (less than eutectoid) **alloy.** Cooling an alloy of this composition is represented by moving down the vertical line yy' in Figure 10.31. At about 875°C, point c, the microstructure will consist entirely of grains of the γ phase, as shown schematically in the figure. In cooling to point d, about 775°C, which is within the $\alpha + \gamma$ phase region, both these phases will coexist as in the schematic microstructure. Most of the small α particles will form along the original γ grain boundaries. The

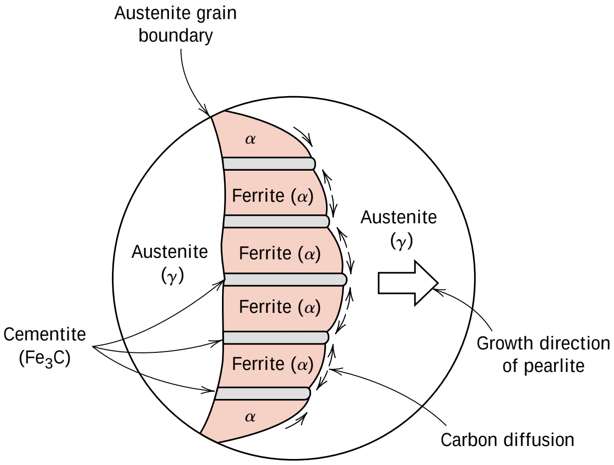

FIGURE 10.30 Schematic representation of the formation of pearlite from austenite; direction of carbon diffusion indicated by arrows.

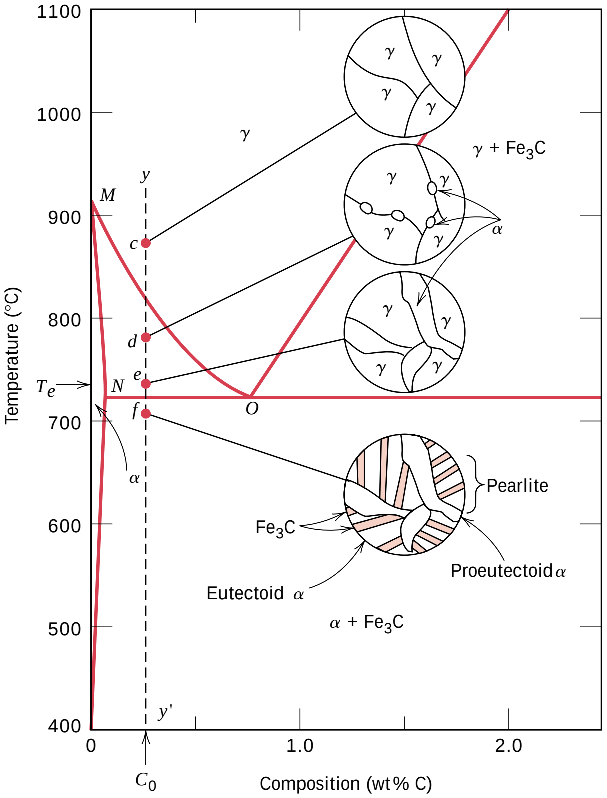

FIGURE 10.31 Schematic representations of the microstructures for an iron–carbon alloy of hypoeutectoid composition C_0 (containing less than 0.76 wt% C) as it is cooled from within the austenite phase region to below the eutectoid temperature.

compositions of both α and γ phases may be determined using the appropriate tie line; these compositions correspond, respectively, to about 0.020 and 0.40 wt% C.

While cooling an alloy through the $\alpha + \gamma$ phase region, the composition of the ferrite phase changes with temperature along the $\alpha - (\alpha + \gamma)$ phase boundary, line MN, becoming slightly richer in carbon. On the other hand, the change in composition of the austenite is more dramatic, proceeding along the $(\alpha + \gamma) - \gamma$ boundary, line MO, as the temperature is reduced.

Cooling from point d to e, just above the eutectoid but still in the $\alpha + \gamma$ region, will produce an increased fraction of the α phase and a microstructure similar to that also shown: the α particles will have grown larger. At this point, the compositions of the α and γ phases are determined by constructing a tie line at the temperature T_e; the α phase will contain 0.022 wt% C, while the γ phase will be of the eutectoid composition, 0.76 wt% C.

As the temperature is lowered just below the eutectoid, to point f, all the γ phase that was present at temperature T_e (and having the eutectoid composition) will transform to pearlite, according to the reaction in Equation 10.19. There will be virtually no change in the α phase that existed at point e in crossing the eutectoid temperature—it will normally be present as a continuous matrix phase surrounding the isolated pearlite colonies. The microstructure at point f will appear as the corresponding schematic inset of Figure 10.31. Thus the ferrite phase will be present both in the pearlite and also as the phase that formed while cooling through the $\alpha + \gamma$ phase region. The ferrite that is present in the pearlite is called *eutectoid ferrite,* whereas the other, that formed above T_e, is termed **proeutectoid** (meaning pre- or before eutectoid) **ferrite,** as labeled in Figure 10.31. Figure 10.32 is a photomicrograph of a 0.38 wt% C steel; large, white regions correspond to the proeutectoid

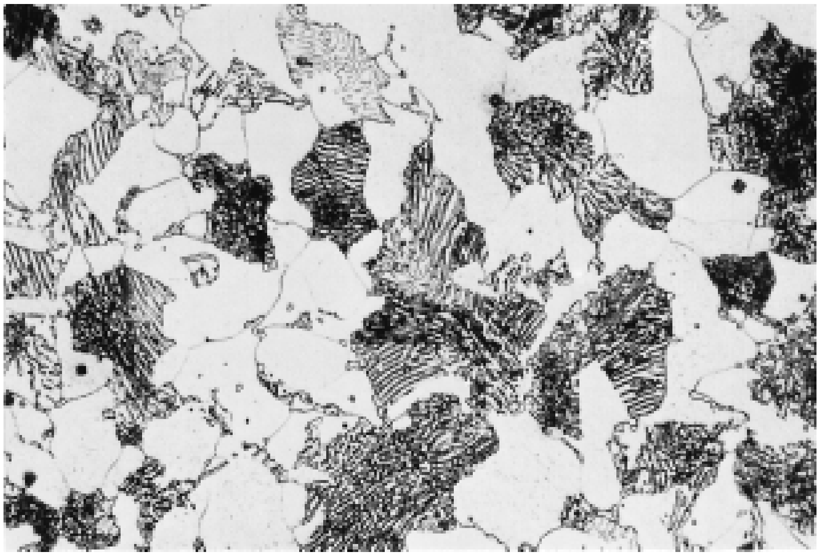

Figure 10.32 Photomicrograph of a 0.38 wt% C steel having a microstructure consisting of pearlite and proeutectoid ferrite. 635×. (Photomicrograph courtesy of Republic Steel Corporation.)

ferrite. For pearlite, the spacing between the α and Fe_3C layers varies from grain to grain; some of the pearlite appears dark because the many close-spaced layers are unresolved at the magnification of the photomicrograph. The chapter-opening photograph for this chapter is a scanning electron micrograph of a hypoeutectoid (0.44 wt% C) steel in which may also be seen both pearlite and proeutectoid ferrite, only at a higher magnification. It should also be noted that two microconstituents are present in these micrographs—proeutectoid ferrite and pearlite—which will appear in all hypoeutectoid iron–carbon alloys that are slowly cooled to a temperature below the eutectoid.

The relative amounts of the proeutectoid α and pearlite may be determined {in a manner similar to that described in Section 10.11 for primary and eutectic microconstituents.} We use the lever rule in conjunction with a tie line that extends from the $\alpha - (\alpha + Fe_3C)$ phase boundary (0.022 wt% C) to the eutectoid composition (0.76 wt% C), inasmuch as pearlite is the transformation product of austenite having this composition. For example, let us consider an alloy of composition C_0' in Figure 10.33. Thus, the fraction of pearlite, W_p, may be determined according to

$$W_p = \frac{T}{T + U}$$

$$= \frac{C_0' - 0.022}{0.76 - 0.022} = \frac{C_0' - 0.022}{0.74} \tag{10.20}$$

Furthermore, the fraction of proeutectoid α, $W_{\alpha'}$, is computed as follows:

$$W_{\alpha'} = \frac{U}{T + U}$$

$$= \frac{0.76 - C_0'}{0.76 - 0.022} = \frac{0.76 - C_0'}{0.74} \tag{10.21}$$

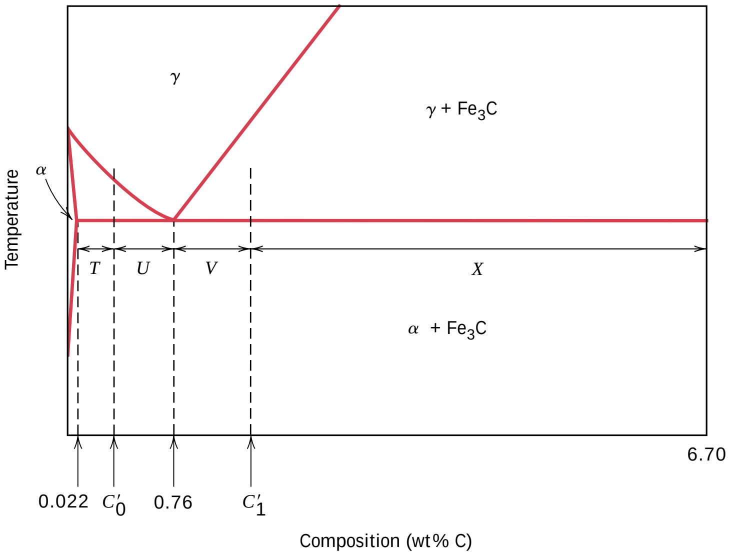

FIGURE 10.33 A portion of the Fe–Fe$_3$C phase diagram used in computations for relative amounts of proeutectoid and pearlite microconstituents for hypoeutectoid (C_0') and hypereutectoid (C_1') compositions.

Of course, fractions of both total α (eutectoid and proeutectoid) and cementite are determined using the lever rule and a tie line that extends across the entirety of the α + Fe$_3$C phase region, from 0.022 to 6.7 wt% C.

HYPEREUTECTOID ALLOYS

Analogous transformations and microstructures result for **hypereutectoid alloys,** those containing between 0.76 and 2.14 wt% C, which are cooled from temperatures within the γ phase field. Consider an alloy of composition C_1 in Figure 10.34 which, upon cooling, moves down the line zz'. At point g only the γ phase will be present with a composition of C_1; the microstructure will appear as shown, having only γ grains. Upon cooling into the γ + Fe$_3$C phase field, say, to point h, the cementite phase will begin to form along the initial γ grain boundaries, similar to the α phase in Figure 10.31, point d. This cementite is called **proeutectoid cementite**—that which forms before the eutectoid reaction. Of course, the cementite composition remains constant (6.70 wt% C) as the temperature changes. However, the composition of the austenite phase will move along line PO toward the eutectoid. As the temperature is lowered through the eutectoid to point i, all remaining austenite of eutectoid composition is converted into pearlite; thus, the resulting microstructure consists of pearlite and proeutectoid cementite as microconstituents (Figure 10.34). In the photomicrograph of a 1.4 wt% C steel (Figure 10.35), note that the proeutectoid cementite appears light. Since it has much the same appearance as proeutectoid ferrite (Figure 10.32), there is some difficulty in distinguishing between hypoeutectoid and hypereutectoid steels on the basis of microstructure.

Relative amounts of both pearlite and proeutectoid Fe$_3$C microconstituents may be computed for hypereutectoid steel alloys in a manner analogous to that for hypoeutectoid materials; the appropriate tie line extends between 0.76 and 6.70 wt% C. Thus, for an alloy having composition C_1' in Figure 10.33, fractions of pearlite W_p and proeutectoid cementite $W_{\mathrm{Fe_3C'}}$ are determined from the following lever rule expressions:

$$W_p = \frac{X}{V + X} = \frac{6.70 - C_1'}{6.70 - 0.76} = \frac{6.70 - C_1'}{5.94} \qquad (10.22)$$

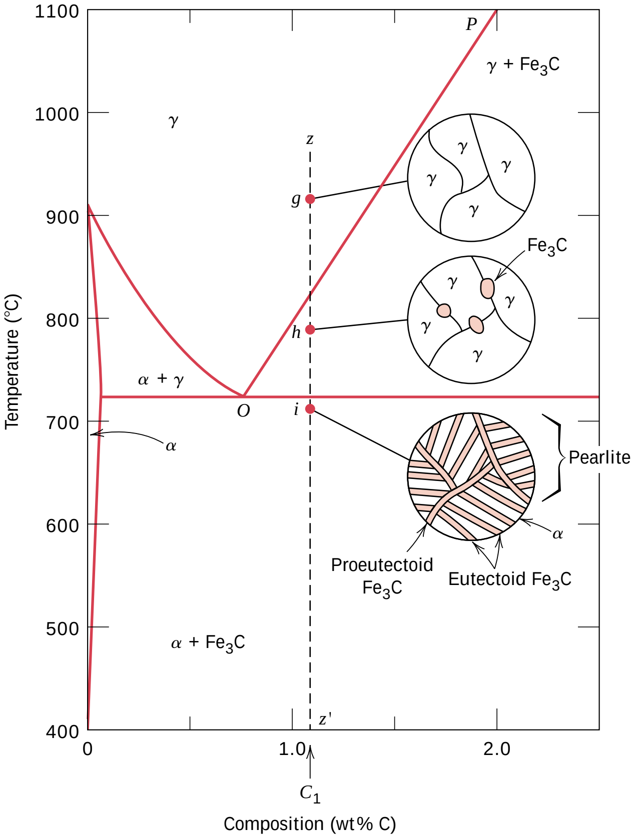
1100
1000
900
800
700
600
500
400
Temperature (°C)
0
1.0
2.0
Composition (wt% C)
C_1
γ
γ + Fe$_3$C
$\alpha + \gamma$
α
α + Fe$_3$C
P
O
z
z'
g
h
i
Fe$_3$C
Pearlite
Proeutectoid Fe$_3$C
Eutectoid Fe$_3$C

FIGURE 10.34 Schematic representations of the microstructures for an iron–carbon alloy of hypereutectoid composition C_1 (containing between 0.76 and 2.14 wt% C), as it is cooled from within the austenite phase region to below the eutectoid temperature.

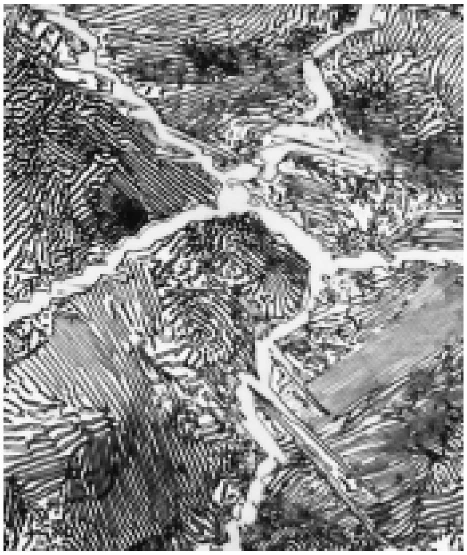

FIGURE 10.35 Photomicrograph of a 1.4 wt% C steel having a microstructure consisting of a white proeutectoid cementite network surrounding the pearlite colonies. 1000×. (Copyright 1971 by United States Steel Corporation.)

and

$$W_{Fe_3C'} = \frac{V}{V + X} = \frac{C_1' - 0.76}{6.70 - 0.76} = \frac{C_1' - 0.76}{5.94} \tag{10.23}$$

EXAMPLE PROBLEM 10.4

For a 99.65 wt% Fe–0.35 wt% C alloy at a temperature just below the eutectoid, determine the following:

(a) The fractions of total ferrite and cementite phases.

(b) The fractions of the proeutectoid ferrite and pearlite.

(c) The fraction of eutectoid ferrite.

SOLUTION

(a) This part of the problem is solved by application of the lever rule expressions employing a tie line that extends all the way across the α + Fe_3C phase field. Thus, C_0' is 0.35 wt% C, and

$$W_\alpha = \frac{6.70 - 0.35}{6.70 - 0.022} = 0.95$$

and

$$W_{Fe_3C} = \frac{0.35 - 0.022}{6.70 - 0.022} = 0.05$$

(b) The fractions of proeutectoid ferrite and pearlite are determined by using the lever rule, and a tie line that extends only to the eutectoid composition (i.e., Equations 10.20 and 10.21). Or

$$W_p = \frac{0.35 - 0.022}{0.76 - 0.022} = 0.44$$

and

$$W_{\alpha'} = \frac{0.76 - 0.35}{0.76 - 0.022} = 0.56$$

(c) All ferrite is either as proeutectoid or eutectoid (in the pearlite). Therefore, the sum of these two ferrite fractions will equal the fraction of total ferrite, that is,

$$W_{\alpha'} + W_{\alpha e} = W_\alpha$$

where $W_{\alpha e}$ denotes the fraction of the total alloy that is eutectoid ferrite. Values for W_α and $W_{\alpha'}$ were determined in parts (a) and (b) as 0.95 and 0.56, respectively. Therefore,

$$W_{\alpha e} = W_\alpha - W_{\alpha'} = 0.95 - 0.56 = 0.39$$

NONEQUILIBRIUM COOLING

In this discussion on the microstructural development of iron–carbon alloys it has been assumed that, upon cooling, conditions of metastable equilibrium[1] have been continuously maintained; that is, sufficient time has been allowed at each new temperature for any necessary adjustment in phase compositions and relative amounts as predicted from the Fe–Fe_3C phase diagram. In most situations these cooling rates are impractically slow and really unnecessary; in fact, on many occasions nonequilibrium conditions are desirable. Two nonequilibrium effects of practical importance are (1) the occurrence of phase changes or transformations at temperatures other than those predicted by phase boundary lines on the phase diagram, and (2) the existence at room temperature of nonequilibrium phases that do not appear on the phase diagram. Both are discussed in the next chapter.

---

[1] The term ‘‘metastable equilibrium’’ is used in this discussion inasmuch as Fe_3C is only a metastable compound.

10.20 THE INFLUENCE OF OTHER ALLOYING ELEMENTS (CD-ROM)

SUMMARY

Equilibrium phase diagrams are a convenient and concise way of representing the most stable relationships between phases in alloy systems. This discussion considered binary phase diagrams for which temperature and composition are variables. Areas, or phase regions, are defined on these temperature-versus-composition plots within which either one or two phases exist. For an alloy of specified composition and at a known temperature, the phases present, their compositions, and relative amounts under equilibrium conditions may be determined. Within two-phase regions, tie lines and the lever rule must be used for phase composition and mass fraction computations, respectively.

Several different kinds of phase diagram were discussed for metallic systems. Isomorphous diagrams are those for which there is complete solubility in the solid phase; the copper–nickel system displays this behavior. {Also discussed for alloys belonging to isomorphous systems were the development of microstructure for both cases of equilibrium and nonequilibrium cooling} and the dependence of mechanical characteristics on composition.

In a eutectic reaction, as found in some alloy systems, a liquid phase transforms isothermally to two different solid phases upon cooling. Such a reaction is noted on the copper–silver and lead–tin phase diagrams. Complete solid solubility for all compositions does not exist; instead, solid solutions are terminal—there is only a limited solubility of each component in the other. {Four different kinds of microstructures that may develop for the equilibrium cooling of alloys belonging to eutectic systems were discussed.}

Other equilibrium phase diagrams are more complex, having intermediate compounds and/or phases, possibly more than a single eutectic, and other reactions including eutectoid, peritectic, and congruent phase transformations. These are found for copper–zinc and magnesium–lead systems.

{Phase diagrams for the Al_2O_3–Cr_2O_3, MgO–Al_2O_3, ZrO_2–CaO, and SiO_2–Al_2O_3 systems were discussed. These diagrams are especially useful in assessing the high-temperature performance of ceramic materials.}

{The Gibbs phase rule was introduced; it is a simple equation that relates the number of phases present in a system at equilibrium with the number of degrees of freedom, the number of components, and the number of noncompositional variables.}

Considerable attention was given to the iron–carbon system, and specifically, the iron–iron carbide phase diagram, which technologically is one of the most important. The development of microstructure in many iron–carbon alloys and steels depends on the eutectoid reaction in which the FCC austenite phase of composition 0.76 wt% C transforms isothermally to the BCC α ferrite phase (0.022 wt% C) and the intermetallic compound, cementite (Fe_3C). The microstructural product of an iron–carbon alloy of eutectoid composition is pearlite, a microconstituent consisting of alternating layers of ferrite and cementite. The microstructures of alloys having carbon contents less than the eutectoid (hypoeutectoid) are comprised of a proeutectoid ferrite phase in addition to pearlite. On the other hand, pearlite and proeutectoid cementite constitute the microconstituents for hypereutectoid alloys—those with carbon contents in excess of the eutectoid composition.

IMPORTANT TERMS AND CONCEPTS

Austenite
Cementite
Component
Congruent transformation
Equilibrium
Eutectic phase
Eutectic reaction
Eutectic structure
Eutectoid reaction
Ferrite
Free energy
Gibbs phase rule
Hypereutectoid alloy
Hypoeutectoid alloy
Intermediate solid solution
Intermetallic compound
Invariant point
Isomorphous
Lever rule
Liquidus line
Metastable
Microconstituent
Pearlite
Peritectic reaction
Phase
Phase diagram
Phase equilibrium
Primary phase
Proeutectoid cementite
Proeutectoid ferrite
Solidus line
Solubility limit
Solvus line
System
Terminal solid solution
Tie line

REFERENCES

ASM Handbook, Vol. 3, *Alloy Phase Diagrams,* ASM International, Materials Park, OH, 1992.

ASM Handbook, Vol. 9, *Metallography and Microstructures,* ASM International, Materials Park, OH, 1985.

Bergeron, C. G. and S. H. Risbud, *Introduction to Phase Equilibria in Ceramics,* American Ceramic Society, Columbus, OH, 1984.

Cook, L. P. and H. F. McMurdie (Editors), *Phase Diagrams for Ceramists,* Vol. VII, American Ceramic Society, Columbus, OH, 1989.

Gordon, P., *Principles of Phase Diagrams in Materials Systems,* McGraw-Hill Book Company, New York, 1968. Reprinted by Krieger Publishing Company, Melbourne, FL, 1983.

Hansen, M. and K. Anderko, *Constitution of Binary Alloys,* 2nd edition, McGraw-Hill Book Company, New York, 1958. *First Supplement* (R. P. Elliott), 1965. *Second Supplement* (F. A. Shunk), 1969. Reprinted by Genium Publishing Corp., Schenectady, NY.

Kingery, W. D., H. K. Bowen, and D. R. Uhlmann, *Introduction to Ceramics,* 2nd edition, John Wiley & Sons, New York, 1976. Chapter 7.

Levin, E. M., C. R. Robbins, and H. F. McMurdie (Editors), *Phase Diagrams for Ceramists,* Vol. I, American Ceramic Society, Columbus, OH, 1964. Also supplementary Volumes II, III, IV, V and VI, published in 1969, 1973, 1981, 1983 and 1987, respectively.

Massalski, T. B. (Editor), *Binary Phase Diagrams,* 2nd edition, ASM International, Materials Park, OH, 1990. Three volumes. On CD-ROM with updates.

Mysen, B. O. (Editor), *Phase Diagrams for Ceramists,* Vol. VIII, American Ceramic Society, Columbus, OH, 1990.

Petzow, G. and G. Effenberg, *Ternary Alloys, A*

Comprehensive Compendium of Evaluated Constitutional Data and Phase Diagrams, VCH Publishers, New York, 1988. Eight volumes.

Rhines, F. N., *Phase Diagrams in Metallurgy—Their Development and Application,* McGraw-Hill Book Company, Inc., New York, 1956.

QUESTIONS AND PROBLEMS

Note: To solve those problems having an asterisk (*) by their numbers, consultation of supplementary topics [appearing only on the CD-ROM (and not in print)] will probably be necessary.

10.1 Cite three variables that determine the microstructure of an alloy.

10.2 What thermodynamic condition must be met for a state of equilibrium to exist?

10.3 For metal alloys, the development of microstructure depends on the phenomenon of diffusion (Figures {10.13} and 10.30). It was noted in Section 6.3 that the driving force for steady-state diffusion is a concentration gradient. However, concentration gradients are normally absent in regions where diffusion is occurring, as represented in Figures {10.13} and 10.30; for these situations, what is the driving force?

10.4 What is the difference between the states of phase equilibrium and metastability?

10.5 Cite the phases that are present and the phase compositions for the following alloys:

(a) 90 wt% Zn–10 wt% Cu at 400°C (750°F).

(b) 75 wt% Sn–25 wt% Pb at 175°C (345°F).

(c) 55 wt% Ag–45 wt% Cu at 900°C (1650°F).

(d) 30 wt% Pb–70 wt% Mg at 425°C (795°F).

(e) 2.12 kg Zn and 1.88 kg Cu at 500°C (930°F).

(f) 37 lb_m Pb and 6.5 lb_m Mg at 400°C (750°F).

(g) 8.2 mol Ni and 4.3 mol Cu at 1250°C (2280°F).

(h) 4.5 mol Sn and 0.45 mol Pb at 200°C (390°F).

10.6 For an alloy of composition 74 wt% Zn–26 wt% Cu, cite the phases present and their compositions at the following temperatures: 850°C, 750°C, 680°C, 600°C, and 500°C.

10.7 Determine the relative amounts (in terms of mass fractions) of the phases for the alloys and temperatures given in Problem 10.5.

10.8 Derive Equations 10.6a and 10.7a, which may be used to convert mass fraction to volume fraction, and vice versa.

10.9 Determine the relative amounts (in terms of volume fractions) of the phases for the alloys and temperatures given in Problem 10.5a, b, and c. Below are given the approximate densities of the various metals at the alloy temperatures:

Metal	*Temperature (°C)*	*Density (g/cm^3)*
Ag	900	9.97
Cu	400	8.77
Cu	900	8.56
Pb	175	11.20
Sn	175	7.22
Zn	400	6.83

10.10 Below is a portion of the H_2O–NaCl phase diagram:

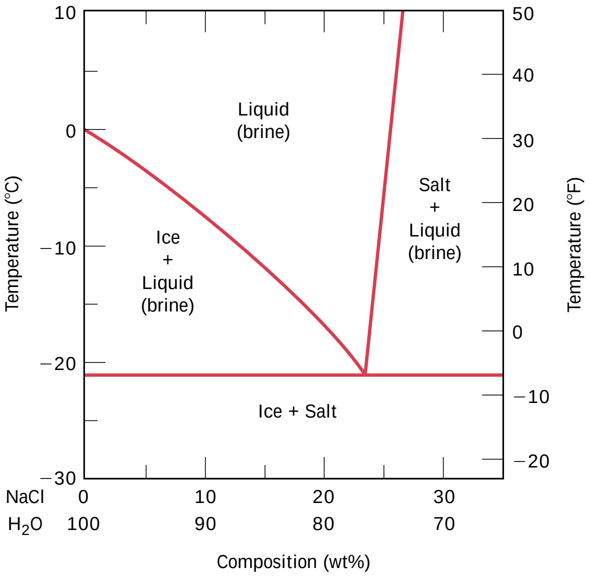

(a) Using this diagram, briefly explain how spreading salt on ice that is at a temperature below 0°C (32°F) can cause the ice to melt.

(b) What concentration of salt is necessary to have a 50% ice–50% liquid brine at −10°C (14°F)?

10.11 A 1.5-kg specimen of a 90 wt% Pb–10 wt% Sn alloy is heated to 250°C (480°F), at which temperature it is entirely an α-phase solid solution (Figure 10.7). The alloy is to be melted to the extent that 50% of the specimen is liquid, the remainder being the α phase. This may be accomplished either by heating the alloy or changing its composition while holding the temperature constant.

(a) To what temperature must the specimen be heated?

(b) How much tin must be added to the 1.5-kg specimen at 250°C to achieve this state?

10.12 Consider the sugar–water phase diagram of Figure 10.1.

(a) How much sugar will dissolve in 1500 g water at 90°C (194°F)?

(b) If the saturated liquid solution in part (a) is cooled to 20°C (68°F), some of the sugar will precipitate out as a solid. What will be the composition of the saturated liquid solution (in wt% sugar) at 20°C?

(c) How much of the solid sugar will come out of solution upon cooling to 20°C?

10.13 Consider a specimen of ice I which is at −10°C and 1 atm pressure. Using Figure 10.38, the pressure–temperature phase diagram for H_2O, determine the pressure to which the specimen must be raised or lowered to cause it **(a)** to melt, and **(b)** to sublime.

10.14 At a pressure of 0.01 atm, determine **(a)** the melting temperature for ice I, and **(b)** the boiling temperature for water.

10.15 A magnesium–lead alloy of mass 5.5 kg consists of a solid α phase that has a composition that is just slightly below the solubility limit at 200°C (390°F).

(a) What mass of lead is in the alloy?

(b) If the alloy is heated to 350°C (660°F), how much more lead may be dissolved in the α phase without exceeding the solubility limit of this phase?

10.16* **(a)** Briefly describe the phenomenon of coring and why it occurs.

(b) Cite one undesirable consequence of coring.

10.17 It is desired to produce a copper–nickel alloy that has a minimum noncold-worked tensile strength of 350 MPa (50,750 psi) and a ductility of at least 48%EL. Is such an alloy possible? If so, what must be its composition? If this is not possible, then explain why.

10.18 Is it possible to have a copper–silver alloy that, at equilibrium, consists of a β phase

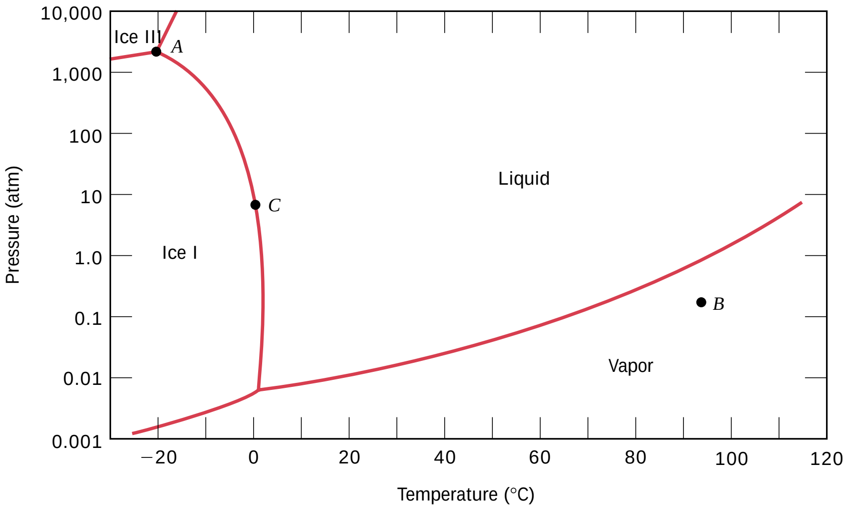

FIGURE 10.38 Logarithm pressure-versus-temperature phase diagram for H_2O.

of composition 92 wt% Ag–8 wt% Cu, and also a liquid phase of composition 76 wt% Ag–24 wt% Cu? If so, what will be the approximate temperature of the alloy? If this is not possible, explain why.

10.19 Is it possible to have a copper–zinc alloy that, at equilibrium, consists of an ϵ phase of composition 80 wt% Zn–20 wt% Cu, and also a liquid phase of composition 95 wt% Zn–5 wt% Cu? If so, what will be the approximate temperature of the alloy? If this is not possible, explain why.

10.20 A copper–nickel alloy of composition 70 wt% Ni–30 wt% Cu is slowly heated from a temperature of 1300°C (2370°F).

(a) At what temperature does the first liquid phase form?

(b) What is the composition of this liquid phase?

(c) At what temperature does complete melting of the alloy occur?

(d) What is the composition of the last solid remaining prior to complete melting?

10.21 A 50 wt% Pb–50 wt% Mg alloy is slowly cooled from 700°C (1290°F) to 400°C (750°F).

(a) At what temperature does the first solid phase form?

(b) What is the composition of this solid phase?

(c) At what temperature does the liquid solidify?

(d) What is the composition of this last remaining liquid phase?

10.22 A 90 wt% Ag–10 wt% Cu alloy is heated to a temperature within the β + liquid phase region. If the composition of the liquid phase is 85 wt% Ag, determine **(a)** the temperature of the alloy, **(b)** the composition of the β phase, and **(c)** the mass fractions of both phases.

10.23 Below are given the solidus and liquidus temperatures for the germanium–silicon system. Construct the phase diagram for this system and label each region.

Composition (wt% Si)	*Solidus Temperature (°C)*	*Liquidus Temperature (°C)*
0	938	938
10	1005	1147
20	1065	1226
30	1123	1278
40	1178	1315
50	1232	1346
60	1282	1367
70	1326	1385
80	1359	1397
90	1390	1408
100	1414	1414

10.24 A 30 wt% Sn–70 wt% Pb alloy is heated to a temperature within the α + liquid phase region. If the mass fraction of each phase is 0.5, estimate **(a)** the temperature of the alloy, and **(b)** the compositions of the two phases.

10.25* When kaolinite clay [$Al_2(Si_2O_5)(OH)_4$] is heated to a sufficiently high temperature, chemical water is driven off.

(a) Under these circumstances what is the composition of the remaining product?

(b) What are the liquidus and solidus temperatures of this material?

10.26 For alloys of two hypothetical metals A and B, there exist an α, A-rich phase and a β, B-rich phase. From the mass fractions of both phases for two different alloys, which are at the same temperature, determine the composition of the phase boundary (or solubility limit) for both α and β phases at this temperature.

Alloy Composition	*Fraction α Phase*	*Fraction β Phase*
60 wt% A–40 wt% B	0.57	0.43
30 wt% A–70 wt% B	0.14	0.86

10.27 A hypothetical A–B alloy of composition 55 wt% B–45 wt% A at some temperature is found to consist of mass fractions of 0.5 for both α and β phases. If the composition of the β phase is 90 wt% B–10 wt% A, what is the composition of the α phase?

10.28 Is it possible to have a copper–silver alloy of composition 50 wt% Ag–50 wt% Cu, which, at equilibrium, consists of α and β phases having mass fractions $W_\alpha = 0.60$ and $W_\beta = 0.40$? If so, what will be the approximate temperature of the alloy? If such an alloy is not possible, explain why.

10.29 For 11.20 kg of a magnesium–lead alloy of composition 30 wt% Pb–70 wt% Mg, is it possible, at equilibrium, to have α and Mg_2Pb phases having respective masses of 7.39 kg and 3.81 kg? If so, what will be the approximate temperature of the alloy? If such an alloy is not possible, explain why.

10.30 At 700°C (1290°F), what is the maximum solubility **(a)** of Cu in Ag? **(b)** Of Ag in Cu?

10.31* A 45 wt% Pb–55 wt% Mg alloy is rapidly quenched to room temperature from an elevated temperature in such a way that the high-temperature microstructure is preserved. This microstructure is found to consist of the α phase and Mg_2Pb, having respective mass fractions of 0.65 and 0.35. Determine the approximate temperature from which the alloy was quenched.

10.32* Is it possible to have a copper–silver alloy in which the mass fractions of primary β and total β are 0.68 and 0.925, respectively, at 775°C (1425°F)? Why or why not?

10.33* For 6.70 kg of a magnesium–lead alloy, is it possible to have the masses of primary α and total α of 4.23 kg and 6.00 kg, respectively, at 460°C (860°F)? Why or why not?

10.34* For a copper–silver alloy of composition 25 wt% Ag–75 wt% Cu and at 775°C (1425°F) do the following:

(a) Determine the mass fractions of the α and β phases.

(b) Determine the mass fractions of primary α and eutectic microconstituents.

(c) Determine the mass fraction of eutectic α.

10.35* The microstructure of a lead–tin alloy at 180°C (355°F) consists of primary β and eutectic structures. If the mass fractions of these two microconstituents are 0.57 and 0.43, respectively, determine the composition of the alloy.

10.36* Consider the hypothetical eutectic phase diagram for metals A and B, which is similar to that for the lead–tin system, Figure 10.7. Assume that (1) α and β phases exist at the A and B extremities of the phase diagram, respectively; (2) the eutectic composition is 47 wt% B–53 wt% A; and (3) the composition of the β phase at the eutectic temperature is 92.6 wt% B–7.4 wt% A. Determine the composition of an alloy that will yield primary α and total α mass fractions of 0.356 and 0.693, respectively.

10.37* Briefly explain why, upon solidification, an alloy of eutectic composition forms a microstructure consisting of alternating layers of the two solid phases.

10.38* For an 85 wt% Pb–15 wt% Mg alloy, make schematic sketches of the microstructure that would be observed for conditions of very slow cooling at the following temperatures: 600°C (1110°F), 500°C (930°F), 270°C (520°F), and 200°C (390°F). Label all phases and indicate their approximate compositions.

10.39* For a 68 wt% Zn–32 wt% Cu alloy, make schematic sketches of the microstructure that would be observed for conditions of very slow cooling at the following temperatures: 1000°C (1830°F), 760°C (1400°F), 600°C (1110°F), and 400°C (750°F). Label all phases and indicate their approximate compositions.

10.40* For a 30 wt% Zn–70 wt% Cu alloy, make schematic sketches of the microstructure that would be observed for conditions of very slow cooling at the following temperatures: 1100°C (2010°F), 950°C (1740°F), 900°C (1650°F), and 700°C (1290°F). Label all phases and indicate their approximate compositions.

10.41 What is the principal difference between congruent and incongruent phase transformations?

10.42 Figure 10.39 is the aluminum–neodymium phase diagram, for which only single-phase regions are labeled. Specify temperature–composition points at which all eutectics, eutectoids, peritectics, and congruent phase transformations occur. Also, for each, write the reaction upon cooling.

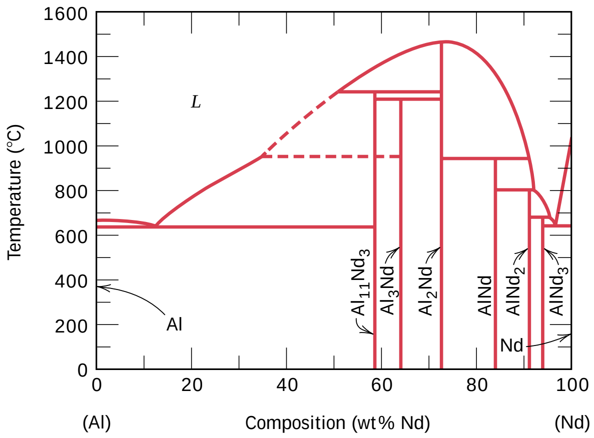

FIGURE 10.39 The aluminum–neodymium phase diagram. (Adapted from *ASM Handbook*, Vol. 3, *Alloy Phase Diagrams*, H. Baker, Editor, 1992. Reprinted by permission of ASM International, Materials Park, OH.)

10.43 Figure 10.40 is a portion of the titanium–copper phase diagram for which only single-phase regions are labeled. Specify all temperature–composition points at which eutectics, eutectoids, peritectics, and congruent phase transformations occur. Also, for each, write the reaction upon cooling.

10.44* For the ZrO_2–CaO system (Figure 10.23), write all eutectic and eutectoid reactions for cooling.

10.45* From Figure 10.22, the phase diagram for the MgO–Al_2O_3 system, it may be noted that the spinel solid solution exists over a range of compositions, which means that it is nonstoichiometric at compositions other than 50 mol% MgO–50 mol% Al_2O_3.

(a) The maximum nonstoichiometry on the Al_2O_3-rich side of the spinel phase field exists at about 2000°C (3630°F) corresponding to approximately 82 mol% (92 wt%) Al_2O_3.

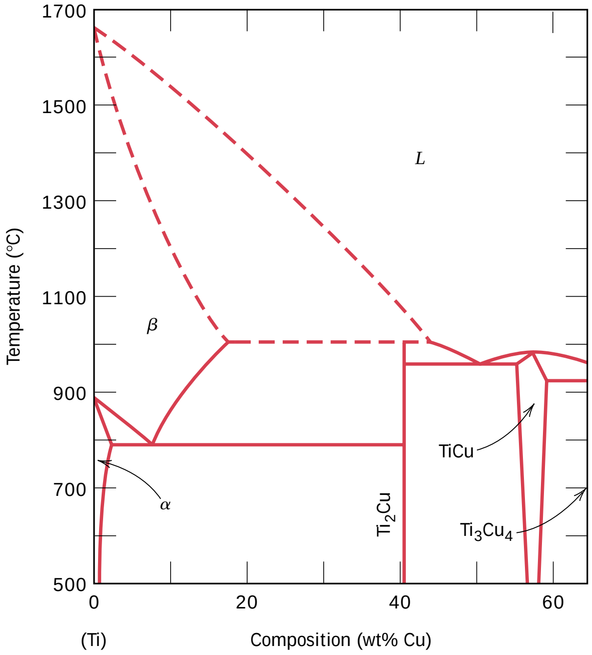

FIGURE 10.40 The titanium–copper phase diagram. (Adapted from *Phase Diagrams of Binary Titanium Alloys*, J. L. Murray, Editor, 1987. Reprinted by permission of ASM International, Materials Park, OH.)

Determine the type of vacancy defect that is produced and the percentage of vacancies that exist at this composition.

(b) The maximum nonstoichiometry on the MgO-rich side of the spinel phase field exists at about 2000°C (3630°F) corresponding to approximately 39 mol% (62 wt%) Al_2O_3. Determine the type of vacancy defect that is produced and the percentage of vacancies that exist at this composition.

10.46* For a ternary system, three components are present; temperature is also a variable. Compute the maximum number of phases that may be present for a ternary system, assuming that pressure is held constant.

10.47* In Figure 10.38 is shown the pressure–temperature phase diagram for H_2O. Apply the Gibbs phase rule at points *A*, *B*, and *C*; that is, specify the number of degrees of freedom at each of the points, that is, the number of externally controllable variables that need be specified to completely define the system.

10.48 Construct the hypothetical phase diagram for metals A and B between temperatures of 600°C and 1000°C given the following information:

- The melting temperature of metal A is 940°C.
- The solubility of B in A is negligible at all temperatures.
- The melting temperature of metal B is 830°C.
- The maximum solubility of A in B is 12 wt% A, which occurs at 700°C.
- At 600°C, the solubility of A in B is 8 wt% A.
- One eutectic occurs at 700°C and 75 wt% B–25 wt% A.
- A second eutectic occurs at 730°C and 60 wt% B–40 wt% A.
- A third eutectic occurs at 755°C and 40 wt% B–60 wt% A.
- One congruent melting point occurs at 780°C and 51 wt% B–49 wt% A.
- A second congruent melting point occurs at 755°C and 67 wt% B–33 wt% A.
- The intermetallic compound AB exists at 51 wt% B–49 wt% A.
- The intermetallic compound AB_2 exists at 67 wt% B–33 wt% A.

10.49* Two intermetallic compounds, AB and AB_2, exist for elements A and B. If the compositions for AB and AB_2 are 34.3 wt% A–65.7 wt% B and 20.7 wt% A–79.3 wt% B, respectively, and element A is potassium, identify element B.

10.50 Compute the mass fractions of α ferrite and cementite in pearlite.

10.51 What is the difference between a phase and a microconstituent?

10.52 **(a)** What is the distinction between hypoeutectoid and hypereutectoid steels?

(b) In a hypoeutectoid steel, both eutectoid and proeutectoid ferrite exist. Explain the difference between them. What will be the carbon concentration in each?

10.53 Briefly explain why a proeutectoid phase forms along austenite grain boundaries. *Hint:* Consult Section 5.8.

10.54 What is the carbon concentration of an iron–carbon alloy for which the fraction of total ferrite is 0.94?

10.55 What is the proeutectoid phase for an iron–carbon alloy in which the mass fractions of total ferrite and total cementite are 0.92 and 0.08, respectively? Why?

10.56 Consider 1.0 kg of austenite containing 1.15 wt% C, cooled to below 727°C (1341°F).

(a) What is the proeutectoid phase?

(b) How many kilograms each of total ferrite and cementite form?

(c) How many kilograms each of pearlite and the proeutectoid phase form?

(d) Schematically sketch and label the resulting microstructure.

10.57 Consider 2.5 kg of austenite containing 0.65 wt% C, cooled to below 727°C (1341°F).

(a) What is the proeutectoid phase?

(b) How many kilograms each of total ferrite and cementite form?

(c) How many kilograms each of pearlite and the proeutectoid phase form?

(d) Schematically sketch and label the resulting microstructure.

10.58 Compute the mass fractions of proeutectoid ferrite and pearlite that form in an iron–carbon alloy containing 0.25 wt% C.

10.59 The microstructure of an iron–carbon alloy consists of proeutectoid ferrite and pearlite; the mass fractions of these two microconstituents are 0.286 and 0.714, respectively. Determine the concentration of carbon in this alloy.

10.60 The mass fractions of total ferrite and total cementite in an iron–carbon alloy are 0.88 and 0.12, respectively. Is this a hypoeutectoid or hypereutectoid alloy? Why?

10.61 The microstructure of an iron–carbon alloy consists of proeutectoid ferrite and pearlite; the mass fractions of these microconstituents are 0.20 and 0.80, respectively. Determine the concentration of carbon in this alloy.

10.62 Consider 2.0 kg of a 99.6 wt% Fe–0.4 wt% C alloy that is cooled to a temperature just below the eutectoid.

(a) How many kilograms of proeutectoid ferrite form?

(b) How many kilograms of eutectoid ferrite form?

(c) How many kilograms of cementite form?

10.63 Compute the maximum mass fraction of proeutectoid cementite possible for a hypereutectoid iron–carbon alloy.

10.64 Is it possible to have an iron–carbon alloy for which the mass fractions of total ferrite and proeutectoid cementite are 0.846 and 0.049, respectively? Why or why not?

10.65 Is it possible to have an iron–carbon alloy for which the mass fractions of total cementite and pearlite are 0.039 and 0.417, respectively? Why or why not?

10.66 Compute the mass fraction of eutectoid ferrite in an iron–carbon alloy that contains 0.43 wt% C.

10.67 The mass fraction of *eutectoid* cementite in an iron–carbon alloy is 0.104. On the basis of this information, is it possible to determine the composition of the alloy? If so, what is its composition? If this is not possible, explain why.

10.68 The mass fraction of *eutectoid* ferrite in an iron–carbon alloy is 0.82. On the basis of this information, is it possible to determine the composition of the alloy? If so, what is its composition? If this is not possible, explain why.

10.69 For an iron–carbon alloy of composition 5 wt% C–95 wt% Fe, make schematic sketches of the microstructure that would be observed for conditions of very slow cooling at the following temperatures: 1175°C (2150°F), 1145°C (2095°F), and 700°C (1290°F). Label the phases and indicate their compositions (approximate).

10.70 Often, the properties of multiphase alloys may be approximated by the relationship

$$E \text{ (alloy)} = E_\alpha V_\alpha + E_\beta V_\beta$$

where E represents a specific property (modulus of elasticity, hardness, etc.), and V is the volume fraction. The subscripts α and β denote the existing phases or microconstituents. Employ the relationship above to determine the approximate Brinell hardness of a 99.80 wt% Fe–0.20 wt% C alloy. Assume Brinell hardnesses of 80 and 280 for ferrite and pearlite, respectively, and that volume fractions may be approximated by mass fractions.

10.71* On the basis of the photomicrograph (i.e., the relative amounts of the microconstituents) for the lead–tin alloy shown in Figure 10.15 and the Pb–Sn phase diagram (Figure 10.7), estimate the composition of the alloy, and then compare this estimate with the composition given in the figure legend of Figure 10.15. Make the following assumptions: (1) the area fraction of each phase and microconstituent in the photomicrograph is equal to its volume fraction; (2) the densities of the α and β phases as well as the eutectic structure are 11.2, 7.3, and 8.7 g/cm^3, respectively; and (3) this photomicrograph represents the equilibrium microstructure at 180°C (356°F).

10.72* A steel alloy contains 97.5 wt% Fe, 2.0 wt% Mo, and 0.5 wt% C.

(a) What is the eutectoid temperature of this alloy?

(b) What is the eutectoid composition?

(c) What is the proeutectoid phase?

Assume that there are no changes in the positions of other phase boundaries with the addition of Mo.

10.73* A steel alloy is known to contain 93.8 wt% Fe, 6.0 wt% Ni, and 0.2 wt% C.

(a) What is the approximate eutectoid temperature of this alloy?

(b) What is the proeutectoid phase when this alloy is cooled to a temperature just below the eutectoid?

(c) Compute the relative amounts of the proeutectoid phase and pearlite. Assume that there are no alterations in the positions of other phase boundaries with the addition of Ni.

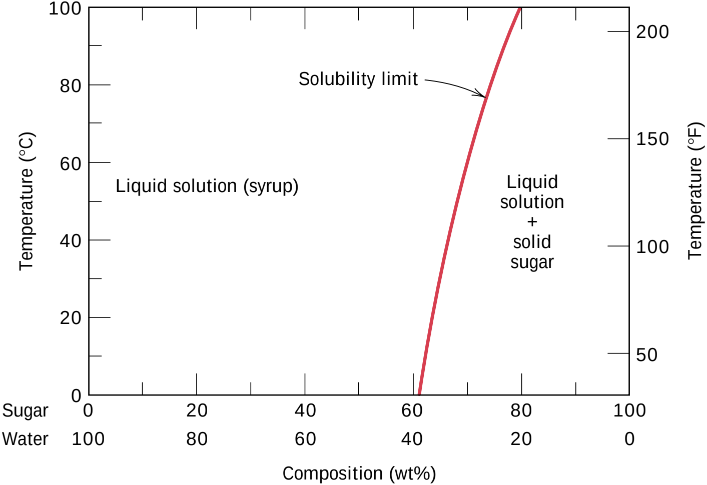

FIGURE 10.1 The solubility of sugar ($C_{12}H_{22}O_{11}$) in a sugar–water syrup.

```
[Loader]
Program=mse5e
CommandLine=PhaseDiagrams
```

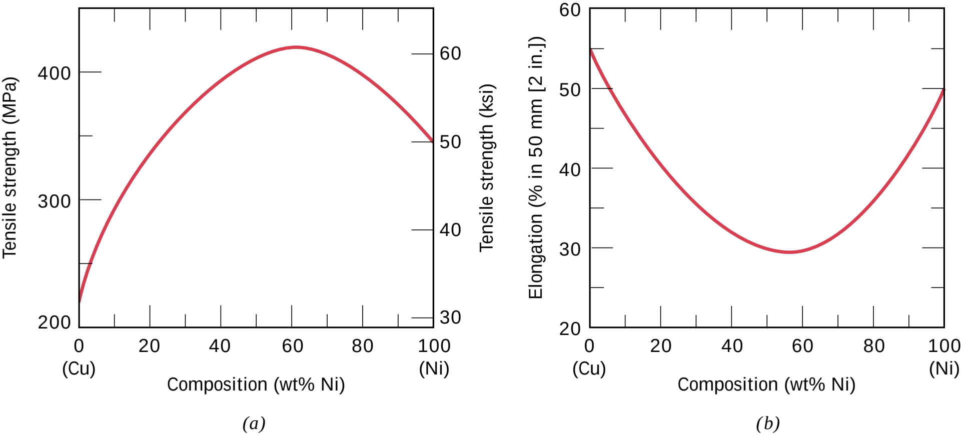

Figure 10.5 For the copper–nickel system, (*a*) tensile strength versus composition, and (*b*) ductility (%EL) versus composition at room temperature. A solid solution exists over all compositions for this system.

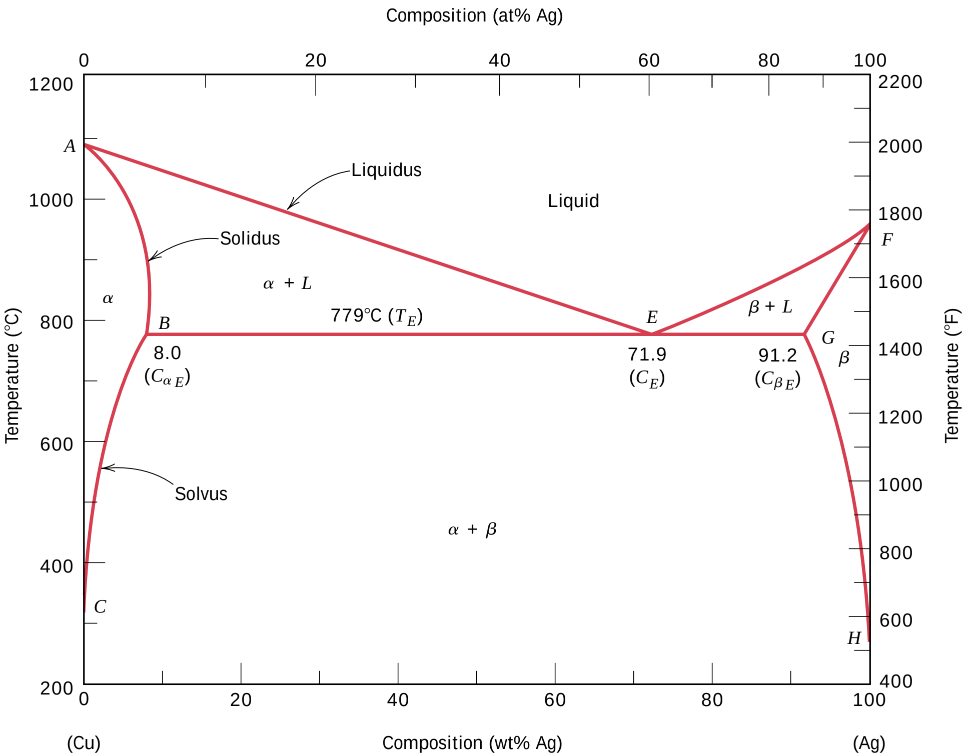

Figure 10.6 The copper–silver phase diagram. (Adapted from *Binary Alloy Phase Diagrams*, 2nd edition, Vol. 1, T. B. Massalski, Editor-in-Chief, 1990. Reprinted by permission of ASM International, Materials Park, OH.)

Chapter 10 / Phase Diagrams

10.8 DEVELOPMENT OF MICROSTRUCTURE IN ISOMORPHOUS ALLOYS

EQUILIBRIUM COOLING

At this point it is instructive to examine the development of microstructure that occurs for isomorphous alloys during solidification. We first treat the situation in which the cooling occurs very slowly, in that phase equilibrium is continuously maintained.

Let us consider the copper–nickel system (Figure 10.2*a*), specifically an alloy of composition 35 wt% Ni–65 wt% Cu as it is cooled from 1300°C. The region of the Cu–Ni phase diagram in the vicinity of this composition is shown in Figure 10.3. Cooling of an alloy of the above composition corresponds to moving down the vertical dashed line. At 1300°C, point *a*, the alloy is completely liquid (of composition 35 wt% Ni–65 wt% Cu) and has the microstructure represented by the circle inset in the figure. As cooling begins, no microstructural or compositional changes will be realized until we reach the liquidus line (point *b*, ~1260°C). At this point, the first solid α begins to form, which has a composition dictated by the tie line drawn at this temperature [i.e., 46 wt% Ni–54 wt% Cu, noted as α(46 Ni)]; the composition of liquid is still approximately 35 wt% Ni–65 wt% Cu [L (35 Ni)], which is different from that of the solid α. With continued cooling, both compositions and relative amounts of each of the phases will change. The compositions of the liquid and α phases will follow the liquidus and solidus lines, respectively. Furthermore, the fraction of the α phase will increase with continued cooling. Note that the overall alloy composition (35 wt% Ni–65 wt% Cu) remains unchanged during cooling even though there is a redistribution of copper and nickel between the phases.

At 1250°C, point *c* in Figure 10.3, the compositions of the liquid and α phases are 32 wt% Ni–68 wt% Cu [L (32 Ni)] and 43 wt% Ni–57 wt% Cu [α(43 Ni)], respectively.

The solidification process is virtually complete at about 1220°C, point *d*; the composition of the solid α is approximately 35 wt% Ni–65 wt% Cu (the overall alloy composition) while that of the last remaining liquid is 24 wt% Ni–76 wt% Cu. Upon crossing the solidus line, this remaining liquid solidifies; the final product then is a polycrystalline α-phase solid solution that has a uniform 35 wt% Ni–65 wt% Cu composition (point *e*, Figure 10.3). Subsequent cooling will produce no microstructural or compositional alterations.

NONEQUILIBRIUM COOLING

Conditions of equilibrium solidification and the development of microstructures, as described in the previous section, are realized only for extremely slow cooling rates. The reason for this is that with changes in temperature, there must be readjust-

Figure 10.3 Schematic representation of the development of microstructure during the equilibrium solidification of a 35 wt% Ni–65 wt% Cu alloy.

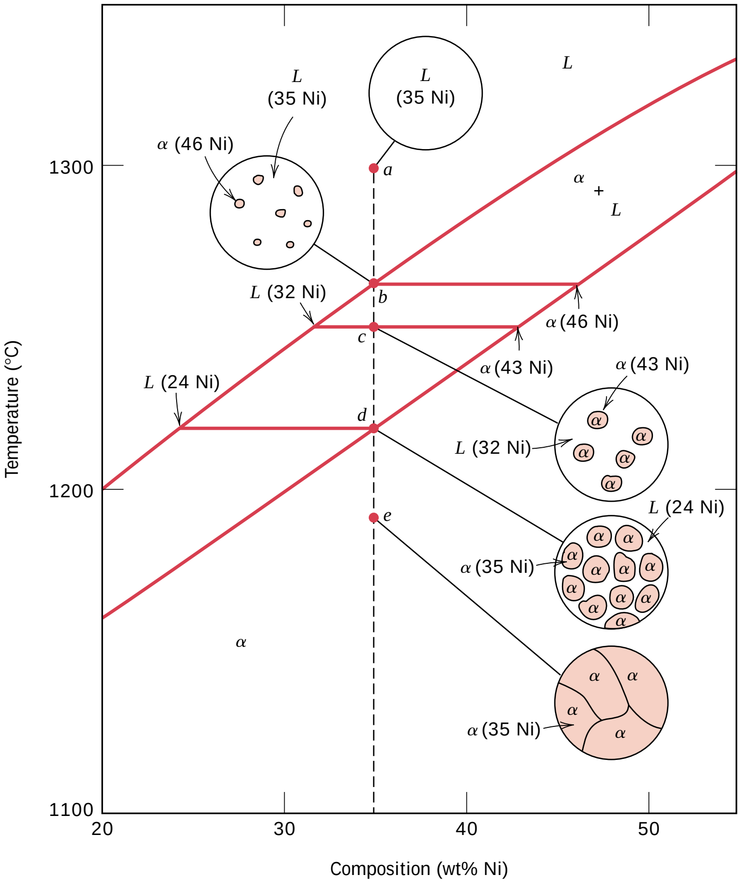

ments in the compositions of the liquid and solid phases in accordance with the phase diagram (i.e., with the liquidus and solidus lines), as discussed. These readjustments are accomplished by diffusional processes, that is, diffusion in both solid and liquid phases and also across the solid–liquid interface. Inasmuch as diffusion is a time-dependent phenomenon (Section 6.3), to maintain equilibrium during cooling, sufficient time must be allowed at each temperature for the appropriate compositional readjustments. Diffusion rates (i.e., the magnitudes of the diffusion coefficients) are especially low for the solid phase and, for both phases, decrease with diminishing temperature. In virtually all practical solidification situations, cooling rates are much too rapid to allow these compositional readjustments and maintenance of equilibrium; consequently, microstructures other than those previously described develop.

Some of the consequences of nonequilibrium solidification for isomorphous alloys will now be discussed by considering a 35 wt% Ni–65 wt% Cu alloy, the same composition that was used for equilibrium cooling in the previous section. The portion of the phase diagram near this composition is shown in Figure 10.4; in addition, microstructures and associated phase compositions at various temperatures upon cooling are noted in the circular insets. In order to simplify this discussion it will be assumed that diffusion rates in the liquid phase are sufficiently rapid such that equilibrium is maintained in the liquid.

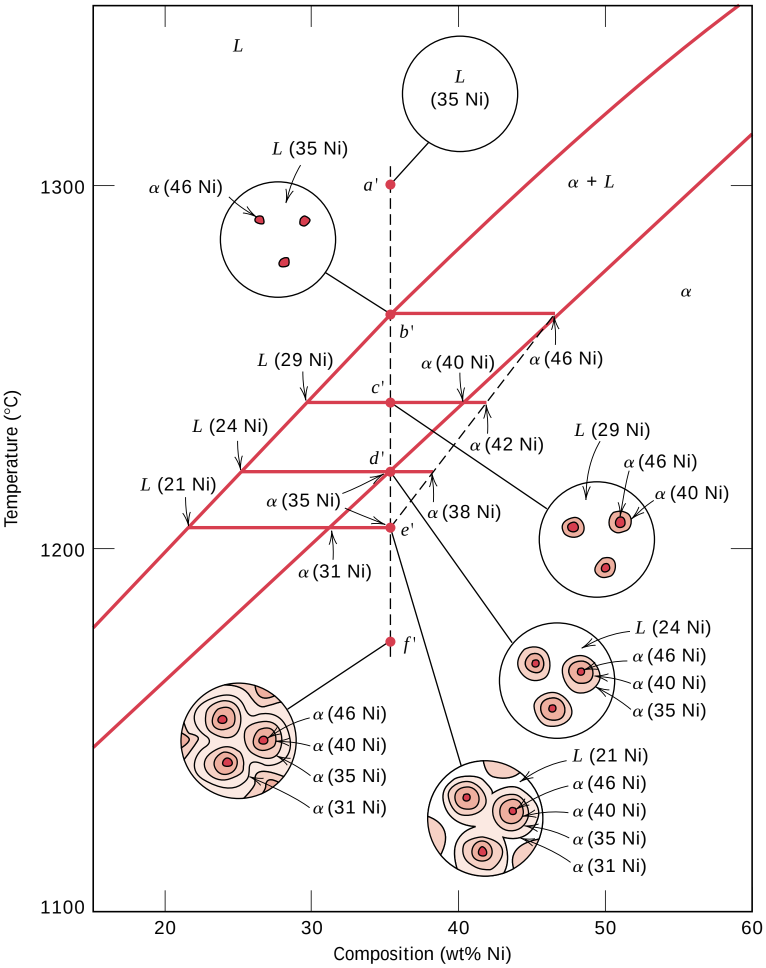
L
L (35 Ni)
L (35 Ni)
α (46 Ni)
a'
α + L
1300
α
b'
L (29 Ni)
α (40 Ni)
α (46 Ni)
c'
L (24 Ni)
α (42 Ni)
L (29 Ni)
d'
α (46 Ni)
L (21 Ni)
α (40 Ni)
α (35 Ni)
α (38 Ni)
e'
1200
α (31 Ni)
L (24 Ni)
α (46 Ni)
f'
α (40 Ni)
α (35 Ni)
α (46 Ni)
α (40 Ni)
L (21 Ni)
α (35 Ni)
α (46 Ni)
α (31 Ni)
α (40 Ni)
α (35 Ni)
α (31 Ni)
1100
20
30
40
50
60
Composition (wt% Ni)
Temperature (°C)

Figure 10.4 Schematic representation of the development of microstructure during the nonequilibrium solidification of a 35 wt% Ni–65 wt% Cu alloy.

Let us begin cooling from a temperature of about 1300°C; this is indicated by point *a*′ in the liquid region. This liquid has a composition of 35 wt% Ni–65 wt% Cu [noted as *L*(35 Ni) in the figure], and no changes occur while cooling through the liquid phase region (moving down vertically from point *a*′). At point *b*′ (approximately 1260°C), α phase particles begin to form, which, from the tie line constructed, have a composition of 46 wt% Ni–54 wt% Cu [α(46 Ni)].

Upon further cooling to point *c*′ (about 1240°C), the liquid composition has shifted to 29 wt% Ni–71 wt% Cu; furthermore, at this temperature the composition of the α phase that solidified is 40 wt% Ni–60 wt% Cu [α(40 Ni)]. However, since diffusion in the solid α phase is relatively slow, the α phase that formed at point *b*′ has not changed composition appreciably—i.e., it is still about 46 wt% Ni—and the composition of the α grains has continuously changed with radial position, from 46 wt% Ni at grain centers to 40 wt% Ni at the outer grain perimeters. Thus, at point *c*′, the *average composition* of the solid α grains that have formed would be some volume weighted average composition, lying between 46 and 40 wt% Ni; for the sake of argument, let us take this average composition to be 42 wt% Ni–58 wt% Cu [α(42 Ni)]. Furthermore, we would also find that, on the basis of lever-rule computations, a greater proportion of liquid is present for these nonequilibrium conditions than for equilibrium cooling. The implication of this nonequilibrium solidification phenomenon is that the solidus line on the phase diagram has been shifted to higher Ni contents—to the average compositions of the α phase (e.g., 42 wt% Ni at 1240°C)—and is represented by the dashed line in Figure 10.4. There is no comparable alteration of the liquidus line inasmuch as it is assumed that equilibrium is maintained in the liquid phase during cooling because of sufficiently rapid diffusion rates.

At point d' (~1220°C) and for equilibrium cooling rates, solidification should be completed. However, for this nonequilibrium situation, there is still an appreciable proportion of liquid remaining, and the α phase that is forming has a composition of 35 wt% Ni [α(35 Ni)]; also the *average* α-phase composition at this point is 38 wt% Ni [α(38 Ni)].

Nonequilibrium solidification finally reaches completion at point e' (~1205°C). The composition of the last α phase to solidify at this point is about 31 wt% Ni; the *average* composition of the α phase at complete solidification is 35 wt% Ni. The inset at point f' shows the microstructure of the totally solid material.

The degree of displacement of the nonequilibrium solidus curve from the equilibrium one will depend on rate of cooling. The slower the cooling rate, the smaller this displacement—that is, the difference between the equilibrium solidus and average solid composition is lower. Furthermore, if the diffusion rate in the solid phase is increased, this displacement will be diminished.

There are some important consequences for isomorphous alloys that have solidified under nonequilibrium conditions. As discussed above, the distribution of the two elements within the grains is nonuniform, a phenomenon termed *segregation;* that is, concentration gradients are established across the grains that are represented by the insets of Figure 10.4. The center of each grain, which is the first part to freeze, is rich in the high-melting element (e.g., nickel for this Cu–Ni system), whereas the concentration of the low-melting element increases with position from this region to the grain boundary. This is termed a *cored* structure, the properties of which are less than optimal; as a casting having a cored structure is reheated, grain boundary regions will melt first inasmuch as they are richer in the low-melting component. This produces a sudden loss in mechanical integrity due to the thin liquid film that separates the grains. Furthermore, this melting may begin at a temperature below the equilibrium solidus temperature of the alloy. Coring may be eliminated by a homogenization heat treatment carried out at a temperature below the solidus point for the particular alloy composition. During this process, atomic diffusion occurs, which produces compositionally homogeneous grains.

10.11 DEVELOPMENT OF MICROSTRUCTURE IN EUTECTIC ALLOYS

Depending on composition, several different types of microstructures are possible for the slow cooling of alloys belonging to binary eutectic systems. These possibilities will be considered in terms of the lead–tin phase diagram, Figure 10.7.

The first case is for compositions ranging between a pure component and the maximum solid solubility for that component at room temperature [20°C (70°F)]. For the lead–tin system, this includes lead-rich alloys containing between 0 and about 2 wt% Sn (for the α phase solid solution), and also between approximately 99 wt% Sn and pure tin (for the β phase). For example, consider an alloy of composition C_1 (Figure 10.9) as it is slowly cooled from a temperature within the

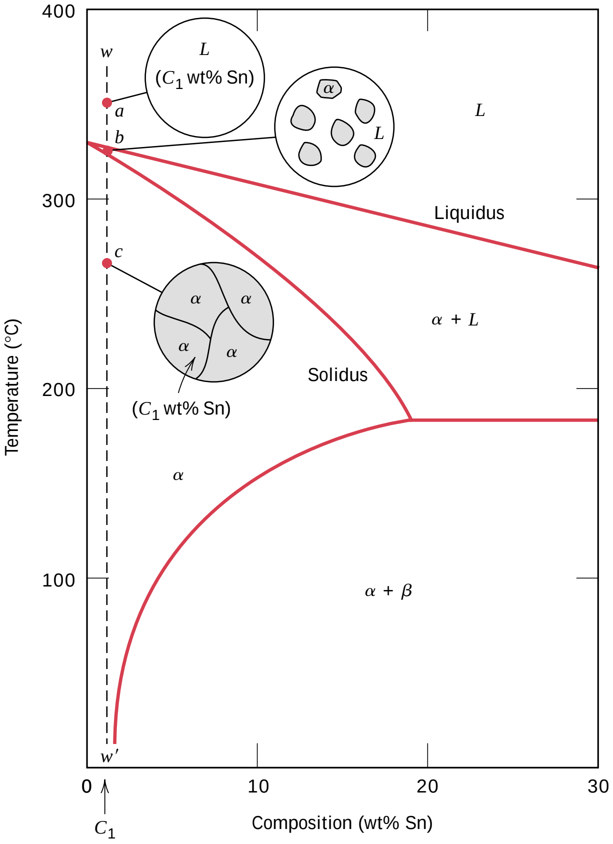

FIGURE 10.9 Schematic representations of the equilibrium microstructures for a lead–tin alloy of composition C_1 as it is cooled from the liquid-phase region.

liquid-phase region, say, 350°C; this corresponds to moving down the dashed vertical line ww' in the figure. The alloy remains totally liquid and of composition C_1 until we cross the liquidus line at approximately 330°C, at which time the solid α phase begins to form. While passing through this narrow $\alpha + L$ phase region, solidification proceeds in the same manner as was described for the copper–nickel alloy in Section 10.8; that is, with continued cooling more of the solid α forms. Furthermore, liquid- and solid-phase compositions are different, which follow along the liquidus and solidus phase boundaries, respectively. Solidification reaches completion at the point where ww' crosses the solidus line. The resulting alloy is polycrystalline with a uniform composition of C_1, and no subsequent changes will occur upon cooling to room temperature. This microstructure is represented schematically by the inset at point c in Figure 10.9.

The second case considered is for compositions that range between the room temperature solubility limit and the maximum solid solubility at the eutectic temperature. For the lead–tin system (Figure 10.7), these compositions extend from about 2 wt% Sn to 18.3 wt% Sn (for lead-rich alloys) and from 97.8 wt% Sn to approximately 99 wt% Sn (for tin-rich alloys). Let us examine an alloy of composition C_2 as it is cooled along the vertical line xx' in Figure 10.10. Down to the intersection of xx' and the solvus line, changes that occur are similar to the previous case, as we pass through the corresponding phase regions (as demonstrated by the insets at points d, e, and f). Just above the solvus intersection, point f, the microstructure consists of α grains of composition C_2. Upon crossing the solvus line, the α solid solubility

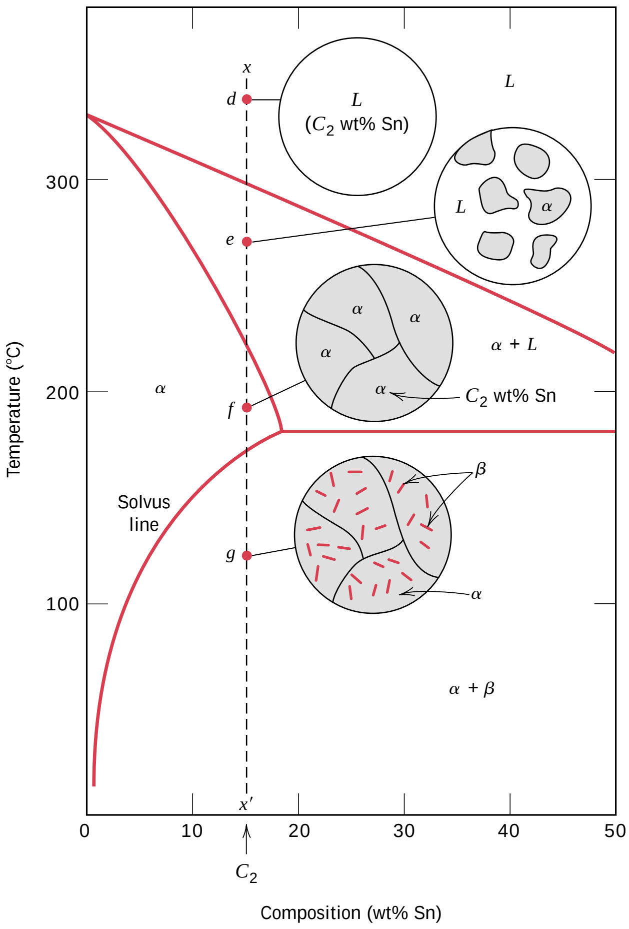

Figure 10.10 Schematic representations of the equilibrium microstructures for a lead–tin alloy of composition C_2 as it is cooled from the liquid-phase region.

is exceeded, which results in the formation of small β phase particles; these are indicated in the microstructure inset at point g. With continued cooling, these particles will grow in size because the mass fraction of the β phase increases slightly with decreasing temperature.

The third case involves solidification of the eutectic composition, 61.9 wt% Sn (C_3 in Figure 10.11). Consider an alloy having this composition that is cooled from a temperature within the liquid-phase region (e.g., 250°C) down the vertical line yy' in Figure 10.11. As the temperature is lowered, no changes occur until we reach the eutectic temperature, 183°C. Upon crossing the eutectic isotherm, the liquid transforms to the two α and β phases. This transformation may be represented by the reaction

$$L\,(61.9\text{ wt\% Sn}) \underset{\text{heating}}{\overset{\text{cooling}}{\rightleftharpoons}} \alpha(18.3\text{ wt\% Sn}) + \beta(97.8\text{ wt\% Sn}) \qquad (10.9)$$

in which the α and β phase compositions are dictated by the eutectic isotherm end points.

During this transformation, there must necessarily be a redistribution of the lead and tin components, inasmuch as the α and β phases have different compositions neither of which is the same as that of the liquid (as indicated in Equation 10.9). This redistribution is accomplished by atomic diffusion. The microstructure

Figure 10.11 Schematic representations of the equilibrium microstructures for a lead–tin alloy of eutectic composition C_3 above and below the eutectic temperature.

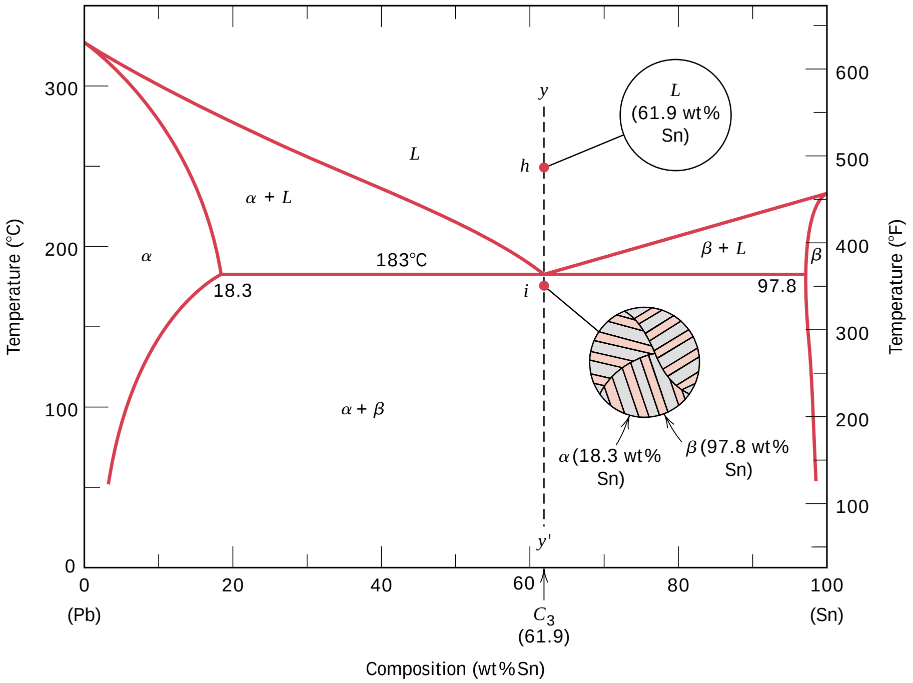

of the solid that results from this transformation consists of alternating layers (sometimes called lamellae) of the α and β phases that form simultaneously during the transformation. This microstructure, represented schematically in Figure 10.11, point *i*, is called a **eutectic structure,** and is characteristic of this reaction. A photomicrograph of this structure for the lead–tin eutectic is shown in Figure 10.12. Subsequent cooling of the alloy from just below the eutectic to room temperature will result in only minor microstructural alterations.

The microstructural change that accompanies this eutectic transformation is represented schematically in Figure 10.13; here is shown the α-β layered eutectic growing into and replacing the liquid phase. The process of the redistribution of lead and tin occurs by diffusion in the liquid just ahead of the eutectic–liquid interface. The arrows indicate the directions of diffusion of lead and tin atoms; lead atoms diffuse toward the α-phase layers since this α phase is lead-rich (18.3 wt% Sn–81.7 wt% Pb); conversely, the direction of diffusion of tin is in the direction

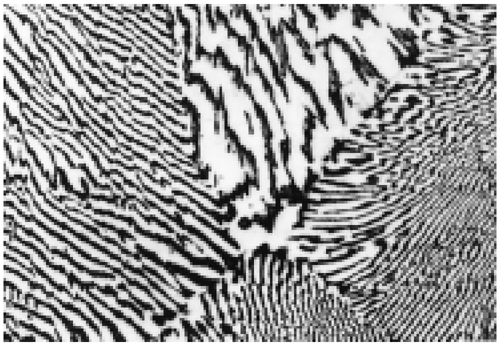

Figure 10.12 Photomicrograph showing the microstructure of a lead–tin alloy of eutectic composition. This microstructure consists of alternating layers of a lead-rich α-phase solid solution (dark layers), and a tin-rich β-phase solid solution (light layers). 375×. (Reproduced with permission from *Metals Handbook*, Vol. 9, 9th edition, *Metallography and Microstructures,* American Society for Metals, Materials Park, OH, 1985.)

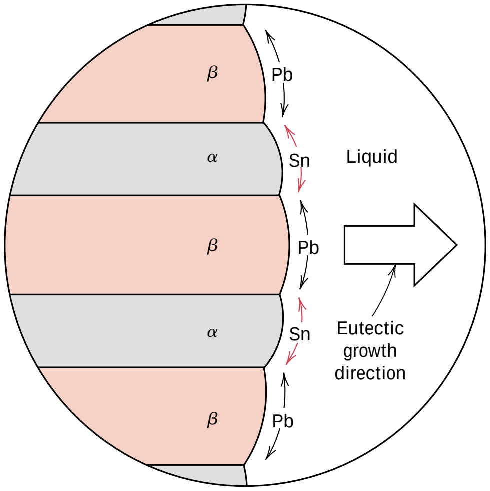

Figure 10.13 Schematic representation of the formation of the eutectic structure for the lead–tin system. Directions of diffusion of tin and lead atoms are indicated by colored and black arrows, respectively.

of the β, tin-rich (97.8 wt% Sn–2.2 wt% Pb) layers. The eutectic structure forms in these alternating layers because, for this lamellar configuration, atomic diffusion of lead and tin need only occur over relatively short distances.

The fourth and final microstructural case for this system includes all compositions other than the eutectic that, when cooled, cross the eutectic isotherm. Consider, for example, the composition C_4, Figure 10.14, which lies to the left of the eutectic; as the temperature is lowered, we move down the line zz', beginning at point j. The microstructural development between points j and l is similar to that for the second case, such that just prior to crossing the eutectic isotherm (point l), the α and liquid phases are present having compositions of approximately 18.3 and 61.9 wt% Sn, respectively, as determined from the appropriate tie line. As the temperature is lowered to just below the eutectic, the liquid phase, which is of the eutectic composition, will transform to the eutectic structure (i.e., alternating α and β lamellae); insignificant changes will occur with the α phase which formed during cooling through the $\alpha + L$ region. This microstructure is represented schematically by the inset at point m in Figure 10.14. Thus, the α phase will be present both in the eutectic structure and also as that phase that formed while cooling through the $\alpha + L$ phase field. To distinguish one α from the other, that which resides in the eutectic structure is called **eutectic** α, while the other that formed prior to crossing the eutectic isotherm is termed **primary** α; both are labeled in Figure 10.14. The photomicrograph in Figure 10.15 is of a lead–tin alloy in which both primary α and eutectic structures are shown.

In dealing with microstructures, it is sometimes convenient to use the term **microconstituent,** that is, an element of the microstructure having an identifiable and characteristic structure. For example, in the point m inset, Figure 10.14, there are two microconstituents, namely, primary α and the eutectic structure. Thus, the eutectic structure is a microconstituent even though it is a mixture of two phases, because it has a distinct lamellar structure, with a fixed ratio of the two phases.

It is possible to compute the relative amounts of both eutectic and primary α microconstituents. Since the eutectic microconstituent always forms from the liquid having the eutectic composition, this microconstituent may be assumed to have a composition of 61.9 wt% Sn. Hence, the lever rule is applied using a tie line between

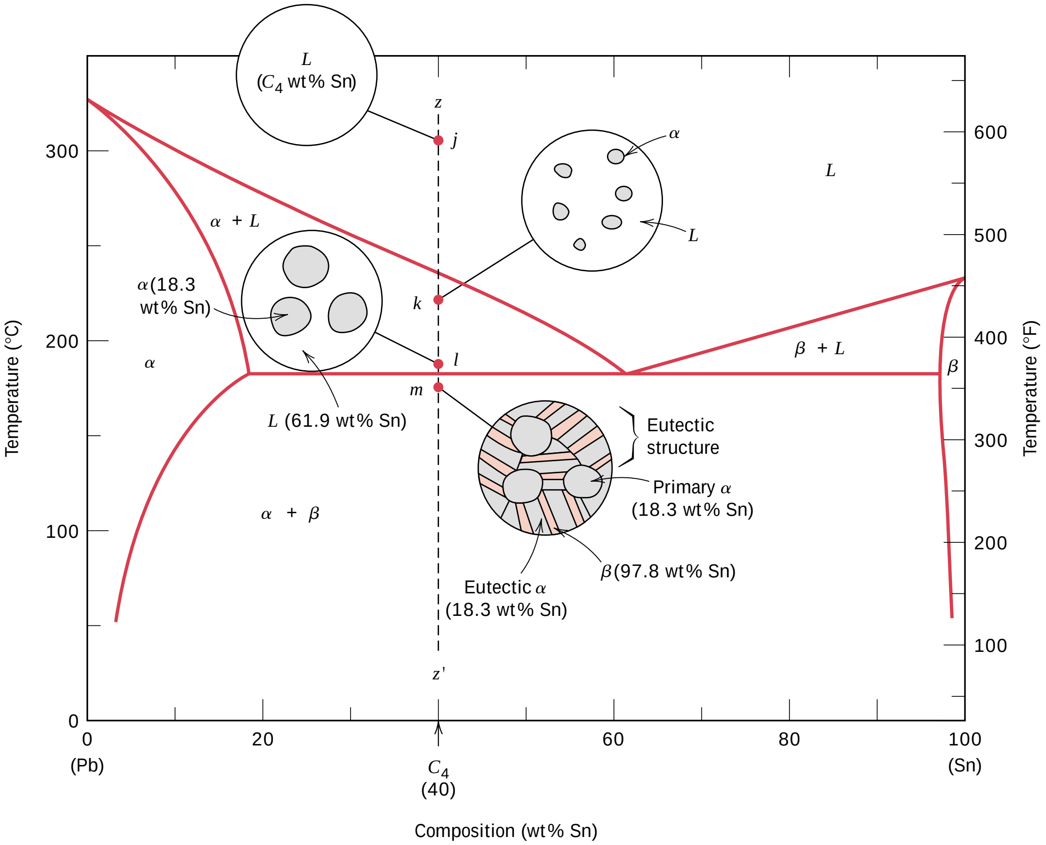
L
(C_4 wt% Sn)
z
j
α
L
300
600
α + L
L
500
α(18.3
wt% Sn)
k
200
400
l
β + L
α
β
m
L (61.9 wt% Sn)
Eutectic
structure
300
Primary α
(18.3 wt% Sn)
α + β
100
200
β(97.8 wt% Sn)
Eutectic α
(18.3 wt% Sn)
100
z'
0
0
(Pb)
20
C_4
(40)
60
80
100
(Sn)
Temperature (°C)
Temperature (°F)
Composition (wt% Sn)

Figure 10.14 Schematic representations of the equilibrium microstructures for a lead–tin alloy of composition C_4 as it is cooled from the liquid-phase region.

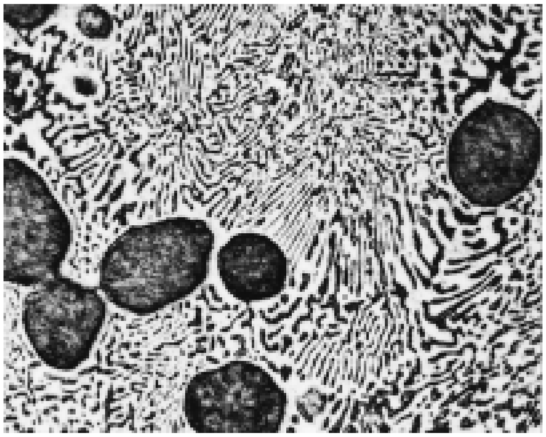

Figure 10.15 Photomicrograph showing the microstructure of a lead–tin alloy of composition 50 wt% Sn–50 wt% Pb. This microstructure is composed of a primary lead-rich α phase (large dark regions) within a lamellar eutectic structure consisting of a tin-rich β phase (light layers) and a lead-rich α phase (dark layers). 400×. (Reproduced with permission from *Metals Handbook*, Vol. 9, 9th edition, *Metallography and Microstructures*, American Society for Metals, Materials Park, OH, 1985.)

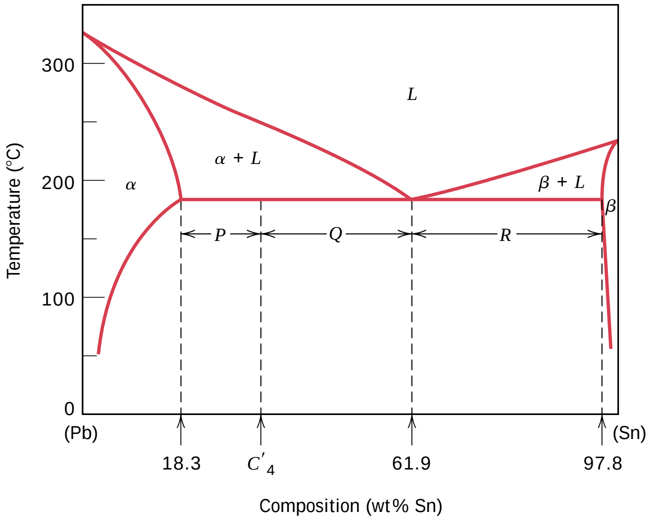

FIGURE 10.16 The lead–tin phase diagram used in computations for relative amounts of primary α and eutectic microconstituents for an alloy of composition C'_4.

the α–($\alpha + \beta$) phase boundary (18.3 wt% Sn) and the eutectic composition. For example, consider the alloy of composition C'_4 in Figure 10.16. The fraction of the eutectic microconstituent W_e is just the same as the fraction of liquid W_L from which it transforms, or

$$W_e = W_L = \frac{P}{P + Q}$$

$$= \frac{C'_4 - 18.3}{61.9 - 18.3} = \frac{C'_4 - 18.3}{43.6} \tag{10.10}$$

Furthermore, the fraction of primary α, $W_{\alpha'}$, is just the fraction of the α phase that existed prior to the eutectic transformation; or, from Figure 10.16,

$$W_{\alpha'} = \frac{Q}{P + Q}$$

$$= \frac{61.9 - C'_4}{61.9 - 18.3} = \frac{61.9 - C'_4}{43.6} \tag{10.11}$$

The fractions of *total* α, W_α (both eutectic and primary), and also of total β, W_β, are determined by use of the lever rule and a tie line that extends *entirely across the* $\alpha + \beta$ *phase field.* Again, for an alloy having composition C'_4,

$$W_\alpha = \frac{Q + R}{P + Q + R}$$

$$= \frac{97.8 - C'_4}{97.8 - 18.3} = \frac{97.8 - C'_4}{79.5} \tag{10.12}$$

and

$$W_\beta = \frac{P}{P + Q + R}$$

$$= \frac{C_4' - 18.3}{97.8 - 18.3} = \frac{C_4' - 18.3}{79.5} \tag{10.13}$$

Analogous transformations and microstructures result for alloys having compositions to the right of the eutectic (i.e., between 61.9 and 97.8 wt% Sn). However, below the eutectic temperature, the microstructure will consist of the eutectic and primary β microconstituents because, upon cooling from the liquid, we pass through the β + liquid phase field.

When, for case 4 (represented in Figure 10.14), conditions of equilibrium are not maintained while passing through the α (or β) + liquid phase region, the following consequences will be realized for the microstructure upon crossing the eutectic isotherm: (1) grains of the primary microconstituent will be cored, that is, have a nonuniform distribution of solute across the grains; and (2) the fraction of the eutectic microconstituent formed will be greater than for the equilibrium situation.

10.15 Ceramic Phase Diagrams

It need not be assumed that phase diagrams exist only for metal–metal systems; in fact, phase diagrams that are very useful in the design and processing of ceramic systems have been experimentally determined for quite a number of these materials. For binary or two-component phase diagrams, it is frequently the case that the two components are compounds that share a common element, often oxygen. These diagrams may have configurations similar to metal–metal systems, and they are interpreted in the same way.

THE Al_2O_3–Cr_2O_3 SYSTEM

One of the relatively simple ceramic phase diagrams is that found for the aluminum oxide–chromium oxide system, Figure 10.21. This diagram has the same form as the isomorphous copper–nickel phase diagram (Figure 10.2*a*), consisting of single liquid and single solid phase regions separated by a two-phase solid–liquid region having the shape of a blade. The Al_2O_3–Cr_2O_3 solid solution is a substitutional one in which Al^{3+} substitutes for Cr^{3+}, and vice versa. It exists for all compositions below the melting point of Al_2O_3 inasmuch as both aluminum and chromium ions have the same charge as well as similar radii (0.053 and 0.062 nm, respectively). Furthermore, both Al_2O_3 and Cr_2O_3 have the same crystal structure.

THE MgO–Al_2O_3 SYSTEM

The phase diagram for the magnesium oxide–aluminum oxide system (Figure 10.22) is similar in many respects to the lead–magnesium diagram (Figure 10.18). There exists an intermediate phase, or better, a compound called *spinel,* which has the chemical formula $MgAl_2O_4$ (or MgO–Al_2O_3). Even though spinel is a distinct compound [of composition 50 mol% Al_2O_3–50 mol% MgO (72 wt% Al_2O_3–28 wt% MgO)], it is represented on the phase diagram as a single-phase field rather than as a vertical line, as for Mg_2Pb (Figure 10.18); that is, there is a range of compositions over which spinel is a stable compound. Thus, spinel is nonstoichiometric (Section

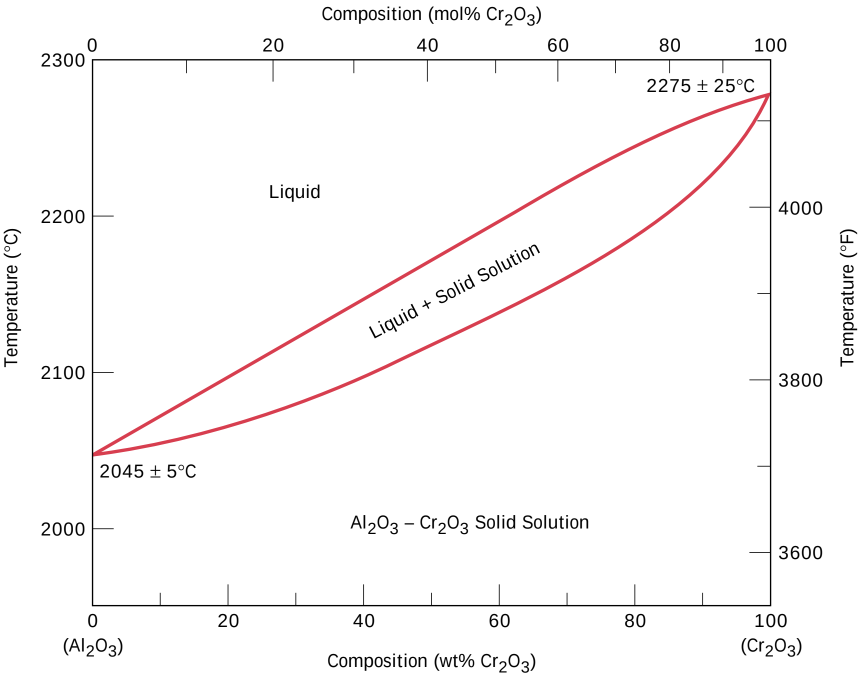

Figure 10.21 The aluminum oxide–chromium oxide phase diagram. (Adapted from E. N. Bunting, "Phase Equilibria in the System Cr_2O_3–Al_2O_3," *Bur. Standards J. Research*, **6,** 1931, p. 948.)

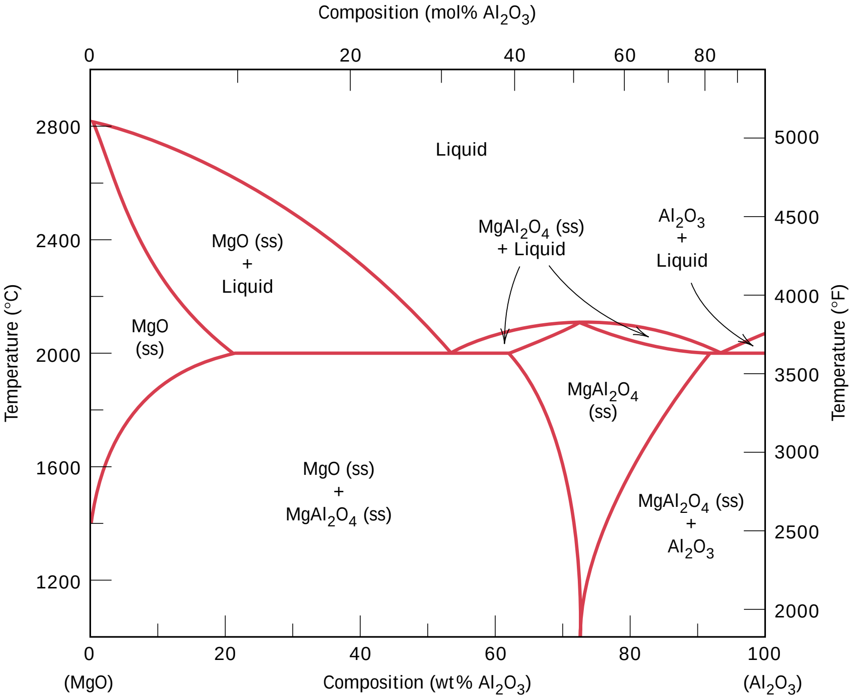

Figure 10.22 The magnesium oxide–aluminum oxide phase diagram; *ss* denotes solid solution. (Adapted from B. Hallstedt, "Thermodynamic Assessment of the System MgO–Al_2O_3," *J. Am. Ceram. Soc.*, **75** [6] 1502 (1992). Reprinted by permission of the American Ceramic Society.)

5.3) for other than the 50 mol% Al_2O_3–50 mol% MgO composition. Furthermore, there is limited solubility of Al_2O_3 in MgO below about 1400°C (2550°F) at the left-hand extremity of Figure 10.22, which is due primarily to the differences in charge and radii of the Mg^{2+} and Al^{3+} ions (0.072 versus 0.053 nm). For the same reasons, MgO is virtually insoluble in Al_2O_3, as evidenced by a lack of a terminal solid solution on the right-hand side of the phase diagram. Also, two eutectics are found, one on either side of the spinel phase field, and stoichiometric spinel melts congruently at about 2100°C (3800°F).

THE ZrO_2–CaO SYSTEM

Another important binary ceramic system is that for zirconium oxide (zirconia) and calcium oxide (calcia); a portion of this phase diagram is shown in Figure 10.23. The horizontal axis extends to only about 31 wt% CaO (50 mol% CaO), at which composition the compound $CaZrO_3$ forms. It is worth noting that one eutectic (2250°C and 23 wt% CaO) and two eutectoid (1000°C and 2.5 wt% CaO, and 850°C and 7.5 wt% CaO) reactions are found for this system.

It may also be observed from Figure 10.23 that ZrO_2 phases having three different crystal structures exist in this system, namely tetragonal, monoclinic,

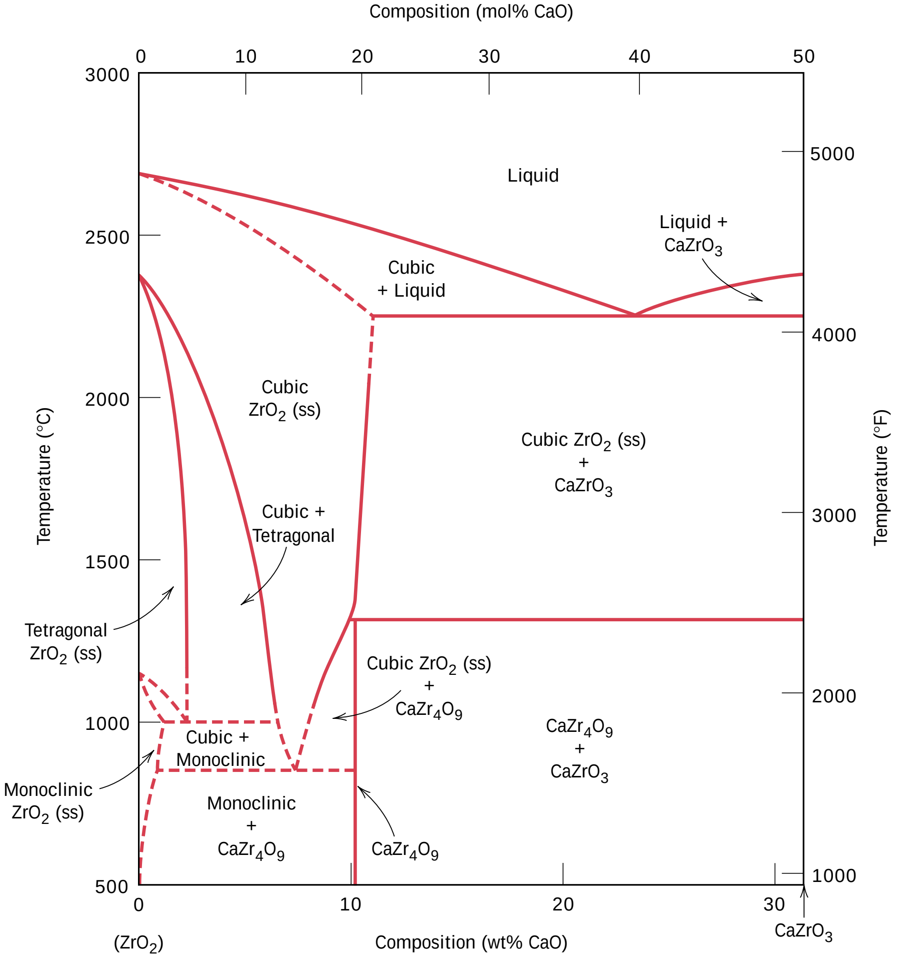

FIGURE 10.23 A portion of the zirconia–calcia phase diagram; *ss* denotes solid solution. (Adapted from V. S. Stubican and S. P. Ray, ''Phase Equilibria and Ordering in the System ZrO_2-CaO,'' *J. Am. Ceram. Soc.*, **60** [11–12] 535 (1977). Reprinted by permission of the American Ceramic Society.)

and cubic. Pure ZrO_2 experiences a tetragonal-to-monoclinic phase transformation at about 1150°C (2102°F). A relatively large volume change accompanies this transformation, resulting in the formation of cracks that render a ceramic ware useless. This problem is overcome by ''stabilizing'' the zirconia by adding between about 3 and 7 wt% CaO. Over this composition range and at temperatures above about 1000°C both cubic and tetragonal phases will be present. Upon cooling to room temperature under normal cooling conditions, the monoclinic and $CaZr_4O_9$ phases do not form (as predicted from the phase diagram); consequently, the cubic and tetragonal phases are retained, and crack formation is circumvented. A zirconia material having a calcia content within the range cited above is termed a *partially stabilized zirconia,* or *PSZ.* Yttrium oxide (Y_2O_3) and magnesium oxide are also used as stabilizing agents. Furthermore, for higher stabilizer contents, only the cubic phase may be retained at room temperature; such a material is fully stabilized.

THE SiO_2–Al_2O_3 SYSTEM

Commercially, the silica-alumina system is an important one since the principal constituents of many ceramic refractories are these two materials. Figure 10.24 shows the SiO_2–Al_2O_3 phase diagram. The polymorphic form of silica that is stable at these temperatures is termed *cristobalite,* the unit cell for which is shown in Figure 3.11. Silica and alumina are not mutually soluble in one another, which is evidenced by the absence of terminal solid solutions at both extremities of the phase diagram. Also, it may be noted that the intermediate compound *mullite,* $3Al_2O_3$–$2SiO_2$, exists, which is represented as a narrow phase field in Figure 10.24;

FIGURE 10.24 The silica–alumina phase diagram. (Adapted from F. J. Klug, S. Prochazka, and R. H. Doremus, ''Alumina-Silica Phase Diagram in the Mullite Region,'' *J. Am. Ceram. Soc.,* **70** [10] 758 (1987). Reprinted by permission of the American Ceramic Society.)

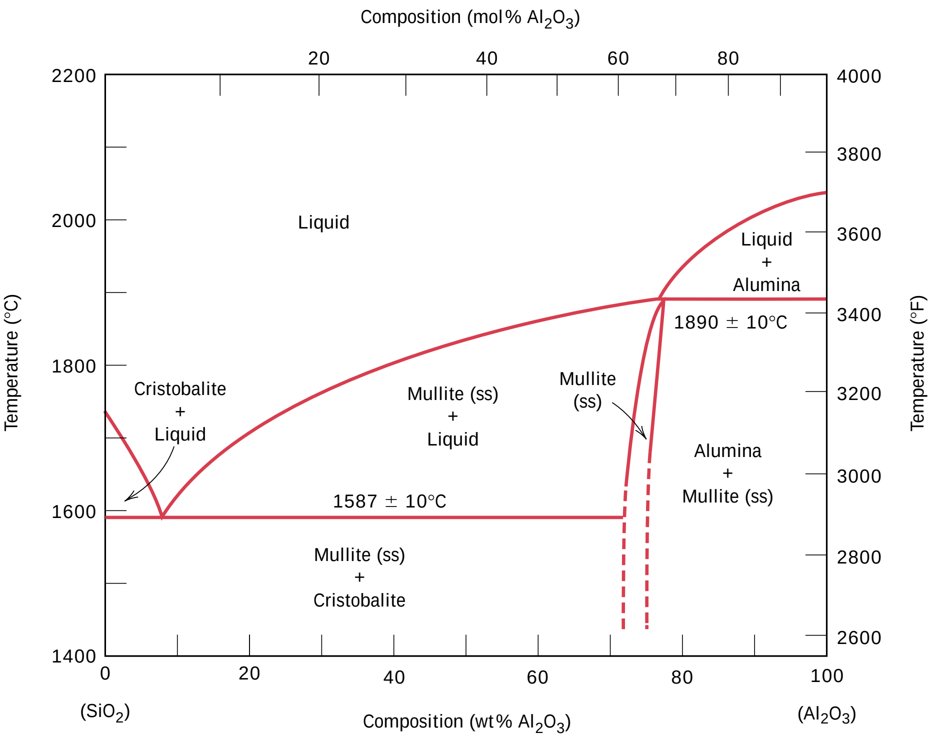

furthermore, mullite melts incongruently at 1890°C (3435°F). A single eutectic exists at 1587°C (2890°F) and 7.7 wt% Al_2O_3. In Section 13.7, refractory ceramic materials, the prime constituents for which are silica and alumina, are discussed.

10.17 THE GIBBS PHASE RULE

The construction of phase diagrams as well as some of the principles governing the conditions for phase equilibria are dictated by laws of thermodynamics. One of these is the **Gibbs phase rule,** proposed by the nineteenth-century physicist J. Willard Gibbs. This rule represents a criterion for the number of phases that will coexist within a system at equilibrium, and is expressed by the simple equation

$$P + F = C + N \tag{10.16}$$

where P is the number of phases present (the phase concept is discussed in Section 10.3). The parameter F is termed the *number of degrees of freedom* or the number of externally controlled variables (e.g., temperature, pressure, composition) which must be specified to completely define the state of the system. Or, expressed another way, F is the number of these variables that can be changed independently without altering the number of phases that coexist at equilibrium. The parameter C in Equation 10.16 represents the number of components in the system. Components are normally elements or stable compounds and, in the case of phase diagrams, are the materials at the two extremities of the horizontal compositional axis (e.g., H_2O and $C_{12}H_{22}O_{11}$, and Cu and Ni for the phase diagrams shown in Figures 10.1 and 10.2*a*, respectively). Finally, N in Equation 10.16 is the number of noncompositional variables (e.g., temperature and pressure).

Let us demonstrate the phase rule by applying it to binary temperature–composition phase diagrams, specifically the copper–silver system, Figure 10.6. Since pressure is constant (1 atm), the parameter N is 1—temperature is the only noncompositional variable. Equation 10.16 now takes the form

$$P + F = C + 1 \tag{10.17}$$

Furthermore, the number of components C is 2 (viz Cu and Ag), and

$$P + F = 2 + 1 = 3$$

or

$$F = 3 - P$$

Consider the case of single-phase fields on the phase diagram (e.g., α, β, and liquid regions). Since only one phase is present, $P = 1$ and

$$\begin{aligned} F &= 3 - P \\ &= 3 - 1 = 2 \end{aligned}$$

This means that to completely describe the characteristics of any alloy that exists within one of these phase fields, we must specify two parameters; these are composition and temperature, which locate, respectively, the horizontal and vertical positions of the alloy on the phase diagram.

For the situation wherein two phases coexist, for example, $\alpha + L$, $\beta + L$, and $\alpha + \beta$ phase regions, Figure 10.6, the phase rule stipulates that we have but one degree of freedom since

$$F = 3 - P$$
$$= 3 - 2 = 1$$

Thus, it is necessary to specify either temperature or the composition of one of the phases to completely define the system. For example, suppose that we decide to specify temperature for the $\alpha + L$ phase region, say, T_1 in Figure 10.25. The compositions of the α and liquid phases (C_α and C_L) are thus dictated by the extremities of the tie line constructed at T_1 across the $\alpha + L$ field. It should be noted that only the nature of the phases is important in this treatment and not the relative phase amounts. This is to say that the overall alloy composition could lie anywhere along this tie line constructed at temperature T_1 and still give C_α and C_L compositions for the respective α and liquid phases.

The second alternative is to stipulate the composition of one of the phases for this two-phase situation, which thereby fixes completely the state of the system. For example, if we specified C_α as the composition of the α phase that is in equilibrium with the liquid (Figure 10.25), then both the temperature of the alloy (T_1) and the composition of the liquid phase (C_L) are established, again by the tie line drawn across the $\alpha + L$ phase field so as to give this C_α composition.

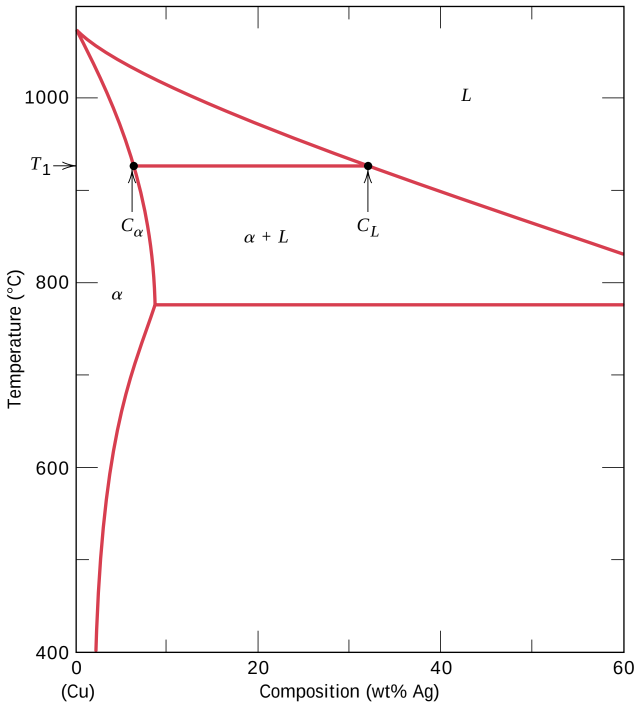

FIGURE 10.25 Enlarged copper-rich section of the Cu–Ag phase diagram in which the Gibbs phase rule for the coexistence of two phases (i.e., α and L) is demonstrated. Once the composition of either phase (i.e., C_α or C_L) or the temperature (i.e., T_1) is specified, values for the two remaining parameters are established by construction of the appropriate tie line.

For binary systems, when three phases are present, there are no degrees of freedom, since

$$F = 3 - P$$
$$= 3 - 3 = 0$$

This means that the compositions of all three phases as well as the temperature are fixed. This condition is met for a eutectic system by the eutectic isotherm; for the Cu–Ag system (Figure 10.6), it is the horizontal line that extends between points B and G. At this temperature, 779°C, the points at which each of the α, L, and β phase fields touch the isotherm line correspond to the respective phase compositions; namely, the composition of the α phase is fixed at 8.0 wt% Ag, that of the liquid at 71.9 wt% Ag, and that of the β phase at 91.2 wt% Ag. Thus, three-phase equilibrium will not be represented by a phase field, but rather by the unique horizontal isotherm line. Furthermore, all three phases will be in equilibrium for any alloy composition that lies along the length of the eutectic isotherm (e.g., for the Cu–Ag system at 779°C and compositions between 8.0 and 91.2 wt% Ag).

One use of the Gibbs phase rule is in analyzing for nonequilibrium conditions. For example, a microstructure for a binary alloy that developed over a range of temperatures and consisting of three phases is a nonequilibrium one; under these circumstances, three phases will exist only at a single temperature.

THE IRON–CARBON SYSTEM

10.20 THE INFLUENCE OF OTHER ALLOYING ELEMENTS

Additions of other alloying elements (Cr, Ni, Ti, etc.) bring about rather dramatic changes in the binary iron–iron carbide phase diagram, Figure 10.26. The extent of these alterations of the positions of phase boundaries and the shapes of the phase fields depends on the particular alloying element and its concentration. One of the important changes is the shift in position of the eutectoid with respect to

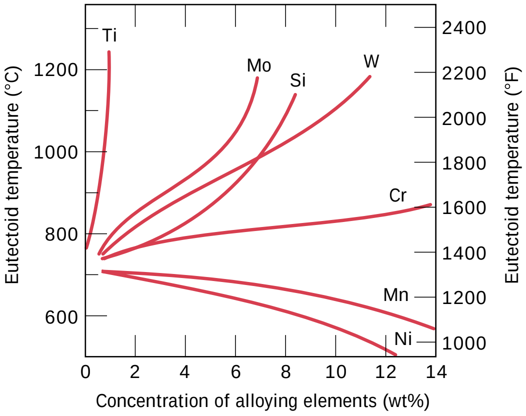

FIGURE 10.36 The dependence of eutectoid temperature on alloy concentration for several alloying elements in steel. (From Edgar C. Bain, *Functions of the Alloying Elements in Steel,* American Society for Metals, 1939, p. 127.)

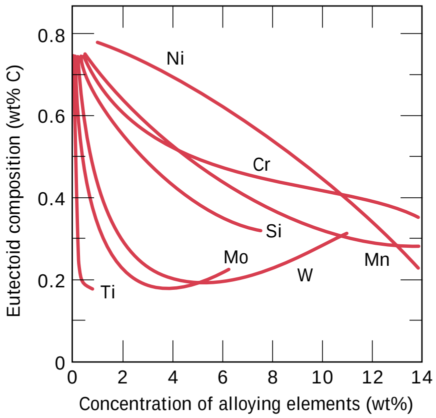

Figure 10.37 The dependence of eutectoid composition (wt% C) on alloy concentration for several alloying elements in steel. (From Edgar C. Bain, *Functions of the Alloying Elements in Steel,* American Society for Metals, 1939, p. 127.)

temperature and to carbon concentration. These effects are illustrated in Figures 10.36 and 10.37, which plot the eutectoid temperature and eutectoid composition (in wt% C) as a function of concentration for several other alloying elements. Thus, other alloy additions alter not only the temperature of the eutectoid reaction but also the relative fractions of pearlite and the proeutectoid phase that form. Steels are normally alloyed for other reasons, however—usually either to improve their corrosion resistance or to render them amenable to heat treatment (see Section 14.6).

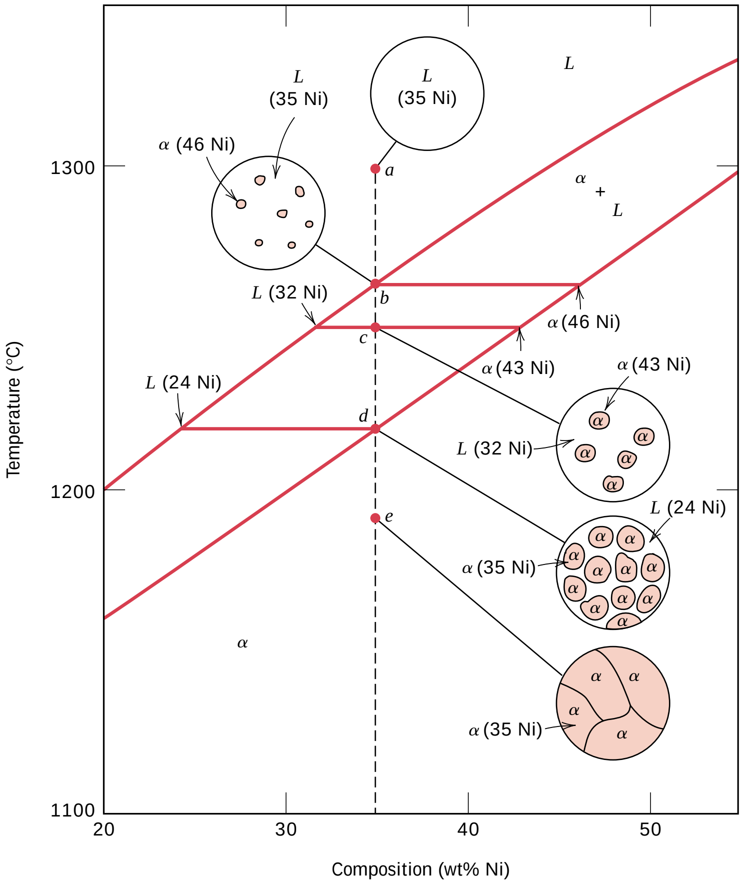
L
(35 Ni)
L
(35 Ni)
L
α (46 Ni)
1300
a
α
+
L
L (32 Ni)
b
α (46 Ni)
c
α (43 Ni)
α (43 Ni)
L (24 Ni)
d
α
L (32 Ni)
α
α
α
α
1200
e
L (24 Ni)
α
α
α
α
α
α
α (35 Ni)
α
α
α
α
α
α
α
α
α
α (35 Ni)
α
Temperature (°C)
1100
20
30
40
50
Composition (wt% Ni)

FIGURE 10.3 Schematic representation of the development of microstructure during the equilibrium solidification of a 35 wt% Ni–65 wt% Cu alloy.

Figure 10.4 Schematic representation of the development of microstructure during the nonequilibrium solidification of a 35 wt% Ni–65 wt% Cu alloy.

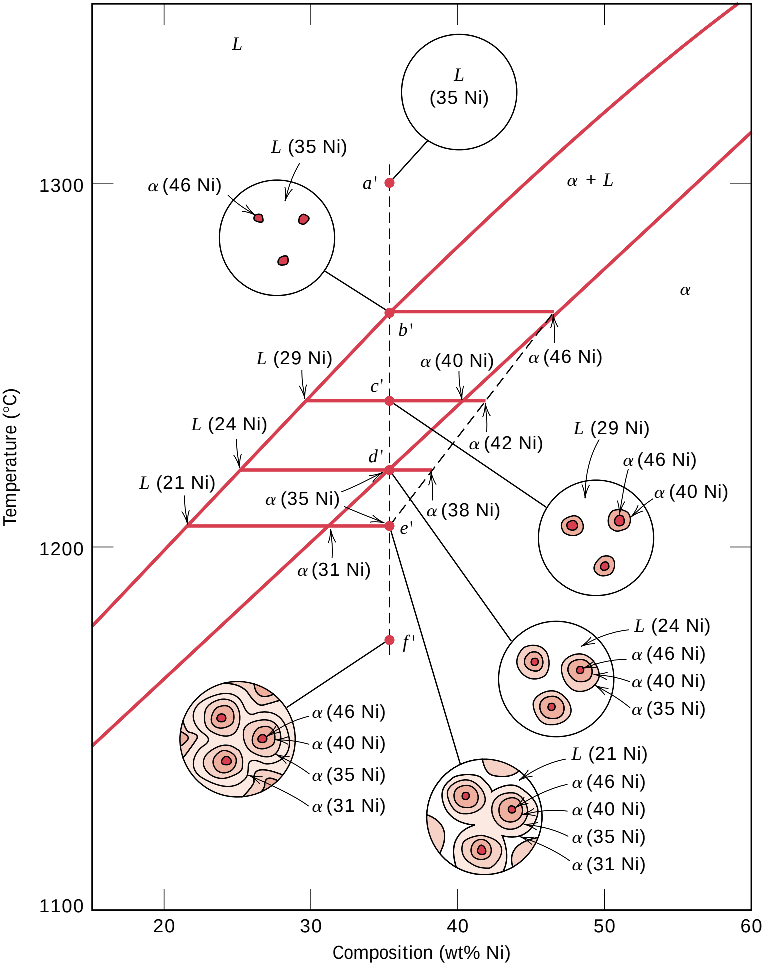

L
L
(35 Ni)
L (35 Ni)
α (46 Ni)
a'
1300
α + L
α
b'
L (29 Ni)
α (40 Ni)
α (46 Ni)
c'
L (24 Ni)
α (42 Ni)
L (29 Ni)
d'
α (46 Ni)
α (40 Ni)
L (21 Ni)
α (35 Ni)
α (38 Ni)
e'
1200
α (31 Ni)
L (24 Ni)
f'
α (46 Ni)
α (40 Ni)
α (35 Ni)
α (46 Ni)
α (40 Ni)
α (35 Ni)
α (31 Ni)
L (21 Ni)
α (46 Ni)
α (40 Ni)
α (35 Ni)
α (31 Ni)
Temperature (°C)
1100
20
30
40
50
60
Composition (wt% Ni)

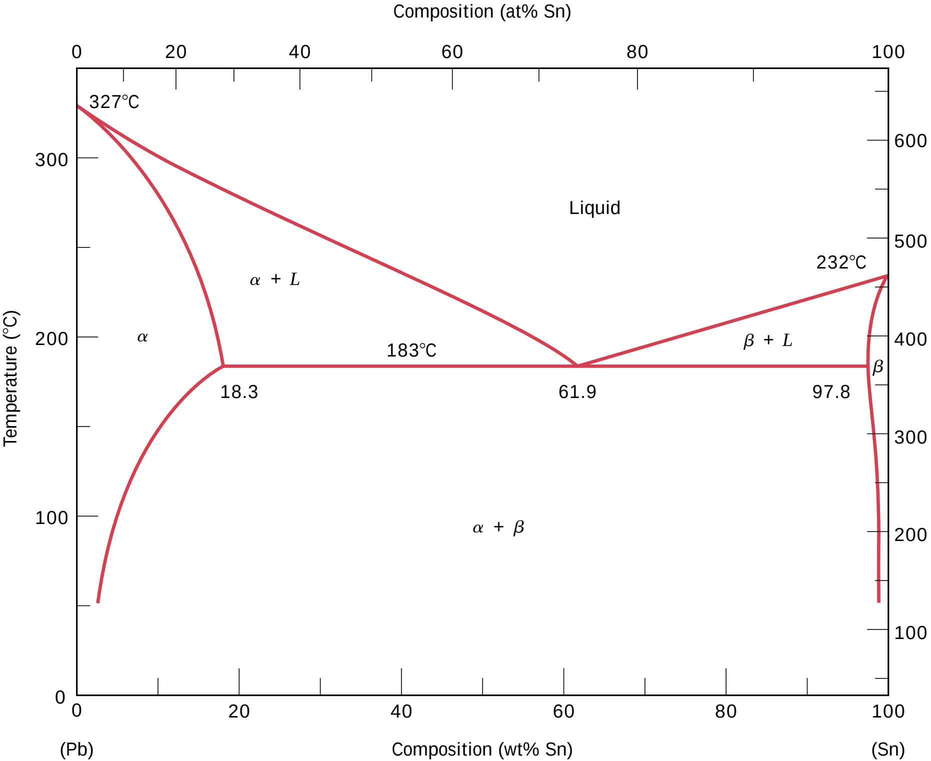

FIGURE 10.7 The lead–tin phase diagram. (Adapted from *Binary Alloy Phase Diagrams,* 2nd edition, Vol. 3, T. B. Massalski, Editor-in-Chief, 1990. Reprinted by permission of ASM International, Materials Park, OH.)

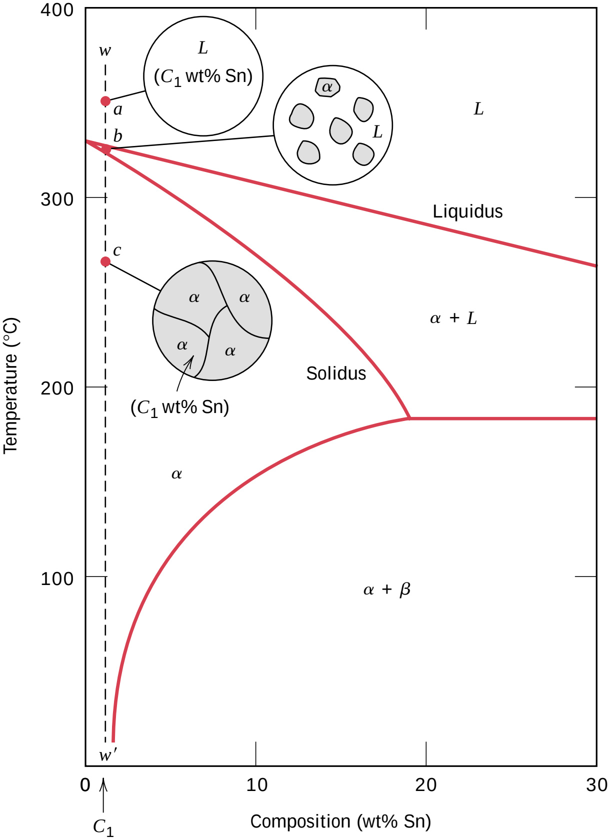
400
300
200
100
Temperature (°C)
0
10
20
30
Composition (wt% Sn)
C_1
w
w′
a
b
c
L
(C_1 wt% Sn)
α
L
L
Liquidus
α + L
α
α
α
α
(C_1 wt% Sn)
Solidus
α
α + β

Figure 10.9 Schematic representations of the equilibrium microstructures for a lead–tin alloy of composition C_1 as it is cooled from the liquid-phase region.

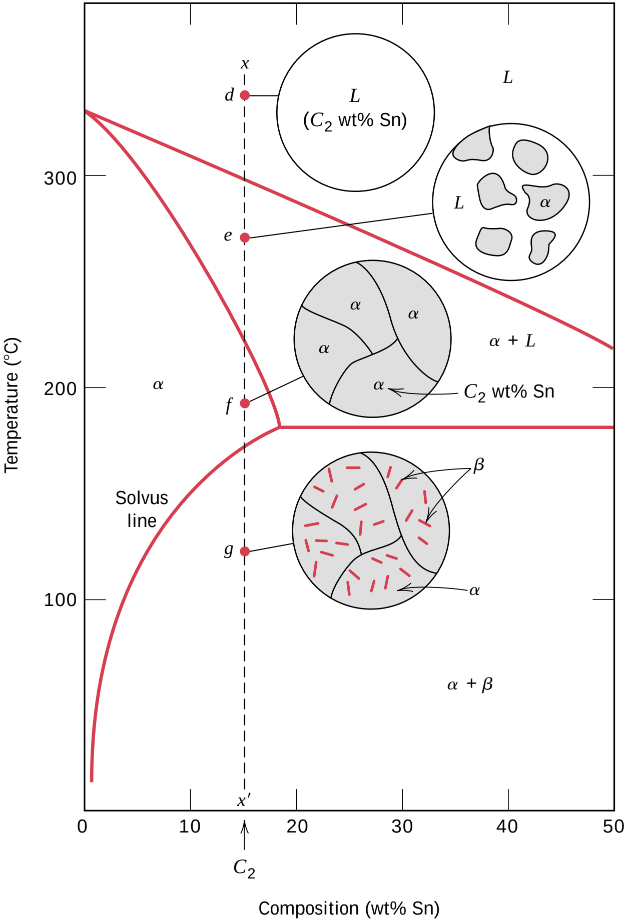
x
d
L
(C_2 wt% Sn)
L
L
α
300
e
α
α
α
α + L
200
α
f
α
C_2 wt% Sn
β
Solvus
line
g
α
100
α + β
x′
0
10
20
30
40
50
C_2
Temperature (°C)
Composition (wt% Sn)

Figure 10.10 Schematic representations of the equilibrium microstructures for a lead–tin alloy of composition C_2 as it is cooled from the liquid-phase region.

Figure 10.11 Schematic representations of the equilibrium microstructures for a lead–tin alloy of eutectic composition C_3 above and below the eutectic temperature.

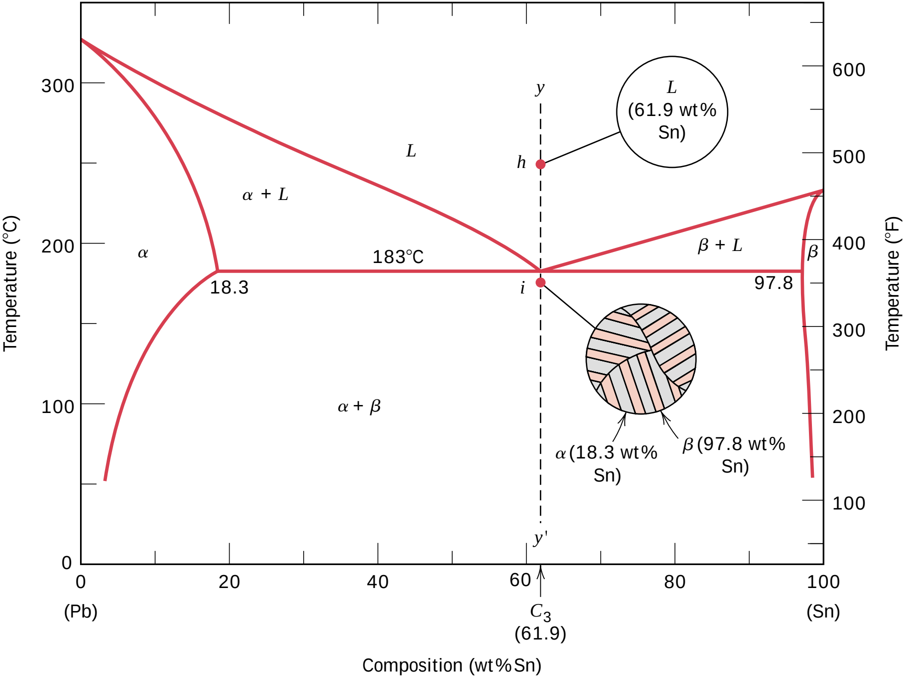

Temperature (°C)
300
200
100
0
Temperature (°F)
600
500
400
300
200
100
L
α + L
α
β + L
β
α + β
183°C
18.3
97.8
y
y'
h
i
L (61.9 wt% Sn)
α (18.3 wt% Sn)
β (97.8 wt% Sn)
0
20
40
60
80
100
(Pb)
(Sn)
C_3 (61.9)
Composition (wt% Sn)

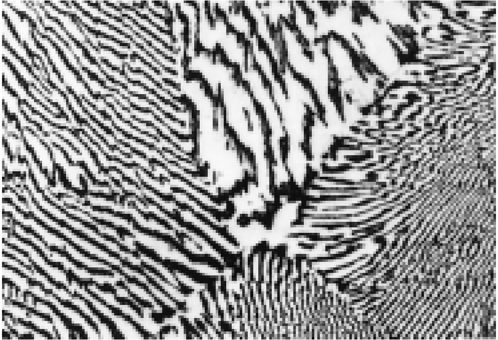

Figure 10.12 Photomicrograph showing the microstructure of a lead–tin alloy of eutectic composition. This microstructure consists of alternating layers of a lead-rich α-phase solid solution (dark layers), and a tin-rich β-phase solid solution (light layers). 375×. (Reproduced with permission from *Metals Handbook*, Vol. 9, 9th edition, *Metallography and Microstructures*, American Society for Metals, Materials Park, OH, 1985.)

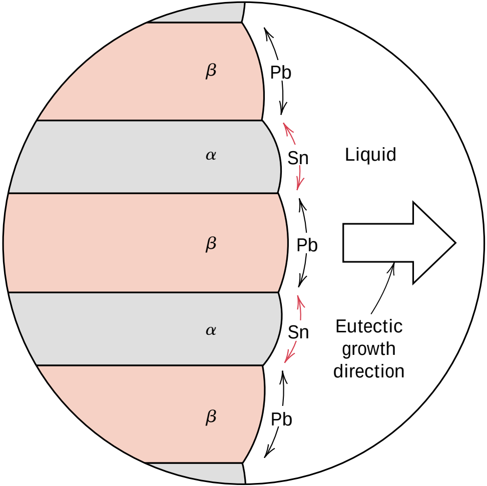
β
Pb
α
Sn
Liquid
β
Pb
α
Sn
Eutectic growth direction
β
Pb

Figure 10.13 Schematic representation of the formation of the eutectic structure for the lead–tin system. Directions of diffusion of tin and lead atoms are indicated by colored and black arrows, respectively.

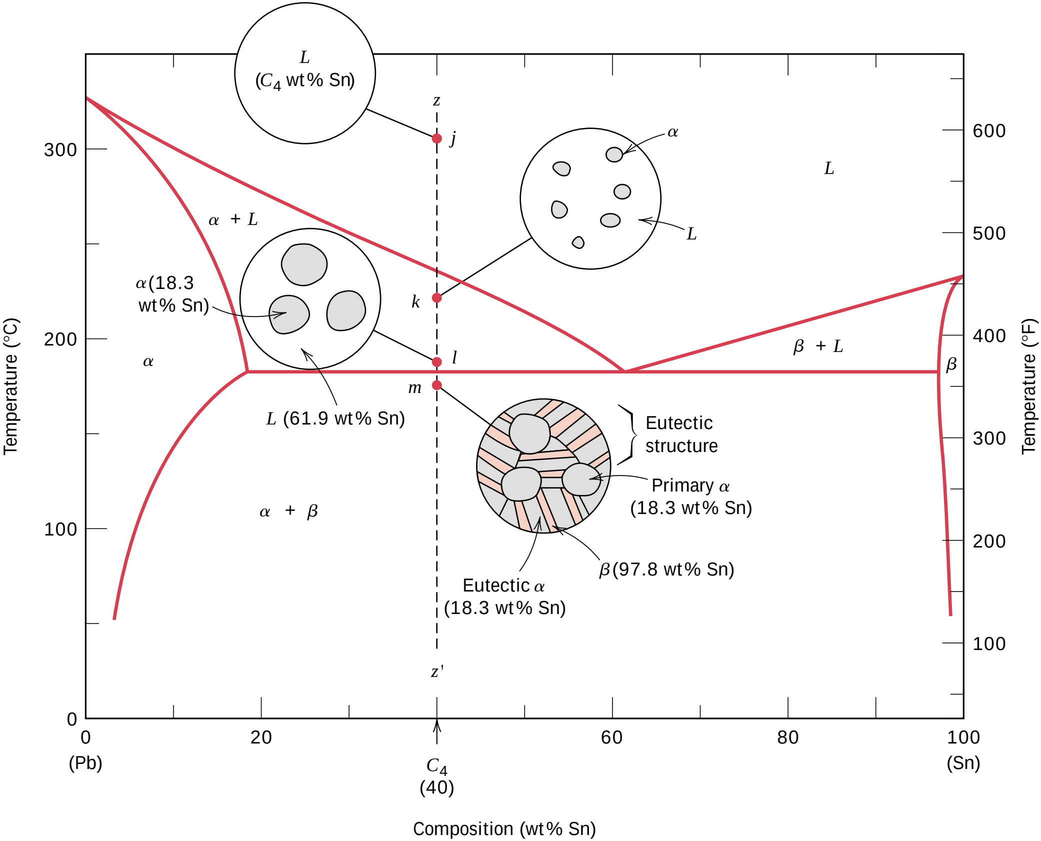
L
(C_4 wt% Sn)
z
j
α
L
L
α + L
α(18.3 wt% Sn)
k
l
m
α
L (61.9 wt% Sn)
β + L
β
Eutectic structure
Primary α (18.3 wt% Sn)
α + β
β(97.8 wt% Sn)
Eutectic α (18.3 wt% Sn)
z'
Temperature (°C)
0
100
200
300
Temperature (°F)
100
200
300
400
500
600
0 (Pb)
20
C_4 (40)
60
80
100 (Sn)
Composition (wt% Sn)

FIGURE 10.14 Schematic representations of the equilibrium microstructures for a lead–tin alloy of composition C_4 as it is cooled from the liquid-phase region.

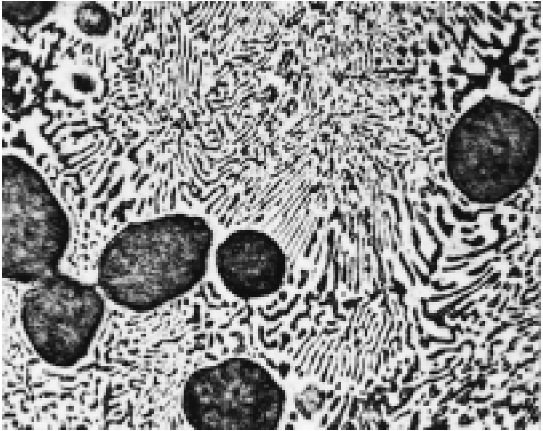

Figure 10.15 Photomicrograph showing the microstructure of a lead–tin alloy of composition 50 wt% Sn–50 wt% Pb. This microstructure is composed of a primary lead-rich α phase (large dark regions) within a lamellar eutectic structure consisting of a tin-rich β phase (light layers) and a lead-rich α phase (dark layers). 400×. (Reproduced with permission from *Metals Handbook*, Vol. 9, 9th edition, *Metallography and Microstructures,* American Society for Metals, Materials Park, OH, 1985.)

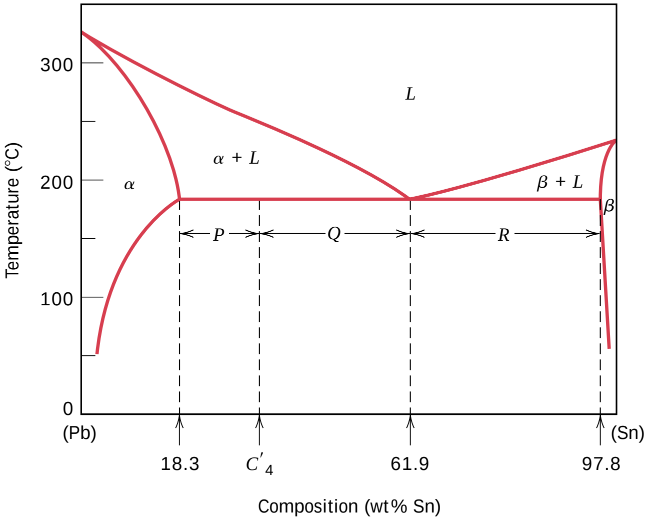

Figure 10.16 The lead–tin phase diagram used in computations for relative amounts of primary α and eutectic microconstituents for an alloy of composition C_4'.

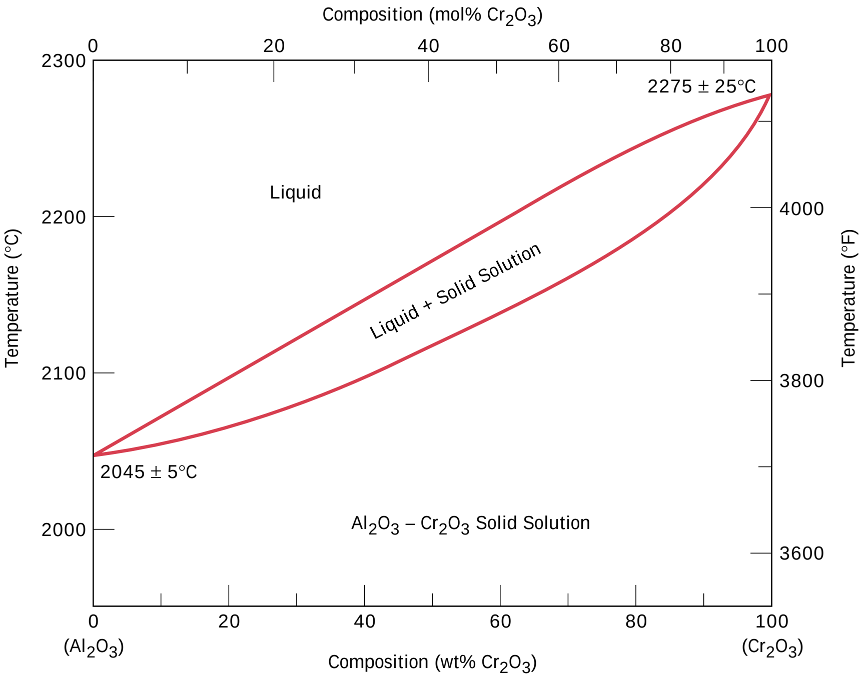

FIGURE 10.21 The aluminum oxide–chromium oxide phase diagram. (Adapted from E. N. Bunting, ''Phase Equilibria in the System Cr_2O_3–Al_2O_3,'' *Bur. Standards J. Research*, **6,** 1931, p. 948.)

FIGURE 10.22 The magnesium oxide–aluminum oxide phase diagram; *ss* denotes solid solution. (Adapted from B. Hallstedt, "Thermodynamic Assessment of the System $MgO–Al_2O_3$," *J. Am. Ceram. Soc.*, **75** [6] 1502 (1992). Reprinted by permission of the American Ceramic Society.)

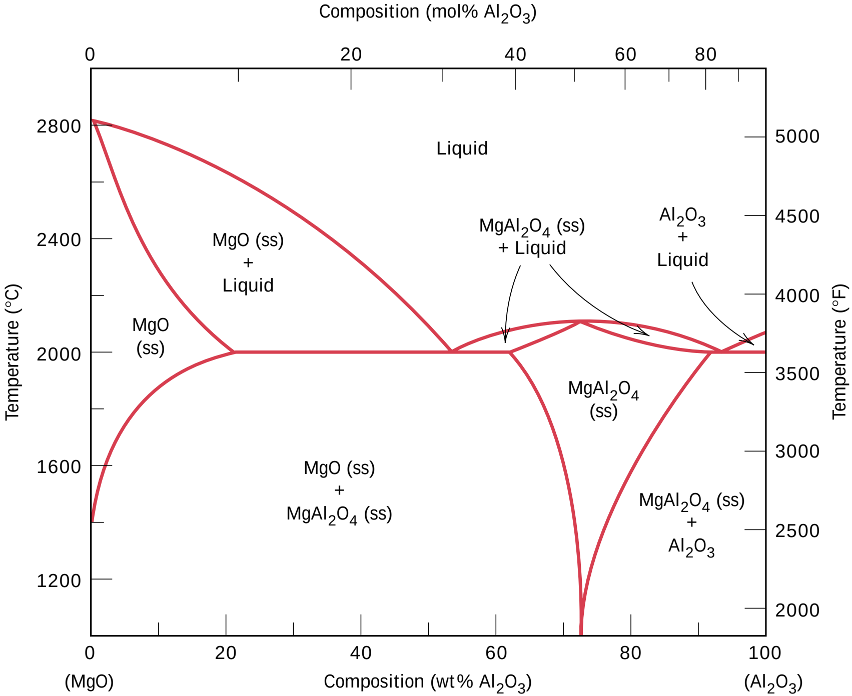

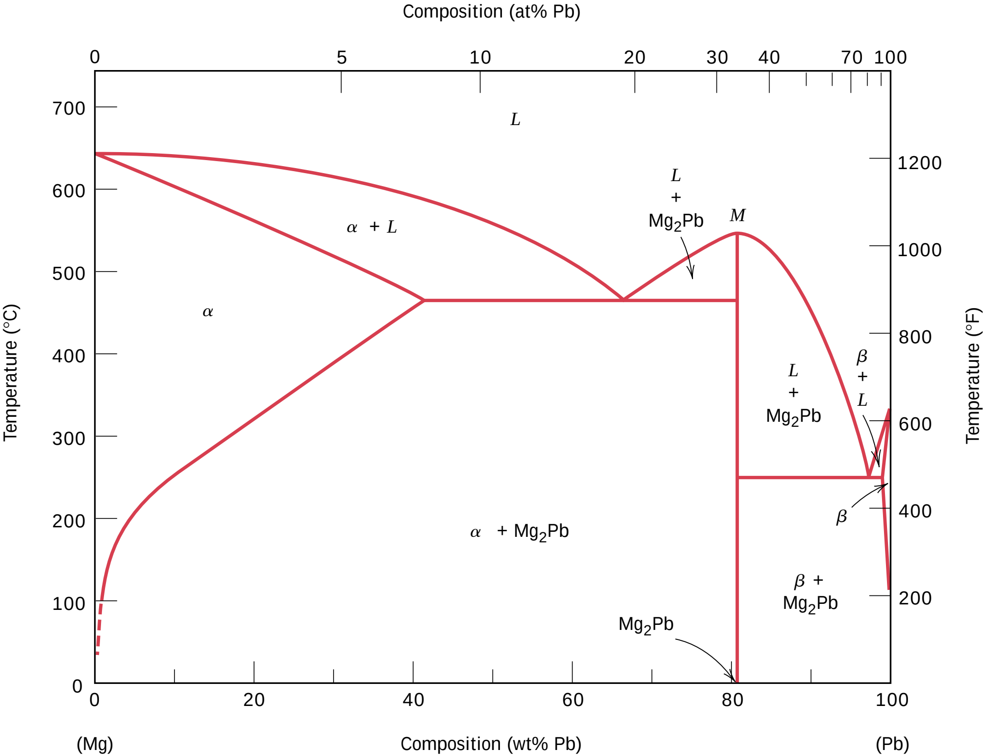

Figure 10.18 The magnesium–lead phase diagram. (Adapted from *Phase Diagrams of Binary Magnesium Alloys*, A. A. Nayeb-Hashemi and J. B. Clark, Editors, 1988. Reprinted by permission of ASM International, Materials Park, OH.)

FIGURE 10.23 A portion of the zirconia–calcia phase diagram; *ss* denotes solid solution. (Adapted from V. S. Stubican and S. P. Ray, ‘‘Phase Equilibria and Ordering in the System ZrO_2-CaO,’’ *J. Am. Ceram. Soc.*, **60** [11–12] 535 (1977). Reprinted by permission of the American Ceramic Society.)

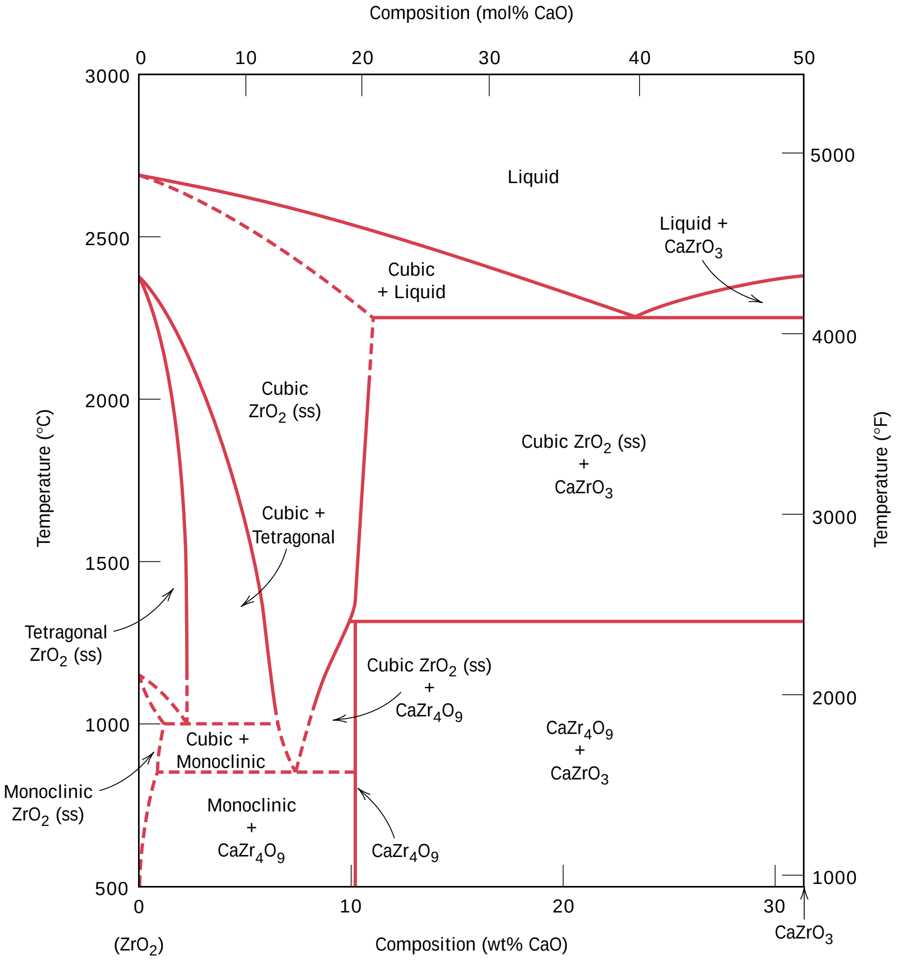

FIGURE 10.24 The silica–alumina phase diagram. (Adapted from F. J. Klug, S. Prochazka, and R. H. Doremus, ''Alumina-Silica Phase Diagram in the Mullite Region,'' *J. Am. Ceram. Soc.*, **70** [10] 758 (1987). Reprinted by permission of the American Ceramic Society.)

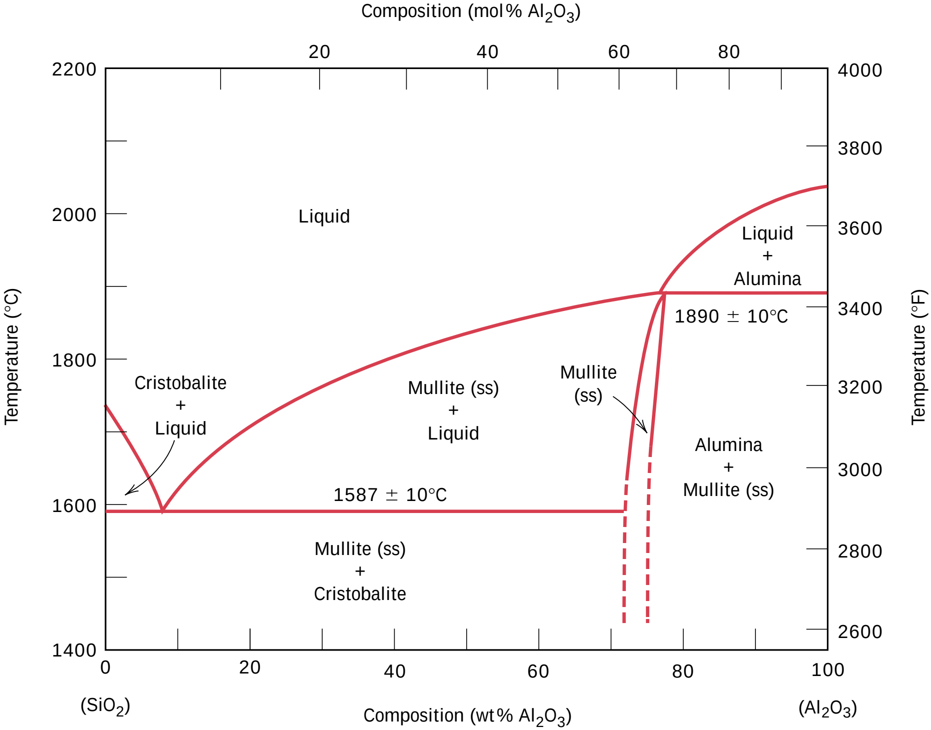

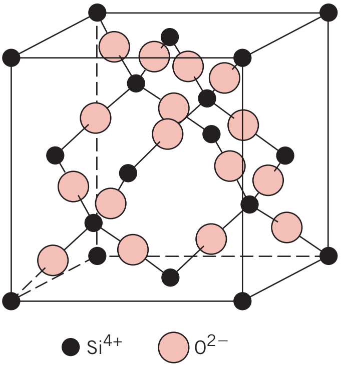
Si^{4+}
O^{2-}

FIGURE 3.11 The arrangement of silicon and oxygen atoms in a unit cell of cristobalite, a polymorph of SiO_2.

Chapter 16 / Corrosion and Degradation of Materials

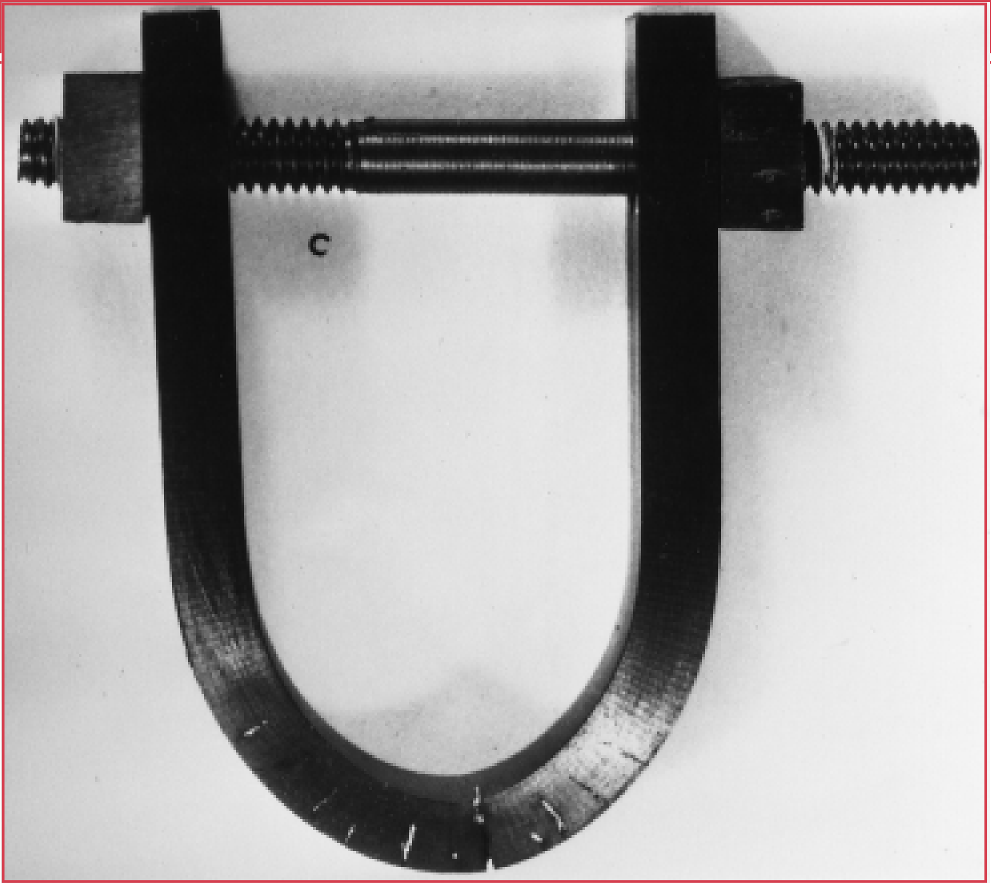

Photograph showing a bar of steel that has been bent into a "horseshoe" shape using a nut-and-bolt assembly. While immersed in seawater, stress corrosion cracks formed along the bend at those regions where the tensile stresses are the greatest. (Photograph courtesy of F. L. LaQue. From F. L. LaQue, *Marine Corrosion, Causes and Prevention.* Copyright © 1975 by John Wiley & Sons, Inc. Reprinted by permission of John Wiley & Sons, Inc.)

Why Study *Corrosion and Degradation of Materials?*

With a knowledge of the types of and an understanding of the mechanisms and causes of corrosion and degradation, it is possible to take measures to prevent them from occurring. For example, we may change the nature of the environment, select a material that is relatively nonreactive, and/or protect the material from appreciable deterioration.

Learning Objectives

After careful study of this chapter you should be able to do the following:

1. **Distinguish between oxidation and reduction electrochemical reactions.**
2. **Describe the following: galvanic couple, standard half-cell, and standard hydrogen electrode.**
3. **Compute the cell potential and write the spontaneous electrochemical reaction direction for two pure metals that are electrically connected and also submerged in solutions of their respective ions.**
4. **Determine metal oxidation rate given the reaction current density.**
5. **Name and briefly describe the two different types of polarization, and specify the conditions under which each is rate controlling.**
6. **For each of the eight forms of corrosion and hydrogen embrittlement, describe the nature of the deteriorative process, and then note the proposed mechanism.**
7. **List five measures that are commonly used to prevent corrosion.**
8. **Explain why ceramic materials are, in general, very resistant to corrosion.**
9. **For polymeric materials discuss (a) two degradation processes that occur when they are exposed to liquid solvents, and (b) the causes and consequences of molecular chain bond rupture.**

16.1 INTRODUCTION

To one degree or another, most materials experience some type of interaction with a large number of diverse environments. Often, such interactions impair a material's usefulness as a result of the deterioration of its mechanical properties (e.g., ductility and strength), other physical properties, or appearance. Occasionally, to the chagrin of a design engineer, the degradation behavior of a material for some application is ignored, with adverse consequences.

Deteriorative mechanisms are different for the three material types. In metals, there is actual material loss either by dissolution **(corrosion)** or by the formation of nonmetallic scale or film (*oxidation*). Ceramic materials are relatively resistant to deterioration, which usually occurs at elevated temperatures or in rather extreme environments; the process is frequently also called corrosion. For polymers, mechanisms and consequences differ from those for metals and ceramics, and the term **degradation** is most frequently used. Polymers may dissolve when exposed to a liquid solvent, or they may absorb the solvent and swell; also, electromagnetic radiation (primarily ultraviolet) and heat may cause alterations in their molecular structure.

The deterioration of each of these material types is discussed in this chapter, with special regard to mechanism, resistance to attack by various environments, and measures to prevent or reduce degradation.

CORROSION OF METALS

Corrosion is defined as the destructive and unintentional attack of a metal; it is electrochemical and ordinarily begins at the surface. The problem of metallic corrosion is one of significant proportions; in economic terms, it has been estimated that approximately 5% of an industrialized nation's income is spent on corrosion prevention and the maintenance or replacement of products lost or contaminated as a result of corrosion reactions. The consequences of corrosion are all too common. Familiar examples include the rusting of automotive body panels and radiator and exhaust components.

Corrosion processes are occasionally used to advantage. For example, etching procedures, as discussed in Section 5.12, make use of the selective chemical reactivity of grain boundaries or various microstructural constituents. Also, the current developed in dry-cell batteries is a result of corrosion processes.

16.2 ELECTROCHEMICAL CONSIDERATIONS

For metallic materials, the corrosion process is normally electrochemical, that is, a chemical reaction in which there is transfer of electrons from one chemical species to another. Metal atoms characteristically lose or give up electrons in what is called an **oxidation** reaction. For example, the hypothetical metal M that has a valence of n (or n valence electrons) may experience oxidation according to the reaction

$$\mathrm{M} \longrightarrow \mathrm{M}^{n+} + ne^{-} \tag{16.1}$$

in which M becomes an $n+$ positively charged ion and in the process loses its n valence electrons; e^{-} is used to symbolize an electron. Examples in which metals oxidize are

$$\mathrm{Fe} \longrightarrow \mathrm{Fe}^{2+} + 2e^{-} \tag{16.2a}$$

$$\mathrm{Al} \longrightarrow \mathrm{Al}^{3+} + 3e^{-} \tag{16.2b}$$

The site at which oxidation takes place is called the **anode;** oxidation is sometimes called an anodic reaction.

The electrons generated from each metal atom that is oxidized must be transferred to and become a part of another chemical species in what is termed a **reduction** reaction. For example, some metals undergo corrosion in acid solutions, which have a high concentration of hydrogen (H^{+}) ions; the H^{+} ions are reduced as follows:

$$2\mathrm{H}^{+} + 2e^{-} \longrightarrow \mathrm{H}_2 \tag{16.3}$$

and hydrogen gas (H_2) is evolved.

Other reduction reactions are possible, depending on the nature of the solution to which the metal is exposed. For an acid solution having dissolved oxygen, reduction according to

$$\mathrm{O}_2 + 4\mathrm{H}^{+} + 4e^{-} \longrightarrow 2\mathrm{H}_2\mathrm{O} \tag{16.4}$$

will probably occur. Or, for a neutral or basic aqueous solution in which oxygen is also dissolved,

$$\mathrm{O}_2 + 2\mathrm{H}_2\mathrm{O} + 4e^{-} \longrightarrow 4(\mathrm{OH}^{-}) \tag{16.5}$$

Any metal ions present in the solution may also be reduced; for ions that can exist in more than one valence state (multivalent ions), reduction may occur by

$$\mathrm{M}^{n+} + e^{-} \longrightarrow \mathrm{M}^{(n-1)+} \tag{16.6}$$

in which the metal ion decreases its valence state by accepting an electron. Or, a metal may be totally reduced from an ionic to a neutral metallic state according to

$$\mathrm{M}^{n+} + ne^{-} \longrightarrow \mathrm{M} \tag{16.7}$$

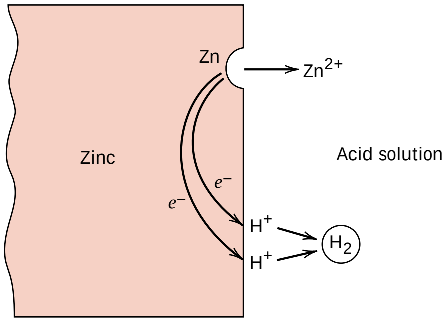

Figure 16.1 The electrochemical reactions associated with the corrosion of zinc in an acid solution. (From M. G. Fontana, *Corrosion Engineering,* 3rd edition. Copyright © 1986 by McGraw-Hill Book Company. Reproduced with permission.)

That location at which reduction occurs is called the **cathode.** Furthermore, it is possible for two or more of the reduction reactions above to occur simultaneously.

An overall electrochemical reaction must consist of at least one oxidation and one reduction reaction, and will be the sum of them; often the individual oxidation and reduction reactions are termed *half-reactions.* There can be no net electrical charge accumulation from the electrons and ions; that is, the total rate of oxidation must equal the total rate of reduction, or all electrons generated through oxidation must be consumed by reduction.

For example, consider zinc metal immersed in an acid solution containing H^+ ions. At some regions on the metal surface, zinc will experience oxidation or corrosion as illustrated in Figure 16.1, and according to the reaction

$$Zn \longrightarrow Zn^{2+} + 2e^- \tag{16.8}$$

Since zinc is a metal, and therefore a good electrical conductor, these electrons may be transferred to an adjacent region at which the H^+ ions are reduced according to

$$2H^+ + 2e^- \longrightarrow H_2 \text{ (gas)} \tag{16.9}$$

If no other oxidation or reduction reactions occur, the total electrochemical reaction is just the sum of reactions 16.8 and 16.9, or

$$\begin{array}{r}
Zn \longrightarrow Zn^{2+} + 2e^- \\
2H^+ + 2e^- \longrightarrow H_2 \text{ (gas)} \\ \hline
Zn + 2H^+ \longrightarrow Zn^{2+} + H_2 \text{ (gas)}
\end{array} \tag{16.10}$$

Another example is the oxidation or rusting of iron in water, which contains dissolved oxygen. This process occurs in two steps; in the first, Fe is oxidized to Fe^{2+} [as $Fe(OH)_2$],

$$Fe + \tfrac{1}{2}O_2 + H_2O \longrightarrow Fe^{2+} + 2OH^- \longrightarrow Fe(OH)_2 \tag{16.11}$$

and, in the second stage, to Fe^{3+} [as $Fe(OH)_3$] according to

$$2Fe(OH)_2 + \tfrac{1}{2}O_2 + H_2O \longrightarrow 2Fe(OH)_3 \tag{16.12}$$

The compound $Fe(OH)_3$ is the all-too-familiar rust.

As a consequence of oxidation, the metal ions may either go into the corroding solution as ions (reaction 16.8), or they may form an insoluble compound with nonmetallic elements as in reaction 16.12.

ELECTRODE POTENTIALS

Not all metallic materials oxidize to form ions with the same degree of ease. Consider the electrochemical cell shown in Figure 16.2. On the left-hand side is a piece of

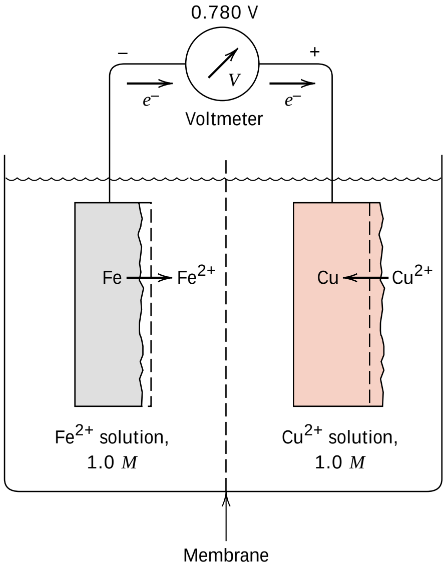

FIGURE 16.2 An electrochemical cell consisting of iron and copper electrodes, each of which is immersed in a 1*M* solution of its ion. Iron corrodes while copper electrodeposits.

pure iron immersed in a solution containing Fe^{2+} ions of 1*M* concentration.[1] The other side of the cell consists of a pure copper electrode in a 1*M* solution of Cu^{2+} ions. The cell halves are separated by a membrane, which limits the mixing of the two solutions. If the iron and copper electrodes are connected electrically, reduction will occur for copper at the expense of the oxidation of iron, as follows:

$$Cu^{2+} + Fe \longrightarrow Cu + Fe^{2+} \tag{16.13}$$

or Cu^{2+} ions will deposit (electrodeposit) as metallic copper on the copper electrode, while iron dissolves (corrodes) on the other side of the cell and goes into solution as Fe^{2+} ions. Thus, the two half-cell reactions are represented by the relations

$$Fe \longrightarrow Fe^{2+} + 2e^- \tag{16.14a}$$

$$Cu^{2+} + 2e^- \longrightarrow Cu \tag{16.14b}$$

When a current passes through the external circuit, electrons generated from the oxidation of iron flow to the copper cell in order that Cu^{2+} be reduced. In addition, there will be some net ion motion from each cell to the other across the membrane. This is called a *galvanic couple*—two metals electrically connected in a liquid **electrolyte** wherein one metal becomes an anode and corrodes, while the other acts as a cathode.

An electric potential or voltage will exist between the two cell halves, and its magnitude can be determined if a voltmeter is connected in the external circuit. A potential of 0.780 V results for a copper–iron galvanic cell when the temperature is 25°C (77°F).

Now consider another galvanic couple consisting of the same iron half-cell connected to a metal zinc electrode that is immersed in a 1*M* solution of Zn^{2+} ions (Figure 16.3). In this case the zinc is the anode and corrodes, whereas the Fe now becomes the cathode. The electrochemical reaction is thus

$$Fe^{2+} + Zn \longrightarrow Fe + Zn^{2+} \tag{16.15}$$

The potential associated with this cell reaction is 0.323 V.

---

[1] Concentration of liquid solutions is often expressed in terms of **molarity,** *M*, the number of moles of solute per million cubic millimeters (10^6 mm^3, or 1000 cm^3) of solution.

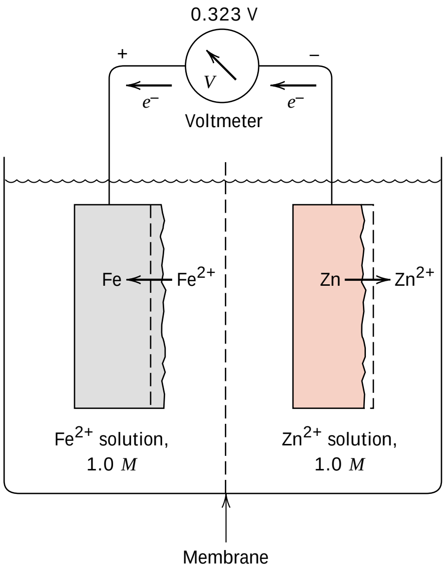
0.323 V
+
–
e^-
e^-
V
Voltmeter
Fe
Fe^{2+}
Zn
Zn^{2+}
Fe^{2+} solution, 1.0 M
Zn^{2+} solution, 1.0 M
Membrane

Figure 16.3 An electrochemical cell consisting of iron and zinc electrodes, each of which is immersed in a 1M solution of its ion. The iron electrodeposits while the zinc corrodes.

Thus, various electrode pairs have different voltages; the magnitude of such a voltage may be thought of as representing the driving force for the electrochemical oxidation–reduction reaction. Consequently, metallic materials may be rated as to their tendency to experience oxidation when coupled to other metals in solutions of their respective ions. A half-cell similar to those described above [i.e., a pure metal electrode immersed in a 1M solution of its ions and at 25°C (77°F)] is termed a **standard half-cell.**

THE STANDARD EMF SERIES

These measured cell voltages represent only differences in electrical potential, and thus it is convenient to establish a reference point, or reference cell, to which other cell halves may be compared. This reference cell, arbitrarily chosen, is the standard hydrogen electrode (Fig. 16.4). It consists of an inert platinum electrode in a 1M

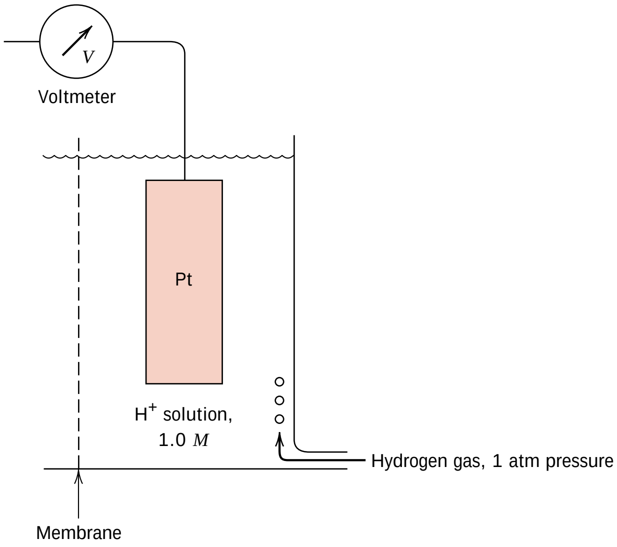
V
Voltmeter
Pt
H^+ solution, 1.0 M
Hydrogen gas, 1 atm pressure
Membrane

Figure 16.4 The standard hydrogen reference half-cell.

Table 16.1 The Standard emf Series

	Electrode Reaction	*Standard Electrode Potential, V^0* (V)
	$Au^{3+} + 3e^- \longrightarrow Au$	+1.420
↑	$O_2 + 4H^+ + 4e^- \longrightarrow 2H_2O$	+1.229
	$Pt^{2+} + 2e^- \longrightarrow Pt$	~+1.2
	$Ag^+ + e^- \longrightarrow Ag$	+0.800
Increasingly inert	$Fe^{3+} + e^- \longrightarrow Fe^{2+}$	+0.771
(cathodic)	$O_2 + 2H_2O + 4e^- \longrightarrow 4(OH^-)$	+0.401
	$Cu^{2+} + 2e^- \longrightarrow Cu$	+0.340
	$2H^+ + 2e^- \longrightarrow H_2$	0.000
	$Pb^{2+} + 2e^- \longrightarrow Pb$	−0.126
	$Sn^{2+} + 2e^- \longrightarrow Sn$	−0.136
	$Ni^{2+} + 2e^- \longrightarrow Ni$	−0.250
	$Co^{2+} + 2e^- \longrightarrow Co$	−0.277
	$Cd^{2+} + 2e^- \longrightarrow Cd$	−0.403
	$Fe^{2+} + 2e^- \longrightarrow Fe$	−0.440
Increasingly active	$Cr^{3+} + 3e^- \longrightarrow Cr$	−0.744
(anodic)	$Zn^{2+} + 2e^- \longrightarrow Zn$	−0.763
	$Al^{3+} + 3e^- \longrightarrow Al$	−1.662
	$Mg^{2+} + 2e^- \longrightarrow Mg$	−2.363
↓	$Na^+ + e^- \longrightarrow Na$	−2.714
	$K^+ + e^- \longrightarrow K$	−2.924

solution of H^+ ions, saturated with hydrogen gas that is bubbled through the solution at a pressure of 1 atm and a temperature of 25°C (77°F). The platinum itself does not take part in the electrochemical reaction; it acts only as a surface on which hydrogen atoms may be oxidized or hydrogen ions may be reduced. The **electromotive force (emf) series** (Table 16.1) is generated by coupling to the standard hydrogen electrode, standard half-cells for various metals and ranking them according to measured voltage. Table 16.1 represents the corrosion tendencies for the several metals; those at the top (i.e., gold and platinum) are noble, or chemically inert. Moving down the table, the metals become increasingly more active, that is, more susceptible to oxidation. Sodium and potassium have the highest reactivities.

The voltages in Table 16.1 are for the half-reactions as *reduction reactions*, with the electrons on the left-hand side of the chemical equation; for oxidation, the direction of the reaction is reversed and the sign of the voltage changed.

Consider the generalized reactions involving the oxidation of metal M_1 and the reduction of metal M_2 as

$$M_1 \longrightarrow M_1^{n+} + ne^- \qquad -V_1^0 \tag{16.16a}$$

$$M_2^{n+} + ne^- \longrightarrow M_2 \qquad +V_2^0 \tag{16.16b}$$

where the V^0's are the standard potentials as taken from the standard emf series. Since metal M_1 is oxidized, the sign of V_1^0 is opposite to that as it appears in Table 16.1. Addition of Equations 16.16a and 16.16b yields

$$M_1 + M_2^{n+} \longrightarrow M_1^{n+} + M_2 \tag{16.17}$$

and the overall cell potential ΔV^0 is

$$\Delta V^0 = V_2^0 - V_1^0 \tag{16.18}$$

For this reaction to occur spontaneously, ΔV^0 must be positive; if it is negative, the spontaneous cell direction is just the reverse of Equation 16.17. When standard half-cells are coupled together, the metal that lies lower in Table 16.1 will experience oxidation (i.e., corrosion), whereas the higher one will be reduced.

INFLUENCE OF CONCENTRATION AND TEMPERATURE ON CELL POTENTIAL

The emf series applies to highly idealized electrochemical cells (i.e., pure metals in 1*M* solutions of their ions, at 25°C). Altering temperature or solution concentration or using alloy electrodes instead of pure metals will change the cell potential, and, in some cases, the spontaneous reaction direction may be reversed.

Consider again the electrochemical reaction described by Equation 16.17. If M_1 and M_2 electrodes are pure metals, the cell potential depends on the absolute temperature T and the molar ion concentrations $[M_1^{n+}]$ and $[M_2^{n+}]$ according to the Nernst equation:

$$\Delta V = (V_2^0 - V_1^0) - \frac{RT}{n\mathscr{F}} \ln \frac{[M_1^{n+}]}{[M_2^{n+}]} \tag{16.19}$$

where R is the gas constant, n is the number of electrons participating in either of the half-cell reactions, and $\mathscr{F}$ is the Faraday constant, 96,500 C/mol—the magnitude of charge per mole (6.023×10^{23}) of electrons. At 25°C (about room temperature),

$$\Delta V = (V_2^0 - V_1^0) - \frac{0.0592}{n} \log \frac{[M_1^{n+}]}{[M_2^{n+}]} \tag{16.20}$$

to give ΔV in volts. Again, for reaction spontaneity, ΔV must be positive. As expected, for 1*M* concentrations of both ion types (that is, $[M_1^{n+}] = [M_2^{n+}] = 1$), Equation 16.19 simplifies to Equation 16.18.

EXAMPLE PROBLEM 16.1

One half of an electrochemical cell consists of a pure nickel electrode in a solution of Ni^{2+} ions; the other is a cadmium electrode immersed in a Cd^{2+} solution.

(a) If the cell is a standard one, write the spontaneous overall reaction and calculate the voltage that is generated.

(b) Compute the cell potential at 25°C if the Cd^{2+} and Ni^{2+} concentrations are 0.5 and 10^{-3} *M*, respectively. Is the spontaneous reaction direction still the same as for the standard cell?

SOLUTION

(a) The cadmium electrode will be oxidized and nickel reduced because cadmium is lower in the emf series; thus, the spontaneous reactions will be

$$\begin{array}{r}
\text{Cd} \longrightarrow \text{Cd}^{2+} + 2e^- \\
\text{Ni}^{2+} + 2e^- \longrightarrow \text{Ni} \\
\hline
\text{Ni}^{2+} + \text{Cd} \longrightarrow \text{Ni} + \text{Cd}^{2+}
\end{array} \tag{16.21}$$

From Table 16.1, the half-cell potentials for cadmium and nickel are, respectively, −0.403 and −0.250 V. Therefore, from Equation 16.18,

$$\Delta V = V^0_{\text{Ni}} - V^0_{\text{Cd}} = -\ 0.250\text{ V} - (-0.403\text{ V}) = +0.153\text{ V}$$

(b) For this portion of the problem, Equation 16.20 must be utilized, since the half-cell solution concentrations are no longer 1*M*. At this point it is necessary to make a calculated guess as to which metal species is oxidized (or reduced). This choice will either be affirmed or refuted on the basis of the sign of ΔV at the conclusion of the computation. For the sake of argument, let us assume that in contrast to part a, nickel is oxidized and cadmium reduced according to

$$\text{Cd}^{2+} + \text{Ni} \longrightarrow \text{Cd} + \text{Ni}^{2+} \tag{16.22}$$

Thus,

$$\begin{aligned}\Delta V &= (V^0_{\text{Cd}} - V^0_{\text{Ni}}) - \frac{RT}{n\mathscr{F}}\ln\frac{[\text{Ni}^{2+}]}{[\text{Cd}^{2+}]}\\ &= -0.403\text{ V} - (-0.250\text{ V}) - \frac{0.0592}{2}\log\left(\frac{10^{-3}}{0.50}\right)\\ &= -0.073\text{ V}\end{aligned}$$

Since ΔV is negative, the spontaneous reaction direction is the opposite to that of Equation 16.22, or the same as that of the standard cell (Equation 16.21).

THE GALVANIC SERIES

Even though Table 16.1 was generated under highly idealized conditions and has limited utility, it nevertheless indicates the relative reactivities of the metals. A more realistic and practical ranking, however, is provided by the **galvanic series,** Table 16.2. This represents the relative reactivities of a number of metals and commercial alloys in seawater. The alloys near the top are cathodic and unreactive, whereas those at the bottom are most anodic; no voltages are provided. Comparison of the standard emf and the galvanic series reveals a high degree of correspondence between the relative positions of the pure base metals.

Most metals and alloys are subject to oxidation or corrosion to one degree or another in a wide variety of environments; that is, they are more stable in an ionic state than as metals. In thermodynamic terms, there is a net decrease in free energy in going from metallic to oxidized states. Consequently, essentially all metals occur in nature as compounds—for example, oxides, hydroxides, carbonates, silicates, sulfides, and sulfates. Two notable exceptions are the noble metals gold and platinum. For them, oxidation in most environments is not favorable, and, therefore, they may exist in nature in the metallic state.

16.3 CORROSION RATES

The half-cell potentials listed in Table 16.1 are thermodynamic parameters that relate to systems at equilibrium. For example, for the discussions pertaining to Figures 16.2 and 16.3, it was tacitly assumed that there was no current flow through the external circuit. Real corroding systems are not at equilibrium; there will be a flow of electrons from anode to cathode (corresponding to the short-circuiting of the electrochemical cells in Figures 16.2 and 16.3), which means that the half-cell potential parameters (Table 16.1) cannot be applied.

Table 16.2 The Galvanic Series

	Platinum
	Gold
	Graphite
	Titanium
	Silver
	316 Stainless steel (passive)
	304 Stainless steel (passive)
↑	Inconel (80Ni–13Cr–7Fe) (passive)
	Nickel (passive)
	Monel (70Ni–30Cu)
Increasingly inert (cathodic)	Copper–nickel alloys
	Bronzes (Cu–Sn alloys)
	Copper
	Brasses (Cu–Zn alloys)
	Inconel (active)
	Nickel (active)
	Tin
	Lead
Increasingly active (anodic)	316 Stainless steel (active)
	304 Stainless steel (active)
↓	Cast iron
	Iron and steel
	Aluminum alloys
	Cadmium
	Commercially pure aluminum
	Zinc
	Magnesium and magnesium alloys

Source: M. G. Fontana, *Corrosion Engineering,* 3rd edition. Copyright 1986 by McGraw-Hill Book Company. Reprinted with permission.

Furthermore, these half-cell potentials represent the magnitude of a driving force, or the tendency for the occurrence of the particular half-cell reaction. However, it should be noted that although these potentials may be used to determine spontaneous reaction directions, they provide no information as to corrosion rates. That is, even though a ΔV potential computed for a specific corrosion situation using Equation 16.20 is a relatively large positive number, the reaction may occur at only an insignificantly slow rate. From an engineering perspective, we are interested in predicting the rates at which systems corrode; this requires the utilization of other parameters, as discussed below.

The corrosion rate, or the rate of material removal as a consequence of the chemical action, is an important corrosion parameter. This may be expressed as the **corrosion penetration rate (CPR),** or the thickness loss of material per unit of time. The formula for this calculation is

$$\mathrm{CPR} = \frac{KW}{\rho A t} \tag{16.23}$$

where W is the weight loss after exposure time t; ρ and A represent the density and exposed specimen area, respectively, and K is a constant, its magnitude depending on the system of units used. The CPR is conveniently expressed in terms of either mils per year (mpy) or millimeters per year (mm/yr). In the first case, $K = 534$ to give

CPR in mpy (where 1 mil = 0.001 in.), and W, ρ, A, and t are specified in units of milligrams, grams per cubic centimeter, square inches, and hours, respectively. In the second case, $K = 87.6$ for mm/yr, and units for the other parameters are the same as for mils per year, except that A is given in square centimeters. For most applications a corrosion penetration rate less than about 20 mpy (0.50 mm/yr) is acceptable.

Inasmuch as there is an electric current associated with electrochemical corrosion reactions, we can also express corrosion rate in terms of this current, or, more specifically, current density—that is, the current per unit surface area of material corroding—which is designated i. The rate r, in units of mol/m^2-s, is determined using the expression

$$r = \frac{i}{n\mathscr{F}} \tag{16.24}$$

where, again, n is the number of electrons associated with the ionization of each metal atom, and $\mathscr{F}$ is 96,500 C/mol.

16.4 PREDICTION OF CORROSION RATES

POLARIZATION

Consider the standard Zn/H_2 electrochemical cell shown in Figure 16.5, which has been short-circuited such that oxidation of zinc and reduction of hydrogen will occur at their respective electrode surfaces. The potentials of the two electrodes will not be at the values determined from Table 16.1 because the system is now a nonequilibrium one. The displacement of each electrode potential from its equilibrium value is termed **polarization,** and the magnitude of this displacement is the *overvoltage*, normally represented by the symbol η. Overvoltage is expressed in terms of plus or minus volts (or millivolts) relative to the equilibrium potential. For example, suppose that the zinc electrode in Figure 16.5 has a potential of −0.621 V after it has been connected to the platinum electrode. The equilibrium potential is −0.763 V (Table 16.1), and, therefore,

$$\eta = -0.621 \text{ V} - (-0.763 \text{ V}) = +0.142 \text{ V}$$

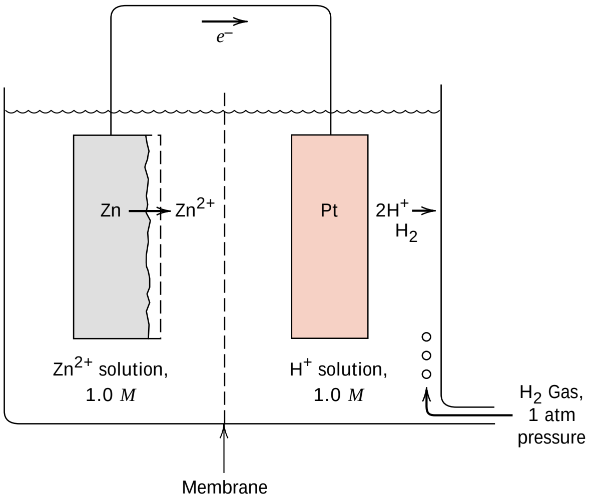

FIGURE 16.5 Electrochemical cell consisting of standard zinc and hydrogen electrodes that has been short-circuited.

There are two types of polarization—activation and concentration—the mechanisms of which will now be discussed since they control the rate of electrochemical reactions.

Activation Polarization

All electrochemical reactions consist of a sequence of steps that occur in series at the interface between the metal electrode and the electrolyte solution. **Activation polarization** refers to the condition wherein the reaction rate is controlled by the one step in the series that occurs at the slowest rate. The term ''activation'' is applied to this type of polarization because an activation energy barrier is associated with this slowest, rate-limiting step.

To illustrate, let us consider the reduction of hydrogen ions to form bubbles of hydrogen gas on the surface of a zinc electrode (Figure 16.6). It is conceivable that this reaction could proceed by the following step sequence:

1. Adsorption of H^+ ions from the solution onto the zinc surface.
2. Electron transfer from the zinc to form a hydrogen atom,

$$H^+ + e^- \longrightarrow H$$

3. Combining of two hydrogen atoms to form a molecule of hydrogen,

$$2H \longrightarrow H_2$$

4. The coalescence of many hydrogen molecules to form a bubble.

The slowest of these steps determines the rate of the overall reaction.

For activation polarization, the relationship between overvoltage η_a and current density i is

$$\eta_a = \pm\beta \log \frac{i}{i_0} \tag{16.25}$$

where β and i_0 are constants for the particular half-cell. The parameter i_0 is termed the *exchange current density,* which deserves a brief explanation. Equilibrium for some particular half-cell reaction is really a dynamic state on the atomic level. That is, oxidation and reduction processes are occurring, but both at the same rate, so that there is no net reaction. For example, for the standard hydrogen cell (Figure

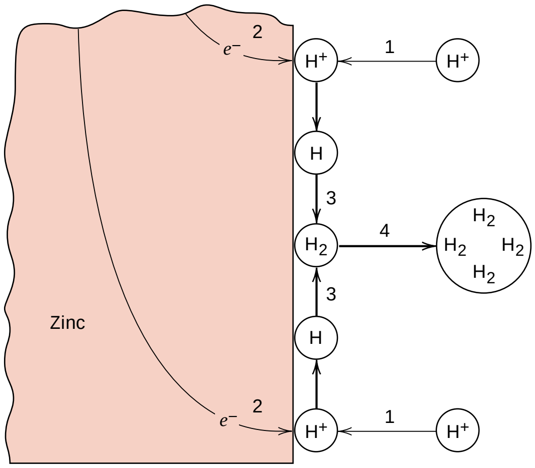

FIGURE 16.6 Schematic representation of possible steps in the hydrogen reduction reaction, the rate of which is controlled by activation polarization. (From M. G. Fontana, *Corrosion Engineering,* 3rd edition. Copyright © 1986 by McGraw-Hill Book Company. Reproduced with permission.)

16.4) reduction of hydrogen ions in solution will take place at the surface of the platinum electrode according to

$$2H^+ + 2e^- \longrightarrow H_2$$

with a corresponding rate r_{red}. Similarly, hydrogen gas in the solution will experience oxidation as

$$H_2 \longrightarrow 2H^+ + 2e^-$$

at rate r_{oxid}. Equilibrium exists when

$$r_{red} = r_{oxid}$$

This exchange current density is just the current density from Equation 16.24 at equilibrium, or

$$r_{red} = r_{oxid} = \frac{i_0}{n\mathscr{F}} \tag{16.26}$$

Use of the term ''current density'' for i_0 is a little misleading inasmuch as there is no net current. Furthermore, the value for i_0 is determined experimentally and will vary from system to system.

According to Equation 16.25, when overvoltage is plotted as a function of the logarithm of current density, straight-line segments result; these are shown in Figure 16.7 for the hydrogen electrode. The line segment with a slope of $+\beta$ corresponds to the oxidation half-reaction, whereas the line with a $-\beta$ slope is for reduction. Also worth noting is that both line segments originate at i_0 (H_2/H^+), the exchange current density, and at zero overvoltage, since at this point the system is at equilibrium and there is no net reaction.

Concentration Polarization

Concentration polarization exists when the reaction rate is limited by diffusion in the solution. For example, consider again the hydrogen evolution reduction reaction. When the reaction rate is low and/or the concentration of H^+ is high, there is always

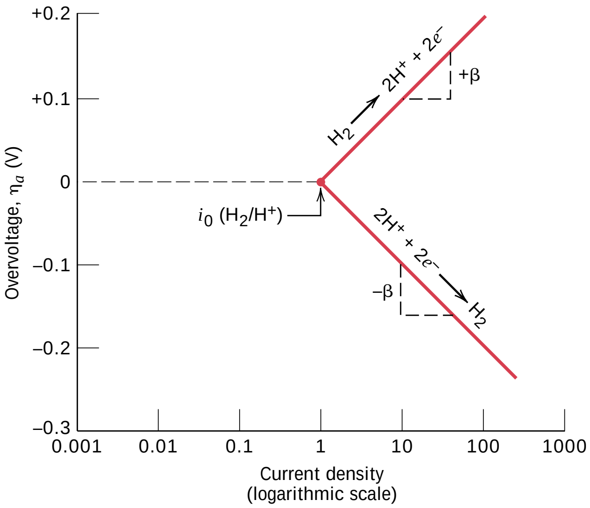

FIGURE 16.7 For a hydrogen electrode, plot of activation polarization overvoltage versus logarithm of current density for both oxidation and reduction reactions. (Adapted from M. G. Fontana, *Corrosion Engineering,* 3rd edition. Copyright © 1986 by McGraw-Hill Book Company. Reproduced with permission.)

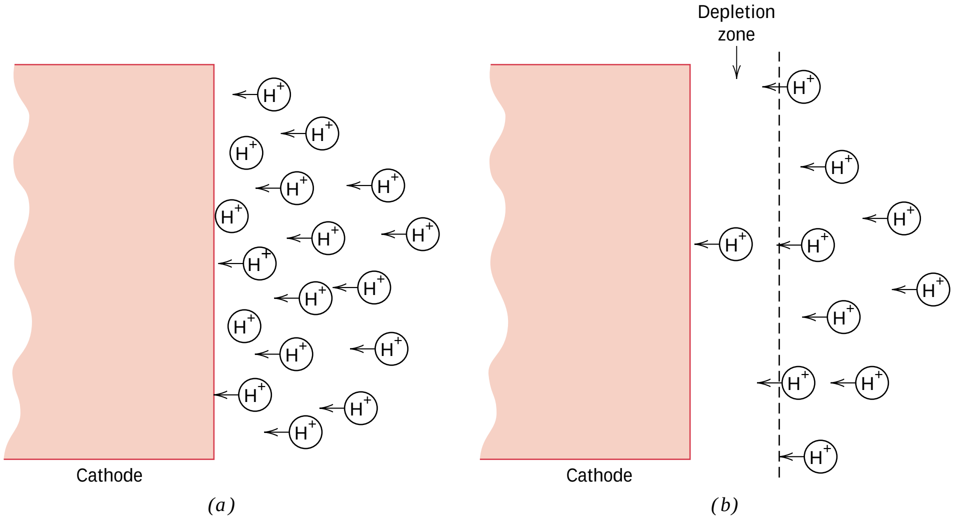

FIGURE 16.8 For hydrogen reduction, schematic representations of the H^+ distribution in the vicinity of the cathode for (*a*) low reaction rates and/or high concentrations, and (*b*) high reaction rates and/or low concentrations wherein a depletion zone is formed that gives rise to concentration polarization. (Adapted from M. G. Fontana, *Corrosion Engineering*, 3rd edition. Copyright © 1986 by McGraw-Hill Book Company. Reproduced with permission.)

an adequate supply of hydrogen ions available in the solution at the region near the electrode interface (Figure 16.8*a*). On the other hand, at high rates and/or low H^+ concentrations, a depletion zone may be formed in the vicinity of the interface, inasmuch as the H^+ ions are not replenished at a rate sufficient to keep up with the reaction (Figure 16.8*b*). Thus, diffusion of H^+ to the interface is rate controlling, and the system is said to be concentration polarized. Concentration polarization generally occurs only for reduction reactions because for oxidation, there is virtually an unlimited supply of metal atoms at the corroding electrode interface.

Concentration polarization data are also normally plotted as overvoltage versus the logarithm of current density; such a plot is represented schematically in Figure 16.9*a*.[2] It may be noted from this figure that overvoltage is independent of current density until i approaches i_L; at this point, η_c decreases abruptly in magnitude.

Both concentration and activation polarization are possible for reduction reactions. Under these circumstances, the total overvoltage is just the sum of both overvoltage contributions. Figure 16.9*b* shows such a schematic η-versus-log i plot.

---

[2] The mathematical expression relating concentration polarization overvoltage η_c and current density i is

$$\eta_c = \frac{2.3RT}{n\mathscr{F}} \log\left(1 - \frac{i}{i_L}\right) \tag{16.27}$$

where R and T are the gas constant and absolute temperature, respectively, n and $\mathscr{F}$ have the same meanings as above, and i_L is the limiting diffusion current density.

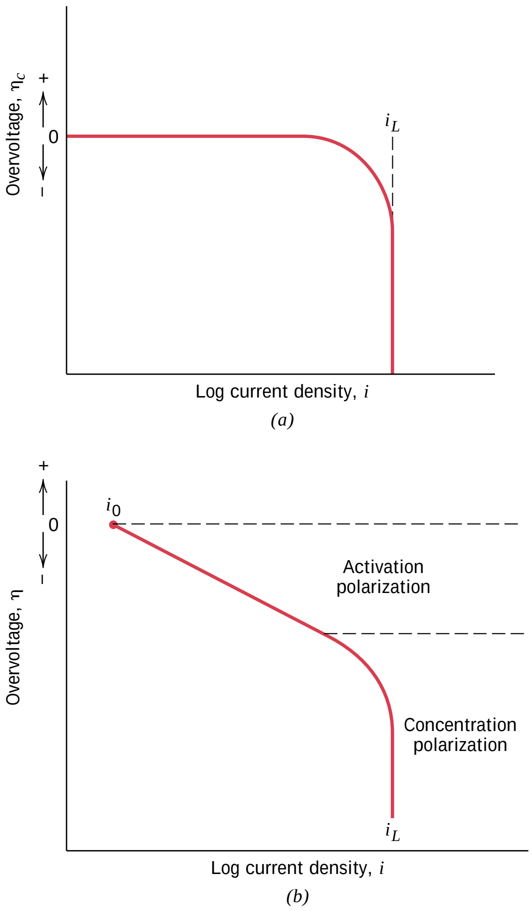

FIGURE 16.9 For reduction reactions, schematic plots of overvoltage versus logarithm of current density for (*a*) concentration polarization, and (*b*) combined activation–concentration polarization.

CORROSION RATES FROM POLARIZATION DATA

Let us now apply the concepts developed above to the determination of corrosion rates. Two types of systems will be discussed. In the first case, both oxidation and reduction reactions are rate limited by activation polarization. In the second case, both concentration and activation polarization control the reduction reaction, whereas only activation polarization is important for oxidation. Case one will be illustrated by considering the corrosion of zinc immersed in an acid solution (see Figure 16.1). The reduction of H^+ ions to form H_2 gas bubbles occurs at the surface of the zinc according to

$$2H^+ + 2e^- \longrightarrow H_2 \tag{16.3}$$

and the zinc oxidizes as

$$Zn \longrightarrow Zn^{2+} + 2e^- \tag{16.8}$$

No net charge accumulation may result from these two reactions; that is, all electrons generated by reaction 16.8 must be consumed by reaction 16.3, which is to say that rates of oxidation and reduction must be equal.

Activation polarization for both reactions is expressed graphically in Figure 16.10 as cell potential referenced to the standard hydrogen electrode (not overvoltage) versus the logarithm of current density. The potentials of the uncoupled

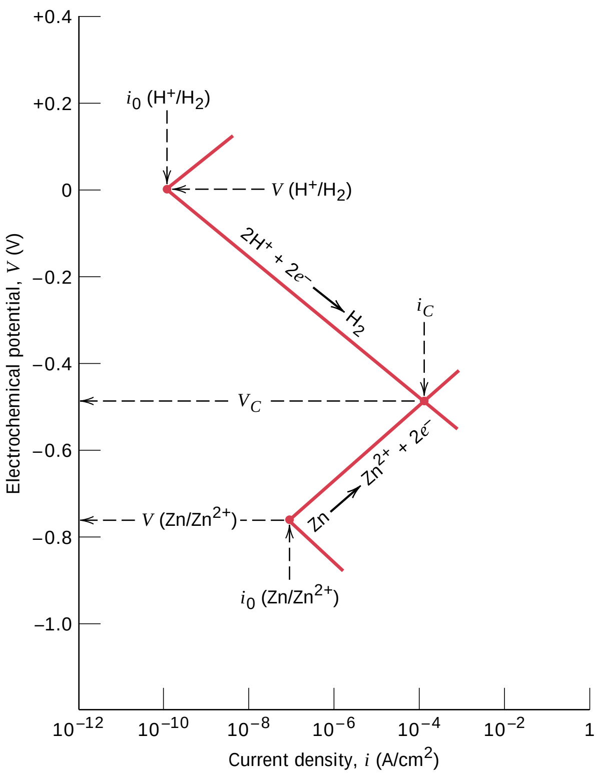

Figure 16.10 Electrode kinetic behavior of zinc in an acid solution; both oxidation and reduction reactions are rate limited by activation polarization. (Adapted from M. G. Fontana, *Corrosion Engineering*, 3rd edition. Copyright © 1986 by McGraw-Hill Book Company. Reproduced with permission.)

hydrogen and zinc half-cells, $V(\text{H}^+/\text{H}_2)$ and $V(\text{Zn}/\text{Zn}^{2+})$, respectively, are indicated, along with their respective exchange current densities, $i_0(\text{H}^+/\text{H}_2)$ and $i_0(\text{Zn}/\text{Zn}^{2+})$. Straight line segments are shown for hydrogen reduction and zinc oxidation. Upon immersion, both hydrogen and zinc experience activation polarization along their respective lines. Also, oxidation and reduction rates must be equal as explained above, which is only possible at the intersection of the two line segments; this intersection occurs at the corrosion potential, designated V_C, and the corrosion current density i_C. The corrosion rate of zinc (which also corresponds to the rate of hydrogen evolution) may thus be computed by insertion of this i_C value into Equation 16.24.

The second corrosion case (combined activation and concentration polarization for hydrogen reduction and activation polarization for oxidation of metal M) is treated in a like manner. Figure 16.11 shows both polarization curves; as above, corrosion potential and corrosion current density correspond to the point at which the oxidation and reduction lines intersect.

EXAMPLE PROBLEM 16.2

Zinc experiences corrosion in an acid solution according to the reaction

$$\text{Zn} + 2\text{H}^+ \longrightarrow \text{Zn}^{2+} + \text{H}_2$$

The rates of both oxidation and reduction half-reactions are controlled by activation polarization.

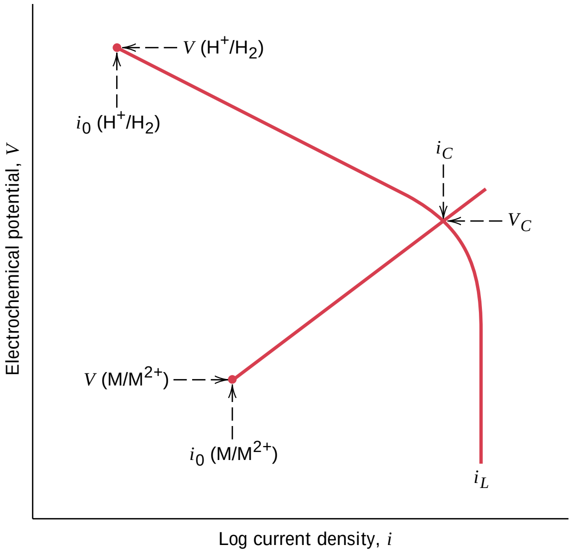

Figure 16.11 Schematic electrode kinetic behavior for metal M; the reduction reaction is under combined activation–concentration polarization control.

(a) Compute the rate of oxidation of Zn (in mol/cm^2-s) given the following activation polarization data:

For Zn	***For Hydrogen***
$V_{(\mathrm{Zn/Zn^{2+}})} = -0.763$ V	$V_{(\mathrm{H^+/H_2})} = 0$ V
$i_0 = 10^{-7}$ A/cm^2	$i_0 = 10^{-10}$ A/cm^2
$\beta = +0.09$	$\beta = -0.08$

(b) Compute the value of the corrosion potential.

SOLUTION

(a) To compute the rate of oxidation for Zn, it is first necessary to establish relationships in the form of Equation 16.25 for the potential of both oxidation and reduction reactions. Next, these two expressions are set equal to one another, and then we solve for the value of i that is the corrosion current density, i_C. Finally, the corrosion rate may be calculated using Equation 16.24. The two potential expressions are as follows: For hydrogen reduction,

$$V_{\mathrm{H}} = V_{(\mathrm{H^+/H_2})} + \beta_{\mathrm{H}} \log\left(\frac{i}{i_{0_{\mathrm{H}}}}\right)$$

and for Zn oxidation,

$$V_{\mathrm{Zn}} = V_{(\mathrm{Zn/Zn^{2+}})} + \beta_{\mathrm{Zn}} \log\left(\frac{i}{i_{0_{\mathrm{Zn}}}}\right)$$

Now, setting $V_{\mathrm{H}} = V_{\mathrm{Zn}}$ leads to

$$V_{(\mathrm{H^+/H_2})} + \beta_{\mathrm{H}} \log\left(\frac{i}{i_{0_{\mathrm{H}}}}\right) = V_{(\mathrm{Zn/Zn^{2+}})} + \beta_{\mathrm{Zn}} \log\left(\frac{i}{i_{0_{\mathrm{Zn}}}}\right)$$

And, solving for log i (i.e., log i_C) leads to

$$\log i_C = \left(\frac{1}{\beta_{\mathrm{Zn}} - \beta_{\mathrm{H}}}\right)[V_{(\mathrm{H^+/H_2})} - V_{(\mathrm{Zn/Zn^{2+}})} - \beta_{\mathrm{H}} \log i_{0_{\mathrm{H}}} + \beta_{\mathrm{Zn}} \log i_{0_{\mathrm{Zn}}}]$$

$$= \left[\frac{1}{0.09 - (-0.08)}\right][0 - (-0.763) - (-0.08)(\log 10^{-10})$$

$$+ (0.09)(\log 10^{-7})]$$

$$= -3.924$$

Or

$$i_C = 10^{-3.924} = 1.19 \times 10^{-4} \text{ A/cm}^2$$

And from Equation 16.24,

$$r = \frac{i_C}{n\mathscr{F}}$$

$$= \frac{1.19 \times 10^{-4} \text{ C/s-cm}^2}{(2)(96{,}500 \text{ C/mol})} = 6.17 \times 10^{-10} \text{ mol/cm}^2\text{-s}$$

(b) Now it becomes necessary to compute the value of the corrosion potential V_C. This is possible by using either of the above equations for V_{H} or V_{Zn} and substituting for i the value determined above for i_C. Thus, using the V_{H} expression yields

$$V_C = V_{(\mathrm{H^+/H_2})} + \beta_{\mathrm{H}} \log\left(\frac{i_C}{i_{0_{\mathrm{H}}}}\right)$$

$$= 0 + (-0.08 \text{ V}) \log\left(\frac{1.19 \times 10^{-4} \text{ A/cm}^2}{10^{-10} \text{ A/cm}^2}\right) = -0.486 \text{ V}$$

This is the same problem that is represented and solved graphically in the voltage-versus-logarithm current density plot of Figure 16.10. It is worth noting that the i_C and V_C we have obtained by this analytical treatment are in agreement with those values occurring at the intersection of the two line segments on the plot.

16.5 PASSIVITY

Some normally active metals and alloys, under particular environmental conditions, lose their chemical reactivity and become extremely inert. This phenomenon, termed **passivity,** is displayed by chromium, iron, nickel, titanium, and many of their alloys. It is felt that this passive behavior results from the formation of a highly adherent and very thin oxide film on the metal surface, which serves as a protective barrier to further corrosion. Stainless steels are highly resistant to corrosion in a rather wide variety of atmospheres as a result of passivation. They contain at least 11% chromium which, as a solid-solution alloying element in iron, minimizes the formation of rust; instead, a protective surface film forms in oxidizing atmospheres. (Stainless steels are susceptible to corrosion in some environments, and therefore are not always ''stainless.'') Aluminum is highly corrosion resistant in many environ-

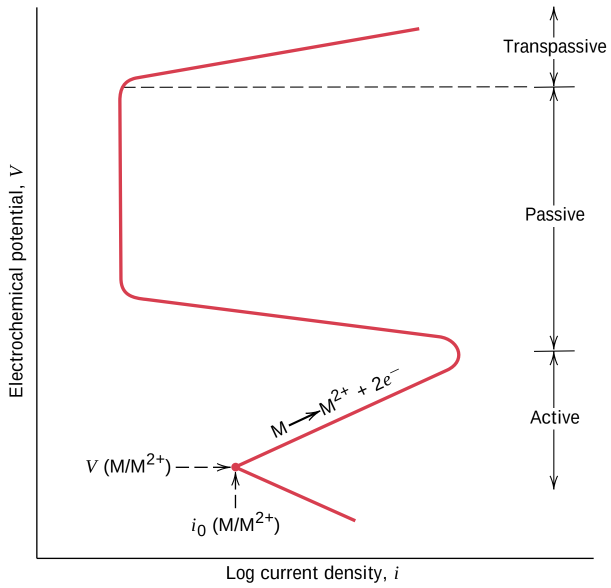

Figure 16.12 Schematic polarization curve for a metal that displays an active–passive transition.

ments because it also passivates. If damaged, the protective film normally reforms very rapidly. However, a change in the character of the environment (e.g., alteration in the concentration of the active corrosive species) may cause a passivated material to revert to an active state. Subsequent damage to a preexisting passive film could result in a substantial increase in corrosion rate, by as much as 100,000 times.

This passivation phenomenon may be explained in terms of polarization potential–log current density curves discussed in the preceding section. The polarization curve for a metal that passivates will have the general shape shown in Figure 16.12. At relatively low potential values, within the ''active'' region the behavior is linear as it is for normal metals. With increasing potential, the current density suddenly decreases to a very low value that remains independent of potential; this is termed the ''passive'' region. Finally, at even higher potential values, the current density again increases with potential in the ''transpassive'' region.

Figure 16.13 illustrates how a metal can experience both active and passive behavior depending on the corrosion environment. Included in this figure is the S-shaped oxidation polarization curve for an active–passive metal M and, in addition, reduction polarization curves for two different solutions, which are labeled 1 and 2. Curve 1 intersects the oxidation polarization curve in the active region at point A, yielding a corrosion current density i_C(A). The intersection of curve 2 at point B is in the passive region and at current density i_C(B). The corrosion rate of metal M in solution 1 is greater than in solution 2 since i_C(A) is greater than i_C(B) and rate is proportional to current density according to Equation 16.24. This difference in corrosion rate between the two solutions may be significant—several orders of magnitude—when one considers that the current density scale in Figure 16.13 is scaled logarithmically.

16.6 ENVIRONMENTAL EFFECTS

The variables in the corrosion environment, which include fluid velocity, temperature, and composition, can have a decided influence on the corrosion properties of

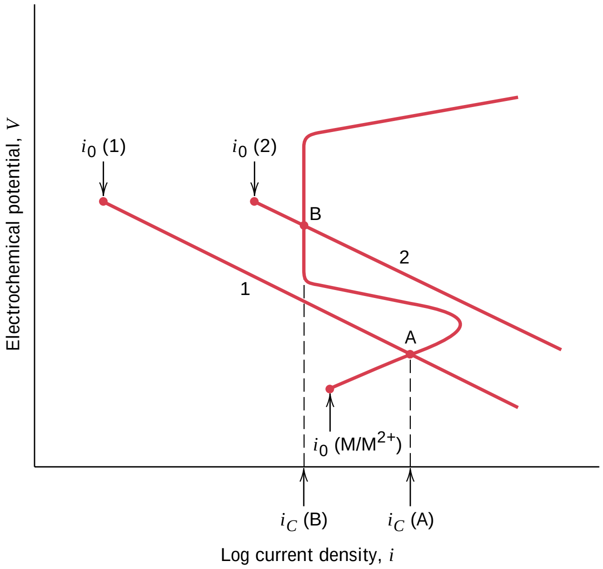

Figure 16.13 Demonstration of how an active–passive metal can exhibit both active and passive corrosion behavior.

the materials that are in contact with it. In most instances, increasing fluid velocity enhances the rate of corrosion due to erosive effects, as discussed later in the chapter. The rates of most chemical reactions rise with increasing temperature; this also holds for the great majority of corrosion situations. Increasing the concentration of the corrosive species (e.g., H^+ ions in acids) in many situations produces a more rapid rate of corrosion. However, for materials capable of passivation, raising the corrosive content may result in an active-to-passive transition, with a considerable reduction in corrosion.

Cold working or plastically deforming ductile metals is used to increase their strength; however, a cold-worked metal is more susceptible to corrosion than the same material in an annealed state. For example, deformation processes are used to shape the head and point of a nail; consequently, these positions are anodic with respect to the shank region. Thus, differential cold working on a structure should be a consideration when a corrosive environment may be encountered during service.

16.7 FORMS OF CORROSION

It is convenient to classify corrosion according to the manner in which it is manifest. Metallic corrosion is sometimes classified into eight forms: uniform, galvanic, crevice, pitting, intergranular, selective leaching, erosion–corrosion, and stress corrosion. The causes and means of prevention of each of these forms are discussed briefly. In addition, we have elected to discuss the topic of hydrogen embrittlement in this section. Hydrogen embrittlement is, in a strict sense, a type of failure rather than a form of corrosion; however, it is often produced by hydrogen that is generated from corrosion reactions.

UNIFORM ATTACK

Uniform attack is a form of electrochemical corrosion that occurs with equivalent intensity over the entire exposed surface and often leaves behind a scale or deposit. In a microscopic sense, the oxidation and reduction reactions occur randomly over the surface. Some familiar examples include general rusting of steel and iron and the tarnishing of silverware. This is probably the most common form of corrosion. It is also the least objectionable because it can be predicted and designed for with relative ease.

GALVANIC CORROSION

Galvanic corrosion occurs when two metals or alloys having different compositions are electrically coupled while exposed to an electrolyte. This is the type of corrosion or dissolution that was described in Section 16.2. The less noble or more reactive metal in the particular environment will experience corrosion; the more inert metal, the cathode, will be protected from corrosion. For example, steel screws corrode when in contact with brass in a marine environment; or if copper and steel tubing are joined in a domestic water heater, the steel will corrode in the vicinity of the junction. Depending on the nature of the solution, one or more of the reduction reactions, Equations 16.3 through 16.7, will occur at the surface of the cathode material. Figure 16.14 shows galvanic corrosion.

Again, the galvanic series (Table 16.2) indicates the relative reactivities, in seawater, of a number of metals and alloys. When two alloys are coupled in seawater, the one lower in the series will experience corrosion. Some of the alloys in the

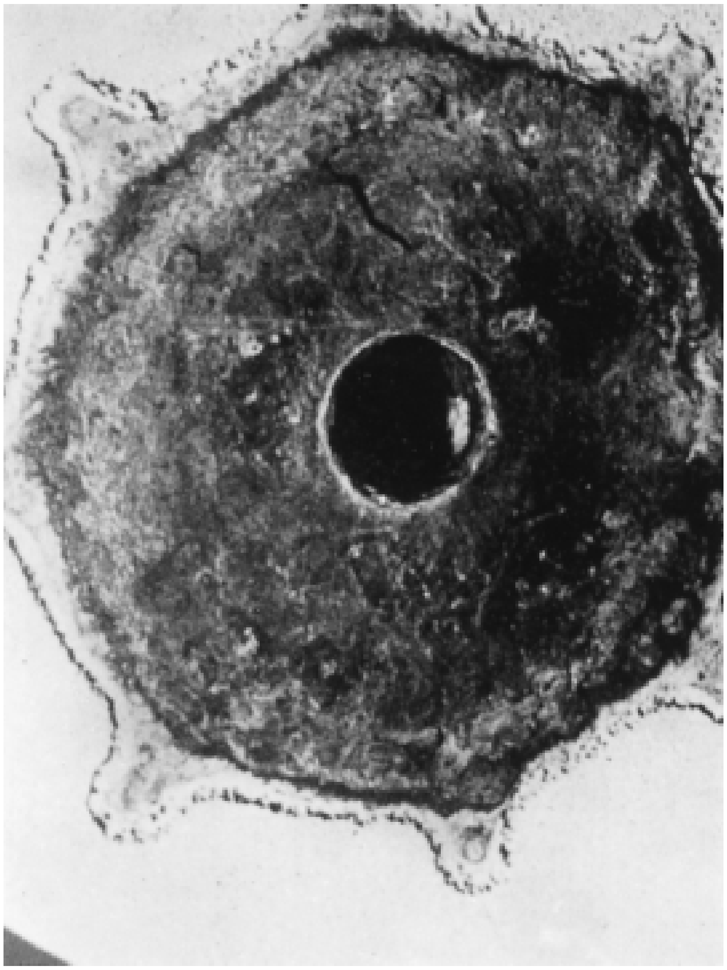

FIGURE 16.14 Galvanic corrosion of a magnesium shell that was cast around a steel core. (Photograph courtesy of LaQue Center for Corrosion Technology, Inc.)

table are grouped in brackets. Generally the base metal is the same for these bracketed alloys, and there is little danger of corrosion if alloys within a single bracket are coupled. It is also worth noting from this series that some alloys are listed twice (e.g., nickel and the stainless steels), in both active and passive states.

The rate of galvanic attack depends on the relative anode-to-cathode surface areas that are exposed to the electrolyte, and the rate is related directly to the cathode–anode area ratio; that is, for a given cathode area, a smaller anode will corrode more rapidly than a larger one. The reason for this is that corrosion rate depends on current density (Equation 16.24), the current per unit area of corroding surface, and not simply the current. Thus, a high current density results for the anode when its area is small relative to that of the cathode.

A number of measures may be taken to significantly reduce the effects of galvanic corrosion. These include the following:

1. If coupling of dissimilar metals is necessary, choose two that are close together in the galvanic series.
2. Avoid an unfavorable anode-to-cathode surface area ratio; use an anode area as large as possible.
3. Electrically insulate dissimilar metals from each other.
4. Electrically connect a third, anodic metal to the other two; this is a form of **cathodic protection,** discussed presently.

CREVICE CORROSION

Electrochemical corrosion may also occur as a consequence of concentration differences of ions or dissolved gases in the electrolyte solution, and between two regions of the same metal piece. For such a *concentration cell,* corrosion occurs in the locale that has the lower concentration. A good example of this type of corrosion occurs in crevices and recesses or under deposits of dirt or corrosion products where the solution becomes stagnant and there is localized depletion of dissolved oxygen. Corrosion preferentially occurring at these positions is called **crevice corrosion** (Figure 16.15). The crevice must be wide enough for the solution to penetrate, yet narrow enough for stagnancy; usually the width is several thousandths of an inch.

The proposed mechanism for crevice corrosion is illustrated in Figure 16.16. After oxygen has been depleted within the crevice, oxidation of the metal occurs at this position according to Equation 16.1. Electrons from this electrochemical reaction are conducted through the metal to adjacent external regions, where they

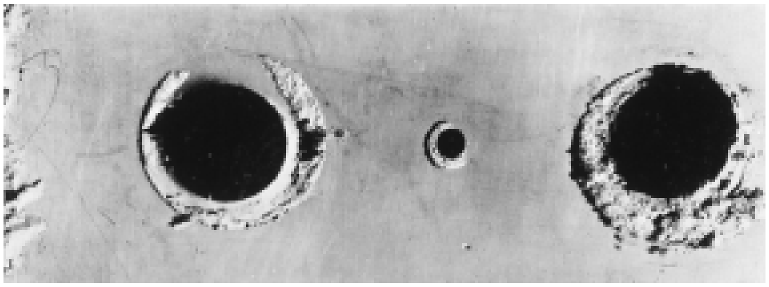

FIGURE 16.15 On this plate, which was immersed in seawater, crevice corrosion has occurred at the regions that were covered by washers. (Photograph courtesy of LaQue Center for Corrosion Technology, Inc.)

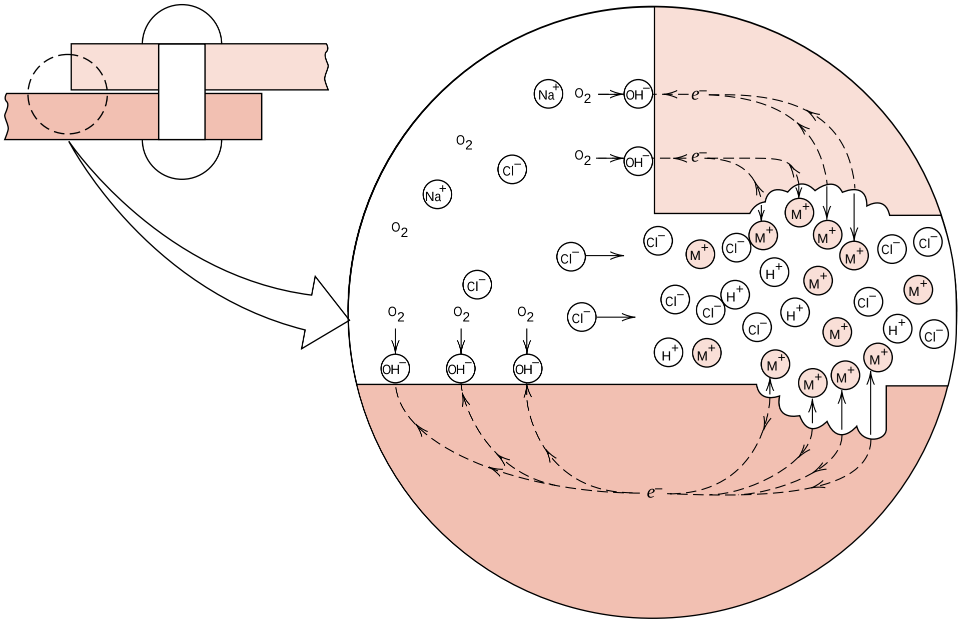

Figure 16.16 Schematic illustration of the mechanism of crevice corrosion between two riveted sheets. (From M. G. Fontana, *Corrosion Engineering*, 3rd edition. Copyright © 1986 by McGraw-Hill Book Company. Reproduced with permission.)

are consumed by reduction—most probably reaction 16.5. In many aqueous environments, the solution within the crevice has been found to develop high concentrations of H^+ and Cl^- ions, which are especially corrosive. Many alloys that passivate are susceptible to crevice corrosion because protective films are often destroyed by the H^+ and Cl^- ions.

Crevice corrosion may be prevented by using welded instead of riveted or bolted joints, using nonabsorbing gaskets when possible, removing accumulated deposits frequently, and designing containment vessels to avoid stagnant areas and ensure complete drainage.

PITTING

Pitting is another form of very localized corrosion attack in which small pits or holes form. They ordinarily penetrate from the top of a horizontal surface downward in a nearly vertical direction. It is an extremely insidious type of corrosion, often going undetected and with very little material loss until failure occurs. An example of pitting corrosion is shown in Figure 16.17.

The mechanism for pitting is probably the same as for crevice corrosion in that oxidation occurs within the pit itself, with complementary reduction at the surface. It is supposed that gravity causes the pits to grow downward, the solution at the pit tip becoming more concentrated and dense as pit growth progresses. A pit may be initiated by a localized surface defect such as a scratch or a slight variation in composition. In fact, it has been observed that specimens having polished surfaces display a greater resistance to pitting corrosion. Stainless steels are somewhat susceptible to this form of corrosion; however, alloying with about 2% molybdenum enhances their resistance significantly.

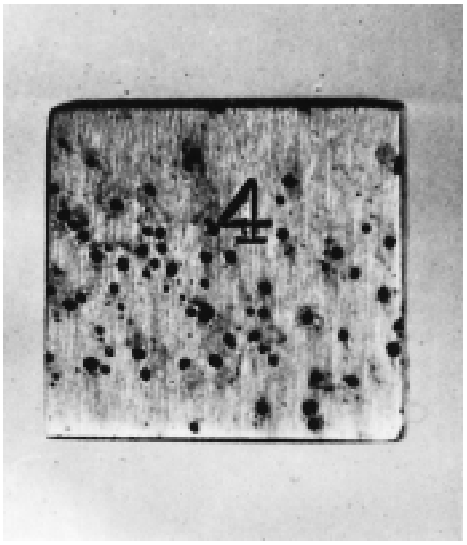

Figure 16.17 The pitting of a 304 stainless steel plate by an acid-chloride solution. (Photograph courtesy of Mars G. Fontana. From M. G. Fontana, *Corrosion Engineering*, 3rd edition. Copyright © 1986 by McGraw-Hill Book Company. Reproduced with permission.)

INTERGRANULAR CORROSION

As the name suggests, **intergranular corrosion** occurs preferentially along grain boundaries for some alloys and in specific environments. The net result is that a macroscopic specimen disintegrates along its grain boundaries. This type of corrosion is especially prevalent in some stainless steels. When heated to temperatures between 500 and 800°C (950 and 1450°F) for sufficiently long time periods, these alloys become sensitized to intergranular attack. It is believed that this heat treatment permits the formation of small precipitate particles of chromium carbide ($Cr_{23}C_6$) by reaction between the chromium and carbon in the stainless steel. These particles form along the grain boundaries, as illustrated in Figure 16.18. Both the chromium and the carbon must diffuse to the grain boundaries to form the precipitates, which leaves a chromium-depleted zone adjacent to the grain boundary. Consequently, this grain boundary region is now highly susceptible to corrosion.

Intergranular corrosion is an especially severe problem in the welding of stainless steels, when it is often termed **weld decay.** Figure 16.19 shows this type of intergranular corrosion.

Figure 16.18 Schematic illustration of chromium carbide particles that have precipitated along grain boundaries in stainless steel, and the attendant zones of chromium depletion.

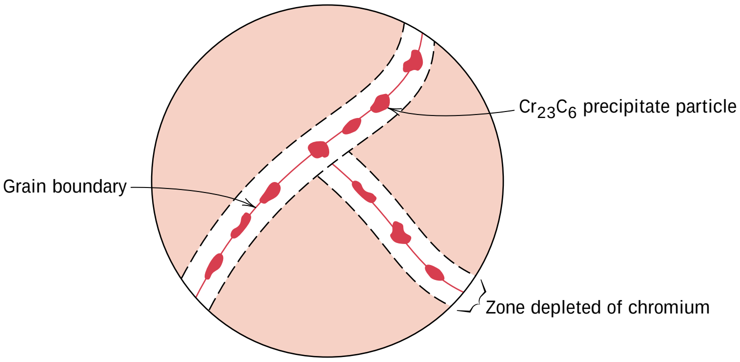

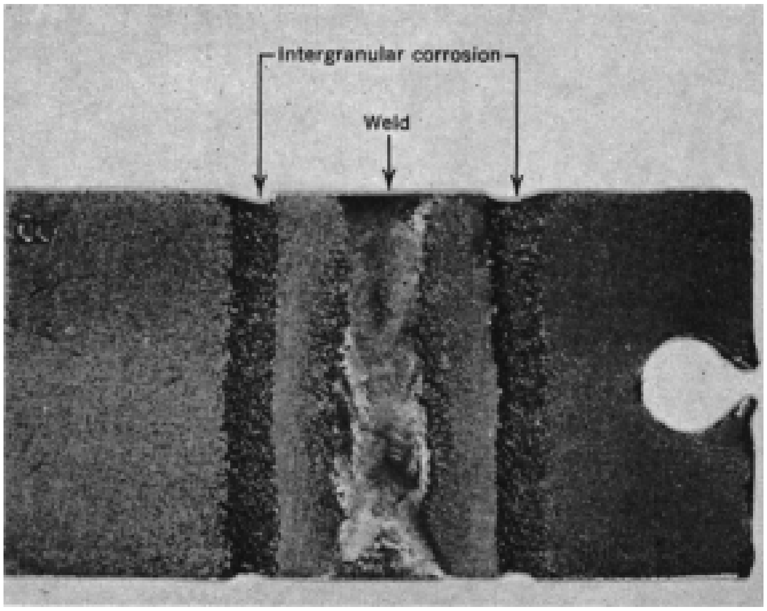

Figure 16.19 Weld decay in a stainless steel. The regions along which the grooves have formed were sensitized as the weld cooled. (From H. H. Uhlig and R. W. Revie, *Corrosion and Corrosion Control,* 3rd edition, Fig. 2, p. 307. Copyright © 1985 by John Wiley & Sons, Inc. Reprinted by permission of John Wiley & Sons, Inc.)

Stainless steels may be protected from intergranular corrosion by the following measures: (1) subjecting the sensitized material to a high-temperature heat treatment in which all the chromium carbide particles are redissolved, (2) lowering the carbon content below 0.03 wt% C so that carbide formation is minimal, and (3) alloying the stainless steel with another metal such as niobium or titanium, which has a greater tendency to form carbides than does chromium so that the Cr remains in solid solution.

SELECTIVE LEACHING

Selective leaching is found in solid solution alloys and occurs when one element or constituent is preferentially removed as a consequence of corrosion processes. The most common example is the dezincification of brass, in which zinc is selectively leached from a copper–zinc brass alloy. The mechanical properties of the alloy are significantly impaired, since only a porous mass of copper remains in the region that has been dezincified. In addition, the material changes from yellow to a red or copper color. Selective leaching may also occur with other alloy systems in which aluminum, iron, cobalt, chromium, and other elements are vulnerable to preferential removal.

EROSION–CORROSION

Erosion–corrosion arises from the combined action of chemical attack and mechanical abrasion or wear as a consequence of fluid motion. Virtually all metal alloys, to one degree or another, are susceptible to erosion–corrosion. It is especially harmful to alloys that passivate by forming a protective surface film; the abrasive action may erode away the film, leaving exposed a bare metal surface. If the coating is not capable of continuously and rapidly reforming as a protective barrier, corrosion may be severe. Relatively soft metals such as copper and lead are also sensitive to this form of attack. Usually it can be identified by surface grooves and waves having contours that are characteristic of the flow of the fluid.

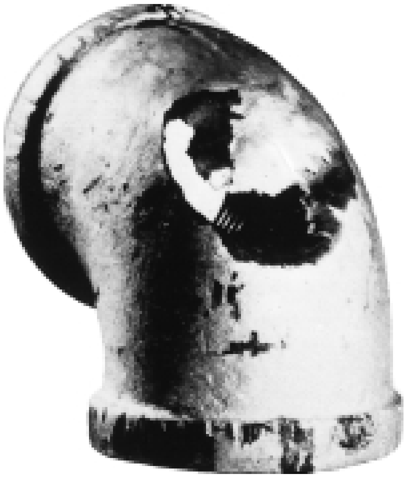

Figure 16.20 Impingement failure of an elbow that was part of a steam condensate line. (Photograph courtesy of Mars G. Fontana. From M. G. Fontana, *Corrosion Engineering,* 3rd edition. Copyright © 1986 by McGraw-Hill Book Company. Reproduced with permission.)

The nature of the fluid can have a dramatic influence on the corrosion behavior. Increasing fluid velocity normally enhances the rate of corrosion. Also, a solution is more erosive when bubbles and suspended particulate solids are present.

Erosion–corrosion is commonly found in piping, especially at bends, elbows, and abrupt changes in pipe diameter—positions where the fluid changes direction or flow suddenly becomes turbulent. Propellers, turbine blades, valves, and pumps are also susceptible to this form of corrosion. Figure 16.20 illustrates the impingement failure of an elbow fitting.

One of the best ways to reduce erosion–corrosion is to change the design to eliminate fluid turbulence and impingement effects. Other materials may also be utilized that inherently resist erosion. Furthermore, removal of particulates and bubbles from the solution will lessen its ability to erode.

STRESS CORROSION

Stress corrosion, sometimes termed stress corrosion cracking, results from the combined action of an applied tensile stress and a corrosive environment; both influences are necessary. In fact, some materials that are virtually inert in a particular corrosive medium become susceptible to this form of corrosion when a stress is applied. Small cracks form and then propagate in a direction perpendicular to the stress (see the chapter-opening photograph for this chapter), with the result that failure may eventually occur. Failure behavior is characteristic of that for a brittle material, even though the metal alloy is intrinsically ductile. Furthermore, cracks may form at relatively low stress levels, significantly below the tensile strength. Most alloys are susceptible to stress corrosion in specific environments, especially at moderate stress levels. For example, most stainless steels stress corrode in solutions containing chloride ions, whereas brasses are especially vulnerable when exposed to ammonia. Figure 16.21 is a photomicrograph in which an example of intergranular stress corrosion cracking in brass is shown.

The stress that produces stress corrosion cracking need not be externally applied; it may be a residual one that results from rapid temperature changes and uneven contraction, or for two-phase alloys in which each phase has a different coefficient of expansion. Also, gaseous and solid corrosion products that are entrapped internally can give rise to internal stresses.

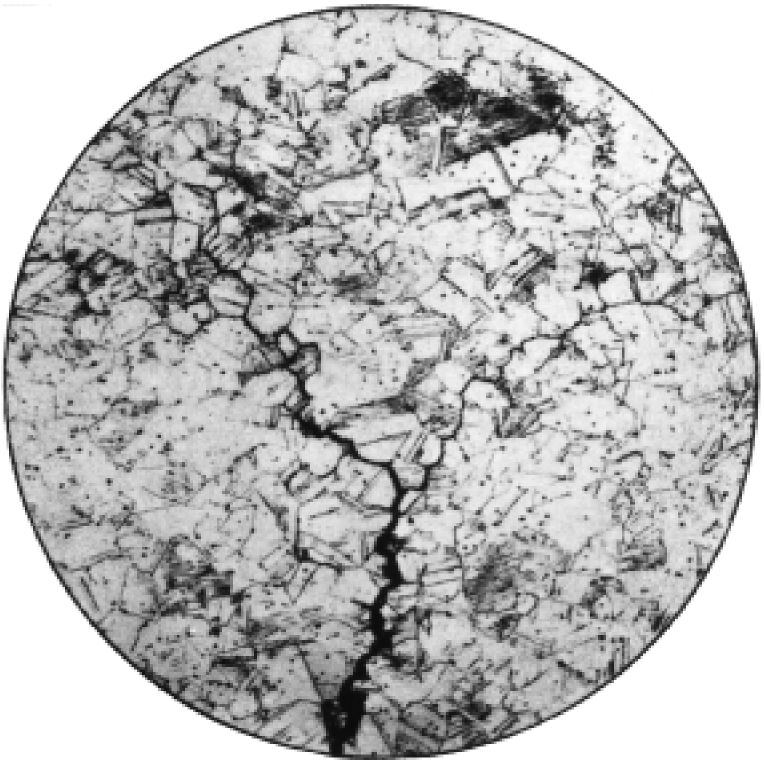

Figure 16.21 Photomicrograph showing intergranular stress corrosion cracking in brass. (From H. H. Uhlig and R. W. Revie, *Corrosion and Corrosion Control,* 3rd edition, Fig. 5, p. 335. Copyright 1985 by John Wiley & Sons, Inc. Reprinted by permission of John Wiley & Sons, Inc.)

Probably the best measure to take in reducing or totally eliminating stress corrosion is to lower the magnitude of the stress. This may be accomplished by reducing the external load or increasing the cross-sectional area perpendicular to the applied stress. Furthermore, an appropriate heat treatment may be used to anneal out any residual thermal stresses.

HYDROGEN EMBRITTLEMENT

Various metal alloys, specifically some steels, experience a significant reduction in ductility and tensile strength when atomic hydrogen (H) penetrates into the material. This phenomenon is aptly referred to as **hydrogen embrittlement;** the terms *hydrogen induced cracking* and *hydrogen stress cracking* are sometimes also used. Strictly speaking, hydrogen embrittlement is a type of failure; in response to applied or residual tensile stresses, brittle fracture occurs catastrophically as cracks grow and rapidly propagate. Hydrogen in its atomic form (H as opposed to the molecular form, H_2) diffuses interstitially through the crystal lattice, and concentrations as low as several parts per million can lead to cracking. Furthermore, hydrogen-induced cracks are most often transgranular, although intergranular fracture is observed for some alloy systems. A number of mechanisms have been proposed to explain hydrogen embrittlement; most of them are based on the interference of dislocation motion by the dissolved hydrogen.

Hydrogen embrittlement is similar to stress corrosion (as discussed in the preceding section) in that a normally ductile metal experiences brittle fracture when exposed to both a tensile stress and a corrosive atmosphere. However, these two phenomena may be distinguished on the basis of their interactions with applied electric currents. Whereas cathodic protection (Section 16.9) reduces or causes a cessation of stress corrosion, it may, on the other hand, lead to the initiation or enhancement of hydrogen embrittlement.

In order for hydrogen embrittlement to occur, some source of hydrogen must be present, and, in addition, the possibility for the formation of its atomic species. Situations wherein these conditions are met include the following: pickling[3] of steels in sulfuric acid; electroplating; and the presence of hydrogen-bearing atmospheres (including water vapor) at elevated temperatures such as during welding and heat treatments. Also, the presence of what are termed ''poisons'' such as sulfur (i.e., H_2S) and arsenic compounds accelerates hydrogen embrittlement; these substances retard the formation of molecular hydrogen and thereby increase the residence time of atomic hydrogen on the metal surface. Hydrogen sulfide, probably the most aggressive poison, is found in petroleum fluids, natural gas, oil-well brines, and geothermal fluids.

High-strength steels are susceptible to hydrogen embrittlement, and increasing strength tends to enhance the material's susceptibility. Martensitic steels are especially vulnerable to this type of failure; bainitic, ferritic, and spheroiditic steels are more resilient. Furthermore, FCC alloys (austenitic stainless steels, and alloys of copper, aluminum, and nickel) are relatively resistant to hydrogen embrittlement, mainly because of their inherently high ductilities. However, strain hardening these alloys will enhance their susceptibility to embrittlement.

Some of the techniques commonly used to reduce the likelihood of hydrogen embrittlement include: reducing the tensile strength of the alloy via a heat treatment; removal of the source of hydrogen; ''baking'' the alloy at an elevated temperature to drive out any dissolved hydrogen; and substitution of a more embrittlement-resistant alloy.

16.8 CORROSION ENVIRONMENTS

Corrosive environments include the atmosphere, aqueous solutions, soils, acids, bases, inorganic solvents, molten salts, liquid metals, and, last but not least, the human body. On a tonnage basis, atmospheric corrosion accounts for the greatest losses. Moisture containing dissolved oxygen is the primary corrosive agent, but other substances, including sulfur compounds and sodium chloride, may also contribute. This is especially true of marine atmospheres, which are highly corrosive because of the presence of sodium chloride. Dilute sulfuric acid solutions (acid rain) in industrial environments can also cause corrosion problems. Metals commonly used for atmospheric applications include alloys of aluminum and copper, and galvanized steel.

Water environments can also have a variety of compositions and corrosion characteristics. Fresh water normally contains dissolved oxygen, as well as other minerals several of which account for hardness. Seawater contains approximately 3.5% salt (predominantly sodium chloride), as well as some minerals and organic matter. Seawater is generally more corrosive than fresh water, frequently producing pitting and crevice corrosion. Cast iron, steel, aluminum, copper, brass, and some stainless steels are generally suitable for freshwater use, whereas titanium, brass, some bronzes, copper–nickel alloys, and nickel–chromium–molybdenum alloys are highly corrosion resistant in seawater.

Soils have a wide range of compositions and susceptibilities to corrosion. Compositional variables include moisture, oxygen, salt content, alkalinity, and acidity, as well as the presence of various forms of bacteria. Cast iron and plain carbon steels, both with and without protective surface coatings, are found most economical for underground structures.

---

[3] *Pickling* is a procedure used to remove surface oxide scale from steel pieces by dipping them in a vat of hot, dilute sulfuric or hydrochloric acid.

Because there are so many acids, bases, and organic solvents, no attempt is made to discuss these solutions. Good references are available that treat these topics in detail.

16.9 CORROSION PREVENTION

Some corrosion prevention methods were treated relative to the eight forms of corrosion; however, only the measures specific to each of the various corrosion types were discussed. Now, some more general techniques are presented; these include material selection, environmental alteration, design, coatings, and cathodic protection.

Perhaps the most common and easiest way of preventing corrosion is through the judicious selection of materials once the corrosion environment has been characterized. Standard corrosion references are helpful in this respect. Here, cost may be a significant factor. It is not always economically feasible to employ the material that provides the optimum corrosion resistance; sometimes, either another alloy and/or some other measure must be used.

Changing the character of the environment, if possible, may also significantly influence corrosion. Lowering the fluid temperature and/or velocity usually produces a reduction in the rate at which corrosion occurs. Many times increasing or decreasing the concentration of some species in the solution will have a positive effect; for example, the metal may experience passivation.

Inhibitors are substances that, when added in relatively low concentrations to the environment, decrease its corrosiveness. Of course, the specific inhibitor depends both on the alloy and on the corrosive environment. There are several mechanisms that may account for the effectiveness of inhibitors. Some react with and virtually eliminate a chemically active species in the solution (such as dissolved oxygen). Other inhibitor molecules attach themselves to the corroding surface and interfere with either the oxidation or the reduction reaction, or form a very thin protective coating. Inhibitors are normally used in closed systems such as automobile radiators and steam boilers.

Several aspects of design consideration have already been discussed, especially with regard to galvanic and crevice corrosion, and erosion–corrosion. In addition, the design should allow for complete drainage in the case of a shutdown, and easy washing. Since dissolved oxygen may enhance the corrosivity of many solutions, the design should, if possible, include provision for the exclusion of air.

Physical barriers to corrosion are applied on surfaces in the form of films and coatings. A large diversity of metallic and nonmetallic coating materials are available. It is essential that the coating maintain a high degree of surface adhesion, which undoubtedly requires some preapplication surface treatment. In most cases, the coating must be virtually nonreactive in the corrosive environment and resistant to mechanical damage that exposes the bare metal to the corrosive environment. All three material types—metals, ceramics, and polymers—are used as coatings for metals.

CATHODIC PROTECTION

One of the most effective means of corrosion prevention is **cathodic protection;** it can be used for all eight different forms of corrosion as discussed above, and may,

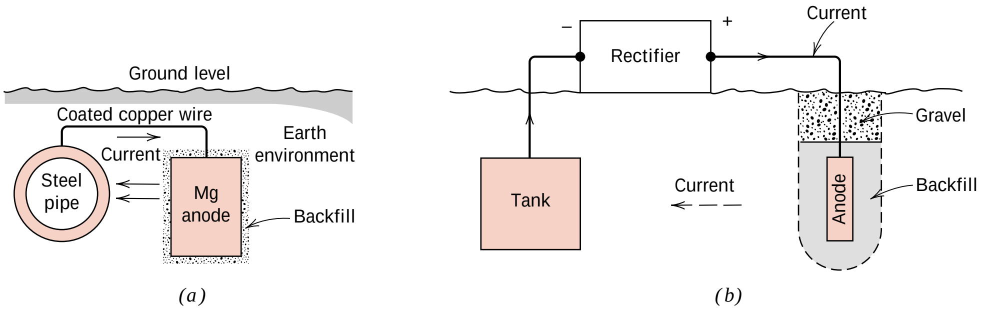
Ground level
Coated copper wire
Current
Earth environment
Steel pipe
Mg anode
Backfill
(a)
Rectifier
–
+
Current
Gravel
Tank
Current
Anode
Backfill
(b)

Figure 16.22 Cathodic protection of (*a*) an underground pipeline using a magnesium sacrificial anode, and (*b*) an underground tank using an impressed current. (From M. G. Fontana, *Corrosion Engineering,* 3rd edition. Copyright © 1986 by McGraw-Hill Book Company. Reproduced with permission.)

in some situations, completely stop corrosion. Again, oxidation or corrosion of a metal M occurs by the generalized reaction

$$M \longrightarrow M^{n+} + ne^- \tag{16.1}$$

Cathodic protection simply involves supplying, from an external source, electrons to the metal to be protected, making it a cathode; the reaction above is thus forced in the reverse (or reduction) direction.

One cathodic protection technique employs a galvanic couple: the metal to be protected is electrically connected to another metal that is more reactive in the particular environment. The latter experiences oxidation, and, upon giving up electrons, protects the first metal from corrosion. The oxidized metal is often called a **sacrificial anode,** and magnesium and zinc are commonly used as such because they lie at the anodic end of the galvanic series. This form of galvanic protection, for structures buried in the ground, is illustrated in Figure 16.22*a*.

The process of *galvanizing* is simply one in which a layer of zinc is applied to the surface of steel by hot dipping. In the atmosphere and most aqueous environments, zinc is anodic to and will thus cathodically protect the steel if there is any surface damage (Figure 16.23). Any corrosion of the zinc coating will proceed at an extremely slow rate because the ratio of the anode-to-cathode surface area is quite large.

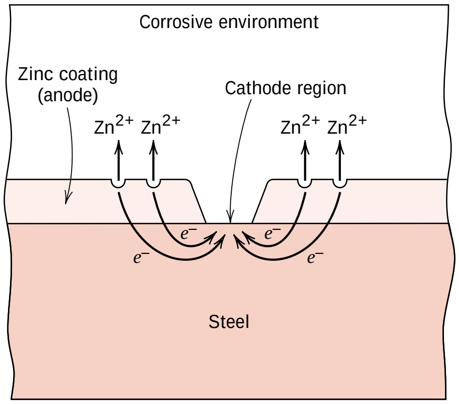
Corrosive environment
Zinc coating (anode)
Cathode region
Zn2+ Zn2+
Zn2+ Zn2+
e−
e−
e−
e−
Steel

Figure 16.23 Galvanic protection of steel as provided by a coating of zinc.

For another method of cathodic protection, the source of electrons is an impressed current from an external dc power source, as represented in Figure 16.22*b* for an underground tank. The negative terminal of the power source is connected to the structure to be protected. The other terminal is joined to an inert anode (often graphite), which is, in this case, buried in the soil; high-conductivity backfill material provides good electrical contact between the anode and surrounding soil. A current path exists between the cathode and anode through the intervening soil, completing the electrical circuit. Cathodic protection is especially useful in preventing corrosion of water heaters, underground tanks and pipes, and marine equipment.

16.10 OXIDATION

The discussion of Section 16.2 treated the corrosion of metallic materials in terms of electrochemical reactions that take place in aqueous solutions. In addition, oxidation of metal alloys is also possible in gaseous atmospheres, normally air, wherein an oxide layer or scale forms on the surface of the metal. This phenomenon is frequently termed *scaling, tarnishing,* or *dry corrosion.* In this section possible mechanisms for this type of corrosion, the types of oxide layers that can form, and the kinetics of oxide formation will be discussed.

MECHANISMS

As with aqueous corrosion, the process of oxide layer formation is an electrochemical one, which may be expressed, for divalent metal M, by the following reaction[4]:

$$M + \tfrac{1}{2}O_2 \longrightarrow MO \qquad (16.28)$$

Furthermore, the above reaction consists of oxidation and reduction half-reactions. The former, with the formation of metal ions,

$$M \longrightarrow M^{2+} + 2e^- \qquad (16.29)$$

occurs at the metal–scale interface. The reduction half-reaction produces oxygen ions as follows:

$$\tfrac{1}{2}O_2 + 2e^- \longrightarrow O^{2-} \qquad (16.30)$$

and takes place at the scale–gas interface. A schematic representation of this metal–scale–gas system is shown in Figure 16.24.

For the oxide layer to increase in thickness via Equation 16.28, it is necessary that electrons be conducted to the scale–gas interface, at which point the reduction reaction occurs; in addition, M^{2+} ions must diffuse away from the metal–scale interface, and/or O^{2-} ions must diffuse toward this same interface (Figure 16.24).[5] Thus, the oxide scale serves both as an electrolyte through which ions diffuse and as an electrical circuit for the passage of electrons. Furthermore, the scale may

---

[4] For other than divalent metals, this reaction may be expressed as

$$aM + \frac{b}{2}O_2 \rightarrow M_aO_b \qquad (16.31)$$

[5] Alternatively, electron holes (Section 12.10) and vacancies may diffuse instead of electrons and ions.

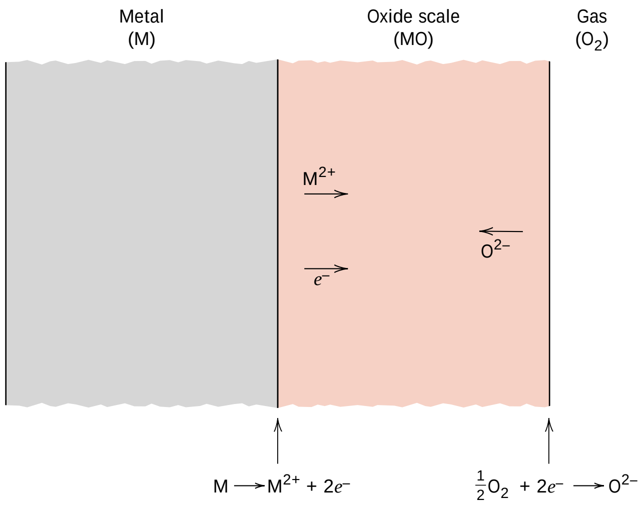
Metal
(M)
Oxide scale
(MO)
Gas
(O_2)
M^{2+}
e^-
O^{2-}
$M \longrightarrow M^{2+} + 2e^-$
$\frac{1}{2}O_2 + 2e^- \longrightarrow O^{2-}$

FIGURE 16.24 Schematic representation of processes that are involved in the gaseous oxidation at a metal surface.

protect the metal from rapid oxidation when it acts as a barrier to ionic diffusion and/or electrical conduction; most metal oxides are highly electrically insulative.

SCALE TYPES

Rate of oxidation (i.e., the rate of film thickness increase) and the tendency of the film to protect the metal from further oxidation are related to the relative volumes of the oxide and metal. The ratio of these volumes, termed the **Pilling–Bedworth ratio,** may be determined from the following expression[6]:

$$\text{P–B ratio} = \frac{A_O \rho_M}{A_M \rho_O} \tag{16.32}$$

where A_O is the molecular (or formula) weight of the oxide, A_M is the atomic weight of the metal, and ρ_O and ρ_M are the oxide and metal densities, respectively. For metals having P–B ratios less than unity, the oxide film tends to be porous and unprotective because it is insufficient to fully cover the metal surface. If the ratio is greater than unity, compressive stresses result in the film as it forms. For a ratio greater than 2–3, the oxide coating may crack and flake off, continually exposing a fresh and unprotected metal surface. The ideal P–B ratio for the formation of a protective oxide film is unity. Table 16.3 presents P–B ratios for metals that form protective coatings and for those that do not. It may be noted from these data that protective coatings normally form for metals having P–B ratios between 1 and 2, whereas nonprotective ones usually result when this ratio is less than 1 or greater than about 2. In addition to the P–B ratio, other factors also influence the oxidation resistance imparted by the film; these include a high degree of adherence between film and metal, comparable coefficients of thermal expansion for metal

---

[6] For other than divalent metals, Equation 16.32 becomes

$$\text{P–B ratio} = \frac{A_O \rho_M}{a A_M \rho_O} \tag{16.33}$$

where a is the coefficient of the metal species for the overall oxidation reaction described by Equation 16.31.

Table 16.3 **Pilling–Bedworth Ratios for a Number of Metals**

Protective		*Nonprotective*	
Ce	1.16	K	0.45
Al	1.28	Li	0.57
Pb	1.40	Na	0.57
Ni	1.52	Cd	1.21
Be	1.59	Ag	1.59
Pd	1.60	Ti	1.95
Cu	1.68	Ta	2.33
Fe	1.77	Sb	2.35
Mn	1.79	Nb	2.61
Co	1.99	U	3.05
Cr	1.99	Mo	3.40
Si	2.27	W	3.40

Source: B. Chalmers, *Physical Metallurgy*. Copyright © 1959 by John Wiley & Sons, New York. Reprinted by permission of John Wiley & Sons, Inc.

and oxide, and, for the oxide, a relatively high melting point and good high-temperature plasticity.

Several techniques are available for improving the oxidation resistance of a metal. One involves application of a protective surface coating of another material that adheres well to the metal and also is itself resistant to oxidation. In some instances, the addition of alloying elements will form a more adherent and protective oxide scale by virtue of producing a more favorable Pilling–Bedworth ratio and/or improving other scale characteristics.

KINETICS

One of the primary concerns relative to metal oxidation is the rate at which the reaction progresses. Inasmuch as the oxide scale reaction product normally remains on the surface, the rate of reaction may be determined by measuring the weight gain per unit area as a function of time.

When the oxide that forms is nonporous and adheres to the metal surface, the rate of layer growth is controlled by ionic diffusion. A *parabolic* relationship exists between the weight gain per unit area W and the time t as follows:

$$W^2 = K_1 t + K_2 \tag{16.34}$$

where K_1 and K_2 are time-independent constants at a given temperature. This weight gain–time behavior is plotted schematically in Figure 16.25. The oxidation of iron, copper, and cobalt follows this rate expression.

In the oxidation of metals for which the scale is porous or flakes off (i.e., for P–B ratios less than about 1 or greater than about 2), the oxidation rate expression is *linear;* that is,

$$W = K_3 t \tag{16.35}$$

where K_3 is a constant. Under these circumstances oxygen is always available for reaction with an unprotected metal surface because the oxide does not act as a

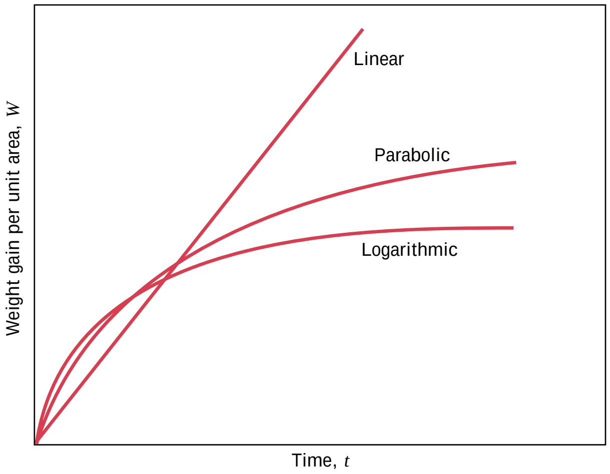

Figure 16.25 Oxidation film growth curves for linear, parabolic, and logarithmic rate laws.

reaction barrier. Sodium, potassium, and tantalum oxidize according to this rate expression and, incidentally, have P–B ratios significantly different from unity (Table 16.3). Linear growth rate kinetics is also represented in Figure 16.25.

Still a third reaction rate law has been observed for very thin oxide layers [generally less than 100 nm (1000 Å)] that form at relatively low temperatures. The dependence of weight gain on time is *logarithmic* and takes the form

$$W = K_4 \log(K_5 t + K_6) \tag{16.36}$$

Again, the K's are constants. This oxidation behavior, also shown in Figure 16.25, has been observed for aluminum, iron, and copper at near-ambient temperatures.

CORROSION OF CERAMIC MATERIALS

Ceramic materials, being compounds between metallic and nonmetallic elements, may be thought of as having already been corroded. Thus, they are exceedingly immune to corrosion by almost all environments, especially at room temperature. Corrosion of ceramic materials generally involves simple chemical dissolution, in contrast to the electrochemical processes found in metals, as described above.

Ceramic materials are frequently utilized because of their resistance to corrosion. Glass is often used to contain liquids for this reason. Refractory ceramics must not only withstand high temperatures and provide thermal insulation but, in many instances, must resist high-temperature attack by molten metals, salts, slags, and glasses. Some of the new technology schemes for convering energy from one form to another that is more useful require relatively high temperatures, corrosive atmospheres, and pressures above the ambient. Ceramic materials are much better suited to withstand most of these environments for reasonable time periods than are metals.

DEGRADATION OF POLYMERS

Polymeric materials also experience deterioration by means of environmental interactions. However, an undesirable interaction is specified as degradation rather than corrosion because the processes are basically dissimilar. Whereas most metallic corrosion reactions are electrochemical, by contrast, polymeric degradation is physiochemical; that is, it involves physical as well as chemical phenomena. Furthermore, a wide variety of reactions and adverse consequences are possible for polymer degradation. Polymers may deteriorate by swelling and dissolution. Covalent bond rupture, as a result of heat energy, chemical reactions, and radiation is also possible, ordinarily with an attendant reduction in mechanical integrity. It should also be mentioned that because of the chemical complexity of polymers, their degradation mechanisms are not well understood.

To briefly cite a couple of examples of polymer degradation, polyethylene, if exposed to high temperatures in an oxygen atmosphere, suffers an impairment of its mechanical properties by becoming brittle. Or, the utility of polyvinyl chloride may be limited because this material may become colored when exposed to high temperatures, although such environments do not affect its mechanical characteristics.

16.11 Swelling and Dissolution

When polymers are exposed to liquids, the main forms of degradation are swelling and dissolution. With swelling, the liquid or solute diffuses into and is absorbed within the polymer; the small solute molecules fit into and occupy positions among the polymer molecules. This forces the macromolecules apart such that the specimen expands or swells. Furthermore, this increase in chain separation results in a reduction of the secondary intermolecular bonding forces; as a consequence, the material becomes softer and more ductile. The liquid solute also lowers the glass transition temperature and, if depressed below the ambient temperature, will cause a once strong material to become rubbery and weak.

Swelling may be considered to be a partial dissolution process in which there is only limited solubility of the polymer in the solvent. Dissolution, which occurs when the polymer is completely soluble, may be thought of as just a continuation of swelling. As a rule of thumb, the greater the similarity of chemical structure between the solvent and polymer, the greater the likelihood of swelling and/or dissolution. For example, many hydrocarbon rubbers readily absorb hydrocarbon liquids such as gasoline. The responses of selected polymeric materials to organic solvents are contained in Tables 16.4 and 16.5.

Swelling and dissolution traits also are affected by temperature as well as characteristics of the molecular structure. In general, increasing molecular weight, increasing degree of crosslinking and crystallinity, and decreasing temperature result in a reduction of these deteriorative processes.

Resistance to attack by acidic and alkaline solutions is, in general, much better for polymers than for metals. A qualitative comparison of the behavior of various polymers in these solutions is also presented in Tables 16.4 and 16.5. Materials that exhibit outstanding resistance to attack by both solution types include polytetrafluoroethylene (and other fluorocarbons) and polyetheretherketone.

16.12 Bond Rupture

Polymers may also experience degradation by a process termed **scission**—the severence or rupture of molecular chain bonds. This causes a separation of chain segments at the point of scission and a reduction in the molecular weight. As previously discussed (Chapter 8), several properties of polymeric materials, including mechanical strength, depend on molecular weight. Consequently, some of the

Table 16.4 **Resistance to Degradation by Various Environments for Selected Plastic Materials**[a]

Material	*Nonoxidizing Acids (20% H_2SO_4)*	*Oxidizing Acids (10% HNO_3)*	*Aqueous Salt Solutions (NaCl)*	*Aqueous Alkalis (NaOH)*	*Polar Solvents (C_2H_5OH)*	*Nonpolar Solvents (C_6H_6)*	*Water*
Polytetrafluoroethylene	S	S	S	S	S	S	S
Nylon 6,6	U	U	S	S	Q	S	S
Polycarbonate	Q	U	S	U	S	U	S
Polyester	Q	Q	S	Q	Q	U	S
Polyetheretherketone	S	S	S	S	S	S	S
Low-density polyethylene	S	Q	S	—	S	Q	S
High-density polyethylene	S	Q	S	—	S	Q	S
Polyethylene terephthalate	S	Q	S	S	S	S	S
Polyphenylene oxide	S	Q	S	S	S	U	S
Polypropylene	S	Q	S	S	S	Q	S
Polystyrene	S	Q	S	S	S	U	S
Polyurethane	Q	U	S	Q	U	Q	S
Epoxy	S	U	S	S	S	S	S
Silicone	Q	U	S	S	S	Q	S

[a] S = satisfactory; Q = questionable; U = unsatisfactory.

Source: Adapted from R. B. Seymour, *Polymers for Engineering Applications,* ASM International, Materials Park, OH, 1987.

Table 16.5 **Resistance to Degradation by Various Environments for Selected Elastomeric Materials**[a]

Material	*Weather-Sunlight Aging*	*Oxidation*	*Ozone Cracking*	*Alkali Dilute/Concentrated*	*Acid Dilute/Concentrated*	*Chlorinated Hydrocarbons, Degreasers*	*Aliphatic Hydrocarbons, Kerosene, Etc.*	*Animal, Vegetable Oils*
Polyisoprene (natural)	D	B	NR	A/C-B	A/C-B	NR	NR	D-B
Polyisoprene (synthetic)	NR	B	NR	C-B/C-B	C-B/C-B	NR	NR	D-B
Butadiene	D	B	NR	C-B/C-B	C-B/C-B	NR	NR	D-B
Styrene-butadiene	D	C	NR	C-B/C-B	C-B/C-B	NR	NR	D-B
Neoprene	B	A	A	A/A	A/A	D	C	B
Nitrile (high)	D	B	C	B/B	B/B	C-B	A	B
Silicone (polysiloxane)	A	A	A	A/A	B/C	NR	D-C	A

[a] A = excellent, B = good, C = fair, D = use with caution, NR = not recommended.

Source: *Compound Selection and Service Guide,* Seals Eastern, Inc., Red Bank, NJ, 1977.

physical and chemical properties of polymers may be adversely affected by this form of degradation. Bond rupture may result from exposure to radiation or to heat, and from chemical reaction.

RADIATION EFFECTS

Certain types of radiation (electron beams, x-rays, β- and γ-rays, and ultraviolet radiation) possess sufficient energy to penetrate a polymer specimen and interact with the constituent atoms or their electrons. One such reaction is *ionization*, in which the radiation removes an orbital electron from a specific atom, converting that atom into a positively charged ion. As a consequence, one of the covalent bonds associated with the specific atom is broken, and there is a rearrangement of atoms or groups of atoms at that point. This bond breaking leads to either scission or crosslinking at the ionization site, depending on the chemical structure of the polymer and also on the dose of radiation. Stabilizers (Section 14.12) may be added to protect polymers from ultraviolet damage.

Not all consequences of radiation exposure are deleterious. Crosslinking may be induced by irradiation to improve the mechanical behavior and degradation characteristics. For example, γ-radiation is used commercially to crosslink polyethylene to enhance its resistance to softening and flow at elevated temperatures; indeed, this process may be carried out on products that have already been fabricated.

CHEMICAL REACTION EFFECTS

Oxygen, ozone, and other substances can cause or accelerate chain scission as a result of chemical reaction. This effect is especially prevalent in vulcanized rubbers that have doubly bonded carbon atoms along the backbone molecular chains, and which are exposed to ozone (O_3), an atmospheric pollutant. One such scission reaction may be represented by

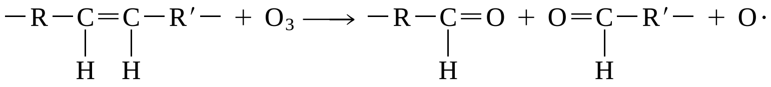

$$-\mathrm{R}-\underset{\mathrm{H}}{\underset{|}{\mathrm{C}}}=\underset{\mathrm{H}}{\underset{|}{\mathrm{C}}}-\mathrm{R}'- + \mathrm{O}_3 \longrightarrow -\mathrm{R}-\underset{\mathrm{H}}{\underset{|}{\mathrm{C}}}=\mathrm{O} + \mathrm{O}=\underset{\mathrm{H}}{\underset{|}{\mathrm{C}}}-\mathrm{R}'- + \mathrm{O}\cdot \tag{16.37}$$

where the chain is severed at the point of the double bond; R and R′ represent groups of atoms bonded to the chain that are unaffected during the reaction. Ordinarily, if the rubber is in an unstressed state, a film will form on the surface, protecting the bulk material from any further reaction. However, when these materials are subjected to tensile stresses, cracks and crevices form and grow in a direction perpendicular to the stress; eventually, rupture of the material may occur. Apparently these cracks result from large numbers of ozone-induced scissions. The elastomers in Table 16.5 are rated as to their resistance to degradation by exposure to ozone.

THERMAL EFFECTS

Thermal degradation corresponds to the scission of molecular chains at elevated temperatures; as a consequence, some polymers undergo chemical reactions in which gaseous species are produced. These reactions are evidenced by a weight loss of material; a polymer's thermal stability is a measure of its resilience to this decomposition. Thermal stability is related primarily to the magnitude of the bonding energies between the various atomic constituents of the polymer: higher bonding energies result in more thermally stable materials. For example, the magnitude of the C—F bond is greater than that of the C—H bond, which in turn is greater than that of the C—Cl bond. The fluorocarbons, having C—F bonds, are among the most thermally resistant polymeric materials and may be utilized at relatively high temperatures.

16.13 WEATHERING

Many polymeric materials serve in applications that require exposure to outdoor conditions. Any resultant degradation is termed *weathering*, which may, in fact, be a combination of several different processes. Under these conditions deterioration is primarily a result of oxidation, which is initiated by ultraviolet radiation from the sun. Some polymers such as nylon and cellulose are also susceptible to water absorption, which produces a reduction in their hardness and stiffness. Resistance to weathering among the various polymers is quite diverse. The fluorocarbons are virtually inert under these conditions; but some materials, including polyvinyl chloride and polystyrene, are susceptible to weathering.

SUMMARY

Metallic corrosion is ordinarily electrochemical, involving both oxidation and reduction reactions. Oxidation is the loss of the metal atom's valence electrons; the resulting metal ions may either go into the corroding solution or form an insoluble compound. During reduction, these electrons are transferred to at least one other chemical species. The character of the corrosion environment dictates which of several possible reduction reactions will occur.

Not all metals oxidize with the same degree of ease, which is demonstrated with a galvanic couple; when in an electrolyte, one metal (the anode) will corrode, whereas a reduction reaction will occur at the other metal (the cathode). The magnitude of the electric potential that is established between anode and cathode is indicative of the driving force for the corrosion reaction.

The standard emf and galvanic series are simply rankings of metallic materials on the basis of their tendency to corrode when coupled to other metals. For the standard emf series, ranking is based on the magnitude of the voltage generated when the standard cell of a metal is coupled to the standard hydrogen electrode at 25°C (77°F). The galvanic series consists of the relative reactivities of metals and alloys in seawater.

The half-cell potentials in the standard emf series are thermodynamic parameters that are valid only at equilibrium; corroding systems are not in equilibrium. Furthermore, the magnitudes of these potentials provide no indication as to the rates at which corrosion reactions occur.

The rate of corrosion may be expressed as corrosion penetration rate, that is, the thickness loss of material per unit of time. Mils per year and millimeters per year are the common units for this parameter. Alternatively, rate is proportional to the current density associated with the electrochemical reaction.

Corroding systems will experience polarization, which is the displacement of each electrode potential from its equilibrium value; the magnitude of the displacement is termed the overvoltage. The corrosion rate of a reaction is limited by polarization, of which there are two types—activation and concentration. Polarization data are plotted as potential versus the logarithm of current density. The corrosion rate for a particular reaction may be computed using the current density associated with the intersection point of oxidation and reduction polarization curves.

A number of metals and alloys passivate, or lose their chemical reactivity, under some environmental circumstances. This phenomenon is thought to involve the formation of a thin protective oxide film. Stainless steels and aluminum alloys exhibit this type of behavior. The active-to-passive behavior may be explained by the alloy's S-shaped electrochemical potential-versus-log current density curve. Intersections with reduction polarization curves in active and passive regions correspond, respectively, to high and low corrosion rates.

Metallic corrosion is sometimes classified into eight different forms: uniform attack, galvanic corrosion, crevice corrosion, pitting, intergranular corrosion, selective leaching, erosion–corrosion, and stress corrosion. Hydrogen embrittlement, a type of failure sometimes observed in corrosion environments, was also discussed.

The measures that may be taken to prevent, or at least reduce, corrosion include material selection, environmental alteration, the use of inhibitors, design changes, application of coatings, and cathodic protection.

Oxidation of metallic materials by electrochemical action is also possible in dry, gaseous atmospheres. An oxide film forms on the surface which may act as a barrier to further oxidation if the volumes of metal and oxide film are similar, that is, if the Pilling–Bedworth ratio is near unity. The kinetics of film formation may follow parabolic, linear, or logarithmic rate laws.

Ceramic materials, being inherently corrosion resistant, are frequently utilized at elevated temperatures and/or in extremely corrosive environments.

Polymeric materials deteriorate by noncorrosive processes. Upon exposure to liquids, they may experience degradation by swelling or dissolution. With swelling, solute molecules actually fit into the molecular structure. Scission, or the severance of molecular chain bonds, may be induced by radiation, chemical reactions, or heat. This results in a reduction of molecular weight and a deterioration of the physical and chemical properties of the polymer.

IMPORTANT TERMS AND CONCEPTS

Activation polarization
Anode
Cathode
Cathodic protection
Concentration polarization
Corrosion
Corrosion penetration rate
Crevice corrosion
Degradation
Electrolyte
Electromotive force (emf) series
Erosion–corrosion
Galvanic corrosion
Galvanic series
Hydrogen embrittlement
Inhibitor
Intergranular corrosion
Molarity
Oxidation
Passivity
Pilling–Bedworth ratio
Pitting
Polarization
Reduction
Sacrificial anode
Scission
Selective leaching
Standard half-cell
Stress corrosion
Weld decay

REFERENCES

ASM Handbook, Vol. 13, *Corrosion,* ASM International, Materials Park, OH, 1987.

Craig, B. D. (Editor), *Handbook of Corrosion Data,* 2nd edition, ASM International, Materials Park, OH, 1995.

Fontana, M. G., *Corrosion Engineering,* 3rd edition, McGraw-Hill Book Company, New York, 1986.

Fontana, M. G. and R. W. Staehle (Editors), *Advances in Corrosion Science and Technology,* Plenum Publishing Corp., New York. In seven volumes, 1970–1980.

Gibala, R. and R. F. Hehemann, *Hydrogen Embrittlement and Stress Corrosion Cracking,* ASM International, Materials Park, OH, 1984.

Jones, D. A., *Principles and Prevention of Corrosion,* 2nd edition, Prentice Hall, Upper Saddle, NJ, 1996.

Marcus, P. and J. Oudar (Editors), *Corrosion Mechanisms in Theory and Practice,* Marcel Dekker, Inc., New York, 1995.

McEvily, A. J., Jr. (Editor), *Atlas of Stress-Corrosion and Corrosion Fatigue Curves,* ASM International, Materials Park, OH, 1990.

Schreir, L. L. (Editor), *Corrosion,* Vol. 1, *Metal/Environment Reactions;* Vol. 2, *Corrosion Control,* 3rd edition, Butterworth-Heinemann Ltd., Oxford, 1994.

Schweitzer, P. A. (Editor), *Corrosion and Corrosion Protection Handbook,* 2nd edition, Marcel Dekker, Inc., New York, 1989.

Schweitzer, P., *Corrosion Resistance Tables,* 4th edition, Marcel Dekker, Inc., New York, 1995. In three volumes.

Uhlig, H. H. and R. W. Revie, *Corrosion and Corrosion Control,* 3rd edition, NACE International, Houston, TX, 1995.

QUESTIONS AND PROBLEMS

16.1 **(a)** Briefly explain the difference between oxidation and reduction electrochemical reactions.

(b) Which reaction occurs at the anode, and which at the cathode?

16.2 **(a)** Write the possible oxidation and reduction half-reactions that occur when magnesium is immersed in each of the following solutions: (i) HCl, (ii) an HCl solution containing dissolved oxygen, (iii) an HCl solution containing dissolved oxygen and, in addition, Fe^{2+} ions.

(b) In which of these solutions would you expect the magnesium to oxidize most rapidly? Why?

16.3 Would you expect iron to corrode in water of high purity? Why or why not?

16.4 Demonstrate that **(a)** the value of $\mathscr{F}$ in Equation 16.19 is 96,500 C/mol, and **(b)** at 25°C (298 K),

$$\frac{RT}{n\mathscr{F}}\ln x = \frac{0.0592}{n}\log x$$

16.5 **(a)** Compute the voltage at 25°C of an electrochemical cell consisting of pure cadmium immersed in a $2 \times 10^{-3}M$ solution of Cd^{2+} ions, and pure iron in a $0.4M$ solution of Fe^{2+} ions.

(b) Write the spontaneous electrochemical reaction.

16.6 A Zn/Zn^{2+} concentration cell is constructed in which both electrodes are pure zinc. The Zn^{2+} concentration for one cell half is $1.0M$, for the other, $10^{-2}M$. Is a voltage generated between the two cell halves? If so, what is its magnitude and which electrode will be oxidized? If no voltage is produced, explain this result.

16.7 An electrochemical cell is composed of pure copper and pure lead electrodes immersed in solutions of their respective divalent ions. For a $0.6M$ concentration, of Cu^{2+}, the lead electrode is oxidized yielding a cell potential of 0.507 V. Calculate the concentration of Pb^{2+} ions if the temperature is 25°C.

16.8 An electrochemical cell is constructed such that on one side a pure nickel electrode is in contact with a solution containing Ni^{2+} ions at a concentration of 3×10^{-3} M. The other cell half consists of a pure Fe electrode that is immersed in a solution of Fe^{2+} ions having a concentration of 0.1 M. At what temperature will the potential between the two electrodes be $+0.140$ V?

16.9 Modify Equation 16.19 for the case in which metals M_1 and M_2 are alloys.

16.10 For the following pairs of alloys that are coupled in seawater, predict the possibility of corrosion; if corrosion is probable, note which alloy will corrode.

(a) Aluminum and magnesium.

(b) Zinc and a low-carbon steel.

(c) Brass (60Cu-40Zn) and Monel (70Ni-30Cu).

(d) Titanium and 304 stainless steel.

(e) Cast iron and 316 stainless steel.

16.11 **(a)** From the galvanic series (Table 16.2), cite three metals or alloys that may be used to galvanically protect nickel in the active state.

(b) Sometimes galvanic corrosion is prevented by making an electrical contact between both metals in the couple and a third metal that is anodic to these other two. Using the galvanic series, name one metal that could be used to protect a copper–aluminum galvanic couple.

16.12 Demonstrate that the constant K in Equation 16.23 will have values of 534 and 87.6 for the CPR in units of mpy and mm/yr, respectively.

16.13 A piece of corroded steel plate was found in a submerged ocean vessel. It was estimated that the original area of the plate was 10 in.^{2} and that approximately 2.6 kg had corroded away during the submersion. Assuming a corrosion penetration rate of 200 mpy for this alloy in seawater, estimate the time of submersion in years. The density of steel is 7.9 g/cm^3.

16.14 A thick steel sheet of area 400 cm^2 is exposed to air near the ocean. After a one-year period it was found to experience a weight loss of 375 g due to corrosion. To what rate of corrosion, in both mpy and mm/yr, does this correspond?

16.15 **(a)** Demonstrate that the CPR is related to the corrosion current density i (A/cm^2) through the expression

$$\text{CPR} = \frac{KAi}{n\rho} \tag{16.38}$$

where K is a constant, A is the atomic weight of the metal experiencing corrosion, n is the number of electrons associated with the ionization of each metal atom, and ρ is the density of the metal.

(b) Calculate the value of the constant K for the CPR in mpy and i in μA/cm^2 (10^{-6} A/cm^2).

16.16 Using the results of Problem 16.15, compute the corrosion penetration rate, in mpy, for the corrosion of iron in citric acid (to form Fe^{2+} ions) if the corrosion current density is 1.15×10^{-5} A/cm^2.

16.17 **(a)** Cite the major differences between activation and concentration polarizations.

(b) Under what conditions is activation polarization rate controlling?

(c) Under what conditions is concentration polarization rate controlling?

16.18 **(a)** Describe the phenomenon of dynamic equilibrium as it applies to oxidation and reduction electrochemical reactions.

(b) What is the exchange current density?

16.19 Briefly explain why concentration polarization is not normally rate controlling for oxidation reactions.

16.20 Lead experiences corrosion in an acid solution according to the reaction

$$Pb + 2H^+ \longrightarrow Pb^{2+} + H_2$$

The rates of both oxidation and reduction half-reactions are controlled by activation polarization.

(a) Compute the rate of oxidation of Pb (in mol/cm^2-s) given the following activation polarization data:

For Lead	***For Hydrogen***
$V_{(Pb/Pb^{2+})} = -0.126$ V	$V_{(H^+/H_2)} = 0$ V
$i_0 = 2 \times 10^{-9}$ A/cm^2	$i_0 = 1.0 \times 10^{-8}$ A/cm^2
$\beta = +0.12$	$\beta = -0.10$

(b) Compute the value of the corrosion potential.

16.21 The corrosion rate is to be determined for some divalent metal M in a solution containing hydrogen ions. The following corrosion data are known about the metal and solution:

For Metal M	***For Hydrogen***
$V_{(M/M^{2+})} = -0.47$ V	$V_{(H^+/H_2)} = 0$ V
$i_0 = 5 \times 10^{-10}$ A/cm^2	$i_0 = 2 \times 10^{-9}$ A/cm^2
$\beta = +0.15$	$\beta = -0.12$

(a) Assuming that activation polarization controls both oxidation and reduction reactions, determine the rate of corrosion of metal M (in mol/cm^2-s).

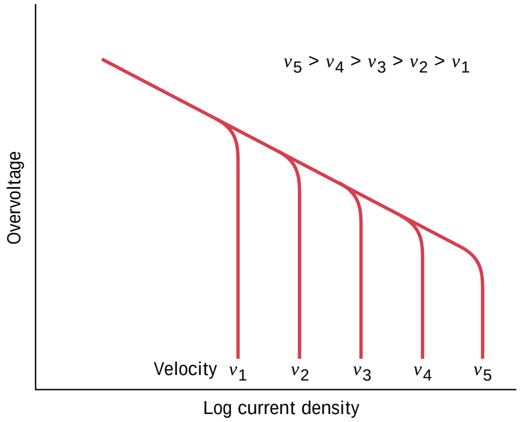

Figure 16.26 Plot of overvoltage versus logarithm of current density for a solution that experiences combined activation–concentration polarization at various solution velocities.

(b) Compute the corrosion potential for this reaction.

16.22 The influence of increasing solution velocity on the overvoltage-versus-log current density behavior for a solution that experiences combined activation–concentration polarization is indicated in Figure 16.26. On the basis of this behavior, make a schematic plot of corrosion rate versus solution velocity for the oxidation of a metal; assume that the oxidation reaction is controlled by activation polarization.

16.23 Briefly describe the phenomenon of passivity. Name two common types of alloy that passivate.

16.24 Why does chromium in stainless steels make them more corrosion resistant in many environments than plain carbon steels?

16.25 For each form of corrosion, other than uniform, do the following:

(a) describe why, where, and the conditions under which the corrosion occurs; and

(b) cite three measures that may be taken to prevent or control it.

16.26 Cite two examples of the beneficial use of galvanic corrosion.

16.27 Briefly explain why cold-worked metals are more susceptible to corrosion than noncold-worked metals.

16.28 Briefly explain why, for a small anode-to-cathode area ratio, the corrosion rate will be higher than for a large ratio.

16.29 For a concentration cell, briefly explain why corrosion occurs at that region having the lower concentration.

16.30 Is Equation 16.23 equally valid for uniform corrosion and pitting? Why or why not?

16.31 **(a)** What are inhibitors?

(b) What possible mechanisms account for their effectiveness?

16.32 Briefly describe the two techniques that are used for galvanic protection.

16.33 Tin cans are made of a steel the inside of which is coated with a thin layer of tin. The tin protects the steel from corrosion by food products in the same manner as zinc protects steel from atmospheric corrosion. Briefly explain how this cathodic protection of tin cans is possible since tin is electrochemically less active than steel in the galvanic series (Table 16.2).

16.34 For each of the metals listed below, compute the Pilling–Bedworth ratio. Also, on the basis of this value, specify whether or not you would expect the oxide scale that forms on the surface to be protective, and then justify your decision. Density data for both the metal and its oxide are also tabulated.

Metal	*Metal Density (g/cm^3)*	*Metal Oxide*	*Oxide Density (g/cm^3)*
Zr	6.51	ZrO_2	5.89
Sn	7.30	SnO_2	6.95
Bi	9.80	Bi_2O_3	8.90

16.35 According to Table 16.3, the oxide coating that forms on silver should be nonprotective, and yet Ag does not oxidize appreciably at room temperature and in air. How do you explain this apparent discrepancy?

16.36 Below, weight gain-time data for the oxidation of copper at an elevated temperature are tabulated.

W (*mg/cm*^{2})	***Time* (*min*)**
0.316	15
0.524	50
0.725	100

(a) Determine whether the oxidation kinetics obey a linear, parabolic, or logarithmic rate expression.

(b) Now compute *W* after a total time of 450 min.

16.37 Below, weight gain–time data for the oxidation of some metal at an elevated temperature are tabulated.

W (*mg/cm*^{2})	***Time* (*min*)**
4.66	20
11.7	50
41.1	175

(a) Determine whether the oxidation kinetics obey a linear, parabolic, or logarithmic rate expression.

(b) Now compute *W* after a time of 1000 min.

16.38 Below, weight gain–time data for the oxidation of some metal at an elevated temperature are tabulated.

W (*mg/cm*^{2})	***Time* (*min*)**
1.90	25
3.67	75
6.40	250

(a) Determine whether the oxidation kinetics obey a linear, parabolic, or logarithmic rate expression.

(b) Now compute *W* after a time of 3500 min.

16.39 From a molecular perspective, explain why increasing crosslinking and crystallinity of a polymeric material will enhance its resistance to swelling and dissolution. Would you expect crosslinking or crystallinity to have the greater influence? Justify your choice.

16.40 List three differences between the corrosion of metals and

(a) the corrosion of ceramics, and

(b) the degradation of polymers.

Design Problems

16.D1 A brine solution is used as a cooling medium in a steel heat exchanger. The brine is circulated within the heat exchanger and contains some dissolved oxygen. Suggest three methods, other than cathodic protection, for reducing corrosion of the steel by the brine. Explain the rationale for each suggestion.

16.D2 Suggest an appropriate material for each of the following applications, and, if necessary, recommend corrosion prevention measures that should be taken. Justify your suggestions.

(a) Laboratory bottles to contain relatively dilute solutions of nitric acid.

(b) Barrels to contain benzene.

(c) Pipe to transport hot alkaline (basic) solutions.

(d) Underground tanks to store large quantities of high purity water.

(e) Architectural trim for high-rise buildings.

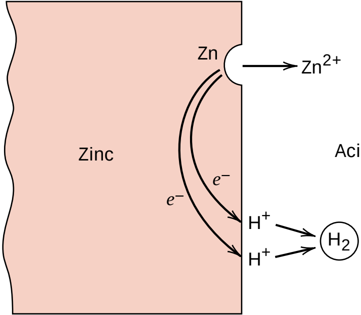
Zn
Zn^{2+}
Zinc
Acid solution
e^-
e^-
H^+
H^+
H_2

FIGURE 16.1 The electrochemical reactions associated with the corrosion of zinc in an acid solution. (From M. G. Fontana, *Corrosion Engineering*, 3rd edition. Copyright © 1986 by McGraw-Hill Book Company. Reproduced with permission.)

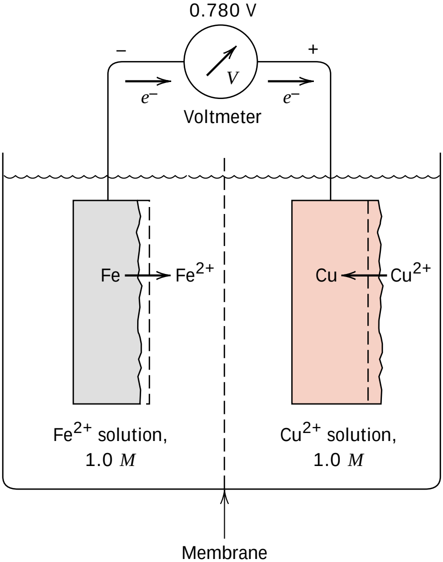
0.780 V
−
+
V
e−
e−
Voltmeter
Fe
Fe2+
Cu
Cu2+
Fe2+ solution,
1.0 M
Cu2+ solution,
1.0 M
Membrane

Figure 16.2 An electrochemical cell consisting of iron and copper electrodes, each of which is immersed in a 1*M* solution of its ion. Iron corrodes while copper electrodeposits.

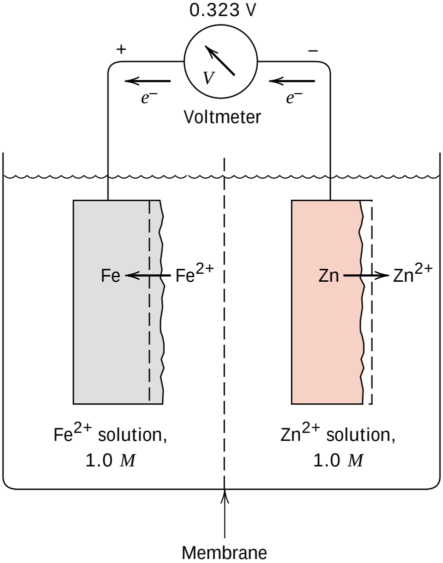
0.323 V
+
−
V
e^-
e^-
Voltmeter
Fe
Fe^{2+}
Zn
Zn^{2+}
Fe^{2+} solution, 1.0 M
Zn^{2+} solution, 1.0 M
Membrane

FIGURE 16.3 An electrochemical cell consisting of iron and zinc electrodes, each of which is immersed in a 1M solution of its ion. The iron electrodeposits while the zinc corrodes.

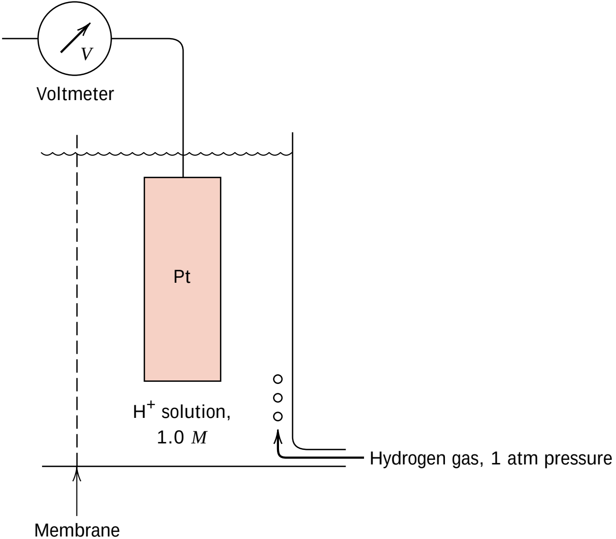
V
Voltmeter
Pt
H+ solution,
1.0 M
Hydrogen gas, 1 atm pressure
Membrane

FIGURE 16.4 The standard hydrogen reference half-cell.

Table 16.1 The Standard emf Series

	Electrode Reaction	*Standard Electrode Potential, V^0 (V)*
	$Au^{3+} + 3e^- \longrightarrow Au$	+1.420
↑	$O_2 + 4H^+ + 4e^- \longrightarrow 2H_2O$	+1.229
	$Pt^{2+} + 2e^- \longrightarrow Pt$	∼+1.2
	$Ag^+ + e^- \longrightarrow Ag$	+0.800
Increasingly inert (cathodic)	$Fe^{3+} + e^- \longrightarrow Fe^{2+}$	+0.771
	$O_2 + 2H_2O + 4e^- \longrightarrow 4(OH^-)$	+0.401
	$Cu^{2+} + 2e^- \longrightarrow Cu$	+0.340
	$2H^+ + 2e^- \longrightarrow H_2$	0.000
	$Pb^{2+} + 2e^- \longrightarrow Pb$	−0.126
	$Sn^{2+} + 2e^- \longrightarrow Sn$	−0.136
	$Ni^{2+} + 2e^- \longrightarrow Ni$	−0.250
	$Co^{2+} + 2e^- \longrightarrow Co$	−0.277
	$Cd^{2+} + 2e^- \longrightarrow Cd$	−0.403
	$Fe^{2+} + 2e^- \longrightarrow Fe$	−0.440
Increasingly active (anodic)	$Cr^{3+} + 3e^- \longrightarrow Cr$	−0.744
	$Zn^{2+} + 2e^- \longrightarrow Zn$	−0.763
	$Al^{3+} + 3e^- \longrightarrow Al$	−1.662
	$Mg^{2+} + 2e^- \longrightarrow Mg$	−2.363
↓	$Na^+ + e^- \longrightarrow Na$	−2.714
	$K^+ + e^- \longrightarrow K$	−2.924

Table 16.2 The Galvanic Series

	Platinum
	Gold
	Graphite
	Titanium
	Silver
	316 Stainless steel (passive) 304 Stainless steel (passive)
↑	Inconel (80Ni–13Cr–7Fe) (passive) Nickel (passive)
Increasingly inert (cathodic)	Monel (70Ni–30Cu) Copper–nickel alloys Bronzes (Cu–Sn alloys) Copper Brasses (Cu–Zn alloys)
	Inconel (active) Nickel (active)
	Tin
	Lead
Increasingly active (anodic)	316 Stainless steel (active) 304 Stainless steel (active)
↓	Cast iron Iron and steel
	Aluminum alloys
	Cadmium
	Commercially pure aluminum
	Zinc
	Magnesium and magnesium alloys

Source: M. G. Fontana, *Corrosion Engineering,* 3rd edition. Copyright 1986 by McGraw-Hill Book Company. Reprinted with permission.

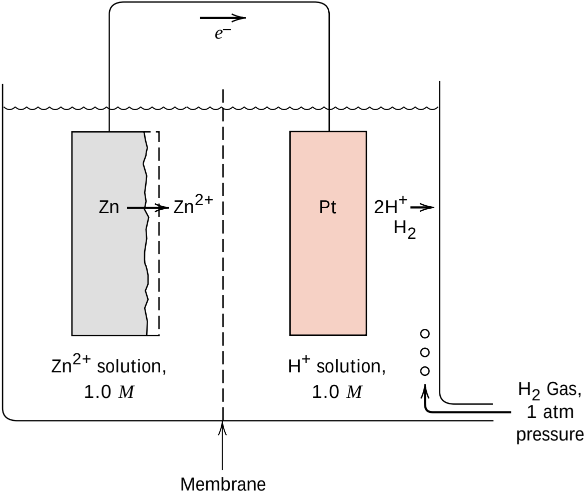
e^-
Zn → Zn^{2+}
Pt
$2H^+$ → H_2
Zn^{2+} solution, 1.0 *M*
H^+ solution, 1.0 *M*
H_2 Gas, 1 atm pressure
Membrane

FIGURE 16.5 Electrochemical cell consisting of standard zinc and hydrogen electrodes that has been short-circuited.

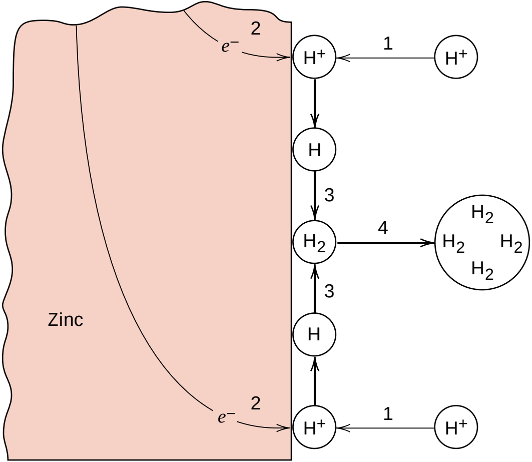
2
e^-
1
H^+
H^+
H
3
H_2
4
H_2
H_2
H_2
H_2
3
Zinc
H
2
e^-
1
H^+
H^+

FIGURE 16.6 Schematic representation of possible steps in the hydrogen reduction reaction, the rate of which is controlled by activation polarization. (From M. G. Fontana, *Corrosion Engineering*, 3rd edition. Copyright © 1986 by McGraw-Hill Book Company. Reproduced with permission.)

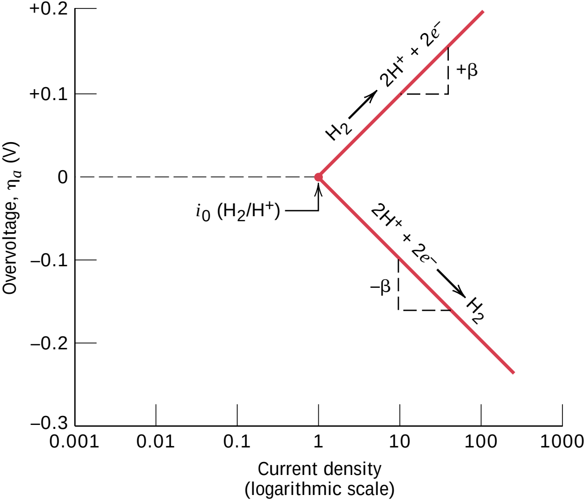

Figure 16.7 For a hydrogen electrode, plot of activation polarization overvoltage versus logarithm of current density for both oxidation and reduction reactions. (Adapted from M. G. Fontana, *Corrosion Engineering*, 3rd edition. Copyright © 1986 by McGraw-Hill Book Company. Reproduced with permission.)

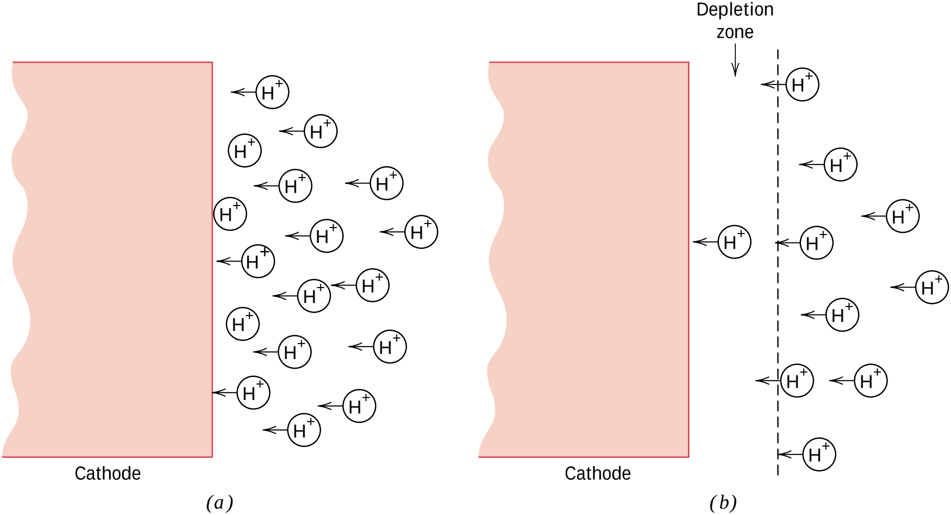

Figure 16.8 For hydrogen reduction, schematic representations of the H^+ distribution in the vicinity of the cathode for (*a*) low reaction rates and/or high concentrations, and (*b*) high reaction rates and/or low concentrations wherein a depletion zone is formed that gives rise to concentration polarization. (Adapted from M. G. Fontana, *Corrosion Engineering*, 3rd edition. Copyright © 1986 by McGraw-Hill Book Company. Reproduced with permission.)

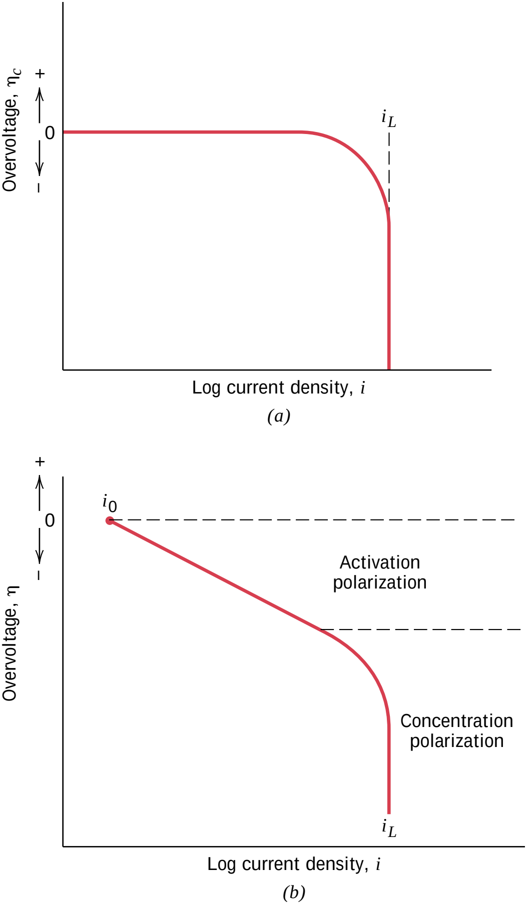

FIGURE 16.9 For reduction reactions, schematic plots of overvoltage versus logarithm of current density for (*a*) concentration polarization, and (*b*) combined activation–concentration polarization.

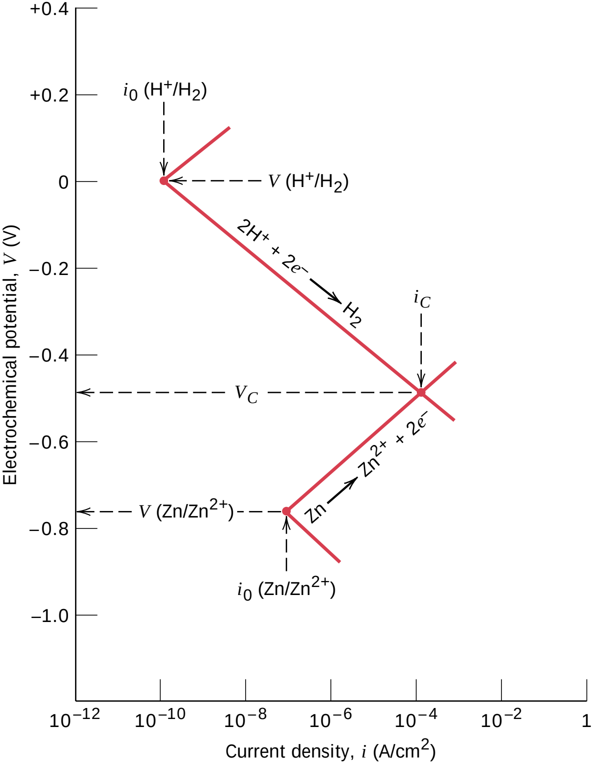

FIGURE 16.10 Electrode kinetic behavior of zinc in an acid solution; both oxidation and reduction reactions are rate limited by activation polarization. (Adapted from M. G. Fontana, *Corrosion Engineering*, 3rd edition. Copyright © 1986 by McGraw-Hill Book Company. Reproduced with permission.)

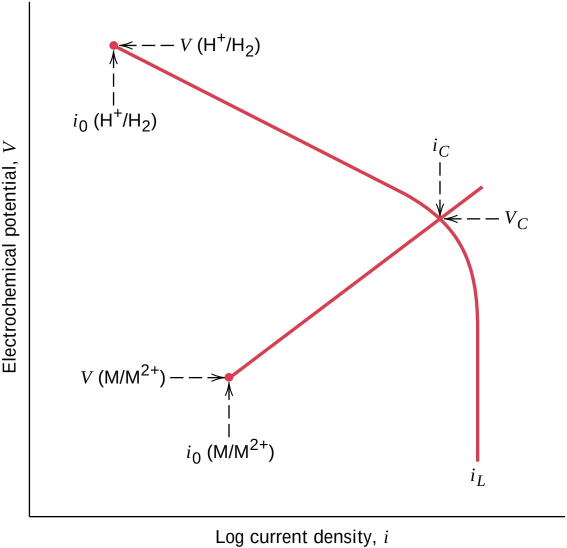

Figure 16.11 Schematic electrode kinetic behavior for metal M; the reduction reaction is under combined activation–concentration polarization control.

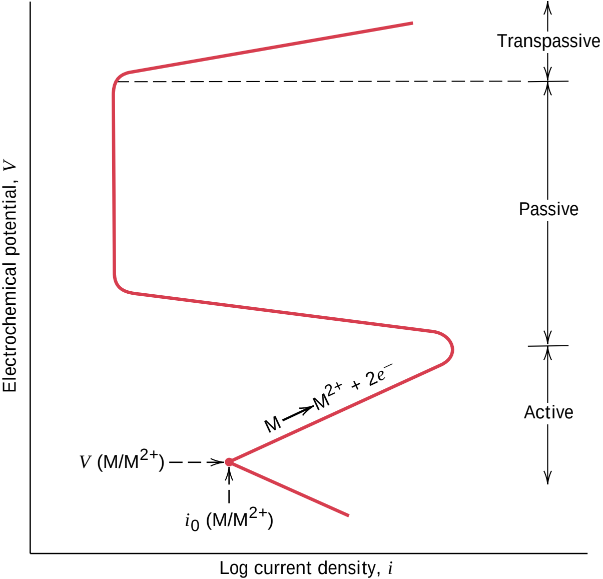

FIGURE 16.12 Schematic polarization curve for a metal that displays an active–passive transition.

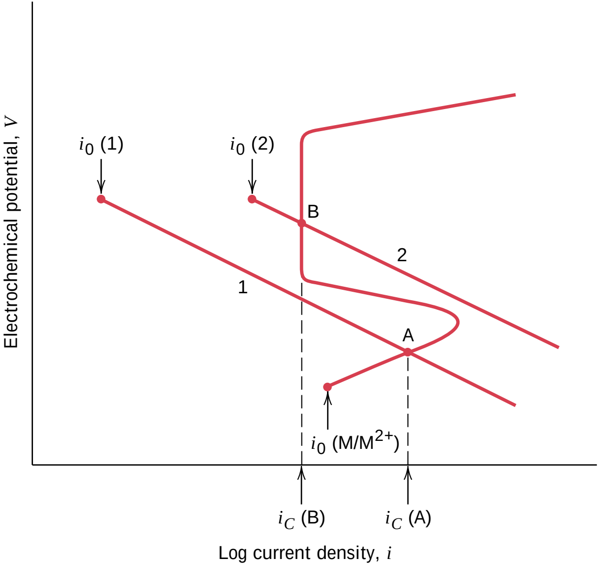

Figure 16.13 Demonstration of how an active–passive metal can exhibit both active and passive corrosion behavior.

FIGURE 16.14
Galvanic corrosion of a magnesium shell that was cast around a steel core. (Photograph courtesy of LaQue Center for Corrosion Technology, Inc.)

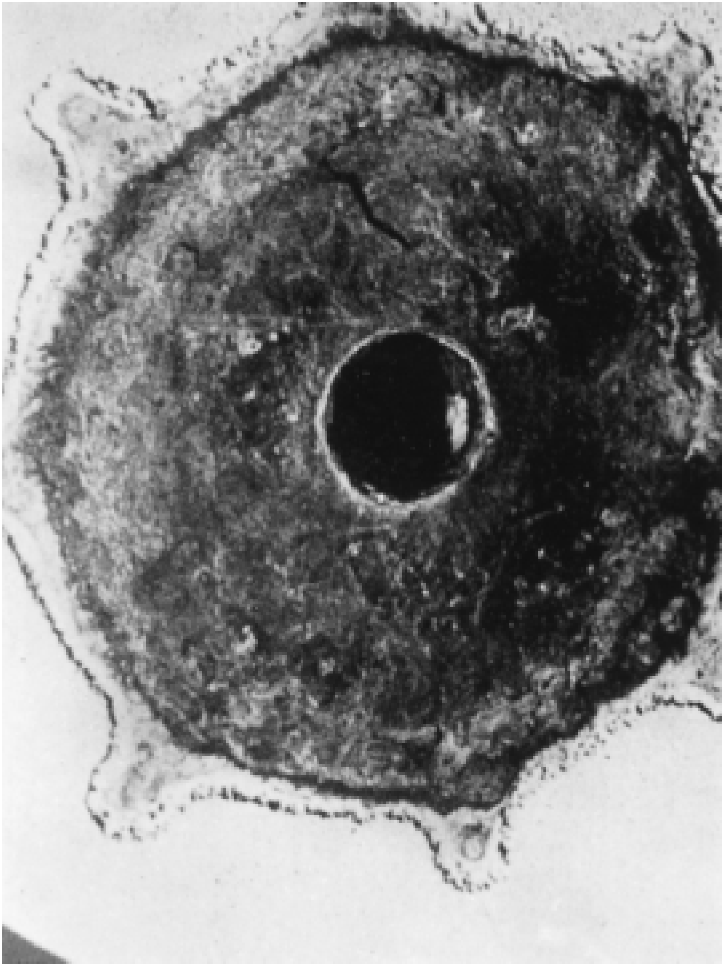

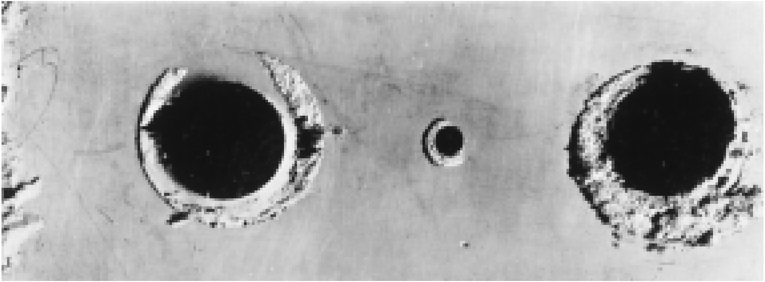

Figure 16.15 On this plate, which was immersed in seawater, crevice corrosion has occurred at the regions that were covered by washers. (Photograph courtesy of LaQue Center for Corrosion Technology, Inc.)

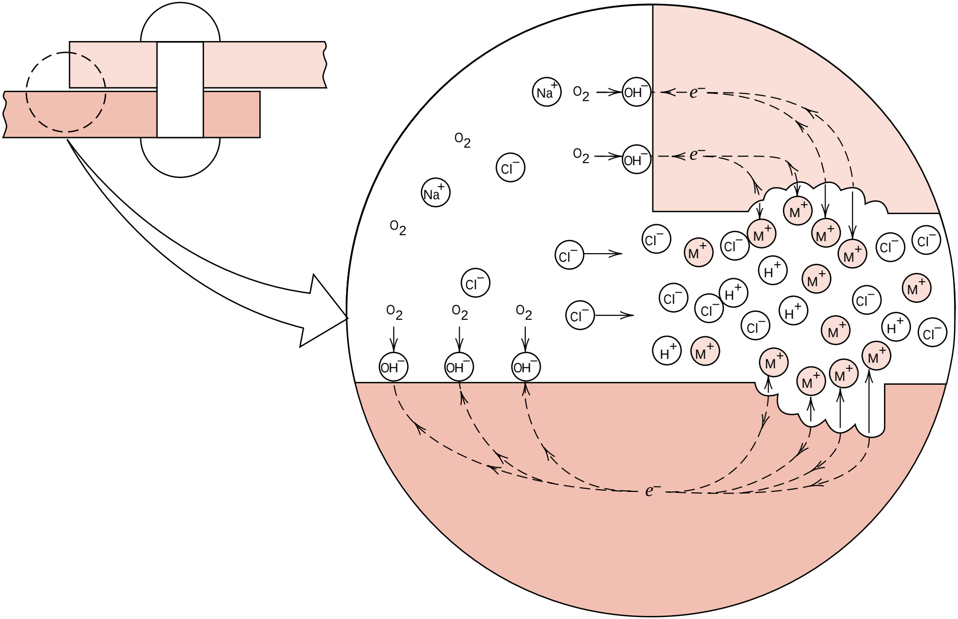
Na+
O2
OH−
e−
O2
Cl−
O2
OH−
e−
Na+
O2
Cl−
M+
Cl−
M+
Cl−
M+
M+
M+
Cl−
Cl−
H+
Cl−
M+
Cl−
H+
Cl−
M+
O2
O2
O2
Cl−
Cl−
H+
Cl−
Cl−
H+
M+
Cl−
OH−
OH−
OH−
H+
M+
M+
M+
M+
M+
e−

FIGURE 16.16 Schematic illustration of the mechanism of crevice corrosion between two riveted sheets. (From M. G. Fontana, *Corrosion Engineering*, 3rd edition. Copyright © 1986 by McGraw-Hill Book Company. Reproduced with permission.)

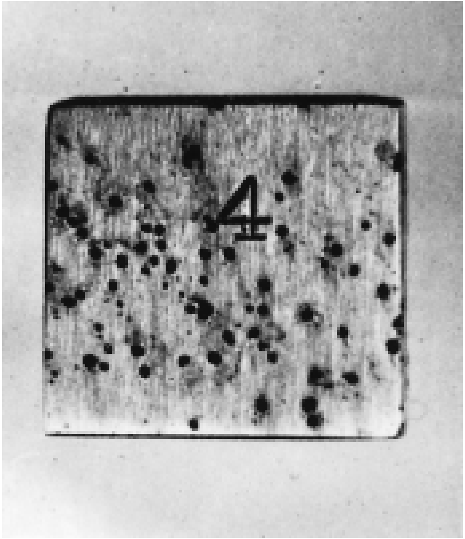

Figure 16.17 The pitting of a 304 stainless steel plate by an acid-chloride solution. (Photograph courtesy of Mars G. Fontana. From M. G. Fontana, *Corrosion Engineering*, 3rd edition. Copyright © 1986 by McGraw-Hill Book Company. Reproduced with permission.)

FIGURE 16.18 Schematic illustration of chromium carbide particles that have precipitated along grain boundaries in stainless steel, and the attendant zones of chromium depletion.

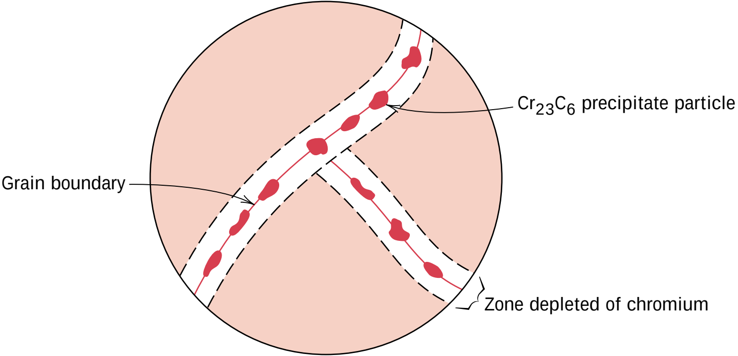
$Cr_{23}C_6$ precipitate particle
Grain boundary
Zone depleted of chromium

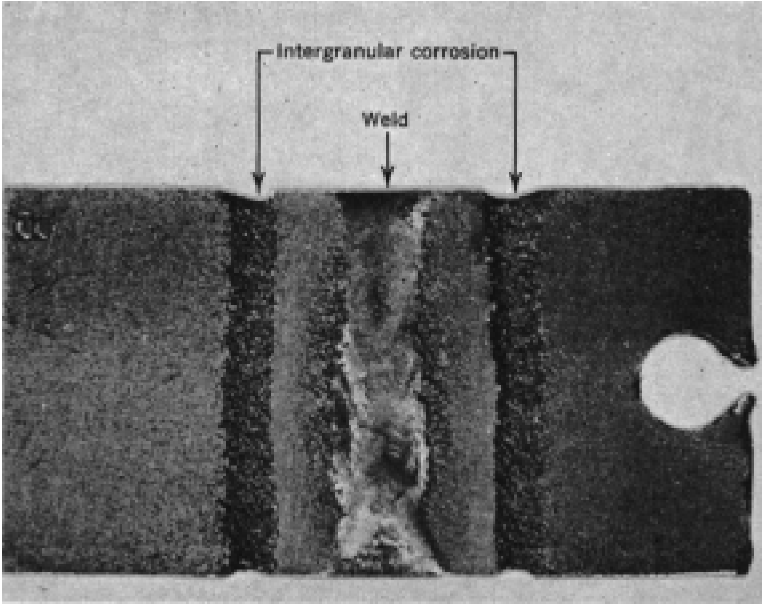

FIGURE 16.19 Weld decay in a stainless steel. The regions along which the grooves have formed were sensitized as the weld cooled. (From H. H. Uhlig and R. W. Revie, *Corrosion and Corrosion Control*, 3rd edition, Fig. 2, p. 307. Copyright © 1985 by John Wiley & Sons, Inc. Reprinted by permission of John Wiley & Sons, Inc.)

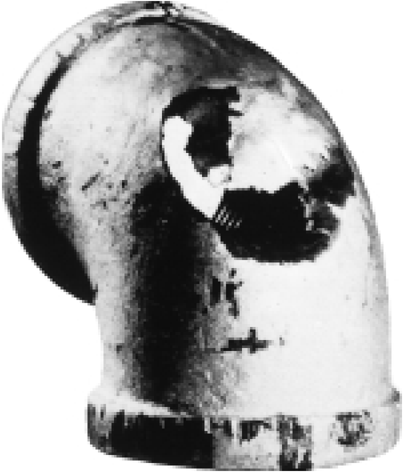

Figure 16.20 Impingement failure of an elbow that was part of a steam condensate line. (Photograph courtesy of Mars G. Fontana. From M. G. Fontana, *Corrosion Engineering*, 3rd edition. Copyright © 1986 by McGraw-Hill Book Company. Reproduced with permission.)

FIGURE 16.21 Photomicrograph showing intergranular stress corrosion cracking in brass. (From H. H. Uhlig and R. W. Revie, *Corrosion and Corrosion Control*, 3rd edition, Fig. 5, p. 335. Copyright 1985 by John Wiley & Sons, Inc. Reprinted by permission of John Wiley & Sons, Inc.)

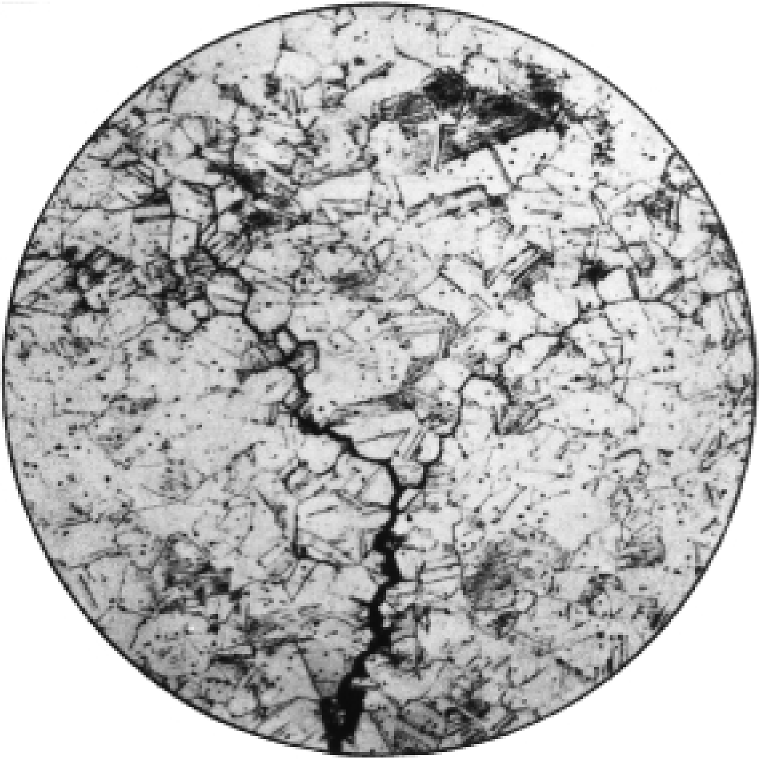

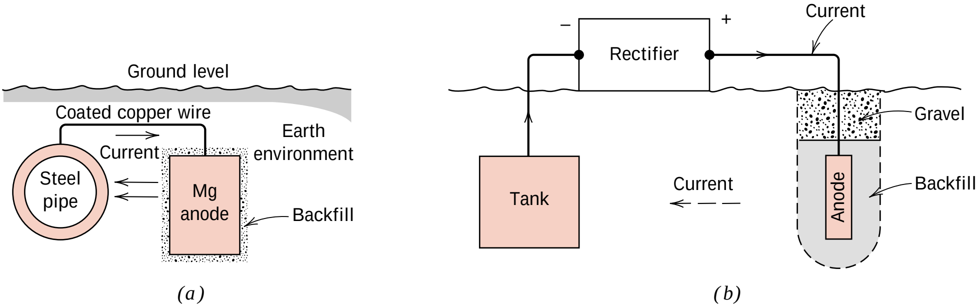
Ground level
Coated copper wire
Current
Steel pipe
Mg anode
Earth environment
Backfill
(a)
Rectifier
−
+
Current
Gravel
Tank
Current
Anode
Backfill
(b)

Figure 16.22 Cathodic protection of (*a*) an underground pipeline using a magnesium sacrificial anode, and (*b*) an underground tank using an impressed current. (From M. G. Fontana, *Corrosion Engineering*, 3rd edition. Copyright © 1986 by McGraw-Hill Book Company. Reproduced with permission.)

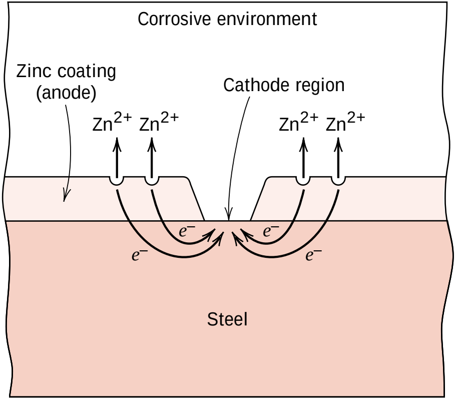
Corrosive environment
Zinc coating (anode)
Cathode region
Zn^{2+} Zn^{2+}
Zn^{2+} Zn^{2+}
e^-
e^-
e^-
e^-
Steel

Figure 16.23 Galvanic protection of steel as provided by a coating of zinc.

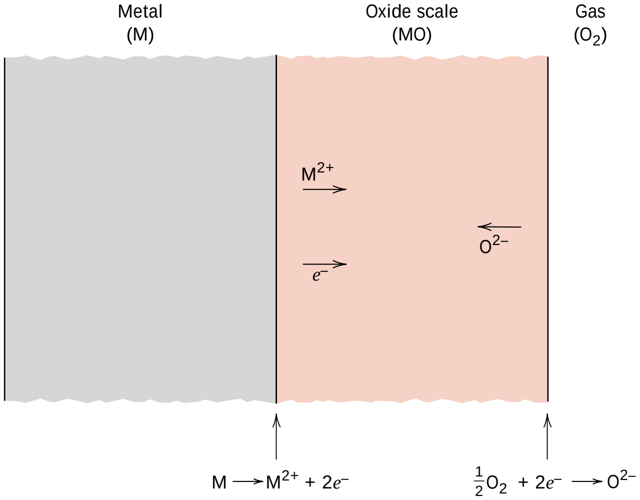
Metal
(M)
Oxide scale
(MO)
Gas
(O_2)
M^{2+}
e^-
O^{2-}
$M \longrightarrow M^{2+} + 2e^-$
$\frac{1}{2}O_2 + 2e^- \longrightarrow O^{2-}$

FIGURE 16.24 Schematic representation of processes that are involved in the gaseous oxidation at a metal surface.

Table 16.3 Pilling–Bedworth Ratios for a Number of Metals

Protective		*Nonprotective*	
Ce	1.16	K	0.45
Al	1.28	Li	0.57
Pb	1.40	Na	0.57
Ni	1.52	Cd	1.21
Be	1.59	Ag	1.59
Pd	1.60	Ti	1.95
Cu	1.68	Ta	2.33
Fe	1.77	Sb	2.35
Mn	1.79	Nb	2.61
Co	1.99	U	3.05
Cr	1.99	Mo	3.40
Si	2.27	W	3.40

Source: B. Chalmers, *Physical Metallurgy*. Copyright © 1959 by John Wiley & Sons, New York. Reprinted by permission of John Wiley & Sons, Inc.

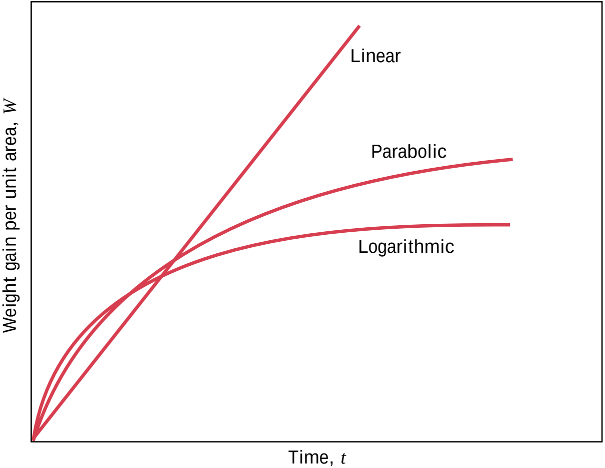

FIGURE 16.25 Oxidation film growth curves for linear, parabolic, and logarithmic rate laws.

Table 16.4 **Resistance to Degradation by Various Environments for Selected Plastic Materials**[a]

Material	*Nonoxidizing Acids ($20\%\ H_2SO_4$)*	*Oxidizing Acids ($10\%\ HNO_3$)*	*Aqueous Salt Solutions (NaCl)*	*Aqueous Alkalis (NaOH)*	*Polar Solvents (C_2H_5OH)*	*Nonpolar Solvents (C_6H_6)*	*Water*
Polytetrafluoroethylene	S	S	S	S	S	S	S
Nylon 6,6	U	U	S	S	Q	S	S
Polycarbonate	Q	U	S	U	S	U	S
Polyester	Q	Q	S	Q	Q	U	S
Polyetheretherketone	S	S	S	S	S	S	S
Low-density polyethylene	S	Q	S	—	S	Q	S
High-density polyethylene	S	Q	S	—	S	Q	S
Polyethylene terephthalate	S	Q	S	S	S	S	S
Polyphenylene oxide	S	Q	S	S	S	U	S
Polypropylene	S	Q	S	S	S	Q	S
Polystyrene	S	Q	S	S	S	U	S
Polyurethane	Q	U	S	Q	U	Q	S
Epoxy	S	U	S	S	S	S	S
Silicone	Q	U	S	S	S	Q	S

[a] S = satisfactory; Q = questionable; U = unsatisfactory.

Source: Adapted from R. B. Seymour, *Polymers for Engineering Applications,* ASM International, Materials Park, OH, 1987.

Table 16.5 Resistance to Degradation by Various Environments for Selected Elastomeric Materials[a]

Material	*Weather-Sunlight Aging*	*Oxidation*	*Ozone Cracking*	*Alkali Dilute/Concentrated*	*Acid Dilute/Concentrated*	*Chlorinated Hydrocarbons, Degreasers*	*Aliphatic Hydrocarbons, Kerosene, Etc.*	*Animal, Vegetable Oils*
Polyisoprene (natural)	D	B	NR	A/C-B	A/C-B	NR	NR	D-B
Polyisoprene (synthetic)	NR	B	NR	C-B/C-B	C-B/C-B	NR	NR	D-B
Butadiene	D	B	NR	C-B/C-B	C-B/C-B	NR	NR	D-B
Styrene-butadiene	D	C	NR	C-B/C-B	C-B/C-B	NR	NR	D-B
Neoprene	B	A	A	A/A	A/A	D	C	B
Nitrile (high)	D	B	C	B/B	B/B	C-B	A	B
Silicone (polysiloxane)	A	A	A	A/A	B/C	NR	D-C	A

[a] A = excellent, B = good, C = fair, D = use with caution, NR = not recommended.

Source: *Compound Selection and Service Guide,* Seals Eastern, Inc., Red Bank, NJ, 1977.

Answers to Selected Problems

Chapter 2

2.3 **(a)** 1.66×10^{-24} g/amu;
(b) 2.73×10^{26} atoms/lb-mol

2.13

$$r_0 = \left(\frac{A}{nB}\right)^{1/(1-n)}$$

$$E_0 = -\frac{A}{\left(\frac{A}{nB}\right)^{1/(1-n)}} + \frac{B}{\left(\frac{A}{nB}\right)^{n/(1-n)}}$$

2.14 **(c)** $r_0 = 0.279$ nm; $E_0 = -4.57$ eV

2.19 63.2% for TiO_2; 1.0% for InSb

Chapter 3

3.3 $V_C = 6.62 \times 10^{-29}$ m^3

3.9 $R = 0.136$ nm

3.12 **(a)** $V_C = 1.40 \times 10^{-28}$ m^3;
(b) $a = 0.323$ nm, $c = 0.515$ nm

3.15 Metal B: face-centered cubic

3.17 **(a)** $n = 8.0$; **(b)** $\rho = 4.96$ g/cm^3

3.20 $V_C = 8.63 \times 10^{-2}$ nm^3

3.29 **(a)** Cesium chloride; **(c)** sodium chloride

3.31 APF = 0.73

3.35 **(a)** $a = 0.421$ nm; $a = 0.424$ nm

3.37 **(a)** ρ (calculated) = 4.11 g/cm^3;
(b) ρ (measured) = 4.10 g/cm^3

3.39 **(a)** $\rho = 4.20$ g/cm^3

3.41 Cesium chloride

3.43 APF = 0.84

3.45 APF = 0.68

3.50 **(a)** Direction 1: [012]; **(b)** Plane 1: (020)

3.52 Direction A: $[0\bar{1}\bar{1}]$; Direction C: [112]

3.53 Direction B: $[2\bar{3}2]$; Direction D: $[13\bar{6}]$

3.54 **(b)** $[\bar{1}\bar{1}0]$, $[\bar{1}10]$, and $[1\bar{1}0]$

3.56 Plane B: $(\bar{1}\bar{1}2)$ or $(11\bar{2})$

3.57 Plane A: $(32\bar{2})$

3.58 Plane B: (221)

3.60 **(a)** $(1\bar{1}00)$

3.64 **(a)** (100) and $(0\bar{1}0)$

3.65 **(c)** [010]

3.66 **(a)** FCC; **(b)** tetrahedral; **(c)** one half

3.68 **(a)** octahedral; **(b)** all

3.70* [100]: LD = 0.71

3.71* [111]: LD = 1.0

3.72* (100): PD = 0.79

3.73* (110): PD = 0.83

3.79* $2\theta = 81.38°$

3.80* $d_{110} = 0.2862$ nm

3.82* **(a)** $d_{321} = 0.1523$ nm; **(b)** $R = 0.2468$ nm

3.84* $d_{110} = 0.2015$ nm; $a = 0.285$ nm

Chapter 4

4.4 $n_n = 23{,}700$

4.6 **(a)** $\overline{M} = 33{,}040$ g/mol; **(c)** $n_n = 785$

4.9 **(a)** $C_{Cl} = 20.3$ wt%

4.11 $L = 1254$ nm; $r = 15.4$ nm

4.16 8530 of both styrene and butadiene mers

4.18 Propylene

4.21 f(isoprene) = 0.88; f(isobutylene) = 0.12

4.28 $\rho = 0.998$ g/cm^3

4.30 **(a)** $\rho_a = 2.000$ g/cm^3, $\rho_c = 2.301$ g/cm^3;
(b) % crystallinity = 87.9%

Chapter 5

5.1 $N_v/N = 2.41 \times 10^{-5}$

5.3 $Q_v = 1.10$ eV/atom

5.4 6.02×10^{28} atoms/m^3

5.9 For FCC, $r = 0.41R$

5.10 **(a)** O^{2-} vacancy; one O^{2-} vacancy for every two Li$^+$ added

5.13 $C_{\text{Pb}} = 10.0$ wt%; $C_{\text{Sn}} = 90.0$ wt%

5.15 $C'_{\text{Sn}} = 72.5$ at%; $C'_{\text{Pb}} = 27.5$ at%

5.18* $C'_{\text{Fe}} = 94.2$ at%; $C'_{\text{Si}} = 5.8$ at%

5.23 $N_{\text{Au}} = 3.36 \times 10^{21}$ atoms/cm^3

5.27 $C_{\text{Nb}} = 35.2$ wt%

5.30 **(a)** FCC: $\mathbf{b} = \frac{a}{2}[110]$;

(b) Al: $|\mathbf{b}| = 0.2862$ nm

5.35 $d \cong 0.07$ mm

5.37 **(a)** $N = 8$

5.D1* $C_{\text{Li}} = 1.537$ wt%

Chapter 6

6.6 $M = 2.6 \times 10^{-3}$ kg/h

6.8 $D = 3.9 \times 10^{-11}$ m^2/s

6.11 $t = 19.7$ h

6.15 $t = 40$ h

6.18 $T = 1152$ K (879°C)

6.21 **(a)** $Q_d = 252.4$ kJ/mol, $D_0 = 2.2 \times 10^{-5}$ m^2/s

(b) $D = 5.3 \times 10^{-15}$ m^2/s

6.24 $T = 1044$ K (771°C)

6.29 $x = 1.6$ mm

6.D1 Not possible

Chapter 7

7.4 $l_0 = 250$ mm (10 in.)

7.7 **(a)** $F = 89{,}400$ N (20,000 lb$_f$)

(b) $l_i = 115.28$ mm (4.511 in.)

7.9 $\Delta l = 0.10$ mm (0.004 in.)

7.12

$$\left(\frac{dF}{dr}\right)_{r_0} = -\frac{2A}{\left(\frac{A}{nB}\right)^{3/(1-n)}} + \frac{(nB)(n+1)}{\left(\frac{A}{nB}\right)^{(n+2)/(1-n)}}$$

7.14 **(a)** $\Delta l = 0.50$ mm (0.02 in.);

(b) $\Delta d = -1.62 \times 10^{-2}$ mm (-6.2×10^{-4} in.); decrease

7.15 $F = 16{,}250$ N (3770 lb$_f$)

7.16 $\nu = 0.280$

7.18 $E = 170.5$ GPa (24.7×10^6 psi)

7.21 **(a)** $\Delta l = 0.10$ mm (4×10^{-3} in.);

(b) $\Delta d = -3.6 \times 10^{-3}$ mm (-1.4×10^{-4} in.)

7.24 Steel

7.27 **(a)** Both elastic and plastic;

(b) $\Delta l = 4.0$ mm (0.16 in.)

7.29 **(b)** $E = 62$ GPa (9×10^6 psi)

(c) $\sigma_y = 285$ MPa (41,500 psi)

(d) $TS = 370$ MPa (53,500 psi)

(e) %EL = 16%

(f) $U_r = 0.66 \times 10^6$ J/m^2 (95.7 in.-lb$_m$/in.^{3})

7.32 Figure 7.12: $U_r = 3.32 \times 10^5$ J/m^3 (47.6 in.-lb$_f$/in.^{3})

7.34 $\sigma_y = 381$ MPa (55,500 psi)

7.39 $\epsilon_T = 0.237$

7.41 $\sigma_T = 440$ MPa (63,700 psi)

7.43 Toughness = 3.65×10^9 J/m^3 (5.29×10^5 in.-lb$_m$/in.^{3})

7.45 $n = 0.134$

7.47 **(a)** ϵ (elastic) $\cong 0.0027$; ϵ (plastic) $\cong 0.0023$

(b) $l_i = 461.1$ mm (18.05 in.)

7.49 $R = 4$ mm

7.50 $F_f = 10{,}100$ N (2165 lb$_f$)

7.52* **(a)** $E_0 = 342$ GPa; **(b)** $E = 280$ GPa

7.54* **(b)** $P = 0.186$

7.59* $E_r(10) = 4.25$ MPa (616 psi)

7.65 **(a)** 125 HB (70 HRB)

7.70 Figure 7.12: $\sigma_w = 125$ MPa (18,000 psi)

7.D2 **(a)** $\Delta x = 2.5$ mm; **(b)** $\sigma = 10$ MPa

Chapter 8

8.10* $\cos \lambda \cos \phi = 0.408$

8.12* **(b)** $\tau_{\text{crss}} = 0.80$ MPa (114 psi)

8.13* $\tau_{\text{crss}} = 0.45$ MPa (65.1 psi)

8.20 $d = 1.48 \times 10^{-2}$ mm

8.21 $d = 6.9 \times 10^{-3}$ mm

8.25 $r_d = 8.25$ mm

8.27 $r_0 = 10.6$ mm (0.424 in.)

8.29 $\tau_{\text{crss}} = 20.2$ MPa (2920 psi)

8.35 **(b)** $t \cong 150$ min

8.36 **(b)** $d = 0.085$ mm

8.45* $TS = 44$ MPa

8.54 Fraction sites vulcanized = 0.180

8.56 Fraction of mer sites crosslinked = 0.47

8.D1 Is possible

8.D6 Cold work to between 21 and 23%CW [to $d_0' \cong 12.8$ mm (0.50 in.)], anneal, then cold work to give a final diameter of 11.3 mm (0.445 in.).

Chapter 9

9.3 $\sigma_m = 2404$ MPa (354,000 psi)

9.7 $\rho_t = 0.39$ nm

9.8 $\sigma_c = 16.2$ MPa

9.10* **(a)** $\sigma_x = 171$ MPa (25,000 psi), $\sigma_y = 247$ MPa (35,800 psi)

(d) $\sigma_x = 41.7$ MPa (6050 psi), $\sigma_y = 126$ MPa (18,300 psi)

9.12* **(a)** $\sigma_m = 170$ MPa (24,650 psi)

9.13* **(a)** $\sigma_m = 120$ MPa (17,400 psi)

9.15* Aluminum 2024-T3: $B \geq 40.6$ mm (1.6 in.); 4340 steel (tempered at 260°C): $B \geq 2.3$ mm (0.10 in.)

9.17 Fracture will not occur

9.19 $a = 24$ mm (0.95 in.)

9.21 Is not subject to detection since $a < 4.0$ mm

9.26 **(b)** −105°C; **(c)** −95°C

9.29 **(a)** $\sigma_{\max} = 275$ MPa (40,000 psi), $\sigma_{\min} = -175$ MPa (−25,500 psi);

(b) $R = -0.64$; **(c)** $\sigma_r = 450$ MPa (65,500 psi)

9.31 $N_f = 1 \times 10^5$ cycles

9.33 **(b)** $S = 250$ MPa; **(c)** $N_f \cong 2.2 \times 10^6$ cycles

9.34 **(a)** $\tau = 130$ MPa; **(c)** $\tau = 195$ MPa

9.36 **(a)** $t = 120$ min; **(c)** $t = 220$ h

9.47 $\Delta\epsilon/\Delta t = 7.0 \times 10^{-3}\ \text{min}^{-1}$

9.48 $\Delta l = 7.1$ mm (0.29 in.)

9.50 $t_r = 36{,}000$ h

9.52* 427°C: $n = 5.3$

9.53* **(a)** $Q_c = 186{,}200$ J/mol

9.55* $\dot{\epsilon}_s = 0.118\ (\text{h})^{-1}$

9.D1* $K_{Ic} = 67.9\ \text{MPa}\sqrt{\text{m}}$ ($62.3\ \text{ksi}\sqrt{\text{in.}}$)

9.D3* $W \geq 4.4$ mm

9.D7* $\sigma_{\max} = 178$ MPa

9.D9* $a_c = 0.25$ in.

9.D14* $T = 991$ K (718°C)

9.D16* For 5 years: $\sigma = 260$ MPa (37,500 psi)

Chapter 10

10.5 **(a)** $\epsilon + \eta$; $C_\epsilon = 87$ wt% Zn-13 wt% Cu, $C_\eta = 97$ wt% Zn-3 wt% Cu;

(c) Liquid; $C_L = 55$ wt% Ag-45 wt% Cu;

(e) $\beta + \gamma$; $C_\beta = 49$ wt% Zn-51 wt% Cu, $C_\gamma = 57$ wt% Zn-43 wt% Cu;

(g) α; $C_\alpha = 63.8$ wt% Ni-36.2 wt% Cu

10.7 **(a)** $W_\epsilon = 0.70$, $W_\eta = 0.30$;

(c) $W_L = 1.0$;

(e) $W_\beta = 0.50$, $W_\gamma = 0.50$;

(g) $W_\alpha = 1.0$

10.9 **(a)** $V_\epsilon = 0.70$, $V_\eta = 0.30$

10.11 **(a)** $T = 300$°C (570°F)

10.12 **(a)** $m_s = 5022$ g;

(b) $C_L = 64$ wt% sugar;

(c) $m_s = 2355$ g

10.13 **(a)** The pressure must be raised to approximately 570 atm

10.18 Is possible

10.21 **(a)** $T = 550$°C (1020°F);

(b) $C_\alpha = 22$ wt% Pb-78 wt% Mg;

(c) $T = 465$°C (870°F);

(d) $C_L = 66$ wt% Pb-34 wt% Mg

10.24 **(a)** $T \cong 230$°C (445°F);

(b) $C_\alpha = 15$ wt% Sn; $C_L = 42$ wt% Sn

10.25* **(a)** $C = 45.9$ wt% Al_2O_3–54.1 wt% SiO_2

10.26 $C_\alpha = 90$ wt% A-10 wt% B; $C_\beta = 20.2$ wt% A-79.8 wt% B

10.28 Not possible

10.32* Is possible

10.35* $C_0 = 82.4$ wt% Sn-17.6 wt% Pb

10.38*

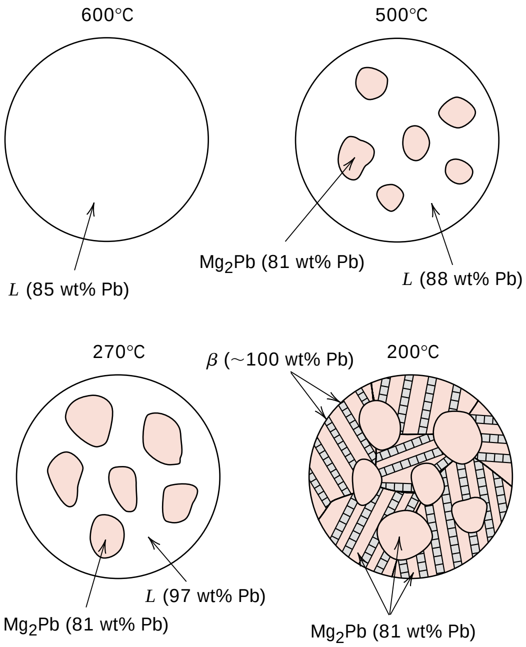

10.42 Eutectics: **(1)** 12 wt% Nd, 632°C, $L \rightarrow \text{Al} + \text{Al}_{11}\text{Nd}_3$;

(2) 97 wt% Nd, 635°C, $L \rightarrow \text{AlNd}_3 + \text{Nd}$;
Congruent melting point: 73 wt% Nd, 1460°C, $L \rightarrow \text{Al}_2\text{Nd}$
Peritectics: **(1)** 59 wt% Nd, 1235°C, $L + \text{Al}_2\text{Nd} \rightarrow \text{Al}_{11}\text{Nd}_3$;

(2) 84 wt% Nd, 940°C, $L + \text{Al}_2\text{Nd} \rightarrow \text{AlNd}$;

(3) 91 wt% Nd, 795°C, $L + \text{AlNd} \rightarrow \text{AlNd}_2$;

(4) 94 wt% Nd, 675°C, $L + \text{AlNd}_2 \rightarrow \text{AlNd}_3$
No eutectoids are present.

10.45* **(a)** 8.1% of Mg^{2+} vacancies

10.47* For point B, $F = 2$

10.54 $C_0' = 0.42$ wt% C

10.57 **(a)** α-ferrite; **(b)** 2.26 kg of ferrite, 0.24 kg of Fe_3C;

(c) 0.38 kg of proeutectoid ferrite, 2.12 kg of pearlite

10.59 $C_0 = 0.55$ wt% C

10.61 $C_0 = 0.61$ wt% C

10.64 Possible

10.67 Two answers are possible: $C_0 = 1.11$ wt% C and 0.72 wt% C

10.70 HB (alloy) = 128

10.73* **(a)** T (eutectoid) = 650°C (1200°F); **(b)** ferrite; **(c)** $W_{\alpha'} = 0.68$, $W_p = 0.32$

Chapter 11

11.2 $t = 305$ s

11.4 $r = 4.42 \times 10^{-3}\ \text{min}^{-1}$

11.6 $y = 0.51$

11.7 **(c)** $t \cong 250$ days

11.10 **(b)** 265 HB (27 HRC)

11.14 **(a)** 50% coarse pearlite and 50% martensite; **(d)** 100% martensite; **(e)** 40% bainite and 60% martensite; **(g)** 100% fine pearlite

11.16 **(a)** martensite; **(c)** bainite; **(e)** ferrite, medium pearlite, bainite, and martensite; **(g)** proeutectoid ferrite, pearlite, and martensite

11.19* **(a)** martensite

11.24* **(a)** martensite; **(c)** martensite, proeutectoid ferrite, and bainite

11.34 **(b)** 180 HB (87 HRB); **(g)** 265 HB (27 HRC)

11.36* **(c)** $TS = 915$ MPa (132,500 psi)

11.37 **(a)** Rapidly cool to about 675°C (1245°F), hold for at least 200 s, then cool to room temperature

11.D1 Not possible

11.D5 Temper at between 400 and 450°C (750 and 840°F) for 1 h

11.D8 For about 10 h at 149°C, or between about 35 and 400 h at 121°C

Chapter 12

12.2 $d = 1.88$ mm

12.5 **(a)** $R = 4.7 \times 10^{-3}\ \Omega$; **(b)** $I = 10.6$ A;

(c) $J = 1.5 \times 10^6\ \text{A/m}^2$; $\mathscr{E} = 2.5 \times 10^{-2}$ V/m

12.12 $\sigma = 0.096\ (\Omega\text{-m})^{-1}$

12.13 **(a)** $n = 1.25 \times 10^{29}\ \text{m}^{-3}$;

(b) 1.48 free electrons/atom

12.16 **(a)** $\rho_0 = 1.58 \times 10^{-8}$ Ω-m, $a = 6.5 \times 10^{-11}$ Ω-m/°C;
(b) $A = 1.12 \times 10^{-6}$ Ω-m;
(c) $\rho = 4.26 \times 10^{-8}$ Ω-m

12.18 $\sigma = 7.3 \times 10^{6}\ (\Omega\text{-m})^{-1}$

12.21 **(b)** for Si, 2.7×10^{-13}; for Ge, 5.6×10^{-10}

12.30 **(a)** $n = 8.9 \times 10^{21}\ \text{m}^{-3}$; **(b)** *p*-type extrinsic

12.33 $\mu_e = 0.50\ \text{m}^2/\text{V-s}$; $\mu_h = 0.02\ \text{m}^2/\text{V-s}$

12.38 $E_g = 1.46$ eV

12.39 **(b)** $\sigma = 3.8 \times 10^{-5}\ (\Omega\text{-m})^{-1}$

12.40 **(a)** $\sigma = 61.4\ (\Omega\text{-m})^{-1}$; **(b)** $n = p = 1.16 \times 10^{21}\ \text{m}^{-3}$

12.45* $B_z = 0.58$ tesla

12.52* $l = 1.6$ mm

12.56* $p_i = 2.26 \times 10^{-30}$ C-m

12.58* **(a)** $V = 17.3$ V; **(b)** $V = 86.5$ V;
(e) $P = 1.75 \times 10^{-7}\ \text{C/m}^2$

12.60* Fraction of ϵ_r due to $P_i = 0.67$

12.D2 $\sigma = 2.44 \times 10^{7} (\Omega\text{-m})^{-1}$

12.D3 Possible; 30 wt% $< C_{\text{Ni}} <$ 32.5 wt%

Chapter 13

13.5 $V_{\text{Gr}} = 11.1$ vol%

13.21* **(a)** $T = 2000$°C (3630°F)

13.23* **(a)** $W_L = 0.86$; **(c)** $W_L = 0.66$

13.24* **(a)** 1890°C (3435°F); between ~77 and 100 wt% Al_2O_3

Chapter 14

14.11 **(a)** 890–920°C (1635–1690°F)

14.12 **(b)** 790–815°C (1450–1500°F)

14.26 **(b)** $Q_{\text{vis}} = 362$ kJ/mol

14.43 **(a)** m(adipic acid) = 117.7 kg
(b) m(polyester) = 153.2 kg

14.D5 Maximum diameter = 75 mm (3 in.)

14.D7 Maximum diameter = 70 mm (2.75 in.)

Chapter 15

15.4 $k_{\max} = 33.3$ W/m-K; $k_{\min} = 29.7$ W/m-K

15.9 $\tau_c = 34.5$ MPa

15.12 Possible

15.14 $E_f = 70.4$ GPa (10.2×10^6 psi); $E_m = 2.79$ GPa (4.04×10^5 psi)

15.17 **(a)** $F_f/F_m = 23.4$;
(b) $F_f = 42{,}676$ N (9590 lb_f), $F_m = 1824$ N (410 lb_f)
(c) $\sigma_f = 445$ MPa (63,930 psi), $\sigma_m = 8.14$ MPa (1170 psi);
(d) $\epsilon = 3.4 \times 10^{-3}$

15.19 $\sigma_{cl}^* = 633$ MPa (91,700 psi)

15.21 $\sigma_{cd}^* = 1340$ MPa (194,400 psi)

15.28 $E_{cl} = 69.1$ GPa (10.0×10^6 psi)

15.D1 Carbon (PAN standard-modulus) and aramid

15.D2 Not possible

Chapter 16

16.5 **(a)** $\Delta V = +0.031$ V;
(b) $Fe^{2+} + Cd \longrightarrow Fe + Cd^{2+}$

16.7 $[Pb^{2+}] = 2.5 \times 10^{-2}\ M$

16.13 $t = 10$ yr

16.16 CPR = 5.24 mpy

16.20 **(a)** $r = 8.0 \times 10^{-14}\ \text{mol/cm}^2\text{-s}$;
(b) $V_C = -\ 0.019$ V

16.34 Sn: P-B ratio = 1.33; protective

16.36 **(a)** Parabolic kinetics; **(b)** $W = 1.51\ \text{mg/cm}^2$

Chapter 17

17.2 $T_f = 49$°C (120°F)

17.4 **(a)** $c_v = 139$ J/kg-K; **(b)** $c_v = 925$ J/kg-K

17.9 $\Delta l = -9.2$ mm (−0.36 in.)

17.14 $T_f = 129.5$°C

17.16 **(b)** $dQ/dt = 9.3 \times 10^8$ J/h

17.24 k(upper) = 26.4 W/m-K

17.28 **(a)** $\sigma = 150$ MPa (21,800 psi); compression

17.29 $T_f = 39$°C (102°F)

17.30 $\Delta d = 0.0251$ mm

17.D1 $T_f = 42.2$°C (108°F)

17.D4 Glass ceramic: $\Delta T_f = 317$°C

Chapter 18

18.1 **(a)** $H = 10{,}000$ A-turns/m;
(b) $B_0 = 1.257 \times 10^{-2}$ tesla;
(c) $B \cong 1.257 \times 10^{-2}$ tesla;
(d) $M = 1.81$ A/m

18.6 **(a)** $\mu = 1.26 \times 10^{-6}$ H/m;
(b) $\chi_m = 6 \times 10^{-3}$

18.8 **(a)** $M_s = 1.45 \times 10^6$ A/m

18.16 4.6 Bohr magnetons/Mn^{2+} ion

18.24 $M_s = 1.69 \times 10^6$ A/m

18.27 **(b)** $\mu_i = 3.0 \times 10^{-3}$ H/m, $\mu_{ri} = 2400$;
(c) $\mu(\text{max}) \cong 9 \times 10^{-3}$ H/m

18.29 **(b)** **(i)** $\mu \cong 1.0 \times 10^{-2}$ H/m; **(iii)** $\chi_m \cong 7954$

18.32 **(a)** 2.5 K: 1.33×10^4 A/m; **(b)** 5.96 K

Chapter 19

19.9 $v = 2.09 \times 10^8$ m/s

19.10 Silica: 0.53; soda-lime glass: 0.33

19.11 Fused silica: $\epsilon_r = 2.13$; polyethylene: $\epsilon_r = 2.28$

19.19 $I'_T/I'_0 = 0.81$

19.21 $l = 67.3$ mm

19.30 $\Delta E = 1.78$ eV

Chapter 20

20.D2 Stiffness: $P = \dfrac{\sqrt{G}}{\rho}$

20.D3 Stiffness $P = \dfrac{\sqrt{E}}{\rho}$; strength: $P = \dfrac{\sigma_y^{2/3}}{\rho}$

20.D6 **(a)** $F = 21.5$ N (4.8 lb_f);
(b) $F = 53.6$ N (12.0 lb_f)

CHAPTER 2

ATOMIC STRUCTURE AND INTERATOMIC BONDING

2.3 (a) In order to determine the number of grams in one amu of material, appropriate manipulation of the amu/atom, g/mol, and atom/mol relationships is all that is necessary, as

$$\begin{aligned}\#\text{g/amu} &= \left(\frac{1\ \text{mol}}{6.023\times 10^{23}\ \text{atoms}}\right)\left(\frac{1\ \text{g/mol}}{1\ \text{amu/atom}}\right)\\ &= 1.66\times 10^{-24}\ \text{g/amu}\end{aligned}$$

2.14 (c) This portion of the problem asks that we determine for a K^+-Cl^- ion pair the interatomic spacing (**r_o**) and the bonding energy (**E_o**). From Equation (2.11) for **E_N**

$$A = 1.436$$

$$B = 5.86\times 10^{-6}$$

$$n = 9$$

Thus, using the solutions from Problem 2.13

$$\begin{aligned}r_o &= \left(\frac{A}{nB}\right)^{1/(1-n)}\\ &= \left[\frac{1.436}{(9)(5.86\times 10^{-6})}\right]^{1/(1-9)} = 0.279\ \text{nm}\end{aligned}$$

and

$$\begin{aligned}E_o &= -\frac{1.436}{\left[\dfrac{1.436}{(9)(5.86\times 10^{-6})}\right]^{1/(1-9)}} + \frac{5.86\times 10^{-6}}{\left[\dfrac{1.436}{(9)(5.86\times 10^{-6})}\right]^{9/(1-9)}}\\ &= -4.57\ \text{eV}\end{aligned}$$

2.19 The percent ionic character is a function of the electronegativities of the ions **X_A** and **X_B** according to Equation (2.10). The electronegativities of the elements are found in Figure 2.7.

For TiO_2, **X_{Ti}** $= 1.5$ and **X_O** $= 3.5$, and therefore,

$$\%IC = \left[1 - \mathbf{e}^{(-0.25)(3.5-1.5)^2}\right]\times 100 = 63.2\%$$

CHAPTER 3

STRUCTURES OF METALS AND CERAMICS

3.3 For this problem, we are asked to calculate the volume of a unit cell of aluminum. Aluminum has an FCC crystal structure (Table 3.1). The FCC unit cell volume may be computed from Equation (3.4) as

$$V_C = 16R^3\sqrt{2} = (16)(0.143 \times 10^{-9}\ \mathrm{m})^3\sqrt{2} = 6.62 \times 10^{-29}\ \mathrm{m}^3$$

3.7 This problem calls for a demonstration that the **APF** for HCP is 0.74. Again, the **APF** is just the total sphere-unit cell volume ratio. For HCP, there are the equivalent of six spheres per unit cell, and thus

$$V_S = 6\left(\frac{4\pi R^3}{3}\right) = 8\pi R^3$$

Now, the unit cell volume is just the product of the base area times the cell height, **c.** This base area is just three times the area of the parallelepiped **ACDE** shown below.

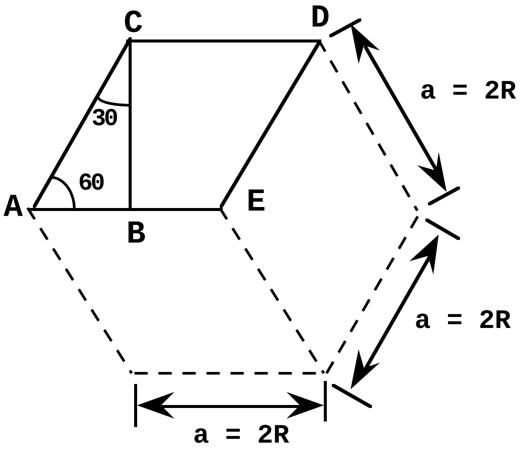

The area of **ACDE** is just the length of $\overline{\mathbf{CD}}$ times the height $\overline{\mathbf{BC}}$. But $\overline{\mathbf{CD}}$ is just **a** or 2**R**, and

$$\overline{BC} = 2R\cos(30^\circ) = \frac{2R\sqrt{3}}{2}$$

Thus, the base area is just

$$\mathrm{AREA} = (3)(\overline{CD})(\overline{BC}) = (3)(2R)\left(\frac{2R\sqrt{3}}{2}\right) = 6R^2\sqrt{3}$$

and since $\mathbf{c} = 1.633\mathbf{a} = 2\mathbf{R}(1.633)$

$$V_C = (\mathrm{AREA})(c) = 6R^2c\sqrt{3} = (6R^2\sqrt{3})(2)(1.633)R = 12\sqrt{3}(1.633)R^3$$

Thus,

$$\mathrm{APF} = \frac{V_S}{V_C} = \frac{8\pi R^3}{12\sqrt{3}(1.633)R^3} = 0.74$$

3.12. (a) This portion of the problem asks that we compute the volume of the unit cell for Zr. This volume may be computed using Equation (3.5) as

$$V_C = \frac{nA_{Zr}}{\rho N_A}$$

Now, for HCP, **n** = 6 atoms/unit cell, and for Zr, $\mathbf{A_{Zr}}$ = 91.2 g/mol. Thus,

$$\begin{aligned} V_C &= \frac{(6 \text{ atoms/unit cell})(91.2 \text{ g/mol})}{(6.51 \text{ g/cm}^3)(6.023 \times 10^{23} \text{ atoms/mol})} \\ &= 1.396 \times 10^{-22} \text{ cm}^3\text{/unit cell} = 1.396 \times 10^{-28} \text{ m}^3\text{/unit cell} \end{aligned}$$

(b) We are now to compute the values of **a** and **c**, given that **c**/**a** = 1.593. From the solution to Problem 3.7, since **a** = 2**R**, then, for HCP

$$V_C = \frac{3\sqrt{3}a^2c}{2}$$

but, since **c** = 1.593**a**

$$V_C = \frac{3\sqrt{3}(1.593)a^3}{2} = 1.396 \times 10^{-22} \text{ cm}^3\text{/unit cell}$$

Now, solving for **a**

$$\begin{aligned} a &= \left[\frac{(2)(1.396 \times 10^{-22} \text{ cm}^3)}{(3)(\sqrt{3})(1.593)}\right]^{1/3} \\ &= 3.23 \times 10^{-8} \text{ cm} = 0.323 \text{ nm} \end{aligned}$$

And finally

$$c = 1.593a = (1.593)(0.323 \text{ nm}) = 0.515 \text{ nm}$$

3.17 In this problem we are given that iodine has an orthorhombic unit cell for which the **a**, **b**, and **c** lattice parameters are 0.479, 0.725, and 0.978 nm, respectively.

(a) Given that the atomic packing factor and atomic radius are 0.547 and 0.177 nm, respectively we are to determine the number of atoms in each unit cell. From the definition of the APF

$$\mathrm{APF} = \frac{V_S}{V_C} = \frac{n\left(\frac{4}{3}\pi R^3\right)}{abc}$$

we may solve for the number of atoms per unit cell, **n**, as

$$
\begin{aligned}
n &= \frac{(\text{APF})abc}{\frac{4}{3}\pi R^3} \\
&= \frac{(0.547)(4.79)(7.25)(9.78)(10^{-24}\ \text{cm}^3)}{\frac{4}{3}\pi(1.77 \times 10^{-8}\ \text{cm})^3} \\
&= 8.0\ \text{atoms/unit cell}
\end{aligned}
$$

(b) In order to compute the density, we just employ Equation (3.5) as

$$
\begin{aligned}
\rho &= \frac{nA_I}{abcN_A} \\
&= \frac{(8\ \text{atoms/unit cell})(126.91\ \text{g/mol})}{[(4.79)(7.25)(9.78) \times 10^{-24}\ \text{cm}^3/\text{unit cell}](6.023 \times 10^{23}\ \text{atoms/mol})} \\
&= 4.96\ \text{g/cm}^3
\end{aligned}
$$

3.22 This question asks that we generate a three-dimensional unit cell for $AuCu_3$ using the Molecule Definition File on the CD-ROM. One set of directions that may be used to construct this unit cell and that are entered on the Notepad are as follows:

```
[DisplayProps]
Rotatez=−30
Rotatey=−15

[AtomProps]
Gold=LtRed,0.14
Copper=LtYellow,0.13

[BondProps]
SingleSolid=LtGray

[Atoms]
Au1=1,0,0,Gold
Au2=0,0,0,Gold
Au3=0,1,0,Gold
Au4=1,1,0,Gold
Au5=1,0,1,Gold
Au6=0,0,1,Gold
Au7=0,1,1,Gold
Au8=1,1,1,Gold
Cu1=0.5,0,0.5,Copper
Cu2=0,0.5,0.5,Copper
Cu3=0.5,1,0.5,Copper
Cu4=1,0.5,0.5,Copper
Cu5=0.5,0.5,1,Copper
Cu6=0.5,0.5,0,Copper
```

```
[Bonds]
B1=Au1,Au5,SingleSolid
B2=Au5,Au6,SingleSolid
B3=Au6,Au2,SingleSolid
B4=Au2,Au1,SingleSolid
B5=Au4,Au8,SingleSolid
B6=Au8,Au7,SingleSolid
B7=Au7,Au3,SingleSolid
B8=Au3,Au4,SingleSolid
B9=Au1,Au4,SingleSolid
B10=Au8,Au5,SingleSolid
B11=Au2,Au3,SingleSolid
B12=Au6,Au7,SingleSolid
```

When saving these instructions, the file name that is chosen should end with a period followed by mdf and the entire file name needs to be enclosed within quotation marks. For example, if one wants to name the file AuCu3, the name by which it should be saved is “AuCu3.mdf”. In addition, the file should be saved as a “Text Document.”

3.27 In this problem we are asked to show that the minimum cation-to-anion radius ratio for a coordination number of six is 0.414. Below is shown one of the faces of the rock salt crystal structure in which anions and cations just touch along the edges, and also the face diagonals.

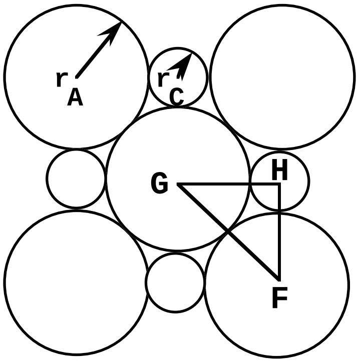

From triangle **FGH,**

$$\overline{\mathrm{GF}} = 2\mathrm{r_A} \quad \text{and} \quad \overline{\mathrm{FH}} = \overline{\mathrm{GH}} = \mathrm{r_A} + \mathrm{r_C}$$

Since **FGH** is a right triangle

$$(\overline{\mathrm{GH}})^2 + (\overline{\mathrm{FH}})^2 = (\overline{\mathrm{FG}})^2$$

or

$$(\mathrm{r_A} + \mathrm{r_C})^2 + (\mathrm{r_A} + \mathrm{r_C})^2 = (2\mathrm{r_A})^2$$

which leads to

$$\mathrm{r_A} + \mathrm{r_C} = \frac{2\mathrm{r_A}}{\sqrt{2}}$$

Or, solving for $\mathbf{r_C}/\mathbf{r_A}$

$$\frac{r_C}{r_A} = \left(\frac{2}{\sqrt{2}} - 1\right) = 0.414$$

3.29 This problem calls for us to predict crystal structures for several ceramic materials on the basis of ionic charge and ionic radii.

(a) For CsI, from Table 3.4

$$\frac{r_{Cs^+}}{r_{I^-}} = \frac{0.170\ \text{nm}}{0.220\ \text{nm}} = 0.773$$

Now, from Table 3.3, the coordination number for each cation (Cs^+) is eight, and, using Table 3.5, the predicted crystal structure is cesium chloride.

(c) For KI, from Table 3.4

$$\frac{r_{K^+}}{r_{I^-}} = \frac{0.138\ \text{nm}}{0.220\ \text{nm}} = 0.627$$

The coordination number is six (Table 3.3), and the predicted crystal structure is sodium chloride (Table 3.5).

3.36 This problem asks that we compute the theoretical density of diamond given that the C—C distance and bond angle are 0.154 nm and 109.5°, respectively. The first thing we need do is to determine the unit cell edge length from the given C—C distance. The drawing below shows the cubic unit cell with those carbon atoms that bond to one another in one-quarter of the unit cell.

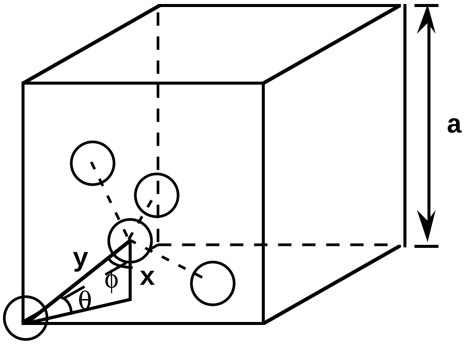

From this figure, ϕ is one-half of the bond angle or $\phi = 109.5°/2 = 54.75°$, which means that

$$\theta = 90° - 54.75° = 35.25°$$

since the triangle shown is a right triangle. Also, $\mathbf{y} = 0.154$ nm, the carbon-carbon bond distance. Furthermore, $\mathbf{x} = \mathbf{a}/4$, and therefore,

$$x = \frac{a}{4} = y \sin\theta$$

Or

$$
\begin{aligned}
a &= 4y \sin\theta = (4)(0.154\ \text{nm})(\sin 35.25^\circ) = 0.356\ \text{nm} \\
&= 3.56 \times 10^{-8}\ \text{cm}
\end{aligned}
$$

The unit cell volume, $\mathbf{V_C}$, is just $\mathbf{a}^3$, that is

$$V_C = a^3 = (3.56 \times 10^{-8}\ \text{cm})^3 = 4.51 \times 10^{-23}\ \text{cm}^3$$

We must now utilize a modified Equation (3.6) since there is only one atom type. There are eight equivalent atoms per unit cell (i.e., one equivalent corner, three equivalent faces, and four interior atoms), and therefore

$$
\begin{aligned}
\rho &= \frac{n' A_C}{V_C N_A} \\
&= \frac{(8\ \text{atoms/unit cell})(12.01\ \text{g/g-atom})}{(4.51 \times 10^{-23}\ \text{cm}^3/\text{unit cell})(6.023 \times 10^{23}\ \text{atoms/g-atom})} \\
&= 3.54\ \text{g/cm}^3
\end{aligned}
$$

The measured density is 3.51 g/cm^3.

3.39 (a) We are asked to compute the density of CsCl. Modifying the result of Problem 3.4, we get

$$
\begin{aligned}
a &= \frac{2r_{Cs^+} + 2r_{Cl^-}}{\sqrt{3}} = \frac{2(0.170\ \text{nm}) + 2(0.181\ \text{nm})}{\sqrt{3}} \\
&= 0.405\ \text{nm} = 4.05 \times 10^{-8}\ \text{cm}
\end{aligned}
$$

From Equation (3.6)

$$\rho = \frac{n'(A_{Cs} + A_{Cl})}{V_C N_A} = \frac{n'(A_{Cs} + A_{Cl})}{a^3 N_A}$$

For the CsCl crystal structure, $\mathbf{n}' = 1$ formula unit/unit cell, and thus

$$
\begin{aligned}
\rho &= \frac{(1\ \text{formula unit/unit cell})(132.91\ \text{g/mol} + 35.45\ \text{g/mol})}{(4.05 \times 10^{-8}\ \text{cm})^3/\text{unit cell}(6.023 \times 10^{23}\ \text{formula units/mol})} \\
&= 4.20\ \text{g/cm}^3
\end{aligned}
$$

(b) This value of the density is greater than the measured density. The reason for this discrepancy is that the ionic radii in Table 3.4, used for this computation, were for a coordination number of six, when, in fact, the coordination number of both Cs$^+$ and Cl$^-$ is eight. Under these circumstances, the actual ionic radii and unit cell volume ($\mathbf{V_C}$) will be slightly greater than calculated values; consequently, the measured density is smaller than the calculated density.

3.45 We are asked in this problem to compute the atomic packing factor for the CsCl crystal structure. This requires that we take the ratio of the sphere volume within the unit cell and the total unit cell volume. From Figure 3.6 there is the equivalent of one Cs and one Cl ion per unit cell; the ionic radii of these two ions are 0.170 nm and 0.181 nm, respectively (Table 3.4). Thus, the sphere volume, $\mathbf{V_S}$, is just

$$V_S = \frac{4}{3}(\pi)[(0.170\text{ nm})^3 + (0.181\text{ nm})^3] = 0.0454\text{ nm}^3$$

For CsCl the unit cell edge length, **a**, in terms of the atomic radii is just

$$\begin{aligned} a &= \frac{2r_{Cs^+} + 2r_{Cl^-}}{\sqrt{3}} = \frac{2(0.170\text{ nm}) + 2(0.181\text{ nm})}{\sqrt{3}} \\ &= 0.405\text{ nm} \end{aligned}$$

Since $\mathbf{V_C} = \mathbf{a}^3$

$$V_C = (0.405\text{ nm})^3 = 0.0664\text{ nm}^3$$

And, finally the atomic packing factor is just

$$\text{APF} = \frac{V_S}{V_C} = \frac{0.0454\text{ nm}^3}{0.0664\text{ nm}^3} = 0.684$$

3.50 (a) We are asked for the indices of the two directions sketched in the figure. For direction **1**, the projection on the **x**-axis is zero (since it lies in the **y-z** plane), while projections on the **y-** and **z**-axes are **b**/2 and **c**, respectively. This is an [012] direction as indicated in the summary below.

	x	y	z
Projections	0a	b/2	c
Projections in terms of **a**, **b**, and **c**	0	1/2	1
Reduction to integers	0	1	2
Enclosure		[012]	

3.51 This problem asks for us to sketch several directions within a cubic unit cell. The $[\bar{1}10]$, $[\bar{1}\bar{2}1]$, and $[0\bar{1}2]$ directions are indicated below.

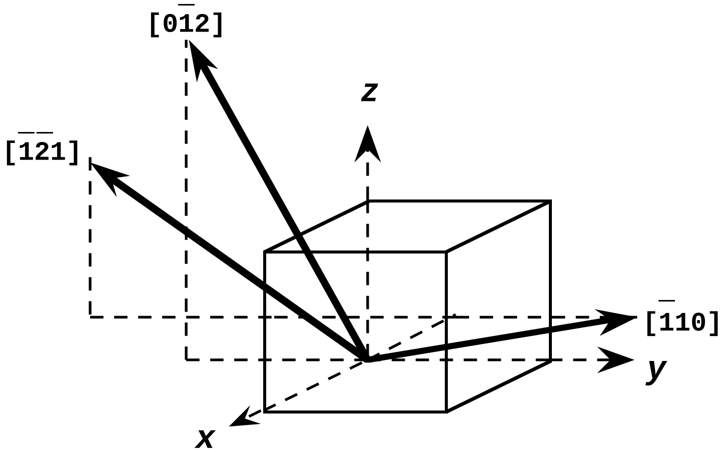

3.53 This problem asks that we determine indices for several directions that have been drawn within a cubic unit cell. Direction **B** is a $[2\bar{3}2]$ direction, the determination of which is summarized as follows.

We first of all position the origin of the coordinate system at the tail of the direction vector; then in terms of this new coordinate system

	x	y	z
Projections	$\frac{2a}{3}$	$-b$	$\frac{2c}{3}$
Projections in terms of **a**, **b**, and **c**	$\frac{2}{3}$	-1	$\frac{2}{3}$
Reduction to integers	2	-3	2
Enclosure		$[2\bar{3}2]$	

Direction **D** is a $[13\bar{6}]$ direction, the determination of which is summarized as follows. We first of all position the origin of the coordinate system at the tail of the direction vector; then in terms of this new coordinate system

	x	y	z
Projections	$\frac{a}{6}$	$\frac{b}{2}$	$-c$
Projections in terms of **a**, **b**, and **c**	$\frac{1}{6}$	$\frac{1}{2}$	-1
Reduction to integers	1	3	-6
Enclosure		$[13\bar{6}]$	

3.56 This problem asks that we determine the Miller indices for planes that have been drawn within a unit cell. For plane **B** we will move the origin of the unit cell one unit cell distance to the right along the **y** axis, and one unit cell distance parallel to the **x** axis; thus, this is a $(\bar{1}\bar{1}2)$ plane, as summarized below.

	x	y	z
Intercepts	$-a$	$-b$	$\frac{c}{2}$
Intercepts in terms of **a**, **b**, and **c**	-1	-1	$\frac{1}{2}$
Reciprocals of intercepts	-1	-1	2
Enclosure		$(\bar{1}\bar{1}2)$	

3.58 For plane **B** we will leave the origin at the unit cell as shown; this is a (221) plane, as summarized below.

	x	y	z
Intercepts	$\frac{a}{2}$	$\frac{b}{2}$	c
Intercepts in terms of **a**, **b**, and **c**	$\frac{1}{2}$	$\frac{1}{2}$	1
Reciprocals of intercepts	2	2	1
Enclosure		(221)	

3.59 The $(1\bar{1}01)$ plane in a hexagonal unit cell is shown below.

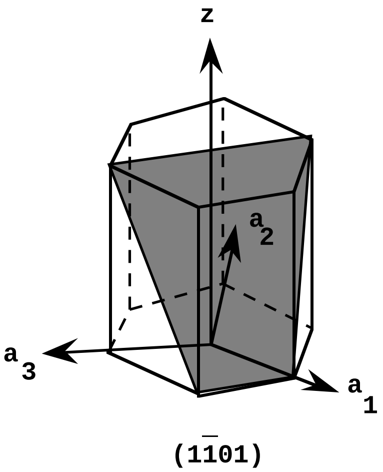

3.60 This problem asks that we specify the Miller indices for planes that have been drawn within hexagonal unit cells.

(a) For this plane we will leave the origin of the coordinate system as shown; thus, this is a $(1\bar{1}00)$ plane, as summarized below.

	$\underline{a_1}$	$\underline{a_2}$	$\underline{a_3}$	$\underline{z}$
Intercepts	a	−a	∞a	∞c
Intercepts in terms of **a**'s and **c**	1	−1	∞	∞
Reciprocals of intercepts	1	−1	0	0
Enclosure		$(1\bar{1}00)$		

3.61 This problem asks for us to sketch several planes within a cubic unit cell. The $(0\bar{1}\bar{1})$ and $(10\bar{2})$ planes are indicated below.

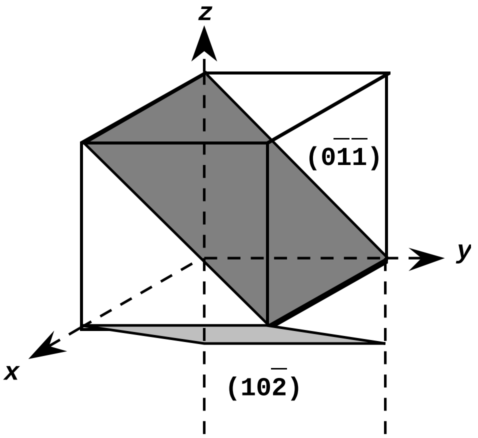

3.63 This problem asks that we represent specific crystallographic planes for various ceramic crystal structures.

(a) A (100) plane for the rock salt crystal structure would appear as

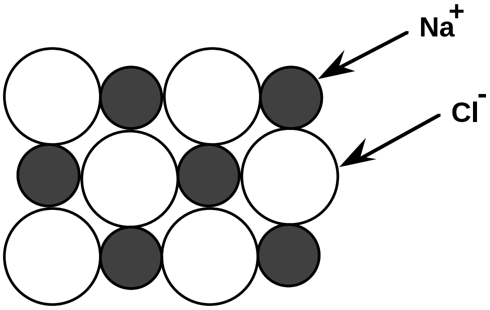

3.64 For the unit cell shown in Problem 3.21 we are asked to determine, from three given sets of crystallographic planes, which are equivalent.

(a) The unit cell in Problem 3.21 is body-centered tetragonal. Only the (100) (front face) and $(0\bar{1}0)$ (left side face) planes are equivalent since the dimensions of these planes within the unit cell (and therefore the distances between adjacent atoms) are the same (namely 0.40 nm × 0.30 nm), which are different than the (001) (top face) plane (namely 0.30 nm × 0.30 nm).

3.66 This question is concerned with the zinc blende crystal structure in terms of close-packed planes of anions.

(a) The stacking sequence of close-packed planes of anions for the zinc blende crystal structure will be the same as FCC (and not HCP) because the anion packing is FCC (Table 3.5).

(b) The cations will fill tetrahedral positions since the coordination number for cations is four (Table 3.5).

(c) Only one-half of the tetrahedral positions will be occupied because there are two tetrahedral sites per anion, and yet only one cation per anion.

3.70* In this problem we are to compute the linear densities of several crystallographic planes for the face-centered cubic crystal structure. For FCC the linear density of the [100] direction is computed as follows:

The linear density, **LD**, is defined by the ratio

$$\mathrm{LD} = \frac{L_c}{L_l}$$

where $\mathbf{L_l}$ is the line length within the unit cell along the [100] direction, and $\mathbf{L_c}$ is line length passing through intersection circles. Now, $\mathbf{L_l}$ is just the unit cell edge length, **a** which, for FCC is related to the atomic radius **R** according to $\mathbf{a} = 2\mathbf{R}\sqrt{2}$ [Equation (3.1)]. Also for this situation, $\mathbf{L_c} = 2\mathbf{R}$ and therefore

$$\mathrm{LD} = \frac{2R}{2R\sqrt{2}} = 0.71$$

3.73* In this problem we are to compute the planar densities of several crystallographic planes for the body-centered cubic crystal structure. Planar density, **PD**, is defined as

$$\mathrm{PD} = \frac{A_c}{A_p}$$

where $\mathbf{A_p}$ is the total plane area within the unit cell and $\mathbf{A_c}$ is the circle plane area within this same plane. For (110), that portion of a plane that passes through a BCC unit cell forms a rectangle as shown below.

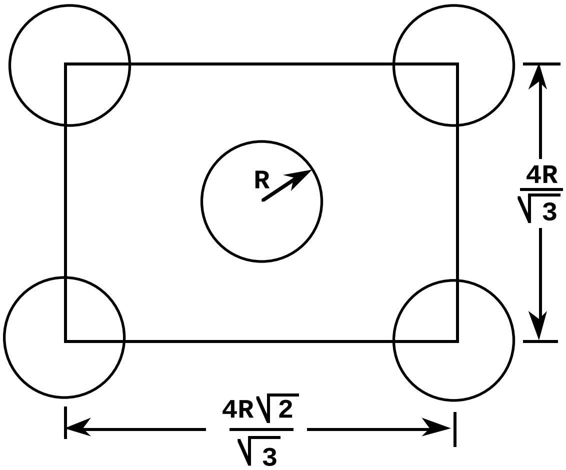

In terms of the atomic radius **R**, the length of the rectangle base is $\frac{4\mathbf{R}\sqrt{2}}{\sqrt{3}}$, whereas the height is $\mathbf{a} = \frac{4\mathbf{R}}{\sqrt{3}}$. Therefore, the area of this rectangle, which is just $\mathbf{A_p}$ is

$$A_p = \left(\frac{4R\sqrt{2}}{\sqrt{3}}\right)\left(\frac{4R}{\sqrt{3}}\right) = \frac{16R^2\sqrt{2}}{3}$$

Now for the number equivalent atoms within this plane. One-fourth of each corner atom and the entirety of the center atom belong to the unit cell. Therefore, there is an equivalent of 2 atoms within the unit cell. Hence

$$A_c = 2(\pi R^2)$$

and

$$\mathrm{PD} = \frac{2\pi R^2}{\dfrac{16R^2\sqrt{2}}{3}} = 0.83$$

3.80* Using the data for aluminum in Table 3.1, we are asked to compute the interplanar spacings for the (110) and (221) sets of planes. From the table, aluminum has an FCC crystal structure and an atomic radius of 0.1431 nm. Using Equation (3.1) the lattice parameter, **a**, may be computed as

$$a = 2R\sqrt{2} = (2)(0.1431\ \mathrm{nm})(\sqrt{2}) = 0.4047\ \mathrm{nm}$$

Now, the $\mathbf{d_{110}}$ interplanar spacing may be determined using Equation (3.11) as

$$d_{110} = \frac{a}{\sqrt{(1)^2 + (1)^2 + (0)^2}} = \frac{0.4047 \text{ nm}}{\sqrt{2}} = 0.2862 \text{ nm}$$

3.84* From the diffraction pattern for α-iron shown in Figure 3.37, we are asked to compute the interplanar spacing for each set of planes that has been indexed; we are also to determine the lattice parameter of Fe for each peak. In order to compute the interplanar spacing and the lattice parameter we must employ Equations (3.11) and (3.10), respectively. For the first peak which occurs at 45.0°

$$d_{110} = \frac{n\lambda}{2 \sin \theta} = \frac{(1)(0.1542 \text{ nm})}{(2)\left(\sin \frac{45.0^\circ}{2}\right)} = 0.2015 \text{ nm}$$

And

$$a = d_{hkl}\sqrt{(h)^2 + (k)^2 + (l)^2} = d_{110}\sqrt{(1)^2 + (1)^2 + (0)^2}$$
$$= (0.2015 \text{ nm})\sqrt{2} = 0.2850 \text{ nm}$$

Similar computations are made for the other peaks which results are tabulated below:

Peak Index	2θ	d_{hkl} (nm)	a (nm)
200	65.1	0.1433	0.2866
211	82.8	0.1166	0.2856

Table 3.1 **Atomic Radii and Crystal Structures for 16 Metals**

Metal	*Crystal Structure*[a]	*Atomic Radius*[b] *(nm)*	*Metal*	*Crystal Structure*	*Atomic Radius (nm)*
Aluminum	FCC	0.1431	Molybdenum	BCC	0.1363
Cadmium	HCP	0.1490	Nickel	FCC	0.1246
Chromium	BCC	0.1249	Platinum	FCC	0.1387
Cobalt	HCP	0.1253	Silver	FCC	0.1445
Copper	FCC	0.1278	Tantalum	BCC	0.1430
Gold	FCC	0.1442	Titanium (α)	HCP	0.1445
Iron (α)	BCC	0.1241	Tungsten	BCC	0.1371
Lead	FCC	0.1750	Zinc	HCP	0.1332

[a] FCC = face-centered cubic; HCP = hexagonal close-packed; BCC = body-centered cubic.

[b] A nanometer (nm) equals 10^{-9} m; to convert from nanometers to angstrom units (Å), multiply the nanometer value by 10.

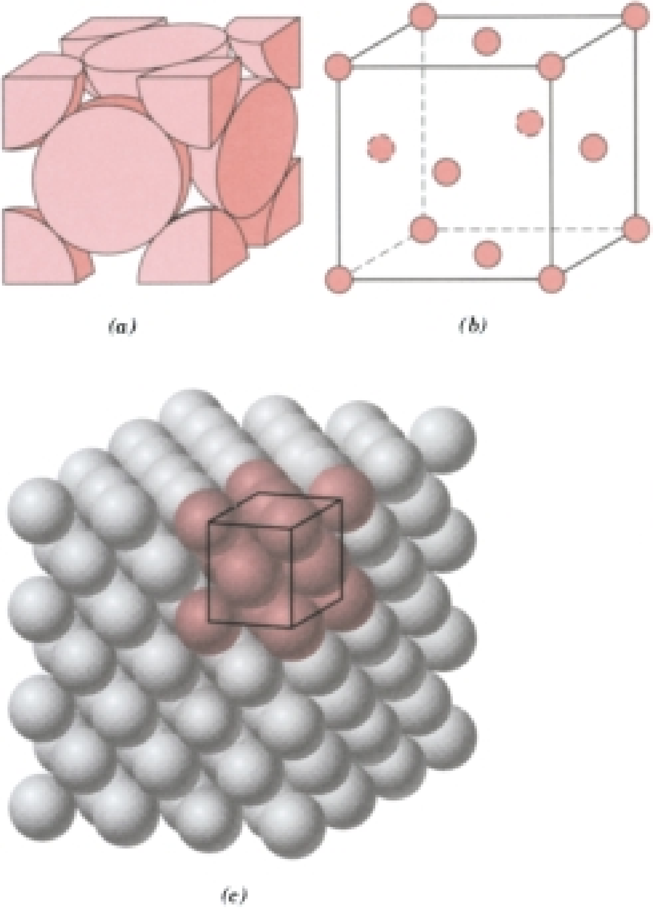

FIGURE 3.1 For the face-centered cubic crystal structure: (*a*) a hard sphere unit cell representation, (*b*) a reduced-sphere unit cell, and (*c*) an aggregate of many atoms. (Figure *c* adapted from W. G. Moffatt, G. W. Pearsall, and J. Wulff, *The Structure and Properties of Materials*, Vol. I, *Structure*, p. 51. Copyright © 1964 by John Wiley & Sons, New York. Reprinted by permission of John Wiley & Sons, Inc.)

Table 3.4 **Ionic Radii for Several Cations and Anions (for a Coordination Number of 6)**

Cation	*Ionic Radius (nm)*	*Anion*	*Ionic Radius (nm)*
Al^{3+}	0.053	Br^{-}	0.196
Ba^{2+}	0.136	Cl^{-}	0.181
Ca^{2+}	0.100	F^{-}	0.133
Cs^{+}	0.170	I^{-}	0.220
Fe^{2+}	0.077	O^{2-}	0.140
Fe^{3+}	0.069	S^{2-}	0.184
K^{+}	0.138		
Mg^{2+}	0.072		
Mn^{2+}	0.067		
Na^{+}	0.102		
Ni^{2+}	0.069		
Si^{4+}	0.040		
Ti^{4+}	0.061		

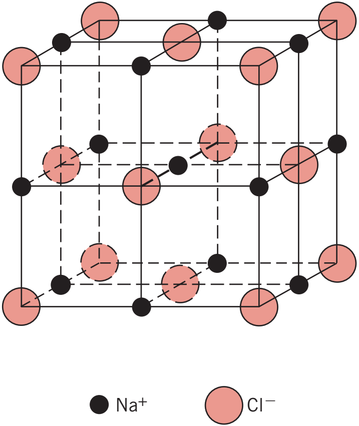

FIGURE 3.5 A unit cell for the rock salt, or sodium chloride (NaCl), crystal structure.

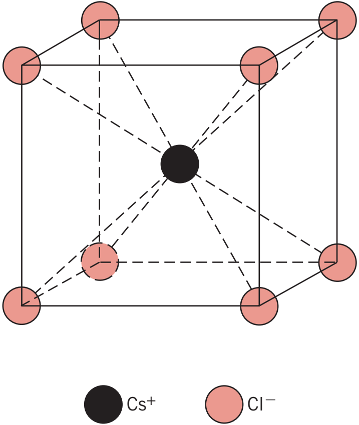

Figure 3.6 A unit cell for the cesium chloride (CsCl) crystal structure.

Table 3.3 Coordination Numbers and Geometries for Various Cation–Anion Radius Ratios (r_C/r_A)

Coordination Number	*Cation–Anion Radius Ratio*	*Coordination Geometry*
2	<0.155	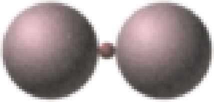
3	0.155–0.225	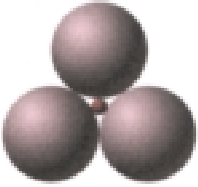
4	0.225–0.414	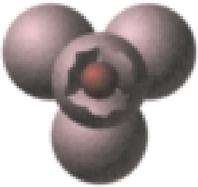
6	0.414–0.732	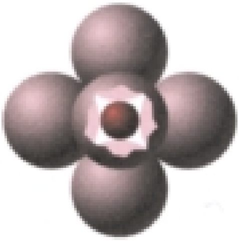
8	0.732–1.0	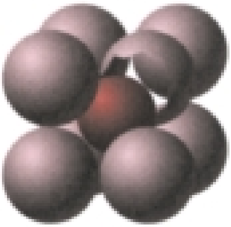

Source: W. D. Kingery, H. K. Bowen, and D. R. Uhlmann, *Introduction to Ceramics*, 2nd edition. Copyright © 1976 by John Wiley & Sons, New York. Reprinted by permission of John Wiley & Sons, Inc.

Table 3.5 Summary of Some Common Ceramic Crystal Structures

Structure Name	Structure Type	Anion Packing	Coordination Numbers: Cation	Coordination Numbers: Anion	Examples
Rock salt (sodium chloride)	AX	FCC	6	6	NaCl, MgO, FeO
Cesium chloride	AX	Simple cubic	8	8	CsCl
Zinc blende (sphalerite)	AX	FCC	4	4	ZnS, SiC
Fluorite	AX_2	Simple cubic	8	4	CaF_2, UO_2, ThO_2
Perovskite	ABX_3	FCC	12(A) 6(B)	6	$BaTiO_3$, $SrZrO_3$, $SrSnO_3$
Spinel	AB_2X_4	FCC	4(A) 6(B)	4	$MgAl_2O_4$, $FeAl_2O_4$

Source: W. D. Kingery, H. K. Bowen, and D. R. Uhlmann, *Introduction to Ceramics*, 2nd edition. Copyright © 1976 by John Wiley & Sons, New York. Reprinted by permission of John Wiley & Sons, Inc.

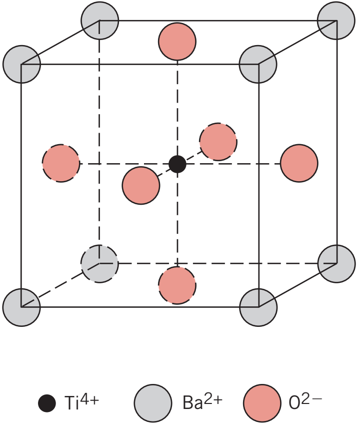

Figure 3.9 A unit cell for the perovskite crystal structure.

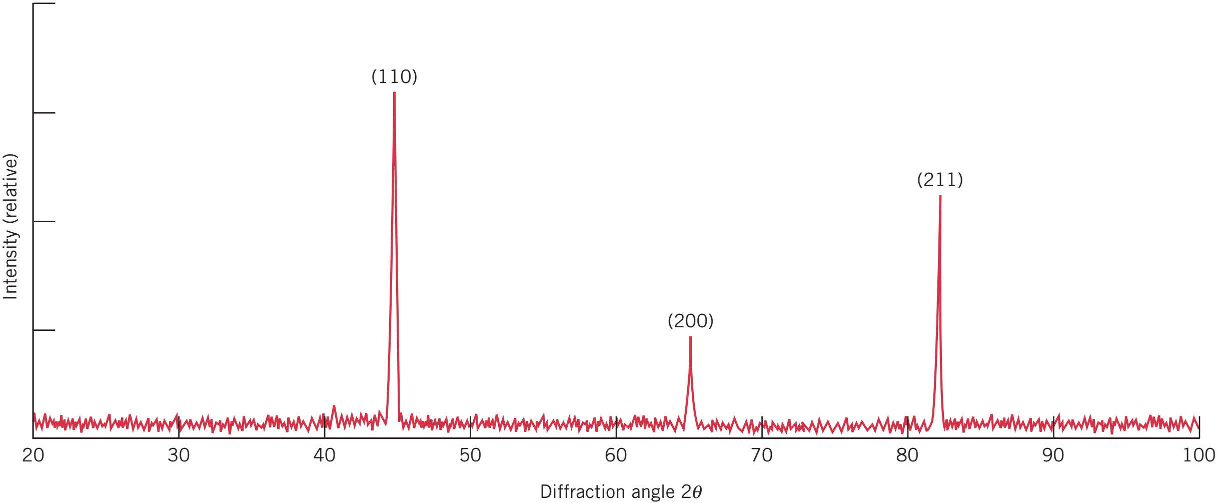

Figure 3.37 Diffraction pattern for polycrystalline α-iron.

CHAPTER 4

POLYMER STRUCTURES

4.4 We are asked to compute the number-average degree of polymerization for polypropylene, given that the number-average molecular weight is 1,000,000 g/mol. The mer molecular weight of polypropylene is just

$$\begin{aligned} m &= 3(A_C) + 6(A_H) \\ &= (3)(12.01\text{ g/mol}) + (6)(1.008\text{ g/mol}) = 42.08\text{ g/mol} \end{aligned}$$

If we let $\mathbf{n_n}$ represent the number-average degree of polymerization, then from Equation (4.4a)

$$n_n = \frac{\overline{M}_n}{m} = \frac{10^6\text{ g/mol}}{42.08\text{ g/mol}} = 23{,}700$$

4.6 (a) From the tabulated data, we are asked to compute $\mathbf{\overline{M}_n}$, the number-average molecular weight. This is carried out below.

Molecular wt Range	Mean M_i	x_i	x_iM_i
8,000–16,000	12,000	0.05	600
16,000–24,000	20,000	0.16	3200
24,000–32,000	28,000	0.24	6720
32,000–40,000	36,000	0.28	10,080
40,000–48,000	44,000	0.20	8800
48,000–56,000	52,000	0.07	3640

$$\overline{M}_n = \sum x_iM_i = 33{,}040\text{ g/mol}$$

(c) Now we are asked to compute $\mathbf{n_n}$ (the number-average degree of polymerization), using the Equation (4.4a). For polypropylene,

$$\begin{aligned} m &= 3(A_C) + 6(A_H) \\ &= (3)(12.01\text{ g/mol}) + (6)(1.008\text{ g/mol}) = 42.08\text{ g/mol} \end{aligned}$$

And

$$n_n = \frac{\overline{M}_n}{m} = \frac{33040\text{ g/mol}}{42.08\text{ g/mol}} = 785$$

4.11 This problem first of all asks for us to calculate, using Equation (4.11), the average total chain length, **L**, for a linear polytetrafluoroethylene polymer having a number-average molecular weight of 500,000 g/mol. It is necessary to calculate the number-average degree of polymerization, $\mathbf{n_n}$, using Equation (4.4a). For PTFE, from Table 4.3, each mer unit has two carbons and four fluorines. Thus,

$$\begin{aligned} m &= 2(A_C) + 4(A_F) \\ &= (2)(12.01\text{ g/mol}) + (4)(19.00\text{ g/mol}) = 100.02\text{ g/mol} \end{aligned}$$

and

$$n_n = \frac{\overline{M}_n}{m} = \frac{500000\text{ g/mol}}{100.02\text{ g/mol}} = 5000$$

which is the number of mer units along an average chain. Since there are two carbon atoms per mer unit, there are two C—C chain bonds per mer, which means that the total number of chain bonds in the molecule, **N**, is just (2)(5000) = 10,000 bonds. Furthermore, assume that for single carbon-carbon bonds, **d** = 0.154 nm and θ = 109° (Section 4.4); therefore, from Equation (4.11)

$$\begin{aligned} L &= Nd\sin\left(\frac{\theta}{2}\right) \\ &= (10{,}000)(0.154\text{ nm})\left[\sin\left(\frac{109^\circ}{2}\right)\right] = 1254\text{ nm} \end{aligned}$$

It is now possible to calculate the average chain end-to-end distance, **r**, using Equation (4.12) as

$$r = d\sqrt{N} = (0.154\text{ nm})\sqrt{10000} = 15.4\text{ nm}$$

4.19 For a poly(styrene-butadiene) alternating copolymer with a number-average molecular weight of 1,350,000 g/mol, we are asked to determine the average number of styrene and butadiene mer units per molecule.

Since it is an alternating copolymer, the number of both types of mer units will be the same. Therefore, consider them as a single mer unit, and determine the number-average degree of polymerization. For the styrene mer, there are eight carbon atoms and eight hydrogen atoms, while the butadiene mer consists of four carbon atoms and six hydrogen atoms. Therefore, the styrene-butadiene combined mer weight is just

$$\begin{aligned} m &= 12(A_C) + 14(A_H) \\ &= (12)(12.01\text{ g/mol}) + (14)(1.008\text{ g/mol}) = 158.23\text{ g/mol} \end{aligned}$$

From Equation (4.4a), the number-average degree of polymerization is just

$$n_n = \frac{\overline{M}_n}{m} = \frac{1350000\text{ g/mol}}{158.23\text{ g/mol}} = 8530$$

Thus, there is an average of 8530 of both mer types per molecule.

4.28 Given that polyethylene has an orthorhombic unit cell with two equivalent mer units, we are asked to compute the density of totally crystalline polyethylene. In order to solve this problem it is necessary to employ Equation (3.5), in which **n** represents the number of mer units within the unit cell (**n** = 2), and **A** is the mer molecular weight, which for polyethylene is just

$$\begin{aligned} A &= 2(A_C) + 4(A_H) \\ &= (2)(12.01\text{ g/mol}) + (4)(1.008\text{ g/mol}) = 28.05\text{ g/mol} \end{aligned}$$

Also, $\mathbf{V_C}$ is the unit cell volume, which is just the product of the three unit cell edge lengths in Figure 4.10. Thus,

$$\begin{aligned} \rho &= \frac{nA}{V_C N_A} \\ &= \frac{(2\text{ mers/uc})(28.05\text{ g/mol})}{(7.41\times10^{-8}\text{ cm})(4.94\times10^{-8}\text{ cm})(2.55\times10^{-8}\text{ cm})/\text{uc}(6.023\times10^{23}\text{ mers/mol})} \\ &= 0.998\text{ g/cm}^3 \end{aligned}$$

Chapter 4 / Polymer Structures

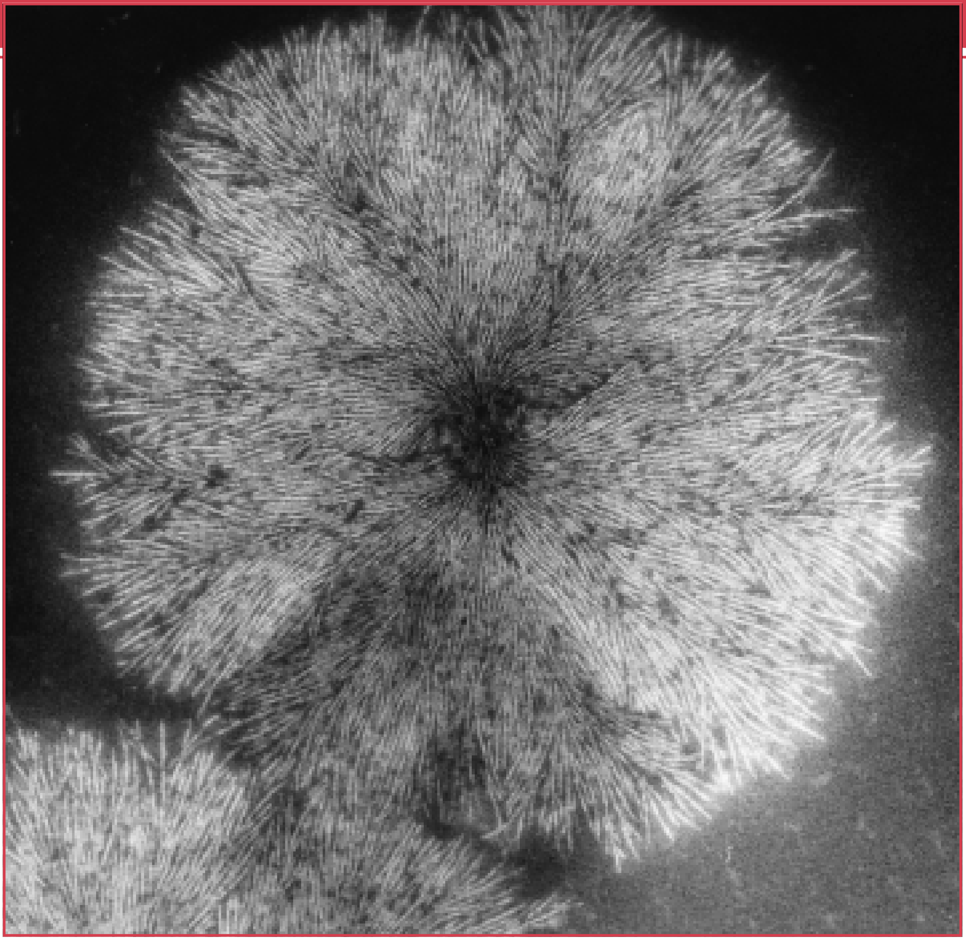

Transmission electron micrograph showing the spherulite structure in a natural rubber specimen. Chain-folded lamellar crystallites approximately 10 nm thick extend in radial directions from the center; they appear as white lines in the micrograph. 30,000×. (Photograph supplied by P. J. Phillips. First published in R. Bartnikas and R. M. Eichhorn, *Engineering Dielectrics*, Vol. IIA, *Electrical Properties of Solid Insulating Materials: Molecular Structure and Electrical Behavior.* Copyright ASTM. Reprinted with permission.)

Why Study *Polymer Structures?*

A relatively large number of chemical and structural characteristics affect the properties and behaviors of polymeric materials. Some of these influences are as follows:

1. Degree of crystallinity of semicrystalline polymers—on density, stiffness, strength, and ductility (Sections 4.11 and 8.18).
2. Degree of crosslinking—on the stiffness of rubber-like materials (Section 8.19).

{3. Polymer chemistry—on melting and glass-transition temperatures (Section 11.17).}

Learning Objectives

After careful study of this chapter you should be able to do the following:

1. **Describe a typical polymer molecule in terms of its chain structure, and, in addition, how the molecule may be generated by repeating mer units.**
2. **Draw mer structures for polyethylene, polyvinyl chloride, polytetrafluoroethylene, polypropylene, and polystyrene.**
3. **Calculate number-average and weight-average molecular weights, and number-average and weight-average degrees of polymerization for a specified polymer.**
4. **Name and briefly describe:**
   - **(a) the four general types of polymer molecular structures;**
   - {**(b) the three types of stereoisomers;**}
   - {**(c) the two kinds of geometrical isomers;**}
   - **(d) the four types of copolymers.**
5. **Cite the differences in behavior and molecular structure for thermoplastic and thermosetting polymers.**
6. **Briefly describe the crystalline state in polymeric materials.**
7. **Briefly describe/diagram the spherulitic structure for a semicrystalline polymer.**

4.1 INTRODUCTION

Naturally occurring polymers—those derived from plants and animals—have been used for many centuries; these materials include wood, rubber, cotton, wool, leather, and silk. Other natural polymers such as proteins, enzymes, starches, and cellulose are important in biological and physiological processes in plants and animals. Modern scientific research tools have made possible the determination of the molecular structures of this group of materials, and the development of numerous polymers, which are synthesized from small organic molecules. Many of our useful plastics, rubbers, and fiber materials are synthetic polymers. In fact, since the conclusion of World War II, the field of materials has been virtually revolutionized by the advent of synthetic polymers. The synthetics can be produced inexpensively, and their properties may be managed to the degree that many are superior to their natural counterparts. In some applications metal and wood parts have been replaced by plastics, which have satisfactory properties and may be produced at a lower cost.

As with metals and ceramics, the properties of polymers are intricately related to the structural elements of the material. This chapter explores molecular and crystal structures of polymers; Chapter 8 discusses the relationships between structure and some of the mechanical properties.

4.2 HYDROCARBON MOLECULES

Since most polymers are organic in origin, we briefly review some of the basic concepts relating to the structure of their molecules. First, many organic materials are *hydrocarbons;* that is, they are composed of hydrogen and carbon. Furthermore, the intramolecular bonds are covalent. Each carbon atom has four electrons that may participate in covalent bonding, whereas every hydrogen atom has only one bonding electron. A single covalent bond exists when each of the two bonding atoms contributes one electron, as represented schematically in Figure 2.10 for a molecule of methane (CH_4). Double and triple bonds between two carbon atoms involve the sharing of two and three pairs of electrons, respectively. For example, in ethylene, which has the chemical formula C_2H_4, the two carbon atoms are doubly bonded together, and each is also singly bonded to two hydrogen atoms, as represented by the structural formula

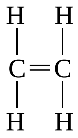

$$\begin{array}{ccc} H & & H \\ \vert & & \vert \\ C & = & C \\ \vert & & \vert \\ H & & H \end{array}$$

where — and = denote single and double covalent bonds, respectively. An example of a triple bond is found in acetylene, C_2H_2:

$$H-C\equiv C-H$$

Molecules that have double and triple covalent bonds are termed **unsaturated.** That is, each carbon atom is not bonded to the maximum (or four) other atoms; as such, it is possible for another atom or group of atoms to become attached to the original molecule. Furthermore, for a **saturated** hydrocarbon, all bonds are single ones (and saturated), and no new atoms may be joined without the removal of others that are already bonded.

Some of the simple hydrocarbons belong to the paraffin family; the chainlike paraffin molecules include methane (CH_4), ethane (C_2H_6), propane (C_3H_8), and butane (C_4H_{10}). Compositions and molecular structures for paraffin molecules are contained in Table 4.1. The covalent bonds in each molecule are strong, but only weak hydrogen and van der Waals bonds exist between molecules, and thus these hydrocarbons have relatively low melting and boiling points. However, boiling temperatures rise with increasing molecular weight (Table 4.1).

Hydrocarbon compounds with the same composition may have different atomic arrangements, a phenomenon termed **isomerism.** For example, there are two iso-

Table 4.1 Compositions and Molecular Structures for Some of the Paraffin Compounds: C_nH_{2n+2}

Name	*Composition*	*Structure*	*Boiling Point* (°*C*)
Methane	CH_4	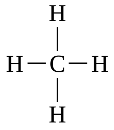 $\begin{array}{ccc} & H & \\ & \vert & \\ H- & C & -H \\ & \vert & \\ & H & \end{array}$	−164
Ethane	C_2H_6	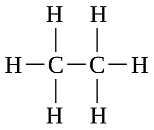 $\begin{array}{cccc} & H & H & \\ & \vert & \vert & \\ H- & C- & C & -H \\ & \vert & \vert & \\ & H & H & \end{array}$	−88.6
Propane	C_3H_8	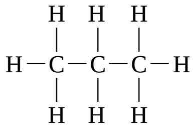 $\begin{array}{ccccc} & H & H & H & \\ & \vert & \vert & \vert & \\ H- & C- & C- & C & -H \\ & \vert & \vert & \vert & \\ & H & H & H & \end{array}$	−42.1
Butane	C_4H_{10}	·	−0.5
Pentane	C_5H_{12}	·	36.1
Hexane	C_6H_{14}	·	69.0

mers for butane; normal butane has the structure

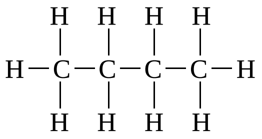

$$\begin{array}{ccccccccc} & & \text{H} & & \text{H} & & \text{H} & & \text{H} & & \\ & & | & & | & & | & & | & & \\ \text{H} & - & \text{C} & - & \text{C} & - & \text{C} & - & \text{C} & - & \text{H} \\ & & | & & | & & | & & | & & \\ & & \text{H} & & \text{H} & & \text{H} & & \text{H} & & \end{array}$$

whereas a molecule of isobutane is represented as follows:

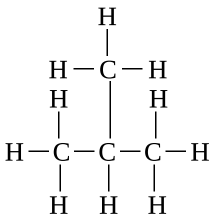

Some of the physical properties of hydrocarbons will depend on the isomeric state; for example, the boiling temperatures for normal butane and isobutane are −0.5 and −12.3°C (31.1 and 9.9°F), respectively.

There are numerous other organic groups, many of which are involved in polymer structures. Several of the more common groups are presented in Table 4.2, where R and R′ represent organic radicals—groups of atoms that remain as a single unit and maintain their identity during chemical reactions. Examples of singly bonded hydrocarbon radicals include the CH_3, C_2H_5, and C_6H_5 (methyl, ethyl, and phenyl) groups.

4.3 Polymer Molecules

The molecules in polymers are gigantic in comparison to the hydrocarbon molecules heretofore discussed; because of their size they are often referred to as **macromolecules.** Within each molecule, the atoms are bound together by covalent interatomic bonds. For most polymers, these molecules are in the form of long and flexible chains, the backbone of which is a string of carbon atoms; many times each carbon atom singly bonds to two adjacent carbons atoms on either side, represented schematically in two dimensions as follows:

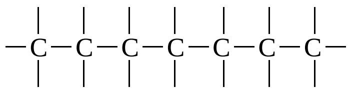

$$\begin{array}{ccccccccccccccc} & | & & | & & | & & | & & | & & | & & | & \\ - & \text{C} & - & \text{C} & - & \text{C} & - & \text{C} & - & \text{C} & - & \text{C} & - & \text{C} & - \\ & | & & | & & | & & | & & | & & | & & | & \end{array}$$

Each of the two remaining valence electrons for every carbon atom may be involved in side-bonding with atoms or radicals that are positioned adjacent to the chain. Of course, both chain and side double bonds are also possible.

These long molecules are composed of structural entities called **mer** units, which are successively repeated along the chain. ''Mer'' originates from the Greek word *meros,* which means part; the term **polymer** was coined to mean many mers. We sometimes use the term **monomer,** which refers to a stable molecule from which a polymer is synthesized.

Table 4.2 Some Common Hydrocarbon Groups

Family	*Characteristic Unit*	*Representative Compound*	
Alcohols	$R{-}OH$	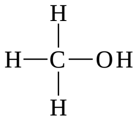	Methyl alcohol
Ethers	$R{-}O{-}R'$	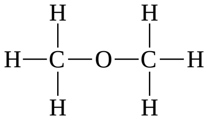	Dimethyl ether
Acids	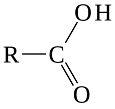	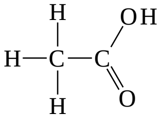	Acetic acid
Aldehydes	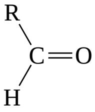	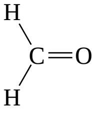	Formaldehyde
Aromatic hydrocarbons	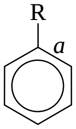 [a]	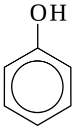	Phenol

[a] The simplified structure 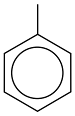 denotes a phenyl group, 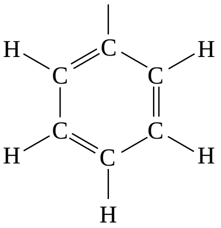

4.4 THE CHEMISTRY OF POLYMER MOLECULES

Consider again the hydrocarbon ethylene (C_2H_4), which is a gas at ambient temperature and pressure, and has the following molecular structure:

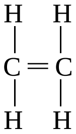

$$\begin{array}{ccc} H & & H \\ | & & | \\ C & = & C \\ | & & | \\ H & & H \end{array}$$

If the ethylene gas is subjected catalytically to appropriate conditions of temperature and pressure, it will transform to polyethylene (PE), which is a solid polymeric material. This process begins when an active mer is formed by the reaction between an initiator or catalyst species (R·) and the ethylene mer unit, as follows:

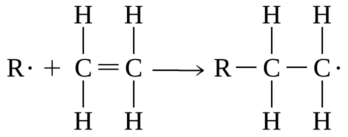

$$R\cdot + \underset{\underset{\textstyle H}{|}}{\overset{\overset{\textstyle H}{|}}{C}} = \underset{\underset{\textstyle H}{|}}{\overset{\overset{\textstyle H}{|}}{C}} \longrightarrow R - \underset{\underset{\textstyle H}{|}}{\overset{\overset{\textstyle H}{|}}{C}} - \underset{\underset{\textstyle H}{|}}{\overset{\overset{\textstyle H}{|}}{C}}\cdot \qquad (4.1)$$

The polymer chain then forms by the sequential addition of polyethylene monomer units to this active initiator-mer center. The active site, or unpaired electron (denoted by ·), is transferred to each successive end monomer as it is linked to the chain. This may be represented schematically as follows:

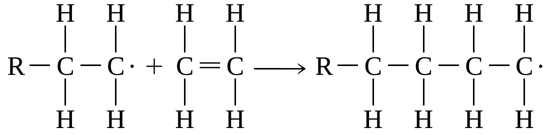

$$R - \underset{\underset{\textstyle H}{|}}{\overset{\overset{\textstyle H}{|}}{C}} - \underset{\underset{\textstyle H}{|}}{\overset{\overset{\textstyle H}{|}}{C}}\cdot + \underset{\underset{\textstyle H}{|}}{\overset{\overset{\textstyle H}{|}}{C}} = \underset{\underset{\textstyle H}{|}}{\overset{\overset{\textstyle H}{|}}{C}} \longrightarrow R - \underset{\underset{\textstyle H}{|}}{\overset{\overset{\textstyle H}{|}}{C}} - \underset{\underset{\textstyle H}{|}}{\overset{\overset{\textstyle H}{|}}{C}} - \underset{\underset{\textstyle H}{|}}{\overset{\overset{\textstyle H}{|}}{C}} - \underset{\underset{\textstyle H}{|}}{\overset{\overset{\textstyle H}{|}}{C}}\cdot \qquad (4.2)$$

The final result, after the addition of many ethylene monomer units, is the polyethylene molecule, a portion of which is shown in Figure 4.1*a*. This representation is not strictly correct in that the angle between the singly bonded carbon atoms is not 180° as shown, but rather close to 109°. A more accurate three-dimensional model is one in which the carbon atoms form a zigzag pattern (Figure 4.1*b*), the C—C bond length being 0.154 nm. In this discussion, depiction of polymer molecules is frequently simplified using the linear chain model.

If all the hydrogen atoms in polyethylene are replaced by fluorine, the resulting polymer is *polytetrafluoroethylene* (PTFE); its mer and chain structures are shown in Figure 4.2*a*. Polytetrafluoroethylene (having the trade name Teflon) belongs to a family of polymers called the fluorocarbons.

Polyvinyl chloride (PVC), another common polymer, has a structure that is a slight variant of that for polyethylene, in which every fourth hydrogen is replaced with a Cl atom. Furthermore, substitution of the CH_3 methyl group

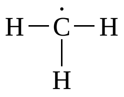

$$H - \overset{\cdot}{\underset{\underset{\textstyle H}{|}}{C}} - H$$

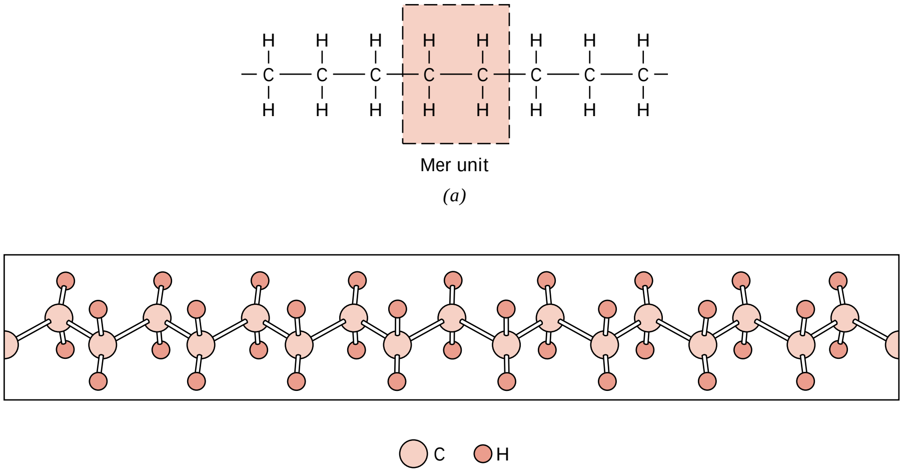

(*b*)

FIGURE 4.1 For polyethylene, (*a*) a schematic representation of mer and chain structures, and (*b*) a perspective of the molecule, indicating the zigzag backbone structure.

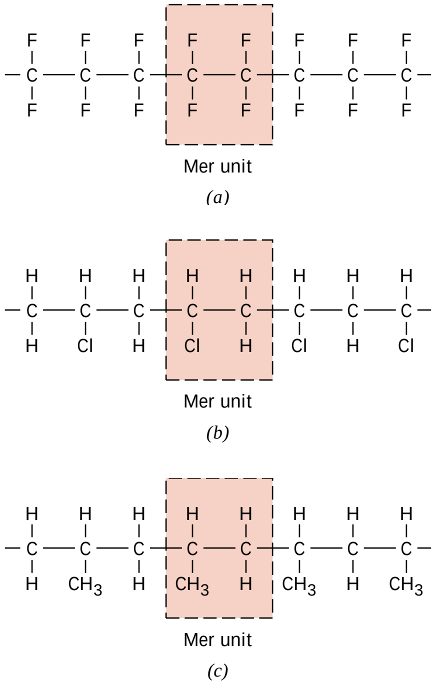

Figure 4.2 Mer and chain structures for (*a*) polytetrafluoroethylene, (*b*) polyvinyl chloride, and (*c*) polypropylene.

for each Cl atom in PVC yields *polypropylene* (PP). Polyvinyl chloride and polypropylene chain structures are also represented in Figure 4.2. Table 4.3 lists mer structures for some of the more common polymers; as may be noted, some of them, for example, nylon, polyester, and polycarbonate, are relatively complex. Mer structures for a large number of relatively common polymers are given in Appendix D.

When all the repeating units along a chain are of the same type, the resulting polymer is called a **homopolymer.** There is no restriction in polymer synthesis that prevents the formation of compounds other than homopolymers; and, in fact, chains may be composed of two or more different mer units, in what are termed **copolymers** (see Section 4.10).

The monomers discussed thus far have an active bond that may react to covalently bond with other monomers, as indicated above for ethylene; such a monomer is termed **bifunctional;** that is, it may bond with two other units in forming the two-dimensional chainlike molecular structure. However, other monomers, such as phenol-formaldehyde (Table 4.3), are **trifunctional;** they have three active bonds, from which a three-dimensional molecular network structure results.

4.5 MOLECULAR WEIGHT

Extremely large molecular weights[1] are to be found in polymers with very long chains. During the polymerization process in which these large macromolecules are

---

[1] ''Molecular mass,'' ''molar mass,'' and ''relative molecular mass'' are sometimes used and are really more appropriate terms than ''molecular weight'' in the context of the present discussion—in actual fact, we are dealing with masses and not weights. However, molecular weight is most commonly found in the polymer literature, and thus will be used throughout this book.

Table 4.3 A Listing of Mer Structures for 10 of the More Common Polymeric Materials

Polymer	*Repeating (Mer) Structure*
Polyethylene (PE)	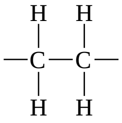 $-\underset{H}{\overset{H}{C}}-\underset{H}{\overset{H}{C}}-$
Polyvinyl chloride (PVC)	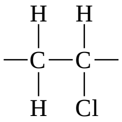 $-\underset{H}{\overset{H}{C}}-\underset{Cl}{\overset{H}{C}}-$
Polytetrafluoroethylene (PTFE)	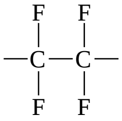 $-\underset{F}{\overset{F}{C}}-\underset{F}{\overset{F}{C}}-$
Polypropylene (PP)	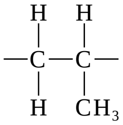 $-\underset{H}{\overset{H}{C}}-\underset{CH_3}{\overset{H}{C}}-$
Polystyrene (PS)	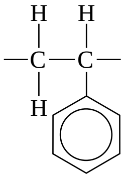
Polymethyl methacrylate (PMMA)	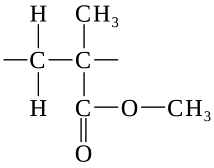
Phenol-formaldehyde (Bakelite)	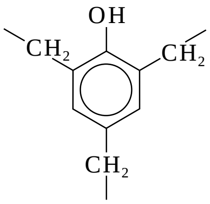
Polyhexamethylene adipamide (nylon 6,6)	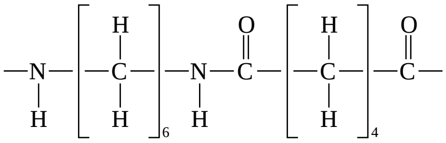 $-\underset{H}{N}-\left[-\underset{H}{\overset{H}{C}}-\right]_6-\underset{H}{N}-\overset{O}{\overset{\|}{C}}-\left[-\underset{H}{\overset{H}{C}}-\right]_4-\overset{O}{\overset{\|}{C}}-$

Table 4.3 **(*Continued*)**

Polymer	***Repeating (Mer) Structure***
Polyethylene terephthalate (PET, a polyester)	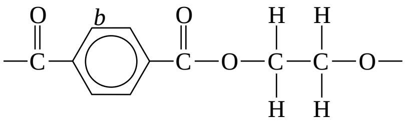
Polycarbonate	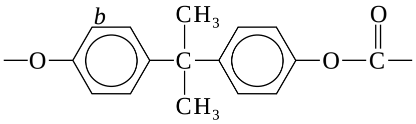

[b] The 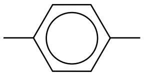 symbol in the backbone chain denotes an aromatic ring as 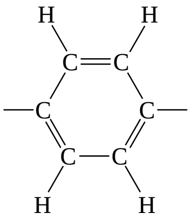

synthesized from smaller molecules, not all polymer chains will grow to the same length; this results in a distribution of chain lengths or molecular weights. Ordinarily, an average molecular weight is specified, which may be determined by the measurement of various physical properties such as viscosity and osmotic pressure.

There are several ways of defining average molecular weight. The number-average molecular weight $\overline{M}_n$ is obtained by dividing the chains into a series of size ranges and then determining the number fraction of chains within each size range (Figure 4.3*a*). This number-average molecular weight is expressed as

$$\overline{M}_n = \Sigma x_i M_i \tag{4.3a}$$

where M_i represents the mean (middle) molecular weight of size range i, and x_i is the fraction of the total number of chains within the corresponding size range.

A weight-average molecular weight $\overline{M}_w$ is based on the weight fraction of molecules within the various size ranges (Figure 4.3*b*). It is calculated according to

$$\overline{M}_w = \Sigma w_i M_i \tag{4.3b}$$

where, again, M_i is the mean molecular weight within a size range, whereas w_i denotes the weight fraction of molecules within the same size interval. Computations for both number-average and weight-average molecular weights are carried out in Example Problem 4.1. A typical molecular weight distribution along with these molecular weight averages are shown in Figure 4.4.

An alternate way of expressing average chain size of a polymer is as the **degree of polymerization** *n*, which represents the average number of mer units in a chain.

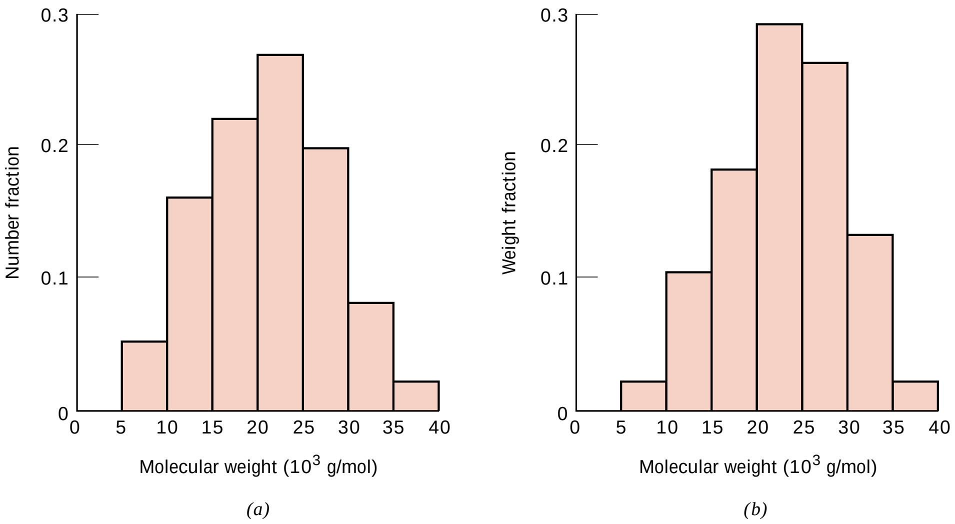

FIGURE 4.3 Hypothetical polymer molecule size distributions on the basis of (*a*) number and (*b*) weight fractions of molecules.

Both number-average (n_n) and weight-average (n_w) degrees of polymerization are possible, as follows:

$$n_n = \frac{\overline{M}_n}{\overline{m}} \tag{4.4a}$$

$$n_w = \frac{\overline{M}_w}{\overline{m}} \tag{4.4b}$$

where $\overline{M}_n$ and $\overline{M}_w$ are the number-average and weight-average molecular weights as defined above, while $\overline{m}$ is the mer molecular weight. For a copolymer (having

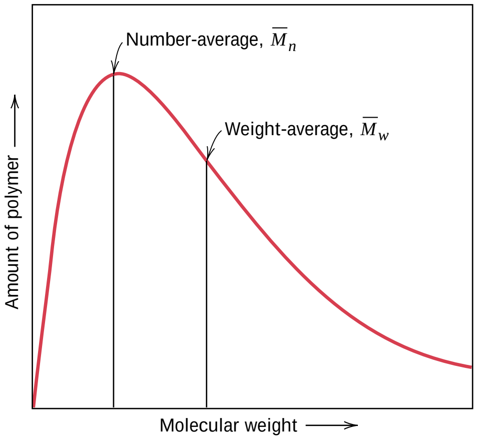

FIGURE 4.4 Distribution of molecular weights for a typical polymer.

two or more different mer units), $\overline{m}$ is determined from

$$\overline{m} = \Sigma f_j m_j \tag{4.5}$$

In this expression, f_j and m_j are, respectively, the chain fraction and molecular weight of mer j.

EXAMPLE PROBLEM 4.1

Assume that the molecular weight distributions shown in Figure 4.3 are for polyvinyl chloride. For this material, compute **(a)** the number-average molecular weight; **(b)** the number-average degree of polymerization; and **(c)** the weight-average molecular weight.

SOLUTION

(a) The data necessary for this computation, as taken from Figure 4.3*a*, are presented in Table 4.4a. According to Equation 4.3a, summation of all the $x_i M_i$ products (from the right-hand column) yields the number-average molecular weight, which in this case is 21,150 g/mol.

(b) To determine the number-average degree of polymerization (Equation 4.4a), it first becomes necessary to compute the mer molecular weight. For PVC, each mer consists of two carbon atoms, three hydrogen atoms, and a

Table 4.4a **Data Used for Number-Average Molecular Weight Computations in Example Problem 4.1**

Molecular Weight Range (g/mol)	*Mean M_i (g/mol)*	x_i	$x_i M_i$
5,000–10,000	7,500	0.05	375
10,000–15,000	12,500	0.16	2000
15,000–20,000	17,500	0.22	3850
20,000–25,000	22,500	0.27	6075
25,000–30,000	27,500	0.20	5500
30,000–35,000	32,500	0.08	2600
35,000–40,000	37,500	0.02	750
			$\overline{M}_n = 21{,}150$

Table 4.4b **Data Used for Weight-Average Molecular Weight Computations in Example Problem 4.1**

Molecular Weight Range (g/mol)	*Mean M_i (g/mol)*	w_i	$w_i M_i$
5,000–10,000	7,500	0.02	150
10,000–15,000	12,500	0.10	1250
15,000–20,000	17,500	0.18	3150
20,000–25,000	22,500	0.29	6525
25,000–30,000	27,500	0.26	7150
30,000–35,000	32,500	0.13	4225
35,000–40,000	37,500	0.02	750
			$\overline{M}_w = 23{,}200$

single chlorine atom (Table 4.3). Furthermore, the atomic weights of C, H, and Cl are, respectively, 12.01, 1.01, and 35.45 g/mol. Thus, for PVC

$$\begin{aligned}\overline{m} &= 2(12.01\text{ g/mol}) + 3(1.01\text{ g/mol}) + 35.45\text{ g/mol}\\ &= 62.50\text{ g/mol}\end{aligned}$$

and

$$n_n = \frac{\overline{M}_n}{\overline{m}} = \frac{21{,}150\text{ g/mol}}{62.50\text{ g/mol}} = 338$$

(c) Table 4.4b shows the data for the weight-average molecular weight, as taken from Figure 4.3*b*. The $w_i M_i$ products for the several size intervals are tabulated in the right-hand column. The sum of these products (Equation 4.3b) yields a value of 23,200 g/mol for $\overline{M}_w$.

Various polymer characteristics are affected by the magnitude of the molecular weight. One of these is the melting or softening temperature; melting temperature is raised with increasing molecular weight (for $\overline{M}$ up to about 100,000 g/mol). At room temperature, polymers with very short chains (having molecular weights on the order of 100 g/mol) exist as liquids or gases. Those with molecular weights of approximately 1000 g/mol are waxy solids (such as paraffin wax) and soft resins. Solid polymers (sometimes termed *high polymers*), which are of prime interest here, commonly have molecular weights ranging between 10,000 and several million g/mol.

4.6 MOLECULAR SHAPE

There is no reason to suppose that polymer chain molecules are strictly straight, in the sense that the zigzag arrangement of the backbone atoms (Figure 4.1*b*) is disregarded. Single chain bonds are capable of rotation and bending in three dimensions. Consider the chain atoms in Figure 4.5*a*; a third carbon atom may lie at any point on the cone of revolution and still subtend about a 109° angle with the bond between the other two atoms. A straight chain segment results when

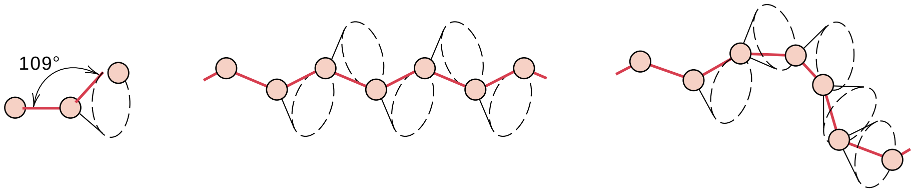

(*a*) (*b*) (*c*)

FIGURE 4.5 Schematic representations of how polymer chain shape is influenced by the positioning of backbone carbon atoms (solid circles). For (*a*), the rightmost atom may lie anywhere on the dashed circle and still subtend a 109° angle with the bond between the other two atoms. Straight and twisted chain segments are generated when the backbone atoms are situated as in (*b*) and (*c*), respectively. (From *Science and Engineering of Materials, 3rd edition,* by D. R. Askeland. © 1994. Reprinted with permission of Brooks/Cole, a division of Thomson Learning. Fax 800 730-2215.)

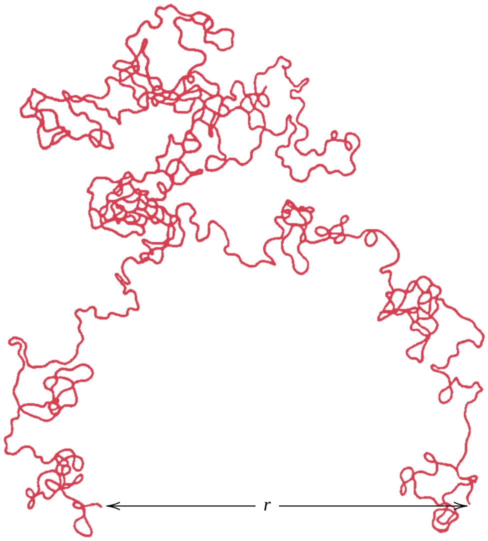

FIGURE 4.6 Schematic representation of a single polymer chain molecule that has numerous random kinks and coils produced by chain bond rotations. (From L. R. G. Treloar, *The Physics of Rubber Elasticity*, 2nd edition, Oxford University Press, Oxford, 1958, p. 47.)

successive chain atoms are positioned as in Figure 4.5*b*. On the other hand, chain bending and twisting are possible when there is a rotation of the chain atoms into other positions, as illustrated in Figure 4.5*c*.[2] Thus, a single chain molecule composed of many chain atoms might assume a shape similar to that represented schematically in Figure 4.6, having a multitude of bends, twists, and kinks.[3] Also indicated in this figure is the end-to-end distance of the polymer chain *r*; this distance is much smaller than the total chain length.

Polymers consist of large numbers of molecular chains, each of which may bend, coil, and kink in the manner of Figure 4.6. This leads to extensive intertwining and entanglement of neighboring chain molecules, a situation similar to that of a fishing line that has experienced backlash from a fishing reel. These random coils and molecular entanglements are responsible for a number of important characteristics of polymers, to include the large elastic extensions displayed by the rubber materials.

Some of the mechanical and thermal characteristics of polymers are a function of the ability of chain segments to experience rotation in response to applied stresses or thermal vibrations. Rotational flexibility is dependent on mer structure and chemistry. For example, the region of a chain segment that has a double bond (C=C) is rotationally rigid. Also, introduction of a bulky or large side group of atoms restricts rotational movement. For example, polystyrene molecules, which have a phenyl side group (Table 4.3), are more resistant to rotational motion than are polyethylene chains.

4.7 MOLECULAR STRUCTURE

The physical characteristics of a polymer depend not only on its molecular weight and shape, but also on differences in the structure of the molecular chains. Modern polymer synthesis techniques permit considerable control over various structural possibilities. This section discusses several molecular structures including linear, branched, crosslinked, and network, in addition to various isomeric configurations.

---

[2] For some polymers, rotation of carbon backbone atoms within the cone may be hindered by bulky side group elements on neighboring chains.

[3] The term *conformation* is often used in reference to the physical outline of a molecule, or molecular shape, that can only be altered by rotation of chain atoms about single bonds.

LINEAR POLYMERS

Linear polymers are those in which the mer units are joined together end to end in single chains. These long chains are flexible and may be thought of as a mass of spaghetti, as represented schematically in Figure 4.7*a*, where each circle represents a mer unit. For linear polymers, there may be extensive van der Waals and hydrogen bonding between the chains. Some of the common polymers that form with linear structures are polyethylene, polyvinyl chloride, polystyrene, polymethyl methacrylate, nylon, and the fluorocarbons.

BRANCHED POLYMERS

Polymers may be synthesized in which side-branch chains are connected to the main ones, as indicated schematically in Figure 4.7*b*; these are fittingly called **branched polymers.** The branches, considered to be part of the main-chain molecule, result from side reactions that occur during the synthesis of the polymer. The chain packing efficiency is reduced with the formation of side branches, which results in a lowering of the polymer density. Those polymers that form linear structures may also be branched.

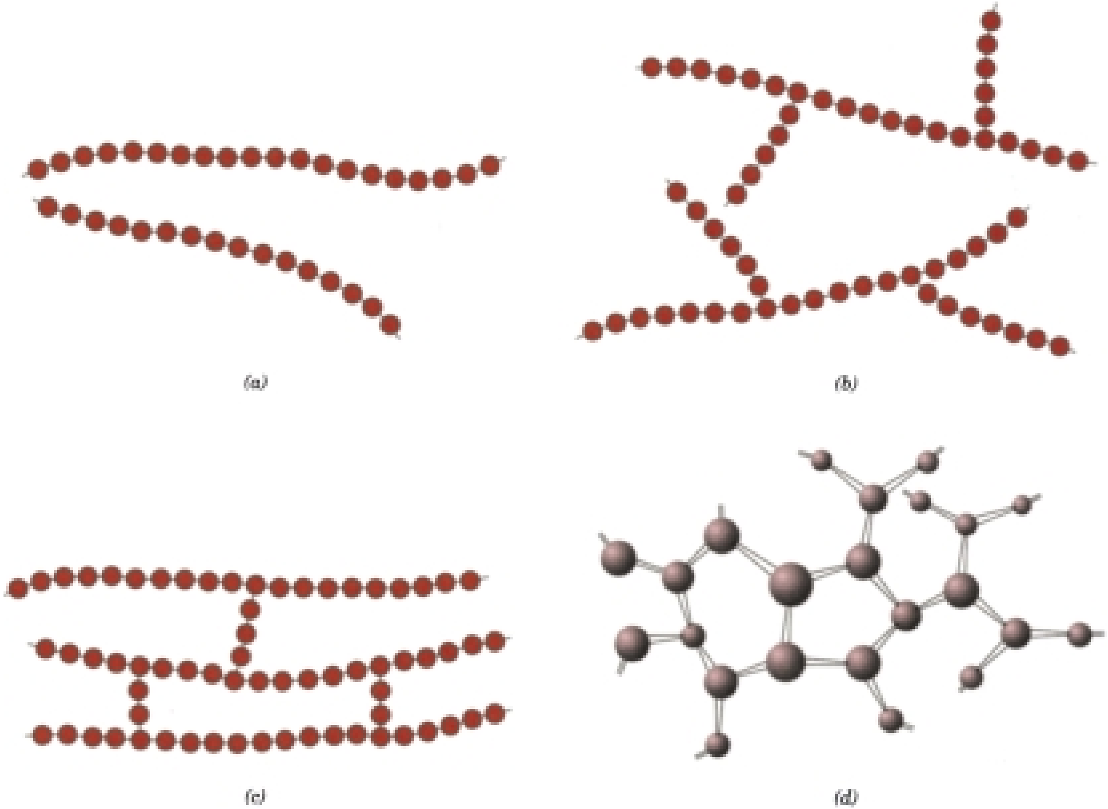

Figure 4.7 Schematic representations of (*a*) linear, (*b*) branched, (*c*) crosslinked, and (*d*) network (three-dimensional) molecular structures. Circles designate individual mer units.

CROSSLINKED POLYMERS

In **crosslinked polymers,** adjacent linear chains are joined one to another at various positions by covalent bonds, as represented in Figure 4.7*c*. The process of crosslinking is achieved either during synthesis or by a nonreversible chemical reaction that is usually carried out at an elevated temperature. Often, this crosslinking is accomplished by additive atoms or molecules that are covalently bonded to the chains. Many of the rubber elastic materials are crosslinked; in rubbers, this is called vulcanization, a process described in Section 8.19.

NETWORK POLYMERS

Trifunctional mer units, having three active covalent bonds, form three-dimensional networks (Figure 4.7*d*) and are termed **network polymers.** Actually, a polymer that is highly crosslinked may be classified as a network polymer. These materials have distinctive mechanical and thermal properties; the epoxies and phenol-formaldehyde belong to this group.

It should be pointed out that polymers are not usually of only one distinctive structural type. For example, a predominantly linear polymer might have some limited branching and crosslinking.

4.8 MOLECULAR CONFIGURATIONS (CD-ROM)

By way of summary of the preceding sections, polymer molecules may be characterized in terms of their size, shape, and structure. Molecular size is specified in terms of molecular weight (or degree of polymerization). Molecular shape relates to the degree of chain twisting, coiling, and bending. Molecular structure depends on the manner in which structural units are joined together. Linear, branched, crosslinked, and network structures are all possible, {in addition to several isomeric configurations (isotactic, syndiotactic, atactic, cis, and trans).} These molecular characteristics are presented in the taxonomic chart, Figure 4.8. It should be noted that some of the structural elements are not mutually exclusive of one another, and, in fact, it may be necessary to specify molecular structure in terms of more than one. For example, a linear polymer may also be isotactic.

4.9 THERMOPLASTIC AND THERMOSETTING POLYMERS

The response of a polymer to mechanical forces at elevated temperatures is related to its dominant molecular structure. And, in fact, one classification scheme for these materials is according to behavior with rising temperature. *Thermoplasts* (or **thermoplastic polymers**) and *thermosets* (or **thermosetting polymers**) are the two subdivisions. Thermoplasts soften when heated (and eventually liquefy) and harden when cooled—processes that are totally reversible and may be repeated. On a molecular level, as the temperature is raised, secondary bonding forces are diminished (by increased molecular motion) so that the relative movement of adjacent chains is facilitated when a stress is applied. Irreversible degradation results when the temperature of a molten thermoplastic polymer is raised to the point at which molecular vibrations become violent enough to break the primary covalent bonds. In addition, thermoplasts are relatively soft. Most linear polymers and those having

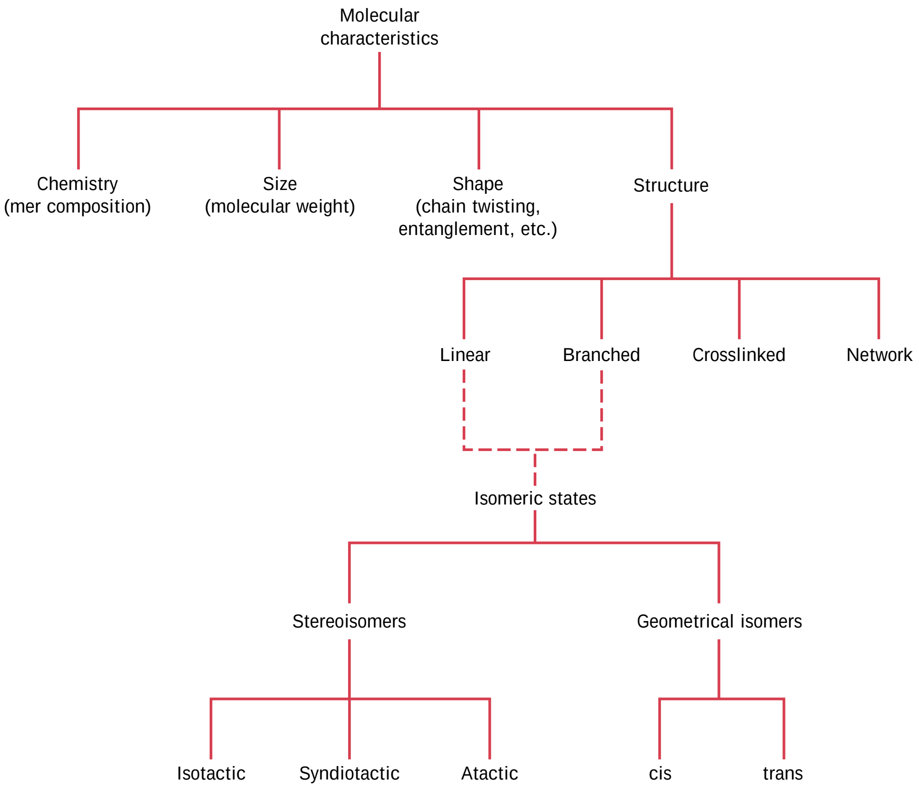
Molecular characteristics
Chemistry (mer composition)
Size (molecular weight)
Shape (chain twisting, entanglement, etc.)
Structure
Linear
Branched
Crosslinked
Network
Isomeric states
Stereoisomers
Geometrical isomers
Isotactic
Syndiotactic
Atactic
cis
trans

Figure 4.8 Classification scheme for the characteristics of polymer molecules.

some branched structures with flexible chains are thermoplastic. These materials are normally fabricated by the simultaneous application of heat and pressure.

Thermosetting polymers become permanently hard when heat is applied and do not soften upon subsequent heating. During the initial heat treatment, covalent crosslinks are formed between adjacent molecular chains; these bonds anchor the chains together to resist the vibrational and rotational chain motions at high temperatures. Crosslinking is usually extensive, in that 10 to 50% of the chain mer units are crosslinked. Only heating to excessive temperatures will cause severance of these crosslink bonds and polymer degradation. Thermoset polymers are generally harder and stronger than thermoplastics, and have better dimensional stability. Most of the crosslinked and network polymers, which include vulcanized rubbers, epoxies, and phenolic and some polyester resins, are thermosetting.

4.10 COPOLYMERS

Polymer chemists and scientists are continually searching for new materials that can be easily and economically synthesized and fabricated, with improved properties or better property combinations than are offered by the homopolymers heretofore discussed. One group of these materials are the copolymers.

Consider a copolymer that is composed of two mer units as represented by ● and ● in Figure 4.9. Depending on the polymerization process and the relative fractions of these mer types, different sequencing arrangements along the polymer chains are possible. For one, as depicted in Figure 4.9*a*, the two different units are randomly dispersed along the chain in what is termed a **random copolymer.** For an **alternating copolymer,** as the name suggests, the two mer units alternate chain

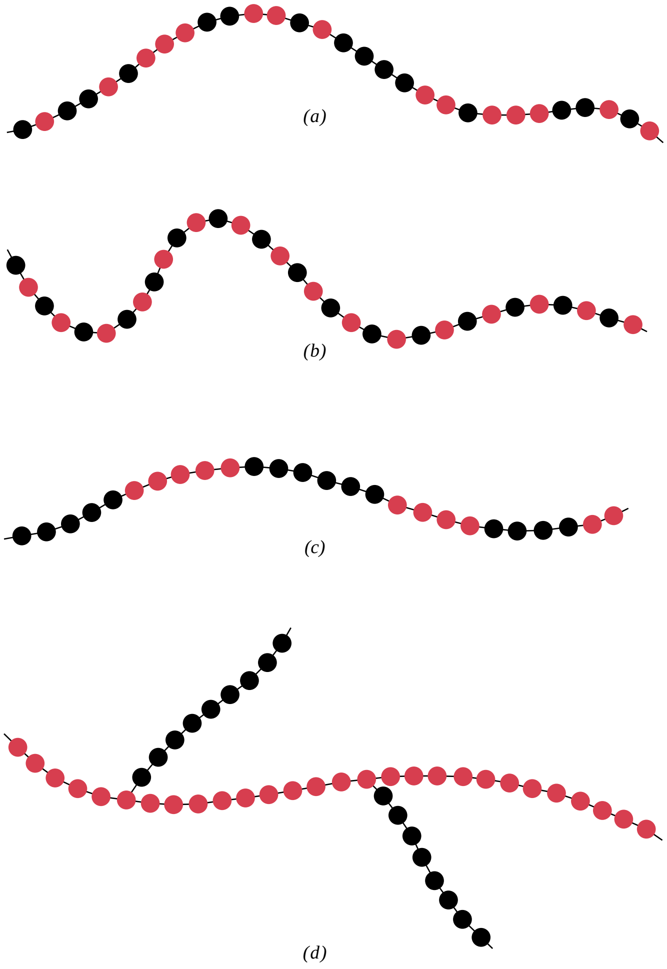

FIGURE 4.9 Schematic representations of (*a*) random, (*b*) alternating, (*c*) block, and (*d*) graft copolymers. The two different mer types are designated by black and colored circles.

positions, as illustrated in Figure 4.9*b*. A **block copolymer** is one in which identical mers are clustered in blocks along the chain (Figure 4.9*c*). And, finally, homopolymer side branches of one type may be grafted to homopolymer main chains that are composed of a different mer; such a material is termed a **graft copolymer** (Figure 4.9*d*).

Synthetic rubbers, discussed in Section 13.13, are often copolymers; chemical repeat units that are employed in some of these rubbers are contained in Table 4.5. Styrene–butadiene rubber (SBR) is a common random copolymer from which automobile tires are made. Nitrile rubber (NBR) is another random copolymer composed of acrylonitrile and butadiene. It is also highly elastic and, in addition, resistant to swelling in organic solvents; gasoline hoses are made of NBR.

4.11 POLYMER CRYSTALLINITY

The crystalline state may exist in polymeric materials. However, since it involves molecules instead of just atoms or ions, as with metals and ceramics, the atomic arrangements will be more complex for polymers. We think of **polymer crystallinity** as the packing of molecular chains so as to produce an ordered atomic array. Crystal structures may be specified in terms of unit cells, which are often quite complex. For example, Figure 4.10 shows the unit cell for polyethylene and its relationship

Table 4.5 **Chemical Repeat Units That Are Employed in Copolymer Rubbers**

Repeat Unit Name	*Repeat Unit Structure*	*Repeat Unit Name*	*Repeat Unit Structure*
Acrylonitrile	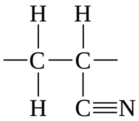 $\begin{array}{cccc} & \mathrm{H} & \mathrm{H} & \\ & \vert & \vert & \\ - & \mathrm{C} - & \mathrm{C} & - \\ & \vert & \vert & \\ & \mathrm{H} & \mathrm{C{\equiv}N} & \end{array}$	*cis*-Isoprene	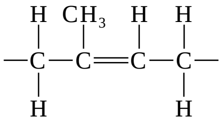 $\begin{array}{cccccc} & \mathrm{H} & \mathrm{CH_3} & \mathrm{H} & \mathrm{H} & \\ & \vert & \vert & \vert & \vert & \\ - & \mathrm{C} - & \mathrm{C} = & \mathrm{C} - & \mathrm{C} & - \\ & \vert & & & \vert & \\ & \mathrm{H} & & & \mathrm{H} & \end{array}$
Styrene	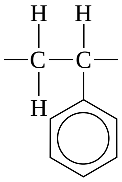	Isobutylene	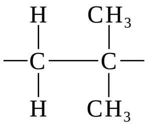 $\begin{array}{cccc} & \mathrm{H} & \mathrm{CH_3} & \\ & \vert & \vert & \\ - & \mathrm{C} - & \mathrm{C} & - \\ & \vert & \vert & \\ & \mathrm{H} & \mathrm{CH_3} & \end{array}$
Butadiene	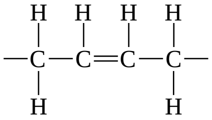 $\begin{array}{cccccc} & \mathrm{H} & \mathrm{H} & \mathrm{H} & \mathrm{H} & \\ & \vert & \vert & \vert & \vert & \\ - & \mathrm{C} - & \mathrm{C} = & \mathrm{C} - & \mathrm{C} & - \\ & \vert & & & \vert & \\ & \mathrm{H} & & & \mathrm{H} & \end{array}$	Dimethylsiloxane	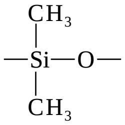 $\begin{array}{cccc} & \mathrm{CH_3} & & \\ & \vert & & \\ - & \mathrm{Si} - & \mathrm{O} & - \\ & \vert & & \\ & \mathrm{CH_3} & & \end{array}$
Chloroprene	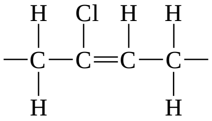 $\begin{array}{cccccc} & \mathrm{H} & \mathrm{Cl} & \mathrm{H} & \mathrm{H} & \\ & \vert & \vert & \vert & \vert & \\ - & \mathrm{C} - & \mathrm{C} = & \mathrm{C} - & \mathrm{C} & - \\ & \vert & & & \vert & \\ & \mathrm{H} & & & \mathrm{H} & \end{array}$		

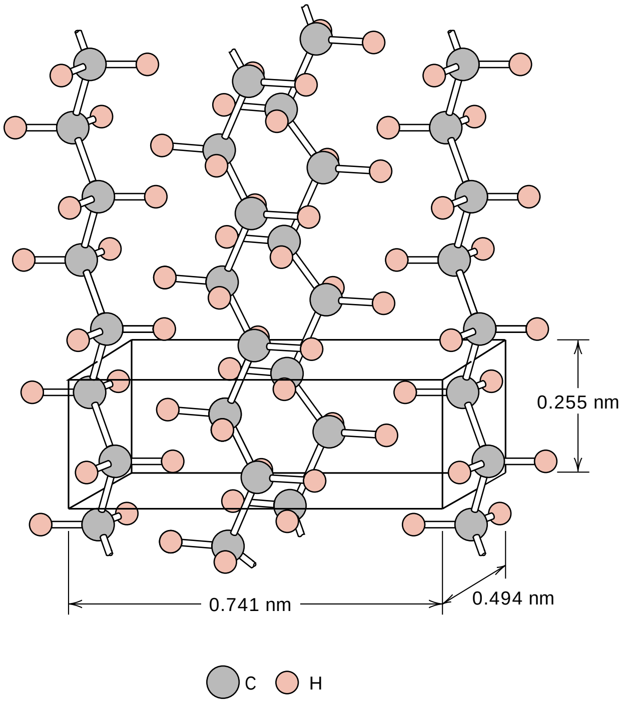

FIGURE 4.10 Arrangement of molecular chains in a unit cell for polyethylene. (Adapted from C. W. Bunn, *Chemical Crystallography*, Oxford University Press, Oxford, 1945, p. 233.)

to the molecular chain structure; this unit cell has orthorhombic geometry (Table 3.6). Of course, the chain molecules also extend beyond the unit cell shown in the figure.

Molecular substances having small molecules (e.g., water and methane) are normally either totally crystalline (as solids) or totally amorphous (as liquids). As a consequence of their size and often complexity, polymer molecules are often only partially crystalline (or semicrystalline), having crystalline regions dispersed within the remaining amorphous material. Any chain disorder or misalignment will result in an amorphous region, a condition that is fairly common, since twisting, kinking, and coiling of the chains prevent the strict ordering of every segment of every chain. Other structural effects are also influential in determining the extent of crystallinity, as discussed below.

The degree of crystallinity may range from completely amorphous to almost entirely (up to about 95%) crystalline; by way of contrast, metal specimens are almost always entirely crystalline, whereas many ceramics are either totally crystalline or totally noncrystalline. Semicrystalline polymers are, in a sense, analogous to two-phase metal alloys, discussed in subsequent chapters.

The density of a crystalline polymer will be greater than an amorphous one of the same material and molecular weight, since the chains are more closely packed together for the crystalline structure. The degree of crystallinity by weight may be determined from accurate density measurements, according to

$$\%\ \text{crystallinity} = \frac{\rho_c(\rho_s - \rho_a)}{\rho_s(\rho_c - \rho_a)} \times 100 \tag{4.10}$$

where ρ_s is the density of a specimen for which the percent crystallinity is to be determined, ρ_a is the density of the totally amorphous polymer, and ρ_c is the density of the perfectly crystalline polymer. The values of ρ_a and ρ_c must be measured by other experimental means.

The degree of crystallinity of a polymer depends on the rate of cooling during solidification as well as on the chain configuration. During crystallization upon cooling through the melting temperature, the chains, which are highly random and entangled in the viscous liquid, must assume an ordered configuration. For this to occur, sufficient time must be allowed for the chains to move and align themselves.

The molecular chemistry as well as chain configuration also influence the ability of a polymer to crystallize. Crystallization is not favored in polymers that are composed of chemically complex mer structures (e.g., polyisoprene). On the other hand, crystallization is not easily prevented in chemically simple polymers such as polyethylene and polytetrafluoroethylene, even for very rapid cooling rates.

For linear polymers, crystallization is easily accomplished because there are virtually no restrictions to prevent chain alignment. Any side branches interfere with crystallization, such that branched polymers never are highly crystalline; in fact, excessive branching may prevent any crystallization whatsoever. Most network and crosslinked polymers are almost totally amorphous; a few crosslinked polymers are partially crystalline. {With regard to stereoisomers, atactic polymers are difficult to crystallize; however, isotactic and syndiotactic polymers crystallize much more easily because the regularity of the geometry of the side groups facilitates the process of fitting together adjacent chains.} Also, the bulkier or larger the side-bonded groups of atoms, the less tendency there is for crystallization.

For copolymers, as a general rule, the more irregular and random the mer arrangements, the greater is the tendency for the development of noncrystallinity.

For alternating and block copolymers there is some likelihood of crystallization. On the other hand, random and graft copolymers are normally amorphous.

To some extent, the physical properties of polymeric materials are influenced by the degree of crystallinity. Crystalline polymers are usually stronger and more resistant to dissolution and softening by heat. Some of these properties are discussed in subsequent chapters.

4.12 POLYMER CRYSTALS

We shall now briefly discuss some of the models that have been proposed to describe the spatial arrangement of molecular chains in polymer crystals. One early model, accepted for many years, is the *fringed-micelle* model (Figure 4.11). It was proposed that a semicrystalline polymer consists of small crystalline regions (**crystallites,** or micelles), each having a precise alignment, which are embedded within the amorphous matrix composed of randomly oriented molecules. Thus a single chain molecule might pass through several crystallites as well as the intervening amorphous regions.

More recently, investigations centered on polymer single crystals grown from dilute solutions. These crystals are regularly shaped, thin platelets (or lamellae), approximately 10 to 20 nm thick, and on the order of 10 μm long. Frequently, these platelets will form a multilayered structure, like that shown in the electron micrograph of a single crystal of polyethylene, Figure 4.12. It is theorized that the molecular chains within each platelet fold back and forth on themselves, with folds occurring at the faces; this structure, aptly termed the **chain-folded model,** is illustrated schematically in Figure 4.13. Each platelet will consist of a number of molecules; however, the average chain length will be much greater than the thickness of the platelet.

Many bulk polymers that are crystallized from a melt form **spherulites.** As implied by the name, each spherulite may grow to be spherical in shape; one of them, as found in natural rubber, is shown in the transmission electron micrograph of the chapter-opening photograph for this chapter. The spherulite consists of an aggregate of ribbonlike chain-folded crystallites (lamellae) approximately 10 nm thick that radiate from the center outward. In this electron micrograph, these

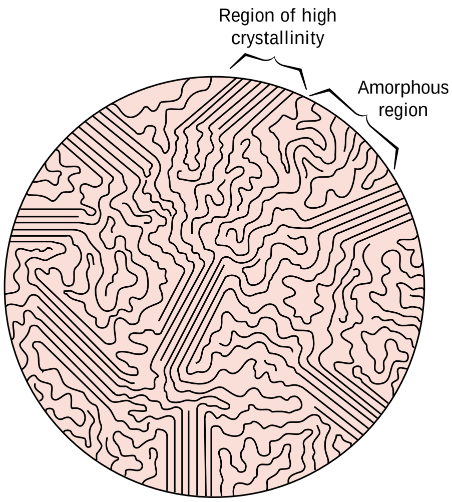

FIGURE 4.11 Fringed-micelle model of a semicrystalline polymer, showing both crystalline and amorphous regions. (From H. W. Hayden, W. G. Moffatt, and J. Wulff, *The Structure and Properties of Materials*, Vol. III, *Mechanical Behavior.* Copyright © 1965 by John Wiley & Sons, New York. Reprinted by permission of John Wiley & Sons, Inc.)

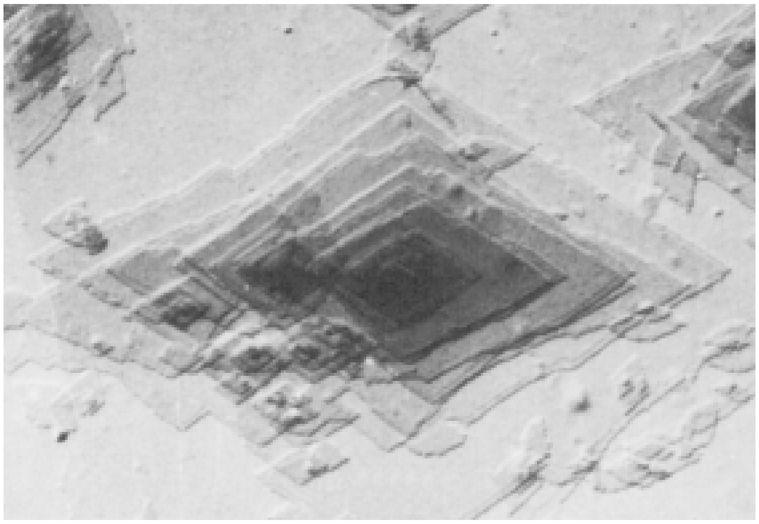

Figure 4.12 Electron micrograph of a polyethylene single crystal. 20,000×. (From A. Keller, R. H. Doremus, B. W. Roberts, and D. Turnbull, Editors, *Growth and Perfection of Crystals.* General Electric Company and John Wiley & Sons, Inc., 1958, p. 498.)

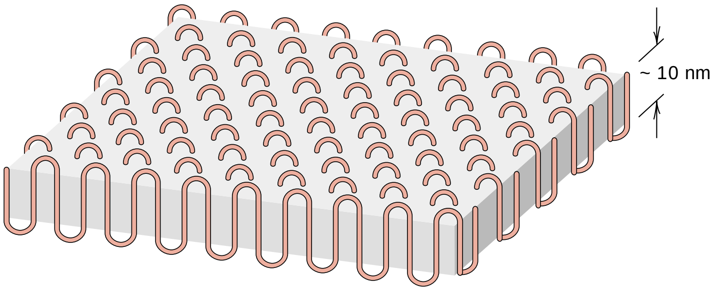

Figure 4.13 The chain-folded structure for a plate-shaped polymer crystallite.

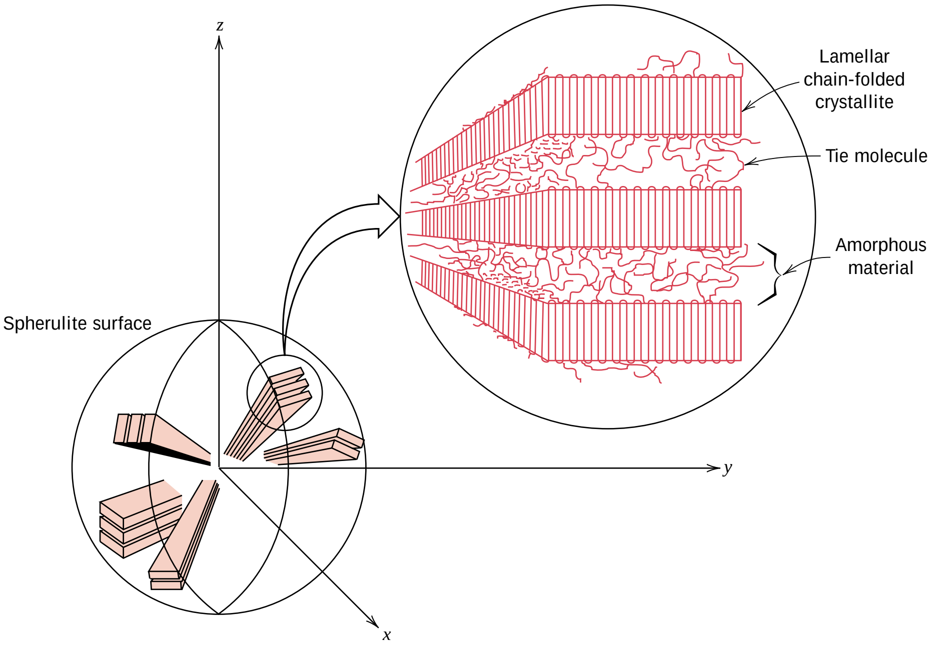
z
Lamellar chain-folded crystallite
Tie molecule
Amorphous material
Spherulite surface
y
x

Figure 4.14 Schematic representation of the detailed structure of a spherulite. (From John C. Coburn, *Dielectric Relaxation Processes in Poly*(*ethylene terephthalate*), Dissertation, University of Utah, 1984.)

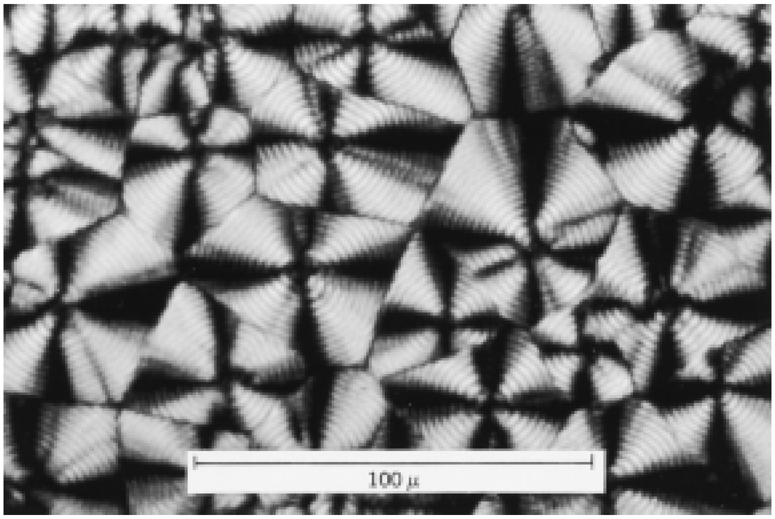

Figure 4.15 A transmission photomicrograph (using cross-polarized light) showing the spherulite structure of polyethylene. Linear boundaries form between adjacent spherulites, and within each spherulite appears a Maltese cross. 525×. (Courtesy F. P. Price, General Electric Company.)

lamellae appear as thin white lines. The detailed structure of a spherulite is illustrated schematically in Figure 4.14; shown here are the individual chain-folded lamellar crystals that are separated by amorphous material. Tie-chain molecules that act as connecting links between adjacent lamellae pass through these amorphous regions.

As the crystallization of a spherulitic structure nears completion, the extremities of adjacent spherulites begin to impinge on one another, forming more or less planar boundaries; prior to this time, they maintain their spherical shape. These boundaries are evident in Figure 4.15, which is a photomicrograph of polyethylene using cross-polarized light. A characteristic Maltese cross pattern appears within each spherulite.

Spherulites are considered to be the polymer analogue of grains in polycrystalline metals and ceramics. However, as discussed above, each spherulite is really composed of many different lamellar crystals and, in addition, some amorphous material. Polyethylene, polypropylene, polyvinyl chloride, polytetrafluoroethylene, and nylon form a spherulitic structure when they crystallize from a melt.

SUMMARY

Most polymeric materials are composed of very large molecules—chains of carbon atoms, to which are side-bonded various atoms or radicals. These macromolecules may be thought of as being composed of mers, smaller structural entities, which are repeated along the chain. Mer structures of some of the chemically simple polymers (e.g., polyethylene, polytetrafluoroethylene, polyvinyl chloride, and polypropylene) were presented.

Molecular weights for high polymers may be in excess of a million. Since all molecules are not of the same size, there is a distribution of molecular weights. Molecular weight is often expressed in terms of number and weight averages. Chain length may also be specified by degree of polymerization, the number of mer units per average molecule.

Several molecular characteristics that have an influence on the properties of polymers were discussed. Molecular entanglements occur when the chains assume twisted, coiled, and kinked shapes or contours. With regard to molecular structure, linear, branched, crosslinked, and network structures are possible, {in addition to isotactic, syndiotactic, and atactic stereoisomers, and the cis and trans geometrical isomers.} The copolymers include random, alternating, block, and graft types.

With regard to behavior at elevated temperatures, polymers are classified as either thermoplastic or thermosetting. The former have linear and branched structures; they soften when heated and harden when cooled. In contrast, thermosets, once having hardened, will not soften upon heating; their structures are crosslinked and network.

When the packing of molecular chains is such as to produce an ordered atomic arrangement, the condition of crystallinity is said to exist. In addition to being entirely amorphous, polymers may also exhibit varying degrees of crystallinity; for the latter case, crystalline regions are interdispersed within amorphous areas. Crystallinity is facilitated for polymers that are chemically simple and that have regular and symmetrical chain structures.

Polymer single crystals may be grown from dilute solutions as thin platelets and having chain-folded structures. Many semicrystalline polymers form spherulites; each spherulite consists of a collection of ribbonlike chain-folded lamellar crystallites that radiate outward from its center.

IMPORTANT TERMS AND CONCEPTS

Alternating copolymer
Atactic configuration
Bifunctional mer
Block copolymer
Branched polymer
Chain-folded model
Cis (structure)
Copolymer
Crosslinked polymer
Crystallite
Degree of polymerization
Graft copolymer
Homopolymer
Isomerism
Isotactic configuration
Linear polymer
Macromolecule
Mer
Molecular chemistry
Molecular structure
Molecular weight
Monomer
Network polymer
Polymer
Polymer crystallinity
Random copolymer
Saturated
Spherulite
Stereoisomerism
Syndiotactic configuration
Thermoplastic polymer
Thermosetting polymer
Trans (structure)
Trifunctional mer
Unsaturated

REFERENCES

Baer, E., ‘‘Advanced Polymers,’’ *Scientific American*, Vol. 255, No. 4, October 1986, pp. 178–190.

Bovey, F. A. and F. H. Winslow (Editors), *Macromolecules: An Introduction to Polymer Science*, Academic Press, New York, 1979.

Cowie, J. M. G., *Polymers: Chemistry and Physics of Modern Materials*, 2nd edition, Chapman and Hall (USA), New York, 1991.

Engineered Materials Handbook, Vol. 2, *Engineering Plastics*, ASM International, Materials Park, OH, 1988.

McCrum, N. G., C. P. Buckley, and C. B. Bucknall, *Principles of Polymer Engineering*, 2nd edition, Oxford University Press, Oxford, 1997. Chapters 0–6.

Rodriguez, F., *Principles of Polymer Systems*, 3rd edition, Hemisphere Publishing Company (Taylor & Francis), New York, 1989.

Rosen, S. L., *Fundamental Principles of Polymeric Materials*, 2nd edition, John Wiley & Sons, New York, 1993.

Rudin, A., *The Elements of Polymer Science and Engineering: An Introductory Text for Engineers and Chemists*, Academic Press, New York, 1982.

Schultz, J., *Polymer Materials Science,* Prentice-Hall, Englewood Cliffs, NJ, 1974.

Seymour, R. B. and C. E. Carraher, Jr., *Polymer Chemistry, An Introduction,* 3rd edition, Marcel Dekker, Inc., New York, 1992.

Sperling, L. H., *Introduction to Physical Polymer Science,* 2nd edition, John Wiley & Sons, New York, 1992.

Young, R. J. and P. Lovell, *Introduction to Polymers,* 2nd edition, Chapman and Hall, London, 1991.

QUESTIONS AND PROBLEMS

Note: To solve those problems having an asterisk (*) by their numbers, consultation of supplementary topics [appearing only on the CD-ROM (and not in print)] will probably be necessary.

4.1 Differentiate between polymorphism and isomerism.

4.2 On the basis of the structures presented in this chapter, sketch mer structures for the following polymers: **(a)** polyvinyl fluoride, **(b)** polychlorotrifluoroethylene, and **(c)** polyvinyl alcohol.

4.3 Compute mer molecular weights for the following: **(a)** polyvinyl chloride, **(b)** polyethylene terephthalate, **(c)** polycarbonate, and **(d)** polydimethylsiloxane.

4.4 The number-average molecular weight of a polypropylene is 1,000,000 g/mol. Compute the number-average degree of polymerization.

4.5 **(a)** Compute the mer molecular weight of polystyrene.

(b) Compute the weight-average molecular weight for a polystyrene for which the weight-average degree of polymerization is 25,000.

4.6 Below, molecular weight data for a polypropylene material are tabulated. Compute **(a)** the number-average molecular weight, **(b)** the weight-average molecular weight, **(c)** the number-average degree of polymerization, and **(d)** the weight-average degree of polymerization.

Molecular Weight Range (g/mol)	x_i	w_i
8,000–16,000	0.05	0.02
16,000–24,000	0.16	0.10
24,000–32,000	0.24	0.20
32,000–40,000	0.28	0.30
40,000–48,000	0.20	0.27
48,000–56,000	0.07	0.11

4.7 Below, molecular weight data for some polymer are tabulated. Compute **(a)** the number-average molecular weight, and **(b)** the weight-average molecular weight. **(c)** If it is known that this material's weight-average degree of polymerization is 780, which one of the polymers listed in Table 4.3 is this polymer? Why? **(d)** What is this material's number-average degree of polymerization?

Molecular Weight Range (g/mol)	x_i	w_i
15,000–30,000	0.04	0.01
30,000–45,000	0.07	0.04
45,000–60,000	0.16	0.11
60,000–75,000	0.26	0.24
75,000–90,000	0.24	0.27
90,000–105,000	0.12	0.16
105,000–120,000	0.08	0.12
120,000–135,000	0.03	0.05

4.8 Is it possible to have a polymethyl methacrylate homopolymer with the following molecular weight data and a weight-average degree of polymerization of 585? Why or why not?

Molecular Weight Range (g/mol)	x_i	w_i
8,000–20,000	0.04	0.01
20,000–32,000	0.10	0.05
32,000–44,000	0.16	0.12
44,000–56,000	0.26	0.25
56,000–68,000	0.23	0.27
68,000–80,000	0.15	0.21
80,000–92,000	0.06	0.09

4.9 High-density polyethylene may be chlorinated by inducing the random substitution of chlorine atoms for hydrogen.

(a) Determine the concentration of Cl (in wt%) that must be added if this substitution occurs for 5% of all the original hydrogen atoms.

(b) In what ways does this chlorinated polyethylene differ from polyvinyl chloride?

4.10 What is the difference between *configuration* and *conformation* in relation to polymer chains?

4.11 For a linear polymer molecule, the total chain length L depends on the bond length between chain atoms d, the total number of bonds in the molecule N, and the angle between adjacent backbone chain atoms θ, as follows:

$$L = Nd \sin\left(\frac{\theta}{2}\right) \tag{4.11}$$

Furthermore, the average end-to-end distance for a series of polymer molecules r in Figure 4.6 is equal to

$$r = d\sqrt{N} \tag{4.12}$$

A linear polytetrafluoroethylene has a number-average molecular weight of 500,000 g/mol; compute average values of L and r for this material.

4.12 Using the definitions for total chain molecule length L (Equation 4.11) and average chain end-to-end distance r (Equation 4.12), for a linear polyethylene determine **(a)** the number-average molecular weight for $L = 2500$ nm; and **(b)** the number-average molecular weight for $r = 20$ nm.

4.13 Make comparisons of thermoplastic and thermosetting polymers **(a)** on the basis of mechanical characteristics upon heating, and **(b)** according to possible molecular structures.

4.14 Some of the polyesters may be either thermoplastic or thermosetting. Suggest one reason for this.

4.15 **(a)** Is it possible to grind up and reuse phenol-formaldehyde? Why or why not?

(b) Is it possible to grind up and reuse polypropylene? Why or why not?

4.16* Sketch portions of a linear polystyrene molecule that are **(a)** syndiotactic, **(b)** atactic, and **(c)** isotactic.

4.17* Sketch cis and trans mer structures for **(a)** butadiene, and **(b)** chloroprene.

4.18 Sketch the mer structure for each of the following alternating copolymers: **(a)** poly (butadiene-chloroprene), **(b)** poly(styrene-methyl methacrylate), and **(c)** poly(acrylonitrile-vinyl chloride).

4.19 The number-average molecular weight of a poly(styrene-butadiene) alternating copolymer is 1,350,000 g/mol; determine the average number of styrene and butadiene mer units per molecule.

4.20 Calculate the number-average molecular weight of a random nitrile rubber [poly(acrylonitrile-butadiene) copolymer] in which the fraction of butadiene mers is 0.30; assume that this concentration corresponds to a number-average degree of polymerization of 2000.

4.21 An alternating copolymer is known to have a number-average molecular weight of 250,000 g/mol and a number-average degree of polymerization of 3420. If one of the mers is styrene, which of ethylene, propylene, tetrafluoroethylene, and vinyl chloride is the other mer? Why?

4.22 **(a)** Determine the ratio of butadiene to styrene mers in a copolymer having a weight-average molecular weight of 350,000 g/mol and weight-average degree of polymerization of 4425.

(b) Which type(s) of copolymer(s) will this copolymer be, considering the following possibilities: random, alternating, graft, and block? Why?

4.23 Crosslinked copolymers consisting of 60 wt% ethylene and 40 wt% propylene may have elastic properties similar to those for natural rubber. For a copolymer of this composition, determine the fraction of both mer types.

4.24 A random poly(isobutylene-isoprene) copolymer has a weight-average molecular weight of 200,000 g/mol and a weight-average degree of polymerization of 3000. Compute the fraction of isobutylene and isoprene mers in this copolymer.

4.25 **(a)** Compare the crystalline state in metals and polymers.

(b) Compare the noncrystalline state as it applies to polymers and ceramic glasses.

4.26 Explain briefly why the tendency of a polymer to crystallize decreases with increasing molecular weight.

4.27* For each of the following pairs of polymers, do the following: (1) state whether or not it is possible to determine if one polymer is more likely to crystallize than the other; (2) if it is possible, note which is the more likely and then cite reason(s) for your choice; and (3) if it is not possible to decide, then state why.

(a) Linear and syndiotactic polyvinyl chloride; linear and isotactic polystyrene.

(b) Network phenol-formaldehyde; linear and heavily crosslinked *cis*-isoprene.

(c) Linear polyethylene; lightly branched isotactic polypropylene.

(d) Alternating poly(styrene-ethylene) copolymer; random poly(vinyl chloride-tetrafluoroethylene) copolymer.

4.28 Compute the density of totally crystalline polyethylene. The orthorhombic unit cell for polyethylene is shown in Figure 4.10; also, the equivalent of two ethylene mer units is contained within each unit cell.

4.29 The density of totally crystalline polypropylene at room temperature is 0.946 g/cm^3. Also, at room temperature the unit cell for this material is monoclinic with lattice parameters

$a = 0.666$ nm $\quad \alpha = 90°$
$b = 2.078$ nm $\quad \beta = 99.62°$
$c = 0.650$ nm $\quad \gamma = 90°$

If the volume of a monoclinic unit cell, V_{mono}, is a function of these lattice parameters as

$$V_{\text{mono}} = abc \sin \beta$$

determine the number of mer units per unit cell.

4.30 The density and associated percent crystallinity for two polytetrafluoroethylene materials are as follows:

ρ (g/cm^3)	Crystallinity (%)
2.144	51.3
2.215	74.2

(a) Compute the densities of totally crystalline and totally amorphous polytetrafluoroethylene.

(b) Determine the percent crystallinity of a specimen having a density of 2.26 g/cm^3.

4.31 The density and associated percent crystallinity for two nylon 6,6 materials are as follows:

ρ (g/cm^3)	Crystallinity (%)
1.188	67.3
1.152	43.7

(a) Compute the densities of totally crystalline and totally amorphous nylon 6,6.

(b) Determine the density of a specimen having 55.4% crystallinity.

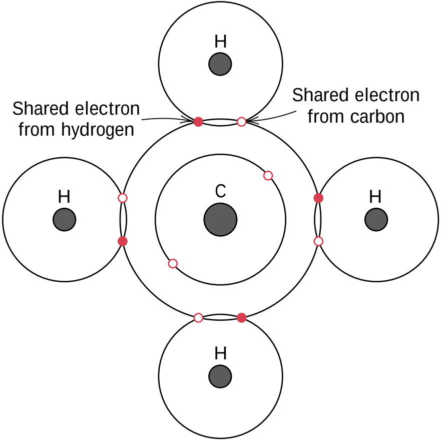
H
Shared electron from hydrogen
Shared electron from carbon
H
C
H
H

FIGURE 2.10 Schematic representation of covalent bonding in a molecule of methane (CH_4).

Table 4.1 **Compositions and Molecular Structures for Some of the Paraffin Compounds: C_nH_{2n+2}**

Name	*Composition*	*Structure*	*Boiling Point (°C)*
Methane	CH_4	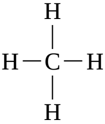 $\mathrm{H-\overset{H}{\underset{H}{C}}-H}$	−164
Ethane	C_2H_6	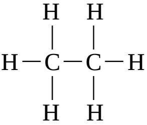 $\mathrm{H-\overset{H}{\underset{H}{C}}-\overset{H}{\underset{H}{C}}-H}$	−88.6
Propane	C_3H_8	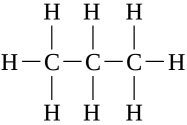 $\mathrm{H-\overset{H}{\underset{H}{C}}-\overset{H}{\underset{H}{C}}-\overset{H}{\underset{H}{C}}-H}$	−42.1
Butane	C_4H_{10}	·	−0.5
Pentane	C_5H_{12}	·	36.1
Hexane	C_6H_{14}	·	69.0

Table 4.2 Some Common Hydrocarbon Groups

Family	*Characteristic Unit*	*Representative Compound*	
Alcohols	$R{-}OH$	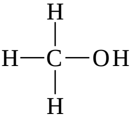 $H{-}\overset{\displaystyle H}{\underset{\displaystyle H}{C}}{-}OH$	Methyl alcohol
Ethers	$R{-}O{-}R'$	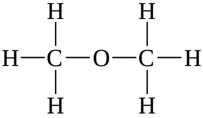 $H{-}\overset{\displaystyle H}{\underset{\displaystyle H}{C}}{-}O{-}\overset{\displaystyle H}{\underset{\displaystyle H}{C}}{-}H$	Dimethyl ether
Acids	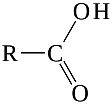	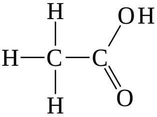	Acetic acid
Aldehydes	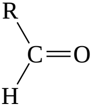	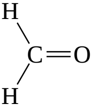	Formaldehyde
Aromatic hydrocarbons	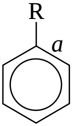 [a]	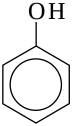	Phenol

---

[a] The simplified structure 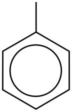 denotes a phenyl group, 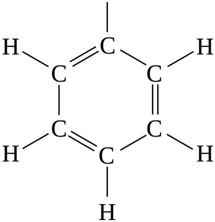

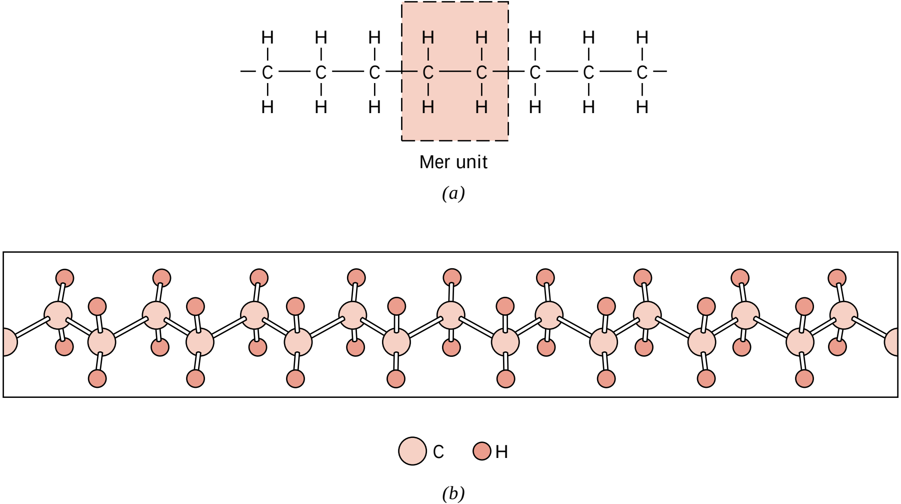

(a)

(b)

Figure 4.1 For polyethylene, (*a*) a schematic representation of mer and chain structures, and (*b*) a perspective of the molecule, indicating the zigzag backbone structure.

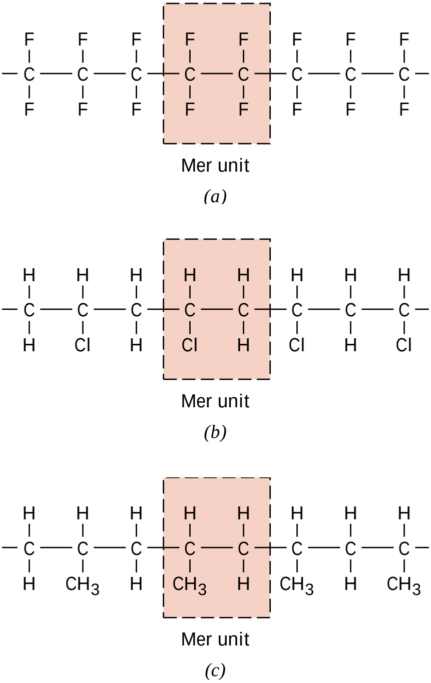
Mer unit
(a)
Mer unit
(b)
Mer unit
(c)

Figure 4.2 Mer and chain structures for (*a*) polytetrafluoroethylene, (*b*) polyvinyl chloride, and (*c*) polypropylene.

```
[Loader]
Program=mse5e
CommandLine=MerPolymers
```

Table 4.3 A Listing of Mer Structures for 10 of the More Common Polymeric Materials

Polymer	*Repeating (Mer) Structure*
Polyethylene (PE)	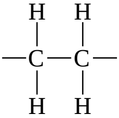 $-\overset{H}{\underset{H}{C}}-\overset{H}{\underset{H}{C}}-$
Polyvinyl chloride (PVC)	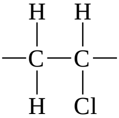 $-\overset{H}{\underset{H}{C}}-\overset{H}{\underset{Cl}{C}}-$
Polytetrafluoroethylene (PTFE)	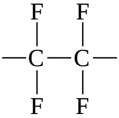 $-\overset{F}{\underset{F}{C}}-\overset{F}{\underset{F}{C}}-$
Polypropylene (PP)	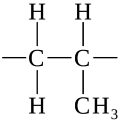 $-\overset{H}{\underset{H}{C}}-\overset{H}{\underset{CH_3}{C}}-$
Polystyrene (PS)	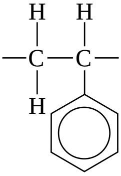
Polymethyl methacrylate (PMMA)	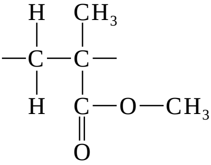
Phenol-formaldehyde (Bakelite)	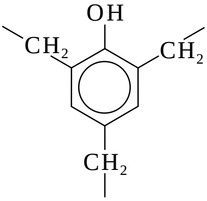
Polyhexamethylene adipamide (nylon 6,6)	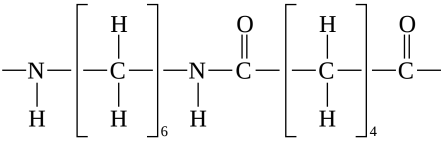 $-\underset{H}{N}-\left[-\overset{H}{\underset{H}{C}}-\right]_6-\underset{H}{N}-\overset{O}{\overset{\Vert}{C}}-\left[-\overset{H}{\underset{H}{C}}-\right]_4-\overset{O}{\overset{\Vert}{C}}-$

Table 4.3 (*Continued*)

Polymer	*Repeating (Mer) Structure*
Polyethylene terephthalate (PET, a polyester)	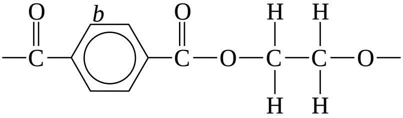
Polycarbonate	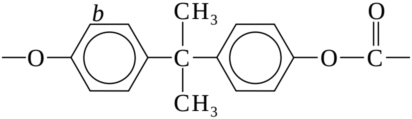

---

[b] The 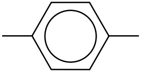 symbol in the backbone chain denotes an aromatic ring as 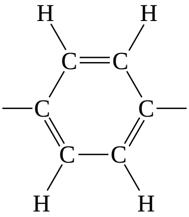

Appendix D / Mer Structures for Common Polymers

Chemical Name	***Mer Chemical Structure***
Epoxy (diglycidyl ether of bisphenol A, DGEPA)	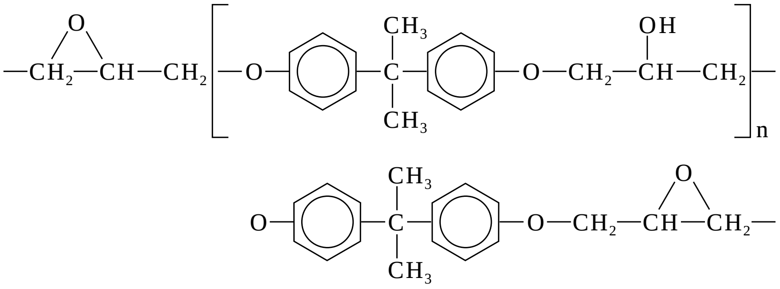
Melamine-formaldehyde (melamine)	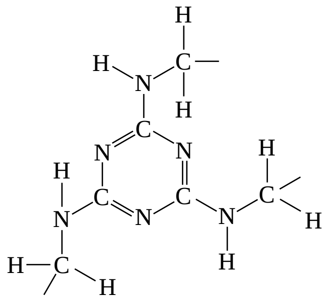
Phenol-formaldehyde (phenolic)	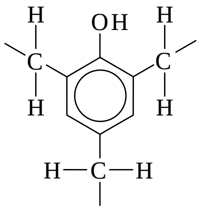
Polyacrylonitrile (PAN)	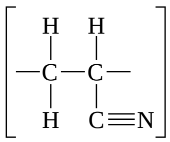
Polyamide-imide (PAI)	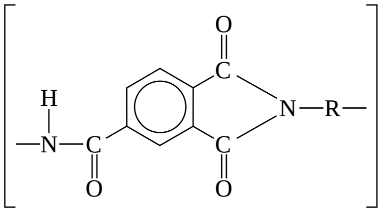

Chemical Name	*Mer Chemical Structure*
Polybutadiene	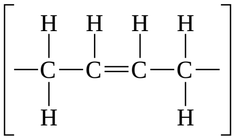 $\left[-\overset{H}{\underset{H}{C}}-\overset{H}{C}=\overset{H}{C}-\overset{H}{\underset{H}{C}}-\right]$
Polybutylene terephthalate (PBT)	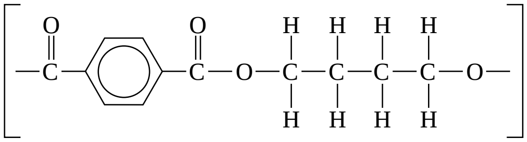
Polycarbonate (PC)	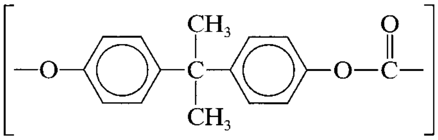
Polychloroprene	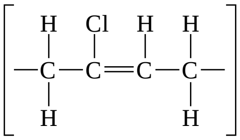 $\left[-\overset{H}{\underset{H}{C}}-\overset{Cl}{C}=\overset{H}{C}-\overset{H}{\underset{H}{C}}-\right]$
Polychlorotrifluoroethylene	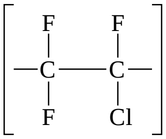 $\left[-\overset{F}{\underset{F}{C}}-\overset{F}{\underset{Cl}{C}}-\right]$
Polydimethyl siloxane (silicone rubber)	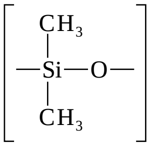 $\left[-\overset{CH_3}{\underset{CH_3}{Si}}-O-\right]$
Polyetheretherketone (PEEK)	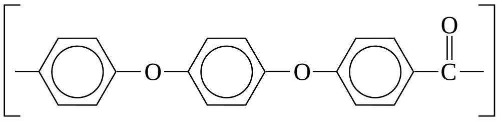
Polyethylene (PE)	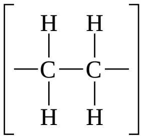 $\left[-\overset{H}{\underset{H}{C}}-\overset{H}{\underset{H}{C}}-\right]$
Polyethylene terephthalate (PET)	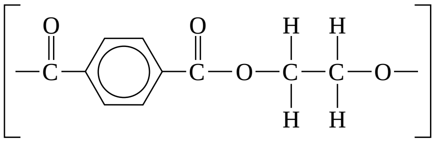

Chemical Name	*Mer Chemical Structure*
Polyhexamethylene adipamide (nylon 6,6)	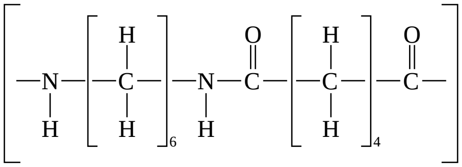 $\left[-\underset{\mathrm{H}}{\underset{\vert}{\mathrm{N}}}-\left[-\overset{\mathrm{H}}{\overset{\vert}{\underset{\mathrm{H}}{\underset{\vert}{\mathrm{C}}}}}-\right]_6-\underset{\mathrm{H}}{\underset{\vert}{\mathrm{N}}}-\overset{\mathrm{O}}{\overset{\Vert}{\mathrm{C}}}-\left[-\overset{\mathrm{H}}{\overset{\vert}{\underset{\mathrm{H}}{\underset{\vert}{\mathrm{C}}}}}-\right]_4-\overset{\mathrm{O}}{\overset{\Vert}{\mathrm{C}}}-\right]$
Polyimide	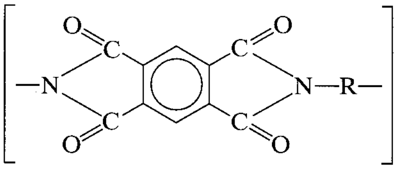
Polyisobutylene	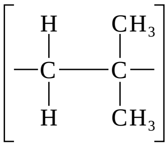 $\left[-\overset{\mathrm{H}}{\overset{\vert}{\underset{\mathrm{H}}{\underset{\vert}{\mathrm{C}}}}}-\overset{\mathrm{CH_3}}{\overset{\vert}{\underset{\mathrm{CH_3}}{\underset{\vert}{\mathrm{C}}}}}-\right]$
cis-Polyisoprene (natural rubber)	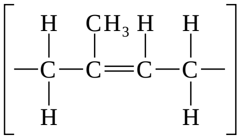 $\left[-\overset{\mathrm{H}}{\overset{\vert}{\underset{\mathrm{H}}{\underset{\vert}{\mathrm{C}}}}}-\overset{\mathrm{CH_3}}{\overset{\vert}{\mathrm{C}}}=\overset{\mathrm{H}}{\overset{\vert}{\mathrm{C}}}-\overset{\mathrm{H}}{\overset{\vert}{\underset{\mathrm{H}}{\underset{\vert}{\mathrm{C}}}}}-\right]$
Polymethyl methacrylate (PMMA)	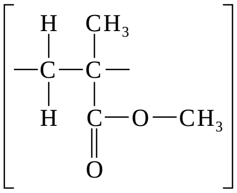 $\left[-\overset{\mathrm{H}}{\overset{\vert}{\underset{\mathrm{H}}{\underset{\vert}{\mathrm{C}}}}}-\overset{\mathrm{CH_3}}{\overset{\vert}{\underset{\underset{\underset{\mathrm{O}}{\Vert}}{\mathrm{C}}-\mathrm{O}-\mathrm{CH_3}}{\underset{\vert}{\mathrm{C}}}}}-\right]$
Polyphenylene oxide (PPO)	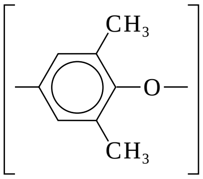
Polyphenylene sulfide (PPS)	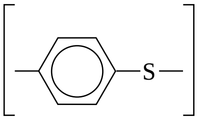
Polyparaphenylene terephthalamide (aramid)	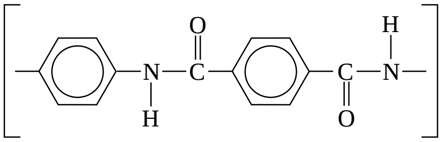

Chemical Name	*Mer Chemical Structure*
Polypropylene (PP)	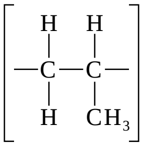 $\left[-\overset{H}{\underset{H}{C}}-\overset{H}{\underset{CH_3}{C}}-\right]$
Polystyrene (PS)	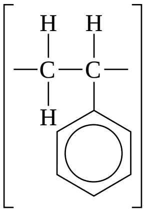
Polytetrafluoroethylene (PTFE)	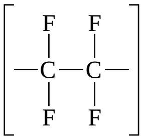 $\left[-\overset{F}{\underset{F}{C}}-\overset{F}{\underset{F}{C}}-\right]$
Polyvinyl acetate (PVAc)	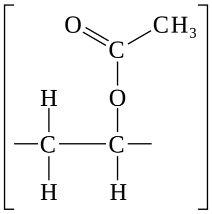
Polyvinyl alcohol (PVA)	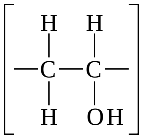 $\left[-\overset{H}{\underset{H}{C}}-\overset{H}{\underset{OH}{C}}-\right]$
Polyvinyl chloride (PVC)	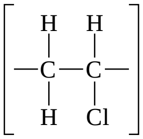 $\left[-\overset{H}{\underset{H}{C}}-\overset{H}{\underset{Cl}{C}}-\right]$
Polyvinyl fluoride (PVF)	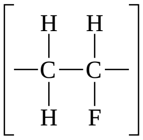 $\left[-\overset{H}{\underset{H}{C}}-\overset{H}{\underset{F}{C}}-\right]$
Polyvinylidene chloride (PVDC)	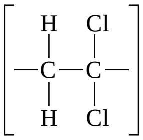 $\left[-\overset{H}{\underset{H}{C}}-\overset{Cl}{\underset{Cl}{C}}-\right]$
Polyvinylidene fluoride (PVDF)	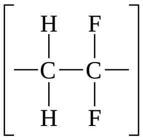 $\left[-\overset{H}{\underset{H}{C}}-\overset{F}{\underset{F}{C}}-\right]$

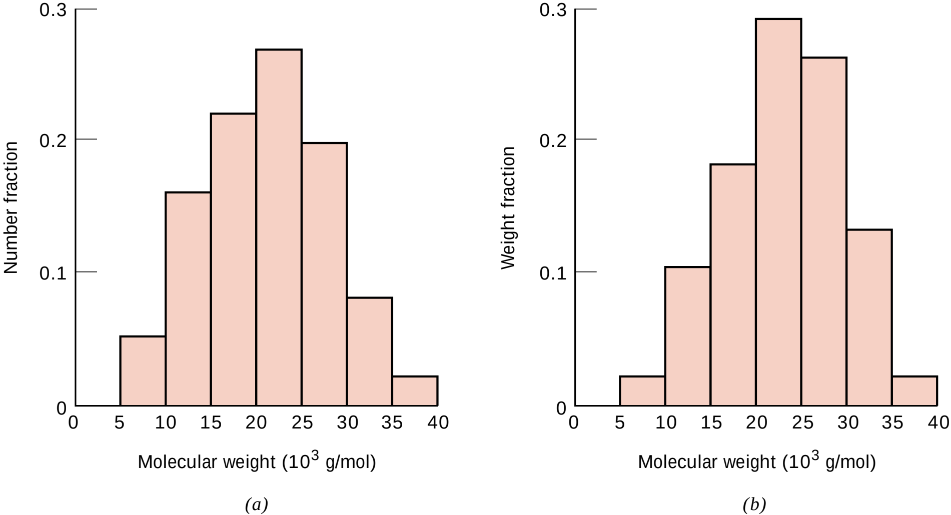

(a) *(b)*

FIGURE 4.3 Hypothetical polymer molecule size distributions on the basis of (*a*) number and (*b*) weight fractions of molecules.

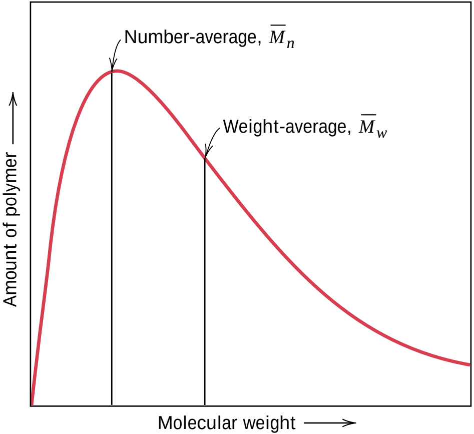

FIGURE 4.4 Distribution of molecular weights for a typical polymer.

Table 4.4a **Data Used for Number-Average Molecular Weight Computations in Example Problem 4.1**

Molecular Weight Range (g/mol)	*Mean M_i (g/mol)*	x_i	x_iM_i
5,000–10,000	7,500	0.05	375
10,000–15,000	12,500	0.16	2000
15,000–20,000	17,500	0.22	3850
20,000–25,000	22,500	0.27	6075
25,000–30,000	27,500	0.20	5500
30,000–35,000	32,500	0.08	2600
35,000–40,000	37,500	0.02	750
			$\overline{M}_n = 21{,}150$

Table 4.4b Data Used for Weight-Average Molecular Weight Computations in Example Problem 4.1

Molecular Weight Range (g/mol)	***Mean M_i (g/mol)***	***w_i***	***$w_i\ M_i$***
5,000–10,000	7,500	0.02	150
10,000–15,000	12,500	0.10	1250
15,000–20,000	17,500	0.18	3150
20,000–25,000	22,500	0.29	6525
25,000–30,000	27,500	0.26	7150
30,000–35,000	32,500	0.13	4225
35,000–40,000	37,500	0.02	750
			$\overline{M}_w = 23{,}200$

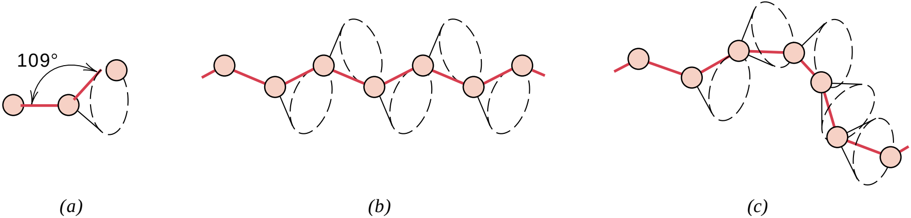

FIGURE 4.5 Schematic representations of how polymer chain shape is influenced by the positioning of backbone carbon atoms (solid circles). For (*a*), the rightmost atom may lie anywhere on the dashed circle and still subtend a 109° angle with the bond between the other two atoms. Straight and twisted chain segments are generated when the backbone atoms are situated as in (*b*) and (*c*), respectively. (From *Science and Engineering of Materials, 3rd edition,* by D. R. Askeland. © 1994. Reprinted with permission of Brooks/Cole, a division of Thomson Learning. Fax 800 730-2215.)

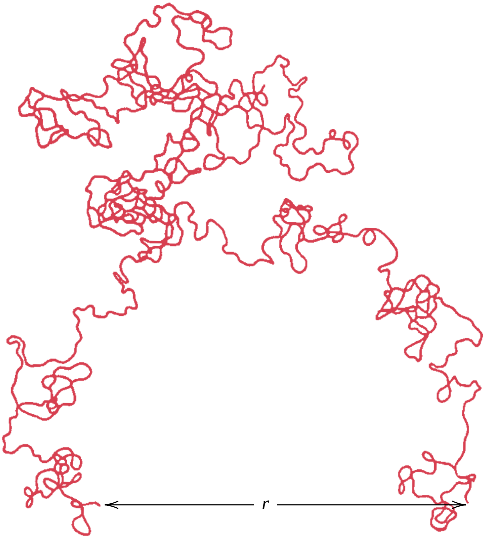

Figure 4.6 Schematic representation of a single polymer chain molecule that has numerous random kinks and coils produced by chain bond rotations. (From L. R. G. Treloar, *The Physics of Rubber Elasticity*, 2nd edition, Oxford University Press, Oxford, 1958, p. 47.)

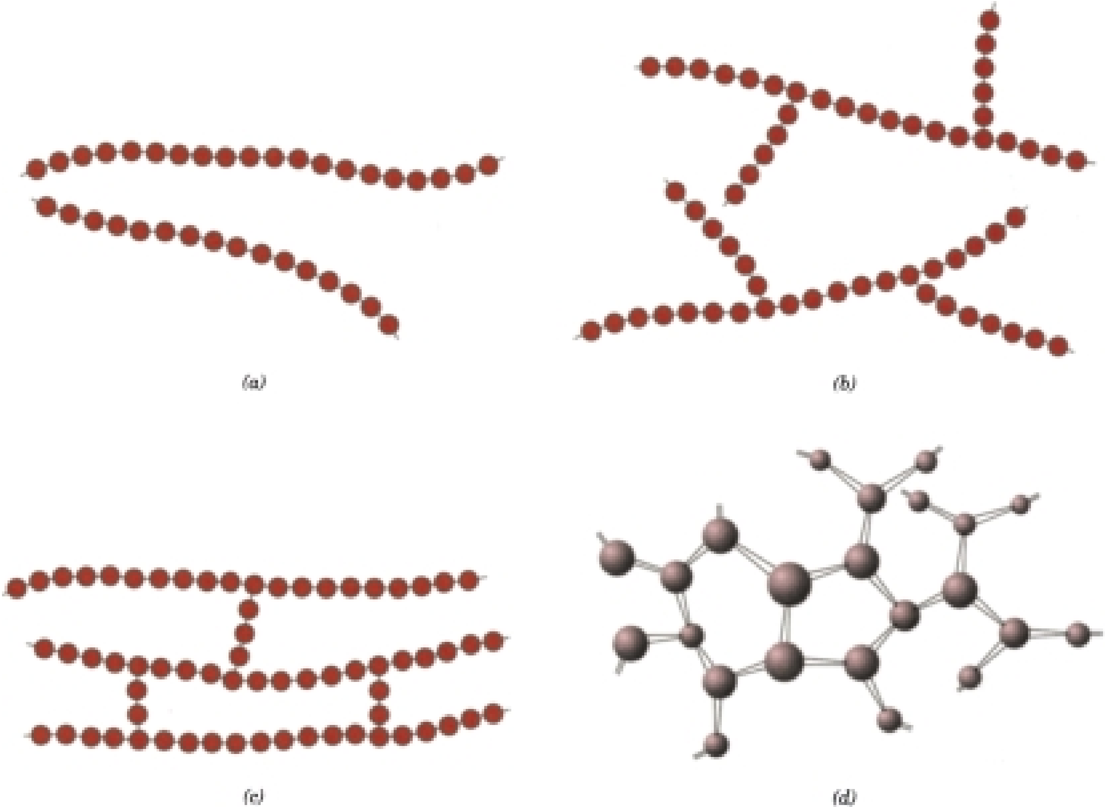

Figure 4.7 Schematic representations of (*a*) linear, (*b*) branched, (*c*) crosslinked, and (*d*) network (three-dimensional) molecular structures. Circles designate individual mer units.

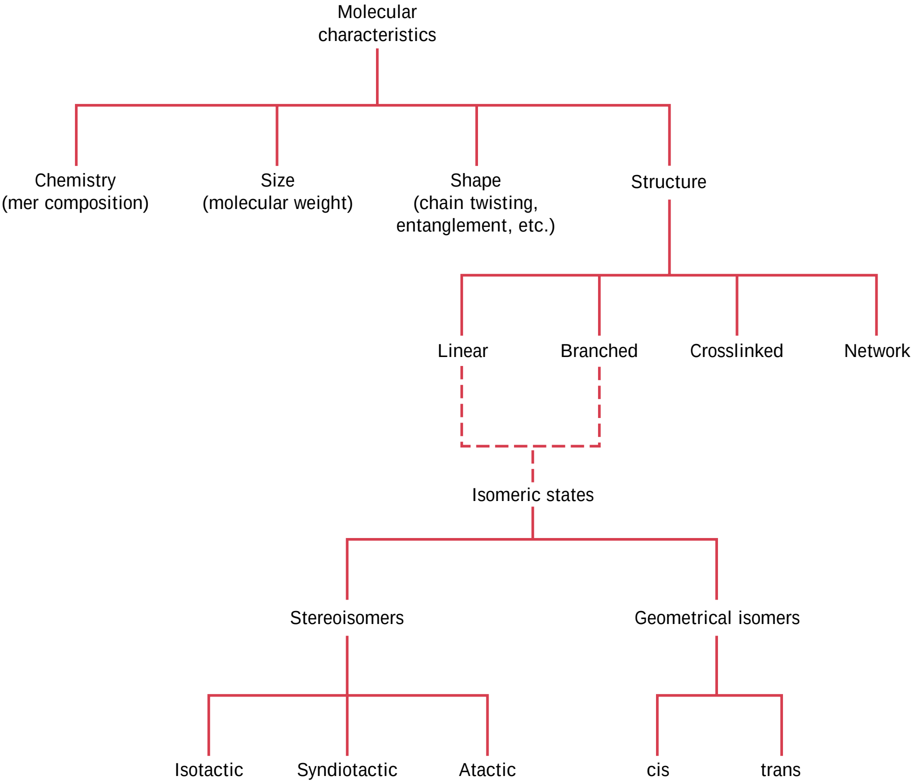
Molecular characteristics
Chemistry (mer composition)
Size (molecular weight)
Shape (chain twisting, entanglement, etc.)
Structure
Linear
Branched
Crosslinked
Network
Isomeric states
Stereoisomers
Geometrical isomers
Isotactic
Syndiotactic
Atactic
cis
trans

FIGURE 4.8 Classification scheme for the characteristics of polymer molecules.

Chapter 4 / Polymer Structures

4.8 MOLECULAR CONFIGURATIONS

For polymers having more than one side atom or group of atoms bonded to the main chain, the regularity and symmetry of the side group arrangement can significantly influence the properties. Consider the mer unit

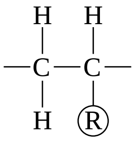

$$\begin{array}{ccccc} & \mathrm{H} & & \mathrm{H} & \\ & | & & | & \\ - & \mathrm{C} & - & \mathrm{C} & - \\ & | & & | & \\ & \mathrm{H} & & \textcircled{R} & \end{array}$$

in which R represents an atom or side group other than hydrogen (e.g., Cl, CH_3). One arrangement is possible when the R side groups of successive mer units bond to alternate carbon atoms as follows:

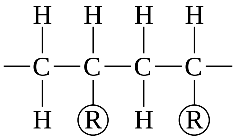

$$\begin{array}{ccccccccc} & \mathrm{H} & & \mathrm{H} & & \mathrm{H} & & \mathrm{H} & \\ & | & & | & & | & & | & \\ - & \mathrm{C} & - & \mathrm{C} & - & \mathrm{C} & - & \mathrm{C} & - \\ & | & & | & & | & & | & \\ & \mathrm{H} & & \textcircled{R} & & \mathrm{H} & & \textcircled{R} & \end{array} \qquad (4.6a)$$

This is designated as a head-to-tail configuration.[4] Its complement, the head-to-head configuration, occurs when R groups bond to adjacent chain atoms:

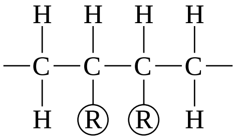

$$\begin{array}{ccccccccc} & \mathrm{H} & & \mathrm{H} & & \mathrm{H} & & \mathrm{H} & \\ & | & & | & & | & & | & \\ - & \mathrm{C} & - & \mathrm{C} & - & \mathrm{C} & - & \mathrm{C} & - \\ & | & & | & & | & & | & \\ & \mathrm{H} & & \textcircled{R} & & \textcircled{R} & & \mathrm{H} & \end{array} \qquad (4.6b)$$

In most polymers, the head-to-tail configuration predominates; often a polar repulsion occurs between R groups for the head-to-head configuration.

Isomerism (Section 4.2) is also found in polymer molecules, wherein different atomic configurations are possible for the same composition. Two isomeric subclasses, stereoisomerism and geometrical isomerism, are topics of discussion in the succeeding sections.

---

[4] The term *configuration* is used in reference to arrangements of units along the axis of the chain, or atom positions that are not alterable except by the breaking and then reforming of primary bonds.

STEREOISOMERISM

Stereoisomerism denotes the situation in which atoms are linked together in the same order (head-to-tail) but differ in their spatial arrangement. For one stereoisomer, all the R groups are situated on the same side of the chain as follows:

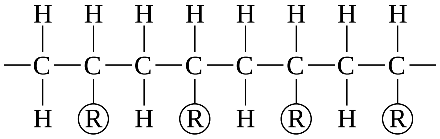

$$\begin{array}{cccccccccccccccc} & \mathrm{H} & & \mathrm{H} & & \mathrm{H} & & \mathrm{H} & & \mathrm{H} & & \mathrm{H} & & \mathrm{H} & & \mathrm{H} \\ & | & & | & & | & & | & & | & & | & & | & & | \\ - & \mathrm{C} & - & \mathrm{C} & - & \mathrm{C} & - & \mathrm{C} & - & \mathrm{C} & - & \mathrm{C} & - & \mathrm{C} & - & \mathrm{C} - \\ & | & & | & & | & & | & & | & & | & & | & & | \\ & \mathrm{H} & & \textcircled{R} & & \mathrm{H} & & \textcircled{R} & & \mathrm{H} & & \textcircled{R} & & \mathrm{H} & & \textcircled{R} \end{array} \qquad (4.7)$$

This is called an **isotactic configuration.**

In a **syndiotactic configuration,** the R groups alternate sides of the chain:

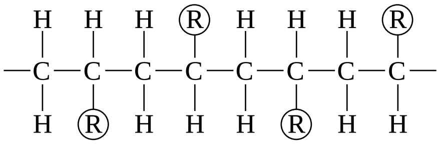

$$\begin{array}{cccccccccccccccc} & \mathrm{H} & & \mathrm{H} & & \mathrm{H} & & \textcircled{R} & & \mathrm{H} & & \mathrm{H} & & \mathrm{H} & & \textcircled{R} \\ & | & & | & & | & & | & & | & & | & & | & & | \\ - & \mathrm{C} & - & \mathrm{C} & - & \mathrm{C} & - & \mathrm{C} & - & \mathrm{C} & - & \mathrm{C} & - & \mathrm{C} & - & \mathrm{C} - \\ & | & & | & & | & & | & & | & & | & & | & & | \\ & \mathrm{H} & & \textcircled{R} & & \mathrm{H} & & \mathrm{H} & & \mathrm{H} & & \textcircled{R} & & \mathrm{H} & & \mathrm{H} \end{array} \qquad (4.8)$$

And for random positioning,

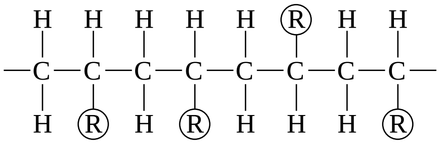

$$\begin{array}{cccccccccccccccc} & \mathrm{H} & & \mathrm{H} & & \mathrm{H} & & \mathrm{H} & & \mathrm{H} & & \textcircled{R} & & \mathrm{H} & & \mathrm{H} \\ & | & & | & & | & & | & & | & & | & & | & & | \\ - & \mathrm{C} & - & \mathrm{C} & - & \mathrm{C} & - & \mathrm{C} & - & \mathrm{C} & - & \mathrm{C} & - & \mathrm{C} & - & \mathrm{C} - \\ & | & & | & & | & & | & & | & & | & & | & & | \\ & \mathrm{H} & & \textcircled{R} & & \mathrm{H} & & \textcircled{R} & & \mathrm{H} & & \mathrm{H} & & \mathrm{H} & & \textcircled{R} \end{array} \qquad (4.9)$$

the term **atactic configuration** is used.

Conversion from one stereoisomer to another (e.g., isotactic to syndiotactic) is not possible by a simple rotation about single chain bonds; these bonds must first be severed, and then, after the appropriate rotation, they are reformed.

In reality, a specific polymer does not exhibit just one of these configurations; the predominant form depends on the method of synthesis.

GEOMETRICAL ISOMERISM

Other important chain configurations, or geometrical isomers, are possible within mer units having a double bond between chain carbon atoms. Bonded to each of the carbon atoms participating in the double bond is a single side-bonded atom or radical, which may be situated on one side of the chain or its opposite. Consider the isoprene mer having the structure

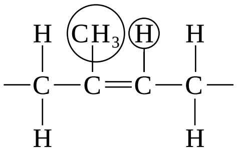

$$\begin{array}{cccccccc} & \mathrm{H} & & \boxed{\mathrm{CH_3}} & & \boxed{\mathrm{H}} & & \mathrm{H} \\ & | & & | & & | & & | \\ - & \mathrm{C} & - & \mathrm{C} & = & \mathrm{C} & - & \mathrm{C} - \\ & | & & & & & & | \\ & \mathrm{H} & & & & & & \mathrm{H} \end{array}$$

in which the CH_3 group and the H atom are positioned on the same side of the chain. This is termed a **cis** structure, and the resulting polymer, *cis*-polyisoprene, is natural rubber. For the alternative isomer

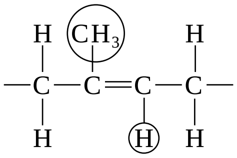

$$\begin{array}{ccccccccc} & \text{H} & & \text{CH}_3 & & & & \text{H} & \\ & | & & | & & & & | & \\ — & \text{C} & — & \text{C} & = & \text{C} & — & \text{C} & — \\ & | & & & & | & & | & \\ & \text{H} & & & & \text{H} & & \text{H} & \end{array}$$

the **trans** structure, the CH_3 and H reside on opposite chain sides. *Trans*-polyisoprene, sometimes called gutta percha, has properties that are distinctly different from natural rubber as a result of this configurational alteration. Conversion of trans to cis, or vice versa, is not possible by a simple chain bond rotation because the chain double bond is extremely rigid.

```
[Loader]
Program=mse5e
CommandLine=isomers
```

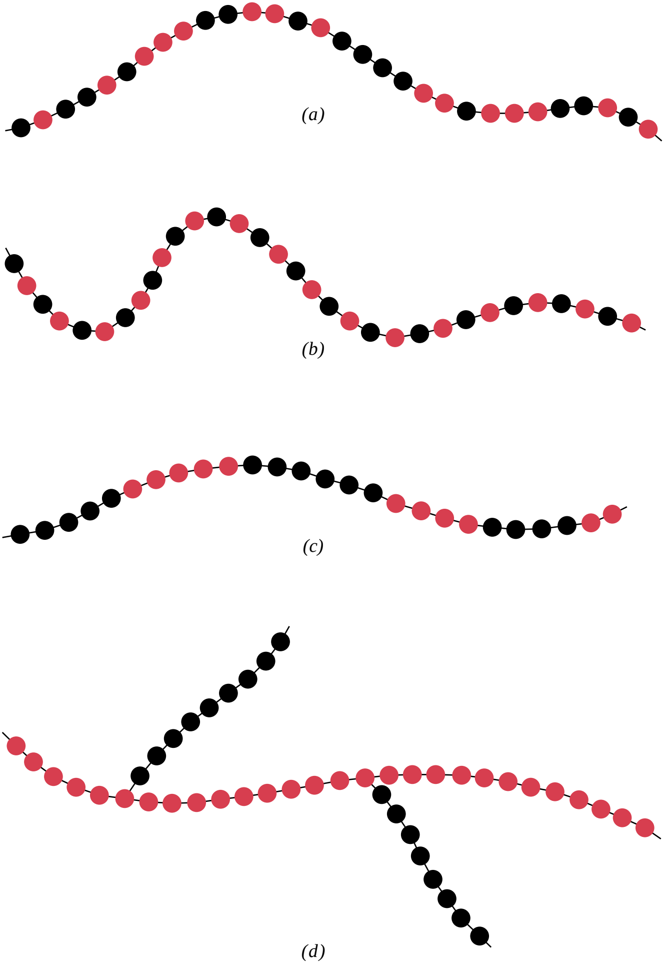

Figure 4.9 Schematic representations of (*a*) random, (*b*) alternating, (*c*) block, and (*d*) graft copolymers. The two different mer types are designated by black and colored circles.

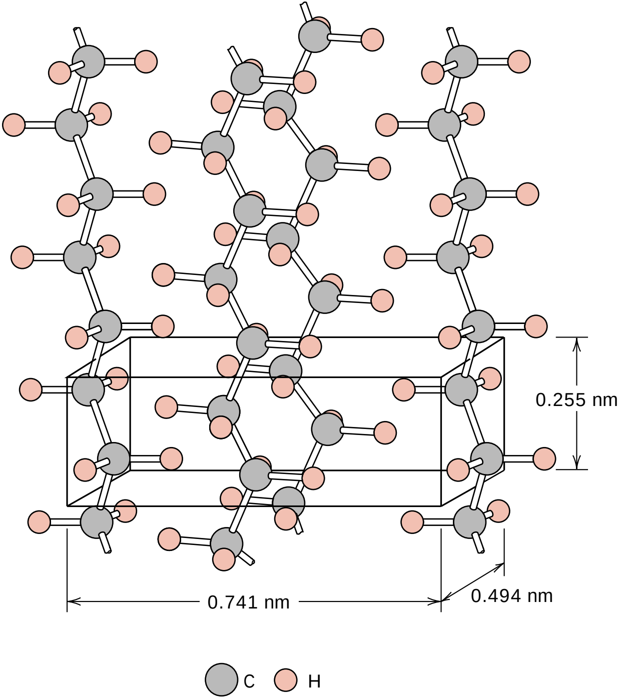
0.255 nm
0.741 nm
0.494 nm
C
H

FIGURE 4.10 Arrangement of molecular chains in a unit cell for polyethylene. (Adapted from C. W. Bunn, *Chemical Crystallography*, Oxford University Press, Oxford, 1945, p. 233.)

Table 4.5 **Chemical Repeat Units That Are Employed in Copolymer Rubbers**

Repeat Unit Name	*Repeat Unit Structure*	*Repeat Unit Name*	*Repeat Unit Structure*
Acrylonitrile	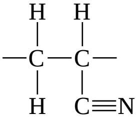 $\begin{array}{ccccc} & H & & H & \\ & \vert & & \vert & \\ - & C & - & C & - \\ & \vert & & \vert & \\ & H & & C{\equiv}N & \end{array}$	*cis*-Isoprene	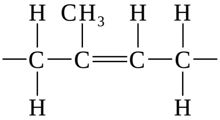 $\begin{array}{ccccccccc} & H & & CH_3 & & H & & H & \\ & \vert & & \vert & & \vert & & \vert & \\ - & C & - & C & = & C & - & C & - \\ & \vert & & & & & & \vert & \\ & H & & & & & & H & \end{array}$
Styrene	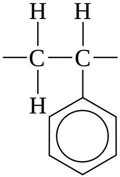	Isobutylene	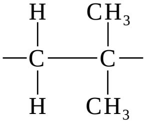 $\begin{array}{ccccc} & H & & CH_3 & \\ & \vert & & \vert & \\ - & C & - & C & - \\ & \vert & & \vert & \\ & H & & CH_3 & \end{array}$
Butadiene	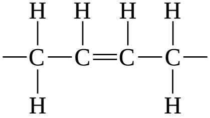 $\begin{array}{ccccccccc} & H & & H & & H & & H & \\ & \vert & & \vert & & \vert & & \vert & \\ - & C & - & C & = & C & - & C & - \\ & \vert & & & & & & \vert & \\ & H & & & & & & H & \end{array}$	Dimethylsiloxane	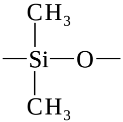 $\begin{array}{ccccc} & CH_3 & & & \\ & \vert & & & \\ - & Si & - & O & - \\ & \vert & & & \\ & CH_3 & & & \end{array}$
Chloroprene	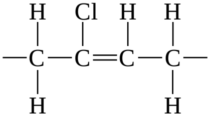 $\begin{array}{ccccccccc} & H & & Cl & & H & & H & \\ & \vert & & \vert & & \vert & & \vert & \\ - & C & - & C & = & C & - & C & - \\ & \vert & & & & & & \vert & \\ & H & & & & & & H & \end{array}$		

```
[Loader]
Program=mse5e
CommandLine=MerRubbers
```

Table 3.6 **Lattice Parameter Relationships and Figures Showing Unit Cell Geometries for the Seven Crystal Systems**

Crystal System	*Axial Relationships*	*Interaxial Angles*	*Unit Cell Geometry*
Cubic	$a = b = c$	$\alpha = \beta = \gamma = 90°$	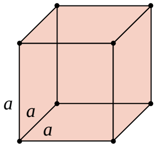
Hexagonal	$a = b \neq c$	$\alpha = \beta = 90°, \gamma = 120°$	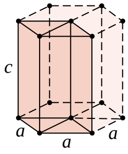
Tetragonal	$a = b \neq c$	$\alpha = \beta = \gamma = 90°$	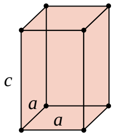
Rhombohedral	$a = b = c$	$\alpha = \beta = \gamma \neq 90°$	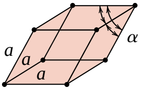
Orthorhombic	$a \neq b \neq c$	$\alpha = \beta = \gamma = 90°$	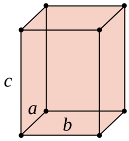
Monoclinic	$a \neq b \neq c$	$\alpha = \gamma = 90° \neq \beta$	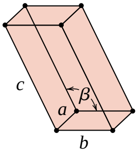
Triclinic	$a \neq b \neq c$	$\alpha \neq \beta \neq \gamma \neq 90°$	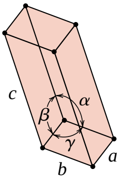

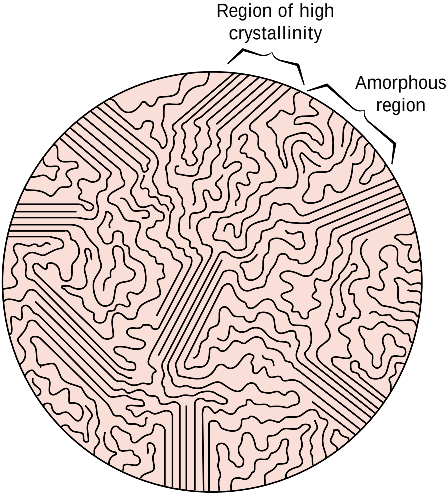
Region of high crystallinity
Amorphous region

Figure 4.11 Fringed-micelle model of a semicrystalline polymer, showing both crystalline and amorphous regions. (From H. W. Hayden, W. G. Moffatt, and J. Wulff, *The Structure and Properties of Materials*, Vol. III, *Mechanical Behavior*. Copyright © 1965 by John Wiley & Sons, New York. Reprinted by permission of John Wiley & Sons, Inc.)

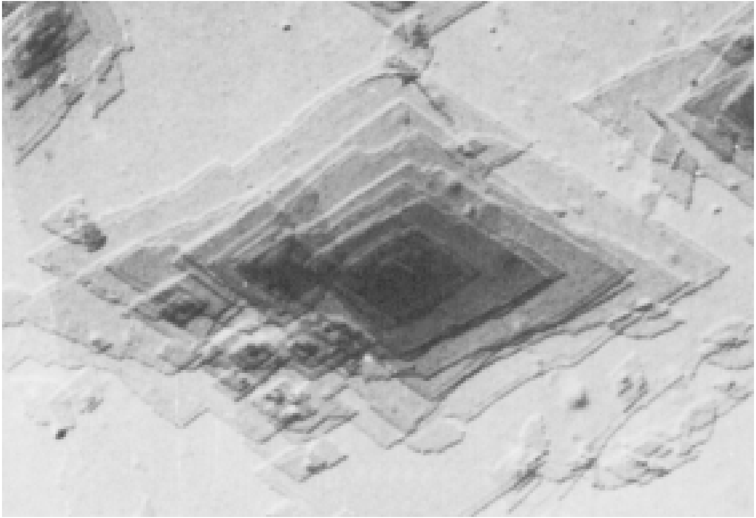

FIGURE 4.12 Electron micrograph of a polyethylene single crystal. 20,000×. (From A. Keller, R. H. Doremus, B. W. Roberts, and D. Turnbull, Editors, *Growth and Perfection of Crystals.* General Electric Company and John Wiley & Sons, Inc., 1958, p. 498.)

FIGURE 4.13 The chain-folded structure for a plate-shaped polymer crystallite.

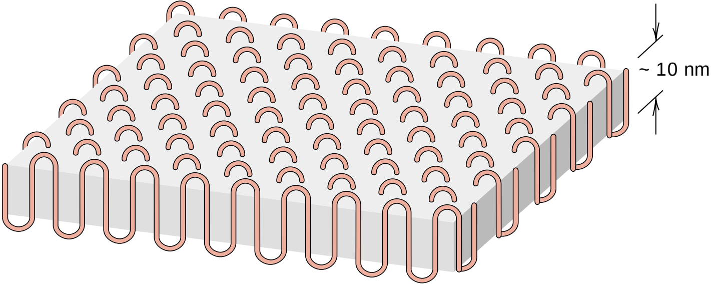

FIGURE 4.14 Schematic representation of the detailed structure of a spherulite. (From John C. Coburn, *Dielectric Relaxation Processes in Poly(ethylene terephthalate)*, Dissertation, University of Utah, 1984.)

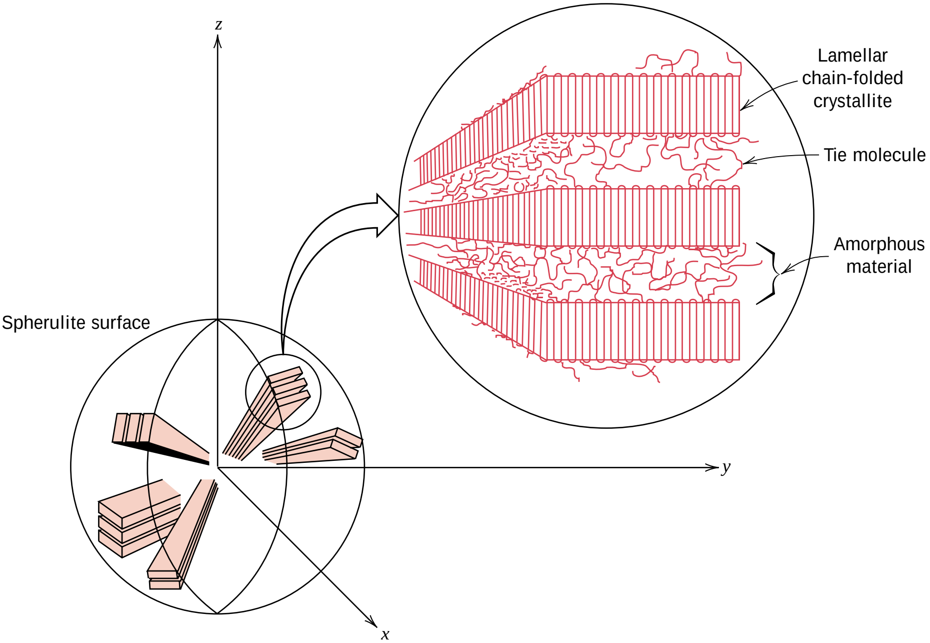

Lamellar chain-folded crystallite
Tie molecule
Amorphous material
Spherulite surface
z
y
x

FIGURE 4.15 A transmission photomicrograph (using cross-polarized light) showing the spherulite structure of polyethylene. Linear boundaries form between adjacent spherulites, and within each spherulite appears a Maltese cross. 525×. (Courtesy F. P. Price, General Electric Company.)

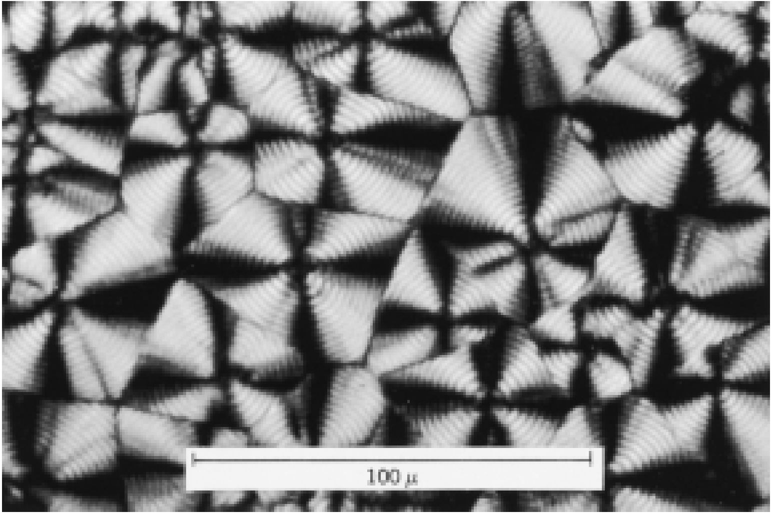

CHAPTER 5

IMPERFECTIONS IN SOLIDS

5.1 In order to compute the fraction of atom sites that are vacant in lead at 600 K, we must employ Equation (5.1). As stated in the problem, $\mathbf{Q_V} = 0.55$ eV/atom. Thus,

$$\frac{N_V}{N} = \exp\left(-\frac{Q_V}{kT}\right) = \exp\left[-\frac{0.55\ \text{eV/atom}}{(8.62 \times 10^{-5}\ \text{eV/atom-K})(600\ \text{K})}\right]$$
$$= 2.41 \times 10^{-5}$$

5.4 This problem calls for a determination of the number of atoms per cubic meter of aluminum. In order to solve this problem, one must employ Equation (5.2),

$$N = \frac{N_A \rho_{Al}}{A_{Al}}$$

The density of Al (from the table inside of the front cover) is 2.71 g/cm^3, while its atomic weight is 26.98 g/mol. Thus,

$$N = \frac{(6.023 \times 10^{23}\ \text{atoms/mol})(2.71\ \text{g/cm}^3)}{26.98\ \text{g/mol}}$$
$$= 6.05 \times 10^{22}\ \text{atoms/cm}^3 = 6.05 \times 10^{28}\ \text{atoms/m}^3$$

5.9 In the drawing below is shown the atoms on the (100) face of an FCC unit cell; the interstitial site is at the center of the edge.

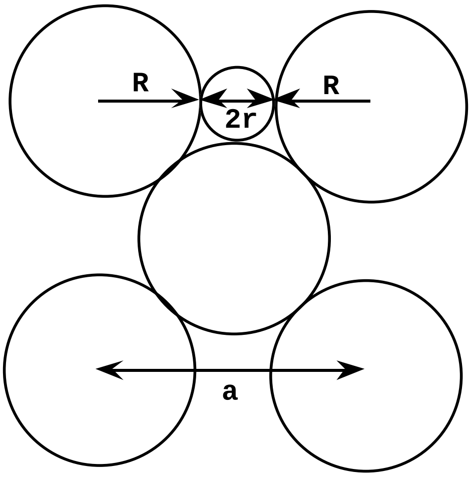

The diameter of an atom that will just fit into this site (2**r**) is just the difference between that unit cell edge length (**a**) and the radii of the two host atoms that are located on either side of the site (**R**);

that is

$$2r = a - 2R$$

However, for FCC **a** is related to **R** according to Equation (3.1) as $\mathbf{a} = 2\mathbf{R}\sqrt{2}$; therefore, solving for **r** gives

$$r = \frac{a - 2R}{2} = \frac{2R\sqrt{2} - 2R}{2} = 0.41R$$

5.10 (a) For Li^+ substituting for Ca^{2+} in CaO, oxygen vacancies would be created. For each Li^+ substituting for Ca^{2+}, one positive charge is removed; in order to maintain charge neutrality, a single negative charge may be removed. Negative charges are eliminated by creating oxygen vacancies, and for every two Li^+ ions added, a single oxygen vacancy is formed.

5.15 This problem asks that we determine the composition, in atom percent, of an alloy that contains 98 g tin and 65 g of lead. The concentration of an element in an alloy, in atom percent, may be computed using Equation (5.5). With this problem, it first becomes necessary to compute the number of moles of both Sn and Pb, for which Equation (5.4) is employed. Thus, the number of moles of Sn is just

$$n_{m_{Sn}} = \frac{m'_{Sn}}{A_{Sn}} = \frac{98\ \text{g}}{118.69\ \text{g/mol}} = 0.826\ \text{mol}$$

Likewise, for Pb

$$n_{m_{Pb}} = \frac{65\ \text{g}}{207.2\ \text{g/mol}} = 0.314\ \text{mol}$$

Now, use of Equation (5.5) yields

$$\begin{aligned} C'_{Sn} &= \frac{n_{m_{Sn}}}{n_{m_{Sn}} + n_{m_{Pb}}} \times 100 \\ &= \frac{0.826\ \text{mol}}{0.826\ \text{mol} + 0.314\ \text{mol}} \times 100 = 72.5\ \text{at\%} \end{aligned}$$

Also,

$$C'_{Pb} = \frac{0.314\ \text{mol}}{0.826\ \text{mol} + 0.314\ \text{mol}} \times 100 = 27.5\ \text{at\%}$$

5.27 This problem asks us to determine the weight percent of Nb that must be added to V such that the resultant alloy will contain 1.55×10^{22} Nb atoms per cubic centimeter. To solve this problem, employment of Equation (5.18) is necessary, using the following values:

$$\begin{aligned} N_1 &= N_{Nb} = 1.55 \times 10^{22}\ \text{atoms/cm}^3 \\ \rho_1 &= \rho_{Nb} = 8.57\ \text{g/cm}^3 \\ \rho_2 &= \rho_V = 6.10\ \text{g/cm}^3 \\ A_1 &= A_{Nb} = 92.91\ \text{g/mol} \\ A_2 &= A_V = 50.94\ \text{g/mol} \end{aligned}$$

Thus

$$
\begin{aligned}
C_{Nb} &= \frac{100}{1 + \dfrac{N_A \rho_V}{N_{Nb} A_{Nb}} - \dfrac{\rho_V}{\rho_{Nb}}} \\
&= \frac{100}{1 + \dfrac{(6.023 \times 20^{23}\ \text{atoms/mole})(6.10\ \text{g/cm}^3)}{(1.55 \times 10^{22}\ \text{atoms/cm}^3)(92.91\ \text{g/mol})} - \left(\dfrac{6.10\ \text{g/cm}^3}{8.57\ \text{g/cm}^3}\right)} \\
&= 35.2\ \text{wt\%}
\end{aligned}
$$

5.30 In this problem we are given a general equation which may be used to determine the Burgers vector and are asked to give Burgers vector representations for specific crystal structures, and then to compute Burgers vector magnitudes.

(a) The Burgers vector will point in that direction having the highest linear density. From Problem 3.70 the linear density for the [110] direction in FCC is 1.0, the maximum possible; therefore for FCC

$$\mathbf{b} = \frac{a}{2}[110]$$

(b) For Al which has an FCC crystal structure, $\mathbf{R} = 0.1431$ nm (Table 3.1) and $\mathbf{a} = 2\mathbf{R}\sqrt{2} = 0.4047$ nm [Equation (3.1)]; therefore

$$
\begin{aligned}
\mathbf{b} &= \frac{a}{2}\sqrt{h^2 + k^2 + l^2} \\
&= \frac{0.4047\ \text{nm}}{2}\sqrt{(1)^2 + (1)^2 + (0)^2} = 0.2862\ \text{nm}
\end{aligned}
$$

5.37 (a) We are asked for the number of grains per square inch ($\mathbf{N}$) at a magnification of 100X, and for an ASTM grain size of 4. From Equation (5.16), $\mathbf{n} = 4$, and

$$N = 2^{(n-1)} = 2^{(4-1)} = 2^3 = 8$$

CHAPTER 6

DIFFUSION

6.8 This problem calls for computation of the diffusion coefficient for a steady-state diffusion situation. Let us first convert the carbon concentrations from wt% to kg C/m^3 using Equation (5.9a); the densities of carbon and iron (from inside the front cover of the book) are 2.25 and 7.87 g/cm^3. For 0.012 wt% C

$$C''_C = \left(\frac{C_C}{\dfrac{C_C}{\rho_C} + \dfrac{C_{Fe}}{\rho_{Fe}}}\right) \times 10^3$$

$$= \left(\frac{0.012}{\dfrac{0.012}{2.25 \text{ g/cm}^3} + \dfrac{99.988}{7.87 \text{ g/cm}^3}}\right) \times 10^3$$

$$= 0.944 \text{ kg C/m}^3$$

Similarly, for 0.0075 wt% C

$$C''_C = \left(\frac{0.0075}{\dfrac{0.0075}{2.25 \text{ g/cm}^3} + \dfrac{99.9925}{7.87 \text{ g/cm}^3}}\right) \times 10^3$$

$$= 0.590 \text{ kg C/m}^3$$

Now, using a form of Equation (6.3)

$$D = -J\left[\frac{x_A - x_B}{C_A - C_B}\right]$$

$$= -(1.40 \times 10^{-8} \text{ kg/m}^2\text{-s})\left[\frac{-10^{-3} \text{ m}}{0.944 \text{ kg/m}^3 - 0.590 \text{ kg/m}^3}\right]$$

$$= 3.95 \times 10^{-11} \text{ m}^2\text{/s}$$

6.13 This problem asks us to compute the nitrogen concentration (**C_x**) at the 1 mm position after a 10 h diffusion time, when diffusion is nonsteady-state. From Equation (6.5)

$$\frac{C_x - C_o}{C_s - C_o} = \frac{C_x - 0}{0.1 - 0} = 1 - \text{erf}\left(\frac{x}{2\sqrt{Dt}}\right)$$

$$= 1 - \text{erf}\left[\frac{10^{-3} \text{ m}}{(2)\sqrt{(2.5 \times 10^{-11} \text{ m}^2\text{/s})(10 \text{ h})(3600 \text{ s/h})}}\right]$$

$$= 1 - \text{erf}(0.527)$$

Using data in Table 6.1 and linear interpolation

z	erf(z)
0.500	0.5205
0.527	y
0.550	0.5633

$$\frac{0.527 - 0.500}{0.550 - 0.500} = \frac{y - 0.5205}{0.5633 - 0.5205}$$

from which

$$y = \mathrm{erf}(0.527) = 0.5436$$

Thus,

$$\frac{C_x - 0}{0.1 - 0} = 1.0 - 0.5436$$

This expression gives

$$C_x = 0.046 \text{ wt\% N}$$

6.15 This problem calls for an estimate of the time necessary to achieve a carbon concentration of 0.45 wt% at a point 5 mm from the surface. From Equation (6.6b),

$$\frac{x^2}{Dt} = \text{constant}$$

But since the temperature is constant, so also is **D** constant, and

$$\frac{x^2}{t} = \text{constant}$$

or

$$\frac{x_1^2}{t_1} = \frac{x_2^2}{t_2}$$

Thus,

$$\frac{(2.5 \text{ mm})^2}{10 \text{ h}} = \frac{(5.0 \text{ mm})^2}{t_2}$$

from which

$$t_2 = 40 \text{ h}$$

6.21 (a) Using Equation (6.9a), we set up two simultaneous equations with $\mathbf{Q_d}$ and $\mathbf{D_o}$ as unknowns. Solving for $\mathbf{Q_d}$ in terms of temperatures $\mathbf{T_1}$ and $\mathbf{T_2}$ (1273 K and 1473 K) and $\mathbf{D_1}$ and $\mathbf{D_2}$ (9.4×10^{-16} and 2.4×10^{-14} m^2/s), we get

$$\begin{aligned} Q_d &= -R\frac{\ln D_1 - \ln D_2}{1/T_1 - 1/T_2} \\ &= -\frac{(8.31 \text{ J/mol-K})[\ln(9.4 \times 10^{-16}) - \ln(2.4 \times 10^{-14})]}{1/(1273 \text{ K}) - 1/(1473 \text{ K})} \\ &= 252{,}400 \text{ J/mol} \end{aligned}$$

Now, solving for $\mathbf{D_o}$ from Equation (6.8)

$$D_o = D_1 \exp\left(\frac{Q_d}{RT_1}\right)$$

$$= (9.4 \times 10^{-16}\ \mathrm{m^2/s}) \exp\left[\frac{252400\ \mathrm{J/mol}}{(8.31\ \mathrm{J/mol\text{-}K})(1273\ \mathrm{K})}\right]$$

$$= 2.2 \times 10^{-5}\ \mathrm{m^2/s}$$

(b) Using these values of $\mathbf{D_o}$ and $\mathbf{Q_d}$, **D** at 1373 K is just

$$D = (2.2 \times 10^{-5}\ \mathrm{m^2/s}) \exp\left[-\frac{252400\ \mathrm{J/mol}}{(8.31\ \mathrm{J/mol\text{-}K})(1373\ \mathrm{K})}\right]$$

$$= 5.4 \times 10^{-15}\ \mathrm{m^2/s}$$

6.29 For this problem, a diffusion couple is prepared using two hypothetical A and B metals. After a 30-h heat treatment at 1000 K, the concentration of A in B is 3.2 wt% at the 15.5-mm position. After another heat treatment at 800 K for 30 h, we are to determine at what position the composition will be 3.2 wt% A. In order to make this determination, we must employ Equation (6.6b) with **t** constant. That is

$$\frac{x^2}{D} = \text{constant}$$

Or

$$\frac{x_{800}^2}{D_{800}} = \frac{x_{1000}^2}{D_{1000}}$$

It is necessary to compute both $\mathbf{D_{800}}$ and $\mathbf{D_{1000}}$ using Equation (6.8), as follows:

$$D_{800} = (1.8 \times 10^{-5}\ \mathrm{m^2/s}) \exp\left[-\frac{152000\ \mathrm{J/mol}}{(8.31\ \mathrm{J/mol\text{-}K})(800\ \mathrm{K})}\right]$$

$$= 2.12 \times 10^{-15}\ \mathrm{m^2/s}$$

$$D_{1000} = (1.8 \times 10^{-5}\ \mathrm{m^2/s}) \exp\left[-\frac{152000\ \mathrm{J/mol}}{(8.31\ \mathrm{J/mol\text{-}K})(1000\ \mathrm{K})}\right]$$

$$= 2.05 \times 10^{-13}\ \mathrm{m^2/s}$$

Now, solving for $\mathbf{x_{800}}$ yields

$$x_{800} = x_{1000}\sqrt{\frac{D_{800}}{D_{1000}}}$$

$$= (15.5\ \mathrm{mm})\sqrt{\frac{2.12 \times 10^{-15}\ \mathrm{m^2/s}}{2.05 \times 10^{-13}\ \mathrm{m^2/s}}}$$

$$= 1.6\ \mathrm{mm}$$

Table 6.1 **Tabulation of Error Function Values**

z	*erf*(*z*)	*z*	*erf*(*z*)	*z*	*erf*(*z*)
0	0	0.55	0.5633	1.3	0.9340
0.025	0.0282	0.60	0.6039	1.4	0.9523
0.05	0.0564	0.65	0.6420	1.5	0.9661
0.10	0.1125	0.70	0.6778	1.6	0.9763
0.15	0.1680	0.75	0.7112	1.7	0.9838
0.20	0.2227	0.80	0.7421	1.8	0.9891
0.25	0.2763	0.85	0.7707	1.9	0.9928
0.30	0.3286	0.90	0.7970	2.0	0.9953
0.35	0.3794	0.95	0.8209	2.2	0.9981
0.40	0.4284	1.0	0.8427	2.4	0.9993
0.45	0.4755	1.1	0.8802	2.6	0.9998
0.50	0.5205	1.2	0.9103	2.8	0.9999

CHAPTER 7

MECHANICAL PROPERTIES

7.4 We are asked to compute the maximum length of a cylindrical titanium alloy specimen that is deformed elastically in tension. For a cylindrical specimen

$$A_o = \pi\left(\frac{d_o}{2}\right)^2$$

where $\mathbf{d_o}$ is the original diameter. Combining Equations (7.1), (7.2), and (7.5) and solving for $\mathbf{l_o}$ leads to

$$\begin{aligned} l_o &= \frac{E\pi d_o^2 \Delta l}{4F} \\ &= \frac{(107 \times 10^9 \text{ N/m}^2)(\pi)(3.8 \times 10^{-3} \text{ m})^2(0.42 \times 10^{-3} \text{ m})}{(4)(2000 \text{ N})} \\ &= 0.25 \text{ m} = 250 \text{ mm } (10 \text{ in.}) \end{aligned}$$

7.9 This problem asks that we calculate the elongation $\Delta\mathbf{l}$ of a specimen of steel the stress-strain behavior of which is shown in Figure 7.33. First it becomes necessary to compute the stress when a load of 23,500 N is applied as

$$\sigma = \frac{F}{A_o} = \frac{F}{\pi\left(\frac{d_o}{2}\right)^2} = \frac{23500 \text{ N}}{\pi\left(\frac{10 \times 10^{-3} \text{ m}}{2}\right)^2} = 300 \text{ MPa } (44{,}400 \text{ psi})$$

Referring to Figure 7.33, at this stress level we are in the elastic region on the stress-strain curve, which corresponds to a strain of 0.0013. Now, utilization of Equation (7.2) yields

$$\Delta l = \varepsilon l_o = (0.0013)(75 \text{ mm}) = 0.10 \text{ mm } (0.004 \text{ in.})$$

7.14 (a) We are asked, in this portion of the problem, to determine the elongation of a cylindrical specimen of aluminum. Using Equations (7.1), (7.2), and (7.5)

$$\frac{F}{\pi\left(\frac{d_o^2}{4}\right)} = E\frac{\Delta l}{l_o}$$

Or

$$\begin{aligned} \Delta l &= \frac{4Fl_o}{\pi d_o^2 E} \\ &= \frac{(4)(48{,}800 \text{ N})(200 \times 10^{-3} \text{ m})}{(\pi)(19 \times 10^{-3} \text{ m})^2(69 \times 10^9 \text{ N/m}^2)} = 0.50 \text{ mm } (0.02 \text{ in.}) \end{aligned}$$

(b) We are now called upon to determine the change in diameter, $\Delta\mathbf{d}$. Using Equation (7.8)

$$\nu = -\frac{\varepsilon_x}{\varepsilon_z} = -\frac{\Delta d/d_o}{\Delta l/l_o}$$

From Table 7.1, for Al, $\nu = 0.33$. Now, solving for $\Delta\mathbf{d}$ yields

$$\Delta d = -\frac{\nu \Delta l d_o}{l_o} = -\frac{(0.33)(0.50\text{ mm})(19\text{ mm})}{200\text{ mm}}$$
$$= -1.6 \times 10^{-2}\text{ mm } (-6.2 \times 10^{-4}\text{ in.})$$

The diameter will decrease.

7.16 This problem asks that we compute Poisson's ratio for the metal alloy. From Equations (7.5) and (7.1)

$$\varepsilon_z = \frac{\sigma}{E} = \frac{F/A_o}{E} = \frac{F}{\pi\left(\frac{d_o}{2}\right)^2 E} = \frac{4F}{\pi d_o^2 E}$$

Since the transverse strain $\varepsilon_\mathbf{x}$ is just

$$\varepsilon_x = \frac{\Delta d}{d_o}$$

and Poisson's ratio is defined by Equation (7.8) then

$$\nu = -\frac{\varepsilon_x}{\varepsilon_z} = -\frac{\Delta d/d_o}{\left(\frac{4F}{\pi d_o^2 E}\right)} = -\frac{d_o \Delta d \pi E}{4F}$$
$$= -\frac{(8 \times 10^{-3}\text{ m})(-5 \times 10^{-6}\text{ m})(\pi)(140 \times 10^{9}\text{ N/m}^2)}{(4)(15{,}700\text{ N})} = 0.280$$

7.21 (a) This portion of the problem asks that we compute the elongation of the brass specimen. The first calculation necessary is that of the applied stress using Equation (7.1), as

$$\sigma = \frac{F}{A_o} = \frac{F}{\pi\left(\frac{d_o}{2}\right)^2} = \frac{5000\text{ N}}{\pi\left(\frac{6 \times 10^{-3}\text{ m}}{2}\right)^2} = 177\text{ MPa } (25{,}000\text{ psi})$$

From the stress-strain plot in Figure 7.12, this stress corresponds to a strain of about 2.0×10^{-3}. From the definition of strain, Equation (7.2),

$$\Delta l = \varepsilon l_o = (2.0 \times 10^{-3})(50\text{ mm}) = 0.10\text{ mm } (4 \times 10^{-3}\text{ in.})$$

(b) In order to determine the reduction in diameter $\Delta\mathbf{d}$, it is necessary to use Equation (7.8) and the definition of lateral strain (i.e., $\varepsilon_\mathbf{x} = \Delta\mathbf{d}/\mathbf{d_o}$) as follows:

$$\Delta d = d_o \varepsilon_x = -d_o \nu \varepsilon_z = -(6\text{ mm})(0.30)(2.0 \times 10^{-3})$$
$$= -3.6 \times 10^{-3}\text{ mm } (-1.4 \times 10^{-4}\text{ in.})$$

7.27 This problem asks us to determine the deformation characteristics of a steel specimen, the stress-strain behavior of which is shown in Figure 7.33.

(a) In order to ascertain whether the deformation is elastic or plastic, we must first compute the stress, then locate it on the stress-strain curve, and, finally, note whether this point is on the elastic or plastic region. Thus,

$$\sigma = \frac{F}{A_o} = \frac{44500 \text{ N}}{\pi\left(\dfrac{10 \times 10^{-3} \text{ m}}{2}\right)^2} = 565 \text{ MPa } (80{,}000 \text{ psi})$$

The 565 MPa point is past the linear portion of the curve, and, therefore, the deformation will be both elastic and plastic.

(b) This portion of the problem asks us to compute the increase in specimen length. From the stress-strain curve, the strain at 565 MPa is approximately 0.008. Thus, from Equation (7.2)

$$\Delta l = \varepsilon l_o = (0.008)(500 \text{ mm}) = 4 \text{ mm } (0.16 \text{ in.})$$

7.29 This problem calls for us to make a stress-strain plot for aluminum, given its tensile load-length data, and then to determine some of its mechanical characteristics.

(a) The data are plotted below on two plots: the first corresponds to the entire stress-strain curve, while for the second, the curve extends just beyond the elastic region of deformation.

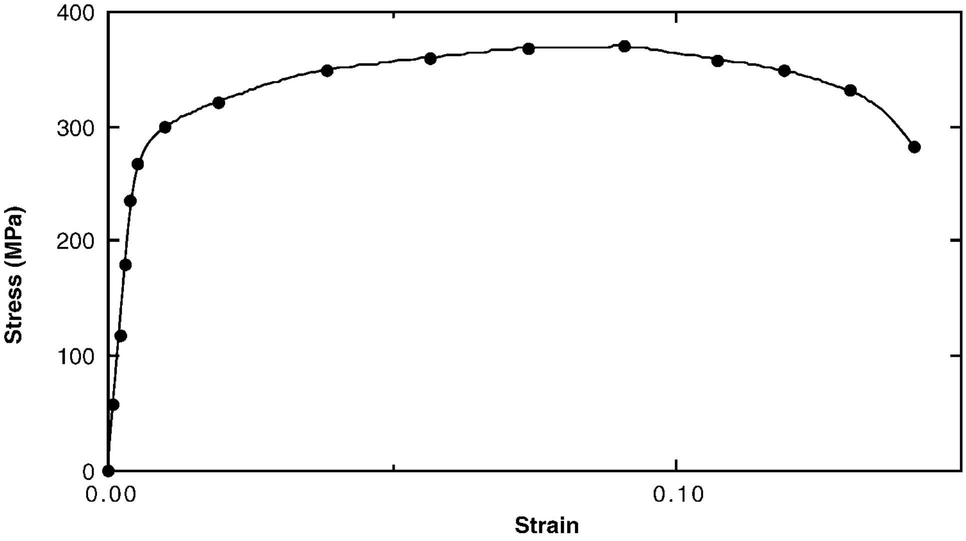

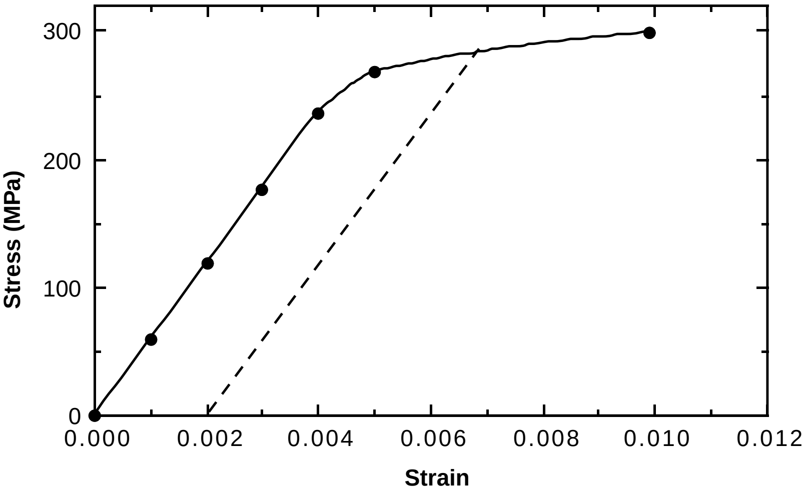

(b) The elastic modulus is the slope in the linear elastic region as

$$E = \frac{\Delta\sigma}{\Delta\varepsilon} = \frac{200\ \text{MPa} - 0\ \text{MPa}}{0.0032 - 0} = 62.5 \times 10^3\ \text{MPa} = 62.5\ \text{GPa}\ (9.1 \times 10^6\ \text{psi})$$

(c) For the yield strength, the 0.002 strain offset line is drawn dashed. It intersects the stress-strain curve at approximately 285 MPa (41,000 psi).

(d) The tensile strength is approximately 370 MPa (54,000 psi), corresponding to the maximum stress on the complete stress-strain plot.

(e) The ductility, in percent elongation, is just the plastic strain at fracture, multiplied by one-hundred. The total fracture strain at fracture is 0.165; subtracting out the elastic strain (which is about 0.005) leaves a plastic strain of 0.160. Thus, the ductility is about 16%EL.

(f) From Equation (7.14), the modulus of resilience is just

$$U_r = \frac{\sigma_y^2}{2E}$$

which, using data computed in the problem yields a value of

$$U_r = \frac{(285\ \text{MPa})^2}{(2)(62.5 \times 10^3\ \text{MPa})} = 6.5 \times 10^5\ \text{J/m}^3\ (93.8\ \text{in.-lb}_f/\text{in.}^3)$$

7.32 This problem asks us to calculate the moduli of resilience for the materials having the stress-strain behaviors shown in Figures 7.12 and 7.33. According to Equation (7.14), the modulus of resilience $\mathbf{U_r}$ is a function of the yield strength and the modulus of elasticity as

$$U_r = \frac{\sigma_y^2}{2E}$$

The values for $\sigma_\mathbf{y}$ and **E** for the brass in Figure 7.12 are 250 MPa (36,000 psi) and 93.9 GPa (13.6×10^6 psi), respectively. Thus

$$U_r = \frac{(250\ \text{MPa})^2}{(2)(93.9 \times 10^3\ \text{MPa})} = 3.32 \times 10^5\ \text{J/m}^3\ (47.6\ \text{in.-lb}_f/\text{in.}^3)$$

7.41 For this problem, we are given two values of $\varepsilon_\mathbf{T}$ and $\sigma_\mathbf{T}$, from which we are asked to calculate the true stress which produces a true plastic strain of 0.25. Employing Equation (7.19), we may set up two simultaneous equations with two unknowns (the unknowns being **K** and **n**), as

$$\log(50{,}000\ \text{psi}) = \log K + n \log(0.10)$$

$$\log(60{,}000\ \text{psi}) = \log K + n \log(0.20)$$

From these two expressions,

$$n = \frac{\log(50{,}000) - \log(60{,}000)}{\log(0.1) - \log(0.2)} = 0.263$$

$$\log K = 4.96 \ \text{ or } K = 91{,}623\ \text{psi}$$

Thus, for $\varepsilon_\mathbf{T} = 0.25$

$$\sigma_T = K(\varepsilon_T)^2 = (91{,}623\ \text{psi})(0.25)^{0.263} = 63{,}700\ \text{psi}\ (440\ \text{MPa})$$

7.45 This problem calls for us to utilize the appropriate data from Problem 7.29 in order to determine the values of **n** and **K** for this material. From Equation (7.32) the slope and intercept of a log σ_T versus log ε_T plot will yield **n** and log **K**, respectively. However, Equation (7.19) is only valid in the region of plastic deformation to the point of necking; thus, only the 7th, 8th, 9th, and 10th data points may be utilized. The log-log plot with these data points is given below.

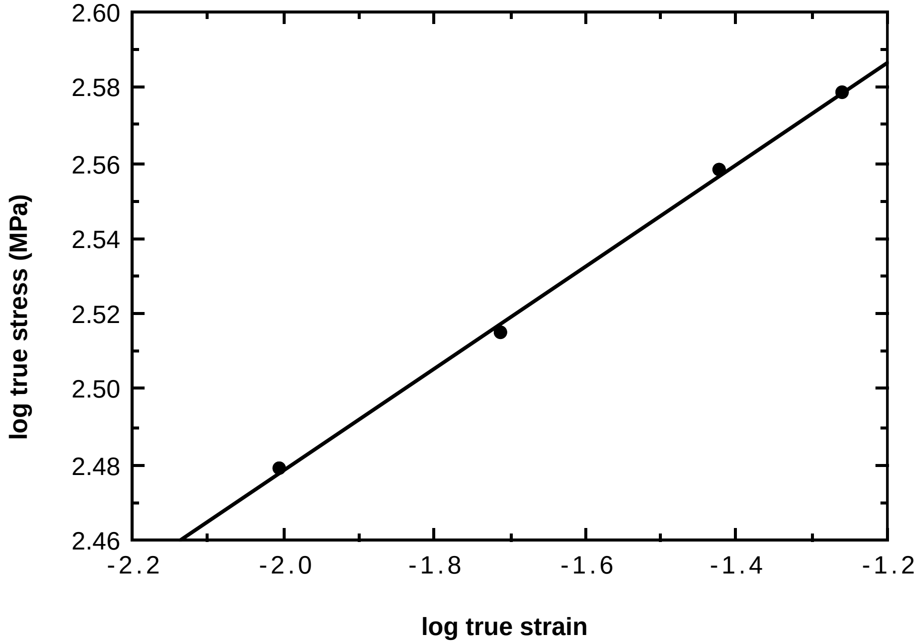

The slope yields a value of 0.136 for **n**, whereas the intercept gives a value of 2.7497 for log **K**, and thus **K** = 562 MPa.

7.50 For this problem, the load is given at which a circular specimen of aluminum oxide fractures when subjected to a three-point bending test; we are then are asked to determine the load at which a specimen of the same material having a square cross-section fractures. It is first necessary to compute the flexural strength of the alumina using Equation (7.20b), and then, using this value, we may calculate the value of $\mathbf{F_f}$ in Equation (7.20a). From Equation (7.20b)

$$\sigma_{fs} = \frac{F_f L}{\pi R^3}$$

$$= \frac{(950\ \text{N})(50 \times 10^{-3}\ \text{m})}{(\pi)(3.5 \times 10^{-3}\ \text{m})^3} = 352 \times 10^6\ \text{N/m}^2 = 352\ \text{MPa}\ (50{,}000\ \text{psi})$$

Now, solving for $\mathbf{F_f}$ from Equation (7.20a), realizing that **b** = **d** = 12 mm, yields

$$F_f = \frac{2\sigma_{fs} d^3}{3L}$$

$$= \frac{(2)(352 \times 10^6\ \text{N/m}^2)(12 \times 10^{-3}\ \text{m})^3}{(3)(40 \times 10^{-3}\ \text{m})} = 10{,}100\ \text{N}\ (2165\ \text{lb}_f)$$

7.54* (a) This part of the problem asks us to determine the flexural strength of nonporous MgO assuming that the value of **n** in Equation (7.22) is 3.75. Taking natural logarithms of both sides of

Equation (7.22) yields

$$\ln \sigma_{fs} = \ln \sigma_o - nP$$

In Table 7.2 it is noted that for **P** = 0.05, $\sigma_{\mathbf{fs}}$ = 105 MPa. For the nonporous material **P** = 0 and, ln $\sigma_{\mathbf{o}}$ = ln $\sigma_{\mathbf{fs}}$. Solving for ln $\sigma_{\mathbf{o}}$ from the above equation gives and using these data gives

$$\begin{aligned}\ln \sigma_o &= \ln \sigma_{fs} + nP \\ &= \ln(105\text{ MPa}) + (3.75)(0.05) = 4.841\end{aligned}$$

or

$$\sigma_o = e^{4.841} = 127\text{ MPa }(18{,}100\text{ psi})$$

(b) Now we are asked to compute the volume percent porosity to yield a $\sigma_{\mathbf{fs}}$ of 62 MPa (9000 psi). Taking the natural logarithm of Equation (7.22) and solving for **P** leads to

$$\begin{aligned}P &= \frac{\ln \sigma_o - \ln \sigma_{fs}}{n} \\ &= \frac{\ln(127\text{ MPa}) - \ln(62\text{ MPa})}{3.75} \\ &= 0.19 \text{ or } 19\text{ vol\%}\end{aligned}$$

7.65 This problem calls for estimations of Brinell and Rockwell hardnesses.

(a) For the brass specimen, the stress-strain behavior for which is shown in Figure 7.12, the tensile strength is 450 MPa (65,000 psi). From Figure 7.31, the hardness for brass corresponding to this tensile strength is about 125 HB or 70 HRB.

7.70 The working stresses for the two alloys, the stress-strain behaviors of which are shown in Figures 7.12 and 7.33, are calculated by dividing the yield strength by a factor of safety, which we will take to be 2. For the brass alloy (Figure 7.12), since $\sigma_{\mathbf{y}}$ = 250 MPa (36,000 psi), the working stress is 125 MPa (18,000 psi), whereas for the steel alloy (Figure 7.33), $\sigma_{\mathbf{y}}$ = 570 MPa (82,000 psi), and, therefore, $\sigma_{\mathbf{w}}$ = 285 MPa (41,000 psi).

FIGURE 7.33 Tensile stress–strain behavior for a plain carbon steel.

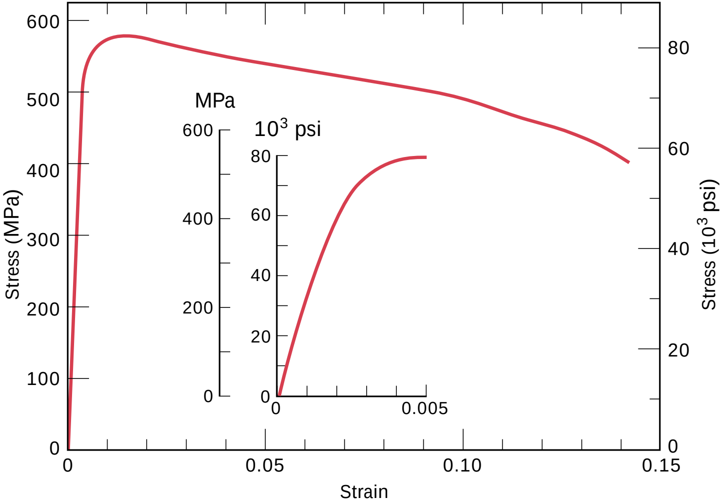

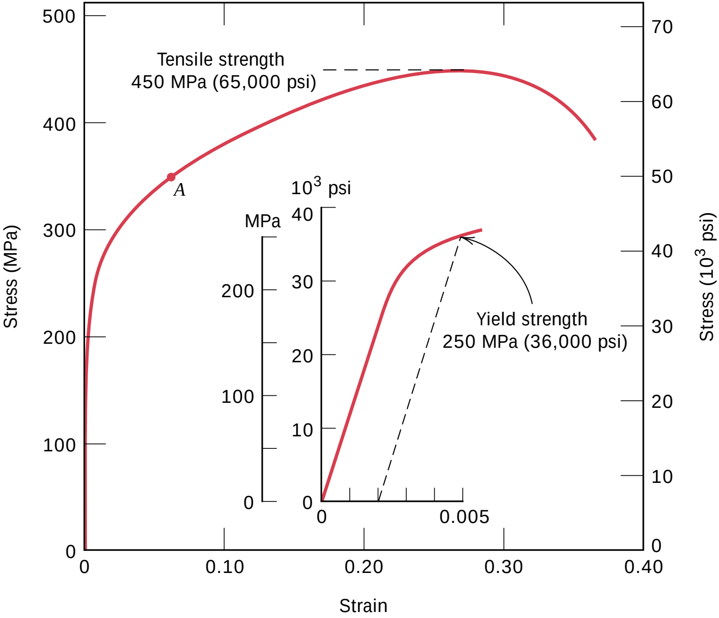

FIGURE 7.12 The stress–strain behavior for the brass specimen discussed in Example Problem 7.3.

Chapter 7 / Mechanical Properties

7.12 INFLUENCE OF POROSITY ON THE MECHANICAL PROPERTIES OF CERAMICS

For some ceramic fabrication techniques (Sections 14.8 and 14.9), the precursor material is in the form of a powder. Subsequent to compaction or forming of these powder particles into the desired shape, pores or void spaces will exist between the powder particles. During the ensuing heat treatment, much of this porosity will be eliminated; however, it is often the case that this pore elimination process is incomplete and some residual porosity will remain (Figure 14.25). Any residual porosity will have a deleterious influence on both the elastic properties and strength. For example, it has been observed for some ceramic materials that the magnitude of the modulus of elasticity E decreases with volume fraction porosity P according to

$$E = E_0(1 - 1.9P + 0.9P^2) \tag{7.21}$$

where E_0 is the modulus of elasticity of the nonporous material. The influence of volume fraction porosity on the modulus of elasticity for aluminum oxide is shown in Figure 7.20; the curve represented in the figure is according to Equation 7.21.

Porosity is deleterious to the flexural strength for two reasons: (1) pores reduce the cross-sectional area across which a load is applied, and (2) they also act as stress concentrators—for an isolated spherical pore, an applied tensile stress is amplified by a factor of 2. The influence of porosity on strength is rather dramatic; for example, it is not uncommon that 10 vol% porosity will decrease the flexural strength by 50% from the measured value for the nonporous material. The degree of the influence of pore volume on flexural strength is demonstrated in Figure 7.21, again for aluminum oxide. Experimentally it has been shown that the flexural strength decreases exponentially with volume fraction porosity (P) as

$$\sigma_{fs} = \sigma_0 \exp(-nP) \tag{7.22}$$

In this expression σ_0 and n are experimental constants.

7.15 VISCOELASTICITY

An amorphous polymer may behave like a glass at low temperatures, a rubbery solid at intermediate temperatures [above the glass transition temperature (Section 11.15)], and a viscous liquid as the temperature is further raised. For relatively small deformations, the mechanical behavior at low temperatures may be elastic; that is, in conformity to Hooke's law, $\sigma = E\epsilon$. At the highest temperatures, viscous or liquidlike behavior prevails. For intermediate temperatures is found a rubbery

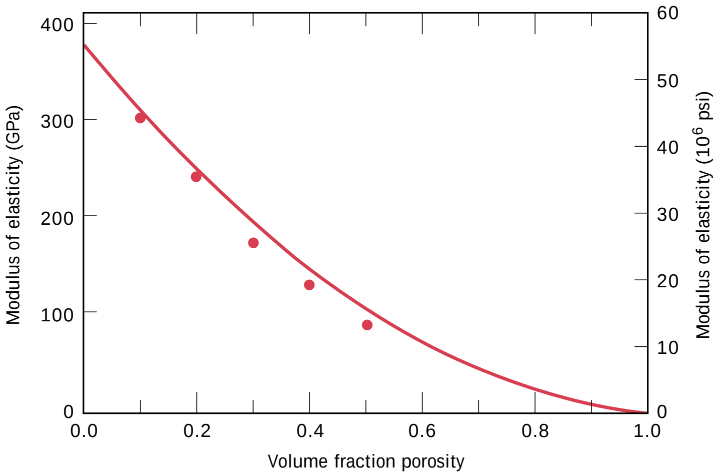

FIGURE 7.20 The influence of porosity on the modulus of elasticity for aluminum oxide at room temperature. The curve drawn is according to Equation 7.21. (From R. L. Coble and W. D. Kingery, ''Effect of Porosity on Physical Properties of Sintered Alumina,'' *J. Am. Ceram. Soc.*, **39,** 11, Nov. 1956, p. 381. Reprinted by permission of the American Ceramic Society.)

solid that exhibits the combined mechanical characteristics of these two extremes; the condition is termed **viscoelasticity.**

Elastic deformation is instantaneous, which means that total deformation (or strain) occurs the instant the stress is applied or released (i.e., the strain is independent of time). In addition, upon release of the external stress, the deformation is totally recovered—the specimen assumes its original dimensions. This behavior is

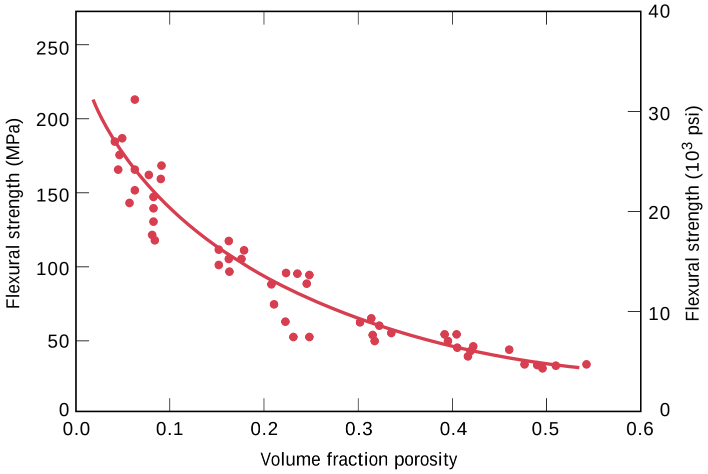

FIGURE 7.21 The influence of porosity on the flexural strength for aluminum oxide at room temperature. (From R. L. Coble and W. D. Kingery, ''Effect of Porosity on Physical Properties of Sintered Alumina,'' *J. Am. Ceram. Soc.*, **39,** 11, Nov. 1956, p. 382. Reprinted by permission of the American Ceramic Society.)

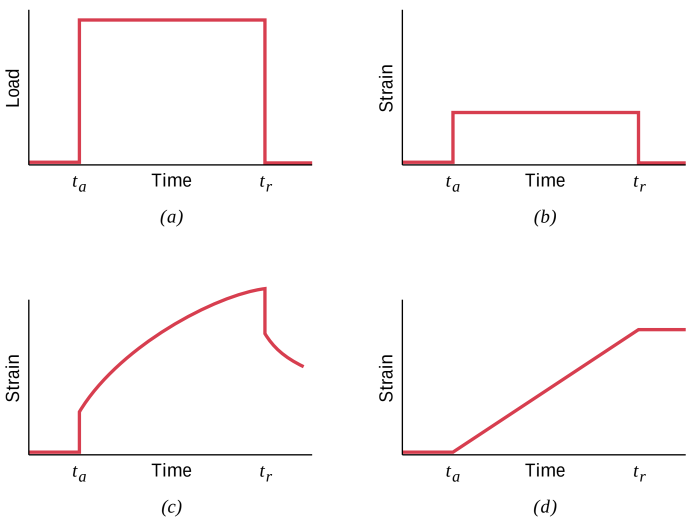

Figure 7.26 (*a*) Load versus time, where load is applied instantaneously at time t_a and released at t_r. For the load–time cycle in (*a*), the strain-versus-time responses are for totally elastic (*b*), viscoelastic (*c*), and viscous (*d*) behavior.

represented in Figure 7.26*b* as strain versus time for the instantaneous load–time curve, shown in Figure 7.26*a*.

By way of contrast, for totally viscous behavior, deformation or strain is not instantaneous; that is, in response to an applied stress, deformation is delayed or dependent on time. Also, this deformation is not reversible or completely recovered after the stress is released. This phenomenon is demonstrated in Figure 7.26*d*.

For the intermediate viscoelastic behavior, the imposition of a stress in the manner of Figure 7.26*a* results in an instantaneous elastic strain, which is followed by a viscous, time-dependent strain, a form of anelasticity (Section 7.4); this behavior is illustrated in Figure 7.26*c*.

A familiar example of these viscoelastic extremes is found in a silicone polymer that is sold as a novelty and known by some as ''silly putty.'' When rolled into a ball and dropped onto a horizontal surface, it bounces elastically—the rate of deformation during the bounce is very rapid. On the other hand, if pulled in tension with a gradually increasing applied stress, the material elongates or flows like a highly viscous liquid. For this and other viscoelastic materials, the rate of strain determines whether the deformation is elastic or viscous.

VISCOELASTIC RELAXATION MODULUS

The viscoelastic behavior of polymeric materials is dependent on both time and temperature; several experimental techniques may be used to measure and quantify this behavior. *Stress relaxation* measurements represent one possibility. With these tests, a specimen is initially strained rapidly in tension to a predetermined and relatively low strain level. The stress necessary to maintain this strain is measured as a function of time, while temperature is held constant. Stress is found to decrease with time due to molecular relaxation processes that take place within the polymer. We may define a **relaxation modulus** $E_r(t)$, a time-dependent elastic modulus for viscoelastic polymers, as

$$E_r(t) = \frac{\sigma(t)}{\epsilon_0} \qquad (7.23)$$

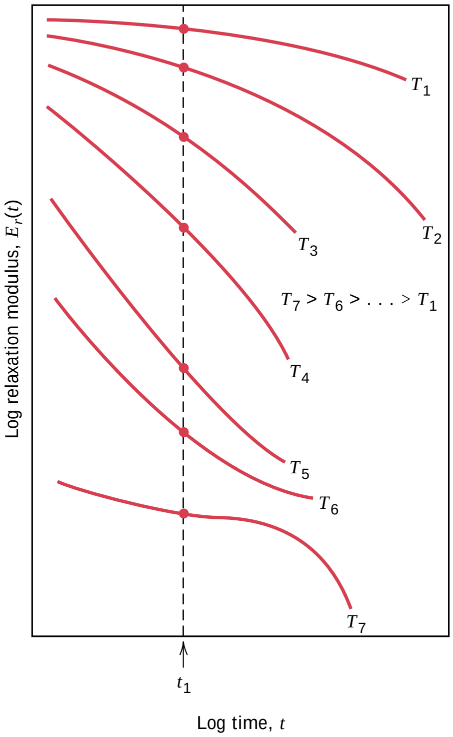

Figure 7.27 Schematic plot of logarithm of relaxation modulus versus logarithm of time for a viscoelastic polymer; isothermal curves are generated at temperatures T_1 through T_7. The temperature dependence of the relaxation modulus is represented as log $E_r(t_1)$ versus temperature.

where $\sigma(t)$ is the measured time-dependent stress and ϵ_0 is the strain level, which is maintained constant.

Furthermore, the magnitude of the relaxation modulus is a function of temperature; and to more fully characterize the viscoelastic behavior of a polymer, isothermal stress relaxation measurements must be conducted over a range of temperatures. Figure 7.27 is a schematic log $E_r(t)$-versus-log time plot for a polymer that exhibits viscoelastic behavior; included are several curves generated at a variety of temperatures. Worth noting from this figure are (1) the decrease of $E_r(t)$ with time (corresponding to the decay of stress, Equation 7.23), and (2) the displacement of the curves to lower $E_r(t)$ levels with increasing temperature.

To represent the influence of temperature, data points are taken at a specific time from the log $E_r(t)$-versus-log time plot—for example, t_1 in Figure 7.27—and then cross-plotted as log $E_r(t_1)$ versus temperature. Figure 7.28 is such a plot for an amorphous (atactic) polystyrene; in this case, t_1 was arbitrarily taken 10 s after the load application. Several distinct regions may be noted on the curve shown in this figure. For the first, at the lowest temperatures, in the glassy region, the material is rigid and brittle, and the value of $E_r(10)$ is that of the elastic modulus, which initially is virtually independent of temperature. Over this temperature range, the strain–time characteristics are as represented in Figure 7.26*b*. On a molecular level, the long molecular chains are essentially frozen in position at these temperatures.

As the temperature is increased, $E_r(10)$ drops abruptly by about a factor of 10^3 within a 20°C (35°F) temperature span; this is sometimes called the leathery, or glass transition region, and the glass transition temperature (T_g, Section 11.16) lies near the upper temperature extremity; for polystyrene (Figure 7.28), $T_g = 100°C$ (212°F). Within this temperature region, a polymer specimen will be leathery; that

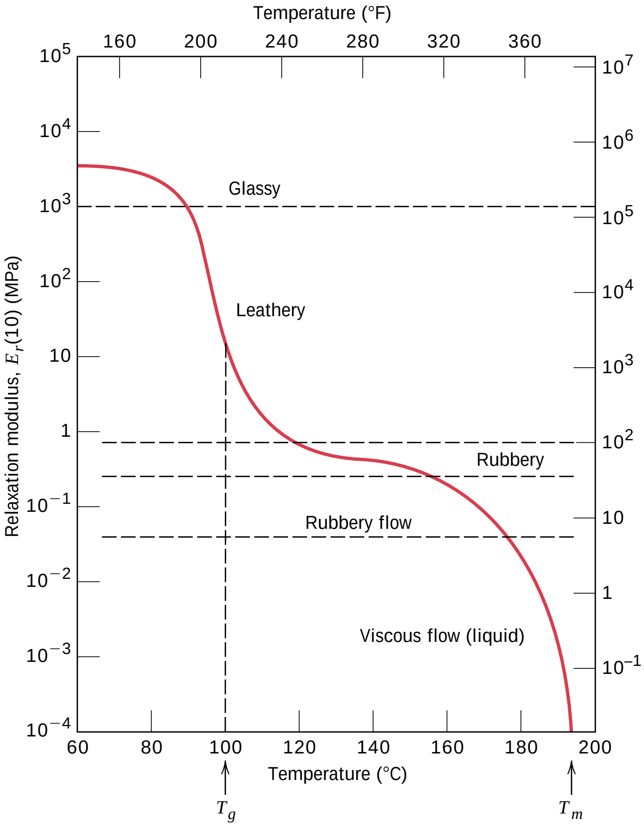

Figure 7.28 Logarithm of the relaxation modulus versus temperature for amorphous polystyrene, showing the five different regions of viscoelastic behavior. (From A. V. Tobolsky, *Properties and Structures of Polymers.* Copyright © 1960 by John Wiley & Sons, New York. Reprinted by permission of John Wiley & Sons, Inc.)

is, deformation will be time dependent and not totally recoverable on release of an applied load, characteristics depicted in Figure 7.26*c*.

Within the rubbery plateau temperature region (Figure 7.28), the material deforms in a rubbery manner; here, both elastic and viscous components are present, and deformation is easy to produce because the relaxation modulus is relatively low.

The final two high-temperature regions are rubbery flow and viscous flow. Upon heating through these temperatures, the material experiences a gradual transition to a soft rubbery state, and finally to a viscous liquid. Within the viscous flow region, the modulus decreases dramatically with increasing temperature; and, again, the strain–time behavior is as represented in Figure 7.26*d*. From a molecular standpoint, chain motion intensifies so greatly that for viscous flow, the chain segments experience vibration and rotational motion quite independently of one another. At these temperatures, any deformation is entirely viscous.

Normally, the deformation behavior of a viscous polymer is specified in terms of viscosity, a measure of a material's resistance to flow by shear forces. Viscosity is discussed for the inorganic glasses in Section 8.16.

The rate of stress application also influences the viscoelastic characteristics. Increasing the loading rate has the same influence as lowering temperature.

The log $E_r(10)$-versus-temperature behavior for polystyrene materials having several molecular configurations is plotted in Figure 7.29. The curve for the amorphous material (curve *C*) is the same as in Figure 7.28. For a lightly crosslinked atactic polystyrene (curve *B*), the rubbery region forms a plateau that extends to

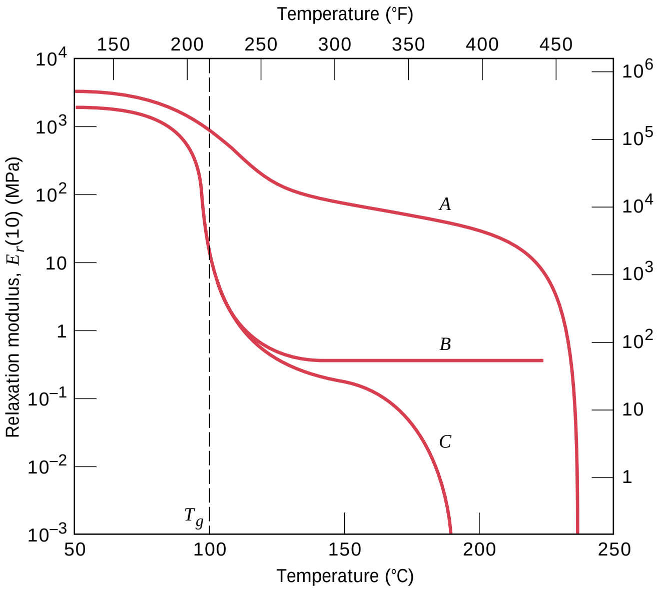

FIGURE 7.29 Logarithm of the relaxation modulus versus temperature for crystalline isotactic (curve A), lightly crosslinked atactic (curve B), and amorphous (curve C) polystyrene. (From A. V. Tobolsky, *Properties and Structures of Polymers.* Copyright © 1960 by John Wiley & Sons, New York. Reprinted by permission of John Wiley & Sons, Inc.)

the temperature at which the polymer decomposes; this material will not experience melting. For increased crosslinking, the magnitude of the plateau $E_r(10)$ value will also increase. Rubber or elastomeric materials display this type of behavior and are ordinarily utilized at temperatures within this plateau range.

Also shown in Figure 7.29 is the temperature dependence for an almost totally crystalline isotactic polystyrene (curve A). The decrease in $E_r(10)$ at T_g is much less pronounced than the other polystyrene materials since only a small volume fraction of this material is amorphous and experiences the glass transition. Furthermore, the relaxation modulus is maintained at a relatively high value with increasing temperature until its melting temperature T_m is approached. From Figure 7.29, the melting temperature of this isotactic polystyrene is about 240°C (460°F).

VISCOELASTIC CREEP

Many polymeric materials are susceptible to time-dependent deformation when the stress level is maintained constant; such deformation is termed *viscoelastic creep.* This type of deformation may be significant even at room temperature and under modest stresses that lie below the yield strength of the material. For example, automobile tires may develop flat spots on their contact surfaces when the automobile is parked for prolonged time periods. Creep tests on polymers are conducted in the same manner as for metals (Chapter 9); that is, a stress (normally tensile) is applied instantaneously and is maintained at a constant level while strain is measured as a function of time. Furthermore, the tests are performed under isothermal conditions. Creep results are represented as a time-dependent *creep modulus* $E_c(t)$, defined by

$$E_c(t) = \frac{\sigma_0}{\epsilon(t)} \tag{7.24}$$

wherein σ_0 is the constant applied stress and $\epsilon(t)$ is the time-dependent strain. The creep modulus is also temperature sensitive and diminishes with increasing temperature.

With regard to the influence of molecular structure on the creep characteristics, as a general rule the susceptibility to creep decreases [i.e., $E_c(t)$ increases] as the degree of crystallinity increases.

7.19 VARIABILITY OF MATERIAL PROPERTIES

COMPUTATION OF AVERAGE AND STANDARD DEVIATION VALUES

An average value is obtained by dividing the sum of all measured values by the number of measurements taken. In mathematical terms, the average $\overline{x}$ of some parameter x is

$$\overline{x} = \frac{\sum_{i=1}^{n} x_i}{n} \tag{7.26}$$

where n is the number of observations or measurements and x_i is the value of a discrete measurement.

Furthermore, the standard deviation s is determined using the following expression:

$$s = \left[\frac{\sum_{i=1}^{n} (x_i - \overline{x})^2}{n - 1}\right]^{1/2} \tag{7.27}$$

where x_i, $\overline{x}$, and n are defined above. A large value of the standard deviation corresponds to a high degree of scatter.

EXAMPLE PROBLEM 7.6

The following tensile strengths were measured for four specimens of the same steel alloy:

Sample Number	Tensile Strength (MPa)
1	520
2	512
3	515
4	522

(a) Compute the average tensile strength.

(b) Determine the standard deviation.

SOLUTION

(a) The average tensile strength ($\overline{TS}$) is computed using Equation 7.26 with $n = 4$:

$$\overline{TS} = \frac{\sum_{i=1}^{4} (TS)_i}{4}$$

$$= \frac{520 + 512 + 515 + 522}{4}$$

$$= 517 \text{ MPa}$$

(b) And for the standard deviation, using Equation 7.27,

$$s = \left[\frac{\sum_{i=1}^{4} \{(TS)_i - \overline{TS}\}^2}{4 - 1} \right]^{1/2}$$

$$= \left[\frac{(520 - 517)^2 + (512 - 517)^2 + (515 - 517)^2 + (522 - 517)^2}{4 - 1} \right]^{1/2}$$

$$= 4.6 \text{ MPa}$$

Figure 7.32 presents the tensile strength by specimen number for this example problem, and also how the data may be represented in graphical form. The tensile strength data point (Figure 7.32*b*) corresponds to the average value

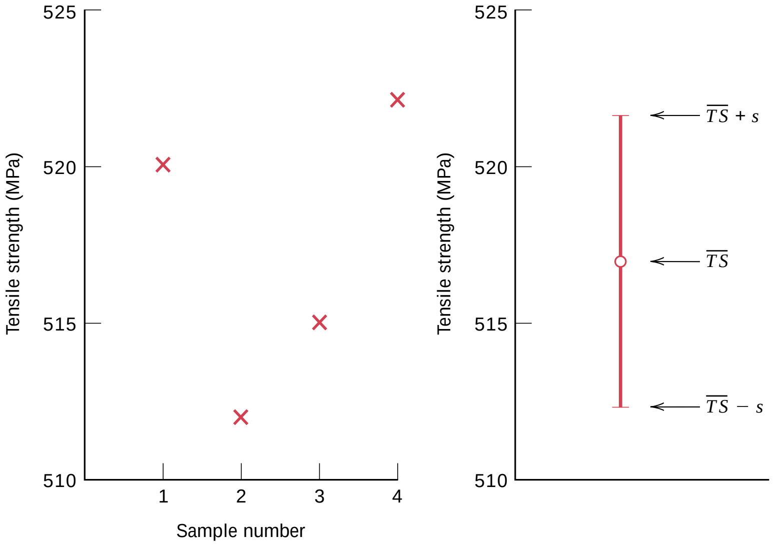

(*a*) (*b*)

FIGURE 7.32 (*a*) Tensile strength data associated with Example Problem 7.6. (*b*) The manner in which these data could be plotted. The data point corresponds to the average value of the tensile strength ($\overline{TS}$); error bars that indicate the degree of scatter correspond to the average value plus and minus the standard deviation ($\overline{TS} \pm s$).

$\overline{TS}$, whereas scatter is depicted by error bars (short horizontal lines) situated above and below the data point symbol and connected to this symbol by vertical lines. The upper error bar is positioned at a value of the average value plus the standard deviation ($\overline{TS} + s$), whereas the lower error bar corresponds to the average minus the standard deviation ($\overline{TS} - s$).

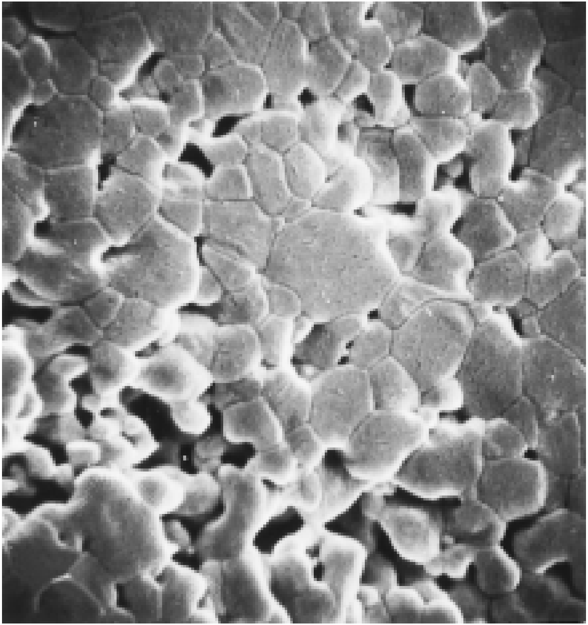

FIGURE 14.25 Scanning electron micrograph of an aluminum oxide powder compact that was sintered at 1700°C for 6 min. 5000×. (From W. D. Kingery, H. K. Bowen, and D. R. Uhlmann, *Introduction to Ceramics*, 2nd edition, p. 483. Copyright © 1976 by John Wiley & Sons, New York. Reprinted by permission of John Wiley & Sons, Inc.)

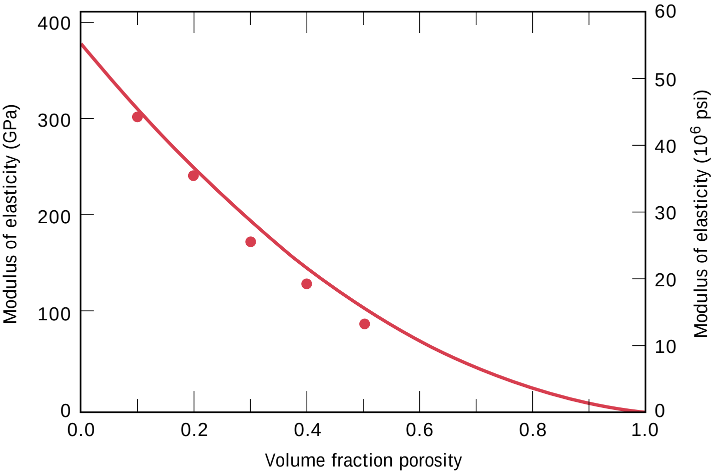

FIGURE 7.20 The influence of porosity on the modulus of elasticity for aluminum oxide at room temperature. The curve drawn is according to Equation 7.21. (From R. L. Coble and W. D. Kingery, ‘‘Effect of Porosity on Physical Properties of Sintered Alumina,’’ *J. Am. Ceram. Soc.*, **39,** 11, Nov. 1956, p. 381. Reprinted by permission of the American Ceramic Society.)

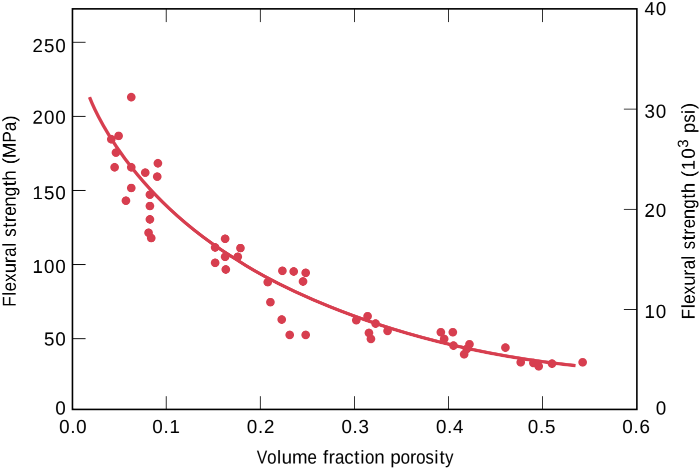

FIGURE 7.21 The influence of porosity on the flexural strength for aluminum oxide at room temperature. (From R. L. Coble and W. D. Kingery, ''Effect of Porosity on Physical Properties of Sintered Alumina,'' *J. Am. Ceram. Soc.*, **39,** 11, Nov. 1956, p. 382. Reprinted by permission of the American Ceramic Society.)

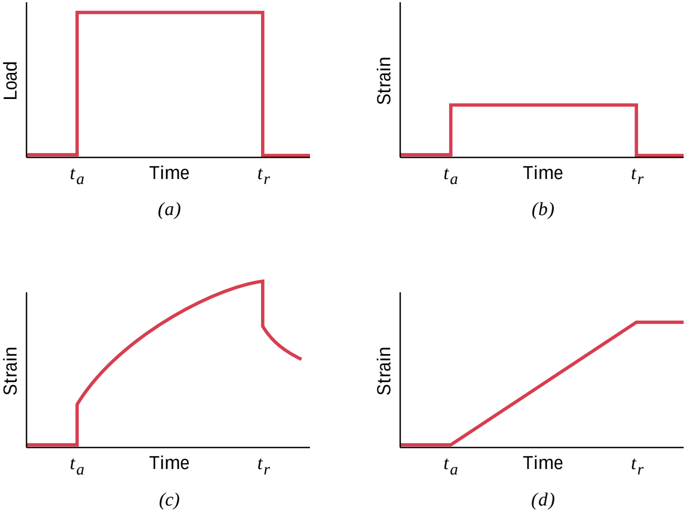

Figure 7.26 (*a*) Load versus time, where load is applied instantaneously at time t_a and released at t_r. For the load–time cycle in (*a*), the strain-versus-time responses are for totally elastic (*b*), viscoelastic (*c*), and viscous (*d*) behavior.

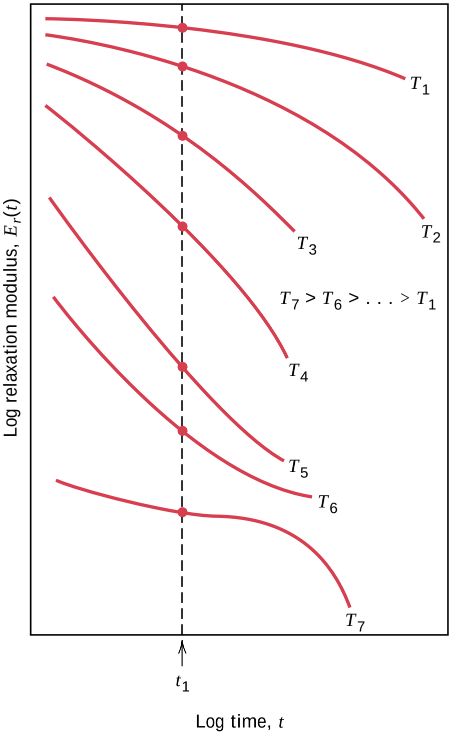

Figure 7.27 Schematic plot of logarithm of relaxation modulus versus logarithm of time for a viscoelastic polymer; isothermal curves are generated at temperatures T_1 through T_7. The temperature dependence of the relaxation modulus is represented as log $E_r(t_1)$ versus temperature.

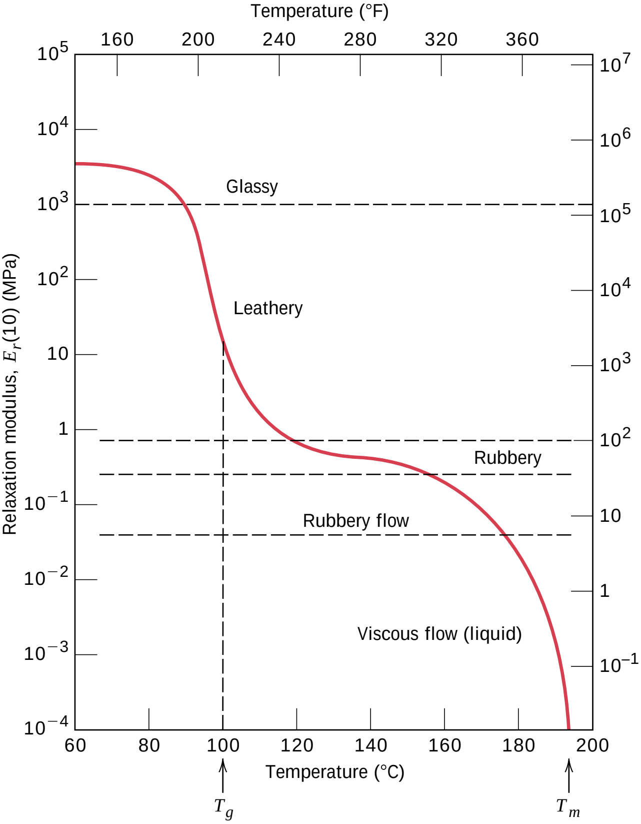

FIGURE 7.28 Logarithm of the relaxation modulus versus temperature for amorphous polystyrene, showing the five different regions of viscoelastic behavior. (From A. V. Tobolsky, *Properties and Structures of Polymers.* Copyright © 1960 by John Wiley & Sons, New York. Reprinted by permission of John Wiley & Sons, Inc.)

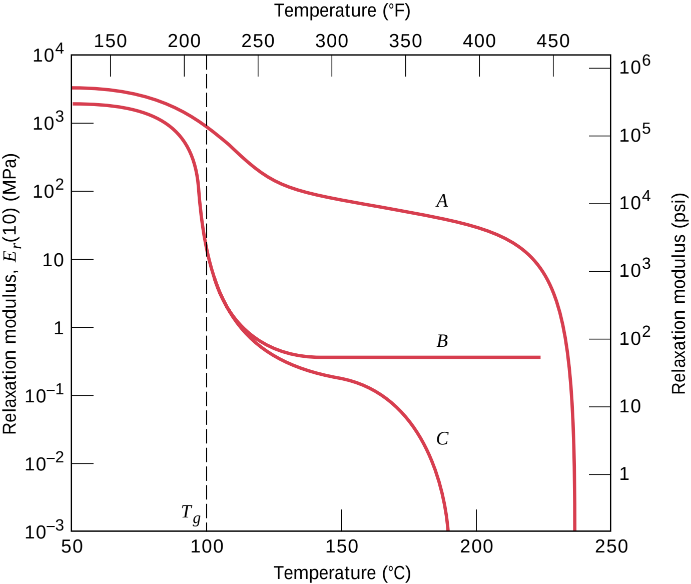

FIGURE 7.29 Logarithm of the relaxation modulus versus temperature for crystalline isotactic (curve *A*), lightly crosslinked atactic (curve *B*), and amorphous (curve *C*) polystyrene. (From A. V. Tobolsky, *Properties and Structures of Polymers*. Copyright © 1960 by John Wiley & Sons, New York. Reprinted by permission of John Wiley & Sons, Inc.)

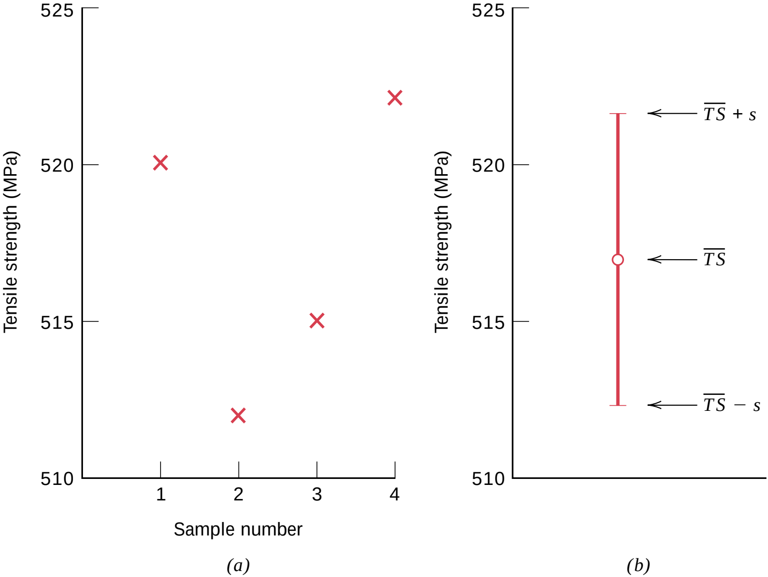

Figure 7.32 (*a*) Tensile strength data associated with Example Problem 7.6. (*b*) The manner in which these data could be plotted. The data point corresponds to the average value of the tensile strength ($\overline{TS}$); error bars that indicate the degree of scatter correspond to the average value plus and minus the standard deviation ($\overline{TS} \pm s$).

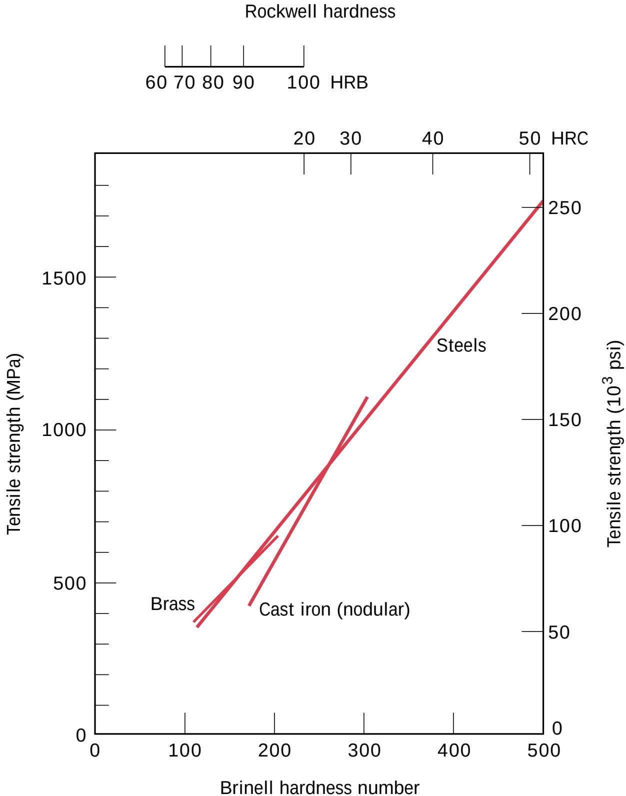

Figure 7.31 Relationships between hardness and tensile strength for steel, brass, and cast iron. (Data taken from *Metals Handbook: Properties and Selection: Irons and Steels,* Vol. 1, 9th edition, B. Bardes, Editor, American Society for Metals, 1978, pp. 36 and 461; and *Metals Handbook: Properties and Selection: Nonferrous Alloys and Pure Metals,* Vol. 2, 9th edition, H. Baker, Managing Editor, American Society for Metals, 1979, p. 327.)

Table 7.2 Room-Temperature Mechanical Properties (in Tension) for Various Materials

	Yield Strength		*Tensile Strength*		
Material	***MPa***	***ksi***	***MPa***	***ksi***	***Ductility, %EL [in 50 mm (2 in.)]***[a]
Metal Alloys[b]					
Molybdenum	565	82	655	95	35
Titanium	450	65	520	75	25
Steel (1020)	180	26	380	55	25
Nickel	138	20	480	70	40
Iron	130	19	262	38	45
Brass (70 Cu–30 Zn)	75	11	300	44	68
Copper	69	10	200	29	45
Aluminum	35	5	90	13	40
Ceramic Materials[c]					
Zirconia (ZrO_2)[d]	—	—	800–1500	115–215	—
Silicon nitride (Si_3N_4)	—	—	250–1000	35–145	—
Aluminum oxide (Al_2O_3)	—	—	275–700	40–100	—
Silicon carbide (SiC)	—	—	100–820	15–120	—
Glass–ceramic (Pyroceram)	—	—	247	36	—
Mullite ($3Al_2O_3$-$2SiO_2$)	—	—	185	27	—
Spinel ($MgAl_2O_4$)	—	—	110–245	16–36	—
Fused silica (SiO_2)	—	—	110	16	—
Magnesium oxide (MgO)[e]	—	—	105	15	—
Soda–lime glass	—	—	69	10	—
Polymers					
Nylon 6,6	44.8–82.8	6.5–12	75.9–94.5	11.0–13.7	15–300
Polycarbonate (PC)	62.1	9.0	62.8–72.4	9.1–10.5	110–150
Polyester (PET)	59.3	8.6	48.3–72.4	7.0–10.5	30–300
Polymethyl methacrylate (PMMA)	53.8–73.1	7.8–10.6	48.3–72.4	7.0–10.5	2.0–5.5
Polyvinyl chloride (PVC)	40.7–44.8	5.9–6.5	40.7–51.7	5.9–7.5	40–80
Phenol-formaldehyde	—	—	34.5–62.1	5.0–9.0	1.5–2.0
Polystyrene (PS)	—	—	35.9–51.7	5.2–7.5	1.2–2.5
Polypropylene (PP)	31.0–37.2	4.5–5.4	31.0–41.4	4.5–6.0	100–600
Polyethylene—high density (HDPE)	26.2–33.1	3.8–4.8	22.1–31.0	3.2–4.5	10–1200
Polytetrafluoroethylene (PTFE)	—	—	20.7–34.5	3.0–5.0	200–400
Polyethylene—low density (LDPE)	9.0–14.5	1.3–2.1	8.3–31.4	1.2–4.55	100–650

[a] For polymers, percent elongation at break.

[b] Property values are for metal alloys in an annealed state.

[c] The tensile strength of ceramic materials is taken as flexural strength (Section 7.10).

[d] Partially stabilized with 3 mol% Y_2O_3.

[e] Sintered and containing approximately 5% porosity.

CHAPTER 8

DEFORMATION AND STRENGTHENING MECHANISMS

8.7 In the manner of Figure 8.6b, we are to sketch the atomic packing for a BCC {110} type plane, and with arrows indicate two different ⟨111⟩ type directions. Such is shown below.

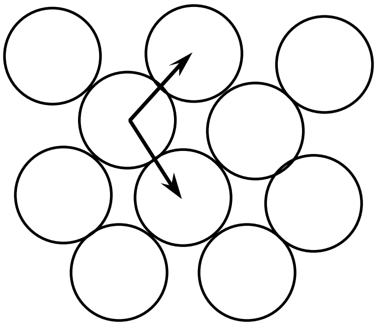

8.10* We are asked to compute the **Schmid factor** for an FCC crystal oriented with its [100] direction parallel to the loading axis. With this scheme, slip may occur on the (111) plane and in the $[1\bar{1}0]$ direction as noted in the figure below.

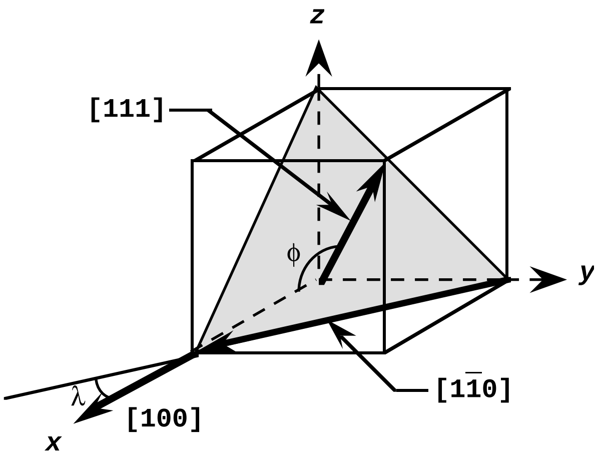

The angle between the [100] and $[1\bar{1}0]$ directions, λ, is 45°. For the (111) plane, the angle between its normal (which is the [111] direction) and the [100] direction, ϕ, is $\tan^{-1}\left(\frac{\mathbf{a}\sqrt{2}}{\mathbf{a}}\right) = 54.74^\circ$; therefore

$$\cos\lambda\cos\phi = \cos(45^\circ)\cos(54.74^\circ) = 0.408$$

8.20 We are asked to determine the grain diameter for an iron which will give a yield strength of 205 MPa (30,000 psi). The best way to solve this problem is to first establish two simultaneous expressions of Equation (8.5), solve for $\sigma_{\mathbf{o}}$ and $\mathbf{k_y}$, and finally determine the value of **d** when $\sigma_{\mathbf{y}} = 205$ MPa. The data pertaining to this problem may be tabulated as follows:

σ_y	d (mm)	$d^{-1/2}$ $(mm)^{-1/2}$
135 MPa	5×10^{-2}	4.47
260 MPa	8×10^{-3}	11.18

The two equations thus become

$$135 \text{ MPa} = \sigma_o + (4.47)k_y$$

$$260 \text{ MPa} = \sigma_o + (11.18)k_y$$

which yield the values, $\boldsymbol{\sigma_o} = 51.7$ MPa and $\mathbf{k_y} = 18.63$ MPa$(mm)^{1/2}$. At a yield strength of 205 MPa

$$205 \text{ MPa} = 51.7 \text{ MPa} + [18.63 \text{ MPa(mm)}^{1/2}]d^{-1/2}$$

or $\mathbf{d}^{-1/2} = 8.23$ $(mm)^{-1/2}$, which gives $\mathbf{d} = 1.48 \times 10^{-2}$ mm.

8.25 This problem stipulates that two previously undeformed cylindrical specimens of an alloy are to be strain hardened by reducing their cross-sectional areas. For one specimen, the initial and deformed radii are 16 mm and 11 mm, respectively. The second specimen with an initial radius of 12 mm is to have the same deformed hardness as the first specimen. We are asked to compute the radius of the second specimen after deformation. In order for these two cylindrical specimens to have the same deformed hardness, they must be deformed to the same percent cold work. For the first specimen

$$\%\text{CW} = \frac{A_o - A_d}{A_o} \times 100 = \frac{\pi r_o^2 - \pi r_d^2}{\pi r_o^2} \times 100$$

$$= \frac{\pi(16 \text{ mm})^2 - \pi(11 \text{ mm})^2}{\pi(16 \text{ mm})^2} \times 100 = 52.7\%\text{CW}$$

For the second specimen, the deformed radius is computed using the above equation and solving for $\mathbf{r_d}$ as

$$r_d = r_o\sqrt{1 - \frac{\%\text{CW}}{100}}$$

$$= (12 \text{ mm})\sqrt{1 - \frac{52.7\%\text{CW}}{100}} = 8.25 \text{ mm}$$

8.27 This problem calls for us to calculate the precold-worked radius of a cylindrical specimen of copper that has a cold-worked ductility of 25%EL. From Figure 8.19(c), copper that has a ductility of 25%EL will have experienced a deformation of about 11%CW. For a cylindrical specimen, Equation (8.6) becomes

$$\%\text{CW} = \left[\frac{\pi r_o^2 - \pi r_d^2}{\pi r_o^2}\right] \times 100$$

Since $\mathbf{r_d} = 10$ mm (0.40 in.), solving for $\mathbf{r_o}$ yields

$$r_o = \frac{r_d}{\sqrt{1 - \frac{\%\text{CW}}{100}}} = \frac{10 \text{ mm}}{\sqrt{1 - \frac{11.0}{100}}} = 10.6 \text{ mm (0.424 in.)}$$

8.35 In this problem, we are asked for the length of time required for the average grain size of a brass material to increase a specified amount using Figure 8.25.

(a) At 500°C, the time necessary for the average grain diameter to increase from 0.01 to 0.1 mm is approximately 3500 min.

(b) At 600°C the time required for this same grain size increase is approximately 150 min.

8.45* This problem gives us the tensile strengths and associated number-average molecular weights for two polymethyl methacrylate materials and then asks that we estimate the tensile strength for $\overline{\mathbf{M}}_{\mathbf{n}} = 30{,}000$ g/mol. Equation (8.9) provides the dependence of the tensile strength on $\overline{\mathbf{M}}_{\mathbf{n}}$. Thus, using the data provided in the problem, we may set up two simultaneous equations from which it is possible to solve for the two constants $\mathbf{TS}_\infty$ and **A**. These equations are as follows:

$$107\text{ MPa} = \text{TS}_\infty - \frac{\text{A}}{40000\text{ g/mol}}$$

$$170\text{ MPa} = \text{TS}_\infty - \frac{\text{A}}{60000\text{ g/mol}}$$

Thus, the values of the two constants are $\mathbf{TS}_\infty = 296$ MPa and $\mathbf{A} = 7.56 \times 10^6$ MPa-g/mol. Substituting these values into an equation for which $\overline{\mathbf{M}}_{\mathbf{n}} = 30{,}000$ g/mol leads to

$$\begin{aligned}\text{TS} &= \text{TS}_\infty - \frac{\text{A}}{30000\text{ g/mol}}\\ &= 296\text{ MPa} - \frac{7.56 \times 10^6\text{ MPa-g/mol}}{30000\text{ g/mol}}\\ &= 44\text{ MPa}\end{aligned}$$

8.54 This problem asks that we compute the fraction of possible crosslink sites in 10 kg of polybutadiene when 4.8 kg of S is added, assuming that, on the average, 4.5 sulfur atoms participate in each crosslink bond. Given the butadiene mer unit in Table 4.5, we may calculate its molecular weight as follows:

$$\begin{aligned}\text{A(butadiene)} &= 4(\text{A}_\text{C}) + 6(\text{A}_\text{H})\\ &= (4)(12.01\text{ g/mol}) + 6(1.008\text{ g/mol}) = 54.09\text{ g/mol}\end{aligned}$$

which means that in 10 kg of butadiene there are $\frac{10000\text{ g}}{54.09\text{ g/mol}} = 184.9$ mol.

For the vulcanization of polybutadiene, there are two possible crosslink sites per mer—one for each of the two carbon atoms that are doubly bonded. Furthermore, each of these crosslinks forms a bridge between two mers. Therefore, we can say that there is the equivalent of one crosslink per mer. Therefore, let us now calculate the number of moles of sulfur ($\mathbf{n}_{\mathbf{sulfur}}$) that react with the butadiene, by taking the mole ratio of sulfur to butadiene, and then dividing this ratio by 4.5 atoms per crosslink; this yields the fraction of possible sites that are crosslinked. Thus

$$\text{n}_\text{sulfur} = \frac{4800\text{ g}}{32.06\text{ g/mol}} = 149.7\text{ mol}$$

And

$$\text{fraction sites crosslinked } = \frac{\dfrac{149.7\text{ mol}}{184.9\text{ mol}}}{4.5} = 0.180$$

8.D1 This problem calls for us to determine whether or not it is possible to cold work steel so as to give a minimum Brinell hardness of 225 and a ductility of at least 12%EL. According to Figure 7.31, a Brinell hardness of 225 corresponds to a tensile strength of 800 MPa (116,000 psi). Furthermore, from Figure 8.19(b), in order to achieve a tensile strength of 800 MPa, deformation of at least 13%CW is necessary. Finally, if we cold work the steel to 13%CW, then the ductility is reduced to only 14%EL from Figure 8.19(c). Therefore, it **is possible** to meet both of these criteria by plastically deforming the steel.

8.D6 This problem stipulates that a cylindrical rod of copper originally 16.0 mm in diameter is to be cold worked by drawing; a cold-worked yield strength in excess of 250 MPa and a ductility of at least 12%EL are required, whereas the final diameter must be 11.3 mm. We are to explain how this is to be accomplished. Let us first calculate the percent cold work and attendant yield strength and ductility if the drawing is carried out without interruption. From Equation (8.6)

$$\%\mathrm{CW} = \frac{\pi\left(\frac{d_o}{2}\right)^2 - \pi\left(\frac{d_d}{2}\right)^2}{\pi\left(\frac{d_o}{2}\right)^2} \times 100$$

$$= \frac{\pi\left(\frac{16\ \mathrm{mm}}{2}\right)^2 - \pi\left(\frac{11.3\ \mathrm{mm}}{2}\right)^2}{\pi\left(\frac{16\ \mathrm{mm}}{2}\right)^2} \times 100 = 50\%\mathrm{CW}$$

At 50%CW, the copper will have a yield strength on the order of 330 MPa (48,000 psi), Figure 8.19(a), which is adequate; however, the ductility will be about 4%EL, Figure 8.19(c), which is insufficient.

Instead of performing the drawing in a single operation, let us initially draw some fraction of the total deformation, then anneal to recrystallize, and, finally, cold work the material a second time in order to achieve the final diameter, yield strength, and ductility.

Reference to Figure 8.19(a) indicates that 21%CW is necessary to give a yield strength of 250 MPa. Similarly, a maximum of 23%CW is possible for 12%EL [Figure 8.19(c)]. The average of these two values is 22%CW, which we will use in the calculations. If the final diameter after the first drawing is $\mathbf{d}'_\mathbf{o}$, then

$$22\%\mathrm{CW} = \frac{\pi\left(\frac{d'_o}{2}\right)^2 - \pi\left(\frac{11.3}{2}\right)^2}{\pi\left(\frac{d'_o}{2}\right)^2} \times 100$$

And, solving for $\mathbf{d}'_\mathbf{o}$ yields $\mathbf{d}'_\mathbf{o} = 12.8$ mm (0.50 in.).

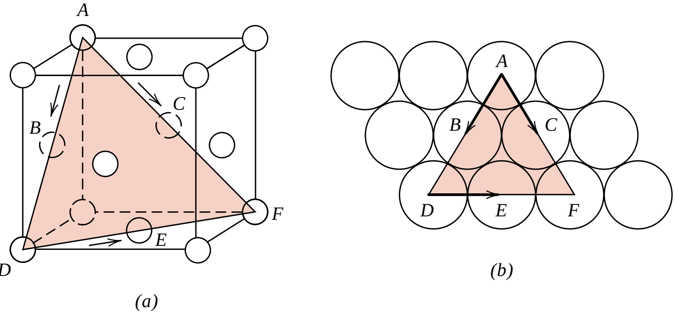

(a)

(b)

FIGURE 8.6 (*a*) A {111}⟨110⟩ slip system shown within an FCC unit cell. (*b*) The (111) plane from (*a*) and three ⟨110⟩ slip directions (as indicated by arrows) within that plane comprise possible slip systems.

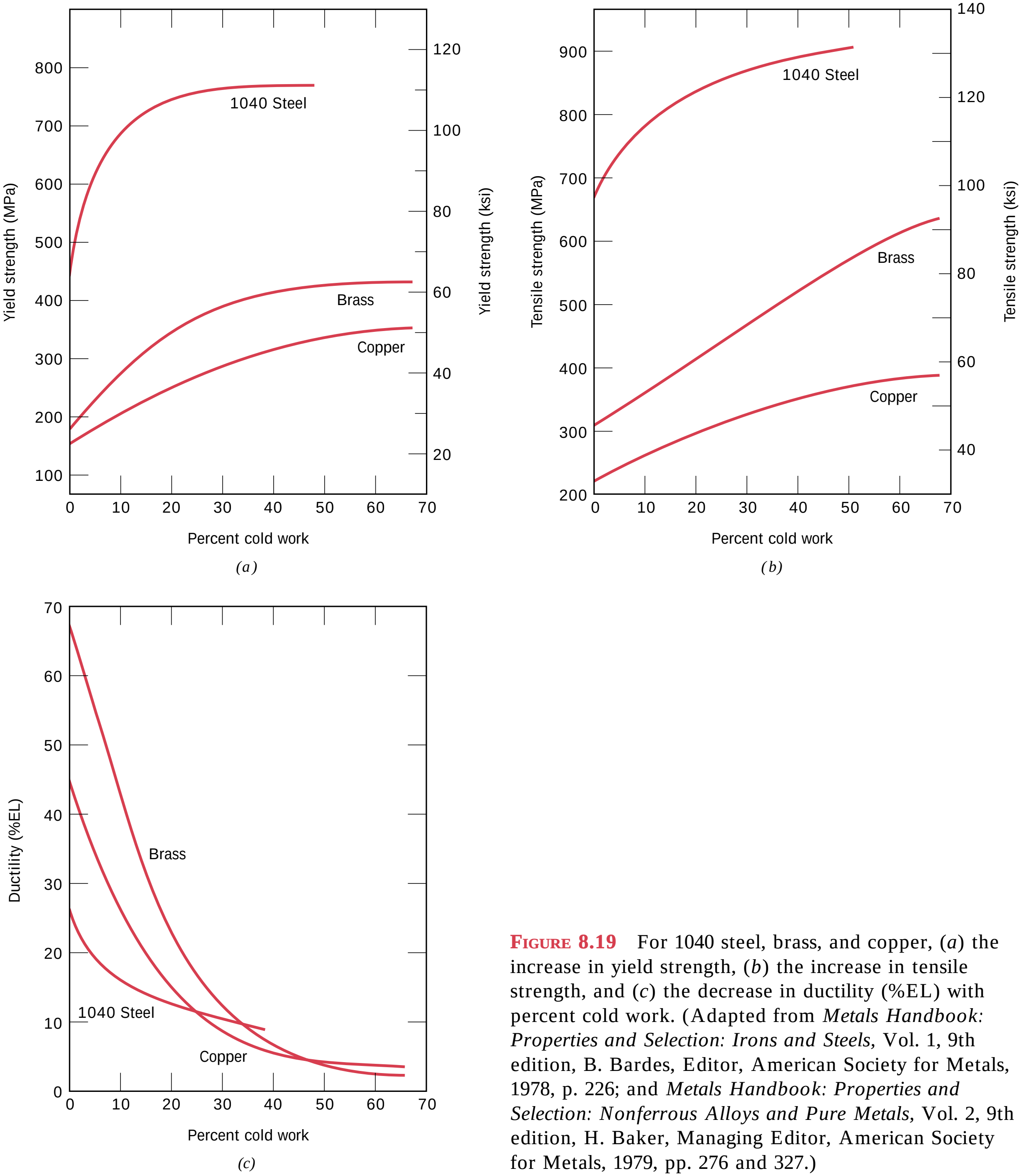

Figure 8.19 For 1040 steel, brass, and copper, (*a*) the increase in yield strength, (*b*) the increase in tensile strength, and (*c*) the decrease in ductility (%EL) with percent cold work. (Adapted from *Metals Handbook: Properties and Selection: Irons and Steels,* Vol. 1, 9th edition, B. Bardes, Editor, American Society for Metals, 1978, p. 226; and *Metals Handbook: Properties and Selection: Nonferrous Alloys and Pure Metals,* Vol. 2, 9th edition, H. Baker, Managing Editor, American Society for Metals, 1979, pp. 276 and 327.)

Chapter 8 / Deformation and Strengthening Mechanisms

8.6 SLIP IN SINGLE CRYSTALS

A further explanation of slip is simplified by treating the process in single crystals, then making the appropriate extension to polycrystalline materials. As mentioned previously, edge, screw, and mixed dislocations move in response to shear stresses applied along a slip plane and in a slip direction. As was noted in Section 7.2, even though an applied stress may be pure tensile (or compressive), shear components exist at all but parallel or perpendicular alignments to the stress direction (Equation 7.4b). These are termed **resolved shear stresses,** and their magnitudes depend not only on the applied stress, but also on the orientation of both the slip plane and direction within that plane. Let ϕ represent the angle between the normal to the slip plane and the applied stress direction, and λ the angle between the slip and stress directions, as indicated in Figure 8.7; it can then be shown that for the resolved shear stress τ_R

$$\tau_R = \sigma \cos\phi \cos\lambda \tag{8.1}$$

where σ is the applied stress. In general, $\phi + \lambda \neq 90°$, since it need not be the case that the tensile axis, the slip plane normal, and the slip direction all lie in the same plane.

A metal single crystal has a number of different slip systems that are capable of operating. The resolved shear stress normally differs for each one because the orientation of each relative to the stress axis (ϕ and λ angles) also differs. However, one slip system is generally oriented most favorably, that is, has the largest resolved shear stress, τ_R(max):

$$\tau_R(\text{max}) = \sigma(\cos\phi \cos\lambda)_{\text{max}} \tag{8.2}$$

In response to an applied tensile or compressive stress, slip in a single crystal commences on the most favorably oriented slip system when the resolved shear stress reaches some critical value, termed the **critical resolved shear stress** τ_{crss}; it represents the minimum shear stress required to initiate slip, and is a property of the material that determines when yielding occurs. The single crystal plastically deforms or yields when $\tau_R(\text{max}) = \tau_{\text{crss}}$, and the magnitude of the applied stress required to initiate yielding (i.e., the yield strength σ_y) is

$$\sigma_y = \frac{\tau_{\text{crss}}}{(\cos\phi \cos\lambda)_{\text{max}}} \tag{8.3}$$

The minimum stress necessary to introduce yielding occurs when a single crystal is oriented such that $\phi = \lambda = 45°$; under these conditions,

$$\sigma_y = 2\tau_{\text{crss}} \tag{8.4}$$

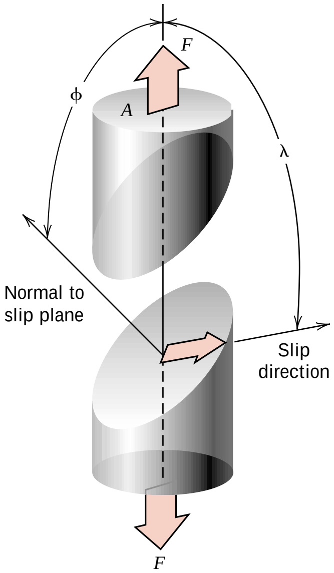

Figure 8.7 Geometrical relationships between the tensile axis, slip plane, and slip direction used in calculating the resolved shear stress for a single crystal.

For a single-crystal specimen that is stressed in tension, deformation will be as in Figure 8.8, where slip occurs along a number of equivalent and most favorably oriented planes and directions at various positions along the specimen length. This slip deformation forms as small steps on the surface of the single crystal that are parallel to one another and loop around the circumference of the specimen as indicated in Figure 8.8. Each step results from the movement of a large number of dislocations along the same slip plane. On the surface of a polished single crystal specimen, these steps appear as lines, which are called slip lines. A zinc single crystal that has been plastically deformed to the degree that these slip markings are discernible is shown in Figure 8.9.

With continued extension of a single crystal, both the number of slip lines and the slip step width will increase. For FCC and BCC metals, slip may eventually begin along a second slip system, that which is next most favorably oriented with

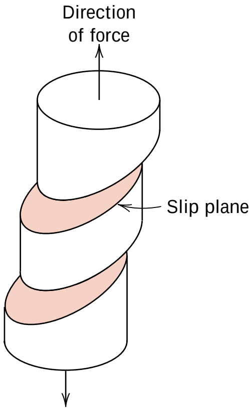

Figure 8.8 Macroscopic slip in a single crystal.

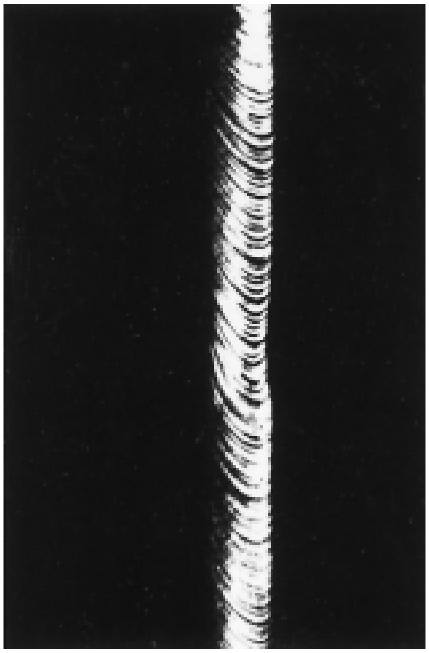

Figure 8.9 Slip in a zinc single crystal. (From C. F. Elam, *The Distortion of Metal Crystals,* Oxford University Press, London, 1935.)

the tensile axis. Furthermore, for HCP crystals having few slip systems, if, for the most favorable slip system, the stress axis is either perpendicular to the slip direction ($\lambda = 90°$) or parallel to the slip plane ($\phi = 90°$), the critical resolved shear stress will be zero. For these extreme orientations the crystal ordinarily fractures rather than deforming plastically.

Example Problem 8.1

Consider a single crystal of BCC iron oriented such that a tensile stress is applied along a [010] direction. **(a)** Compute the resolved shear stress along a (110) plane and in a $[\bar{1}11]$ direction when a tensile stress of 52 MPa (7500 psi) is applied. **(b)** If slip occurs on a (110) plane and in a $[\bar{1}11]$ direction, and the critical resolved shear stress is 30 MPa (4350 psi), calculate the magnitude of the applied tensile stress necessary to initiate yielding.

Solution

(a) A BCC unit cell along with the slip direction and plane as well as the direction of the applied stress are all shown in the accompanying diagram (*a*). As indicated, ϕ, the angle between the (110) plane normal and the [010] direction is 45°. From the triangle ABC in diagram (*b*), λ, the angle between the $[\bar{1}11]$ and [010] directions is $\tan^{-1}(a\sqrt{2}/a) = 54.7°$, a being the unit cell length. Thus according to Equation 8.1,

$$\tau_R = \sigma \cos \phi \cos \lambda = (52 \text{ MPa})(\cos 45°)(\cos 54.7°)$$

$$= 21.3 \text{ MPa } (3060 \text{ psi})$$

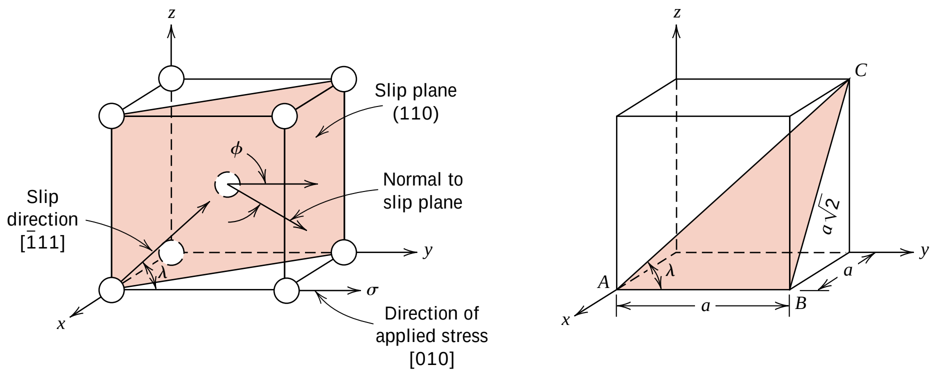
z
Slip plane (110)
ϕ
Normal to slip plane
Slip direction [$\bar{1}$11]
y
σ
λ
x
Direction of applied stress [010]
z
C
$a\sqrt{2}$
A
λ
a
B
x
y

(a) *(b)*

(b) The yield strength σ_y may be computed from Equation 8.3; ϕ and λ will be the same as for part a, and

$$\sigma_y = \frac{30 \text{ MPa}}{(\cos 45^\circ)(\cos 54.7^\circ)} = 73.4 \text{ MPa } (10{,}600 \text{ psi})$$

8.8 DEFORMATION BY TWINNING

In addition to slip, plastic deformation in some metallic materials can occur by the formation of mechanical twins, or *twinning*. The concept of a twin was introduced in Section 5.8; that is, a shear force can produce atomic displacements such that on one side of a plane (the twin boundary), atoms are located in mirror image positions of atoms on the other side. The manner in which this is accomplished is demonstrated in Figure 8.12. Here, open circles represent atoms that did not move, and dashed and solid circles represent original and final positions, respectively, of

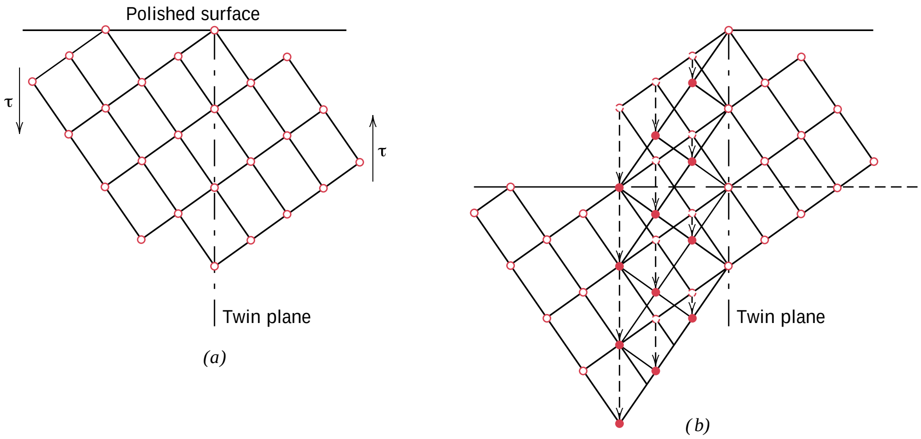
Polished surface
τ
τ
Twin plane
Twin plane

(a) *(b)*

FIGURE 8.12 Schematic diagram showing how twinning results from an applied shear stress τ. In (*b*), open circles represent atoms that did not change position; dashed and solid circles represent original and final atom positions, respectively. (From G. E. Dieter, *Mechanical Metallurgy*, 3rd edition. Copyright © 1986 by McGraw-Hill Book Company, New York. Reproduced with permission of McGraw-Hill Book Company.)

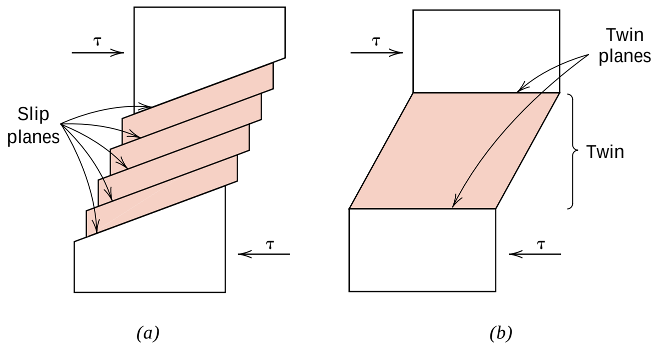

FIGURE 8.13 For a single crystal subjected to a shear stress τ, (*a*) deformation by slip; (*b*) deformation by twinning.

atoms within the twinned region. As may be noted in this figure, the displacement magnitude within the twin region (indicated by arrows) is proportional to the distance from the twin plane. Furthermore, twinning occurs on a definite crystallographic plane and in a specific direction that depend on crystal structure. For example, for BCC metals, the twin plane and direction are (112) and [111], respectively.

Slip and twinning deformations are compared in Figure 8.13 for a single crystal that is subjected to a shear stress τ. Slip ledges are shown in Figure 8.13*a*, the formation of which were described in Section 8.6; for twinning, the shear deformation is homogeneous (Figure 8.13*b*). These two processes differ from one another in several respects. First of all, for slip, the crystallographic orientation above and below the slip plane is the same both before and after the deformation; whereas for twinning, there will be a reorientation across the twin plane. In addition, slip occurs in distinct atomic spacing multiples, whereas the atomic displacement for twinning is less than the interatomic separation.

Mechanical twinning occurs in metals that have BCC and HCP crystal structures, at low temperatures, and at high rates of loading (shock loading), conditions under which the slip process is restricted; that is, there are few operable slip systems. The amount of bulk plastic deformation from twinning is normally small relative to that resulting from slip. However, the real importance of twinning lies with the accompanying crystallographic reorientations; twinning may place new slip systems in orientations that are favorable relative to the stress axis such that the slip process can now take place.

8.18a FACTORS THAT INFLUENCE THE MECHANICAL PROPERTIES OF SEMICRYSTALLINE POLYMERS (DETAILED VERSION)

A number of factors influence the mechanical characteristics of polymeric materials. For example, we have already discussed the effect of temperature and strain rate on stress–strain behavior (Section 7.13, Figure 7.24). Again, increasing the temperature or diminishing the strain rate leads to a decrease in the tensile modulus, a reduction in tensile strength, and an enhancement of ductility.

In addition, several structural/processing factors have decided influences on the mechanical behavior (i.e., strength and modulus) of polymeric materials. An increase in strength results whenever any restraint is imposed on the process illustrated in Figure 8.27; for example, extensive chain entanglements or a significant degree of intermolecular bonding inhibit relative chain motions. It should be noted that even though secondary intermolecular (e.g., van der Waals) bonds are much weaker than the primary covalent ones, significant intermolecular forces result from the formation of large numbers of van der Waals interchain bonds. Furthermore, the modulus rises as both the secondary bond strength and chain alignment increase. We now discuss how several structural/processing factors [viz. molecular weight, degree of crystallinity, predeformation (drawing), and heat treating] affect the mechanical behavior of polymers.

MOLECULAR WEIGHT

The magnitude of the tensile modulus does not seem to be directly influenced by molecular weight. On the other hand, for many polymers it has been observed that tensile strength increases with increasing molecular weight. Mathematically, TS is a function of the number-average molecular weight according to

$$TS = TS_{\infty} - \frac{A}{\overline{M}_n} \tag{8.9}$$

where TS_{∞} is the tensile strength at infinite molecular weight and A is a constant. The behavior described by this equation is explained by increased chain entanglements with rising $\overline{M}_n$.

DEGREE OF CRYSTALLINITY

For a specific polymer, the degree of crystallinity can have a rather significant influence on the mechanical properties, since it affects the extent of the intermolecular secondary bonding. For crystalline regions in which molecular chains are closely packed in an ordered and parallel arrangement, extensive secondary bonding ordinarily exists between adjacent chain segments. This secondary bonding is much less prevalent in amorphous regions, by virtue of the chain misalignment. As a consequence, for semicrystalline polymers, tensile modulus increases significantly with degree of crystallinity. For example, for polyethylene, the modulus increases approximately an order of magnitude as the crystallinity fraction is raised from 0.3 to 0.6.

Furthermore, increasing the crystallinity of a polymer generally enhances its strength; in addition, the material tends to become more brittle. The influence of chain chemistry and structure (branching, stereoisomerism, etc.) on degree of crystallinity was discussed in Chapter 4.

The effects of both percent crystallinity and molecular weight on the physical state of polyethylene are represented in Figure 8.28.

PREDEFORMATION BY DRAWING

On a commercial basis, one of the most important techniques used to improve mechanical strength and tensile modulus is permanently deforming the polymer in tension. This procedure is sometimes termed *drawing*, and corresponds to the neck extension process illustrated schematically in Figure 7.25. In terms of property alterations, drawing is the polymer analog of strain hardening in metals. It is an important stiffening and strengthening technique that is employed in the production of fibers and films. During drawing the molecular chains slip past one another and become highly oriented; for semicrystalline materials the chains assume conformations similar to that represented schematically in Figure 8.27*e*.

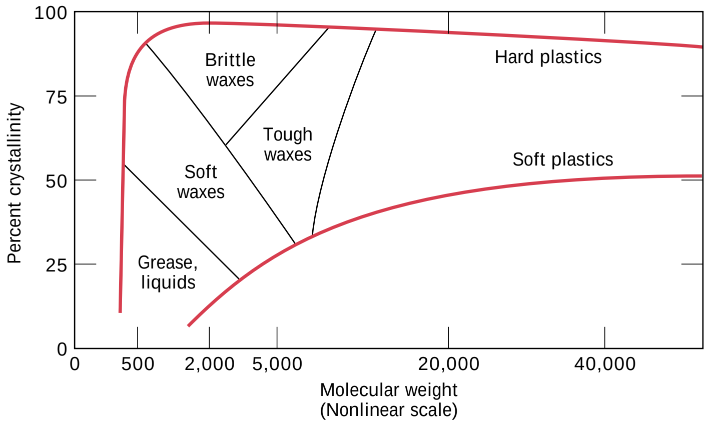

Figure 8.28 The influence of degree of crystallinity and molecular weight on the physical characteristics of polyethylene. (From R. B. Richards, ''Polyethylene—Structure, Crystallinity and Properties,'' *J. Appl. Chem.*, **1,** 370, 1951.)

Degrees of strengthening and stiffening will depend on the extent of deformation (or extension) of the material. Furthermore, the properties of drawn polymers are highly anisotropic. For those materials drawn in uniaxial tension, tensile modulus and strength values are significantly greater in the direction of deformation than in other directions. Tensile modulus in the direction of drawing may be enhanced by up to approximately a factor of three relative to the undrawn material. At an angle of 45° from the tensile axis the modulus is a minimum; at this orientation the modulus has a value on the order of one-fifth that of the undrawn polymer.

Tensile strength parallel to the direction of orientation may be improved by a factor of at least two to five relative to that of the unoriented material. On the other hand, perpendicular to the alignment direction, tensile strength is reduced by on the order of one-third to one-half.

For an amorphous polymer that is drawn at an elevated temperature, the oriented molecular structure is retained only when the material is quickly cooled to the ambient; this procedure gives rise to the strengthening and stiffening effects described in the previous paragraph. On the other hand, if, after stretching, the polymer is held at the temperature of drawing, molecular chains relax and assume random conformations characteristic of the predeformed state; as a consequence, drawing will have no effect on the mechanical characteristics of the material.

HEAT TREATING

Heat treating (or annealing) of semicrystalline polymers leads to modifications in crystallite size and perfection, as well as the spherulite structure. For undrawn materials that are subjected to constant-time heat treatments, increasing the annealing temperature leads to the following: (1) an increase in tensile modulus, (2) an increase in yield strength, and (3) a reduction in ductility. It should be noted that these annealing effects are opposite to those typically observed for metallic materials (Section 8.13)—i.e., weakening, softening, and enhanced ductility.

For some polymer fibers that have been drawn, the influence of annealing on the tensile modulus is contrary to that for undrawn materials—i.e., modulus decreases with increased annealing temperature due to a loss of chain orientation and strain-induced crystallinity.

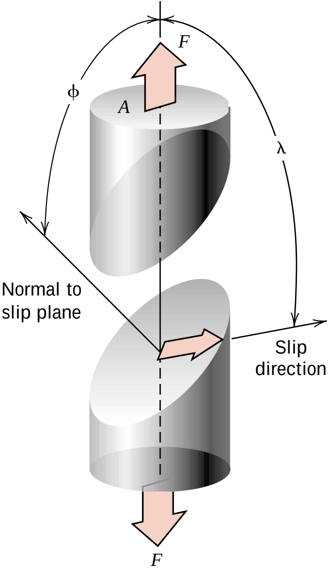
F
ϕ
A
λ
Normal to slip plane
Slip direction
F

Figure 8.7 Geometrical relationships between the tensile axis, slip plane, and slip direction used in calculating the resolved shear stress for a single crystal.

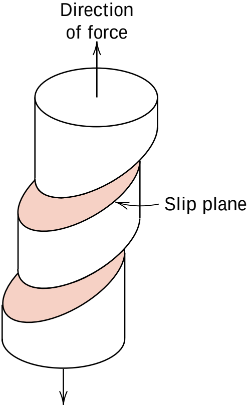
Direction of force
Slip plane

FIGURE 8.8 Macroscopic slip in a single crystal.

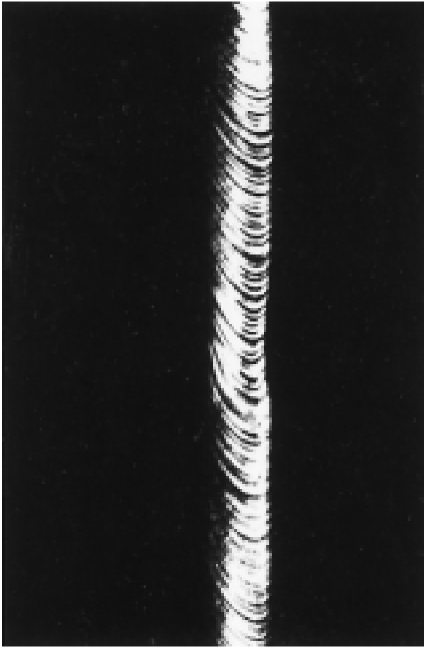

FIGURE 8.9 Slip in a zinc single crystal. (From C. F. Elam, *The Distortion of Metal Crystals,* Oxford University Press, London, 1935.)

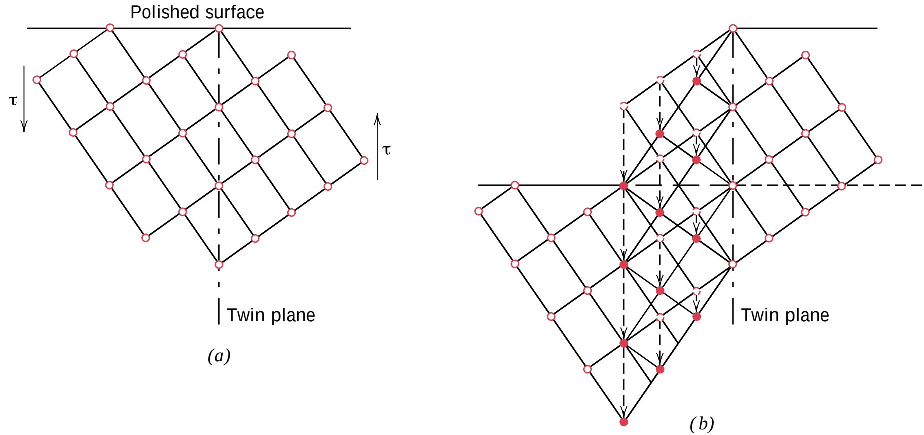
Polished surface
τ
τ
Twin plane
(a)
Twin plane
(b)

FIGURE 8.12 Schematic diagram showing how twinning results from an applied shear stress τ. In (*b*), open circles represent atoms that did not change position; dashed and solid circles represent original and final atom positions, respectively. (From G. E. Dieter, *Mechanical Metallurgy*, 3rd edition. Copyright © 1986 by McGraw-Hill Book Company, New York. Reproduced with permission of McGraw-Hill Book Company.)

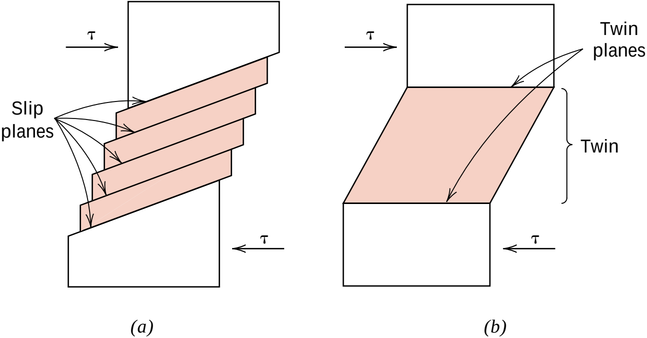
τ
Slip planes
τ
τ
Twin planes
Twin
τ

(a) *(b)*

FIGURE 8.13 For a single crystal subjected to a shear stress τ, (*a*) deformation by slip; (*b*) deformation by twinning.

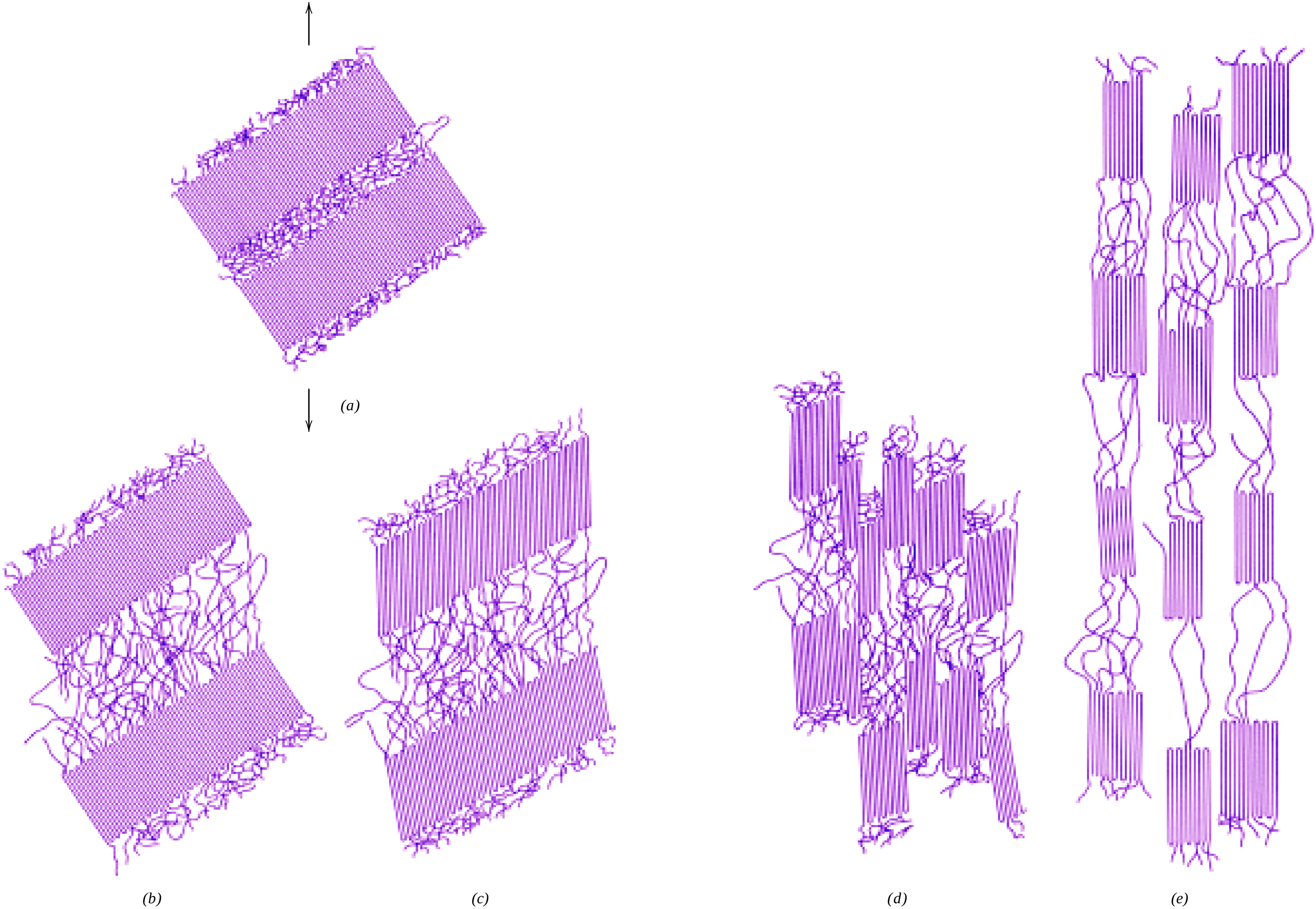

FIGURE 8.27 Stages in the deformation of a semicrystalline polymer. (*a*) Two adjacent chain-folded lamellae and interlamellar amorphous material before deformation. (*b*) Elongation of amorphous tie chains during the first stage of deformation. (*c*) Tilting of lamellar chain folds during the second stage. (*d*) Separation of crystalline block segments during the third stage. (*e*) Orientation of block segments and tie chains with the tensile axis in the final deformation stage. (From Jerold M. Schultz, *Polymer Materials Science*, copyright © 1974, pp. 500–501. Reprinted by permoission of Prentice-Hall, Inc., Englewood Cliffs, NJ.)

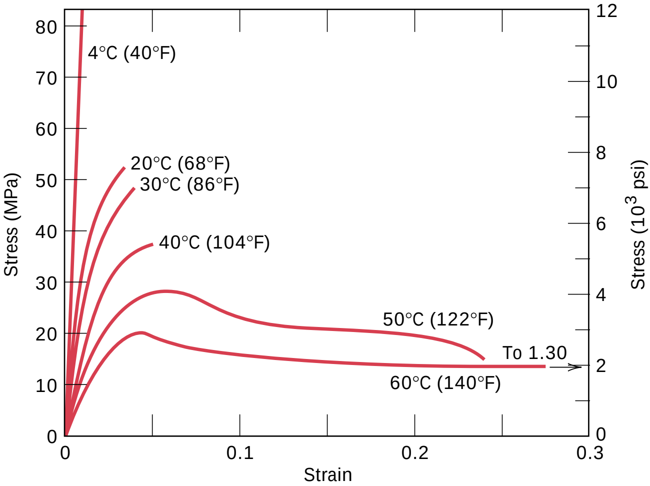

FIGURE 7.24 The influence of temperature on the stress–strain characteristics of polymethyl methacrylate. (From T. S. Carswell and H. K. Nason, ‘‘Effect of Environmental Conditions on the Mechanical Properties of Organic Plastics,’’ *Symposium on Plastics*, American Society for Testing and Materials, Philadelphia, 1944. Copyright, ASTM. Reprinted with permission.)

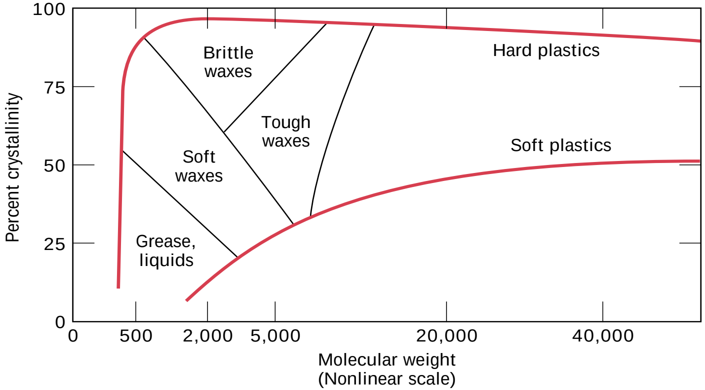

FIGURE 8.28 The influence of degree of crystallinity and molecular weight on the physical characteristics of polyethylene. (From R. B. Richards, ‘‘Polyethylene—Structure, Crystallinity and Properties,’’ *J. Appl. Chem.*, **1,** 370, 1951.)

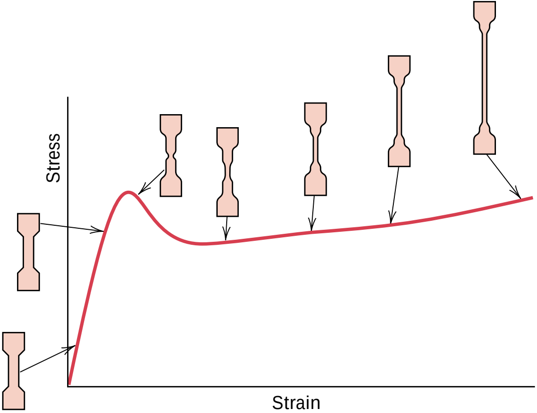

Figure 7.25 Schematic tensile stress–strain curve for a semicrystalline polymer. Specimen contours at several stages of deformation are included. (From Jerold M. Schultz, *Polymer Materials Science*, copyright © 1974, p. 488. Reprinted by permission of Prentice-Hall, Inc., Englewood Cliffs, NJ.)

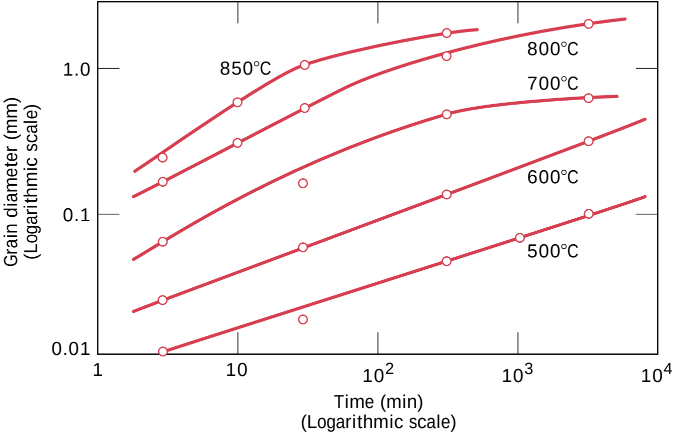

Figure 8.25 The logarithm of grain diameter versus the logarithm of time for grain growth in brass at several temperatures. (From J. E. Burke, ''Some Factors Affecting the Rate of Grain Growth in Metals.'' Reprinted with permission from *Metallurgical Transactions*, Vol. 180, 1949, a publication of The Metallurgical Society of AIME, Warrendale, Pennsylvania.)

CHAPTER 9

FAILURE

9.7 We are asked for the critical crack tip radius for an Al_2O_3 material. From Equation (9.1b)

$$\sigma_m = 2\sigma_o\left(\frac{a}{\rho_t}\right)^{1/2}$$

Fracture will occur when σ_m reaches the fracture strength of the material, which is given as **E**/10; thus

$$\frac{E}{10} = 2\sigma_o\left(\frac{a}{\rho_t}\right)^{1/2}$$

Or, solving for ρ_t

$$\rho_t = \frac{400a\sigma_o^2}{E^2}$$

From Table 7.1, **E** = 393 GPa, and thus,

$$\rho_t = \frac{(400)(2 \times 10^{-3}\ \text{mm})(275\ \text{MPa})^2}{(393 \times 10^3\ \text{MPa})^2}$$

$$= 3.9 \times 10^{-7}\ \text{mm} = 0.39\ \text{nm}$$

9.8 We may determine the critical stress required for the propagation of a surface crack in soda-lime glass using Equation (9.3); taking the value of 69 GPa (Table 7.1) as the modulus of elasticity, we get

$$\sigma_c = \sqrt{\frac{2E\gamma_s}{\pi a}}$$

$$= \sqrt{\frac{(2)(69 \times 10^9\ \text{N/m}^2)(0.30\ \text{N/m})}{(\pi)(5 \times 10^{-5}\ \text{m})}} = 16.2 \times 10^6\ \text{N/m}^2 = 16.2\ \text{MPa}$$

9.12* This problem deals with a tensile specimen, a drawing of which is provided.

(a) In this portion of the problem it is necessary to compute the stress at point **P** when the applied stress is 100 MPa (14,500 psi). In order to determine the stress concentration it is necessary to consult Figure 9.8c. From the geometry of the specimen, **w**/**h** = (25 mm)/(20 mm) = 1.25; furthermore, the **r**/**h** ratio is (3 mm)/(20 mm) = 0.15. Using the **w**/**h** = 1.25 curve in Figure 9.8c, the $\mathbf{K_t}$ value at **r**/**h** = 0.15 is 1.7. And since $\mathbf{K_t} = \frac{\sigma_m}{\sigma_o}$, then

$$\sigma_m = K_t\sigma_o = (1.7)(100\ \text{MPa}) = 170\ \text{MPa}\ (24{,}650\ \text{psi})$$

9.15* This problem calls for us to determine the value of **B**, the minimum component thickness for which the condition of plane strain is valid using Equation (9.12) for the metal alloys listed in Table 9.1.

For the 2024-T3 aluminum alloy

$$B = 2.5\left(\frac{K_{Ic}}{\sigma_y}\right)^2 = (2.5)\left(\frac{44\ \text{MPa}\sqrt{\text{m}}}{345\ \text{MPa}}\right)^2 = 0.041\ \text{m} = 41\ \text{mm}\ (1.60\ \text{in.})$$

For the 4340 alloy steel tempered at 260°C

$$B = (2.5)\left(\frac{50\ \text{MPa}\sqrt{\text{m}}}{1640\ \text{MPa}}\right)^2 = 0.0023\ \text{m} = 2.3\ \text{mm}\ (0.09\ \text{in.})$$

9.19 For this problem, we are given values of $\mathbf{K_{Ic}}$, $\boldsymbol{\sigma}$, and $\mathbf{Y}$ for a large plate and are asked to determine the minimum length of a surface crack that will lead to fracture. All we need do is to solve for $\mathbf{a_c}$ using Equation (9.14); therefore

$$a_c = \frac{1}{\pi}\left(\frac{K_{Ic}}{Y\sigma}\right)^2 = \frac{1}{\pi}\left[\frac{55\ \text{MPa}\sqrt{\text{m}}}{(1)(200\ \text{MPa})}\right]^2 = 0.024\ \text{m} = 24\ \text{mm}\ (0.95\ \text{in.})$$

9.26 This problem first provides a tabulation of Charpy impact data for a ductile cast iron.

(a) The plot of impact energy versus temperature is shown below.

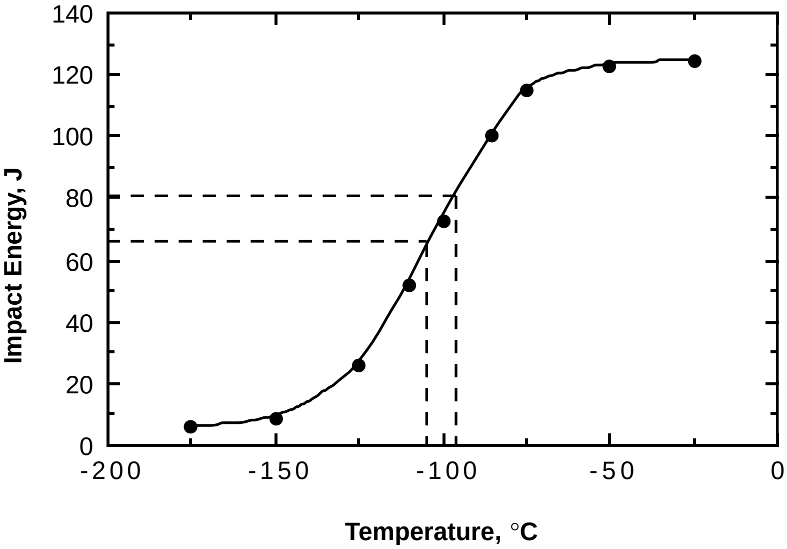

(b) This portion of the problem asks us to determine the ductile-to-brittle transition temperature as that temperature corresponding to the average of the maximum and minimum impact energies. From these data, this average is

$$\text{Average} = \frac{124\ \text{J} + 6\ \text{J}}{2} = 65\ \text{J}$$

As indicated on the plot by the one set of dashed lines, the ductile-to-brittle transition temperature according to this criterion is about −105°C.

(c) Also as noted on the plot by the other set of dashed lines, the ductile-to-brittle transition temperature for an impact energy of 80 J is about −95°C.

9.31 We are asked to determine the fatigue life for a cylindrical red brass rod given its diameter (8.0 mm) and the maximum tensile and compressive loads (+7500 N and −7500 N, respectively). The first thing that is necessary is to calculate values of $\sigma_{\mathbf{max}}$ and $\sigma_{\mathbf{min}}$ using Equation (7.1). Thus

$$\sigma_{\max} = \frac{F_{\max}}{A_o} = \frac{F_{\max}}{\pi\left(\dfrac{d_o}{2}\right)^2}$$

$$= \frac{7500\ \text{N}}{(\pi)\left(\dfrac{8.0 \times 10^{-3}\ \text{m}}{2}\right)^2} = 150 \times 10^6\ \text{N/m}^2 = 150\ \text{MPa (22,500 psi)}$$

$$\sigma_{\min} = \frac{F_{\min}}{\pi\left(\dfrac{d_o}{2}\right)^2}$$

$$= \frac{-7500\ \text{N}}{(\pi)\left(\dfrac{8.0 \times 10^{-3}\ \text{m}}{2}\right)^2} = -150 \times 10^6\ \text{N/m}^2 = -150\ \text{MPa}\ (-22{,}500\ \text{psi})$$

Now it becomes necessary to compute the stress amplitude using Equation (9.23) as

$$\sigma_a = \frac{\sigma_{\max} - \sigma_{\min}}{2} = \frac{150\ \text{MPa} - (-150\ \text{MPa})}{2} = 150\ \text{MPa (22,500 psi)}$$

From Figure 9.46 for the red brass, the number of cycles to failure at this stress amplitude is about 1×10^5 cycles.

9.33 This problem first provides a tabulation of fatigue data (i.e., stress amplitude and cycles to failure) for a brass alloy.

(a) These fatigue data are plotted below.

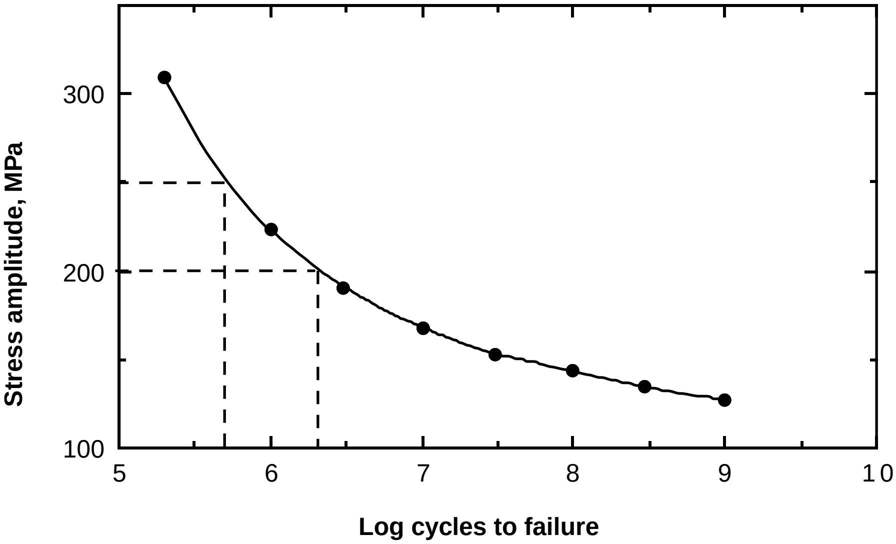

(b) As indicated by one set of dashed lines on the plot, the fatigue strength at 5×10^5 cycles [$\log(5 \times 10^5) = 5.7$] is about 250 MPa.

(c) As noted by the other set of dashed lines, the fatigue life for 200 MPa is about 2×10^6 cycles (i.e., the log of the lifetime is about 6.3).

9.34 We are asked to compute the maximum torsional stress amplitude possible at each of several fatigue lifetimes for the brass alloy, the fatigue behavior of which is given in Problem 9.33. For each lifetime, first compute the number of cycles, and then read the corresponding fatigue strength from the above plot.

(a) Fatigue lifetime = (1 yr)(365 days/yr)(24 h/day)(60 min/h)(1500 cycles/min) = 7.9×10^8 cycles. The stress amplitude corresponding to this lifetime is about 130 MPa.

(c) Fatigue lifetime = (24 h)(60 min/h)(1200 cycles/min) = 2.2×10^6 cycles. The stress amplitude corresponding to this lifetime is about 195 MPa.

9.48 This problem asks that we determine the total elongation of a low carbon-nickel alloy that is exposed to a tensile stress of 40 MPa (5800 psi) at 538°C for 5000 h; the instantaneous and primary creep elongations are 1.5 mm (0.06 in.).

From the 538°C line in Figure 9.43, the steady-state creep rate, $\dot{\varepsilon}_{\mathbf{s}}$, is about 0.15%/1000 h (or 1.5×10^{-4}%/h) at 40 MPa. The steady-state creep strain, $\varepsilon_{\mathbf{s}}$, therefore, is just the product of $\dot{\varepsilon}_{\mathbf{s}}$ and time as

$$\begin{aligned}\varepsilon_s &= \dot{\varepsilon}_s \times (\text{time})\\ &= (1.5 \times 10^{-4}\%/\text{h})(5000\ \text{h}) = 0.75\% = 7.5 \times 10^{-3}\end{aligned}$$

Strain and elongation are related as in Equation (7.2); solving for the steady-state elongation, $\Delta \mathbf{l}_{\mathbf{s}}$, leads to

$$\Delta l_s = l_o \varepsilon_s = (750\ \text{mm})(7.5 \times 10^{-3}) = 5.6\ \text{mm}\ (0.23\ \text{in.})$$

Finally, the total elongation is just the sum of this $\Delta \mathbf{l}_{\mathbf{s}}$ and the total of both instantaneous and primary creep elongations [i.e., 1.5 mm (0.06 in.)]. Therefore, the total elongation is 7.1 mm (0.29 in.).

9.52* The slope of the line from a $\log \dot{\varepsilon}_{\mathbf{s}}$ versus $\log \sigma$ plot yields the value of **n** in Equation (9.33); that is

$$n = \frac{\Delta \log \dot{\varepsilon}_s}{\Delta \log \sigma}$$

We are asked to determine the values of **n** for the creep data at the three temperatures in Figure 9.43. This is accomplished by taking ratios of the differences between two $\log \dot{\varepsilon}_{\mathbf{s}}$ and $\log \sigma$ values. Thus for 427°C

$$n = \frac{\Delta \log \dot{\varepsilon}_s}{\Delta \log \sigma} = \frac{\log(10^{-1}) - \log(10^{-2})}{\log(85\ \text{MPa}) - \log(55\ \text{MPa})} = 5.3$$

and for 538°C

$$n = \frac{\Delta \log \dot{\varepsilon}_s}{\Delta \log \sigma} = \frac{\log(1.0) - \log(10^{-2})}{\log(59\ \text{MPa}) - \log(23\ \text{MPa})} = 4.9$$

9.55* This problem gives $\dot{\varepsilon}_s$ values at two different temperatures and 70 MPa (10,000 psi), and the stress exponent $\mathbf{n} = 7.0$, and asks that we determine the steady-state creep rate at a stress of 50 MPa (7250 psi) and 1250 K.

Taking the natural logarithm of Equation (9.34) yields

$$\ln \dot{\varepsilon}_s = \ln K_2 + n \ln \sigma - \frac{Q_c}{RT}$$

With the given data there are two unknowns in this equation—namely $\mathbf{K_2}$ and $\mathbf{Q_c}$. Using the data provided in the problem we can set up two independent equations as follows:

$$\ln[1.0 \times 10^{-5}\ (\mathrm{h})^{-1}] = \ln K_2 + (7.0)\ln(70\ \mathrm{MPa}) - \frac{Q_c}{(8.31\ \mathrm{J/mol\text{-}K})(977\ \mathrm{K})}$$

$$\ln[2.5 \times 10^{-3}\ (\mathrm{h})^{-1}] = \ln K_2 + (7.0)\ln(70\ \mathrm{MPa}) - \frac{Q_c}{(8.31\ \mathrm{J/mol\text{-}K})(1089\ \mathrm{K})}$$

Now, solving simultaneously for $\mathbf{K_2}$ and $\mathbf{Q_c}$ leads to $\mathbf{K_2} = 2.55 \times 10^5\ (\mathrm{h})^{-1}$ and $\mathbf{Q_c} = 436{,}000$ J/mol. Thus it is now possible to solve for $\dot{\varepsilon}_\mathbf{s}$ at 50 MPa and 1250 K using Equation (9.34) as

$$\dot{\varepsilon}_\mathbf{s} = K_2\sigma^n \exp\left(-\frac{Q_c}{RT}\right)$$

$$\dot{\varepsilon}_\mathbf{s} = [2.55 \times 10^5\ (\mathrm{h})^{-1}](50\ \mathrm{MPa})^{7.0} \exp\left(-\frac{436000\ \mathrm{J/mol}}{(8.31\ \mathrm{J/mol\text{-}K})(1250\ \mathrm{K})}\right)$$

$$= 0.118\ (\mathrm{h})^{-1}$$

9.D1* This problem asks us to calculate the minimum $\mathbf{K_{Ic}}$ necessary to ensure that failure will not occur for a flat plate given an expression from which $\mathbf{Y(a/W)}$ may be determined, the internal crack length, 2**a** (20 mm), the plate width, **W** (90 mm), and the value of σ (375 MPa). First we must compute the value of $\mathbf{Y(a/W)}$ using Equation (9.10), as follows:

$$Y(a/W) = \left[\frac{W}{\pi a}\tan\frac{\pi a}{W}\right]^{1/2}$$

$$= \left[\frac{90\ \mathrm{mm}}{(\pi)(10\ \mathrm{mm})}\tan\frac{(\pi)(10\ \mathrm{mm})}{90\ \mathrm{mm}}\right]^{1/2} = 1.021$$

Now, using Equation (9.11) it is possible to determine $\mathbf{K_{Ic}}$; thus

$$K_{Ic} = Y(a/W)\sigma\sqrt{\pi a}$$

$$= (1.021)(375\ \mathrm{MPa})\sqrt{(\pi)(10 \times 10^{-3}\ \mathrm{m})} = 67.9\ \mathrm{MPa}\sqrt{\mathrm{m}}\ (62.3\ \mathrm{ksi}\sqrt{\mathrm{in.}})$$

9.D7* We are asked in this problem to estimate the maximum tensile stress that will yield a fatigue life of 2.5×10^7 cycles, given values of $\mathbf{a_o}$, $\mathbf{a_c}$, **m**, **A**, and **Y**. Since **Y** is independent of crack length we may utilize Equation (9.31) which, upon integration, takes the form

$$N_f = \frac{1}{A\pi^{m/2}(\Delta\sigma)^m Y^m}\int_{a_o}^{a_c} a^{-m/2}\,da$$

And for **m** = 3.5

$$N_f = \frac{1}{A\pi^{1.75}(\Delta\sigma)^{3.5}Y^{3.5}} \int_{a_o}^{a_c} a^{-1.75}da$$
$$= -\frac{1.33}{A\pi^{1.75}(\Delta\sigma)^{3.5}Y^{3.5}}\left[\frac{1}{a_c^{0.75}} - \frac{1}{a_o^{0.75}}\right]$$

Now, solving for $\Delta\sigma$ from this expression yields

$$\Delta\sigma = \left\{\frac{1.33}{N_f A\pi^{1.75}Y^{3.5}}\left[\frac{1}{a_o^{0.75}} - \frac{1}{a_c^{0.75}}\right]\right\}^{1/3.5}$$
$$= \left\{\frac{1.33}{(2.5 \times 10^7)(2 \times 10^{-14})(\pi)^{1.75}(1.4)^{3.5}}\left[\frac{1}{(1.5 \times 10^{-4})^{0.75}} - \frac{1}{(4.5 \times 10^{-3})^{0.75}}\right]\right\}^{1/3.5}$$
$$= 178 \text{ MPa}$$

This 178 MPa will be the maximum tensile stress since we can show that the minimum stress is a compressive one—when $\sigma_{\mathbf{min}}$ is negative, $\Delta\sigma$ is taken to be $\sigma_{\mathbf{max}}$. If we take $\sigma_{\mathbf{max}}$ = 178 MPa, and since $\sigma_{\mathbf{m}}$ is stipulated in the problem to have a value of 25 MPa, then from Equation (9.21)

$$\sigma_{\text{min}} = 2\sigma_{\text{m}} - \sigma_{\text{max}} = 2(25 \text{ MPa}) - 178 \text{ MPa} = -128 \text{ MPa}$$

Therefore $\sigma_{\mathbf{min}}$ is negative and we are justified in taking $\sigma_{\mathbf{max}}$ to be 178 MPa.

9.D16* We are asked in this problem to calculate the stress levels at which the rupture lifetime will be 5 years and 20 years when an 18-8 Mo stainless steel component is subjected to a temperature of 500°C (773 K). It first becomes necessary, using the specified temperature and times, to calculate the values of the Larson-Miller parameter at each temperature. The values of $\mathbf{t_r}$ corresponding to 5 and 20 years are 4.38×10^4 h and 1.75×10^5 h, respectively. Hence, for a lifetime of 5 years

$$T(20 + \log t_r) = 773[20 + \log(4.38 \times 10^4)] = 19.05 \times 10^3$$

And for $\mathbf{t_r}$ = 20 years

$$T(20 + \log t_r) = 773[20 + \log(1.75 \times 10^5)] = 19.51 \times 10^3$$

Using the curve shown in Figure 9.47, the stress values corresponding to the five- and twenty-year lifetimes are approximately 260 MPa (37,500 psi) and 225 MPa (32,600 psi), respectively.

Chapter 9 / Failure

9.3 DUCTILE FRACTURE

FRACTOGRAPHIC STUDIES

Much more detailed information regarding the mechanism of fracture is available from microscopic examination, normally using scanning electron microscopy. Studies of this type are termed *fractographic*. The scanning electron microscope is preferred for fractographic examinations since it has a much better resolution and depth of field than does the optical microscope; these characteristics are necessary to reveal the topographical features of fracture surfaces.

When the fibrous central region of a cup-and-cone fracture surface is examined with the electron microscope at a high magnification, it will be found to consist of numerous spherical ‘‘dimples’’ (Figure 9.4*a*); this structure is characteristic of fracture resulting from uniaxial tensile failure. Each dimple is one half of a microvoid that formed and then separated during the fracture process. Dimples also form on the 45° shear lip of the cup-and-cone fracture. However, these will be elongated or C-shaped, as shown in Figure 9.4*b*. This parabolic shape may be indicative of shear failure. Furthermore, other microscopic fracture surface features are also possible. Fractographs such as those shown in Figures 9.4*a* and 9.4*b* provide valuable information in the analyses of fracture, such as the fracture mode, the stress state, and the site of crack initiation.

9.5a PRINCIPLES OF FRACTURE MECHANICS (DETAILED VERSION)

Brittle fracture of normally ductile materials, such as that shown in the chapter-opening photograph of this chapter, has demonstrated the need for a better understanding of the mechanisms of fracture. Extensive research endeavors over the past several decades have led to the evolution of the field of **fracture mechanics.** This subject allows quantification of the relationships between material properties, stress level, the presence of crack-producing flaws, and crack propagation mechanisms. Design engineers are now better equipped to anticipate, and thus prevent, structural failures. The present discussion centers on some of the fundamental principles of the mechanics of fracture.

STRESS CONCENTRATION

The fracture strength of a solid material is a function of the cohesive forces that exist between atoms. On this basis, the theoretical cohesive strength of a brittle elastic solid has been estimated to be approximately $E/10$, where E is the modulus of elasticity. The experimental fracture strengths of most engineering materials normally lie between 10 and 1000 times below this theoretical value. In the 1920s, A. A. Griffith proposed that this discrepancy between theoretical cohesive strength

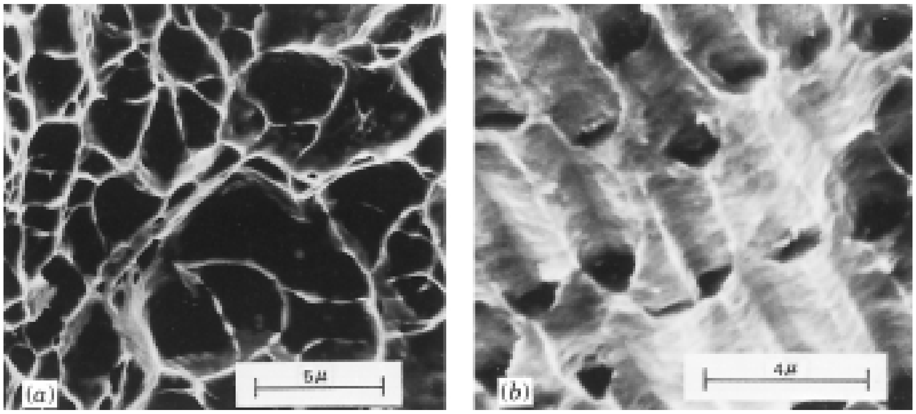

Figure 9.4 (*a*) Scanning electron fractograph showing spherical dimples characteristic of ductile fracture resulting from uniaxial tensile loads. 3300×. (*b*) Scanning electron fractograph showing parabolic-shaped dimples characteristic of ductile fracture resulting from shear loading. 5000×. (From R. W. Hertzberg, *Deformation and Fracture Mechanics of Engineering Materials*, 3rd edition. Copyright © 1989 by John Wiley & Sons, New York. Reprinted by permission of John Wiley & Sons, Inc.)

and observed fracture strength could be explained by the presence of very small, microscopic flaws or cracks that always exist under normal conditions at the surface and within the interior of a body of material. These flaws are a detriment to the fracture strength because an applied stress may be amplified or concentrated at the tip, the magnitude of this amplification depending on crack orientation and geometry. This phenomenon is demonstrated in Figure 9.7, a stress profile across a cross

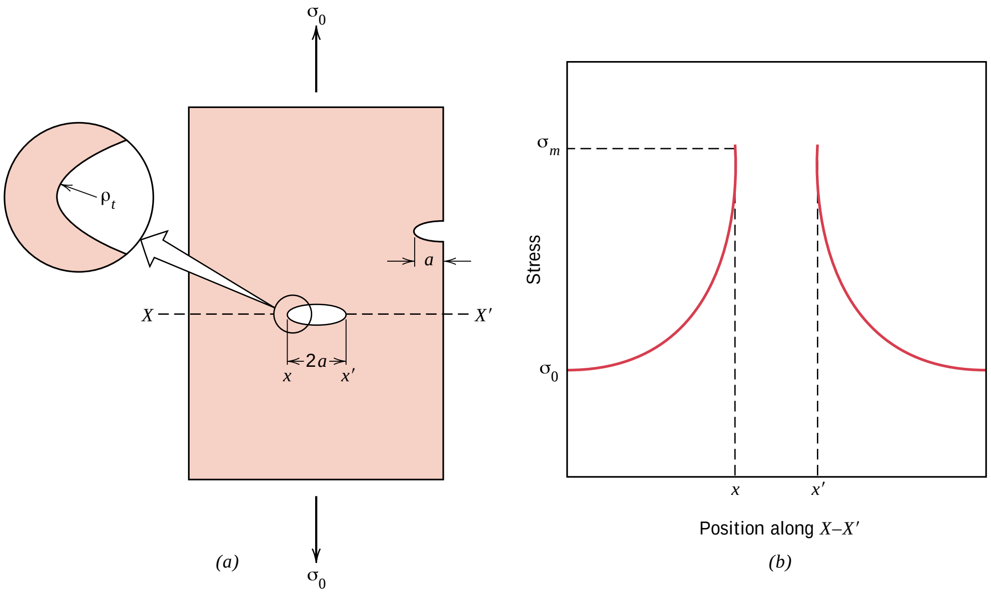

Figure 9.7 (*a*) The geometry of surface and internal cracks. (*b*) Schematic stress profile along the line X–X' in (*a*), demonstrating stress amplification at crack tip positions.

section containing an internal crack. As indicated by this profile, the magnitude of this localized stress diminishes with distance away from the crack tip. At positions far removed, the stress is equal to the nominal stress σ_0, or the applied load divided by the specimen cross-sectional area (perpendicular to this load). Due to their ability to amplify an applied stress in their locale, these flaws are sometimes called **stress raisers.**

If it is assumed that a crack has an elliptical shape (or is circular) and is oriented perpendicular to the applied stress, the maximum stress at the crack tip, σ_m, is equal to

$$\sigma_m = \sigma_0 \left[1 + 2 \left(\frac{a}{\rho_t} \right)^{1/2} \right] \tag{9.1a}$$

where σ_0 is the magnitude of the nominal applied tensile stress, ρ_t is the radius of curvature of the crack tip (Figure 9.7*a*), and a represents the length of a surface crack, or half of the length of an internal crack. For a relatively long microcrack that has a small tip radius of curvature, the factor $(a/\rho_t)^{1/2}$ may be very large (certainly much greater than unity); under these circumstances Equation 9.1a takes the form

$$\sigma_m = 2\sigma_0 \left(\frac{a}{\rho_t} \right)^{1/2} \tag{9.1b}$$

Furthermore, σ_m will be many times the value of σ_0.

Sometimes the ratio σ_m/σ_0 is denoted as the *stress concentration factor* K_t:

$$K_t = \frac{\sigma_m}{\sigma_0} = 2 \left(\frac{a}{\rho_t} \right)^{1/2} \tag{9.2}$$

which is simply a measure of the degree to which an external stress is amplified at the tip of a crack.

By way of comment, it should be said that stress amplification is not restricted to these microscopic defects; it may occur at macroscopic internal discontinuities (e.g., voids), at sharp corners, and at notches in large structures. Figure 9.8 shows theoretical stress concentration factor curves for several simple and common macroscopic discontinuities.

Furthermore, the effect of a stress raiser is more significant in brittle than in ductile materials. For a ductile material, plastic deformation ensues when the maximum stress exceeds the yield strength. This leads to a more uniform distribution of stress in the vicinity of the stress raiser and to the development of a maximum stress concentration factor less than the theoretical value. Such yielding and stress redistribution do not occur to any appreciable extent around flaws and discontinuities in brittle materials; therefore, essentially the theoretical stress concentration will result.

Griffith then went on to propose that all brittle materials contain a population of small cracks and flaws that have a variety of sizes, geometries, and orientations. Fracture will result when, upon application of a tensile stress, the theoretical cohesive strength of the material is exceeded at the tip of one of these flaws. This leads to the formation of a crack that then rapidly propagates. If no flaws were present, the fracture strength would be equal to the cohesive strength of the material. Very

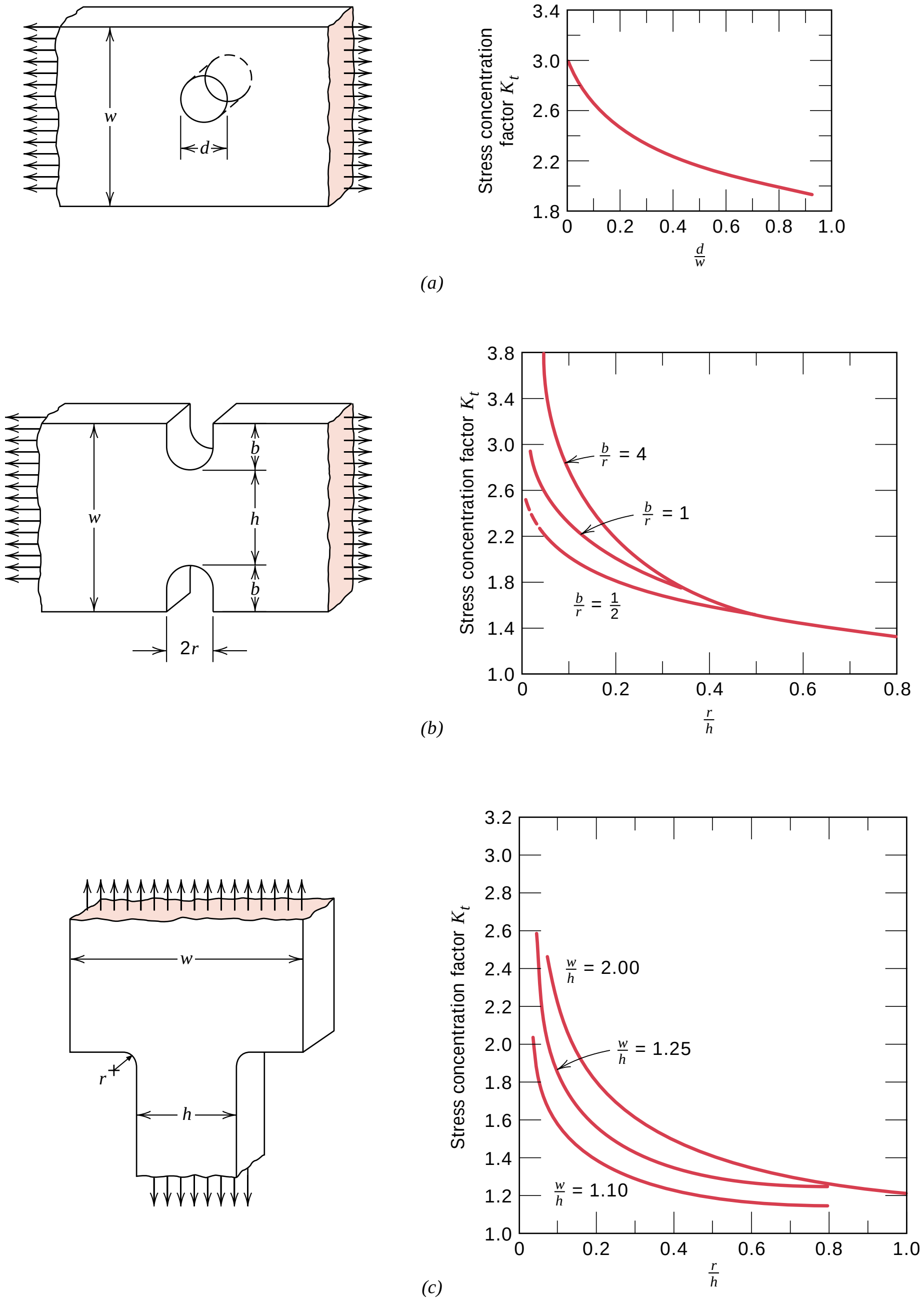

FIGURE 9.8 Theoretical stress concentration factor curves for three simple geometrical shapes. (From G. H. Neugebauer, *Prod. Eng.* (NY), Vol. 14, pp. 82–87, 1943.)

small and virtually defect-free metallic and ceramic whiskers have been grown with fracture strengths that approach their theoretical values.

GRIFFITH THEORY OF BRITTLE FRACTURE

During the propagation of a crack, there is a release of what is termed the *elastic strain energy*, some of the energy that is stored in the material as it is elastically deformed. Furthermore, during the crack extension process, new free surfaces are created at the faces of a crack, which give rise to an increase in surface energy of the system. Griffith developed a criterion for crack propagation of an elliptical crack (Figure 9.7*a*) by performing an energy balance using these two energies. He demonstrated that the critical stress σ_c required for crack propagation in a brittle material is described by

$$\sigma_c = \left(\frac{2E\gamma_s}{\pi a}\right)^{1/2} \tag{9.3}$$

where

E = modulus of elasticity

γ_s = specific surface energy

a = one half the length of an internal crack

Worth noting is that this expression does not involve the crack tip radius ρ_t, as does the stress concentration equation (Equation 9.1); however, it is assumed that the radius is sufficiently sharp (on the order of the interatomic spacing) so as to raise the local stress at the tip above the cohesive strength of the material.

The previous development applies only to completely brittle materials, for which there is no plastic deformation. Most metals and many polymers do experience some plastic deformation during fracture; thus, crack extension involves more than producing just an increase in the surface energy. This complication may be accommodated by replacing γ_s in Equation 9.3 by $\gamma_s + \gamma_p$, where γ_p represents a plastic deformation energy associated with crack extension. Thus,

$$\sigma_c = \left[\frac{2E(\gamma_s + \gamma_p)}{\pi a}\right]^{1/2} \tag{9.4a}$$

For highly ductile materials, it may be the case that $\gamma_p \gg \gamma_s$ such that

$$\sigma_c = \left(\frac{2E\gamma_p}{\pi a}\right)^{1/2} \tag{9.4b}$$

In the 1950s, G. R. Irwin chose to incorporate both γ_s and γ_p into a single term, $\mathcal{G}_c$, as

$$\mathcal{G}_c = 2(\gamma_s + \gamma_p) \tag{9.5}$$

$\mathcal{G}_c$ is known as the *critical strain energy release rate.* Incorporation of Equation 9.5 into Equation 9.4a after some rearrangement leads to another expression for the Griffith cracking criterion as

$$\mathcal{G}_c = \frac{\pi\sigma^2 a}{E} \tag{9.6}$$

Thus, crack extension occurs when $\pi\sigma^2 a/E$ exceeds the value of $\mathcal{G}_c$ for the particular material under consideration.

EXAMPLE PROBLEM 9.1

A relatively large plate of a glass is subjected to a tensile stress of 40 MPa. If the specific surface energy and modulus of elasticity for this glass are 0.3 J/m^2 and 69 GPa, respectively, determine the maximum length of a surface flaw that is possible without fracture.

SOLUTION

To solve this problem it is necessary to employ Equation 9.3. Rearrangement of this expression such that a is the dependent variable, and realizing that σ = 40 MPa, γ_s = 0.3 J/m^2, and E = 69 GPa leads to

$$\begin{aligned} a &= \frac{2E\gamma_s}{\pi\sigma^2} \\ &= \frac{(2)(69 \times 10^9 \text{ N/m}^2)(0.3 \text{ N/m})}{\pi(40 \times 10^6 \text{ N/m}^2)^2} \\ &= 8.2 \times 10^{-6} \text{ m} = 0.0082 \text{ mm} = 8.2\ \mu\text{m} \end{aligned}$$

STRESS ANALYSIS OF CRACKS

As we continue to explore the development of fracture mechanics, it is worthwhile to examine the stress distributions in the vicinity of the tip of an advancing crack. There are three fundamental ways, or modes, by which a load can operate on a crack, and each will affect a different crack surface displacement; these are illustrated in Figure 9.9. Mode I is an opening (or tensile) mode, whereas modes II and III are sliding and tearing modes, respectively. Mode I is encountered most frequently, and only it will be treated in the ensuing discussion on fracture mechanics.

For this mode I configuration, the stresses acting on an element of material are shown in Figure 9.10. Using elastic theory principles and the notation indicated, tensile (σ_x and σ_y)[1] and shear (τ_{xy}) stresses are functions of both radial distance r

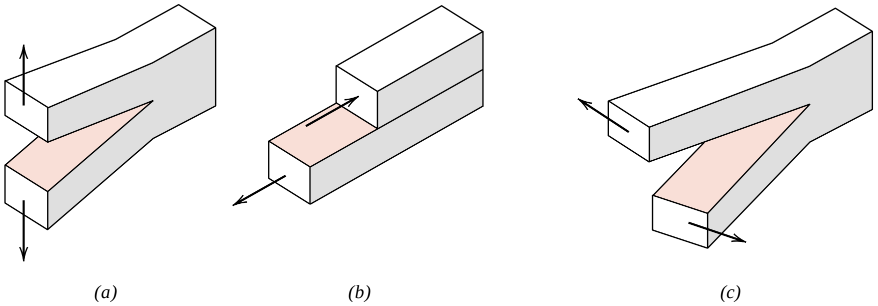
(a) (b) (c)

FIGURE 9.9 The three modes of crack surface displacement. (*a*) Mode I, opening or tensile mode; (*b*) mode II, sliding mode; and (*c*) mode III, tearing mode.

---

[1] This σ_y denotes a tensile stress parallel to the y-direction and should not be confused with the yield strength (Section 7.6), which uses the same symbol.

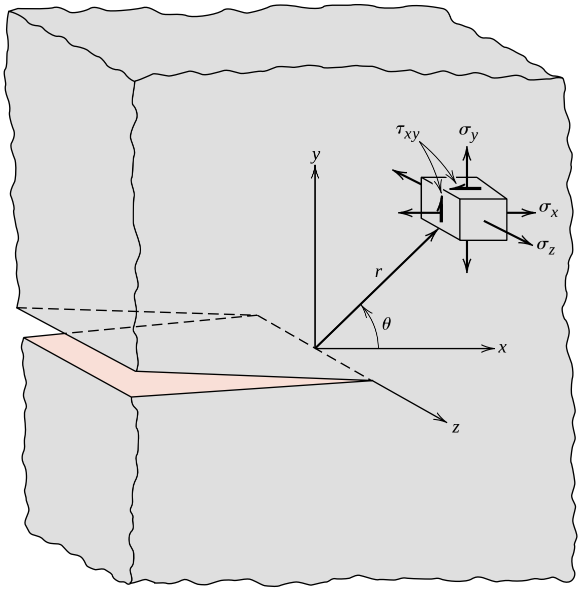

FIGURE 9.10 The stresses acting in front of a crack that is loaded in a tensile mode I configuration.

and the angle θ as follows:[2]

$$\sigma_x = \frac{K}{\sqrt{2\pi r}} f_x(\theta) \tag{9.7a}$$

$$\sigma_y = \frac{K}{\sqrt{2\pi r}} f_y(\theta) \tag{9.7b}$$

$$\tau_{xy} = \frac{K}{\sqrt{2\pi r}} f_{xy}(\theta) \tag{9.7c}$$

If the plate is thin relative to the dimensions of the crack, then $\sigma_z = 0$, or a condition of *plane stress* is said to exist. At the other extreme (a relatively thick plate), $\sigma_z = \nu(\sigma_x + \sigma_y)$, and the state is referred to as **plane strain** (since $\epsilon_z = 0$); ν in this expression is Poisson's ratio.

In Equations 9.7, the parameter K is termed the **stress intensity factor;** its use provides for a convenient specification of the stress distribution around a flaw. It

---

[2] The $f(\theta)$ functions are as follows:

$$f_x(\theta) = \cos\frac{\theta}{2}\left(1 - \sin\frac{\theta}{2}\sin\frac{3\theta}{2}\right)$$

$$f_y(\theta) = \cos\frac{\theta}{2}\left(1 + \sin\frac{\theta}{2}\sin\frac{3\theta}{2}\right)$$

$$f_{xy}(\theta) = \sin\frac{\theta}{2}\cos\frac{\theta}{2}\cos\frac{3\theta}{2}$$

should be noted that this stress intensity factor and the stress concentration factor K_t in Equation 9.2, although similar, are not equivalent.

The stress intensity factor is related to the applied stress and the crack length by the following equation:

$$K = Y\sigma\sqrt{\pi a} \tag{9.8}$$

Here Y is a dimensionless parameter or function that depends on both the crack and specimen sizes and geometries, as well as the manner of load application. More will be said about Y in the discussion that follows. Moreover, it should be noted that K has the unusual units of MPa$\sqrt{\text{m}}$ (psi$\sqrt{\text{in.}}$ [alternatively ksi$\sqrt{\text{in.}}$]).

FRACTURE TOUGHNESS

In the previous discussion, a criterion was developed for the crack propagation in a brittle material containing a flaw; fracture occurs when the applied stress level exceeds some critical value σ_c (Equation 9.3). Similarly, since the stresses in the vicinity of a crack tip can be defined in terms of the stress intensity factor, a critical value of K exists that may be used to specify the conditions for brittle fracture; this critical value is termed the **fracture toughness** K_c, and, from Equation 9.8, is defined by

$$K_c = Y(a/W)\sigma_c\sqrt{\pi a} \tag{9.9b}$$

Here σ_c again is the critical stress for crack propagation, and we now represent Y as a function of both crack length (a) and component width (W)—i.e., as $Y(a/W)$.

Relative to this $Y(a/W)$ function, as the a/W ratio approaches zero (i.e., for very wide planes and short cracks), $Y(a/W)$ approaches a value of unity. For example, for a plate of infinite width having a through-thickness crack, Figure 9.11*a*, $Y(a/W) = 1.0$; while for a plate of semi-infinite width containing an edge crack of length a (Figure 9.11*b*), $Y(a/W) \cong 1.1$. Mathematical expressions for $Y(a/W)$ (often relatively complex) in terms of a/W are required for components of finite dimensions. For example, for a center-cracked (through-thickness) plate of width W

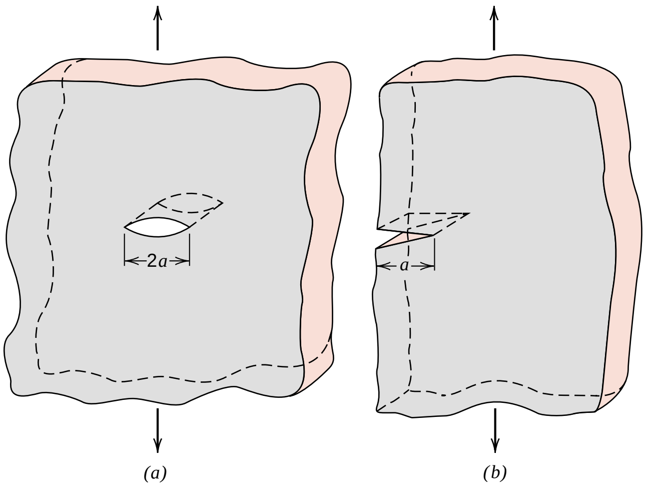

FIGURE 9.11 Schematic representations of (*a*) an interior crack in a plate of infinite width, and (*b*) an edge crack in a plate of semi-infinite width.

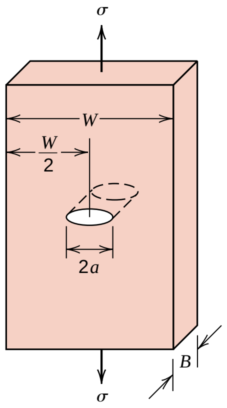

Figure 9.12 Schematic representation of a flat plate of finite width having a through-thickness center crack.

(Figure 9.12)

$$Y(a/W) = \left(\frac{W}{\pi a}\tan\frac{\pi a}{W}\right)^{1/2} \tag{9.10}$$

Here the $\pi a/W$ argument for the tangent is expressed in radians, not degrees. It is often the case for some specific component-crack configuration that $Y(a/W)$ is plotted versus a/W (or some variation of a/W). Several of these plots are shown in Figures 9.13*a*, *b*, and *c*; included in the figures are equations that are used to determine K_cs.

By definition, fracture toughness is a property that is the measure of a material's resistance to brittle fracture when a crack is present. Its units are the same as for the stress intensity factor (i.e., MPa$\sqrt{\text{m}}$ or psi$\sqrt{\text{in.}}$).

For relatively thin specimens, the value of K_c will depend on and decrease with increasing specimen thickness B, as indicated in Figure 9.14. Eventually, K_c becomes independent of B, at which time the condition of plane strain is said to exist.[3] The constant K_c value for thicker specimens is known as the **plane strain fracture toughness** K_{Ic}, which is also defined by[4]

$$K_{Ic} = Y\sigma\sqrt{\pi a} \tag{9.11}$$

It is the fracture toughness normally cited since its value is always less than K_c. The I subscript for K_{Ic} denotes that this critical value of K is for mode I crack displacement, as illustrated in Figure 9.9*a*. Brittle materials, for which appreciable plastic deformation is not possible in front of an advancing crack, have low K_{Ic} values and are vulnerable to catastrophic failure. On the other hand, K_{Ic} values are relatively large for ductile materials. Fracture mechanics is especially useful in

---

[3] Experimentally, it has been verified that for plane strain conditions

$$B \geq 2.5\left(\frac{K_{Ic}}{\sigma_y}\right)^2 \tag{9.12}$$

where σ_y is the 0.002 strain offset yield strength of the material.

[4] In the ensuing discussion we will use Y to designate $Y(a/W)$, in order to simplify the form of the equations.

FIGURE 9.13 Y calibration curves for three simple crack-plate geometries. (Copyright ASTM. Reprinted with permission.)

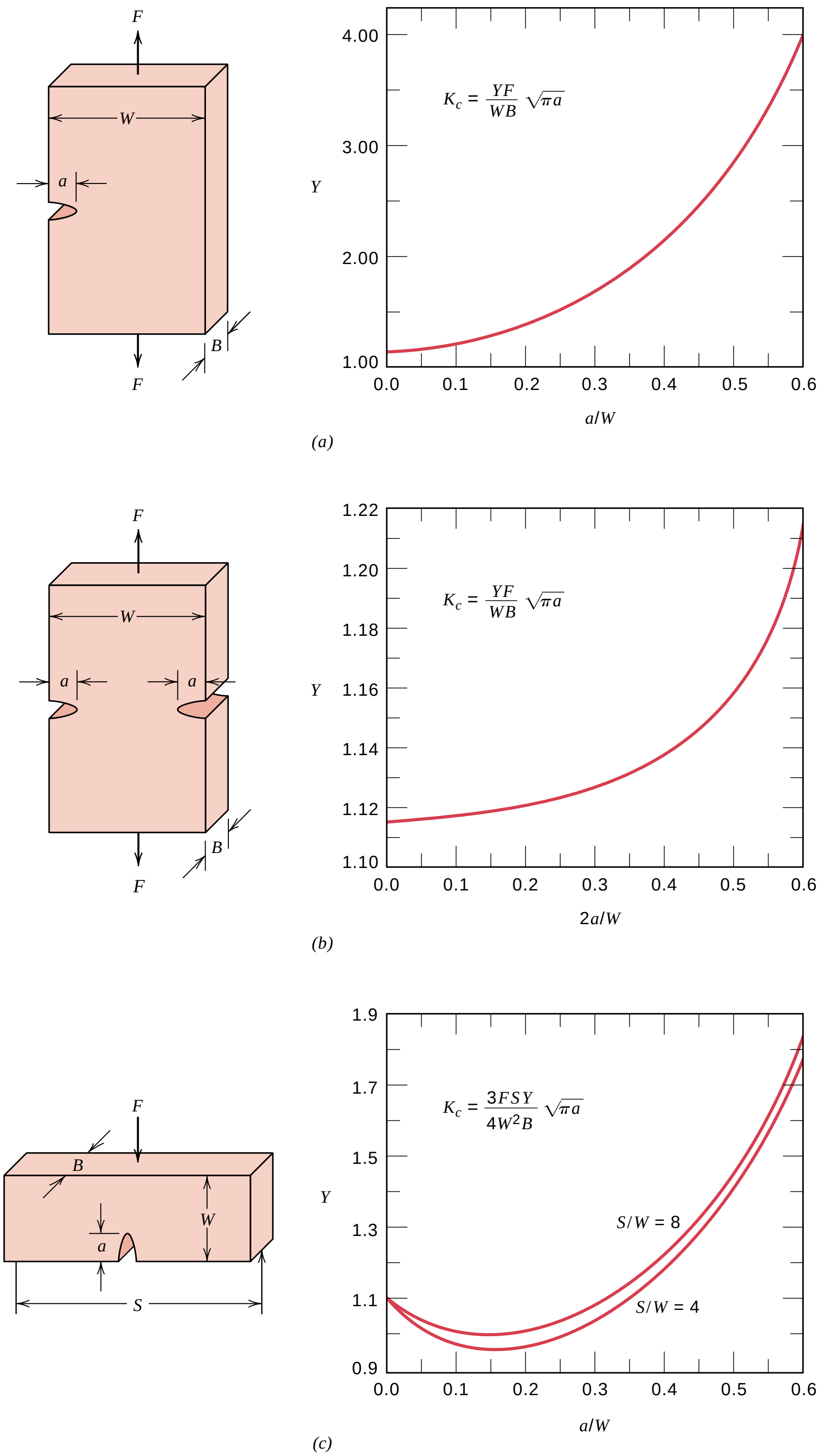

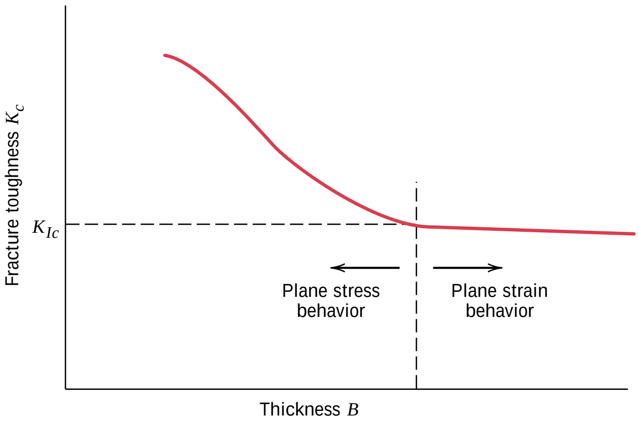

Figure 9.14 Schematic representation showing the effect of plate thickness on fracture toughness.

predicting catastrophic failure in materials having intermediate ductilities. Plane strain fracture toughness values for a number of different materials are presented in Table 9.1; a more extensive list of K_{Ic} values is contained in Table B.5 of Appendix B.

The stress intensity factor K in Equations 9.7 and the plane strain fracture toughness K_{Ic} are related to one another in the same sense as are stress and yield strength. A material may be subjected to many values of stress; however, there is a specific stress level at which the material plastically deforms—that is, the yield strength. Likewise, a variety of K's are possible, whereas K_{Ic} is unique for a particular material, and indicates the conditions of flaw size and stress necessary for brittle fracture.

Several different testing techniques are used to measure K_{Ic}.[6] Virtually any specimen size and shape consistent with mode I crack displacement may be utilized, and accurate values will be realized provided that the Y scale parameter in Equation 9.11 has been properly determined.

The plane strain fracture toughness K_{Ic} is a fundamental material property that depends on many factors, the most influential of which are temperature, strain rate, and microstructure. The magnitude of K_{Ic} diminishes with increasing strain rate and decreasing temperature. Furthermore, an enhancement in yield strength wrought by solid solution or dispersion additions or by strain hardening generally produces a corresponding decrease in K_{Ic}. Furthermore, K_{Ic} normally increases with reduction in grain size as composition and other microstructural variables are maintained constant. Yield strengths are included for some of the materials listed in Table 9.1.

DESIGN USING FRACTURE MECHANICS

According to Equations 9.9b and 9.11, three variables must be considered relative to the possibility for fracture of some structural component—viz. the fracture toughness (K_c) or plane strain fracture toughness (K_{Ic}), the imposed stress (σ), and the flaw size (a), assuming, of course, that Y has been determined. When designing a component, it is first important to decide which of these variables are constrained by the application and which are subject to design control. For example, material selection (and hence K_c or K_{Ic}) is often dictated by factors such as density (for

---

[6] See for example ASTM Standard E 399, ''Standard Test Method for Plane Strain Fracture Toughness of Metallic Materials.''

Table 9.1 **Room-Temperature Yield Strength and Plane Strain Fracture Toughness Data for Selected Engineering Materials**

	Yield Strength		K_{Ic}	
Material	***MPa***	***ksi***	***MPa*** $\sqrt{m}$	***ksi*** $\sqrt{in.}$
	Metals			
Aluminum Alloy[a] (7075-T651)	495	72	24	22
Aluminum Alloy[a] (2024-T3)	345	50	44	40
Titanium Alloy[a] (Ti-6Al-4V)	910	132	55	50
Alloy Steel[a] (4340 tempered @ 260°C)	1640	238	50.0	45.8
Alloy Steel[a] (4340 tempered @ 425°C)	1420	206	87.4	80.0
	Ceramics			
Concrete	—	—	0.2–1.4	0.18–1.27
Soda-Lime Glass	—	—	0.7–0.8	0.64–0.73
Aluminum Oxide	—	—	2.7–5.0	2.5–4.6
	Polymers			
Polystyrene (PS)	—	—	0.7–1.1	0.64–1.0
Polymethyl Methacrylate (PMMA)	53.8–73.1	7.8–10.6	0.7–1.6	0.64–1.5
Polycarbonate (PC)	62.1	9.0	2.2	2.0

[a] **Source:** Reprinted with permission, *Advanced Materials and Processes,* ASM International, © 1990.

lightweight applications) or the corrosion characteristics of the environment. Or, the allowable flaw size is either measured or specified by the limitations of available flaw detection techniques. It is important to realize, however, that once any combination of two of the above parameters is prescribed, the third becomes fixed (Equations 9.9b and 9.11). For example, assume that K_{Ic} and the magnitude of a are specified by application constraints; therefore, the design (or critical) stress σ_c must be

$$\sigma_c \leq \frac{K_{Ic}}{Y\sqrt{\pi a}} \tag{9.13}$$

On the other hand, if stress level and plane strain fracture toughness are fixed by the design situation, then the maximum allowable flaw size a_c is

$$a_c = \frac{1}{\pi}\left(\frac{K_{Ic}}{\sigma Y}\right)^2 \tag{9.14}$$

A number of nondestructive test (NDT) techniques have been developed that permit detection and measurement of both internal and surface flaws. Such NDT methods are used to avoid the occurrence of catastrophic failure by examining structural components for defects and flaws that have dimensions approaching the critical size.

EXAMPLE PROBLEM 9.2

A structural component in the form of a very wide plate, as shown in Figure 9.11*a*, is to be fabricated from a 4340 steel. Two sheets of this alloy, each having a different heat treatment and thus different mechanical properties, are available. One, denoted material A, has a yield strength of 860 MPa (125,000 psi) and a plane strain fracture toughness of 98.9 MPa$\sqrt{\text{m}}$ (90 ksi$\sqrt{\text{in.}}$). For the other, material Z, σ_y and K_{Ic} values are 1515 MPa (220,000 psi) and 60.4 MPa$\sqrt{\text{m}}$ (55 ksi$\sqrt{\text{in.}}$), respectively.

(a) For each alloy, determine whether or not plane strain conditions prevail if the plate is 10 mm (0.39 in.) thick.

(b) It is not possible to detect flaw sizes less than 3 mm, which is the resolution limit of the flaw detection apparatus. If the plate thickness is sufficient such that the K_{Ic} value may be used, determine whether or not a critical flaw is subject to detection. Assume that the design stress level is one half of the yield strength; also, for this configuration, the value of Y is 1.0.

SOLUTION

(a) Plane strain is established by Equation 9.12. For material A,

$$B = 2.5\left(\frac{K_{Ic}}{\sigma_y}\right)^2 = 2.5\left(\frac{98.9\ \text{MPa}\sqrt{\text{m}}}{860\ \text{MPa}}\right)^2$$

$$= 0.033\ \text{m} = 33\ \text{mm}\ (1.30\ \text{in.})$$

Thus, plane strain conditions *do not* hold for material A because this value of B is greater than 10 mm, the actual plate thickness; the situation is one of plane stress and must be treated as such.

And for material Z,

$$B = 2.5\left(\frac{60.4\ \text{MPa}\sqrt{\text{m}}}{1515\ \text{MPa}}\right)^2 = 0.004\ \text{m} = 4.0\ \text{mm}\ (0.16\ \text{in.})$$

which is less than the actual plate thickness, and therefore the situation is one of plane strain.

(b) We need only determine the critical flaw size for material Z because the situation for material A is not plane strain, and K_{Ic} may not be used. Employing Equation 9.14 and taking σ to be $\sigma_y/2$,

$$a_c = \frac{1}{\pi}\left(\frac{60.4\ \text{MPa}\sqrt{\text{m}}}{(1)(1515/2)\ \text{MPa}}\right)^2$$

$$= 0.002\ \text{m} = 2.0\ \text{mm}\ (0.079\ \text{in.})$$

Therefore, the critical flaw size for material Z is not subject to detection since it is less than 3 mm.

DESIGN EXAMPLE 9.1

Consider the thin-walled spherical tank of radius r and thickness t (Figure 9.15) that may be used as a pressure vessel.

(a) One design of such a tank calls for yielding of the wall material prior to failure as a result of the formation of a crack of critical size and its subsequent rapid propagation. Thus, plastic distortion of the wall may be observed and the pressure within the tank released before the occurrence of catastrophic failure. Consequently, materials having large critical crack lengths are desired. On the basis of this criterion, rank the metal alloys listed in Table B.5, Appendix B, as to critical crack size, from longest to shortest.

(b) An alternative design that is also often utilized with pressure vessels is termed *leak-before-break*. Using principles of fracture mechanics, allowance is made for the growth of a crack through the thickness of the vessel wall prior to the occurrence of rapid crack propagation (Figure 9.15). Thus, the crack will completely penetrate the wall without catastrophic failure, allowing for its detection by the leaking of pressurized fluid. With this criterion the critical crack length a_c (i.e., one-half of the total internal crack length) is taken to be equal to the pressure vessel thickness t. Allowance for $a_c = t$ instead of $a_c = t/2$ assures that fluid leakage will occur prior to the buildup of dangerously high pressures. Using this criterion, rank the metal alloys in Table B.5, Appendix B as to the maximum allowable pressure.

For this spherical pressure vessel, the circumferential wall stress σ is a function of the pressure p in the vessel and the radius r and wall thickness t according to

$$\sigma = \frac{pr}{2t} \tag{9.15}$$

For both parts (a) and (b) assume a condition of plane strain.

SOLUTION

(a) For the first design criterion, it is desired that the circumferential wall stress be less than the yield strength of the material. Substitution of σ_y for σ in Equation 9.11, and incorporation of a factor of safety N leads to

$$K_{Ic} = Y\left(\frac{\sigma_y}{N}\right)\sqrt{\pi a_c} \tag{9.16}$$

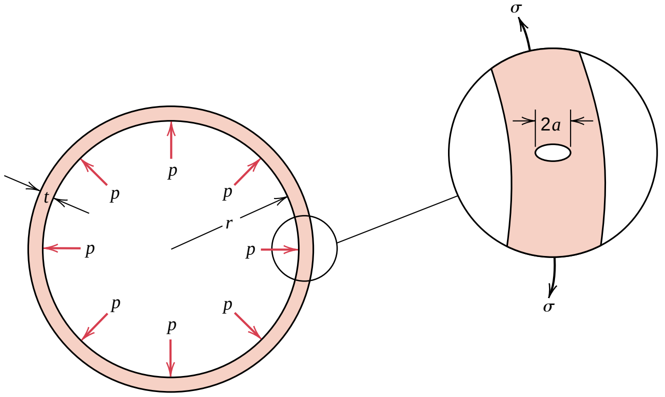

FIGURE 9.15 Schematic diagram showing the cross section of a spherical tank that is subjected to an internal pressure p, and that has a radial crack of length $2a$ in its wall.

Table 9.2 Ranking of Several Metal Alloys Relative to Critical Crack Length (Yielding Criterion) for a Thin-Walled Spherical Pressure Vessel

Material	$\left(\frac{K_{Ic}}{\sigma_y}\right)^2$ *(mm)*
Medium carbon (1040) steel	43.1
AZ31B magnesium	19.6
2024 aluminum (T3)	16.3
Ti-5Al-2.5Sn titanium	6.6
4140 steel (tempered @ 482°C)	5.3
4340 steel (tempered @ 425°C)	3.8
Ti-6Al-4V titanium	3.7
17-7PH steel	3.4
7075 aluminum (T651)	2.4
4140 steel (tempered @ 370°C)	1.6
4340 Steel (tempered @ 260°C)	0.93

where a_c is the critical crack length. Solving for a_c yields the following expression:

$$a_c = \frac{N^2}{Y^2\pi}\left(\frac{K_{Ic}}{\sigma_y}\right)^2 \tag{9.17}$$

Therefore, the critical crack length is proportional to the square of the K_{Ic}-σ_y ratio, which is the basis for the ranking of the metal alloys in Table B.5. The ranking is provided in Table 9.2, where it may be seen that the medium carbon (1040) steel with the largest ratio has the longest critical crack length, and, therefore, is the most desirable material on the basis of this criterion.

(b) As stated previously, the leak-before-break criterion is just met when one-half of the internal crack length is equal to the thickness of the pressure vessel—i.e., when $a = t$. Substitution of $a = t$ into Equation 9.11 gives

$$K_{Ic} = Y\sigma\sqrt{\pi t} \tag{9.18}$$

And, from Equation 9.15

$$t = \frac{pr}{2\sigma} \tag{9.19}$$

The stress is replaced by the yield strength, inasmuch as the tank should be designed to contain the pressure without yielding; furthermore, substitution of Equation 9.19 into Equation 9.18, after some rearrangement, yields the following expression:

$$p = \frac{2}{Y^2\pi r}\left(\frac{K_{Ic}^2}{\sigma_y}\right) \tag{9.20}$$

Hence, for some given spherical vessel of radius r, the maximum allowable pressure consistent with this leak-before-break criterion is proportional to K_{Ic}^2/σ_y. The same several materials are ranked according to this ratio in Table 9.3; as may be noted, the medium carbon steel will contain the greatest pressures.

Table 9.3 **Ranking of Several Metal Alloys Relative to Maximum Allowable Pressure (Leak-Before-Break Criterion) for a Thin-Walled Spherical Pressure Vessel**

Material	$\frac{K_{Ic}^2}{\sigma_y}$ *(MPa-m)*
Medium carbon (1040) steel	11.2
4140 steel (tempered @ 482°C)	6.1
Ti-5Al-2.5Sn titanium	5.8
2024 aluminum (T3)	5.6
4340 steel (tempered @ 425°C)	5.4
17-7PH steel	4.4
AZ31B magnesium	3.9
Ti-6Al-4V titanium	3.3
4140 steel (tempered @ 370°C)	2.4
4340 steel (tempered @ 260°C)	1.5
7075 aluminum (T651)	1.2

Of the eleven metal alloys that are listed in Table B.5, the medium carbon steel ranks first according to both yielding and leak-before-break criteria. For these reasons, many pressure vessels are constructed of medium carbon steels, when temperature extremes and corrosion need not be considered.

9.6 BRITTLE FRACTURE OF CERAMICS

STATIC FATIGUE

Under some circumstances, fracture of ceramic materials will occur by the slow propagation of cracks, when stresses are static in nature, and the right-hand side of Equation 9.11 is less than K_{Ic}. This phenomenon is called *static fatigue,* or *delayed fracture;* use of the term ''fatigue'' is somewhat misleading inasmuch as fracture may occur in the absence of cyclic stresses (metal fatigue is discussed later in this chapter). It has been observed that this type of fracture is especially sensitive to environmental conditions, specifically when moisture is present in the atmosphere. Relative to mechanism, a stress–corrosion process probably occurs at the crack tips; that is, the combination of an applied tensile stress and material dissolution leads to a sharpening and lengthening of the cracks until, ultimately, one crack grows to a size capable of rapid propagation according to Equation 9.3. Furthermore, the duration of stress application preceding fracture diminishes with increasing stress. Consequently, when specifying the static fatigue strength, the time of stress application should also be stipulated. Silicate glasses are especially susceptible to this type of fracture; it has also been observed in other ceramic materials to include porcelain, portland cement, high-alumina ceramics, barium titanate, and silicon nitride.

9.12a CRACK INITIATION AND PROPAGATION (DETAILED VERSION)

The process of fatigue failure is characterized by three distinct steps: (1) crack initiation, wherein a small crack forms at some point of high stress concentration; (2) crack propagation, during which this crack advances incrementally with each stress cycle; and (3) final failure, which occurs very rapidly once the advancing crack has reached a critical size. The fatigue life N_f, the total number of cycles to failure, therefore can be taken as the sum of the number of cycles for crack initiation N_i and crack propagation N_p:

$$N_f = N_i + N_p \tag{9.25}$$

The contribution of the final failure step to the total fatigue life is insignificant since it occurs so rapidly. Relative proportions to the total life of N_i and N_p depend on the particular material and test conditions. At low stress levels (i.e., for high-cycle fatigue), a large fraction of the fatigue life is utilized in crack initiation. With increasing stress level, N_i decreases and the cracks form more rapidly. Thus, for low-cycle fatigue (high stress levels), the propagation step predominates (i.e., $N_p > N_i$).

Cracks associated with fatigue failure almost always initiate (or nucleate) on the surface of a component at some point of stress concentration. Crack nucleation sites include surface scratches, sharp fillets, keyways, threads, dents, and the like. In addition, cyclic loading can produce microscopic surface discontinuities resulting from dislocation slip steps which may also act as stress raisers, and therefore as crack initiation sites.

Once a stable crack has nucleated, it then initially propagates very slowly and, in polycrystalline metals, along crystallographic planes of high shear stress; this is sometimes termed *stage I propagation* (Figure 9.28). This stage may constitute a large or small fraction of the total fatigue life depending on stress level and the nature of the test specimen; high stresses and the presence of notches favor a short-lived stage I. In polycrystalline metals, cracks normally extend through only several grains during this propagation stage. The fatigue surface that is formed during stage I propagation has a flat and featureless appearance.

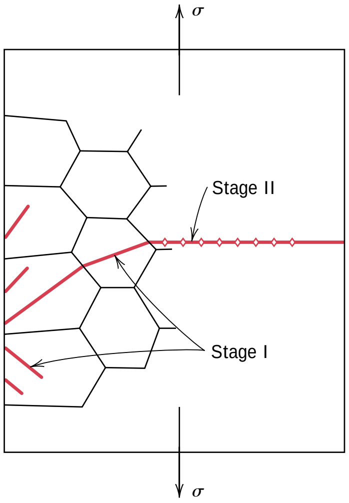

FIGURE 9.28 Schematic representation showing stages I and II of fatigue crack propagation in polycrystalline metals. (Copyright ASTM. Reprinted with permission.)

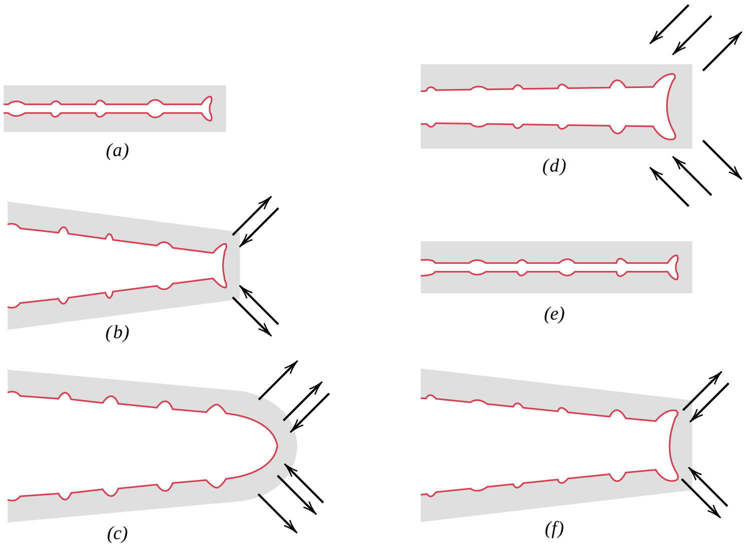

Figure 9.29 Fatigue crack propagation mechanism (stage II) by repetitive crack tip plastic blunting and sharpening; (*a*) zero or maximum compressive load, (*b*) small tensile load, (*c*) maximum tensile load, (*d*) small compressive load, (*e*) zero or maximum compressive load, (*f*) small tensile load. The loading axis is vertical. (Copyright ASTM. Reprinted with permission.)

Eventually, a second propagation stage (*stage II*) takes over, wherein the crack extension rate increases dramatically. Furthermore, at this point there is also a change in propagation direction to one that is roughly perpendicular to the applied tensile stress (see Figure 9.28). During this stage of propagation, crack growth proceeds by a repetitive plastic blunting and sharpening process at the crack tip, a mechanism illustrated in Figure 9.29. At the beginning of the stress cycle (zero or maximum compressive load), the crack tip has the shape of a sharp double-notch (Figure 9.29*a*). As the tensile stress is applied (Figure 9.29*b*), localized deformation occurs at each of these tip notches along slip planes that are oriented at 45° angles relative to the plane of the crack. With increased crack widening, the tip advances by continued shear deformation and the assumption of a blunted configuration (Figure 9.29*c*). During compression, the directions of shear deformation at the crack tip are reversed (Figure 9.29*d*) until, at the culmination of the cycle, a new sharp double-notch tip has formed (Figure 9.29*e*). Thus, the crack tip has advanced a one-notch distance during the course of a complete cycle. This process is repeated with each subsequent cycle until eventually some critical crack dimension is achieved that precipitates the final failure step and catastrophic failure ensues.

The region of a fracture surface that formed during stage II propagation may be characterized by two types of markings termed *beachmarks* and *striations.* Both of these features indicate the position of the crack tip at some point in time and appear as concentric ridges that expand away from the crack initiation site(s), frequently in a circular or semicircular pattern. Beachmarks (sometimes also called ''clamshell marks'') are of macroscopic dimensions (Figure 9.30), and may be observed with the unaided eye. These markings are found for components that experienced interruptions during stage II propagation—for example, a machine that operated only during normal work-shift hours. Each beachmark band represents a period of time over which crack growth occurred.

On the other hand, fatigue striations are microscopic in size and subject to observation with the electron microscope (either TEM or SEM). Figure 9.31 is an electron fractograph which shows this feature. Each striation is thought to represent the advance distance of the crack front during a single load cycle. Striation width depends on, and increases with, increasing stress range.

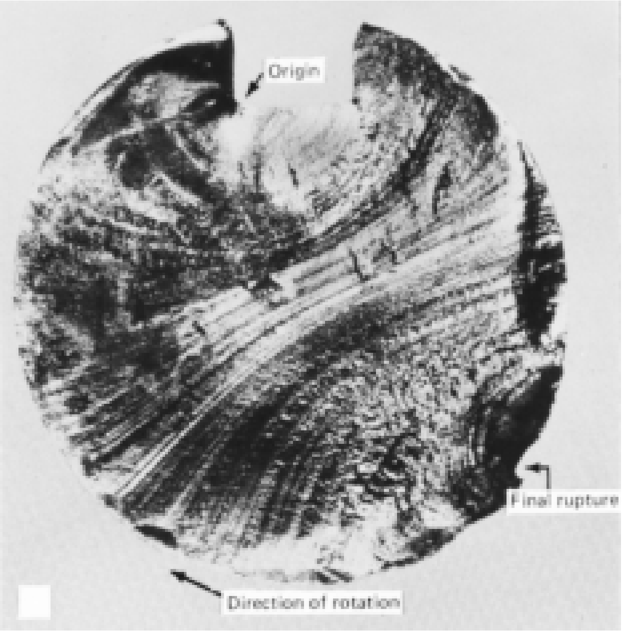

FIGURE 9.30 Fracture surface of a rotating steel shaft that experienced fatigue failure. Beachmark ridges are visible in the photograph. (Reproduced with permission from D. J. Wulpi, *Understanding How Components Fail,* American Society for Metals, Materials Park, OH, 1985.)

At this point it should be emphasized that although both beachmarks and striations are fatigue fracture surface features having similar appearances, they are nevertheless different, both in origin and size. There may be literally thousands of striations within a single beachmark.

Often the cause of failure may be deduced after examination of the failure surfaces. The presence of beachmarks and/or striations on a fracture surface confirms that the cause of failure was fatigue. Nevertheless, the absence of either or both does not exclude fatigue as the cause of failure.

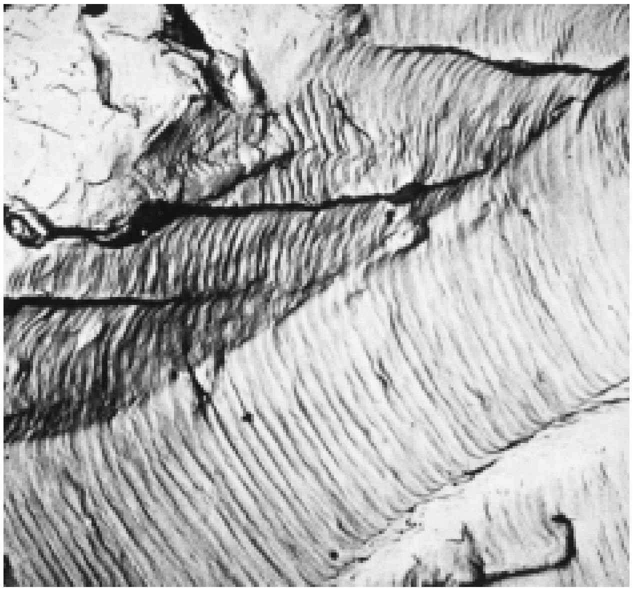

FIGURE 9.31 Transmission electron fractograph showing fatigue striations in aluminum. Magnification unknown. (From V. J. Colangelo and F. A. Heiser, *Analysis of Metallurgical Failures,* 2nd edition. Copyright © 1987 by John Wiley & Sons, New York. Reprinted by permission of John Wiley & Sons, Inc.)

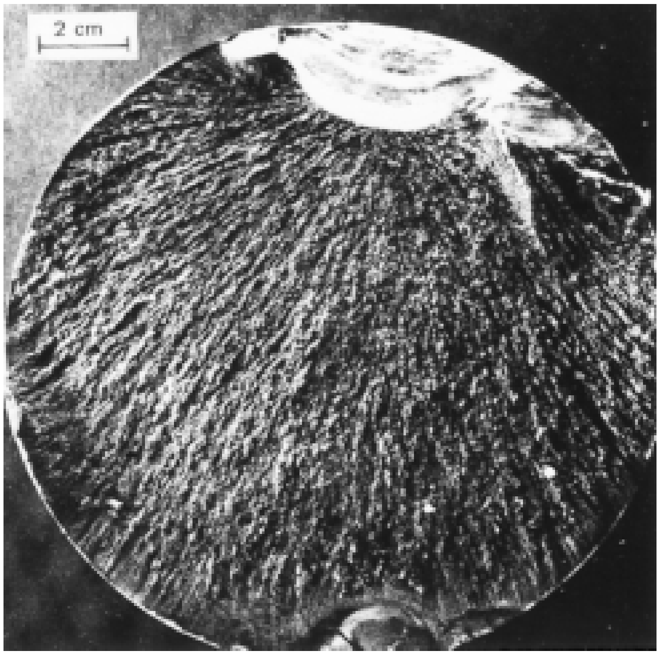

FIGURE 9.32 Fatigue failure surface. A crack formed at the top edge. The smooth region also near the top corresponds to the area over which the crack propagated slowly. Rapid failure occurred over the area having a dull and fibrous texture (the largest area). Approximately 0.5 ×. (Reproduced by permission from *Metals Handbook: Fractography and Atlas of Fractographs,* Vol. 9, 8th edition, H. E. Boyer, Editor, American Society for Metals, 1974.)

One final comment regarding fatigue failure surfaces: Beachmarks and striations will not appear on that region over which the rapid failure occurs. Rather, the rapid failure may be either ductile or brittle; evidence of plastic deformation will be present for ductile, and absent for brittle, failure. This region of failure may be noted in Figure 9.32.

9.13 CRACK PROPAGATION RATE

Even though measures may be taken to minimize the possibility of fatigue failure, cracks and crack nucleation sites will always exist in structural components. Under the influence of cyclic stresses, cracks will inevitably form and grow; this process, if unabated, can ultimately lead to failure. The intent of the present discussion is to develop a criterion whereby fatigue life may be predicted on the basis of material and stress state parameters. Principles of fracture mechanics (Section 9.5) will be employed inasmuch as the treatment involves determination of a maximum crack length that may be tolerated without inducing failure. It should be noted that this discussion relates to the domain of high-cycle fatigue, that is, for fatigue lives greater than about 10^4 to 10^5 cycles.

Results of fatigue studies have shown that the life of a structural component may be related to the rate of crack growth. During stage II propagation, cracks may grow from a barely perceivable size to some critical length. Experimental techniques are available which are employed to monitor crack length during the cyclic stressing. Data are recorded and then plotted as crack length a versus the number of cycles N.[9] A typical plot is shown in Figure 9.33, where curves are

---

[9] The symbol N in the context of Section 9.10 represents the number of cycles to fatigue failure; in the present discussion it denotes the number of cycles associated with some crack length prior to failure.

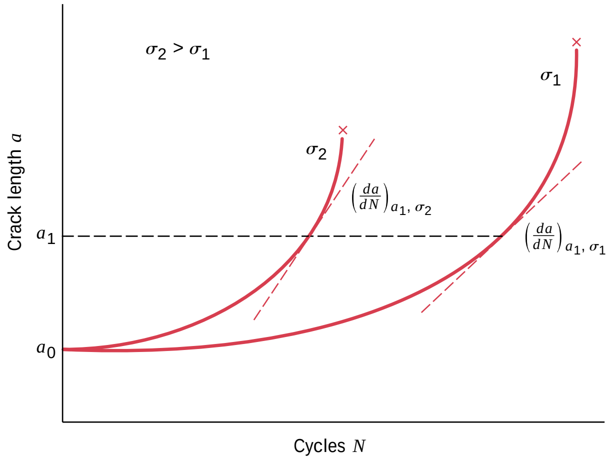

Figure 9.33 Crack length versus the number of cycles at stress levels σ_1 and σ_2 for fatigue studies. Crack growth rate da/dN is indicated at crack length a_1 for both stress levels.

included from data generated at two different stress levels; the initial crack length a_0 for both sets of tests is the same. Crack growth rate da/dN is taken as the slope at some point of the curve. Two important results are worth noting: (1) initially, growth rate is small, but increases with increasing crack length; and (2) growth rate is enhanced with increasing applied stress level and for a specific crack length (a_1 in Figure 9.33).

Fatigue crack propagation rate during stage II is a function of not only stress level and crack size but also material variables. Mathematically, this rate may be expressed in terms of the stress intensity factor K (developed using fracture mechanics in Section 9.5) and takes the form

$$\frac{da}{dN} = A(\Delta K)^m \tag{9.26}$$

The parameters A and m are constants for the particular material, which will also depend on environment, frequency, and the stress ratio (R in Equation 9.24). The value of m normally ranges between 1 and 6.

Furthermore, ΔK is the stress intensity factor range at the crack tip, that is,

$$\Delta K = K_{\max} - K_{\min} \tag{9.27a}$$

or, from Equation 9.8,

$$\Delta K = Y \Delta\sigma \sqrt{\pi a} = Y(\sigma_{\max} - \sigma_{\min})\sqrt{\pi a} \tag{9.27b}$$

Since crack growth stops or is negligible for a compression portion of the stress cycle, if $\sigma_{\min}$ is compressive, then $K_{\min}$ and $\sigma_{\min}$ are taken to be zero; that is, $\Delta K = K_{\max}$ and $\Delta\sigma = \sigma_{\max}$. Also note that $K_{\max}$ and $K_{\min}$ in Equation 9.27a represent stress intensity factors, not the fracture toughness K_c nor the plane strain fracture toughness K_{Ic}.

The typical fatigue crack growth rate behavior of materials is represented schematically in Figure 9.34 as the logarithm of crack growth rate da/dN versus the logarithm of the stress intensity factor range ΔK. The resulting curve has a

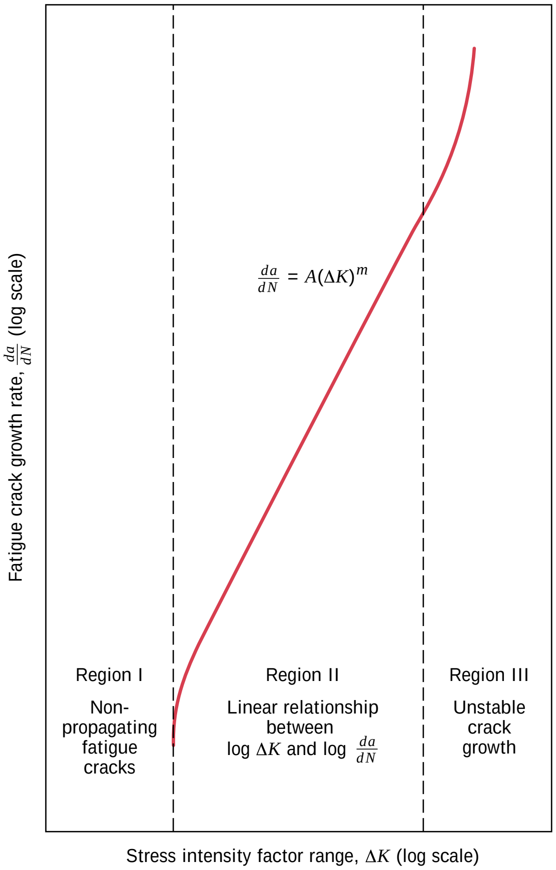

Figure 9.34 Schematic representation of logarithm fatigue crack propagation rate da/dN versus logarithm stress intensity factor range ΔK. The three regions of different crack growth response (I, II, and III) are indicated. (Reprinted with permission from ASM International, Metals Park, OH 44073-9989. W. G. Clark, Jr., ''How Fatigue Crack Initiation and Growth Properties Affect Material Selection and Design Criteria,'' *Metals Engineering Quarterly*, Vol. 14, No. 3, 1974.)

sigmoidal shape which may be divided into three distinct regions, labeled I, II, and III. In region I (at low stress levels and/or small crack sizes), preexisting cracks will not grow with cyclic loading. Furthermore, associated with region III is accelerated crack growth, which occurs just prior to the rapid fracture.

The curve is essentially linear in region II, which is consistent with Equation 9.26. This may be confirmed by taking the logarithm of both sides of this expression, which leads to

$$\log\left(\frac{da}{dN}\right) = \log[A(\Delta K)^m] \tag{9.28a}$$

$$\log\left(\frac{da}{dN}\right) = m \log \Delta K + \log A \tag{9.28b}$$

Indeed, according to Equation 9.28b, a straight-line segment will result when $\log(da/dN)$-versus-log ΔK data are plotted; the slope and intercept correspond to the values of m and $\log A$, respectively, which may be determined from test data that have been represented in the manner of Figure 9.34. Figure 9.35 is one such plot for a Ni–Mo–V steel alloy. The linearity of the data may be noted, which verifies the power law relationship of Equation 9.26. Furthermore, the slope yields

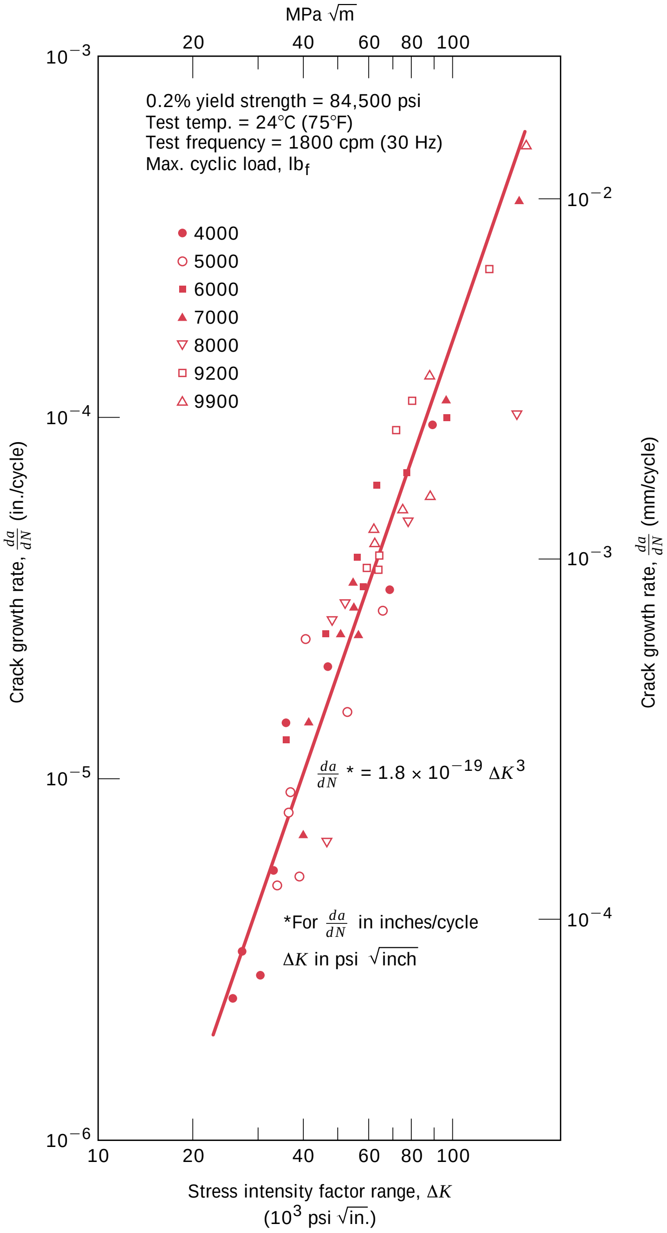

FIGURE 9.35 Logarithm crack growth rate versus logarithm stress intensity factor range for a Ni–Mo–V steel. (Reprinted by permission of the Society for Experimental Mechanics, Inc.)

a value of 3 for m; A is approximately 1.8×10^{-14}, as taken from the extrapolated intercept for da/dN in in./cycle and ΔK in psi$\sqrt{\text{in.}}$

One of the goals of failure analysis is to be able to predict fatigue life for some component, given its service constraints and laboratory test data. We are now able to develop an analytical expression for N_f, due to stage II, by integration of Equation 9.26. Rearrangement is first necessary as follows:

$$dN = \frac{da}{A(\Delta K)^m} \tag{9.29}$$

which may be integrated as

$$N_f = \int_0^{N_f} dN = \int_{a_0}^{a_c} \frac{da}{A(\Delta K)^m} \tag{9.30}$$

The limits on the second integral are between the initial flaw length a_0, which may be measured using nondestructive examination techniques, and the critical crack length a_c determined from fracture toughness tests.

Substitution of the expression for ΔK (Equation 9.27b) leads to

$$\begin{aligned} N_f &= \int_{a_0}^{a_c} \frac{da}{A(Y\Delta\sigma\sqrt{\pi a})^m} \\ &= \frac{1}{A\pi^{m/2}(\Delta\sigma)^m} \int_{a_0}^{a_c} \frac{da}{Y^m a^{m/2}} \end{aligned} \tag{9.31}$$

Here it is assumed that $\Delta\sigma$ (or $\sigma_{\text{max}} - \sigma_{\text{min}}$) is constant; furthermore, in general Y will depend on crack length a and therefore cannot be removed from within the integral.

A word of caution: Equation 9.31 presumes the validity of Equation 9.26 over the entire life of the component; it ignores the time taken to initiate the crack and also for final failure. Therefore, this expression should only be taken as an estimate of N_f.

Design Example 9.2

A relatively large sheet of steel is to be exposed to cyclic tensile and compressive stresses of magnitudes 100 MPa and 50 MPa, respectively. Prior to testing, it has been determined that the length of the largest surface crack is 2.0 mm (2×10^{-3} m). Estimate the fatigue life of this sheet if its plane strain fracture toughness is 25 MPa$\sqrt{\text{m}}$ and the values of m and A in Equation 9.26 are 3.0 and 1.0×10^{-12}, respectively, for $\Delta\sigma$ in MPa and a in m. Assume that the parameter Y is independent of crack length and has a value of 1.0.

Solution

It first becomes necessary to compute the critical crack length a_c, the integration upper limit in Equation 9.31. Equation 9.14 is employed for this computation, assuming a stress level of 100 MPa, since this is the maximum tensile stress. Therefore,

$$\begin{aligned} a_c &= \frac{1}{\pi}\left(\frac{K_{Ic}}{\sigma Y}\right)^2 \\ &= \frac{1}{\pi}\left(\frac{25\ \text{MPa}\sqrt{\text{m}}}{(100\ \text{MPa})(1)}\right)^2 = 0.02\ \text{m} \end{aligned}$$

We now want to solve Equation 9.31 using 0.002 m as the lower integration limit a_0, as stipulated in the problem. The value of $\Delta\sigma$ is just 100 MPa, the magnitude of the tensile stress, since $\sigma_{\min}$ is compressive. Therefore, integration yields

$$N_f = \frac{1}{A\pi^{m/2}(\Delta\sigma)^m}\int_{a_0}^{a_c}\frac{da}{Y^m a^{m/2}}$$

$$= \frac{1}{A\pi^{3/2}(\Delta\sigma)^3\,Y^3}\int_{a_0}^{a_c} a^{-3/2}\,da$$

$$= \frac{1}{A\pi^{3/2}(\Delta\sigma)^3\,Y^3}(-2)a^{-1/2}\Big|_{a_0}^{a_c}$$

$$= \frac{2}{A\pi^{3/2}(\Delta\sigma)^3\,Y^3}\left(\frac{1}{\sqrt{a_0}} - \frac{1}{\sqrt{a_c}}\right)$$

$$= \frac{2}{(1.0\times10^{-12})(\pi)^{3/2}(100)^3(1)^3}\left(\frac{1}{\sqrt{0.002}} - \frac{1}{\sqrt{0.02}}\right)$$

$$= 5.49\times10^6 \text{ cycles}$$

9.15 ENVIRONMENTAL EFFECTS

Environmental factors may also affect the fatigue behavior of materials. A few brief comments will be given relative to two types of environment-assisted fatigue failure: thermal fatigue and corrosion fatigue.

Thermal fatigue is normally induced at elevated temperatures by fluctuating thermal stresses; mechanical stresses from an external source need not be present. The origin of these thermal stresses is the restraint to the dimensional expansion and/or contraction that would normally occur in a structural member with variations in temperature. The magnitude of a thermal stress developed by a temperature change ΔT is dependent on the coefficient of thermal expansion α_l and the modulus of elasticity E according to

$$\sigma = \alpha_l E\,\Delta T \tag{9.32}$$

(The topics of thermal expansion and thermal stresses are discussed in Sections 17.3 and 17.5.) Of course, thermal stresses will not arise if this mechanical restraint is absent. Therefore, one obvious way to prevent this type of fatigue is to eliminate, or at least reduce, the restraint source, thus allowing unhindered dimensional changes with temperature variations, or to choose materials with appropriate physical properties.

Failure that occurs by the simultaneous action of a cyclic stress and chemical attack is termed **corrosion fatigue.** Corrosive environments have a deleterious influence and produce shorter fatigue lives. Even the normal ambient atmosphere will affect the fatigue behavior of some materials. Small pits may form as a result of chemical reactions between the environment and material, which serve as points of stress concentration, and therefore as crack nucleation sites. In addition, crack propagation rate is enhanced as a result of the corrosive environment. The nature of the stress cycles will influence the fatigue behavior; for example, lowering the load application frequency leads to longer periods during which the opened crack is in contact with the environment and to a reduction in the fatigue life.

Several approaches to corrosion fatigue prevention exist. On one hand, we can take measures to reduce the rate of corrosion by some of the techniques discussed in Chapter 16, for example, apply protective surface coatings, select a more corrosion-resistant material, and reduce the corrosiveness of the environment. And/or it might be advisable to take actions to minimize the probability of normal fatigue failure, as outlined above, for example, reduce the applied tensile stress level and impose residual compressive stresses on the surface of the member.

9.17a STRESS AND TEMPERATURE EFFECTS (DETAILED VERSION)

Both temperature and the level of the applied stress influence the creep characteristics (Figure 9.41). At a temperature substantially below $0.4T_m$, and after the initial deformation, the strain is virtually independent of time. With either increasing stress or temperature, the following will be noted: (1) the instantaneous strain at the time of stress application increases; (2) the steady-state creep rate is increased; and (3) the rupture lifetime is diminished.

The results of creep rupture tests are most commonly presented as the logarithm of stress versus the logarithm of rupture lifetime. Figure 9.42 is one such plot for a nickel alloy in which a linear relationship can be seen to exist at each temperature. For some alloys and over relatively large stress ranges, nonlinearity in these curves is observed.

Empirical relationships have been developed in which the steady-state creep rate as a function of stress and temperature is expressed. Its dependence on stress can be written

$$\dot{\epsilon}_s = K_1\sigma^n \tag{9.33}$$

where K_1 and n are material constants. A plot of the logarithm of $\dot{\epsilon}_s$ versus the logarithm of σ yields a straight line with slope of n; this is shown in Figure 9.43 for a nickel alloy at three temperatures. Clearly, a straight line segment is drawn at each temperature.

Now, when the influence of temperature is included,

$$\dot{\epsilon}_s = K_2\sigma^n \exp\left(-\frac{Q_c}{RT}\right) \tag{9.34}$$

where K_2 and Q_c are constants; Q_c is termed the activation energy for creep.

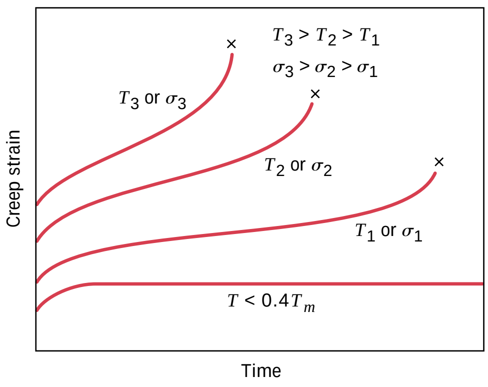

FIGURE 9.41 Influence of stress σ and temperature T on creep behavior.

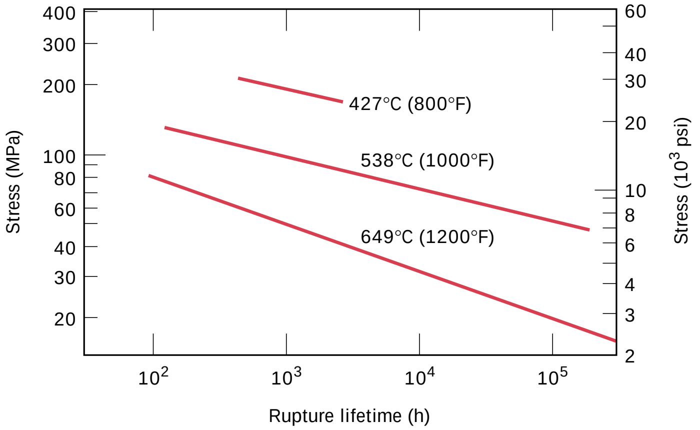

FIGURE 9.42 Stress (logarithmic scale) versus rupture lifetime (logarithmic scale) for a low carbon–nickel alloy at three temperatures. (From *Metals Handbook: Properties and Selection: Stainless Steels, Tool Materials and Special-Purpose Metals*, Vol. 3, 9th edition, D. Benjamin, Senior Editor, American Society for Metals, 1980, p. 130.)

Several theoretical mechanisms have been proposed to explain the creep behavior for various materials; these mechanisms involve stress-induced vacancy diffusion, grain boundary diffusion, dislocation motion, and grain boundary sliding. Each leads to a different value of the stress exponent n in Equation 9.33. It has been possible to elucidate the creep mechanism for a particular material by comparing its experimental n value with values predicted for the various mechanisms. In addition, correlations have been made between the activation energy for creep (Q_c) and the activation energy for diffusion (Q_d, Equation 6.8).

Creep data of this nature are represented pictorially for some well-studied systems in the form of stress–temperature diagrams, which are termed *deformation*

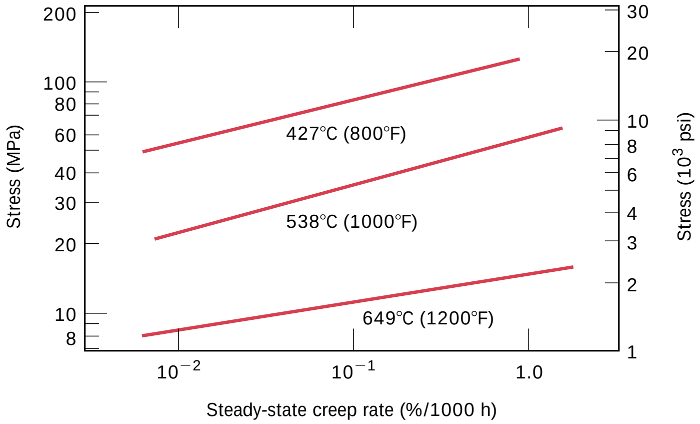

FIGURE 9.43 Stress (logarithmic scale) versus steady-state creep rate (logarithmic scale) for a low carbon–nickel alloy at three temperatures. (From *Metals Handbook: Properties and Selection: Stainless Steels, Tool Materials and Special-Purpose Metals*, Vol. 3, 9th edition, D. Benjamin, Senior Editor, American Society for Metals, 1980, p. 131.)

mechanism maps. These maps indicate stress–temperature regimes (or areas) over which various mechanisms operate. Constant strain rate contours are often also included. Thus, for some creep situation, given the appropriate deformation mechanism map and any two of the three parameters—temperature, stress level, and creep strain rate—the third parameter may be determined.

9.18 DATA EXTRAPOLATION METHODS

The need often arises for engineering creep data that are impractical to collect from normal laboratory tests. This is especially true for prolonged exposures (on the order of years). One solution to this problem involves performing creep and/or creep rupture tests at temperatures in excess of those required, for shorter time periods, and at a comparable stress level, and then by making a suitable extrapolation to the in-service condition. A commonly used extrapolation procedure employs the Larson–Miller parameter, defined as

$$T(C + \log t_r) \tag{9.35}$$

where C is a constant (usually on the order of 20), for T in Kelvin and the rupture lifetime t_r in hours. The rupture lifetime of a given material measured at some specific stress level will vary with temperature such that this parameter remains constant. Or, the data may be plotted as the logarithm of stress versus the Larson–Miller parameter, as shown in Figure 9.44. Utilization of this technique is demonstrated in the following design example.

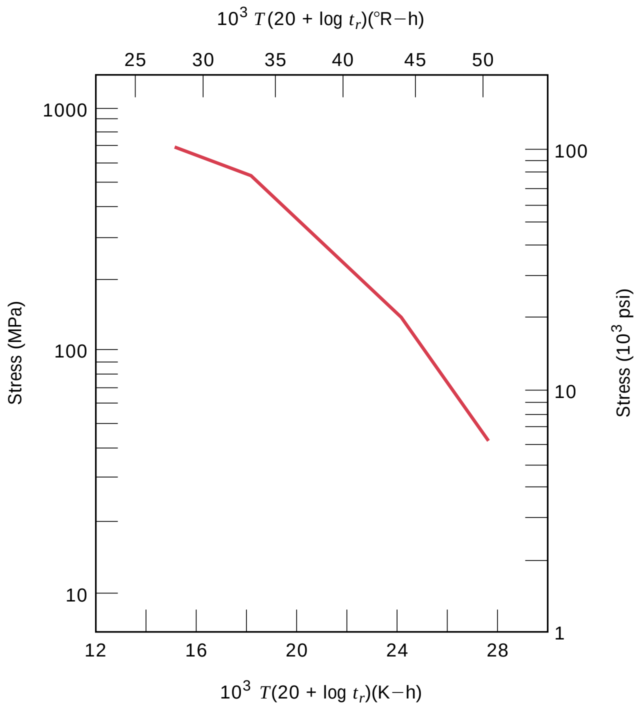

FIGURE 9.44 Logarithm stress versus the Larson–Miller parameter for an S-590 iron. (From F. R. Larson and J. Miller, *Trans. ASME*, **74,** 765, 1952. Reprinted by permission of ASME.)

DESIGN EXAMPLE 9.3

Using the Larson–Miller data for S-590 iron shown in Figure 9.44, predict the time to rupture for a component that is subjected to a stress of 140 MPa (20,000 psi) at 800°C (1073 K).

SOLUTION

From Figure 9.44, at 140 MPa (20,000 psi) the value of the Larson–Miller parameter is 24.0×10^3, for T in K and t_r in h; therefore,

$$\begin{aligned} 24.0 \times 10^3 &= T(20 + \log t_r) \\ &= 1073(20 + \log t_r) \end{aligned}$$

and, solving for the time,

$$\begin{aligned} 22.37 &= 20 + \log t_r \\ t_r &= 233 \text{ h } (9.7 \text{ days}) \end{aligned}$$

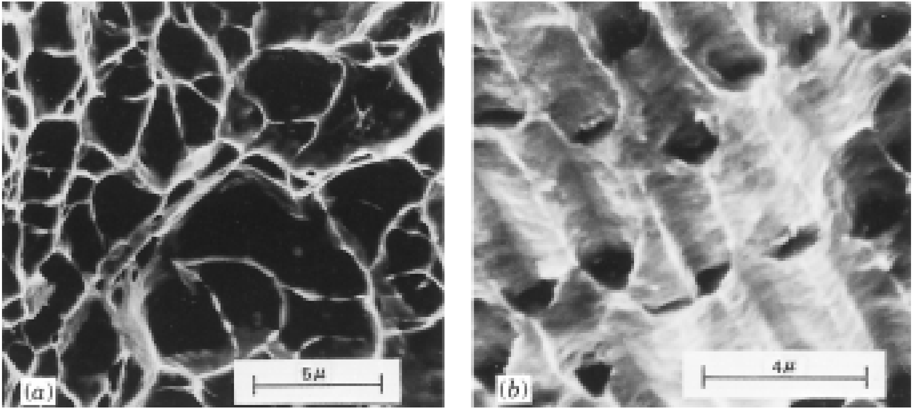

FIGURE 9.4 (*a*) Scanning electron fractograph showing spherical dimples characteristic of ductile fracture resulting from uniaxial tensile loads. 3300×. (*b*) Scanning electron fractograph showing parabolic-shaped dimples characteristic of ductile fracture resulting from shear loading. 5000×. (From R. W. Hertzberg, *Deformation and Fracture Mechanics of Engineering Materials*, 3rd edition. Copyright © 1989 by John Wiley & Sons, New York. Reprinted by permission of John Wiley & Sons, Inc.)

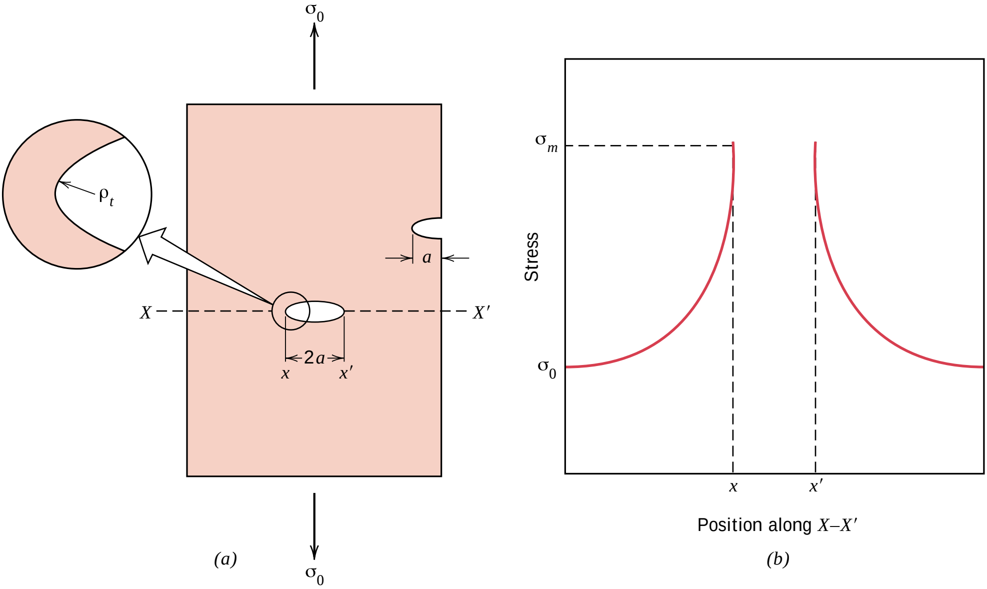
σ0
ρt
a
X
X′
2a
x
x′
(a)
σ0
σm
Stress
σ0
x
x′
Position along X–X′
(b)

FIGURE 9.7 (*a*) The geometry of surface and internal cracks. (*b*) Schematic stress profile along the line X–X' in (*a*), demonstrating stress amplification at crack tip positions.

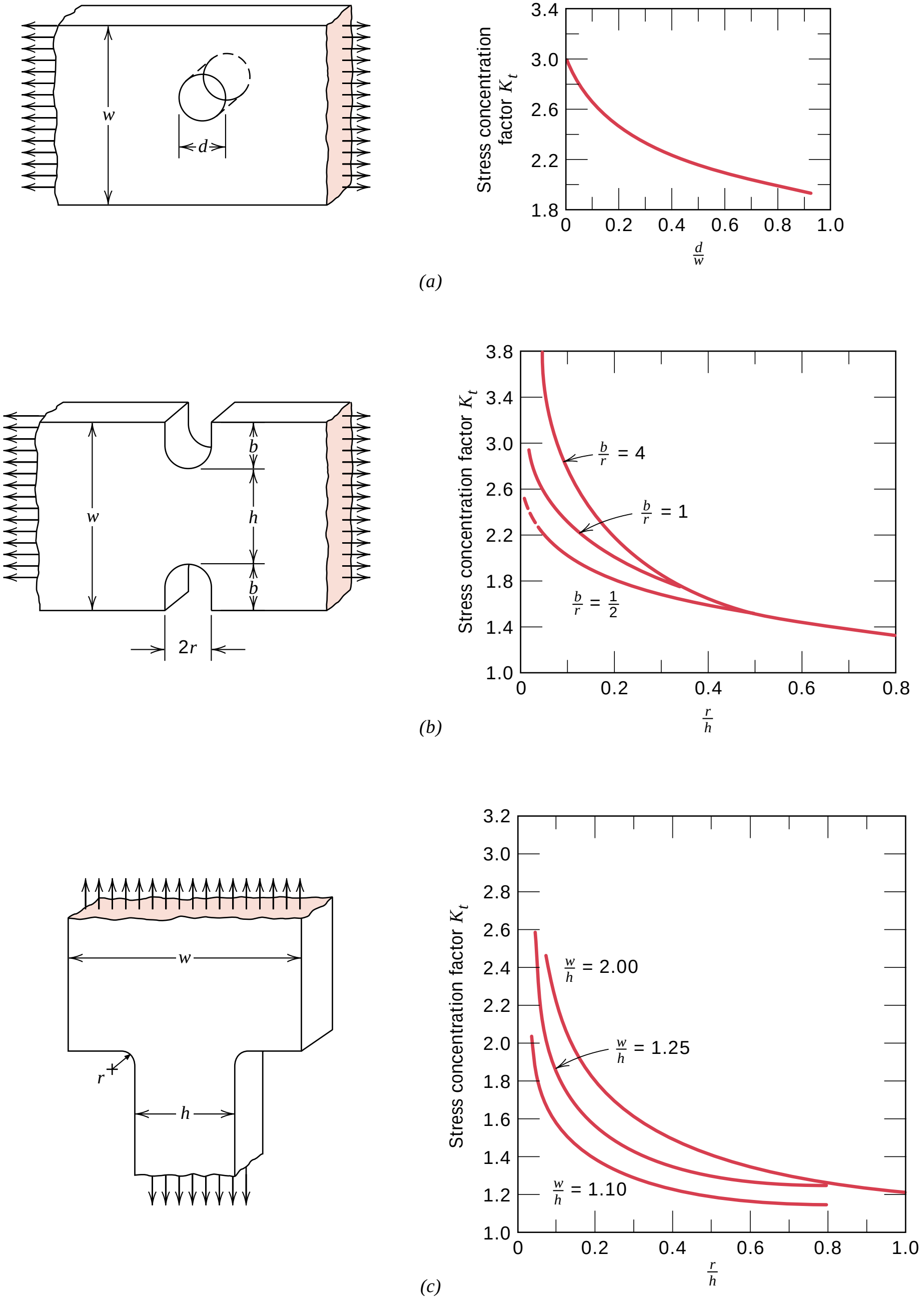

FIGURE 9.8 Theoretical stress concentration factor curves for three simple geometrical shapes. (From G. H. Neugebauer, *Prod. Eng.* (NY), Vol. 14, pp. 82–87, 1943.)

FIGURE 9.9 The three modes of crack surface displacement. (*a*) Mode I, opening or tensile mode; (*b*) mode II, sliding mode; and (*c*) mode III, tearing mode.

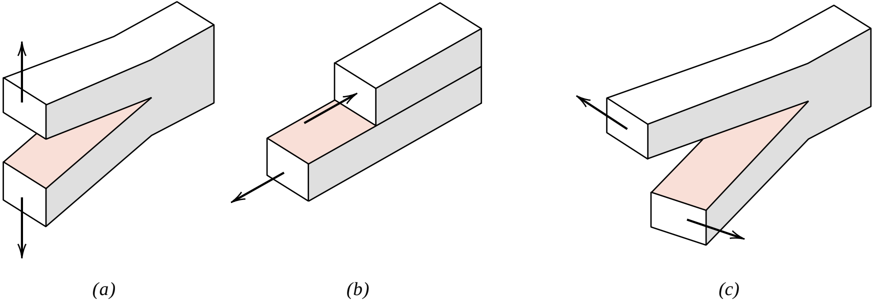

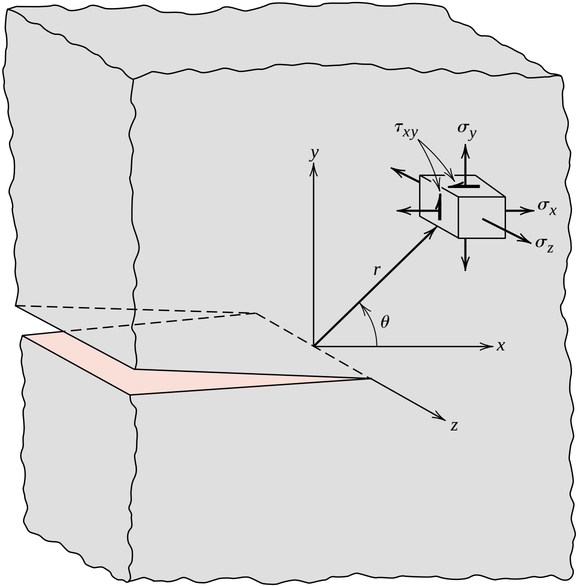
τ_{xy}
σ_y
y
σ_x
σ_z
r
θ
x
z

Figure 9.10 The stresses acting in front of a crack that is loaded in a tensile mode I configuration.

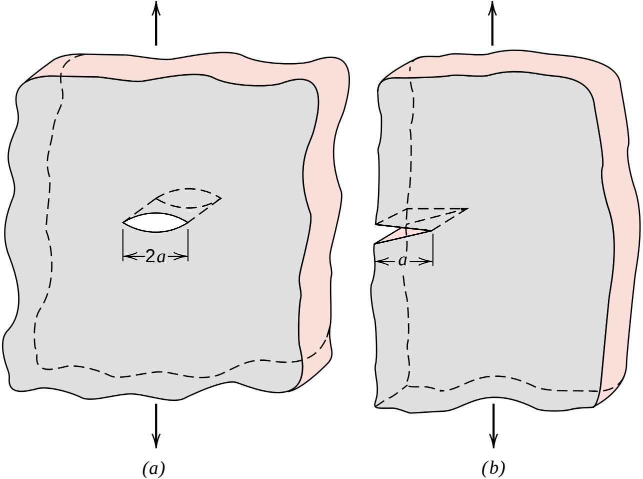

Figure 9.11 Schematic representations of (*a*) an interior crack in a plate of infinite width, and (*b*) an edge crack in a plate of semi-infinite width.

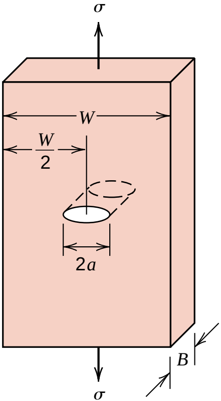
σ
W
$\frac{W}{2}$
$2a$
B
σ

Figure 9.12 Schematic representation of a flat plate of finite width having a through-thickness center crack.

Figure 9.13 Y calibration curves for three simple crack-plate geometries. (Copyright ASTM. Reprinted with permission.)

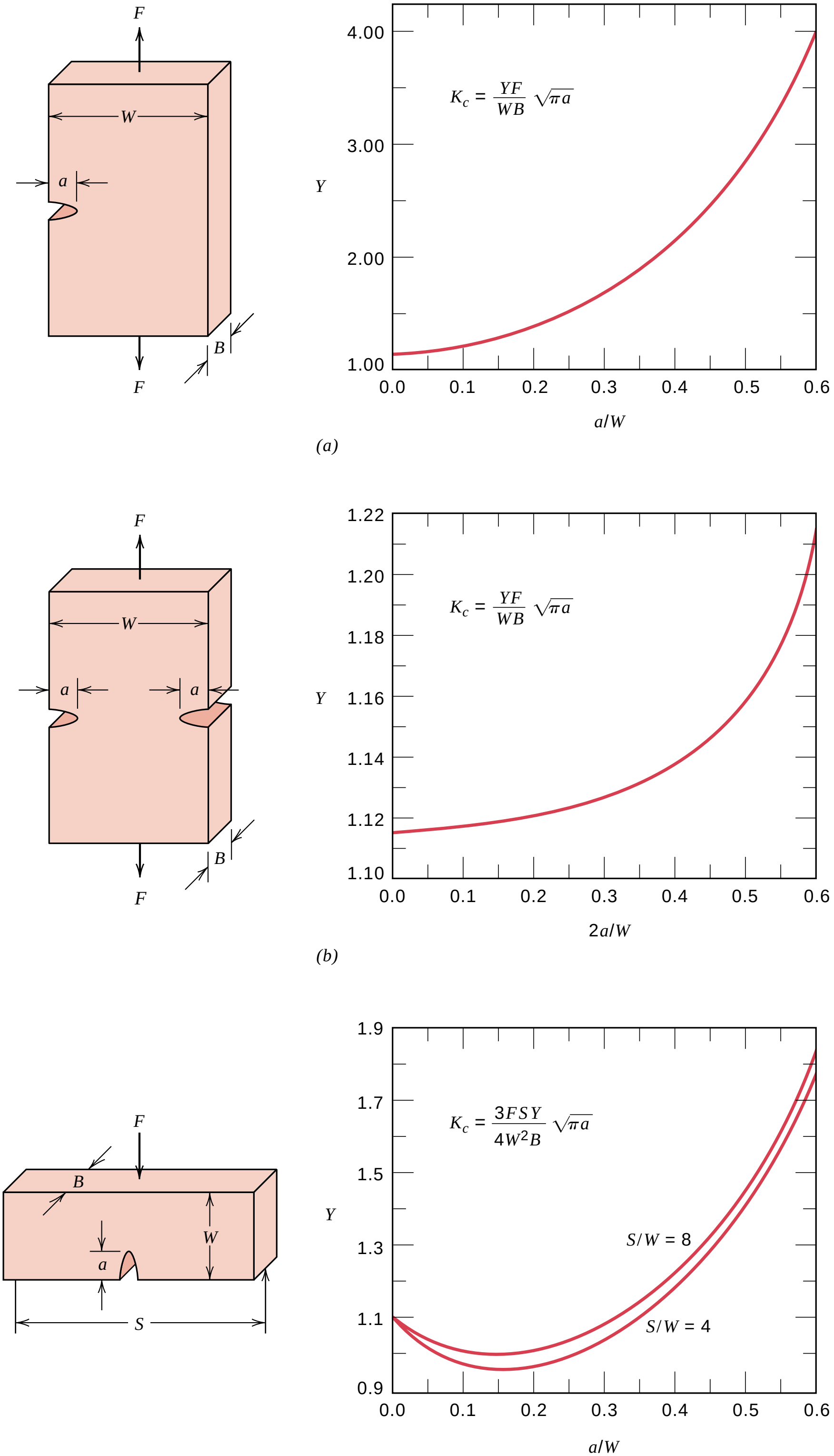

(a)

(b)

(c)

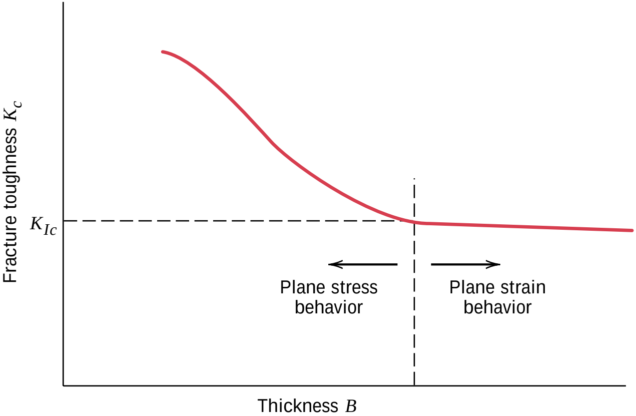

FIGURE 9.14 Schematic representation showing the effect of plate thickness on fracture toughness.

Table 9.1 Room-Temperature Yield Strength and Plane Strain Fracture Toughness Data for Selected Engineering Materials

	Yield Strength		K_{Ic}	
Material	***MPa***	***ksi***	$MPa\sqrt{m}$	$ksi\sqrt{in.}$
Metals				
Aluminum Alloy[a] (7075-T651)	495	72	24	22
Aluminum Alloy[a] (2024-T3)	345	50	44	40
Titanium Alloy[a] (Ti-6Al-4V)	910	132	55	50
Alloy Steel[a] (4340 tempered @ 260°C)	1640	238	50.0	45.8
Alloy Steel[a] (4340 tempered @ 425°C)	1420	206	87.4	80.0
Ceramics				
Concrete	—	—	0.2–1.4	0.18–1.27
Soda-Lime Glass	—	—	0.7–0.8	0.64–0.73
Aluminum Oxide	—	—	2.7–5.0	2.5–4.6
Polymers				
Polystyrene (PS)	—	—	0.7–1.1	0.64–1.0
Polymethyl Methacrylate (PMMA)	53.8–73.1	7.8–10.6	0.7–1.6	0.64–1.5
Polycarbonate (PC)	62.1	9.0	2.2	2.0

[a] **Source:** Reprinted with permission, *Advanced Materials and Processes*, ASM International, © 1990.

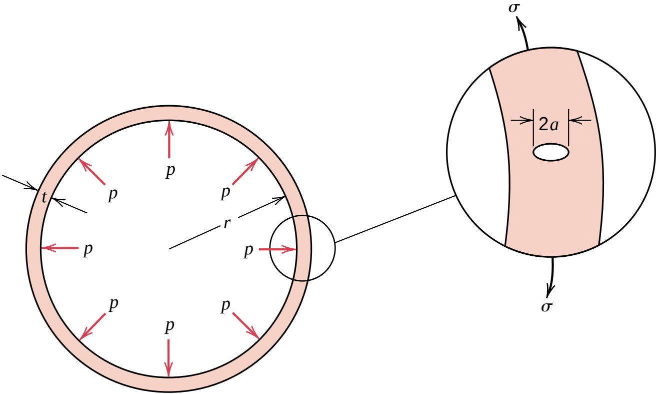

FIGURE 9.15 Schematic diagram showing the cross section of a spherical tank that is subjected to an internal pressure *p*, and that has a radial crack of length 2*a* in its wall.

Table 9.2 Ranking of Several Metal Alloys Relative to Critical Crack Length (Yielding Criterion) for a Thin-Walled Spherical Pressure Vessel

Material	$\left(\frac{K_{Ic}}{\sigma_y}\right)^2$ (*mm*)
Medium carbon (1040) steel	43.1
AZ31B magnesium	19.6
2024 aluminum (T3)	16.3
Ti-5Al-2.5Sn titanium	6.6
4140 steel (tempered @ 482°C)	5.3
4340 steel (tempered @ 425°C)	3.8
Ti-6Al-4V titanium	3.7
17-7PH steel	3.4
7075 aluminum (T651)	2.4
4140 steel (tempered @ 370°C)	1.6
4340 Steel (tempered @ 260°C)	0.93

Table 9.3 Ranking of Several Metal Alloys Relative to Maximum Allowable Pressure (Leak-Before-Break Criterion) for a Thin-Walled Spherical Pressure Vessel

Material	$\frac{K_{Ic}^2}{\sigma_y}$ (*MPa-m*)
Medium carbon (1040) steel	11.2
4140 steel (tempered @ 482°C)	6.1
Ti-5Al-2.5Sn titanium	5.8
2024 aluminum (T3)	5.6
4340 steel (tempered @ 425°C)	5.4
17-7PH steel	4.4
AZ31B magnesium	3.9
Ti-6Al-4V titanium	3.3
4140 steel (tempered @ 370°C)	2.4
4340 steel (tempered @ 260°C)	1.5
7075 aluminum (T651)	1.2

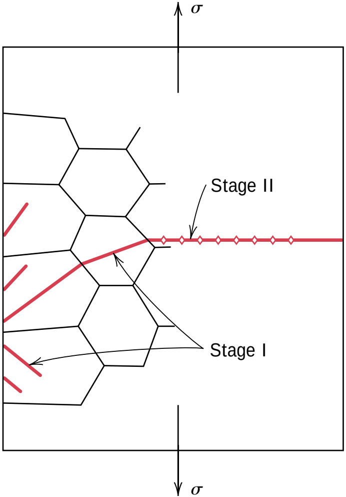
σ
Stage II
Stage I
σ

Figure 9.28 Schematic representation showing stages I and II of fatigue crack propagation in polycrystalline metals. (Copyright ASTM. Reprinted with permission.)

FIGURE 9.29 Fatigue crack propagation mechanism (stage II) by repetitive crack tip plastic blunting and sharpening; (*a*) zero or maximum compressive load, (*b*) small tensile load, (*c*) maximum tensile load, (*d*) small compressive load, (*e*) zero or maximum compressive load, (*f*) small tensile load. The loading axis is vertical. (Copyright ASTM. Reprinted with permission.)

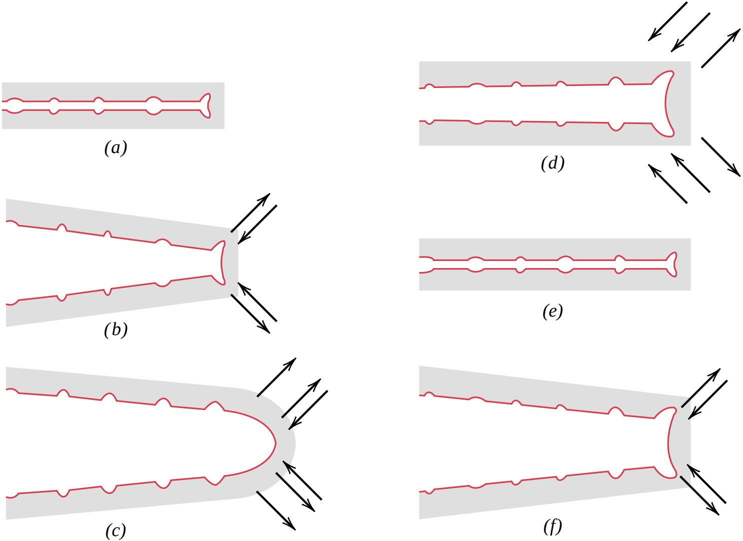

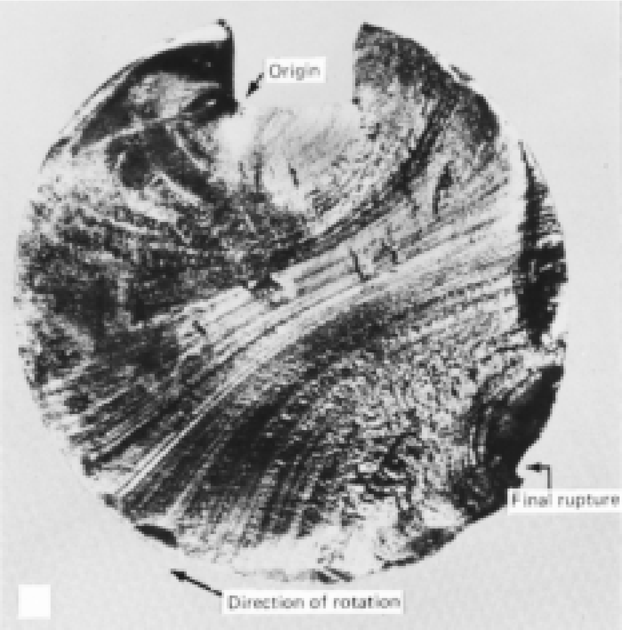
Origin
Final rupture
Direction of rotation

FIGURE 9.30 Fracture surface of a rotating steel shaft that experienced fatigue failure. Beachmark ridges are visible in the photograph. (Reproduced with permission from D. J. Wulpi, *Understanding How Components Fail,* American Society for Metals, Materials Park, OH, 1985.)

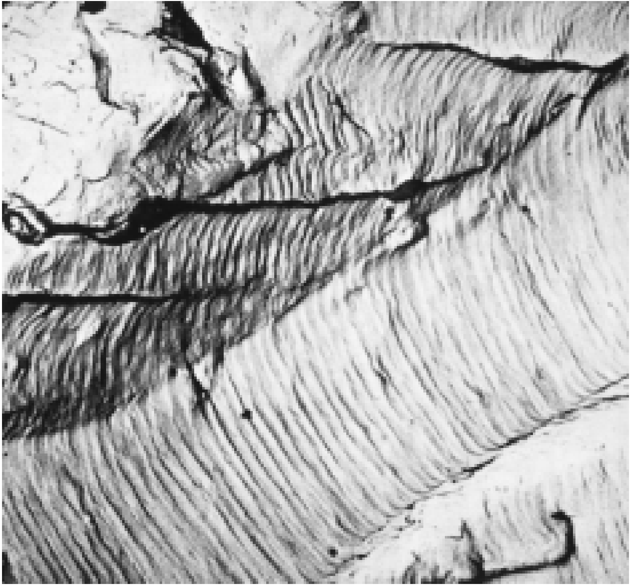

FIGURE 9.31 Transmission electron fractograph showing fatigue striations in aluminum. Magnification unknown. (From V. J. Colangelo and F. A. Heiser, *Analysis of Metallurgical Failures*, 2nd edition. Copyright © 1987 by John Wiley & Sons, New York. Reprinted by permission of John Wiley & Sons, Inc.)

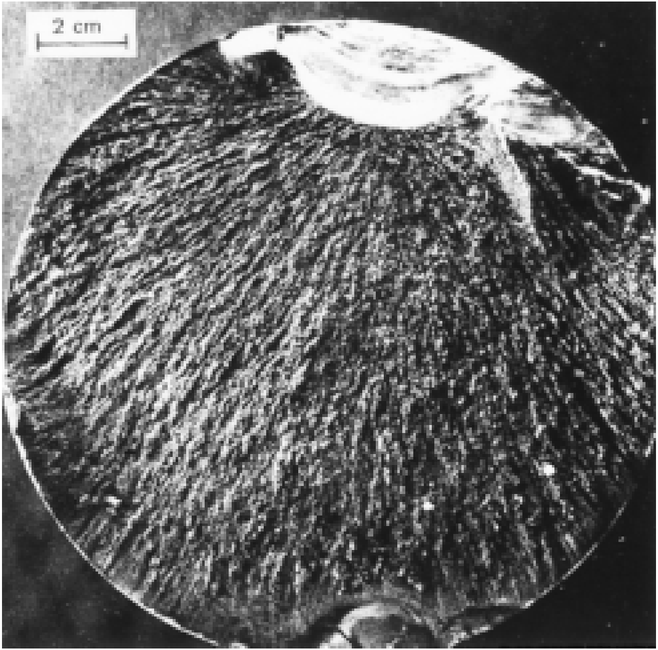

FIGURE 9.32 Fatigue failure surface. A crack formed at the top edge. The smooth region also near the top corresponds to the area over which the crack propagated slowly. Rapid failure occurred over the area having a dull and fibrous texture (the largest area). Approximately 0.5 ×. (Reproduced by permission from *Metals Handbook: Fractography and Atlas of Fractographs*, Vol. 9, 8th edition, H. E. Boyer, Editor, American Society for Metals, 1974.)

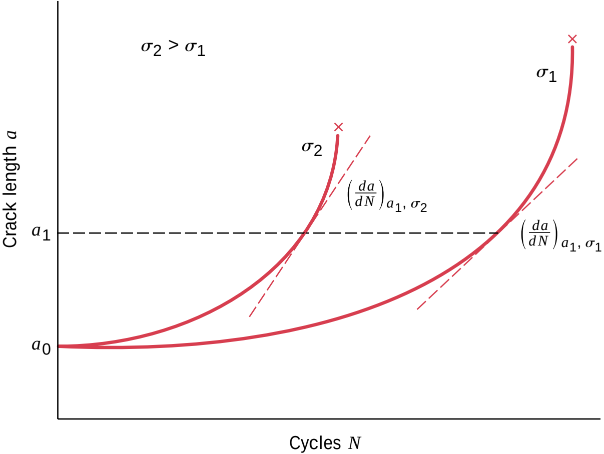

FIGURE 9.33 Crack length versus the number of cycles at stress levels σ_1 and σ_2 for fatigue studies. Crack growth rate da/dN is indicated at crack length a_1 for both stress levels.

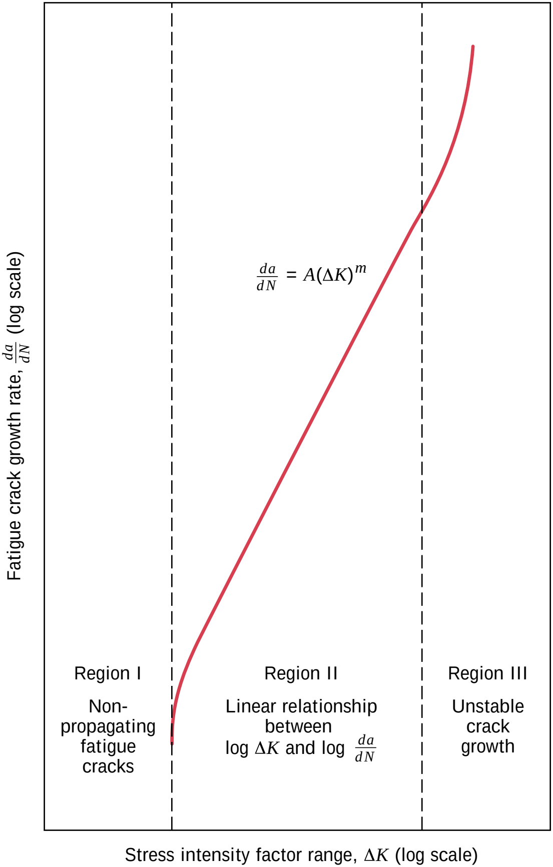

FIGURE 9.34 Schematic representation of logarithm fatigue crack propagation rate da/dN versus logarithm stress intensity factor range ΔK. The three regions of different crack growth response (I, II, and III) are indicated. (Reprinted with permission from ASM International, Metals Park, OH 44073-9989. W. G. Clark, Jr., ‘‘How Fatigue Crack Initiation and Growth Properties Affect Material Selection and Design Criteria,’’ *Metals Engineering Quarterly*, Vol. 14, No. 3, 1974.)

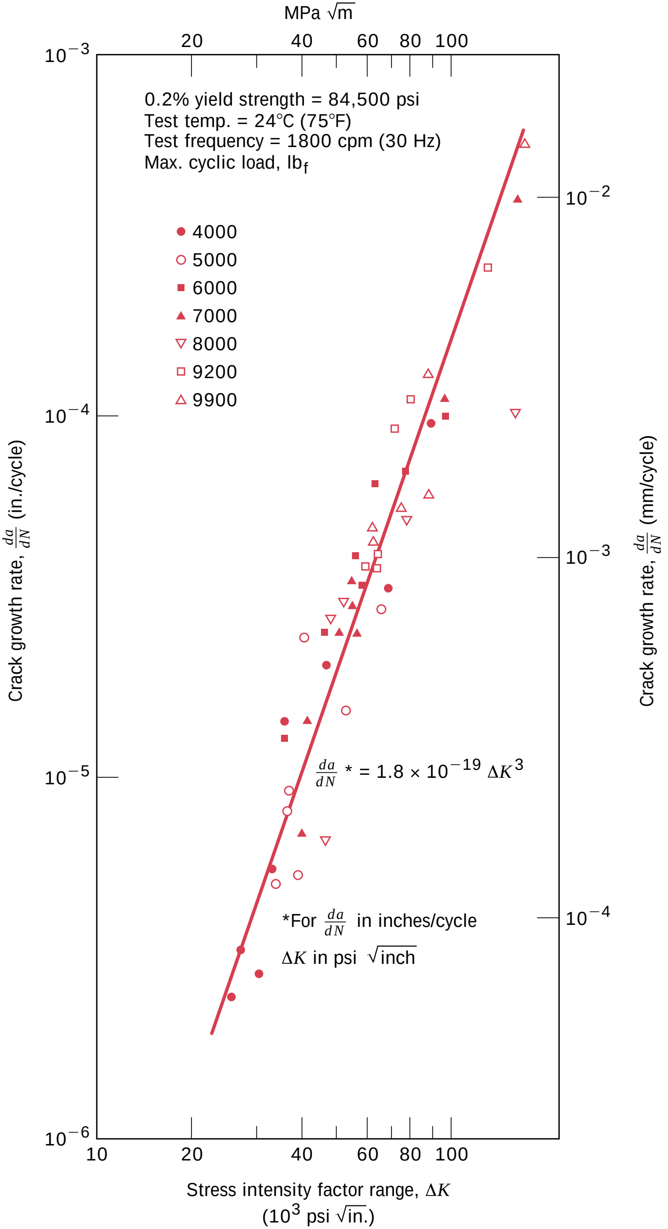

FIGURE 9.35 Logarithm crack growth rate versus logarithm stress intensity factor range for a Ni–Mo–V steel. (Reprinted by permission of the Society for Experimental Mechanics, Inc.)

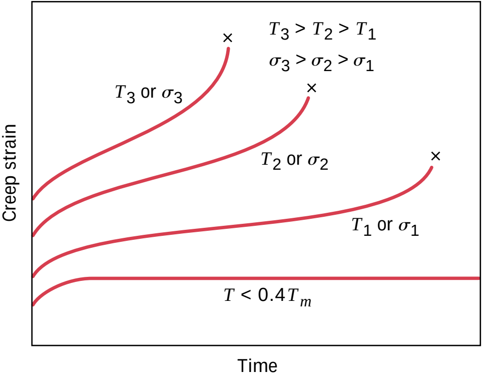

FIGURE 9.41 Influence of stress σ and temperature T on creep behavior.

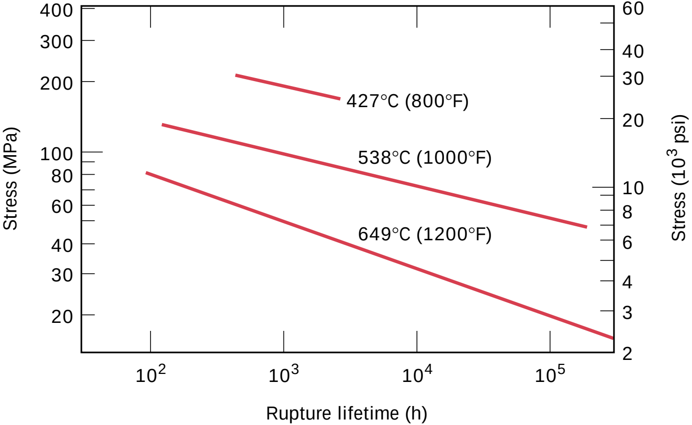

FIGURE 9.42 Stress (logarithmic scale) versus rupture lifetime (logarithmic scale) for a low carbon–nickel alloy at three temperatures. (From *Metals Handbook: Properties and Selection: Stainless Steels, Tool Materials and Special-Purpose Metals*, Vol. 3, 9th edition, D. Benjamin, Senior Editor, American Society for Metals, 1980, p. 130.)

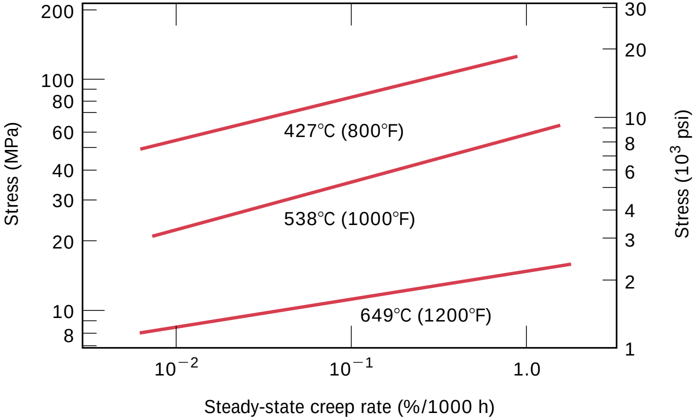

FIGURE 9.43 Stress (logarithmic scale) versus steady-state creep rate (logarithmic scale) for a low carbon–nickel alloy at three temperatures. (From *Metals Handbook: Properties and Selection: Stainless Steels, Tool Materials and Special-Purpose Metals*, Vol. 3, 9th edition, D. Benjamin, Senior Editor, American Society for Metals, 1980, p. 131.)

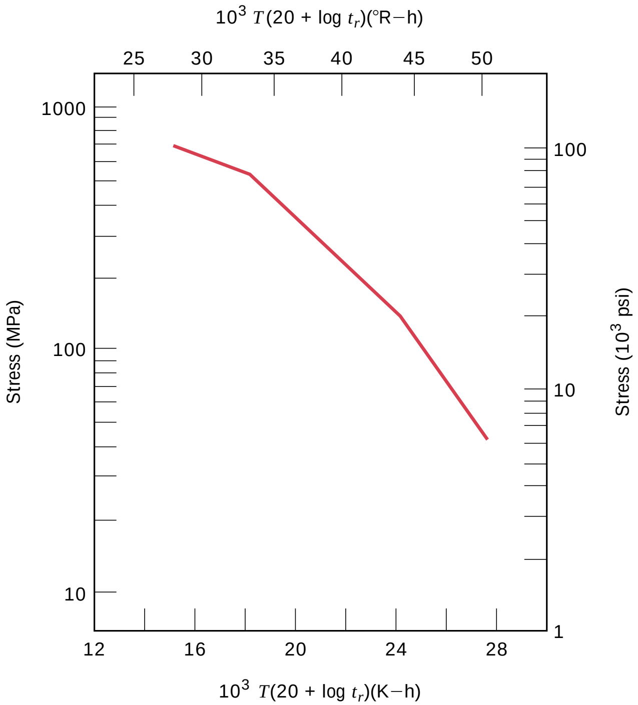

FIGURE 9.44 Logarithm stress versus the Larson–Miller parameter for an S-590 iron. (From F. R. Larson and J. Miller, *Trans. ASME*, **74,** 765, 1952. Reprinted by permission of ASME.)

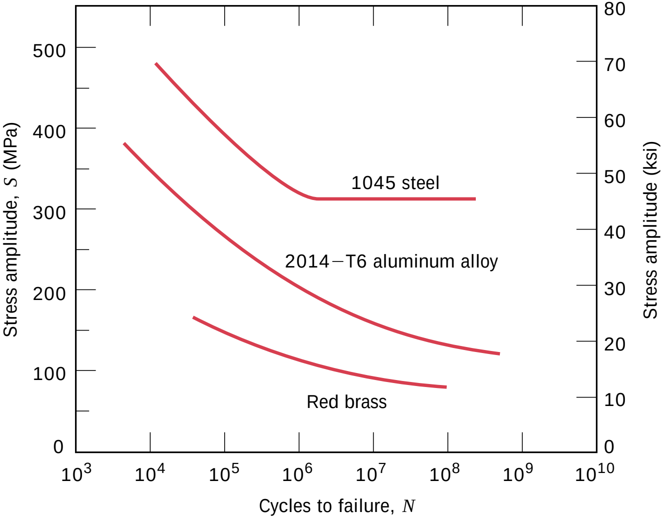

FIGURE 9.46 Stress magnitude S versus the logarithm of the number N of cycles to fatigue failure for red brass, an aluminum alloy, and a plain carbon steel. (Adapted from H. W. Hayden, W. G. Moffatt, and J. Wulff, *The Structure and Properties of Materials*, Vol. III, *Mechanical Behavior*, p. 15. Copyright © 1965 by John Wiley & Sons, New York. Reprinted by permission of John Wiley & Sons, Inc. Also adapted from *ASM Handbook*, Vol. 2, *Properties and Selection: Nonferrous Alloys and Special-Purpose Materials*, 1990. Reprinted by permission of ASM International.)

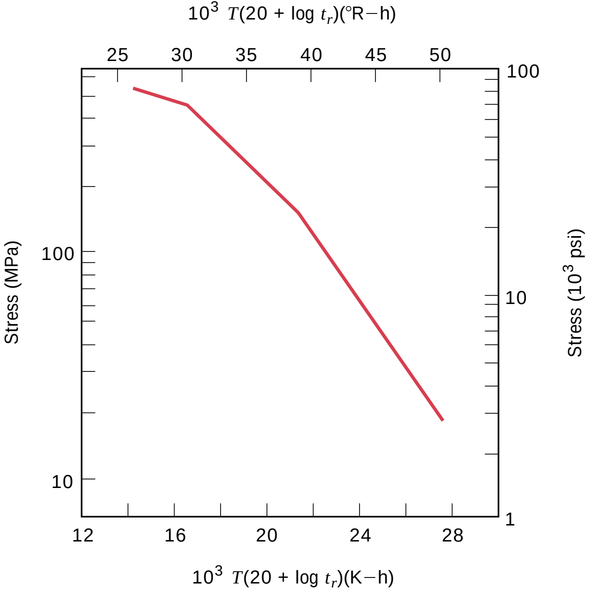

FIGURE 9.47 Logarithm stress versus the Larson–Miller parameter for an 18-8 Mo stainless steel. (From F. R. Larson and J. Miller, *Trans. ASME*, **74,** 765, 1952. Reprinted by permission of ASME.)

CHAPTER 10

PHASE DIAGRAMS

10.5 This problem asks that we cite the phase or phases present for several alloys at specified temperatures.

(a) For an alloy composed of 90 wt% Zn-10 wt% Cu and at 400°C, from Figure 10.17, ε and η phases are present, and

$$C_\varepsilon = 87 \text{ wt\% Zn-13 wt\% Cu}$$

$$C_\eta = 97 \text{ wt\% Zn-3 wt\% Cu}$$

(c) For an alloy composed of 55 wt% Ag-45 wt% Cu and at 900°C, from Figure 10.6, only the liquid phase is present; its composition is 55 wt% Ag-45 wt% Cu.

10.7 This problem asks that we determine the phase mass fractions for the alloys and temperatures in Problem 10.5.

(a) For an alloy composed of 90 wt% Zn-10 wt% Cu and at 400°C, ε and η phases are present, and

$$C_o = 90 \text{ wt\% Zn}$$

$$C_\varepsilon = 87 \text{ wt\% Zn}$$

$$C_\eta = 97 \text{ wt\% Zn}$$

Therefore, using modified forms of Equation (10.2b) we get

$$W_\varepsilon = \frac{C_\eta - C_o}{C_\eta - C_\varepsilon} = \frac{97 - 90}{97 - 87} = 0.70$$

$$W_\eta = \frac{C_o - C_\varepsilon}{C_\eta - C_\varepsilon} = \frac{90 - 87}{97 - 87} = 0.30$$

(c) For an alloy composed of 55 wt% Ag-45 wt% Cu and at 900°C, since only the liquid phase is present, then $\mathbf{W_L} = 1.0$.

10.9 This problem asks that we determine the phase volume fractions for the alloys and temperatures in Problem 10.5a, b, and c. This is accomplished by using the technique illustrated in Example Problem 10.3, and the results of Problem 10.7.

(a) This is a Cu-Zn alloy at 400°C, wherein

$$C_\varepsilon = 87 \text{ wt\% Zn-13 wt\% Cu}$$

$$C_\eta = 97 \text{ wt\% Zn-3 wt\% Cu}$$

$$W_\varepsilon = 0.70$$

$$W_\eta = 0.30$$

$$\rho_{Cu} = 8.77 \text{ g/cm}^3$$

$$\rho_{Zn} = 6.83 \text{ g/cm}^3$$

Using these data it is first necessary to compute the densities of the ε and η phases using Equation (5.10a). Thus

$$\rho_\varepsilon = \frac{100}{\dfrac{C_{Zn(\varepsilon)}}{\rho_{Zn}} + \dfrac{C_{Cu(\varepsilon)}}{\rho_{Cu}}}$$

$$= \frac{100}{\dfrac{87}{6.83\ \text{g/cm}^3} + \dfrac{13}{8.77\ \text{g/cm}^3}} = 7.03\ \text{g/cm}^3$$

$$\rho_\eta = \frac{100}{\dfrac{C_{Zn(\eta)}}{\rho_{Zn}} + \dfrac{C_{Cu(\eta)}}{\rho_{Cu}}}$$

$$= \frac{100}{\dfrac{97}{6.83\ \text{g/cm}^3} + \dfrac{3}{8.77\ \text{g/cm}^3}} = 6.88\ \text{g/cm}^3$$

Now we may determine the $\mathbf{V}_\varepsilon$ and $\mathbf{V}_\eta$ values using Equation 10.6. Thus,

$$V_\varepsilon = \frac{\dfrac{W_\varepsilon}{\rho_\varepsilon}}{\dfrac{W_\varepsilon}{\rho_\varepsilon} + \dfrac{W_\eta}{\rho_\eta}}$$

$$= \frac{\dfrac{0.70}{7.03\ \text{g/cm}^3}}{\dfrac{0.70}{7.03\ \text{g/cm}^3} + \dfrac{0.30}{6.88\ \text{g/cm}^3}} = 0.70$$

$$V_\eta = \frac{\dfrac{W_\eta}{\rho_\eta}}{\dfrac{W_\varepsilon}{\rho_\varepsilon} + \dfrac{W_\eta}{\rho_\eta}}$$

$$= \frac{\dfrac{0.30}{6.88\ \text{g/cm}^3}}{\dfrac{0.70}{7.03\ \text{g/cm}^3} + \dfrac{0.30}{6.88\ \text{g/cm}^3}} = 0.30$$

10.12 (a) We are asked to determine how much sugar will dissolve in 1500 g of water at 90°C. From the solubility limit curve in Figure 10.1, at 90°C the maximum concentration of sugar in the syrup is about 77 wt%. It is now possible to calculate the mass of sugar using Equation (5.3) as

$$C_{sugar}(\text{wt\%}) = \frac{m_{sugar}}{m_{sugar} + m_{water}} \times 100$$

$$77\ \text{wt\%} = \frac{m_{sugar}}{m_{sugar} + 1500\ \text{g}} \times 100$$

Solving for $\mathbf{m_{sugar}}$ yields $\mathbf{m_{sugar}} = 5022$ g.

(b) Again using this same plot, at 20°C the solubility limit (or the concentration of the saturated solution) is about 64 wt% sugar.

(c) The mass of sugar in this saturated solution at 20°C (**m'_{sugar}**) may also be calculated using Equation (5.3) as follows:

$$64 \text{ wt\%} = \frac{m'_{sugar}}{m'_{sugar} + 1500 \text{ g}} \times 100$$

which yields a value for **m'_{sugar}** of 2667 g. Subtracting the latter from the former of these sugar concentrations yields the amount of sugar that precipitated out of the solution upon cooling **m''_{sugar}**; that is

$$m''_{sugar} = m_{sugar} - m'_{sugar} = 5022 \text{ g} - 2667 \text{ g} = 2355 \text{ g}$$

10.21 Upon cooling a 50 wt% Pb-50 wt% Mg alloy from 700°C and utilizing Figure 10.18:

(a) The first solid phase forms at the temperature at which a vertical line at this composition intersects the **L**-(α + **L**) phase boundary—i.e., about 550°C;

(b) The composition of this solid phase corresponds to the intersection with the α-(α + **L**) phase boundary, of a tie line constructed across the α + **L** phase region at 550°C—i.e., 22 wt% Pb-78 wt% Mg;

(c) Complete solidification of the alloy occurs at the intersection of this same vertical line at 50 wt% Pb with the eutectic isotherm—i.e., about 465°C;

(d) The composition of the last liquid phase remaining prior to complete solidification corresponds to the eutectic composition—i.e., about 66 wt% Pb-34 wt% Mg.

10.24 (a) We are given that the mass fractions of α and liquid phases are both 0.5 for a 30 wt% Sn-70 wt% Pb alloy and asked to estimate the temperature of the alloy. Using the appropriate phase diagram, Figure 10.7, by trial and error with a ruler, a tie line within the α + **L** phase region that is divided in half for an alloy of this composition exists at about 230°C.

(b) We are now asked to determine the compositions of the two phases. This is accomplished by noting the intersections of this tie line with both the solidus and liquidus lines. From these intersections, $\mathbf{C}_\alpha$ = 15 wt% Sn, and $\mathbf{C}_\mathbf{L}$ = 42 wt% Sn.

10.28 This problem asks if it is possible to have a Cu-Ag alloy of composition 50 wt% Ag-50 wt% Cu that consists of mass fractions $\mathbf{W}_\alpha$ = 0.60 and $\mathbf{W}_\beta$ = 0.40. Such an alloy is **not** possible, based on the following argument. Using the appropriate phase diagram, Figure 10.6, and, using Equations (10.1) and (10.2) let us determine $\mathbf{W}_\alpha$ and $\mathbf{W}_\beta$ at just below the eutectic temperature and also at room temperature. At just below the eutectic, $\mathbf{C}_\alpha$ = 8.0 wt% Ag and $\mathbf{C}_\beta$ = 91.2 wt% Ag; thus,

$$W_\alpha = \frac{C_\beta - C_o}{C_\beta - C_\alpha} = \frac{91.2 - 50}{91.2 - 8} = 0.50$$

$$W_\beta = 1.0 - W_\alpha = 1.0 - 0.5 = 0.50$$

Furthermore, at room temperature, $\mathbf{C}_\alpha$ = 0 wt% Ag and $\mathbf{C}_\beta$ = 100 wt% Ag; employment of Equations (10.1) and (10.2) yields

$$W_\alpha = \frac{C_\beta - C_o}{C_\beta - C_\alpha} = \frac{100 - 50}{100 - 0} = 0.50$$

And, $\mathbf{W}_\beta$ = 0.50. Thus, the mass fractions of the α and β phases, upon cooling through the $\alpha + \beta$ phase region will remain approximately constant at about 0.5, and will never have values of $\mathbf{W}_\alpha$ = 0.60 and $\mathbf{W}_\beta$ = 0.40 as called for in the problem.

10.35* This problem asks that we determine the composition of a Pb-Sn alloy at 180°C given that $\mathbf{W}_{\beta'} =$ 0.57 and $\mathbf{W_e} = 0.43$. Since there is a primary β microconstituent present, then we know that the alloy composition, $\mathbf{C_o}$, is between 61.9 and 97.8 wt% Sn (Figure 10.7). Furthermore, this figure also indicates that $\mathbf{C}_\beta = 97.8$ wt% Sn and $\mathbf{C_{eutectic}} = 61.9$ wt% Sn. Applying the appropriate lever rule expression for $\mathbf{W}_{\beta'}$

$$W_{\beta'} = \frac{C_o - C_{eutectic}}{C_\beta - C_{eutectic}} = \frac{C_o - 61.9}{97.8 - 61.9} = 0.57$$

and solving for $\mathbf{C_o}$ yields $\mathbf{C_o} = 82.4$ wt% Sn.

10.47* We are asked to specify the value of **F** for Gibbs phase rule at point B on the pressure-temperature diagram for H_2O. Gibbs phase rule in general form is

$$P + F = C + N$$

For this system, the number of components, **C**, is 1, whereas **N**, the number of noncompositional variables, is 2—viz. temperature and pressure. Thus, the phase rule now becomes

$$P + F = 1 + 2 = 3$$

Or

$$F = 3 - P$$

where **P** is the number of phases present at equilibrium.

At point B on the figure, only a single (vapor) phase is present (i.e., **P** = 1), or

$$F = 3 - P = 3 - 1 = 2$$

which means that both temperature and pressure are necessary to define the system.

10.54 This problem asks that we compute the carbon concentration of an iron-carbon alloy for which the fraction of total ferrite is 0.94. Application of the lever rule [of the form of Equation (10.12)] yields

$$W_\alpha = 0.94 = \frac{C_{Fe_3C} - C'_o}{C_{Fe_3C} - C_\alpha} = \frac{6.70 - C'_o}{6.70 - 0.022}$$

and solving for $\mathbf{C'_o}$

$$C'_o = 0.42 \text{ wt\% C}$$

10.59 This problem asks that we determine the carbon concentration in an iron-carbon alloy, given the mass fractions of proeutectoid ferrite and pearlite. From Equation (10.20)

$$W_p = 0.714 = \frac{C'_o - 0.022}{0.74}$$

which yields $\mathbf{C'_o} = 0.55$ wt% C.

10.64 This problem asks if it is possible to have an iron-carbon alloy for which $\mathbf{W}_\alpha = 0.846$ and $\mathbf{W}_{\mathbf{Fe_3C'}} = 0.049$. In order to make this determination, it is necessary to set up lever rule expressions for these two mass fractions in terms of the alloy composition, then to solve for the alloy composition of each; if both alloy composition values are equal, then such an alloy is possible. The expression for the mass fraction of total ferrite is

$$W_\alpha = \frac{C_{Fe_3C} - C_o}{C_{Fe_3C} - C_\alpha} = \frac{6.70 - C_o}{6.70 - 0.022} = 0.846$$

Solving for this $\mathbf{C_o}$ yields $\mathbf{C_o} = 1.05$ wt% C. Now for $\mathbf{W}_{\mathbf{Fe_3C'}}$ we utilize Equation (10.23) as

$$W_{Fe_3C'} = \frac{C_1' - 0.76}{5.94} = 0.049$$

This expression leads to $\mathbf{C_1'} = 1.05$ wt% C. And, since $\mathbf{C_o} = \mathbf{C_1'}$, this alloy is possible.

10.70 This problem asks that we determine the approximate Brinell hardness of a 99.8 wt% Fe-0.2 wt% C alloy. First, we compute the mass fractions of pearlite and proeutectoid ferrite using Equations (10.20) and (10.21), as

$$W_p = \frac{C_o' - 0.022}{0.74} = \frac{0.20 - 0.022}{0.74} = 0.24$$

$$W_{\alpha'} = \frac{0.76 - C_o'}{0.74} = \frac{0.76 - 0.20}{0.74} = 0.76$$

Now, we compute the Brinell hardness of the alloy as

$$\begin{aligned} HB_{alloy} &= HB_{\alpha'} W_{\alpha'} + HB_p W_p \\ &= (80)(0.76) + (280)(0.24) = 128 \end{aligned}$$

10.73* We are asked to consider a steel alloy of composition 93.8 wt% Fe, 6.0 wt% Ni, and 0.2 wt% C.

(a) From Figure 10.36, the eutectoid temperature for 6 wt% Ni is approximately 650°C (1200°F).

(b) From Figure 10.37, the eutectoid composition is approximately 0.62 wt% C. Since the carbon concentration in the alloy (0.2 wt%) is less than the eutectoid, the proeutectoid phase is ferrite.

(c) Assume that the α-($\alpha + Fe_3C$) phase boundary is at a negligible carbon concentration. Modifying Equation (10.21) leads to

$$W_{\alpha'} = \frac{0.62 - C_o'}{0.62 - 0} = \frac{0.62 - 0.20}{0.62} = 0.68$$

Likewise, using a modified Equation (10.20)

$$W_p = \frac{C_o' - 0}{0.62 - 0} = \frac{0.20}{0.62} = 0.32$$

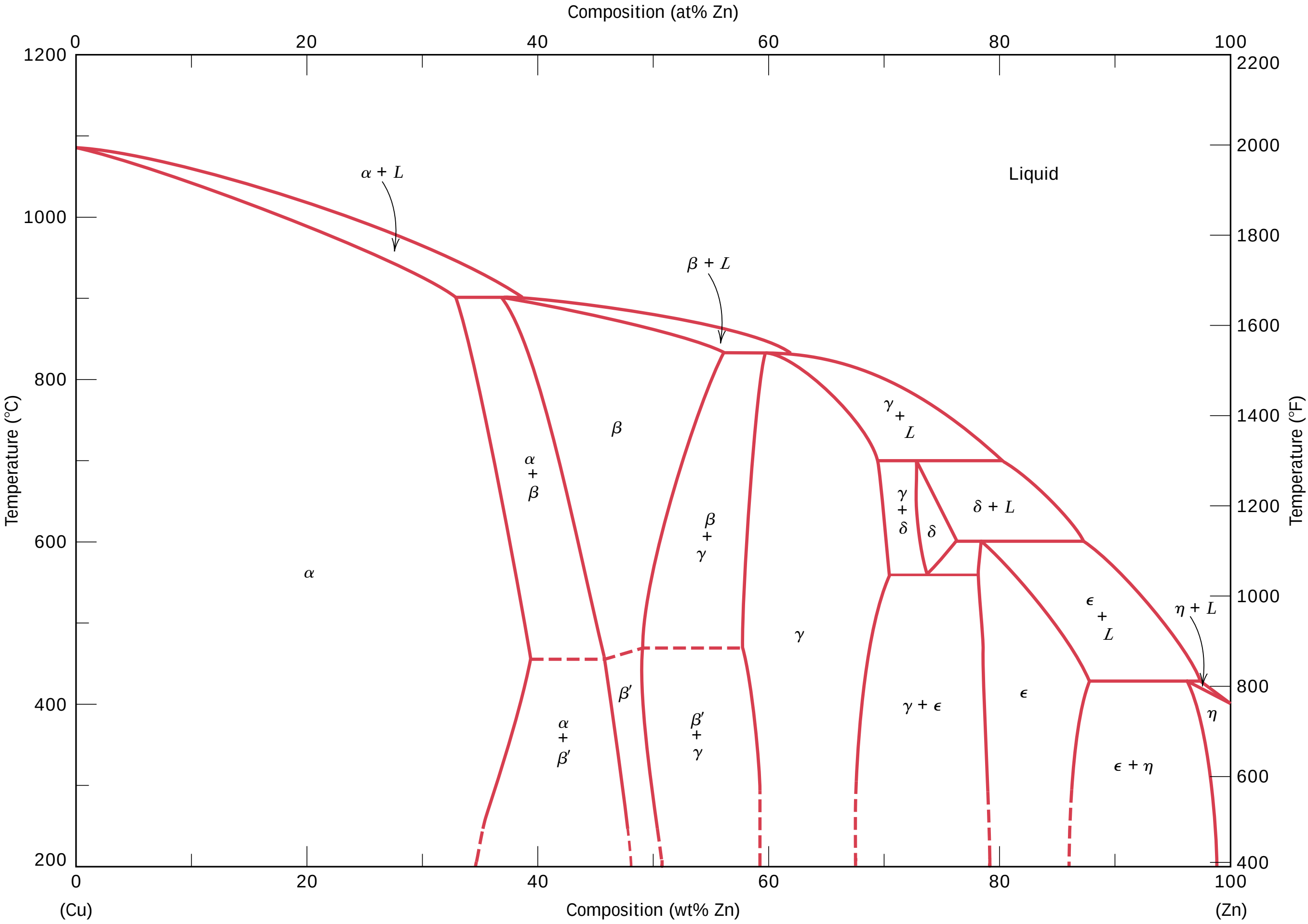

Figure 10.17 The copper–zinc phase diagram. (Adapted from *Binary Alloy Phase Diagrams*, 2nd edition, Vol. 2, T. B. Massalski, Editor-in-Chief, 1990. Reprinted by permission of ASM International, Materials Park, OH.)

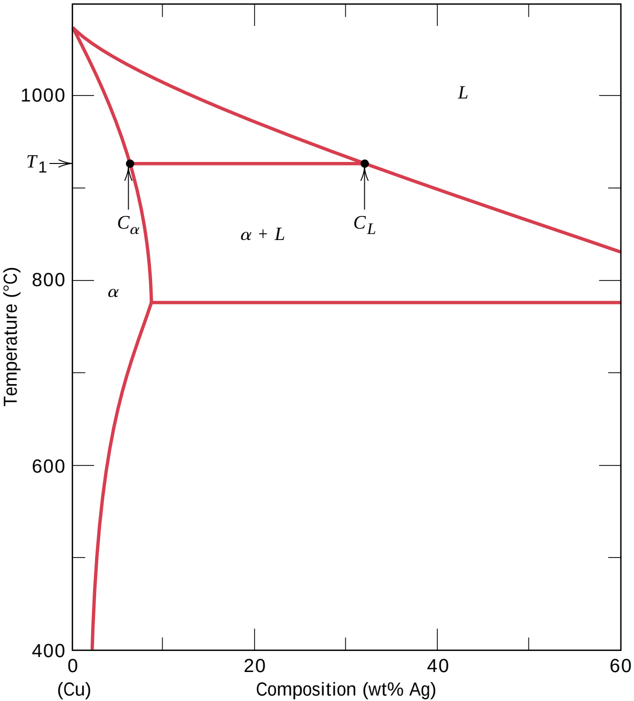

FIGURE 10.25 Enlarged copper-rich section of the Cu–Ag phase diagram in which the Gibbs phase rule for the coexistence of two phases (i.e., α and L) is demonstrated. Once the composition of either phase (i.e., C_α or C_L) or the temperature (i.e., T_1) is specified, values for the two remaining parameters are established by construction of the appropriate tie line.

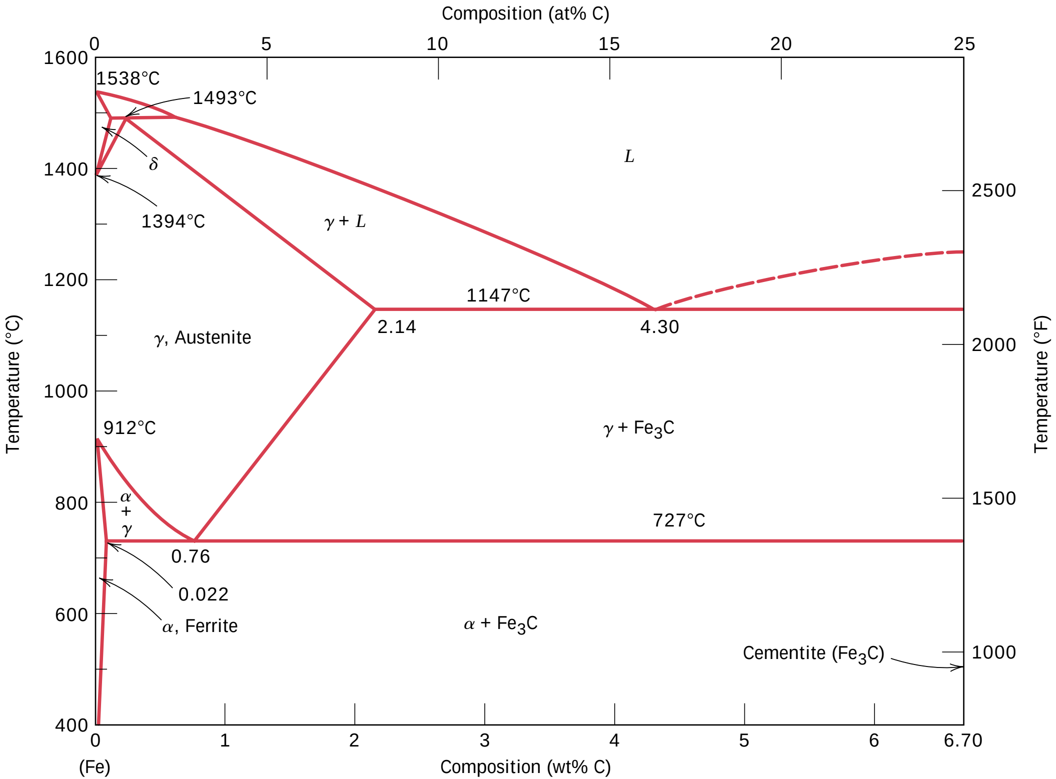

Figure 10.26 The iron–iron carbide phase diagram. (Adapted from *Binary Alloy Phase Diagrams*, 2nd edition, Vol. 1, T. B. Massalski, Editor-in-Chief, 1990. Reprinted by permission of ASM International, Materials Park, OH.)

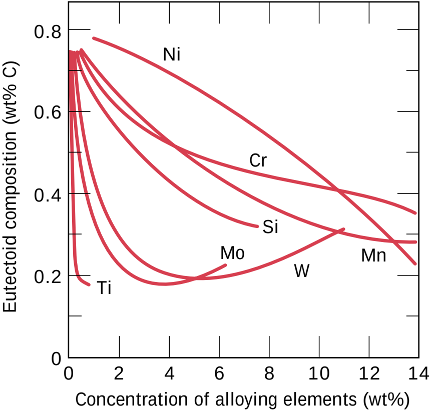

FIGURE 10.37 The dependence of eutectoid composition (wt% C) on alloy concentration for several alloying elements in steel. (From Edgar C. Bain, *Functions of the Alloying Elements in Steel*, American Society for Metals, 1939, p. 127.)

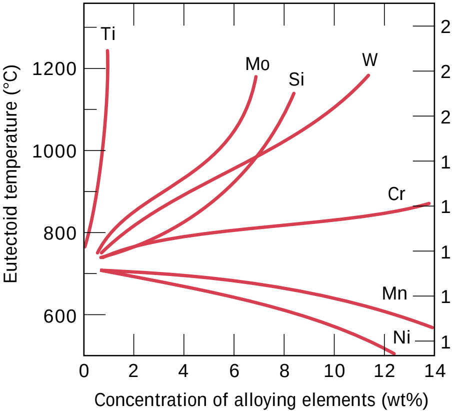

FIGURE 10.36 The dependence of eutectoid temperature on alloy concentration for several alloying elements in steel. (From Edgar C. Bain, *Functions of the Alloying Elements in Steel*, American Society for Metals, 1939, p. 127.)

CHAPTER 11

PHASE TRANSFORMATIONS

11.4 This problem gives us the value of **y** (0.40) at some time **t** (200 min), and also the value of **n** (2.5) for the recrystallization of an alloy at some temperature, and then asks that we determine the rate of recrystallization at this same temperature. It is first necessary to calculate the value of **k** in Equation (11.1) as

$$\begin{aligned} k &= -\frac{\ln(1-y)}{t^n} \\ &= -\frac{\ln(1-0.4)}{(200\ \text{min})^{2.5}} = 9.0 \times 10^{-7} \end{aligned}$$

At this point we want to compute $\mathbf{t_{0.5}}$, the value of **t** for **y** = 0.5, also using Equation (11.1). Thus

$$\begin{aligned} t_{0.5} &= \left[-\frac{\ln(1-0.5)}{k}\right]^{1/n} \\ &= \left[-\frac{\ln(1-0.5)}{9.0 \times 10^{-7}}\right]^{1/2.5} = 226.3\ \text{min} \end{aligned}$$

And, therefore, from Equation (11.2), the rate is just

$$\text{rate} = \frac{1}{t_{0.5}} = \frac{1}{226.3\ \text{min}} = 4.42 \times 10^{-3}\ (\text{min})^{-1}$$

11.7 This problem asks us to consider the percent recrystallized versus logarithm of time curves for copper shown in Figure 11.2.

(a) The rates at the different temperatures are determined using Equation (11.2), which rates are tabulated below:

Temperature (°C)	Rate $(\text{min})^{-1}$
135	0.105
119	4.4×10^{-2}
113	2.9×10^{-2}
102	1.25×10^{-2}
88	4.2×10^{-3}
43	3.8×10^{-5}

(b) These data are plotted below as ln rate versus the reciprocal of absolute temperature.

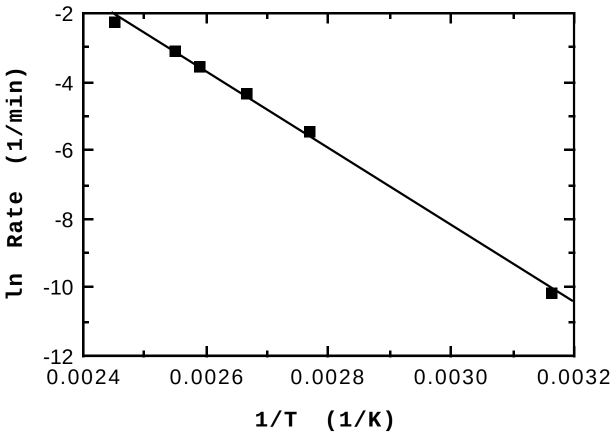

The activation energy, **Q**, is related to the slope of the line drawn through the data points as

$$Q = -\text{Slope}(R)$$

where **R** is the gas constant. The slope of this line is -1.126×10^4 K, and thus

$$\begin{aligned} Q &= -(-1.126 \times 10^4 \text{ K})(8.31 \text{ J/mol-K}) \\ &= 93{,}600 \text{ J/mol} \end{aligned}$$

(c) At room temperature (20°C), $1/\mathbf{T} = 3.41 \times 10^{-3}\ \text{K}^{-1}$. Extrapolation of the data in the plot to this $1/\mathbf{T}$ value gives

$$\ln(\text{rate}) \cong -12.8$$

or

$$\text{rate} \cong e^{-12.8} = 2.76 \times 10^{-6}\ (\text{min})^{-1}$$

But since

$$\text{rate} = \frac{1}{t_{0.5}}$$

then

$$\begin{aligned} t_{0.5} &= \frac{1}{\text{rate}} \cong \frac{1}{2.76 \times 10^{-6}\ (\text{min})^{-1}} \\ &\cong 3.62 \times 10^5 \text{ min} \cong 250 \text{ days} \end{aligned}$$

11.15 Below is shown an isothermal transformation diagram for a eutectoid iron-carbon alloy, with a time-temperature path that will produce (a) 100% coarse pearlite.

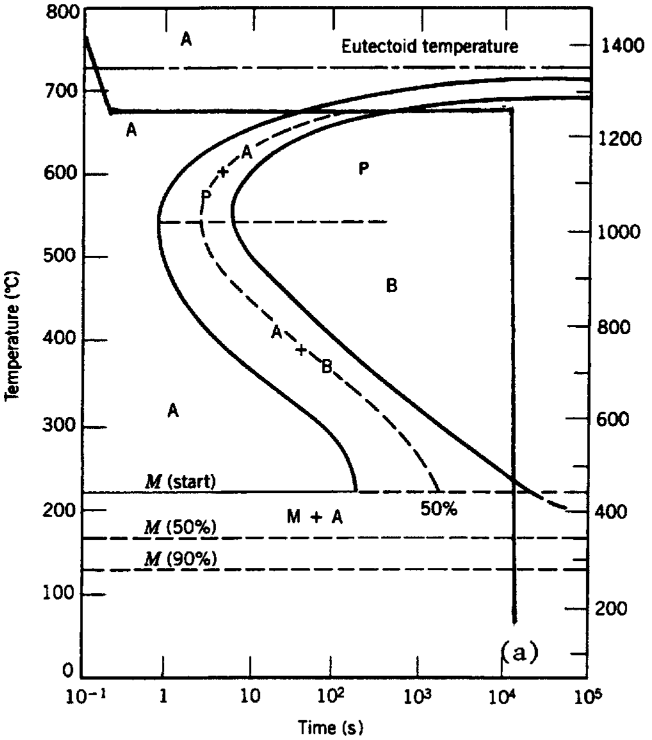

11.18 Below is shown an isothermal transformation diagram for a 0.45 wt% C iron-carbon alloy, with a time-temperature path that will produce (b) 50% fine pearlite and 50% bainite.

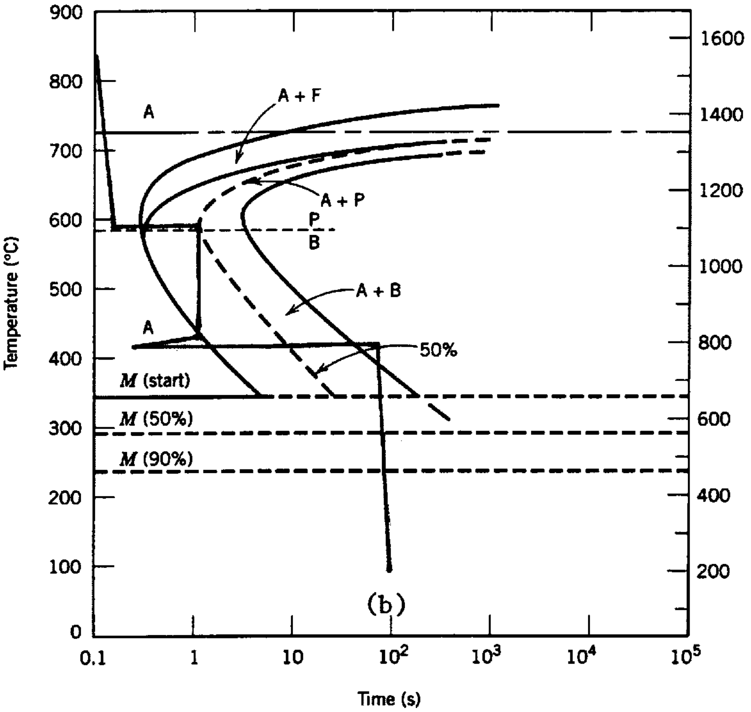

11.20* Below is shown a continuous cooling transformation diagram for a 1.13 wt% C iron-carbon alloy, with a continuous cooling path that will produce (a) fine pearlite and proeutectoid cementite.

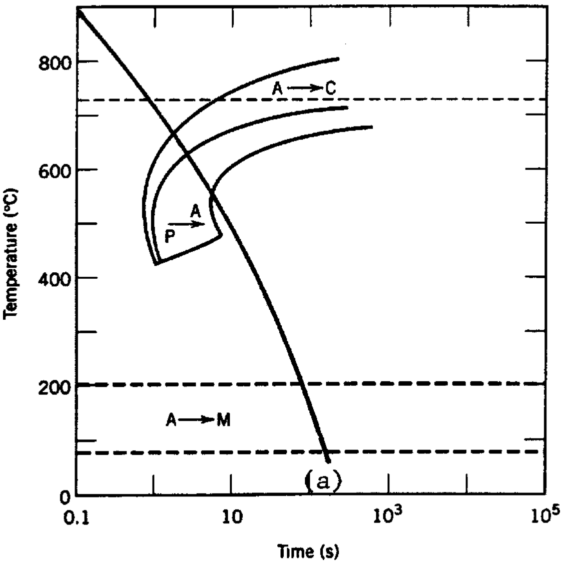

11.34 This problem asks for estimates of Rockwell hardness values for specimens of an iron-carbon alloy of eutectoid composition that have been subjected to some of the heat treatments described in Problem 11.14.

(b) The microstructural product of this heat treatment is 100% spheroidite. According to Figure 11.22(a) the hardness of a 0.76 wt% C alloy with spheroidite is about 87 HRB.

(g) The microstructural product of this heat treatment is 100% fine pearlite. According to Figure 11.22(a), the hardness of a 0.76 wt% C alloy consisting of fine pearlite is about 27 HRC.

11.37 For this problem we are asked to describe isothermal heat treatments required to yield specimens having several Brinell hardnesses.

(a) From Figure 11.22(a), in order for a 0.76 wt% C alloy to have a Rockwell hardness of 93 HRB, the microstructure must be coarse pearlite. Thus, utilizing the isothermal transformation diagram for this alloy, Figure 11.14, we must rapidly cool to a temperature at which coarse pearlite forms (i.e., to about 675°C), allowing the specimen to isothermally and completely transform to coarse pearlite. At this temperature an isothermal heat treatment for at least 200 s is required.

11.D1 This problem inquires as to the possibility of producing an iron-carbon alloy of eutectoid composition that has a minimum hardness of 90 HRB and a minimum ductility of 35%RA. If the alloy is possible, then the continuous cooling heat treatment is to be stipulated.

According to Figures 11.22(a) and (b), the following is a tabulation of Rockwell B hardnesses and percents reduction of area for fine and coarse pearlites and spheroidite for a 0.76 wt% C alloy.

Microstructure	HRB	%RA
Fine pearlite	>100	22
Coarse pearlite	93	29
Spheroidite	88	68

Therefore, none of the microstructures meets both of these criteria. Both fine and coarse pearlites are hard enough, but lack the required ductility. Spheroidite is sufficiently ductile, but does not meet the hardness criterion.

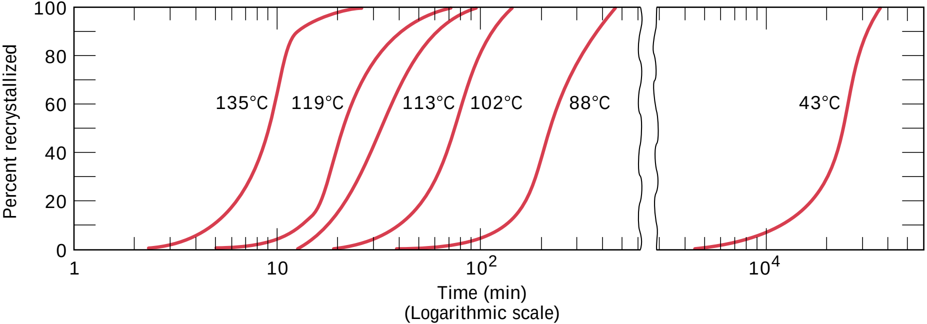

FIGURE 11.2 Percent recrystallization as a function of time and at constant temperature for pure copper. (Reprinted with permission from *Metallurgical Transactions*, Vol. 188, 1950, a publication of The Metallurgical Society of AIME, Warrendale, Pennsylvania. Adapted from B. F. Decker and D. Harker, ‘‘Recrystallization in Rolled Copper,’’ *Trans. AIME*, **188,** 1950, p. 888.)

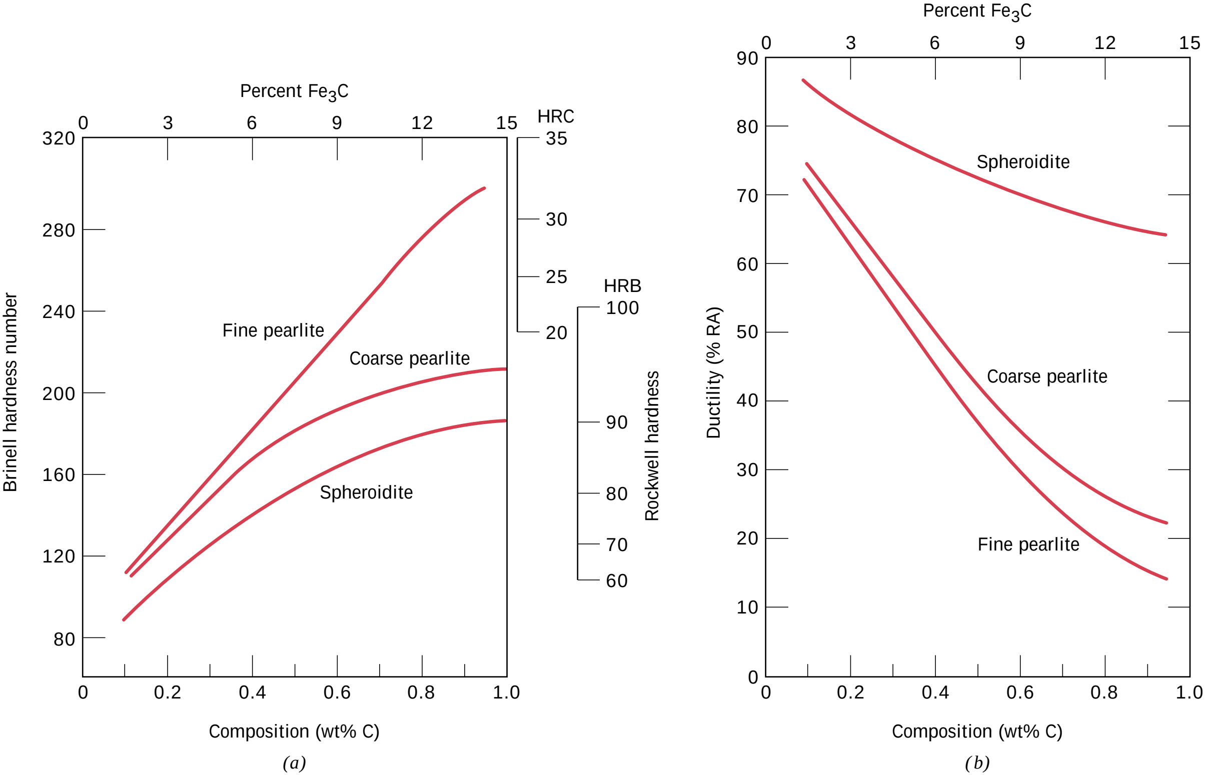

Figure 11.22 (*a*) Brinell and Rockwell hardness as a function of carbon concentration for plain carbon steels having fine and coarse pearlite as well as spheroidite microstructures. (*b*) Ductility (%RA) as a function of carbon concentration for plain carbon steels having fine and coarse pearlite as well as spheroidite microstructures. (Data taken from *Metals Handbook: Heat Treating,* Vol. 4, 9th edition, V. Masseria, Managing Editor, American Society for Metals, 1981, pp. 9 and 17.)

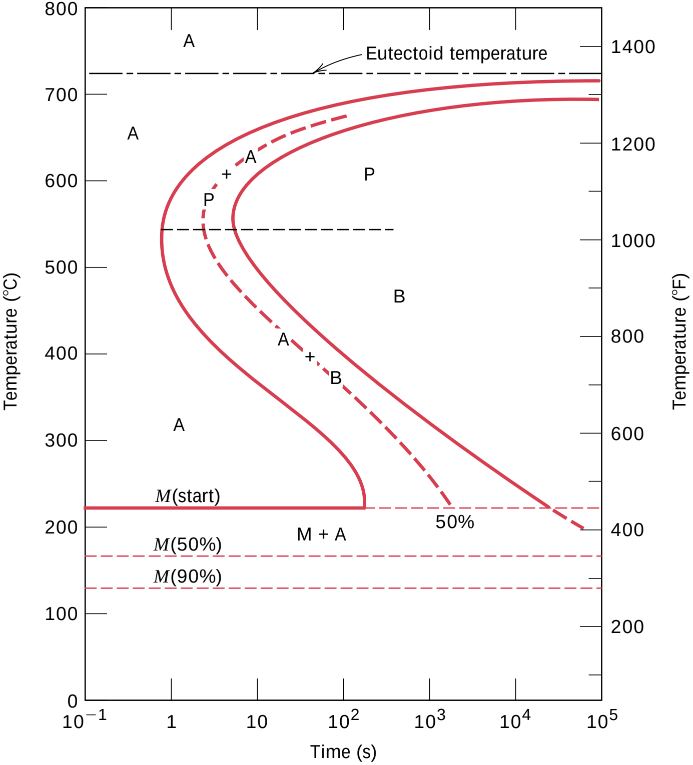

Figure 11.14 The complete isothermal transformation diagram for an iron–carbon alloy of eutectoid composition: A, austenite; B, bainite; M, martensite; P, pearlite.

CHAPTER 12

ELECTRICAL PROPERTIES

12.5 (a) In order to compute the resistance of this copper wire it is necessary to employ Equations (12.2) and (12.4). Solving for the resistance in terms of the conductivity,

$$R = \frac{\rho l}{A} = \frac{l}{\sigma A}$$

From Table 12.1, the conductivity of copper is 6.0×10^7 (Ω-m)$^{-1}$, and

$$R = \frac{l}{\sigma A} = \frac{2\text{ m}}{[6.0 \times 10^7\ (\Omega\text{-m})^{-1}](\pi)\left(\frac{3 \times 10^{-3}\text{ m}}{2}\right)^2}$$

$$= 4.7 \times 10^{-3}\ \Omega$$

(b) If **V** = 0.05 V then, from Equation (12.1)

$$I = \frac{V}{R} = \frac{0.05\text{ V}}{4.7 \times 10^{-3}\ \Omega} = 10.6\text{ A}$$

(c) The current density is just

$$J = \frac{I}{A} = \frac{I}{\pi\left(\frac{d}{2}\right)^2} = \frac{10.6\text{ A}}{\pi\left(\frac{3 \times 10^{-3}\text{ m}}{2}\right)^2} = 1.5 \times 10^6\text{ A/m}^2$$

(d) The electric field is just

$$E = \frac{V}{l} = \frac{0.05\text{ V}}{2\text{ m}} = 2.5 \times 10^{-2}\text{ V/m}$$

12.13 (a) The number of free electrons per cubic meter for copper at room temperature may be computed using Equation (12.8) as

$$n = \frac{\sigma}{|e|\mu_e}$$

$$= \frac{6.0 \times 10^7\ (\Omega\text{-m})^{-1}}{(1.602 \times 10^{-19}\text{ C})(0.0030\text{ m}^2/\text{V-s})}$$

$$= 1.25 \times 10^{29}\text{ m}^{-3}$$

(b) In order to calculate the number of free electrons per copper atom, we must first determine the number of copper atoms per cubic meter, $\mathbf{N_{Cu}}$. From Equation (5.2)

$$N_{Cu} = \frac{N_A \rho'}{A_{Cu}}$$

Note: in the above expression, density is represented by ρ' in order to avoid confusion with resistivity which is designated by ρ. Thus

$$N_{Cu} = \frac{(6.023 \times 10^{23} \text{ atoms/mol})(8.94 \text{ g/cm}^3)(10^6 \text{ cm}^3/\text{m}^3)}{63.55 \text{ g/mol}}$$

$$= 8.47 \times 10^{28} \text{ m}^{-3}$$

The number of free electrons per copper atom is just

$$\frac{n}{N} = \frac{1.25 \times 10^{29} \text{ m}^{-3}}{8.47 \times 10^{28} \text{ m}^{-3}} = 1.48$$

12.18 This problem asks for us to compute the room-temperature conductivity of a two-phase Cu-Sn alloy. It is first necessary for us to determine the volume fractions of the α and ε phases, after which the resistivity (and subsequently, the conductivity) may be calculated using Equation (12.12). Weight fractions of the two phases are first calculated using the phase diagram information provided in the problem.

We might represent the phase diagram near room temperature as shown below.

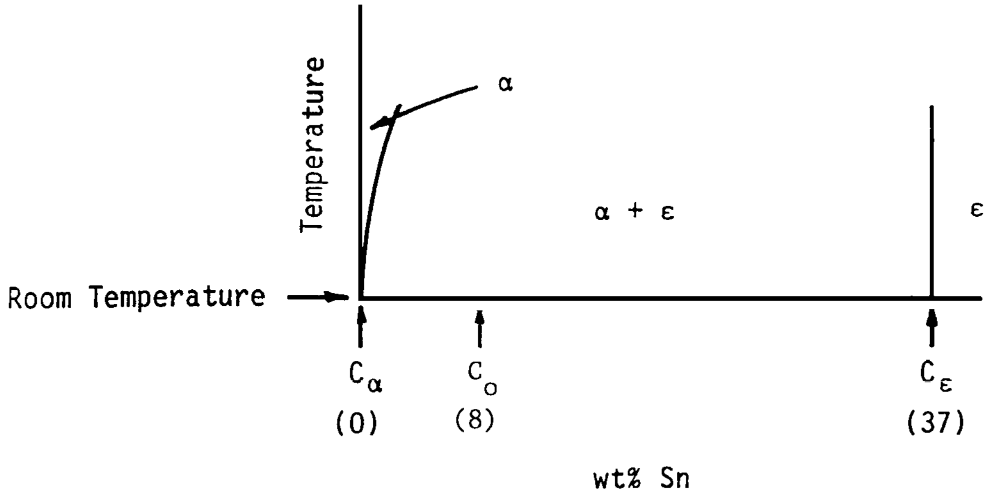

Applying the lever rule to this situation

$$W_\alpha = \frac{C_\varepsilon - C_o}{C_\varepsilon - C_\alpha} = \frac{37 - 8}{37 - 0} = 0.784$$

$$W_\varepsilon = \frac{C_o - C_\alpha}{C_\varepsilon - C_\alpha} = \frac{8 - 0}{37 - 0} = 0.216$$

We must now convert these mass fractions into volume fractions using the phase densities given in the problem. (Note: in the following expressions, density is represented by ρ' in order to avoid confusion with resistivity which is designated by ρ.) Utilization of Equations (10.6a) and (10.6b) leads to

$$
\begin{aligned}
V_\alpha &= \frac{\dfrac{W_\alpha}{\rho'_\alpha}}{\dfrac{W_\alpha}{\rho'_\alpha} + \dfrac{W_\varepsilon}{\rho'_\varepsilon}} \\
&= \frac{\dfrac{0.784}{8.94\text{ g/cm}^3}}{\dfrac{0.784}{8.94\text{ g/cm}^3} + \dfrac{0.216}{8.25\text{ g/cm}^3}} \\
&= 0.770
\end{aligned}
$$

$$
\begin{aligned}
V_\varepsilon &= \frac{\dfrac{W_\varepsilon}{\rho'_\varepsilon}}{\dfrac{W_\alpha}{\rho'_\alpha} + \dfrac{W_\varepsilon}{\rho'_\varepsilon}} \\
&= \frac{\dfrac{0.216}{8.25\text{ g/cm}^3}}{\dfrac{0.784}{8.94\text{ g/cm}^3} + \dfrac{0.216}{8.25\text{ g/cm}^3}} \\
&= 0.230
\end{aligned}
$$

Now, using Equation (12.12)

$$
\begin{aligned}
\rho &= \rho_\alpha V_\alpha + \rho_\varepsilon V_\varepsilon \\
&= (1.88 \times 10^{-8}\ \Omega\text{-m})(0.770) + (5.32 \times 10^{-7}\ \Omega\text{-m})(0.230) \\
&= 1.368 \times 10^{-7}\ \Omega\text{-m}
\end{aligned}
$$

Finally, for the conductivity

$$\sigma = \frac{1}{\rho} = \frac{1}{1.368 \times 10^{-7}\ \Omega\text{-m}} = 7.31 \times 10^6\ (\Omega\text{-m})^{-1}$$

12.30 (a) In this problem, for a Si specimen, we are given **p** and σ, while $\mu_\mathbf{h}$ and $\mu_\mathbf{e}$ are included in Table 12.2. In order to solve for **n** we must use Equation (12.13), which, after rearrangement, leads to

$$
\begin{aligned}
n &= \frac{\sigma - p|e|\mu_h}{|e|\mu_e} \\
&= \frac{10^3\ (\Omega\text{-m})^{-1} - (1.0 \times 10^{23}\ \text{m}^{-3})(1.602 \times 10^{-19}\ \text{C})(0.05\ \text{m}^2/\text{V-s})}{(1.602 \times 10^{-19}\ \text{C})(0.14\ \text{m}^2/\text{V-s})} \\
&= 8.9 \times 10^{21}\ \text{m}^{-3}
\end{aligned}
$$

(b) This material is **p**-type extrinsic since **p** (1.0×10^{23} m^{-3}) is greater than **n** (8.9×10^{21} m^{-3}).

12.38 For this problem, we are given conductivity values at two different temperatures for an intrinsic semiconductor, and are then asked to determine its band gap energy. It is possible, using

Equation (12.18), to set up two independent equations with **C** and $\mathbf{E_g}$ as unknowns. At 20°C

$$\ln \sigma = C - \frac{E_g}{2kT}$$

$$\ln[1.0\,(\Omega\text{-m})^{-1}] = C - \frac{E_g}{(2)(8.62 \times 10^{-5}\ \text{eV/atom-K})(293\ \text{K})}$$

or

$$C = 19.80E_g$$

At 373 K

$$\ln[500\,(\Omega\text{-m})^{-1}] = C - \frac{E_g}{(2)(8.62 \times 10^{-5}\ \text{eV/atom-K})(373\ \text{K})}$$

$$6.21 = C - 15.55E_g$$

From these two expressions

$$E_g = 1.46\ \text{eV}$$

12.45* In this problem we are asked to determine the magnetic field required to produce a Hall voltage of -1.0×10^{-7} V, given that $\sigma = 1.5 \times 10^{7}\ (\Omega\text{-m})^{-1}$, $\mu_\mathbf{e} = 0.0020\ \text{m}^2\text{/V-s}$, $\mathbf{I_x} = 45$ A, and $\mathbf{d} = 35$ mm. Combining Equations (12.21) and (12.23b), and after solving for $\mathbf{B_z}$, we get

$$\begin{aligned} B_z &= \frac{|V_H|\sigma d}{I_x \mu_e} \\ &= \frac{(|-1.0 \times 10^{-7}\ \text{V}|)[1.5 \times 10^{7}\ (\Omega\text{-m})^{-1}](35 \times 10^{-3}\ \text{m})}{(45\ \text{A})(0.0020\ \text{m}^2\text{/V-s})} \\ &= 0.58\ \text{tesla} \end{aligned}$$

12.52* We want to compute the plate spacing of a parallel-plate capacitor as the dielectric constant is increased from 2.5 to 4.0, while maintaining the capacitance constant. Combining Equations (12.29) and (12.30) yields

$$C = \frac{\varepsilon_r \varepsilon_o A}{l}$$

Now, let us use the subscripts **1** and **2** to denote the initial and final states, respectively. Since $\mathbf{C_1} = \mathbf{C_2}$, then

$$\frac{\varepsilon_{r1}\varepsilon_o A}{l_1} = \frac{\varepsilon_{r2}\varepsilon_o A}{l_2}$$

And, solving for $\mathbf{l_2}$

$$l_2 = \frac{\varepsilon_{r2} l_1}{\varepsilon_{r1}} = \frac{(4.0)(1\ \text{mm})}{2.5} = 1.6\ \text{mm}$$

12.58* (a) We want to solve for the voltage when $\mathbf{Q} = 3.5 \times 10^{-11}$ C, $\mathbf{A} = 160\ \text{mm}^2$, $\mathbf{l} = 3.5$ mm, and $\varepsilon_\mathbf{r} = 5.0$. Combining Equations (12.27), (12.29), and (12.30) yields

$$\frac{Q}{V} = \varepsilon_r \varepsilon_o \frac{A}{l}$$

And, solving for **V**

$$
\begin{aligned}
V &= \frac{Ql}{\varepsilon_r \varepsilon_o A} \\
&= \frac{(3.5 \times 10^{-11}\ \mathrm{C})(3.5 \times 10^{-3}\ \mathrm{m})}{(5.0)(8.85 \times 10^{-12}\ \mathrm{F/m})(160\ \mathrm{mm}^2)(1\ \mathrm{m}^2/10^6\ \mathrm{mm}^2)} \\
&= 17.3\ \mathrm{V}
\end{aligned}
$$

(b) For this same capacitor, if a vacuum is used

$$
\begin{aligned}
V &= \frac{Ql}{\varepsilon_o A} \\
&= \frac{(3.5 \times 10^{-11}\ \mathrm{C})(3.5 \times 10^{-3}\ \mathrm{m})}{(8.85 \times 10^{-12}\ \mathrm{F/m})(160 \times 10^{-6}\ \mathrm{m}^2)} \\
&= 86.5\ \mathrm{V}
\end{aligned}
$$

(e) The polarization is determined using Equations (12.35) and (12.6) as

$$
\begin{aligned}
P &= \varepsilon_o(\varepsilon_r - 1)\frac{V}{l} \\
&= \frac{(8.85 \times 10^{-12}\ \mathrm{F/m})(5.0 - 1)(17.3\ \mathrm{V})}{3.5 \times 10^{-3}\ \mathrm{m}} \\
&= 1.75 \times 10^{-7}\ \mathrm{C/m}^2
\end{aligned}
$$

12.D2 This problem asks that we determine the electrical conductivity of an 80 wt% Cu-20 wt% Zn alloy at −150°C using information contained in Figures 12.8 and 12.35. In order to solve this problem it is necessary to employ Equation (12.9) which is of the form

$$\rho_{\mathrm{total}} = \rho_t + \rho_i$$

since it is assumed that the alloy is undeformed. Let us first determine the value of $\boldsymbol{\rho_i}$ at room temperature (25°C), a value which will be independent of temperature. From Figure (12.8), at 25°C and for pure Cu, $\boldsymbol{\rho_t(25)} = 1.75 \times 10^{-8}\ \Omega$-m. Now, since it is assumed that the curve in Figure 12.35 was generated also at room temperature, we may take ρ as $\boldsymbol{\rho_{\mathrm{total}}(25)}$ at 80 wt% Cu-20 wt% Zn which has a value of $5.3 \times 10^{-8}\ \Omega$-m. Thus

$$
\begin{aligned}
\rho_i &= \rho_{\mathrm{total}}(25) - \rho_t(25) \\
&= 5.3 \times 10^{-8}\ \Omega\text{-m} - 1.75 \times 10^{-8}\ \Omega\text{-m} = 3.55 \times 10^{-8}\ \Omega\text{-m}
\end{aligned}
$$

Finally, we may determine the resistivity at −150°C, $\boldsymbol{\rho_{\mathrm{total}}(-150)}$, by taking the resistivity of pure Cu at −150°C from Figure 12.8, which gives us $\boldsymbol{\rho_t(-150)} = 0.55 \times 10^{-8}\ \Omega$-m. Therefore

$$
\begin{aligned}
\rho_{\mathrm{total}}(-150) &= \rho_i + \rho_t(-150) \\
&= 3.55 \times 10^{-8}\ \Omega\text{-m} + 0.55 \times 10^{-8}\ \Omega\text{-m} = 4.10 \times 10^{-8}\ \Omega\text{-m}
\end{aligned}
$$

And, using Equation (12.4) the conductivity is calculated as

$$\sigma = \frac{1}{\rho} = \frac{1}{4.10 \times 10^{-8}\ \Omega\text{-m}} = 2.44 \times 10^{7}\ (\Omega\text{-m})^{-1}$$

Table 12.1 Room-Temperature Electrical Conductivities for Nine Common Metals and Alloys

Metal	*Electrical Conductivity* $[(\Omega\text{-}m)^{-1}]$
Silver	6.8×10^7
Copper	6.0×10^7
Gold	4.3×10^7
Aluminum	3.8×10^7
Iron	1.0×10^7
Brass (70 Cu–30 Zn)	1.6×10^7
Platinum	0.94×10^7
Plain carbon steel	0.6×10^7
Stainless steel	0.2×10^7

Table 12.2 **Band Gap Energies, Electron and Hole Mobilities, and Intrinsic Electrical Conductivities at Room Temperature for Semiconducting Materials**

Material	*Band Gap (eV)*	*Electrical Conductivity* $[(\Omega\text{-}m)^{-1}]$	*Electron Mobility* $(m^2/V\text{-}s)$	*Hole Mobility* $(m^2/V\text{-}s)$
		Elemental		
Si	1.11	4×10^{-4}	0.14	0.05
Ge	0.67	2.2	0.38	0.18
		III–V Compounds		
GaP	2.25	—	0.05	0.002
GaAs	1.42	10^{-6}	0.85	0.45
InSb	0.17	2×10^{4}	7.7	0.07
		II–VI Compounds		
CdS	2.40	—	0.03	—
ZnTe	2.26	—	0.03	0.01

Chapter 12 / Electrical Properties

12.13 THE HALL EFFECT

For some material, it is on occasion desired to determine its majority charge carrier type, concentration, and mobility. Such determinations are not possible from a simple electrical conductivity measurement; a **Hall effect** experiment must also be conducted. This Hall effect is a result of the phenomenon whereby a magnetic field applied perpendicular to the direction of motion of a charged particle exerts a force on the particle perpendicular to both the magnetic field and the particle motion directions.

In demonstrating the Hall effect, consider the specimen geometry shown in Figure 12.18, a parallelepiped specimen having one corner situated at the origin of a Cartesian coordinate system. In response to an externally applied electric field, the electrons and/or holes move in the x direction and give rise to a current I_x. When a magnetic field is imposed in the positive z direction (denoted as B_z), the resulting force brought to bear on the charge carriers will cause them to be deflected in the y direction—holes (positively charged carriers) to the right specimen face and electrons (negatively charged carriers) to the left face, as indicated in the figure. Thus, a voltage, termed the *Hall voltage* V_H, will be established in the y direction. The magnitude of V_H will depend on I_x, B_z, and the specimen thickness d as follows:

$$V_H = \frac{R_H I_x B_z}{d} \tag{12.21}$$

In this expression R_H is termed the *Hall coefficient*, which is a constant for a given material. For metals, wherein conduction is by electrons, R_H is negative and equal to

$$R_H = \frac{1}{n|e|} \tag{12.22}$$

Thus, n may be determined, inasmuch as R_H may be measured using Equation 12.21 and the magnitude of e, the charge on an electron, is known.

Furthermore, from Equation 12.8, the electron mobility μ_e is just

$$\mu_e = \frac{\sigma}{n|e|} \tag{12.23a}$$

Or, using Equation 19.22,

$$\mu_e = |R_H|\sigma \tag{12.23b}$$

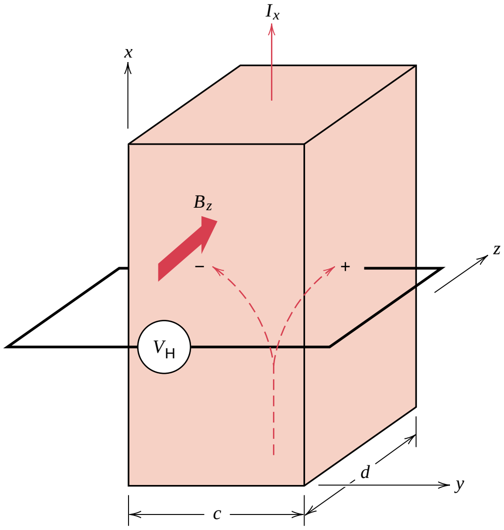

FIGURE 12.18 Schematic demonstration of the Hall effect. Positive and/or negative charge carriers that are part of the I_x current are deflected by the magnetic field B_z and give rise to the Hall voltage, V_H.

Thus, the magnitude of μ_e may also be determined if the conductivity σ has also been measured.

For semiconducting materials, the determination of majority carrier type and computation of carrier concentration and mobility are more complicated and will not be discussed here.

EXAMPLE PROBLEM 12.4

The electrical conductivity and electron mobility for aluminum are 3.8×10^7 $(\Omega\text{-m})^{-1}$ and 0.0012 m^2/V-s, respectively. Calculate the Hall voltage for an aluminum specimen that is 15 mm thick for a current of 25 A and a magnetic field of 0.6 tesla (imposed in a direction perpendicular to the current).

SOLUTION

The Hall voltage V_H may be determined using Equation 12.21. However, it first becomes necessary to compute the Hall coefficient (R_H) from Equation 12.23b as

$$R_H = -\frac{\mu_e}{\sigma}$$

$$= -\frac{0.0012 \text{ m}^2/\text{V-s}}{3.8 \times 10^7 \, (\Omega\text{-m})^{-1}} = -3.16 \times 10^{-11} \text{ V-m/A-tesla}$$

Now, employment of Equation 12.21 leads to

$$V_H = \frac{R_H I_x B_z}{d}$$

$$= \frac{(-3.16 \times 10^{-11} \text{ V-m/A-tesla})(25 \text{ A})(0.6 \text{ tesla})}{15 \times 10^{-3} \text{ m}}$$

$$= -3.16 \times 10^{-8} \text{ V}$$

12.14 SEMICONDUCTOR DEVICES

The unique electrical properties of semiconductors permit their use in devices to perform specific electronic functions. Diodes and transistors, which have replaced old-fashioned vacuum tubes, are two familiar examples. Advantages of semiconductor devices (sometimes termed solid-state devices) include small size, low power consumption, and no warmup time. Vast numbers of extremely small circuits, each consisting of numerous electronic devices, may be incorporated onto a small silicon chip. The invention of semiconductor devices, which has given rise to miniaturized circuitry, is responsible for the advent and extremely rapid growth of a host of new industries in the past few years.

THE *p–n* RECTIFYING JUNCTION

A rectifier, or **diode**, is an electronic device that allows the current to flow in one direction only; for example, a rectifier transforms an alternating current into direct current. Before the advent of the *p–n* junction semiconductor rectifier, this operation was carried out using the vacuum tube diode. The *p–n* **rectifying junction** is constructed from a single piece of semiconductor that is doped so as to be *n*-type on one side and *p*-type on the other (Figure 12.19*a*). If pieces of *n*- and *p*-type materials are joined together, a poor rectifier results, since the presence of a surface between the two sections renders the device very inefficient. Also, single crystals of semiconducting materials must be used in all devices because electronic phenomena that are deleterious to operation occur at grain boundaries.

Before the application of any potential across the *p–n* specimen, holes will be the dominant carriers on the *p*-side, and electrons will predominate in the *n*-region,

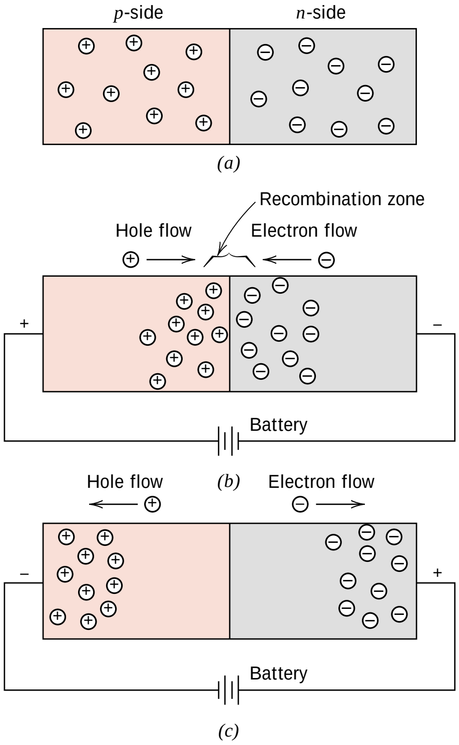

FIGURE 12.19 For a *p–n* rectifying junction, representations of electron and hole distributions for (*a*) no electrical potential, (*b*) forward bias, and (*c*) reverse bias.

as illustrated in Figure 12.19*a*. An external electric potential may be established across a *p*–*n* junction with two different polarities. When a battery is used, the positive terminal may be connected to the *p*-side, and the negative terminal to the *n*-side; this is referred to as a **forward bias.** The opposite polarity (minus to *p* and plus to *n*) is termed **reverse bias.**

The response of the charge carriers to the application of a forward-biased potential is demonstrated in Figure 12.19*b*. The holes on the *p*-side and the on the *n*-side are attracted to the junction. As electrons and holes encounter one another near the junction, they continuously recombine and annihilate one another, according to

$$\text{electron} + \text{hole} \longrightarrow \text{energy} \tag{12.24}$$

Thus for this bias, large numbers of charge carriers flow across the semiconductor and to the junction, as evidenced by an appreciable current and a low resistivity. The current–voltage characteristics for forward bias are shown on the right-hand half of Figure 12.20.

For reverse bias (Figure 12.19*c*), both holes and electrons, as majority carriers, are rapidly drawn away from the junction; this separation of positive and negative charges (or polarization) leaves the junction region relatively free of mobile charge carriers. Recombination will not occur to any appreciable extent, so that the junction is now highly insulative. Figure 12.20 also illustrates the current–voltage behavior for reverse bias.

The rectification process in terms of input voltage and output current is demonstrated in Figure 12.21. Whereas voltage varies sinusoidally with time (Figure 12.21*a*), maximum current flow for reverse bias voltage I_R is extremely small in comparison to that for forward bias I_F (Figure 12.21*b*). Furthermore, correspondence between I_F and I_R and the imposed maximum voltage ($\pm V_0$) is noted in Figure 12.20.

At high reverse bias voltages, sometimes on the order of several hundred volts, large numbers of charge carriers (electrons and holes) are generated. This gives rise to a very abrupt increase in current, a phenomenon known as *breakdown,* also shown in Figure 12.20, and discussed in more detail in Section 12.21.

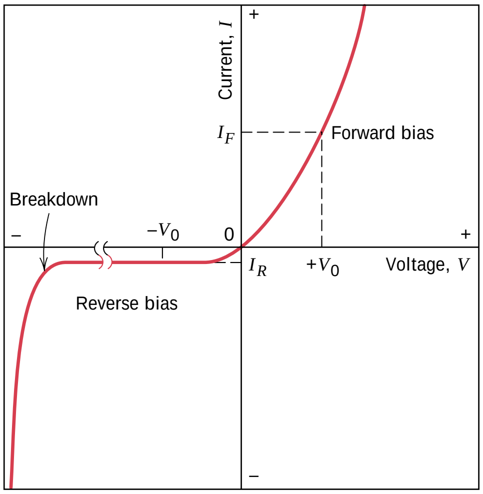

FIGURE 12.20 The current–voltage characteristics of a *p*–*n* junction for forward and reverse biases. The phenomenon of breakdown is also shown.

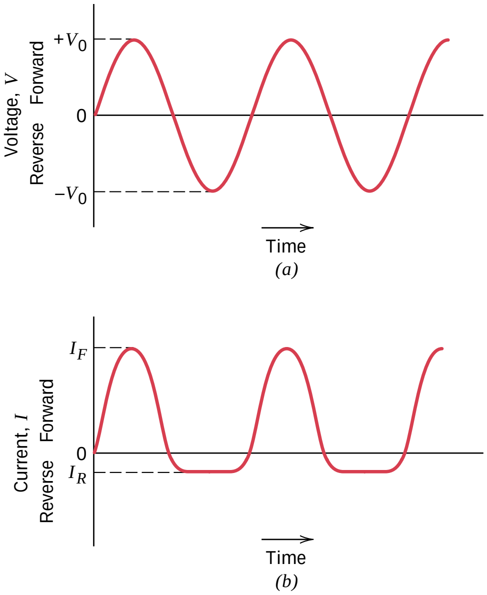

Figure 12.21 (*a*) Voltage versus time for the input to a *p–n* rectifying junction. (*b*) Current versus time, showing rectification of voltage in (*a*) by a *p–n* rectifying junction having the voltage–current characteristics shown in Figure 12.20.

THE TRANSISTOR

Transistors, which are extremely important semiconducting devices in today's microelectronic circuitry, are capable of two primary types of function. First, they can perform the same operation as their vacuum tube precursor, the triode; that is, they can amplify an electrical signal. In addition, they serve as switching devices in computers for the processing and storage of information. The two major types are the **junction** (or bimodal) **transistor** and the *metal-oxide-semiconductor field-effect transistor* (abbreviated as **MOSFET**).

Junction Transistors

The junction transistor is composed of two *p–n* junctions arranged back to back in either the *n–p–n* or the *p–n–p* configuration; the latter variety is discussed here. Figure 12.22 is a schematic representation of a *p–n–p* junction transistor along with

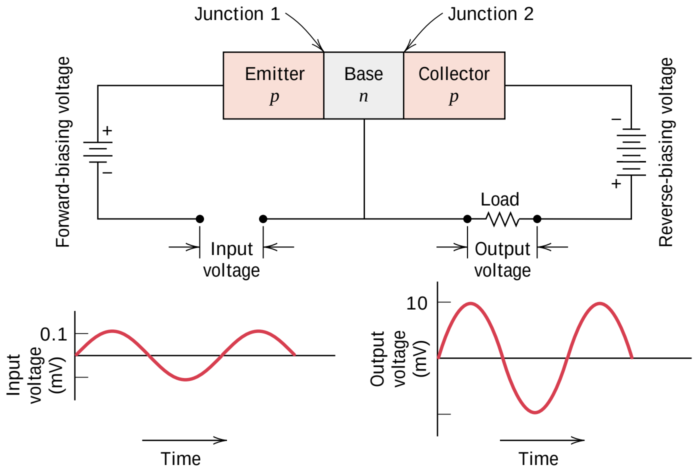
Junction 1
Junction 2
Emitter
p
Base
n
Collector
p
Forward-biasing voltage
Reverse-biasing voltage
+
−
−
+
Load
Input voltage
Output voltage
Input voltage (mV)
0.1
Time
Output voltage (mV)
10
Time

Figure 12.22 Schematic diagram of a *p–n–p* junction transistor and its associated circuitry, including input and output voltage–time characteristics showing voltage amplification. (Adapted from A. G. Guy, *Essentials of Materials Science*, McGraw-Hill Book Company, New York, 1976.)

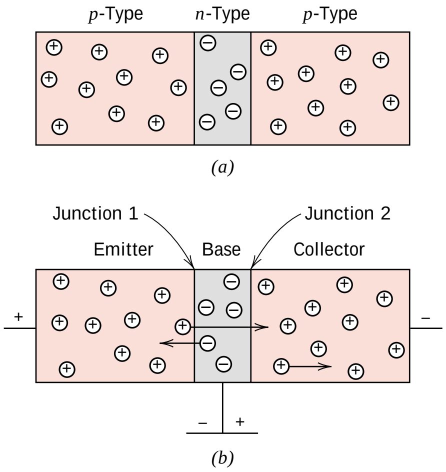

Figure 12.23 For a junction transistor (p–n–p type), the distributions and directions of electron and hole motion (*a*) when no potential is applied and (*b*) with appropriate bias for voltage amplification.

its attendant circuitry. A very thin *n*-type *base* region is sandwiched in between *p*-type *emitter* and *collector* regions. The circuit that includes the emitter–base junction (junction 1) is forward biased, whereas a reverse bias voltage is applied across the base–collector junction (junction 2).

Figure 12.23 illustrates the mechanics of operation in terms of the motion of charge carriers. Since the emitter is *p*-type and junction 1 is forward biased, large numbers of holes enter the base region. These injected holes are minority carriers in the *n*-type base, and some will combine with the majority electrons. However, if the base is extremely narrow and the semiconducting materials have been properly prepared, most of these holes will be swept through the base without recombination, then across junction 2 and into the *p*-type collector. The holes now become a part of the emitter–collector circuit. A small increase in input voltage within the emitter–base circuit produces a large increase in current across junction 2. This large increase in collector current is also reflected by a large increase in voltage across the load resistor, which is also shown in the circuit (Figure 12.22). Thus, a voltage signal that passes through a junction transistor experiences amplification; this effect is also illustrated in Figure 12.22 by the two voltage–time plots.

Similar reasoning applies to the operation of an n–p–n transistor, except that electrons instead of holes are injected across the base and into the collector.

The MOSFET

One variety of MOSFET consists of two small islands of *p*-type semiconductor that are created within a substrate of *n*-type silicon, as shown in cross section in Figure 12.24; the islands are joined by a narrow *p*-type channel. Appropriate metal connections (source and drain) are made to these islands; an insulating layer of silicon dioxide is formed by the surface oxidation of the silicon. A final connector (gate) is then fashioned onto the surface of this insulating layer.

The operation of a MOSFET differs from that of the junction transistor in that a single type of charge carrier (either electron or hole) is active. The conductivity of the channel is varied by the presence of an electric field imposed on the gate. For example, imposition of a positive field on the gate will drive charge carriers (in this case holes) out of the channel, thereby reducing the electrical conductivity. Thus, a small alteration in the field at the gate will

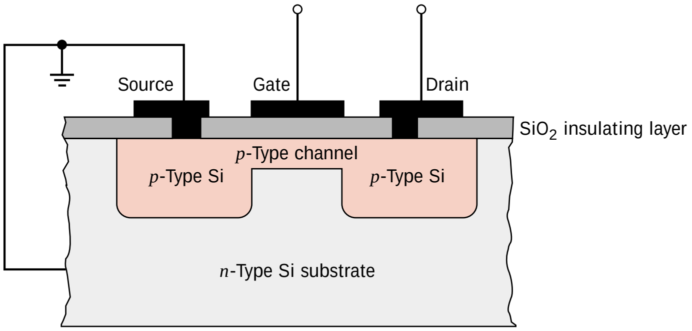

FIGURE 12.24 Schematic cross-sectional view of a MOSFET transistor.

produce a relatively large variation in current between the source and the drain. In some respects, then, the operation of a MOSFET is very similar to that described for the junction transistor. The primary difference is that the gate current is exceedingly small in comparison to the base current of a junction transistor. MOSFETs are, therefore, used where the signal sources to be amplified cannot sustain an appreciable current.

Semiconductors in Computers

In addition to their ability to amplify an imposed electrical signal, transistors and diodes may also act as switching devices, a feature utilized for arithmetic and logical operations, and also for information storage in computers. Computer numbers and functions are expressed in terms of a binary code (i.e., numbers written to the base 2). Within this framework, numbers are represented by a series of two states (sometimes designated 0 and 1). Now, transistors and diodes within a digital circuit operate as switches that also have two states—on and off, or conducting and nonconducting; ''off'' corresponds to one binary number state, and ''on'' to the other. Thus, a single number may be represented by a collection of circuit elements containing transistors that are appropriately switched.

MICROELECTRONIC CIRCUITRY

During the past few years, the advent of microelectronic circuitry, where thousands of electronic components and circuits are incorporated into a very small space, has revolutionized the field of electronics. This revolution was precipitated, in part, by aerospace technology, which necessitated computers and electronic devices that were small and had low power requirements. As a result of refinement in processing and fabrication techniques, there has been an astonishing depreciation in the cost of integrated circuitry. Consequently, at the time of this writing, personal computers are affordable to a large segment of the population in the United States. Also, the use of **integrated circuits** has become infused into many other facets of our lives—calculators, communications, watches, industrial production and control, and all phases of the electronics industry.

Inexpensive microelectronic circuits are mass produced by using some very ingenious fabrication techniques. The process begins with the growth of relatively large cylindrical single crystals of high-purity silicon from which thin circular wafers are cut. Many microelectronic or integrated circuits, sometimes called ''chips,'' are prepared on a single wafer; a photograph of one such wafer containing numerous chips is shown in Figure 20.20. A chip is rectangular,

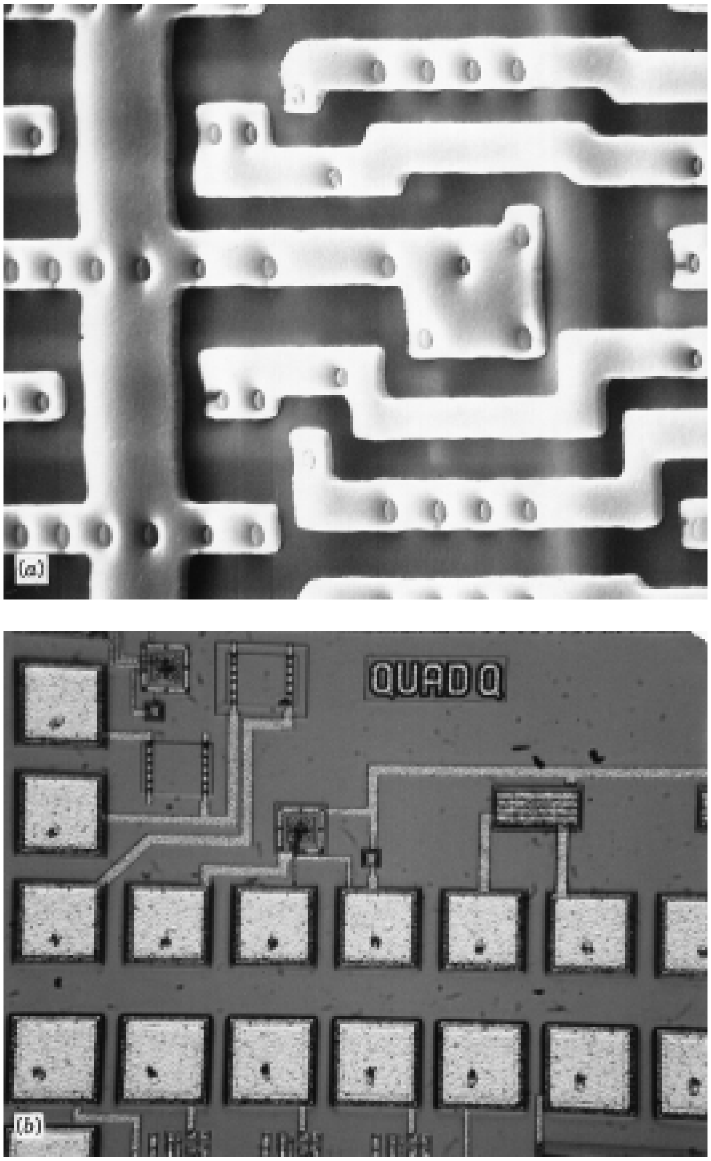

Figure 12.25 (*a*) Scanning electron micrograph showing a small region of a microprocessing chip (a 0.5 MB selected address device). The narrow, white regions are an aluminum top layer that serves as the wiring for this device. The gray regions are diffusion-layer doped silicon that have been coated with an interlayer dielectric. Approximately 2000×. (*b*) An optical photomicrograph showing a portion of a circuit that is used to test microprocessing chips. The narrow, light regions are aluminum connectors, while the white, square areas are test pads (semiconductor devices); test circuits (also composed of semiconductor devices) appear in the upper left-hand corner of the photograph. Approximately 50×. (Both photographs courtesy of Nick Gonzales of National Semiconductor Corporation, West Jordan, Utah.)

typically on the order of 6 mm ($\frac{1}{4}$ in.) on a side and contains thousands of circuit elements: diodes, transistors, resistors, and capacitors. One such microprocessor chip is shown in its entirety in Figure 20.22*b*; also shown are the numerous electrical leads that are used to connect this chip to its leadframe, which in turn is bonded to a printed circuit board. Enlarged photographs of microprocessor chips at different magnifications are presented in Figures 12.25*a* and 12.25*b*; these micrographs reveal the intricacy of integrated circuits. At this time, 175,000,000 component chips are being produced, and memory capabilities currently double about every 12 months.

Microelectronic circuits consist of many layers that lie within or are stacked on top of the silicon wafer in a precisely detailed pattern. Using photolithographic techniques, for each layer, very small elements are masked in accordance with a microscopic pattern. Circuit elements are constructed by the selective introduction of specific materials (by diffusion or ion implantation) into unmasked regions to create localized *n*-type, *p*-type, high-resistivity, or conductive areas. This procedure is repeated layer by layer until the total integrated circuit has been fabricated, as illustrated in the MOSFET schematic (Figure 12.24). Elements of integrated circuits are shown in Figure 12.25 and in the chapter-opening photograph for this chapter.

DIELECTRIC BEHAVIOR

A **dielectric** material is one that is electrically insulating (nonmetallic) and exhibits or may be made to exhibit an electric dipole structure; that is, there is a separation of positive and negative electrically charged entities on a molecular or atomic level. This concept of an electric dipole was introduced in Section 2.7. As a result of dipole interactions with electric fields, dielectric materials are utilized in capacitors.

12.17 CAPACITANCE

When a voltage is applied across a capacitor, one plate becomes positively charged, the other negatively charged, with the corresponding electric field directed from the positive to the negative. The **capacitance** C is related to the quantity of charge stored on either plate Q by[2]

$$C = \frac{Q}{V} \tag{12.27}$$

where V is the voltage applied across the capacitor. The units of capacitance are coulombs per volt, or farads (F).

Now, consider a parallel-plate capacitor with a vacuum in the region between the plates (Figure 12.26*a*). The capacitance may be computed from the relationship

$$C = \epsilon_0 \frac{A}{l} \tag{12.28}$$

---

[2] By convention, the uppercase "C" is used to represent both capacitance and the unit of charge, coulomb. To minimize confusion in this discussion, the capacitance designation will be italicized, as C.

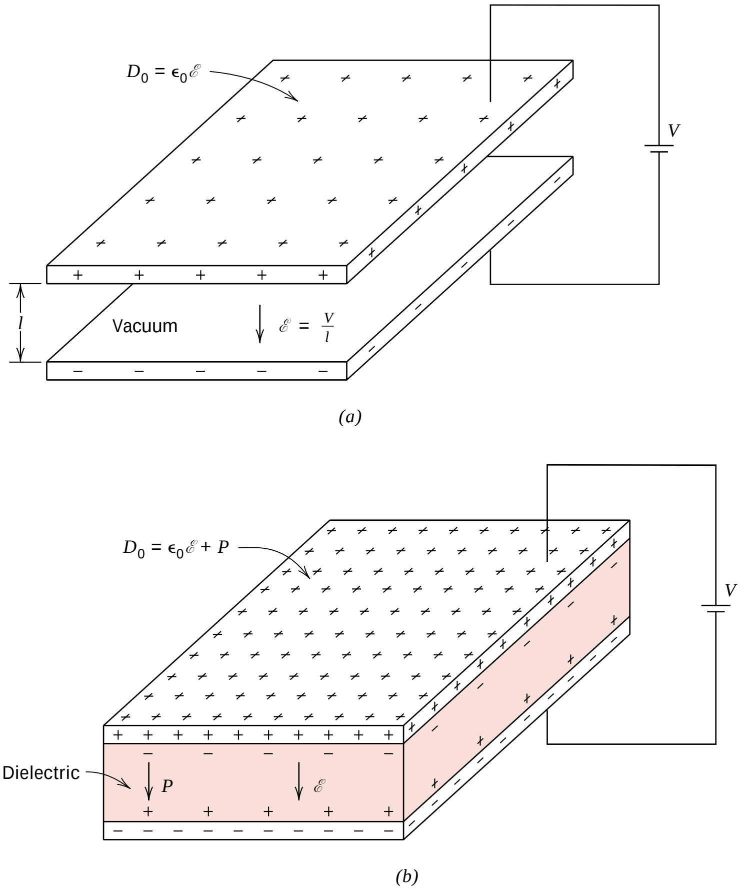
$D_0 = \epsilon_0 \mathscr{E}$
V
Vacuum
$\mathscr{E} = \frac{V}{l}$
l
(a)
$D_0 = \epsilon_0 \mathscr{E} + P$
V
Dielectric
P
$\mathscr{E}$
(b)

Figure 12.26 A parallel-plate capacitor (*a*) when a vacuum is present and (*b*) when a dielectric material is present. (From K. M. Ralls, T. H. Courtney, and J. Wulff, *Introduction to Materials Science and Engineering.* Copyright © 1976 by John Wiley & Sons, Inc. Reprinted by permission of John Wiley & Sons, Inc.)

where A represents the area of the plates and l is the distance between them. The parameter ϵ_0, called the **permittivity** of a vacuum, is a universal constant having the value of 8.85×10^{-12} F/m.

If a dielectric material is inserted into the region within the plates (Figure 12.26*b*), then

$$C = \epsilon \frac{A}{l} \tag{12.29}$$

where ϵ is the permittivity of this dielectric medium, which will be greater in magnitude than ϵ_0. The relative permittivity ϵ_r, often called the **dielectric constant,** is equal to the ratio

$$\epsilon_r = \frac{\epsilon}{\epsilon_0} \tag{12.30}$$

which is greater than unity and represents the increase in charge storing capacity by insertion of the dielectric medium between the plates. The dielectric constant is one material property that is of prime consideration for capacitor design. The ϵ_r values of a number of dielectric materials are contained in Table 12.4.

Table 12.4 Dielectric Constants and Strengths for Some Dielectric Materials

Material	*Dielectric Constant* 60 Hz	*Dielectric Constant* 1 MHz	*Dielectric Strength (V/mil)*[a]
		Ceramics	
Titanate ceramics	—	15–10,000	50–300
Mica	—	5.4–8.7	1000–2000
Steatite ($MgO-SiO_2$)	—	5.5–7.5	200–350
Soda–lime glass	6.9	6.9	250
Porcelain	6.0	6.0	40–400
Fused silica	4.0	3.8	250
		Polymers	
Phenol-formaldehyde	5.3	4.8	300–400
Nylon 6,6	4.0	3.6	400
Polystyrene	2.6	2.6	500–700
Polyethylene	2.3	2.3	450–500
Polytetrafluoroethylene	2.1	2.1	400–500

[a] One mil = 0.001 in. These values of dielectric strength are average ones, the magnitude being dependent on specimen thickness and geometry, as well as the rate of application and duration of the applied electric field.

12.18 FIELD VECTORS AND POLARIZATION

Perhaps the best approach to an explanation of the phenomenon of capacitance is with the aid of field vectors. To begin, for every electric dipole, there is a separation between a positive and a negative electric charge as demonstrated in Figure 12.27. An electric dipole moment p is associated with each dipole as follows:

$$p = qd \tag{12.31}$$

where q is the magnitude of each dipole charge and d is the distance of separation between them. In reality, a dipole moment is a vector that is directed from the negative to the positive charge, as indicated in Figure 12.27. In the presence of an electric field $\mathscr{E}$, which is also a vector quantity, a force (or torque) will come to bear on an electric dipole to orient it with the applied field; this phenomenon is illustrated in Figure 12.28. The process of dipole alignment is termed **polarization.**

Again, returning to the capacitor, the surface charge density D, or quantity of charge per unit area of capacitor plate (C/m^2), is proportional to the electric field.

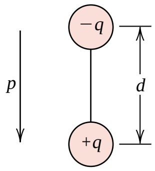

FIGURE 12.27 Schematic representation of an electric dipole generated by two electric charges (of magnitude q) separated by the distance d; the associated polarization vector p is also shown.

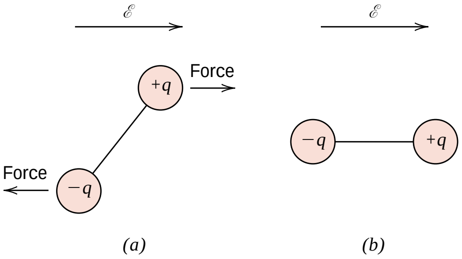

FIGURE 12.28 (*a*) Imposed forces (torque) acting on a dipole by an electric field. (*b*) Final dipole alignment with the field.

When a vacuum is present, then

$$D_0 = \epsilon_0 \mathscr{E} \tag{12.32}$$

the constant of proportionality being ϵ_0. Furthermore, an analogous expression exists for the dielectric case, that is,

$$D = \epsilon \mathscr{E} \tag{12.33}$$

Sometimes, D is also called the **dielectric displacement.**

The increase in capacitance, or dielectric constant, can be explained using a simplified model of polarization within a dielectric material. Consider the capacitor in Figure 12.29*a*, the vacuum situation, wherein a charge of $+Q_0$ is stored on the top plate, and $-Q_0$ on the bottom one. When a dielectric is introduced and an electric field is applied, the entire solid within the plates becomes polarized (Figure 12.29*c*). As a result of this polarization, there is a net accumulation of negative charge of magnitude $-Q'$ at the dielectric surface near the positively charged plate and, in a similar manner, a surplus of $+Q'$ charge at the surface adjacent to the negative plate. For the region of dielectric removed from these surfaces, polarization effects are not important. Thus, if each plate and its adjacent dielectric surface are considered to be a single entity, the induced charge from the dielectric ($+Q'$ or $-Q'$) may be thought of as nullifying some of the charge that originally existed on the plate for a vacuum ($-Q_0$ or $+Q_0$). The voltage imposed across the plates is maintained at the vacuum value by increasing the charge at the negative (or bottom) plate by an amount $-Q'$, and the top plate by $+Q'$. Electrons are caused to flow from the positive to the negative plate by the external voltage source such that the proper voltage is reestablished. And so the charge on each plate is now $Q_0 + Q'$, having been increased by an amount Q'.

In the presence of a dielectric, the surface charge density on the plates of a capacitor may also be represented by

$$D = \epsilon_0 \mathscr{E} + P \tag{12.34}$$

where P is the *polarization*, or the increase in charge density above that for a vacuum because of the presence of the dielectric; or, from Figure 12.29*c*, $P = Q'/A$, where A is the area of each plate. The units of P are the same as for D (C/m^2).

The polarization P may also be thought of as the total dipole moment per unit volume of the dielectric material, or as a polarization electric field within the dielectric that results from the mutual alignment of the many atomic or molecular dipoles with the externally applied field $\mathscr{E}$. For many dielectric materials, P is

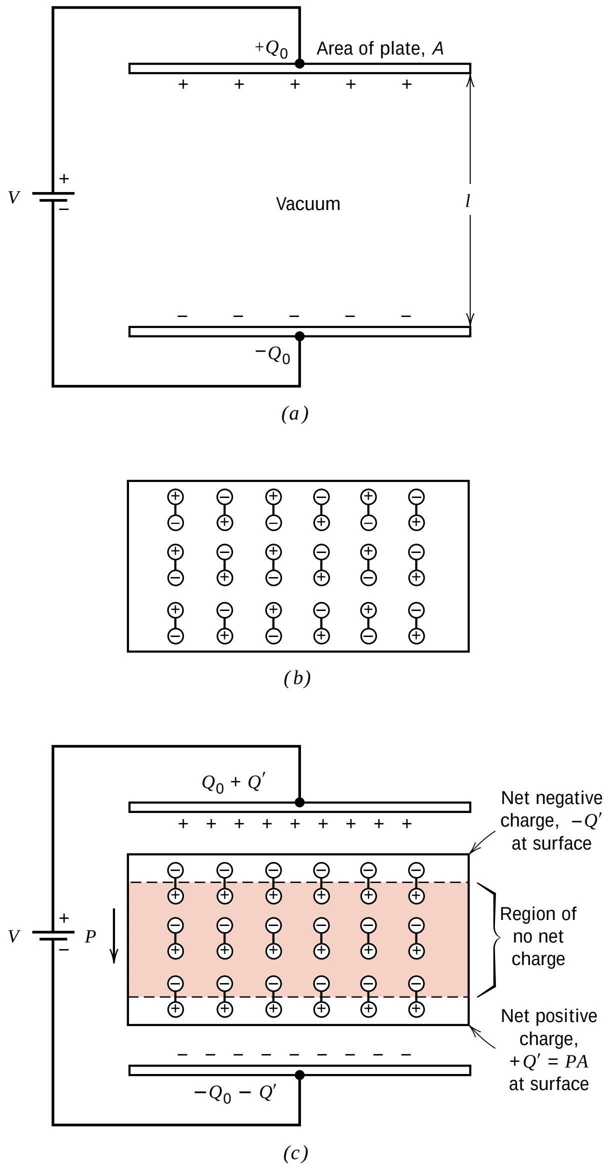
$+Q_0$
Area of plate, A
V
Vacuum
l
$-Q_0$
(a)
(b)
$Q_0 + Q'$
Net negative charge, $-Q'$ at surface
V
P
Region of no net charge
Net positive charge, $+Q' = PA$ at surface
$-Q_0 - Q'$
(c)

Figure 12.29 Schematic representations of (*a*) the charge stored on capacitor plates for a vacuum, (*b*) the dipole arrangement in an unpolarized dielectric, and (*c*) the increased charge storing capacity resulting from the polarization of a dielectric material. (Adapted from A. G. Guy, *Essentials of Materials Science*, McGraw-Hill Book Company, New York, 1976.)

proportional to $\mathscr{E}$ through the relationship

$$P = \epsilon_0(\epsilon_r - 1)\mathscr{E} \tag{12.35}$$

in which case ϵ_r is independent of the magnitude of the electric field.

Table 12.5 lists the several dielectric parameters along with their units.

EXAMPLE PROBLEM 12.5

Consider a parallel-plate capacitor having an area of 6.45×10^{-4} m^2 (1 in.^{2}) and a plate separation of 2×10^{-3} m (0.08 in.) across which a potential of 10 V

Table 12.5 Primary and Derived Units for Various Electrical Parameters and Field Vectors

Quantity	*Symbol*	*SI Units* Derived	*SI Units* Primary
Electric potential	V	volt	kg-m^2/s^2-C
Electric current	I	ampere	C/s
Electric field strength	$\mathscr{E}$	volt/meter	kg-m/s^2-C
Resistance	R	ohm	kg-m^2/s-C^2
Resistivity	ρ	ohm-meter	kg-m^3/s-C^2
Conductivity	σ	(ohm-meter)$^{-1}$	s-C^2/kg-m^3
Electric charge	Q	coulomb	C
Capacitance	C	farad	s^2-C^2/kg-m^2
Permittivity	ϵ	farad/meter	s^{2}C^2/kg-m^3
Dielectric constant	ϵ_r	ratio	ratio
Dielectric displacement	D	farad-volt/m^2	C/m^2
Electric polarization	P	farad-volt/m^2	C/m^2

is applied. If a material having a dielectric constant of 6.0 is positioned within the region between the plates, compute

(a) The capacitance.

(b) The magnitude of the charge stored on each plate.

(c) The dielectric displacement D.

(d) The polarization.

SOLUTION

(a) Capacitance is calculated using Equation 12.29; however, the permittivity ϵ of the dielectric medium must first be determined from Equation 12.30 as follows:

$$\epsilon = \epsilon_r \epsilon_0 = (6.0)(8.85 \times 10^{-12}\ \text{F/m})$$
$$= 5.31 \times 10^{-11}\ \text{F/m}$$

Thus, the capacitance is

$$C = \epsilon \frac{A}{l} = (5.31 \times 10^{-11}\ \text{F/m})\left(\frac{6.45 \times 10^{-4}\ \text{m}^2}{2 \times 10^{-3}\ \text{m}}\right)$$
$$= 1.71 \times 10^{-11}\ \text{F}$$

(b) Since the capacitance has been determined, the charge stored may be computed using Equation 12.27, according to

$$Q = CV = (1.71 \times 10^{-11}\ \text{F})(10\ \text{V}) = 1.71 \times 10^{-10}\ \text{C}$$

(c) The dielectric displacement is calculated from Equation 12.33, which yields

$$D = \epsilon \mathscr{E} = \epsilon \frac{V}{l} = \frac{(5.31 \times 10^{-11}\ \text{F/m})(10\ \text{V})}{2 \times 10^{-3}\ \text{m}}$$
$$= 2.66 \times 10^{-7}\ \text{C/m}^2$$

(d) Using Equation 12.34, the polarization may be determined as follows:

$$P = D - \epsilon_0 \mathscr{E} = D - \epsilon_0 \frac{V}{l}$$

$$= 2.66 \times 10^{-7}\ \mathrm{C/m^2} - \frac{(8.85 \times 10^{-12}\ \mathrm{F/m})(10\ \mathrm{V})}{2 \times 10^{-3}\ \mathrm{m}}$$

$$= 2.22 \times 10^{-7}\ \mathrm{C/m^2}$$

12.19 TYPES OF POLARIZATION

Again, polarization is the alignment of permanent or induced atomic or molecular dipole moments with an externally applied electric field. There are three types or sources of polarization: electronic, ionic, and orientation. Dielectric materials ordinarily exhibit at least one of these polarization types depending on the material and also the manner of the external field application.

ELECTRONIC POLARIZATION

Electronic polarization may be induced to one degree or another in all atoms. It results from a displacement of the center of the negatively charged electron cloud relative to the positive nucleus of an atom by the electric field (Figure 12.30*a*). This polarization type is found in all dielectric materials, and, of course, exists only while an electric field is present.

IONIC POLARIZATION

Ionic polarization occurs only in materials that are ionic. An applied field acts to displace cations in one direction and anions in the opposite direction, which gives rise to a net dipole moment. This phenomenon is illustrated in Figure 12.30*b*. The magnitude of the dipole moment for each ion pair p_i is equal to the product of the relative displacement d_i and the charge on each ion, or

$$p_i = qd_i \tag{12.36}$$

ORIENTATION POLARIZATION

The third type, **orientation polarization,** is found only in substances that possess permanent dipole moments. Polarization results from a rotation of the permanent moments into the direction of the applied field, as represented in Figure 12.30*c*. This alignment tendency is counteracted by the thermal vibrations of the atoms, such that polarization decreases with increasing temperature.

The total polarization P of a substance is equal to the sum of the electronic, ionic, and orientation polarizations (P_e, P_i, and P_o, respectively), or

$$P = P_e + P_i + P_o \tag{12.37}$$

It is possible for one or more of these contributions to the total polarization to be either absent or negligible in magnitude relative to the others. For example, ionic polarization will not exist in covalently bonded materials in which no ions are present.

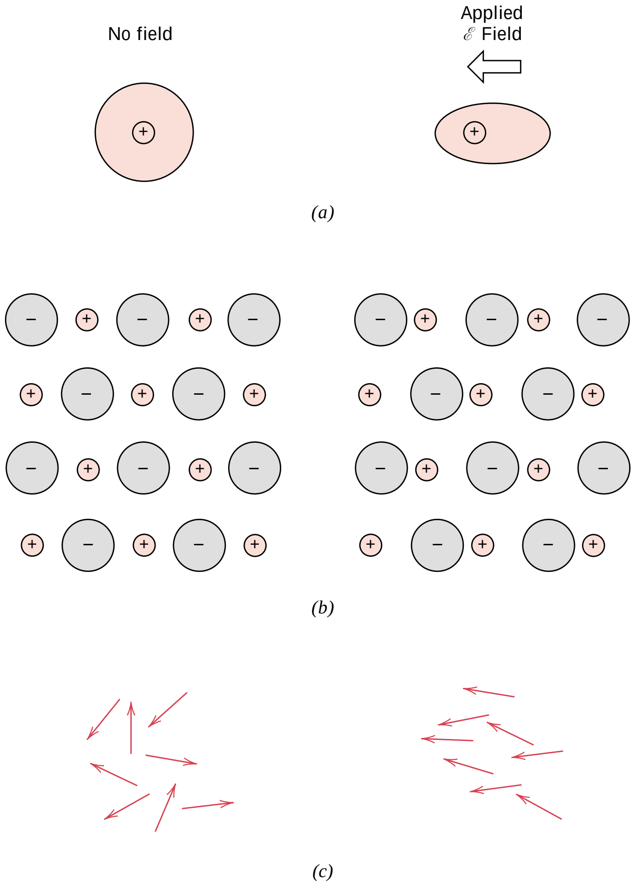

FIGURE 12.30 (*a*) Electronic polarization that results from the distortion of an atomic electron cloud by an electric field. (*b*) Ionic polarization that results from the relative displacement of electrically charged ions in response to an electric field. (*c*) Response of permanent electric dipoles (arrows) to an applied electric field, producing orientation polarization. (From O. H. Wyatt and D. Dew-Hughes, *Metals, Ceramics and Polymers*, Cambridge University Press, 1974.)

12.20 FREQUENCY DEPENDENCE OF THE DIELECTRIC CONSTANT

In many practical situations the current is alternating (ac); that is, an applied voltage or electric field changes direction with time, as indicated in Figure 12.21*a*. Now, consider a dielectric material that is subject to polarization by an ac electric field. With each direction reversal, the dipoles attempt to reorient with the field, as illustrated in Figure 12.31, a process requiring some finite time. For each polarization type, some minimum reorientation time exists, which depends on the ease with which the particular dipoles are capable of realignment. A **relaxation frequency** is taken as the reciprocal of this minimum reorientation time.

A dipole cannot keep shifting orientation direction when the frequency of the applied electric field exceeds its relaxation frequency, and therefore, will not make a contribution to the dielectric constant. The dependence of ϵ_r on the field frequency is represented schematically in Figure 12.32 for a dielectric medium that exhibits all three types of polarization; note that the frequency axis is scaled logarithmically. As indicated in Figure 12.32, when a polarization mechanism ceases to function, there is an abrupt drop in the dielectric constant; otherwise, ϵ_r is virtually frequency independent. Table 12.4 gave values of the dielectric constant at 60 Hz and 1 MHz; these provide an indication of this frequency dependence at the low end of the frequency spectrum.

The absorption of electrical energy by a dielectric material that is subjected to an alternating electric field is termed *dielectric loss*. This loss may be important at

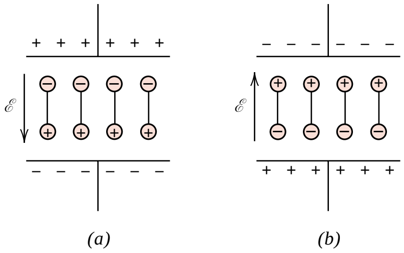

Figure 12.31 Dipole orientations for (*a*) one polarity of an alternating electric field and (*b*) for the reversed polarity. (From Richard A. Flinn and Paul K. Trojan, *Engineering Materials and Their Applications*, 4th edition. Copyright © 1990 by John Wiley & Sons, Inc. Adapted by permission of John Wiley & Sons, Inc.)

electric field frequencies in the vicinity of the relaxation frequency for each of the operative dipole types for a specific material. A low dielectric loss is desired at the frequency of utilization.

12.21 DIELECTRIC STRENGTH

When very high electric fields are applied across dielectric materials, large numbers of electrons may suddenly be excited to energies within the conduction band. As a result, the current through the dielectric by the motion of these electrons increases dramatically; sometimes localized melting, burning, or vaporization produces irreversible degradation and perhaps even failure of the material. This phenomenon is known as dielectric breakdown. The **dielectric strength,** sometimes called the breakdown strength, represents the magnitude of an electric field necessary to produce breakdown. Table 12.4 presented dielectric strengths for several materials.

12.22 DIELECTRIC MATERIALS

A number of ceramics and polymers are utilized as insulators and/or in capacitors. Many of the ceramics, including glass, porcelain, steatite, and mica, have dielectric constants within the range of 6 to 10 (Table 12.4). These materials also exhibit a high degree of dimensional stability and mechanical strength. Typical applications include powerline and electrical insulation, switch bases, and light receptacles. The titania (TiO_2) and titanate ceramics, such as barium titanate ($BaTiO_3$), can be

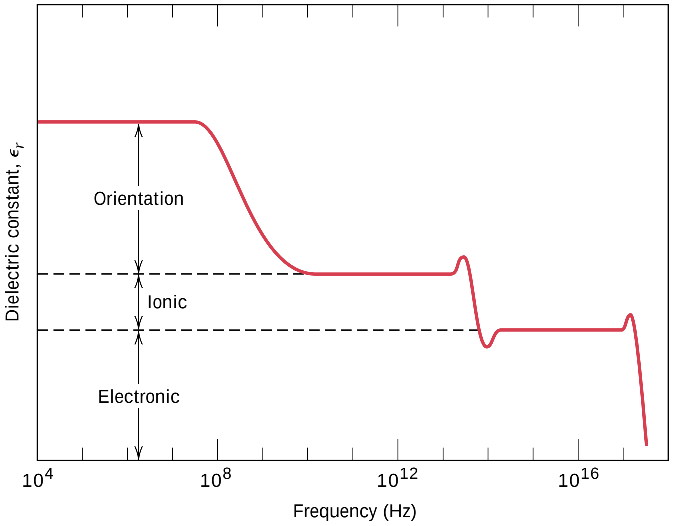

Figure 12.32 Variation of dielectric constant with frequency of an alternating electric field. Electronic, ionic, and orientation polarization contributions to the dielectric constant are indicated.

made to have extremely high dielectric constants, which render them especially useful for some capacitor applications.

The magnitude of the dielectric constant for most polymers is less than for ceramics, since the latter may exhibit greater dipole moments; ϵ_r values for polymers generally lie between 2 and 5. These materials are commonly utilized for insulation of wires, cables, motors, generators, and so on, and, in addition, for some capacitors.

OTHER ELECTRICAL CHARACTERISTICS OF MATERIALS

Two other relatively important and novel electrical characteristics that are found in some materials deserve brief mention, namely, ferroelectricity and piezoelectricity.

12.23 FERROELECTRICITY

The group of dielectric materials called **ferroelectrics** exhibit spontaneous polarization, that is, polarization in the absence of an electric field. They are the dielectric analogue of ferromagnetic materials, which may display permanent magnetic behavior. There must exist in ferroelectric materials permanent electric dipoles, the origin of which is explained for barium titanate, one of the most common ferroelectrics. The spontaneous polarization is a consequence of the positioning of the Ba^{2+}, Ti^{4+}, and O^{2-} ions within the unit cell, as represented in Figure 12.33. The Ba^{2+} ions are located at the corners of the unit cell, which is of tetragonal symmetry (a cube that has been elongated slightly in one direction). The dipole moment results from the relative displacements of the O^{2-} and Ti^{4+} ions from their symmetrical positions as shown in the side view of the unit cell. The O^{2-} ions are located near, but slightly

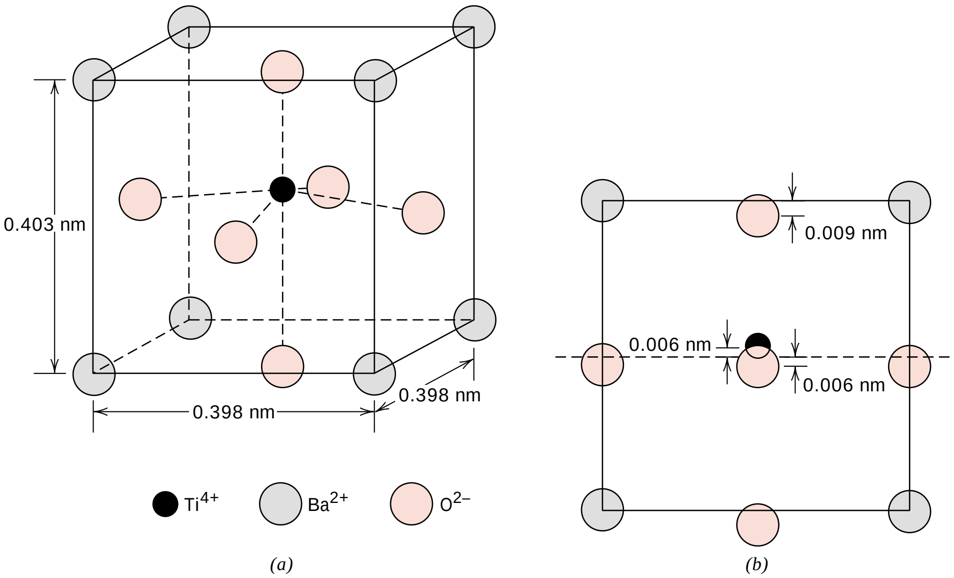

FIGURE 12.33 A barium titanate ($BaTiO_3$) unit cell (*a*) in an isometric projection, and (*b*) looking at one face, which shows the displacements of Ti^{4+} and O^{2-} ions from the center of the face.

below, the centers of each of the six faces, whereas the Ti^{4+} ion is displaced upward from the unit cell center. Thus, a permanent ionic dipole moment is associated with each unit cell. However, when barium titanate is heated above its *ferroelectric Curie temperature* [120°C (250°F)], the unit cell becomes cubic, and all ions assume symmetric positions within the cubic unit cell; the material now has a perovskite crystal structure (Section 3.6), and the ferroelectric behavior ceases.

Spontaneous polarization of this group of materials results as a consequence of interactions between adjacent permanent dipoles wherein they mutually align, all in the same direction. For example, with barium titanate, the relative displacements of O^{2-} and Ti^{4+} ions are in the same direction for all the unit cells within some volume region of the specimen. Other materials display ferroelectricity; these include Rochelle salt ($\mathrm{NaKC_4H_4O_6 \cdot 4H_2O}$), potassium dihydrogen phosphate ($\mathrm{KH_2PO_4}$), potassium niobate ($\mathrm{KNbO_3}$), and lead zirconate–titanate ($\mathrm{Pb[ZrO_3, TiO_3]}$). Ferroelectrics have extremely high dielectric constants at relatively low applied field frequencies; for example, at room temperature, ϵ_r for barium titanate may be as high as 5000. Consequently, capacitors made from these materials can be significantly smaller than capacitors made from other dielectric materials.

12.24 PIEZOELECTRICITY

An unusual property exhibited for a few ceramic materials is piezoelectricity, or, literally, pressure electricity: polarization is induced and an electric field is established across a specimen by the application of external forces. Reversing the sign of an external force (i.e., from tension to compression) reverses the direction of the field. The piezoelectric effect is demonstrated in Figure 12.34.

Piezoelectric materials are utilized in transducers, devices that convert electrical energy into mechanical strains, or vice versa. Familiar applications that employ piezoelectrics include phonograph pickups, microphones, ultrasonic generators, strain gages, and sonar detectors. In a phonograph cartridge, as the stylus traverses the grooves on a record, a pressure variation is imposed on a piezoelectric material located in the cartridge, which is then transformed into an electric signal, and amplified before going to the speaker.

Piezoelectric materials include titanates of barium and lead, lead zirconate ($\mathrm{PbZrO_3}$), ammonium dihydrogen phosphate ($\mathrm{NH_4H_2PO_4}$), and quartz. This property is characteristic of materials having complicated crystal structures with a low degree of symmetry. The piezoelectric behavior of a polycrystalline specimen may be improved by heating above its Curie temperature and then cooling to room temperature in a strong electric field.

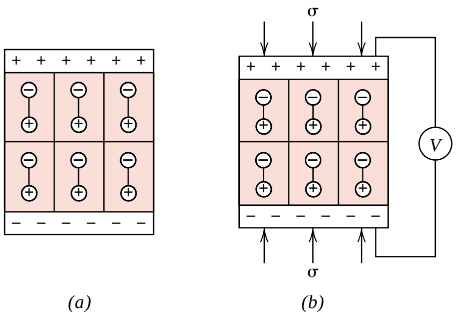

(a) (b)

Figure 12.34 (*a*) Dipoles within a piezoelectric material. (*b*) A voltage is generated when the material is subjected to a compressive stress. (From *Elements of Materials Science and Engineering* by Van Vlack, © 1989. Reprinted by permission of Prentice-Hall, Inc., Upper Saddle River, NJ.)

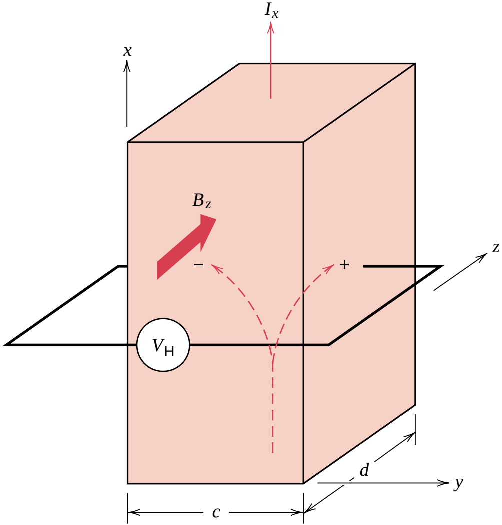

FIGURE 12.18 Schematic demonstration of the Hall effect. Positive and/or negative charge carriers that are part of the I_x current are deflected by the magnetic field B_z and give rise to the Hall voltage, V_H.

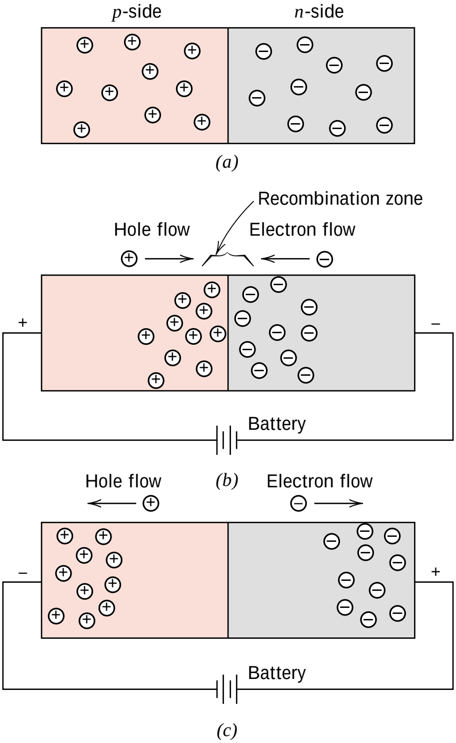
p-side
n-side
(a)
Recombination zone
Hole flow
Electron flow
+
−
Battery
(b)
Hole flow
Electron flow
−
+
Battery
(c)

Figure 12.19 For a p–n rectifying junction, representations of electron and hole distributions for (*a*) no electrical potential, (*b*) forward bias, and (*c*) reverse bias.

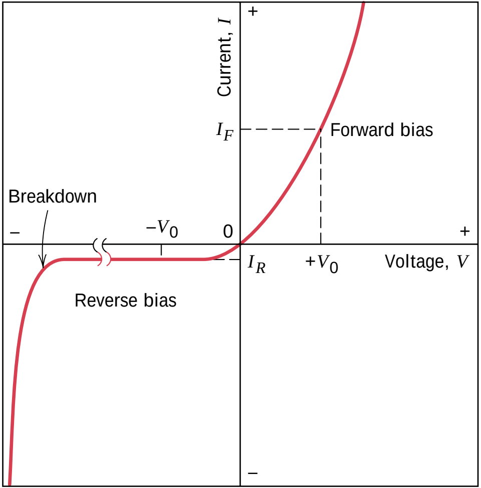

FIGURE 12.20 The current–voltage characteristics of a p–n junction for forward and reverse biases. The phenomenon of breakdown is also shown.

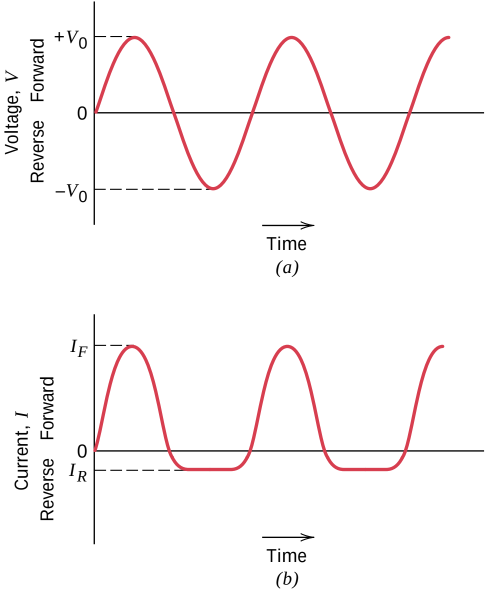

(a)

(b)

Figure 12.21 (*a*) Voltage versus time for the input to a *p*–*n* rectifying junction. (*b*) Current versus time, showing rectification of voltage in (*a*) by a *p*–*n* rectifying junction having the voltage–current characteristics shown in Figure 12.20.

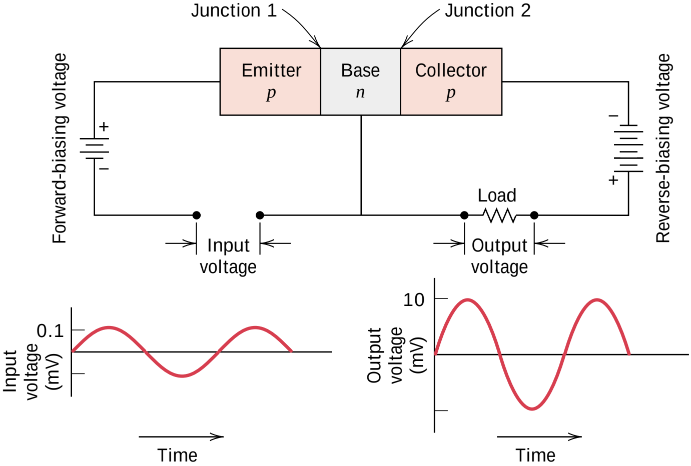
Junction 1
Junction 2
Emitter
p
Base
n
Collector
p
Forward-biasing voltage
+
–
–
+
Reverse-biasing voltage
Load
Input voltage
Output voltage
0.1
Input voltage (mV)
Time
10
Output voltage (mV)
Time

Figure 12.22 Schematic diagram of a *p*–*n*–*p* junction transistor and its associated circuitry, including input and output voltage–time characteristics showing voltage amplification. (Adapted from A. G. Guy, *Essentials of Materials Science*, McGraw-Hill Book Company, New York, 1976.)

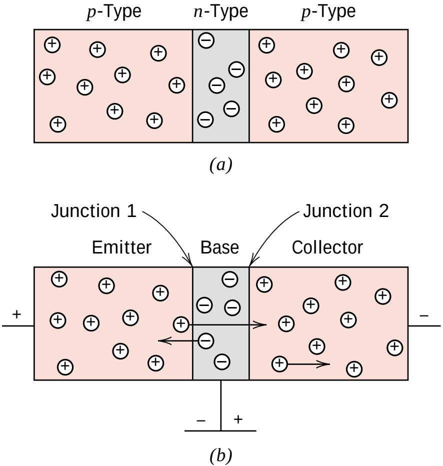
p-Type
n-Type
p-Type
(*a*)
Junction 1
Junction 2
Emitter
Base
Collector
+
–
–
+
(*b*)

FIGURE 12.23 For a junction transistor (*p*–*n*–*p* type), the distributions and directions of electron and hole motion (*a*) when no potential is applied and (*b*) with appropriate bias for voltage amplification.

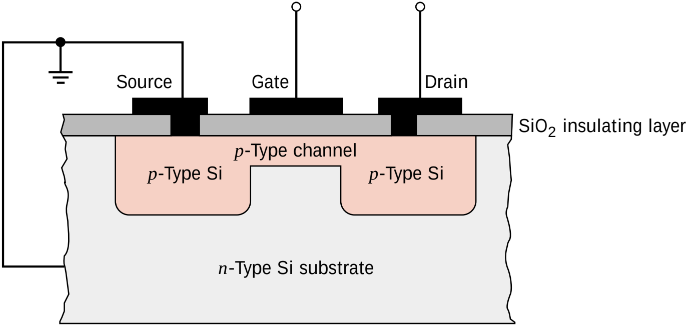
Source
Gate
Drain
SiO$_2$ insulating layer
p-Type channel
p-Type Si
p-Type Si
n-Type Si substrate

FIGURE 12.24 Schematic cross-sectional view of a MOSFET transistor.

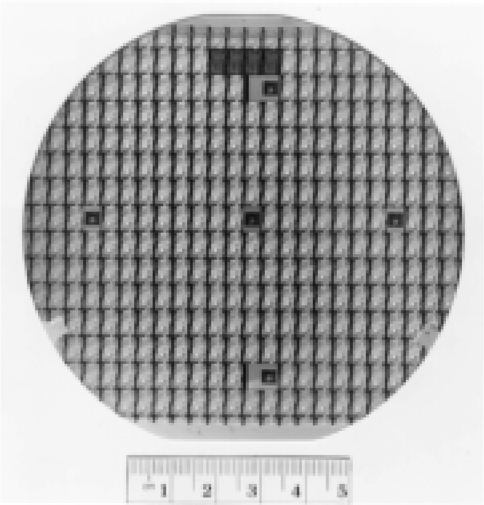

FIGURE 20.20 Photograph of a 100-mm-diameter (4-in.-diameter) silicon wafer. Each of the small rectangles shown is an individual IC chip or die.

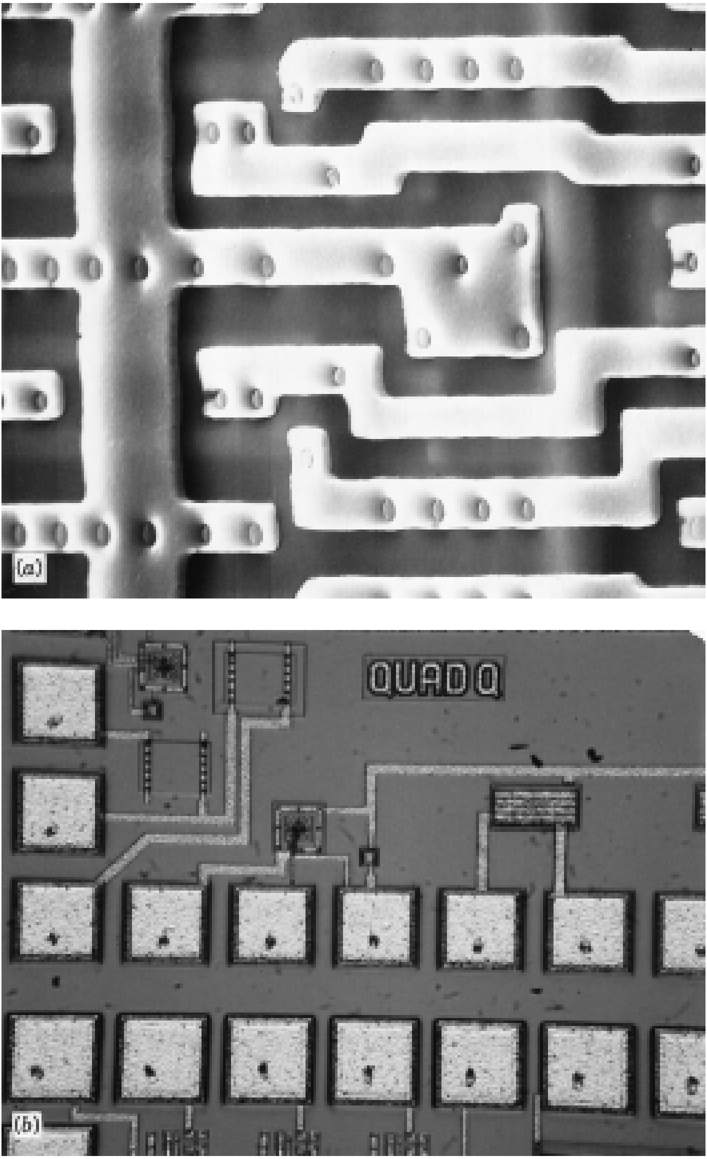

Figure 12.25 (*a*) Scanning electron micrograph showing a small region of a microprocessing chip (a 0.5 MB selected address device). The narrow, white regions are an aluminum top layer that serves as the wiring for this device. The gray regions are diffusion-layer doped silicon that have been coated with an interlayer dielectric. Approximately 2000×. (*b*) An optical photomicrograph showing a portion of a circuit that is used to test microprocessing chips. The narrow, light regions are aluminum connectors, while the white, square areas are test pads (semiconductor devices); test circuits (also composed of semiconductor devices) appear in the upper left-hand corner of the photograph. Approximately 50×. (Both photographs courtesy of Nick Gonzales of National Semiconductor Corporation, West Jordan, Utah.)

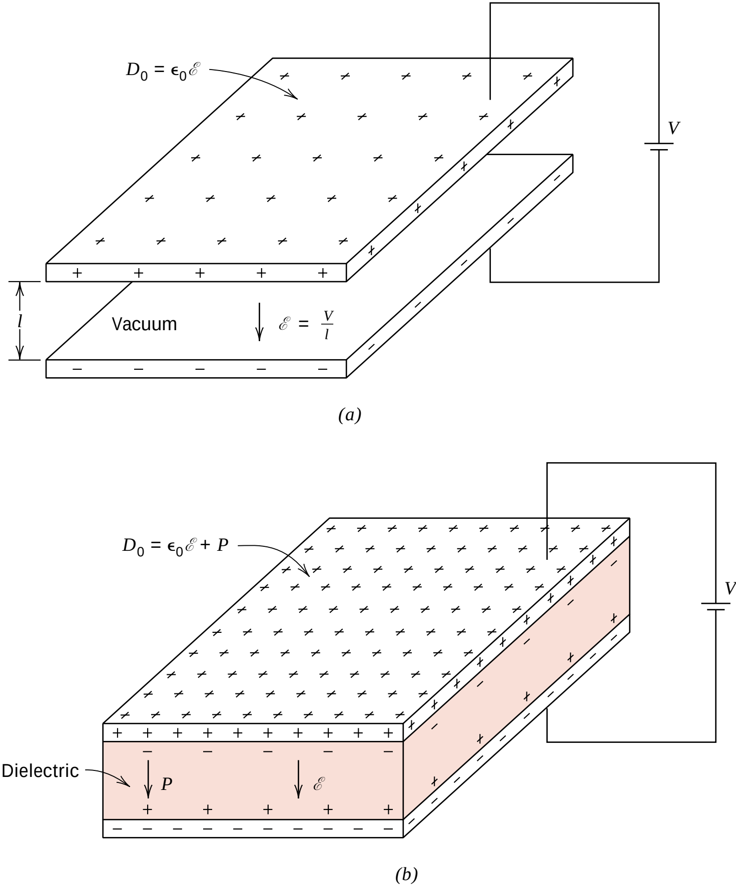
D₀ = ϵ₀ℰ
V
l
Vacuum
ℰ = V/l
(a)
D₀ = ϵ₀ℰ + P
V
Dielectric
P
ℰ
(b)

Figure 12.26 A parallel-plate capacitor (*a*) when a vacuum is present and (*b*) when a dielectric material is present. (From K. M. Ralls, T. H. Courtney, and J. Wulff, *Introduction to Materials Science and Engineering.* Copyright © 1976 by John Wiley & Sons, Inc. Reprinted by permission of John Wiley & Sons, Inc.)

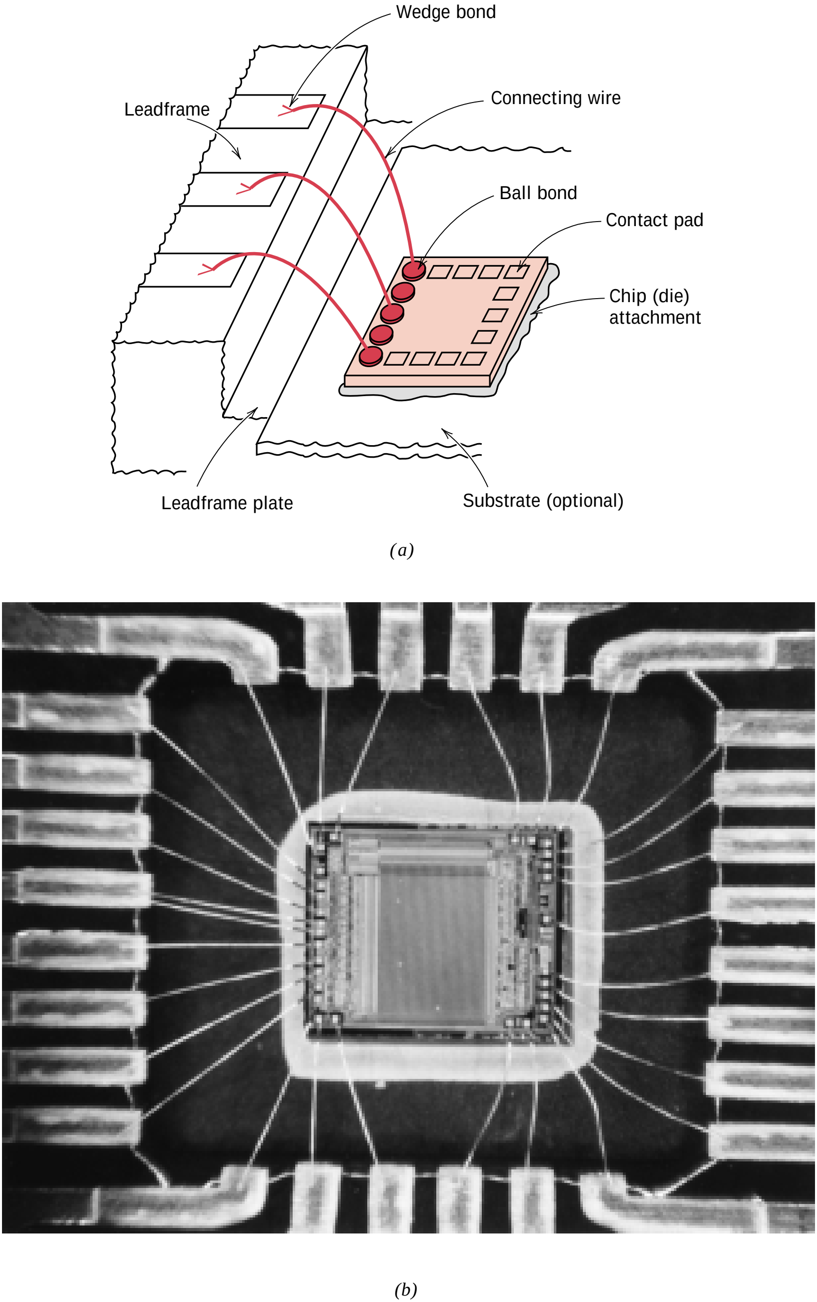
Wedge bond
Leadframe
Connecting wire
Ball bond
Contact pad
Chip (die) attachment
Leadframe plate
Substrate (optional)
(a)
(b)

FIGURE 20.22 (*a*) Schematic diagram showing the IC chip, its attachment to the substrate (or leadframe plate), and the connecting wires that run to the leadframe contact leads. (Adapted from *Electronic Materials Handbook*, Vol. 1, *Packaging*, C. A. Dostal, editor, ASM International, 1989, p. 225.) (*b*) Photograph showing a portion of a leadframe package. Included is the IC chip along with its connecting wires. One end of each wire is bonded to a chip pad; the other wire extremity is bonded to a leadframe contact lead. $7\frac{1}{2}\times$. (Photograph courtesy of National Semiconductor Corporation.)

Table 12.4 **Dielectric Constants and Strengths for Some Dielectric Materials**

	Dielectric Constant		*Dielectric Strength*
Material	*60 Hz*	*1 MHz*	*(V/mil)*[a]
		Ceramics	
Titanate ceramics	—	15–10,000	50–300
Mica	—	5.4–8.7	1000–2000
Steatite (MgO–SiO_2)	—	5.5–7.5	200–350
Soda–lime glass	6.9	6.9	250
Porcelain	6.0	6.0	40–400
Fused silica	4.0	3.8	250
		Polymers	
Phenol-formaldehyde	5.3	4.8	300–400
Nylon 6,6	4.0	3.6	400
Polystyrene	2.6	2.6	500–700
Polyethylene	2.3	2.3	450–500
Polytetrafluoroethylene	2.1	2.1	400–500

[a] One mil = 0.001 in. These values of dielectric strength are average ones, the magnitude being dependent on specimen thickness and geometry, as well as the rate of application and duration of the applied electric field.

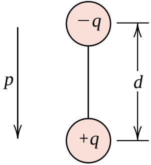

FIGURE 12.27 Schematic representation of an electric dipole generated by two electric charges (of magnitude q) separated by the distance d; the associated polarization vector p is also shown.

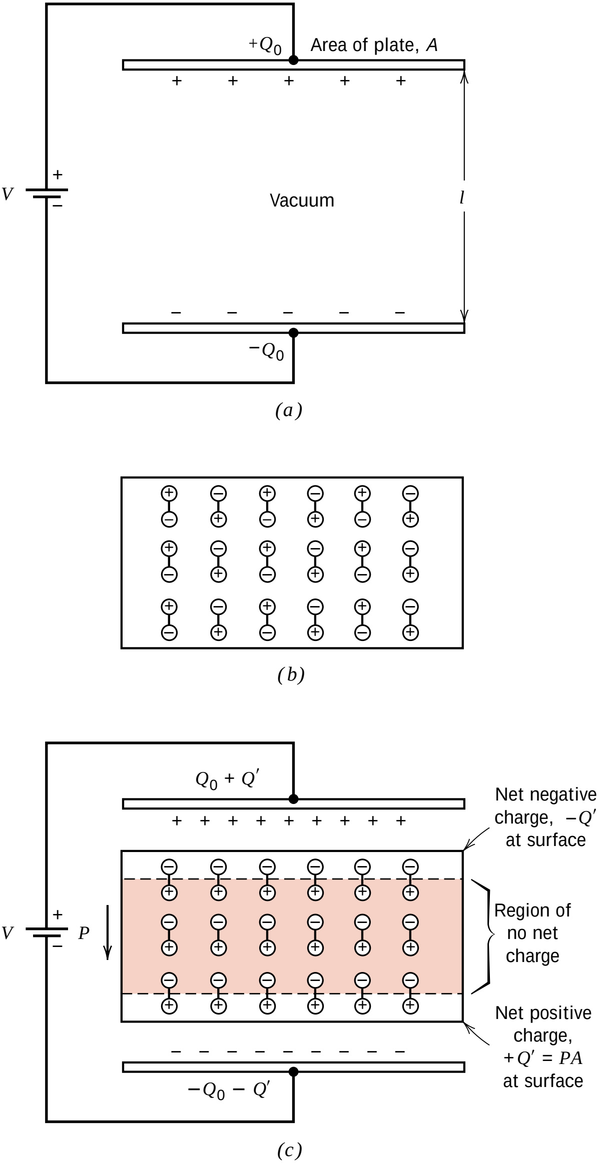
+Q_0
Area of plate, A
V
+
−
Vacuum
l
−Q_0
(a)
(b)
Q_0 + Q′
Net negative charge, −Q′ at surface
Region of no net charge
P
Net positive charge, +Q′ = PA at surface
−Q_0 − Q′
(c)

FIGURE 12.29 Schematic representations of (*a*) the charge stored on capacitor plates for a vacuum, (*b*) the dipole arrangement in an unpolarized dielectric, and (*c*) the increased charge storing capacity resulting from the polarization of a dielectric material. (Adapted from A. G. Guy, *Essentials of Materials Science*, McGraw-Hill Book Company, New York, 1976.)

Table 12.5 Primary and Derived Units for Various Electrical Parameters and Field Vectors

Quantity	*Symbol*	*SI Units*	
		Derived	*Primary*
Electric potential	V	volt	kg-m^2/s^2-C
Electric current	I	ampere	C/s
Electric field strength	$\mathscr{E}$	volt/meter	kg-m/s^2-C
Resistance	R	ohm	kg-m^2/s-C^2
Resistivity	ρ	ohm-meter	kg-m^3/s-C^2
Conductivity	σ	(ohm-meter)$^{-1}$	s-C^2/kg-m^3
Electric charge	Q	coulomb	C
Capacitance	C	farad	s^2-C^2/kg-m^2
Permittivity	ϵ	farad/meter	s^{2}C^2/kg-m^3
Dielectric constant	ϵ_r	ratio	ratio
Dielectric displacement	D	farad-volt/m^2	C/m^2
Electric polarization	P	farad-volt/m^2	C/m^2

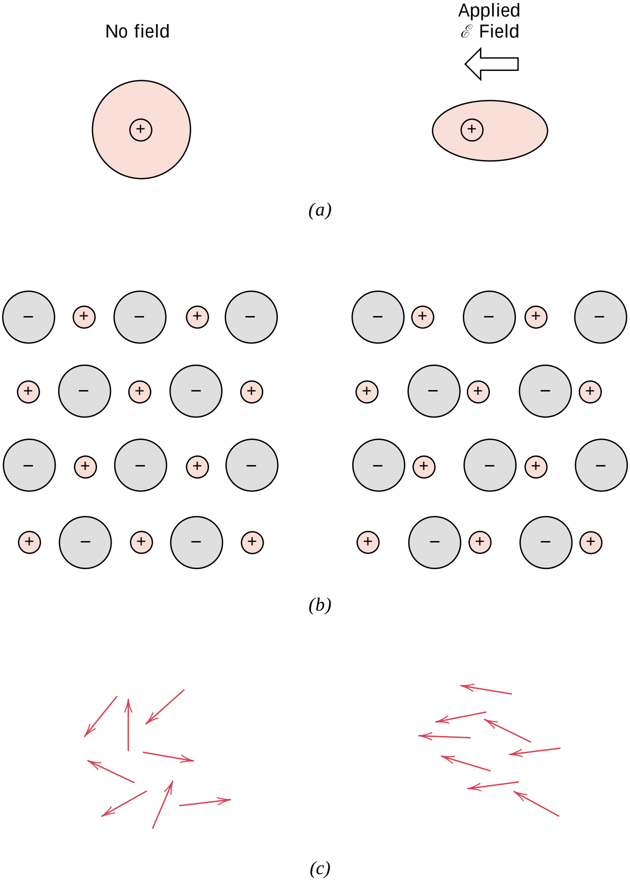

FIGURE 12.30 (*a*) Electronic polarization that results from the distortion of an atomic electron cloud by an electric field. (*b*) Ionic polarization that results from the relative displacement of electrically charged ions in response to an electric field. (*c*) Response of permanent electric dipoles (arrows) to an applied electric field, producing orientation polarization. (From O. H. Wyatt and D. Dew-Hughes, *Metals, Ceramics and Polymers*, Cambridge University Press, 1974.)

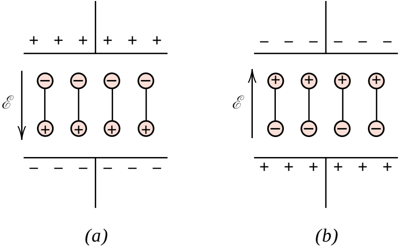

FIGURE 12.31 Dipole orientations for (*a*) one polarity of an alternating electric field and (*b*) for the reversed polarity. (From Richard A. Flinn and Paul K. Trojan, *Engineering Materials and Their Applications*, 4th edition. Copyright © 1990 by John Wiley & Sons, Inc. Adapted by permission of John Wiley & Sons, Inc.)

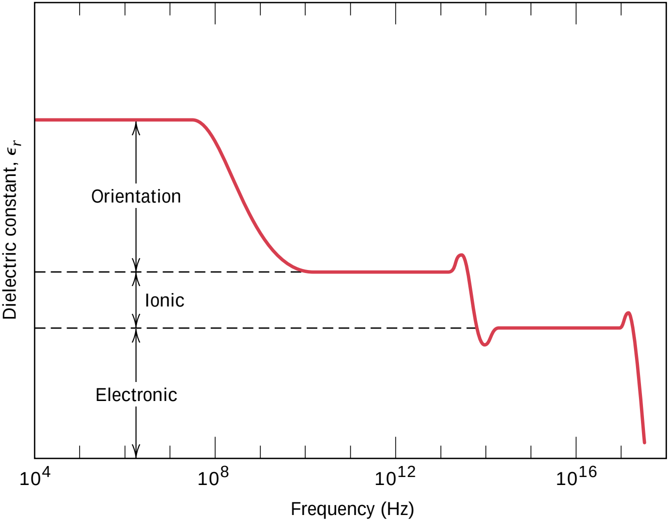

Figure 12.32 Variation of dielectric constant with frequency of an alternating electric field. Electronic, ionic, and orientation polarization contributions to the dielectric constant are indicated.

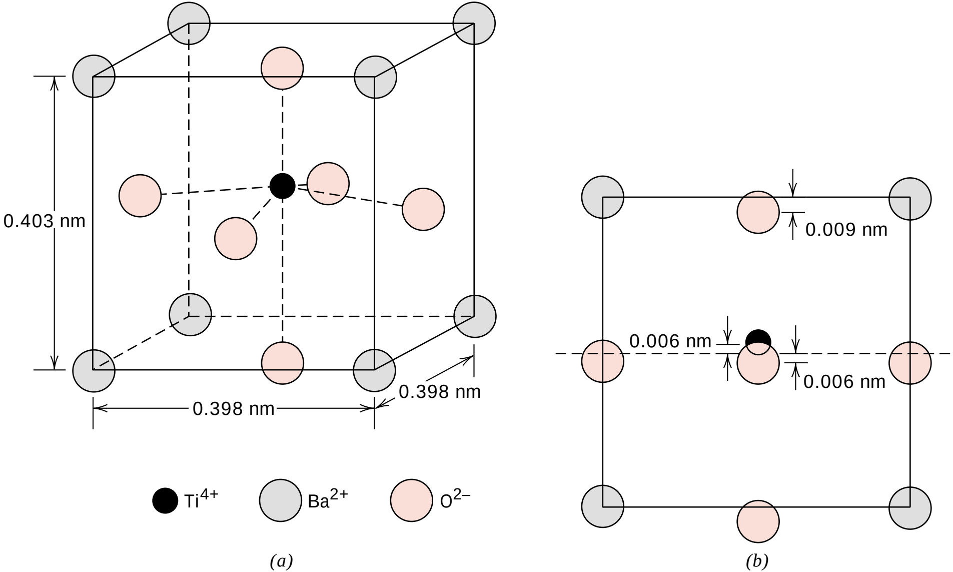
0.403 nm
0.398 nm
0.398 nm
Ti4+
Ba2+
O2−
0.009 nm
0.006 nm
0.006 nm
(a)
(b)

FIGURE 12.33 A barium titanate ($BaTiO_3$) unit cell (*a*) in an isometric projection, and (*b*) looking at one face, which shows the displacements of Ti^{4+} and O^{2-} ions from the center of the face.

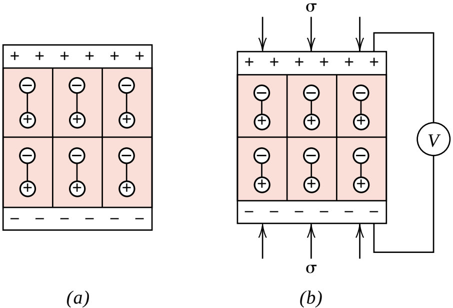

FIGURE 12.34 (*a*) Dipoles within a piezoelectric material. (*b*) A voltage is generated when the material is subjected to a compressive stress. (From *Elements of Materials Science and Engineering* by Van Vlack, © 1989. Reprinted by permission of Prentice-Hall, Inc., Upper Saddle River, NJ.)

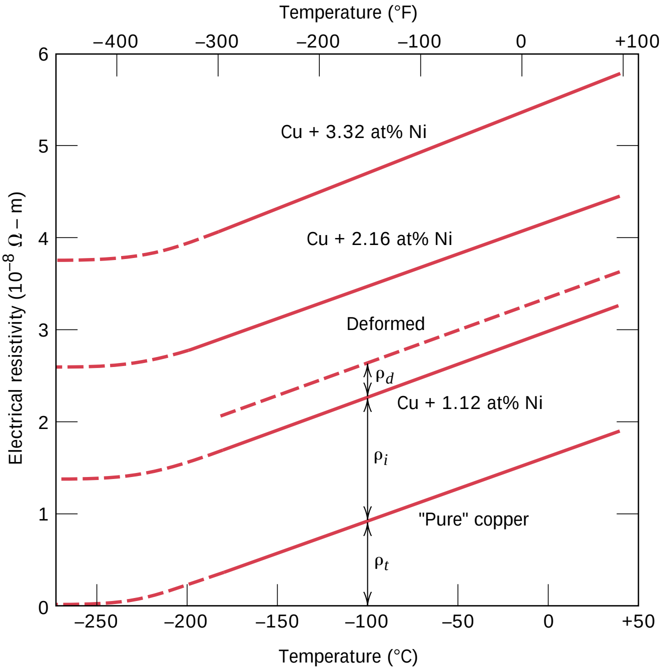

FIGURE 12.8 The electrical resistivity versus temperature for copper and three copper–nickel alloys, one of which has been deformed. Thermal, impurity, and deformation contributions to the resistivity are indicated at −100°C. [Adapted from J. O. Linde, *Ann. Physik*, **5,** 219 (1932); and C. A. Wert and R. M. Thomson, *Physics of Solids*, 2nd edition, McGraw-Hill Book Company, New York, 1970.]

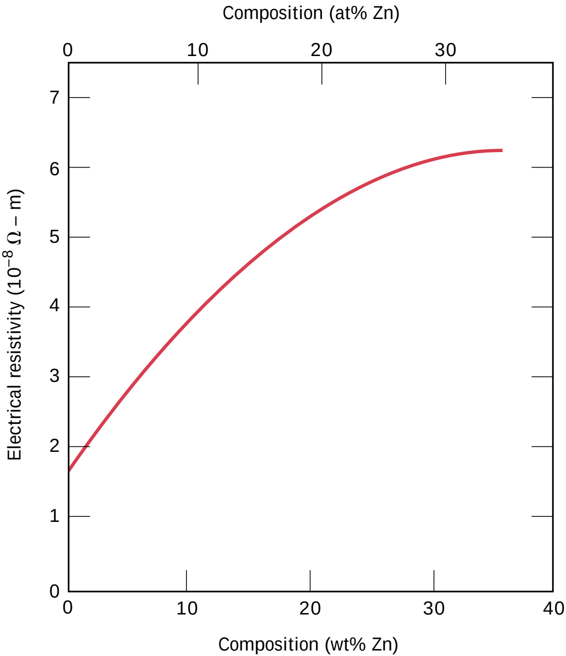

Figure 12.35 Room-temperature electrical resistivity versus composition for copper–zinc alloys. (Adapted from *Metals Handbook: Properties and Selection: Nonferrous Alloys and Pure Metals*, Vol. 2, 9th edition, H. Baker, Managing Editor, American Society for Metals, 1979, p. 315.)

CHAPTER 13

TYPES AND APPLICATIONS OF MATERIALS

13.5 We are asked to compute the volume percent graphite in a 3.5 wt% C cast iron. It first becomes necessary to compute mass fractions using the lever rule. From the iron-carbon phase diagram (Figure 13.2), the tie-line in the α and graphite phase field extends from essentially 0 wt% C to 100 wt% C. Thus, for a 3.5 wt% C cast iron

$$W_\alpha = \frac{C_{Gr} - C_o}{C_{Gr} - C_\alpha} = \frac{100 - 3.5}{100 - 0} = 0.965$$

$$W_{Gr} = \frac{C_o - C_\alpha}{C_{Gr} - C_\alpha} = \frac{3.5 - 0}{100 - 0} = 0.035$$

Conversion from weight fraction to volume fraction of graphite is possible using Equation (10.6a) as

$$V_{Gr} = \frac{\dfrac{W_{Gr}}{\rho_{Gr}}}{\dfrac{W_\alpha}{\rho_\alpha} + \dfrac{W_{Gr}}{\rho_{Gr}}}$$

$$= \frac{\dfrac{0.035}{2.3\ \text{g/cm}^3}}{\dfrac{0.965}{7.9\ \text{g/cm}^3} + \dfrac{0.035}{2.3\ \text{g/cm}^3}}$$

$$= 0.111 \text{ or } 11.1\,\text{vol\%}$$

13.21* In this problem we are asked to find the maximum temperatures to which magnesia-alumina refractories may be heated before a liquid phase will appear.

(a) For a spinel-bonded alumina material of composition 95 wt% Al_2O_3-5 wt% MgO we must use Figure 10.22. According to this phase diagram, the maximum temperature without a liquid phase corresponds to the temperature of the eutectic isotherm on the Al_2O_3-rich side of the phase diagram, which is approximately 2000°C (3630°F).

13.23* This problem calls for us to compute the mass fractions of liquid for four refractory materials at 1600°C. In order to solve this problem it is necessary that we use the SiO_2-Al_2O_3 phase diagram (Figure 10.24), in conjunction with tie-lines and the lever rule at 1600°C.

(a) For $\mathbf{C_o} = 6$ wt% Al_2O_3 the mass fraction of liquid $\mathbf{W_L}$ is just

$$W_L = \frac{C_o - C_{SiO_2}}{C_L - C_{SiO_2}}$$

$$= \frac{6 - 0}{7 - 0} = 0.86$$

FIGURE 13.2 The true equilibrium iron–carbon phase diagram with graphite instead of cementite as a stable phase. (Adapted from *Binary Alloy Phase Diagrams*, T. B. Massalski, Editor-in-Chief, 1990. Reprinted by permission of ASM International, Materials Park, OH.)

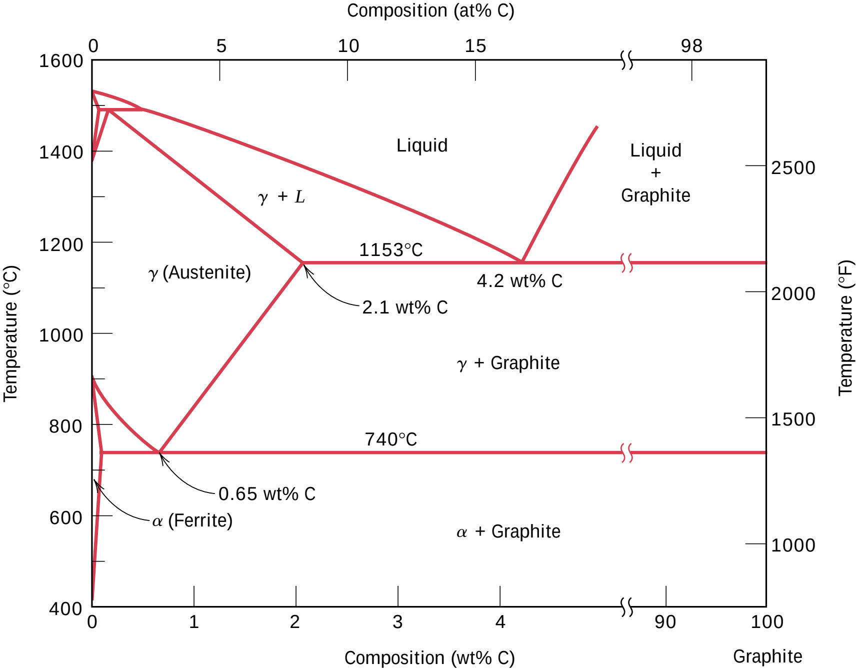

CHAPTER 14

SYNTHESIS, FABRICATION, AND PROCESSING OF MATERIALS

14.19 (a) This part of the problem calls for us to construct a radial hardness profile for a 50 mm (2 in.) diameter cylindrical specimen of an 8640 steel that has been quenched in moderately agitated oil. In the manner of Example Problem 14.1, the equivalent distances and hardnesses tabulated below were determined from Figures 14.8 and 14.11.

Radial Position	Equivalent Distance, mm (in.)	HRC Hardness
Surface	7 (5/16)	54
3/4 R	11 (7/16)	50
Midradius	14 (9/16)	45
Center	16 (10/16)	44

The resulting profile is plotted below.

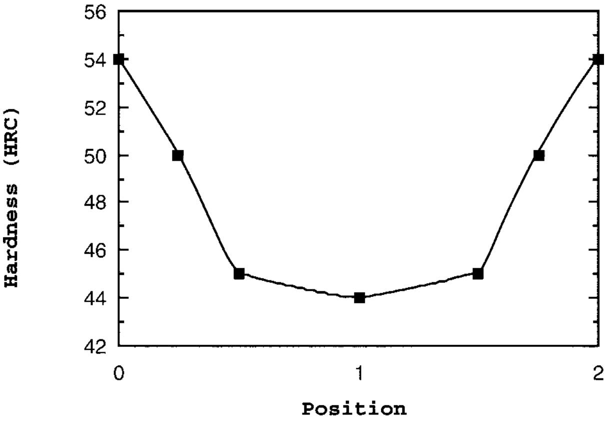

14.26 (a) Below is shown the logarithm viscosity versus reciprocal of temperature plot for the borosilicate glass, using the data in Figure 14.16.

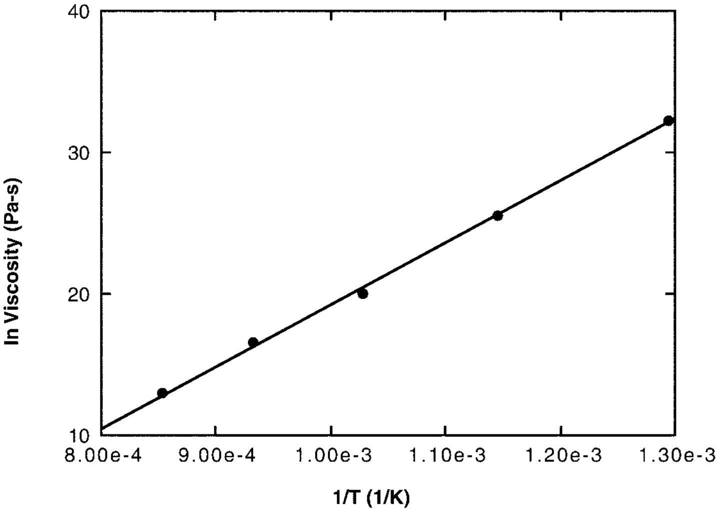

(b) Solving for the activation energy, $\mathbf{Q_{vis}}$, from the equation given in the problem, we get

$$Q_{\text{vis}} = RT \ln \eta + RT \ln A$$

The activation energy, $\mathbf{Q_{vis}}$, may be computed from this plot according to

$$Q_{\text{vis}} = R \left[\frac{\Delta \ln \eta}{\Delta \left(\frac{1}{T} \right)} \right]$$

where **R** is the gas constant, and $\Delta \ln \eta / \Delta(1/\mathbf{T})$ is the slope of the line that has been constructed. The value of this slope is 4.36×10^4. Therefore,

$$\begin{aligned} Q_{\text{vis}} &= (8.31 \text{ J/mol-K})(4.36 \times 10^4) \\ &= 362{,}000 \text{ J/mol} \end{aligned}$$

14.43 (a) This problem asks that we determine how much adipic acid must be added to 50.0 kg of ethylene glycol to produce a linear chain structure of polyester according to Equation 14.5. Since the chemical formulas are provided in this equation we may calculate the molecular weights of each of these materials as follows:

$$\begin{aligned} A(\text{adipic}) &= 6(A_C) + 10(A_H) + 4(A_O) \\ &= 6(12.01 \text{ g/mol}) + 10(1.008 \text{ g/mol}) + 4(16.00 \text{ g/mol}) = 146.14 \text{ g/mol} \\ A(\text{glycol}) &= 2(A_C) + 6(A_H) + 2(A_O) \\ &= 2(12.01 \text{ g/mol}) + 6(1.008 \text{ g/mol}) + 2(16.00 \text{ g/mol}) = 62.07 \text{ g/mol} \end{aligned}$$

The 50.0 kg mass of ethylene glycol equals 50,000 g or $\frac{50000 \text{ g}}{62.07 \text{ g/mol}} = 805.5$ mol. According to Equation (14.5), each mole of adipic acid used requires one mole of ethylene glycol, which is equivalent to (805.5 mol)(146.14 g/mol) = 1.177×10^5 g = 117.7 kg.

(b) Now we are asked for the mass of the resulting polyester. Inasmuch as one mole of water is given off for every mer unit produced, this corresponds to 805.5 moles or (805.5 mol)(18.02 g/mol) = 14,500 g or 14.5 kg since the molecular weight of water is 18.02 g/mol. The mass of polyester is just the sum of the masses of the two reactant materials (as computed in part a) minus the mass of water released, or

$$\text{mass(polyester)} = 50.0 \text{ kg} + 117.7 \text{ kg} - 14.5 \text{ kg} = 153.2 \text{ kg}$$

14.D1 A one-inch diameter steel specimen is to be quenched in moderately agitated oil. We are to decide which of five different steels will have surface and center hardnesses of at least 55 and 50 HRC, respectively.

In moderately agitated oil, the equivalent distances from the quenched end for a one-inch diameter bar for surface and center positions are 3 mm (1/8 in.) and 8 mm (11/32 in.), respectively [Figure 14.11(b)]. The hardnesses at these two positions for the alloys cited (as determined using Figure 14.8) are given below.

Alloy	Surface Hardness (HRC)	Center Hardness (HRC)
1040	50	30
5140	55	47
4340	57	57
4140	56	54
8640	56	52.5

Thus, alloys 4340, 4140, and 8640 will satisfy the criteria for both surface and center hardnesses.

14.D5 We are asked to determine the maximum diameter possible for a cylindrical piece of 4140 steel that is to be quenched in moderately agitated oil such that the microstructure will consist of at least 50% martensite throughout the entire piece. From Figure 14.8, the equivalent distance from the quenched end of a 4140 steel to give 50% martensite (or a 42.5 HRC hardness) is 26 mm (1–1/16 in.). Thus, the quenching rate at the center of the specimen should correspond to this equivalent distance. Using Figure 14.11(b), the center specimen curve takes on a value of 26 mm (1–1/16 in.) equivalent distance at a diameter of about 75 mm (3 in.).

FIGURE 14.8 Hardenability curves for five different steel alloys, each containing 0.4 wt% C. Approximate alloy compositions (wt%) are as follows: 4340–1.85 Ni, 0.80 Cr, and 0.25 Mo; 4140–1.0 Cr and 0.20 Mo; 8640–0.55 Ni, 0.50 Cr, and 0.20 Mo; 5140–0.85 Cr; 1040 is an unalloyed steel. (Adapted from figure furnished courtesy Republic Steel Corporation.)

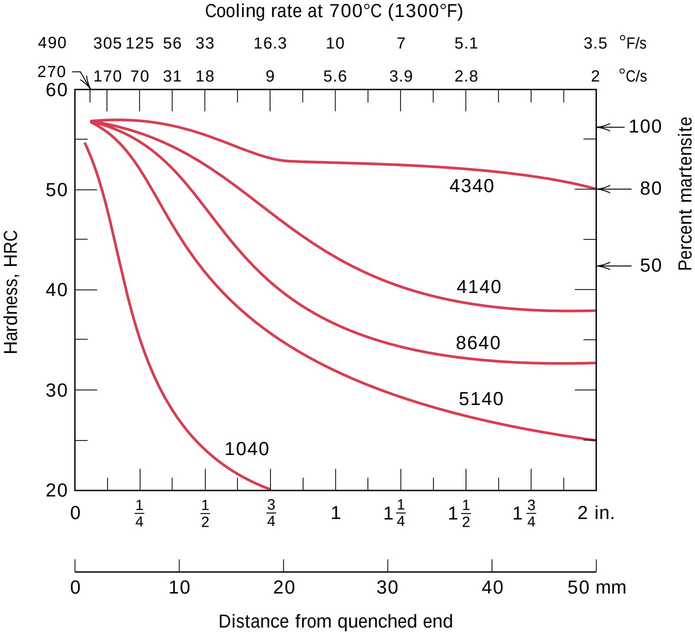

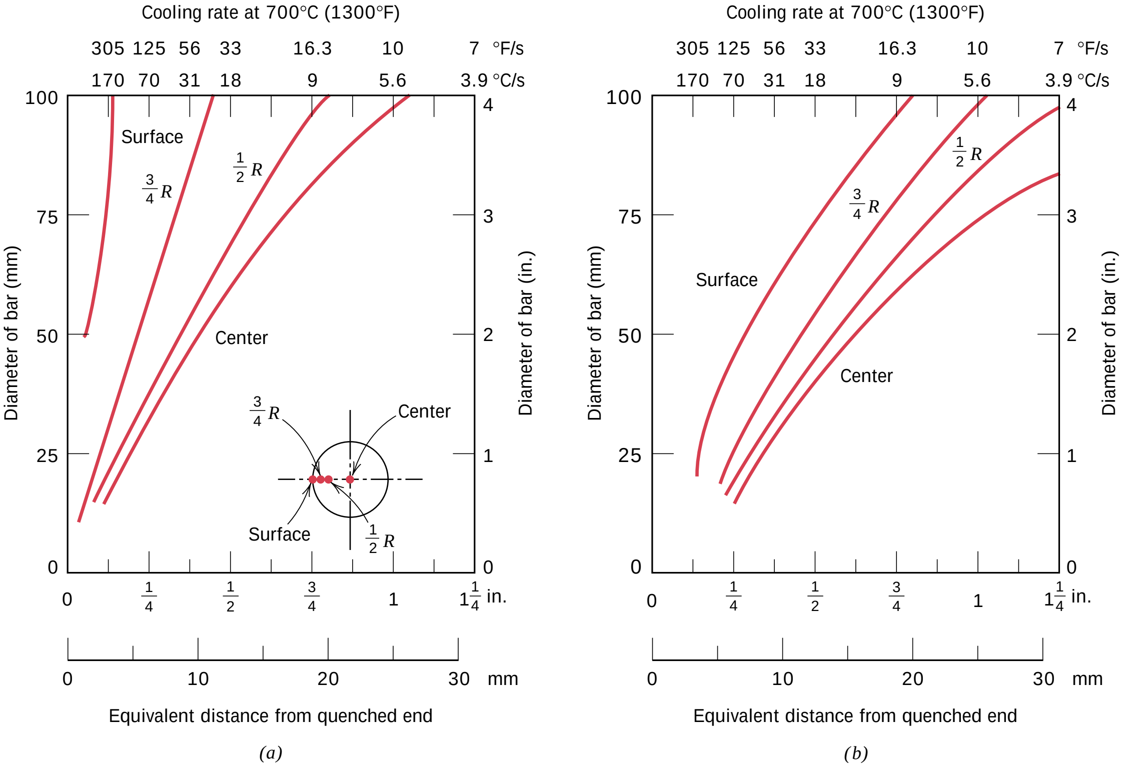

FIGURE 14.11 Cooling rate as a function of diameter at surface, three-quarters radius ($\frac{3}{4}R$), midradius ($\frac{1}{2}R$), and center positions for cylindrical bars quenched in mildly agitated (*a*) water and (*b*) oil. Equivalent Jominy positions are included along the bottom axis. (Adapted from *Metals Handbook: Properties and Selection: Irons and Steels,* Vol. 1, 9th edition, B. Bardes, Editor, American Society for Metals, 1978, p. 492.)

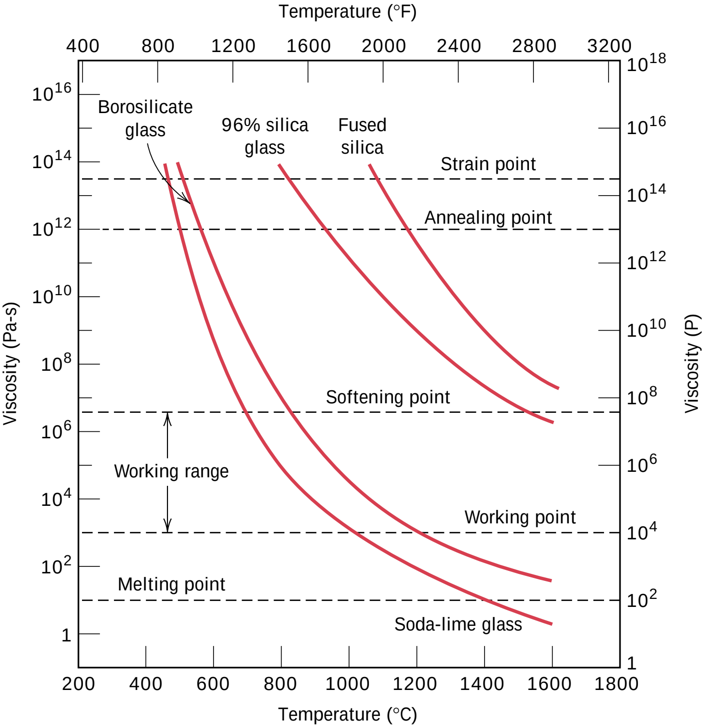

FIGURE 14.16 Logarithm of viscosity versus temperature for fused silica and several silica glasses. (From E. B. Shand, *Engineering Glass, Modern Materials,* Vol. 6, Academic Press, New York, 1968, p. 262.)

CHAPTER 15

COMPOSITES

15.4 This problem asks for the maximum and minimum thermal conductivity values for a TiC-Co cermet. Using a modified form of Equation (15.1) the maximum thermal conductivity $\mathbf{k_c(u)}$ is calculated as

$$\begin{aligned} k_c(u) &= k_m V_m + k_p V_p = k_{Co} V_{Co} + k_{TiC} V_{TiC} \\ &= (69\ \mathrm{W/m\text{-}K})(0.15) + (27\ \mathrm{W/m\text{-}K})(0.85) = 33.3\ \mathrm{W/m\text{-}K} \end{aligned}$$

The minimum thermal conductivity $\mathbf{k_c(l)}$ will be

$$\begin{aligned} k_c(l) &= \frac{k_{Co} k_{TiC}}{V_{Co} k_{TiC} + V_{TiC} k_{Co}} \\ &= \frac{(69\ \mathrm{W/m\text{-}K})(27\ \mathrm{W/m\text{-}K})}{(0.15)(27\ \mathrm{W/m\text{-}K}) + (0.85)(69\ \mathrm{W/m\text{-}K})} \\ &= 29.7\ \mathrm{W/m\text{-}K} \end{aligned}$$

15.12 This problem asks for us to determine if it is possible to produce a continuous and oriented aramid fiber-epoxy matrix composite having longitudinal and transverse moduli of elasticity of 57.1 GPa and 4.12 GPa, respectively, given that the modulus of elasticity for the epoxy is 2.4 GPa. Also, from Table 15.4 the value of **E** for aramid fibers is 131 GPa. The approach to solving this problem is to calculate two values of $\mathbf{V_f}$ using the data and Equations (15.10b) and (15.16); if they are the same then this composite is possible.

For the longitudinal modulus $\mathbf{E_{cl}}$,

$$\begin{aligned} E_{cl} &= E_m[1 - V_{fl}] + E_f V_{fl} \\ 57.1\ \mathrm{GPa} &= (2.4\ \mathrm{GPa})[1 - V_{fl}] + (131\ \mathrm{GPa})V_{fl} \end{aligned}$$

Solving this expression for $\mathbf{V_{fl}}$ yields $\mathbf{V_{fl}} = 0.425$.

Now, repeating this procedure for the transverse modulus $\mathbf{E_{ct}}$

$$\begin{aligned} E_{ct} &= \frac{E_m E_f}{[1 - V_{ft}]E_f + V_{ft} E_m} \\ 4.12\ \mathrm{GPa} &= \frac{(2.4\ \mathrm{GPa})(131\ \mathrm{GPa})}{[1 - V_{ft}](131\ \mathrm{GPa}) + V_{ft}(2.4\ \mathrm{GPa})} \end{aligned}$$

Solving this expression for $\mathbf{V_{ft}}$ leads to $\mathbf{V_{ft}} = 0.425$. Thus, since $\mathbf{V_{fl}}$ and $\mathbf{V_{ft}}$ are equal, the proposed composite is possible.

15.17 The problem stipulates that the cross-sectional area of a composite, $\mathbf{A_c}$, is 320 mm^2 (0.50 $\mathrm{in.}^2$), and the longitudinal load, $\mathbf{F_c}$, is 44,500 N (10,000 $\mathrm{lb_f}$) for the composite described in Problem 15.11.

(a) First, we are asked to calculate the $\mathbf{F_f/F_m}$ ratio. According to Equation (15.11)

$$\frac{F_f}{F_m} = \frac{E_f V_f}{E_m V_m} = \frac{(131\ \mathrm{GPa})(0.30)}{(2.4\ \mathrm{GPa})(0.70)} = 23.4$$

Or, $\mathbf{F_f} = 23.4\mathbf{F_m}$

(b) Now, the actual loads carried by both phases are called for. Since

$$\begin{aligned} F_f + F_m &= F_c = 44{,}500\ \mathrm{N} \\ 23.4F_m + F_m &= 44{,}500\ \mathrm{N} \end{aligned}$$

which leads to

$$F_m = 1824\ \text{N}\ (410\ \text{lb}_f)$$
$$F_f = 44{,}500\ \text{N} - 1824\ \text{N} = 42{,}676\ \text{N}\ (9590\ \text{lb}_f)$$

(c) To compute the stress on each of the phases, it is first necessary to know the cross-sectional areas of both fiber and matrix. These are determined as

$$A_f = V_f A_c = (0.30)(320\ \text{mm}^2) = 96\ \text{mm}^2\ (0.15\ \text{in.}^2)$$
$$A_m = V_m A_c = (0.70)(320\ \text{mm}^2) = 224\ \text{mm}^2\ (0.35\ \text{in.}^2)$$

Now, for the stresses,

$$\sigma_f = \frac{F_f}{A_f} = \frac{42676\ \text{N}}{(96\ \text{mm}^2)} = 445\ \text{MPa}\ (63{,}930\ \text{psi})$$
$$\sigma_m = \frac{F_m}{A_m} = \frac{1824\ \text{N}}{(224\ \text{mm}^2)} = 8.14\ \text{MPa}\ (1170\ \text{psi})$$

(d) The strain on the composite is the same as the strain on each of the matrix and fiber phases, as

$$\varepsilon_m = \frac{\sigma_m}{E_m} = \frac{8.14\ \text{MPa}}{2.4 \times 10^3\ \text{MPa}} = 3.39 \times 10^{-3}$$
$$\varepsilon_f = \frac{\sigma_f}{E_f} = \frac{445\ \text{MPa}}{131 \times 10^3\ \text{MPa}} = 3.39 \times 10^{-3}$$

15.21 In this problem, for an aligned glass fiber-epoxy matrix composite, we are asked to compute the longitudinal tensile strength given the following: the average fiber diameter (0.010 mm), the average fiber length (2.5 mm), the volume fraction of fibers (0.40), the fiber fracture strength (3500 MPa), the fiber-matrix bond strength (75 MPa), and the matrix stress at composite failure (8.0 MPa). It is first necessary to compute the value of the critical fiber length using Equation (15.3). If the fiber length is much greater than $\mathbf{l_c}$, then we may determine $\sigma^*_{\mathbf{cl}}$ using Equation (15.17), otherwise, use of either Equation (15.18) or (15.19) is necessary. Thus,

$$l_c = \frac{\sigma_f^* d}{2\tau_c} = \frac{(3500\ \text{MPa})(0.010\ \text{mm})}{2(75\ \text{MPa})} = 0.233\ \text{mm}\ (0.0093\ \text{in.})$$

Inasmuch as $l > \mathbf{l_c}$ (2.5 mm > 0.233 mm), but $\mathbf{l}$ is not much greater than $\mathbf{l_c}$, then use of Equation (15.18) is necessary. Therefore,

$$\begin{aligned}\sigma^*_{cd} &= \sigma_f^* V_f \left[1 - \frac{l_c}{2l}\right] + \sigma'_m(1 - V_f)\\ &= (3500\ \text{MPa})(0.40)\left[1 - \frac{0.233\ \text{mm}}{(2)(2.5\ \text{mm})}\right] + (8.0\ \text{MPa})(1 - 0.40)\\ &= 1340\ \text{MPa}\ (194{,}400\ \text{psi})\end{aligned}$$

15.D1 In order to solve this problem, we want to make longitudinal elastic modulus and tensile strength computations assuming 50 vol% fibers for all three fiber materials, in order to see which meet the stipulated criteria [i.e., a minimum elastic modulus of 50 GPa (7.3 $\times 10^6$ psi), and a minimum tensile strength of 1300 MPa (189,000 psi)]. Thus, it becomes necessary to use Equations (15.10b) and (15.17) with $\mathbf{V_m} = 0.5$ and $\mathbf{V_f} = 0.5$, $\mathbf{E_m} = 3.1$ GPa, and $\sigma^*_{\mathbf{m}} = 75$ MPa.

For glass, $\mathbf{E_f} = 72.5$ GPa and $\sigma_{\mathbf{f}}^* = 3450$ MPa. Therefore,

$$\begin{aligned} E_{cl} &= E_m(1 - V_f) + E_f V_f \\ &= (3.1 \text{ GPa})(1 - 0.5) + (72.5 \text{ GPa})(0.5) = 37.8 \text{ GPa } (5.48 \times 10^6 \text{ psi}) \end{aligned}$$

Since this is less than the specified minimum, glass is not an acceptable candidate.

For carbon (PAN standard-modulus), $\mathbf{E_f} = 230$ GPa and $\sigma_{\mathbf{f}}^* = 4000$ MPa (the average of the range of values in Table B.4), thus

$$E_{cl} = (3.1 \text{ GPa})(0.5) + (230 \text{ GPa})(0.5) = 116.6 \text{ GPa } (16.9 \times 10^6 \text{ psi})$$

which is greater than the specified minimum. In addition, from Equation (15.17)

$$\begin{aligned} \sigma_{cl}^* &= \sigma_m'(1 - V_f) + \sigma_f^* V_f \\ &= (30 \text{ MPa})(0.5) + (4000 \text{ MPa})(0.5) = 2015 \text{ MPa } (292{,}200 \text{ psi}) \end{aligned}$$

which is also greater than the minimum. Thus, carbon (PAN standard-modulus) is a candidate.

For aramid, $\mathbf{E_f} = 131$ GPa and $\sigma_{\mathbf{f}}^* = 3850$ MPa (the average of the range of values in Table B.4), thus

$$E_{cl} = (3.1 \text{ GPa})(0.5) + (131 \text{ GPa})(0.5) = 67.1 \text{ GPa } (9.73 \times 10^6 \text{ psi})$$

which value is greater than the minimum. Also, from Equation (15.17)

$$\begin{aligned} \sigma_{cl}^* &= \sigma_m'(1 - V_f) + \sigma_f^* V_f \\ &= (50 \text{ MPa})(0.5) + (3850 \text{ MPa})(0.5) = 1950 \text{ MPa } (283{,}600 \text{ psi}) \end{aligned}$$

which is also greater than the minimum strength value. Therefore, of the three fiber materials, both the carbon (PAN standard-modulus) and the aramid meet both minimum criteria.

15.D3 This problem asks us to determine whether or not it is possible to produce a continuous and oriented glass fiber-reinforced polyester having a tensile strength of at least 1400 MPa in the longitudinal direction, and a maximum specific gravity of 1.65. We will first calculate the minimum volume fraction of fibers to give the stipulated tensile strength, and then the maximum volume fraction of fibers possible to yield the maximum permissible specific gravity; if there is an overlap of these two fiber volume fractions then such a composite is possible.

With regard to tensile strength, from Equation (15.17)

$$\begin{aligned} \sigma_{cl}^* &= \sigma_m'(1 - V_f) + \sigma_f^* V_f \\ 1400 \text{ MPa} &= (15 \text{ MPa})(1 - V_f) + (3500 \text{ MPa})(V_f) \end{aligned}$$

Solving for $\mathbf{V_f}$ yields $\mathbf{V_f} = 0.397$. Therefore, $\mathbf{V_f} > 0.397$ to give the minimum desired tensile strength.

Now, upon consideration of the specific gravity, ρ, we employ the following relationship:

$$\begin{aligned} \rho_c &= \rho_m(1 - V_f) + \rho_f V_f \\ 1.65 &= 1.35(1 - V_f) + 2.50(V_f) \end{aligned}$$

And, solving for $\mathbf{V_f}$ from this expression gives $\mathbf{V_f} = 0.261$. Therefore, it is necessary for $\mathbf{V_f} < 0.261$ in order to have a composite specific gravity less than 1.65.

Hence, such a composite is **not** possible since there is no overlap of the fiber volume fractions as computed using the two stipulated criteria.

Chapter 15 / Composites

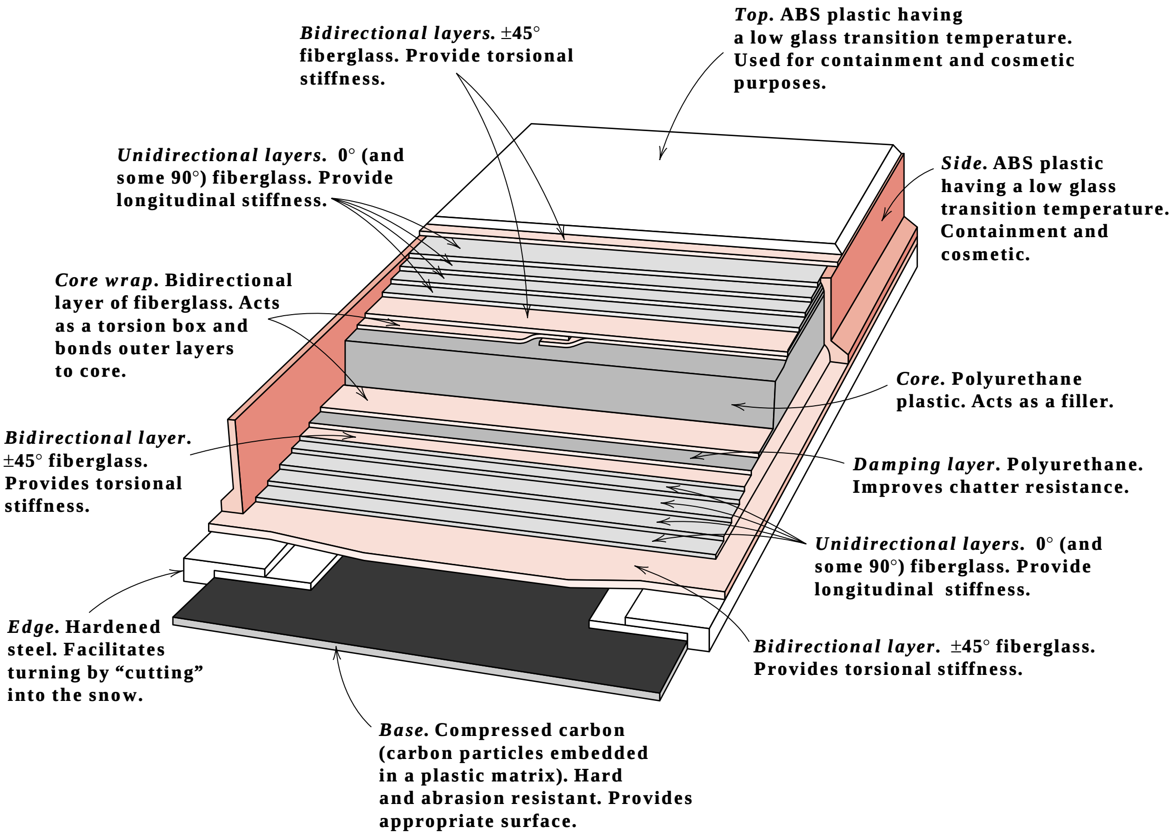
Top. ABS plastic having a low glass transition temperature. Used for containment and cosmetic purposes.
Bidirectional layers. ±45° fiberglass. Provide torsional stiffness.
Unidirectional layers. 0° (and some 90°) fiberglass. Provide longitudinal stiffness.
Side. ABS plastic having a low glass transition temperature. Containment and cosmetic.
Core wrap. Bidirectional layer of fiberglass. Acts as a torsion box and bonds outer layers to core.
Core. Polyurethane plastic. Acts as a filler.
Bidirectional layer. ±45° fiberglass. Provides torsional stiffness.
Damping layer. Polyurethane. Improves chatter resistance.
Unidirectional layers. 0° (and some 90°) fiberglass. Provide longitudinal stiffness.
Edge. Hardened steel. Facilitates turning by "cutting" into the snow.
Bidirectional layer. ±45° fiberglass. Provides torsional stiffness.
Base. Compressed carbon (carbon particles embedded in a plastic matrix). Hard and abrasion resistant. Provides appropriate surface.

One relatively complex composite material is the modern ski. In this illustration, a cross-section of a high-performance snow ski, are shown the various components. The function of each component is noted, as well as the material that is used in its construction. (Courtesy of Evolution Ski Company, Salt Lake City, Utah.)

Why Study *Composites?*

With a knowledge of the various types of composites, as well as an understanding of the dependence of their behaviors on the characteristics, relative amounts, geometry/distribution, and properties of the constituent phases, it is possible to design materials having property combinations that are better than those found in the metal alloys, ceramics, and polymeric materials. For example, in Design Example 15.1, we discuss how a filament-wound tubular shaft is designed that meets specified stiffness requirements.

Learning Objectives

After careful study of this chapter you should be able to do the following:

1. **Name the three main divisions of composite materials, and cite the distinguishing feature of each.**
2. **Cite the difference in strengthening mechanism for large-particle and dispersion-strengthened particle-reinforced composites.**
3. **Name the three different types of fiber-reinforced composites on the basis of fiber length and orientation; comment on the distinctive mechanical characteristics for each type.**
4. **Calculate longitudinal modulus and longitudinal strength for an aligned and continuous fiber-reinforced composite.**
5. **Compute longitudinal strengths for discontinuous and aligned fibrous composite materials.**
6. **Note the three common fiber reinforcements used in polymer-matrix composites, and, for each, cite both desirable characteristics and limitations.**
7. **Cite the desirable features of metal-matrix composites.**
8. **Note the primary reason for the creation of ceramic-matrix composites.**
9. **Name and briefly describe the two subclassifications of structural composites.**

15.1 INTRODUCTION

Many of our modern technologies require materials with unusual combinations of properties that cannot be met by the conventional metal alloys, ceramics, and polymeric materials. This is especially true for materials that are needed for aerospace, underwater, and transportation applications. For example, aircraft engineers are increasingly searching for structural materials that have low densities, are strong, stiff, and abrasion and impact resistant, and are not easily corroded. This is a rather formidable combination of characteristics. Frequently, strong materials are relatively dense; also, increasing the strength or stiffness generally results in a decrease in impact strength.

Material property combinations and ranges have been, and are yet being, extended by the development of composite materials. Generally speaking, a composite is considered to be any multiphase material that exhibits a significant proportion of the properties of both constituent phases such that a better combination of properties is realized. According to this **principle of combined action,** better property combinations are fashioned by the judicious combination of two or more distinct materials. Property trade-offs are also made for many composites.

Composites of sorts have already been discussed; these include multiphase metal alloys, ceramics, and polymers. For example, pearlitic steels (Section 10.19) have a microstructure consisting of alternating layers of α ferrite and cementite (Figure 10.29). The ferrite phase is soft and ductile, whereas cementite is hard and very brittle. The combined mechanical characteristics of the pearlite (reasonably high ductility and strength) are superior to those of either of the constituent phases. There are also a number of composites that occur in nature. For example, wood consists of strong and flexible cellulose fibers surrounded and held together by a stiffer material called lignin. Also, bone is a composite of the strong yet soft protein collagen and the hard, brittle mineral apatite.

A composite, in the present context, is a multiphase material that is artificially made, as opposed to one that occurs or forms naturally. In addition, the constituent phases must be chemically dissimilar and separated by a distinct interface. Thus, most metallic alloys and many ceramics do not fit this definition because their multiple phases are formed as a consequence of natural phenomena.

In designing composite materials, scientists and engineers have ingeniously combined various metals, ceramics, and polymers to produce a new generation of

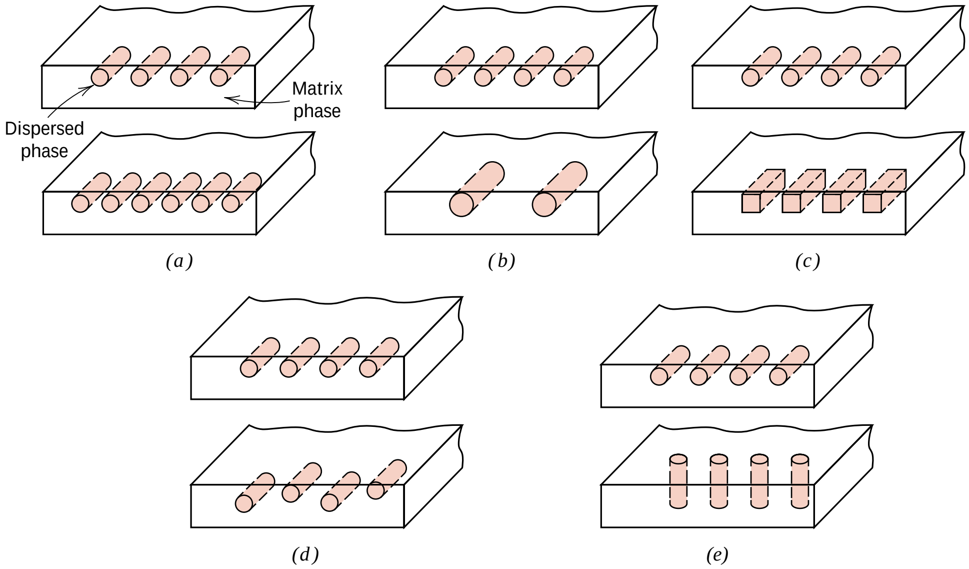
Matrix phase
Dispersed phase
(a)
(b)
(c)
(d)
(e)

Figure 15.1 Schematic representations of the various geometrical and spatial characteristics of particles of the dispersed phase that may influence the properties of composites: (*a*) concentration, (*b*) size, (*c*) shape, (*d*) distribution, and (*e*) orientation. (From Richard A. Flinn and Paul K. Trojan, *Engineering Materials and Their Applications,* 4th edition. Copyright © 1990 by John Wiley & Sons, Inc. Adapted by permission of John Wiley & Sons, Inc.)

extraordinary materials. Most composites have been created to improve combinations of mechanical characteristics such as stiffness, toughness, and ambient and high-temperature strength.

Many composite materials are composed of just two phases; one is termed the **matrix,** which is continuous and surrounds the other phase, often called the **dispersed phase.** The properties of composites are a function of the properties of the constituent phases, their relative amounts, and the geometry of the dispersed phase. ''Dispersed phase geometry'' in this context means the shape of the particles and the particle size, distribution, and orientation; these characteristics are represented in Figure 15.1.

One simple scheme for the classification of composite materials is shown in Figure 15.2, which consists of three main divisions—particle-reinforced, fiber-rein-

Figure 15.2 A classification scheme for the various composite types discussed in this chapter.

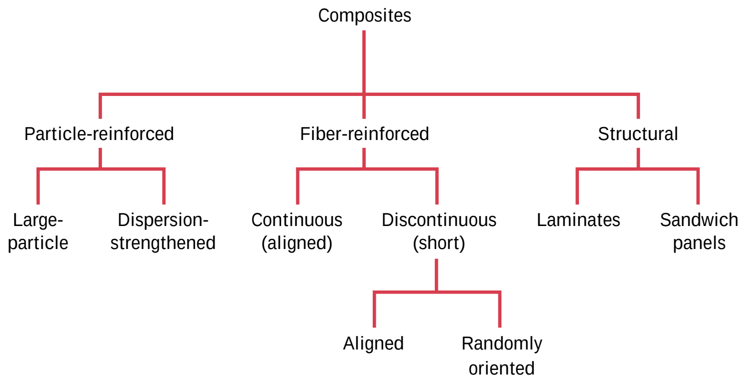
Composites
Particle-reinforced
Fiber-reinforced
Structural
Large-particle
Dispersion-strengthened
Continuous (aligned)
Discontinuous (short)
Laminates
Sandwich panels
Aligned
Randomly oriented

forced, and structural composites; also, at least two subdivisions exist for each. The dispersed phase for particle-reinforced composites is equiaxed (i.e., particle dimensions are approximately the same in all directions); for fiber-reinforced composites, the dispersed phase has the geometry of a fiber (i.e., a large length-to-diameter ratio). Structural composites are combinations of composites and homogenous materials. The discussion of the remainder of this chapter will be organized according to this classification scheme.

PARTICLE-REINFORCED COMPOSITES

As noted in Figure 15.2, **large-particle** and **dispersion-strengthened composites** are the two subclassifications of particle-reinforced composites. The distinction between these is based upon reinforcement or strengthening mechanism. The term ''large'' is used to indicate that particle–matrix interactions cannot be treated on the atomic or molecular level; rather, continuum mechanics is used. For most of these composites, the particulate phase is harder and stiffer than the matrix. These reinforcing particles tend to restrain movement of the matrix phase in the vicinity of each particle. In essence, the matrix transfers some of the applied stress to the particles, which bear a fraction of the load. The degree of reinforcement or improvement of mechanical behavior depends on strong bonding at the matrix–particle interface.

For dispersion-strengthened composites, particles are normally much smaller, having diameters between 0.01 and 0.1 μm (10 and 100 nm). Particle–matrix interactions that lead to strengthening occur on the atomic or molecular level. The mechanism of strengthening is similar to that for precipitation hardening discussed in Section 11.11. Whereas the matrix bears the major portion of an applied load, the small dispersed particles hinder or impede the motion of dislocations. Thus, plastic deformation is restricted such that yield and tensile strengths, as well as hardness, improve.

15.2 LARGE-PARTICLE COMPOSITES

Some polymeric materials to which fillers have been added (Section 14.12) are really large-particle composites. Again, the fillers modify or improve the properties of the material and/or replace some of the polymer volume with a less expensive material—the filler.

Another familiar large-particle composite is concrete, being composed of cement (the matrix), and sand and gravel (the particulates). Concrete is the discussion topic of a succeeding section.

Particles can have quite a variety of geometries, but they should be of approximately the same dimension in all directions (equiaxed). For effective reinforcement, the particles should be small and evenly distributed throughout the matrix. Furthermore, the volume fraction of the two phases influences the behavior; mechanical properties are enhanced with increasing particulate content. Two mathematical expressions have been formulated for the dependence of the elastic modulus on the volume fraction of the constituent phases for a two-phase composite. These **rule of mixtures** equations predict that the elastic modulus should fall between an upper bound represented by

$$E_c(u) = E_m V_m + E_p V_p \tag{15.1}$$

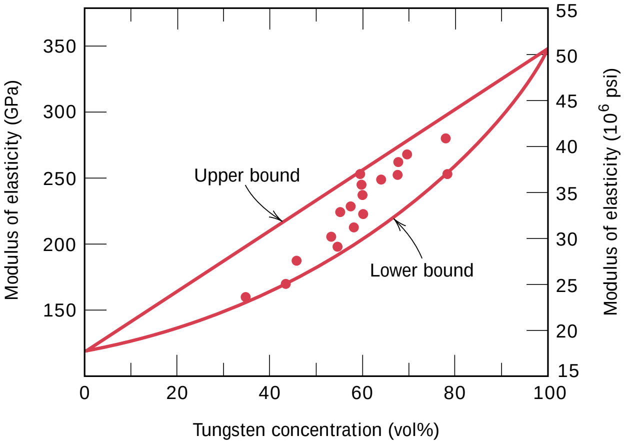

Figure 15.3 Modulus of elasticity versus volume percent tungsten for a composite of tungsten particles dispersed within a copper matrix. Upper and lower bounds are according to Equations 15.1 and 15.2; experimental data points are included. (From R. H. Krock, *ASTM Proceedings*, Vol. 63, 1963. Copyright ASTM. Reprinted with permission.)

and a lower bound, or limit,

$$E_c(l) = \frac{E_m E_p}{V_m E_p + V_p E_m} \tag{15.2}$$

In these expressions, E and V denote the elastic modulus and volume fraction, respectively, whereas the subscripts c, m, and p represent composite, matrix, and particulate phases. Figure 15.3 plots upper- and lower-bound E_c-versus-V_p curves for a copper–tungsten composite, in which tungsten is the particulate phase; experimental data points fall between the two curves. Equations analogous to 15.1 and 15.2 for fiber-reinforced composites are derived in Section 15.5.

Large-particle composites are utilized with all three material types (metals, polymers, and ceramics). The **cermets** are examples of ceramic–metal composites. The most common cermet is the cemented carbide, which is composed of extremely hard particles of a refractory carbide ceramic such as tungsten carbide (WC) or titanium carbide (TiC), embedded in a matrix of a metal such as cobalt or nickel. These composites are utilized extensively as cutting tools for hardened steels. The hard carbide particles provide the cutting surface but, being extremely brittle, are not themselves capable of withstanding the cutting stresses. Toughness is enhanced by their inclusion in the ductile metal matrix, which isolates the carbide particles from one another and prevents particle-to-particle crack propagation. Both matrix and particulate phases are quite refractory, to withstand the high temperatures generated by the cutting action on materials that are extremely hard. No single material could possibly provide the combination of properties possessed by a cermet. Relatively large volume fractions of the particulate phase may be utilized, often exceeding 90 vol%; thus the abrasive action of the composite is maximized. A photomicrograph of a WC–Co cemented carbide is shown in Figure 15.4.

Both elastomers and plastics are frequently reinforced with various particulate materials. Our use of many of the modern rubbers would be severely restricted without reinforcing particulate materials such as carbon black. Carbon black consists of very small and essentially spherical particles of carbon, produced by the combustion of natural gas or oil in an atmosphere that has only a limited air supply. When added to vulcanized rubber, this extremely inexpensive material enhances tensile strength, toughness, and tear and abrasion resistance. Automobile tires contain on

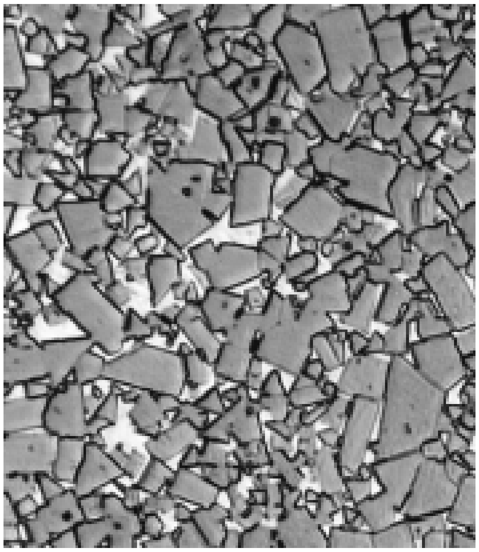

FIGURE 15.4 Photomicrograph of a WC–Co cemented carbide. Light areas are the cobalt matrix; dark regions, the particles of tungsten carbide. 100×. (Courtesy of Carboloy Systems Department, General Electric Company.)

the order of 15 to 30 vol% of carbon black. For the carbon black to provide significant reinforcement, the particle size must be extremely small, with diameters between 20 and 50 nm; also, the particles must be evenly distributed throughout the rubber and must form a strong adhesive bond with the rubber matrix. Particle reinforcement using other materials (e.g., silica) is much less effective because this special interaction between the rubber molecules and particle surfaces does not exist. Figure 15.5 is an electron micrograph of a carbon black-reinforced rubber.

CONCRETE

Concrete is a common large-particle composite in which both matrix and dispersed phases are ceramic materials. Since the terms ''concrete'' and ''cement'' are some-

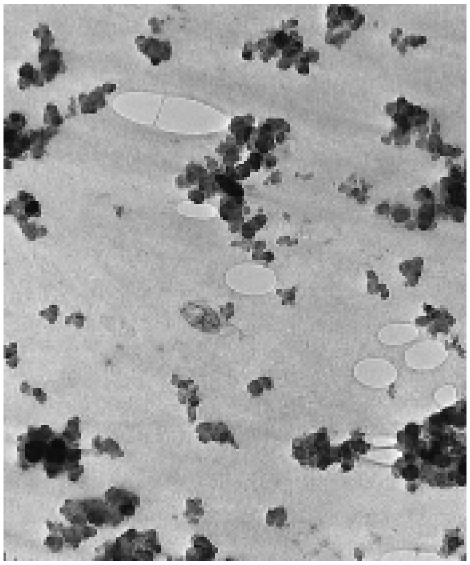

FIGURE 15.5 Electron micrograph showing the spherical reinforcing carbon black particles in a synthetic rubber tire tread compound. The areas resembling water marks are tiny air pockets in the rubber. 80,000×. (Courtesy of Goodyear Tire & Rubber Company.)

times incorrectly interchanged, perhaps it is appropriate to make a distinction between them. In a broad sense, concrete implies a composite material consisting of an aggregate of particles that are bound together in a solid body by some type of binding medium, that is, a cement. The two most familiar concretes are those made with portland and asphaltic cements, where the aggregate is gravel and sand. Asphaltic concrete is widely used primarily as a paving material, whereas portland cement concrete is employed extensively as a structural building material. Only the latter is treated in this discussion.

Portland Cement Concrete

The ingredients for this concrete are portland cement, a fine aggregate (sand), a coarse aggregate (gravel), and water. The process by which portland cement is produced and the mechanism of setting and hardening were discussed very briefly in Section 13.9. The aggregate particles act as a filler material to reduce the overall cost of the concrete product because they are cheap, whereas cement is relatively expensive. To achieve the optimum strength and workability of a concrete mixture, the ingredients must be added in the correct proportions. Dense packing of the aggregate and good interfacial contact are achieved by having particles of two different sizes; the fine particles of sand should fill the void spaces between the gravel particles. Ordinarily these aggregates comprise between 60 and 80% of the total volume. The amount of cement–water paste should be sufficient to coat all the sand and gravel particles, otherwise the cementitious bond will be incomplete. Furthermore, all the constituents should be thoroughly mixed. Complete bonding between cement and the aggregate particles is contingent upon the addition of the correct quantity of water. Too little water leads to incomplete bonding, and too much results in excessive porosity; in either case the final strength is less than the optimum.

The character of the aggregate particles is an important consideration. In particular, the size distribution of the aggregates influences the amount of cement–water paste required. Also, the surfaces should be clean and free from clay and silt, which prevent the formation of a sound bond at the particle surface.

Portland cement concrete is a major material of construction, primarily because it can be poured in place and hardens at room temperature, and even when submerged in water. However, as a structural material, there are some limitations and disadvantages. Like most ceramics, portland cement concrete is relatively weak and extremely brittle; its tensile strength is approximately 10 to 15 times smaller than its compressive strength. Also, large concrete structures can experience considerable thermal expansion and contraction with temperature fluctuations. In addition, water penetrates into external pores, which can cause severe cracking in cold weather as a consequence of freeze–thaw cycles. Most of these inadequacies may be eliminated or at least improved by reinforcement and/or the incorporation of additives.

Reinforced Concrete

The strength of portland cement concrete may be increased by additional reinforcement. This is usually accomplished by means of steel rods, wires, bars (rebar), or mesh, which are embedded into the fresh and uncured concrete. Thus, the reinforcement renders the hardened structure capable of supporting greater tensile, compressive, and shear stresses. Even if cracks develop in the concrete, considerable reinforcement is maintained.

Steel serves as a suitable reinforcement material because its coefficient of thermal expansion is nearly the same as that of concrete. In addition, steel is not rapidly corroded in the cement environment, and a relatively strong adhesive bond is formed between it and the cured concrete. This adhesion may be enhanced by the incorporation of contours into the surface of the steel member, which permits a greater degree of mechanical interlocking.

Portland cement concrete may also be reinforced by mixing into the fresh concrete fibers of a high-modulus material such as glass, steel, nylon, and polyethylene. Care must be exercised in utilizing this type of reinforcement, since some fiber materials experience rapid deterioration when exposed to the cement environment.

Still another reinforcement technique for strengthening concrete involves the introduction of residual compressive stresses into the structural member; the resulting material is called **prestressed concrete.** This method utilizes one characteristic of brittle ceramics—namely, that they are stronger in compression than in tension. Thus, to fracture a prestressed concrete member, the magnitude of the precompressive stress must be exceeded by an applied tensile stress.

In one such prestressing technique high-strength steel wires are positioned inside the empty molds and stretched with a high tensile force, which is maintained constant. After the concrete has been placed and allowed to harden, the tension is released. As the wires contract, they put the structure in a state of compression because the stress is transmitted to the concrete via the concrete-wire bond that is formed.

Another technique is also utilized in which stresses are applied after the concrete hardens; it is appropriately called *posttensioning.* Sheet metal or rubber tubes are situated inside and pass through the concrete forms, around which the concrete is cast. After the cement has hardened, steel wires are fed through the resulting holes, and tension is applied to the wires by means of jacks attached and abutted to the faces of the structure. Again, a compressive stress is imposed on the concrete piece, this time by the jacks. Finally, the empty spaces inside the tubing are filled with a grout to protect the wire from corrosion.

Concrete that is prestressed should be of a high quality, having a low shrinkage and a low creep rate. Prestressed concretes, usually prefabricated, are commonly used for highway and railway bridges.

15.3 DISPERSION-STRENGTHENED COMPOSITES

Metals and metal alloys may be strengthened and hardened by the uniform dispersion of several volume percent of fine particles of a very hard and inert material. The dispersed phase may be metallic or nonmetallic; oxide materials are often used. Again, the strengthening mechanism involves interactions between the particles and dislocations within the matrix, as with precipitation hardening. The dispersion strengthening effect is not as pronounced as with precipitation hardening; however, the strengthening is retained at elevated temperatures and for extended time periods because the dispersed particles are chosen to be unreactive with the matrix phase. For precipitation-hardened alloys, the increase in strength may disappear upon heat treatment as a consequence of precipitate growth or dissolution of the precipitate phase.

The high-temperature strength of nickel alloys may be enhanced significantly by the addition of about 3 vol% of thoria (ThO_2) as finely dispersed particles; this material is known as thoria-dispersed (or TD) nickel. The same effect is produced in the aluminum–aluminum oxide system. A very thin and adherent alumina coating is caused to form on the surface of extremely small (0.1 to 0.2 μm thick) flakes of aluminum, which are dispersed within an aluminum metal matrix; this material is termed sintered aluminum powder (SAP).

FIBER-REINFORCED COMPOSITES

Technologically, the most important composites are those in which the dispersed phase is in the form of a fiber. Design goals of **fiber-reinforced composites** often include high strength and/or stiffness on a weight basis. These characteristics are expressed in terms of **specific strength** and **specific modulus** parameters, which correspond, respectively, to the ratios of tensile strength to specific gravity and modulus of elasticity to specific gravity. Fiber-reinforced composites with exceptionally high specific strengths and moduli have been produced that utilize low-density fiber and matrix materials.

As noted in Figure 15.2, fiber-reinforced composites are subclassified by fiber length. For short fiber, the fibers are too short to produce a significant improvement in strength.

15.4 INFLUENCE OF FIBER LENGTH

The mechanical characteristics of a fiber-reinforced composite depend not only on the properties of the fiber, but also on the degree to which an applied load is transmitted to the fibers by the matrix phase. Important to the extent of this load transmittance is the magnitude of the interfacial bond between the fiber and matrix phases. Under an applied stress, this fiber–matrix bond ceases at the fiber ends, yielding a matrix deformation pattern as shown schematically in Figure 15.6; in other words, there is no load transmittance from the matrix at each fiber extremity.

Some critical fiber length is necessary for effective strengthening and stiffening of the composite material. This critical length l_c is dependent on the fiber diameter d and its ultimate (or tensile) strength σ_f^*, and on the fiber–matrix bond strength (or the shear yield strength of the matrix, whichever is smaller) τ_c according to

$$l_c = \frac{\sigma_f^* d}{2\tau_c} \tag{15.3}$$

For a number of glass and carbon fiber–matrix combinations, this critical length is on the order of 1 mm, which ranges between 20 and 150 times the fiber diameter.

When a stress equal to σ_f^* is applied to a fiber having just this critical length, the stress–position profile shown in Figure 15.7*a* results; that is, the maximum fiber load is achieved only at the axial center of the fiber. As fiber length l increases,

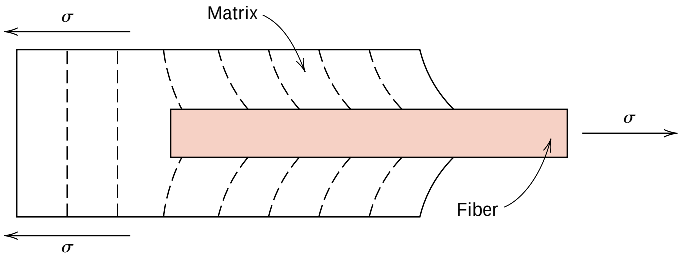

FIGURE 15.6 The deformation pattern in the matrix surrounding a fiber that is subjected to an applied tensile load.

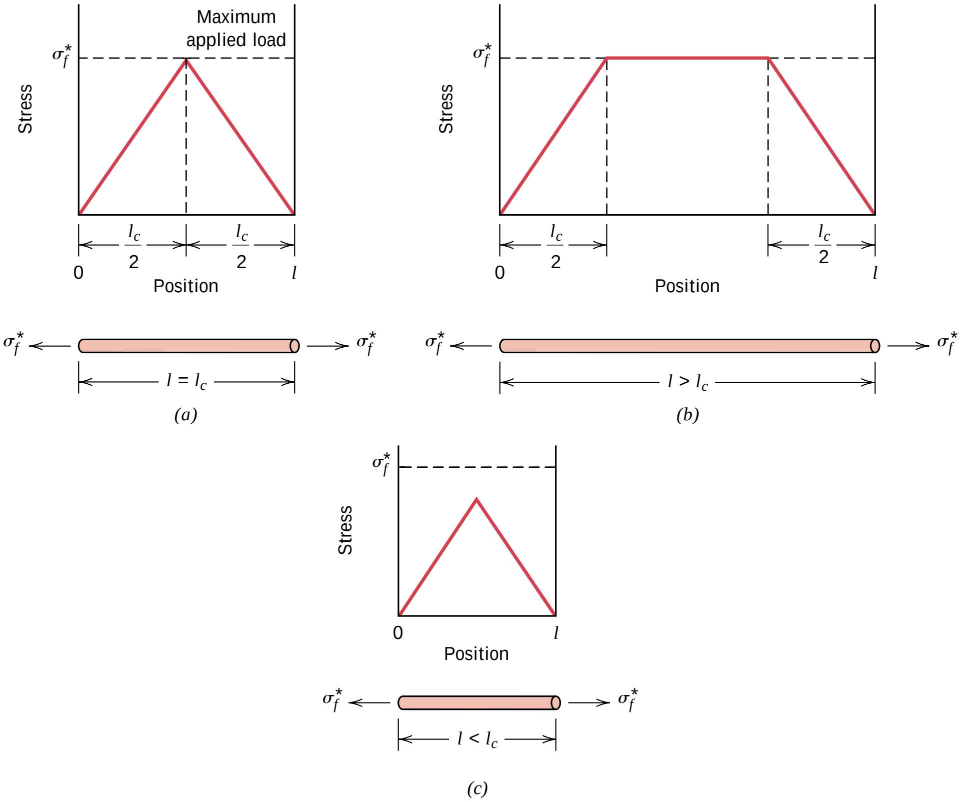

Figure 15.7 Stress–position profiles when fiber length l (a) is equal to the critical length l_c, (b) is greater than the critical length, and (c) is less than the critical length for a fiber-reinforced composite that is subjected to a tensile stress equal to the fiber tensile strength σ_f^*.

the fiber reinforcement becomes more effective; this is demonstrated in Figure 15.7*b*, a stress–axial position profile for $l > l_c$ when the applied stress is equal to the fiber strength. Figure 15.7*c* shows the stress–position profile for $l < l_c$.

Fibers for which $l \gg l_c$ (normally $l > 15l_c$) are termed *continuous; discontinous* or *short fibers* have lengths shorter than this. For discontinuous fibers of lengths significantly less than l_c, the matrix deforms around the fiber such that there is virtually no stress transference and little reinforcement by the fiber. These are essentially the particulate composites as described above. To affect a significant improvement in strength of the composite, the fibers must be continuous.

15.5 INFLUENCE OF FIBER ORIENTATION AND CONCENTRATION

The arrangement or orientation of the fibers relative to one another, the fiber concentration, and the distribution all have a significant influence on the strength and other properties of fiber-reinforced composites. With respect to orientation, two extremes are possible: (1) a parallel alignment of the longitudinal axis of the fibers in a single direction, and (2) a totally random alignment. Continuous fibers are normally aligned (Figure 15.8*a*), whereas discontinuous fibers may be aligned

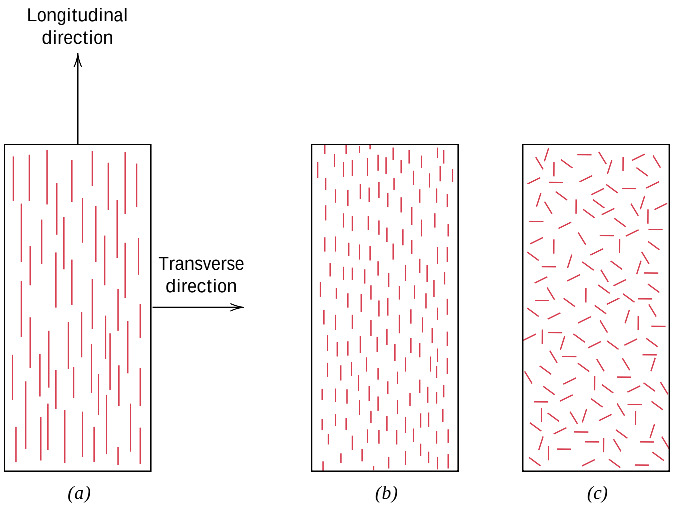

Figure 15.8 Schematic representations of (*a*) continuous and aligned, (*b*) discontinous and aligned, and (*c*) discontinous and randomly oriented fiber-reinforced composites.

(Figure 15.8*b*), randomly oriented (Figure 15.8*c*), or partially oriented. Better overall composite properties are realized when the fiber distribution is uniform.

CONTINUOUS AND ALIGNED FIBER COMPOSITES

Tensile Stress–Strain Behavior—Longitudinal Loading

Mechanical responses of this type of composite depend on several factors to include the stress–strain behaviors of fiber and matrix phases, the phase volume fractions, and, in addition, the direction in which the stress or load is applied. Furthermore, the properties of a composite having its fibers aligned are highly anisotropic, that is, dependent on the direction in which they are measured. Let us first consider the stress–strain behavior for the situation wherein the stress is applied along the direction of alignment, the **longitudinal direction,** which direction is indicated in Figure 15.8*a*.

To begin, assume the stress versus strain behaviors for fiber and matrix phases that are represented schematically in Figure 15.9*a*; in this treatment we consider the fiber to be totally brittle and the matrix phase to be reasonably ductile. Also indicated in this figure are fracture strengths in tension for fiber and matrix, σ_f^* and σ_m^*, respectively, and their corresponding fracture strains, ϵ_f^* and ϵ_m^*; furthermore, it is assumed that $\epsilon_m^* > \epsilon_f^*$, which is normally the case.

A fiber-reinforced composite consisting of these fiber and matrix materials will exhibit the uniaxial stress–strain response illustrated in Figure 15.9*b*; the fiber and matrix behaviors from Figure 15.9*a* are included to provide perspective. In the initial Stage I region, both fibers and matrix deform elastically; normally this portion of the curve is linear. Typically, for a composite of this type, the matrix yields and deforms plastically (at ϵ_{ym}, Figure 15.9*b*) while the fibers continue to stretch elastically, inasmuch as the tensile strength of the fibers is significantly higher than the yield strength of the matrix. This process constitutes Stage II as noted in the figure, which stage is ordinarily very nearly linear, but of diminished slope relative to Stage I. Furthermore, in passing from Stage I to Stage II, the proportion of the applied load that is borne by the fibers increases.

The onset of composite failure begins as the fibers start to fracture, which corresponds to a strain of approximately ϵ_f^* as noted in Figure 15.9*b*. Composite failure is not catastrophic for a couple of reasons. First of all, not all fibers fracture at the same time, since there will always be considerable variations in the fracture

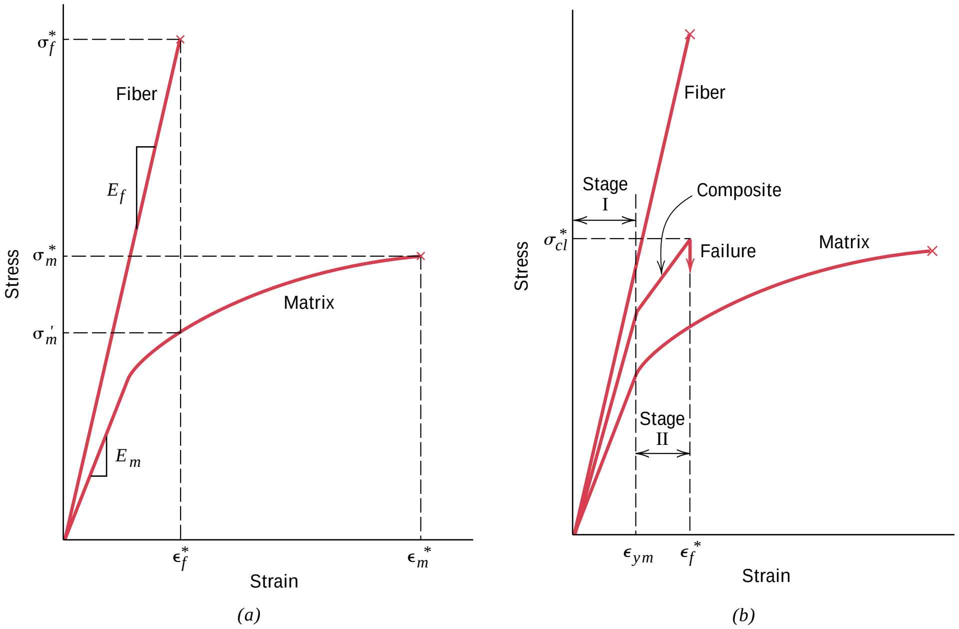

Figure 15.9 (*a*) Schematic stress–strain curves for brittle fiber and ductile matrix materials. Fracture stresses and strains for both materials are noted. (*b*) Schematic stress–strain curve for an aligned fiber-reinforced composite that is exposed to a uniaxial stress applied in the direction of alignment; curves for the fiber and matrix materials shown in part (*a*) are also superimposed.

strength of brittle fiber materials (Section 9.6). In addition, even after fiber failure, the matrix is still intact inasmuch as $\epsilon_f^* < \epsilon_m^*$ (Figure 15.9*a*). Thus, these fractured fibers, which are shorter than the original ones, are still embedded within the intact matrix, and consequently are capable of sustaining a diminished load as the matrix continues to plastically deform.

Elastic Behavior—Longitudinal Loading

Let us now consider the elastic behavior of a continuous and oriented fibrous composite that is loaded in the direction of fiber alignment direction. First of all, it is assumed that the fiber–matrix interfacial bond is very good, such that deformation of both matrix and fibers is the same (an *isostrain* situation). Under these conditions, the total load sustained by the composite F_c is equal to the loads carried by the matrix phase F_m and the fiber phase F_f, or

$$F_c = F_m + F_f \tag{15.4}$$

From the definition of stress, Equation 7.1, $F = \sigma A$; and thus expressions for F_c, F_m, and F_f in terms of their respective stresses (σ_c, σ_m, and σ_f) and cross-sectional areas (A_c, A_m, and A_f) are possible. Substitution of these into Equation 15.4 yields

$$\sigma_c A_c = \sigma_m A_m + \sigma_f A_f \tag{15.5}$$

and then, dividing through by the total cross-sectional area of the composite, A_c, we have

$$\sigma_c = \sigma_m \frac{A_m}{A_c} + \sigma_f \frac{A_f}{A_c} \tag{15.6}$$

where A_m/A_c and A_f/A_c are the area fractions of the matrix and fiber phases, respectively. If the composite, matrix, and fiber phase lengths are all equal, A_m/A_c is equivalent to the volume fraction of the matrix, V_m; and likewise for the fibers, $V_f = A_f/A_c$. Equation 15.6 now becomes

$$\sigma_c = \sigma_m V_m + \sigma_f V_f \tag{15.7}$$

The previous assumption of an isostrain state means that

$$\epsilon_c = \epsilon_m = \epsilon_f \tag{15.8}$$

and when each term in Equation 15.7 is divided by its respective strain,

$$\frac{\sigma_c}{\epsilon_c} = \frac{\sigma_m}{\epsilon_m} V_m + \frac{\sigma_f}{\epsilon_f} V_f \tag{15.9}$$

Furthermore, if composite, matrix, and fiber deformations are all elastic, then $\sigma_c/\epsilon_c = E_c$, $\sigma_m/\epsilon_m = E_m$, and $\sigma_f/\epsilon_f = E_f$, the E's being the moduli of elasticity for the respective phases. Substitution into Equation 15.9 yields an expression for the modulus of elasticity of a continuous and aligned fibrous composite *in the direction of alignment* (or *longitudinal direction*), E_{cl}, as

$$E_{cl} = E_m V_m + E_f V_f \tag{15.10a}$$

or

$$E_{cl} = E_m (1 - V_f) + E_f V_f \tag{15.10b}$$

since the composite consists of only matrix and fiber phases; that is, $V_m + V_f = 1$.

Thus, E_{cl} is equal to the volume-fraction weighted average of the moduli of elasticity of the fiber and matrix phases. Other properties, including density, also have this dependence on volume fractions. Equation 15.10a is the fiber analogue of Equation 15.1, the upper bound for particle-reinforced composites.

It can also be shown, for longitudinal loading, that the ratio of the load carried by the fibers to that carried by the matrix is

$$\frac{F_f}{F_m} = \frac{E_f V_f}{E_m V_m} \tag{15.11}$$

The demonstration is left as a homework problem.

EXAMPLE PROBLEM 15.1

A continuous and aligned glass fiber-reinforced composite consists of 40 vol% of glass fibers having a modulus of elasticity of 69 GPa (10×10^6 psi) and 60 vol% of a polyester resin that, when hardened, displays a modulus of 3.4 GPa (0.5×10^6 psi).

(a) Compute the modulus of elasticity of this composite in the longitudinal direction.

(b) If the cross-sectional area is 250 mm^2 (0.4 in.^{2}) and a stress of 50 MPa (7250 psi) is applied in this longitudinal direction, compute the magnitude of the load carried by each of the fiber and matrix phases.

(c) Determine the strain that is sustained by each phase when the stress in part b is applied.

SOLUTION

(a) The modulus of elasticity of the composite is calculated using Equation 15.10a:

$$E_{cl} = (3.4\text{ GPa})(0.6) + (69\text{ GPa})(0.4)$$
$$= 30\text{ GPa } (4.3 \times 10^6\text{ psi})$$

(b) To solve this portion of the problem, first find the ratio of fiber load to matrix load, using Equation 15.11; thus,

$$\frac{F_f}{F_m} = \frac{(69\text{ GPa})(0.4)}{(3.4\text{ GPa})(0.6)} = 13.5$$

or $F_f = 13.5F_m$.

In addition, the total force sustained by the composite F_c may be computed from the applied stress σ and total composite cross-sectional area A_c according to

$$F_c = A_c\sigma = (250\text{ mm}^2)(50\text{ MPa}) = 12{,}500\text{ N } (2900\text{ lb}_\text{f})$$

However, this total load is just the sum of the loads carried by fiber and matrix phases, that is

$$F_c = F_f + F_m = 12{,}500\text{ N } (2900\text{ lb}_\text{f})$$

Substitution for F_f from the above yields

$$13.5F_m + F_m = 12{,}500\text{ N}$$

or

$$F_m = 860\text{ N } (200\text{ lb}_\text{f})$$

whereas

$$F_f = F_c - F_m = 12{,}500\text{ N} - 860\text{ N} = 11{,}640\text{ N } (2700\text{ lb}_\text{f})$$

Thus, the fiber phase supports the vast majority of the applied load.

(c) The stress for both fiber and matrix phases must first be calculated. Then, by using the elastic modulus for each (from part a), the strain values may be determined.

For stress calculations, phase cross-sectional areas are necessary:

$$A_m = V_mA_c = (0.6)(250\text{ mm}^2) = 150\text{ mm}^2\ (0.24\text{ in.}^2)$$

and

$$A_f = V_fA_c = (0.4)(250\text{ mm}^2) = 100\text{ mm}^2\ (0.16\text{ in.}^2)$$

Thus,

$$\sigma_m = \frac{F_m}{A_m} = \frac{860\text{ N}}{150\text{ mm}^2} = 5.73\text{ MPa } (833\text{ psi})$$

$$\sigma_f = \frac{F_f}{A_f} = \frac{11{,}640\text{ N}}{100\text{ mm}^2} = 116.4\text{ MPa } (16{,}875\text{ psi})$$

Finally, strains are computed as

$$\epsilon_m = \frac{\sigma_m}{E_m} = \frac{5.73 \text{ MPa}}{3.4 \times 10^3 \text{ MPa}} = 1.69 \times 10^{-3}$$

$$\epsilon_f = \frac{\sigma_f}{E_f} = \frac{116.4 \text{ MPa}}{69 \times 10^3 \text{ MPa}} = 1.69 \times 10^{-3}$$

Therefore, strains for both matrix and fiber phases are identical, which they should be, according to Equation 15.8 in the previous development.

Elastic Behavior—Transverse Loading

A continuous and oriented fiber composite may be loaded in the **transverse direction;** that is, the load is applied at a 90° angle to the direction of fiber alignment as shown in Figure 15.8*a*. For this situation the stress σ to which the composite as well as both phases are exposed is the same, or

$$\sigma_c = \sigma_m = \sigma_f = \sigma \tag{15.12}$$

This is termed an *isostress* state. Also, the strain or deformation of the entire composite ϵ_c is

$$\epsilon_c = \epsilon_m V_m + \epsilon_f V_f \tag{15.13}$$

but, since $\epsilon = \sigma/E$,

$$\frac{\sigma}{E_{ct}} = \frac{\sigma}{E_m} V_m + \frac{\sigma}{E_f} V_f \tag{15.14}$$

where E_{ct} is the modulus of elasticity in the transverse direction. Now, dividing through by σ yields

$$\boxed{\frac{1}{E_{ct}} = \frac{V_m}{E_m} + \frac{V_f}{E_f}} \tag{15.15}$$

which reduces to

$$\boxed{E_{ct} = \frac{E_m E_f}{V_m E_f + V_f E_m} = \frac{E_m E_f}{(1 - V_f)E_f + V_f E_m}} \tag{15.16}$$

Equation 15.16 is analogous to the lower-bound expression for particulate composites, Equation 15.2.

EXAMPLE PROBLEM 15.2

Compute the elastic modulus of the composite material described in Example Problem 15.1, but assume that the stress is applied perpendicular to the direction of fiber alignment.

SOLUTION

According to Equation 15.16,

$$E_{ct} = \frac{(3.4 \text{ GPa})(69 \text{ GPa})}{(0.6)(69 \text{ GPa}) + (0.4)(3.4 \text{ GPa})}$$

$$= 5.5 \text{ GPa } (0.81 \times 10^6 \text{ psi})$$

This value for E_{ct} is slightly greater than that of the matrix phase but, from Example Problem 15.1a, only approximately one-fifth of the modulus of elasticity along the fiber direction (E_{cl}), which indicates the degree of anisotropy of continuous and oriented fiber composites.

Longitudinal Tensile Strength

We now consider the strength characteristics of continuous and aligned fiber-reinforced composites that are loaded in the longitudinal direction. Under these circumstances, strength is normally taken as the maximum stress on the stress–strain curve, Figure 15.9*b*; often this point corresponds to fiber fracture, and marks the onset of composite failure. Table 15.1 lists typical longitudinal tensile strength values for three common fibrous composites. Failure of this type of composite material is a relatively complex process, and several different failure modes are possible. The mode that operates for a specific composite will depend on fiber and matrix properties, and the nature and strength of the fiber–matrix interfacial bond.

If we assume that $\epsilon_f^* < \epsilon_m^*$ (Figure 15.9*a*), which is the usual case, then fibers will fail before the matrix. And once the fibers have fractured, the majority of the load that was borne by the fibers is now transferred to the matrix. This being the case, it is possible to adapt the expression for the stress on this type of composite, Equation 15.7, into the following expression for the longitudinal strength of the composite, σ_{cl}^*:

$$\sigma_{cl}^* = \sigma_m'(1 - V_f) + \sigma_f^* V_f \tag{15.17}$$

Here σ_m' is the stress in the matrix at fiber failure (as illustrated in Figure 15.9*a*) and, as previously, σ_f^* is the fiber tensile strength.

Transverse Tensile Strength

The strengths of continuous and unidirectional fibrous composites are highly anisotropic, and such composites are normally designed to be loaded along the high-strength, longitudinal direction. However, during in-service applications transverse tensile loads may also be present. Under these circumstances, premature failure may result inasmuch as transverse strength is usually extremely low—it sometimes lies below the tensile strength of the matrix. Thus, in actual fact, the reinforcing effect of the fibers is a negative one. Typical transverse tensile strengths for three unidirectional composites are contained in Table 15.1.

Table 15.1 Typical Longitudinal and Transverse Tensile Strengths for Three Unidirectional Fiber-Reinforced Composites. The Fiber Content for Each is Approximately 50 Vol%

Material	*Longitudinal Tensile Strength (MPa)*	*Transverse Tensile Strength (MPa)*
Glass–Polyester	700	20
Carbon (High Modulus)–Epoxy	1000	35
Kevlar–Epoxy	1200	20

Source: D. Hull and T. W. Clyne, *An Introduction to Composite Materials,* 2nd edition, Cambridge University Press, 1996, p. 179.

Whereas longitudinal strength is dominated by fiber strength, a variety of factors will have a significant influence on the transverse strength; these factors include properties of both the fiber and matrix, the fiber–matrix bond strength, and the presence of voids. Measures that have been employed to improve the transverse strength of these composites usually involve modifying properties of the matrix.

DISCONTINUOUS AND ALIGNED FIBER COMPOSITES

Even though reinforcement efficiency is lower for discontinuous than for continuous fibers, discontinuous and aligned fiber composites (Figure 15.8*b*) are becoming increasingly more important in the commercial market. Chopped glass fibers are used most extensively; however, carbon and aramid discontinuous fibers are also employed. These short fiber composites can be produced having moduli of elasticity and tensile strengths that approach 90% and 50%, respectively, of their continuous fiber counterparts.

For a discontinuous and aligned fiber composite having a uniform distribution of fibers and in which $l > l_c$, the longitudinal strength (σ^*_{cd}) is given by the relationship

$$\sigma^*_{cd} = \sigma^*_f V_f \left(1 - \frac{l_c}{2l}\right) + \sigma'_m (1 - V_f) \tag{15.18}$$

where σ^*_f and σ'_m represent, respectively, the fracture strength of the fiber and the stress in the matrix when the composite fails (Figure 15.9*a*).

If the fiber length is less than critical ($l < l_c$), then the longitudinal strength ($\sigma^*_{cd'}$) is given by

$$\sigma^*_{cd'} = \frac{l\tau_c}{d} V_f + \sigma'_m (1 - V_f) \tag{15.19}$$

where d is the fiber diameter and τ_c is the smaller of either the fiber–matrix bond strength or the matrix shear yield strength.

DISCONTINUOUS AND RANDOMLY ORIENTED FIBER COMPOSITES

Normally, when the fiber orientation is random, short and discontinuous fibers are used; reinforcement of this type is schematically demonstrated in Figure 15.8*c*. Under these circumstances, a ''rule-of-mixtures'' expression for the elastic modulus similar to Equation 15.10a may be utilized, as follows:

$$E_{cd} = KE_f V_f + E_m V_m \tag{15.20}$$

In this expression, K is a fiber efficiency parameter, which depends on V_f and the E_f/E_m ratio. Of course, its magnitude will be less than unity, usually in the range 0.1 to 0.6. Thus, for random fiber reinforcement (as with oriented), the modulus increases in some proportion of the volume fraction of fiber. Table 15.2, which gives some of the mechanical properties of unreinforced and reinforced polycarbonates for discontinuous and randomly oriented glass fibers, provides an idea of the magnitude of the reinforcement that is possible.

By way of summary, then, aligned fibrous composites are inherently anisotropic, in that the maximum strength and reinforcement are achieved along the alignment

Table 15.2 **Properties of Unreinforced and Reinforced Polycarbonates with Randomly Oriented Glass Fibers**

		Fiber Reinforcement (vol%)		
Property	***Unreinforced***	***20***	***30***	***40***
Specific gravity	1.19–1.22	1.35	1.43	1.52
Tensile strength [MPa (ksi)]	59–62 (8.5–9.0)	110 (16)	131 (19)	159 (23)
Modulus of elasticity [GPa (10^6 psi)]	2.24–2.345 (0.325–0.340)	5.93 (0.86)	8.62 (1.25)	11.6 (1.68)
Elongation (%)	90–115	4–6	3–5	3–5
Impact strength, notched Izod (lb_f/in.)	12–16	2.0	2.0	2.5

Source: Adapted from Materials Engineering's *Materials Selector*, copyright © Penton/IPC.

(longitudinal) direction. In the transverse direction, fiber reinforcement is virtually nonexistent: fracture usually occurs at relatively low tensile stresses. For other stress orientations, composite strength lies between these extremes. The efficiency of fiber reinforcement for several situations is presented in Table 15.3; this efficiency is taken to be unity for an oriented fiber composite in the alignment direction, and zero perpendicular to it.

When multidirectional stresses are imposed within a single plane, aligned layers that are fastened together one on top of another at different orientations are frequently utilized. These are termed *laminar composites,* which are discussed in Section 15.14.

Applications involving totally multidirectional applied stresses normally use discontinuous fibers, which are randomly oriented in the matrix material. Table 15.3 shows that the reinforcement efficiency is only one fifth that of an aligned composite in the longitudinal direction; however, the mechanical characteristics are isotropic.

Consideration of orientation and fiber length for a particular composite will depend on the level and nature of the applied stress as well as fabrication cost.

Table 15.3 **Reinforcement Efficiency of Fiber-Reinforced Composites for Several Fiber Orientations and at Various Directions of Stress Application**

Fiber Orientation	***Stress Direction***	***Reinforcement Efficiency***
All fibers parallel	Parallel to fibers	1
	Perpendicular to fibers	0
Fibers randomly and uniformly distributed within a specific plane	Any direction in the plane of the fibers	$\frac{3}{8}$
Fibers randomly and uniformly distributed within three dimensions in space	Any direction	$\frac{1}{5}$

Source: H. Krenchel, *Fibre Reinforcement,* Copenhagen: Akademisk Forlag, 1964 [33].

Production rates for short-fiber composites (both aligned and randomly oriented) are rapid, and intricate shapes can be formed that are not possible with continuous fiber reinforcement. Furthermore, fabrication costs are considerably lower than for continuous and aligned; fabrication techniques applied to short-fiber composite materials include compression, injection, and extrusion molding, which are described for unreinforced polymers in Section 14.13.

15.6 The Fiber Phase

An important characteristic of most materials, especially brittle ones, is that a small-diameter fiber is much stronger than the bulk material. As discussed in Section 9.6, the probability of the presence of a critical surface flaw that can lead to fracture diminishes with decreasing specimen volume, and this feature is used to advantage in the fiber-reinforced composites. Also, the materials used for reinforcing fibers have high tensile strengths.

On the basis of diameter and character, fibers are grouped into three different classifications: *whiskers, fibers,* and *wires.* **Whiskers** are very thin single crystals that have extremely large length-to-diameter ratios. As a consequence of their small size, they have a high degree of crystalline perfection and are virtually flaw free, which accounts for their exceptionally high strengths; they are the strongest known materials. In spite of these high strengths, whiskers are not utilized extensively as a reinforcement medium because they are extremely expensive. Moreover, it is difficult and often impractical to incorporate whiskers into a matrix. Whisker materials include graphite, silicon carbide, silicon nitride, and aluminum oxide; some mechanical characteristics of these materials are given in Table 15.4.

Materials that are classified as **fibers** are either polycrystalline or amorphous and have small diameters; fibrous materials are generally either polymers or ceramics (e.g., the polymer aramids, glass, carbon, boron, aluminum oxide, and silicon carbide). Table 15.4 also presents some data on a few materials that are used in fiber form.

Fine wires have relatively large diameters; typical materials include steel, molybdenum, and tungsten. Wires are utilized as a radial steel reinforcement in automobile tires, in filament-wound rocket casings, and in wire-wound high-pressure hoses.

15.7 The Matrix Phase

The **matrix phase** of fibrous composites may be a metal, polymer, or ceramic. In general, metals and polymers are used as matrix materials because some ductility is desirable; for ceramic-matrix composites (Section 15.10), the reinforcing component is added to improve fracture toughness. The discussion of this section will focus on polymer and metal matrices.

For fiber-reinforced composites, the matrix phase serves several functions. First, it binds the fibers together and acts as the medium by which an externally applied stress is transmitted and distributed to the fibers; only a very small proportion of an applied load is sustained by the matrix phase. Furthermore, the matrix material should be ductile. In addition, the elastic modulus of the fiber should be much higher than that of the matrix. The second function of the matrix is to protect the individual fibers from surface damage as a result of mechanical abrasion or chemical reactions with the environment. Such interactions may introduce surface flaws capable of forming cracks, which may lead to failure at low tensile stress levels. Finally, the matrix separates the fibers and, by virtue of its relative softness and

Table 15.4 **Characteristics of Several Fiber-Reinforcement Materials**

Material	*Specific Gravity*	*Tensile Strength [GPa (10^6 psi)]*	*Specific Strength (GPa)*	*Modulus of Elasticity [GPa (10^6 psi)]*	*Specific Modulus (GPa)*
		Whiskers			
Graphite	2.2	20 (3)	9.1	700 (100)	318
Silicon nitride	3.2	5–7 (0.75–1.0)	1.56–2.2	350–380 (50–55)	109–118
Aluminum oxide	4.0	10–20 (1–3)	2.5–5.0	700–1500 (100–220)	175–375
Silicon carbide	3.2	20 (3)	6.25	480 (70)	150
		Fibers			
Aluminum oxide	3.95	1.38 (0.2)	0.35	379 (55)	96
Aramid (Kevlar 49)	1.44	3.6–4.1 (0.525–0.600)	2.5–2.85	131 (19)	91
Carbon[a]	1.78–2.15	1.5–4.8 (0.22–0.70)	0.70–2.70	228–724 (32–100)	106–407
E-Glass	2.58	3.45 (0.5)	1.34	72.5 (10.5)	28.1
Boron	2.57	3.6 (0.52)	1.40	400 (60)	156
Silicon carbide	3.0	3.9 (0.57)	1.30	400 (60)	133
UHMWPE (Spectra 900)	0.97	2.6 (0.38)	2.68	117 (17)	121
		Metallic Wires			
High-strength steel	7.9	2.39 (0.35)	0.30	210 (30)	26.6
Molybdenum	10.2	2.2 (0.32)	0.22	324 (47)	31.8
Tungsten	19.3	2.89 (0.42)	0.15	407 (59)	21.1

[a] The term ''carbon'' instead of ''graphite'' is used to denote these fibers, since they are composed of crystalline graphite regions, and also of noncrystalline material and areas of crystal misalignment.

plasticity, prevents the propagation of brittle cracks from fiber to fiber, which could result in catastrophic failure; in other words, the matrix phase serves as a barrier to crack propagation. Even though some of the individual fibers fail, total composite fracture will not occur until large numbers of adjacent fibers, once having failed, form a cluster of critical size.

It is essential that adhesive bonding forces between fiber and matrix be high to minimize fiber pull-out. In fact, bonding strength is an important consideration in the choice of the matrix–fiber combination. The ultimate strength of the composite depends to a large degree on the magnitude of this bond; adequate bonding is essential to maximize the stress transmittance from the weak matrix to the strong fibers.

15.8 POLYMER–MATRIX COMPOSITES

Polymer-matrix composites (*PMCs*) consist of a polymer resin[1] as the matrix, with fibers as the reinforcement medium. These materials are used in the greatest diversity of composite applications, as well as in the largest quantities, in light of their room-temperature properties, ease of fabrication, and cost. In this section the various classifications of PMCs are discussed according to reinforcement type (i.e., glass, carbon, and aramid), along with their applications and the various polymer resins that are employed.

GLASS FIBER-REINFORCED POLYMER (GFRP) COMPOSITES

Fiberglass is simply a composite consisting of glass fibers, either continuous or discontinuous, contained within a polymer matrix; this type of composite is produced in the largest quantities. The composition of the glass that is most commonly drawn into fibers (sometimes referred to as *E-glass*) is contained in Table 13.10; fiber diameters normally range between 3 and 20 μm. Glass is popular as a fiber reinforcement material for several reasons:

1. It is easily drawn into high-strength fibers from the molten state.
2. It is readily available and may be fabricated into a glass-reinforced plastic economically using a wide variety of composite-manufacturing techniques.
3. As a fiber, it is relatively strong, and when embedded in a plastic matrix, it produces a composite having a very high specific strength.
4. When coupled with the various plastics, it possesses a chemical inertness that renders the composite useful in a variety of corrosive environments.

The surface characteristics of glass fibers are extremely important because even minute surface flaws can deleteriously affect the tensile properties, as discussed in Section 9.6. Surface flaws are easily introduced by rubbing or abrading the surface with another hard material. Also, glass surfaces that have been exposed to the normal atmosphere for even short time periods generally have a weakened surface layer that interferes with bonding to the matrix. Newly drawn fibers are normally coated during drawing with a ''size,'' a thin layer of a substance that protects the fiber surface from damage and undesirable environmental interactions. This size is ordinarily removed prior to composite fabrication and replaced with a ''coupling agent'' or finish that promotes a better bond between the fiber and matrix.

There are several limitations to this group of materials. In spite of having high strengths, they are not very stiff and do not display the rigidity that is necessary for some applications (e.g., as structural members for airplanes and bridges). Most fiberglass materials are limited to service temperatures below 200°C (400°F); at higher temperatures, most polymers begin to flow or to deteriorate. Service temperatures may be extended to approximately 300°C (575°F) by using high-purity fused silica for the fibers and high-temperature polymers such as the polyimide resins.

Many fiberglass applications are familiar: automotive and marine bodies, plastic pipes, storage containers, and industrial floorings. The transportation industries are utilizing increasing amounts of glass fiber-reinforced plastics in an effort to decrease vehicle weight and boost fuel efficiencies. A host of new applications are being used or currently investigated by the automotive industry.

---

[1] The term ''resin'' is used in this context to denote a high-molecular-weight reinforcing plastic.

CARBON FIBER-REINFORCED POLYMER (CFRP) COMPOSITES

Carbon is a high-performance fiber material that is the most commonly used reinforcement in advanced (i.e., nonfiberglass) polymer-matrix composites. The reasons for this are as follows:

1. Carbon fibers have the highest specific modulus and specific strength of all reinforcing fiber materials.
2. They retain their high-tensile modulus and high strength at elevated temperatures; high-temperature oxidation, however, may be a problem.
3. At room temperature carbon fibers are not affected by moisture or a wide variety of solvents, acids, and bases.
4. These fibers exhibit a diversity of physical and mechanical characteristics, allowing composites incorporating these fibers to have specific engineered properties.
5. Fiber and composite manufacturing processes have been developed that are relatively inexpensive and cost effective.

Use of the term ''carbon fiber'' may seem perplexing inasmuch as carbon is an element, and, as noted in Section 3.9, the stable form of crystalline carbon at ambient conditions is graphite, having the structure represented in Figure 3.17. Carbon fibers are not totally crystalline, but are composed of both graphitic and noncrystalline regions; these areas of noncrystallinity are devoid of the three-dimensional ordered arrangement of hexagonal carbon networks that is characteristic of graphite (Figure 3.17).

Manufacturing techniques for producing carbon fibers are relatively complex and will not be discussed. However, three different organic precursor materials are used—rayon, polyacrylonitrile (PAN), and pitch. Processing technique will vary from precursor to precursor, as will also the resultant fiber characteristics.

One classification scheme for carbon fibers is according to tensile modulus; on this basis the four classes are standard, intermediate, high, and ultrahigh moduli. Furthermore, fiber diameters normally range between 4 and 10 μm; both continuous and chopped forms are available. In addition, carbon fibers are normally coated with a protective epoxy size that also improves adhesion with the polymer matrix.

Carbon-reinforced polymer composites are currently being utilized extensively in sports and recreational equipment (fishing rods, golf clubs), filament-wound rocket motor cases, pressure vessels, and aircraft structural components—both military and commercial, fixed wing and helicopters (e.g., as wing, body, stabilizer, and rudder components).

ARAMID FIBER-REINFORCED POLYMER COMPOSITES

Aramid fibers are high-strength, high-modulus materials that were introduced in the early 1970s. They are especially desirable for their outstanding strength-to-weight ratios, which are superior to metals. Chemically, this group of materials is known as poly paraphenylene terephthalamide. There are a number of aramid materials; trade names for two of the most common are Kevlar and Nomex. For the former, there are several grades (viz. Kevlar 29, 49, and 149) which have different mechanical behaviors. During synthesis, the rigid molecules are aligned in the

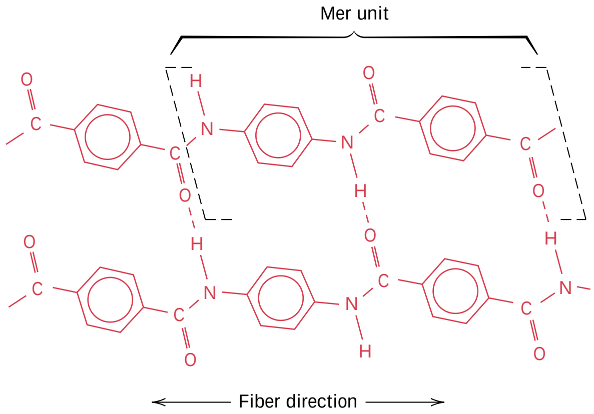

Figure 15.10 Schematic representation of mer and chain structures for aramid (Kevlar) fibers. Chain alignment with the fiber direction and hydrogen bonds that form between adjacent chains are also shown. (From F. R. Jones, Editor, *Handbook of Polymer-Fibre Composites.* Copyright © 1994 by Addison Wesley Longman. Reprinted with permission.)

direction of the fiber axis, as liquid crystal domains (Section 13.16); the mer chemistry and mode of chain alignment are represented in Figure 15.10. Mechanically, these fibers have longitudinal tensile strengths and tensile moduli (Table 15.4) that are higher than other polymeric fiber materials; however, they are relatively weak in compression. In addition, this material is known for its toughness, impact resistance, and resistance to creep and fatigue failure. Even though the aramids are thermoplastics, they are, nevertheless, resistant to combustion and stable to relatively high temperatures; the temperature range over which they retain their high mechanical properties is between −200 and 200°C (−330 and 390°F). Chemically, they are susceptible to degradation by strong acids and bases, but they are relatively inert in other solvents and chemicals.

The aramid fibers are most often used in composites having polymer matrices; common matrix materials are the epoxies and polyesters. Since the fibers are relatively flexible and somewhat ductile, they may be processed by most common textile operations. Typical applications of these aramid composites are in ballistic products (bullet-proof vests), sporting goods, tires, ropes, missile cases, pressure vessels, and as a replacement for asbestos in automotive brake and clutch linings, and gaskets.

The properties of continuous and aligned glass-, carbon-, and aramid-fiber reinforced epoxy composites are included in Table 15.5. Thus, a comparison of the mechanical characteristics of these three materials may be made in both longitudinal and transverse directions.

OTHER FIBER REINFORCEMENT MATERIALS

Glass, carbon, and the aramids are the most common fiber reinforcements incorporated in polymer matrices. Other fiber materials that are used to much lesser degrees are boron, silicon carbide, and aluminum oxide; tensile moduli, tensile strengths, specific strengths, and specific moduli of these materials in fiber form are contained in Table 15.4. Boron fiber-reinforced polymer composites have been used in military aircraft components, helicopter rotor blades, and some sporting goods. Silicon carbide and alumina fibers are utilized in tennis rackets, circuit boards, and rocket nose cones.

POLYMER MATRIX MATERIALS

The roles assumed by the polymer matrix are outlined in Section 15.7. In addition, the matrix often determines the maximum service temperature, since it normally

Table 15.5 Properties of Continuous and Aligned Glass-, Carbon-, and Aramid-fiber Reinforced Epoxy-matrix Composites in Longitudinal and Transverse Directions. In All Cases the Fiber Volume Fraction is 0.60

Property	***Glass (E-glass)***	***Carbon (High Strength)***	***Aramid (Kevlar 49)***
Specific gravity	2.1	1.6	1.4
Tensile modulus			
Longitudinal [GPa (10^6 psi)]	45 (6.5)	145 (21)	76 (11)
Transverse [GPa (10^6 psi)]	12 (1.8)	10 (1.5)	5.5 (0.8)
Tensile strength			
Longitudinal [MPa (ksi)]	1020 (150)	1240 (180)	1380 (200)
Transverse [MPa (ksi)]	40 (5.8)	41 (6)	30 (4.3)
Ultimate tensile strain			
Longitudinal	2.3	0.9	1.8
Transverse	0.4	0.4	0.5

Source: Adapted from R. F. Floral and S. T. Peters, ''Composite Structures and Technologies,'' tutorial notes, 1989.

softens, melts, or degrades at a much lower temperature than the fiber reinforcement.

The most widely utilized and least expensive polymer resins are the polyesters and vinyl esters;[2] these matrix materials are used primarily for glass fiber-reinforced composites. A large number of resin formulations provide a wide range of properties for these polymers. The epoxies are more expensive and, in addition to commercial applications, are also utilized extensively in PMCs for aerospace applications; they have better mechanical properties and resistance to moisture than the polyesters and vinyl resins. For high-temperature applications, polyimide resins are employed; their continuous-use, upper-temperature limit is approximately 230°C (450°F). And finally, high-temperature thermoplastic resins offer the potential to be used in future aerospace applications; such materials include polyetheretherketone (PEEK), polyphenylene sulfide (PPS), and polyetherimide (PEI).

15.9 METAL–MATRIX COMPOSITES

As the name implies, for **metal-matrix composites** (*MMC*s), the matrix is a ductile metal. These materials may be utilized at higher service temperatures than their base metal counterparts; furthermore, the reinforcement may improve specific stiffness, specific strength, abrasion resistance, creep resistance, thermal conductivity, and dimensional stability. Some of the advantages of these materials over the polymer-matrix composites include higher operating temperatures, nonflammability, and greater resistance to degradation by organic fluids. Metal-matrix composites are much more expensive than PMCs, and, therefore, their (MMC) use is somewhat restricted.

The superalloys, as well as alloys of aluminum, magnesium, titanium, and copper, are employed as matrix materials. The reinforcement may be in the form of particulates, both continuous and discontinuous fibers, and whiskers; concentrations

---

[2] The chemistry and typical properties of some of the matrix materials discussed in this section are included in Appendices B, D, and E.

Table 15.6 Properties of Several Metal-Matrix Composites Reinforced with Continuous and Aligned Fibers

Fiber	*Matrix*	*Fiber Content* (*vol%*)	*Density* (g/cm^3)	*Longitudinal Tensile Modulus* (*GPa*)	*Longitudinal Tensile Strength* (*MPa*)
Carbon	6061 Al	41	2.44	320	620
Boron	6061 Al	48	—	207	1515
SiC	6061 Al	50	2.93	230	1480
Alumina	380.0 Al	24	—	120	340
Carbon	AZ31 Mg	38	1.83	300	510
Borsic	Ti	45	3.68	220	1270

Source: Adapted from J. W. Weeton, D. M. Peters, and K. L. Thomas, *Engineers' Guide to Composite Materials,* ASM International, Materials Park, OH, 1987.

normally range between 10 and 60 vol%. Continuous fiber materials include carbon, silicon carbide, boron, alumina, and the refractory metals. On the other hand, discontinuous reinforcements consist primarily of silicon carbide whiskers, chopped fibers of alumina and carbon, and particulates of silicon carbide and alumina. In a sense, the cermets (Section 15.2) fall within this MMC scheme. In Table 15.6 are presented the properties of several common metal-matrix, continuous and aligned fiber-reinforced composites.

Some matrix–reinforcement combinations are highly reactive at elevated temperatures. Consequently, composite degradation may be caused by high-temperature processing, or by subjecting the MMC to elevated temperatures during service. This problem is commonly resolved either by applying a protective surface coating to the reinforcement or by modifying the matrix alloy composition.

Normally the processing of MMCs involves at least two steps: consolidation or synthesis (i.e., introduction of reinforcement into the matrix), followed by a shaping operation. A host of consolidation techniques are available, some of which are relatively sophisticated; discontinuous fiber MMCs are amenable to shaping by standard metal-forming operations (e.g., forging, extrusion, rolling).

Recently, some of the automobile manufacturers have introduced engine components consisting of an aluminum-alloy matrix that is reinforced with alumina and carbon fibers; this MMC is light in weight and resists wear and thermal distortion. Aerospace structural applications include advanced aluminum alloy metal-matrix composites; boron fibers are used as the reinforcement for the Space Shuttle Orbiter, and continuous graphite fibers for the Hubble Telescope.

The high-temperature creep and rupture properties of some of the superalloys (Ni- and Co-based alloys) may be enhanced by fiber reinforcement using refractory metals such as tungsten. Excellent high-temperature oxidation resistance and impact strength are also maintained. Designs incorporating these composites permit higher operating temperatures and better efficiencies for turbine engines.

15.10 CERAMIC–MATRIX COMPOSITES

As discussed in Chapter 13, ceramic materials are inherently resilient to oxidation and deterioration at elevated temperatures; were it not for their disposition to brittle fracture, some of these materials would be ideal candidates for use in high-temperature and severe-stress applications, specifically for components in automobile and aircraft gas turbine engines. Fracture toughness values for ceramic materials are low and typically lie between 1 and 5 $\text{MPa}\sqrt{\text{m}}$ (0.9 and 4.5 $\text{ksi}\sqrt{\text{in.}}$), Table 9.1 and Table B.5, Appendix B. By way of contrast, K_{Ic} values for most metals are much higher (15 to greater than 150 $\text{MPa}\sqrt{\text{m}}$ [14 to >140 $\text{ksi}\sqrt{\text{in.}}$]).

The fracture toughnesses of ceramics have been improved significantly by the development of a new generation of **ceramic-matrix composites** (*CMC*s)—particulates, fibers, or whiskers of one ceramic material that have been embedded into a matrix of another ceramic. Ceramic-matrix composite materials have extended fracture toughnesses to between about 6 and 20 $\text{MPa}\sqrt{\text{m}}$ (5.5 and 18 $\text{ksi}\sqrt{\text{in.}}$).

In essence, this improvement in the fracture properties results from interactions between advancing cracks and dispersed phase particles. Crack initiation normally occurs with the matrix phase, whereas crack propagation is impeded or hindered by the particles, fibers, or whiskers. Several techniques are utilized to retard crack propagation, which are discussed as follows.

One particularly interesting and promising toughening technique employs a phase transformation to arrest the propagation of cracks and is aptly termed *transformation toughening.* Small particles of partially stabilized zirconia (Section 10.15) are dispersed within the matrix material, often Al_2O_3 or ZrO_2 itself. Typically, CaO, MgO, Y_2O_3, and CeO are used as stabilizers. Partial stabilization allows retention of the metastable tetragonal phase at ambient conditions rather than the stable monoclinic phase; these two phases are noted on the ZrO_2-$ZrCaO_3$ phase diagram, Figure 10.23. The stress field in front of a propagating crack causes these metastably retained tetragonal particles to undergo transformation to the stable monoclinic phase. Accompanying this transformation is a slight particle volume increase, and the net result is that compressive stresses are established on the crack surfaces near the crack tip that tend to pinch the crack shut, thereby arresting its growth. This process is demonstrated schematically in Figure 15.11.

Other recently developed toughening techniques involve the utilization of ceramic whiskers, often SiC or Si_3N_4. These whiskers may inhibit crack propagation by (1) deflecting crack tips, (2) forming bridges across crack faces, (3) absorbing energy during pull-out as the whiskers debond from the matrix, and/or (4) causing a redistribution of stresses in regions adjacent to the crack tips.

In general, increasing fiber content improves strength and fracture toughness; this is demonstrated in Table 15.7 for SiC whisker-reinforced alumina. Furthermore,

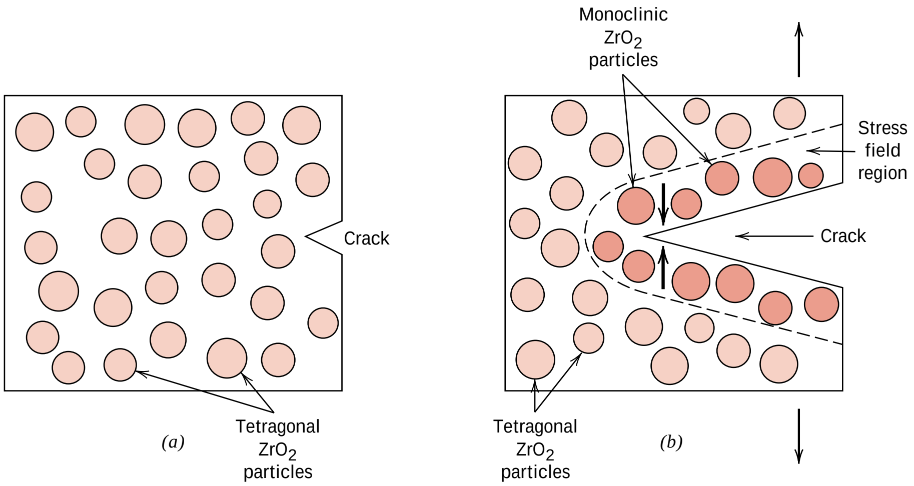
Crack
Tetragonal ZrO_2 particles
(a)
Monoclinic ZrO_2 particles
Stress field region
Crack
Tetragonal ZrO_2 particles
(b)

Figure 15.11 Schematic demonstration of transformation toughening. (*a*) A crack prior to inducement of the ZrO_2 particle phase transformation. (*b*) Crack arrestment due to the stress-induced phase transformation.

Table 15.7 **Room-Temperature Fracture Strengths and Fracture Toughnesses for Various SiC Whisker Contents in Al_2O_3**

Whisker Content (*vol%*)	*Fracture Strength* (*MPa*)	*Fracture Toughness* ($MPa\sqrt{m}$)
0	—	4.5
10	455 ± 55	7.1
20	655 ± 135	7.5–9.0
40	850 ± 130	6.0

Source: Adapted from *Engineered Materials Handbook*, Vol. 1, *Composites*, C. A. Dostal, Senior Editor, ASM International, Materials Park, OH, 1987.

there is a considerable reduction in the scatter of fracture strengths for whisker-reinforced ceramics relative to their unreinforced counterparts. In addition, these CMCs exhibit improved high-temperature creep behavior and resistance to thermal shock (i.e., failure resulting from sudden changes in temperature).

Ceramic-matrix composites may be fabricated using hot pressing, hot isostatic pressing, and liquid phase sintering techniques. Relative to applications, SiC whisker-reinforced aluminas are being utilized as cutting tool inserts for machining hard metal alloys; tool lives for these materials are greater than for cemented carbides (Section 15.2).

15.11 CARBON–CARBON COMPOSITES

One of the most advanced and promising engineering material is the carbon fiber-reinforced carbon-matrix composite, often termed a **carbon–carbon composite;** as the name implies, both reinforcement and matrix are carbon. These materials are relatively new and expensive and, therefore, are not currently being utilized extensively. Their desirable properties include high-tensile moduli and tensile strengths that are retained to temperatures in excess of 2000°C (3630°F), resistance to creep, and relatively large fracture toughness values. Furthermore, carbon–carbon composites have low coefficients of thermal expansion and relatively high thermal conductivities; these characteristics, coupled with high strengths, give rise to a relatively low susceptibility to thermal shock. Their major drawback is a propensity to high-temperature oxidation.

The carbon–carbon composites are employed in rocket motors, as friction materials in aircraft and high-performance automobiles, for hot-pressing molds, in components for advanced turbine engines, and as ablative shields for re-entry vehicles.

The primary reason that these composite materials are so expensive is the relatively complex processing techniques that are employed. Preliminary procedures are similar to those used for carbon-fiber, polymer-matrix composites. That is, the continuous carbon fibers are laid down having the desired two- or three-dimensional pattern; these fibers are then impregnated with a liquid polymer resin, often a phenolic; the workpiece is next formed into the final shape, and the resin is allowed to cure. At this time the matrix resin is ‘‘pyrolyzed,’’ that is, converted into carbon by heating in an inert atmosphere; during pyrolysis, molecular components consisting of oxygen, hydrogen, and nitrogen are driven off, leaving behind large carbon chain molecules. Subsequent heat treatments at higher temperatures will cause this carbon matrix to densify and increase in strength. The resulting composite, then, consists of the original carbon fibers that remained essentially unaltered, which are contained in this pyrolyzed carbon matrix.

15.12 HYBRID COMPOSITES

A relatively new fiber-reinforced composite is the **hybrid,** which is obtained by using two or more different kinds of fibers in a single matrix; hybrids have a better all-around combination of properties than composites containing only a single fiber type. A variety of fiber combinations and matrix materials are used, but in the most common system, both carbon and glass fibers are incorporated into a polymeric resin. The carbon fibers are strong and relatively stiff and provide a low-density reinforcement; however, they are expensive. Glass fibers are inexpensive and lack the stiffness of carbon. The glass–carbon hybrid is stronger and tougher, has a higher impact resistance, and may be produced at a lower cost than either of the comparable all-carbon or all-glass reinforced plastics.

There are a number of ways in which the two different fibers may be combined, which will ultimately affect the overall properties. For example, the fibers may all be aligned and intimately mixed with one another; or laminations may be constructed consisting of layers, each of which consists of a single fiber type, alternating one with another. In virtually all hybrids the properties are anisotropic.

When hybrid composites are stressed in tension, failure is usually noncatastrophic (i.e., does not occur suddenly). The carbon fibers are the first to fail, at which time the load is transferred to the glass fibers. Upon failure of the glass fibers, the matrix phase must sustain the applied load. Eventual composite failure concurs with that of the matrix phase.

Principal applications for hybrid composites are lightweight land, water, and air transport structural components, sporting goods, and lightweight orthopedic components.

15.13 PROCESSING OF FIBER-REINFORCED COMPOSITES

To fabricate continuous fiber-reinforced plastics that meet design specifications, the fibers should be uniformly distributed within the plastic matrix and, in most instances, all oriented in virtually the same direction. In this section newly developed techniques (pultrusion, filament winding, and prepreg production processes) by which useful products of these materials are manufactured will be discussed.

PULTRUSION

Pultrusion is used for the manufacture of components having continuous lengths and a constant cross-sectional shape (i.e., rods, tubes, beams, etc.). With this technique, illustrated schematically in Figure 15.12, continuous fiber *rovings*, or *tows,*[3] are first impregnated with a thermosetting resin; these are then pulled through a steel die that preforms to the desired shape and also establishes the resin/fiber ratio. The stock then passes through a curing die that is precision machined so as to impart

---

[3] A roving, or tow, is a loose and untwisted bundle of continuous fibers that are drawn together as parallel strands.

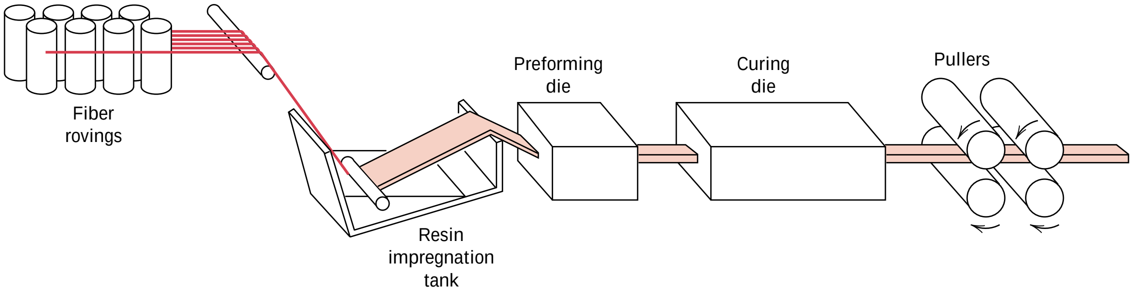
Fiber
rovings
Resin
impregnation
tank
Preforming
die
Curing
die
Pullers

Figure 15.12 Schematic diagram showing the pultrusion process.

the final shape; this die is also heated in order to initiate curing of the resin matrix. A pulling device draws the stock through the dies and also determines the production speed. Tubes and hollow sections are made possible by using center mandrels or inserted hollow cores. Principal reinforcements are glass, carbon, and aramid fibers, normally added in concentrations between 40 and 70 vol%. Commonly used matrix materials include polyesters, vinyl esters, and epoxy resins.

Pultrusion is a continuous process that is easily automated; production rates are relatively high, making it very cost effective. Furthermore, a wide variety of shapes are possible, and there is really no practical limit to the length of stock that may be manufactured.

PREPREG PRODUCTION PROCESSES

Prepreg is the composite industry's term for continuous fiber reinforcement preimpregnated with a polymer resin that is only partially cured. This material is delivered in tape form to the manufacturer, who then directly molds and fully cures the product without having to add any resin. It is probably the composite material form most widely used for structural applications.

The prepregging process, represented schematically for thermoset polymers in Figure 15.13, begins by collimating a series of spool-wound continuous fiber tows.

Figure 15.13 Schematic diagram illustrating the production of prepreg tape using thermoset polymers.

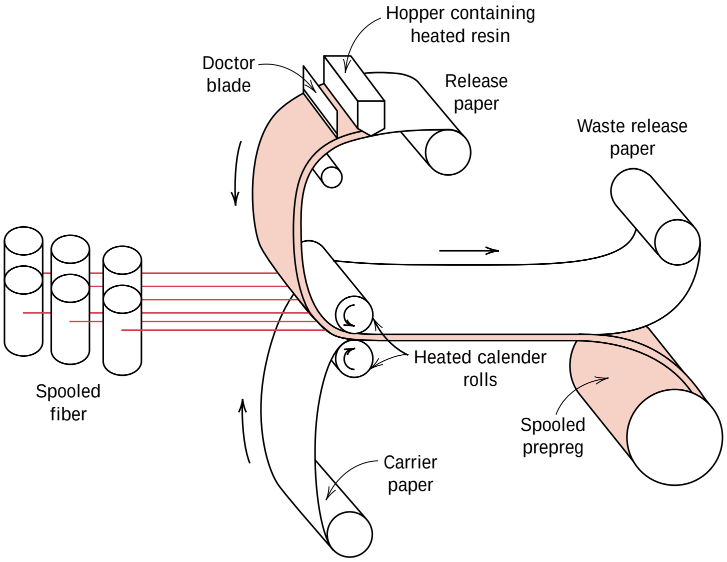
Hopper containing
heated resin
Doctor
blade
Release
paper
Waste release
paper
Spooled
fiber
Heated calender
rolls
Spooled
prepreg
Carrier
paper

These tows are then sandwiched and pressed between sheets of release and carrier paper using heated rollers, a process termed ‘‘calendering.’’ The release paper sheet has been coated with a thin film of heated resin solution of relatively low viscosity so as to provide for its thorough impregnation of the fibers. A ‘‘doctor blade’’ spreads the resin into a film of uniform thickness and width. The final prepreg product—the thin tape consisting of continuous and aligned fibers embedded in a partially cured resin—is prepared for packaging by winding onto a cardboard core. As shown in Figure 15.13, the release paper sheet is removed as the impregnated tape is spooled. Typical tape thicknesses range between 0.08 and 0.25 mm (3×10^{-3} and 10^{-2} in.), tape widths range between 25 and 1525 mm (1 and 60 in.), whereas resin content usually lies between about 35 and 45 vol%.

At room temperature the thermoset matrix undergoes curing reactions; therefore, the prepreg is stored at 0°C (32°F) or lower. Also, the time in use at room temperature (or ‘‘out-time’’) must be minimized. If properly handled, thermoset prepregs have a lifetime of at least six months and usually longer.

Both thermoplastic and thermosetting resins are utilized; carbon, glass, and aramid fibers are the common reinforcements.

Actual fabrication begins with the ‘‘lay-up’’—laying of the prepreg tape onto a tooled surface. Normally a number of plies are laid up (after removal from the carrier backing paper) to provide the desired thickness. The lay-up arrangement may be unidirectional, but more often the fiber orientation is alternated to produce a cross-ply or angle-ply laminate. Final curing is accomplished by the simultaneous application of heat and pressure.

The lay-up procedure may be carried out entirely by hand (hand lay-up), wherein the operator both cuts the lengths of tape and then positions them in the desired orientation on the tooled surface. Alternately, tape patterns may be machine cut, then hand laid. Fabrication costs can be further reduced by automation of prepreg lay-up and other manufacturing procedures (e.g., filament winding, as discussed below), which virtually eliminates the need for hand labor. These automated methods are essential for many applications of composite materials to be cost effective.

FILAMENT WINDING

Filament winding is a process by which continuous reinforcing fibers are accurately positioned in a predetermined pattern to form a hollow (usually cylindrical) shape. The fibers, either as individual strands or as tows, are first fed through a resin bath and then continuously wound onto a mandrel, usually using automated winding equipment (Figure 15.14). After the appropriate number of layers have been applied, curing is carried out either in an oven or at room temperature, after which the mandrel is removed. As an alternative, narrow and thin prepregs (i.e., tow pregs) 10 mm or less in width may be filament wound.

Various winding patterns are possible (i.e., circumferential, helical, and polar) to give the desired mechanical characteristics. Filament-wound parts have very high strength-to-weight ratios. Also, a high degree of control over winding uniformity and orientation is afforded with this technique. Furthermore, when automated, the process is most economically attractive. Common filament-wound structures include rocket motor casings, storage tanks and pipes, and pressure vessels.

Manufacturing techniques are now being used to produce a wide variety of structural shapes that are not necessarily limited to surfaces of revolution (e.g., I-beams). This technology is advancing very rapidly because it is very cost effective.

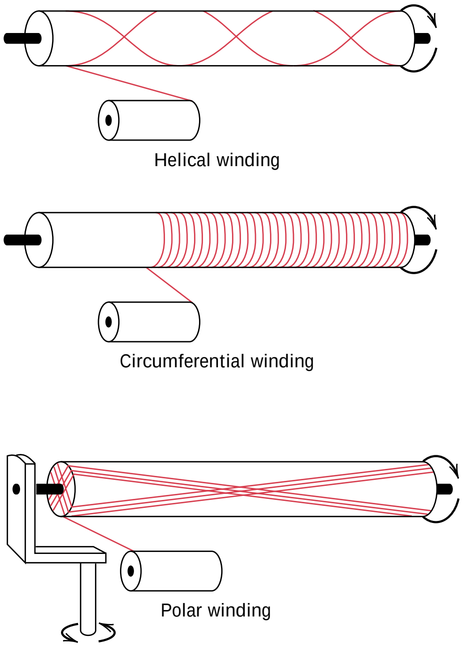

Figure 15.14 Schematic representations of helical, circumferential, and polar filament winding techniques. (From N. L. Hancox, Editor, *Fibre Composite Hybrid Materials*, The Macmillan Company, New York, 1981.)

Design Example 15.1

A tubular filament-wound composite shaft is to be designed that has an outside diameter of 70 mm (2.75 in.), an inside diameter of 50.8 mm (2.0 in.) and a length of 1.22 m (4 ft). The mechanical characteristic of prime importance is bending stiffness in terms of the longitudinal modulus of elasticity; strength and fatigue resistance are not significant parameters for this application when filament composites are utilized. Stiffness is to be specified as maximum allowable deflection in bending; when subjected to three-point bending as in Figure 7.18 (i.e., support points at both tube extremities and load application at the longitudinal midpoint), a load of 890 N (200 $\mathrm{lb_f}$) is to produce an elastic deflection of no more than 0.330 mm (0.013 in.) at the midpoint position.

A circumferential winding pattern is to be used similar to that shown in Figure 15.14. Furthermore, the winding pitch of the fibers, expressed in terms of the angle θ, Figure 15.15, should be relatively small, in order to maximize stiffness in the longitudinal direction; this particular design calls for $\theta = 15°$. Possible fiber materials are glass, and carbon in standard-, intermediate-, and high-modulus grades. The matrix material is to be an epoxy resin, and the maximum allowable fiber volume fraction is 0.60.

This design problem calls for us to do the following:

(a) Decide which of the four fiber materials, when embedded in the epoxy matrix, meet the stipulated criteria.

(b) Of these possibilities, select the one fiber material that will yield the lowest-cost filament-wound composite material (assuming fabrication costs are the same for all fibers).

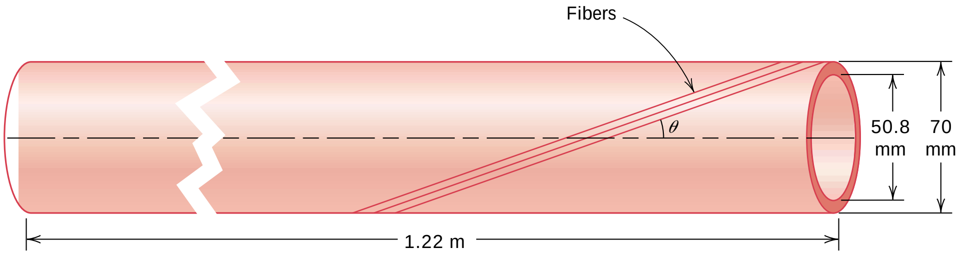

Figure 15.15 Schematic representation of a filament wound composite shaft, which is the subject of Design Example 15.1.

Elastic modulus, density, and cost data for the fiber and matrix materials are contained in Table 15.8.

Solution

(a) It first becomes necessary to determine the required longitudinal modulus of elasticity for this composite material, consistent with the stipulated criteria. This computation necessitates the use of the three-point deflection expression

$$\Delta y = \frac{FL^3}{48EI} \tag{15.21}$$

in which Δy is the midpoint deflection, F is the applied force, L is the support point separation distance, E is the modulus of elasticity, and I is the cross-sectional moment of inertia. For a tube having inside and outside diameters of d_i and d_o, respectively

$$I = \frac{\pi}{64}(d_o^4 - d_i^4) \tag{15.22}$$

and

$$E = \frac{4FL^3}{3\pi\,\Delta y\,(d_o^4 - d_i^4)} \tag{15.23}$$

For this shaft design

$$F = 890 \text{ N}$$

$$L = 1.22 \text{ m}$$

$$\Delta y = 0.330 \text{ mm}$$

$$d_o = 70 \text{ mm}$$

$$d_i = 50.8 \text{ mm}$$

Table 15.8 Elastic Modulus, Density, and Cost Data for Glass and Various Carbon Fibers and Epoxy Resin

Material	*Elastic Modulus (GPa)*	*Density (g/cm^3)*	*Cost ($/kg)*
Glass fibers	72.5	2.58	2.50
Carbon fibers (standard modulus)	230	1.80	35.00
Carbon fibers (intermediate modulus)	285	1.80	70.00
Carbon fibers (high modulus)	400	1.80	175.00
Epoxy resin	2.4	1.14	9.00

Thus, the required longitudinal modulus of elasticity for this shaft is

$$E = \frac{4(890\ \text{N})(1.22\ \text{m})^3}{3\pi(0.33 \times 10^{-3}\ \text{m})[(70 \times 10^{-3}\ \text{m})^4 - (50.8 \times 10^{-3}\ \text{m})^4]}$$

$$= 120\ \text{GPa}\ (17.4 \times 10^6\ \text{psi})$$

The next step is to determine the fiber and matrix volume fractions for each of the four candidate fiber materials. This is possible using a rule-of-mixtures expression, similar to Equation 15.10, which must be modified to take into account that the continuous fibers are filament wound and that the fiber orientation is not parallel to the shaft's longitudinal axis. Thus, from Equation 15.10 we may write an expression for the longitudinal modulus of elasticity of this composite shaft E_{cs} as

$$E_{cs} = (\cos\theta)(E_m V_m + E_f V_f) \tag{15.24a}$$

where, again, θ is the winding pitch (Figure 15.15). Inasmuch as $\theta = 15°$, and cos $(15°) = 0.966$, then

$$E_{cs} = 0.966(E_m V_m + E_f V_f) \tag{15.24b}$$

Upon consultation of Table 15.8 it is obvious that a 120 GPa modulus of elasticity value for a glass-fiber filament-wound composite is not possible since E for glass fibers (i.e., 72.5 GPa) is significantly below this value. Furthermore, in Table 15.9 is given a tabulation of the V_m and V_f values required for $E_{cs} = 120$ GPa; Equation 15.24b and the moduli data in Table 15.8 were used in these computations. Hence, all three carbon fiber types are still possibilities inasmuch as for none of them is it necessary for V_f to be greater than 0.60.

(b) At this point it becomes necessary to determine the volume of fibers and matrix for each of the three carbon types. The total tube volume V_c in centimeters is

$$V_c = \frac{\pi L}{4}(d_o^2 - d_i^2) \tag{15.25}$$

$$= \frac{\pi(122\ \text{cm})}{4}[(7\ \text{cm})^2 - (5.08\ \text{cm})^2]$$

$$= 2222\ \text{cm}^3\ (134.3\ \text{in.}^3)$$

Thus, fiber and matrix volumes result from products of this value and the V_f and V_m values cited in Table 15.9. These volume values are presented in Table 15.10, which are then converted into masses using densities (Table 15.8), and finally, into material costs, from the per unit mass cost (also given in Table 15.8).

As may be noted in Table 15.10, the material of choice (i.e., the least expensive) is the standard-modulus carbon-fiber composite; the relatively low cost per unit

Table 15.9 Fiber and Matrix Volume Fractions for Three Carbon Fiber Types As Required to Give a Composite Modulus of 120 GPa

Fiber Type	V_f	V_m
Standard modulus	0.535	0.465
Intermediate modulus	0.431	0.569
High modulus	0.306	0.694

Table 15.10 **Fiber and Matrix Volumes, Masses, and Costs and Total Material Cost for Three Carbon Fiber-Epoxy-Matrix Composites**

Fiber Type	*Fiber Volume* (cm^3)	*Fiber Mass* (*kg*)	*Fiber Cost* ($)	*Matrix Volume* (cm^3)	*Matrix Mass* (*kg*)	*Matrix Cost* ($)	*Total Cost* ($)
Standard modulus	1189	2.14	74.90	1033	1.18	10.60	85.50
Intermediate modulus	958	1.72	120.70	1264	1.44	12.96	133.66
High modulus	680	1.22	214.20	1542	1.76	15.82	230.00

mass of this fiber material offsets its relatively low modulus of elasticity and required high volume fraction.

STRUCTURAL COMPOSITES

A **structural composite** is normally composed of both homogeneous and composite materials, the properties of which depend not only on the properties of the constituent materials but also on the geometrical design of the various structural elements. Laminar composites and sandwich panels are two of the most common structural composites; only a relatively superficial examination is offered here for them.

15.14 Laminar Composites

A **laminar composite** is composed of two-dimensional sheets or panels that have a preferred high-strength direction such as is found in wood and continuous and aligned fiber-reinforced plastics. The layers are stacked and subsequently cemented together such that the orientation of the high-strength direction varies with each successive layer (Figure 15.16). For example, adjacent wood sheets in plywood are aligned with the grain direction at right angles to each other. Laminations may also

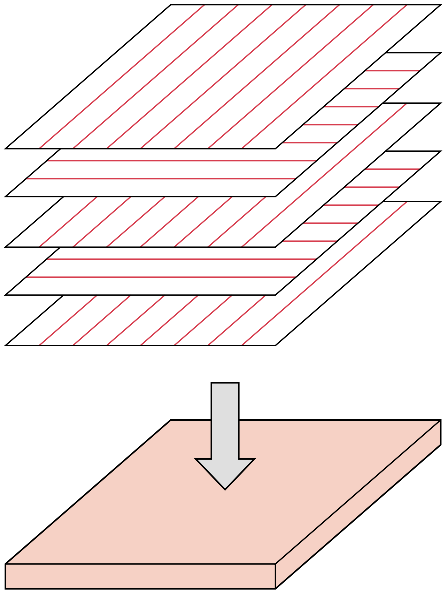

Figure 15.16 The stacking of successive oriented, fiber-reinforced layers for a laminar composite.

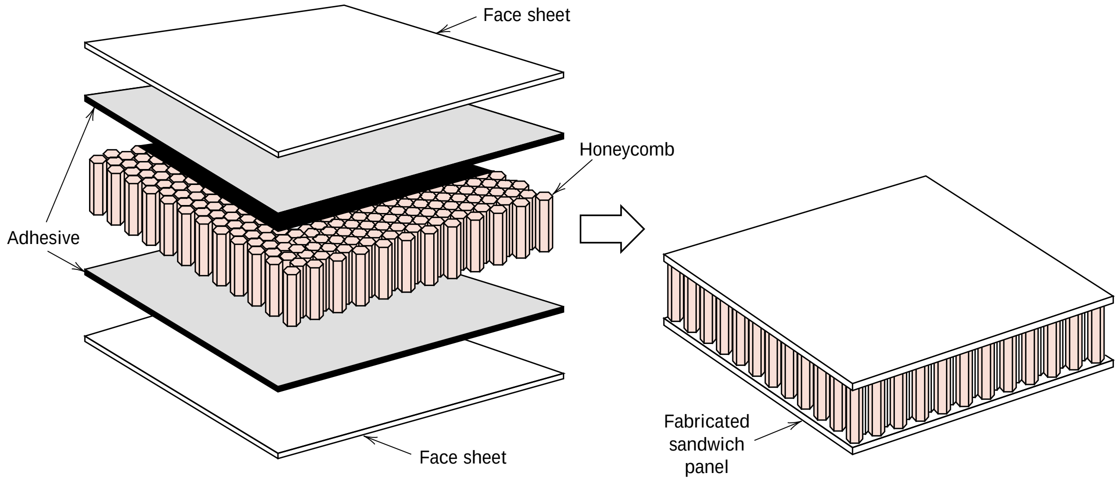

Figure 15.17 Schematic diagram showing the construction of a honeycomb core sandwich panel. (Reprinted with permission from *Engineered Materials Handbook,* Vol. 1, *Composites,* ASM International, Metals Park, OH, 1987.)

be constructed using fabric material such as cotton, paper, or woven glass fibers embedded in a plastic matrix. Thus a laminar composite has relatively high strength in a number of directions in the two-dimensional plane; however, the strength in any given direction is, of course, lower than it would be if all the fibers were oriented in that direction. One example of a relatively complex laminated structure is the modern ski (see the schematic diagram on the chapter-opening page for this chapter).

15.15 Sandwich Panels

Sandwich panels, considered to be a class of structural composites, consist of two strong outer sheets, or faces, separated by a layer of less-dense material, or core, which has lower stiffness and lower strength. The faces bear most of the in-plane loading, and also any transverse bending stresses. Typical face materials include aluminum alloys, fiber-reinforced plastics, titanium, steel, and plywood.

Structurally, the core serves two functions. First, it separates the faces and resists deformations perpendicular to the face plane. Secondly, it provides a certain degree of shear rigidity along planes that are perpendicular to the faces. Various materials and structures are utilized for cores, including foamed polymers, synthetic rubbers, inorganic cements, as well as balsa wood.

Another popular core consists of a ''honeycomb'' structure—thin foils that have been formed into interlocking hexagonal cells, with axes oriented perpendicular to the face planes. The material of which the honeycomb is made may be similar to the face material. Figure 15.17 shows a cutaway view of a honeycomb core sandwich panel.

Sandwich panels are found in a wide variety of applications; they include roofs, floors, and walls of buildings; and, in aircraft, for wings, fuselage, and tailplane skins.

SUMMARY

Composites are artificially produced multiphase materials having a desirable combination of the best properties of the constituent phases. Usually, one phase (the matrix) is continuous and completely surrounds the other (the dispersed phase). In this discussion, composites were classified as particle-reinforced, fiber-reinforced, and structural composites.

Large-particle and dispersion-strengthened composites fall within the particle-reinforced classification. For dispersion strengthening, improved strength is achieved by extremely small particles of the dispersed phase, which inhibit dislocation motion; that is, the strengthening mechanism involves interactions that may be treated on the atomic level. The particle size is normally greater with large-particle composites, whose mechanical characteristics are enhanced by reinforcement action.

Concrete, a type of large-particle composite, consists of an aggregate of particles bonded together with cement. In the case of portland cement concrete, the aggregate consists of sand and gravel; the cementitious bond develops as a result of chemical reactions between the portland cement and water. The mechanical strength of this concrete may be improved by reinforcement methods (e.g., embedment into the fresh concrete of steel rods, wires, etc.). Additional reinforcement is possible by the imposition of residual compressive stresses using prestressing and posttensioning techniques.

Of the several composite types, the potential for reinforcement efficiency is greatest for those that are fiber reinforced. With these composites an applied load is transmitted and distributed among the fibers via the matrix phase, which in most cases is at least moderately ductile. Significant reinforcement is possible only if the matrix–fiber bond is strong. On the basis of diameter, fiber reinforcements are classified as whiskers, fibers, or wires. Since reinforcement discontinues at the fiber extremities, reinforcement efficiency depends on fiber length. For each fiber–matrix combination, there exists some critical length; the length of continuous fibers greatly exceeds this critical value, whereas shorter fibers are discontinuous.

Fiber arrangement is also crucial relative to composite characteristics. The mechanical properties of continuous and aligned fiber composites are highly anisotropic. In the alignment direction, reinforcement and strength are a maximum; perpendicular to the alignment, they are a minimum. The stress–strain behavior for longitudinal loading was discussed. Composite rule-of-mixture expressions for the modulus in both longitudinal and transverse orientations were developed; in addition, an equation for longitudinal strength was also cited.

For short and discontinuous fibrous composites, the fibers may be either aligned or randomly oriented. Significant strengths and stiffnesses are possible for aligned short-fiber composites in the longitudinal direction. Despite some limitations on reinforcement efficiency, the properties of randomly oriented short-fiber composites are isotropic.

Fibrous-reinforced composites are sometimes classified according to matrix type; within this scheme are three classifications—viz. polymer-, metal-, and ceramic-matrix. Polymer-matrix are the most common, which may be reinforced with glass, carbon, and aramid fibers. Service temperatures are higher for metal-matrix composites, which also utilize a variety of fiber and whisker types. The objective of many polymer- and metal-matrix composites is a high specific strength and/or specific modulus, which requires matrix materials having low densities. With ceramic-matrix composites, the design goal is increased fracture toughness. This is achieved by interactions between advancing cracks and dispersed phase particles; transformation toughening is one such technique for improving K_{Ic}. Other more advanced composites are carbon–carbon (carbon fibers embedded in a pyrolyzed carbon matrix) and the hybrids (containing at least two different fiber types).

Several composite processing techniques have been developed that provide a uniform fiber distribution and a high degree of alignment. With pultrusion, components of continuous length and constant cross section are formed as resin-impregnated fiber tows are pulled through a die. Composites utilized for many structural applications are commonly prepared using a lay-up operation (either hand or automated), wherein prepreg tape plies are laid down on a tooled surface and are subsequently fully cured by the simultaneous application of heat and pressure. Some hollow structures may be fabricated using automated filament winding procedures, whereby resin-coated strands or tows or prepreg tape are continuously wound onto a mandrel, followed by a curing operation.

Two general kinds of structural composites were discussed: the laminar composites and sandwich panels. The properties of laminar composites are virtually isotropic in a two-dimensional plane. This is made possible with several sheets of a highly anisotropic composite, which are cemented onto one another such that the high-strength direction is varied with each successive layer. Sandwich panels consist of two strong and stiff sheet faces that are separated by a core material or structure. These structures combine relatively high strengths and stiffnesses with low densities.

IMPORTANT TERMS AND CONCEPTS

Carbon–carbon composite
Ceramic-matrix composite
Cermet
Concrete
Dispersed phase
Dispersion-strengthened composite
Fiber
Fiber-reinforced composite
Hybrid composite
Laminar composite
Large-particle composite
Longitudinal direction
Matrix phase
Metal-matrix composite
Polymer-matrix composite
Prepreg
Prestressed concrete
Principle of combined action
Reinforced concrete
Rule of mixtures
Sandwich panel
Specific modulus
Specific strength
Structural composite
Transverse direction
Whisker

REFERENCES

Agarwal, B. D. and L. J. Broutman, *Analysis and Performance of Fiber Composites,* 2nd edition, John Wiley & Sons, New York, 1990.

Ashbee, K. H. G., *Fundamental Principles of Fiber Reinforced Composites,* 2nd edition, Technomic Publishing Company, Inc., Lancaster, PA, 1993.

Broutman, L. J. and R. H. Krock, *Modern Composite Materials,* Addison-Wesley Publishing Co., Reading, MA, 1967.

Chawla, K. K., *Composite Materials,* Springer-Verlag, New York, 1993.

Chou, T. W., R. L. McCullough, and R. B. Pipes, ‘‘Composites,’’ *Scientific American,* Vol. 255, No. 4, October 1986, pp. 192–203.

Engineered Materials Handbook, Vol. 1, *Composites,* ASM International, Metals Park, OH, 1987.

Folkes, M. J., *Short Fibre Reinforced Thermoplastics,* John Wiley & Sons, New York, 1982.

Hollaway, L. (Editor), *Handbook of Polymer Composites for Engineers,* Woodhead Publishing Ltd., Cambridge, 1994.

Hull, D. and T. W. Clyne, *An Introduction to Composite Materials,* 2nd edition, Cambridge University Press, Cambridge, 1996.

Jones, F. R. (Editor), *Handbook of Polymer-Fibre Composites,* Longman Scientific & Technical, Harlow, England (reprinted by Halstead Press, a division of John Wiley & Sons, New York), 1994.

Kelly, A. and N. H. Macmillan, *Strong Solids*, 3rd edition, Clarendon Press, Oxford, 1986.

Piggott, M. R., *Load-Bearing Fibre Composites*, Pergamon Press, Oxford, 1980.

Richardson, M. O. W. (Editor), *Polymer Engineering Composites*, Applied Science Publishers, Ltd., London, 1977.

Schwartz, M. M. (Editor), *Composite Materials Handbook*, 2nd edition, McGraw-Hill Book Company, New York, 1992.

Sheldon, R. P., *Composite Polymeric Materials*, Applied Science Publishers, London, 1982.

Strong, A. B., *Fundamentals of Composites: Materials, Methods, and Applications*, Society of Manufacturing Engineers, Dearborn, MI, 1989.

Strong, A. B., *High Performance and Engineering Thermoplastic Composites*, Technomic Publishing Company, Lancaster, PA, 1993.

Weeton, J. W. (Editor), *Engineers' Guide to Composite Materials*, American Society for Metals, Metals Park, OH, 1986.

Woishnis, W. A. (Editor), *Engineering Plastics and Composites*, 2nd edition, ASM International, Materials Park, OH, 1993.

QUESTIONS AND PROBLEMS

15.1 Cite the general difference in strengthening mechanism between large-particle and dispersion-strengthened particle-reinforced composites.

15.2 Cite one similarity and two differences between precipitation hardening and dispersion strengthening.

15.3 The mechanical properties of aluminum may be improved by incorporating fine particles of aluminum oxide (Al_2O_3). Given that the moduli of elasticity of these materials are, respectively, 69 GPa (10×10^6 psi) and 393 GPa (57×10^6 psi), plot modulus of elasticity versus the volume percent of Al_2O_3 in Al from 0 to 100 vol%, using both upper- and lower-bound expressions.

15.4 Estimate the maximum and minimum thermal conductivity values for a cermet that contains 85 vol% titanium carbide (TiC) particles in a cobalt matrix. Assume thermal conductivities of 27 and 69 W/m-K for TiC and Co, respectively.

15.5 A large-particle composite consisting of tungsten particles within a copper matrix is to be prepared. If the volume fractions of tungsten and copper are 0.60 and 0.40, respectively, estimate the upper limit for the specific stiffness of this composite given the data below.

	Specific Gravity	***Modulus of Elasticity (GPa)***
Copper	8.9	110
Tungsten	19.3	407

15.6 **(a)** What is the distinction between matrix and dispersed phases in a composite material?

(b) Contrast the mechanical characteristics of matrix and dispersed phases for fiber-reinforced composites.

15.7 **(a)** What is the distinction between cement and concrete?

(b) Cite three important limitations that restrict the use of concrete as a structural material.

(c) Briefly explain three techniques that are utilized to strengthen concrete by reinforcement.

15.8 For a polymer-matrix fiber-reinforced composite,

(a) list three functions of the matrix phase;

(b) compare the desired mechanical characteristics of matrix and fiber phases; and

(c) cite two reasons why there must be a strong bond between fiber and matrix at their interface.

15.9 For some glass fiber–epoxy matrix combination, the critical fiber length–fiber diameter ratio is 50. Using the data in Table 15.4, determine the fiber-matrix bond strength.

15.10 **(a)** For a fiber-reinforced composite, the efficiency of reinforcement η is dependent on fiber length l according to

$$\eta = \frac{l - 2x}{l}$$

where x represents the length of the fiber at each end that does not contribute to the load transfer. Make a plot of η versus l to $l = 40$ mm (1.6 in.) assuming that $x = 0.75$ mm (0.03 in.).

(b) What length is required for a 0.80 efficiency of reinforcement?

15.11 A continuous and aligned fiber-reinforced composite is to be produced consisting of 30 vol% aramid fibers and 70 vol% of a polycarbonate matrix; mechanical characteristics of these two materials are as follows:

	Modulus of Elasticity [GPa (psi)]	***Tensile Strength [MPa (psi)]***
Aramid fiber	131 (19×10^6)	3600 (520,000)
Polycarbonate	2.4 (3.5×10^5)	65 (9425)

Also, the stress on the polycarbonate matrix when the aramid fibers fail is 45 MPa (6500 psi).
For this composite, compute

(a) the longitudinal tensile strength, and

(b) the longitudinal modulus of elasticity.

15.12 Is it possible to produce a continuous and oriented aramid fiber-epoxy matrix composite having longitudinal and transverse moduli of elasticity of 57.1 GPa (8.28×10^6 psi) and 4.12 GPa (6×10^5 psi), respectively? Why or why not? Assume that the modulus of elasticity of the epoxy is 2.4 GPa (3.50×10^5 psi).

15.13 **(a)** Calculate and compare the specific longitudinal strengths of the glass-fiber, carbon-fiber, and aramid-fiber reinforced epoxy composites in Table 15.5 with the following alloys: tempered (315°C) 440A martensitic stainless steel, normalized 1020 plain-carbon steel, 2024-T3 aluminum alloy, cold-worked (HO2 temper) C36000 free-cutting brass, rolled AZ31B magnesium alloy, and annealed Ti-6Al-4V titanium alloy.

(b) Compare the specific moduli of the same three fiber-reinforced epoxy composites with the same metal alloys. Densities (i.e., specific gravities), tensile strengths, and moduli of elasticity for these metal alloys may be found in Tables B.1, B.4, and B.2, respectively, in Appendix B.

15.14 For a continuous and oriented fiber-reinforced composite, the moduli of elasticity in the longitudinal and transverse directions are 19.7 and 3.66 GPa (2.8×10^6 and 5.3×10^5 psi), respectively. If the volume fraction of fibers is 0.25, determine the moduli of elasticity of fiber and matrix phases.

15.15 **(a)** Verify that Equation 15.11, the expression for the fiber load–matrix load ratio (F_f/F_m), is valid.

(b) What is the F_f/F_c ratio in terms of E_f, E_m, and V_f?

15.16 In an aligned and continuous glass fiber-reinforced nylon 6,6 composite, the fibers are to carry 94% of a load applied in the longitudinal direction.

(a) Using the data provided, determine the volume fraction of fibers that will be required.

(b) What will be the tensile strength of this composite? Assume that the matrix stress at fiber failure is 30 MPa (4350 psi).

	Elastic Modulus [GPa (psi)]	***Tensile Strength [MPa (psi)]***
Glass fiber	72.5 (10.5×10^6)	3,400 (4.9×10^5)
Nylon 6,6	3.0 (4.35×10^5)	76 (11,000)

15.17 Assume that the composite described in Problem 15.11 has a cross-sectional area of 320 mm^2 (0.50 in.^{2}) and is subjected to a longitudinal load of 44,500 N (10,000 lb$_f$).

(a) Calculate the fiber–matrix load ratio.

(b) Calculate the actual loads carried by both fiber and matrix phases.

(c) Compute the magnitude of the stress on each of the fiber and matrix phases.

(d) What strain is experienced by the composite?

15.18 A continuous and aligned fiber-reinforced composite having a cross-sectional area of 1130 mm^2 (1.75 in.^{2}) is subjected to an external tensile load. If the stresses sustained by the fiber and matrix phases are 156 MPa (22,600 psi) and 2.75 MPa (400 psi), respectively, the force sustained by the fiber phase is 74,000 N (16,600 lb$_f$) and the total longitudinal strain is 1.25×10^{-3}, determine

(a) the force sustained by the matrix phase,

(b) the modulus of elasticity of the composite material in the longitudinal direction, and

(c) the moduli of elasticity for the fiber and matrix phases.

15.19 Compute the longitudinal strength of an aligned carbon fiber-epoxy matrix composite having a 0.25 volume fraction of fibers, assuming the following:

(1) an average fiber diameter of 10×10^{-3} mm (3.94×10^{-4} in.),

(2) an average fiber length of 5 mm (0.20 in.),

(3) a fiber fracture strength of 2.5 GPa (3.625×10^{5} psi),

(4) a fiber-matrix bond strength of 80 MPa (11,600 psi),

(5) a matrix stress at fiber failure of 10.0 MPa (1450 psi), and

(6) a matrix tensile strength of 75 MPa (11,000 psi).

15.20 It is desired to produce an aligned carbon fiber-epoxy matrix composite having a longitudinal tensile strength of 750 MPa (109,000 psi). Calculate the volume fraction of fibers necessary if

(1) the average fiber diameter and length are 1.2×10^{-2} mm (4.7×10^{-4} in.) and 1 mm (0.04 in.), respectively;

(2) the fiber fracture strength is 5000 MPa (725,000 psi);

(3) the fiber-matrix bond strength is 25 MPa (3625 psi); and

(4) the matrix stress at fiber failure is 10 MPa (1450 psi).

15.21 Compute the longitudinal tensile strength of an aligned glass fiber-epoxy matrix composite in which the average fiber diameter and length are 0.010 mm (4×10^{-4} in.) and 2.5 mm (0.10 in.), respectively, and the volume fraction of fibers is 0.40. Assume that

(1) the fiber-matrix bond strength is 75 MPa (10,900 psi),

(2) the fracture strength of the fibers is 3500 MPa (508,000 psi), and

(3) the matrix stress at fiber failure is 8.0 MPa (1160 psi).

15.22 **(a)** From the moduli of elasticity data in Table 15.2 for glass fiber-reinforced polycarbonate composites, determine the value of the fiber efficiency parameter for each of 20, 30, and 40 vol% fibers.

(b) Estimate the modulus of elasticity for 50 vol% glass fibers.

15.23 Cite one desirable characteristic and one less desirable characteristic for each of (1) discontinuous-oriented, and (2) discontinuous-random fiber-reinforced composites.

15.24 **(a)** List four reasons why glass fibers are most commonly used for reinforcement.

(b) Why is the surface perfection of glass fibers so important?

(c) What measures are taken to protect the surface of glass fibers?

15.25 Cite the distinction between carbon and graphite.

15.26 **(a)** Cite several reasons why fiberglass-reinforced composites are utilized extensively.

(b) Cite several limitations of this type of composite.

15.27 **(a)** What is a hybrid composite?

(b) List two important advantages of hybrid composites over normal fiber composites.

15.28 **(a)** Write an expression for the modulus of elasticity for a hybrid composite in which all fibers of both types are oriented in the same direction.

(b) Using this expression, compute the longitudinal modulus of elasticity of a hybrid composite consisting of aramid and glass fibers in volume fractions of 0.30 and 0.40, respectively, within a polyester resin matrix [E_m = 2.5 GPa (3.6×10^{5} psi)].

15.29 Derive a generalized expression analogous to Equation 15.16 for the transverse modulus of elasticity of an aligned hybrid composite consisting of two types of continuous fibers.

15.30 Briefly describe pultrusion, filament winding, and prepreg production fabrication processes; cite the advantages and disadvantages of each.

15.31 Briefly describe laminar composites. What is the prime reason for fabricating these materials?

15.32 **(a)** Briefly describe sandwich panels.

(b) What is the prime reason for fabricating these structural composites?

(c) What are the functions of the faces and the core?

Design Problems

15.D1 It is desired to produce an aligned and continuous fiber-reinforced epoxy composite having a maximum of 50 vol% fibers. In addition, a minimum longitudinal modulus of elasticity of 50 GPa (7.3×10^6 psi) is required, as well as a minimum tensile strength of 1300 MPa (189,000 psi). Of E-glass, carbon (PAN standard modulus), and aramid fiber materials, which are possible candidates and why? The epoxy has a modulus of elasticity of 3.1 GPa (4.5×10^5 psi) and a tensile strength of 75 MPa (11,000 psi). In addition, assume the following stress levels on the epoxy matrix at fiber failure: E-glass—70 MPa (10,000 psi); carbon (PAN standard modulus)—30 MPa (4350 psi); and aramid—50 MPa (7250 psi). Other fiber data are contained in Tables B.2 and B.4 in Appendix B.

15.D2 It is desired to produce a continuous and oriented carbon fiber-reinforced epoxy having a modulus of elasticity of at least 83 GPa (12×10^6 psi) in the direction of fiber alignment. The maximum permissible specific gravity is 1.40. Given the following data, is such a composite possible? Why or why not? Assume that composite specific gravity may be determined using a relationship similar to Equation 15.10a.

	Specific Gravity	***Modulus of Elasticity [GPa (psi)]***
Carbon fiber	1.80	260 (37×10^6)
Epoxy	1.25	2.4 (3.5×10^5)

15.D3 It is desired to fabricate a continuous and aligned glass fiber-reinforced polyester having a tensile strength of at least 1400 MPa (200,000 psi) in the longitudinal direction. The maximum possible specific gravity is 1.65. Using the following data, determine if such a composite is possible. Justify your decision. Assume a value of 15 MPa for the stress on the matrix at fiber failure.

	Specific Gravity	***Tensile Strength [MPa (psi)]***
Glass fiber	2.50	3500 (5×10^5)
Polyester	1.35	50 (7.25×10^3)

15.D4 It is necessary to fabricate an aligned and discontinuous carbon fiber-epoxy matrix composite having a longitudinal tensile strength of 1900 MPa (275,000 psi) using 0.45 volume fraction of fibers. Compute the required fiber fracture strength assuming that the average fiber diameter and length are 8×10^{-3} mm (3.1×10^{-4} in.) and 3.5 mm (0.14 in.), respectively. The fiber-matrix bond strength is 40 MPa (5800 psi), and the matrix stress at fiber failure is 12 MPa (1740 psi).

15.D5 A filament-wound tubular shaft is to be designed that has an outside diameter of 76.2 mm (3.0 in.) and a length of 1.82 m (6 ft). The mechanical characteristic of prime importance is bending stiffness in terms of the longitudinal modulus of elasticity. Stiffness is to be specified as maximum allowable deflection in bending; when subjected to three-point bending as in Figure 7.18, a load of 667 N (150 lb_f) is to produce an elastic deflection of no more than 0.84 mm (0.033 in.) at the midpoint position.

A circumferential winding pattern is to be used, and the winding pitch of fibers (θ in Figure 15.15) is to be 20°. Possible fiber materials are glass, and carbon in standard-, intermediate-, and high-modulus grades. The matrix material is to be an epoxy resin, and fiber volume fraction called for is 0.50.

(a) Decide which of the four fiber materials are possible candidates for this application, and for each candidate determine the required inside diameter consistent with the above criteria.

(b) For each candidate, determine the required cost, and on this basis, specify the fiber that would be the most inexpensive to use.

Elastic modulus, density, and cost data for the fiber and matrix materials are contained in Table 15.8.

15.D6 Using the *E-Z Solve* software included on the CD-ROM that is associated with this book, construct a routine for the design of a tubular filament-wound composite shaft (Design Example 15.1). Values of the following parameters should be incorporated into the routine:

$F = 650$ N
$L = 1.0$ m
$\Delta y = 0.45$ mm
$d_o = 60$ mm
$d_i = 45$ mm
$\theta = 20°$
Maximum $V_f = 0.60$

The user is allowed to input values of density, elastic modulus, and cost (dollars per kilogram) for both fiber and matrix phases, and the routine determines whether or not the fiber and matrix phases selected meet the design criteria, and, if so, what the shaft will cost.

15.D7 Composite materials are now being utilized extensively in sports equipment.

(a) Make a list of at least four different sports implements that are made of or contain composites.

(b) For one of these implements, write an essay in which you do the following: (1) cite the materials that are used for matrix and dispersed phases, and, if possible, the proportions of each phase; (2) note the nature of the dispersed phase (e.g., continuous fibers); and (3) describe the process by which the implement is fabricated.

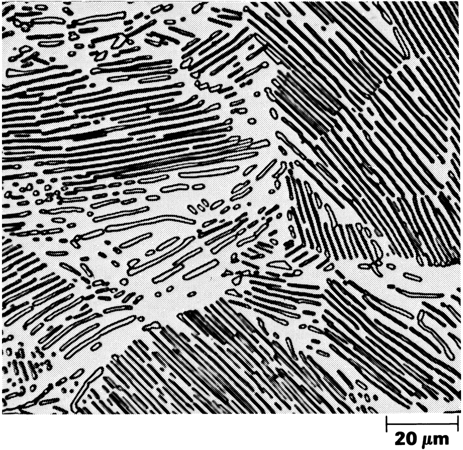

FIGURE 10.29 Photomicrograph of a eutectoid steel showing the pearlite microstructure consisting of alternating layers of α ferrite (the light phase) and Fe_3C (thin layers most of which appear dark). 500×. (Reproduced with permission from *Metals Handbook*, Vol. 9, 9th edition, *Metallography and Microstructures*, American Society for Metals, Materials Park, OH, 1985.)

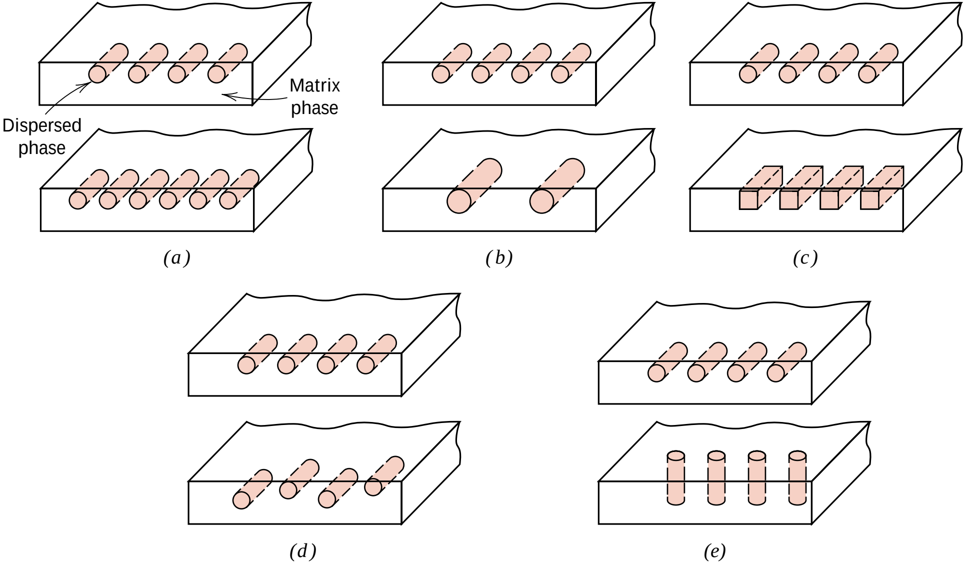

Figure 15.1 Schematic representations of the various geometrical and spatial characteristics of particles of the dispersed phase that may influence the properties of composites: (*a*) concentration, (*b*) size, (*c*) shape, (*d*) distribution, and (*e*) orientation. (From Richard A. Flinn and Paul K. Trojan, *Engineering Materials and Their Applications,* 4th edition. Copyright © 1990 by John Wiley & Sons, Inc. Adapted by permission of John Wiley & Sons, Inc.)

FIGURE 15.2 A classification scheme for the various composite types discussed in this chapter.

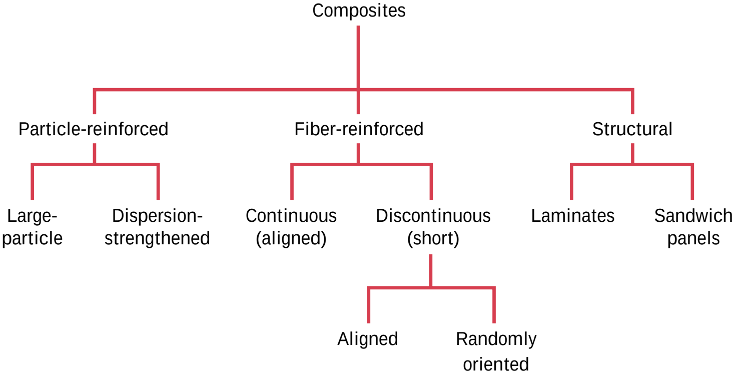
Composites
Particle-reinforced
Fiber-reinforced
Structural
Large-particle
Dispersion-strengthened
Continuous (aligned)
Discontinuous (short)
Laminates
Sandwich panels
Aligned
Randomly oriented

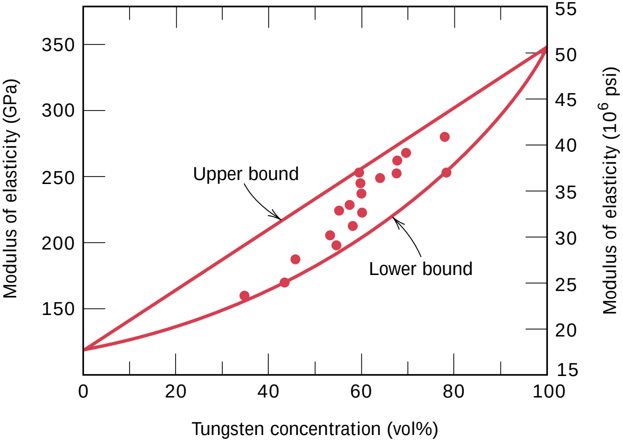

Figure 15.3 Modulus of elasticity versus volume percent tungsten for a composite of tungsten particles dispersed within a copper matrix. Upper and lower bounds are according to Equations 15.1 and 15.2; experimental data points are included. (From R. H. Krock, *ASTM Proceedings*, Vol. 63, 1963. Copyright ASTM. Reprinted with permission.)

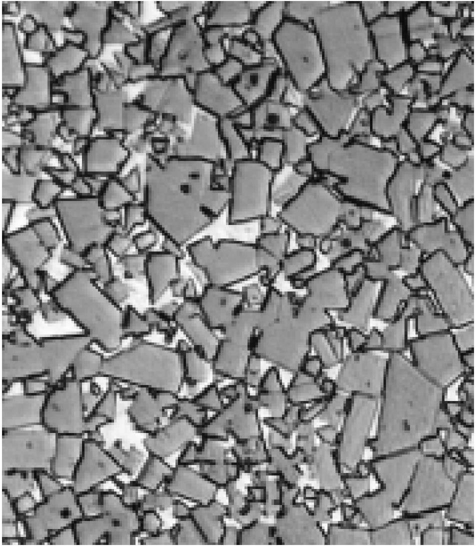

Figure 15.4 Photomicrograph of a WC–Co cemented carbide. Light areas are the cobalt matrix; dark regions, the particles of tungsten carbide. 100×. (Courtesy of Carboloy Systems Department, General Electric Company.)

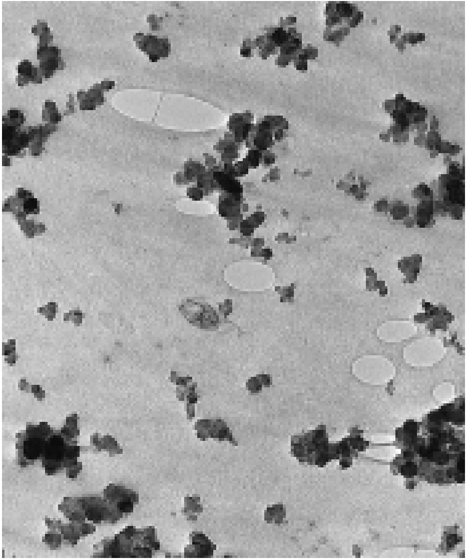

Figure 15.5 Electron micrograph showing the spherical reinforcing carbon black particles in a synthetic rubber tire tread compound. The areas resembling water marks are tiny air pockets in the rubber. 80,000×. (Courtesy of Goodyear Tire & Rubber Company.)

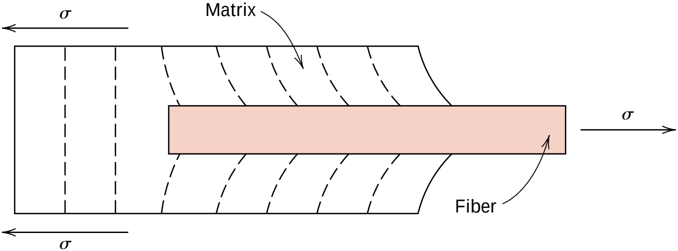
σ
Matrix
σ
Fiber
σ

Figure 15.6 The deformation pattern in the matrix surrounding a fiber that is subjected to an applied tensile load.

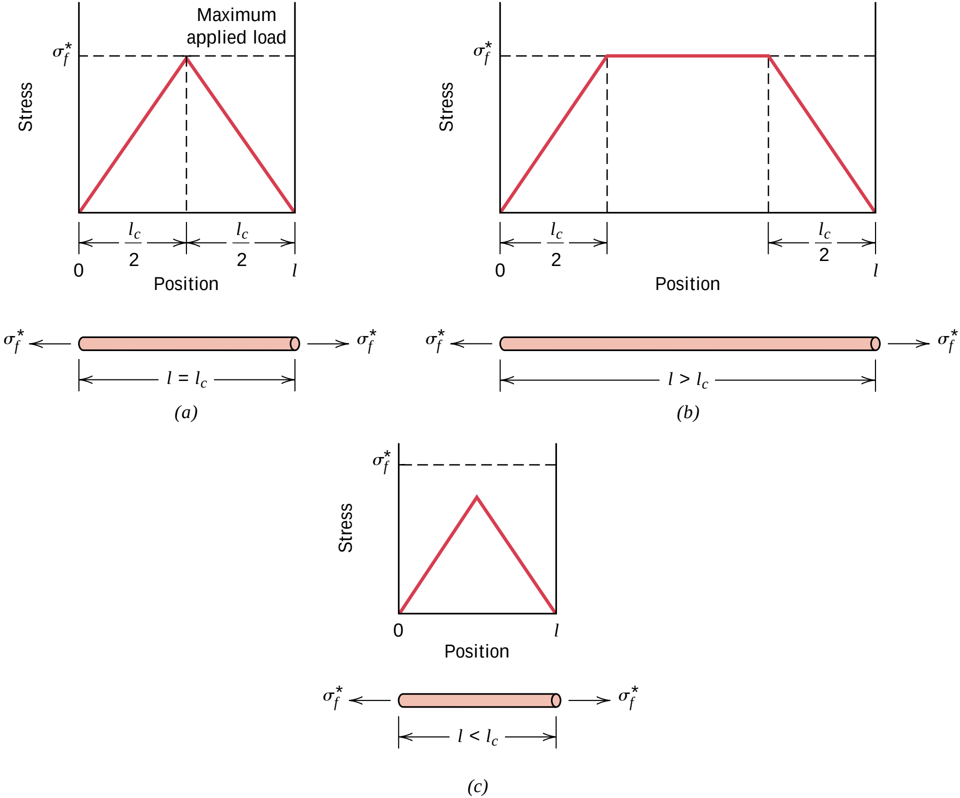
Maximum applied load
σ*f
Stress
lc/2
lc/2
0
l
Position
σ*f
σ*f
l = lc
(a)
σ*f
Stress
lc/2
lc/2
0
l
Position
σ*f
σ*f
l > lc
(b)
σ*f
Stress
0
l
Position
σ*f
σ*f
l < lc
(c)

Figure 15.7 Stress–position profiles when fiber length l (a) is equal to the critical length l_c, (b) is greater than the critical length, and (c) is less than the critical length for a fiber-reinforced composite that is subjected to a tensile stress equal to the fiber tensile strength σ_f^*.

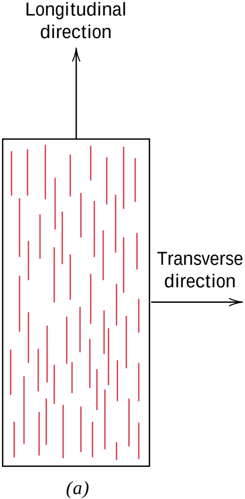
Longitudinal direction
Transverse direction
(a)

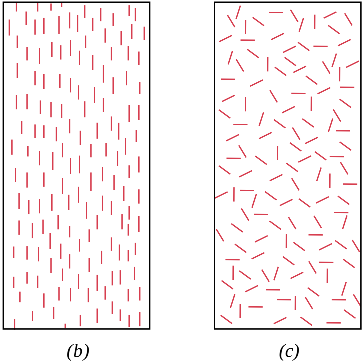

Figure 15.8 Schematic representations of (*a*) continuous and aligned, (*b*) discontinous and aligned, and (*c*) discontinuous and randomly oriented fiber-reinforced composites.

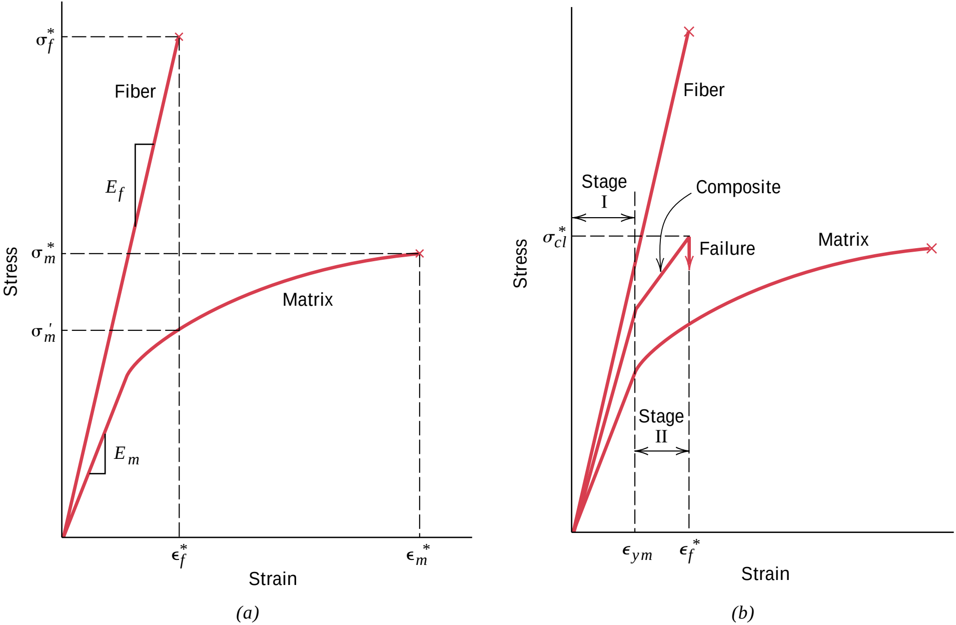

Figure 15.9 (*a*) Schematic stress–strain curves for brittle fiber and ductile matrix materials. Fracture stresses and strains for both materials are noted. (*b*) Schematic stress–strain curve for an aligned fiber-reinforced composite that is exposed to a uniaxial stress applied in the direction of alignment; curves for the fiber and matrix materials shown in part (*a*) are also superimposed.

Table 15.1 Typical Longitudinal and Transverse Tensile Strengths for Three Unidirectional Fiber-Reinforced Composites. The Fiber Content for Each is Approximately 50 Vol%

Material	*Longitudinal Tensile Strength* (*MPa*)	*Transverse Tensile Strength* (*MPa*)
Glass–Polyester	700	20
Carbon (High Modulus)–Epoxy	1000	35
Kevlar–Epoxy	1200	20

Source: D. Hull and T. W. Clyne, *An Introduction to Composite Materials*, 2nd edition, Cambridge University Press, 1996, p. 179.

Table 15.2 Properties of Unreinforced and Reinforced Polycarbonates with Randomly Oriented Glass Fibers

		Fiber Reinforcement (***vol%***)		
Property	***Unreinforced***	***20***	***30***	***40***
Specific gravity	1.19–1.22	1.35	1.43	1.52
Tensile strength [MPa (ksi)]	59–62 (8.5–9.0)	110 (16)	131 (19)	159 (23)
Modulus of elasticity [GPa (10^6 psi)]	2.24–2.345 (0.325–0.340)	5.93 (0.86)	8.62 (1.25)	11.6 (1.68)
Elongation (%)	90–115	4–6	3–5	3–5
Impact strength, notched Izod (lb_f/in.)	12–16	2.0	2.0	2.5

Source: Adapted from Materials Engineering's *Materials Selector*, copyright © Penton/IPC.

Table 15.3 **Reinforcement Efficiency of Fiber-Reinforced Composites for Several Fiber Orientations and at Various Directions of Stress Application**

Fiber Orientation	*Stress Direction*	*Reinforcement Efficiency*
All fibers parallel	Parallel to fibers	1
	Perpendicular to fibers	0
Fibers randomly and uniformly distributed within a specific plane	Any direction in the plane of the fibers	$\frac{3}{8}$
Fibers randomly and uniformly distributed within three dimensions in space	Any direction	$\frac{1}{5}$

Source: H. Krenchel, *Fibre Reinforcement*, Copenhagen: Akademisk Forlag, 1964 [33].

Table 15.4 Characteristics of Several Fiber-Reinforcement Materials

Material	*Specific Gravity*	*Tensile Strength [GPa (10^6 psi)]*	*Specific Strength (GPa)*	*Modulus of Elasticity [GPa (10^6 psi)]*	*Specific Modulus (GPa)*
		Whiskers			
Graphite	2.2	20 (3)	9.1	700 (100)	318
Silicon nitride	3.2	5–7 (0.75–1.0)	1.56–2.2	350–380 (50–55)	109–118
Aluminum oxide	4.0	10–20 (1–3)	2.5–5.0	700–1500 (100–220)	175–375
Silicon carbide	3.2	20 (3)	6.25	480 (70)	150
		Fibers			
Aluminum oxide	3.95	1.38 (0.2)	0.35	379 (55)	96
Aramid (Kevlar 49)	1.44	3.6–4.1 (0.525–0.600)	2.5–2.85	131 (19)	91
Carbon[a]	1.78–2.15	1.5–4.8 (0.22–0.70)	0.70–2.70	228–724 (32–100)	106–407
E-Glass	2.58	3.45 (0.5)	1.34	72.5 (10.5)	28.1
Boron	2.57	3.6 (0.52)	1.40	400 (60)	156
Silicon carbide	3.0	3.9 (0.57)	1.30	400 (60)	133
UHMWPE (Spectra 900)	0.97	2.6 (0.38)	2.68	117 (17)	121
		Metallic Wires			
High-strength steel	7.9	2.39 (0.35)	0.30	210 (30)	26.6
Molybdenum	10.2	2.2 (0.32)	0.22	324 (47)	31.8
Tungsten	19.3	2.89 (0.42)	0.15	407 (59)	21.1

---

[a] The term ‘‘carbon’’ instead of ‘‘graphite’’ is used to denote these fibers, since they are composed of crystalline graphite regions, and also of noncrystalline material and areas of crystal misalignment.

Table 13.10 **Compositions and Characteristics of Some of the Common Commercial Glasses**

	Composition (wt%)						
Glass Type	SiO_2	Na_2O	CaO	Al_2O_3	B_2O_3	***Other***	***Characteristics and Applications***
Fused silica	>99.5						High melting temperature, very low coefficient of expansion (shock resistant)
96% Silica (Vycor)	96				4		Thermally shock and chemically resistant—laboratory ware
Borosilicate (Pyrex)	81	3.5		2.5	13		Thermally shock and chemically resistant—ovenware
Container (soda–lime)	74	16	5	1		4MgO	Low melting temperature, easily worked, also durable
Fiberglass	55		16	15	10	4MgO	Easily drawn into fibers—glass–resin composites
Optical flint	54	1				37PbO, $8K_2O$	High density and high index of refraction—optical lenses
Glass–ceramic (Pyroceram)	43.5	14		30	5.5	$6.5TiO_2$, $0.5As_2O_3$	Easily fabricated; strong; resists thermal shock—ovenware

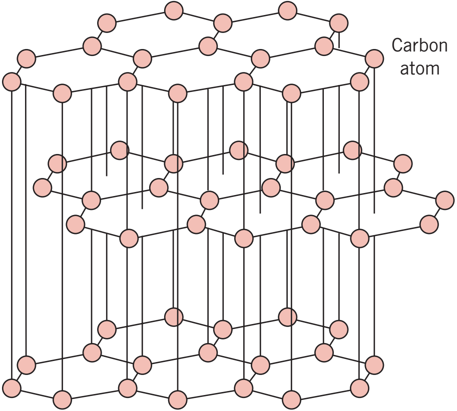
Carbon atom

FIGURE 3.17 The structure of graphite.

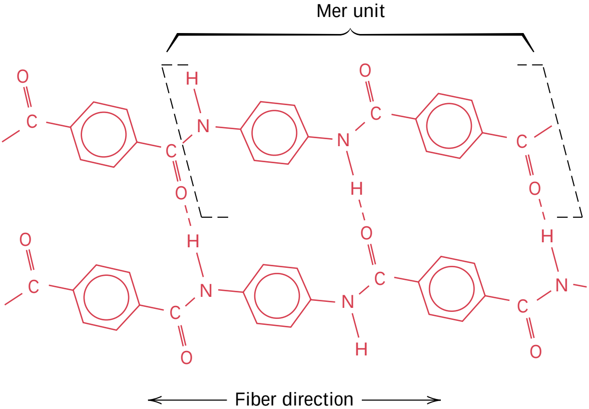
Mer unit
O
C
H
N
C
O
N
H
O
C
C
O
H
N
O
C
N
H
C
N
C
O
H
N
C
O
Fiber direction

FIGURE 15.10 Schematic representation of mer and chain structures for aramid (Kevlar) fibers. Chain alignment with the fiber direction and hydrogen bonds that form between adjacent chains are also shown. (From F. R. Jones, Editor, *Handbook of Polymer-Fibre Composites.* Copyright © 1994 by Addison Wesley Longman. Reprinted with permission.)

Table 15.5 **Properties of Continuous and Aligned Glass-, Carbon-, and Aramid-fiber Reinforced Epoxy-matrix Composites in Longitudinal and Transverse Directions. In All Cases the Fiber Volume Fraction is 0.60**

Property	*Glass (E-glass)*	*Carbon (High Strength)*	*Aramid (Kevlar 49)*
Specific gravity	2.1	1.6	1.4
Tensile modulus			
Longitudinal [GPa (10^6 psi)]	45 (6.5)	145 (21)	76 (11)
Transverse [GPa (10^6 psi)]	12 (1.8)	10 (1.5)	5.5 (0.8)
Tensile strength			
Longitudinal [MPa (ksi)]	1020 (150)	1240 (180)	1380 (200)
Transverse [MPa (ksi)]	40 (5.8)	41 (6)	30 (4.3)
Ultimate tensile strain			
Longitudinal	2.3	0.9	1.8
Transverse	0.4	0.4	0.5

Source: Adapted from R. F. Floral and S. T. Peters, ‘‘Composite Structures and Technologies,’’ tutorial notes, 1989.

Table 15.6 Properties of Several Metal-Matrix Composites Reinforced with Continuous and Aligned Fibers

Fiber	*Matrix*	*Fiber Content (vol%)*	*Density (g/cm^3)*	*Longitudinal Tensile Modulus (GPa)*	*Longitudinal Tensile Strength (MPa)*
Carbon	6061 Al	41	2.44	320	620
Boron	6061 Al	48	—	207	1515
SiC	6061 Al	50	2.93	230	1480
Alumina	380.0 Al	24	—	120	340
Carbon	AZ31 Mg	38	1.83	300	510
Borsic	Ti	45	3.68	220	1270

Source: Adapted from J. W. Weeton, D. M. Peters, and K. L. Thomas, *Engineers' Guide to Composite Materials*, ASM International, Materials Park, OH, 1987.

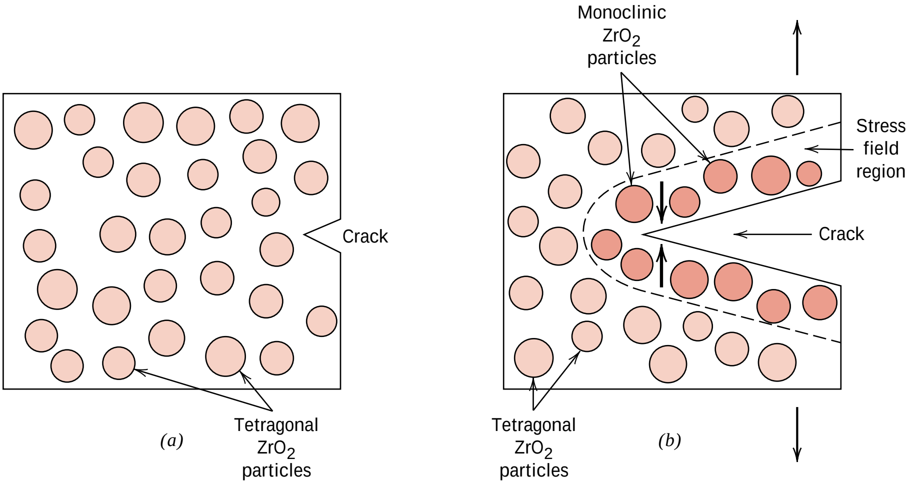
Crack
Tetragonal ZrO_2 particles
(a)
Monoclinic ZrO_2 particles
Stress field region
Crack
Tetragonal ZrO_2 particles
(b)

Figure 15.11 Schematic demonstration of transformation toughening. (*a*) A crack prior to inducement of the ZrO_2 particle phase transformation. (*b*) Crack arrestment due to the stress-induced phase transformation.

Table 15.7 Room-Temperature Fracture Strengths and Fracture Toughnesses for Various SiC Whisker Contents in Al_2O_3

Whisker Content (*vol%*)	*Fracture Strength* (*MPa*)	*Fracture Toughness* ($MPa\sqrt{m}$)
0	—	4.5
10	455 ± 55	7.1
20	655 ± 135	7.5–9.0
40	850 ± 130	6.0

Source: Adapted from *Engineered Materials Handbook*, Vol. 1, *Composites*, C. A. Dostal, Senior Editor, ASM International, Materials Park, OH, 1987.

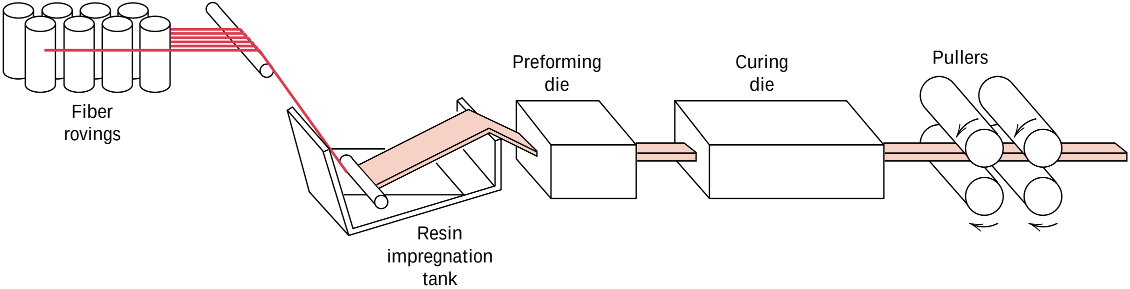
Fiber rovings
Preforming die
Curing die
Pullers
Resin impregnation tank

Figure 15.12 Schematic diagram showing the pultrusion process.

FIGURE 15.13 Schematic diagram illustrating the production of prepreg tape using thermoset polymers.

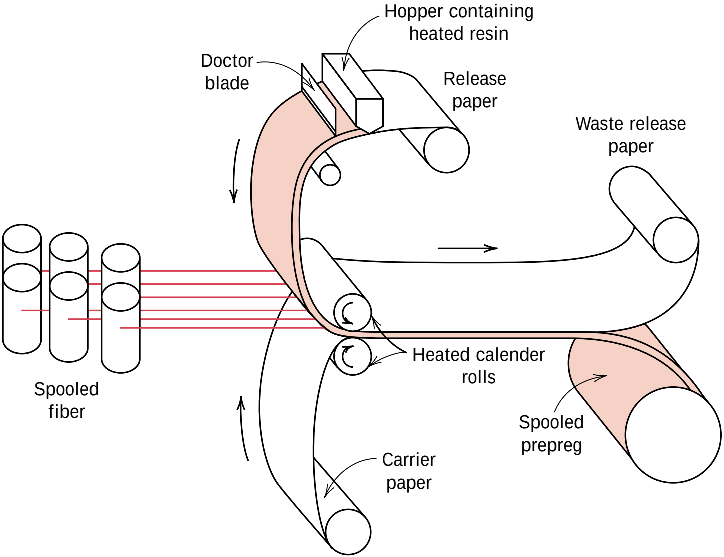
Hopper containing heated resin
Doctor blade
Release paper
Waste release paper
Spooled fiber
Heated calender rolls
Spooled prepreg
Carrier paper

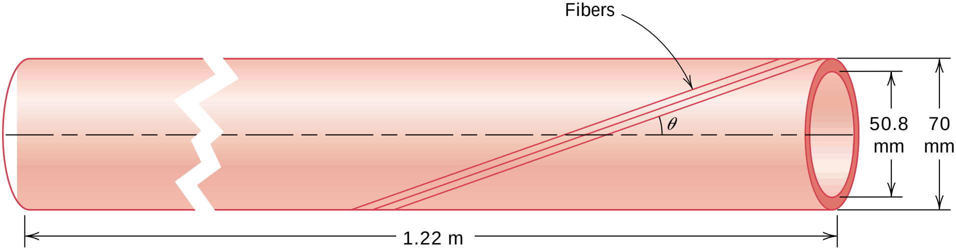
Fibers
θ
50.8 mm
70 mm
1.22 m

FIGURE 15.15 Schematic representation of a filament wound composite shaft, which is the subject of Design Example 15.1.

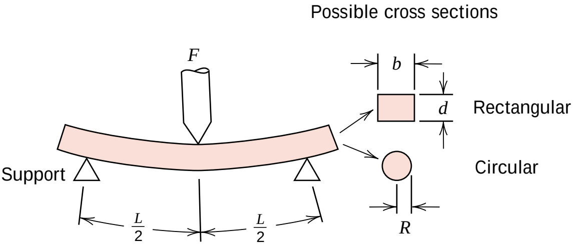
Possible cross sections
F
b
d
Rectangular
Circular
R
Support
L/2
L/2

σ = stress = $\frac{Mc}{I}$

where M = maximum bending moment

c = distance from center of specimen to outer fibers

I = moment of inertia of cross section

F = applied load

	M	c	I	σ
Rectangular	$\frac{FL}{4}$	$\frac{d}{2}$	$\frac{bd^3}{12}$	$\frac{3FL}{2bd^2}$
Circular	$\frac{FL}{4}$	R	$\frac{\pi R^4}{4}$	$\frac{FL}{\pi R^3}$

FIGURE 7.18 A three-point loading scheme for measuring the stress–strain behavior and flexural strength of brittle ceramics, including expressions for computing stress for rectangular and circular cross sections.

Table 15.8 **Elastic Modulus, Density, and Cost Data for Glass and Various Carbon Fibers and Epoxy Resin**

Material	*Elastic Modulus* (*GPa*)	*Density* (*g/cm³*)	*Cost* (*$/kg*)
Glass fibers	72.5	2.58	2.50
Carbon fibers (standard modulus)	230	1.80	35.00
Carbon fibers (intermediate modulus)	285	1.80	70.00
Carbon fibers (high modulus)	400	1.80	175.00
Epoxy resin	2.4	1.14	9.00

Table 15.9 Fiber and Matrix Volume Fractions for Three Carbon Fiber Types As Required to Give a Composite Modulus of 120 GPa

Fiber Type	V_f	V_m
Standard modulus	0.535	0.465
Intermediate modulus	0.431	0.569
High modulus	0.306	0.694

Table 15.10 Fiber and Matrix Volumes, Masses, and Costs and Total Material Cost for Three Carbon Fiber-Epoxy-Matrix Composites

Fiber Type	*Fiber Volume* (cm^3)	*Fiber Mass* (*kg*)	*Fiber Cost* (*$*)	*Matrix Volume* (cm^3)	*Matrix Mass* (*kg*)	*Matrix Cost* (*$*)	*Total Cost* (*$*)
Standard modulus	1189	2.14	74.90	1033	1.18	10.60	85.50
Intermediate modulus	958	1.72	120.70	1264	1.44	12.96	133.66
High modulus	680	1.22	214.20	1542	1.76	15.82	230.00

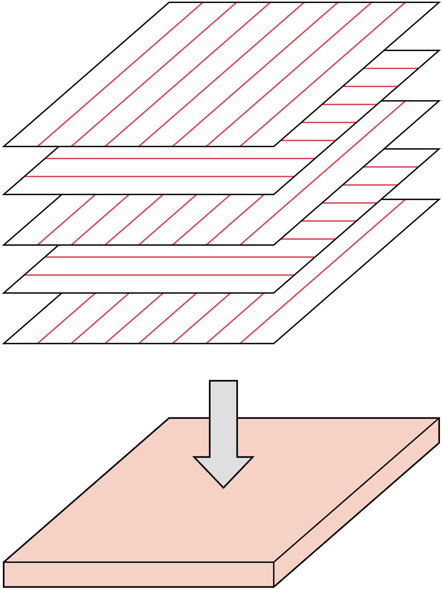

Figure 15.16 The stacking of successive oriented, fiber-reinforced layers for a laminar composite.

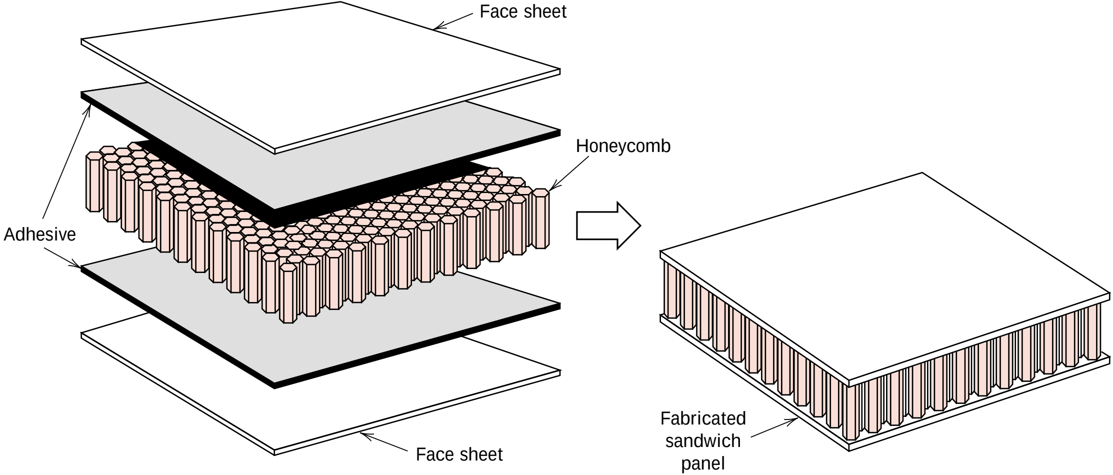
Face sheet
Honeycomb
Adhesive
Face sheet
Fabricated sandwich panel

FIGURE 15.17 Schematic diagram showing the construction of a honeycomb core sandwich panel. (Reprinted with permission from *Engineered Materials Handbook*, Vol. 1, *Composites*, ASM International, Metals Park, OH, 1987.)

```
[Loader]
Program=ezsolve
```

CHAPTER 16

CORROSION AND DEGRADATION OF MATERIALS

16.5 (a) We are asked to compute the voltage of a nonstandard Cd-Fe electrochemical cell. Since iron is lower in the emf series (Table 16.1), we will begin by assuming that iron is oxidized and cadmium is reduced, as

$$\mathrm{Fe} + \mathrm{Cd}^{2+} \longrightarrow \mathrm{Fe}^{2+} + \mathrm{Cd}$$

and

$$\begin{aligned}\Delta V &= (V^{\circ}_{\mathrm{Cd}} - V^{\circ}_{\mathrm{Fe}}) - \frac{0.0592}{2}\log\frac{[\mathrm{Fe}^{2+}]}{[\mathrm{Cd}^{2+}]}\\ &= [-0.403\ \mathrm{V} - (-0.440\ \mathrm{V})] - \frac{0.0592}{2}\log\left[\frac{0.40}{2\times10^{-3}}\right]\\ &= -0.031\ \mathrm{V}\end{aligned}$$

(b) Since the $\Delta \mathbf{V}$ is negative, the spontaneous cell direction is just the reverse of that above, or

$$\mathrm{Fe}^{2+} + \mathrm{Cd} \longrightarrow \mathrm{Fe} + \mathrm{Cd}^{2+}$$

16.13 This problem calls for us to compute the time of submersion of a steel piece. In order to solve this problem, we must first rearrange Equation (16.23), as

$$t = \frac{KW}{\rho A(\mathrm{CPR})}$$

Thus,

$$\begin{aligned}t &= \frac{(534)(2.6\times10^{6}\ \mathrm{mg})}{(7.9\ \mathrm{g/cm^3})(10\ \mathrm{in.^2})(200\ \mathrm{mpy})}\\ &= 8.8\times10^{4}\ \mathrm{h} = 10\ \mathrm{yr}\end{aligned}$$

16.20 (a) This portion of the problem asks that we compute the rate of oxidation for Pb given that both the oxidation and reduction reactions are controlled by activation polarization, and also given the polarization data for both lead oxidation and hydrogen reduction. The first thing necessary is to establish relationships of the form of Equation (16.25) for the potentials of both oxidation and reduction reactions. Next we will set these expressions equal to one another, and then solve for the value of **i** which is really the corrosion current density, $\mathbf{i_c}$. Finally, the corrosion rate may be calculated using Equation (16.24). The two potential expressions are as follows:
For hydrogen reduction

$$V_H = V_{(H^+/H_2)} + \beta_H \log\left(\frac{i}{i_{o_H}}\right)$$

And for Pb oxidation

$$V_{Pb} = V_{(Pb/Pb^{2+})} + \beta_{Pb} \log\left(\frac{i}{i_{o_{Pb}}}\right)$$

Setting $\mathbf{V_H} = \mathbf{V_{Pb}}$ and solving for log $\mathbf{i}$ (log $\mathbf{i_c}$) leads to

$$\log i_c = \left(\frac{1}{\beta_{Pb} - \beta_H}\right)[V_{(H^+/H_2)} - V_{(Pb/Pb^{2+})} - \beta_H \log i_{o_H} + \beta_{Pb} \log i_{o_{Pb}}]$$

$$= \left[\frac{1}{0.12 - (-0.10)}\right][0 - (-0.126) - (-0.10)\{\log(1.0 \times 10^{-8})\} + (0.12)\{\log(2 \times 10^{-9})\}]$$

$$= -7.809$$

Or

$$i_c = 10^{-7.809} = 1.55 \times 10^{-8} \text{ A/cm}^2$$

And from Equation (16.24)

$$r = \frac{i_c}{nF}$$

$$= \frac{1.55 \times 10^{-8} \text{ C/s-cm}^2}{(2)(96500 \text{ C/mol})} = 8.03 \times 10^{-14} \text{ mol/cm}^2\text{-s}$$

16.34 For this problem we are given, for three metals, their densities, chemical formulas, and oxide densities, and are asked to compute the Pilling-Bedworth ratios, and then specify whether or not the oxide scales that form will be protective. The general form of the equation used to calculate this ratio is Equation (16.33) [or Equation (16.32)]. For tin, oxidation occurs by the reaction

$$Sn + O_2 \longrightarrow SnO_2$$

and therefore

$$\text{P-B ratio} = \frac{A_{SnO_2}\rho_{Sn}}{A_{Sn}\rho_{SnO_2}}$$

$$= \frac{(150.69 \text{ g/mol})(7.30 \text{ g/cm}^3)}{(118.69 \text{ g/mol})(6.95 \text{ g/cm}^3)} = 1.33$$

Hence, the film would most likely be protective since the ratio lies between one and two.

16.36 For this problem we are given weight gain-time data for the oxidation of Cu at an elevated temperature.

(a) We are first asked to determine whether the oxidation kinetics obey a parabolic, linear, or logarithmic rate expression, expressions which are described by Equations (16.34), (16.35), and (16.36), respectively. One way to make this determination is by trial and error. Let us assume that the parabolic relationship is valid; that is, from Equation (16.34)

$$W^2 = K_1 t + K_2$$

which means that we may establish three simultaneous equations using the three sets of given $\mathbf{W}$ and $\mathbf{t}$ values, then using two combinations of two pairs of equations, solve for $\mathbf{K_1}$ and $\mathbf{K_2}$; if $\mathbf{K_1}$ and $\mathbf{K_2}$ have the same values for both solutions, then the kinetics are parabolic. If the values are not identical then the other kinetic relationships need to be explored. Thus, the three equations are

$$(0.316)^2 = 0.100 = 15K_1 + K_2$$

$$(0.524)^2 = 0.275 = 50K_1 + K_2$$

$$(0.725)^2 = 0.526 = 100K_1 + K_2$$

From the first two equations $\mathbf{K_1} = 5 \times 10^{-3}$ and $\mathbf{K_2} = 0.025$; these same two values are obtained using the last two equations. Hence, the oxidation rate law is parabolic.

(b) Since a parabolic relationship is valid, this portion of the problem calls for us to determine **W** after a total time of 450 min. Again, using Equation (16.34) and the values of $\mathbf{K_1}$ and $\mathbf{K_2}$

$$\begin{aligned} W^2 &= K_1 t + K_2 \\ &= (0.005)(450\text{ min}) + 0.025 = 2.28 \end{aligned}$$

Or $\mathbf{W} = \sqrt{2.28} = 1.51\text{ mg/cm}^2$.

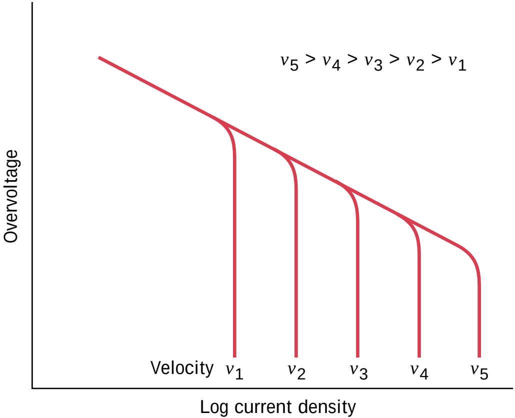

FIGURE 16.26 Plot of overvoltage versus logarithm of current density for a solution that experiences combined activation–concentration polarization at various solution velocities.

CHAPTER 17

THERMAL PROPERTIES

17.4 (a) For aluminum, $\mathbf{C_v}$ at 50 K may be approximated by Equation (17.2), since this temperature is significantly below the Debye temperature. The value of $\mathbf{C_v}$ at 30 K is given, and thus, we may compute the constant **A** as

$$A = \frac{C_v}{T^3} = \frac{0.81\ \text{J/mol-K}}{(30\ \text{K})^3} = 3 \times 10^{-5}\ \text{J/mol-K}^4$$

Therefore, at 50 K

$$C_v = AT^3 = (3 \times 10^{-5}\ \text{J/mol-K}^4)(50\ \text{K})^3 = 3.75\ \text{J/mol-K}$$

and

$$c_v = (3.75\ \text{J/mol-K})(1\ \text{mol}/26.98\ \text{g})(1000\ \text{g/kg}) = 139\ \text{J/kg-K}$$

(b) Since 425 K is above the Debye temperature, a good approximation for $\mathbf{C_v}$ is

$$\begin{aligned} C_v &= 3R \\ &= (3)(8.31\ \text{J/mol-K}) = 24.9\ \text{J/mol-K} \end{aligned}$$

And, converting this to specific heat

$$c_v = (24.9\ \text{J/mol-K})(1\ \text{mol}/26.98\ \text{g})(1000\ \text{g/kg}) = 925\ \text{J/kg-K}$$

17.14 This problem asks for us to determine the temperature to which a cylindrical rod of tungsten 10.000 mm in diameter must be heated in order for it to just fit into a 9.988 mm diameter circular hole in a plate of 316 stainless steel, assuming that the initial temperature is 25°C. This requires the use of Equation (17.3a), which is applied to the diameters of the rod and hole. That is

$$\frac{d_f - d_o}{d_o} = \alpha_l(T_f - T_o)$$

Solving this expression for $\mathbf{d_f}$ yields

$$d_f = d_o[1 + \alpha_l(T_f - T_o)]$$

Now all we need do is to establish expressions for $\mathbf{d_f}$(316 stainless) and $\mathbf{d_f}$(W), set them equal to one another, and solve for $\mathbf{T_f}$. According to Table 17.1, α_l (316 stainless) = $16.0 \times 10^{-6}\ (^\circ\text{C})^{-1}$ and α_l(W) = $4.5 \times 10^{-6}\ (^\circ\text{C})^{-1}$. Thus

$$\begin{gathered} d_f(316\ \text{stainless}) = d_f(\text{W}) \\ (9.988\ \text{mm})[1 + \{16.0 \times 10^{-6}\ (^\circ\text{C})^{-1}\}(T_f - 25^\circ\text{C})] \\ = (10.000\ \text{mm})[1 + \{4.5 \times 10^{-6}\ (^\circ\text{C})^{-1}\}(T_f - 25^\circ\text{C})] \end{gathered}$$

Now solving for $\mathbf{T_f}$ gives $\mathbf{T_f}$ = 129.5°C.

17.24 This problem asks that we treat a porous material as a composite wherein one of the phases is a pore phase, and that we estimate upper and lower limits for the room-temperature thermal conductivity of a magnesium oxide material having a 0.30 volume fraction of pores. The upper limit of **k** (**k**) may be determined using Equation (15.1) with thermal conductivity substituted for the elastic modulus, **E**. From Table 17.1, the value of **k** for MgO is 37.7 W/m-K, while for still air in the pore phase, **k** = 0.02 W/m-K. Thus

$$\begin{aligned} k_{\text{upper}} &= V_p k_{\text{air}} + V_{\text{MgO}} k_{\text{MgO}} \\ &= (0.30)(0.02\ \text{W/m-K}) + (0.70)(37.7\ \text{W/m-K}) = 26.4\ \text{W/m-K} \end{aligned}$$

For the lower limit we employ a modification of Equation (15.2) as

$$\begin{aligned} k_{\text{lower}} &= \frac{k_{\text{air}} k_{\text{MgO}}}{V_p k_{\text{MgO}} + V_{\text{MgO}} k_{\text{air}}} \\ &= \frac{(0.02\ \text{W/m-K})(37.7\ \text{W/m-K})}{(0.30)(37.7\ \text{W/m-K}) + (0.70)(0.02\ \text{W/m-K})} = 0.067\ \text{W/m-K} \end{aligned}$$

17.29 We want to heat the copper wire in order to reduce the stress level from 70 MPa to 35 MPa; in doing so, we reduce the stress in the wire by 70 MPa − 35 MPa = 35 MPa, which will be a compressive stress (i.e., $\sigma = -35$ MPa). Taking a value for **E** of 110 GPa (Table 7.1) and solving for **T_f** from Equation (17.8)

$$\begin{aligned} T_f &= T_o - \frac{\sigma}{E\alpha_1} \\ &= 20^\circ\text{C} - \frac{-35\ \text{MPa}}{(110 \times 10^3\ \text{MPa})[17 \times 10^{-6}\ (^\circ\text{C})^{-1}]} \\ &= 20^\circ\text{C} + 19^\circ\text{C} = 39^\circ\text{C}\ (101^\circ\ \text{F}) \end{aligned}$$

17.D1 This problem stipulates that 1025 steel railroad tracks are laid at a temperature of 10°C We are asked to determine the hottest possible temperature that can be tolerated without the introduction of thermal stresses if the rails are 11.9 m long, and for a joint space of 4.6 mm. For these railroad tracks, each end is allowed to expand one-half of the joint space distance, or the track may expand a total of this distance (4.6 mm). Equation (17.3a) is used to solve for **T_f**, where α_l for the 1025 steel is found in Table 17.1. Thus,

$$\begin{aligned} T_f &= \frac{\Delta l}{\alpha_l l_o} + T_o \\ &= \frac{4.6 \times 10^{-3}\ \text{m}}{[12.0 \times 10^{-6}\ (^\circ\text{C})^{-1}]\,(11.9\ \text{m})} + 10^\circ\text{C} \\ &= 32.2^\circ\text{C} + 10^\circ\text{C} = 42.2^\circ\text{C}\ (108^\circ\text{F}) \end{aligned}$$

CHAPTER 18

MAGNETIC PROPERTIES

18.1 This problem concerns a coil of wire 0.20 m long that has 200 turns and carries 10 A.

(a) We may calculate the magnetic field strength generated by this coil using Equation (18.1) as

$$\begin{aligned} H &= \frac{NI}{l} \\ &= \frac{(200 \text{ turns})(10 \text{ A})}{0.2 \text{ m}} = 10{,}000 \text{ A-turns/m} \end{aligned}$$

(b) In a vacuum, the flux density is determined from Equation (18.3). Thus,

$$\begin{aligned} B_o &= \mu_o H \\ &= (1.257 \times 10^{-6} \text{ H/m})(10{,}000 \text{ A-turns/m}) = 1.257 \times 10^{-2} \text{ tesla} \end{aligned}$$

(c) When a bar of titanium is positioned within the coil, we must use an expression that is a combination of Equations (18.5) and (18.6) in order to compute the flux density given the magnetic susceptibility. Inasmuch as $\chi_\mathbf{m} = 1.81 \times 10^{-4}$ (Table 18.2), then

$$\begin{aligned} B &= \mu_o H + \mu_o M = \mu_o H + \mu_o \chi_m H = \mu_o H(1 + \chi_m) \\ &= (1.257 \times 10^{-6} \text{ H/m})(10{,}000 \text{ A-turns/m})(1 + 1.81 \times 10^{-4}) \\ &\cong 1.257 \times 10^{-2} \text{ tesla} \end{aligned}$$

which is essentially the same result as part (b). This is to say that the influence of the titanium bar within the coil makes an imperceptible difference in the magnitude of the **B** field.

(d) The magnetization is computed from Equation (18.6):

$$M = \chi_m H = (1.81 \times 10^{-4})(10{,}000 \text{ A-turns/m}) = 1.81 \text{ A/m}$$

18.4 For this problem, we want to convert the volume susceptibility of silver (i.e., 2.38×10^{-5}) into other systems of units.

For the mass susceptibility

$$\begin{aligned} \chi_m \text{(kg)} &= \frac{\chi_m}{\rho(\text{kg/m}^3)} \\ &= \frac{-2.38 \times 10^{-5}}{10.49 \times 10^3 \text{ kg/m}^3} = -2.27 \times 10^{-9} \end{aligned}$$

For the atomic susceptibility

$$\begin{aligned} \chi_m(\text{a}) &= \chi_m \text{(kg)} \times [\text{atomic weight (in kg)}] \\ &= (-2.27 \times 10^{-9})(0.10787 \text{ kg/mol}) = -2.45 \times 10^{-10} \end{aligned}$$

18.6 This problem stipulates that the magnetic flux density within a bar of some material is 0.435 tesla at an **H** field of 3.44×10^5 A/m.

(a) We are first of all asked to compute the magnetic permeability of this material. This is possible using Equation (18.2) as

$$\mu = \frac{B}{H} = \frac{0.435 \text{ tesla}}{3.44 \times 10^5 \text{ A/m}} = 1.2645 \times 10^{-6} \text{ H/m}$$

(b) The magnetic susceptibility is calculated as

$$\chi_m = \frac{\mu}{\mu_o} - 1 = \frac{1.2645 \times 10^{-6} \text{ H/m}}{1.257 \times 10^{-6} \text{ H/m}} - 1$$
$$= 6 \times 10^{-3}$$

18.27 (a) The **B-H** data provided in the problem are plotted below.

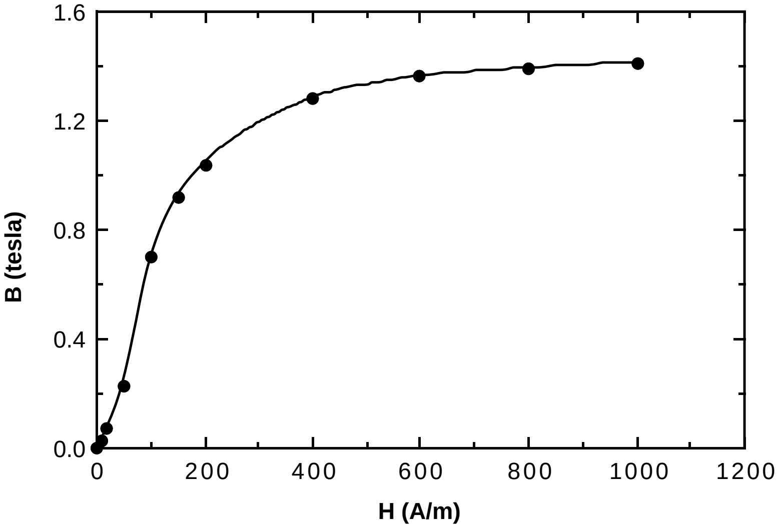

(b) This portion of the problem asks for us to determine values of the initial permeability and initial relative permeability. The first four data points are plotted below.

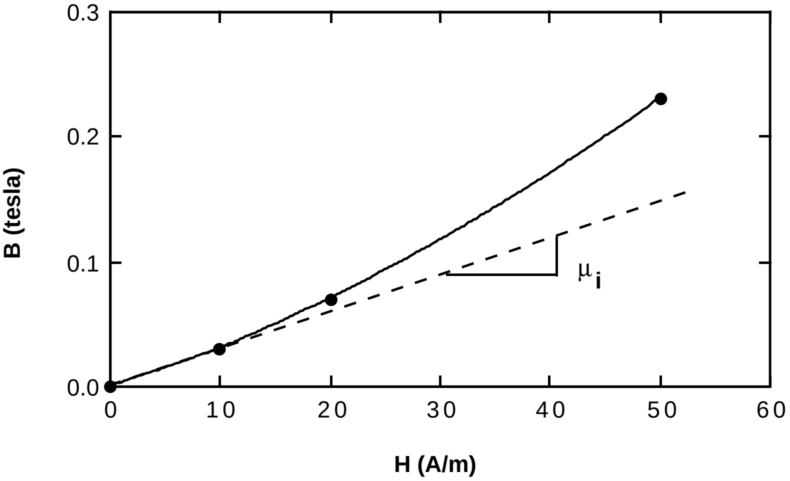

The slope of the initial portion of the curve is μ_i (as shown), is

$$\mu_i = \frac{\Delta B}{\Delta H} = \frac{(0.15 - 0)\text{ tesla}}{(50 - 0)\text{ A/m}} = 3.0 \times 10^{-3}\text{ H/m}$$

Also, the initial relative permeability [Equation (18.4)] is just

$$\mu_{ri} = \frac{\mu_i}{\mu_o} = \frac{3.0 \times 10^{-3}\text{ H/m}}{1.257 \times 10^{-6}\text{ H/m}} = 2400$$

(c) The maximum permeability is the tangent to the **B-H** curve having the greatest slope; it is drawn on the plot below, and designated as μ**(max)**.

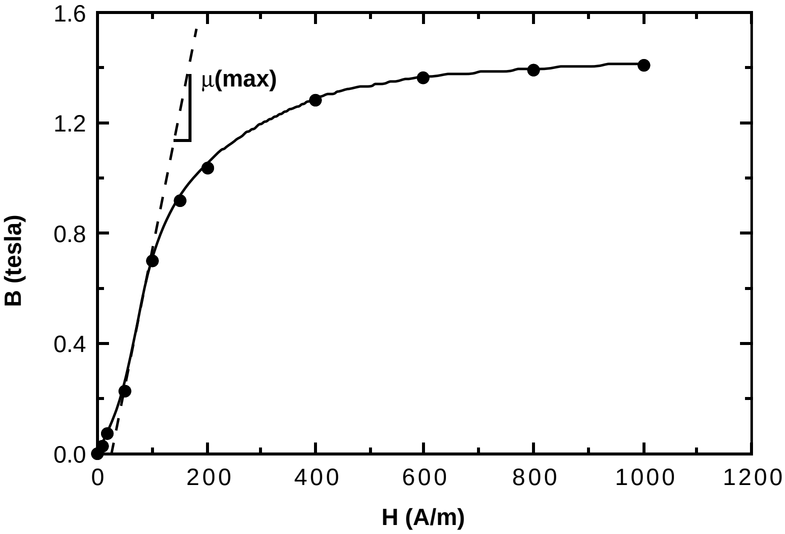

The value of μ**(max)** is

$$\mu(\text{max}) = \frac{\Delta B}{\Delta H} = \frac{(1.3 - 0.3)\text{ tesla}}{(160 - 45)\text{ A-m}} = 8.70 \times 10^{-3}\text{ H/m}$$

18.32 (a) Given Equation (18.12) and the data in Table 18.7, we are asked to calculate the critical magnetic fields for tin at 1.5 and 2.5 K. From the table, for Sn, $\mathbf{T_C} = 3.72$ K and $\mathbf{B_C(0)} = 0.0305$ tesla. Thus, from Equation (18.3)

$$H_C(0) = \frac{B_C(0)}{\mu_o}$$

$$= \frac{0.0305\text{ tesla}}{1.257 \times 10^{-6}\text{ H/m}} = 2.43 \times 10^4\text{ A/m}$$

Now, solving for $\mathbf{H_C(2.5)}$ using Equation (18.12) yields

$$H_C(T) = H_C(0)\left[1 - \frac{T^2}{T_C^2}\right]$$

$$H_C(2.5) = (2.43 \times 10^4\text{ A/m})\left[1 - \frac{(2.5\text{ K})^2}{(3.72\text{ K})^2}\right] = 1.33 \times 10^4\text{ A/m}$$

(b) Now we are to determine the temperature to which lead must be cooled in a magnetic field of 20,000 A/m in order for it to be superconductive. The value of **H_C(0)** must first be determined using **B_C(0)** given in the table (i.e., 0.0803 tesla); thus

$$H_C(0) = \frac{B_C(0)}{\mu_o} = \frac{0.0803 \text{ tesla}}{1.257 \times 10^{-6} \text{ H/m}} = 6.39 \times 10^4 \text{ A/m}$$

Since **T_C** $= 7.19$ K we may solve for **T** using Equation (18.12) as

$$T = T_C\sqrt{1 - \frac{H_C(T)}{H_C(0)}}$$

$$= (7.19 \text{ K})\sqrt{1 - \frac{20000 \text{ A/m}}{63900 \text{ A/m}}} = 5.96 \text{ K}$$

Table 18.2 Room-Temperature Magnetic Susceptibilities for Diamagnetic and Paramagnetic Materials

Diamagnetics		*Paramagnetics*	
Material	*Susceptibility* χ_m *(volume) (SI units)*	*Material*	*Susceptibility* χ_m *(volume) (SI units)*
Aluminum oxide	-1.81×10^{-5}	Aluminum	2.07×10^{-5}
Copper	-0.96×10^{-5}	Chromium	3.13×10^{-4}
Gold	-3.44×10^{-5}	Chromium chloride	1.51×10^{-3}
Mercury	-2.85×10^{-5}	Manganese sulfate	3.70×10^{-3}
Silicon	-0.41×10^{-5}	Molybdenum	1.19×10^{-4}
Silver	-2.38×10^{-5}	Sodium	8.48×10^{-6}
Sodium chloride	-1.41×10^{-5}	Titanium	1.81×10^{-4}
Zinc	-1.56×10^{-5}	Zirconium	1.09×10^{-4}

Table 18.7 **Critical Temperatures and Magnetic Fluxes for Selected Superconducting Materials**

Material	*Critical Temperature T_C (K)*	*Critical Magnetic Flux Density B_C (tesla)*[a]
	Elements[b]	
Tungsten	0.02	0.0001
Titanium	0.40	0.0056
Aluminum	1.18	0.0105
Tin	3.72	0.0305
Mercury (α)	4.15	0.0411
Lead	7.19	0.0803
	Compounds and Alloys[b]	
Nb-Ti alloy	10.2	12
Nb-Zr alloy	10.8	11
$PbMo_6S_8$	14.0	45
V_3Ga	16.5	22
Nb_3Sn	18.3	22
Nb_3Al	18.9	32
Nb_3Ge	23.0	30
	Ceramic Compounds	
$YBa_2Cu_3O_7$	92	—
$Bi_2Sr_2Ca_2Cu_3O_{10}$	110	—
$Tl_2Ba_2Ca_2Cu_3O_{10}$	125	—
$HgBa_2Ca_2Cu_2O_8$	153	—

[a] The critical magnetic flux density ($\mu_0 H_C$) for the elements was measured at 0 K. For alloys and compounds, the flux is taken as $\mu_0 H_{C2}$ (in teslas), measured at 0 K.

[b] **Source:** Adapted with permission from *Materials at Low Temperatures*, R. P. Reed and A. F. Clark, Editors, American Society for Metals, Metals Park, OH, 1983.

CHAPTER 19

OPTICAL PROPERTIES

19.9 We want to compute the velocity of light in calcium fluoride given that $\varepsilon_\mathbf{r} = 2.056$ and $\chi_\mathbf{m} = -1.43 \times 10^{-5}$. The velocity is determined using Equation (19.8); but first, we must calculate the values of ε and μ for calcium fluoride. According to Equation (12.30)

$$\varepsilon = \varepsilon_r\varepsilon_o = (2.056)(8.85 \times 10^{-12}\ \text{F/m}) = 1.82 \times 10^{-11}\ \text{F/m}$$

Now, utilizing Equations (18.4) and (18.7)

$$\begin{aligned}\mu &= \mu_o(\chi_m + 1)\\ &= (1.257 \times 10^{-6}\ \text{H/m})(1 - 1.43 \times 10^{-5}) = 1.257 \times 10^{-6}\ \text{H/m}\end{aligned}$$

And, finally

$$\begin{aligned}v &= \frac{1}{\sqrt{\varepsilon\mu}}\\ &= \frac{1}{\sqrt{(1.82 \times 10^{-11}\ \text{F/m})(1.257 \times 10^{-6}\ \text{H/m})}}\\ &= 2.09 \times 10^{8}\ \text{m/s}\end{aligned}$$

19.11 This problem asks for us, using data in Table 19.1, to estimate the dielectric constants for silica glass, soda-lime glass, PTFE, polyethylene, and polystyrene, and then to compare these values with those cited in Table 12.4 and briefly explain any discrepancies. From Equation (19.10)

$$\varepsilon_r = n^2$$

Thus, for fused silica, since $\mathbf{n} = 1.458$

$$\varepsilon_r = (1.458)^2 = 2.13$$

When we compare this value with that given in Table 12.4 at a frequency of 1 MHz (i.e., $\varepsilon_\mathbf{r} = 3.8$) there is a significant discrepancy. The reason for this is that, for this material, an ionic component to the dielectric constant is present at 1 MHz, which is absent at frequencies within the visible electromagnetic spectrum, frequencies which are on the order 10^9 MHz. This effect may be noted in Figure 12.32.

19.19 In this problem we are asked to calculate the fraction of nonreflected light transmitted through a 20 mm thickness of transparent material, given that the fraction transmitted through a 10 mm width is 0.90. From Equation (19.18), the fraction of nonreflected light transmitted is just $\mathbf{I'_T}/\mathbf{I'_o}$. Using this expression we must first determine the value of β as

$$\begin{aligned}\beta &= -\frac{1}{x}\ln\left(\frac{I'_T}{I'_o}\right)\\ &= -\left(\frac{1}{10\ \text{mm}}\right)\ln(0.90) = 1.05 \times 10^{-2}\ \text{mm}^{-1}\end{aligned}$$

Now, solving for $\frac{\mathbf{I'_T}}{\mathbf{I'_o}}$ when $\mathbf{x} = 20$ mm

$$\frac{I'_T}{I'_o} = \exp(-\beta x)$$

$$\exp[-(1.05 \times 10^{-2}\ \text{mm}^{-1})(20\ \text{mm})] = 0.81$$

19.30 This problem asks for the difference in energy between metastable and ground electron states for a ruby laser. The wavelength of the radiation emitted by an electron transition from the metastable to ground state is cited as 0.6943 μm. The difference in energy between these states, Δ**E**, may be determined from Equation (19.6), as

$$
\begin{aligned}
\Delta E &= h\nu = \frac{hc}{\lambda} \\
&= \frac{(4.13 \times 10^{-15}\ \text{eV-s})(3 \times 10^{8}\ \text{m/s})}{6.943 \times 10^{-7}\ \text{m}} \\
&= 1.78\ \text{eV}
\end{aligned}
$$

Chapter 19 / Optical Properties

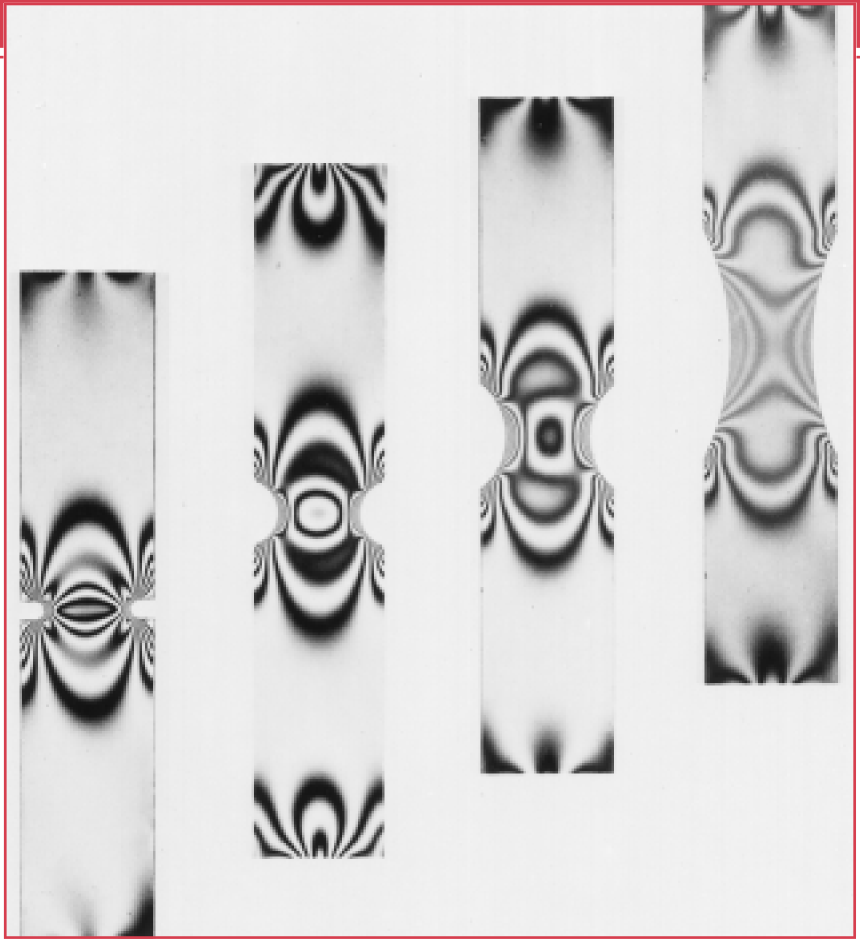

The four notched and transparent rods shown in this photograph demonstrate the phenomenon of *photoelasticity*. When elastically deformed, the optical properties (e.g., index of refraction) of a photoelastic specimen become anisotropic. Using a special optical system and polarized light, the stress distribution within the specimen may be deduced from interference fringes that are produced. These fringes within the four photoelastic specimens shown in the photograph indicate how the stress concentration and distribution change with notch geometry for an axial tensile stress. (Photograph courtesy of Measurements Group, Inc., Raleigh, North Carolina, U.S.)

Why Study the *Optical Properties* of Materials?

When materials are exposed to electromagnetic radiation, it is sometimes important to be able to predict and alter their responses. This is possible when we are familiar with their optical properties, and understand the mechanisms responsible for their optical behaviors. For example, in Section 19.14 on optical fiber materials, we note that the performance of optical fibers is increased by introducing a gradual variation of the index of refraction (i.e., a graded index) at the outer surface of the fiber. This is accomplished by the addition of specific impurities in controlled concentrations.

Learning Objectives

After careful study of this chapter you should be able to do the following:

1. **Compute the energy of a photon given its frequency and the value of Planck's constant.**
2. **Briefly describe electronic polarization that results from electromagnetic radiation-atomic interactions. Cite two consequences of electronic polarization.**
3. **Briefly explain why metallic materials are opaque to visible light.**
4. **Define *index of refraction.***
5. **Describe the mechanism of photon absorption for (a) high-purity insulators and semiconductors, and (b) insulators and semiconductors that contain electrically active defects.**
6. **For inherently transparent dielectric materials, note three sources of internal scattering that can lead to translucency and opacity.**
7. **Briefly describe the construction and operation of ruby and semiconductor lasers.**

19.1 INTRODUCTION

By ''optical property'' is meant a material's response to exposure to electromagnetic radiation and, in particular, to visible light. This chapter first discusses some of the basic principles and concepts relating to the nature of electromagnetic radiation and its possible interactions with solid materials. Next to be explored are the optical behaviors of metallic and nonmetallic materials in terms of their absorption, reflection, and transmission characteristics. The final sections outline luminescence, photoconductivity, and light amplification by stimulated emission of radiation (laser), the practical utilization of these phenomena, and optical fibers in communications.

BASIC CONCEPTS

19.2 ELECTROMAGNETIC RADIATION

In the classical sense, electromagnetic radiation is considered to be wavelike, consisting of electric and magnetic field components that are perpendicular to each other and also to the direction of propagation (Figure 19.1). Light, heat (or radiant energy), radar, radio waves, and x-rays are all forms of electromagnetic radiation. Each is characterized primarily by a specific range of wavelengths, and also according to the technique by which it is generated. The *electromagnetic spectrum* of radiation spans the wide range from γ-rays (emitted by radioactive materials) having wavelengths on the order of 10^{-12} m (10^{-3} nm), through x-rays, ultraviolet, visible, infrared, and finally radio waves with wavelengths as long as 10^5 m. This spectrum, on a logarithmic scale, is shown in Figure 19.2.

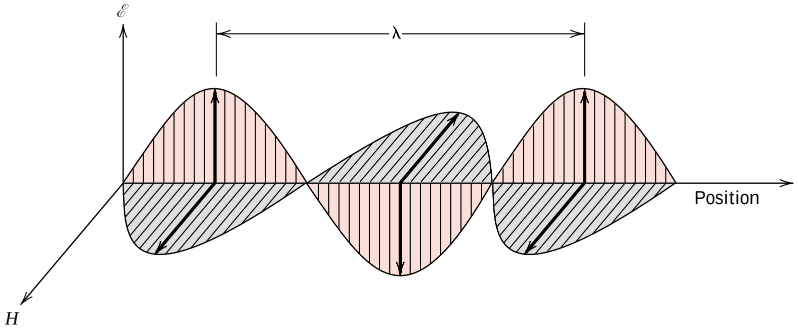

FIGURE 19.1 An electromagnetic wave showing electric field $\mathscr{E}$ and magnetic field H components, and the wavelength λ.

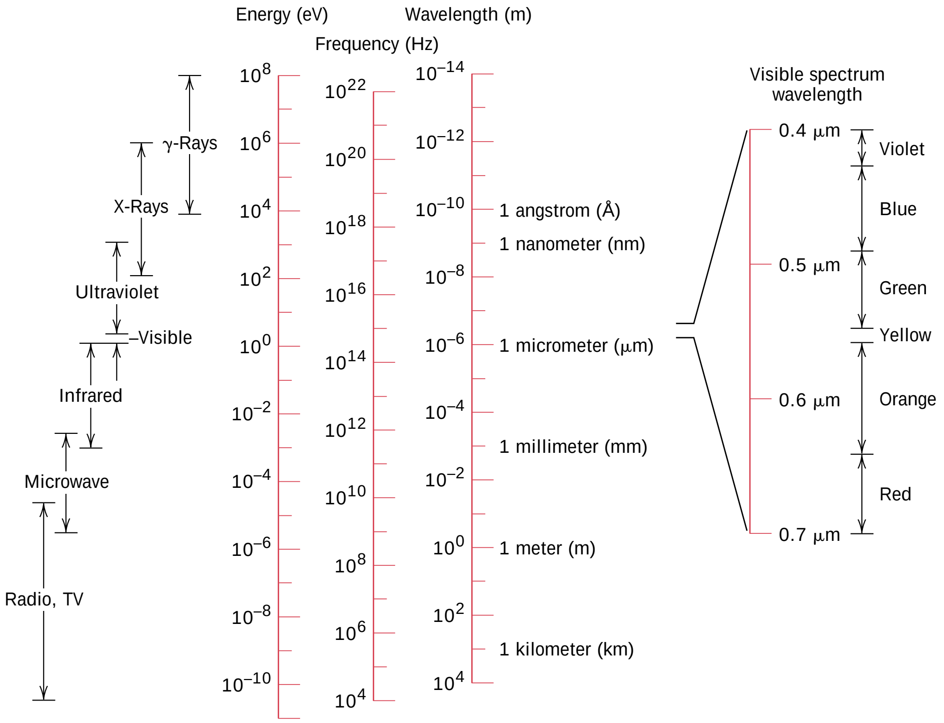
Energy (eV)
Frequency (Hz)
Wavelength (m)
γ-Rays
X-Rays
Ultraviolet
Visible
Infrared
Microwave
Radio, TV
10^8
10^6
10^4
10^2
10^0
10^-2
10^-4
10^-6
10^-8
10^-10
10^22
10^20
10^18
10^16
10^14
10^12
10^10
10^8
10^6
10^4
10^-14
10^-12
10^-10
10^-8
10^-6
10^-4
10^-2
10^0
10^2
10^4
1 angstrom (Å)
1 nanometer (nm)
1 micrometer (μm)
1 millimeter (mm)
1 meter (m)
1 kilometer (km)
Visible spectrum wavelength
0.4 μm
0.5 μm
0.6 μm
0.7 μm
Violet
Blue
Green
Yellow
Orange
Red

Figure 19.2 The spectrum of electromagnetic radiation, including wavelength ranges for the various colors in the visible spectrum.

Visible light lies within a very narrow region of the spectrum, with wavelengths ranging between about 0.4 μm (4×10^{-7} m) and 0.7 μm. The perceived color is determined by wavelength; for example, radiation having a wavelength of approximately 0.4 μm appears violet, whereas green and red occur at about 0.5 and 0.65 μm, respectively. The spectral ranges for the several colors are included in Figure 19.2. White light is simply a mixture of all colors. The ensuing discussion is concerned primarily with this visible radiation, by definition the only radiation to which the eye is sensitive.

All electromagnetic radiation traverses a vacuum at the same velocity, that of light, namely, 3×10^8 m/s (186,000 miles/s). This velocity, c, is related to the electric permittivity of a vacuum ϵ_0 and the magnetic permeability of a vacuum μ_0 through

$$c = \frac{1}{\sqrt{\epsilon_0 \mu_0}} \qquad (19.1)$$

Thus, there is an association between the electromagnetic constant c and these electrical and magnetic constants.

Furthermore, the frequency ν and the wavelength λ of the electromagnetic radiation are a function of velocity according to

$$c = \lambda \nu \qquad (19.2)$$

Frequency is expressed in terms of hertz (Hz), and 1 Hz = 1 cycle per second. Ranges of frequency for the various forms of electromagnetic radiation are also included in the spectrum (Figure 19.2).

Sometimes it is more convenient to view electromagnetic radiation from a quantum-mechanical perspective, in that the radiation, rather than consisting of waves, is composed of groups or packets of energy, which are called **photons.** The energy E of a photon is said to be quantized, or can only have specific values, defined by the relationship

$$E = h\nu = \frac{hc}{\lambda} \tag{19.3}$$

where h is a universal constant called **Planck's constant,** which has a value of 6.63×10^{-34} J-s. Thus, photon energy is proportional to the frequency of the radiation, or inversely proportional to the wavelength. Photon energies are also included in the electromagnetic spectrum (Figure 19.2).

When describing optical phenomena involving the interactions between radiation and matter, an explanation is often facilitated if light is treated in terms of photons. On other occasions, a wave treatment is more appropriate; at one time or another, both approaches are used in this discussion.

19.3 LIGHT INTERACTIONS WITH SOLIDS

When light proceeds from one medium into another (e.g., from air into a solid substance), several things happen. Some of the light radiation may be transmitted through the medium, some will be absorbed, and some will be reflected at the interface between the two media. The intensity I_0 of the beam incident to the surface of the solid medium must equal the sum of the intensities of the transmitted, absorbed, and reflected beams, denoted as I_T, I_A, and I_R, respectively, or

$$I_0 = I_T + I_A + I_R \tag{19.4}$$

Radiation intensity, expressed in watts per square meter, corresponds to the energy being transmitted per unit of time across a unit area that is perpendicular to the direction of propagation.

An alternate form of Equation 19.4 is

$$T + A + R = 1 \tag{19.5}$$

where T, A, and R represent, respectively, the transmissivity (I_T/I_0), absorptivity (I_A/I_0), and reflectivity (I_R/I_0), or the fractions of incident light that are transmitted, absorbed, and reflected by a material; their sum must equal unity, since all the incident light is either transmitted, absorbed, or reflected.

Materials that are capable of transmitting light with relatively little absorption and reflection are **transparent**—one can see through them. **Translucent** materials are those through which light is transmitted diffusely; that is, light is scattered within the interior, to the degree that objects are not clearly distinguishable when viewed through a specimen of the material. Those materials that are impervious to the transmission of visible light are termed **opaque.**

Bulk metals are opaque throughout the entire visible spectrum; that is, all light radiation is either absorbed or reflected. On the other hand, electrically insulating materials can be made to be transparent. Furthermore, some semiconducting materials are transparent whereas others are opaque.

19.4 ATOMIC AND ELECTRONIC INTERACTIONS

The optical phenomena that occur within solid materials involve interactions between the electromagnetic radiation and atoms, ions, and/or electrons. Two of the most important of these interactions are electronic polarization and electron energy transitions.

ELECTRONIC POLARIZATION

One component of an electromagnetic wave is simply a rapidly fluctuating electric field (Figure 19.1). For the visible range of frequencies, this electric field interacts with the electron cloud surrounding each atom within its path in such a way as to induce electronic polarization, or to shift the electron cloud relative to the nucleus of the atom with each change in direction of electric field component, as demonstrated in Figure 12.30*a*. Two consequences of this polarization are: (1) some of the radiation energy may be absorbed, and (2) light waves are retarded in velocity as they pass through the medium. The second consequence is manifested as refraction, a phenomenon to be discussed in Section 19.5.

ELECTRON TRANSITIONS

The absorption and emission of electromagnetic radiation may involve electron transitions from one energy state to another. For the sake of this discussion, consider an isolated atom, the electron energy diagram for which is represented in Figure 19.3. An electron may be excited from an occupied state at energy E_2 to a vacant and higher-lying one, denoted E_4, by the absorption of a photon of energy. The change in energy experienced by the electron, ΔE, depends on the radiation frequency as follows:

$$\Delta E = h\nu \tag{19.6}$$

where, again, h is Planck's constant. At this point it is important that several concepts be understood. First, since the energy states for the atom are discrete, only specific ΔE's exist between the energy levels; thus, only photons of frequencies correspond-

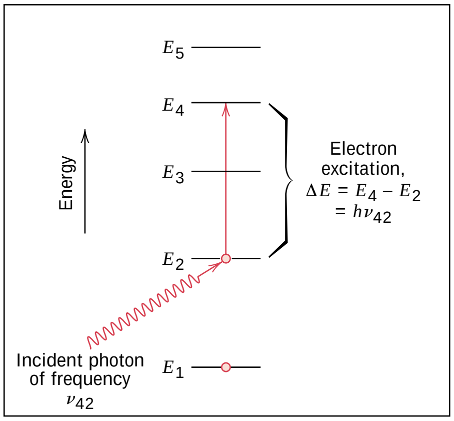
E_5
E_4
E_3
E_2
E_1
Energy
Electron excitation, $\Delta E = E_4 - E_2 = h\nu_{42}$
Incident photon of frequency ν_{42}

FIGURE 19.3 For an isolated atom, a schematic illustration of photon absorption by the excitation of an electron from one energy state to another. The energy of the photon ($h\nu_{42}$) must be exactly equal to the difference in energy between the two states ($E_4 - E_2$).

ing to the possible ΔE's for the atom can be absorbed by electron transitions. Furthermore, all of a photon's energy is absorbed in each excitation event.

A second important concept is that a stimulated electron cannot remain in an **excited state** indefinitely; after a short time, it falls or decays back into its **ground state,** or unexcited level, with a reemission of electromagnetic radiation. Several decay paths are possible, and these are discussed later. In any case, there must be a conservation of energy for absorption and emission electron transitions.

As the ensuing discussions show, the optical characteristics of solid materials that relate to absorption and emission of electromagnetic radiation are explained in terms of the electron band structure of the material (possible band structures were discussed in Section 12.5) and the principles relating to electron transitions, as outlined in the preceding two paragraphs.

OPTICAL PROPERTIES OF METALS

Consider the electron energy band schemes for metals as illustrated in Figures 12.4*a* and 12.4*b*; in both cases a high-energy band is only partially filled with electrons. Metals are opaque because the incident radiation having frequencies within the visible range excites electrons into unoccupied energy states above the Fermi energy, as demonstrated in Figure 19.4*a*; as a consequence, the incident radiation is absorbed, in accordance with Equation 19.6. Total absorption is within a very thin outer layer, usually less than 0.1 μm; thus only metallic films thinner than 0.1 μm are capable of transmitting visible light.

All frequencies of visible light are absorbed by metals because of the continuously available empty electron states, which permit electron transitions as in Figure 19.4*a*. In fact, metals are opaque to all electromagnetic radiation on the low end of the frequency spectrum, from radio waves, through infrared, the visible, and into about the middle of the ultraviolet radiation. Metals are transparent to high-frequency (x- and γ-ray) radiation.

Most of the absorbed radiation is reemitted from the surface in the form of visible light of the same wavelength, which appears as reflected light; an electron

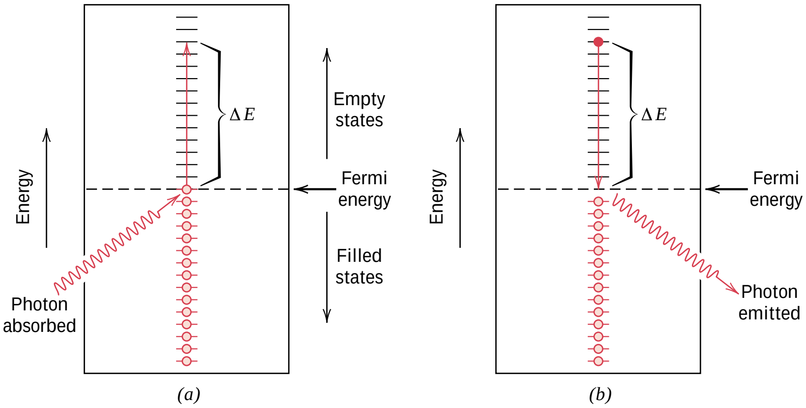

Figure 19.4 (*a*) Schematic representation of the mechanism of photon absorption for metallic materials in which an electron is excited into a higher-energy unoccupied state. The change in energy of the electron ΔE is equal to the energy of the photon. (*b*) Reemission of a photon of light by the direct transition of an electron from a high to a low energy state.

transition accompanying reradiation is shown in Figure 19.4*b*. The reflectivity for most metals is between 0.90 and 0.95; some small fraction of the energy from electron decay processes is dissipated as heat.

Since metals are opaque and highly reflective, the perceived color is determined by the wavelength distribution of the radiation that is reflected and not absorbed. A bright silvery appearance when exposed to white light indicates that the metal is highly reflective over the entire range of the visible spectrum. In other words, for the reflected beam, the composition of these reemitted photons, in terms of frequency and number, is approximately the same as for the incident beam. Aluminum and silver are two metals that exhibit this reflective behavior. Copper and gold appear red-orange and yellow, respectively, because some of the energy associated with light photons having short wavelengths is not reemitted as visible light.

OPTICAL PROPERTIES OF NONMETALS

By virtue of their electron energy band structures, nonmetallic materials may be transparent to visible light. Therefore, in addition to reflection and absorption, refraction and transmission phenomena also need to be considered.

19.5 REFRACTION

Light that is transmitted into the interior of transparent materials experiences a decrease in velocity, and, as a result, is bent at the interface; this phenomenon is termed **refraction.** The **index of refraction** n of a material is defined as the ratio of the velocity in a vacuum c to the velocity in the medium v, or

$$n = \frac{c}{v} \tag{19.7}$$

The magnitude of n (or the degree of bending) will depend on the wavelength of the light. This effect is graphically demonstrated by the familiar dispersion or separation of a beam of white light into its component colors by a glass prism. Each color is deflected by a different amount as it passes into and out of the glass, which results in the separation of the colors. Not only does the index of refraction affect the optical path of light, but also, as explained below, it influences the fraction of incident light that is reflected at the surface.

Just as Equation 19.1 defines the magnitude of c, an equivalent expression gives the velocity of light v in a medium as

$$v = \frac{1}{\sqrt{\epsilon\mu}} \tag{19.8}$$

where ϵ and μ are, respectively, the permittivity and permeability of the particular substance. From Equation 19.7, we have

$$n = \frac{c}{v} = \frac{\sqrt{\epsilon\mu}}{\sqrt{\epsilon_0\mu_0}} = \sqrt{\epsilon_r\mu_r} \tag{19.9}$$

where ϵ_r and μ_r are the dielectric constant and the relative magnetic permeability, respectively. Since most substances are only slightly magnetic, $\mu_r \cong 1$, and

$$n \cong \sqrt{\epsilon_r} \tag{19.10}$$

Thus, for transparent materials, there is a relation between the index of refraction and the dielectric constant. As already mentioned, the phenomenon of refraction is related to electronic polarization (Section 19.4) at the relatively high frequencies for visible light; thus, the electronic component of the dielectric constant may be determined from index of refraction measurements using Equation 19.10.

Since the retardation of electromagnetic radiation in a medium results from electronic polarization, the size of the constituent atoms or ions has a considerable influence on the magnitude of this effect—generally, the larger an atom or ion, the greater will be the electronic polarization, the slower the velocity, and the greater the index of refraction. The index of refraction for a typical soda–lime glass is approximately 1.5. Additions of large barium and lead ions (as BaO and PbO) to a glass will increase *n* significantly. For example, highly leaded glasses containing 90 wt% PbO have an index of refraction of approximately 2.1.

For crystalline ceramics that have cubic crystal structures, and for glasses, the index of refraction is independent of crystallographic direction (i.e., it is isotropic). Noncubic crystals, on the other hand, have an anisotropic *n*; that is, the index is greatest along the directions that have the highest density of ions. Table 19.1 gives refractive indices for several glasses, transparent ceramics, and polymers. Average values are provided for the crystalline ceramics in which *n* is anisotropic.

19.6 REFLECTION

When light radiation passes from one medium into another having a different index of refraction, some of the light is scattered at the interface between the two media

Table 19.1 Refractive Indices for Some Transparent Materials

Material	*Average Index of Refraction*
Ceramics	
Silica glass	1.458
Borosilicate (Pyrex) glass	1.47
Soda–lime glass	1.51
Quartz (SiO_2)	1.55
Dense optical flint glass	1.65
Spinel ($MgAl_2O_4$)	1.72
Periclase (MgO)	1.74
Corundum (Al_2O_3)	1.76
Polymers	
Polytetrafluoroethylene	1.35
Polymethyl methacrylate	1.49
Polypropylene	1.49
Polyethylene	1.51
Polystyrene	1.60

even if both are transparent. The reflectivity R represents that fraction of the incident light which is reflected at the interface, or

$$R = \frac{I_R}{I_0} \tag{19.11}$$

where I_0 and I_R are the intensities of the incident and reflected beams, respectively. If the light is normal (or perpendicular) to the interface, then

$$R = \left(\frac{n_2 - n_1}{n_2 + n_1}\right)^2 \tag{19.12}$$

where n_1 and n_2 are the indices of refraction of the two media. If the incident light is not normal to the interface, R will depend on the angle of incidence. When light is transmitted from a vacuum or air into a solid s, then

$$R = \left(\frac{n_s - 1}{n_s + 1}\right)^2 \tag{19.13}$$

since the index of refraction of air is very nearly unity. Thus, the higher the index of refraction of the solid, the greater is the reflectivity. For typical silicate glasses, the reflectivity is approximately 0.05. Just as the index of refraction of a solid depends on the wavelength of the incident light, so also does the reflectivity vary with wavelength. Reflection losses for lenses and other optical instruments are minimized significantly by coating the reflecting surface with very thin layers of dielectric materials such as magnesium fluoride (MgF_2).

19.7 ABSORPTION

Nonmetallic materials may be opaque or transparent to visible light; and, if transparent, they often appear colored. In principle, light radiation is absorbed in this group of materials by two basic mechanisms, which also influence the transmission characteristics of these nonmetals. One of these is electronic polarization (Section 19.4). Absorption by electronic polarization is important only at light frequencies in the vicinity of the relaxation frequency of the constituent atoms. The other mechanism involves valence band-conduction band electron transitions, which depends on the electron energy band structure of the material; band structures for semiconductors and insulators were discussed in Section 12.5.

Absorption of a photon of light may occur by the promotion or excitation of an electron from the nearly filled valence band, across the band gap, and into an empty state within the conduction band, as demonstrated in Figure 19.5*a*; a free electron in the conduction band and a hole in the valence band are created. Again, the energy of excitation ΔE is related to the absorbed photon frequency through Equation 19.6. These excitations with the accompanying absorption can take place only if the photon energy is greater than that of the band gap E_g, that is, if

$$h\nu > E_g \tag{19.14}$$

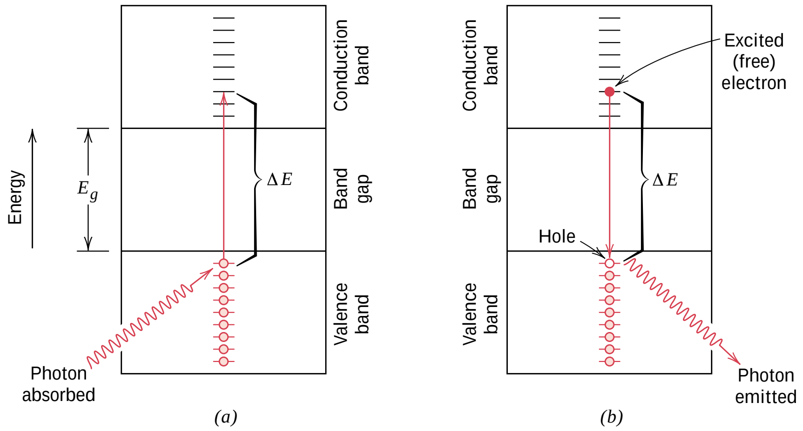

Figure 19.5 (*a*) Mechanism of photon absorption for nonmetallic materials in which an electron is excited across the band gap, leaving behind a hole in the valence band. The energy of the photon absorbed is ΔE, which is necessarily greater than the band gap energy E_g. (*b*) Emission of a photon of light by a direct electron transition across the band gap.

or, in terms of wavelength,

$$\frac{hc}{\lambda} > E_g \tag{19.15}$$

The minimum wavelength for visible light, $\lambda(\text{min})$, is about 0.4 μm, and since $c = 3 \times 10^8$ m/s and $h = 4.13 \times 10^{-15}$ eV-s, the maximum band gap energy $E_g(\text{max})$ for which absorption of visible light is possible is just

$$\begin{aligned} E_g(\text{max}) &= \frac{hc}{\lambda(\text{min})} \\ &= \frac{(4.13 \times 10^{-15}\text{ eV-s})(3 \times 10^8\text{ m/s})}{4 \times 10^{-7}\text{ m}} \\ &= 3.1\text{ eV} \end{aligned} \tag{19.16a}$$

Or, no visible light is absorbed by nonmetallic materials having band gap energies greater than about 3.1 eV; these materials, if of high purity, will appear transparent and colorless.

On the other hand, the maximum wavelength for visible light, $\lambda(\text{max})$, is about 0.7 μm; computation of the minimum band gap energy $E_g(\text{min})$ for which there is absorption of visible light is according to

$$\begin{aligned} E_g(\text{min}) &= \frac{hc}{\lambda(\text{max})} \\ &= \frac{(4.13 \times 10^{-15}\text{ eV-s})(3 \times 10^8\text{ m/s})}{7 \times 10^{-7}\text{ m}} = 1.8\text{ eV} \end{aligned} \tag{19.16b}$$

This result means that all visible light is absorbed by valence band to conduction band electron transitions for those semiconducting materials that have band gap energies less than about 1.8 eV; thus, these materials are opaque. Only a portion of the visible spectrum is absorbed by materials having band gap energies between 1.8 and 3.1 eV; consequently, these materials appear colored.

Every nonmetallic material becomes opaque at some wavelength, which depends on the magnitude of its E_g. For example, diamond, having a band gap of 5.6 eV, is opaque to radiation having wavelengths less than about 0.22 μm.

Interactions with light radiation can also occur in dielectric solids having wide band gaps, involving other than valence band-conduction band electron transitions. If impurities or other electrically active defects are present, electron levels within the band gap may be introduced, such as the donor and acceptor levels (Section 12.11), except that they lie closer to the center of the band gap. Light radiation of specific wavelengths may be emitted as a result of electron transitions involving these levels within the band gap. For example, consider Figure 19.6*a* which shows the valence band-conduction band electron excitation for a material that has one such impurity level. Again, the electromagnetic energy that was absorbed by this electron excitation must be dissipated in some manner; several mechanisms are possible. For one, this dissipation may occur via direct electron and hole recombination according to the reaction

$$\text{electron} + \text{hole} \longrightarrow \text{energy}\ (\Delta E) \tag{19.17}$$

which is represented schematically in Figure 19.5*b*. In addition, multiple-step electron transitions may occur, which involve impurity levels lying within the band gap. One possibility, as indicated in Figure 19.6*b*, is the emission of two photons; one is emitted as the electron drops from a state in the conduction band to the impurity level, the other as it decays back into the valence band. Or, alternatively, one of

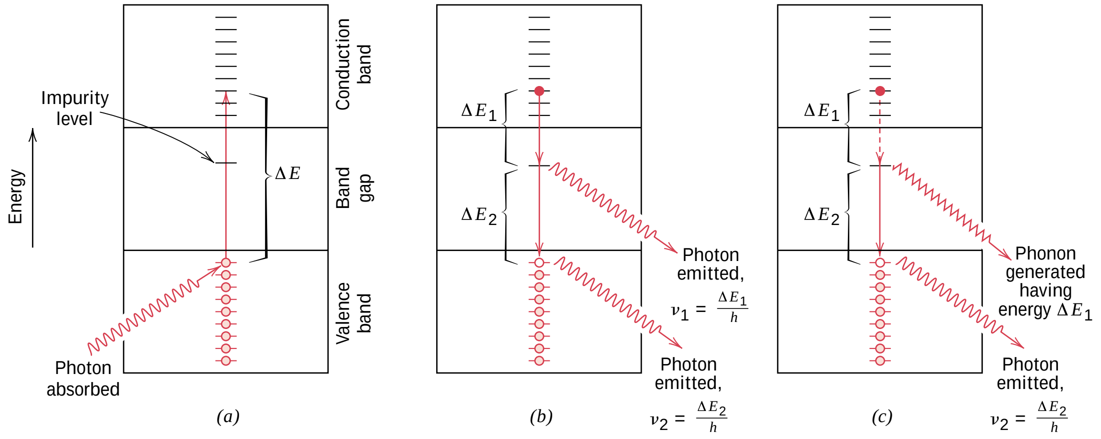
Impurity level
Energy
Conduction band
Band gap
Valence band
ΔE
Photon absorbed
ΔE_1
ΔE_2
Photon emitted, $\nu_1 = \frac{\Delta E_1}{h}$
Photon emitted, $\nu_2 = \frac{\Delta E_2}{h}$
ΔE_1
ΔE_2
Phonon generated having energy ΔE_1
Photon emitted, $\nu_2 = \frac{\Delta E_2}{h}$

(*a*) (*b*) (*c*)

FIGURE 19.6 (*a*) Photon absorption via a valence band-conduction band electron excitation for a material that has an impurity level that lies within the band gap. (*b*) Emission of two photons involving electron decay first into an impurity state, and finally into the ground state. (*c*) Generation of both a phonon and a photon as an excited electron falls first into an impurity level and finally back to its ground state.

the transitions may involve the generation of a phonon (Figure 19.6*c*), wherein the associated energy is dissipated in the form of heat.

The intensity of the net absorbed radiation is dependent on the character of the medium as well as the path length within. The intensity of transmitted or nonabsorbed radiation I'_T continuously decreases with distance x that the light traverses:

$$I'_T = I'_0 e^{-\beta x} \tag{19.18}$$

where I'_0 is the intensity of the nonreflected incident radiation and β, the *absorption coefficient* (in mm^{-1}), is characteristic of the particular material; furthermore, β varies with wavelength of the incident radiation. The distance parameter x is measured from the incident surface into the material. Materials that have large β values are considered to be highly absorptive.

19.8 TRANSMISSION

The phenomena of absorption, reflection, and transmission may be applied to the passage of light through a transparent solid, as shown in Figure 19.7. For an incident beam of intensity I_0 that impinges on the front surface of a specimen of thickness l and absorption coefficient β, the transmitted intensity at the back face I_T is

$$I_T = I_0(1 - R)^2 e^{-\beta l} \tag{19.19}$$

where R is the reflectance; for this expression, it is assumed that the same medium exists outside both front and back faces. The derivation of Equation 19.19 is left as a homework problem.

Thus, the fraction of incident light that is transmitted through a transparent material depends on the losses that are incurred by absorption and reflection. Again, the sum of the reflectivity R, absorptivity A, and transmissivity T, is unity according to Equation 19.5. Also, each of the variables R, A, and T depends on light wavelength. This is demonstrated over the visible region of the spectrum for a green glass in Figure 19.8. For example, for light having a wavelength of 0.4 μm, the

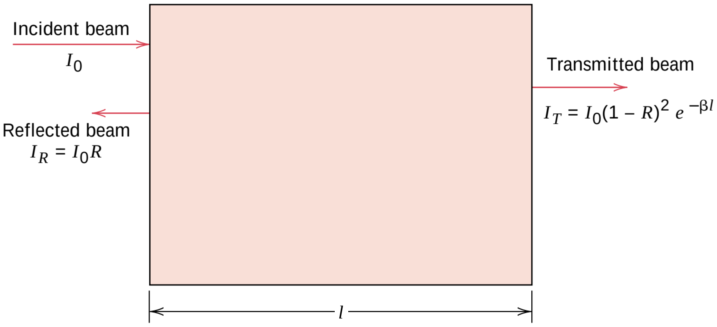

FIGURE 19.7 The transmission of light through a transparent medium for which there is reflection at front and back faces, as well as absorption within the medium. (Adapted from R. M. Rose, L. A. Shepard, and J. Wulff, *The Structure and Properties of Materials,* Vol. 4, *Electronic Properties.* Copyright © 1966 by John Wiley & Sons, New York. Reprinted by permission of John Wiley & Sons, Inc.)

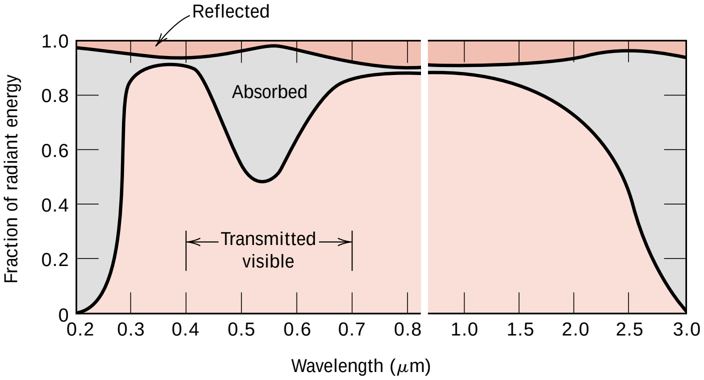

Figure 19.8 The variation with wavelength of the fractions of incident light transmitted, absorbed, and reflected through a green glass. (From W. D. Kingery, H. K. Bowen, and D. R. Uhlmann, *Introduction to Ceramics*, 2nd edition. Copyright © 1976 by John Wiley & Sons, New York. Reprinted by permission of John Wiley & Sons, Inc.)

fractions transmitted, absorbed, and reflected are approximately 0.90, 0.05, and 0.05, respectively. However, at 0.55 μm, the respective fractions have shifted to about 0.50, 0.48, and 0.02.

19.9 COLOR

Transparent materials appear colored as a consequence of specific wavelength ranges of light that are selectively absorbed; the **color** discerned is a result of the combination of wavelengths that are transmitted. If absorption is uniform for all visible wavelengths, the material appears colorless; examples include high-purity inorganic glasses and high-purity and single-crystal diamonds and sapphire.

Usually, any selective absorption is by electron excitation. One such situation involves semiconducting materials that have band gaps within the range of photon energies for visible light (1.8 to 3.1 eV). Thus, the fraction of the visible light having energies greater than E_g is selectively absorbed by valence band–conduction band electron transitions. Of course, some of this absorbed radiation is reemitted as the excited electrons drop back into their original, lower-lying energy states. It is not necessary that this reemission occur at the same frequency as that of the absorption. As a result, the color depends on the frequency distribution of both transmitted and reemitted light beams.

For example, cadmium sulfide (CdS) has a band gap of about 2.4 eV; hence, it absorbs photons having energies greater than about 2.4 eV, which correspond to the blue and violet portions of the visible spectrum; some of this energy is reradiated as light having other wavelengths. Nonabsorbed visible light consists of photons having energies between about 1.8 and 2.4 eV. Cadmium sulfide takes on a yellow-orange color because of the composition of the transmitted beam.

With insulator ceramics, specific impurities also introduce electron levels within the forbidden band gap, as discussed above. Photons having energies less than the band gap may be emitted as a consequence of electron decay processes involving impurity atoms or ions as demonstrated in Figures 19.6*b* and 19.6*c*. Again, the color of the material is a function of the distribution of wavelengths that is found in the transmitted beam.

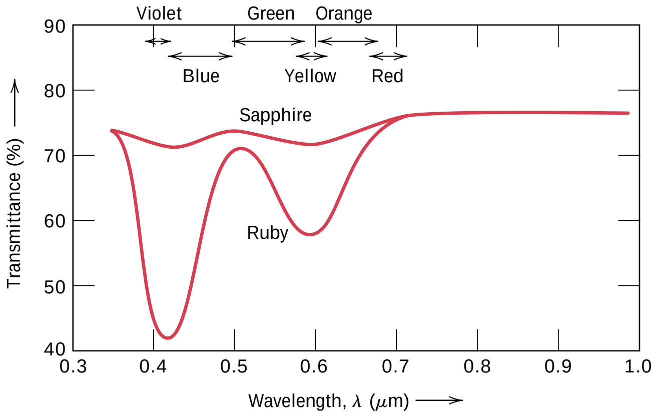

FIGURE 19.9 Transmission of light radiation as a function of wavelength for sapphire (single-crystal aluminum oxide) and ruby (aluminum oxide containing some chromium oxide). The sapphire appears colorless, while the ruby has a red tint due to selective absorption over specific wavelength ranges. (Adapted from ‘‘The Optical Properties of Materials,’’ by A. Javan. Copyright © 1967 by Scientific American, Inc. All rights reserved.)

For example, high-purity and single-crystal aluminum oxide or sapphire is colorless. Ruby, which has a brilliant red color, is simply sapphire to which has been added 0.5 to 2% of chromium oxide (Cr_2O_3). The Cr^{3+} ion substitutes for the Al^{3+} ion in the Al_2O_3 crystal structure and, furthermore, introduces impurity levels within the wide energy band gap of the sapphire. Light radiation is absorbed by valence band-conduction band electron transitions, some of which is then reemitted at specific wavelengths as a consequence of electron transitions to and from these impurity levels. The transmittance as a function of wavelength for sapphire and ruby is presented in Figure 19.9. For the sapphire, transmittance is relatively constant with wavelength over the visible spectrum, which accounts for the colorlessness of this material. However, strong absorption peaks (or minima) occur for the ruby, one in the blue-violet region (at about 0.4 μm), and the other for yellow-green light (at about 0.6 μm). That nonabsorbed or transmitted light mixed with reemitted light imparts to ruby its deep-red color.

Inorganic glasses are colored by incorporating transition or rare earth ions while the glass is still in the molten state. Representative color–ion pairs include Cu^{2+}, blue-green; Co^{2+}, blue–violet; Cr^{3+}, green; Mn^{2+}, yellow; and Mn^{3+}, purple. These colored glasses are also used as glazes, decorative coatings on ceramic ware.

19.10 OPACITY AND TRANSLUCENCY IN INSULATORS

The extent of translucency and opacity for inherently transparent dielectric materials depends to a great degree on their internal reflectance and transmittance characteristics. Many dielectric materials that are intrinsically transparent may be made translucent or even opaque because of interior reflection and refraction. A transmitted light beam is deflected in direction and appears diffuse as a result of multiple scattering events. Opacity results when the scattering is so extensive that virtually none of the incident beam is transmitted, undeflected, to the back surface.

This internal scattering may result from several different sources. Polycrystalline specimens in which the index of refraction is anisotropic normally appear translu-

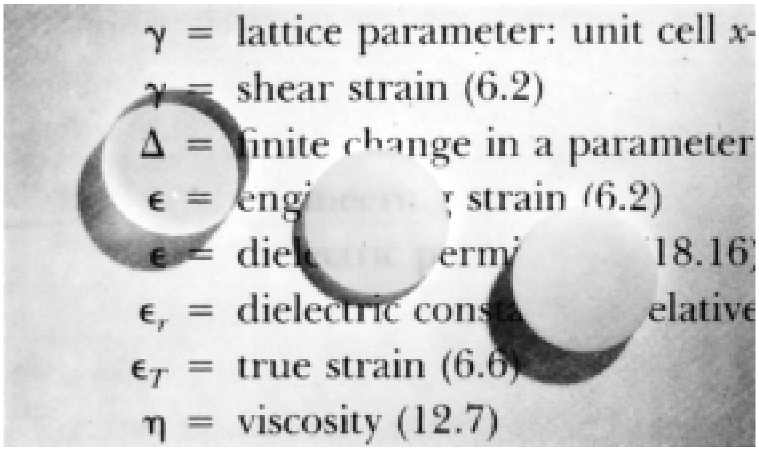
γ = lattice parameter: unit cell x-
γ = shear strain (6.2)
Δ = finite change in a parameter
ϵ = engineering strain (6.2)
ϵ = dielectric permi 18.16)
ϵ_r = dielectric consta elative
ϵ_T = true strain (6.6)
η = viscosity (12.7)

Figure 19.10 Photograph showing the light transmittance of three aluminum oxide specimens. From left to right: single-crystal material (sapphire), which is transparent; a polycrystalline and fully dense (nonporous) material, which is translucent; and a polycrystalline material that contains approximately 5% porosity, which is opaque. (Specimen preparation, P. A. Lessing; photography by J. Telford.)

cent. Both reflection and refraction occur at grain boundaries, which causes a diversion in the incident beam. This results from a slight difference in index of refraction *n* between adjacent grains that do not have the same crystallographic orientation.

Scattering of light also occurs in two-phase materials in which one phase is finely dispersed within the other. Again, the beam dispersion occurs across phase boundaries when there is a difference in the refractive index for the two phases; the greater this difference, the more efficient is the scattering.

As a consequence of fabrication or processing, many ceramic pieces contain some residual porosity in the form of finely dispersed pores. These pores also effectively scatter light radiation.

Figure 19.10 demonstrates the difference in optical transmission characteristics of single-crystal, fully dense polycrystalline, and porous (~5% porosity) aluminum oxide specimens. Whereas the single crystal is totally transparent, polycrystalline and porous materials are, respectively, translucent and opaque.

For intrinsic polymers (without additives and impurities), the degree of translucency is influenced primarily by the extent of crystallinity. Some scattering of visible light occurs at the boundaries between crystalline and amorphous regions, again as a result of different indices of refraction. For highly crystalline specimens, this degree of scattering is extensive, which leads to translucency, and, in some instances, even opacity. Highly amorphous polymers are completely transparent.

APPLICATIONS OF OPTICAL PHENOMENA

19.11 LUMINESCENCE

Some materials are capable of absorbing energy and then reemitting visible light in a phenomenon called **luminescence.** Photons of emitted light are generated from electron transitions in the solid. Energy is absorbed when an electron is promoted to an excited energy state; visible light is emitted when it falls back to a lower energy state if 1.8 eV $< h\nu <$ 3.1 eV. The absorbed energy may be supplied as higher-energy electromagnetic radiation (causing valence band–conduction band transitions, Figure 19.6*a*) such as ultraviolet light, or other sources such as high energy electrons, or by heat, mechanical, or chemical energy. Furthermore, luminescence is classified according to the magnitude of the delay time between absorption and reemission events. If reemission occurs for times much less than one second, the phenomenon is termed **fluorescence;** for longer times, it is called **phosphorescence.** A number of materials can be made to fluoresce or phosphoresce; these include some sulfides, oxides, tungstates, and a few organic materials. Ordinarily, pure materials do not display these phenomena, and to induce them, impurities in controlled concentrations must be added.

Luminescence has a number of commercial applications. Fluorescent lamps consist of a glass housing, coated on the inside with specially prepared tungstates or silicates. Ultraviolet light is generated within the tube from a mercury glow discharge, which causes the coating to fluoresce and emit white light. The picture viewed on a television screen is the product of luminescence. The inside of the screen is coated with a material that fluoresces as an electron beam inside the picture tube very rapidly traverses the screen. Detection of x-rays and γ-rays is also possible; certain phosphors emit visible light or glow when introduced into a beam of the radiation that is otherwise invisible.

Some *p*–*n* rectifying junctions, as described in Section 12.14, may also be used to generate visible light in a process termed **electroluminescence.** When a forward-biased potential is applied across the device, electrons and holes will annihilate one another within the recombination region according to Equation 19.17. Under some circumstances the energy produced will appear as visible light. Such diodes that luminesce visible light are the familiar *light-emitting diodes* (*LED*s), which are used for digital displays. The characteristic color of an LED depends on the particular semiconducting material that is used.

19.12 PHOTOCONDUCTIVITY

The conductivity of semiconducting materials depends on the number of free electrons in the conduction band and also the number of holes in the valence band, according to Equation 12.13. Thermal energy associated with lattice vibrations can promote electron excitations in which free electrons and/or holes are created, as described in Section 12.6. Additional charge carriers may be generated as a consequence of photon-induced electron transitions in which light is absorbed; the attendant increase in conductivity is called **photoconductivity.** Thus, when a specimen of a photoconductive material is illuminated, the conductivity increases.

This phenomenon is utilized in photographic light meters. A photoinduced current is measured, and its magnitude is a direct function of the intensity of the incident light radiation, or the rate at which the photons of light strike the photoconductive material. Of course, visible light radiation must induce electronic transitions in the photoconductive material; cadmium sulfide is commonly utilized in light meters.

Sunlight may be directly converted into electrical energy in solar cells, which also employ semiconductors. The operation of these devices is, in a sense, the reverse of that for the light-emitting diode. A *p*–*n* junction is used in which photoexcited electrons and holes are drawn away from the junction, in opposite directions, and become part of an external current.

19.13 LASERS

All the radiative electron transitions heretofore discussed are spontaneous; that is, an electron falls from a high energy state to a lower one without any external provocation. These transition events occur independently of one another and at random times, producing radiation that is incoherent; that is, the light waves are out of phase with one another. With lasers, however, coherent light is generated by electron transitions initiated by an external stimulus; in fact, **"laser"** is just the acronym for light amplification by stimulated emission of radiation.

Although there are several different varieties of laser, the principles of operation are explained using the solid-state ruby laser. Ruby is simply a single crystal of Al_2O_3 (sapphire) to which has been added on the order of 0.05% Cr^{3+} ions. As previously explained (Section 19.9), these ions impart to ruby its characteristic red color; more important, they provide electron states that are essential for the laser to function. The ruby laser is in the form of a rod, the ends of which are flat, parallel, and highly polished. Both ends are silvered such that one is totally reflecting and the other partially transmitting.

The ruby is illuminated with light from a xenon flash lamp (Figure 19.11). Before this exposure, virtually all the Cr^{3+} ions are in their ground states; that is, electrons fill the lowest energy levels, as represented schematically in Figure 19.12. However, photons of wavelength 0.56 μm from the xenon lamp excite electrons from the Cr^{3+} ions into higher energy states. These electrons can decay back into their ground state by two different paths. Some fall back directly; associated photon emissions are not part of the laser beam. Other electrons decay into a metastable intermediate state (path EM, Figure 19.12), where they may reside for up to 3 ms before spontaneous emission (path MG). In terms of electronic processes, 3 ms is a relatively long time, which means that a large number of these metastable states may become occupied. This situation is indicated in Figure 19.13*b*.

The initial spontaneous photon emission by a few of these electrons is the stimulus that triggers an avalanche of emissions from the remaining electrons in the metastable state (Figure 19.13*c*). Of the photons directed parallel to the long axis of the ruby rod, some are transmitted through the partially silvered end; others, incident to the totally silvered end, are reflected. Photons that are not emitted in this axial direction are lost. The light beam repeatedly travels back and forth along the rod length, and its intensity increases as more emissions are stimulated. Ultimately, a high intensity, coherent, and highly collimated laser light beam of

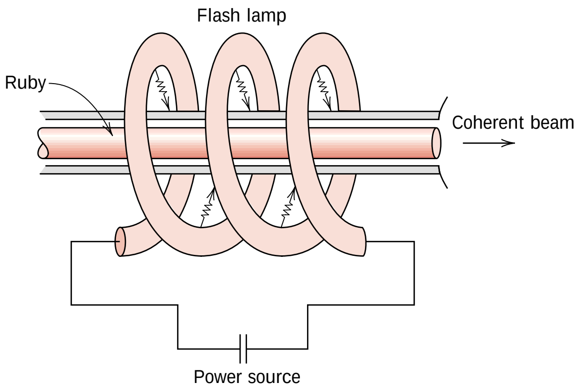

FIGURE 19.11 Schematic diagram of the ruby laser and xenon flash lamp. (From R. M. Rose, L. A. Shepard, and J. Wulff, *The Structure and Properties of Materials*, Vol. 4, *Electronic Properties*. Copyright © 1966 by John Wiley & Sons, New York. Reprinted by permission of John Wiley & Sons, Inc.)

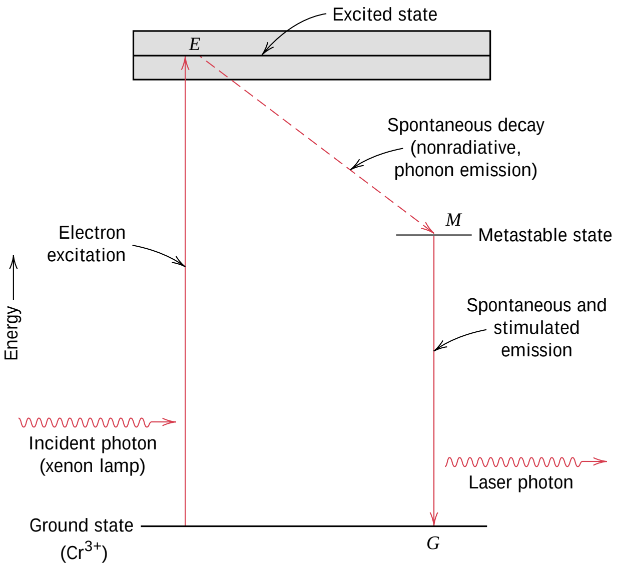
Excited state
E
Spontaneous decay
(nonradiative,
phonon emission)
M
Metastable state
Electron
excitation
Energy
Spontaneous and
stimulated
emission
Incident photon
(xenon lamp)
Laser photon
Ground state
(Cr^{3+})
G

Figure 19.12 Schematic energy diagram for the ruby laser, showing electron excitation and decay paths.

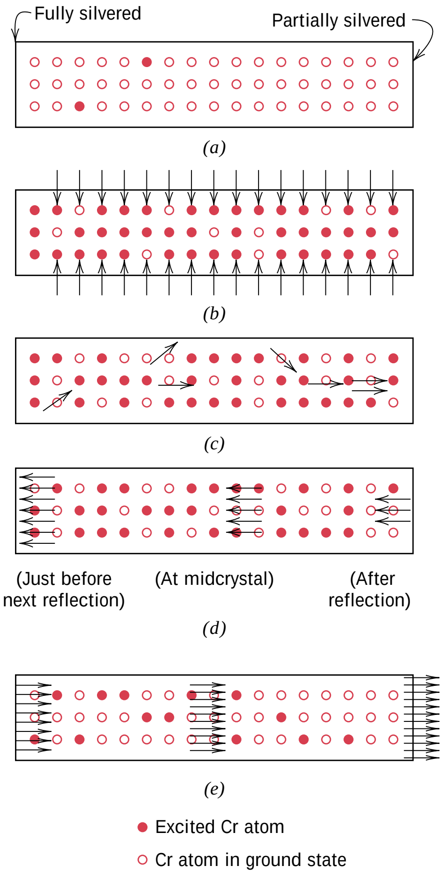
Fully silvered
Partially silvered
(a)
(b)
(c)
(Just before
next reflection)
(At midcrystal)
(After
reflection)
(d)
(e)
● Excited Cr atom
○ Cr atom in ground state

Figure 19.13 Schematic representations of the stimulated emission and light amplification for a ruby laser. (*a*) The chromium ions before excitation. (*b*) Electrons in some chromium atoms are excited into higher energy states by the xenon light flash. (*c*) Emission from metastable electron states is initiated or stimulated by photons that are spontaneously emitted. (*d*) Upon reflection from the silvered ends, the photons continue to stimulate emissions as they traverse the rod length. (*e*) The coherent and intense beam is finally emitted through the partially silvered end. (From R. M. Rose, L. A. Shepard, and J. Wulff, *The Structure and Properties of Materials,* Vol. 4, *Electronic Properties.* Copyright © 1966 by John Wiley & Sons, New York. Reprinted by permission of John Wiley & Sons, Inc.)

short duration is transmitted through the partially silvered end of the rod (Figure 19.13*e*). This monochromatic red beam has a wavelength of 0.6943 μm.

Semiconducting materials such as gallium arsenide may also be used as lasers that are employed in compact disk players and in the modern telecommunications industry. One requirement of these semiconducting materials is that the wavelength λ associated with the band gap energy E_g must correspond to visible light; that is, from a modification of Equation 19.3, viz.,

$$\lambda = \frac{hc}{E_g} \tag{19.20}$$

λ must lie between 0.4 and 0.7 μm. A voltage applied to the material excites electrons from the valence band, across the band gap, and into the conduction band; correspondingly, holes are created in the valence band. This process is demonstrated in Figure 19.14*a*, which shows the energy band scheme over some region of the semiconducting material, along with several holes and excited electrons. Subsequently, a few of these excited electrons and holes spontaneously recombine. For each recombination event, a photon of light having a wavelength given by Equation 19.20 is emitted (Figure 19.14*a*). One such photon will stimulate the recombination of other excited electron–hole pairs, Figure 19.14*b*–*f*, and the production of additional photons that have the same wavelength and are all in phase with one another and with the original photon; thus, a monochromatic and coherent beam results. As with the ruby laser (Figure 19.13), one end of the semiconductor laser is totally reflecting; at this end, the beam is reflected back into the material so that additional recombinations will be stimulated. The other end of the laser is partially reflecting, which allows for some of the beam to escape. Furthermore, with this type of laser, a continuous beam is produced inasmuch as a constant applied voltage ensures that there is always a steady source of holes and excited electrons.

The semiconductor laser is composed of several layers of semiconducting materials that have different compositions and are sandwiched between a heat sink and a metal conductor; a typical arrangement is represented schematically in Figure 19.15. The compositions of the layers are chosen so as to confine both the excited electrons and holes as well as the laser beam to within the central gallium arsenide layer.

A variety of other substances may be used for lasers, including some gases and glasses. Table 19.2 lists several common lasers and their characteristics. Laser applications are diverse. Since laser beams may be focused to produce localized heating, they are used in some surgical procedures and for cutting, welding, and machining metals. Lasers are also used as light sources for optical communication systems. Furthermore, because the beam is highly coherent, they may be utilized for making very precise distance measurements.

19.14 Optical Fibers in Communications

The communications field has recently experienced a revolution with the development of optical fiber technology; at present, virtually all telecommunications are transmitted via this medium rather than through copper wires. Signal transmission through a metallic wire conductor is electronic (i.e., by electrons), whereas using optically transparent fibers, signal transmission is *photonic*, that is, using photons of electromagnetic or light radiation. Use of fiber-optic systems has improved speed of transmission, information density, and transmission distance, with a reduction

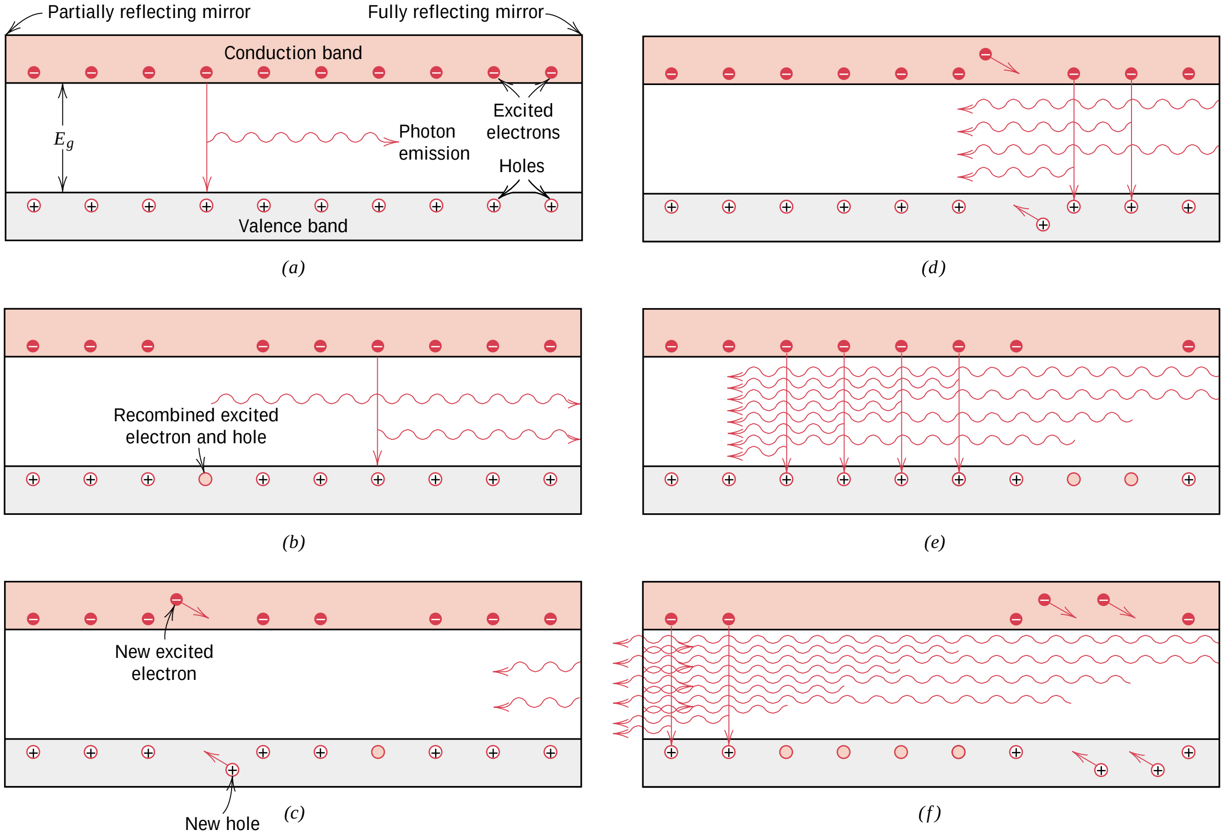
Partially reflecting mirror
Fully reflecting mirror
Conduction band
E_g
Photon emission
Excited electrons
Holes
Valence band
(a)
(d)
Recombined excited electron and hole
(b)
(e)
New excited electron
New hole
(c)
(f)

Figure 19.14 For the semiconductor laser, schematic representations of the stimulated recombination of excited electrons in the conduction band with holes in the valence band that gives rise to a laser beam. (*a*) One excited electron recombines with a hole; the energy associated with this recombination is emitted as a photon of light. (*b*) The photon emitted in (*a*) stimulates the recombination of another excited electron and hole resulting in the emission of another photon of light. (*c*) The two photons emitted in (*a*) and (*b*), having the same wavelength and being in phase with one another, are reflected by the fully reflecting mirror, back into the laser semiconductor. In addition, new excited electrons and new holes are generated by a current that passes through the semiconductor. (*d*) and (*e*) In proceeding through the semiconductor, more excited electron-hole recombinations are stimulated, which give rise to additional photons of light that also become part of the monochromatic and coherent laser beam. (*f*) Some portion of this laser beam escapes through the partially reflecting mirror at one end of the semiconducting material. (Adapted from ''Photonic Materials,'' by J. M. Rowell. Copyright © 1986 by Scientific American, Inc. All rights reserved.)

in error rate; furthermore, there is no electromagnetic interference with fiber optics. With regard to speed, optical fibers can transmit, in one second, information equivalent to three episodes of your favorite television program. Or relative to information density, two small optical fibers can transmit the equivalent of 24,000 telephone calls simultaneously. Furthermore, it would require 30,000 kg (33 tons) of copper to transmit the same amount of information as only 0.1 kg ($\frac{1}{4}$ lb_m) of optical fiber material.

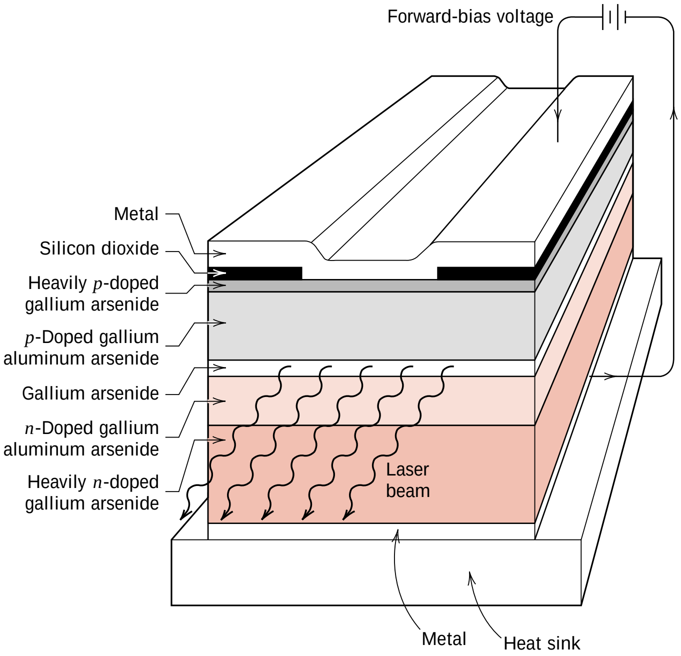
Forward-bias voltage
Metal
Silicon dioxide
Heavily *p*-doped gallium arsenide
p-Doped gallium aluminum arsenide
Gallium arsenide
n-Doped gallium aluminum arsenide
Heavily *n*-doped gallium arsenide
Laser beam
Metal
Heat sink

FIGURE 19.15 Schematic diagram showing the layered cross section of a GaAs semiconducting laser. Holes, excited electrons, and the laser beam are confined to the GaAs layer by the adjacent *n*- and *p*-type GaAlAs layers. (Adapted from "Photonic Materials," by J. M. Rowell. Copyright © 1986 by Scientific American, Inc. All rights reserved.)

The present treatment will center on the characteristics of optical fibers; however, it is thought worthwhile to first briefly discuss the components and operation of the transmission system. A schematic diagram showing these components is presented in Figure 19.16. The information (i.e., telephone conversation) in electronic form must first be digitized into bits, that is, 1's and 0's; this is accomplished

Table 19.2 Characteristics and Applications of Several Types of Lasers

Laser	***Type***	***Common Wavelengths*** (μ***m***)	***Max. Output Power*** (***W***)[a]	***Applications***
He-Ne	Gas	0.6328, 1.15, 3.39	0.0005–0.05 (CW)	Line-of sight communications, recording/playback of holograms
CO_2	Gas	9.6, 10.6	500–15,000 (CW)	Heat treating, welding, cutting, scribing, marking
Argon	Gas ion	0.488, 0.5145	0.005–20 (CW)	Surgery, distance measurements, holography
HeCd	Metal vapor	0.441, 0.325	0.05–0.1	Light shows, spectroscopy
Dye	Liquid	0.38–1.0	0.01 (CW) 1×10^6 (P)	Spectroscopy, pollution detection
Ruby	Solid state	0.694	(P)	Pulsed holography, hole piercing
Nd-YAG	Solid state	1.06	1000 (CW) 2×10^8 (P)	Welding, hole piercing, cutting
Nd-Glass	Solid state	1.06	5×10^{14} (P)	Pulse welding, hole piercing
Diode	Semiconductor	0.33–40	0.6 (CW) 100 (P)	Bar-code reading, CDs and video disks, optical communications

[a] "CW" denotes continuous; "P" denotes pulsed.

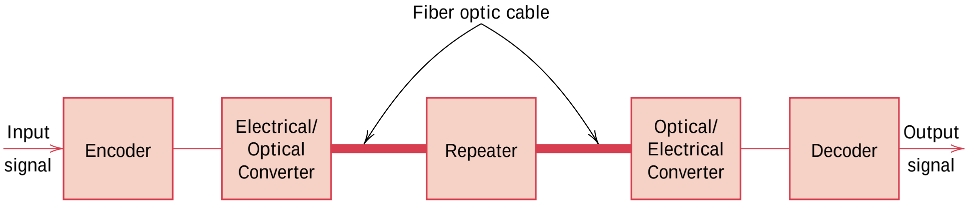

Figure 19.16 Schematic diagram showing the components of an optical fiber communications system.

in the encoder. It is next necessary to convert this electrical signal into an optical (photonic) one, which takes place in the electrical-to-optical converter (Figure 19.16). This converter is normally a semiconductor laser, as described in the previous section, which emits monochromatic and coherent light. The wavelength normally lies between 0.78 and 1.6 μm, which is in the infrared region of the electromagnetic spectrum; absorption losses are low within this range of wavelengths. The output from this laser converter is in the form of pulses of light; a binary 1 is represented by a high-power pulse (Figure 19.17*a*), whereas a 0 corresponds to a low-power pulse (or the absence of one), Figure 19.17*b*. These photonic pulse signals are then fed into and carried through the fiber-optical cable (sometimes called a ''waveguide'') to the receiving end. For long transmissions, repeaters may be required; these are devices that amplify and regenerate the signal. Finally, at the receiving end the photonic signal is reconverted to an electronic one, and is then decoded (undigitized).

The heart of this communication system is the optical fiber. It must guide these light pulses over long distances without significant signal power loss (i.e., attenuation) and pulse distortion. Fiber components are the core, cladding, and coating; these are represented in the cross-section profile, Figure 19.18. The signal passes through the core, whereas the surrounding cladding constrains the light rays to travel within the core; the outer coating protects core and cladding from damage that might result from abrasion and external pressures.

High-purity silica glass is used as the fiber material; fiber diameters normally range between about 5 and 100 μm. The fibers are relatively flaw free, and, thus, remarkably strong; during production the continuous fibers are tested to ensure that they meet minimum strength standards.

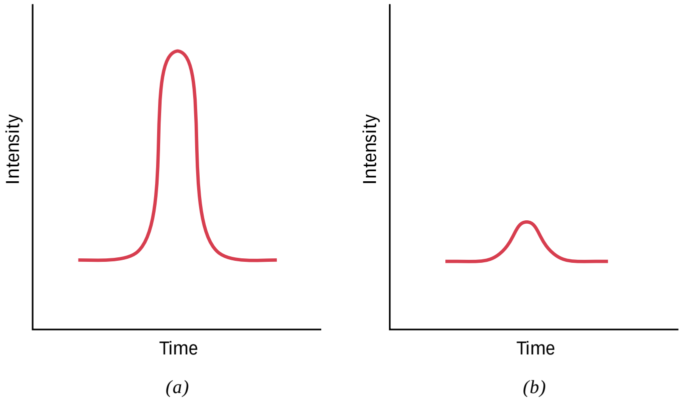

Figure 19.17 Digital encoding scheme for optical communications. (*a*) A high-power pulse of photons corresponds to a ''one'' in the binary format. (*b*) A low-power photon pulse represents a ''zero.''

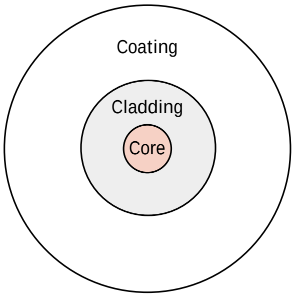

Figure 19.18 Schematic cross section of an optical fiber.

Containment of the light to within the fiber core is made possible by total internal reflection; that is, any light rays traveling at oblique angles to the fiber axis are reflected back into the core. Internal reflection is accomplished by varying the index of refraction of the core and cladding glass materials. In this regard, two design types are employed. With one type (termed ‘‘step-index’’), the index of refraction of the cladding is slightly lower than that of the core; the index profile and the manner of internal reflection are shown in Figures 19.19*b* and 19.19*d*. For this design, the output pulse will be broader than the input one (Figures 19.19*c* and *e*), a phenomenon that is undesirable since it limits the rate of transmission. Pulse broadening results because various light rays, although being injected at approximately the same instant, arrive at the output at different times; they traverse different trajectories, and, thus, have a variety of path lengths.

Pulse broadening is largely avoided by utilization of the other or ‘‘graded-index’’ design. Here, impurities such as boron oxide (B_2O_3) or germanium dioxide (GeO_2) are added to the silica glass such that the index of refraction is made to vary parabolically across the cross section (Figure 19.20*b*). Thus, the velocity of light within the core varies with radial position, being greater at the periphery than at the center. Consequently, light rays that traverse longer path lengths through the outer periphery of the core travel faster in this lower index material, and arrive at the output at approximately the same time as undeviated rays that pass through the center portion of the core.

Exceptionally pure and high-quality fibers are fabricated using advanced and sophisticated processing techniques, which will not be discussed. Impurities and

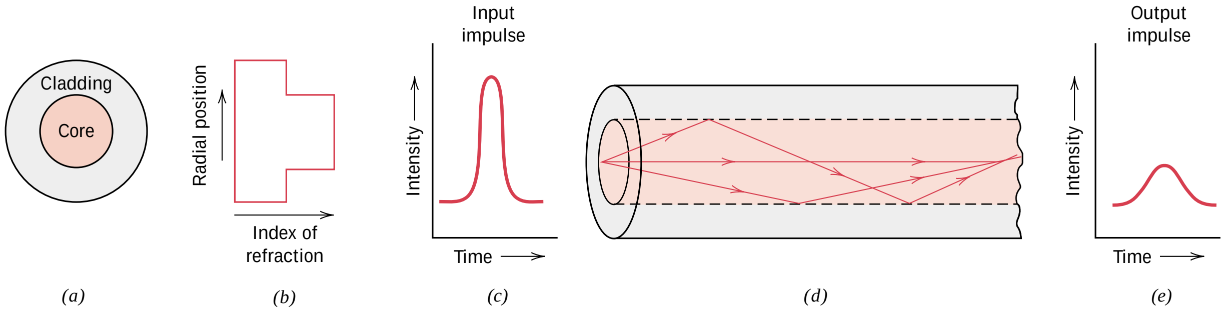

Figure 19.19 Step-index optical fiber design. (*a*) Fiber cross section. (*b*) Fiber radial index of refraction profile. (*c*) Input light pulse. (*d*) Internal reflection of light rays. (*e*) Output light pulse. (Adapted from S. R. Nagel, *IEEE Communications Magazine*, Vol. 25, No. 4, p. 34, 1987.)

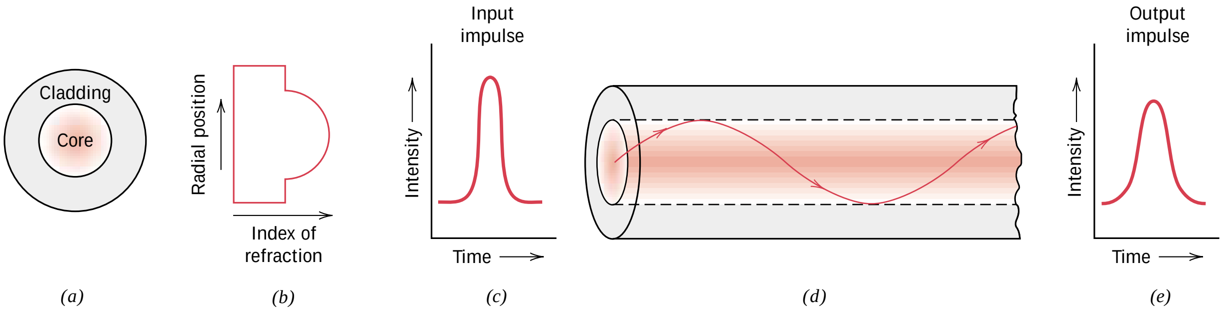

Figure 19.20 Graded-index optical fiber design. (*a*) Fiber cross section. (*b*) Fiber radial index of refraction profile. (*c*) Input light pulse. (*d*) Internal reflection of a light ray. (*e*) Output light pulse. (Adapted from S. R. Nagel, *IEEE Communications Magazine*, Vol. 25, No. 4, p. 34, 1987.)

other defects that absorb, scatter, and thus attenuate the light beam must be eliminated. The presence of copper, iron, and vanadium is especially detrimental; their concentrations are reduced to on the order of several parts per billion. Likewise, water and hydroxyl contaminant contents are extremely low. Uniformity of fiber cross-sectional dimensions and core roundness are critical; tolerances of these parameters to within a micrometer over 1 km (0.6 mile) of length are possible. In addition, bubbles within the glass and surface defects have been virtually eliminated. The attenuation of light in this glass material is imperceptibly small. For example, the power loss through a sixteen-kilometer (ten-mile) thickness of optical fiber glass is equivalent to the power loss through a twenty five-millimeter (one-inch) thickness of ordinary window glass!

SUMMARY

The optical behavior of a solid material is a function of its interactions with electromagnetic radiation having wavelengths within the visible region of the spectrum. Possible interactive phenomena include refraction, reflection, absorption, and transmission of incident light.

Metals appear opaque as a result of the absorption and then reemission of light radiation within a thin outer surface layer. Absorption occurs via the excitation of electrons from occupied energy states to unoccupied ones above the Fermi energy level. Reemission takes place by decay electron transitions in the reverse direction. The perceived color of a metal is determined by the spectral composition of the reflected light.

Nonmetallic materials are either intrinsically transparent or opaque. Opacity results in relatively narrow band gap materials as a result of absorption whereby a photon's energy is sufficient to promote valence band–conduction band electron transitions. Transparent nonmetals have band gaps greater than about 3 eV.

For wide-band gap insulators that contain impurities, decay processes involving excited electrons to states within the band gap are possible with the emission of photons having energies less than the band gap energy. These materials appear colored, and the color depends on the distribution of wavelength ranges in the transmitted beam.

Light radiation experiences refraction in transparent materials; that is, its velocity is retarded and the light beam is bent at the interface. Index of refraction is the ratio of the velocity of light in a vacuum to that in the particular medium. The phenomenon of refraction is a consequence of electronic polarization of the atoms or ions, which is induced by the electric field component of the light wave.

When light passes from one transparent medium to another having a different index of refraction, some of it is reflected at the interface. The degree of the reflectance depends on the indices of refraction of both media, as well as the angle of incidence.

Some light absorption occurs in even transparent materials as a consequence of electronic polarization.

Normally transparent materials may be made translucent or even opaque if the incident light beam experiences interior reflection and/or refraction. Translucency and opacity as a result of internal scattering may occur (1) in polycrystalline materials that have an anisotropic index of refraction, (2) in two-phase materials, (3) in materials containing small pores, and (4) in highly crystalline polymers.

Three other important optical phenomena were discussed: luminescence, photoconductivity, and light amplification by stimulated emission of radiation (lasers). With luminescence, energy is absorbed as a consequence of electron excitations, which is reemitted as visible light. The electrical conductivity of some semiconductors may be enhanced by photoinduced electron transitions, whereby additional free electrons and holes are generated. Coherent and high-intensity light beams are produced in lasers by stimulated electron transitions.

This chapter concluded with a discussion of the use of optical fibers in our modern telecommunications. Using fiber-optic technology, transmission of information is interference free, rapid, and intense.

IMPORTANT TERMS AND CONCEPTS

Absorption
Color
Electroluminescence
Excited state
Fluorescence
Ground state
Index of refraction
Laser
Luminescence
Opaque
Phosphorescence
Photoconductivity
Photon
Planck’s constant
Reflection
Refraction
Translucent
Transmission
Transparent

REFERENCES

Azaroff, L. V. and J. J. Brophy, *Electronic Processes in Materials*, McGraw-Hill Book Company, New York, 1963, Chapter 14. Reprinted by TechBooks, Marietta, OH.

Javan, A., ‘‘The Optical Properties of Materials,’’ *Scientific American*, Vol. 217, No. 3, September 1967, pp. 238–248.

Kingery, W. D., H. K. Bowen, and D. R. Uhlmann, *Introduction to Ceramics*, 2nd edition, John Wiley & Sons, New York, 1976, Chapter 13.

Ralls, K. M., T. H. Courtney, and J. Wulff, *Introduction to Materials Science and Engineering*, John Wiley & Sons, New York, 1976, Chapter 27.

Rowell, J. M., ‘‘Photonic Materials,’’ *Scientific American*, Vol. 255, No. 4, October 1986, pp. 146–157.

QUESTIONS AND PROBLEMS

19.1 Briefly discuss the similarities and differences between photons and phonons.

19.2 Electromagnetic radiation may be treated from the classical or the quantum-mechanical perspective. Briefly compare these two viewpoints.

19.3 Visible light having a wavelength of 6×10^{-7} m appears orange. Compute the frequency and energy of a photon of this light.

19.4 Distinguish between materials that are opaque, translucent, and transparent in terms of their appearance and light transmittance.

19.5 **(a)** Briefly describe the phenomenon of electronic polarization by electromagnetic radiation. **(b)** What are two consequences of electronic polarization in transparent materials?

19.6 **(a)** In ionic materials, how does the size of the component ions affect the extent of electronic polarization? **(b)** Which of the following oxide materials when added to fused silica (SiO_2) will increase its index of refraction: Al_2O_3, TiO_2, NiO, MgO? Why? You may find Table 3.4 helpful.

19.7 **(a)** Briefly explain why metals are opaque to electromagnetic radiation having photon energies within the visible region of the spectrum. **(b)** Why are metals transparent to high-frequency x-ray and γ-ray radiation?

19.8 Can a material have an index of refraction less than unity? Why or why not?

19.9 Compute the velocity of light in calcium fluoride (CaF_2), which has a dielectric constant ϵ_r of 2.056 (at frequencies within the visible range) and a magnetic susceptibility of -1.43×10^{-5}.

19.10 The indices of refraction of fused silica and a soda–lime glass within the visible spectrum are 1.458 and 1.51, respectively. For each of these materials determine the fraction of the relative dielectric constant at 60 Hz that is due to electronic polarization, using the data of Table 12.4. Neglect any orientation polarization effects.

19.11 Using the data in Table 19.1, estimate the dielectric constants for silica glass (fused silica), soda–lime glass, polytetrafluoroethylene, polyethylene, and polystyrene, and compare these values with those cited in Table 12.4. Briefly explain any discrepancies.

19.12 Briefly describe the phenomenon of dispersion in a transparent medium.

19.13 It is desired that the reflectivity of light at normal incidence to the surface of a transparent medium be less than 5.0%. Which of the following materials in Table 19.1 are likely candidates: soda–lime glass, Pyrex glass, periclase, spinel, polystyrene, and polypropylene? Justify your selections.

19.14 Briefly explain how reflection losses of transparent materials are minimized by thin surface coatings.

19.15 Briefly describe the three absorption mechanisms in nonmetallic materials.

19.16 Will the elemental semiconductors silicon and germanium be transparent to visible light? Why or why not? Their band gap energies are given in Table 12.2.

19.17 Zinc telluride has a band gap of 2.26 eV. Over what range of wavelengths of visible light is it transparent?

19.18 Briefly explain why the magnitude of the absorption coefficient (β in Equation 19.18) depends on the radiation wavelength.

19.19 The fraction of nonreflected radiation that is transmitted through a 10-mm thickness of a transparent material is 0.90. If the thickness is increased to 20 mm, what fraction of light will be transmitted?

19.20 Derive Equation 19.19, starting from other expressions given in the chapter.

19.21 The transmissivity T of a transparent material 20 mm thick to normally incident light is 0.85. If the index of refraction of this material is 1.6, compute the thickness of material that will yield a transmissivity of 0.75. All reflection losses should be considered.

19.22 Briefly explain what determines the characteristic color of **(a)** a metal and **(b)** a transparent nonmetal.

19.23 Briefly explain why some transparent materials appear colored while others are colorless.

19.24 The index of refraction of quartz is anisotropic. Suppose that visible light is passing from one grain to another of different crystallographic orientation and at normal incidence to the grain boundary. Calculate the reflectivity at the boundary if the indices of refraction for the two grains are 1.544 and 1.553.

19.25 Briefly explain why amorphous polymers are transparent, while predominantly crystalline polymers appear opaque or, at best, translucent.

19.26 **(a)** In your own words describe briefly the phenomenon of luminescence.
(b) What is the distinction between fluorescence and phosphorescence?

19.27 **(a)** In your own words, briefly describe the phenomenon of photoconductivity. **(b)** Would the semiconductor zinc selenide, which has a band gap of 2.58 eV, be photoconductive when exposed to visible light radiation? Why or why not?

19.28 Briefly explain the operation of a photographic lightmeter.

19.29 In your own words, describe how a ruby laser operates.

19.30 Compute the difference in energy between metastable and ground electron states for the ruby laser.

Design Problem

19.D1 Gallium arsenide (GaAs) and gallium phosphide (GaP) are compound semiconductors that have room-temperature band gap energies of 1.42 and 2.25 eV, respectively, and form solid solutions in all proportions. Furthermore, the band gap of the alloy increases approximately linearly with GaP additions (in mol%). Alloys of these two materials are used for light-emitting diodes wherein light is generated by conduction band-to-valence band electron transitions. Determine the composition of a GaAs-GaP alloy that will emit orange light having a wavelength of 0.60 μm.

FIGURE 19.1
An electromagnetic wave showing electric field $\mathscr{E}$ and magnetic field H components, and the wavelength λ.

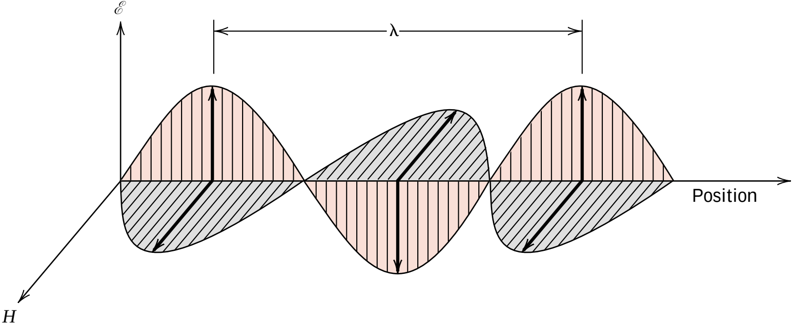
$\mathscr{E}$
λ
Position
H

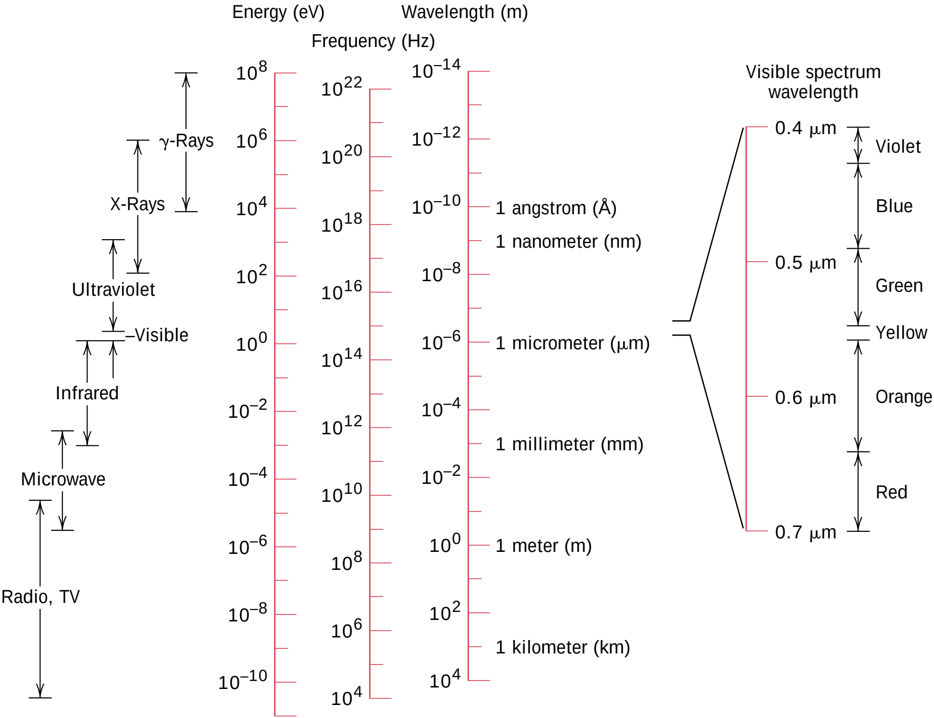

Energy (eV)
Wavelength (m)
Frequency (Hz)
γ-Rays
X-Rays
Ultraviolet
–Visible
Infrared
Microwave
Radio, TV
10^8
10^6
10^4
10^2
10^0
10^–2
10^–4
10^–6
10^–8
10^–10
10^22
10^20
10^18
10^16
10^14
10^12
10^10
10^8
10^6
10^4
10^–14
10^–12
10^–10
1 angstrom (Å)
1 nanometer (nm)
10^–8
10^–6
1 micrometer (μm)
10^–4
1 millimeter (mm)
10^–2
10^0
1 meter (m)
10^2
1 kilometer (km)
10^4
Visible spectrum wavelength
0.4 μm
0.5 μm
0.6 μm
0.7 μm
Violet
Blue
Green
Yellow
Orange
Red

Figure 19.2 The spectrum of electromagnetic radiation, including wavelength ranges for the various colors in the visible spectrum.

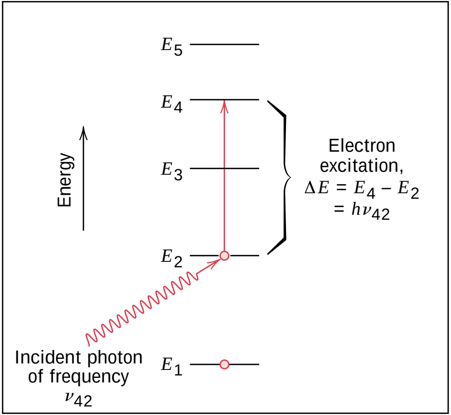

E_5
E_4
E_3
E_2
E_1
Energy
Electron excitation,
$\Delta E = E_4 - E_2$
$= h\nu_{42}$
Incident photon of frequency ν_{42}

Figure 19.3 For an isolated atom, a schematic illustration of photon absorption by the excitation of an electron from one energy state to another. The energy of the photon ($h\nu_{42}$) must be exactly equal to the difference in energy between the two states ($E_4 - E_2$).

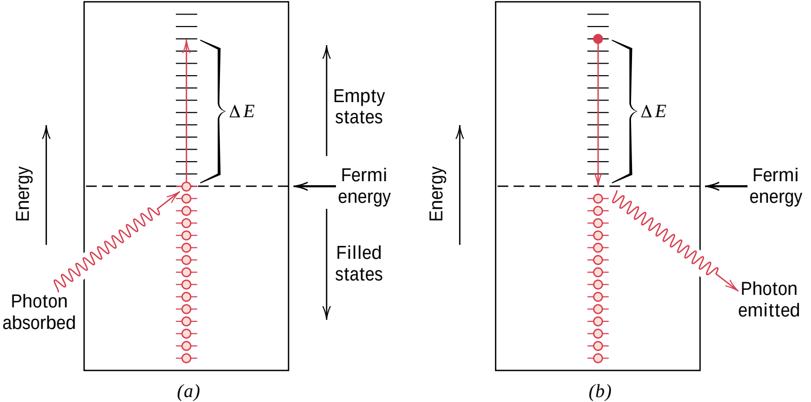
Energy
ΔE
Empty states
Fermi energy
Filled states
Photon absorbed
(a)
Energy
ΔE
Fermi energy
Photon emitted
(b)

FIGURE 19.4 (*a*) Schematic representation of the mechanism of photon absorption for metallic materials in which an electron is excited into a higher-energy unoccupied state. The change in energy of the electron ΔE is equal to the energy of the photon. (*b*) Reemission of a photon of light by the direct transition of an electron from a high to a low energy state.

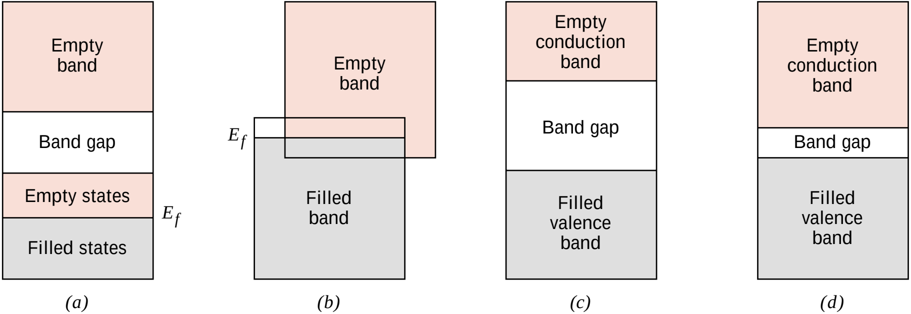
Empty band
Band gap
Empty states
Filled states
E_f
Empty band
E_f
Filled band
Empty conduction band
Band gap
Filled valence band
Empty conduction band
Band gap
Filled valence band
(a)
(b)
(c)
(d)

FIGURE 12.4 The various possible electron band structures in solids at 0 K. (*a*) The electron band structure found in metals such as copper, in which there are available electron states above and adjacent to filled states, in the same band. (*b*) The electron band structure of metals such as magnesium, wherein there is an overlap of filled and empty outer bands. (*c*) The electron band structure characteristic of insulators; the filled valence band is separated from the empty conduction band by a relatively large band gap ($>$2 eV). (*d*) The electron band structure found in the semiconductors, which is the same as for insulators except that the band gap is relatively narrow ($<$2 eV).

Table 19.1 Refractive Indices for Some Transparent Materials

Material	*Average Index of Refraction*
Ceramics	
Silica glass	1.458
Borosilicate (Pyrex) glass	1.47
Soda–lime glass	1.51
Quartz (SiO_2)	1.55
Dense optical flint glass	1.65
Spinel ($MgAl_2O_4$)	1.72
Periclase (MgO)	1.74
Corundum (Al_2O_3)	1.76
Polymers	
Polytetrafluoroethylene	1.35
Polymethyl methacrylate	1.49
Polypropylene	1.49
Polyethylene	1.51
Polystyrene	1.60

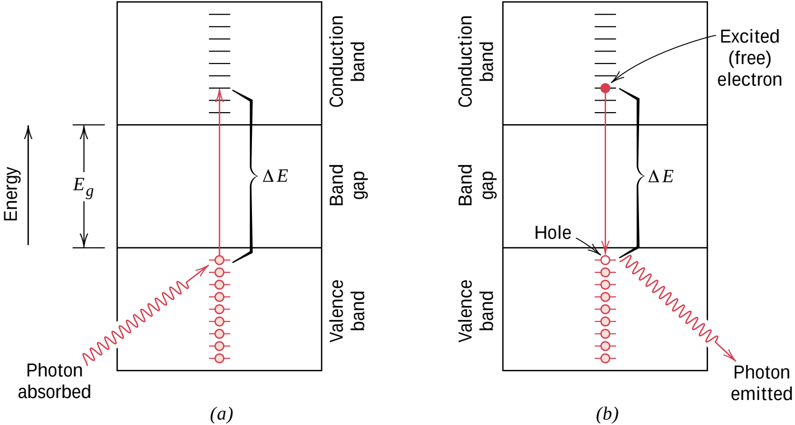
Energy
E_g
ΔE
Conduction band
Band gap
Valence band
Photon absorbed
(a)
Excited (free) electron
ΔE
Hole
Conduction band
Band gap
Valence band
Photon emitted
(b)

Figure 19.5 (*a*) Mechanism of photon absorption for nonmetallic materials in which an electron is excited across the band gap, leaving behind a hole in the valence band. The energy of the photon absorbed is ΔE, which is necessarily greater than the band gap energy E_g. (*b*) Emission of a photon of light by a direct electron transition across the band gap.

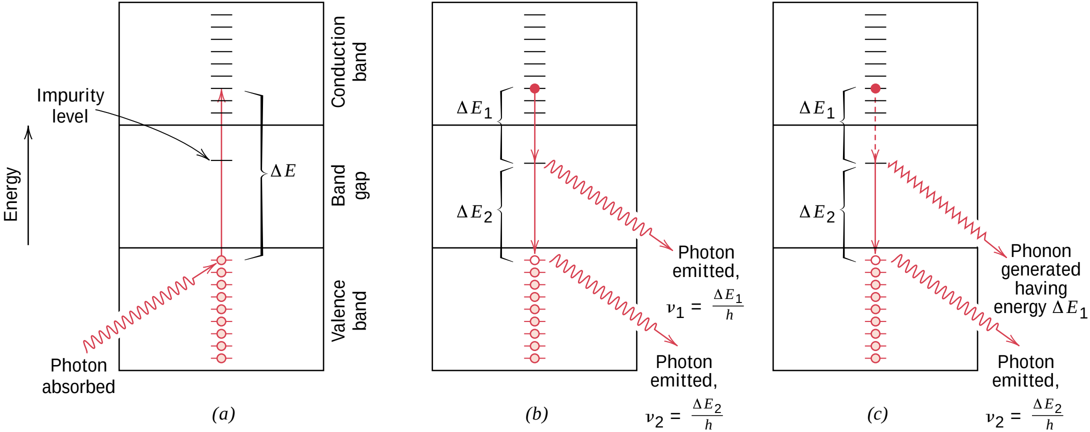
Energy
Impurity level
Conduction band
Band gap
Valence band
ΔE
Photon absorbed
(a)
ΔE_1
ΔE_2
Photon emitted, $\nu_1 = \frac{\Delta E_1}{h}$
Photon emitted, $\nu_2 = \frac{\Delta E_2}{h}$
(b)
ΔE_1
ΔE_2
Phonon generated having energy ΔE_1
Photon emitted, $\nu_2 = \frac{\Delta E_2}{h}$
(c)

FIGURE 19.6 (*a*) Photon absorption via a valence band-conduction band electron excitation for a material that has an impurity level that lies within the band gap. (*b*) Emission of two photons involving electron decay first into an impurity state, and finally into the ground state. (*c*) Generation of both a phonon and a photon as an excited electron falls first into an impurity level and finally back to its ground state.

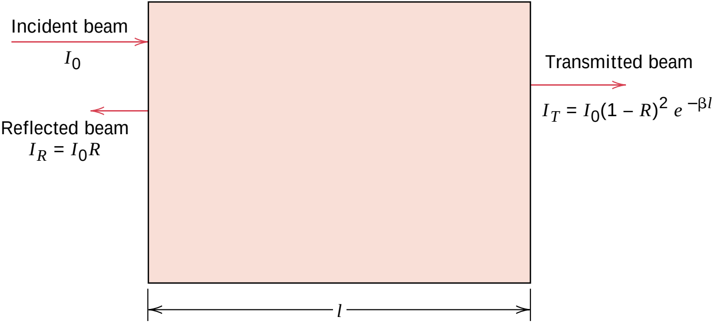
Incident beam
I_0
Reflected beam
$I_R = I_0 R$
Transmitted beam
$I_T = I_0(1 - R)^2 e^{-\beta l}$
l

FIGURE 19.7 The transmission of light through a transparent medium for which there is reflection at front and back faces, as well as absorption within the medium. (Adapted from R. M. Rose, L. A. Shepard, and J. Wulff, *The Structure and Properties of Materials*, Vol. 4, *Electronic Properties*. Copyright © 1966 by John Wiley & Sons, New York. Reprinted by permission of John Wiley & Sons, Inc.)

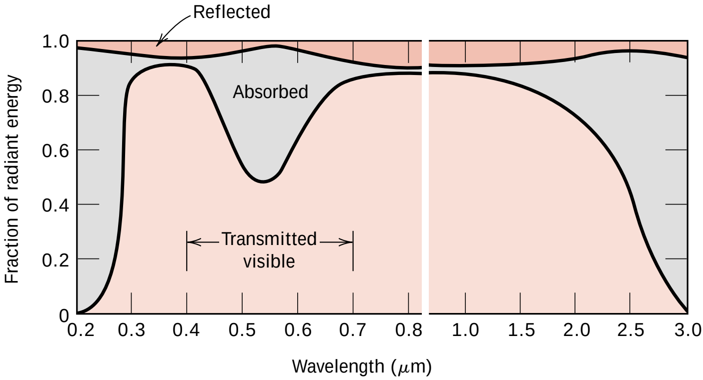

FIGURE 19.8 The variation with wavelength of the fractions of incident light transmitted, absorbed, and reflected through a green glass. (From W. D. Kingery, H. K. Bowen, and D. R. Uhlmann, *Introduction to Ceramics*, 2nd edition. Copyright © 1976 by John Wiley & Sons, New York. Reprinted by permission of John Wiley & Sons, Inc.)

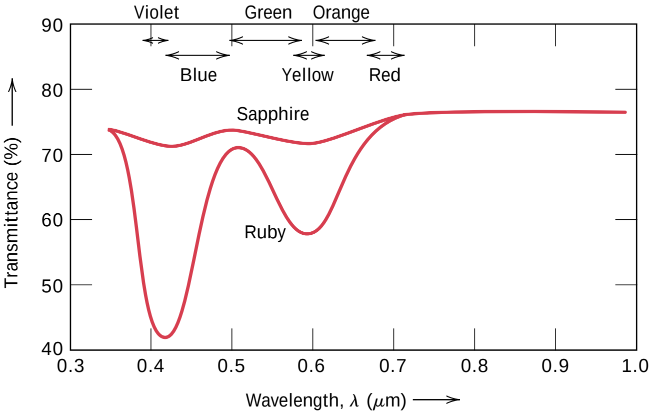

Figure 19.9 Transmission of light radiation as a function of wavelength for sapphire (single-crystal aluminum oxide) and ruby (aluminum oxide containing some chromium oxide). The sapphire appears colorless, while the ruby has a red tint due to selective absorption over specific wavelength ranges. (Adapted from ''The Optical Properties of Materials,'' by A. Javan. Copyright © 1967 by Scientific American, Inc. All rights reserved.)

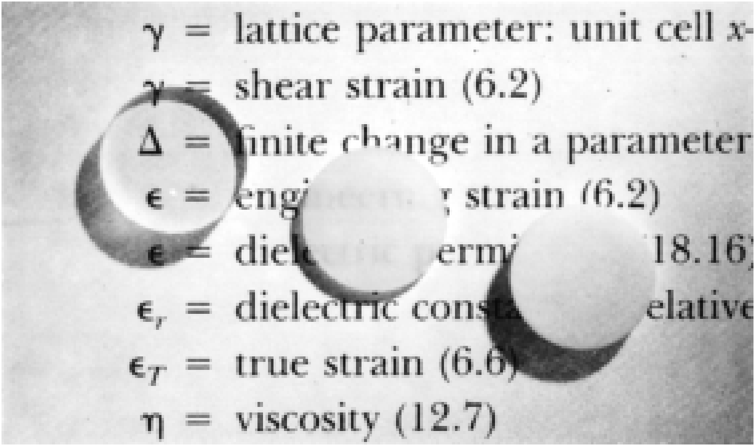

FIGURE 19.10 Photograph showing the light transmittance of three aluminum oxide specimens. From left to right: single-crystal material (sapphire), which is transparent; a polycrystalline and fully dense (nonporous) material, which is translucent; and a polycrystalline material that contains approximately 5% porosity, which is opaque. (Specimen preparation, P. A. Lessing; photography by J. Telford.)

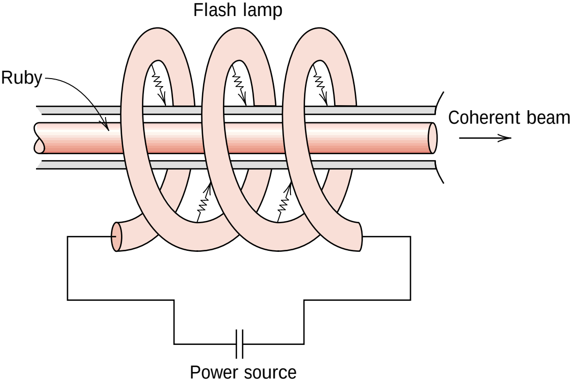
Flash lamp
Ruby
Coherent beam
Power source

FIGURE 19.11 Schematic diagram of the ruby laser and xenon flash lamp. (From R. M. Rose, L. A. Shepard, and J. Wulff, *The Structure and Properties of Materials,* Vol. 4, *Electronic Properties.* Copyright © 1966 by John Wiley & Sons, New York. Reprinted by permission of John Wiley & Sons, Inc.)

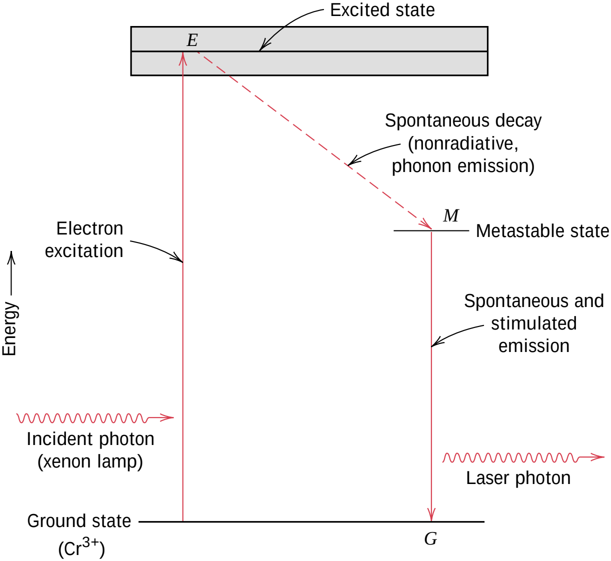
Excited state
E
Spontaneous decay (nonradiative, phonon emission)
M
Metastable state
Electron excitation
Energy
Spontaneous and stimulated emission
Incident photon (xenon lamp)
Laser photon
Ground state (Cr^{3+})
G

FIGURE 19.12 Schematic energy diagram for the ruby laser, showing electron excitation and decay paths.

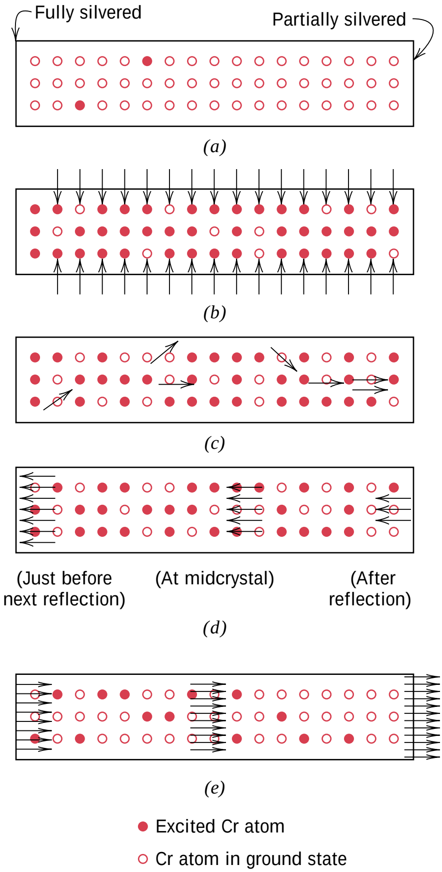
Fully silvered
Partially silvered
(a)
(b)
(c)
(Just before next reflection)
(At midcrystal)
(After reflection)
(d)
(e)
● Excited Cr atom
○ Cr atom in ground state

FIGURE 19.13 Schematic representations of the stimulated emission and light amplification for a ruby laser. (*a*) The chromium ions before excitation. (*b*) Electrons in some chromium atoms are excited into higher energy states by the xenon light flash. (*c*) Emission from metastable electron states is initiated or stimulated by photons that are spontaneously emitted. (*d*) Upon reflection from the silvered ends, the photons continue to stimulate emissions as they traverse the rod length. (*e*) The coherent and intense beam is finally emitted through the partially silvered end. (From R. M. Rose, L. A. Shepard, and J. Wulff, *The Structure and Properties of Materials*, Vol. 4, *Electronic Properties.* Copyright © 1966 by John Wiley & Sons, New York. Reprinted by permission of John Wiley & Sons, Inc.)

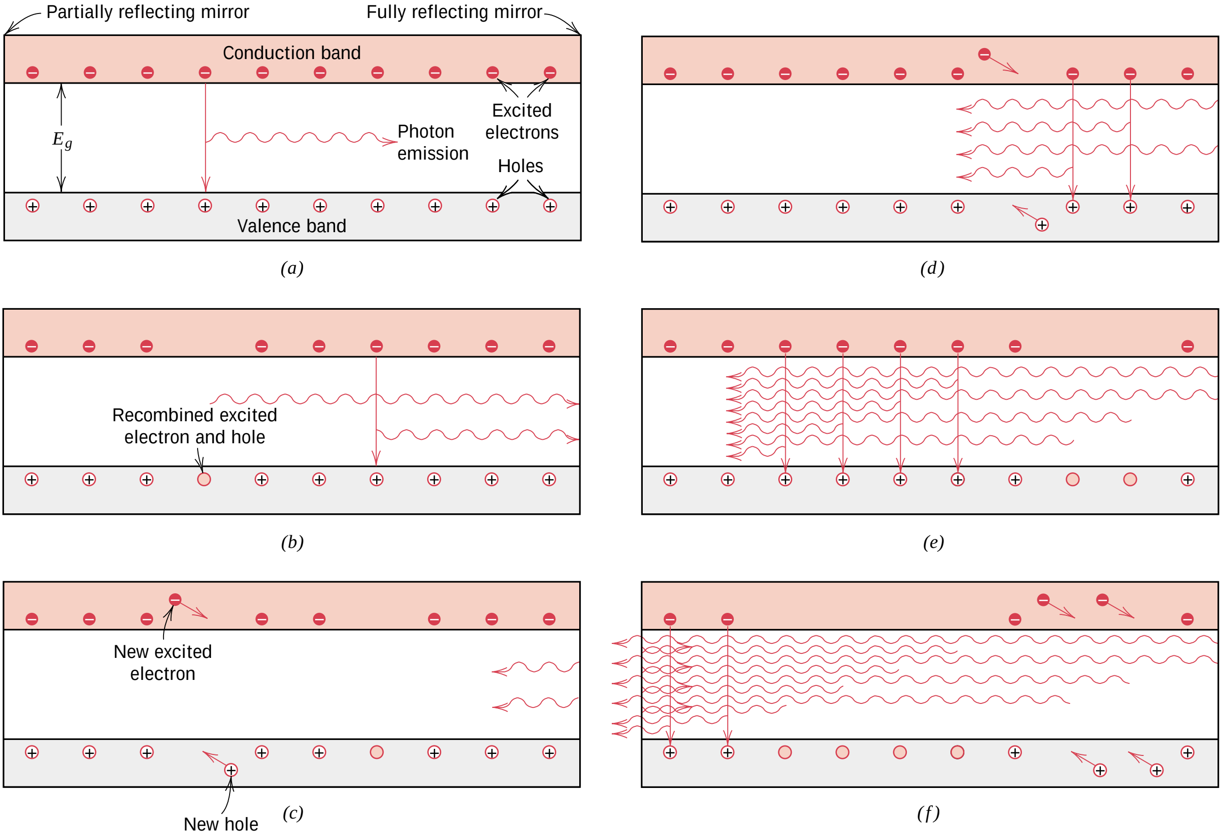
Partially reflecting mirror
Fully reflecting mirror
Conduction band
E_g
Photon emission
Excited electrons
Holes
Valence band
(a)
(d)
Recombined excited electron and hole
(b)
(e)
New excited electron
New hole
(c)
(f)

FIGURE 19.14 For the semiconductor laser, schematic representations of the stimulated recombination of excited electrons in the conduction band with holes in the valence band that gives rise to a laser beam. (*a*) One excited electron recombines with a hole; the energy associated with this recombination is emitted as a photon of light. (*b*) The photon emitted in (*a*) stimulates the recombination of another excited electron and hole resulting in the emission of another photon of light. (*c*) The two photons emitted in (*a*) and (*b*), having the same wavelength and being in phase with one another, are reflected by the fully reflecting mirror, back into the laser semiconductor. In addition, new excited electrons and new holes are generated by a current that passes through the semiconductor. (*d*) and (*e*) In proceeding through the semiconductor, more excited electron-hole recombinations are stimulated, which give rise to additional photons of light that also become part of the monochromatic and coherent laser beam. (*f*) Some portion of this laser beam escapes through the partially reflecting mirror at one end of the semiconducting material. (Adapted from ''Photonic Materials,'' by J. M. Rowell. Copyright © 1986 by Scientific American, Inc. All rights reserved.)

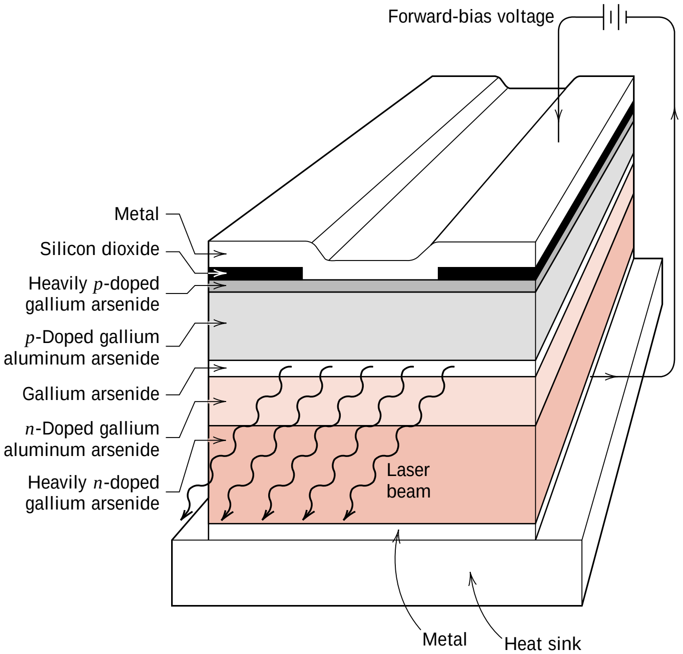
Forward-bias voltage
Metal
Silicon dioxide
Heavily *p*-doped gallium arsenide
p-Doped gallium aluminum arsenide
Gallium arsenide
n-Doped gallium aluminum arsenide
Heavily *n*-doped gallium arsenide
Laser beam
Metal
Heat sink

FIGURE 19.15 Schematic diagram showing the layered cross section of a GaAs semiconducting laser. Holes, excited electrons, and the laser beam are confined to the GaAs layer by the adjacent *n*- and *p*-type GaAlAs layers. (Adapted from "Photonic Materials," by J. M. Rowell. Copyright © 1986 by Scientific American, Inc. All rights reserved.)

Table 19.2 Characteristics and Applications of Several Types of Lasers

Laser	*Type*	*Common Wavelengths* (μ*m*)	*Max. Output Power* (*W*)[a]	*Applications*
He-Ne	Gas	0.6328, 1.15, 3.39	0.0005–0.05 (CW)	Line-of sight communications, recording/ playback of holograms
CO_2	Gas	9.6, 10.6	500–15,000 (CW)	Heat treating, welding, cutting, scribing, marking
Argon	Gas ion	0.488, 0.5145	0.005–20 (CW)	Surgery, distance measurements, holography
HeCd	Metal vapor	0.441, 0.325	0.05–0.1	Light shows, spectroscopy
Dye	Liquid	0.38–1.0	0.01 (CW) 1×10^6 (P)	Spectroscopy, pollution detection
Ruby	Solid state	0.694	(P)	Pulsed holography, hole piercing
Nd-YAG	Solid state	1.06	1000 (CW) 2×10^8 (P)	Welding, hole piercing, cutting
Nd-Glass	Solid state	1.06	5×10^{14} (P)	Pulse welding, hole piercing
Diode	Semiconductor	0.33–40	0.6 (CW) 100 (P)	Bar-code reading, CDs and video disks, optical communications

[a] "CW" denotes continuous; "P" denotes pulsed.

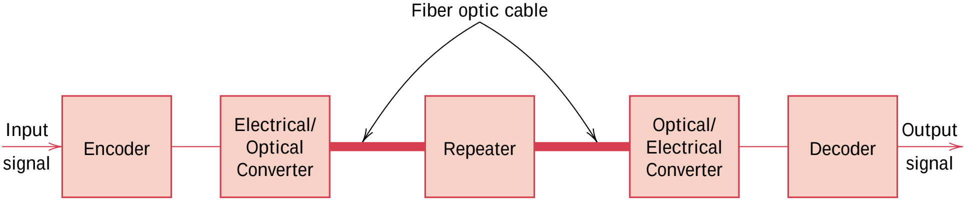
Fiber optic cable
Input signal
Encoder
Electrical/ Optical Converter
Repeater
Optical/ Electrical Converter
Decoder
Output signal

Figure 19.16 Schematic diagram showing the components of an optical fiber communications system.

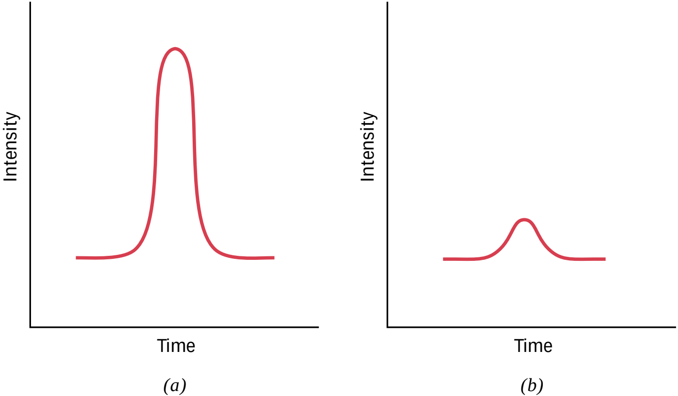

(a) *(b)*

Figure 19.17 Digital encoding scheme for optical communications. (*a*) A high-power pulse of photons corresponds to a ‘‘one’’ in the binary format. (*b*) A low-power photon pulse represents a ‘‘zero.’’

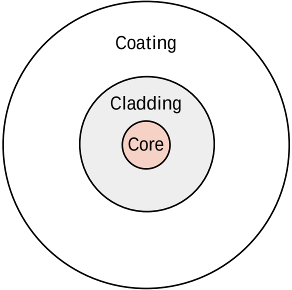
Coating
Cladding
Core

Figure 19.18 Schematic cross section of an optical fiber.

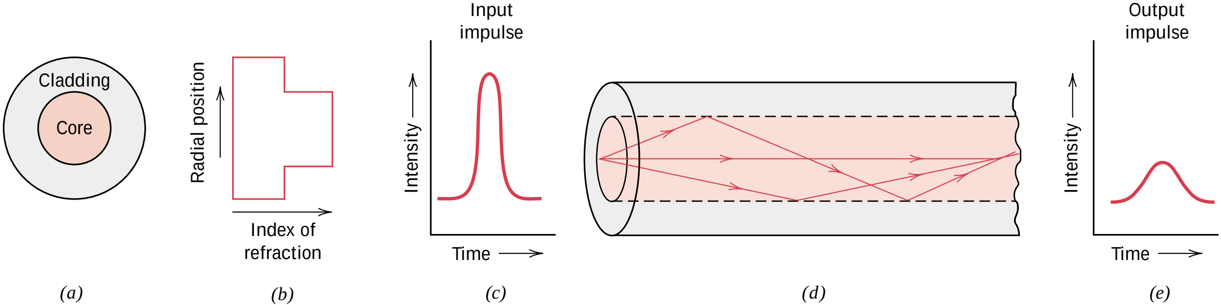
Cladding
Core
Radial position
Index of refraction
Input impulse
Intensity
Time
Output impulse
Intensity
Time
(a)
(b)
(c)
(d)
(e)

FIGURE 19.19 Step-index optical fiber design. (*a*) Fiber cross section. (*b*) Fiber radial index of refraction profile. (*c*) Input light pulse. (*d*) Internal reflection of light rays. (*e*) Output light pulse. (Adapted from S. R. Nagel, *IEEE Communications Magazine*, Vol. 25, No. 4, p. 34, 1987.)

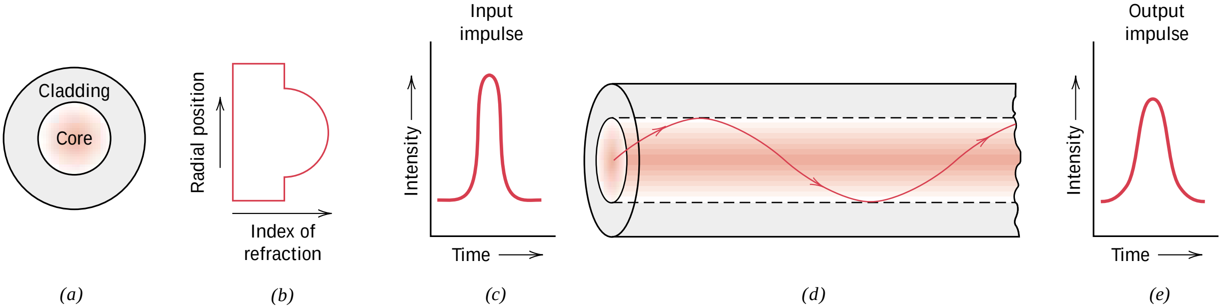
Cladding
Core
Radial position
Index of refraction
Input impulse
Intensity
Time
Output impulse
Intensity
Time
(a)
(b)
(c)
(d)
(e)

Figure 19.20 Graded-index optical fiber design. (*a*) Fiber cross section. (*b*) Fiber radial index of refraction profile. (*c*) Input light pulse. (*d*) Internal reflection of a light ray. (*e*) Output light pulse. (Adapted from S. R. Nagel, *IEEE Communications Magazine*, Vol. 25, No. 4, p. 34, 1987.)

CHAPTER 20

MATERIALS SELECTION AND DESIGN CONSIDERATIONS

20.D3 (a) This portion of the problem asks that we derive a performance index expression for strength analogous to Equation (20.9) for a cylindrical cantilever beam that is stressed in the manner shown in the accompanying figure. The stress on the unfixed end, σ, for an imposed force, **F**, is given by the expression [Equation (20.24) in the textbook]

$$\sigma = \frac{FLr}{I} \tag{20.D1}$$

where **L** and **r** are the rod length and radius, respectively, and **I** is the moment of inertia; for a cylinder the expression for **I** is provided in Figure 7.18:

$$I = \frac{\pi r^4}{4} \tag{20.D2}$$

Substitution for **I** into Equation (20.D1) leads to

$$\sigma = \frac{4FL}{\pi r^3} \tag{20.D3}$$

Now, the mass **m** of some given quantity of material is the product of its density (ρ) and volume. Inasmuch as the volume of a cylinder is just $\pi \mathbf{r}^2 \mathbf{L}$, then

$$m = \pi r^2 L \rho \tag{20.D4}$$

From this expression, the radius is just

$$r = \sqrt{\frac{m}{\pi L \rho}} \tag{20.D5}$$

Inclusion of Equation (20.D5) into Equation (20.D3) yields

$$\sigma = \frac{4F\pi^{1/2}L^{5/2}\rho^{3/2}}{m^{3/2}} \tag{20.D6}$$

And solving for the mass gives

$$m = (16\pi F^2 L^5)^{1/3} \frac{\rho}{\sigma^{2/3}} \tag{20.D7}$$

To ensure that the beam will not fail, we replace stress in Equation (20.D7) with the yield strength ($\sigma_\mathbf{y}$) divided by a factor of safety (**N**) as

$$m = (16\pi F^2 L^5 N^2)^{1/3} \frac{\rho}{\sigma_y^{2/3}} \tag{20.D8}$$

Thus, the best materials to be used for this cylindrical cantilever beam when strength is a consideration are those having low $\frac{\rho}{\sigma_y^{2/3}}$ ratios. Furthermore, the strength performance index, **P**, is just the reciprocal of this ratio, or

$$P = \frac{\sigma_y^{2/3}}{\rho} \tag{20.D9}$$

The second portion of the problem asks for an expression for the stiffness performance index. Let us begin by consideration of Equation (20.25) which relates δ, the elastic deflection at the unfixed end, to the force (**F**), beam length (**L**), the modulus of elasticity (**E**), and moment of inertia (**I**) as

$$\delta = \frac{FL^3}{3EI} \tag{20.25}$$

Again, Equation (20.D2) gives an expression for **I** for a cylinder, which when substituted into Equation (20.25) yields

$$\delta = \frac{4FL^3}{3\pi E r^4} \tag{20.D10}$$

And, substitution of the expression for **r** [Equation (20.D5)] into Equation (20.D10), leads to

$$\begin{aligned}\delta &= \frac{4FL^3}{3\pi E\left(\sqrt{\dfrac{m}{\pi L\rho}}\right)^4} \\ &= \frac{4FL^5\pi\rho^2}{3Em^2}\end{aligned} \tag{20.D11}$$

Now solving this expression for the mass **m** yields

$$m = \left(\frac{4FL^5\pi}{3\delta}\right)^{1/2}\frac{\rho}{\sqrt{E}} \tag{20.D12}$$

Or, for this cantilever situation, the mass of material experiencing a given deflection produced by a specific force is proportional to the $\frac{\rho}{\sqrt{\mathbf{E}}}$ ratio for that material. And, finally, the stiffness performance index, **P**, is just the reciprocal of this ratio, or

$$P = \frac{\sqrt{E}}{\rho} \tag{20.D13}$$

(b) Here we are asked to select those metal alloys in the database that have stiffness performance indices greater than 3.0 (in SI units). (**Note:** for this performance index of 3.0, density has been taken in terms of g/cm^3 rather than in the SI units of kg/m^3.) Seventeen metal alloys satisfy this criterion; they and their $\sqrt{\mathbf{E}}/\rho$ values are listed below, and ranked from highest to lowest value.

Alloy	Condition	$\frac{\sqrt{E}}{\rho}$
AZ31B Mg	Rolled	3.790
AZ31B Mg	Extruded	3.790
AZ91D Mg	As cast	3.706
356.0 Al	As cast, high production	3.163
356.0 Al	As cast, custom	3.163
356.0 Al	T6	3.163
6061 Al	O	3.077
6061 Al	T6	3.077
6061 Al	T651	3.077
2024 Al	O	3.072
2024 Al	T3	3.072
2024 Al	T351	3.072
1100 Al	O	3.065
1100 Al	H14	3.065
7075 Al	O	3.009
7075 Al	T6	3.009
7075 Al	T651	3.009

(c) We are now asked to do a cost analysis on the above alloys. Below are tabulated the $\rho/\sqrt{\mathbf{E}}$ ratio, the relative material cost ($\bar{\mathbf{c}}$), and the product of these two parameters; also those alloys for which cost data are provided are ranked, from least to most expensive.

Alloy	Condition	$\frac{\rho}{\sqrt{E}}$	$\bar{c}$	$\bar{c}\left(\frac{\rho}{\sqrt{E}}\right)$
AZ91D Mg	As cast	0.2640	5.4	1.43
6061 Al	T6	0.3250	7.6	2.47
356.0 Al	As cast, high production	0.3162	7.9	2.50
6061 Al	T651	0.3250	8.7	2.83
AZ31B Mg	Extruded	0.2640	12.6	3.33
1100 Al	O	0.3263	12.3	4.01
AZ31B Mg	Rolled	0.2640	15.7	4.14
7075 Al	T6	0.3323	13.4	4.45
2024 Al	T3	0.3255	14.1	4.59
356.0 Al	As cast, custom	0.3162	15.7	4.96
356.0 Al	T6	0.3162	16.6	5.25
2024 Al	T351	0.3255	16.2	5.27
1100 Al	H14	0.3263	–	–
2024 Al	O	0.3255	–	–
6061 Al	O	0.3250	–	–
7075 Al	O	0.3323	–	–
7075 Al	T651	0.3323	–	–

It is up to the student to select the best metal alloy to be used for this cantilever beam on a stiffness-per-mass basis, including the element of cost, and other relevant considerations.

20.D6 (a) This portion of the problem asks that we compute the maximum tensile load that may be applied to a spring constructed of a $\frac{1}{4}$ hard 304 stainless steel such that the total deflection is less than 5 mm; there are 10 coils in the spring, whereas, its center-to-center diameter is 15 mm, and the wire diameter is 2.0 mm. The total spring deflection δ_s may be determined by combining Equations (20.14) and (20.15); solving for the load **F** from the combined equation leads to

$$F = \frac{\delta_s d^4 G}{8 N_c D^3}$$

However, it becomes necessary to determine the value of the shear modulus **G**. This is possible using Equation (7.9) and values of the modulus of elasticity (193 GPa) and Poisson's ratio (0.30) as taken from Tables B.2 and B.3 in Appendix B. Thus

$$\begin{aligned} G &= \frac{E}{2(1+\nu)} \\ &= \frac{193 \text{ GPa}}{2(1+0.30)} = 74.2 \text{ GPa} \end{aligned}$$

Substitution of this value and values of the other parameters into the above equation for **F** leads to

$$\begin{aligned} F &= \frac{(5 \times 10^{-3} \text{ m})(2 \times 10^{-3} \text{ m})^4 (74.2 \times 10^9 \text{ N/m}^2)}{(8)(10 \text{ coils})(15 \times 10^{-3} \text{ m})^3} \\ &= 22.0 \text{ N } (5.1 \text{ lb}_f) \end{aligned}$$

(b) We are now asked to compute the maximum tensile load that may be applied without any permanent deformation of the spring wire. This requires that we combine Equations (20.12) and (20.13), and then solve for **F**. However, it is first necessary to calculate the shear yield strength and substitute it for τ in Equation (20.12). The problem statement stipulates that $\tau_y = 0.6\,\sigma_y$. From Table B.4 in Appendix B, we note that the tensile yield strength for this alloy in the 1/4 hardened state is 515 MPa; thus $\tau_y = 309$ MPa. Thus, solving for **F** as outlined above

$$\begin{aligned} F &= \frac{\pi \tau_y d^3}{(1.6)(8)(D)\left(\dfrac{D}{d}\right)^{-0.140}} \\ &= \frac{\pi (309 \times 10^6 \text{ N/m}^2)(2 \times 10^{-3} \text{ m})^3}{(1.6)(8)(15 \times 10^{-3} \text{ m})\left(\dfrac{15 \times 10^{-3} \text{ m}}{2 \times 10^{-3} \text{ m}}\right)^{-0.140}} \\ &= 53.6 \text{ N } (12.5 \text{ lb}_f) \end{aligned}$$

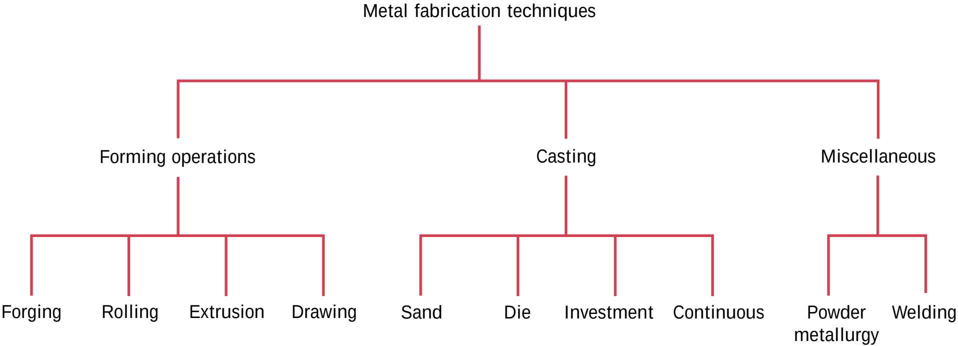
Metal fabrication techniques
Forming operations
Casting
Miscellaneous
Forging
Rolling
Extrusion
Drawing
Sand
Die
Investment
Continuous
Powder metallurgy
Welding

FIGURE 14.1 Classification scheme of metal fabrication techniques discussed in this chapter.

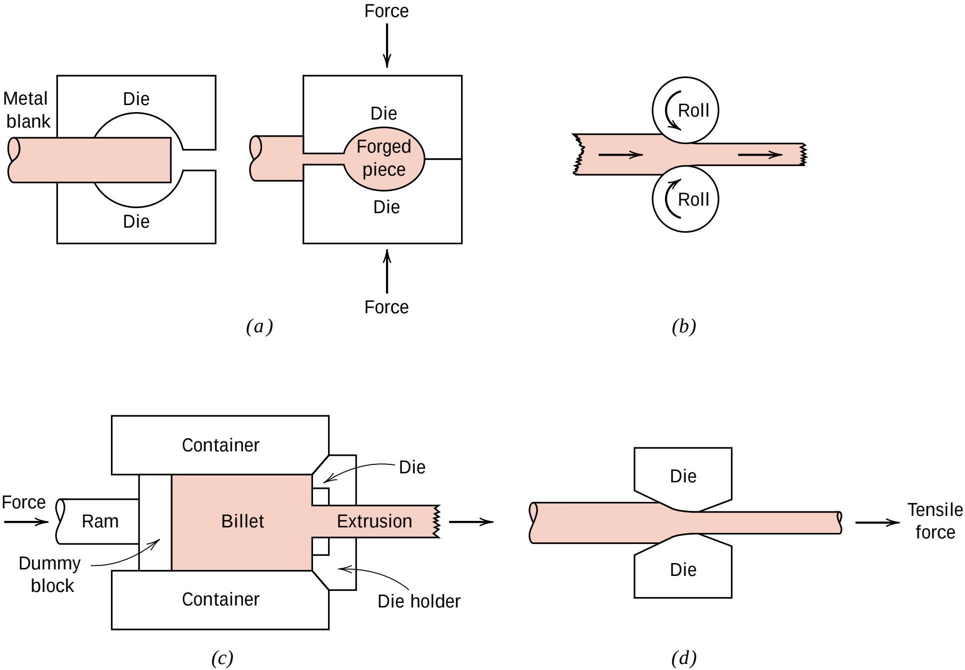
Force
Metal blank
Die
Die
Die
Forged piece
Die
Force
(a)
Roll
Roll
(b)
Container
Die
Force
Ram
Billet
Extrusion
Dummy block
Container
Die holder
(c)
Die
Die
Tensile force
(d)

Figure 14.2 Metal deformation during (*a*) forging, (*b*) rolling, (*c*) extrusion, and (*d*) drawing.

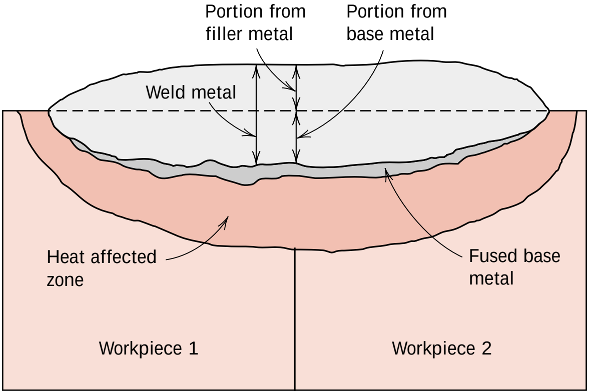
Portion from filler metal
Portion from base metal
Weld metal
Heat affected zone
Fused base metal
Workpiece 1
Workpiece 2

FIGURE 14.3 Schematic cross-sectional representation showing the zones in the vicinity of a typical fusion weld. (From *Iron Castings Handbook*, C. F. Walton and T. J. Opar, Editors, 1981.)

FIGURE 14.4 The iron–iron carbide phase diagram in the vicinity of the eutectoid, indicating heat treating temperature ranges for plain carbon steels. (Adapted from *Metals Handbook*, T. Lyman, Editor, American Society for Metals, 1948, p. 661.)

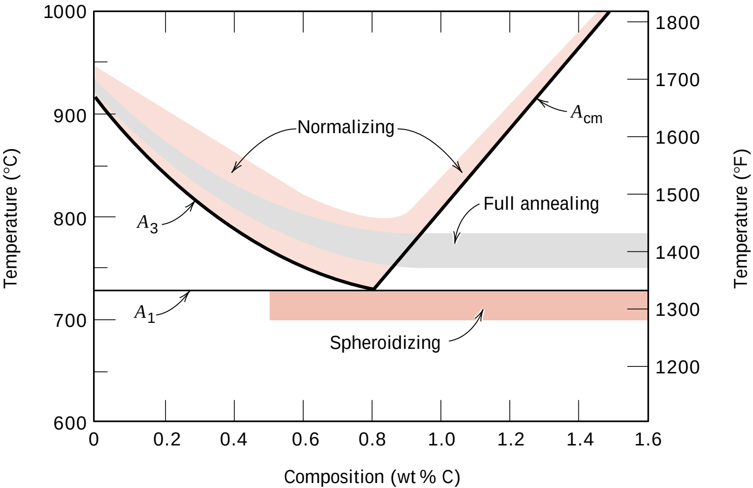

FIGURE 11.18 Moderately rapid and slow cooling curves superimposed on a continuous cooling transformation diagram for a eutectoid iron–carbon alloy.

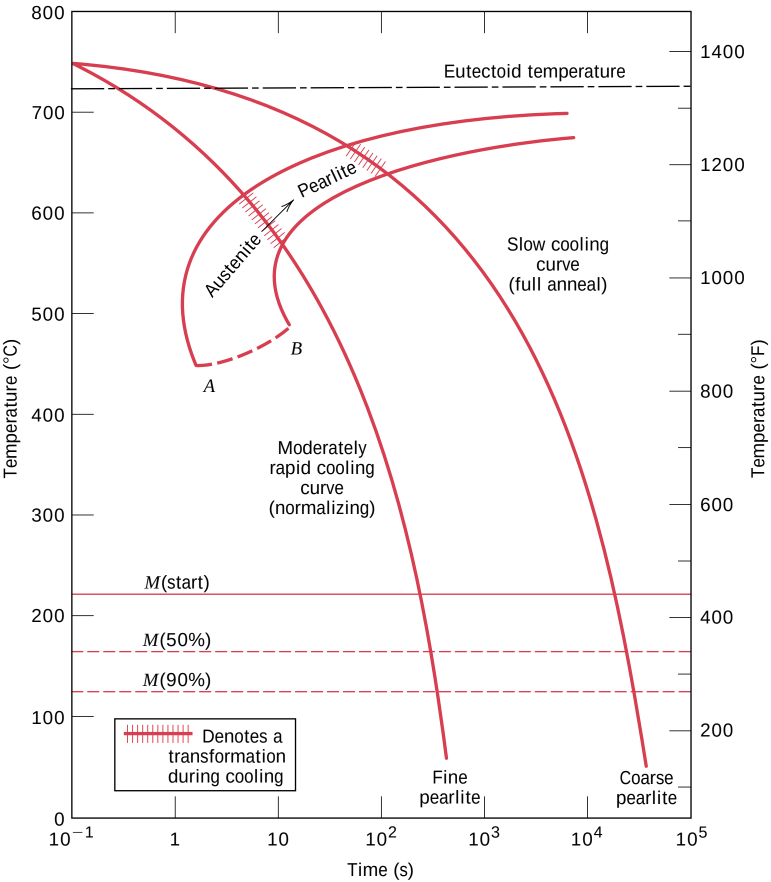

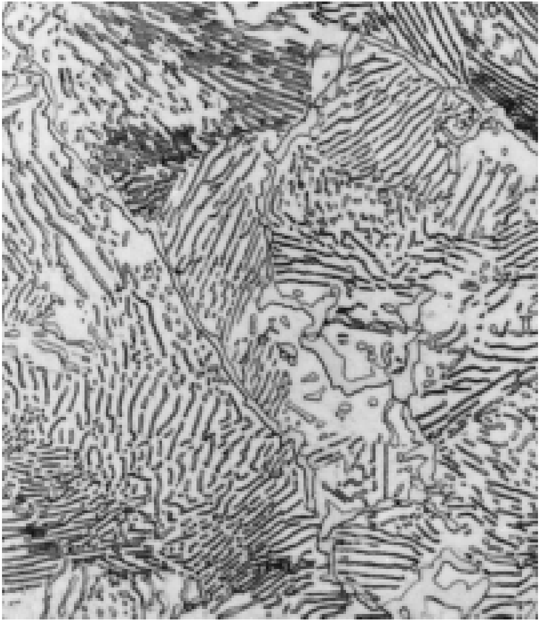

Figure 11.11 A photomicrograph of a pearlitic steel that has partially transformed to spheroidite. 1400×. (Courtesy of United States Steel Corporation.)

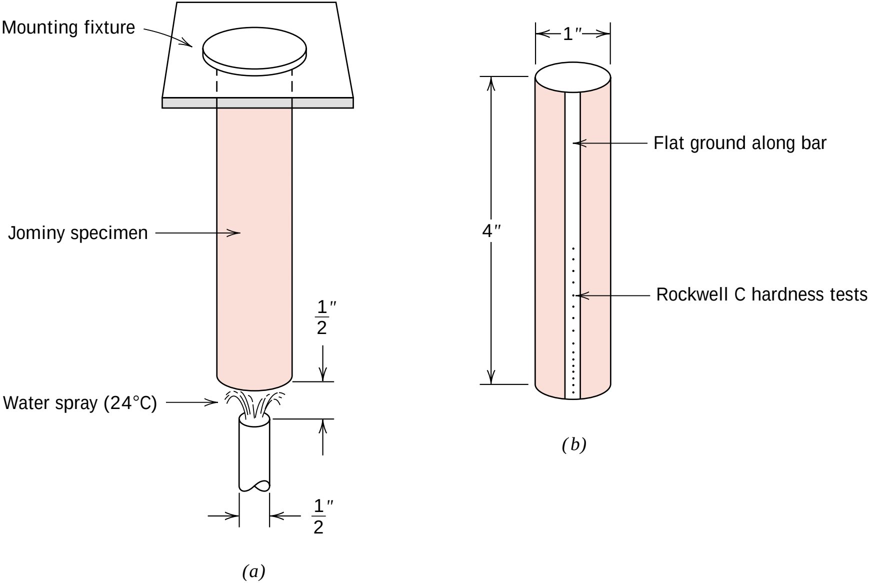
Mounting fixture
Jominy specimen
1″/2
Water spray (24°C)
1″/2
(a)
1″
4″
Flat ground along bar
Rockwell C hardness tests
(b)

FIGURE 14.5 Schematic diagram of Jominy end-quench specimen (*a*) mounted during quenching and (*b*) after hardness testing from the quenched end along a ground flat. (Adapted from A. G. Guy, *Essentials of Materials Science.* Copyright 1978 by McGraw-Hill Book Company, New York.)

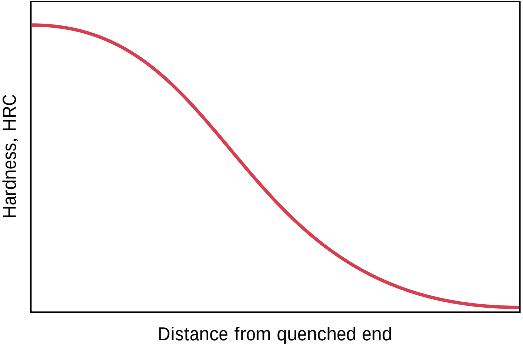

FIGURE 14.6 Typical hardenability plot of Rockwell C hardness as a function of distance from the quenched end.

FIGURE 14.7 Correlation of hardenability and continuous cooling information for an iron–carbon alloy of eutectoid composition. (Adapted from H. Boyer, Editor, *Atlas of Isothermal Transformation and Cooling Transformation Diagrams*, American Society for Metals, 1977, p. 376.)

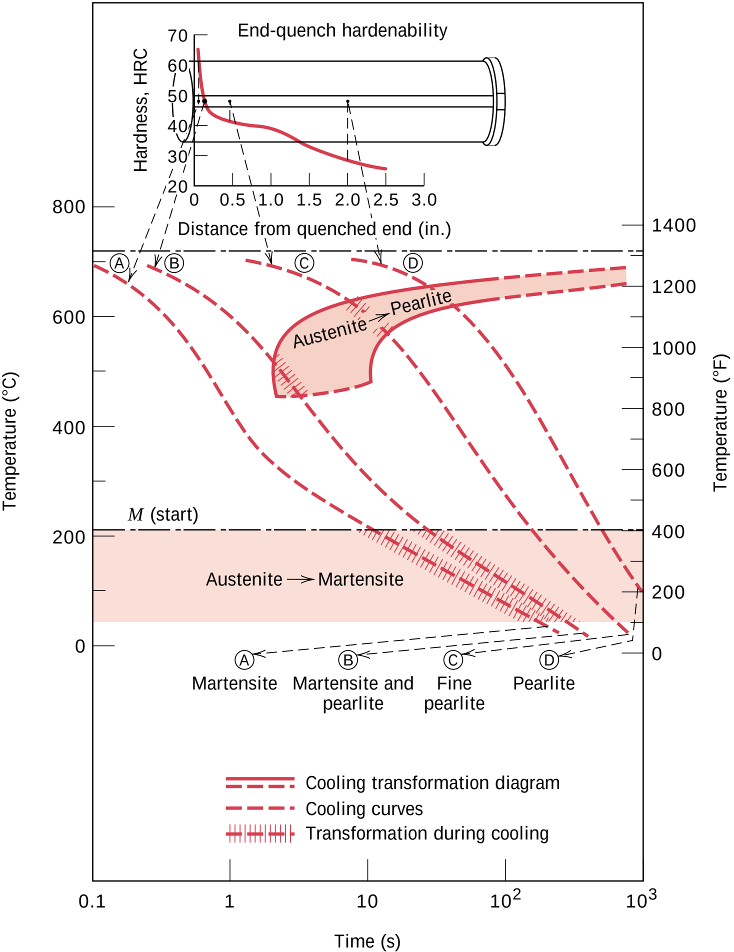

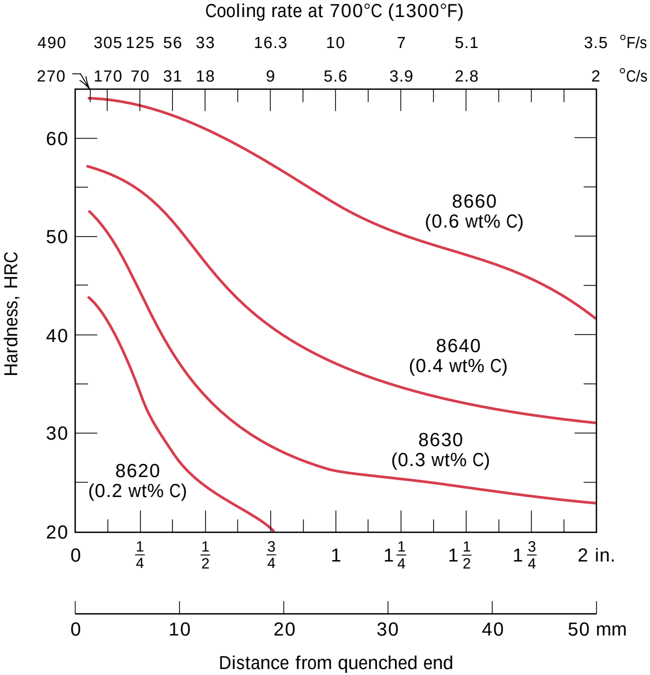

Figure 14.9 Hardenability curves for four 8600 series alloys of indicated carbon content. (Adapted from figure furnished courtesy Republic Steel Corporation.)

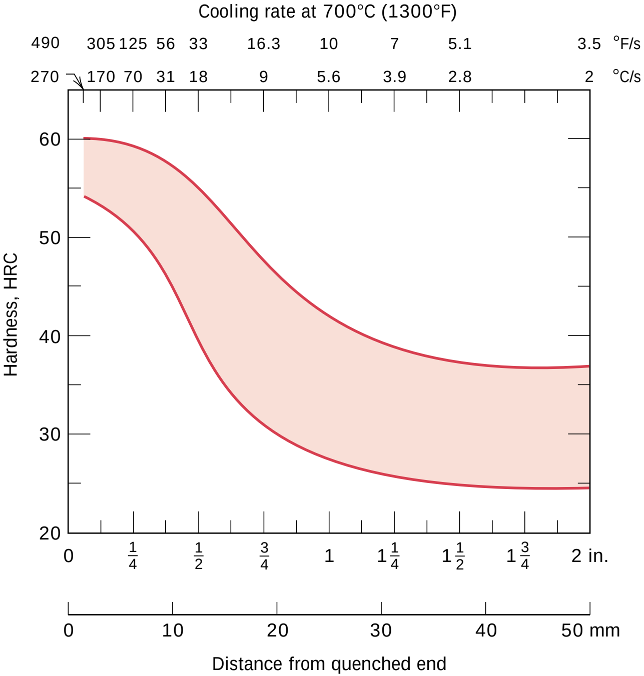

Figure 14.10 The hardenability band for an 8640 steel indicating maximum and minimum limits. (Adapted from figure furnished courtesy Republic Steel Corporation.)

FIGURE 14.12 Radial hardness profiles for (*a*) 50 mm (2 in.) diameter cylindrical 1040 and 4140 steel specimens quenched in mildly agitated water, and (*b*) 50 and 100 mm (2 and 4 in.) diameter cylindrical specimens of 4140 steel quenched in mildly agitated water.

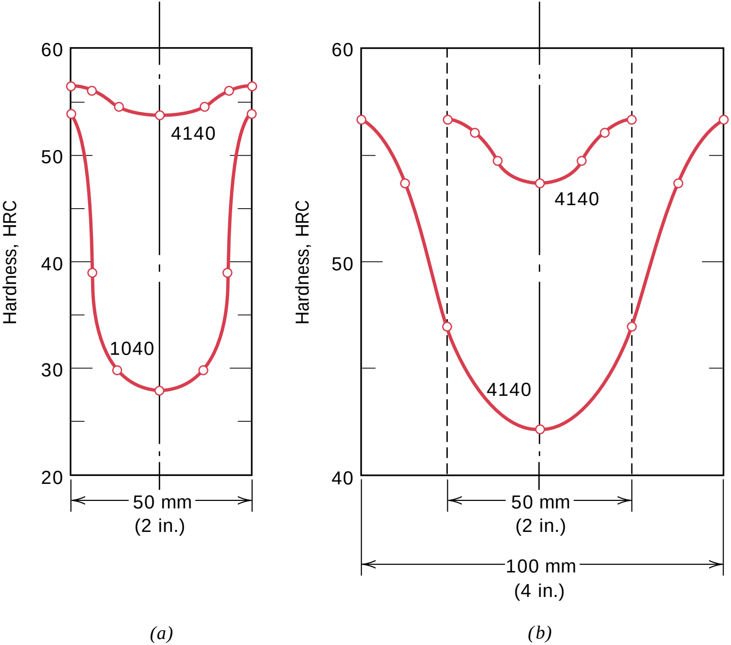

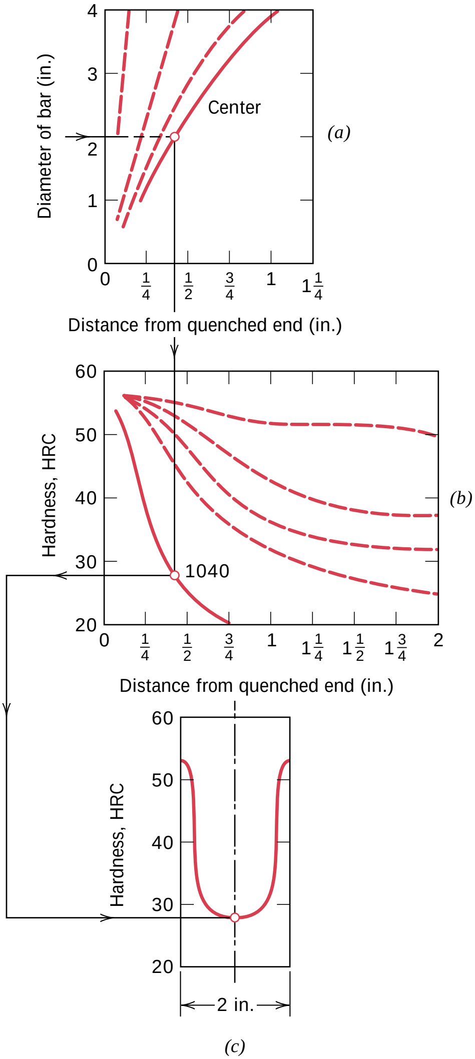

FIGURE 14.13 Use of hardenability data in the generation of hardness profiles. (*a*) The cooling rate at the center of a water-quenched 50 mm (2 in.) diameter specimen is determined. (*b*) The cooling rate is converted into an HRC hardness for a 1040 steel. (*c*) The Rockwell hardness is plotted on the radial hardness profile.

Table 14.1 Surface Hardnesses for Oil-Quenched Cylinders of 1060 Steel Having Various Diameters

Diameter (*in.*)	*Surface Hardness* (*HRC*)
0.5	59
1	34
2	30.5
4	29

Table 14.2 Rockwell C Hardness (Surface) and Percent Elongation Values for 1-in. Diameter Cylinders of Six Steel Alloys, in the As-Quenched Condition and for Various Tempering Heat Treatments

	As-Quenched	*Tempered at 540°C (1000°F)*		*Tempered at 595°C (1100°F)*		*Tempered at 650°C (1200°F)*	
Alloy Designation/ Quenching Medium	*Hardness (HRC)*	*Hardness (HRC)*	*Ductility (%EL)*	*Hardness (HRC)*	*Ductility (%EL)*	*Hardness (HRC)*	*Ductility (%EL)*
1040/oil	23	(12.5)[a]	26.5	(10)[a]	28.2	(5.5)[a]	30.0
1040/water	50	(17.5)[a]	23.2	(15)[a]	26.0	(12.5)[a]	27.7
4130/water	51	31	18.5	26.5	21.2	—	—
4140/oil	55	33	15.5	30	19.5	27.5	21.0
4150/oil	62	**38**	**14.0**	35.5	15.7	30	18.7
4340/oil	57	**38**	**14.2**	35.5	16.5	29	20.0
6150/oil	60	**38**	**14.5**	33	16.0	31	18.7

[a] These hardness values are only approximate because they are less than 20 HRC.

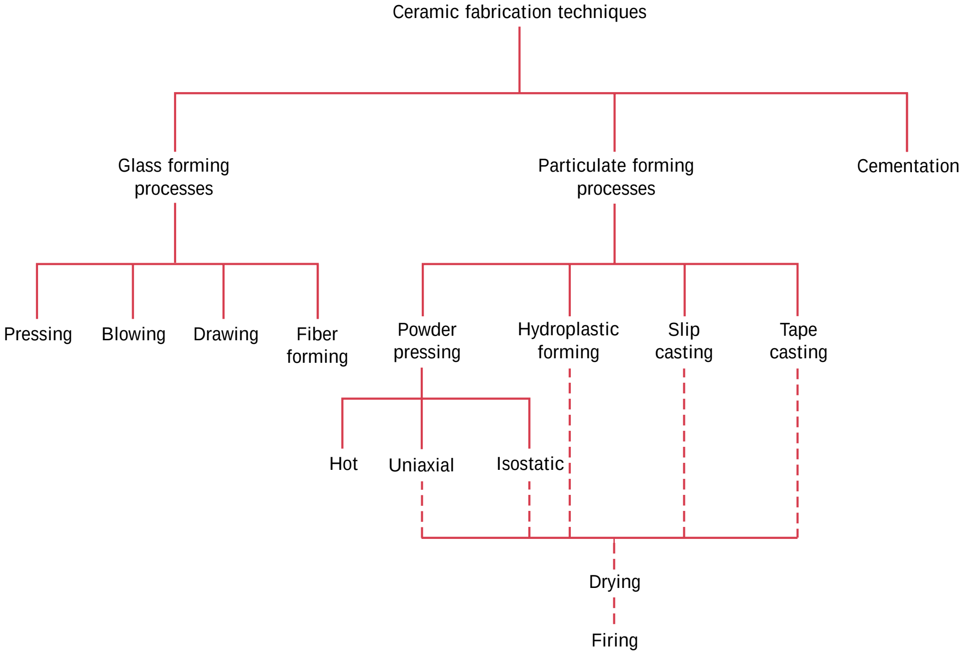
Ceramic fabrication techniques
Glass forming processes
Particulate forming processes
Cementation
Pressing
Blowing
Drawing
Fiber forming
Powder pressing
Hydroplastic forming
Slip casting
Tape casting
Hot
Uniaxial
Isostatic
Drying
Firing

FIGURE 14.14 A classification scheme for the ceramic-forming techniques discussed in this chapter.

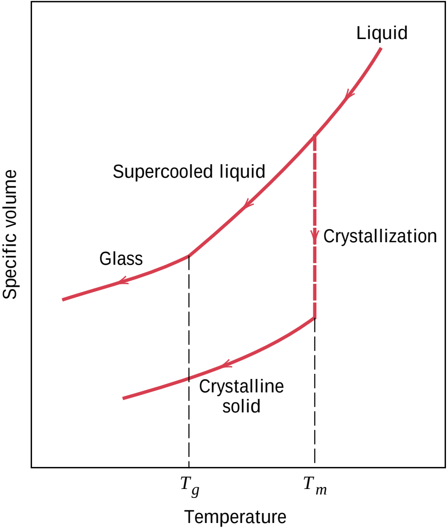

Figure 14.15 Contrast of specific volume-versus-temperature behavior of crystalline and noncrystalline materials. Crystalline materials solidify at the melting temperature T_m. Characteristic of the noncrystalline state is the glass transition temperature T_g.

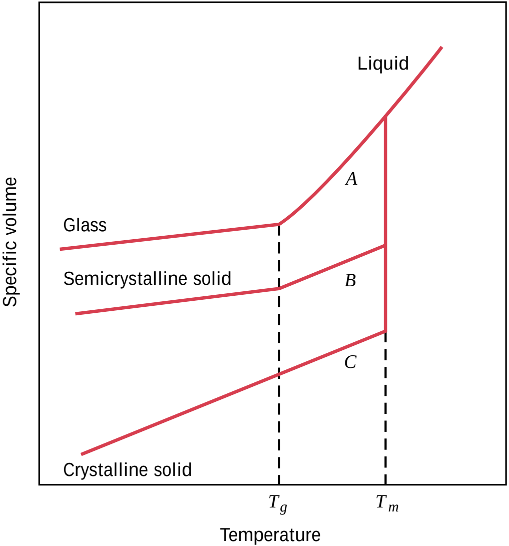

FIGURE 11.36 Specific volume versus temperature, upon cooling from the liquid melt, for totally amorphous (curve *A*), semicrystalline (curve *B*), and crystalline (curve *C*) polymers.

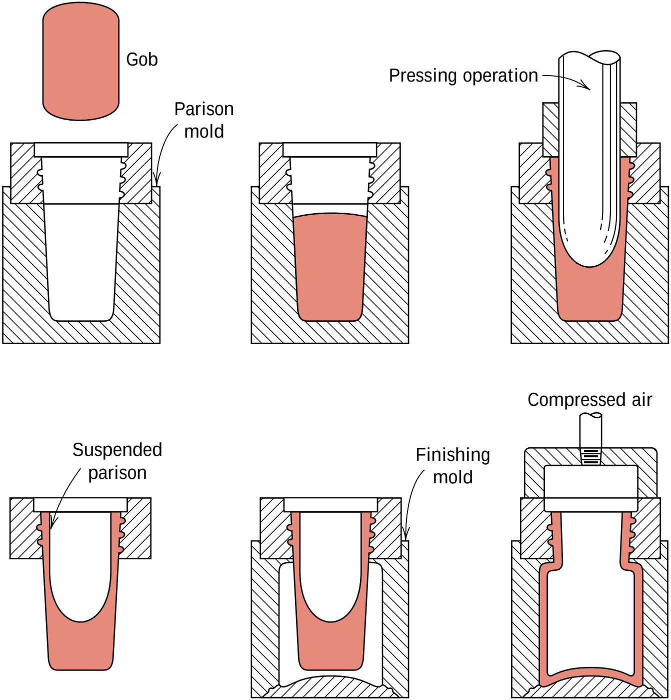
Gob
Parison mold
Pressing operation
Compressed air
Suspended parison
Finishing mold

Figure 14.17 The press-and-blow technique for producing a glass bottle. (Adapted from C. J. Phillips, *Glass: The Miracle Maker*. Reproduced by permission of Pitman Publishing Ltd., London.)

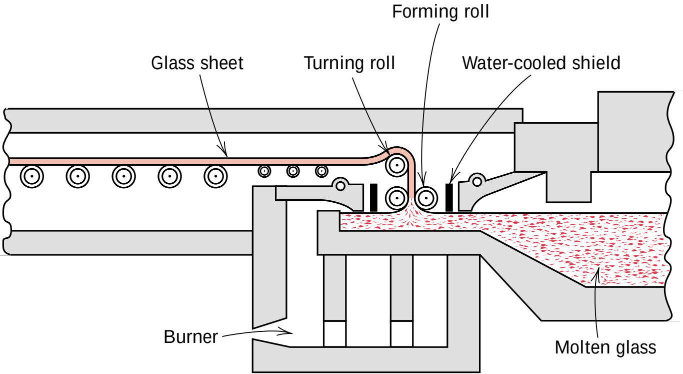
Forming roll
Glass sheet
Turning roll
Water-cooled shield
Burner
Molten glass

FIGURE 14.18 A process for the continuous drawing of sheet glass. (From W. D. Kingery, *Introduction to Ceramics*. Copyright © 1960 by John Wiley & Sons, New York. Reprinted by permission of John Wiley & Sons, Inc.)

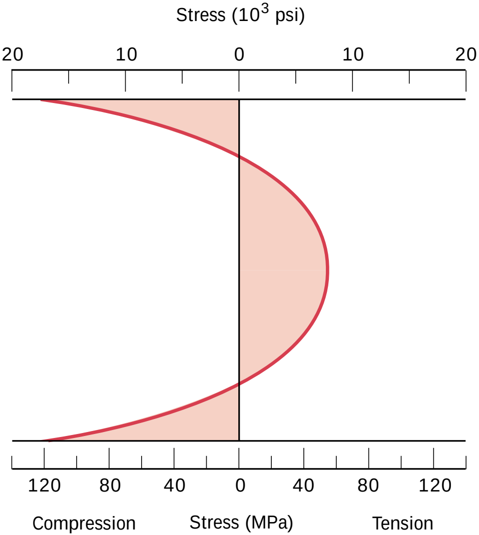

Figure 14.19 Room-temperature residual stress distribution over the cross section of a tempered glass plate. (From W. D. Kingery, H. K. Bowen, and D. R. Uhlmann, *Introduction to Ceramics*, 2nd edition. Copyright © 1976 by John Wiley & Sons, New York. Reprinted by permission of John Wiley & Sons, Inc.)

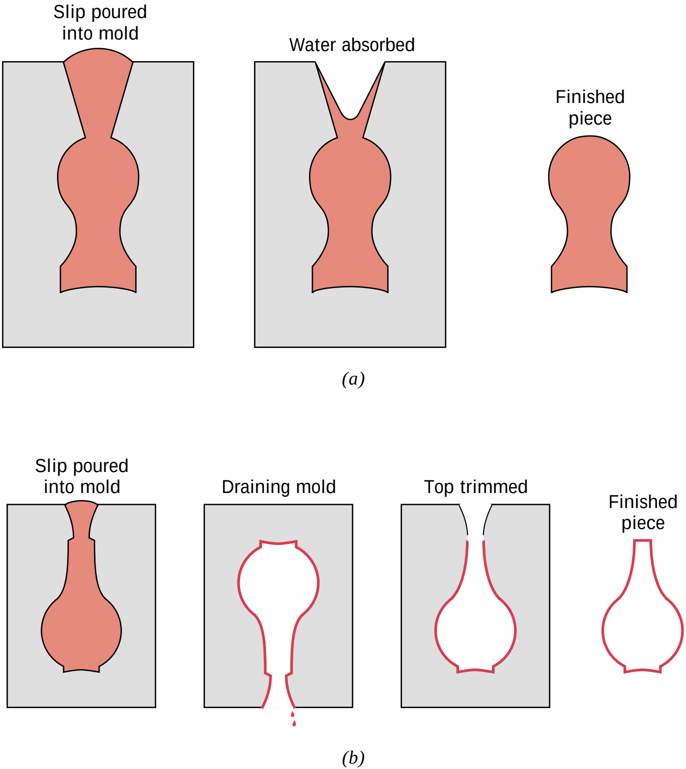
Slip poured into mold
Water absorbed
Finished piece
(a)
Slip poured into mold
Draining mold
Top trimmed
Finished piece
(b)

Figure 14.20 The steps in (*a*) solid and (*b*) drain slip casting using a plaster of paris mold. (From W. D. Kingery, *Introduction to Ceramics*. Copyright © 1960 by John Wiley & Sons, New York. Reprinted by permission of John Wiley & Sons, Inc.)

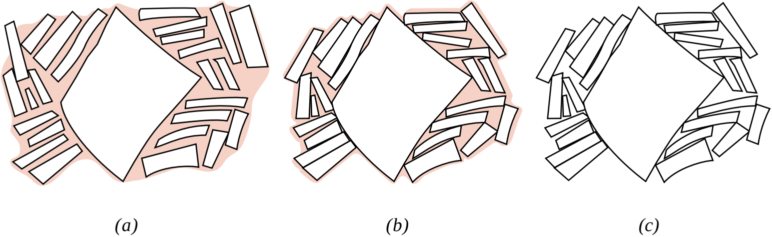

FIGURE 14.21 Several stages in the removal of water from between clay particles during the drying process. (*a*) Wet body. (*b*) Partially dry body. (*c*) Completely dry body. (From W. D. Kingery, *Introduction to Ceramics*. Copyright © 1960 by John Wiley & Sons, New York. Reprinted by permission of John Wiley & Sons, Inc.)

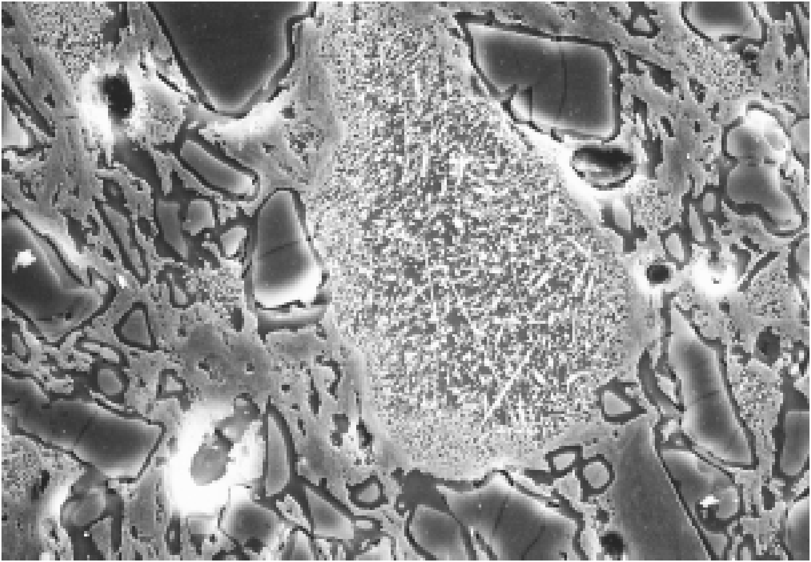

FIGURE 14.22 Scanning electron micrograph of a fired porcelain specimen (etched 15 s, 5°C, 10% HF) in which may be seen the following features: quartz grains (large dark particles) which are surrounded by dark glassy solution rims; partially dissolved feldspar regions (small unfeatured areas); mullite needles; and pores (dark holes with white border regions). Also, cracks within the quartz particles may be noted, which were formed during cooling, as a result of the difference in shrinkage between the glassy matrix and the quartz. 1500×. (Courtesy of H. G. Brinkies, Swinburne University of Technology, Hawthorn Campus, Hawthorn, Victoria, Australia.)

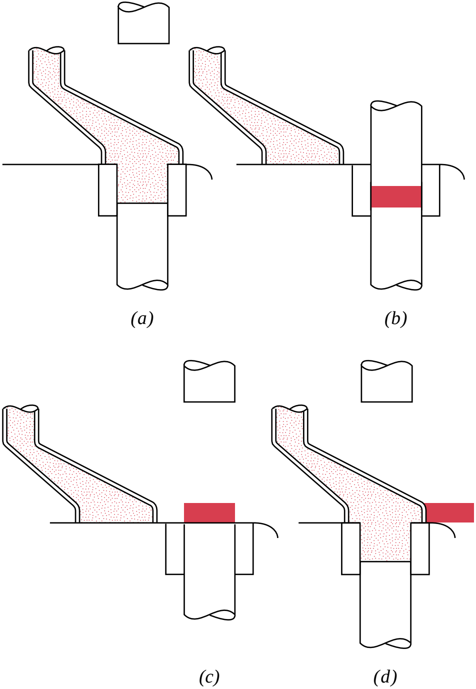

FIGURE 14.23 Schematic representation of the steps in uniaxial powder pressing. (*a*) The die cavity is filled with powder. (*b*) The powder is compacted by means of pressure applied to the top die. (*c*) The compacted piece is ejected by rising action of the bottom punch. (*d*) The fill shoe pushes away the compacted piece, and the fill step is repeated. (From W. D. Kingery, Editor, *Ceramic Fabrication Processes*, MIT Press. Copyright © 1958 by the Massachusetts Institute of Technology.)

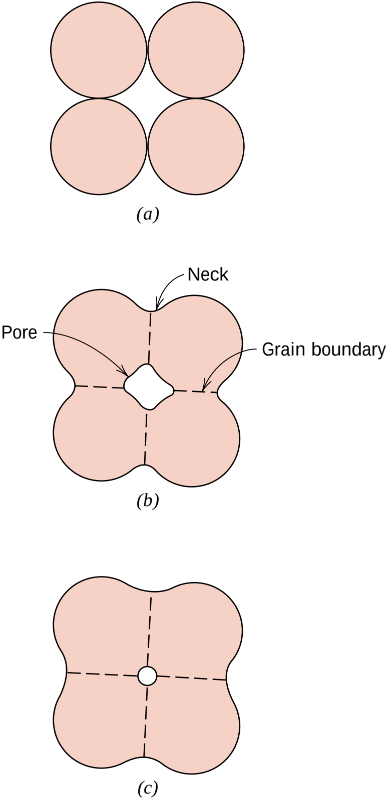
Neck
Pore
Grain boundary
(a)
(b)
(c)

Figure 14.24 For a powder compact, microstructural changes that occur during firing. (*a*) Powder particles after pressing. (*b*) Particle coalescence and pore formation as sintering begins. (*c*) As sintering proceeds, the pores change size and shape.

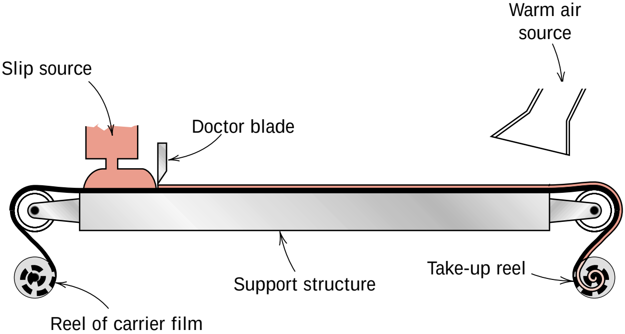
Warm air source
Slip source
Doctor blade
Take-up reel
Support structure
Reel of carrier film

FIGURE 14.26 Schematic diagram showing the tape casting process using a doctor blade. (From D. W. Richerson, *Modern Ceramic Engineering,* 2nd edition, Marcel Dekker, Inc., NY, 1992. Reprinted from *Modern Ceramic Engineering,* 2nd edition, p. 472 by courtesy of Marcel Dekker, Inc.)

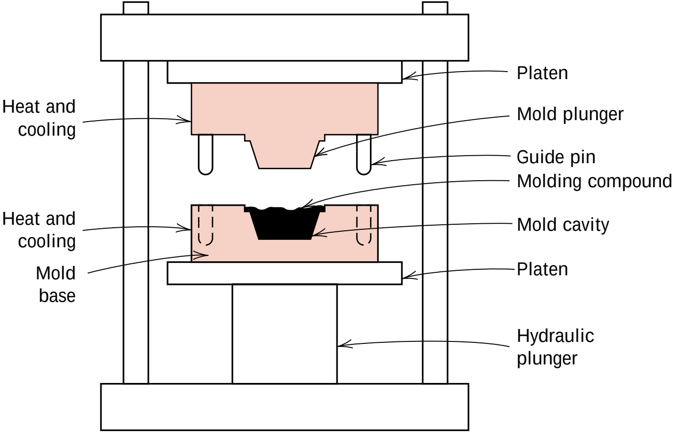
Platen
Heat and cooling
Mold plunger
Guide pin
Molding compound
Heat and cooling
Mold cavity
Mold base
Platen
Hydraulic plunger

Figure 14.27 Schematic diagram of a compression molding apparatus. (From F. W. Billmeyer, Jr., *Textbook of Polymer Science*, 3rd edition. Copyright © 1984 by John Wiley & Sons, New York. Reprinted by permission of John Wiley & Sons, Inc.)

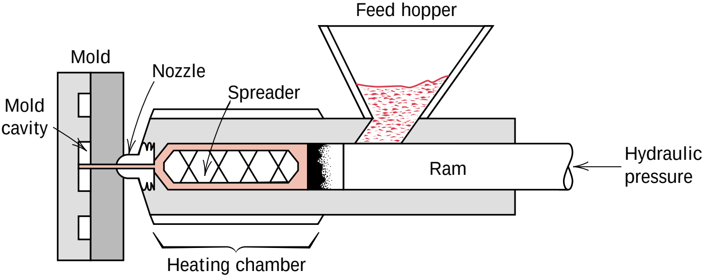
Feed hopper
Mold
Nozzle
Spreader
Mold cavity
Ram
Hydraulic pressure
Heating chamber

Figure 14.28 Schematic diagram of an injection molding apparatus. (Adapted from F. W. Billmeyer, Jr., *Textbook of Polymer Science*, 2nd edition. Copyright © 1971 by John Wiley & Sons, New York. Reprinted by permission of John Wiley & Sons, Inc.)

Table 13.3 **Designations, Compositions, and Applications for Six Tool Steels**

AISI Number	*UNS Number*	*Composition (wt%)*[a] *C*	*Cr*	*Ni*	*Mo*	*W*	*V*	*Typical Applications*
M1	T11301	0.85	3.75	0.30 max	8.70	1.75	1.20	Drills, saws; lathe and planer tools
A2	T30102	1.00	5.15	0.30 max	1.15	—	0.35	Punches, embossing dies
D2	T30402	1.50	12	0.30 max	0.95	—	1.10 max	Cutlery, drawing dies
O1	T31501	0.95	0.50	0.30 max	—	0.50	0.30 max	Shear blades, cutting tools
S1	T41901	0.50	1.40	0.30 max	0.50 max	2.25	0.25	Pipe cutters, concrete drills
W1	T72301	1.10	0.15 max	0.20 max	0.10 max	0.15 max	0.10 max	Blacksmith tools, wood-working tools

[a] The balance of the composition is iron. Manganese concentrations range between 0.10 and 1.4 wt%, depending on alloy; silicon concentrations between 0.20 and 1.2 wt% depending on alloy.

Source: Adapted from *ASM Handbook*, Vol. 1, *Properties and Selection: Irons, Steels, and High-Performance Alloys*, 1990. Reprinted by permission of ASM International, Materials Park, OH.

Table 13.4 Designations, Compositions, Mechanical Properties, and Typical Applications for Austenitic, Ferritic, Martensitic, and Precipitation-Hardenable Stainless Steels

				Mechanical Properties			
AISI Number	*UNS Number*	*Composition (wt%)*[a]	*Condition*[b]	*Tensile Strength [MPa (ksi)]*	*Yield Strength [MPa (ksi)]*	*Ductility [%EL in 50 mm (2 in.)]*	*Typical Applications*
			Ferritic				
409	S40900	0.08 C, 11.0 Cr, 1.0 Mn, 0.50 Ni, 0.75 Ti	Annealed	380 (55)	205 (30)	20	Automotive exhaust components, tanks for agricultural sprays
446	S44600	0.20 C, 25 Cr, 1.5 Mn	Annealed	515 (75)	275 (40)	20	Valves (high temperature), glass molds, combustion chambers
			Austenitic				
304	S30400	0.08 C, 19 Cr, 9 Ni, 2.0 Mn	Annealed	515 (75)	205 (30)	40	Chemical and food processing equipment, cryogenic vessels
316L	S31603	0.03 C, 17 Cr, 12 Ni, 2.5 Mo, 2.0 Mn	Annealed	485 (70)	170 (25)	40	Welding construction
			Martensitic				
410	S41000	0.15 C, 12.5 Cr, 1.0 Mn	Annealed Q & T	485 (70) 825 (120)	275 (40) 620 (90)	20 12	Rifle barrels, cutlery, jet engine parts
440A	S44002	0.70 C, 17 Cr, 0.75 Mo, 1.0 Mn	Annealed Q & T	725 (105) 1790 (260)	415 (60) 1650 (240)	20 5	Cutlery, bearings, surgical tools
			Precipitation Hardenable				
17-7PH	S17700	0.09 C, 17 Cr, 7 Ni, 1.0 Al, 1.0 Mn	Precipitation hardened	1450 (210)	1310 (190)	1–6	Springs, knives, pressure vessels

[a] The balance of the composition is iron.

[b] Q & T denotes quenched and tempered.

Source: Adapted from *ASM Handbook*, Vol. 1, *Properties and Selection: Irons, Steels, and High-Performance Alloys*, 1990. Reprinted by permission of ASM International, Materials Park, OH.

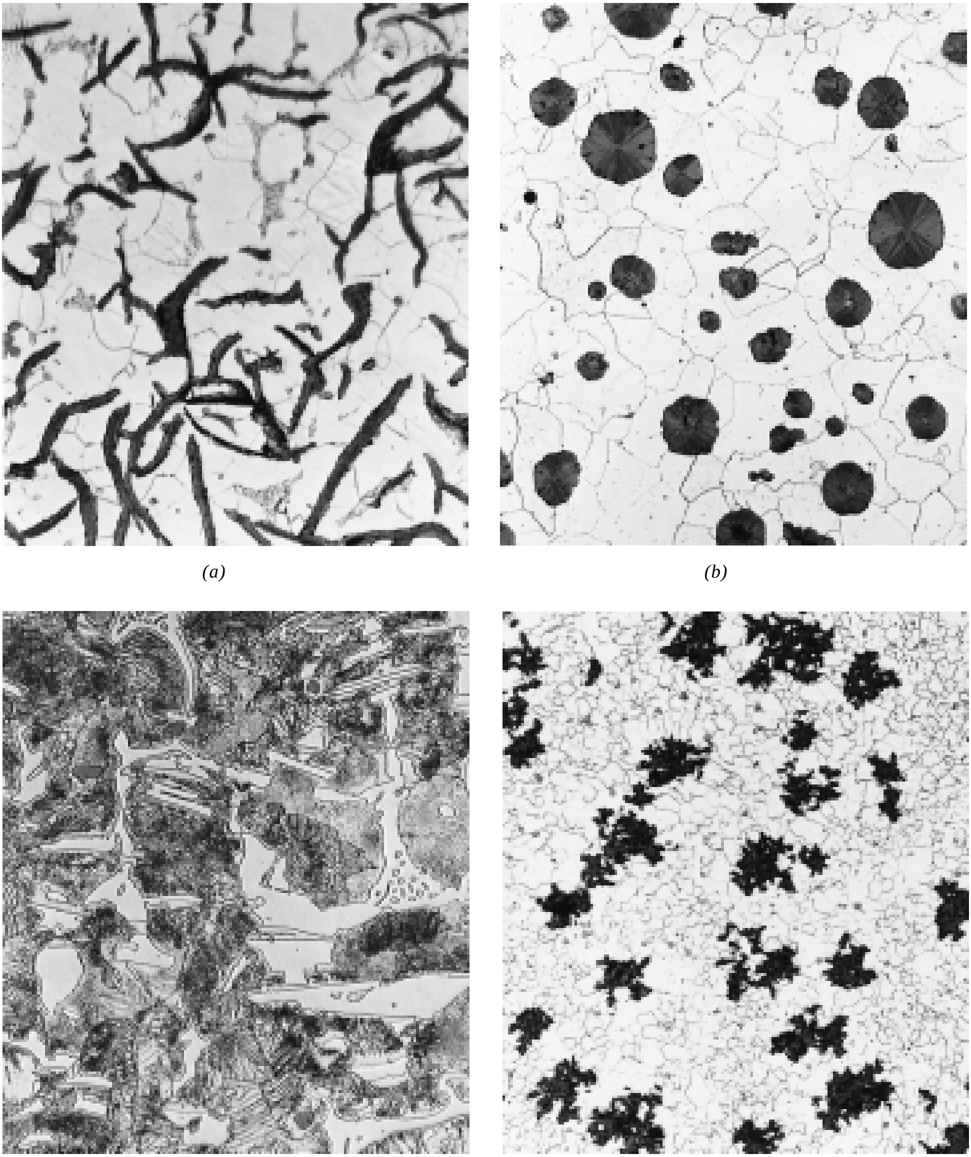

(a) (b)

(c) (d)

Figure 13.3 Optical photomicrographs of various cast irons. (*a*) Gray iron: the dark graphite flakes are embedded in an α-ferrite matrix. 500×. (Courtesy of C. H. Brady, National Bureau of Standards, Washington, DC.) (*b*) Nodular (ductile) iron: the dark graphite nodules are surrounded by an α-ferrite matrix. 200×. (Courtesy of C. H. Brady and L. C. Smith, National Bureau of Standards, Washington, DC.) (*c*) White iron: the light cementite regions are surrounded by pearlite, which has the ferrite–cementite layered structure. 400×. (Courtesy of Amcast Industrial Corporation.) (*d*) Malleable iron: dark graphite rosettes (temper carbon) in an α-ferrite matrix. 150×. (Reprinted with permission of the Iron Castings Society, Des Plaines, IL.)

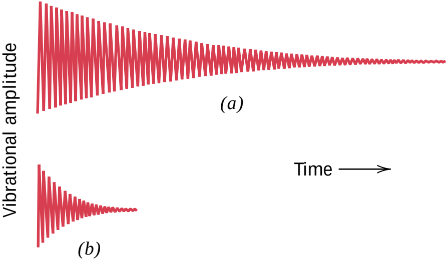

FIGURE 13.4 Comparison of the relative vibrational damping capacities of (*a*) steel and (*b*) gray cast iron. (From *Metals Engineering Quarterly*, February 1961. Copyright 1961 American Society for Metals.)

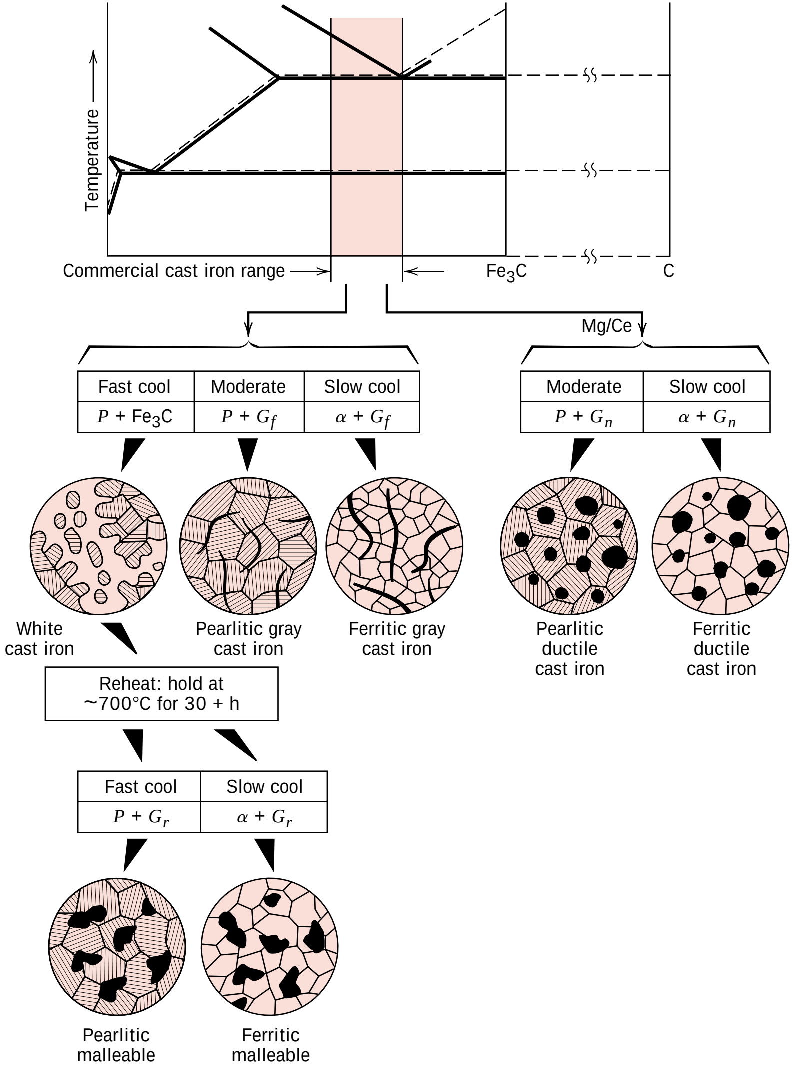
Temperature
Commercial cast iron range
Fe$_3$C
C
Mg/Ce
Fast cool
Moderate
Slow cool
P + Fe$_3$C
$P + G_f$
$\alpha + G_f$
Moderate
Slow cool
$P + G_n$
$\alpha + G_n$
White cast iron
Pearlitic gray cast iron
Ferritic gray cast iron
Pearlitic ductile cast iron
Ferritic ductile cast iron
Reheat: hold at ~700°C for 30 + h
Fast cool
Slow cool
$P + G_r$
$\alpha + G_r$
Pearlitic malleable
Ferritic malleable

Figure 13.5 From the iron–carbon phase diagram, composition ranges for commercial cast irons. Also shown are microstructures that result from a variety of heat treatments. G_f, flake graphite; G_r, graphite rosettes; G_n, graphite nodules; P, pearlite; α, ferrite. (Adapted from W. G. Moffatt, G. W. Pearsall, and J. Wulff, *The Structure and Properties of Materials*, Vol. 1, *Structure*, p. 195. Copyright © 1964 by John Wiley & Sons, New York. Reprinted by permission of John Wiley & Sons, Inc.)

Table 13.5 **Designations, Minimum Mechanical Properties, Approximate Compositions, and Typical Applications for Various Gray, Nodular, and Malleable Cast Irons**

				Mechanical Properties			
Grade	***UNS Number***	***Composition (wt%)***[a]	***Matrix Structure***	***Tensile Strength [MPa (ksi)]***	***Yield Strength [MPa (ksi)]***	***Ductility [%EL in 50 mm (2 in.)]***	***Typical Applications***
				Gray Iron			
SAE G1800	F10004	3.40–3.7 C, 2.55 Si, 0.7 Mn	Ferrite + Pearlite	124 (18)	—	—	Miscellaneous soft iron castings in which strength is not a primary consideration
SAE G2500	F10005	3.2–3.5 C, 2.20 Si, 0.8 Mn	Ferrite + Pearlite	173 (25)	—	—	Small cylinder blocks, cylinder heads, pistons, clutch plates, transmission cases
SAE G4000	F10008	3.0–3.3 C, 2.0 Si, 0.8 Mn	Pearlite	276 (40)	—	—	Diesel engine castings, liners, cylinders, and pistons
				Ductile (Nodular) Iron			
ASTM A536							
60-40-18	F32800	3.5–3.8 C, 2.0–2.8 Si, 0.05 Mg, $<$0.20 Ni, $<$0.10 Mo	Ferrite	414 (60)	276 (40)	18	Pressure-containing parts such as valve and pump bodies
100-70-03	F34800		Pearlite	689 (100)	483 (70)	3	High-strength gears and machine components
120-90-02	F36200		Tempered martensite	827 (120)	621 (90)	2	Pinions, gears, rollers, slides
				Malleable Iron			
32510	F22200	2.3–2.7 C, 1.0–1.75 Si, $<$0.55 Mn	Ferrite	345 (50)	224 (32)	10	General engineering service at normal and elevated temperatures
45006	—	2.4–2.7 C, 1.25–1.55 Si, $<$0.55 Mn	Ferrite + Pearlite	448 (65)	310 (45)	6	

[a] The balance of the composition is iron.

Source: Adapted from *ASM Handbook*, Vol. 1, *Properties and Selection: Irons, Steels, and High-Performance Alloys*, 1990. Reprinted by permission of ASM International, Materials Park, OH.

Table 13.6 Compositions, Mechanical Properties, and Typical Applications for Eight Copper Alloys

				Mechanical Properties			
Alloy Name	***UNS Number***	***Composition (wt%)***[a]	***Condition***	***Tensile Strength [MPa (ksi)]***	***Yield Strength [MPa (ksi)]***	***Ductility [%EL in 50 mm (2 in.)]***	***Typical Applications***
			Wrought Alloys				
Electrolytic tough pitch	C11000	0.04 O	Annealed	220 (32)	69 (10)	45	Electrical wire, rivets, screening, gaskets, pans, nails, roofing
Beryllium copper	C17200	1.9 Be, 0.20 Co	Precipitation hardened	1140–1310 (165–190)	690–860 (100–125)	4–10	Springs, bellows, firing pins, bushings, valves, diaphragms
Cartridge brass	C26000	30 Zn	Annealed Cold-worked (H04 hard)	300 (44) 525 (76)	75 (11) 435 (63)	68 8	Automotive radiator cores, ammunition components, lamp fixtures, flashlight shells, kickplates
Phosphor bronze, 5% A	C51000	5 Sn, 0.2 P	Annealed Cold-worked (H04 hard)	325 (47) 560 (81)	130 (19) 515 (75)	64 10	Bellows, clutch disks, diaphragms, fuse clips, springs, welding rods
Copper-nickel, 30%	C71500	30 Ni	Annealed Cold-worked (H02 hard)	380 (55) 515 (75)	125 (18) 485 (70)	36 15	Condenser and heat-exchanger components, saltwater piping
			Cast Alloys				
Leaded yellow brass	C85400	29 Zn, 3 Pb, 1 Sn	As cast	234 (34)	83 (12)	35	Furniture hardware, radiator fittings, light fixtures, battery clamps
Tin bronze	C90500	10 Sn, 2 Zn	As cast	310 (45)	152 (22)	25	Bearings, bushings, piston rings, steam fittings, gears
Aluminum bronze	C95400	4 Fe, 11 Al	As cast	586 (85)	241 (35)	18	Bearings, gears, worms, bushings, valve seats and guards, pickling hooks

[a] The balance of the composition is copper.

Source: Adapted from *ASM Handbook*, Vol. 2, *Properties and Selection: Nonferrous Alloys and Special-Purpose Materials*, 1990. Reprinted by permission of ASM International, Materials Park, OH.

Table 13.7 **Compositions, Mechanical Properties, and Typical Applications for Several Common Aluminum Alloys**

				Mechanical Properties			
Aluminum Association Number	***UNS Number***	***Composition (wt%)***[a]	***Condition (Temper Designation)***	***Tensile Strength [MPa (ksi)]***	***Yield Strength [MPa (ksi)]***	***Ductility [%EL in 50 mm (2 in.)]***	***Typical Applications/ Characteristics***
			Wrought, Nonheat-Treatable Alloys				
1100	A91100	0.12 Cu	Annealed (O)	90 (13)	35 (5)	35–45	Food/chemical handling & storage equipment, heat exchangers, light reflectors
3003	A93003	0.12 Cu, 1.2 Mn, 0.1 Zn	Annealed (O)	110 (16)	40 (6)	30–40	Cooking utensils, pressure vessels and piping
5052	A95052	2.5 Mg, 0.25 Cr	Strain hardened (H32)	230 (33)	195 (28)	12–18	Aircraft fuel & oil lines, fuel tanks, appliances, rivets, and wire
			Wrought, Heat-Treatable Alloys				
2024	A92024	4.4 Cu, 1.5 Mg, 0.6 Mn	Heat treated (T4)	470 (68)	325 (47)	20	Aircraft structures, rivets, truck wheels, screw machine products
6061	A96061	1.0 Mg, 0.6 Si, 0.30 Cu, 0.20 Cr	Heat treated (T4)	240 (35)	145 (21)	22–25	Trucks, canoes, railroad cars, furniture, pipelines
7075	A97075	5.6 Zn, 2.5 Mg, 1.6 Cu, 0.23 Cr	Heat treated (T6)	570 (83)	505 (73)	11	Aircraft structural parts and other highly stressed applications
			Cast, Heat-Treatable Alloys				
295.0	A02950	4.5 Cu, 1.1 Si	Heat treated (T4)	221 (32)	110 (16)	8.5	Flywheel and rear-axle housings, bus and aircraft wheels, crankcases
356.0	A03560	7.0 Si, 0.3 Mg	Heat treated (T6)	228 (33)	164 (24)	3.5	Aircraft pump parts, automotive transmission cases, water-cooled cylinder blocks
			Aluminum–Lithium Alloys				
2090	—	2.7 Cu, 0.25 Mg, 2.25 Li, 0.12 Zr	Heat treated, cold worked (T83)	455 (66)	455 (66)	5	Aircraft structures and cryogenic tankage structures
8090	—	1.3 Cu, 0.95 Mg, 2.0 Li, 0.1 Zr	Heat treated, cold worked (T651)	465 (67)	360 (52)	—	Aircraft structures that must be highly damage tolerant

[a] The balance of the composition is aluminum.

Source: Adapted from *ASM Handbook*, Vol. 2, *Properties and Selection: Nonferrous Alloys and Special-Purpose Materials*, 1990. Reprinted by permission of ASM International, Materials Park, OH.

Table 13.8 Compositions, Mechanical Properties, and Typical Applications for Six Common Magnesium Alloys

				Mechanical Properties			
ASTM Number	***UNS Number***	***Composition (wt%)***[a]	***Condition***	***Tensile Strength [MPa (ksi)]***	***Yield Strength [MPa (ksi)]***	***Ductility [%EL in 50 mm (2 in.)]***	***Typical Applications***
				Wrought Alloys			
AZ31B	M11311	3.0 Al, 1.0 Zn, 0.2 Mn	As extruded	262 (38)	200 (29)	15	Structures and tubing, cathodic protection
HK31A	M13310	3.0 Th, 0.6 Zr	Strain hardened, partially annealed	255 (37)	200 (29)	9	High strength to 315°C (600°F)
ZK60A	M16600	5.5 Zn, 0.45 Zr	Artificially aged	350 (51)	285 (41)	11	Forgings of maximum strength for aircraft
				Cast Alloys			
AZ91D	M11916	9.0 Al, 0.15 Mn, 0.7 Zn	As cast	230 (33)	150 (22)	3	Die-cast parts for automobiles, luggage, and electronic devices
AM60A	M10600	6.0 Al, 0.13 Mn	As cast	220 (32)	130 (19)	6	Automotive wheels
AS41A	M10410	4.3 Al, 1.0 Si, 0.35 Mn	As cast	210 (31)	140 (20)	6	Die castings requiring good creep resistance

[a] The balance of the composition is magnesium.

Source: Adapted from *ASM Handbook*, Vol. 2, *Properties and Selection: Nonferrous Alloys and Special-Purpose Materials*, 1990. Reprinted by permission of ASM International, Materials Park, OH.

Table 13.9 **Compositions, Mechanical Properties, and Typical Applications for Several Common Titanium Alloys**

				Average Mechanical Properties			
Alloy Type	***Common Name (UNS Number)***	***Composition (wt%)***	***Condition***	***Tensile Strength [MPa (ksi)]***	***Yield Strength [MPa (ksi)]***	***Ductility [%EL in 50 mm (2 in.)]***	***Typical Applications***
Commercially pure	Unalloyed (R50500)	99.1 Ti	Annealed	484 (70)	414 (60)	25	Jet engine shrouds, cases and airframe skins, corrosion-resistant equipment for marine and chemical processing industries
α	Ti-5Al-2.5Sn (R54520)	5 Al, 2.5 Sn, balance Ti	Annealed	826 (120)	784 (114)	16	Gas turbine engine casings and rings; chemical processing equipment requiring strength to temperatures of 480°C (900°F)
Near α	Ti-8Al-1Mo-1V (R54810)	8 Al, 1 Mo, 1 V, balance Ti	Annealed (duplex)	950 (138)	890 (129)	15	Forgings for jet engine components (compressor disks, plates, and hubs)
α-β	Ti-6Al-4V (R56400)	6 Al, 4 V, balance Ti	Annealed	947 (137)	877 (127)	14	High-strength prosthetic implants, chemical-processing equipment, airframe structural components
α-β	Ti-6Al-6V-2Sn (R56620)	6 Al, 2 Sn, 6 V, 0.75 Cu, balance Ti	Annealed	1050 (153)	985 (143)	14	Rocket engine case airframe applications and high-strength airframe structures
β	Ti-10V-2Fe-3Al	10 V, 2 Fe, 3 Al, balance Ti	Solution + aging	1223 (178)	1150 (167)	10	Best combination of high strength and toughness of any commercial titanium alloy; used for applications requiring uniformity of tensile properties at surface and center locations; high-strength airframe components

Source: Adapted from *ASM Handbook*, Vol. 2, *Properties and Selection: Nonferrous Alloys and Special-Purpose Materials*, 1990. Reprinted by permission of ASM International, Materials Park, OH.

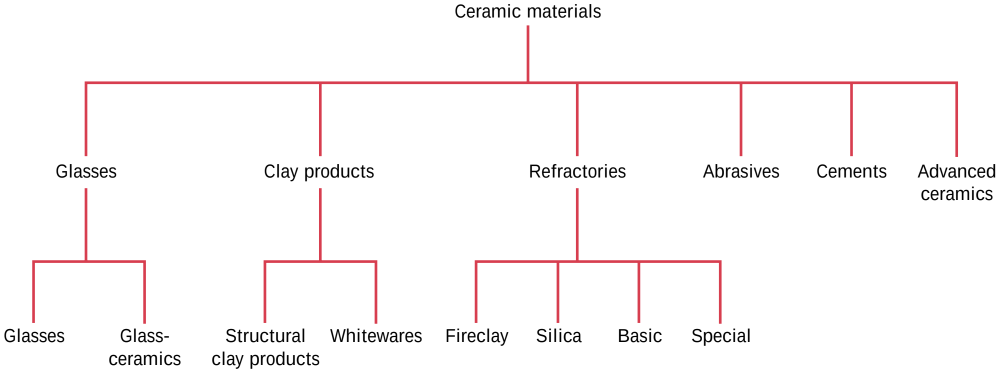
Ceramic materials
Glasses
Clay products
Refractories
Abrasives
Cements
Advanced ceramics
Glasses
Glass-ceramics
Structural clay products
Whitewares
Fireclay
Silica
Basic
Special

FIGURE 13.6 Classification of ceramic materials on the basis of application.

Table 13.11 Compositions of Five Common Ceramic Refractory Materials

Refractory Type	Composition (wt%)							Apparent Porosity (%)
	Al_2O_3	SiO_2	MgO	Cr_2O_3	Fe_2O_3	CaO	TiO_2	
Fireclay	25–45	70–50	0–1		0–1	0–1	1–2	10–25
High-alumina fireclay	90–50	10–45	0–1		0–1	0–1	1–4	18–25
Silica	0.2	96.3	0.6			2.2		25
Periclase	1.0	3.0	90.0	0.3	3.0	2.5		22
Periclase–chrome ore	9.0	5.0	73.0	8.2	2.0	2.2		21

Source: From W. D. Kingery, H. K. Bowen, and D. R. Uhlmann, *Introduction to Ceramics*, 2nd edition. Copyright © 1976 by John Wiley & Sons, New York. Reprinted by permission of John Wiley & Sons, Inc.

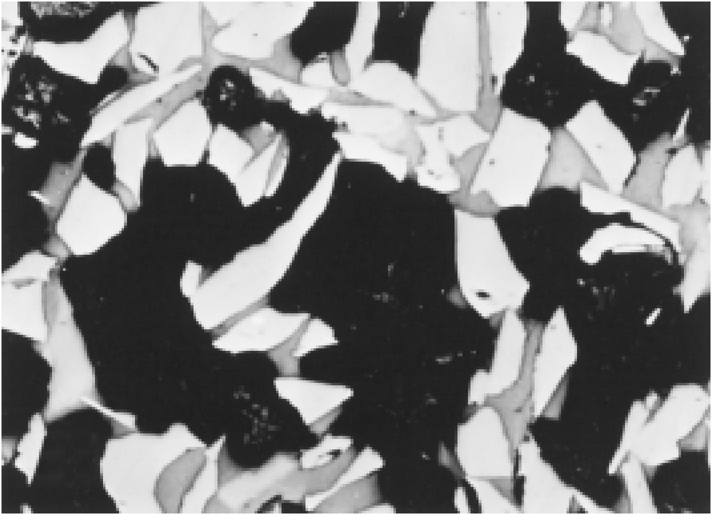

FIGURE 13.7 Photomicrograph of an aluminum oxide bonded ceramic abrasive. The light regions are the Al_2O_3 abrasive grains; the gray and dark areas are the bonding phase and porosity, respectively. 100×. (From W. D. Kingery, H. K. Bowen, and D. R. Uhlmann, *Introduction to Ceramics*, 2nd edition, p. 568. Copyright © 1976 by John Wiley & Sons. Reprinted by permission of John Wiley & Sons, Inc.)

Chapter 13 / Types and Applications of Materials

13.7 REFRACTORIES

FIRECLAY REFRACTORIES

The primary ingredients for the fireclay refractories are high-purity fireclays, alumina and silica mixtures usually containing between 25 and 45 wt% alumina. According to the SiO_2–Al_2O_3 phase diagram, Figure 10.24, over this composition range the highest temperature possible without the formation of a liquid phase is 1587°C (2890°F). Below this temperature the equilibrium phases present are mullite and silica (cristobalite). During refractory service use the presence of a small amount of a liquid phase may be allowable without compromising mechanical integrity. Above 1587°C the fraction of liquid phase present will depend on refractory composition. Upgrading the alumina content will increase the maximum service temperature, allowing for the formation of a small amount of liquid.

Fireclay bricks are used principally in furnace construction, to confine hot atmospheres, and to thermally insulate structural members from excessive temperatures. For fireclay brick, strength is not ordinarily an important consideration, because support of structural loads is usually not required. Some control is normally maintained over the dimensional accuracy and stability of the finished product.

SILICA REFRACTORIES

The prime ingredient for silica refractories, sometimes termed acid refractories, is silica. These materials, well known for their high-temperature load-bearing capacity, are commonly used in the arched roofs of steel- and glass-making furnaces; for these applications, temperatures as high as 1650°C (3000°F) may be realized. Under these conditions some small portion of the brick will actually exist as a liquid. The presence of even small concentrations of alumina has an adverse influence on the performance of these refractories, which may be explained by the silica–alumina phase diagram, Figure 10.24. Since the eutectic composition (7.7 wt% Al_2O_3) is very near to the silica extremity of the phase diagram, even small additions of Al_2O_3 lower the liquidus temperature significantly, which means that substantial amounts of liquid may be present at temperatures in excess of 1600°C (2910°F). Thus, the alumina content should be held to a minimum, normally to between 0.2 and 1.0 wt%.

These refractory materials are also resistant to slags that are rich in silica (called acid slags) and are often used as containment vessels for them. On the other hand, they are readily attacked by slags composed of a high proportion of CaO and/or MgO (basic slags), and contact with these oxide materials should be avoided.

BASIC REFRACTORIES

The refractories that are rich in periclase, or magnesia (MgO), are termed basic; they may also contain calcium, chromium, and iron compounds. The presence of silica is deleterious to their high-temperature performance. Basic refractories are especially resistant to attack by slags containing high concentrations of MgO and CaO, and find extensive use in some steel-making open hearth furnaces.

SPECIAL REFRACTORIES

There are yet other ceramic materials that are used for rather specialized refractory applications. Some of these are relatively high-purity oxide materials, many of which may be produced with very little porosity. Included in this group are alumina, silica, magnesia, beryllia (BeO), zirconia (ZrO_2), and mullite ($3Al_2O_3$–$2SiO_2$). Others include carbide compounds, in addition to carbon and graphite. Silicon carbon (SiC) has been used for electrical resistance heating elements, as a crucible material, and in internal furnace components. Carbon and graphite are very refractory, but find limited application because they are susceptible to oxidation at temperatures in excess of about 800°C (1470°F). As would be expected, these specialized refractories are relatively expensive.

13.10 ADVANCED CERAMICS

Up until the past 50 or so years, the most important ceramic materials were termed the ''traditional ceramics,'' those that have been heretofore discussed in this chapter. Of late, significant progress has been made in understanding the fundamental character of these materials and of the phenomena that occur in them that are responsible for their unique properties. Consequently, a new generation of these materials has evolved, and the term ''ceramic'' has taken on a much broader meaning. Some of these, the ''advanced ceramics,'' have begun and will continue to establish a prominent niche in our advanced technologies. In particular, electrical, magnetic, and optical properties and property combinations unique to ceramics have been exploited in a host of new products. To one degree or another, these new materials have a rather dramatic effect on our lives; electronic, computer, communication, aerospace, and a host of other industries rely on their use. Some of these will now be discussed.

HEAT ENGINE APPLICATIONS

Advanced ceramic materials are just beginning to be used in automobile internal combustion engines. The principal advantages of these new materials over the conventional metal alloys include: the ability to withstand higher operating temperatures, thereby increasing fuel efficiency; excellent wear and corrosion resistance; lower frictional losses; the ability to operate without a cooling system; and lower densities, which result in decreased engine weights. Such engines are still in the developmental stage; however, ceramic engine blocks as well as valves, cylinder liners, pistons, bearings, and other components have been demonstrated. Furthermore, research is also being conducted on automobile gas turbine engines that employ ceramic rotors, stators, regenerators, and combustion housings.

On the basis of their desirable physical and chemical characteristics mentioned above, advanced ceramic materials will, at some future time, most certainly be utilized in jet aircraft engines. Of particular significance are the relatively low densities of these materials, which will result in turbine blades that are lighter than their superalloy counterparts, and which will also lead to other light-weight components. Materials presently under consideration for use in ceramic heat engines include silicon nitride (Si_3N_4), silicon carbide (SiC), and zirconia (ZrO_2).

The wear resistance and/or high-temperature deterioration characteristics of some metal heat engine parts currently in use have been improved significantly by using ceramic surface coatings. For example, superalloy aircraft turbine engine components are protected by a zirconia thermal barrier coating. The successful performance of these coatings is dependent on the establishment of a strong bond between the ceramic and its metal substrate that must be maintained during thermal cycling.

The chief drawback to the use of ceramics in heat engines is their disposition to brittle and catastrophic failure, due to their relatively low fracture toughnesses. Techniques are currently being developed to enhance the toughness characteristics of these materials; these involve ceramic-matrix composites, which are discussed in Section 15.10.

Furthermore, improved material processing techniques are necessary so as to produce materials that have specific microstructures and, therefore, uniform and reliable mechanical and corrosion-resistant characteristics at elevated temperatures. Several key issues relative to processing include starting ceramic powder characterization (i.e., purity, particle size, and size distribution); powder synthesis and processing; improved densification techniques; and property (e.g., mechanical, physical, and chemical) evaluation. In addition, it is important to develop a methodology whereby more reliable service life predictions may be made for these materials.

CERAMIC ARMOR

Some of the new advanced ceramics are being used in armor systems to protect military personnel and vehicles from ballistic projectiles. The chief consideration in these applications is the weight of the protective material required to thwart projectile impact. On a per weight basis, some ceramic materials are highly armor efficient.

Most ceramic armor systems consist of one or more outer ceramic facing plates that are combined with a ductile and softer backing sheet. Upon impact, the facing plates must be hard enough to fracture the high-velocity projectile, which upon impact also causes brittle fracture of the plate itself. Ceramic armor materials include alumina (Al_2O_3), boron carbide (B_4C), silicon carbide (SiC), and titanium diboride (TiB_2).

The armor backing must absorb the remaining projectile kinetic energy by deformation and, in addition, restrain continued penetration of projectile and ceramic fragments. Aluminum and laminates of synthetic fibers embedded in a plastic matrix are commonly used.

ELECTRONIC PACKAGING

The electronics industry is continually looking for new materials to keep up with its ever changing technologies. Of particular interest is the packaging of integrated circuits (ICs). For some package designs, the ICs are mounted on a substrate material that must be electrically insulating, have appropriate dielectric characteristics (i.e., low dielectric constant), as well as dissipate heat generated by electrical currents that pass through the electronic components (i.e., be thermally conductive). As the IC electronic components become packed closer together, this dissipation of heat becomes an increasingly more critical consideration.

Aluminum oxide has been the standard-bearer substrate material; its chief limitation, however, is a relatively low thermal conductivity. As a general rule, materials that are poor electrical conductors are also poor thermal conductors, and vice versa. Exceptions (i.e., electrical insulators and thermal conductors) are high-purity ceramic materials that have simple crystal structures; these include boron nitride (BN), silicon carbide (SiC), and aluminum nitride (AlN). Currently, the most promising substrate alternative is AlN, which has a thermal conductivity a factor of 10 better than that for alumina. Furthermore, the thermal expansion of AlN is very close to the silicon IC chips for which it serves as a substrate.

A detailed case study relative to materials that are used in electronic packages is contained in Chapter 20.

13.16 ADVANCED POLYMERIC MATERIALS

A number of new polymers having unique and desirable combinations of properties have been developed over the past several years; many have found niches in new technologies and/or have satisfactorily replaced other materials. Some of these include ultrahigh molecular weight polyethylene, liquid crystal polymers, and thermoplastic elastomers. Each of these will now be discussed.

ULTRAHIGH MOLECULAR WEIGHT POLYETHYLENE

Ultrahigh molecular weight polyethylene (*UHMWPE*) is a linear polyethylene that has an extremely high molecular weight. Its typical $\overline{M}_w$ is approximately 4×10^6 g/mol, which is an order of magnitude (i.e., factor of ten) greater than that of high-density polyethylene. In fiber form, UHMWPE has the tradename Spectra. Some of the extraordinary characteristics of this material are as follows:

1. An extremely high impact resistance.
2. Outstanding resistance to wear and abrasion.
3. A very low coefficient of friction.
4. A self-lubricating and nonstick surface.
5. Very good chemical resistance to normally encountered solvents.
6. Excellent low-temperature properties.
7. Outstanding sound damping and energy absorption characteristics.
8. Electrically insulating and excellent dielectric properties.

However, since this material has a relatively low melting temperature, its mechanical properties diminish rapidly with increasing temperature.

This unusual combination of properties leads to numerous and diverse applications for this material, including: bullet-proof vests, composite military helmets, fishing line, ski bottom surfaces, golf ball cores, bowling alley and ice skating rink surfaces, biomedical prostheses (Section 20.8), blood filters, marking pen nibs, bulk material handling equipment (for coal, grain, cement, gravel, etc.), bushings, pump impellers, and valve gaskets.

LIQUID CRYSTAL POLYMERS

The **liquid crystal polymers** (*LCP*s) are a group of chemically complex and structurally distinct materials that have unique properties and are utilized in diverse applications. Discussion of the chemistry of these materials is beyond the scope of this book. Suffice it to say that LCPs are composed of extended, rod-shaped, and rigid molecules. In terms of molecular arrangement, these materials do not fall within any of conventional liquid, amorphous, crystalline, semicrystalline classifications, but may be considered as a new state of matter—the liquid crystalline state, being neither crystalline nor liquid. In the melt (or liquid) condition, whereas other polymer molecules are randomly oriented, LCP molecules can become aligned in highly ordered configurations. As solids, this molecular alignment remains, and, in addition, the molecules form in domain structures having characteristic intermolecu-

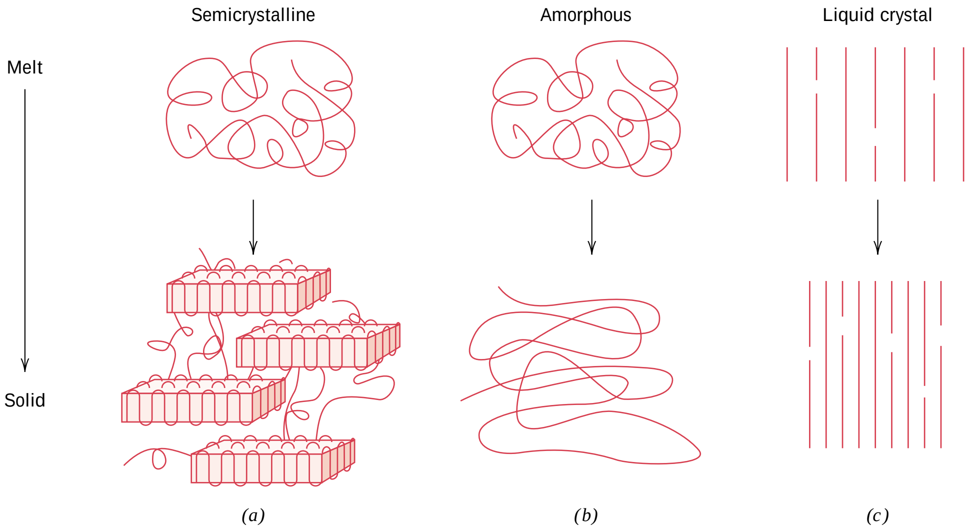

Figure 13.9 Schematic representations of the molecular structures in both melt and solid states for (*a*) semicrystalline, (*b*) amorphous, and (*c*) liquid crystal polymers. (Adapted from G. W. Calundann and M. Jaffe, ''Anisotropic Polymers, Their Synthesis and Properties,'' Chapter VII in *Proceedings of the Robert A. Welch Foundation Conferences on Polymer Research,* 26th Conference, Synthetic Polymers, Nov. 1982.)

lar spacings. A schematic comparison of liquid crystals, amorphous polymers, and semicrystalline polymers in both melt and solid states is illustrated in Figure 13.9. Furthermore, there are three types of liquid crystals, based on orientation and positional ordering—smectic, nematic, and cholesteric; distinctions among these types are also beyond the scope of this discussion.

The principal use of liquid crystal polymers is in *liquid crystal displays* (*LCD*s), on digital watches, laptop computers, and for other digital displays. Here cholesteric types of LCPs are employed which, at room temperature, are fluid liquids, transparent, and optically anisotropic. The displays are composed of two sheets of glass between which is sandwiched the liquid crystal material. The outer face of each glass sheet is coated with a transparent and electrically conductive film; in addition, into this film on the side that is to be viewed are etched the character-forming number/letter elements. A voltage applied through the conductive films (and thus between these two glass sheets) over one of these character-forming regions causes a disruption of the orientation of the LCP molecules in this region, a darkening of this LCP material, and, in turn, the formation of a visible character.

Some of the nematic type of liquid crystal polymers are rigid solids at room temperature and, on the basis of an outstanding combination of properties and processing characteristics, have found widespread use in a variety of commercial applications. For example, these materials exhibit the following behaviors:

1. Excellent thermal stability; they may be used to temperatures as high as 230°C (450°F).
2. Stiff and strong; their tensile moduli range between 10 and 24 GPa (1.4×10^6 and 3.5×10^6 psi), while tensile strengths are from 125 to 255 MPa (18,000 to 37,000 psi).

3. High impact strengths, which are retained upon cooling to relatively low temperatures.
4. Chemical inertness to a wide variety of acids, solvents, bleaches, etc.
5. Inherent flame resistance and combustion products that are relatively nontoxic.

The thermal stability and chemical inertness of these materials are explained by extremely high intermolecular interactions.

The following may be said about their processing and fabrication characteristics:

1. All conventional processing techniques available for thermoplastic materials may be used.
2. Extremely low shrinkage and warpage during molding.
3. Exceptional dimensional repeatability from part to part.
4. Low melt viscosity, which permits molding of thin sections and/or complex shapes.
5. Low heats of fusion; this results in rapid melting and subsequent cooling, which shortens molding cycle times.
6. Anisotropic finished-part properties; molecular orientation effects are produced from melt flow during molding.

These materials are used extensively by the electronics industry (interconnect devices, relay and capacitor housings, brackets, etc.), by the medical equipment industry (in components to be repeatedly sterilized), and in photocopiers and fiber-optic components.

THERMOPLASTIC ELASTOMERS

The **thermoplastic elastomers** (*TPE*s or *TE*s) are a type of polymeric material that, at ambient conditions, exhibits elastomeric (or rubbery) behavior, yet is thermoplastic in nature (Section 4.9). By way of contrast, most elastomers heretofore discussed are thermosets, since they become crosslinked during vulcanization. Of the several varieties of TPEs, one of the best known and widely used is a block copolymer consisting of block segments of a hard and rigid thermoplastic mer (commonly styrene [S]), and a soft and flexible elastic mer (often butadiene [B] or isoprene [I]). These two block types alternate positions—for a common molecule, hard polymerized segments are located at chain ends, whereas the soft central region consists of polymerized butadiene or isoprene units. These TPEs are frequently termed *styrenic block copolymers*, and chain chemistries for the two (S-B-S and S-I-S) types are shown in Figure 13.10.

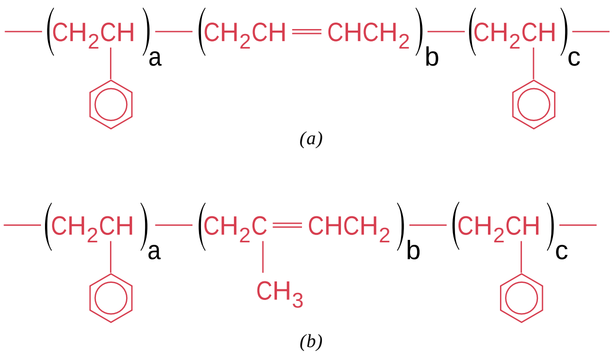

FIGURE 13.10 Representations of the chain chemistries for (*a*) styrene-butadiene-styrene (S-B-S), and (*b*) styrene-isoprene-styrene (S-I-S) thermoplastic elastomers.

At ambient temperatures, the soft, amorphous, central (butadiene or isoprene) segments impart the rubbery, elastomeric behavior to the material. Furthermore, for temperatures below the T_m of the hard (styrene) component, hard chain-end segments from numerous adjacent chains aggregate together to form rigid domain regions. These domains are ''physical crosslinks'' that act as anchor points so as to restrict soft-chain segment motions; they function in much the same way as ''chemical crosslinks'' for the thermoset elastomers. In Figure 13.11 is presented a schematic illustration for the structure of this TPE type.

The tensile modulus of this TPE material is subject to alteration; increasing the number of soft-component blocks per chain will lead to a decrease in modulus and, therefore, a diminishment of stiffness. Furthermore, the useful temperature range lies between T_g of the soft and flexible component and T_m of the hard, rigid one; for the styrenic block copolymers this range is between about −70°C (−95°F) and 100°C (212°F).

In addition to the styrenic block copolymers, there are other types of TPEs, including thermoplastic olefins, copolyesters, thermoplastic polyurethanes, and elastomeric polyamides.

The chief advantage of the TPEs over the thermoset elastomers is that upon heating above T_m of the hard phase, they melt (i.e., the physical crosslinks disappear), and, therefore, they may be processed by conventional thermoplastic forming techniques (e.g., blow molding, injection molding, etc.); thermoset polymers do not experience melting, and, consequently, forming is normally more difficult. Furthermore, since the melting-solidification process is reversible and repeatable for thermoplastic elastomers, TPE parts may be reformed into other shapes. In other words,

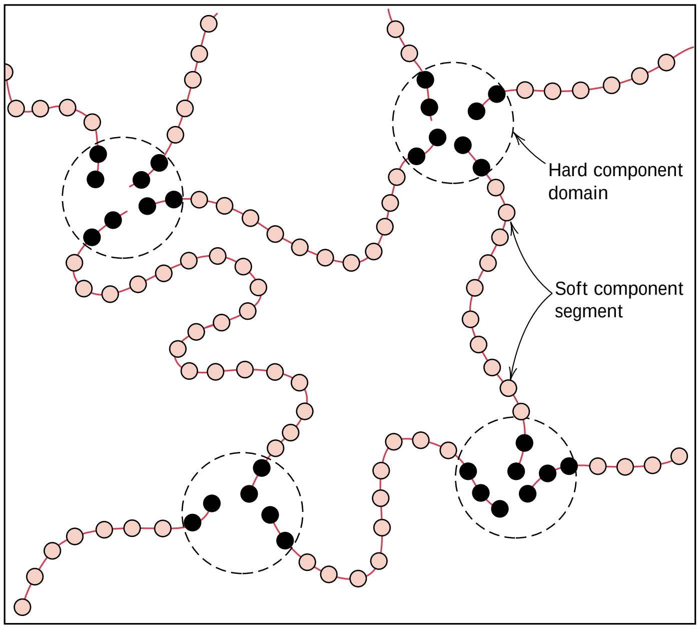

FIGURE 13.11 Schematic representation of the molecular structure for a thermoplastic elastomer. This structure consists of ''soft'' (i.e., butadiene or isoprene) mer center-chain segments and ''hard'' (i.e., styrene) domains (chain ends), which act as physical crosslinks at room temperature. (From *Science and Engineering of Materials, 3rd edition,* by D. R. Askeland. © 1994. Reprinted with permission of Brooks/Cole, a division of Thomson Learning. Fax 800 730-2215.)

they are recyclable; thermoset elastomers are, to a large degree, nonrecyclable. Scrap that is generated during forming procedures may also be recycled, which results in lower production costs than with thermosets. In addition, tighter controls may be maintained on part dimensions for TPEs, and TPEs have lower densities.

In quite a variety of applications, the thermoplastic elastomers have replaced the conventional thermoset elastomers. Typical uses for the TPEs include automotive exterior trim (bumpers, fascia, etc.), automotive underhood components (electrical insulation and connectors, and gaskets), shoe soles and heels, sporting goods, appliance parts, medical devices, and as components in sealants, caulking, and adhesives.

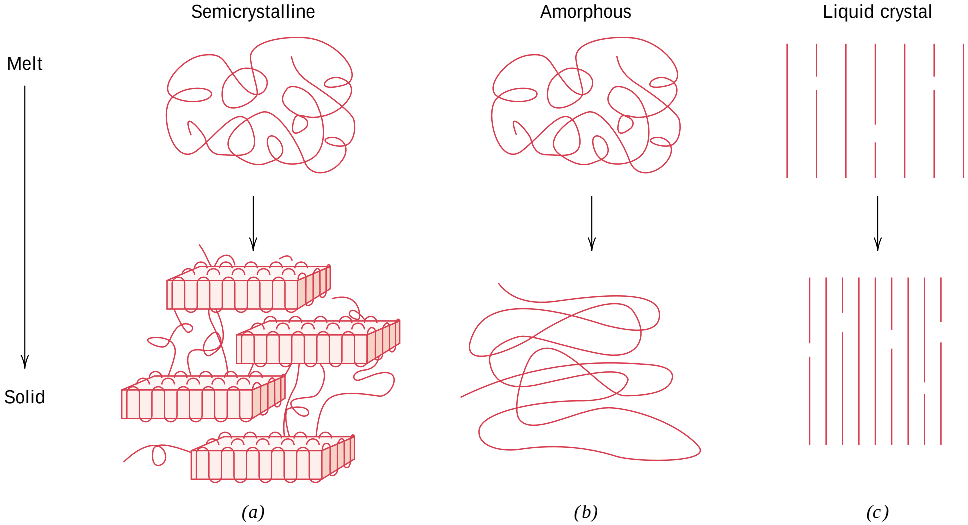
Semicrystalline
Amorphous
Liquid crystal
Melt
Solid
(a)
(b)
(c)

Figure 13.9 Schematic representations of the molecular structures in both melt and solid states for (*a*) semicrystalline, (*b*) amorphous, and (*c*) liquid crystal polymers. (Adapted from G. W. Calundann and M. Jaffe, ‘‘Anisotropic Polymers, Their Synthesis and Properties,’’ Chapter VII in *Proceedings of the Robert A. Welch Foundation Conferences on Polymer Research*, 26th Conference, Synthetic Polymers, Nov. 1982.)

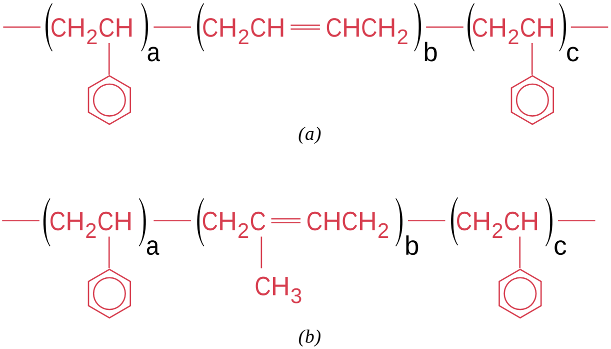
CH2CH
a
CH2CH=CHCH2
b
CH2CH
c
CH2C=CHCH2
CH3

(a)

(b)

Figure 13.10 Representations of the chain chemistries for (*a*) styrene-butadiene-styrene (S-B-S), and (*b*) styrene-isoprene-styrene (S-I-S) thermoplastic elastomers.

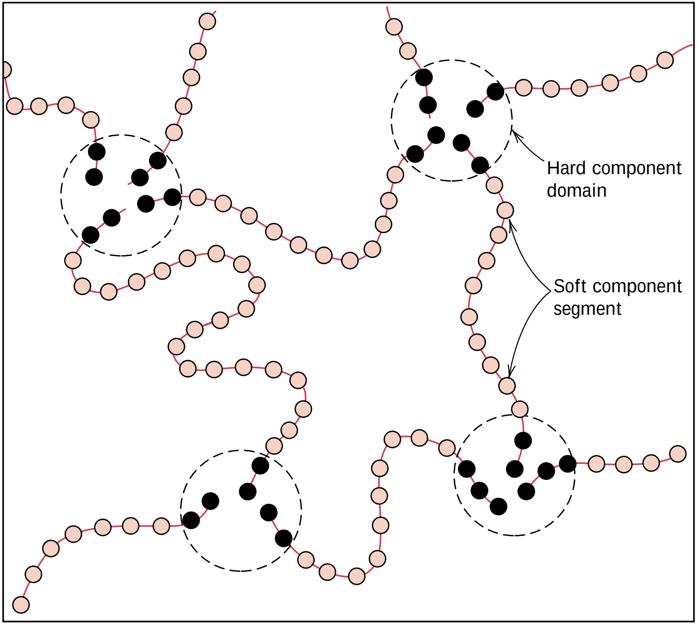

FIGURE 13.11 Schematic representation of the molecular structure for a thermoplastic elastomer. This structure consists of ‘‘soft’’ (i.e., butadiene or isoprene) mer center-chain segments and ‘‘hard’’ (i.e., styrene) domains (chain ends), which act as physical crosslinks at room temperature. (From *Science and Engineering of Materials, 3rd edition*, by D. R. Askeland. © 1994. Reprinted with permission of Brooks/Cole, a division of Thomson Learning. Fax 800 730-2215.)

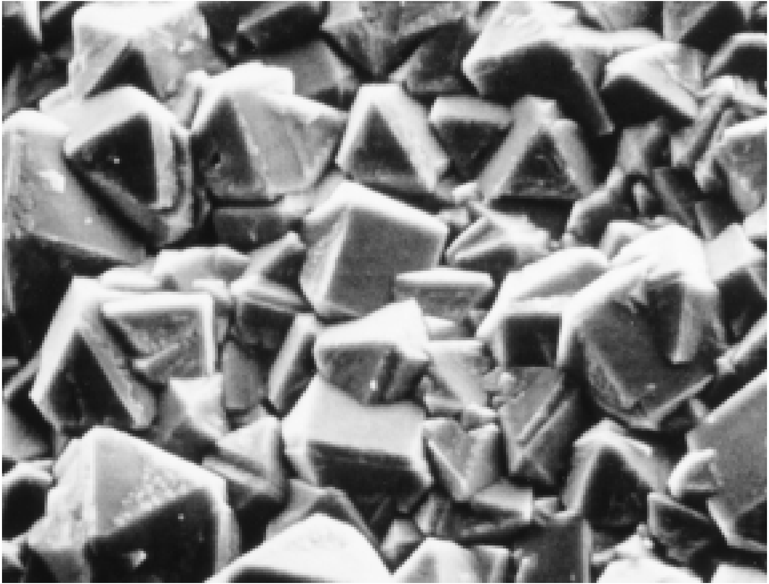

FIGURE 13.8 Scanning electron micrograph of a diamond thin film in which is shown numerous multifaceted microcrystals. 1000×. (Photograph courtesy of the Norton Company.)

Table 13.12 Trade Names, Characteristics, and Typical Applications for a Number of Plastic Materials

Material Type	*Trade Names*	*Major Application Characteristics*	*Typical Applications*
		Thermoplastics	
Acrylonitrile-butadiene-styrene (ABS)	Abson Cycolac Kralastic Lustran Novodur Tybrene	Outstanding strength and toughness, resistant to heat distortion; good electrical properties; flammable and soluble in some organic solvents	Refrigerator linings, lawn and garden equipment, toys, highway safety devices
Acrylics (polymethyl methacrylate)	Acrylite Diakon Lucite Plexiglas	Outstanding light transmission and resistance to weathering; only fair mechanical properties	Lenses, transparent aircraft enclosures, drafting equipment, outdoor signs
Fluorocarbons (PTFE or TFE)	Teflon Fluon Halar Halon Hostaflon TF	Chemically inert in almost all environments, excellent electrical properties; low coefficient of friction; may be used to 260°C (500°F); relatively weak and poor cold-flow properties	Anticorrosive seals, chemical pipes and valves, bearings, antiadhesive coatings, high-temperature electronic parts
Polyamides (nylons)	Nylon Durethan Herox Nomex Ultramid Zytel	Good mechanical strength, abrasion resistance, and toughness; low coefficient of friction; absorbs water and some other liquids	Bearings, gears, cams, bushings, handles, and jacketing for wires and cables
Polycarbonates	Baylon Iupilon Lexan Makrolon Merlon Nuclon	Dimensionally stable; low water absorption; transparent; very good impact resistance and ductility; chemical resistance not outstanding	Safety helmets, lenses, light globes, base for photographic film
Polyethylene	Alathon Alkathene Ethron Fortiflex Hi-fax Petrothene Rigidex Zendel	Chemically resistant, and electrically insulating; tough and relatively low coefficient of friction; low strength and poor resistance to weathering	Flexible bottles, toys, tumblers, battery parts, ice trays, film wrapping materials

Table 13.12 ***(Continued)***

Material Type	*Trade Names*	*Major Application Characteristics*	*Typical Applications*
Polypropylene	Bexphane Herculon Meraklon Moplen Poly-pro Pro-fax Propathene	Resistant to heat distortion; excellent electrical properties and fatigue strength; chemically inert; relatively inexpensive; poor resistance to UV light	Sterilizable bottles, packaging film, TV cabinets, luggage
Polystyrene	Carinex Celatron Hostyren Lustrex Styron Vestyron	Excellent electrical properties and optical clarity; good thermal and dimensional stability; relatively inexpensive	Wall tile, battery cases, toys, indoor lighting panels, appliance housings
Vinyls	Darvic Exon Geon Pee Vee Cee Pliovic Saran Tygon	Good low-cost, general-purpose materials; ordinarily rigid, but may be made flexible with plasticizers; often copolymerized; susceptible to heat distortion	Floor coverings, pipe, electrical wire insulation, garden hose, phonograph records
Polyester (PET or PETE)	Celanar Crastin Dacron Hylar Melinex Mylar Terylem	One of the toughest of plastic films; excellent fatigue and tear strength, and resistance to humidity, acids, greases, oils, and solvents	Magnetic recording tapes, clothing, automotive tire cords, beverage containers
		Thermosetting Polymers	
Epoxies	Araldite Epikote Epon Epi-rez Lekutherm Nepoxide	Excellent combination of mechanical properties and corrosion resistance; dimensionally stable; good adhesion; relatively inexpensive; good electrical properties	Electrical moldings, sinks, adhesives, protective coatings, used with fiberglass laminates
Phenolics	Bakelite Amberol Arofene Durite Resinox	Excellent thermal stability to over 150°C (300°F); may be compounded with a large number of resins, fillers, etc.; inexpensive	Motor housings, telephones, auto distributors, electrical fixtures
Polyesters	Aropol Baygal Derakane Laguval Laminac Selectron	Excellent electrical properties and low cost; can be formulated for room- or high-temperature use; often fiber reinforced	Helmets, fiberglass boats, auto body components, chairs, fans

Source: Adapted from C. A. Harper, Editor, *Handbook of Plastics and Elastomers.* Copyright © 1975 by McGraw-Hill Book Company. Reproduced with permission.

Table 13.13 Tabulation of Important Characteristics and Typical Applications for Five Commercial Elastomers

Chemical Type	*Trade (Common) Name*	*Elongation (%)*	*Useful Temperature Range* [°C (°F)]	*Major Application Characteristics*	*Typical Applications*
Natural polyisoprene	Natural Rubber (NR)	500–760	−60 to 120 (−75 to 250)	Excellent physical properties; good resistance to cutting, gouging, and abrasion; low heat, ozone, and oil resistance; good electrical properties	Pneumatic tires and tubes; heels and soles; gaskets
Styrene–butadiene copolymer	GRS, Buna S (SBR)	450–500	−60 to 120 (−75 to 250)	Good physical properties; excellent abrasion resistance; not oil, ozone, or weather resistant; electrical properties good, but not outstanding	Same as natural rubber
Acrylonitrile–butadiene copolymer	Buna A, Nitrile (NBR)	400–600	−50 to 150 (−60 to 300)	Excellent resistance to vegetable, animal, and petroleum oils; poor low-temperature properties; electrical properties not outstanding	Gasoline, chemical, and oil hose; seals and O-rings; heels and soles
Chloroprene	Neoprene (CR)	100–800	−50 to 105 (−60 to 225)	Excellent ozone, heat, and weathering resistance; good oil resistance; excellent flame resistance; not as good in electrical applications as natural rubber	Wire and cable; chem. tank linings; belts, hoses, seals, and gaskets
Polysiloxane	Silicone (VMQ)	100–800	−115 to 315 (−175 to 600)	Excellent resistance to high and low temperatures; low strength; excellent electrical properties	High- and low-temperature insulation; seals, diaphragms; tubing for food and medical uses

Sources: Adapted from: C. A. Harper, Editor, *Handbook of Plastics and Elastomers.* Copyright © 1975 by McGraw-Hill Book Company, reproduced with permission; and Materials Engineering's *Materials Selector,* copyright Penton/IPC.

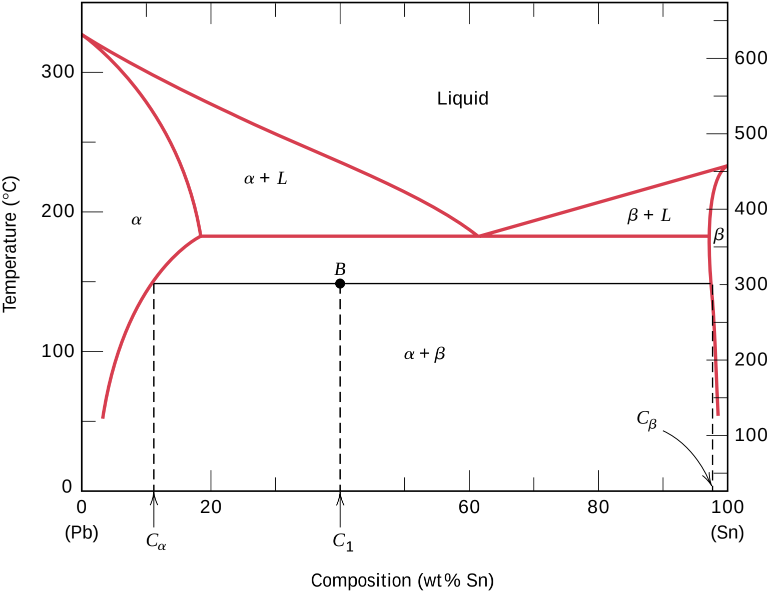

FIGURE 10.8 The lead–tin phase diagram. For a 40 wt% Sn–60 wt% Pb alloy at 150°C (point *B*), phase compositions and relative amounts are computed in Example Problems 10.2 and 10.3.

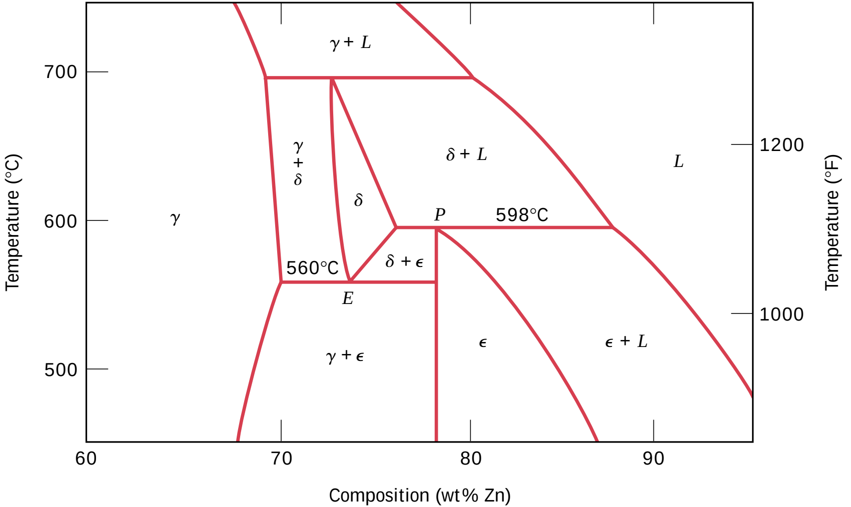

Figure 10.19 A region of the copper–zinc phase diagram that has been enlarged to show eutectoid and peritectic invariant points, labeled *E* (560°C, 74 wt% Zn) and *P* (598°C, 78.6 wt% Zn), respectively. (Adapted from *Binary Alloy Phase Diagrams*, 2nd edition, Vol. 2, T. B. Massalski, Editor-in-Chief, 1990. Reprinted by permission of ASM International, Materials Park, OH.)

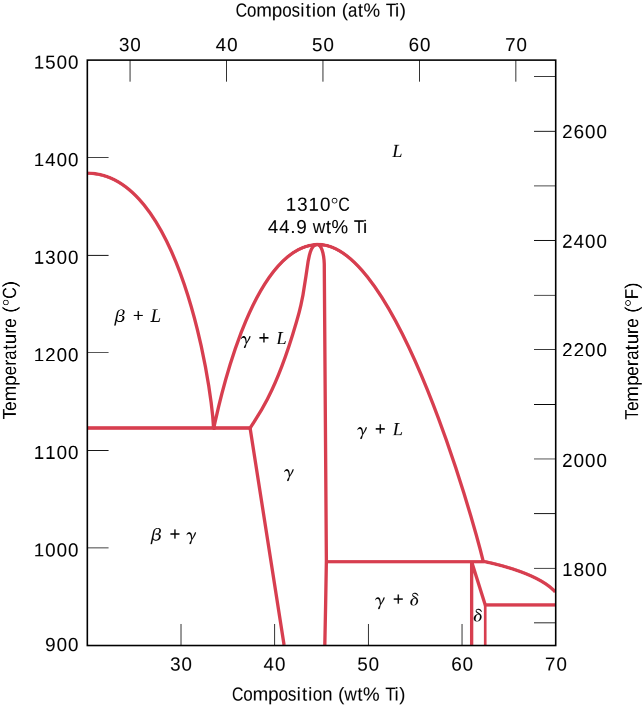

FIGURE 10.20 A portion of the nickel–titanium phase diagram on which is shown a congruent melting point for the γ phase solid solution at 1310°C and 44.9 wt% Ti. (Adapted from *Phase Diagrams of Binary Nickel Alloys*, P. Nash, Editor, 1991. Reprinted by permission of ASM International, Materials Park, OH.)

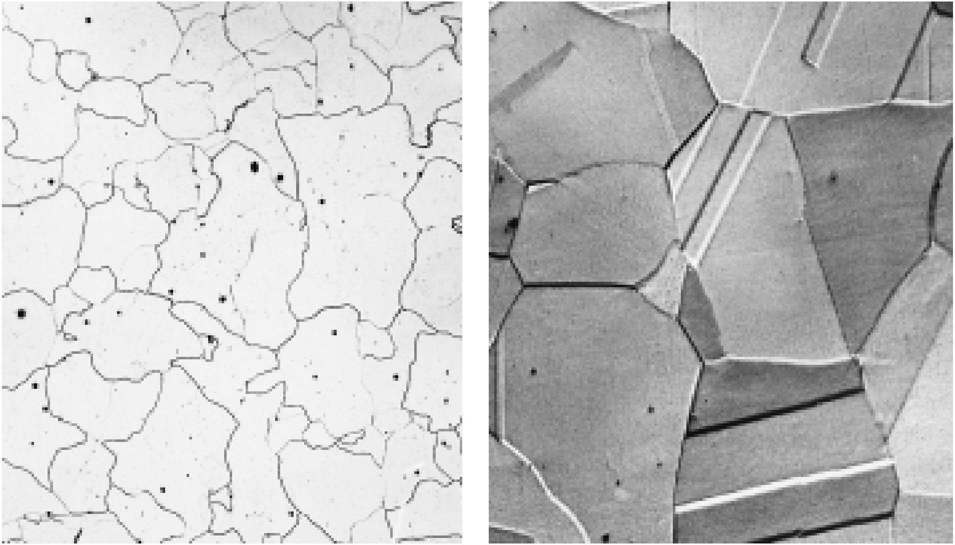

(a) *(b)*

Figure 10.27 Photomicrographs of (*a*) α ferrite (90×) and (*b*) austenite (325×). (Copyright 1971 by United States Steel Corporation.)

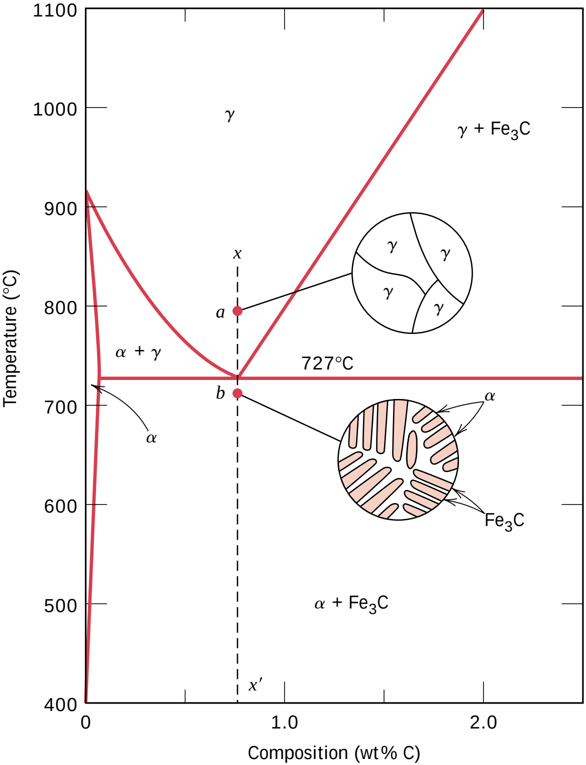
1100
1000
900
800
700
600
500
400
Temperature (°C)
0
1.0
2.0
Composition (wt% C)
γ
γ + Fe3C
α + γ
α + Fe3C
727°C
x
x′
a
b
α
γ
γ
γ
γ
α
Fe3C

FIGURE 10.28 Schematic representations of the microstructures for an iron–carbon alloy of eutectoid composition (0.76 wt% C) above and below the eutectoid temperature.

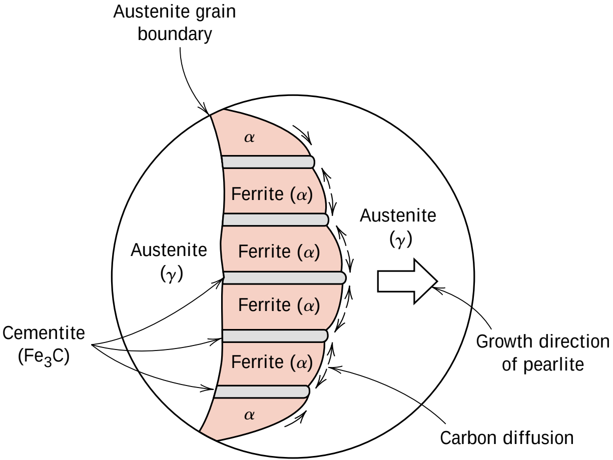
Austenite grain boundary
α
Ferrite (α)
Ferrite (α)
Ferrite (α)
Ferrite (α)
α
Austenite (γ)
Austenite (γ)
Cementite (Fe_3C)
Growth direction of pearlite
Carbon diffusion

Figure 10.30 Schematic representation of the formation of pearlite from austenite; direction of carbon diffusion indicated by arrows.

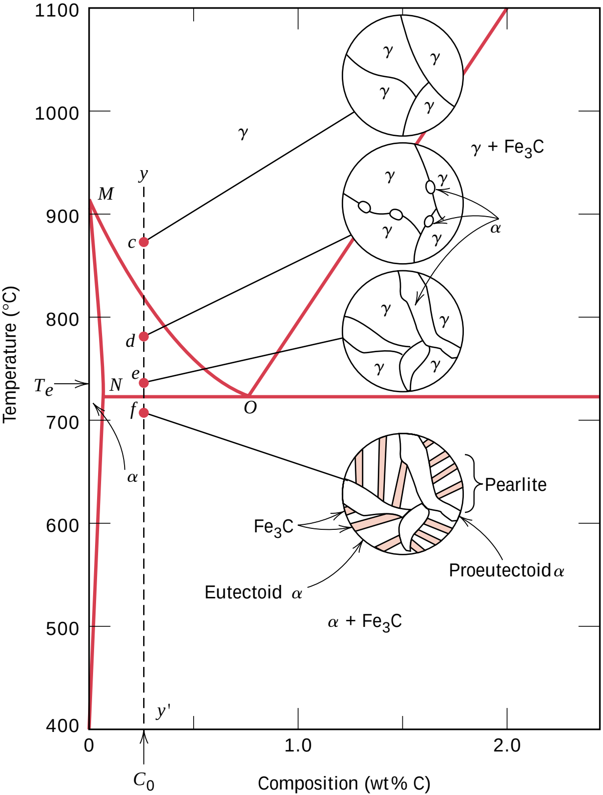
1100
1000
900
800
700
600
500
400
Temperature (°C)
T_e
M
N
O
y
y'
c
d
e
f
α
γ
γ + Fe$_3$C
α + Fe$_3$C
Pearlite
Fe$_3$C
Eutectoid α
Proeutectoid α
0
1.0
2.0
C_0
Composition (wt% C)

Figure 10.31 Schematic representations of the microstructures for an iron–carbon alloy of hypoeutectoid composition C_0 (containing less than 0.76 wt% C) as it is cooled from within the austenite phase region to below the eutectoid temperature.

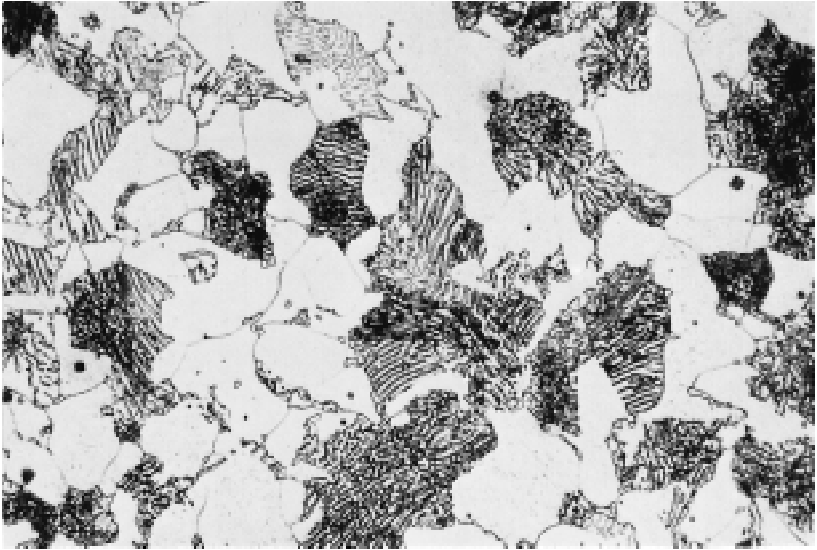

Figure 10.32 Photomicrograph of a 0.38 wt% C steel having a microstructure consisting of pearlite and proeutectoid ferrite. 635×. (Photomicrograph courtesy of Republic Steel Corporation.)

Figure 10.33 A portion of the Fe–Fe_3C phase diagram used in computations for relative amounts of proeutectoid and pearlite microconstituents for hypoeutectoid (C_0') and hypereutectoid (C_1') compositions.

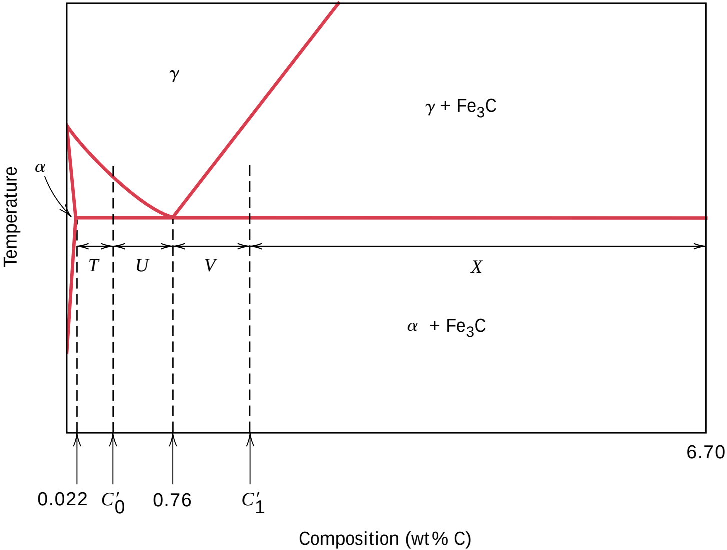

γ
γ + Fe_3C
α
Temperature
T
U
V
X
α + Fe_3C
6.70
0.022
C_0'
0.76
C_1'
Composition (wt% C)

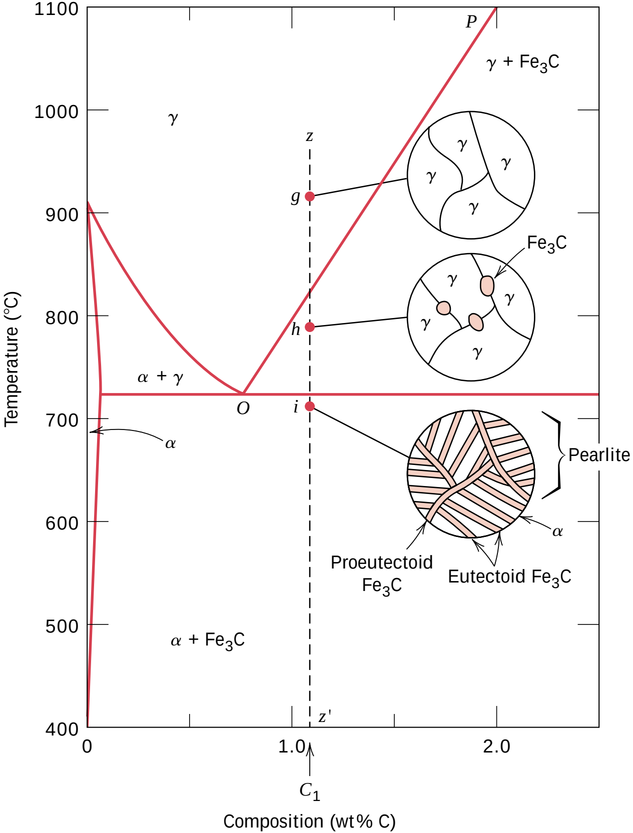
1100
1000
900
800
700
600
500
400
Temperature (°C)
0
1.0
2.0
C_1
Composition (wt% C)
P
$\gamma + Fe_3C$
γ
z
g
h
i
O
z'
$\alpha + \gamma$
α
$\alpha + Fe_3C$
Fe_3C
Pearlite
Proeutectoid Fe_3C
Eutectoid Fe_3C

Figure 10.34 Schematic representations of the microstructures for an iron–carbon alloy of hypereutectoid composition C_1 (containing between 0.76 and 2.14 wt% C), as it is cooled from within the austenite phase region to below the eutectoid temperature.

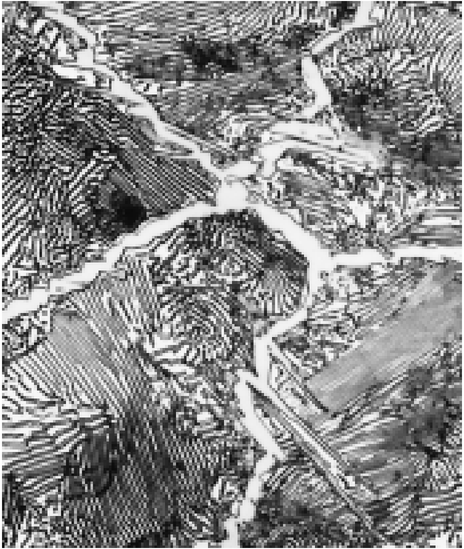

Figure 10.35 Photomicrograph of a 1.4 wt% C steel having a microstructure consisting of a white proeutectoid cementite network surrounding the pearlite colonies. 1000×. (Copyright 1971 by United States Steel Corporation.)

FIGURE 10.38 Logarithm pressure-versus-temperature phase diagram for H_2O.

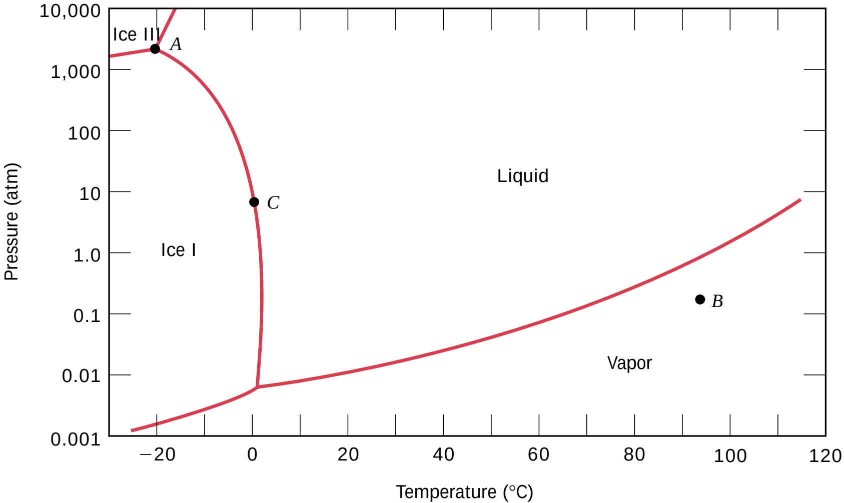

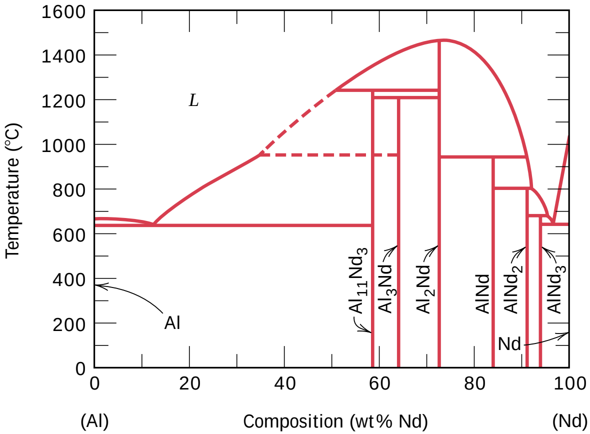

FIGURE 10.39 The aluminum–neodymium phase diagram. (Adapted from *ASM Handbook*, Vol. 3, *Alloy Phase Diagrams*, H. Baker, Editor, 1992. Reprinted by permission of ASM International, Materials Park, OH.)

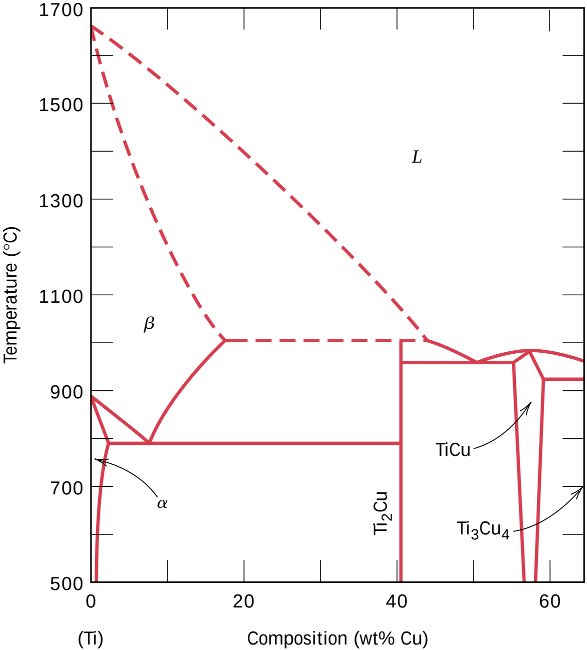

Figure 10.40 The titanium–copper phase diagram. (Adapted from *Phase Diagrams of Binary Titanium Alloys*, J. L. Murray, Editor, 1987. Reprinted by permission of ASM International, Materials Park, OH.)

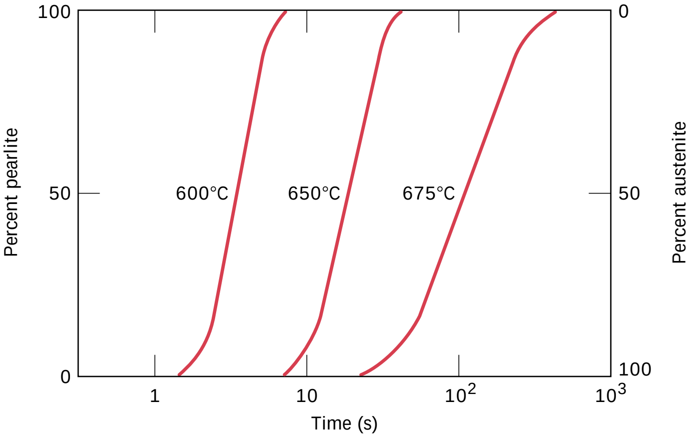

FIGURE 11.3 For an iron–carbon alloy of eutectoid composition (0.76 wt% C), isothermal fraction reacted versus the logarithm of time for the austenite-to-pearlite transformation.

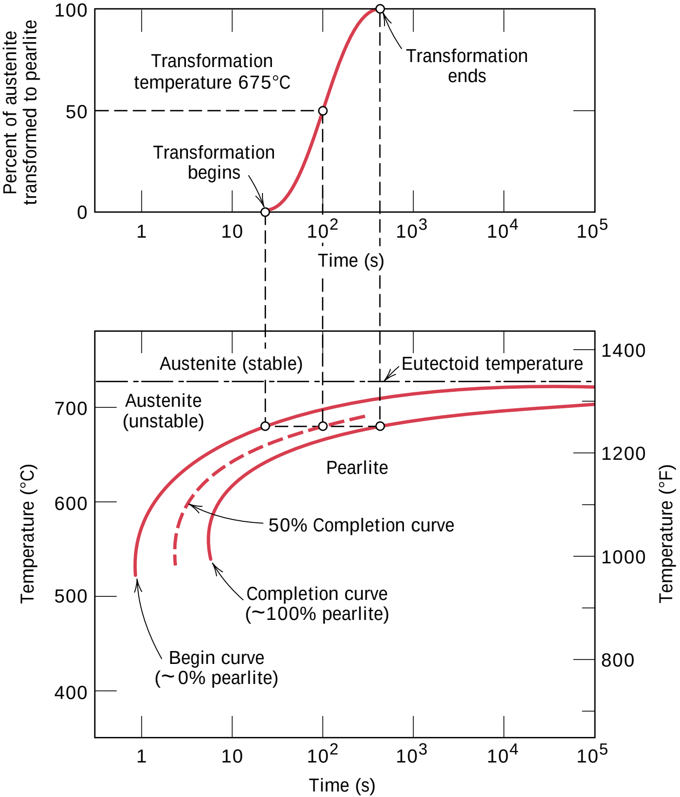

FIGURE 11.4 Demonstration of how an isothermal transformation diagram (bottom) is generated from percent transformation-versus-logarithm of time measurements (top). (Adapted from H. Boyer, Editor, *Atlas of Isothermal Transformation and Cooling Transformation Diagrams*, American Society for Metals, 1977, p. 369.)

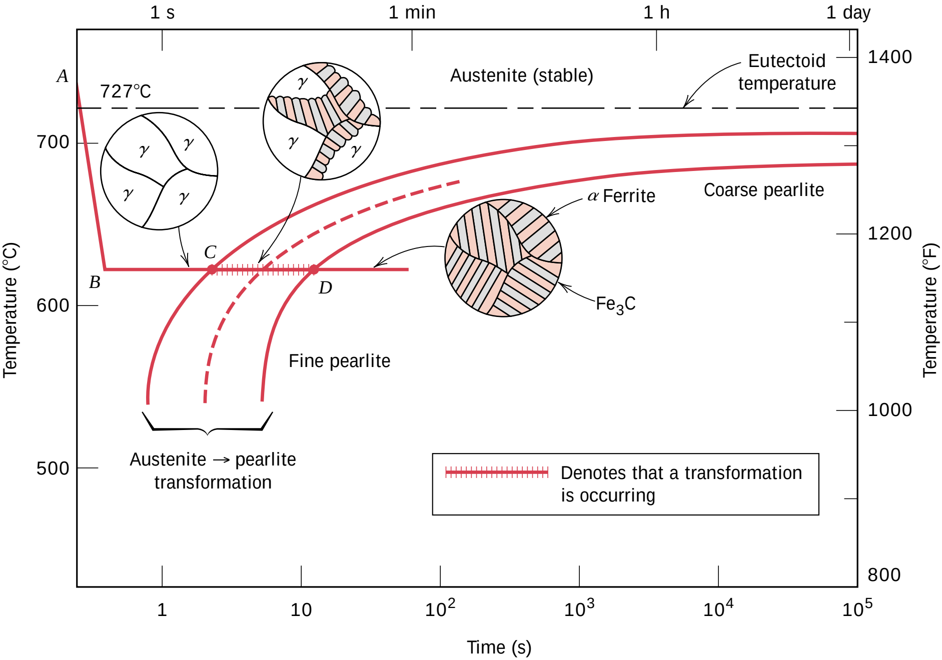

Figure 11.5 Isothermal transformation diagram for a eutectoid iron–carbon alloy, with superimposed isothermal heat treatment curve (*ABCD*). Microstructures before, during, and after the austenite-to-pearlite transformation are shown. (Adapted from H. Boyer, Editor, *Atlas of Isothermal Transformation and Cooling Transformation Diagrams,* American Society for Metals, 1977, p. 28.)

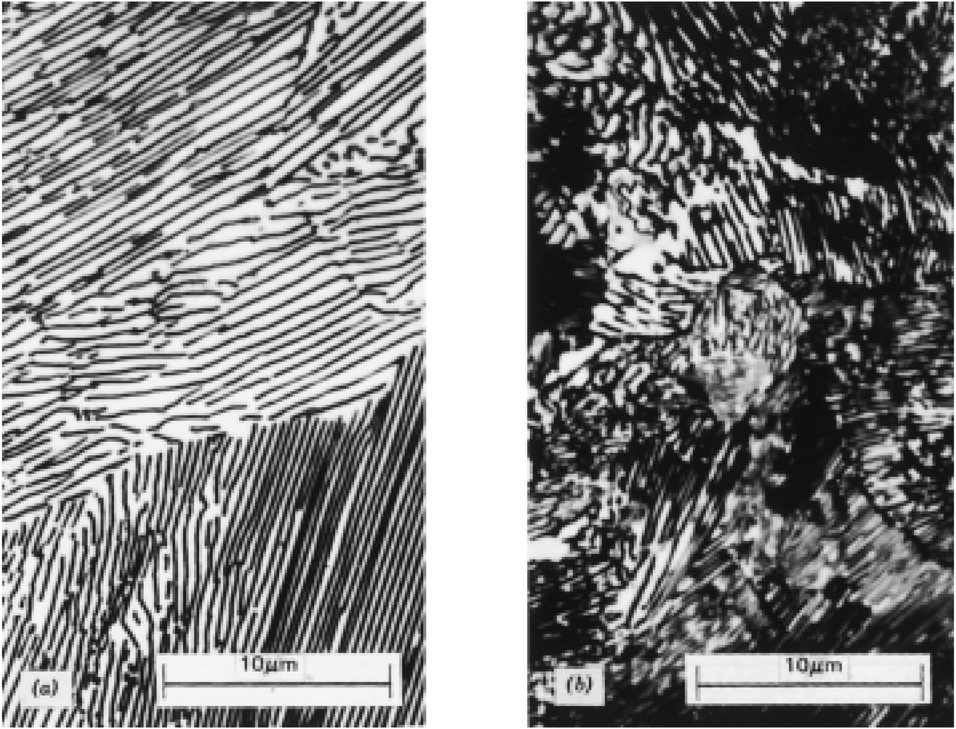

Figure 11.6 Photomicrographs of (*a*) coarse pearlite and (*b*) fine pearlite. 3000×. (From K. M. Ralls, et al., *An Introduction to Materials Science and Engineering*, p. 361. Copyright © 1976 by John Wiley & Sons, New York. Reprinted by permission of John Wiley & Sons, Inc.)

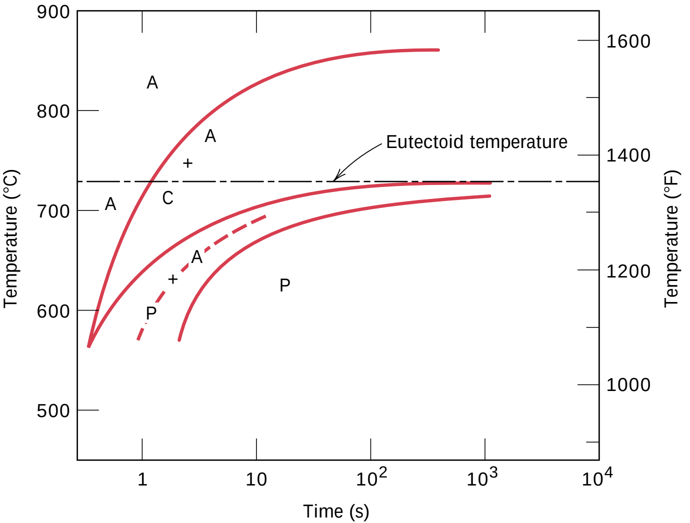

FIGURE 11.7 Isothermal transformation diagram for a 1.13 wt% C iron–carbon alloy: A, austenite; C, proeutectoid cementite; P, pearlite. (Adapted from H. Boyer, Editor, *Atlas of Isothermal Transformation and Cooling Transformation Diagrams*, American Society for Metals, 1977, p. 33.)

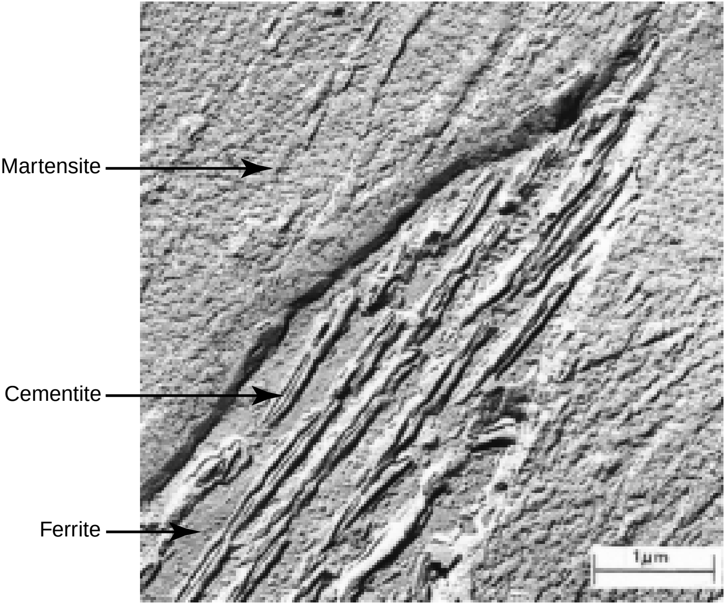

FIGURE 11.8 Replica transmission electron micrograph showing the structure of bainite. A grain of bainite passes from lower left to upper right-hand corners, which consists of elongated and needle-shaped particles of Fe_3C within a ferrite matrix. The phase surrounding the bainite is martensite. (Reproduced with permission from *Metals Handbook,* Vol. 8, 8th edition, *Metallography, Structures and Phase Diagrams,* American Society for Metals, Materials Park, OH, 1973.)

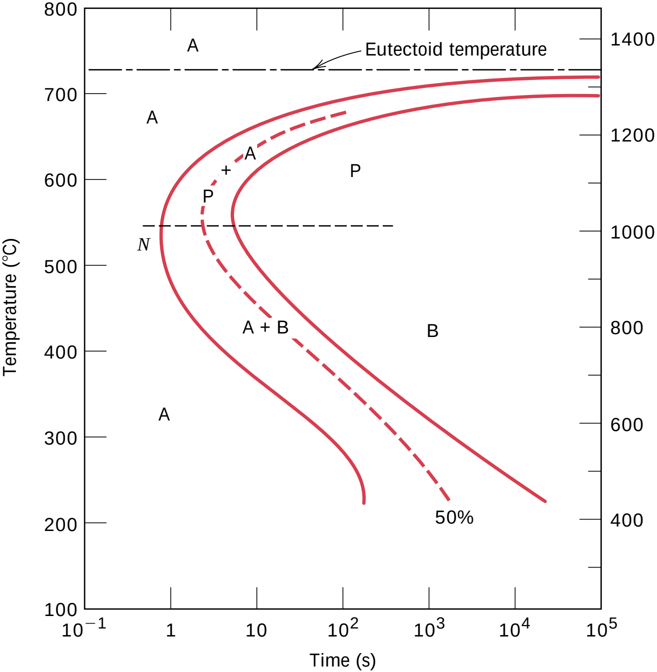

FIGURE 11.9 Isothermal transformation diagram for an iron–carbon alloy of eutectoid composition, including austenite-to-pearlite (A–P) and austenite-to-bainite (A–B) transformations. (Adapted from H. Boyer, Editor, *Atlas of Isothermal Transformation and Cooling Transformation Diagrams*, American Society for Metals, 1977, p. 28.)

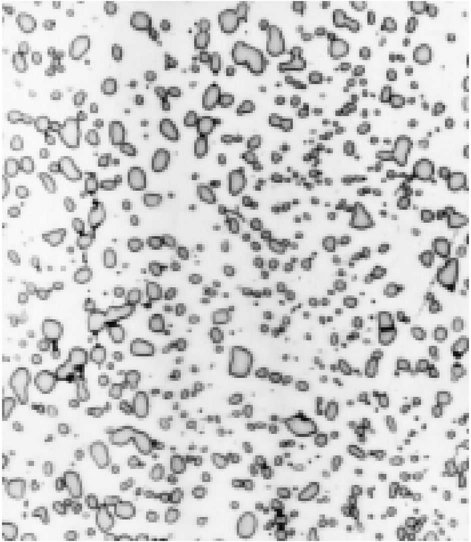

Figure 11.10 Photomicrograph of a steel having a spheroidite microstructure. The small particles are cementite; the continuous phase is α ferrite. 1000×. (Copyright 1971 by United States Steel Corporation.)

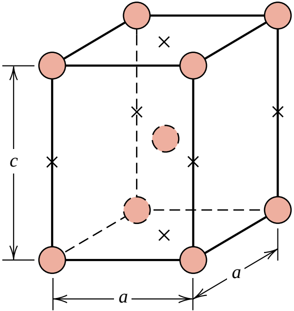

Figure 11.12 The body-centered tetragonal unit cell for martensitic steel showing iron atoms (circles) and sites that may be occupied by carbon atoms (crosses). For this tetragonal unit cell, $c > a$.

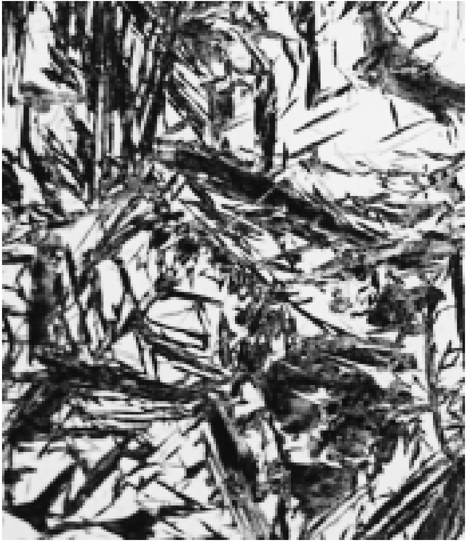

FIGURE 11.13 Photomicrograph showing the martensitic microstructure. The needle-shaped grains are the martensite phase, and the white regions are austenite that failed to transform during the rapid quench. 1220×. (Photomicrograph courtesy of United States Steel Corporation.)

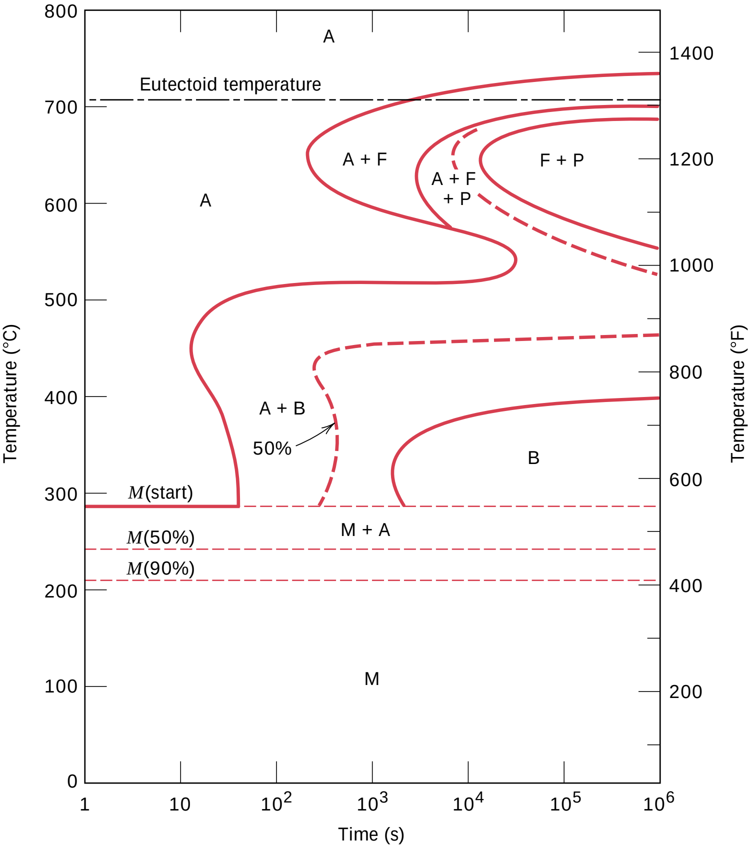

FIGURE 11.15 Isothermal transformation diagram for an alloy steel (type 4340): A, austenite; B, bainite; P, pearlite; M, martensite; F, proeutectoid ferrite. (Adapted from H. Boyer, Editor, *Atlas of Isothermal Transformation and Cooling Transformation Diagrams*, American Society for Metals, 1977, p. 181.)

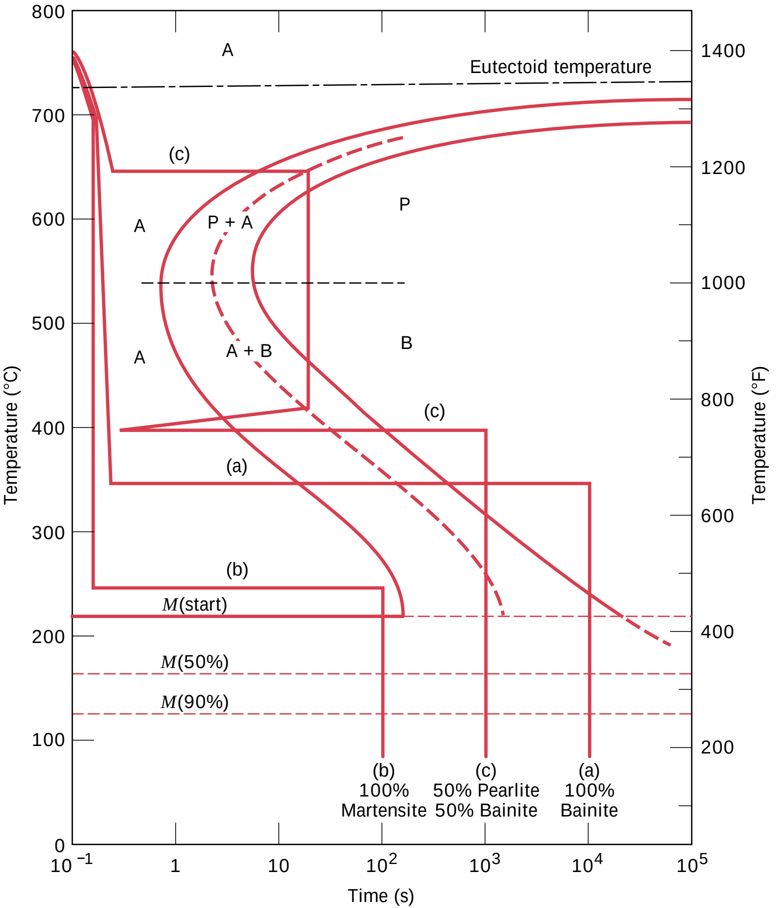

FIGURE 11.16 Isothermal transformation diagram for an iron–carbon alloy of eutectoid composition and the isothermal heat treatments (a), (b), and (c) in Example Problem 11.1.

Chapter 11 / Phase Transformations

11.6 CONTINUOUS COOLING TRANSFORMATION DIAGRAMS

Isothermal heat treatments are not the most practical to conduct because an alloy must be rapidly cooled to and maintained at an elevated temperature from a higher temperature above the eutectoid. Most heat treatments for steels involve the continuous cooling of a specimen to room temperature. An isothermal transformation diagram is valid only for conditions of constant temperature, which diagram must be modified for transformations that occur as the temperature is constantly changing. For continuous cooling, the time required for a reaction to begin and end is delayed. Thus the isothermal curves are shifted to longer times and lower temperatures, as indicated in Figure 11.17 for an iron–carbon alloy of eutectoid composition. A plot containing such modified beginning and ending reaction curves is termed a **continuous cooling transformation** (CCT) **diagram.** Some control may be maintained over the rate of temperature change depending on the cooling environment. Two cooling curves corresponding to moderately fast and slow rates are superimposed and labeled in Figure 11.18, again for a eutectoid steel. The transformation starts after a time period corresponding to the intersection of the cooling curve with the beginning reaction curve and concludes upon crossing the completion transformation curve. The microstructural products for the moderately rapid and slow cooling rate curves in Figure 11.18 are fine and coarse pearlite, respectively.

Normally, bainite will not form when an alloy of eutectoid composition or, for that matter, any plain carbon steel is continuously cooled to room temperature. This is because all the austenite will have transformed to pearlite by the time the bainite transformation has become possible. Thus, the region representing the austenite–pearlite transformation terminates just below the nose (Figure 11.18) as indicated by the curve AB. For any cooling curve passing through AB in Figure 11.18, the transformation ceases at the point of intersection; with continued cooling, the unreacted austenite begins transforming to martensite upon crossing the M(start) line.

With regard to the representation of the martensitic transformation, the M(start), M(50%), and M(90%) lines occur at identical temperatures for both isothermal and continuous cooling transformation diagrams. This may be verified for an iron–carbon alloy of eutectoid composition by comparison of Figures 11.14 and 11.17.

For the continuous cooling of a steel alloy, there exists a critical quenching rate, which represents the minimum rate of quenching that will produce a totally martensitic structure. This critical cooling rate, when included on the continuous transformation diagram, will just miss the nose at which the pearlite transformation begins, as illustrated in Figure 11.19. As the figure also shows, only martensite will exist for quenching rates greater than the critical; in addition, there will be a range

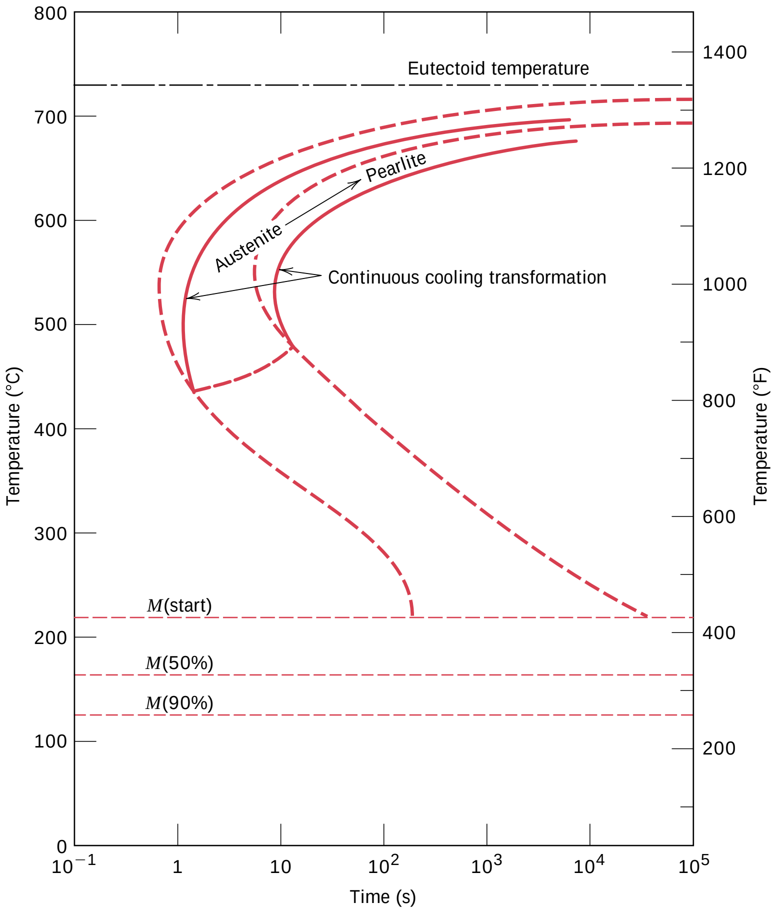

FIGURE 11.17 Superimposition of isothermal and continuous cooling transformation diagrams for a eutectoid iron–carbon alloy. (Adapted from H. Boyer, Editor, *Atlas of Isothermal Transformation and Cooling Transformation Diagrams,* American Society for Metals, 1977, p. 376.)

of rates over which both pearlite and martensite are produced. Finally, a totally pearlitic structure develops for low cooling rates.

Carbon and other alloying elements also shift the pearlite (as well as the proeutectoid phase) and bainite noses to longer times, thus decreasing the critical cooling rate. In fact, one of the reasons for alloying steels is to facilitate the formation of martensite so that totally martensitic structures can develop in relatively thick cross sections. Figure 11.20 shows the continuous cooling transformation diagram for the same alloy steel the isothermal transformation diagram for which is presented in Figure 11.15. The presence of the bainite nose accounts for the possibility of formation of bainite for a continuous cooling heat treatment. Several cooling curves superimposed on Figure 11.20 indicate the critical cooling rate, and also how the transformation behavior and final microstructure are influenced by the rate of cooling.

Interestingly enough, the critical cooling rate is diminished even by the presence of carbon. In fact, iron–carbon alloys containing less than about 0.25 wt% carbon are not normally heat treated to form martensite because quenching rates too rapid to be practical are required. Other alloying elements that are particularly effective in rendering steels heat treatable are chromium, nickel, molybdenum, manganese, silicon, and tungsten; however, these elements must be in solid solution with the austenite at the time of quenching.

Figure 11.18 Moderately rapid and slow cooling curves superimposed on a continuous cooling transformation diagram for a eutectoid iron–carbon alloy.

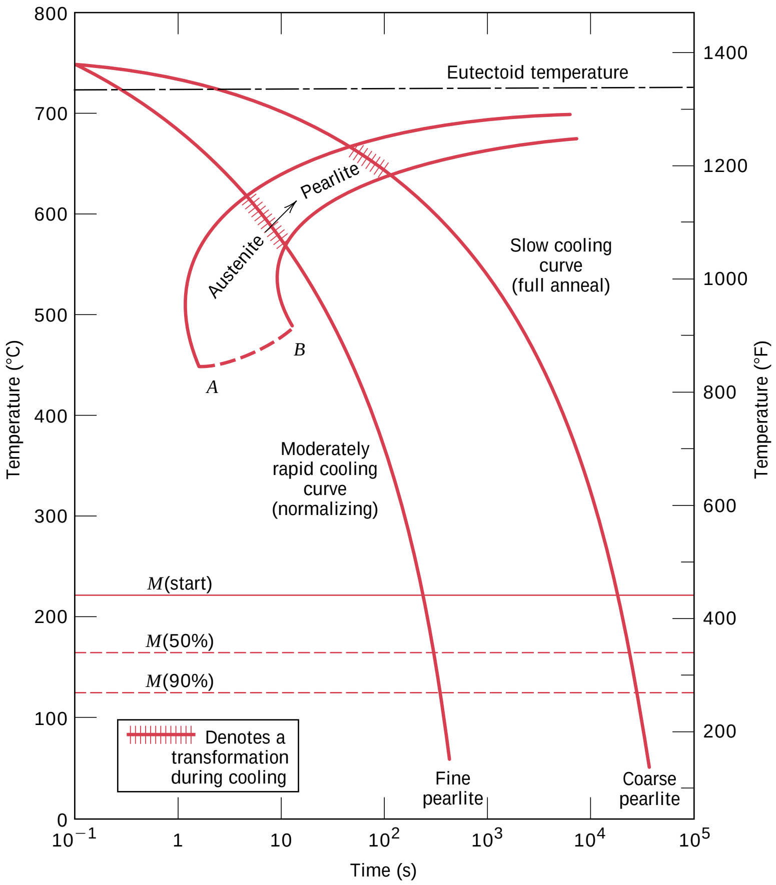

In summary, isothermal and continuous transformation diagrams are, in a sense, phase diagrams in which the parameter of time is introduced. Each is experimentally determined for an alloy of specified composition, the variables being temperature and time. These diagrams allow prediction of the microstructure after some time period for constant temperature and continuous cooling heat treatments, respectively.

11.17 FACTORS THAT INFLUENCE MELTING AND GLASS TRANSITION TEMPERATURES

MELTING TEMPERATURE

During melting of a polymer there will necessarily occur a rearrangement of the molecules in the transformation from ordered to disordered molecular states. Molecular chemistry and structure will influence the ability of the polymer chain molecules to make these rearrangements, and, therefore, will also affect the melting temperature.

Chain stiffness, which is controlled by the ease of rotation about the chemical bonds along the chain, has a pronounced effect. The presence of double-chain bonds and aromatic groups lowers chain flexibility and causes an increase in T_m. Furthermore, the size and type of side groups influence chain rotational freedom

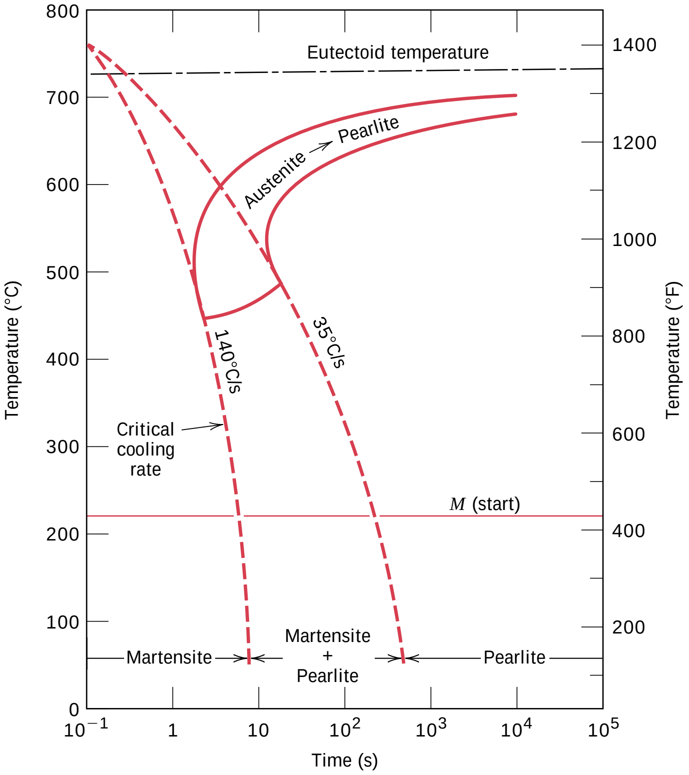

FIGURE 11.19 Continuous cooling transformation diagram for a eutectoid iron–carbon alloy and superimposed cooling curves, demonstrating the dependence of the final microstructure on the transformations that occur during cooling.

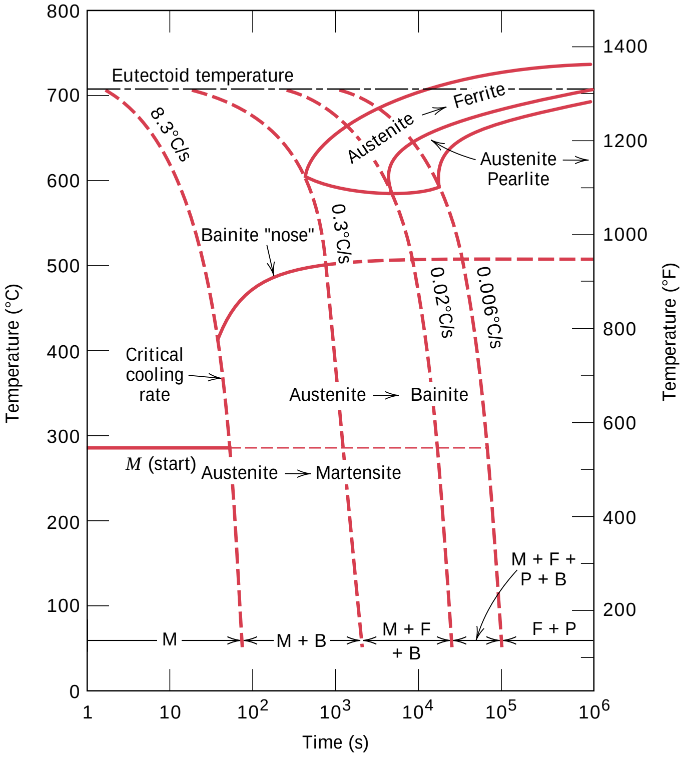

FIGURE 11.20 Continuous cooling transformation diagram for an alloy steel (type 4340) and several superimposed cooling curves demonstrating dependency of the final microstructure of this alloy on the transformations that occur during cooling. (Adapted from H. E. McGannon, Editor, *The Making, Shaping and Treating of Steel*, 9th edition, United States Steel Corporation, Pittsburgh, 1971, p. 1096.)

and flexibility; bulky or large side groups tend to restrict molecular rotation and raise T_m. For example, polypropylene has a higher melting temperature than polyethylene (175°C versus 115°C, Table 11.1); the CH_3 methyl side group for polypropylene is larger than the H atom found on polyethylene. The presence of polar side groups (viz. Cl, OH, and CN), even though not excessively large, leads to significant intermolecular bonding forces and relatively high T_ms. This may be verified by comparing the melting temperatures of polypropylene (175°C) and polyvinyl chloride (212°C).

For a specific polymer, melting temperature will also depend on molecular weight. At relatively low molecular weights, increasing $\overline{M}$ (or chain length) raises T_m (Figure 11.37). Furthermore, the melting of a polymer takes place over a range of temperatures, and, thus, there will exist a range of T_ms, rather than a single melting temperature. This is because, every polymer will be composed of molecules having a variety of molecular weights (Section 4.5), and because T_m depends on molecular weight. For most polymers, this melting temperature range will normally be on the order of several degrees Celsius. Those melting temperatures cited in Table 11.1 and Appendix E are near the high ends of these ranges.

Degree of branching will also affect the melting temperature of a polymer. The introduction of side branches introduces defects into the crystalline material and lowers the melting temperature. High-density polyethylene, being a predominately linear polymer, has a higher melting temperature (137°C, Table 11.1) than low-density polyethylene (115°C) which has some branching.

GLASS TRANSITION TEMPERATURE

Upon heating through the glass transition temperature, the amorphous solid polymer transforms from a rigid to a rubbery state. Correspondingly, the molecules which are virtually frozen in position below T_g begin to experience rotational and translational motions above T_g. Thus, the value of the glass transition temperature will depend on molecular characteristics that affect chain stiffness; most of these factors and their influences are the same as for the melting temperature, as discussed above. Again, chain flexibility is diminished and T_g is increased by the following:

1. The presence of bulky side groups; from Table 11.1, the respective values for polypropylene and polystyrene are −18°C and 100°C.

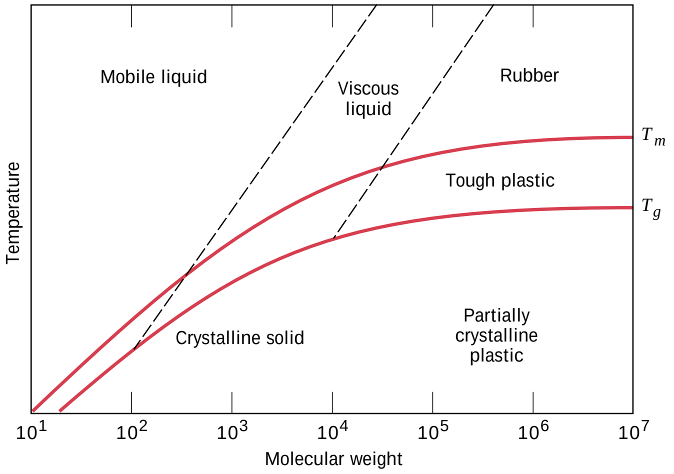

Figure 11.37 Dependence of polymer properties as well as melting and glass transition temperatures on molecular weight. (From F. W. Billmeyer, Jr., *Textbook of Polymer Science*, 3rd edition. Copyright © 1984 by John Wiley & Sons, New York. Reprinted by permission of John Wiley & Sons, Inc.)

2. Polar side atoms or groups of atoms; this may be confirmed by comparing T_g values for polyvinyl chloride and polypropylene (87°C versus −18°C).
3. Double-chain bonds and aromatic chain groups which tend to stiffen the molecular backbone.

Increasing the molecular weight also tends to raise the glass transition temperature, as noted in Figure 11.37. A small amount of branching will tend to lower T_g; on the other hand, a high density of branches reduces chain mobility, and elevates the glass transition temperature. Some amorphous polymers are crosslinked, which has been observed to elevate T_g; crosslinks restrict molecular motion. With a high density of crosslinks, molecular motion is virtually disallowed; long-range molecular motion is prevented, to the degree that these polymers do not experience a glass transition or its accompanying softening.

From the preceding discussion it is evident that essentially the same molecular characteristics raise and lower both melting and glass transition temperatures; normally the value of T_g lies somewhere between 0.5 and $0.8T_m$ (in Kelvin). Consequently, for a homopolymer, it is not possible to independently vary both T_m and T_g. A greater degree of control over these two parameters is possible by the synthesis and utilization of copolymeric materials.

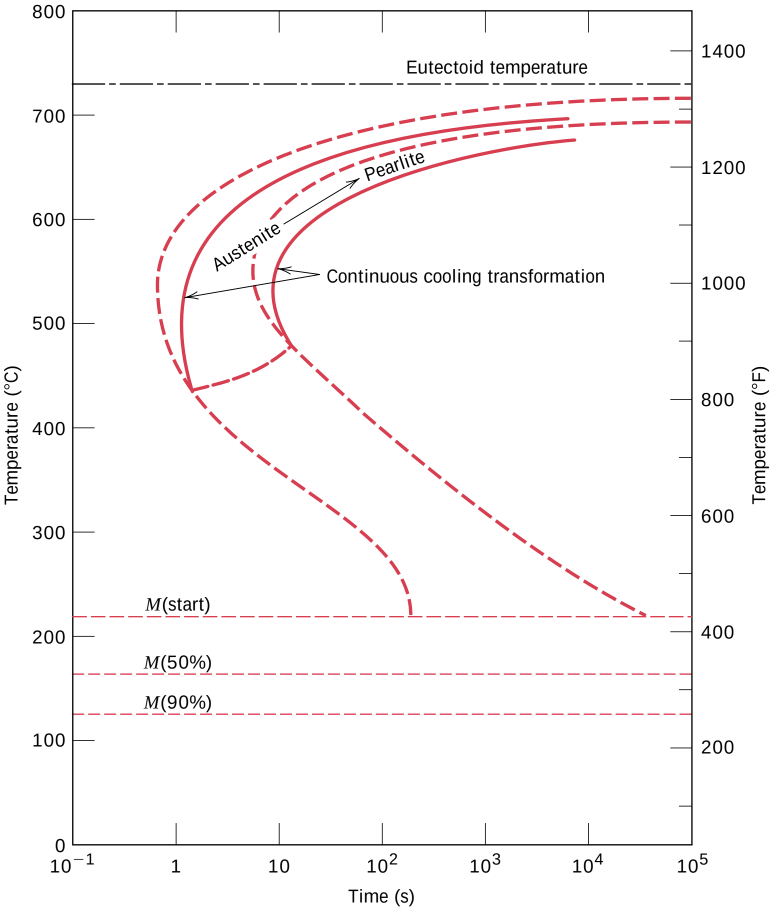

FIGURE 11.17 Superimposition of isothermal and continuous cooling transformation diagrams for a eutectoid iron–carbon alloy. (Adapted from H. Boyer, Editor, *Atlas of Isothermal Transformation and Cooling Transformation Diagrams*, American Society for Metals, 1977, p. 376.)

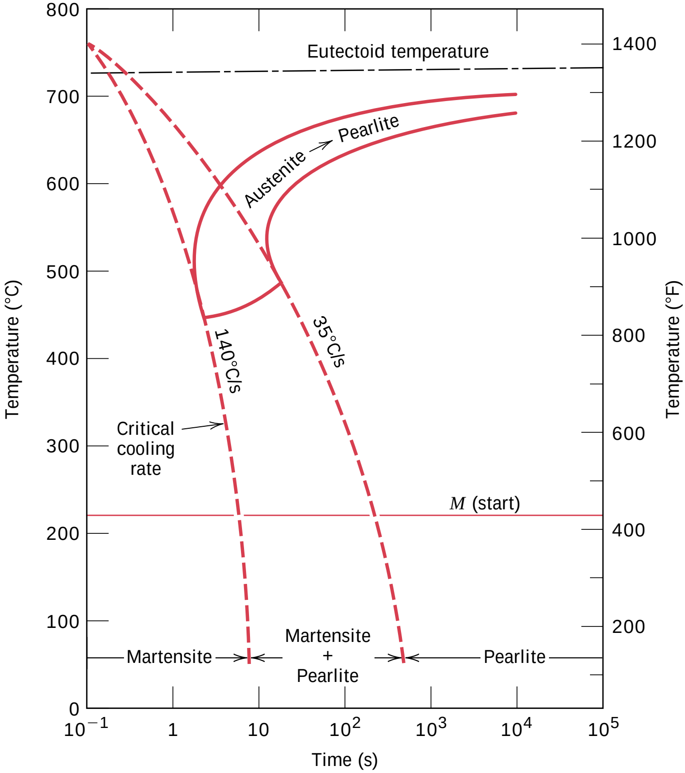

FIGURE 11.19 Continuous cooling transformation diagram for a eutectoid iron–carbon alloy and superimposed cooling curves, demonstrating the dependence of the final microstructure on the transformations that occur during cooling.

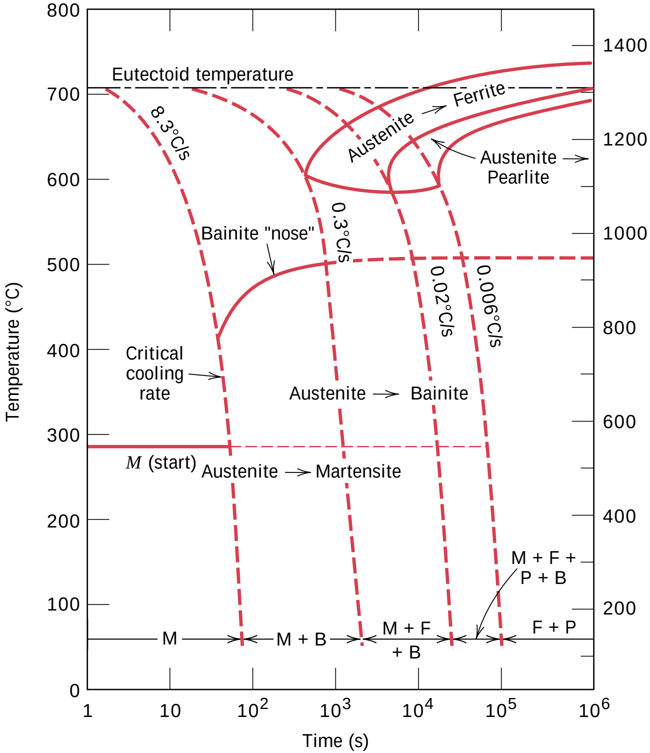

FIGURE 11.20 Continuous cooling transformation diagram for an alloy steel (type 4340) and several superimposed cooling curves demonstrating dependency of the final microstructure of this alloy on the transformations that occur during cooling. (Adapted from H. E. McGannon, Editor, *The Making, Shaping and Treating of Steel*, 9th edition, United States Steel Corporation, Pittsburgh, 1971, p. 1096.)

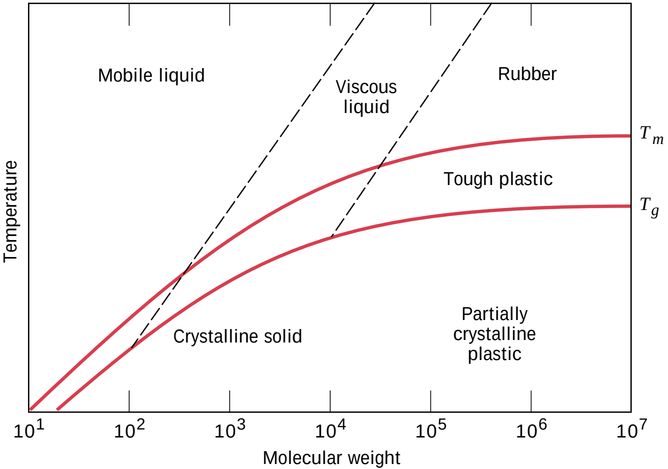

FIGURE 11.37 Dependence of polymer properties as well as melting and glass transition temperatures on molecular weight. (From F. W. Billmeyer, Jr., *Textbook of Polymer Science*, 3rd edition. Copyright © 1984 by John Wiley & Sons, New York. Reprinted by permission of John Wiley & Sons, Inc.)

Table 11.1 Melting and Glass Transition Temperatures for Some of the More Common Polymeric Materials

Material	*Glass Transition Temperature* [*°C* (*°F*)]	*Melting Temperature* [*°C* (*°F*)]
Polyethylene (low density)	−110 (−165)	115 (240)
Polytetrafluoroethylene	−97 (−140)	327 (620)
Polyethylene (high density)	−90 (−130)	137 (279)
Polypropylene	−18 (0)	175 (347)
Nylon 6,6	57 (135)	265 (510)
Polyester (PET)	69 (155)	265 (510)
Polyvinyl chloride	87 (190)	212 (415)
Polystyrene	100 (212)	240 (465)
Polycarbonate	150 (300)	265 (510)

Appendix E / Glass Transition and Melting Temperatures for Common Polymeric Materials

Polymer	***Glass Transition Temperature [°C (°F)]***	***Melting Temperature [°C (°F)]***
Aramid	375 (705)	~640 (~1185)
Polyimide (thermoplastic)	280–330 (535–625)	[a]
Polyamide-imide	277–289 (530–550)	[a]
Polycarbonate	150 (300)	265 (510)
Polyetheretherketone	143 (290)	334 (635)
Polyacrylonitrile	104 (220)	317 (600)
Polystyrene		
• Atactic	100 (212)	[a]
• Isotactic	100 (212)	240 (465)
Polybutylene terephthalate	—	220–267 (428–513)
Polyvinyl chloride	87 (190)	212 (415)
Polyphenylene sulfide	85 (185)	285 (545)
Polyethylene terephthalate	69 (155)	265 (510)
Nylon 6,6	57 (135)	265 (509)
Polymethyl methacrylate		
• Syndiotactic	3 (35)	105 (220)
• Isotactic	3 (35)	45 (115)
Polypropylene		
• Isotactic	−10 (15)	175 (347)
• Atactic	−18 (0)	175 (347)
Polyvinylidene chloride	−17 (1)	198 (390)
• Atactic	−18 (0)	175 (347)
Polyvinyl fluoride	−20 (−5)	200 (390)
Polyvinylidene fluoride	−35 (−30)	—
Polychloroprene (chloroprene rubber or neoprene)	−50 (−60)	80 (175)
Polyisobutylene	−70 (−95)	128 (260)
cis-Polyisoprene	−73 (−100)	28 (80)
Polybutadiene		
• Syndiotactic	−90 (−130)	154 (310)
• Isotactic	−90 (−130)	120 (250)
High density polyethylene	−90 (−130)	137 (279)
Polytetrafluoroethylene	−97 (−140)	327 (620)
Low density polyethylene	−110 (−165)	115 (240)
Polydimethylsiloxane (silicone rubber)	−123 (−190)	−54 (−65)

[a] These polymers normally exist at least 95% noncrystalline.

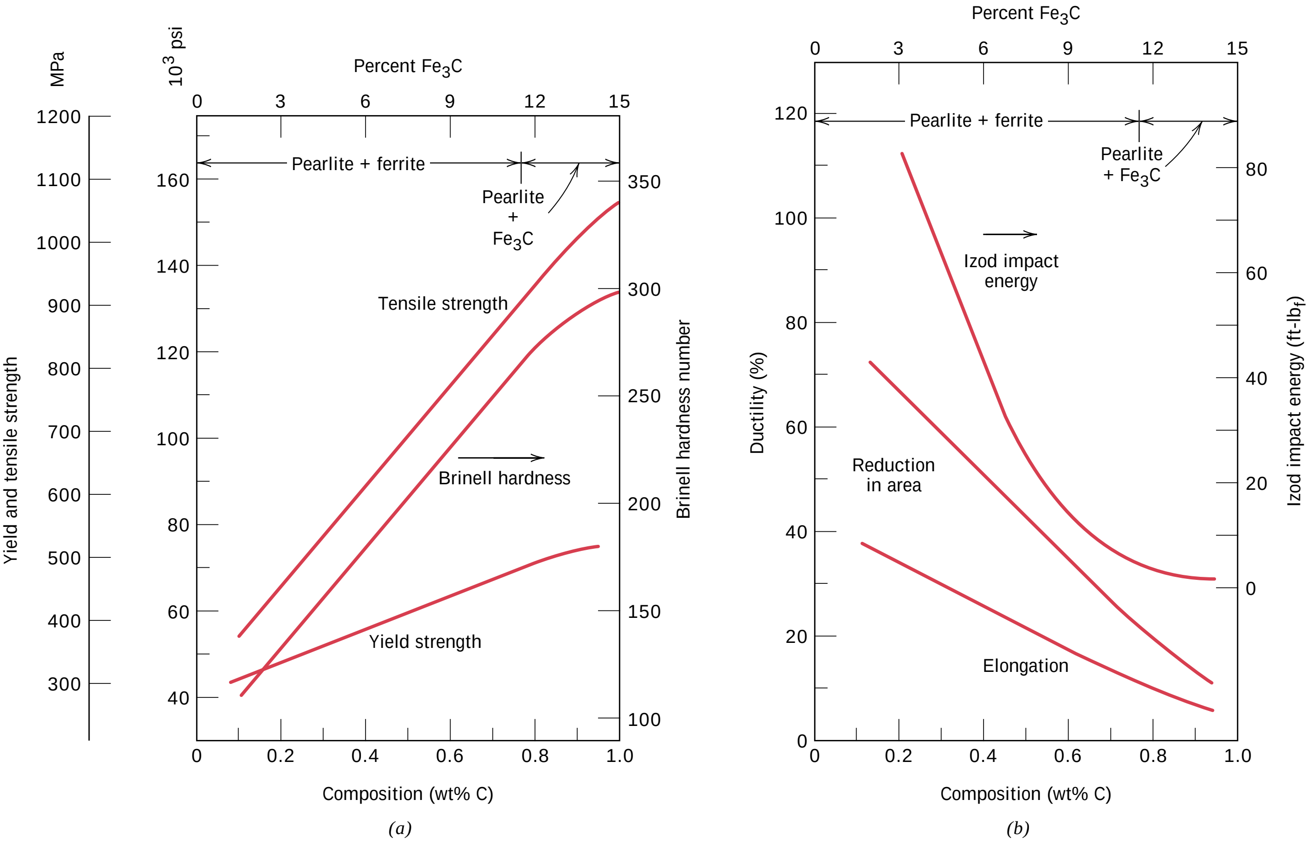

Figure 11.21 (*a*) Yield strength, tensile strength, and Brinell hardness versus carbon concentration for plain carbon steels having microstructures consisting of fine pearlite. (*b*) Ductility (%EL and %RA) and Izod impact energy versus carbon concentration for plain carbon steels having microstructures consisting of fine pearlite. (Data taken from *Metals Handbook: Heat Treating*, Vol. 4, 9th edition, V. Masseria, Managing Editor, American Society for Metals, 1981, p. 9.)

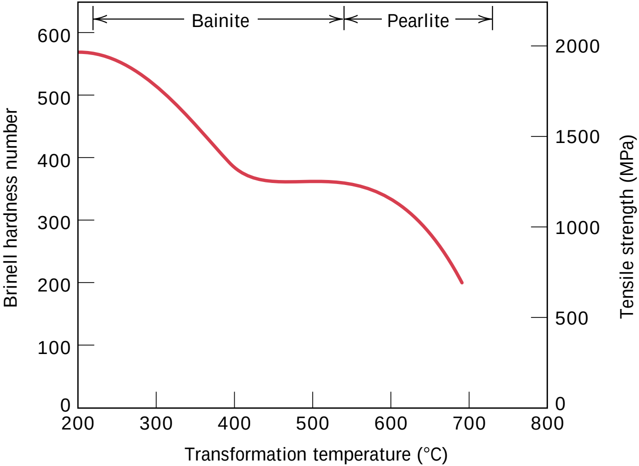

FIGURE 11.23 Brinell hardness and tensile strength as a function of isothermal transformation temperature for an iron–carbon alloy of eutectoid composition, taken over the temperature range at which bainitic and pearlitic microstructures form. (Adapted from E. S. Davenport, ''Isothermal Transformation in Steels,'' *Trans. ASM,* **27,** 1939, p. 847. Reprinted by permission of ASM International.)

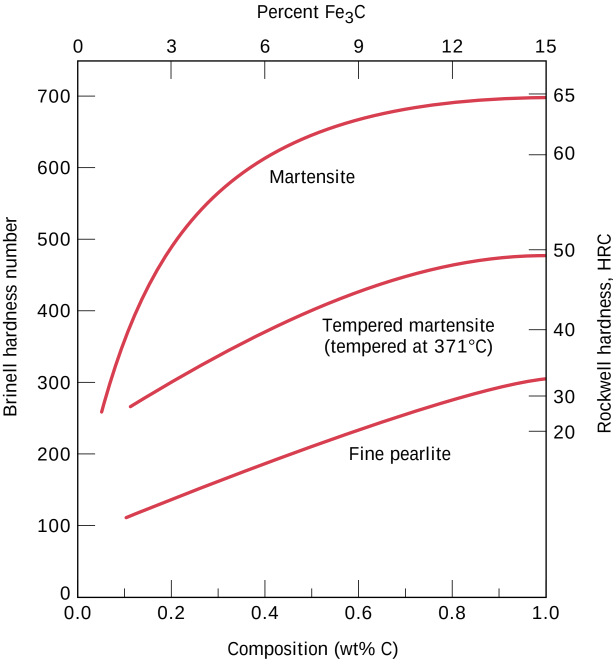

Figure 11.24 Hardness as a function of carbon concentration for plain carbon martensitic, tempered martensitic [tempered at 371°C (700°F)], and pearlitic steels. (Adapted from Edgar C. Bain, *Functions of the Alloying Elements in Steel*, American Society for Metals, 1939, p. 36; and R. A. Grange, C. R. Hribal, and L. F. Porter: *Metall. Trans. A*, Vol. 8A, p. 1776.)

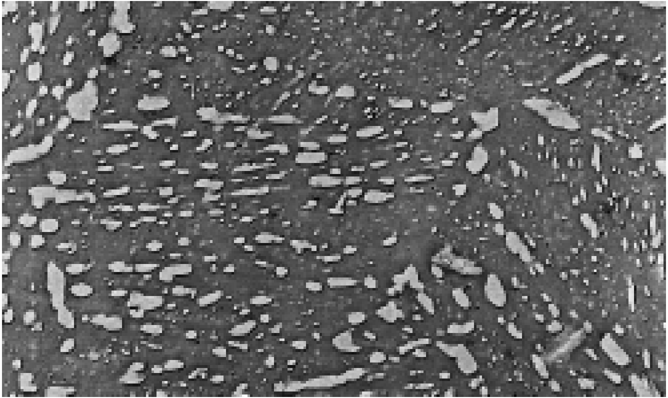

Figure 11.25 Electron micrograph of tempered martensite. Tempering was carried out at 594°C (1100°F). The small particles are the cementite phase; the matrix phase is α ferrite. 9300×. (Copyright 1971 by United States Steel Corporation.)

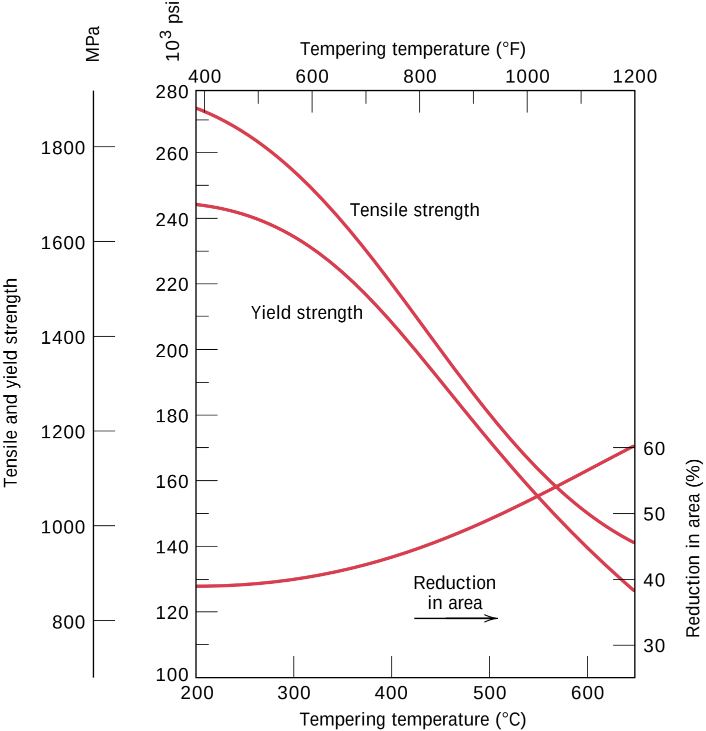

FIGURE 11.26 Tensile and yield strengths and ductility (%RA) versus tempering temperature for an oil-quenched alloy steel (type 4340). (Adapted from figure furnished courtesy Republic Steel Corporation.)

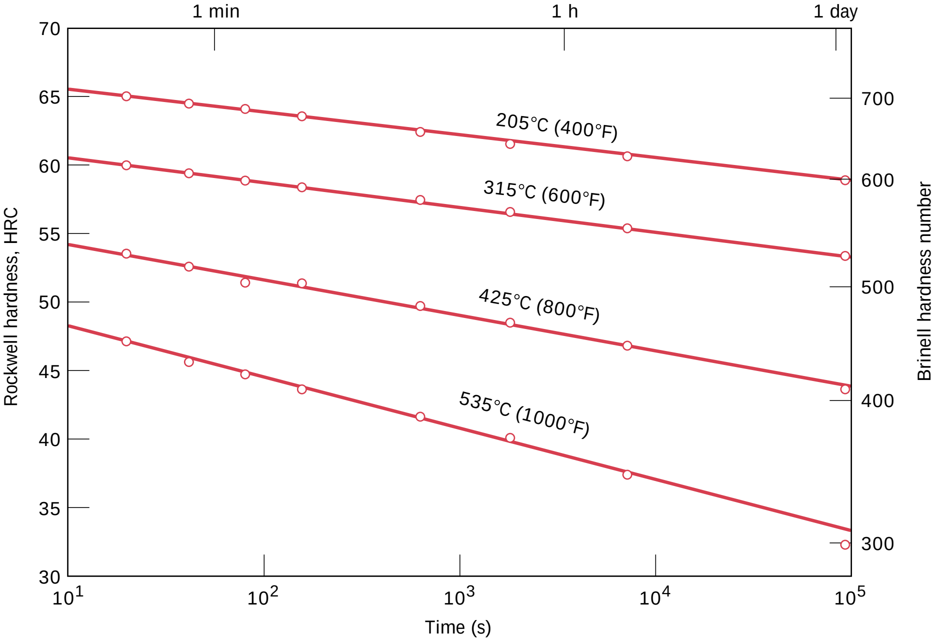

Figure 11.27 Hardness versus tempering time for a water-quenched eutectoid plain carbon (1080) steel. (Adapted from Edgar C. Bain, *Functions of the Alloying Elements in Steel*, American Society for Metals, 1939, p. 233.)

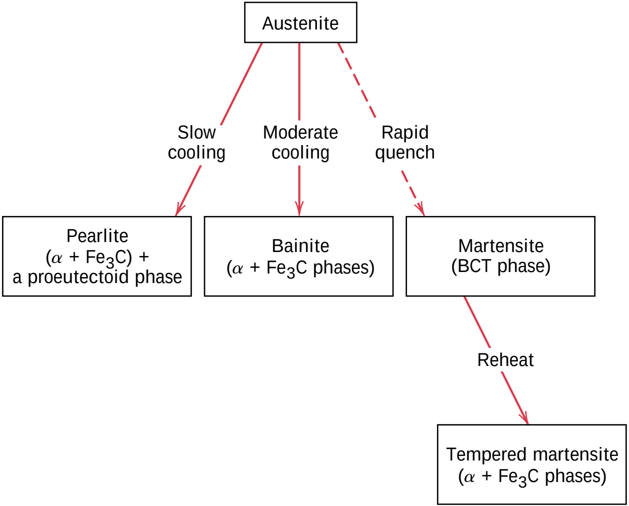
Austenite
Slow cooling
Moderate cooling
Rapid quench
Pearlite
(α + Fe3C) +
a proeutectoid phase
Bainite
(α + Fe3C phases)
Martensite
(BCT phase)
Reheat
Tempered martensite
(α + Fe3C phases)

FIGURE 11.28 Possible transformations involving the decomposition of austenite. Solid arrows, transformations involving diffusion; dashed arrow, diffusionless transformation.

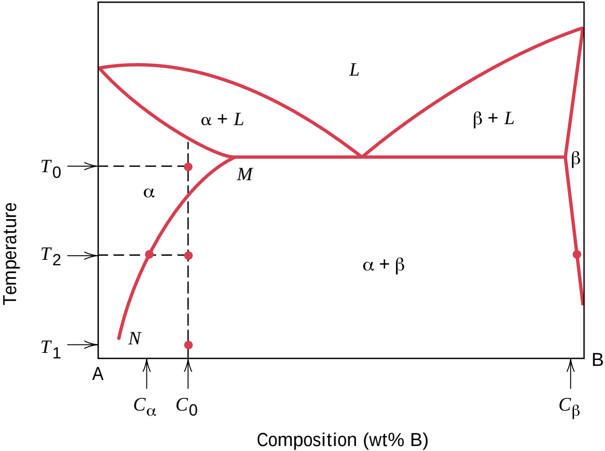
L
α + L
β + L
β
M
α
α + β
N
T_0
T_2
T_1
Temperature
A
B
C_α
C_0
C_β
Composition (wt% B)

Figure 11.29 Hypothetical phase diagram for a precipitation hardenable alloy of composition C_0.

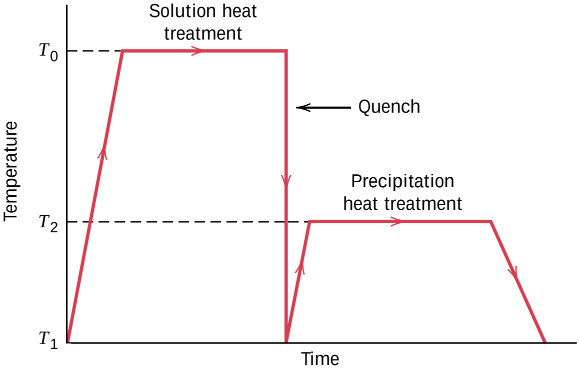

Figure 11.30 Schematic temperature-versus-time plot showing both solution and precipitation heat treatments for precipitation hardening.

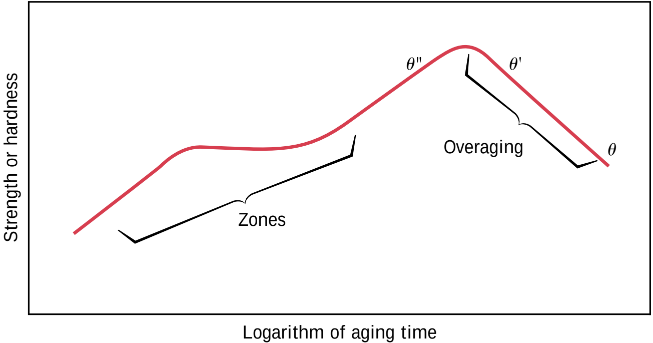

FIGURE 11.31 Schematic diagram showing strength and hardness as a function of the logarithm of aging time at constant temperature during the precipitation heat treatment.

FIGURE 11.32 The aluminum-rich side of the aluminum–copper phase diagram. (Adapted from J. L. Murray, *International Metals Review*, **30,** 5, 1985. Reprinted by permission of ASM International.)

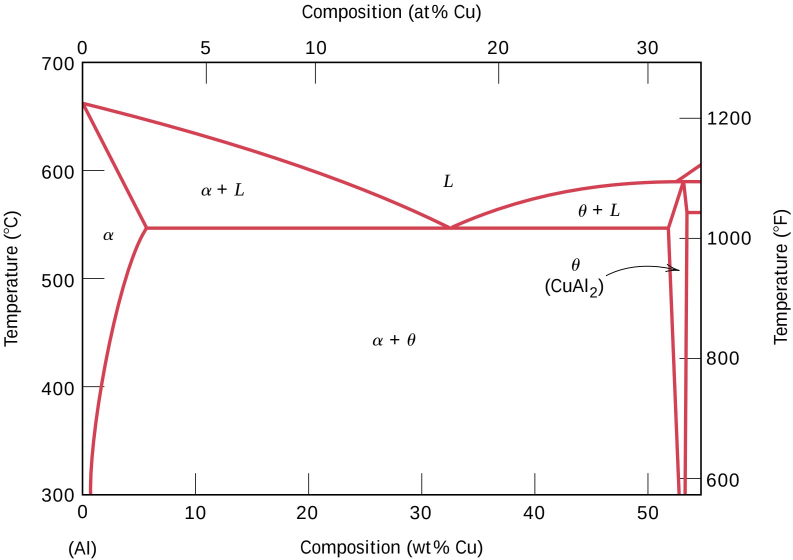

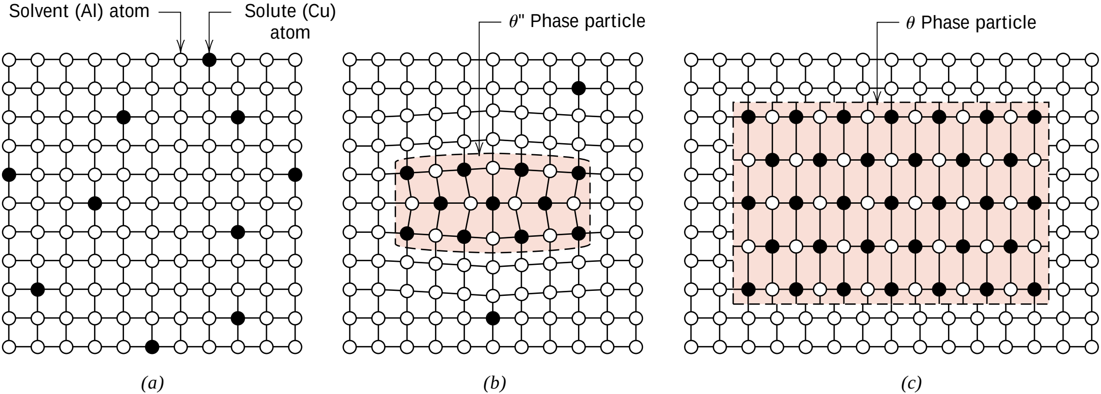
Solvent (Al) atom
Solute (Cu) atom
θ" Phase particle
θ Phase particle
(a)
(b)
(c)

FIGURE 11.33 Schematic depiction of several stages in the formation of the equilibrium precipitate (θ) phase. (*a*) A supersaturated α solid solution. (*b*) A transition, θ'', precipitate phase. (*c*) The equilibrium θ phase, within the α matrix phase. Actual phase particle sizes are much larger than shown here.

FIGURE 11.34 The precipitation hardening characteristics of a 2014 aluminum alloy (0.9 wt% Si, 4.4 wt% Cu, 0.8 wt% Mn, 0.5 wt% Mg) at four different aging temperatures: (*a*) tensile strength, and (*b*) ductility (%EL). (Adapted from *Metals Handbook: Properties and Selection: Nonferrous Alloys and Pure Metals*, Vol. 2, 9th edition, H. Baker, Managing Editor, American Society for Metals, 1979, p. 41.)

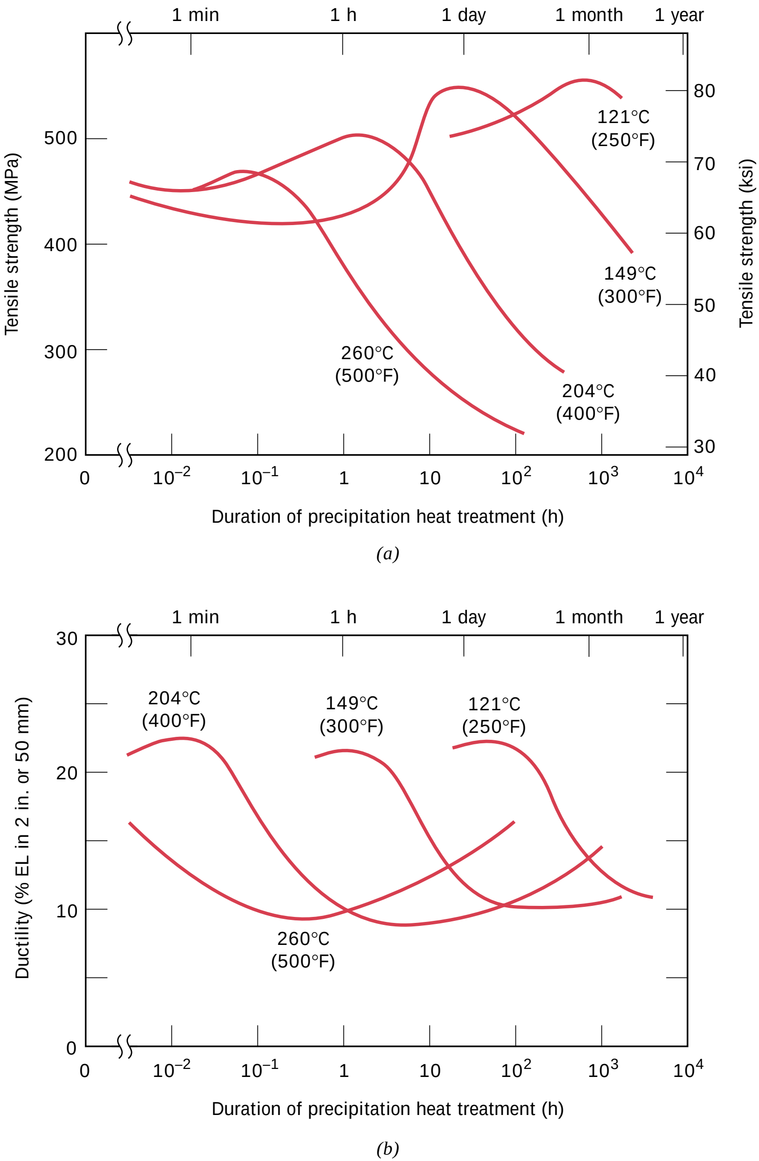

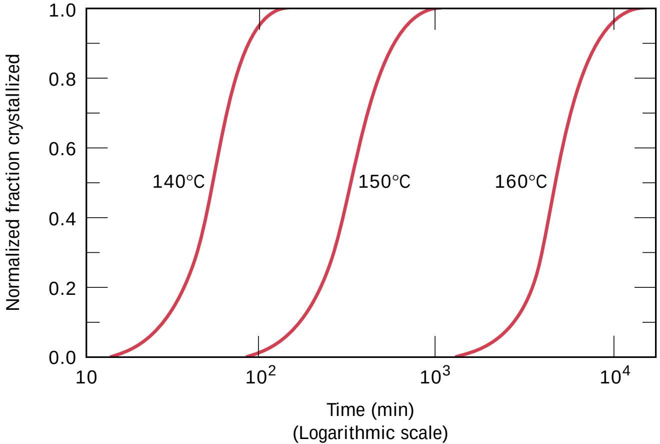

Figure 11.35 Plot of normalized fraction crystallized versus the logarithm of time for polypropylene at constant temperatures of 140°C, 150°C, and 160°C. (Adapted from P. Parrini and G. Corrieri, *Makromol. Chem.*, **62,** 83, 1963. Reprinted by permission of Hüthig & Wepf Publishers, Zug, Switzerland.)

Figure 11.38 Isothermal transformation diagram for a 0.45 wt% C iron–carbon alloy: A, austenite; B, bainite; F, proeutectoid ferrite; M, martensite; P, pearlite. (Adapted from *Atlas of Time-Temperature Diagrams for Irons and Steels*, G. F. Vander Voort, Editor, 1991. Reprinted by permission of ASM International, Materials Park, OH.)

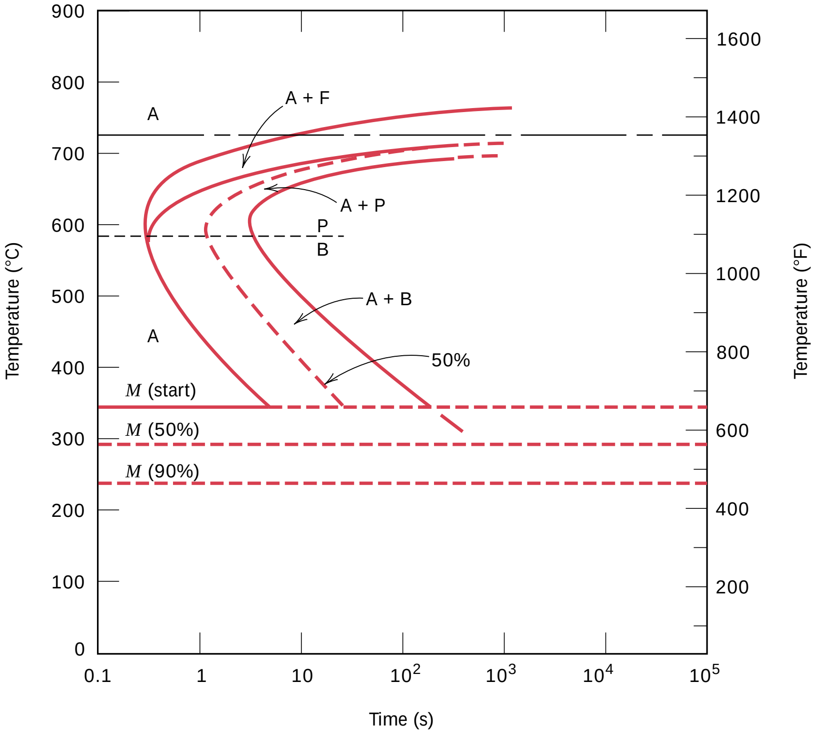

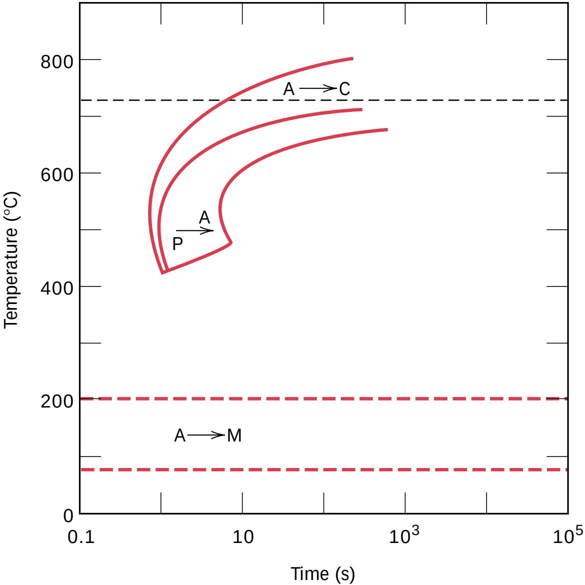

FIGURE 11.39 Continuous cooling transformation diagram for a 1.13 wt% C iron–carbon alloy.

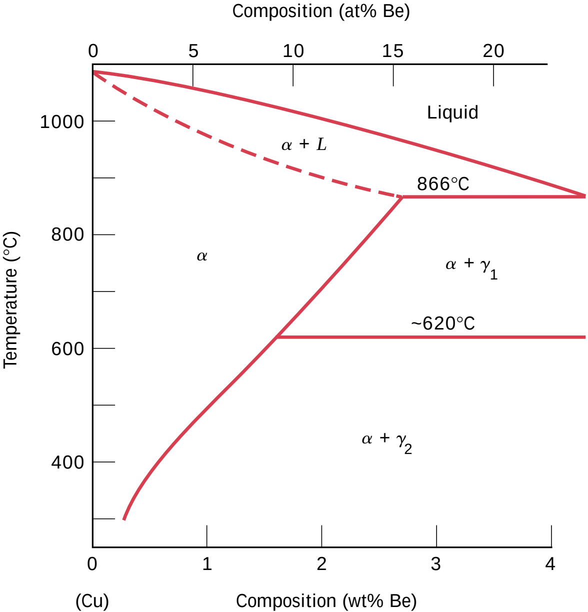

Figure 11.40 The copper-rich side of the copper–beryllium phase diagram. (Adapted from *Binary Alloy Phase Diagrams*, 2nd edition, Vol. 2, T. B. Massalski, Editor-in-Chief, 1990. Reprinted by permission of ASM International, Materials Park, OH.)

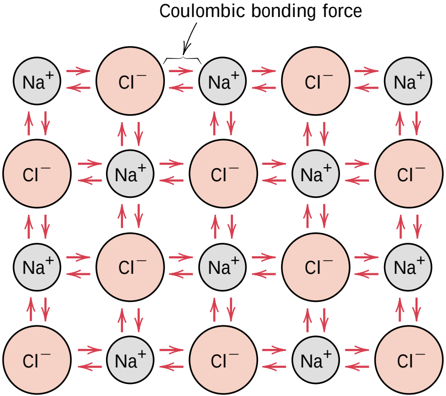
Coulombic bonding force
Na+
Cl−
Na+
Cl−
Na+
Cl−
Na+
Cl−
Na+
Cl−
Na+
Cl−
Na+
Cl−
Na+
Cl−
Na+
Cl−
Na+
Cl−

FIGURE 2.9 Schematic representation of ionic bonding in sodium chloride (NaCl).

Table 2.3 **Bonding Energies and Melting Temperatures for Various Substances**

		Bonding Energy		
Bonding Type	*Substance*	*kJ/mol (kcal/mol)*	*eV/Atom, Ion, Molecule*	*Melting Temperature (°C)*
Ionic	NaCl	640 (153)	3.3	801
	MgO	1000 (239)	5.2	2800
Covalent	Si	450 (108)	4.7	1410
	C (diamond)	713 (170)	7.4	>3550
Metallic	Hg	68 (16)	0.7	−39
	Al	324 (77)	3.4	660
	Fe	406 (97)	4.2	1538
	W	849 (203)	8.8	3410
van der Waals	Ar	7.7 (1.8)	0.08	−189
	Cl_2	31 (7.4)	0.32	−101
Hydrogen	NH_3	35 (8.4)	0.36	−78
	H_2O	51 (12.2)	0.52	0

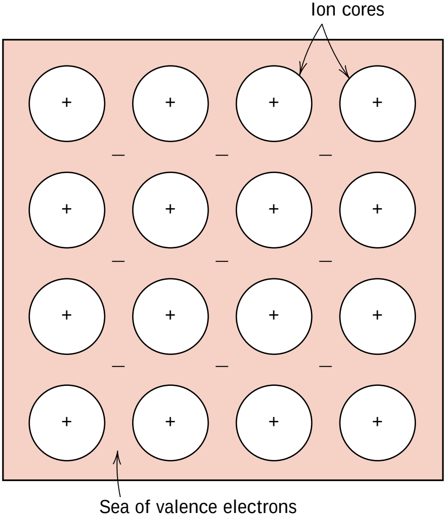
Ion cores
+
−
Sea of valence electrons

FIGURE 2.11 Schematic illustration of metallic bonding.

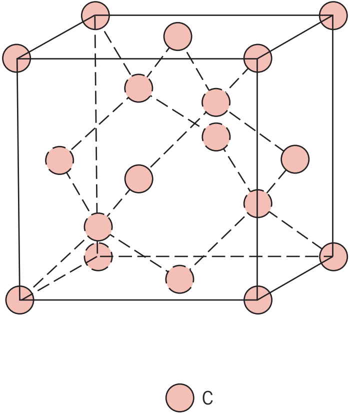

FIGURE 3.16 A unit cell for the diamond cubic crystal structure.

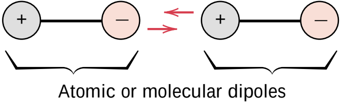
+
–
+
–
Atomic or molecular dipoles

FIGURE 2.12 Schematic illustration of van der Waals bonding between two dipoles.

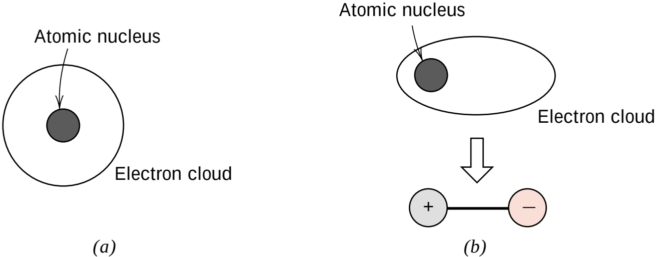
Atomic nucleus
Electron cloud
Atomic nucleus
Electron cloud
+
−
(a)
(b)

Figure 2.13 Schematic representations of (*a*) an electrically symmetric atom and (*b*) an induced atomic dipole.

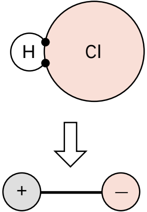

FIGURE 2.14 Schematic representation of a polar hydrogen chloride (HCl) molecule.

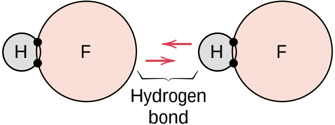
H
F
H
F
Hydrogen
bond

Figure 2.15 Schematic representation of hydrogen bonding in hydrogen fluoride (HF).

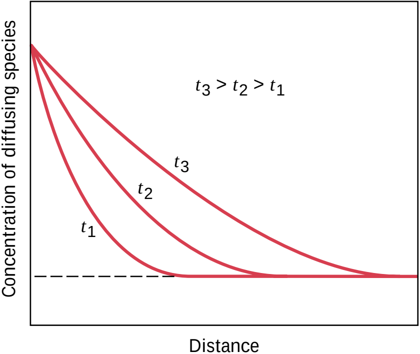

Figure 6.5 Concentration profiles for nonsteady-state diffusion taken at three different times, t_1, t_2, and t_3.

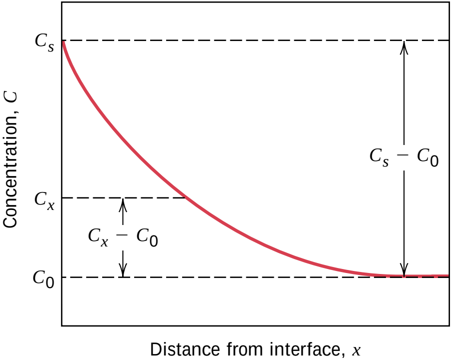

FIGURE 6.6 Concentration profile for nonsteady-state diffusion; concentration parameters relate to Equation 6.5.

Table 6.2 A Tabulation of Diffusion Data

Diffusing Species	Host Metal	$D_0(m^2/s)$	Activation Energy Q_d		Calculated Values	
			kJ/mol	eV/atom	T(°C)	$D(m^2/s)$
Fe	α-Fe (BCC)	2.8×10^{-4}	251	2.60	500	3.0×10^{-21}
					900	1.8×10^{-15}
Fe	γ-Fe (FCC)	5.0×10^{-5}	284	2.94	900	1.1×10^{-17}
					1100	7.8×10^{-16}
C	α-Fe	6.2×10^{-7}	80	0.83	500	2.4×10^{-12}
					900	1.7×10^{-10}
C	γ-Fe	2.3×10^{-5}	148	1.53	900	5.9×10^{-12}
					1100	5.3×10^{-11}
Cu	Cu	7.8×10^{-5}	211	2.19	500	4.2×10^{-19}
Zn	Cu	2.4×10^{-5}	189	1.96	500	4.0×10^{-18}
Al	Al	2.3×10^{-4}	144	1.49	500	4.2×10^{-14}
Cu	Al	6.5×10^{-5}	136	1.41	500	4.1×10^{-14}
Mg	Al	1.2×10^{-4}	131	1.35	500	1.9×10^{-13}
Cu	Ni	2.7×10^{-5}	256	2.65	500	1.3×10^{-22}

Source: E. A. Brandes and G. B. Brook (Editors), *Smithells Metals Reference Book*, 7th edition, Butterworth-Heinemann, Oxford, 1992.

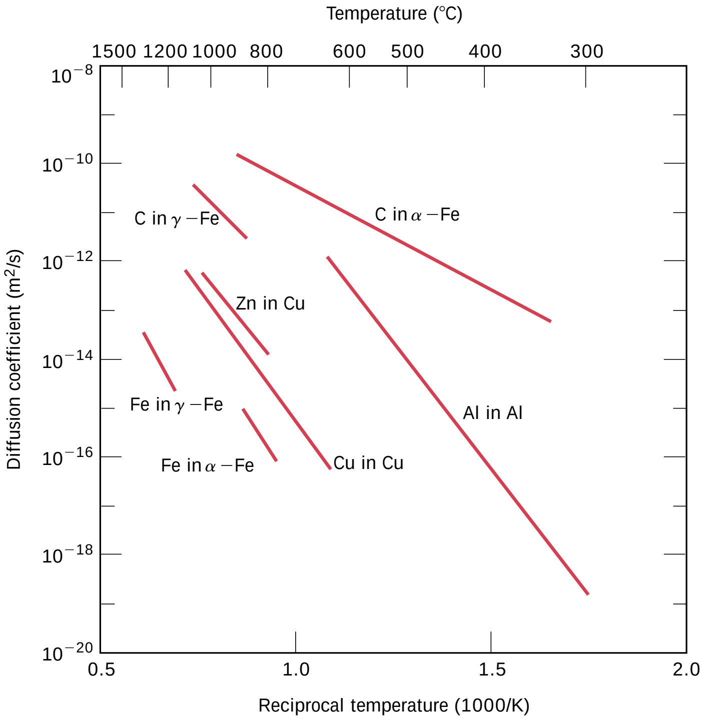

FIGURE 6.7 Plot of the logarithm of the diffusion coefficient versus the reciprocal of absolute temperature for several metals. [Data taken from E. A. Brandes and G. B. Brook (Editors), *Smithells Metals Reference Book*, 7th edition, Butterworth-Heinemann, Oxford, 1992.]

```
[Loader]
Program=mse5e
CommandLine=DiffusionCoef
```

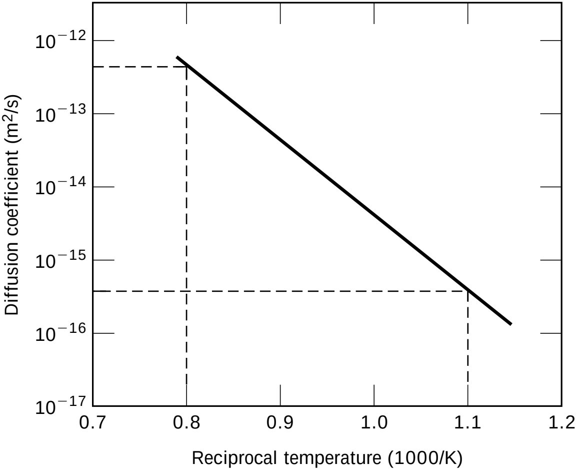

FIGURE 6.8 Plot of the logarithm of the diffusion coefficient versus the reciprocal of absolute temperature for the diffusion of copper in gold.

```
[Loader]
Program=mse5e
CommandLine=DesignProblem
```

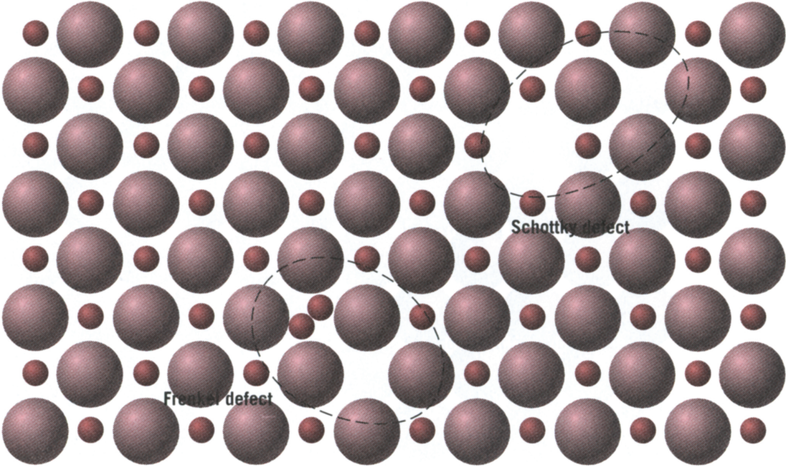
Schottky defect
Frenkel defect

Figure 5.3 Schematic diagram showing Frenkel and Schottky defects in ionic solids. (From W. G. Moffatt, G. W. Pearsall, and J. Wulff, *The Structure and Properties of Materials*, Vol. 1, *Structure*, p. 78. Copyright © 1964 by John Wiley & Sons, New York. Reprinted by permission of John Wiley & Sons, Inc.)

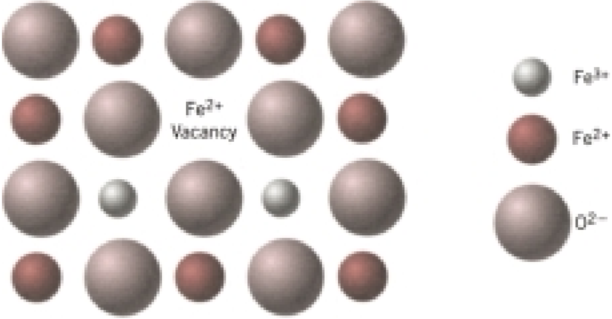
Fe^{2+}
Vacancy
Fe^{3+}
Fe^{2+}
O^{2-}

Figure 5.4 Schematic representation of an Fe^{2+} vacancy in FeO that results from the formation of two Fe^{3+} ions.

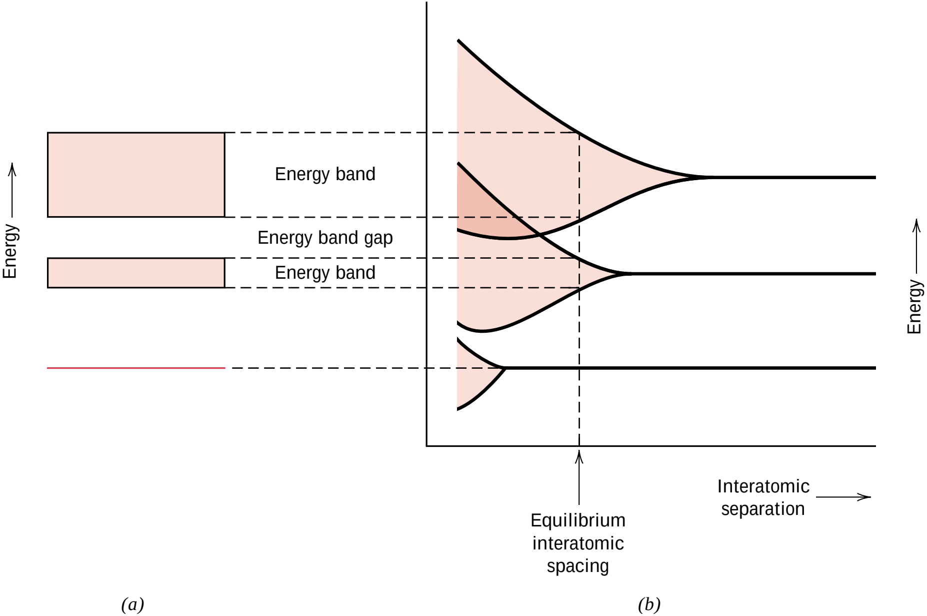
Energy
Energy band
Energy band gap
Energy band
Energy
Equilibrium interatomic spacing
Interatomic separation
(a)
(b)

Figure 12.3 (*a*) The conventional representation of the electron energy band structure for a solid material at the equilibrium interatomic separation. (*b*) Electron energy versus interatomic separation for an aggregate of atoms, illustrating how the energy band structure at the equilibrium separation in (*a*) is generated. (From Z. D. Jastrzebski, *The Nature and Properties of Engineering Materials,* 3rd edition. Copyright © 1987 by John Wiley & Sons, Inc. Reprinted by permission of John Wiley & Sons, Inc.)

FIGURE 12.5 For a metal, occupancy of electron states (*a*) before and (*b*) after an electron excitation.

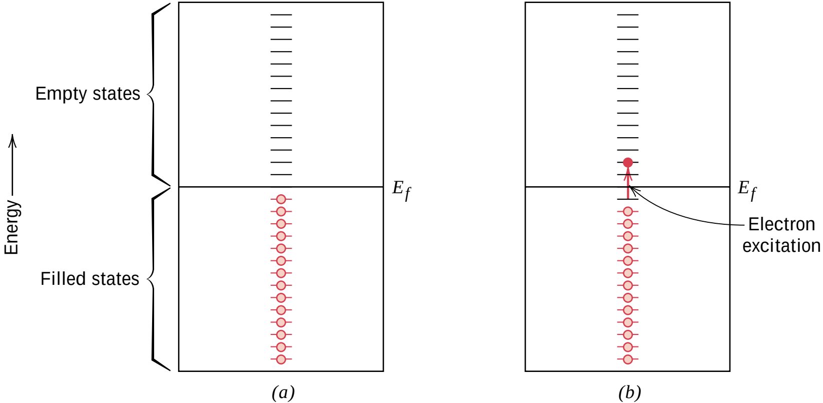
Energy
Empty states
Filled states
E_f
E_f
Electron excitation
(a)
(b)

FIGURE 12.6 For an insulator or semiconductor, occupancy of electron states (*a*) before and (*b*) after an electron excitation from the valence band into the conduction band, in which both a free electron and a hole are generated.

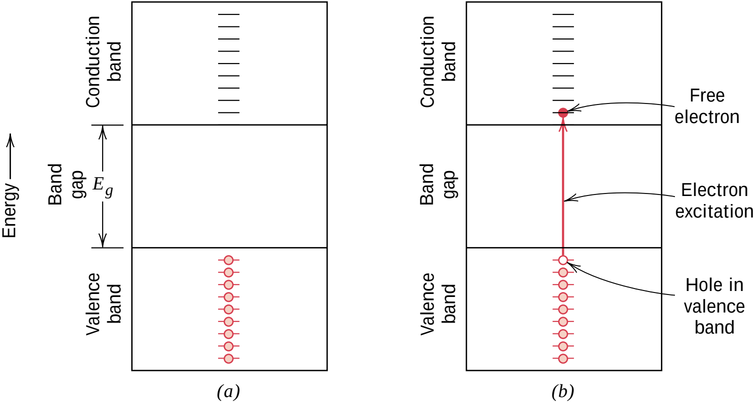
Energy
Conduction band
Band gap
E_g
Valence band
(a)
Conduction band
Band gap
Valence band
Free electron
Electron excitation
Hole in valence band
(b)

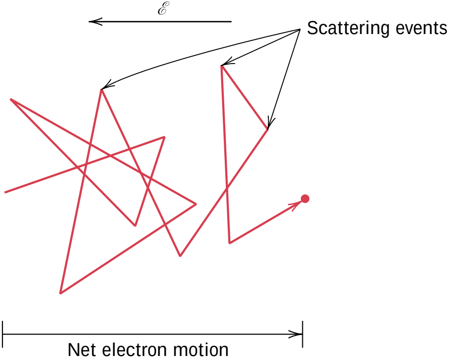
$\mathscr{E}$
Scattering events
Net electron motion

FIGURE 12.7 Schematic diagram showing the path of an electron that is deflected by scattering events.

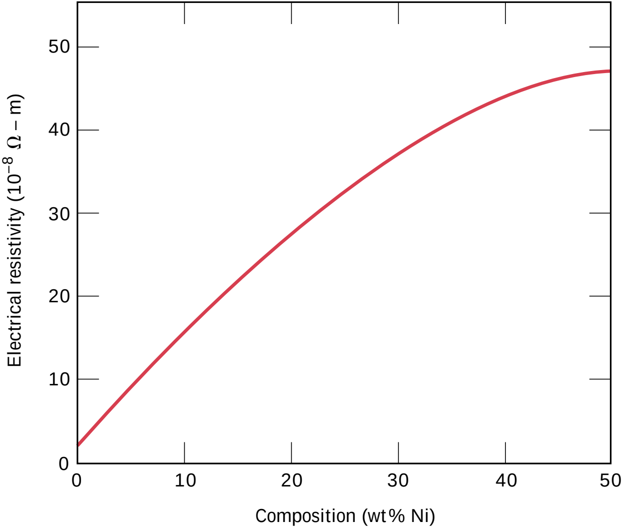

Figure 12.9 Room-temperature electrical resistivity versus composition for copper–nickel alloys.

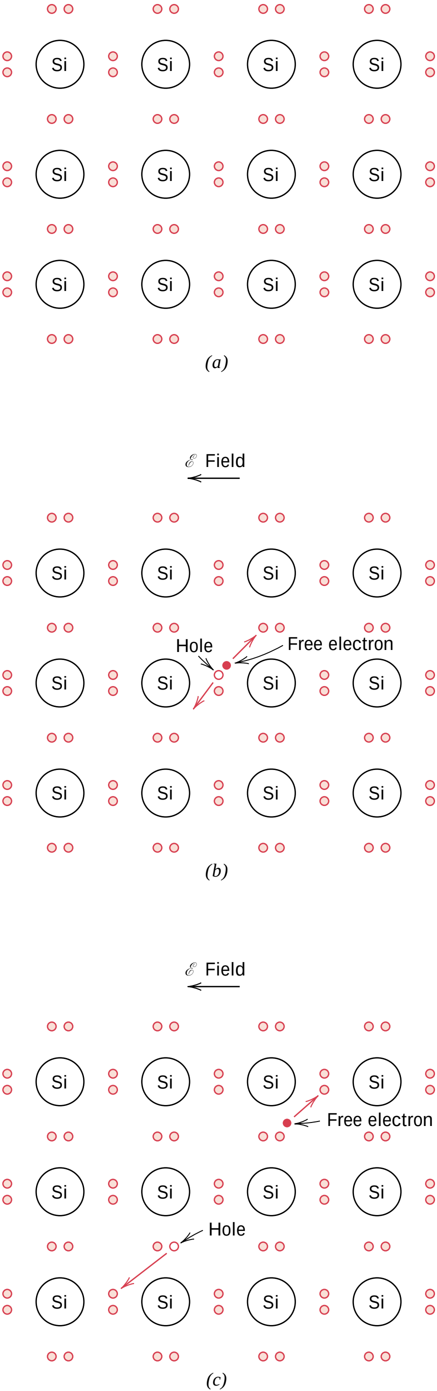
Si
(a)
ℰ Field
Hole
Free electron
(b)
ℰ Field
Free electron
Hole
(c)

Figure 12.10 Electron bonding model of electrical conduction in intrinsic silicon: (*a*) before excitation; (*b*) and (*c*) after excitation (the subsequent free-electron and hole motions in response to an external electric field).

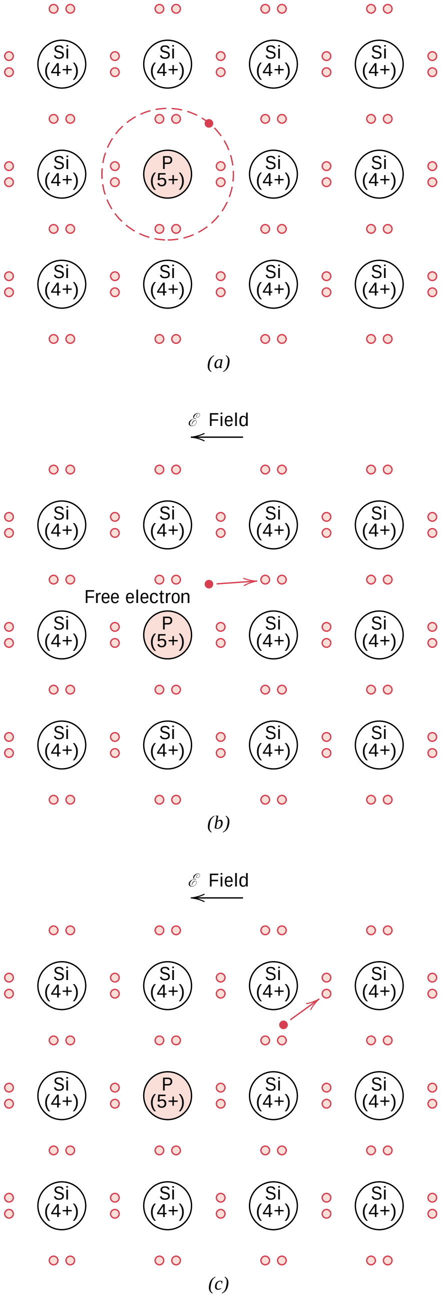

Figure 12.11 Extrinsic *n*-type semiconduction model (electron bonding). (*a*) An impurity atom such as phosphorus, having five valence electrons, may substitute for a silicon atom. This results in an extra bonding electron, which is bound to the impurity atom and orbits it. (*b*) Excitation to form a free electron. (*c*) The motion of this free electron in response to an electric field.

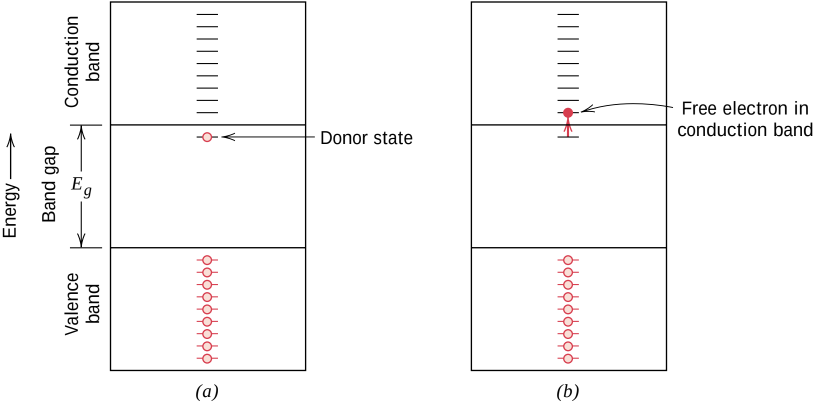
Conduction band
Band gap
E_g
Energy
Valence band
Donor state
Free electron in conduction band
(a)
(b)

FIGURE 12.12 (*a*) Electron energy band scheme for a donor impurity level located within the band gap and just below the bottom of the conduction band. (*b*) Excitation from a donor state in which a free electron is generated in the conduction band.

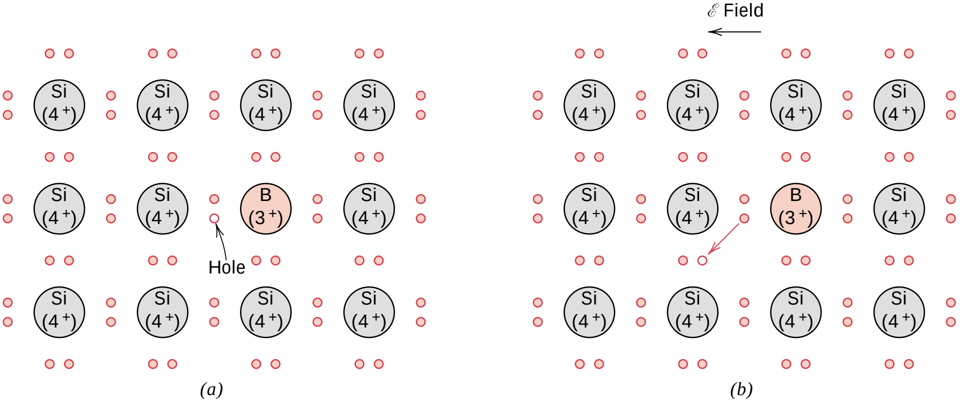

Figure 12.13 Extrinsic p-type semiconduction model (electron bonding). (*a*) An impurity atom such as boron, having three valence electrons, may substitute for a silicon atom. This results in a deficiency of one valence electron, or a hole associated with the impurity atom. (*b*) The motion of this hole in response to an electric field.

Figure 12.14 (*a*) Energy band scheme for an acceptor impurity level located within the band gap and just above the top of the valence band. (*b*) Excitation of an electron into the acceptor level, leaving behind a hole in the valence band.

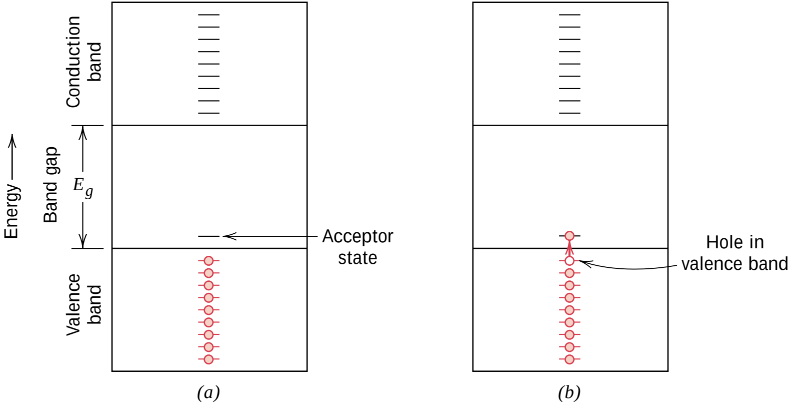
Energy
Conduction band
Band gap
E_g
Valence band
Acceptor state
Hole in valence band
(a)
(b)

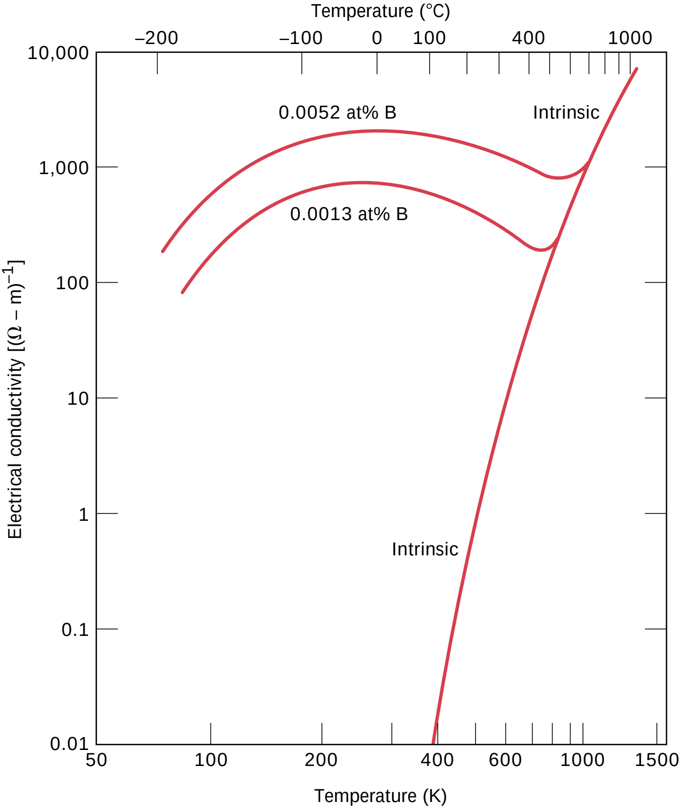

FIGURE 12.15 The temperature dependence of the electrical conductivity (log–log scales) for intrinsic silicon and boron-doped silicon at two doping levels. [Adapted from G. L. Pearson and J. Bardeen, *Phys. Rev.*, **75,** 865 (1949).]

FIGURE 12.16 The logarithm of carrier (electron and hole) concentration as a function of the reciprocal of the absolute temperature for intrinsic silicon and two boron-doped silicon materials. (Adapted from G. L. Pearson and J. Bardeen, *Phys. Rev.*, **75,** 865, 1949.)

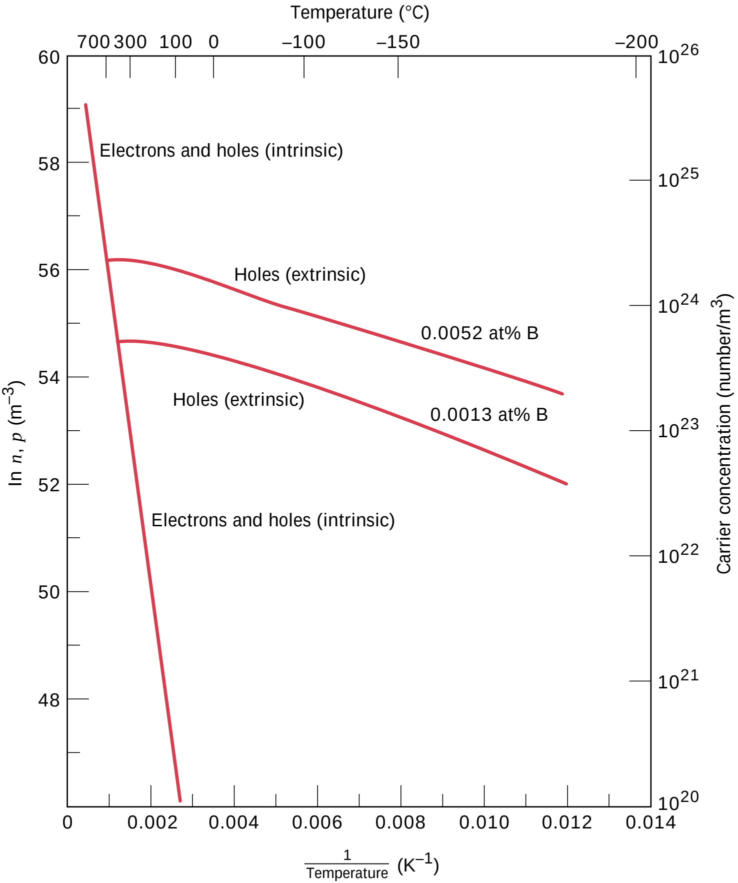

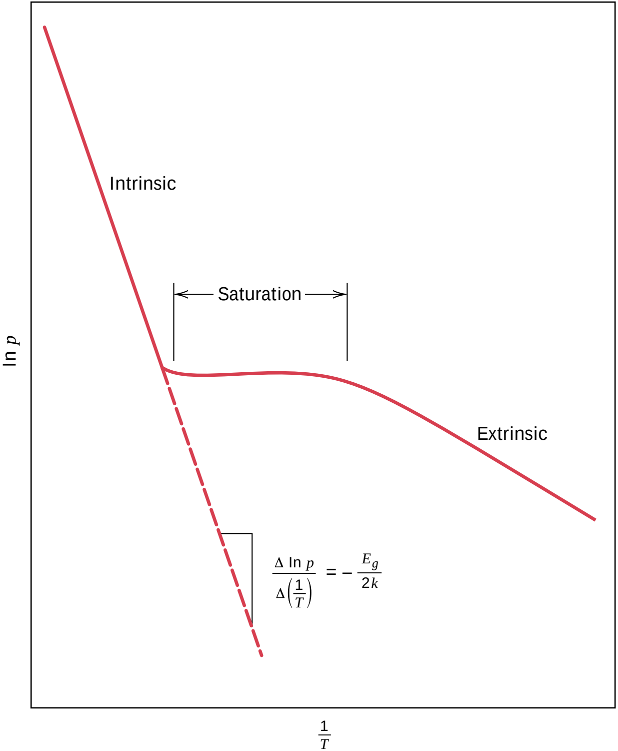

Figure 12.17 Schematic plot of the natural logarithm of hole concentration as a function of the reciprocal of absolute temperature for a p-type semiconductor that exhibits extrinsic, saturation, and intrinsic behavior.

Table 12.3 Typical Room-Temperature Electrical Conductivities for 13 Nonmetallic Materials

Material	*Electrical Conductivity* $[(\Omega\text{-}m)^{-1}]$
Graphite	3×10^4–2×10^5
Ceramics	
Concrete (dry)	10^{-9}
Soda–lime glass	10^{-10}–10^{-11}
Porcelain	10^{-10}–10^{-12}
Borosilicate glass	$\sim 10^{-13}$
Aluminum oxide	$<10^{-13}$
Fused silica	$<10^{-18}$
Polymers	
Phenol-formaldehyde	10^{-9}–10^{-10}
Polymethyl methacrylate	$<10^{-12}$
Nylon 6,6	10^{-12}–10^{-13}
Polystyrene	$<10^{-14}$
Polyethylene	10^{-15}–10^{-17}
Polytetrafluoroethylene	$<10^{-17}$

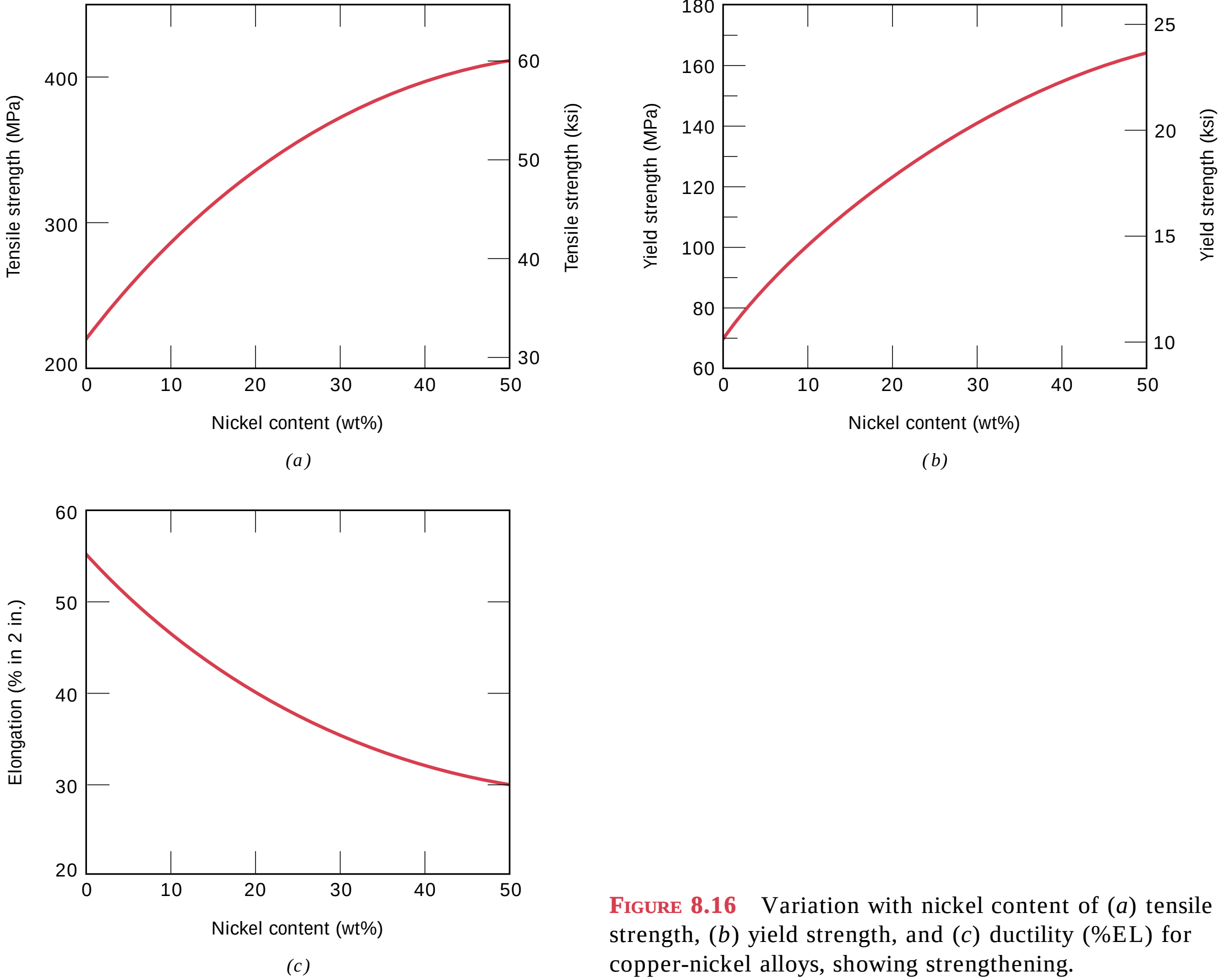

(a)

(b)

(c)

FIGURE 8.16 Variation with nickel content of (*a*) tensile strength, (*b*) yield strength, and (*c*) ductility (%EL) for copper-nickel alloys, showing strengthening.

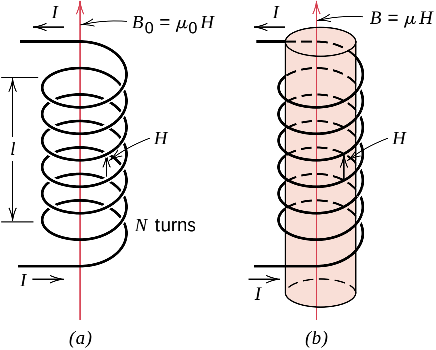

FIGURE 18.3 (*a*) The magnetic field H as generated by a cylindrical coil is dependent on the current I, the number of turns N, and the coil length l, according to Equation 18.1. The magnetic flux density B_0 in the presence of a vacuum is equal to $\mu_0 H$, where μ_0 is the permeability of a vacuum, $4\pi \times 10^{-7}$ H/m. (*b*) The magnetic flux density B within a solid material is equal to μH, where μ is the permeability of the solid material. (Adapted from A. G. Guy, *Essentials of Materials Science,* McGraw-Hill Book Company, New York, 1976.)

Table 18.1 Magnetic Units and Conversion Factors for the SI and cgs–emu Systems

		SI Units			
Quantity	***Symbol***	***Derived***	***Primary***	***cgs–emu Unit***	***Conversion***
Magnetic induction (flux density)	B	tesla (Wb/m^2)[a]	kg/s-C	gauss	1 Wb/m^2 = 10^4 gauss
Magnetic field strength	H	amp-turn/m	C/m-s	oersted	1 amp-turn/m = $4\pi \times 10^{-3}$ oersted
Magnetization	M (SI) I (cgs–emu)	amp-turn/m	C/m-s	maxwell/cm^2	1 amp-turn/m = 10^{-3} maxwell/cm^2
Permeability of a vacuum	μ_0	henry/m[b]	kg-m/C^2	Unitless (emu)	$4\pi \times 10^{-7}$ henry/m = 1 emu
Relative permeability	μ_r (SI) μ' (cgs–emu)	Unitless	Unitless	Unitless	$\mu_r = \mu'$
Susceptibility	χ_m (SI) χ'_m (cgs–emu)	Unitless	Unitless	Unitless	$\chi_m = 4\pi\chi'_m$

[a] Units of the weber (Wb) are volt-seconds.

[b] Units of the henry are webers per ampere.

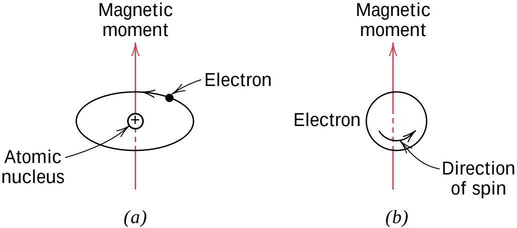
Magnetic moment
Electron
Atomic nucleus
(a)
Magnetic moment
Electron
Direction of spin
(b)

Figure 18.4 Demonstration of the magnetic moment associated with (*a*) an orbiting electron and (*b*) a spinning electron.

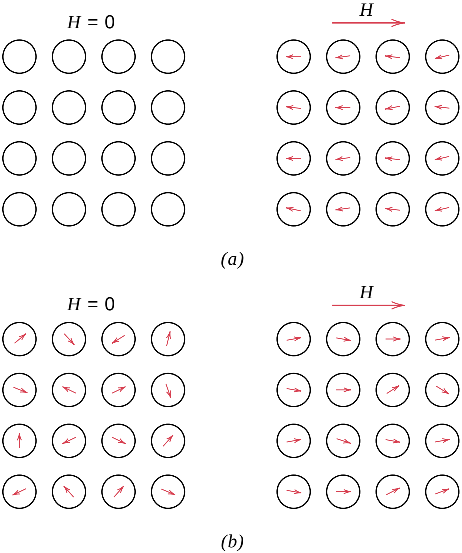

Figure 18.5 (*a*) The atomic dipole configuration for a diamagnetic material with and without a magnetic field. In the absence of an external field, no dipoles exist; in the presence of a field, dipoles are induced that are aligned opposite to the field direction. (*b*) Atomic dipole configuration with and without an external magnetic field for a paramagnetic material.

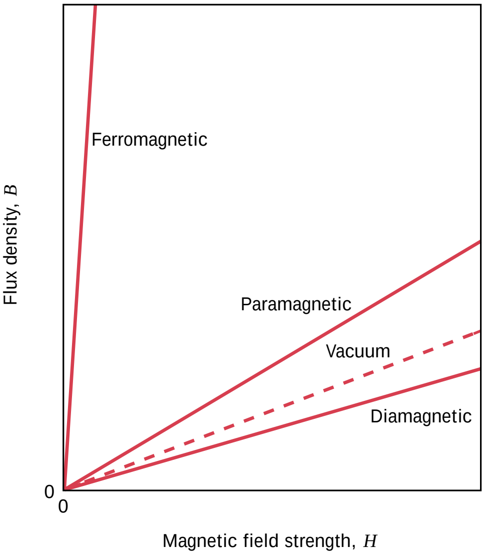

FIGURE 18.6 Schematic representation of the flux density B versus the magnetic field strength H for diamagnetic, paramagnetic, and ferromagnetic materials.

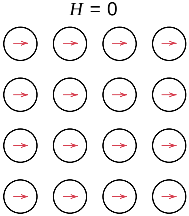

FIGURE 18.7 Schematic illustration of the mutual alignment of atomic dipoles for a ferromagnetic material, which will exist even in the absence of an external magnetic field.

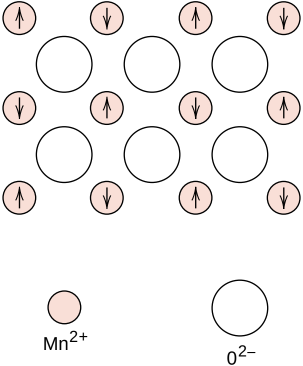

Figure 18.8 Schematic representation of antiparallel alignment of spin magnetic moments for antiferromagnetic manganese oxide.

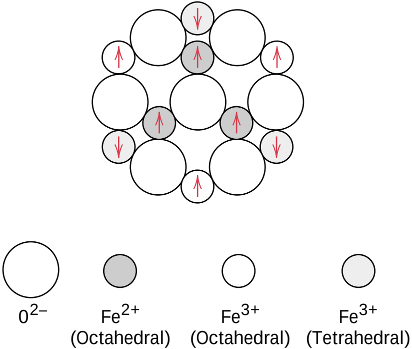
O2–
Fe2+
(Octahedral)
Fe3+
(Octahedral)
Fe3+
(Tetrahedral)

FIGURE 18.9 Schematic diagram showing the spin magnetic moment configuration for Fe^{2+} and Fe^{3+} ions in Fe_3O_4. (From Richard A. Flinn and Paul K. Trojan, *Engineering Materials and Their Applications*, 4th edition. Copyright © 1990 by John Wiley & Sons, Inc. Adapted by permission of John Wiley & Sons, Inc.)

Table 18.3 The Distribution of Spin Magnetic Moments for Fe^{2+} and Fe^{3+} Ions in a Unit Cell of Fe_3O_4[a]

Cation	*Octahedral Lattice Site*	*Tetrahedral Lattice Site*	*Net Magnetic Moment*
Fe^{3+}	↑ ↑ ↑ ↑ ↑ ↑ ↑ ↑	↓ ↓ ↓ ↓ ↓ ↓ ↓ ↓	Complete cancellation
Fe^{2+}	↑ ↑ ↑ ↑ ↑ ↑ ↑ ↑	—	↑ ↑ ↑ ↑ ↑ ↑ ↑ ↑

[a] Each arrow represents the magnetic moment orientation for one of the cations.

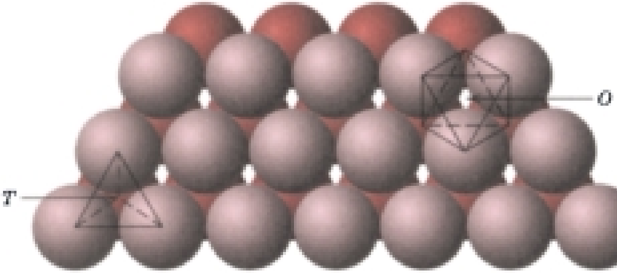

FIGURE 3.30 The stacking of one plane of close-packed spheres (anions) on top of another; tetrahedral and octahedral positions between the planes are designated by *T* and *O*, respectively. (From W. G. Moffatt, G. W. Pearsall, and J. Wulff, *The Structure and Properties of Materials,* Vol. 1, *Structure.* Copyright © 1964 by John Wiley & Sons, New York. Reprinted by permission of John Wiley & Sons, Inc.)

Table 18.4 Net Magnetic Moments for Six Cations

Cation	*Net Spin Magnetic Moment (Bohr magnetons)*
Fe^{3+}	5
Fe^{2+}	4
Mn^{2+}	5
Co^{2+}	3
Ni^{2+}	2
Cu^{2+}	1

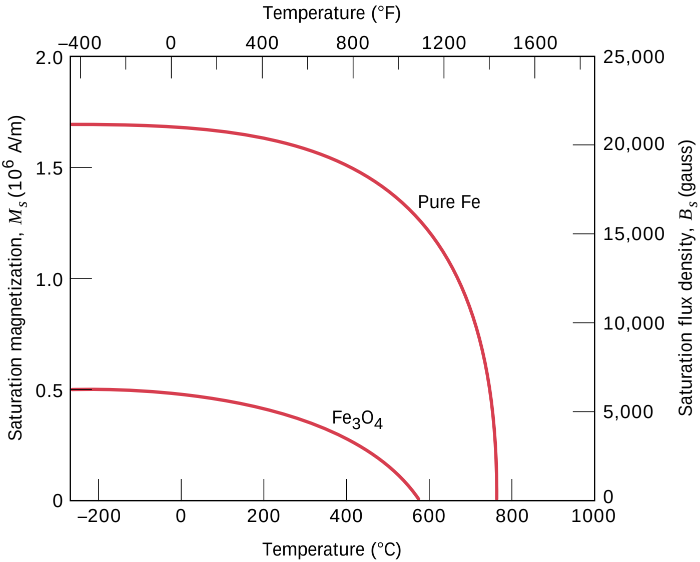

FIGURE 18.10 Plot of saturation magnetization as a function of temperature for iron and Fe_3O_4. [Adapted from J. Smit and H. P. J. Wijn, *Ferrites.* Copyright © 1959 by N. V. Philips Gloeilampenfabrieken, Eindhoven (Holland). Reprinted by permission.]

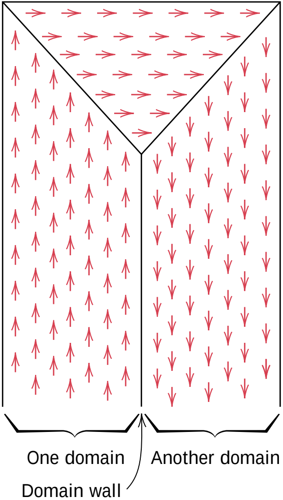
One domain
Another domain
Domain wall

Figure 18.11 Schematic depiction of domains in a ferromagnetic or ferrimagnetic material; arrows represent atomic magnetic dipoles. Within each domain, all dipoles are aligned, whereas the direction of alignment varies from one domain to another.

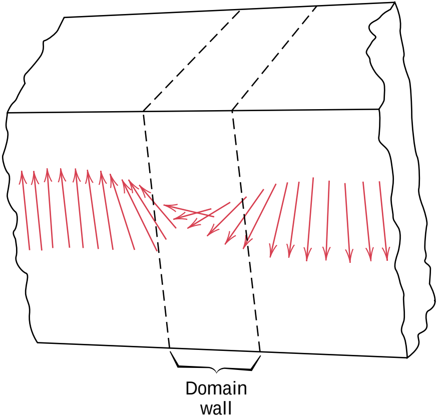

FIGURE 18.12 The gradual change in magnetic dipole orientation across a domain wall. (From W. D. Kingery, H. K. Bowen, and D. R. Uhlmann, *Introduction to Ceramics*, 2nd edition. Copyright © 1976 by John Wiley & Sons, New York. Reprinted by permission of John Wiley & Sons, Inc.)

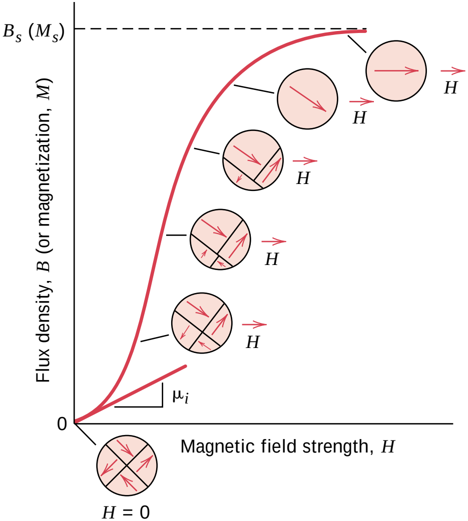

B_s (M_s)
Flux density, B (or magnetization, M)
H
H
H
H
H
μ_i
0
Magnetic field strength, H
H = 0

FIGURE 18.13 The B-versus-H behavior for a ferromagnetic or ferrimagnetic material that was initially unmagnetized. Domain configurations during several stages of magnetization are represented. Saturation flux density B_s, magnetization M_s, and initial permeability μ_i are also indicated. (Adapted from O. H. Wyatt and D. Dew-Hughes, *Metals, Ceramics and Polymers*, Cambridge University Press, 1974.)

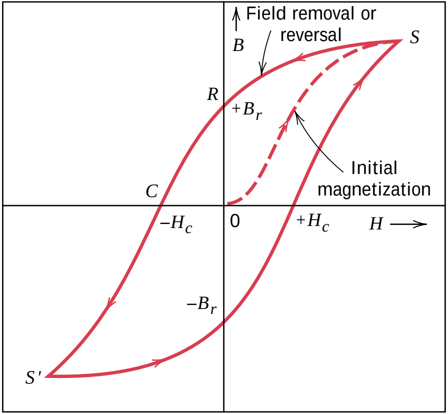

Figure 18.14 Magnetic flux density versus the magnetic field strength for a ferromagnetic material that is subjected to forward and reverse saturations (points S and S'). The hysteresis loop is represented by the solid curve; the dashed curve indicates the initial magnetization. The remanence B_r and the coercive force H_c are also shown.

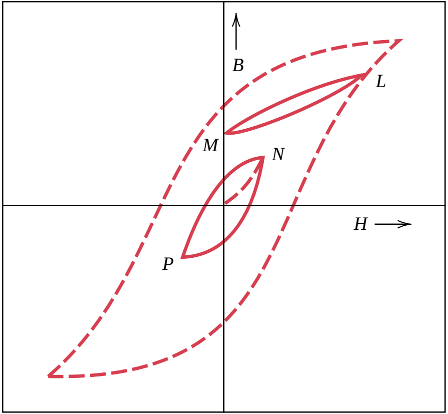

FIGURE 18.15 A hysteresis curve at less than saturation (curve NP) within the saturation loop for a ferromagnetic material. The B–H behavior for field reversal at other than saturation is indicated by curve LM.

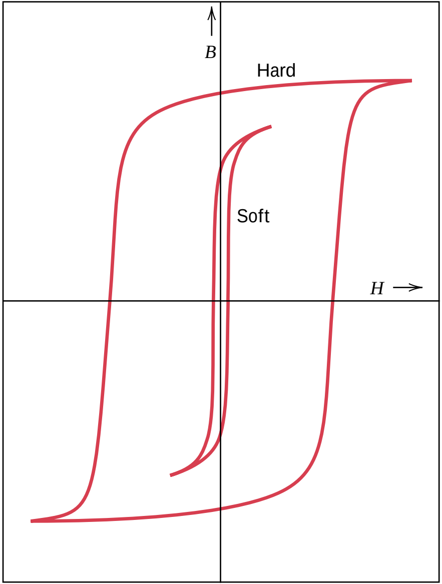

FIGURE 18.16 Schematic magnetization curves for soft and hard magnetic materials. (From K. M. Ralls, T. H. Courtney, and J. Wulff, *Introduction to Materials Science and Engineering*. Copyright © 1976 by John Wiley & Sons, New York. Reprinted by permission of John Wiley & Sons, Inc.)

Table 18.5 **Typical Properties for Several Soft Magnetic Materials**

Material	*Composition (wt%)*	*Initial Relative Permeability* μ_i	*Saturation Flux Density* B_s *[tesla (gauss)]*	*Hysteresis Loss/Cycle* [J/m^3 (erg/cm^3)]	*Resistivity* ρ (Ω-*m*)
Commercial iron ingot	99.95Fe	150	2.14 (21,400)	270 (2700)	1.0×10^{-7}
Silicon–iron (oriented)	97Fe, 3Si	1400	2.01 (20,100)	40 (400)	4.7×10^{-7}
45 Permalloy	55Fe, 45Ni	2500	1.60 (16,000)	120 (1200)	4.5×10^{-7}
Supermalloy	79Ni, 15Fe, 5Mo, 0.5Mn	75,000	0.80 (8000)	—	6.0×10^{-7}
Ferroxcube A	48$MnFe_2O_4$, 52$ZnFe_2O_4$	1400	0.33 (3300)	~40 (~400)	2000
Ferroxcube B	36$NiFe_2O_4$, 64$ZnFe_2O_4$	650	0.36 (3600)	~35 (~350)	10^7

Source: Adapted from *Metals Handbook: Properties and Selection: Stainless Steels, Tool Materials and Special-Purpose Metals,* Vol. 3, 9th edition, D. Benjamin, Senior Editor, American Society for Metals, 1980.

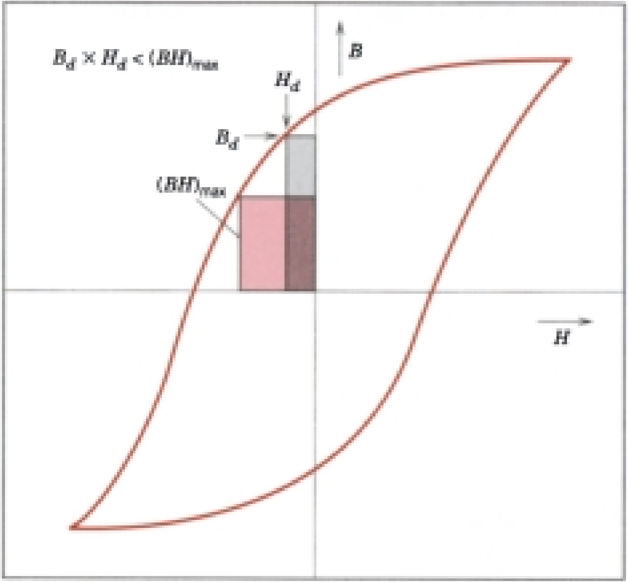
$B_d \times H_d < (BH)_{max}$
B
H_d
B_d
$(BH)_{max}$
H

FIGURE 18.17 Schematic magnetization curve that displays hysteresis. Within the second quadrant are drawn two B-H energy product rectangles; the area of that rectangle labeled $(BH)_{max}$ is the largest possible, which is greater than the area defined by B_d-H_d.

Table 18.6 Typical Properties for Several Hard Magnetic Materials

Material	***Composition (wt%)***	***Remanence B_r [tesla (gauss)]***	***Coercivity H_c [amp-turn/m (Oe)]***	***$(BH)_{max}$ [kJ/m^3 (MGOe)]***	***Curie Temperature T_c [°C (°F)]***	***Resistivity ρ (Ω-m)***
Tungsten steel	92.8 Fe, 6 W, 0.5 Cr, 0.7 C	0.95 (9500)	5900 (74)	2.6 (0.33)	760 (1400)	3.0×10^{-7}
Cunife	20 Fe, 20 Ni, 60 Cu	0.54 (5400)	44,000 (550)	12 (1.5)	410 (770)	1.8×10^{-7}
Sintered alnico 8	34 Fe, 7 Al, 15 Ni, 35 Co, 4 Cu, 5 Ti	0.76 (7600)	125,000 (1550)	36 (4.5)	860 (1580)	—
Sintered ferrite 3	$BaO\text{-}6Fe_2O_3$	0.32 (3200)	240,000 (3000)	20 (2.5)	450 (840)	$\sim 10^4$
Cobalt rare earth 1	$SmCo_5$	0.92 (9200)	720,000 (9,000)	170 (21)	725 (1340)	5.0×10^{-7}
Sintered neodymium-iron-boron	$Nd_2Fe_{14}B$	1.16 (11,600)	848,000 (10,600)	255 (32)	310 (590)	1.6×10^{-6}

Source: Adapted from *ASM Handbook*, Vol. 2, *Properties and Selection: Nonferrous Alloys and Special-Purpose Materials*. Copyright © 1990 by ASM International. Reprinted by permission of ASM International, Materials Park, OH.

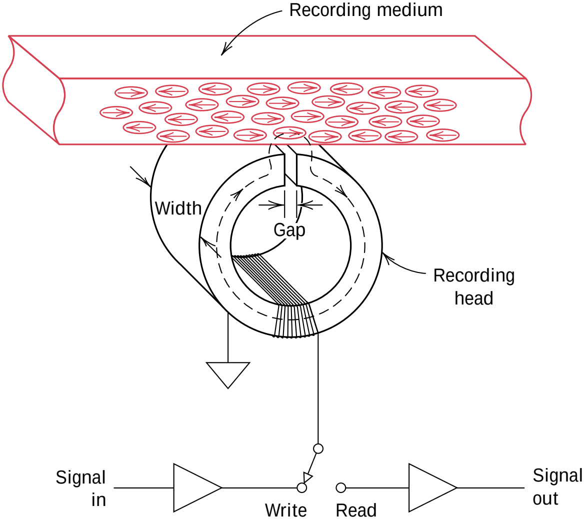
Recording medium
Width
Gap
Recording head
Signal in
Write
Read
Signal out

FIGURE 18.18 Schematic representation showing how information is stored and retrieved using a magnetic storage medium. (From J. U. Lemke, *MRS Bulletin*, Vol. XV, No. 3, p. 31, 1990. Reprinted with permission.)

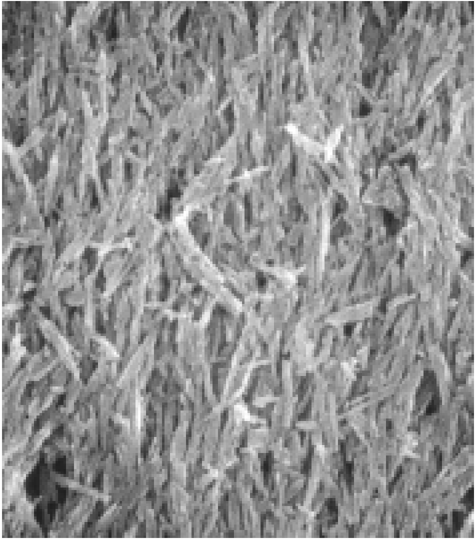

FIGURE 18.19 A scanning electron micrograph showing the microstructure of a magnetic storage disk. Needle-shaped particles of γ-Fe_2O_3 are oriented and embedded within an epoxy phenolic resin. 8000×. (Photograph courtesy of P. Rayner and N. L. Head, IBM Corporation.)

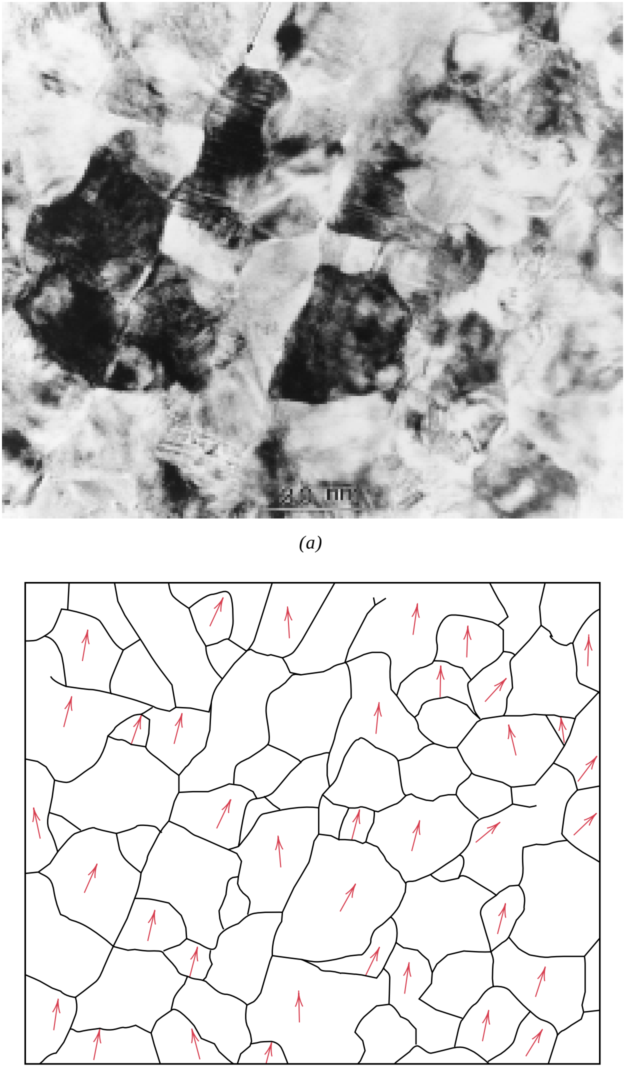

(a)

(b)

Figure 18.20 (*a*) A high-resolution transmission electron micrograph showing the microstructure of a cobalt–chromium–platinum thin film that is used as a high-density magnetic storage medium. The arrow at the top indicates the motion direction of the medium. 500,000×. (*b*) A representation of the grain structure for the electron micrograph in (*a*); the arrows in some of the grains indicate the texture, or the direction of easy magnetization. (From M. R. Kim, S. Guruswamy, and K. E. Johnson, *J. Appl. Phys.*, Vol. 74, No. 7, p. 4646, 1993. Reprinted with permission.)

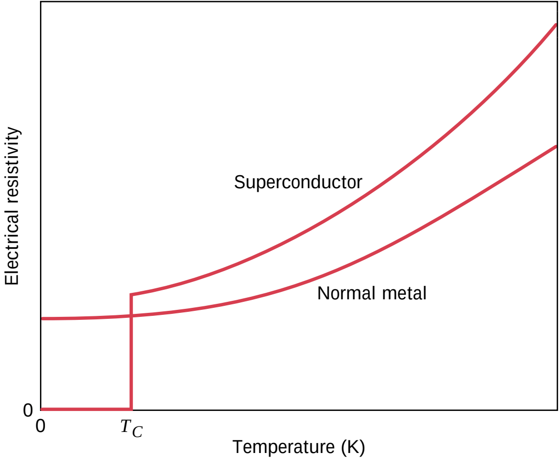

FIGURE 18.21 Temperature dependence of the electrical resistivity for normally conducting and superconducting materials in the vicinity of 0 K.

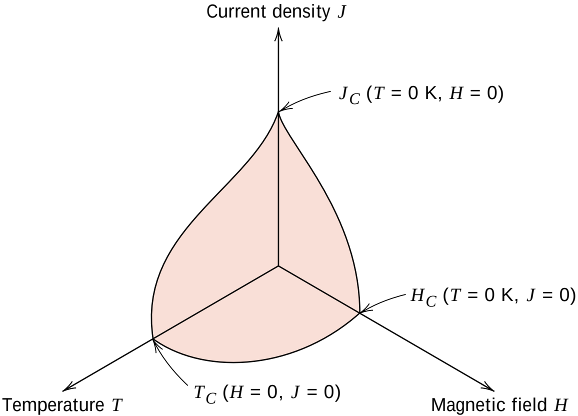
Current density J
J_C (T = 0 K, H = 0)
H_C (T = 0 K, J = 0)
T_C (H = 0, J = 0)
Temperature T
Magnetic field H

FIGURE 18.22 Critical temperature, current density, and magnetic field boundary separating superconducting and normal conducting states (schematic).

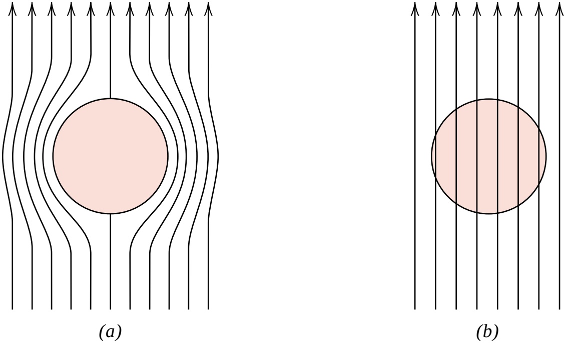

FIGURE 18.23 Representation of the Meissner effect. (*a*) While in the superconducting state, a body of material (circle) excludes a magnetic field (arrows) from its interior. (*b*) The magnetic field penetrates the same body of material once it becomes normally conductive.

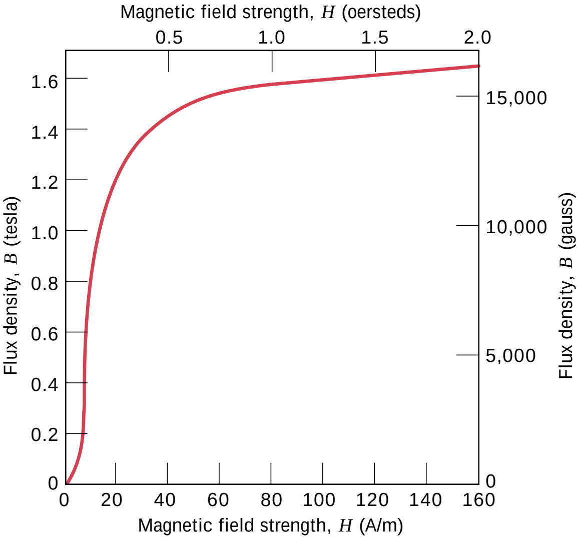

FIGURE 18.24 Initial magnetization B-versus-H curve for an iron-silicon alloy.

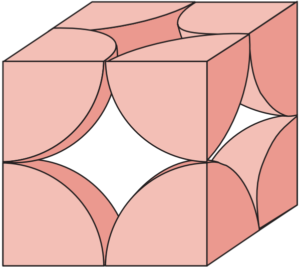

FIGURE 3.40 Hard-sphere unit cell representation of the simple cubic crystal structure.

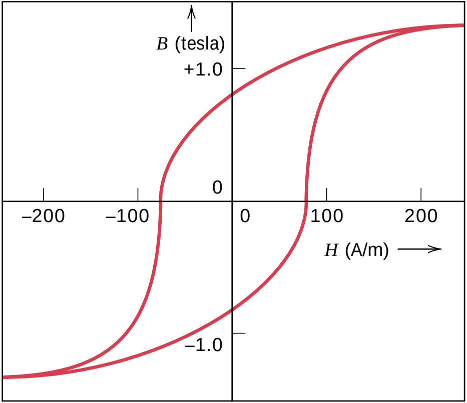

Figure 18.25 Complete magnetic hysteresis loop for a steel alloy.

```
[Loader]
Program=mse5e
CommandLine=crystals
```

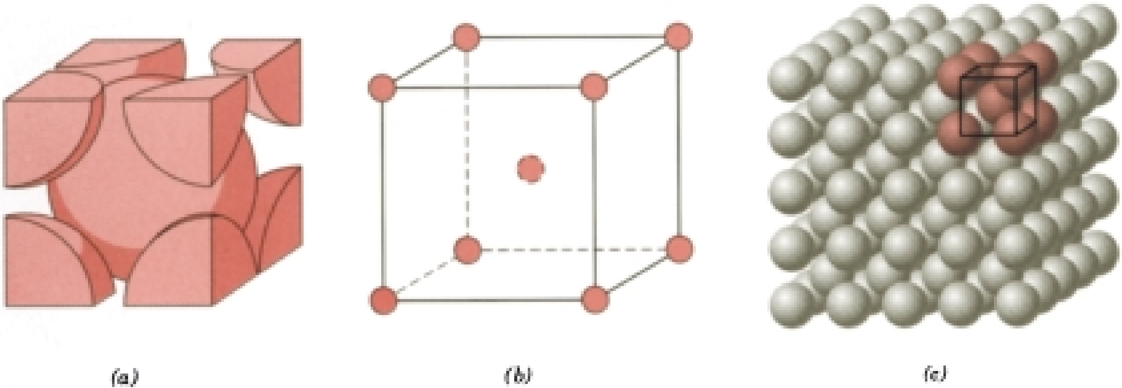

FIGURE 3.2 For the body-centered cubic crystal structure, (*a*) a hard sphere unit cell representation, (*b*) a reduced-sphere unit cell, and (*c*) an aggregate of many atoms. (Figure (*c*) from W. G. Moffatt, G. W. Pearsall, and J. Wulff, *The Structure and Properties of Materials*, Vol. I, *Structure*, p. 51. Copyright © 1964 by John Wiley & Sons, New York. Reprinted by permission of John Wiley & Sons, Inc.)

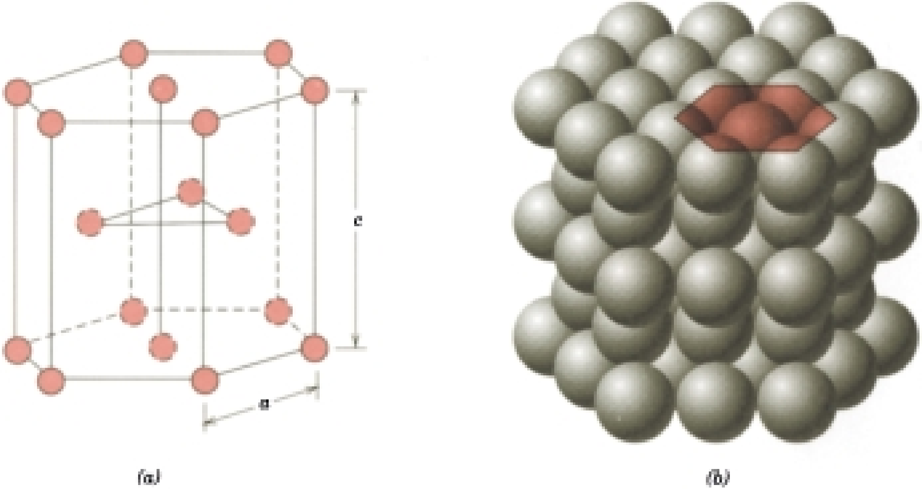

Figure 3.3 For the hexagonal close-packed crystal structure, (*a*) a reduced-sphere unit cell (*a* and *c* represent the short and long edge lengths, respectively), and (*b*) an aggregate of many atoms. (Figure (*b*) from W. G. Moffatt, G. W. Pearsall, and J. Wulff, *The Structure and Properties of Materials*, Vol. I, *Structure*, p. 51. Copyright © 1964 by John Wiley & Sons, New York. Reprinted by permission of John Wiley & Sons, Inc.)

Table 3.2 **For Several Ceramic Materials, Percent Ionic Character of the Interatomic Bonds**

Material	*Percent Ionic Character*
CaF_2	89
MgO	73
NaCl	67
Al_2O_3	63
SiO_2	51
Si_3N_4	30
ZnS	18
SiC	12

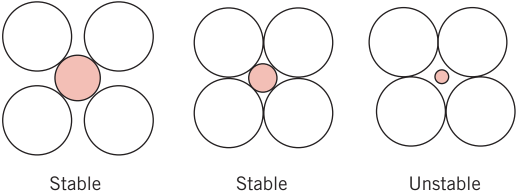

Stable

Stable

Unstable

Figure 3.4 Stable and unstable anion–cation coordination configurations. Open circles represent anions; colored circles denote cations.

```
[Loader]
Program=mse5e
CommandLine=ceramics
```

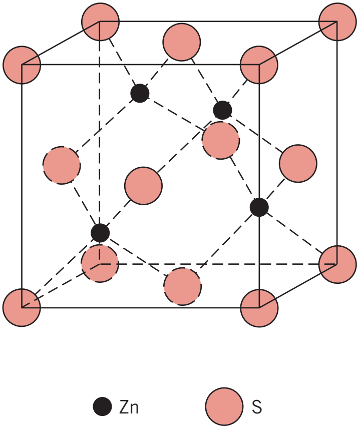

FIGURE 3.7 A unit cell for the zinc blende (ZnS) crystal structure.

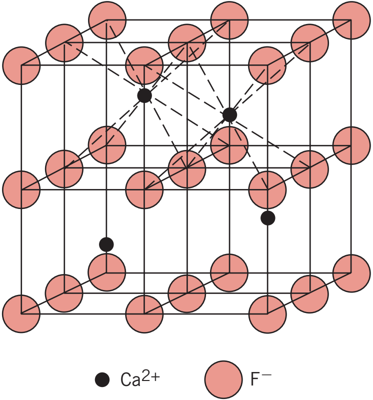

FIGURE 3.8 A unit cell for the fluorite (CaF_2) crystal structure.

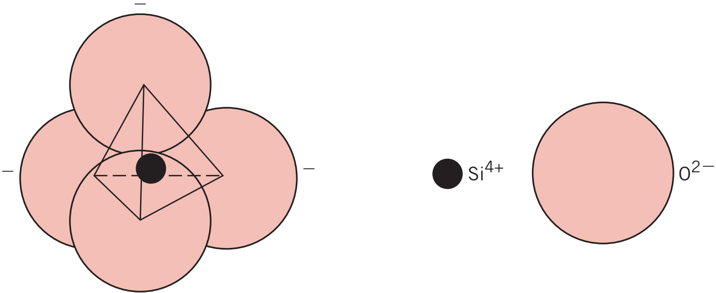

Figure 3.10 A silicon–oxygen (SiO_4^{4-}) tetrahedron.

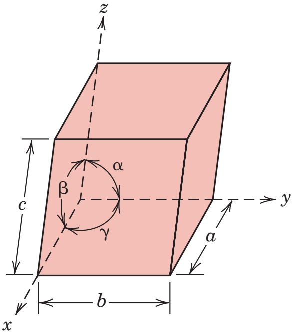

FIGURE 3.19 A unit cell with x, y, and z coordinate axes, showing axial lengths (a, b, and c) and interaxial angles (α, β, and γ).

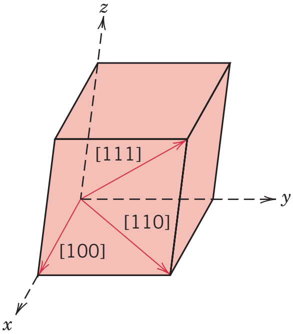
z
y
x
[111]
[110]
[100]

FIGURE 3.20 The [100], [110], and [111] directions within a unit cell.

```
[Loader]
Program=mse5e
CommandLine=directions
```

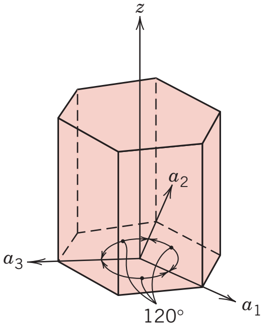
z
a_2
a_3
a_1
120°

Figure 3.21 Coordinate axis system for a hexagonal unit cell (Miller–Bravais scheme).

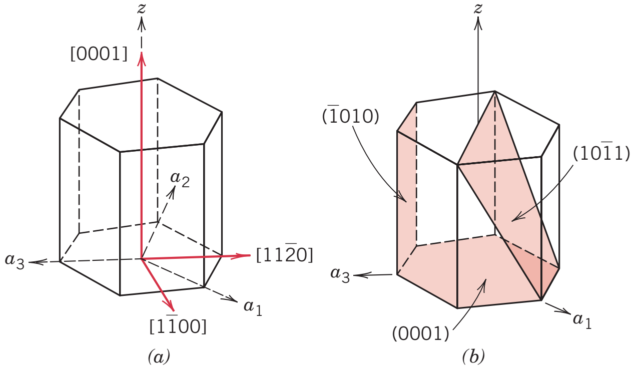
z
[0001]
a_2
a_3
$[11\bar{2}0]$
a_1
$[1\bar{1}00]$
(a)
z
$(\bar{1}010)$
$(10\bar{1}1)$
a_3
a_1
(0001)
(b)

Figure 3.22 For the hexagonal crystal system, (*a*) [0001], $[1\bar{1}00]$, and $[11\bar{2}0]$ directions, and (*b*) the (0001), $(10\bar{1}1)$, and $(\bar{1}010)$ planes.

```
[Loader]
Program=mse5e
CommandLine=planes
```

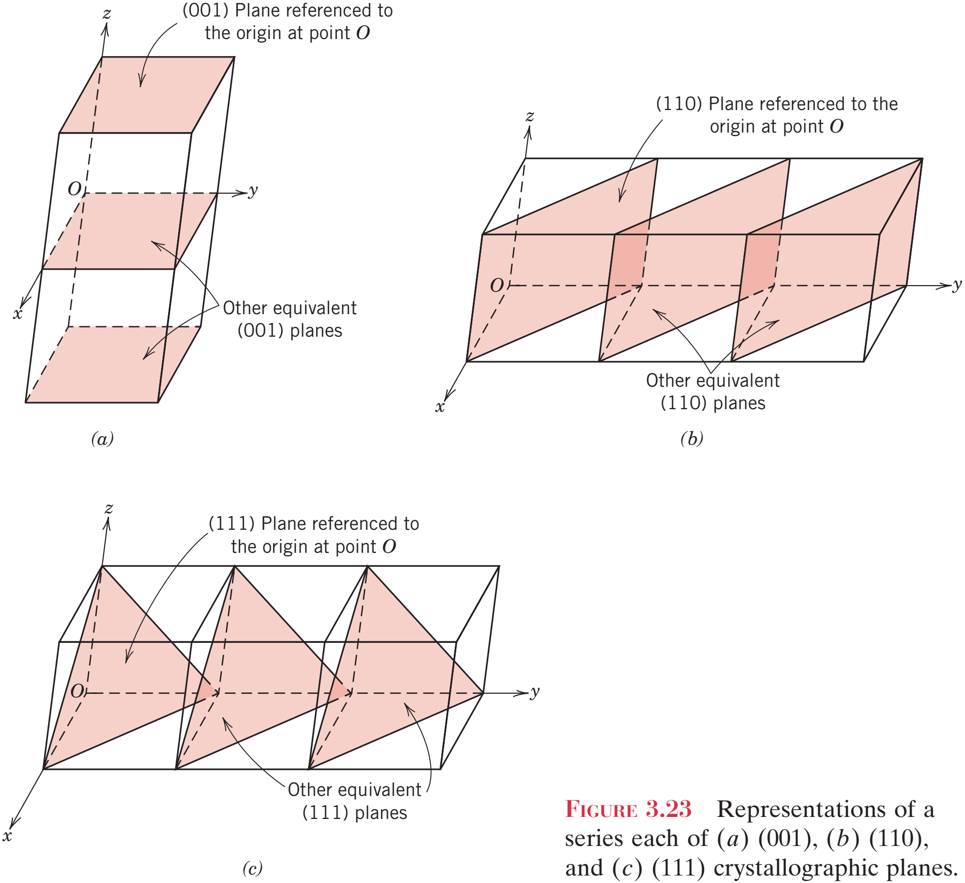
(001) Plane referenced to the origin at point O
z
O
y
x
Other equivalent (001) planes
(a)
(110) Plane referenced to the origin at point O
z
O
y
x
Other equivalent (110) planes
(b)
(111) Plane referenced to the origin at point O
z
O
y
x
Other equivalent (111) planes
(c)

FIGURE 3.23 Representations of a series each of (*a*) (001), (*b*) (110), and (*c*) (111) crystallographic planes.

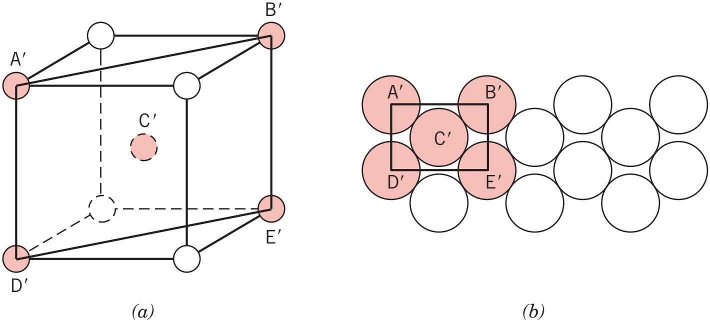

(a) (b)

Figure 3.25 (*a*) Reduced-sphere BCC unit cell with (110) plane. (*b*) Atomic packing of a BCC (110) plane. Corresponding atom positions from (*a*) are indicated.

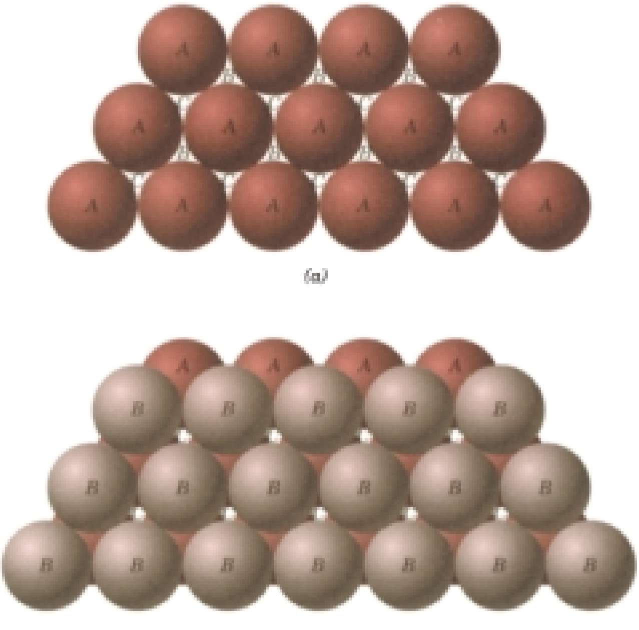

(a)

(b)

Figure 3.27 (*a*) A portion of a close-packed plane of atoms; *A*, *B*, and *C* positions are indicated. (*b*) The *AB* stacking sequence for close-packed atomic planes. (Adapted from W. G. Moffatt, G. W. Pearsall, and J. Wulff, *The Structure and Properties of Materials*, Vol. I, *Structure*, p. 50. Copyright © 1964 by John Wiley & Sons, New York. Reprinted by permission of John Wiley & Sons, Inc.)

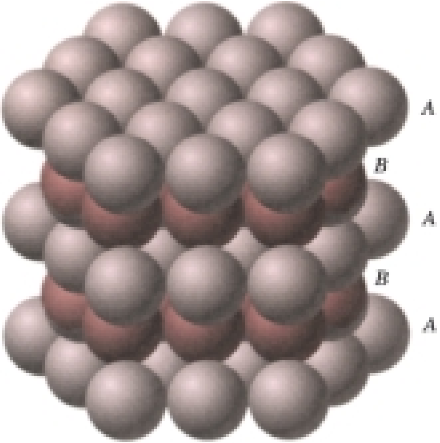

FIGURE 3.28 Close-packed plane stacking sequence for hexagonal close-packed. (Adapted from W. G. Moffatt, G. W. Pearsall, and J. Wulff, *The Structure and Properties of Materials,* Vol. I, *Structure,* p. 51. Copyright © 1964 by John Wiley & Sons, New York. Reprinted by permission of John Wiley & Sons, Inc.)

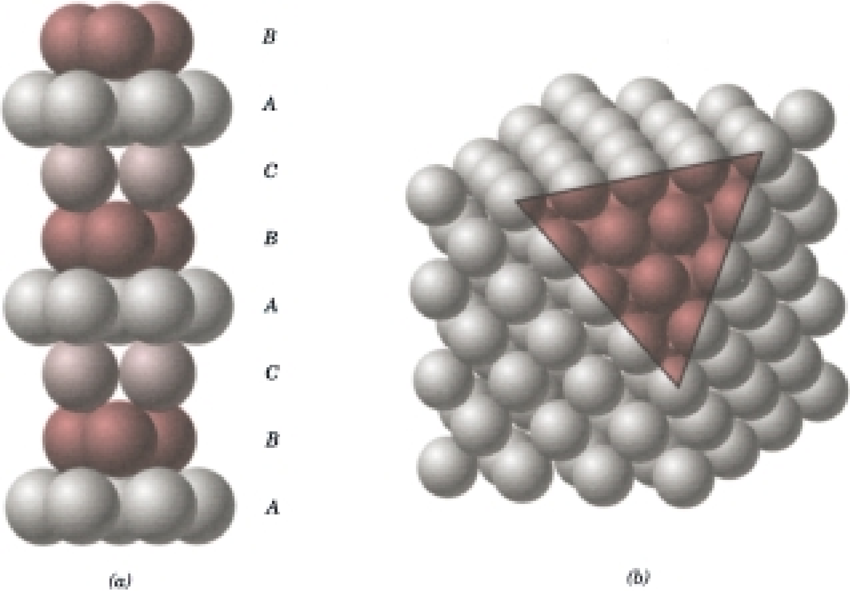

FIGURE 3.29 (*a*) Close-packed stacking sequence for face-centered cubic. (*b*) A corner has been removed to show the relation between the stacking of close-packed planes of atoms and the FCC crystal structure; the heavy triangle outlines a (111) plane. (Figure (*b*) from W. G. Moffatt, G. W. Pearsall, and J. Wulff, *The Structure and Properties of Materials,* Vol. I, *Structure,* p. 51. Copyright © 1964 by John Wiley & Sons, New York. Reprinted by permission of John Wiley & Sons, Inc.)

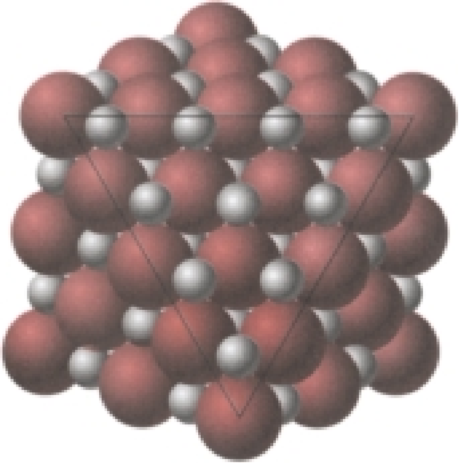

FIGURE 3.31 A section of the rock salt crystal structure from which a corner has been removed. The exposed plane of anions (light spheres inside the triangle) is a {111}-type plane; the cations (dark spheres) occupy the interstitial octahedral positions.

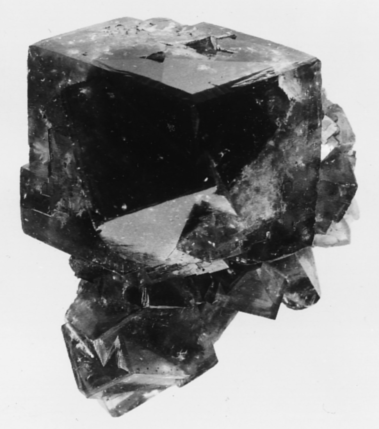

Figure 3.32 Photograph showing several single crystals of fluorite, CaF_2. (Smithsonian Institution photograph number 38181P.)

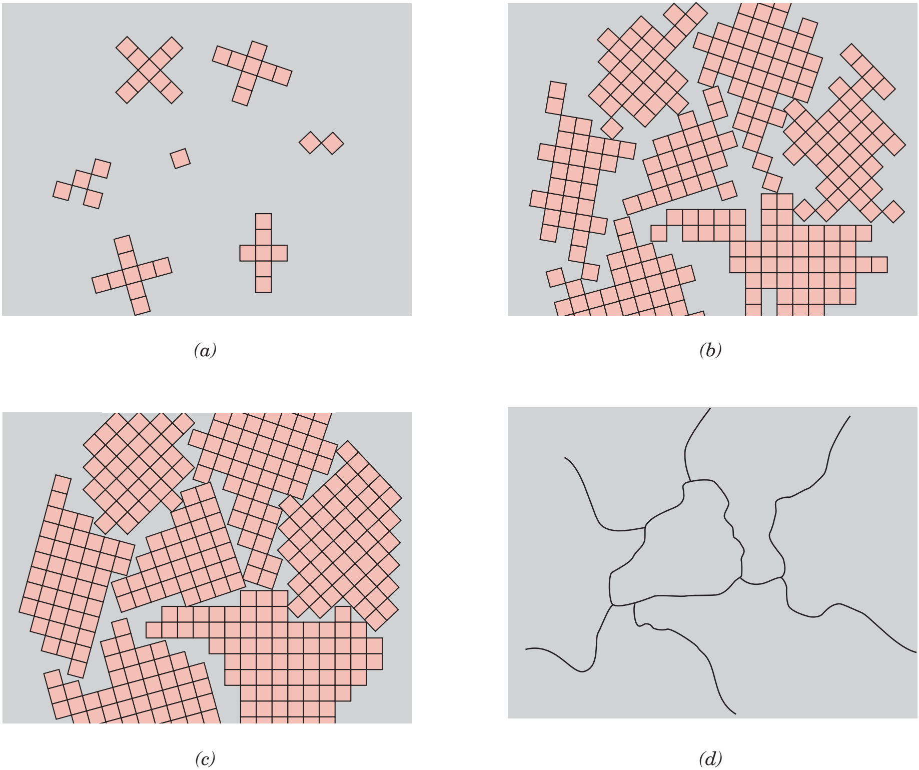

Figure 3.33 Schematic diagrams of the various stages in the solidification of a polycrystalline material; the square grids depict unit cells. (*a*) Small crystallite nuclei. (*b*) Growth of the crystallites; the obstruction of some grains that are adjacent to one another is also shown. (*c*) Upon completion of solidification, grains having irregular shapes have formed. (*d*) The grain structure as it would appear under the microscope; dark lines are the grain boundaries. (Adapted from W. Rosenhain, *An Introduction to the Study of Physical Metallurgy,* 2nd edition, Constable & Company Ltd., London, 1915.)

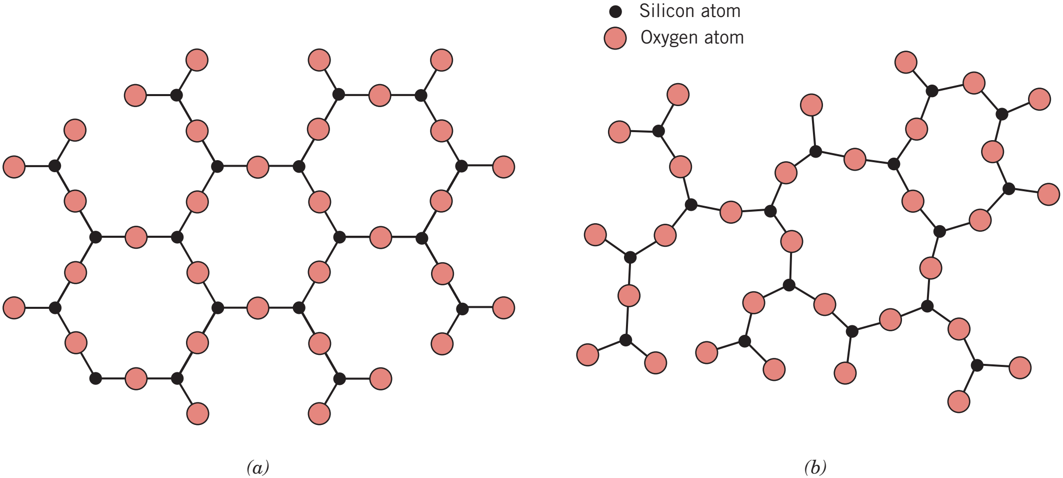
Silicon atom
Oxygen atom
(a)
(b)

FIGURE 3.38 Two-dimensional schemes of the structure of (*a*) crystalline silicon dioxide and (*b*) noncrystalline silicon dioxide.

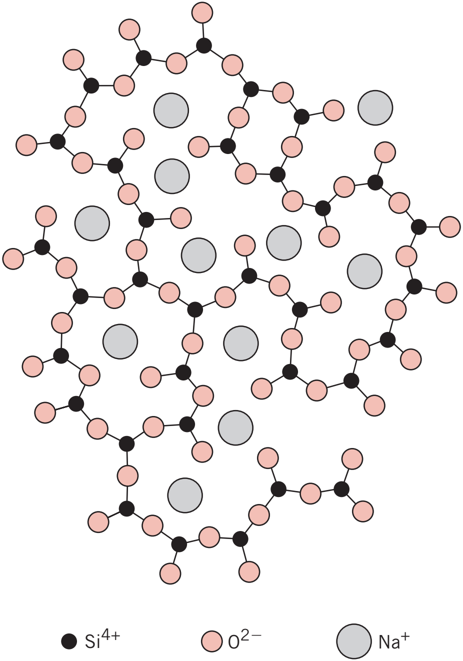

FIGURE 3.39 Schematic representation of ion positions in a sodium–silicate glass.

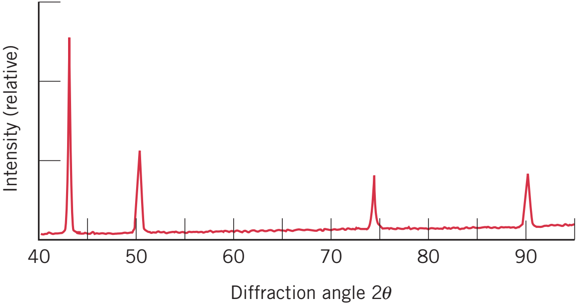

FIGURE 3.41 Diffraction pattern for polycrystalline copper.

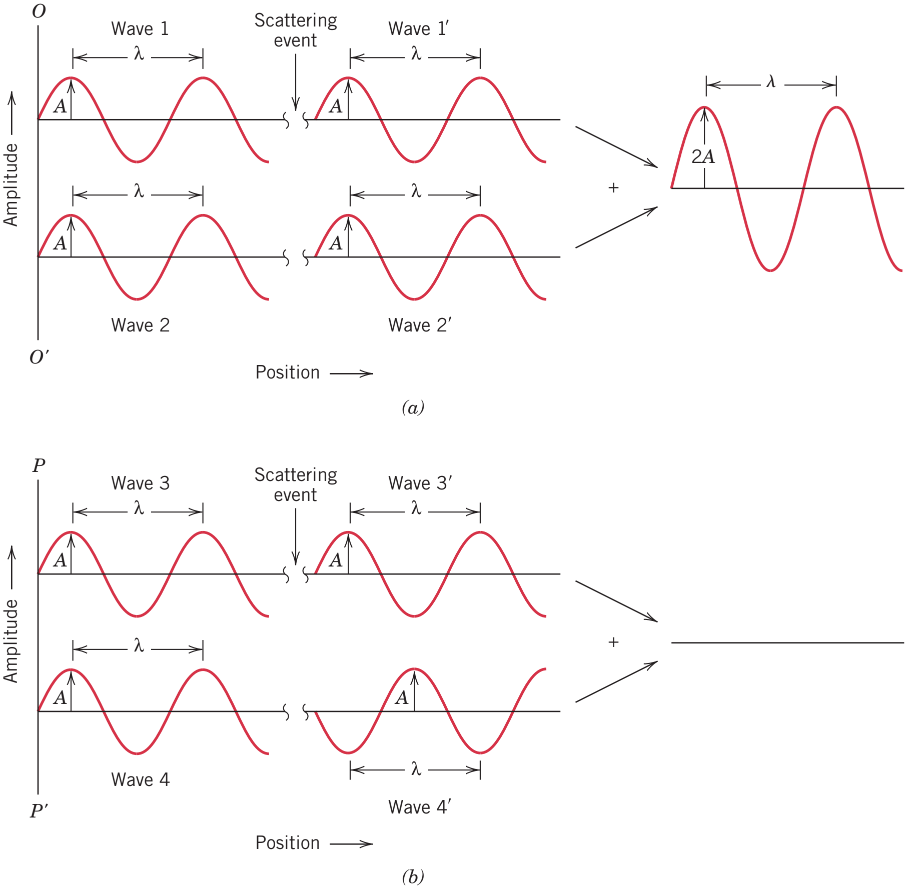
O
Wave 1
λ
A
Scattering event
Wave 1′
λ
A
Amplitude
λ
A
Wave 2
λ
A
Wave 2′
O′
+
λ
2A
Position
(a)
P
Wave 3
λ
A
Scattering event
Wave 3′
λ
A
Amplitude
λ
A
Wave 4
A
λ
Wave 4′
P′
+
Position
(b)

Figure 3.34 (*a*) Demonstration of how two waves (labeled 1 and 2) that have the same wavelength λ and remain in phase after a scattering event (waves 1′ and 2′) constructively interfere with one another. The amplitudes of the scattered waves add together in the resultant wave. (*b*) Demonstration of how two waves (labeled 3 and 4) that have the same wavelength and become out of phase after a scattering event (waves 3′ and 4′) destructively interfere with one another. The amplitudes of the two scattered waves cancel one another.

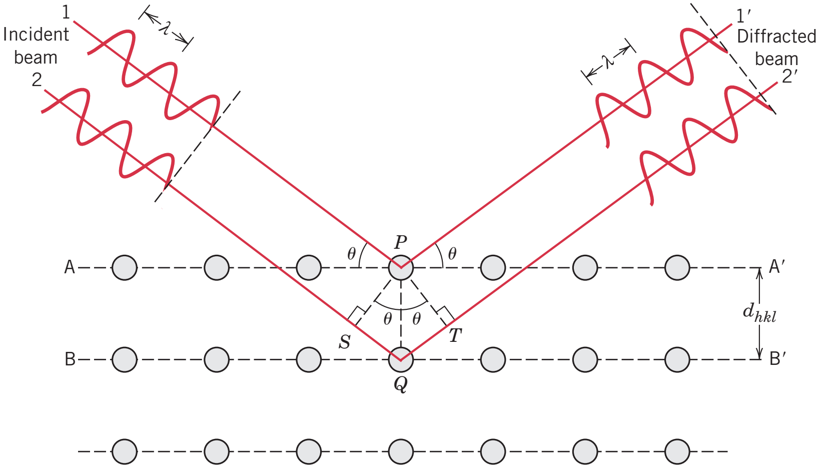
1
Incident beam
2
λ
λ
1′
Diffracted beam
2′
θ
P
θ
A
A′
θ
θ
S
T
d_{hkl}
B
B′
Q

FIGURE 3.35 Diffraction of x-rays by planes of atoms (A–A′ and B–B′).

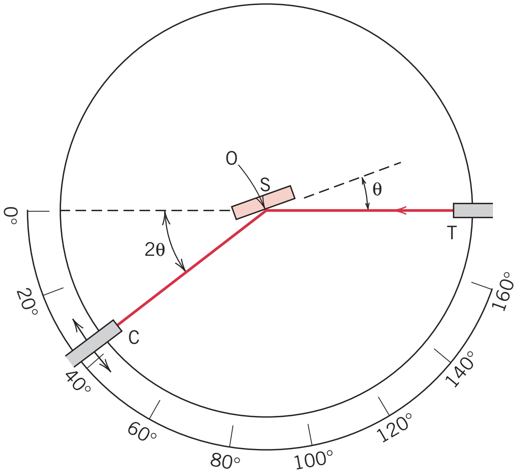
O
S
θ
T
0°
2θ
C
20°
40°
60°
80°
100°
120°
140°
160°

FIGURE 3.36 Schematic diagram of an x-ray diffractometer; T = x-ray source, S = specimen, C = detector, and O = the axis around which the specimen and detector rotate.

Figure 7.10 (*a*) Typical stress–strain behavior for a metal showing elastic and plastic deformations, the proportional limit *P*, and the yield strength σ_y, as determined using the 0.002 strain offset method. (*b*) Representative stress–strain behavior found for some steels demonstrating the yield point phenomenon.

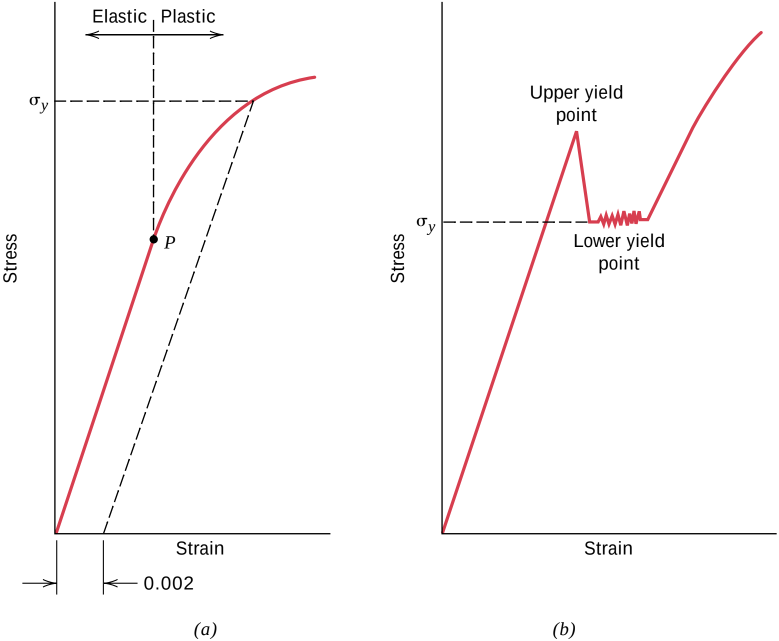

FIGURE 7.11 Typical engineering stress–strain behavior to fracture, point *F*. The tensile strength *TS* is indicated at point *M*. The circular insets represent the geometry of the deformed specimen at various points along the curve.

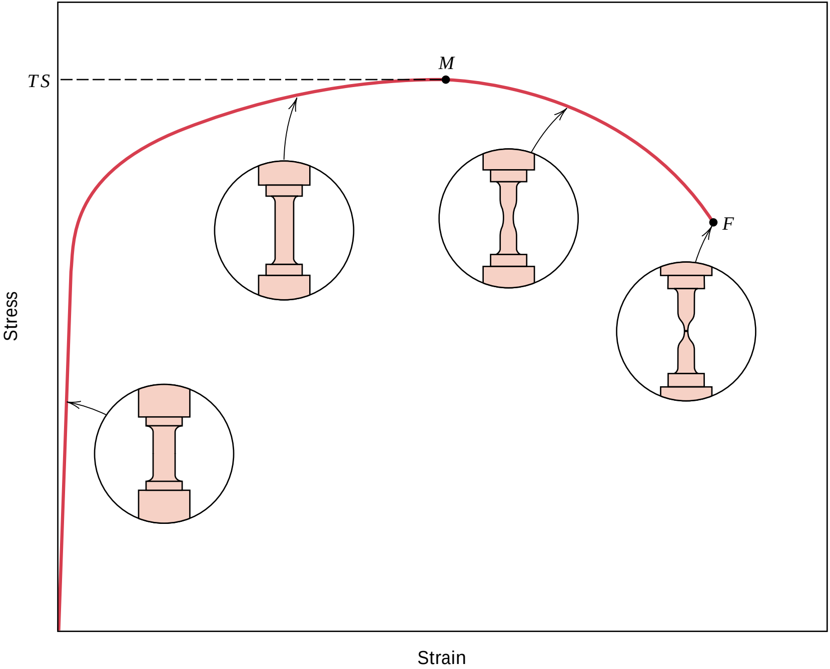

FIGURE 7.14 Engineering stress–strain behavior for iron at three temperatures.

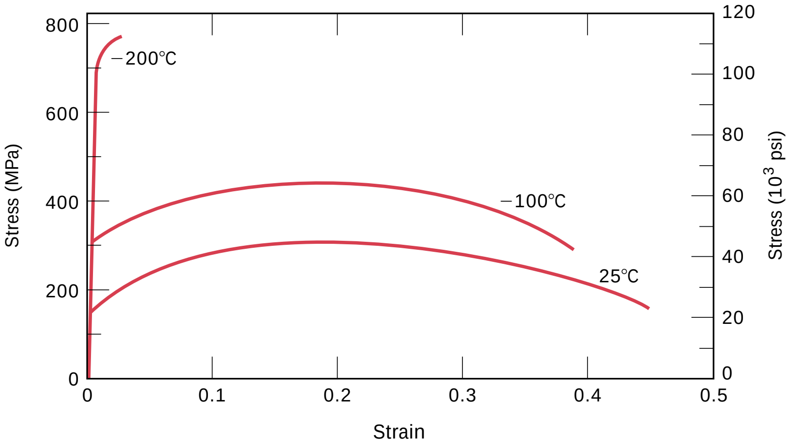

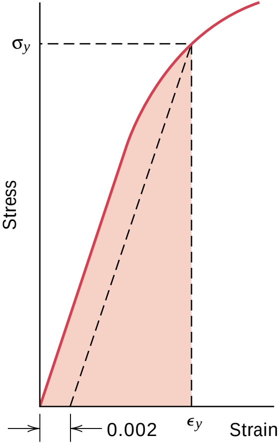

FIGURE 7.15 Schematic representation showing how modulus of resilience (corresponding to the shaded area) is determined from the tensile stress–strain behavior of a material.

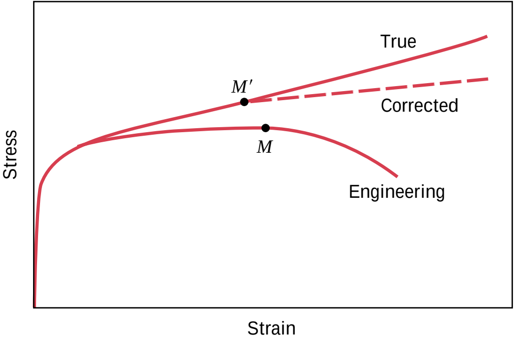

Figure 7.16 A comparison of typical tensile engineering stress–strain and true stress–strain behaviors. Necking begins at point M on the engineering curve, which corresponds to M' on the true curve. The ‘‘corrected’’ true stress–strain curve takes into account the complex stress state within the neck region.

Table 7.3 **Tabulation of *n* and *K* Values (Equation 7.19) for Several Alloys**

		K	
Material	***n***	***MPa***	***psi***
Low-carbon steel (annealed)	0.26	530	77,000
Alloy steel (Type 4340, annealed)	0.15	640	93,000
Stainless steel (Type 304, annealed)	0.45	1275	185,000
Aluminum (annealed)	0.20	180	26,000
Aluminum alloy (Type 2024, heat treated)	0.16	690	100,000
Copper (annealed)	0.54	315	46,000
Brass (70Cu–30Zn, annealed)	0.49	895	130,000

Source: From *Manufacturing Processes for Engineering Materials* by Seope Kalpakjian, © 1997. Reprinted by permission of Prentice-Hall, Inc., Upper Saddle River, NJ.

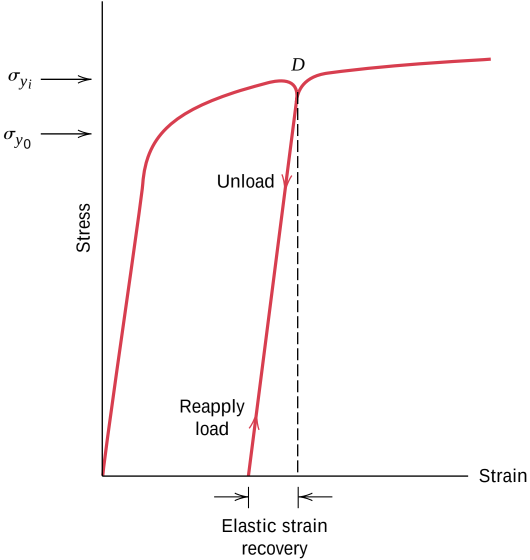

FIGURE 7.17 Schematic tensile stress–strain diagram showing the phenomena of elastic strain recovery and strain hardening. The initial yield strength is designated as σ_{y_0}; σ_{y_i} is the yield strength after releasing the load at point *D*, and then upon reloading.

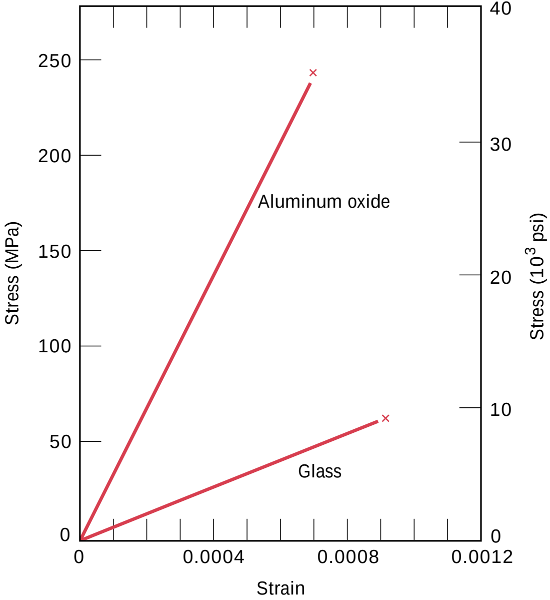

FIGURE 7.19 Typical stress–strain behavior to fracture for aluminum oxide and glass.

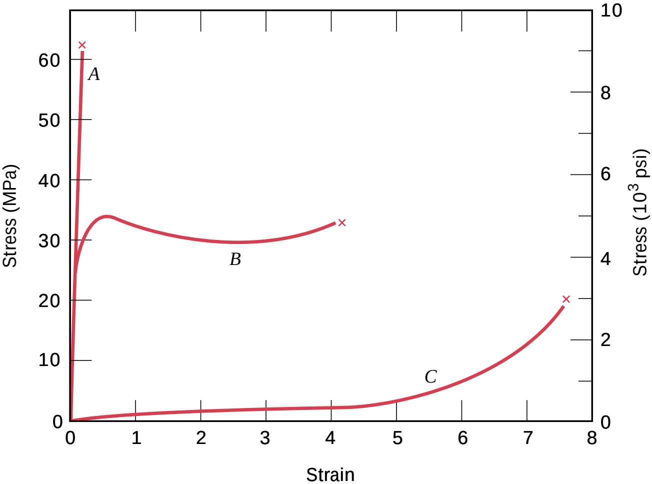

Figure 7.22 The stress–strain behavior for brittle (curve *A*), plastic (curve *B*), and highly elastic (elastomeric) (curve *C*) polymers.

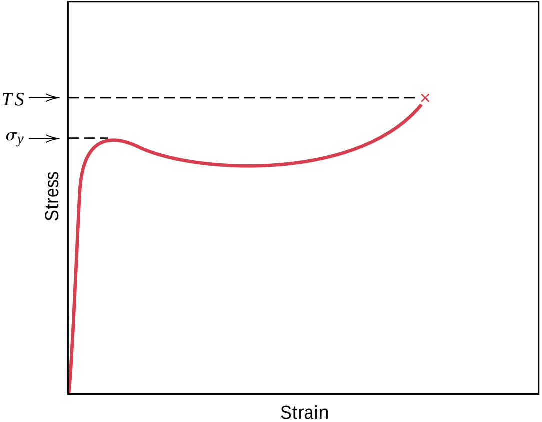

FIGURE 7.23 Schematic stress–strain curve for a plastic polymer showing how yield and tensile strengths are determined.

```
[Loader]
Program=mse5e
CommandLine=TensilePolymers
```

Table 7.4 **Hardness Testing Techniques**

		Shape of Indentation			
Test	***Indenter***	***Side View***	***Top View***	***Load***	***Formula for Hardness Number***[a]
Brinell	10-mm sphere of steel or tungsten carbide	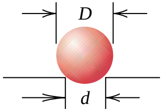	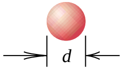	P	$\mathrm{HB} = \dfrac{2P}{\pi D[D - \sqrt{D^2 - d^2}]}$
Vickers microhardness	Diamond pyramid	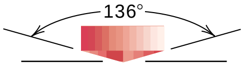	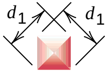	P	$\mathrm{HV} = 1.854P/d_1^2$
Knoop microhardness	Diamond pyramid	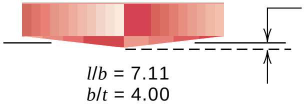	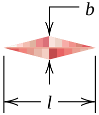	P	$\mathrm{HK} = 14.2P/l^2$
Rockwell and Superficial Rockwell	Diamond cone $\frac{1}{16}$, $\frac{1}{8}$, $\frac{1}{4}$, $\frac{1}{2}$ in. diameter steel spheres	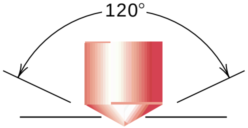 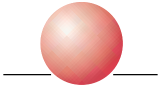	 	60 kg 100 kg 150 kg } Rockwell 15 kg 30 kg 45 kg } Superficial Rockwell	

[a] For the hardness formulas given, P (the applied load) is in kg, while D, d, d_1, and l are all in mm.

Source: Adapted from H. W. Hayden, W. G. Moffatt, and J. Wulff, *The Structure and Properties of Materials*, Vol. III, *Mechanical Behavior*. Copyright © 1965 by John Wiley & Sons, New York. Reprinted by permission of John Wiley & Sons, Inc.

Table 7.5a Rockwell Hardness Scales

Scale Symbol	*Indenter*	*Major Load (kg)*
A	Diamond	60
B	$\frac{1}{16}$ in. ball	100
C	Diamond	150
D	Diamond	100
E	$\frac{1}{8}$ in. ball	100
F	$\frac{1}{16}$ in. ball	60
G	$\frac{1}{16}$ in. ball	150
H	$\frac{1}{8}$ in. ball	60
K	$\frac{1}{8}$ in. ball	150

Table 7.5b Superficial Rockwell Hardness Scales

Scale Symbol	*Indenter*	*Major Load (kg)*
15N	Diamond	15
30N	Diamond	30
45N	Diamond	45
15T	$\frac{1}{16}$ in. ball	15
30T	$\frac{1}{16}$ in. ball	30
45T	$\frac{1}{16}$ in. ball	45
15W	$\frac{1}{8}$ in. ball	15
30W	$\frac{1}{8}$ in. ball	30
45W	$\frac{1}{8}$ in. ball	45

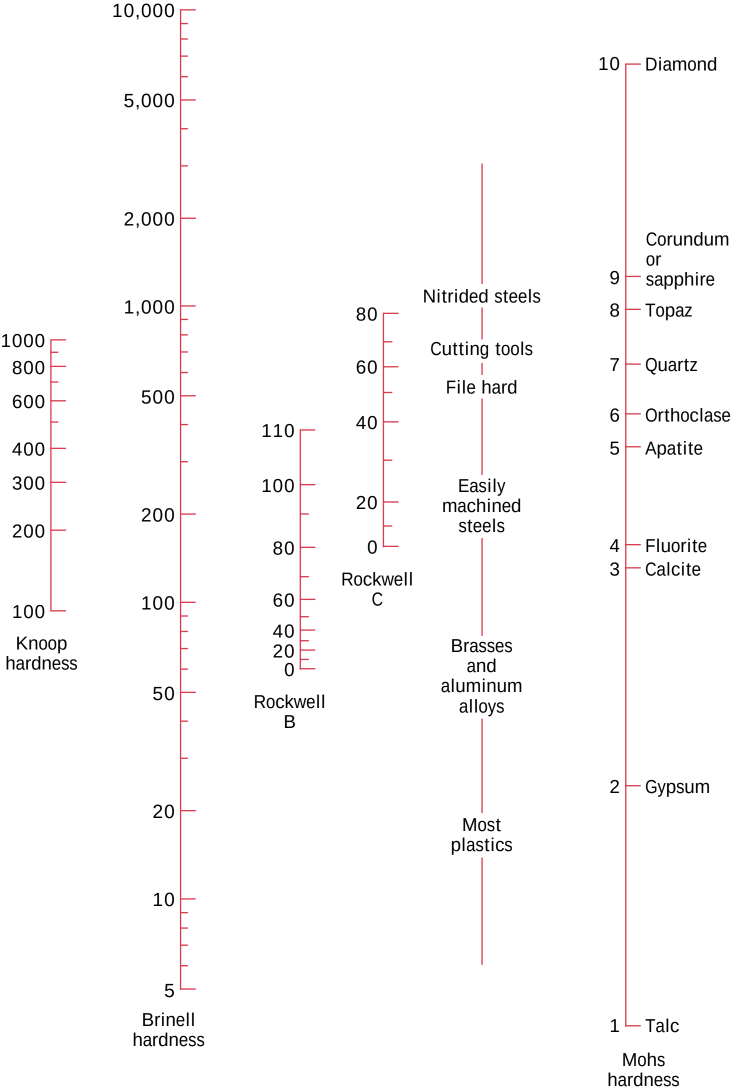

Figure 7.30 Comparison of several hardness scales. (Adapted from G. F. Kinney, *Engineering Properties and Applications of Plastics,* p. 202. Copyright © 1957 by John Wiley & Sons, New York. Reprinted by permission of John Wiley & Sons, Inc.)

Table 7.6 Approximate Knoop Hardness (100 g load) for Seven Ceramic Materials

Material	*Approximate Knoop Hardness*
Diamond (carbon)	7000
Boron carbide (B_4C)	2800
Silicon carbide (SiC)	2500
Tungsten carbide (WC)	2100
Aluminum oxide (Al_2O_3)	2100
Quartz (SiO_2)	800
Glass	550

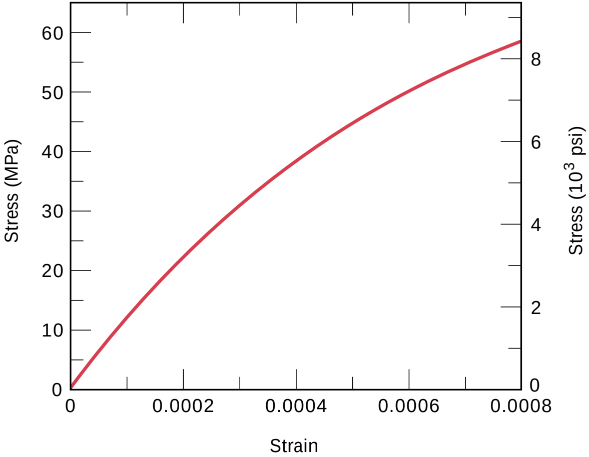

FIGURE 7.34 Tensile stress–strain behavior for a gray cast iron.

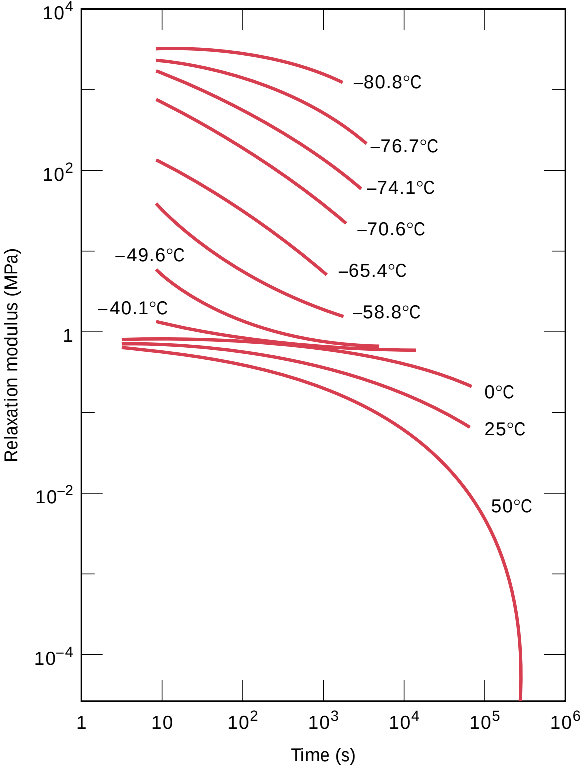

FIGURE 7.35 Logarithm of relaxation modulus versus logarithm of time for polyisobutylene between −80 and 50°C. (Adapted from E. Catsiff and A. V. Tobolsky, ‘‘Stress-Relaxation of Polyisobutylene in the Transition Region [1,2],’’ *J. Colloid Sci.*, **10,** 377 [1955]. Reprinted by permission of Academic Press, Inc.)

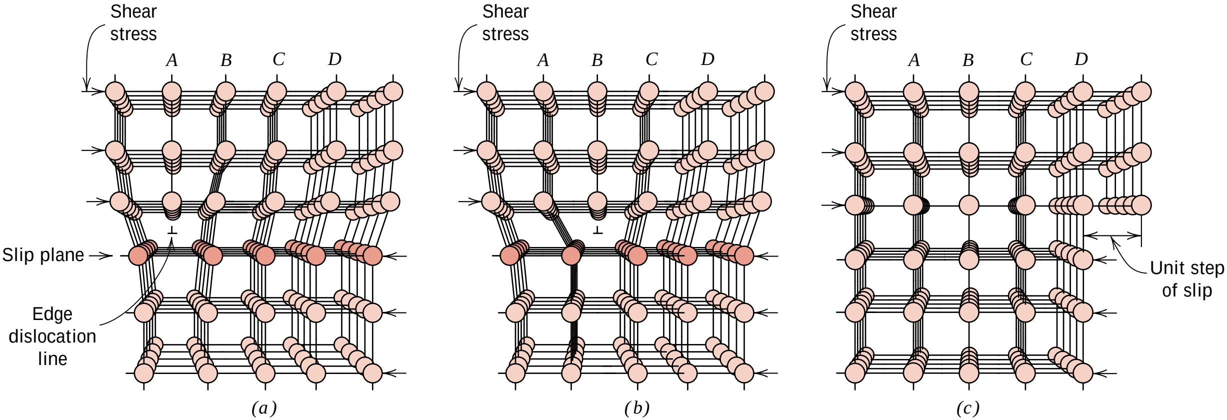
Shear stress
A
B
C
D
Slip plane
Edge dislocation line
Unit step of slip
(a)
(b)
(c)

Figure 8.1 Atomic rearrangements that accompany the motion of an edge dislocation as it moves in response to an applied shear stress. (*a*) The extra half-plane of atoms is labeled *A*. (*b*) The dislocation moves one atomic distance to the right as *A* links up to the lower portion of plane *B*; in the process, the upper portion of *B* becomes the extra half-plane. (*c*) A step forms on the surface of the crystal as the extra half-plane exits. (Adapted from A. G. Guy, *Essentials of Materials Science*, McGraw-Hill Book Company, New York, 1976, p. 153.)

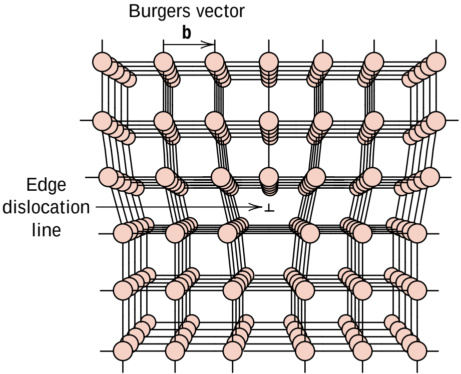
Burgers vector
b
Edge dislocation line
⊥

FIGURE 5.7 The atom positions around an edge dislocation; extra half-plane of atoms shown in perspective. (Adapted from A. G. Guy, *Essentials of Materials Science*, McGraw-Hill Book Company, New York, 1976, p. 153.)

FIGURE 5.8 (*a*) A screw dislocation within a crystal. (*b*) The screw dislocation in (*a*) as viewed from above. The dislocation line extends along line *AB*. Atom positions above the slip plane are designated by open circles, those below by solid circles. (Figure (*b*) from W. T. Read, Jr., *Dislocations in Crystals*, McGraw-Hill Book Company, New York, 1953.)

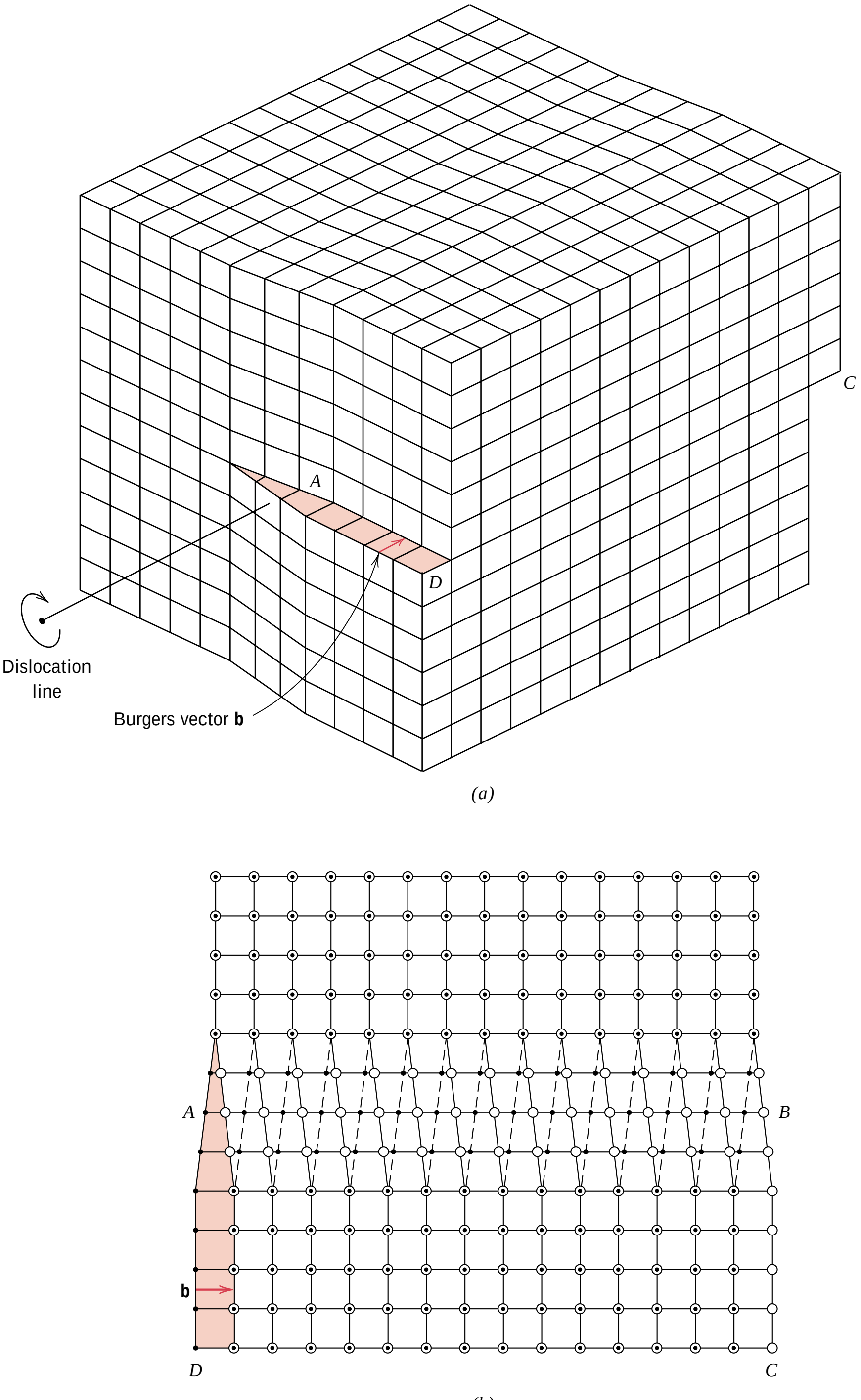
C
A
D
Dislocation line
Burgers vector **b**
(a)
A
B
b
D
C
(b)

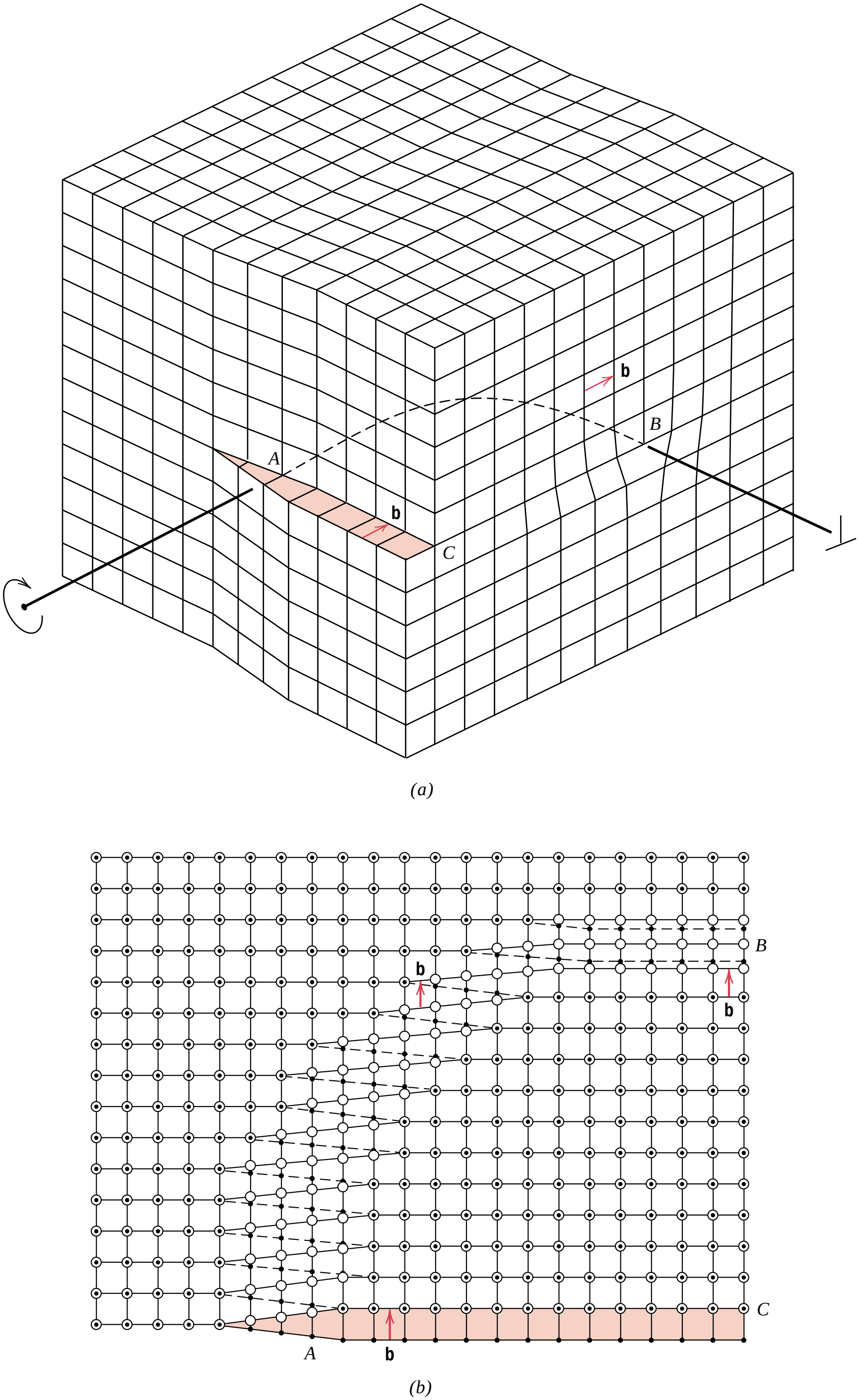

(a)

(b)

FIGURE 5.9 (*a*) Schematic representation of a dislocation that has edge, screw, and mixed character. (*b*) Top view, where open circles denote atom positions above the slip plane. Solid circles, atom positions below. At point *A*, the dislocation is pure screw, while at point *B*, it is pure edge. For regions in between where there is curvature in the dislocation line, the character is mixed edge and screw. (Figure (*b*) from W. T. Read, Jr., *Dislocations in Crystals*, McGraw-Hill Book Company, New York, 1953.)

```
[Loader]
Program=mse5e
CommandLine=Dislocations
```

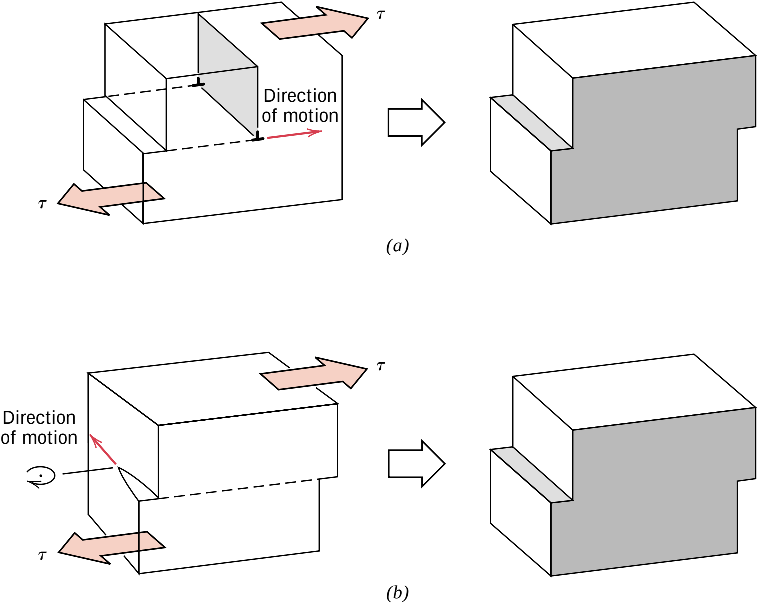

FIGURE 8.2 The formation of a step on the surface of a crystal by the motion of (*a*) an edge dislocation and (*b*) a screw dislocation. Note that for an edge, the dislocation line moves in the direction of the applied shear stress τ; for a screw, the dislocation line motion is perpendicular to the stress direction. (Adapted from H. W. Hayden, W. G. Moffatt, and J. Wulff, *The Structure and Properties of Materials,* Vol. III, *Mechanical Behavior,* p. 70. Copyright © 1965 by John Wiley & Sons, New York. Reprinted by permission of John Wiley & Sons, Inc.)

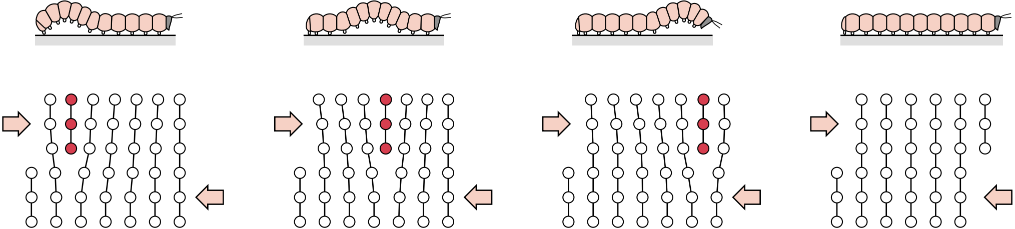

FIGURE 8.3 Representation of the analogy between caterpillar and dislocation motion.

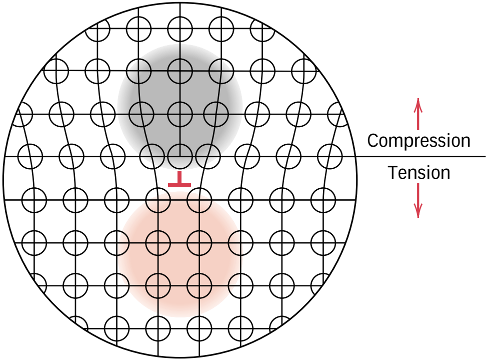

Figure 8.4 Regions of compression (dark) and tension (colored) located around an edge dislocation. (Adapted from W. G. Moffatt, G. W. Pearsall, and J. Wulff, *The Structure and Properties of Materials*, Vol. I, *Structure*, p. 85. Copyright © 1964 by John Wiley & Sons, New York. Reprinted by permission of John Wiley & Sons, Inc.)

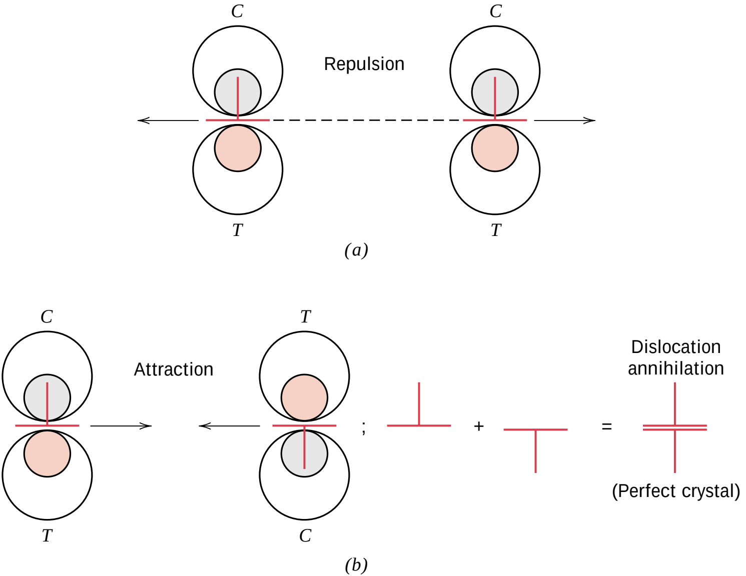
C
Repulsion
C
T
T
(a)
C
Attraction
T
Dislocation annihilation
;
+
=
(Perfect crystal)
T
C
(b)

Figure 8.5 (*a*) Two edge dislocations of the same sign and lying on the same slip plane exert a repulsive force on each other; *C* and *T* denote compression and tensile regions, respectively. (*b*) Edge dislocations of opposite sign and lying on the same slip plane exert an attractive force on each other. Upon meeting, they annihilate each other and leave a region of perfect crystal. (Adapted from H. W. Hayden, W. G. Moffatt, and J. Wulff, *The Structure and Properties of Materials*, Vol. III, *Mechanical Behavior*, p. 75. Copyright © 1965 by John Wiley & Sons, New York. Reprinted by permission of John Wiley & Sons.)

Table 8.1 Slip Systems for Face-Centered Cubic, Body-Centered Cubic, and Hexagonal Close-Packed Metals

Metals	*Slip Plane*	*Slip Direction*	*Number of Slip Systems*
Face-Centered Cubic			
Cu, Al, Ni, Ag, Au	$\{111\}$	$\langle 1\bar{1}0\rangle$	12
Body-Centered Cubic			
α-Fe, W, Mo	$\{110\}$	$\langle \bar{1}11\rangle$	12
α-Fe, W	$\{211\}$	$\langle \bar{1}11\rangle$	12
α-Fe, K	$\{321\}$	$\langle \bar{1}11\rangle$	24
Hexagonal Close-Packed			
Cd, Zn, Mg, Ti, Be	$\{0001\}$	$\langle 11\bar{2}0\rangle$	3
Ti, Mg, Zr	$\{10\bar{1}0\}$	$\langle 11\bar{2}0\rangle$	3
Ti, Mg	$\{10\bar{1}1\}$	$\langle 11\bar{2}0\rangle$	6

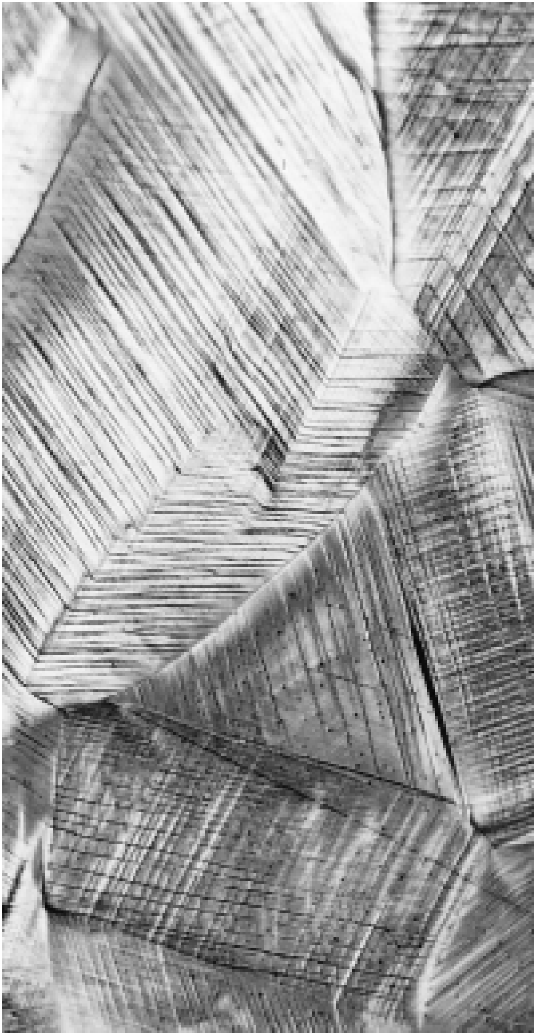

FIGURE 8.10 Slip lines on the surface of a polycrystalline specimen of copper that was polished and subsequently deformed. 173×. (Photomicrograph courtesy of C. Brady, National Bureau of Standards.)

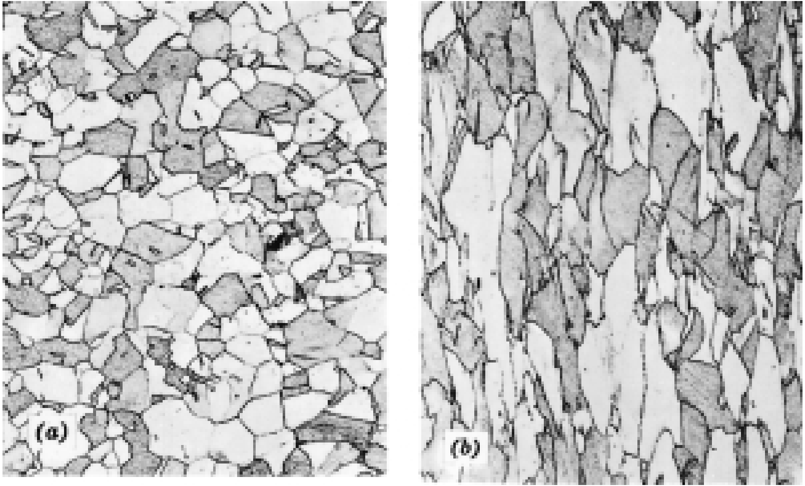

Figure 8.11 Alteration of the grain structure of a polycrystalline metal as a result of plastic deformation. (*a*) Before deformation the grains are equiaxed. (*b*) The deformation has produced elongated grains. 170×. (From W. G. Moffatt, G. W. Pearsall, and J. Wulff, *The Structure and Properties of Materials,* Vol. I, *Structure,* p. 140. Copyright © 1964 by John Wiley & Sons, New York. Reprinted by permission of John Wiley & Sons, Inc.)

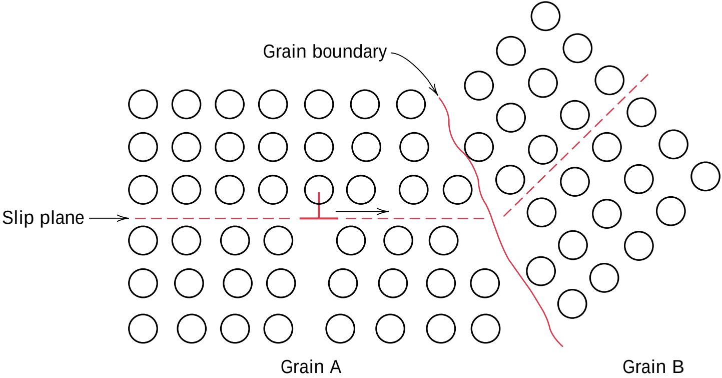
Grain boundary
Slip plane
Grain A
Grain B

FIGURE 8.14 The motion of a dislocation as it encounters a grain boundary, illustrating how the boundary acts as a barrier to continued slip. Slip planes are discontinuous and change directions across the boundary. (From *A Textbook of Materials Technology* by Van Vlack, © 1973. Reprinted by permission of Prentice-Hall, Inc., Upper Saddle River, NJ.)

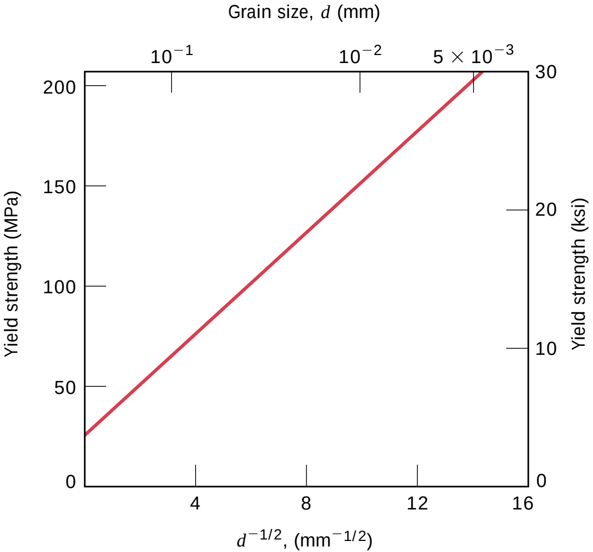

FIGURE 8.15 The influence of grain size on the yield strength of a 70 Cu–30 Zn brass alloy. Note that the grain diameter increases from right to left and is not linear. (Adapted from H. Suzuki, ‘‘The Relation Between the Structure and Mechanical Properties of Metals,’’ Vol. II, *National Physical Laboratory, Symposium No. 15*, 1963, p. 524.)

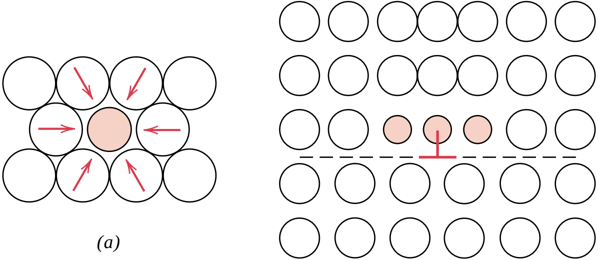

(a) (b)

FIGURE 8.17 (*a*) Representation of tensile lattice strains imposed on host atoms by a smaller substitutional impurity atom. (*b*) Possible locations of smaller impurity atoms relative to an edge dislocation such that there is partial cancellation of impurity–dislocation lattice strains.

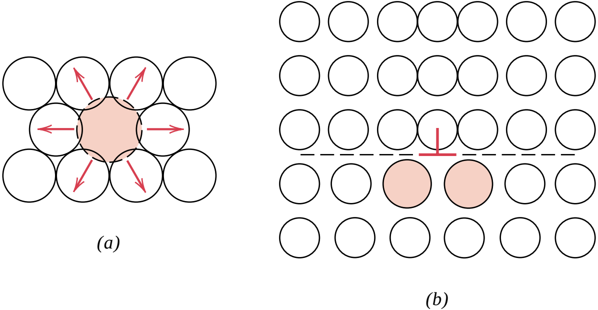

FIGURE 8.18 (*a*) Representation of compressive strains imposed on host atoms by a larger substitutional impurity atom. (*b*) Possible locations of larger impurity atoms relative to an edge dislocation such that there is partial cancellation of impurity–dislocation lattice strains.

```
[Loader]
Program=mse5e
CommandLine=SolidSolution
```

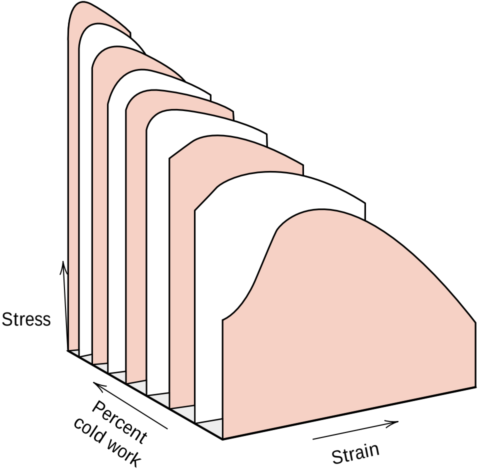

FIGURE 8.20 The influence of cold work on the stress–strain behavior for a low-carbon steel. (From *Metals Handbook: Properties and Selection: Irons and Steels*, Vol. 1, 9th edition, B. Bardes, Editor, American Society for Metals, 1978, p. 221.)

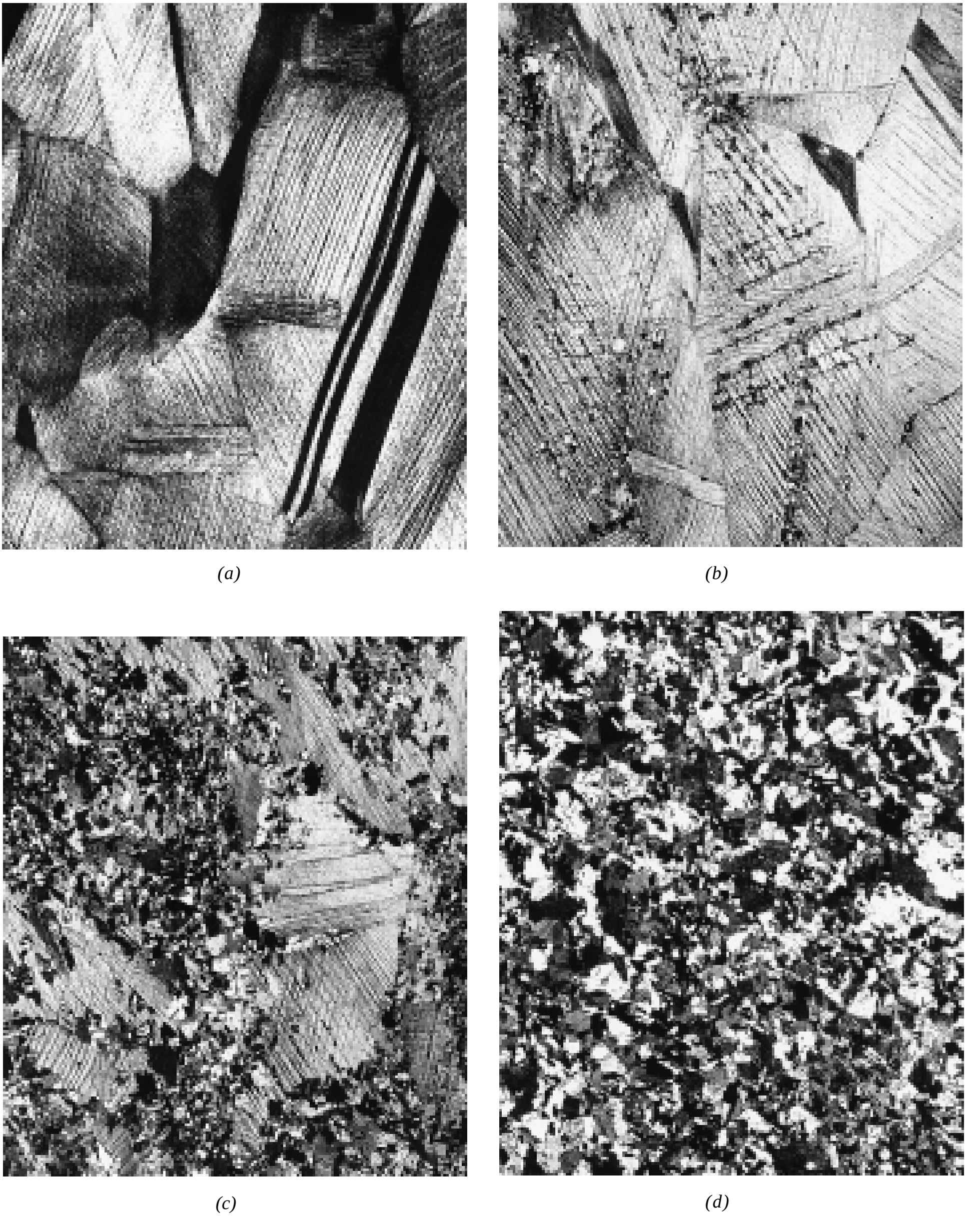

FIGURE 8.21 Photomicrographs showing several stages of the recrystallization and grain growth of brass. (*a*) Cold-worked (33%CW) grain structure. (*b*) Initial stage of recrystallization after heating 3 s at 580°C (1075°F); the very small grains are those that have recrystallized. (*c*) Partial replacement of cold-worked grains by recrystallized ones (4 s at 580°C). (*d*) Complete recrystallization (8 s at 580°C). (*e*) Grain growth after 15 min at 580°C. (*f*) Grain growth after 10 min at 700°C (1290°F). All photomicrographs 75×. (Photomicrographs courtesy of J. E. Burke, General Electric Company.)

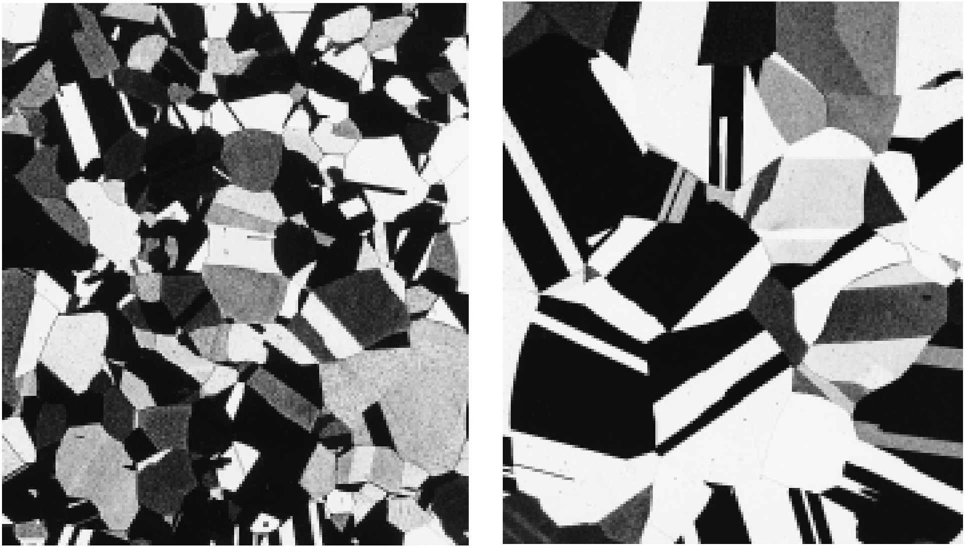

(e) (f)

FIGURE 8.21 (*continued*)

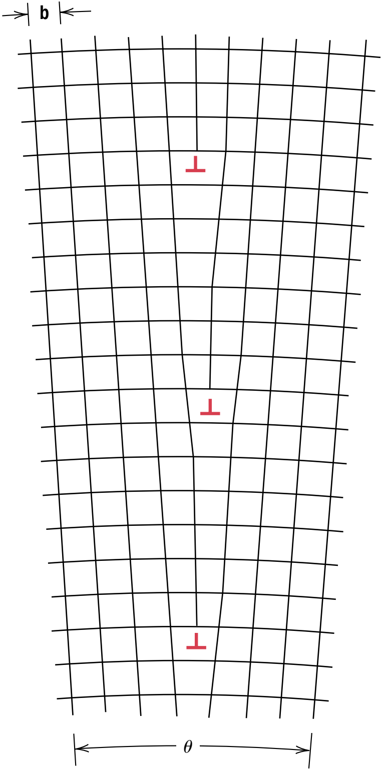

Figure 5.12 Demonstration of how a tilt boundary having an angle of misorientation θ results from an alignment of edge dislocations.

Figure 8.22 The influence of annealing temperature on the tensile strength and ductility of a brass alloy. Grain size as a function of annealing temperature is indicated. Grain structures during recovery, recrystallization, and grain growth stages are shown schematically. (Adapted from G. Sachs and K. R. Van Horn, *Practical Metallurgy, Applied Metallurgy and the Industrial Processing of Ferrous and Nonferrous Metals and Alloys*, American Society for Metals, 1940, p. 139.)

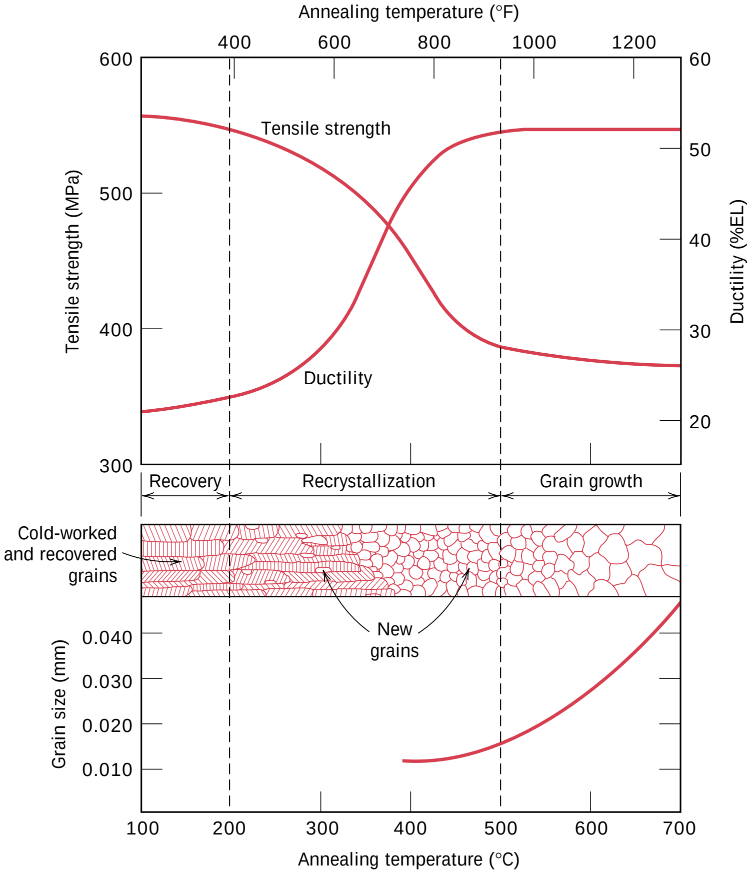

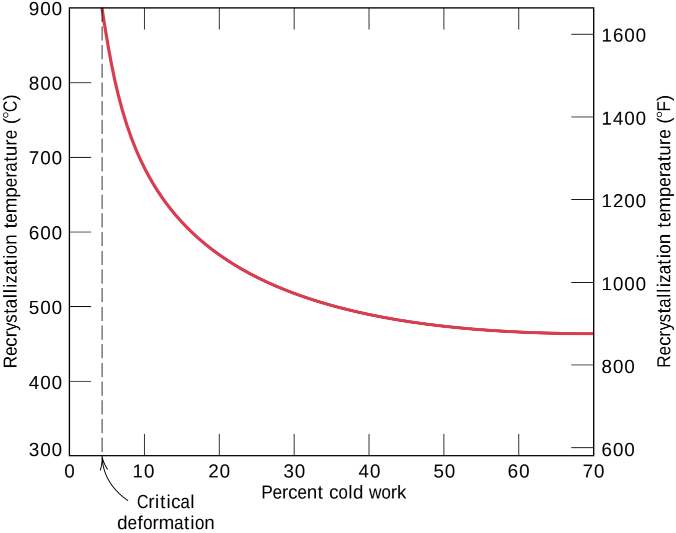

Figure 8.23 The variation of recrystallization temperature with percent cold work for iron. For deformations less than the critical (about 5%CW), recrystallization will not occur.

Table 8.2 **Recrystallization and Melting Temperatures for Various Metals and Alloys**

	Recrystallization Temperature		*Melting Temperature*	
Metal	***°C***	***°F***	***°C***	***°F***
Lead	−4	25	327	620
Tin	−4	25	232	450
Zinc	10	50	420	788
Aluminum (99.999 wt%)	80	176	660	1220
Copper (99.999 wt%)	120	250	1085	1985
Brass (60 Cu–40 Zn)	475	887	900	1652
Nickel (99.99 wt%)	370	700	1455	2651
Iron	450	840	1538	2800
Tungsten	1200	2200	3410	6170

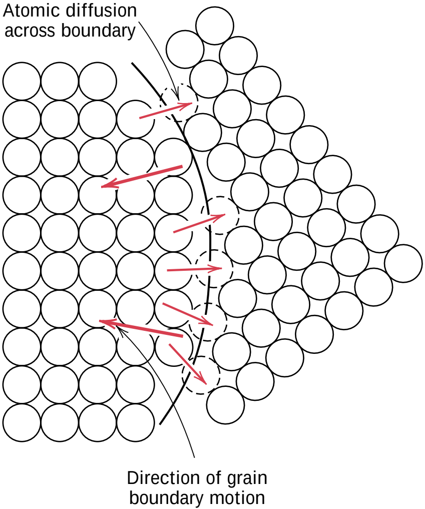
Atomic diffusion across boundary
Direction of grain boundary motion

FIGURE 8.24 Schematic representation of grain growth via atomic diffusion. (From *Elements of Materials Science and Engineering* by Van Vlack, © 1989. Reprinted by permission of Prentice-Hall, Inc., Upper Saddle River, NJ.)

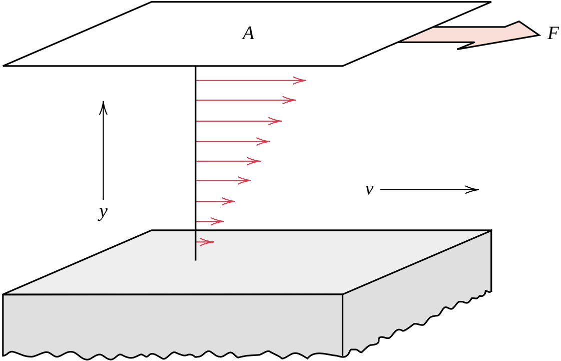

FIGURE 8.26 Representation of the viscous flow of a liquid or fluid glass in response to an applied shear force.

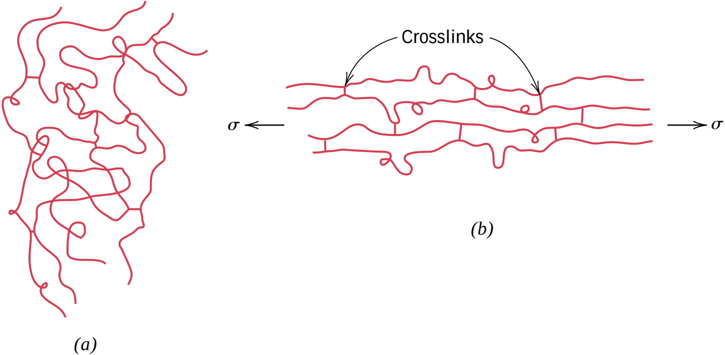

FIGURE 8.29 Schematic representation of crosslinked polymer chain molecules (*a*) in an unstressed state and (*b*) during elastic deformation in response to an applied tensile stress. (Adapted from Z. D. Jastrzebski, *The Nature and Properties of Engineering Materials,* 3rd edition. Copyright © 1987 by John Wiley & Sons, New York. Reprinted by permission of John Wiley & Sons, Inc.)

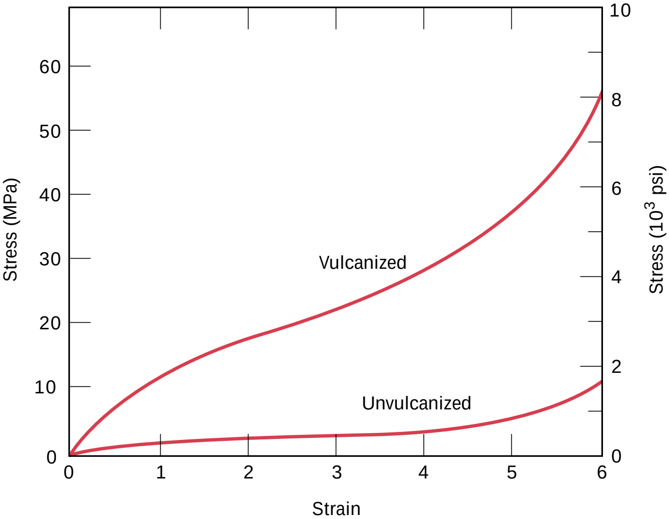

FIGURE 8.30 Stress–strain curves to 600% elongation for unvulcanized and vulcanized natural rubber.

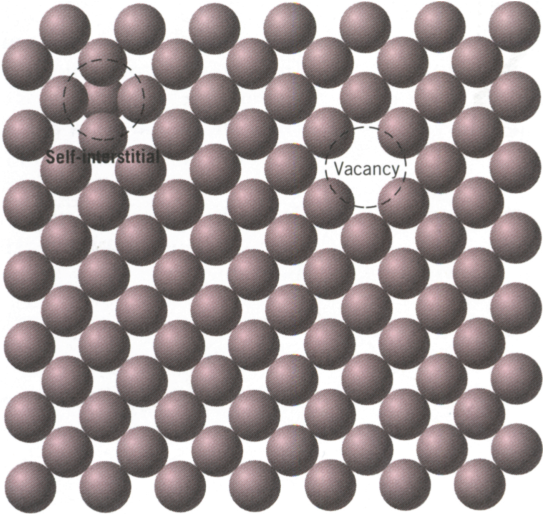

FIGURE 5.1 Two-dimensional representations of a vacancy and a self-interstitial. (Adapted from W. G. Moffatt, G. W. Pearsall, and J. Wulff, *The Structure and Properties of Materials,* Vol. I, *Structure,* p. 77. Copyright © 1964 by John Wiley & Sons, New York. Reprinted by permission of John Wiley & Sons, Inc.)

Figure 5.2 Schematic representations of cation and anion vacancies and a cation interstitial. (From W. G. Moffatt, G. W. Pearsall, and J. Wulff, *The Structure and Properties of Materials,* Vol. 1, *Structure,* p. 78. Copyright © 1964 by John Wiley & Sons, New York. Reprinted by permission of John Wiley & Sons, Inc.)

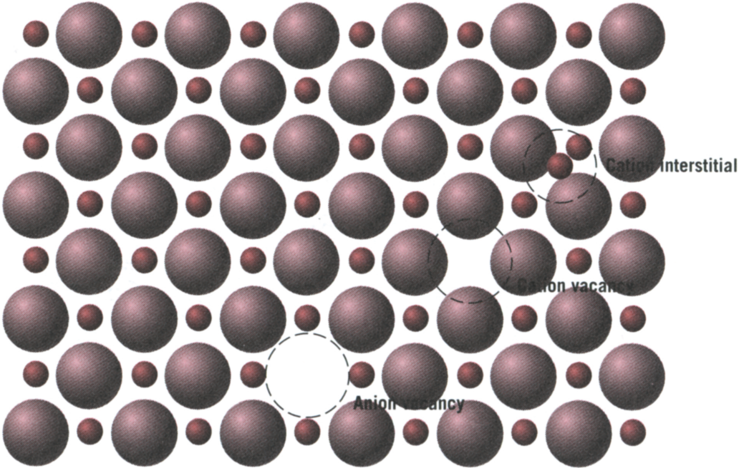
Cation interstitial
Cation vacancy
Anion vacancy

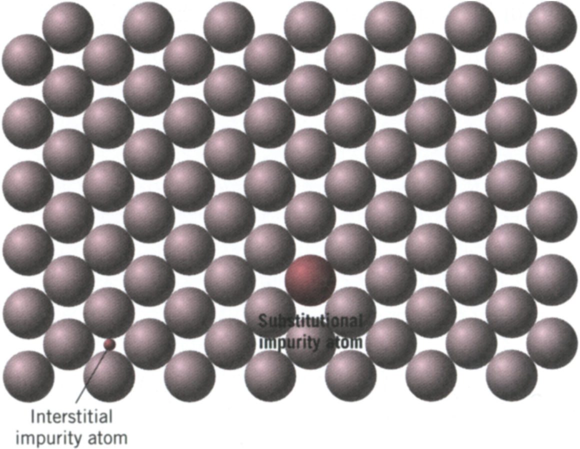
Substitutional impurity atom
Interstitial impurity atom

FIGURE 5.5 Two-dimensional schematic representations of substitutional and interstitial impurity atoms. (Adapted from W. G. Moffatt, G. W. Pearsall, and J. Wulff, *The Structure and Properties of Materials*, Vol. I, *Structure*, p. 77. Copyright © 1964 by John Wiley & Sons, New York. Reprinted by permission of John Wiley & Sons, Inc.)

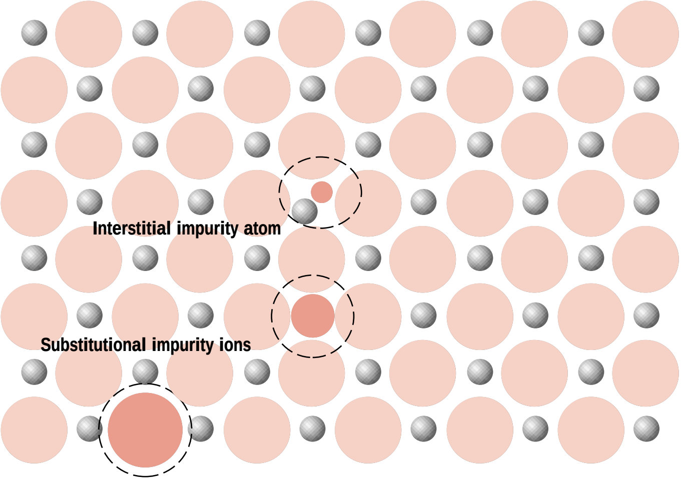
Interstitial impurity atom
Substitutional impurity ions

FIGURE 5.6 Schematic representations of interstitial, anion-substitutional, and cation-substitutional impurity atoms in an ionic compound. (Adapted from W. G. Moffatt, G. W. Pearsall, and J. Wulff, *The Structure and Properties of Materials*, Vol. 1, *Structure*, p. 78. Copyright © 1964 by John Wiley & Sons, New York. Reprinted by permission of John Wiley & Sons, Inc.)

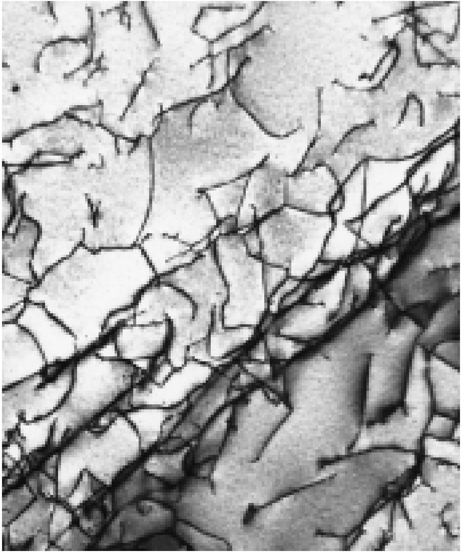

FIGURE 5.10 A transmission electron micrograph of a titanium alloy in which the dark lines are dislocations. 51,450×. (Courtesy of M. R. Plichta, Michigan Technological University.)

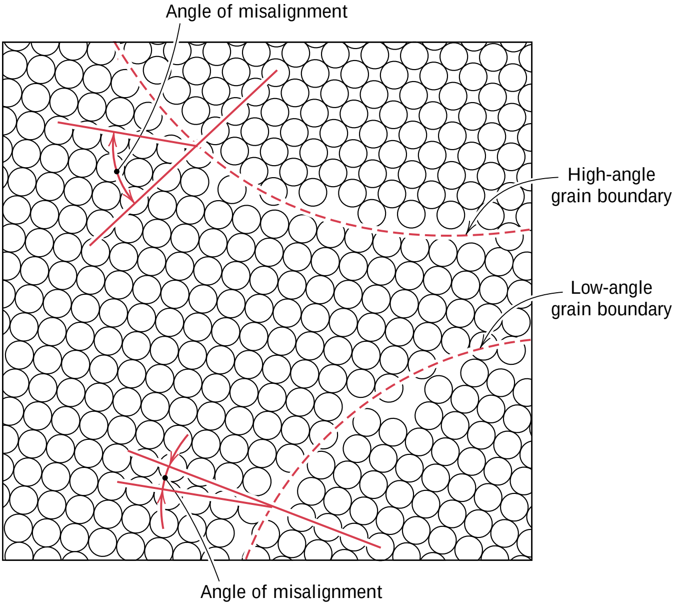
Angle of misalignment
High-angle
grain boundary
Low-angle
grain boundary
Angle of misalignment

FIGURE 5.11 Schematic diagram showing low- and high-angle grain boundaries and the adjacent atom positions.

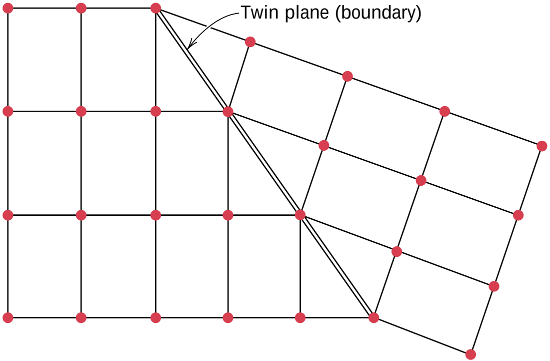
Twin plane (boundary)

FIGURE 5.13 Schematic diagram showing a twin plane or boundary and the adjacent atom positions (dark circles).

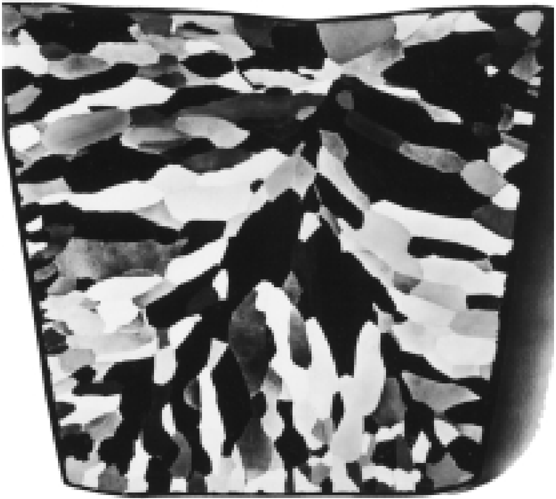

FIGURE 5.14 High-purity polycrystalline lead ingot in which the individual grains may be discerned. 0.7×. (Reproduced with permission from *Metals Handbook,* Vol. 9, 9th edition, *Metallography and Microstructures,* American Society for Metals, Metals Park, OH, 1985.)

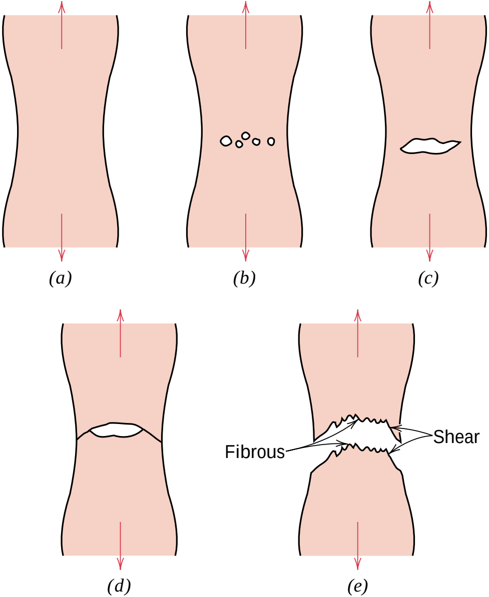

FIGURE 9.2 Stages in the cup-and-cone fracture. (*a*) Initial necking. (*b*) Small cavity formation. (*c*) Coalescence of cavities to form a crack. (*d*) Crack propagation. (*e*) Final shear fracture at a 45° angle relative to the tensile direction. (From K. M. Ralls, T. H. Courtney, and J. Wulff, *Introduction to Materials Science and Engineering*, p. 468. Copyright © 1976 by John Wiley & Sons, New York. Reprinted by permission of John Wiley & Sons, Inc.)

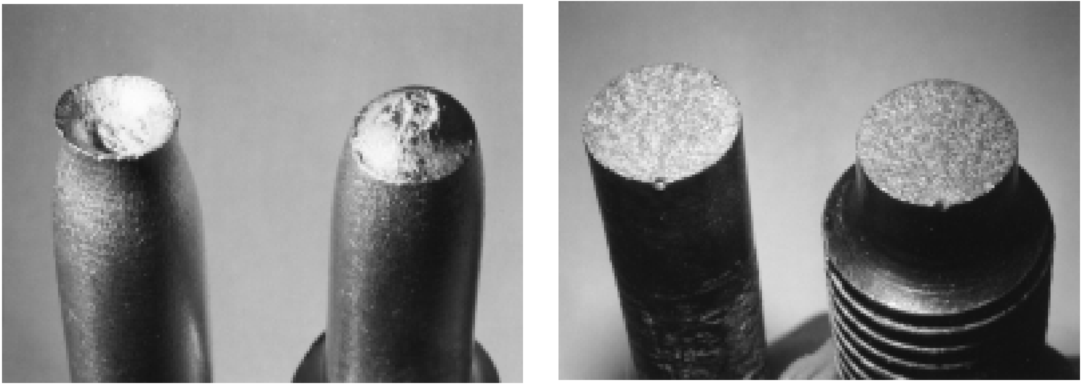

(a) *(b)*

Figure 9.3 (*a*) Cup-and-cone fracture in aluminum. (*b*) Brittle fracture in a mild steel.

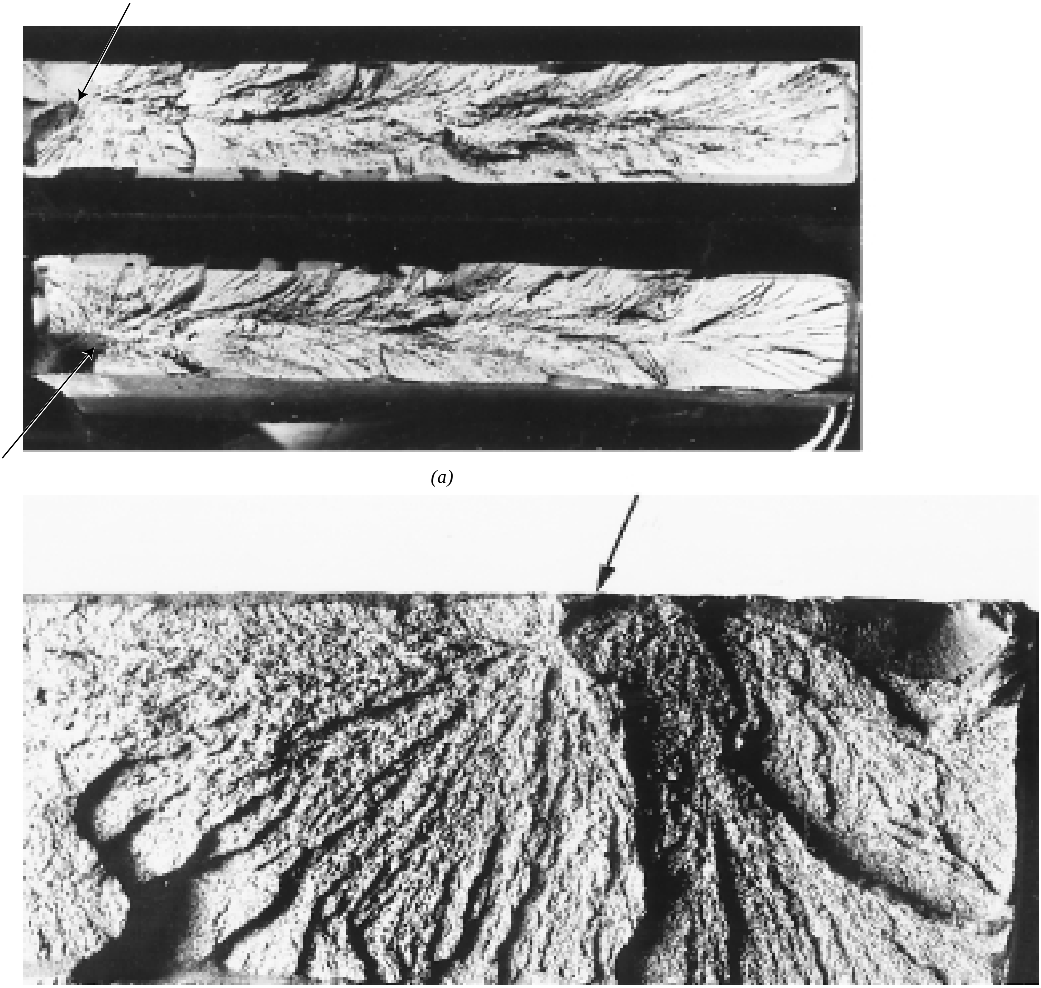

(a)

(b)

FIGURE 9.5 (*a*) Photograph showing V-shaped ‘‘chevron’’ markings characteristic of brittle fracture. Arrows indicate origin of crack. Approximately actual size. (From R. W. Hertzberg, *Deformation and Fracture Mechanics of Engineering Materials,* 3rd edition. Copyright © 1989 by John Wiley & Sons, New York. Reprinted by permission of John Wiley & Sons, Inc. Photograph courtesy of Roger Slutter, Lehigh University.) (*b*) Photograph of a brittle fracture surface showing radial fan-shaped ridges. Arrow indicates origin of crack. Approximately 2×. (Reproduced with permission from D. J. Wulpi, *Understanding How Components Fail,* American Society for Metals, Materials Park, OH, 1985.)

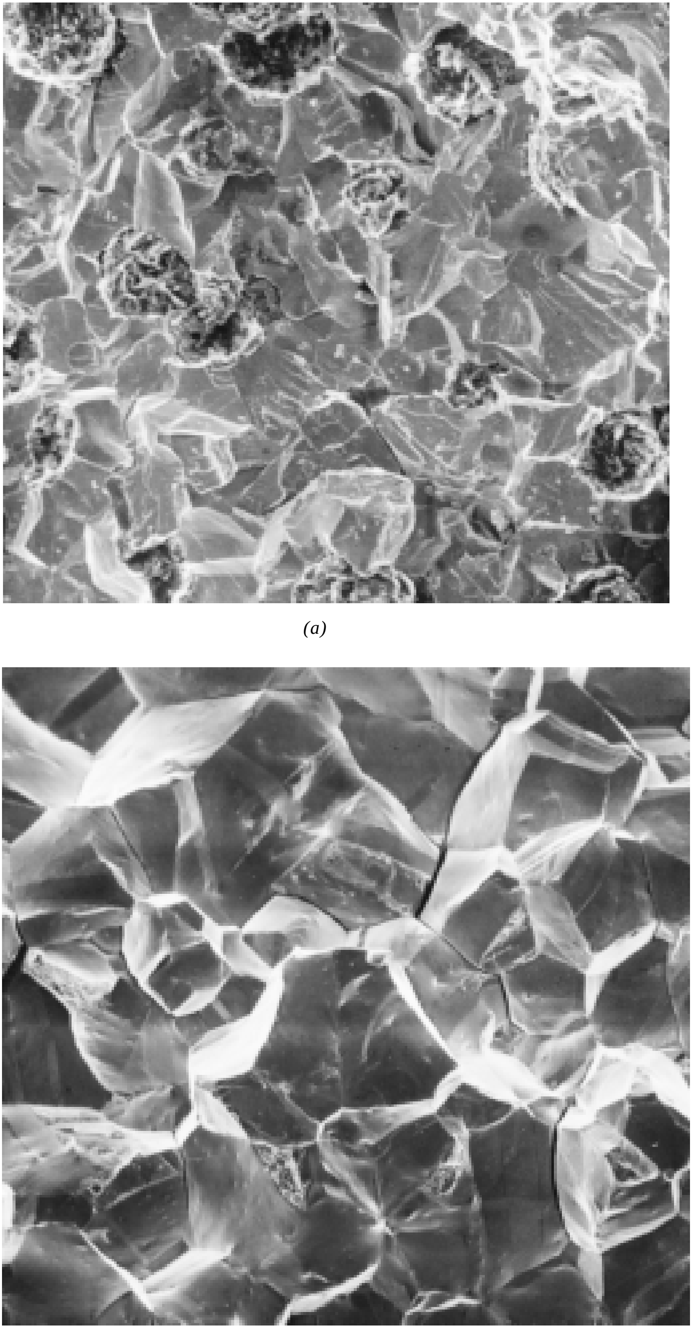

(a)

(b)

Figure 9.6 (*a*) Scanning electron fractograph of ductile cast iron showing a transgranular fracture surface. Magnification unknown. (From V. J. Colangelo and F. A. Heiser, *Analysis of Metallurgical Failures,* 2nd edition. Copyright © 1987 by John Wiley & Sons, New York. Reprinted by permission of John Wiley & Sons, Inc.) (*b*) Scanning electron fractograph showing an intergranular fracture surface. 50×. (Reproduced with permission from *ASM Handbook,* Vol. 12, *Fractography,* ASM International, Materials Park, OH, 1987.)

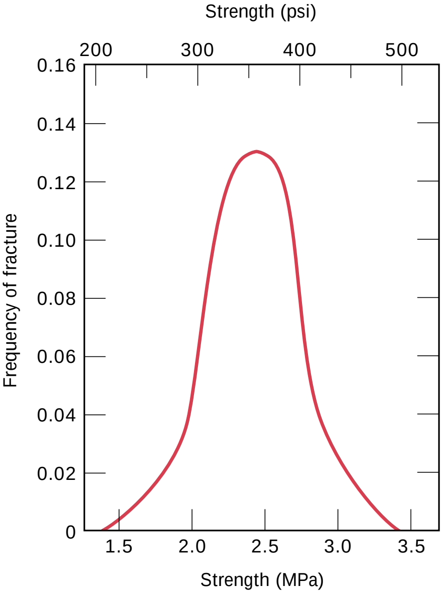

FIGURE 9.16 The frequency distribution of observed fracture strengths for a portland cement. (From W. Weibull, *Ing. Vetensk. Akad.*, Proc. 151, No. 153, 1939.)

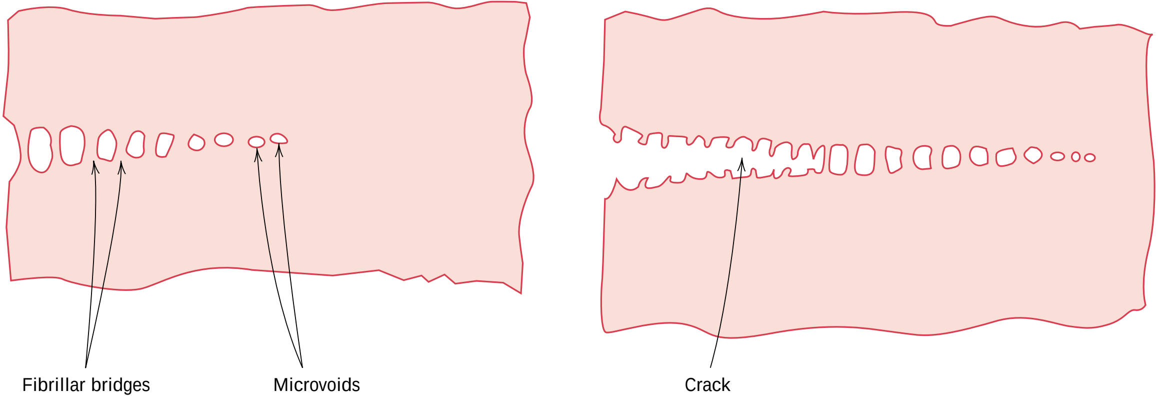
Fibrillar bridges
Microvoids
Crack

(a) *(b)*

FIGURE 9.17 Schematic drawings of (*a*) a craze showing microvoids and fibrillar bridges, and (*b*) a craze followed by a crack. (From J. W. S. Hearle, *Polymers and Their Properties*, Vol. 1, *Fundamentals of Structure and Mechanics*, Ellis Horwood, Ltd., Chichester, West Sussex, England, 1982.)

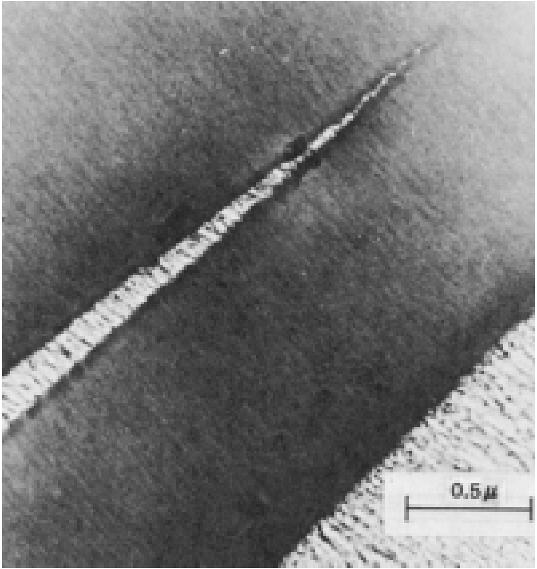

FIGURE 9.18 Photomicrograph of a craze in polyphenylene oxide. (From R. P. Kambour and R. E. Robertson, "The Mechanical Properties of Plastics," in *Polymer Science, A Materials Science Handbook*, A. D. Jenkins, Editor. Reprinted with permission of Elsevier Science Publishers.)

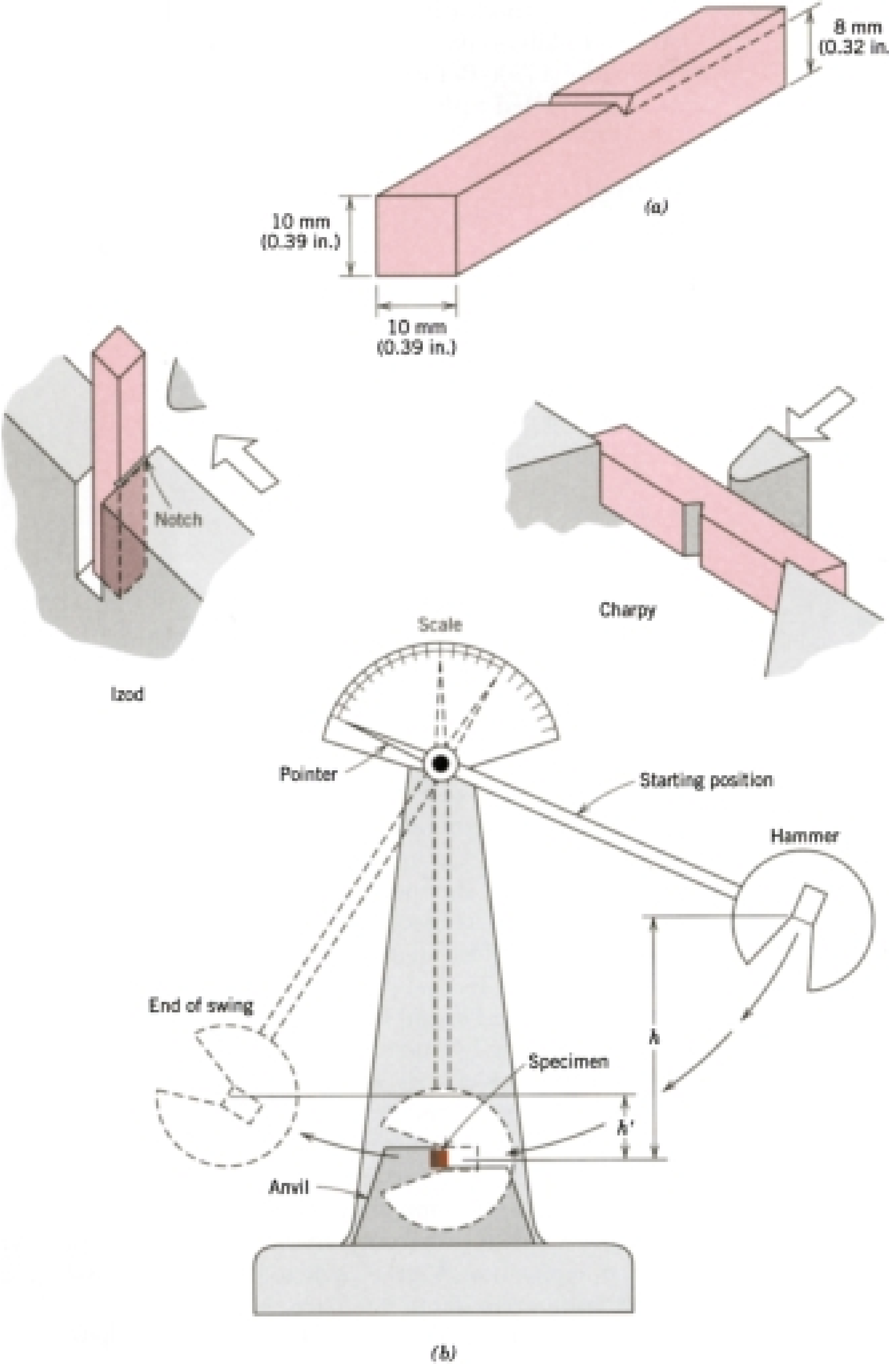
8 mm
(0.32 in.
10 mm
(0.39 in.)
10 mm
(0.39 in.)
(a)
Notch
Izod
Charpy
Scale
Pointer
Starting position
Hammer
End of swing
Specimen
h
h'
Anvil
(b)

FIGURE 9.19 (*a*) Specimen used for Charpy and Izod impact tests. (*b*) A schematic drawing of an impact testing apparatus. The hammer is released from fixed height *h* and strikes the specimen; the energy expended in fracture is reflected in the difference between *h* and the swing height *h*′. Specimen placements for both Charpy and Izod tests are also shown. (Figure (*b*) adapted from H. W. Hayden, W. G. Moffatt, and J. Wulff, *The Structure and Properties of Materials*, Vol. III, *Mechanical Behavior*, p. 13. Copyright © 1965 by John Wiley & Sons, New York. Reprinted by permission of John Wiley & Sons, Inc.)

FIGURE 9.20 Temperature dependence of the Charpy V-notch impact energy (curve *A*) and percent shear fracture (curve *B*) for an A283 steel. (Reprinted from *Welding Journal*. Used by permission of the American Welding Society.)

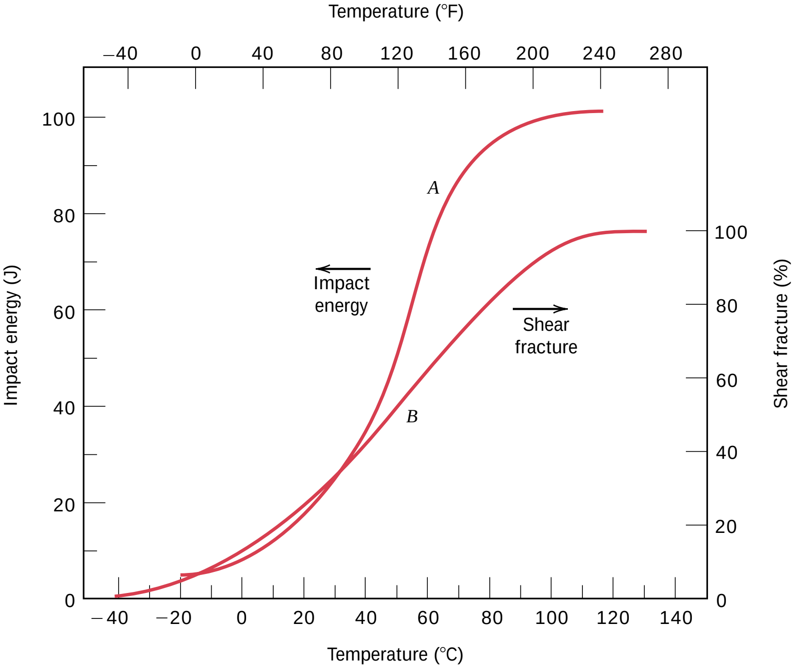

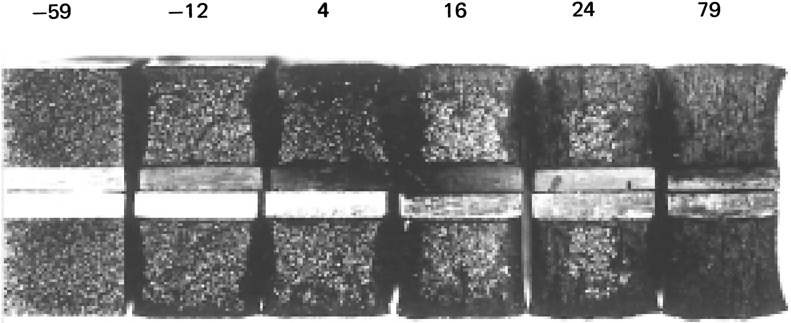

Figure 9.21 Photograph of fracture surfaces of A36 steel Charpy V-notch specimens tested at indicated temperatures (in °C). (From R. W. Hertzberg, *Deformation and Fracture Mechanics of Engineering Materials*, 3rd edition, Fig. 9.6, p. 329. Copyright © 1989 by John Wiley & Sons, Inc., New York. Reprinted by permission of John Wiley & Sons, Inc.)

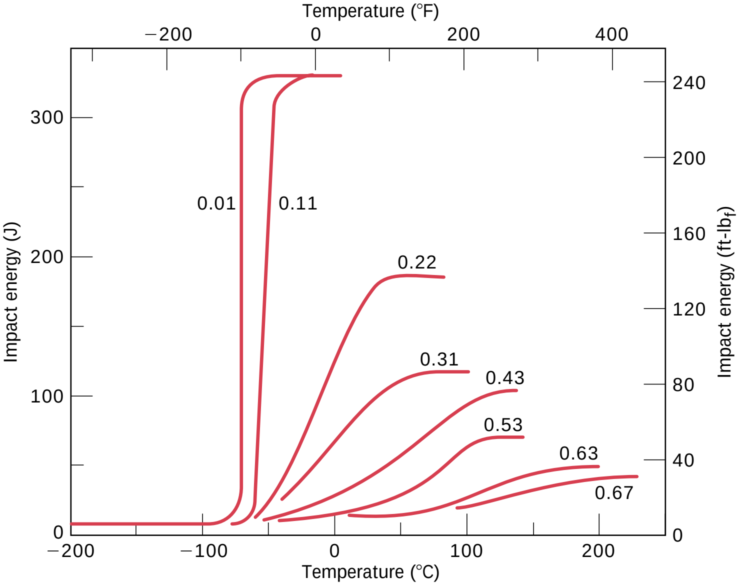

Figure 9.22 Influence of carbon content on the Charpy V-notch energy-versus-temperature behavior for steel. (Reprinted with permission from ASM International, Metals Park, OH 44073-9989, USA; J. A. Reinbolt and W. J. Harris, Jr., "Effect of Alloying Elements on Notch Toughness of Pearlitic Steels," *Transactions of ASM*, Vol. 43, 1951.)

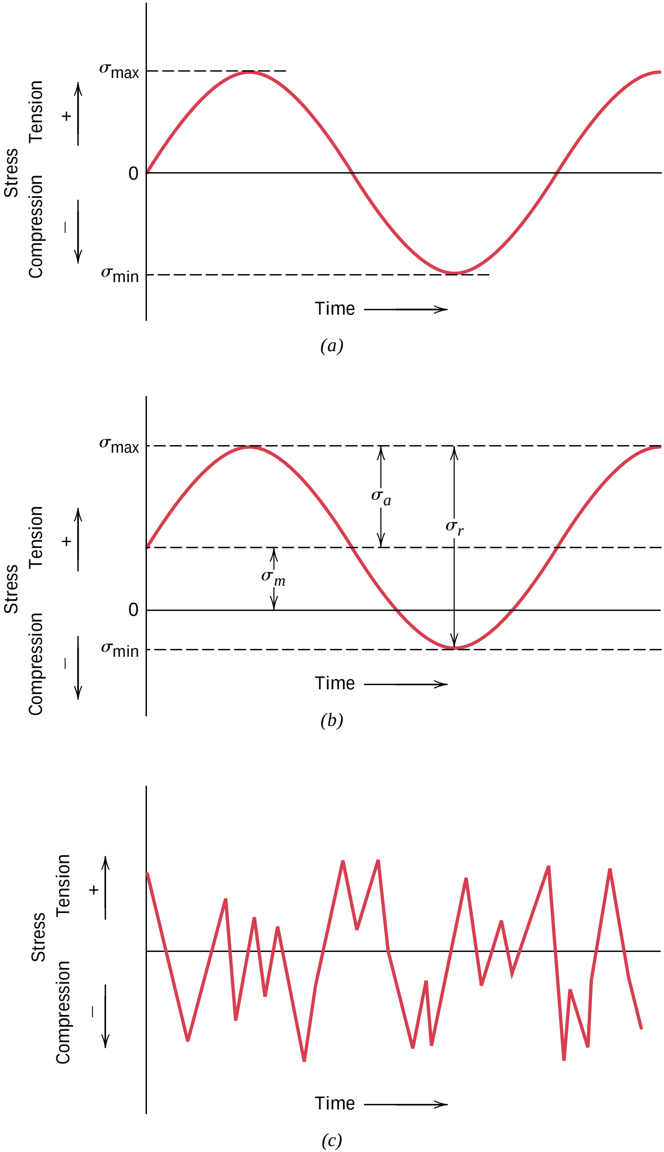

Figure 9.23 Variation of stress with time that accounts for fatigue failures. (*a*) Reversed stress cycle, in which the stress alternates from a maximum tensile stress (+) to a maximum compressive stress (−) of equal magnitude. (*b*) Repeated stress cycle, in which maximum and minimum stresses are asymmetrical relative to the zero stress level; mean stress σ_m, range of stress σ_r, and stress amplitude σ_a are indicated. (*c*) Random stress cycle.

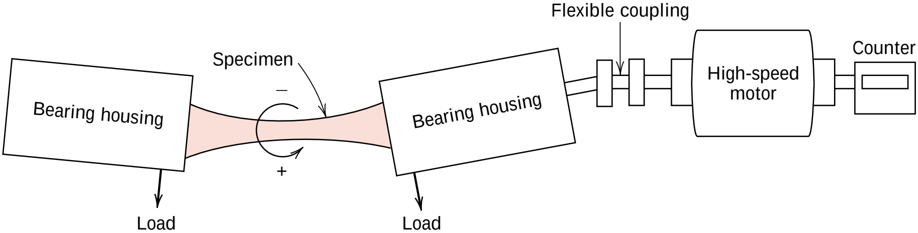
Flexible coupling
Counter
Specimen
High-speed motor
Bearing housing
Bearing housing
–
+
Load
Load

Figure 9.24 Schematic diagram of fatigue testing apparatus for making rotating-bending tests. (From *Materials Science in Engineering,* fourth edition, by Keyser, Carl A., © 1986. Reprinted by permission of Prentice-Hall, Inc., Upper Saddle River, NJ.)

FIGURE 9.26 Fatigue *S*–*N* probability of failure curves for a 7075-T6 aluminum alloy; *P* denotes the probability of failure. (From G. M. Sinclair and T. J. Dolan, *Trans.*, *ASME*, **75,** 1953, p. 867. Reprinted with permission of the American Society of Mechanical Engineers.)

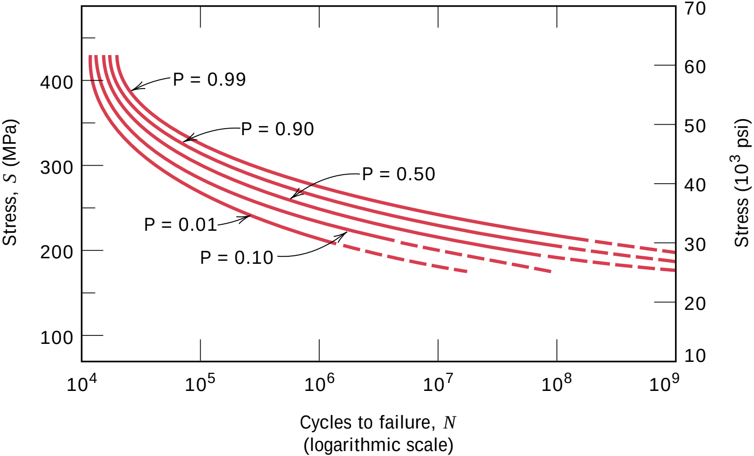

FIGURE 9.27 Fatigue curves (stress amplitude versus the number of cycles to failure) for polyethylene terephthalate (PET), nylon, polystyrene (PS), polymethyl methacrylate (PMMA), polypropylene (PP), polyethylene (PE), and polytetrafluoroethylene (PTFE). The testing frequency was 30 Hz. (From M. N. Riddell, "A Guide to Better Testing of Plastics," *Plast. Eng.*, Vol. 30, No. 4, p. 78, 1974.)

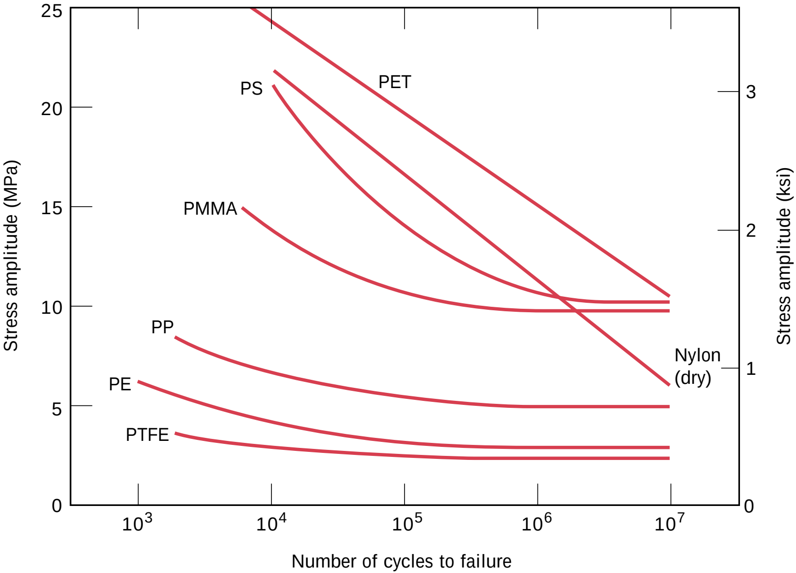

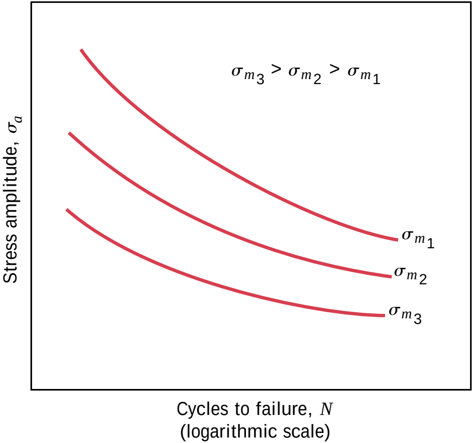

FIGURE 9.36 Demonstration of influence of mean stress σ_m on S–N fatigue behavior.

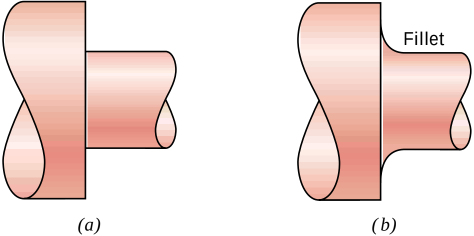

(a) (b)

Figure 9.37 Demonstration of how design can reduce stress amplification. (*a*) Poor design: sharp corner. (*b*) Good design: fatigue lifetime improved by incorporating rounded fillet into a rotating shaft at the point where there is a change in diameter.

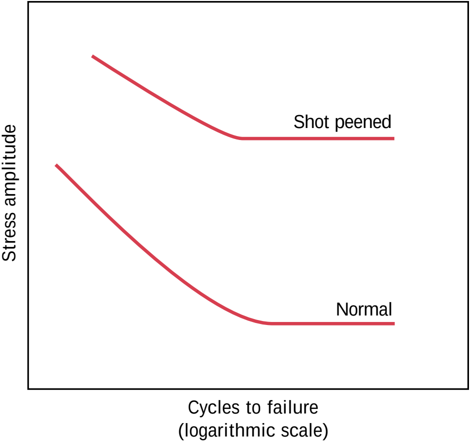

FIGURE 9.38 Schematic S–N fatigue curves for normal and shot-peened steel.

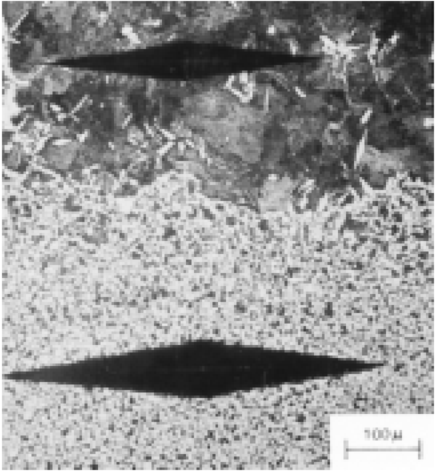

Figure 9.39 Photomicrograph showing both core (bottom) and carburized outer case (top) regions of a case-hardened steel. The case is harder as attested by the smaller microhardness indentation. 100×. (From R. W. Hertzberg, *Deformation and Fracture Mechanics of Engineering Materials,* 3rd edition. Copyright © 1989 by John Wiley & Sons, New York. Reprinted by permission of John Wiley & Sons, Inc.)

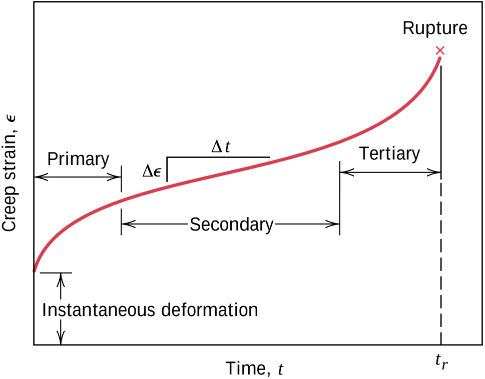

Figure 9.40 Typical creep curve of strain versus time at constant stress and constant elevated temperature. The minimum creep rate $\Delta\epsilon/\Delta t$ is the slope of the linear segment in the secondary region. Rupture lifetime t_r is the total time to rupture.

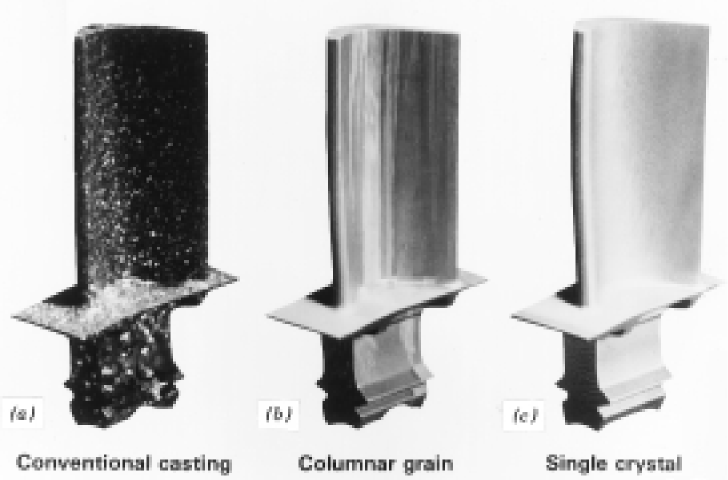
(a)
(b)
(c)
Conventional casting
Columnar grain
Single crystal

Figure 9.45 (*a*) Polycrystalline turbine blade that was produced by a conventional casting technique. High-temperature creep resistance is improved as a result of an oriented columnar grain structure (*b*) produced by a sophisticated directional solidification technique. Creep resistance is further enhanced when single-crystal blades (*c*) are used. (Courtesy of Pratt & Whitney.)

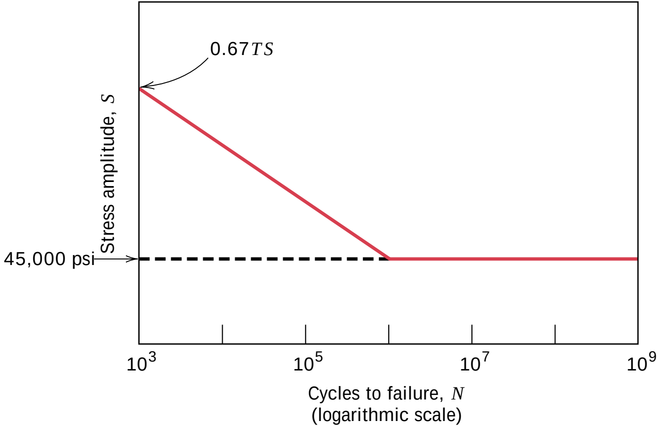

Figure 20.9 Shear stress amplitude versus logarithm of the number of cycles to fatigue failure for typical ferrous alloys.

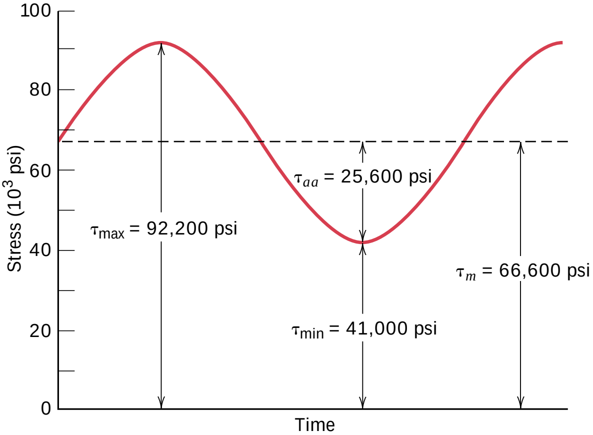

FIGURE 20.10 Shear stress versus time for an automobile valve spring.

Table 20.3 **Mechanical Characteristics of Human Long Bone Both Parallel and Perpendicular to the Bone Axis**

Property	*Parallel to Bone Axis*	*Perpendicular to Bone Axis*
Elastic modulus, GPa (psi)	17.4 (2.48×10^6)	11.7 (1.67×10^6)
Ultimate strength, tension, MPa (ksi)	135 (19.3)	61.8 (8.96)
Ultimate strength, compression, MPa (ksi)	196 (28.0)	135 (19.3)
Elongation at fracture	3–4%	—

Source: From D. F. Gibbons, ‘‘Biomedical Materials,’’ pp. 253–254, in *Handbook of Engineering in Medicine and Biology*, D. G. Fleming, and B. N. Feinberg, CRC Press, Boca Raton, Florida, 1976. With permission.

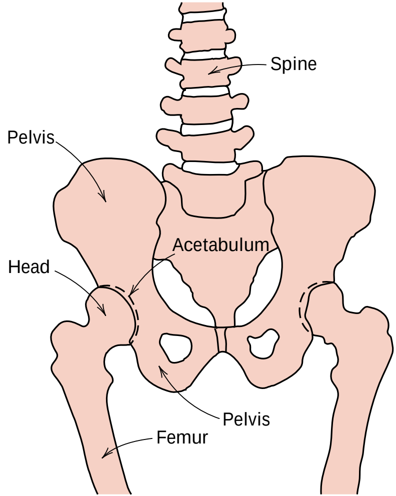
Spine
Pelvis
Acetabulum
Head
Pelvis
Femur

Figure 20.11 Schematic diagram of human hip joints and adjacent skeletal components.

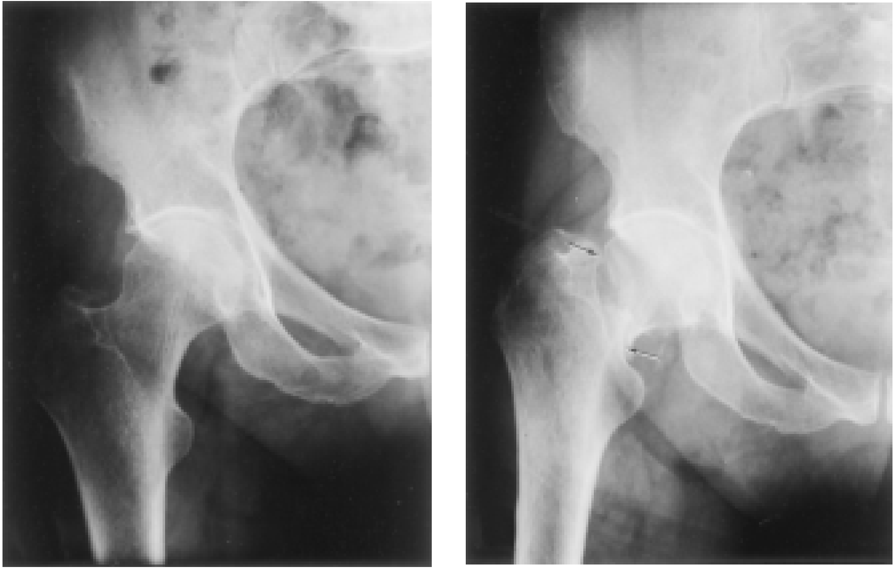

(a) (b)

FIGURE 20.12 X-Rays of (*a*) a normal hip joint and (*b*) a fractured hip joint. The arrows in (*b*) show the two ends of the fracture line through the femoral neck.

FIGURE 20.13 (*a*) Schematic diagram and (*b*) x-ray of an artificial total hip replacement.

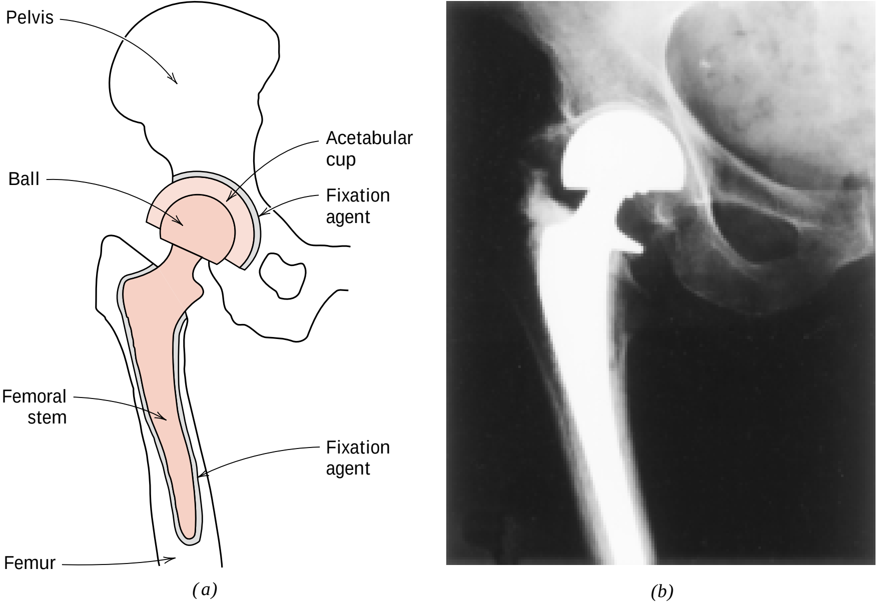
Pelvis
Acetabular cup
Ball
Fixation agent
Femoral stem
Fixation agent
Femur
(*a*)
(*b*)

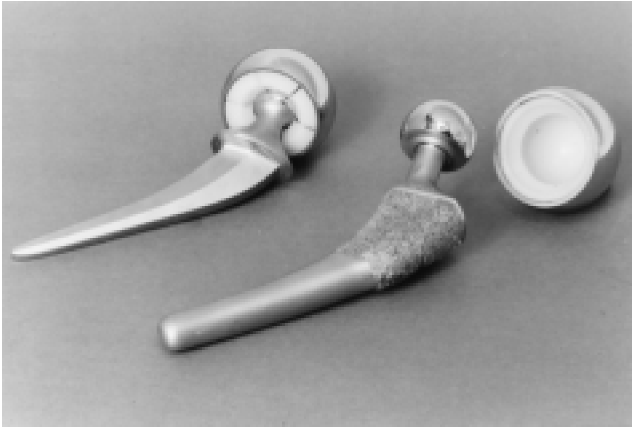

FIGURE 20.14 Photograph showing two artificial total hip replacement designs.

Table 20.4 Mechanical and Corrosion Characteristics of Three Metal Alloys That Are Commonly Used for the Femoral Stem Component of the Prosthetic Hip

Alloy	*Elastic Modulus [GPa (psi)]*	*0.2% Yield Strength [MPa (ksi)]*	*Tensile Strength [MPa (ksi)]*	*Elongation at Fracture (%)*	*Fatigue Strength or Limit, 10^7 Cycles [MPa (ksi)]*	*Corrosion Rate (mpy)*[a]
316L Stainless steel (cold worked)	196 (28.4×10^6)	700 (102)	875 (127)	12	383 (55.5)	0.001–0.002
MP35N (hot forged)	230 (33.4×10^6)	1000 (145)	1200 (174)	13	500 (72.5)	0.0012–0.002
Ti-6Al-4V (hot forged)	120 (17.4×10^6)	950 (138)	1075 (156)	13	580 (84.1)	0.007–0.04

[a] mpy means mils per year, or 0.001 in./yr

Sources: From Gladius Lewis, *Selection of Engineering Materials*, © 1990, p. 189. Adapted by permission of Prentice Hall, Englewood Cliffs, New Jersey. And D. F. Gibbons, ‘‘Materials for Orthopedic Joint Prostheses,’’ Ch. 4, p. 116, in *Biocompatibility of Orthopedic Implants*, Vol. I, D. F. Williams, CRC Press, Boca Raton, Florida, 1982. With permission.

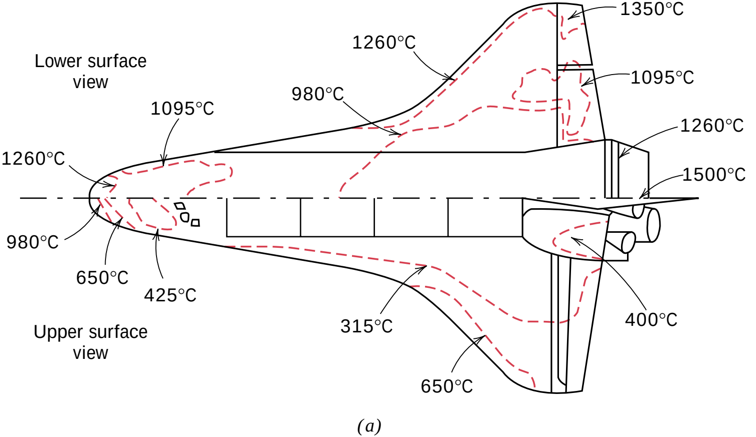
1350°C
1260°C
Lower surface view
1095°C
980°C
1095°C
1260°C
1260°C
1500°C
980°C
650°C
425°C
Upper surface view
315°C
400°C
650°C
(a)

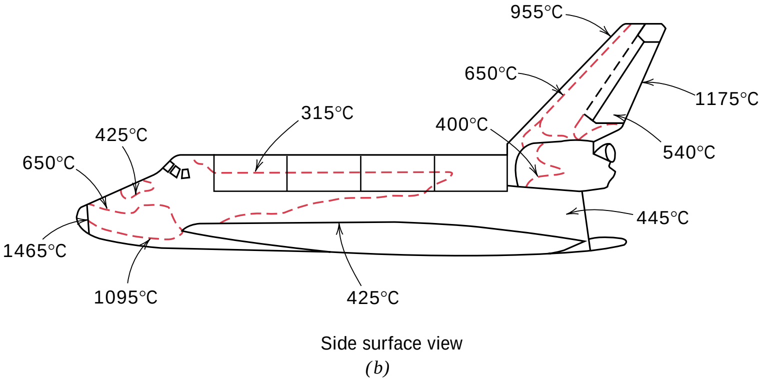
955°C
650°C
1175°C
315°C
400°C
425°C
540°C
650°C
445°C
1465°C
1095°C
425°C
Side surface view
(b)

Figure 20.15 Approximate maximum outer surface temperature profiles for the Space Shuttle Orbiter during reentry: (*a*) upper and lower views; (*b*) side view. (From "The Shuttle Orbiter Thermal Protection System," L. J. Korb, C. A. Morant, R. M. Calland, and C. S. Thatcher, *Ceramic Bulletin*, No. 11, Nov. 1981, p. 1188. Copyright 1981. Reprinted by permission of the American Ceramic Society.)

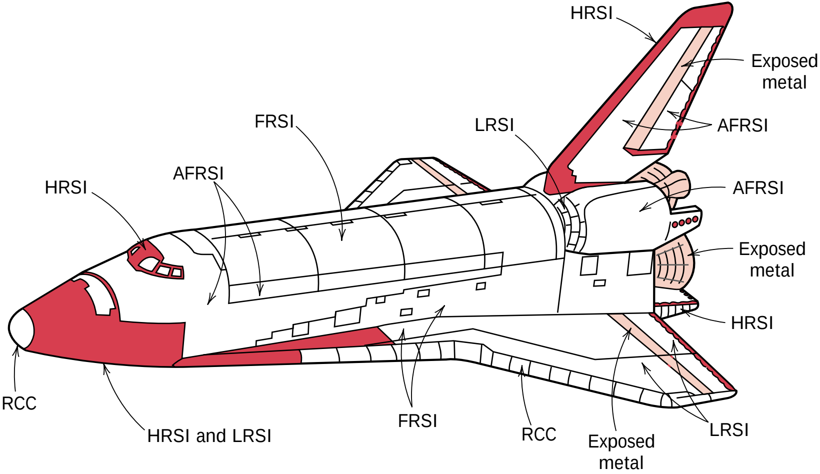
HRSI
Exposed metal
AFRSI
FRSI
LRSI
AFRSI
HRSI
AFRSI
Exposed metal
HRSI
RCC
HRSI and LRSI
FRSI
RCC
Exposed metal
LRSI

FIGURE 20.16 Locations of the various components of the thermal protection system on the Space Shuttle Orbiter: FRSI, felt reusable surface insulation; AFRSI, advanced flexible reusable surface insulation; LRSI, low-temperature reusable surface insulation; HRSI, high-temperature reusable surface insulation; RCC, reinforced carbon–carbon composite. (Adapted from L. J. Korb, C. A. Morant, R. M. Calland, and C. S. Thatcher, ‘‘The Shuttle Orbiter Thermal Protection System,’’ *Ceramic Bulletin*, No. 11, Nov. 1981, p. 1189. Copyright 1981. Reprinted by permission of the American Ceramic Society.)

Table 20.5 Thermal Protection Systems Employed on the Space Shuttle Orbiter

Material Generic Name	*Minimum Operating Temperature, °C (°F)*	*Maximum Operating Temperature, °C (°F)*	*Material Composition*	*Orbiter Locations*
Felt reusable surface insulation (FRSI)	−130 (−200)	400 (750)	Nylon felt, silicone rubber coating	Wing upper surface, upper sides, cargo bay doors
Advanced flexible reusable surface insulation (AFRSI)	−130 (−200)	815 (1500)	Quartz batting sandwiched between quartz and glass fabrics	Upper surface regions
Low-temperature reusable surface insulation (LRSI)	−130 (−200)	650 (1200)	Silica tiles, borosilicate glass coating	Upper wing surfaces, tail surfaces, upper vehicle sides
High-temperature reusable insulation (HRSI)	−130 (−200)	1260 (2300)	Silica tiles, borosilicate glass coating with SiB_4 added	Lower surfaces and sides, tail leading and trailing edges
Reinforced carbon–carbon (RCC)	No lower limit identified	1650 (3000)	Pyrolized carbon–carbon, coated with SiC	Nose cap and wing leading edges

Source: Adapted from L. J. Korb, C. A. Morant, R. M. Calland and C. S. Thatcher, ''The Shuttle Orbiter Thermal Protection System,'' *Ceramic Bulletin*, No. 11, Nov. 1981, p. 1188. Copyright 1981. Reprinted by permission of the American Ceramic Society.

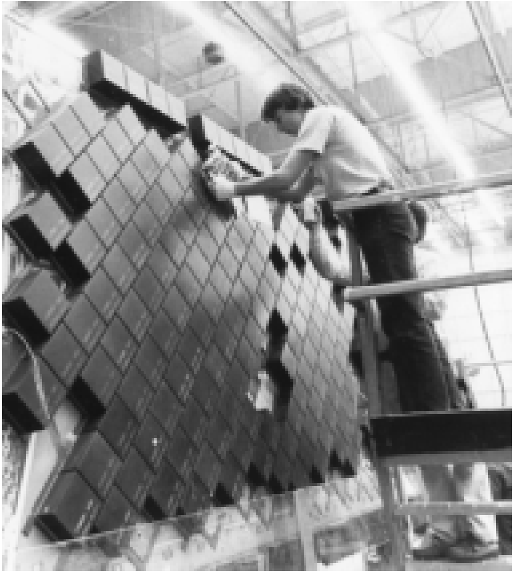

FIGURE 20.17 Photograph showing the installation of thermal protection ceramic tiles on the Space Shuttle Orbiter. [Photograph courtesy the National Aeronautics and Space Administration (NASA).]

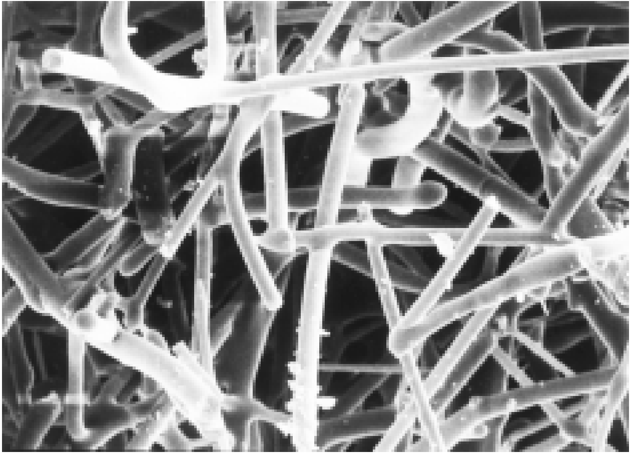

FIGURE 20.18 Scanning electron micrograph of a Space Shuttle Orbiter ceramic tile showing silica fibers that were bonded to one another during a sintering heat treatment. 750×. (Photograph provided courtesy of Lockheed Aerospace Ceramics Systems, Sunnyvale, California.)

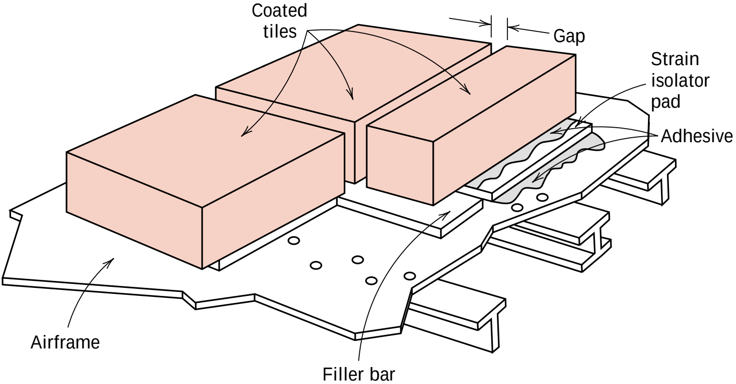
Coated tiles
Gap
Strain isolator pad
Adhesive
Airframe
Filler bar

FIGURE 20.19 Schematic cross section of the tile component of the Space Shuttle Orbiter's thermal protection system. (From L. J. Korb, C. A. Morant, R. M. Calland, and C. S. Thatcher, ''The Shuttle Orbiter Thermal Protection System,'' *Ceramic Bulletin*, No. 11, Nov. 1981, p. 1189. Copyright 1981. Reprinted by permission of the American Ceramic Society.)

FIGURE 20.21 Photograph of a leadframe on which the central plate and contact leads are labeled. 2×. (Leadframe supplied by National Semiconductor Corporation. Photograph by Dennis Haynes.)

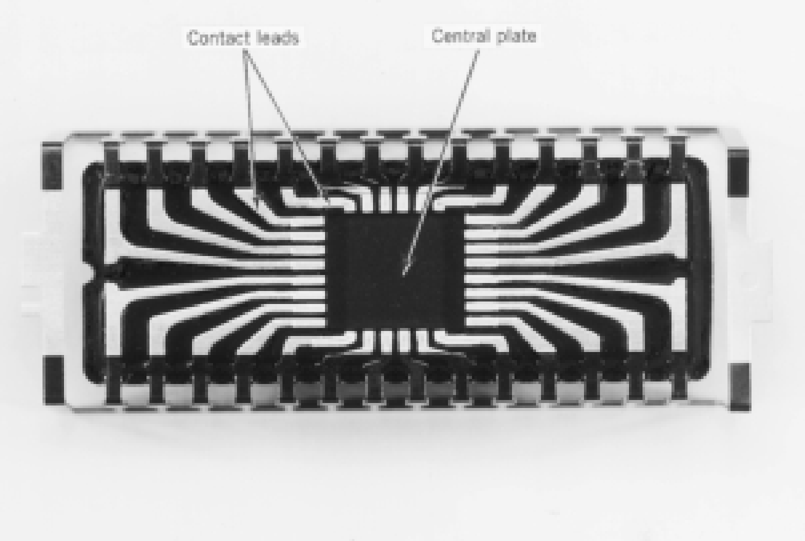
Contact leads
Central plate

Table 20.6 **Designations, Compositions, Electrical and Thermal Conductivities, and Coefficients of Thermal Expansion for Common IC Leadframe Alloys**

Alloy Designation	*Composition (wt%)* *Fe*	*Ni*	*Co*	*Cu*	*Other*	*Electrical Conductivity* $[10^6\ (\Omega\text{-}m)^{-1}]$	*Thermal Conductivity (W/m-K)*	*Coefficient of Thermal Expansion*[a] $[10^{-6}\ (^\circ C)^{-1}]$
C19400	2.35			Balance	0.03 P, 0.12 Zn, 0.03 Pb (max)	39.4	260	16.3
C19500	1.5		0.8	Balance	0.6 Sn, 0.03 P	29.1	200	16.9
Kovar (ASTM F15)	54	29	17			2.0	17	5.1
Alloy 42 (ASTM F30)	58	42				1.4	12	4.9

[a] Coefficient of thermal expansion values are averages measured between 20°C and 300°C.

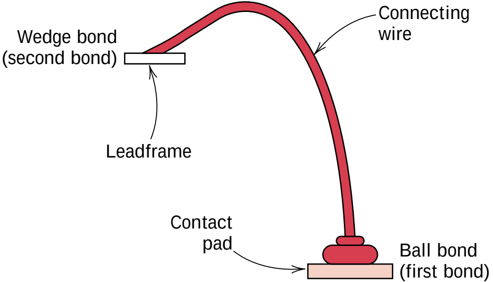
Wedge bond
(second bond)
Connecting wire
Leadframe
Contact pad
Ball bond
(first bond)

Figure 20.23 Schematic diagram showing a connecting wire that is ball bonded to the IC contact pad and wedge bonded to the leadframe. (Adapted from *Electronic Materials Handbook*, Vol. 1, *Packaging*, C. A. Dostal, editor, ASM International, 1989, p. 225.)

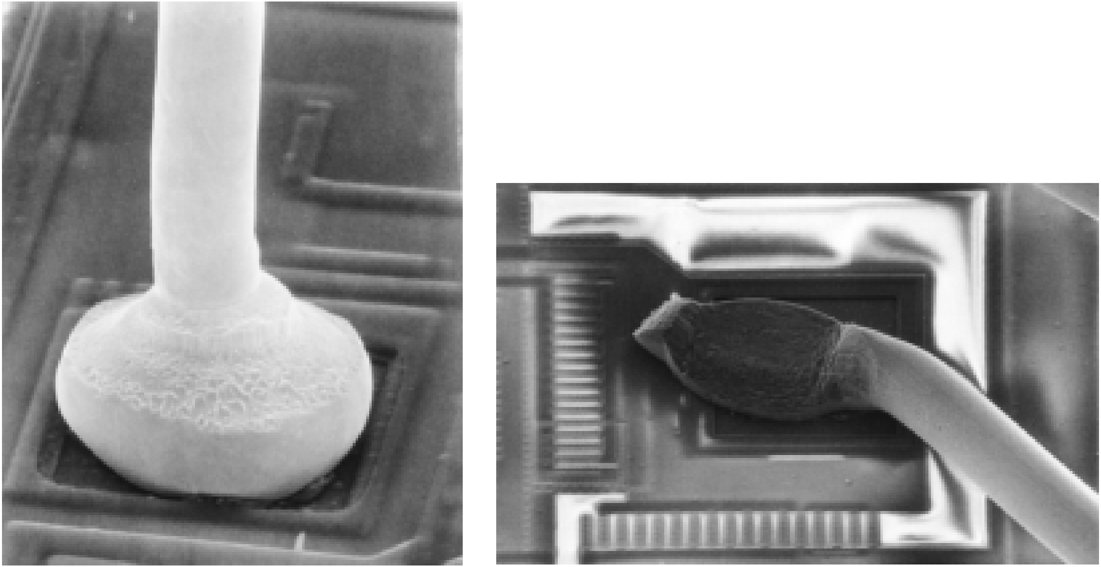
(*a*) (*b*)

Figure 20.24 Scanning electron micrographs of (*a*) a ball bond (475×), and (*b*) a wedge bond (275×). (Photographs courtesy of National Semiconductor Corporation.)

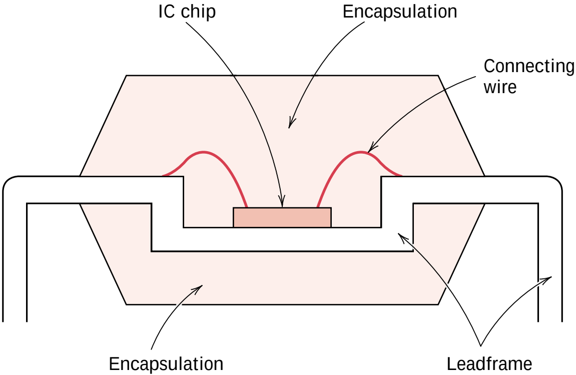
IC chip
Encapsulation
Connecting wire
Encapsulation
Leadframe

Figure 20.25 Schematic diagram showing an encapsulated IC leadframe package. (Adapted from *Electronic Materials Handbook*, Vol. 1, *Packaging*, C. A. Dostal, editor, ASM International, 1989, p. 241.)

Table 20.7 **Property Comparisons of Four Classes of Polymers Used for IC Package Encapsulation**

	Epoxy Resins	*Silicones*	*Polyurethanes*	*Polysulphides*
Dielectric strength	Good	Good	Good	Good
Elastic modulus	High	Low	Wide range	Low
Tensile strength	High	Low	Wide range	—
Precursor viscosity	Low	Low	Low	High
Adhesion to package	Excellent	Poor (to ceramics)	Good	Good
Moisture diffusion rate	High	High	Low	Very low

Source: From C. R. M. Grovenor, *Microelectronic Materials*. Copyright © 1989 by Institute of Physics Publishing, Bristol.

FIGURE 20.26 Schematic diagram of a complete tape-bonded (TAB) leadframe. (From *Electronic Materials Handbook*, Vol. 1, *Packaging*, C. A. Dostal, editor, ASM International, 1989, p. 233.)

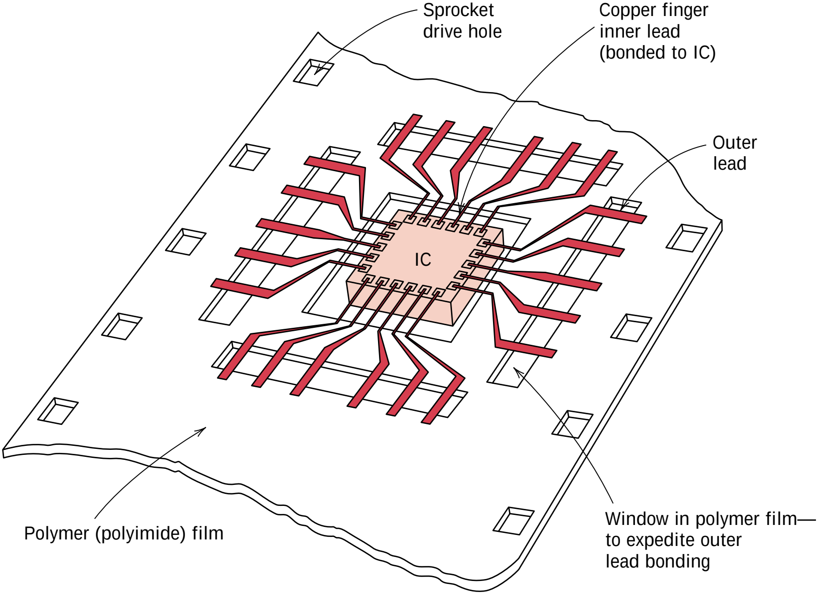
Sprocket drive hole
Copper finger inner lead (bonded to IC)
Outer lead
IC
Polymer (polyimide) film
Window in polymer film—to expedite outer lead bonding

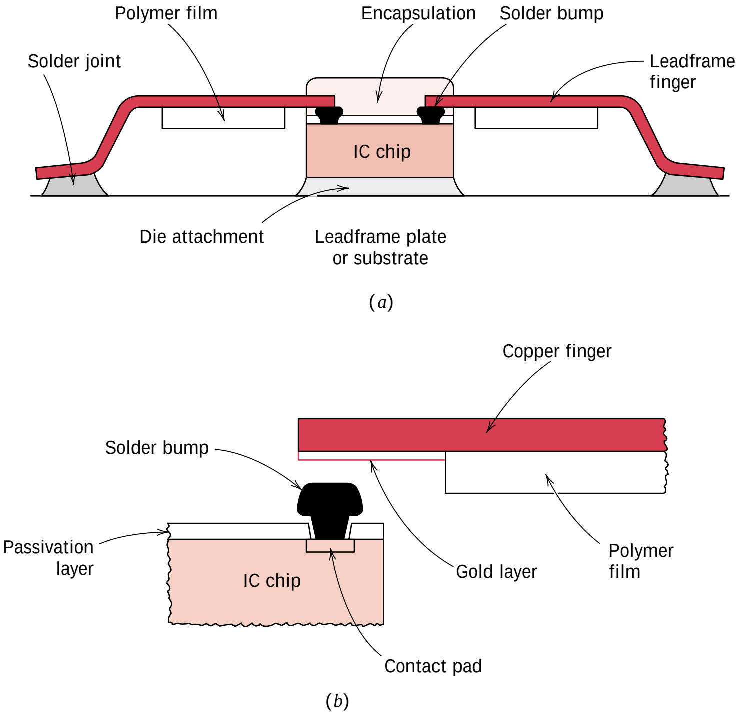
Polymer film
Encapsulation
Solder bump
Solder joint
Leadframe finger
IC chip
Die attachment
Leadframe plate or substrate
(a)
Copper finger
Solder bump
Passivation layer
IC chip
Gold layer
Polymer film
Contact pad
(b)

FIGURE 20.27 Schematic diagrams showing (*a*) the cross section of an encapsulated TAB leadframe package, and (*b*) how bonding between the IC chip and a copper finger is achieved with a solder bump. (Adapted from *Electronic Materials Handbook*, Vol. 1, *Packaging*, C. A. Dostal, editor, ASM International, 1989, pp. 233, 234.)

Appendix C / Costs and Relative Costs for Selected Engineering Materials

This appendix contains price information for the same set of materials for which the properties are included in Appendix B. The collection of valid cost data for materials is an extremely difficult task, which explains the dearth of materials-pricing information in the literature. One reason for this is that there are three pricing tiers: manufacturer, distributor, and retail. Under most circumstances, we have cited distributor prices. For some materials (e.g., specialized ceramics such as silicon carbide and silicon nitride), it was necessary to use manufacturer's prices. In addition, there may be significant variation in the cost for a specific material. There are several reasons for this. First, each vendor has its own pricing scheme. Furthermore, cost will depend on quantity of material purchased and, in addition, how it was processed or treated. We have endeavored to collect data for relatively large orders—i.e., quantities on the order of 900 kg (2000 lb_m) for materials that are ordinarily sold in bulk lots—and, also, for common shapes/treatments. When possible, we obtained price quotes from at least three distributors/manufacturers.

This pricing information was collected between May and August of 1998. Cost data are in U.S. dollars per kilogram; in addition, these data are expressed as both price ranges and single-price values. The absence of a price range (i.e., when a single value is cited) means that either the variation is small, or that, on the basis of limited data, it is not possible to identify a range of prices. Furthermore, inasmuch as material prices change over time, it was decided to use a relative cost index; this index represents the per-unit mass cost (or average per-unit mass cost) of a material divided by the average per-unit mass cost of a common engineering material—A36 plain carbon steel. Although the price of a specific material will vary over time, the price ratio between that material and another will, most likely, change more slowly.

Material/Condition	***Cost ($US/kg)***	***Relative Cost***
PLAIN CARBON AND LOW ALLOY STEELS		
Steel alloy A36		
• Plate, hot rolled	0.50–0.90	1.00
• Angle bar, hot rolled	1.15	1.6
Steel alloy 1020		
• Plate, hot rolled	0.50–0.60	0.8
• Plate, cold rolled	0.85–1.45	1.6
Steel alloy 1040		
• Plate, hot rolled	0.75–0.85	1.1
• Plate, cold rolled	1.30	1.9

Material/Condition	*Cost* (*$US/kg*)	*Relative Cost*
Steel alloy 4140		
• Bar, normalized	1.75–1.95	2.6
• H grade (round), normalized	2.85–3.05	4.2
Steel alloy 4340		
• Bar, annealed	2.45	3.5
• Bar, normalized	3.30	4.7
STAINLESS STEELS		
Stainless alloy 304		
• Plate, hot finished and annealed	2.15–3.50	4.0
Stainless alloy 316		
• Plate, hot finished and annealed	3.00–4.40	5.3
• Round, cold drawn and annealed	6.20	8.9
Stainless alloy 440A		
• Plate, annealed	4.40–5.00	6.7
Stainless alloy 17-7PH		
• Plate, cold rolled	6.85–10.00	12.0
CAST IRONS		
Gray irons (all grades)		
• High production	1.20–1.50	1.9
• Low production	3.30	4.7
Ductile irons (all grades)		
• High production	1.45–1.85	2.4
• Low production	3.30–5.00	5.9
ALUMINUM ALLOYS		
Alloy 1100		
• Sheet, annealed	7.25–10.00	12.3
Alloy 2024		
• Sheet, T3 temper	8.80–11.00	14.1
• Bar, T351 temper	11.35	16.2
Alloy 6061		
• Sheet, T6 temper	4.40–6.20	7.6
• Bar, T651 temper	6.10	8.7
Alloy 7075		
• Sheet, T6 temper	9.00–9.70	13.4
Alloy 356		
• As cast, high production	4.40–6.60	7.9
• As cast, custom pieces	11.00	15.7
• T6 temper, custom pieces	11.65	16.6
COPPER ALLOYS		
Alloy C11000 (electrolytic tough pitch), sheet	4.00–7.00	7.9
Alloy C17200 (beryllium–copper), sheet	25.00–47.00	51.4
Alloy C26000 (cartridge brass), sheet	3.50–4.85	6.0
Alloy C36000 (free-cutting brass), sheet, rod	3.20–4.00	5.1
Alloy C71500 (copper–nickel, 30%), sheet	8.50–9.50	12.9
Alloy C93200 (bearing bronze)		
• Bar	4.50–6.50	7.9
• As cast, custom piece	12.20	17.4

Material/Condition	*Cost ($US/kg)*	*Relative Cost*
MAGNESIUM ALLOYS		
Alloy AZ31B		
• Sheet (rolled)	11.00	15.7
• Extruded	8.80	12.6
Alloy AZ91D (as cast)	3.80	5.4
TITANIUM ALLOYS		
Commercially pure		
• ASTM grade 1, annealed	28.00–65.00	66.4
Alloy Ti-5Al-2.5V	90.00–130.00	157
Alloy Ti-6Al-4V	55.00–130.00	132
PRECIOUS METALS		
Gold, bullion	9,500–10,250	14,100
Platinum, bullion	11,400–14,400	18,400
Silver, bullion	170–210	271
REFRACTORY METALS		
Molybdenum		
• Commercially pure, sheet and rod	85.00–115.00	143
Tantalum		
• Commercially pure, sheet and rod	390–440	593
Tungsten		
• Commercially pure, sheet	77.50	111
• Commercially pure, rod ($\frac{1}{2}$–$\frac{3}{8}$ in. dia.)	97.00–135.00	166
MISCELLANEOUS NONFERROUS ALLOYS		
Nickel 200	19.00–25.00	31.4
Inconel 625	20.00–29.00	35.0
Monel 400	15.50–16.50	22.9
Haynes alloy 25	85.50–103.50	135
Invar	17.25–19.75	26.4
Super invar	22.00–33.00	39.3
Kovar	30.75–39.75	50.4
Chemical lead		
• Ingot	1.20	1.7
• Plate	1.55–1.95	2.5
Antimonial lead (6%)		
• Ingot	1.50	2.1
• Plate	2.00–2.70	3.4
Tin, commercial purity (99.9+%), ingot	6.85–8.85	11.2
Solder (60Sn-40Pb), bar	5.50–7.50	9.3
Zinc, commercial purity		
• Ingot	1.20	1.7
• Anode	1.65–2.45	2.9
Zirconium, reactor grade 702 (plate)	44.00–48.50	66.1
GRAPHITE, CERAMICS, AND SEMICONDUCTING MATERIALS		
Aluminum oxide		
• Calcined powder, 99.8% pure, particle size between 0.4 and 5 μm	1.40–1.60	2.1
• Ball grinding media, 99% pure, $\frac{1}{4}$ in. dia.	28.65	41
• Ball grinding media, 96% pure, $\frac{1}{4}$ in. dia.	29.75	42.5
• Ball grinding media, 90% pure, $\frac{1}{4}$ in. dia.	15.20	21.7

Material/Condition	***Cost*** (***$US/kg***)	***Relative Cost***
Concrete, mixed	0.04	0.06
Diamond		
• Natural, 1/3 carat, industrial grade	36,000–90,000	90,000
• Synthetic, 30–40 mesh, industrial grade	18,750	27,000
• Natural, powder, 45 μm, polishing abrasive	5,000	7,100
Gallium arsenide		
• Mechanical grade, 75 mm dia. wafers, ~625 μm thick	1650–2700	3100
• Prime grade, 75 mm dia. wafers, ~625 μm thick	8500–10,000	13,200
Glass, borosilicate (Pyrex), plate	8.50–17.00	18.2
Glass, soda–lime, plate	1.75–2.35	2.9
Glass ceramic (Pyroceram), plate	12.25–19.25	22.5
Graphite		
• Powder, synthetic, 99% pure, particle size ~10 μm	5.00	7.1
• Powder, synthetic, 99.7% pure, particle size ~10 μm	7.50	10.7
• Extruded, high purity, fine (<0.75 mm) particle size	6.00–7.00	9.3
• Isostatically pressed parts, high purity, ~20 μm particle size	15.00–25.50	29
Silica, fused, plate	315–395	500
Silicon		
• Test grade, undoped, 100 mm dia. wafers, ~425 μm thick	900–2000	2070
• Prime grade, undoped, 100 mm dia. wafers, ~425 μm thick	2075–2525	3300
Silicon carbide		
• α-phase sinterable powder, particle size between 1 and 10 μm	22.00–58.00	57.1
• α-phase, polishing abrasive	4.50–21.50	18.6
• β-phase sinterable powder, particle size between 1 and 10 μm	40.00–100.00	100
• β-phase, polishing abrasive, 1200 to 400 mesh	8.00–22.00	21.4
• α-phase ball grinding media, 1/4 in. dia., sintered	250.00	360
Silicon nitride		
• Sinterable powder, submicron particle size	100.00	143
• Balls, unfinished, 0.25 in. to 0.50 in. in diameter, hot isostatic pressed	875–1100	1400
• Balls, finished ground, 0.25 in. to 0.50 in. diameter, hot isostatic pressed	2000–4000	4300
Zirconia, partially stabilized (3 mol% Y_2O_3)		
• Sinterable powder, submicron particle size	45.00–50.00	68
• Sinterable powder, particle size greater than a micron	22.00–33.00	39.3
• Ball grinding media, 15 mm dia., sintered	125.00–175.00	215

Material/Condition	*Cost ($US/kg)*	*Relative Cost*
POLYMERS		
Butadiene-acrylonitrile (nitrile) rubber		
• Raw and unprocessed	2.90	4.1
• Extruded sheet ($^1/_4$ to $^1/_8$ in. thick)	9.90–10.50	14.6
• Calendered sheet ($^1/_4$ to $^1/_8$ in. thick)	8.40	12.0
Styrene-butadiene (SBR) rubber		
• Raw and unprocessed	1.20	1.7
• Extruded sheet ($^1/_4$ to $^1/_8$ in. thick)	7.60–12.20	14.1
• Calendered sheet ($^1/_4$ to $^1/_8$ in. thick)	6.80	9.7
Silicone rubber		
• Raw and unprocessed	5.50	7.9
• Extruded sheet ($^1/_4$ to $^1/_8$ in. thick)	12.60–26.20	27.7
• Calendered sheet ($^1/_4$ to $^1/_8$ in. thick)	31.50–38.50	50.0
Epoxy resin, raw form	3.00–4.00	5.0
Nylon 6,6		
• Raw form	4.40–6.00	7.4
• Extruded	9.40	13.4
Phenolic resin, raw form	6.50–12.00	13.2
Polybutylene terephthalate (PBT)		
• Raw form	4.00	5.7
• Sheet	9.75	13.9
Polycarbonate (PC)		
• Raw form	4.85–5.30	7.3
• Sheet	7.00–10.00	12.1
Polyester (thermoset), raw form	1.50–4.40	4.2
Polyetheretherketone (PEEK), raw form	90.00–110.00	143
Polyethylene		
• Low density (LDPE), raw form	1.20–1.35	1.8
• High density (HDPE), raw form	1.00–1.70	1.9
• Ultrahigh molecular weight (UHMWPE), raw form	3.00–8.50	8.2
Polyethylene terephthalate (PET)		
• Raw form	1.90–2.10	2.9
• Sheet	3.30–7.70	7.9
Polymethyl methacrylate (PMMA)		
• Raw form	2.40	3.4
• Calendered sheet	4.20	6.0
• Cell cast	5.85	8.4
Polypropylene (PP), raw form	0.85–1.65	1.8
Polystyrene (PS), raw form	1.00–1.10	1.5
Polytetrafluoroethylene (PTFE)		
• Raw form	20.00–26.50	33.2
• Sheet	38.00	54
Polyvinyl chloride (PVC), raw form	1.40–2.80	3.0
FIBER MATERIALS		
Aramid (Kevlar 49), continuous	31.00	44.3
Carbon (PAN precursor), continuous		
• Standard modulus	31.50–41.50	52.1
• Intermediate modulus	70.00–105.00	125
• High modulus	175.00–225.00	285
E glass, continuous	1.90–3.30	3.7

Material/Condition	***Cost*** **(*$US/kg*)**	***Relative Cost***
COMPOSITE MATERIALS		
Aramid (Kevlar 49) continuous-fiber, epoxy prepreg	55.00–62.00	84
Carbon continuous-fiber, epoxy prepreg		
• Standard modulus	40.00–60.00	71
• Intermediate modulus	100.00–130.00	164
• High modulus	200.00–275.00	340
E-glass continuous-fiber, epoxy prepreg	22.00	31.4
Woods		
Douglas fir	0.54–0.60	0.8
Red oak	2.55–3.35	4.2

Chapter 1 / Introduction

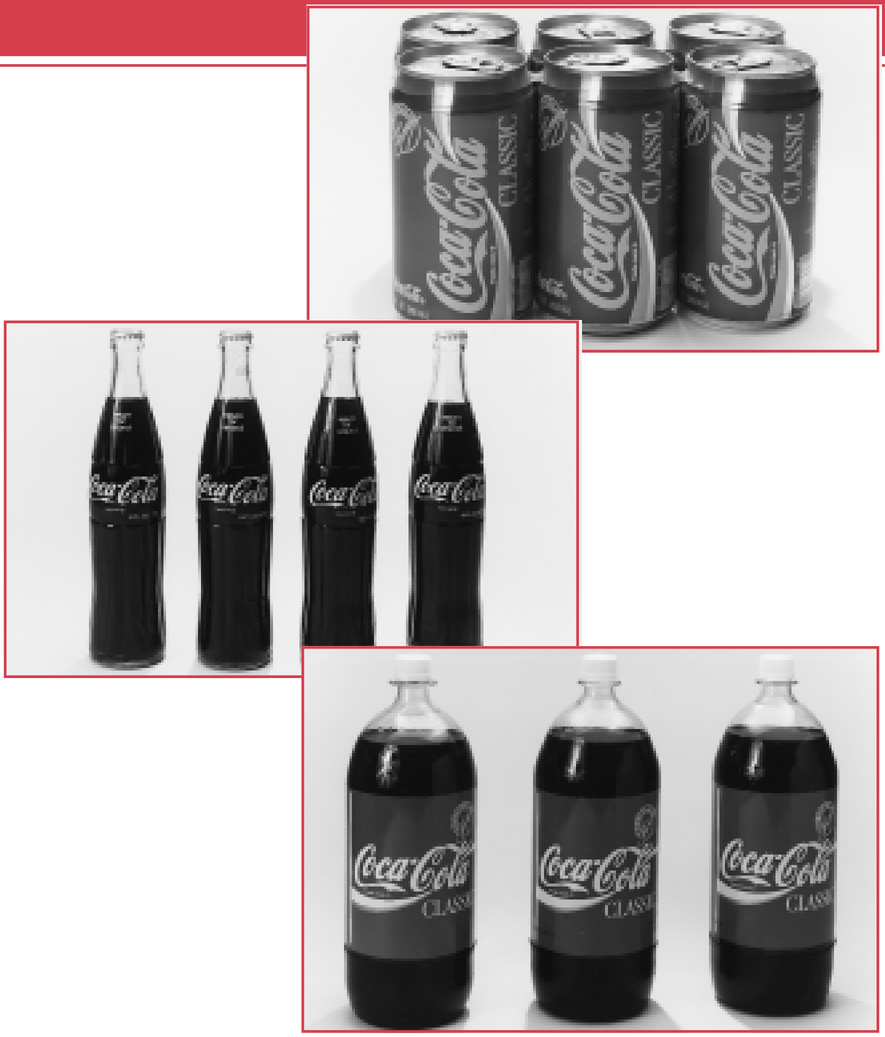

A familiar item that is fabricated from three different material types is the beverage container. Beverages are marketed in aluminum (metal) cans (top), glass (ceramic) bottles (center), and plastic (polymer) bottles (bottom). (Permission to use these photographs was granted by the Coca-Cola Company.)

Learning Objectives

After careful study of this chapter you should be able to do the following:

1. **List six different property classifications of materials that determine their applicability.**
2. **Cite the four components that are involved in the design, production, and utilization of materials, and briefly describe the interrelationships between these components.**
3. **Cite three criteria that are important in the materials selection process.**
4. **(a) List the three primary classifications of solid materials, and then cite the distinctive chemical feature of each.**
   (b) Note the other three types of materials and, for each, its distinctive feature(s).

1.1 HISTORICAL PERSPECTIVE

Materials are probably more deep-seated in our culture than most of us realize. Transportation, housing, clothing, communication, recreation, and food production—virtually every segment of our everyday lives is influenced to one degree or another by materials. Historically, the development and advancement of societies have been intimately tied to the members' ability to produce and manipulate materials to fill their needs. In fact, early civilizations have been designated by the level of their materials development (i.e., Stone Age, Bronze Age).

The earliest humans had access to only a very limited number of materials, those that occur naturally: stone, wood, clay, skins, and so on. With time they discovered techniques for producing materials that had properties superior to those of the natural ones; these new materials included pottery and various metals. Furthermore, it was discovered that the properties of a material could be altered by heat treatments and by the addition of other substances. At this point, materials utilization was totally a selection process, that is, deciding from a given, rather limited set of materials the one that was best suited for an application by virtue of its characteristics. It was not until relatively recent times that scientists came to understand the relationships between the structural elements of materials and their properties. This knowledge, acquired in the past 60 years or so, has empowered them to fashion, to a large degree, the characteristics of materials. Thus, tens of thousands of different materials have evolved with rather specialized characteristics that meet the needs of our modern and complex society; these include metals, plastics, glasses, and fibers.

The development of many technologies that make our existence so comfortable has been intimately associated with the accessibility of suitable materials. An advancement in the understanding of a material type is often the forerunner to the stepwise progression of a technology. For example, automobiles would not have been possible without the availability of inexpensive steel or some other comparable substitute. In our contemporary era, sophisticated electronic devices rely on components that are made from what are called semiconducting materials.

1.2 MATERIALS SCIENCE AND ENGINEERING

The discipline of *materials science* involves investigating the relationships that exist between the structures and properties of materials. In contrast, *materials engineering* is, on the basis of these structure–property correlations, designing or engineering the structure of a material to produce a predetermined set of properties. Throughout this text we draw attention to the relationships between material properties and structural elements.

''Structure'' is at this point a nebulous term that deserves some explanation. In brief, the structure of a material usually relates to the arrangement of its internal components. Subatomic structure involves electrons within the individual atoms and interactions with their nuclei. On an atomic level, structure encompasses the organization of atoms or molecules relative to one another. The next larger structural realm, which contains large groups of atoms that are normally agglomerated together, is termed ''microscopic,'' meaning that which is subject to direct observation using some type of microscope. Finally, structural elements that may be viewed with the naked eye are termed ''macroscopic.''

The notion of ''property'' deserves elaboration. While in service use, all materials are exposed to external stimuli that evoke some type of response. For example, a specimen subjected to forces will experience deformation; or a polished metal surface will reflect light. Property is a material trait in terms of the kind and magnitude of response to a specific imposed stimulus. Generally, definitions of properties are made independent of material shape and size.

Virtually all important properties of solid materials may be grouped into six different categories: mechanical, electrical, thermal, magnetic, optical, and deteriorative. For each there is a characteristic type of stimulus capable of provoking different responses. Mechanical properties relate deformation to an applied load or force; examples include elastic modulus and strength. For electrical properties, such as electrical conductivity and dielectric constant, the stimulus is an electric field. The thermal behavior of solids can be represented in terms of heat capacity and thermal conductivity. Magnetic properties demonstrate the response of a material to the application of a magnetic field. For optical properties, the stimulus is electromagnetic or light radiation; index of refraction and reflectivity are representative optical properties. Finally, deteriorative characteristics indicate the chemical reactivity of materials. The chapters that follow discuss properties that fall within each of these six classifications.

In addition to structure and properties, two other important components are involved in the science and engineering of materials, viz. ''processing'' and ''performance.'' With regard to the relationships of these four components, the structure of a material will depend on how it is processed. Furthermore, a material's performance will be a function of its properties. Thus, the interrelationship between processing, structure, properties, and performance is linear, as depicted in the schematic illustration shown in Figure 1.1. Throughout this text we draw attention to the relationships among these four components in terms of the design, production, and utilization of materials.

We now present an example of these processing-structure-properties-performance principles with Figure 1.2, a photograph showing three thin disk specimens placed over some printed matter. It is obvious that the optical properties (i.e., the light transmittance) of each of the three materials are different; the one on the left is transparent (i.e., virtually all of the reflected light passes through it), whereas the disks in the center and on the right are, respectively, translucent and opaque. All of these specimens are of the same material, aluminum oxide, but the leftmost one is what we call a single crystal—that is, it is highly perfect—which gives rise to its transparency. The center one is composed of numerous and very small single

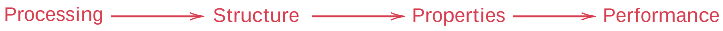

FIGURE 1.1 The four components of the discipline of materials science and engineering and their linear interrelationship.

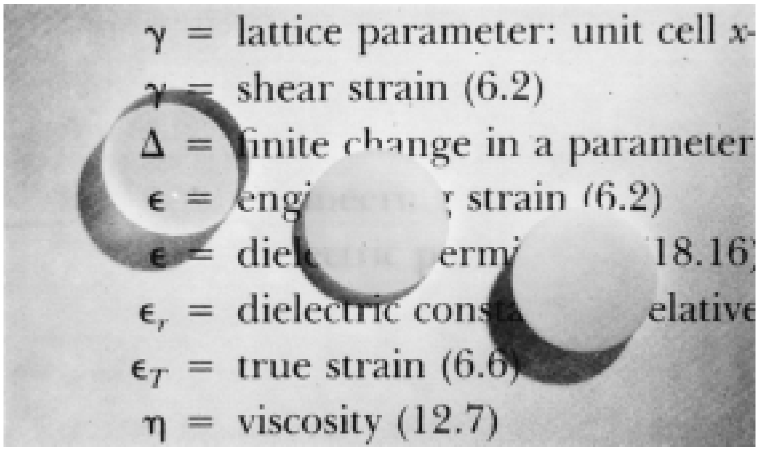

Figure 1.2 Photograph showing the light transmittance of three aluminum oxide specimens. From left to right: single-crystal material (sapphire), which is transparent; a polycrystalline and fully dense (nonporous) material, which is translucent; and a polycrystalline material that contains approximately 5% porosity, which is opaque. (Specimen preparation, P. A. Lessing; photography by J. Telford.)

crystals that are all connected; the boundaries between these small crystals scatter a portion of the light reflected from the printed page, which makes this material optically translucent. And finally, the specimen on the right is composed not only of many small, interconnected crystals, but also of a large number of very small pores or void spaces. These pores also effectively scatter the reflected light and render this material opaque.

Thus, the structures of these three specimens are different in terms of crystal boundaries and pores, which affect the optical transmittance properties. Furthermore, each material was produced using a different processing technique. And, of course, if optical transmittance is an important parameter relative to the ultimate in-service application, the performance of each material will be different.

1.3 Why Study Materials Science and Engineering?

Why do we study materials? Many an applied scientist or engineer, whether mechanical, civil, chemical, or electrical, will at one time or another be exposed to a design problem involving materials. Examples might include a transmission gear, the superstructure for a building, an oil refinery component, or an integrated circuit chip. Of course, materials scientists and engineers are specialists who are totally involved in the investigation and design of materials.

Many times, a materials problem is one of selecting the right material from the many thousands that are available. There are several criteria on which the final decision is normally based. First of all, the in-service conditions must be characterized, for these will dictate the properties required of the material. On only rare occasions does a material possess the maximum or ideal combination of properties. Thus, it may be necessary to trade off one characteristic for another. The classic example involves strength and ductility; normally, a material having a high strength will have only a limited ductility. In such cases a reasonable compromise between two or more properties may be necessary.

A second selection consideration is any deterioration of material properties that may occur during service operation. For example, significant reductions in mechanical strength may result from exposure to elevated temperatures or corrosive environments.

Finally, probably the overriding consideration is that of economics: What will the finished product cost? A material may be found that has the ideal set of properties but is prohibitively expensive. Here again, some compromise is inevitable. The cost of a finished piece also includes any expense incurred during fabrication to produce the desired shape.

The more familiar an engineer or scientist is with the various characteristics and structure–property relationships, as well as processing techniques of materials, the more proficient and confident he or she will be to make judicious materials choices based on these criteria.

1.4 CLASSIFICATION OF MATERIALS

Solid materials have been conveniently grouped into three basic classifications: metals, ceramics, and polymers. This scheme is based primarily on chemical makeup and atomic structure, and most materials fall into one distinct grouping or another, although there are some intermediates. In addition, there are three other groups of important engineering materials—composites, semiconductors, and biomaterials. Composites consist of combinations of two or more different materials, whereas semiconductors are utilized because of their unusual electrical characteristics; biomaterials are implanted into the human body. A brief explanation of the material types and representative characteristics is offered next.

METALS

Metallic materials are normally combinations of metallic elements. They have large numbers of nonlocalized electrons; that is, these electrons are not bound to particular atoms. Many properties of metals are directly attributable to these electrons. Metals are extremely good conductors of electricity and heat and are not transparent to visible light; a polished metal surface has a lustrous appearance. Furthermore, metals are quite strong, yet deformable, which accounts for their extensive use in structural applications.

CERAMICS

Ceramics are compounds between metallic and nonmetallic elements; they are most frequently oxides, nitrides, and carbides. The wide range of materials that falls within this classification includes ceramics that are composed of clay minerals, cement, and glass. These materials are typically insulative to the passage of electricity and heat, and are more resistant to high temperatures and harsh environments than metals and polymers. With regard to mechanical behavior, ceramics are hard but very brittle.

POLYMERS

Polymers include the familiar plastic and rubber materials. Many of them are organic compounds that are chemically based on carbon, hydrogen, and other nonmetallic elements; furthermore, they have very large molecular structures. These materials typically have low densities and may be extremely flexible.

COMPOSITES

A number of composite materials have been engineered that consist of more than one material type. Fiberglass is a familiar example, in which glass fibers are embedded within a polymeric material. A composite is designed to display a combination of the best characteristics of each of the component materials. Fiberglass acquires strength from the glass and flexibility from the polymer. Many of the recent material developments have involved composite materials.

SEMICONDUCTORS

Semiconductors have electrical properties that are intermediate between the electrical conductors and insulators. Furthermore, the electrical characteristics of these materials are extremely sensitive to the presence of minute concentrations of impurity atoms, which concentrations may be controlled over very small spatial regions. The semiconductors have made possible the advent of integrated circuitry that has totally revolutionized the electronics and computer industries (not to mention our lives) over the past two decades.

BIOMATERIALS

Biomaterials are employed in components implanted into the human body for replacement of diseased or damaged body parts. These materials must not produce toxic substances and must be compatible with body tissues (i.e., must not cause adverse biological reactions). All of the above materials—metals, ceramics, polymers, composites, and semiconductors—may be used as biomaterials. {For example, in Section 20.8 are discussed some of the biomaterials that are utilized in artificial hip replacements.}

1.5 ADVANCED MATERIALS

Materials that are utilized in high-technology (or high-tech) applications are sometimes termed *advanced materials.* By high technology we mean a device or product that operates or functions using relatively intricate and sophisticated principles; examples include electronic equipment (VCRs, CD players, etc.), computers, fiber-optic systems, spacecraft, aircraft, and military rocketry. These advanced materials are typically either traditional materials whose properties have been enhanced or newly developed, high-performance materials. Furthermore, they may be of all material types (e.g., metals, ceramics, polymers), and are normally relatively expensive. In subsequent chapters are discussed the properties and applications of a number of advanced materials—for example, materials that are used for lasers, integrated circuits, magnetic information storage, liquid crystal displays (LCDs), fiber optics, and the thermal protection system for the Space Shuttle Orbiter.

1.6 MODERN MATERIALS' NEEDS

In spite of the tremendous progress that has been made in the discipline of materials science and engineering within the past few years, there still remain technological challenges, including the development of even more sophisticated and specialized materials, as well as consideration of the environmental impact of materials production. Some comment is appropriate relative to these issues so as to round out this perspective.

Nuclear energy holds some promise, but the solutions to the many problems that remain will necessarily involve materials, from fuels to containment structures to facilities for the disposal of radioactive waste.

Significant quantities of energy are involved in transportation. Reducing the weight of transportation vehicles (automobiles, aircraft, trains, etc.), as well as increasing engine operating temperatures, will enhance fuel efficiency. New high-strength, low-density structural materials remain to be developed, as well as materials that have higher-temperature capabilities, for use in engine components.

Furthermore, there is a recognized need to find new, economical sources of energy, and to use the present resources more efficiently. Materials will undoubtedly play a significant role in these developments. For example, the direct conversion of solar into electrical energy has been demonstrated. Solar cells employ some rather complex and expensive materials. To ensure a viable technology, materials that are highly efficient in this conversion process yet less costly must be developed.

Furthermore, environmental quality depends on our ability to control air and water pollution. Pollution control techniques employ various materials. In addition, materials processing and refinement methods need to be improved so that they produce less environmental degradation, that is, less pollution and less despoilage of the landscape from the mining of raw materials. Also, in some materials manufacturing processes, toxic substances are produced, and the ecological impact of their disposal must be considered.

Many materials that we use are derived from resources that are nonrenewable, that is, not capable of being regenerated. These include polymers, for which the prime raw material is oil, and some metals. These nonrenewable resources are gradually becoming depleted, which necessitates: 1) the discovery of additional reserves, 2) the development of new materials having comparable properties with less adverse environmental impact, and/or 3) increased recycling efforts and the development of new recycling technologies. As a consequence of the economics of not only production but also environmental impact and ecological factors, it is becoming increasingly important to consider the ‘‘cradle-to-grave’’ life cycle of materials relative to the overall manufacturing process.

{The roles that materials scientists and engineers play relative to these, as well as other environmental and societal issues, are discussed in more detail in Chapter 21.}

REFERENCES

The October 1986 issue of *Scientific American,* Vol. 255, No. 4, is devoted entirely to various advanced materials and their uses. Other references for Chapter 1 are textbooks that cover the basic fundamentals of the field of materials science and engineering.

Ashby, M. F. and D. R. H. Jones, *Engineering Materials 1, An Introduction to Their Properties and Applications,* 2nd edition, Pergamon Press, Oxford, 1996.

Ashby, M. F. and D. R. H. Jones, *Engineering Materials 2, An Introduction to Microstructures, Processing and Design,* Pergamon Press, Oxford, 1986.

Askeland, D. R., *The Science and Engineering of Materials,* 3rd edition, Brooks/Cole Publishing Co., Pacific Grove, CA, 1994.

Barrett, C. R., W. D. Nix, and A. S. Tetelman, *The Principles of Engineering Materials,* Prentice Hall, Inc., Englewood Cliffs, NJ, 1973.

Flinn, R. A. and P. K. Trojan, *Engineering Materials and Their Applications,* 4th edition, John Wiley & Sons, New York, 1990.

Jacobs, J. A. and T. F. Kilduff, *Engineering Materials Technology,* 3rd edition, Prentice Hall, Upper Saddle River, NJ, 1996.

McMahon, C. J., Jr. and C. D. Graham, Jr., *Introduction to Engineering Materials: The Bicycle and the Walkman,* Merion Books, Philadelphia, 1992.

Murray, G. T., *Introduction to Engineering Materials—Behavior, Properties, and Selection,* Marcel Dekker, Inc., New York, 1993.

Ohring, M., *Engineering Materials Science,* Academic Press, San Diego, CA, 1995.

Ralls, K. M., T. H. Courtney, and J. Wulff, *Introduction to Materials Science and Engineering,* John Wiley & Sons, New York, 1976.

Schaffer, J. P., A. Saxena, S. D. Antolovich, T. H. Sanders, Jr., and S. B. Warner, *The Science and*

Design of Engineering Materials, 2nd edition, WCB/McGraw-Hill, New York, 1999.

Shackelford, J. F., *Introduction to Materials Science for Engineers,* 5th edition, Prentice Hall, Inc., Upper Saddle River, NJ, 2000.

Smith, W. F., *Principles of Materials Science and Engineering,* 3rd edition, McGraw-Hill Book Company, New York, 1995.

Van Vlack, L. H., *Elements of Materials Science and Engineering,* 6th edition, Addison-Wesley Publishing Co., Reading, MA, 1989.

Processing → Structure → Properties → Performance

FIGURE 1.1 The four components of the discipline of materials science and engineering and their linear interrelationship.

FIGURE 1.2
Photograph showing the light transmittance of three aluminum oxide specimens. From left to right: single-crystal material (sapphire), which is transparent; a polycrystalline and fully dense (nonporous) material, which is translucent; and a polycrystalline material that contains approximately 5% porosity, which is opaque. (Specimen preparation, P. A. Lessing; photography by J. Telford.)

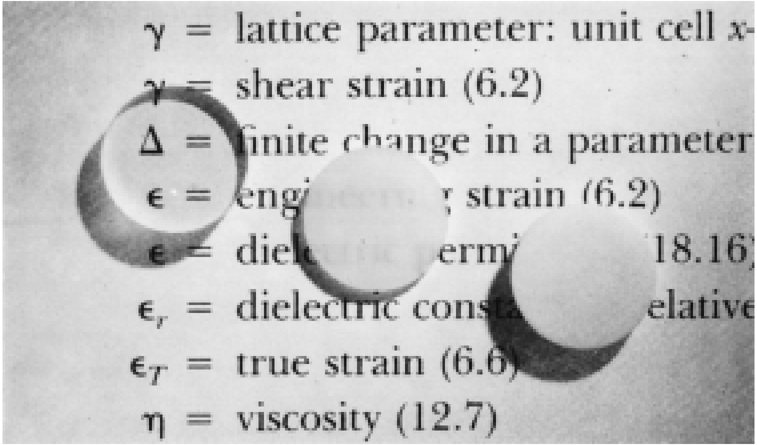
γ = lattice parameter: unit cell x-
γ = shear strain (6.2)
Δ = finite change in a parameter
ϵ = eng strain (6.2)
ϵ = diel erm 18.16
ϵ_r = dielectric const elative
ϵ_T = true strain (6.6)
η = viscosity (12.7)

Chapter 21 / Economic, Environmental, and Societal Issues in Materials Science and Engineering

Used aluminum beverage cans that are to be recycled. These cans will be crushed and pressed into bales (shown in the background) and then shredded into small pieces. Ferrous and nonferrous metal contaminants are next eliminated, and the decorative coating is removed in a delacquering operation. A thermomechanical process then separates can bodies (alloy 3004) from the lids (alloy 5182). The final recycling stages include melting, refining, casting, and rolling. (Photograph courtesy Alcoa.)

Why Study *Economic, Environmental, and Societal Issues in Materials Science and Engineering?*

It is essential for the engineer to know about and understand economic issues simply because the company/institution for which he/she works must realize a profit from the products it manufactures. Materials engineering decisions have economic consequences, with regard to both material and production costs.

An awareness of environmental and societal issues is important for the engineer inasmuch as over time, greater demands are being made on the world's natural resources. Furthermore, levels of pollution are ever increasing. Materials engineering decisions have impacts on the consumption of raw materials and energy, on the contamination of our water and atmosphere, and on the ability of the consumer to recycle or dispose of spent products. The quality of life for this and future generations will depend, to some degree, on how these issues are addressed by the global engineering community.

Learning Objectives

After careful study of this chapter you should be able to do the following:

1. **List and briefly discuss three factors over which an engineer has control that affect the cost of a product.**
2. **Diagram the total materials cycle, and briefly discuss relevant issues that pertain to each stage of this cycle.**
3. **List the two inputs and five outputs for the life cycle analysis/assessment scheme.**
4. **Cite issues that are relevant to the "green design" philosophy of product design.**
5. **Discuss recyclability/disposability issues relative to (a) metals, (b) glass, (c) plastics and rubber, and (d) composite materials.**

21.1 INTRODUCTION

In previous chapters, we dealt with a variety of materials science and materials engineering issues to include criteria that may be employed in the materials selection process. Many of these selection criteria relate to material properties or property combinations—mechanical, electrical, thermal, corrosion, etc.; the performance of some component will depend on the properties of the material from which it is made. Processability or ease of fabrication of the component may also play a role in the selection process. Virtually the entirety of this book, in one way or another, has addressed these property and fabrication issues.

In engineering practice there are other important criteria that must be considered in the development of a marketable product. Some of these are economic in nature, which, to some degree, are unrelated to scientific principles and engineering practice, and yet are significant if a product is to be competitive in the commercial marketplace. Other criteria that should be addressed involve environmental and societal issues—i.e., pollution, disposal, recycling, energy, etc. This final chapter offers relatively brief overviews of economic, environmental, and societal considerations that are important in engineering practice.

ECONOMIC CONSIDERATIONS

It goes without saying that engineering practice involves utilizing scientific principles to design components and systems that perform reliably and satisfactorily. Another critical driving force in engineering practice is that of economics; simply stated, the company or institution must realize a profit from the products that it manufactures and sells. The engineer might design the perfect component; however, as manufactured, it must be offered for sale at a price that is attractive to the consumer, and, in addition, return a suitable profit to the company. Only a brief overview of important economic considerations as they apply to the materials engineer will be provided. The student may want to consult references provided at the end of this chapter that address engineering economics in detail.

There are three factors over which the materials engineer has control and which affect the cost of a product; they are (1) component design, (2) the material(s) used, and (3) the manufacturing technique(s) that are employed. These factors are interrelated in that component design may affect which material is used, and both component design and the material used will influence the choice of manufacturing technique(s). Economic considerations for each of these factors is now briefly discussed.

21.2 Component Design

Some fraction of the cost of a component is associated with its design. In this context, component design is the specification of size, shape, and configuration, which will affect in-service component performance. For example, if mechanical forces are present, then stress analyses may be required. Detailed drawings of the component must be prepared; computers are normally employed, using software that has been generated for this specific function.

It is often the case that a single component is part of a complex device or system consisting of a large number of components (e.g., the television, automobile, VCR, etc.). Thus, design must take into consideration each component's contribution to the efficient operation of the complete system.

Component design is a highly iterative process that involves many compromises and trade-offs. The engineer should keep in mind that an optimal component design may not be possible due to system constraints.

21.3 Materials

In terms of economics, we want to select the material or materials having the appropriate combination(s) of properties which are the least expensive. Once a family of materials has been selected that satisfy the design constraints, cost comparisons of the various candidate materials may be made on the basis of cost per part. Material price is usually quoted per unit mass. The part volume may be determined from its dimensions and geometry, which is then converted into mass using the density of the material. In addition, during manufacturing there ordinarily is some unavoidable material waste, which should also be taken into account in these computations. Current prices for a wide variety of engineering materials are contained in Appendix C.

21.4 Manufacturing Techniques

As already stated, the choice of manufacturing process will be influenced by both the material selected and part design. The entire manufacturing process will normally consist of primary and secondary operations. Primary operations are those that convert the raw material into a recognizable part (e.g., casting, plastic forming, powder compaction, molding, etc.), whereas secondary ones are those subsequently employed to produce the finished part (e.g., heat treatments, welding, grinding, drilling, painting, decorating). The major cost considerations for these processes include capital equipment, tooling, labor, repairs, machine downtime, and waste. Of course, within this cost analysis, rate of production is an important consideration. If this particular part is one component of a system, then assembly costs must also be addressed. And, finally, there will undoubtedly be costs associated with inspection and packaging of the final product.

As a sidelight, there are also other factors not directly related to design, material, or manufacturing that figure into the product selling price. These factors include labor fringe benefits, supervisory and management labor, research and development, property and rent, insurance, profit, taxes, and so on.

ENVIRONMENTAL AND SOCIETAL CONSIDERATIONS

Our modern technologies and the manufacturing of their associated products impact our societies in a variety of ways—some are positive, others are adverse. Furthermore, these impacts are economic and environmental in type, and international in scope inasmuch as (1) the resources required for a new technology often come from many different countries, (2) the economic prosperity resulting from technological development is global in extent, and (3) environmental impacts may extend beyond the boundaries of a single country.

Materials play a crucial role in this technology-economy-environment scheme. A material that is utilized in some end product and then discarded passes through several stages or phases; these stages are represented in Figure 21.1, which is sometimes termed the ‘‘total materials cycle’’ or just ‘‘materials cycle,’’ and represents the ‘‘cradle-to-grave’’ life circuit of a material. Beginning on the far left side of Figure 21.1, raw materials are extracted from their natural earthly habitats by mining, drilling, harvesting, etc. These raw materials are then purified, refined, and converted into bulk forms such as metals, cements, petroleum, rubber, fibers, etc. Further synthesis and processing results in products that are what may be termed ‘‘engineered materials’’; examples include metal alloys, ceramic powders, glass, plastics, composites, semiconductors, elastomers. Next, these engineered materials are further shaped, treated, and assembled into products, devices, and appliances that are ready for the consumer—this constitutes the ‘‘product design, manufacture, assembly’’ stage of Figure 21.1. The consumer purchases these products and uses them (the ‘‘applications’’ stage) until they wear out or become obsolete, and are

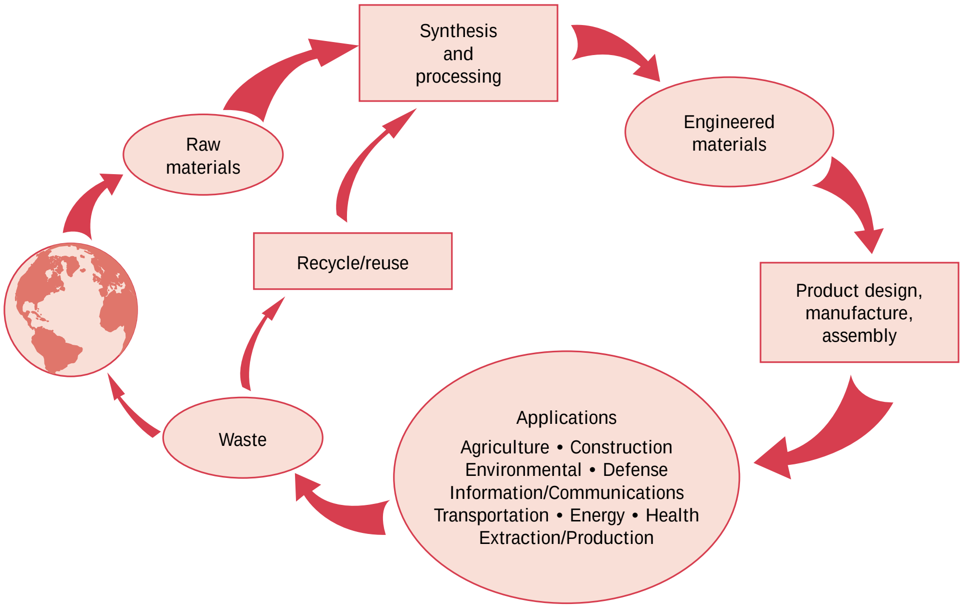
Synthesis and processing
Engineered materials
Raw materials
Recycle/reuse
Product design, manufacture, assembly
Waste
Applications
Agriculture • Construction
Environmental • Defense
Information/Communications
Transportation • Energy • Health
Extraction/Production

Figure 21.1 Schematic representation of the total materials cycle. (Adapted from M. Cohen, *Advanced Materials & Processes,* Vol. 147, No. 3, p. 70, 1995. Copyright © 1995 by ASM International. Reprinted by permission of ASM International, Materials Park, OH.)

discarded. At this time the product constituents may either be recycled/reused (whereby they reenter the materials cycle) or disposed of as waste, normally being either incinerated or dumped as solid waste in municipal land-fills—as such, they return to the earth and complete the materials cycle.

It has been estimated that worldwide, on the order of 15 billion tons of raw materials are extracted from the earth every year; some of these are renewable and some are not. Over time, it is becoming more apparent that the earth is virtually a closed system relative to its constituent materials, and that its resources are finite. In addition, as our societies mature and populations increase, the available resources become scarcer, and greater attention must be paid to more effective utilization of these resources relative to this materials cycle.

Furthermore, energy must be supplied at each cycle stage; in the United States it has been estimated that approximately one-half of the energy consumed by manufacturing industries goes to produce and fabricate materials. Energy is a resource that, to some degree, is limited in supply and measures must be taken to conserve and more effectively utilize it in the production, application, and disposal of materials.

And, finally, there are interactions with and impacts on the natural environment at all stages of the materials cycle. The condition of the earth's atmosphere, water, and land depends to a large extent on how carefully we traverse this materials cycle. Some ecological damage and landscape spoilage undoubtedly result during the extraction of raw materials phase. Pollutants may be generated that are expelled into the air and water during the synthesis and processing stage; in addition, any toxic chemicals that are produced need to be disposed of or discarded. The final product, device, or appliance should be designed such that during its lifetime, any impact on the environment is minimal; furthermore, at the end of its life that, at best, provision be made for recycling of its component materials, or at least for their disposal with little ecological degradation (i.e., it should be biodegradable).

Recycling of used products rather than disposing of them as waste is a desirable approach for several reasons. First of all, using recycled material obviates the need to extract raw materials from the earth, and thus conserves natural resources and eliminates any associated ecological impact from the extraction phase. Second, energy requirements for the refinement and processing of recycled materials are normally less than for their natural counterparts; for example, approximately 28 times as much energy is required to refine natural aluminum ores than to recycle aluminum beverage can scrap. And, finally, there is no need to dispose of recycled materials.

Thus, this materials cycle (Figure 21.1) is really a system that involves interactions and exchanges among materials, energy, and the environment.

In many countries, environmental problems and issues are being addressed by the establishment of standards that are mandated by governmental regulatory agencies. Furthermore, from an industrial perspective, it becomes incumbent for engineers to propose viable solutions to existing and potential environmental concerns.

Correcting any environmental problems associated with manufacturing will influence product price. That is, manufacturing cost is normally greater for a ''green'' (or ''environmentally friendly'') product than for its equivalent that is produced under conditions wherein environmental issues are minimized. Thus, a company must confront the dilemma of this potential economic-environmental trade-off and then decide the relative importance of economics and of environmental impact.

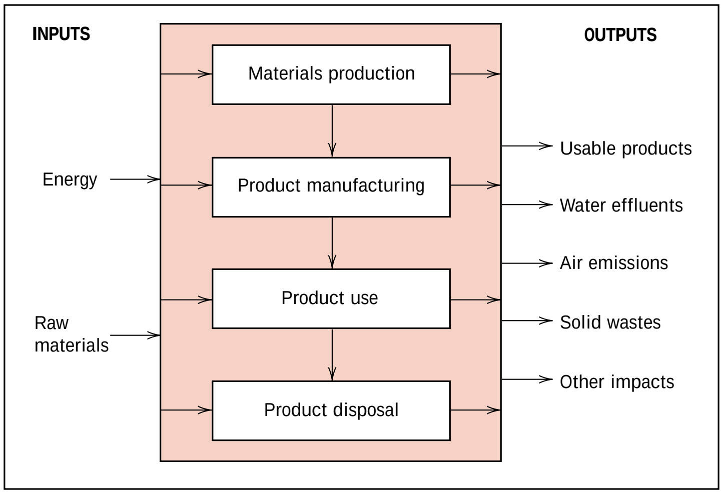

FIGURE 21.2 Schematic representation of an input/output inventory for the life-cycle assessment of a product. (Adapted from J. L. Sullivan and S. B. Young, *Advanced Materials & Processes,* Vol. 147, No. 2, p. 38, 1995. Copyright © 1995 by ASM International. Reprinted by permission of ASM International, Materials Park, OH.)

One approach that is being implemented by industry to improve the environmental performance of products is termed *life cycle analysis/assessment.* With this approach to product design, consideration is given to the cradle-to-grave environmental assessment of the product, from material extraction to product manufacture to product use, and, finally, to recycling and disposal; sometimes this approach is also labeled as ''green design.'' One important phase of this approach is to quantify the various inputs (e.g., materials and energy) and outputs (e.g., wastes) for each phase of the life cycle; this is represented schematically in Figure 21.2. In addition, an assessment is conducted relative to the impact on both global and local environments in terms of the effects on the ecology, human health, and resource reserves.

21.5 RECYCLING ISSUES IN MATERIALS SCIENCE AND ENGINEERING

Important stages in the materials cycle where materials science and engineering plays a significant role are recycling and disposal. The issues of recyclability and disposability are important when new materials are being designed and synthesized. Furthermore, during the materials selection process, the ultimate disposition of the materials employed should be an important criterion. Let us conclude this section by briefly discussing several of these recyclability/disposability issues.

From an environmental perspective, the ideal material should be either totally recyclable or completely biodegradable. Recyclable means that a material, after having completed its life cycle in one component, could be reprocessed, could reenter the materials cycle, and could be reused in another component—a process that could be repeated an indefinite number of times. By completely biodegradable, we mean that, by interactions with the environment (natural chemicals, microorganisms, oxygen, heat, sunlight, etc.), the material deteriorates and returns to virtually the same state in which it existed prior to the initial processing. Engineering materials exhibit varying degrees of recyclability and biodegradability.

METALS

Most metal alloys (e.g., Fe, Cu), to one degree or another experience corrosion and are also biodegradable. However, some metals (e.g., Hg, Pb) are toxic and, when land-filled, may present health hazards. Furthermore, alloys of most metals are recyclable; on the other hand it is not feasible to recycle all alloys of every metal. In addition, the quality of alloys that are recycled tends to diminish with each cycle.

Product designs should allow for the dismantling of components composed of different alloys. Another of the problems of recycling involves separation of various alloys types (e.g., aluminum from ferrous alloys) after dismantling and shredding; in this regard, some rather ingenious separation techniques have been devised (e.g., magnetic and gravity). Joining of dissimilar alloys presents contamination problems; for example, if two similar alloys are to be joined, welding is preferred over bolting or riveting. Coatings (paints, anodized layers, claddings, etc.) may also act as contaminants, and render the material nonrecyclable.

Aluminum alloys are very corrosion resistant, and, therefore, nonbiodegradable. Fortunately, however, they may be recycled; in fact, aluminum is the most important recyclable nonferrous metal. Since aluminum is not easily corroded, it may be totally reclaimed. A low ratio of energy is required to refine recycled aluminum relative to its primary production. In addition, there is a large number of commercially available alloys that have been designed to accommodate impurity contamination. The primary sources of recycled aluminum are used beverage cans and scrapped automobiles.

GLASS

The one ceramic material that is consumed by the general public in the greatest quantities is glass, in the form of containers. Glass is a relatively inert material, and, as such, it does not decompose; thus, it is not biodegradable. A significant proportion of municipal land-fills consists of waste glass; so also does incinerator residue.

In addition, there is not a significant economic driving force for recycling glass. Its basic raw materials (sand, soda ash, and limestone) are inexpensive and readily available. Furthermore, salvaged glass (also called ‘‘cullet’’) must be sorted by color (clear, amber, and green), by type (plate versus container), and by composition (lime, lead, and borosilicate [or Pyrex]); these sorting procedures are time-consuming and expensive. Therefore, scrap glass has a low market value, which diminishes its recyclability. Advantages of utilizing recycled glass include more rapid and increased production rates and a reduction in pollutant emissions.

PLASTICS AND RUBBER

One of the reasons that synthetic polymers (including rubber) are so popular as engineering materials lies with their chemical and biological inertness. On the down side, this characteristic is really a liability when it comes to waste disposal. Polymers are not biodegradable, and, as such, they constitute a significant land-fill component; major sources of waste are from packaging, junk automobiles, automobile tires, and domestic durables. Biodegradable polymers have been synthesized, but they are relatively expensive to produce. On the other hand, since some polymers are combustible and do not yield appreciable toxic or polluting emissions, they may be disposed of by incineration.

Thermoplastic polymers, specifically polyethylene terephthalate, polyethylene, and polypropylene, are those most amenable to reclamation and recycling, since they may be reformed upon heating. Sorting by type and color is necessary. In the United States, type sorting of packaging materials is facilitated using a number

Table 21.1 **Recycle Codes, Uses of the Virgin Material, and Recycled Products for Several Commercial Polymers**

Recycle Code	*Polymer Name*	*Uses of Virgin Material*	*Recycled Products*
1	Polyethylene terephthalate (PET or PETE)	Plastic beverage containers, mouthwash jars, peanut butter and salad dressing bottles	Liquid-soap bottles, strapping, fiberfill for winter coats, surfboards, paint brushes, fuzz on tennis balls, soft-drink bottles, film, egg cartons, skis, carpets, boats
2	High-density polyethylene (HDPE)	Milk, water and juice containers, grocery bags, toys, liquid detergent bottles	Soft-drink bottle base caps, flower pots, drain pipes, signs, stadium seats, trash cans, recycling bins, traffic-barrier cones, golf bag liners, detergent bottles, toys
3	Polyvinyl chloride or vinyl (V)	Clear food packaging, shampoo bottles	Floor mats, pipes, hose, mud flaps
4	Low-density polyethylene (LDPE)	Bread bags, frozen-food bags, grocery bags	Garbage can liners, grocery bags, multipurpose bags
5	Polypropylene (PP)	Ketchup bottles, yogurt containers and margarine tubs, medicine bottles	Manhole steps, paint buckets, videocassette storage cases, ice scrapers, fast food trays, lawn mower wheels, automobile battery parts
6	Polystyrene (PS)	Videocassette cases, compact disc jackets, coffee cups; knives, spoons, and forks; cafeteria trays, grocery store meat trays, and fast-food sandwich containers	License plate holders, golf course and septic tank drainage systems, desktop accessories, hanging files, food service trays, flower pots, trash cans, videocassettes

Source: American Plastics Council.

identification code; for example, a ‘‘1’’ denotes high-density polyethylene (HDPE). Table 21.1 presents these recycling code numbers and their associated materials. Also included in the table are uses of virgin and recycled materials. Plastics recycling is complicated by the presence of fillers (Section 14.12) that were added to modify the original properties. The recycled plastic is less costly than the original material, and quality and appearance are generally degraded with each recycle. Typical applications for recycled plastics include shoe soles, tool handles, and industrial products such as pallets.

The recycling of thermoset resins is much more difficult since these materials are not easily remolded or reshaped due to their crosslinked or network structures. Some thermosets are ground up and added to the virgin molding material prior to processing; as such, they are recycled as filler materials.

Rubber materials present some disposal and recycling challenges. When vulcanized, they are thermoset materials, which makes chemical recycling difficult. In addition, they may also contain a variety of fillers. The major source of rubber scrap in the United States is discarded automobile tires, which are highly nonbiodegradable. Scrap tires have been utilized as a fuel for some industrial applications (e.g., cement plants), but yield dirty emissions. Recycled rubber tires that have been split and reshaped are used in a variety of applications such as automotive bumper guards, mud flaps, door mats, and conveyor rollers; and, of course, used tires may also be recapped. In addition, rubber tires may be ground into small chunks that are then recombined into the desired shape using some type of adhesive; the resulting material may be used in a number of nondemanding applications such as place mats and rubber toys.

The most viable recyclable alternatives to the traditional rubber materials are the thermoplastic elastomers (Section 13.16). Being thermoplastic in nature they are not chemically crosslinked and, thus, are easily reshaped. Furthermore, production energy requirements are lower than for the thermoset rubbers since a vulcanization step is not required in their manufacture.

COMPOSITE MATERIALS

Composites are inherently difficult to recycle because they are multiphase in nature. The two or more phases/materials that constitute the composite are normally intermixed on a very fine scale; consequently, complete phase/material separation is virtually impossible, and recycling procedures that require material separation are impractical.

SUMMARY

The economics of engineering is very important in product design and manufacturing. To minimize product cost, materials engineers must take into account component design, what materials are used, and manufacturing processes. Other significant economic factors include fringe benefits, labor, insurance, profit, etc.

Environmental and societal impacts of production are becoming significant engineering issues. In this regard, the material cradle-to-grave life cycle is an important consideration; this cycle consists of extraction, synthesis/processing, product design/manufacture, application, and disposal stages. Materials, energy, and environmental interactions/exchanges are important factors in the efficient operation of the materials cycle. The earth is a closed system in that its materials resources are finite; to some degree, the same may be said of energy resources. Environmental issues involve ecological damage, pollution, and waste disposal. Recycling of used products and the utilization of green design obviate some of these environmental problems.

Recyclability and disposability issues were addressed in the context of materials science and engineering. Ideally, a material should be at best recyclable, and at least biodegradable or disposable. The recyclability and disposability of metal alloys, glasses, polymers, and composites were also discussed.

REFERENCES

Engineering Economics

Cassimatis, P. A., *Concise Introduction to Engineering Economics*, Routledge, Chapman and Hall, New York, 1988.

Park, C. S., *Contemporary Engineering Economics*, 2nd edition, Addison-Wesley Publishing Company, Menlo Park, CA, 1997.

Riggs, J. L. and T. M. West, *Engineering Economics*, 3rd edition, McGraw-Hill Book Company, New York, 1986.

Steiner, H. M., *Engineering Economic Principles*, McGraw-Hill, New York, 1992.

White, J. A., K. E. Case, D. B. Pratt, and M. H. Agee, *Principles of Engineering Economics Analysis*, 4th edition, John Wiley & Sons, New York, 1998.

Societal

Cohen, M., ‘‘Societal Issues in Materials Science and Technology,’’ *Materials Research Society Bulletin,* September, 1994, pp. 3–8.

Materials Science and Engineering for the 1990s, National Academy Press, Washington, DC, 1989.

Environmental

Carless, J., *Taking Out the Trash,* Island Press, Washington, DC, 1992.

Dutson, T. E., *Recycling Solid Waste, The First Choice for Private and Public Sector Management,* Quorum Books, Westport, CT, 1993.

Smith, P. I. S., *Recycling Waste,* Scholium International, Inc., Port Washington, NY, 1976.

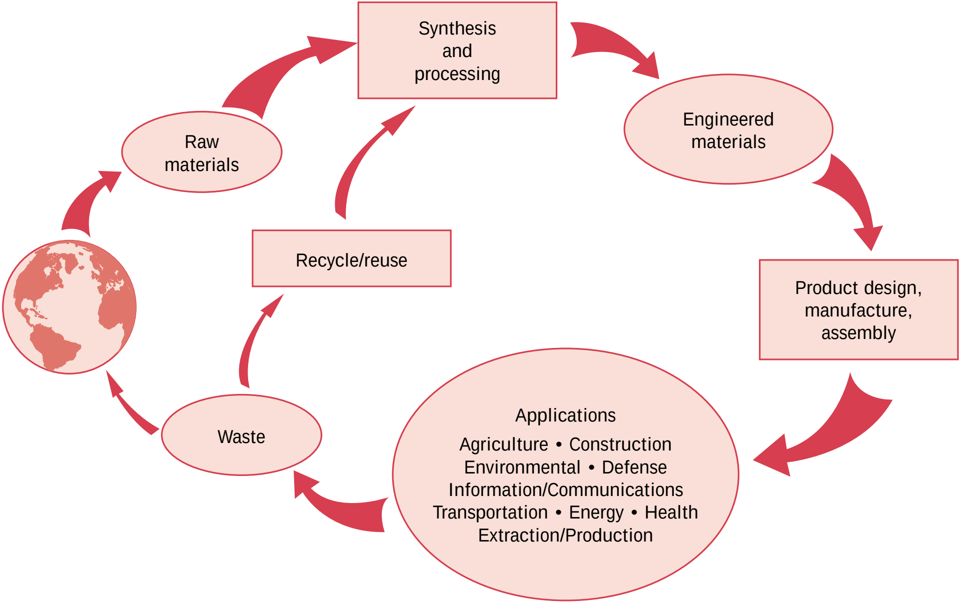
Synthesis and processing
Engineered materials
Product design, manufacture, assembly
Applications
Agriculture • Construction
Environmental • Defense
Information/Communications
Transportation • Energy • Health
Extraction/Production
Waste
Recycle/reuse
Raw materials

Figure 21.1 Schematic representation of the total materials cycle. (Adapted from M. Cohen, *Advanced Materials & Processes*, Vol. 147, No. 3, p. 70, 1995. Copyright © 1995 by ASM International. Reprinted by permission of ASM International, Materials Park, OH.)

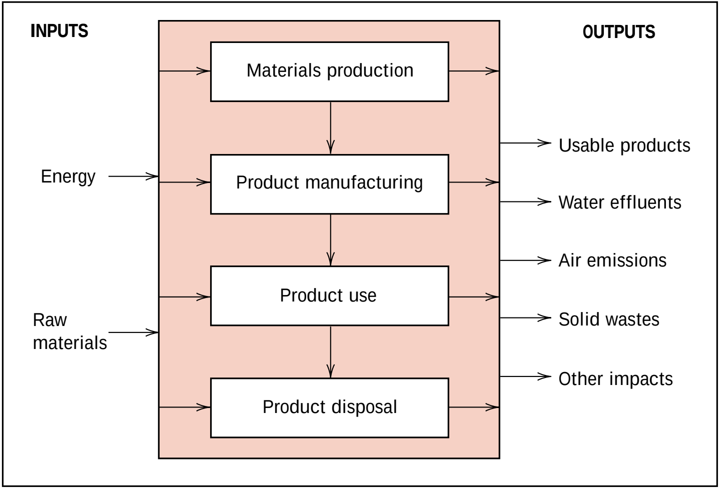
INPUTS
OUTPUTS
Materials production
Product manufacturing
Product use
Product disposal
Energy
Raw materials
Usable products
Water effluents
Air emissions
Solid wastes
Other impacts

FIGURE 21.2 Schematic representation of an input/output inventory for the life-cycle assessment of a product. (Adapted from J. L. Sullivan and S. B. Young, *Advanced Materials & Processes*, Vol. 147, No. 2, p. 38, 1995. Copyright © 1995 by ASM International. Reprinted by permission of ASM International, Materials Park, OH.)

Table 21.1 **Recycle Codes, Uses of the Virgin Material, and Recycled Products for Several Commercial Polymers**

Recycle Code	*Polymer Name*	*Uses of Virgin Material*	*Recycled Products*
1	Polyethylene terephthalate (PET or PETE)	Plastic beverage containers, mouthwash jars, peanut butter and salad dressing bottles	Liquid-soap bottles, strapping, fiberfill for winter coats, surfboards, paint brushes, fuzz on tennis balls, soft-drink bottles, film, egg cartons, skis, carpets, boats
2	High-density polyethylene (HDPE)	Milk, water and juice containers, grocery bags, toys, liquid detergent bottles	Soft-drink bottle base caps, flower pots, drain pipes, signs, stadium seats, trash cans, recycling bins, traffic-barrier cones, golf bag liners, detergent bottles, toys
3	Polyvinyl chloride or vinyl (V)	Clear food packaging, shampoo bottles	Floor mats, pipes, hose, mud flaps
4	Low-density polyethylene (LDPE)	Bread bags, frozen-food bags, grocery bags	Garbage can liners, grocery bags, multipurpose bags
5	Polypropylene (PP)	Ketchup bottles, yogurt containers and margarine tubs, medicine bottles	Manhole steps, paint buckets, videocassette storage cases, ice scrapers, fast food trays, lawn mower wheels, automobile battery parts
6	Polystyrene (PS)	Videocassette cases, compact disc jackets, coffee cups; knives, spoons, and forks; cafeteria trays, grocery store meat trays, and fast-food sandwich containers	License plate holders, golf course and septic tank drainage systems, desktop accessories, hanging files, food service trays, flower pots, trash cans, videocassettes

Source: American Plastics Council.

Appendix A / The International System of Units (SI)

Units in the *International System of Units* fall into two classifications: base and derived. Base units are fundamental and not reducible. Table A.1 lists the base units of interest in the discipline of materials science and engineering.

Derived units are expressed in terms of the base units, using mathematical signs for multiplication and division. For example, the SI units for density are kilogram per cubic meter (kg/m^3). For some derived units, special names and symbols exist; for example, N is used to denote the newton, the unit of force, which is equivalent to 1 $kg\text{-}m/s^2$. Table A.2 contains a number of the important derived units.

It is sometimes necessary, or convenient, to form names and symbols that are decimal multiples or submultiples of SI units. Only one prefix is used when a multiple of an SI unit is formed, which should be in the numerator. These prefixes and their approved symbols are given in Table A.3. Symbols for all units used in this book, SI or otherwise, are contained inside the front cover.

Table A.1 **The SI Base Units**

Quantity	*Name*	*Symbol*
Length	meter, metre	m
Mass	kilogram	kg
Time	second	s
Electric current	ampere	A
Thermodynamic temperature	kelvin	K
Amount of substance	mole	mol

Table A.2 Some of the SI Derived Units

Quantity	*Name*	*Formula*	*Special Symbol*[a]
Area	square meter	m^2	—
Volume	cubic meter	m^3	—
Velocity	meter per second	m/s	—
Density	kilogram per cubic meter	kg/m^3	—
Concentration	moles per cubic meter	mol/m^3	—
Force	newton	$kg\text{-}m/s^2$	N
Energy	joule	$kg\text{-}m^2/s^2$, N-m	J
Stress	pascal	$kg/m\text{-}s^2$, N/m^2	Pa
Strain	—	m/m	—
Power, radiant flux	watt	$kg\text{-}m^2/s^3$, J/s	W
Viscosity	pascal-second	kg/m-s	Pa-s
Frequency (of a periodic phenomenon)	hertz	s^{-1}	Hz
Electric charge	coulomb	A-s	C
Electric potential	volt	$kg\text{-}m^2/s^2\text{-}C$	V
Capacitance	farad	$s^2\text{-}C/kg\text{-}m^2$	F
Electric resistance	ohm	$kg\text{-}m^2/s\text{-}C^2$	Ω
Magnetic flux	weber	$kg\text{-}m^2/s\text{-}C$	Wb
Magnetic flux density	tesla	kg/s-C, Wb/m^2	(T)

[a] Special symbols in parentheses are approved in the SI but not used in this text; here, the name is used.

Table A.3 SI Multiple and Submultiple Prefixes

Factor by Which Multiplied	*Prefix*	*Symbol*
10^9	giga	G
10^6	mega	M
10^3	kilo	k
10^{-2}	centi[a]	c
10^{-3}	milli	m
10^{-6}	micro	μ
10^{-9}	nano	n
10^{-12}	pico	p

[a] Avoided when possible.

Table A.1 The SI Base Units

Quantity	*Name*	*Symbol*
Length	meter, metre	m
Mass	kilogram	kg
Time	second	s
Electric current	ampere	A
Thermodynamic temperature	kelvin	K
Amount of substance	mole	mol

Table A.2 Some of the SI Derived Units

Quantity	*Name*	*Formula*	*Special Symbol*[a]
Area	square meter	m^2	—
Volume	cubic meter	m^3	—
Velocity	meter per second	m/s	—
Density	kilogram per cubic meter	kg/m^3	—
Concentration	moles per cubic meter	mol/m^3	—
Force	newton	$kg\text{-}m/s^2$	N
Energy	joule	$kg\text{-}m^2/s^2$, N-m	J
Stress	pascal	$kg/m\text{-}s^2$, N/m^2	Pa
Strain	—	m/m	—
Power, radiant flux	watt	$kg\text{-}m^2/s^3$, J/s	W
Viscosity	pascal-second	kg/m-s	Pa-s
Frequency (of a periodic phenomenon)	hertz	s^{-1}	Hz
Electric charge	coulomb	A-s	C
Electric potential	volt	$kg\text{-}m^2/s^2\text{-}C$	V
Capacitance	farad	$s^2\text{-}C/kg\text{-}m^2$	F
Electric resistance	ohm	$kg\text{-}m^2/s\text{-}C^2$	Ω
Magnetic flux	weber	$kg\text{-}m^2/s\text{-}C$	Wb
Magnetic flux density	tesla	kg/s-C, Wb/m^2	(T)

[a] Special symbols in parentheses are approved in the SI but not used in this text; here, the name is used.

Table A.3 SI Multiple and Submultiple Prefixes

Factor by Which Multiplied	*Prefix*	*Symbol*
10^9	giga	G
10^6	mega	M
10^3	kilo	k
10^{-2}	centi[a]	c
10^{-3}	milli	m
10^{-6}	micro	μ
10^{-9}	nano	n
10^{-12}	pico	p

[a] Avoided when possible.

Index

Page numbers in *italics* refer to the glossary.

A
Abrasive ceramics, 422, 425
Abrasives, *480*
Absorption coefficient, S–308
Absorption of light:
  in metals, S–302
  in nonmetals, S–303—S–310
Absorptivity, S–300
ABS polymer, 429
$A_mB_nX_p$ crystal structures, 43
Acceptors, 382, *480*
Acetabulum, S–340
Acetabular cup, S–344
Acetic acid, 80
Acetylene, 78
Acid rain, as corrosion environment, S–231
Acids, 80
Acid slags, S–110
Acrylics, *see* Polymethyl methacrylate
Acrylonitrile, *see* Polyacrylonitrile (PAN)
Acrylonitrile-butadiene rubber, 431
Acrylonitrile-butadiene-styrene (ABS), 429
Activation energy, *480*
  for creep, S–63—S–64
  for diffusion, 136
  for viscous flow, S–159
  phase transformations, 326–327
Activation polarization, S–215—S–216, *480*
Addition polymerization, S–150—S–151, *480*
Additives, polymer, S–151—S–153
Adhesives, 433, *480*
Advanced ceramics, 422, S–111—S–113
Advanced flexible reusable surface insulation (AFRSI), S–347—S–348
Advanced materials, 6
Advanced polymers, S–113—S–117
Age hardening, *see* Precipitation hardening
Air, as quenching medium, S–132
AISI/SAE steel designation scheme, 406
Akermanite, S–1
Alcohols, 80
Aldehydes, 80
Alkali metals, 17
Alkaline earth metals, 17
Allotropy, 49, *480*
Alloys, 402, *480*. *See also* Solid solutions; specific alloys
  atomic weight equations, S–15
  cast, 414
  composition specification, 110–111
  compositions for various, 467–468
  costs, 469–471
  defined, 107
  density equations, S–15
  density values, 441–443
  ductility values, 449–451
  electrical resistivity values, 464–466
  fracture toughness values, 454
  heat treatable, 414
  high-temperature, 268–269
  linear coefficient of thermal expansion values, 455–456
  modulus of elasticity values, 444–446
  Poisson's ratio values, 448
  specific heat values, 462–463
  strengthening, *see* Strengthening of metals
  tensile strength values, 449–451
  thermal conductivity values, 459–460
  wrought, 414
  yield strength values, 449–451
Alloy steels, 338, 403, *480*. *See also* Steels
Alnico, S–283
α Iron, *see* Ferrite (α)
Alternating copolymers, 91, 92, *480*
Alumina, *see* Aluminum oxide
Aluminosilicates, S–142
Aluminum:
  atomic radius and crystal structure, 33
  bonding energy and melting temperature, 22
  elastic and shear moduli, 154
  electrical conductivity, 374, 376
  Poisson's ratio, 154
  recrystallization temperature, 217
  slip systems, 204
  superconducting critical temperature, S–290
  thermal properties, S–251
  used beverage cans, S–368
  yield and tensile strengths, ductility, 165
Aluminum alloys, 416–418
  fatigue behavior, 276
  integrated circuits, S–352
  plane strain fracture toughness, 244, 454, S–49
  precipitation hardening, 323, 349–351
  properties and applications, 417
Aluminum-copper alloys, phase diagram, 350
Aluminum-lithium alloys, 417, 418
Aluminum-neodymium phase diagram, 319
Aluminum nitride, use in electronic packaging, S–112—S–113

Aluminum oxide:
  electrical conductivity, 389
  flexural strength, 165
  hardness, 182
  index of refraction, S–304
  modulus of elasticity, 154
  plane strain fracture toughness, 244, S–49, 454
  Poisson's ratio, 154
  sintered microstructure, S–148
  stress-strain behavior, 173
  thermal properties, S–251
  translucency, 4, S–311
  use in artificial hip, S–344
  use in ceramic armor, S–112
  use in electronic packaging, S–112
  as whiskers and fibers, S–181
Aluminum oxide-chromium oxide phase diagram, S–77, S–78
Ammonia, bonding energy and melting temperature, 22
Amorphous materials, 31, 64–65, *480*
Anelasticity, 157, *480*
Anions, 38, *480*
Anisotropy, 63–64, *480*
  of elastic modulus, 64, 158, 188–189
Annealing, S–87, S–124, S–125—S–126, *480*
  ferrous alloys, S–125—S–126
  glass, S–140—S–141, *480*
Annealing point, glass, S–139, *480*
Annealing twins, 117
Anodes, S–206, *480*
  area effect, galvanic corrosion, S–225
  sacrificial, S–233, *490*
Antiferromagnetism, S–272, *480*
  temperature dependence, S–276
Aramid:
  cost, as a fiber, 473
  fiber-reinforced polymer-matrix composites, S–183—S–184
  melting and glass transition temperatures, 479
  mer structure, S–184, 477
  properties as fiber, S–181
Argon, bonding energy and melting temperature, 22
Aromatic hydrocarbons (chain groups), 80, S–87
Artificial aging, 351, *480*
Artificial hip replacement, materials selection, S–341—S–345
Asphaltic concrete, S–168
ASTM standards, 148
Atactic configuration, S–12, *480*
Athermal transformation, 337, *480*
Atomic bonding, *see* Bonding
Atomic force micrograph, 9, S–20
Atomic mass, 10
Atomic mass unit (amu), 10–11, *480*
Atomic models:
  Bohr, 11, 13, *481*
  wave-mechanical, 12–13, *494*
Atomic number, 10, *480*
Atomic packing factor, 34, *480*
Atomic point defects, 103, 105–107
Atomic radii, of selected metals, 33
Atomic structure, 10–18
Atomic vibrations, 118, S–248—S–249, *480*
Atomic weight, 10, *480*
  metal alloys, equations for, S–15
Atom percent, 110–111, *480*
Austenite, 302–304, *481*
  transformations, 327–339, S–85—S–87
    summary, 346–347
Austenitic stainless steels, 407–408
Austenitizing, S–126, *481*
Automobile valve spring design, S–332—S–339
Average value, 183, S–28
Avogadro's number, 11
Avrami equation, 325, 353
AX crystal structures, 41–42
A_mX_p crystal structures, 42–43

B

Bainite, 332–333, 347, S–85, *481*
  mechanical properties, 342, 343
Bakelite, *see* Phenol-formaldehyde (Bakelite)
Band gap, 370
Band gap energy, *481*
  determination, 385
  selected semiconductors, 377
Bands, *see* Energy bands
Barcol hardness, 182
Barium titanate:
  crystal structure, 43, 44, S–108
  as dielectric, S–107
  as ferroelectric, S–108—S–109
Base (transistor), S–95—S–96
Basic refractories, S–110—S–111
Basic slags, S–111
Beachmarks (fatigue), 261, S–55—S–56
Bend strength, 172. *See also* flexural strength
Beryllia, S–111
Beryllium-copper alloys, 416
Beverage containers, 1, S–367
  stages of production, S–118
Bifunctional mers, 82, *481*
Bimetallic strips, S–260
Binary eutectic alloys, 292–297, S–70—S–77
  tensile strength, 362
Binary isomorphous alloys, 286–287, S–67—S–70
  mechanical properties, 292
  microstructure development, equilibrium cooling, S–67, S–68
  microstructure development, nonequilibrium cooling, S–67—S–70
Biocompatibility, S–341—S–342
Biomaterials, 6
Block copolymers, 92, *481*
Blowing, of glass, S–139—S–140
Blow molding, plastics, S–155
Body-centered cubic structure, 34–35, *481*
  slip systems, 204
  twinning in, S–35
Bohr atomic model, 11, 13, *481*
Bohr magneton, S–268, *481*
Boltzmann's constant, 104, *481*
Bonding:
  carbon-carbon, 81
  cementitious, 426–427
  covalent, 22–23, 38, *482*
  hybrid *sp*, 16
  hydrogen, 25, 26, *486*
  ionic, 20–22, 38, *486*
  metallic, 23–24, *487*
  van der Waals, *see* van der Waals bonding
Bonding energy, 20, *481*
  and melting temperature for selected materials, 21, 22

Bonding forces, 18–19
Bond rupture, in polymers, S–238, S–240—S–241
Bone:
  as composite, S–163
  mechanical properties, S–339
Boron carbide:
  in ceramic armor, S–112
  hardness, 182
Boron:
  boron-doped silicon semiconductors, 381–382, 383–385
  fiber-reinforced composites, S–184, S–186
  properties as a fiber, S–181
Boron nitride, S–112
Borosilicate glass:
  composition, 423
  electrical conductivity, 389
  viscosity, S–138
Borsic fiber-reinforced composites, S–186
Bragg's law, S–6—S–8, *481*
Branched polymers, 89, *481*
Brass, 414, 415, *481*
  annealing behavior, 216
  elastic and shear moduli, 154
  electrical conductivity, 374, 395
  fatigue behavior, 276
  phase diagrams, 298–299
  Poisson's ratio, 154
  recrystallization temperature, 217
  stress corrosion, 229, 230
  stress-strain behavior, 163
  thermal properties, S–251
  yield and tensile strengths, ductility, 165
Brazing, S–123, *481*
Breakdown, dielectric, S–94, S–107
Brinell hardness tests, 179
Brittle fracture, 164–165, 235–236, 238–240, *481*
  ceramics, 248–249
Brittle materials, thermal shock, S–257—S–258
Bronze, 416, *481*
Buckminsterfullerene, S–3—S–4
Burgers vector, 112, 113, 114, 124, *481*
Butadiene:
  degradation resistance, S–239
  melting and glass transition temperatures, 479
  mer structure, 93, 476
Butane, 78–79

C

Cadmium sulfide:
  color, S–309
  electrical characteristics, 377
Calcination, 426, *481*
Calendering, S–191
Cantilever beam, materials selection, S–364
Capacitance, S–99—S–100, *481*
Capacitors, S–99—S–103
Carbon:
  vs. graphite, S–181, S–183
  polymorphism, 47–48, 49
Carbon black, as reinforcement in rubbers, 432, S–166—S–167
Carbon-carbon composites, S–188, S–351, *481*
Carbon diffusion, in steels, 306–307, 345
Carbon fiber-reinforced polymer-matrix composites, S–183, S–185
Carbon fibers, S–183
  properties as fiber, S–181
Carburizing, 134, *481*
Case-hardened gear, 126
Case hardening, 126, 265, *481*
Cast alloys, 414
Casting techniques:
  metals, S–121—S–122
  plastics, S–155
  slip, S–143—S–144
  tape, S–149
Cast irons, 305, 403, 409–414, *481*
  annealing, S–126
  compositions, mechanical properties, and applications, 412
  graphite formation in, 409–410
  heat treatment effect on microstructure, 413
  phase diagram, 409, 413
  stress-strain behavior (gray), 188
Cathodes, S–207, *481*
Cathodic protection, S–225, S–232—S–234, *481*
Cations, 38, *481*
Cemented carbide, S–166, S–167
Cementite, 302–303, *481*
  decomposition, 409, 413
  proeutectoid, 310–311
  in white iron, 410, 411
Cementitious bond, 426–427
Cements, 422, 425–427, *481*
Ceramic armor, S–112
Ceramic-matrix composites, S–186—S–188, *481*
Ceramics, 5, *481*. *See also* Glass
  advanced, S–111—S–113
  application-classification scheme, 422
  brittle fracture, 248–249
  coefficient of thermal expansion values, S–251, 457
  color, S–309—S–310
  corrosion, S–237
  costs, 471–472
  crystal structures, 38–44, 60–61
    summary, 44
  defects, 105–107
  defined, 5
  density computation, 45–46
  density values, 443
  elastic modulus values, 154, 446
  electrical conductivity values for selected, 389
  electrical resistivity values, 466
  fabrication techniques classification, S–137
  flexural strength values, 165, 452
  fracture toughness values, 244, S–49, 454–455
  impurities in, 109–110
  indices of refraction, S–304
  as insulators, 389, S–101, S–107
  magnetic, S–272—S–276
  mechanical properties of, 171–173
  phase diagrams, S–77—S–81
  plastic deformation, 220–221
  Poisson's ratio values, 154, 448
  porosity, S–147—S–148
  porosity, influence on properties, S–22
  silicates, 46–47, S–1—S–3
  specific heat values, S–251, 463
  as superconductors, S–289—S–290

Ceramics (*Continued*)
  thermal conductivity values, S–251, 460
  thermal properties, S–251, S–253, S–255, S–257—S–258
  traditional *vs.* new, S–111
  translucency and opacity, S–310—S–311
Ceramic tile systems (Space Shuttle), S–348—S–351
Cercor (glass ceramic), 423
Cermets, S–166—S–167, *481*
Cesium chloride structure, 41–42, 44
Chain-folded model, 95–96, *481*
Chain-reaction polymerization, S–150—S–151, *481*
Chain stiffening/stiffness, 88, S–87, S–89—S–90
Charge carriers:
  majority *vs.* minority, 381
  temperature variation, 384–386
Charpy impact test, 251–254, *481*
Chevron markings, 238–239
Chips, semiconductor, S–97—S–99, S–351—S–352
Chlorine, bonding energy and melting temperature, 22
Chloroprene, mer structure, 93, 476
Chloroprene rubber:
  characteristics and applications, 431
  melting and glass transition temperatures, 479
Chrome-vanadium steels, S–337—S–339
cis, S–12, *482*
Clay products, 422, 424, S–142—S–145
  characteristics, S–142
  drying and firing, 424, S–144—S–145
  fabrication, S–142—S–144
Cleavage, 238
Clinker, 426
Close-packed crystal structures:
  ceramics, 60–61
  metals, 58–59
Coarse pearlite, 331, S–85, S–87, *482*
Coatings (polymer), 433
Cobalt:
  atomic radius and crystal structure, 33
  Curie temperature, S–276
  as ferromagnetic material, S–270
Cobalt-nickel-chromium-molybdenum alloy, for artificial hips, S–343—S–344
Coercivity (coercive force), S–279, *482*
Cold work, percent, 210
Cold working, *see* Strain hardening
Collector, S–96
Color, *482*
  metals, S–303
  nonmetals, S–309—S–310
Colorants, S–152, *482*
Compact disc, S–367
Component, 282, S–81, *482*
Composites:
  aramid fiber-reinforced polymer, S–183—S–184
  carbon-carbon, S–188, S–351
  carbon fiber-reinforced polymer, S–183
  ceramic-matrix, S–186—S–188
  classification scheme, S–164—S–165
  costs, 474
  definition, 5, S–163
  dispersion-strengthened, S–169
  elastic behavior:
    longitudinal, S–173—S–174
    transverse, S–176
  fiber-reinforced, *see* Fiber-reinforced composites
  glass fiber-reinforced polymer, S–182
  hybrid, S–189, *486*
  laminar, S–164, S–179, S–195—S–196, *487*
  large-particle, S–164, S–165—S–169
  metal-matrix, S–185—S–186
  particle-reinforced, S–165—S–169
  production processes, S–189—S–192
  properties, glass-, carbon-, aramid-fiber reinforced, S–185
  rule of mixtures expressions, S–165—S–166, S–174, S–176, S–177, S–178, S–194
  strength:
    longitudinal, S–177
    transverse, S–177
  stress-strain behavior, S–172—S–173
  structural, S–195—S–196
Composition, *482*
  conversion equations, S–14—S–17, 123, 124
  specification of, 110–111
Compression molding, plastics, S–153—S–154
Compression tests, 151
Compressive deformation, 150, 170–171
Computers, semiconductors in, 97–99
Concentration, 110, *482. See also* Composition
Concentration cells, S–225
Concentration gradient, 131, *482*
Concentration polarization, S–216—S–217, *482*
Concentration profile, 130, *482*
Concrete, S–167—S–169, *482*
  electrical conductivity, 389
  plane strain fracture toughness, 244, S–49, 454
Condensation polymerization, S–151, *482*
Conducting polymers, 390
Conduction:
  electronic, 368, 368–372
  ionic, 368, 389–390
Conduction band, 370, *482*
Conductivity, *see* Electrical conductivity; Thermal conductivity
Configuration, polymer, S–11—S–13
Conformation, polymer, 88
Congruent phase transformations, 301, *482*
Constitutional diagrams, *see* Phase diagrams
Continuous casting, S–122
Continuous cooling transformation diagrams, S–85—S–88, *482*
  4340 steel, S–88
  0.76 wt% C steel, S–86
  1.13 wt% C steel, 361
Continuous fibers, S–171
Conventional hard magnetic materials, S–282—S–283
Conversion factors, magnetic units, S–267
Cooling rate, of cylindrical rounds, S–133

Coordination numbers, 34, 35, 38–40, 46, *482*
Copolymers, 82, 91–92, *482*
  styrenic block, S–115—S–116
Copper:
  atomic radius and crystal structure, 33
  diffraction pattern, 75
  elastic and shear moduli, 154
  electrical conductivity, 374
  OFHC, 376
  Poisson's ratio, 154
  recrystallization, 217, 326
  slip systems, 204
  thermal properties, S–251
  yield and tensile strengths, ductility, 165
Copper alloys, 414–416
  for integrated circuit fabrication, S–354—S–355
  properties and applications of, 415
Copper-beryllium alloys, 376
  phase diagram, 363
Copper-nickel alloys:
  ductility *vs.* composition, 209, 292
  electrical conductivity, 375–376
  phase diagrams, 286–287
  tensile strength *vs.* composition, 209, 292
  yield strength *vs.* composition, 209
Copper-silver phase diagram, 292–294, S–82
Copper-titanium phase diagram, 319
Coring, S–70
Corningware (glass ceramic), 423
Corrosion, *482*
  ceramic materials, S–237
  electrochemistry of, S–206—S–212
  environmental effects, S–222—S–223
  environments, S–231—S–232
  forms of, S–223—S–231
  galvanic series, S–212, S–213
  integrated circuits, S–354
  overview of, S–205
  passivity, S–221—S–222
  rates, S–212—S–214
    prediction, S–214—S–221
Corrosion fatigue, S–62, S–342, *482*
Corrosion inhibitors, S–232
Corrosion penetration rate, S–213, *482*
  artificial hip alloys, S–344
  minimum for body implant materials, S–342
Corrosion prevention, S–232—S–234
Corundum, 425. *See also* Aluminum oxide
  crystal structure, 73
Cost of various materials, 469–474
Coulombic force, 21, *482*
Covalency, degree of, 23
Covalent bonding, 22–23, 38, 77, *482*
Crack formation, 236
  fatigue and, 260–262, S–54—S–57
  glass, S–141
Crack propagation, 236. *See also* Fracture mechanics
  in brittle fracture, 238
  in ceramics, 248–249, S–53
  in ductile fracture, 236–237
  fatigue and, 260–262, S–54—S–62
  Griffith theory, S–41—S–42
Crack propagation rate, S–57—S–62
Cracks:
  stable *vs.* unstable, 236
  stress analysis of, 239–242, S–38—S–41, S–43—S–45
Crack surface displacement modes, 243, 244, S–43
Crazing, 250, 251
Creep, 265–269, S–63—S–66, *482*
  ceramics, 269
  influence of temperature and stress on, 267–268, S–63—S–65
  mechanisms, S–64—S–65
  in polymers, 269, S–27
  stages of, 266
  steady-state rate, 266
  viscoelastic, S–27
Creep modulus, S–27
Creep rupture tests, 267
  data extrapolation, S–65—S–66
Crevice corrosion, S–225—S–226, S–342, *482*
Cristobalite, 47, S–80
Critical cooling rate, S–85—S–88
Critical fiber length, S–170—S–171
Critical resolved shear stress, S–31, *482*
  as related to dislocation density, 230
Critical stress, 242, 245, S–42, S–49
Critical temperature (superconductivity), S–288, S–290
Crosslinking, 89–90, *482*
  elastomers, 225–226
  influence on viscoelastic behavior, S–26—S–27
  thermosetting polymers, 91
Crystalline materials, 31, 62, *482*
  defects, 103–107
  single crystals, 62, *491*
Crystallinity, polymers, 92–95, *482*
  influence on mechanical properties, 224, S–36, S–37
Crystallites, 95, *482*
Crystallization (polymers), 353–354
Crystallographic directions, 51–54
  families, 53
Crystallographic planes, 54–58
  atomic arrangements, 57, 58
  close-packed, 58–61
  diffraction by, S–7—S–8
  families, 57
Crystal structures, 31–37, *482*. *See also* Body-centered cubic structure; Close-packed crystal structures; Face-centered cubic structure; Hexagonal close-packed structure
  ceramics, 38–44
  close-packed, 58–61
  determination by x-ray diffraction, S–6—S–10
  selected metals, 33
  types, 33–35, 41–44, 58–61
Crystal systems, 49–50, *482*
Cubic crystal system, 49, 50
Cubic ferrites, S–273—S–275
Cunife, S–283
Cup-and-cone fracture, 237, S–38
Curie temperature, S–276, *482*
  ferroelectric, S–109
  ferromagnetic, S–250
Curing, plastics, S–153
Current density, 367
Cyclic stresses, 255–257

D
Damping capacity, steel *vs.* cast iron, 413
Data scatter, 183
Debye temperature, S–249—S–250
Decarburization, 143
Defects, *see also* Dislocations
  atomic vibrations and, 118
  dependence of properties on, 102
  in ceramics, 105–107
  interfacial, 115–118
  point, 103–111, *489*
  volume, 118
Defect structure, 105, *483*
Deformation:
  elastic, *see* Elastic deformation
  elastomers, 224
  plastic, *see* Plastic deformation
Deformation mechanism maps, S–64—S–65
Degradation of polymers, S–237—S–240, *483*
Degree of polymerization, 84, *483*
Degrees of freedom, S–81
Delayed fracture, S–53
Density:
  computation for ceramics, 45–46
  computation for metal alloys, S–15
  computation for metals, 37
  of dislocations, 201
  polymers, 443–444
  relation to percent crystallinity for polymers, 94
  values for various materials, 441–444
Design, S–325. *See also* Materials selection
  component, S–370
Design examples:
  cold work and recrystallization, 217–218
  conductivity of an *n*-type semiconductor, 387–388
  cubic mixed-ferrite magnet, S–275—S–276
  creep rupture lifetime for an S-590 steel, S–66
  fatigue life prediction, S–61—S–62
  filament-wound composite shaft, S–192—S–195
  nonsteady-state diffusion, 139–140
  spherical pressure vessel (failure of), 245–248, S–51—S–53
  steel shaft, alloy/heat treatment of, S–135—S–136
  tensile-testing apparatus, 184–185
Design factor, 183
Design guidelines, S–328
Design stress, 183, *483*
Devitrification, 423, *483*
Dezincification, of brass, S–228
Diamagnetism, S–268—S–269, *483*
Diamond, 48, 427
  as abrasive, 425
  bonding energy and melting temperature, 22
  cost, 472
  films, 427, 428
  hardness, 181, 182
  thermal conductivity value, 460
Diamond cubic structure, 48
Die (silicon), S–352
Die bonding, S–354
Die casting, S–120, S–122
Dielectric breakdown, S–94, S–107
Dielectric constant, S–100—S–101, *483*
  frequency dependence, S–106—S–107
  relationship to refractive index, S–303—S–304
  selected ceramics and polymers, S–101
Dielectric displacement, S–102, *483*
Dielectric loss, S–106
Dielectric materials, S–99, S–107, *483*
Dielectric strength, S–107, *483*
  selected ceramics and polymers, S–101
Diffraction, S–6, *483*
Diffraction angle, S–9
Diffractometers, S–8
Diffusion, 127, *483*
  grain growth and, 218
  interstitial, 95, *486*
  in ionic materials, 141
  mechanisms, 127–129
  and microstructure development, S–68—S–70, S–72—S–74, 306–307
  nonsteady-state, 132–135, *488*
  in polymers, 141
  short-circuit, 141
  steady-state, 130–131, *492*
  vacancy, 129, *494*
Diffusion coefficient, 131, *483*
  relation to ionic mobility, 390
  temperature dependence, 136–139
  values for various metal systems, 136
Diffusion couples, 127
Diffusion flux, 130, *483*
Digitization of information/signals, S–285—S–287, S–317—S–318
Dimethyl ether, 80
Dimethylsiloxane, 93, 431, 432, 476. *See also* Silicones; Silicone rubber
  melting and glass transition temperatures, 479
Diode, S–93, *483*
Dipole moment, S–101
Dipoles:
  electric, 25, *483*
  induced, 25–26
  magnetic, S–264—S–265
  permanent, 26, S–105
Directional solidification, 269
Directions, *see* Crystallographic directions
Discontinuous fibers, S–171
Dislocation density, 201, 228, 230, *483*
Dislocation etch pits, 197
Dislocation line, 111–112, 113, 114, *483*
Dislocation motion, 199–200
  caterpillar locomotion analogy, 200
  in ceramics, 220
  at grain boundaries, 207
  influence on strength, 206–208
  in polymers, 112
  recovery and, 213
Dislocations, 111–114, *483*
  characteristics of, 201–202
  interactions, 201–202
  multiplication, 203
  at phase boundaries, 340, 344
  plastic deformation and, 160, 199–206
  strain fields, 201
Dispersed phase, S–164, *483*
  definition, S–164

Dispersed phase (*Continued*)
  geometry, S–164
Dispersion-strengthened composites, S–169, *483*
Disposal of materials, S–371—S–372
Domain growth, S–278
  iron single crystal, S–263
Domains, S–271, S–276—S–279, *483*
Domain walls, S–277
Donors, 381, *483*
Doping, 383, 385–387, *483*
Double bonds, 77–78
Drain casting, S–143, S–144
Drawing:
  glass, S–139, S–140
  influence on polymer properties, 224, S–36—S–37
  metals, S–121, *483*
  polymer fibers, S–155, *483*
Drift velocity, electron, 373
Driving force, 131, *483*
  electrochemical reactions, S–209
  grain growth, 218
  recrystallization, 213
  sintering, S–147
  steady-state diffusion, 131
Dry corrosion, S–234
Drying, clay products, S–144—S–145
Ductile fracture, 164–165, 236–237, *483*
Ductile iron, 410, 411, *483*
  compositions, mechanical properties, and applications, 412
Ductile-to-brittle transition, 253–254, *483*
  polymers, 249, 254
  and temper embrittlement, 346
Ductility, 164–165, *483*
  artificial hip materials, S–344
  fine and coarse pearlite, 342
  precipitation hardened aluminum alloy, 352
  selected materials, 449–453
  selected metals, 165
  spheroidite, 342
  tempered martensite, 345
Durometer hardness, 180, 182

E

Economics, materials selection:
  considerations in materials engineering, S–369—S–370
  torsionally stressed shaft, S–330—S–331
  tubular filament-wound shaft, S–193—S–195
Eddy currents, S–281
Edge dislocations, 111–112, 199–200, *483*. *See also* Dislocations
  interactions, 202
E-glass, S–181, S–182
Elastic deformation, 153–160, *483*
Elastic modulus, *see* Modulus of elasticity
Elastic recovery, *483*
Elastic strain energy, S–41—S–42
Elastic strain recovery, 170, *483*
Elastomers, 174, 431–432, *483*
  in composites, S–166
  deformation, 224–225
  thermoplastic, S–115—S–117
  trade names, properties and applications, 431
Electrical conduction:
  in insulators and semiconductors, 371–372
  in metals, 371
Electrical conductivity, 367, 373–374, *484*
  influence of impurities, 375
  influence of plastic deformation, 375
  influence of temperature, 374–375
  integrated circuit lead-frame materials, S–355
  selected ceramics and polymers, 389
  selected metals, 374
  selected semiconductors, 377
    temperature variation, 383–387, 397
Electrical resistivity, 366, *490*. *See also* Electrical conductivity
  values for various materials, 464–467
Electric dipole moment, S–101
Electric dipoles, *see* Dipoles
Electric field, 367, 373, *484*
Electrochemical cells, S–208—S–209
Electrochemical reactions, S–206—S–212
Electrodeposition, S–208
Electrode potentials, S–207—S–209
  values of, S–210
Electroluminescence, S–312, *484*
Electrolytes, S–208, *484*
Electromagnetic radiation, S–298—S–300
  interactions with atoms/electrons, S–301—S–302
Electromagnetic spectrum, S–298—S–299
Electron band structure, *see* Energy bands
Electron cloud, 12, 23
Electron configurations, 15–16, *484*
  elements, 16
  periodic table and, 17
  stable, 15
Electronegativity, 18, 23, *484*
  influence on solid solubility, 108
  values for the elements, 18
Electroneutrality, 106, *484*
Electron gas, 371
Electronic conduction, 367, 368–372
Electronic packaging:
  advanced ceramics in, S–112—S–113
  case study, materials selection, S–351—S–361
Electronic polarization, S–105, S–106, S–301, S–305, *489*
Electron microscopy, S–17—S–20
Electron mobility, 372–373
  selected semiconductors, 377
Electron orbitals, 11
Electron probability distribution, 12, 13
Electrons, 10
  conduction process, 378, S–95—S–96
  energy bands, *see* Energy bands
  energy levels, 11–14
  free, *see* Free electrons
  scattering, 373, S–249
  in semiconductors, 377–383
    temperature variation of concentration, 383–387
  spin, 14, S–268
  valence, 15
Electron states, *484*
Electron transitions, S–301—S–302
  metals, S–302
  nonmetals, S–305—S–307
Electron volt, 21, *484*
Electropositivity, 18, *484*

Elongation, percent, 164
  selected materials, 449–453
  selected metals, 165
  selected polymers, 165
Embrittlement:
  hydrogen, S–230—S–231
  temper, 345–346
Emf series, S–209—S–211
Emitter, S–96
Endurance limit, 258. *See also* Fatigue limit
Energy:
  activation, *see* Activation energy
  bonding, 20–22, *481*
  current concerns about, 6–7, S–372—S–373
  free, 284, 285, *485*
  grain boundary, 116–117
  photon, S–300
  surface, 115
  vacancy formation, 104
Energy band gap, *see* Band gap
Energy bands, 368–370
  structures for metals, insulators, and semiconductors, 370
Energy levels (states), 11–14, 368–369
Energy and materials, S–372
Energy product, magnetic, S–282
Engineering stress/strain, 149–151, *492*
Entropy, 225, 284
Environmental considerations and materials, S–371—S–376
Epoxies:
  degradation resistance, S–239
  for integrated circuit fabrication, S–359—S–360
  mer structure, 475
  polymer-matrix composites, S–185
  trade names, characteristics, applications, 430
Equilibrium:
  definition of, 284
  phase, 284–285, *484*
Equilibrium diagrams, *see* Phase diagrams
Erosion-corrosion, S–228—S–229, *484*
Error bars, S–30
Error function, Gaussian, 133
Etching, S–17
Etch pits, 197
Ethane, 78
Ethers, 80
Ethylene, 77–78
  polymerization, 81
Eutectic isotherm, 294
Eutectic phase, S–72, *484*
Eutectic reactions, 294, S–72, *484*
  iron-iron carbide system, 305
Eutectic structure, S–73, *484*
Eutectic systems:
  binary, 292–297, S–70—S–77
  microstructure development, S–70—S–77
Eutectoid, shift of position, S–83—S–84
Eutectoid ferrite, 308
Eutectoid reactions, 298, 300–301, *484*
  iron-iron carbide system, 305
  kinetics, 328–329
Eutectoid steel, microstructure changes/development, 305–307
Exchange current density, S–215
Excited states, S–302, *484*
Exhaustion, in extrinsic semiconductors, 386
Expansion, thermal, *see* Thermal expansion
Extrinsic semiconductors, 379–383, *484*
  saturation, 386
Extrusion, *484*
  clay products, S–143
  metals, S–120—S–121
  polymers, S–155

F

Fabrication:
  ceramics, S–136—S–137
  clay products, S–142—S–144
  fiber-reinforced composites, S–189—S–192
  integrated circuits, S–351—S–361
  metals, S–119—S–124
Face-centered cubic structure, 33–34, *484*
  anion stacking, 60–61
  close-packed planes, 58–59
  slip systems, 203–204
Factor of safety, 184, 246, S–51, S–326
Failure, mechanical, *see* Creep; Fatigue; Fracture
Faraday constant, S–211
Fatigue, 255–265, S–54—S–63, *484*
  automobile valve springs, S–335—S–336
  corrosion, S–62—S–63
  crack initiation and propagation, 260–263, S–54—S–61
  cyclic stresses, 255–257
  environmental effects, S–62
  low- and high-cycle, 259
  polymers, 260
  probability curves, 259
  thermal, S–62
Fatigue life, 259, *484*
  factors that affect, 263–265
  prediction, S–60—S–62
Fatigue limit, 258, S–335, S–336, *484*
Fatigue strength, 258, *484*
  artificial hip materials, S–342, S–344
Fatigue testing, 257
  S–N curves, 257–259, 260, 276, S–336
Feldspar, S–142
Felt reusable surface insulation (FRSI), S–347—S–348
Fermi energy, 370, 381, 396, S–250, *484*
Ferrimagnetism, S–272—S–276, *484*
  temperature dependence, S–276—S–277
Ferrite (α), 302–304, *484*
  eutectoid/proeutectoid, 281, 308–309, *490*
  from decomposition of cementite, 409
Ferrites (magnetic ceramics), S–272—S–276, *484*
  Curie temperature, S–276
  as magnetic storage, S–285—S–286
Ferritic stainless steels, 407, 408
Ferroelectricity, S–108—S–109, *484*
Ferroelectric materials, S–109
Ferromagnetic domain walls, 117
Ferromagnetism, S–270—S–271, *484*
  temperature dependence, S–276
Ferrous alloys, *484. See also* Cast irons; Iron; Steels
  annealing, S–125—S–126

Ferrous alloys (*Continued*)
  classification, 305, 403
  continuous cooling transformation diagrams, S–85—S–88
  costs, 469–470
  hypereutectoid, 310–312, *486*
  hypoeutectoid, 307–309, *486*
  isothermal transformation diagrams, 328–339
  microstructures, 305–312
  mechanical properties of, 339–343, 444–445, 448, 449–450
Fiber efficiency parameter, S–178
Fiberglass, 423
Fiberglass-reinforced composites, S–182
Fiber-reinforced composites, S–170, *484*
  continuous and aligned, S–171—S–178
  discontinuous and aligned, S–178
  discontinuous and randomly oriented, S–178—S–179
  fiber length effect, S–170—S–171
  fiber orientation/concentration effect, S–171—S–180
  fiber phase, S–180—S–181
  longitudinal loading, S–172—S–176, S–177
  matrix phase, S–180—S–181
  processing, S–189—S–192
  reinforcement efficiency, S–179
  transverse loading, S–176—S–177
Fibers, 432, *484*
  coefficient of thermal expansion values, 458
  in composites, S–164—S–165
    continuous *vs.* discontinuous, S–171
    fiber phase, S–180, S–181
    length effect, S–170—S–171
    orientation and concentration, S–171—S–179
  costs, 473
  density values, 444
  elastic modulus values, S–181, 447
  electrical resistivity values, 467
  optical, S–318—S–320
  polymer, 432
  properties of selected, S–181
  specific heat values, 464
  spinning, S–155
  tensile strength values, S–181, 453
  thermal conductivity values, 461
Fibrous refractory composite insulation (FRCI), S–349
Fick's first law, 131, S–254, *484*
Fick's second law, 132, S–261, *485*
Fictive temperature, S–137
Field ion microscopy, 102
Filament winding, S–191—S–192
Filler bars, Space Shuttle, S–350
Fillers, S–152, *485*
Films:
  diamond, 427, 428
  polymer, 433
Fine pearlite, 331, 340, 342, *485*
Fireclay refractories, S–110
Firing, 424, S–145, *485*
Fixation agents, S–345
Flame retardants, S–152—S–153, *485*
Flexural strength, 171–172, *485*
  influence of porosity on, ceramics, S–22, S–23
  values for selected ceramics, 165, 452
Fluorescence, S–312, *485*
Fluorite single crystals, 62
Fluorite structure, 42–43
Fluorocarbons, 81
  trade names, characteristics, applications, 429, 431
Foams, 433–434, *485*
Forces:
  bonding, 18–20
  coulombic, 21, *482*
Forging, S–120, *485*
Formaldehyde, 80
Forming operations, metals, S–119—S–121
Forsterite, S–1
Forward bias, S–94, S–95—S–96, *485*
Fractographic investigations, S–38
Fractographs:
  cup-and-cone fracture surfaces, S–39
  fatigue striations, 262, S–56
  intergranular fracture, 240
  transgranular fracture, 240
Fracture, *see also* Brittle fracture; Ductile fracture; Impact fracture testing
  delayed, S–53
  fundamentals of, 235–236
  polymers, 249–250
  types, 164–165, 236–238
Fracture mechanics, 328, S–38, S–41—S–42, *485*
  applied to ceramics, 248
  crack propagation rate, S–57—S–62
  Griffith theory, 239–241, S–38—S–39, S–41—S–42
  polymers, 250
  stress analysis of cracks, S–43—S–45
  use in design, 245–248, S–48—S–53
Fracture profiles, 236
Fracture strength, 162. *See also* Flexural strength
  ceramics, 172
  distribution of, 248–249
  influence of porosity, S–22, S–23
  influence of specimen size, 248, S–180
Fracture toughness, 167, 242–245, S–45—S–48, *485*
  ceramic-matrix composites, S–187—S–188
  values for selected materials, 244, S–49, 454–455
Free electrons, 371–373, *485*
  contributions to heat capacity, S–250
  role in heat conduction, S–254
Free energy, 284, 285, *485*
Frenkel defects, 106, *485*
Fringed-micelle model, 95
Full annealing, S–87, S–126, *485*
Fullerenes, S–3—S–4
Functional groups, 79, 80
Furnace heating elements, 376
Fused silica, 65
  characteristics, 423, S–138
  dielectric properties, S–101
  electrical conductivity, 389
  flexural strength, 165
  index of refraction, S–304
  modulus of elasticity, 154
  thermal properties, S–251

G

Gadolinium, S–270
Gallium arsenide:
  cost, 472
  diffraction pattern, 30

Gallium arsenide (*Continued*)
  electrical characteristics, 377
  for lasers, S–315, S–317
  for light-emitting diodes, S–323
Gallium phosphide:
  electrical characteristics, 377
  for light-emitting diodes, S–323
Galvanic corrosion, S–224—S–225, *485*
Galvanic couples, S–208
Galvanic series, S–212, S–213, *485*
Galvanized steel, 422, S–233
Garnets, S–274
Gas constant, 104, *485*
Gating system, S–121
Gauge length, 149
Gaussian error function, 133
Geometrical isomerism, 91, S–12—S–13
Germanium:
  crystal structure, 48
  electrical characteristics, 377, 397
Gibbs phase rule, S–81—S–83, *485*
Gilding metal, 415
Glass:
  as amorphous material, 64–65
  annealing, S–126, S–140
  blowing, S–139, S–140
  classification, 422
  color, S–310
  commercial; compositions and characteristics, 423
  corrosion resistance, S–237
  cost, 472
  dielectric properties, S–101
  electrical conductivity, 389
  flexural strength, 165
  forming techniques, S–139—S–140
  hardness, 182
  heat treatment, S–140—S–141
  for integrated circuit fabrication, S–359
  melting point, S–138
  modulus of elasticity, 154, 443
  optical flint, 423
  plane strain fracture toughness, 244, S–49, 454
  refractive index, S–304
  soda-lime, composition, 423
  softening point, S–138
  strain point, S–138
  stress-strain behavior, 173
  structure, 65
  surface crack propagation, 248
  tempering, S–139—S–140
  thermal properties, S–251
  viscous properties, S–138—S–139
  working point, S–138, *494*
Glass-ceramics, 423, *485*
  composition and properties, 423
  flexural strength, 165, 452
  microstructure, 401
  modulus of elasticity, 154, 446
Glass fibers, 423, S–182
  fiberglass-reinforced composites, S–182, S–185
  forming, S–139
  properties as fiber, S–181
Glass transition, polymers, 354, 355
Glass transition temperature, 354–355, S–137—S–138, *485*
  factors that affect, polymers, S–89—S–90
  values for selected polymers, 356, 479
Gold, 421
  AFM micrograph of surface, 9
  atomic radius and crystal structure, 33
  electrical conductivity, 374
  for integrated circuit fabrication, S–357
  slip systems, 204
  thermal properties, S–251
Goodman's law, S–336
Graft copolymers, 92, *485*
Grain boundaries, 62, 115–117, *485*
Grain boundary energy, 116–117
Grain growth, 218–219, *485*
Grains, *485*
  definition, 62
  distortion during plastic deformation, 204–205
Grain size, *485*
  dependence on time, 219
  determination, 119–120
  mechanical properties and, 219
  reduction, and strengthening of metals, 206–207
  refinement of by annealing, S–126
Grain size number (ASTM), 120
Graphite:
  in cast irons, 409–411
  compared to carbon, S–181, S–183
  cost, 472
  from decomposition of cementite, 409
  electrical conductivity, 389
  properties/applications, 427–428
  properties as whisker, S–181
  as a refractory, S–111
  structure of, 48
Gray cast iron, 410, 411, *485*
  compositions, mechanical properties, and applications, 412
Green ceramic bodies, S–144, *485*
Green products, S–372
Griffith theory of brittle fracture, S–41—S–42
Ground state, 15, S–302, *485*
Gutta percha, S–13

H

Half-cells, standard, S–209—S–210
Half-reactions, S–207
Hall coefficient, S–91
Hall effect, S–91—S–92, *485*
Hall-Petch equation, 207
Hall voltage, S–91
Halogens, 17
Hardenability, S–127—S–131, *485*
Hardenability band, S–130—S–131
Hardenability curves, S–127—S–131
Hard magnetic materials, S–282—S–284, *485*
  properties, S–283
Hardness, *485*
  bainite, pearlite *vs.* transformation temperature, 343
  ceramics, 181, 182
  comparison of scales, 180–181
  conversion diagram, 181
  correlation with tensile strength, 180, 182
  fine and coarse pearlite, spheroidite, 340, 342
  pearlite, martensite, tempered martensite, 343
  polymers, 182
  tempered martensite, 343, 346
Hardness tests, 177–180
  summary of tests, 178
Hard sphere model, 32
Head-to-head configuration, S–11

Head-to-tail configuration, S–11
Heat affected zone, S–123
Heat capacity, S–248—S–250, *485*
  temperature dependence, S–249—S–250
  vibrational contribution, S–248—S–249
Heat flux, S–253
Heat transfer:
  mechanism, S–248—S–249, S–254
  nonsteady-state, S–261
Heat treatable, definition of, 414
Heat treatments, 126. *See also* Annealing; Phase transformations
  dislocation reduction, 201
  glass, S–140—S–141
  hydrogen embrittlement, S–231
  intergranular corrosion and, S–227
  polymer morphology, 223
  polymer properties, S–37
  for precipitation hardening, 347–349
  recovery, recrystallization, and grain growth during, 213–219
  steel, S–126—S–136
Hermetic sealing, S–354
Hertz, S–300
Hexagonal close-packed structure, 35–36, *485*
  anion stacking, 60
  close-packed planes, 58–59
  slip systems, 203–204
  twinning in, S–35
Hexagonal crystal system, 49, 50
  direction indices, 53–54
  planar indices, 57–58
Hexagonal ferrites, S–274
Hexane, 78
High carbon steels, 403, 405
High-cycle fatigue, 259–260
High polymers, 87, *485*
High-strength, low-alloy (HSLA) steels, 404–405, *485*
High-temperature reusable surface insulation (HRSI), S–347, S–348, S–350
High-temperature superconductors, S–289—S–290
Hip joint, anatomy, S–339—S–341
Hip joint replacement, materials selection, S–341—S–345
Holes, 371, 377–379, *485*
  mobility, selected semiconductors, 377
  temperature dependence of concentration, 383–387
Homopolymers, 82, *486*
Honeycomb structure, S–196
Hooke's law, 153, S–22
Hot pressing, S–147
Hot working, 215, S–119, *486*. *See also* Heat treatments
HSLA (high-strength, low-alloy) steels, 404–405, *485*
Hybrid composites, S–189, *486*
Hydration, of cement, 426
Hydrocarbons, 77–79
Hydrogen:
  diffusive purification, 131, 143, 145
  reduction, S–215
Hydrogen bonding, 22, 25, 26, *486*
Hydrogen chloride, 26, 29
Hydrogen electrode, S–209—S–210
Hydrogen embrittlement, S–230—S–231, *486*
Hydrogen fluoride, 26, 29
Hydrogen induced cracking, S–230
Hydrogen stress cracking, S–230
Hydroplastic forming, S–143, *486*
Hydroplasticity, S–142
Hydrostatic powder pressing, S–146
Hypereutectoid alloys, 310–312, *486*
Hypoeutectoid alloys, 307–310, *486*
Hysteresis, S–278—S–280
Hysteresis, ferromagnetic, *486*
  soft and hard magnetic materials, S–280—S–282

I

Impact energy, 251, *486*
  fine pearlite, 341
  temperature dependence, 253
Impact fracture testing, 250–255
Impact strength, polymers, 254
Imperfections, *see* Defects; Dislocations
Impurities:
  in ceramics, 109–110
  diffusion, 127–128
  electrical conductivity, 375–376
  in metals, 107–109
  thermal conductivity, S–255
Incongruent phase transformation, 301
Index of refraction, S–303—S–304, *486*
  selected materials, S–304
Indices, Miller, 54–57, *488*
Indium antimonide, electrical characteristics, 377
Induced dipoles, 25
Inert gases, 17
Inhibitors, S–232, *486*
Initial permeability, S–278
Injection molding, S–154
Insulators (electrical), *486*. *See also* Dielectric materials
  ceramics and polymers as, 389, S–107—S–108
  color, S–309—S–310
  defined, 368
  electron band structure, 370, 371–372
  translucency and opacity, S–310—S–311
Insulators (thermal), Space Shuttle thermal protection system, S–345—S–351
Integrated circuits, S–97—S–99, *486*
  advanced ceramics in, S–112—S–113
  fabrication, S–351—S–361
  materials selection, S–351—S–361
  scanning electron micrograph, 365, S–98
Interatomic bonding, 20–24
Interatomic separation, 19, 20
Interdiffusion, 127, *486*
Interfacial defects, 115–118
Interfacial energy, 118
Intergranular corrosion, S–227—S–228, *486*
Intergranular fracture, 238, 240, *486*
Intermediate solid solutions, 298, 301, *486*
Intermetallic compounds, 69, 298, 350, S–358, *486*
Interplanar spacing, cubic crystals, S–8
Interstitial diffusion, 129, *486*
Interstitial impurity defects, 108

Interstitials:
  in ceramics, 105
  self-, 104, *491*
Interstitial solid solutions, 108, 109, *486*
Intrinsic conductivity, 379
  temperature variation, 383–386
Intrinsic semiconductors, 377–379, *486*
Invar, S–251, S–253
Invariant point, 294, *486*
Inverse lever rule, 298–290, *487*
Inverse spinel structure, S–273
Ion cores, 23
Ionic bonding, 20–22, *486*
  in ceramics, 38
Ionic character (percent), 23, 38
Ionic conduction, 368, 389–390
Ionic polarization, S–105, S–106, *489*
Ionic radii, 38, 41
Iridium, 421
Iron, *see also* Ferrous alloys; Steels
  atomic radius and crystal structure, 33
  bonding energy and melting temperature, 22
  Curie temperature, S–276
  diffraction pattern, S–10
  electrical conductivity, 374
  ferrite (α), 302–304, *484*
  as ferromagnetic material, S–270, S–271
  magnetic properties, S–281
  polymorphism, 49
  recrystallization temperature, 217
  slip systems, 204
  stress-strain behavior, 166
  thermal properties, S–251
  yield and tensile strengths, ductility, 165
Iron-carbon alloys, *see* Ferrous alloys
Iron-iron carbide alloys, 302–305
Iron-silicon alloys, magnetic properties, S–281
Isobutane, 79
Isobutylene, 93
Isomerism, 78, *486*
  geometrical, S–12—S–13, 91
  stereoisomerism, S–12, 91
Isomorphous systems, 286, *486*
  binary, *see* Binary isomorphous alloys
Isoprene, S–12
Isostatic powder pressing, S–146
Isostrain, in fiber-reinforced composites, S–173
Isostress, in fiber-reinforced composites, S–176
Isotactic configuration, S–12, *486*
Isothermal transformation diagrams, 328–339, *486*
  4340 alloy steel, 337
  0.45 wt% C steel, 360
  0.76 wt% C steel, 336
Isotopes, 10, *486*
Isotropic materials, 63–64, S–179, *486*
Izod impact test, 251–252, *486*

J

Jominy end-quench test, S–127, S–128, *487*
Junction transistors, S–95—S–96, *487*

K

Kaolinite clay, S–1—S–3, S–142
Kevlar, *see* Aramid
Kinetics, 325–326, *487*
  crystallization of polymers, 353–354
  oxidation, S–236—S–237
  phase transformations, 325–326
Knoop hardness, 178, 180
Kovar, S–253
  thermal properties, S–251
  for integrated circuit fabrication, S–354, S–355

L

Lamellae, 95
Laminar composites, S–179, S–195—S–196, *487*
Large-particle composites, S–165—S–169, *487*
Larson-Miller parameter, S–65
Lasers, S–313—S–315, S–316, S–317, *487*
  semiconductor, S–315, S–316, S–317, S–318
  types, characteristics, and applications, S–317
Laser beam welding, S–123—S–124
Lattice parameters, 49, 50, *487*
Lattices, 32, *487*
Lattice strains, 201–202, 208–210, 351, *487*
Lattice waves, S–248—S–249
Layered silicates, S–1—S–3
Lay-up, in prepreg processing, S–191
Lead, 421
  atomic radius and crystal structure, 33
  recrystallization temperature, 217
  superconducting critical temperature, S–290
Leadframe design, S–353—S–354, S–356
Lead-tin phase diagram, 294–296, S–70—S–77
Lead zirconate, S–109
Lead-zirconate-titanate, S–109
Leak-before-break design, 246, S–51
Leathery region, polymers, S–25—S–26
LEDs (light emitting diodes), S–312
Lever rule, 289–290, *487*
Life cycle analysis/assessment, S–373
Light:
  absorption, S–305—S–308
  reflection, S–304—S–305
  refraction, S–303—S–304
  scattering, S–310—S–311
  transmission, S–308
Light-emitting diodes, S–312
Lime, 425, 427
Linear atomic density, S–4—S–5
Linear coefficient of thermal expansion, S–62, S–250—S–253, S–258, *493*
  values for leadframe materials, S–355
  values for selected materials, S–251, 455–458
Linear defects, 111–114
Linear polymers, 89, *487*
Liquid crystal polymers, S–113—S–115, *487*
Liquidus line, 286, 287, 294, 295, *487*
Liquidus temperatures, Ge-Si system, 317
Lodestone (magnetite), S–264, S–273
Longitudinal direction, S–172, *487*
Longitudinal loading, composites, S–173—S–174
Lost-wax casting, S–122

Low-angle grain boundaries, 115–116, 207
Low-carbon steels, 403
Low-cycle fatigue, 259
Lower critical temperature, S–125, *487*
Lower yield point, 160, 161
Low-temperature reusable surface insulation (LRSI), S–347, S–348, S–350
Luminescence, S–311—S–312, *487*

M

Macromolecules, 79, *487*
Magnesia, *see* Magnesium oxide
Magnesium:
  elastic and shear moduli, 154
  Poisson's ratio, 154
  slip systems, 204
Magnesium alloys, 418, 419
Magnesium fluoride, optical properties, S–305
Magnesium-lead phase diagram, 300
Magnesium oxide:
  bonding energy and melting temperature, 22
  flexural strength, 165
  index of refraction, S–304
  modulus of elasticity, 154
  thermal properties, S–251
Magnesium oxide-aluminum oxide phase diagram, S–78
Magnetic ceramics, S–273—S–275
Magnetic dipoles, S–264—S–265
Magnetic domains, *see* Domains
Magnetic energy product, S–282
Magnetic field strength, S–265, S–267, *487*
Magnetic field vectors, S–265—S–267
Magnetic flux density, S–265, S–267, *487*
  critical values for superconductors, S–290
Magnetic hysteresis, S–277—S–279
  soft and hard magnetic materials, S–280—S–282
Magnetic induction, *see* Magnetic flux density
Magnetic materials:
  hard, S–282—S–284
  neodymium-iron-boron alloys, S–284
  samarium-cobalt alloys, S–283—S–284
  soft, S–280—S–281
Magnetic moments, S–267—S–268
  cations, S–274
Magnetic permeability, S–266, S–267, S–299, S–303
Magnetic storage, S–284—S–286
Magnetic susceptibility, S–267, *487*
  selected diamagnetic and paramagnetic materials, S–270
  various units for, S–267, S–293
Magnetic units, conversion factors, S–267
Magnetism:
  basic concepts, S–264—S–268
  electron spin and, S–268
Magnetite (lodestone), S–264, S–273
Magnetization, S–266—S–267, *487*
  saturation, S–271, S–275, *491*
Majority charge carriers, 381
Malleability, *see* Ductility
Malleable cast iron, 411, 414, *487*
  compositions, mechanical properties, and applications, 412
Manganese oxide, as antiferromagnetic material, S–272
Manufacturing techniques, economics, S–370
Martensite, 334–337, S–85, 347, *487*
  alloying to favor formation of, S–86, S–88
  crystal structure, 335
  hardness, 342–343
  hardness *vs.* carbon content, 343
  tempering of, 344–345
Martensitic stainless steels, 407–408
Materials:
  advanced, 6
  classification of, 5–6
  costs, S–193, S–331, 469–474
  current and future needs, 6–7
  disposal of, S–372—S–373
  economic considerations, S–370
  engineered, S–371
  historical development of, 2
  nonrenewable sources of, 7, S–372
  total cycle, S–371—S–372
Materials engineering, 2–4, 149, S–325
Materials science, 2–3
Materials selection, S–325
  case studies:
    artificial hip replacement, S–339—S–345
    integrated circuit packaging, S–351—S–361
    Space Shuttle thermal protection, S–345—S–351
    valve spring design, S–332—S–339
    torsionally stressed cylindrical shaft, S–325—S–332
Materials selection charts, S–327, S–328—S–329
Matrix phase, *487*
  definition, S–164
  fiber-reinforced composites, S–180—S–181
Matthiessen's rule, 374, *487*
Mean stress, 256, 263
Mechanical properties, *see also* specific mechanical properties
  grain size and, 219
  variability, 183, S–28—S–30
Mechanical twin, 117, S–35. *See also* Twinning
Mechanics of materials, 153
Medium carbon steels, 405
Meissner effect, S–289
Melamine-formaldehyde, mer structure, 475
Melting (polymers), 354
Melting point (temperature), S–138
  and bonding energy for selected materials, 22
  factors that affect (polymers), S–87, S–89—S–90
  glasses, *487*
  polymers, 354–355, 356, 479
Melt spinning, S–155
Mercury:
  bonding energy and melting temperature, 22
  superconducting critical temperature, S–290
Mer units, 79, *487*
  bifunctional and trifunctional, 82
  table of, 83–84, 475–478
Metal alloys, *see* Alloys
Metallic bonding, 23–24, *487*
Metallic glasses, 394, S–367
Metallographic examination, S–17

Metal-matrix composites, S–185—S–186, *487*
Metals, *see also* Alloys; Crystalline materials
  corrosion, *see* Corrosion
  costs, 469–471
  crystal structure, *see* Crystal structures
  defined, 5, *487*
  density values, 441–443
  elastic modulus values, 154, 444–446
  as electrical conductors, 367
  electrical resistivity values, 464–466
  electron band structure, 370
  fabrication, S–119—S–124
  fracture toughness for selected, 244, S–49, 454
  linear coefficient of thermal expansion values, S–251, 455–456
  optical properties, S–302—S–303
  oxidation, S–234—S–237
  Poisson's ratio for selected, 154, 448
  shear moduli, 154
  specific heat values, S–251, 462–463
  strengthening, *see* Strengthening of metals
  thermal conductivity values, S–251, 459–460
Metastability, *487*
  of microstructures, 327
Metastable states, 285
Methane, 22, 78
Methyl alcohol, 80
Methyl group, 81
Mica, S–2
  dielectric constant and dielectric strength, S–101
Micelles, 95
Microconstituents, *see also* specific microconstituent phases:
  definition, S–74, *487*
  in eutectic alloys, S–74—S–77
  in steel alloys, 306–311
Microcracks, 239, 241, S–39—S–40
  in ceramics, 248–249
Microelectronics, S–97—S–99
  materials selection for, S–351—S–361
Microhardness tests, 180
Micron, 119
Microscopy, 118–119, S–17—S–21, *487*
Microstructure, 119, *487*
  austenite, 304
  bainite, 333
  bonded ceramic abrasive, 426
  brass during recrystallization and grain growth, 214–215
  carbon-black-reinforced rubber, S–167
  cast irons, 411, 413
  cemented carbide, S–167
  coarse and fine pearlite, 331
  craze in polyphenylene oxide, 251
  development in eutectic alloys, S–70—S–77
  development in iron-carbon alloys, 305–312
  development in isomorphous alloys:
    equilibrium cooling, S–67, S–68
    nonequilibrium cooling, S–67—S–70
  eutectic (lead-tin), S–73
  ferrite (α), 304
  glass-ceramic, 401
  gray cast iron, 411
  hypereutectoid steel alloy, 311
  hypoeutectoid steel alloy, 281, 309
  influence of cooling rate, S–129
  integrated circuit, 365, S–98
  magnetic storage disk, S–286, S–287
  martensite, 336
  metastable, 285
  microscopic examination, 118–119, S–17—S–21
  pearlite, 307, 331
  pearlite partially transformed to spheroidite, 335
  polycrystalline metal before and after deformation, 205
  porcelain, S–146
  precipitation-hardened aluminum alloy, 323
  silica fibers, Space Shuttle tile, S–349
  single-phase iron-chromium alloy, S–19
  sintered ceramic, S–148
  spheroidite, 334
  spherulite (natural rubber), 76
  stress corrosion in brass, S–230
  tempered martensite, 344
Microvoids, S–39, 250
Miller-Bravais index system, 53–54
Miller indices, 54–57, *488*
Minority charge carriers, 381
Mixed dislocations, 112, 114, 199, *488*. *See also* Dislocations
Mobility, of charge carriers, 372–373, *488*
  ionic, 390
  values for selected semiconductors, 377
Modulus of elasticity, 153–156, *488*
  anisotropy, 64, 188
  artificial hip alloys, S–344
  atomic bonding and, 155–156, 189
  copper reinforced with tungsten, S–166
  dependence of cohesive strength on, S–38
  directionality dependence for cubic crystals, 188–189
  influence of porosity on, in ceramics, S–22, S–23
  relation to shear modulus, 158
  selected ceramics, 154, 446
  selected fiber-reinforcement materials, S–181, 447
  selected metals, 154, 444–446
  selected polymers, 154, 446–447
  temperature dependence, 156
  and thermal fatigue, S–62
  and thermal stresses, S–257, S–258
  values for various materials, 444–447
Modulus of resilience, 166
Modulus of rupture, 172. *See also* Flexural strength
Mohs hardness scale, 176, 181
Molarity, S–208, *488*
Molding, plastics, S–153—S–155, *488*
Mole, 11, *488*
Molecular chemistry, polymers, 80–82, *488*
Molecular configurations, polymers, S–11—S–13
Molecular mass, 82

Molecular materials, 26–27
Molecular shape, polymers, 87–88
Molecular structure, polymers, 88–90, *488*
Molecular weight, *488*
  influence on polymer melting/glass transition temperatures, S–89—S–90
  influence on mechanical behavior, polymers, 224, S–36, S–37
  number-average, 84, 86–87
  weight-average, 84, 86–87
Molecular weight distribution, 84–85
Molecules:
  definition, 26, *488*
  polar, 25–26, *489*
Molybdenum, 419
  atomic radius and crystal structure, 33
  density, 442
  modulus of elasticity, 445
  Poisson’s ratio, 448
  properties as wire, S–181
  slip systems, 204
  thermal properties, 456, 460, 463
  yield strength, tensile strength, ductility, 165, 451
Moment of inertia, 172, 193, S–193, S–326
Monel, 421
Monoclinic crystal system, 49, 50
Monomers, 79, *488*
MOSFET transistors, S–95, S–96—S–97, *488*
Mullite, S–80, S–111
  flexural strength, 165
  modulus of elasticity, 154
  Poisson’s ratio, 154
Multiphase transformations, *see* Phase transformations
Muntz metal, 415
Muscovite (mica), S–2

N

Natural aging, 351, *488*
Natural rubber (polyisoprene), S–12—S–13, 431
  degradation resistance, S–239
  melting and glass transition temperatures, 479
  stress-strain behavior, 226
  thermal properties, S–251
NBR, *see* Nitrile rubber (NBR)
Necking, 161
  complex stress state in, 168
  criterion for, 193
  in ductile fracture, 236–237
  polymers, 176
Néel temperature, S–276
Neodymium-aluminum phase diagram, 319
Neodymium-iron-boron magnets, S–284
Neoprene rubber, 431, S–239
Nernst equation, S–211
Network formers (glass), 65
Network modifiers (glass), 66
Network polymers, 89, 90, *488*
Network solids, S–4
Neutrons, 10
Nichrome, 376
Nickel, 421
  atomic radius and crystal structure, 33
  Curie temperature, S–276
  elastic and shear moduli, 154
  as ferromagnetic material, S–270, S–271—S–272
  Poisson’s ratio, 154
  recrystallization temperature, 217
  slip systems, 204
  thermal properties, S–251
  thoria-dispersed (TD), S–169
  yield and tensile strengths, ductility, 165
Nickel ferrite, S–274
Niobium, 419
Niobium alloys, as superconductors, S–289, S–290
Nitrile rubber (NBR), 92, 93
  characteristics and applications, 431, 432
  degradation resistance, S–239
Noble metals, 421
Nodular iron, *see* Ductile iron
Noncrystalline materials, 31, 64–65, *488*
Nondestructive testing, 245, S–49—S–50
Nonequilibrium cooling, 312–313
Nonequilibrium solidification, S–67—S–70
Nonferrous alloys, 414–422, *488*. *See also* specific nonferrous alloys
Nonsteady-state diffusion, 132–135, *488*
Nonstoichiometry, 106
Normalizing, S–87, S–125—S–126, *488*
Notches, effect of, 241, S–40
Notch toughness, 167, 251
n-p-n Junction transistors, S–95—S–96
n-Type semiconductors, 380–381, *488*
Nucleation, 325, *488*
Number-average molecular weight, 84–86
Nylon, fatigue behavior, 260
Nylon 6,6: 83
  degradation resistance, S–239
  density, 101, 443
  dielectric constant and dielectric strength, S–101
  electrical conductivity, 389
  mechanical properties, 154, 165
  melting and glass transition temperatures, 356, 479
  thermal properties, S–251
Nylons, trade names, characteristics, and applications, 429

O

Octahedral position, 60–61, S–273—S–274, *488*
Ohm’s law, 366, 367, *488*
Oil, as quenching medium, S–132—S–133
Opacity, S–300, *488*
  in insulators, S–310—S–311
  in semiconductors, S–306—S–307
Optical fibers, S–318—S–320
Optical flint glass, composition and properties, 423, S–304
Optical microscopy, S–17, S–18, S–19
Optical properties, S–298
  of metals, S–302—S–303
  of nonmetals, S–303—S–311
Ordered solid solution, 298, 415
Orientation polarization, S–105—S–106, *489*
Orthorhombic crystal system, 49, 50
Osmium, 421
Overaging, 349, *488*
Overvoltage, S–214, S–215—S–218
Oxidation, S–206—S–207, *488*
  kinetics, S–236—S–237
  metals, S–234—S–237

Ozone, degradation of polymers, S–240

P

Palladium, 131, 421
Paraffins, 78
Paramagnetism, S–270, *488*
Parisons, S–139, S–155
Particle-reinforced composites, S–165—S–170, *488*
Particulate magnetic recording media, S–285
Pascal-seconds, 220
Passivity, S–221—S–222, *488*
Pauli exclusion principle, 15, *488*
Pearlite, 306, *488*
  coarse, 331, *482*
  colonies, 306
  as composite, S–163
  fine, 331, 341, *485*
  formation, 306–307, 328–331, S–85, S–87, 347
  hardness *vs.* transformation temperature, 343
  mechanical properties, 340, 341, 342, 343
Pentane, 78
Performance (materials), 3
Performance index, S–327—S–331
Periclase, 424, S–110, *see* Magnesium oxide
Periodic table, 17–18, *488*
Peritectic reaction, 298, *488*
Permalloy (45), magnetic properties, S–281
Permanent dipoles, 25–26, S–106
Permeability, S–266, S–267, S–299, S–303, *488*
Permittivity, 21, S–100, S–299, S–303, *488*
Perovskite structure, 43–44, S–108, S–289
PET, *see* Polyester(s)
Phase boundaries, 117
Phase diagrams, 285–291, *489*
  binary eutectic systems, 292–297, S–70—S–77
  binary isomorphous systems, 286–287, 292, S–67—S–70
  ceramic systems, S–77—S–81
  congruent phase transformations, 301
  definitions/basic concepts, 282–285
  eutectoid and peritectic reactions, 298, 300–301
  intermediate phases in, 297–298
  interpretation, 288–291
  specific:
    aluminum-copper, 350
    aluminum-neodymium, 319
    aluminum oxide-chromium oxide, S–78
    cast iron, 413
    copper-beryllium, 363
    copper-nickel, 287
    copper-silver, 293, S–82
    copper-zinc, 299, 300
    iron-carbide (graphite), 409
    iron-iron carbide, 303
    lead-tin, 295, S–70—S–77
    magnesium-lead, 300
    magnesium oxide-aluminum oxide, S–78
    nickel-titanium, 302
    silica-alumina, S–80
    sugar-water, 283
    titanium-copper, 319
    water (pressure-temperature), 316
    water-sodium chloride, 315
    zirconia-calcia, S–79—S–80
  ternary, 301
Phase equilibria, 284–285, *489*
Phases, 283–284, *489*
Phase transformation diagrams:
  continuous cooling, S–85—S–87, 361, *482*
  isothermal, 328–339, 360, *486*
Phase transformation rate, 325–326
  martensitic transformation, 335–336
  temperature dependence, 326
Phase transformations, *489*
  athermal, 337
  classification, 325
  multiphase, 327
Phenol, 80
Phenol-formaldehyde (Bakelite):
  dielectric constant and dielectric strength, S–101
  electrical conductivity, 389
  mechanical properties, 154, 165
  mer structure, 83, 475
  thermal properties, S–251
Phenolics, trade names, characteristics, applications, 430
Phenyl group, 80
Phonons, S–249, S–254, S–255, *489*
Phosphorescence, S–312, *489*
Photoconductivity, S–312, *489*
Photoelasticity, S–297
Photomicrographs, 119, *489*
Photonic signal, S–315
Photons, S–249, S–300, *489*
Pickling, of steels, S–231
Piezoelectricity, S–109, *489*
Piezoelectric materials, S–109
Pilling-Bedworth ratio, S–235—S–236, *489*
  selected metals, S–236
Pitting corrosion, S–226—S–227, S–342, *489*
Plain carbon steels, 338, 403, *489*
Planar atomic density, S–4—S–6
Planck's constant, S–301, *489*
Planes, *see* Crystallographic planes
Plane strain, 243, S–44, *489*
Plane strain fracture toughness, 243, S–46, S–48, *489*
  ceramic-matrix composites, S–188
  selected materials, 244, S–49, 454–455
Plane stress, S–44
Plaster of paris, S–122, S–143, 425
Plastic deformation, 160–166, *489*
  ceramics, 220–221
  dislocation motion and, 199–206, S–31—S–34
  in fracture, S–42
  influence on electrical conductivity, 375
  polycrystalline materials, 204–206
  semicrystalline polymers, 221–223
  twinning, S–34—S–35
Plasticizers, S–152, *489*
Plastics, *489*
  characteristics and applications, 428–431
  in composites, S–166
  forming techniques, S–153—S–155
Platinum, 421
  atomic radius and crystal structure, 33
  electrical conductivity, 374
Plexiglas, *see* Polymethyl methacrylate
Plywood, S–195

p-n-p Junction transistors, S–95—S–96
p-n Rectifying junctions, S–93—S–95, *490*
Point defects, 103–111, *489*
Poise, 220
Poisson's ratio, 158–160, *489*
  values for various materials, 154, 448–449
Polarization, S–101—S–103, *489*. *See also* Electronic polarization; Ionic polarization; Orientation polarization
Polarization (corrosion), S–214—S–218, *489*
  corrosion rates from, S–218—S–221
Polar molecules, 25–26, *489*
Polar moment of inertia, S–326
Polyacrylonitrile (PAN):
  mer structure, 93, 475
  carbon fibers, S–183
Polyamide-imide (PAI), mer structure, 475
Polybutadiene, *see* Butadiene
Polybutylene terephthalate (PBT), mer structure, 476
Polycarbonates:
  density, 443
  degradation resistance, S–239
  mechanical properties, 154, 165
  melting and glass transition temperatures, 356, 479
  mer structure, *front cover*, 84, 476
  reinforced *vs.* unreinforced properties, S–179
  trade names, characteristics, applications, 429
Polychloroprene, *see* Chloroprene; Chloroprene rubber
Polychlorotrifluoroethylene, mer structure, 476
Polycrystalline materials, 62, *489*
  plastic deformation, 204–206
Polydimethylsiloxane, 431–432
  degradation resistance, S–239
  mer structure, 432, 476
Polyester(s):
  degradation resistance (PET), S–239
  density (PET), 444
  fatigue behavior (PET), 260
  mechanical properties (PET), 154, 165
  melting and glass transition temperatures (PET), 356, 479
  mer structure (PET), *back cover*, 84, 476
  in polymer-matrix composites, S–185
  recycle code and products (PET), S–375
  trade names, characteristics, applications, 430
Polyetheretherketone (PEEK), S–185
  degradation resistance, S–239
  melting and glass transition temperatures, 479
  mer structure, 476
Polyetherimide (PEI), S–185
Polyethylene, 81, 83
  crystal structure of, 93
  degradation resistance, S–239
  density, 443
  dielectric constant and dielectric strength, S–101
  electrical conductivity, 389
  fatigue behavior, 260
  index of refraction, S–304
  mechanical properties, 154, 165
  melting and glass transition temperatures, 356, 479
  recycle codes and products, S–375
  single crystals, 96
  thermal properties, S–251
  trade names, characteristics, applications, 429
  ultrahigh molecular weight, *see* Ultrahigh molecular weight polyethylene
Polyethylene terephthalate (PET), *see* Polyester(s)
Polyhexamethylene adipamide, *see* Nylon 6,6
Polyimides:
  glass transition temperature, 479
  for integrated circuit fabrication, S–360
  mer structure, 477
  polymer-matrix composites, S–185
Polyisobutylene:
  melting and glass transition temperatures, 479
  mer structure, 93, 477
  relaxation modulus, 195
Polyisoprene, *see* Natural rubber (polyisoprene)
Polymer-matrix composites, S–182—S–185, *489*
Polymerization, 81, S–150—S–151
  degree of, 84
Polymers, 5, 79, *489*. *See also* Plastics
  as additives, 433
  classification, molecular characteristics, 91
  coefficient of thermal expansion values, S–251, 457
  conducting, 390
  costs, 473
  crosslinking, *see* Crosslinking
  crystallinity, 92–95, *482*
  crystallization, 353–354
  crystals, 95–97
  defined, 5, 79
  deformation:
    elastic, 221
    plastic, 221–223
  degradation of, S–237—S–241
  density, 94
  density values, 443–444
  ductility values, 165, 452–453
  elastic modulus values, 154, 446–447
  elastomers, 431–432
  electrical properties, 389, 390, S–101, 466
  fibers, 432–433
  fracture mechanics, 250
  fracture toughness values, 244, S–49, 455
  glass transition, 354
  glass transition temperatures, 356, 479
  as insulators, 389, S–107—S–108
  for integrated circuit fabrication, S–359
  liquid crystal, S–113—S–115
  mechanical properties, 173–175, 181–182
    factors that affect, 223–224, S–35—S–37
    values of, 446–447, 448, 452–453
  melting, 354
  melting temperatures, 356, 479
  miscellaneous applications, 433–434
  molecular chemistry, 80–82

- Polymers (*Continued*)
  - molecular configurations, S–11—S–13
  - molecular shape, 87–88
  - molecular structure, 88–90
  - molecular weight, 82–87
  - natural, 77
  - opacity and translucency, S–311
  - Poisson's ratio values, 154, 448
  - radiation effects, S–240
  - refraction indices, S–304
  - semicrystalline, 94–96, 221–223, 224, S–36
  - specific heat values, S–251, 463–464
  - spherulites in, 76, 95–97, 223
  - stereoisomerism, S–12, 91
  - stress-strain behavior, 173–176
  - swelling and dissolution, S–238
  - tensile strength values, 165, 452–453
  - thermal conductivity values, S–251, 460–461
  - thermal properties, S–253, S–256
  - thermoplastic, *see* Thermoplastic polymers
  - thermosetting, *see* Thermosetting polymers
  - types of, 77
  - viscoelasticity, S–22—S–27
  - weathering, S–241
  - yield strength values, 165, 452–453
- Polymethyl methacrylate:
  - density, 444
  - electrical conductivity, 389
  - fatigue behavior, 260
  - fixation agent for artificial hip, S–345
  - index of refraction, S–304
  - mechanical properties, 447, 453
  - melting and glass transition temperatures, 479
  - mer structure, 83, 477
  - plane strain fracture toughness, 244, S–49, 455
  - stress-strain behavior as function of temperature, 175
  - trade names, characteristics, applications, 429
- Polymorphic transformations, in iron, 302–303
- Polymorphism, 49, *489*
- Polyparaphenylene terephthalamide, *see* Aramid
- Polyphenylene oxide (PPO), mer structure, 477
- Polyphenylene sulfide (PPS), S–185
  - melting and glass transition temperatures, 479
  - mer structure, 477
- Polypropylene, 81–82
  - degradation resistance, S–239
  - density, 444
  - fatigue behavior, 260
  - index of refraction, S–304
  - kinetics of crystallization, 353
  - mechanical properties, 447, 453
  - melting and glass transition temperatures, 356, 479
  - mer structure, 83, 478
  - recycle code and products, S–375
  - thermal properties, S–251
  - trade names, characteristics, applications, 430
- Polystyrene:
  - degradation resistance, S–239
  - density, 444
  - dielectric properties, S–101
  - electrical conductivity, 389
  - fatigue behavior, 260
  - index of refraction, S–304
  - mechanical properties, 447, 448, 453
  - melting and glass transition temperatures, 356, 479
  - mer structure, 83, 478
  - plane strain fracture toughness, 244, S–49, 455
  - thermal properties, S–251
  - trade names, characteristics, applications, 430
  - viscoelastic behavior, S–26—S–27
- Polysulphides, for integrated circuit fabrication, S–360
- Polytetrafluoroethylene, 81
  - degradation resistance, S–239
  - density, 444
  - dielectric constant and dielectric strength, S–101
  - electrical conductivity, 389
  - fatigue behavior, 260
  - index of refraction, S–304
  - mechanical properties, 447, 448, 453
  - melting and glass transition temperatures, 356, 479
  - mer structure, 83, 478
  - thermal properties, S–251
- Polyurethane, for integrated circuit fabrication, S–360
- Polyvinyl acetate, mer structure, 478
- Polyvinyl alcohol, mer structure, 478
- Polyvinyl chloride:
  - density, 444
  - mechanical properties, 447, 448, 453
  - melting and glass transition temperatures, 356, 479
  - mer structure, 83, 478
  - recycle code and products, S–375
- Polyvinyl fluoride:
  - melting and glass transition temperatures, 479
  - mer structure, 478
- Polyvinylidene chloride:
  - melting and glass transition temperatures, 479
  - mer structure, 478
- Polyvinylidene fluoride:
  - glass transition temperature, 479
  - mer structure, 478
- Porcelain, 424
  - dielectric constant and dielectric strength, S–101
  - electrical conductivity, 389
  - microstructure, S–146
- Porosity:
  - formation during sintering, S–147—S–148
  - influence on flexural strength, ceramics, S–22—S–23
  - influence on modulus of elasticity, ceramics, S–22—S–23
  - influence on thermal conductivity, S–255
  - optical translucency and opacity, S–311
  - refractory ceramics, 425
- Portland cement, 426
  - fracture strength distribution, 249
- Portland cement concrete, S–168
- Posttensioned concrete, S–169
- Potassium chloride, 29
- Powder metallurgy, S–122, *489*
- Powder pressing, ceramics, S–145—S–147

Powder x-ray diffraction techniques, S–8—S–9
Precipitation-hardenable stainless steels, 408, 409
Precipitation hardening, 347–352, *489*
  heat treatments, 347–349
  mechanism, 349–351
Prepreg production processes, S–190—S–191, *489*
Pressing:
  glass, S–139
  powder ceramics, S–145—S–146
Prestressed concrete, S–169, *489*
Primary bonds, 20–24, *490*
Primary creep, 266
Primary phase, S–74, *490*
Principal quantum number, 12
Principle of combined action, S–163, *490*
Process annealing, S–124, *490*
Processing, materials, 3
Proeutectoid cementite, 310, 311, *490*
Proeutectoid ferrite, 308, 309, *490*
Propane, 78
Properties, *490*
  categories of, 3
Proportional limit, 161, *490*
Protons, 10
PTFE, *see* Polytetrafluoroethylene
p-Type semiconductors, 381–383, *490*
Pultrusion, S–189—S–190
Purple plague, S–358
Pyrex glass:
  composition, 423
  index of refraction, S–304
  mechanical properties, 446, 448, 452
  thermal properties, S–251
  thermal shock, S–258
Pyroceram:
  composition, 423
  density, 443
  flexural strength, 452
  modulus of elasticity, 446
  Poisson's ratio, 448

Q
Quantum mechanics, 11, *490*
Quantum numbers, 12–14, *490*
  magnetic, 14, S–268
Quartz, 47, S–142
  hardness, 182
  index of refraction, S–304
  as piezoelectric material, S–109
Quenching media, S–132—S–133

R
Radiation effects, polymers, S–240
Random copolymers, 91, 92, *490*
Range of stress, 256
Reaction cured glass, S–350
Recombination, electron-hole, S–94, S–306, S–307
Recovery, 213, *490*
Recrystallization, 213–218, S–124, *490*
  effect on properties, 216
  kinetics for copper, 326
Recrystallization temperature, 215–217, *490*
  dependence on percent cold work, 216
  selected metals and alloys, 217
Rectification, S–93—S–95
Rectifying junctions, S–93—S–94, *490*
Recycling:
  issues in materials science and engineering, S–373—S–376
  of composite materials, S–376
  of glass, S–374
  of metals, S–373—S–374
  of plastics and rubber, S–374—S–376
Recycling codes and products, S–375
Reduction (electrochemical), S–206, *490*
Reduction in area, percent, 164
Reflection, S–304—S–305, *490*
Reflectivity, S–300, S–305
Refraction, S–303—S–304, *490*
  index of, S–303, *486*
Refractories (ceramics), 422, 424–425, S–110—S–111, *490*
  corrosion, S–237
Refractory metals, 419
  creep resistance, 269
Reinforced carbon-carbon composites, S–347, S–348, S–351
Reinforced concrete, S–168—S–169, *490*
Reinforcement efficiency, table of, S–179
Relative permeability, S–266, S–267, *490*
Relative permittivity, *see* Dielectric constant
Relaxation frequency, S–106, *490*
Relaxation modulus, S–24—S–27, *490*
Relaxation time, 194
Remanence (remanent induction), S–279, *490*
Repeated stress cycle, 255, 256
Residual stresses, S–125, *490. See also* Thermal stresses
  glass, S–140
  martensitic steels, 344
Resilience, 166, *490*
Resin, polymer, S–182
Resistance (electrical), 366
Resistivity, *see* Electrical resistivity
Resolved shear stresses, S–31—S–32, *490*
Retained austenite, 335
Reverse bias, S–94, *490*
Reversed stress cycle, 255, 256, S–335
Rhodium, 421
Rhombohedral crystal system, 49, 50
Rochelle salt, S–109
Rock salt structure, 41, 42
Rockwell hardness tests, 147, 177–179
Rolling, of metals, 120, 121, *490*
Rouge, 425
Rovings, S–189
Rubbers, 90, 92, 93
  natural, *see* Natural rubber (polyisoprene)
  synthetic, 92, 93, 431–432
  trade names, characteristics, and applications, 431
Rubbery region, polymers, S–26
Ruby, *see also* Aluminum oxide
  lasers, S–313
  optical characteristics, S–310
Rule of mixtures, *490*
  composites, S–165—S–166, S–174, S–176, S–177, S–178, S–194
  electrical resistivity, 375
Rupture, 266, *490*
Rupture lifetime, 267
  extrapolation of, S–65—S–66
Rust, S–207
Ruthenium, 421

S

Sacrificial anodes, S–233, *490*
Safe stress, 184, *491*
Safety factors, 184, 246, S–51, S–326
Samarium-cobalt magnets, S–283
Sand casting, S–121—S–122
Sandwich panels, S–196, *491*
Sapphire, *see also* Aluminum oxide
  optical transmittance, S–310
Saturated hydrocarbons, 78, *491*
Saturation, extrinsic semiconductors, 386
Saturation magnetization, S–271, S–275, S–278, *491*
  temperature dependence, S–277
SBR, *see* Styrene-butadiene rubber
Scaling, S–234
Scanning electron microscopy, S–20, *491*
Scanning probe microscopy, S–20—S–21, *491*
Schmid factor, 229
Schottky defect, 106, *491*
Scission, S–238, *491*
Scleroscope hardness, 180
Screw dislocations, 112, 113, 199, 200, *491*. *See also* Dislocations
Seawater, as corrosion environment, S–231
Secant modulus, 155
Secondary bonds, 24–26, *491*
Secondary creep, 266
Segregation, S–70
Selection of materials, *see* Materials selection
Selective leaching, S–228, *491*
Self-diffusion, 127, *491*
Self-interstitials, 104, *491*
SEM, *see* Scanning electron microscopy
Semiconductor devices, S–93—S–99
Semiconductor lasers, S–315, S–316, S–317
Semiconductors:
  band structure, 370
  in computers, S–97—S–99
  costs, 472
  defined, 6, 370, *491*
  extrinsic, 379–383, *484*
  fullerenes as, S–4
  intrinsic, 377–379, *486*
  light absorption, S–305—S–308
  n-type, 380–381, *488*
  p-type, 381–383, *490*
  temperature dependence of conductivity, 383–387
    of germanium, 397
Semicrystalline polymers, 94–95
  deformation mechanisms:
    elastic, 221
    plastic, 221–223
Severity of quench, S–132
Shape memory effect, S–367
Shear deformation, 150, 170–171
Shear modulus, 156–157
  performance of torsionally stressed shaft, S–332
  relationship to elastic modulus, 158
  selected metals, 154
  spring design, S–333
Shear strain, 152, *491*
Shear strength, S–326
Shear stress, 152, *491*
  resolved, S–31—S–32
  resolved from tensile stress, 152–153
  springs, S–332—S–333
Shear tests, 152
Shot peening, 264, S–338
Shrinkage, clay products, S–144—S–145
Silica, 47
  crystalline and noncrystalline structures, 65
  fibers, Space Shuttle tiles, S–348—S–349
  fibers for optical communications, S–318—S–320
  fused, *see* Fused silica
  as refractory, S–110
Silica-alumina phase diagram, S–80
Silica glasses, 65–66
  viscosity, S–138
Silicates:
  glasses, 65–66
  layered, S–1—S–3
  tetrahedral structure, 47
  types and structures, 46–47, S–1—S–3, 65–66
Silicon:
  bonding energy and melting temperature, 22
  carrier concentration *vs.* temperature, 385
  conduction in, 378
  conductivity *vs.* temperature, 384
  cost, 472
  electrical characteristics, 377
  linear coefficient of thermal expansion, S–354
  wafer, S–352
Silicon carbide:
  as abrasive, 425
  as advanced ceramic, S–111—S–112
  flexural strength, 165, 452
  hardness, 182
  modulus of elasticity, 154, 446
  oxidation protection, Space Shuttle, S–351
  properties as whiskers and fibers, S–181
  as refractory, S–111
Silicon dioxide, *see* Silica
Silicone rubber, 432
  characteristics and applications, 431
  degradation resistance, S–239
Silicones:
  for integrated circuit fabrication, S–360
  use on Space Shuttle, S–347—S–348, S–350
Silicon nitride:
  as advanced ceramic, S–111
  flexural strength, 165, 452
  modulus of elasticity, 154, 446
  properties as a whisker, S–181
Silicon tetraboride, S–350
Silly putty, S–24
Silver, 421
  atomic radius and crystal structure, 33
  electrical conductivity, 374, 376
  slip systems, 204
  thermal properties, S–251
Simple cubic crystal structure, 68
Single crystals, 62, *491*
  slip in, S–31—S–33
Sintered aluminum powder (SAP), S–170
Sintering, S–147—S–148, *491*
SI units, 439–440
Ski, cross-section, S–162
Slip, 160, 200, *491*
  compared to twinning, S–35

Slip (*Continued*)
  polycrystalline materials, 204–205
  single crystals, S–31—S–33
Slip casting, S–143—S–144, *491*
Slip direction, 203
Slip lines, 204–205
Slip plane, 200, 203
Slip systems, 203–204, *491*
  selected metals, 204
Small-angle grain boundaries, 115–116, 207
Societal considerations, materials science, S–371—S–376
Soda-lime glasses:
  composition, 423
  dielectric properties, S–101
  electrical conductivity, 389
  thermal properties, S–251
  thermal shock, S–258
  viscosity, S–138
Sodium chloride:
  bonding energy and melting temperature, 22
  ionic bonding, 21
  structure, 41, 42
Sodium-silicate glass, 65
Softening point, S–139, *491*
Soft magnetic materials, S–280—S–281, *491*
  properties, S–281
Soils, as corrosion environments, S–231—S–232
Solder bumps, S–361
Soldering, S–123, *491*
  integrated circuit packaging, S–354, S–361
Solid-solution strengthening, 208–210, 292, 343, *491*
Solid solutions, 107–109, *491*
  in ceramics, 109–110
  intermediate, 298, *486*
  interstitial, 108–109, *486*
  ordered, 298, 415
  terminal, 297, *493*
Solidus line, 286, 287, 293, *491*
Solubility limit, 283, *491*
  factors that influence for solid phase, 108
Solutes, *491*
  defined, 107
Solution heat treatment, 348, *491*
Solvents, *492*
  defined, 107
Solvus line, 293, *492*
Space Shuttle Orbiter, S–324, S–345
Space Shuttle thermal protection, S–247
  materials selection, S–345—S–351
Specific heat, S–248, *492*
  values for selected materials, S–251, 462–464
Specific modulus, 418, S–170, *492*
  selected fiber-reinforcement materials, S–181
Specific strength, 416, 418, S–170, *492*
  selected fiber-reinforcement materials, S–181
Sphalerite structure, 42, 44
Spheroidite, 334, *492*
  hardness and ductility, 342
Spheroidization, S–126, *492*
Spherulites, in polymers, 76, 95–96, *492*
  alteration during deformation, 223
  photomicrograph of polyethylene, 97
  transmission electron micrograph, 76
Spinel, 61, S–77
  flexural strength, 165
  index of refraction, S–304
  modulus of elasticity, 154
  structure, 61
  thermal properties, S–251
Spin magnetic moment, 14, S–268
Spinnerettes, S–155
Spinning, polymer fibers, S–155, *492*
Spring design, materials selection, S–332—S–339
Stabilized zirconia, S–80, S–187
Stabilizers, S–152, *492*
Stacking faults, 117
Stainless steels, 407–408, *492*. *See also* Ferrous alloys; specific steels
  for artificial hips, S–343—S–344
  compositions, properties, and applications for selected, 408
  creep resistance, 269
  electrical conductivity, 374
  passivity, S–221
  thermal properties, S–251
  weld decay, S–227—S–228
Standard deviation, 183, S–28—S–29
Standard emf series, S–209—S–210
Standard half-cells, S–209, *492*
Static fatigue, S–53
Steady-state creep rate, 266
Steatite, dielectric properties, S–101
Steels, 305. *See also* Alloy steels; Stainless steels
  AISI/SAE designation scheme, 405–406
  classification, 338, 402–403
  costs, 469–470
  elastic and shear moduli, 154
  electrical conductivity, 374
  fatigue behavior (1045), 276
  heat treatments, S–125—S–133
  impact energy, 255
  magnetic properties, S–283
  overview of types, 402–407
  plane strain fracture toughness, 244, S–49, 454
  Poisson's ratio, 154
  properties as wires (fiber reinforcement), S–181
  for springs, S–337, S–366
  thermal properties, S–251
  yield and tensile strengths, ductility (1020), 165
Step reaction polymerization, S–151, *482*
Stereoisomerism, *492*
  polymers, S–12
Sterling silver, 107, 421
Stiffness, *see* Modulus of elasticity
Stoichiometry, 106, *492*
Strain, 151. *See also* Stress-strain behavior
  engineering, 149, *492*
  lattice, 201, 208–210, 351, *487*
  shear, 152, *491*
  true, 168, *493*
Strain energy release rate, S–42
Strain hardening, 171, 210–212, S–120, *482*, *492*
  corrosion and, S–223
  influence on electrical resistivity, 375
  influence on mechanical properties, 211, 212
  recrystallization after, 213–216
Strain-hardening exponent, 169, 212

- Strain-hardening exponent (*Continued*)
  - determination of, 193
  - selected metal alloys, 169
- Strain isolator pads, S–350
- Strain point (glass), S–139, *492*
- Strength, 161
  - flexural, 171–172, *485*
  - fracture, 162
  - shear, S–326
  - for a torsionally stressed shaft, S–326—S–331
- Strengthening of metals:
  - grain size reduction, 206–208
  - mechanism, 206
  - solid-solution strengthening, 208–210
  - strain hardening, *see* Strain hardening
- Stress, *see also* Stress-strain behavior
  - critical, 242, S–42
  - effect on creep, 267–268, S–63—S–64
  - engineering, 149, *492*
  - mean (fatigue), 256, 263
  - normal (resolved from pure tensile), 152–153
  - range (fatigue), 256
  - residual, *see* Residual stresses
  - safe, 184, *491*
  - shear, 152, 153, S–31, *491*
  - shear (resolved from pure tensile), 152–153
  - thermal, *see* Thermal stresses
  - true, 167–168, *493*
  - working, 184
- Stress amplitude, 256–257, S–338
- Stress analysis of cracks, S–43—S–45
- Stress concentration, 239–241, S–38—S–41, 251, 263, *492*
  - polymers, 249
- Stress concentration factor, 241, S–40, S–41
- Stress corrosion cracking, S–204, S–229—S–230, S–342, *492*
  - in ceramics, S–53
- Stress intensity factor, S–44, S–45, S–48, *492*
  - and fatigue crack propagation rate, S–58—S–59
- Stress raisers, 241, S–40, 263, *492*
  - in ceramics, 248, S–22
- Stress ratio, 257
- Stress relaxation measurements, S–24
- Stress relief annealing, S–125, *492*
- Stress state, geometric considerations, 152–153
- Stress-strain behavior:
  - ceramics, 173
  - composite, fibrous (longitudinal), S–173
  - elastic deformation, 153–157
  - natural rubber, vulcanized and unvulcanized, 226
  - nonlinear, 155
  - plain carbon steel, 188
  - plastic deformation, 160–166
  - polymers, 173–176
  - true, 168
- Striations (fatigue), 261–262, S–55—S–56
- Structural clay products, 422, 424, S–142, *492*
- Structural composites, S–195—S–196, *492*
- Structure, 3
  - atomic, 10–16
  - definition, *492*
- Structures, crystal, *see* Crystal structures
- Styrene, 93
- Styrene-butadiene rubber (SBR), 92, 93
  - characteristics and applications, 431–432
  - degradation resistance, S–239
- Styrenic block copolymers, S–115—S–116
- Styrofoam, S–256
- Substitutional impurity defects, 108
- Substitutional solid solutions, 108, 109, *492*
- Superalloys, 421
  - creep resistance, 269
  - fiber reinforcement, S–185—S–186
- Superconductivity, S–287—S–291, *492*
  - applications, S–290—S–291
- Superconductors, S–287
  - critical properties, S–290
  - high-temperature, S–289—S–290
  - types I and II, S–289
- Supercooling, 327, *492*
- Superficial Rockwell hardness tests, 177, 179
- Superheating, 327, *492*
- Super Invar, S–251, S–253
- Supermalloy, magnetic properties, S–281
- Surface energy, 115
- Susceptibility, magnetic, S–267
- Symbols, list, xix–xxi
- Syndiotactic configuration, S–12, *492*
- Synthetic rubbers, 92–93, 431–432, S–239
- Systems:
  - definition, 282, *492*
  - homogeneous *vs.* heterogeneous, 284

T

- Talc, S–2
- Tangent modulus, 155
- Tantalum, 419, 421
- Tape automated bonding, S–360—S–361
- Tape casting, S–149
- Tarnishing, S–234
- Tear strength, polymers, 181–182
- Teflon, *see* Polytetrafluoroethylene
- TEM, 30, 115, S–19—S–20, *493*
- Temperature gradient, S–253
  - thermal stresses, S–257
- Temper designation, 416, *492*
- Tempered martensite, 344–345, *492*
  - hardness *vs.* carbon content, 343
  - mechanical properties *vs.* tempering temperature, 345–346
- Temper embrittlement, 345–346
- Tempering:
  - glass, 249, S–141, S–160
  - steels, 344–346
- Tensile strength, 161–163, *493*
  - artificial hip materials, S–342, S–344
  - correlation with hardness, 180, 182
  - fibrous composites, S–177
  - fine pearlite, 341
  - influence of recrystallization on, 216
  - precipitation hardened aluminum alloy, 352
  - selected fiber-reinforcement materials, S–181
  - tempered martensite, 345
  - values for various materials, 165, 449–453
  - wire, as a function of diameter, S–337
- Tensile test apparatus, 149, 151
- Tensile tests, 149–151. *See also* Stress-strain behavior

Terminal solid solutions, 297, *493*
Ternary phase diagrams, 301
Tertiary creep, 266
Tetragonal crystal system, 49, 50
Tetrahedral position, 60–61, S–273—S–274, *493*
Textile fibers, 432–433
Thermal conduction, S–249, S–254
Thermal conductivity, S–253—S–256, *493*
  influence of impurities, S–255
  of leadframe materials, S–355
  selected materials, S–251, 459–461
Thermal diffusivity, S–261
Thermal expansion, S–250—S–253
  linear coefficient of, S–62, S–250, S–256—S–258, *493*
  relation to bonding, S–252
  selected materials, S–251, S–355, 455–458
  volume coefficient of, S–251
Thermal fatigue, S–62, *493*
Thermal insulation, for Space Shuttle thermal protection system, S–345—S–351
Thermally activated processes, 327, *493*
Thermal properties, S–248. *See also* specific thermal properties
  selected materials, S–251, 455–464
Thermal protection system (Space Shuttle), S–247
  materials selection for, S–345—S–351
Thermal shock, S–140—S–141, S–253, *493*
  brittle materials, S–257—S–258
  maximum temperature change without, S–262
Thermal shock resistance, S–258
Thermal stresses, S–62, S–256, *493*
  glass, S–140
Thermal tempering (glass), S–141, *493*
Thermoplastic elastomers, S–115—S–117, *493*
Thermoplastic polymers, 90, *493*
  characteristics and applications, 429–430
  degradation resistance, S–239
  forming techniques, S–153—S–155
Thermosetting polymers, 90–91, *493*
  characteristics and applications, 430
  degradation resistance, S–239
  forming techniques, S–153—S–155
Thin film magnetic recording media, S–284—S–287
Thoria-dispersed (TD) nickel, S–169
Tie lines, 288, *493*
Tilt boundaries, 115–116
Time-temperature-transformation diagrams, *see* Isothermal transformation diagrams
Tin, 421
  recrystallization temperature, 217
  superconducting critical temperature, S–290
Tin cans, S–245
Titanium:
  atomic radius and crystal structure, 33
  elastic and shear moduli, 154
  Poisson's ratio, 154
  slip systems, 204
  superconducting critical temperature, S–290
  yield and tensile strengths, ductility, 165
Titanium alloys, 418–419, 420
  for artificial hips, S–343—S–344
  plane strain fracture toughness, 244, S–49, 454
  properties and applications of, 420
Titanium-copper phase diagram, 319
Titanium diboride, S–112
Tool steels, 405, 407
Torque, 149–150, S–326
Torsion, 152
Torsional deformation, 150
Torsional tests, 170
Torsionally stressed shaft, case study, S–325—S–332
Toughness, 167, *493*
Tows, S–189
Trade names:
  selected elastomers, 431
  selected plastics, 429–430
trans, S–13, *493*
Transdermal patch, S–367
Transducers, S–109
Transfer molding, plastics, S–153—S–154
Transformation rate, *493*
Transformation toughening, S–187
Transgranular fracture, 238, 240, *493*
Transient creep, 266
Transistors, S–95—S–99
Transition metals, 17
Transition temperature, ductile-brittle, *see* Ductile-to-brittle transition
Translucency, S–300, *493*
  insulators, S–310—S–311
Transmission, S–308
Transmission electron microscopy, 30, 115, S–19—S–20, *493*
Transmissivity, S–300
Transparency, S–300, *493*
Transverse bending test, 171–172
  equation for maximum deflection, 193
Transverse direction, S–172, S–176, *493*
Transverse loading, composites, S–176, S–177
Triclinic crystal system, 49, 50
  anisotropy in, 63
Tridymite, 47
Trifunctional mers, 82, *493*
True stress/strain, 167–168, *493*
T-T-T diagrams, *see* Isothermal transformation diagrams
Tungsten, 419
  atomic radius and crystal structure, 33
  bonding energy and melting temperature, 22
  elastic and shear moduli, 154
  Poisson's ratio, 154
  properties as wire, S–181
  recrystallization temperature, 217
  slip systems, 204
  superconducting critical temperature, S–290
  thermal properties, S–251
Tungsten carbide:
  as abrasive, 425
  hardness, 182
Turbine blades, 269
Twin boundaries, 117
Twinning, S–34—S–35
  compared to slip, S–35

Twins, 117
Twisting moment, S–326

U

UHMWPE (Ultrahigh molecular weight polyethylene), S–113, *493*
  for artificial hips, S–344
  properties as a fiber, S–181
Uniaxial powder pressing, S–146, S–147
Unidirectional solidification, 269
Uniform corrosion, S–223—S–224
Unit cells, 32, *493*. *See also* Crystal structures
  crystal systems, 49, 50
Units:
  electrical and dielectric parameters, S–104
  magnetic parameters, S–267
  SI, 439–440
Unsaturated hydrocarbons, 78, *494*
UNS designation scheme, 405, 406
Upper critical temperature, S–125, *494*
Upper yield point, 160, 161

V

Vacancies, 103–104, *494*
  in ceramics, 105
  diffusion, 129, *494*
  equilibrium number, 104
Valence band, 370, *494*
Valence electrons, 15, *494*
Valve spring design, S–332—S–339
van der Waals bonding, 24–26, *494*
  in clays, S–1
  hydrocarbons, 78
  in polymers, 89, 221, 223, S–36
Vibrational heat capacity, S–248—S–249
Vibrations, atomic, 118, S–248—S–249
Vickers hardness tests, 178, 180
Video cassette recorders, 284, S–367
Vinyl esters, polymer-matrix composites, S–185
Vinyls, 430
Viscoelastic creep, S–27
Viscoelasticity, 157, S–22—S–28, *494*
Viscoelastic relaxation modulus, S–24—S–27, *490*
Viscosity, 220–221, S–159, *494*
  temperature dependence for glasses, S–138—S–139
Viscous flow:
  in ceramics, 220
  in polymers, S–26
Visible spectrum, S–299
Vision (glass ceramic), 423
Vitreous silica, *see* Fused silica
Vitrification, S–145, *494*
Volume defects, 118
Volume expansion coefficient, S–251—S–252
Volume fraction (phase), 291
Vulcanization, 90, 226, *494*
Vycor, 423

W

Water:
  as corrosion environment, S–231
  bonding energy and melting temperature, 22
  hydrogen bonding in, 26
  phase diagram, 316
  as quenching medium, S–132—S–133
Wave-mechanical atomic model, 12, *494*
Weathering, of polymers, S–241
Weight-average molecular weight, 84
Weight percent, 110–111, S–14—S–17, *494*
Weld decay, S–227—S–228, *494*
Welding, S–123—S–124, *494*
Whiskers, 242, S–41, S–180, S–181, *494*
White cast iron, 410, 411, 413, *494*
Whitewares, 424, *494*
Wiedemann-Franz constant, S–254, S–260
  values of, for metals, S–251
Wiedemann-Franz law, S–254
Wire bonding, S–353, S–356, S–358
Wires, S–180, S–181
Wood:
  as composite, S–163
  cost, 474
  density, 444
  electrical resistivity, 467
  modulus of elasticity, 447
  specific heat, 464
  tensile strength, 453
  thermal conductivity, 461
  thermal expansion coefficient, 458
Work hardening, *see* Strain hardening
Working point (glass), S–138, *494*
Working range, S–138
Working stress, 184
Wrought alloys, 414, *494*
Wüstite, 106, 397, 399

X

X-ray diffraction, S–6—S–10
X-rays, 298, 299

Y

Yielding, 161, *494*
Yield point phenomenon, 160, 161
Yield strength, 160, 161, 174, *494*
  artificial hip materials, S–342, S–344
  dependence on grain size (brass), 208
  fine pearlite, 341
  in shear, spring design, S–333
  tempered martensite, 345
  values for various materials, 165, 449–453
Young's modulus, *see* Modulus of elasticity
Yttrium barium copper oxide, S–289, S–290
Yttrium iron garnet (YIG), S–275, S–294

Z

Zinc:
  atomic radius and crystal structure, 33
  recrystallization, 217
  slip systems, 204
Zinc alloys, 421–422
Zinc blende structure, 42, 43
Zinc telluride, electrical characteristics, 377
Zirconia, S–111
  flexural strength, 165
  modulus of elasticity, 154
  stabilized, S–80
  transformation toughening, S–187
Zirconia-calcia phase diagram, S–79
Zirconium:
  alloys, 422
  slip systems, 204